OHBM 2024
JUNE 23~27, SEOUL, KOREA

ABSTRACTS

Sunday, June 23 – Thursday, June 27
COEX CONVENTION & EXHIBITION CENTER | SEOUL

30TH ANNUAL MEETING OF THE
ORGANIZATION FOR HUMAN BRAIN MAPPING

Poster No 451

Association of amygdala volume and autistic traits in monozygotic twins: Controlling for confounds

Neda Sadeghi[1], Tonya White[1]

[1]*National Institute of Mental Health, Bethesda, MD*

Introduction: Autism is a complex neurodevelopmental disorder that is characterized by difficulties in social interaction and a pattern of restrictive and repetitive behaviors. There has been an increasing interest in studying the role of the amygdala in autism, especially given that it is a component structure of the "social brain" (Brothers, L. 1990; Baron-Cohen, S., et al., 2000; Zalla, T. et al., 2013; Sharp, T.H., et al., 2023). However, findings related to the amygdala have been mixed. This could be due to many reasons such as differences related to confounding factors, i.e., age, sex, race, etc. In addition, studies that utilize neuroimaging suffer from scanner induced variability. To control for these potential biases, we used monozygotic (MZ) twin data from Adolescent Brain Cognitive Development (ABCD) study (Iacono, W.G., et al., 2018) to assess the relationship between autistic traits (scores on Social Responsiveness Scale (SRS); Constantino, J.N. et al., 2003) and amygdala volume. Using MZ twin data provides a unique opportunity to control for many confounds.

Methods: We analyzed data from 372 pairs of MZ twins (Male: 191, Female: 181; age 9-10 years). Autistic traits were measured using the SRS short form. This measure assesses the severity of social difficulties across the spectrum of autistic symptoms, including children with ASD, subclinical symptoms, and typically developing (Constantino, J.N. et al., 2003). Higher SRS scores indicate greater autistic symptoms. For each twin pair, difference between SRS scores was calculated. Neuroimaging data were collected, processed, and quality checked by ABCD Data Analysis, Informatics & Resource Center (DAIRC). T1-weighted images were collected on 3-Tesla scanners (Casey, B.J., et al., 2018). FreeSurfer was used to extract subcortical and cortical regions of interests. We used the available volumetric measures for amygdala. The difference between volumetric measures of left and right amygdala within each twin pair was calculated and normalized by their average score to create a relative difference in volume between twins. Linear regression was performed to assess the relationship between differences in SRS scores in relation to differences in amygdala volume in twin pairs.

Results: Autistic traits as measured by SRS were negatively correlated with left amygdala volume (Beta=-3.39, 95%CI = -6.45, -0.35, p=0.029), however, there was no association between SRS and right amygdala volume (Beta=-2.34, 95% CI=-6.16, 1.48, p=0.23; Figure 1). We noticed two outliers in the SRS measure, we repeated the analysis after removing these outliers and the result was no longer significant for left amygdala (Beta=-2.42408, 95% CI= -5.25, 0.40, p=0.093; Figure 2).

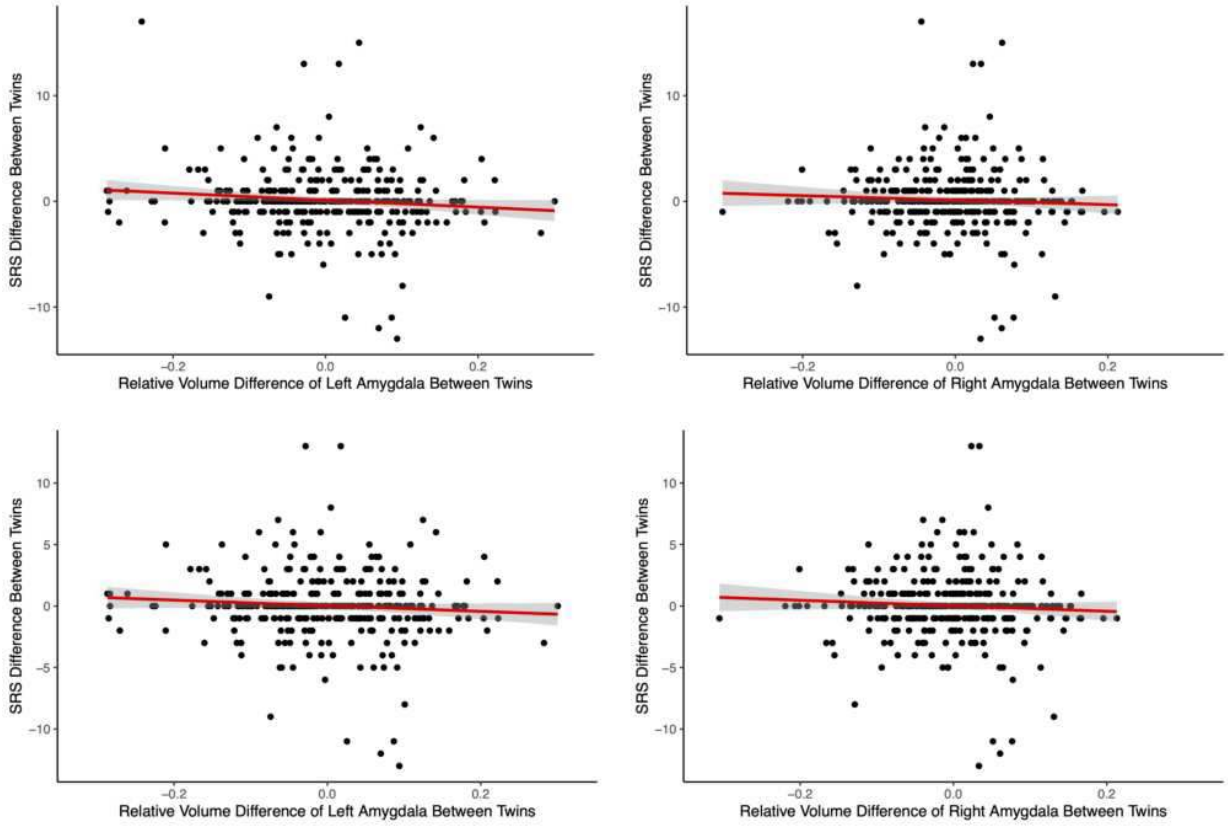

Conclusions: We found a negative association between SRS and volume of left amygdala, indicating an increased amygdala volume in a twin is associated with a lower SRS score. However, even though we found a significant association between SRS and relative size of left amygdala, the effect size is small, and after removing two outlier data points, the result was no longer significant. Since the ABCD study excluded subjects with moderate to severe autism, our study focused on those with mild or subclinical symptoms. Thus, our findings may not be true for those with more severe autistic symptoms. Our study provides a mechanism to control for potential cofounds and biases when evaluating neuroimaging correlates of autistic symptoms.

References

1. Baron-Cohen, S., et al., (2000). The amygdala theory of autism. Neuroscience & Biobehavioral Reviews, 24(3), pp.355-364.
2. Brothers, L. (1990). The social brain: a project for integrating primate behavior and neurophysiology in a new domain. Concepts Neurosci. 1, 27–51.
3. Casey, B.J., et al., (2018). The Adolescent Brain Cognitive Development (ABCD) study: Imaging acquisition across 21 sites. Developmental Cognitive Neuroscience, 32: p. 43-54.
4. Constantino, J.N. et al., (2003). Autistic traits in the general population: a twin study. Archives of general psychiatry, 60(5), pp.524-530.
5. Constantino, J.N. et al., (2012), Social responsiveness scale: SRS-2.
6. Iacono, W.G., et al., (2018). The utility of twins in developmental cognitive neuroscience research: How twins strengthen the ABCD research design. Developmental Cognitive Neuroscience, 32: p. 30-42.
7. Sharp, T.H., et al., (2023). The subcortical correlates of autistic traits in school-age children: a population-based neuroimaging study. Molecular Autism, 14(1), pp.1-12.
8. Zalla, T. et al., (2013). The amygdala and the relevance detection theory of autism: an evolutionary perspective. Frontiers in human neuroscience, 7, p.894.

Poster No 452

Atypical Activation Networks in Prosody Processing for ASD By Activation Networks Mapping

Pinyuan Hu[1], Xinyu Zhang[2], Suyu Zhong[1], Xiaochen Sun[2]

[1]Beijing University of Posts and Telecommunications, Beijing, Beijing, [2]Beijing Language and Culture University, Beijing, China

Introduction: Autism Spectrum Disorders (ASD) exhibit atypical perception and expression of prosody compared to healthy individuals. These distinctions may imply atypical functional connectivity patterns during prosody processing. However, existing literature reports a significant heterogeneity in activation patterns, with limited exploration of the distant network effects on the brain during prosody processing. Here, we integrated heterogeneous research on prosody with activation network mapping (ANM)[1] to explore the atypical functional connectivity patterns of ASD based on the Autism Brain Imaging Data Exchange (ABIDE) dataset[2]. These findings might provide new insights about the ASD neural mechanism.

Methods: 300 ASD and 433 healthy control (HC) were included (16 sites). Studies published from 1 November 1992 to 14 June 2018 were identified by a literature search of PubMed using the following combination of search terms: ('prosody' OR 'emotional prosody' OR 'affective prosody' OR 'linguistic prosody') AND ('fMRI' OR 'functional MRI' OR 'functional magnetic resonance imaging' OR 'PET' OR 'positron emission tomography' OR 'neuroimaging')[3]. Then, 4-mm-radius sphere centered on each activation coordinate were generated. For each study, a combined seed was generated by merging all the spheres reported in this study. Subsequently, for each subject in each ABIDE site, we computed Pearson's correlation coefficient between the average time course of all voxels within the combined seed and the time course of every voxel in the whole brain. The resulting subject-level correlation maps were then transformed into Fisher z maps and averaged after regressing out gender and age to create a site-level mean Fisher z map[4]. After regressing out site effects, we created the study-level mean Fisher z map by a weighted average of the site-level mean Fisher z maps. Then, study-level mean Fisher z maps that belong to the same group (ASD or HC, affective prosody or linguistic prosody) were compared against zero using a voxel-wised one-sample t-test. To quantify the group differences in prosody-related functional connectivity patterns, we conducted a voxel-wised two-sample t-test on the study-level mean Fisher z maps of the two groups.

(1) Literature related to affective or linguistic prosody
(2) Include healthy adult subjects
(3) Studies on fMRI/PET
(4) Include control tasks
(5) Tasks with subjective judgment and perception (exclude production and reading tasks)
(6) Tasks involving passive listening
(7) Reported activation coordinates
(8) Excluded audiovisual integration and binaural listening studies

Table 1. Literature including criteria. As a results, 45 and 23 articles were included for affective and linguistic prosody respectively. Finally, we extracted 969 affective prosody activation coordinates and 637 linguistic prosody activation coordinates from the included literatures.

Results: Figure 1 showed the activation networks for affective prosody and linguistic prosody respectively. For the affective prosody, the typical activation network mainly located in superior temporal gyrus, cingulate gyrus and frontal regions for HC (Fig. 1A), while there are an expanded activation networks in ASD group, including the supramarginal gyrus, postcentral gyrus and superior temporal gyrus, parietal lobe and cerebellum (Fig. 1 B). As shown in the Figure 1 C, the differences between two group in affective prosody activation networks is in inferior frontal gyrus and precentral gyrus. Figure 1 D-F showed the results about linguistic prosody activity network. More specifically, the HC activation network of linguistic prosody mainly focus on bilateral temporal lobe and cerebellar regions (Fig. 1 D). The ASD activation network of linguistic prosody included regions such as cingulate gyrus, angular gyrus, sub-gyral, fusiform gyrus, temporal gyrus and negative correlations in occipital lobe and cerebellum (Fig.1 E). The two-sample t-tests indicated significantly differences in linguistic prosody activity networks including right angular, middle temporal gyrus and para hippocampal gyrus.

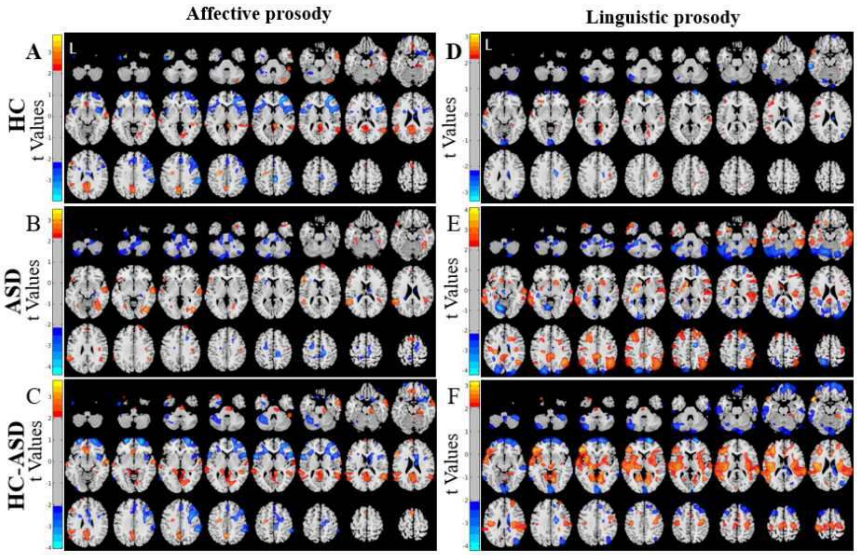

Figure 1. Activation network mapping results of affective and linguistic prosody. (A) Affective prosody activation network on healthy cohort. (B) Affective prosody activation network on ASD cohort. (C) Group differences in affective prosody activation network between HC and ASD. (D) Linguistic prosody activation network on healthy cohort. (E) Linguistic prosody activation network on ASD cohort. (F) Group differences in linguistic prosody activation network between HC and ASD. Regions survived after alphasim multicompriation corretion were showed (voxel-level $p < 0.05$, cluster level $p < 0.05$)

Conclusions: Our study indicates that there are significant differences in activation network patterns between the ASD and HC groups during prosody processing. Specifically, the ASD group consistently exhibits higher positive correlations in the temporal lobe compared to the healthy group, while demonstrating consistently higher negative correlations in certain cerebellar regions. In summary, utilizing activation network mapping, we observed distinct functional network connectivity patterns, providing valuable insights into the neural mechanisms underlying ASD.

References

1. Peng S, et al. (2022), 'Activation network mapping for integration of heterogeneous fMRI findings'. Nature Human Behaviour, vol. 6, no. 10, pp. 1417-1429.
2. Di Martino A, et al. (2017), 'Enhancing studies of the connectome in autism using the autism brain imaging data exchange II'. Scientific data, vol. 4, no. 1, pp. 1-15.
3. Belyk M, et al. (2014), 'Perception of affective and linguistic prosody: an ALE meta-analysis of neuroimaging studies'. Social cognitive and affective neuroscience, vol. 9, no. 9, pp. 1395-1403.
4. Dansereau C, et al. (2017), 'Statistical power and prediction accuracy in multisite resting-state fMRI connectivity'. Neuroimage, vol. 149, pp. 220-232.

Poster No 453

Mapping brain structural laterity abnormalities and multiscale cascade in ASD and DD/ID children

Shujie Geng[1], Yuan Dai[2], Yuqi Liu[2], Yue Zhang[1], Jianfeng Feng[1], Fei Li[2], Miao Cao[1]

[1]Institute of Science and Technology for Brain inspired Intelligence, Fudan University, Shanghai, China, [2]Shanghai Jiao Tong University School of Medicine, Shanghai, China

Introduction: Autism spectrum disorder (ASD) and developmental delay/intellectual disability (DD/ID) are both typical neurodevelopmental disorders with early onset and highly heritable. However, high co-occurring prevalence rate of ASD and DD/ID and overlapping symptoms prevent the effective diagnosis and treatments, making the identification of sufficient biomarkers for discrimination important. Brain asymmetry establishes early since fetal period, whose abnormality has been found associated with the core symptoms in ASD children and adults. However, the multi-scale cascade about the atypical development of brain asymmetry during early childhood of ASD and DD/ID, which might characterize the comorbidity and difference between, remains unclear. To 1) characterize the individual brain asymmetry patterns of ASD and DD/ID at early life stage, 2) explore whether structural brain asymmetries could differentiate ASD and DD/ID from each other and 3) link them to gene expression profiles and clinical manifestations.

Methods: Using the sMRI data of 1030 children under 8 years old from Shanghai Autism Early Development Cohort, including 563 children diagnosed as ASD with DD/ID (3.98±1.22 years, 472 males), 212 children diagnosed as ASD without DD/ID (3.24±1.15 years, 184 males), 36 children with DD/ID only (4.42±1.4 years, 25 males) and 219 age-matched typically developing children (4.42±1.62 years, 107 males), we obtained the individual gender-specific atypical development deviations of gray matter volume (GMV) asymmetry in ASD and DD/ID based-on normative models. One-sample T test was utilized to identify significant regional GMV deviations and the summed T values of 7 networks were performed. Two unsupervised algorithms, K-means and t-SNE, were conducted to test whether ASD and DD/ID can differentiate from each other with GMV asymmetry deviations as features. The canonical correlation analysis (CCA) was done to explore the group-specific associations between GMV asymmetry deviations and clinical performance. The inter-regional similarity analysis was performed to identify the associations between GMV asymmetry deviations and genome expression data from Allen Human Brain Atlas (AHBA) dataset. The identified gene lists were functionally annotated by gene enrichment analysis.

Results: ASD-common pattern of the GMV rightward laterality were found in inferior parietal cortex and precentral cortex (Fig.1.a). Similar structural asymmetry patterns were found among ASD and DD/ID children (Fig.1.b) and clustering algorithm cannot distinguish one group from others (Fig.1.c). The GMV laterality of ASD without DD/ID were linked to ASD symptoms whereas ASD with DD/ID linking to both ASD symptoms and verbal IQ with brain loading as shown in Fig.1. d. The GMV laterality of ASD with and without DD/ID are associated with shared and unique gene expression profiles and intellectual genes showed opposite effects (Fig.2)

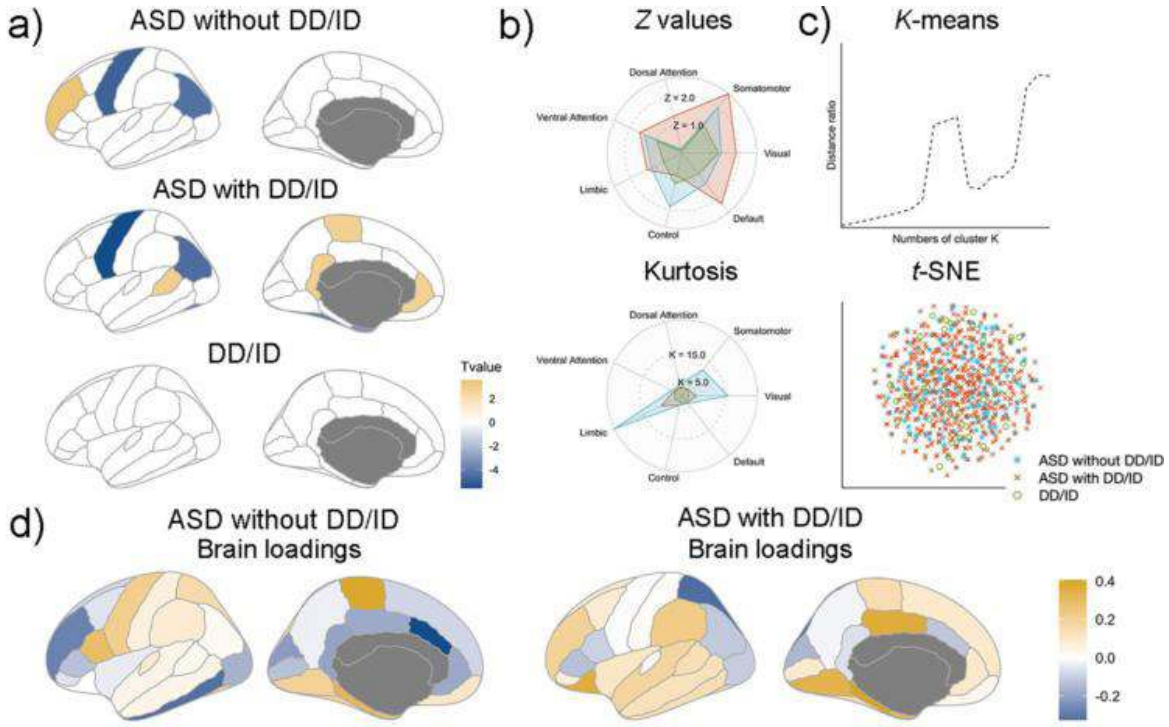

Figure1. The GMV asymmetry deviations derived from normative model and their associations with clinical performances.

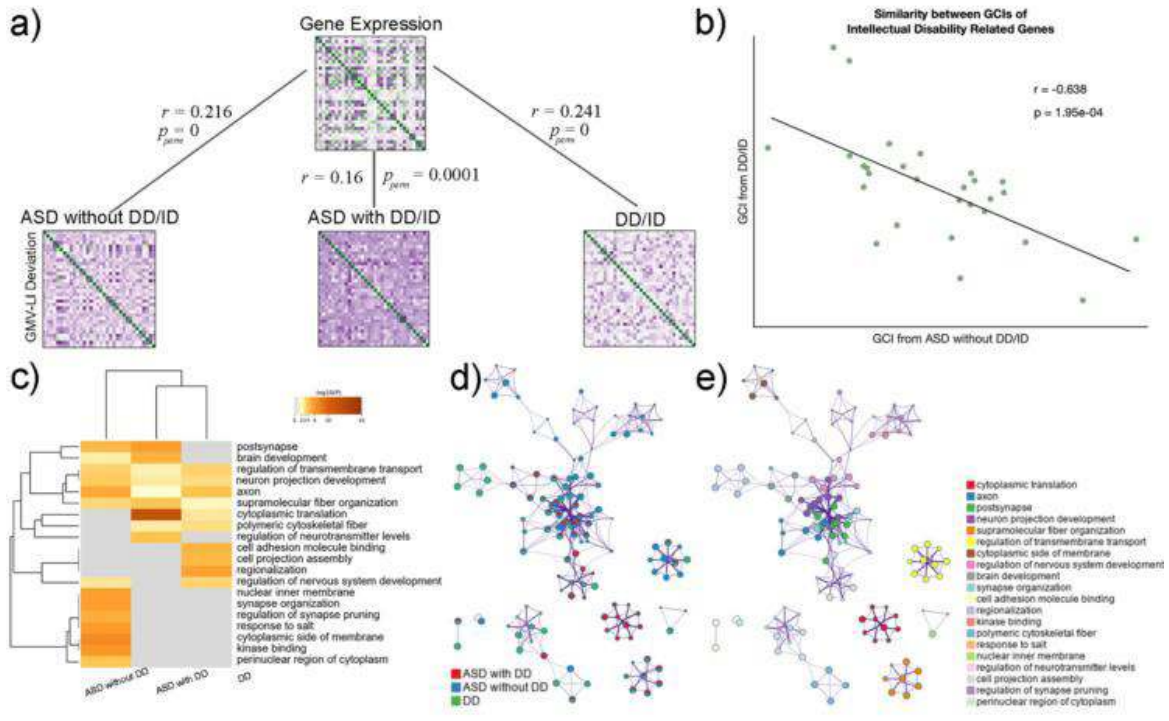

Figure2. The associations between GMV asymmetry deviations and gene expresion profiles.

Conclusions: Our study improves understanding of ASD concurrent with DD/ID from the perspective of multiscale cascade. For ASD and DD/ID young children, globally similar and regionally subtle changed structural laterality derived from divergent gene effects and linked to diagnostic-specific behavioral deficits.

References

1. Arnatkevičiūtė, A., B. D. Fulcher and A. Fornito (2019). "A practical guide to linking brain-wide gene expression and neuroimaging data." Neuroimage 189: 353-367.
2. Burt, J. B., M. Helmer, M. Shinn, A. Anticevic and J. D. Murray (2020). "Generative modeling of brain maps with spatial autocorrelation." NeuroImage 220: 117038.

3. Cao, M., H. Huang and Y. He (2017). "Developmental connectomics from infancy through early childhood." Trends in neurosciences 40(8): 494-506.
4. Dai, Y., Y. Liu, L. Zhang, T. Ren, H. Wang, J. Yu, X. Liu, Z. Chen, L. Deng and M. Tao (2022). "Shanghai Autism Early Development: An Integrative Chinese ASD Cohort." Neuroscience Bulletin 38(12): 1603-1607.
5. Karolis, V. R., M. Corbetta and M. Thiebaut de Schotten (2019). "The architecture of functional lateralisation and its relationship to callosal connectivity in the human brain." Nature communications 10(1): 1-9.
6. Li, J., J. Seidlitz, J. Suckling, F. Fan, G.-J. Ji, Y. Meng, S. Yang, K. Wang, J. Qiu and H. Chen (2021). "Cortical structural differences in major depressive disorder correlate with cell type-specific transcriptional signatures." Nature communications 12(1): 1-14.
7. Lombardo, M. V., M.-C. Lai and S. Baron-Cohen (2019). "Big data approaches to decomposing heterogeneity across the autism spectrum." Molecular psychiatry 24(10): 1435-1450.
8. Lombardo, M. V., T. Pramparo, V. Gazestani, V. Warrier, R. A. Bethlehem, C. Carter Barnes, L. Lopez, N. E. Lewis, L. Eyler and K. Pierce (2018). "Large-scale associations between the leukocyte transcriptome and BOLD responses to speech differ in autism early language outcome subtypes." Nature neuroscience 21(12): 1680-1688.
9. Postema, M. C., D. Van Rooij, E. Anagnostou, C. Arango, G. Auzias, M. Behrmann, S. Calderoni, R. Calvo, E. Daly and C. Deruelle (2019). "Altered structural brain asymmetry in autism spectrum disorder in a study of 54 datasets." Nature communications 10(1): 1-12.
10. Rutherford, S., S. M. Kia, T. Wolfers, C. Fraza, M. Zabihi, R. Dinga, P. Berthet, A. Worker, S. Verdi and H. G. Ruhe (2022). "The normative modeling framework for computational psychiatry." Nature Protocols: 1-24.
11. Xie, Y., Z. Xu, M. Xia, J. Liu, X. Shou, Z. Cui, X. Liao and Y. He (2022). "Alterations in connectome dynamics in autism spectrum disorder: A harmonized mega-and meta-analysis study using the Autism Brain Imaging Data Exchange Dataset." Biological Psychiatry 91(11): 945-955.

Poster No 454

Childhood trauma is associated with accelerated brain aging: a transdiagnostic structural MRI study

Lan Zhou[1], Jan-Bernard Marsman[1], Marieke Begemann[1]

[1]University Medical Center of Groningen, Groningen, Groningen

Introduction: Childhood trauma is an important transdiagnostic risk factor for the development of psychopathology and cognitive impairment later in life. Accelerated biological aging is one of the potential underlying mechanisms. Prior research has mainly focused on the relation of childhood trauma with physical aging and genetic aging, yet the relationship between childhood trauma and brain aging has remained unexplored. In the current study, we investigated the association between childhood trauma and brain aging measures in a transdiagnostic sample.

Methods: We included 518 participants: 241 bipolar-I patients, 113 schizophrenia-spectrum patients and 164 healthy individuals without a psychiatric history, ranging from 18 to 79 years. Participants filled in the Childhood Trauma Questionnaire – Short Form. Anatomical T1 MRI scans were acquired at 3T, and regional brain morphology was assessed using FreeSurfer. Neuroanatomical age was predicted by sex-specific machine learning models trained to individually estimate age from the structural magnetic resonance imaging of 35,683 healthy controls5. Differences between predicted neuroanatomical age and chronological age, referred to as the "brain age gap estimation" (BrainAGE), were calculated. As BrainAGE values are often overestimated in younger individuals and underestimated in older individuals, adjustments for chronological age were made within a bias-adjustment brain age framework, with elevated values indicating accelerated brain aging. Linear regression analyses were conducted to investigate the association between childhood trauma severity with the adjusted BrainAGE, while controlling for sex and diagnosis.

Results: Group-level analyses showed that the brain age gap was + 0.67 years in the total sample, + 1.35 years in BPD, + 0.57 years in SZ and + 0.19 years in healthy controls. In the total sample, childhood trauma severity was associated with brain age acceleration, $\beta = 0.046$, $p = 0.034$, independent of the diagnosed psychiatric condition. A categorical approach showed a similar dose response pattern of more pronounced brain age acceleration in individuals reporting multiple forms of trauma and across quartiles of cumulative trauma scores. A similar pattern was revealed within the bipolar subgroup, whereas such patterns did not reach significance among individuals in the schizophrenia-spectrum or the healthy control group.

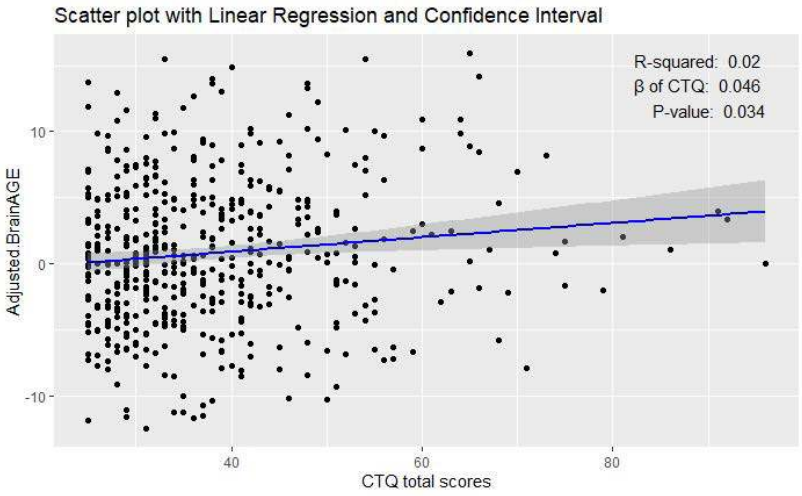

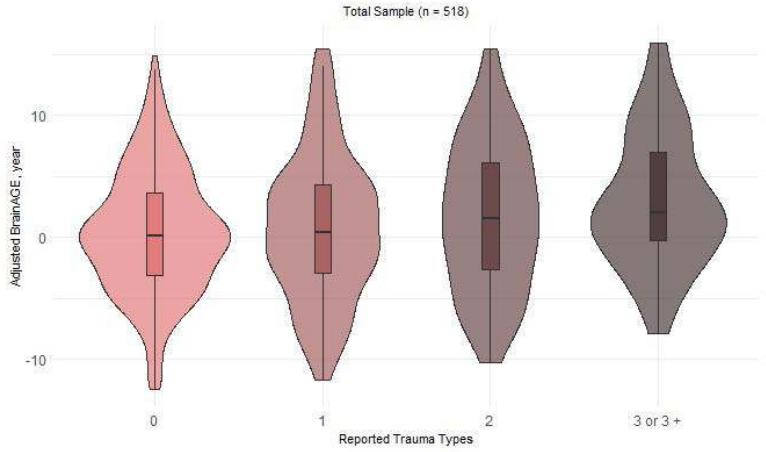

Conclusions: We observed that childhood trauma severity was linked to accelerated brain aging, across transdiagnostic boundaries. These results suggest that acceleration of the ageing trajectory may be an important mechanism by which childhood trauma contributes to the neuroanatomical signature of various mental disorders, which in turn is linked to cognitive and functional deficits. Gaining insight into the mechanisms behind normal and accelerated brain aging may not only elucidate the various factors influencing gray matter abnormalities in patients, but also aid in individualizing treatment.

References

1. Beheshti, I. (2019). Bias-adjustment in neuroimaging-based brain age frameworks: A robust scheme. NeuroImage: Clinical, 24, 102063.
2. Hamlat, E. J. (2023). Early life adversity predicts an accelerated cellular aging phenotype through early timing of puberty. Psychological Medicine, 1-9.
3. Holm, M. C. (2023). Linking brain maturation and puberty during early adolescence using longitudinal brain age prediction in the ABCD cohort. Developmental Cognitive Neuroscience, 60, 101220.
4. McLaughlin, K. A. (2020). Mechanisms linking childhood trauma exposure and psychopathology: a transdiagnostic model of risk and resilience. BMC medicine, 18(1), 1-11.
5. Yang, G. (2022). Association of unhealthy lifestyle and childhood adversity with acceleration of aging among UK biobank participants. JAMA Network Open, 5(9), e2230690-e2230690.
6. Yu, Y. (2023). Brain-Age Prediction: Systematic Evaluation of Site Effects, and Sample Age Range and Size. bioRxiv, 2023-11.

Poster No 455

Neural Activation and Connectivity underlying Face Encoding and Retrieval under Threat-of-Shock

Sarah Buehler[1], Millie Lowther[1], Peter Kirk[1], Paulina Lukow[1], Oliver Robinson[1]

[1]UCL, London, United Kingdom

Introduction: There is mixed evidence pointing to alterations in emotional face recognition in pathological and experimentally induced anxiety. We investigated this by manipulating anxiety levels using threat-of-shock, distinctly at the encoding and

retrieval stage. Based on previous studies, we hypothesized that the ability to recognize (i.e., retrieve) faces is reduced when these are perceived (i.e., encoded) under threat-of-shock (Bolton & Robinson/2017/Learning & Memory/24/532-542; Garibbo et al./2019/Social Cognitive and Affective Neuroscience/14/1087-1096).

Methods: We analysed behavioural and fMRI data in 92 participants as they completeted a face recognition task under threat-of-shock. We investigated behaviour using an ANOVA and meta-analysis (our N=92, N=86 in Bolton & Robinson, 2017; N=32 in Garibbo et al., 2019, total N=210). For the underlying neural correlates, we assessed neural activation in our sample and combined with Garibbo et al., 2019 at the whole-brain level and in predefined regions of interest (ROIs; anterior cingulate cortex, hippocampus). Further, we investigated how functional connectivity is modulated using a generalized psychophysiological interaction (gPPI) analysis of the bilateral amygdala and dorsomedial prefrontal cortex, which are relevant to anxiety.

Results: In our sample (N=92) we found a significant main effect of encoding state (F=4.246, p=0.042, ηp2=0.044), with more accurate retrieval for faces encoded during safety (M=0.668, sd=0.172) compared to threat-of-shock (M=0.652, sd=0.157), which was supported by a meta-analysis (Cohen's d=0.26, z=3.52, p<0.001). At the neural level, a whole brain analysis revealed that this behavioural effect was associated with a significant cluster in the posterior cingulate cortex (voxel-wise threshold=p<0.001, cluster-level significance threshold=p<0.05). Interestingly, the strength of activation in the posterior cingulate cortex (PCC) cluster during encoding was significantly negatively correlated with the recognition accuracy of those faces at the behavioural level (t=-2.795, df=90, p=0.006, R=-0.28). This suggests that those individuals who had higher PCC activation while encoding faces under threat-of-shock were subsequently worse at remembering those faces. In a combined whole brain mega-analysis of the current study sample (N=92) and a previous sample from Garibbo et al. (2019: N=32) we found that both the PCC and a cluster in the anterior cingulate cortex (ACC) were significantly more active when encoding under threat-of-shock compared to safety. However, we found no significant functional connectivity results in our psychophysiological interaction analysis.

Conclusions: Threat-of-shock induced anxiety during the encoding stage appears to robustly impair subsequent face recognition. This may result from the attentional demands of a heightened anxious arousal state competing with the attentional resources required to encode faces, which are subsequently retrieved less accurately. The underlying neural activation we observed in the posterior and anterior cingulate regions might signal the tuning of selective attention to internal, self-relevant cues and increase with arousal state (Abraham et al., 2013; Daley et al., 2020; Leech & Sharp, 2014). It is well-established that posterior and anterior cingulate regions have reciprocal connections with subcortical structures that are involved in processing interoceptive signals, such as the heart beat (Northoff et al., 2006), which allows them to control attentional allocation to interoceptive arousal signals (Stern et al., 2017). Therefore, we propose a potential extension to the influential attentional control theory (Eysenck et al., 2007), which posits that anxiety reduces goal-directed attentional processing, and suggest that this may be paralleled by an increase in internally directed attention.

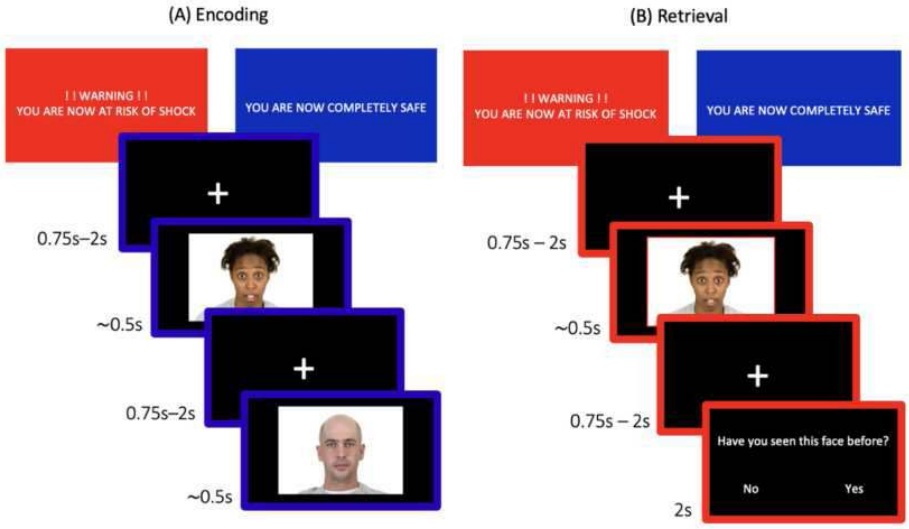

Figure 1. Threat-of-Shock potentiated Face Recognition Task: *During every block an encoding condition (A) was followed by a retrieval condition (B), alternating between a threat-of-shock state (red) and safe control state (blue). At both (A) and (B), a warning slide was presented to inform participants which state they were entering, and a coloured frame reminded them throughout each condition (red for ToS, blue for safe). Emotional face stimuli were presented during (A) encoding (18 unseen) and (B) retrieval (18 seen and 18 unseen) for approximately 0.5 seconds and with inter-stimulus intervals (ISI) of 0.75-2 seconds. During the retrieval condition (B) Participants were asked if they have seen the face before and respond (Yes/No) with a button-press.*

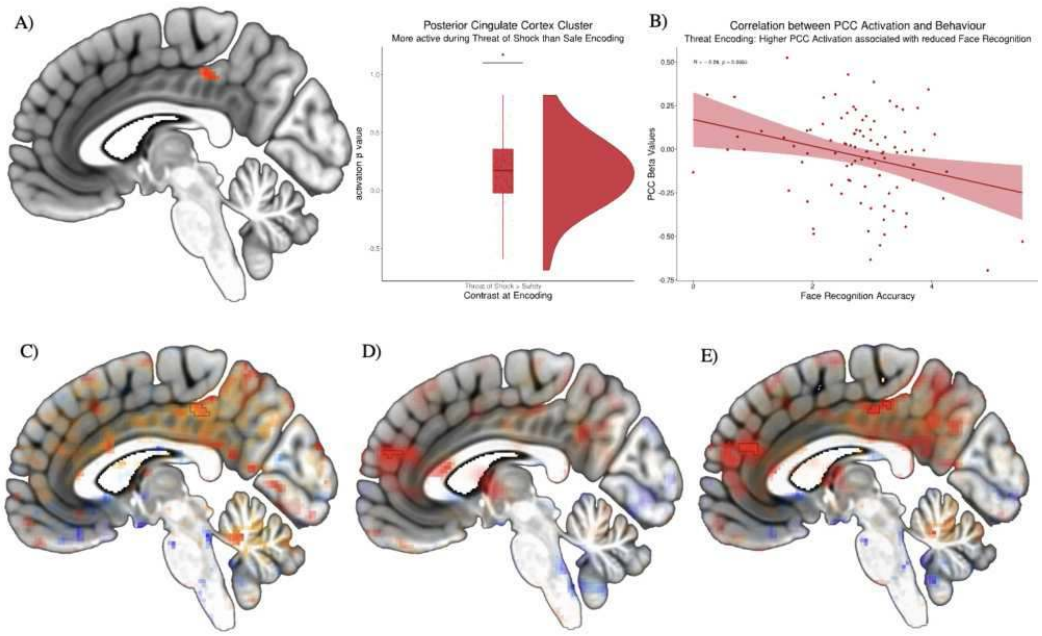

Figure 4. Whole-brain analysis of neural activation *shows that when encoding under threat-of-shock compared to safety A) a cluster (t-statistic map in red) in the posterior cingulate cortex (PCC) was more active and B) the strength of that activation significantly correlates with reduced face recognition at the behavioural level. Further, when we combined C) the current study, see unthresholded group-level map with significant PCC cluster outlined in black, with D) the within-subject results from Garibbo et al. (2019), see unthresholded group-level map with significant anterior cingulate cortex (ACC) cluster outlined in black, in E) a whole brain mega-analysis, we found that when encoding under threat-of-shock compared to safety both the ACC and PCC are significantly more active, outlined in black on the unthresholded combined group-level map.*

References

1. Cox RW (1996). AFNI: software for analysis and visualization of functional magnetic resonance neuroimages. Comput Biomed Res 29(3):162-173. doi:10.1006/cbmr.1996.0014
2. https://pubmed.ncbi.nlm.nih.gov/8812068/

Poster No 456

Predicting Treatment Outcomes in MDD using Baseline Resting-state Data: A Meta-Analysis

Yanyao Zhou[1], Charlene Lam[1]

[1]*The University of Hong Kong, Hong Kong, Hong Kong*

Introduction: Current pharmacological and psychotherapeutic interventions for major depressive disorder (MDD) demonstrate limited and heterogeneous efficacy, benefiting some patients. Past studies have attempted to find biomarkers, such as genetic variants, to improve treatment efficacy and better predict patient response to the treatments. Resting-state functional connectivity (rsFC) at the baseline may offer particular promise as a predictive biomarker of the treatment outcome for MDD interventions. However, findings regarding the effect of baseline rsFC on predicting the treatment outcome have been mixed. In order to draw more robust conclusions regarding rsFC's potential as a biomarker for MDD treatment response, this meta-analysis systematically evaluates the evidence for baseline rsFC as a predictor of treatment outcomes in MDD interventions.

Methods: We targeted MDD literature published between 2013 and 2023. Articles were included if they: 1) examined adult patients (>18 years old) with MDD; 2) tested antidepressants, psychotherapies like cognitive behavioral therapy, or non-invasive brain stimulation treatments; and 3) reported correlation coefficients indicating the relationship between baseline between-network and/or within-network rsFC and treatment outcomes. We generated a pooled predictive coefficient for different types of rsFC connections, if such type of rsFC connection contains predictive coefficients extracted from at least three different samples.

Results: From 15 included studies, pooled coefficients were generated for three rsFC connections: 1) between the frontoparietal network (FPN) and the default mode network (DMN); 2) between the FPN and the ventral attention network (VAN); and 3) within the DMN. The rsFC between the FPN and VAN emerged as the strongest predictor of treatment outcomes in MDD interventions, demonstrating an overall moderate to large effect. The effect size was 0.41 (95% CI: 0.23 – 0.59)

for fixed effects and 0.45 (95% CI: 0.13 – 0.78) for random effects. The other two types of rsFC connections also showed predictive value, albeit with small to moderate effects. The effect size of the rsFC connection between the DMN and FPN was -0.17 (95% CI: -0.26 – -0.07) for fixed effects and -0.21 (95% CI: -0.46 – 0.05) for random effects. As for the rsFC connection within the DMN, the effect size was 0.19 (95% CI: 0.07 – 0.32) for fixed effects and 0.14 (95% CI: -0.13 – 0.41) for random effects. Both the rsFC between the FPN and VAN and the rsFC within the DMN exhibited positive associations with treatment outcomes. In contrast, the rsFC between the FPN and DMN showed a negative association with treatment outcomes. Notably, substantial heterogeneity was observed across the three connection types, as well as in study design and data analysis approaches.

Conclusions: Significant heterogeneity was observed in effect size and direction of prediction, as well as the design and analysis pipelines across studies. However, rsFC still predicted outcomes with at least a small to moderate effect across different intervention types. RsFC demonstrates potential as a predictive biomarker; however, further research is needed to explore its full capabilities. This includes conducting studies with larger sample sizes, incorporating a wider range of MDD interventions, and employing more precise and consistent methodologies.

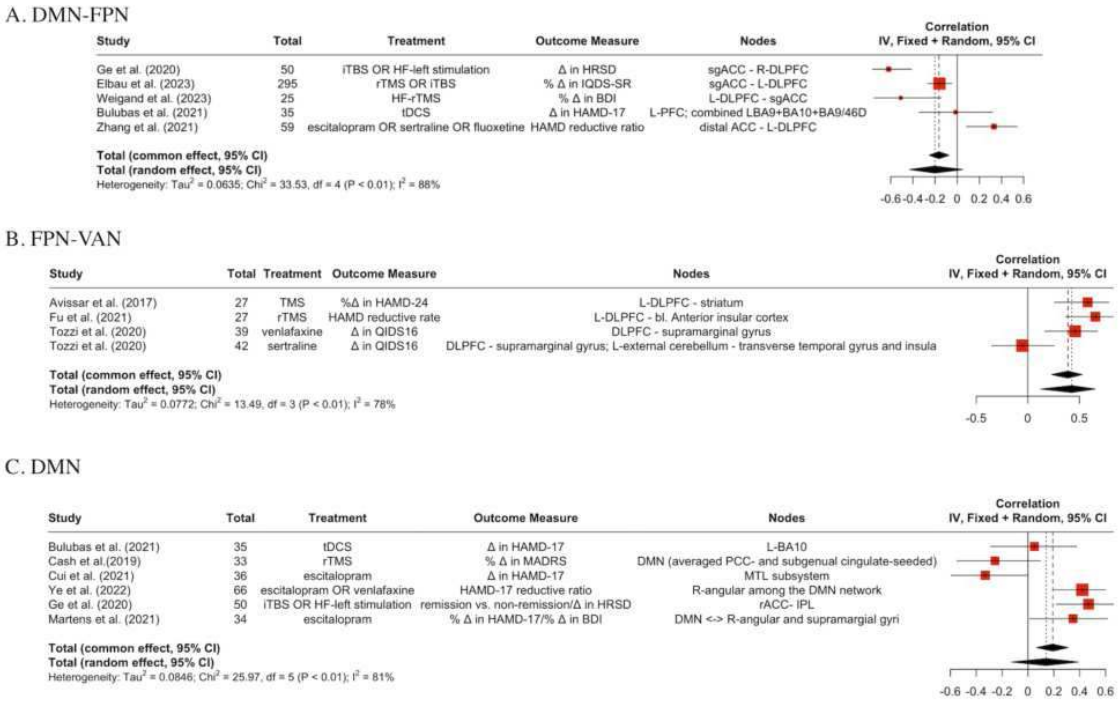

Figure 1. Pooled Pearson Correlation Coefficient for Different Types of rsFC Connection

Note. DMN = default mode network; FPN = frontoparietal network; VAN = ventral attention network

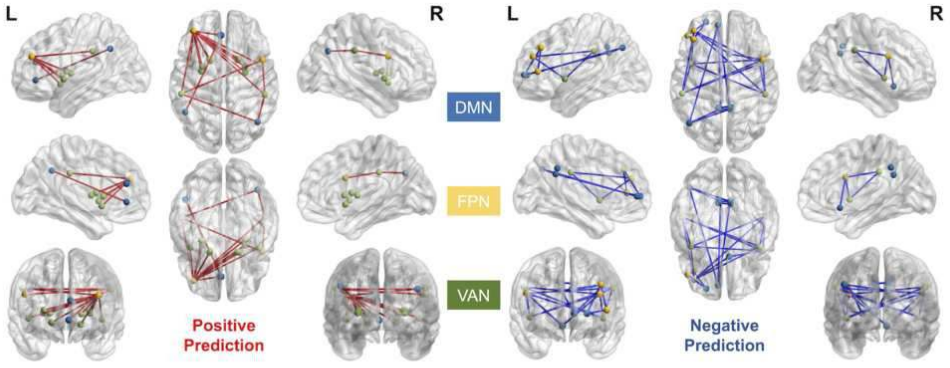

Figure 2. Nodes Involved in the rsFC Connection Predicting Treatment Outcomes with Different Directions

Note. DMN = default mode network; FPN = frontoparietal network; VAN = ventral attention network

References
1. Fadel, E., Boeker, H., Gaertner, M., Richter, A., Kleim, B., Seifritz, E., . . . Wade-Bohleber, L. M. (2021). Differential alterations in resting state functional connectivity associated with depressive symptoms and early life adversity. Brain sciences, 11(5), 591.
2. Kaiser, R. H., Andrews-Hanna, J. R., Wager, T. D., & Pizzagalli, D. A. (2015). Large-scale network dysfunction in major depressive disorder: a meta-analysis of resting-state functional connectivity. JAMA psychiatry, 72(6), 603–611.
3. Long, Z., Du, L., Zhao, J., Wu, S., Zheng, Q., & Lei, X. (2020). Prediction on treatment improvement in depression with resting state connectivity: a coordinate-based meta-analysis. Journal of Affective Disorders, 276, 62–68.
4. Nord, C. L. (2021). Predicting response to brain stimulation in depression: a roadmap for biomarker discovery. Current Behavioral Neuroscience Reports, 8(1), 11–19.

Poster No 457

Multivariate associations between psychiatric drug intake and GMV in psychosis and depression

Clara Weyer[1,2], David Popovic[3,1,4], Anne Ruef[1], Lisa Hahn[1], Elif Sarişik[3,1,4], John Fanning[1,4], Joseph Kambeitz[5], Raimo K. Salokangas[6], Jarmo Hietala[6], Alessandro Bertolino[7], Stefan Borgwardt[8,9], Paolo Brambilla[10,11], Rachel Upthegrove[12,13], Stephen J. Wood[14], Rebecca Lencer[15], Eva Meisenzahl[16], Nikolaos Koutsouleris[1,3,17]

[1]Department of Psychiatry and Psychotherapy, LMU University Hospital, LMU Munich, Munich, Germany, [2]Graduate School of Systemic Neurosciences, LMU Munich, Planegg-Martinsried, Germany, [3]Max-Planck Institute of Psychiatry, Munich, Germany, [4]International Max Planck Research School for Translational Psychiatry (IMPRS-TP), Munich, Germany, [5]Department of Psychiatry and Psychotherapy, University of Cologne, Cologne, Bavaria, [6]Department of Psychiatry, University of Turku, Turku, Finland, [7]Department of Basic Medical Science, Neuroscience and Sense Organs, University of Bari Aldo Moro, Bari, Bari, [8]Department of Psychiatry and Psychotherapy, University of Lübeck, Lübeck, Germany, [9]University of Basel, Department of Psychiatry (Psychiatric University Hospital, UPK), Basel, Switzerland, [10]Department of Neurosciences and Mental Health, Fondazione IRCCS Ca' Granda Ospedale Maggiore Policli, Milan, Italy, [11]Department of Pathophysiology and Transplantation, University of Milan, Milan, Italy, [12]Institute of Mental Health, University of Birmingham, Birmingham, United Kingdom, [13]Early Intervention Service, Birmingham Women's and Children's NHS Foundation Trust, Birmingham, United Kingdom, [14]Centre for Youth Mental Health, University of Melbourne, Melbourne, Australia, [15]Institute for Translational Psychiatry, University Münster, Münster, Germany, [16]Department of Psychiatry and Psychotherapy, Medical Faculty, Heinrich Heine University, Düsseldorf, Germany, [17]Institute of Psychiatry, Psychology and Neuroscience, King's College London, London, United Kingdom

Introduction: Psychiatric medication, including antipsychotics and antidepressants, is widely prescribed, even in young and adolescent populations at early or subthreshold disease stages. However, its impact on brain structure remains elusive. Elucidating the relationship between psychiatric medication and structural brain changes could enhance the understanding of the potential benefits and risks associated with such treatment. Therefore, the aim of this study is to investigate the associations between psychiatric medication intake and longitudinal grey matter volume (GMV) changes in a transdiagnostic sample of young individuals at early stages of psychosis or depression using an unbiased data-driven approach.

Methods: The study sample comprised 247 participants (mean [SD] age = 25.06 [6.13] years, 50.61% male), consisting of young, minimally medicated individuals at clinical high-risk states for psychosis, individuals with recent-onset depression or psychosis, and healthy control individuals. Participants were recruited as part of the multicentric PRONIA (Personalised Prognostic Tools for Early Psychosis Management) study. Structural magnetic resonance imaging was used to obtain whole-brain voxel-wise GMV for all participants at two timepoints (mean [SD] time between scans = 11.15 [4.93] months). The multivariate sparse partial least squares (SPLS) algorithm was embedded in a nested cross-validation framework to identify parsimonious associations between the cumulative intake of psychiatric medication, including commonly prescribed antipsychotics and antidepressants, and change in GMV between both timepoints, while additionally factoring in age, sex, and diagnosis. Furthermore, we correlated the retrieved SPLS results to personality domains (NEO-FFI) and childhood trauma (CTQ).

Results: SPLS analysis revealed significant associations between the antipsychotic classes of benzamides, butyrophenones and thioxanthenes and longitudinal GMV decreases in cortical regions including the insula, posterior superior temporal sulcus as well as cingulate, postcentral, precentral, orbital and frontal gyri. These brain regions corresponded most closely to the dorsal and ventral attention, somatomotor, salience and default network. Furthermore, the medication signature was negatively associated with the personality domains extraversion, agreeableness and conscientiousness and positively associated with the CTQ domains emotional and physical neglect.

Conclusions: Antipsychotic treatment over a period of one year was linked to distinct GMV reductions in key cortical hubs. These patterns were already visible in young individuals at early or subthreshold stages of mental illness and were further linked to childhood neglect and personality traits. Hence, a better and more in-depth understanding of the structural

brain implications of medicating young and adolescent individuals might lead to more cautious, sustainable and targeted treatment strategies.

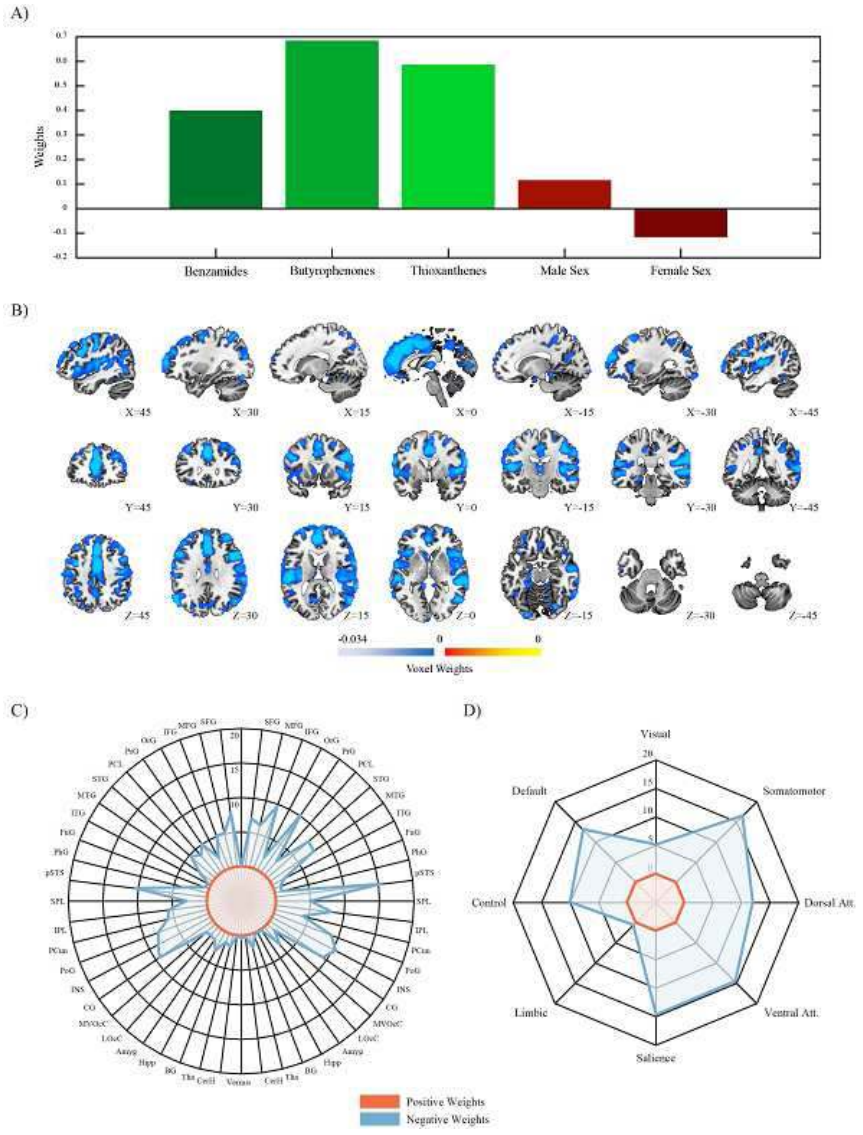

References

1. Koutsouleris, N., Kambeitz-Ilankovic, L., Ruhrmann, S., Rosen, M., Ruef, A., Dwyer, D. B., Paolini, M., Chisholm, K., Kambeitz, J., Haidl, T., Schmidt, A., Gillam, J., Schultze-Lutter, F., Falkai, P., Reiser, M., Riecher-Rössler, A., Upthegrove, R., Hietala, J., Salokangas, R. K. R., Pantelis, C., ... PRONIA Consortium (2018). Prediction Models of Functional Outcomes for Individuals in the Clinical High-Risk State for Psychosis or With Recent-Onset Depression: A Multimodal, Multisite Machine Learning Analysis. JAMA psychiatry, 75(11), 1156–1172. https://doi.org/10.1001/jamapsychiatry.2018.2165
2. Monteiro, J. M., Rao, A., Shawe-Taylor, J., Mourão-Miranda, J., & Alzheimer's Disease Initiative (2016). A multiple hold-out framework for Sparse Partial Least Squares. Journal of neuroscience methods, 271, 182–194. https://doi.org/10.1016/j.jneumeth.2016.06.011
3. Popovic, D., Ruef, A., Dwyer, D. B., Antonucci, L. A., Eder, J., Sanfelici, R., Kambeitz-Ilankovic, L., Oztuerk, O. F., Dong, M. S., Paul, R., Paolini, M., Hedderich, D., Haidl, T., Kambeitz, J., Ruhrmann, S., Chisholm, K., Schultze-Lutter, F., Falkai, P., Pergola, G., Blasi, G., ... PRONIA Consortium (2020). Traces of Trauma: A Multivariate Pattern Analysis of Childhood Trauma, Brain Structure, and Clinical Phenotypes. Biological psychiatry, 88(11), 829–842. https://doi.org/10.1016/j.biopsych.2020.05.020

Poster No 458

Perturbation in silico Indicates the Crucial Role of NAc in Abstinence from Meth Addiction

Jiaqi Zhang[1], Yaoyao Du[2], Jun Liu[2], Tianzi Jiang[1]

[1]Brainnetome Center, Institute of Automation, Chinese Academy of Sciences, Beijing, Beijing, [2]Department of Radiology, Second Xiangya Hospital of Central South University, Changsha, Hunan, China, Changsha, Hunan

Introduction: Methamphetamine (MA) addiction imposes a significant public health burden and various intervention methods have limited therapeutic efficacy. To explore an innovative and effective intervention strategy, we carried out a one-year longitudinal study for 62 MA users. MRI scans and MA craving questionnaires (MCQs) were collected before (MA1) and after long-term abstinence (MA2). We established the whole-brain computational models to investigate crucial regions associated with abstinence from methamphetamine addiction. To the best of our knowledge, the application of this approach to investigate MA addiction is currently lacking in the existing studies. Our work may serve as a reference for the practical application of this approach in future addiction therapeutics.

Methods: Probabilistic Metastable Substates (PMS) Brain activity is not static, so to capture its metastable nature, we employed the PMS method, which is consistent with previous literature. By leveraging the PMS, we were able to identify and characterize recurrent substates, enabling us to quantitatively assess the brain's state for subsequent model fitting and in silico perturbations. First, we obtained phase coherence matrices (dFC). Then, we extracted the leading eigenvectors to capture the temporal evolution of dFC. Lastly, we applied the k-means clustering algorithm to identify the PMS space. In our subsequent analysis, we selected a cluster solution with k = 8, as it is the smallest number of clusters that could effectively distinguish the three distinct groups of subjects. Whole-Brain Computational Model The brain can be conceptualized as a complex network, with nodes representing specific brain regions and edges representing the structural connectivity obtained via diffusion MRI. Here, each of the N = 246 brain regions was modeled as the Hopf model, which is a canonical model for characterizing features of brain dynamics and studying perturbation dynamics. To simulate the dynamics of the entire brain, we coupled each Hopf model with the empirical structure connectivity and adjusted the strength of these connections using a global coupling parameter. This coupling parameter played a crucial role in scaling the constraints imposed by the structural connectivity, allowing for a more accurate representation of the brain's dynamics. Before conducting a model fitting to determine the optimal model, it is essential to establish a measurement that can quantitatively assess the distance between simulated data and empirical data. In alignment with prior literature, we adopted the symmetrized Kullback-Leibler (KL) distance as our distance metric.

Results: 1. We quantitatively characterized the brain states and identified the significant brain states related to craving scores, indicating distinct spatiotemporal functional patterns among the three cohorts, namely the MA1, MA2, and HC. 2. We constructed whole-brain computational models and identified the nucleus accumbens (NAc) as a potential intervention target through in silico perturbations for each region across the whole brain, which is aligned with previous clinical experiments. Our observations of the underlying functional alterations also indicated reduced craving scores and improved cognitive functions. 3. We observed that the impact of perturbing other brain regions across the whole brain was related to their connectivity with NAc in the context of MA1, suggesting the ability of NAc to identify other potential intervention targets. Notably, this relationship was absent within the context of MA2, suggesting a potential decrease in the abstinence influence of the nucleus accumbens, or possibly that NAc has recovered during long-term abstinence.

Conclusions: In summary, our findings not only offer a new perspective highlighting the central role of NAc in abstinence from methamphetamine addiction but also offer potential avenues for advanced translational interventions in addiction therapy.

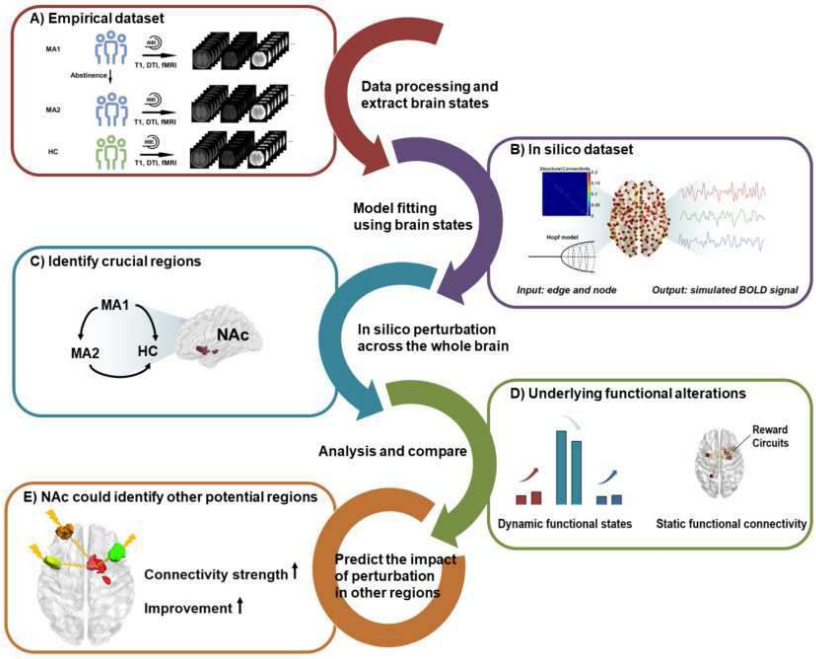

References
1. Breakspear, M. (2017). "Dynamic models of large-scale brain activity." Nature neuroscience 20(3): 340-352.
2. Deco, G., et al. (2017). "The dynamics of resting fluctuations in the brain: metastability and its dynamical cortical core." Scientific reports 7(1): 3095.
3. Deco, G., et al. (2019). "Awakening: Predicting external stimulation to force transitions between different brain states." Proceedings of the National Academy of Sciences 116(36): 18088-18097.
4. Du, Y., et al. (2022). "Changes in ALFF and ReHo values in methamphetamine abstinent individuals based on the Harvard-Oxford atlas: A longitudinal resting-state fMRI study." Addiction Biology 27(1): e13080.
5. Fan, L., et al. (2016). "The human brainnetome atlas: a new brain atlas based on connectional architecture." Cerebral cortex 26(8): 3508-3526.
6. Fox, M. D., et al. (2014). "Resting-state networks link invasive and noninvasive brain stimulation across diverse psychiatric and neurological diseases." Proceedings of the National Academy of Sciences 111(41): E4367-E4375.

Poster No 459

Homotopic functional connectivity disruptions in schizophrenia and their associated gene expression

Yuan Ji[1]

[1]*Department of Radiology, Tianjin Medical University General Hospital, Tianjin, China*

Introduction: Although abnormal voxel-mirrored homotopic connectivity (VMHC) has been detected in individuals diagnosed with schizophrenia, disparities in the relevant findings exist. Furthermore, our understanding of its connection with brain gene expression profiles remains limited.

Methods: In this study, we conducted transcription-neuroimaging association analyses using gene expression data from the Allen Human Brain Atlas. These analyses included case-control comparisons of VMHC differences in both the discovery phase (meta-analysis, including 9 studies with a total of 386 patients and 357 controls) and the replication phase (separate group-level comparisons within two datasets, including a total of 258 patients and 287 controls). Our objective was to pinpoint genes associated to VMHC changes. To further illuminate the findings, we performed enrichment analyses to delineate the biological functions and unique expression patterns of these genes. Additionally, we utilized Neurosynth decoding analysis to investigate the relationship between VMHC alterations in schizophrenia and cognitive processes.

Results: Across both the discovery and replication phases, individuals with schizophrenia consistently displayed VMHC alterations compared to control subjects. These changes were found to be associated with a series of cognitive-related processes. Notably, when employing meta-regression analysis, it was revealed that the duration of illness exhibited a negative correlation with VMHC abnormalities specifically within the cerebellum and the postcentral/precentral gyrus. The abnormal VMHC patterns were also consistently associated to a set of 1,287 genes, which enriched for fundamental biological processes like regulation of cell communication, nervous system development, and cell communication. Moreover, these genes showed higher expression levels in astrocytes and immune cells, and they displayed enrichment in numerous cortical regions across different developmental time periods.

Conclusions: These results could enhance our grasp of the molecular mechanisms that underlie VMHC changes in individuals with schizophrenia.

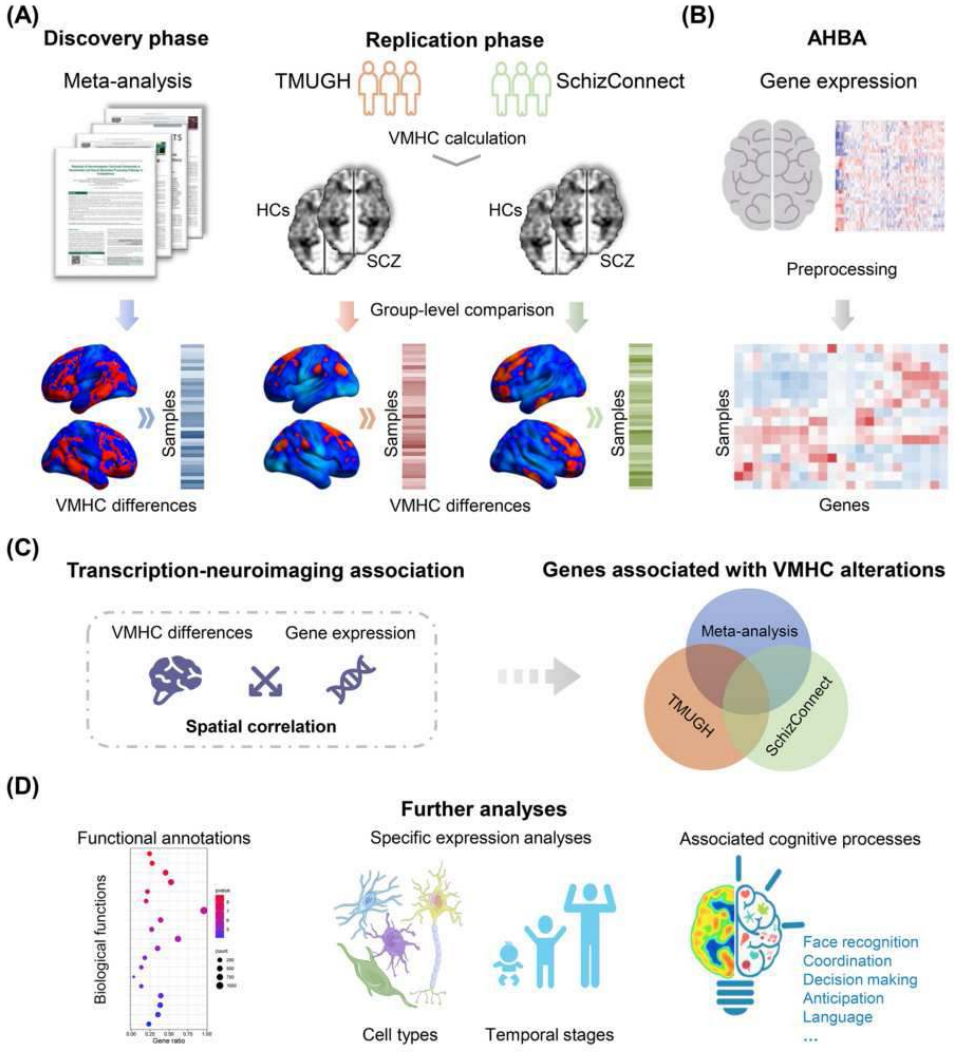

Figure 1 Flowchart for the design of this study.

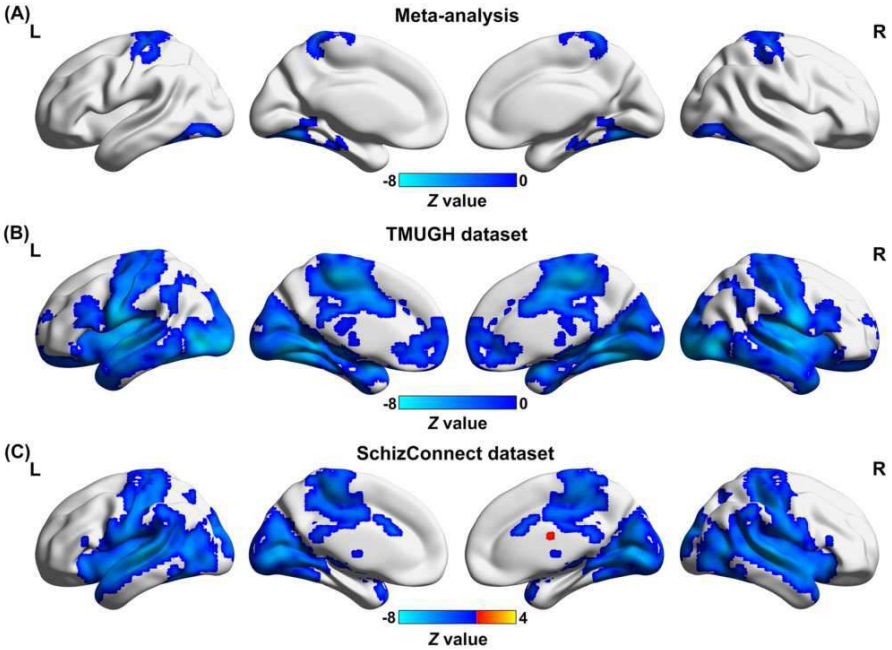

Figure 2 VMHC alterations in patients with schizophrenia. Case-control VMHC differences in the meta-analysis, TMUGH dataset, and SchizConnect dataset are shown in (A), (B), and (C), respectively.

References

1. Arnatkeviciute, A., R. D. Markello, B. D. Fulcher, B. Misic and A. Fornito (2023). "Toward Best Practices for Imaging Transcriptomics of the Human Brain." Biol Psychiatry 93(5): 391-404.
2. Butler, P. D., S. M. Silverstein and S. C. Dakin (2008). "Visual perception and its impairment in schizophrenia." Biol Psychiatry 64(1): 40-47.
3. Chang, X., Y. B. Xi, L. B. Cui, H. N. Wang, J. B. Sun, Y. Q. Zhu, P. Huang, G. Collin, K. Liu, M. Xi, S. Qi, Q. R. Tan, D. M. Miao and H. Yin (2015). "Distinct inter-hemispheric dysconnectivity in schizophrenia patients with and without auditory verbal hallucinations." Sci Rep 5: 11218.
4. Chen, C., H. Huang, X. Qin, L. Zhang, B. Rong, G. Wang and H. Wang (2022). "Reduced inter-hemispheric auditory and memory-related network interactions in patients with schizophrenia experiencing auditory verbal hallucinations." Front Psychiatry 13: 956895.
5. Crow, T. J. (1997). "Schizophrenia as failure of hemispheric dominance for language." Trends Neurosci 20(8): 339-343.
6. Fornito, A., A. Zalesky, C. Pantelis and E. T. Bullmore (2012). "Schizophrenia, neuroimaging and connectomics." Neuroimage 62(4): 2296-2314.
7. Guo, W., F. Liu, J. Chen, R. Wu, L. Li, Z. Zhang, H. Chen and J. Zhao (2018). "Treatment effects of olanzapine on homotopic connectivity in drug-free schizophrenia at rest." World J Biol Psychiatry 19(sup3): S106-s114.
8. Hawrylycz, M., J. A. Miller, V. Menon, D. Feng, T. Dolbeare, A. L. Guillozet-Bongaarts, A. G. Jegga, B. J. Aronow, C. K. Lee, A. Bernard, M. F. Glasser, D. L. Dierker, J. Menche, A. Szafer, F. Collman, P. Grange, K. A. Berman, S. Mihalas, Z. Yao, L. Stewart, A. L. Barabási, J. Schulkin, J. Phillips, L. Ng, C. Dang, D. R. Haynor, A. Jones, D. C. Van Essen, C. Koch and E. Lein (2015). "Canonical genetic signatures of the adult human brain." Nat Neurosci 18(12): 1832-1844.
9. Hoptman, M. J., X. N. Zuo, D. D'Angelo, C. J. Mauro, P. D. Butler, M. P. Milham and D. C. Javitt (2012). "Decreased interhemispheric coordination in schizophrenia: a resting state fMRI study." Schizophr Res 141(1): 1-7.
10. McCutcheon, R. A., T. Reis Marques and O. D. Howes (2020). "Schizophrenia-An Overview." JAMA Psychiatry 77(2): 201-210.
11. Raudvere, U., L. Kolberg, I. Kuzmin, T. Arak, P. Adler, H. Peterson and J. Vilo (2019). "g:Profiler: a web server for functional enrichment analysis and conversions of gene lists (2019 update)." Nucleic Acids Res 47(W1): W191-w198.

Poster No 460

Transcriptional Vulnerability of Immune Genes Underlying Mental Disorders' Cortical Abnormality

WenBIn Qu[1], Peng Ren[1], lili sun[1], Xia Liang[2]

[1]School of Life Science and Technology, Harbin Institute of Technology, Harbin, Heilongjiang, [2]Laboratory for Space Environment and Physical Sciences, Harbin Institute of Technology, Harbin, Heilongjiang

Introduction: Cortical thickness abnormalities are a well-documented neuroimaging phenotype in various mental disorders, highlighting both commonalities and specificities among these disorder[1,2]. The interconnection between the nervous system and the immune system plays a critical role in brain development[3,4], abnormal brain immune responses[5] and the development of mental illness[6]. However, no study has systematically characterized the contribution of the immune gene transcriptome to vulnerability to abnormal cortical thickness. Our study used the cortical thickness abnormality maps of six mental disorders from the ENIGMA consortium and the gene transcriptome data from Allen Human Brain Atlas (AHBA) to construct a cortical thickness-gene transcriptome covariation map. These findings could reveal the commonality and specificity of immune gene transcriptome vulnerability in different mental disorders and revolutionize our understanding of mental disorders.

Methods: In this study, we used structural MRI dataset from the ENIGMA consortium[7] on case-control differences of nearly 15,000 cases and over 22,000 controls for six disorders-ADHD, ASD, BD, MDD, OCD, SCZ (Fig.1a), and the whole-brain gene transcriptome of the AHBA (dataset1) and selected 976 immune-related gene (dataset2)[6]. We firstly used partial least squares to construct transcriptome-cortical thickness abnormality covariation patterns on gene datasets (Fig.1d)[8,9]. Then, we used principal component analysis to identify PC1 in cortical thickness across the six diseases and construct common covariation patterns to identify common features among the six diseases and classified the six mental disorders using hierarchical clustering and constructed disorder-specific patterns of co-variation to identify differences across mental disorders. Gene set enrichment analysis[10,11] was used to enrich pathways involved in the most significant 50% of genes. Immune class bias was analyzed using the rank sum test.

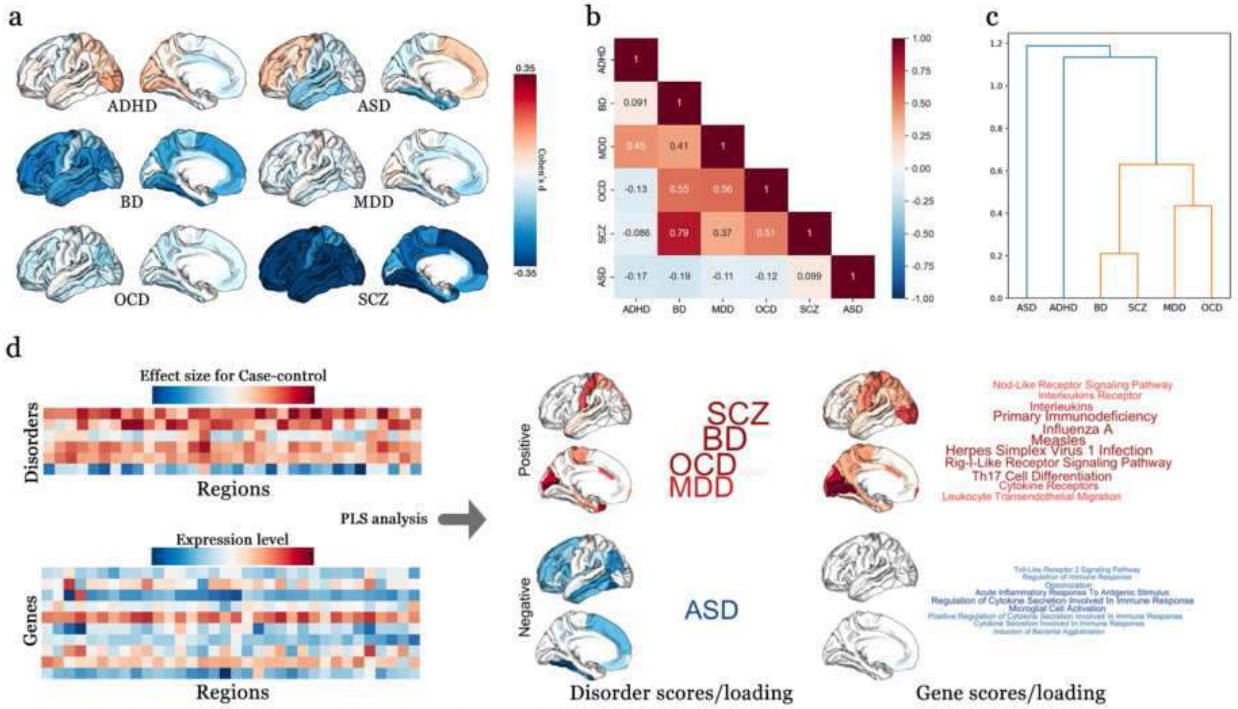

Fig.1| Classification of abnormal cortical thickness, abnormal cortical thickness-immune gene transcriptome common covariation patterns a, Abnormal group differences (Cohen's d) in cortical thickness among case-control subjects for six mental disorders collected from the ENIGMA consortium, vnormalized using z-score. b, Classification of six mental disorders using pairwise correlations of group differences and hierarchical clustering (c). d, PLS analysis was used to construct covariation patterns of cortical thickness abnormalities and immune gene transcriptomes. The score pattern is obtained by projecting the original matrix to the weights obtained by singular value decomposition. Score expresses the degree of abnormal gene expression/cortical thickness in a brain region. Loading is calculated as the Pearson correlation between the original matrix and the score pattern obtained from PLS analysis. Loading indicates the contribution of each variable to the PLS scoring pattern. The example in the figure comes from the common covariation matrix of six disorders. We used permutation test that preserved spatial autocorrelation to assess significance (i.e., the null hypothesis that there is spatial autocorrelation in the covariation pattern), and used Bootstrap resampling method to evaluate the contribution of cortical thickness abnormalities and gene transcriptomes to the covariation pattern. Examination of abnormal cortical thickness-immune gene transcriptome covariation patterns across mental disorders (P_{spin}=0.0190; bootstrap-estimated 95% confidence interval (CI) = (0.68, 0.87), one tailed).

Results: Hierarchical clustering based on the between-disorder Pearson correlation in cortical thickness abnormalities revealed that ASD and ADHD exist alone, while the other four diseases cluster into one cluster (Fig. 1a-c). PLS analysis on cross-disorder pattern showed a gradient from the prefrontal lobe (negative) to the occipital lobe (positive) (Fig.1d). We found that pathways with negative covariation are mainly concentrated in innate immunity, such as microglia activation, macrophage activation. In contrast, the pathways mainly focus on adaptive immunity, such as T cell differentiation regulation and lymph node development (P<0.05). The covariation pattern of ADHD is similar to the common covariation pattern, with the most positive/negative part appearing in the pericalcarine gyrus and temporal pole respectively (Fig.2a). The gradient pattern of cortical thickness-immune covariation in ASD is characterized by the frontal lobe (positive) and the temporal lobe (negative) (Fig.2b). The most negative parts of the other four disorders appear in the lateral parietal lobe and medial occipital lobe, while the positive part of the gene score is similar to the pattern of ASD, and the temporal lobe also shows positivity (Fig.2c). ASD showed a significant bias towards adaptive immunity in positive brain areas (P<0.001) while ADHD and the other four disorders did not show a bias toward innate/adaptive immunity (Fig.2a-c, dataset2). The immune pathway is also negative for ADHD and ASD (accounting for 33.8% and 37.8% respectively), but for the covariation patterns of the other four disorders, we did not observe the involvement of significant immune gene pathways (Fig.2d-f, dataset1).

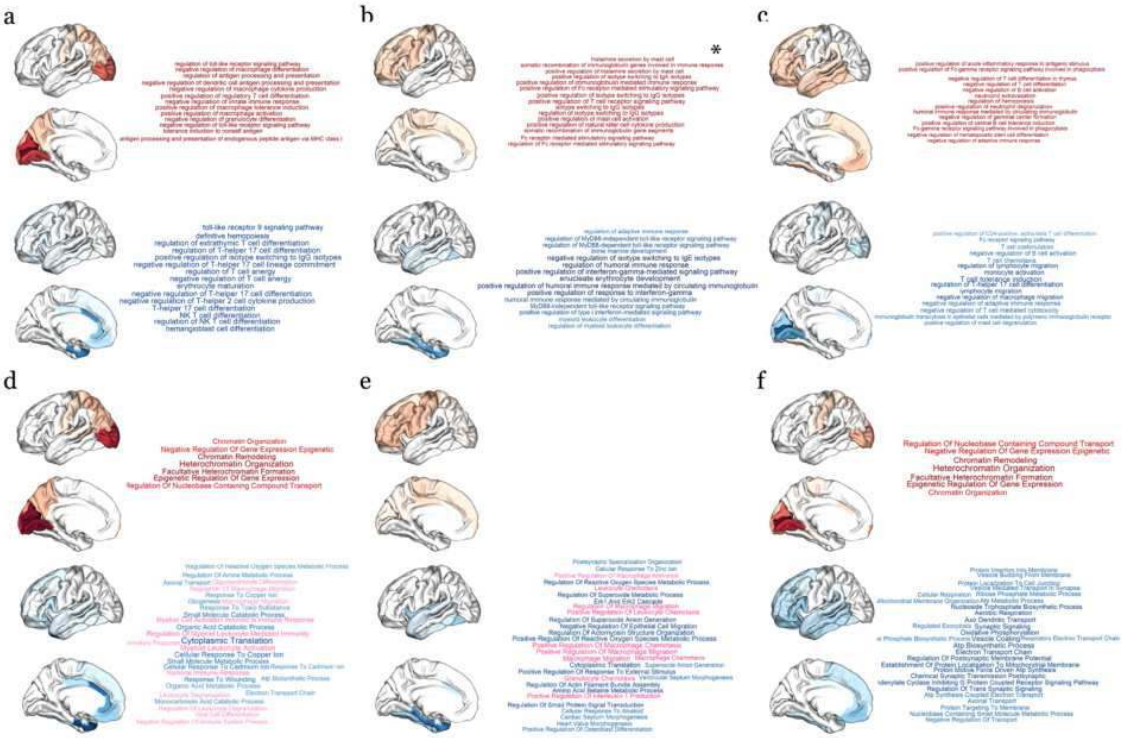

Fig.2| Abnormal cortical thickness-immune gene transcriptome-specific covariation patterns and AHBA gene transcriptome validation The 976 immune genes screened were used to conduct PLS covariation analysis with abnormal cortical thickness patterns of ADHD (a), ASD (b) and other four types of disorders (c). Only the positive pathway for ASD was significant in the rank sum test. The brain gradient map is the gene score pattern map, and the word cloud map is the visualization result of the most significant load of positive and negative genes. d, e, f, On a larger data set, we verified the importance of the immune mechanism in the covariation pattern, and the immune-involved pathways are highlighted in pink. There is no significant pathway in the positive part of ASD's covariation pattern (e). Statistical analysis of the immune covariation patterns of ADHD (P_{spin}<0.001; bootstrap-estimated 95% CI = (0.67, 0.86), one tailed), ASD (P_{spin}=0.16; bootstrap-estimated 95% CI = (0.59, 0.82), one tailed), and the four other disorders (P_{spin}<0.0001; bootstrap-estimated 95% CI = (-0.55, -0.84), one tailed) was performed using the Bootstrap resampling method and permutation tests that preserved spatial autocorrelation.

Conclusions: Covariation mechanism formed between gene transcriptome and cortical thickness abnormalities could align with mental disorder subtypes (ADHD, ASD and the other four disorders). These findings provide evidence for further elucidating the vulnerability mechanisms of mental disorders.

References

1. The Brainstorm Consortium. (2018), Analysis of shared heritability in common disorders of the brain. Science, 360, eaap8757.
2. Romero, C. (2022), Exploring the genetic overlap between twelve psychiatric disorders. Nature Genetics, 54, 1795–1802.
3. Boulanger, L. M. (2009), Immune Proteins in Brain Development and Synaptic Plasticity. Neuron, 64, 93–109.
4. Graeber, M. B. (2010), Changing Face of Microglia. Science, 330, 783–788.
5. Salam, A. P. (2018), Trained innate immunity: a salient factor in the pathogenesis of neuroimmune psychiatric disorders. Molecular Psychiatry, 23, 170–176.
6. Chen, Y. (2023), Neuroimmune transcriptome changes in patient brains of psychiatric and neurological disorders. Molecular Psychiatry, 28, 710–721.
7. Larivière, S. (2021),The ENIGMA Toolbox: multiscale neural contextualization of multisite neuroimaging datasets. Nature Methods, 18, 698–700.
8. Krishnan, A. (2011), Partial Least Squares (PLS) methods for neuroimaging: A tutorial and review. NeuroImage, 56, 455–475.
9. Hansen, J. Y. (2021), Mapping gene transcription and neurocognition across human neocortex. Nature Human Behaviour, 5, 1240–1250 .
10. Subramanian, A. (2005), Gene set enrichment analysis: a knowledge-based approach for interpreting genome-wide expression profiles. Proceedings of the National Academy of Sciences of the United States of America, 102, 15545–15550.
11. Mootha, V. K. (2003), PGC-1α-responsive genes involved in oxidative phosphorylation are coordinately downregulated in human diabetes. Nature Genetics, 34, 267–273.

Poster No 461

Preliminary evidence for altered brain-heart communication during anxiogenic movies

Peter Kirk[1], Oliver Robinson[1]

[1]*UCL, London, United Kingdom*

Introduction: During states of anxiety, fundamental threat circuitry in the brain can increase heart rate via alterations in autonomic balance (increased sympathetic activity and parasympathetic withdrawal) and may serve to promote interoceptive integration and awareness of cardiac signals. Moreover, evidence indicates pathological anxiety could be associated with increased communication between the brain and the heart. Yet, this phenomenon remains not well understood. For instance, studies in this area have been conducted within the confines of tightly-controlled experimental paradigms. Whether anxiety impacts brain-heart communication outside of such experimental settings, and in relatively more naturalistic contexts, is less clear.

Methods: Using a suspenseful movie fMRI paradigm (n=29 healthy volunteers; Caltech Conte dataset; Kliemann et al., 2022), we predicted that brain responses across an anxiety-relevant 'defensive response network' would show increased coherence with cardiac responses heart rate as a function of induced anxiety. That is, the coherence between brain activity and heart rate would be greater as participants watched a suspenseful movie clip compared to a non-suspenseful movie clip and during rest.

Results: Counter to our predictions, we found decreased coherence between heart rate and brain responses during increased anxiety, namely in amygdala-prefrontal circuitry (figure 1). Specifically, we demonstrated that suspenseful movie-watching was associated with reduced coherence between heart rate and: amygdala-dorsomedial prefrontal dynamic connectivity; amygdala-subgenual anterior cingulate dynamic connectivity; precuneus activity; vmPFC activity; and bilateral putamen activity.

Conclusions: Here, we found preliminary evidence for anxiety-relevant alterations in the coherence between heart rate and amygdala-prefrontal responding during movie-watching. However, effects were in the inverse direction to which we hypothesized. We posit that anxiety-relevant decreases in brain-heart coherence may be underpinned by parasympathetic withdrawal or decreased interoceptive awareness during suspenseful movie-watching.

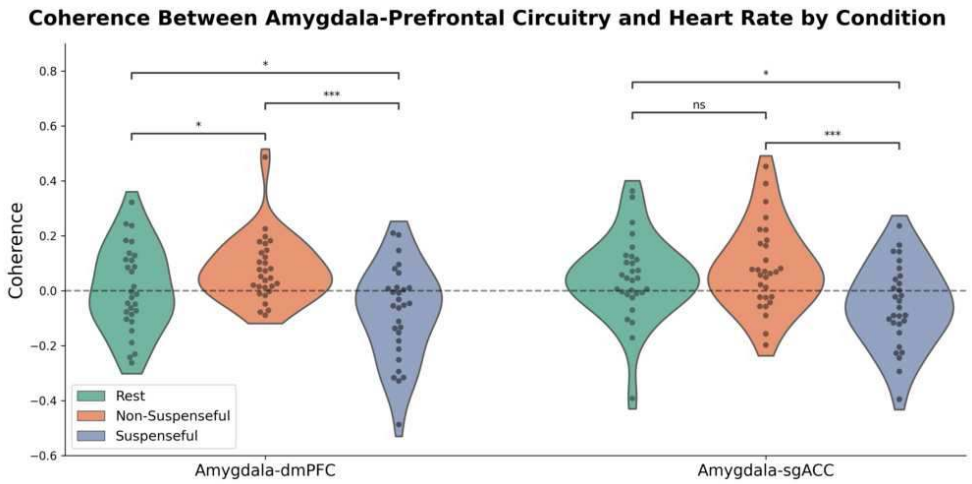

References

1. Kliemann, D., Adolphs, R., Armstrong, T., Galdi, P., Kahn, D. A., Rusch, T., Enkavi, A. Z., Liang, D., Lograsso, S., Zhu, W., Yu, R., Nair, R., Paul, L. K., & Tyszka, J. M. (2022). Caltech Conte Center, a multimodal data resource for exploring social cognition and decision-making. Scientific Data, 9(1), Article 1.

Poster No 462

Exploring brain temperature and free water as markers of neuroinflammation in major depression

Ben Moloney[1], Anna Forsyth[1], Rachael Sumner[1], Nicholas Hoeh[1], Frederick Sundram[1], Suresh Muthukumaraswamy[1], Joanne Lin[1]

[1]*University of Auckland, Auckland, New Zealand*

Introduction: Major depressive disorder (MDD) is a psychiatric condition affecting over 300 million people worldwide (World Health Organization, 2017). MDD is characterized by persistently low mood and motivation, loss of interest in activities, and, in severe cases, suicidality. Inflammation is thought to play a role in worsening depressive symptoms and inhibiting response to antidepressant medications through direct effects on the brain (Miller & Raison, 2016). However, current methods for measuring inflammation inside the brain, like lumbar puncture and positron emission tomography (PET) imaging, are invasive and not clinically feasible. Measuring neuroinflammation in vivo may allow for the a precise diagnosis and treatment of MDD cases with an inflammatory component than would otherwise be achievable by measuring peripheral inflammation. Regional brain temperature and metabolite concentrations measured using magnetic resonance spectroscopy (MRS) and diffusion metrics derived from neurite orientation density and dispersion index imaging (NODDI), such as free water, are sensitive to neuroinflammation and so may be clinically useful in identifying and monitoring it in MDD (Oestreich & O'Sullivan, 2022; Plank et al., 2022). This exploratory study aims to determine if there is a difference between these markers in the anterior cingulate cortex (ACC) and right insula in MDD compared to controls and whether this is associated with chronic low-grade peripheral inflammation.

Methods: Participants with MDD (n=25) who were moderately depressed and receiving pharmacological antidepressant therapy and healthy controls (n=13) were recruited. Participants with MDD were stratified into low and high peripheral inflammation subgroups based on their serum high-sensitivity C-reactive protein (hs-CRP) being consistently ≤ 1 mg/L or ≥ 3mg/L, respectively. MRS and diffusion-weighted imaging data were collected on a 3T Siemens Vida Fit scanner for each participant. Local temperature and N-acetyl aspartate, myoinositol, and choline levels relative to total creatine were measured in voxels placed in the dorsal anterior cingulate cortex (dACC) and right anterior insula. NODDI metrics, including the cerebrospinal fluid (CSF) volume fraction, a measure of free water, were extracted from the anterior cingulate gyrus and the right insula using masks derived from the Harvard-Oxford cortical structural atlas (Desikan et al., 2006). Metrics between MDD and control groups were compared using two-tailed independent sample t-tests. For metrics that differed significantly between groups, post-hoc comparisons were carried out between low and high peripheral inflammation MDD subgroups.

Results: Data from 23 participants in the MDD group and 12 participants in the control group were included in MRS analyses, and data from all participants were included in NODDI analyses. Participants in the MDD group (M=38.45, SD=0.43) exhibited significantly higher temperature in the dACC than the control group (M = 38.09, SD = 0.31), t(29) = -2.78, p=0.009. The CSF volume fraction was also significantly higher in the anterior cingulate gyrus of the MDD group (M = 0.036, SD = 0.011) than the control group (M=0.026, SD=0.008), t(32) = -3.19, p = 0.003. No significant difference between these markers in the low and high peripheral inflammation MDD subgroups was identified.

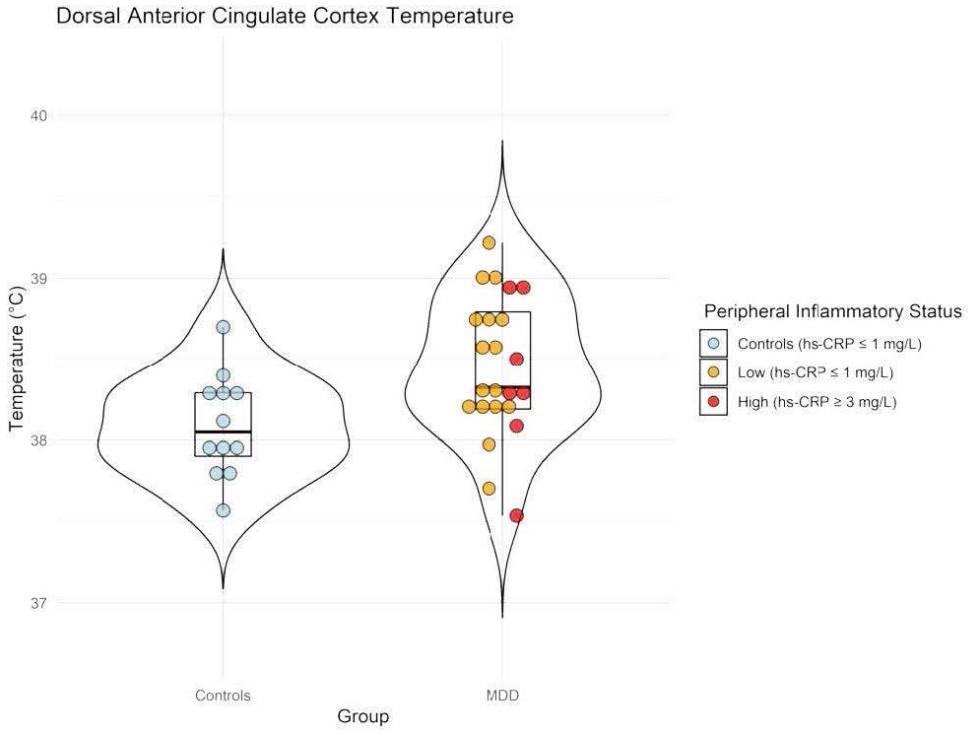

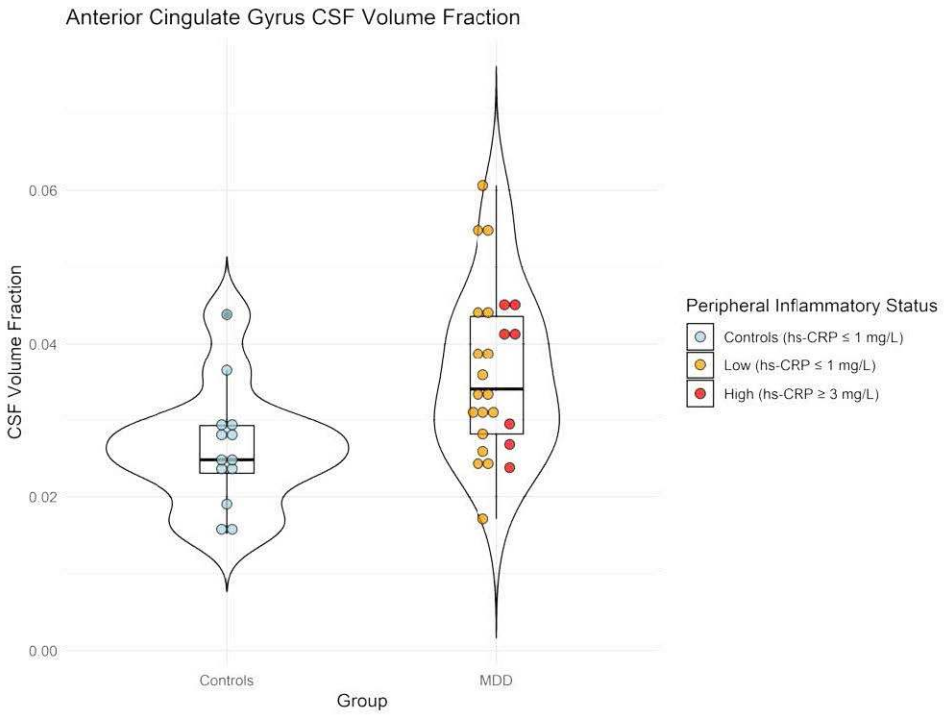

Conclusions: These results indicate that neuroinflammation may be occurring in the ACC in MDD, and that this may not be reflected by consistently elevated serum hs-CRP. This finding is consistent with post-mortem and positron emission tomography studies identifying neuroinflammation in the ACC in MDD (Enache et al., 2019). To further investigate ACC temperature and free water as markers of neuroinflammation in MDD, longitudinal research is required that tests them in relation to the effects of central nervous system anti-inflammatories and elucidates relationships with symptom profiles and outcomes for patients.

References

1. Desikan, R. S. (2006), 'An automated labeling system for subdividing the human cerebral cortex on MRI scans into gyral based regions of interest', NeuroImage, vol. 31 no. 3, pp. 968-980
2. Enache, D. (2019), 'Markers of central inflammation in major depressive disorder: A systematic review and meta-analysis of studies examining cerebrospinal fluid, positron emission tomography and post-mortem brain tissue', Brain, Behavior, and Immunity, vol. 81, pp. 24-40
3. Miller, A. H. (2016), 'The role of inflammation in depression: from evolutionary imperative to modern treatment target', Nature Reviews Immunology, vol. 16, no. 1, pp. 22-34
4. Oestreich, L. K. L. (2022), 'Transdiagnostic In Vivo Magnetic Resonance Imaging Markers of Neuroinflammation' Biological Psychiatry: Cognitive Neuroscience and Neuroimaging. vol. 7, no. 7, pp. 638-658
5. Plank, J. R. (2022), 'Brain temperature as an indicator of neuroinflammation induced by typhoid vaccine: Assessment using whole-brain magnetic resonance spectroscopy in a randomised crossover study', NeuroImage: Clinical, vol. 35
6. World Health Organisation. (2017), 'Depression and Other Common Mental Disorders: Global Health Estimates'

Poster No 463

Machine Learning Study on Dissociative Symptoms and the Relationship with Structural Brain Regions

John Fanning[1], Caroline Plett[1], Anne Ruef[1], Joseph Kambeitz[2], Raimo K. Salokangas[3], Jarmo Hietala[3], Alessandro Bertolino[4], Stefan Borgwardt[5], Paolo Brambilla[6], Rachel Upthegrove[7], Stephen J. Wood[8], Rebecca Lencer[9], Eva Meisenzahl[10], Peter Falkai[11], Lisa Hahn[1], Nikolaos Koutsouleris[1]

[1]Department of Psychiatry and Psychotherapy, LMU University Hospital, LMU Munich, Munich, Bavaria, [2]Department of Psychiatry and Psychotherapy, University of Cologne, Cologne, Bavaria, [3]Department of Psychiatry, University of Turku, Turku, Finland, [4]Department of Basic Medical Science, Neuroscience and Sense Organs, University of Bari Aldo Moro, Bari, Bari, [5]Department of Psychiatry and Psychotherapy, University of Lübeck, Lübeck, Germany, [6]Department of Neurosciences and Mental Health, Fondazione IRCCS Ca' Granda Ospedale Maggiore Policli, Milan, Italy, [7]Institute of Mental Health, University of Birmingham, Birmingham, United Kingdom, [8]Centre for Youth Mental Health, University of Melbourne, Melbourne, Australia, [9]Institute for Translational Psychiatry, University Münster, Münster, Germany, [10]Department of Psychiatry and Psychotherapy,

Medical Faculty, Heinrich Heine University, Düsseldorf, Germany, [11]Department of Psychiatry and Psychotherapy, LMU University Hospital, LMU Munich, Munich, Germany

Introduction: Depersonalization and derealization are highly distressing symptoms that are not only confined to trauma-related diagnoses, such as post-traumatic stress disorder, but also frequently emerge in psychotic and affective conditions. Structural brain imaging studies have identified associations between regional brain volumes and these dissociative symptoms; however, there is a lack of evidence whether the presence of these symptoms in early-stage affective and psychotic patients can be predicted at the individual level using brain imaging data. In this study we attempt to predict the presence of the two dissociative symptoms using structural imaging as well as explore how closely related the measured brain patterns relate to childhood trauma and/or life events.

Methods: The current study employed a machine learning-based approach to predict the presence of derealization (n = 605) and depersonalization (n = 602) using structural brain imaging of patients collected from the multisite PRONIA study cohort. The sample consisted of healthy controls and patients with recent-onset psychosis, recent-onset depression, and clinical high-risk of developing psychosis. We created support vector machines with a 10-fold nested cross validation scheme to facilitate the prediction of our sample for each of the symptoms seperately. Additionally, the decision scores derived from these models were correlated with the Childhood Trauma Questionnaire and the Cologne Chart of Life Events.

Results: Two stratifications of the sample were created to independently analyze derealization and depersonalization symptom presence as assessed by SPI-A O8 and SPI-A F6 scores, respectively. Balanced accuracy in the support vector machine models using structural imaging for derealization symptoms was 58.7% (sensitivity = 80.0%, specificity = 37.6%), and 54.5% for depersonalization symptoms (sensitivity: 66.4%, specificity: 42.5%). Furthermore, the decisions scores from the models showed no significant relationships between either of the trauma-based questionnaires.

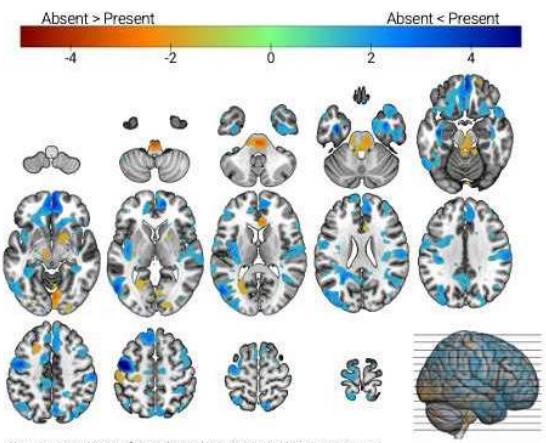

Figure 1a. Mosaic of Sign-based Consistency Map on MNI152 standard for the Derealization model.

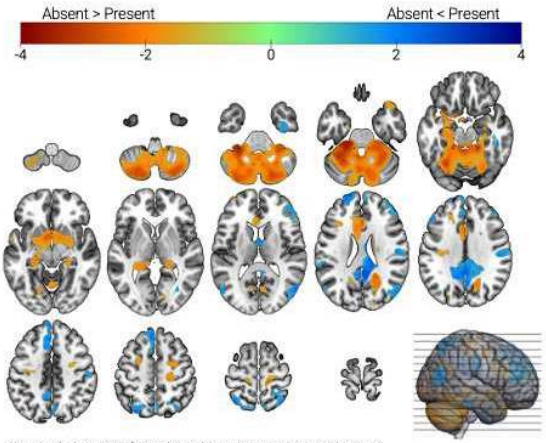

Figure 1b. Mosaic of Sign-based Consistency Map on MNI152 standard for the Depersonalization model.

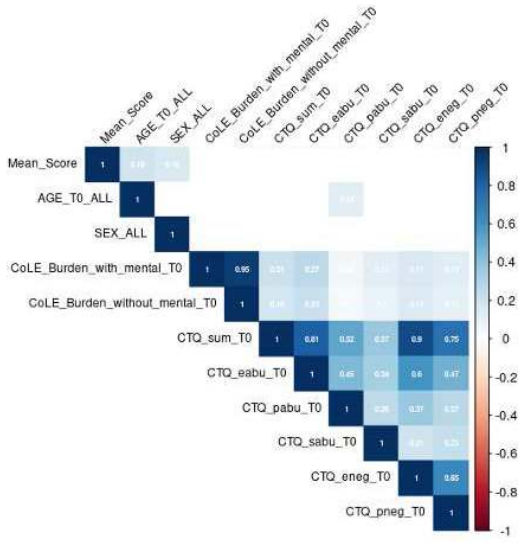

Figure 2. Correlation matrix showing the relationship between the decision scores and the items from the Cologne Chart of Life Events and the Childhood Trauma Questionnaire.

Conclusions: The machine learning analyses identified a signal using structural brain imaging to identify dissociative symptoms in a trans-diagnostic sample of early-stage affective and psychotic patients. However, both models showed poor performance predicting the presence of either symptom, which suggests that the SPI-A may be an ineffective tool to fully assess these symptoms. This notion is supported from the correlational analyses, in which no significant relationships were found. Future investigations could use different questionnaires like the Dissociative Experiences Scale to find a more robust measure for the prediction of these symptoms.

References

1. Büetiger, J.R. (2020). 'Trapped in a Glass Bell Jar: Neural Correlates of Depersonalization and Derealization in Subjects at Clinical High-Risk of Psychosis and Depersonalization–Derealization Disorder', Frontiers in Psychiatry, vol. 11
2. Lotfinia, S. (2020). 'Structural and functional brain alterations in psychiatric patients with dissociative experiences: A systematic review of magnetic resonance imaging studies', Journal of Psychiatric Research, vol. 128, pp. 5-15
3. Lyssenko, L. (2018), 'Dissociation in Psychiatric Disorders: A Meta-Analysis of Studies Using the Dissociative Experiences Scale', The American Journal of Psychiatry, vol. 175, no. 1, pp. 37-46

Poster No 464

Thalamic Subnuclei Connectivity in Major Depressive Disorder: A 7-Tesla Diffusion MRI Study

Weijian Liu[1], Jurjen Heij[2], Shu Liu[1], Luka Liebrand[3], Matthan Caan[3], Wietske van der Zwaag[4], Dick Veltman[5], Lin Lu[6], Moji Aghajani[7], Guido Wingen[1]

[1]Amsterdam UMC location University of Amsterdam, Amsterdam, North Netherlands, [2]Spinoza Centre for Neuroimaging, KNAW, Amsterdam, North Netherlands, [3]Amsterdam Neuroscience, Amsterdam, North Netherlands, [4]Spinoza Centre for Neuroimaging, KNAW, Amsrwedam, North Netherlands, [5]Amsterdam UMC location Vrije Universiteit Amsterdam, Department of Psychiatry, Amsterdam, North Netherlands, [6]Peking University Sixth Hospital, Beijing, Beijing, [7]Amsterdam UMC location Vrije Universiteit Amsterdam, Amsterdam, North Netherlands

Introduction: The thalamus serves as a central relay station within the brain, and thalamic connectional anomalies are increasingly thought to be present in major depressive disorder (MDD). However, the use of conventional MRI scanners and acquisition techniques has prevented a thorough examination of the thalamus and its subnuclear connectional profile. We combined ultra-high field diffusion MRI acquired at 7.0 Tesla to map the white matter connectivity of thalamic subnuclei.

Methods: Fifty-three MDD patients and 12 healthy controls (HCs) were involved in the final analysis. Freesurfer was used to segment the thalamus into 14 subnuclei: anteroventral nucleus (AV), lateral nucleus (LTR), ventral anterior nucleus (VA), ventral lateral anterior nucleus (VLa), ventral lateral posterior nucleus (VLp), ventral posterolateral nucleus (VPL), intralaminar nucleus (ITL), medial nucleus (MED), lateral geniculate nucleus (LGN), medical geniculate nucleus (MGN), limitans (suprageniculate) nucleus (L-SG), pulvinar medial nucleus (PuM), pulvinar lateral nucleus (PuL), and pulvinar inferior nucleus (Pul). MRtrix was used to perform the preprocessing and tractography. Fractional anisotropy (FA), axial diffusivity (AD), mean diffusivity (MD), radial diffusivity (RD), and streamline count (SC) of thalamic subnuclear tracts were measured as proxies of white matter integrity. Bayesian analysis of covariance (ANCOVA) was used to assess group differences in white matter metrics for each thalamic subnuclear tract. Age, gender, and intracranial volume (ICV) were regarded as covariates. The Bayesian factor (BF) was interpreted using the following evidence categories: BF < 3 (and its reciprocal) indicates anecdotal evidence for Hypothesis 1; BF ≥ 3 corresponds to moderate evidence; BF ≥ 10 suggests strong evidence; BF ≥ 30 represents very strong evidence; and BF ≥ 100 indicates extreme evidence. Only results with BF ≥ 3 for group effects are reported.

Results: All tracts with moderate or greater evidence in Bayesian ANCOVA are presented, and they essentially project into regions reported in previous literature or anatomical evidence (Figure 1). Bayesian ANCOVA identified very strong evidence that MDD patients have lower SC of tracts spanning from left PuM than HC participants (Figure 2. A). Similarly, moderate evidence that MDD patients have lower AD of tracts spanning from left VLa than HC participants were identified (Figure 2. B). Furthermore, lower FA of tracts spanning from right ITL was observed in MDD patients compared to HCs, with moderate evidence (Figure 2. C). Strong evidence that severe MDD patients have lower FA of tracts spanning from right Pul than non-severe MDD was identified by the Bayesian ANCOVA (Figure 2. D). Moderate evidence was found by the Bayesian ANCOVA that medicated MDD patients have higher AD in tracts spanning from the right VLa compared to MDD patients not taking any psychotropic medications (Figure 2. E). Compared to patients with typical MDD, the Bayesian ANCOVA analysis provided moderate evidence that patients with atypical MDD exhibit higher RD in tracts spanning from right Pul (Figure 2. F). MDD patients with high anxiety had four higher DTI indicators (AD of tracts spanning from right VLa, right VPL, right ITL, and left MED) than MDD patients with low anxiety, which was determined to be moderate evidence by Bayesian ANCOVA (Figure 2. G-J). The Bayesian ANCOVA identified moderate evidence that MDD patients with adult age of onset had higher SC of tracts

spanning from left PuM than MDD patients with juvenile age of onset (Figure 2. K). For SC of tracts spanning from left LGN, moderate evidence was found that MDD patients with adult age of onset had lower values than those with juvenile age of onset (Figure 2. L).

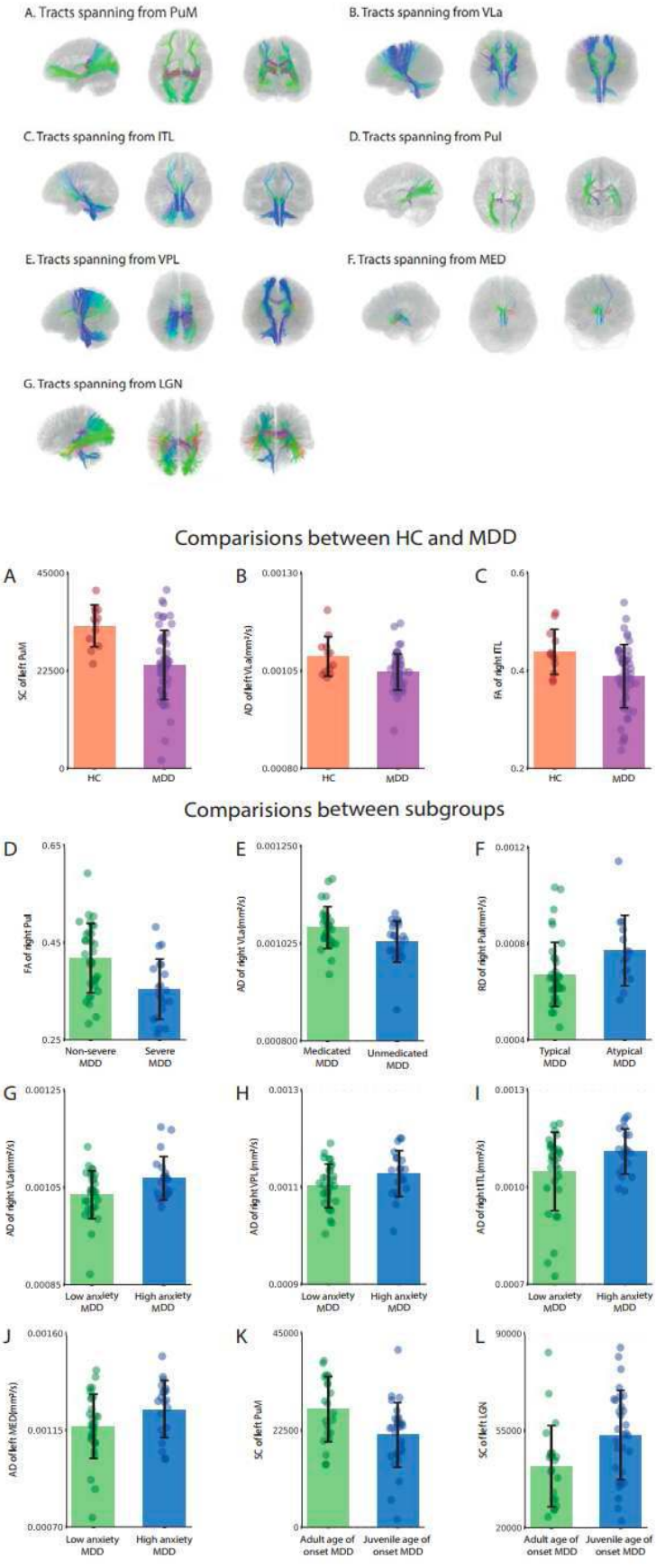

Conclusions: MDD and several clinical characteristics are related to perturbed thalamic subnuclear connectivity with cortical and subcortical circuits that govern sensory processing, emotional function, and goal-directed behavior.

References

1. Basser, P. J., J. Mattiello, and D. LeBihan. (1994). "MR Diffusion Tensor Spectroscopy and Imaging." Biophysical Journal 66 (1): 259–67.
2. Fischl, Bruce. 2012. "FreeSurfer." NeuroImage 62 (2): 774–81.
3. Iglesias, Juan Eugenio, Ricardo Insausti, Garikoitz Lerma-Usabiaga, Martina Bocchetta, Koen Van Leemput, Douglas N. Greve, Andre van der Kouwe, Bruce Fischl, César Caballero-Gaudes, and Pedro M. Paz-Alonso. (2018). "A Probabilistic Atlas of the Human Thalamic Nuclei Combining Ex Vivo MRI and Histology." NeuroImage 183 (December): 314–26.
4. Lee, Michael D., and Eric-Jan Wagenmakers. (2014). Bayesian Cognitive Modeling: A Practical Course. Cambridge university press.
5. Otte, C., S. M. Gold, B. W. Penninx, C. M. Pariante, A. Etkin, M. Fava, D. C. Mohr, and A. F. Schatzberg. 2016. "Major Depressive Disorder." Nat Rev Dis Primers 2 (September): 16065.
6. Smith, Robert E., Jacques-Donald Tournier, Fernando Calamante, and Alan Connelly. (2012). "Anatomically-Constrained Tractography: Improved Diffusion MRI Streamlines Tractography through Effective Use of Anatomical Information." NeuroImage 62 (3): 1924–38.
7. Strotmann, Barbara, Robin M. Heidemann, Alfred Anwander, Marcel Weiss, Robert Trampel, Arno Villringer, and Robert Turner. (2014). "High-Resolution MRI and Diffusion-Weighted Imaging of the Human Habenula at 7 Tesla." Journal of Magnetic Resonance Imaging 39 (4): 1018–26.
8. Zhang, Yuxuan, Yingli Zhang, Hui Ai, Nicholas T Van Dam, Long Qian, Gangqiang Hou, and Pengfei Xu. 2022. "Microstructural Deficits of the Thalamus in Major Depressive Disorder." Brain Communications 4 (5): fcac236.

Poster No 465

Common spatial patterns link network correlates of cocaine use disorder and D2/3 receptor densities

Jocelyn Ricard[1], Loic Labache[2], Ashlea Segal[2], Elvisha Dhamala[3], Carrisa Cocuzza[2], Grant Jones[4], Sarah Yip[2], Sidhant Chopra[2], Avram Holmes[5]

[1]Stanford University, Stanford, CA, [2]Yale University, New Haven, CT, [3]Feinstein Institutes for Medical Research, Glen Oaks, NY, [4]Harvard University, Cambridge, MA, [5]Department of Psychiatry, Brain Health Institute, Rutgers University, Piscataway, NJ

Introduction: Prior work on the development and maintenance of substance use has largely focused on cortico-striatal circuits and associated aspects of the dopamine system, with relatively less attention on corresponding alterations within and across large-scale functional brain networks (Koob et al., 2010). Critically, the functional connectome correlates of substance use and their specificity to dopamine receptor densities relative to other metabotropic receptors classes remains to be established.

Methods: In an open-access dataset of participants with cocaine use disorder (n=69) and healthy matched controls (n=62) (Angeles-Valdez et al., 2022), we characterized brain-wide functional connectivity (FC) for each subject by computing pairwise Pearson correlations between timeseries extracted from 432 regions. To comprehensively delineate brain-wide alterations in FC, we examine group differences at each edge, using the Network Based Statistic (Zalesky et al., 2010) to correct for multiple comparisons. We present the results at three different scales: (a) the level of individual connections (i.e., where edges are either under- or over-connected, or hypo- versus hyperconnectivity, respectively); (b) the level of individual brain regions, to identify specific brain areas which had a high number of significant connections, and (c) the level of large-scale functional brain networks, analyzed both within- and between- networks. Further, we studied the relationship between the observed FC signatures of cocaine use and the spatial distribution of a broad range of normative neurotransmitter receptor and transporter bindings as assessed through positron emission tomography (PET) using an open-access toolbox, neuromaps (Markello et al., 2022).

Results: Our analyses identified a widespread profile of FC differences between individuals with cocaine use disorder and matched healthy comparison participants (8.8% of total edges; 8,185 edges; pFWE=0.025). Broadly, we observed reduced between-network connectivity linking default network and subcortical regions in participants with cocaine use disorder. Higher within-network connectivity in the default network was also evident in participants with cocaine use disorder (Figure 1). Furthermore, our observations revealed consistent replicable associations between signatures of cocaine use and normative spatial density of dopamine D2/3 receptors (Figure 2).

Conclusions: Our analyses revealed a widespread profile of altered connectivity in individuals with cocaine use disorder that extends across the functional connectome and implicates multiple circuits. This profile is robustly coupled with normative dopamine D2/3 receptors densities. Thus, this work has broad implications on the neurobiological mechanisms of cocaine use disorder and potential development of personalized interventions.

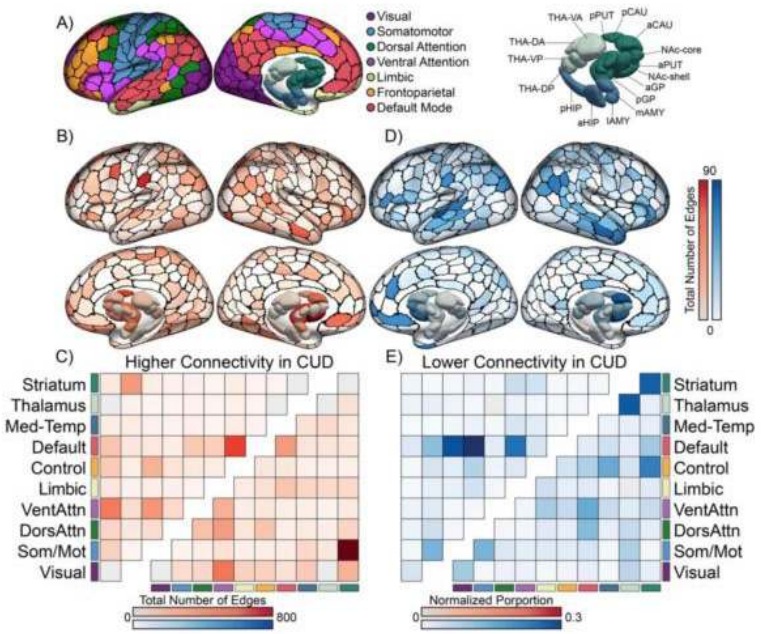

Figure 1. Whole brain atypical functional connectivity in cocaine use disorder. A widespread network of affected connections exists between individuals with cocaine use disorder and healthy matched controls, extending across the functional connectome. A) Schaefer 7-network (Schaefer et al., 2018, Yeo et al., 2011) and Tian subcortex parcellations (Scale II) (Tian et al., 2020) from left to right: a Indicates anterior; AMY, amygdala; CAU, caudate nucleus; d, dorsal; DA, dorsoanterior; DMN, default mode network; DorsAttn, dorsal attention network; DP, dorsoposterior; FPN, frontoparietal network; GP, globus pallidus; HIP, hippocampus; l, lateral; Lim, cortical limbic network; m, medial; MTL, medial-temporal lobe (amygdala and hippocampus); NAc, nucleus accumbens; p, posterior; SomMot, somatomotor network; Stri, striatum; PUT, putamen; THA, thalamus. B) Images with a red color scale represent number of significant edges where individuals with cocaine use disorder show hyperconnectivity. B) Images with a red color scale represent number of significant negative edges of NBS network where individuals with cocaine use disorder show hypoconnectivity. C) Heatmap quantified using raw total edge count (upper triangle) and normalized proportion of edges based upon network size (lower triangle) within the NBS component that fall within each of the canonical networks. The darker red indicates higher connectivity in cocaine use disorder. D) Images with a blue color scale represent number of significant negative edges of NBS network where individuals with cocaine use disorder show hypoconnectivity. E) Heatmap quantified using raw total edge count (upper triangle) and normalized proportion of edges based upon network size (lower triangle) within the NBS component that fall within each of the canonical networks. Darker blue color indicates lower connectivity in cocaine use disorder.

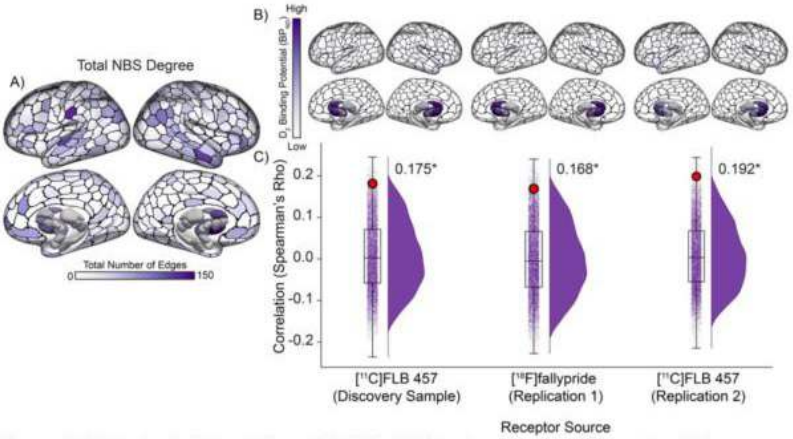

Figure 2. Whole-brain Network Based Statistic (NBS) network and spatial overlap of $D_{2/3}$ receptor density in cocaine use disorder. A) Visualization of the total (positive + negative) number of significant edges at each region within the NBS component (**Fig. 1B** + **1D**) where change in fcMRI was significantly correlated with the spatial $D_{2/3}$ receptor density in a discovery sample (Sandiego 2015, p_{spin}=0.019) and two replication samples (Jaworska 2020, p_{spin}=0.030 and Smith 2017, p_{spin}=0.013), respectively). B) $D_{2/3}$ binding potential of PET samples for each receptor source, i.e., discovery sample and replication samples. C) Each violin-box plot contains (from left to right) distribution of 10k spin-test null correlations between each edge of the NBS component and the spatial density of $D_{2/3}$ receptors. Red dot indicates significant spearman's correlation. *'s reflect statistical significance at the threshold p_{spin}<0.05. Discovery Sample: Sandiego et al., (2015) (8); Replication 1: Jaworska et al., 2020 (9); Replication 2: Smith et al., 2017 (10).

References
1. Angeles-Valdez, D., et al., (2022). The Mexican magnetic resonance imaging dataset of patients with cocaine use disorder: SUDMEX CONN. Scientific data, 9(1), 133.
2. Jaworska, N., et al., (2020). Extra-striatal D2/3 receptor availability in youth at risk for addiction. Neuropsychopharmacology, 45(9), 1498-1505.
3. Koob, G. F., et al., (2010). Neurocircuitry of addiction. Neuropsychopharmacology, 35(1), 217-238.
4. Markello, R. D., et al., (2022). Neuromaps: structural and functional interpretation of brain maps. Nature Methods, 19(11), 1472-1479.
5. Sandiego, C. M., et al., (2015). Reference region modeling approaches for amphetamine challenge studies with [11C] FLB 457 and PET. Journal of Cerebral Blood Flow & Metabolism, 35(4), 623-629.
6. Schaefer, A., et al., (2018). Local-global parcellation of the human cerebral cortex from intrinsic functional connectivity MRI. Cerebral cortex, 28(9), 3095-3114.
7. Smith, C. T., et al., (2017). The impact of common dopamine D2 receptor gene polymorphisms on D2/3 receptor availability: C957T as a key determinant in putamen and ventral striatum. Translational psychiatry, 7(4), e1091-e1091.
8. Tian, Y., et al., (2020). Topographic organization of the human subcortex unveiled with functional connectivity gradients. Nature neuroscience, 23(11), 1421-1432.
9. Thomas Yeo, B. T., et al., (2011). The organization of the human cerebral cortex estimated by intrinsic functional connectivity. Journal of neurophysiology, 106(3), 1125-1165.
10. Zalesky, A., et al., (2010). Network-based statistic: identifying differences in brain networks. Neuroimage, 53(4), 1197-1207.

Poster No 466

Connectivity changes after ketamine in treatment resistant depression and receptor expression

Jen Evans[1], Carlos Zarate[2]

[1]NIH, Bethesda, MD, [2]National Institute of Mental Health/NIH, Bethesda, MD

Introduction: The rapid acting antidepressant ketamine is described as being a glutamatergic modulator (Zarate, 2017) but its exact mechanism of action remains an active area of research. Recent developments in making neurotransmitter atlases available enables the investigation of the overlap of functional changes and receptor density. Robust changes in the BOLD signal have been measured after a ketamine infusion (McMillan, 2020) but most studies have been performed in healthy volunteers with drug doses that differ from that administered in clinical treatment. Here we investigate functional connectivity changes administration in unmedicated patients with treatment resistant major depression in conjunction with receptor density maps.

Methods: Fourteen patients (mean age 35 years, [19-61]) with treatment resistant major depression underwent a double-blind placebo cross-over trial where they received either a 40 minute infusion of either 0.5 mg/kg racemic ketamine or saline placebo while they were being scanned in a 3T Siemens Skyra scanner with 1 week between each infusion. Briefly, a 15 minute eyes closed resting state scan was acquired prior to (baseline) and from approximately 20-35 minutes after the start of the infusion (post). Multi-echo fMRI data (3mm isotropic, TR: 2.08 s, TEs: 13,27,47 ms, FA: 75 degrees) was preprocessed with afni_proc with slice-timing correction, motion alignment, registration to MNI space, and spatial smoothing to 4mm and anaticor. Correlation matrices were generated for each scan using 3dNetcorr (Taylor, 2013) using the Schaefer 100 parcellation (Schafer, 2018) and split into positive and negative change matrices. Neuromaps was used to generate receptor density maps following Hansen et al., 2022. Receptor densities were correlated against correlation changes using python's scipy.stats module.

Results: Figure 1a illustrates the group average correlation change (baseline – post) matrices for the ketamine (ket) and placebo (pbo) sessions. The post-ketamine scan has widespread connectivity changes, which show regional specificity. Figure 1b shows the spatial locations of the positive and negative edges of the correlation changes. For reference, figure 2a shows the spatial distribution of glutamate receptors displayed using the same functional parcellation. The connectivity changes during the ketamine infusion are correlated against the density of glutamate receptors in figure 2b, demonstrating a weak but significant correlation between the negative edges (R2 :0.08 p: 0.004) but not for the positive (R2 :0.02 p: 0.13). Several other receptors also demonstrate significant relations notably serotonin (5HT*), mu opioid (MOR), cannabinoid (CB1) and muscarinic (M1). Interestingly, there was not a strong relation with functional changes and NMDA receptors which have also been implicated in ketamine's mechanism of action. Comparable motion values were measured between paired ketamine and placebo scans suggesting that this result is not an effect of increased motion during drug administration.

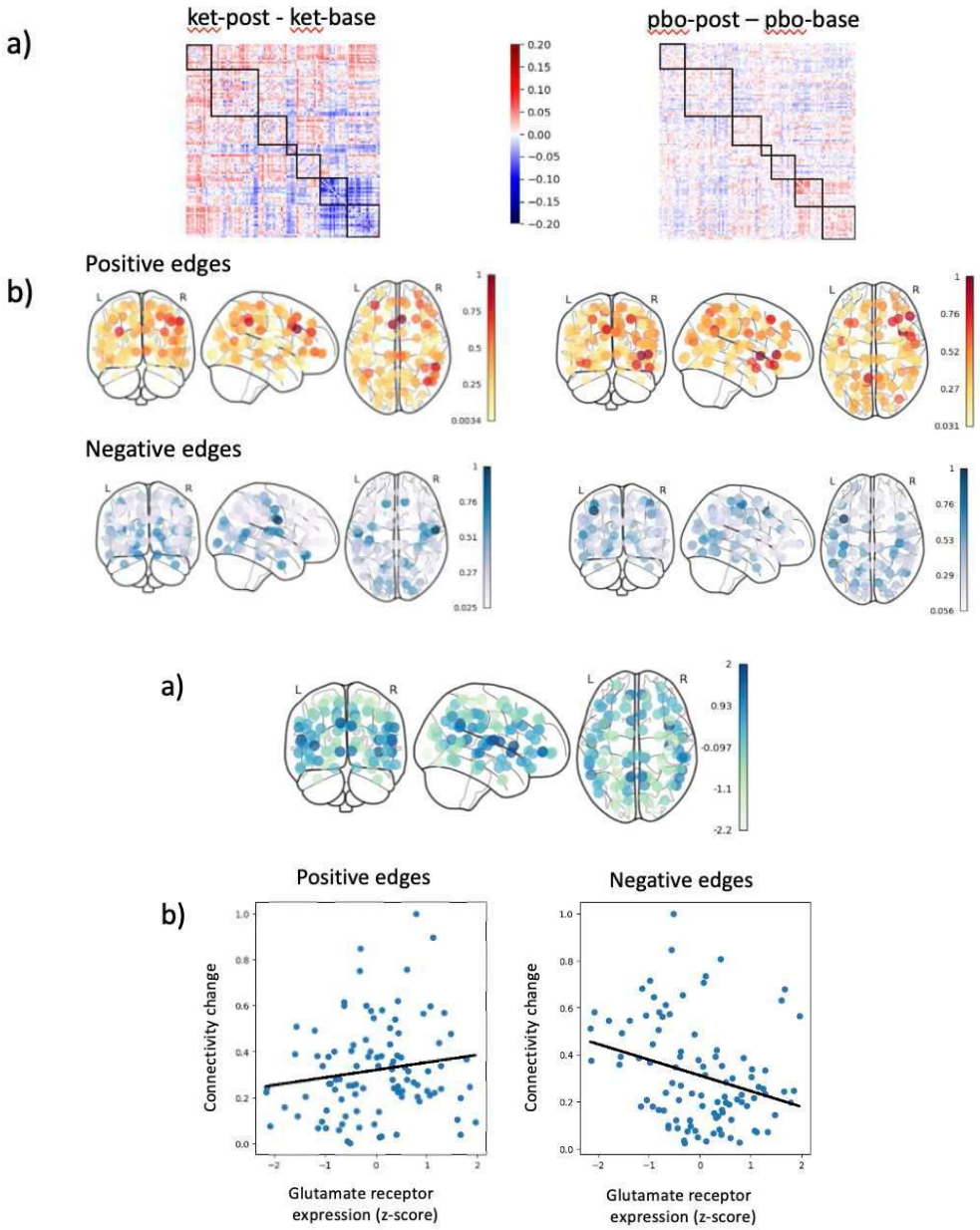

Conclusions: The very early functional connectivity changes expressed by this depressed patient sample during a ketamine infusion reflect glutamatergic receptors involvement commensurate with ketamine's expected mechanism of action. Relating functional changes to the neurotransmitter architecture may be a step towards bridging preclinical development of drugs and their application in the clinic. Further, using individualized correlations with behavioral changes may help investigate differences in behavioral response.

References

1. Hansen J.Y. Nat. Neurosci. 25, 1569–1581 (2022).
2. Nugent, AC. (2019) Mol Psychiatry Jul;24(7):1040-1052.
3. McMillan, R. (2020) Reviews in the Neurosciences, vol. 31, no. 5
4. Schaefer, A., (2018), Cereb Cortex, Sep 1;28(9):3095-3114
5. Taylor, PT (2013) Brain Connectivity 3:5;523-35.
6. Zarate, CA, (2017) Molecular Psychiatry,volume 22:324–327

Poster No 467

Resting State Functional Connectivity in Cannabis Users: The Moderating Role of Cannabis Attitudes

Emese Kroon[1], Yara Toenders[1], Lauren Kuhns[2], Janna Cousijn[1], Francesca Filbey[3]

[1]Erasmus University Rotterdam, Rotterdam, Zuid-Holland, [2]University of Amsterdam, Amsterdam, Noord-Holland, [3]University of Texas at Dallas, Dallas, TX

Introduction: The global increase in lenient cannabis policy has been paralleled by reduced harm perception, which appears to affect cannabis use initiation and persistent use[1]. Substance use disorders have been associated with altered resting-state functional connectivity (RSFC) in various neural networks, including the executive control network (ECN), salience network (SN), and default mode network (DMN). These alterations are thought to result in increased salience of substance-related cues and introspective processes, combined with a lack of control over the motivational urges to use[2]. However, studies on RSFC in cannabis users are limited and yield inconsistent results. Furthermore, given evidence from the growing field of cultural neuroscience - demonstrating interactions between sociocultural factors and brain mechanisms[3] - it is likely that similar sociocultural factors affect the brain processes underlying substance use. Nevertheless, it is unclear how cannabis attitudes may affect brain processes including RSFC underlying cannabis use and cannabis use disorder (CUD)

Methods: RSFC within the ECN, SN, and DMN was assessed in 110 near-daily cannabis users with CUD and 79 closely matched controls aged 18-30 from The Netherlands and Texas, USA. Matched scan sequences were used to record an 8-minute T2* functional scan assessing BOLD responses while resting with eyes closed. Participants completed an adapted version of the cannabis culture questionnaire[4], assessing the perceived benefits and harms of cannabis use from their personal, friends-family's and country-state's perspective and reported on their cannabis use (gram/week) and DSM-5 CUD symptoms count. After preprocessing, mean time series were extracted from each of the pre-defined ROI templates of the networks of interest[5] before the activity time series from each network were regressed out of the individual timeseries, resulting in an individual within-network RSFC map for each network of interest. Permutation tests were used to assess 1) group differences in within-network RSFC, 2) associations between the measures of cannabis use and 3) within-network RSFC in the CUD group, and whether cannabis attitudes moderated these associations. Site was added as a covariate to all models to control for potential effects of scanner differences.

Results: RSFC within the dorsal SN was lower in the CUD group than controls, and heavier cannabis use within the CUD group was associated with lower dorsal SN RSFC. Perceived benefits and harms of cannabis use moderated associations of cannabis use (Fig. 1) and CUD severity (Fig. 2) with within-network RSFC of multiple networks of interest. The association between CUD scores and ventral DMN RSFC was less negative in those perceiving more positive country-state attitudes. The association between CUD scores and anterior SN RSFC was positive in those perceiving less negative country-state attitudes, while this association was negative in those perceiving more negative country-state attitudes. Focusing on personal negative attitudes, the association between cannabis use and both dorsal DMN and left ECN RSFC appears to be more negative in those with more negative attitudes. Looking at personal positive attitudes, the pattern is reversed: the association between cannabis use and dorsal DMN RSFC is more positive in those with more positive attitudes.

Conclusions: These results indicate that while positive and negative attitudes appear to have opposite moderating effects when assessed within the same brain region, the direction of the effect is highly dependent on the network/area and show that results from a specific region can be conflicting dependent on its role in different networks. Our findings highlight the importance of considering individual differences in the perceived harms and benefits of cannabis use as a factor in the associations between brain functioning and heaviness of cannabis use and CUD severity.

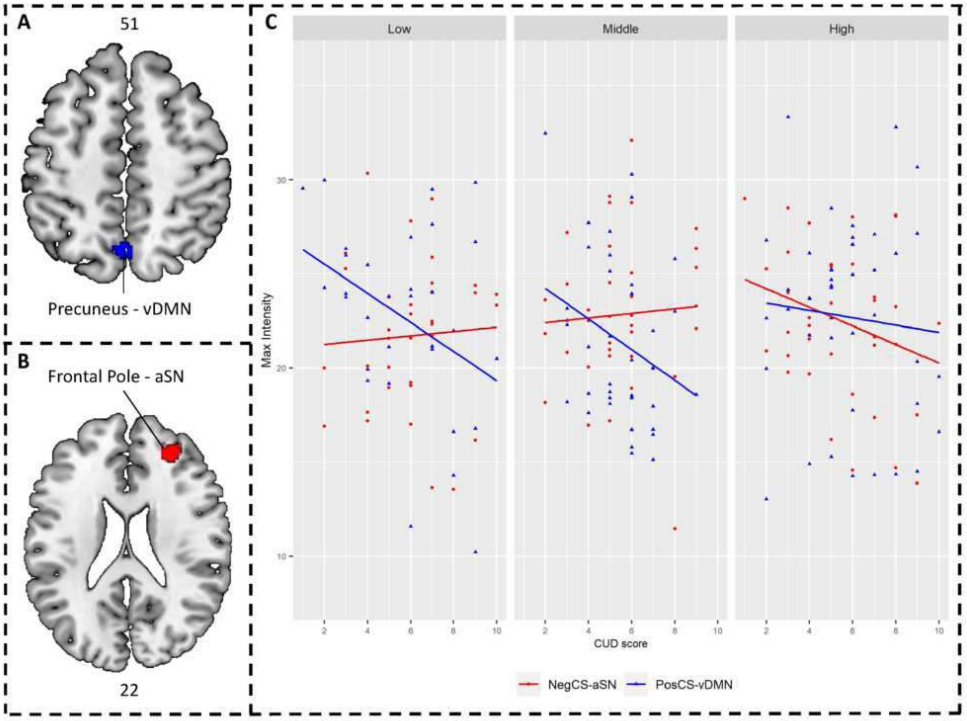

Figure 1. Associations between within-network resting state functional connectivity and CUD scores: the moderating role of cannabis attitudes. A) transversal view of the precuneus cluster as part of the ventral default mode network (vDMN), image MNI Z-coordinate = 51, B) transversal view of the frontal pole cluster as part of the anterior salience network (aSN), image MNI Z-coordinate = 22, C) moderating effects of negative country/state (NegCS) and positive country/state (PosCS) attitudes on the associations between maximum extracted cluster intensity (y-axis) and CUD scores (x-axis). A tertiary split was used to visualize the effect of the continuous culture variables.

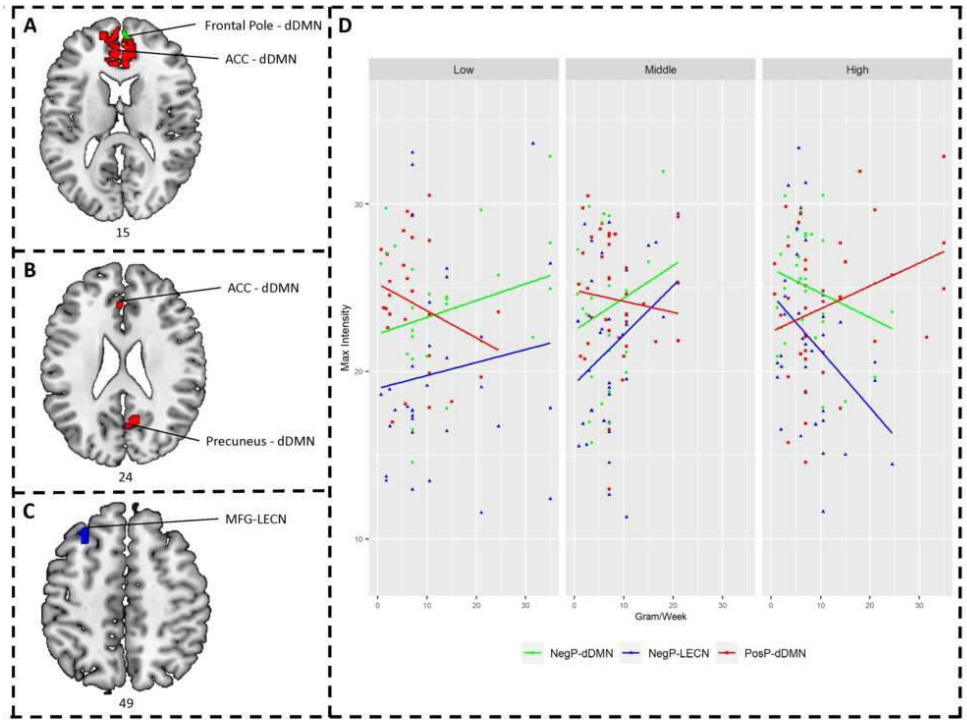

Figure 2. Associations between within-network resting state functional connectivity and gram/week: the moderating role of cannabis attitudes. A) transversal view of the anterior cingulate cortex (ACC) and the frontal pole clusters as part of the dorsal default mode network (dDMN), image MNI Z-coordinate = 15, B) transversal view of the ACC and the precuneus clusters as part of dDMN, image MNI Z-coordinate = 24, C) transversal view of the medial frontal gyrus (MFG) cluster as part of the lateral executive control network (LECN), image MNI Z-coordinate = 49, D) moderating effects of personal negative (NegP) and personal positive (PosP) attitudes on the associations between maximum extracted cluster intensity (y-axis) and grams of cannabis used per week (gram/week; x-axis). A tertiary split was used to visualize the effect of the continuous culture variables.

References
1. Holm, S., Tolstrup, J., Thylstrup, B., Hesse, M., 2016. Neutralization and glorification: Cannabis culture-related beliefs predict cannabis use initiation. Drugs: Education, Prevention and Policy 23, 48–53. https://doi.org/10.3109/09687637.2015.1087967
2. Zhang, R., Volkow, N.D., 2019. Brain default-mode network dysfunction in addiction. Neuroimage 200, 313–331. https://doi.org/10.1016/j.neuroimage.2019.06.036
3. Ames, D.L., Fiske, S.T., 2010. Cultural neuroscience. Asian J Soc Psychol 13, 72–82. https://doi.org/10.1111/j.1467-839X.2010.01301.x
4. Holm, S., Tolstrup, J., Thylstrup, B., Hesse, M., 2016. Neutralization and glorification: Cannabis culture-related beliefs predict cannabis use initiation. Drugs: Education, Prevention and Policy 23, 48–53. https://doi.org/10.3109/09687637.2015.1087967
5. Shirer, W.R., Ryali, S., Rykhlevskaia, E., Menon, V., Greicius, M.D., 2012. Decoding subject-driven cognitive states with whole-brain connectivity patterns. Cerebral Cortex 22, 158–165. https://doi.org/10.1093/cercor/bhr099

Poster No 469

Comparing data-driven subtypes of depression informed by symptom and neuroimaging data

Kayla Hannon[1], Luca Balogh[2], Fyzeen Ahmad[3], Petra Lenzini[1], Aristeidis Sotiras[1], Janine Bijsterbosch[1]

[1]Washington University in St Louis, St Louis, MO, [2]University of Amsterdam, Amsterdam, North Holland, [3]University of Minnesota, Minneapolis, MN

Introduction: The wide heterogeneity of depression (both clinically and neurobiologically) points to the presence of subtypes within the disorder. However, efforts to subtype depression have failed to converge on a consensus. Our study aims to compare several previously developed data-driven depression subtyping approaches informed by either symptom or neuroimaging data within the same subject space. We leverage the rich symptom and neuroimaging data in the UK Biobank (UKB). We evaluate similarities in resulting subtypes on subject cluster assignment agreement and sensitivity to differentiation of clinical and biological phenotypes.

Methods: Subtyping approaches: We applied the subtyping approaches of two studies that clustered on symptom data [Maglanoc et al 2019 & Lamers et al 2010]. Briefly, Maglanoc et al performed Gaussian mixture discriminant analysis on symptom questions using Bayesian Information criterion to determine the optimal cluster solution. Lamers et al performed latent class analysis on symptom questions with Akaike Information criterion for cluster optimization. We also applied the subtyping approaches of two studies that clustered on functional neuroimaging data [Price et al 2017 & Drysdale et al 2017]. Price et al performed a group iterative multiple model estimation (GIMME) on functional networks, determining clusters using the walktrap algorithm. Drysdale et al performed hierarchical clustering on functional nodes related to depression measures, with an optimal solution based on the variance ratio criterion. Please see the pre-registration, accepted as a stage 1 registered report, for more details [Hannon et al 2023]. We applied these approaches in the same UKB sample (N=2299) who have been identified to have moderate to severe recurrent depression [Smith et al 2013]. We evaluated the agreement of the resulting cluster solutions between approaches using the Adjusted Rand Index (ARI). Sensitivity to Phenotype Differentiation: To determine which domain of phenotypes each subtyping approach is sensitive to, we evaluated the cluster solutions on the same demographic information, clinical measures, and structural neuroimaging measures (only including measures not used to drive any of the clustering approaches). We performed ANOVAs within each approach for a within-approach evaluation of phenotype differentiation, using false discovery rate correction across all phenotypes. We performed linear models with regressors for each subtype to extract variance explained (R2) measures for each subtyping approach. The resulting R2 were used to compare subtyping approaches and assess phenotype sensitivity. We determined significance by creating a null distribution of permuted ΔR2, then taking the maximum permuted ΔR2 across all possible pairs of combinations for each of 2000 shuffles. A ΔR2 was significant accounting for multiple comparisons if larger than the equivalent maximum permuted ΔR2.

Results: The optimal subtype solutions ranged from 2 to 8 clusters (Fig 1A). The agreement between clustering approaches was minimal (ARI<0.023; Fig. 1B), indicating that there was functionally no overlap of cluster solutions between any subtyping approach, even when clustered on similar data. All of the cluster approaches showed significant within-method cluster differences (Fig 2A&B). The two symptom-based cluster approaches were more sensitive to clinical and imaging phenotypes than the neuroimaging-based cluster approaches (Fig 2C&D), although the phenotype sensitivity patterns were largely inconsistent (Fig 2E).

A

Approach	Number of clusters (k)
Drysdale	3
Price	2
Maglanoc	8
Lamers	5

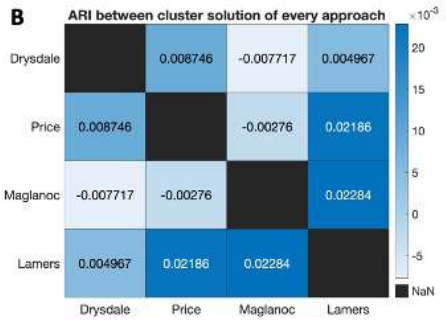

Figure 1. A) The optimal number of clusters determined for each subtyping approach. **B)** the Adjusted Rand Index (ARI) between each cluster solution for each approach.

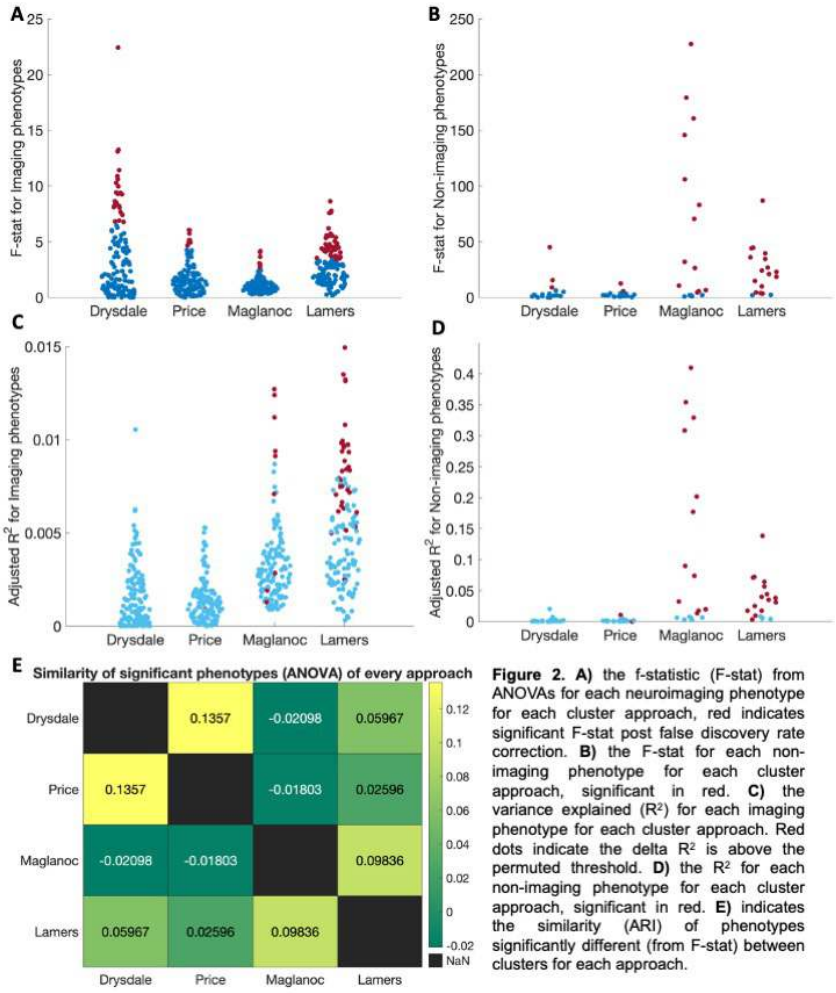

Figure 2. A) the f-statistic (F-stat) from ANOVAs for each neuroimaging phenotype for each cluster approach, red indicates significant F-stat post false discovery rate correction. **B)** the F-stat for each non-imaging phenotype for each cluster approach, significant in red. **C)** the variance explained (R^2) for each imaging phenotype for each cluster approach. Red dots indicate the delta R^2 is above the permuted threshold. **D)** the R^2 for each non-imaging phenotype for each cluster approach, significant in red. **E)** indicates the similarity (ARI) of phenotypes significantly different (from F-stat) between clusters for each approach.

Conclusions: We find a lack of agreement on depression subtypes across approaches, which demonstrates the impact of analytical decisions in subtyping efforts. Different subtyping approaches were sensitive to different phenotypes, indicating they were parsing different domains of heterogeneity. In all, this work indicates different subtyping approaches capture different sources of heterogeneity that do not have a direct relationship to other sources of heterogeneity.

References

1. Drysdale, Andrew T, Logan Grosenick, Jonathan Downar, Katharine Dunlop, Farrokh Mansouri, Yue Meng, Robert N Fetcho, et al. 2017. "Resting-State Connectivity Biomarkers Define Neurophysiological Subtypes of Depression." Nat. Med. 23 (1): 28–38. https://doi.org/10.1038/nm.4246.

2. Hannon, Kayla, Luca Balogh, Fyzeen Ahmad, Petra Lenzini, Aristeidis Sotiras, and Janine Bijsterbosch. 2023. “Comparing Data-Driven Subtypes of Depression Informed by Clinical and Neuroimaging Data: A Registered Report.” https://doi.org/10.17605/OSF.IO/W54DA.
3. Lamers, Femke, Peter de Jonge, Willem A. Nolen, Johannes H. Smit, Frans G. Zitman, Aartjan T. F. Beekman, and Brenda W. J. H. Penninx. 2010. “Identifying Depressive Subtypes in a Large Cohort Study: Results From the Netherlands Study of Depression and Anxiety (NESDA).” The Journal of Clinical Psychiatry 71 (12): 1582–89. https://doi.org/10.4088/JCP.09m05398blu.
4. Maglanoc, Luigi A., Nils Inge Landrø, Rune Jonassen, Tobias Kaufmann, Aldo Córdova-Palomera, Eva Hilland, and Lars T. Westlye. 2019. “Data-Driven Clustering Reveals a Link Between Symptoms and Functional Brain Connectivity in Depression.” Biological Psychiatry: Cognitive Neuroscience and Neuroimaging 4 (1): 16–26. https://doi.org/10.1016/j.bpsc.2018.05.005.
5. Price, Rebecca B, Kathleen Gates, Thomas E Kraynak, Michael E Thase, and Greg J Siegle. 2017. “Data-Driven Subgroups in Depression Derived from Directed Functional Connectivity Paths at Rest.” Neuropsychopharmacology 42 (13): 2623–32. https://doi.org/10.1038/npp.2017.97.
6. Smith, Daniel J., Barbara I. Nicholl, Breda Cullen, Daniel Martin, Zia Ul-Haq, Jonathan Evans, Jason M. R. Gill, et al. 2013. “Prevalence and Characteristics of Probable Major Depression and Bipolar Disorder within UK Biobank: Cross-Sectional Study of 172,751 Participants.” PloS One 8 (11): e75362. https://doi.org/10.1371/journal.pone.0075362.

Poster No 470

Dysregulation among insula, postcentral gyrus, and precuneus and its association with suicide risk

Yoojin Lee[1], Jessica Gilbert[1], Carlos Zarate[1], Elizabeth Ballard[1]

[1]NIMH/NIH, Bethesda, MD

Introduction: Suicide is a serious public health concern in the US, underscoring the need for objective markers of the suicidal behaviors. Research links aggressive impulsivity to suicide(Mann et al., 2003; Gvion et al., 2014), possibly tied to reduced brain function in sensory regulating regions (Lalovic et al., 2022), such as prefrontal cortex, precuneus, and insula (Alacreu-Crespo et al., 2020; Brown et al., 2020; Cao et al., 2015; Dombrovski et al., 2013; Sankar et al., 2022). However, limited knowledge is available on the association between the impulsive aggression, suicidal behavior, and brain regions responsible for the sensory and emotional regulation, specifically when considering the temporal dynamics of the suicidal behavior. This study examines whether trait-like aggression and impulsivity, along with task-oriented impulsivity measures, could moderate resting-state magnetoencephalographic (MEG) power and effective connectivity.

Methods: Initial recruitment included 121 participants across four groups: recent suicidal crisis (HR; n=14), suicide attempt history excluding the last year (LR; n=41), anxiety/mood disorders without suicidal history (CC; n=38), and no psychiatric/suicidal history (MR; n=28). Impulsivity was assessed through two measurements: trait impulsivity, measured using the Barratt Impulsiveness Scale (BIS), and risk-taking impulsivity, evaluated using the Balloon Analogue Rating Task (BART). Additionally, trait-like aggression was measured using the Buss-Perry Aggression Scale (BPA). Linear mixed effects models probed differences in resting-state MEG power between HR group and LR, CC, and MR groups across delta (2-4Hz), theta (4-8Hz), alpha (9-14Hz), beta (15-29Hz), and gamma (30-58Hz) bands in sensory regulating and decision-making brain regions, such as the prefrontal cortex, precuneus, insula, and post-central gyrus. This study also explored the interactions between the resting-state MEG power and aggressive impulsivity measures in those regions. Dynamic causal modeling (DCM), a generative model that seeks to find hidden neural states from measured brain responses using a Bayesian perspective (Stephan et al., 2010), was used to assess the extrinsic connectivity between sensory/emotion-regulating brain regions. The CMM_NMDA model of DCM was used to assess the fast (α-amino-3-hydroxy-5-methyl-4-isoxazolepropionic acid (AMPA)-mediated) and slow (N-methyl-D-aspartate (NMDA)-mediated) glutamatergic signaling (Moran et al., 2011).

Results: The HR group did not show the difference in resting-state MEG power, compared to LR, CC, and MR groups. However, HR group with high trait-like aggression or impulsivity scores showed reduced MEG power in regions responsible for sensory/emotion regulation, compared to HR group with low scores. Those regions included the precuneus (delta), supra marginal gyrus (theta), angular gyrus, middle frontal gyrus, inferior frontal gyrus (alpha), precuneus, and inferior frontal gyrus (beta), voxel-based corrected ps<.05. For the gamma band, postcentral gyrus showed a trend-level reduction, voxel-based corrected p=.09. Compared to LR, CC, and MR groups, HR group showed downregulated glutamatergic feedback between the precuneus (PRE) and insula (INS), posterior probability(pp) > .95. High trait-like impulsivity yielded reduced PRE to INS feedback, whereas high risk-taking impulsivity upregulated glutamatergic feedback from INS to the postcentral gyrus (PCG) and between PCG and INS, pps > .95. The results indicate dysregulated glutamatergic connectivity in brain regions related to the sensory regulation, with implications for suicide risk.

Conclusions: Investigating various impulsivity types and their connection to suicide risk while considering temporal dynamics of suicidal behaviors could be crucial for the suicide research. The study suggests that the glutamatergic-mediated sensory and emotion-regulation processes may serve as significant markers of suicide risk, which can be evaluated in future longitudinal studies.

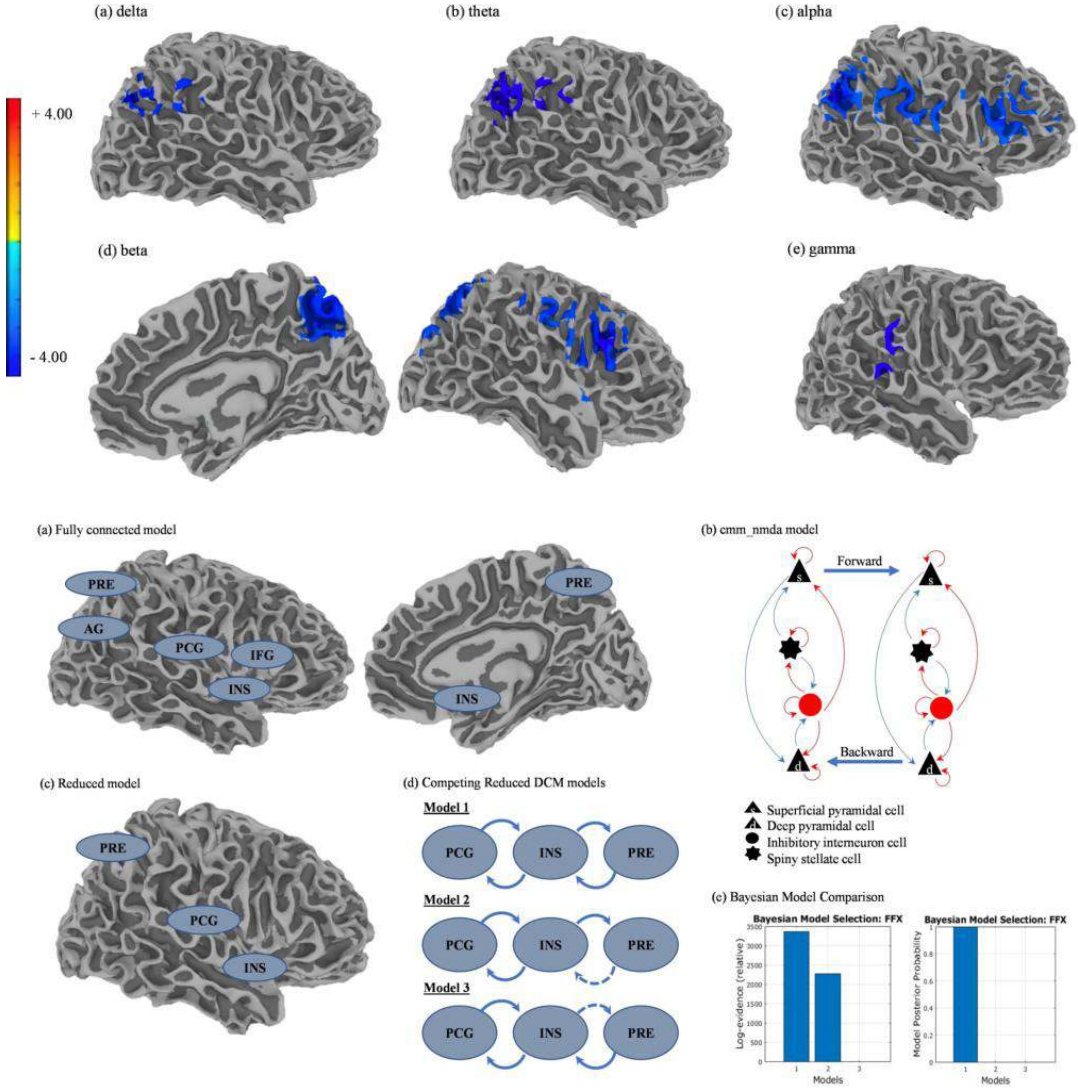

References

1. Alacreu-Crespo, A. (2020) 'Prefrontal activation in suicide attempters during decision making with emotional feedback', Translational Psychiatry, 10(1), p. 313.
2. Brown, V. M. (2020) 'Ventromedial prefrontal value signals and functional connectivity during decision-making in suicidal behavior and impulsivity', Neuropsychopharmacology, 45(6), pp. 1034-1041.
3. Cao, J. (2015) 'Abnormal regional homogeneity in young adult suicide attempters with no diagnosable psychiatric disorder: a resting state functional magnetic imaging study', Psychiatry Research, 231(2), pp. 95-102.
4. Dombrovski, A. Y. (2013) 'Reward signals, attempted suicide, and impulsivity in late-life depression', JAMA Psychiatry, 70(10), p. 1.
5. Gvion, Y. (2014) 'Aggression-impulsivity, mental pain, and communication difficulties in medically serious and medically non-serious suicide attempters', Comprehensive Psychiatry, 55(1), pp. 40-50.
6. Lalovic, A., Wang, S., Keilp, J. G., Bowie, C. R., Kennedy, S. H. & Rizvi, S. J. (2022) 'A qualitative systematic review of neurocognition in suicide ideators and attempters: Implications for cognitive-based psychotherapeutic interventions', Neuroscience and Biobehavioral Reviews, 132, pp. 92-109.
7. Mann, J. J. (2003) 'Neurobiology of suicidal behaviour', Nature Reviews Neuroscience, 4(10), pp. 819-828.
8. Moran, R. J. (2011) 'Consistent spectral predictors for dynamic causal models of steady-state responses', Neuroimage, 55(4), pp. 1694-1708.
9. Sankar, A. (2022) 'Graph theory analysis of whole brain functional connectivity to assess disturbances associated with suicide attempts in bipolar disorder', Translational Psychiatry, 12(1), p. 7.
10. Stephan, K. E. (2010) 'Ten simple rules for dynamic causal modeling', Neuroimage, 49(4), pp. 3099-3109.

Poster No 471

Dynamic Functional Connectivity Changes Associated with Rumination by CBT in depression

Nariko Katayama[1], Kazushi Shinagawa[2], Yuki Kobayashi[1], Jinichi Hirano[1], Atsuo Nakagawa[3,4], Kei Kamiya[5], Miyuki Tajima[1], Yuri Terasawa[2], Satoshi Umeda[2], Toshiaki Kikuchi[1], Masaru Mimura[1], Hiroyuki Uchida[1]

[1]Department of Neuropsychiatry, Keio University school of Medicine, Shinjuku, Tokyo, [2]Department of Psychology, Keio University, Mita, Tokyo, [3]Department of Neuropsychiatry, St. Marianna University School of Medicine, Kawasaki, Kanagawa, [4]Department of Neuropsychiatry, Keio University school of Medicine, Tokyo, Japan, [5]Keio University School of Medicine, [35] Shinanomachi, Shinjuku-ku

Introduction: Rumination is the repetitive brooding about their symptoms, causes, meanings, and consequences of depression, and has recently been identified as one of the most important risk factors for chronicity and relapse or recurrence of depression. Depressed patients are easily trapped in a thinking process of abstract, repetitive, negative, nonfunctional rumination. Cognitive-behavioral therapy (CBT) is one of the psychotherapies with established efficacy for depression that also approaches biased cognition and rumination. However, the mechanism by which treatments for depression improve rumination has not yet been clearly elucidated by functional brain imaging studies. In the present study, we compared resting-state functional brain imaging with time-varying functional connectivity (TVFC) analysis to investigate the temporal network changes related to rumination in depressed patients and healthy controls, and to identify treatment mechanisms specific to CBT.

Methods: Patients with a DSM-V diagnosis of major depressive disorder and healthy controls were eligible for the study. Depressed patients were assigned to a cognitive-behavioral therapy group, a pharmacotherapy group, a repetitive transcranial magnetic stimulation (TMS) group, or an electroconvulsive therapy (ECT) group, depending on the treatment they received. Participants underwent fMRI imaging at baseline and at the end of treatment. Participants underwent resting-fMRI and were assessed rumination (Rumination response score: RRS) at baseline and at the end of treatment. The CBT group underwent individual sessions once a week for about 50 min for 16 weeks based on Beck's manual. fMRI images were preprocessed by fMRI prep, divided into ROIs (Automated Anatomical Labeling: AAL2), and time-series data were extracted. After principal component analysis (PCA), the states were estimated by TVFC analysis using the hidden Markov model (HMM) method. States of the estimated brain network were compared between depressed patients and healthy controls, and indicators correlated with RRS were extracted (Pearson correlation analysis). Group-by-time interaction effect was examined by ANOVA and a within-group comparison before and after treatment was performed as a post-hoc analysis. The study was approved by the Ethics Committee of Keio University School of Medicine to assure ethical considerations and protection of the privacy of the participants.

Results: A total of 138 adult participants, 80 patients with moderate to severe major depressive disorder and 58 healthy controls, were included in this study. Twelve states of brain networks were estimated and significant differences in the number of occurrences of state 9 and state 12 was found between the depressed patients and the healthy group (figure1). State 9 was mainly insula network activity, and state 12 was predominantly default mode network activity. The number of occurrences of state 12 was positively correlated with RRS ($p=0.001$). The number of occurrences of state 9 and state 12, and the transition probability had group-by-time interaction effect ($p=0.01$, $p=0.055$, $p=0.011$, respectively). The number of occurrences of state 12 changed significantly before and after treatment in the CBT group ($p=0.047$) (figure2).

Figure 1

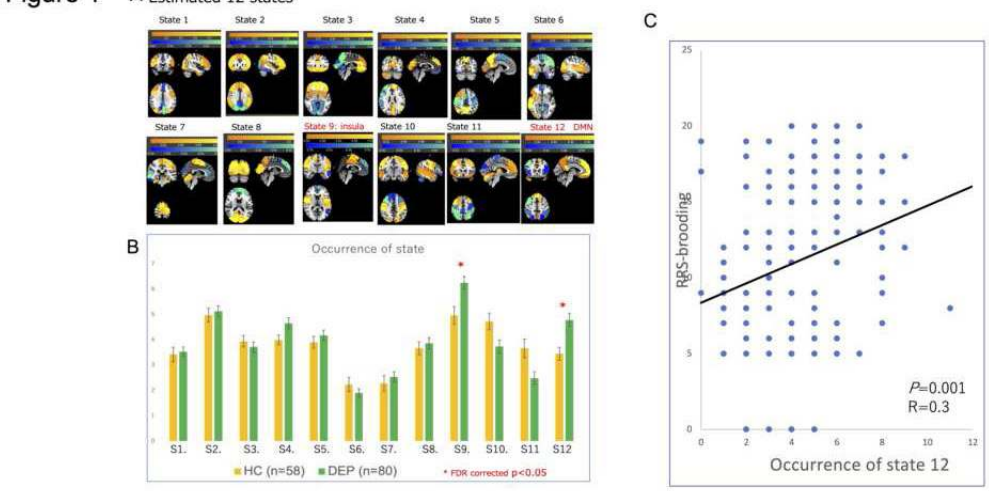

A) Estimated 12 states by TVFC analysis. State9 was insula network and state 12 was DMN activity mainly. B) Number of occurrence of states compared between MDD and healthy controls. The occurrence of state 9 and state 12 were higher in MDD group than HC group. C) The number of occurrences of state 12 was positively correlated with brooding score of RRS.

Figure 2

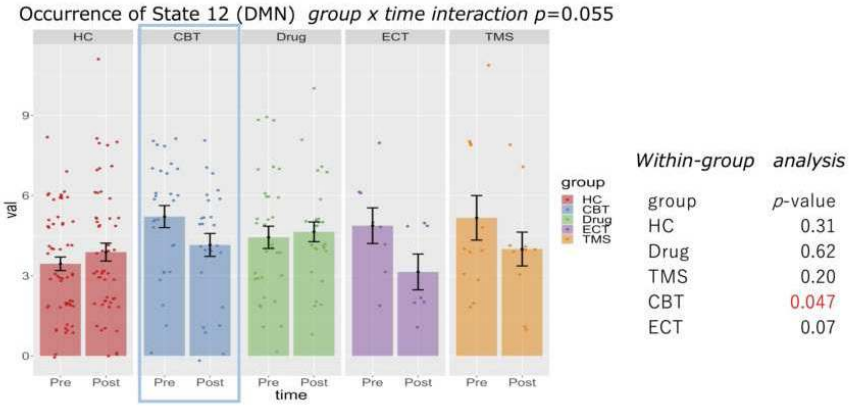

The number of occurrences of state 12 had a trend of group-by-time interaction effect (p=0.055) and changed significantly before and after treatment in the CBT group (p=0.047).

Conclusions: CBT differed from other treatments in reducing the number of DMN occurrences and the probability of transitions between networks, suggesting that these changes may be related to unique therapeutic mechanisms of CBT, such as its effect on rumination. In the treatment of depressed patients with diverse symptoms, the findings of this large-scale brain imaging study are expected to contribute to the establishment of more effective treatments and therapeutic strategies.

References

1. Nolen-Hoeksema, S., Wisco, B.E., Lyubomirsky, S., 2008. Rethinking Rumination. Perspectives on psychological science : a journal of the Association for Psychological Science 3, 400-424.
2. Watkins, E.R., Mullan, E., Wingrove, J., Rimes, K., Steiner, H., Bathurst, N., Eastman, R.,Scott, J., 2011. Rumination-focused cognitive-behavioural therapy for residual depression: phase II randomised controlled trial. The British journal of psychiatry : the journal of mental science 199, 317-322.
3. Hui-Xia Zhoua,b,c, Xiao Chena,b,c, Yang-Qian Shena, Le Lia,b,c, Ning-Xuan Chena,b,c, Zhi-Chen Zhua,b,c, Francisco Xavier Castellanose,f, Chao-Gan Yan.2020. Rumination and the default mode network: Meta-analysis of brain imaging studies and implications for depression. NeuroImage 206 (2020) 116287

Poster No 472

Effects of Exercise on Structural and Functional Brain Patterns in Schizophrenia

Lukas Roell[1]

[1]*Department of Psychiatry and Psychotherapy, LMU Hospital Munich, Munich, Bavaria*

Introduction: Aerobic exercise as an adjunct therapy for schizophrenia leads to additional improvements in psychiatric symptoms and cognitive performance. However, the neural mechanisms underlying these clinical improvements are not fully understood. Therefore, our aim was to identify exercise-induced structural and functional adaptations at the neural level that underlie the clinical rehabilitation processes of patients with schizophrenia. Insights into the neural mechanisms induced by aerobic exercise can contribute to a better understanding of the pathophysiology of schizophrenia and may provide a basis for optimizing current treatment approaches.

Methods: We analyzed comprehensive clinical and MRI data of 100 patients with schizophrenia from the ESPRIT C3 study (NCT03466112) and the BrainTrain study (NCT05956327). These large-scale randomized controlled trials investigate the effect of an aerobic exercise program on stationary bicycles compared to flexibility, strengthening, and balance training on various health outcomes in patients with schizophrenia. We acquired multimodal MRI at baseline and post-intervention, comprising T1- and T2-weighted structural MRI, resting-state functional MRI, diffusion-tensor imaging (DTI), arterial spin labeling (ASL) and magnetic resonance spectroscopy (MRS) of the hippocampus. At both timepoints, we computed global and regional brain volumes, cortical thickness, cortical gyrification, static and dynamic functional connectivity, structural connectivity, global and regional brain perfusion, and relevant neurotransmitter concentrations in the hippocampus, aiming to identify neural mechanisms that drive a clinical response after exercise in schizophrenia.

Results: First, we identified compensatory relationships between aerobic fitness and functional connectivity within the default mode network and the cortical-striatal-thalamic-cerebellar network. Additionally, associations with symptom severity were present for the latter. Second, we found positive effects of aerobic exercise on the structural and functional organization of the default mode network, the cortical-striatal-thalamic-cerebellar network, and the cortical-striatal-pallidal-thalamic-cortical loop. Adaptations within the de-fault mode network were related to improvements in overall disorder severity. Third, we discovered positive associations between patients' aerobic fitness and the volume of the hippocampus, particularly prominent in the hippocampal subregions CA1-4 and DG. However, we did not find stable relationships with symptom severity and cognitive performance. Fourth, we observed exercise-induced increases in the hippocampal subfields CA1-4 and DG, but could not detect volume increases in the total hippocampus. However, these effects were not associated with relevant clinical parameters.

Conclusions: In summary, we identified four neural entities in schizophrenia – the hippocampus, the default-mode network, the cortical-striatal-thalamic-cerebellar network, and the cortical-striatal-pallidal-thalamic-cortical loop – that exhibit beneficial adaptations as a result of aerobic exercise. While we were able to demonstrate a few associations between these neural changes and clinical improvements, further large-scale randomized controlled exercise studies in patients with schizophrenia are warranted to elucidate the clinical relevance of these neural adaptations.

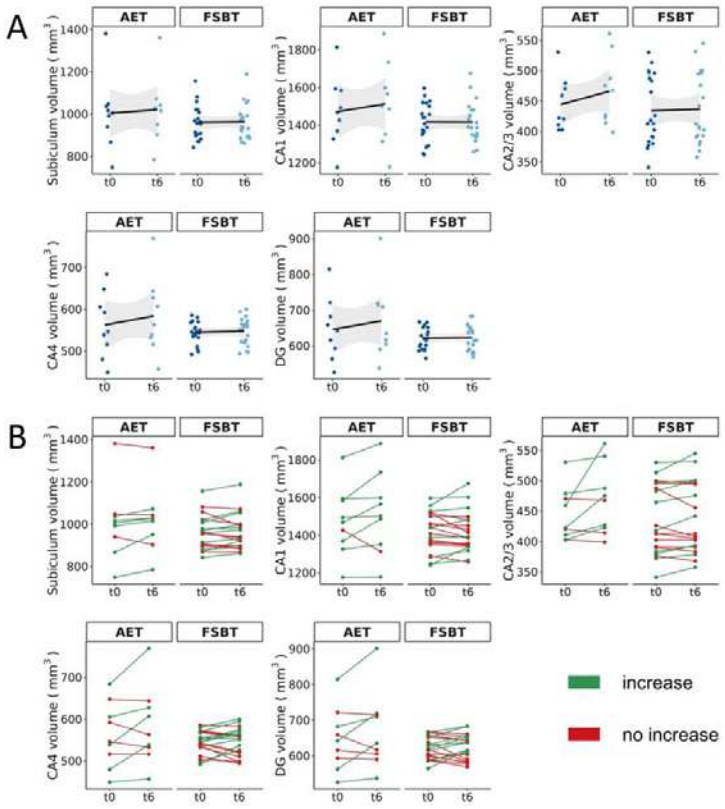

Exercise-induced volume changes of the HF subfields. (A) Mean volume changes. (B) Individual volume changes.

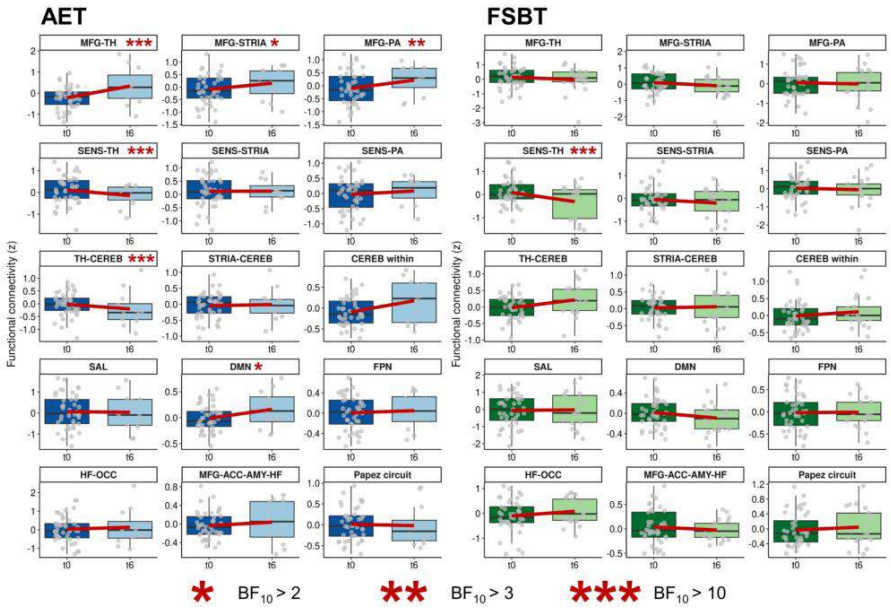

Exercise effects on functional connectivity in schizophrenia-related brain circuits. AET: aerobic exercise training, FSBT: flexibility, strength, and balance training.

References

1. Roell L, et al (2022). Association between aerobic fitness and the functional connectome in patients with schizophrenia. Eur Arch Psychiatry Clin Neurosci;272(7):1253-1272. 10.1007/s00406-022-01411-x.
2. Maurus I, Roell L, et al (2022). Fitness is positively associated with hippocampal formation subfield volumes in schizophrenia: a multiparametric magnetic resonance imaging study. Transl Psychiatry;12(1):388. 10.1038/s41398-022-02155-x.
3. Roell L, et al (2023). Effects of Exercise on Structural and Functional Brain Patterns in Schizophrenia—Data From a Multicenter Randomized-Controlled Study. Schizophrenia Bulletin. 10.1093/schbul/sbad113.
4. Roell, L., Fischer, T., et al. (2023), Effects of aerobic exercise on hippocampal formation volume in people with schizophrenia – a systematic review and meta-analysis with original data from a randomized-controlled trial. OSF Preprints, 2023. DOI: osf.io/y2phs [under review]

Poster No 473

Neuroanatomy of obsessive-compulsive disorder: from lesional connectivity to primary dysfunction

Nelson Descalço[1,2,3], Gonçalo Cotovio[1,2,4], Jaime Caballero-Insaurriaga[1], Ana Maia[1,2,4], Francisco Faro Viana[1], Nuno Loução[1], João Valente Duarte[1], Catarina Fonseca[2], João Ramos[5], José Oliveira[1,2], J. Bernardo Barahona-Corrêa[1,2], Albino J. Oliveira-Maia[1,2]

[1]Champalimaud Research and Clinical Centre, Champalimaud Foundation, Lisbon, Portugal, [2]NOVA Medical School, Faculdade de Ciências Médicas, NMS, FCM, Universidade NOVA de Lisboa, Lisbon, Portugal, [3]Psychiatry and Mental Health Department, Hospital Garcia de Orta, Almada, Portugal, [4]Department of Psychiatry and Mental Health, Centro Hospitalar de Lisboa Ocidental, Lisbon, Portugal, [5]Department of Neurorradiology, Centro Hospitalar de Lisboa Ocidental, Lisbon, Portugal

Introduction: Lesional neuropsychiatric syndromes offer a unique avenue to explore the intricate relationship between structural brain changes and brain function in complex disorders. Techniques such as functional lesion connectivity mapping (fLCM) can be employed for this purpose, using resting-state functional connectivity data from extensive databases of healthy individuals to construct a network of brain regions functionally connected to lesioned areas. Obsessive-compulsive disorder (OCD) cases are predominantly idiopathic but can emerge after brain lesions. In an ongoing work, we have found that lesions associated with OCD-like symptoms are more frequently situated in the bilateral orbitofrontal cortex (OFC) and right middle and superior temporal lobe. Furthermore, these lesions exhibit a distinctive pattern of brain functional connectivity compared to control lesions, with preferential connectivity to the OFC and ventral basal ganglia, bilaterally. However, fLCM predominantly leverages on functional connectivity patterns largely driven by cortical regions, neglecting the characterization of white matter (WM) pathways. Structural disconnections arising from brain lesions can be explored using structural LCM (sLCM) methods resorting to normative connectomes constructed from diffusion imaging data. Here, we aim to 1) examine whether focal brain lesions associated with OCD symptoms converge on a specific structural connectivity network, and whether it is shared with lesional OCD functional connectivity networks; and 2) investigate whether WM regions identified with sLCM exhibit microstructural abnormalities in patients with primary OCD.

Methods: For aim 1, we performed a systematic literature search following PRISMA guidelines to identify lesion locations associated with OCD and those eligible were traced onto a standard space (N=40). Structural disconnection maps for each brain lesion were computed using BCBToolKit with a structural normative connectome (N=178) and compared to structural disconnection maps from a lesional control cohort (N=608) not selected for a specific neuropsychiatric syndrome. We used a voxel-wise permutation-based two-sample t-test of 5000 permutations, two-tailed and $\alpha<0.05$, with threshold-free cluster enhancement (TFCE). Voxels were labelled using the JHU WM tractography atlas. For aim 2, we used multishell diffusion images from a multicentric case-control study of age- and sex-matched patients with primary OCD (N=70) and healthy controls (N=69). Diffusion data were preprocessed and reconstructed using generalized q-sampling imaging in DSI Studio. Deterministic tractography was performed for the WM tracts identified in the previous aim. Mean fractional anisotropy (FA), a diffusion tensor metric of WM fiber integrity, was calculated for each tract, and group differences were tested using a two-sample t-test, correcting for multiple comparisons (False Discovery Rate of 10%).

Results: When looking into sLCM, compared to control lesions, OCD-associated lesions exhibit a significantly higher probability of structural disconnection to the corpus callosum, forceps minor, anterior thalamic radiation, uncinate fasciculus, inferior fronto-occipital fasciculus, and cingulum. Consistently, patients with primary OCD had significantly lower mean FA values than the control cohort for the forceps minor ($p=0.022$), cingulum ($p=0.028$), corpus callosum ($p=0.044$), and right anterior thalamic radiation ($p=0.044$).

Conclusions: Our findings support that OCD-associated brain lesions are linked to a pattern of structural dysconnectivity affecting major associative pathways of the frontal lobe with the thalamus, the temporal and occipital lobes, and interhemispheric pathways. Additionally, our study suggests that these pathways are altered in patients with primary OCD, mainly due to abnormal WM integrity compared to healthy controls. This is consistent with the current neurobiological model of dysfunctional cortico-striato-thalamo-cortical circuits in OCD.

References

1. Yeh, Fang-Cheng, et al. “Deterministic diffusion fiber tracking improved by quantitative anisotropy.” (2013): e80713. PLoS ONE 8(11): e80713. doi:10.1371/journal.pone.0080713

Poster No 474

Network control energy within the salience network underlies multi-task switching

Johannes Wiesner[1], Anastasia Benedyk[1], Jamila Andoh[1], Maximilian Lueckel[2], Anais Buhl[1], Linden Parkes[3], Lorenzo Caciagli[4], Xiaosong He[5], Dani Bassett[6], Emanuel Schwarz[1], Andreas Meyer-Lindenberg[1], Heike Tost[1], Urs Braun[1]

[1]Central Institute of Mental Health, Mannheim, Baden-Württemberg, [2]Neuroimaging Center (NIC), Focus Program Translational Neuroscience, Johannes Gutenberg University, Mainz, Germany, [3]Rutgers University, Philadelphia, PA, [4]University of Bern, Bern, Bern, [5]University of Science and Technology of China, Hefei, Anhui, [6]UPenn, Philadelphia, PA

Introduction: Network Control Theory (NCT) is able to model the brain as a dynamical system that transitions through various discrete states. While previous research has focused on the identification of brain networks that are tightly coupled to certain behavioral domains, less research has been done on addressing the question which networks facilitate switching between these bio-behavioral domains (Insel et al., 2010). Here, we used a Multi-Task control theory framework in order to identify a set of regions of interests (ROIs) that is relatively more involved in steering the brain into any specific target state than the rest of the brain. We then investigated behavioral, neuromodulatory, topological and behavioral correlates of these ROIs leading to possible implications for patients in the mood-psychosis spectrum.

Methods: We used task fMRI and DWI data from the HCP dataset from 763 subjects that had completed all fMRI tasks and all tasks of the NIH toolbox (Glasser et al., 2013). SPM12 was used to compute T-maps for all conditions of interest ("Working Memory", "Emotional Regulation", "Reward Processing", "Social Processing"). DWI data was reconstructed in DSI-Studio using q-space diffeomorphic reconstruction (Yeh & Tseng, 2011). A Glasser Atlas with additional subcortical regions from the Tian Atlas (Glasser et al., 2016; Tian et al., 2020) was used to both parcellate the T-maps and to obtain structural connectivity matrices using deterministic fiber-tracking. For each subject, optimal control energy was computed for all possible state-to-state-transitions using previously described methods (Braun et al., 2021). Random intercept models were set up for each brain region to obtain both estimates for the average energy input across the entire sample and for each individual subject. Otsu's method was used to obtain ROIs with particularly high energy inputs (Otsu, 1979). We correlated our statistical image with the salience network map derived from neurosynth. To investigate possible links to cognitive functioning, subjects' control energy inputs of our identified network were correlated with relevant measures of fluid intelligence using univariate and multivariate methods. Finally, we tested for differences in receptor densities for each of the major ascending neuromodulatory systems as well as for modal and average controllability differences between our ROIs and the rest of the brain.

Results: We identified an extended network of regions that showed a positive correlation with the salience network map from neurosynth ($r = 0.16$, $p < 0.01$). ROIs were also significantly correlated with higher D2 receptor density ($U = 20507$, $p < 0.01$), higher modal ($W = 0$, $p < 0.01$), and lower average controllability values ($W = 2692$, $p < .01$). Finally, higher energy in the ROIs was significantly correlated with worse performance in the Card Sorting test ($\rho = -.07$, $p < .05$) and the Flanker Test ($\rho = -.08$, $p < .05$).

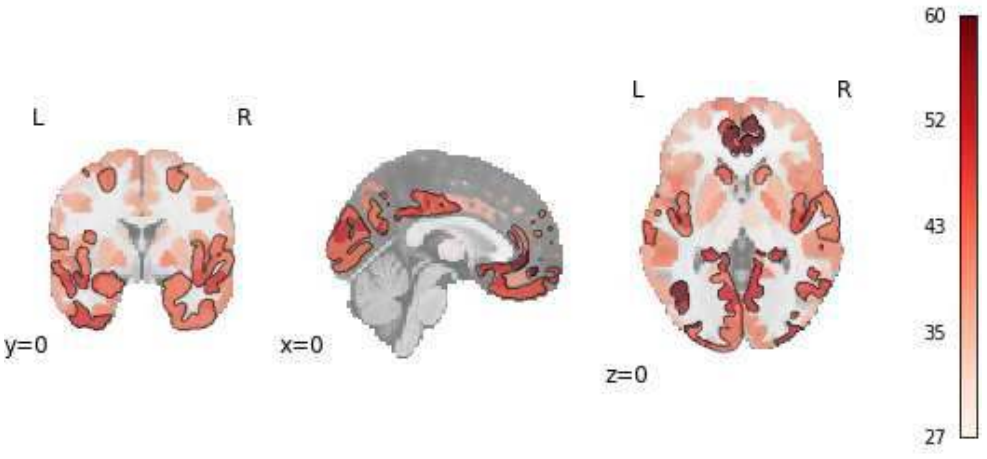

Conclusions: Our results support the hypothesis that the salience network plays a crucial role in the control of brain state transitions. The finding that our ROIs are associated with higher D2 receptor expression density supports previous works stating that these receptors are important for facilitating segregation in brain-state dynamics (Shine et al., 2019). This is further supported by the finding of higher modal controllability in the identified network. These findings, and the identified link between control energy and cognitive functioning, highlights the salience network as a promising target for further investigation in a larger clinical sample with a particular focus on patients in the mood-psychosis spectrum.

References
1. Braun, U. (2021), 'Brain network dynamics during working memory are modulated by dopamine and diminished in schizophrenia', Nature Communications, 12(1), 3478
2. Glasser, M. F. (2016), 'A multi-modal parcellation of human cerebral cortex', Nature, 536(7615), 171–178
3. Glasser, M. F. (2013), 'The minimal preprocessing pipelines for the Human Connectome Project', NeuroImage, 80, 105–124
4. Otsu, N. (1979), 'A Threshold Selection Method from Gray-Level Histograms', IEEE Transactions on Systems, Man, and Cybernetics, 9(1), 62–66
5. Tian, Y. (2020), 'Topographic organization of the human subcortex unveiled with functional connectivity gradients', Nature Neuroscience, 23(11), 1421–1432
6. Yeh, F. C. (2011), 'NTU-90: A high angular resolution brain atlas constructed by q-space diffeomorphic reconstruction', NeuroImage, 58(1), 91–99

Poster No 475

Dynamic functional connectivity analysis: uncovering disorder signatures in anorexia nervosa

Monica Di Giuliano[1], Feliberto de la Cruz[2], Andy Schumann[1], Karl- Jürgen Bär[1], Katrin Rieger[1]

[1]Klinikum Universität, Jena, Thuringia, [2]Jena University Hospital, Jena, Germany

Introduction: The maintenance and non-stationary switching between brain states is crucial for self-regulation, cognitive and emotional processes. These states represent stable neural conditions persisting over specific periods and have been studied to gain insights into neurological and neuropsychiatric disorders, utilizing methods like dynamic functional connectivity analysis (dFC). Nevertheless, the potential benefits of analyzing dFC have not been fully dived into regarding anorexia nervosa (AN), a severe and prominent mental disorder primarily affecting adolescent girls and young women, with the highest mortality rate among all psychiatric conditions. Underlying psychological and biological mechanisms driving dFC in AN - at whole brain level - are still to be elucidated. In this work our goal is to investigate the whole brain dFC in patients with AN and their relationship with disorder-defining characteristics, such as body mass index.

Methods: We collected resting state fMRI data from 18 acute AN patients and 22 healthy controls (HCs), matched by age and gender. The sequence parameters were: TR = 484 ms, TE = 30 ms, voxels = 2.5 mm3, 1,900 whole brain volume sets. Data preprocessing was performed using the 'afni_proc.py' script. We extracted the average time series of 300 regions-of-interest exploiting a well-validated parcellation model[1], on the whole brain level. We adopted a sliding-window approach with 60 s window length and the onset of each window progressively shifted by 20 s (~40 TR) from that of the previous window (total number of windows = 44). In each window, we computed the Pearson's correlation between all parcellated brain regions, generating a symmetric FC matrix, whose values were then transformed to z score. All dFC matrices were concatenated across all participants, and k-means clustering was performed to identify a set of brain states. The elbow method was used to identify the optimal number of kernels: this procedure results in five cluster centroids used to classify the dFC matrices for each subject. For each brain state, we computed different dynamic features (dwell time, flexibility index, fraction of time spent).

Results: Among the five identified brain functional states in both HCs and AN, state 3 stands out as clinically relevant in AN (Fig.1A, left). The time spent for patients and HCs was significantly different ($p < 0.01$) in state 3. We also observed a trend ($p < 0.1$) for the dwell time in state 3, with AN patients spending approximately 5 consecutive windows, compared to 4 for HCs. This state exhibited a strong coupling between ventral attention (VAN) – somotomotor (SMN) networks as well as by a weak coupling between dorsal attention with default mode and limbic networks (Fig.1A, right). Another finding was the robust correlation ($p = 0.003$) between body mass index and the time spent in state 3 (Fig. 2B), suggesting potential clinical significance for this specific brain state.

Conclusions: The VAN system is salient for alteration of bodily signalling processing as well as low interoception, highlighting the possibility of a role in disconnection of large brain networks during self-representation and environmental salience processing[2]. Accordingly, the SMN is important for body image disturbances, as well as responsible for the failure of integrating visual and somatosensory perceptual information. Given the functional connectivity pattern between the VAN and SMN networks during state 3, we suggest that patients are less able to redirect and shift their focus from body-related stimuli to non-bodily-relate environmental stimuli. Therefore, brain states allow us to draw a peculiar therapeutical and interventional attention on the role of attentional and interoceptive bodily mechanisms in shaping and maintaining AN psychopathology. Notably, these mechanisms can be uncovered during dynamic functional connectivity changes in the whole brain, which appear to be less plastic and disrupted in AN.

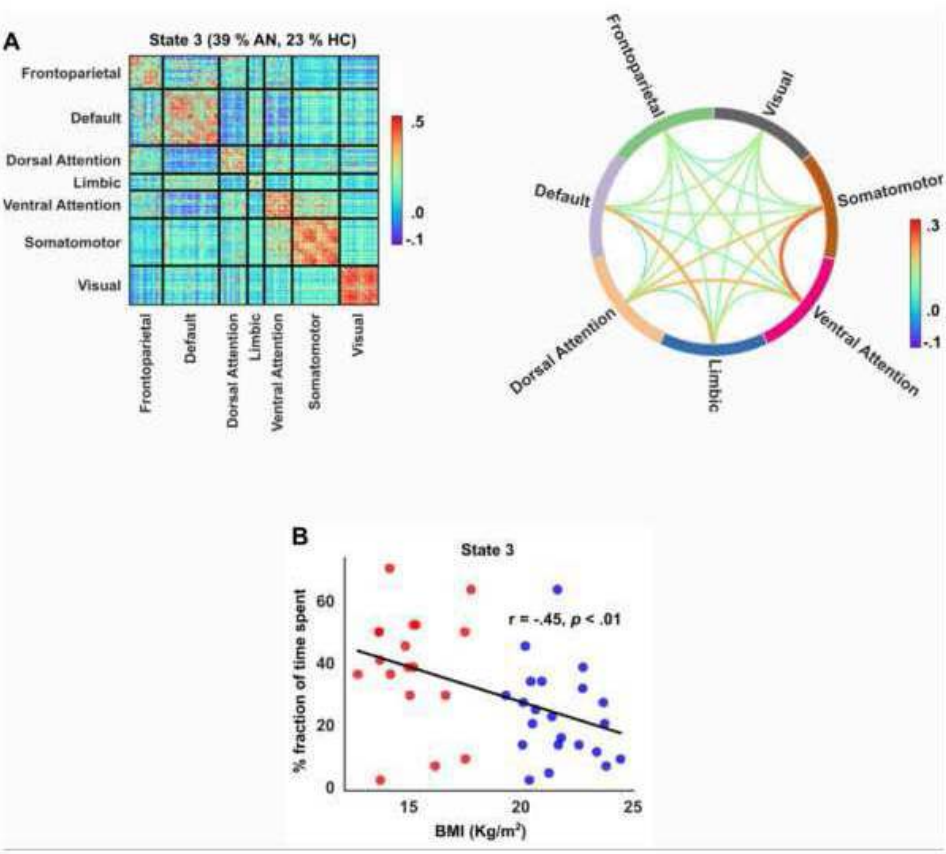

Fig 1. Among the 5 brain functional states identified in both healthy individuals and those with anorexia nervosa, state 3 appears to have clinical relevance in anorexia disease.
A. Brain state represented in matrix and chord diagrams. The brain state is symmetrically organized by functional networks, with colors indicating the average strength and direction of the pairwise correlation between two regions. Red indicates a positive correlation, while blue indicates a negative correlation. Notably, patients spent nearly 40% of their time in this state, contrasting with the 23% observed in healthy participants. For simplicity, the chord diagram displays only the average functional coupling between networks. In this diagram, one can easily observe the strong coupling between ventral attention (VAN) and somotomotor (SMN) networks as well as the weak coupling between other relevant networks, like the dorsal attention and default mode networks.
B. Association of the percentage of time spent in this clinically relevant brain state and body-mass-index.

References
1. Schaefer, A., Kong, R., Gordon, E. M., Laumann, T. O., Zuo, X. N., Holmes, A. J., ... & Yeo, B. T. (2018). Local-global parcellation of the human cerebral cortex from intrinsic functional connectivity MRI. Cerebral cortex, 28(9), 3095-3114.
2. Kim, D. J., Moussa-Tooks, A. B., Bolbecker, A. R., Apthorp, D., Newman, S. D., O'Donnell, B. F., & Hetrick, W. P. (2020). Cerebellar–cortical dysconnectivity in resting-state associated with sensorimotor tasks in schizophrenia. Human Brain Mapping, 41(11), 3119-3132.

Poster No 476

The protective effects of secure attachment despite childhood maltreatment on brain and behavior

Katharina Brosch[1,2], Vincent Hammes[2], Paula Usemann[2], Elvisha Dhamala[1], Frederike Stein[2], Florian Thomas-Odenthal[2], Lea Teutenberg[2], Susanne Meinert[3], Kira Flinkenflügel[3], Katharina Thiel[3], Alexandra Winter[3], Janik Goltermann[3], Tim Hahn[3], Hamidreza Jamalabadi[2], Benjamin Straube[2], Andreas Jansen[2], Udo Dannlowski[3], Axel Krug[2,4], Igor Nenadic[2], Tilo Kircher[2], Nina Alexander[2]

[1]Institute of Behavioral Science, Feinstein Institutes for Medical Research, Manhasset, NY, [2]Department of Psychiatry and Psychotherapy, University of Marburg, Marburg, Germany, [3]Institute for Translational Psychiatry, University of Münster, Münster, Germany, [4]Department of Psychiatry and Psychotherapy, University Hospital Bonn, Bonn, Germany

Introduction: Childhood maltreatment (CM) is a traumatic interpersonal experience and survivors may struggle to form secure attachments even into adulthood. Individuals with a history of CM who are securely attached can therefore be described as interpersonally resilient. While CM constitutes a strong risk factor for major depressive disorder, secure attachment conversely has been associated with improved mental well-being and decreased depressive symptoms. CM and secure attachment have been independently associated with distinct alterations in brain structure. However, it is unclear how interpersonal resilience is associated with changes in behavior and brain structure. This study investigated the clinical outcomes and neural correlates of interpersonal resilience as defined by a secure attachment style in adulthood despite a history of CM.

Methods: We investigated behavioral outcomes and gray matter volume (GMV) in a sample of N=1317 adults with and without a history of depression, aged 18–65. Participants were drawn from the FOR2107 study investigating the neurobiology of affective and psychotic disorders. On the behavioral level, we investigated perceived stress, self-reported depressive symptoms (Beck Depression inventory, BDI), rater-based depressive symptoms (Hamilton Depression Rating Scale, HAM-D), resilience (RS-25), global symptom severity (SCL-90) and global assessment of functioning (GAF). Brain structural data (3T magnetic resonance imaging) were analyzed using voxel-based morphometry. We applied a 2x2 factorial design (CM x attachment style) and investigated the main and interaction effects on behavior and brain. CM was assessed using the childhood trauma questionnaire (CTQ), and subjects were classified as maltreated or non-maltreated according to established cut-off scales. Accordingly, attachment style was assessed using the relationship scales questionnaire (RSQ), and participants were classified as securely or insecurely attached, resulting in four groups differing in experiences of maltreatment and attachment style. The group with CM and a secure attachment style was termed interpersonally resilient.

Results: On a phenotypic level, both CM and secure attachment exerted opposing main effects on all behavioral outcomes, i.e., CM was associated with worse psychopathological outcomes (i.e., higher perceived stress, higher self-reported and rater based depressive scores, lower resilience, higher global symptom severity and lower global functioning), whereas the opposite was observed with secure attachment. Additionally, we detected interaction effects for BDI, GAF and SCL-90, such that interpersonally resilient individuals showed significantly lower self-reported depressive symptoms, higher global functioning scores, and lower global symptom severity (Figure 1). At the brain level, we detected a significant interaction effect of CM x attachment in a cluster comprising the left supramarginal gyrus: Interpersonally resilient individuals exhibited significantly larger GMV in this area (Figure 2).

Figure 1. Phenotypical effects of attachment style and childhood maltreatment

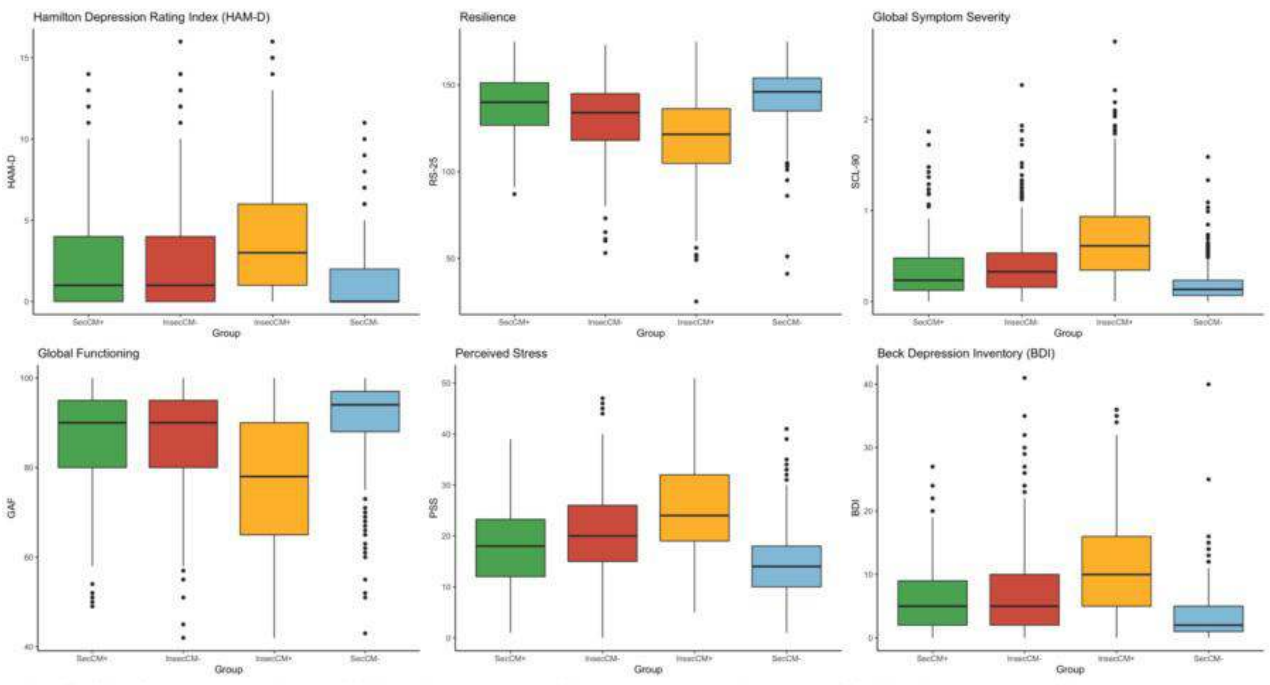

Note: SecCM+ = Securely attached with history of Childhood Maltreatment, InsecCM- = Insecurely attached without a history of Childhood Maltreatment, InsecCM+ = Insecurely attached with a history of Childhood Maltreatment, SecCM- = Securely attached without a history of Childhood Maltreatment.

Figure 2. Significant interaction effect of CM x attachment in the left supramarginal gyrus and volume per group

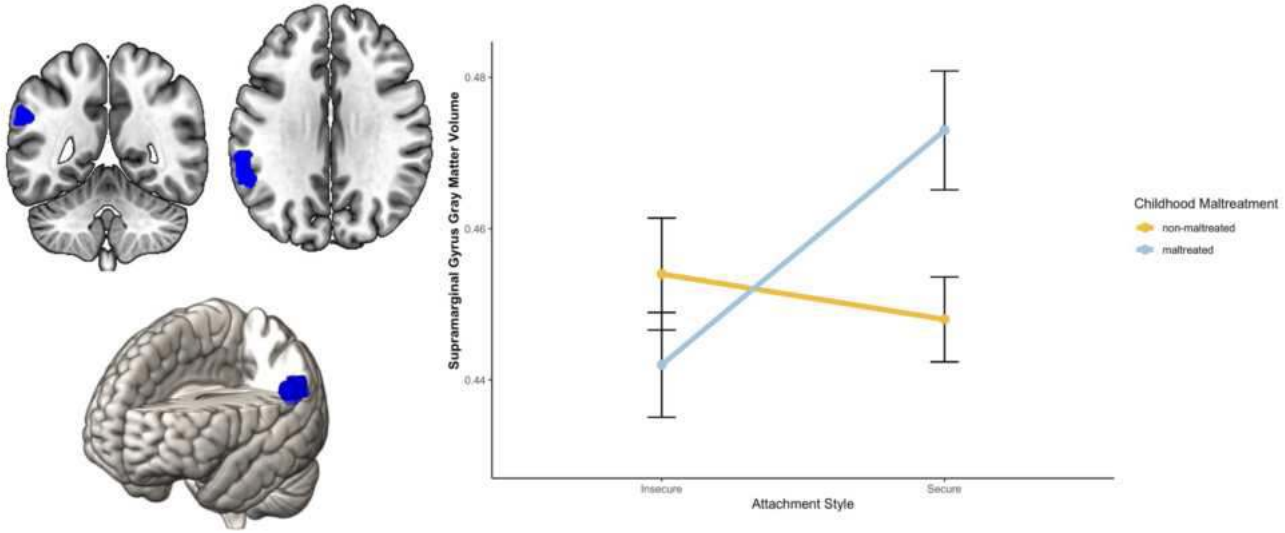

Note: Estimated marginal means depicted (values adjusted for covariates). Error bars indicate two standard errors of the mean symbolize the estimated marginal means for the cluster (adjusted for covariates).

Conclusions: Our results shed light on the behavioral and neural correlates of interpersonal resilience. The supramarginal gyrus is part of the somatosensory association cortex and further considered to be part of the mirror neuron system. Increased volume in this area might constitute a neural compensatory mechanism to CM and aid interpersonally resilient individuals in more adaptively processing semantic information and tactile sensory integration. Our results further demonstrate that risk (i.e., CM) and protective factors (i.e., secure attachment) not only have independent but also interdependent influences. Interpersonally resilient individuals had better psychopathological outcomes, highlighting the importance of secure attachment as a resilience factor in mitigating the negative effects of CM. This suggests that treatment interventions targeted at developing and strengthening secure attachments may improve mental well-being.

References

1. Acosta, H. et al., (2018). A voxel-based morphometry study on adult attachment style and affective loss. Neuroscience, 392, 219–229. https://doi.org/10.1016/J.NEUROSCIENCE.2018.06.045
2. Betz, L. T., et al., (2022). Disentangling the impact of childhood abuse and neglect on depressive affect in adulthood: A machine learning approach in a general population sample. Journal of Affective Disorders, 315, 17–26. https://doi.org/10.1016/J.JAD.2022.07.042
3. Darling Rasmussen, P., et al., (2018). Attachment as a Core Feature of Resilience: A Systematic Review and Meta-Analysis. Psychological Reports, 122(4), 1259–1296. https://doi.org/10.1177/0033294118785577
4. Muller, R. T., et al., (2012). Attachment as a Mediator between Childhood Maltreatment and Adult Symptomatology. Journal of Family Violence, 27(3), 243–255. https://doi.org/10.1007/s10896-012-9417-5
5. Nanni, V., et al., (2012). Childhood maltreatment predicts unfavorable course of illness and treatment outcome in depression: A meta-analysis. American Journal of Psychiatry, 169(2), 141–151. https://doi.org/10.1176/appi.ajp.2011.11020335
6. Nemeroff, C. B. (2016). Paradise Lost: The Neurobiological and Clinical Consequences of Child Abuse and Neglect. Neuron, 89(5), 892–909. https://doi.org/10.1016/j.neuron.2016.01.019

Poster No 477

Association between physical frailty and incident depression: a prospective study

Rongtao Jiang[1], Stephanie Noble[2], Matthew Rosenblatt[1], Jean Ye[1], Vince Calhoun[3], Jing Sui[4], Dustin Scheinost[1]

[1]Yale University, New Haven, CT, [2]Northeastern University, Boston, MA, [3]Georgia State University, Atlanta, GA, [4]State Key Laboratory of Cognitive Neuroscience and Learning, Beijing Normal University, Beijing, China

Introduction: Identifying modifiable risk factors that prevent depression constitutes a public health priority[1]. Cross-sectional studies have demonstrated strong associations between physical frailty and depression, pointing towards physical frailty as one potential target[2]. However, the evidence from prospective, longitudinal studies is limited. This study investigates the prospective association between physical frailty and incident depression and the potential mechanisms driven by inflammatory markers and brain structure.

Methods: This study included 352,277 participants (37-73 years, who were free of depression at baseline and within the 2-year follow-up period) from UK Biobank, of whom 11,269 developed depression during the 12.25-year follow-up. Physical frailty was

defined using the following five criteria: weight loss, exhaustion, weakness (low grip strength), physical inactivity, and slow walking speed[2-4]. Participants were deemed pre-frail if they fulfilled one or two criteria or frail if they fulfilled three or more[5,6]. Cox proportional hazard models were used to estimate the association between frailty status and depression incidence. Mediation analyses were performed to examine the role of regional grey matter volume (GMV) and nine inflammatory markers in mediating the relationships.

Results: Compared with non-frail individuals, pre-frail (hazard ratio (HR)=1.60, [95% CI 1.53-1.66]) and frail (HR=3.20, [2.98-3.43]) individuals had increased risk for incident depression independent of sociodemographic, lifestyle, and metabolic factors during the 12.25-year follow-up period (Figure 1A). Altogether, pre-frail and frail individuals accounted for 20.58% and 13.16% of depression cases by population attributable fraction analyses[7]. The HR of depression increased from 1.45 to 4.37 for participants fulfilling one to five frailty components, and no evidence of non-linearity was observed (Figure 1B). Age and sex showed significant interactions with physical frailty on depression. Specifically, higher risks were observed in males and individuals younger than 65 years than their counterparts (Figure 1C). All five components defining frailty showed individual and independent associations with incident depression, with exhaustion showing the strongest effect (Figure 1D). Associations were also observed between eight of the nine inflammatory markers and incident depression (Bonferroni corrected P<0.05, Figure 2A), whereas significant non-linear associations were only observed for leukocytes (P<0.001), platelets (P=0.03), and neutrophils (P=0.04), with plateauing slopes at lower exposure and linear trends at higher levels. Six out of the nine inflammatory markers significantly mediated the prospective association between physical frailty and depression incidence while adjusting for covariates and multiple comparisons (Figure 2B). Further, the neuroimaging analyses revealed 46 and 7 brain regions significantly associated with physical frailty and depression symptoms (measured by PHQ-9 scores), respectively (Figure 2C). Five brain regions were consistently identified by both physical frailty and depressive symptom scores, and the association map of frailty was significantly similar to that of depression symptoms, indicating a shared neurobiological basis (r=0.568, P=9.25×10-11). Further analysis indicated that the mean GMV of these 5 brain regions significantly mediated the association between physical frailty and depressive symptoms (P<0.001).

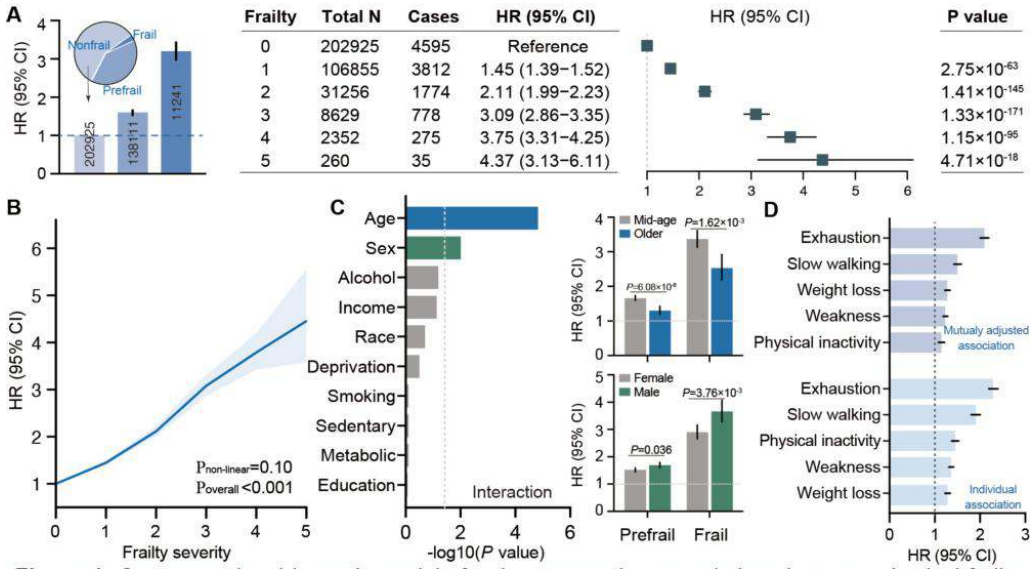

Figure 1. Cox proportional hazards models for the prospective associations between physical frailty and incident depression. (**A**) Three mutually exclusive groups of frailty, pre-frailty, and non-frailty were defined for participants fulfilling three or more, one or two, or no criteria, respectively. Compared with non-frail individuals, those with pre-frailty and frailty were at higher risk of developing depression after adjustment for covariates during the 12-year follow-up period. When physical frailty was modeled as an ordinal variable, the depression risk increased along with the number of frailty indicators. (**B**) No evidence of non-linearity was supported. (**C**) Among all confounds, only age and sex showed significant interaction with physical frailty on depression incidence (Bonferroni corrected P<0.05), with more pronounced effects observed in males and middle-aged people (≤65 years) than in females and older people, respectively. (**D**) Each of the five components of physical frailty showed significant associations with the risk of depression, even in mutually adjusting models where all five components are simultaneously modeled as exposures. HR, Hazard Ratio.

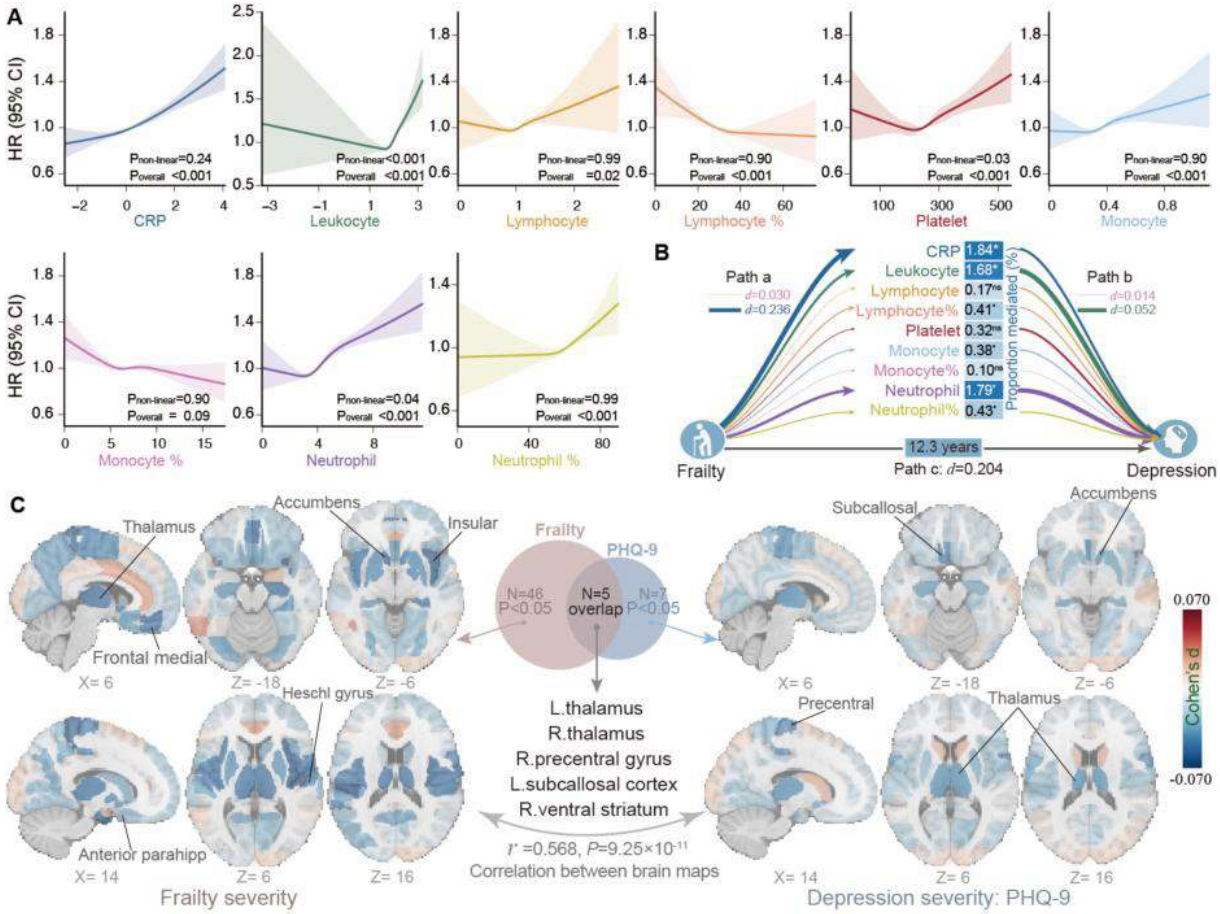

Figure 2. The mediating role of nine inflammatory markers and regional GMVs in the association between frailty and depression. (**A**) The exposure-response curve between inflammatory markers and risk of depression incidence. Cox proportional hazards models revealed significant linear associations between eight of the nine inflammatory markers (except monocyte percentage) and incident depression during the 12-year follow-up period. Significant non-linear associations were only observed for leukocytes (P<0.001), platelets (P=0.03), and neutrophils (P=0.04). (**B**) Six out of the nine inflammatory markers significantly mediated the prospective association between physical frailty and depression incidence while adjusting for covariates and multiple comparisons. Path thickness indicates the strength of associations, and numerical values for the largest and smallest effect sizes are provided for reference. The numbers in the rectangles represent the mediated variance. (**C**) The neuroimaging analyses revealed 46 and 7 regional brain regions significantly associated with physical frailty and depression symptoms (measured by PHQ-9 scores), respectively, while adjusting for potential covariates. Five brain regions, including left and right thalamus, right precentral gyrus, left subcallosal cortex, and right ventral striatum, were consistently identified by both physical frailty and PHQ-9 scores, and the association map of frailty was significantly similar to that of depression symptoms, indicating a shared neurobiological basis (r=0.568, P=9.25×10^{-11}). HR, Hazard Ratio. PHQ-9, 9-item patient health questionnaires.

Conclusions: The present findings suggest that frailty may be a risk factor for depression, and the associations can be explained by brain structure and systemic inflammation. Given the scarcity of curative treatment for depression and the high disease burden[8], routine surveillance and assessment of physical frailty from middle age may provide cost-effective targets for monitoring and potentially mitigating the onset of depression.

References

1. Firth J, Solmi M, Wootton RE, et al. A meta-review of "lifestyle psychiatry": the role of exercise, smoking, diet and sleep in the prevention and treatment of mental disorders. World psychiatry : official journal of the World Psychiatric Association 2020; 19(3): 360-80.
2. Jiang R, Noble S, Sui J, et al. Associations of physical frailty with health outcomes and brain structure in 483 033 middle-aged and older adults: a population-based study from the UK Biobank. Lancet Digit Health 2023; 5(6): e350-e9.
3. Hanlon P, Nicholl BI, Jani BD, Lee D, McQueenie R, Mair FS. Frailty and pre-frailty in middle-aged and older adults and its association with multimorbidity and mortality: a prospective analysis of 493 737 UK Biobank participants. Lancet Public Health 2018; 3(7): e323-e32.
4. Petermann-Rocha F, Hanlon P, Gray SR, et al. Comparison of two different frailty measurements and risk of hospitalisation or death from COVID-19: findings from UK Biobank. BMC Med 2020; 18(1): 355.
5. Petermann-Rocha F, Lyall DM, Gray SR, et al. Associations between physical frailty and dementia incidence: a prospective study from UK Biobank. The Lancet Healthy Longevity 2020; 1(2): e58-e68.
6. Zheng Z, Lv Y, Rong S, Sun T, Chen L. Physical Frailty, Genetic Predisposition, and Incident Parkinson Disease. JAMA Neurol 2023; 80(5): 455-61.
7. Mansournia MA, Altman DG. Population attributable fraction. BMJ 2018; 360: k757.
8. Smith K. Mental health: a world of depression. Nature 2014; 515(7526): 181.

Poster No 478

Associations of adolescent versus young adult cannabis use with longitudinal neurocognitive change

Hugh Garavan[1], Emma Pearson[1], Bader Chaarani[1], Robert Althoff[1], Alexandra Potter[1], Matthew Albaugh[1]

[1]*University of Vermont, Burlington, VT*

Introduction: Leveraging approximately ten years of prospective longitudinal data on 704 participants, we examined the effects of adolescent versus young adult cannabis initiation on MRI-assessed cortical thickness development and behavior.

Methods: Participants were drawn from the IMAGEN study[1], a longitudinal study of ~2,000 youth conducted across eight European sites. We identified IMAGEN participants who reported being cannabis-naïve at baseline (age 14) and had data available at baseline, age 19, and age 22 follow-up visits. Cannabis use was assessed with the self-report European School Survey Project on Alcohol and Drugs[2]. T1-weighted MR images were processed through the CIVET pipeline.

Results: Associations between adolescent cannabis use (14-19 years) and cortical thickness change were observed primarily in dorso- and ventrolateral portions of the prefrontal cortex. In contrast, the extent of cannabis initiation during young adulthood (from 19-22 years in those naïve to cannabis up to age 19) showed a quite different pattern of associations. Here, cannabis use levels between 19 and 22 years of age were associated with thickness change in temporal and cortical midline areas including vmPFC. Of note, brain changes related to adolescent use persisted into young adulthood with adolescent use levels correlating with cortical thickness at age 22 even after controlling for cannabis use levels between ages 21 and 22. Further, the adolescent-related effects mediated the association between adolescent cannabis use and past-month cocaine, ecstasy, and cannabis use at age 22. In contrast to these adolescent effects, the extent of cannabis initiation during young adulthood (from 19 to 22 years) had an indirect effect on psychotic symptoms at age 22 through thickness change in temporal areas.

Conclusions: These results suggest that the developmental timing of cannabis exposure may have a marked effect on neuroanatomical correlates of cannabis use as well as on associated behavioral sequelae. Brains regions showing cannabis-related associations tended to be those showing the largest neurodevelopmental change giving insight into why different associations might be observed across different age ranges. Finally, we will present initial results examining cannabis use among the ABCD study participants.

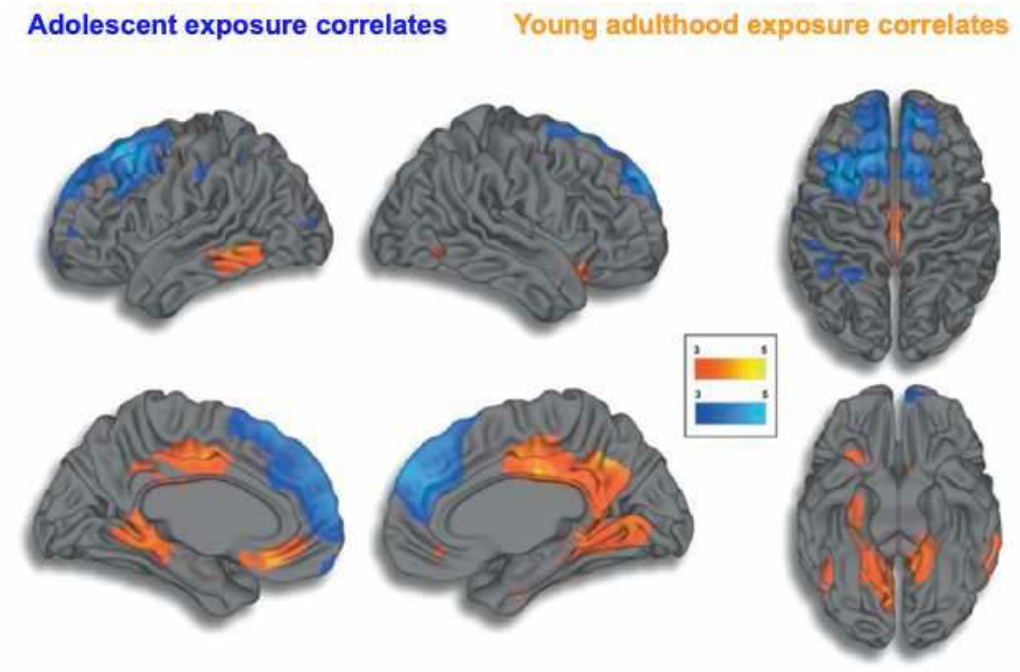

References

1. Sherif T, Rioux P, Rousseau ME, Kassis N, Beck N, Adalat R, et al. CBRAIN: a web- based, distributed computing platform for collaborative neuroimaging research. Front Neuroinform. 2014;8:54.

Poster No 480

Resting-state fMRI links longitudinal brain activity changes to cognitive function in depression

Zi-You Qiu[1], Vincent Chin-Hung Chen[2,3], Yuan-Hsiung Tsai[2,4], Jun-Cheng Weng[1,3]

[1]Department of Medical Imaging and Radiological Sciences, Chang Gung University, Taoyuan, Taiwan, [2]School of Medicine, Chang Gung University, Taoyuan, Taiwan, [3]Department of Psychiatry, Chang Gung Memorial Hospital, Chiayi, Taiwan, [4]Department of Diagnostic Radiology, Chang Gung Memorial Hospital, Chiayi, Taiwan

Introduction: Depression is a prevalent disorder in the general population. Indeed, 3.8% of the population, including 5% of adults and 5.7% of adults older than 60 years old, have depression[1]. It thus represents a serious public health concern. In addition, depression can be categorized according to severity as mild, moderate, or severe. Individuals with severe depression often experience suicidal ideation (SI), and over 700,000 people die because of suicide every year. In the study, we aimed to investigate whether there was a longitudinal association between brain function alterations and neuropsychological assessment changes in in depressed patients with SI and without SI (NS).

Methods: We recruited 68 subjects from Chiayi Chang Gung Memorial Hospital. The subjects were divided into four groups: 27 depressed patients without suicidal ideation (NS), 18 depressed patients suicidal ideation (SI), and 13 depressed patients with SI converted to NS (improved). All subjects underwent resting-state fMRI at baseline (TP1) and one year later (TP2) after receiving therapy. They also underwent four neuropsychological assessments, including the Hamilton Depression Rating Scale (HAM-D)[2], Hospital Anxiety and Depression Scale (HADS)[3], Beck Scale for Suicide Ideation (BSS)[4], and Ruminative Responses Scale (RRS)[5], that yielded scale scores. The mean amplitude of low-frequency fluctuations (mfALFF) and mean regional homogeneity (mReHo) were used to obtain functional indices. Multiple regression analysis was also used to examine the association between brain function alterations and neuropsychological assessment changes in each group.

Results: In multiple regression analysis, differences in mfALFF/mReHo over time were compared with differences in assessment scores. We found several positive and negative correlations between mfALFF/mReHo alterations and assessment score changes after treatment. There was a negative correlation between the ΔmReHo of the precentral gyrus and ΔHAMD scores in the SI group (Fig. 1a). There were negative correlations of ΔmfALFF and ΔmReHo in the precuneus with ΔHAMD scores in the improved group (Fig. 1b, 1c). We found a positive correlation between ΔmfALFF of the caudate and ΔHADS-A scores in the improved group (Fig. 2a). We also found a positive correlation between ΔmReHo of the insula and ΔHADS-A scores in the improved group (Fig. 2b). There was a negative correlation of ΔmfALFF and ΔmReHo of the inferior parietal lobe with ΔHADS-A scores in the improved group (Fig. 1d, 1e). There was a positive correlation between ΔmfALFF of the superior temporal gyrus and ΔBSS scores in the SI group (Fig. 2c). There was a negative correlation between ΔmfALFF of the thalamus and ΔRRS scores in the SI group (Fig. 1f). There were negative correlations of ΔmfALFF of the ACC and insula with ΔRRS scores in the improved group (Fig. 1g, 1h) (corrected p value of all results < 0.05).

Conclusions: This longitudinal study investigated brain function alterations in depressed patients with three trajectories of SI at two time points. In multiple regression analysis, we found several associations between functional mapping changes and neuropsychological assessment changes in each group. Our findings provide more information about potential neural biomarkers of various depressive disorders. In the future, machine learning or deep learning could be included to enhance the ease and accuracy of diagnosis.

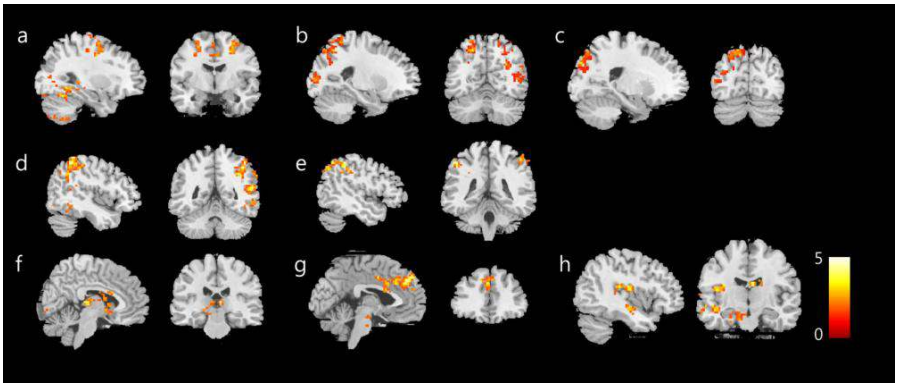

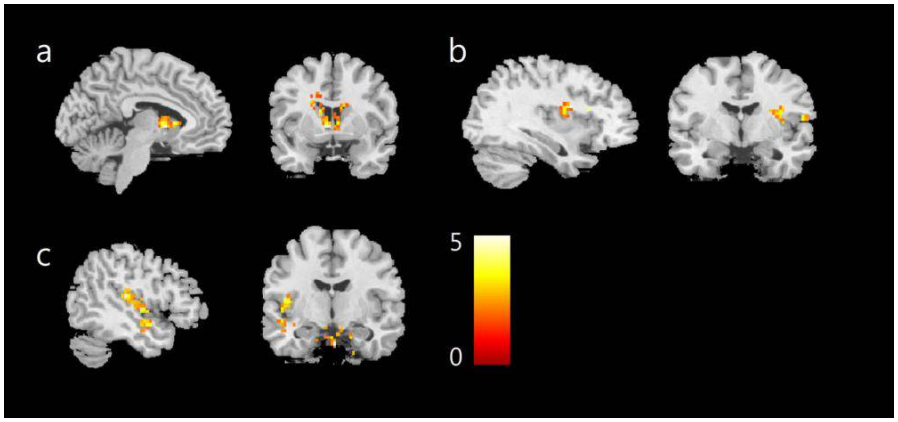

References

1. Woody, C.A., et al., A systematic review and meta-regression of the prevalence and incidence of perinatal depression. J Affect Disord, 2017. 219: p. 86-92.
2. Zimmerman, M., et al., Severity classification on the Hamilton Depression Rating Scale. J Affect Disord, 2013. 150(2): p. 384-8.
3. Annunziata, M.A., et al., Hospital Anxiety and Depression Scale (HADS) accuracy in cancer patients. Supportive Care in Cancer, 2020. 28: p. 3921+.
4. Kliem, S., et al., German Beck Scale for Suicide Ideation (BSS): psychometric properties from a representative population survey. BMC Psychiatry, 2017. 17(1): p. 389.
5. Parola, N., et al., Psychometric properties of the Ruminative Response Scale-short form in a clinical sample of patients with major depressive disorder. Patient Prefer Adherence, 2017. 11: p. 929-937.

Poster No 481

Non-linear Impact of Symptom Severity on Effect Size of Neuro-Symptom Variations in Psychosis

Kangjoo Lee[1], Clara Fonteneau[1], Ally Price[1], Lucie Berkovitch[1], Jie Lisa Ji[1], Zailyn Tamayo[1], Yvette Afriyie-Agyemang[1,2], Amber Howell[1], Grega Repovš[3], John D. Murray[1,4], Youngsun Cho[1], Alan Anticevic[1]

[1]Yale University School of Medicine, New Haven, CT, [2]University of Pittsburgh, Pittsburgh PA, [3]University of Ljubljana, Ljubljana, Slovenia, [4]Dartmouth University, Hanover, NH

Introduction: The identification of neural circuit abnormalities associated with psychiatric symptoms is crucial for the development of neural markers, where the reproducibility of neural-to-symptom mapping plays a key issue (Greicius 2008). While large sample sizes are critical for discovering and replicating brain-behavior associations with small effect sizes (Marek 2022), strong brain-behavior associations can be found using dense sampling in a small number of subjects exhibiting severe symptoms (Siegel 2023; Lynch 2023). It remains unclear whether the characteristics of studied samples, such as symptom severity, and sample size have a unique or additive impact on the reproducibility of neuro-symptom relationship across psychiatric spectra.

Methods: We analyzed resting-state functional magnetic resonance imaging (rs-fMRI) and 32 symptom variables from 1,218 young individuals (8-21 y/o) from the Philadelphia Neurodevelopmental Cohort dataset (Fig 1). Among them, 350 subjects were identified as the psychosis spectrum group using raw scales (Calkins 2015). Principal component analysis (PCA) of clinical variables allowed the identification of five reproducible data-driven symptom PCs (Fig. 1) and the corresponding individual PC scores. Varying the sample size ratio (r=a/b, a: psychosis, b: non-psychosis), the pooled standard deviation (SD) of combined sample (a+b) was estimated (Fig 2). For a given ratio (r), we selected a random number (a) of subjects from the psychosis group and a random set of subjects (b=a/r) from the non-psychosis group across 1,000 permutations. Next, to study the impact of symptom severity on effect sizes in neural data (Fig. 2), we computed Pearson's correlation between the rs-fMRI time-course in each parcel and time-courses in all the other parcels of the brain, which were then averaged and Fisher's Z-transformed to estimate global brain connectivity (GBC) for each parcel (Cole-Anticevic Brain Network Parcellation; Ji 2021). For a given ratio, Glass's δ was computed for each parcel per permutation, using individual GBC values from the psychosis versus non-psychosis groups, and then averaged across 1,000 permutations. Finally, we computed how much the effect sizes estimated from the true group comparisons (δ_test) deviates from the effect sizes estimated from the null group comparisons (δ_null).

Results: Five symptom PCs exhibiting prominent symptom variances were reproducible, representing global psychopathology, cognitive, negative symptoms, lifetime delusion, and lifetime hallucination, as demonstrated by the loading profiles and their correlation to the raw symptom scores (Fig. 1). The distribution of individual PC scores, except PC2, from the psychosis group

exhibited a large variance compared to that of the non-psychosis group (Fig. 2A). A robust estimation of pooled SD based on a random subsampling (random 350 subjects from the non-psychosis group to match the number of subjects in the psychosis group) confirmed that this observation is independent of the sample size (gray lines, 1,000 permutations). The sample ratio (r) impacts the pooled SD of symptom PC scores (Fig. 2B), suggesting a combined effect of data quality and sample size on behavioral effects. Using neural data, our data shows a nonlinear curve of effect size deviation as a function of sample size ratio, suggesting a plateau effect.

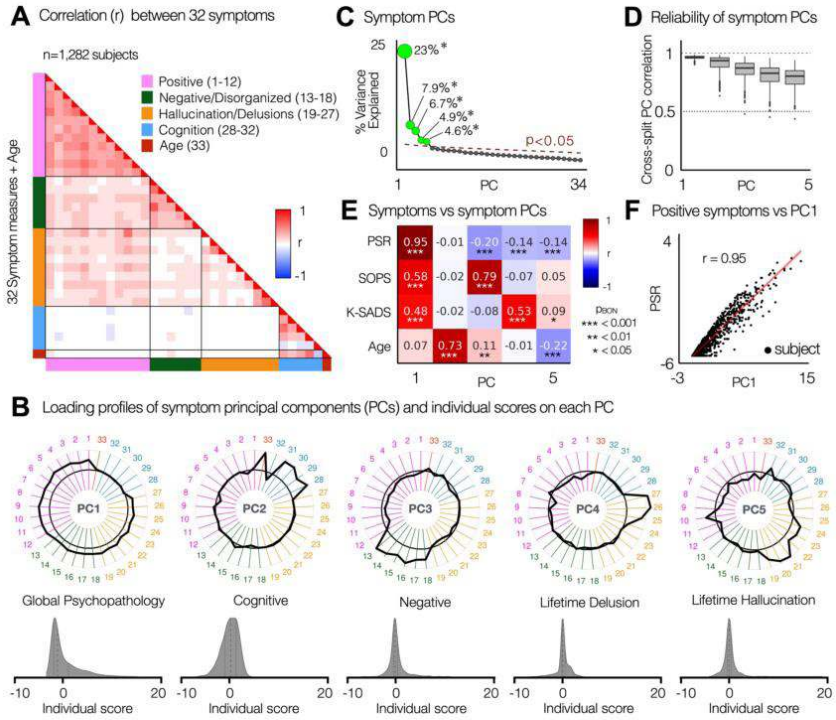

Figure 1. The principal variations of psychopathology are reliable and characterized by distinct symptom domains and individual score distributions. (A) Correlation structure between 32 symptoms across 1,282 subjects in the PNC dataset: the Prime Screen Revised for positive sub-psychosis (PSR), Negative and Disorganized Subscores (SOPS), the Kiddie-Schedule for Affective Disorders and Schizophrenia (KSADS), and the Penn computerized neurocognitive battery (Penn CNB). (B) The geometry of the first five symptom PCs estimated from the 32 symptom measures. The distribution of individual subjects' scores for each PC is presented at the bottom of each PC geometry. (C) Scree plot of PCs. (D) Reliability of PCs estimated by Pearson's correlation between the PC geometries that are independently estimated from split-halves. Subjects were divided into two splits with equal numbers (n=641) in each permutation for which PCA was performed independently. 1,000 permutations. (E) The correlation between the individual PC scores and summary statistics of symptom measures for each individual, which were obtained from the PSR (positive symptoms), SOPS (negative symptoms), K-SADS (endorsement of having hallucination/delusion), or age at the time of scan as a covariate. Bonferroni corrected p-value estimated for each correlation coefficient is annotated in the heat-map. (F) An example scatter plot between the symptom PC 1 and the summary statistic of PSR scores, which showed the largest correlation in (E).

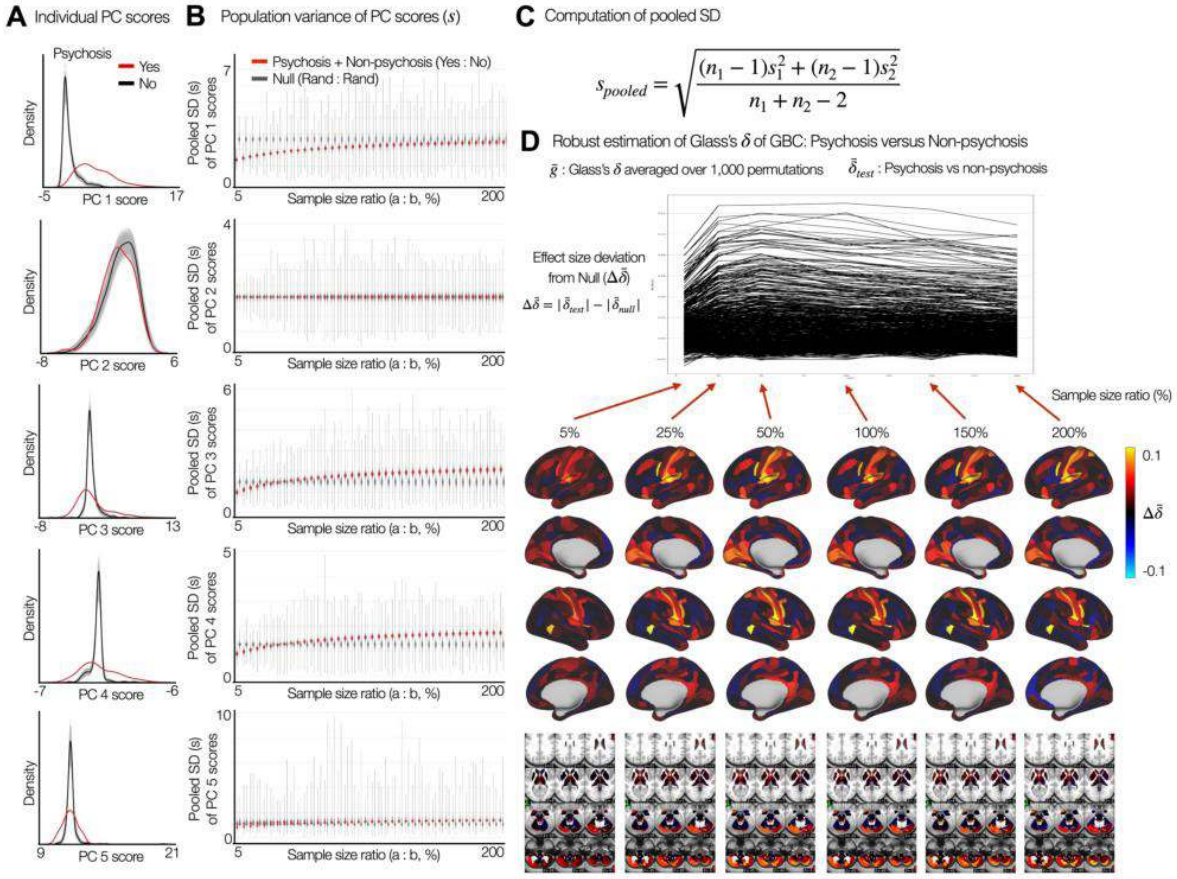

Figure 2. The number of individuals with severe symptoms in studied samples impacts effect sizes of neuro-symptom relationship. (A-B) The proportion of individuals with severe symptoms in a studied sample impacts the estimation of effect sizes in behavioral data. **(A)** In the entire PNC cohort (n=1218), individuals with psychosis (n=350, in red) show a higher variance and extreme PC scores in comparison to those without psychosis (n=932, in black). For a robust estimation of variance without a bias in sample size difference, we used subsampling of non-psychosis groups with equal numbers (n=350) with 1,000 permutations (in gray). Psychosis spectrum group was identified if individuals meet any of the following criteria: (1) age-adjusted PRIME Screen-Revised total score (PSR Z-score >= 2) or extreme score on a single item, (2) age-adjusted Scale of Prodromal Symptoms (SOPS Z-score >= 2), (3) Hallucination and/or delusions endorsed on the Kiddie-Schedule for Affective Disorders and Schizophrenia (K-SADS;: yes or no) [5]. **(B)** Sample variance of PC scores shows a non-linear increase with the ratio of sample sizes (a : b, %) from psychosis (a) and non-psychosis (b) groups. Pooled standard deviation (SD) is used for the calculation of effect sizes (e.g. Glass's δ). Null distribution of the pooled standard deviation of PC scores were obtained for each ratio, by selecting two random groups without considering the psychosis versus non-psychosis criteria. (C) Computation of the pools standard deviation (SD). **(D)** The proportion of individuals with severe symptoms in a studied sample impacts the estimation of effect sizes in static functional connectivity measured by GBC. Each line indicates results from a parcel. Comparing groups of psychosis vs non-psychosis.

Conclusions: We identified reproducible, data-driven clinical dimensions that have different contributions in psychosis versus non-psychosis groups. Symptom severity combined with sample size ratio exhibited an reproducible effect of psychiatric illnesses in both behavioral and neural data. Testing the hypothesis that neuro-symptom reproducibility plateaus under specific conditions combining symptom severity and sample size may allow us to derive a data-driven estimation of multivariate thresholds that meets the criteria of reproducibility.

References

1. Calkins ME et al. (2015), The Philadelphia Neurodevelopmental Cohort: constructing a deep phenotyping collaborative. Journal of Child Psychology Psychiatry. 56(12):1356-1369. doi: 10.1111/jcpp.12416.
2. Greicius M. (2008), Resting-state functional connectivity in neuropsychiatric disorders. Current Opinion Neurology. 21(4):424-30. doi: 10.1097/WCO.0b013e328306f2c5.
3. Ji JL et al. (2021), Mapping brain-behavior space relationships along the psychosis spectrum. Elife. 10:e66968. doi: 10.7554/eLife.66968. Erratum in: Elife. 2022 Apr 05;11
4. Lynch CJ et al. (2023), Expansion of a frontostriatal salience network in individuals with depression. bioRxiv. 14:2023.08.09.551651. doi: 10.1101/2023.08.09.551651.
5. Marek S et al. (2022), Reproducible brain-wide association studies require thousands of individuals. Nature. 603(7902):654-660. doi: 10.1038/s41586-022-04492-9. Epub 2022 Mar 16. Erratum in: Nature. 2022 May;605(7911):E11.
6. Siegel JS et al. (2023), Psilocybin desynchronizes brain networks. medRxiv. 24:2023.08.22.23294131. doi: 10.1101/2023.08.22.23294131.

Poster No 482

Increasing prefrontal gray matter volume correlates with reduction of negative symptoms in psychosis

Dirk Wildgruber[1], Klaus Hesse[2], Kathrin Eckstein[2], Janina Richter[2], Mark-Christian Eberle[2], Lina Hawlik[2], Peter Martus[3], Benjamin Kreifelts[2], Michael Erb[4], Stefan Klingberg[2]

[1]University Tuebingen, Germany, Tuebingen, Germany, [2]Department of Psychiatry and Psychotherapy, University Tuebingen, Germany, Tuebingen, Germany, [3]Institute for Clinical Epidemiology and Applied Biometry, University Tuebingen, Germany, Tuebingen, Germany, [4]Department of Biomedical Magnetic Resonance, University Tuebingen, Germany, Tuebingen, Germany

Introduction: Besides psychotic symptoms (hallucinations, delusions), cognitive deficits and negative symptoms may occur in patients with psychotic disorders. Negative symptoms (blunted affect, alogia, anhedonia, avolition, social withdrawal) are the most important predictors of long-term impairment in social functioning and quality of life. Moreover, negative symptoms respond poorly to pharmacological and psychotherapeutic intervention available to date. This study evaluated the efficacy of an innovative cognitive behavioral therapy to reduce negative symptoms in patients with psychosis. The new approach (MOSAIC-therapy) combines individual sessions of cognitive behavioral therapy (CBT) and corresponding social skills group trainings. Change goals were identified in individual CBT sessions and corresponding interactions were practiced in the social environment of the group. In turn, experiences from group sessions were taken up in individual CBT to promote transfer to everyday life. In addition to changes in negative symptoms (PANSS-neg) and social functioning (SSPA, TBM) psychotherapy-related changes of gray matter volume were evaluated using voxel-based morphometry (VBM).

Methods: MOSAIC (30 sessions individual CBT & 30 group trainings within 8 months) was compared with SUPPORT (supportive talks and enjoyable group activities without specific therapeutic goals in the same timeframe) in a randomized controlled trial. Sixty patients with psychotic disorders with marked negative symptoms participated (PANSS negative syndrome > 10), of which 54 patients completed the intervention (27 per group). Assessments for the primary (PANSS-neg) and secondary endpoints (SSPA, TBM) were carried out before therapy initiation (T0) and after completion of the interventions (T2). The investigator was blind to information on which therapy the patient had received. Specific treatment effects of MOSAIC as compared to SUPPORT were evaluated using t-tests, in which the differences in post- and pre-intervention data (T2-T0) were tested for mean differences ($p < 0.05$). In addition, both groups were tested separately for significant pre-post effects ($p < 0.05$). Furthermore, pre- and post-interventional structural MRI data (3T) were assessed for therapy-related changes of gray matter volume using SPM12 (www.fil.ion.ucl.ac.uk/spm, CAT12-Toolbox, $p < 0.05$).

Results: No significant differences were observed between MOSAIC and SUPPORT for PANSS-neg ($p = 0.36$, Cohen's $d = 0.1$), SSPA ($p = 0.30$, $d = 0.14$) and TBM ($p = 0.07$, $d = 0.40$). However, pre-post comparisons showed reduction of negative symptoms as well as increase of social functioning within each group with moderate to large effect sizes (Fig. 1): MOSAIC: PANSS-neg ($p < 0.001$, $d = 0.82$), SSPA ($p = 0.006$, $d = 0.52$), TBM ($p = 0.03$, $d = 0.37$). SUPPORT: PANSS-neg ($p = 0.005$, $d = 0.53$), SSPA ($p = 0.007$, $d = 0.51$), TBM ($p = 0.28$, $d = 0.11$). Regarding VBM correlates of psychotherapy-related changes, no interaction between time (T2 vs. T0) and group (MOSAIC vs. SUPPORT) was observed, whereas the extent of individual reduction of negative symptoms (across both groups) correlated with increased gray matter volume (T2 > T0) in the bilateral ventromedial prefrontal cortex (vmPFC) and the left temporal pole (Fig. 2).

Conclusions: MOSAIC showed no significant difference in efficacy compared to SUPPORT. However, reduction of negative symptoms occured in both groups. These results indicate that patients with negative symptoms can benefit significantly from intensive psychotherapy combining individual sessions and group trainings that are focused on increase of motivation and social interaction. The observed correlation between the extent of individual symptom reduction and increase of gray matter volume within the bilateral vmPFC and the left TP indicates a link between clinical improvement and neuroplastic changes presumably involving psychotherapy-related formation of new synaptic connections within regions underlying social motivational processing.

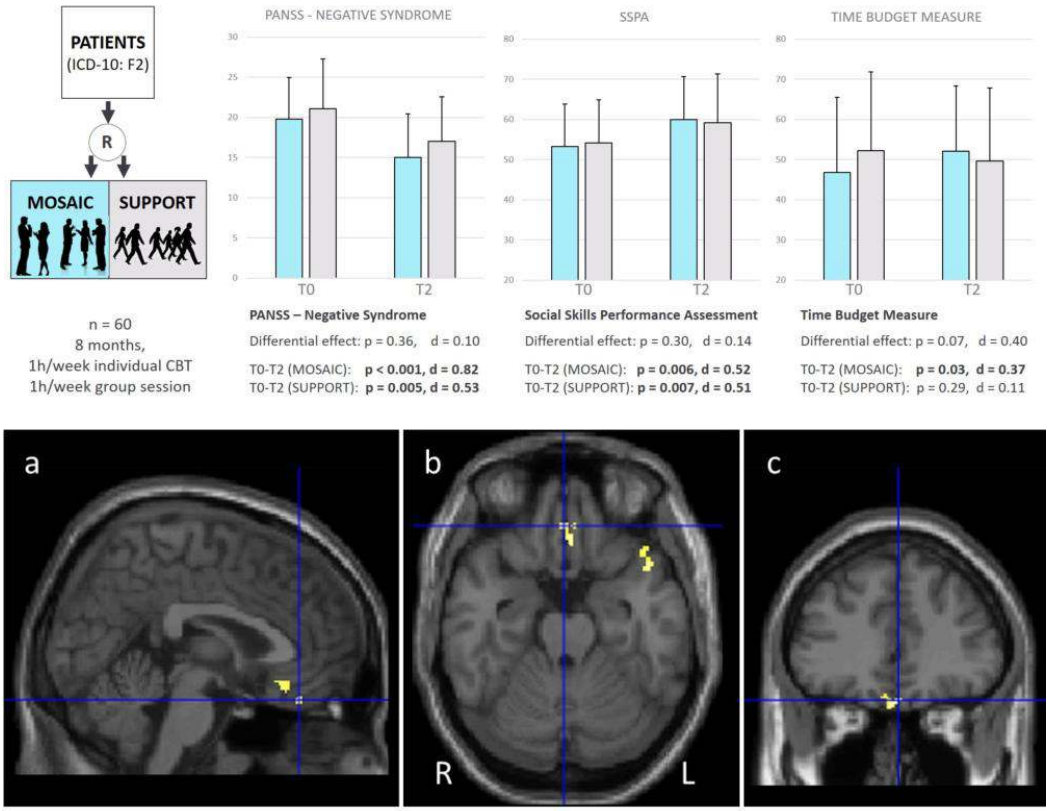

References

1. Kirkpatrick et al. (2006), The NIMH-MATRICS consensus statement on negative symptoms. Schizophrenia Bulletin, 32: 214-219.
2. Lang et al. (2013), Psychopathological long-term outcome of schizophrenia - a review. Acta Psychiatrica Scandinavica, 127: 173-182.
3. Siegel et al. (2006), Prognostic variables at intake and long-term level of function in schizophrenia. American Journal of Psychiatry, 163: 433-441.
4. Milev, et al. (2005), Predictive values of neurocognition and negative symptoms on functional outcome in schizophrenia: A longitudinal first-episode study with 7-year follow-up. Am J. Psychiatry, 162: 495-506.
5. Fusar-Poli et al. (2015) Treatments of Negative Symptoms in Schizophrenia: Meta-Analysis of 168 Randomized Placebo-Controlled Trials. Schizophrenia Bulletin, 41: 892–899.
6. Leucht et al. (2009), How effective are second-generation antipsychotic drugs? A meta-analysis of placebo-controlled trials. Molecular Psychiatry, 14: 429-447.
7. Turner et al. (2014), Psychological Interventions for Psychosis: A Meta-Analysis of Comparative Outcome Studies. Am J Psychiatry, 171: 523-538.
8. Kay et al. (1987), The positive and negative syndrome scale (PANSS) for schizophrenia. Schizophrenia Bulletin, 13: 261-276.
9. Marder et al. (1997), The effects of risperidone on the five dimensions of schizophrenia derived by factor analysis: Combined results of the North American trials. J. Clin. Psychiatry, 58: 538–546.
10. Patterson et al. (2001), Social skills performance assessment among older patients with schizophrenia. Schizophrenia Research, 48: 351–360.
11. Jolley et al. (2006), A validation of a new measure of activity in psychosis. Schizophrenia Research, 85: 288-295.
12. Howard et al., (2020), Mapping the interconnected neural systems underlying motivation and emotion: A key step toward understanding the human affectome, Neuroscience & Biobehavioral Reviews, 113: 204-226.

Poster No 483

Alterations in functional network dynamics following ketamine treatment in major depression

Brandon Taraku[1], Jason Nomi[2], Artemis Zavaliangos-Petropulu[2], Noor Al-Sharif[2], Paloma Pfeiffer[2], Randall Espinoza[2], Katherine Narr[3]

[1]UCLA, Los Angeles, CA, [2]University of California, Los Angeles, Los Angeles, CA, [3]University of California Los Angeles, Los Angeles, CA

Introduction: Ketamine, an N-methyl-D-aspartate receptor (NMDAR) antagonist, produces rapid antidepressant effects in major depressive disorder (MDD). Recent investigations show that patients with MDD exhibit altered resting brain network dynamics that manifest as increased transitions between the central executive (CEN) and default mode (DMN) networks (Belleau et al., 2022), and increased dwell time in fronto-insular brain networks, which associate with rumination (Kaiser et

al., 2019). We thus used Co-Activation Pattern (CAP) analysis (Liu et al., 2013) to determine how ketamine affects the dynamic properties of resting brain networks and the relationships with therapeutic effects in patients with treatment resistant depression (TRD).

Methods: Participants included 58 TRD patients (mean age=40.7 years, female=28) and 56 healthy controls (HC) (mean age=32.8 years, female=32). TRD patients received 4 serial ketamine infusions (SKI) (0.5 mg/kg) over 2 weeks. MRI scans included structural (T1/T2w) and resting state fMRI(acquisition time:13min, TR:0.8s, VS:2mm isotropic), and clinical scales included the Hamilton Depression Rating scale (HDRS) and Rumination and Reflection Scale (RRS). MRI and clinical data were collected at baseline for all participants, and 24hrs after the last ketamine infusion for TRD patients. MRI preprocessing included the HCP minimal preprocessing pipeline(Glasser et al., 2013), followed by global signal regression and band-pass filtering [0.01 – 0.1 Hz]. fMRI data, parcellated using the Schaefer 400 atlas(Schaefer et al., 2018) plus 54 subcortical regions(Tian et al., 2020), were z-scored to normalize BOLD activity. CAP analysis included k-means clustering in MATLAB across a range of clustering solutions to find the optimal cluster number. Here, the cluster validity index was computed(Allen et al., 2014), and an L-curve was fitted to the range of clustering scores using least squares regression to determine the 'elbow' point. For the optimal cluster number, CAP metrics were computed including 1) the fraction of time spent in a CAP (F), and 2) the transition probability from one CAP to another (T). Statistical analyses addressed changes in CAP metrics over time in TRD patients using paired t-tests, and associations with mood scores using Pearson correlations. CAP metrics showing significant SKI effects were compared between TRD and HC at baseline with independent sample t-tests controlling for age and sex. Bonferroni correction addressed multiple comparisons.

Results: Six CAP clusters were revealed as optimal (Fig 1). Significant decreases in F for visual (VN) CAP (t=-3.57, p=7.37E-04) and increases in F for CEN CAP (t=3.26, p=1.90E-03) occurred post SKI. Follow-up analyses for CEN and VN CAPs found significant increases in T from salience (SN) to CEN (t=3.65, p=5.79E-04), and decreases in T from SN to VN (t=-3.04, p=3.60E-03). Decreases in F for SN CAP were significantly correlated with improvements in RRS (r=-0.402, p=1.90E-03). Baseline analyses revealed significantly lower F for CEN CAP (t=-3.55, p=5.70E-04) and lower T from SN to CEN (t=-2.44, p=0.016) and higher T from SN to VN (t=3.08, p=2.60E-03) for TRD compared to HCs (Fig 2).

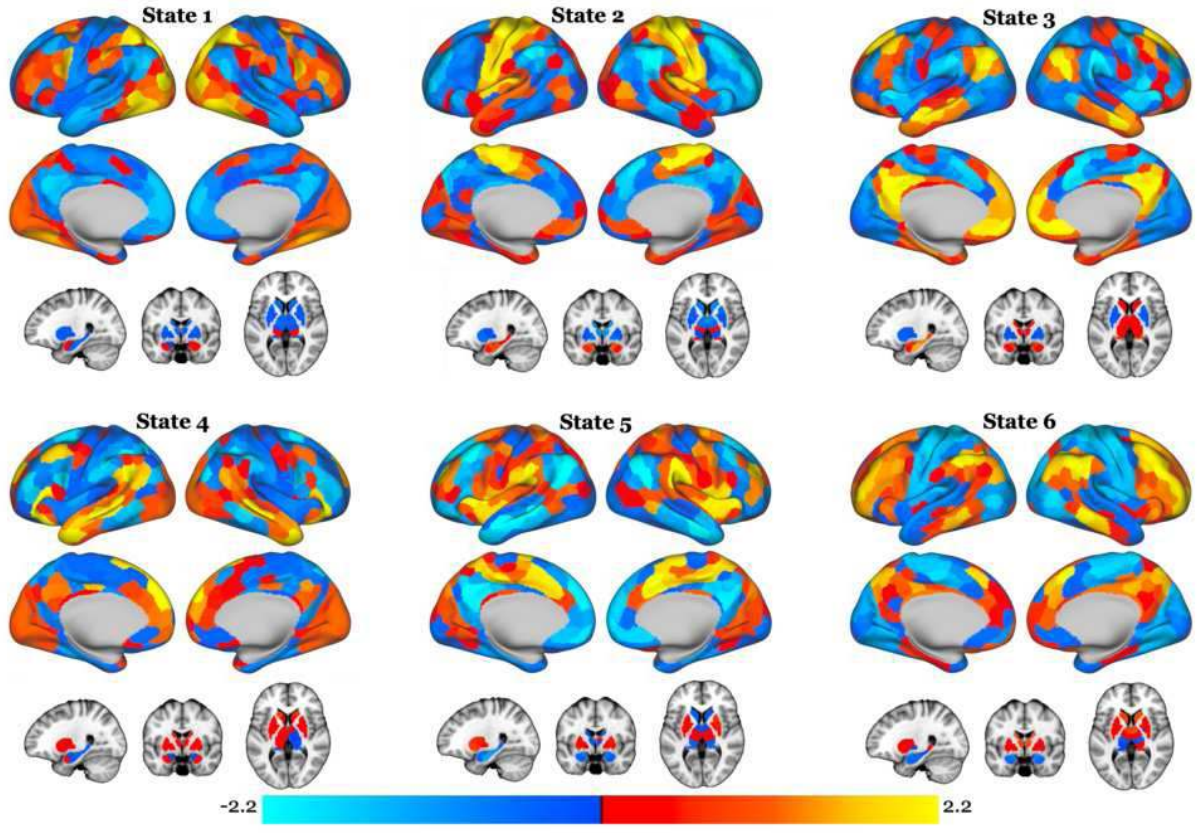

Figure 1: CAP states determined from optimal number of clusters. Colors represent z-scores for each state to show which regions are relatively more active and inactive. State 1 shows activation in the visual network (VN), dorsal attention network (DAN) and amygdala. State 2 shows activation in the somatomotor network (SMN), amygdala, and hippocampus. State 3 shows activation in the default mode network (DMN), amygdala and hippocampus. State 4 shows activation in ventral DMN structures, VN, amygdala and striatum. State 5 shows activation in the salience network (SN), and some striatum and thalamic structures. State 6 shows activation in the central executive network (CEN), striatum and some DMN and thalamus.

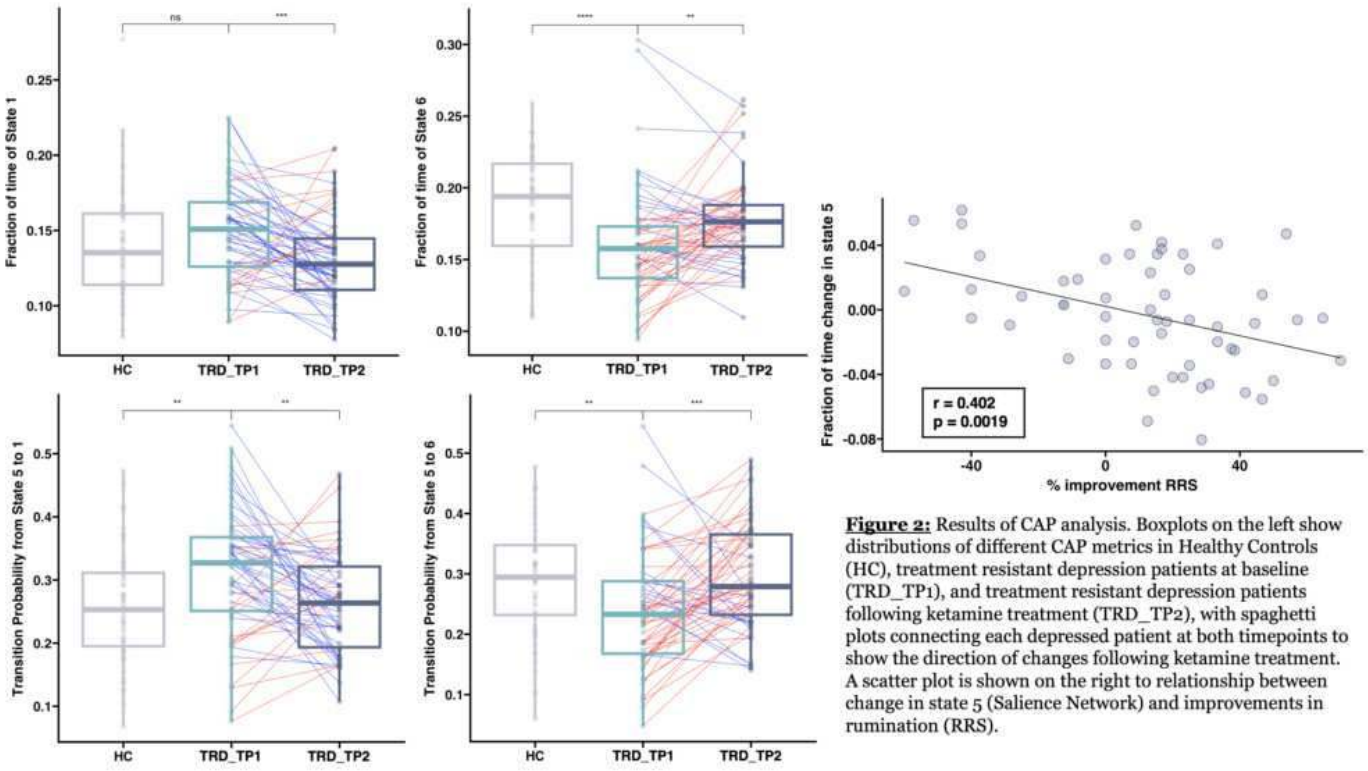

Figure 2: Results of CAP analysis. Boxplots on the left show distributions of different CAP metrics in Healthy Controls (HC), treatment resistant depression patients at baseline (TRD_TP1), and treatment resistant depression patients following ketamine treatment (TRD_TP2), with spaghetti plots connecting each depressed patient at both timepoints to show the direction of changes following ketamine treatment. A scatter plot is shown on the right to relationship between change in state 5 (Salience Network) and improvements in rumination (RRS).

Conclusions: Results suggest that SKI primarily affects network dynamics between VN, CEN and SN in TRD, and that SN transitions account for these dynamics. These findings support the hypothesis that the SN acts as mediator by switching between large scale brain networks(Menon & Uddin, 2010), and suggest this pattern is modulated by ketamine. Cross sectional results suggest that ketamine normalizes baseline differences between patients and HCs including decreased occurrences of CEN and SN to CEN transitions, and increased SN to VN transitions. Findings align with prior research suggesting decreased CEN activity in MDD is linked with emotion regulation(Brakowski et al., 2017) and CAP findings that showed increased occurrences of states involving the insula, a key hub of the SN, associate with rumination (Kaiser et al., 2019).

References

1. Allen, E. A., Damaraju, E., Plis, S. M., Erhardt, E. B., Eichele, T., & Calhoun, V. D. (2014). Tracking whole-brain connectivity dynamics in the resting state. Cerebral Cortex, 24(3), 663–676.
2. Belleau, E. L., Bolton, T. A. W., Kaiser, R. H., Clegg, R., Cárdenas, E., Goer, F., Pechtel, P., Beltzer, M., Vitaliano, G., Olson, D. P., Teicher, M. H., & Pizzagalli, D. A. (2022). Resting state brain dynamics: Associations with childhood sexual abuse and major depressive disorder. NeuroImage. Clinical, 36, 103164.
3. Brakowski, J., Spinelli, S., Dörig, N., Bosch, O. G., Manoliu, A., Holtforth, M. G., & Seifritz, E. (2017). Resting state brain network function in major depression - Depression symptomatology, antidepressant treatment effects, future research. Journal of Psychiatric Research, 92, 147–159.
4. Glasser, M. F., Sotiropoulos, S. N., Wilson, J. A., Coalson, T. S., Fischl, B., Andersson, J. L., Xu, J., Jbabdi, S., Webster, M., Polimeni, J. R., Van Essen, D. C., Jenkinson, M., & WU-Minn HCP Consortium. (2013). The minimal preprocessing pipelines for the Human Connectome Project. NeuroImage, 80, 105–124.
5. Kaiser, R. H., Kang, M. S., Lew, Y., Van Der Feen, J., Aguirre, B., Clegg, R., Goer, F., Esposito, E., Auerbach, R. P., Hutchison, R. M., & Pizzagalli, D. A. (2019). Abnormal frontoinsular-default network dynamics in adolescent depression and rumination: a preliminary resting-state co-activation pattern analysis. Neuropsychopharmacology: Official Publication of the American College of Neuropsychopharmacology, 44(9), 1604–1612.
6. Liu, X., Chang, C., & Duyn, J. H. (2013). Decomposition of spontaneous brain activity into distinct fMRI co-activation patterns. Frontiers in Systems Neuroscience, 7, 101.
7. Menon, V., & Uddin, L. Q. (2010). Saliency, switching, attention and control: a network model of insula function. Brain Structure & Function, 214(5-6), 655–667.
8. Schaefer, A., Kong, R., Gordon, E. M., Laumann, T. O., Zuo, X.-N., Holmes, A. J., Eickhoff, S. B., &
9. Yeo, B. T. T. (2018). Local-Global Parcellation of the Human Cerebral Cortex from Intrinsic Functional Connectivity MRI. Cerebral Cortex, 28(9), 3095–3114.
10. Tian, Y., Margulies, D. S., Breakspear, M., & Zalesky, A. (2020). Topographic organization of the human subcortex unveiled with functional connectivity gradients. Nature Neuroscience, 23(11), 1421–1432.

Poster No 484

Amygdala downregulation training using fMRI neurofeedback in post-traumatic stress disorder

Zhiying Zhao[1], Or Duek[2], Rebecca Seidemann[2], Charles Gordon[2], Christopher Walsh[2], Emma Romaker[2], William Koller[2], Mark Horvath[2], Jitendra Awasthi[2], Ilan Harpaz-Rotem[2], Michelle Hampson[2]

[1]University of Macau, Macau, Macau, [2]Yale University School of Medicine, New Haven, CT

Introduction: Post-traumatic stress disorder (PSTD) is a psychiatric disorder with a high prevalence worldwide[1]. Recent neuroimaging studies have revealed a relationship between PTSD symptoms and dysregulated amygdala activity and have suggested that normalizing amygdala activity may be therapeutic[2]. We explored whether fMRI NF could improve amygdala regulation by conducting a clinical trial (NCT03574974) in which PTSD patients were trained to down-regulate their amygdala activity following trauma recall.

Methods: Individuals with PTSD symptoms were recruited and screened through the VA. They were assessed using the Clinician-Administered PTSD Scale for DSM-5 (CAPS-5). Those eligible were assigned to receive either Real or Sham feedback. During three feedback sessions, they were instructed to downregulate the feedback signal after listening to personal trauma scripts. Participants also underwent three additional imaging sessions to assess changes in control over amygdala activity at the following timepoints: baseline, post-NF, and 30 days post-NF. During these sessions, they performed down-regulation after trauma recall in the absence of a feedback signal. This served as our primary measurement for improvement in amygdala activity control.

Results: 25 PTSD patients (14 Real, 11 Sham) completed this randomized, double-blind trial. Although the Real group showed greater improvement in amygdala control than the Sham group at the post-training time point, this difference was not significant. However, at the 30day follow-up time point, the Real group had significantly greater improvement in amygdala control than the Sham group: Cohen's d = 0.986; t17 = 2.146, p = 0.047, two-tailed. Clinical improvements were also qualitatively larger and increased over time in the Real group, although this was not significant.

Conclusions: In this mechanistic study, we found improved control over amygdala activity after neurofeedback training. Although not significant in this small sample, the clinical changes induced were also promising. These data support the growing literature suggesting that neurofeedback of amygdala activity has therapeutic potential for PTSD[3,4].

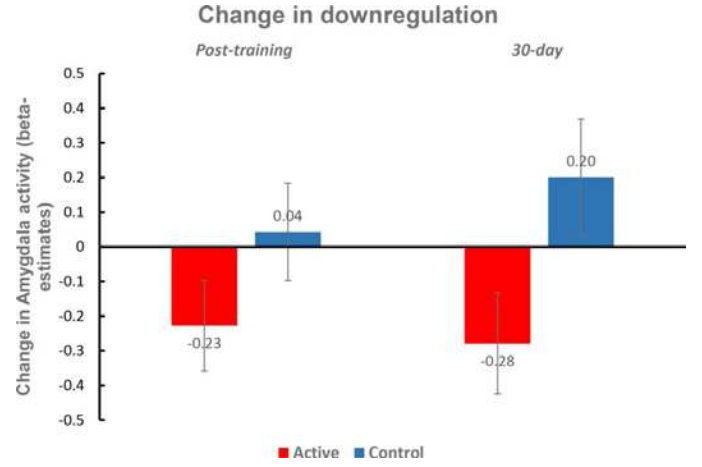

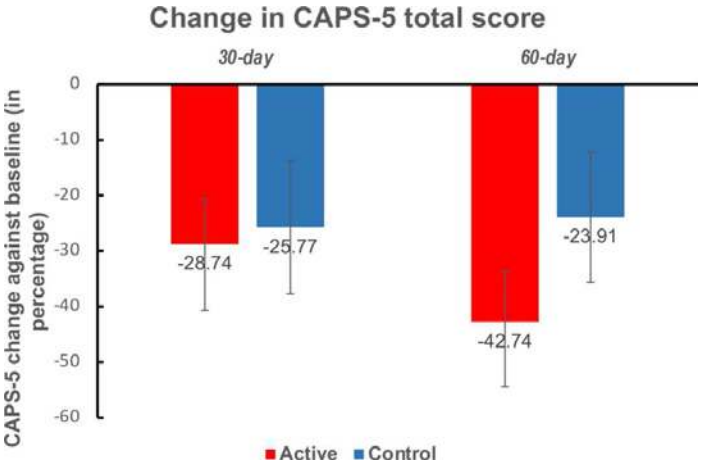

References
1. Atwoli L, et al. Curr Opin Psychiatry. 2015;28(4):307-311.
2. Diamond DM, et al. J Neurosci Res. 2016;94(6):437-444.
3. Fruchtman T, et al. PsyArXiv. 2019.
4. Nicholson AA, et al. HBM. 2017;38(1):541-560.

Poster No 485

Right superior frontal gyrus: A potential marker for predicting the efficay in schizophrenia

Yongfeng Yang[1], Xue Li[1], Hongyan Yu[1], Qing Liu[1], Luwen Zhang[1], Xi Su[1], Bing Liu[2], Luxian Lv[1], Wenqiang Li[1]

[1]The Second Affiliated Hospital of Xinxiang Medical University, Xinxiang, Henan, [2]Beijing Normal University, Beijing, Beijing

Introduction: Schizophrenia is a severe chronic mental disorder with a lifetime prevalence of about 1%. Antipsychotic drug treatment for schizophrenia can alter brain structure and function, but it is unclear if specific regional changes are associated with treatment outcome. Little is known about the effects of antipsychotics on brain tissue density or functional connectivity (FC) Therefore, we examined the effects of antipsychotic drug treatment on regional grey matter (GM) density, white matter (WM) density, and FC as well as associations between regional changes and treatment efficacy.

Methods: We examined the effects of antipsychotic drug treatment on regional grey matter (GM) density, white matter (WM) density, and functional connectivity (FC) as well as associations between regional changes and treatment efficacy. SZ patients (n=163) and health controls (HCs) (n=131) were examined by structural magnetic resonance imaging (sMRI) at baseline, and a subset of SZ patients (n=77) were re-examined after 8 weeks of second-generation antipsychotic treatment to assess changes in regional GM and WM density. In addition, 88 SZ patients and 81 HCs were examined by resting-state functional MRI (rs-fMRI) at baseline and the patients were re-examined post-treatment to examine FC changes. The Positive and Negative Syndrome Scale (PANSS) and MATRICS Consensus Cognitive Battery (MCCB) were applied to measure psychiatric symptoms and cognitive impairments in SZ. SZ patients were then stratified into response and non-response groups according to PANSS score change (≥50% decrease or <50% decrease, respectively).

Results: The demographic and clinical characteristics of the 163 SZ patients and 131 HCs are analyses. There were no significant differences in age or sex ratio between the total SZ and HC cohorts, while years of education was significantly lower in the patient cohort. Regions exhibiting WM density reductions included the inferior frontal gyrus, orbital gyrus, inferior temporal gyrus, parahippocampal gyrus, cingulate, medioventral occipital cortex, lateral occipital cortex, basal ganglia, and thalamus. The GM density of the right cingulate gyrus, WM density of the right superior frontal gyrus (SFG) plus 5 other WM tracts were reduced in the response group (n=44) compared to the non-response group (n=33). The FC values between the right anterior cingulate and both paracingulate gyrus and left thalamus were reduced in the entire SZ group (n=88) after treatment, while FC between the right inferior temporal gyrus (ITG) and right medial superior frontal gyrus (SFGmed) was increased in the response group. Partial correlation analyses with age, sex, illness duration, and years of education as covariates yielded no significant relationships between clinical scores and individual FC changes.

Conclusions: These findings suggest that the right SFG is a critical target of antipsychotic drugs and that WM density and FC alterations within this region could be used as potential indicators in predicting the treatment outcome of antipsychotics of SZ.

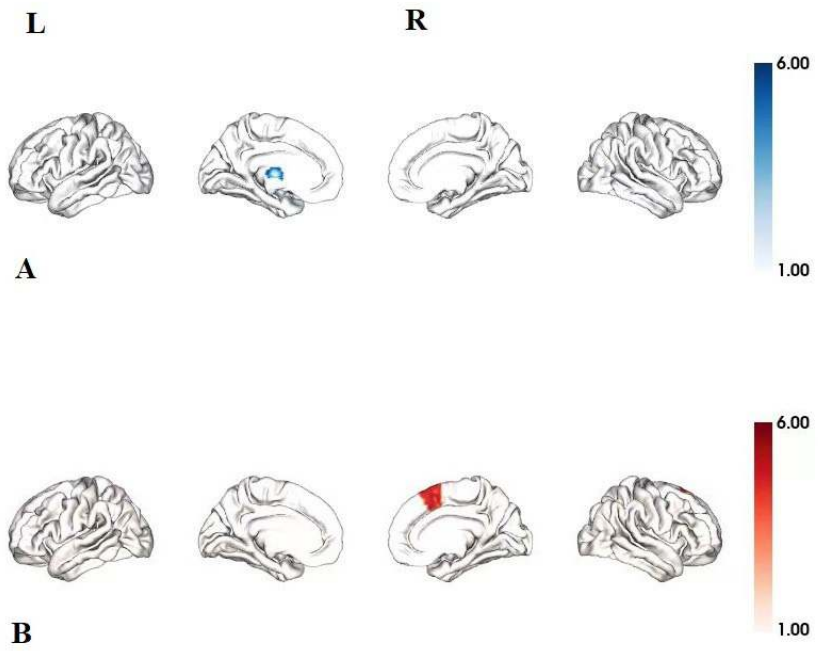

Fig. FC Changes before and after treatment in the SZ. FC between the ITG and the right medial SFG (SFGmed) was strengthened in the response group.

References

1. Li, X.(2023), 'Abnormalities of Regional Brain Activity in Patients With Schizophrenia: A Longitudinal Resting-State fMRI Study, Schizophrenia Bulltin', vol. 49, no.5, pp.1336-1344.
2. Yang Y. Y. (2022) 'Abnormal patterns of regional homogeneity and functional connectivity across the adolescent first-episode, adult first-episode and adult chronic schizophrenia'. Neuroimage: Clinical, vol, 36. pp.103198.
3. Fan, L.Z., (2016) 'The Human Brainnetome Atlas: A new brain atlas based on connectional architecture', Cereb Cortex, vol. 26, pp. 3508-3526.
4. Zhang Z., (2021) 'Dynamic functional connectivity and its anatomical substrate reveal treatment outcome in first-episode drug-naïve schizophrenia', Translation Psychiatry .vol. 11, no. 1, pp.282.

Poster No 486

The functional connectivity changes of amygdala linked with anxiety in schizophrenia and prodrome

Tzuhan Tseng[1], Ching-Lun Tsai[2], Hsien-Yuan Lane[3], Wei-Fen Ma[4], Cheng-Hao Tu[5]

[1]School of Chinese Medicine, China medical university, Taichung, Taiwan, [2]Department of Public Health, China Medical University, Taichung, Taiwan, [3]Department of Psychiatry, China Medical University Hospital, Taichung, Taiwan, [4]School of Nursing, China Medical University, Taichung, Taiwan, [5]Graduate Institute of Acupuncture Science, China Medical University, Taichung, Taiwan

Introduction: Clinically, schizophrenia has a strong association with imbalances in emotional control that 38.3% of patients diagnosed with anxiety disorders and related conditions (Achim et al., 2011; Foussias et al., 2015). Previous study indicated that the emotional deficits in schizophrenia stem from disturbances in the neural networks encompassing the amygdala (Friston, 1998). Thus, functional dysconnectivity of the amygdala networks may serve as a pivotal etiological factor of anxiety in schizophrenia. Furthermore, it has been observed that different levels of anxiety were correlated with distinct patterns of functional connectivity (FC) strength between the right amygdala and the dorsomedial prefrontal cortex (Kim et al., 2011). Thus, we hypothesized that patients with schizophrenia and prodromal participants may have abnormal resting-state FC in the right amygdala networks when compared with healthy controls, and dysfunctional connectivity of right amygdala may be associated with different levels of anxiety.

Methods: Eighty-six Participants (26 schizophrenia patients, 25 prodromal participants, and 35 healthy controls) were included in this study. The anxiety levels of the participants were assessed by the State-Trait Anxiety Inventory in Chinese Mandarin. Participants with trait scores exceeding 60 was considered as high anxiety level. Each participant underwent a whole-

brain anatomical scan and 200 continuous whole-brain resting-state fMRI scans (2.5 seconds per scan). The images were preprocessed using Data Processing Assistant for Resting-state fMRI (DPARSF). The seed region of right amygdala was placed at MNI coordinates x=22, y=-6, and z=-18 as a 3mm radius spheres. The averaged time-activity series were extracted from the seed region, and FC maps (r-to-z value converted) of seed region were generated. The statistical analysis for standardized FC maps were conducted using SPM12. The flexible factorial design was utilized with group and anxiety factor as between-subject factors. The changes were deemed as significant if the family-wise error rate corrected cluster $p < 0.05$ (the cluster forming threshold was in uncorrected voxel $p < 0.005$).

Results: For the group effect, a significant increased FC between the amygdala and the middle frontal gyrus (MFG) has been found in schizophrenia patients compared to healthy controls, whereas prodromal subjects revealed FC values between them. For the anxiety effect, a significant increased FC has been found in ventrolateral prefrontal cortex (vlPFC) between subjects with high and low anxiety, in both prodromal subjects and healthy controls. The high anxiety subjects in prodromal and healthy groups revealed positive FC in vlPFC, while low anxiety subjects revealed negative FC in vlPFC. Moreover, high anxiety subjects exhibited a positive FC between amygdala and precuneus in schizophrenia group, whereas negative FC in precuneus were observed in both prodromal and healthy groups. Notably, the prodromal group revealed FC value between schizophrenia and healthy groups.

Conclusions: In the current study, we found altered FCs in MFG and precuneus in both schizophrenia patients and prodromal subjects, which may associate with the progression from normal state to illness onset. Moreover, altered FC have also been found in the vlPFC between different anxiety levels in prodromal subjects and healthy controls. Considering the precuneus and vlPFC were involved in emotional control, the FC changes between the right amygdala and these emotion-modulating regions highlight the intricate relationship between anxiety and pathophysiological changes in individuals with schizophrenia and those in the prodromal stage. Future researches are needed to include longitudinal studies to track FC changes in amygdala over time, especially in high-anxiety individuals transitioning from the prodromal stage to diagnosed schizophrenia.

References

1. Achim, A. M.(2011). How prevalent are anxiety disorders in schizophrenia? A meta-analysis and critical review on a significant association. Schizophrenia bulletin, 37(4), 811-821. doi:10.1093/schbul/sbp148.
2. Foussias, G. (2015).Dissecting negative symptoms in schizophrenia: opportunities for translation into new treatments. Journal of psychopharmacology (Oxford, England), 29(2), 116-126.doi:10.1177/0269881114562092.
3. Friston K. J. (1998). The disconnection hypothesis. Schizophrenia research, 30(2), 115–125. https://doi-org.autorpa.cmu.edu.tw:8443/10.1016/s0920-9964(97)00140-0
4. Kim, M. J.(2011). Anxiety dissociates dorsal and ventral medial prefrontal cortex functional connectivity with the amygdala at rest. Cerebral cortex (New York, N.Y. : 1991), 21(7), 1667-1673. doi:10.1093/cercor/bhq237.

Poster No 487

Unveiling causal interactions between depression and alcohol use from adolescence to young adulthood

Xuefei Wang[1]

[1]*Fudan University, Shanghai, China*

Introduction: Depression is one of the most common mental disorders, and alcohol use disorder often co-occurs with depression. However, little is known about the direction of the relationship between the two diseases. Most of the research on alcohol use and depression has been conducted in adults, and the findings may not necessarily apply to adolescents. Our study aims to longitudinally track the relationship between alcohol use and depression from adolescence to early adulthood.

Methods: We analyzed the IMAGEN dataset at baseline (14 years old), Follow-up 1 (16 years old), Follow-up 2 (19 years old), and Follow-up 3 (23 years old) to assess the partial correlations between alcohol consumption and depression, controlling for covariates such as gender, handedness, and imaging sites. We then employed cross-lagged panel analysis and a modified Mendelian randomization analysis to investigate the causal interactions. This new MR approach employed polygenic risk scores (PRS) as the instrumental variable that integrates the contributions of multiple genetic variations while accounting for pleiotropic SNPs. In addition, we employed a mediation analysis to investigate shared neural mechanisms, extracting participants' average brain activation in regions of interest (ROIs) comprising the bilateral Inferior Frontal Cortex (IFC) and Caudate during reward anticipation in the Monetary Incentive Delay (MID) task, as well as in the Stop-Signal Task (SST). The masks in the current study with $t > 5$ in the contrasts of large win vs. no win in MID and stop success vs. go success in SST.

Results: Depression and alcohol consumption frequency were significantly positively correlated at baseline ($r = 0.139$, $p = 4.11E-10$). The correlation gradually decreased over time and became negative. However, depression and harmful alcohol use

remained significantly positively correlated at all time points (baseline: r = 0.106, p = 1.15E-06) (Figure 1a). Instrumental PRS of depression at both baseline and follow-up 3 showed positive correlations with alcohol abuse, while instrumental PRS for alcohol drinking at Follow-up 3 displayed a negative correlation with depression scores (Figure 1b). In the Stop-Signal Task, the left inferior orbitofrontal cortex (OFC) may mediate the positive correlation between Major Depressive Disorder Polygenic Risk Scores (MDD PRS) and harmful alcohol use (βmediation = 7.55E-4, p = 4E-3). Conversely, in the Monetary Incentive Delay (MID) task, right Caudate may mediate the negative correlation between Alcohol Polygenic Risk Scores (ALCO PRS) and dep8_FU3 (βmediation = -440, p = 0.017) (Figure 2).

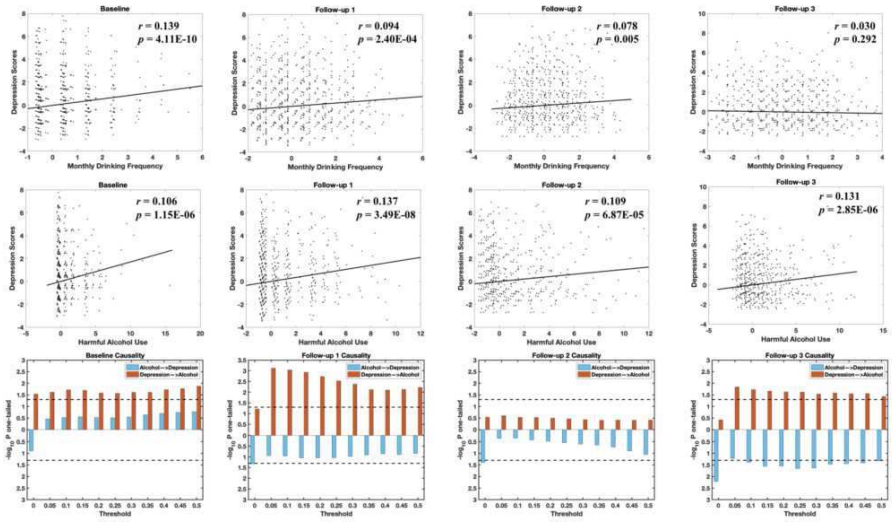

Figure 1a-b. Correlation between depression scores and drinking behaviors, represented by mean plus residuals.
Figure 1c. The causal interaction between depression and alcohol consumption.

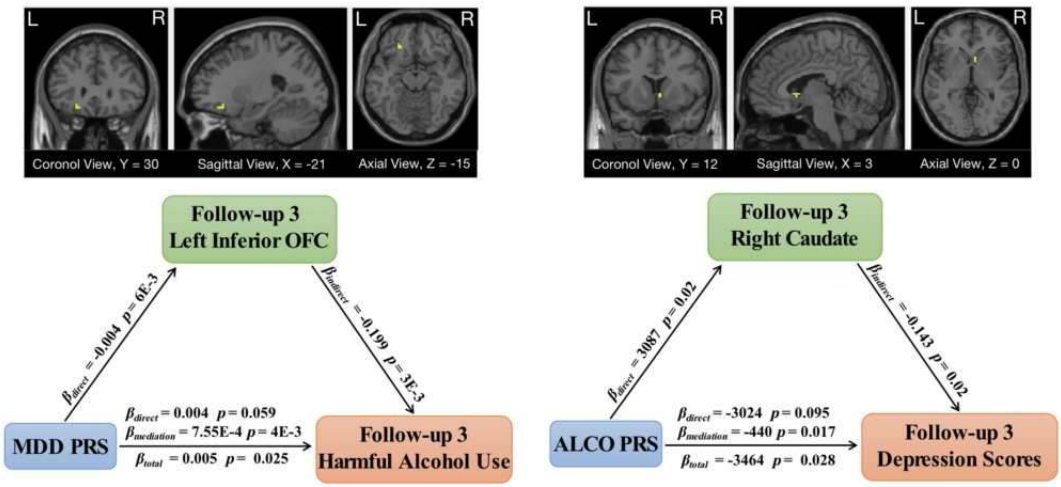

Figure 2. The results of mediation analysis. The p-values of the mediation effects were obtained with 10000 times bootstrap samplings.

Conclusions: Depression has a positive predictive effect on harmful alcohol use, while moderate alcohol consumption in early adulthood can alleviate depression. This mutual causal interactions could help to a better understanding and management of the relationship between alcohol consumption and depressive symptoms, ultimately enhancing the mental health of adolescents and young adults.

References

1. Fernandes GS, Lewis G, Hammerton G, et al. (2020), 'Alcohol consumption and internalising disorders in young adults of ALSPAC: a population-based study', J Epidemiol Community Health, vol. 74, no. 2, pp. 1023–1027.
2. Li J, Wang H, Li M, et al. (2020), 'Effect of alcohol use disorders and alcohol intake on the risk of subsequent depressive symptoms: a systematic review and meta-analysis of cohort studies', Addiction, vol. 115, no. 6, pp. 1224–1243.
3. Turner S, Mota N, Bolton J, Sareen J. (2018), 'Self-medication with alcohol or drugs for mood and anxiety disorders: a narrative review of the epidemiological literature', Depress Anxiety, vol. 35, no. 7, pp. 851–860.
4. Burgess S, Foley CN, Allara E, Staley JR, Howson JM. (2020), 'A robust and efficient method for Mendelian randomization with hundreds of genetic variants', Nat Commun, vol. 11, no. 6, pp.1–11.

Poster No 488

Neurobiological mapping of abnormal gray matter developmental trajectories in psychosis

Natalia García-San-Martín[1], Richard Bethlehem[2], Agoston Mihalik[2], Jakob Seidlitz[3], Isaac Sebenius[2], Claudio Alemán-Morillo[1], Lena Dorfschmidt[3], Golia Shafiei[4], Víctor Ortiz-García de la Foz[5], Kate Merritt[6], Anthony David[6], Sarah Morgan[2], Miguel Ruiz-Veguilla[7], Rosa Ayesa-Arriola[5], Javier Vázquez-Bourgon[5], Aaron Alexander-Bloch[4], Bratislav Misic[8], Edward Bullmore[2], John Suckling[2], Benedicto Crespo-Facorro[5,7,1], Rafael Romero-García[1,2]

[1]University of Seville, Seville, Spain, [2]University of Cambridge, Cambridge, United Kingdom, [3]The Children's Hospital of Philadelphia, Philadelphia, PA, [4]University of Pennsylvania, Philadelphia, PA, [5]Marqués de Valdecilla University Hospital, Cantabria, Spain, [6]University College London, London, United Kingdom, [7]Virgen del Rocío University Hospital, Seville, Spain, [8]McGill University, Montreal, Canada

Introduction: The psychosis spectrum encompasses a heterogeneous range of clinical conditions associated with abnormal brain development. The molecular and micro-architectural attributes that account for structural deviations from typical neurodevelopment are still unknown.

Methods: MRI data (T1-w) from first-degree relatives of schizophrenia (SCZ) and schizoaffective disorder (SAD) patients (n=160; age=42.3±15.7), chronic SCZ-SAD patients (n=587; age=37.2±12), and healthy controls (HC; n =38,232; age=51.9±23.7) were obtained from ABCD, ASRB, BSNIP, UCLA CNP LA5c, MCIC, and UKB datasets. Individuals who had Psychotic Experiences (PE) rated as 'suspected', 'definite', or 'clinical' if they had additional signs of social impairment or help-seeking, formed the PE group (ALSPAC cohort; n=157; age=21.5±1.4). HC (n=269; age=22.3±1.5) were rated as not having had PEs. Individuals who had experienced a First Episode of Psychosis (n=352; age=31.4±8.8), along with their HC (n=195; age=30.6±7.7), were obtained from PAFIP cohort. We used GAMLSS (Stasinopoulos & Rigby, 2007) to benchmark regional cortical volumes of psychosis-related groups against normative trajectories from ~100,000 participants (Bethlehem et al., 2022). Thus, age, sex, and site-normalized measures of cortical atypicalities across the lifespan ranked brain volumes within a range of 0 to 1 (centiles), which were compared with HC using the Wilcoxon test (FDR-corrected). Following Hansen et al., 2022 methodology, we explored the associations between centiles and the spatial maps of 46 neurobiological features classified under 6 types: neurotransmitter, cell type, layer thickness, microstructure, cortical expansion, and metabolism. The Principal Component Analysis-Canonical Correlation Analysis (PCA-CCA) model captured associations (weights) between the neurobiological maps and the regional centiles that the resulting linear combination of the maps constituted the predicted centiles (Mihalik et al., 2022). A spatial autocorrelation-preserving permutation test (spin test) was used to assess the statistical significance of the models and weights. Finally, a set of loadings was computed to ascertain the extent to which each neurobiological feature contributed to the predicted centiles.

Results: We found a generalized decrease in centiles across all groups compared to HC (Fig. 1a top). The relatives showed significant decreases in a great number of regions, while FEP and chronic in the majority of them (Fig. 1a middle). The PCA-CCA predicted centiles closely resembled empirical centiles for significant models (Fig. 1a bottom; all groups except PE; Pspin<0.05), where the groups with the lowest centiles, FEP and chronic, revealed the strongest correlation between them (Fig. 1b). All models exhibited significant loadings (Fig. 2a; Pspin<0.05). Groups with the lowest centiles showed a greater number of significant negative loadings. Synapse density and 5-HT2A stood out in all groups, neurotransmitters and cortical expansion in relatives and the chronic group, metabolism and microstructure in FEP, and layer thickness in the chronic group. The greatest negative overlapping loadings across all groups indicated a high presence of neurotransmitters, excitatory neurons, synapse density, and metabolism in regions where centiles are consistently low (Fig. 2b). The greatest positive loadings, consistent across all groups except chronic, indicating a high presence of neurotransmitters and cell types in regions closer to neurotypical centiles.

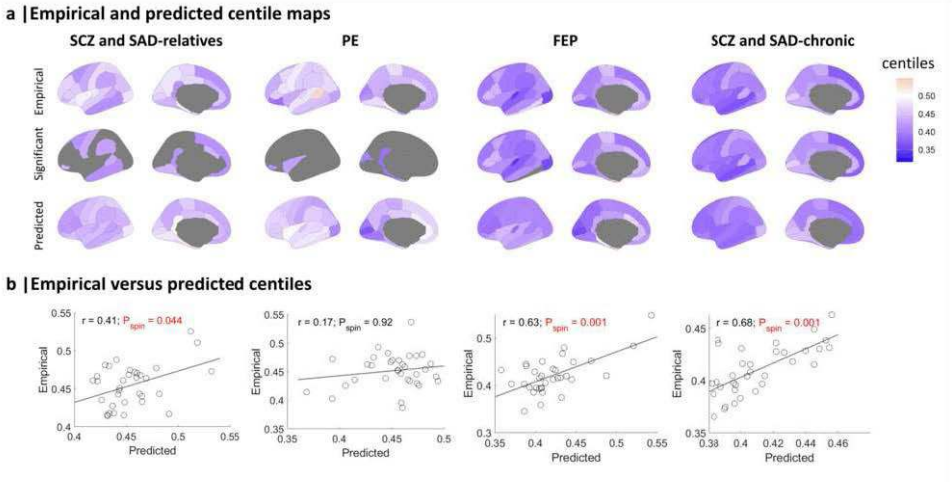

Fig. 1 | Empirical, significant, and predicted centiles. **a**, Maps of empirical MRI-derived centiles (top), empirical centiles that exhibit significant differences from HC (P<0.05) (middle), and predicted PCA-CCA-derived centiles from neurobiological features (bottom). **b**, Correlation between empirical and predicted regional centiles. Non-significant models are denoted as n.s (P_{spin}>0.05).

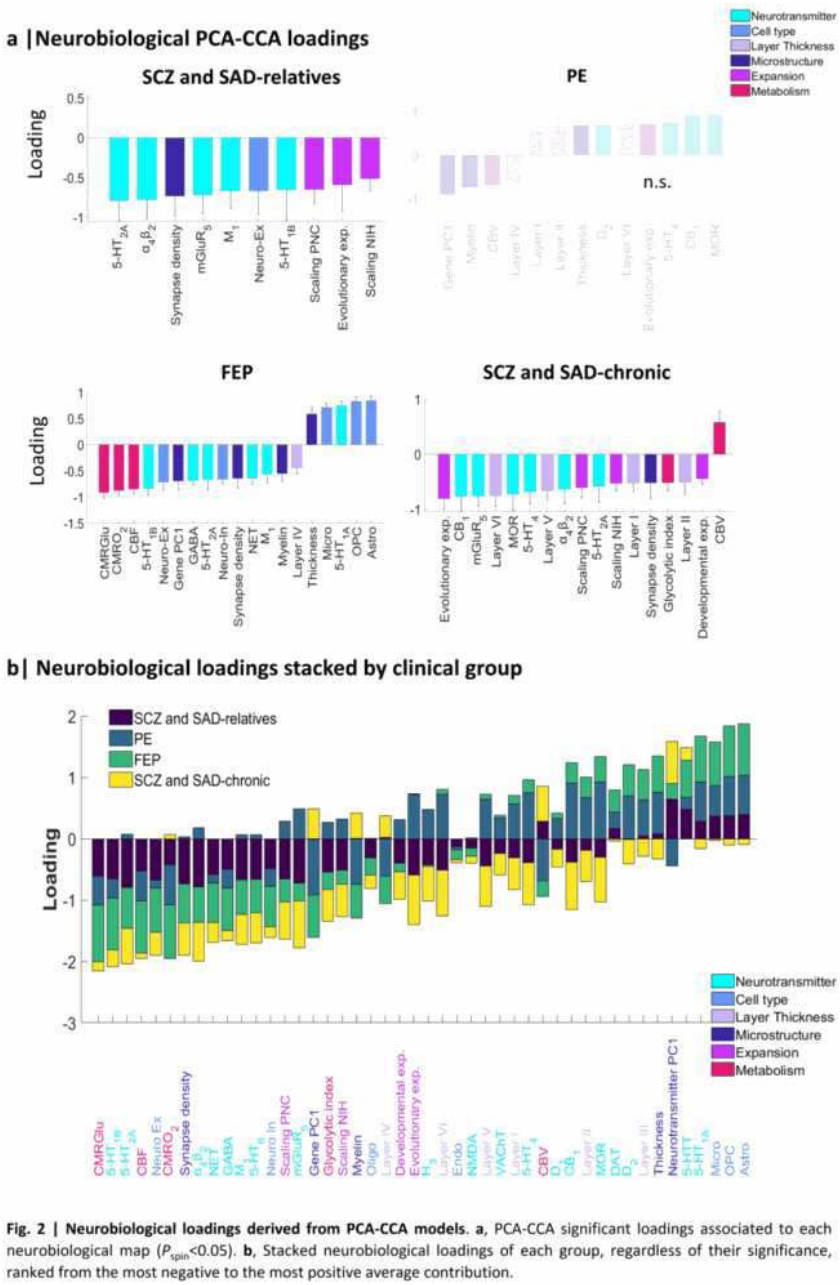

Fig. 2 | Neurobiological loadings derived from PCA-CCA models. **a**, PCA-CCA significant loadings associated to each neurobiological map (P_{spin}<0.05). **b**, Stacked neurobiological loadings of each group, regardless of their significance, ranked from the most negative to the most positive average contribution.

Conclusions: We identified group-specific volume deviations below the expected trajectory for different psychosis-related groups based on a normative centile method. We revealed an overlapping spatial distribution of the neurobiological features, which are highly co-localized with the abnormal developmental trajectories. These findings help understand the vulnerability factors that may underlie atypical brain maturation in different conditions and stages of psychosis.

References

1. Bethlehem, R. A. I., Seidlitz, J., White, S. R., Vogel, J. W., Anderson, K. M., Adamson, C., Adler, S., Alexopoulos, G. S., Anagnostou, E., Areces-Gonzalez, A., Astle, D. E., Auyeung, B., Ayub, M., Bae, J., Ball, G., Baron-Cohen, S., Beare, R., Bedford, S. A., Benegal, V., ... Alexander-Bloch, A. F. (2022). Brain charts for the human lifespan. Nature, 604(7906), 525–533. https://doi.org/10.1038/s41586-022-04554-y
2. Hansen, J. Y., Shafiei, G., Markello, R. D., Smart, K., Cox, S. M. L., Nørgaard, M., Beliveau, V., Wu, Y., Gallezot, J. D., Aumont, É., Servaes, S., Scala, S. G., DuBois, J. M., Wainstein, G., Bezgin, G., Funck, T., Schmitz, T. W., Spreng, R. N., Galovic, M., ... Misic, B. (2022). Mapping neurotransmitter systems to the structural and functional organization of the human neocortex. Nature Neuroscience, 25(11), 1569–1581. https://doi.org/10.1038/s41593-022-01186-3
3. Mihalik, A., Chapman, J., Adams, R. A., Winter, N. R., Ferreira, F. S., Shawe-Taylor, J., & Mourão-Miranda, J. (2022). Canonical Correlation Analysis and Partial Least Squares for Identifying Brain–Behavior Associations: A Tutorial and a Comparative Study. In Biological Psychiatry: Cognitive Neuroscience and Neuroimaging (Vol. 7, Issue 11, pp. 1055–1067). Elsevier Inc. https://doi.org/10.1016/j.bpsc.2022.07.012
4. Stasinopoulos, D. M., & Rigby, R. A. (2007). Generalized Additive Models for Location Scale and Shape (GAMLSS) in R. Journal of Statistical Software, 23(7). https://doi.org/10.18637/jss.v023.i07

Poster No 489

Extending imaging-transcriptomics: from decoding group-based findings to individual brains

Min Tae Park[1], Lena Palaniyappan[1], Mallar Chakravarty[1]

[1]McGill University, Montreal, Canada

Introduction: Imaging transcriptomics has been pivotal in linking variation in brain structure to spatial gene expression (in the Allen Human Brain Atlas (AHBA)[1], for example), uncovering novel insights regarding the molecular mechanisms of neuroanaomical diversity[2]. These methods have focused on correlating group-based findings (i.e. effect sizes of case-control comparisons) with the AHBA. Building on this, a pertinent question arises: can these group-based correlations be replicated or observed in individual brains? Determining whether the generalizations at the group level with imaging transcriptomics also hold true at the individual level may provide a more nuanced and personalized understanding of brain function and neurobiology. We tested this hypothesis using brain MRI scans from healthy controls (HC) and patients with schizophrenia (SCZ).

Methods: We hypothesized that we could infer gene expression, or transcriptomic "representation" maps using individual MRI data and multiple structural phenotypes. The goal is to identify transcriptomic signatures of brain structure in individual brains and identify broad pathway level correlations to brain structure. Publicly available MRI datasets consisting of HC and SCZ were gathered, standard pipelines (CIVET) were used to measure cortical thickness (CT), surface area (SA), cortical volume (CV), and curvature (CC) across 40,892 vertices per hemisphere. After quality control, total sample size was n=1152 (HC=606, FEP=101, SCZ=445). We correlated individual phenotypes separately with AHBA gene expression measures across ~1,000 matched vertices for ~15k genes. We focused on CT-gene correlations given the recent focus. For each individual's gene correlations, we examined enrichment of gene sets including: 1) Schizophrenia genes (120 genes from 2022 PGC GWAS3), 2) Cell types, and 3) Biological pathways. Enrichment testing was done using the AUCell R package. Group differences in individual measures of enrichment were tested using mixed-effects models, taking age, sex as fixed effects and dataset as random effect.

Results: Examining imaging-gene correlations across the four phenotypes reveals CT with the most variable correlations across genes (Figure). We did not find significant enrichment of SCZ genes in SCZ patients. Cell-type enrichment analysis demonstrates the oligodendrocyte precursor cell (OPC) enrichment as significantly greater in SCZ compared to HC (t=3.93, p=8.97E-05), replicating previous group-level comparison with imaging-transcriptomic analysis3. Astrocyte enrichment was significantly lesser in SCZ (t=-2.447, p=1.46E-02).

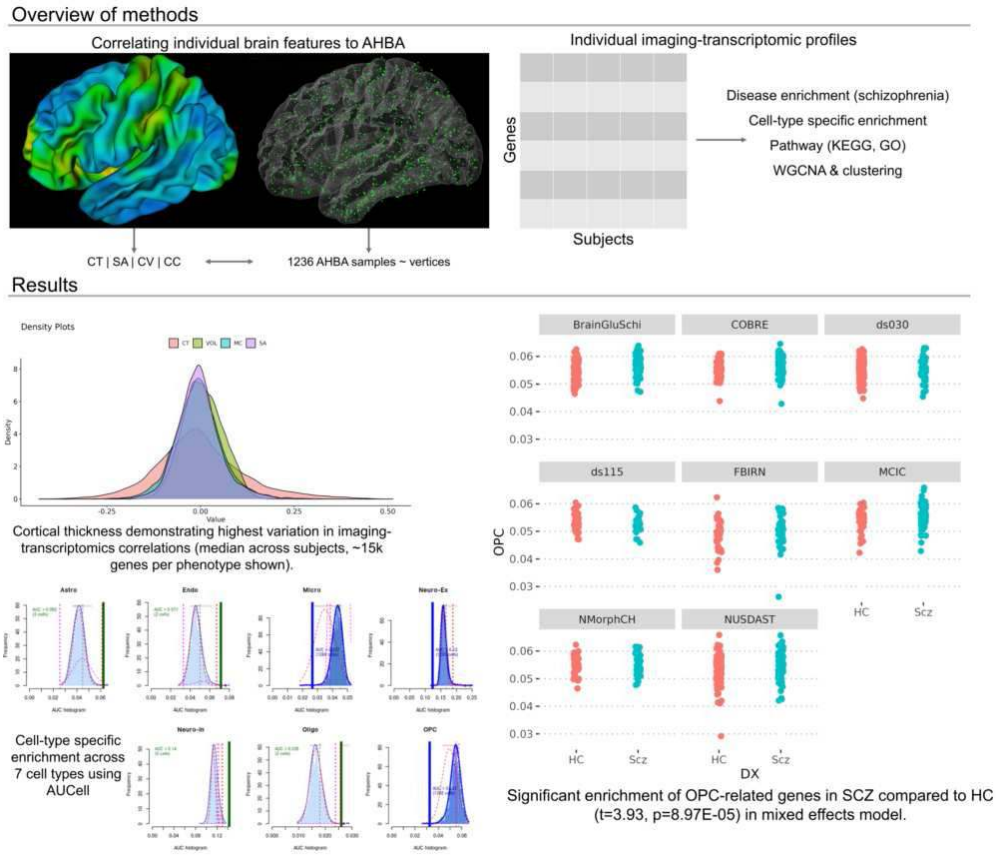

Conclusions: Aligning individual MRIs to the AHBA may recapitulate imaging-transcriptomic correlations observed at the group level. Notably, we did not find significant enrichment of SCZ genes in SCZ patients compared to HC–suggesting a cumulative effect of group-based testing in gene enrichment analysis, while individual patient correlations with SCZ genes may be few in number. We replicated previous findings of cell-type enrichment in SCZ, specifically within OPC, astrocytes. Extending imaging transcriptomics into individuals appears to be feasible, and likely to provide more nuanced insights into individual neurobiology with possible clinical applications in the future.

References

1. Hawrylycz MJ, Lein ES, Guillozet-Bongaarts AL, et al. An anatomically comprehensive atlas of the adult human brain transcriptome. Nature. 2012;489(7416):391-399.
2. Arnatkeviciute A, Fulcher BD, Bellgrove MA, Fornito A. Imaging Transcriptomics of Brain Disorders. Biological Psychiatry Global Open Science. 2021.
3. Trubetskoy V, Pardiñas AF, Qi T, et al. Mapping genomic loci implicates genes and synaptic biology in schizophrenia. Nature. 2022;604(7906):502-508.
4. Di Biase MA, Geaghan MP, Reay WR, et al. Cell type-specific manifestations of cortical thickness heterogeneity in schizophrenia. Molecular psychiatry. 2022;27(4):2052-2060.

Poster No 490

Neuroticism Heterogeneity in Item-Level Associations with Resting-State Functional Connectivity

Masaya Misaki[1,2], Heekyeong Park[3,1], Fan Chun Chieh[4,1], Wesley Thompson[4,1], Martin Paulus[1]

[1]Laureate Institute for Brain Research, Tulsa, OK, [2]Oxley College of Health Sciences, University of Tulsa, Tulsa, OK, [3]University of North Texas at Dallas, Dallas, TX, [4]University of California San Diego, San Diego, CA

Introduction: Neuroticism, a personality trait marked by negative affect and dysregulation[1], is linked to poor mental health outcomes[2] and significantly overlaps with symptoms of mood and anxiety disorders[3]. A genetic study[4] reveals that neuroticism is not genetically uniform but comprises various distinct genetic correlates, with certain traits linked to depression and others to anxiety. This indicates a complex, multi-genetic structure of neuroticism. Yet, the relationship between this heterogeneity and individuals' neurofunctional traits is not well understood. To explore the heterogeneity of neuroticism in

its neurofunctional underpinnings, the present study examines resting-state functional connectivity (RSFC) associations with neuroticism item scores using the UK Biobank data.

Methods: The UK Biobank data from the first imaging visit of 33,194 participants (17,274 females, mean age = 63.6 [SD = 7.7]) were analyzed. The RSFC matrix provided by the UK Biobank represents a partial correlation between 55 independent components, containing 1,485 values. Neuroticism was assessed using the Eysenck Personality Questionnaire (12 items). We employed a machine learning (ML) predictive modeling approach to associate RSFC with neuroticism scores. An ML model was trained on whole-brain FC values to predict neuroticism scores, using three-fold cross-validation and controlling for confounding factors such as scan location, sex, age, motion, signal-to-noise ratio, and T1-EPI discrepancies. We utilized an automated machine learning (AutoML) approach that addresses the Combined Algorithm Selection and Hyperparameter Optimization (CASH) problem by automatically searching for and optimizing feature selection, model algorithm, and hyperparameters. Specifically, the H2O AutoML software package[5], known for its comprehensive algorithm selection and optimization capabilities, was used.

Results: Classification accuracies were significant for all items ($p < 5x10\text{-}8$). A previous GWAS[4] identified four items each in the depressed-affect and worry clusters. The present result showed that items within the worry cluster showed higher classification accuracy compared to those in the depressed-affect cluster. Figure 1A illustrates the similarity patterns of the items, as measured by the correlation between the RSFC weights of the ML models. Notably, items within the same genetic cluster exhibit tight grouping. Figure 1B presents the correlation between RSFC pattern similarities and genetic correlations for each item pair. A high concordance was observed between RSFC pattern correlations and genetic correlations, $r = 0.834$ ($p < 0.0001$), suggesting a genetic basis for RSFC neuroticism subtypes. The RSFC signatures were distinctly different between the 'depressed affect' and 'worry' clusters (Fig. 2), indicating separate neural circuits for these subcomponents.

Conclusions: This study highlights the intricate relationship between genetic traits and RSFC patterns in neuroticism, demonstrating the distinct neural circuits involved in its different facets. The contrasting RSFC signatures between the "depressed affect" and "worry" clusters reveal the complexity of the neurofunctional basis of neuroticism. Specifically, RSFCs associated with depressed affect are distributed throughout the brain, while those associated with worry are concentrated in the cerebellum and caudate. The cerebellum, with its connections to the amygdala and prefrontal cortex[6], plays a critical role in modulating fear and anxiety responses. In comparison, the caudate, which is involved in reward processing and stress responses, is integral to the pathophysiology of anxiety disorders. These findings indicate that self-report measures of neuroticism may not fully capture its biological complexity, suggesting the potential for more comprehensive approaches to personality research that integrate neurofunctional data.

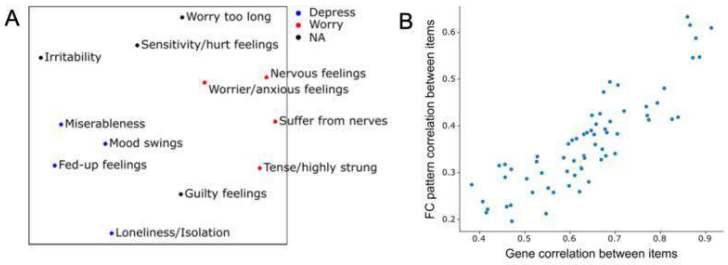

Figure 1. Visualization of the similarities in RSFC patterns associated with different neuroticism items. A. Multidimensional scaling is used to map the similarity space of RSFC patterns onto a two-dimensional plane, where blue dots represent items in the 'depressed affect' cluster and red dots represent items in the 'worry' cluster. B. The plot shows the relationship between genetic correlations and RSFC correlations for each pair of neuroticism items, highlighting the neurobiological linkage between genetic and neural connectivity profiles.

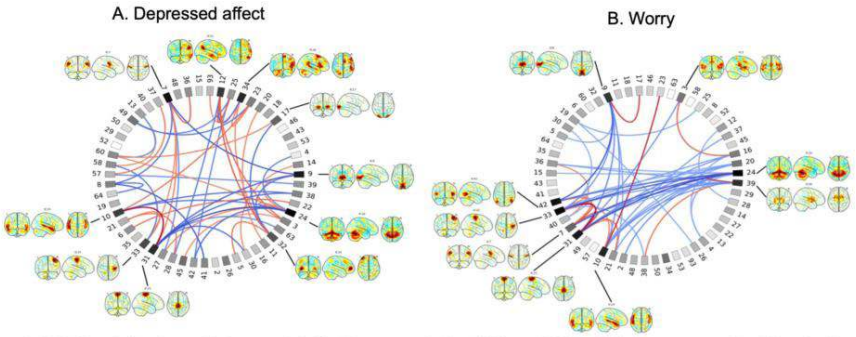

Figure 2. RSFC weights in prediction models for 'Depressed affect' (A) and 'Worry' (B) item scores. Red lines indicate positive weights, blue lines indicate negative weights. The shading intensity of the nodes corresponds to connectivity density, represented by the mean absolute values of FCs linked to each node, highlighting regions of high connectivity influence. Node numbers refer to independent component indices in the UK Biobank data.

References

1. Revelle W, Wilt J, Condon DM. Individual Differences and Differential Psychology. The Wiley-Blackwell Handbook of Individual Differences; 2011. p. 1-38.
2. Jeronimus BF, Kotov R, Riese H, et al. (2016), 'Neuroticism's prospective association with mental disorders halves after adjustment for baseline symptoms and psychiatric history, but the adjusted association hardly decays with time: a meta-analysis on 59 longitudinal/ prospective studies with 443 313 participants', Psychological medicine, vol. 46, no. 14, pp. 2883-2906.
3. Jylhä P, Isometsä E (2006), 'The relationship of neuroticism and extraversion to symptoms of anxiety and depression in the general population', Depression and Anxiety, vol. 23, no. 5, pp. 281-289.
4. Nagel M, Watanabe K, Stringer S, et al. (2018), 'Item-level analyses reveal genetic heterogeneity in neuroticism', Nature communications, vol. 9, no. 1, p. 905.
5. LeDell E, Poirier S. H2o automl: Scalable automatic machine learning. Proceedings of the AutoML Workshop at ICML. Volume 2020: ICML; 2020.
6. Nieto SJ, Patriquin MA, Nielsen DA, et al. (2016), 'Don't worry; be informed about the epigenetics of anxiety', Pharmacology, biochemistry, and behavior, vol. 146-147, pp. 60-72.

Poster No 491

Functional gradients of striatum and its linkage with frontal cortical function in cocaine addiction

Ran Zhang[1], Feng Zhou[1], Ting Xu[2], Debo Dong[1], Yawei Qi[1], Qinghua He[1]

[1]Southwest University, Chongqing, China, [2]University of Electronic Science and Technology of China, Chengdu, Sichuan, China

Introduction: Dysregulated striatal function and executive control deficits are typically characterized in the development and perpetuation of cocaine addiction, as evidenced by animal models and human neuroimaging studies. Recently, connectome gradient-based approaches have emerged as a promising alternative to traditional parcellation-based methods for indicating continuous variations in neural organization across cortical and subcortical systems. These approaches pose huge potential in offering a novel perspective on elucidating dysfunction of striatum in cocaine addiction. Here we systematically examined the abnormalities of intra-striatal and striatal-cerebral cortex functional connectome gradient in cocaine users and revealed the effect of repetitive transcranial magnetic stimulation (rTMS) on striatal function, to facilitate the understanding about functional connectome hierarchy of striatum in cocaine addiction and treatment targets.

Methods: In the present study, we investigated cocaine use disorder (CUD)-related alterations in the intra-striatal and striatal-cerebral cortex functional gradient using resting-state functional magnetic resonance imaging (MRI) data from 85 participants (41 patients and 44 healthy controls (HC)). To validate our findings, we included two groups of patients with cocaine addiction, who were randomly assigned to receive either active or sham rTMS treatment over the left dorsolateral prefrontal cortex (dlPFC) and underwent pre- and post-treatment assessments. Based on the observed gradient changes, we used the left caudate cluster as seed to compute Pearson' correlation coefficient between each voxel in the cerebral cortex, and then compared these functional connectivity (FC) patterns between different groups to clarify the FC associated with principle gradient alterations.

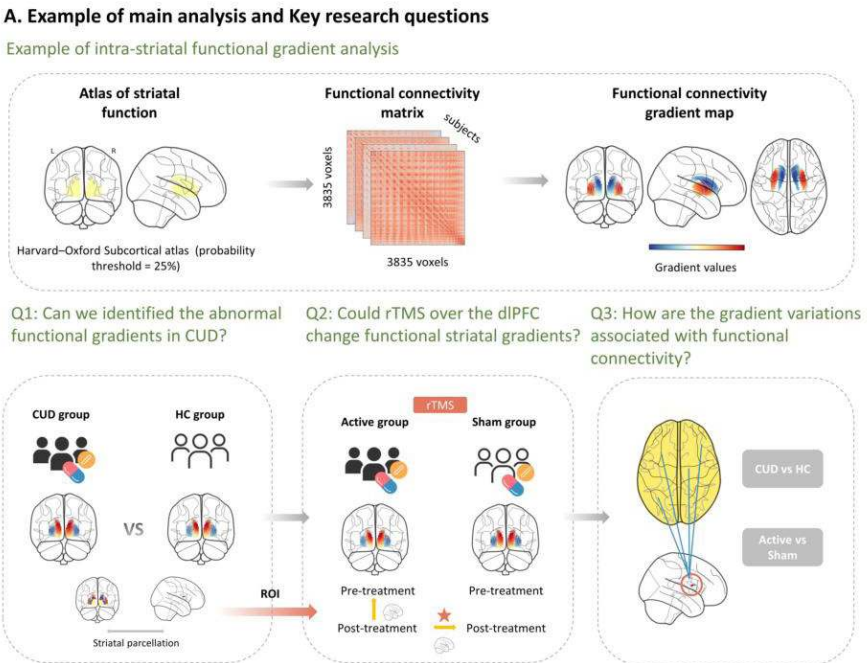

Results: Consistent with previous studies, our findings confirmed the presence of the primary intra-striatal gradient that delineates fundamental anatomical subdivisions. This gradient follows a gradual axis extending from the caudate to the nucleus accumbens and ultimately to the caudal putamen. Compared to the HC group, CUD group exhibited increased abnormal gradient values mostly in the left caudate (x/y/z: -8/6/14, T = 4.86, pfwe-voxel < 0.05), with the same findings observed in their striatal-cortical functional gradient maps. To further validate our findings, we conducted the same functional gradient analysis in an independent longitudinal MRI study that examined the effectiveness of rTMS over the dlPFC for CUD. Results demonstrated a significant group × time interaction effect ($F(1,42) = 4.75$, $p = 0.03$, partial $\eta 2=0.10$). Post-hoc tests revealed that active rTMS led to significantly lower gradient values in the left dorsal caudate relative to sham stimulation ($t42 = -1.88$, $p = 0.07$). Given that patients receiving active rTMS had an alteration in abnormal gradient values, the left dorsal caudate-based FC analysis was conducted to show whether the gradient variations are associated with FC. Results showed that both the CUD group and the active treatment group exhibited alternative FC to several prefrontal regions (e.g., dlPFC), in comparison to the control groups.

Conclusions: Our study characterized the functional gradient of striatal function in patients with CUD and revealed the aberrant gradient values specifically in the left dorsal striatum. In addition, we identified that rTMS treatment may have a beneficial effect on the neural activity within the dorsal stratum. These findings suggest that alterations in striatal organization could serve as a neurobiological trait marker across cocaine addiction and may further enhance the progress of developing new potential therapeutics.

References

1. Angeles-Valdez, D., Rasgado-Toledo, J., Issa-Garcia, V., Balducci, T., Villicaña, V., Valencia, A., ... & Garza-Villarreal, E. A. (2022). The Mexican magnetic resonance imaging dataset of patients with cocaine use disorder: SUDMEX CONN. Scientific data, 9(1), 133.
2. Garza-Villarreal, E. A., Alcala-Lozano, R., Fernandez-Lozano, S., Morelos-Santana, E., Dávalos, A., Villicaña, V., ... & Gonzalez-Olvera, J. J. (2021). Clinical and functional connectivity outcomes of 5-Hz repetitive transcranial magnetic stimulation as an add-on treatment in cocaine use disorder: a double-blind randomized controlled trial. Biological Psychiatry: Cognitive Neuroscience and Neuroimaging, 6(7), 745-757.
3. Hu, Y., Salmeron, B. J., Gu, H., Stein, E. A., & Yang, Y. (2015). Impaired functional connectivity within and between frontostriatal circuits and its association with compulsive drug use and trait impulsivity in cocaine addiction. JAMA psychiatry, 72(6), 584-592.
4. Oldehinkel, M., Llera, A., Faber, M., Huertas, I., Buitelaar, J. K., Bloem, B. R., ... & Beckmann, C. F. (2022). Mapping dopaminergic projections in the human brain with resting-state fMRI. Elife, 11, e71846.
5. Marquand, A. F., Haak, K. V., & Beckmann, C. F. (2017). Functional corticostriatal connection topographies predict goal-directed behaviour in humans. Nature human behaviour, 1(8), 0146.

Poster No 492

Cortico-Striatal White Matter Dysconnectivity Across Phases of Psychosis

Hyungyou Park[1], Minah Kim[2], Kang Ik Cho[3], Minji Ha[4], Moonyoung Jang[2], Sunghyun Park[2], Jun Soo Kwon[4]

[1]Seoul National University, Seoul, Seoul, [2]Department of Neuropsychiatry, Seoul National University Hospital, Seoul, Seoul, [3]Department of Psychiatry, Psychiatry Neuroimaging Laboratory, Brigham and Women's Hospital, Harvard, Boston, MA, [4]Department of Brain and Cognitive Sciences, Seoul National University College of Natural Sciences, Seoul, Seoul

Introduction: Dysfunction of the striatum and its upstream cortex is central to the pathophysiology of psychosis in its clinical stages. Cortical projections, either segregated or integrated, regulate striatal functions; however, the anatomical disruptions of cortico-striatal connections in psychosis remain poorly understood. The aim of this study was to elucidate alterations in white matter (WM) connectivity between the cerebral cortices and the striatum and their association with symptomatology in different phases of psychosis.

Methods: Datasets were collected from 277 healthy controls (HCs), 162 participants at clinical high risk for psychosis (CHR), 132 patients with first-episode psychosis (FEP), and 173 patients with chronic schizophrenia (CSZ). All participants underwent T1 and diffusion-weighted imaging (DWI) scans at four sites using five different acquisition parameter sets. Retrospective harmonization was performed on all DWI data to minimize site-specific variation, and probabilistic tractography was then used to examine cortico-striatal WM connectivity. Connectivity values showing significant group differences were subjected to regression analysis to demonstrate their associations with symptom severity.

Results: Reduced striatal WM connectivity with the temporal cortex was significantly presented in FEP patients compared to other groups. In CSZ patients, connectivity of executive (dorsal frontal) and occipital cortices was significantly diminished relative to HCs and CHR individuals. Furthermore, decreased executive connectivity was negatively associated with the severity of both positive and negative symptoms in CSZ patients.

Conclusions: This study highlights the disrupted striatal WM connectivity in the executive (dorsal) circuit as a significant pathological and symptomatic underpinning in CSZ, along with the involvement of temporal (ventral) connectivity in the early stage of psychosis. Demonstrating specific WM dysconnectivity across phases of psychosis, these findings provide the anatomical basis of cortico-striatal dysfunctions, particularly integration of executive and sensory inputs, throughout the disease progression.

References

1. Haber SN. Corticostriatal circuitry. Dialogues Clin Neurosci 2016; 18(1): 7-21.
2. Tziortzi AC, Haber SN, Searle GE, et al. Connectivity-based functional analysis of dopamine release in the striatum using diffusion-weighted MRI and positron emission tomography. Cereb Cortex 2014; 24(5): 1165-77.
3. Cetin Karayumak S, Bouix S, Ning L, et al. Retrospective harmonization of multi-site diffusion MRI data acquired with different acquisition parameters. Neuroimage 2019; 184: 180-200.

Poster No 493

Influence of reward sensitivity on resting-state networks in OCD patients and healthy controls

Daniela Costa[1], Celina Gomes[2], Pedro Morgado[1], Maria Picó-Pérez[3]

[1]Life and Health Sciences Research Institute (ICVS), Braga, Portugal, [2]Clinical Academic Center – Braga, Braga, Portugal, [3]Jaume I University, Castelló de la Plana, Spain

Introduction: Motivational tendencies are fundamental to improving performance and goal achievement, even more so in the context of psychiatric disorders. Despite this, personality from the perspective of inhibition and approach behavior has rarely been studied in the context of obsessive-compulsive disorder (OCD), and never in association with brain imaging. Thus, in this study we aim to explore the association between reward sensitivity as measured by the Behavioral Inhibition/Behavioral Activation Scales (BIS/BAS; Moreira et al., 2015) and resting-state network connectivity in OCD patients compared to a matched control sample.

Methods: Twenty-nine OCD patients and 22 controls participated in the study. Sociodemographic and clinical data was collected, as well as the BIS/BAS and the Yale-Brown Obsessive-Compulsive Scale (Y-BOCS). Groups were compared on these variables using independent-sample t-tests in JASP, and Pearson's r correlations between the BIS/BAS and the Y-BOCS were performed for the patient group. Neuroimaging data was acquired in a Siemens Verio 3T, and preprocessed using fMRIPrep 20.2.5 (Esteban et al., 2019), which is based on Nipype 1.6.1 (Gorgolewski et al., 2011). Resting-state network (RSN) maps were analyzed voxel-wise through a probabilistic Independent Component Analysis (ICA) as implemented in Multivariate Exploratory Linear Optimized Decomposition into Independent Components (MELODIC), distributed with FSL (Beckmann & Smith, 2004). Only components visually identified to represent typical RSNs (Horowitz-Kraus et al., 2015) were used in further statistical analyses, which included: the primary visual network, higher visual network, dorsal attention network (DAN), basal ganglia network, default mode network (DMN), limbic network, auditory network, and cerebellar network. Finally, the RSNs functional connectivity (FC) was first compared between groups, using independent samples t-tests within a non-parametric permutation procedure implemented in the randomise tool of FSL (Winkler et al., 2014), and a threshold-free cluster enhancement (TFCE) correction at an α=.05. For each contrast, 5000 permutations were performed. Then, multiple regression analyses were also performed including either BIS or BAS subscales in the model in interaction with group.

Results: Groups were matched on age, education level, and sex/gender distribution. Patients with OCD presented higher behavioral inhibition but no differences in the BAS subscales, and a significant positive correlation between the BIS and Y-BOCS Obsessions. Regarding the RSNs group comparison, OCD patients presented increased FC in the primary visual, the higher visual and the basal ganglia networks (see Figure 1). Regarding BIS/BAS associations, BIS scores were positively associated with DMN FC in patients with OCD. Also in patients, the primary visual network FC was negatively associated with BAS Reward Responsiveness and BAS Drive, while BAS Drive was also negatively associated with the FC of the DMN, the higher visual, the auditory and the basal ganglia networks, and BAS Fun Seeking was negatively associated with limbic network FC. On the other hand, BAS Reward Responsiveness was positively associated with the FC of the basal ganglia network in patients (see Figure 2).

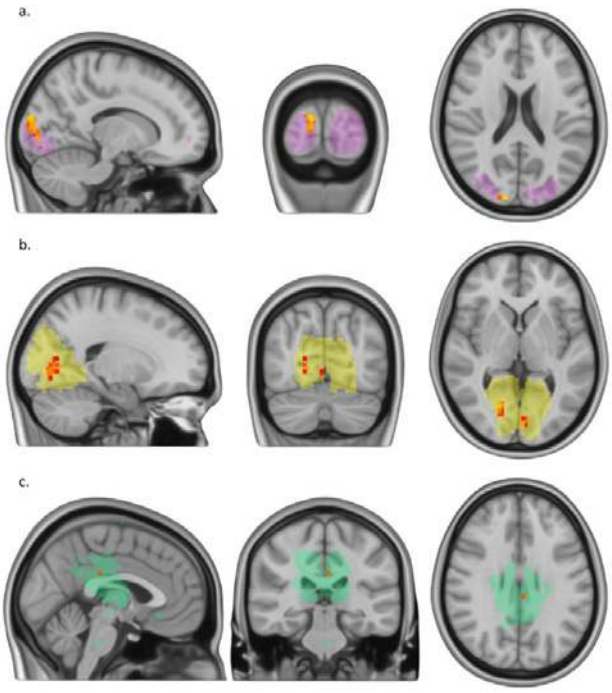

Figure 1. Increased functional connectivity in OCD patients compared to controls in higher visual (a), primary visual (b), and basal ganglia networks (c).

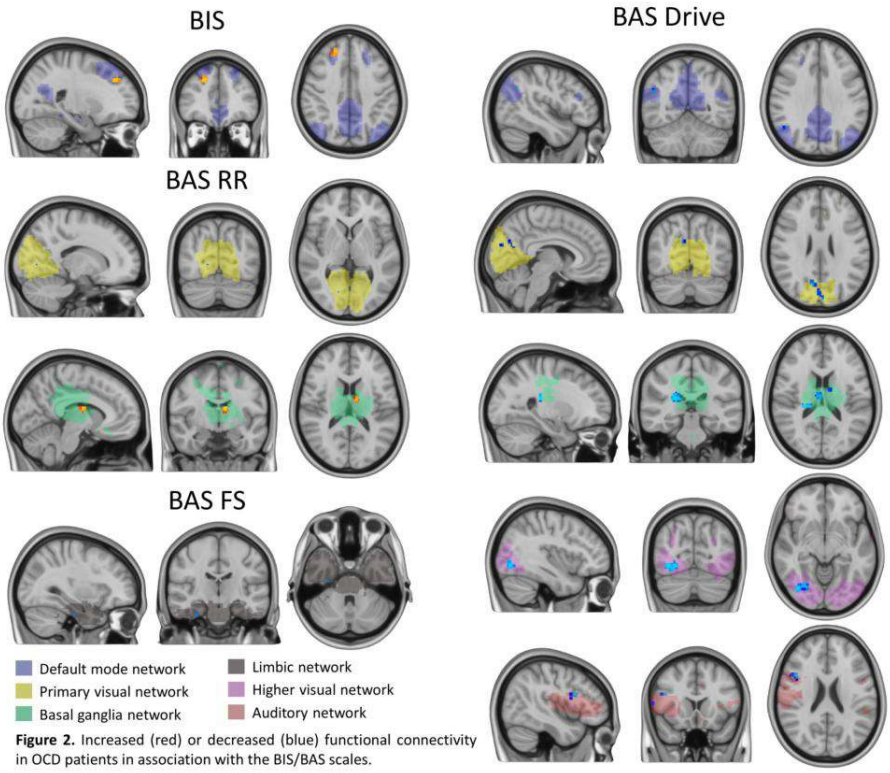

Figure 2. Increased (red) or decreased (blue) functional connectivity in OCD patients in association with the BIS/BAS scales.

Conclusions: We found significant differences between patients and controls at the behavioral level on the BIS scale but not on the BAS subscales, while at the brain-level, there were widespread associations between both BIS and BAS subscales and RSNs FC. The RSNs found to be associated with BIS/BAS have been previously reported to be critically involved in motivated behavior and in the pathophysiology of OCD, such as the basal ganglia and the limbic network, but also the DMN and the visual networks. This approach could help identify different neuropsychological and neural profiles within OCD, which could eventually guide individualized treatment selection depending on each patient's characteristics.

References

1. Beckmann, C. F., & Smith, S. M. (2004). Probabilistic Independent Component Analysis for Functional Magnetic Resonance Imaging. IEEE Transactions on Medical Imaging, 23(2), 137–152. https://doi.org/10.1109/TMI.2003.822821
2. Esteban, O., Markiewicz, C. J., Blair, R. W., Moodie, C. A., Isik, A. I., Erramuzpe, A., Kent, J. D., Goncalves, M., DuPre, E., Snyder, M., Oya, H., Ghosh, S. S., Wright, J., Durnez, J., Poldrack, R. A., & Gorgolewski, K. J. (2019). fMRIPrep: a robust preprocessing pipeline for functional MRI. Nature Methods, 16(1), 111–116. https://doi.org/10.1038/s41592-018-0235-4
3. Gorgolewski, K., Burns, C. D., Madison, C., Clark, D., Halchenko, Y. O., Waskom, M. L., & Ghosh, S. S. (2011). Nipype: A flexible, lightweight and extensible neuroimaging data processing framework in Python. Frontiers in Neuroinformatics, 5, 13. https://doi.org/10.3389/FNINF.2011.00013/ABSTRACT
4. Horowitz-Kraus, T., Difrancesco, M., Kay, B., Wang, Y., & Holland, S. K. (2015). Increased resting-state functional connectivity of visual- and cognitive-control brain networks after training in children with reading difficulties. NeuroImage: Clinical, 8, 619–630. https://doi.org/10.1016/J.NICL.2015.06.010
5. Moreira, D., Almeida, F., Pinto, M., Segarra, P., & Barbosa, F. (2015). Data concerning the psychometric properties of the behavioral inhibition/behavioral activation scales for the portuguese population. Psychological Assessment, 27(3), 1117–1122. https://doi.org/10.1037/pas0000108
6. Winkler, A. M., Ridgway, G. R., Webster, M. A., Smith, S. M., & Nichols, T. E. (2014). Permutation inference for the general linear model. Neuroimage, 92(100), 381. https://doi.org/10.1016/J.NEUROIMAGE.2014.01.060

Poster No 494

Transcriptional and neurochemical profiles of cerebral blood flow changes in psychosis and prodrome

Samuel Knight[1], Leyla Abbasova[1], Yashar Zeighami[2], Daniel Martins[1], Fernando Zelaya[1], Ottavia Dipasquale[3], Thomas Liu[4], David Shin[5], Matthijs Bossong[6], Matilda Azis[1], Mathilde Antoniades[7], Alice Egerton[1], Paul Allen[1], Owen O'Daly[1], Philip McGuire[8], Gemma Modinos[1]

[1]King's College London, London, United Kingdom, [2]Douglas Research Centre, Montreal, Quebec, [3]Olea Medical, La Ciotat, France, [4]UC San Diego, San Diego, CA, [5]GEHeathCare, Menlo Park, CA, [6]University Medical Center Utrecht, Utrecht, Netherlands, [7]University of Pennsylvania, Philadelphia, PA, [8]Oxford University, Oxford, United Kingdom

Introduction: In vivo investigations have demonstrated resting regional cerebral blood flow (rCBF) alterations in patients with schizophrenia (SCZ) and individuals at clinical high-risk for psychosis (CHR)(du Sert et al. 2023). Understanding how these differences in rCBF are related to dysfunction at the genetic or molecular level has the potential to inform the discovery of new therapeutic strategies. Recently, several tools have become available to combine MRI and genetic data: the Allen Human Brain Atlas (AHBA) and neurochemical data derived from PET atlases. These approaches have yet to be applied to investigate the underlying molecular mechanisms of rCBF alterations in psychosis. The study aimed to determine the gene expression and neuroreceptor density profiles that correspond to rCBF phenotypes in CHR and SCZ, thereby gaining insight into the cellular and molecular mechanisms underlying these alterations.

Methods: Participants included 122 patients with SCZ and 116 healthy controls (HC1), and 129 CHR individuals and 58 healthy controls (HC2). Due to differences in scanning modality, pre-processing, and sample characteristics, each clinical group was compared to its own matched group of healthy controls, and not between clinical groups. rCBF maps from all participants were estimated from arterial spin labelling (ASL) data and pre-processed using the CBFBIRN pipeline(Shin et al. 2014) ('SCZ and HC1') and the ASL Toolbox (all participants)(Mato et al. 2015). SPM12 was used to derive case-control t-stat maps of and 'SCZvsHC1' and 'CHRvsHC2' comparisons. Unthresholded case-control rCBF difference maps and receptor atlases were segmented into the same standard space (Schaefer+Xiao atlases, 100 cortical and 22 subcortical regions)(Schaefer et al. 2018; Xiao et al. 2019) (Figure 1a). We next looked for spatial associations between rCBF t-stat maps and gene expression data, accessed via the AHBA, as well as neuroreceptor binding distribution of 19 freely available PET atlases across 9 neurotransmitter systems (Hansen et al. 2022). Gene expression correlations with rCBF maps were assessed with Spearman's rank correlations, and a dominance regression analysis was used to determine the unique contribution of mean receptor binding values to the prediction of mean rCBF differences in each region. Significance of all analyses was assessed against FDR-corrected spatial autocorrelation-preserving null models.

Results: The rCBF profile of both 'SCZvsHC1' and 'CHRvsHC2' alterations was found to track the distribution of astrocytes, oligodendrocyte precursor and vascular leptomeningeal cell gene markers (pFDR<0.05)(Figure 1b). Receptor distribution significantly predicted 'SCZvsHC1' and 'CHRvsHC2' difference patterns (R2adj = .514, pFDR<.01; R2adj = .611, pFDR<0.01 respectively) (Figure 1c). Dopamine D1 and D2 and GABA-A receptors, as well as dopamine and acetylcholine transporters contributed most to 'SCZvsHC1' rCBF differences, while 5-HT1a, muscarinic 1, norepinephrine, CB1, and NMDA receptors, and dopamine transporter contributed most to the prediction of 'CHRvsHC2' rCBF differences.

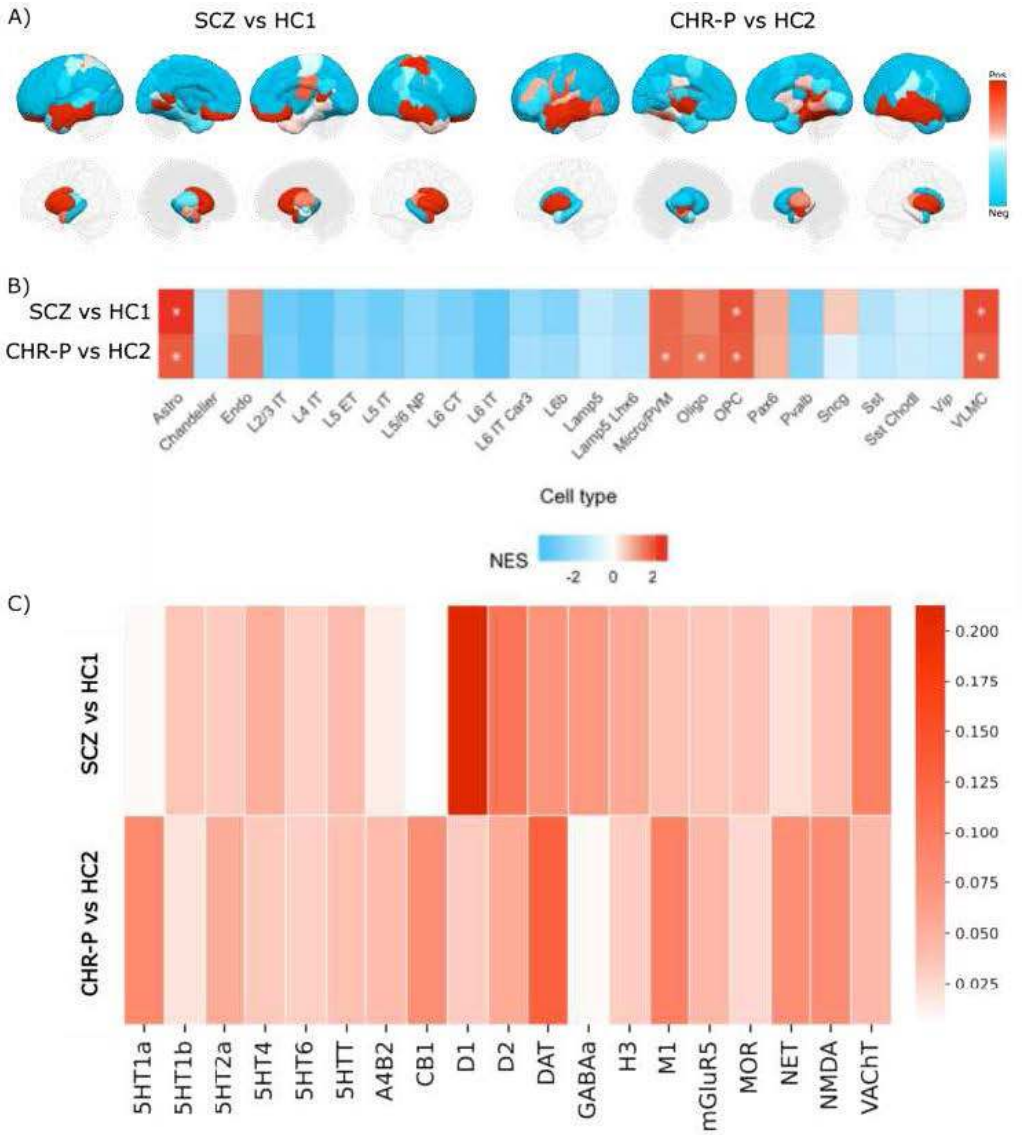

Figure 1. A) case-control regional cerebral blood flow (rCBF) unthresholded t-stat maps z-scored and parcellated into 100 cortical (Schaefer) and 22 subcortical (Xiao) 2x2x2mm atlas, mean intensity mapped across each region. B) Spearman correlations between case-control rCBF maps and cell type enrichments. Significant ($P_{FDR} < 0.05$) enrichments are indicated with white asterisks and tiles are coloured by net enrichment score (NES). C) Dominance analysis of unique contribution of predictors (PET maps) to case-control rCBF phenotypes. Each PET map parcellated into same 122 region atlas space and z-scored. Individual dominance of each predictor adds to total R^2_{adj}. SCZ vs HC1 (R^2_{adj}=.514, P_{FDR}<.01), CHR-P vs HC2 (R^2_{adj}=.611, P_{FDR}<0.01)

Conclusions: In summary, our findings implicate cell types involved in stress response and neuroinflammation, as well as dopamine, GABA-A, and NMDA receptor systems as distinct cellular and neurochemical signatures of SCZ- and CHR-associated rCBF profiles. Such hypothesis-generating approaches could be utilised in future to guide the non-invasive stratification of mechanisms of risk, which may be amenable to pharmacological intervention.

References

1. Percie du Sert, O., (2023), 'Cerebral blood flow in schizophrenia: A systematic review and meta-analysis of MRI-based studies', Progress in Neuro-Psychopharmacology and Biological Psychiatry, 121, 110669
2. Shin, David D, (2014), 'Robust and Fast Quantification of CBF measures for Multiphase PCASL using Bayesian Nonlinear Model Fitting'. Proceedings of the International Society for Magnetic Resonance in Medicine, 22
3. Mato Abad V, (2016), 'ASAP (Automatic Software for ASL Processing): A toolbox for processing Arterial Spin Labeling images'. Magnetic Resonance Imaging. Apr;34(3):334-44.
4. Schaefer, A. (2018), 'Local-Global Parcellation of the Human Cerebral Cortex from Intrinsic Functional Connectivity MRI'. Cerebral Cortex 28, no. 9: 3095–3114.
5. Xiao, Y. (2019), 'An Accurate Registration of the BigBrain Dataset with the MNI PD25 and ICBM152 Atlases'. Scientific Data 6, no. 1: 210.
6. Hansen, J.Y., (2022), 'Mapping neurotransmitter systems to the structural and functional organization of the human neocortex'. Nature Neuroscience 25, 1569–1581.

Poster No 495

Childhood maltreatment is associated with cortical thickness in adults with alcohol use disorder

Cagdas Türkmen[1], Haoye Tan[1], Sarah Gerhardt[1], Emilie Bougelet[1], Maria Bernardo[1], Noah Machunze[1], Yasmin Grauduszus[2], Maurizio Sicorello[3], Traute Demirakca[2], Falk Kiefer[1], Sabine Vollstädt-Klein[1]

[1]Department of Addictive Behaviour and Addiction Medicine, Central Institute of Mental Health, Mannheim, Germany, [2]Department of Neuroimaging, Central Institute of Mental Health, Mannheim, Germany, [3]Department of Psychosomatic Medicine and Psychotherapy, Central Institute of Mental Health, Mannheim, Germany

Introduction: Previous studies have established a connection between childhood maltreatment (CM) and alcohol use disorder (AUD), both of which are associated with alterations in gray matter volume (GMV) and cortical thickness (CT). Yet, limited research has assessed the neurobiological impact of CM specifically within the context of AUD, as well as the role of maltreatment type (i.e. abuse or neglect) and timing. Thus, this study aimed to test the following hypotheses: 1) Adults with AUD, compared to healthy controls, exhibit reduced GMV and CT in specific regions. 2) Within the AUD group, CM is associated with a decrease in GMV and CT in the altered regions from hypothesis 1. 3) Specific types and timings of CM are associated with a decrease in GMV and CT in the altered regions from hypothesis 1 (explorative).

Methods: Structural MRI data were collected with a 3 Tesla whole-body tomograph from 35 adults with AUD (age[mean]: 40; 31% female) and 28 healthy controls (age[mean]: 36; 61% female) with varying degrees of CM. Images were obtained using a transaxial T1-weighed image acquisition (voxel size 1x1x1 mm3, FoV 232 x 256 mm2, TR = 2000ms, TE = 3.03 ms, TI 900 ms, flip angle = 9°). Voxel-wise and regional GMV and CT were estimated using voxel- and surface-based morphometry in the SPM12 and CAT12 software. CT was estimated based on the projection-based thickness method. Preprocessing was performed using CAT12 to assess image quality. In addition to whole-brain voxel-wise analyses, we defined bilateral amygdala and hippocampus as regions of interest (ROIs) based on existing findings. CM was assessed using the Childhood Trauma Questionnaire (CTQ), and the brief German version of the Maltreatment and Abuse Chronology interview, which additionally examined timing. Alcohol dependence severity was assessed using the Alcohol Dependence Scale (ADS), the scores of which were used to assess a potential interaction with CM on GMV or CT. A two-sample t-test was used to assess hypothesis 1 (voxel-wise-$p < 0.001$ with cluster corrections by SPM random field theory, corresponding to $pFWE < 0.05$). Hypothesis 2 was examined using partial correlation, controlling for age, gender, and transcranial volume (only for GMV). For hypothesis 3, we used random forest regression to identify important ages for maltreatment type, and performed follow-up correlation analyses. The significance levels of analyses were $p < 0.05$.

Results: Relative to the healthy controls, the AUD group had significantly reduced CT in a cluster encompassing the left inferior frontal gyrus, left circular sulcus of the insula, and subcentral gyrus and sulci (C1), and in a cluster comprising the central sulcus and precentral gyrus (C2). No group differences in GMV were found. A higher severity of CM, as indicated by higher CTQ sum scores, was significantly associated with a CT decrease in cluster C1. There was no interaction between CTQ sum scores and ADS scores on CT in cluster C1. No significant associations between CTQ sum scores and ROI volumes (amygdala and hippocampus) or CT in C2 were found. Type and timing analyses revealed a significant association between higher abuse at ages 13 to 15 and reduced CT in cluster C1.

Conclusions: Abuse during early adolescence is associated with reduced CT in regions involved in response inhibition in adults with AUD, indicating the potential relevance of cognitive pathways in the risk association between CM and AUD. Prevention and intervention strategies for CM-exposed individuals with AUD should incorporate cognitive functioning as a treatment target. Longitudinal designs with larger sample sizes are needed to confirm and expand upon current findings.

Poster No 496

Longitudinal rs-fMRI changes reveal local brain function in patients with schizophrenia

Song Liu[1], Yong Han[1], Han Shi[1], Xiaoge Guo[1], Xiujuan Wang[1], Luxian Lv[1], Wenqiang Li[1], Yongfeng Yang[1]

[1]the Second Affiliated Hospital of Xinxiang Medical University, Xinxiang, HENAN

Introduction: Schizophrenia (SZ) is a serious psychiatric disorder that affects 1% of the world's population and the main symptoms can be classified as positive, negative, and general psychopathology symptoms [1,2]. Regional brain function is measured by assessing ALFF, fALFF, and ReHo [3,4]. These 3 voxel based metrics define brain functional characteristics from different perspectives and show a progressive relationship that allows for more sensitive identification of regional abnormalities. A reliable brain atlas reflecting this subdivision is essential to quantitatively investigate the functional and

structural characteristics of the human brain. We used Brainnetome Atlas [5]to investigate the changes in rs-fMRI indicators before and after treatment in SZ patients and their association with symptoms and cognitive function.

Methods: This study recruited 109 patients with SZ from the Second Affiliated Hospital of Xinxiang Medical College. Collect their baseline and 8-week post-treatment imaging, PANSS and MATRICS consensus cognitive test (MCCB) data. The patient meets the clinical diagnostic criteria for SZ in DSM-IV of the United States, and is confirmed by two attending physicians or more psychiatrists. Preprocess the original image of the patient, and then calculate individual ALFF, fALFF, and ReHo to evaluate functional activity. Statistical analysis was conducted using Matlab2020a, and statistical charts were conducted using PyCharm software based on Python. All continuous variables are represented by the mean SD. Map the resting fMRI indicators (ALFF, fALFF, and ReHo) calculated by SZ patients to Brainnetome Atlas in Matlab software, and extract the mean values of each brain region in the map for analysis. To determine the differences in resting fMRI indicators between baseline and 8-week treatment patients, we used paired sample t-tests for analysis and performed Bonferroni correction on the results. Then, Pearson correlation analysis was performed on the baseline resting fMRI indicators of brain regions that underwent changes after treatment with PANSS reduction rate, Spearman correlation analysis was performed on MCCB reduction rate (MCCB reduction rates did not conform to normal distribution), and Bonferroni correction was performed on the results.

Results: Compared with baseline, after 8 weeks of treatment, the brain regions with increased ALFF were distributed in the frontal lobe, parietal lobe, insula gyrus, cingulate gyrus, and basal ganglia; The brain regions with reduced ALFF are distributed in the temporal and occipital lobes; The increased brain area of fALFF is distributed in the temporal lobe, cingulate gyrus, basal ganglia, and thalamus; The brain regions with decreased fALFF are distributed in the frontal, temporal, parietal, and occipital lobes; The increased brain area of ReHo is distributed in the frontal lobe; The brain regions with reduced ReHo are distributed in the frontal lobe, temporal lobe, parietal lobe, insular gyrus, and occipital lobe (Figure 1). The correlation analysis between baseline resting fMRI indicators and PANSS and MCCB reduction rates in brain regions that underwent changes after treatment is shown in Figure 2.

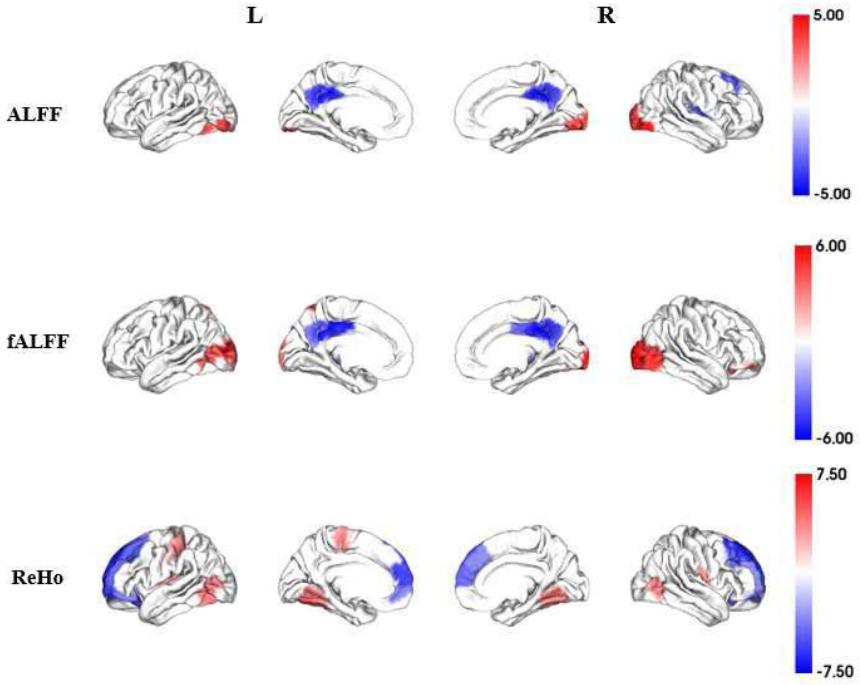

Figure 1: Brain regions with changes in imaging indicators before and after treatment

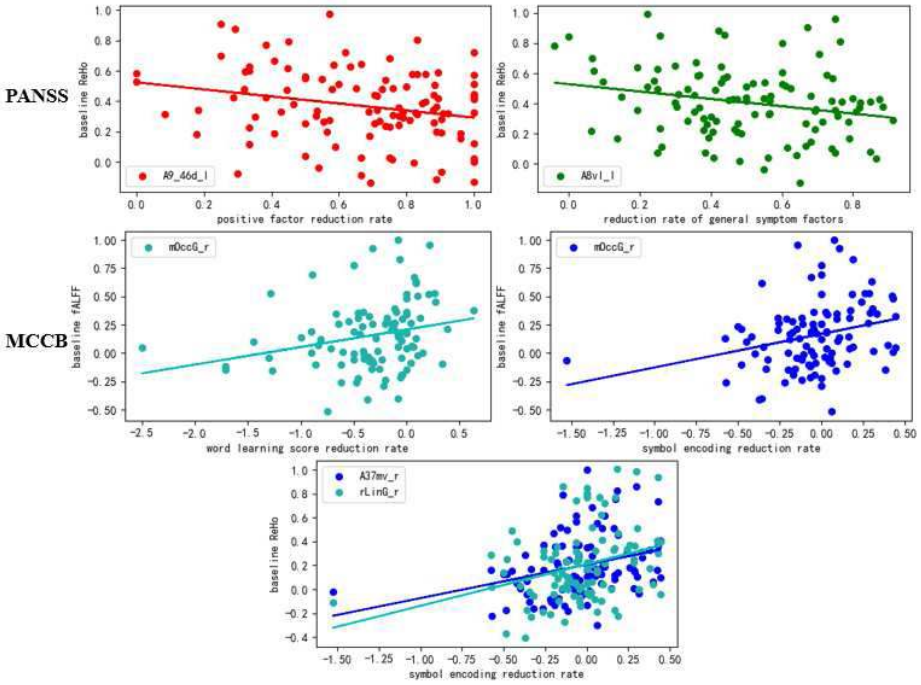

Figure 2: Correlation between baseline imaging indicators and scales of brain regions with differences before and after treatment

Conclusions: This study found that the brain regions with changes in local brain function before and after treatment were mainly concentrated in the frontal lobe, temporal lobe, and occipital lobe. Two subregions of the middle frontal gyrus were negatively correlated with the reduction rate of positive factors and general symptoms, respectively. The two subregions of the occipital lobe were positively correlated with word learning and symbol encoding in MCCB.These findings provide new evidence for the hypothesis of abnormal SZ functional activity and potential neurobiological objective indicators for clinical diagnosis and efficacy prediction.

References

1. Marder, SR.,2019a, 'Schizophrenia', The New England Journal of Medicine, vol. 381, no. 18, pp. 1753-1761
2. Kim, J-H.,2012a, 'Evaluation of the factor structure of symptoms in patients with schizophrenia', Psychiatry Research, vol. 197, no. 3, pp. 285–289
3. Yu-Feng Z., 2007a, 'Altered baseline brain activity in children with ADHD revealed by resting-state functional MRI', Brain and Development, vol. 29, no.2, pp. 83–91
4. Zang Y., 2004a, 'Regional homogeneity approach to fMRI data analysis', NeuroImage, vol. 22, no. 1, pp. 394–400
5. Fan LZ. (2016a), 'The Human Brainnetome Atlas: A New Brain Atlas Based on Connectional Architecture', Cerebral Cortex, vol. 26, no. 8, pp. 3508-26

Poster No 497

A Comparative Machine Learning Study of Connectivity-Based Biomarkers of Schizophrenia

Victoria Shevchenko[1], R. Austin Benn[1], Robert Scholz[1,2,3], Wei Wei[1], Carla Pallavicini[1], Ulysse Klatzmann[1], Francesco Alberti[1], Theodore Satterthwaite[4], Demian Wassermann[5], Pierre-Louis Bazin[6], Daniel Margulies[1]

[1]Université Paris Cité, INCC UMR 8002, CNRS, Paris, France, [2]Max Planck School of Cognition, Leipzig, Germany, [3]Wilhelm Wundt Institute for Psychology, Leipzig University, Leipzig, Germany, [4]University of Pennsylvania, Perelman School of Medicine, Philadelphia, PA, USA, [5]Université Paris-Saclay, Inria, CEA, Paris, France, [6]Full brain picture Analytics, Leiden, The Netherlands

Introduction: Functional connectivity holds promise as a biomarker of psychiatric disorders. Yet, its high dimensionality, combined with small sample sizes in clinical research, increases the risk of overfitting when the aim is prediction (Serin et al., 2021). Recently, low-dimensional representations of the connectome such as cortical gradients (Jung et al., 2022; Margulies et al., 2016) and gradient dispersion (Bethlehem et al., 2020) have been proposed, with studies noting consistent gradient and dispersion differences in psychiatric conditions (Dong et al., 2021; Pasquini et al., 2022; Xia et al., 2022). However, it is unknown which of these derivatives has the highest predictive capacity and how they compare to raw connectivity. Our study

evaluates which connectome features -- functional connectivity, gradients, or gradient dispersion -- best predict schizophrenia (Figure 1A) and analyzes the impact of feature quantity on model selection.

Methods: We compiled resting state fMRI data from three open-source datasets: COBRE (Aine et al., 2017), UCLA Consortium for Neuropsychiatric Phenomics (Poldrack et al., 2016) and SRPBS multidisorder MRI dataset (Tanaka et al., 2021), totaling 996 individuals. After excluding 40 subjects due to motion artifacts (FD > 0.5mm), the sample included 248 patients with schizophrenia and 688 controls. Preprocessing of MRI data was done with fMRIPrep 20.2.1 (Esteban et al., 2019) with BOLD timeseries parcellated using Schaefer parcellation (1000 parcels). We correlated (Pearson) region-wise timeseries to produce connectivity matrices. To compute cortical gradients, we z-transformed and thresholded (10%) the matrices and applied principal component analysis (PCA). Next, we computed gradient dispersion using two distinct approaches: 1. Bethlehem et al. (2020) and 2. K-Nearest Neighbors. We refer to these two types of dispersion as centroid and neighborhood dispersion, respectively. Next, for each subject, we concatenated the flattened matrices, 200 gradients and centroid and neighborhood dispersion in one array. We applied PCA to each feature type separately across subjects. To ensure that more than 1 component is extracted from each feature type, we retained 20% of variance except for the centroid dispersion for which all variance was included. We fitted L2-regularized logistic regression on the training set and computed permutation component importance (Figure 1C, see caption). Finally, we inverse transformed component importance for each feature type to obtain feature importance which was used to select 100-10000 features per feature type for further assessments of model performance. Using Pycaret, we fit 13 models on the subsets (for the list of models, see Figure 2D). The analytic workflow used to compute component and feature permutation importance is depicted in Figure 1.

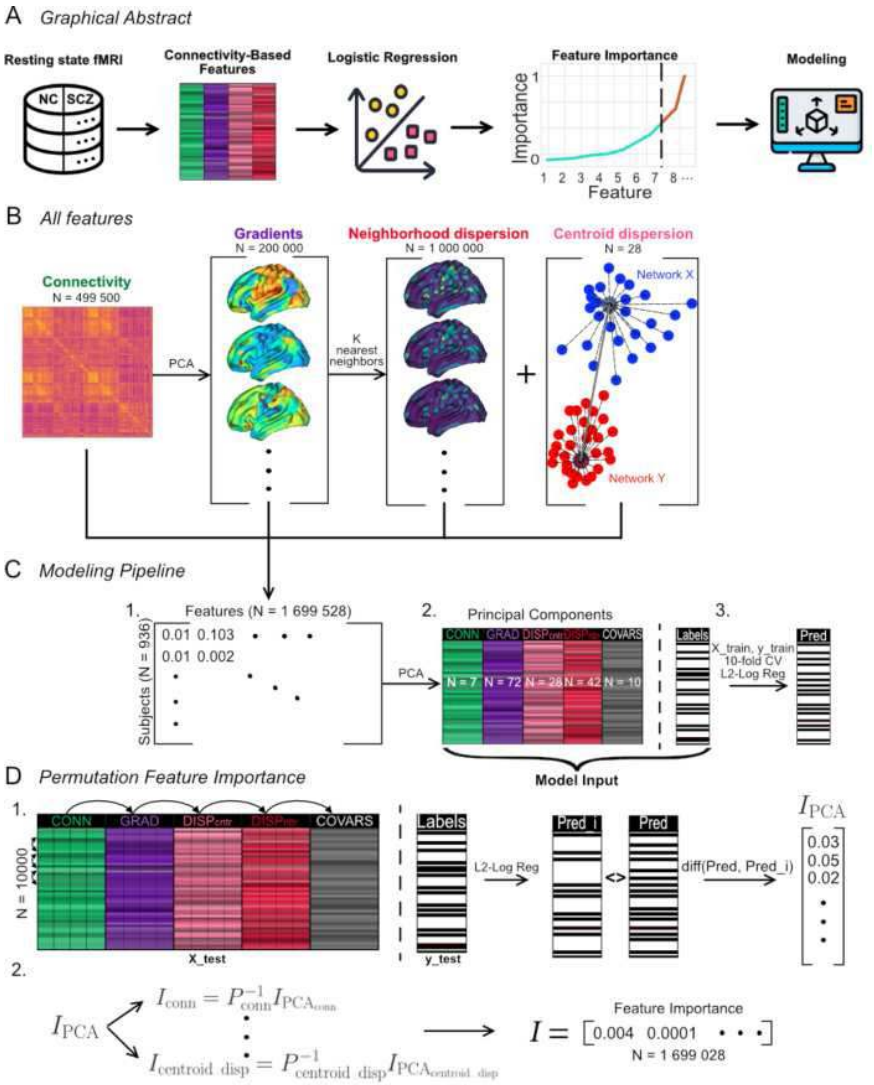

Figure 1. A: Graphical abstract of the study. Schematic images: Flaticon.com. **B:** The types of predictors tested in this work (left to right): connectivity matrices (vectorized), macroscale cortical gradients, neighborhood dispersion and centroid dispersion. **C:** All features were vectorized and concatenated to form a [936 x 1699528] matrix (1). PCA was applied separately to each feature type to retain 20% of variance (in the case of centroid dispersion, we retained all variance) (2). The principal components of the features and diagnosis labels were divided into a training (75%) and testing sets (N_scz/N_controls = 0.35 in both). L2-regularized logistic regression was fit on the data. 10-fold cross-validation (CV) was used to assess model performance on the train set (3). All data transformations were applied within a Scikit-Learn pipeline. **D:** Permutation component importance (N_permutations = 10000) was computed for each principal component using the testing set: X_test, y_test (1). For each feature type, component importance was inverse transformed to obtain feature importance in the feature space, I (2).

Results: Our analyses yielded unexpected results. Out of all feature types tested in this study, connectivity had the largest component permutation importance (Figure 2A) and consistently showed the best predictive performance (Figure 2B). Connectivity also performed better across different numbers of features selected based on the importance in the feature space (Figure 2C). In addition, as the number of features increased, linear models tended to outperform more complex models.

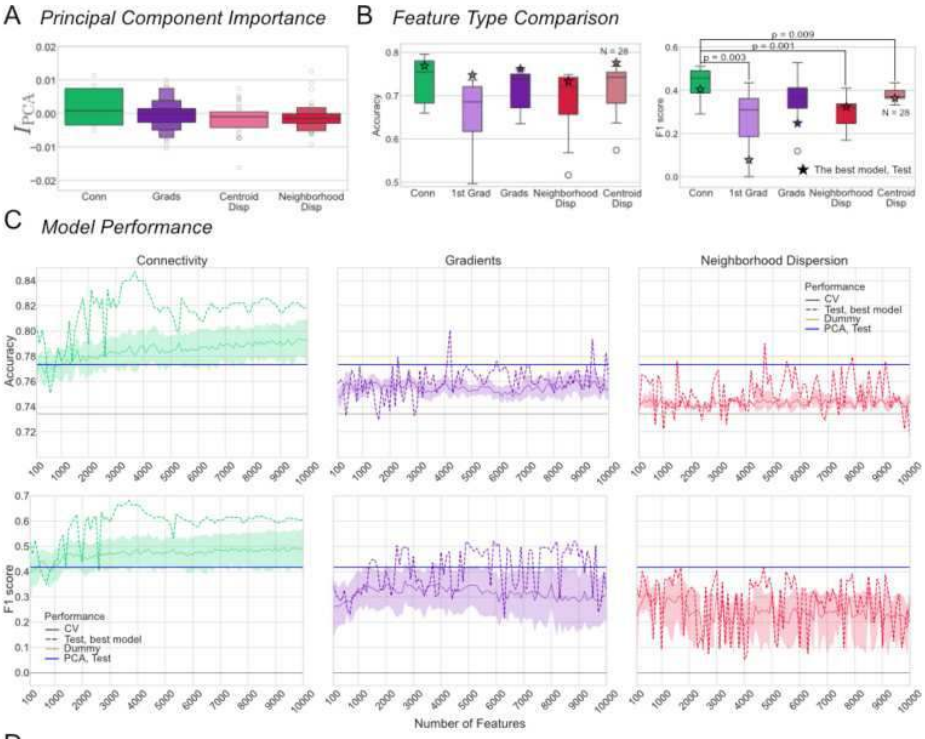

Figure 2. A: Permutation importance across feature types. **B:** Accuracy and F1 score across 13 models (mean cross CV folds; the models performing worse than the dummy classifier were excluded) fit on 936 features with the highest permutation importance from connectivity, the principal gradient, all gradients, neighborhood dispersion and the 28 values of centroid dispersion (light red). P-values indicate significant difference as per Mann-Whitney U test, alpha = 0.013 (connectivity vs. all: Bonferroni-corrected). The stars denote the performance of the best model as identified based on mean accuracy across 10 CV folds.**C:** CV and test performance across models for N features ranging from 100 to 10000 for connectivity (left), gradients (middle), and neighborhood dispersion (right). Horizontal lines represent test performance of the logistic regression on all principal components (blue), and the performance of the dummy classifier (brown). Connectivity manifested the best performance among all feature types. **D:** Relative density of fits where the corresponding model was identified as best. Larger area indicates that the corresponding model had the highest CV accuracy more often. As the number of features increases, linear models yield better accuracy. The legend includes all models that were tested in this study; the models in black were never identified as the best.

Conclusions: The emergence of novel connectivity-based methods broadens our toolkit for predicting psychiatric disorders, but it also necessitates empirical testing. Surprisingly, our findings indicate that functional connectivity outperforms its more recent, low-dimensional derivatives such as cortical gradients and gradient dispersion in predicting schizophrenia. This suggests that the information within the connectome's specific edges is crucial for distinguishing between neurotypical individuals and those with schizophrenia. Further transdiagnostic studies are necessary to establish whether this tendency is consistent across the psychiatric spectrum.

References

1. Aine, C. J. et al. (2017). Multimodal Neuroimaging in Schizophrenia: Description and Dissemination. Neuroinformatics, 15(4), 343–364.
2. Bethlehem, R. A. I. et al. (2020). Dispersion of functional gradients across the adult lifespan. NeuroImage, 222, 117299.
3. Dong, D. et al. Compressed sensorimotor-to-transmodal hierarchical organization in schizophrenia. Psychological Medicine, 1–14.
4. Esteban, O. et al. (2019). fMRIPrep: a robust preprocessing pipeline for functional MRI. Nature Methods, 16(1), 111–116.
5. Margulies, D. S. et al. (2016). Situating the default-mode network along a principal gradient of macroscale cortical organization. Proceedings of the National Academy of Sciences of the United States of America, 113(44), 12574–12579.
6. Pasquini, L. et al. (2022). Dysfunctional Cortical Gradient Topography in Treatment-Resistant Major Depressive Disorder. Biological Psychiatry. Cognitive Neuroscience and Neuroimaging. https://doi.org/10.1016/j.bpsc.2022.10.009

7. Poldrack RA et al. (2016) A phenome-wide examination of neural and cognitive function. Scientific data 3(1). Springer Science and Business Media LLC: 160110.
8. Serin, E. et al. (2021). NBS-Predict: A prediction-based extension of the network-based statistic. NeuroImage, 244, 118625.
9. Tanaka, S. C., et al. (2021). A multi-site, multi-disorder resting-state magnetic resonance image database. Scientific Data, 8(1), 227.

Poster No 498

Shared and Distinct Brain Alterations in Youth with Internalising or Externalising Disorders

Sophie Townend[1], Marlene Staginnus[1], Yidian Gao[2], Barbara Franke[3,4,5], Martine Hoogman[3,4,5], Lianne Schmaal[6,7], Dick Veltman[8], Elena Pozzi[6,7], Janna Marie Bas-Hoogendam[9,10,11], Nynke Groenewold[12,13], Dan Stein[12,14], Nic van der Wee[10,11], Moji Aghajani[15,8], Charlotte Cecil[16,17], Eduard Klapwijk[18,19], Arielle Baskin-Sommers[20], Daniel Pine[21], Sophia Thomopoulos[22], Neda Jahanshad[22], Paul Thompson[22], Esther Walton[1], Stephane De Brito[2], Graeme Fairchild[1], ENIGMA consortium[23]

[1]Department of Psychology, University of Bath, Bath, United Kingdom, [2]Centre for Human Brain Health and Institute for Mental Health, University of Birmingham, Birmingham, United Kingdom, [3]Department of Cognitive Neuroscience, Radboud University Medical Center, Nijmegen, Netherlands, [4]Department of Psychiatry, Radboud University Medical Center, Nijmegen, Netherlands, [5]Donders Institute for Brain, Cognition and Behaviour, Radboud University, Nijmegen, Netherlands, [6]Orygen, Parkville, Australia, [7]Centre for Youth Mental Health, The University of Melbourne, Parkville, Australia, [8]Department of Psychiatry, Amsterdam University Medical Centers, Vrije Universiteit Medical Center, Amsterdam, Netherlands, [9]Institute of Psychology, Leiden University, Leiden, Netherlands, [10]Department of Psychiatry, Leiden University Medical Center, Leiden, Netherlands, [11]Leiden Institute for Brain and Cognition, Leiden, Netherlands, [12]Department of Psychiatry and Mental Health, Neuroscience Institute, University of Cape Town, Cape Town, South Africa, [13]South African Medical Research Council (SA-MRC) Unit on Child and Adolescent Health, Department of Paediatrics and Child Health, Red Cross War Memorial Children's Hospital, University of Cape Town, Cape Town, South Africa, [14]South African Medical Research Council Unit on Risk & Resilience in Mental Disorders, University of Cape Town, Cape Town, South Africa, [15]Leiden University, Institute of Education & Child Studies, Section Forensic Family & Youth Care, Leiden, Netherlands, [16]Department of Child and Adolescent Psychiatry/ Psychology, Erasmus Medical Centre, Rotterdam, Netherlands, [17]Department of Epidemiology, Erasmus Medical Centre, Rotterdam, Netherlands, [18]Erasmus School of Social and Behavioural Sciences, Erasmus University Rotterdam, Rotterdam, Netherlands, [19]Brain and Development Research Center, Leiden University, Leiden, Netherlands, [20]Department of Psychology, Yale University, New Haven, CT, [21]National Institute of Mental Health (NIMH), National Institutes of Health (NIH), Bethesda, MD, [22]Imaging Genetics Center, Mark and Mary Stevens Neuroimaging and Informatics Institute, USC, Marina del Rey, CA, [23]Imaging Genetics Center, Mark and Mary Stevens Neuroimaging and Informatics Institute, Marina del Rey, CA, CA

Introduction: Externalising and internalising disorders are common in youth but are often studied in isolation, preventing an investigation of the transdiagnostic vulnerability which may underlie them. Recent studies have attempted to identify unique versus shared neurobiological alterations across these disorders (e.g., Durham et al., 2021; Gold et al., 2016; Goodkind et al., 2015; Yu et al., 2023), but results have been inconsistent, likely due to heterogeneous sample selection and methods. Using data from the ENIGMA consortium, we conducted a mega-analysis to identify shared and distinct cortical and subcortical alterations between internalising (anxiety disorders and depression) and externalising (attention-deficit/hyperactivity disorder [ADHD] and conduct disorder [CD]) disorders in youth.

Methods: Structural T1-weighted MRI data from healthy controls (n=4,743) and patients with anxiety disorders (n=1,044), depression (n=504), ADHD (n=1,317) and CD (n=1,172) aged 4-21 years were collated from 67 international samples. Using ENIGMA protocols, we assessed group differences in regional cortical thickness and surface area (34 regions, averaged across hemispheres), and subcortical volume (7 regions, averaged across hemispheres) using general linear models. We adjusted for age, sex, and intracranial volume [ICV] (where appropriate). False-discovery rate correction was applied for each outcome measure, and site effects were adjusted for using ComBat (Radua et al., 2020). Sensitivity analyses explored the impact of IQ and medication status.

Results: We observed transdiagnostic effects, with all four disorders characterised by lower surface area in the insula, entorhinal cortex, and middle temporal gyrus, and lower amygdala volume (Cohen's ds=0.07-0.24). All disorders were also associated with global reductions in total surface area and ICV (ds=0.11-0.25). Externalising-specific (i.e., CD and ADHD) reductions in surface area were observed in several fronto-parietal regions (ds=0.08-0.13), but no internalising-specific (i.e., anxiety disorders and depression) effects were identified. Disorder-specific alterations were identified for ADHD, CD, and anxiety disorders, but not for depression. Overall, six out of 34 regions showed case-control differences in cortical thickness, but there were more widespread effects for surface area and subcortical volume. Of the disorder-specific effects observed for surface area and subcortical volume, most were specific to CD. Most group differences in surface area and cortical

thickness survived adjustment for IQ, but were more affected by medication status adjustment, while the opposite was true for subcortical volumes.

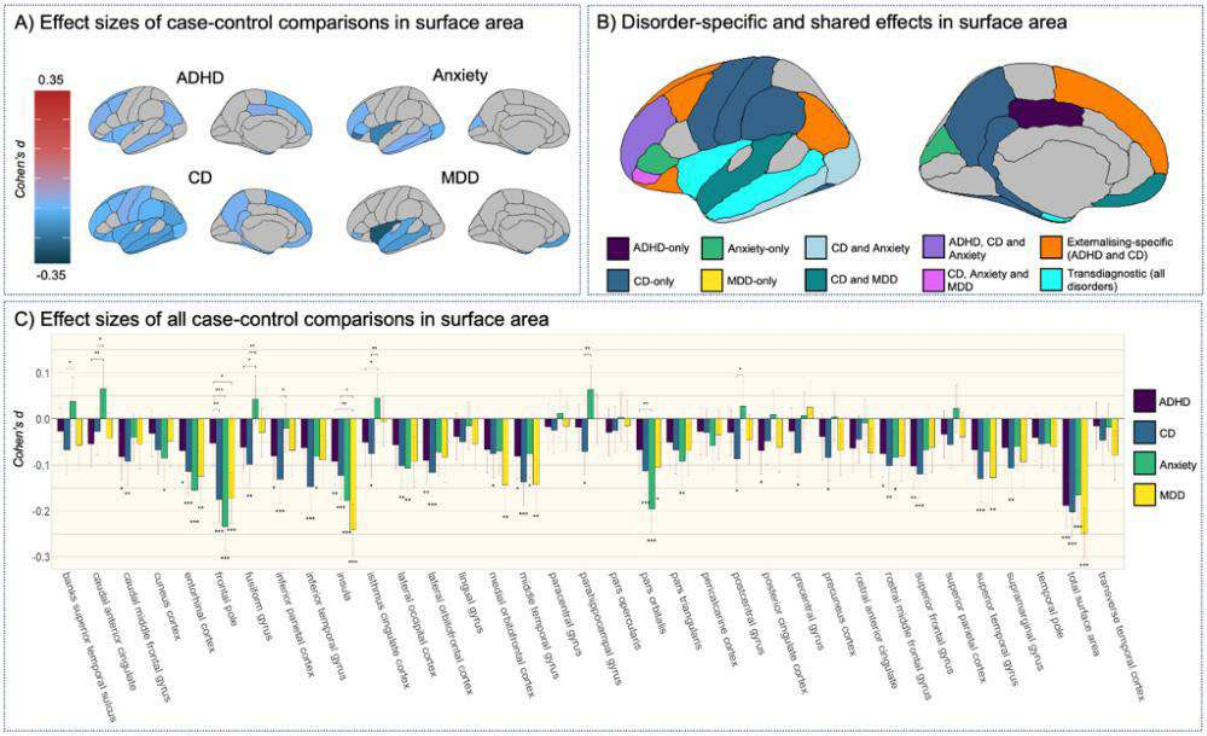

Figure 1. Disorder-specific and shared effects in surface area. (A) Cohen's d maps indicating case-control differences in surface area for each disorder separately, where blue represents a decrease and red represents an increase relative to controls. (B) Brain maps showing case-control effects in surface area which are specific or shared across disorders. (C) Cohen's d effect sizes for all case-control comparisons in surface area. All analyses are adjusted for age, sex and intracranial volume. Error bars represent 95% confidence intervals. ADHD = Attention-Deficit/Hyperactivity Disorder; CD = Conduct Disorder; MDD = Major Depressive Disorder. * P <.05 corrected, ** P <.005 corrected, *** P <.001 corrected.

Conclusions: In the first mega-analysis to investigate structural brain alterations in internalising and externalising disorders in youth, both disorder-specific and shared effects were found, including transdiagnostic effects on surface area and subcortical volume. These findings may guide future research into the neural mechanisms of transdiagnostic vulnerability, as well as understanding how specific disorders map onto distinct brain networks.

References

1. Caspi, A., Houts, R. M., Belsky, D. W., Goldman-Mellor, S. J., Harrington, H., Israel, S., ... & Moffitt, T. E. (2014). The p factor: one general psychopathology factor in the structure of psychiatric disorders? Clinical Psychological Science, 2(2), 119-137.
2. Durham, E. L., Jeong, H. J., Moore, T. M., Dupont, R. M., Cardenas-Iniguez, C., Cui, Z., ... & Kaczkurkin, A. N. (2021). Association of gray matter volumes with general and specific dimensions of psychopathology in children. Neuropsychopharmacology, 46(7), 1333-1339.
3. Gold, A. L., Brotman, M. A., Adleman, N. E., Lever, S. N., Steuber, E. R., Fromm, S. J., ... & Leibenluft, E. (2016). Comparing brain morphometry across multiple childhood psychiatric disorders. Journal of the American Academy of Child & Adolescent Psychiatry, 55(12), 1027-1037.
4. Goodkind, M., Eickhoff, S. B., Oathes, D. J., Jiang, Y., Chang, A., Jones-Hagata, L. B., ... & Etkin, A. (2015). Identification of a common neurobiological substrate for mental illness. JAMA Psychiatry, 72(4), 305-315.
5. Radua, J., Vieta, E., Shinohara, R., Kochunov, P., Quidé, Y., Green, M. J., ... & Pineda-Zapata, J. (2020). Increased power by harmonizing structural MRI site differences with the ComBat batch adjustment method in ENIGMA. NeuroImage, 218, 116956.
6. Yu, G., Liu, Z., Wu, X., Becker, B., Zhang, K., Fan, H., ... & Zhang, J. (2023). Common and disorder-specific cortical thickness alterations in internalizing, externalizing and thought disorders during early adolescence: an Adolescent Brain and Cognitive Development study. Journal of Psychiatry and Neuroscience, 48(5), E345-E356.

Poster No 499

Gray matter correlates of MDD: a cross-cohort investigation of replicability and generalizability

Janik Goltermann[1], Udo Dannlowski[2], Klaus Berger[3], Tilo Kircher[4], Tim Hahn[2]

[1]University of Münster, Münster, NRW, Germany, [2]Institute for Translational Psychiatry, Münster, North Rhine Westphalia, [3]Institute of Epidemiology and Social Medicine, University of Münster, Münster, NRW, Germany, [4]University of Marburg, Marburg, Germany

Introduction: Major depressive disorder (MDD) is one of the leading causes of disability worldwide[1] and is still insufficiently treated, with approximately one third of patients being treatment-resistent[2]. Despite the societal relevance of depression and

a plethora of research over the past decades, the neurobiological underpinnings of the disorder are still poorly understood. Previous neuroimaging studies have yielded highly heterogeneous results, even across large consortia[3–5] and effect sizes appear to be subtle at most[6]. In addition, the validity of brain-behavior findings in general have been questioned due to reports of underpowered study samples, overestimated effect sizes and overall low replicability[7]. These findings make it highly relevant to systematically investigate the replicability of the neural correlates of psychiatric disorders, such as depression and assess their generalizability to independent cohorts.

Methods: Three independent cohorts totaling N=4021 adult participants were analyzed, including lifetime MDD patients (n=1764) and health control (HC) individuals (n=2257). Cohorts were from the MACS (n=1799), the MNC (n=1198) and the BiDirect study (n=1024). Lifetime MDD diagnosis was determined using structured interviews, conducted by clinically trained raters. Brain-wide association between MDD and gray matter voxel-based morphometry was tested using general linear models, controlling for age, sex and total intracranial volume. Cross-cohort replicability was assessed by inspecting the congruence of significant voxels between the three cohorts, at a liberal uncorrected threshold of $p<.001$ and using a stringent FWE-corrected threshold of $pFWE<.05$. Cross-cohort generalizability was investigated using a cross-validation framework, iterating through the three cohorts as independent test sets.

Results: Using an uncorrected threshold of $p<.001$ an overlap in significance congruently between all three cohorts was found in clusters distributed mainly across the thalamus, insula, as well as the lingual, fusiform and parahippocampal gyri (a total of k=787 voxels; Figure 1). When correcting for multiple comparisons at $pFWE<.05$ no voxels showed significant effects congruently across all three cohorts. However, all pairwise combinations of cohorts showed an overlap in congruent significance even at this level in some areas, located mainly within the thalamus, insula, orbitofrontal cortex, and the fusiform and lingual gyri. All observed effect sizes were small, with maximum explained variance of the diagnosis effect up to partial $R^2=.01$. Inspecting the threshold-free cohort-wise generalizability of the diagnosis effect using cross-validation yielded largely generalizable effects across cohorts (Figure 2). Largest and most robust generalization was achieved within bilateral insulae. Effects within the parahippocampal-lingual compound, the thalamus, the cerebellum, and widespread prefrontal clusters generalized between some cohort combinations but not others.

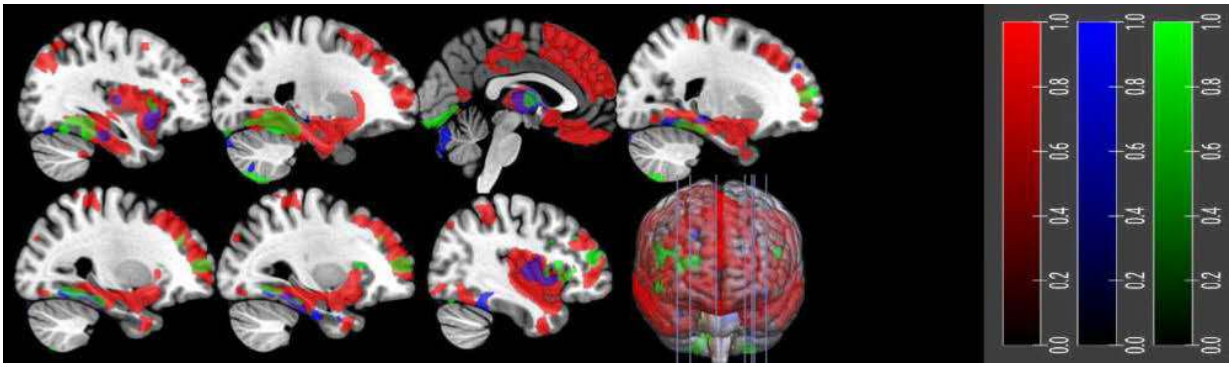

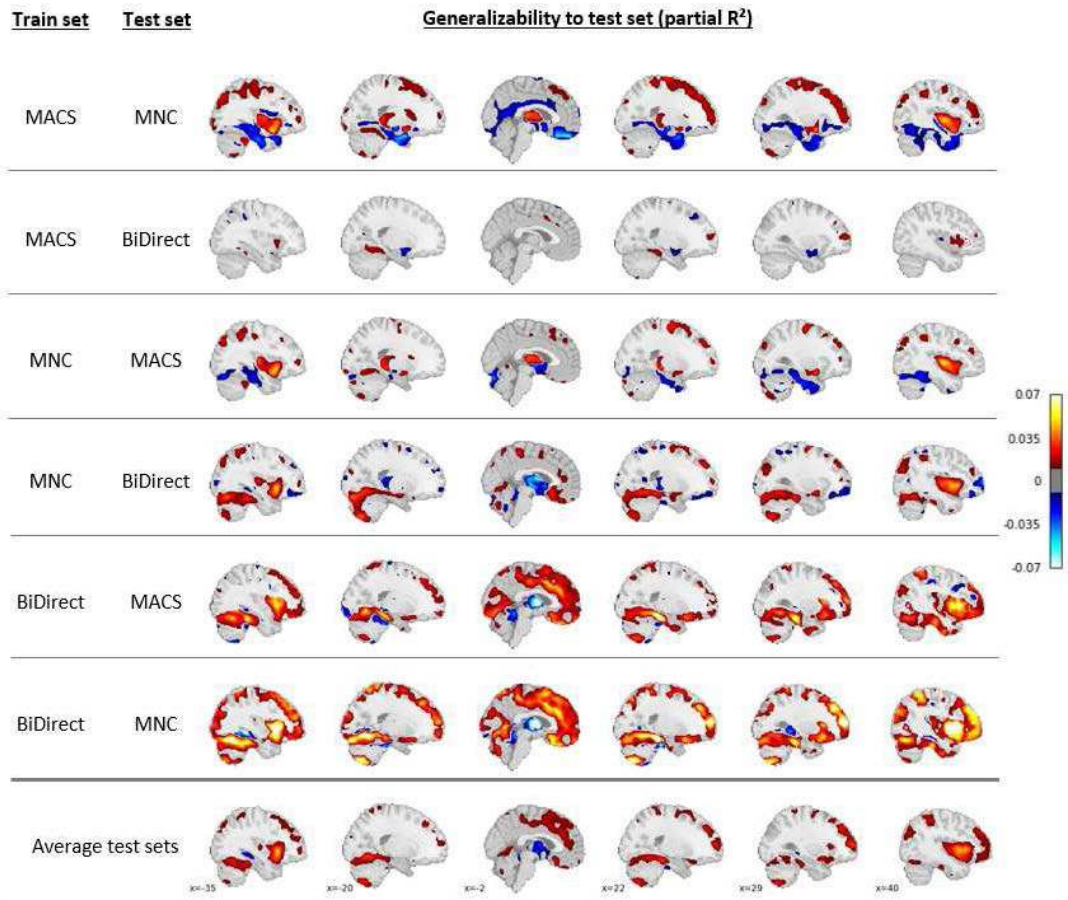

Conclusions: Gray matter correlates of depression are in part replicable and even generalizable between well-powered independent cohorts, despite the small magnitude of effects. Evidence implies a network containing the insula, thalamus and a lingual-parahippocampal complex. Most robust effects were found for the insula, while little evidence was found for a replicable or generalizable effect located within the hippocampus, opposed to a variety of previous findings. The most important limitation is the relatively low demographic diversity across cohorts (German, caucasian and comparably high socioeconomic status). Nevertheless, our findings demonstrate the need of replication efforts and the potential utility of cross-validation for univariate analyses in order to ensure the generalizability of findings, thus counteracting current concerns of low replicability.

References

1. Friedrich M (2017): Depression Is the Leading Cause of Disability Around the World. JAMA 317: 1517.
2. McLachlan G (2018): Treatment resistant depression: what are the options? BMJ 363: k5354.
3. Harris MA, Cox SR, de Nooij L, Barbu MC, Adams MJ, Shen X, et al. (2022): Structural neuroimaging measures and lifetime depression across levels of phenotyping in UK biobank. Transl Psychiatry 12. https://doi.org/10.1038/s41398-022-01926-w
4. Frodl T, Janowitz D, Schmaal L, Tozzi L, Dobrowolny H, Stein DJ, et al. (2017): Childhood adversity impacts on brain subcortical structures relevant to depression. J Psychiatr Res 86: 58–65.
5. Gray JP, Müller VI, Eickhoff SB, Fox PT (2020): Multimodal Abnormalities of Brain Structure and Function in Major Depressive Disorder: A Meta-Analysis of Neuroimaging Studies. Am J Psychiatry 177: 422–434.
6. Winter NR, Leenings R, Ernsting J, Sarink K, Fisch L, Emden D, et al. (2022): Quantifying Deviations of Brain Structure and Function in Major Depressive Disorder Across Neuroimaging Modalities. JAMA Psychiatry. https://doi.org/10.1001/jamapsychiatry.2022.1780
7. Marek S, Tervo-Clemmens B, Calabro FJ, Montez DF, Kay BP, Hatoum AS, et al. (2022): Reproducible brain-wide association studies require thousands of individuals. Nature 603: 654–660.

Poster No 500

Effects of Pregnenolone on Functional Connectivity of Dorsolateral Prefrontal Cortex in Depression

Che Liu[1], Sherwood Brown[2], Jayme Palka[2], Francesca Filbey[1]

[1]Center for BrainHealth, School of Behavioral and Brain Sciences, University of Texas at Dallas, Dallas, TX, [2]Department of Psychiatry, UT Southwestern Medical Center, Dallas, TX

Introduction: Pregnenolone is an endogenous neurosteroid and the precursor to all other neurosteroids in the brain. In patients with depression, lower levels of cerebrospinal fluid (CSF) pregnenolone were linked to depressed states (George, Guidotti et al. 1994). Previous clinical trials showed that adjunctive pregnenolone treatment improved depressive symptoms in patients with bipolar disorder (Osuji, Vera-Bolanos et al. 2010, Brown, Park et al. 2014), and reduced negative symptoms such as blunted affect, alogia and anhedonia (Marx, Keefe et al. 2009, Ritsner, Bawakny and Kreinin 2014) in patients with schizophrenia. However, to date, little research has examined its effect on resting state functional connectivity (rsFC), especially in patients with major depressive disorder (MDD). The dorsolateral prefrontal cortex (DLPFC), a key node of executive control network, is thought to be responsible for regulation of negative emotion (Phillips, Drevets et al. 2003, Koenigs and Grafman 2009), plays a critical role in the pathophysiology of depression (Koenigs and Grafman 2009), and is a target to treat depression (Koenigs and Grafman 2009, Kupfer, Frank and Phillips 2012). A post-mortem study showed that the endogenous production of steroids (i.e., dehydroepiandrosterone and its sulfate metabolite) is altered in the DLPFC of patients with MDD (Qi, Luchetti et al. 2018). Thus, FC of DLPFC may serve as markers for dose-dependent pregnenolone treatment.

Methods: In a cross-over clinical trial, twelve adult women (mean ± SD= 46.08 ± 6.96, range: 36-57 years) with mild or moderate MDD underwent three treatment conditions in a randomized order: 500mg/day, 800 mg/day pregnenolone and placebo. Each treatment lasted for 7 days with a 14-day washout period between treatments. Structural MRI and 6-min rsfMRI data were collected after completion of each treatment condition using a 3-T Philips Achieva scanner. Depressive symptoms were assessed using Hamilton Rating Scale for Depression (HRSD) at baseline (mean ± SD= 12.67 ± 4.03, range: 6-21). The DLPFC mainly corresponds to Brodmann area (BA)9 and BA46 (Jung, Lambon Ralph and Jackson 2022). The left and right BA9 and BA46 were selected as the seed regions and used to conduct seed-based voxel-wise connectivity analyses. Data were preprocessed and analyzed using CONN toolbox (v.22a). The rsfMRI data of one participant was excluded due to excessive head motion. Repeated measures analyses of covariances (ANCOVA) controlling for the sequence orders were conducted for the comparisons between treatment conditions. A whole-brain voxel-level uncorrected $P<.001$, cluster-level P-FDR<.05 and a minimum cluster size of 10 voxels were used to identify significant clusters.

Results: Compared to placebo, pregnenolone dose 500mg/day increased FC of right BA46 with posterior and anterior cingulate gyri (P-FDR=.005) and left anterior supramarginal gyrus (P-FDR=.031), of right BA9 with precuneus (P-FDR=.040), but reduced FC between right BA46 and bilateral occipital poles (P-FDR=.005). However, FC of BA46 or 9 did not significantly differ between pregnenolone dose 800mg/day and placebo. Compared to pregnenolone dose 500mg/day, lower FC were found following higher dose 800 mg/day between right BA9 and precuneus (P-FDR≤.005), between left BA46 and left frontal pole (P-FDR=.0497), and between right BA46 and left frontal pole (P-FDR=.0003) and temporooccipital part of left inferior temporal gyrus (P-FDR=.024).

Conclusions: Administration of pregnenolone 500mg/day could represent a new potential treatment for women with MDD. Quantifying FC of DLPFC holds the promise for the prediction of pregnenolone response in depression. In addition, higher FC of DLPFC also predicted better symptom scores after treatment.

References

1. Brown, E. S., J. Park, C. E. Marx, L. S. Hynan, C. Gardner, D. Davila, A. Nakamura, P. Sunderajan, A. Lo and T. Holmes (2014), 'A randomized, double-blind, placebo-controlled trial of pregnenolone for bipolar depression', Neuropsychopharmacology, vol. 39, no. 12, pp. 2867-2873.
2. George, M. S., A. Guidotti, D. Rubinow, B. Pan, K. Mikalauskas and R. M. Post (1994), 'CSF neuroactive steroids in affective disorders: pregnenolone, progesterone, and DBI', Biol Psychiatry, vol. 35, no. 10, pp. 775-780.
3. Jung, J., M. A. Lambon Ralph and R. L. Jackson (2022), 'Subregions of DLPFC Display Graded yet Distinct Structural and Functional Connectivity', J Neurosci, vol. 42, no. 15, pp. 3241-3252.
4. Koenigs, M. and J. Grafman (2009), 'The functional neuroanatomy of depression: distinct roles for ventromedial and dorsolateral prefrontal cortex', Behav Brain Res, vol. 201, no. 2, pp. 239-243.
5. Kupfer, D. J., E. Frank and M. L. Phillips (2012), 'Major depressive disorder: new clinical, neurobiological, and treatment perspectives', Lancet, vol. 379, no. 9820, pp. 1045-1055.
6. Marx, C. E., R. S. Keefe, R. W. Buchanan, R. M. Hamer, J. D. Kilts, D. W. Bradford, J. L. Strauss, J. C. Naylor, V. M. Payne, J. A. Lieberman, A. J. Savitz, L. A. Leimone, L. Dunn, P. Porcu, A. L.
7. Morrow and L. J. Shampine (2009), 'Proof-of-concept trial with the neurosteroid pregnenolone targeting cognitive and negative symptoms in schizophrenia', Neuropsychopharmacology, vol. 34, no. 8, pp. 1885-1903.
8. Osuji, I. J., E. Vera-Bolanos, T. J. Carmody and E. S. Brown (2010), 'Pregnenolone for cognition and mood in dual diagnosis patients', Psychiatry Res, vol. 178, no. 2, pp. 309-312.
9. Phillips, M. L., W. C. Drevets, S. L. Rauch and R. Lane (2003), 'Neurobiology of emotion perception II: Implications for major psychiatric disorders', Biol Psychiatry, vol. 54, no. 5, pp. 515-528.
10. Qi, X. R., S. Luchetti, R. W. H. Verwer, A. A. Sluiter, M. R. J. Mason, J. N. Zhou and D. F. Swaab (2018), 'Alterations in the steroid biosynthetic pathways in the human prefrontal cortex in mood disorders: A post-mortem study', Brain Pathol, vol. 28, no. 4, pp. 536-547.
11. Ritsner, M. S., H. Bawakny and A. Kreinin (2014), 'Pregnenolone treatment reduces severity of negative symptoms in recent-onset schizophrenia: an 8-week, double-blind, randomized add-on two-center trial', Psychiatry Clin Neurosci, vol. 68, no. 6, pp. 432-440.

This page left intentionally blank

Poster No 501

Altered Cortical Gyrification as a Marker of Treatment Resistance in Patients with First-Episode Psychosis

Moonyoung Jang[1], Jun Soo Kwon[2], Minah Kim[1]

[1]Department of Neuropsychiatry, Seoul National University Hospital, Seoul, Seoul, [2]Department of Brain and Cognitive Sciences, Seoul National University College of Natural Sciences, Seoul, Seoul

Introduction: Predicting resistance to drug treatment in the early stages of schizophrenia can improve patient outcomes and ultimately enable more personalized therapies, potentially leading to healthcare cost savings. Currently, there is no biomarker that accurately predicts the prognosis of first-episode psychosis patients. Alterations in gyrification represent abnormal neurodevelopmental processes and have the potential to identify treatment resistance at the onset of the illness. However, only a few studies have explored the gyrification patterns of first-episode psychosis, and none of them suggested alterations in gyrification as a predictive marker of treatment resistance. This study aims to investigate cortical gyrification as a viable biomarker candidate for predicting resistance to drug treatment in the first-episode of schizophrenia.

Methods: A cohort of 101 individuals diagnosed with first-episode psychosis and an equivalent number of age- and sex-matched healthy controls underwent T1-weighted magnetic resonance imaging scans immediately after their initial contact. Patients received treatment in a naturalistic clinical setting, and treatment resistance was assessed at the last follow-up. Treatment resistance was defined as either taking clozapine or exhibiting moderate to severe symptoms despite of taking more than two types of antipsychotics in sufficient amounts and duration at their last follow-up point, based on Treatment Response and Resistance in Psychosis Working Group Consensus criteria. Cortical gyrification was calculated using the local gyrification index in a vertex-wise manner across the entire cortical surface, employing Freesurfer pipeline. Local gyrification indices were compared across treatment-resistant patients, non-treatment-resistant patients, and healthy controls.

Results: Patients with first-episode psychosis exhibited hypogyria compared to healthy controls in three clusters: (1) precuneus, cuneus, and lingual gyrus, (2) precentral and postcentral gyrus, and (3) insula. Patients classified as treatment-resistant showed significant reduction in cortical gyrification compared to healthy controls in a cluster including precuneus, cuneus, and lingual gyri. Meanwhile, patients not categorized as treatment-resistant exhibited significantly reduced cortical gyrification compared to healthy controls in a cluster including precentral and postcentral areas (all clusters significant at $P < 0.05$).

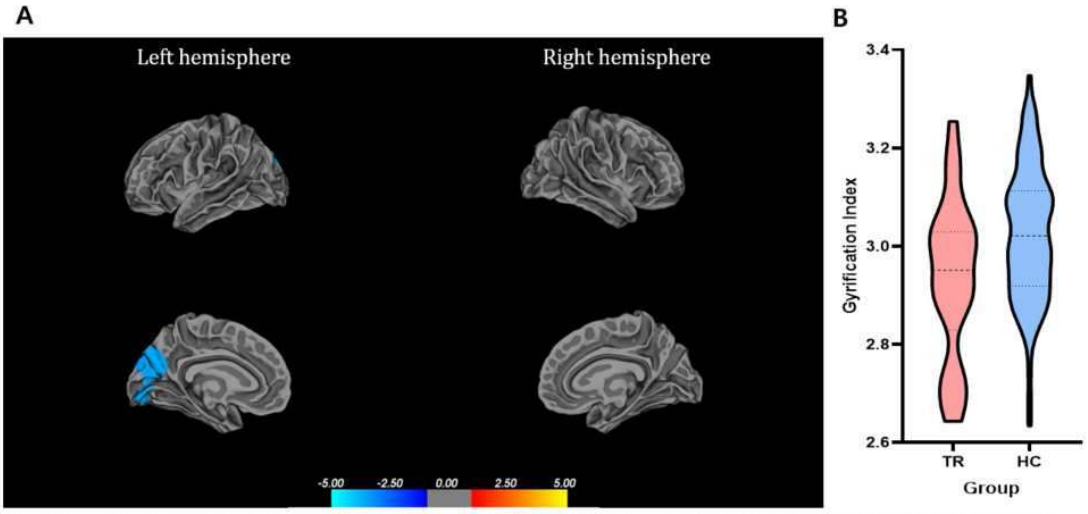

Figure1. A Group differences in the local gyrification index between the first-episode psychosis patients classified as treatment resistant and healthy controls. A statistical maps of the left and right hemispheres are shown in the lateral and medial views, respectively. The maps are shown for the clusters with significantly reduced local gyrification index in the patient group after clusterwise correction for multiple comparisons ($p < 0.05$). B Bar graph of mean local gyrification index values extracted from the left superior parietal cluster showing significant group differences. The error bars indicate 95% confidence intervals. $^{**}p < 0.01$.

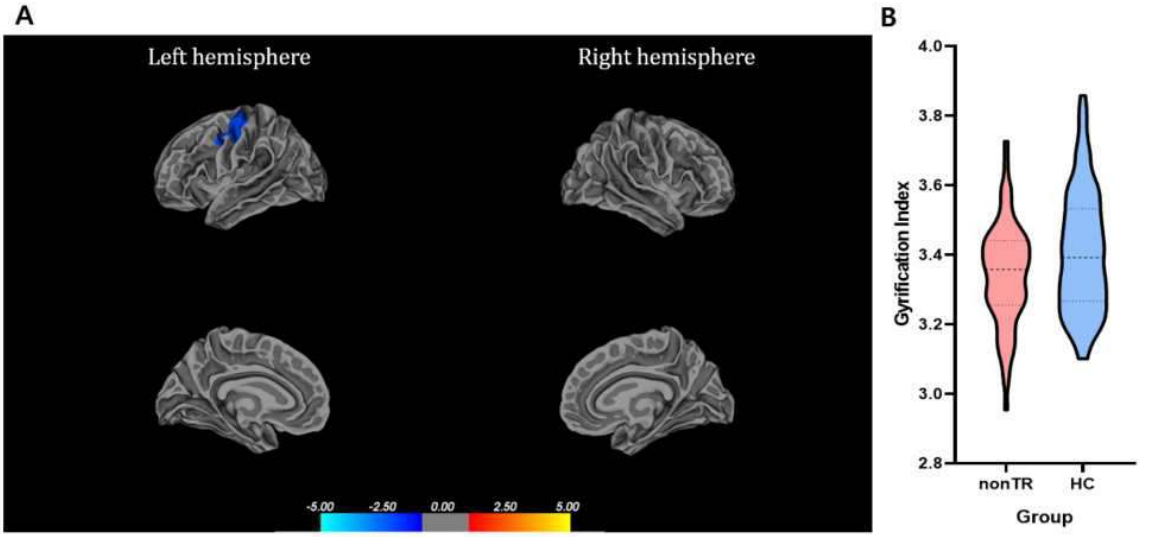

Figure2. A Group differences in the local gyrification index between the first-episode psychosis patients not classified as treatment resistant and healthy controls. A statistical maps of the left and right hemispheres are shown in the lateral and medial views, respectively. The maps are shown for the clusters with significantly reduced local gyrification index in patient group after clusterwise correction for multiple comparisons ($p < 0.05$). B Bar graph of mean local gyrification index values extracted from the left precentral cluster showing significant group differences. The error bars indicate 95% confidence intervals. $^{**}p < 0.01$.

Conclusions: The present study revealed that the treatment-resistant group exhibited hypogyria in the parieto-occipital region, consistent with previous findings in patients with first-episode psychosis who showed poor response to initial antipsychotic treatments and in asymptomatic individuals at a genetic high risk for schizophrenia. Conversely, patients not classified as treatment-resistant exhibited hypogyria in the fronto-parietal region, aligning with previous findings in first-episode psychosis patients. The observed disparities in gyrification patterns between the two groups suggest the presence of discrete neurodevelopmental anomalies underlying these distinct groups. These findings indicate that cortical gyrification may serve as a promising biomarker for early prediction of treatment resistance in conventional antipsychotic interventions within the context of psychotic disorders.

References

1. Ajnakina, O., et al. (2021), 'Structural Covariance of Cortical Gyrification at Illness Onset in Treatment Resistance: A Longitudinal Study of First-Episode Psychoses', Schizophr Bull, 47 (6), 1729-39.
2. Das, T., et al. (2018), 'Disorganized Gyrification Network Properties During the Transition to Psychosis', JAMA Psychiatry, 75 (6), 613-22.
3. Fond, G., et al. (2015), 'The promise of biological markers for treatment response in first-episode psychosis: a systematic review', Schizophr Bull, 41 (3), 559-73.
4. Howes, O. D., et al. (2017), 'Treatment-Resistant Schizophrenia: Treatment Response and Resistance in Psychosis (TRRIP) Working Group Consensus Guidelines on Diagnosis and Terminology', Am J Psychiatry, 174 (3), 216-29.
5. Palaniyappan, L., et al. (2013), 'Cortical folding defects as markers of poor treatment response in first-episode psychosis', JAMA Psychiatry, 70 (10), 1031-40.
6. Park, I., et al. (2021), 'Reduced cortical gyrification in the posteromedial cortex in unaffected relatives of schizophrenia patients with high genetic loading', NPJ Schizophr, 7 (1), 17.
7. Sasabayashi, D., et al. (2020), 'Increased brain gyrification in the schizophrenia spectrum', Psychiatry Clin Neurosci, 74 (1), 70-76.
8. Schaer, M., et al. (2008), 'A surface-based approach to quantify local cortical gyrification', IEEE Trans Med Imaging, 27 (2), 161-70.

Poster No 502

Age-Dependent Microstructural Changes in Major Depressive Disorder: A Fixel-Based Analysis Study

Shi-Ming Wang[1,2], Fan Huang[2,3,4], Chih-Mao Huang[2,3,4], Shwu-Hua Lee[5,6], Chemin Lin[7,6,8]

[1]Department of Computer Science, National Yang Ming Chiao Tung University, Hsinchu, Taiwan, [2]Department of Biological Science and Technology, National Yang Ming Chiao Tung University, Hsinchu, Taiwan, [3]Center for intelligent Drug Systems and Smart Bio-devices, National Yang Ming Chiao Tung University, Hsinchu, Taiwan, [4]Interdisciplinary neuroscience PhD program, National Yang Ming Chiao Tung University, Hsinchu, Taiwan, [5]Community Medicine Research Center, Linkou Chang Gung Memorial Hospital, Taoyuan, Taiwan, [6]College of Medicine, Chang Gung University, Taoyuan, Taiwan, [7]Department of Psychiatry, Keelung Chang Gung Memorial Hospital, Keelung, Taiwan, [8]Community Medicine Research Center, Chang Gung Memorial Hospital, Keelung, Taiwan

Introduction: Late-life depression (LLD) is one of the most common psychiatric illnesses affecting the growing population of older adults, associated with an increased risk of age-related cognitive declines[1] and progression of dementia[2]. It has been firmly established that Major Depressive Disorder (MDD) is associated with structural brain abnormalities[3-5]. Prior studies using Diffusion Tensor Imaging (DTI) have revealed a wide range of white matter abnormalities in adults with MDD[6-8]. In this study, we employed Fixel-Based Analysis (FBA), a novel diffusion model based on Constrained Spherical Deconvolution (CSD), to examine the specificity of LLD brain microstructure[9]. By utilizing FBA to conduct a fiber-specific investigation of white matter alterations, we aim to further unveil the interplay between the progression of MDD in the aging brain.

Methods: We included 85 patients with major depressive disorder (MDD) and 67 healthy controls (HC). The MDD group consisted of 26 middle-aged (mean age 51.5 years; men/women = 6/20) and 59 elderly individuals (mean age 66.8 years; men/women = 20/39). The HC group comprised 26 middle-aged (mean age 49.1 years; men/women = 7/19) and 41 elderly participants (mean age 68.4 years; men/women = 16/25). High-resolution images were obtained using a GE HC 3T Discovery MR750 scanner. T1-weighted images: TR/TE=8.24/3.2 ms, resolution voxel size = 0.5 x 0.5 x 1 mm^3, 160 slices, inversion time=450 ms, flip angle=12°, matrix size = 512 x 512. DWI utilized a spin-echo EPI sequence with: TR/TE=4500/84 ms, voxel size = 0.98 x 0.98 x 4 mm^3, matrix size = 256 x 256, 29 slices, b-values of 0 and 1000 s/mm^2 across 32 directions. Intracranial volume calculations (ICV) from T1-weighted images were performed using FSL's Brain Extraction Tool. We implemented fixel-based analysis adhering to protocols outlined by MRtrix3[9]. For subsequent analysis, the three main FBA metrics-fiber density (FD), fiber cross-section (FC), and the combined measure of fiber density and cross-section (FDC)-were computed. For tract-based analysis, we delineated 72 fiber tracts using the automated TractSeg approach[10]. We conducted a statistical comparison of FBA metrics between MDD patients and healthy controls, with ICV, age and gender as covariates. For each participant, mean FD, FC, and FDC values within each tract of interest (TOI) were computed. To assess the interplay between disease presence and age, a two-factor ANOVA was employed. This analysis delineated the effects and interactions between these two crucial factors (p-value < 0.05).

Results: Fig.1.A indicates that after adjusting for age and gender, patients with MDD exhibit significantly lower FD in the bilateral Fornix (FX) compared to healthy individuals. Fig.1.B and 1.C demonstrate widespread white matter alterations across three different FBA metrics as a function of age between individuals with MDD and healthy controls., Patients with MDD showed changes in inter-hemispheric and intra-hemispheric connectivity with age. Fig.2.A highlights significant disease effects on FD within the corpus callosum (CC) and the bilateral FX. Additionally, the FD result showed interaction between disease progression and age within the right optic radiation (OR), right parieto-occipital pontine (POPT), right striato-occipital (ST OCC), right striato-parietal (ST PAR), and right thalamo-occipital (T OCC) tracts. Fig.2.B reveals FC interactions between disease and age in the right anterior thalamic radiation (ATR), left OR, left ST OCC, and left T OCC. In Fig.2.C, FDC result showed interaction of disease and age in the left ATR, suggesting that these changes in the ATR may modulate by both disease progression and aging.

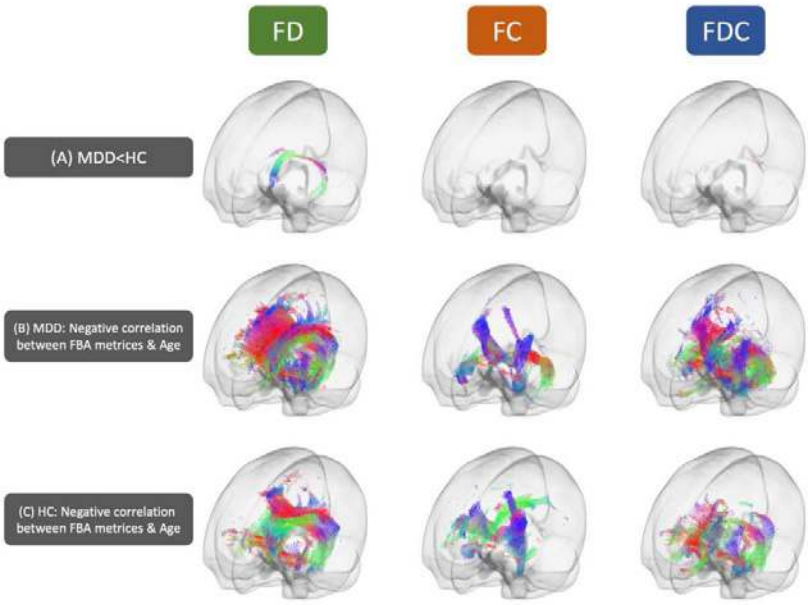

Figure 1. Fixel-based analysis results visualized within glass brain, with colors marking fixel directions, thresholded by FWE-corrected p-values.

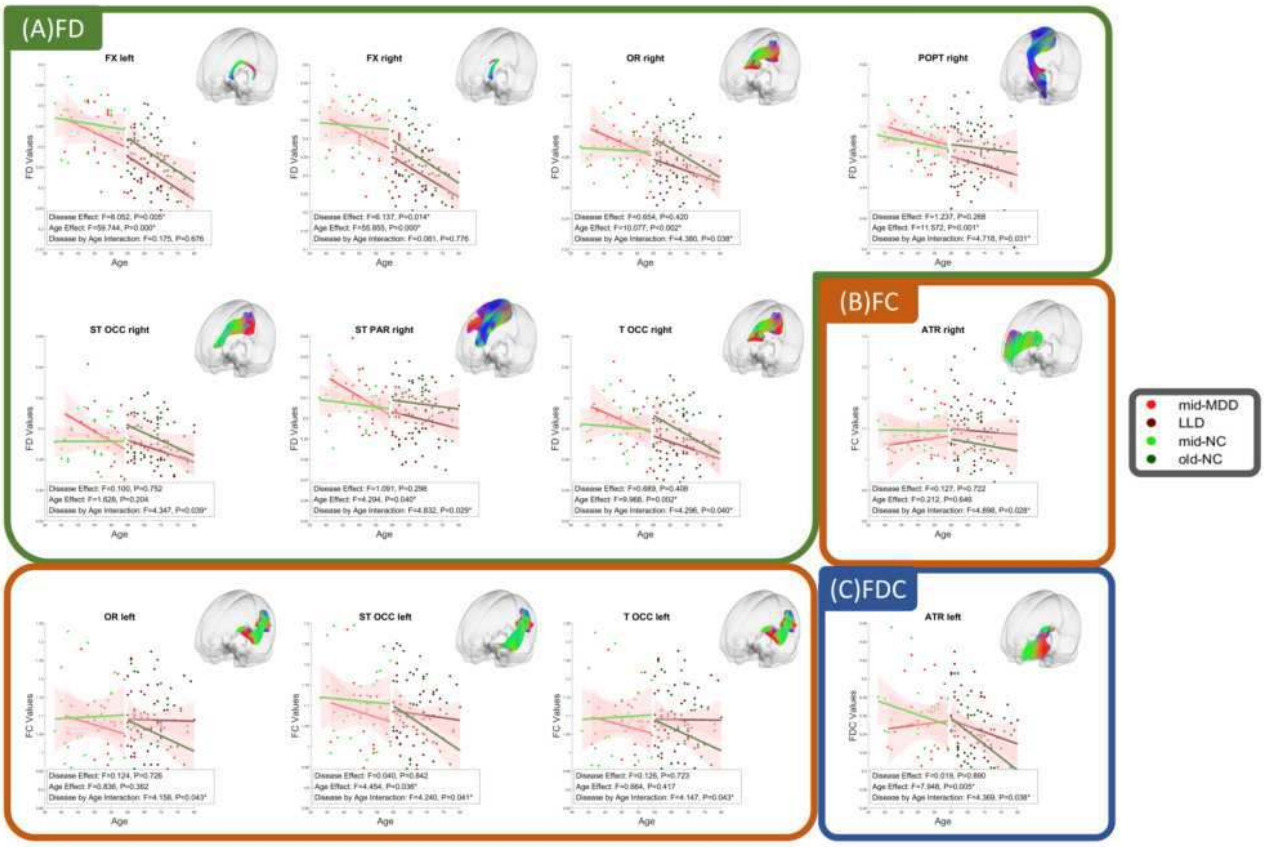

Figure 2. This figure displays the distribution of mean FBA metrics for key fiber bundles from a two-way ANOVA analysis, overlaid on glass brain with color-coded fixel orientations.

Conclusions: Our findings imply microstructural changes in the depressive brain are dynamic and age-dependent. The study underscores the need for considering age in neurological disease progression and white matter integrity, advocating for more targeted treatments.

References

1. John, A., et al., Affective problems and decline in cognitive state in older adults: a systematic review and meta-analysis. Psychological medicine, 2019. 49(3): p. 353-365.
2. Asmer, M.S., et al., Meta-analysis of the prevalence of major depressive disorder among older adults with dementia. The Journal of clinical psychiatry, 2018. 79(5): p. 15460.
3. Lin, C., et al., Automatic diagnosis of late-life depression by 3D convolutional neural networks and cross-sample Entropy analysis from resting-state fMRI. Brain Imaging and Behavior, 2023. 17(1): p. 125-135.
4. Lin, C., et al., Greater white matter hyperintensities and the association with executive function in suicide attempters with late-life depression. Neurobiology of aging, 2021. 103: p. 60-67.
5. Patil, A.U., et al., Review of EEG-based neurofeedback as a therapeutic intervention to treat depression. Psychiatry Research: Neuroimaging, 2023: p. 111591.
6. Chen, G., et al., Disorganization of white matter architecture in major depressive disorder: a meta-analysis of diffusion tensor imaging with tract-based spatial statistics. Scientific reports, 2016. 6(1): p. 21825.
7. Liao, Y., et al., Is depression a disconnection syndrome? Meta-analysis of diffusion tensor imaging studies in patients with MDD. Journal of Psychiatry and Neuroscience, 2013. 38(1): p. 49-56.
8. Murphy, M.L. and T. Frodl, Meta-analysis of diffusion tensor imaging studies shows altered fractional anisotropy occurring in distinct brain areas in association with depression. Biology of mood & anxiety disorders, 2011. 1: p. 1-12.
9. Raffelt, D.A., et al., Investigating white matter fibre density and morphology using fixel-based analysis. Neuroimage, 2017. 144: p. 58-73.
10. Wasserthal, J., P. Neher, and K.H. Maier-Hein, TractSeg-Fast and accurate white matter tract segmentation. NeuroImage, 2018. 183: p. 239-253.

Poster No 503

3D CNN Classification Model to Identify Bipolar Disorders and Major Depressive Disorders by Rs-fMRI

Jaimie Yeh[1], Albert Yang[1,2,3,4]

[1]Institute of Brain Science, National Yang Ming Chiao Tung University, Taipei City, Taiwan, [2]Digital Medicine and Smart Healthcare Research Center, National Yang Ming Chiao Tung University, Taipei City, Taiwan, [3]Department of Medical Research, Taipei Veterans General Hospital, Taipei City, Taiwan, [4]Brain Research Center, National Yang Ming Chiao Tung University, Taipei City, Taiwan

Introduction: Bipolar disorder (BD) and major depressive disorder (MDD) are prevalent psychiatric disorders that present similar clinical symptoms during depressive episodes. Distinguishing between depressed BD and MDD based on clinical symptoms is a considerable challenge, which makes the clinical treatment more difficult. Consequently, biomarkers that are capable of accurately discerning between these two disorders assume paramount importance in clinical diagnostics. Resting-state functional magnetic resonance imaging (rs-fMRI) provides diagnostic markers for studying affective disorders. Although several rs-fMRI studies have reported abnormal functional connectivity between individuals with BD and those with MDD, most have focused on identifying relevant brain alterations at the group level. Machine learning techniques offer significant practical value in predicting diagnoses and clinical outcomes at the individual level. Furthermore, deep learning applications, such as the three-dimensional convolutional neural network (3D CNN) classification model, provide a more comprehensive approach by incorporating spatio-temporal features. In this study, we aimed to utilize 3D CNN methodologies to identify neuroimaging feature differences between individuals with BD and individuals with MDD, which can help in clinical diagnosis and treatment strategies.

Methods: Rs-fMRI data were obtained from the Taiwan Aging and Mental Illness cohort, encompassing 99 individuals with BD (age: 50.66 ± 10.35; 34% in males), 90 individuals with MDD (age: 54.11 ± 13.57; 33% in males), and 193 healthy controls (HCs; age: 50.07 ± 11.37; 35% in males). The whole brain voxelwise functional connectivity map was computed for each participant. We applied z-transformation to improve the normality of the data. Subsequently, 90 functional connectivity maps for each participant were delineated based on the Automated Anatomical Labeling (AAL) atlas. The 3D characteristics of each functional connectivity map were retained for subsequent model training. Hierarchical 3D CNN classification models were applied to each functional connectivity map. Initially, we classified between the HCs and individuals with affective disorders (i.e., BD and MDD). Next, we performed 3D CNN classification models to differentiate between individuals with BD and those with MDD. Based on the outcomes of these two steps, we were able to identify critical brain features for the differential diagnosis of affective disorders.

Results: In the classification of HCs and individuals with affective disorders, our results revealed that 3D CNN models, constructed using brain regions such as the right superior temporal gyrus, rolandic operculum, insula, hippocampus, parahippocampal gyrus, thalamus, lingual gyrus, fusiform gyrus, precentral gyrus, middle frontal gyrus, and the left caudate nucleus, achieved accuracy values ranging from 80% to 88%. Additionally, the f1-score values for these models were found to be within the range of 80% to 89%. Afterward, 3D CNN models constructed using the left supplementary motor area, medial orbital part of superior frontal gyrus, and orbital part of superior frontal gyrus for classifying individuals with BD and individuals with MDD demonstrated accuracy values of 72%, 71%, and 70%, respectively. Correspondingly, the f1-score values for these classifications were observed to be 70%, 71%, and 67%.

Conclusions: Our findings offer a promising approach for integrating rs-fMRI data with 3D CNN techniques for the individual-level classification of affective disorders. Moreover, the observed abnormalities in these brain regions may serve as potential imaging markers for distinguishing patients with MDD and BD from HCs. These biomarkers could also contribute to differentiating individuals with BD from those with MDD. Overall, this study provides a comprehensive understanding of the neurobiology of affective disorders and lays a foundation for developing more precise and personalized diagnostic tools.

References

1. Delvecchio, G. (2012), 'Common and distinct neural correlates of emotional processing in Bipolar Disorder and Major Depressive Disorder: A voxel-based meta-analysis of functional magnetic resonance imaging studies', European Neuropsychopharmacology, vol. 22, no. 2, pp. 100-113
2. Gong, J. (2020), 'Common and distinct patterns of intrinsic brain activity alterations in major depression and bipolar disorder: voxel-based meta-analysis', Translational Psychiatry, vol. 10, no. 353
3. Han, K.M. (2019), 'Differentiating between bipolar and unipolar depression in functional and structural MRI studies', Progress in Neuro-Psychopharmacology and Biological Psychiatry, vol. 91, pp. 20-27
4. Jiang, X. (2020), 'Common and distinct neural activities in frontoparietal network in first-episode bipolar disorder and major depressive disorder: Preliminary findings from a follow-up resting state fMRI study', Journal of Affective Disorders, vol. 260, pp. 653-659
5. Kim, Y.K. (2018), 'Application of machine learning classification for structural brain MRI in mood disorders: Critical review from a clinical perspective', Progress in Neuro-Psychopharmacology and Biological Psychiatry, vol. 80, pp. 71-80

Poster No 504

Advanced Machine Learning for Brain Age Gap Estimation in Anorexia Nervosa: A Neuroimaging Approach

Yubraj Gupta[1], Andy Schumann[2], Feliberto de la Cruz[1], Karl- Jürgen Bär[2]

[1]Jena University Hospital, Jena, Germany, [2]Klinikum Universität, Jena, Thuringia

Introduction: Anorexia Nervosa (AN) is a condition that primarily affects young women, leading to significant weight loss and cognitive deficits. Accurate and early detection of these neurobiological changes is vital. This study aims to develop a Brain Age Gap Estimation (BrainAGE) model using ML to investigate accelerated brain ageing in AN. BrainAGE, a proven biomarker in conditions like Alzheimer's, is utilized here to determine if AN is linked to faster brain ageing, thereby serving as an effective tool for assessing brain health in AN patients.

Methods: We developed a BrainAGE model for AN leveraging structural magnetic resonance imaging (sMRI) from 2887 healthy female controls (HC, ages 18-40) and 44 female AN patients of equivalent age. HC data spanned eight global databases, ensuring diverse brain morphology representation, vital for model training and the discernment of AN-induced deviations (Figure 1(a)). AN data was sourced exclusively from Jena University Hospital (JUH). Each sMRI sample was processed via FreeSurfer v.7.3.2, utilizing 'recon-all' to automate morphological feature extraction. This workflow provided 378 features, including volumetric, surface area, and curvature measures from cortical/sub-cortical structures, guided by the Desikan-Killiany atlas. To predict chronological age, we implemented Support Vector Regression (SVR) and Gaussian Process Regression (GPR), forming an N x P feature matrix (N = 2887, P = 378). We applied 10-fold cross-validation and PCA for dimensionality reduction, maintaining 99% feature variance, and identified 257 independent features. Hyperparameter tuning was conducted for both SVR and GPR models, optimizing epsilon, gamma, kernel, regularization parameters (SVR), and lengthscale, noise, and kernels (GPR). Data was partitioned into training, validation, and a 44-HC-JUH-DATA hold-out set. Models were trained on 2799 HC samples, validated, and tested on the hold-out and 44 AN samples. Statistical analysis included Pearson's correlation coefficient (PCC), MAE, MSE, and RMSE to assess prediction accuracy and infer potential brain ageing in AN.

Results: In our study, SVR and GPR were leveraged to develop a BrainAGE model, demonstrating high efficacy with and without PCA dimensionality reduction for the prediction of age. Particularly, GPR showed superior performance. Figure 2(a) shows the obtained actual vs predicted BrainAGE prediction for validation, hold-out and patients. According to Figure 1(b), the GPR model achieved notable correlation scores across all groups, affirming the significance of the full feature set for age prediction. Figure 2(b)'s boxplot displays prediction error distributions, with the validation and 44-HC-JUH-DATA hold-out sets showing tight interquartile ranges and minimal median errors, indicating precise age estimations. Conversely, the AN patient group exhibited increased median errors and variability, with significant differences from the hold-out set ($p = 0.0254$) and validation set ($p = 0.0010$), suggesting altered brain ageing in AN using GPR without PCA (Figure 2(b), Figure 1(c)). Further, Figure 2(c)'s bar chart reveals that while the validation set achieved a strong correlation (0.84), indicating accurate age predictions, the AN patient group presented higher MSE (28.16) and lower correlation (0.42), implying potential brain structure differences in AN using GPR without PCA. This underlines that, despite the models' accuracy with healthy data, predictions for AN patients indicate a potential acceleration in brain ageing.

a.)

Model	Gender	Samples	Age (years)
Brain Genomics Superstruct Project (GSP)	F	940	21.44 ± 2.76
HCP Young Adult Project		606	29.55 ± 3.60
ID1000 AOMIC Project		483	22.85 ± 1.68
Jena University Hospital (JUH)		405	24.71 ± 4.82
PIOP2 AOMIC Project		128	21.82 ± 1.75
PIOP1 AOMIC Project		120	22.37 ± 1.68
BeijingEnhanced Project		107	21.24 ± 1.97
IXI – Information eXtraction from Images Project		98	29.76 ± 5.47

b.)

Group	Model	PCC	MAE	MSE	RMSE
Validation (44-samples)	SVR with PCA (257 features)	**0.84**	2.03	**6.04**	**2.46**
	SVR without PCA	0.81	2.16	7.49	2.74
	GPR with PCA (257 features)	0.83	2.05	6.33	2.52
	GPR without PCA	**0.84**	**2.02**	6.20	2.49
44-HC-JUH-DATA (44-samples)	SVR with PCA (257 features)	**0.77**	2.65	13.95	3.73
	SVR without PCA	**0.77**	2.62	14.96	3.87
	GPR with PCA (257 features)	0.76	2.64	13.78	3.71
	GPR without PCA	**0.77**	**2.60**	**13.36**	**3.66**
AN patients (44-samples) (JHU-DATA)	SVR with PCA (257 features)	**0.37**	4.39	27.76	5.27
	SVR without PCA	0.39	4.40	27.68	5.26
	GPR with PCA (257 features)	0.43	**4.37**	**27.44**	**5.24**
	GPR without PCA	0.42	4.42	28.16	5.31

c.)

Group	Val vs HC (*P*)	Val vs ANX (*P*)	HC vs ANX (*P*)
SVR with PCA (257 features)	0.4128	0.0027	0.0552
SVR without PCA	0.5578	0.0038	0.0270
GPR with PCA (257 features)	0.4429	0.0017	0.0356
GPR without PCA	**0.3959**	**0.0010**	**0.0254**

Notes: Val: Validation, HC: Healthy control, ANX: Anorexia, Statistical significant ***P*** value

Figure 1: (a) Shows the number of female sMRI samples acquired from eight different databases. (b) Illustrates the comparative performance of GPR and SVR in predicting brain age, both with and without the application of PCA. (c) Presents the statistical significance of the discrepancies in brain age prediction errors across different cohorts.

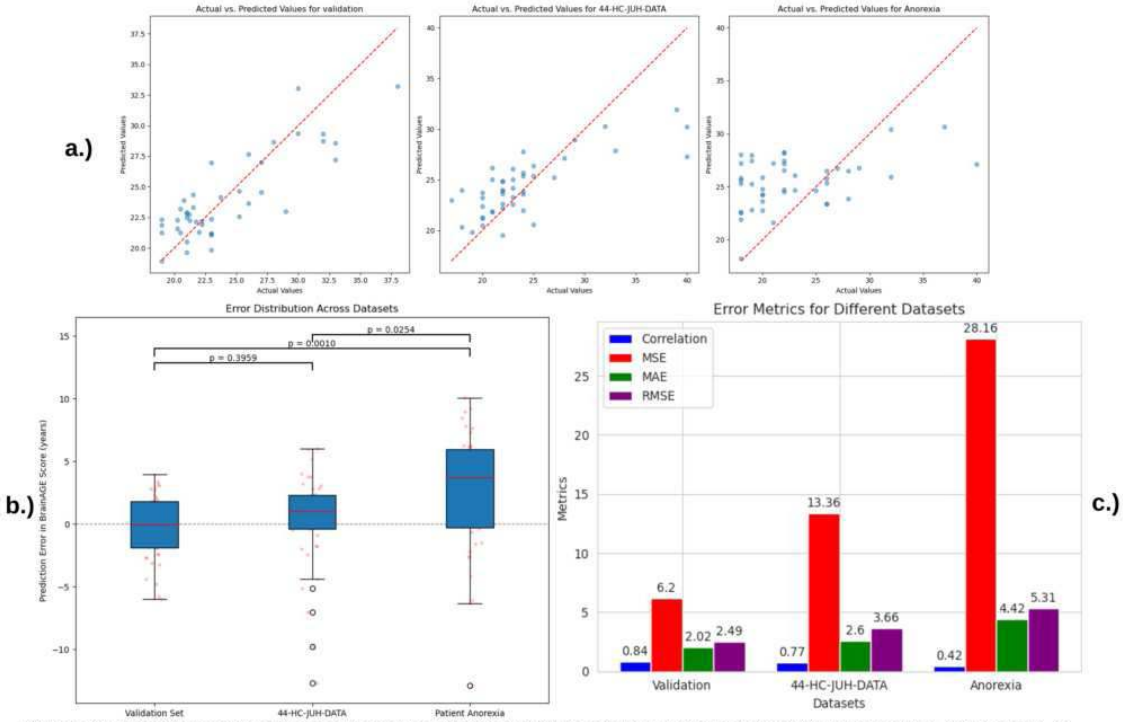

Figure 2: (a) Presents a scatter plot comparing actual versus predicted ages for the validation dataset, 44-HC-JUH-DATA, and Anorexia, as derived from the Gaussian Process Regression (GPR) model without the application of PCA. (b) Illustrates the distribution of prediction errors across all datasets, inclusive of their respective p-values, as obtained from the GPR model without PCA. (c) Displays the performance metrics achieved by the GPR model, which was implemented without the incorporation of PCA.

Conclusions: The models' ability to discern between healthy and atypical brain development in AN patients demonstrates the value of BrainAGE in neurodevelopmental assessment. The observed prediction errors in AN patients align with the hypothesis of accelerated brain ageing, establishing Brain Age Gap Estimation as a viable biomarker for monitoring AN. These findings may inform precision medicine strategies for AN, emphasizing the role of ML in psychiatric evaluation.

References
1. Cole, J.H., 2018. Brain age predicts mortality. Molecular psychiatry, 23(5), pp.1385-1392.
2. Cole, J.H., 2020. Multimodality neuroimaging brain-age in UK biobank: relationship to biomedical, lifestyle, and cognitive factors. Neurobiology of aging, 92, pp.34-42.
3. Franke, K., 2010. Estimating the age of healthy subjects from T1-weighted MRI scans using kernel methods: exploring the influence of various parameters. Neuroimage, 50(3), pp.883-892.
4. Griffiths-King, D., 2023. Predicting 'Brainage'in late childhood to adolescence (6-17yrs) using structural MRI, morphometric similarity, and machine learning. Scientific Reports, 13(1), p.15591.
5. Koutsouleris, N., 2014. Accelerated brain aging in schizophrenia and beyond: a neuroanatomical marker of psychiatric disorders. Schizophrenia bulletin, 40(5), pp.1140-1153.
6. Lombardi, A., 2021. Brain age prediction with morphological features using deep neural networks: results from predictive analytic competition 2019. Frontiers in Psychiatry, 11, p.619629.

Poster No 505

Functional and Structural Hierarchy in Individuals at Ultra High Risk for Developing Psychosis

Thuan Tinh Nguyen[1,2,3], Siwei Liu[1,2], Chen Hao Wang[1], Michael Chee[1,2], Jimmy Lee[4], Juan Helen Zhou[1,2,5,6]

[1]Centre for Sleep and Cognition, Yong Loo Lin School of Medicine, National University of Singapore, Singapore, Singapore, [2]Centre for Translational Magnetic Resonance Research, Yong Loo Lin School of Medicine, National University of Singapore, Singapore, Singapore, [3]Integrative Sciences and Engineering Programme (ISEP), NUS Graduate School, National University of Singapore, Singapore, Singapore, [4]Department of Psychosis, Institute of Mental Health, Singapore, Singapore, [5]Integrative Sciences and Engineering Programme (ISEP), NUS Graduate School, National University of S, Singapore, Singapore, [6]Department of Electrical and Computer Engineering, National University of Singapore, Singapore, Singapore

Introduction: Research on individuals at ultra high risk for psychosis (UHR) demonstrates grey matter reduction and brain functional dysconnectivity, suggesting potential for predicting psychosis transition[1,2]. Gradient-based studies showed compressed functional hierarchy in schizophrenia[3], yet no exploration of UHR-associated changes. This project aims to compare functional and structural cortical topography between UHR and control groups and within UHR groups with different transition outcomes. We expect to see group differences in functional hierarchy, larger effect sizes with functional measures compared to structural, and more severe functional changes in converters.

Methods: We used data from Longitudinal Youth-at-Risk Study (LYRIKS) dataset[4] and retained 79 scans for the UHR positive (21.5±3.6 years, 52 males) and 43 scans (21.7±4.1 years, 20 males) for the control groups for further analysis. The Comprehensive Assessment of At Risk Mental State (CAARMS) was used to identify UHR individuals. All participants were followed up longitudinally for two years; UHR participants were assigned to either those who converted to psychosis during the course of the study (N=10, 19.3±3.3 years, 7 males) and those who did not (N=69, 21.8±3.6 years, 45 males). The preprocessing pipeline was applied to resting state fMRI data following previous work[1]. Functional connectivity (FC) matrices were computed among 400 regions using Pearson's correlation[5]. We derived individual-level gradients from extracted FC matrices using Brainspace Toolbox[6]. For the top 2 gradients, values from 400 regions were averaged into 7 networks using a functional parcellation[7]. To extract reliable morphology estimates, images were automatically processed using FreeSurfer[8]. Based on the individual surface and volume templates, five structural features (surface area, cortical thickness, gray matter volume, Gaussian curvature, and mean curvature) were extracted. The morphometric similarity matrix was constructed for each individual and used as input to calculate morphometric similarity gradient following previous work[9]. To investigate structural and functional hierarchy of control and UHR subjects, we performed a series of t-test to see whether specific network gradients differed across groups. To study whether brain hierarchy correlated with disease severity, we calculated the Spearman correlation between gradients and total CAARMS score, which measures the severity of the symptoms. All analyses were controlled for age, sex, handedness, ethnicity.

Results: The top two functional gradients separate the visual-somatomotor regions as well as the unimodal-transmodal regions (Fig. 1A). There was no difference between the two groups across all networks (FDR-corrected p-value>0.05; Fig. 1B, 1C). The same comparison between the control and the UHR positive population, now separated into the nonconverters and converters, returned no difference across groups. There was also no significant correlation between CAARMS score and gradients (FDR-corrected p-value>0.05). The top two morphometric gradients correspond to the top two gradients reported in previous study[9] (Fig. 2A). Similarly, we observed no difference between controls and UHR participants across all networks (FDR-corrected p-value>0.05; Fig. 2B, 2C). There was also no difference in across conversion status or disease severity.

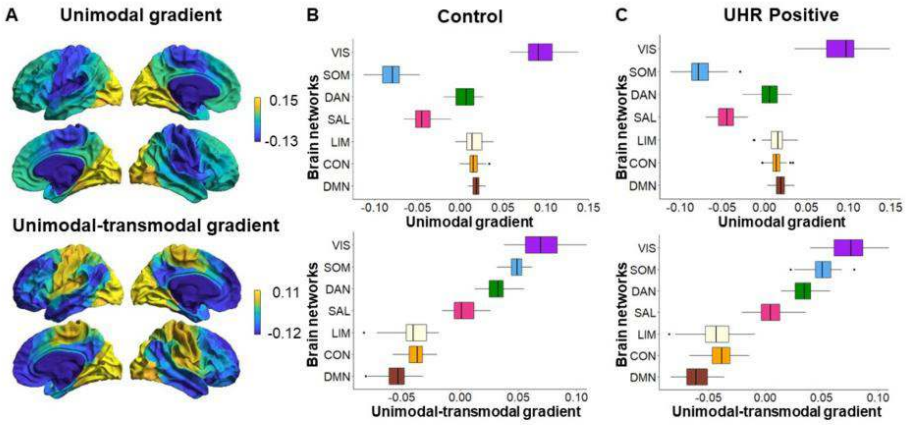

Figure 1. No difference in functional organization between control and UHR participants. (A) Top two group-level gradient values in arbitrary units (B) Top two gradient values distribution in Yeo's 7 networks in the control groups (C) Top two gradient values distribution in Yeo's 7 networks in the UHR participants. Abbreviations: CON: Control, DAN: Dorsal Attention, DMN: Default Mode, LIM: Limbic, SAL: Salience/ Ventral Attention, SOM: Somatomotor, VIS: Visual.

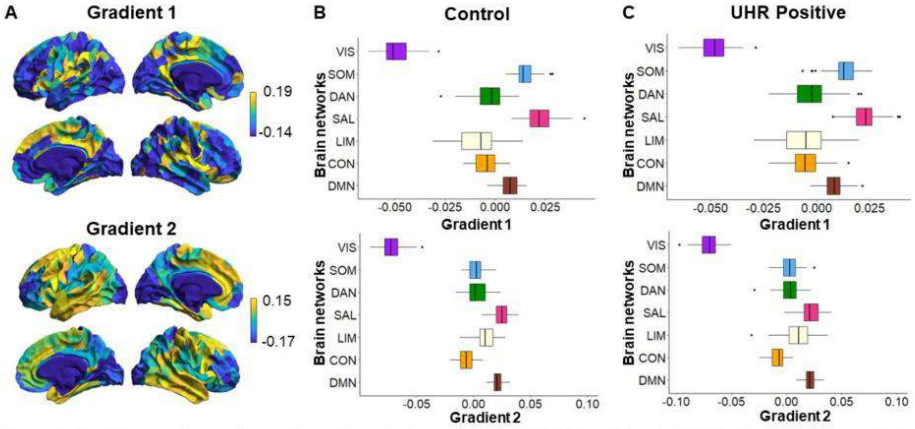

Figure 2. No difference in morphometric gradients between control and UHR participants. (A) Top two group-level gradient values in arbitrary units (B) Top two gradient values distribution in Yeo's 7 networks in the control groups (C) Top two gradient values distribution in Yeo's 7 networks in the UHR participants. Abbreviations: CON: Control, DAN: Dorsal Attention, DMN: Default Mode, LIM: Limbic, SAL: Salience/ Ventral Attention, SOM: Somatomotor, VIS: Visual.

Conclusions: Surprisingly, both functional and morphometric gradients didn't differentiate the control and UHR positive groups or predict conversion status or disease severity. The small sample size, particularly for converters, may have contributed to this. It is also plausible that disruptions in cortical hierarchy emerge later in advanced disease stages. Larger studies are needed to confirm changes in hierarchy and identify the specific point in disease progression when they manifest.

Poster No 506

Aberrations in the Ventral Tegmental Area predict depression severity in the general population

Sarah Khalife[1], Lena Oestreich[1], Steffen Bollmann[1], Andrew Zalesky[2]

[1]University of Queensland, Brisbane, Queensland, [2]The University of Melbourne, Melbourne, Victoria

Introduction: Approximately 300 million individuals are affected by major depression worldwide, making it one of the leading causes of disability (WHO, 2017). A growing body of literature indicates that many depression symptoms, such as loss of motivation and anhedonia may be attributed to the influence of inflammatory cytokines on mesolimbic dopamine signaling (Felger et al., 2017). Midbrain dopaminergic neurons originating from the ventral tegmental area (VTA) are among the areas most susceptible to these negative consequences of inflammatory cytokines. As such, it is conceivable that depression may be caused by dopaminergic neuron depletion and/or dysfunction in the VTA, possibly as a sequelae of inflammation. Here we set out to test whether diffusion MRI and Quantitative Susceptibility Mapping (QSM) markers sensitive transient processes, together with microstructural markers, can predict depression severity across the general population.

Methods: We included 8,249 participants with varying degrees of depression severity from the UK biobank (Sudlow et al., 2015). Diffusion weighted imaging (DWI), QSM and T1-weighted images were included in the analyses. Pre-processing of DWI and QSM data was performed by the UK biobank (Alfaro-Almagro et al., 2018). Free-water correction was applied to the pre-processed DWI data (Pasternak et al., 2009). The VTA was delineated with the Levinson-Bari Limbic Brainstem Atlas (Levinson et al., 2023) and co-registered to DWI subject space. Estimates of the DWI metrics free-water (FW), isotropic volume fraction (ISOVF), Intra-cellular volume fraction (ICVF) and orientation dispersion index (ODI), as well as magnetic susceptibility derived from QSM were extracted from the VTA. Depression symptomatology was evaluated using the Recent Depressive Symptoms questionnaire, assessing the severity of depressed mood, disinterest, restlessness, and tiredness on a 4-point Likert scale within the past two weeks (Dutt et al., 2022). Multiple linear regression analysis was conducted to estimate associations between the MRI-derived metrics in the VTA and depression severity while controlling for age, age squared and sex.

Results: Participants ranged in age from 46 to 82 years (M=64.1, SD=7.7). The variance inflation factor (VIF) for FW (VIF=28) and ISOVF (VIF=28), indicated the presence of multicollinearity. Due to ease of interpretation in the context of the other neurite orientation and dispersion density imaging (NODDI) metrics ICVF and ODI, FW was removed from the regression model while ISOVF was kept in the model. The overall model was significant ($F(7,8248)=41.53$, $p<0.001$) and explained 3.32% of the variance in depression severity. The predictors ODI and magnetic susceptibility independently contributed to depression severity ($\beta=1.17$, $p=0.002$ and $\beta=0.42$, $p=0.002$, respectively), such that depression severity increased with increasing ODI and magnetic susceptibility. ISOVF contributed negatively to depression severity ($\beta= -0.48$, $p=0.027$), such that depression severity increased with decreasing ISOVF.

Conclusions: ISOVF, which estimates the amount of extracellular volume, was negatively associated with depression severity. In gray matter, glial cells in the extracellular space transport nutrients and energy to neurons and may influence how well neurons function and communicate. A decrease in ISOVF could therefore suggest functional aberrations of dopaminergic neurons originating from VTA with increasing depression severity. The positive association between magnetic susceptibility and depression severity is suggestive of increased iron content in the VTA, which may reflect neurodegeneration in this area as depressive symptoms worsen. In conclusion, transient markers sensitive to extracellular processes derived from diffusion MRI and QSM in the VTA are predictive of depression severity across the general population. Future studies may wish to examine whether these estimates can be utilized for diagnostic classification of major depression.

References

1. Alfaro-Almagro, F. (2018). 'Image processing and Quality Control for the first 10,000 brain imaging datasets from UK Biobank'. NeuroImage, 166, 400–424.
2. Dutt, R. (2022). 'Mental health in the UK Biobank: A roadmap to self-report measures and neuroimaging correlates'. HUMAN BRAIN MAPPING, 43(2), 816–832.
3. Felger, J. C. (2017). 'Inflammation Effects on Motivation and Motor Activity: Role of Dopamine'. Neuropsychopharmacology, 42(1), Article 1.
4. Levinson, S. (2023). 'A structural connectivity atlas of limbic brainstem nuclei'. Frontiers in Neuroimaging, 1, 1009399.
5. Pasternak, O. (2009). 'Free water elimination and mapping from diffusion MRI'. Magnetic Resonance in Medicine, 62(3), 717–730.
6. Sudlow, C. (2015). 'UK Biobank: An Open Access Resource for Identifying the Causes of a Wide Range of Complex Diseases of Middle and Old Age'. PLOS Medicine, 12(3), e1001779.
7. World Health Organization. (2017). 'Depression and other common mental disorders: Global health estimates'. World Health Organization; WHO IRIS.

Poster No 507

Global Signal Topography Alterations and Gene Expression in Major Depressive Disorder

Huaijin Gao[1], Rui Qian[1], Wen Zhu[1], Chengjiaao Liao[1], Dan Wu[1], Zhiyong Zhao[1]

[1]Zhejiang University, Hangzhou, Zhejiang

Introduction: The global signal (GS) refers to the average signal of the gray matter voxels, reflecting an overall fluctuation of the global BOLD activity[1]. Conventionally, GS has been regarded as a non-neuronal signal, but recent evidence demonstrated its link to human cognition[2] and clinical diseases[1]. Transcription-neuroimaging association analyses have been used to uncover the genes associated with imaging phenotypes in the brain. Previous studies established connections between gene expression and functional changes in individuals with major depressive disorder (MDD)[3,4]. However, GS topography alteration in MDD patients and its genetic basis remain unclear. This study combined the Chinese REST-meta-MDD database and Allen Human Brain Atlas (AHBA) gene data to investigate the MDD-related alterations in GS topography and their associations with gene expression.

Methods: Resting-state fMRI data of 821 MDD patients and 757 NCs from the REST-meta-MDD consortium were screened and divided into three paired subgroups: 177 recurrent MDD (RMDD) and 392 NCs, 227 first-episode drug-naïve (FEDN) MDD and 388 NCs, and 117 FEDN and 72 RMDD. A standardized DPARSF processing parameters[5] was used to preprocess individual-level MRI image. Then, GS and averaged time series of each region were extracted for each subject by using a whole-brain grey matter mask and a Dos-160 atlas[6] respectively, and their Pearson correlation coefficients (GSCORR) were calculated as the indicator of GS topography[7]. We used linear mixed models to compare regional GSCORR differences between groups. Then, partial least squares (PLS) regression analysis was performed to detect the relationship between GSCORR alterations and gene expression from the AHBA[8] data. Finally, the genes were ranked based on their weights, and a Gene Ontology (GO) enrichment analysis was conducted using GOrilla (http://cbl-gorilla.cs.technion.ac.il). Benjamini-Hochberg false discovery rate (FDR) correction was used to control false discoveries.

Results: Total MDD and RMDD both showed decreased GSCORR in the temporal lobe, precentral gyrus, parietal lobe, and post occipital sulcus compared with NC. RMDD also showed decreased GSCORR in the ventral prefrontal cortex and inferior temporal lobe compared with NC and FEDN (Figure 1). No significant difference was observed between FEDN and NC. In the PLS regression analysis, the first gene component (PLS1), with the largest explained variance, showed distinct expression patterns in two MMD subtypes. Specifically, the PLS1 exhibited high expression in lateral cerebellum and precuneus for FEDN, and high expression in inferior parietal lobe and prefrontal cortex and low expression in middle insula for RMDD. Regional gene expressions of PLS1 were positively correlated with GS topography alterations in both FEDN and RMDD. Moreover, the PLS1 exhibited enrichment in biological processes related to learning or memory and neurotransmitter receptor activity in RMDD but not FEDN (Figure 2), and was enriched in biological processes related to synaptic transmission and neuron projection development in two MDD subgroups.

Conclusions: This study revealed decreased GSCORR in MDD-related regions in RMDD compared with NC and FEDN, which were not observed in FEDN compared to NC, suggesting these alterations may be associated with depression severity[5]. Consistent with previous studies[9], transcription-neuroimaging analyses exhibited an association between GSCORR changes and genes enriched in chemical synaptic transmission and neuron projection development. Moreover, the difference between FEDN and RMDD in GSCORR alterations might be associated with specific biological processes such as learning or memory and neurotransmitter receptor activity, which agreed with prior findings[10]. In summary, our findings suggest that first-episode and recurrent MDD show different alterations in GS topography, which may be supported by distinct molecular basis.

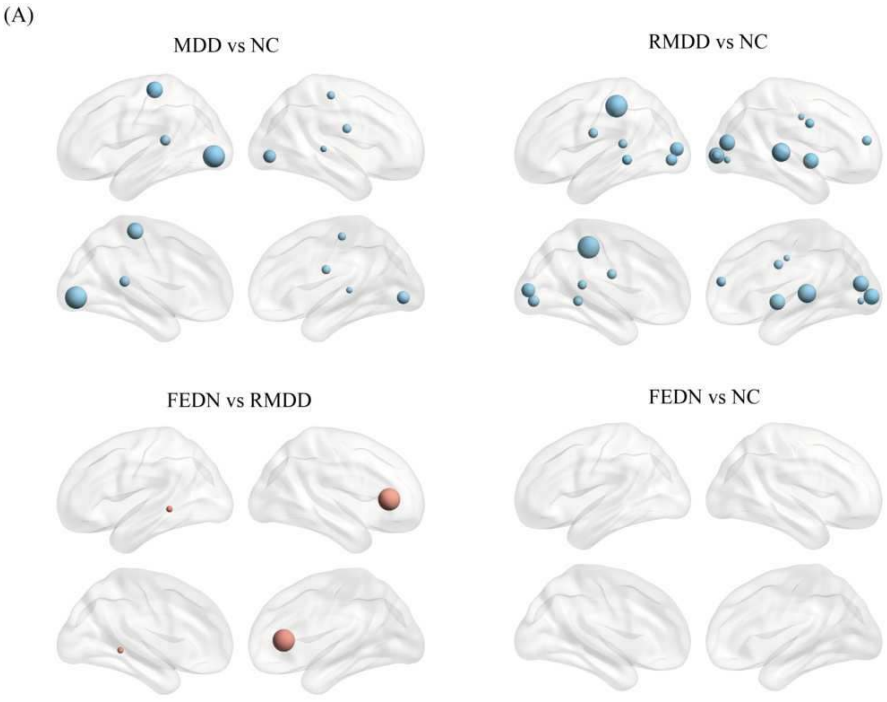

Figure 1. GSCORR differences between groups. The size and color (red/blue) of the node represents the t-value, and the change (increase/decrease) of GSCORR in former than latter groups, respectively.

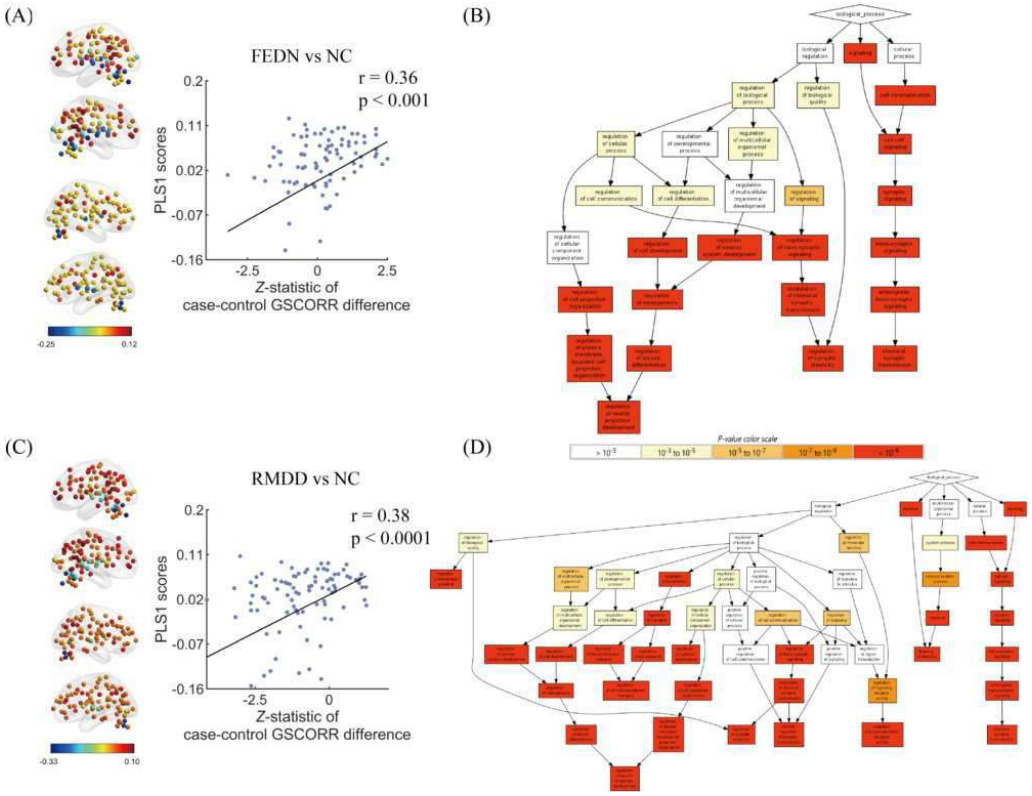

Figure 2. Association between GSCORR alterations and gene expression. Differences between FEDN and RMDD in PLS1 enrichment were involved in biological process of learning or memory and neurotransmitter.

References

1. Chen, Pindong (2023), "Altered Global Signal Topography in Alzheimer's Disease." eBioMedicine 89 (March): 104455.
2. Chen, Xiaodan (2018), "Topological Analyses of Functional Connectomics: A Crucial Role of Global Signal Removal, Brain Parcellation, and Null Models." Human Brain Mapping 39 (11): 4545–64.
3. Xue, Kaizhong (2022), "Local Dynamic Spontaneous Brain Activity Changes in First-Episode, Treatment-Naïve Patients with Major Depressive Disorder and Their Associated Gene Expression Profiles." Psychological Medicine 52 (11): 2052–61.
4. Zhu, Wenshuang (2023), "Genes Associated with Spontaneous Brain Activity Changes in Clinically Different Patients with Major Depressive Disorder: A Transcription-neuroimaging Association Study." CNS Neuroscience & Therapeutics, June, cns.14311.
5. Yan, Chao-Gan (2019), "Reduced Default Mode Network Functional Connectivity in Patients with Recurrent Major Depressive Disorder." Proceedings of the National Academy of Sciences 116 (18): 9078–83.
6. Dosenbach, Nico U. F. 2010. "Prediction of Individual Brain Maturity Using fMRI." Science (New York, N.Y.) 329 (5997): 1358–61.
7. Power, Jonathan D. (2012), "Spurious but Systematic Correlations in Functional Connectivity MRI Networks Arise from Subject Motion." NeuroImage 59 (3): 2142–54.
8. Hawrylycz, Michael J. 2012. "An Anatomically Comprehensive Atlas of the Adult Human Brain Transcriptome." Nature 489 (7416): 391–99.
9. Howard, David M. (2019), "Genome-Wide Meta-Analysis of Depression Identifies 102 Independent Variants and Highlights the Importance of the Prefrontal Brain Regions." Nature Neuroscience 22 (3): 343–52.
10. Xia, Mingrui (2022), "Connectome Gradient Dysfunction in Major Depression and Its Association with Gene Expression Profiles and Treatment Outcomes." Molecular Psychiatry 27 (3): 1384–93.

Poster No 508

Longitudinal Brain Age in First-Episode Mania Youth Treated with Lithium or Quetiapine

Laura Han[1], Niousha Dehestani[2], Chao Suo[3], Michael Berk[4], Lianne Schmaal[5]

[1]University of Melbourne, Melbourne, VIC, [2]Deakin University, Centre for Social and Early Emotional Development, School of Psychology, Faculty, Melbourne, Australia, [3]Turner Institute for Brain and Mental Health, School of Psychological Science and Monash Biomedical, Melbourne, Australia, [4]Deakin University, IMPACT, The Institute for Mental and Physical Health and Clinical Translation, Sc, Melbourne, Australia, [5]Centre for Youth Mental Health, The University of Melbourne, Parkville, VIC, Australia., Melbourne, Australia

Introduction: Bipolar disorder is increasingly viewed as a disorder involving deviations from typical brain development[1]. Treatment of the disorder may involve pharmacological therapy with lithium or quetiapine. However, it is unclear if these

agents have neuroprotective effects, especially in early stages of bipolar and schizoaffective disorders. If we can identify interventions with neuroprotective properties during the early stages of illness onset, i.e., after an initial first-episode of mania (FEM), we can potentially limit aberrations in neurodevelopmental trajectories. With these knowledge gaps in mind, we examined whether an age-related multivariate measure of brain structure (i.e., the brain age gap or BAG): a) differs in young individuals after a FEM compared to controls at baseline, b) improves following treatment, and c) is differentially affected by lithium or quetiapine. Finally, we explored whether improvements in clinical symptoms demonstrate parallel improvements in BAG, regardless of treatment.

Methods: Patients were randomized to lithium (n=21) or quetiapine (n=18) monotherapy[2]. T1-weighted scans were acquired at baseline, 3 months (patients only) and 12 months. Brain age predictions for controls (n=29) and patients (15-26 years) were derived using a deep learning model trained on one of the largest and most diverse assembled datasets to date (N=53,542; https://github.com/estenhl/pyment-public)[3]. To examine test-retest reliability of the predictions generated by the model, we evaluated the intraclass correlation coefficients (ICCs) between baseline and 12-month follow-up brain age and BAG in controls. To examine changes in BAG in response to treatment over time, we performed linear mixed models with BAG as outcome and treatment group (quetiapine, lithium), time (baseline, 3 months, 12 months), age, and sex as fixed effects, while estimating random effects for patient ID. To investigate potential differential effects of quetiapine versus lithium treatment, a treatment by time interaction was included. To explore whether changes in BAG were associated with changes in clinical measures in patients (regardless of treatment), we computed repeated measures correlations (rmcorr package in R)[4].

Results: A higher baseline BAG was found in FEM patients compared to controls (+1.86 year, p=0.04; Cohen's d=0.52 [SE=0.25], CI 95% [0.03 to 1.01]). Test-retest reliability was high for both brain age predictions: ICC=0.86, p<.0001 [95% CI: 0.72 - 0.93] and BAG: ICC=0.83, p<.0001 [0.67 - 0.91]. No significant effects of time or treatment group, nor any interaction between the two, were observed throughout the course of the study (Figure 1). Collapsed across treatment groups, significant longitudinal correlations were found between BAG and bipolar depression severity (rrm(51) = -0.30, 95% CI [-0.54, 0.16], p = 0.02)[5] and quality of life (QLS Total: rrm(49) = 0.32, 95% CI [-0.08, 0.52], p = 0.02)[6] in patients (Figure 2).

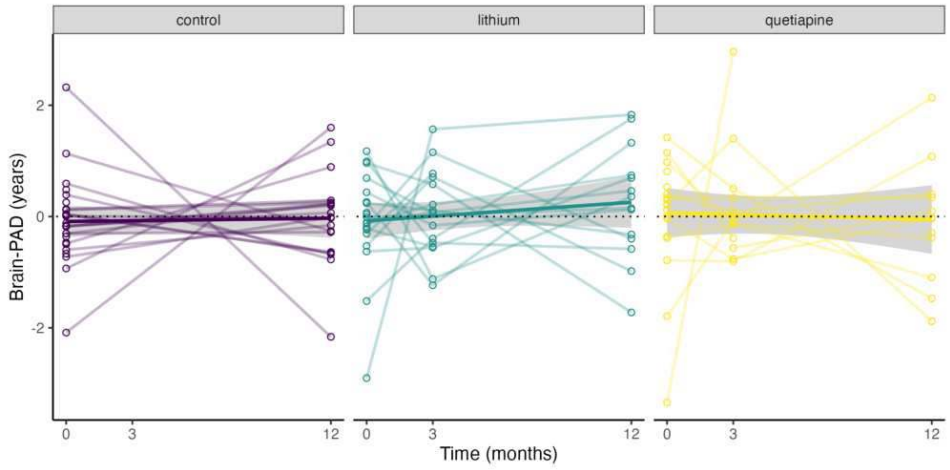

Figure 1. Longitudinal brain age gap by treatment group.

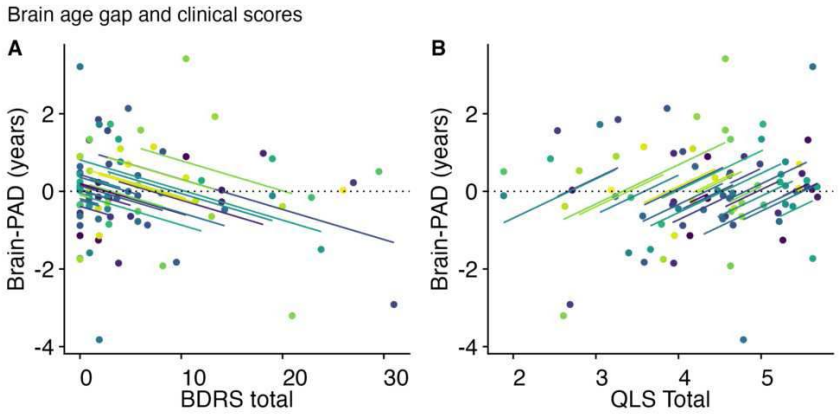

Figure 2. Longitudinal correlations between the brain age gap and clinical scores.

Conclusions: This is the first longitudinal study to characterize BAG following a FEM in young individuals receiving lithium or quetiapine treatment. At baseline, individuals showed older appearing brains compared to controls. However, BAG remained stable and administration of lithium or quetiapine did not change BAG during the first year following a FEM, regardless of treatment group. Longitudinal correlations between BAG and bipolar depressive symptoms, as well as quality of life were found, suggesting compensatory mechanisms. To understand whether potential reversible effects become apparent later in the trajectory of bipolar and schizoaffective disorders, a more extended follow-up period with a larger sample is warranted.

References

1. Kloiber, S. et al. Neurodevelopmental pathways in bipolar disorder. Neurosci. Biobehav. Rev. 112, 213–226 (2020).
2. Berk, M. et al. Quetiapine v. lithium in the maintenance phase following a first episode of mania: randomised controlled trial. Br. J. Psychiatry 210, 413–421 (2017).
3. Leonardsen, E. H. et al. Deep neural networks learn general and clinically relevant representations of the ageing brain. Neuroimage 256, 119210 (2022).
4. Bakdash, J. Z. & Marusich, L. R. Repeated Measures Correlation. Front. Psychol. 8, 456 (2017).
5. Berk, M. et al. The Bipolar Depression Rating Scale (BDRS): its development, validation and utility. Bipolar Disord. 9, 571–579 (2007).
6. Heinrichs, D. W., Hanlon, T. E. & Carpenter, W. T., Jr. The Quality of Life Scale: an instrument for rating the schizophrenic deficit syndrome. Schizophr. Bull. 10, 388–398 (1984).

Poster No 509

Orbitofrontal sulcal patterns in catatonia

Mylène Moyal[1], Alexandre Haroche[2], David Attali[1], Sylvain Charron[3], Clément Debacker[3], Boris Chaumette[1], Anton Iftimovici[1], Alice Le berre[1], Matthieu Raoelison[4], Ghita Dadi[1], Sylvain Leroy[1], Catherine Oppenheim[2], Arnaud Cachia[5], Marion Plaze[2]

[1]GHU Paris Psychiatrie et Neurosciences, Paris, Ile de France, [2]GHU Paris Psychiatrie et Neurosciences, Paris, France, [3]Institut de Psychiatrie et Neurosciences de Paris, Paris, France, [44]Université Paris Cité, Laboratory for the Psychology of Child Development and Education, CNRS, Paris, Ile de France, [5]LaPsyDé, Paris

Introduction: Catatonia is a psychomotor syndrome frequently observed in disorders with neurodevelopmental impairments, including psychiatric disorders such as schizophrenia. The orbitofrontal cortex (OFC) has been repeatedly associated with catatonia including GABAergic deficits during negative emotional processing and poor connectivity with medial prefrontal cortices along with reduced local cortical surface area and increased local gyrification index. The OFC presents with an important inter-individual morphological variability, with three distinct H-shaped sulcal patterns, type I, II, III, based on the continuity of the medial and lateral orbital sulci, see Figure 1. The OFC sulcal pattern are determined in utero, during third semester of gestation and previous studies reported a stability after birth of the sulcal pattern. As opposed to quantitative features of the cortical sheet (e.g., thickness, surface area or curvature) taking decades to reach the levels measured in adult, the qualitative sulcal patterns of the cortex anatomy in postnatal life are a proxy for earlier developmental events. Types II and III sulcal pattern have been identified as neurodevelopmental risk factors for schizophrenia. The sulcal pattern of the OFC has never been investigated in catatonia despite the role of the OFC in the pathophysiology of catatonia and the increasingly documented neurodevelopmental component of catatonia.

Methods: In this context, we performed a retrospective analysis of the OFC sulcal pattern in carefully selected homogeneous and matched subgroups of schizophrenia and schizo-affective patients with catatonia (N=58) or without catatonia (N=65), and healthy controls (N=82). The classification of OFC sulcal pattern followed the standard visual inspection procedure of Chiavaras and Petrides, based on the continuity of the medial orbital sulcus (MOS) and lateral orbital sulcus (LOS), see figure 1. Classification of the sulcal pattern type was blind to the diagnoses and the sulcal pattern in the contralateral hemisphere by 2 independent raters with 3D slicer sotfware. We added measure of global brain volume, found to be related to the sulcation of the prefrontal cortex to ensure that the difference in sulcal patterns was not related to brain size. Multinomial logistic regressions were used to compare the distribution of OFC sulcal pattern in the left and right hemispheres with group and gender as categorical factor and age as continuous covariate. Post-hoc comparisons, with Tukey correction for multiple tests, were used to investigate distribution differences between pairs of subgroups. This study was authorized by the data protection delegation of the GHU-Paris Psychiatry and Neurosciences under reference number D22-R003.

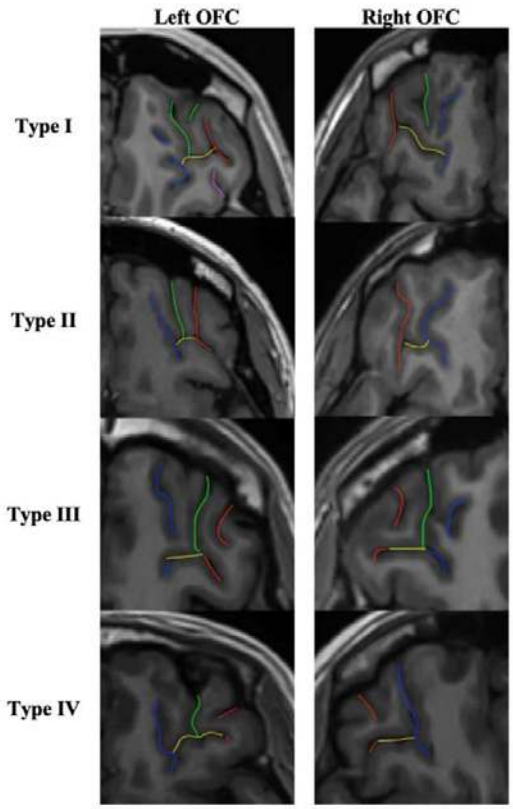

Figure. 1. OFC sulcal pattern classification. Red sulci= lateral orbital sulcus, blue sulci= medial orbital sulcus, yellow sulci= transverse orbital sulcus, green and purple= intermediate and posterior sulcus

Results: Logistic regression analyses revealed a group effect on OFC sulcal pattern in the left (χ^2=18.1; p<.001) and right (χ^2=28.3; p<.001) hemispheres, see Figure 2. Catatonia patients were found to have more type III and less type I in both hemispheres compared to healthy controls and more type III on the left hemisphere compared to schizophrenia patients without catatonia. In addition, the catatonia severity rating scale score was found to be higher in the type III (t ratio=-3.105; p=.02).

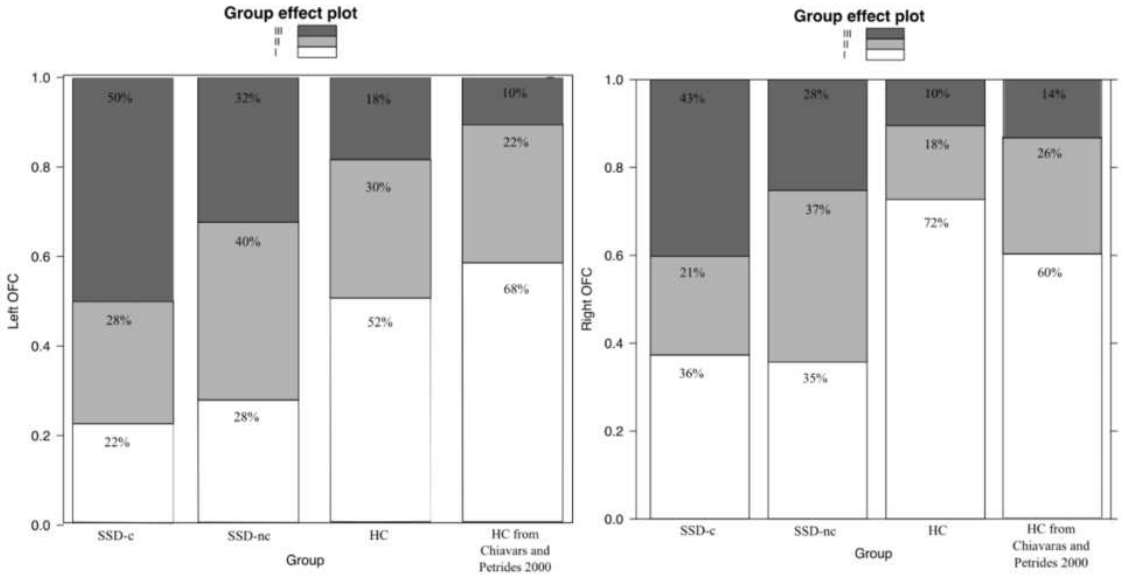

Figure. 2. OFC sulcal pattern distribution. Abbreviations: SSD=Schizophrenia; SSD-c=Schizophrenia patients with catatonia; SSD-nc=Schizophrenia patients without catatonia, HC=Healthy Control

Conclusions: This is the first study to provide evidence of abnormal OFC sulcal patterns in schizophrenia and schizo-affective patients with catatonia, with more type III than in healthy subjects and in patients without catatonia, supporting a neurodevelopmental component of catatonia, at least in schizophrenia and schizo-affective patients. Catatonia neurodevelopmental component is increasingly recognized and needs to be further investigate notably in non-psychosis catatonia patients. Such investigations aim to enhance patient characterization and delve deeper into the underlying pathophysiological mechanisms of catatonia.

References

1. Bartholomeusz, et al. 2013. « Sulcogyral Patterns and Morphological Abnormalities of the Orbitofrontal Cortex in Psychosis ». Progress in Neuro-Psychopharmacology and Biological Psychiatry 44 (juillet): 168-77. https://doi.org/10.1016/j.pnpbp.2013.02.010.
2. Cachia, et al. 2021. « Towards Deciphering the Fetal Foundation of Normal Cognition and Cognitive Symptoms From Sulcation of the Cortex ». Frontiers in Neuroanatomy 15 (septembre): 712862. https://doi.org/10.3389/fnana.2021.712862.
3. Chakirova et al. 2010. « Orbitofrontal Morphology in People at High Risk of Developing Schizophrenia ». European Psychiatry 25 (6): 366-72. https://doi.org/10.1016/j.eurpsy.2010.03.001.
4. Cropley et al. 2015. « Investigation of Orbitofrontal Sulcogyral Pattern in Chronic Schizophrenia ». Psychiatry Research: Neuroimaging 234 (2): 280-83. https://doi.org/10.1016/j.pscychresns.2015.09.001.
5. Hauptman et al. 2023. « Catatonia in Neurodevelopmental Disorders: Assessing Catatonic Deterioration from Baseline ». The Lancet Psychiatry, janvier, S2215036622004369. https://doi.org/10.1016/S2215-0366(22)00436-9.
6. Heckers et al. 2023. « Catatonia ». Édité par Allan H. Ropper. New England Journal of Medicine 389 (19): 1797-1802. https://doi.org/10.1056/NEJMra2116304.
7. Hirjak et al. 2019. « Cortical Contributions to Distinct Symptom Dimensions of Catatonia ». Schizophrenia Bulletin 45 (6): 1184-94. https://doi.org/10.1093/schbul/sby192.
8. Isomura et al. 2017. « Altered Sulcogyral Patterns of Orbitofrontal Cortex in a Large Cohort of Patients with Schizophrenia ». Npj Schizophrenia 3 (1): 3. https://doi.org/10.1038/s41537-016-0008-y.
9. Lavoie et al 2014. « Sulcogyral Pattern and Sulcal Count of the Orbitofrontal Cortex in Individuals at Ultra High Risk for Psychosis ». Schizophrenia Research 154 (1-3): 93-99. https://doi.org/10.1016/j.schres.2014.02.008.
10. Nakamura et al. 2020. « Orbitofrontal Sulcogyral Pattern as a Transdiagnostic Trait Marker of Early Neurodevelopment in the Social Brain ». Clinical EEG and Neuroscience 51 (4): 275-84. https://doi.org/10.1177/1550059420904180.
11. Northoff et al. 2004. « Orbitofrontal Cortical Dysfunction in Akinetic Catatonia: A Functional Magnetic Resonance Imaging Study During Negative Emotional Stimulation ». Schizophrenia Bulletin 30 (2): 405-27. https://doi.org/10.1093/oxfordjournals.schbul.a007088.
12. Northoff et al. 2002. « What Catatonia Can Tell Us about "Top-down Modulation": A Neuropsychiatric Hypothesis ». Behavioral and Brain Sciences 25 (5): 555-77.

Poster No 510

Brain criticality predicts PTSD psychotherapy response

Remko van Lutterveld[1], Myrthe Sterk[1], Cristian Spitoni[2], Elbert Geuze[1]

[1]Brain Research and Innovation Centre, Ministry of Defence, Utrecht, Netherlands, [2]Mathematical Institute, Utrecht University, Utrecht, Netherlands

Introduction: Trauma-focused psychotherapy is an effective treatment for post-traumatic stress disorder (PTSD). However, about half of patients are treatment resistant, which highlights the need for biomarkers of prospective treatment response. Recently, there is increased interest in characterizing the order and disorder of brain activity. Operating close to the border between order and disorder is theorized to present optimal information processing, and this can be analyzed using the concept of brain criticality. In the current study, we studied if brain criticality is related to prospective psychotherapy treatment response, hypothesizing that prospective treatment responders' brains operate closer to criticality.

Methods: Resting-state functional magnetic resonance imaging scans were acquired from 46 male veterans with PTSD around the start of treatment (median age 36 years). Therapy consisted of trauma-focused cognitive behavioral therapy (tf-CBT), eye movement desensitization and reprocessing (EMDR), or a combination thereof. Treatment response was assessed using the Clinician-Administered PTSD Scale, and criticality was assessed using Ising temperature, which was obtained by fitting the entire dataset to an Ising model, after which we personalized the obtained model by adusting the Ising temperature for each individual. Ising temperature was assessed for seven canonical brain networks (i.e., the visual, somatomotor, dorsal attention, ventral attention, limbic, frontoparietal and default mode networks). Differences between treatment responders and non-responders were statistically analyzed using a mixed ANOVA with age as covariate.

Results: Groups did not differ significantly in PTSD symptomatology, age, education level, handedness, type and amount of received treatment, and medication use. Criticality analysis showed that the brains of both groups operated in a supercritical state, and that prospective responders were closer to criticality than non-responders ($P = 0.014$), while no significant interaction effect between group and region was observed ($P = 0.608$).

Conclusions: The brains of prospective PTSD psychotherapy treatment responders operate closer to criticality than non-responders, and this effect seems to occur across the entire brain instead of in separate canonical brain networks. These results show that effective psychotherapy might be mediated by brains operating closer to criticality, resulting in increased information processing, which in turn facilitates effectiveness of psychotherapy.

Poster No 511

Beyond Theta-Beta Ratio: EEG Microstate D as a Target for ADHD Neurofeedback

Victor Férat[1], Marie-Pierre Deiber[2,3], Roland Hasler[2], Nader Perroud[2,3], Christoph Michel[1,4], Tomas Ros[1,4]

[1]Functional Brain Mapping Laboratory, Department of Fundamental Neurosciences, Geneva, Switzerland, [2]Department of Psychiatry, Faculty of Medicine, University of Geneva, Geneva, Switzerland, [3]Division of Psychiatric Specialties, Department of Psychiatry, University Hospitals of Geneva, Geneva, Switzerland, [4]Center for Biomedical Imaging, Lausanne, Switzerland

Introduction: Attention-Deficit/Hyperactivity Disorder (ADHD) is a mental disorder marked by persistent inattention, hyperactivity, and impulsivity, significantly impacting daily life. First-line treatments, like psychostimulants, though effective, come with side effects, leading some to seek alternatives for long-term remission. Neurofeedback (NFB), allowing self-regulation of neurophysiology, stands out. NFB, especially Theta-Beta ratio (TBR)-based protocols, has been common for ADHD. However, recent studies (Arns et al., 2018) challenge TBR's consistency in ADHD diagnosis, supported by a meta-analysis (Arns, 2014). This highlights the need for exploring new diagnostic and treatment markers. In a recent study (Férat et al., 2022a), EEG microstate analysis (Michel, 2018) emerged as a novel framework, revealing increased microstate D presence in ADHD individuals. Building on this, our study explores EEG microstate (Hernandez, 2015) D as a potential therapy for ADHD individuals. This research promises to enhance understanding and offer alternative, potentially more effective approaches in managing ADHD symptoms through neurofeedback interventions tailored to specific neurophysiological markers.

Methods: In this clinical study, a crossover design was employed. 19 participants with ADHD underwent two randomly ordered neurofeedback sessions, one aiming to increase microstate D and the other to decrease it. Comprehensive clinical assessments, self-report questionnaires, resting-state EEG recordings, and continuous performance tasks were administered before and after each neurofeedback session. EEG was continuously recorded throughout the 2 neurofeedback sessions using a 64 electrode cap.The five grand average EEG microstate topographies obtained from dataset 2 of Férat et al. 2022 (Férat et al., 2022a) were used as template to estimate in real time the coverage of microstate D. A score was estimated by comparing the real-time value to the one at rest. A visual feedback consisting of a rectangular gauge placed horizontally in the center of the screen was used to inform participants. When the feedback value was negative, the gauge filled linearly to the left, gradually filling completely for a feedback value of -1. Similarly, when the feedback value was positive, the gauge filled to the right, gradually filling completely for a feedback value of 1.

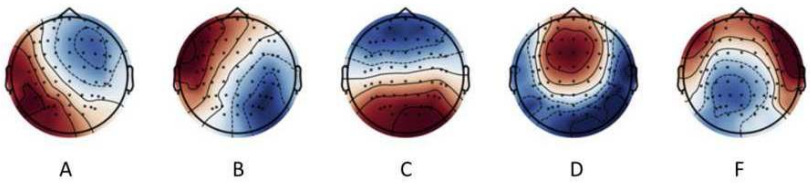

Figire. EEG microstate topographies

Results: Among the twenty individuals with ADHD enrolled, two dropped out before the neurofeedback sessions. After artifact rejection, data from 16 participants for the up-regulation session, 13 for the down-regulation session, and 12 for the comparative analysis of both were analyzed. During the up-regulation phase, a significant increase in the presence of microstate D was observed compared to baseline. However, no significant differences were found during the down-regulation phase. When comparing the two phases, a trend suggested the specificity of the neurofeedback protocol, with neurofeedback-specific effects observed. In addition, during each execution of the continuous performance task, an increase in the presence of microstate D was observed, regardless of the neurofeedback direction. No adverse effects were reported throughout the study.

Conclusions: These findings suggest that neurofeedback targeting microstate D does not induce significant adverse effects. The exclusion of some subjects highlights the technical intricacies of microstate neurofeedback, which heavily relies online

data quality. The non-specific results indicate the efficacy of the protocol in increasing the presence of microstate D in individuals with ADHD but less effectiveness in reducing it. The analyses underscore the potential specificity of microstate neurofeedback, with distinctions between up-regulation and down- regulation sessions. Moreover, the increased presence of microstate D during continuous performance tasks supports the existing literature on its association with attentional functions in the human brain.

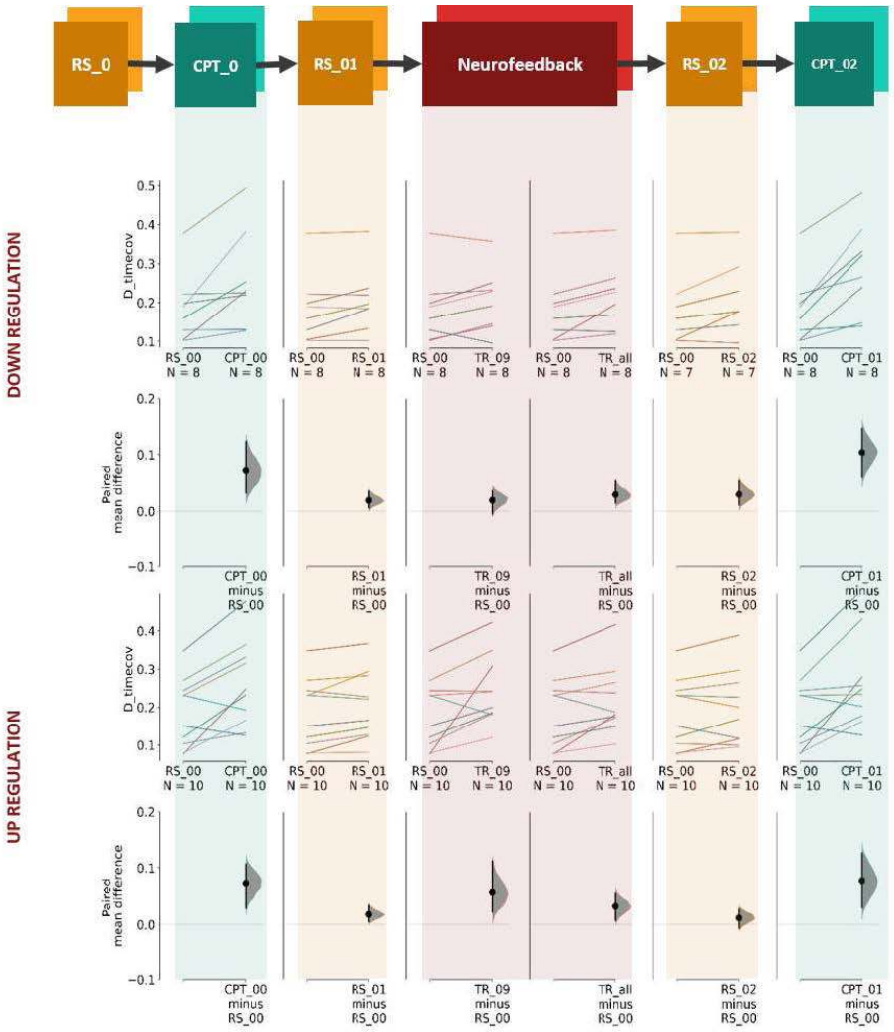

Figure. EEG microstate D time coverage during Up and Down regulation sessions and during each task

References

1. Arns, M. (2014), 'Evaluation of neurofeedback in ADHD: the long and winding road', Biological Psychology, vol. 95, pp. 108-115.
2. Arns, M. (2018), 'Electroencephalographic biomarkers as predictors of methylphenidate response in attention-deficit/hyperactivity disorder', European Neuropsychopharmacology, vol. 28, no. 8.
3. Férat, A. (2022a), 'Electroencephalographic microstates as novel functional biomarkers for adult attention-deficit/hyperactivity disorder', Biological Psychiatry: Cognitive Neuroscience and Neuroimaging, vol. 7, no. 8, pp. 814-823.
4. Férat, A. (2022b), 'Pycrostates: a Python library to study EEG microstates', Journal of Open Source Software, vol. 7, no. 78, p. 4564.
5. Hernandez, J. (2015), 'Towards using microstate-neurofeedback for the treatment of psychotic symptoms in schizophrenia: a feasibility study in healthy participants', Brain Topography, vol. 29, no. 2, pp. 308-332.
6. Michel, C. (2018), 'EEG microstates as a tool for studying the temporal dynamics of whole-brain neuronal networks: A review', NeuroImage, vol. 180, pp. 577-593.

Poster No 512

A possible white matter compensating mechanism of relatives of people affected by psychosis

Yaron Caspi[1]

[1]UMC Utrecht Brain Center, Department of Psychiatry, University Medical Center Utrecht, Utrecht, The Netherlands

Introduction: Extensive findings concerning subjects diagnosed with psychosis (D), their first-degree relatives, and the general population fit the 'Familial Risk' model. I.e., some alterations in the brain of the D group will be detected to a lesser extent in the brain of their relatives[1,2]. An alternative, though not mutually exclusive, model ('Compensating Mechanisms') suggests that relatives of the D group will exhibit some features different from those of the affected probands but also different from the general population[3]. Since such a model might represent some plasticity or resilience[3,4] features of the relatives' brains, it is valuable to consider the evidence. This abstract presents such evidence based on a recent publication[5].

Methods: We used the Diffusion Tensor Imaging (DTI) results from the three epochs of the Utrecht GROUP cohort. Namely, a D group (82 people), a control group (89 people), and relatives (all siblings) (122 people) that had two or three consecutive scans and passed our quality control[6,7]. For each individual, we averaged the results of the different epochs and calculated a set of diffusivity measures (for 48 distinct tracts) for four different diffusivity modes (Fractional Anisotropy (FA), mean diffusivity (MD), Axial Diffusivity (AD), and Radial Diffusivity (RD)), and a set of connectivity measures (thirteen graph matrix measures) for four different modes of connectivity matrix calculation: (a) deterministic tracking algorithm; (b) probabilistic tracking algorithm; (c) sampling FA along the tracts obtained from the deterministic algorithm; (d) sampling FA along the tracts obtained from the probabilistic algorithm. We analyzed these results (diffusivity and connectivity) on two levels. First, we used analysis of covariance (ANCOVA) Measure ~ Age + Ggroup followed by Tukey's test analysis (for representative results see Fig. 1). Second, we directly calculated the age-dependent epoch-averaged slope for each group, fitted the data to one out of three linear models (independent variables – Age, Age + Sex, Age + Sex + GROUP) based on quality of fit, and studied cases where the p-value of the model slope was below 0.05. Finally, we calculated scoring results for each diffusivity mode and the four connectivity matrix calculation methods. E.g., for the ANCONA analysis, the score was equal to ((0.05- T)*M) for each relevant measure from each analysis mode. T is the Tukey's False Discovery Rate (FDR) corrected p-value. The multiplication factor (M) was equal to 1, 0.5, and 1/3 for cases where only one, two, or three of the three group comparisons had a p-value below 0.05. Finally, we summed up the scores for all measures related to each diffusivity or connectivity analysis mode. Such scoring calculation, which represents the main results of this study, identified a general pattern of difference between the three groups.

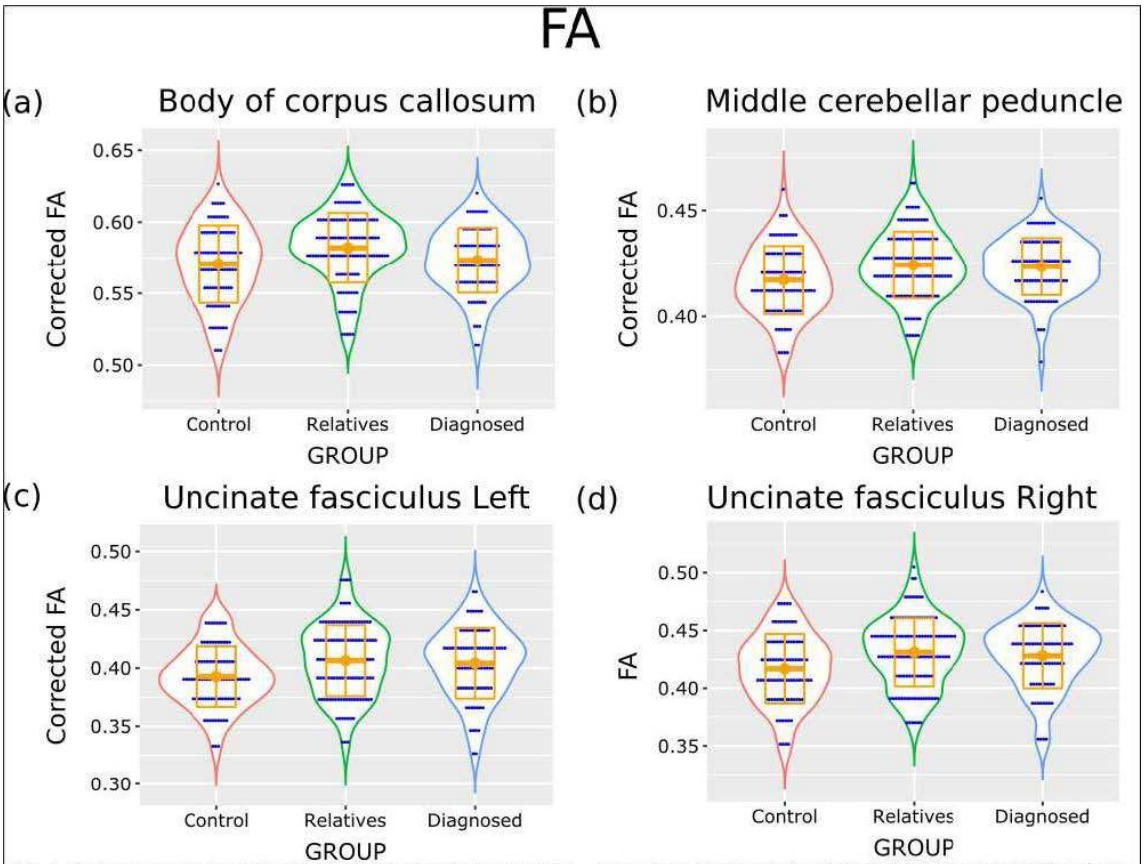

Fig. 1. **Tukey's test comparisons analysis of FA results — largest effect.** Violin plots for four corrected FA values measures that showed the larges Tukey's test difference (FDR corrected p-value below 0.05) when comparing one of the three possible comparisons between the different groups. I.e., the control-diagnosed groups, control-relatives groups, and relative-diagnosed groups. Orange squares represent the median data values, and orange boxes represent SD. For the body of the corpus callosum, the figure represents values after correction for sex and age. For the middle cerebellar peduncle and the left uncinate fasciculus the figures represent values after correction for sex alone. No correction was applied for the right uncinate fasciculus.

Results: For score results, see Fig. 2. For Tukey's test, the scoring results of the FA stood as an almost unique characteristic, showing scores sum differences between the relatives and the other two groups (mainly the general population). Only the scores sum of connectivity measures using deterministic tractography supports the 'Familial Risk' model. For the epoch-averaged slope analysis, only for AD and RD, the scoring system supports a naive 'Familial Risk' model where the value of the relatives' group is intermediate between that of the control and that of the diagnosed group. By contrast, the relatives' group showed either the most or the least epoch-averaged age-dependent behavior relative to the two other groups for FA, MD, and three of the four connectivity modalities.

	Tukey's test comparisons			Slope Analysis		
	C-D	R-D	C-R	C	R	D
FA	0	0.050±0.013 (0.075 ± 0.012)	**0.057±0.007 (0.623±0.018)**	0.188±0.013	**0.451±0.023**	0.282±0.023
MD	0	0	0	0048±0.016	0.033±0.016	**0.092±0.021**
AD	0	0	0	**0.261±0.015**	0.128±0.014	0.052±0.008
RD	0	0	0	0.057±0.016	0.131±0.036	**0.156±0.035**
Deterministic Connectivity	**0.155±0.026**	0	0	**0.100****	0*	0*
Deterministic Connectivity - FA along tracts Probabilistic	0	0	0	**0.332±0.043**	0.039±0.016	0.094±0.024
Probabilistic Connectivity	0	0	0	**0.066±0.026**	0*	0.004±0.002
Probabilistic Connectivity - FA along tracts	0	0	0	**0.285±0.035**	0*	0.006±0.003

Fig 2. - **Sum of Scores analysis.** C-D—aggregate comparison between the control and the diagnosed groups. R-D—aggregate comparison between the relatives and diagnosed groups. C-R—aggregate comparison between the control and relatives groups. C—control group. R - Relatives group. D—diagnosed group. For Tukey's test comparisons analysis, bold represents the largest value. For FA the value in the parenthesis represent similar analysis to the score analysis but including all tracts with FDR corrected p-value below 0.1 instead of 0.05. In this case, the formula for calculating the score was adjusted accordingly, replacing the value 0.05 by 0.1 (see "Methods" section). For the epoch-averaged slope analysis, bold represents the largest value, and an underline the smallest. *Standard deviation (SD) could not be calculated since all values are 0. **SD could not be calculated since there is only one value.

Conclusions: We showed evidence for a putative white matter-based structural compensation mechanism in relatives' brains. Such a mechanism might protect the relatives group against the deleterious load associated with their genetic background. These findings contribute to the growing discussion about brain plasticity in psychiatry[8].

References

1. Skudlarski P, Schretlen DJ, Thaker GK, Stevens MC, Keshavan MS, Sweeney JA, et al. (2013), 'Diffusion Tensor Imaging White Matter Endophenotypes in Patients With Schizophrenia or Psychotic Bipolar Disorder and Their Relatives', American Journal of Psychiatry, vol 170 no. 8, pp. 886–898
2. Hilker R, Helenius D, Fagerlund B, Skytthe A, Christensen K, Werge TM, et al. (2018), 'Heritability of Schizophrenia and Schizophrenia Spectrum Based on the Nationwide Danish Twin Register', Biological Psychiatry, vol 83 no. 6, pp. 492–498.
3. Dazzan P (2018), 'Not just risk: there is also resilience and we should understand its neurobiological basis'. Schizophrenia Research, vol. 193, pp. 293–294
4. Hess JL, Tylee DS, Mattheisen M, Børglum AD, Als TD, Grove J, et al. (2021), 'A polygenic resilience score moderates the genetic risk for schizophrenia'. Molecular Psychiatry, vol. 26 no. 3, pp. 800–815
5. Caspi Y (2022), 'A Possible White Matter Compensating Mechanism in the Brain of Relatives of People Affected by Psychosis Inferred from Repeated Long-Term DTI Scans'. Schizophrenia Bulletin Open, vol. 3, no. 1, pp. sgac055
6. Korver N, Quee PJ, Boos HBM, Simons CJP, de Haan L. (2012), 'Genetic Risk and Outcome of Psychosis (GROUP), a multi site longitudinal cohort study focused on gene-environment interaction: objectives, sample characteristics, recruitment and assessment methods', International journal of methods in psychiatric research, vol. 21, no. 3, pp. 205–221
7. Boos HBM, Mandl RCW, van Haren NEM, Cahn W, van Baal GCM, Kahn RS, et al. (2013), 'Tract-based diffusion tensor imaging in patients with schizophrenia and their non-psychotic siblings', European Neuropsychopharmacology, vol. 23, no. 4, pp. 295–304
8. Chen X, Tan W, Cheng Y, Huang D, Liu D, Zhang J, et al. (2023), 'Polygenic risk for schizophrenia and the language network: Putative compensatory reorganization in unaffected siblings', Psychiatry Research, vol. 326, pp. 115319

Poster No 513

Cortical morphometric similarity gradient in schizophrenia

Yong Han[1], Xiujuan Wang[2], Zhilu Zhou[3], Xue Li[4], Song Liu[5], Wenqiang Li[4], Luxian Lv[4], Yongfeng Yang[4]

[1]The Second Affiliated Hospital of Xinxiang Medical University, No.388, Jianshe Middle Road, Xinxiang, XinXiang, Henan, [2]The Second Affiliated Hospital of Xinxiang Medical University, Xinxiang, Xinxiang, [3]The Second Affiliated Hospital of Xinxiang Medical University, Xinxiang, Henan, [4]the Second Affiliated Hospital of Xinxiang Medical University, Xinxiang, HENAN, [5]The second affiliated hospital of Xinxiang medical university, xinxiang, Xinxiang City, Henan Province

Introduction: Recent research has indicated that functional network gradient changes are present in schizophrenia (SCZ). However, it is still completely unknown whether changes to the cortical morphometric similarity (MS) network gradient exist and how these changes relate to transcriptional profiles and clinical phenomenology.

Methods: The MS network was constructed in this study, and the gradient of the network was computed in 203 patients with SCZ and 201 healthy controls who shared the same demographics in terms of age and gender. To examine irregularities in the MS network gradient, between-group comparisons were carried out, and partial least squares regression analysis was used to study the relationships between the MS network gradient-based variations in SCZ and gene expression patterns and clinical phenotype.

Results: In contrast to healthy controls, the principal MS gradient of patients with SCZ was primarily significantly lower in sensorimotor areas, and higher in more areas. In addition, the aberrant gradient pattern was spatially linked with the genes enriched for neurobiologically significant pathways and preferential expression in various brain regions and cortical layers. Furthermore, there were strong positive connections between the principal MS network gradient and the symptomatologic score in SCZ individuals.

Conclusions: These findings showed changes in principal MS network gradient in SCZ and offered potential molecular explanations for the structural changes underpinning SCZ.

References

1. Marder, S.R. (2019), 'Schizophrenia', The New England journal of medicine, vol. 381, no.18,pp. 1753–1761
2. Chong, H.Y. (2016), 'Global economic burden of schizophrenia: a systematic review', Neuropsychiatric disease and treatment, vol. 12, pp. 357–373
3. Howes, O.D. (2014), 'Schizophrenia: an integrated sociodevelopmental-cognitive model', Lancet (London, England), vol. 383, no. 9929, pp. 1677–1687
4. Bora, E. (2011). 'Neuroanatomical abnormalities in schizophrenia: a multimodal voxelwise meta-analysis and meta-regression analysis', Schizophrenia research, vol. 127, no.1-3, pp. 46–57
5. Amann, B.L. (2016), 'Brain structural changes in schizoaffective disorder compared to schizophrenia and bipolar disorder', Acta psychiatrica Scandinavica,vol. 133, no. 1, pp. 23–33
6. Haijma, S.V. (2013), 'Brain volumes in schizophrenia: a meta-analysis in over 18 000 subjects', Schizophrenia bulletin, vol. 39, no. 5, pp. 1129–1138
7. Shepherd, A.M. (2012), 'Systematic meta-review and quality assessment of the structural brain alterations in schizophrenia', Neuroscience and biobehavioral reviews, vol. 36, no. 4, pp. 1342–1356
8. Winkler, A.M. (2010), 'Cortical thickness or grey matter volume? The importance of selecting the phenotype for imaging genetics studies', NeuroImage, vol. 53, no. 3, pp. 1135–1146
9. Margulies, D.S. (2016), 'Situating the default-mode network along a principal gradient of macroscale cortical organization', Proceedings of the National Academy of Sciences of the United States of America, vol. 113, no. 44, pp. 12574–12579

Poster No 514

Cognitive impairment in anti-LGI1 encephalitis is linked to structural brain network reorganization

Stephan Krohn[1], Leonie Müller-Jensen[2], Joseph Kuchling[2], Amy Romanello[1], Carsten Finke[1]

[1]Charité - Universitätsmedizin Berlin, Berlin, Germany, [2]Charité-Universitätsmedizin Berlin, Berlin, Berlin

Introduction: Anti-leucine-rich glioma-inactivated 1 encephalitis (LGI1-EN) represents a severe autoimmune disease of the central nervous system that frequently causes seizures, psychiatric symptoms, and long-term cognitive impairment. Although traditionally conceptualized as a form of "limbic" encephalitis, prior studies on (i) the persistence of cognitive symptoms and (ii) alterations of functional brain networks have increasingly suggested the involvement of extra-limbic brain structures in LGI1-EN. However, it remains largely unknown how cognitive impairment in LGI1-EN relates to structural brain networks connecting limbic and extra-limbic brain systems.

Methods: Here we applied diffusion-weighted neuroimaging to analyze the structural connectomes of 25 patients with LGI1-EN and 25 age-and sex-matched healthy control participants (HC). To this end, we used anatomically constrained probabilistic tractography with density normalization through participant-specific fiber density proportionality coefficients, resulting in weighted and symmetrical connectivity matrices. Topological characteristics of these matrices were assessed as node degree and betweenness centrality (BC) using the Brain Connectivity Toolbox. Moreover, we developed a new region-to-network mapping procedure, in which each anatomical region from the Desikan-Killiany atlas is assigned to a functional system from the Multiresolution Intrinsic Segmentation Template. Cognitive performance was assessed with standardized neuropsychological tests and summarized as composite scores in the domains of visuospatial memory, verbal episodic memory, attention, executive functions, and working memory. To analyze brain-wide connectome organization, we furthermore developed a novel topology deviation index (TDI), given by the nonparametric correlation distance between a whole-brain reference distribution of BC values in HC and each individual connectome.

Results: Patients with LGI1-EN exhibited a reduction in whole-brain structural connectivity ($t = -2.16$, $p = 0.036$, $d = -0.61$) as well as a characteristic pattern of cortico-subcortical hypoconnectivity beyond the limbic system: In line with previous findings,

connectivity reductions clustered in the hippocampus, but also strongly affected the caudate, accumbens, and thalamus as well as a variety of cortical areas including salience, frontoparietal, motor, default mode, and visual areas. Furthermore, LGI1-EN was characterized by a topological reorganization of structural brain networks, which involved a bidirectional shift in the relative importance of individual brain regions in the network (Fig. 1). Specifically, patients showed increased BC in the amygdala bilaterally as well as in a variety of cortical areas (strongest effects: inferior parietal cortex and parahippocampal gyrus). Conversely, patients showed decreased BC in deep gray matter areas, with strongest effects in the hippocampal formations. Here again, network mapping suggested that extra-limbic systems are strongly affected by this topological reorganization, most notably the salience and frontoparietal network. Importantly, this topological reorganization –as assessed by the TDI– was linked to cognitive impairment in a domain-specific manner (Fig. 2): While we observed no relationship between TDI and working memory or visuospatial memory, higher topological deviation in LGI1-EN was associated with impaired cognitive performance in the domains of attention ($r = -0.47$, $n = 21$, $p_{corr} = 0.050$), verbal episodic memory ($r = -0.57$, $n = 21$, $p_{corr} = 0.026$), and executive functions ($r = -0.60$, $n = 17$, $p_{corr} = 0.026$).

Conclusions: LGI1-EN is characterized by multi-domain cognitive impairment that is associated with a topological reorganization of structural brain networks. These findings link cognitive symptoms to structural alterations that go beyond individual brain regions and instead characterize LGI1-EN as a network disease that involves both limbic and extra-limbic brain systems.

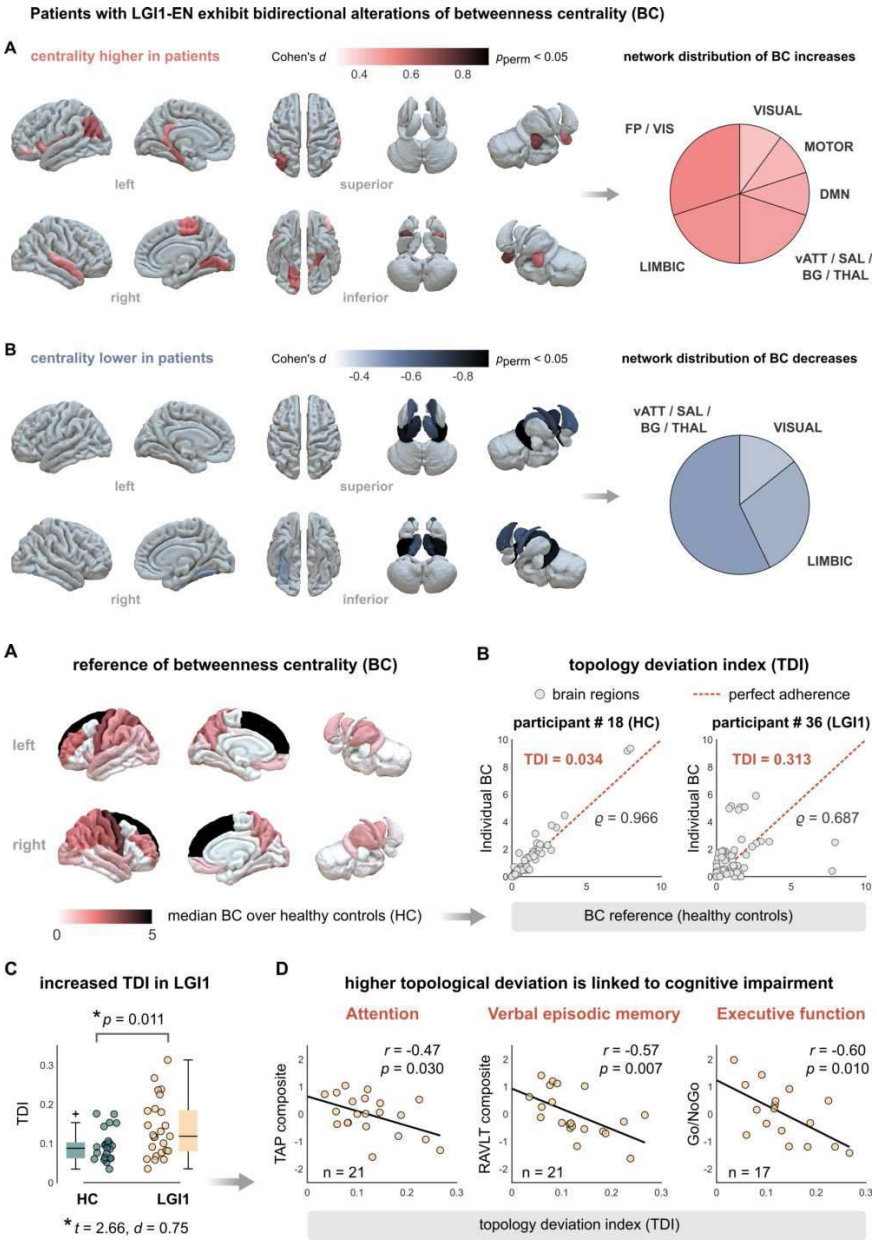

References
1. Desikan RS. An automated labeling system for subdividing the human cerebral cortex on MRI scans into gyral based regions of interest. NeuroImage. 2006;31(3):968-980. doi:10.1016/j.neuroimage.2006.01.021
2. Finke C. Evaluation of Cognitive Deficits and Structural Hippocampal Damage in Encephalitis With Leucine-Rich, Glioma-Inactivated 1 Antibodies. JAMA Neurol. 2017;74(1):50. doi:10.1001/jamaneurol.2016.4226
3. Heine J. Beyond the limbic system: disruption and functional compensation of large-scale brain networks in patients with anti-LGI1 encephalitis. J Neurol Neurosurg Psychiatry. 2018;89(11):1191-1199. doi:10.1136/jnnp-2017-317780
4. Tüzün E. Limbic Encephalitis and Variants: Classification, Diagnosis and Treatment. The Neurologist. 2007;13(5):261-271. doi:10.1097/NRL.0b013e31813e34a5
5. Urchs S. MIST: A multi-resolution parcellation of functional brain networks. MNI Open Res. 2019;1:3. doi:10.12688/mniopenres.12767.2

Poster No 515

Polygenic risk of depression and resting state connectivity of subgenual ACC in young adults

Huey-Ting Li[1], Yu Chen[2], Xingguang Luo[2], Jaime Ide[2], Chiang-Shan Li[2]

[1]Yale University, Hamden, CT, [2]Yale University School of Medicine, New Haven, CT

Introduction: Genetic variants may confer risks for depression by modulating brain structure and function. Converging evidence has associated depression with brain network dysfunction and highlighted the role of frontolimbic circuits in the pathophysiology of depression. In particular, prior evidence has underscored a key role of the subgenual anterior cingulate cortex (sgACC) in depression. However, the great majority of previous studies were conducted in clinical samples, where the effects of the duration, outcome, and comorbidities of depression could not be readily distinguished from those conferred by genetic risks. Here, we built on the literature and examined how the resting state functional connectivity (rsFC) of the sgACC was associated with polygenic risks (PRS) for depression in a neurotypical sample curated from the Human Connectome Project (HCP).

Methods: We followed published routines and computed seed-based whole-brain sgACC rsFC and PRS of 717 young adults curated from the HCP (a total of 489 subjects were excluded because of missing or questionable imaging or clinical data). The PRS was computed for individuals of the initial cohort of 1,206 young adults using a base sample of 170,756 unrelated cases with major depressive disorder and 329,443 unrelated healthy controls from the meta-analysis of GWAS of 33 UK Biobank cohorts of the Psychiatric Genomics Consortium (Howard et al., 2018). Participants completed the Achenbach Adult Self Report (Achenbach et al., 2003), including the DSM-oriented subscale of depression (14 items). The age- and sex- adjusted depression T score was used in the analyses, with higher T scores indicating higher severity of depressive symptoms. Participants were also evaluated with the Semi-Structured Assessment for the Genetics of Alcoholism (SSAGA). As in our previous studies (Li et al., 2022), we performed a principal component analysis on the 15 interrelated drinking metrics and identified one principal component (PC1) with an eigenvalue > 1 that accounted for 50.54% of the variance. SSAGA also collected household income data, which could serve as a surrogate of socioeconomic factors that may influence the development of depression. We performed whole-brain regression against PRS and severity of depression symptoms in a single model for all subjects and for men and women alone, controlling for age, sex (for all), race, drinking PC1, and household income, and evaluated the results at a corrected threshold. For findings obtained in men or women alone, we followed up with slope tests to confirm sex differences.

Results: In whole-brain regressions, higher PRS were correlated with weaker sgACC rsFC with bilateral superior frontal gyri (SFG) and bilateral precuneus/posterior cingulate cortex, and higher depression T scores were correlated with weaker rsFC between sgACC and right cerebellum (CBL) across all subjects (Fig. 1A). In men alone, higher PRS were correlated with stronger sgACC-left CBL and weaker sgACC-left SFG rsFC, and higher depression T scores were correlated with weaker sgACC rsFC with bilateral CBL and insula (Fig. 1B). In women alone, higher PRS were correlated with stronger sgACC rsFC with bilateral lingual and calcarine gyri (Fig. 1C). For those clusters identified in men and women alone, we confirmed sex differences in the correlations (with slope t's $\geq$ 2.40 and p's $\leq$ 0.017; Fig. 2).

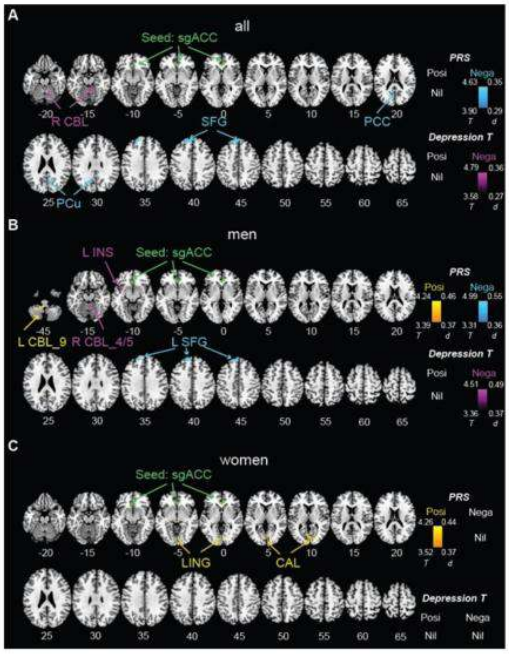

Figure 1. Seed-based whole-brain rsFC of sgACC (green) in correlation with polygenic risk score (PRS) and depression *T* score for **(A)** all subjects, **(B)** men, and **(C)** women. PRS and depression *T* score were modeled together, with age, sex (for all subjects), race, drinking principal component (PC1), and household income as covariates. The results were evaluated at voxel $p < 0.001$, uncorrected in combination with cluster $p < 0.05$ family-wise error (FWE) corrected. Warm color: in positive (Posi) correlation with PRS; Cool color: in negative correlation with PRS; Violet: in negative (Nega) correlation with depression score; Color bar shows voxel *T* and Cohen's *d* values. L: left; R: right; CBL: cerebellum; sgACC: subgenual anterior cingulate cortex; PCu: precuneus; PCC: posterior cingulate cortex; SFG: superior frontal gyrus; INS: insula; LING: lingual gyrus; CAL: calcarine sulcus.

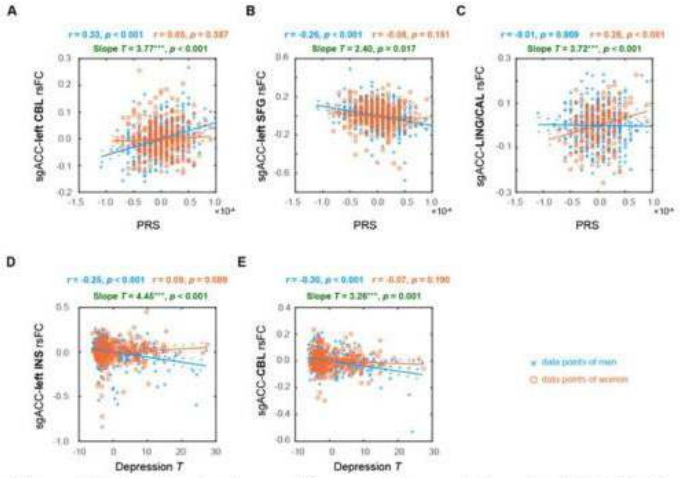

Figure 2. Scatter plots showing sex differences in the correlations of sgACC rsFC with PRS and depression *T* score. **(A)** PRS vs. sgACC-left CBL rsFC; **(B)** PRS vs. sgACC-left SFG rsFC; **(C)** PRS vs. sgACC-LING/CAL rsFC; **(D)** Depression *T* vs. sgACC-left INS rsFC; **(E)** Depression *T* vs. sgACC-CBL rsFC. The data points represent residuals. Solid and dashed lines (men: in blue; women: in orange) represent the regressions and 95% confidence intervals, respectively. The coefficients *r* and *p* values for the correlations as well as slope *t* and *p* values for sex differences in the correlations are presented on top of each panel. Slope test $^{***}p < 0.05/5 = 0.01$ for multiple comparisons. *Note*: sgACC: subgenual anterior cingulate cortex; rsFC: resting state functional connectivity; PRS: polygenic risk score; CBL: cerebellum; SFG: superior frontal gyrus; LING: lingual gyrus; CAL: calcarine gyrus; INS: insula.

Conclusions: Our findings collectively highlighted the pivotal role of distinct sgACC-based networks in the genetic predisposition to depression and the clinical manifestation of depression. The findings also suggest sex differences in the neural markers of the genetic risks of depression. Distinguishing the risk from severity markers of depression may have implications in developing early diagnostics and effective treatments for individuals at risk for depression.

References

1. Achenbach, T.M., Dumenci, L., Rescorla, L., 2003. Ratings of relations between DSM-IV diagnostic categories and items of the Adult Self-Report (ASR) and Adult Behavior Checklist (ABCL). Research Center for Children, Youth and Families.
2. Howard, D.M., Adams, M.J., Shirali, M., Clarke, T.-K., Marioni, R.E., Davies, G., Coleman, J.R., Alloza, C., Shen, X., Barbu, M.C., 2018. Genome-wide association study of depression phenotypes in UK Biobank identifies variants in excitatory synaptic pathways. Nature communications 9, 1470.
3. Li, G., Chen, Y., Chaudhary, S., Tang, X., Li, C.R., 2022. Loss and frontal striatal reactivities characterize alcohol use severity and rule-breaking behavior in young adult drinkers. Biol Psychiatry Cogn Neurosci Neuroimaging. 7(10):1007-1016.

Poster No 516

Investigating Glymphatic Dysfunction in Neuropsychiatric Systemic Lupus Erythematosus by dMRI

Yi Ting Hsieh[1], Chih-Chin Heather Hsu[2], Ni-Jung Chang[3], Jyh-Wen Chai[3], Ching-Po Lin[2,4]

[1]School of Medicine, College of Medicine, National Yang Ming Chiao Tung University, Taipei, Taiwan, [2]Institute of Neuroscience, National Yang Ming Chiao Tung University, Taipei, Taiwan, [3]Department of Radiology, Taichung Veterans General Hospital, Taichung, Taiwan, [4]Department of Education and Research, Taipei City Hospital, Taipei, Taiwan

Introduction: Neuropsychiatric systemic lupus erythematosus (NPSLE) significantly impacts the nervous system and mortality rates. Despite the typical presentation of white matter hyperintensity (WMH) on routine MRI scans in NPSLE patients, the macrostructure appears normal in 50% of cases, posing challenges in disease assessment and treatment[1]. Previous research has proposed that the NPSLE autoantibodies can traverse the blood-brain barrier and induce glymphatic system abnormalities[2]. Additionally, NPSLE patients commonly experienced hypoperfusion in the area served by the middle cerebral artery (MCA)[3,4]. In this study, we investigated regional variations in three glymphatic system stages in NPSLE patients without abnormal WMH: 1) perivascular space (PVS) enlargement depicted by PVS mapping; 2) interstitial fluid stagnation assessed by free water (FW) mapping; and 3) decrease in glymphatic clearance efficiency evaluated by diffusion tensor image analysis along the perivascular space (ALPS). Our goal is to identify imaging biomarkers indicative of NPSLE, as well as improve its diagnosis and treatment.

Methods: There were 27 female patients (age 22-63 y/o) in the NPSLE group and 34 age-matched females in the normal control group (NC). All participants underwent cognitive assessment, including Montreal Cognitive Assessment (MoCA), Mini Mental Status Examination (MMSE), and Frontal Assessment Battery (FAB). MRI images were acquired on a Siemens MAGNETOM Aera 1.5T MRI scanner, including 1 mm...3 isotropic T1w image (TR/TE=2800/3.98 ms, TI=930 ms), T2w image (TR/TE=3000/280 ms), FLAIR image (TR/TE=5000/350 ms, TI=1800 ms), and diffusion-weighted image (TR/TE=10000/107 ms, 30 directions with NEX=3). Firstly, the UBO detector[5] was used for WMH mapping. Next, an enhanced contrast method[6] with automatic PVS quantification[7] was utilized for PVS mapping. The PVS volume was normalized by total intracranial volume as PVS volume fraction (PVSVF). Single shell FW algorithm was used via DIPY (https://dipy.org/). The mean FW values calculation excluded the PVS and WMH maps[8]. ALPS evaluated the diffusivity along the medullary perivenous space in the plane of the lateral ventricle body[9]. The 3D brain MRI arterial atlas[10] was applied on WMH, PVS, and FW for evaluation of regional variation. Last, we analyzed group differences by the Mann-Whitney U test with Bonferroni correction for multiple comparisons.

Results: NPSLE and NC groups showed age-related increases in brain WMH volume without significant group differences (Fig. 1A). There were no differences between groups in whole brain PVSVF and FW mean values (Fig. 1B and 1C). In arterial subregions: medial lenticulostriate (MLS) of anterior cerebral artery (ACA) and lateral lenticulostriate (LLS) of MCA, FW mean values were significantly higher in the NPSLE group (Fig. 1E). ALPS reduced significantly in the NPSLE group (Fig.1D). In the cognitive assessment results for the NPSLE group (Fig. 2), whole brain PVSVF and WMH volume negatively correlated with all assessments, while ALPS and FW correlated positively. Only PVSVF had a significant negative correlation with MMSE. In ACA subregion, significant negative correlations were between MMSE and PVSVF and between MoCA and WMH volume, while MoCA positively correlated with FW.

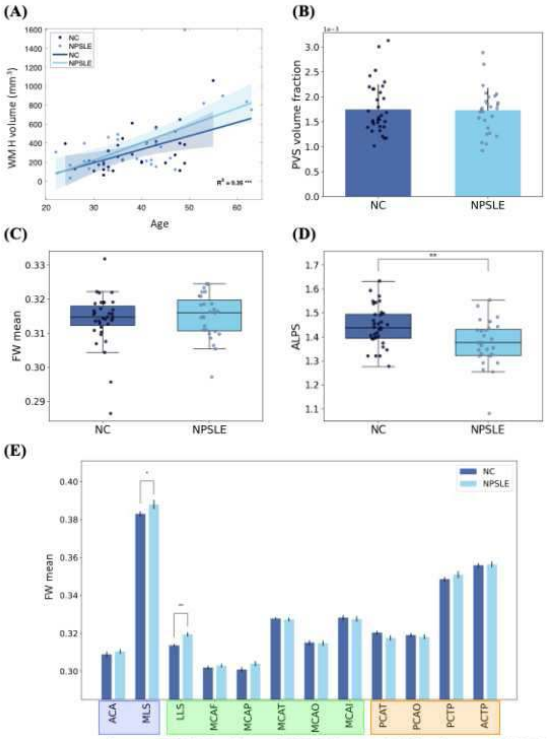

Fig.1 The group comparison of WMH volume, PVSVF, mean FW values and ALPS. (A) Age-related WMH volume change. Fitting curves with a 95% CI are separated into two colors representing different groups. (B, C, D) group differences in PVSVF, mean FW and ALPS. Asterisks are shown if there are significant differences between the two groups. *p<0.05, **<0.01. (E) mean FW differences in arterial subregions. Subregions can be grouped into three main arterial supplies: ACA (colored in blue), MCA(colored in green), and PCA (colored in orange). Asterisks are shown if there are significant differences between the two groups. *p<0.05, **<0.05 with Bonferroni correction.

NPSLE: Neuropsychiatric systemic lupus erythematosus ; NC: normal control; WMH:white matter hyperintensity ; PVSVF: perivascular space volume fraction ;FW: free water; ALPS: diffusion tensor image analysis along the perivascular space ; ACA: Anterior Cerebral Artery ; MCA: Middle Cerebral Artery ; PCA: Posterior Cerebral Artery ;

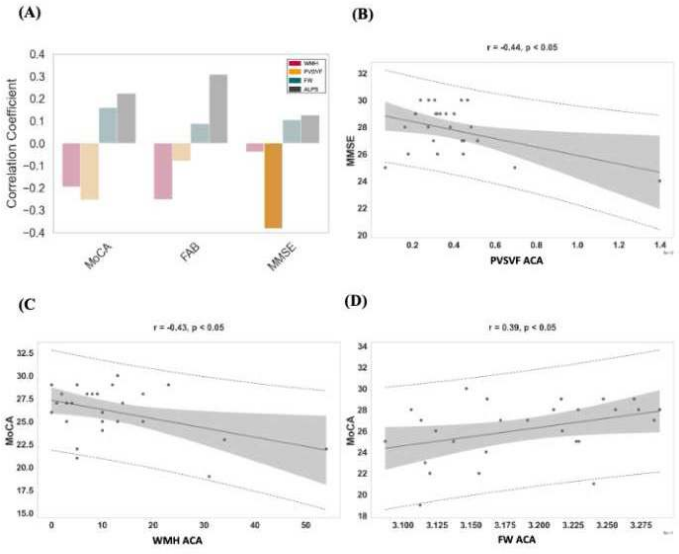

Fig.2 Correlations between glymphatic image markers and cognitive assessments of the NPSLE group. (A) The correlations between image markers and cognitive assessments. The translucent bars indicate a lack of significant correlations. (B, C, D) Significant correlations between image markers and cognitive assessments are found in the ACA region. The dashed line represents the 95% prediction limits and the grey patch indicates 95% confidence limits. The solid line is the fitting line of the data.

WMH: white matter hyperintensity; PVSVF: perivascular space volume fraction; FW: free water; ALPS: diffusion tensor image analysis along the perivascular space; ACA: Anterior Cerebral Artery.

Conclusions: The study unveiled the glymphatic abnormalities in NPSLE patients. While global PVSVF showed no significant differences, localized glymphatic dysfunction in specific arterial subregions, along with reduced waste clearance efficiency, were evident in NPSLE patients. Cognitive assessments suggested glymphatic abnormalities may contribute to NPSLE-related cognitive impairment. Correlation trends with ALPS and PVSVF support glymphatic dysfunction's role in cognitive decline. Intriguingly, a positive FW correlation challenged prior assumptions of the expectations of deteriorating brain function. Our findings provide valuable insights into the pathophysiology of NPSLE.

References

1. Bertsias, G. K.(2010). Pathogenesis, diagnosis, and management of neuropsychiatric SLE manifestations. Nat Rev Rheumatol, vol. 6, no. 6, pp. 358-367.
2. Ota. (2022). Central Nervous System Systemic Lupus Erythematosus: Pathophysiologic, Clinical, and Imaging Features. Radiographics, vol. 42, no. 1, pp. 212-232.
3. Shen. (1999). Regional Cerebral Blood Flow in Patients with Systemic Lupus Erythematosus, Journal of Neuroimaging, vol. 9
4. Tian. (2022). The Underlying Role of the Glymphatic System and Meningeal Lymphatic Vessels in Cerebral Small Vessel Disease. Biomolecules, vol. 12, no.6, pp.748.
5. Jiang. (2018). UBO Detector - A cluster-based, fully automated pipeline for extracting white matter hyperintensities. Neuroimage, vol. 174, pp. 539-549.
6. Sepehrband. (2019). Image processing approaches to enhance perivascular space visibility and quantification using MRI. Sci Rep, vol. 9, no. 1, pp. 12351.
7. Frangi. (1998). Multiscale vessel enhancement filtering. In: Wells, W.M., Colchester, A., Delp, S. (eds) Medical Image Computing and Computer-Assisted Intervention. MICCAI'98. MICCAI 1998. Lecture Notes in Computer Science, vol 1496.Springer, Berlin, Heidelberg.
8. Smith. (2004). Advances in functional and structural MR image analysis and implementation as FSL. Neuroimage, vol. 23, Suppl 1, S208-219.
9. Taoka. (2017). Evaluation of glymphatic system activity with the diffusion MR technique: diffusion tensor image analysis along the perivascular space (DTI-ALPS) in Alzheimer's disease cases. Jpn J Radiol, vol. 35, no. 4, pp. 172-178.
10. Liu. (2023). Digital 3D Brain MRI Arterial Territories Atlas. Sci Data, vol. 10, no. 1, pp. 74.

Poster No 517

Pathways linking physical and mental health: The role of brain structure and lifestyle factors

Ye Tian[1], Andrew Zalesky[2]

[1]University of Melbourne, Carlton South, Victoria, [2]The University of Melbourne, Melbourne, Victoria

Introduction: Depression and anxiety are common mental health problems. They are not only highly comorbid with each other; the prevalence of depression and anxiety is also high in individuals with a chronic physical health condition. Multiple putative biological and psychosocial pathways have been proposed, attempting to explain the link between physical and mental health problems. However, the brain is rarely considered in these models, albeit that depression and anxiety are commonly associated with alterations in brain structure and function. We sought to understand mechanisms of neurobiology in the concurrent manifestation of physical and mental health.

Methods: Multimodal brain imaging (structural and diffusion-weighted MRI), physiological, blood- and urine-derived markers from 18, 128 individuals (7,455 males) participating in the UK Biobank were used in this study. Physical health was assessed for each body organ (cardiovascular, pulmonary, musculoskeletal, immune, renal, hepatic and metabolic) using organ-specific phenotypes (40-70 years, mean 53.7 ± 7.3). Brain imaging was acquired at 4-14 years follow-up (45-83 years, mean 62.7 ± 7.5). Normative models were used to assess the extent to which each individual's organ health and function deviated from an age- and sex-specific normative references ranges (mean and centiles). Structural equation modeling was used to test the significance of pathways from physical health to mental health via structural alterations in brain gray and white matter. Lifestyles factors that can influence symptoms of depression, anxiety and neuroticism via influencing organ health and brain structure were identified.

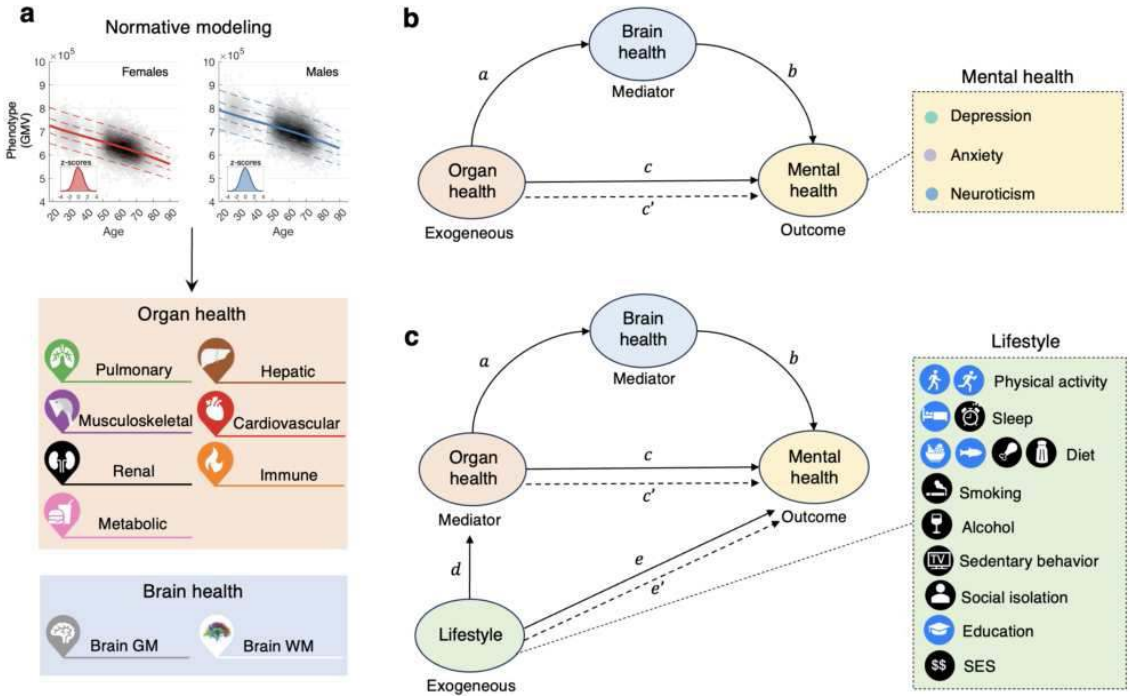

Results: We found multiple significant pathways through which poor organ health may lead to poor brain health, which in turns lead to poor mental health. In general, the brain showed strong mediating effect on organs that had strong direct effect on mental health outcome, which is mostly exemplified by the musculoskeletal and immune systems. However, specific pathways were observed linking specific organ systems and mental health, exemplified by pulmonary and cardiovascular systems. Specifically, we found that GM showed significant mediating effect on pulmonary-depression and pulmonary-neuroticism but not pulmonary-anxiety associations, whereas WM showed significant mediating effect on associations of cardiovascular-anxiety and cardiovascular-neuroticism, but not cardiovascular-depression. We found that lifestyle exposure had impact on depression and neuroticism via influencing organ health and brain structure. However, the mediation effects were not significant for anxiety. Significant pathways were identified for all 7 organ systems for depression via GM, but not via WM. In contrast, significant pathways leading to neuroticism were mainly through WM and were evident for 5 organ systems including immune, musculoskeletal, metabolic, hepatic and pulmonary system. Notably, we found that while some lifestyle factors, including physical activity, sedentary behavior, diet, sleep quality, degree of education and socioeconomic inequality, influenced mental health via influencing multiple body and brain systems, some other lifestyle factors, particularly of smoking and alcohol intake, had more specific path affecting mental health through metabolic and pulmonary system, and musculoskeletal and hepatic system, respectively.

Conclusions: In conclusion, our work provides an integrated model linking physical health, neurobiology and mental health outcome. Our findings suggest a crucial role of the brain in mediating the relationship between physical and mental health, which is an important step toward bridging the mind-body dualism. The modifiable lifestyle factors identified from this study can potentially inform the development of targeted interventions to improve both physical and mental health synergistically.

References

1. Kessler, R.C., et al. Anxious and non-anxious major depressive disorder in the World Health Organization World Mental Health Surveys. Epidemiol Psychiatr Sci 24, 210-226 (2015).
2. Gold, S.M., et al. Comorbid depression in medical diseases. Nature Reviews Disease Primers 6, 69 (2020).
3. Roy-Byrne, P.P., et al. Anxiety disorders and comorbid medical illness. Gen Hosp Psychiatry 30, 208-225 (2008).
4. Schmaal, L., et al. Cortical abnormalities in adults and adolescents with major depression based on brain scans from 20 cohorts worldwide in the ENIGMA Major Depressive Disorder Working Group. Molecular psychiatry 22, 900-909 (2017).
5. Harrewijn, A., et al. Cortical and subcortical brain structure in generalized anxiety disorder: findings from 28 research sites in the ENIGMA-Anxiety Working Group. Translational psychiatry 11, 502 (2021).
6. Winter, N.R., et al. Quantifying Deviations of Brain Structure and Function in Major Depressive Disorder Across Neuroimaging Modalities. JAMA psychiatry 79, 879-888 (2022).
7. van Velzen, L.S., et al. White matter disturbances in major depressive disorder: a coordinated analysis across 20 international cohorts in the ENIGMA MDD working group. Molecular psychiatry 25, 1511-1525 (2020).

Poster No 518

Multimodal-based machine learning approach to classify features of addiction using EEG

Ji-Yoon Lee[1], Myeong Seop Song[1], Woo-Young Ahn[1], Jung-Seok Choi[2]

[1]Seoul National University, Seoul, Korea, Republic of, [2]Samsung Medical Center, Seoul, Korea, Republic of

Introduction: Addictions have recently been classified as substance use disorder (SUD) and behavioral addiction (BA), but the concept of BA is still debatable. Therefore, it is necessary to conduct further neuroscientific research to understand the mechanisms of BA to the same extent as SUD. The present study used machine learning (ML) algorithms to investigate the neuropsychological and neurophysiological aspects of addictions in individuals with internet gaming disorder (IGD) and alcohol use disorder (AUD).

Methods: We developed three models for distinguishing individuals with IGD from those with AUD, individuals with IGD from healthy controls (HCs), and individuals with AUD from HCs using ML algorithms, including L1-norm support vector machine, random forest, and L1-norm logistic regression (LR). Three distinct feature sets were used for model training: a unimodal-electroencephalography (EEG) feature set combined with sensor- and source-level feature; a unimodal-neuropsychological feature (NF) set included sex, age, depression, anxiety, impulsivity, and general cognitive function, and a multimodal (EEG + NF) feature set.

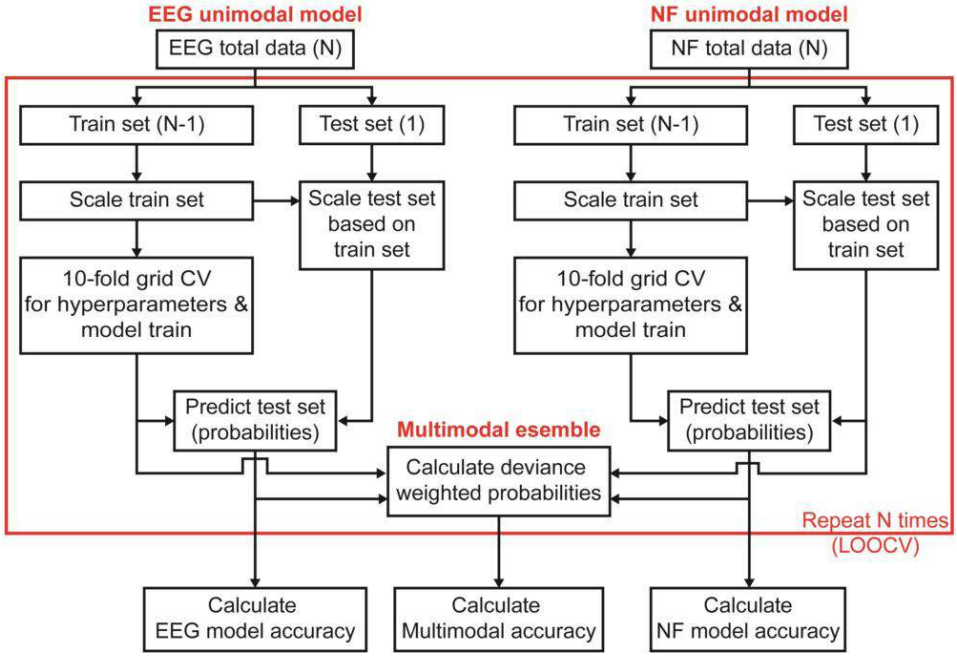

Fig. 1. Flowchart for calculating the accuracy of each algorithm and illustration of different feature set combinations based on cross-validation (CV) deviances.

Results: The LR model with the multimodal feature set used for the classification of IGD and AUD outperformed the other models (accuracy: 0.712). The important features selected by the model highlighted that the IGD group had differential delta and beta source connectivity between right intrahemispheric regions and distinct sensor-level EEG activities. Among the NFs, sex and age were the important features for good model performance.

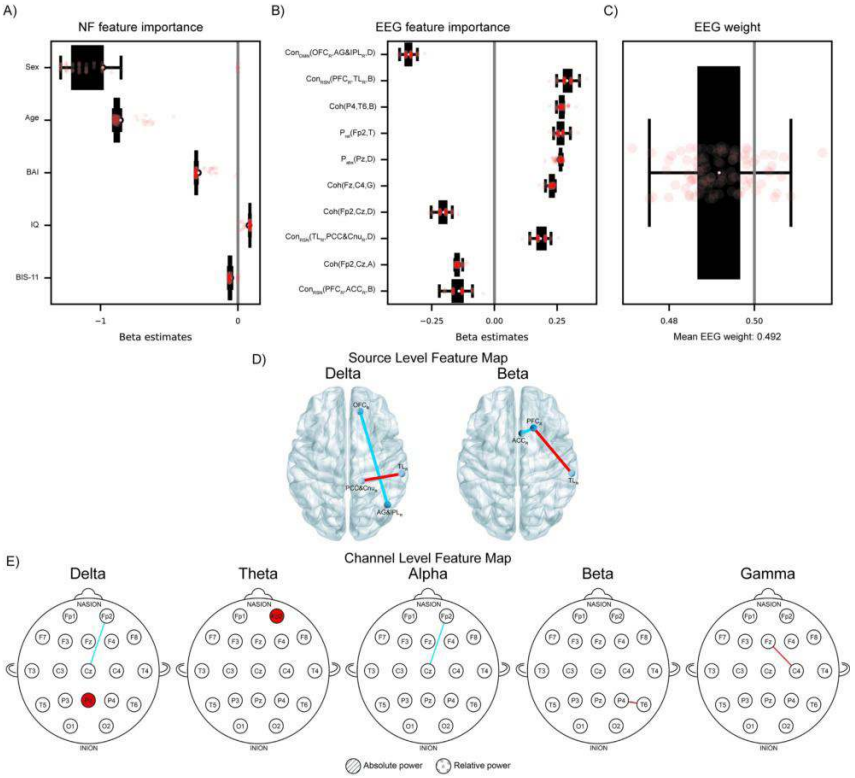

Fig. 2. Feature importance according to beta coefficients: comparison between internet gaming disorder (IGD) and alcohol use disorder (AUD).

Conclusions: This is the first study to develop ML models to distinguish among patients with IGD, patients with AUD, and HCs using multimodal feature sets, including sensor- and source-level EEG and NFs. In particular, the changes delta and beta source-level FC within the right hemisphere can serve as a neurophysiological indicator for distinguishing between IGD and AUD. Notably, individuals with IGD and AUD have similar neuropsychological symptoms despite their dissociable neurophysiological mechanisms. Furthermore, the multimodal ML model for distinguishing IGD from HCs emphasizes the potential utility of ML models for diagnosing IGD. In conclusion, our findings enhance our understanding of the utility of ML techniques for detecting IGD based on neurophysiological and neuropsychological similarities and differences between IGD (a BA) and AUD (a SUD).

References

1. Alavi, S. S. (2012). Behavioral Addiction versus Substance Addiction: Correspondence of Psychiatric and Psychological Views. International Journal of Preventive Medicine, 3(4), 290-294.
2. Choi, S. W. (2014). Similarities and differences among Internet gaming disorder, gambling disorder and alcohol use disorder: a focus on impulsivity and compulsivity. Journal of Behavioral Addictions, 3(4), 246-253. https://doi.org/10.1556/JBA.3.2014.4.6.
3. Kamarajan, C. (2020). Random Forest Classification of Alcohol Use Disorder Using EEG Source Functional Connectivity, Neuropsychological Functioning, and Impulsivity Measures. Behavioral Sciences, 10(3), 62. https://doi.org/10.3390/bs10030062.
4. Kinreich, S. (2021). Predicting risk for Alcohol Use Disorder using longitudinal data with multimodal biomarkers and family history: a machine learning study. Molecular Psychiatry, 26(4), 1133-1141. https://doi.org/10.1038/s41380-019-0534-x.
5. Lee, J. Y. (2022). Enhanced resting-state EEG source functional connectivity within the default mode and reward-salience networks in internet gaming disorder. Psychological Medicine, 52(11), 2189-2197. https://doi.org/10.1017/S0033291722000137.
6. Mumtaz, W. (2018). A review on EEG-based methods for screening and diagnosing alcohol use disorder. Cognitive Neurodynamics, 12(2), 141-156. https://doi.org/10.1007/s11571-017-9465-x.
7. Park, M. (2020). Neurophysiological and Cognitive Correlates of Error Processing Deficits in Internet Gaming Disorder. Cerebral Cortex, 30(9), 4914-4921. https://doi.org/10.1093/cercor/bhaa083.
8. Park, S. M. (2021). Identification of Major Psychiatric Disorders From Resting-State Electroencephalography Using a Machine Learning Approach. Frontiers in Psychiatry, 12. https://doi.org/10.3389/fpsyt.2021.707581.
9. Park, S. M. (2020). Respiratory sinus arrhythmia biofeedback alters heart rate variability and default mode network connectivity in major depressive disorder: A preliminary study. International Journal of Psychophysiology, 158, 225-237. https://doi.org/10.1016/j.ijpsycho.2020.10.008.
10. Park, S. M. (2017). Neural connectivity in Internet gaming disorder and alcohol use disorder: A resting-state EEG coherence study. Scientific Reports, 7(1), 1333. https://doi.org/10.1038/s41598-017-01419-7.
11. Son, K. L. (2015). Neurophysiological features of Internet gaming disorder and alcohol use disorder: a resting-state EEG study. Translational Psychiatry, 5(9), e628-e628. https://doi.org/10.1038/tp.2015.124.

Poster No 519

ECT-related textural change in the gray matter of the limbic system in psychosis patients

Eugenie Choe[1,2], Minah Kim[1,3], Jun Soo Kwon[4,1,3]

[1]Department of Neuropsychiatry, Seoul National University Hospital, Seoul, Korea, Republic of, [2]Department of Clinical Pharmacology and Therapeutics, Seoul National University College of Medicine, Seoul, Korea, Republic of, [3]Department of Psychiatry, Seoul National University College of Medicine, Seoul, Korea, Republic of, [4]Department of Brain and Cognitive Sciences, Seoul National University College of Natural Sciences, Seoul, Korea, Republic of

Introduction: Even though electroconvulsive therapy (ECT) is an important treatment modality for psychosis, ECT in psychosis is relatively less investigated than in depression. It is evident from non-human studies that ECT may induce histopathological alterations of the gray matter. While most studies that investigated structural changes in the brain related to ECT exposure in psychotic patients focused on macrostructural changes, such as volumetric change, such macrostructural measures are relatively crude to capture more subtle changes, such as tissue characteristics. We therefore adopted texture analysis, a methodology widely used to reflect microstructures of the brain in many pathological conditions (e.g. brain tumor, Alzheimer's disease, etc.), as a way to non-invasively quantify microstructural changes induced by ECT in psychosis patients. Especially, we focused on the limbic system, which is widely known to be involved in the effect of ECT in depression, a psychiatric condition more extensively explored in studies on ECT. Hence, we hypothesized that, in psychosis patients also, there would be microstructural changes in the gray matter of the limbic system after ECT and those changes would be correlated with clinical response.

Methods: Our dataset includes 36 schizophrenia or schizoaffective disorder patients who were treated with both ECT and medication, and 27 patients treated with medication only. Structural MRI data were acquired before and after ECT from the ECT group, and from the medication only group, twice with time interval same as that of the ECT group. After preprocessing and segmentation or parcellation, regions of interest (ROI) that constitute the limbic system were identified. For each ROI, each timepoint, and each participant, gray matter volume was estimated, and MRI texture was computed using Gray Level Size Zone Matrix (GLSZM). After feature selection from multiple interdependent GLSZM features, group-time interactions of change in volume and texture features were estimated with repeated-measures mixed model. Repeated-measures correlations between clinical variables and texture features that showed statistically significant group-time interactions were calculated. Statistical significance was set as FDR-adjusted $p < 0.05$.

Results: Among twelve ROIs that constitute the limbic system, seven showed significant group-time interactions in terms of volumetric change. Among the GLSZM texture-ROI pairs, group-time interactions of Large Area Emphasis of left hippocampus and that of right amygdala reached statistical significance. For the ECT group, repeated-measures correlation revealed negative correlation between changes in multiple clinical variables and changes in Large Area Emphasis feature for both left hippocampus and right amygdala. On the other hand, medication only group did not show any significant correlation between clinical changes and changes in texture. There was also significant positive correlation between volumetric changes and change in texture in the ECT group.

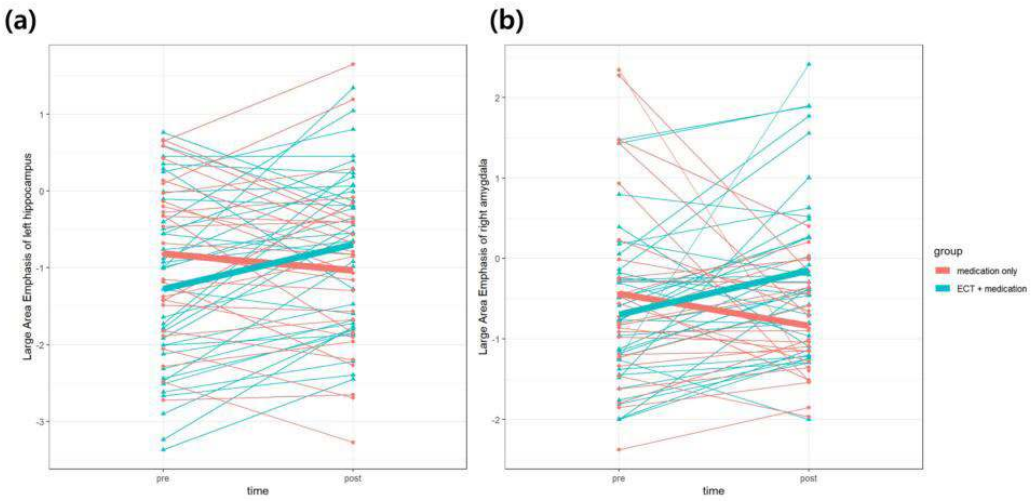

Figure 1 Group-time interaction in (a) Large Area Emphasis of left hippocampus, and (b) Large Area Emphasis of right amygdala
Thick lines represent the mean of every path in each group.

Conclusions: Our data is in accordance with the literature in which hippocampus and amygdala have repeatedly been mentioned as key regions of ECT-related macrostructural alterations, regardless of the diagnosis of interest. Our results additionally suggest that these regions undergo more subtle, microstructural changes, and these changes are correlated with clinical response. Our study therefore implies that alteration in limbic structures constitutes a key role in the effect of ECT not only in depression but also in psychosis. It also supports that change in tissue characteristics as a result of ECT-induced neuroplasticity is one of the core mechanisms of ECT.

References

1. Cano, M. (2023), 'Understanding the Mechanisms of Action of Electroconvulsive Therapy: Revisiting Neuroinflammatory and Neuroplasticity Hypotheses', JAMA Psychiatry, vol. 80, no. 6, pp. 643-644
2. Kassner, A. (2010), 'Texture Analysis: A Review of Neurologic MR Imaging Applications', American Journal of Neuroradiology, vol. 31, no. 5, pp. 809-816
3. Leaver, A.M. (2022), 'Parsing the Network Mechanisms of Electroconvulsive Therapy', Biological Psychiatry, vol. 92, pp. 193-203
4. Lee, S. (2020), 'Magnetic Resonance Imaging Texture Predicts Progression to Dementia due to Alzheimer Disease Earlier than Hippocampal Volume', Journal of Psychiatry and Neuroscience, vol 45, no. 1, pp. 7-14
5. Jiang, Y. (2022), 'Structural and Functional MRI Brain Changes in Patients with Schizophrenia Following Electroconvulsive Therapy: A Systematic Review', Current Neuropharmacology, vol 20, pp. 1241-1252
6. Moon, S.Y. (2023), 'Magnetic Resonance Texture Analysis Reveals Stagewise Nonlinear Alterations of the Frontal Gray Matter in Patients with Early Psychosis', Molecular Psychiatry, online ahead of print
7. Moon, S.Y. (2021), 'Systematic Review of the Neural Effect of Electroconvulsive Therapy in Patients with Schizophrenia: Hippocampus and Insula as the Key Regions of Modulation', Psychiatry Investigation, vol. 18, no. 6, pp. 486-499

Poster No 520

Sustained Attention Evokes Disordered Topology in Brain Connectomics in OCD

Mario Yacou[1], John Kopchick[2], Phillip Easter[3], David Rosenberg[3], Vaibhav Diwadkar[3]

[1]Wayne State University, Sterling Heights, MI, [2]Wayne State University, Department of Psychiatry, Detroit, MI, [3]Wayne State University, Detroit, MI

Introduction: Obsessive-compulsive disorder (OCD) is characterized by excessive anxiety-inducing thoughts (obsessions) leading to repetitive anxiety-reducing behaviors (compulsions); these symptoms can impact cognitive domains like attention (Menzies et al., 2007). Indeed, our recent work in OCD shows how variations in sustained attention demand impact effective connectivity in the ascending thalamocortical relay (Yacou et al., 2022). However, these impacts have not been investigated using connectomic measures such as graph theory (Rubinov & Sporns, 2010). Our current investigation addresses this lacuna. Here we used graph theoretic analysis to characterize dysfunctional topology of brain network repertoires in OCD. Topology was studied by focusing on changes in the Betweenness Centrality (BC) of nodes under varying attention demand. BC was chosen because as a metric for approximating the number of the shortest functional paths that traverse through the node, it provides a lucid index of a node's integrative role in the network (Rubinov & Sporns, 2010).

Methods: Thirty-eight OCD subjects (Age: 11.08 – 22.81 yrs.; Mean Age: 16.53 yrs.; 18 males) and 44 healthy controls (HC, Age: 11.16 – 23.53 yrs.; Mean Age: 16.30 yrs.; 21 males) provided informed consent or assent to participate in the fMRI study (Siemens Verio 3T) using a modified version of the Continuous Performance Task, Identical Pairs (CPT-IP) (Figure 1). Participants detected repeating instances of rapidly presented two-digit or three-digit numbers (50 ms, 250 ms SOA) blocked into extended trials (120 s duration). The extended blocks were specifically used to induce sustained attention over extended periods of activity. Numerical magnitude (2- or 3-digit) provided a simple manipulation of attention demand. fMRI data were processed using typical methods (SPM12). For each participant and condition, fMRI time series were extracted from the 246-nodes and following summarization of functional connectivity (zero lag bivariate correlations), BC of each node was estimated. Then, on each node, we conducted a two-factor ANOVA to investigate main effects of group (OCD ≠ HC), the main effect of attentional load (Low ≠ High), and, of specific interest in this study, any interactions between the two factors (group and attentional load).

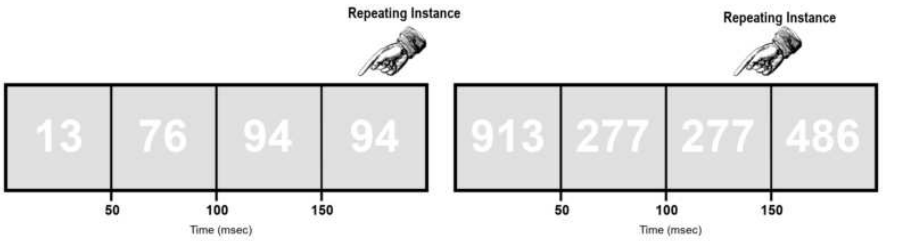

(a) Task paradigm depicting the 2-digit (low) attention demand condition

(b) Task paradigm depicting the 3-digit (high) attention demand condition

Figure 1

(a) and (b). The paradigm employed and the low and high demand conditions are schematically depicted. Participants performed a continuous performance task, identical pairs version (CPT-IP) task paradigm, and identified repeating instances of either 2- or 3-digit numbers (blocked in 120 s epochs). The magnitude of targets constitutes a parametric manipulation of attention demands: low (2-digit) or high (3-digit) attention demand.

Results: The most salient results from the ANOVA revealed nine nodes with statistically significant interactions between group and attention demand (Figure 2). As seen, in six frontal-parietal lobes, the insula and the putamen, an increase in attention demand lead to an increase in the integrative importance in HC but a decrease in the same in OCD. In a single thalamic node, we observed an inverse pattern.

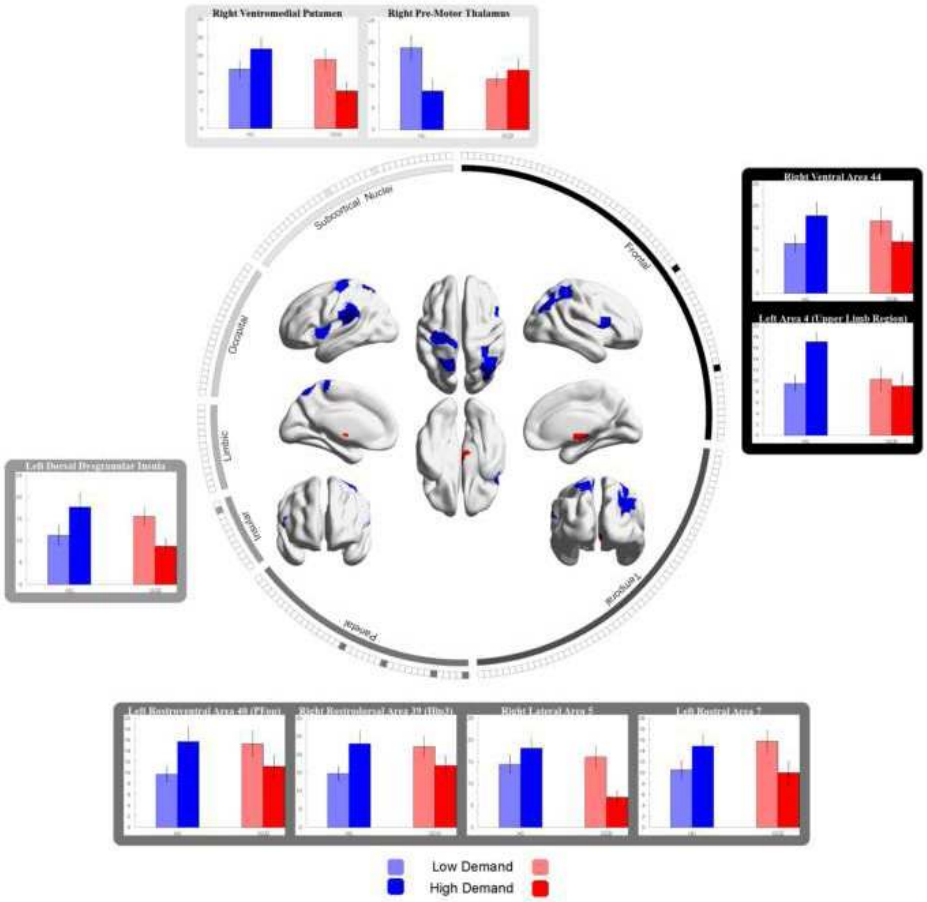

Figure 2

Figure showcases nine brain nodes where statistically significant interactions between the two independent variables (group & attentional load) on the dependent variable (Betweenness Centrality (BC)). The statistical results were obtained from a 2-factor ANOVA on BC means and plotted as nine unique column graphs. Within each column graph, low attentional demand load is indicated as a translucent red (OCD) or blue (HC) color. In contrast, the high attention demand load is indicated as a solid red (OCD) or blue (HC) color. Inside the connectome, the brain maps visually depict the overall interaction effect: 1) blue shading indicates a direct relationship for HC and an inverse relationship for OCD (i.e., as attentional load increases from low to high, BC decreases in OCD) 2). While red shading indicates an inverse relationship for HC and a direct relationship for OCD, which occurred in only one node (Right Pre-Motor Thalamus). The inner circle is divided into seven segments indicating the brain region (i.e., Frontal). Grayscale is also used to indicate each segment, with grayscale intensity increasing in a clockwise order (Black to white). The outer circle further divides each segment into their individual, respective nodes (246 nodes total).

Conclusions: To our knowledge, this is the first evidence of task-induced disruptions in the network topology of the OCD brain, and our work complements and extends upon existing applications of graph theory to the resting state (Li et al., 2022). It appears that the OCD brain does not flexibly increase the integrative role of key frontal, parietal and striatal regions in response to increases in attention demand. Conversely, an aberrant increase in the BC of thalamic nodes in OCD suggests a replication of the abnormalities of the ascending relay (from the thalamus to the cortex) previously discovered in the disorder. More generally, given that the brain is prepared to flexibly respond to imposed tasks (Park & Friston, 2013), a combination of graph theory and parametric tasks can reveal compelling expressions in psychiatric conditions (Meram et al., 2023).

References

1. Li, X., Li, H., Jiang, X., Li, J., Cao, L., Liu, J., . . . Gong, Q. (2022). Characterizing multiscale modular structures in medication-free obsessive-compulsive disorder patients with no comorbidity. Hum Brain Mapp, 43(7), 2391-2399. doi: 10.1002/hbm.25794
2. Menzies, L., Achard, S., Chamberlain, S. R., Fineberg, N., Chen, C. H., del Campo, N., . . . Bullmore, E. (2007). Neurocognitive endophenotypes of obsessive-compulsive disorder. Brain, 130(Pt 12), 3223-3236. doi: 10.1093/brain/awm205
3. Meram, E. D., Baajour, S., Chowdury, A., Kopchick, J., Thomas, P., Rajan, U., . . . Diwadkar, V. A. (2023). The topology, stability, and instability of learning-induced brain network repertoires in schizophrenia. Network Neuroscience, 7(1), 184-212. doi: 10.1162/netn_a_00278
4. Park, H. J., & Friston, K. (2013). Structural and functional brain networks: from connections to cognition. Science, 342(6158), 1238411. doi: 10.1126/science.1238411
5. Rubinov, M., & Sporns, O. (2010). Complex network measures of brain connectivity: uses and interpretations. Neuroimage, 52(3), 1059-1069. doi: 10.1016/j.neuroimage.2009.10.003
6. Yacou, M. A., Chowdury, A., Easter, P., Hanna, G. L., Rosenberg, D. R., & Diwadkar, V. A. (2022). Sustained attention induces altered effective connectivity of the ascending thalamo-cortical relay in obsessive-compulsive disorder. Front Psychiatry, 13, 869106. doi: 10.3389/fpsyt.2022.869106

Poster No 521

Effects of continuous theta burst stimulation in mild-to-moderate obsessive compulsive disorder

Junjie Bu[1], Yueling Liu[1], Rui Ni[2], Jiafang Liu[1], Chunyan Zhu[1]

[1]Anhui Medical University, Hefei, Anhui, [2]Imperial College London, London, London

Introduction: Obsessive-compulsive disorder (OCD) is a clinically heterogeneous psychiatric disorder characterized by pathologically activated brain activity. Currently, first-line treatments for OCD fail to bring response in up to 60% of patients, indicating the refractory nature of OCD. Meanwhile, over 70% of the patients have only mild-to-moderate severity, their symptoms will develop into severe OCD without timely treatment, resulting in a greater burden on clinical treatment. Continuous theta burst stimulation (cTBS) can non-invasively induce inhibitory effects on the underlying cortex; hence, it is considered a potential treatment for inhibiting aberrantly hyperactivated brain regions in patients with obsessive-compulsive disorder (OCD). This is the first study to investigate the effectiveness of cTBS in the treatment of mild-to-moderate OCD in a preliminary study with an external validation design across two centers.

Methods: In the first preliminary experiment conducted at the Hangzhou Seventh People's Hospital Center (Hangzhou, China), 50 inpatients with DSM-5 (Diagnostic and Statistical Manual, 5th edition) diagnosis of OCD, having a total Yale-Brown Obsessive-Compulsive Scale (YBOCS) score of >16 or obsession/compulsion subscale of >10, were enrolled to receive cTBS (10 sessions/day for five continuous days) or sham over the personalized right pre-supplementary motor area (preSMA) based on the functional connectivity map of the PreSMA and the subthalamic nucleus according to prior research by our group[1]. Each session contained 1800 pulses in a continuous train of 600 theta bursts, while each burst contained three pulses at 50 Hz, repeated at 5 Hz. Patients in the sham group received stimulation through a placebo coil, which led to similar skin sensations and significantly reduced biological activity compared with active stimulation. In the external validation experiment conducted at the Anhui Mental Health Center (Hefei, China), 32 outpatients with lesser OCD severity received a cTBS session per day for 15 consecutive days to generalize the treatment effects. Each session contained 1800 cTBS pulses. According to previous study, responders are defined as patients who showed a ≥35% decrease in YBOCS and remission as patients who showed a post-treatment YBOCS score of ≤14. OCD can be classified as mild, moderate, or severe: mild, 6–15 points (O-YBOCS or C-YBOCS 6–9 points); moderate, 16–25 points (O-YBOCS or C-YBOCS 10–14 points); severe, ≥25 points (O-YBOCS, YBOCS, or C-YBOCS >15 points).

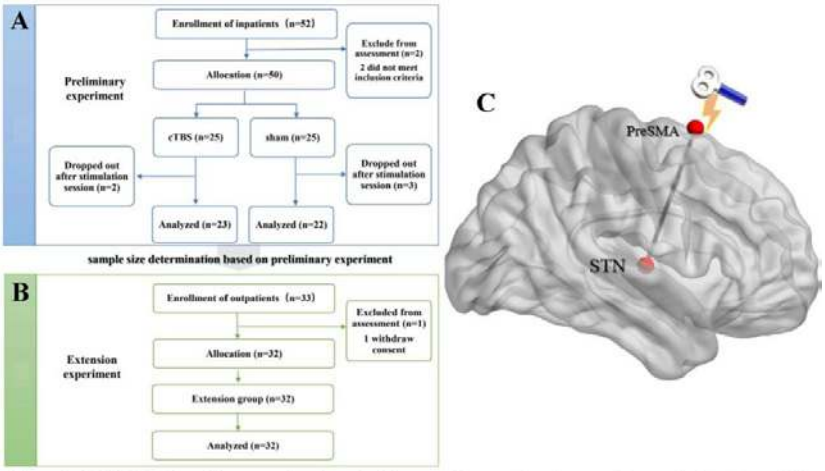

Figure 1. CONSORT flow diagram and schematic diagram of personalized targets from a single subject. (A) Preliminary experiment. (B) Extension experiment based on the preliminary experiment. To achieve a statistical power of 0.99, 30 patients are required in the outpatient group. (C) First, we defined two regions of interest (ROIs), the preSMA (pre-supplementary motor area) and STN (subthalamic nucleus). Second, we normalized each individual's T1 image to MNI space and the inverse transformation was applied to the STN and preSMA. Finally, STN to preSMA functional connectivity in resting state was performed in individual space. The preSMA voxel with the highest correlation value was selected as the personalized cTBS target.

Results: In the preliminary experiment, there was a marginally significant difference in the YBOCS improvement between the groups. The response and remission rates in the cTBS group were 56·52% and 57·14%, respectively, significantly higher than those in the sham group ($\chi2=3·94$, $p=0·047$; $\chi2=5·41$, $p=0·02$, respectively). Further analysis revealed significant YBOCS improvement in patients with moderate OCD ($F=9·45$, $p=0·005$, $\eta2=0·27$) than those with severe OCD ($F=0·16$, $p=0·69$, $\eta2=0·01$). In the extension experiment, YBOCS scores significantly decreased after treatment ($t=5·56$, $p<0·001$, Cohen's $d=0·98$). The extension group had a response rate of 50% and a remission rate of 56·52%. Additionally, a significant difference in YBOCS scores before and after cTBS intervention was found in patients with mild-to-moderate OCD, but not in those with severe OCD (mild: $t=2·57$, $p=0·03$, Cohen's $d=0·86$; moderate: $t=4·70$, $p<0·001$, Cohen's $d=1·08$; severe: $t=2·02$, $p=0·14$, Cohen's $d=1·01$). No severe adverse reactions were observed.

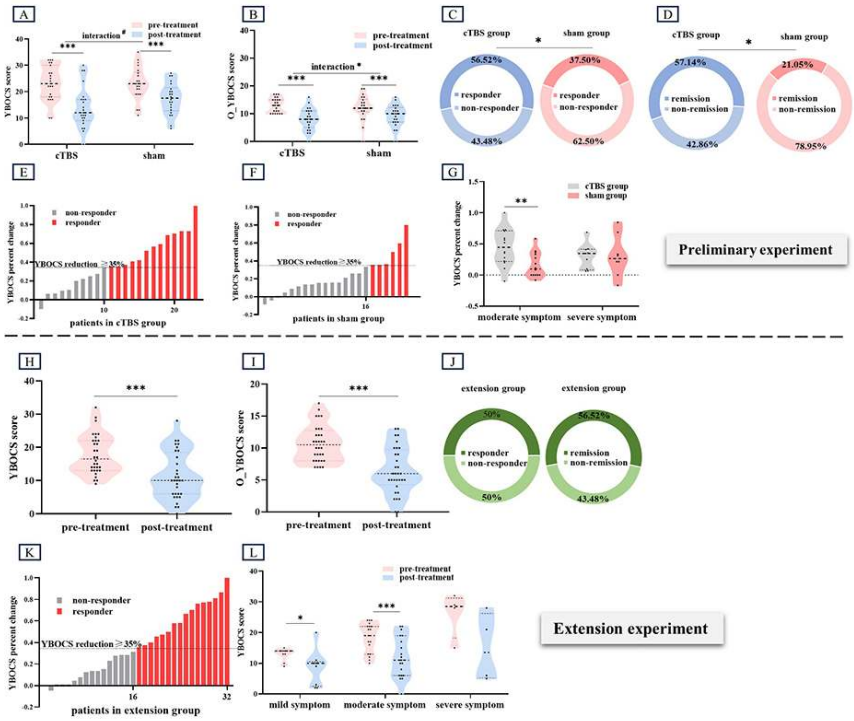

Figure 2. Continuous theta burst stimulation (cTBS) intervention effects on obsessive-compulsive symptoms in the preliminary experiment and extension experiment. Changes of YBOCS and O_YBOCS in the preliminary experiment (A, B) and in the extension group (H, I). Response rate and remission rate between groups in the preliminary experiment (C, D) and in the extension group (J). Individual distribution of responders and non-responders according to the reduction rate of YBOCS in cTBS group (E) , sham group (F) and extension group (K). Grouped analysis in the preliminary experiment (G) and in the extension group (L). YBOCS reduction= (pre-treatment – post-treatment)/pre-treatment. YBOCS, Yale-Brown obsessive-compulsive scale. O_YBOCS, obsessive subscale of YBOCS. $^{\#}p<0.1$, * $p<0.05$, ** $p<0.01$, *** $p<0.001$.

Conclusions: This is the first preliminary study with an external validation design across two centers to determine the treatment effects of cTBS over the right preSMA in patients with OCD, especially mild-to-moderate OCD. The treatment effect of cTBS was comparable to that of the first-line method for OCD. Therefore, cTBS can be applied as an effective alternative for OCD within a certain range of symptom severity.

References

1. Ji, GJ. et al. (2017), 'Dynamic aftereffects in supplementary motor network following inhibitory transcranial magnetic stimulation protocols', Neuroimage, vol. 149, pp. 285-294

Poster No 522

Mozart's music affects the frontal theta activity related to response suppression in SHE patients

Chenxi Qiu[1], Ying Liu[1], Xinjian Su[1], Sijia Guo[1], Xiaoting Hao[2], Jing Lu[1]

[1]School of Life Science and Technology, University of Electronic Science and Technology of China, Chengdu, China, [2]Department of Neurology, West China Hospital, Sichuan University, Chengdu, China

Introduction: As reported, focal frontal lobe lesions have impaired Stroop performance indexing the response suppression[1,2], which has been shown reflected by frontal theta oscillation in the research on adults[3]. As the rarer frontal lobe epilepsy (FLE)[4], patients with sleep-related hypermotor epilepsy (SHE) have worse cognitive deficits related to frontal lobe, such as attention, executive functioning, and response inhibition[5]. Meanwhile, as an effective means, music may increase response suppression function in adults by reducing theta oscillation[6]. Among them, music composed by Mozart has been widely used in potential music therapy for epileptic patients[7]. However, whether Mozart's music can improve response suppression function in SHE patients, and the mechanism of how it works still need to be explored. Therefore, we measured the effects of Mozart's music on the behavioral and electroencephalographic parameters of SHE patients, nocturnal epilepsy (NE) patients, and healthy controls (HCs). This study provided evidence for the mechanism that how music interventions affect response suppression function in SHE patients.

Methods: 22 SHE patients, 21 NE patients, and 21 healthy controls were enrolled. Patients executed a visual GoNoGo task of 12 min (pre-test), followed by approximately 8 min of Mozart's music while wearing the earphones, and finally another 12 min of the GoNoGo task (post-test). Electroencephalogram (EEG) and behavior data such as accuracy rates and reaction times were recorded. We used the non-parametric test to assess the behavior data of response suppression between three groups in the pre-test and between the pre- and post-test in each group. Then we segmented the consistent EEG data into 1000ms epochs and performed time-frequency analysis in frontal electrodes. The paired t-test was used to indicate the changes between Go and NoGo trials at pre-and post-test.

Results: The different accuracy and reaction times of the GoNoGo tasks in three groups before listening to Mozart's music are shown in Figure 1. The multiple comparisons results showed that the SHE group had a slower reaction time than the other two groups (WSHE vs NE=14.26, WSHE vs HCs=16.77, $p<0.05$), and the accuracy shows no significance in the three groups. After Mozart's music stimulus, the SHE group had the higher accuracy ($W= 130.0$, $p<0.05$) and faster reaction time ($W= -110.0$, $p<0.05$), other two groups had no significant alteration. Time-frequency results were illustrated in Figure 2, which indicated that the theta power in the frontal region decreased in the SHE group from 0ms to 500ms at NoGo minus Go trials ($t=2.14$, $p<0.05$). Meanwhile, there was no significant difference in theta power in the frontal region in the NE and HCs groups.

Conclusions: Studies found that the focal frontal lobe lesions in SHE patients were potentially accompanied by a decrease in response suppression[1,2,5]. However, SHE patients showed higher accuracy and faster reaction time after Mozart's music stimulus, which indicated that Mozart's music improved the inhibitory control ability. Besides, the Mozart's music reduced the frontal theta power in the SHE patients. Previously, the abnormal frontal theta power were observed of SHE patients in the interictal period[8], this is related to response suppression function in adults. It suggested that this abnormal activity in SHE patients may also reflect response suppression function. Meanwhile, some studies reported that frequent responses make patients susceptible to false alarms[9] and it may contribute to the higher frontal theta power which likely reflect the coding of a "surprise signal". Therefore, the decrease it might illustrate the reduction of "surprise" in SHE patients. In conclusion, our findings contribute to a better understanding of inhibitory control ability in SHE patients and mechanisms by which musical interventions affect response suppression in them.

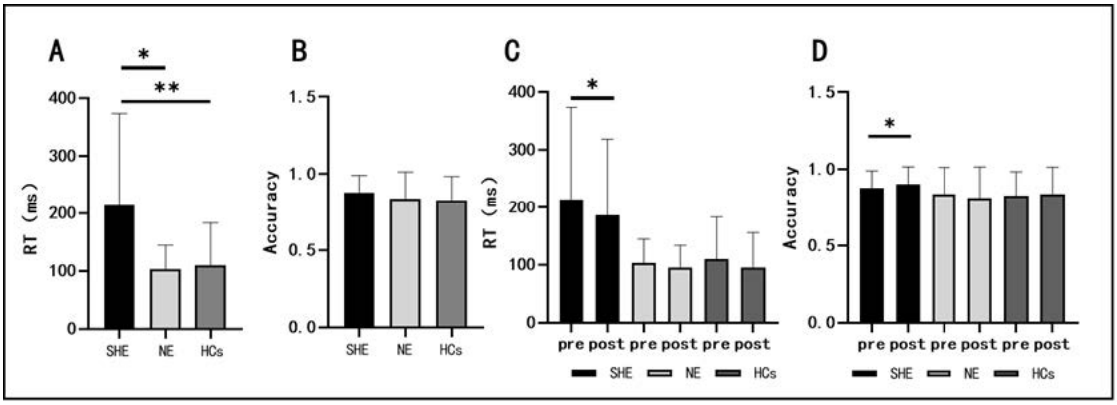

Figure 1. A. Three group's reaction time; B. Three group's accuracies; C. Three group's reaction time at pre-post test; D. Three group's accuracies at pre-post test. *p<0.05, **p<0.01.

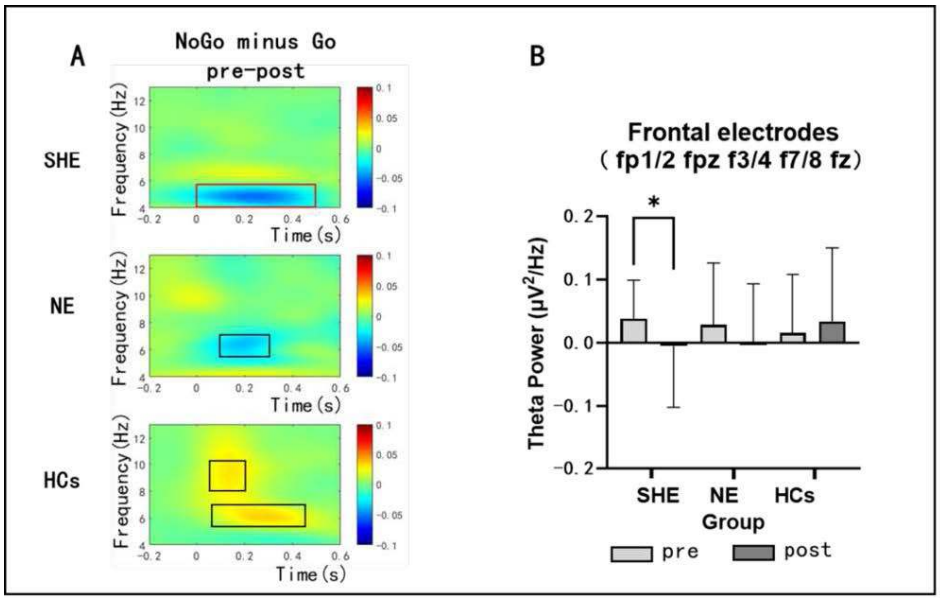

Figure 2. A. The changes in theta power in frontal electrodes of three groups at NoGo minus Go trials at pre- and post-test; B. The average theta power in different time-frequency windows. *p<0.05.

References

1. Stuss, D. T., D. Floden, M. Alexander, B. Levine and D. Katz (2001), 'Stroop performance in focal lesion patients: dissociation of processes and frontal lobe lesion location', Neuropsychologia, vol. 39, no. 8, pp. 771-786.
2. Demakis, G. J. (2004), 'Frontal lobe damage and tests of executive processing: a meta-analysis of the category test, stroop test, and trail-making test', Journal of clinical and experimental neuropsychology, vol. 26, no. 3, pp. 441-450.
3. Cohen, M. X. and T. H. Donner (2013), 'Midfrontal conflict-related theta-band power reflects neural oscillations that predict behavior', Journal of neurophysiology, vol. 110, no. 12, pp. 2752-2763.
4. Tinuper, P., F. Bisulli, J. Cross, D. Hesdorffer, P. Kahane, L. Nobili, F. Provini, I. E. Scheffer, L. Tassi and L. Vignatelli (2016), 'Definition and diagnostic criteria of sleep-related hypermotor epilepsy', Neurology, vol. 86, no. 19, pp. 1834-1842.
5. Licchetta, L., R. Poda, L. Vignatelli, T. Pippucci, C. Zenesini, V. Menghi, B. Mostacci, S. Baldassari, F. Provini and P. Tinuper (2018), 'Profile of neuropsychological impairment in Sleep-related Hypermotor Epilepsy', Sleep Medicine, vol. 48, no., pp. 8-15.
6. Lu, J., A. Moussard, S. Guo, Y. Lee, G. M. Bidelman, S. Moreno, C. Skrotzki, J. Bugos, D. Shen and D. Yao (2022), 'Music training modulates theta brain oscillations associated with response suppression', Annals of the New York Academy of Sciences, vol. 1516, no. 1, pp. 212-221.
7. Ding, R., H. Tang, Y. Liu, Y. Yin, B. Yan, Y. Jiang, P.-J. Toussaint, Y. Xia, A. C. Evans and D. Zhou (2023), 'Therapeutic effect of tempo in Mozart's "Sonata for two pianos"(K. 448) in patients with epilepsy: An electroencephalographic study', Epilepsy & Behavior, vol. 145, no., pp. 109323.
8. Jiang, Y.-l., C.-g. Song, H.-m. Zhou, B. Feng, J.-j. Zhao, Y. Liu, Y.-l. Man, J. Han, S.-b. Liu and W. Jiang (2022), 'Rare variants in GABRG2 associated with sleep-related hypermotor epilepsy', Journal of Neurology, vol. 269, no. 9, pp. 4939-4954.
9. Dippel, G., W. Chmielewski, M. Mückschel and C. Beste (2016), 'Response mode-dependent differences in neurofunctional networks during response inhibition: an EEG-beamforming study', Brain Structure and Function, vol. 221, no., pp. 4091-4101.
10. Cavanagh, J. F. and M. J. Frank (2014), 'Frontal theta as a mechanism for cognitive control', Trends in cognitive sciences, vol. 18, no. 8, pp. 414-421.

Poster No 523

Predicting panic disorder with machine learning of resting-state fMRI features

Junhyung Kim[1], Byung-Hoon Kim[2]

[1]Department of Psychiatry, Korea University College of Medicine, Seoul, Republic of Korea, [2]Department of Psychiatry,Yonsei University College of Medicine, Seoul, Republic of Korea

Introduction: Panic Disorder (PD) is a condition marked by unexpected, intense panic attacks, often in minimally threatening situations.[1] PD can significantly disrupt daily life. While neuroimaging has identified PD-related brain regions, using these findings to predict or classify PD remains a relatively unexplored area. This study employs radiomics to classify PD using fMRI-derived features like regional homogeneity (ReHo) and fractional amplitude of low-frequency fluctuation (fALFF).[2] These features, reflecting brain activity and connectivity, are integrated with machine learning models to determine PD diagnosis. The aim is to evaluate the effectiveness of these models in distinguishing PD patients from healthy controls, focusing on the relative importance of various fMRI-derived features. This approach could deepen our understanding of PD's neurobiological aspects in young adults.

Methods: This study at Korea University Guro Hospital involved 29 patients with PD and 28 healthy adults, categorized into Panic and CON groups. Participants underwent psychiatric evaluations, including the Mini-International Neuropsychiatric Interview, to screen for psychiatric illnesses and drug use. The study, ethically approved (2021GR0321), utilized various scales like the Panic Disorder Severity Scale (PDSS) and Hospital Anxiety and Depression Scale (HADS) to assess anxiety severity and traits. Imaging data were collected using a 3 T Philips Ingenia scanner, capturing coronal anatomical and functional images. Data preprocessing focused on resting-state brain functional radiomic features like ReHo and fALFF. These features were extracted for 14 brain regions of interest (ROIs) related to anxiety disorders. The dataset was processed using Python libraries pandas and scikit-learn, then split into training and test sets, with the former normalized for stable training. Six machine learning models were employed, including Logistic Regression, Support Vector Machine, Random Forest, and eXtreme Gradient Boosting (XGBoost). Model optimization used GridSearchCV for hyperparameter tuning, and performance was evaluated using the F1 score. The study's final evaluation of the test dataset involved measuring accuracy and F1 score, along with the average and standard deviation of predicted class probabilities.

Results: The distributions of age, sex, and marital status between the two groups did not vary significantly. The PD group had more years of education than the CON group. Except for the LSAS-fear and LSAS-avoidance subscale scores, psychological characteristics associated with anxiety differed significantly. The accuracy of the logistic regression (LogReg), SVM, random forest (RF), multi-layer perceptron (MLP), and the extreme gradient boosting (XGBoost) for classifying the PD group was 0.315, 0.315, 0.515, 0.616, and 0.616, respectively. The F1 score, which reflects both the sensitivity and specificity of the model by computing the harmonic mean of the precision and recall scores, also resulted in a similar trend with the accuracy and the balanced accuracy, demonstrating 0.530, 0.530, 0.626, 0.714 and 0.714 for the LogReg, SVM, RF, MLP, and XGBoost models, respectively.

Conclusions: It could be seen that the XGBoost model resulted in the best classification performance on the test data in terms of all three metrics evaluated.

References

1. Locke Ab, Kirst N, Shultz CG. Diagnosis and management of generalized anxiety disorder and panic disorder in adults. Am Fam Physician. (2015) 91:617–24.
2. Zou, Q. H. et al. An improved approach to detection of amplitude of low-frequency fluctuation (ALFF) for resting-state fMRI: Fractional ALFF. J. Neurosci. Methods (2008) 172: 137–141

Poster No 524

Increasing gamma oscillation reflects the effect of music therapy on overall psychiatric symptoms

liju wang[1], Jiaxian Chen[2], Ting Liu[3], Lujie Wang[4], Sijia Guo[2], Jing Lu[1]

[1]School of Life Science and Technology, University of Electronic Science and Technology of China, Chengdu, China, [2]School of Life Science and Technology, University of Electronic Science and Technology of China, Chengdu, Sichuan, [3]Chengdu Dekang Hospital, Chengdu, Sichuan, [4]Musicology Department, Sichuan Conservatory of Music, Chengdu, Sichuan

Introduction: Previous studies have shown that patients with schizophrenia have a decrease in gamma oscillation, which is closely related to their cognitive deficits such as attentional distraction, decreased executive function, and social difficulties[1], [2]. Music therapy as an adjunctive therapy to improve cognitive function in schizophrenia patients was proved by clinical

behavioral evidence[3-5], but the neuroimaging evidence is still insufficient. In our work, schizophrenia accepted a five-week combined group music therapy which united receptive and active music training, integrating singing, composing, and listening, and required patients to cooperate in a group to complete music therapy tasks[6]. We calculated the gamma-band power spectral densities of electroencephalography (EEG) signals in the music therapy group and visual art therapy group (control group) before and after therapy to study the neural mechanism of music therapy for schizophrenia.

Methods: We recruited a total of 32 patients with schizophrenia from Chengdu Dekang Hospital in Sichuan Province, including 17 in the music therapy group and 15 in the visual art therapy group. There was no significant difference in age and clinical diagnostic performance between the two groups. The therapy schedule was designed by Professor Wang Lujie, a professional music therapist from the Sichuan Conservatory of Music, and the schedule was five weeks long, with two sessions per week, each session lasting 45 minutes (more therapy details are shown in Figure 1). Behavioral scales of the Standardized Rating Scale for Chronic Psychosis (SRCP) and resting-state EEG data were collected. Then, the Welch method was used to calculate power spectral density (PSD) in the gamma band and statistically analyzed the PSD values and behavioral data using t-tests before and after five-week therapy.

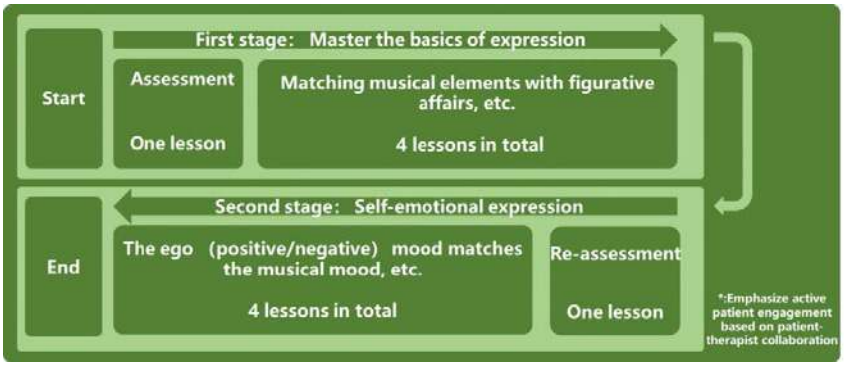

Figure 1. The Music Therapy Schedule.

Results: After therapy, the SRCP scores of both the music and visual art therapy group significantly decreased (music therapy group: $p < 0.0001$, $t = -8.899$; visual art therapy group: $p = 0.0004$, $t = -4.583$, Figure 2. A). Moreover, the decline in scores in the music therapy group was greater than that in the visual art therapy group ($p = 0.0363$, $t = 2.192$, Figure 2. B). The gamma-band PSD values in the prefrontal lobes increased after the music therapy ($p = 0.0480$, $t = 2.1415$, Figure 2. C) and this change was linearly correlated with (the change of SRCP score/ Original SRCP score) ($p < 0.0001$, $r = -0.8601$, Figure 2. D), whereas there was no significant change in the gamma-band PSD after the visual art therapy.

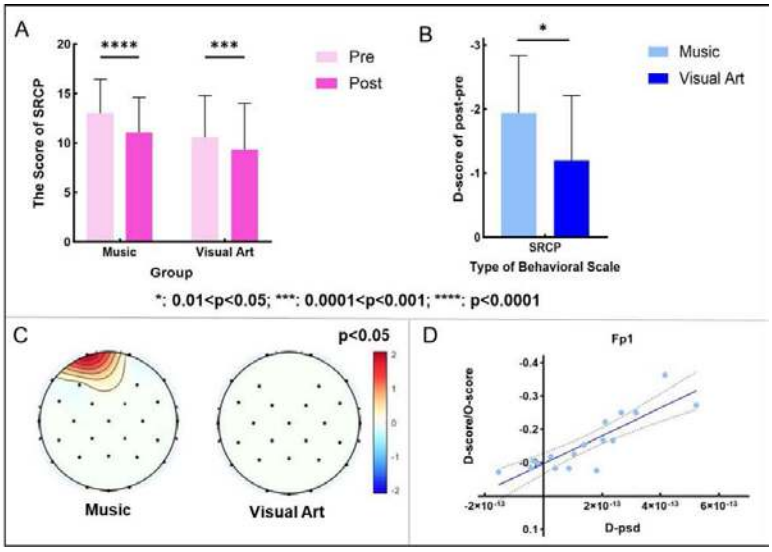

Figure 2. A & B. Changes in the SRCP scores and post-pre scale differences. C & D. PSD variation of post-pre test and its negative correlation with score changes in music therapy group.

Conclusions: Consistent with previous research results[7,8], both music and visual art therapy can effectively help schizophrenia patients relieve their psychiatric symptoms, while music therapy showed better and more significant overall psychiatric symptom intervention effects than visual art therapy. Meanwhile, for the music therapy group, the increase in the prefrontal gamma power spectrum was linearly correlated with the change in the SRCP score, revealing that improvement in overall

psychiatric symptoms was accompanied by stronger gamma oscillation, so we infer that music therapy may improve overall psychiatric symptoms by increasing prefrontal gamma oscillation.

References

1. Cohen, N. S. (2015), 'Music therapy handbook', Journal of Music Therapy, vol. 52, no. 2, pp. 319-321.
2. Spencer KM, N. P., Perlmutter R, et al (2004), 'Neural synchrony indexes disordered perception and cognition in schizophrenia', Proc Natl Acad Sci U S A, vol. 101, no., pp. 5.
3. Jia, R., D. Liang, J. Yu, et al. (2020), 'The effectiveness of adjunct music therapy for patients with schizophrenia: A meta-analysis', Psychiatry Research, vol. 293, no.
4. Lim, K., O.-H. Peh, Z. Yang, et al. (2021), 'Large-scale evaluation of the Positive and Negative Syndrome Scale (PANSS) symptom architecture in schizophrenia', Asian Journal of Psychiatry, vol. 62, no.
5. Pedersen, I. N., L. O. Bonde, N. J. Hannibal, et al. (2021), 'Music Therapy vs. Music Listening for Negative Symptoms in Schizophrenia: Randomized, Controlled, Assessor- and Patient-Blinded Trial', Frontiers in Psychiatry, vol. 12, no.
6. Silverman, M. J. and J. Leonard (2012), 'Effects of active music therapy interventions on attendance in people with severe mental illnesses: Two pilot studies', The Arts in Psychotherapy, vol. 39, no. 5, pp. 390-396.
7. Gold, C., T. Heldal, T. Dahle, et al. (2005), 'Music therapy for schizophrenia or schizophrenia-like illnesses - art. no. CD004025.pub2', Cochrane database of systematic reviews (Online), vol. 2, no., pp. CD004025.
8. Tseng, P.-T., Y.-W. Chen, P.-Y. Lin, et al. (2016), 'Significant treatment effect of adjunct music therapy to standard treatment on the positive, negative, and mood symptoms of schizophrenic patients: a meta-analysis', BMC Psychiatry, vol. 16, no. 1.

Poster No 526

Lysergic acid diethylamide alters white matter microstructure in patients with depression

Mihai Avram[1], Aurore Menegaux[2], Felix Müller[3], Hannes Zaczek[3], Alexandra Korda[1], Helena Rogg[1], Anna Becker[3], Laura Ley[3], Matthias Liechti[3], Stefan Borgwardt[1]

[1]University of Lübeck, Lübeck, Germany, [2]Technical University of Munich, Munich, Bayern, [3]University Hospital Basel, Basel, Switzerland

Introduction: Mounting evidence indicates that psychedelics like psilocybin and lysergic acid diethylamide (LSD) may be used as psychiatric medicines in the treatment of several mental disorders[1,2,3]. While the most consistent findings from modern clinical studies indicate significant antidepressant potential for psilocybin[1], recent findings also hint at LSD's antidepressant effects[2]. The clinical trial NCT03866252 directly investigated LSD as a therapeutic agent in the treatment of major depression (MDD) and compared the effects of two low (2 x 25µg) and two moderate-to-high doses (2 x 100µg or 200µg in the second session) with promising results. While it is unclear how LSD might induce antidepressant effects, increased neuroplasticity has been suggested as a possible candidate[4]. Intriguingly, rapid-induced neuroplastic effects have been reported in white matter (WM) in healthy subjects following distinct interventions5. Changes in WM can be assessed with diffusion-tensor imaging (DTI) in vivo, which quantifies fractional anisotropy (FA), a summary measure of WM microstructure integrity, and mean diffusivity (MD), reflecting the average mobility of water molecules.

Methods: The data used in this study were derived from the clinical trial NCT03866252, which evaluated 61 patients with MDD. Patients were randomly allocated to the low- (LD-LSD) or high-dose LSD group (HD-LSD). DTI data were available for 38 MDD patients, consisting of two sessions: pre- and post-intervention. DTI data were analyzed with FSL. Preprocessing steps included image distortion correction, eddy current and motion correction, and quality checks (visual inspection and quad/squad). Three patients were excluded following quality control. The remaining participants (N=35; 17 HD-LSD) did not differ in age (p=.36) or sex (p=.63). We used tract-based spatial statistics (TBSS) to quantify FA and MD. To evaluate group differences, we first used a 2-way mixed effect ANOVA (2 groups, 2 levels per subject – pre/post) to test for group-by-time interactions for each measure (i.e., FA, MD). Significant interactions were followed by two-sample t-tests based on the post-pre difference to identify the direction of change. Finally, post-intervention FA values were extracted from areas reflecting group differences and correlated with changes from baseline in the Inventory of Depressive Symptomatology (ΔIDS-C, clinician-rated) and Beck's Depression Inventory (ΔBDI) at 2, 6, and 12 weeks after the second intervention.

Results: A 2-way mixed effect ANOVA demonstrated a significant group-by-time interaction for FA in areas covering parts of the internal and external capsule, sagittal stratum, and fornix/stria-terminalis. This analysis was followed by a two-sample t-test, which demonstrated increased post-intervention FA values in the HD-LSD group in the same areas. Next, we extracted FA values from the regions reflecting group differences from the post-intervention scans and correlated them with ΔIDS-C and ΔBDI, respectively, at 2, 6, and 12 weeks after the second intervention. Symptom relief was significantly associated with post-intervention FA-values at 2 (ΔIDS-C: r=-.51, p=.03; ΔBDI: r=-.67, p=.003), 6 (ΔIDS-C: r=-.53, p=.03; ΔBDI: r=-.43, p=.09), and 12 weeks post-intervention (ΔIDS-C: r=-.71, p=.002; ΔBDI: r=-.63, p=.009) in the HD-LSD group only. No significant correlations were found for the LD-LSD group. Finally, the group-by-time interaction for MD was not significant.

Conclusions: We investigated LSD-induced changes in DTI-derived measures reflecting white matter integrity in MDD patients. While we did not find significant changes in MD, we observed higher FA values after treatment in the HD-LSD group. Remarkably, the increase in FA correlated with symptom improvement at 2, 6, and 12 weeks after intervention. Results indicate that two moderate-to-high doses of LSD induce structural changes related to symptom relief in MDD. Such changes may reflect LSD-induced neuroplasticity.

References

1. Carhart-Harris, R., Giribaldi, B., Watts, R., Baker-Jones, M., Murphy-Beiner, A., Murphy, R., ... & Nutt, D. J. (2021). Trial of psilocybin versus escitalopram for depression. New England Journal of Medicine, 384(15), 1402-1411.
2. Holze, F., Gasser, P., Müller, F., Dolder, P. C., & Liechti, M. E. (2023). Lysergic acid diethylamide–assisted therapy in patients with anxiety with and without a life-threatening illness: a randomized, double-blind, placebo-controlled phase II study. Biological Psychiatry, 93(3), 215-223.
3. Bogenschutz, M. P., Ross, S., Bhatt, S., Baron, T., Forcehimes, A. A., Laska, E., ... & Worth, L. (2022). Percentage of heavy drinking days following psilocybin-assisted psychotherapy vs placebo in the treatment of adult patients with alcohol use disorder: a randomized clinical trial. JAMA psychiatry, 79(10), 953-962
4. Calder AE, Hasler G. (2023). Towards an understanding of psychedelic-induced neuroplasticity. Neuropsychopharmacology. 248(1):104-112.
5. Sampaio-Baptista C, Johansen-Berg H. (2017). White Matter Plasticity in the Adult Brain. Neuron. 96(6):1239-1251.

Poster No 527

Unveiling Compromised Control Networks in Insomnia: Insights from Functional and Structural MRI

Yun Tian[1], Haobo Zhang[2], Shiyan Yang[3], Shuo Wang[1], Linman Weng[1], Lei Xu[3]

[1]Southwest University, Chongqing, Chongqing, [2]Southwest University, Chongqing, Chongqing, [3]Southwest University, Chongqing, China

Introduction: Insomnia, a prevalent sleep disorder, not only affects sleep quality but also potentially impacts daytime functioning and brain dynamics(Van Someren, 2021). However, a comprehensive understanding of changes in brain networks, both functionally and structurally, among individuals with insomnia remains incomplete. This study aims to explore functional and structural alterations in cerebral networks among insomnia patients, utilizing functional magnetic resonance imaging (fMRI) and structural magnetic resonance imaging (sMRI) to provide evidence supporting the link between insomnia and cerebral networks.

Methods: We recruited 43 diagnosed insomnia patients and 41 healthy control volunteers for resting-state fMRI and sMRI scans. Fmriprep, along with embedded FreeSurfer, was used to preprocess resting-state images and structural images (Esteban et al., 2019; Fischl, 2012). For structural metrics, differences between healthy and insomnia groups were analyzed across nine indices covering whole-brain measures, including curvature index, folding index, Gaussian curvature, grey matter volume, mean curvature, vertex count, surface area, cortical thickness standard deviation, and mean cortical thickness. Regarding functional images, differences between healthy and insomnia groups in provincial hub and connector hub of eight brain networks were investigated from a functional hub perspective (Bertolero et al., 2018). FDR correction was applied.

Results: Insomnia participants exhibited structural abnormalities solely in the right inferior orbital frontal gyrus of the control network, showing significantly lower values in curvature index, folding index, Gaussian curvature, grey matter volume, mean curvature, vertex count, cortical surface area, and cortical thickness standard deviation compared to the healthy group, with only mean thickness showing no significant differences (Fig 1). Simultaneously, the fMRI data unveiled a notable decrease in connector hub strength (specifically in the right dorsal prefrontal cortex) within the control network among insomnia patients (Fig 2). Conversely, no substantial differences were detected in the provincial hub.

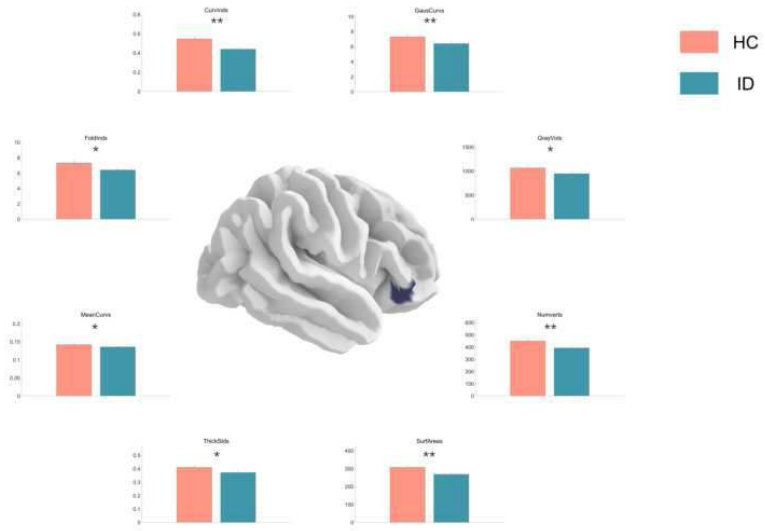

Fig. 1 Abnormalities in cortical structure in insomnia patients

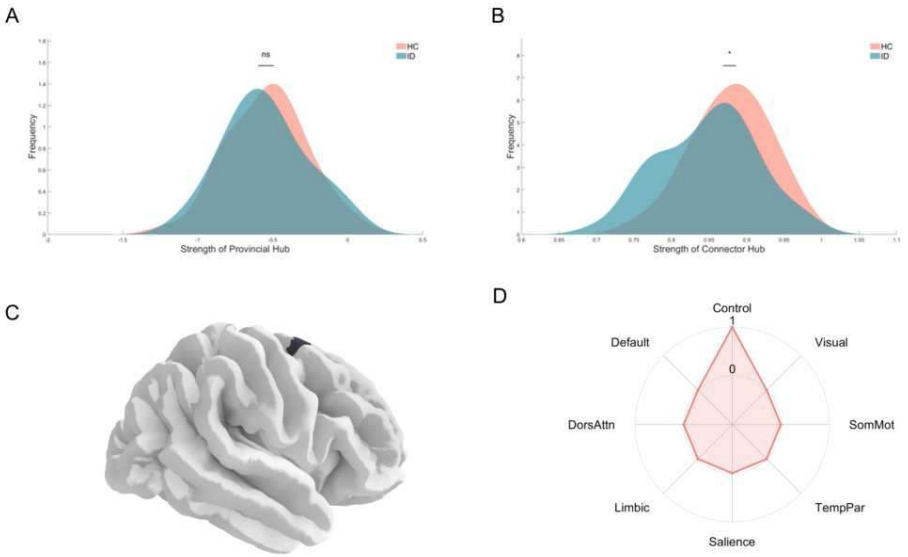

Fig 2. Abnormalities in functional network hubs in insomnia patients

Conclusions: This study provides evidence of impaired functionality and structure in control networks among insomnia patients, supporting the association between insomnia and control networks. These findings hold promise for advancing our understanding of the pathophysiological mechanisms underlying insomnia and may offer potential neurobiological targets for future interventions and treatments.

References

1. Bertolero, M. A. (2018). A mechanistic model of connector hubs, modularity and cognition. Nat Hum Behav, 2(10), 765-777.
2. Esteban, O. (2019). fMRIPrep: a robust preprocessing pipeline for functional MRI. Nat Methods, 16(1), 111-116.
3. Fischl, B. (2012). FreeSurfer. Neuroimage, 62(2), 774-781.
4. Van Someren, E. J. W. (2021). Brain mechanisms of insomnia: new perspectives on causes and consequences. Physiol Rev, 101(3), 995-1046.

Poster No 528

Decomposing cortical thickness heterogeneity by evaluating PRS of psychiatric and medical disorders

Hadis Jameei[1], William Reay[2], Rebecca Cooper[1], Sina Mansour L[1], Murray Cairns[2], Andrew Zalesky[1], Maria Di Biase[1]

[1]University of Melbourne, Melbourne, VIC, [2]University of Newcastle, Newcastle, NSW

Introduction: A common feature of neuropsychiatric disorders is reduced cortical thickness, yet the extent and spatial distribution of these reductions are heterogeneous across patients, even within diagnostic groups. To understand this variability from an etiological standpoint, recent studies have examined common genetic risk variants of distinct psychiatric disorders, revealing significant, albeit weak, associations with cortical thickness. We speculate that variability is better explained by genetic risk profiles for diverse psychiatric and non-psychiatric conditions, which are overrepresented in psychiatric populations. Here, we evaluate polygenic risk correlations between psychiatric disorders and commonly comorbid chronic diseases and test their effects on deviations in brain cortical thickness variation.

Methods: This study comprises healthy adults with available genotype and magnetic resonance imaging data from the UK Biobank (N=7,873, age=56±8, 45% male). Polygenic risk scores (PRSs) were computed for 21 binary traits, including 5 psychiatric traits and 16 chronic medical conditions overrepresented amongst individuals with a psychiatric diagnosis (Figure 1). Normative models constructed with Generalized Additive Models for Location, Scale and Shape (GAMLSS) calculated person-specific cortical thickness deviations from the median for a given age/sex. Linear regressions tested pair-wise correlations between disorder PRSs, and associations between each PRS with regional cortical thickness deviations. Spatial correspondence (Spin) tests evaluated overlap between traits in terms of their PRS associations with regional deviation profiles. A permutation test was devised to account for the degree of trait-pair PRS correlations in assessing spatial correspondence.

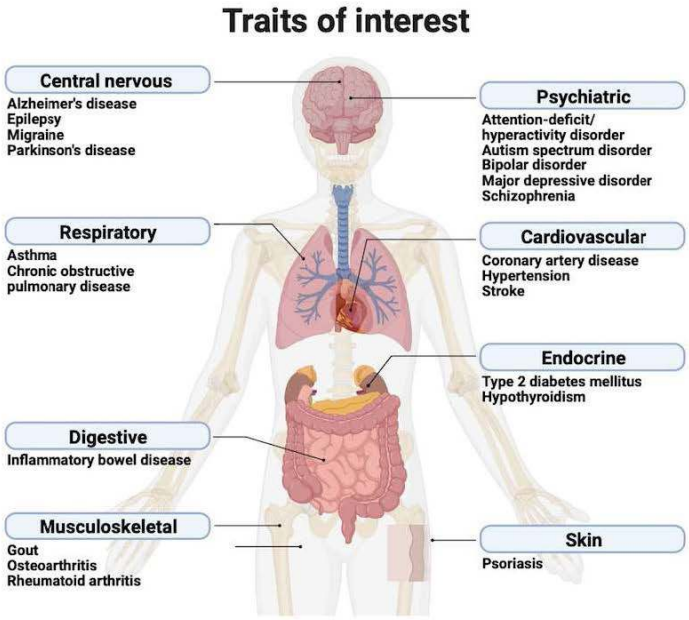

Figure 1. Psychiatric disorders and chronic disorders selected for this study

Results: Polygenic risk for the 16 chronic medical conditions exhibited smaller pair-wise correlations across individuals compared to psychiatric disorders, suggesting greater diagnostic specificity and/or more distinct etiologies. Out of 90 psychiatric-psychiatric and psychiatric-chronic trait pairs, 13 pairs departed from expected patterns of genetic and spatial convergence (Figure 2). Of 12 psychiatric-chronic trait pairs that were genetically correlated, only 2 (17%) revealed significant spatial correspondence in their regional distributions of cortical thickness deviations (r range=0.36-0.39; $p<0.05$). In contrast, 3 (4%) trait pairs exhibited stronger associations in regional cortical deviation profiles relative to that expected by their genetic correlations (r range=0.41-0.44; $p<0.05$).

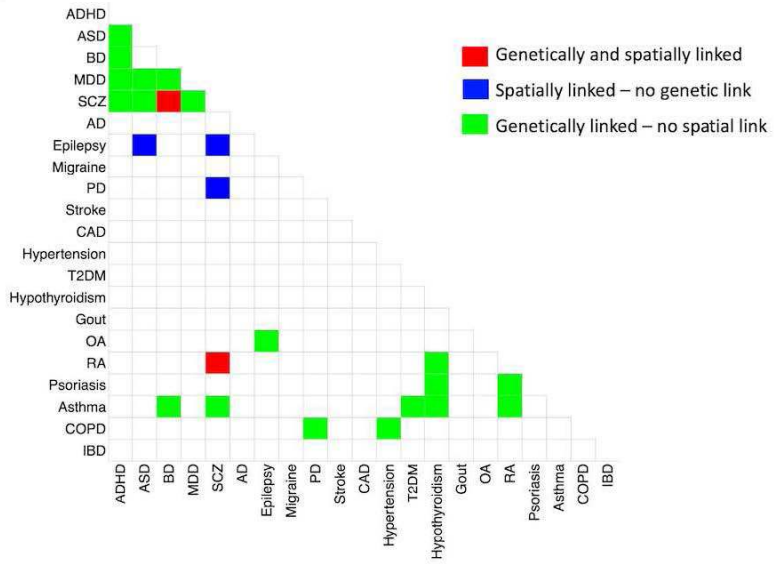

Figure 2. Genetic and spatial links between disorder pairs. Abbreviations: AD = Alzheimer's disease, ADHD = attention-deficit/hyperactivity disorder, ASD = autism spectrum disorder, BD = bipolar disorder, CAD = coronary artery disease, COPD = chronic obstructive pulmonary disease, IBD = inflammatory bowel disease, MDD = major depressive disorder, OA = osteoarthritis, PD = Parkinson's disease, RA = rheumatoid arthritis, SCZ = schizophrenia, T2DM = type 2 diabetes mellitus

Conclusions: Psychiatric disorders with shared genetic components can exhibit varied cortical deviation profiles, consistent with pleiotropic-like effects.6 Conversely, chronic diseases with distinct genetic bases to psychiatric disorders can map to similar deviation profiles of cortical thickness. Our results suggest that moving beyond analyses of single genetic traits leads to improved characterization of complex relationships between genetic architecture and phenotypic variability in cortical thickness. These advancements can help toward developing predictive models of neuro-phenotypic outcomes in psychiatry.

References

1. Jameei, H. (2023), 'Linking Polygenic Risk of Schizophrenia to Variation in Magnetic Resonance Imaging Brain Measures: A Comprehensive Systematic Review,' Schizophrenia Bulletin.
2. Cattarinussi, G. (2022), 'The effect of polygenic risk scores for major depressive disorder, bipolar disorder and schizophrenia on morphological brain measures: A systematic review of the evidence,' Journal of Affective Disorders, vol. 2022, no. 310, pp. 213-222
3. Sudlow, C (2015), 'UK biobank: an open access resource for identifying the causes of a wide range of complex diseases of middle and old age,' PLoS Med, vol. 12, no. 3, pp. 1001779
4. Kurki, M.I. (2023), 'FinnGen provides genetic insights from a well-phenotyped isolated population,' Nature, vol. 613, no. 7944 (2023), pp. 508-518
5. Trubetskoy, V. 'Mapping genomic loci implicates genes and synaptic biology in schizophrenia,' Nature, vol. 604, no. 7906, pp. 502-508
6. Lee, P.H. (2021), 'Pleiotropy and Cross-Disorder Genetics Among Psychiatric Disorders. Biological Psychiatry,' vol. 89, no. 1, pp. 20-31

Poster No 529

Parsing heterogeneity in white matter integrity along the progression of psychosis

Galya Iseli[1,2], Sarah Ulrich[3,4], Philipp Staempfli[5,6], Erich Studerus[7], Anita Riecher-Rössler[8], Philipp Homan[9], Stefan Kaiser[10], Stefan Borgwardt[11], Matthias Kirschner[10], André Schmidt[12]

[1]Department of Clinical Research (DKF), University Psychiatric Clinics, Translational Neurosciences, Basel, Switzerland, [2]Division of Cognitive Neuroscience, Department of Biomedicine University of Basel, Basel, Switzerland, [3]Experimental Clinical Affective Neuroscience Lab (ECANL), Department of Clinical Research (DKF)), Basel, Switzerland, [4]Center for Affective, Stress and Sleep Disorders, University Psychiatric Clinics (UPK), Basel, Switzerland, [5]Psychiatric University Hospital Zurich, Zurich, Switzerland, [6]MR-Center of the Psychiatric Hospital and the Department of Child and Adolescent Psychiatry, University of Zurich, Zürich, Switzerland, [7]Division of Personality and Developmental Psychology, University of Basel, Basel, Switzerland, [8]Faculty of Medicine, University of Basel, Basel, Switzerland, [9]Department of Psychiatry, Psychotherapy and Psychosomatics, Psychiatric University Hospital Zurich, Basel, Switzerland, [10]Division of Adult Psychiatry, Department of Psychiatry, Geneva University Hospitals, Geneva, Switzerland, [11]University of Lübeck, Lübeck, Germany, [12]University of Basel, Department of Clinical Research (DKF), University Psychiatric Clinics (UPK), Basel, Switzerland

Introduction: Psychosis develops along a continuum ranging from subclinical psychotic experiences in healthy volunteers from the general population and individuals at clinical high risk to patients with clinically relevant psychosis. Each stage along the continuum demonstrates heterogeneity in clinical profiles and outcome features. While previous research also indicated structural brain heterogeneity at both ends of the continuum, it remains unknown whether it evolves with disease progression and whether divergence from the norm is associated with more adverse clinical features.

Methods: Data of 212 participants collected at three different centers was included in this post-hoc analysis. Samples ranging from five different groups of disease progression were collected at the Department of Psychiatry (UPK) of the University of Basel, the University Hospital of Psychiatry, Bern and the Department of Psychiatry, Psychotherapy and Psychosomatics at the Psychiatric Hospital, University of Zurich: healthy controls (HC, n = 59), schizotypal (SPT, n = 27), at risk mental state (ARMS, n = 35), first episode psychosis (FEP, n = 50), and patients diagnosed with schizophrenia (SZ, n = 41). Structural brain heterogeneity of diffusion tensor imaging (DTI) parameters including fractional anisotropy (FA), mean diffusivity (MD) and fiber density (FD) was computed using the person-based similarity index (PBSI) scores, a novel index that expresses an individual's similarity towards others of the same group. Besides comparing the different DTI PBSIs across groups using the Kruskal-Wallis test, normalized PBSIs were further converted into z-scores (z-nPBSI) indicating deviators to the normative reference. Furthermore, age, sex and diagnostic group adjusted ANCOVAs were performed to determine whether individuals with deviating PBSIs differ in verbal IQ (MWT-B), psychiatric symptoms (BPRS, SANS) and general ability to function (GAF) compared to subjects with non-deviating PBSIs.

Results: Across diagnostic groups significant differences in the PBSI were found for all three diffusion measures FA (H = 51.81, p < 0.001). MD (H = 44.49, p < 0.001), and FD (H = 55.80, p < 0.001) (Figure 1). Group differences in FA heterogeneity were found between ARMS-SPT (U = -2.87, p = 0.04), FEP-SZ (U = -4.04, p = <0.001), ARMS-SZ (U = -6.13, p = <0.001), and HC-SZ (U = -6.25, p = <0.001). For MD significant differences were found between HC-SPT (U = -3.39, p = 0.007), FEP-SPT (U = -3.56, p = 0.003), HC-ARMS (U = -4.02, p = <0.001), ARMS-FEP (U = 4.17, p = <0.001), HC-SZ (U = -4.74, p = <0.001), and FEP-SZ (U = -4.87, p = <0.001). For FD, FEP-SZ (U = -2.91, p = 0.03), FEP-SPT (U = -4.31, p = <0.001), ARMS-SZ (U = -4.81, p = <0.001), HC-SZ (U = -4.51, p = <0.001), HC-SPT (U = -5.67, p = <0.001), and ARMS-SPT (U = -5.88, p = <0.001) differed significantly. For FA, SZ showed the greatest percentage of deviators (24.390%) followed by SPT (14.815%), HC (8.475%), FEP (8%) and ARMS (2.857%). For MD 22.5% deviators in SZ, 20% in ARMS, 11.111% in SPT 8% in FEP, and 6.780% in HC. And for FD 25.926% in SPT, 14.634% in SZ, followed by 13.793% in HC, 5.714% in ARMS, and 8.0% in FEP. Across all DTI parameters, the number of deviators differed significantly across the groups (χ^2 = 11.24, df = 1, p = 0.02). Post-hoc comparisons revealed significant differences between the groups HC-SPT (OR = 2.94, p = 0.04), FEP-SZ (OR = 2.8, p = 0.04) and SPT-FEP (OR = 3.64, p = 0.02). Furthermore, there were statistical trends for lower GAF scores in SZ patients (F (1,1) = 3.61, p = 0.08) and individuals with SPT (F (1,1) = 3.66, p = 0.07) who exhibited deviating PBSIs compared to those with non-deviating PBSIs.

Conclusions: Our results indicate progressive increases in structural brain heterogeneity. Further large-scale studies are encouraged to examine those with marked deviance from normative data reveal more severe clinical features. Such approaches may enable improved prognosis of disease progression and treatment guidance.

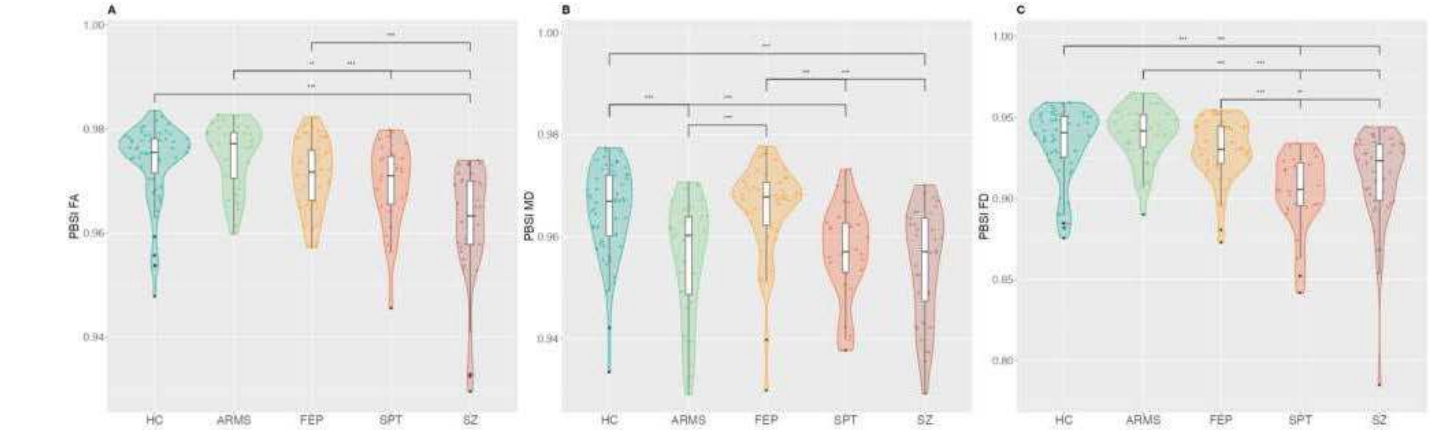

Figure 1: PBSIs for fractional anisotropy (A), mean diffusivity (B), and fiber density (C). Significant group differences after Bonferroni correction (* = 0.05, ** = 0.01, *** = 0.001).

References

1. Baldwin, H., et al., Neuroanatomical heterogeneity and homogeneity in individuals at clinical high risk for psychosis. Translational Psychiatry, 2022. 12(1): p. 297
2. Cavelti, M., et al., Formal thought disorder is related to aberrations in language-related white matter tracts in patients with schizophrenia. Psychiatry Res Neuroimaging, 2018. 279: p. 40-50

3. Kirschner, M., et al., Ventral Striatal Dysfunction and Symptom Expression in Individuals With Schizotypal Personality Traits and Early Psychosis. Schizophr Bull, 2018. 44(1): p. 147-157
4. Riecher-Rossler, A., et al., [The Basel Screening Instrument for Psychosis (BSIP): development, structure, reliability and validity]. Fortschr Neurol Psychiatr, 2008. 76(4): p. 207-16
5. Riecher-Rossler, A., et al., The Basel early-detection-of-psychosis (FEPSY)-study--design and preliminary results. Acta Psychiatr Scand, 2007. 115(2): p. 114-25
6. Schmidt, A., et al., Structural Network Disorganization in Subjects at Clinical High Risk for Psychosis. Schizophrenia Bulletin, 2016. 43(3): p. 583-591
7. Schmidt, A., et al., Brain Diffusion Changes in Emerging Psychosis and the Impact of State-Dependent Psychopathology. Neurosignals, 2015. 23(1): p. 71-83
8. Stampfli, P., et al., Subtle white matter alterations in schizophrenia identified with a new measure of fiber density. Scientific Reports, 2019. 9(1): p. 4636

Poster No 530

A Novel Cognition-guided Neurofeedback Protocol for Methamphetamine Abuse Treatment

Huixing Gou[1], Junjie Bu[2], Xiaochu Zhang[1]

[1]University of Science and Technology of China, Hefei, Anhui, [2]Anhui Medical University, Hefei, Anhui

Introduction: The World Drug Report 2023 reveals a global rise in methamphetamine (meth) production and usage. In China, meth predominant among illicit substance. Meth abusers (MAS) exhibit cognitive deficits, especially in response inhibition (Potvin et al., 2018). Intense craving and recurrent relapse is the key feature of MAS, often triggered by exposure to cues associated with addiction drug (Carter et al., 1999). Recent studies have explored methods as virtual reality cue exposure therapy (Wang et al., 2019) and electrical stimulation (Ekhtiari et al., 2022) to reduce meth cue reactivity (CR), but these suffer from lack of effective tracking or short tracking times. Neurofeedback (NF) is seen as a promising avenue to ameliorate MA-related impairments (Paulus et al., 2020). Our previous work developed a cognition-guided NF protocol, successfully deactivated nicotine CR in nicotine-dependent participants with significant effects on craving and smoking (Bu et al., 2019, 2021). This study aims to further develop this cognition-guided NF protocol, assess its efficacy in MA and compare it with the current routine treatment (RT) in Chinese compulsory rehabilitation centers.

Methods: We collected two data samples (Sample I and II) who met DSM-V criteria. Sample I (investigate cognition-guided NF effects for MA), consisting of Real-Feedback Group I (Real-NFG I, n = 31) and Yoke-Feedback Group (Yoke-NFG, received feedback based on Real-NFG I participant brain activity patterns, n = 32). Sample II (compare with RT), including Real-Feedback Group II (Real-NFG II, n = 16) and Routine-Treatment Group (RT-Group, completed normal labor production as usual, n = 16). This study employed a randomized double-blind controlled design. See more details in Fig. 1.

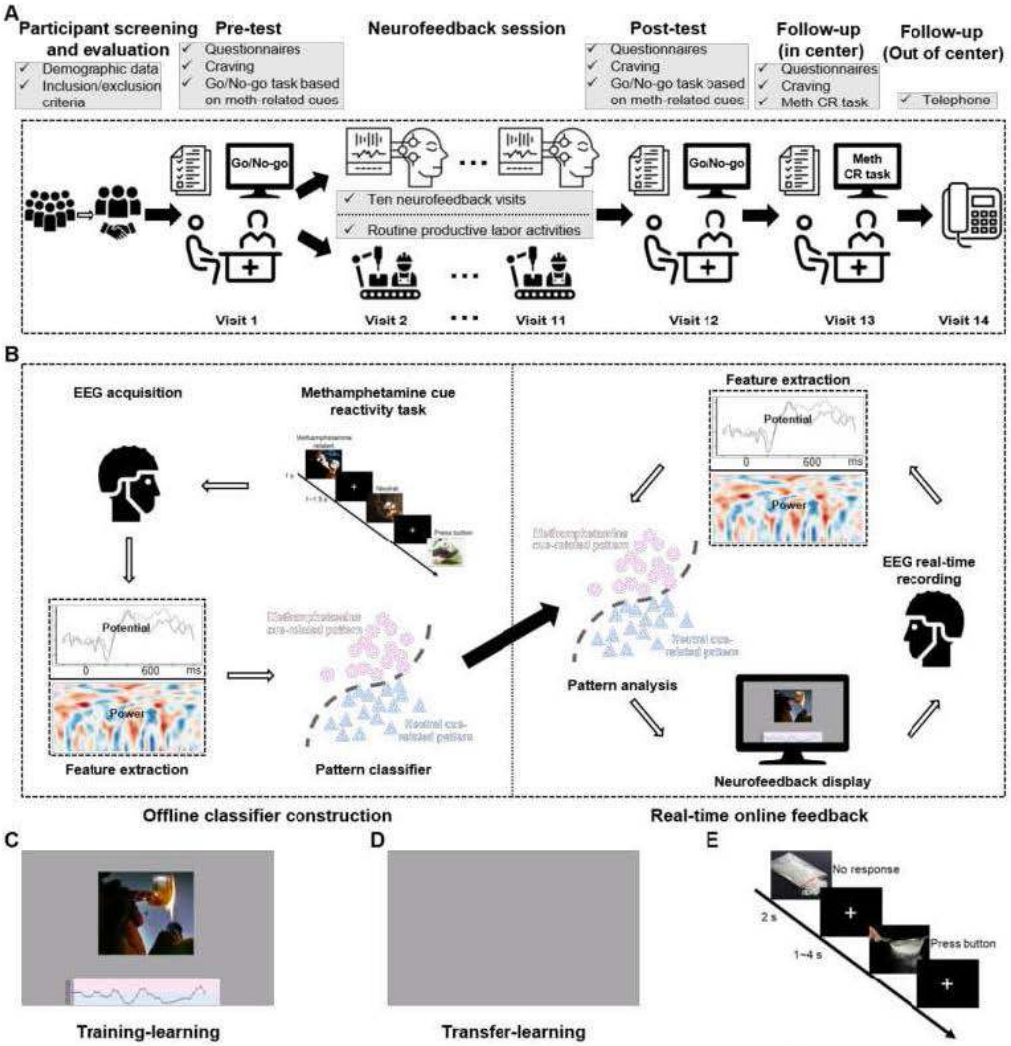

Figure 1. **Experimental procedure and task paradigms.** (A) Experimental procedure. Comprised of six stages: (i) Participants screening and evaluation; (ii) Pre-test (Visit 1); (iii) NF session (From Visit 2 to Visit 11); (iv) Post-test (Visit 12); (v) Follow-up in center (Visit 13, after 3-month, only Sample I included); (vi) Follow-up out of center (Visit 14, 6-month after discharge, only Sample I included). (B) NF paradigm. The NF paradigm comprised two modules: offline classifier construction (based on meth CR task) and real-time online feedback (10 cycles, 8 training-learning cycles, and 2 transfer-learning cycles). (C) Screenshot of NF training-learning cycle. The real-time decoded probabilistic score of the participant's brain reactivity pattern matching the meth cue-related brain reactivity pattern, is illustrated through the line chart at the bottom of the screen (red: 0.5-1; blue: 0-0.5). Concurrently, the meth cue picture at the screen's top updated according to the line chart (closed-loop). Elevated probabilistic score corresponded to updates involving pictures of heightened craving. (D) Screenshot presentation during NF transfer-learning. The screen stayed all-blank without feedback. (E) Go/No-go task based on meth-related cues. In the 'Drug No-go' condition, participants press the 'space' bar for neutral pictures and refrain from responding to meth-related pictures.

Results: Short-term effects Real-NFG I had a significantly better NF performance than Yoke-NFG (Fig. 2A). A two-way mixed-design ANOVA showed a significant group*Visit interaction for both training-learning ($F = 6.057$, $p = 0.017$), transfer-learning ($F = 7.144$, $p = 0.009$) probabilistic score, d-prime of Go/No-go task (Fig. 2B). And negative correlation was observed between them in Real-NFG I (Fig. 2C). Craving was significantly reduced in Real-NFG than Yoke-NFG ($t = -2.106$, $p = 0.041$). Moreover, cluster-based ERP analyses yielded a significant increase in N2 for Real-NFG I ($t = 2.285$, $p = 0.031$) but not for Yoke-NFG ($t = -0.610$, $p = 0.547$). Long-term effects Craving in Real-NFG I significantly decreased compared with Yoke-NFG (Fig. 2D), and this reduction was correlated with NF performance in Real-NFG I ($r = -0.380$, $p = 0.035$) but not in Yoke-NFG ($r = -0.108$, $p = 0.556$). Moreover, the two groups exhibited significant differences in beta time-frequency (TF) power change (Fig. 2E), and this change correlated with NF performance ($r = -0.430$, $p = 0.022$) and craving ($r = 0.437$, $p = 0.020$) in Real-NFG I but not in Yoke-NFG (NF: $r = 0.136$, $p = 0.472$; craving: $r = 0.259$, $p = 0.166$). Furthermore, significant group differences emerged in changes of questionnaires of BDI ($t = 2.164$, $p = 0.035$) and BIS ($t = 2.627$, $p = 0.011$). Notably, the Real-NFG was more likely not to contact old friends who used meth (Fig. 2F). Effects prediction SVM predicts short-term effects with 79.31% accuracy (Fig. 2G) and long-term with 78.57% accuracy (Fig. 2H). Effects replication Real-NFG II significantly deactivated the NF probabilistic score (Fig. 2I), increased d-prime (Fig. 2J). And positive correlation between them was observed ($r = -0.344$, $p = 0.192$). Moreover, the effects prediction classifier built in Sample I has an accuracy of 75% in Sample II (Fig. 2K).

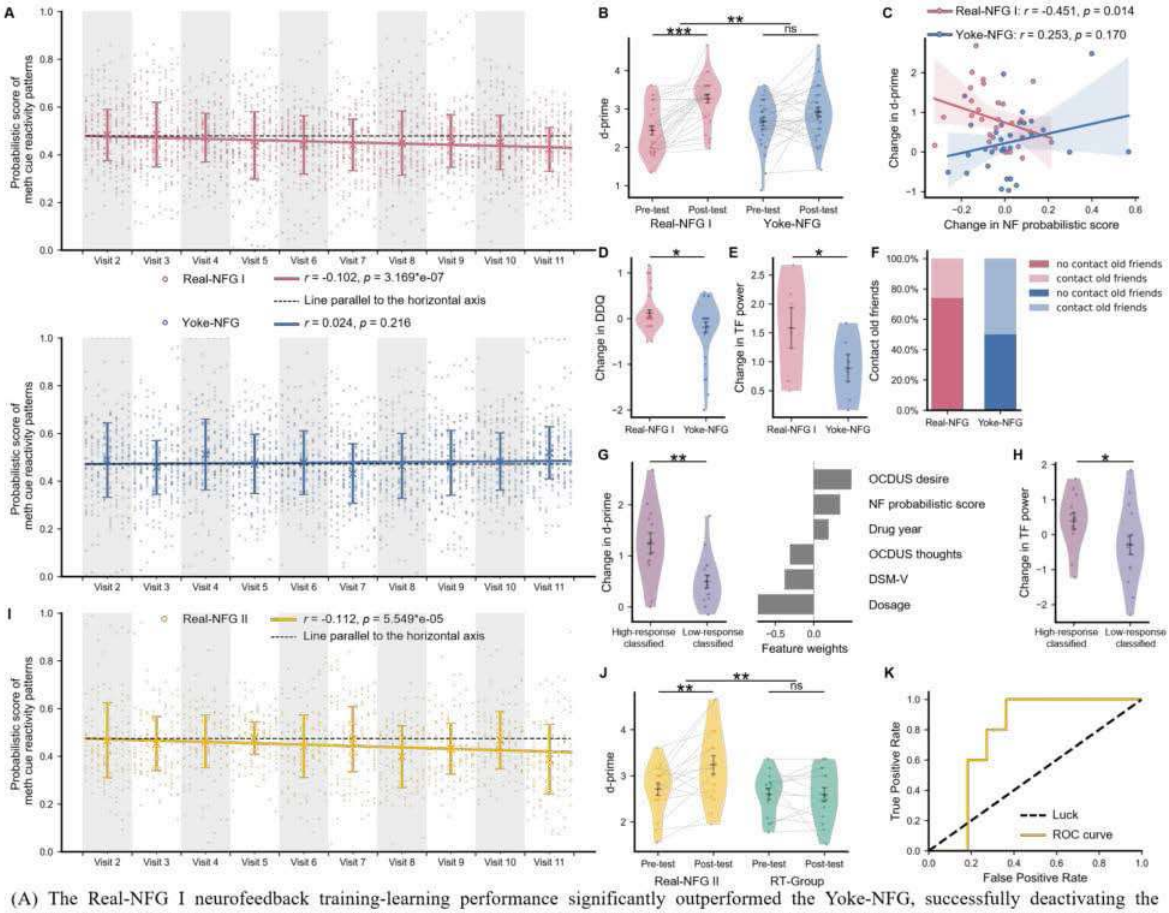

(A) The Real-NFG I neurofeedback training-learning performance significantly outperformed the Yoke-NFG, successfully deactivating the neurofeedback signal in ten neurofeedback Visits. Each neurofeedback Visit consisted of 8 training-learning cycles, and each hollow circle represents the average probabilistic score for one participant across one training-learning cycle. (B) D-prime in the 'drug No-go' condition for the Real-NFG I and the Yoke-NFG ($F = 8.733$, $p = 0.005$). (C) The change in the probabilistic score of meth cue reactivity patterns is positively related with the change in d-prime in the Real-NFG I, but not in the Yoke-NFG. (D) Change in craving (Drug Desired Questionnaire, DDQ, $t = 2.305$, $p = 0.025$). (E) Change of TF power ($t = 2.012$, $p < 0.050$). (F) Situation of contact with old friends who used meth after discharge of Real-NFG I (23.3%) and Yoke-NFG (50.0%, $p = 0.030$). (G) Short-term effects prediction. Real-NFG I were categorized into high- and low-response groups based on the median change in d-prime. Then employing leave-one-out cross-validation with SVM (linear kernel function) to predict participant's response level to the NF intervention. Changes in d-prime depending on whether participants in Real-NFG I were labeled as high-response or low-response by the classifier (left). Feature weights of the prediction model (right). (H) Long-term effects prediction. Similar to the short-term effects prediction, but based on TF power but not d-prime with SVM (rbf kernel function). (I) The NF probabilistic score significantly deactivated from Visit 2 to Visit. (J) D-prime in the 'drug No-go' condition for the Real-NFG II and the RT-Group ($t = -3.225$, $p = 0.003$). (K) ROC curves for Real-NFG II response classification (AUC = 76.36%).

Conclusions: We deactivated meth CR in MAS by cognition-guided NF, thereby enhancing their RI capability. Participants' baseline NF performance and information could predict the intervention effects. Furthermore, we achieved effects replication in a separate data sample. All of these results suggest that our NF protocol is a promising avenue for drug addiction.

References

1. Bu, J. (2021). 'A Novel Cognition-Guided Neurofeedback BCI Dataset on Nicotine Addiction', Frontiers in Neuroscience, vol. 15, p. 647844
2. Bu, J. (2019). 'Effect of deactivation of activity patterns related to smoking cue reactivity on nicotine addiction', Brain, vol. 142, no. 6, pp. 1827–1841
3. Carter, B. L. (1999). 'Meta-analysis of cue-reactivity in addiction research', Addiction, vol. 94, no. 3, pp. 327–340
4. Ekhtiari, H. (2022). 'Transcranial direct current stimulation to modulate fMRI drug cue reactivity in methamphetamine users: A randomized clinical trial', Human Brain Mapping, vol. 43, no. 17, pp. 5340–5357
5. Paulus, M. P. (2020). 'Neurobiology, Clinical Presentation, and Treatment of Methamphetamine Use Disorder: A Review', JAMA Psychiatry, vol. 77, no. 9, p. 959
6. Potvin, S. (2018). 'Cognitive deficits in individuals with methamphetamine use disorder: A meta-analysis', Addictive Behaviors, vol. 80, pp. 154–160
7. Wang, Y. (2019). 'A virtual reality counterconditioning procedure to reduce methamphetamine cue-induced craving', Journal of Psychiatric Research, vol. 116, pp. 88–94

Poster No 531

Distinct brain functional networks are associated with state- and trait-depression

Wei Zhang[1], Rosie Dutt[2], Daphne Lew[1], Deanna Barch[1], Janine Bijsterbosch[1]

[1]Washington University in St. Louis, Saint Louis, MO, [2]Washington University in St. Louis; University of Chicago, Saint Louis, MO; Chicago, IL

Introduction: Depression is a significant contributor to global disability, affecting over 300 million people worldwide[1]. Despite its broad recognition as a disorder involving large-scale brain networks, the foundational brain mechanisms remain elusive. Although some evidence points to altered connectivity patterns within major brain networks, prior findings often display inconsistency[2,3] or lack replication[4], offering, at best, a partial explanation for a limited proportion of the observed variance[5]. This inconsistency presents an enduring challenge in comprehensively understanding the etiology of depression. One potential contributing factor to this challenge may be the conflation of state (current symptoms; variable) and trait (general propensity; stable) depression. Addressing this issue, this study aims to disentangle state and trait depression, seeking to identify potentially dissociable resting-state correlates for these interconnected yet distinct constructs.

Methods: We analyzed longitudinal data from the UK Biobank, using the resting-state fMRI data (scan1 and follow-up scan2), and depression assessments with Recent Depressive Scale (RDS)[6] at baseline, scan1 and scan2. We differentiated trait from state depression, defining "trait" as individuals in remission (i.e., RDSscan1≤5) with a prior history (i.e., RDSbaseline≥7), and "state" as significant longitudinal fluctuation between two scans (i.e., RDS|scan2-scan1|≥3). We identified N=311 and N=265 participants for state and trait groups, respectively, and selected the same number of control participants with minimal RDS across all time points (RDSbaseline≤5 & RDSscan1≤5 & RDSscan2≤5) and matched on covariates (i.e., sex, age, head motion, scanning site and alcohol intake frequency), using optimal pair matching. The resting-state data were decomposed into a set of 15 modes (i.e., resting-state networks), using Probabilistic Functional Modes (PROFUMO)7. Each mode is described by a spatial map (from which the spatial overlap was estimated as the correlation between each pair of mode spatial maps8), network matrix (i.e., connectivity matrix - estimated as the partial correlation between mode time-courses), and mode amplitude (indicative of overall BOLD signal fluctuations). We obtained these PROFUMO outputs separately per scan per participant. After removing 2 spurious modes, we conducted two separate linear regression models to estimate group differences (i.e., state vs. control, trait vs. control; Fig 1A) in all PROFUMO outputs while accounting for covariates. We also repeated statistical analyses for two subgroups with stricter definitions of "state" (i.e., adding RDSbaseline≤5; N=148) and "trait" (adding PHQonline≥5; N=193) to replicate our findings. False Discover Rate (FDR) was applied to account for multiple testing within each class of PROFUMO output.

Figure 1

A. Group Comparison Equations

State vs. Control

$$^{abs}IDP_{scan2\text{-}scan1} = \beta_1 Group + \beta_2 RDS_{scan1} + \beta_3 Age_{scan1} + \beta_4 Sex_{scan1} + \beta_5 Head\_Motion_{scan1} + \beta_6 Alcohol\_Intake_{scan1}$$

Trait vs. Control

$$IDP_{scan1} = \beta_1 Group + \beta_2 Age_{scan1} + \beta_3 Sex_{scan1} + \beta_4 Head\_Motion_{scan1} + \beta_5 Alcohol\_Intake_{scan1}$$

IDP = imaging derived phenotypes, here are PROFUMO outputs (amplitude, network matrix, spatial map)
abs = absolute value ; scan2-scan1 = changes in IDP between two scans

B. PROFUMO Modes

Mode 8 (M8) and mode 10 (M10) were considered noise modes and thus removed from subsequent analyses.

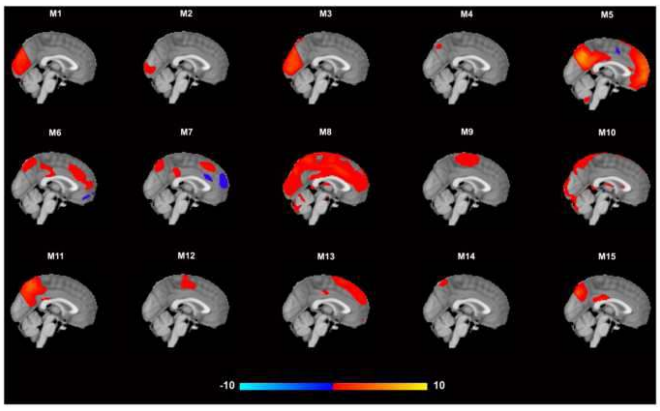

Results: After FDR corrections, we found no significant differences in network matrix (i.e., temporal coupling between modes) or spatial overlap matrix (i.e., similarity of spatial maps between modes) between state and control groups, nor between trait and control groups. However, we observed significantly smaller magnitude of changes in amplitude of the primary and

sensorimotor cortices in individuals with state depression in contrast to controls (β=-0.02, pFDR=0.036), and significantly higher amplitude in the primary visual cortex in individuals with trait depression in contrast to controls (β=0.04, pFDR=0.02). These results replicated in subgroups with stricter definitions of state/trait (p's<0.03).

Figure 2. Group Comparisons in PROFUMO Amplitude

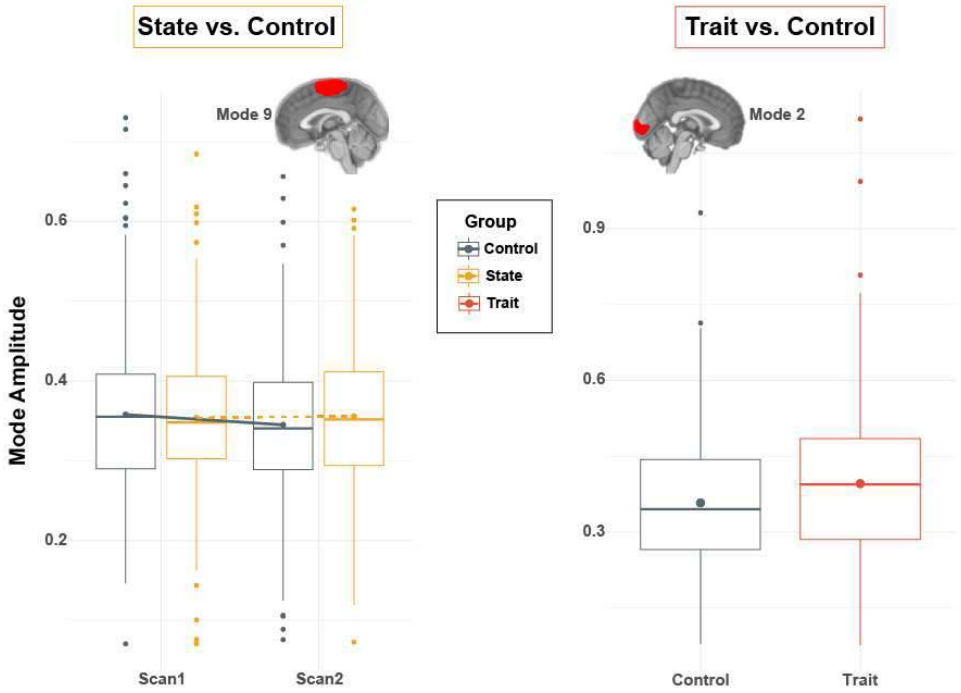

Conclusions: Our findings show that both state and trait depression are associated with abnormal amplitudes of large-scale resting-state networks. Although the motor areas and visual cortex have been consistently implicated in depression symptoms[9,10], our data suggest that these brain circuits may play different roles in differentiating state vs. trait depression experiences.

References

1. Friedrich MJ. Depression Is the Leading Cause of Disability Around the World. JAMA. 2017;317(15):1517. doi:10.1001/jama.2017.3826
2. Greene AS, Shen X, Noble S, et al. Brain–phenotype models fail for individuals who defy sample stereotypes. Nature. 2022;609(7925):109-118. doi:10.1038/s41586-022-05118-w
3. Tozzi L, Zhang X, Chesnut M, Holt-Gosselin B, Ramirez CA, Williams LM. Reduced functional connectivity of default mode network subsystems in depression: Meta-analytic evidence and relationship with trait rumination. Neuroimage Clin. 2021;30:102570. doi:10.1016/j.nicl.2021.102570
4. Kennis M, Gerritsen L, van Dalen M, Williams A, Cuijpers P, Bockting C. Prospective biomarkers of major depressive disorder: a systematic review and meta-analysis. Mol Psychiatry. 2020;25(2):321-338. doi:10.1038/s41380-019-0585-z
5. Schmaal L. The Search for Clinically Useful Neuroimaging Markers of Depression—A Worthwhile Pursuit or a Futile Quest? JAMA Psychiatry. 2022;79(9):845-846. doi:10.1001/jamapsychiatry.2022.1606
6. Dutt RK, Hannon K, Easley TO, Griffis JC, Zhang W, Bijsterbosch JD. Mental health in the UK Biobank: A roadmap to self-report measures and neuroimaging correlates. Hum Brain Mapp. 2022;43(2):816-832. doi:10.1002/hbm.25690
7. Harrison SJ, Bijsterbosch JD, Segerdahl AR, et al. Modelling subject variability in the spatial and temporal characteristics of functional modes. NeuroImage. 2020;222:117226. doi:10.1016/j.neuroimage.2020.117226
8. Bijsterbosch JD, Beckmann CF, Woolrich MW, Smith SM, Harrison SJ. The relationship between spatial configuration and functional connectivity of brain regions revisited. Ivry RB, Honey C, Margulies DS, Seidlitz J, eds. eLife. 2019;8:e44890. doi:10.7554/eLife.44890
9. Ray D, Bezmaternykh D, Mel'nikov M, Friston KJ, Das M. Altered effective connectivity in sensorimotor cortices is a signature of severity and clinical course in depression. Proceedings of the National Academy of Sciences. 2021;118(40):e2105730118. doi:10.1073/pnas.2105730118
10. Wu F, Lu Q, Kong Y, Zhang Z. A Comprehensive Overview of the Role of Visual Cortex Malfunction in Depressive Disorders: Opportunities and Challenges. Neuroscience Bulletin. 2023;39(9):1426. doi:10.1007/s12264-023-01052-7

Poster No 532

Cognition-mediated genetic influences on psychotic symptoms in adolescence

Sarah Chang[1], Dylan Hughes[1], Sullivan Salone[1], Jinhan Zhu[2], Mahnoor Hyat[2], Jennifer Forsyth[3], Carrie Bearden[4]

[1]University of California, Los Angeles, Los Angeles, CA, [2]University of Washington, Seattle, WA, [3]University of Washington, Seattle, CA, [4]University of California at Los Angeles, Los Angeles, CA

Introduction: Across domains of cognitive deficits in schizophrenia (SCZ), attention is among the most significantly impaired. Deficits are present long before onset of overt illness (Reichenberg et al. 2010), and are also observed in unaffected first-degree relatives (Egan et al. 2000). Collectively, findings suggest that attention impairments and accompanying alterations in neurodevelopment may reflect genetic liability to SCZ. While hundreds of genome-wide significant variants associated with SCZ diagnosis have been identified (Trubetskoy et al. 2022), less is known about the genetic etiology of psychotic symptoms across development, and variants implicated in SCZ may be developmentally dynamic. For example, previous work in adolescence shows that polygenic scores (PGS) for ADHD, but not SCZ, are associated with subthreshold psychotic symptoms (Hughes et al. 2023). This study seeks to extend these findings by evaluating whether attention and/or attention-related functional connectivity (FC) may partially explain the effect of genetic risk for ADHD on psychotic-like experiences (PLEs) in adolescence.

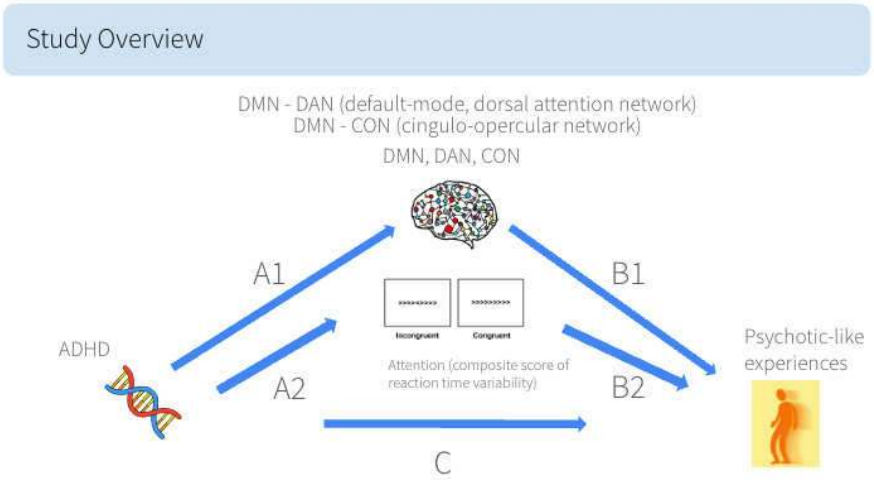

Methods: For a visual representation of these analyses, please see Figure 1. This study leveraged data from 5,385 adolescents of European descent from the Adolescent Brain and Cognitive Development (ABCD) study, spanning 5 yearly study visits (age at baseline study visit: 9-11, female: 49.75%) (Casey et al. 2018). Using linear mixed models, we evaluated associations between ADHD genetic risk, attention, attention-related FC, and psychotic-like experiences. Secondly, we hypothesized that attention or attention-related FC would mediate the relationship between genetic risk and PLEs. Attention was quantified using variability in reaction time (intra-individual variability; IIV) from the NIH Toolbox cognitive battery (Chang et al. 2022). For the ABCD study, MRI acquisition and processing has been described previously (Hagler et al. 2018). Using resting state scans, we focused on within-network FC of three attention-related networks (dorsal attention network, cingulo-opercular network, and default mode network) and between-network FC of the default mode-dorsal attention networks and default mode-cingulo-opercular networks. To address motion and physiological artifacts, we removed resting state scans with framewise displacement (FD) larger than 5mm or had more than half of their volumes censored (due to volumes with framewise displacement >0.3mm or derivative of root mean square variance over voxels >50), consistent with Chen et al. 2023. Genetic risk was estimated using PRS-continuous shrinkage (PRS-CS) and ancestral population was estimated via principal components analysis and random forest classification (Ge et al. 2019). PLEs were measured via the Prodromal Questionnaire - Brief Child Version (Karcher et al. 2018).

Results: We found that greater ADHD PGS was associated with worse attention (ie. greater IIV; β=0.07 [CI: 0.05,0.1]; q=3.81e-10) and more severe psychotic-like experiences (β=0.1 [0.08,0.12], q<2e-16). Worse attention (ie., greater IIV) was also associated with more severe psychotic-like experiences (β=0.1 [0.08,0.11]; q<2e-16). Moreover, we found that worse attention partially mediated the relationship between ADHD PGS and psychotic-like experiences, explaining 7% of the association, according to 10,000 simulation bootstrapping (indirect effect = 0.64 [0.43,0.85], q<2e-16). We also found that reduced within-network dorsal attention network FC (β=0.08 [0.04,0.11]; q=4.18e-5) and weaker between-network default mode-dorsal attention FC (β = - 0.04 [-0.08, -0.01]; q=0.033) was associated with more severe psychotic-like experiences, but had no relationship with ADHD PGS.

Conclusions: Cognitive deficits are non-responsive to current treatments for schizophrenia, motivating this research. Understanding the pathophysiology of cognitive deficits during the early stages of psychosis may be critical for early intervention.

References

1. Reichenberg, A. (2010), 'The assessment of neuropsychological functioning in schizophrenia', Dialogues in Clinical Neuroscience, vol. 12, no. 3, pp. 383-392
2. Egan, M.F. (2000), 'Relative risk of attention deficits in siblings of patients with schizophrenia', American Journal of Psychiatry, vol. 157, no. 8, pp. 1309-1316
3. Trubetskoy, V. (2022), 'Mapping genomic loci implicates genes and synaptic biology in schizophrenia', Nature, vol. 604, no. 7906, pp. 502-508
4. Hughes, D.E. (2023), 'Genetic patterning for child psychopathology is distinct from that for adults and implicates fetal cerebellar development', Nature Neuroscience, vol. 26, no. 6, pp. 959-969
5. Casey, B.J. (2018), 'The Adolescent Brain Cognitive Development (ABCD) study: Imaging acquisition across 21 sites', Developmental Cognitive Neuroscience, vol. 32, pp 43-54.
6. Luciana, M. (2018), 'Adolescent neurocognitive development and impacts of substance use: Overview of the adolescent brain cognitive development (ABCD) baseline neurocognition battery', Developmental Cognitive Neuroscience, vol. 32, pp 67-79.
7. Hagler D.J. (2019), 'Image processing and analysis methods for the Adolescent Brain Cognitive Development Study', Neuroimage, vol. 202, no 116091.
8. Chen, J. (2022), 'Shared and unique brain network features predict cognitive, personality and mental health scores in the ABCD study', Nature Communications, vol. 13, no. 1, pp. 2217
9. Ge, T. (2019), 'Polygenic prediction via Bayesian regression and continuous shrinkage priors', Nature Communications, vol. 10, no. 1, pp 1776
10. Karcher, N.R. (2018), 'Assessment of the Prodromal Questionnaire - Brief Child Version for Measurement of Self-reported Psychoticlike Experiences in Childhood', JAMA Psychiatry, vol. 75, no. 8, pp 853-861

Poster No 533

Task fMRI Investigation of Pain Processing in Adolescent Cannabis Use

Tram Nguyen[1], Gustavo Delgado[2], Samuel Holzman[2], Russell Tobe[3], Vilma Gabbay[4], Benjamin Ely[5]

[1]Albert Einstein College of Medicine, Bronx, NY, [2]Albert Einstein College of Medicine, Bronx, NY, [3]Nathan S. Kline Institute for Psychiatric Research, Orangeburg, NY, [4]University of Miami Miller School of Medicine, Miami, FL, [5]Albert Einstein College of Medicine, New York, NY

Introduction: Despite growing evidence for biobehavioral relationships between pain and cannabis use (Yanes et al. 2018, Gogulski and Craft 2022), there has been sparse research on pain circuitry in adolescent cannabis use. Here, we examined pain processing among adolescent cannabis users and non-users.

Methods: Our study is on-going and recruiting adolescents in the New York City metropolitan area. In this preliminary analysis, we included data from 25 subjects (age: 15.4 ± 2.5 years; 84% female). History of cannabis use was determined from clinician-based interviews, self-reported measures, and urine toxicology screens. MRI was performed on a 3T Siemens Skyra using protocols similar to those of the Human Connectome Project (HCP) Lifespan studies (Van Essen et al. 2012), including anatomical T1w MPRAGE and T2w SPACE (0.9mm isotropic) and fMRI (2.3mm isotropic, TR=1s, 5x multiband). Our electric pain paradigm based on a published protocol (Ma et al. 2016) incorporated out-of-scanner and in-scanner portions (see also our related abstract detailing the task and associations with psychiatric symptoms: Ely BA et al. "Pain Response and Associations with Psychiatric Symptoms Using an Affordable Electric Shock Task"). Pre-scan, an electrode was placed on the dorsal surface of the right foot, and stimulation (100Hz, 0.5ms pulses) was calibrated (0.25V steps, max 10V) to determine when shocks were first painlessly felt (innocuous threshold), became painful (pain threshold), and were as painful as could be tolerated (maximum threshold). Thresholds were confirmed and adjusted as needed in scanner. The task comprised three 5-minute runs, each with 10 trials. For each trial (Fig. 1), the subject was first shown a cue, followed by a fixation cross, then received an electric shock. Post-shock, the subject rated pain level on a 0-10 Visual Analogue Scale. Trials were separated by jittered fixation. Preprocessing steps included motion correction, normalization to MNI space, and mild spatial smoothing (FWHM=4mm). Subject-level data were analyzed using an event-related GLM, as implemented in FSL FEAT (Woolrich et al. 2001), to model neural responses during 1) cues preceding painful vs. non-painful shocks, 2) receipt of painful vs. non-painful shocks, and 3) post-shock pain ratings. At the group level, mixed effects models with FLAME1+2 (Woolrich et al. 2004) and outlier de-weighting were performed. Neural activation across phases of pain processing was compared between cannabis users and non-users as well as correlated with cannabis use frequency across the full sample. Results were controlled for multiple comparisons using cluster-based inference at $Z>2.58$, $p<0.05$.

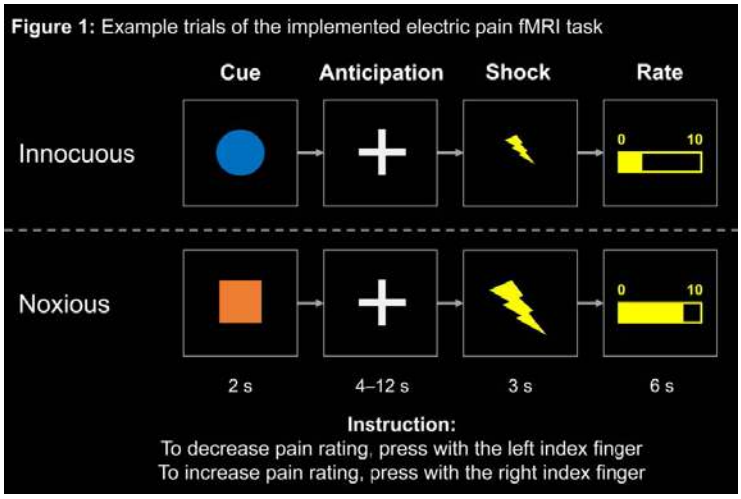

Results: Adolescent cannabis users and non-users exhibited similar neural activation while viewing painful vs. non-painful cues. When experiencing painful vs. non-painful shocks, cannabis users showed stronger activation in the right frontal gyrus, frontal pole, insula, caudate, and bilateral paracingulate gyri (Fig. 2A). During pain rating, the bilateral precentral and postcentral gyri had stronger activation among cannabis users (Fig. 2B). Heavier cannabis use correlated with activation of the right frontal gyrus during shock (Fig. 2C) and the left precentral gyrus during pain rating (Fig. 2D).

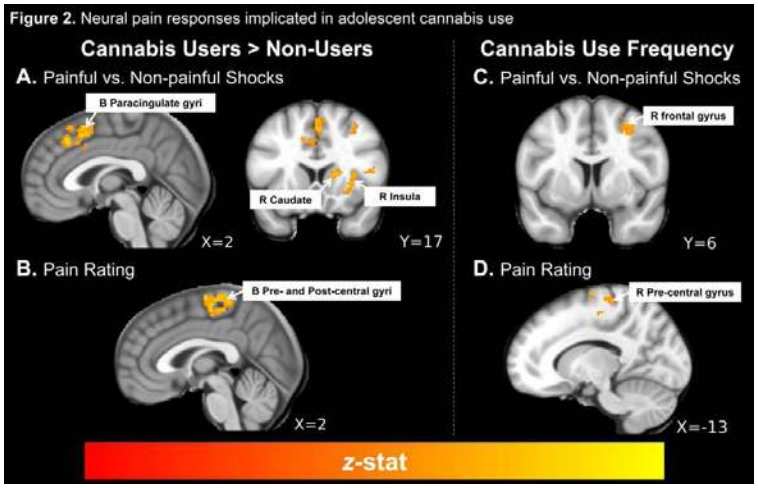

Conclusions: We found that experiencing and rating pain elicited stronger neural responses in adolescent cannabis users than non-users. Though preliminary, these results align with converging evidence for cannabis-associated alterations in pain processing in youth. Recruitment for this study is ongoing, with future analyses to include a larger sample and examine the role of comorbid cannabis use and depression in pain processing.

References

1. Gogulski, H. Y. and R. M. Craft (2022). "Adolescent THC exposure: effects on pain-related, exploratory, and consummatory behaviors in adult male vs. female rats." Psychopharmacology (Berl) 239(5): 1563-1578.
2. Ma, Y. et al. (2016). "Serotonin transporter polymorphism alters citalopram effects on human pain responses to physical pain." Neuroimage 135: 186-196.
3. Van Essen, D. C et al. (2012). "The Human Connectome Project: a data acquisition perspective." Neuroimage 62(4): 2222-2231.
4. Woolrich, M. W. et al. (2004). "Multilevel linear modelling for FMRI group analysis using Bayesian inference." Neuroimage 21(4): 1732-1747.
5. Woolrich, M. W. et al. (2001). "Temporal autocorrelation in univariate linear modeling of FMRI data." Neuroimage 14(6): 1370-1386.
6. Yanes, J. A. et al. (2018). "Neuroimaging meta-analysis of cannabis use studies reveals convergent functional alterations in brain regions supporting cognitive control and reward processing." J Psychopharmacol 32(3): 283-295.

Poster No 534

COVID-19 affects white matter microstructure in healthy populations and major depressive disorder

Taipeng Sun[1], Yonggui Yuan[2], Chenguang Jiang[2], Wenhao Jiang[2], Gang Chen[2], Wei Xu[2], Linlin You[2], Yue Zhou[2]

[1]ZhongDa Hospital, School of Medicine, Southeast University, Nanjing, Jiangsu, [2]ZhongDa Hospital; School of Medicine, Southeast University, Nanjing, Jiangsu

Introduction: Coronavirus disease-2019(COVID-19) infection has been reported to be associated with multiple neuropsychiatric complications including depression, insomnia, cognitive impairment, and anosmia. However, information on brain alterations in individuals affected by COVID-19 is limited. Consistently, Major Depressive Disorder (MDD) patients also have specific structural and functional brain abnormalities, but the effect of COVID-19 on the brain structure and function in MDD remains undefined.

Methods: We enrolled 2 populations (healthy population and MDD), four cohorts: 57 healthy controls (HC) post- COVID-19 infection, 108 age- and gender-matched HC pre-COVID-19 infection; 79 MDD post- COVID-19 infection, 165 age- and gender-matched MDD pre-COVID-19 infection. For all subjects, we acquired T1-weighted MRI, fMRI, and diffusion tensor imaging (DTI), calculated regional cortical thickness, surface area, subcortical volume, Amplitude of Low-Frequency Fluctuations (ALFF), regional homogeneity (ReHo), functional connectivity (FC), and fractional anisotropy (FA) to quantify Gray and white matter structural and functional abnormalities. Group comparisons were analyzed with ANCOVA, and Bonferroni correction was applied for multiple comparisons.

Results: We found widespread decreased FA values (PBonferroni<0.05) in post-COVID-19 infected HC compared to pre-COVID-19 infected HC in 20 white matter tracts, and 2 FC (left Superior longitudinal fasciculus-left Anterior thalamic radiation, left Superior longitudinal fasciculus-left Uncinate fasciculus) were significantly decreased (PBonferroni<0.05) in post-COVID-19 infected HC. ALFF and ReHo values in white matter tracts between HC pre- and post-COVID-19 infection had no significant differences after Bonferroni correction. In gray matter, there were no significant differences in cortical thickness, surface area, subcortical volume, ALFF, ReHo, and FC between HC pre- and post-COVID-19 infection. Our study also found FA values were decreased in bilateral Superior longitudinal fasciculus, left Anterior thalamic radiation, left Cingulum (cingulate gyrus), and Forceps minor in post-COVID-19 infected MDD compared to pre-COVID-19 infected MDD (PBonferroni<0.05). ALFF values in left Cingulum hippocampus and right Uncinate fasciculus had significant differences after Bonferroni correction between MDD pre- and post-COVID-19 infection. In gray matter, we found ALFF values were increased in left Amygdala, left Parahippocampal gyrus, and bilateral Supplementary motor area, and decreased in left Angular gyrus in post-COVID-19 infected MDD compared to pre-COVID-19 infected MDD. Other gray matter indicator (cortical thickness, surface area, subcortical volume, ReHo, FC) had no significant differences among two MDD groups.

Conclusions: COVID-19 significantly impairs the microstructure of white matter fibers in healthy individuals, and exacerbated white matter microstructural injury of MDD. Of note, the appearance of COVID-19 induced functional impairment may precede structure impairment of gray matter in MDD. Above all, our study results highlighted that the impact of COVID-19 on white matter is sensitive compared to gray matter, and the potential influence of COVID-19 in future neuroimaging studies should be fully considered, especially in white matter studies.

References

1. Ballering AV.(2022)," Persistence of somatic symptoms after COVID-19 in the Netherlands: an observational cohort study". Lancet. 2022. 400(10350),pp,452-461
2. Segal A.(2023), " Regional, circuit and network heterogeneity of brain abnormalities in psychiatric disorders". Nat Neurosci. 2023. 26(9),pp,1613-1629.

Poster No 535

Brain Gene Expression of Insomnia Disorder is Associated with Brain Function, rather than Structure

Haobo Zhang[1,2], Haonan Sun[1,2], Jiatao Li[1,2], Zhangwei Lv[1,2], Lei Xu[1,2]

[1]Sleep and NeuroImaging Center, Faculty of Psychology, Southwest University, Chongqing, China, [2]Key Laboratory of Cognition and Personality of Ministry of Education, Chongqing, China

Introduction: The etiology of insomnia disorder (ID) is very complex and potentially influenced by genetic factors (Jansen & Watanabe, 2019; Madrid-Valero et al., 2021). However, the ID is highly polygenic, determined by many combinations of variants in many genes that each individually have a very small effect (Van Someren, 2021). Previous research has highlighted the abnormalities of specific brain regions among ID, including altered brain function and/or structure (Spiegelhalder et al., 2013).

In this context, an interesting question is whether the observed abnormalities in brain structure and function, obtained by neuroimaging techniques, are influenced by genetic factors in ID. Therefore, we want compare the different contribution of gene expression in functional and structural neuroimaging in ID, which is an interesting topic, by magnetic resonance imaging (MRI) and Allen Human Brain Atlas (AHBA) (Hawrylycz et al., 2012).

Methods: The data included 264 ID (58 male, M = 39.08, SD = 15.49) recruited from three hospitals in Chongqing according to DSM-V diagnostic criteria and 129 healthy controls (HC, 101 male, M = 38.91, SD = 14.44). Resting-state functional images and high-resolution structural images were acquired for each subject. After preprocessing, we calculated amplitude of low-frequency fluctuation, fractional ALFF, and regional homogeneity. Then, with human Brainnetome (BN) atlas, three functional measures and gray matter volume (GMV) were calculated for 210 brain cortical regions. For AHBA data, we obtained the Gene Expression after processing according to the guide of previous study (Arnatkeviciute et al., 2019). We used two-sample t-test to assess the differences in ALFF, fALFF, ReHo and GMV between groups. Converting T-values to Cohen's d effect for observing the differences. The p-values were adjusted using the false discover rate (FDR, $p < 0.05$). We utilized Principal Component Analysis (PCA) to extract the first principal component (funcPC1) among three functional measures. Similarly, the first principal component was extracted from the gene expression matrix (genePC1). Using Spearman's rank correlation analysis to investigate the association between whole brain gene expression and brain abnormalities, and significant ID-related genes. Finally, we annotated the function of ID-related genes by enrichment analysis.

Results: Compared to the healthy group, the IDs exhibited similar difference patterns in three functional measures, there was an increase in neuronal activity in lateral regions and a decrease in activity in medial regions. Furthermore, PCA was applied to extract the first principal component of effect sizes for three functional measures, which explained 71% variance of functional brain abnormalities in ID. In terms of GMV, decreased GMV in frontal cortex and increased GMV in temporal cortex were observed (Figure 1). The correlation analysis revealed that genePC1 was negatively correlated with funcPC1, but not with GMV differences. Then, it was observed that the gene expression of 1336 genes exhibited significant positive correlations with funcPC1, while gene expression of 1550 genes showed significant negative correlations with funcPC1 (Figure 2). For funcPC1+ genes, we observed enriched pathways such as development, synaptic transmission, and regulation processes. For funcPC1- genes, significant enrichment was mainly found for transport processes and signal transmission.

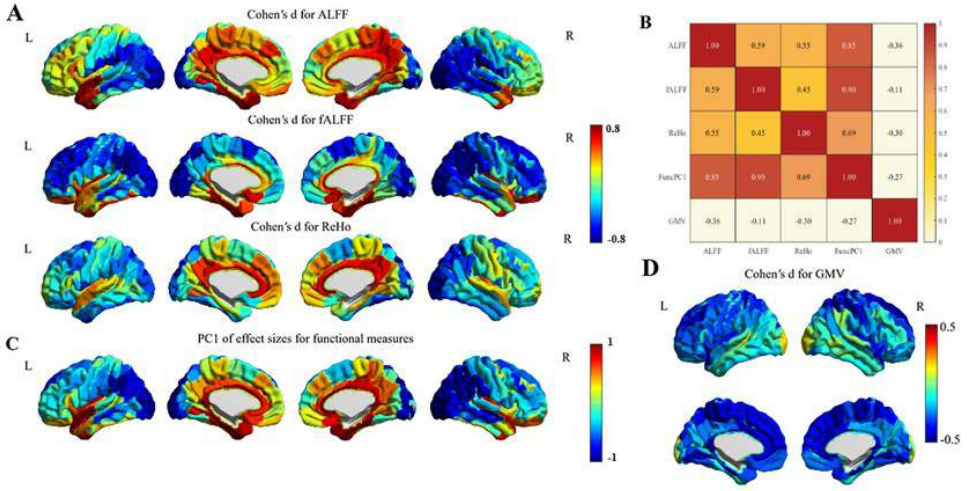

Figure 1. Brain differences between patients and the control across 210 cortical regions. A) Differences for functional brain measures including amplitude of low-frequency fluctuation (ALFF), fractional ALFF (fALFF), and regional homogeneity (ReHo); B) the correlations between case-control differences; C) the first principle component of effect sizes for three functional measures (funcPC1); D) differences for gray matter volume (GMV).

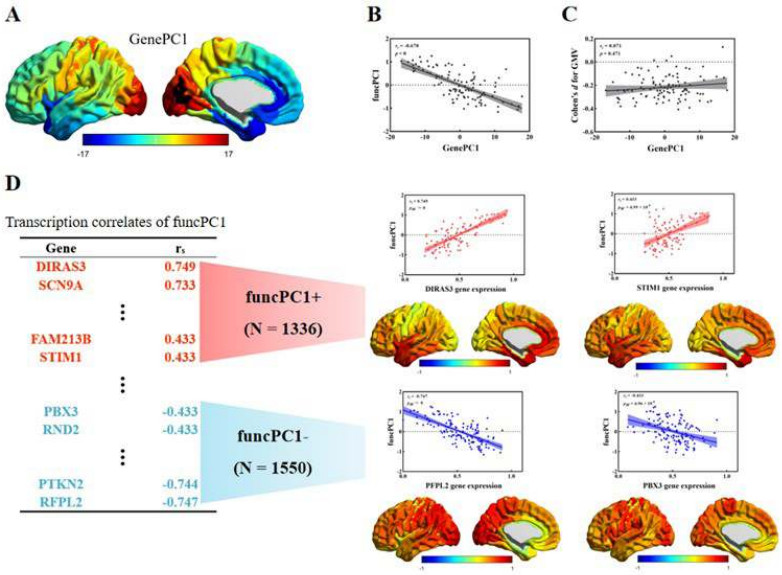

Figure 2. Relations of gene expression with case-control differences for 105 cortical regions (Left hemisphere). A) The first principal component of gene expression (GenePC1); B) Relationships between GenePC1 and the first principal component of three functional measures (funcPC1); C) Relationships between GenePC1 and gray matter volume (GMV) differences; D) Genes positively or negatively related to funcPC1 (funcPC1+ or funcPC1-), with descending order of *r*. The four images in the lower right corner show the highest and lowest correlation genes in the whole brain expression patterns and correlation maps of funcPC1+ and funcPC1-, respectively. p_{BF}, the *p* values corrected by Bonferroni multiple testing correction; r_s, Spearman's correlation coefficient.

Conclusions: Gene expression is associated with functional, but not structural brain abnormalities in ID. Additionally, ID-related genes are enriched in brain tissue, cortex, cells, and biological pathways. The above findings suggest that abnormal brain gene expression may lead to dysfunction of the HPA axis, neurotransmitter disorders and hyper-arousal in ID. Future studies focusing on the classification of insomnia subtypes should be based on brain structure rather than brain function, which maybe more effective.

References

1. Arnatkeviciute, A., Fulcher, B. D., & Fornito, A. (2019). A practical guide to linking brain-wide gene expression and neuroimaging data. Neuroimage, 189, 353-367. https://doi.org/10.1016/j.neuroimage.2019.01.011
2. Hawrylycz, M. J., Lein, E. S., Guillozet-Bongaarts, A. L., Shen, E. H., Ng, L., Miller, J. A., van de Lagemaat, L. N., Smith, K. A., Ebbert, A., Riley, Z. L., Abajian, C., Beckmann, C. F., Bernard, A., Bertagnolli, D., Boe, A. F., Cartagena, P. M., Chakravarty, M. M., Chapin, M., Chong, J., Dalley, R. A., David Daly, B., Dang, C., Datta, S., Dee, N., Dolbeare, T. A., Faber, V., Feng, D., Fowler, D. R., Goldy, J., Gregor, B. W., Haradon, Z., Haynor, D. R., Hohmann, J. G., Horvath, S., Howard, R. E., Jeromin, A., Jochim, J. M., Kinnunen, M., Lau, C., Lazarz, E. T., Lee, C., Lemon, T. A., Li, L., Li, Y., Morris, J. A., Overly, C. C., Parker, P. D., Parry, S. E., Reding, M., Royall, J. J., Schulkin, J., Sequeira, P. A., Slaughterbeck, C. R., Smith, S. C., Sodt, A. J., Sunkin, S. M., Swanson, B. E., Vawter, M. P., Williams, D., Wohnoutka, P., Zielke, H. R., Geschwind, D. H., Hof, P. R., Smith, S. M., Koch, C., Grant, S. G. N., & Jones, A. R. (2012). An anatomically comprehensive atlas of the adult human brain transcriptome. Nature, 489(7416), 391-399. https://doi.org/10.1038/nature11405
3. Jansen, P. R., & Watanabe, K. (2019). Genome-wide analysis of insomnia in 1,331,010 individuals identifies new risk loci and functional pathways. 51(3), 394-403. https://doi.org/10.1038/s41588-018-0333-3
4. Madrid-Valero, J. J., Rubio-Aparicio, M., Gregory, A. M., Sánchez-Meca, J., & Ordoñana, J. R. (2021). The heritability of insomnia: Systematic review and meta-analysis of twin studies. Sleep Med Rev, 58, 101437. https://doi.org/10.1016/j.smrv.2021.101437
5. Spiegelhalder, K., Regen, W., Baglioni, C., Riemann, D., & Winkelman, J. W. (2013). Neuroimaging studies in insomnia. Curr Psychiatry Rep, 15(11), 405. https://doi.org/10.1007/s11920-013-0405-0
6. Van Someren, E. J. W. (2021). Brain mechanisms of insomnia: new perspectives on causes and consequences. Physiol Rev, 101(3), 995-1046. https://doi.org/10.1152/physrev.00046.2019

Poster No 536

Functional connectivity alterations in depression and their associations with gene expression

Rui Qian[1], Huaijin Gao[1], Chengjiaao Liao[1], Wen Zhu[1], Minmin Wang[2], Dan Wu[1], Zhiyong Zhao[1]

[1]Zhejiang University, Hangzhou, China, [2]Qiushi Academy for Advanced Studies, Zhejiang University, Hangzhou, China

Introduction: Major Depressive Disorder (MDD) has persisted as one of the predominant psychiatric disorders for over a century, exerting a substantial adverse impact on patients' life. Previous studies have reported aberrant functional

connectivity strength (FCS) in MDD, which exhibited distinct patterns in first-episode, drug-naïve (FEDN) and recurrent MDD (RMDD)[1,2]. However, the molecular basis of FCS differences between first-episode and recurrent MDD remains unexplored. Recent studies have demonstrated a close relationship between FCS and gene expression in the brain cortex of healthy populations[3]. Therefore, this study aims to explore the genetic basis underlying the differences of FCS among different MDD subtypes.

Methods: Resting-state fMRI data from the REST-meta-MDD Consortium were utilized in this study, comprising four paired groups: 848 MDD and 794 normal control (NC), 232 FEDN and 394 NC, 189 RMDD and 427 NC, 119 FEDN and 72 RMDD. The brain was divided into 116 regions of interest (ROI) according to Anatomical Automatic Labeling (AAL) atlas, and then ROI-wise FCS was calculated using Pearson correlation with a threshold of $R \geq 0.25$[4]. Finally, we compared differences between groups using a linear mixed model controlling age, sex, education and head motion as covariates, and site as a random factor[5]. False Discovery Rate (FDR) correction was used to control false positive discoveries. The ROI-wise gene expression profile was obtained from the AHBA database using abagen toolbox[6] with AAL atlas. Then, partial least squares (PLS) regression analysis[7] was employed to explore the association between transcriptional profiles and FCS differences. Finally, the genes were ranked based on corrected weights reflecting their contribution to the PLS regression component, and further were applied to enrichment analysis to identify enriched Gene Ontology terms using Gorilla[8] (http://cbl-gorilla.cs.technion.ac.il/), considering all three ontology categories: biological process, molecular function, and cellular component.

Results: Significant increase in FCS was observed in the left angular gyrus in total MDD and in the right posterior cingulate gyrus, left and right thalamus, and cerebellum in RMDD compared to NC (Fig. 1). No significant difference was found between FEDN and NC and between FEDN and RMDD. The first PLS component (PLS1) showed the highest interpretable variance among all components (25.4% for FEDN vs. NC, 35.9% for RMDD vs. NC). The PLS1 showing positive correlation with FCS alteration in FEDN displayed high expression in the frontal lobe and primary motor cortex but low expression in the occipital and temporal lobes (Fig. 2a), while that in RMDD showed low expression across the entire brain, especially in the frontal and parietal regions (Fig. 2b). Moreover, the PLS1 gene sequence enriched in the biological process of the electron transport chain for FEDN (Fig. 2c), whereas it enriched in the biological process of regulation of nucleic acid-related metabolic processes for RMDD (Fig. 2d).

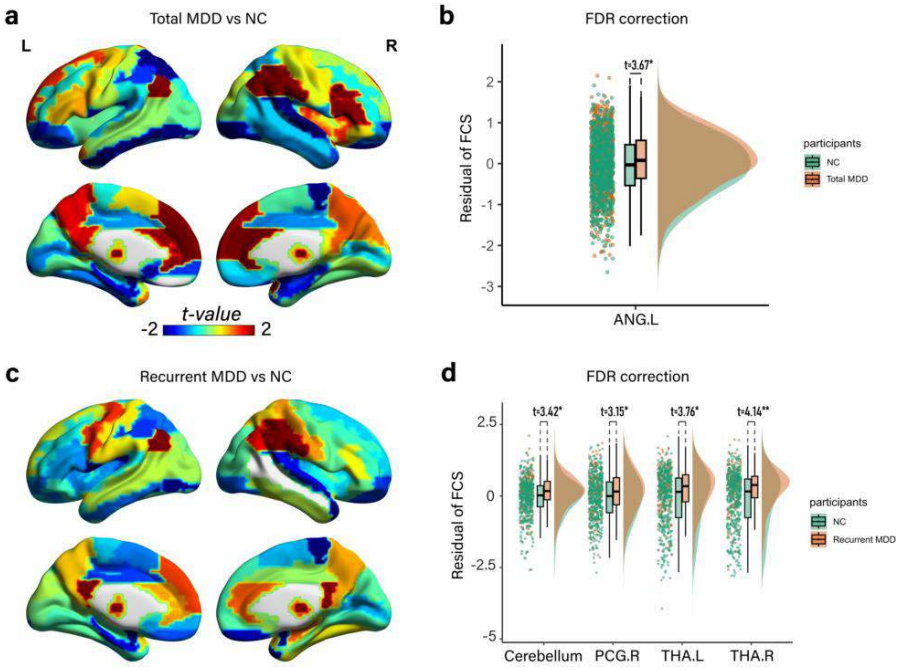

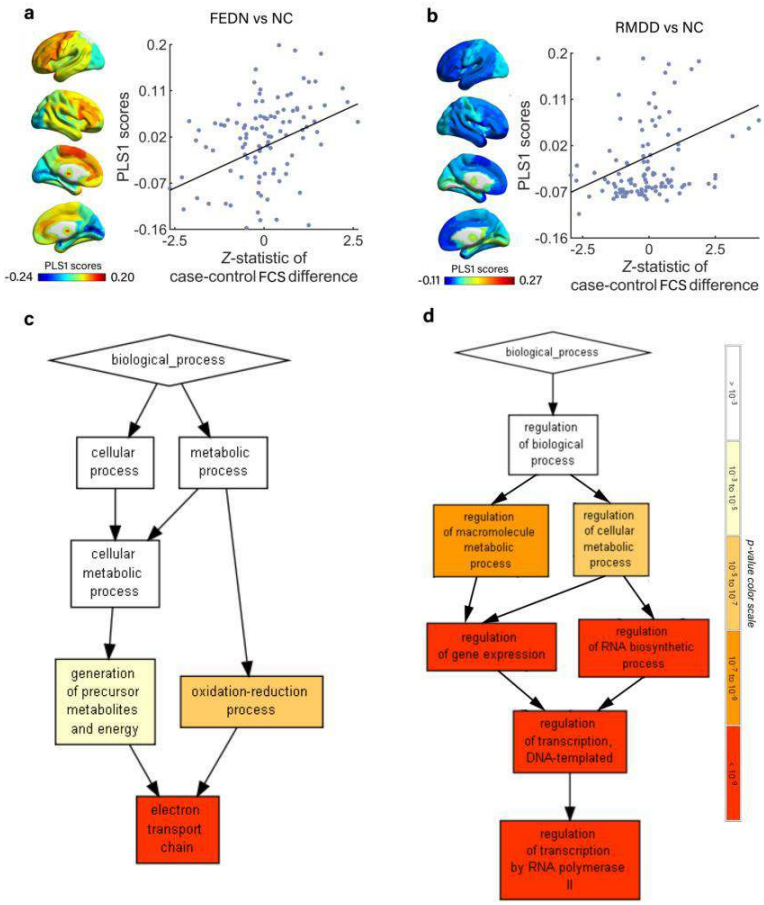

Conclusions: We found RMDD showed FCS values increase in several brain regions, while FEDN had no significant alterations compared with NC. This supported previous findings that FEDN and RMDD differed in functional connectivity abnormality[2]. Moreover, transcription-neuroimaging association analysis demonstrated that the genes related to FCS alterations of MDD subtypes enriched in distinct biological processes, specifically electron transposition in the mitochondrion for FEDN and nucleic acid metabolism for RMDD, which were related to mitochondrial dysfunction and epigenetic modification role as molecular pathways of MDD[9]. These findings offer new insights into the biological substrates underlying FCS differences between MDD patients and NC.

References

1. Shi, Y., Li, J., Feng, Z., et al. (2020). Abnormal functional connectivity strength in first-episode, drug-naive adult patients with major depressive disorder. Progress in Neuropsychopharmacology & Biological Psychiatry, 97, 109759. https://doi.org/10.1016/j.pnpbp.2019.109759
2. Yan, C. G., Chen, X., Li, L., et al. (2019). Reduced default mode network functional connectivity in patients with recurrent major depressive disorder. Proceedings of the National Academy of Sciences of the United States of America, 116(18), 9078-9083. https://doi.org/10.1073/pnas.1900390116
3. Zhu, D., Yuan, T., Gao, J., Xu, Q., Xue, K., Zhu, W., Tang, J., Liu, F., Wang, J., & Yu, C. (2021). Correlation between cortical gene expression and resting-state functional network centrality in healthy young adults. Human Brain Mapping, 42(7), 2236-2249. https://doi.org/10.1002/hbm.25362
4. Tomasi, D., & Volkow, N. D. (2010). Functional connectivity density mapping. Proceedings of the National Academy of Sciences of the United States of America, 107(21), 9885-9890. https://doi.org/10.1073/pnas.1001414107
5. Luo, C., Islam, M. N., Sheils, N. E., Buresh, J., Reps, J., Schuemie, M. J., ... Chen, Y. (2022). DLMM as a lossless one-shot algorithm for collaborative multi-site distributed linear mixed models. Nature Communications, 13(1), 1678. https://doi.org/10.1038/s41467-022-29160-4
6. Markello, R. D., Arnatkeviciute, A., Poline, J. B., Fulcher, B. D., Fornito, A., & Misic, B. (2021). Standardizing workflows in imaging transcriptomics with the abagen toolbox. eLife, 10, e72129. https://doi.org/10.7554/eLife.72129
7. Abdi, H., & Williams, L. J. (2013). Partial least squares methods: partial least squares correlation and partial least square regression. Methods in Molecular Biology, 930, 549-579. https://doi.org/10.1007/978-1-62703-059-5_23
8. Eden, E., Navon, R., Steinfeld, I., Lipson, D., & Yakhini, Z. (2009). GOrilla: a tool for discovery and visualization of enriched GO terms in ranked gene lists. BMC Bioinformatics, 10, 48. https://doi.org/10.1186/1471-2105-10-48
9. Fries, G. R., Saldana, V. A., Finnstein, J., & Rein, T. (2023). Molecular pathways of major depressive disorder converge on the synapse. Molecular Psychiatry, 28(1), 284-297. https://doi.org/10.1038/s41380-022-01806-1

Poster No 537

Functional Network Dysconnectivity in Schizophrenia Independent of Medication and Illness Duration

Kyle Jensen[1,2], Adithya Ram Ballem[1,2], Pablo Andrés-Camazón[3,1], Shalaila Haas[4,1], Jiayu Chen[1,2], Zening Fu[1,2], Vince Calhoun[1,2], Armin Iraji[1,2]

[1]Tri-institutional Center for Translational Research in Neuroimaging and Data Science (TReNDS), Atlanta, GA, [2]Georgia State University, Atlanta, GA, [3]Hospital General Universitario Gregorio Marañón, Madrid, Spain, [4]Icahn School of Medicine at Mount Sinai, New York, NY

Introduction: Recent efforts in neuroscience seek to re-define schizophrenia (SZ) as a disorder of the brain by identifying abnormalities in functional circuitry. Symptoms of SZ (e.g., psychosis) are believed to be caused by disruptions in cortical-subcortical-cerebellar circuitry[1]. Resting-state functional magnetic resonance imaging (rs-fMRI) has been used to investigate and identify abnormal functional network connectivity (FNC) linked to SZ[2]. Specifically, previous studies have highlighted patterns of SZ-related aberrant cerebello-thalamo-cortical connectivity (CTCC) in networks involving the motor cortices, thalamic and subthalamic nuclei, the cerebellum, and the prefrontal cortex[2,3]. However, these results are likely influenced by various confounds including changes in the brain over time due to cortical atrophy[4] as well as the effects of medication usage[5]. The current study seeks to disentangle the effects of medication and duration of illness through a data-driven approach to examine whole-brain FNC in individuals with SZ.

Methods: rs-fMRI as well as demographic and clinical features from a large multisite dataset (18 individual sites aggregated from multiple prior studies) was used in the current analyses. In order to investigate the impact of medication and duration of illness, participants with SZ were excluded from the analysis if they lacked this information. Our clinical dataset included 1288 participants (729 Male; mean age 34.96 ± 11.73 years; 45.89% Caucasian, 22.05% African American, 26.63% Asian, 5.43% Other), with 362 individuals with SZ (242 Male; mean age 39.10 ± 12.11 years; mean duration of illness 18.32 ± 12.26 years; mean chlorpromazine equivalence dosage (CPZ) 398.12 ± 332.72 mg), and 926 individuals considered typical controls (487 Males; mean age 33.34 ± 11.18 years). We applied multivariate-objective optimization ICA with reference (MOO-ICAR) and our recently developed multi-spatial-scale intrinsic connectivity networks (ICNs) optimized from 100K+ human participants[6] to identify 105 subject-specific ICNs from preprocessed rs-fMRI data. Postprocessing was performed on the ICN time courses, including steps to remove additional noise effects through detrending, despiking, regression of head motion, and band-pass filtering [0.01-0.15 Hz]. A subject-specific functional network connectivity (FNC) matrix was calculated by a Pearson correlation between all pairs of the 105 ICNs. We conducted a statistical case/control comparison to identify differences in FNC between individuals with SZ and controls. For each FNC, a general linear model was applied, correcting for age, sex, race, imaging site, head motion, CPZ, and duration of illness. We adjusted for multiple comparisons using the false discovery rate (FDR) correction.

Results: Widespread disruptions in functional circuitry were observed across the whole brain in individuals with SZ, indicated by statistically significant case/control differences in visual (VIS), cerebellar (CB), temporal (TM), subcortical (SC), sensorimotor (SM), and higher cognitive (HC) domains (see Fig 1).

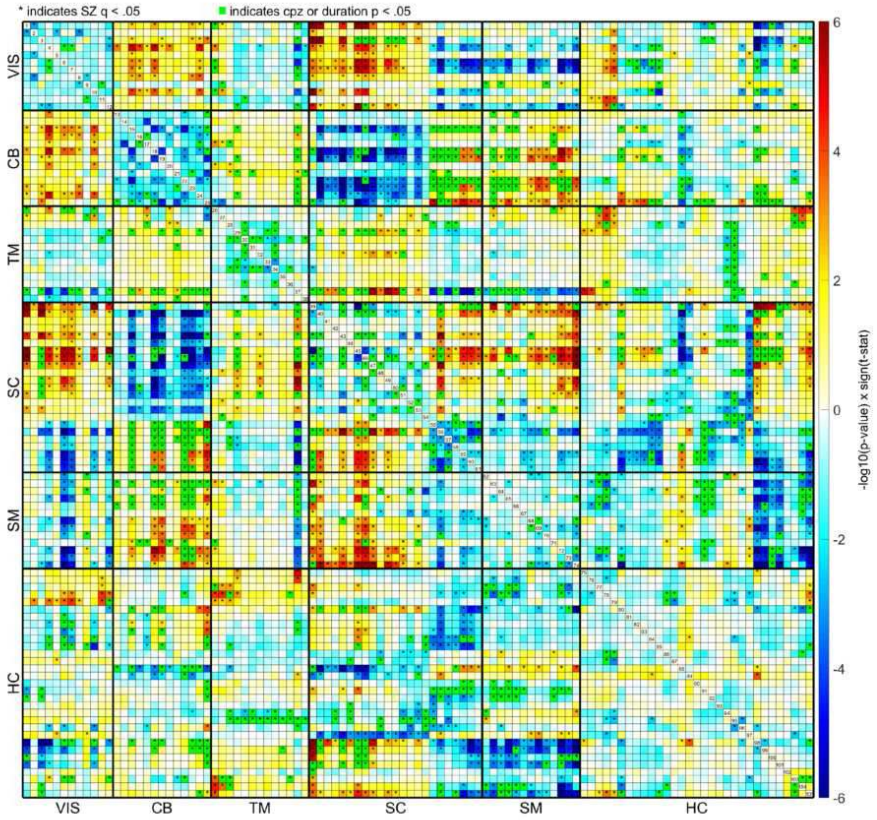

Figure 1 | Results of the general linear model (GLM) for each combination of the 105 Neuromark intrinsic connectivity networks (ICNs). Significant ($q < 0.05$) schizophrenia/control group associations with functional network connectivity (FNC) are marked with an asterisk. Significant ($q < 0.05$) schizophrenia/control group associations with FNC which are also associated with medication or duration of illness ($p < 0.05$) are highlighted in green.

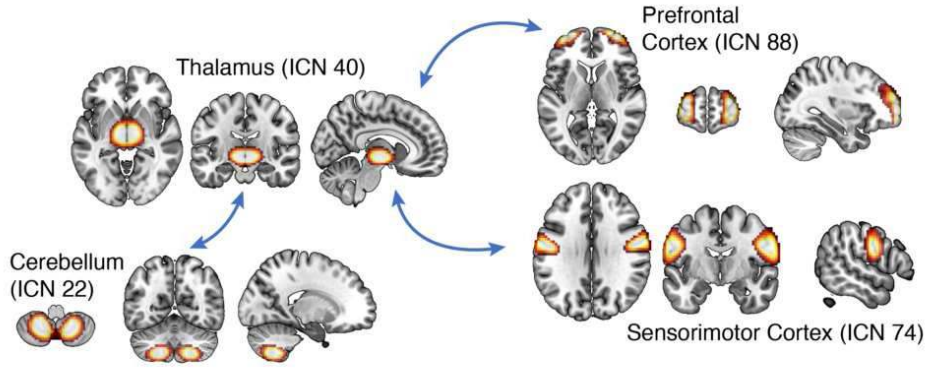

Figure 2 | Spatial maps for notable intrinsic connectivity networks (ICNs) consistent with a CTCC model of schizophrenia are displayed above. Notably we observed dysconnectivity between these ICNs independent of medication and duration of illness.

Conclusions: The patterns of dysconnectivity in functional circuitry observed between CB, SC, and cortical ICNs lends further insight into a CTCC model of SZ (See Fig 2). Furthermore, while medication and duration of illness remain pervasive confounds in SZ research, our analytical approach enabled us to observe many patterns of dysconnectivity associated with SZ which were unrelated to these effects. An increased understanding of the neural underpinnings of SZ will undoubtedly improve diagnosis and treatment outcomes.

References

1. K. J. Friston, "The disconnection hypothesis," Schizophr. Res., vol. 30, no. 2, pp. 115–125, Mar. 1998, doi: 10.1016/S0920-9964(97)00140-0.
2. A. Harikumar et al., "Revisiting Functional Dysconnectivity: a Review of Three Model Frameworks in Schizophrenia," Curr. Neurol. Neurosci. Rep., Nov. 2023, doi: 10.1007/s11910-023-01325-8.

3. K. M. Jensen et al., “A whole-brain Neuromark resting-state fMRI analysis of first-episode and early psychosis: Evidence of aberrant cortical-subcortical-cerebellar functional circuitry.” OSF, Oct. 06, 2023. doi: https://doi.org/10.31234/osf.io/7kdt4.
4. L. E. DeLisi, K. U. Szulc, H. C. Bertisch, M. Majcher, and K. Brown, “Understanding structural brain changes in schizophrenia,” Dialogues Clin. Neurosci., vol. 8, no. 1, pp. 71–78, Mar. 2006.
5. B.-C. Ho, N. C. Andreasen, S. Ziebell, R. Pierson, and V. Magnotta, “Long-term Antipsychotic Treatment and Brain Volumes: A Longitudinal Study of First-Episode Schizophrenia,” Arch. Gen. Psychiatry, vol. 68, no. 2, pp. 128–137, Feb. 2011, doi: 10.1001/archgenpsychiatry.2010.199.
6. A. Iraji et al., “Canonical and Replicable Multi-Scale Intrinsic Connectivity Networks in 100k+ Resting-State fMRI Datasets,” Neuroscience, preprint, Sep. 2022. doi: 10.1101/2022.09.03.506487.

Poster No 538

Delineating pharmacological treatment effect on brain state in schizophrenia using normative models

Rixing Jing[1], Xiao Lin[2], Yanxi Huo[1], Peng Li[2]

[1]Beijing Information Science and Technology University, Beijing, Beijing, [2]Peking University Sixth Hospital, Beijing, Beijing

Introduction: Schizophrenia is diagnosed exclusively based on symptoms, and the clinical and biological heterogeneity makes it difficult to fully and accurately assess pharmacological treatment effects on the brain state (Lin et al., 2021; Mehta et al., 2021). As a promising approach, normative modeling highlights the value of understanding individual variation relative to group means (Marquand, Rezek, Buitelaar, & Beckmann, 2016; Rutherford et al., 2022). In this study, we aimed to map deviations using normative modeling technique on dynamic functional connectome for individuals to investigate the pharmacological treatment effect in schizophrenia.

Methods: In this study, resting state fMRI scans were acquired in 689 individuals from two datasets. Dataset 1 (the Cambridge Centre for Ageing and Neuroscience, Cam-CAN) included 652 healthy individuals. Dataset 2 included 37 patients with schizophrenia from the Peking University Sixth Hospital. All patients underwent two experimental sessions. The first session began before beginning antipsychotic treatment. The second session occurred on the last day of 6 weeks of antipsychotic treatment. The fMRI preprocessing protocol was common and similar to our previous study (Lin et al., 2021; Taylor et al., 2017). For each individual, we computed dynamic functional connectivity (FC) matrices between all pairs of regions of the Human Brainnetome Atlas (Fan et al., 2016) using a sliding time window method (window length=60s) . Then, each FC matrix was decomposed into 17 networks based on Yeo-17 network template (Yeo et al., 2011). The average FC connection strength (aFCS, mean of FC strength from all window-wise FC matrices) and fluctuation characteristic of connection strength (fFCS, average change of the window-wise FC strength) for each Yeo-17 network was yielded from time-varying dynamic FC matrices. Finally, each individual’s dynamic FC pattern was represented by 34 features. Based on Cam-CAN dataset, we built normative models of 34 features using quantile regression to estimate the normative range, and mapped the deviations of the brain characteristics of each patient before treatment (bSCZ) or after treatment(aSCZ) (Jing et al., 2023). Then, we tested whether deviations from these models were related to psychiatric symptoms in patients with schizophrenia to investigated the pharmacological treatment effect on deviation distributions.

Results: Fig1A showed the overall deviation scores for 37 patients across 17 brain networks at the individual level before and after treatment. Fig1B shows the coefficients of variation (the ratio of the standard deviation to the absolute mean value at group level) at network-level for bSCZ and aSCZ, and the brain networks of the patients converged (the drug made them develop in one direction) in aFCS variability after treatment. In Fig2, we analyzed the predictive effects of baseline clinical symptoms for the change of deviations in patients ($p<0.05$). For aFCS in Fig2A, the severity of depressive symptoms at baseline could negatively predict the deviation changes. These results suggested that, the brain networks of those patients with milder depressive symptoms were more likely to be placed back to the normal range in clinical therapy. As for fFCS in Fig2B, the severity of overall symptoms and the positive symptoms at baseline could negatively predict the dynamic fluctuations deviations of dorsal and ventral attention, salience, control, and default mode networks.

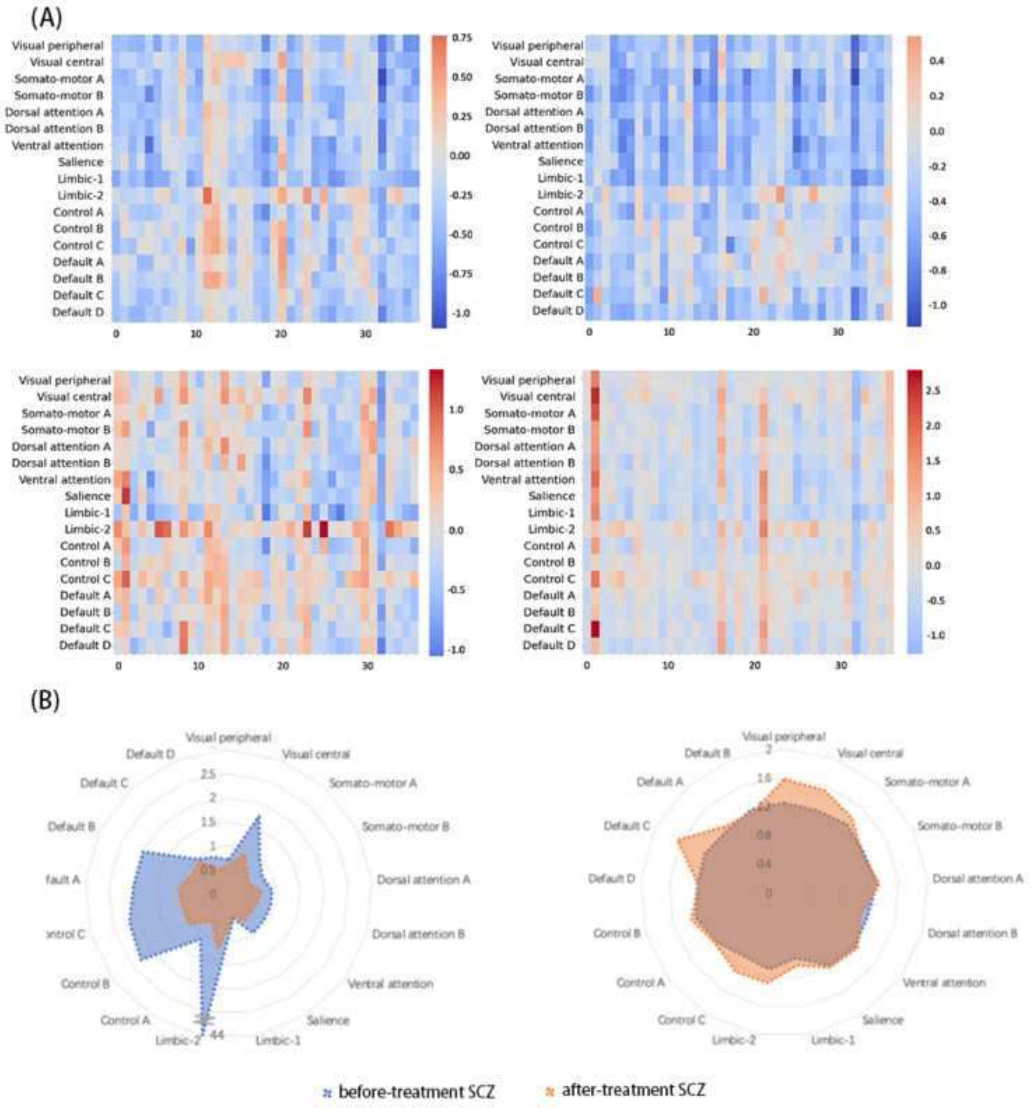

Fig1. The brain network changes after treatment. (A) Up: The deviation scores of the average FC connection strength across 17 brain networks at the individual level in patients with schizophrenia at before (left) and after treatment (right); Bottom: The deviation scores of the fluctuation characteristic of connection strength across 17 brain networks at the individual level in patients with schizophrenia at before (left) and after treatment (right). (B) The coefficients of variation for the average FC connection strength (left) and the fluctuation characteristic of connection strength (right) at the network level for patients at before and after treatment.

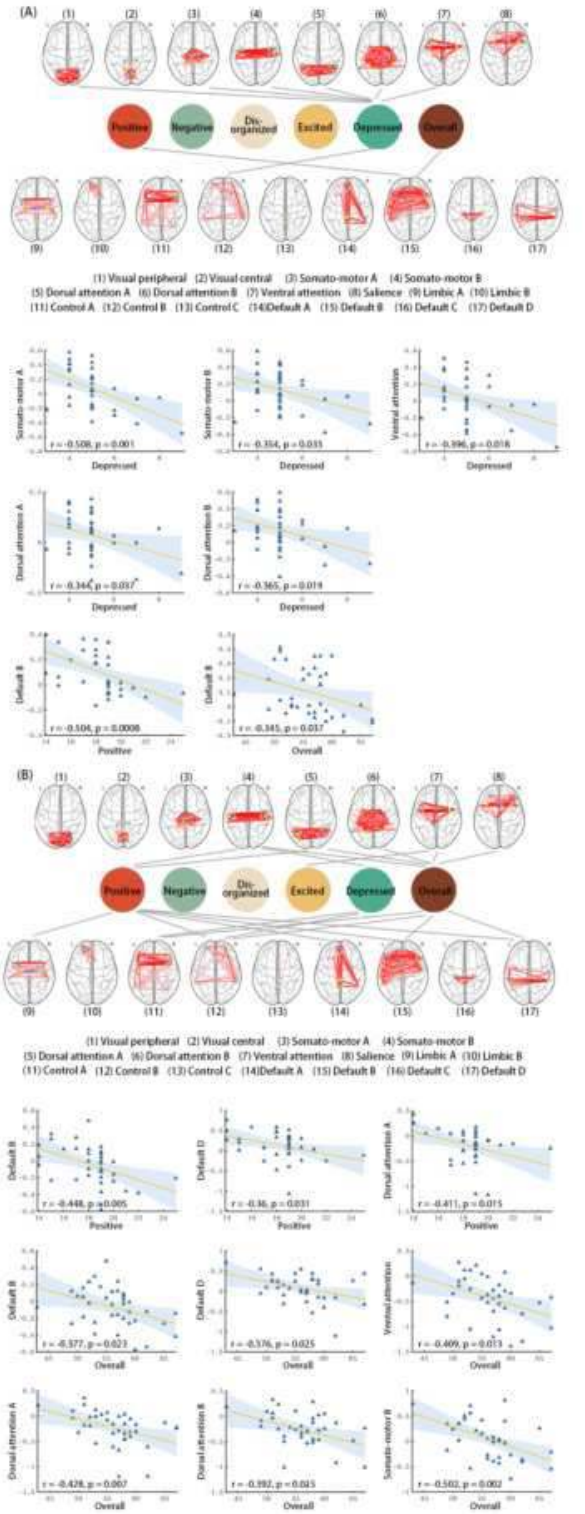

Fig2. The predictive effect of baseline clinical symptoms for the change of deviations of the brain network. (A) The correlation and the specific shows between the clinical profile with the deviation changes of the average connection strength across 17 brain networks; (B) The correlation and the specific shows between the clinical profile with the deviation changes of the fluctuation characteristic of connection strength across 17 brain networks. The gray lines represent the negative correlations between baseline clinical profiles with the deviation changes of the brain networks.

Conclusions: This study adopted a normative model to assess brain changes affected by pharmacological treatment in patients with schizophrenia. We found that the baseline severity of symptoms, especially the depressive and the overall symptoms, could predict the deviation of the brain networks after treatment. Our study suggested that modeling brain states as deviations from the normative range may assist in understanding the heterogeneity of the illness pathology as well as the treatment response.

References

1. Fan, L., Li, H., Zhuo, J., Zhang, Y., Wang, J., Chen, L., . . . Jiang, T. (2016). The Human Brainnetome Atlas: A New Brain Atlas Based on Connectional Architecture. Cerebral Cortex (New York, N.Y.: 1991), 26(8), 3508-3526.
2. Jing, R., Lin, X., Ding, Z., Chang, S., Shi, L., Liu, L., . . . Lu, L. (2023). Heterogeneous brain dynamic functional connectivity patterns in first-episode drug-naive patients with major depressive disorder. Human Brain Mapping, 44(8), 3112-3122.
3. Lin, X., Deng, J., Dong, G., Li, S., Wu, P., Sun, H., . . . Li, P. (2021). Effects of Chronic Pharmacological Treatment on Functional Brain Network Connectivity in Patients with Schizophrenia. Psychiatry Research, 295, 113338.
4. Marquand, A. F., Rezek, I., Buitelaar, J., & Beckmann, C. F. (2016). Understanding Heterogeneity in Clinical Cohorts Using Normative Models: Beyond Case-Control Studies. Biological Psychiatry, 80(7), 552-561.
5. Mehta, U. M., Ibrahim, F. A., Sharma, M. S., Venkatasubramanian, G., Thirthalli, J., Bharath, R. D., . . . Keshavan, M. S. (2021). Resting-state functional connectivity predictors of treatment response in schizophrenia - A systematic review and meta-analysis. Schizophrenia Research, 237, 153-165.
6. Rutherford, S., Kia, S. M., Wolfers, T., Fraza, C., Zabihi, M., Dinga, R., . . . Marquand, A. F. (2022). The normative modeling framework for computational psychiatry. Nature Protocols, 17(7), 1711-1734.
7. Taylor, J. R., Williams, N., Cusack, R., Auer, T., Shafto, M. A., Dixon, M., . . . Henson, R. N. (2017). The Cambridge Centre for Ageing and Neuroscience (Cam-CAN) data repository: Structural and functional MRI, MEG, and cognitive data from a cross-sectional adult lifespan sample. Neuroimage, 144(Pt B), 262-269. doi:10.1016/j.neuroimage.2015.09.018
8. Yeo, B. T. T., Krienen, F. M., Sepulcre, J., Sabuncu, M. R., Lashkari, D., Hollinshead, M., . . . Buckner, R. L. (2011). The organization of the human cerebral cortex estimated by intrinsic functional connectivity. Journal of Neurophysiology, 106(3), 1125-1165.

Poster No 539

IL-1beta moderated the relations of MFG-insula/mACC connectivity and depressive symptoms in BDII-D

Yuan Cao[1], Paulo Lizano[2], Hongqi Xiao[3], Meng Li[1], Zhiyun Jia[4], Changjian Qiu[3], Martin Walter[1]

[1]Jena University Hospital, Jena, Germany, [2]Beth Israel Deaconess Medical Center of Harvard Medical School, Boston, MA, [3]Mental Health Center of West China Hospital, Chengdu, China, [4]Sichuan University West China Hospital, Chengdu, Sichuan

Introduction: Bipolar disorder depression (BDD) is a chronic and challenging mental health condition characterized by profound mood disturbances, cognitive impairment, and a higher risk of suicide[1]. Approximately 60% of bipolar disorder (BD) experience their first mood episode as depression, and 17% of BDD individuals were diagnosed with unipolar depression in primary care[2,3]. Our previous study has unveiled the relationships between reduced gray matter volumes (GMVs) of the middle frontal gyrus (MFG), superior frontal gyrus (SFG), middle temporal pole, cerebellum, insula, and caudate and inflammation, childhood adversity, and psychiatric symptoms in BDII-D[4]. Additionally, our previous indicated that higher interleukin (IL)-1β levels were related to greater depressive symptoms and smaller volumes of MFG[4,5]. Whether alterations in brain structure correspondingly usher in impairments in brain function, whether there is a link between such brain functional alterations and inflammation, childhood adversity, and psychiatric symptoms, and whether IL-1β plays a moderate role between brain functional alterations and psychiatric symptoms, are aspects that need to be explored but have not yet been fully revealed.

Methods: Using the CONN toolbox, we assessed brain activity and functional connectivity in 147 BDII-D individuals and 150 healthy controls (HCs). Partial correlation with multiple comparison correction identified significant relationships between brain functional alterations and inflammation, childhood adversity, and psychiatric symptoms. Moderated analysis delved into the role of IL-1β.

Results: Compared to HCs, BDII-D individuals displayed significantly lower amplitude of low-frequency fluctuation (ALFF) in the frontal and insular regions but higher ALFF in the occipital-temporal area. Significant differences in FC were observed in the seed regions of MFG and insula. Within BDII-D, lower ALFF of the right insula was significantly correlated with higher IL-6 level ($r = -0.316$, $q = 0.0021$), CRP level ($r = -0.448$, $q < 0.001$), emotional abuse scores ($r = -0.376$, $q = 0.002$), and emotional neglect scores ($r = -0.304$, $q = 0.004$). Lower ALFF of the MFG significantly related to higher CRP ($r = -0.309$, $q = 0.002$) and childhood physical abuse score ($r = -0.256$, $q = 0.027$). For seeds derived from ALFF results, we observed higher MFG-mACC FC was significantly related to higher IL-1β ($r = 0.289$, $q = 0.016$). Moreover, there were positive relationships between higher HAMD score and higher FC value between the right MFG and right insula ($r = 0.22$, $q = 0.036$) and higher FC value between the right MFG and medial anterior cingulate cortex (mACC) ($r = 0.327$, $q < 0.001$). . Moreover, IL-1β moderated associations between higher MFG-mACC ($\beta = 2.68$, 95%CI 0.60-4.77, $p = 0.01$) and MFG-insula ($\beta = 3.53$, 95%CI 1.085-5.968, $p = 0.005$) connectivity and greater depressive symptoms.

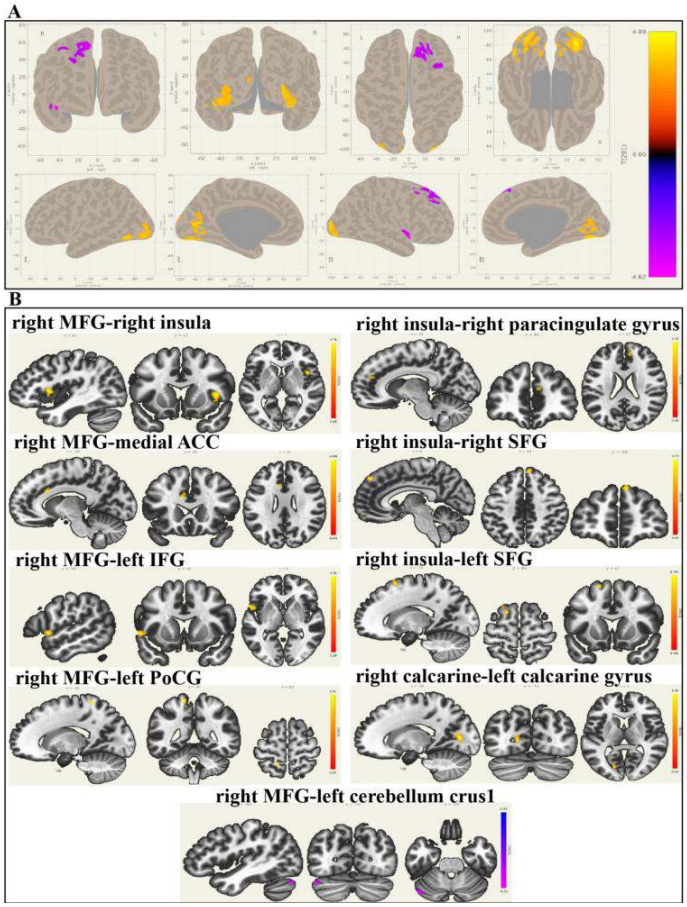

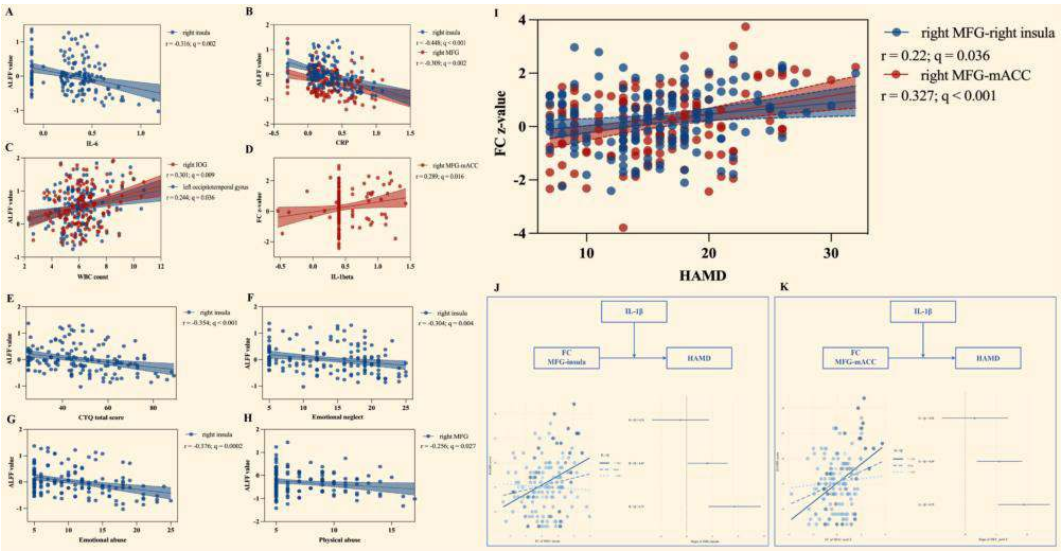

Conclusions: Our study reveals abnormal function alterations in the right MFG, and insula associated with elevated inflammation, childhood adversity, and depressive symptoms in BDII-D. Importantly, IL-1β plays a moderated role in the relationship between MFG-related FC and depressive symptoms.

References

1. Vieta E. (2018), 'Bipolar disorders', Nature reviews Disease primers, vol. 4, no.1, pp. 1-16
2. Bauer MS, (2022), 'Bipolar disorder', Annals of Internal Medicine, vol.175, no. 7, pp. ITC97-ITC112
3. Mitchell PB, (2008), 'Diagnostic guidelines for bipolar depression: a probabilistic approach', Bipolar disorders, vol. 10, no, 1p2, pp. 144-152
4. Cao Y, (2023), 'Effects of inflammation, childhood adversity, and psychiatric symptoms on brain morphometrical phenotypes in bipolar II depression', Psychological Medicine vol. 6, pp. 1-10
5. Cao Y, (2023), 'Brain-derived subgroups of bipolar II depression associate with inflammation and choroid plexus morphology', Psychiatry Clin Neurosci, vol. 77, no. 11, pp. 613-621

Poster No 540

Systematic organization of cortical thickness co-alterations in substance use disorders

Sofie Valk[1], Foivos Georgiadis[2], Meike Hettwer[3], Sophia Thomopoulos[4], Paul Thompson[5], Scott Mackey[6], Patricia Conrod[7], Hugh Garavan[8], Clara Moreau[9], Boris Bernhardt[10], Matthias Kirschner[11], ENIGMA Addiction Working Group[12]

[1]Max Planck Institute for Human Cognitive and Brain Sciences, Leipzig, Germany, [2]University of Zurich, Zurich, Switzerland, [3]Forschungszentrum Jülich, Jülich, North Rhine-Westphalia, [4]USC, Marina del Rey, CA, [5]USC, Marina Del Rey, CA, [6]The University of Vermont, Burlington, VT, [7]University of Montreal, Montreal, Quebec, [8]University of Vermont, Burlington, VT, [9]University of Southern California, Los Angeles, CA, [10]Montreal Neurological Institute and Hospital, Montreal, Quebec, [11]Geneva University Hospitals (HUG), Thonex, Geneva, [12]UCLA, Burlington, Vermont

Introduction: Substance use disorders are highly comorbid with other neuropsychiatric disorders and share with them widespread structural brain alterations (Eaton, Rodriguez-Seijas, Carragher, & Krueger, 2015; Mackey et al., 2019; Reich-Erkelenz, Schmitt, & Falkai, 2015). Previous work has shown that structural alterations across neuropsychiatric conditions are organized in a systematic fashion, linked to the intrinsic organization of the human connectome (Hettwer et al., 2022). However, to what extent similar coordinated co-alteration effects extend to substance use disorders remains to be established. Here, we investigated substance use co-alteration networks (pathological structural covariance) to elucidate concordant macroscale principles of illness and substance-use effects across the cortex.

Methods: We derived maps of case-control differences in cortical thickness from 2,847 patients with six substance use disorders (SUDs: alcohol, amphetamines, cocaine, opioids, cannabis, and nicotine; Fig. 1A) and 1,951 non-affected individuals from the Enhancing NeuroImaging Genetics through Meta-Analysis (ENIGMA) Addiction Working Group (Thompson et al., 2020; Mackey, 2020). We investigated substance use co-alteration networks via inter-regional SUD association with cortical thickness (Fig. 1B). Hub regions are regions that show high co-alteration profiles across disorders and were computed as the sum of top 20% covariance strengths in each region. Next, we identified potential substance use co-alteration epicenters, i.e., regions whose normative connectivity profiles (based on data from the Human Connectome Project, (Van Essen et al., 2013)) are correlated with substance use co-alteration hubs. Last, we compared the effects of substance use disorder-related co-alterations and neuropsychiatric disease-related co-alterations based on prior work (Hettwer et al., 2022). To do so, we probed regional embedding and inter-relational organizational axes (Vos de Wael et al., 2020).

Results: We identified organizational principles of shared cortical thickness alterations across SUDs (SUDcov). Co-alteration network hubs followed normative functional ($r=0.527$, $p_{spin}<0.05$) and structural ($r=0.314$, $p_{spin}<0.05$) connectivity patterns (Fig. 1C). Functional epicenters included temporal regions, precuneus, right frontal cortex and hippocampus and amygdala, and structural epicenters were found in posterior/mid cingulate, preSMA, right sensory-motor regions, and the thalamus (Fig. 1C). We observed a high overlap between SUDcov and structural covariance patterns of cortical thickness, except in inferior temporal areas and mOFC (Fig. 2A and B). Similar associations were observed when comparing SUDcov with neuropsychiatric cross-disorder impact (Fig. 2C). Studying low-dimensional organizations of SUDcov, the primary gradient of substance use disorder differentiated OFC, inferior temporal regions, and anterior cingulate from the rest of the cortex and mirrored the second covariance and neuropsychiatric co-alteration gradients ($p_{spin}<0.05$). The second SUDcov gradient differentiated parietal and OFC areas from the rest of the cortex (Fig 2DE). Overall, SUD co-alterations varied stronger along G2cov (median $r=0.25$) relative to G1cov (median $r=0.15$), and the reverse was observed in neuropsychiatric co-alteration gradients (G1 median $r=0.33$, G2 median $r=0.15$). Hierarchical clustering of SUD and neuropsychiatric co-alteration patterns further underlined this differentiation (Fig. 2F).

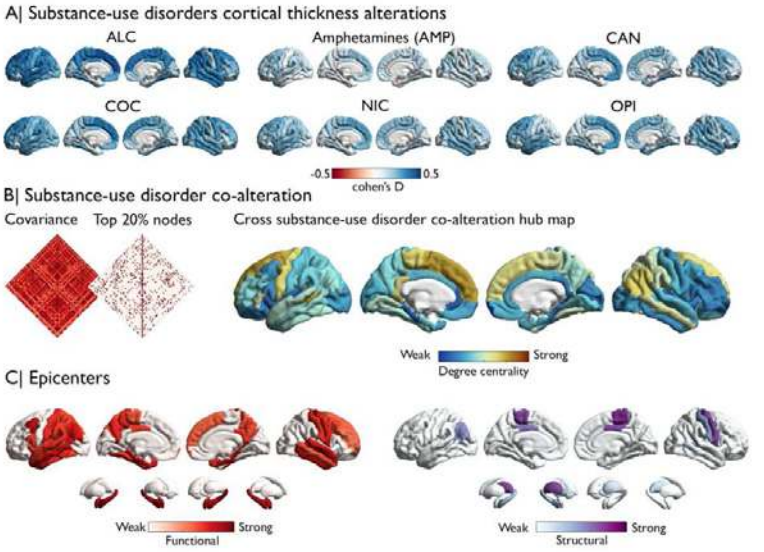

Figure 1. Cross-substance use disorder covariance. A) Cohen's d map of substance use disorder association with cortical thickness; B) Cross-substance-use disorder co-alteration and hub map based on the top 20% of nodes; C) Functional and structural cortical and subcortical epicenters of cross-substance-use disorder co-alterations.

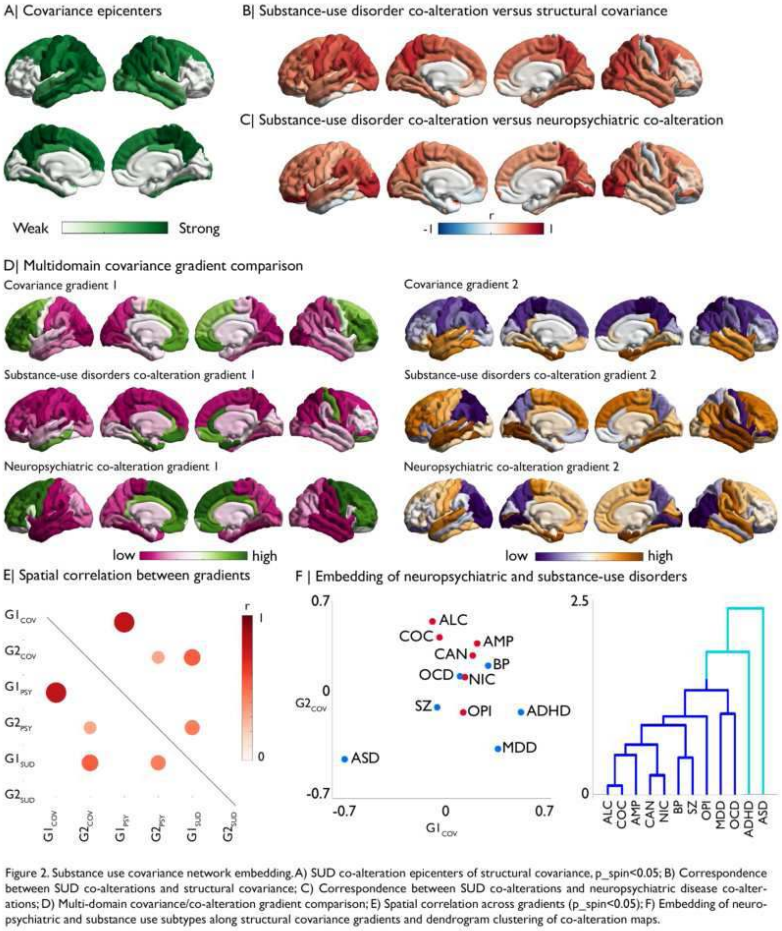

Figure 2. Substance use covariance network embedding. A) SUD co-alteration epicenters of structural covariance, p_spin<0.05; B) Correspondence between SUD co-alterations and structural covariance; C) Correspondence between SUD co-alterations and neuropsychiatric disease co-alterations; D) Multi-domain covariance/co-alteration gradient comparison; E) Spatial correlation across gradients (p_spin<0.05); F) Embedding of neuropsychiatric and substance use subtypes along structural covariance gradients and dendrogram clustering of co-alteration maps.

Conclusions: The shared association of SUDs with cortical thickness covaries in a network-like fashion. These patterns partly mirror those of normative structural covariance, underscoring the differentiation between inferior/paralimbic and superior regions of the cerebral cortex by SUDs as probed by a gradient framework (Valk et al., 2020). We observed differentiation between SUDs versus neuropsychiatric co-alteration networks, possibly related to a differentiation between co-morbidity and neurodevelopment (Hettwer et al., 2022).

References
1. Eaton, N. R., Rodriguez-Seijas, C., Carragher, N., & Krueger, R. F. (2015). Transdiagnostic factors of psychopathology and substance use disorders: a review. Soc Psychiatry Psychiatr Epidemiol, vol. 50, no. 2, pp. 171-182
2. Hettwer, M. D., Lariviere, S., Park, B. Y., van den Heuvel, O. A., Schmaal, L., Andreassen, O. A., . . . Valk, S. L. (2022). Coordinated cortical thickness alterations across six neurodevelopmental and psychiatric disorders. Nat Commun, vol. 13, no. 1, pp. 6851
3. Mackey, S., Allgaier, N., Chaarani, B., Spechler, P., Orr, C., Bunn, J., . . . Group, E. A. W. (2019). Mega-Analysis of Gray Matter Volume in Substance Dependence: General and Substance-Specific Regional Effects. Am J Psychiatry, vol. 176, no. 2, pp. 119-128
4. Reich-Erkelenz, D., Schmitt, A., & Falkai, P. (2015). Unravelling basic mechanisms in addiction and neuropsychiatric disorders. Eur Arch Psychiatry Clin Neurosci, vol. 265, no. 8, pp. 633-635
5. Thompson, P. M., Jahanshad, N., Ching, C. R. K., Salminen, L. E., Thomopoulos, S. I., Bright, J., . . . Enigma Consortium. (2020). ENIGMA and global neuroscience: A decade of large-scale studies of the brain in health and disease across more than 40 countries. Transl Psychiatry, vol. 10, no. 1, pp. 100
6. Valk, S. L., Xu, T., Margulies, D. S., Masouleh, S. K., Paquola, C., Goulas, A., . . . Eickhoff, S. B. (2020). Shaping brain structure: Genetic and phylogenetic axes of macroscale organization of cortical thickness. Sci Adv, vol. 6, no. 39
7. Van Essen, D. C., Smith, S. M., Barch, D. M., Behrens, T. E., Yacoub, E., Ugurbil, K., & WU Consortium. (2013). The WU-Minn Human Connectome Project: an overview. Neuroimage, vol. 80, pp. 62-79
8. Vos de Wael, R., Benkarim, O., Paquola, C., Larivière, S., Royer, J., Tavakol, S., . . . Bernhardt, B. C. (2020). BrainSpace: a toolbox for the analysis of macroscale gradients in neuroimaging and connectomics datasets. Nat Commun Biology.

Poster No 541

Normative Modelling of Molecular-Functional Circuits Captures Transdiagnostic Heterogeneity

Timothy Lawn[1], Alessio Giacomel[1], Daniel Martins[2], Mattia Veronese[3], Matthew Howard[1], Federico Turkheimer[1], Ottavia Dipasquale[2]

[1]King's College London, London, London, [2]King's College London, London, United Kingdom, [3]University of Padua, Padua, Italy

Introduction: Clinical neuroscience aims to delineate the neurobiology underpinning the symptoms of various disorders, with the ultimate goal of developing mechanistically informed treatments for these conditions. This has been hindered by the hierarchical organisation of the brain and heterogeneity of psychiatric disorders[1,2]. However, advances in multimodal analytic techniques – such as Receptor Enriched Analysis of Connectivity by Targets(REACT) – have allowed integration of functional dynamics from fMRI with the brain's receptor landscape, providing novel trans-hierarchical insights[2,3]. Similarly, normative modelling of brain features has allowed translational neuroscience to move beyond group-average differences between patients and controls and characterise deviations from health at an individual level[4]. Here, we bring these novel methods together in order to address these two longstanding translational barriers in clinical neuroscience.

Methods: We utilise healthy data from the CamCAN5 and UCLA phenomics6 datasets(N=607), and patients suffering from Schizophrenia(SCHZ), Bipolar-disorder(BPD), and ADHD from the latter(N=119). Transdiagnostic symptom scores were dimensionally reduced using principal components analysis. REACT3 was used create functional networks enriched with group average receptor/transporter distributions of the main modulatory (noradrenaline, dopamine, serotonin, acetylcholine), inhibitory(GABA), and excitatory(glutamate) neurotransmitter systems, which were parcellated using a custom atlas. Next, using hierarchical Bayesian regression within the predictive clinical neuroscience toolbox[7], we generated normative models of these molecular-enriched networks. Using these models, we characterised deviations from normality within a held out subset of healthy controls(30%) as well the patients. This produced a deviation score for each subject, molecular system, and brain region. We analysed these deviation scores to examine between group differences using ROI-wise ANOVAs and summary brain-wide deviation metrics; between-subject similarity and how this relates to transdiagnostic symptomatology; and transdiagnostic network-symptom relationships through mass-univariate permutation based correlation analyses.

Results: We identified four principal components which explained 68.9% of the total variance in symptom scores. Broadly, our results align with accounts of excitatory-inhibitory imbalance in schizophrenia and bipolar disorder, with between group analyses showing significantly greater negative deviations in glutamatergic and GABAergic systems, driven primarily by SCHZ and BPD. Between subject similarity analyses emphasised the substantial overlap in symptoms and deviations across these disorders transdiagnostically, with levels of within-group similarity significantly correlating with the brain-wide negative glutamatergic and GABAergic network deviations as well as principal component 2(PC2: primarily capturing psychotic symptoms) across multiple receptor systems(fig-1). Finally, across all patients, both the cholinergic and glutamatergic deviations across widespread regions including cingulate, insular, and opercular cortices correlated with PC2, such that those with more negative deviations had greater symptom scores(fig-2).

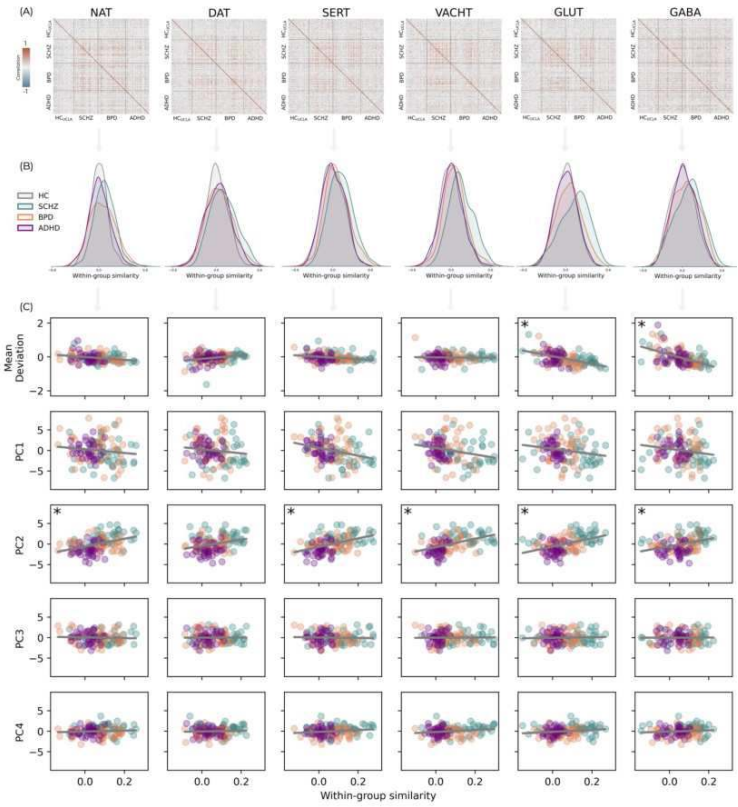

Fig-1: (A) Matrices of between-subject correlations of deviation scores across ROIs for each pair of individuals within and between groups. (B) The correlation coefficients for within group similarity displayed as density plots. (C) the relationship between patients similarity to the other patients in their diagnostic group and the overall deviation burden categorised by mean deviation *z* score across their whole brain (top row) as well as each symptom component. Asterisks denote relationships that are significant following Bonferroni correction ($p < 0.05/30$).

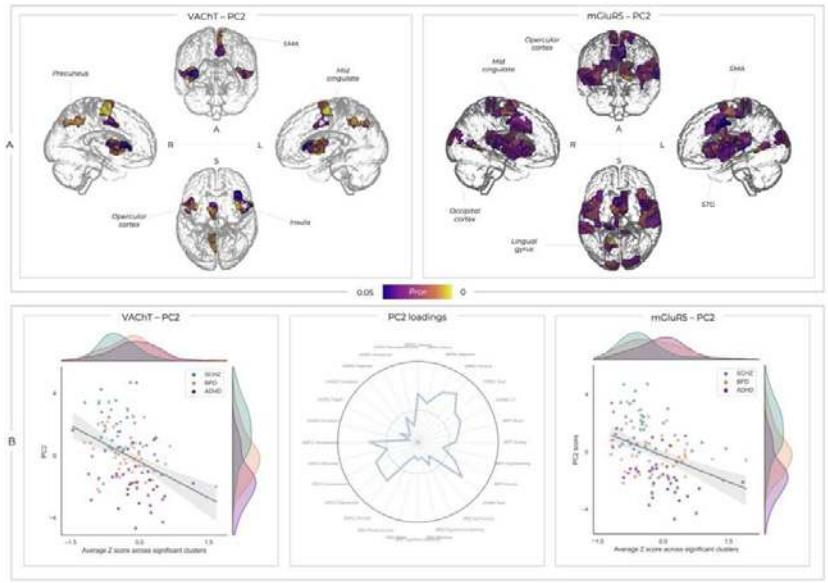

Fig-2: (A) Only two deviation-symptom relationships were significant. Significant p_{FDR} values are shown for the relationships between PC2 and deviations within the VAChT- and mGluR5-enriched networks (A); anterior view, L; left view, R; right view, S; superior view). SMA; supplementary motor area, STG; superior temporal gyrus.(B) The same relationships shown in the brain plots, with Z values averaged across the significant clusters and correlated with PC2 symptom scores. The loadings for PC2 are shown in the middle. The dotted grey line indicates zero, with positive loadings outside this and negative loadings inside.

Conclusions: The integration of novel functional-molecular neuroimaging techniques, normative modelling, and a transdiagnostic perspective utilised here offers methodological and theoretical progress towards an understanding of the shared neurobiological foundations that underpin psychiatric conditions. Our transdiagnostic approach moves away from case-control analyses and offers an interesting way to situate clinical groups or individuals within between-subject similarity and deviation-symptom landscapes, which when scaled up across diagnoses, symptomatology, and molecular systems may offer novel perspectives on how complex aberrations of affect and cognition map onto dysfunction spanning molecular and systems level readouts.

References
1. Nour, M. M., Liu, Y. & Dolan, R. J. Functional neuroimaging in psychiatry and the case for failing better. Neuron 110, 2524–2544 (2022).
2. Lawn, T. et al. From neurotransmitters to networks: Transcending organisational hierarchies with molecular-informed functional imaging. Neuroscience & Biobehavioral Reviews 150, 105193 (2023).
3. Dipasquale, O. et al. Receptor-Enriched Analysis of functional connectivity by targets (REACT): A novel, multimodal analytical approach informed by PET to study the pharmacodynamic response of the brain under MDMA. Neuroimage 195, 252–260 (2019).
4. Marquand, A. F. et al. Conceptualizing mental disorders as deviations from normative functioning. Mol Psychiatry 24, 1415–1424 (2019).
5. Taylor, J. R. et al. The Cambridge Centre for Ageing and Neuroscience (Cam-CAN) data repository: Structural and functional MRI, MEG, and cognitive data from a cross-sectional adult lifespan sample. Neuroimage 144, 262–269 (2017).
6. Poldrack, R. A. et al. A phenome-wide examination of neural and cognitive function. Sci Data 3, 160110 (2016).
7. Rutherford, S. et al. The normative modeling framework for computational psychiatry. Nat Protoc 17, 1711–1734 (2022).

Poster No 542

Striatal Functional Hypoconnectivity in Schizophrenia Negative Symptoms: Longitudinal Findings

Tal Geffen[1], Samyogita Hardikar[2], Jonathan Smallwood[3], Mariia Kaliuzhna[4], Fabien Carruzzo[4], Teresa Katthagen[1], Stefan Kaiser[5], Florian Schlagenhauf[1,6]

[1]Charité – Universitätsmedizin Berlin, Department of Psychiatry and Psychotherapy, Berlin, Germany, [2]Max Planck Institute for Human Cognitive and Brain Sciences, Department of Neurology, Leipzig, Germany, [3]Department of Psychology, Queen's University, Ontario, Canada, [4]University of Geneva, Clinical and Experimental Psychopathology Laboratory, Faculty of Medicine, Geneva, Switzerland, [5]Division of Adult Psychiatry, Department of Psychiatry, Geneva University Hospitals, Basel, Basel, [6]Bernstein Center for Computational Neuroscience, Berlin, Germany

Introduction: Negative symptoms like apathy and diminished expression are persistent challenges in schizophrenia (SZ), with limited treatment options and significant impacts on daily life[1]. Research in this area has been limited, and functional connectivity findings are heterogeneous. SZ is linked to striatal abnormalities, especially in reward and motivation processes[2]. Here we investigate whole-brain connectivity of striatal subregions in schizophrenia patients (SZP) in a longitudinal rsfMRI study across two centers with the aim of discovering striatal connectivity aberrations as potential biomarkers of negative symptoms in SZP.

Methods: Participants in the longitudinal study were assessed at baseline (T1) and at three months (T2) with 9.8 minutes rsfMRI, and at nine months (T3) for clinical follow-up, only for SZ patients (SZP). The study was conducted in Berlin and Geneva. Assessments included the Brief Negative Symptom Scale (BNSS; 3) and the Brief Assessment of Cognition in Schizophrenia (BACS; 4). We investigated seed-to-whole brain rsfMRI connectivity using the functional division of the striatum into associative (STR_Asoc: cognition), limbic (STR_Limb: motivation), and sensorimotor (STR_Sens: locomotion) regions[5] via CONN toolbox v.19.c[6]. First (A), we assessed group differences between SZP and controls for all six bilateral striatal seeds. Associations with cognition/negative symptoms were tested with Pearson correlation clusters with significant group differences. Furthermore (B), within the SPZ group, separate group-level GLMs were used with the three negative symptoms sub-scales as independent variables to identify regions relevant for symptoms outside areas displaying group differences. Lastly (C), within SZP we used a GLM to predict negative symptoms at T3 with striatal connectivity measures from T1. The re-test stability of connectivity measures after three months (T2) was assessed using intraclass correlation ICC(2,1) for clusters showing group differences (A) and clusters associated with negative symptoms in SZP (B). FWE correction was used at the cluster and voxel level, and Bonferroni correction for multiple comparisons for the number of seed regions.

Results: SZP with severe psychotic symptoms (PANSS positive > 4) were excluded; all SZP had stable symptoms. 143 participants (77 SZP/66 age, sex, and parental education matched healthy controls, HC) completed rsfMRI. At T2, 111 participants (56 SZP/55 HC) were involved, and 60 SZP completed clinical measures at T3. At T1, 11 clusters showed hypoconnectivity in SPZ compared to HC. Connectivity measures from four of these clusters showed above moderate re-test stability (ICC(2,1)>0.3) over three months, indicating stable hypoconnectivity of STR_Asoc and STR_Sens with frontal, parietal, and cerebellar areas (Fig.1). Notably, hypoconnectivity between bilateral STR_Asoc and the right Superior Frontal Gyrus (SFG_r) [for both seeds: $T(139) \leq -5.86$, $pFWE*6<0.001$; $ICC(2,1) \geq 0.44$, $n=111$] correlated positively with cognition in SZP [$r(73)=0.26$, $p=0.03$]. Analysis B revealed hypoconnectivity between STR_Sens_r and the right Superior Parietal Lobule (SPL_r) in SZP, associated with stronger BNSS diminished expression severity [$T(74)=-5.13$, $pFWE*18= 0.023$; $ICC(2,1)=0.32$, $n=56$]. Analysis C showed that connectivity between STR_Sens_r and SPL_r at T1 could predict stronger BNSS diminished expression severity nine months later [$T(57)= -3.7$, $p<0.001$] (Fig.2).

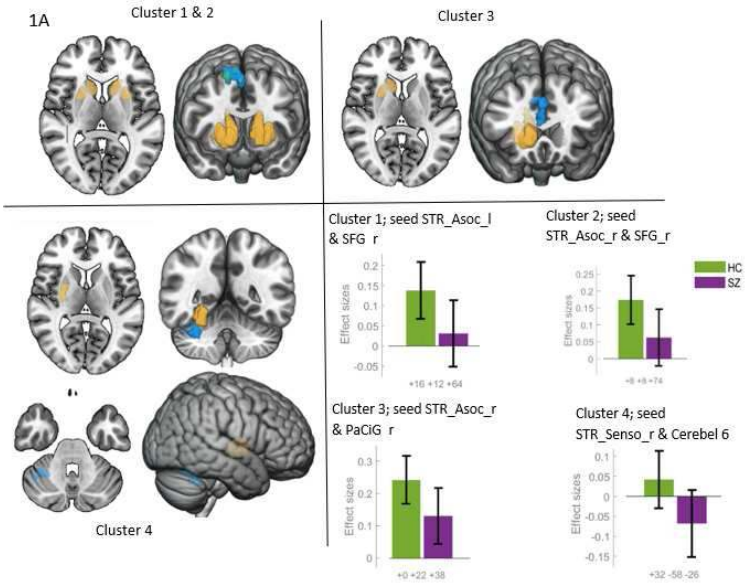

Fig. 1A (up): Clusters showing significant connectivity alterations in SZP compared to controls. Significant connectivity alterations with three striatal seeds (yellow) to brain clusters (blue). The four clusters showed sig. stability between T1 and T2 measures (ICC(2,1) <0.3). SZP showed hypoconnectivity in comparison to HC. Cluster 1 (green) & 2 (blue) have similar anatomical locations. The first three clusters presented weaker positive connectivity and the fourth stronger negative connectivity. The group effect size for SZP and HC is presented for each cluster, together with the center of the cluster MNI coordinate. **Fig. 1B (right):** Among SZP: positive Pearson's correlation between connectivity values (cluster 1: STR_Asoc_l and SFG_r) with BACS total Z score (cognition) among SZP in T1 (r(73)=0.26, p<0.03). In all analyses, we controlled for average-motion and center.

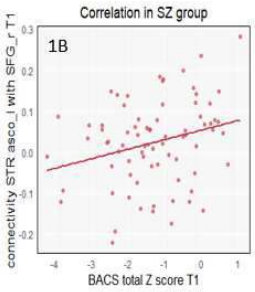

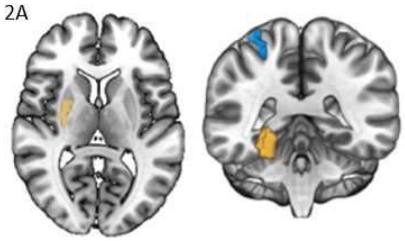

Fig.2A: Using only SZP in T1, with BNSS diminished expression as an independent variable, hypoconnectivity between the STR_Sens_r (yellow) to the SPL_r (MNI: [+28, -46, +58]) was found (T(74) = -5.13, pFWE*18= 0.023). **Fig.2B:** Negative Spearman partial correlation between connectivity values (STR_Sens_r with SPL_r) with BNSS diminished expression at T1 ((r(73)= -0.49, p <0.001). **Fig.2C:** Negative spearman partial correlation between connectivity values (STR_sens_r with SPL_r) at T1 with BNSS diminished expression at T3 (r(56) = -0.39, p = 0.002). In all analyses, we controlled for average-motion and center.

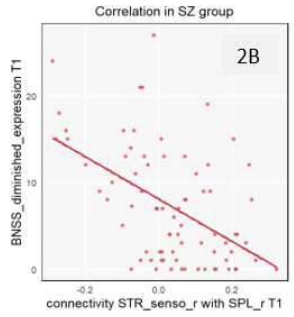

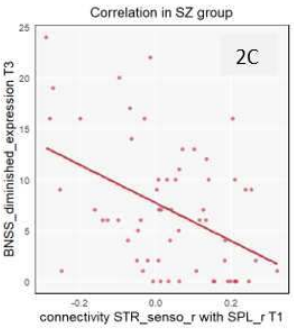

Conclusions: Our study aimed to identify robust striatal connectivity aberrations linked to negative symptoms. We found that hypoconnectivity between STR_Sens_r and SPL_r in SZP, related to diminished expression at T1, was stable from T1 to T2 and could predict symptoms nine months later across two centers. This suggests that such a connectivity pattern is worth further investigation as a potential biomarker. Additionally, the association of cognitive and symptom measures with the relevant functional striatal sub-parcels strengthens the validity of our findings.

References

1. Kirkpatrick, B. (2014). 'Developing concepts in negative symptoms: primary vs secondary and apathy vs expression', The Journal of Clinical Psychiatry, vol. 75, Suppl 1, pp. 3-7.
2. Katthagen, T., Kaminski, J., Heinz, A., Buchert, R., & Schlagenhauf, F. (2020). 'Striatal dopamine and reward prediction error signaling in unmedicated schizophrenia patients', Schizophrenia Bulletin, vol. 46, no. 6, pp. 1535-1546.
3. Strauss, G.P., Keller, W.R., Buchanan, R.W., Gold, J.M., Fischer, B.A., McMahon, R.P., Catalano, L.T., Culbreth, A.J., Carpenter, W.T., & Kirkpatrick, B. (2012b). 'Next-generation negative symptom assessment for clinical trials: validation of the Brief Negative Symptom Scale', Schizophrenia Research, vol. 142, pp. 88-92.
4. Keefe, R.S., Harvey, P.D., Goldberg, T.E., Gold, J.M., Walker, T.M., Kennel, C., & Hawkins, K. (2008). 'Norms and standardization of the Brief Assessment of Cognition in Schizophrenia (BACS)', Schizophrenia Research, vol. 102, nos. 1-3, pp. 108-115.
5. Martinez, D., Slifstein, M., Broft, A., Mawlawi, O., Hwang, D.R., Huang, Y., ... & Laruelle, M. (2003). 'Imaging human mesolimbic dopamine transmission with positron emission tomography. Part II: amphetamine-induced dopamine release in the functional subdivisions of the striatum', Journal of Cerebral Blood Flow & Metabolism, vol. 23, no. 3, pp. 285-300.
6. Whitfield-Gabrieli, S., & Nieto-Castanon, A. (2012). 'Conn: A functional connectivity toolbox for correlated and anticorrelated brain networks', Brain Connectivity. DOI: 10.1089/brain.2012.0073

Poster No 543

A novel imagery script-based retrieval-extinction procedure to prevent nicotine addiction

Li Yang[1], Jiafang Liu[1], Junjie Bu[1]

[1]Anhui Medical University, Hefei, Anhui

Introduction: Memory retrieval-extinction procedure is a promising paradigm for drug addiction intervention[1]. However, individuals with addiction tend to relapse easily upon returning to real-life settings, and the lack of transferability in the intervention effects may be attributed to the low contextuality of drug cues. Meanwhile, the vivid imagery scripts derived from nicotine addicts' smoking experiences in real life emphasize individual active participation and situational diversity[2]. Consequently, we developed a novel imagery script-based retrieval-extinction paradigm and evaluated its effectiveness on nicotine addiction.

Methods: The study was conducted by a single-blind randomized clinical trial design (Figure 1). Fifty-seven nicotine addicts were randomly assigned to imagery script-based retrieval-extinction (R-E) group (N=29) and control group (N=28). Each participant individually underwent the construction of smoking and neutral imagery scripts earlier according to Imagery Scripts Builder Manual. Subsequently, these imagery scripts were transformed into audio recordings using a speech synthesis system for the following retrieval-extinction training. During retrieval-extinction training, R-E group underwent 5-min memory retrieval, 10-min delay and 60-min extinction, while control group underwent 5-min no memory retrieval, 10-min delay and 60-min extinction. At retrieval stage, addicts were asked to vividly imagine scenes from smoking imagery scripts in R-E group, but neutral imagery scripts in control group. Imagery scripts cue reactivity task with EEG recording, smoking imagery vividness and cue-induced smoking craving were assessed at pre-intervention, post-intervention, 1-day, 1-week, and 1-month follow-up. Daily cigarette consumption was being recorded at pre-intervention, post-intervention, 1-week, 1-month, 3-month, 6-month, and 12-month follow-up.

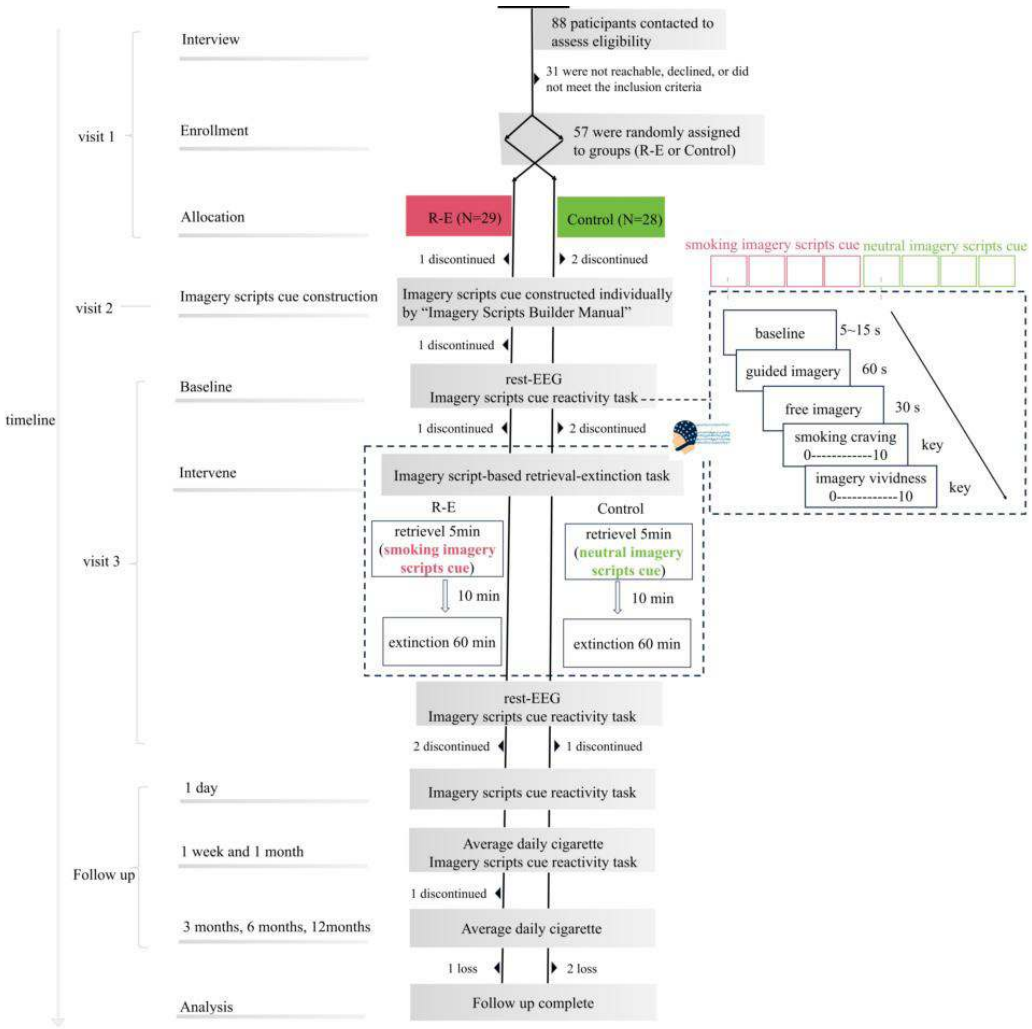

Figure 1. Experimental design. EEG (electroencephalogram). Follow-up tests were performed at 1 day, 1 week, 1 month, 3 months, 6 months, and 12 months after the intervention.

Results: Short-term effects of retrieval-extinction training on smoking imagery vividness and craving There was a significant group × time interaction effect for smoking imagery vividness scores ($F(1,45) = 10.282$, $p = 0.002$; group: R-E, control groups; time: pre-intervention, post-intervention, 1-day follow-up)(Figure 2a). Also, there was a significant group × time interaction effect for cue-induced smoking craving ($F(1,45) = 15.182$, $p < 0.001$)(Figure 2b). Moreover, the significant correlation between smoking imagery vividness scores and cue-induced smoking craving at pre-intervention ($r = 0.581$, $p = 0.003$) was broken at post-intervention and 1-day follow-up in R-E group (Figure 2c). EEG microstate mechanisms of retrieval-extinction training There was a significant group × time interaction effect for EEG microstate C duration ($F(1,45) = 9.592$, $p = 0.003$; group: R-E, control groups; time: pre-intervention, post-intervention), with R-E group showing a significant reduction of microstate C duration at post-intervention (Figure 2d). The reduction of microstate C duration being significantly correlated with the reduction of cue-induced smoking craving in R-E group ($r = 0.432$, $p = 0.035$)(Figure 2e). Long-term effects of retrieval-extinction training on smoking behavior There was a significant group × time interaction effect for daily cigarette consumption ($F(5,205) = 6.997$, $p < 0.001$; group: R-E, control groups; time: pre-intervention, 1-week, 1-month, 3-month, 6-month, 12-month follow-up) (Figure 2f). At 1-week and 1-month follow-up, smoking imagery vividness scores and cue-induced craving were significantly lower in R-E group than in control group (Figure 2g,h). Moreover, smoking imagery vividness scores and cue-induced craving were no longer significantly correlated in R-E group (Figure 2i,j).

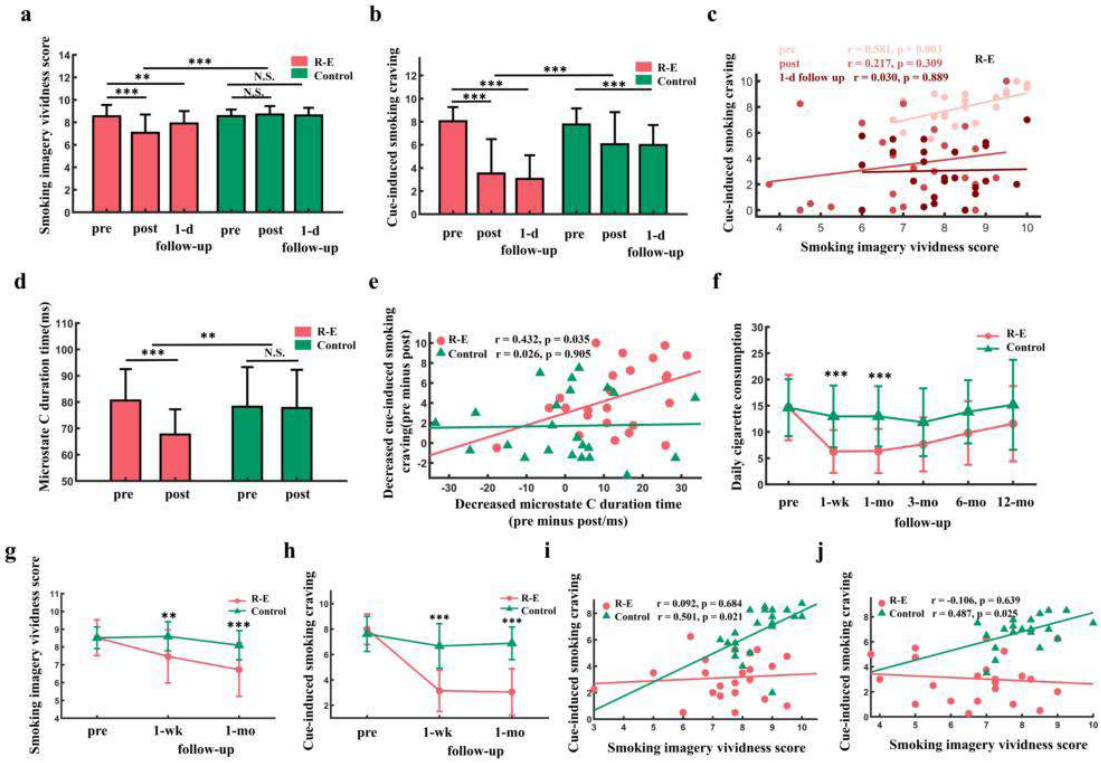

Figure 2. Short- and long-term effects of imagery scripts cue retrieval-extinction training on nicotine addiction memory. (a) Short-term changes in smoking imagery vividness score. (b) Short-term changes in cue-induced smoking craving. (c) The relationship between smoking imagery vividness score and cue-induced smoking craving in the R-E group. (d) Changes in the duration of EEG microstate C before and after intervention. (e) The relationship between EEG microstate C duration and cue-induced smoking craving (pre minus post). (f) Long-term changes in daily cigarette intake. (g) Long-term changes in smoking imagery vividness score. (h) Long-term changes in cue-induced smoking craving. (i) The relationship between smoking imagery vividness score and cue-induced smoking craving after 1 week. (j) The relationship between smoking imagery vividness score and cue-induced smoking craving after 1 month. **: p< 0.01; ***: p<0.001; N.S.: no significant difference.

Conclusions: We developed a novel imagery script-based retrieval-extinction training, which produced short- and long-term effects on smoking craving and smoking behavior. These results suggest that this novel imagery script-based retrieval-extinction intervention is a promising treatment for addiction.

References

1. Xue, Y.X. (2012), 'A Memory Retrieval-Extinction Procedure to Prevent Drug Craving and Relapse', Science, vol. 336, no. 6078, pp. 241-245
2. Buff, C. (2018), 'Directed threat imagery in generalized anxiety disorder', Psychological Medicine, vol. 48, no. 4, pp. 617-628

Poster No 544

Investigating the neurobiological basis of psychopathology using bi-factor models: reliably general

Martin Gell[1,2], Mauricio Hoffmann[3,4], Tyler Moore[5], Aki Nikolaidis[6], Ruben Gur[5], Giovanni Salum[4,7,8], Michael Milham[6,9], Simon Eickhoff[10,2], Robert Langner[10,2], Veronika Müller[10,2], Theodore Satterthwaite[5]

[1]Department of Psychiatry, Psychotherapy, and Psychosomatics, RWTH Aachen University Hospital, Aachen, Germany, [2]Research Centre Juelich, Institute of Neuroscience and Medicine (INM7), Juelich, Germany, [3]Department of Neuropsychiatry, Universidade Federal de Santa Maria, Santa Maria, Brazil, [4]Universidade Federal do Rio Grande do Sul, Porto Alegre, Brazil, [5]University of Pennsylvania, Philadelphia, PA, [6]Child Mind Institute, New York, NY, [7]National Institute of Developmental Psychiatry for Children and Adolescents (INCT-CNPq), São Paulo, Brazil, [8]Child Mind Institute, New York, United States, [9]Nathan S. Kline Institute for Psychiatric Research, Orangeburg, NY, [10]Institute for Systems Neuroscience, Medical Faculty, Heinrich-Heine University Düsseldorf, Düsseldorf, North Rhine-Westphalia

Introduction: Despite sustained efforts to uncover the neurobiological basis of mental health disorders, finding links to specific syndromes using neuroimaging has remained challenging. Factors contributing to this include both high comorbidity among disorders and heterogeneity within diagnostic categories1. In response, models that separate the shared (or general, transdiagnostic) and the unique (or specific) dimensions of psychopathology2 have become an important area of research. Such bi-factor models offer the possibility to disentangle the general and unique biological underpinnings of

psychopathology. However, to investigate associations between individual differences in neurobiology and psychopathology such dimensions also require sufficient test-retest reliability, as it sets an upper bound on effect size3 and determines signal-to-noise ratio in machine learning analyses4. Here we evaluated the reliability of 11 published bi-factor models in two large developmental datasets from the global north and south and investigated the impact of reliability on their associations with brain structure and function.

Methods: We used items from the Child Behaviour Checklist (CBCL) to fit 11 bi-factor models in the ABCD5 (n = 5526, ages 9-10 at baseline, mean retest interval = 12 months) and BHRC6 (n = 772, ages 6-14 at baseline, mean retest interval = 8 months) datasets. CBCL items were configured to load on a single general factor and a varying number of specific factors as defined in all published models7. Test-retest reliability was then assessed using correlation, after regressing out participant age, timepoint and their interaction. Sensitivity analyses were performed using alternative reliability metrics (hierarchical omega and factor determinacy) and shorter retest intervals. Next, we used resting-state functional connectivity (FC) and cortical thickness (CT) to predict general and specific factors as well as summary scores in the ABCD dataset. Predictions were performed with linear ridge regression within nested 2-fold cross-validation using matched discovery (n=3,525) and replication (n=3,447) samples8. Using Mplus, bi-factor models were fit separately in each sample to avoid data leakage and improve replicability. Preprocessed resting-state fMRI data and CT maps were acquired from the ABCD BIDS Community Collection9 and parcellated using the Glasser atlas10. FC was then calculated using Pearson correlation between the time series of all parcels.

Results: For all 11 models, the general "P" factor captured most variance across CBCL items (ABCD = 57-78%; BHRC = 60-79%) and had generally higher reliability (test-retest rABCD = 0.7 - 0.76; rBHRC = 0.55 - 0.59) than specific factors (rABCD = 0.36 - 0.61; rBHRC = 0.14 - 0.47) in both datasets (Fig. 1). Despite the favourable psychometric properties, p-factors could be predicted using FC (Fig. 2A) or CT with a comparable prediction accuracy to externalising and attention factors. Notably, p-factors also showed equivalent prediction accuracy and reliability to many standard CBCL summary scores (esp. total problems, attention, internalising and rule-breaking), which combine all sources of variance and ignore the multidimensional structure parsed by the bi-factor models (Fig. 2B).

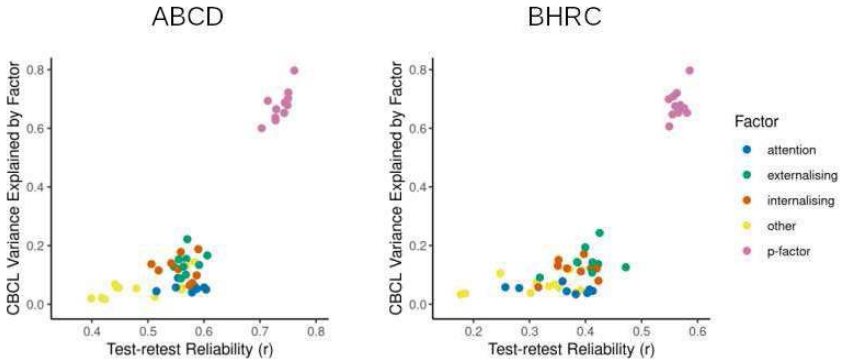

Figure 1. Variance explained in CBCL items and reliability of general and specific factors from all models in both samples.

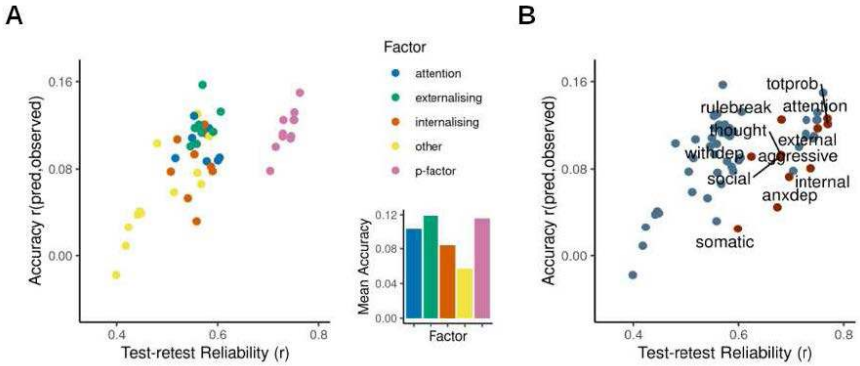

Figure 2. ABCD functional connectivity-based prediction accuracy of general and specific factors from all models and their test-retest reliability (A) and overlayed with CBCL summary scores in red (B)

Conclusions: Here we demonstrate that while capturing most of the reliable variance in CBCL, general psychopathology factors showed comparable associations with brain structure and function to specific factors and summary scores. Across

all bi-factor models, many specific factors displayed low test-retest reliability that will substantially attenuate associations and make comparisons between factors hard to interpret. These results suggest that deeper phenotyping is necessary to better characterise the variance unique to specific dimensions. Finally, while bi-factor models are better suited to address phenotypic complexity and heterogeneity in psychopathology, general factors exhibit predictive utility comparable to that of the CBCL total summary score.

References

1. Feczko, E. & Fair, D. A. Methods and Challenges for Assessing Heterogeneity. Biol. Psychiatry 88, 9–17 (2020).
2. Kotov, R. et al. The Hierarchical Taxonomy of Psychopathology (HiTOP): A dimensional alternative to traditional nosologies. Journal of Abnormal Psychology 126, 454–477 (2017).
3. Spearman, C. Correlation calculated from faulty data. Br. J. Psychol. 3, 271–295 (1910).
4. Gell, M. et al. The Burden of Reliability: How Measurement Noise Limits Brain-Behaviour Predictions. 2023.02.09.527898 Preprint at https://doi.org/10.1101/2023.02.09.527898 (2023).
5. Volkow, N. D. et al. The conception of the ABCD study: From substance use to a broad NIH collaboration. Dev. Cogn. Neurosci. 32, 4–7 (2018).
6. Salum, G. A. et al. High risk cohort study for psychiatric disorders in childhood: rationale, design, methods and preliminary results. Int. J. Methods Psychiatr. Res. 24, 58–73 (2015).
7. Hoffmann, M. et al. Reliability and validity of bifactor models of dimensional psychopathology in youth. J. Psychopathol. Clin. Sci. 131, 407–421 (2022).
8. Feczko, E. et al. Adolescent Brain Cognitive Development (ABCD) Community MRI Collection and Utilities. 2021.07.09.451638 Preprint at https://doi.org/10.1101/2021.07.09.451638 (2021).
9. Fair, D. A., Dosenbach, N. U. F., Moore, A. H., Satterthwaite, T. D. & Milham, M. P. Developmental Cognitive Neuroscience in the Era of Networks and Big Data: Strengths, Weaknesses, Opportunities, and Threats. Annu. Rev. Dev. Psychol. 3, 249–275 (2021).
10. Glasser, M. F. et al. A multi-modal parcellation of human cerebral cortex. Nature 536, 171–178 (2016).

Poster No 545

Contextualized network dysfunction in schizophrenia: Granger Causality to Graph Theory

Kalyyanee Nanaaware[1], John Kopchick[2], Asadur Chowdury[2], Patricia Thomas[2], Usha Rajan[2], Dalal Khatib[2], Luay Haddad[2], Alireza Amirsadri[2], Jeffrey Stanley[2], Vaibhav Diwadkar[2]

[1]Wayne State University School of Medicine, Detroit, MI, [2]Wayne State University, Department of Psychiatry, Detroit, MI

Introduction: In-degree and out-degree centrality are graph theoretic metrics that approximate the flow of information in a directed graph (Rubinov and Sporns, 2010). Such metrics are useful in understanding disordered task-driven connectomics in schizophrenia (Meram et al., 2023). Here, we used a learning paradigm (Stanley et al., 2017) with distinct task conditions (encoding, retrieval) to evoke brain network interactions in a group of controls (HC) and schizophrenia patients (SCZ). From a reduced network of co-activated nodes (dACC, dlPFC, Hippocampus, Superior Parietal, Inferior Temporal, Fusiform), we derived a directed graph where the edges between these six vertices were estimated using Wiener-Granger Causality (Baajour et al., 2020; Bressler and Seth, 2011). From these, the in- and out-degree centrality of each node was estimated before conducting parametric analyses.

Methods: fMRI data were collected in 55 participants (31 patients, Siemens Verio 3T). During the task, participants encoded object-location associations (ENCoding) and were tested in separate blocks (RETrieval) using location cues. fMRI data were preprocessed using typical methods (SPM 12). A co-activated network (HC ∩ SCZ) was identified using a conjunction analyses based on the minimum inference statistic (Nichols et al., 2005). Time series from these (dACC, dlPFC, HPC, ITG, SPC, FG) were extracted from each participant. Next, in each participant inter-node causality was estimated from time series using multi-variate autoregressive models (MVAR, consistent with Weiner Granger Causality). From the resultant directed graphs in each participant (6 vertices, 30 unique edges), we estimated the in- and out-degree centrality of each vertex for each of encoding and retrieval, and in each of the early and late phases of the paradigm. As the paradigm evoked negatively accelerated learning, we studied in-group (HC vs SCZ) and inter-phase (early learning vs. late learning) differences on degree centrality in an analyses of variance framework (separately for ENC and RET).

Results: Figure 1 provides a comprehensive overview of our results. During ENC, a) the in-degree centrality of the dlPFC increased over the course of learning, and was higher in SCZ while b) the out-degree centrality of the SPC increased over the course of learning. During RET, we observe a) an interaction on the in-degree centrality in the dlPFC, wherein in controls in decreased over time, but in patients it increased; b) the out-degree centrality of the FG decreased over time.

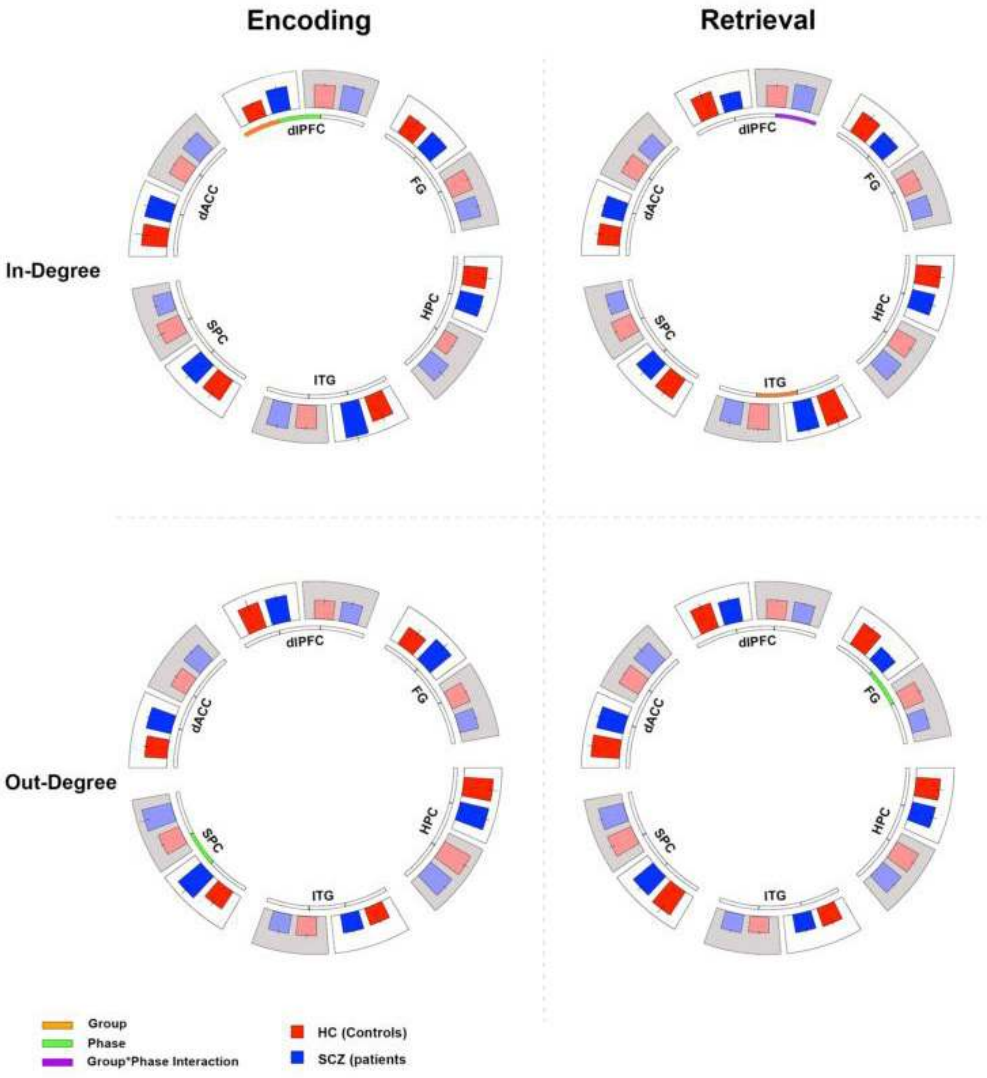

Figure 1. The circular bar graphs depict each node's mean In-degree and Out-degree centrality (top and bottom rows) during ENCoding and RETrieval (left and right columns)(± sem) and phase (Early and Late where the latter is shaded in gray). Controls (HC) are depicted in red, and patients (SCZ) are in blue. The color code is used to indicate any significant effects associated with the ANOVA (Main Effect of Group: ; Main Effect of Phase: ; Group x Phase Interaction:). As seen, during Encoding SCZ showed a significant increase in in-degree centrality of the dlPFC. In addition, the in-degree centrality of the dlPFC increased over time. During this condition, we also see that the out-degree centrality of the SPC increased over time. During Retrieval, we observed two effects on in-degree centrality. First, for the dlPFC the measure decreased over time in HC but increased over time in SCZ. Next, for the ITG, in-degree centrality was lower in SCZ. Finally, we also noted a decrease in out-degree centrality of the FG over time.

Conclusions: Effects during ENC and RET were somewhat distinct in terms of node specificity and patterns. During ENC, the dlPFC showed higher in-degree centrality in SCZ, suggestive of increased "flow" of information into this region. This increase may be seen as a class of "compensatory" response, often seen in the illness (Zovetti et al., 2022). In SCZ, we also observed reduced in-degree centrality of the ITG during RET. This effect is notable in that the retrieval cue (in part originating in the SPC and the dlPFC) must engage the retrieval of the object identity (an ITG related function). The ancillary effects of phase and the interaction between group and phase (dlPFC during RET) highlight a) the complex set of directed functional interactions that accrue in the brain during learning and b) the highly contextualized nature of connectivity deficits evoked in schizophrenia.

References

1. Baajour, S.J. (2020) Disordered directional brain network interactions during learning dynamics in schizophrenia revealed by multivariate autoregressive models. Human brain mapping 41(13), 3594-3607.
2. Bressler, S.L. (2011), Wiener-Granger causality: a well established methodology. NeuroImage 58(2), 323-329.
3. Meram, E.D. (2023), The topology, stability, and instability of learning-induced brain network repertoires in schizophrenia. Network Neuroscience 7(1), 184-212.
4. Nichols, T. (2005), Valid conjunction inference with the minimum statistic. NeuroImage 25(3), 653-660.
5. Rubinov, M. (2010), Complex network measures of brain connectivity: uses and interpretations. NeuroImage 52(3), 1059-1069.
6. Stanley, J.A. (2017), Functional dynamics of hippocampal glutamate during associative learning assessed with in vivo 1H functional magnetic resonance spectroscopy. NeuroImage 153, 189-197.
7. Zovetti, N. (2022), Inefficient white matter activity in Schizophrenia evoked during intra and inter-hemispheric communication. Translational psychiatry 12(1), 449.

Poster No 546

Unique neural signatures of childhood sexual abuse in gray matter volume and cortical thickness

Vincent Hammes[1], Katharina Brosch[2], Paula Usemann[1], Florian Thomas-Odenthal[1], Lea Teutenberg[1], Frederike Stein[1], Janik Goltermann[3], Susanne Meinert[3], Kira Flinkenflügel[3], Alexandra Winter[3], Nils Winter[3], Katharina Thiel[3], Tim Hahn[3], Elvisha Dhamala[2], Axel Krug[1], Udo Dannlowski[3], Igor Nenadic[1], Andreas Jansen[1], Tilo Kircher[1], Nina Alexander[1]

[1]University of Marburg, Marburg, Hesse, [2]Feinstein Institutes for Medical Research, Glen Oaks, NY, [3]University of Münster, Münster, North Rhine-Westphalia

Introduction: Individuals who experienced childhood sexual abuse (CSA) are characterized by higher general trauma load and worse health outcomes compared to other types of maltreatment (i.e., physical and emotional neglect, physical and emotional abuse)[1,7]. Specifically, CSA is associated with an increased risk to develop several psychiatric disorders, such as major depressive disorder (MDD), anxiety disorder and post-traumatic stress disorder[7]. CSA-specific effects on brain morphometry, including thinning of the somatosensory cortex and gray matter volume (GMV) loss in the visual cortex, have previously been reported[2,5]. However, previous studies are limited by methodological issues, such as not accounting for general trauma load, and are comprised of small sample sizes. Further, studies comparing CSA to individuals with no maltreatment might only detect general effects of childhood maltreatment instead of specific CSA effects. Given these current limitations, we have an insufficient understanding of the effects of CSA on brain morphometry. In this study, to reliably identify unique effects of CSA on brain morphometry, we chose a novel approach and compared sexually abused individuals to non-sexually abused individuals who were matched on overall trauma load.

Methods: Healthy and depressed participants were drawn from the longitudinal FOR2107 cohort study investigating the neurobiology of major psychiatric disorders[3]. We investigated n = 195 individuals with a history of CSA and selected a 1:1 matched sample of maltreated individuals without a history of CSA (nCSA), matched for age, sex, diagnostic group distribution and trauma load. Additionally, we compared the CSA group to an age, sex and diagnostic group distribution matched sample with no history of maltreatment (Control) to explore general maltreatment effects, resulting in a total sample of 585 individuals. The sample included men and women aged 18 - 65 with and without a lifetime diagnosis of MDD. History of CSA and other types of maltreatment were assessed using the Childhood Trauma Questionnaire (CTQ) (8). We investigated brain structural differences between the three groups in GMV and cortical thickness using voxel-based morphometry and surface-based analyses, applying threshold-free cluster enhancement (TFCE).

Results: Individuals with a history of CSA exhibited significantly larger GMV in the right cerebellum (Figure 1A) compared to nCSA and further showed widespread cortical thickness increases in areas encompassing fronto-parietal regions (Figure 2A). Exploring general effects of childhood maltreatment, individuals with a history of CSA exhibited significantly larger GMV in the bilateral anterior cingulate gyrus and superior medial frontal gyrus (Figure 1B) and widespread cortical thickness increases in areas encompassing fronto-parietal regions (Figure 2B) compared to the non-maltreated Control group.

Figure 1

Clusters exhibiting significantly larger GMV (TFCE, p_{FWE}-corrected) in CSA compared to: ***A*** *nCSA, and* ***B*** *Control*

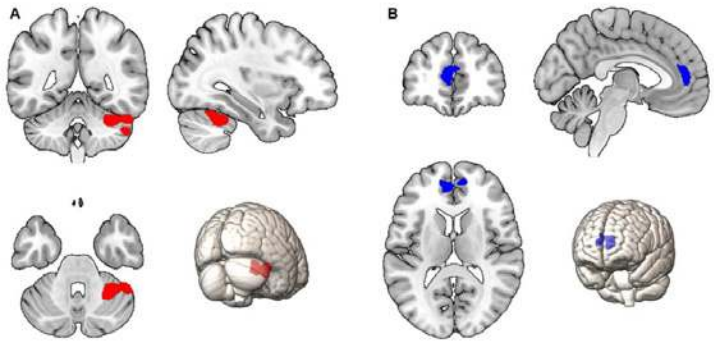

Note. **A** CSA > nCSA group comparison; significant cluster encompasses parts of the right exterior cerebellum (k=1225, TFCE=917.92, p_{FWE}=0.025, x/y/z=33/-48/-32). **B** CSA > Control group comparison; significant cluster encompasses parts of the left anterior cingulate gyrus and left superior medial frontal gyrus (k=842, TFCE=1007.25, p_{FWE}=0.024, x/y/z=-04/46/12).

Figure 2

Clusters exhibiting significantly larger cortical thickness (TFCE, p_{FWE}-corrected) in CSA compared to ***A*** *nCSA and* ***B*** *Control*

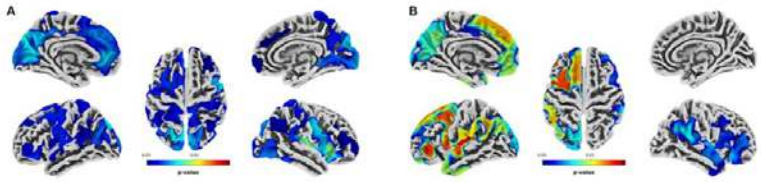

Note. Warmer colors represent lower *p*-values (threshold $p < 0.05$). **A** *CSA > nCSA* group comparison, significant clusters encompass regions of the bilateral superiorfrontal gyrus, pre- and postcentral gyri, supramarginal gyri, superiorparietal cortex, right precuneus and left inferior parietal cortex and insula. **B** *CSA > Control* group comparison, significant clusters encompass regions of the bilateral superiorfrontal gyrus, supramarginal gyrus, superiortemporal gyrus, inferior- and superiorparietal gyri as well as the insula.

Conclusions: This is the largest study so far to examine the neurobiological correlates of childhood sexual abuse in comparison to matched maltreated individuals without a history of CSA in a representative sample with high trauma load. Our findings indicate a unique neural signature of childhood sexual abuse, evident by larger GMV in the cerebellum and greater cortical thickness in fronto-parietal regions. These alterations in brain morphometry might set the ground for a variety of psychiatric disorders, as especially the cerebellum has been implicated in social, cognitive and emotional processes and alterations might impair normal functioning[4,6]. The results of our study thus emphasize the importance of distinguishing specific traumatic subtypes in future research.

References

1. Hailes, H.P., et al. (2019), "Long-term outcomes of childhood sexual abuse: an umbrella review." The Lancet Psychiatry.
2. Heim, C.M. (2013), "Decreased cortical representation of genital somatosensory field after childhood sexual abuse." American Journal of Psychiatry.
3. Kircher, T. (2019), "Neurobiology of the major psychoses: a translational perspective on brain structure and function-the FOR2107 consortium." European archives of psychiatry and clinical neuroscience vol. 269,8.
4. Schmahmann, J. D. (2019), "The theory and neuroscience of cerebellar cognition." Annual review of neuroscience.
5. Tomoda, A. (2009), "Childhood sexual abuse is associated with reduced gray matter volume in visual cortex of young women." Biological psychiatry vol. 66,7.
6. Van Overwalle, F. (2020), "Consensus paper: cerebellum and social cognition." The Cerebellum.
7. Walker, E.A. (1999), "Adult health status of women with histories of childhood abuse and neglect." The American journal of medicine.
8. Wingenfeld, K. (2010), "The German version of the Childhood Trauma Questionnaire (CTQ): preliminary psychometric properties." Psychotherapie, Psychosomatik, Medizinische Psychologie.

Poster No 547

Clinical Correlates of Neural Patterns following Real-time fMRI Neurofeedback in Anorexia Nervosa

Soo-Eun Lee[1], Anna Zilverstand[2], Tim Hendrickson[2], Kelsey Hagan[1], Bryon Mueller[2], Carol Peterson[2], Ann Haynos[1]

[1]Virginia Commonwealth University, Richmond, VA, [2]University of Minnesota, Minneapolis, MN

Introduction: Anorexia nervosa (AN) is a serious eating disorder characterized by emotion regulation difficulties and excessive self-control (Haynos & Fruzzetti, 2011; Pauligk et al., 2021). Real-time fMRI neurofeedback (rt-fMRI NF) is a novel brain-based tool that allows individuals to view and purposefully alter their neural activity, thus improving their emotion regulation skills (Emmert et al., 2016). Our group conducted a study comparing the effects of rt-fMRI NF targeting amygdala downregulation to sham feedback on emotion regulation and eating pathology among individuals with AN. In our previous findings, participants receiving rt-fMRI NF did not differ from sham feedback group in amygdala regulation but demonstrated less DLPFC engagement when instructed to regulate emotions. Further, the rt-fMRI NF group exhibited a linear pattern of decreasing negative affect, whereas the sham group exhibited a quadratic pattern of negative affect that initially declined and then later rebounded. Following these previous results, the current study explored the clinical implications of regional brain activity patterns in both groups. Specifically, we observed whether increased DLPFC activity in the sham group might signify a momentarily effective, but ultimately dysfunctional strategy for regulating emotions in individuals with AN.

Methods: Participants with acute or weight-restored AN (n=23) were randomized to participate in rt-fMRI neurofeedback (n=11) or a sham condition (n=12) and completed one or two scanning sessions. During fMRI sessions, participants engaged in an emotion regulation task which presented with negative pictures and instructed to either 1) regulate their emotional responses (regulate condition) or 2) simply view the images (view condition). In the regulate condition, NF participants received real-time feedback for their amygdala activation, while the sham group received non-contingent feedback linked to previous participants' activation patterns. Before and after the scans, participants completed self-reported assessments measuring positive and negative affect (PANAS), emotion dysregulation (S-DERS), state-trait anxiety (STAI), and eating disorders symptoms (CHEDS). Pearson's correlation analysis was employed to examine the relationship between DLPFC brain activity and these clinical variables both before (time 1) and after (time 2) the initial fMRI scan.

Results: In the sham group, increased activation in the right DLPFC during the regulate condition was significantly correlated with lower emotion dysregulation (r= -0.664, p= .013) and anxiety (r= -0.752, p= .003) at time 1 and lower anxiety at time 2 (r= -0.780, p= .002). Notably, there were no significant correlations between DLPFC activation and clinical variables observed for the NF group (ps > .05), suggesting that the consistent decrease in negative affect previously observed in the NF group likely involves different neural and psychological mechanisms than those associated with DLPFC activity and associated cognitive control.

Conclusions: Individuals with AN demonstrate an inclination toward excessive control over their negative emotions (Pauligk et al., 2021). Our findings for the sham group align with this pattern, suggesting that the tendency toward over-control (i.e., heightened engagement of the DLPFC) may yield short-term effects. However, based on our prior findings demonstrating a subsequent rebound of negative affect in the sham group, the positive short-term effects of cognitive control in AN may lead to longer-term negative consequences. Conversely, rt-fMRI NF targeting down-regulation of the amygdala appears to divert individuals from employing their typical over-control strategy of involving the DLPFC and may introduce alternative emotion regulation mechanisms, such as enhancing emotional or interoceptive awareness. Future studies should further investigate how neurofeedback introduces alternative mechanisms for emotion regulation and their potential efficacy for individuals with AN.

References

1. Emmert, K., Kopel, R., Sulzer, J., Brühl, A. B., Berman, B. D., Linden, D. E., Horovitz, S. G., Breimhorst, M., Caria, A., & Frank, S. (2016). Meta-analysis of real-time fMRI neurofeedback studies using individual participant data: How is brain regulation mediated? Neuroimage, 124, 806-812.
2. Haynos, A. F., & Fruzzetti, A. E. (2011). Anorexia nervosa as a disorder of emotion dysregulation: Evidence and treatment implications. Clinical Psychology: Science and Practice, 18(3), 183.
3. Pauligk, S., Seidel, M., Fürtjes, S., King, J. A., Geisler, D., Hellerhoff, I., Roessner, V., Schmidt, U., Goschke, T., & Walter, H. (2021). The costs of over-control in anorexia nervosa: evidence from fMRI and ecological momentary assessment. Translational Psychiatry, 11(1), 304.

Poster No 548

Neurotransmitter and cellular translation of neuroimaging phenotypes in healthy and abnormal brain

Amir Ebneabbasi[1], Mortaza Afshani[2], Arman Seyed-Ahmadi[3], Varun Warrier[4], Richard Bethlehem[5], Timothy Rittman[1]

[1]Department of Clinical Neurosciences, University of Cambridge, Cambridge, Cambridgeshire, [2]Shahid Beheshti University, Tehran, Tehran, [3]Department of Statistics, University of British Columbia, Vancouver, Canada, Vancouver, British Columbia, [4]Autism Research Centre, Department of Psychiatry, University of Cambridge, Cambridge, Cambridgeshire, [5]Autism Research Centre, Department of Psychiatry, University of Cambridge, Cambridge, United Kingdom

Introduction: Technological advances allow for high-resolution neuroimaging. Magnetoencephalography (MEG) and magnetic resonance imaging (MRI) measure neural oscillations and morphology that can be considered proxies of cognitive and emotional status in health and disease (Rittman, 2020; Vidaurre et al., 2018). Nonetheless, how those system-level measures relate to underlying neurophysiological processes is not completely understood (Larivière et al., 2021; Seidlitz et al., 2020). Previous work has begun associating image-derived phenotypes with neurotransmitter systems using positron emission tomography (PET) radiotracers (Hansen et al., 2022; Park et al., 2022). Here, we tested the hypothesis that functional and morphological imaging markers in healthy individuals and psychiatric disorders are associated with specific molecular and cellular processes assessed by gene expression data.

Methods: We used openly-available large-scale datasets [Human Connectome Project (HCP-MEG), Enhancing NeuroImaging Genetics through Meta-Analysis (ENIGMA), Allen Human Brain Atlas (AHBA)] and unsupervised learning to specify whether the spatial patterns of healthy neural function (frequency-specific power maps: delta, theta, alpha, beta, low- and high-gamma) and abnormal cortical structure (disorder-specific atrophy maps: deletion syndrome, autism spectrum, attention-

deficit hyperactivity, high-risk psychosis, schizophrenia, bipolar, major depressive and obsessive-compulsive disorder), are co-located with topographic distributions of gene expression. Specifically, partial least square (PLS) with brain region bootstrapping and spatial permutation was leveraged to rank the predictor weights of brain genes. Then, we considered fast gene set enrichment analysis (FGSEA) (Subramanian et al., 2005) to explore whether neurotransmitter-specific gene sets (GABA, glutamate, dopamine, serotonin, histamine, aspartate, glycine, epinephrine, norepinephrine, acetylcholine) and cell-specific gene sets (inhibitory/excitatory neurons, intermediate progenitors, microglia, oligodendrocyte, radial glia, astrocytes and vascular cells) (Bhaduri et al., 2021) were within the extreme bounds of the PLS-ranked genes. We leveraged agglomerative hierarchical clustering to calculate the similarity of oscillation and atrophy maps based on the underlying molecular and cellular underpinnings. Finally, we used different gene pre-processing thresholds (differential stability: $r \geq 0.1$, $r \geq 0.2$, $r \geq 0.4$) and multimarker analysis of genomic annotation (MAGMA) for robustness and sensitivity analysis, respectively.

Results: Our findings showed that frequency-specific power maps mostly derive from inhibitory/excitatory neurotransmitters (GABA and glutamate) and their related neurons. In addition, disorder-specific atrophy maps are mainly co-located with serotoninergic/dopaminergic pathways. Neurodevelopmental diseases spatially intersected with immune cell expression and psychiatric disorders with genes expressed in interneuron cells. Analyses were replicated using different gene pre-processing thresholds, with Kendall's coefficients of concordance being satisfactory. We also observed that serotonin/dopamine are highlighted in the genome-wide association studies (GWAS) of psychiatric disorders.

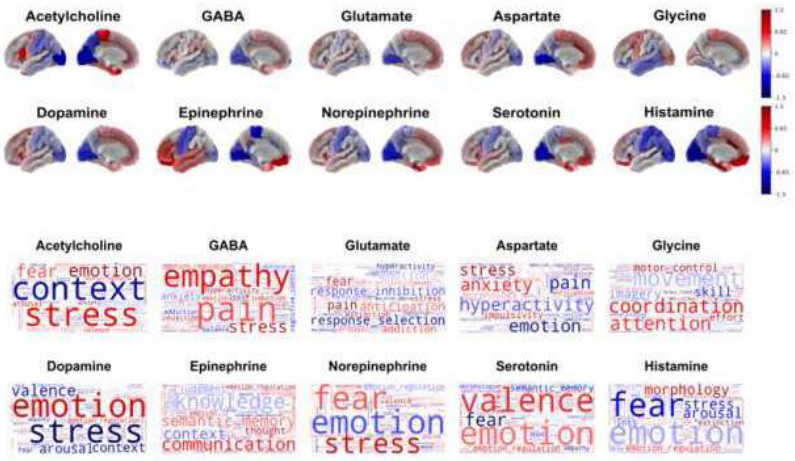

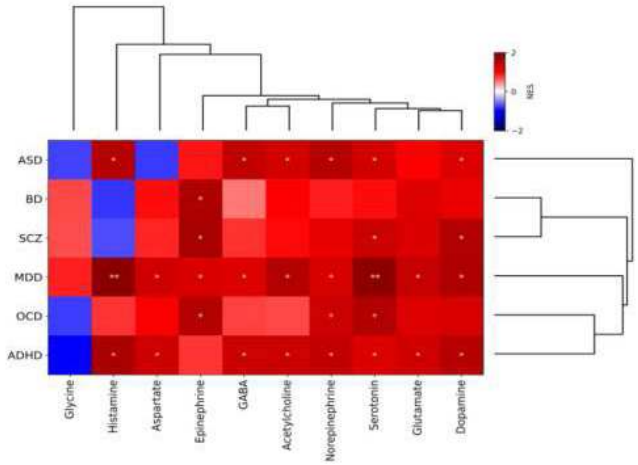

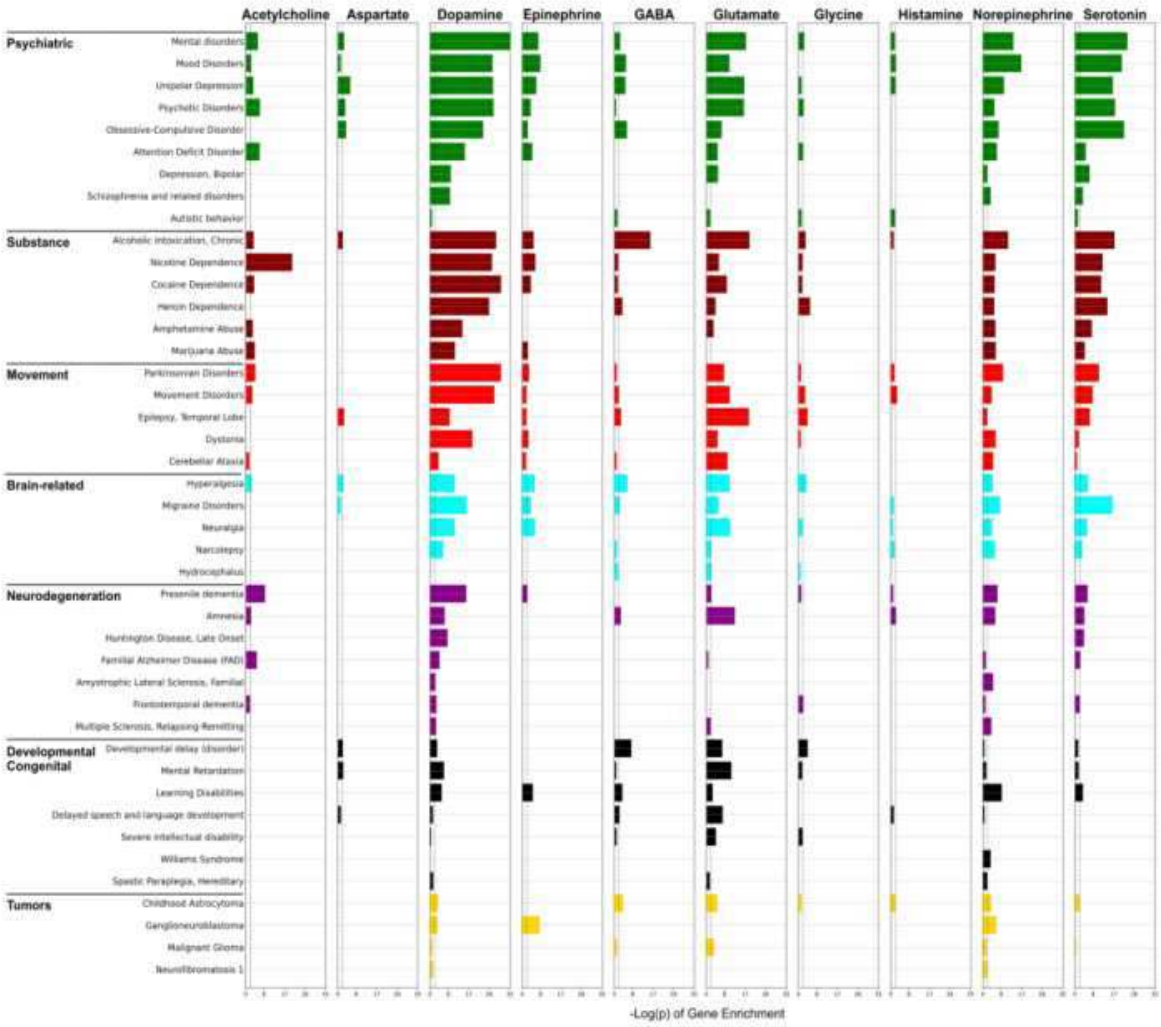

Conclusions: The present study indicates that functional and structural image-derived phenotypes reflect underlying transcriptional processes. Understanding the molecular and cellular underpinnings of neuroimaging changes in this way will provide critical insights into neuropsychiatric disease for developing novel therapeutic targets and biomarkers.

References

1. Bhaduri, A., Sandoval-Espinosa, C., Otero-Garcia, M., Oh, I., Yin, R., Eze, U. C., . . . Kriegstein, A. R. (2021). An atlas of cortical arealization identifies dynamic molecular signatures. Nature, 598(7879), 200-204. doi:10.1038/s41586-021-03910-8
2. Hansen, J. Y., Shafiei, G., Markello, R. D., Smart, K., Cox, S. M. L., Nørgaard, M., . . . Misic, B. (2022). Mapping neurotransmitter systems to the structural and functional organization of the human neocortex. Nature Neuroscience, 25(11), 1569-1581. doi:10.1038/s41593-022-01186-3
3. Larivière, S., Paquola, C., Park, B.-y., Royer, J., Wang, Y., Benkarim, O., . . . Bernhardt, B. C. (2021). The ENIGMA Toolbox: multiscale neural contextualization of multisite neuroimaging datasets. Nature Methods, 18(7), 698-700. doi:10.1038/s41592-021-01186-4
4. Park, B.-y., Kebets, V., Larivière, S., Hettwer, M. D., Paquola, C., van Rooij, D., . . . Bernhardt, B. C. (2022). Multiscale neural gradients reflect transdiagnostic effects of major psychiatric conditions on cortical morphology. Communications Biology, 5(1), 1024. doi:10.1038/s42003-022-03963-z
5. Rittman, T. (2020). Neurological update: neuroimaging in dementia. Journal of Neurology, 267(11), 3429-3435. doi:10.1007/s00415-020-10040-0
6. Seidlitz, J., Nadig, A., Liu, S., Bethlehem, R. A. I., Vértes, P. E., Morgan, S. E., . . . Raznahan, A. (2020). Transcriptomic and cellular decoding of regional brain vulnerability to neurogenetic disorders. Nature Communications, 11(1), 3358. doi:10.1038/s41467-020-17051-5
7. Subramanian, A., Tamayo, P., Mootha, V. K., Mukherjee, S., Ebert, B. L., Gillette, M. A., . . . Mesirov, J. P. (2005). Gene set enrichment analysis: A knowledge-based approach for interpreting genome-wide expression profiles. Proceedings of the National Academy of Sciences, 102(43), 15545. doi:10.1073/pnas.0506580102
8. Vidaurre, D., Abeysuriya, R., Becker, R., Quinn, A. J., Alfaro-Almagro, F., Smith, S. M., & Woolrich, M. W. (2018). Discovering dynamic brain networks from big data in rest and task. NeuroImage, 180(Pt B), 646-656. doi:10.1016/j.neuroimage.2017.06.077

Poster No 549

The reproducibility of grey matter volume differences in psychiatric disorders

Trang Cao[1], James Pang[1], Ashlea Segal[2], Sidhant Chopra[2], Mehul Gajwani[3], Alex Fornito[1]

[1]Monash University, Clayton, Victoria, [2]Yale University, New Haven, CT, [3]Monash University, Clayton, VIC

Introduction: Voxel-based morphometry (VBM)[1] has been used extensively to study anatomical differences between people with psychiatric illness and healthy controls. However, the results of these studies have often been difficult to replicate[2–6], which may be driven in part by the well-known clinical heterogeneity within psychiatric disorders. Despite this heterogeneity, a fundamental assumption in psychiatric neuroimaging is that each disorder is associated with some core neural phenotype that should be replicable and consistent across different samples and study locations. If such a consistent phenotype cannot be identified, there may be questionable value in ongoing attempts to examine group differences in small, individual studies. Here, we investigated the degree to which five psychiatric disorders––Autism Spectrum Disorder (ASD), Bipolar Disorder (BD), Mood Disorder (MDD), Schizoaffective (SCA), and Schizophrenia (SCZ)––show consistent neuroanatomical phenotypes by examining correlations between disorder- and site-specific maps of grey matter volume alterations.

Methods: We used 19 neuroimaging datasets of T1-weighted images acquired at 31 different sites across the five disorders. The final sample consisted of 1595 healthy controls (HC) and 1664 cases (ASD, N=265; BD, N=222; MDD, N=248; SCA, N=187; SCZ, N=742) taken from a larger pool of individuals after performing additional quality control checks. We only considered data from adult samples (aged 18-60 years) and sites with at least 20 individuals in each control and patient group. We estimated case-control differences in grey matter volume (GMV) separately for each site using VBM, implemented via the Computational Anatomy Toolbox[7]. We then created a common mask from all sites and adjusted for site-specific effects using the data harmonization method, ComBat[8]. We ran general linear models, taking into account total intracranial volume (TIV), sex, and age as covariates, and estimated t-statistics within each brain mask to quantify the magnitude of voxel-level case-control differences in GMV. To examine the consistency of the spatial patterns of GMV differences, we then calculate Pearson correlation (r) of the resulting t-maps between each pair of sites separately for each disorder. To investigate whether site differences in sample characteristics influenced consistency estimates, we used Mantel tests to quantify the similarity between site-by-site correlation matrices of GMV differences and matrices corresponding to differences in site-specific properties, including the number of participants, age, sex, age of illness onset, illness duration, medication exposure, scanner manufacturer, and voxel resolution.

Results: Statistical t-maps quantifying GMV reductions in ASD, BD, and MDD show low consistency, having correlation medians of 0.15 ($-0.01 \leq r \leq 0.81$), 0.05 ($-0.11 \leq r \leq 0.31$), and 0.06 ($-0.18 \leq r \leq 0.19$), respectively (Fig 1). Correlations for SCA and SCZ indicated higher consistency having medians of 0.2 ($-0.08 \leq r \leq 0.38$, $-0.06 \leq r \leq 0.5$, respectively). Mantel tests revealed no significant correlation between the site-by-site consistency of GMV differences and variations in clinical and demographic characteristics of the samples.

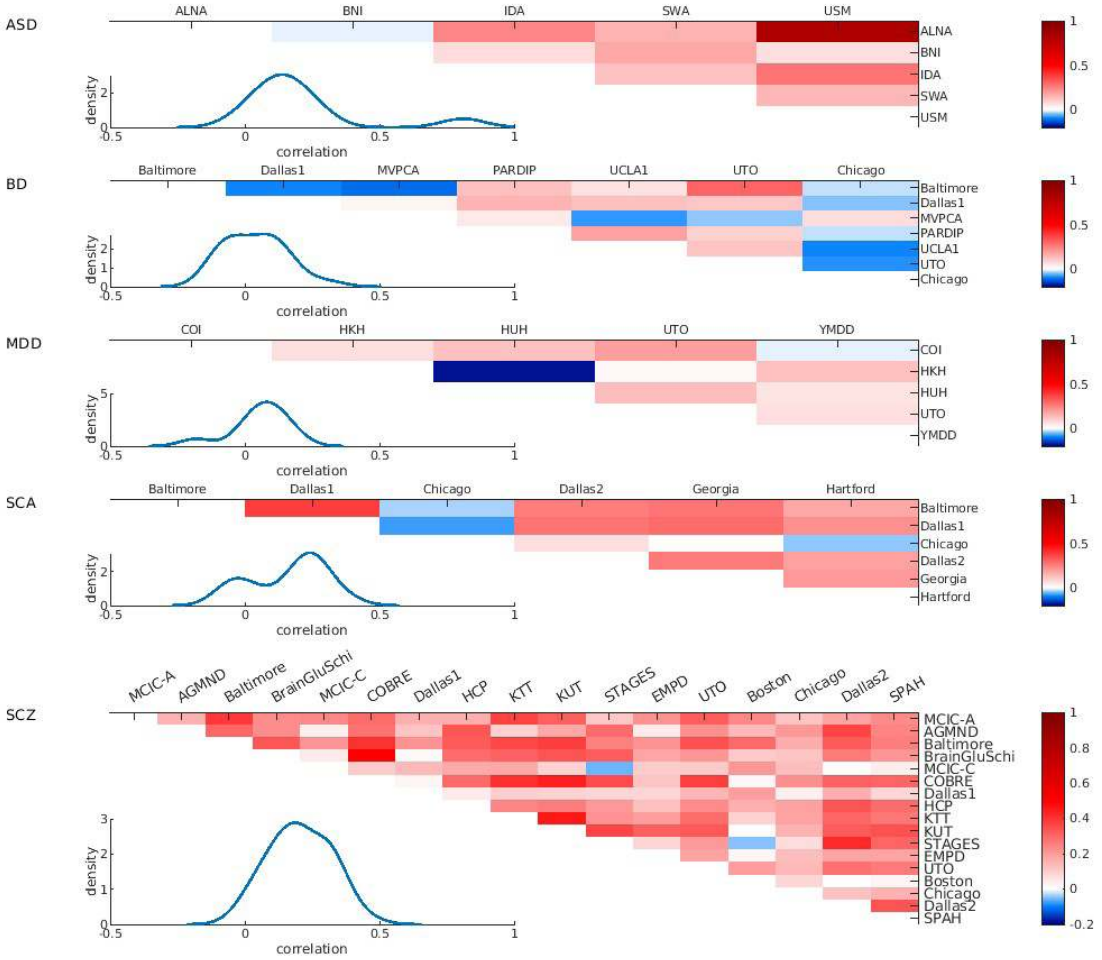

Figure 1: For each disorder, the upper panel shows the between-site correlation matrix of the t-maps and the lower panel shows the kernel density estimation of all elements of the between-site correlation matrix.

Conclusions: Our results suggest the SCZ and SCA show some evidence for a consistent core neuroanatomical phenotype, whereas ASD, BD, and MDD show no such evidence. This lack of consistency may reflect an extreme clinical and biological heterogeneity in these disorders or a limited capacity for VBM to detect the underlying disease phenotype, highlighting the need for more careful analysis and interpretation of psychiatric neuroimaging findings .

References

1. Alnæs, Dag, Tobias Kaufmann, Dennis van der Meer, Aldo Córdova-Palomera, Jaroslav Rokicki, Torgeir Moberget, Francesco Bettella, et al. 2019. 'Brain Heterogeneity in Schizophrenia and Its Association With Polygenic Risk'. JAMA Psychiatry 76 (7): 739–48. https://doi.org/10.1001/jamapsychiatry.2019.0257.
2. Ashburner, J., and K. J. Friston. 2000. 'Voxel-Based Morphometry--the Methods'. NeuroImage 11 (6 Pt 1): 805–21. https://doi.org/10.1006/nimg.2000.0582.
3. Brugger, Stefan P., and Oliver D. Howes. 2017. 'Heterogeneity and Homogeneity of Regional Brain Structure in Schizophrenia: A Meta-Analysis'. JAMA Psychiatry 74 (11): 1104–11. https://doi.org/10.1001/jamapsychiatry.2017.2663.
4. Cattarinussi, Giulia, Parnia Pouya, David Antonio Grimaldi, Mahta Zare Dini, Fabio Sambataro, Paolo Brambilla, and Giuseppe Delvecchio. 2024. 'Cortical Alterations in Relatives of Patients with Bipolar Disorder: A Review of Magnetic Resonance Imaging Studies'. Journal of Affective Disorders 345 (January): 234–43. https://doi.org/10.1016/j.jad.2023.10.097.
5. Fortin, Jean-Philippe, Nicholas Cullen, Yvette I. Sheline, Warren D. Taylor, Irem Aselcioglu, Philip A. Cook, Phil Adams, et al. 2018. 'Harmonization of Cortical Thickness Measurements across Scanners and Sites'. NeuroImage 167 (February): 104–20. https://doi.org/10.1016/j.neuroimage.2017.11.024.
6. Gaser, Christian, Robert Dahnke, Paul M. Thompson, Florian Kurth, Eileen Luders, and Alzheimer's Disease Neuroimaging Initiative. 2022. 'CAT – A Computational Anatomy Toolbox for the Analysis of Structural MRI Data'. bioRxiv. https://doi.org/10.1101/2022.06.11.495736.
7. Li, Xiaoyi, Kai Zhang, Xiao He, Jinyun Zhou, Chentao Jin, Lesang Shen, Yuanxue Gao, Mei Tian, and Hong Zhang. 2021. 'Structural, Functional, and Molecular Imaging of Autism Spectrum Disorder'. Neuroscience Bulletin 37 (7): 1051–71. https://doi.org/10.1007/s12264-021-00673-0.
8. Zhuo, Chuanjun, Gongying Li, Xiaodong Lin, Deguo Jiang, Yong Xu, Hongjun Tian, Wenqiang Wang, and Xueqin Song. 2019. 'The Rise and Fall of MRI Studies in Major Depressive Disorder'. Translational Psychiatry 9 (1): 1–14. https://doi.org/10.1038/s41398-019-0680-6.

Poster No 550

Past Medication Use Continues to Affect Resting-State Connectivity in Obsessive-Compulsive Disorder

Anders Lillevik Thorsen[1,2,3], Chris Vriend[3,4], Niels de Joode[3,4], Petra Pouwels[3,4], Feng Liu[5], Maria Otaduy[6], Bruno Pastorello[6], Frances Robertson[7], Jonathan Ipser[7], Seonjoo Lee[5], Dianne Hezel[5], Page van Meter[5], Marcelo Batistuzzo[6], Marcelo Hoexter[6], Karthik Sheshachala[8], Janardhanan Narayanaswamy[8], Ganesan Venkatasubramanian[8], Christine Lochner[9], Euripedes Miguel[6], Y.C. Janardhan Reddy[8], Roseli Shavitt[6], Dan Stein[7], Melanie Wall[5], Helen Blair Simpson[5], Odile van den Heuvel[3,4]

[1]Haukeland University Hospital, Bergen, Norway, [2]University of Bergen, Bergen, Norway, [3]Amsterdam UMC, Amsterdam, Netherlands, [4]Amsterdam Neuroscience, Amsterdam, Netherlands, [5]Columbia University, and New York State Psychiatric Institute, New York, NY, [6]Universidade de São Paulo, São Paulo, Brazil, [7]University of Cape Town, Cape Town, South Africa, [8]National Institute of Mental Health & Neurosciences (NIMHANS), Bangalore, India, [9]Stellenbosch University, Stellenbosch, South Africa

Introduction: Obsessive-compulsive disorder (OCD) is associated with altered functional connectivity (FC) within and between key brain networks (Stein et al., 2019; Thorsen & van den Heuvel, 2023). However, the magnitude and direction of these alterations is inconsistent and likely influenced by medication use, age, data acquisition and processing procedures (Stein et al., 2019). A notable limitation of most previous studies is low sample size. ENIGMA-OCD attempted to address this through a mega-analysis which found less somatomotor network FC in adults with OCD vs healthy controls (HC), which was driven by patients using selective serotonin reuptake inhibitors (SSRI) or serotonin norepinephrine reuptake inhibitors (SNRI, Bruin et al., 2023). However, such mega-analyses are limited by lack of harmonized data collection. Here, we present findings from the Global OCD study (Pouwels et al. 2023; Simpson et al., 2020), which compares network FC in adult individuals with OCD and HC using harmonized data acquisition and processing procedures across five sites and continents based on a preregistered analysis plan (https://osf.io/b3vz5).

Methods: FC between and within the visual, somatomotor, dorsal attention, ventral attention, limbic, frontoparietal and default mode networks was compared between 259 currently unmedicated (for a minimum of 6 weeks) adults with OCD and 251 age, sex matched HC (mean age 29.79 (SD 8.03), 56% female). Connectivity was estimated in grayordinate fsLR32k space, providing optimal spatial resolution and minimized blurring between regions (Coalson et al., 2018). Denoising included ICA-AROMA noise components, mean cerebrospinal fluid and white matter signals, detrending, and bandpass filtering (0.009-0.08 Hz). FC was estimated between regions of the Schaefer 400 cortical parcellation and 36 subcortical regions from the Brainnetome atlas. ComBat was used to adjust for site differences in FC, permutation-based linear models adjusted for age, sex and years of education were used for statistical analyses, and the false discovery rate was used to adjust for multiple comparisons.

Results: No significant differences in FC were found between adults with OCD and HC. Among individuals with OCD, those with previous use of medication (n=112, including n=99 SSRI, n=4 SNRI, n=9 both), compared to 147 medication naive patients, showed significantly weaker FC between the ventral attention and default mode network and between the ventral attention and limbic network ($pFDR<.03$, $d\geq0.43$). Post-hoc tests showed that more days since last SSRI/SNRI use was related to stronger FC between the ventral attention and default mode network (uncorrected $p<.03$, $r=.12$). Furthermore, previously medicated, but not medication naive, patients also showed significantly weaker FC between the ventral attention and limbic network and between the ventral attention and default mode network compared to HC (uncorrected $p<.02$, $d\geq-0.35$). Medication naive patients showed less severe symptoms of OCD (Yale-Brown Obsessive-Compulsive Scale), depression (Hamilton Depression Rating Scale) and anxiety (Hamilton Anxiety Rating Scale) than previously medicated patients (uncorrected $p<.04$, $d\geq0.28$), but the difference in ventral attention-limbic and ventral attention-default mode FC versus medication naïve patients remained after adjusting for these variables.

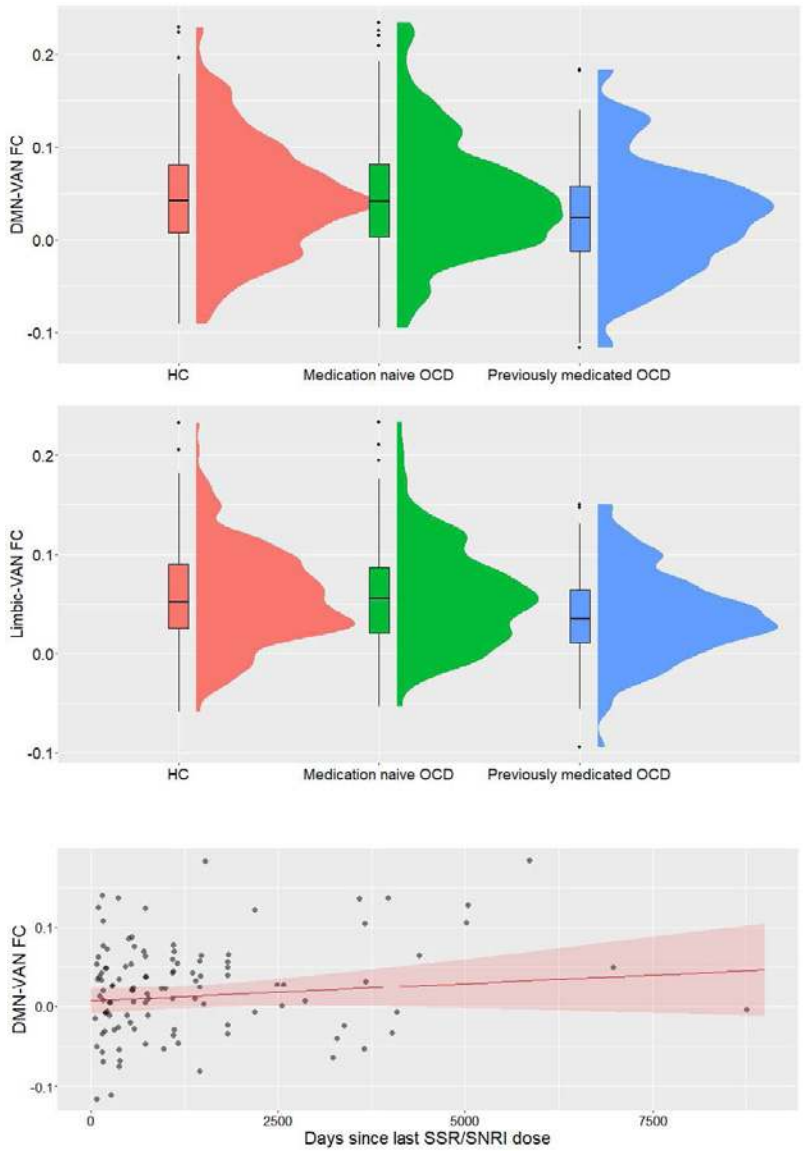

Conclusions: The overall difference in network FC between unmedicated adults with OCD and HC is small and not significant in this relatively large multicenter study with harmonized data collection and processing. Comparions between previously medicated and medication naïve individuals with OCD suggests that previous use of SSRI/SNRI continues to be associated with network FC after a minimum of a six-week wash-out period.

References

1. Bruin, W. B. (2023). The functional connectome in obsessive-compulsive disorder: resting-state mega-analysis and machine learning classification for the ENIGMA-OCD consortium. Molecular Psychiatry, 1-13.
2. Coalson, T. S. (2018). The impact of traditional neuroimaging methods on the spatial localization of cortical areas. Proceedings of the National Academy of Sciences, 115(27)
3. Pouwels, P. J. (2023). Global multi-center and multi-modal magnetic resonance imaging study of obsessive-compulsive disorder: Harmonization and monitoring of protocols in healthy volunteers and phantoms. International Journal of Methods in Psychiatric Research, 32(1), e1931.
4. Simpson, H. B. (2020). Toward identifying reproducible brain signatures of obsessive-compulsive profiles: rationale and methods for a new global initiative. BMC Ppsychiatry, 20, 1-14
5. Stein, D. J. (2019). Obsessive–compulsive disorder. Nature reviews Disease Primers, 5(1)
6. Thorsen, A. L. (2023). Neuroanatomy of obsessive-compulsive and related disorders. In Tolin, D. (Ed.) Oxford Handbook of Obsessive Compulsive and Related Disorders, Second Edition. Oxford University Press.

Poster No 551

White Matter Abnormalities and Differential Treatment Outcomes to CBT or Antidepressant Medication

Jack Gomberg[1], Jungho Cha[1], Juna Khang[1], Boadie Dunlop[2], Edward Craighead[2], Helen Mayberg[1], Ki Sueng Choi[1]

[1]Icahn School of Medicine at Mount Sinai, New York, NY, [2]Emory University, Atlanta, GA

Introduction: First-line treatment for major depressive disorder (MDD) includes cognitive behavioral therapy (CBT) and/or antidepressant medications (ADM).[1] However, these treatments can be highly effective in one patient but ineffective in another with similar MDD symptom presentations.[2–4] Previous treatment selection biomarker studies using resting state fMRI (rsfMRI) implicate differential functional connectivity (FC) from the subcallosal cingulate (SCC) to the left anterior insula, left ventromedial prefrontal, and left periaqueductal gray in CBT and medication remitters.[5] Structural white matter (WM) abnormalities that might mediate these functional connectivity patterns are unknown. Therefore, we evaluated pretreatment WM integrity in treatment naïve MDD patients as a function of differential 3-month clinical outcome to monotherapy with CBT or ADM.

Methods: Diffusion-weighted imaging (DWI) was collected in 167 treatment naïve MDD patients randomized to 12 weeks of CBT or ADM. Subjects were grouped into CBT or ADM remitters (HDRS17 score <7 at 10 and 12 weeks) and CBT or ADM failure (HDRS score improvement <30%). A Whole brain fractional anisotropy (FA) map was calculated for each subject using the Fdt toolbox in FMRIB, and standard Tract-Based Spatial Statistics (TBSS) analysis was performed for preprocessing. A voxel-wise 2 x 2 ANOVA: treatment (CBT/ADM) by outcome (remitter/nonresponder) was performed using the AFNI 3dMVM toolbox. Furthermore, FA values from significant regions in 2 x 2 ANOVA were extracted and analyzed post hoc for treatment group-specific correlations with HDRS17 scores and previously published SCC functional connectivity.

Results: A significant treatment by outcome interaction was identified, affecting WM tracts adjacent to the left anterior insula, left supplementary motor area, and left anterior/posterior hippocampus ($p < 0.001$). ADM remitters and CBT nonresponders show higher FA values in the left insula and SMA compared to both ADM nonresponders and CBT remitters, similar to the pattern of functional connectivity biomarkers. In contrast, ADM remitters and CBT nonresponders show lower FA in the left anterior and posterior hippocampus than ADM nonresponders and CBT remitters. In post hoc analysis, the left anterior insula showed significant anticorrelation between HDRS17 score improvement and FA value ($r=-0.364$, $p=0.008$) in the CBT treatment group but no significant correlation in the ADM group. The hippocampal findings showed significant anticorrelation for HDRS17 score improvement and FA value in the ADM group in both anterior ($r=-0.244$, $p=0.009$) and posterior ($r=-0.202$, $p=0.031$) subregions. The SMA revealed no significant correlation in either treatment groups. Finally, the insula and anterior hippocampus showed no significant correlation with past rsfMRI SCC FC biomarkers. The posterior hippocampus FA finding significantly correlated with FC findings in the SCC FC with the PAG ($r=0.311$, $p=0.002$), insula ($r=0.294$, $p=0.003$), and ventromedial prefrontal cortex ($r=0.241$, $p=0.016$). The SMA showed significant anticorrelation with the insular FC finding ($r=-0.253$, $p=0.011$).

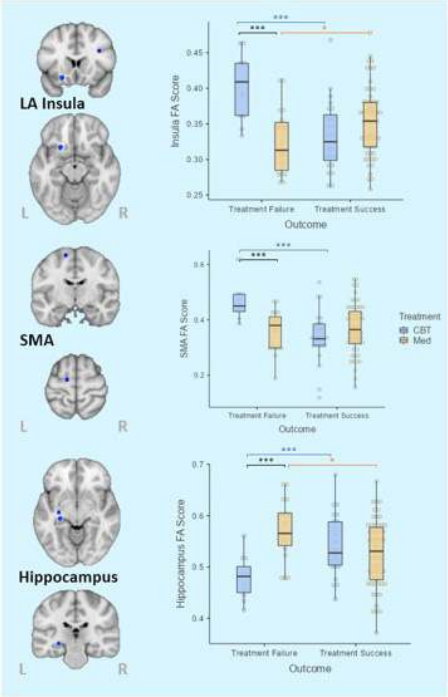

Figure 1. ANOVA 2x2 Analysis Treatment Selection White Matter Biomarker

A significant treatment by outcome interaction was identified adjacent to the left anterior insula, left supplementary motor area, and left hippocampus (p<0.001). (Post hoc: ***p<0.001; **p<0.005; *p<0.05)

Correlation Matrix CBT ONLY		HAMD % Change
HAMD % Change	Pearson's r	—
	p-value	—
Insula (shiny)	Pearson's r	−0.364 **
	p-value	0.008
Ant Hippocampus (shiny)	Pearson's r	0.180
	p-value	0.202
Post Hippocampus (shiny)	Pearson's r	0.215
	p-value	0.126
SMA (shiny)	Pearson's r	−0.158
	p-value	0.262

Correlation Matrix ADM ONLY		HAMD % Change
HAMD % Change	Pearson's r	—
	p-value	—
Insula (shiny)	Pearson's r	0.166
	p-value	0.075
Ant Hippocampus (shiny)	Pearson's r	−0.244 **
	p-value	0.009
Post Hippocampus (shiny)	Pearson's r	−0.202 *
	p-value	0.031
SMA (shiny)	Pearson's r	0.083
	p-value	0.376

Table 1: Group specific correlations

Significant correlation between HDRS17 score change and FA score split by treatment groups was identified in the insula for CBT group and the anterior/posterior hippocampus in the ADM group. (***p<0.001; **p<0.005; *p<0.05)

Conclusions: These findings identify differential WM integrity in WM tracts adjacent to the insula, SMA, and hippocampus in remitters and failures to CBT and ADM. As with functional connectivity findings, WM integrity may define imaging biotypes that impact the capacity to respond to first-line MDD treatments and guide optimal treatment selection. Furthermore, the differential outcomes between treatment groups for the FA correlations suggest differences in the underlying treatment mechanisms within depression circuit pathophysiology. Finally, the correlation of posterior hippocampal and SMA FA findings with past SCC FC biomarkers suggests a relationship between functional and structural findings in MDD.

References

1. Gundlach A, Knight KD. American Psychiatric Association: Practice Guideline for the Treatment of Patients With Major Depressive Disorder, 3rd ed. Am Psychiatr Assoc. Published online 2010.
2. Dunlop BW. Evidence-Based Applications of Combination Psychotherapy and Pharmacotherapy for Depression. Focus J Life Long Learn Psychiatry. 2016;14(2):156-173. doi:10.1176/appi.focus.20150042
3. Gelenberg AJ, Freeman MP, Markowitz JC, et al. WORK GROUP ON MAJOR DEPRESSIVE DISORDER. Published online 2010.
4. Collins FS, Varmus H. A New Initiative on Precision Medicine. N Engl J Med. 2015;372(9):793-795. doi:10.1056/NEJMp1500523
5. Dunlop BW, Rajendra JK, Craighead WE, et al. Functional Connectivity of the Subcallosal Cingulate Cortex And Differential Outcomes to Treatment With Cognitive-Behavioral Therapy or Antidepressant Medication for Major Depressive Disorder. Am J Psychiatry. 2017;174(6):533-545. doi:10.1176/appi.ajp.2016.16050518
6. Guo Q, Duan J, Cai S, Zhang J, Chen T, Yang H. Desynchronized white matter function and structure in drug-naive first-episode major depressive disorder patients. Front Psychiatry. 2023;13:1082052. doi:10.3389/fpsyt.2022.1082052

Poster No 552

Longitudinal stability of individual differences in functional connectivity in psychopathology

Brian Kraus[1], Richard Zinbarg[1], Robin Nusslock[1], Michelle Craske[2], Caterina Gratton[3]

[1]Northwestern University, Evanston, IL, [2]University of California, Los Angeles, Los Angeles, CA, [3]Florida State University, Tallahassee, FL

Introduction: Internalizing psychopathology is characterized by elevated negative affect, such as major depressive disorder (MDD) which shows significant symptom fluctuations over time. "Precision" fMRI has demonstrated that functional connectivity (FC) is reliable within individuals across sessions with >40 minutes of artifact free data at each session. This method can be used to identify idiosyncratic areas of FC which greatly deviate from canonical network FC, which we call network variants. However, while network variants are highly stable in neurotypical individuals ($r > .9$; Kraus et al., 2021), they have not yet been explored in psychiatric contexts where temporal changes in symptoms occur. Here, we sought to evaluate the stability of network variants in individuals diagnosed with internalizing disorders versus healthy controls.

Methods: The current study followed participants longitudinally from ages 18-19 to 21-22 (see Young et al., 2021). At baseline and the 3-year follow-up visits, 150 participants completed approximately 65 minutes of resting-state and task fMRI scans. The data from these scans was processed using fMRIPrep (Esteban et al., 2019). FC processing was performed using custom scripts which included nuisance regression and censoring high motion frames (fFD > .1; (Gratton et al., 2020)), and mapping functional data to surface space. Building off our past work (Kraus et al., 2021), task scans were modeled with a GLM and the residuals were combined with rest to estimate network variants for each participant. Only participants with >40 minutes of fMRI data after censoring at each timepoint were analyzed. To estimate network variants, the pairwise correlation between the timeseries of each vertex on the surface and every other vertex was calculated. Next, a row-wise correlation was performed between each participant's matrix and an independent group-average matrix. In the resulting spatial map, a low value denoted that a given vertex had a very dissimilar FC profile from what would typically be expected in the group-average at that location, and vice-versa. For analysis, variant maps were estimated at baseline and 3-year follow-up for individuals who had met lifetime criteria for anxiety or depressive disorders versus healthy controls. To quantify similarity over time, each individual's variant map was correlated longitudinally with their own map as well as every other individual's map. Then, the mean value for the correlation between each individual and every other individual was compared to each individual's actual longitudinal correlation using a paired t-test.

Results: The longitudinal stability of network variants was not significantly different between healthy controls ($r = .85$) and the lifetime depressive disorder group ($r = .85$, $t(87) = .12$, $p = .91$, $d = .03$), or the lifetime disorder anxiety group ($r = .86$, $t(89) = .92$, $p = .36$, $d = .19$). In each group, network variant maps for an individual looked significantly more similar to the same person at a 3-year longitudinal follow up than to other individuals in the study: healthy controls ($t(71) = 50.46$, $p < .001$, $d = 5.94$), the lifetime depressive disorder group ($t(16) = 28.1$, $p < .001$, $d = 6.82$), and the lifetime disorder anxiety group ($t(18) = 26.78$, $p < .001$, $d = 6.14$). Thus, variant maps showed similar stability over time for those in the anxiety and depressive groups versus the healthy controls, and all three groups' variant maps were much more similar to themselves over time versus other individuals in their group.

Conclusions: These findings suggest that network variants are trait-like in their stability within individuals, regardless of psychiatric history. This suggests that network variants, and likely FC in general, are more sensitive to longitudinally stable factors and less to shorter-term changes associated with fluctuations in psychopathology symptoms. Future work will have to determine the temporal relationship between FC and psychiatric symptoms.

References

1. Esteban, O. (2019). fMRIPrep: A robust preprocessing pipeline for functional MRI. Nature Methods, 16(1), 111–116.
2. Gratton, C. (2020). Removal of high frequency contamination from motion estimates in single-band fMRI saves data without biasing functional connectivity. NeuroImage, 116866.
3. Kraus, B. T. (2021). Network variants are similar between task and rest states. NeuroImage, 229, 117743.
4. Young, K. S. (2021). Dysregulation of threat neurociruitry during fear extinction: The role of anhedonia. Neuropsychopharmacology, 1–8.

Poster No 553

The structural connectome constrains in vivo synaptic density loss in schizophrenia

Sidhant Chopra[1], Patrick Worhunsky[1], Mika Naganawa[1], Gustavo Angarita[1], Kelly Cosgrove[1], Deepak D'Souza[1], David Matuskey[1], Nabeel Nabulsi[1], Yiyun Huang[1], Richard Carson[1], Irina Esterlis[1], Patrick Skosnik[1], Avram Holmes[2], Rajiv Radhakrishnan[1]

[1]Yale University, New Haven, CT, [2]Department of Psychiatry, Brain Health Institute, Rutgers University, Piscataway, NJ

Introduction: Converging genetic, post-mortem and neuroimaging evidence suggests the loss of synapses is fundamental to schizophrenia pathogenesis. The synaptic vesicle glycoprotein 2A radioligand [11C]UCB-J allows the examination of synaptic density in vivo using positron emission tomography (PET)[1], with recent studies showing large and widespread lower synaptic density in individuals with schizophrenia[2,3]. However, the mechanisms explaining the anatomical distribution of these alterations remain elusive. The brain's different regions are connected by a complex structural network of axonal fibers, responsible for propagating action potentials and transporting biological molecules[4]. They may also act as conduits for the progression of synaptic loss, such that illness processes originating in one area can propagate to affect other vulnerable areas[5]. Here, we investigate whether the brain's axonal fibers act as conduits for synaptic density loss in schizophrenia, as observed in other neurological syndromes.

Methods: Using PET parametric images of [11C]UCB-J binding potential from 117 individuals (92 healthy controls and 25 individuals with schizophrenia), we generated brain-wide voxel-level group difference maps. We derived representative functional and structural connectivity patterns from an independent control group (N=100). General linear models were used to assess group differences in synaptic density adjusting for age and sex (Fig1). We derived representative inter-regional functional coupling and structural connectivity patterns from an independent age-matched healthy control group (N=323) using resting-state functional MRI and diffusion-weighted imaging. We used coordinated deformation models6 to predict the extent of brain change in each of 332 parcellated areas by the changes observed in areas to which the index region is either structurally connected or functionally coupled (Fig2). To locate potential focal sources of the observed lower synaptic density, we used a network diffusion model7, sequentially using each brain region as a seed (Fig3).

Results: We found a widespread pattern of lower synaptic density in individuals with schizophrenia (p_FWE<.05; Fig1), with peaks located in temporal, frontal, cingulate cortices, and thalamic and striatal regions. Our results demonstrated that regional synaptic density differences were strongly correlated with estimates of lower synaptic density predicted using a model constrained by structural connectivity (r=.58; p_FWE<.01). Associations between empirical and predicted synaptic density estimates were much lower for models considering only binary structural connectivity or constrained by functional coupling. Finally, we identified the left temporal pole as putative epicenters of the pathological spread of synaptic loss (Fig3).

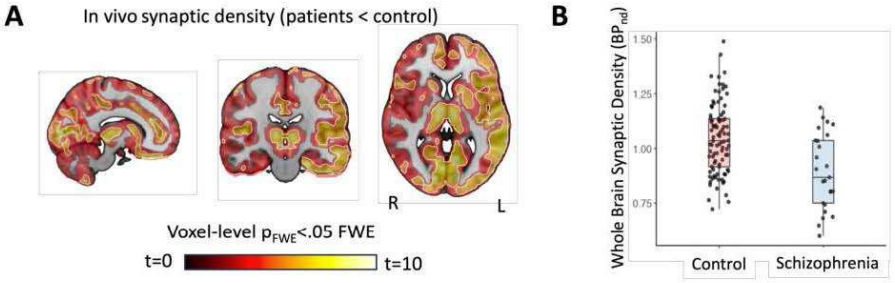

Figure 1 – Lower synaptic density in individuals with Schizophrenia. **(A)** Voxel-wise map of group-differences in synaptic density between patients and controls, while adjusting the model of age and sex. Greater test-statistic (t) indicated lower synaptic density in patients compared to controls. White border indicates voxel-level FWE statistical significance at $p < 0.05$. **(B)** Whole brain mean synaptic density values plotted for each group. BPnd=Binding potential of tracer, using the centrum semiovale as a reference region.

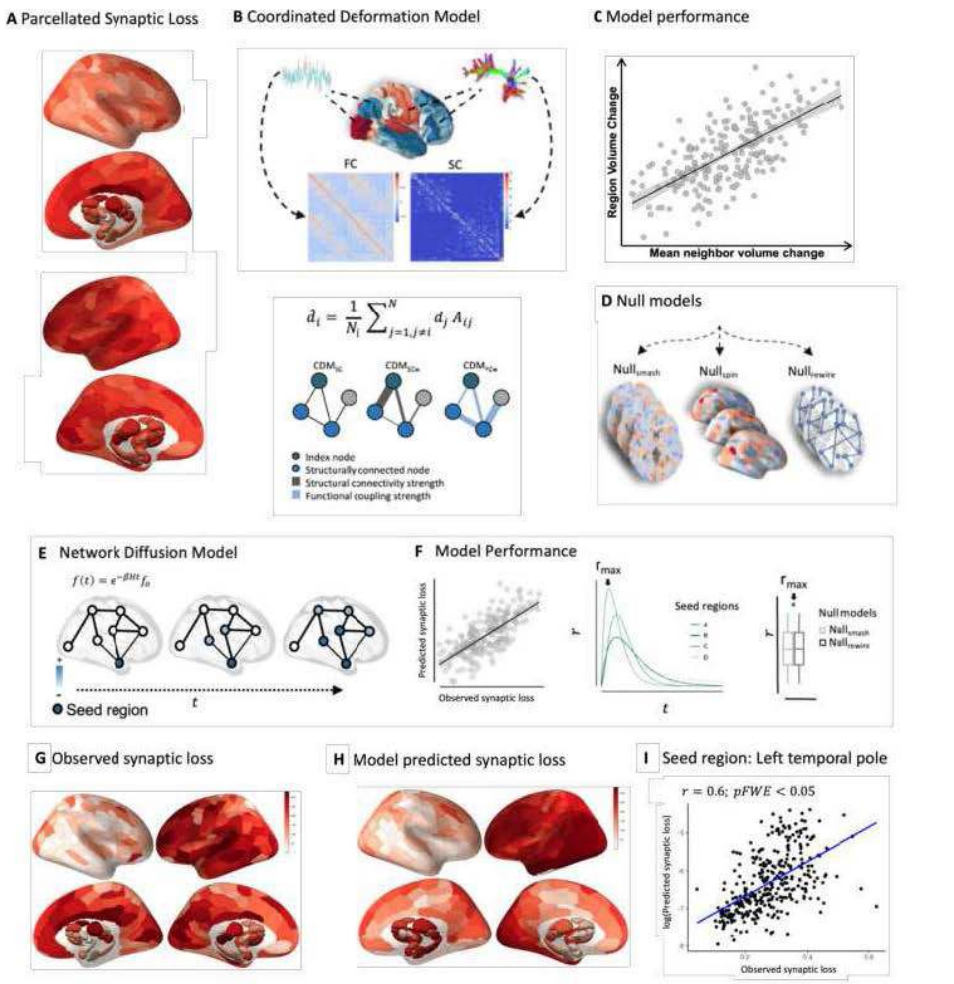

Figure 2 – Coordinated Deformation Models (CDM). **(A)** Contrast statistics from Fig1A projected onto a 332-region brain parcellation. **(B)** Independent healthy sample's diffusion and functional MRI data used to derive average Functional Coupling (FC) and Structural Connectivity (SC) matrices and modeling synaptic density changes in connected regions, weighted by by SC or FC. **(C)** Model performance assessed using Spearman correlation between observed and CDM-predicted synaptic alterations. **(D)** Performance also compared to null models considering spatial connectivity properties. **(E)** Network Diffusion Model (NDM). Epicenters identified as potential sources of pathological synaptic loss with spread determined through NDM simulations. **(F)** Maximum correlation retained between simulated and observed GMV alterations, compared against null models. **(G)** Observed and **(H)** predicted rank-ordered synaptic alteration maps. **(I)** Scatter plot showcasing observed vs. predicted synaptic alterations with the left temporal pole as the starting seed.

Conclusions: Our findings highlight a robust and central role of white matter fibers on the spread of pathology in schizophrenia, mirroring findings reported in other neurological conditions. They also align with volumetric findings in individuals with schizophrenia, suggesting that temporal regions may play a critical role in the origins of brain dysfunction and indicate that the structural connectome may represent a fundamental constraint on synaptic pathology.

References

1. Finnema, S. J. et al. Imaging synaptic density in the living human brain. Science translational medicine 8, 348ra396-348ra396 (2016).
2. Radhakrishnan, R. et al. In vivo evidence of lower synaptic vesicle density in schizophrenia. Molecular Psychiatry, doi:10.1038/s41380-021-01184-0 (2021).
3. Onwordi, E. C. et al. Synaptic density marker SV2A is reduced in schizophrenia patients and unaffected by antipsychotics in rats. Nature Communications 11, 246, doi:10.1038/s41467-019-14122-0 (2020).
4. Sporns, O., Tononi, G. & Kötter, R. The Human Connectome: A Structural Description of the Human Brain. PLOS Computational Biology 1, e42, doi:10.1371/journal.pcbi.0010042 (2005).
5. Vogel, J. W. et al. Spread of pathological tau proteins through communicating neurons in human Alzheimer's disease. Nature Communications 11, 2612, doi:10.1038/s41467-020-15701-2 (2020).
6. Chopra, S. et al. Network-Based Spreading of Gray Matter Changes Across Different Stages of Psychosis. JAMA Psychiatry, doi:10.1001/jamapsychiatry.2023.3293 (2023).
7. Raj, A., Kuceyeski, A. & Weiner, M. A network diffusion model of disease progression in dementia. Neuron 73, 1204-1215, doi:10.1016/j.neuron.2011.12.040 (2012).

Poster No 554

A mega-analysis of functional connectivity and network changes in youth major depression

Nga Yan Tse[1], Aswin Ratheesh[2], Robin Cash[1], Andrew Zalesky[1]

[1]Department of Psychiatry, The University of Melbourne, Carlton, Victoria, [2]Orygen, Parkville, Victoria

Introduction: Major depressive disorder (MDD) has a lifetime prevalence of 11.1-14.6%[1,2] and represents the leading cause of disability due to mental health conditions for young people aged 10-24 years worldwide[3,4]. Functional neuroimaging can delineate the neural substrates of psychiatric, cognitive, and neurological disorders and potentially provide targets for treatment[5-8]. Youth MDD research however lag behind that in adults where existing resting-state functional MRI (rs-fMRI) studies have yielded inconsistent findings[9]. Further, mega-analysis, involving compilation of independent cohort datasets and offering unprecedented advantages of improved generalizability and increased statistical power, has remained unexplored in youth MDD.

Methods: Here, we conducted the first mega-analysis of functional connectivity (FC) changes in youth MDD, encompassing 810 raw, unprocessed T1 and rs-fMRI images collated from 7 international sites (n=440 youths with MDD and 370 healthy controls aged between 12-25 years). Standardized fMRIprep pre-processing, quality control, and COMBAT harmonization were completed for all fMRI data. Whole-brain FC (connectomes) were mapped for each individual based on the Schaefer Yeo 7-network 400 functional atlas. Using impartial, whole-brain-based statistical inference termed network-based statistic (NBS)[10], mega-analyses of between-group and symptom severity-related connectivity differences were conducted at the scale of functional connections and canonical networks. All NBS analyses were adjusted for age and sex and corrected for family-wise error at p<.05. Linear support vector machines with ridge regularization and leave-one-site-out cross validation were applied to build predictive models of diagnostic status and symptom severity (as measured by the Montgomery-Asberg Depression Rating Scale). Accuracy was tested on unseen datasets kept out of the model training to ensure robustness to inter-site variability. Supplementary analyses were conducted to ensure findings are not biased by global signal regression, atlas choice, or potential head motion differences.

Results: Our analyses consistently implicated core nodes of the default mode network (DMN) in youth MDD, particularly the rostral/subgenual anterior cingulate, medial prefrontal cortex, posterior cingulate, and precuneus (Fig. 1-2). Altered connectivity of components of the limbic, and dorsal (DAN) and ventral attentional (VAN) networks also tended to emerge, localizing to the orbitofrontal cortex, insula, striatum, and intraparietal sulcus/superior parietal cortex (Fig. 1-2). Strikingly, these regions have been implicated as rich-club nodes in past literature and consistently demonstrated a higher level of hubness in our analyses, supporting extensive earlier studies reporting hub involvement in early psychopathology development. Critically, individual variation in FC within these networks of regions was significantly associated with depression symptom severity (r=-.58 and r=.65 for hypo- and hyper-connected regions; both p<.001), supporting the clinical importance of these connectivity alterations. Consistently, our machine learning analysis further demonstrated that these FC features provided capacity to classify diagnostic status and depression severity in a generalizable and robust fashion beyond site-specific confounds with good accuracy (averaged cross-validated AUC=73% and r=.63).

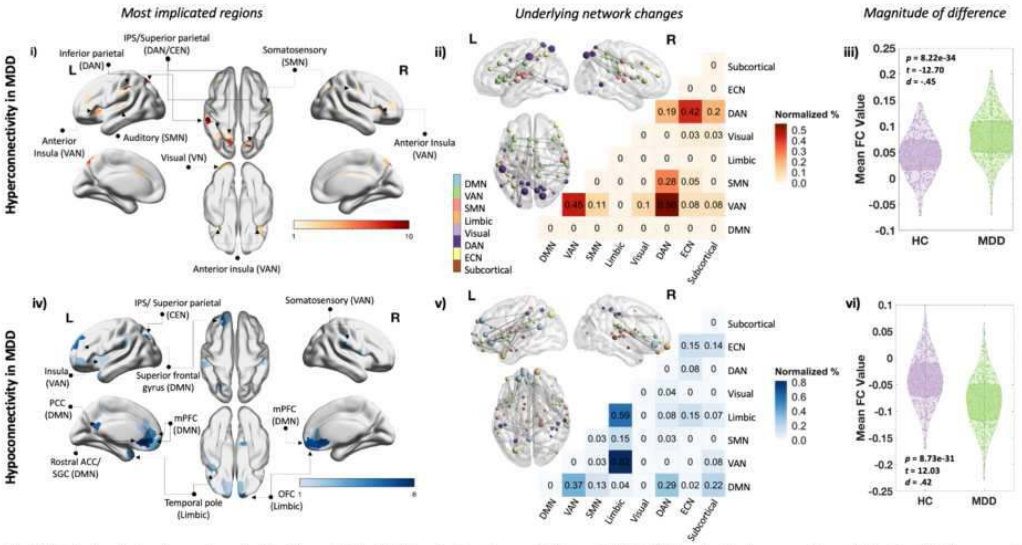

Fig. 1. i) Cortical renderings show regions significantly associated with higher functional connectivity in youth MDD. **ii)** Networks showing connections with significantly higher connectivity strength in youth MDD. Nodes are colored according to 7 canonical functional networks. Matrix displays proportion of connections with significantly higher connectivity strength between pairs of canonical networks, normalized by the total number of possible connections within or between each pair of networks. **iii)** Significantly higher mean connectivity values of all significant hyper-connections (as shown in 1ii) in MDD compared to the healthy comparison. **iv-vi)** Same as i-iii) but for lower functional connectivity in the MDD relative to healthy comparison group.

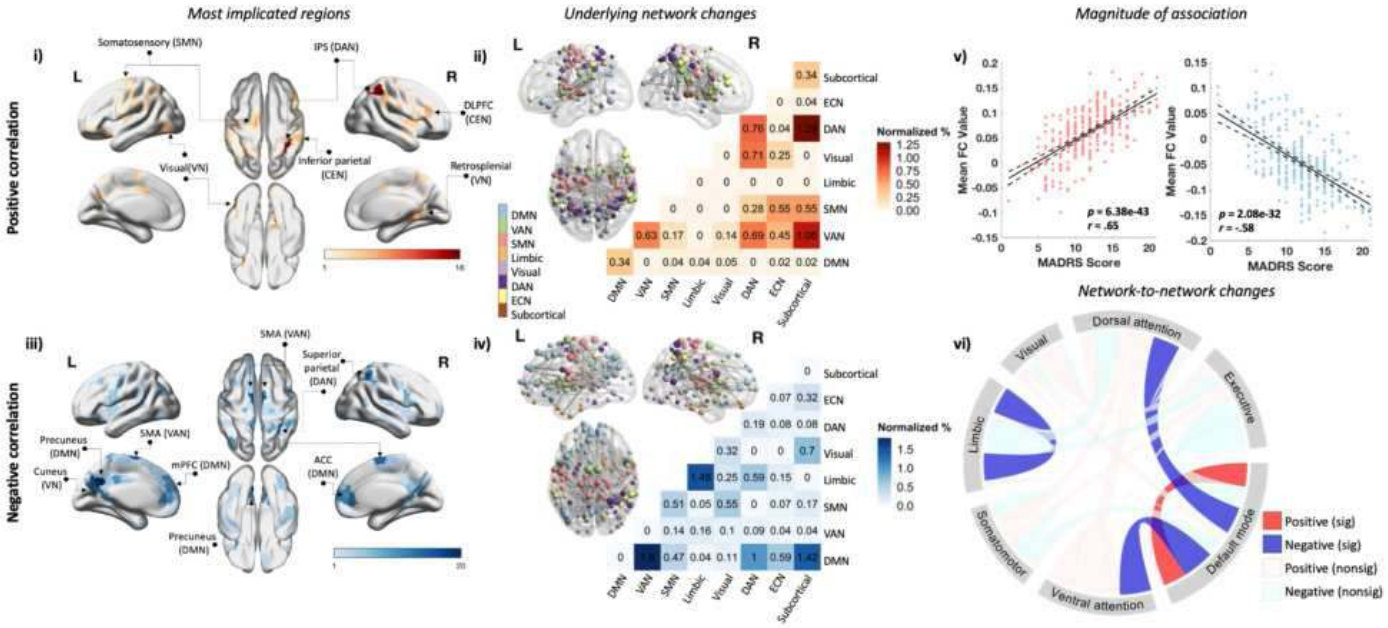

Fig. 2. i) Cortical renderings display regions significantly associated with more severe depression symptoms (i.e., higher total MADRS scores). **ii)** Networks containing connections significantly associated with higher total MADRS scores. Nodes are colored according to 7 canonical functional networks. Matrix displays proportion of connections with significant association with higher total MADRS scores between pairs of canonical networks, normalized by the total number of possible connections within or between each pair of networks. **iii-iv)** Same as i-ii) but for negative association with total MADRS scores. **v)** Scatterplots illustrate the magnitude of correlations between mean connectivity strength of all significant positive and negative connections and MADRS scores, respectively. **vi)** Circular network visualization shows significant correlation between mean intra- (within the limbic and DMN) and inter- (DMN-VAN and DMN-DAN) network connectivity and depression symptom severity. Line width reflects the size of correlation coefficient.

Conclusions: Our data-driven, connectome-wide FC and machine learning analyses converge to implicate robust involvement of hub regions within the DMN, DAN, VAN, and limbic network. Adolescence, coinciding with a protracted period of significant plastic changes and psychosocial transitions, represents a unique window of increased vulnerability to altered hub development. This may in turn confer risks for altered network dynamics and discoordination of a myriad of processes centred on the attentional, affective, and introspective systems, and ultimately early emergence of youth MDD.

References

1. Kessler, R.C., Bromet, E.J. (2013), 'The epidemiology of depression across cultures', Annu Rev Public Health,vol. 34, pp. 119-138. doi:10.1146/annurev-publhealth-031912-114409
2. Kovess-Masfety, V., Alonso, J., Angermeyer, M., et al (2013), 'Irritable mood in adult major depressive disorder: Results from the world mental health surveys', Depress Anxiety, vol. 30, no. 4, pp. 395-406. doi:10.1002/da.22033
3. Gore, F.M., Bloem, P.J.N., Patton, G.C., et al (2011), 'Global burden of disease in young people aged 10-24 years: A systematic analysis', The Lancet, vol. 377, no. 9783, pp. 2093-2102. doi:10.1016/S0140-6736(11)60512-6
4. Vos, T., Allen, C., Arora, M., et al (2016), 'Global, regional, and national incidence, prevalence, and years lived with disability for 310 diseases and injuries, 1990–2015: a systematic analysis for the Global Burden of Disease Study 2015', The Lancet, vol. 388, no. 10053, pp. 1545-1602. doi:10.1016/S0140-6736(16)31678-6
5. Menon, V. (2011), 'Large-scale brain networks and psychopathology: A unifying triple network model', Trends Cogn Sci, vol. 15, no. 10, pp. 483-506. doi:10.1016/j.tics.2011.08.003
6. Bressler, S.L., Menon, V. (2010), 'Large-scale brain networks in cognition: emerging methods and principles', Trends Cogn Sci, vol. 14, no. 6, pp. 277-290. doi:10.1016/j.tics.2010.04.004
7. Siddiqi, S.H., Taylor, S.F., Cooke, D., Pascual-Leone, A., George, M.S., Fox, M.D. (2020), 'Distinct symptom-specific treatment targets for circuit-based neuromodulation', American Journal of Psychiatry, vol. 177, no. 5, pp. 435-446. doi:10.1176/appi.ajp.2019.19090915
8. Siddiqi, S.H., Schaper, F.L.W.V.J., Horn, A., et al (2021), 'Brain stimulation and brain lesions converge on common causal circuits in neuropsychiatric disease', Nat Hum Behav, vol. 5, no. 12, pp. 1707-1716. doi:10.1038/s41562-021-01161-1
9. Tse, N.Y., Ratheesh, A., Ganesan, S., Zalesky, A., Cash, R.F.H. (2023), 'Functional dysconnectivity in youth depression: Systematic review, meta-analysis, and network-based integration', Neurosci Biobehav Rev, vol. 153, no. 105394. doi:10.1016/j.neubiorev.2023.105394
10. Zalesky, A., Fornito, A., Bullmore, E.T. (2010), 'Network-based statistic: Identifying differences in brain networks', Neuroimage, vol. 53, no. 4, pp. 1197-1207. doi:10.1016/j.neuroimage.2010.06.041

Poster No 555

Prefrontal Cortex-based Schizophrenia Phenotypes Linked to Variation in Williams Syndrome Gene LIMK1

Shane Kippenhan[1], Michael Gregory[1], Daniel Eisenberg[1], Tiffany Nash[1], Carolyn Mervis[2], Bhaskar Kolachana[1], Destiny Wright[1], Madeline Garvey[1], Philip Kohn[1], Karen Berman[1]

[1]NIMH, National Institutes of Health, Bethesda, MD, [2]University of Louisville, Louisville, KY

Introduction: LIMK1, one of ~26 genes hemideleted in Williams syndrome (WS), is vital to the neural processes of axonal migration, synaptic plasticity, and the regulation of dendritic spines, all of which critically depend on LIMK1's role in modulating cofilin and actin polymerization[1]. In WS, this gene has been associated with structural and functional alterations of the inferior parietal sulcus[2], but recent work suggests that LIMK1 may also be important in pathophysiologies of other neuropsychiatric conditions, including schizophrenia, which is associated with dorsolateral prefrontal cortex (DLPFC) dysfunction[3,4]. For example, a study of post-mortem DLPFC samples from individuals with schizophrenia found increased expression of LIMK1 as well as decreased dendritic spine density in cortical layer 3[5]. Additionally, in mouse models of schizophrenia, schizophrenia-like behaviors and spine alterations were both rescued by LIMK1 inhibition[6]. Here, we tested whether variations in LIMK1 expression were related to DLPFC structure and function – leveraging naturally occurring expression differences that are present in individuals with rare 7q11.23 copy number variations (CNVs) as well as in the general population, wherein differences are present as a function of LIMK1 haplotype. In each case, we tested whether LIMK1 variation was associated with structural or functional DLPFC changes that were consistent with known schizophrenia phenotypes.

Methods: We first studied regional gray-matter volume (GMV) with respect to 7q11.23 copy number in three groups: (1) children and adolescents with WS (having only one copy of LIMK1 and, thus, reduced LIMK1 expression; N=30, 79 longitudinal visits, mean age=12.8±3.2 years, 20 females), (2) typically developing (TD) individuals (with two copies of LIMK1; N=94, 288 visits, age=12.8±3.2 years, 47 females), and (3) children and adolescents with 7q11.23 Duplication syndrome ([Dup7]; with three copies of LIMK1 and increased LIMK1 expression; N=16, 35 visits, age=14.1±3.1 years, 9 females). We also performed a similarly structured copy number-based fMRI study of a spatial working memory task (again testing across WS, TD, and Dup7 groups). Finally, we examined the relationship between GMV and LIMK1 expression in two separate samples of healthy participants from the general population, one sample from NIMH (255 participants, age=33.0±9.7 years, 142 females), and another from the Human Connectome Project (216 participants, age = 29.3±3.7 years, 140 females). Each of these two general population cohorts was stratified according to a LIMK1 haplotype that has been shown to robustly predict imputed LIMK1 expression in the cerebral cortex(2).

Results: In the copy number-based structural study, there was an association between DLPFC GMV and LIMK1 copy number (and, thus, gene expression) that was consistent with the previously reported schizophrenia-based phenotype: lower DLPFC GMV was associated with increasing LIMK1 copy number (i.e., higher expression; $p<0.001$). In the fMRI study, we found an association between LIMK1 copy number and working memory-related activation that was also consistent with the schizophrenia phenotype: reduced DLPFC activation was related to increased copy number/LIMK1 expression ($p<0.001$). Finally, in each of the two general population cohorts stratified by LIMK1 haplotype, we found reduced DLPFC GMV in the haplotype group linked to higher LIMK1 expression ($p<0.005$ in both discovery and replication cohorts).

Conclusions: Here, we provide in vivo evidence in humans that LIMK1 function is relevant to hallmark schizophrenia brain phenotypes in the DLPFC, including reduced gray matter volume and working memory hypoactivation. Given prior preclinical studies showing that normalization of LIMK1 activity can enhance dendritic spine density and improve neural function, these findings may have implications for understanding mechanisms of pathology in neuropsychiatric disorders, perhaps even for future therapeutic approaches.

References

1. Todorovski Z. LIMK1 regulates long-term memory and synaptic plasticity via the transcriptional factor CREB. Mol Cell Biol. 2015;35(8):1316-28.
2. Kippenhan JS. Dorsal visual stream and LIMK1: hemideletion, haplotype, and enduring effects in children with Williams syndrome. J Neurodev Disord. 2023;15(1):29.
3. Rubinstein DY. Spatiotemporal Alterations in Working Memory-Related Beta Band Neuromagnetic Activity of Patients With Schizophrenia On and Off Antipsychotic Medication: Investigation With MEG. Schizophr Bull. 2023;49(3):669-78.
4. Smucny J. Mechanisms underlying dorsolateral prefrontal cortex contributions to cognitive dysfunction in schizophrenia. Neuropsychopharmacology. 2022;47(1):292-308.
5. Datta D. Altered expression of CDC42 signaling pathway components in cortical layer 3 pyramidal cells in schizophrenia. Biol Psychiatry. 2015;78(11):775-85.
6. Chen P. Spine impairment in mice high-expressing neuregulin 1 due to LIMK1 activation. Cell Death Dis. 2021;12(4):403.

Poster No 556

Unaltered frontoparietal white matter connectivity in first-episode psychosis patients

Jongrak Kim[1], Hyungyou Park[1], Inkyung Park[1], Moonyoung Jang[2], Sunghyun Park[2], Minah Kim[2], Jun Soo Kwon[3]

[1]Seoul National University, Seoul, Seoul, [2]Department of Neuropsychiatry, Seoul National University Hospital, Seoul, Seoul, [3]Department of Brain and Cognitive Sciences, Seoul National University College of Natural Sciences, Seoul, Seoul

Introduction: The Superior Longitudinal Fasciculus (SLF), a component of the frontoparietal network (FPN) comprising white matter, establishes connections between the frontal and parietal lobes and plays a role in various facets of first-episode psychosis (FEP) according to functional and structural studies. Previous neuroimaging investigations have demonstrated structural abnormalities in a whole SLF bundle among FEP patients. However, there remains an insufficient comprehension of the white matter (WM) integrity pertaining to its three distinct anatomical sub-components, utilizing a suitable methodology. Hence, this study seeks to determine whether compromised WM integrity is observable in the sub-components of the SLF among FEP patients through better technique.

Methods: In this study, we obtained diffusion-weighted imaging data from 39 individuals experiencing first-episode psychosis (FEP) and 110 healthy controls (HCs) at Seoul National University Hospital (SNUH). We then processed this data into diffusion tensor imaging using FSL. Whole-brain deterministic tractography was subsequently executed by StarTrack, employing two algorithms (Richardson-Lucy and Euler algorithm). Within the TrackVis program, we accurately reconstructed the three subdivisions of the superior longitudinal fasciculus (SLF), designated as SLF I, II, and III, relying on their anatomical characteristics. From these reconstructed SLF subdivisions on both sides, we evaluated three diffusion indices (fractional anisotropy, FA; mean diffusivity, MD; radial diffusivity, RD). These indices were then subjected to a comparative analysis between the two groups using R statistical programs.

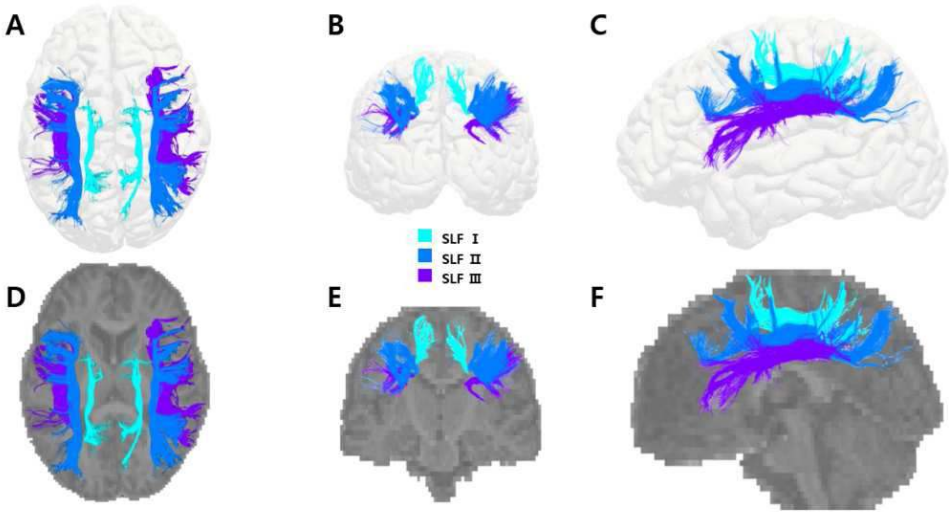

Figure 1. Reconstructing the three sub-divisions of superior longitudinal fasciculus (SLF Ⅰ, Ⅱ, and Ⅲ) through Deterministic Tractography in an individual.
SLF Ⅰ (azure), Ⅱ (blue), and Ⅲ (purple) are depicted within the axial (superior) (A) and coronal (posterior) (B) views, representing both hemispheres. The sagittal view (C) specifically focuses on the left hemisphere. (D), (E), and (F) present the same views as above, but are located in the B0-image.

Results: Among a total of 18 diffusivities (six SLF subcomponents for three DTI indices; FA, MD, and RD), there is no significant difference between FEP patients and HCs in white matter (WM) integrity within the subdivisions of SLFs (SLF I, II, and III), as determined by ANOVA. This analysis controls for age, sex, and the total number (sum of all six subcomponents) of streamlines, applying multiple comparison corrections.

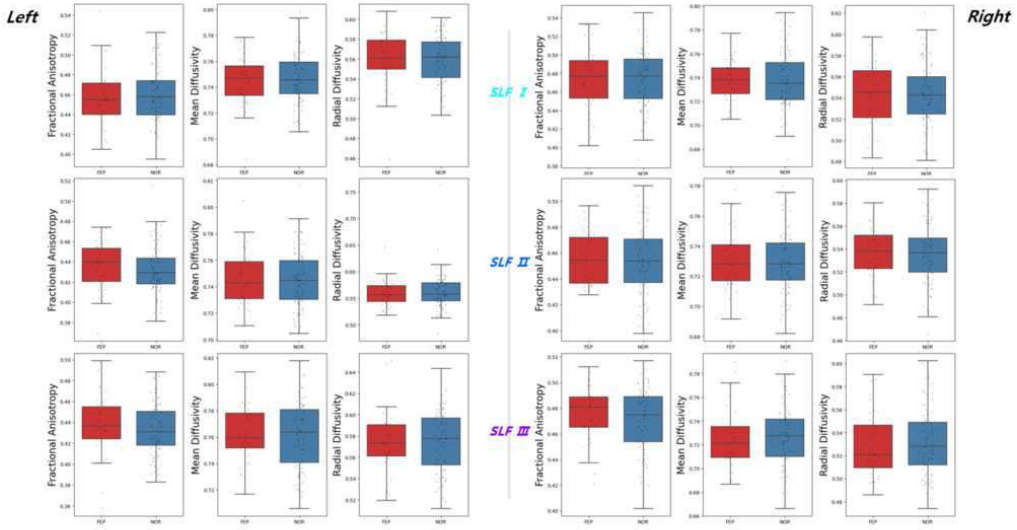

Figure 2. Between-group differences in Fractional Anisotropy, Mean Diffusivity, and Radial Diffusivity for the three sub-divisions of superior longitudinal fasciculus (SLF Ⅰ, Ⅱ, and Ⅲ) in both hemisphere.
FEP patients are shown as red squares and HCs are shown as blue squares. The black bars represent the group means.

Conclusions: Our study reveals that the SLF sub-divisions in FEP patients did not display noteworthy differences in comparison to those in HCs. These findings do not provide the substantiated early progressive modifications in white matter (WM) integrity within the SLF of FEP patients. Nonetheless, we posit that significant alterations may become apparent during the chronic phases of psychosis rather than in the initial stages, aligning with some studies suggesting relatively intact connectivity in the frontoparietal network (FPN) of early psychosis patients. This perspective contributes to a novel understanding of the pathophysiology of FEP within the segmented SLF WM architecture.

References

1. Catani, M., et al. (2002), 'Virtual in vivo interactive dissection of white matter fasciculi in the human brain', Neuroimage, vol. 17, no. 1, pp. 77-94
2. Cavelti, M., et al. (2018), 'Formal thought disorder is related to aberrations in language-related white matter tracts in patients with schizophrenia', Psychiatry Research: Neuroimaging, vol. 279, pp. 40-50
3. Dell'acqua, F., et al. (2010), 'A modified damped Richardson-Lucy algorithm to reduce isotropic background effects in spherical deconvolution', Neuroimage, vol. 49, no. 2, pp. 1446-1458
4. Hecht, E. E., et al. (2015), 'Virtual dissection and comparative connectivity of the superior longitudinal fasciculus in chimpanzees and humans', Neuroimage, vol. 108, pp. 124-137
5. Lee, J., et al. (2022), 'White matter microstructure of superior longitudinal fasciculus II is associated with intelligence and treatment response of negative symptoms in patients with schizophrenia', Schizophrenia, vol. 8, no. 1, pp. 43
6. Lewis, D. A., et al. (2000), 'Catching up on schizophrenia: natural history and neurobiology', Neuron, vol. 28, no. 2, pp. 325-334.
7. Schmidt, A., et al. (2014), 'Approaching a network connectivity-driven classification of the psychosis continuum: a selective review and suggestions for future research', Frontiers in Human Neuroscience, vol. 8, pp. 1047
8. Thiebaut de Schotten, M., et al. (2011), 'A lateralized brain network for visuospatial attention', Nature Neuroscience, vol. 14, no. 10, pp. 1245-1246
9. Whitford, T. J., et al. (2015), 'Cingulum bundle integrity associated with delusions of control in schizophrenia: Preliminary evidence from diffusion-tensor tractography', Schizophrenia Research, vol. 161, no. 1, pp. 36-41

Poster No 557

Social app use modulates functional connectivity in social anxiety disorder individuals differently

Hesun Erin Kim[1], Yesol Cho[1], Byung-Hoon Kim[1], Kyunghee Ham[1], Eunji Kim[1], Soomin Kim[1], Seungmin Lee[1], Bohyun Park[1], Jae-Jin Kim[1]

[1]*Yonsei University, Seoul, Korea, Republic of*

Introduction: Recently, researchers have started to recognize the value of digital phenotyping, data from smart devices that quantifies moment-by-moment of one's daily life, to understand various disorders. Social anxiety disorder (SAD), characterized by an intense fear of social situations, is one of the most common anxiety disorders that impacts various aspects of one's life (Hidalgo et al., 2001; Lochner et al., 2003; Schneier and Goldmark, 2015). The present investigation took a data-driven approach to understand how social app use (daily duration and weekday-weekend consistency) changes resting-state functional connectivity (rsFC) differently in SAD and healthy controls (HC).

Methods: 32 SAD patients and 29 HC underwent two 5min rsfMRI sessions, approx. two months apart. Within the two-month period, timeseries data of all smartphone apps were passively collected. All apps that included messaging and posting features (i.e., Instagram, WhatsApp) were selected. For the overall use, the daily average duration (DURdaily) was computed. To examine the weekday-weekend pattern of social app use, data were segmented by time epochs (12am-12am, 6 hours apart) and by week type (weekday; weekend). Then, the Euclidean distance was calculated (DURpattern). To identify neural regions where the rsFC change were related to social app use metrics differently between groups, a data-driven whole-brain connectome multivariate pattern analysis (MVPA) was performed. For each identified region, a post-hoc seed-to-voxel analysis was implemented to verify the directionality of the rsFC. Results were set at a height-level threshold of $P<0.001$, and a cluster threshold of false discovery rate corrected $PFDR< 0.05$.

Results: MVPA identified rsFC changes, time2 - time1, of bilateral precuneus and posterior cingulate cortex (PCC) were associated with DURdaily differently between the group. Post-hoc analysis showed that rsFC changes between precuneus with bilateral supplementary motor area (SMA) and right precentral gyrus, and between PCC and left SMA, right occipital cortex (OCC), right precentral gyrus and right postcentral gyrus were all negatively modulated by the DURdaily in HC, whereas none of the rsFC changes showed significant relationship in SAD. In association with DURpattern, left insula was identified. Post-hoc analysis indicated modulatory effects of DURpattern on the rsFC change between insula and bilateral OCC, bilateral fusiform gyrus, and right superior parietal lobule were all significantly positive for HC, while the effects on the rsFC change with the right OCC and bilateral fusiform gyrus were significantly negative in SAD (Fig1).

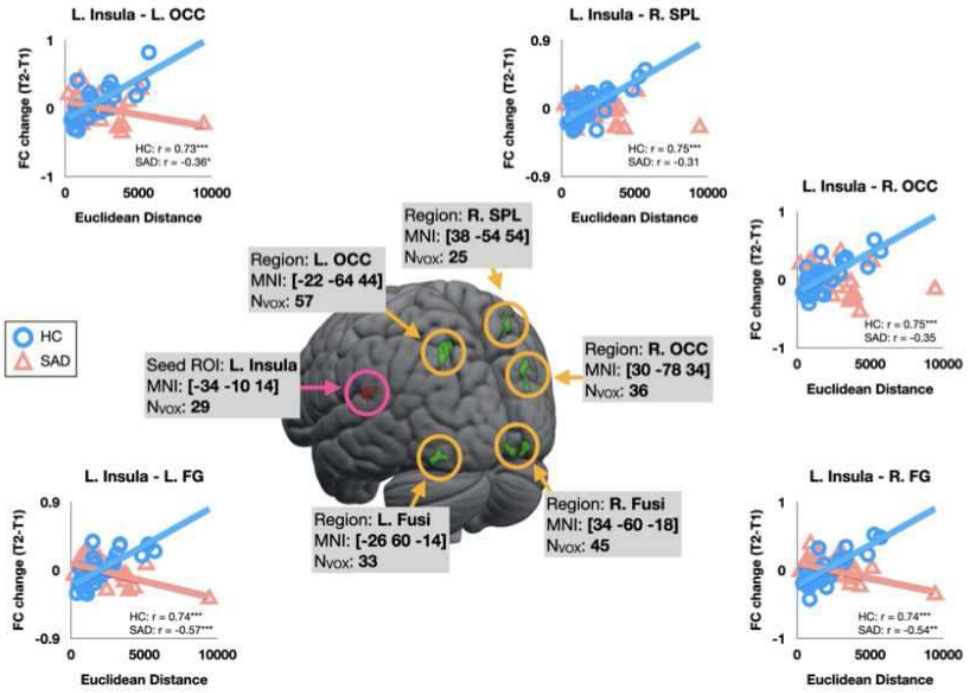

Figure 1. Neural regions showing resting-state functional connectivity (rsFC) change with respect to the consistency pattern of social app use between weekdays and weekends ($DUR_{PATTERN}$) and group. Data-driven whole-brain connectome multivariate pattern analysis revealed different modulatory effects of $DUR_{PATTERN}$ on insula-based rsFC change in healthy control and social anxiety disorder. Abbreviations. HC, healthy control; SAD, social anxiety disorder; R, right; L, left; MNI, Montreal Neurological Index; N_{VOX}, number of voxels; FC, functional connectivity; T1, time 1; T2, time 2; OCC, occipital cortex; SPL, superior parietal lobule; FG, fusiform gyrus. *p < 0.05, **p < 0.01, ***p < 0.001.

Conclusions: In HC, the rsFC between default-mode network (DMN) and motor/somatosensory, visual regions decreased as the DURdaily of social app was higher, whereas for SAD, no significant effects were found. As members of the DMN, PCC/precuneus is associated with well-being and happiness (Buckner et al., 2008). Results seem to suggest that longer use negatively affects self-relevant sensory information processing but for HC only; perhaps it is because SAD individuals find comfort in non-in-person interactions. Additionally, modulatory effects of weekday-weekend inconsistency were identified in the insular-based rsFC, and showed group differences. Insula is a hub that processes interoceptive information, and is necessary for emotion regulation (Dionisio et al., 2019; Price and Hooven, 2018). Results showed opposite effects of week type inconsistency between groups in insular-OCC and -fusiform gyrus. In HC, greater inconsistency was related to increased rsFCs with insula, whereas it was related to decreased insular rsFCs in SAD. It could be communicating that inconsistent use of social app between week types is associated with lower visual interoceptive awareness, triggering maladaptive emotion regulation in SAD. Together, the findings highlight social app use modulates the neural connectivity of SAD differently.

References

1. Buckner, R. L., Andrews-Hanna, J. R., & Schacter, D. L. (2008). The brain's default network: anatomy, function, and relevance to disease. Annals of the New York Academy of Sciences, 1124, 1-38. doi:10.1196/annals.1440.011
2. Dionisio, S., Mayoglou, L., Cho, S. M., Prime, D., Flanigan, P. M., Lega, B., . . . Nair, D. (2019). Connectivity of the human insula: A cortico-cortical evoked potential (CCEP) study. Cortex, 120, 419-442. doi:10.1016/j.cortex.2019.05.019
3. Hidalgo, R. B., Barnett, S. D., & Davidson, J. R. (2001). Social anxiety disorder in review: two decades of progress. International Journal of Neuropsychopharmacology, 4(3), 279-298. doi:10.1017/s1461145701002504
4. Lochner, C., Mogotsi, M., du Toit, P. L., Kaminer, D., Niehaus, D. J., & Stein, D. J. (2003). Quality of life in anxiety disorders: a comparison of obsessive-compulsive disorder, social anxiety disorder, and panic disorder. Psychopathology, 36(5), 255-262. doi:10.1159/000073451
5. Price, C. J., & Hooven, C. (2018). Interoceptive Awareness Skills for Emotion Regulation: Theory and Approach of Mindful Awareness in Body-Oriented Therapy (MABT). Frontiers in Psychology, 9, 798. doi:10.3389/fpsyg.2018.00798
6. Schneier, F., & Goldmark, J. (2015). Social Anxiety Disorder. In D. J. Stein & B. Vythilingum (Eds.), Anxiety Disorders and Gender (pp. 49-67). Cham, Switzerland: Springer International Publishing.

Poster No 558

Regional Heterogeneity of Brain Morphometrical Changes in recreational Ketamine Use Individuals

YI-HSUAN LIU[1], Kun-Hsien Chou[1,2], Pei-Lin Lee[3], Chia-Chun Hung[4,5], Li-Hung Chang[1], Marc Potenza[6,7,8,9,10], Chiang-Shan Li[6], Tony Szu-Hsien Lee[11,5,12], Ching-Po Lin[1,3,13,14]

[1]Institute of Neuroscience, National Yang Ming Chiao Tung University, Taipei, Taiwan, [2]Brain Research Center, National Yang Ming Chiao Tung University, Taipei, Taiwan, [3]Center for Healthy Longevity and Aging Sciences, National Yang Ming Chiao Tung University, Taipei, Taiwan, [4]Continuing Education Master's Program of Addiction Prevention and Treatment, National Taiwan Normal, Taipei, Taiwan, [5]Center for Addiction Prevention and Policy Research, National Taiwan Normal University, Taipei, Taiwan, [6]Department of Psychiatry, School of Medicine, Yale University, New Haven, CT, [7]The Child Study Center, School of Medicine, Yale University, New Haven, CT, [8]Department of Neuroscience and the The Wu Tsai Institute, Yale University, New Haven, CT, [9]The Connecticut Council on Problem Gambling, Wethersfield, CT, [10]The Connecticut Mental Health Center, New Haven, CT, [11]Department of Health Promotion and Health Education, National Taiwan Normal University, Taipei, Taiwan, [12]Continuing Education Master's Program of Addiction Prevention and Treatment, National Taiwan Normal University, Taipei, Taiwan, [13]Department of Education and Research, Taipei City Hospital, Taipei, Taiwan, [14]Institute of Biomedical Engineering and Nanomedicine, National Health Research Institutes, Miaoli, Taiwan

Introduction: The engagement in recreational substance use during youth can exert significant and enduring effects on brain development. Among the array of recreational substances in Taiwan, ketamine stands out as particularly prevalent among young individuals, due to its affordability, easy accessibility, and relatively minor legal consequences[1]. Although our comprehension of the neurobiological alterations associated with ketamine abuse has advanced considerably[2,3], there exists a notable gap in knowledge concerning brain changes resulting from early, non-medical exposure to ketamine. To address this gap, we recruited participants with early ketamine exposure from the community. Given the distinctive characteristics of these individuals, it is crucial to emphasize individual brain structure alterations to elucidate the impact of early-stage ketamine use. Hence, in this study, we employ a personalized analytical approach with structural T1-weighted MRI anatomical scans to pinpoint subtle yet significant changes in gray matter volume among a cohort of young adults with early exposure to recreational ketamine use.

Methods: Participants consisted of 174 individuals from Taiwan, including 53 ketamine use (KU) and 121 healthy controls (HC) [Table 1]. T1-weighted MRI anatomical scans were preprocessed using the VBM pipeline[4]. We extract regional gray matter volume (GMV) from 1060 brain areas and map them into nine corresponded large-scale brain networks[5,6,7]. For individual-level analyses, we employed a w-score approach to identify extreme regional GMV changes for each participant[8]. A general linear model was constructed using healthy controls to obtain beta coefficient estimates of GMV for each ROI, incorporating covariates such as age, sex, and education. This model was applied to individuals with ketamine use further, wherein we calculated residuals for the 1060 brain regions per participant and transformed them into corresponding W-scores. To provide a summary of individual variation in KU, w-scores were summarized by counting how many subjects had an extreme deviation (extreme deviation defined as $p < 0.001$, $|z| > 3.29$) at a given ROI, and then dividing by the group size to show the frequency of individuals with extreme deviations at that brain area. For group-level analyses, we employed an ANCOVA model to identify brain regions with significant between-group difference in GMV using the same statistic threshold ($p < 0.001$) as in the individual analysis. Subsequently, to control for the varying number of regions within networks, we divided the number of significantly different areas to the total within each.

	Subject	Sex	Age				Education				TIV			
Group	Number	M:F	Mean	Std	Max	Min	Mean	Std	Max	Min	Mean	Std	Max	Min
KU	53	41:12	21.17	4.73	38.55	17.16	9.68	2.30	16	6	1446.63	138.00	1718.09	1139.30
HC	121	75:46	24.23	4.85	37.18	17.58	13.72	2.59	18	6	1471.76	126.82	1790.22	1203.83

KU: Participants with Ketamine use
HC: Healthy controls

Results: Upon examination of individual-level w-scores, our analysis uncovered that KU exhibits more extensive alterations in regional GMV, a phenomenon potentially obscured by conventional case-control group-level analysis (Fig 1. (a)). The most substantial impact is also observed in the frontoparietal, somatomotor, visual, dorsal attention, and default networks (Fig 1. (b)).

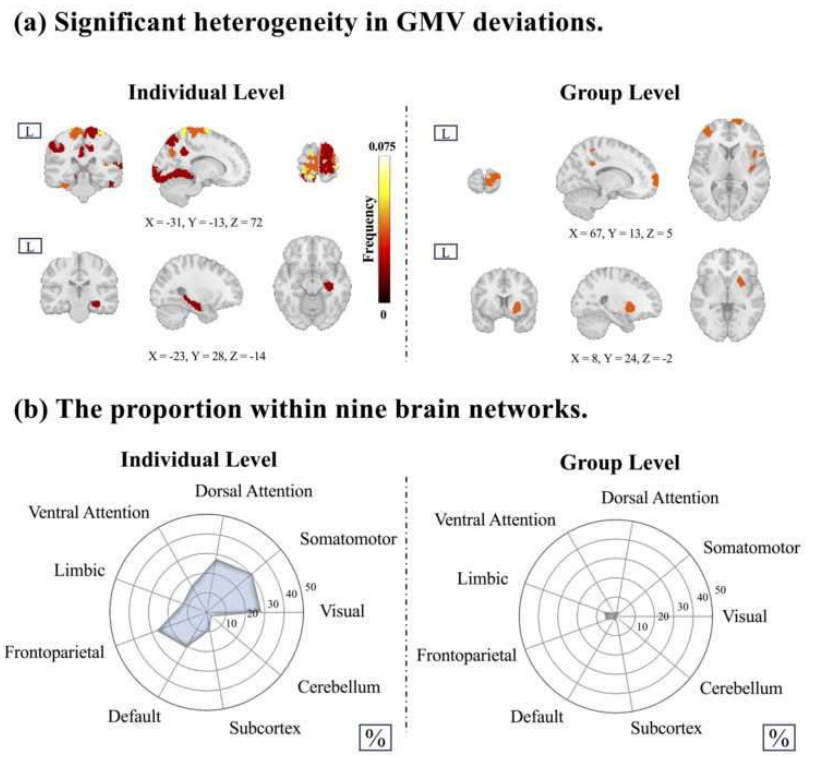

Fig 1: **Regional heterogeneity in extreme gray matter volume (GMV) deviations among individuals using recreational Ketamine, analyzed at individual and group levels.**
(a) It depicts regions exhibiting extreme GMV deviations, which indicate individual variability, as shown on the left side of the brain maps. The frequency of individuals with significant deviations in each brain area was identified, with extreme deviations defined as $p < 0.001$ and $|z| > 3.29$. Group variability is presented and assessed on the right side of the brain maps using a group based ANCOVA analysis ($p < 0.001$). (b) The percentage of significant brain deviation areas across nine brain networks is illustrated using a Radar map, calculated as the number of significant deviation areas divided by the total number of brain areas within each network.

Conclusions: In our investigation, we have identified morphometric heterogeneity throughout the brains of individuals with early exposure to ketamine. Remarkably, the networks involved deviate from the conventional findings associated with addiction, particularly those related to reward networks. This discovery suggests that employing individual-level analysis might unveil subtle yet significant anatomical changes among a cohort of young adults with early exposure to recreational ketamine use. These initial findings provide a glimpse into the potential nuanced direct impact of ketamine or the possibility of serving as an early biomarker for the essential brain networks associated with addiction. Further research is indispensable to validate and gain deeper insights into the implications of these preliminary observations.

References

1. Pan, W. H., Wu, K. C. C., Chen, C. Y., Chu, Y. R., Wu, S. C., Jou, S., ... & Chen, W. J. (2021), 'First-time offenders for recreational ketamine use under a new penalty system in Taiwan: incidence, recidivism and mortality in national cohorts from 2009 to 2017', Addiction, vol. 116, no. 7, pp. 1770-178.
2. Liu, L., Huang, H., Li, Y., Zhang, R., Wei, Y., & Wu, W. (2021), 'Severe encephalatrophy and related disorders from long-term ketamine abuse: a case report and literature review', Frontiers in Psychiatry, vol. 12, 707326.
3. Strous, J. F., Weeland, C. J., van der Draai, F. A., Daams, J. G., Denys, D., Lok, A., ... & Figee, M. (2022), 'Brain changes associated with long-term ketamine abuse, a systematic review', Frontiers in neuroanatomy, vol. 8.
4. Gaser, C., Dahnke, R., Thompson, P. M., Kurth, F., Luders, E., & Alzheimer's Disease Neuroimaging Initiative. (2022), 'CAT–A computational anatomy toolbox for the analysis of structural MRI data', biorxiv, 2022-06.
5. Schaefer, A., Kong, R., Gordon, E. M., Laumann, T. O., Zuo, X. N., Holmes, A. J., ... & Yeo, B. T. (2018), 'Local-global parcellation of the human cerebral cortex from intrinsic functional connectivity MRI', Cerebral cortex, vol. 28, no. 9, pp. 3095-3114.
6. Tian, Y., Margulies, D. S., Breakspear, M., & Zalesky, A. (2020), 'Topographic organization of the human subcortex unveiled with functional connectivity gradients', Nature neuroscience, vol. 23, no. 11, pp. 1421-1432.
7. Buckner, R. L., Krienen, F. M., Castellanos, A., Diaz, J. C., & Yeo, B. T. (2011), 'The organization of the human cerebellum estimated by intrinsic functional connectivity', Journal of neurophysiology, vol. 106, no. 5, pp. 2322-2345.
8. Segal, A., Parkes, L., Aquino, K., Kia, S. M., Wolfers, T., Franke, B., ... & Fornito, A. (2023), 'Regional, circuit and network heterogeneity of brain abnormalities in psychiatric disorders', Nature Neuroscience, vol. 26, no. 9, pp. 1613-1629.

Poster No 559

Cortico-thalamo-cerebellar triple network dysconnectivity across the psychosis risks

Minji Ha[1], Inkyung Park[1], Taekwan Kim[2], Wu Jeong Hwang[1], Sunghyun Park[3], Minah Kim[3], Jun Soo Kwon[1]

[1]Department of Brain and Cognitive Sciences, Seoul National University College of Natural Sciences, Seoul, Korea, Republic of, [2]Department of Bio and Brain Engineering, Information & Electronics Research Institute, Korea Advance, Daejeon, Korea, Republic of, [3]Department of Neuropsychiatry, Seoul National University Hospital, Seoul, Korea, Republic of

Introduction: Cerebellar dysconnectivity has been consistently reported in patients with psychosis, along with concurrent disruptions in the thalamus and associative cortical regions. These disruptions are associated with the triple network model for psychopathology, which explains psychopathological phenomena as abnormal interactions within the salience network (SAL), default mode network (DMN), and executive central network (ECN). However, the pattern of cerebellar functional network interactions with the cortical and thalamic networks across the different stages of psychosis risk within the triple network model still remains largely unknown

Methods: Resting-state fMRI data from 241 participants, including 37 first-episode psychosis (FEP), 63 clinical high risk (CHR), 41 unaffected relatives (URs), and 100 healthy controls (HCs), were used. To capture the network properties of thalamus and cerebellum, we used the parcellated thalamic and cerebellar networks maps derived from FC to cortical networks using winner-take-all approach. Then, we computed and compared the functional connectivity (FC) between cerebellar and cortical triple networks, as well as between thalamic and cerebellar triple networks, across the groups.

Results: Compared to the HCs, FEP showed more widespread dysconnectivity between networks across different regions, while CHR showed dysconnectivity primarily between the networks within the same region. URs, although not significantly different from HCs, displayed a unique FC patterns of triple networks compared to the other clinical groups. In our exploratory analysis aimed at investigating the association between error-based learning performance and the triple network FC in FEP, we found a statistically significant correlation between the FC of cerebellar SAL and thalamic SAL and the accuracy of the CANTAB Spatial Working Meory task.

Conclusions: Our findings expand the classical triple network model to include the cerebellar and thalamic networks, potentially indicating the role of cerebellar network in predicting functional impairment and that of thalamic network in inappropriate information processing in psychosis. Distinct patterns of dysfunctional network connectivity across the psychosis risks suggest the necessity for further research to investigate a large-scale triple network model as a potential marker for early psychosis pathophysiology.

References

1. Moberget, T., & Ivry, R. B. (2019). Prediction, Psychosis, and the Cerebellum. Biological psychiatry. Cognitive neuroscience and neuroimaging, 4(9), 820–831.
2. Ha, M. (2023). Aberrant cortico-thalamo-cerebellar network interactions and their association with impaired cognitive functioning in patients with schizophrenia. Schizophrenia, 9(1).
3. Dong, D. (2017). Dysfunction of large-scale brain networks in schizophrenia: A meta-analysis of resting-state functional connectivity. Schizophrenia Bulletin, 44(1), 168–181.
4. O'Neill, A. (2018). Dysconnectivity of large-scale functional networks in early psychosis: A meta-analysis. Schizophrenia Bulletin, 45(3), 579–590.
5. Kim, M. (2022). Large-scale thalamocortical triple network dysconnectivities in patients with first-episode psychosis and individuals at risk for psychosis. Schizophrenia Bulletin, 49(2), 375–384.
6. Sokolov, A. (2017). The Cerebellum: Adaptive Prediction for Movement and Cognition. Trends in cognitive sciences, 21(5), 313–332.
7. Hwang, K. (2017). The Human Thalamus Is an Integrative Hub for Functional Brain Networks. The Journal of neuroscience : the official journal of the Society for Neuroscience, 37(23), 5594–5607.

Poster No 560

Changes in parents' brain by parenting stress and depression

Jihyun Bae[1], Yong Jeon Cheong[1], Seonkyoung Lee[1], Ji Hyeong Ro[1], Minyoung Jung[1]

[1]Korea Brain Research Institude, Daegu, Korea, Republic of

Introduction: Despite happiness from child-rearing, it is challenging and stressful. Psychological stress, specifically due to parenting, can cause depression. However, it is largely unknown how parenting stress (PS) and depression interact each other and whether their interaction affects the morphological features of parenting brain. In this study, we aim to investigate whether there is a causal relationship between the PS-depression interaction on the brain structure of primary caregivers.

Methods: This study includes 179 participants who are primary caregivers of elementary school children (170 female, mean age [SD] = 40.84 [3.09] years old). The structural magnetic resonance imaging (MRI) data was acquired by 3T. The brain was parcellated into 68 cortical regions via the FreeSurfer toolbox. To assess the level of PS and depression, the participants were asked to complete self-report questionnaires, 1) Korean Parenting Stress Index Forth Edition (K-PSI-4) and 2) Korean-Beck Depression Inventory II (BDI-II). The PSI consists of a 'child domain' and a 'parent domain' that affects the overall stress of the parent, each of which contains a subscale. First, we performed partial correlation analyses between PS, depression, and brain structures using primary caregiver's sex, age, handedness, number of children, intracranial volume, and child's sex as covariates. Second, we divided depression into three levels (top 20%, middle 60%, and bottom 20%) and conducted ANCOVA. Finally, we performed a structural equation model (SEM) analysis to explore causal relationship between PS, depression, and the brain. The institutional research board of the Korea Brain Research Institute granted ethical approval for this study (KBRI-202206-HR-001).

Results: The significant positive correlations were found between 14 subscales of PS and BDI at FDR q<0.05. PS negatively correlated to right fusiform gyrus area (FFG): PSI child domain (Adaptability : r=-0.244, Acceptability : r = -0.258, Child domain : r = -0.258, q<0.05). Additionally, depression scores showed negative correlation with the left entorhinal cortex area (ERC) (r=-0.246, q<0.05). We found that 3 groups divided by depression level were significantly different for the right FFG (F=3.334, p<0.05) and left ERC (F=5.676, p<0.01) area: 1) compared with low depression group, high depression group had significantly smaller sizes in the right FFG and ERC, and 2) high depression group showed significant area reduction in the right FFG compared with middle depression group. SEM analysis showed that PS increased by depression led to area reduction in the right FFG area (NFI = 0.970, CFI = 0.986, RMSEA = 0.067). For the child and parent domains, depression increased by PS led to reduction in the ERC area (PSI child domain : NFI = 0.975, CFI = 0.987, RMSEA = 0.074; PSI parent domain : NFI = 0.961, CFI = 0.993, RMSEA = 0.033).

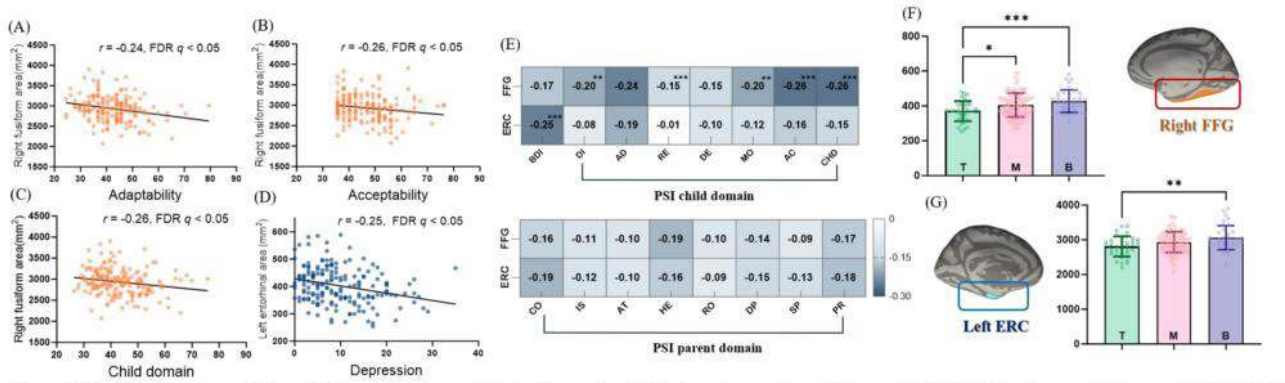

Figure 1. The Significant association with Parenting stress relates to Depression & Brain cortex surface (A) Between AD & right FFG surface area; (B) Between AC & right FFG surface area; (C) Between CHD & right FFG surface area; (D)Between Depression & left ERC surface area; (E) overall correlations across BDI & PSI subscales with Brian; (F) Right FFG and (G) left ERC depending on depression level(Top 20%, Middle 60%, Bottom 20%).

Abbr. FFG = fusiform gyrus, ERC = entorhinal cortex, PSI = parenting stress index, DE = demandingness, MO = mood, AC = acceptability, CHD = child domain, CO = competence, IS = isolation, AT = attachment, HE = health, RO = role restriction, DP = depression, SP = spouse

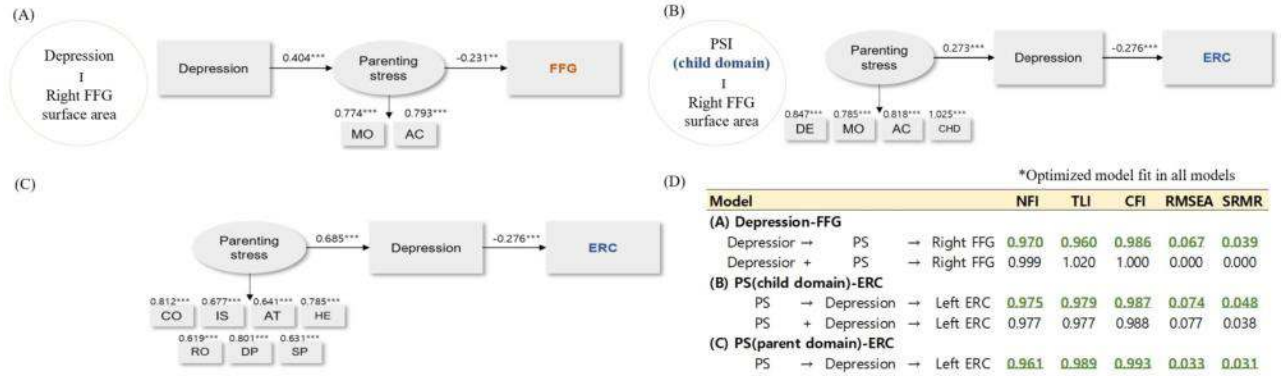

Model				NFI	TLI	CFI	RMSEA	SRMR
(A) Depression-FFG								
Depression	→	PS	→ Right FFG	0.970	0.960	0.986	0.067	0.039
Depression	+	PS	→ Right FFG	0.999	1.020	1.000	0.000	0.000
(B) PS(child domain)-ERC								
PS	→	Depression	→ Left ERC	0.975	0.979	0.987	0.074	0.048
PS	+	Depression	→ Left ERC	0.977	0.977	0.988	0.077	0.038
(C) PS(parent domain)-ERC								
PS	→	Depression	→ Left ERC	0.961	0.989	0.993	0.033	0.031
PS	+	Depression	→ Left ERC	0.961	0.987	0.992	0.037	0.030

Figure 2. Best model for each SEM analysis. (A) Depression to FFG; (B) PS (child domain) to ERC; (C) PS (parent domain) to ERC; (D) Comparison table of hypothesized models' pathways.

Conclusions: In the current study, we demonstrated that both PS and depression affected the brain structure of primary caregivers. The mutual positive relation between PS and depression led to reduction of the brain area, especially in ERC and FFG. Given these areas involve information processing and memory formation, we suggest that PS and depression may affect the cognitive function. In future, we are going to investigate how PS and depression influence the brain function using resting-state functional MRI data.

References
1. Noriuchi, M. (2019), 'The orbitofrontal cortex modulates parenting stress in the maternal brain', Scientific reports, 9(1), 1658.
2. Fang, Y. (2022). 'Parent, child, and situational factors associated with parenting stress: A systematic review', European Child & Adolescent Psychiatry, 1-19.
3. Wang, J. (2017). 'Electroconvulsive therapy selectively enhanced feedforward connectivity from fusiform face area to amygdala in major depressive disorder', Social cognitive and affective neuroscience, 12(12), 1983-1992.
4. Li, X. (2020). 'Effect of emotional enhancement of memory on recollection process in young adults: the influence factors and neural mechanisms', Brain Imaging and Behavior, 14, 119-129

Poster No 561

Examining meta-matching as a tool to predict Obsessive-Compulsive Disorder

Luke Hearne[1], Andrew Zalesky[2], Paul Fitzgerald[3], Oscar Murphy[4], Ye Tian[5], Minah Kim[6], Sunah Choi[7], Jun Soo Kwon[8], Luca Cocchi[9]

[1]QIMR Berghofer Medical Research Institute, Herston, Queensland, [2]The University of Melbourne, Melbourne, Victoria, [3]Australian National University, Caberra, ACT, [4]Monash University, Melbourne, Victoria, [5]University of Melbourne, Carlton South, Victoria, [6]Department of Neuropsychiatry, Seoul National University Hospital, Seoul, Seoul, [7]Seoul National University, Seoul, Seoul, [8]Department of Brain and Cognitive Sciences, Seoul National University College of Natural Sciences, Seoul, Seoul, [9]QIMR Berghofer Medical Research Institute, Brisbane, Queensland

Introduction: A core goal of cognitive neuroscience is to predict individual differences in cognition and psychiatric symptoms from brain imaging data. A key question is whether large predictive models trained on general population datasets can generalize to patient populations. A recent approach, termed 'meta-matching' has furthered this idea (He et al., 2022) by leveraging the observation that most phenotypes are correlated. Therefore, brain features that can predict specific phenotypes in the large, population-based dataset are likely useful in predicting new phenotypes in an independent dataset. In the current work, we test this hypothesis explicitly by attempting to classify OCD status in a clinical sample of moderate size (N=334). We started by contrasting the predictive ability of meta-matching and baseline logistic regression models. We investigate the predictive weights generated by the model and examine them in the cortico-striatal system, a well-known biological correlate of OCD (Naze et al., 2023).

Methods: The study used data pooled across three independent clinical datasets collected in Brisbane, Melbourne and Seoul (N = 334, nOCD = 189, nHC = 145) (Kim et al., 2019; Naze et al., 2023). Brain imaging data were preprocessed using fMRIprep (Esteban et al., 2018), and functional connectivity data, used as features in the predictive models, were estimated using Nilearn. We contrasted two models in their ability to classify OCD diagnoses correctly. The first baseline model used logistic regression, whereas the second model used the openly available meta-matching model (He et al., 2022). In short, this model is a fully connected feedforward deep neural network that uses functional connectivity data to predict 67 non-brain imaging phenotypes (Figure 1A). We tested both models in a 10-fold cross-validation scheme repeated 100 times. We calculated predictive feature weights (PFWs) for each connectivity edge using the Haufe transformation. Specifically, we tested four functional connectivity pathways associated with OCD (Naze et al., 2023) with seed regions stemming from the nucleus accumbens, dorsal caudate, ventral putamen and dorsal putamen.

Results: Both meta-matching (mean accuracy = 62.76%) and logistic regression models (mean accuracy = 62.12%) demonstrated higher performance than shuffled permutations ($p < 0.0001$) (Figure 1B). When compared directly, the meta-matching model performed slightly better than the logistic regression (Cohen's $d = 0.498$). Our analysis revealed that predictive feature weights (PFWs) were significantly lower than would be expected from the shuffled permutations for three of the four cortico-striatal pathways of interest (nucleus accumbens $p = 0.045$, dorsal caudate $p < 0.001$, dorsal putamen $p < 0.001$; ventral putamen $p = 1.0$) (Figure 2). Moreover, the dorsal caudate pathway had larger negative PFWs than would be expected from any random set of brain regions (cortical or subcortical, $p = 0.008$).

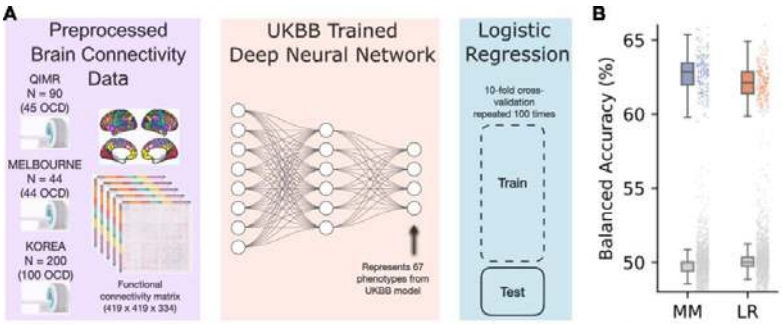

Figure 1. Comparison of model accuracy. **A.** Schematic of the Meta-Matching model pipeline. Preprocessed connectivity data were fed into an independently trained deep neural network (He et al., 2022). The outputs of the network, representing phenotypes in the UKBB, were entered into a logstic regression model to classify OCD status (clinical diagnosis or healthy control). The baseline comparison model skipped the intermediary neural network. **B.** Balanced accuracy for the meta-matching (MM, blue) and logistic regression models (LR, orange) compared to shuffled permutations (grey). Both models outperformed the shuffle permutations, and meta-matching demonstrated a small boost in prediction accuracy compared to logistic regression models.

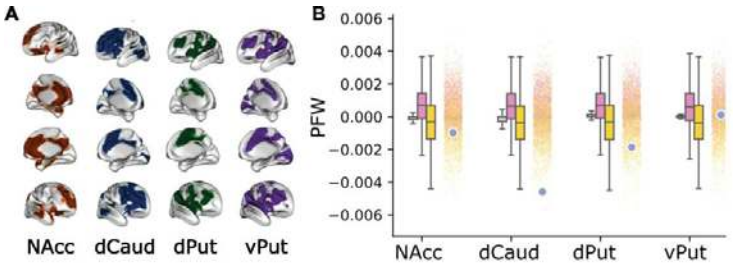

Figure 2. Comparison of model accuracy. A. The four cortico-striatal pathways of interest, Nacc = nucleus accumbens, dCaud = dorsal caudate, vPut = ventral putamen and dPut = dorsal putamen. We derived the regions of interest from an independent dataset of 250 healthy controls (HCP, Naze et al., 2023). **B.** Comparison of predictive feature weights (PFW, y-axis) within each pathway of interest (x-axis) to shuffled permutations (grey data), random subcortical-cortical weights (pink data) and random cortical weights (yellow data). The nucleus accumbens, dorsal caudate, and dorsal putamen demonstrated lower predictive weights than the shuffled data, but only the dorsal caudate had values with lower magnitude than all three null models.**C.** Scatter plots comparing model PFWs (x-axis) and cortical gene expression maps (y-axis) for GRID2, ADCK1, KIT and WDR7.

Conclusions: The recently proposed Meta-matching framework (He et al., 2022) is a promising technique for increasing the validity of predictive models trained in small clinical datasets. Meta-matching performance was similar to a typical logistic regression model; the small prediction boost (< 1%) is not clinically significant and is substantially smaller than the performance noted in the original paper (He et al., 2022). Despite the above caveats, the performance of the meta-matching model is impressive, given the lack of OCD patients and OCD-relevant measurements (e.g., symptom scales) available in the training dataset. In line with prior work, cortico-striatal pathways were disrupted in OCD and, therefore among the best predictors for classifying group status. To improve model performance it is likely that meta-matching models will need to be trained for specific purposes, for example, models that tap into variance associated with mental health symptoms. Such models will likely increase the predictive power of this method.

References

1. Esteban, O., Markiewicz, C. J., Blair, R. W., Moodie, C. A., Isik, A. I., Erramuzpe, A., Kent, J. D., Goncalves, M., DuPre, E., Snyder, M., Oya, H., Ghosh, S. S., Wright, J., Durnez, J., Poldrack, R. A., & Gorgolewski, K. J. (2018). fMRIPrep: A robust preprocessing pipeline for functional MRI. Nature Methods, 1. https://doi.org/10.1038/s41592-018-0235-4
2. He, T., An, L., Chen, P., Chen, J., Feng, J., Bzdok, D., Holmes, A. J., Eickhoff, S. B., & Yeo, B. T. T. (2022). Meta-matching as a simple framework to translate phenotypic predictive models from big to small data. Nature Neuroscience, 25(6), Article 6. https://doi.org/10.1038/s41593-022-01059-9
3. Kim, M., Kwak, S., Yoon, Y. B., Kwak, Y. B., Kim, T., Cho, K. I. K., Lee, T. Y., & Kwon, J. S. (2019). Functional connectivity of the raphe nucleus as a predictor of the response to selective serotonin reuptake inhibitors in obsessive-compulsive disorder. Neuropsychopharmacology, 44(12), Article 12. https://doi.org/10.1038/s41386-019-0436-2
4. Naze, S., Hearne, L. J., Roberts, J. A., Sanz-Leon, P., Burgher, B., Hall, C., Sonkusare, S., Nott, Z., Marcus, L., Savage, E., Robinson, C., Tian, Y. E., Zalesky, A., Breakspear, M., & Cocchi, L. (2023). Mechanisms of imbalanced frontostriatal functional connectivity in obsessive-compulsive disorder. Brain, 146(4), 1322–1327. https://doi.org/10.1093/brain/awac425

Poster No 562

Cortical Gyrification Abnormalities in Pediatric and Adult Obsessive-Compulsive Disorder

Inkyung Park[1], Minah Kim[2], Minji Ha[1], Dan Stein[3], Odile van den Heuvel[4], Paul Thompson[5], Jun Soo Kwon[2]

[1]Seoul National University, Seoul, South Korea, [2]Seoul National University Hospital, Seoul, South Korea, [3]University of Cape Town, Cape Town, South Africa, [4]Amsterdam UMC, Vrije Universiteit Amsterdam, Department of Psychiatry, and Department of Anatomy and, Amsterdam, Netherlands, [5]USC, Marina Del Rey, CA

Introduction: To better understand the complexities of obsessive-compulsive disorder (OCD), it is crucial to identify more homogeneous subtypes of patients with OCD based on biological evidence. The age of onset has been used as a criterion for subtyping, reliably distinguishing between early-onset and late-onset OCD subgroups in accordance with distinct neurodevelopmental perspectives. Cortical folding is primarily determined during the embryonic and early postnatal developmental period and maintains its pattern relatively stable over the lifespan, thus serving as a reliable neurobiological marker for early neurodevelopmental deficits in psychiatric illnesses. The presence of gyrification abnormalities in both adult early-onset OCD and pediatric OCD patients was investigated to categorize OCD into more biologically-based and homogeneous subtypes based on underlying neurodevelopmental origins.

Methods: The local Gyrification Index (lGI) data from 2611 OCD patients and 2723 HCs, collected from 32 sites (52 datasets) worldwide as part of the ENIGMA OCD Working Group, were pooled for mega-analyses. Whole-brain lGI data were harmonized using ComBat to account for site and scanner effects within a mega-analysis framework. The vertex-wise lGI group comparisons were conducted between pediatric OCD patients and pediatric HCs, as well as among adult patients with early-onset OCD, late-onset OCD, and adult HCs using a general linear model implemented in Freesurfer while controlling for age and sex.

Results: Adult patients with early-onset OCD displayed significantly greater gyrification in the bilateral fronto-parietal cortex. This included clusters with peak vertices in the left caudal middle frontal, postcentral, lateral orbitofrontal, and another caudal middle frontal gyri, as well as in the right precentral and inferior parietal gyri. Conversely, adult patients with late-onset OCD exhibited significantly reduced gyrification in corresponding regions, with peak vertices located in the left precentral and lingual gyri, as well as the right superior frontal and inferior temporal gyri. Adult patients with early-onset OCD showed significant hypergyrification compared to those with late-onset OCD in similar but more extensive regions of fronto-parietal, temporal, medial occipital, and cingulate regions. In pediatric OCD patients compared to pediatric HCs, significantly increased gyrification was also observed in bilateral fronto-parietal, temporal, and cingulate regions. Furthermore, hypergyrification in the left precentral, left posterior cingulate, right postcentral, and right superior frontal clusters was significantly correlated with an earlier age of onset, even after correction for multiple comparisons.

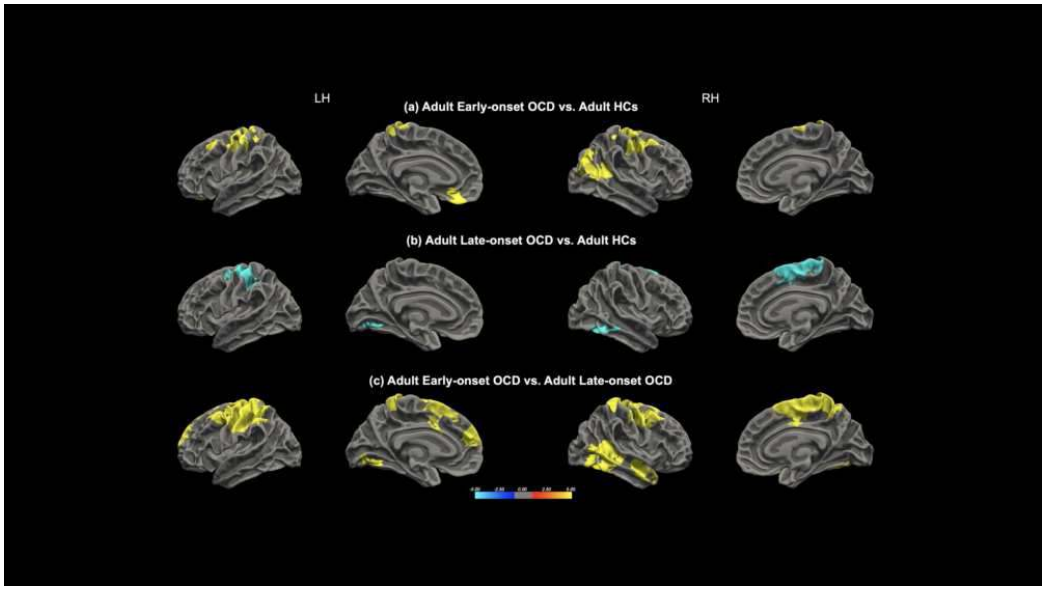

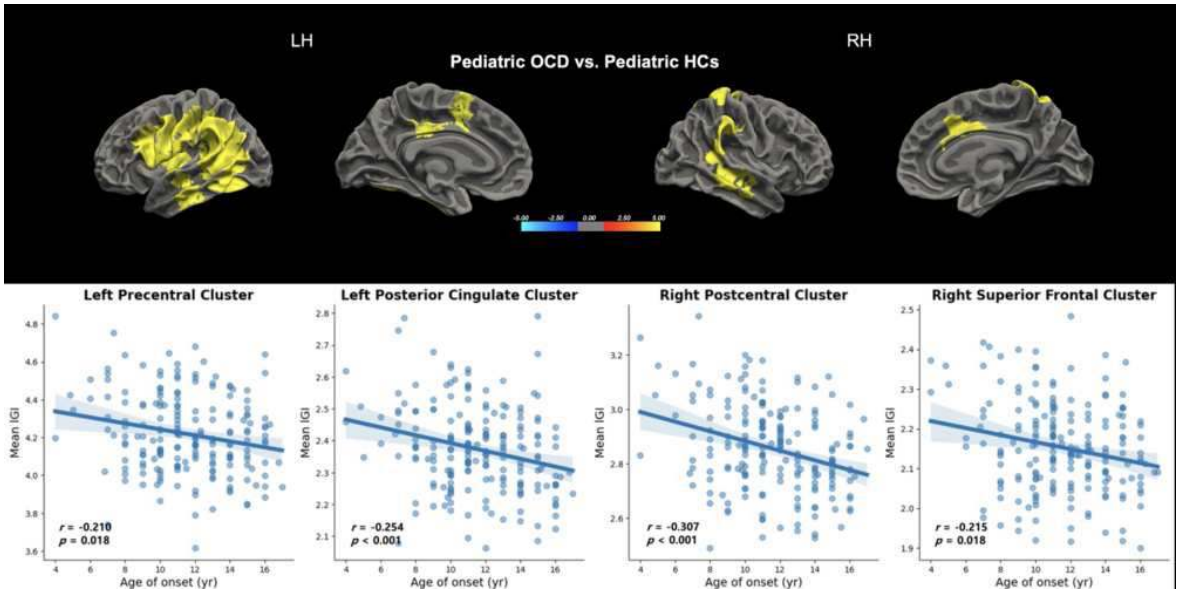

Conclusions: Adult early-onset OCD patients consistently exhibited increased cortical gyrification, predominantly in fronto-parietal and cingulate regions. Additionally, more widespread hypergyrification deficits were consistently found in pediatric OCD patients, and the increased gyrification in the fronto-parietal and cingulate cortices was further correlated with the age of onset in pediatric OCD patients. Our findings, which consistently implicate abnormal hypergyrification in both adult early-onset OCD and pediatric OCD group, provide a potential neurobiological marker that can help categorize patients with OCD into more neurodevelopmentally homogeneous subtypes. This could enhance our understanding of the neurodevelopmental deficits contributing to the etiology of early-onset OCD, aligning with existing evidence suggesting that early-onset OCD has a greater neurodevelopmental loading than late-onset OCD.

References

1. Armstrong, E., Schleicher, A., Omran, H., Curtis, M., & Zilles, K. (1995). The ontogeny of human gyrification. Cerebral Cortex, 5(1), 56–63. doi: 10.1093/cercor/5.1.56
2. Fan, Q., Palaniyappan, L., Tan, L., Wang, J., Wang, X., Li, C., ... Liddle, P. F. (2013). Surface anatomical profile of the cerebral cortex in obsessive–compulsive disorder: A study of cortical thickness, folding and surface area. Psychological Medicine, 43(5), 1081–1091. doi: 10.1017/S0033291712001845
3. Geller, D., Biederman, J., Jones, J., Park, K., Schwartz, S., Shapiro, S., & Coffey, B. (1998). Is juvenile obsessive–compulsive disorder a developmental subtype of the disorder? A review of the pediatric literature. Journal of the American Academy of Child and Adolescent Psychiatry, 37(4), 420–427. doi: 10.1097/00004583-199804000-00020
4. Insel, T. R. (2014). The NIMH Research Domain Criteria (RDoC) project: Precision medicine for psychiatry. The American Journal of Psychiatry, 171(4), 395–397. doi: 10.1176/appi.ajp.2014.14020138
5. Park, I., Ha, M., Kim, T., Lho, S., Moon, S., Kim, M., & Kwon, J. (2022). Cortical gyrification differences between early- and late-onset obsessive–compulsive disorder: Neurobiological evidence for neurodevelopmentally distinct subtypes. Psychological Medicine, 1-10. doi:10.1017/S0033291722003129
6. Schaer, M., Cuadra, M. B., Tamarit, L., Lazeyras, F., Eliez, S., & Thiran, J. P. (2008). A surface-based approach to quantify local cortical gyrification. IEEE Transactions on Medical Imaging, 27(2), 161–170. doi: 10.1109/TMI.2007.903576
7. Taylor, S. (2011). Early versus late onset obsessive–compulsive disorder: Evidence for distinct subtypes. Clinical Psychology Review, 31(7), 1083–1100. doi: 10.1016/j.cpr.2011.06.007
8. Zilles, K., Palomero-Gallagher, N., & Amunts, K. (2013). Development of cortical folding during evolution and ontogeny. Trends in Neurosciences, 36(5), 275–284. doi: 10.1016/j.tins.2013.01.006

Poster No 563

Associations between multimodal brain age and the emergence of internalising symptoms in adolescence

Niamh MacSweeney[1,2,3], Dani Beck[1,2,3], Lucy Whitmore[4], Kathryn Mills[4], Lars Westlye[5], Tilmann von Soest[1], Christian Tamnes[1,2,3]

[1]PROMENTA Research Center, Department of Psychology, University of Oslo, Oslo, Norway, [2]NORMENT, Division of Mental Health and Addiction, Oslo University Hospital & Institute of Clinical Medicine, University of Oslo, Oslo, Norway, [3]Division of Mental Health and Substance Abuse, Diakonhjemmet Hospital, Oslo, Norway, [4]University of Oregon, Eugene, OR, [5]NORMENT, Division of Mental Health and Addiction, Oslo University Hospital & Institute of Clinical M, Oslo, Norway

Introduction: Adolescence is the period of greatest risk for the onset of internalising symptoms, particularly in females[1,2]. How variations in patterns of brain maturation relate to the emergence of these difficulties remains unclear due to inconsistent findings in recent longitudinal studies[3–6]. Prior work has focused on group-level differences in brain maturation using unimodal approaches, limiting the quantification of deviations from typical development at an individual level. Brain age prediction allows us to assess individual deviations from age-expected patterns (i.e., brain age gap (BAG)), indirectly informative of brain maturational patterns, and how this relates to the development of internalising difficulties. Using the Adolescent Brain Cognitive Development (ABCD) Study data (N = ~11,880, 9-10-years at baseline), we examined cross-sectional and longitudinal associations between multi-modal brain age models trained independently on T1-weighted (T1), diffusion tensor (DTI), and resting-state functional (rs-fMRI) MRI data, and self-reported youth internalising symptoms. Although we expected deviations from typical brain development to be associated with greater internalising symptoms, we did not hypothesise about the directionality of this relationship given that both accelerated and delayed patterns of brain maturation have been reported. However, we expected these associations to be stronger in females due to the higher incidence of mood difficulties in females.

Methods: Age prediction was calculated for each MRI modality separately using XGBoost regression[7]. We used ~50% of the ABCD data (baseline and 2-year follow-up: N= ~9,000 observations) as the test sample, and ~50% for model training (N = ~7,200) and ten-fold cross-validation (N=~1,200). In the training set, R2, RSME, and MAE values were used to assess model accuracy and an age-bias correction was applied. Within each modality, BAG was calculated by subtracting chronological age from predicted age, producing T1-BAG, DTI-BAG, and fMRI-BAG for each participant. Internalising symptoms were measured using the Brief Problem Monitor Internalising Scale at 3-year follow-up. For each MRI modality, univariate latent-change score models[8] were estimated to test 1) whether baseline BAG was associated with later internalising symptoms, and 2) to what extent change in BAG between timepoints (ΔBAG) related to internalising symptoms. We ran multi-group analyses to explore sex differences. We also accounted for earlier internalising symptoms at 6-month follow-up in our models.

Results: As shown in Figure 1, the brain age model performance for DTI was the most accurate (r=0.66, p<0.001, 95% CI=[0.65, 0.67], MAE=0.71), followed by T1 (r=0.59, p<0.001, 95% CI=[0.57, 0.60], MAE=0.79) and rs-fMRI (r=0.41, p <0.001, 95% CI=[0.39, 0.43], MAE=0.89). Although baseline T1-BAG was not significantly associated with later youth internalising difficulties, ΔT1-BAG was significantly associated with internalising symptoms at follow-up (ß =0.13, p<0.001). Similar results were found for the fMRI-BAG model, whereby ΔfMRI-BAG (ß=0.04, p=0.007), but not baseline fMRI-BAG, was related to later internalising symptoms. These associations remained significant when accounting for earlier internalising difficulties. Our multi-group analyses showed that these effects were significant in females only. The DTI-BAG measures were not found to be associated with youth internalising difficulties.

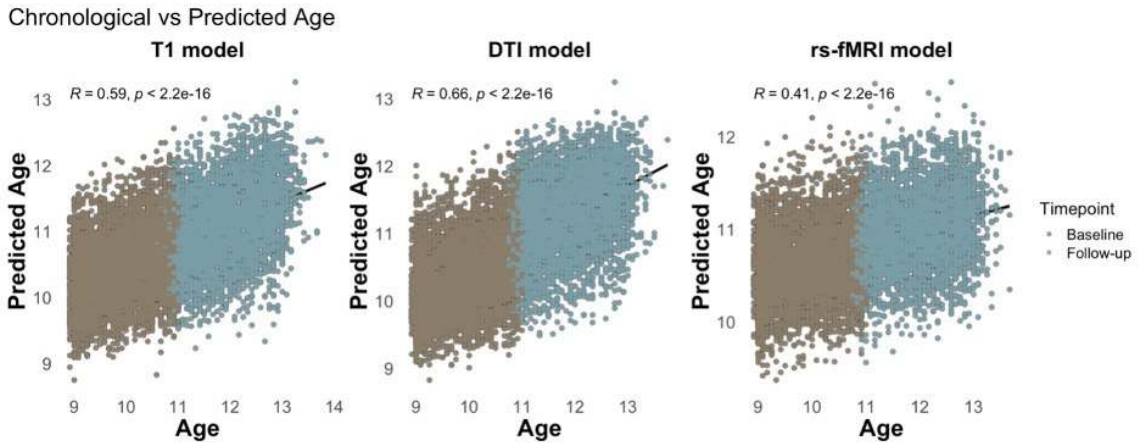

Figure 1: Multimodal brain age prediction. Performance of T1, DTI, and rs-fMRI brain age models.

Conclusions: Our findings suggest that the rate of structural and functional brain maturation is associated with the emergence of mood difficulties in female youth. Female youth that exhibit faster brain ageing over time (ΔBAG), but not older-looking brains to begin with, may be at an increased risk for the onset of internalising symptoms. This pattern of brain maturation could reflect the beginning of a negative developmental trajectory and thus, may be a key window of opportunity for intervention.

References

1. Ref 6: Bos, M.G.N (2018), 'Emerging depression in adolescence coincides with accelerated frontal cortical thinning'. Journal of Child Psychology and Psychiatry. vol. 59, no. 6, pp. 994–1002.

2. Ref 7: Chen, T. (2016), 'XGBoost: A Scalable Tree Boosting System'. Proceedings of the 22nd ACM SIGKDD International Conference on Knowledge Discovery and Data Mining pp. 785–94.
3. Ref 4: Ho T.C (2022) 'Multi-level predictors of depression symptoms in the Adolescent Brain Cognitive Development (ABCD) study. Journal of Child Psychology and Psychiatry.
4. Ref 1: Keyes K. (2023) 'Annual Research Review: Sex, gender, and internalizing conditions among adolescents in the 21st century – trends, causes, consequences', Child Psychology Psychiatry vol.17
5. Ref 8: Kievit, R. A (2018) 'Developmental cognitive neuroscience using latent change score models: A tutorial and applications', Developmental Cognitive Neuroscience, Vo. 33, pp. 99–117.
6. Ref 2: Solmi, M. (2022), 'Age at onset of mental disorders worldwide: large-scale meta-analysis of 192 epidemiological studies'. Mol Psychiatry. Vol. 27, No. 1, pp.281–95.
7. Ref 3: Toenders, Y. J (2022), 'Predicting Depression Onset in Young People Based on Clinical, Cognitive, Environmental, and Neurobiological Data'. Biological Psychiatry: Cognitive Neuroscience and Neuroimaging, Vo. 7, No. 4, pp. 376–84.
8. Ref 5: Whittle, S, (2020), 'Internalizing and Externalizing Symptoms Are Associated With Different Trajectories of Cortical Development During Late Childhood'. Journal of the American Academy of Child & Adolescent Psychiatry. Vol. 59, No. 1, pp.177–85.

Poster No 564

The mediation role of brain structure in the meditation treatment of Schizophrenia: an RCT study

Qing Wang[1], Ting Xue[2], Donghong Cui[3]

[1]Shanghai Mental Health Center, Shanghai, [Select a State], [2]Shanghai Mental Health Center, Shanghai Jiao Tong University School of Medicine, Shanghai, Shanghai, [3]Shanghai Key Laboratory of Psychotic Disorders, Shanghai, China

Introduction: Schizophrenia (SZ), characterized by complex cognitive and behavioral disturbances, represents a significant challenge in mental health[1]. Emerging research has highlighted the therapeutic potential of meditation, a practice rooted in ancient Eastern traditions, particularly in the context of mental disorders. This practice, involving heightened awareness and a focus on the present, has shown promise in the modulation of neurological functions. Recent scientific endeavors have begun to unravel the benefits of meditation in managing conditions like anxiety and depression. However, its efficacy in schizophrenia remains under-explored. We designed a randomized controlled trial (RCT) to study the treatment effect of meditation and the mediation role of brain structural changes for the chronic SZ patients afflicted with persistent hallucinations and delusions, the design of this study has been illustrated in Fig. 1. The results showed that, 3-month meditation can slightly improve the positive and negative symptoms, but not significant while 8-month meditation can significantly improve the PANSS score by 10.6 (p=0.008). We have further estimated the average treatment effect (ATE = 10.2, p=0.003) of 8-month meditation with overlap weighting[2], which allows for causal interpretation. In addition, we discovered the mediation role of rh_lingual thickness and lh_caudalanteriorcingulate for the 3-month negative PANSS decrease. This study has demonstrated the effectiveness of meditation for chronic SZ patients and reported its average treatment effect. The rh_lingual and lh_caudalanteriorcingulate seems to play a mediator role for such treatment effects, which calls for further investigation of their structural and functional roles in the underlying mechanism.

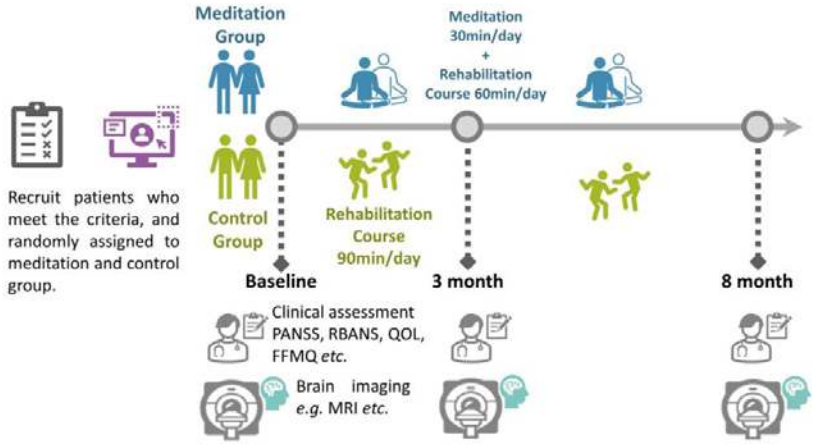

Figure 1 The study design of the random controlled trial (RCT) for assessing the effect of meditation for Schizophrenia patients. This study has been approved by the ethics committee of medical research in the Minzheng hospital (*YJZXLL2017005*) , where this study has been carried out and written informed consents were obtained from all patients. This trial has been registered on Chinese Clinical Trail Registry with ID: *ChiCTR1800014913*, more details can be found there. In general, 64 Schizophrenia patients who meet the criteria have been recruited and randomized into 2 groups: meditation group and control group, the main outcome of this study is the decrease of PANSS (Positive and Negative Syndrome Scale). Demographic, PANSS, RBANS(Repeatable Battery for the Assessment of Neuropsychological Status), FFMQ (Five Factor Meditation Questionnaire) and MRI (Magnetic Resonance Imaging) have been collected at baseline, 3 month and 8 month, respectively.

Methods: The study design has been illustrated in Fig. 1. To estimate the treatment effects of meditation, we focus on PANSS score (positive, negative, sum) decrease of 3 months and 8 months. For the estimation of the average treatment effect (ATE), we use overlap weighting to estimate ATE[2]. All these models have been tested with missing data imputed and excluded. For the mediator analysis, we first test the treatment effect on brain structure (freesurfer 7.0.3 results[3]) and then the effect of brain structures on the final PANSS changes. All the model details and results are illustrated in Fig. 2.

(a) Estimate the (causal) treatment effect of meditation:

Outcomes: PANSS_sum_dec_8, PANSS_positive_dec_8, PANSS_negative_dec_8, PANSS_sum_dec_3, PANSS_positive_dec_3, PANSS_negative_dec_3

Outcome Models: **outcome** = age + **treatment** + age_of_onset + duration + BMI_0 + smoking + education + family_income+ PANSS_0+ RBANS_sum_0+ FFMQ_0

(b)

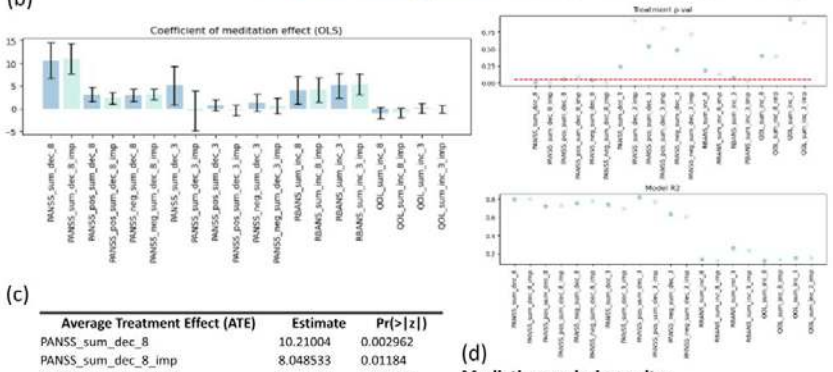

(c)

Average Treatment Effect (ATE)	Estimate	Pr(>|z|)
PANSS_sum_dec_8	10.21004	0.002962
PANSS_sum_dec_8_imp	8.048533	0.01184
PANSS_pos_sum_dec_8	5.031437	0.000233
PANSS_pos_sum_dec_8_imp	4.060313	0.000147
PANSS_neg_sum_dec_8	2.933043	0.23163
PANSS_neg_sum_dec_8_imp	3.063891	0.13725
PANSS_sum_dec_3	4.669992	0.220085
PANSS_sum_dec_3_imp	1.608685	0.67045
PANSS_pos_sum_dec_3	2.735215	0.053968
PANSS_pos_sum_dec_3_imp	2.07297	0.134308
PANSS_neg_sum_dec_3	0.636821	0.776659
PANSS_neg_sum_dec_3_imp	0.004263	0.9984

(d)

Mediation analysis results:

Treatment-> rh_lingual ->PANSS_negative_sum_3
Coef: 0.06/-3.32, p-val: 0.035/0.068
Treatment-> lh_caudalanteriorcingulate volume -> PANSS_negative_sum_3
Coef: 238.53/-3.54, and p-val: 0.035/0.051
Treatment-> lh_caudalanteriorcingulate_area_3-> PANSS_negative_sum_3
coef : 78.47/-3.24, and p-val: 0.034/0.076

Figure 2. The results of this study. (a) The model specifications; (b) Conditional average treatment effects estimated with ordinary least square; (c) Average treatment effect estimated by propensity score and overlap weighting; (d) The mediation effect of brain structures on these meditation effects.

Results: The results show that: 1) 8-month meditation can significantly reduce the PANSS score of SZ patients by 10.61 (p=0.008) while 3 month meditation can only reduce PANSS score by 5.08 (p=0.235, not significant), this trend is the same for both positive PANSS decrease and negative PANSS decrease. 2) The average treatment effect (PANSS decrease) of 8-month meditation is 10.21 (p=0.003) for PANSS sum, 5.03 (p=0.0002) for PANSS positive and 2.93 (p=0.232) for PANSS negative. The results are stable with or without multiple imputation. 3) Meditation can increase can significantly increase the rh_lingual volume by 0.06 (p=0.035) and such changes can reduce the 3-month PANSS negative score by 3.32 (p=0.068). Both lh_ caudalanteriorcingulate volume and area has similar effects on 3month PANSS negative score.

Conclusions: In summary, we carried out an RCT to study the effect of meditation for chronic Schizophrenia (SZ) patients, and 8-month meditation can significantly reduce the PANSS score by about 10. The conditional treatment effect and the average treatment effect are similar. In addition, we discovered 2 potential brain structural mediators : the right hemisphere lingual gyrus (may involve in the visual hallucinations) and left hemisphere caudal anterior cingulate cortex (emotional dysregulation etc.) These findings lead to further investigation of the functional changes related to these regions. Our papers are currently under review and more results and details will be shared during 2024 OHBM meeting.

References

1. Sheng Jialing, et al. CNS Neuroscience & Therapeutics, no. 1, 25 (2019): 147–50.
2. Li Fan, et al. American Journal of Epidemiology, no. 1, 188 (2019): 250-257.
3. Esteban Oscar, et al. Nature Protocols 15, no. 7 (2020): 2186–2202.

Poster No 565

One Week Antidepressant Efficacy Revealed by EEG Analysis

Yueheng Peng[1], Yan Peng[2], Guangying Wang[1], Fali Li[3], Peng Xu[3]

[1]University of Electronic Science and Technology of China, Chengdu, Sichuan, [2]West China Second University Hospital, Chengdu, Sichuan, [3]School of life Science and technology, University of Electronic Science and Technology of China, Chengdu, Sichuan

Introduction: The treatment of major depressive disorder (MDD) was widely investigated, but their efficacy was evaluated by clinical scales, such as Hamilton Depression Scale and Patient Health Questionnaire-9, which were highly depended on patients' subjective feeling and required at least four weeks after baseline to reflect the medication efficacy. Under this situation, researchers began to look for electroencephalogram biomarkers to sensitively and objectively evaluate short-term efficacy, which potentially facilitates treatment selection and reduces time cost. In recent years, EEG analysis has been widely explored, utilizing multiple different tasks such as emotional face presentation and working memory, which might reflect differences in brain functioning between depression patients and healthy controls. In our current study, based on the eyes-open EEG recorded during tasks, the corresponding event-related potential (ERP) at baseline and week1 was investigated to reveal the efficacy of one-week medication. Related brain networks were constructed to further demonstrate the brain changes after one-week medication.

Methods: In this study, there were twenty-five medication-free depressed patients received medicine for two months. At the last week, all patients were divided into responders and non-responders based on Hamilton Depression Scale. 21-channel eyes-open EEG datasets were collected during tasks at baseline and after one-week treatment. Concretely, the binaural acoustic stimuli was of 40-ms duration. The tones were presented in five different intensity levels: 60, 70, 80, 90 and 100 dB. 100 times of each intensity level were presented in a random order with a randomized inter-stimulus interval of 1600-2100 ms. Thereafter, the EEG datasets collected during the tasks were further pre-processed into artifact-free 1-s-length segments by adopting procedures, including the reference electrode standardization technique re-referencing, [1, 10] Hz offline-bandpass filtering, baseline correction and artifact removal, etc. Subsequently, the corresponding ERPs were statistically compared under different phases. Eventually, corresponding EEG networks were constructed by using Phase Locking Value (PLV) and then statistically compared between the two stages.

Results: On one hand, Fig. 1 illustrated the ERP amplitude of N100 and P200 between baseline and week1 in responder arm. Obvious reduction after taking medicine for one week could be observed. Specifically, the amplitudes of both N100 and P200 reduced. Conversely, no significant difference in ERP amplitude between week0 and week1 in non-responder group could be found. On the other hand, Fig. 2 showed the topological differences of related EEG networks (derived from 100 dB N100) between week0 and week1 for the responder cohort, where the blue solid line indicates enhancement (week0week1). As we can see, there was a significant reduction after one week treatment, illustrating that the medication alleviated the activity of

related brain regions. In contrast, after one-week medication, no significant changes in network patterns could be observed in non-responders.

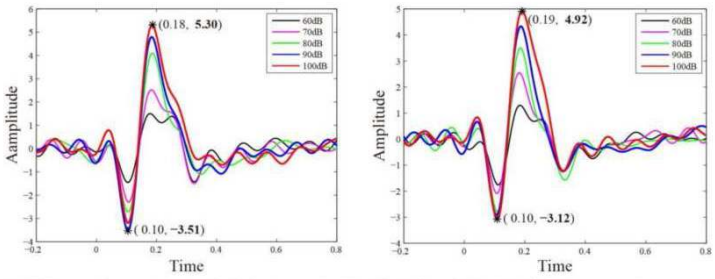

Fig. 1. ERP waveforms at electrode Cz between the Week0 (left) and Week1 (right) in responder group.

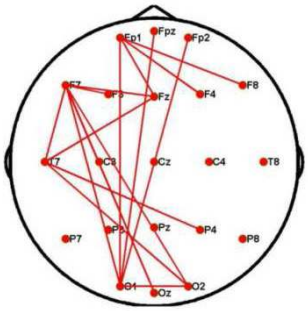

Fig. 2. Topological network differences between Week0 and Week1.

Conclusions: Our present study revealed that after one-week medication, the ERP amplitude of responders decreased. And the corresponding brain network difference between week0 and week1 further demonstrated that the short-term treatment attenuated the activity of frontal-parietal lobes, which might help doctors to adjust therapeutic regimen at the initial stage of a certain long-term treatment.

References

1. Y, Zhang. (2020), 'Identification of psychiatric disorder subtypes from functional connectivity patterns in resting-state electroencephalography', Nature Biomedical Engineering, vol. 5, no. 4, pp. 309-323
2. F, de Aguiar Neto. (2019), 'Depression biomarkers using non-invasive EEG: A review', Neuroscience and Biobehavioral Reviews, vol. 105, pp. 83-93
3. G, Simon. (2001), 'Choosing a first-line antidepressant: Equal on average does not mean equal for everyone', Jama, vol. 286, no. 23, pp. 3003-3004
4. F, Li. (2019), 'Differentiation of schizophrenia by combining the spatial EEG brain network patterns of rest and task P300', IEEE Transactions on Neural Systems and Rehabilitation Engineering, vol. 27, no. 4, pp. 594-602
5. T, Zhang. (2016), 'Structural and functional correlates of motor imagery BCI performance: Insights from the patterns of fronto-parietal attention network', NeuroImage, vol. 134, pp. 475-485
6. W, Wu. (2020), 'An electroencephalographic signature predicts antidepressant response in major depression', Nature Biotechnology, vol. 38, no. 4, pp. 439-447

Poster No 566

Personalized white matter system index for schizophrenia: a multilevel sib-pair analysis

Ming-Hsuan Lu[1], Wen-Yih Tseng[2], Chang-Le Chen[3], Tzung-Jeng Hwang[1,4], Chih-Min Liu[1,4]

[1]Department of Psychiatry, National Taiwan University Hospital, Taipei, Taiwan, [2]Institute of Medical Device and Imaging, College of Medicine, National Taiwan University, Taipei, Taiwan, [3]Department of Bioengineering, University of Pittsburgh, Pittsburgh, PA, [4]Department of Psychiatry, College of Medicine, National Taiwan Univeristy, Taipei, Taiwan

Introduction: Schizophrenia is a heterogeneous disorder characterized by highly individual structural changes involving the whole brain. White matter microstructural abnormality, as measured with diffusion MRI, is a robust endophenotype for schizophrenia at the group level. However, white matter microstructure is highly heritable and sensitive to multiple factors other than schizophrenia. Therefore, white matter changes relevant to schizophrenia are often obscured and indiscernible in individuals. We developed a multilevel analytic approach to extract the personalized disease-relevant features from diffusion MRI and to quantify the systems-level enrichment of disease features in five white matter systems, including two

association systems (corticolimbic and corticocortical), two projection systems (frontostriatal and corticothalamic), and the commissural system.

Methods: Using diffusion spectrum imaging, we characterized generalized fractional anisotropy (GFA) of 76 fibers in patients with schizophrenia (SCZ, n = 97) and their unaffected siblings (Sib, n = 90). Following normative modeling (reference group n = 482), we derived GFA z-scores of 45 fibers with high reliability. To extract disease-relevant features, we subtracted GFA z-scores of siblings from those of patients in sib-pairs. To quantify the systems-level enrichment of white matter changes, we derived normalized enrichment scores (NES) and false discovery rate (FDR), either from GFA z-scores from patients only or from disease-relevant features (SCZ subtracted by Sib), of the five systems. Cognitive functions were assessed with the Continuous Performance Test (CPT) and the Weschler's Adult Intelligence Test - III (WAIS-III). Symptoms were profiled using the Positive and Negative Syndrome Scale (PANSS). Association of systems-level white matter hypointegrity (NES) with cognitive functions (WAIS-III IQ and CPT d') and symptom severity (PANSS) were evaluated using linear regression, with age and gender as covariates. For symptom severity, IQ was also included as a covariate since it is associated with both symptom severity and white matter microstructure.

Results: At the level of individual tracts, bilateral fornix, bilateral orbitofrontal-striatal fibers, and some commissural fibers showed significantly lower GFA in patients compared with unaffected siblings. Of the five systems, corticolimbic, frontostriatal, and commissural system had more systems-level hypointegrity in both disease-relevant NES and patient-only NES than in sibling-only NES (% subjects with NES > 2, corresponding approximately to FDR < 0.05: Corticolimbic SCZ-Sib = 21.8%, SCZ = 24%, Sib = 16.1%; Frontostriatal SCZ-Sib = 24.1%, SCZ = 19.5%, Sib = 11.0%; Commissural SCZ-Sib = 23.0%, SCZ = 23.0%, Sib = 20.7%; Corticocortical SCZ-Sib = 9.2%, SCZ = 16.1%, Sib = 11.5%; Corticothalamic SCZ-Sib = 9.2%, SCZ = 6.9%, Sib = 10.3%). NES of these three systems were included for association tests with cognitive functions and symptom severity. Disease-relevant systems-level corticolimbic hypointegrity was associated with IQ (p = 0.0191, beta = 4.591) and perceptual sensitivity (CPT d' z-score, p = 0.0143, beta = 0.358), indicating that schizophrenic brains with white matter changes concentrated within the corticolimbic system may have cognitive functions preserved. In terms of symptom severity, disease-relevant systems-level corticolimbic hypointegrity was associated with excitement/hostility (p = 0.0087, beta = 0.210) and depression/anxiety (p = 0.0162, beta = 0.280), suggesting that corticolimbic-specific hypointegrity presents with aggression and mood symptoms in schizophrenia. The associations held for disease-relevant NES but not patient-only NES.

Conclusions: At the systems level, corticolimbic-specific white matter hypointegrity is associated with preserved cognitive functions, aggression, and mood symptoms in schizophrenia. The personalized white matter system index may inform disease subtyping and patient stratification.

References

1. Chen, C.L. et al. (2022), 'Detection of advanced brain aging in schizophrenia and its structural underpinning by using normative brain age metrics', NeuroImage: Clinical, vol. 34, no. 103003.
2. Chen, Y.J. et al. (2015), 'Automatic whole brain tract-based analysis using predefined tracts in a diffusion spectrum imaging template and an accurate registration strategy', Human Brain Mapping, vol. 36, no. 9, pp. 3441-3458.
3. Koshiyama, D. et al. (2020), 'White matter microstructural alterations across four major psychiatric disorders: mega-analysis study in 2937 individuals', Molecular Psychiatry, vol. 25, no. 4, pp. 883-895.
4. Lv, J. et al. (2021), 'Individual deviations from normative models of brain structure in a large cross-sectional schizophrenia cohort', Molecular Psychiatry, vol. 26, no. 7, pp. 3512-3523.
5. Tseng, I.W.Y. et al. (2021), 'Microstructural differences in white matter tracts across middle to late adulthood: a diffusion MRI study on 7167 UK Biobank participants', Neurobiolgy of Aging. vol. 98, pp. 160-172.

Poster No 567

Aberrant dynamic functional connectivity of the subcortical structures in subthreshold depression

Siying Zhang[1], Qiwen Lin[1], Changyi Kuang[1], Yuanyun He[1], Bingqing Jiao[1], Huiyuan Huang[2], Lijun Ma[1], Jiabao Lin[1]

[1]School of Public Health and Management, Guangzhou University of Chinese Medicine, Guangzhou, Guangdong Province, [2]Guangzhou University of Chinese medicine, Guangzhou, Guangdong Province

Introduction: Subthreshold depression (StD) could be a significant precursor and a risk factor for major depressive disorder (Zhang et al., 2022). StD individuals generally show mild depressive symptoms in clinical practice, but they do not meet the standardized diagnostic criteria for major depressive disorder (Rodriguez et al., 2012). Previous studies based on functional magnetic resonance imaging (fMRI) have demonstrated that StD appears to be closely correlated with subcortical regions. A study revealed that functional connectivity (FC) was increased between the default mode network and ventral striatum in StD patients compared with healthy controls (Hwang et al., 2016). And Peng et al (2020) found decreased FC between the left amygdala and both the cognitive control network and left insula in individuals with StD. However, these studies mainly

focused on static FC but ignored the temporal dynamics of FC. Recent studies have suggested that dynamic FC (dFC) may reveal a great deal of information regarding the brain's time-varying neural activity (Calhoun et al., 2014; Rashid et al., 2016). Therefore, the present study attempted to investigate the differences in the dFC of the subcortical regions between the StD individuals and healthy controls.

Methods: In this study, all neuroimaging data used were obtained from the Southwest University Longitudinal Imaging Multimodal (SLIM) Brain Data Repository (Liu et al., 2017) and this study was approved by the Research Ethics Committee of the Brain Imaging Center of Southwest University. Participants with Beck Depression Inventory (BDI) scores between 14-29 were entered into the StD group, and those with BDI scores between 0-6 belonged to the healthy control (HC) group. After screening, there were 50 participants in the StD group and 50 participants in the HC group. The two groups were matched for age, gender, state anxiety score, trait anxiety score, and mean framewise displacement (FD, representing head motion) (Table 1). Sixteen subcutaneous nuclei were extracted as the regions of interest (ROIs) using the Harvard–Oxford subcortical structural 25% probability atlas. The dFC analysis was carried out using the sliding-window approach (Allen et al., 2014) by DynamicBC toolbox (Liao et al., 2014). For each sliding window, a whole-brain FC map of each ROI was obtained by calculating the Person correlation coefficient between each ROI and each voxel of the whole brain. Then, based on all windows, we computed the variance of each ROI's FC maps (the variance value in each voxel). Finally, between-group comparisons of the variance were performed using the two-sample t-test within DPABI (Yan et al., 2016). These analyses were carried out with multiple comparisons correction using GRF correction (voxel-level $p < 0.001$, cluster-level $p < 0.05$).

Table 1 Demographics characteristic between HC and StD groups.

	HC	StD	*P*-value
Gender(M/F)	25/25	23/27	0.689[a]
Age	19.84±0.91	20±1.39	0.896[b]
BDI	3.46±2.06	16.82±2.81	< 0.001[b]
Trait Anxiety	45.30±4.15	46.90±5.60	0.108[c]
State Anxiety	39.88±6.64	42.02±8.07	0.151[c]
Mean FD	0.06±0.03	0.06±0.02	0.710[b]

Data are presented as mean±SD. HC, healthy control; StD, subthreshold depression; M/F, male/female; BDI, Beck Depression Inventory; FD, framewise displacement. The *p*-value was attained by conducting three tests: (a) a Chi-square test; (b) a Mann–Whitney test; (c) a two-sample *t*-test.

Results: Compared with the HC group, we found that the StD group showed significantly decreased dFC variance of subcutaneous nuclei with the whole brain. Those brain region pairs include the following: (1) the left caudate with the left median cingulate gyrus (MCG), left cerebellum (CBM), and left superior parietal gyrus (SPG); (2) the right caudate with the right/left thalamus and left CBM; (3) the left amygdala with the left supramarginal gyrus (SMG) and left MCG; (4) the left brainstem with the right posterior central gyrus (PCG); (5) the right putamen with the left SMG; (6) the right pallidum with the left inferior frontal gyrus (IFG) and left SMG (Table 2 and Figure 1).

Table 2 Cluster locations and peak coordinates corresponding to the significant difference of dFC of subcortical ROI between StD group and HC group. The *t* value refers to the statistical difference in the brain cluster.

	Seed region (Subcortical ROI)	Cluster location	MNI coordinate			Cluster size (voxels)	Peak *t* value
			X	Y	Z		
StD<HC	CAU.L	CBM.L	-33	-48	-30	56	-4.13
		MCG.L	0	-6	33	30	-4.10
		SPG.L	-15	-42	57	22	-4.32
	CAU.R	THA.L/R	12	-27	3	41	-4.10
		CBM.L	-27	-51	-36	22	-4.60
	AMY.L	SMG.L	-48	-24	21	20	-3.86
		MCG.L	-12	12	33	19	-4.24
	BSM.R	PCG.R	27	-30	54	22	-4.43
	PUT.R	SMG.L	-63	-33	30	63	-4.81
	PAL.R	IFG.L	-54	15	-9	18	-4.17
		SMG.L	-63	-30	42	18	-4.14

Abbreviation: HC, healthy control; StD, subthreshold depression; MNI, Montreal Neurological Institute; R, right; L, left; CAU, caudate; AMY, amygdala; BSM, brainstem; PUT, putamen; PAL, pallidum; CBM, cerebellum; MCG, median cingulate gyrus; SPG, superior parietal gyrus; CBM, cerebellum; THA, thalamus; SMG, supramarginal gyrus; PCG, postcentral gyrus; IFG, inferior frontal gyrus.

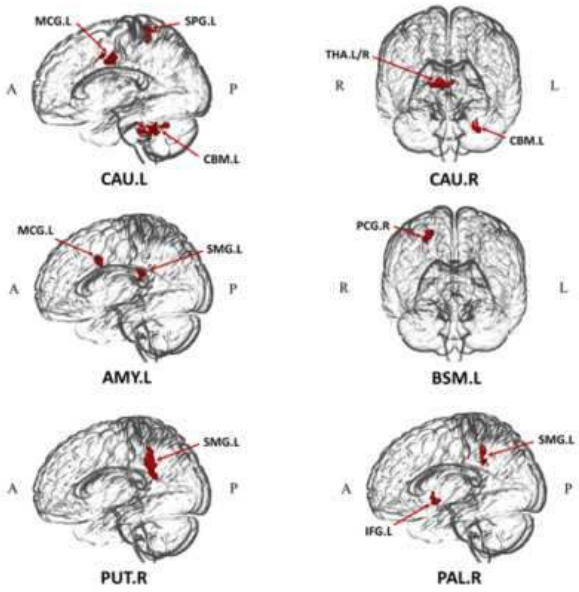

Figure 1 Regions showing significant differences (StD<HC) in dFC variance of subcutaneous nuclei between the StD group and the HC group (GRF correction, voxel-level $p < 0.001$, cluster-level $p < 0.05$). A, Anterior; P, Posterior; R, Right; L, Left; CAU.L, left caudate; CAU.R, right caudate; AMY.L, left amygdala; BSM.L, left brainstem; PUT.R, right putamen; PAL.R, right pallidum; MCG.L, left median cingulate gyrus; SPG.L, left superior parietal gyrus; CBM.L, left cerebellum; THA.L/R, left/right thalamus; SMG.L, left supramarginal gyrus; PCG.R, right postcentral gyrus; IFG.L, left inferior frontal gyrus.

Conclusions: In summary, we found the StD group exhibited a significant reduction in temporal variability of dFC in the extensive subcutaneous nucleus compared to the HC group, highlighting an aberrant dFC pattern in StD. Importantly, these dysfunctional regions are particularly involved in the dFC of caudate with MCG and amygdala with MCG, mainly associated with emotional processing functions. Our findings supported and extended the understanding of the subcortical structures in StD.

References

1. Allen, E. A., E. Damaraju, S. M. Plis, E. B. Erhardt, T. Eichele and V. D. Calhoun (2014). "Tracking Whole-Brain Connectivity Dynamics in the Resting State." Cerebral Cortex 24(3): 663-676.
2. Bi, R., W. X. Dong, Z. X. Zheng, S. J. Li and D. D. Zhang (2022). "Altered motivation of effortful decision-making for self and others in subthreshold depression." Depression and Anxiety 39(8-9): 633-645.
3. Calhoun, V. D., R. Miller, G. Pearlson and T. Adali (2014). "The Chronnectome: Time-Varying Connectivity Networks as the Next Frontier in fMRI Data Discovery." Neuron 84(2): 262-274.

4. Hwang, J. W., S. C. Xin, Y. M. Ou, W. Y. Zhang, Y. L. Liang, J. Chen, X. Q. Yang, X. Y. Chen, T. W. Guo, X. J. Yang, W. H. Ma, J. Li, B. C. Zhao, Y. Tu and J. Kong (2016). "Enhanced default mode network connectivity with ventral striatum in subthreshold depression individuals." Journal of Psychiatric Research 78: 56-56.
5. Liao, W., G. R. Wu, Q. Xu, G. J. Ji, Z. Zhang, Y. F. Zang and G. Lu (2014). "DynamicBC: a MATLAB toolbox for dynamic brain connectome analysis." Brain connectivity 4(10): 780–790.
6. Liu, W., D. T. Wei, Q. L. Chen, W. J. Yang, J. Meng, G. R. Wu, T. Y. Bi, Q. L. Zhang, X. N. Zuo and J. Qiu (2017). "Longitudinal test-retest neuroimaging data from healthy young adults in southwest China." Scientific Data 4: 170017.
7. Peng, X. L., W. K. W. Lau, C. Y. Wang, L. F. Ning and R. B. Zhang (2020). "Impaired left amygdala resting state functional connectivity in subthreshold depression individuals." Scientific Reports 10(1).
8. Rashid, B., M. R. Arbabshirani, E. Damaraju, M. S. Cetin, R. Miller, G. D. Pearlson and V. D. Calhoun (2016). "Classification of schizophrenia and bipolar patients using static and dynamic resting-state fMRI brain connectivity." Neuroimage 134: 645-657.
9. Yan, C. G., X. D. Wang, X. N. Zuo and Y. F. Zang (2016). "DPABI: Data Processing & Analysis for (Resting-State) Brain Imaging." Neuroinformatics 14(3): 339-351.
10. Zhang, R. B., X. L. Peng, X. Q. Song, J. X. Long, C. Y. Wang, C. C. Zhang, R. W. Huang and T. M. C. Lee (2023). "The prevalence and risk of developing major depression among individuals with subthreshold depression in the general population." Psychological Medicine 53(8): 3611-3620.

Poster No 568

Right hippocampal reduction in major depression in international federated analysis

Wenhao jiang[1], Javier Romero[2], Sandeep Panta[2], Jay Fournier[3], Jing Sui[4], Vince Calhoun[5], Jessica Turner[6]

[1]ZhongDa Hospital; School of Medicine, Southeast University, Nanjing, Jiangsu, [2]Georgia State University, Atlanta, GA, [3]The Ohio State University Wexner Medical Center, Columbus, OH, [4]Beijing Normal University, Beijing, China, [5]GSU/GATech/Emory, Decatur, GA, [6]Ohio State University Wexner Medical Center, Columbus, OH

Introduction: Hippocampal volumes tend to be decreased in major depressive disorder (MDD); the ENIGMA MDD meta-analysis of subcortical volumes in 1728 individuals with MDD and over 7000 healthy volunteers found the mean hippocampal volume was reduced in recurrent rather than first episode MDD, but did not show a relationship with depression severity. They did not find effects of severity using the subset which had that data, and they examined the average volumes only. We aimed to replicate those findings in an international, independent sample, examining both left and right hippocampal volumes and with symptom scores. In these analyses, we tested the abillty of a federated analysis platform, COINSTAC, do perform a decentralized regression across the individual sites. The goal of the COINSTAC platform is to bring the analysis to the data, rather than the data to the analysis. In this case, the volumes could be shared but the images could not; we tested the COINSTAC single-shot regression algorithm against a combined analysis. The use of the federated platform allows the potential for more complex analyses on these datasets in the future, to do decentralized machine learning and individual predictions.

Methods: Data from twelve independent sites or studies were included in this analysis. The datasets were pre-existing and collected under IRB approval at each institution. All sites used 3T scanners and collected T1-weighted images with a fixed protocol for that site. The original images could not be aggregated at one location; each site processed their own data through Freesurfer 7.2, and performed visual QC on the segmentations. Left, right, and total hippocampal volume, as well as intracranial volume (ICV) were provided for each participant. Each site included age, sex, diagnosis (MDD or none), and Hamilton's Depression Scale (HAM-D) scores. The total dataset comprised 931 subjects, of whom 602 with MDD, 324 were men, 607 were women. The age range was limited to 18 to 55 in all datasets, with an overall mean age of 31.8 years. The HAM-D scores ranged from 0 to 39 with a median value of 15. The first combined analysis modeled each of left, right, and total hippocampal volumes against diagnosis status, age, sex, and ICV, with site as a random effect. The second analysis regressed HAMD scores for all subjects without considering diagnosis. Analyses that were not done in COINSTAC were done in R using the lme4 package. The COINSTAC analysis did a "single-shot" regression of each of these analyses, which is an automatic, separate analysis on each site's data and a weighted average of the results.

Results: The effects of MDD, sex, and ICV on the total hippocampal volume were significant. The effects of sex and ICV were as expected: women had smaller volumes, and a larger ICV correlated with a larger hippocampal volume. The effect of age in this sample was not significant. Those with MDD on average had a smaller volume ($t(770.2) = -1.98$, $p < .048$). A similar pattern was found in the right hippocampus: the MDD group had a smaller volume ($t(831)=-2.4$, $p=.017$), as well as sex and ICV effects. The same analysis in the left hippocampus, however, found significant effects of sex and ICV only. The HAM-D effect was significant only for the right hippocampus ($t(856) =-2.28$, $p= 0.023$). The federated analysis found comparable single-site results, though the single-shot combination of all sites was not as powerful as the combined analysis.

Conclusions: We extended the original ENIGMA MDD analysis and found that the effects are primarily in the right hippocampal volume. We also found a relationship with symptom severity scores in the same structure. The federated analysis serves as a proof of principle, a foundation for future analyses including cross-site harmonization using ComBat or other techniques, as well as iterative approaches such as machine-learning analyses on the original, unshared images.

Poster No 569

Understanding the functional organization of the thalamocortical connectivity in Chronic SCZ

Harin Oh[1], Han Byul Cho[2], Shinwon Park[3], Sunah Choi[1], Jungha Lee[1], Minah Kim[4,5], Seok-Jun Hong[6,7], Jun Soo Kwon[8,5,9]

[1]Seoul National University, Seoul, Seoul, [2]Center for Neuroscience Imaging Research, Institute for Basic Science, Suwon-si, Gyeonggi-do, [3]Child Mind Institute, New York, NY, [4]Department of Neuropsychiatry, Seoul National University Hospital, Seoul, Seoul, [5]Department of Psychiatry Seoul National University College of Medicine, Seoul, Korea, Republic of, [6]Sungkyunkwan University, Gyeonggi-do, Suwon-si, [7]Department of Biomedical Engineering, Suwon, Korea, Republic of, [8]Department of Brain and Cognitive Sciences, Seoul National University College of Natural Sciences, Seoul, Seoul, [9]Department of Neuropsychiatry, Seoul National University Hospital, Seoul, Korea, Republic of

Introduction: Schizophrenia is a chronic psychiatric disorder with diverse heterogeneity in symptoms and subtypes. Despite such heterogeneity, one consistent finding is the disruption of thalamocortical functional connectivity throughout the disease progression, particularly characterized by reduced connectivity between the thalamus and prefrontal cortex (PFC), and increased connectivity with somatosensory and motor cortex[1,2,3]. Prior research has shown that increased and decreased connectivities are inversely correlated. Patients with greater connectivity to somatosensory areas tend to have reduced connectivity to the PFC, indicating an interconnected relationship between these connectivities and potential dysfunction stemming from a shared mechanism[4]. However, the clinical significance of this dysconnectivity is not fully understood; for instance, their correlation with specific symptoms or their potential as a diagnostic indicator remains uncertain due to current analytical limitations enabling to look at two ROIs at a time. Thus, major focus has been given to identifying the potential cause between the reduced PFC-thalamus and increased somatosensory-thalamus dysconnectivity patterns. Understanding the relationship between two dysconnectivities is crucial, as prefrontal-thalamic connectivity is heavily involved in higher-order functions, while somatosensory-thalamic connectivity plays a critical role in sensory processing and motor coordination[5,6]. To clarify the association between higher order and sensory processing in chronic schizophrenia, exploring the functional hierarchy and organization of those changes could be advantageous. Hence, this study aims to investigate thalamic functional gradient to identify the association between thalamic dysconnectivity patterns in chronic schizophrenia.

Methods: We acquired resting state fMRI images from 63 chronic schizophrenia patients (SCZ, mean age=33.4yrs, M/F=36/27) and 70 healthy individuals (HC, mean age=25.5yrs, M/F=39/31). Thalamic functional connectome method was adapted from Haak[7] for analysis with thalamus as inner region of interest (ROI) and the prefrontal cortex and somatosensory cortex as outer ROIs. The thalamocortical connectivity matrix was extracted from individual subjects, followed by construction of similarity matrix and manifold learning. We extracted two thalamic gradient maps that are known to reflect the thalamic structure (gradient 1) and the hierarchy of behavioral characterization ranging from perception to cognition (gradient 2)[8]. Statistical differences were calculated, with age as covariate, between schizophrenia patients and healthy individuals. Further analysis was performed to examine the functional network disturbances associated to thalamic dysconnectivity in chronic schizophrenia.

Results: Two thalamic gradients presented different patterns (Fig 1A), which showed a statistical (MANOVA) difference in the left thalamus from SCZ compared to HC. The group difference from statistically significant voxel regions showed a greater decrease in the 1st gradient and an increase in the 2nd gradient (Fig 1D). The ANOVA analysis of individual gradients indicated that the second gradient of the left thalamus exhibited a compression within SCZ in comparison to HC at a trend level. Moreover, functional network distribution within the 2nd gradient unveiled a significantly gradient decrease in the visual and default mode networks, while an increase in the frontoparietal network (Fig 2B). This indicates a segregation of visual network and frontoparietal network in patients.

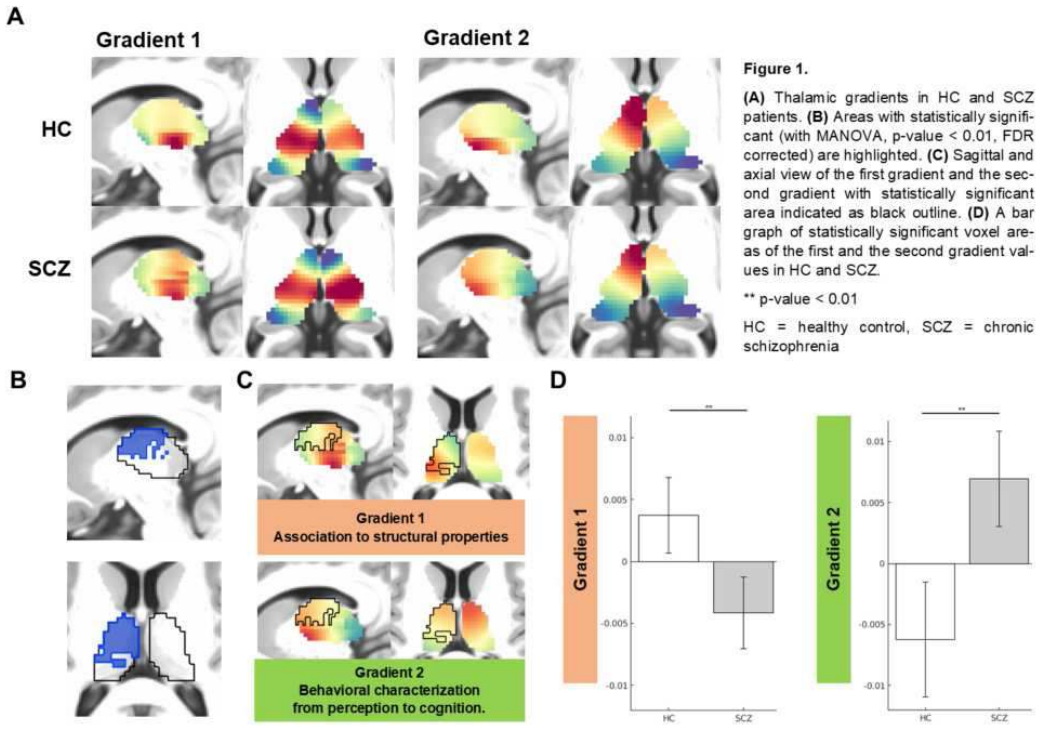

Figure 1.

(A) Thalamic gradients in HC and SCZ patients. **(B)** Areas with statistically significant (with MANOVA, p-value < 0.01, FDR corrected) are highlighted. **(C)** Sagittal and axial view of the first gradient and the second gradient with statistically significant area indicated as black outline. **(D)** A bar graph of statistically significant voxel areas of the first and the second gradient values in HC and SCZ.

** p-value < 0.01

HC = healthy control, SCZ = chronic schizophrenia

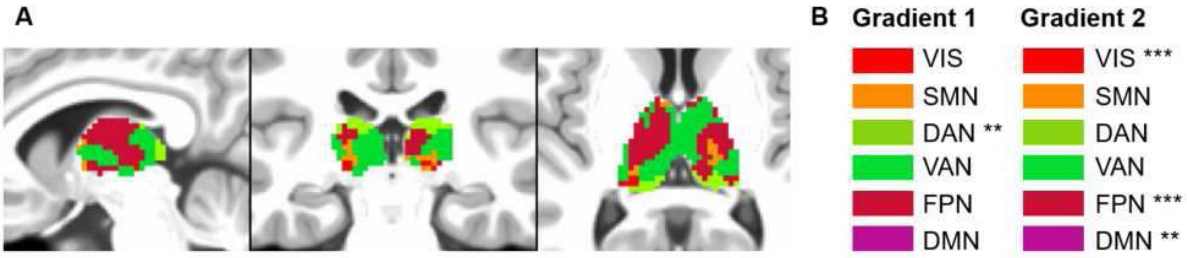

Figure 2. **(A)** Sagittal, coronal, axial view of the thalamic functional network atlas created using winner-takes-it-all method from Yeo's 7 functional network atlas and localized thalamus area from Gordon 333 atlas[10].. **(B)** Figure legend showing the 7 functional networks with statistical group difference at individual network levels are highlighted with asterisk.
** p-value < 0.01; *** p-value <0.001 (Bonferroni corrected)

Conclusions: Our result aligns with previous studies demonstrating changes in the 2nd gradient, which is known to reflect the functional hierarchy of thalamocortical connectivity patterns[8,9]. Our findings offer insights into the issues related to sensory to cognition processing proposed in chronic schizophrenia at the level of neuroimaging-informed functional networks.

References

1. Woodward, N. D., Karbasforoushan, H. & Heckers, S., 2012. Thalamocortical dysconnectivity in schizophrenia. The American Journal of Psychiatry, 169(10), pp. 1092-1099.
2. Anticevic, A. et al., 2015. Association of Thalamic Dysconnectivity and Conversion to Psychosis in Youth and Young Adults at Elevated Clinical Risk. JAMA Psychiatry, 72(9), pp. 882-891.
3. Xi, C. et al., 2020. Schizophrenia patients and their healthy siblings share decreased prefronto-thalamic connectivity but not increased sensorimotor-thalamic connectivity. Schizophrenia Research, Volume 222, pp. 354-361.
4. Ramsay, I. S., 2019. An Activation Likelihood Estimate Meta-analysis of Thalamocortical Dysconnectivity in Psychosis. Biological Psychiatry: Cognitive neuroscience and neuroimaging, 4(10), pp. 859-869.
5. Parnaudeau, S., Bolkan, S. S. & Kellendonk, C., 2018. The Mediodorsal Thalamus: An Essential Partner of the Prefrontal Cortex for Cognition. Biological Psychiatry, 82(8), pp. 648-656.
6. Kumar, V. J., Beckmann, C. F., Scheffler, K. & Grodd, W., 2022. Relay and higher-order thalamic nuclei show an intertwined functional association with cortical-networks. Communications Biology, Volume 5, p. 1187.
7. Haak, K. V., Marquand, A. F. & Beckmann, C. F., 2018. Connectopic mapping with resting-state fMRI. NeuroImage, Volume 170, pp. 83-94.
8. Yang, S. et al., 2020. The thalamic functional gradient and its relationship to structural basis and cognitive relevance. NeuroImage, Volume 218, p. 116960.
9. Fan, Y.-S.et al., 2023. Macroscale Thalamic Functional Organization Disturbances and Underlying Core Cytoarchitecture in Early-Onset Schizophrenia. Schizophrenia Bulletin, 49(5), p. 1375–1386.
10. Gordon, E. M. et al., 2016. Generation and Evaluation of a Cortical Area Parcellation from Resting-State Correlations. Cerebral Cortex, 26(1), p. 288–303.

Poster No 570

Multisite Tractometry Study Reveals Microstructural Abnormalities Along Tracts in Bipolar Disorder

Leila Nabulsi[1], Bramsh Chandio[1], Genevieve McPhilemy[2], Fiona Martyn[2], Gloria Roberts[3], Brian Hallahan[2], Udo Dannlowski[4], Tilo Kircher[5], Benno Haarman[6], Philip Mitchell[3], Colm McDonald[2], Dara Cannon[2], Ole Andreassen[7], Christopher Ching[8], Paul Thompson[9], ENIGMA Bipolar Disorder Working Group[1]

[1]University of Southern California, Los Angeles, CA, [2]University of Galway, Galway, Galway, [3]Discipline of Psychiatry and Mental Health, University of New South Wales, Sydney, New South Wales, Sydney, New South Wales, [4]Institute for Translational Psychiatry, Münster, North Rhine Westphalia, [5]Department of Psychiatry and Psychotherapy, University of Marburg, Marburg, Hesse, [6]Department of Psychiatry, University Medical Center Groningen, University of Groningen, Groningen, Groningen, Groningen, [7]NORMENT, Oslo, Norway, [8]Imaging Genetics Center, Mark and Mary Stevens Neuroimaging & Informatics Institute, USC, Los Angeles, CA, [9]Imaging Genetics Center, Keck School of Medicine of University of Southern California, Los Angeles, CA

Introduction: Methods to more finely map the brain circuitry alterations associated with bipolar disorder (BD) hold promise for identifying new potential biomarkers that could one day support more impactful treatments for BD and related mental illness. Prior diffusion MRI studies have reported subtle abnormalities in the brain's white matter (WM) microstructure by analyzing data within specific regions of interest (Favre 2019). However, there is a need for a more detailed 3D spatial assessment of microstructural differences along WM tracts in BD. A significant advancement would involve integrating tractometry data from multiple scanning sites to better detect subtle effects and improve replication of findings across larger international datasets. In this multisite study using diffusion MRI tractometry, we applied the BUndle ANalytics (BUAN) method (Chandio 2020), which offers a sophisticated analytic approach to tractography. BUAN enables the extraction and mapping of fiber bundles, facilitating the detection and visualization of microstructural irregularities across 3D representations of fiber tracts.

Methods: Diffusion-weighted 3D brain MRI scans of 148 participants diagnosed with BD (age: 36.8+13.5 y) and 259 psychiatrically-healthy controls (age: 37.7+13.7 y), were drawn from 6 independent scanning sites. Scans were corrected for subject motion and eddy-current distortions (Leemans 2009). Deterministic (non-tensor) constrained spherical deconvolution (CSD) was used to account for crossing fibers within voxels (Jeurissen 2014; ExploreDTI), and fractional anisotropy (FA) was calculated at each voxel. Individual whole-brain tractograms underwent streamline-based registration to a bundle atlas template in MNI space (Yeh 2018). Bundle extraction was performed using the auto-calibrated version of RecoBundles and a standard WM tract atlas (Yeh 2018; Chandio 2020). A tract profile for each extracted bundle was generated using the BUAN software package, whereby each profile consisted of 100 segments per subject (Chandio 2020). By treating variations across scanning sites and imaging protocols as random effects, we investigated microstructural abnormalities along WM tracts between BD and controls.

Results: Significant differences between BD and controls were detected in mean FA across several WM tracts (F1). Lower FA values were detected in fronto-limbic, interhemispheric, and posterior pathways in the BD group relative to controls; specifically, in localized regions of the cingulum and the fornix, and in regions within the corpus callosum (middle portion and forceps minor) and the fronto-parietal tract. Several long-range intra-hemispheric WM tracts exhibited lower FA in BD compared to controls in localized segments – specifically, in the extreme capsule, the arcuate, uncinate, inferior-fronto occipital, medial- and middle-longitudinal fasciculi. Higher FA was observed in posterior bundles in BD relative to controls. The incremental inclusion of additional sites progressively enhanced the detection of group differences, as revealed by quantile-quantile plots.

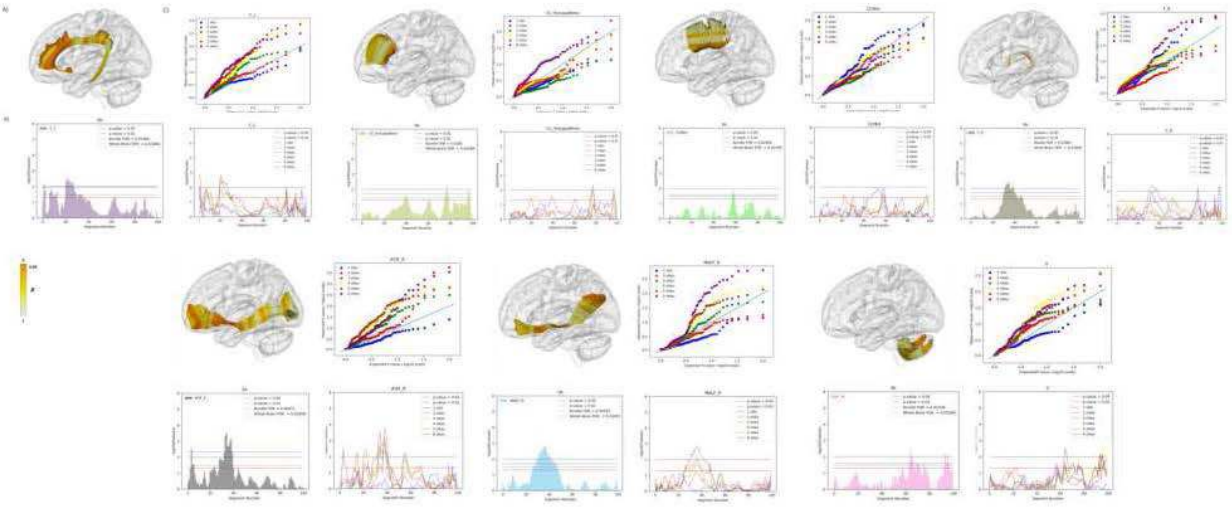

Figure 1. Along-tract microstructure (FA) alterations localized in BD. Compared to healthy controls, participants with BD exhibited altered FA in several bundles. Some are depicted here: C=cingulum; CC=corpus callosum; F=fornix; IFOF=inferior fronto-occipital fasciculus; MdLF=medial longitudinal fasciculus; V=vermis; L=left; R=right; Mid=middle; FA=fractional anisotropy. A) Significant p-values are shown in dark orange on each bundle. B) In each main plot, on the x-axis, segments along the length of the tract are shown and the y-axis shows the negative logarithm of the p-values. P-values between or above the two horizontal lines on the plot imply nominally significant (uncorrected) group differences at that location along the tract. The FDR adjusted threshold is plotted in blue; the whole-brain FDR threshold for each tract is plotted in green. The QQ plots in C) show that adding sites generally boosts the significance, for tracts where effects are identified.

Conclusions: Using an advanced along-tract analytic method, we conducted fine-scale spatial mapping of regional WM microstructure differences in BD, relative to controls, integrating data across sites in the largest such study to date. By integrating tractography and anatomical information, BUAN captured unique effects along WM tracts, offering more anatomical specificity than region-of-interest based analyses, and providing valuable insights into anatomical variations that may assist in disease classification. The tracts implicated here connect regions with important functional roles in the regulation of emotions, motivation, decision-making, and cognitive control, all impaired in BD. Effect sizes for each tract increased with the incremental inclusion of more samples. These findings advance our understanding of the neural underpinnings of BD and offer valuable leads for refining disease classification frameworks.

References

1. Chandio, B.Q. et al. (2020), 'Bundle analytics, a computational framework for investigating the shapes and profiles of brain pathways across populations', Scientific Reports, vol. 10, no. 17149, pp. 1-18.
2. Favre, P., Pauling, M., Stout, J., Hozer, F., Sarrazin, S., Abé, C., ... & Houenou, J. (2019), 'Widespread white matter microstructural abnormalities in bipolar disorder: evidence from mega-and meta-analyses across 3033 individuals', Neuropsychopharmacology, vol. 44, no. 13, pp. 2285-229.
3. Jeurissen, B., Tournier, J. D., Dhollander, T., Connelly, A., & Sijbers, J. (2014), 'Multi-tissue constrained spherical deconvolution for improved analysis of multi-shell diffusion MRI data', NeuroImage, vol. 103, pp. 411-426.
4. Leemans, A., Jeurissen, B., Sijbers, J., & Jones, D. K. (2009), 'ExploreDTI: a graphical toolbox for processing, analyzing, and visualizing diffusion MR data', Proc Intl Soc Mag Reson Med, Vol. 17, no. 1, p. 3537.
5. Tournier, J. D., Calamante, F., & Connelly, A. (2007), 'Robust determination of the fibre orientation distribution in diffusion MRI: non-negativity constrained super-resolved spherical deconvolution', NeuroImage, vol. 35, no. 4, pp. 1459-1472.
6. Yeh, F-C. (2018), 'Population-averaged atlas of the macroscale human structural connectome and its network topology', NeuroImage, vol. 178, pp. 57-68.

Poster No 571

Predictors of Conversion to Psychosis also Predict Transition to High Risk: An ABCD Study Analysis

Jason Smucny[1], Avery Wood[2], Ian Davidson[2], Cameron Carter[3]

[1]University of California, Davis, Sacramento, CA, [2]University of California Davis, Sacramento, CA, [3]University of California Irvine, Irvine, CA

Introduction: Previous work has identified a set of risk factors that significantly predict conversion to psychosis in adolescents at clinical high risk (CHR) for the disorder (Cannon et al. 2016). It is unknown, however, if these same factors also predict transition to a high risk state in preteens aged 12-13.

Methods: A logistic regression (LR) model was used to fit a binary CHR outcome, defined as having a highest distress score ≥2 on any Prodromal Questionnaire-Brief Child (PQ-BC) version (Karcher et al. 2018) question at Adolescent Brain and Cognitive

Development (ABCD) study (https://abcd.org) year 4 (with concurrent distress scores <2 at year 3). Features included age, having a first-degree relative with psychosis, Rey Auditory Verbal Learning Test (RAVLT) n correct trials, NIH Toolbox Pattern Recognition test raw score, n negative life events, n trauma types, and showing a significant drop in grades from the previous year. Site-adjusted overall fractional anisotropy (FA), diffusivity, and cortical thickness were included as MRI predictors in a separate model.

Results: 5237 children were included in analyses. The LR model was significant (p<.001, R2=.042) with 65% accuracy (67% of non-"transitioners" and 52% of transitioners). Including MRI features improved LR model fit (R2 = .051) but not accuracy (65%) with FA and cortical thickness being significant predictors. Machine learning (xgboost with random forest) using all features improved accuracy to 82% (85% of non-transitioners and 52% of transitioners).

Conclusions: These findings suggest that factors previously shown to predict conversion to psychosis in CHRs may also predict transition to a pseudo-CHR state in preteens. Model prediction may be enhanced by incorporating MRI-based features and using machine learning.

References

1. Cannon T.D. (2016). An Individualized Risk Calculator for Research in Prodromal Psychosis. American Journal of Psychiatry vol. 173, no 10, pp. 980-988.
2. Karcher N.R. (2018). Assessment of the Prodromal Questionnaire–Brief Child Version for Measurement of Self-reported Psychoticlike Experiences in Childhood. JAMA Psychiatry vol. 75, no. 8, pp. 853-861.

Poster No 572

The structural connectivity provides the underlying configuration for multiple disorders

Weiyang Shi[1,2], Zhenwei Dong[1,3], Ming Song[1], Yu Zhang[2], Tianzi Jiang[1,2,3]

[1]Brainnetome Center, Institute of Automation, Chinese Academy of Sciences, Beijing, China, [2]Research Center for Augmented Intelligence, Zhejiang Lab, Hangzhou, China, [3]School of Artificial Intelligence, University of Chinese Academy of Sciences, Beijing, China

Introduction: The structural connectivity (SC) has been thought to have intricate relationships with abnormal patterns of multiple brain disorders (Hansen et al., 2022a). Describing these relationships to uncover underlying principles and utilizing it to gain new insights into these diseases has been a focal point of research in this field. In this study, we introduce the spectral energy to valid the intrinsic coupling between the abnormal cortical patterns of multiple disorders and SC. Furthermore, by employing the network control theory (Parkes et al., 2023), we emphasize the SC informed relationships between neurotransmitter receptors/transporters and disorders.

Methods: The group average SC and the statistical pathological maps (effect sizes for case-control differences, Cohen's d) of cortical thickness for eight disorders were obtained from ENIGMA Toolbox (Larivière et al., 2021) which are mapped to DK atlas with 68 cortical ROIs. The density maps of 19 neurotransmitter receptors/transporters, estimated using PET images collected across several studies, were extracted from neuromaps (Markello et al., 2022; Hansen et al., 2022b). To quantify the relationship between specific signal pattern x (representing an abnormal map associated with a disorder) and SC, we introduced the concept of SC-spectral energy. A smaller spectral energy value indicates a stronger coupling between the signal x and the SC architecture (Fig. 1A). To further investigate the SC-informed relationships between receptors and disorders, we considered the density maps of receptors as a priori variables and utilized the network control theory (Parkes et al., 2023; Luppi et al., 2023) to calculate the transition energy from the healthy state to the disorder patterns (Fig. 1B). The spin tests (Váša et al., 2018) were used to performed statistical tests cross this study.

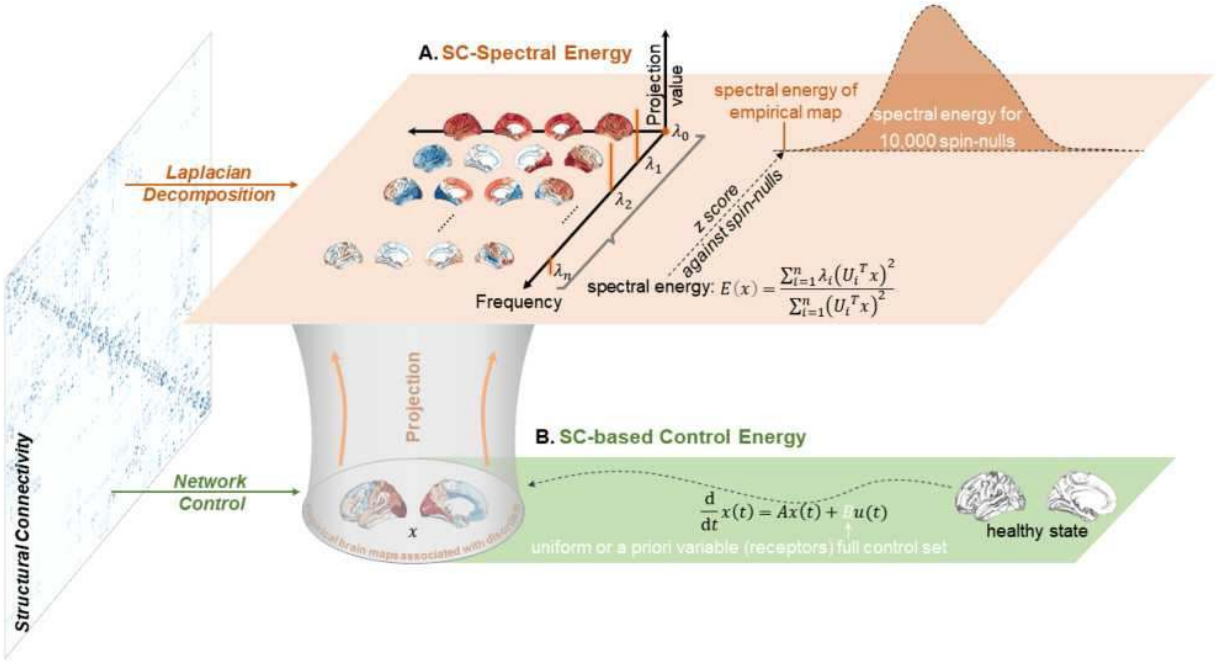

Figure 1. The framework for investigating the relationships between disorder-associated cortical thickness abnormal patterns and SC. A. SC-spectral energy. The SC-spectral energy of a specific signal x is the sum of the frequency-specific harmonic energy λ_i weighted by the projection coefficient of the signal in corresponding harmonic of the SC, i.e., $(U_i^T x)^2$. Here, the harmonic U_i and its corresponding energy λ_i represent the i-th minimum eigenvalue and the corresponding eigenvector of the Laplacian matrix of SC. **B. SC-based network control energy.** This calculates the accumulated energy u required for the transition from the healthy state to different disorder states. Using a uniform full control set *B*, we evaluate the relationship between SC-spectral energy and network control energy across disorders. Additionally, by utilizing the distribution maps of different receptors as a priori to set the control set, we examine the SC-informed relationships between receptors and disorders. The matrix *A* in the figure represents the adjacent matrix, which in this context represents the SC.

Results: To evaluate the coupling between SC and the abnormal patterns of cortical thickness for eight brain disorders (see Fig. 2A for details), we calculated the SC-spectral energy of these patterns (Fig. 2B), respectively. The spectral energy of the diseases suggests a significant coupling between these abnormal spatial patterns and the white matter topological network of brain (p_spin< 0.05, FDR corrected), except for epilepsy, which demonstrated a trend with p=0.051. Based on network control theory, we further estimated the network control energy (NCE) required for transitions from the healthy state to the 8 disorder patterns, respectively. The NCE showed a significant correlation with the SC- spectral energy across disorders, with a Spearman's correlation coefficient of ρ=1.0 (Fig. 2B). By considering the 19 neurotransmitter receptors/transporters as a priori distributions for the control set, we evaluated the NCE required by each disorder when using empirical receptor maps (Fig. 2D) and compared these values to their respective null surrogates (Fig. 2E). The NCE required for a specific disorder under the setting of control set with specific receptor was observed to be lower than its corresponding null spins, suggesting that this receptor contributes to the emergence of the abnormal pattern through SC, such as D1 to MDD, D2 to SZ, and so on (blue pairs in Fig. 2E with p_spin< 0.05, uncorrected). Conversely, higher NCE requirements indicate that the corresponding receptor may potentially counteract specific disease patterns through SC (red pairs in Fig. 2E with p_spin< 0.05, uncorrected).

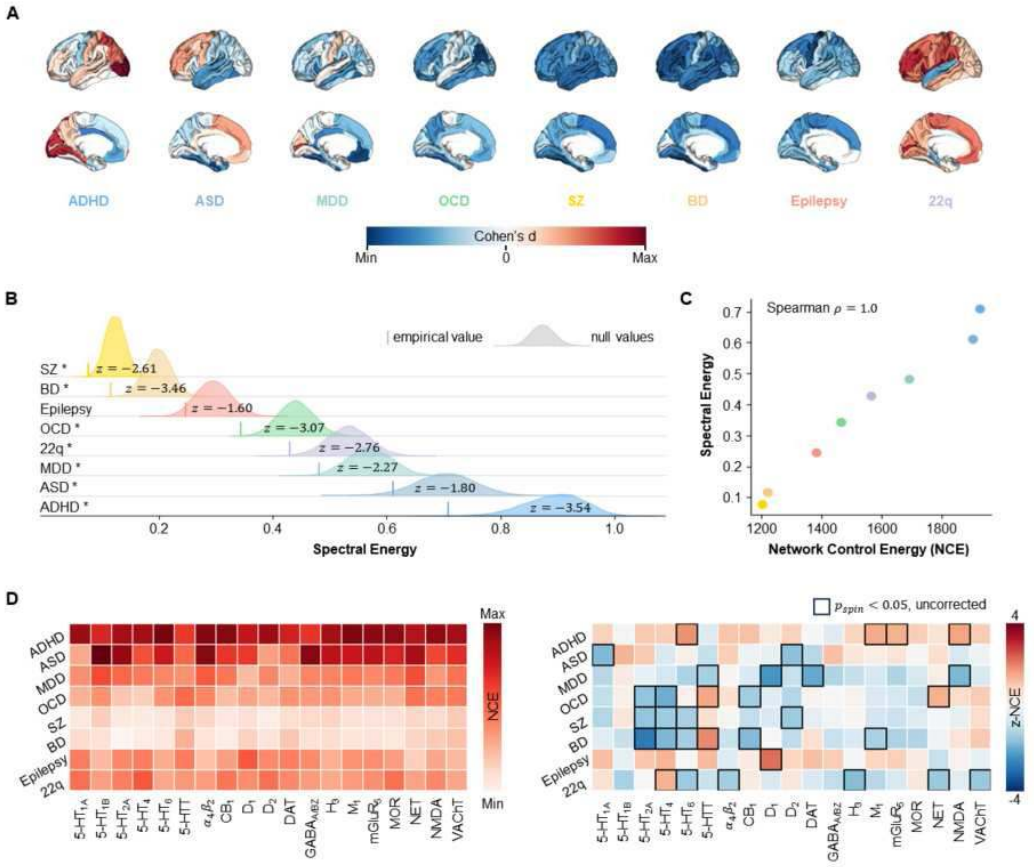

Figure 2. SC provides the substrate for various disorders. A. Abnormal cortical thickness patterns for eight disorders. From left to right: abnormal patterns of attention deficit hyperactivity disorder (ADHD), autism spectrum disorder (ASD), Major depressive disorder (MDD), obsessive-compulsive disorder (OCD), Schizophrenia (SZ), bipolar disorder (BD), Epilepsy, and 22q11.2 deletion syndrome (22q). **B. The SC-spectral energy for each disorder.** Seven out of eight disorders exhibit coupling with SC. * indicates statistical significance ($p_{spin} < 0.05$ after FDR correction). **C. Correlation between SC-spectral energy and SC based network control energy (NCE) across the eight disorders.** The SC-spectral energy shows a significant correlation with NCE (uniform full control set) with Spearman's correlation coefficient of $\rho = 1.0$. **D. SC-informed relationship between disorders and neurotransmitter receptors/transporters.** Left: NCE required for transition from the healthy state to a disorder state using different a priori receptors/transporters density maps for the control set. Right: The standardized NCE score for each disorder-receptor/transporter pair relative to setting the distribution of the control set with spin nulls of the corresponding receptor/transporter density map.

Conclusions: This study provides a novel perspective on characterizing the coupling between disease-related brain abnormal patterns and SC using a novel spectral energy approach. By emphasizing the relationship between diseases and receptors bridged by SC, rather than relying solely on spatial correlations, the study also highlights the significance of utilizing brain's structural topological organization to better understand brain diseases and develop effective therapeutic interventions.

References

1. Hansen, J.Y. (2022a), 'Local molecular and global connectomic contributions to cross-disorder cortical abnormalities', Nature Communications, 13(1), p. 4682.
2. Hansen, J.Y. (2022b), 'Mapping neurotransmitter systems to the structural and functional organization of the human neocortex', Nature Neuroscience, 25(11), pp. 1569–1581.
3. Larivière, S. (2021), 'The ENIGMA Toolbox: multiscale neural contextualization of multisite neuroimaging datasets', Nature Methods, 18(7), pp. 698–700.
4. Luppi, A.I. (2023), 'Transitions between cognitive topographies: contributions of network structure, neuromodulation, and disease'. bioRxiv, p. 2023.03.16.532981.
5. Markello, R.D. (2022), 'Neuromaps: structural and functional interpretation of brain maps', Nature Methods, 19(11), pp. 1472–1479.
6. Parkes, L. (2023), 'Using network control theory to study the dynamics of the structural connectome', bioRxiv: The Preprint Server for Biology, p. 2023.08.23.554519.
7. Váša, F. (2018), 'Adolescent Tuning of Association Cortex in Human Structural Brain Networks', Cerebral Cortex, 28(1), pp. 281–294.

Poster No 573

Diffusion-based brain correlates of adolescent resilience

Tiffany Ngan[1], Benjamin Sipes[1], Angela Jakary[1], Tara Samson[1], Yi Li[1], Eva Henje[2], Tony Yang[1], Olga Tymofiyeva[1]

[1]University of California, San Francisco, San Francisco, CA, [2]University of Umeå, Umeå

Introduction: Adolescent mental health has been an important growing concern over the past several years, especially following large post-COVID-19 increases in anxiety and depression[1]. Elucidating the neural correlates of mental wellbeing has become even more crucial, and resilience, described as "the ability to cope effectively and adapt in the face of loss, hardship or adversity"[2], has been established as a protective factor against mental illness[3]. However, structural and functional neuroimaging findings and approaches to operationalize resilience have been varied[4]. In this study we investigated two brain regions that have previously been associated with measures of resilience, the anterior cingulate cortex (ACC) and the insula, using a myelin-dependent node strength metric derived from DTI connectomics. We first hypothesized that resilience would be negatively associated with depression. We also hypothesized that trait resilience would be associated with node strengths of the ACC and the insula.

Methods: Healthy adolescents 14-18 years old (N=56 [42 female], mean age=16.16 years, SD=1.33 years) were recruited as a part of our research team's ongoing NIH-funded BrainChange study. Participants did not have any prior psychiatric diagnoses. Resilience was measured using the Connor-Davidson Resilience 10-item scale (CD-RISC, score range 0-40). Depression was measured using the Reynolds Adolescent Depression Scale-2 (RADS-2, score range 30-120). MRI data was acquired using a 3T GE MRI scanner at UCSF's Mission Bay campus. The scan included a T1-weighted sequence and a DTI sequence with 30 directions. The node strength was calculated as the sum of the connections from the hypothesized region to all other brain regions weighted by the average fractional anisotropy (FA) along the tractography streamlines[5].

Results: Trait resilience and depression were negatively correlated (r=-0.33, p=0.01, Figure 1). We also found that ACC and insula node strength were positively correlated (r=0.27, p=0.04). Trait resilience was negatively correlated to node strength of the ACC (r=-0.34, p=0.01). No significant correlations were observed for the insula. We did not correct for multiple comparisons due to the exploratory nature of this project.

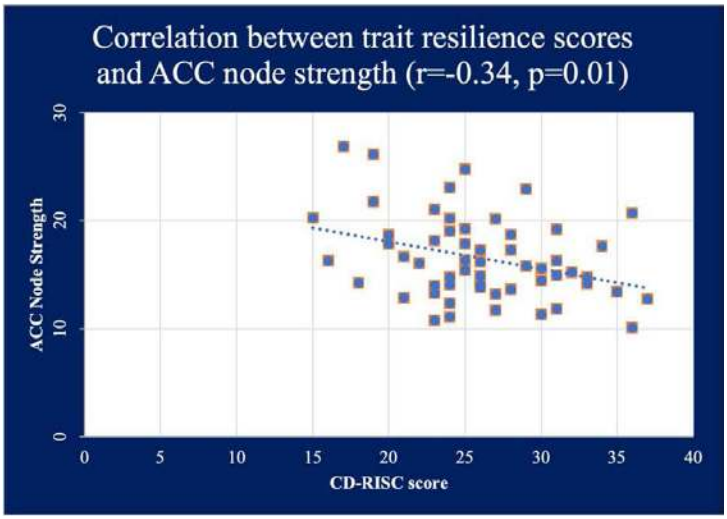

Conclusions: Our hypothesis that resilience would be negatively correlated with depression was confirmed, as was our hypothesis that resilience would be correlated with ACC node strength. This indicates that there are fewer and weaker connections to the ACC in individuals high in resilience, supporting it as a region of interest. The ACC is most functionally connected to areas implicated in both top-down and bottom-up emotion regulation[6], so our findings align with prior research showing that brain regions active in resilient individuals recruit areas implicated in emotional flexibility[7]. Existing literature has been mixed regarding whether or not higher activation in the ACC is indicative of higher or lower psychopathology, although this generally varies depending on which subregion of the ACC is being studied, as well as the type of mental health disorder. Previous research has found higher activation in the subgenual ACC in individuals diagnosed with major depressive disorder[8], which, given that we found more and stronger connections to the ACC in those lower in resilience, could indicate that the subgenual ACC is the driving force behind our observed results. Additionally, the positive relationship between ACC and insula node strength could reflect the involvement of the development of the salience network[9] in adolescent resilience. Future directions include determining which subregions within the ACC contributed to our findings, as well as exploring other imaging metrics (e.g. resting state functional connectivity measures) to facilitate comparison to existing literature on resilience.

References
1. Block, J., & Kremen, A. M. (1996). IQ and ego-resiliency: conceptual and empirical connections and separateness. Journal of personality and social psychology, 70(2), 349.
2. Connolly, C. G., Wu, J., Ho, T. C., Hoeft, F., Wolkowitz, O., Eisendrath, S., ... & Yang, T. T. (2013). Resting-state functional connectivity of subgenual anterior cingulate cortex in depressed adolescents. Biological psychiatry, 74(12), 898-907.
3. Mesman E, Vreeker A, Hillegers M. Resilience and mental health in children and adolescents: an update of the recent literature and future directions. Current Opinion in Psychiatry. 2021 Nov 1;34(6):586-592. doi: 10.1097/YCO.0000000000000741. PMID: 34433193; PMCID: PMC8500371.
4. Panchal, U., Salazar de Pablo, G., Franco, M. et al. The impact of COVID-19 lockdown on child and adolescent mental health: systematic review. European Child & Adolescent Psychiatry 32, 1151–1177 (2023). https://doi.org/10.1007/s00787-021-01856-w
5. Rubinov M, Sporns O. Complex Network Measures of Brain Connectivity: Uses and Interpretations. NeuroImage 52(3):1059–1069. 2010.
6. Seeley, W. W. (2019). The salience network: a neural system for perceiving and responding to homeostatic demands. Journal of Neuroscience, 39(50), 9878-9882.
7. Stevens, F. L., Hurley, R. A., & Taber, K. H. (2011). Anterior cingulate cortex: unique role in cognition and emotion. The Journal of neuropsychiatry and clinical neurosciences, 23(2), 121-125.
8. Waugh, C. E., Wager, T. D., Fredrickson, B. L., Noll, D. C., & Taylor, S. F. (2008). The neural correlates of trait resilience when anticipating and recovering from threat. Social cognitive and affective neuroscience, 3(4), 322-332.
9. Zhang, L., Rakesh, D., Cropley, V., & Whittle, S. (2023). Neurobiological correlates of resilience during childhood and adolescence–A systematic review. Clinical Psychology Review, 102333.

Poster No 574

Reduced cortical thickness in behavioral addictions

Hongsheng Xie[1,2], Fei Zhu[2,3], Qiyong Gong[2,3], Zhiyun Jia[1,2]

[1]Department of Nuclear Medicine, Sichuan University West China Hospital, Chengdu, China, [2]Research Unit of Psychoradiology, Chinese Academy of Medical Sciences, Chengdu, China, [3]Department of Radiology and Huaxi MR Research Center (HMRRC), Functional and Molecular Imaging Key Laboratory of Sichuan Province, West China Hospital, Sichuan University, Chengdu, China

Introduction: Behavioral addictions (BAs) are disorders similar to substance addiction, which are characterized by excessive and uncontrollable engagement in specific activities instead of a psychoactive drug. BAs include gambling disorder, internet gaming disorder, and smartphone addiction[1]. Individuals with BAs can display a variety of symptoms, including cravings, a lack of control, and withdrawal symptoms. Currently, many neuroimaging studies have found structural brain alterations in BAs, such as decreased grey matter volume in the orbitofrontal cortex (OFC), putamen, and supplementary motor area[2,3]. However, these findings are often not consistent, thus, a meta-analysis is needed to confirm and extend previous findings. This study aimed to investigate the altered cortical thickness (CTh) pattern in BAs. We hypothesized that altered CTh could be found in key brain regions involved in reward, executive, and/or affective function.

Methods: Search strategy and selection criteria This study followed the PRISMA guideline, and the protocol was registered on PROSPERO (CRD42023421271)[4]. We searched five databases (PubMed, Embase, Web of Science, PsychINFO, and CNKI) from inception to May 1, 2023 for CTh studies. The key search words were as follows: (behavioral addiction OR gambling disorder OR internet gaming disorder OR phone addiction) AND (cortical thickness OR surface-based morphometry). More details can be found on PROSPERO. Meta-analyses We used the SDM-PSI to investigate the altered CTh in the BAs group[5]. Briefly, the peak coordinates with t-scores from primary studies were used to create the combined effect-size signed map. A p-value of 0.005 was used to generate significant clusters with peak MNI coordinates[6]. Additionally, meta-regression was conducted to explore the association between addiction severity and CTh alterations. Control analyses Potential sources of heterogeneity were analyzed, including age, male proportion, and education. Reproducibility and publication bias were assessed by Jack-knife sensitivity analysis and Egger's test, respectively[7].

Results: Study characteristics From 415 records, 10 studies with 11 datasets (343 individuals with BAs and 355 HCs) were eventually included (Figure 1). The mean age in the BA group was older (23.65 vs 23.57, $p = 0.03$), but there was no significant difference in sex (0.68 vs 0.65, $p = 0.87$) or education (14.91 vs 15.00, $p = 0.59$) between the two groups. Meta-analyses The BA group showed thinner CTh in the bilateral precuneus/cuneus, right superior occipital gyrus, right postcentral gyrus, right OFC, and left dorsolateral prefrontal cortex (DLPFC, Figure 2, all $p < 0.005$). No thicker regional CTh was found in the BA group. The meta-regression analysis showed that the right postcentral gyrus and precuneus cortex were negatively associated with standard addiction severity (both $p < 0.0005$). Control analyses Age, sex, and education showed no effects on our results. The Jackknife sensitivity analysis showed that all clusters were preserved in most combinations. The DLPFC, OFC, and postcentral gyrus were preserved in 9 out of 11 combinations. The Egger test did not show significant publication bias in all clusters (all $p > 0.05$).

Author (year)	Type	Sex (M/F)		Age (years)		Education (years)		Severity of symptoms		
		Patient	HC	Patient	HC	Patient	HC	Scale	Original score	Standardized score
Wang et al. (2018)	IGD	27/11	37/29	20.7 ± 2.1	21.3 ± 2.0	15.0 ± 1.8	14.4 ± 2.1	IAT	64.4 ± 10.5	64.4 ± 10.5
Wang et al. (2019)	IGD	29/33	37/34	20.9 ± 1.6	21.3 ± 2.1	14.3 ± 2.1	14.6 ± 1.8	IAT	62.9 ± 10.8	62.9 ± 10.8
Wang et al. (2018)	IGD	48/0	32/0	20.6 ± 1.0	21.1 ± 2.2	14.5 ± 0.9	15.0 ± 2.1	IAT	68.9 ± 8.2	68.9 ± 8.2
Lee et al. (2018)	IGD	45/0	35/0	23.8 ± 1.5	23.4 ± 1.7	NR	NR	IAT	65.8 ± 10.6	65.8 ± 10.6
He et al. (2021)	IGD	20/6	20/6	20.5 ± 2.1	20.7 ± 2.2	NR	NR	NR	NR	NA
Li et al. (2019)	IGD	27/22	27/23	21.9 ± 2.2	22.6 ± 2.0	15.7 ± 2.2	15.6 ± 1.4	IAT	62.2 ± 10.7	62.2 ± 10.7
Liu et al. (2018)	IGD	14/9	14/5	20.8 ± 2.2	21.3 ± 2.0	13.5 ± 2.6	14.1 ± 2.4	IAT	65.0 ± 9.8	65.0 ± 9.8
Hirjak et al. (2022)	SPA	5/14	7/15	21.9 ± 2.9	22.9 ± 3.3	15.1 ± 3.1	15.4 ± 2.5	SPAI	52.8 ± 10.1	50.8 ± 9.7
Bouchard et al. (2021)	GD	9/8	NR	41.2 ± 16.7	NR	NR	NR	SOGS	10.1 ± 3.8	50.5 ± 19.0
Grant et al. (2015)	GD	10/6	13/4	47.8 ± 13.7	41.0 ± 14.3	16.9 ± NR	17.2 ± NR	G-SAS	33.6 ± 6.5	70.0 ± 13.5

Abbreviation: GD, Gambling disorder; G-SAS, Gambling Symptom Assessment Scale; IAT, Internet addiction test; IGD, Internet gaming disorder; NA, not available; NR, not reported; SOGS, South Oaks Gambling Screen; SPA, Smartphone addiction; SPAI, Smartphone Addiction Inventory

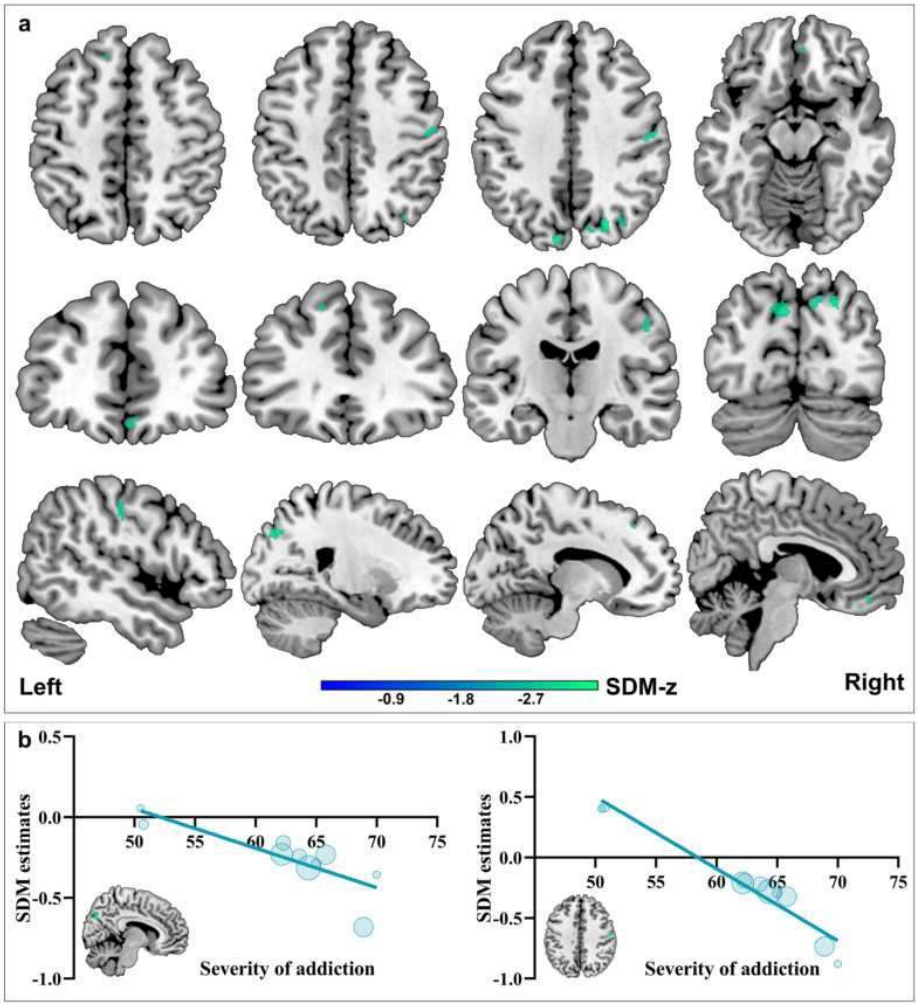

Figure 2. Results of meta-analyses. (a) Thinner cortical thickness (blue–green) was found in the left precuneus (peak MNI = -10, -80, 34), right precuneus (peak MNI = 24, -76, 38), right superior occipital gyrus (peak MNI = 32, -72, 38), right postcentral gyrus (peak MNI = 54, -14, 42), right orbitofrontal cortex (peak MNI = 4, 44, -16), and left dorsolateral prefrontal cortex (peak MNI = -16, 36, 54). **(b)** The right postcentral gyrus (peak MNI = 52, -14, 38) and precuneus cortex (peak MNI = 18, -74, 38) were negatively associated with standard addiction severity.

Conclusions: This meta-analysis investigated the altered CTh pattern in BAs and found reproducible reduced CTh in key brain regions within the default mode, executive control, and sensorimotor networks. More importantly, the CTh of precuneus and postcentral gyrus appear to be associated with the severity of BAs. These findings provide potential support for the addiction model of disruptions in decision-making and self-control[8,9]. In conclusion, our study enhances the understanding of the neurobiological mechanisms underlying BAs and offers valuable insights into strategies for recovery from and prevention of BAs.

References
1. American Psychiatric Association (2013), 'Diagnostic and statistical manual for mental disorders-5', American Psychiatric Association.
2. Solly JE, Hook RW, Grant JE, et al., (2022), 'Structural grey matter differences in Problematic Usage of the Internet: a systematic review and meta-analysis', Molecular Psychiatry, vol. 27, no. 2, pp. 1000-1009
3. Clark L, Boileau I, Zack M, (2019), 'Neuroimaging of reward mechanisms in Gambling disorder: an integrative review', Mol Psychiatry, vol. 24, no. 5, pp. 674-693
4. Moher D, Liberati A, Tetzlaff J, et al., (2009), 'Preferred reporting items for systematic reviews and meta-analyses: the PRISMA statement', PLoS Med, vol. 6, no. 7, pp. e1000097
5. Radua J, Rubia K, Canales-Rodríguez EJ, et al., (2014), 'Anisotropic kernels for coordinate-based meta-analyses of neuroimaging studies', Front Psychiatry, vol. 5, no. pp. 13
6. Radua J, Mataix-Cols D, Phillips ML, et al., (2012), 'A new meta-analytic method for neuroimaging studies that combines reported peak coordinates and statistical parametric maps', European Psychiatry, vol. 27, no. 8, pp. 605-611
7. Egger M, Smith GD, Schneider M, et al., (1997), 'Bias in meta-analysis detected by a simple, graphical test', BMJ, vol. 315, no. 7109, pp. 629
8. Volkow ND, Koob GF, McLellan AT, (2016), 'Neurobiologic Advances from the Brain Disease Model of Addiction', N Engl J Med, vol. 374, no. 4, pp. 363-371
9. Groman SM, Massi B, Mathias SR, et al., (2019), 'Model-Free and Model-Based Influences in Addiction-Related Behaviors', Biol Psychiatry, vol. 85, no. 11, pp. 936-945

Poster No 575

Cognition-related connectome gradient dysfunctions in first-episode major depressive disorder

Qian Zhang[1], Aoxiang Zhang[2], Youjin Zhao[2], Qiyong Gong[3]

[1]Huaxi MR Research Center (HMRRC), Department of Radiology, West China Hospital of Sichuan University, Chengdu, [2]Huaxi MR Research Center (HMRRC), Department of Radiology, West China Hospital of Sichuan University, Chengdu, China, [3]Huaxi MR Research Center, Chengdu, China

Introduction: Functional abnormalities in subcortical networks are believed to be implicated in pathophysiology of clinical symptoms and cognitive impairments in patients with major depressive disorder (MDD)[1]. While significant progress has been made in characterizing discrete large-scale functional network alterations in MDD patients, the continuous spatial patterns of inter-region connectivity, especially alterations in subcortical function, remain less well-understood. By introducing functional gradient mapping, a novel approach to depict spatial organization of brain function by capturing patterns of functional connectivity similarity[2], the present study evaluated subcortical gradients in MDD patients and their association with cognitive features.

Methods: Utilizing functional gradient mapping approach, we investigated the organization patterns and between-group differences in the principal subcortical gradient in 145 never-treated first-episode MDD patients and 145 healthy controls (HCs) across all subcortical voxels (global), three main systems (limbic, thalamic, and basal ganglia), subcortical structural subregions, and functional subregions related to different cortical functional networks. The degree of connectivity similarity and the relative spatial position of each subcortical regions along the principal gradient were represented by principal gradient values[3]. We also examined the associations of significant gradient alterations with clinical and cognitive features of MDD patients and HCs, as well as the spatial and functional connectivity measurements. All reported P values were FDR corrected.

Results: Overall, MDD patients showed a relatively compressed and disturbed gradient organization than HCs, with limbic and BG regions located at both ends ((K-S stat=0.06, P<0.001, Fig. 1a). Specifically, MDD patients had lower principal gradient values in thalamus (t=-5.972, P<0.001) and limbic system (t=-15.916, P<0.001) but higher values in BG (t=15.121, P<0.001) than HCs (Fig. 1a). These gradient alterations manifested as spatial rearrangements of gradient values within each respective structural (Fig. 1a) and functional (Fig. 1b) subregions, which were further associated with intrinsic Euclidian distance (r=-0.204, P<0.001) and functional connectivity patterns (r=0.413, P<0.001) (Fig. 2a). Furthermore, lower gradient values in thalamic subregion projecting to default mode network were associated with higher principal gradient values in BG subregion projecting to ventral attention network (r=-0.596, P<0.001), and these gradient alterations were correlated with poorer episodic memory performance in MDD patients (both P<0.05, Fig. 2b).

Figure 1. Principal gradient alterations of the subcortical-cortical functional connectome.

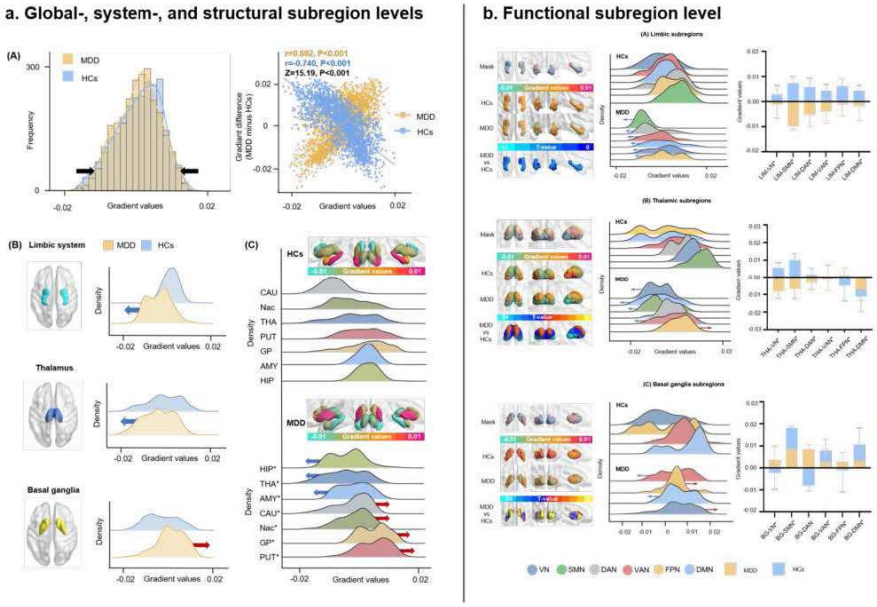

Figure 2. Results of the correlation analyses.

a. Associations between gradient alterations and spatial and functional connectivity measurements

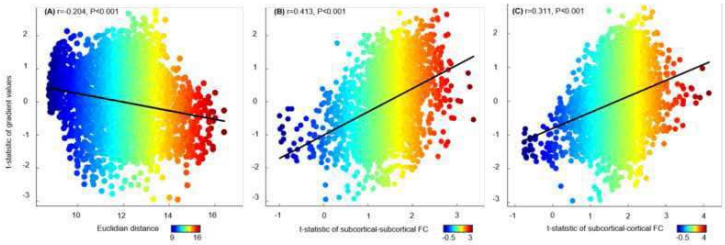

b. Associations between gradient alterations and cognitive features

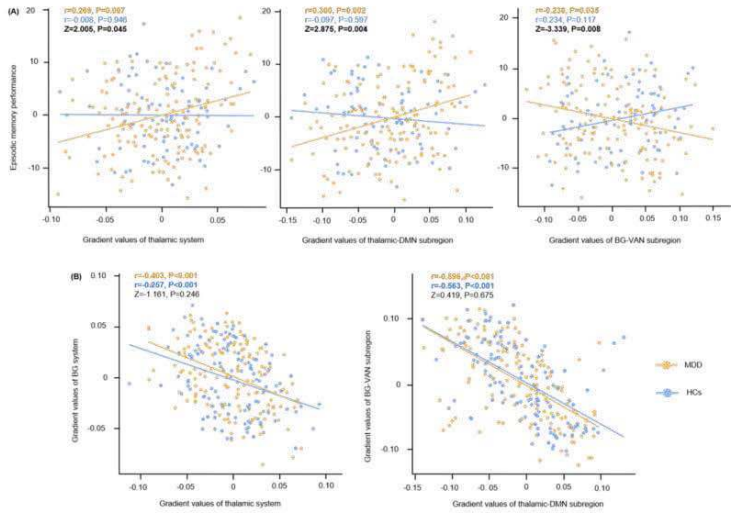

Conclusions: In addition to MDD-related cortical connectome gradient dysfunction revealed by previous study[4], we identified multiscale alterations in both organization and changing patterns of the principal subcortical gradient, which captured spatial disorganizations and functional disturbance of the subcortical-cortical connectome in MDD patients. Notably, opposing gradient alterations in thalamic and BG regions synergistically impact the episodic memory performance in MDD patients, reflecting the neuropathological mechanisms implicated in memory processing. Collectively, our findings revealed an internally differentiated and clinically relevant pattern of subcortical gradient dysfunction in MDD, which enhanced our understanding of MDD-related hierarchical disturbances in subcortical function and may provide potential neuro-biomarkers for cognitive impairments in MDD.

References
1. Mulders, P.C. (2015), 'Resting-state functional connectivity in major depressive disorder: A review', Neuroscience and Biobehavioral Reviews, vol. 56, pp. 330-344.
2. Vos de Wael, R. (2020), 'BrainSpace: a toolbox for the analysis of macroscale gradients in neuroimaging and connectomics datasets', Communications Biology, vol. 3, no.1, pp. 103.
3. Huntenburg, J.M. (2018), 'Large-Scale Gradients in Human Cortical Organization', Trends in Cognitive Sciences, vol. 22, no. 1, pp. 21-31.
4. Xia, M. (2022), 'Connectome gradient dysfunction in major depression and its association with gene expression profiles and treatment outcomes', Molecular Psychiatry, vol. 27, no. 3, pp. 1384-1393.

Poster No 576

The Gender-specific Brain Functional Activation Patterns in Bipolar Depression with Anhedonia

Xiaoqin Wang[1], Yi Xia[1], Rui Yan[1], Hao Sun[1], Yinghong Huang[1], Qing Lu[2], Zhijian Yao[1]

[1]The Affiliated Brain Hospital of Nanjing Medical University, Nanjing, Jiangsu, [2]Southeast University, Nanjing, Jiangsu

Introduction: As a cross-diagnostic symptom, anhedonia is found in depression states of major depressive disorder and bipolar disorder, as well as other disorders. More than half of patients with bipolar depression (BD) suffer from anhedonia. The application of neuroimaging techniques in psychiatric disorders helps us understand the neural mechanism of anhedonia symptoms in BD patients. Although the conclusion is not entirely consistent, the dysfunction of the reward-related regions in BD has been widely described. However, past studies about anhedonia symptoms in BD ignored the unique role of gender on the reward-related regions. Past preclincal evidence points to an important role for gender in reward-related regions. In this study, the role of sex differences in the reward circuit was considered when investigating the brain's functional characteristics in bipolar disorder with anhedonia symptoms. We aim to explore the sex differences in regional brain neuroimaging activity features in BD patients with high anhedonia symptoms. We proposed that neural functional characteristics in patients with BD and anhedonia symptoms may be sexually dimorphic.

Methods: The resting-fMRI by applying fractional amplitude of low-frequency fluctuation (fALFF) method was estimated in 263 patients with BD (174 high anhedonia [HA], 89 low anhedonia [LA]) and 213 healthy controls (HC). To parse out the effects of sex and anhedonia to patients with BD, we entered all of the voxel-based comparisons of the whole brain into a 3 (HA, LA, HC) × 2 (male, female) analysis of variance (ANOVA) model in the Statistical Parametric Mapping (SPM12) software

Results: Regarding the group effect (HA, LA, HC), the fALFF values were significantly difference in the right superior temporal pole, left inferior occipital gyrus, right STG, right SFG pars orbital, right precuneus, left angular, right middle cingulum gyrus (MCG), left supplementary motor area (SMA), left middle frontal gyrus (MFG). A simple post-hoc analysis shows that the fALFF values of right MCG and left SMA ($p < 0.001$, FDR corrected) were significantly higher in the HA group than in LA. In terms of the sex effect (male, female), the fALFF values were significantly difference in the left insula, right rolandic operculum, right right superior temporal gyrus (STG), left calcarine, left medial superior frontal gyrus (SFG) and right SMA. For the sex-by-group interaction, there were significant differences in the fALFF values among the six groups in the right hippocampus, left medial occipital gyrus, right insula and bilateral MCG. A simple post-hoc analysis shows that the fALFF values of all these regions were significantly higher in the HA group than LA in males ($p < 0.001$, FDR corrected). The fALFF values of the right hippocampus ($p < 0.001$, FDR corrected) were significantly lower in the HA group than LA in females.

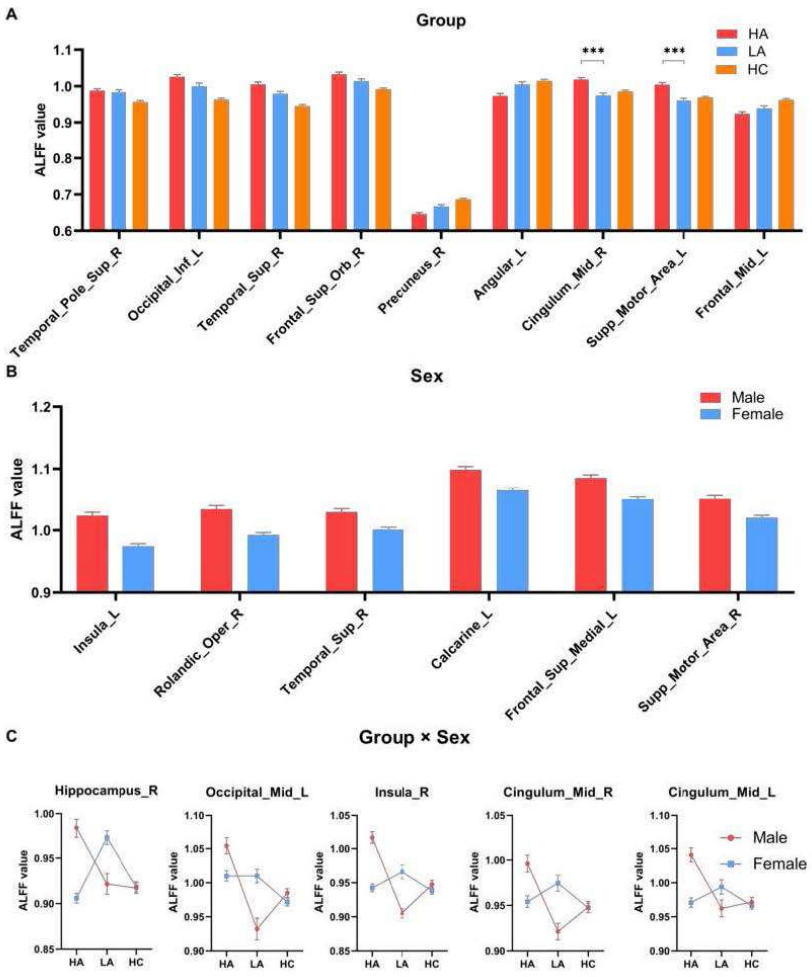

Conclusions: These results suggested that the pattern of high activation could be a marker of anhedonia symptom in male BD, and the sex differences should be considered in future studies of BD with anhedonia symptoms.

Poster No 577

Neurotransmitter-related interhemispheric disconnectivity in depression with and without anxiety

Wen Zhu[1], Huaijin Gao[1], Rui Qian[1], Chengjiaao Liao[1], Dan Wu[1], Zhiyong Zhao[1]

[1]Zhejiang University, Hangzhou, China

Introduction: Anxiety exacerbates major depressive disorder (MDD), leading to adverse outcomes such as lower socioeconomic status and impaired adaptive functioning[1]. Prior studies have reported alterations in interhemispheric functional connectivity in MDD[2], but the impact of post-depression anxiety on this connectivity remains unexplored so far. Moreover, recent evidence indicates that neurotransmitters, such as serotonin (5-HT), norepinephrine (NE) and dopamine (DA), play a pivotal role in the neural mechanisms of depression[3], and show a close association with interhemispheric functional connectivity[4]. Consequently, the primary objective of this study is to examine how depression and anxiety impact interhemispheric functional connectivity and to explore their association with neurotransmitter receptors.

Methods: We screened resting-state fMRI (rs-fMRI) data of MDD patients with anxiety (N = 334) and without anxiety (N = 145) and normal controls (NCs, N = 307) with matched age, sex, education and head motion from the Chinese REST-meta-MDD database. The rs-fMRI images were preprocessed at each site using a standardized DPARSF processing pipeline[5], including slice timing correction, realignment, segmentation, signal regression of white matter and CSF, normalization, smoothing, and filtering (0.01- 0.1Hz). We computed voxel-mirrored homotopic connectivity (VMHC) by calculating the Pearson correlation coefficient between each voxel's residual time series and its symmetrical interhemispheric counterpart, which were then Fisher z-transformed before group-level analysis. Inter-group comparisons used voxel-wise linear mixed models, followed

by Gaussian random field (GRF) correction with voxel-wise p-value < 0.01 and cluster-wise p-value < 0.05. Neurotransmitter receptor density data were obtained from a recent report[6] that collated data from a large number of PET studies involving over 1,200 healthy adults, and it provided the density of 19 unique neurotransmitter receptors and transporters in the Schaefer-100 atlas. Then, normalized density (z-scored) was derived for each of the 19 receptors and transporters across the 100 regions[4]. Finally, we assessed the relationship between VMHC alterations in MDD and neurotransmitter receptor density using Pearson correlation across the 100 regions (FDR correction).

Results: Compared with NCs, non-anxious MDD showed lower VMHC values in posterior cingulate cortex (PCC), while anxious MDD displayed decreased VMHC values in PCC, inferior frontal gyrus (IFG), medial prefrontal cortex (mPFC), middle frontal gyrus (MFG) and parahippocampal gyrus (PHG) (Fig.1). The non-anxious and anxious MDD subgroups did not show significant alterations in the VMHC. Moreover, the VMHC difference between non-anxious MDD and NC group negatively correlated with densities of 5-HT4 receptor, while the VMHC difference between anxious MDD and NC positively correlated with densities of 5-HT2a, H3, M1 and mGluR5 receptors. (Fig.2)

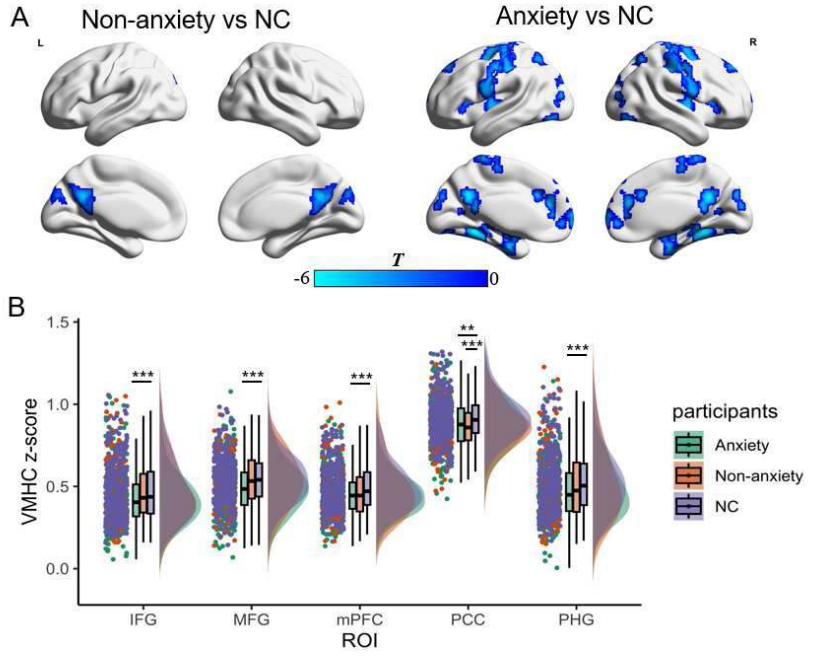

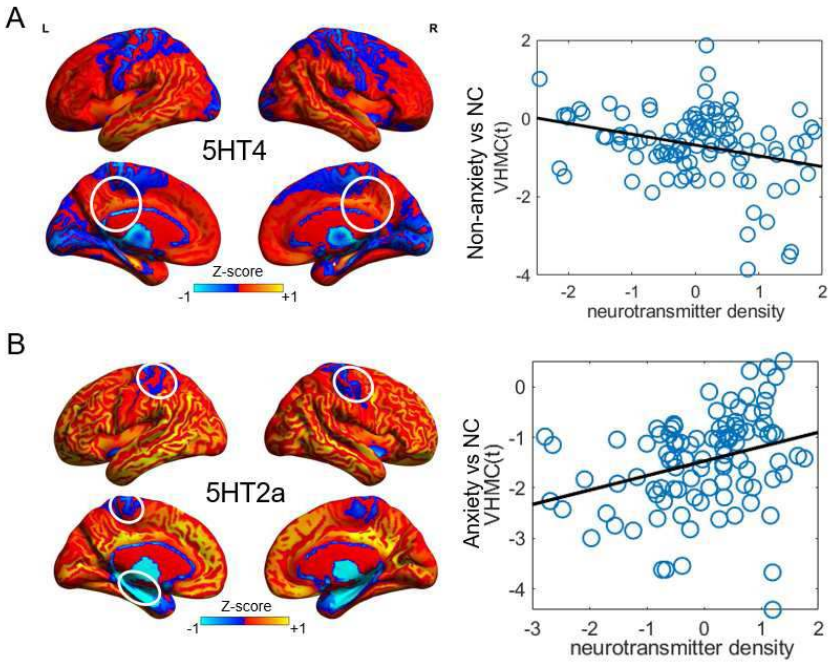

Conclusions: We found decreased VMHC in PCC in both non-anxious and anxious MDD compared with NC, indicating this alteration may be specific to depressive symptom[7,8]. Moreover, we observed anxious-specific decreases in the VMHC of

mPFC, MFG, PHG and IFG, suggesting a more severe interhemispheric functional connectivity impairment in anxiety than depression[7]. Importantly, we found significant links between VMHC changes and neurotransmitter density. The depression-related receptor (5-HT4) is involved in serotonin release and further affects cognitive functions[9], while anxiety-related receptors (5-HT2a, H3, M1, and mGluR5) may influence the release of 5-HT, glutamate and GABA, related to emotional regulation[10]. In summary, our findings uncovered different patterns of interhemispheric disconnectivity in MDD with and without anxiety, which was associated with distinct neurotransmitter systems.

References

1. Gili, M., García Toro, et al. (2013), 'Functional impairment in patients with major depressive disorder and comorbid anxiety disorder', The Canadian Journal of Psychiatry, 58(12), 679–686. https://doi.org/10.1177/070674371305801205
2. Yang, H., Wang, C., Ji, G., et al. (2019), 'Aberrant interhemispheric functional connectivity in first-episode, drug-naïve major depressive disorder', Brain Imaging and Behavior, 13, 1302–1310. https://doi.org/10.1007/s11682-018-9917-x
3. Liu, Y., Zhao, J., & Guo, W. (2018), 'Emotional roles of monoaminergic neurotransmitters in major depressive disorder and anxiety disorders', Frontiers in Psychology, 9, 2201. https://doi.org/10.3389/fpsyg.2018.02201
4. Liao, Z., Banaschewski, T., Bokde, A. L., et al. (2023). 'Hemispheric asymmetry in cortical thinning reflects intrinsic organization of the neurotransmitter systems and homotopic functional connectivity', Proceedings of the National Academy of Sciences, 120(42), e2306990120. https://doi.org/10.1073/pnas.2306990120
5. Yan, C. G., & Zang, Y. F. (2010), 'DPARSF: a MATLAB toolbox for "pipeline" data analysis of resting-state fMRI', Frontiers in Systems Neuroscience, 4, 1377. http://dx.doi.org/10.3389/fnsys.2010.00013
6. Hansen, J. Y., et al. (2022), 'Mapping neurotransmitter systems to the structural and functional organization of the human neocortex', Nature Neuroscience, 25(11), 1569–1581. https://doi.org/10.1038/s41593-022-01186-3
7. Yan, C.G., Chen, X., Li, L., et al. (2019). 'Reduced Default Mode Network Functional Connectivity in Patients with Recurrent Major Depressive Disorder', Proceedings of the National Academy of Sciences of the United States of America, 116(18), 9078-9083. https://doi.org/10.1073/pnas.1900390116
8. Cheng, W., Rolls, E. T., Qiu, J., et al. (2018), 'Increased functional connectivity of the posterior cingulate cortex with the lateral orbitofrontal cortex in depression', Translational Psychiatry, 8(1), 90. https://doi.org/10.1038/41398-018-0139-1
9. Hillhouse, T. M., & Porter, J. H. (2015). 'A brief history of the development of antidepressant drugs: From monoamines to glutamate', Experimental and Clinical Psychopharmacology, 23(1), 1. https://doi.org/10.1037/a0038550
10. Royse, S. K., Lopresti, B. J., et al. (2023). 'Beyond monoamines: II. Novel applications for PET imaging in psychiatric disorders', Journal of Neurochemistry, 164(3), 401-443. https://doi.org/10.1111/jnc.15657

Poster No 578

Graph Convolutional Network Model for Discrimination of Major Depressive Disorder

Kei Kamiya[1], Miyuki Tajima[1], Yuki Kobayashi[1], Yoshimi Arai[1], Risa Ogata[1], Mika Yamagishi[1], Hana Nishida[1], Shun Kudo[1], Akihiro Takamiya[1,2,3], Nariko Katayama[1], Bun Yamagata[1], Masaru Mimura[1], Jinichi Hirano[1]

[1]Department of Neuropsychiatry, Keio University school of Medicine, Shinjuku, Tokyo, [2]Neuropsychiatry, Department of Neurosciences, Leuven Brain Institute, KU Leuven, Belgium, [3]Hills Joint Research Laboratory for Future Preventive Medicine and Wellness, Keio University School, Tokyo, Japan

Introduction: Major depressive disorder (MDD) is considered one of the most socially and economically burdensome illnesses. A recent study of the functional connectome has revealed quantitative differences in the brain networks of individuals with MDD, contributing to identifying potential biological markers (Chai et al., 2023). Machine learning has emerged as a pivotal tool in medical research, with numerous models developed for MDD (Qin et al., 2018). However, these models often face limitations, such as limited sample sizes and a scarcity of advanced models employing deep learning techniques. Addressing these gaps, our study aims to develop a deep learning-based discrimination model for MDD utilizing Functional Connectivity (FC) data derived from a dataset comprising over a thousand samples.

Methods: Dataset: We have used the MDD who was diagnosed by DSM-V and Healthy Control (HC) images from the following data set: Longitudinal MRI study Identifying the Neural Substrates of Remission/Recovery in Mood Disorders (L/R) and the Strategic International Brain Science Research Promotion Program (Brain/MINDS Beyond) MRI data set. Image acquisition and preprocessing: We used resting state functional MRI (rsfMRI) images, which mainly consist of two different scan protocols (non-multiband based SRPB protocol (TR = 2500 msec) (https://bicr.atr.jp/rs-fmri-protocol-2/) and multiband-based HARP protocol (TR = 800 msec) (https://bicr.atr.jp/rs-fmri-protocol-2/)). rsfMRI was obtained from six different scanners. SRPB protocol images were preprocessed by fMRI prep (Esteban et al., 2019), and HARP protocol images were preprocessed by the HCP pipeline. (Glasser, et al. 2013) After preprocessing, we extracted the FC matrix based on the AAL2 (Automated Anatomical Labeling) atlas using Nilearn (https://nilearn.github.io/stable/index.html). To harmonize the scanner effect, NeuroCombat was applied for FC data (Sun et al., 2022). Model building: Using the preprocessed FC matrix, we built a binary prediction model for discriminating the MDD or HC. We used a Graph Convolutional Networks (GCN) model, a deep learning technique on graph-structured data. In this study, we conducted a stratified 10-fold cross-validation. For a 10-fold training/test split, the model was

fit to the training data, and the predictive value was assessed using the test data over all splits (10 times). Balanced accuracy (Average of True Positive Rate and True Negative Rate), accuracy, sensitivity, specificity, and Area Under Curve (AUC) value were calculated to evaluate the overall results. The Pytorch Geometric extension library was used for model building. The flow of analysis was shown in Figure 1.

Figure 1. Flow of the analysis

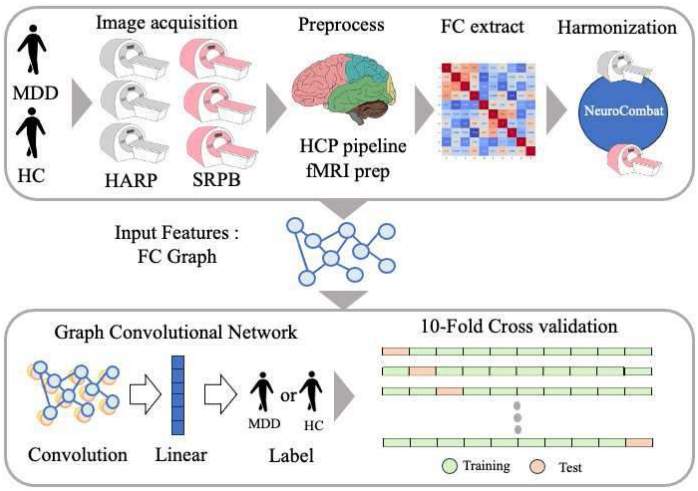

Results: We finally utilized 430 MDD and 586 HC images for model building. Our final models showed 63.6 ± 5.1% balanced accuracy. The accuracy was 65.44 ± 5.01 %, sensitivity was 51.2 ± 11.2 %, specificity was 75.9 ± 10.7 %, and the AUC value was 0.636, respectively (Figure 2).

Figure 2 : Results of Final model

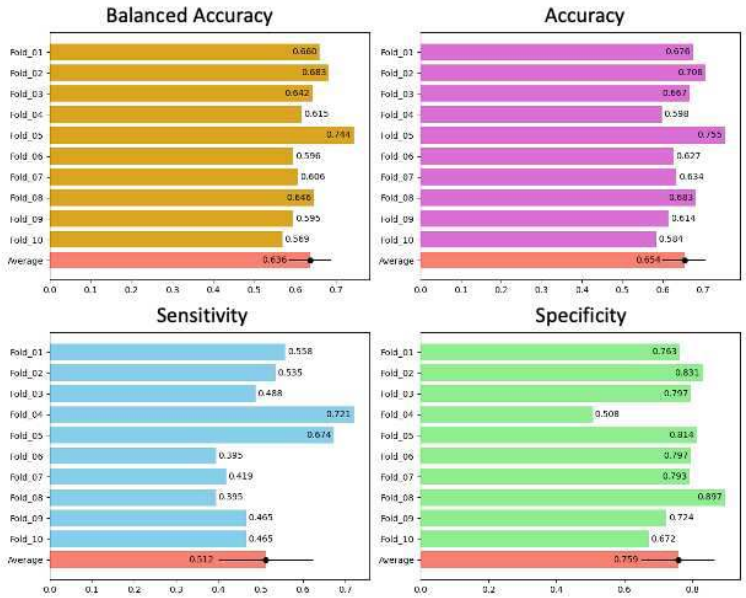

Conclusions: The model trained using GCN showed an accuracy of 65.44%, about 8% higher than the baseline (57.6%, 586/1016). To the best of our knowledge, only one prior study has created a disease discrimination model for MDD using a sample size exceeding a thousand (Qin et al., 2018). While the accuracy of our study is lower compared to this previous research (Qin et al., 2018)., this may be due to our use of two imaging protocols with different temporal resolutions.

References

1. Ya Chai(2023), 'Functional connectomics in depression: insights into therapies.', Trends in Cognitive Sciences, vol. 27, no.9, pp. 814-832
2. Kun Qin(2022), 'Using graph convolutional network to characterize individuals with major depressive disorder across multiple imaging sites.', eBioMedicine, vol. 78
3. Esteban, O.(2019), 'fMRIPrep: a robust preprocessing pipeline for functional MRI.', Nature Methods, vol. 16, pp. 111–116
4. Glasser, M. F.(2013), 'The minimal preprocessing pipelines for the Human Connectome Project.', Neuroimage, vol. 80, pp. 105–124
5. Sun(2022), 'A comparison of methods to harmonize cortical thickness measurements across scanners and sites.' Neuroimage, vol. 261, pp. 1-19

Poster No 579

Convergent Task-State Brain Functional Network Profile Linking Behavioral Symptoms

Yunman Xia[1], Gunter Schumann[2]

[1]Fudan University, Shanghai, China, [2]Centre for Population Neuroscience and Stratified Medicine, Berlin, Germany

Introduction: Mental illness accounts for nearly 30% of the disease burden among non-communicable diseases worldwide[1]. Extensive research efforts have been directed toward understanding the pathological mechanisms underlying psychiatric symptoms and developing effective clinical treatments[2,3]. However, due in part to the complexity of behavioral symptoms and the limitation of sample size, establishing robust and generalizable neuroimaging biomarkers remains challenging. Previous work has identified a shared brain functional network that exhibits a positive relationship with behavioral symptoms during early adolescence[4]. Here, we aim to leverage follow-up data of this longitudinal neuroimaging cohort to identify cross-disorder associated brain functional network profiles in young adults.

Methods: First, we utilized task-fMRI data and clinical measurements obtained from approximately 1000 healthy young adults (from IMAGEN cohort, aged 19 years) to explore the associations between task-state functional brain connectivity and various behavioral symptoms. Specifically, we employed the CONN toolbox to estimate the condition-specific functional connectome derived from the Monetary Incentive Delay (MID)[5] and Stop signal task (SST)[6]. The behavioral symptoms were assessed by the Development and Well-Being Assessment[7] and Strengths and Difficulties Questionnaire[8]. Then we applied the connectome-based predictive model (CPM)[9] to predict behavioral symptoms using whole-brain functional connectome. The CPM was iterated 1,000 times, and the edges that were present in over 95% of predicted models and both related to the externalizing and internalizing symptoms were selected. Subsequently, we validated the behavioral implications of these cross-disorder associated edges in the clinical populations (STRATIFY and ESTRA dataset, N=513, aged 18–26, case/control=288/225). The case-control comparisons involving these edges were conducted, while controlling for site effects, sex, and head motion.

Results: We found that task-based functional connectivity (FC) could significantly predict the majority of externalizing and internalizing symptoms at 19 years of age (Fig.1a and b). We delineated two distinct network profiles comprising FCs displaying either positive or negative relationships with both externalizing and internalizing symptoms, respectively (Fig.1c). The FCs exhibiting positive relationships with behavioral symptoms were primarily localized within brain regions such as the dorsal posterior cingulate cortex (dorsal PCC), inferior frontal gyrus (IFG), dorsolateral prefrontal cortex (DLPFC), and cerebellum. However, the FCs demonstrating negative relationships were localized within regions including dorsal PCC, DLPFC, IFG, angular gyrus (AG), and cerebellum. Moreover, we observed notable group differences in functional network profiles that exhibited negative associations with symptoms between healthy and clinical samples. Specifically, the whole clinical samples and subsets with alcohol use disorder (AUD), eating disorder (ED), and major depression disorder (MDD) all exhibited significant higher behavioral symptoms and weaker connections than healthy people (Fig.2a and b). In addition, we identified different patterns of individual FC profiles across specific disorders (Fig.2c), such as the weaker FC between fusiform and visuomotor regions in the AUD group, the weaker FC between AG and DLPFC in the ED group, and the weaker FC between AG and cerebellum in the MDD group.

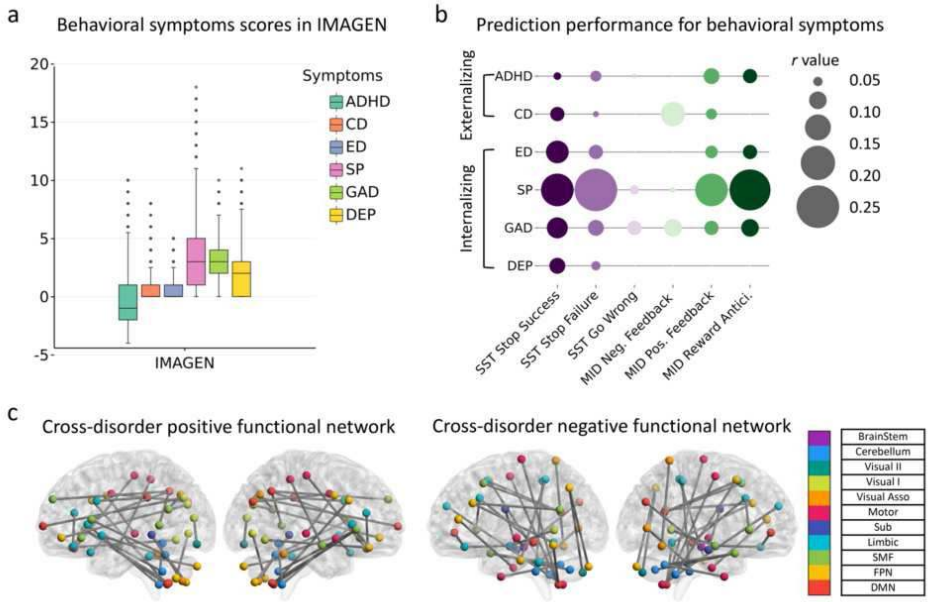

Figure 1. Identification of task-based functional connectome related to behavioral symptoms. (**a**) Behavioral symptoms are categorized into externalizing symptoms, including attention-deficit/hyperactivity disorder (ADHD) and conduct disorder (CD), and internalizing symptoms, which comprise eating disorder (ED), specific phobia (SP), general anxiety disorder (GAD), and depression (DEP). (**b**) The predictive performance for behavioral symptoms using task-based connectome-based predictive models. The task-based functional connectome was obtained from the SST (go-wrong, stop-success, and stop-failure conditions) and MID task (reward anticipation, positive reward feedback, and negative reward feedback conditions). Predictive performance was estimated through a multiple regression model, in which a higher r value indicates better predictive performance. (**c**) Functional brain networks demonstrating significant associations with both externalizing and internalizing symptoms. The node color represents its functional network attribution in the Shen 268 functional brain template.

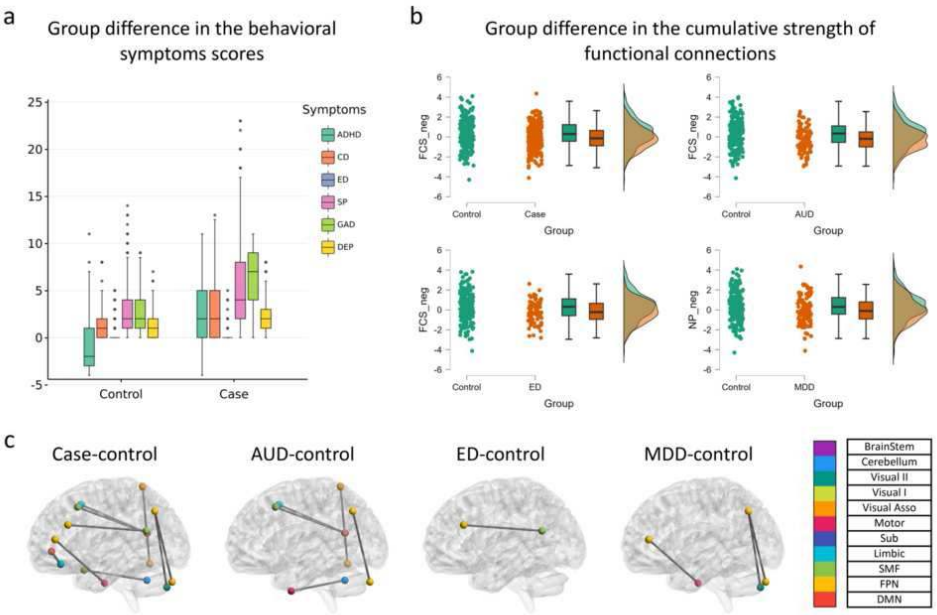

Figure 2. (**a**) Significant group differences between case and control were seen in the scores of attention-deficit/hyperactivity disorder (ADHD), conduct disorder (CD), specific phobia (SP), general anxiety disorder (GAD), and depression (DEP). (**b**) Significant group differences were seen in the functional network profiles demonstrating negative cross-disorder associations, controlling the site effects, sex, and head motion. The case group includes participants diagnosed with alcohol use disorder (AUD, N=98), eating disorder (ED, N=79), and major depression disorder (MDD, N=104). (**c**) For each functional connection exhibiting negative cross-disorder associations, specific disorders showed different patterns in the group differences. The node color represents its functional network attribution in the Shen 268 functional brain template.

Conclusions: Our findings identified a reliable neuroimaging biomarker underlying the symptoms across multiple mental disorders, which holds implications for early prevention and therapeutics in psychiatry. We aim to further simulate this brain biomarker in computational brain models and then manipulate brain models to alter the brain biomarker associated with symptoms.

References
1. World Health Organization. Health statistics and information systems. Estimates for 2000–2012
2. McCutcheon, R. A. (2020), 'Dopamine and glutamate in schizophrenia: biology, symptoms and treatment', World Psychiatry, 19(1), 15-33
3. Chavanne, A. V. (2021), 'The overlapping neurobiology of induced and pathological anxiety: a meta-analysis of functional neural activation', American Journal of Psychiatry, 178(2), 156-164
4. Xie, C. (2023), 'A shared neural basis underlying psychiatric comorbidity', Nature Medicine, 29(5), Article 5
5. Knutson, B. (2001), 'Dissociation of reward anticipation and outcome with event-related fMRI', NeuroReport, 12, 3683–3687
6. Bari, A. (2013), 'Inhibition and impulsivity: behavioral and neural basis of response control', Progress in Neurobiology,108, 44–79
7. Goodman, R. (2000), 'The Development and Well-being Assessment: description and initial validation of an integrated assessment of child and adolescent psychopathology', Journal of Child Psychology and Psychiatry, 41, 645–655
8. Goodman, R. (1997), 'The Strengths and Difficulties Questionnaire: a research note', Journal of Child Psychology and Psychiatry, 38, 581–586
9. Shen, X. (2017), 'Using connectome-based predictive modeling to predict individual behavior from brain connectivity', Nature Protocols, 12(3), Article 3

Poster No 580

Dynamic Coactivation Pattern Analysis Reveals Altered Brain State Dynamics in Cocaine use disorder

Benjamin Klugah-Brown[1], Xing Yao[1], Pan Wang[1], Bharat Biswal[2]

[1]University of Electronic Science and Technology of China, Chengdu, Sichuan, [2]New Jersey Institute of Technology, Newark, NJ

Introduction: Illicit substance use poses a pervasive global health challenge, affecting millions worldwide (SAMSHA, 2019). Cocaine addiction, characterized by severe neurobiological and neuropsychiatric consequences, necessitates a deeper understanding of its neural underpinnings (Volkow et al., 2019). Resting-state functional magnetic resonance images (rsfMRI) studies have highlighted the importance of investigating functional network connectivity characteristics (Kelly et al., 2011; Ma et al., 2015) to gain a more comprehensive understanding of the dynamic nature of brain function in cocaine used disorder (CUD).

Methods: This study employed dynamic coactivation pattern (CAP) analysis (Liu & Duyn, 2013), a data-driven approach, to explore the spatial and temporal dynamics of brain states in CUD. Using rsfMRI data from 56 CUD and 57 healthy control (HC) subjects, we identified six CAP states and compared their temporal dynamics between the two groups. Additionally, we integrated dynamic findings with stationary functional network connectivity (FNC), revealing nuanced changes in activation and connectivity within functional networks linked to CAP states.

Results: Five CAP states exhibited spatial similarity between CUD and HC, while state 6 showed opposing spatial patterns. Specifically, state 6 in the CUD group displayed stronger activation in the frontoparietal and visual networks. This heightened activation in the frontoparietal network, commonly associated with higher-order cognitive functions, suggests that cocaine may have induced neural excitation in the brain's resting state. Temporal dynamics analysis revealed significant differences in CUD. The fraction of time and counts spent in the default mode network (DMN) and frontoparietal network (FPN) were reduced, indicating potential dysfunction within executive and decision-making processes. Conversely, increased activation in the ventral attention network (VAN) suggests heightened attention to drug-related cues. Clinical correlations uncovered associations between CAP states and the duration of cocaine use. A significant negative association was observed with state 5, while a positive association was found with state 6. These findings underscore the intricate interplay between neural adaptations and cocaine use patterns in CUD. Integration with stationary FNC revealed network-specific changes. Notably, state 1 exhibited alterations in the control network, state 3 in the DMN, state 4 in the dorsal attention network, and state 5 in the visual network. These findings highlight the complexity of neural adaptations in CUD.

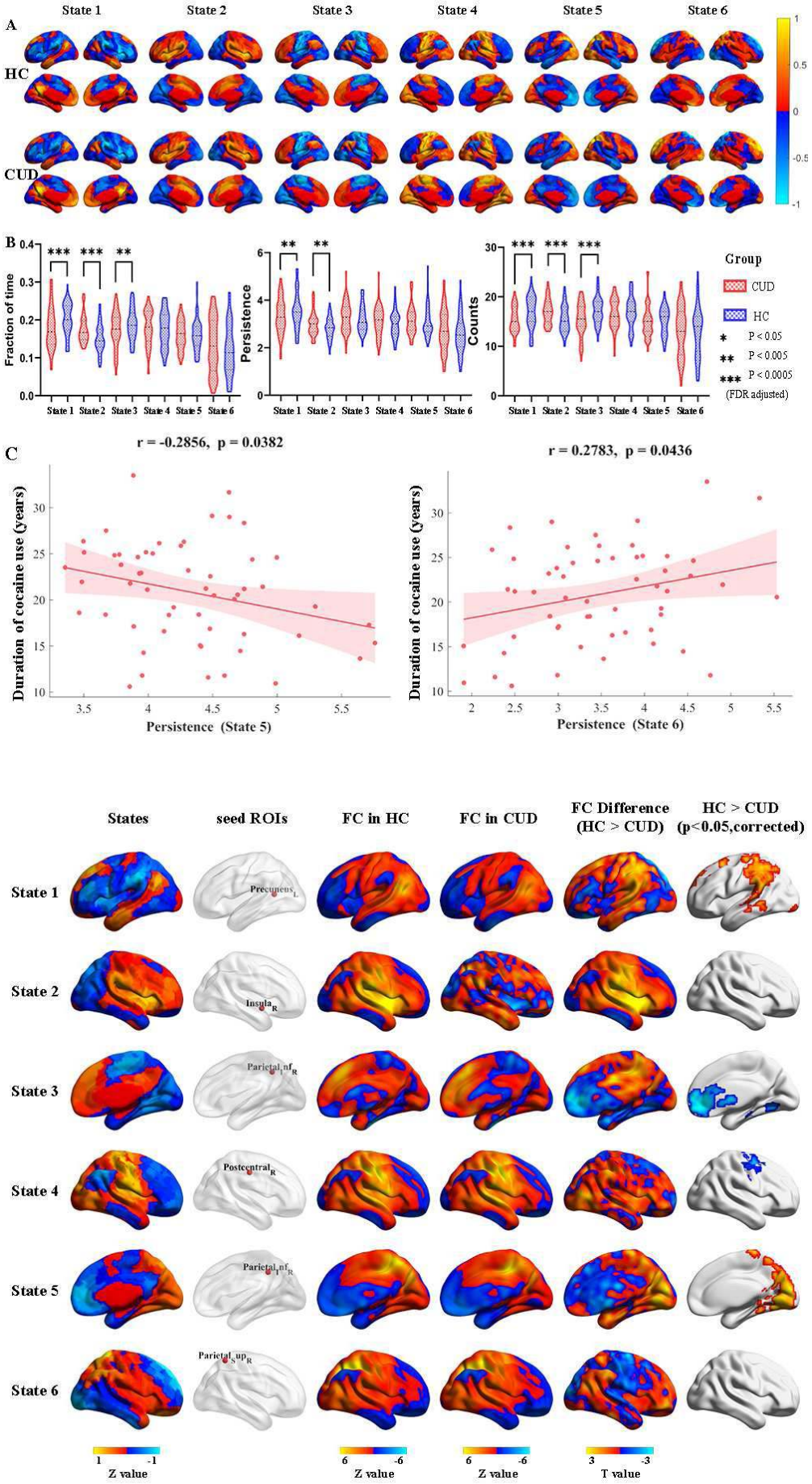
A
State 1
State 2
State 3
State 4
State 5
State 6
HC
CUD
1
0.5
0
-0.5
-1
B
Fraction of time
Persistence
Counts
Group
CUD
HC
* P < 0.05
** P < 0.005
*** P < 0.0005
(FDR adjusted)
C
r = -0.2856, p = 0.0382
Duration of cocaine use (years)
Persistence (State 5)
r = 0.2783, p = 0.0436
Duration of cocaine use (years)
Persistence (State 6)
States
seed ROIs
FC in HC
FC in CUD
FC Difference (HC > CUD)
HC > CUD (p<0.05,corrected)
State 1
State 2
State 3
State 4
State 5
State 6
Precuneus L
Insula R
Parietal_inf R
Postcentral R
Parietal_inf R
Parietal_sup R
Z value
Z value
Z value
T value

Conclusions: This research highlights the dynamic nature of neural alterations in CUD, providing a foundation for understanding the disease's neurobiology. Dynamic CAP analysis proved instrumental in unraveling the temporal intricacies of brain states linked to cocaine addiction. The findings contribute to advancing diagnostic strategies for CUD, emphasizing the need for a comprehensive approach to address the dynamic interplay of neural changes in addiction.

References

1. Kelly, C., Zuo, X. N., Gotimer, K., Cox, C. L., Lynch, L., Brock, D., Imperati, D., Garavan, H., Rotrosen, J., Castellanos, F. X., & Milham, M. P. (2011). Reduced interhemispheric resting state functional connectivity in cocaine addiction. Biological Psychiatry, 69(7), 684–692. https://doi.org/10.1016/j.biopsych.2010.11.022
2. Liu, X., & Duyn, J. H. (2013). Time-varying functional network information extracted from brief instances of spontaneous brain activity. Proceedings of the National Academy of Sciences of the United States of America, 110(11). https://doi.org/10.1073/pnas.1216856110
3. Ma, L., Steinberg, J. L., Cunningham, K. A., Lane, S. D., Bjork, J. M., Neelakantan, H., Price, A. E., Narayana, P. A., Kosten, T. R., Bechara, A., & Moeller, F. G. (2015). Inhibitory behavioral control: A stochastic dynamic causal modeling study comparing cocaine dependent subjects and controls. NeuroImage: Clinical, 7, 837–847. https://doi.org/10.1016/j.nicl.2015.03.015
4. SAMSHA. (2019). Key substance use and mental health indicators in the United States: Results from the 2019 National Survey on Drug Use and Health. HHS Publication No. PEP19-5068, NSDUH Series H-54, 170.
5. Volkow, N. D., Michaelides, M., & Baler, R. (2019). The neuroscience of drug reward and addiction. Physiological Reviews, 99(4). https://doi.org/10.1152/physrev.00014.2018

Poster No 581

Gray Matter Alterations in Young Unmedicated Patients with Bipolar II and Unipolar Depression

Idy Wing Yi Chou[1], Hanna LU[1], Arthur DP Mak[2], Linda Chiu Wa Lam[3]

[1]The Chinese University of Hong Kong, Hong Kong SAR, China, [2]University of Cambridge, London, United Kingdom, [3]The Chinese University of Hong Kong, Hong Kong, Hong Kong

Introduction: This study aimed to investigate multi-scale gray matter (GM) alterations in young, unmedicated individuals with bipolar II depression (BPII) and unipolar depression (UD) compared to healthy controls (HC) using gray matter volume, cortical thickness, pial surface area, and local gyrification index measures.

Methods: The study included 27 individuals with BPII (mean age = 23.1), 27 individuals with UD (mean age = 24.0), and 27 HC (mean age = 23.1). All patients were unmedicated and clinically depressed as assessed by the Montgomery-Åsberg Depression Rating Scale (MADRS). High-resolution structural magnetic resonance imaging (MRI) scans were acquired. Freesurfer was used for image preprocessing and extraction of GM volume, cortical thickness, pial surface area, and local gyrification index (LGI). The Desikan-Killiany atlas was used for cortical parcellation for ROI-based analysis. Vertex-wise analysis was performed for LGI.

Results: Our findings revealed significant GM alterations in both BPII and UD compared to HC. Individuals with BPII exhibited lower cortical thickness at right superior parietal cortex compared to HC ($p = 0.03$), while UD displayed reduced cortical thickness at right caudal anterior cingulate cortex ($p = 0.002$) and posterior cingulate cortex ($p = 0.03$) compared to HC. Additionally, BPII showed higher LGI at the right middle temporal cortex (ROI-based analysis; $p = 0.03$) and right precentral cortex (vertex-wise analysis; $p = 0.04$) compared to UD.

Conclusions: Conclusions: Our study provides evidence of extensive GM alterations in BPII and UD across multi-scale measures. These findings are clinically significant. Firstly, the two groups of patients exhibited distinctive patterns of structural changes, indicative of possible early detection of the BPII and UD using these neuromarkers. Secondly, our findings in young, unmedicated adults with BPII and UD suggest that the observed structural alterations are not solely attributable to medication effects, but occur early in the course of the illness. Indeed, cortical thinning is known to be associated with illness course and symptom burden, such as the number of hypomanic episodes (Abe et al., 2022). Early intervention targeting the identified brain regions may hold promise in mitigating or preventing these pathological processes. This is particularly significant because existing research on high-risk cohorts typically does not show apparent gray matter changes (Hajek et al., 2015). The observed structural differences are in line with the current understanding of the pathophysiological underpinnings of BPII and UD. Cortical thinning in the right superior parietal cortex in BPII is possibly associated with deficits in executive processes such as attention and working memory (Corbetta & Shulman, 2002), which are central to emotion regulation (Wadlinger & Isaacowitz, 2011). UD displayed reduced cortical thickness at the right cingulate cortex, which may imply impairments in emotional responses from the disrupted processing of reward and punishment information (Rolls, 2019) and emotional words (Maddock, Garrett, & Buonocore, 2003). Moreover, UD had reduced gyrification at the right middle temporal and precentral cortex compared to BPII, suggesting difficulties in interpreting and conveying emotional expression (Goghari, Macdonald, &

Sponheim, 2011; Manelis, Huppert, Rodgers, Swartz, & Phillips, 2019). Future studies with larger sample sizes and collaborative efforts are warranted to confirm and extend our results.

References

1. Corbetta, M., & Shulman, G. L. (2002). Control of goal-directed and stimulus-driven attention in the brain. Nat Rev Neurosci, 3(3), 201-215. doi:10.1038/nrn755
2. Goghari, V. M., Macdonald, A. W., 3rd, & Sponheim, S. R. (2011). Temporal lobe structures and facial emotion recognition in schizophrenia patients and nonpsychotic relatives. Schizophr Bull, 37(6), 1281-1294. doi:10.1093/schbul/sbq046
3. Maddock, R. J., Garrett, A. S., & Buonocore, M. H. (2003). Posterior cingulate cortex activation by emotional words: fMRI evidence from a valence decision task. Hum Brain Mapp, 18(1), 30-41. doi:10.1002/hbm.10075
4. Manelis, A., Huppert, T. J., Rodgers, E., Swartz, H. A., & Phillips, M. L. (2019). The role of the right prefrontal cortex in recognition of facial emotional expressions in depressed individuals: fNIRS study. J Affect Disord, 258, 151-158. doi:10.1016/j.jad.2019.08.006
5. Rolls, E. T. (2019). The cingulate cortex and limbic systems for action, emotion, and memory. Handb Clin Neurol, 166, 23-37. doi:10.1016/B978-0-444-64196-0.00002-9
6. Wadlinger, H. A., & Isaacowitz, D. M. (2011). Fixing our focus: training attention to regulate emotion. Pers Soc Psychol Rev, 15(1), 75-102. doi:10.1177/1088868310365565

Poster No 582

Comparing Four Brain Age Algorithms in Predicting Cognition in Bipolar Disorder and Healthy Persons

Hui Xin Ng[1], Lisa Eyler[1]

[1]*University of California San Diego, La Jolla, CA*

Introduction: Our study compares four Brain Age algorithms in their ability to predict level of cognitive performance among individuals with bipolar disorder (BD) versus healthy comparisons (HC). We investigate whether higher brain-predicted age difference (brain-PAD) is linked to poorer cognition in BD, given BD's neuropathological similarities to brain aging (Baecker et al., 2021). We expected the BD group to exhibit a stronger negative correlation between brain-PAD and cognition. We hypothesized that algorithms trained on more granular data would better capture group differences in the strength of the brain-PAD-cognition relationship and exhibit more robust brain-PAD-cognition associations, irrespective of group.

Methods: Dataset: The dataset includes 38 HC and 33 individuals with BD, who met the criteria for BD I and were euthymic. Groups were comparable in terms of age, sex, and education. Cognitive performance was assessed using the Delis-Kaplan Executive Function System (DKEFS) test. Cognitive scores included: Trails Visual Scanning Omission Errors (Misses) and Commission Errors (False Alarm), Trails Completion Times (Number Sequencing, Letter-Number, Motor Speed), Color Word Interference (Color Naming, Word Reading, Inhibition, Inhibition/Switching). Image acquisition: General Electric Signa EXCITE 3.0 Tesla whole-body imaging system in a one session with a variety of T1-weighted and T2-weighted structural and functional sequences. Algorithm Types: 3 algorithms were selected due to their large training sets, public code and diversity of training data granularity and algorithm type: PHOTON-BA (Freesurfer parcellated T1-weighted scans; Han et al., 2021), BrainageR (voxel-based T1-weighted scans; Cole et al., 2018), MIDI (axial T2-weighted and axial diffusion-weighted scans; Wood et al., 2022). UCSD Multimodal, a locally developed ridge regression model, included multiple modalities like T1-weighted MRI, DTI, CBF, task fMRI, and rsMRI. Statistical Analysis: Principal component analysis (PCA) on cognitive scores resulting in a first component (PC1) accounted for 44.5% of variance. We demographically-corrected each algorithm's brain-PAD by adjusting for sex, age, and their interaction; residuals from respective linear models were used in subsequent analyses to test our hypotheses. Residual brain-PAD (rbrain-PAD), group, and their interaction were used as predictors of PC1. Interaction term effect sizes were compared. A model with only rbrain-PAD was then fit given the prior non-significance of group and interaction. We compared effect sizes across simplified models.

Results: In the model with group, rbrain-PAD and their interaction, we found no significant associations of rbrain-PAD or group with PC1 across all algorithms (all p's >0.05). There was no significant interaction of group and rbrain-PAD across the algorithms, but effect sizes of the interaction varied, with the strongest association seen for BrainageR (b= -0.06, t= -1.98, p= 0.05, ηp2= 0.056); MIDI (b= -0.09, t= -1.73, p= 0.08, ηp2=0.043); UCSD Multimodal (b = -0.04, t= -0.99, p= 0.32, ηp2= 0.015); PHOTON-BA (b= 0.00015, t= 0.004, p= 0.99, ηp2= 0.00). With BD and HC groups combined as a follow-up, we found that rbrain-PAD was significantly related to cognition for one algorithm (BrainageR; b=-0.04, t= -2.62, $p < 0.05$, ηp2= 0.091) but not others (MIDI b = -0.04, t= -1.84, p= 0.07, ηp2= 0.047;UCSD Multimodal b= -0.03, t= -1.69, p= 0.09, ηp2= 0.040; PHOTON-BA b = -0.03, t= 0.08, ηp2= 0.043).

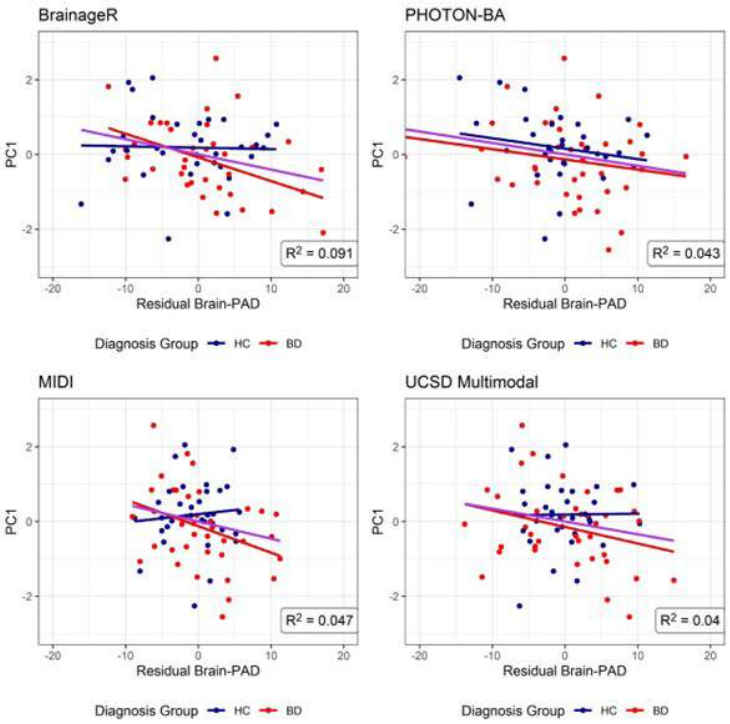

Figure 1. There was no significant interaction between diagnosis and residual brain-PAD. Across all brain age algorithms, the BD group shows a non-significant negative trend between residual brain-PAD and cognition. Some algorithms (e.g., BrainageR and MIDI) are better able to detect the differential strength in the relationship between residual brain-PAD and cognition in BD as demonstrated by their larger non-significant effect sizes. The residual brain-PAD from BrainageR (b=-0.04, t= -2.62, $p < 0.05$, $\eta_p^2 = 0.091$) showed the strongest overall relationship to cognitive performance.

Conclusions: Contrary to our hypothesis, we did not see significantly stronger negative brain-PAD-cognition link in BD compared to HC across all algorithms, but ones trained on raw data like BrainageR and MIDI show potential in detecting a overall brain-PAD-cognition relationship and differential strength of that relationship in BD. BrainageR performed the best in both aspects, showing its potential for revealing deeper relationships between brain aging and cognition among those with serious mental illness such as BD.

References

1. Baecker, L., Garcia-Dias, R., Vieira, S., Scarpazza, C., & Mechelli, A. (2021). Machine learning for brain age prediction: Introduction to methods and clinical applications. eBioMedicine, 72. https://doi.org/10.1016/j.ebiom.2021.103600
2. Cole J.H., Ritchie S.J., Bastin M.E., et al (2018) Brain age predicts mortality. Mol Psychiatry 23:1385– 1392
3. Han, L. K. M., Dinga, R., Hahn, T., Ching, C. R. K., Eyler, L. T., Aftanas, L., Aghajani, M., Aleman, A., Baune, B. T., Berger, K., Brak, I., Filho, G. B., Carballedo, A., Connolly, C. G., Couvy-Duchesne, B., Cullen, K. R., Dannlowski, U., Davey, C. G., Dima, D., … Schmaal, L. (2021). Brain aging in major depressive disorder: Results from the ENIGMA major depressive disorder working group. Molecular Psychiatry, 26(9), Article 9. https://doi.org/10.1038/s41380-020-0754-0
4. Wood, D. A., Kafiabadi, S., Busaidi, A. A., Guilhem, E., Montvila, A., Lynch, J., Townend, M., Agarwal, S., Mazumder, A., Barker, G. J., Ourselin, S., Cole, J. H., & Booth, T. C. (2022). Accurate brain-age models for routine clinical MRI examinations. NeuroImage, 249, 118871. https://doi.org/10.1016/j.neuroimage.2022.118871

Poster No 583

Deviating from the norm: Neuroanatomical dissimilarity in depression is linked to symptom severity

Lukas Sempach[1], Sarah Ulrich[1], Laura Han[2,3], Elena Pozzi[2,3], Dick Veltman[4], Lianne Schmaal[2,3], Paul Thompson[5], André Schmidt[1], for the ENIGMA Major Depressive Disorder Working Group[6]

[1]Department of Clinical Research, University Psychiatric Clinics, University of Basel, Basel, Switzerland, [2]Centre for Youth Mental Health, The University of Melbourne, Parkville, VIC, Australia, [3]Orygen, Parkville, VIC, Australia, [4]Amsterdam UMC location Vrije Universiteit Amsterdam, Department of Psychiatry, Amsterdam, North Netherlands, [5]Imaging Genetics Center, Keck School of Medicine of University of Southern California, Los Angeles, CA, [6]https://enigma.ini.usc.edu/ongoing/enigma-mdd-working-group/, International

Introduction: Major depressive disorder (MDD) is a disabling disorder characterized by a heterogeneous phenotype encompassing a spectrum of symptom profiles. MDD varies in clinical characteristics such as frequency and duration of episodes, response to medication, and stability of remission (Cuijpers et al. 2020). This clinical heterogeneity also implies heterogeneity in the underlying pathophysiology. In terms of neurostructural hallmarks of MDD, large-scale studies have provided evidence for the presence of several structural differences in MDD patients compared to healthy individuals (Schmaal et al. 2017; 2016). These differences, albeit detectable, are small in terms of effect size, a common observation to neuroanatomical differences between MDD patients and healthy individuals (Winter et al. 2022). Heightened neurostructural heterogeneity in MDD patients might be a factor contributing to these subtle group differences. Thus, decomposing variance across neurostructural measures and distinct brain regions in MDD has the potential to map different neuroanatomical phenotypes onto different clinical phenotypes. This study aims to investigate and quantify the neurostructural heterogeneity in MDD patients, providing insights into variance differences and linking them to clinical measures.

Methods: This collaborative effort by the ENIGMA MDD consortium quantified neurostructural heterogeneity in MDD patients (N=3641) and healthy individuals (N=4876) from 40 international sites. Heterogeneity was computed as region-specific and global variance, based on structural magnetic resonance imaging (MRI) measures of subcortical volume (SV), cortical surface area (SA), and cortical thickness (CT). Neuroimaging data were preprocessed following standardized ENIGMA protocols and harmonized using neuroComBat (Fortin et al. 2018) and all analyses were performed on data matched for age and sex. Region-specific differences in variance were measured using the Coefficient of Variation (CV) and the Variability Ratio (VR). To assess variance globally, the Person-Based Similarity Index (PBSI) was calculated (Doucet et al. 2019). A lower PBSI score indicates higher neurostructural variance in the subject's brain profile. Lastly, a normative modelling approach was applied computing the norm-PBSI indicating the 'normativeness' of neuroanatomical brain profiles of MDD patients. Deviating norm-PBSI scores were identified (> -2 SD) and clinical features of non-deviating and deviating MDD patients were compared.

Results: MDD patients demonstrated increased variance (CV > 1) in the CT of 6 temporal lobe brain regions ($p < .05$). No region-specific variance differences were observed for SA and SV. The PBSI revealed increased heterogeneity in the CT profiles of MDD patients (PBSI-MDD = 0.801, PBSI-HC = 0.807, $p < .001$, $d = 0.21$). Again, no differences in heterogeneity between the groups were observed for SA and SV profiles. The norm-PBSI analysis identified deviating MDD patients across all three domains: 193 (5.87%) for SV, 173 (5.25%) for CT, and 153 (4.63%) for SA. Compared to non-deviators in CT, MDD patients with deviating CT profiles reported higher severity of depressive symptoms ($p < .03$). And MDD patients with deviating SA profiles experienced less episodes than non-deviators in SA ($p < .02$).

Conclusions: This examination of both regional and global neuroanatomical heterogeneity demonstrates an increase in CT variance among MDD patients. Notably, MDD patients with a neuroanatomical phenotype reflecting most pronounced heterogeneity in CT (norm deviators) exhibited the highest symptom burden. Together, these findings serve as an initial benchmark, shedding light on the clinical significance of neuroanatomical heterogeneity in MDD patients, which may foster stratification and treatment guidance in the future. Further longitudinal investigations are required to confirm the effect of CT heterogeneity on symptomatology.

References

1. Cuijpers, P. (2020), "A Network Meta-Analysis of the Effects of Psychotherapies, Pharmacotherapies and Their Combination in the Treatment of Adult Depression." World Psychiatry : Official Journal of the World Psychiatric Association (WPA) 19 (1): 92–107.
2. Doucet, G.E. (2019), "Person-Based Brain Morphometric Similarity Is Heritable and Correlates With Biological Features." Cerebral Cortex 29 (2): 852–62.
3. Fortin, J.P. (2018), "Harmonization of Cortical Thickness Measurements across Scanners and Sites." NeuroImage 167 (February): 104–20.
4. Schmaal, L. (2017), "Cortical Abnormalities in Adults and Adolescents with Major Depression Based on Brain Scans from 20 Cohorts Worldwide in the ENIGMA Major Depressive Disorder Working Group." Molecular Psychiatry 22 (6): 900–909.
5. Schmaal, L. (2016), "Subcortical Brain Alterations in Major Depressive Disorder: Findings from the ENIGMA Major Depressive Disorder Working Group." Molecular Psychiatry 21 (6): 806–12.
6. Winter, N.R. (2022), "Quantifying Deviations of Brain Structure and Function in Major Depressive Disorder Across Neuroimaging Modalities." JAMA Psychiatry 79 (9).

Poster No 584

Changes in Model-Based and Model-Free Control Predict Future Drinking Trajectories in Young Adults

Hao Chen[1], Sören Kuitunen-Paul[2], Maria Garbusow[3], Quentin Huys[4], Andreas Heinz[3], Michael Rapp[5], Michael Smolka[1]

[1]Department of Psychiatry and Psychotherapy, Technische Universität Dresden, Dresden, Germany, [2]Chair of Clinical Psychology and Psychotherapy, Technische Universität Chemnitz, Chemnitz, Germany, [3]Department of Psychiatry and Psychotherapy, Charité – Universitätsmedizin Berlin, Berlin, Germany, [4]Division of Psychiatry; Max Planck UCL Centre for Computational Psychiatry and Ageing Research, UCL, London, UK, [5]Area of Excellence Cognitive Sciences, University of Potsdam, Postdam, Germany

Introduction: Building on our previous findings on the link between imbalanced model-based/model-free (MB/MF) control and the development of drinking behaviour between ages 18 and 21, this study investigates whether changes in MB/MF control over these years are consequences of alcohol consumption or whether they consistently act as predisposing factors, potentially predicting drinking patterns from ages 21 to 24.

Methods: In this six-year longitudinal study, we tracked a community sample of young men, starting at age 18. Participants underwent functional magnetic resonance imaging at ages 18 and 21 while performing a two-step sequential decision-making task to evaluate imbalances in MB and MF control. Drinking behaviours were annually assessed through an interview-based binge drinking score, measured in grams of alcohol per occasion, and biannually through a self-reported consumption score using the Alcohol Use Disorders Identification Test. To assess the effects of drinking on MB/MF control, we analysed total alcohol consumption between ages 18 and 21 using area under the curve calculations and examined its correlation with changes in the two-step decision-making parameters. To investigate how MB/MF control predicts future drinking behaviour, latent growth curve models were employed to explore the influence of these parameters on drinking trajectories from ages 21 to 24.

Results: We found no associations between the total amount of alcohol consumption from ages 18 to 21 and any change in the parameters of the two-step task, indicating that drinking behaviour does not affect the imbalance in MB/MF control. The MB behavioural score exhibited a protective effect against the development of the binge drinking score: a higher MB behavioural score was associated with diminished progression in the binge drinking score. In addition, an increased MF behavioural score was linked to a higher binge drinking score at age 21, but it did not predict further development of binge drinking. In terms of the consumption score, as expected, we observed that an enhanced MF reward prediction error (RPE) in the ventral striatum (VS) was associated with escalated consumption score development. However, the MF RPE signal in the ventromedial prefrontal cortex (vmPFC) showed an inverse association with the development of the consumption score. This unexpected association was elucidated by further mediation analysis, which indicated that the MF RPE signal in the vmPFC partially mediated the relationship between the MF RPE in the VS and the development of the consumption score.

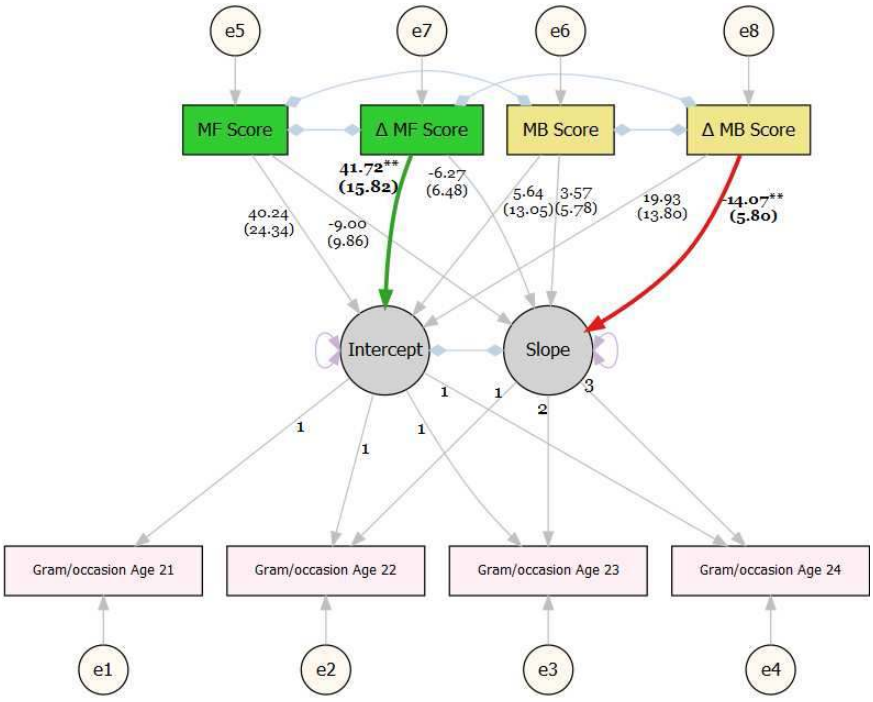

Conclusions: Our findings suggest that changes in MB behavioural control and MF RPE signals are not consequences of earlier drinking, but rather they predispose individuals to the development of drinking behaviours from ages 21 to 24. These findings suggest potential avenues for developing targeted prevention strategies that modulate MB and MF controls to mitigate the risk of future drinking behaviours.

References

1. Chen, H., Mojtahedzadeh, N., Belanger, M. J., Nebe, S., Kuitunen-Paul, S., Sebold, M., Garbusow, M., Huys, Q. J. M., Heinz, A., Rapp, M. A., & Smolka, M. N. (2021). Model-Based and Model-Free Control Predicts Alcohol Consumption Developmental Trajectory in Young Adults: A 3-Year Prospective Study. Biological psychiatry, 89(10), 980–989. https://doi.org/10.1016/j.biopsych.2021.01.009

Poster No 585

Shared and distinct patterns of dFC variability of thalamo-cortical circuit in BDD and MDD patients

Fengmei Lu[1], Wei Luo[1], Yue Yu[1], Zongling He[1], Huafu Chen[1]

[1]The Clinical Hospital of Chengdu Brain Science Institute, MOE Key Lab for Neuroinformation, UESTC, Chengdu, China

Introduction: Bipolar disorder (BD) is a chronic, severe and lifelong psychiatric disorder with a prevalence of 1~2% (Kessing & Andersen, 2017). Though BD has a manic episode, depressive episode is the most common feature of BD that overlaps with major depressive disorder (MDD) and is mainly manifested as depressed mood, loss of interest, insomnia or hypersomnia. Thus, it is difficult to distinguish between BD during a depressive episode (BDD) and MDD due to similar clinical symptoms (Chen et al., 2022; Evans, 2000; Redlich et al., 2015; Smith & Craddock, 2011). Evidence has indicated abnormalities of thalamo-cortical functional connectivity (FC) in bipolar disorder during a depressive episode (BDD) and major depressive disorder (MDD). However, the dynamic FC (dFC) within this system is poorly understood. This study aims to provide more precise thalamic subregions to explore the disrupted thalamo-cortical dFC patterns between BDD and MDD, using the Human Brainnetome Atlas combined with a sliding-window approach.

Methods: A total of 250 subjects including 95 MDD patients, 58 BDD patients and 97 healthy controls (HCs) were recruited. The rs-fMRI data were obtained with a 3T GE Discovery MR750 scanner. Data were preprocessed by the Data Processing and Analysis of Brain Imaging (DPABI) toolkit (v5.1, http://rfmri.org/dpabi). After preprocessing, we defined 16 seeds of the thalamus according to the Human Brainnetome Atlas (HBA, http://atlas.brainnetome.org) (L. Fan et al., 2016; Y. Fan et al., 2015). To identify the dFC variability, a sliding-window dFC approach was applied with the Dynamic Brain Connectome (DynamicBC) toolbox. To explore the differences in dFC variability patterns of each thalamus subregions with the rest of the brain among the three groups, one-way ANOVA model was conducted on the dFC variance in z value at each voxel, with age, gender, educational level, mean FD and the variance of FD as covariates. Next, to examine the differences among the three groups (i.e. BDD vs. MDD, BDD vs. HCs, MDD vs. HCs), the brain clusters showing significant group differences were defined as regions of interest (ROIs) for post-hoc analysis, with age, gender, educational level, mean FD and the variance of FD as covariates. Correlation analysis was performed between altered dFC variability and clinical data (including course of illness, age of first onset, number of depression episodes, duration of single episode, number of mania episodes, HAMD score, and BRMS score) in MDD and BDD, regressing out the age, gender, educational level, mean FD, the variance of FD and total medication load index. Further, classification analysis with a linear support vector machine model was conducted.

Results: Compared with HCs, both patients revealed increased dFC variability between thalamus subregions with hippocampus (HIP), angular gyrus and caudate, and only BDD showed increased dFC variability of the thalamus with superior frontal gyrus (SFG), HIP, insula, middle cingulate gyrus and postcentral gyrus (Figure 1). Compared with MDD and HCs, only BDD exhibited enhanced dFC variability of the thalamus with SFG and superior temporal gyrus (Figure 1). Further, the number of depressive episodes in MDD was significantly positively associated with altered dFC variability (Figure 2A). Finally, the disrupted dFC variability could distinguish BDD from MDD with 83.44% classification accuracy (Figure 2B).

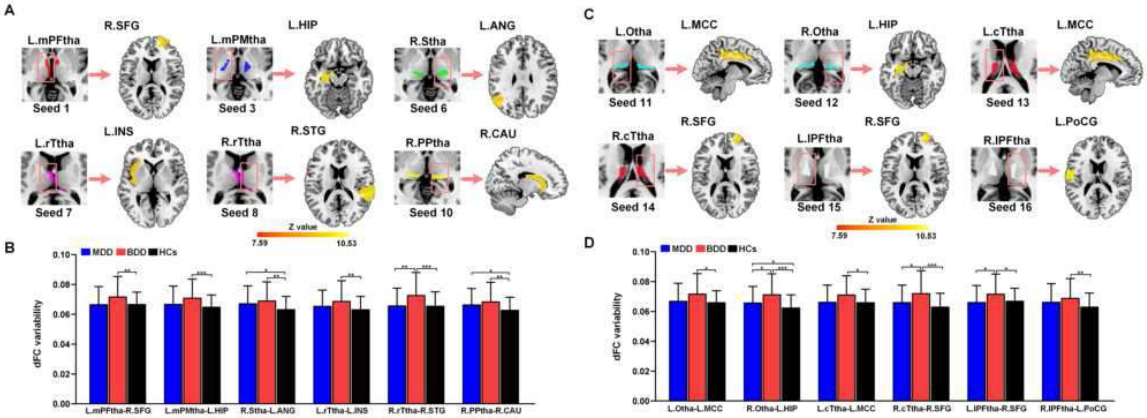

Figure 1. Significant group differences of dFC variability for the thalamus seeds among three groups (MDD, BDD and HCs)

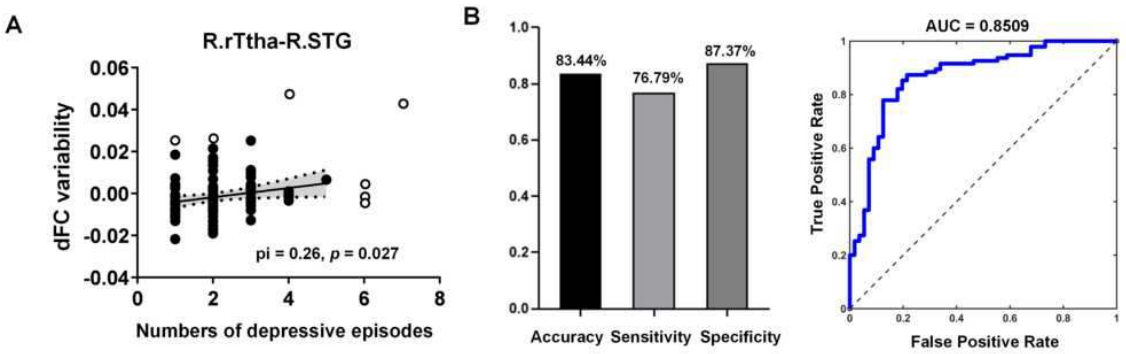

Figure 2. (A) Significant correlation between altered dFC variability and number of depressive episodes in MDD group. (B) The SVM classification results and the ROC curve based on the significant different dFC variability maps.

Conclusions: Our findings support and extend the role of thalamo-cortical circuit in the shared neuropathological mechanisms of the two mood disorders. Discriminative disorder-specific altered dFC in thalamo-cortical circuit were found in BDD. Notably, excesssive varibalitiy in thalamus-related salience and sensory perception system was observed in BDD. Our findings give further evidence to suggest the deficits in the cognitive, emotional as well as sensory and perception processes in BDD.

References

1. Chen, H. (2022). Dimensional Analysis of Atypical Functional Connectivity of Major Depression Disorder and Bipolar Disorder. Cerebral Cortex, 32(6), 1307-1317.
2. Evans, D. L. (2000). Bipolar disorder: diagnostic challenges and treatment considerations. Journal of Clinical Psychiatry, 61, 26-31.
3. Fan, L. (2016). The Human Brainnetome Atlas: A New Brain Atlas Based on Connectional Architecture. Cerebral cortex, 26(8), 3508-3526.
4. Fan, Y. (2015). Functional Connectivity-Based Parcellation of the Thalamus: An Unsupervised Clustering Method and Its Validity Investigation. Brain Connectivity, 5(10).
5. Kessing, L. (2017). Evidence for clinical progression of unipolar and bipolar disorders. Acta Psychiatrica Scandinavica, 135(1), 51-64.
6. Redlich, R. (2015). Reward processing in unipolar and bipolar depression: a functional MRI study. Neuropsychopharmacology, 40(11), 2623-2631.
7. Smith, D. J. (2011). Unipolar and bipolar depression: different of the same? British Journal of Psychiatry, 199(199), 272-274.

Poster No 586

Reconfiguration of Structure-Function Coupling in Diverse Subgroups of Adolescents with Depression

Ming Xu[1], Xuemei Li[2], Teng Teng[2], Yang Huang[2], Mengqi Liu[2], Yicheng Long[3], Fajin Lv[2], Dongmei Zhi[4], Xiang Li[5], Aichen Feng[6], Shan Yu[5], Xinyu Zhou[2], Jing Sui[7]

[1]Chinese Academy of Sciences, Beijing, Beijing, [2]The First Affiliated Hospital of Chongqing Medical University, Chongqing, Chongqing, [3]The Second Xiangya Hospital of Central South University, Changsha, Hunan, [4]Beijing Normal University, Beijing, Select a State, [5]Brainnetome Center and National Laboratory of Pattern Recognition, Institute of Automation, Chinese, Beijing, Beijing, [6]Institute of Automation, Chinese Academy of Sciences, Beijing, Select a State, [7]Beijing Normal University, Beijing, China

Introduction: The presence of major depressive disorder (MDD) during adolescence is associated with elevated rates of self-harm and suicide, which induces significant adverse impact on brain development(Vigo et al., 2016; Vos et al., 2020). Existing findings have suggested that the neurobiological basis of depressive symptom profiles in adolescents is related to complex interactions between environment and multimodal brain development (Redlich et al., 2018; Steingard et al., 1996). However, beyond the functional or structural impairment in cortex or connectivity, whether the structure-function coupling (SC-FC coupling) is disrupted in adolescent MDD, and how such disrupted coupling differ in various MDD subgroups with different clinical characters and environmental stressors remain underexplored. To this end, this study aimed to determine how the SC-FC coupling alters in adolescents with MDD and 3 types of sub-groups.

Methods: In this cross-sectional case-control clinical neuroimaging study, we collected the resting-state functional magnetic resonance images (fMRI) and diffusion MRI data of 187 adolescents with MDD and 120 healthy controls aged 10 to 18 years in Chongqing, China. Structure-function coupling was calculated for each brain region of each subject using whole-brain structure and function connectivity as did in (Zamani Esfahlani et al., 2022)(Fig 1). Primary analyses included the group differences in terms of structure-function coupling of adolescent MDD and HCs. Secondary analyses included differences among 3 types of MDD subgroups (Fig 2), i.e., subgroups with or without suicide attempt (SA+ / SA−), with or without non-suicidal self-injury (NSSI+ / NSSI−), with or without major life events (MLE+ / MLE−).

Results: Adolescent MDD overall showed increased structure-function coupling in visual network, post default mode network and insula (Cohen's d ranged from 0.411 to 0.614, pFDR <.05) (Fig 1C). Regions with group-differed SC-FC coupling (pFDR < 0.05, 246 tests) were labeled in the Manhattan plot (Fig1D). Fig 1E shows significantly increased SC-FC coupling in adolescent MDD in five anatomical structures. More importantly, we identified subgroup-specific alterations in SC-FC coupling. Particularly, the parahippocampal (A35/36c_L) coupling decreased in MDD with suicide attempt (SA+, Fig 2A, B) with partial η2 0.045, 90% CI 0.023 to 0.116, pFDR = .004; while compared with NSSI+ and HC, SC-FC coupling increased in subregions of right insula (dIa_R) with partial η2 0.057, 90% CI 0.017 to 0.104, pFDR = .010, and left thalamus (cTtha_L) with partial η2 0.059, 90% CI 0.018 to 0.106, pFDR = .009) in NSSI− (Fig 2C, D). Remarkably, subgroup variations of SC-FC coupling were most prominent in MDD subgroups related to major life events, in which unique frontal-limbic coupling increases (e.g., medial frontal gyrus (A8vl_L), orbital gyrus (A14m_L/A14m_R), and amygdala (lAmyg_R) etc.) were observed in MLE+ subgroup with patial η2 ranged from 0.045 to 0.068, pFDR < .05 (Fig 2E, F).

Conclusions: Compared to typical developed adolescent, the brain functional communications in adolescent MDD were bound more tightly by anatomical pathways, especially in default mode network, visual network, and insula, which may link to the impaired cross-network dynamics in MDD. Furthermore, the patterns of aberrant structure-function change also interacted with the clinical characters, suggesting potential heterogeneity in neuropathology of the MDD. Collectively, the findings contribute to identification of the common and subgroup-specific neurophysiological markers in adolescent MDD, highlighting the role of adversity exposure in sculpting brain development during adolescence.

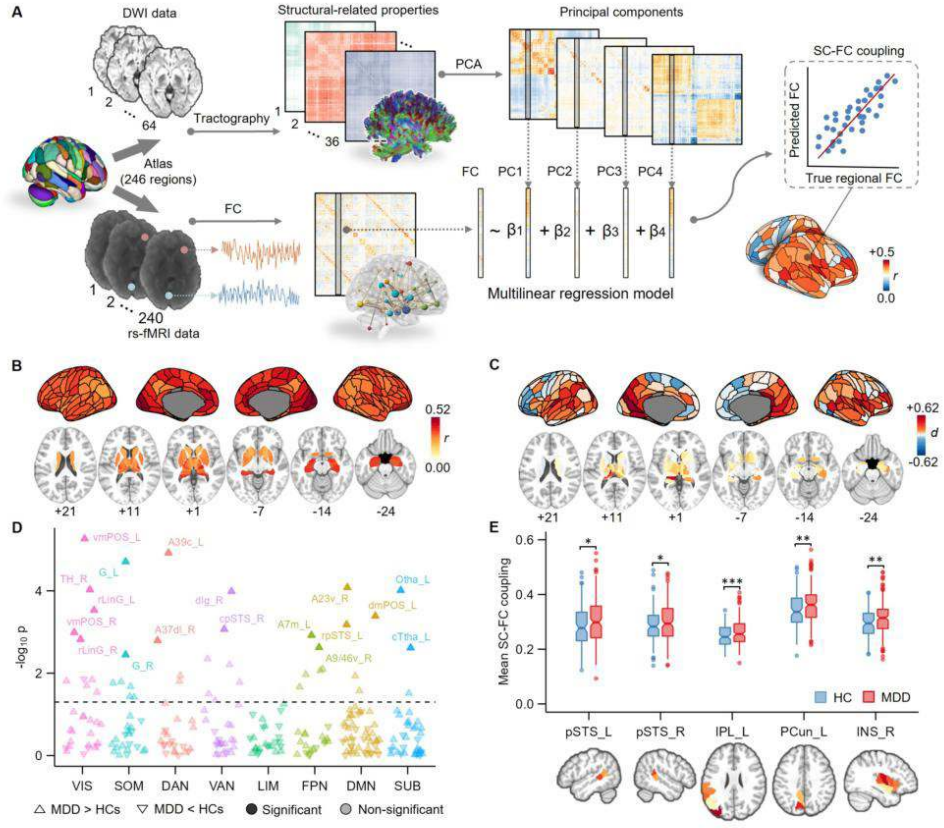

Figure 1. (**A**) The pipeline for calculating the SC-FC coupling of each brain region. (**B**) The group-averaged SC-FC coupling of HCs (n = 101). (**C**) The differences of SC-FC coupling (measured as Cohen's d) between adolescent MDD and HCs at each brain region. (**D**) Manhattan plot of SC-FC coupling differences between adolescent MDD and HCs. Regions with group-differed SC-FC coupling (p_{FDR} < 0.05, 246 tests) were labeled in the plot. The dashed horizontal line indicated $\log_{10}$P = .05 (uncorrected). (**E**) The mean SC-FC coupling of five anatomical structures were significantly increased in adolescent MDD (p_{FDR} < 0.05, 48 tests).

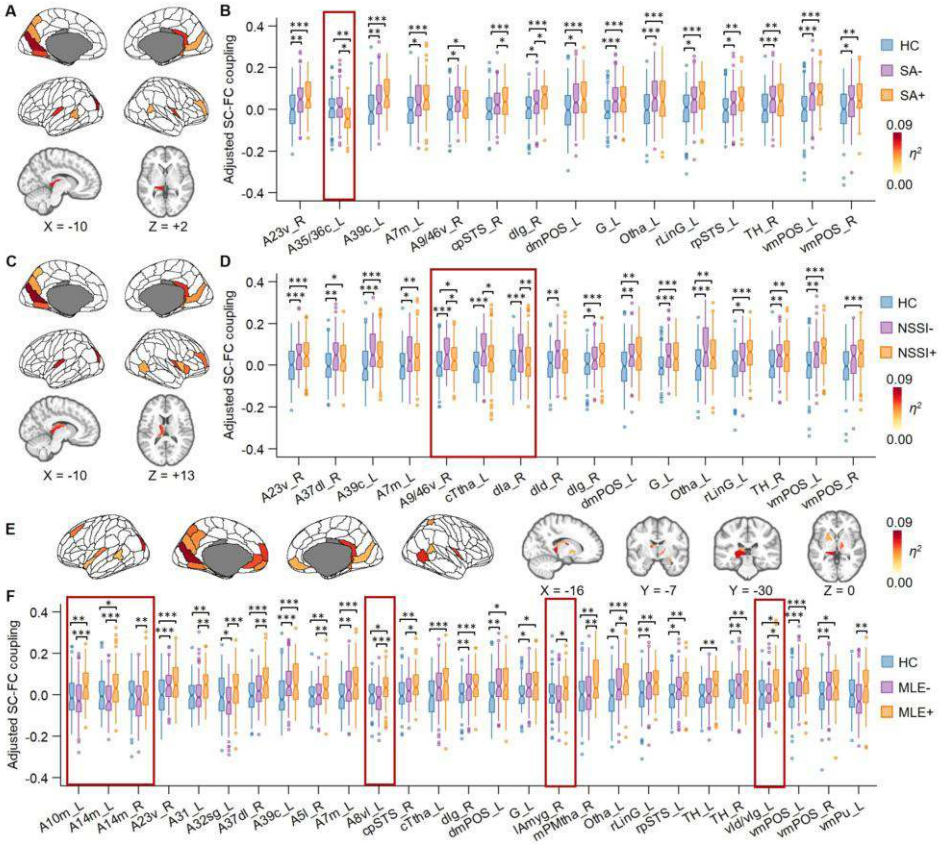

Figure 2. (**A**) Regions with significant differences of SC-FC coupling among HCs, SA+ and SA−. (**B**) *Post-hoc* comparisons of SC-FC coupling among HCs, SA+ and SA−. (**C**) Regions with significant differences of SC-FC coupling among HCs, NSSI+ and NSSI−. (**D**) *Post-hoc* comparisons of SC-FC coupling among HCs, NSSI+ and NSSI−. (**E**) Regions with significant differences of SC-FC coupling among HCs, MLE+ and MLE−. (**F**) *Post-hoc* comparisons of SC-FC coupling among HCs, MLE+ and MLE−.

References
1. Hearne, L. J., Lin, H. Y., Sanz-Leon, P., Tseng, W. I., Gau, S. S., Roberts, J. A., & Cocchi, L. (2021). ADHD symptoms map onto noise-driven structure-function decoupling between hub and peripheral brain regions. Mol Psychiatry, 26(8), 4036-4045.
2. Jiang, H., Zhu, R., Tian, S., Wang, H., Chen, Z., Wang, X., Shao, J., Qin, J., Shi, J., Liu, H., Chen, Y., Yao, Z., & Lu, Q. (2020). Structural-functional decoupling predicts suicide attempts in bipolar disorder patients with a current major depressive episode. Neuropsychopharmacology, 45(10), 1735-1742.
3. Redlich, R., Opel, N., Bürger, C., Dohm, K., Grotegerd, D., Förster, K., Zaremba, D., Meinert, S., Repple, J., Enneking, V., Leehr, E., Böhnlein, J., Winters, L., Froböse, N., Thrun, S., Emtmann, J., Heindel, W., Kugel, H., Arolt, V., . . . Dannlowski, U. (2018). The Limbic System in Youth Depression: Brain Structural and Functional Alterations in Adolescent In-patients with Severe Depression. Neuropsychopharmacology, 43(3), 546-554.
4. Steingard, R. J., Renshaw, P. F., Yurgelun-Todd, D., Appelmans, K. E., Lyoo, I. K., Shorrock, K. L., Bucci, J. P., Cesena, M., Abebe, D., Zurakowski, D., Poussaint, T. Y., & Barnes, P. (1996). Structural Abnormalities in Brain Magnetic Resonance Images of Depressed Children. Journal of the American Academy of Child & Adolescent Psychiatry, 35(3), 307-311.
5. Vigo, D., Thornicroft, G., & Atun, R. (2016). Estimating the true global burden of mental illness. Lancet Psychiatry, 3(2), 171-178.
6. Vos, T., Lim, S. S., Abbafati, C., Abbas, K. M., Abbasi, M., Abbasifard, M., Abbasi-Kangevari, M., Abbastabar, H., Abd-Allah, F., Abdelalim, A., Abdollahi, M., Abdollahpour, I., Abolhassani, H., Aboyans, V., Abrams, E. M., Abreu, L. G., Abrigo, M. R. M., Abu-Raddad, L. J., Abushouk, A. I., . . . Murray, C. J. L. (2020). Global burden of 369 diseases and injuries in 204 countries and territories, 1990-2019: a systematic analysis for the Global Burden of Disease Study 2019. The Lancet, 396(10258), 1204-1222.
7. Zamani Esfahlani, F., Faskowitz, J., Slack, J., Mišić, B., & Betzel, R. F. (2022). Local structure-function relationships in human brain networks across the lifespan. Nature Communications, 13(1), 2053.

Poster No 587

Decoding Dynamic Neural Patterns of MDD: A Preliminary Surface-Based MRI Study of Temporal Stability

Xue-Ying Li[1], Chao-Gan Yan[2]

[1]Department of Psychology, University of Chinese Academy of Sciences, Beijing, China, [2]Institute of Psychology, Chinese Academy of Sciences, Beijing, China

Introduction: Depression poses a common mental health challenge worldwide. While it inflicts substantial burdens and suffering on patients, their families, and society, clinically useful biomarkers for depression diagnosis and treatment response remain elusive. Temporal stability describes the consistency of dynamic functional connectivity in the brain over time and is a key indicator for characterizing the topological properties of brain functional networks. Temporal stability and dynamic functional connectivity, as newly developed approaches, have been increasingly used to measure impact of depressive disorders or interventions on brain functions. Previous studies indicate correlation between these dynamic functional indices and symptomatic improvements in major depressive disorder (MDD) patients. However, clear and powerful conclusions differentiating the dynamic features in brain functional activity between MDD patients and healthy individuals are still lacking, and there is a lack of large-scale surface-based MRI studies to understand the relationship between disease courses and specific symptoms of MDD. In an ongoing study, we utilized a cross-sectional study design to directly compare the dynamic patterns in brain functional activity between MDD patients and healthy individuals, and further explore their relationship with symptoms and long-term prognosis.

Methods: This study utilized a large multi-site MRI database aggregated by the Depression Imaging REsearch ConsorTium (DIRECT), including MDD (n = 1583) and healthy controls (n = 1308). All participants underwent structural and resting-state functional MRI scans, and depression patients were assessed with HAMD by clinicians. To investigate the temporal stability of the whole-brain functional network, we reconstructed the cortical surface mesh and applied preprocessing based on surface space to resting-state functional MRI data. Vertex-wise dynamic functional connectivity was calculated, establishing the temporal stability of the whole-brain functional network. Stability maps were compared through two-sample t-tests, corrected using permutation tests with Threshold Free Cluster Enhancement (TFCE). Subsequently, regions with significant stability differences were chosen as seeds to calculate their whole-brain dynamic functional connectivity maps. These maps were statistically compared between MDD patients and healthy controls using the same methods to explore the sources of observed stability differences. Significant results yeild from 3 seeds (showed by arrows and letters in Figure 1). Additionally, correlation analyses were conducted between stability values of significant regions in MDD patients and HAMD-17 item scores, as well as disease duration, unraveling potential associations between stability differences and clinical manifestations.

Results: We found that, compared to healthy subjects, depressed patients exhibited decreased stability in brain areas of visual and somatomotor networks. This reduced stability was primarily contributed by a decrease in dynamic functional connectivity across widespread brain regions of dorsal attention, visual, somatomotor, and frontoparietal networks. Notably, stability in the somatosensory cortex positively correlated with their HAMD scores of insomnia and insight of illness in MDD patients. On the other hand, we observed increased stability in the frontoparietal and limbic networks in MDD patients. This increase could be

partially attributed to enhanced dynamic functional connectivity between right insula and left precuneus, and associated with the severity of general somatic symptom in MDD patients.

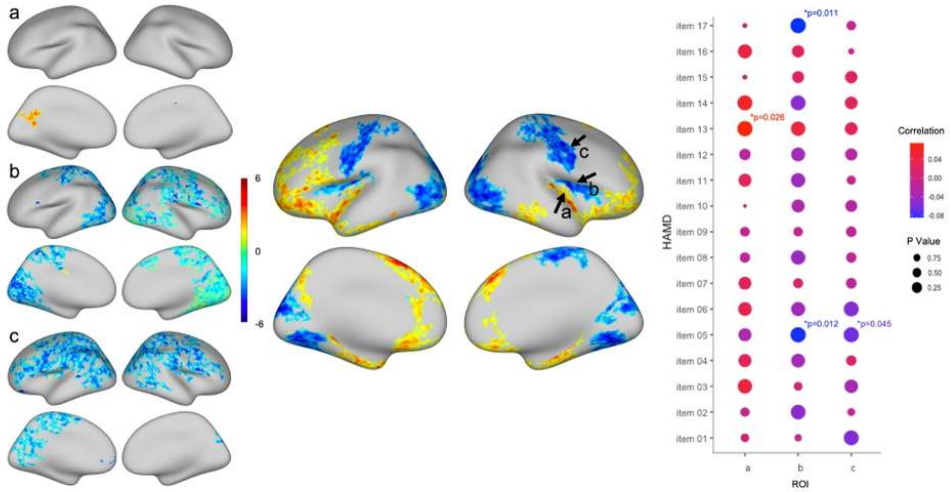

Figure 1. Dynamic functional patterns associated with symptoms in MDD. The middle column shows the comparison results of temporal stability between MDD patients and healthy controls survived multiple comparison correction. Red indicates increased functional stability in MDD patients compared to healthy controls, while blue indicates decreased stability in MDD. Subsequently, significant clusters were selected as regions of interest (ROIs) for dynamic functional connectivity analysis, resulting in three ROIs denoted as a, b, and c, as indicated by arrows. **The left column** displays the corrected results from the comparison of dynamic functional connectivity between MDD patients and healthy controls, corresponding to the ROI a, b, and c in the middle column. **The right column** illustrates the correlation between stability values of ROIs a, b, and c and HAMD-17 item scores. Significantly correlated items include item 05 (insomnia), item 13 (somatic symptoms), and item 17 (illness insight).

Conclusions: This study provides preliminary evidence on associations between differentiating dynamic patterns of MDD and specific symptoms. Future examinations of these results in relation to disease courses and recurrence hold promise for identifying MRI-based biomarkers for depression treatment targets.

References

1. Li L, Lu B, Yan CG. Stability of dynamic functional architecture differs between brain networks and states. Neuroimage. 2020 Aug 1;216:116230. doi: 10.1016/j.neuroimage.2019.116230. Epub 2019 Sep 29. PMID: 31577959.
2. Gerlach AR, Karim HT, Peciña M, Ajilore O, Taylor WD, Butters MA, Andreescu C. MRI predictors of pharmacotherapy response in major depressive disorder. Neuroimage Clin. 2022;36:103157. doi: 10.1016/j.nicl.2022.103157. Epub 2022 Aug 17. PMID: 36027717; PMCID: PMC9420953.
3. Li X, Zhang Y, Meng C, Zhang C, Zhao W, Zhu DM, Zhu J. Functional stability predicts depressive and cognitive improvement in major depressive disorder: A longitudinal functional MRI study. Prog Neuropsychopharmacol Biol Psychiatry. 2021 Dec 20;111:110396. doi: 10.1016/j.pnpbp.2021.110396. Epub 2021 Jul 2. PMID: 34217754.
4. Xiao Chen, Bin Lu, Hui-Xian Li, Xue-Ying Li, Yu-Wei Wang, Francisco Xavier Castellanos, Li-Ping Cao, Ning-Xuan Chen, Wei Chen, Yu-Qi Cheng, Shi-Xian Cui, Zhao-Yu Deng, Yi-Ru Fang, Qi-Yong Gong, Wen-Bin Guo, Zheng-Jia-Yi Hu, Li Kuang, Bao-Juan Li, Le Li, Tao Li, Tao Lian, Yi-Fan Liao, Yan-Song Liu, Zhe-Ning Liu, Jian-Ping Lu, Qing-Hua Luo, Hua-Qing Meng, Dai-Hui Peng, Jiang Qiu, Yue-Di Shen, Tian-Mei Si, Yan-Qing Tang, Chuan-Yue Wang, Fei Wang, Hua-Ning Wang, Kai Wang, Xiang Wang, Ying Wang, Zi-Han Wang, Xiao-Ping Wu, Chun-Ming Xie, Guang-Rong Xie, Peng Xie, Xiu-Feng Xu, Hong Yang, Jian Yang, Shu-Qiao Yao, Yong-Qiang Yu, Yong-Gui Yuan, Ke-Rang Zhang, Wei Zhang, Zhi-Jun Zhang, Jun-Juan Zhu, Xi-Nian Zuo, Jing-Ping Zhao, Yu-Feng Zang, the DIRECT consortium, Chao-Gan Yan, The DIRECT consortium and the REST-meta-MDD project: towards neuroimaging biomarkers of major depressive disorder, Psychoradiology, Volume 2, Issue 1, March 2022, Pages 32–42,

Poster No 588

Structural Connectivity of the Central Olfactory System in Clinical High-Risk for Psychosis

Jun Seo Hwang[1], Hyungyou Park[1], Sunah Choi[1], Kang Ik Cho[2], Yoo Bin Kwak[1], Moonyoung Jang[3], Sunghyun Park[3], Minah Kim[3,4], Jun Soo Kwon[1,3,4,5]

[1]Department of Brain and Cognitive Sciences, Seoul National University College of Natural Sciences, Seoul, Korea, Republic of, [2]Department of Psychiatry, Psychiatry Neuroimaging Laboratory, Brigham and Women's Hospital, Harvard, Boston, MA, [3]Department of Neuropsychiatry, Seoul National University Hospital, Seoul, Korea, Republic of, [4]Department of Psychiatry, Seoul National University College of Medicine, Seoul, Korea, Republic of, [5]Institute of Human Behavioral Medicine, SNU-MRC, Seoul, Korea, Republic of

Introduction: Olfactory dysfunction has been reported in patients diagnosed with schizophrenia and individuals at clinical high-risk for psychosis (CHR). However, the neural basis of olfactory dysfunction in CHR individuals, especially in terms of structural connectivity, remains unexplored. Olfactory processing, particularly higher-order functions such as odor identification, depends on the integration of information from several brain regions within the central olfactory system. This study aims to investigate the relationship between structural connectivity and olfactory dysfunction in CHR individuals.

Methods: Forty-six CHR individuals and 60 healthy controls (HC) were included in the study. Olfactory function was assessed using the Korean version of the Sniffin' Sticks Test (KVSS) in all participants. Subsequently, T1, T2, and diffusion-weighted magnetic resonance imaging (MRI) data were acquired from a subset of this group, comprising 26 CHR individuals and 49 HCs. Probabilistic tractography was then used to examine the structural connectivity of the central olfactory system.

Results: CHR individuals exhibited significantly lower odor identification (OI) scores compared to HCs. Although there were some trends of difference in structural connectivity, no significant differences were found between the primary olfactory cortex and any of the secondary olfactory brain regions. Additionally, there was no significant linear correlation between OI score and structural connectivity.

Conclusions: Olfactory dysfunction was observed in CHR individuals, consistent with previous findings. Preliminary evidence suggests structural connectivity differences in the central olfactory system. Further research is needed to understand the underlying mechanisms of olfactory dysfunction in psychotic disorders.

References

1. Fjaeldstad, A.W. (2021), 'Validation of Olfactory Network Based on Brain Structural Connectivity and Its Association With Olfactory Test Scores', Frontiers in systems neuroscience, 15, 638053
2. Hong, S.C. (1999), 'Development of KVSS test (Korean version of Sniffin' Sticks Test)', Korean Journal of Otorhinolaryngology-Head and Neck Surgery, 42(7), 855-860

Poster No 589

The neural signature of trait impulsivity in methamphetamine use disorder

Gangliang Zhong[1], Tianzhen Chen[1], Hang Su[1], Jiang Du[1], Min Zhao[1,2,3]

[1]Shanghai Jiao Tong University, Shanghai, China, [2]Shanghai Key Laboratory of Psychotic Disorders, Shanghai Mental Health Center, Shanghai, China, [3]CAS Center for Excellence in Brain Science and Intelligence Technology (CEBSIT), Chinese Academy of Sciences, Shanghai, China

Introduction: Methamphetamine (MA) is a widely abused illicit drug with significant global prevalence[1]. The detrimental impact of drug abuse on mortality rates necessitates improved prevention efforts based on known biological mechanisms. Excessive impulsivity has been consistently identified as a key psychological factor in addiction disorders, as well as in other neuropsychiatric and neurological conditions[2]. While research has shown that high trait impulsivity is associated with addictive disorders, the search for reliable brain-based predictors of impulsivity for future prevention remains ongoing. Understanding the neural mechanisms underlying impulsivity can aid in the development of personalized and innovative treatment approaches. Connectome-based predictive modeling (CPM), a recently developed whole-brain approach, was employed to identify impulsive connections associated with MA addiction. Impulsive behavior can stem from both heightened motivation and reduced motivation (apathy), representing failures in information processing or response control. The Barratt Impulsiveness Scale (BIS-11)[3], a widely used self-report scale, captures this heterogeneity through three subscales. CPM has been previously utilized to identify neural markers of impulsivity in opioid and cocaine addiction using functional connectivity data acquired during neurocognitive tasks[4,5]. However, its application in predicting impulsivity in addiction has not been explored.

Methods: A group of MA-using individuals (n=44) underwent resting-state functional magnetic resonance imaging (rsfMRI) scans. Trait impulsivity during abstinence was assessed using the BIS-11, which measures non-planning impulsiveness, motor impulsiveness, and cognitive impulsiveness. CPM with leave-one-out cross-validation was performed to identify neural networks predictive of trait impulsivity. This approach utilizes group connectivity matrices and behavioral data (in this case, trait impulsivity) to generate a predictive model of the behavioral data[6,7]. Regression analyses, such as Pearson's correlation or partial correlation, are employed to correlate edges and behavioral data from the training dataset, revealing positive and negative predictive networks. Follow-up analyses were conducted to assess the specificity of the identified impulsivity connections. To determine clinical relevance, the strength of the MA impulsivity network was compared with that of healthy subjects (n=35). The stability of these networks over time and in relation to pre- and post-treatment was tested in an independent brain intervention dataset (n=25).

Results: CPM identified an MA non-impulsivity network characterized by stronger within-network connectivity between the prefrontal cortex, dorsal and ventral striatum, hippocampus, and nucleus accumbens. The overall CPM model successfully predicted non-planning impulsivity, as evidenced by a significant correspondence between predicted and actual non-impulsivity values ($r = -0.59$, $df = 43$, $p < 0.001$) (Figure 1). This MA impulsivity network was anatomically distinct from the identified healthy impulsivity network. Connectivity strength in the independent sample remained unchanged with rTMS treatment, and strength at pretreatment and posttreatment assessments significantly predicted impulsivity ($p < 0.001$).

Conclusions: The identification of brain-based predictors of impulsivity enhances our understanding of addiction and can improve interventions and clinical practice. By tailoring therapies to individual neural function or neuromarkers, these findings can directly impact treatment approaches. The results indicate that changes in established neural networks contribute to variations in treatment outcomes for substance use disorder. Thus, understanding the neural mechanisms of impulsivity in addiction can aid in developing personalized treatment approaches.

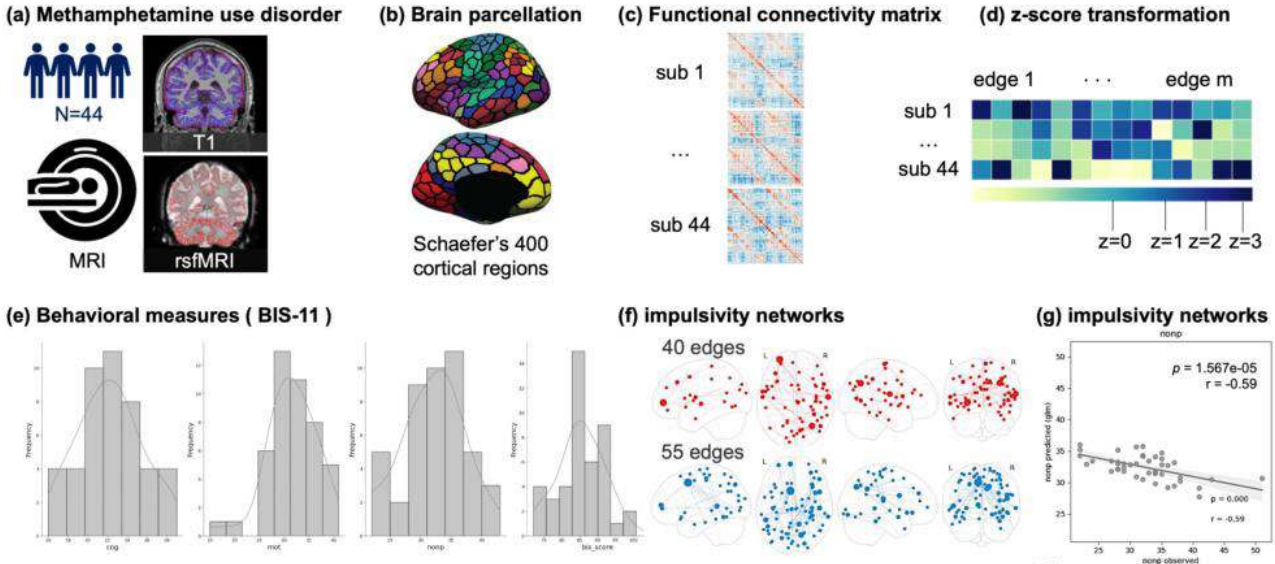

Figure 1. Connectome-based predictive modeling (CPM) performance and positive and negative impulsivity networks. CPM [6,7] is a data-driven machine learning approach that utilizes whole-brain functional connectivity data ("connectomes") to generate brain-behavior models. Unlike previous machine learning approaches, CPM does not require a priori selection of networks. It serves as both a predictive tool and a method for identifying networks associated with specific behaviors, referred to as "neural fingerprints." Consequently, CPM can also be used to identify novel treatment targets [6]. (a) Participants and neuroimaging data. (b) Network nodes were defined using the Schaefer 400-node brain atlas. (c) Whole-brain functional connectivity. (d) z-score transformed connectivity matrix data. (e) Impulsivity data, including three subscales: non-planning impulsiveness, motor impulsiveness, and cognitive impulsiveness. (f) Positive (red) and negative (blue) impulsivity networks are shown. Larger spheres indicate nodes with more edges, while smaller spheres indicate nodes with fewer edges. (g) The graph illustrates the correspondence between actual (x-axis) and predicted (y-axis) impulsivity values generated using CPM.

References

1. Dalley, J. W., & Robbins, T. W. (2017). Fractionating impulsivity: neuropsychiatric implications. Nature Reviews. Neuroscience, 18(3), 158-171. https://doi.org/10.1038/nrn.2017.8
2. Finn, E. S., Shen, X., Scheinost, D., Rosenberg, M. D., Huang, J., Chun, M. M., Papademetris, X., & Constable, R. T. (2015). Functional connectome fingerprinting: identifying individuals using patterns of brain connectivity. Nat Neurosci, 18(11), 1664-1671. https://doi.org/10.1038/nn.4135
3. Lichenstein, S. D., Scheinost, D., Potenza, M. N., Carroll, K. M., & Yip, S. W. (2021). Dissociable neural substrates of opioid and cocaine use identified via connectome-based modelling. Molecular Psychiatry, 26(8), 4383-4393. https://doi.org/10.1038/s41380-019-0586-y
4. Patton, J. H., Stanford, M. S., & Barratt, E. S. (1995). Factor structure of the Barratt impulsiveness scale. J Clin Psychol, 51(6), 768-774. https://doi.org/10.1002/1097-4679(199511)51:6<768::aid-jclp2270510607>3.0.co;2-1
5. Shen, X., Finn, E. S., Scheinost, D., Rosenberg, M. D., Chun, M. M., Papademetris, X., & Constable, R. T. (2017). Using connectome-based predictive modeling to predict individual behavior from brain connectivity. Nat Protoc, 12(3), 506-518. https://doi.org/10.1038/nprot.2016.178
6. United Nations Office on Drugs and Crime (2023): World Drug Report 2023. www.unodc.org/unodc/en/data-and-analysis/world-drug-report-2023.html
7. Yip, S. W., Scheinost, D., Potenza, M. N., & Carroll, K. M. (2019). Connectome-Based Prediction of Cocaine Abstinence. The American Journal of Psychiatry, 176(2), 156-164. https://doi.org/10.1176/appi.ajp.2018.17101147

Poster No 590

Fingerprints of Psychiatric Symptoms in the Stomach-Brain Axis

Leah Banellis[1], Ignacio Rebollo[2], Micah Allen[3]

[1]Aarhus University, Aarhus C, Midtjylland, [2]German Institute of Human Nutrition, Potsdam-Rebrücke, Nuthetal, [3]Aarhus University, Lystrup, Denmark

Introduction: Pioneering research on brain-body interactions has revealed the existence of functional coupling between the rhythmic activities of the stomach and brain (Rebollo et al., 2018; Rebollo & Tallon-Baudry, 2021). While major breakthroughs support a pivotal role of the gut and enteric nervous system in psychopathology (Clapp et al., 2017; Margolis et al., 2021), the mental health implications of this recently discovered stomach-brain axis are unknown. We hypothesised that stomach-brain coupling in trans-diagnostic cortical networks would index individual differences in mental health, and in particular with anxiogenic factors.

Methods: We estimated stomach-brain phase-coupling (Rebollo et al., 2018; Rebollo & Tallon-Baudry, 2021) by combining resting-state functional brain imaging (3 Tesla, TR=1.4, 600 volumes) with electrogastrography (Koch & Stern, 2003) in the largest brain-body study to date, with 199 individuals. To assess a spectrum of psychiatric dimensions, we sampled participants exhibiting a distribution of symptoms from subclinical to clinically significant. Specifically, the psychiatric assessment battery incorporated 37 scores across 16 validated scales including broad symptoms such as anxiety, depression, fatigue, autism, and ADHD. We then utilised multivariate prediction techniques known as Canonical Correlation Analysis (Mihalik et al., 2022) to estimate stomach-brain fingerprints indexing these mental health profiles.

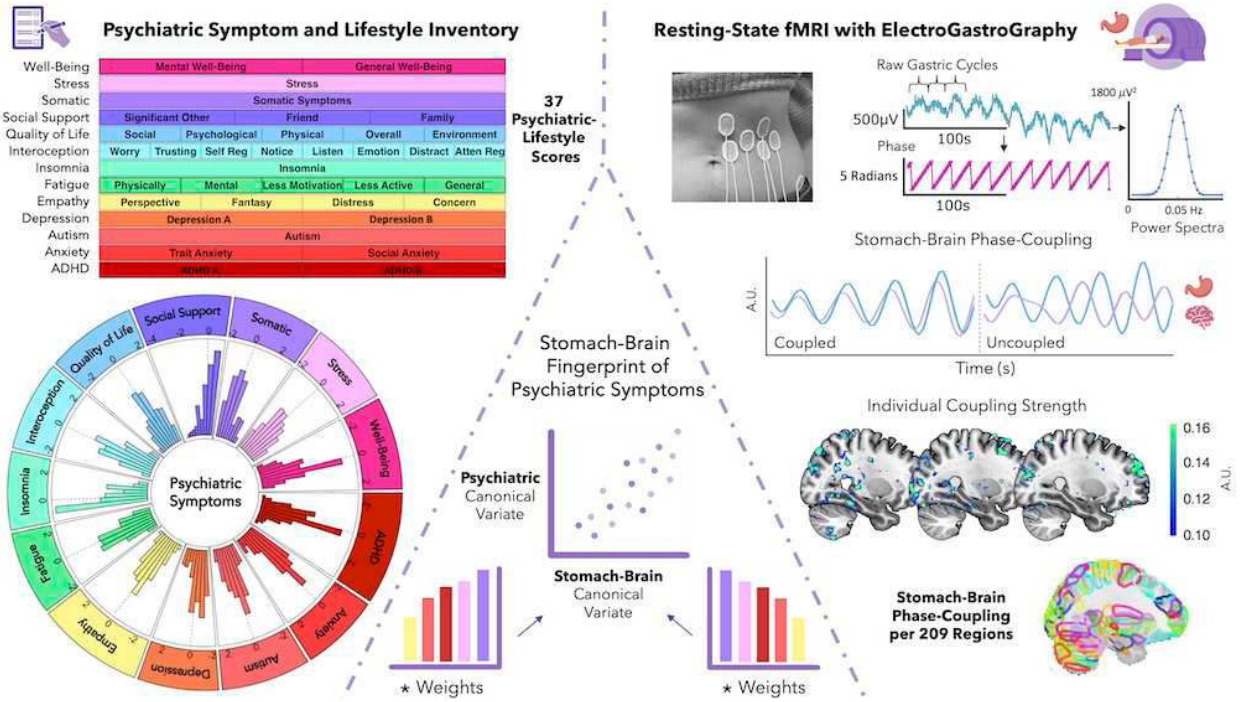

Results: We observed a robust, cross-validated stomach-brain fingerprint indexing psychiatric symptoms in attentional and control networks. Specifically, healthier mental states-characterised by a continuum of transdiagnostic symptoms, including lower levels of anxiety, depression, stress, and fatigue, as well as higher well-being and quality of life-are associated with weaker stomach-brain connections in key frontal and parietal regions. Crucially, this link is exclusive to the stomach-brain axis, controlling for brain connectivity, neural variability, bodily mass, and gastric function.

Conclusions: We discovered a unique stomach-brain biomarker of mental health, highlighting a previously unknown interoceptive component of psychiatric illness. By elucidating the complex interactions between the stomach and the brain in psychiatric illness, our findings lay the groundwork for novel diagnostic and therapeutic strategies targeting disordered brain-stomach interactions. This includes not only innovations like non-invasive vagus nerve stimulation, which recent studies such as Müller et al (2022) have found to modulate stomach-brain coupling, but also the exploration of innovative new mechanical and pharmacological interventions to remedy aberrant stomach-brain interactions (Mayeli et al., 2023; Nord et al., 2021). This breakthrough contributes significantly to multidisciplinary research on the gastrointestinal-brain axis and opens new avenues for therapeutic, diagnostic, and classification strategies in mental health.

References
1. Clapp, M. (2017). Gut Microbiota's Effect on Mental Health: The Gut-Brain Axis. Clinics and Practice, 7(4), Article 4.
2. Koch, K. L. (2003). Handbook of Electrogastrography. Oxford University Press.
3. Margolis, K. G. (2021). The Microbiota-Gut-Brain Axis: From Motility to Mood. Gastroenterology, 160(5), 1486–1501.
4. Mayeli, A. (2023). Parieto-occipital ERP indicators of gut mechanosensation in humans. Nature Communications, 14(1), Article 1.
5. Mihalik, A. (2022). Canonical Correlation Analysis and Partial Least Squares for Identifying Brain–Behavior Associations: A Tutorial and a Comparative Study. Biological Psychiatry: Cognitive Neuroscience and Neuroimaging, 7(11), 1055–1067.
6. Müller, S. J. (2022). Vagus nerve stimulation increases stomach-brain coupling via a vagal afferent pathway. Brain Stimulation, 15(5), 1279–1289.
7. Nord, C. L. (2021). A Causal Role for Gastric Rhythm in Human Disgust Avoidance. Current Biology, 31(3), 629-634.e3.
8. Rebollo, I. (2018). Stomach-brain synchrony reveals a novel, delayed-connectivity resting-state network in humans. eLife, 7, e33321.
9. Rebollo, I. (2021). The sensory and motor components of the cortical hierarchy are coupled to the rhythm of the stomach during rest. Journal of Neuroscience, 42(11), 2202–2220.

Poster No 591

Longitudinal changes in structural connectivity in young people at high risk for bipolar disorder

Gloria Roberts[1], Alistair Perry[2], Kate Ridgway[1], Vivian Leung[1], Megan Campbell[3], Rhoshel Lenroot[4], Philip Mitchell[1], Michael Breakspear[3]

[1]University of New South Wales, Sydney, New South Wales, [2]University of Cambridge, Cambridge, UK, [3]University of Newcastle, Newcastle, New South Wales, [4]University of New Mexico, Albuquerque, NM

Introduction: Recent studies of patients with bipolar disorder or at high genetic risk reveal structural dysconnections among key brain networks supporting cognitive and affective processes (Perry, Roberts et al. 2019). Understanding the longitudinal trajectories of these networks across the peak age range of bipolar disorder onset could inform mechanisms of illness onset or resilience.

Methods: Longitudinal diffusion-weighted MRI and phenotypic data were acquired at baseline and after 2 years in 183 individuals ages 12–30 years in two cohorts: 97 unaffected individuals with a first-degree relative with bipolar disorder (the high-risk group) and 86 individuals with no family history of mental illness (the control group). Whole-brain structural networks were derived using tractography, and longitudinal changes in these networks were studied using network-based statistics and mixed linear models.

Results: Both groups showed widespread longitudinal changes, comprising both increases and decreases in structural connectivity, consistent with a shared neurodevelopmental process. On top of these shared changes, high-risk participants showed weakening of connectivity in a network encompassing the left inferior and middle frontal areas, left striatal and thalamic structures, the left fusiform, and right parietal and occipital regions. Connections among these regions strengthened in the control group, whereas they weakened in the high-risk group, shifting toward a cohort with established bipolar disorder. There was marginal evidence for even greater network weakening in those who had their first manic or hypomanic episode before follow-up.

Conclusions: Neurodevelopment from adolescence into early adulthood is associated with a substantial reorganization of structural brain networks. Differences in these maturational processes occur in a multisystem network in individuals at high genetic risk of bipolar disorder. This may represent a novel candidate to understand resilience and predict conversion to bipolar disorder.

References
1. Perry*, Roberts*, et al. Connectomics of bipolar disorder: a critical review, and evidence for dynamic instabilities within interoceptive networks. Mol Psychiatry. 2019;24(9):1296-1318
2. DOI:10.1038/s41380-018-0267-2

Poster No 593

Aversive conditioning in patients with schizophrenia spectrum disorders using fMRI: A pilot study

Jimmy Jensen[1]

[1]Kristianstad University, Kristianstad, Sweden

Introduction: Abnormal functioning in the brain´s reward systems and prediction systems are reported in patients with schizophrenia spectrum disorders. The current study aimed to examine neural responses, particularly in the ventral striatum, as patients learned aversive associations in a Pavlovian conditiong paradigm.

Methods: Functional magnetic resonance images were obtained using a 3T GE signa HDx scanner. In the Pavlovian conditioning the conditioned stimulus (CS+), a coloured circle, was followed by an unconditioned stimulus (US). The US consisted of an unpleasant high noise in 50% of the trials. A control stimulus (CS-), a circle of another colour as compared to the CS+, was followed by a low not unpleasant sound in 50% of the trials. Twelve unmedicated patients with schizophrenia spectrum disorders and twelve healthy control subjects, matched on age, gender and IQ, underwent the conditioning paradigm using fMRI.

Results: No significant activation differences in the ventral striatum were obtained comparing the patients and the healthy controls using the contrast [CS+>CS-] (peak Z= 1.81; pSVC=n.s in the right ventral striatum). No significant correlations between symptoms and neural responses in the ventral striatum were found among the patients (all p>0.09).

Conclusions: In summary, the study yielded no significant differences in activations in the ventral striatum comparing patients with schizophrenia spectrum disorders and healthy controls in an aversive conditioning paradigm. However, the lack of effect might due to the low statistical power in this pilot study.

Poster No 594

DCE-MRI shows higher Blood–Brain Barrier leakage in first-episode Schizophrenia Spectrum Disorders

Joanna Moussiopoulou[1], Vladislav Yakimov[1], Boris Rauchmann[1], Hannah Toth[1], Julian Melcher[1], Iris Jäger[1], Isabel Lutz[1], Marcel Kallweit[1], Boris Papazov[2], Klaus Seelos[3], Amir Dehsarvi[4], Lukas Röll[1], Elias Wagner[1], Nicolai Franzmeier[4], Daniel Keeser[1,5]

[1]Department of Psychiatry and Psychotherapy, LMU University Hospital, Munich, Germany, [2]Department of Radiology, LMU University Hospital, Munich, Germany, [3]Institute of Neuroradiology, LMU University Hospital, Munich, Germany, [4]Institute for Stroke and Dementia Research (ISD), LMU University Hospital, Munich, Germany, [5]NeuroImaging Core Unit Munich (NICUM), Munich, Germany

Introduction: Previous studies that investigated disruptions in CNS barriers in schizophrenia spectrum disorders (SSD) mainly focused on changes in the cerebrospinal fluid (CSF), that only indirectly and inadequately allows conclusions about the blood-brain barrier (BBB). Dynamic contrast-enhanced MRI represents a sensitive method for investigating subtle barrier breakdown. Only one study so far investigated BBB breakdown in SSD with DCE-MRI, in a relatively small cohort. We hypothesized higher leakage in SSD compared to HC, that is indicative for a clinical sub-phenotype of SSD.

Methods: 45 people with SSD and 42 age- and sex-matched healthy controls (HC) were included in the study and 41 SSD and 40 HC were included in the final analyses. Structural and DCE-MRI were performed cross-sectionally. Clinical characterization, cognitive assessments, blood and CSF analysis were conducted. The analysis software ROCKETSHIP was used for DCE-MRI quantification and pharmacokinetic modelling (Patlak method) was implemented. The volume transfer constant Ktrans was calculated and Ktrans maps were compared between the groups to detect group differences in BBB leakage. Within the SSD cohort, the association of leakage with clinical characteristics was investigated.

Results: Group comparisons of Ktrans maps showed higher leakage in the SSD cohort compared to HC on a whole brain level in multiple widely distributed brain regions. The effect was stronger in first episode compared to multiple episode SSD patients. No association was detected between leakage and cognition, psychopathology, peripheral inflammation and Albumin serum/CSF ratio.

Conclusions: This is the study with the largest cohort to investigate the blood-brain barrier (BBB) in SSD with DCE-MRI, allowing direct exploration of the BBB, compared to a healthy control group and the first study to implement this modality in a multimodal approach, with CSF, blood, clinical and cognitive assessments. The results provide the first in vivo evidence of higher BBB leakage on a whole brain level compared to HC.

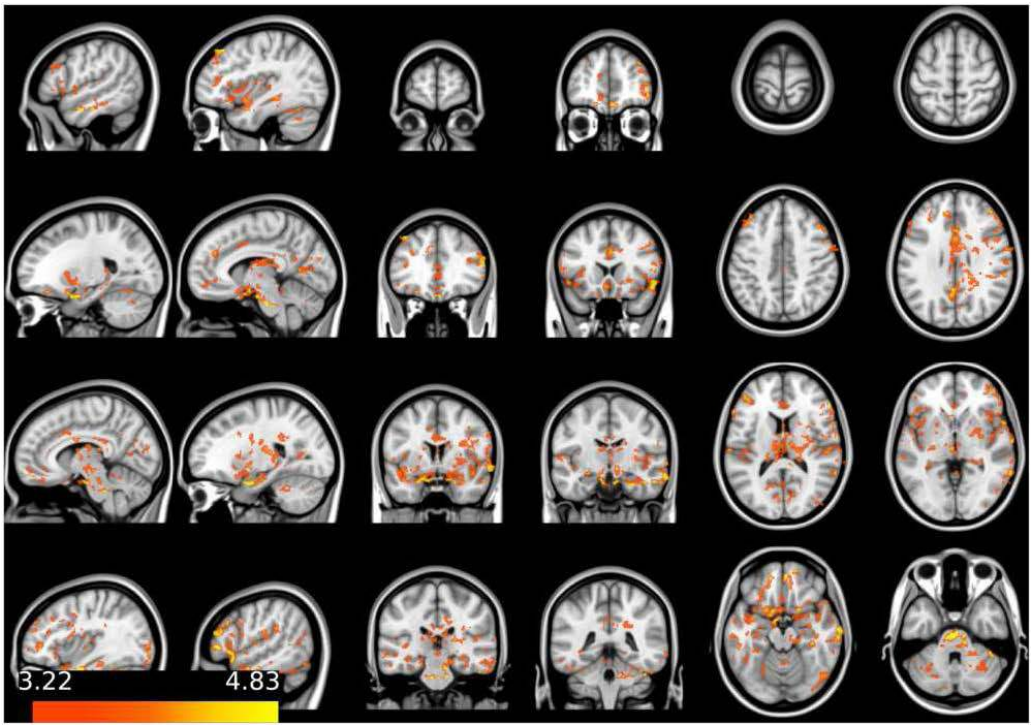

Fig. SSD vs. HC Ktrans map comparison (SPM12)

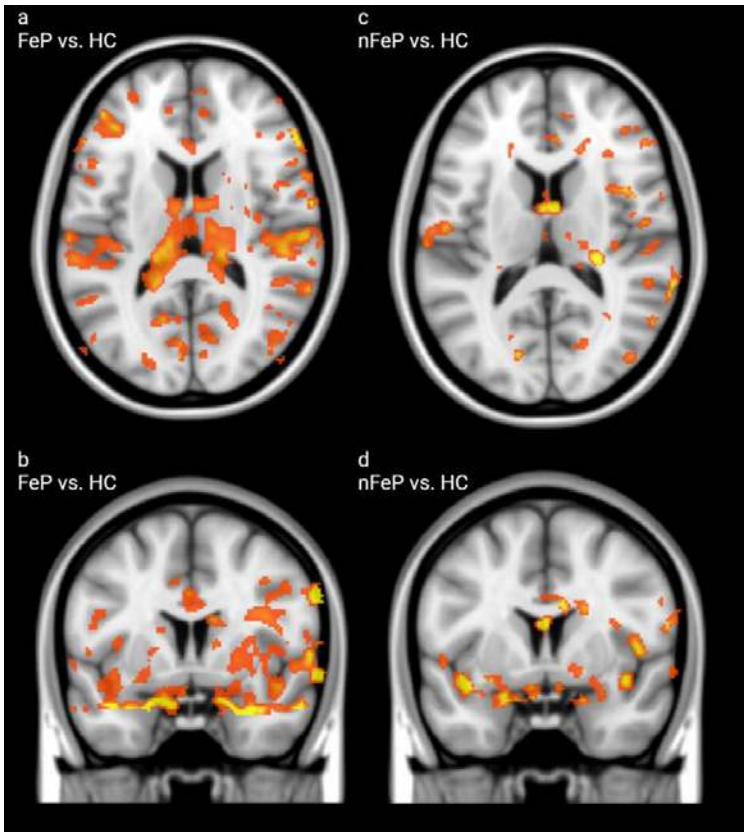

FEP vs. nFEP SSD vs. HC Ktrans map comparison (SPM12)

References

1. Barnes, S.R., et al., ROCKETSHIP: a flexible and modular software tool for the planning, processing and analysis of dynamic MRI studies. BMC Med Imaging, 2015. 15: p. 19.
2. Patlak, C.S., R.G. Blasberg, and J.D. Fenstermacher, Graphical evaluation of blood-to-brain transfer constants from multiple-time uptake data. J Cereb Blood Flow Metab, 1983. 3(1): p. 1-7.

Poster No 595

Predicting Future Recurrence in Affective Disorders from Brain-Age Gaps in a 9-Year Follow-Up

Nils Winter[1], Katharina Förster[2], Thomas Frodl[3], Klaus Berger[4], Philipp Kanske[5], Jan Ernsting[6], Ramona Leenings[7], Carlotta Barkhau[7], Maximilian Konowski[1], Lukas Fisch[7], Daniel Emden[7], Udo Dannlowski[7], Tim Hahn[7], Dominik Grotegerd[8]

[1]University of Münster, Münster, North-Rhine Westphalia, [2]University of Dresden, Dresden, Saxony, [3]RWTH Aachen University, Aachen, North-Rhine Westphalia, [4]Institute of Epidemiology and Social Medicine, University of Münster, Münster, NRW, Germany, [5]Clinical Psychology and Behavioral Neuroscience, Technische Universität Dresden, Dresden, Germany, [6]University of Münster, Münster, NRW, [7]Institute for Translational Psychiatry, Münster, North Rhine Westphalia, [8]Institute for Translational Psychiatry, University of Münster, Münster, North Rhine-Westphalia

Introduction: Affective disorders contribute immensely to the global burden of disease worldwide (Murray et al., 2012; Paykel et al., 2005). Recently, a novel multivariate biomarker has emerged in the field of neuroimaging that aims at quantifying the age-associated biological changes that occur in the brain (Cole et al., 2019). The underlying hypothesis of the brain age prediction paradigm is that this brain age gap (BAG) may serve as a marker of disease risk and there are a number of studies emphasizing an association between brain age gaps and clinically relevant variables (Bittner et al., 2021; Elliott et al., 2019). We investigated associations of the brain age gap with disease course over nine years in patients with affective disorders in a long-term prospective design.

Methods: At two time-points, we acquired T1-weighted MRI images (mean [SD] follow-up period 8.98 [2.20] years) of patients with affective disorders (N = 38) and healthy controls (HC: N = 37) at two sites (Dublin, UK; Münster, Germany). Using a publicly available, uncertainty-aware brain age prediction model trained on a sample of over 10,000 individuals of the German National Cohort (GNC), we estimated individual BAG at two time-points (baseline and follow-up) using gray matter segments derived from MRI images (Hahn et al., 2022). In short, in contrast to existing brain age models, the MCCQR-NN model provides accurate estimations of predictive uncertainty in high-dimensional neuroimaging data while ensuring state-of-the-art model performance. It is therefore especially suited for the detection of subtle brain age changes, e.g., in clinical cohorts. Employing linear-mixed-effects models, we tested main effects of diagnosis at follow-up and hospitalizations during follow-up on BAG at baseline and follow-up, as well as the interaction of diagnosis and hospitalization with time respectively. In an exploratory analysis, we tested if BAG at baseline was predictive of further hospitalizations during the nine-year follow-up using logistic regression and 10-fold nested cross-validation. All brain age predictions and machine learning analyses were made using the Python package PHOTONAI (Leenings et al., 2021).

Results: MDD patients showed a larger BAG compared to HC (MDD>HC: p=.039, MDD vs. BD: n.s.), while BD patients only showed a tendency for a larger BAG (p=.066). In the Münster subsample (N=52), patients with hospitalizations showed a higher BAG compared to patients without hospitalizations (p=.001). No significant group-by-time interaction could be detected. However, an increased baseline BAG was linked to the number of hospitalizations during follow-up (p=.018). Employing machine learning to predict hospitalization based on the baseline BAG resulted in a classification accuracy of 64.3%, yet this did not reach statistical significance.

Conclusions: Using a state-of-the-art brain age prediction model trained on T1-weighted MRI images of 10,000 individuals, we calculated and compared brain age gaps in a sample of 75 patients with affective disorders and healthy controls, measured at two time points with a mean follow-up length of nine years. Our results show that BAG did not change over time as a function of patients' course of disease. The present study rather suggests that a higher estimation of biological ageing (higher BAG) predicts future hospitalizations. Therefore, BAG may indicate a patient's vulnerability to future recurrence.

References

1. Murray, C. J. L., Vos, T., Lozano, R., Naghavi, M., Flaxman, A. D., Michaud, C., Ezzati, M., Shibuya, K., Salomon, J. A., Abdalla, S., Aboyans, V., Abraham, J., Ackerman, I., Aggarwal, R., Ahn, S. Y., Ali, M. K., Alvarado, M., Anderson, H. R., Anderson, L. M., … Memish, Z. A. (2012). Disability-adjusted life years (DALYs) for 291 diseases and injuries in 21 regions, 1990-2010: A systematic analysis for the Global Burden of Disease Study 2010. Lancet, 380(9859), 2197–2223.
2. Paykel, E. S., Brugha, T., & Fryers, T. (2005). Size and burden of depressive disorders in Europe. European Neuropsychopharmacology: The Journal of the European College of Neuropsychopharmacology, 15(4), 411–423.
3. Cole, J. H., Marioni, R. E., Harris, S. E., & Deary, I. J. (2019). Brain age and other bodily 'ages': Implications for neuropsychiatry. Molecular Psychiatry, 24(2), 266–281.
4. Bittner, N., Jockwitz, C., Franke, K., Gaser, C., Moebus, S., Bayen, U. J., Amunts, K., & Caspers, S. (2021). When your brain looks older than expected: Combined lifestyle risk and BrainAGE. Brain Structure & Function, 226(3), 621–645.
5. Elliott, M. L., Belsky, D. W., Knodt, A. R., Ireland, D., Melzer, T. R., Poulton, R., Ramrakha, S., Caspi, A., Moffitt, T. E., & Hariri, A. R. (2019). Brain-age in midlife is associated with accelerated biological aging and cognitive decline in a longitudinal birth cohort. Molecular Psychiatry, 1–10.

6. Hahn, T., Ernsting, J., Winter, N. R., Holstein, V., Leenings, R., Beisemann, M., Fisch, L., Sarink, K., Emden, D., Opel, N., Redlich, R., Repple, J., Grotegerd, D., Meinert, S., Hirsch, J. G., Niendorf, T., Endemann, B., Bamberg, F., Kröncke, T., ... Berger, K. (2022). An uncertainty-aware, shareable, and transparent neural network architecture for brain-age modeling. Science Advances.
7. Leenings, R., Winter, N. R., Plagwitz, L., Holstein, V., Ernsting, J., Sarink, K., Fisch, L., Steenweg, J., Kleine-Vennekate, L., Gebker, J., Emden, D., Grotegerd, D., Opel, N., Risse, B., Jiang, X., Dannlowski, U., & Hahn, T. (2021). PHOTONAI—A Python API for rapid machine learning model development. PLOS ONE, 16(7), e0254062.

Poster No 596

Abnormal cortical glutamate and GABA in individuals with depression and schizophrenia: an MRS study

Shitong Xiang[1], Chao Xie[1], Yijie Zhao[1], Yuchao Jiang[1], Chun Shen[1], Yuzhu Li[1], Xiao Chang[1], Jianfeng Feng[1]

[1]Fudan University, Shanghai, Shanghai

Introduction: Comorbidity in psychiatry, the co-occurrence of two or more psychiatric conditions, has received increasing attention given its high prevalence and persistence (Krueger & Eaton, 2015). Schizophrenia (SCZ) is a major psychiatric disorder and global leading cause of disability. Depressive symptoms commonly occur in schizophrenia and have a significant impact on the distress and burden of the illness (Upthegrove, Marwaha, & Birchwood, 2017). A substantial neuropharmacological evidence suggested a glutamate hypothesis for SCZ (Uno & Coyle, 2019) and a glutamate hypothesis for depression (Sanacora, Treccani, & Popoli, 2012). Our recent studies revealed a shared trajectory in the development of SCZ and depression, specifically associated with structural abnormalities in the anterior cingulate cortex (Chen et al., 2023; Jiang et al., 2023). However, there has been little analysis of underlying neurochemical mechanisms.

Methods: Here, we utilized 7-Tesla proton magnetic resonance spectroscopy (1H-MRS) to assess the concentrations of glutamate (Glu) and γ-amino-butyric acid (GABA) in dorsal anterior cingulate cortex (dACC, Fig. 1a) of healthy participants and individuals with major depression disorder (MDD) or schizophrenia (SCZ). Briefly, participants underwent whole-brain T1-weighted MR and single-voxel proton MRS scans using a 7T Terra MRI (Siemens). LCModel (version 6.3-IL, Provencher, 1993) was used to processed the MRS data with an automated fitting routine. Individual component fitted spectra for the metabolites between 1.2 and 4.2 ppm were extracted for inspection. The concentrations of those metabolites were quantified relative to Cr+PCr (creatine plus phosphocreatine). After quality control, total 128 aged 18-55 years old participants (52 healthy controls, 40 patients with MDD and 36 patients with SCZ) were including in the following analysis. Besides sex and age, the concentration of N-acetylaspartate (NAA, a measure of neuronal integrity) and total intracranial volume were controlled as additional confounders.

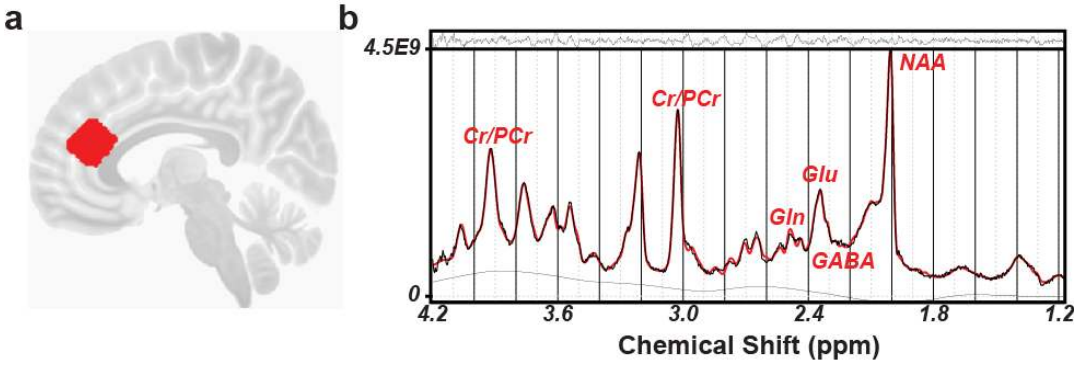

Fig.1 An illustration for the MRS data acquisition.

Results: In the dACC, the levels of Glu and GABA were significantly lower in both MDD group and SCZ group compared to the healthy controls (for Glu, MDD vs healthy controls: $t87 = -2.742$, $p = 0.007$, Cohen's $d = -0.583$, SCZ vs healthy controls: $t83 = -2.126$, $p = 0.037$, Cohen's $d = -0.466$; for GABA, MDD vs healthy controls: $t87 = -2.202$, $p = 0.030$, Cohen's $d = -0.468$, SCZ vs healthy controls: $t83 = -4.531$, $p < 0.001$, Cohen's $d = -0.994$; Fig. 2a). Notably, there were positive relationships between Glu and GABA in the dACC among all healthy control group ($r48 = 0.304$, $p = 0.032$), MDD group ($r36 = 0.589$, $p < 0.001$) and SCZ group ($r32 = 0.506$, $p = 0.002$) (Fig. 2b). Interestingly, the correlation within the patient groups showed an increasing trend, but the difference of intergroup comparisons was under the statistical significance threshold. In addition to the correlation analysis above, the comparison analysis on the ratio between Glu and GABA suggested that both patients with MDD and SCZ established a higher contrast of excitatory and inhibitory neurotransmission than that in healthy controls (MDD vs healthy controls: $t87 = 2.112$, $p = 0.038$, Cohen's $d = 0.449$; SCZ vs healthy controls: $t83 = -3.523$, $p = 0.001$, Cohen's $d = 0.773$).

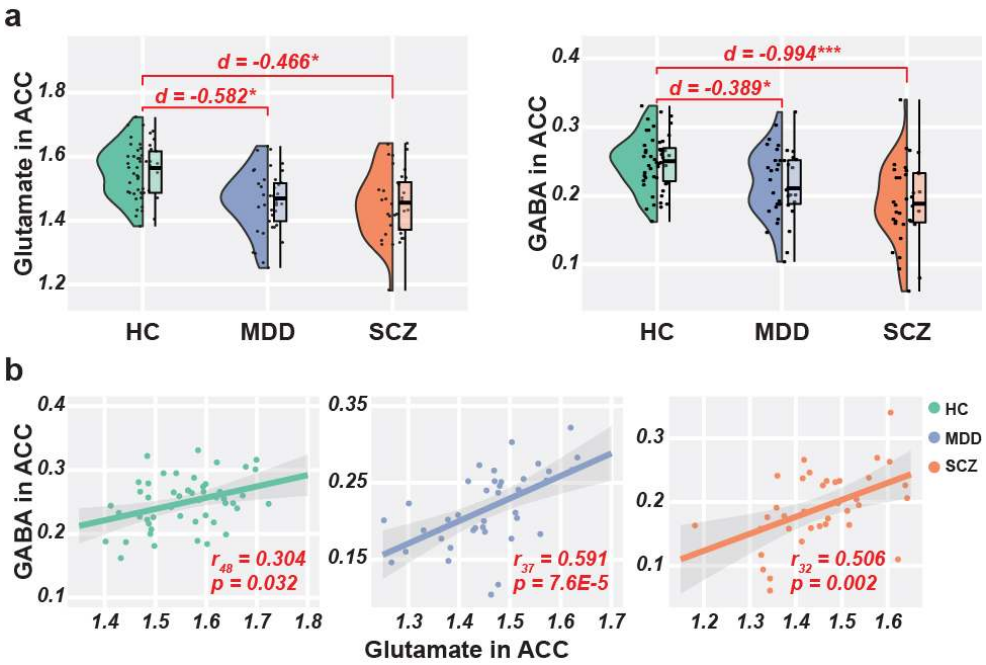

Fig.2 Abnormal cortical cneurochemical indices of the levels Glu and GABA among both patients with major depression disorder and schizophrenia.

Conclusions: Altogether, this 7T MRS study has demonstrated that SCZ and MDD are shared common neurochemical indices in the dACC, suggestive of the deceased levels of Glu and GABA. Moreover, an altered ratio between the neurometabolites Glu and GABA in this region implicated in an abnormal excitatory/inhibitory balance, hence supporting the glutamate hypothesises of these psychiatric disorders and suggesting a converged underlying neurochemical mechanisms.

References

1. Chen, D., Wang, X., Voon, V., Jiang, Y., Lo, C.-Y. Z., Wang, L., . . . Feng, J. (2023). Neurophysiological stratification of major depressive disorder by distinct trajectories. Nature Mental Health, 1(11), 863-875.
2. Jiang, Y., Wang, J., Zhou, E., Palaniyappan, L., Luo, C., Ji, G., . . . Feng, J. (2023). Neuroimaging biomarkers define neurophysiological subtypes with distinct trajectories in schizophrenia. Nature Mental Health, 1(3), 186-199.
3. Krueger, R. F., & Eaton, N. R. (2015). Transdiagnostic factors of mental disorders. World Psychiatry Official Journal of the World Psychiatric Association, 14(1), 27-29.
4. Provencher, S. W. (1993). Estimation of metabolite concentrations from localized in vivo proton NMR spectra. Magn Reson Med, 30(6), 672-679.
5. Sanacora, G., Treccani, G., & Popoli, M. (2012). Towards a glutamate hypothesis of depression: an emerging frontier of neuropsychopharmacology for mood disorders. Neuropharmacology, 62(1), 63-77.
6. Uno, Y., & Coyle, J. T. (2019). Glutamate hypothesis in schizophrenia. Psychiatry Clin Neurosci, 73(5), 204-215.
7. Upthegrove, R., Marwaha, S., & Birchwood, M. (2017). Depression and Schizophrenia: Cause, Consequence, or Trans-diagnostic Issue? Schizophr Bull, 43(2), 240-244.

Poster No 597

White matter microstructure in major depressive disorder is associated with lymphocyte count

Susanne Meinert[1], Anna-Lena Boller[1], Tilo Kircher[2], Udo Dannlowski[3], Judith Alferink[1]

[1]University of Münster, Münster, NRW, [2]Department of Psychiatry and Psychotherapy, University of Marburg, Marburg, Hesse, [3]Institute for Translational Psychiatry, Münster, North Rhine Westphalia

Introduction: In major depressive disorder (MDD), white matter abnormalities and immunological influences are discussed in its pathogenesis. Studies have found altered fibre microstructure as measured by fractional anisotropy (FA) in the corpus callosum and superior longitudinal fasciculus in MDD[1]. In addition, immune system imbalances are described in these patients[2]. Inflammatory processes could exert neurotoxic influences on the fibre structure, which is why both pathophysiological processes are closely intertwined[3]. Since differential immune responses in MDD should be most apparent when confronted with stress, it is not surprising that previous studies have already linked childhood maltreatment experiences with changes in fibre structure as well as inflammatory processes[1,4]. The aim of this study was to describe the interactions between childhood maltreatment, fibre structure, and the immune system.

Methods: N=159 age- and sex-matched MDD and healthy controls (HC) from the FOR2107 consortium were analysed, half of whom were classified as maltreated. Maltreatment was defined as two Childhood Trauma Questionnaire (CTQ) subscales that exceed defined thresholds[5] (N=40 HC_CTQ-, N=40 HC_CTQ+, N=39 MDD_CTQ-, N=40 MDD_CTQ+). Four novel lymphocyte subtypes were combined using principal component analysis (KMO=.618, Bartlett-$\chi^2(6)$<.001). Factor loadings were compared between the diagnosis (MDD vs. HC) and maltreatment (yes vs. no) groups. Diffusion tensor imaging was collected for all participants. Using tract-based spatial statistics, FA was associated with lymphocyte factor loadings. Associations between FA and lymphocyte factor loadings were compared between diagnosis and maltreatment groups. All DTI analyses were performed in a region-of-interest (ROI) analysis in the corpus callosum and the superior longitudinal fasciculus (ptfce-FWE<.05), in addition to an exploratory whole-brain approach (ptfce-FWE<.10).

Results: A lymphocyte factor was found (eigenvalue=1.99, 49.7%). The lymphocyte factor did not differ between MDD and HC (p=.217). However, there was a main effect of maltreatment (p=.026, η^2=.032) and a diagnosis x maltreatment interaction (p=.015, η^2=.038). While no difference was found in HC with or without maltreatment, MDD patients with adverse childhood experiences had fewer immune cells than those without such experiences. Moreover, the lymphocyte factor was negatively associated with FA (ptfce-FWE=.021) in the corpus callosum. Using the exploratory threshold, the corpus callosum was confirmed in addition to the corona radiata and the thalamic radiation in the whole-brain approach (ptfce-FWE=.076). No effects were found in the superior longitudinal fasciculus (ptfce-FWE=.084) and no diagnosis and/or maltreatment interactions were present.

Conclusions: A negative association was found between the combination of novel lymphocyte counts and white matter microstructure of the corpus callosum. This association did not differ between MDD and HC or as a function of maltreatment status. Nevertheless, differences in lymphocyte count were evident between maltreated and nonmaltreated MDD. This could contribute to the heterogeneity of neurobiological findings in depressed patients. Future longitudinal and experimental studies should build on this work to use knowledge of immunological processes to initiate new therapeutic developments.

References

1. Meinert S, Repple J, Nenadic I, Krug A, Jansen A, Grotegerd D, et al. Reduced fractional anisotropy in depressed patients due to childhood maltreatment rather than diagnosis. Neuropsychopharmacology : official publication of the American College of Neuropsychopharmacology. 2019;44(12):2065–72.
2. Otte C, Gold SM, Penninx BWJH, Pariante CM, Etkin A, Fava M, et al. Major depressive disorder. Nature reviews Disease primers. 2016;2:16065.
3. O'Donovan A, Bahorik A, Sidney S, Launer LJ, Yaffe K. Relationships of inflammation trajectories with white matter volume and integrity in midlife. Brain, behavior, and immunity. 2021;91:81–8.
4. Osborn M, Widom CS. Do documented records and retrospective reports of childhood maltreatment similarly predict chronic inflammation? Psychological Medicine. 2020;50(14):2406–15.
5. Walker EA, Gelfand A, Katon WJ, Koss MP, Von Korff M, Bernstein D, et al. Adult health status of women with histories of childhood abuse and neglect. The American Journal of Medicine. 1999 Oct;107(4):332–9.

Poster No 598

EEG microstates reveal brain network dynamics changes with circuit-targeted TMS on anhedonia

QiangYan Che[1], Xinyu Huang[1], Xingyu Zhao[1], Ya Fang[1], Rong Ye[1], Fengqiong Yu[1]

[1]*Anhui Medical University, Hefei, Anhui*

Introduction: A growing body of neuroimaging studies have implicated anhedonia as a core symptom of major depressive disorder that results from dysfunction in the brain's reward circuitry. These studies have inspired the use of transcranial magnetic stimulation (TMS) targeted to sites connected to the reward circuit as a treatment for anhedonia. Yet its mechanism of action is still not known. High temporal resolution of Electroencephalography (EEG) "microstates" as a tool for studying the temporal dynamics of whole-brain neuronal networks. Therefore, the aim of this study is to investigate the therapeutic impact of circuit-targeted TMS on network dynamics in depressive patients along with anhedonia as well as to explore relationship between microstates and therapeutic efficacy.

Methods: 49 patients of major depressive disorder (MDD) along with anhedonia symptoms age =22.5±7.7, were enrolled for this randomized, sham-controlled, double-blind trial. We also recruited 15 age - and sex-matched healthy controls. patients were randomly assigned to either Active TMS group(26 subjects) or Sham group (23 subjects). Each participant received once-daily session of TMS treatment for 15 days with10 Hz frequency and 100% motor threshold, using either active or sham coil. Stimulation was localized to the site of strongest left dorsolateral prefrontal cortex (DLPFC)–nucleus accumbens (NAcc) network by functional magnetic resonance imaging. The Hamilton depression rating scale (HAMD) was used to measure depression severity, the temporal experience pleasure scale (TEPS) to measure anhedonia symptoms. Polarity-insensitive

modified k-means clustering was used to segment EEG microstates into four canonical microstates (A-D). Independent samples t-tests were used to compare the microstate characteristics between patients and healthy controls. Linear mixed effects models tested for within-subject differences over time and microstate features between Active group and Sham group. To understand the relationship between TMS clinic efficacy and microstate characteristics. Linear mixed effects models were used to test for differences in microstate metrics over time between responder and non-responder groups.

Results: Compared with healthy controls, patients show a decreased metrics of microstate C(Occurrence P=0.0002,PFDR=0.002,Cohen's d=1.12;Contribution P=0.004, PFDR =0.025, Cohen's d=0.84)and increased metrics of microstate D(Duration P= 0.006,PFDR=0.025,Cohen's d=0.81;Contribution P=0.015, PFDR =0.046, Cohen's d=0.71) . Linear mixed effects models reveal significant interaction effect of group × time on the microstate C (Occurrence F= 5.053,p =0.029; Contribution F =5.006, p =0.030) reflecting increases over time in microstate C on Active group. Clinical response to TMS was associated with increases in features of microstate C(Occurrence F=6.075,p= 0.012; Duration F=4.875,p= 0.037)and decreases in features of microstate D(Occurrence F=5.158,p= 0.032; Contribution F=7.418,p= 0.012; Duration F=4.4079,p= 0.046) . Non-responders showed no significant changes in any microstate. Linear mixed effects models also show significant interaction effect of group × time on the TEPS total score(F =6.724, p =0.013) reflecting increases over time in TEPS total score on Active TMS group, as well as the main effect of time(F =11.692, p =0.001).

Conclusions: Reduction of metrics microstate C in depressive patients with anhedonia symptoms can be selective modulated through intervention with TMS targeting the left DLPFC–NAcc network. Our finding suggests that microstate C may be closely related to the reward network and anhedonia severity. Furthermore, we identify the changes of microstate C and D are associated with effectiveness of outcome for circuit-based TMS with anhedonia symptoms. Overall, resting-state EEG microstates seems a promising tool for monitoring illness severity and evaluating treatment efficacy through objective neurophysiological biomarkers in psychiatric disorders.

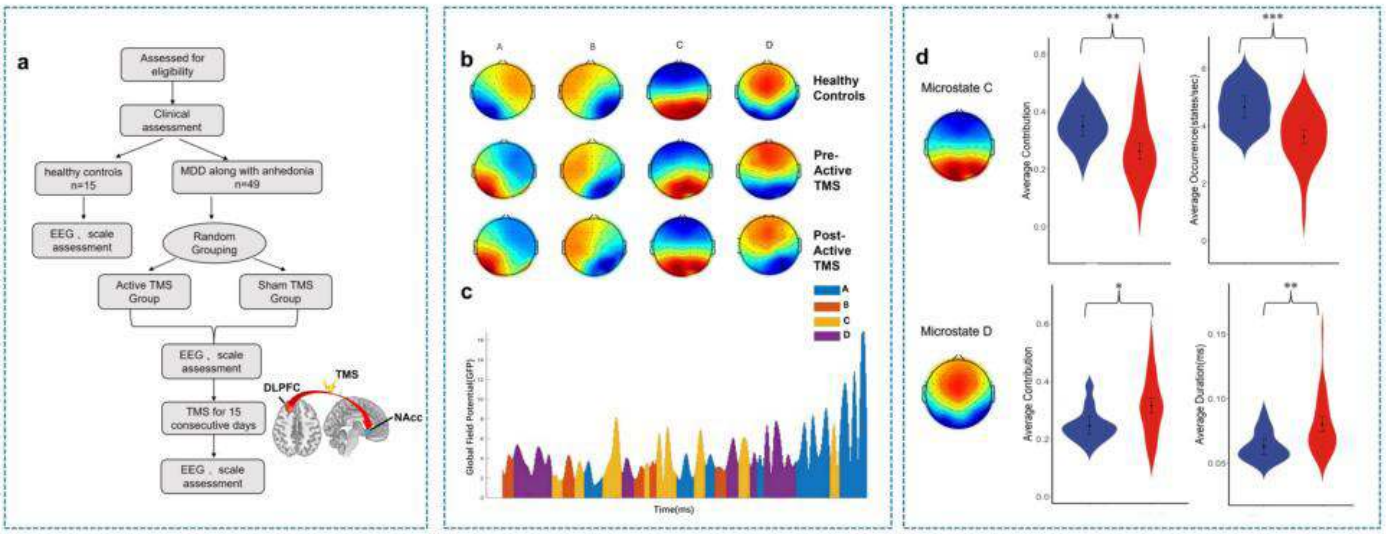

Fig. 1. Study Workflow ,Microstate Topographies , Representation and Microstate changes in patients of Major Depressive Disorder(MDD) along with anhedonia and healthy controls . a) Diagram illustrating randomization of depressed patients with anhedonia to the Active and Sham groups and treatment flowchart. b) 4 clustered prototype microstate voltage maps. In Figure b, the top row represents the EEG microstate topographies of the healthy control group, the middle row represents the topographies before connectivity-directed TMS treatment, and the bottom row represents topographies after 15 days of connectivity-directed TMS treatment. c) Representative sample from one subject after Active TMS treatment over a 2 s microstate segmentation of EEG transformed into its Global Field Potential (GFP). K-means clustering utilizes the EEG signal at GFP peaks. d) Violin plots showing the metric of microstate C and D in each of the two groups. In violin plots, black points are medians, error bars are 95%confidence interval. Blue is the HC group, red is MDD along with anhedonia. The figure displays uncorrected p-values .*: $p < 0.05$, **: $p < 0.01$.

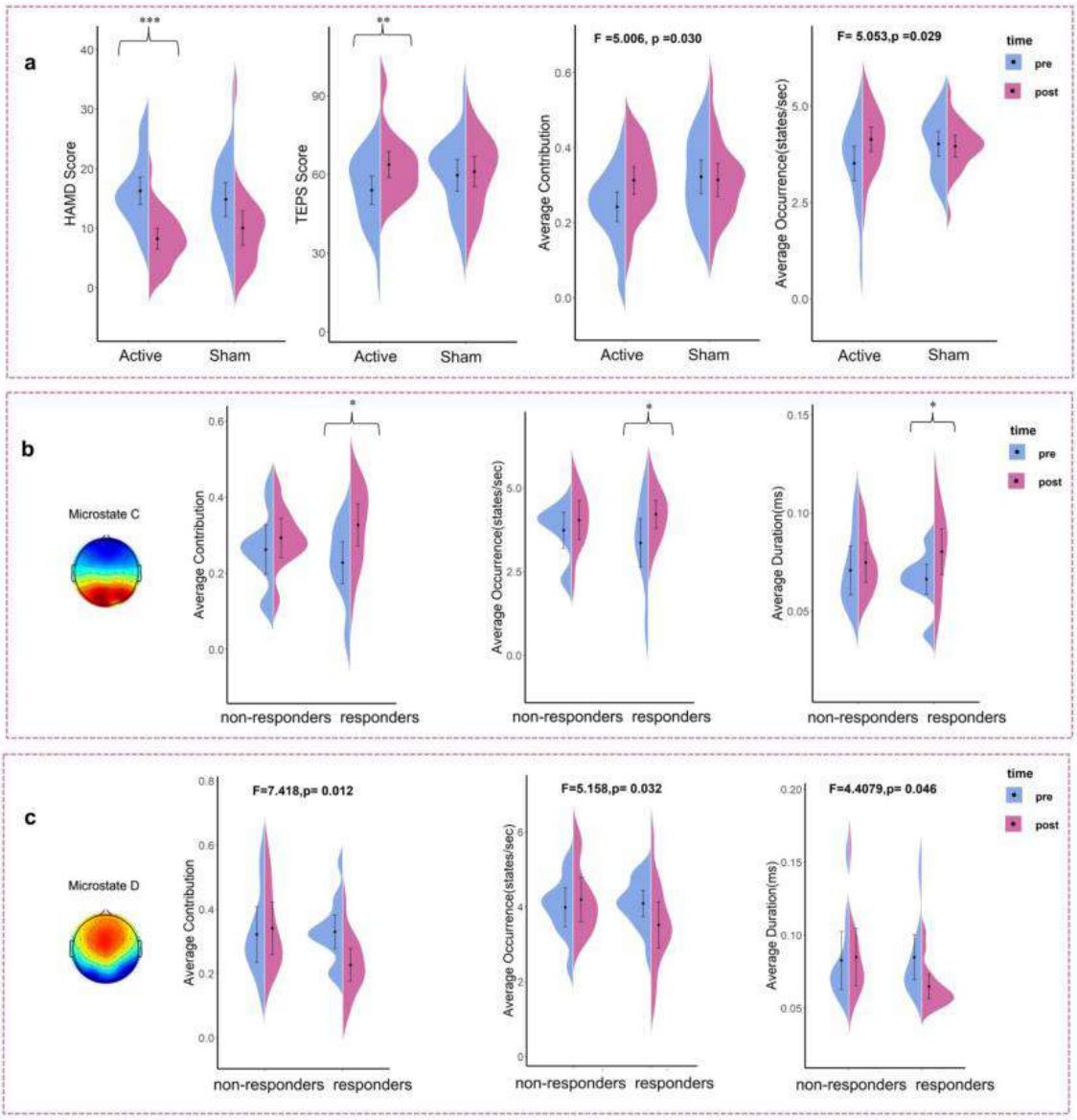

Fig. 2. Categorical Microstate Changes After TMS Course and clinical symptoms improvement . a) Violin plots show that Individually targeted repetitive transcranial magnetic stimulation (rTMS) of the left dorsolateral prefrontal cortex (DLPFC) improved anhedonia and general symptoms of depression. There is a significant interaction effect of group × time on the average Contribution and Occurrence of microstate C. b) Compared with non-responders, responders(HAMD decrease ≥50% after treatment) show a increased metrics of microstate C. c) Linear mixed effects models reveal significant interaction effect of group × time on the microstate D. This reflects decreases over time in microstate D on responders group. In violin plots, black points are medians, error bars are 95%confidence interval. Sky blue is pre-treatment, pink is post-treatment. The figure displays uncorrected p-values .*: $p < 0.05$, **: $p < 0.01$., ***:$p<0.001$.

References

1. Britz, J.(2010), "BOLD correlates of EEG topography reveal rapid resting-state network dynamics," Neuroimage, vol. 52, no. 4, pp. 1162-1170.
2. Gold, M. C. (2022), "Large-scale EEG neural network changes in response to therapeutic TMS," Brain Stimulation, vol. 15, no. 2, pp. 316-325.
3. Michel, C. M. (2018), "EEG microstates as a tool for studying the temporal dynamics of whole-brain neuronal networks: A review," Neuroimage, vol. 180, pp. 577-593.
4. Murphy, M. (2020), "Abnormalities in electroencephalographic microstates are state and trait markers of major depressive disorder," Neuropsychopharmacology, vol. 45, no. 12, pp. 2030-2037.Poulsen 2018, "Microstate EEGlab toolbox: an introductory guide", bioRxiv:289850.
5. Treadway, M. T. (2011), "Reconsidering anhedonia in depression: Lessons from translational neuroscience," Neuroscience and Biobehavioral Reviews, vol. 35, no. 3, pp. 537-555.
6. Williams L. M. (2017), "Defining biotypes for depression and anxiety based on large-scale circuit dysfunction: a theoretical review of the evidence and future directions for clinical translation," Depression and anxiety, vol. 34, no. 1, pp. 9-24.
7. Wang, X. (2021), "Therapeutic efficacy of connectivity-directed transcranial magnetic stimulation on anticipatory anhedonia," (in eng), Depression and anxiety, vol. 38, no. 9, pp. 972-984.

Poster No 599

Quantitative analysis of MRI-visible perivascular spaces in schizophrenia

Hagyeong Yu[1], Changmin Ryu[1], Junghwa Kang[1], Yoonho Nam[1], Tae Young Lee[2]

[1]Division of Biomedical Engineering, Hankuk University of Foreign Studies, Yongin, South Korea, [2]Department of Neuropsychiatry, Pusan National University Yangsan Hospital, Yangsan, South Korea

Introduction: Schizophrenia is a complex neuropsychiatric disorder characterized by diverse symptoms affecting cognitive, emotional, and social functioning. The glymphatic system, a network of dilated PVS (dPVS) and vessels in the brain responsible for clearing waste products and facilitating cerebrospinal fluid flow, has gained increasing attention in neuroimaging research. However, there are not many studies focused on dPVS when it comes to schizophrenia. By using dPVS imaging as a tool for assessing the glymphatic system in the brain, valuable insights into its functionality and potential implications for neurological conditions like schizophrenia may be expected. In this study, we investigated dPVS in schizophrenia subgroups by a visual and volumetric assessment using our automatic pipeline.

Methods: We collected 3D T1-weighted images of subjects categorized into schizophrenia subgroups. The subgroups include 66 patients with first-episode psychosis (FEP), 31 patients with treatment-resistant schizophrenia (TRS), 48 patients classified as clinical high risk for psychosis (CHR), 25 patients with major depressive disorder (MD), and 90 healthy control subjects (HC). For volumetric assessment, we segmented the dPVS included in the regions of interest (ROI), specifically basal ganglia (BG) and white matter (WM), using deep learning-based automatic pipeline. Then, the volumes and numbers of dPVS were calculated for each subject and subgroup. To provide the dPVS volume fraction, the dPVS volumes were divided by the individual brain volumes of each patient. In addition, to compare the dPVS distributions between subgroups, we performed a nonlinear fully deformable registration to MNI space with FSL Anat. For statistical analysis, Student's t-test was used to compare healthy control group with each schizophrenia subgroup. A p-value ≤0.05 was considered as statistically significant.

Results: Our findings reveal differences in dPVS numbers and volumes among schizophrenia subgroups, especially in treatment-resistant schizophrenia(TRS) which showed smaller dPVS volumes compared to other groups in both WM and BG. Figure 2a shows the quantitative differences in dPVS volumes among the various subgroups. Notably, TRS showed relatively small dPVS volumes and numbers compared to other groups for both WM ($p \leq 0.05$) and BG ($p \leq 0.05$). Figure 2b shows the group averaged dPVS maps, offering a visual representation of the distribution of dPVS of each subgroup.

Conclusions: We have investigated the volumes and numbers of dPVS in schizophrenia subgroups. While dPVS volumes in TRS have been observed to be significantly smaller than other subgroups, further research is needed to fully explain the underlying mechanisms driving these volume differences. Our results indicate that the quantification of dPVS may hold promise in distinguishing different schizophrenia subgroups. While this study contributes to our understanding of PVS in schizophrenia, ongoing research is essential to clarify the mechanisms underpinning the observed differences and to determine the clinical relevance of dPVS quantification as a diagnostic tool for schizophrenia.

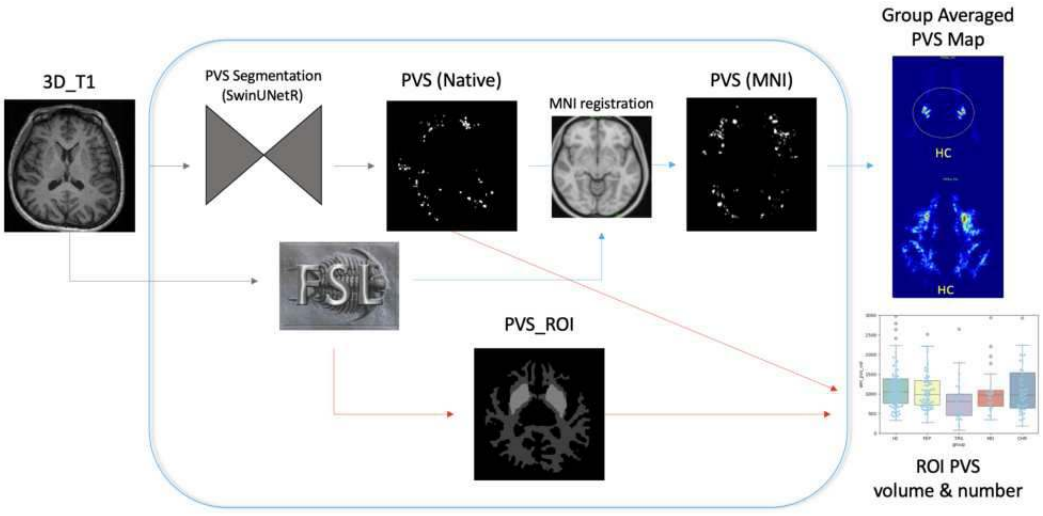

Figure 1. Overview workflow of the processing pipeline for dPVS quantification.

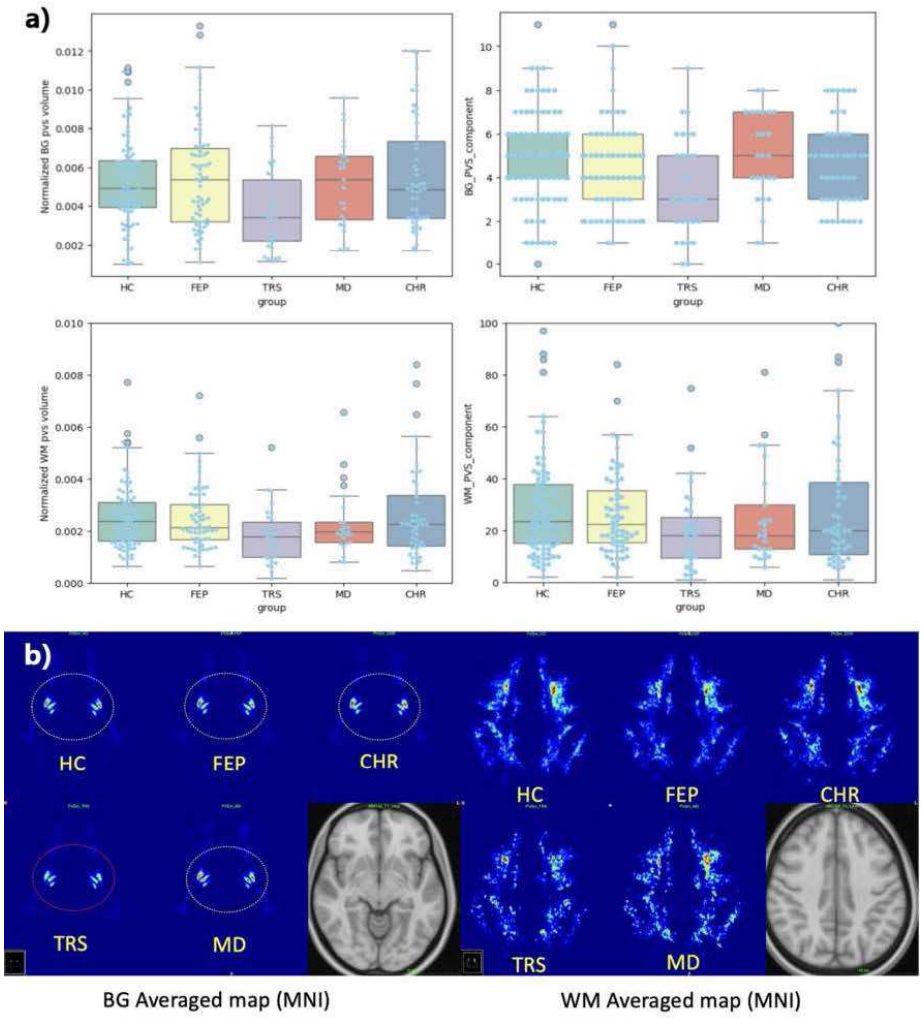

Figure 2. a) Boxplots showing counts and differences in normalized volumes of dPVS in the BG and WM. b) Group-averaged dPVS maps displaying the distribution of dPVS in the BG and WM.

References

1. Li, X., Lin, Z., Liu, C., Bai, R., Wu, D. and Yang, J. (2023), Glymphatic Imaging in Pediatrics. J Magn Reson Imaging. https://doi.org/10.1002/jmri.29040
2. Sotgiu MA, Lo Jacono A, Barisano G, Saderi L, Cavassa V, Montella A, Crivelli P, Carta A and Sotgiu S (2023) Brain perivascular spaces and autism: clinical and pathogenic implications from an innovative volumetric MRI study. Front. Neurosci. 17:1205489. doi: 10.3389/fnins.2023.1205489

Poster No 600

Cerebral network connectivity in OCD: Impacts of certain and uncertain action – reaction mapping

Giulia Gargano[1], John Kopchick[2], Phillip Easter[1], David Rosenberg[1], Jeffrey Stanley[2], Vaibhav Diwadkar[1]

[1]Wayne State University, Detroit, MI, [2]Wayne State University, Department of Psychiatry, Detroit, MI

Introduction: Obsessive-compulsive disorder (OCD) is a complex psychiatric condition characterized by the presence of recurrent and unwanted thoughts (obsessions) and/or stereotypical behaviors (compulsions)(Stein et al., 2019). OCD symptoms are associated with specific cognitive biases, particularly higher sensitivity to threats and a greater intolerance of uncertainty (Tolin et al., 2003; van den Hout & Kindt, 2004). The notion of uncertainty is essential in predictive processing models (PPM) of the brain, where uncertainty represents a challenge to coordinated brain network responses, and evokes the recruitment of the brain's predictive hierarchies (from sensory processing to heteromodal regions) (Muzik & Diwadkar, 2023). Here, we evaluated the effect of certainty and uncertainty of the reaction – action cycle on brain network connectivity using a simple uni-manual response task. Participants (OCD and typical controls, TC) used their forefinger to respond to a briefly presented stimulus. Certainty (and uncertainty) was manipulated by varying the response instruction (see Methods).

Methods: 37 OCD patients and 26 healthy controls (HC) performed the task during fMRI acquisition (3T Siemens Verio). The task manipulated the uncertainty of the reaction-action cycle by varying response mode: a) Uncertain: Responding to only specific presented stimuli (green squares in a admixture of rapidly presented green and red squares) vs. b) Certain: Responding to every presented stimulus (Certain). After preprocessing (SPM12) using established methods, time-series were extracted from functionally defined 246-region atlas (Fan et al., 2016). Functional connectivity analysis (based on zero-lag correlations) were conducted to estimated condition-induced connectivity between all 30,012 pairs of regions in each participant's fMRI data. Next, data for each pathway were analyzed in an Analysis of Variance (ANOVA) framework to determine a) main effects of condition (Response Mode: Uncertain vs. Certain); b) main effects of group (HC vs OCD); and c) any interaction between group and condition.

Results: Uncertainty (relative to Certainty) drove increased connectivity within the anterior heteromodal cortices, whereas the converse effect was observed in posterior regions (main effect of condition Figure 1a). OCD patients (relative to controls) displayed a loss of connectivity in cortical structures related to cognitive and motor control (main effect of group, Figure 1b). Finally, a complex interactive pattern emerged (Figure 1c) where in TC, an increase in uncertainty evoked a loss of connectivity in cross-cerebral pathways, with the converse effect observed in OCD.

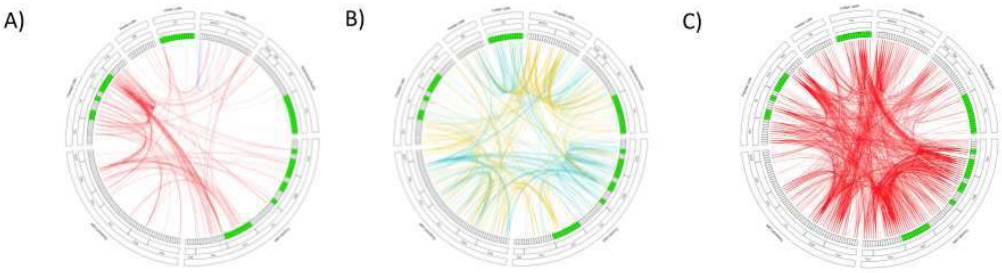

Figure 1. Functional connectivity results after analysis of variance (Anova) for A) effect of group; B) effect of condition (Certain/Uncertain); C) effect of interaction between group and condition. Significant effects are shown for $p<0.01$. All pairs are organized to reflect macro-areas; green pointers indicate known dysfunctional regions in OCD. **A)** Red indicates greater connectivity in HCs; blue indicates greater connectivity in OCDs. **B)** Gold indicates greater connectivity during the Certain response mode, turquoise indicates greater connectivity during the Uncertain response mode. **C)** Red represents (HC_C – HC_U) > (OCD_C – OCD_U); blue represents (HC_C – HC_U) < (OCD_C – OCD_C).

Conclusions: Certainty in the action-reaction cycle drives smooth patterns of network connectivity in the human brain (as is evident from the main effect of condition in Figure 1a and the pattern of connectivity changes seen in TC in Figure 1c) and the effects are broadly consistent with the idea of how the brain forms predictive heirarchies. Moreover, it appears that sensitivity of the OCD brain to changes in the certainty of the action-reaction cycle is profoundly altered. Here, increased uncertainty drives increased connectivity (Figure 1c). More generally, it appears that predictive processing in the OCD brain may be substantially altered by the clinical nature of the condition's symptoms. Our ongoing studies and analyses are addressing these questions.

References

1. Fan, L. (2016). The Human Brainnetome Atlas: A New Brain Atlas Based on Connectional Architecture. Cerebral Cortex, 26(8), 3508-3526.
2. Muzik, O. (2023). Depth and hierarchies in the predictive brain: From reaction to action. Wiley Interdisciplinary Reviews: Cognitive Science, e1664.
3. Stein, D. J. (2019). Obsessive–compulsive disorder. Nature reviews Disease primers, 5(1), 52.
4. Tolin, D. F. (2003). Intolerance of uncertainty in obsessive-compulsive disorder. J Anxiety Disord, 17(2), 233-242.
5. van den Hout, M. (2004). Obsessive-compulsive disorder and the paradoxical effects of perseverative behaviour on experienced uncertainty. J Behav Ther Exp Psychiatry, 35(2), 165-181.

Poster No 601

Amygdala-related abnormalities are hemisphere-specific and associated with symptoms of schizophrenia

Qiongyu Yan[1], Teng Liang[1], Ziwei Zhang[1], Zeyu Shen[1], Wenchao Zhou[1], Shaojie Shi[1], Lin Tian[2], Chun Meng[1]

[1]School of Life Science and Technology, University of Electronic Science and Technology of China, Chengdu, Sichuan, [2]Department of Psychiatry, The Affiliated Wuxi Mental Health Center of Nanjing Medical University, Wuxi, Jiangsu

Introduction: Amygdala plays a key role in emotional function. Particularly basolateral amygdala (BLA), which can regulate nucleus accumbens by facilitating the release of dopamine (Floresco et al., 2001), is involved in mesolimbic dopaminergic pathway (Reynolds, 1983; Kröner et al., 2005). The lateral asymmetry of amygdala is susceptible for dysfunctions in schizophrenia (SZ) (Reynolds, 1983), such as decreased grey matter volume of left BLA and functional connectivity of right BLA (Zheng et al., 2019; Zhang et al., 2020). It remains unclear how the wiring pattern and underlying white matter microstructure of amygdala are altered and associated with dysfunctions in SZ, considering mesolimbic dopaminergic pathway involving cortex, BLA and striatum (Grèzes et al., 2014; Avecillas-Chasin et al., 2023).

Methods: T1 weighted and Diffusion MRI (64 gradient directions with b=1000s/mm^2, plus 1 B0) were analyzed for 109 SZ and 105 matched healthy controls (HC), using FSL6.0 and MRtrix3.0. All patients were diagnosed by the DSM-IV, with symptom severity assessed by PANSS. The written informed consent was obtained from each subject and this study was approved by the local ethics committee. The methods of this study were illustrated in Figure 1. In the bilateral brain, we segmented amygdala voxels into mixed- or dominant-wiring types (Levitt et al., 2020), based on probabilistic tractography from cortex and striatum respectively as well as apriori and connectivity-based segmentation of 7 subregions (Tziortzi et al., 2014). For example, one amygdala voxel, if ≥70% tractography streamlines coming from the same subregion, was labeled as a dominant-wiring voxel, otherwise it was labeled as a mixed-wiring voxel (Tziortzi et al., 2014). The group differences of mixed-wiring voxel number were tested using a general linear model while controlling for age, gender and bilateral amygdala voxel number. Then, we focused on the orbitofrontal-amygdala-striatal part of mesolimbic dopamine pathway (Figure 2a, involving amygdala's dominant-wiring voxels of orbitofrontal subregion), and applied the Fixel (Raffelt et al., 2017) and Tensor model to investigate the microstructure of amygdala and white matter streamlines. We tested group differences of the Fixel and Tensor metrics using a general linear model while controlling for age and gender. Further, we examined Pearson correlations between abnormalities and PANSS as well as illness duration while controlling for age and gender.

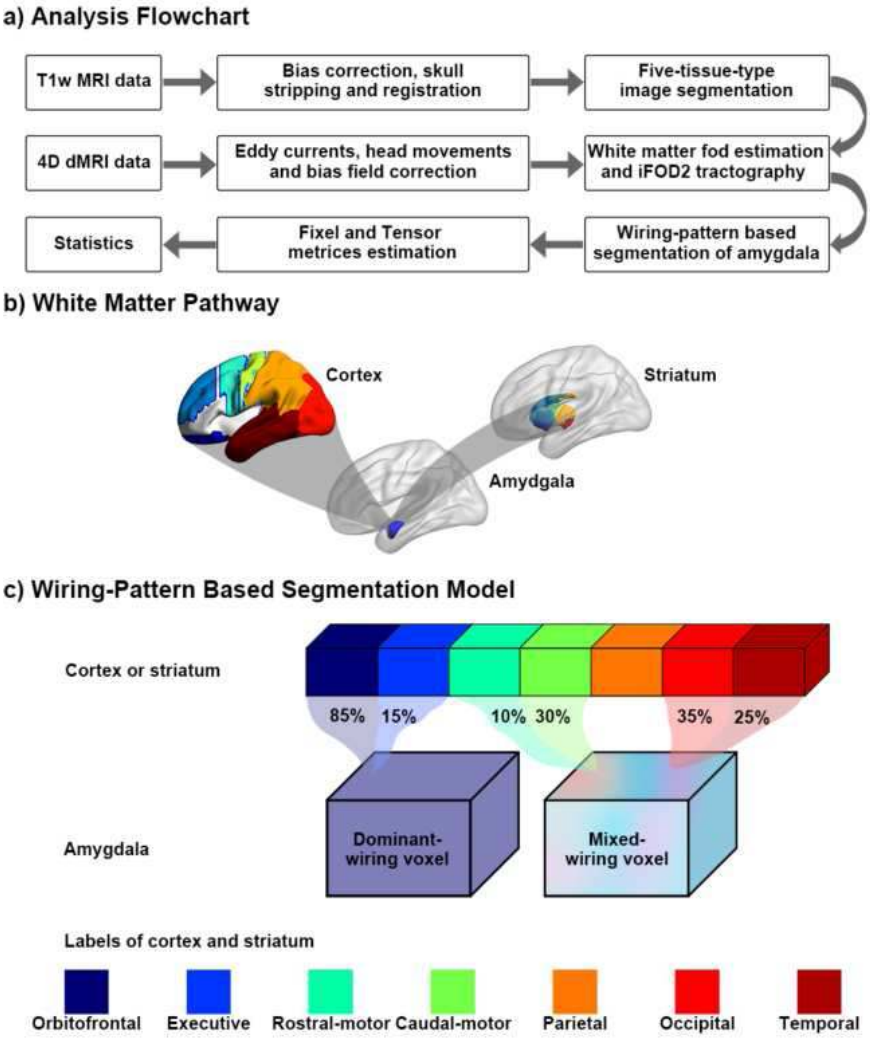

Figure 1. Methods. a) The analysis flowchart of this study. b) The mesolimbic dopaminergic white matter pathway in this study including cortex, striatum and amygdala. The cortex involved 7 subregions obtained from Tziortzi et al., while the striatum involved 7 subregions for each subject obtained by using connectivity-based segmentation[9]. c) The wiring-pattern based segmentation model of this study. The segmentation was processed on the voxels of amygdala using cortical subregions or striatal subregions. The voxels of amygdala were divided into dominant-wiring voxel or mixed-wiring voxel. Take the cortical-amygdala segmentation for example: if the connectivity between a voxel of amygdala and one cortical subregion is ≥ 70%, this voxel will be classified as a dominant-wiring voxel. If the connectivity of a voxel of amygdala with any cortical subregion is < 70%, this voxel will be classified as a mixed-wiring voxel. For the cortex and the striatum, different colors represent the labels of different subregions, as shown at the bottom of the figure.

Results: As shown in Figure 2, SZ displayed reduced number of mixed-wiring voxels defined by amygdala-striatum connectivity in left hemisphere, but no significant mixed-wiring result was found for amygdala-cortex connectivity or right hemisphere. Left amygdala's mixed-wiring changes were associated with PANSS general symptom. Besides, reduced FA of right amygdala was found and related to PANSS negative symptom as well as illness duration in SZ based on Tensor model. Further, we observed significantly reduced fibre density (FD) and FDC (a combination of fibre density and area of fibre cross-section) of right striatum-amygdala based on Fixel model, which correlated with PANSS positive symptom in SZ. The attenuated mixed-wiring pattern may reflect decreased ability to integrate information, while the damaged Tensor- and Fixel-based microstructure characteristics could infer potential white matter degeneration and dysconnectivity, in schizophrenia.

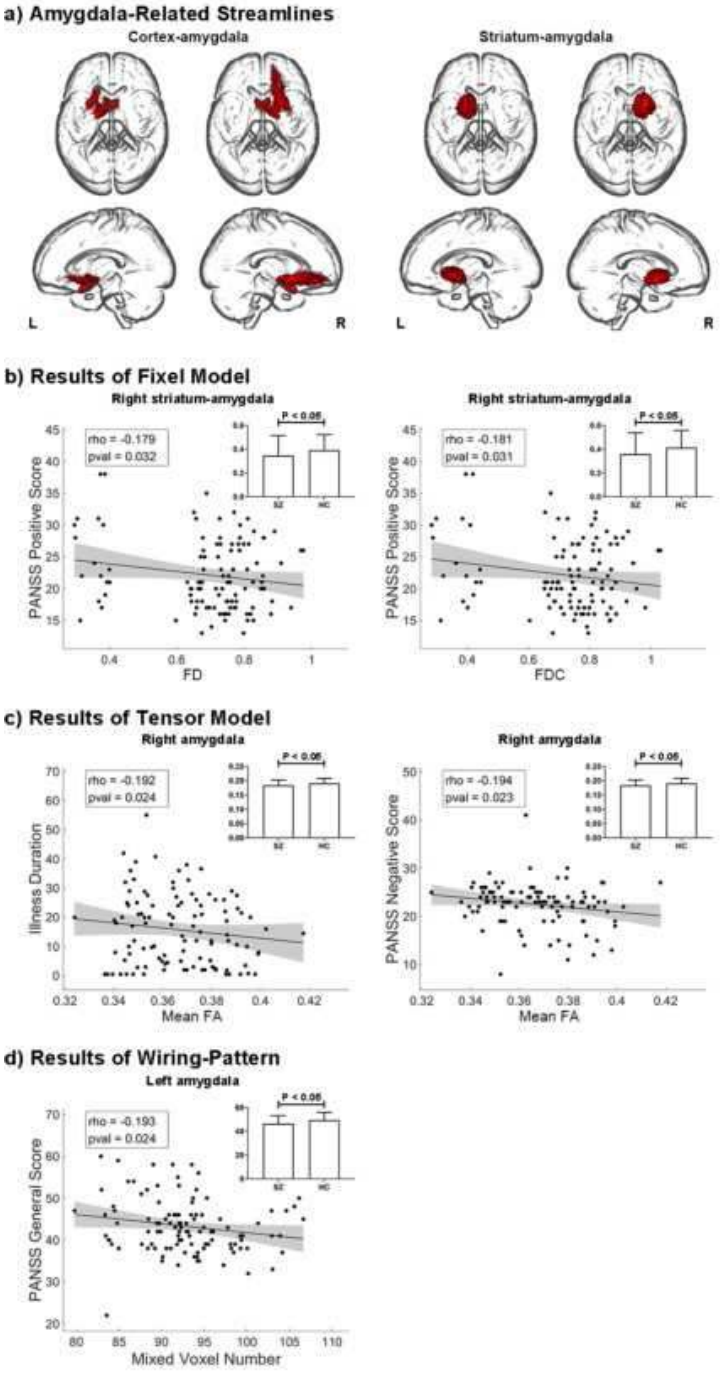

Figure 2. Results. a) Visualization of white matter streamline related to orbitofrontal amygdala, including orbitofrontal cortex, orbitofrontal amygdala (which is defined by the dominant-wiring voxels that strongly connect to the orbitofrontal cortex), and orbitofrontal striatum (individually identified using connectivity-based segmentation[9]). The four plots on the left are visualization of streamlines between the cortex and amygdala in the left and right hemisphere. The four plots on the right are visualization of streamlines between the striatum and amygdala in the left and right hemisphere. The visualization of streamlines was obtained from all subjects in this study. b) Fixel results of streamlines between right striatum and right amygdala, while controlling age and gender for group comparison and correlation analyses. c) Tensor results of right amygdala, while controlling age and gender for group comparison and correlation analyses. d) Wiring pattern results of left amygdala connecting with striatum, while controlling age, gender and voxel number of left amygdala for group comparison; for correlation analyses age and gender was controlled.

Conclusions: Our results provide novel evidence about abnormal mixed-wiring pattern and microstructural changes in amygdala of SZ, which confirm amygdala-related lateralization. The hemisphere-specific changes in white matter of mesolimbic dopamine pathway and amygdala were selectively associated with schizophrenia symptoms and illness duration, which help better understand disrupted emotion and dopaminergic function of schizophrenia.

References

1. Avecillas-Chasin, J.M. et al. (2023) 'Connectivity-based parcellation of the amygdala and identification of its main white matter connections', Scientific Reports, 13(1), p. 1305. Available at: https://doi.org/10.1038/s41598-023-28100-6.

2. Floresco, S.B. et al. (2001) 'Dopamine D 1 and NMDA Receptors Mediate Potentiation of Basolateral Amygdala-Evoked Firing of Nucleus Accumbens Neurons', The Journal of Neuroscience, 21(16), pp. 6370–6376. Available at: https://doi.org/10.1523/JNEUROSCI.21-16-06370.2001.
3. Grèzes, J. et al. (2014) 'A direct amygdala-motor pathway for emotional displays to influence action: A diffusion tensor imaging study: A Direct Limbic Motor Anatomical Pathway', Human Brain Mapping, 35(12), pp. 5974–5983. Available at: https://doi.org/10.1002/hbm.22598.
4. Kröner, S. et al. (2005) 'Dopamine Modulates Excitability of Basolateral Amygdala Neurons In Vitro', Journal of Neurophysiology.
5. Levitt, J.J. et al. (2020) 'Miswiring of Frontostriatal Projections in Schizophrenia', Schizophrenia Bulletin, 46(4), pp. 990–998. Available at: https://doi.org/10.1093/schbul/sbz129.
6. Raffelt, D.A. et al. (2017) 'Investigating white matter fibre density and morphology using fixel-based analysis', NeuroImage, 144, pp. 58–73. Available at: https://doi.org/10.1016/j.neuroimage.2016.09.029.
7. Reynolds, G.P. (1983) 'Increased concentrations and lateral asymmetry of amygdala dopamine in schizophrenia', Nature, 305(5934), pp. 527–529. Available at: https://doi.org/10.1038/305527a0.
8. Tziortzi, A.C. et al. (2014) 'Connectivity-Based Functional Analysis of Dopamine Release in the Striatum Using Diffusion-Weighted MRI and Positron Emission Tomography', Cerebral Cortex, 24(5), pp. 1165–1177. Available at: https://doi.org/10.1093/cercor/bhs397.
9. Zhang, M. et al. (2020) 'Abnormal amygdala subregional-sensorimotor connectivity correlates with positive symptom in schizophrenia', NeuroImage: Clinical, 26, p. 102218. Available at: https://doi.org/10.1016/j.nicl.2020.102218.
10. Zheng, F. et al. (2019) 'Study on the sub-regions volume of hippocampus and amygdala in schizophrenia', Quantitative Imaging in Medicine and Surgery, 9(6), pp. 1025–1036. Available at: https://doi.org/10.21037/qims.2019.05.21.

Poster No 602

Alterations in AMPA and GABA signal transmission in the hippocampus in major depression

Jessica Gilbert[1], Carlos Zarate[1]

[1]NIMH/NIH, Bethesda, MD

Introduction: Patients with major depression (MD) exhibit deficits in working memory (WM) and disrupted neuroplasticity within the hippocampus. Hippocampal memory processes, hypothesized to be supported by gamma oscillatory activity, can be measured using tasks such as the n-back. Gamma rhythms are considered to be a proxy measure of excitation-inhibition balance (Buzsáki and Wang 2012), and changes in gamma in the psychiatric state are thought to reflect dysregulation of homeostatic balance. An emerging pathophysiological feature of MDD includes changes in gamma band rhythms (Fitzgerald and Watson 2018). This study used an n-back task in tandem with magnetoencephalography (MEG) to assess WM network-level differences between MDs and healthy participants (HCs).

Methods: MEG data were recorded using a CTF 275-channel system while participants (MDD=39, HC=21) completed an n-back task. Accuracy and reaction time (RT) were calculated for the 0-, 1-, and 2-back conditions, and Mann-Whitney tests were used to examine behavioral differences. MEG source-level gamma (30-58 Hz) power was projected using the multiple sparse priors algorithm in SPM12 using two peristimulus time windows of interest: -500-0 ms and 0-500 ms, corresponding to the maintenance and retrieval periods of the task. Linear mixed effects models tested for group (MD and HC), condition (0-, 1-, and 2-back), and group-by-condition interactions. Dynamic causal modeling (DCM) was used to model effective connectivity between regions of interest identified from the group-level results, including the cingulate, orbitofrontal cortex, and hippocampus, using a biophysical that included parameters governing AMPA, NMDA, and GABA signaling. Parametric empirical Bayesian analysis was used to identify parameters that differed between groups, using a posterior probably of ≥0.95.

Results: There were significant differences for 2-back accuracy and RT between groups, with MDs having lower accuracy (MD mean=74.03+21.42, HC mean=89.24+9.70, p=0.01) and increased RT (MD mean=0.49+0.23, HC mean=0.3+0.16, p=0.03) relative to HCs. In gamma, increasing WM load was associated with increasing power in bilateral intraparietal sulcus for the 0-to-1-back and 0-to-2-back conditions during the maintenance period across groups (pFDR<0.05). In addition, MDs had increased gamma power in brain regions including the cingulate, orbitofrontal cortex, and hippocampus during maintenance compared to HCs (pFDR<0.05). No significant gamma effects were found during the retrieval period. For the connectivity analysis, significantly increased AMPA time constants in all regions of interest and increased GABA time constants in hippocampus were found for MDs compared to HCs. The inverse of time constants are rate constants, suggesting slower AMPA and GABA signal transmission in these regions in MDs. In addition, the membrane capacitance of superficial and deep pyramidal cells was elevated for MDs compared to HCs, suggesting slower voltage change for these modeled cell types. Finally, the AMPA-mediated connectivity between orbitofrontal cortex and cingulate was reduced for MDs compared to HCs.

Conclusions: These results are consistent with studies reporting WM deficits at higher cognitive loads in individuals with MD. Dysregulated gamma oscillations, potentially mediated by AMPA and GABA signaling deficits in key brain network nodes supporting mood and WM performance, could account for these performance differences. Hippocampal neuroplasticity

deficits in particular might be explained by slower AMPA and GABA signal transmission and altered homeostatic balance within this region. Future work will examine the relationship between depression severity and connectivity metrics in MDs.

References
1. Buzsáki, G. and X.-J. Wang (2012). "Mechanisms of Gamma Oscillations." Annual Review of Neuroscience 35(1): 203-225.
2. Fitzgerald, P. J. and B. O. Watson (2018). "Gamma oscillations as a biomarker for major depression: an emerging topic." Translational Psychiatry 8(1): 177.

Poster No 603

Combining Neuroimaging and Genetics Provides Pathobiological Insights for Bipolar Disorder

Nadine Parker[1], Kevin O'Connell[1], Alexey Shadrin[1], Espen Hagen[1], Pravesh Parekh[1], Paul Thompson[2], Anders Dale[3], Christopher Ching[2], Ole Andreassen[1]

[1]University of Oslo, Oslo, Norway, [2]University of Southern California, Marina Del Rey, CA, [3]University of California San Diego, San Diego, CA

Introduction: Bipolar disorder (BD) is associated with brain structure and genetic variation (Hibar et al., 2016, 2018; Mullins et al., 2021). These associations can be leveraged to understand the disorder's pathophysiology, its treatment, and ultimately improve diagnostic prediction. Here we test associations between structural MRI measures and the genetic liability to BD.

Methods: Using data from 35,660 UK Biobank participants [52.91% female, mean age(sd)=63.55 (7.53)], we determined the associations between FreeSurfer derived measures (i.e., cortical thickness, surface area, and subcortical volumes) in regions of interest (ROI) (Desikan et al., 2006; Fischl et al., 2002) and BD (Mullins et al., 2021) polygenic risk scores (PRS; using LDpred2-auto (Privé et al., 2020)). Next, using a subsample of patients from the ENIGMA BD working group [n=267, 58.05% female, mean age (sd)=34.53 (12.04)], we examined how each ROI is associated with the PRS for BD in a case-only analysis. With an additional sample of 748 healthy controls [44.39% female, mean age (sd)=33.81 (9.84)] from the ENIGMA BD group we tested the interaction between BD status and PRS in significant ROIs identified in the case-only analysis. We also tested for underlying clinical and biological factors by (1) stratifying analysis based on medication use (i.e., anti-depressants, lithium, first and second generation antipsychotics, anti-epileptics, and no medication) and (2) assessing associations with pathway-specific PRS for neural cell types using genes from post-mortem fetal (Bhaduri et al., 2021) and adult (Lake et al., 2018) brain. All linear models included age, age2, sex, scanner, genetic batch, and the first 20 genetic principal components as covariates. Models with brain volumes as outcomes also included intracranial volume as a covariate.

Results: The large cohort level analysis, using the UK Biobank sample, revealed that the BD PRS was associated with reductions in thickness and volume but increased surface area across ROI. In our case-only analysis, positive associations were observed between the BD PRS and thickness in six ROIs in the temporal lobe. Interactions between PRS and BD status were observed for cortical thickness in three of these regions [right inferior temporal (beta (se)=-0.06 (0.02), p_fdr=0.02), left middle temporal (beta (se)=-0.06 (0.02), p_fdr=0.02), and left fusiform (beta (se)=-0.05 (0.01), p_fdr=0.03)]. The positive association for BD patients was strongest among those taking antidepressants and lithium. Additionally, among the six regions associated with the BD PRS, the adult microglia PRS was significantly associated with temporal pole thickness (beta (se)=0.35 (0.10), p_fdr =0.04) in BD.

Conclusions: Structural brain measures are associated with the genetic liability to BD with variability when testing in large non-clinical cohorts compared to BD patients only. Part of this variability may be explained by BD treatment with differing medication effects. Additionally, microglial cells may play a role in mediating the genetically associated variations in brain structure among BD patients. These findings illustrate the importance of combining neuroimaging and genetics to improve our understanding of BD with implications for improved diagnostics.

References
1. Bhaduri, A., Sandoval-Espinosa, C., Otero-Garcia, M., Oh, I., Yin, R., Eze, U. C., Nowakowski, T. J., & Kriegstein, A. R. (2021). An Atlas of Cortical Arealization Identifies Dynamic Molecular Signatures. Nature, 598(7879), 200-204.
2. Desikan, R. S., Ségonne, F., Fischl, B., Quinn, B. T., Dickerson, B. C., Blacker, D., Buckner, R. L., Dale, A. M., Maguire, R. P., Hyman, B. T., Albert, M. S., & Killiany, R. J. (2006). An automated labeling system for subdividing the human cerebral cortex on MRI scans into gyral based regions of interest. NeuroImage, 31(3), 968–980.
3. Fischl, B., Salat, D. H., Busa, E., Albert, M., Dieterich, M., Haselgrove, C., Kouwe, A. van der, Killiany, R., Kennedy, D., Klaveness, S., Montillo, A., Makris, N., Rosen, B., & Dale, A. M. (2002). Whole Brain Segmentation: Automated Labeling of Neuroanatomical Structures in the Human Brain. Neuron, 33(3), 341–355.

4. Hibar, D. P., Westlye, L. T., Doan, N. T., Jahanshad, N., Cheung, J. W., Ching, C. R. K., Versace, A., Bilderbeck, A. C., Uhlmann, A., Mwangi, B., Krämer, B., Overs, B., Hartberg, C. B., Abé, C., Dima, D., Grotegerd, D., Sprooten, E., Bøen, E., Jimenez, E., ... Andreassen, O. A. (2018). Cortical abnormalities in bipolar disorder: An MRI analysis of 6503 individuals from the ENIGMA Bipolar Disorder Working Group. Molecular Psychiatry, 23(4), 932–942.
5. Hibar, D. P., Westlye, L. T., van Erp, T. G. M., Rasmussen, J., Leonardo, C. D., Faskowitz, J., Haukvik, U. K., Hartberg, C. B., Doan, N. T., Agartz, I., Dale, A. M., Gruber, O., Krämer, B., Trost, S., Liberg, B., Abé, C., Ekman, C. J., Ingvar, M., Landén, M., ... Andreassen, O. A. (2016). Subcortical volumetric abnormalities in bipolar disorder. Molecular Psychiatry, 21(12), Article 12.
6. Lake, B. B., Chen, S., Sos, B. C., Fan, J., Kaeser, G. E., Yung, Y. C., Duong, T. E., Gao, D., Chun, J., Kharchenko, P. V., & Zhang, K. (2018). Integrative single-cell analysis of transcriptional and epigenetic states in the human adult brain. Nature Biotechnology.
7. Mullins, N., Forstner, A. J., O'Connell, K. S., et al., (2021). Genome-wide association study of more than 40,000 bipolar disorder cases provides new insights into the underlying biology. Nature Genetics, 53(6).
8. Privé, F., Arbel, J., & Vilhjálmsson, B. J. (2020). LDpred2: Better, faster, stronger. Bioinformatics, 36(22–23), 5424–5431.

Poster No 604

Linking individual brain variability to clinical phenotypes for early detection of bipolar disorders

Junneng Shao[1], Wei Zhang[1], Ting Wang[1], Qian Liao[1], Cong Pei[1], Lien Wang[1], Shui Tian[2], Zhilu Chen[3], Zhijian Yao[3], Qing Lu[1]

[1]School of Biological Sciences & Medical Engineering, Southeast University, Nanjing, China, [2]Nanjing Medical University, Nanjing, China, [3]Department of Psychiatry, the Affiliated Nanjing Brain Hospital of Nanjing Medical University, Nanjing, China

Introduction: Bipolar disorder (BD) with a depressive episode and unipolar disorder (UD; i.e., major depressive disorder) share similar clinical profile (Phillips & Kupfer, 2013) and consequently, individuals with BD are commonly misdiagnosed as UD (de Almeida & Phillips, 2013). Misdiagnosis can lead to inappropriate treatment, poor prognosis and subsequent complication, such as increased risk of suicide and long-term medical costs (de Almeida & Phillips, 2013; Siegel-Ramsay et al., 2022). Evidence has been shown that clinical characteristics, such as age of onset, anxiety and cognitive, may be clinical precursors of BD (Bolton, Warner, Harriss, Geddes, & Saunders, 2021; Faedda et al., 2019). Therefore, we tried to find objective biomarkers that could distinguish BD from MDD early in the course of the disease by linking clinical phenotypes with brain neuroimaging.

Methods: A total of 166 healthy controls, 184 UD patients, 148 BD patients, and 72 patients who were initially strictly diagnosed as UD during scanning and then transformed to BD during follow-up (tBD) were enrolled in the study. Firstly, to exclude the effects of age and gender, we constructed a normative model of brain changes with age and gender based on a large publicly available dataset of HC (N=1112). Then, the individual deviation of each patient in brain structure (GMV) and function (ALFF) could be obtained from these normative models (Figure 1c). Secondly, we included age of onset, family history of psychosis, number of episodes, and five subfactor scores of HAMD-17 as clinical characteristics. Here, we combined sparse multivariate canonical correlation analysis (smCCA) with joint independent component analysis (joint ICA) to identify latent brain structure-function patterns that correlate clinical characteristics and whole-brain personalization deviations (z-scores) across all patients (Figure 1d). Finally, we compared the distribution of these latent patterns across the three groups of patients.

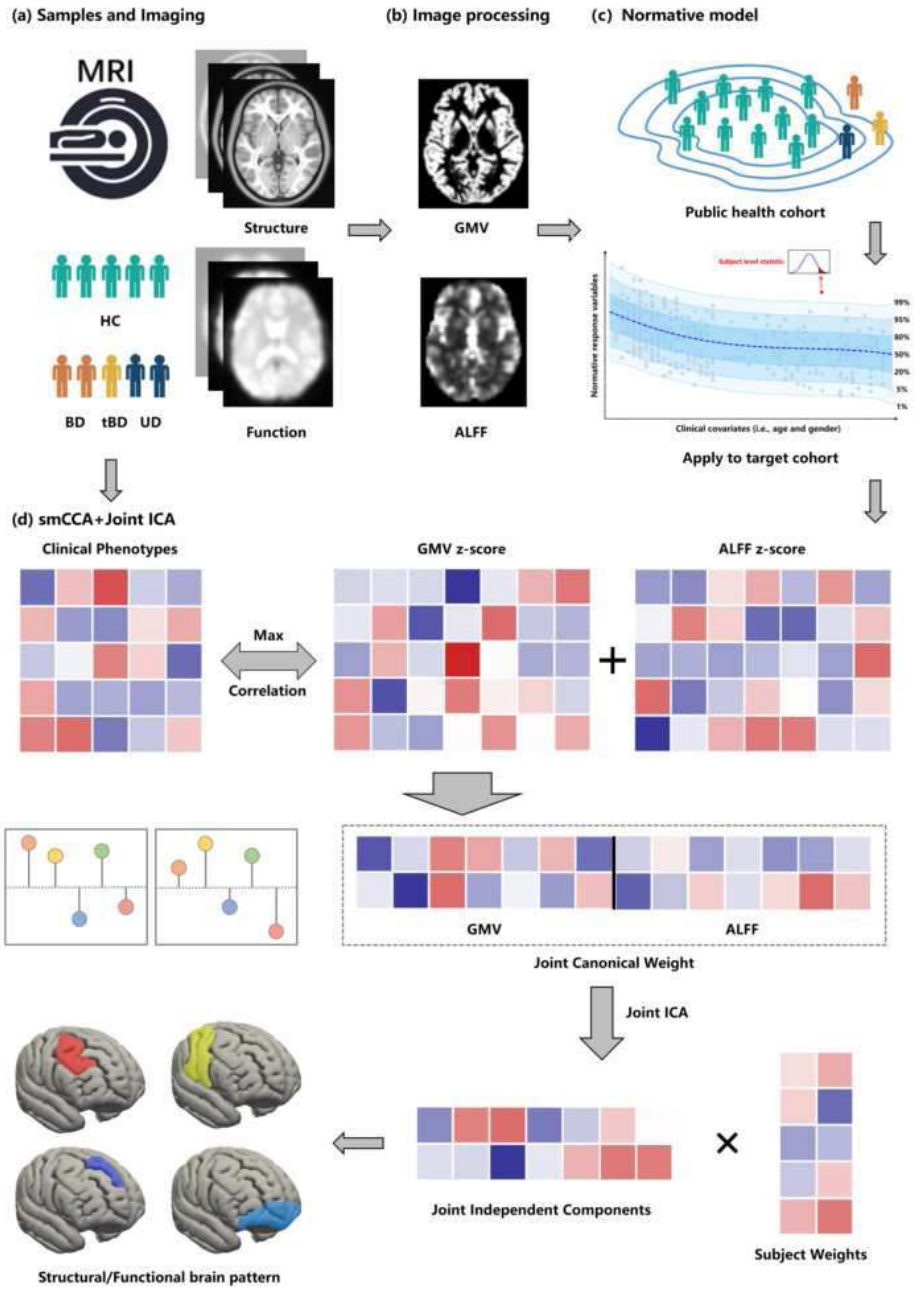

Results: Our analysis revealed two latent patterns (Figure 2): 1) Pattern 1 was associated with age at onset. This pattern mainly involved the high ALFF deviation of limbic and subcortical network in functional brain; low GMV deviation of visual network and high GMV deviation of executive control network and temporoparietal network in structural brain. 2) Pattern 2 was associated with retardation, cognitive impairment and anxiety/somatization. This pattern mainly involved high ALFF deviation of visual and dorsal attention network, and low ALFF deviation of ventral attention and subcortical network in functional brain; high GMV deviation of default mode network A, subcortical network and low GMV deviation of visual network and default mode network B. The results of one-way ANOVA showed that there were significant differences in the subject weights of pattern GMV_1 (p = 0.0015), GMV_2 (p = 0.0067) and ALFF_2 (p = 0.0369) among the three groups above (FDR correction). Post-hoc analysis results showed that there were significant differences in these three modes between BD and UD group (p = 2.8e-04, p = 0.0048, p = 0.0143, respectively). Furthermore, we found that there is a significant difference in pattern GMV_2 between the tBD and UD group (p = 0.0339), but no difference between the tBD and BD group.

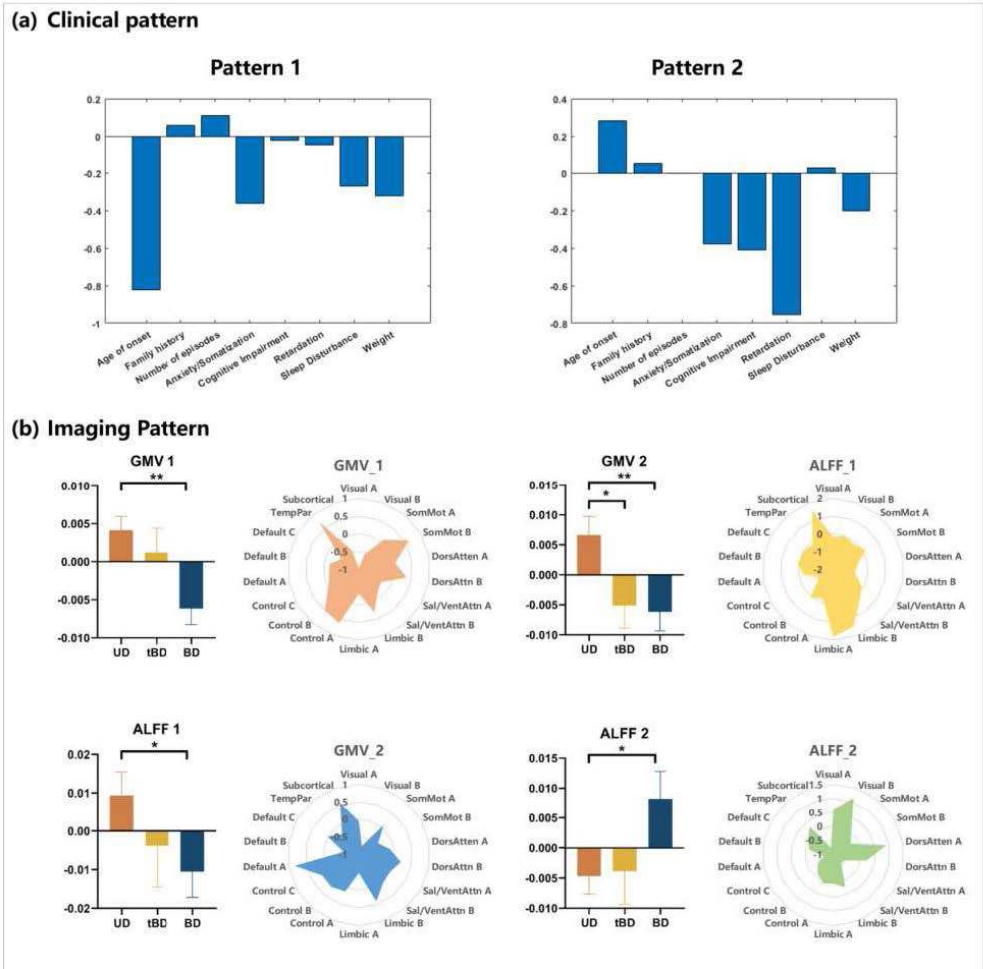

Conclusions: We revealed two latent brain structural-functional patterns associated with clinical phenotypes in patients with UD and BD. Our study showed that these patterns can help identify the differences between UD and BD patients, and hold the promise of timely identification of BD patients early in the course of the disease.

References

1. Bolton, S., Warner, J., Harriss, E., Geddes, J., & Saunders, K. E. A. (2021). Bipolar disorder: Trimodal age-at-onset distribution. Bipolar Disord, 23(4), 341-356. doi:10.1111/bdi.13016
2. de Almeida, J. R. C., & Phillips, M. L. (2013). Distinguishing between Unipolar Depression and Bipolar Depression: Current and Future Clinical and Neuroimaging Perspectives. Biological Psychiatry, 73(2), 111-118. doi:10.1016/j.biopsych.2012.06.010
3. Faedda, G. L., Baldessarini, R. J., Marangoni, C., Bechdolf, A., Berk, M., Birmaher, B., . . . Correll, C. U. (2019). An International Society of Bipolar Disorders task force report: Precursors and prodromes of bipolar disorder. Bipolar Disord, 21(8), 720-740. doi:10.1111/bdi.12831
4. Phillips, M. L., & Kupfer, D. J. (2013). Bipolar disorder diagnosis: challenges and future directions. Lancet, 381(9878), 1663-1671. doi:10.1016/S0140-6736(13)60989-7
5. Siegel-Ramsay, J. E., Bertocci, M. A., Wu, B., Phillips, M. L., Strakowski, S. M., & Almeida, J. R. C. (2022). Distinguishing between depression in bipolar disorder and unipolar depression using magnetic resonance imaging: a systematic review. Bipolar Disorders, 24(5), 474-498. doi:10.1111/bdi.13176

Poster No 605

Neural Oscillatory Patterns Show Reliable Early Identification of Bipolar from Unipolar Depression

Yi Xia[1], Xiaoqin Wang[1], Lingling Hua[1], Zhilu Chen[1], Yingying Huang[1], Moxuan Song[1], Zhijian Yao[1]

[1]The Affiliated Brain Hospital of Nanjing Medical University, Nanjing, Jiangsu

Introduction: Response inhibition is a key neurocognitive factor contributing to impulsivity in bipolar disorder (BD) and unipolar disorder (UD). However, the neurological mechanism under response inhibition impairment is unclear in mood disorders. We explored the common and differential alterations of neural circuits associated with response inhibition in BD and UD and whether the oscillatory signatures can be used as early biomarkers in BD.

Methods: 39 patients with BD, 36 patients with UD, 29 patients who were initially diagnosed as UD and then transformed into BD (tBD), and 36 healthy controls performed a Go/No-Go task during MEG scanning. We carried out time-frequency and connectivity analysis on MEG data. Further, we performed machine learning using oscillatory features as input to identify bipolar from unipolar depression at the early clinical stage.

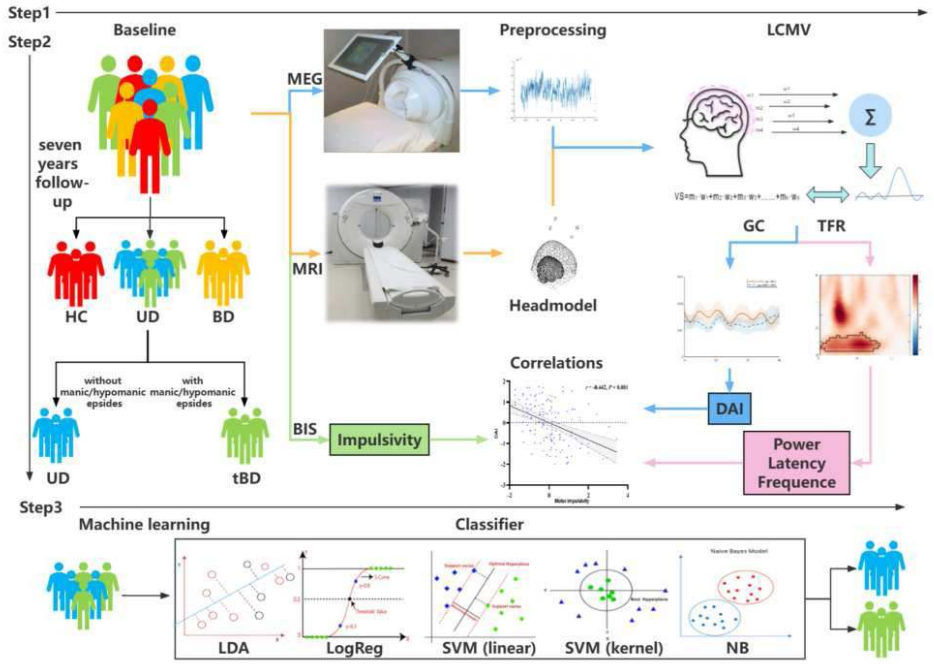

Results: Compared to healthy controls, patients had reduced rIFG-to-pre-SMA connectivity and delayed activity of rIFG. Among patients, lower beta power and higher peak frequency were observed in BD patients than in UD patients. Motor impulsivity was related to power and latency of activity in rIFG and strength of functional connectivity between rIFG and pre-SMA. These changes enabled accurate classification between BD and UD with an accuracy of approximately 80%.

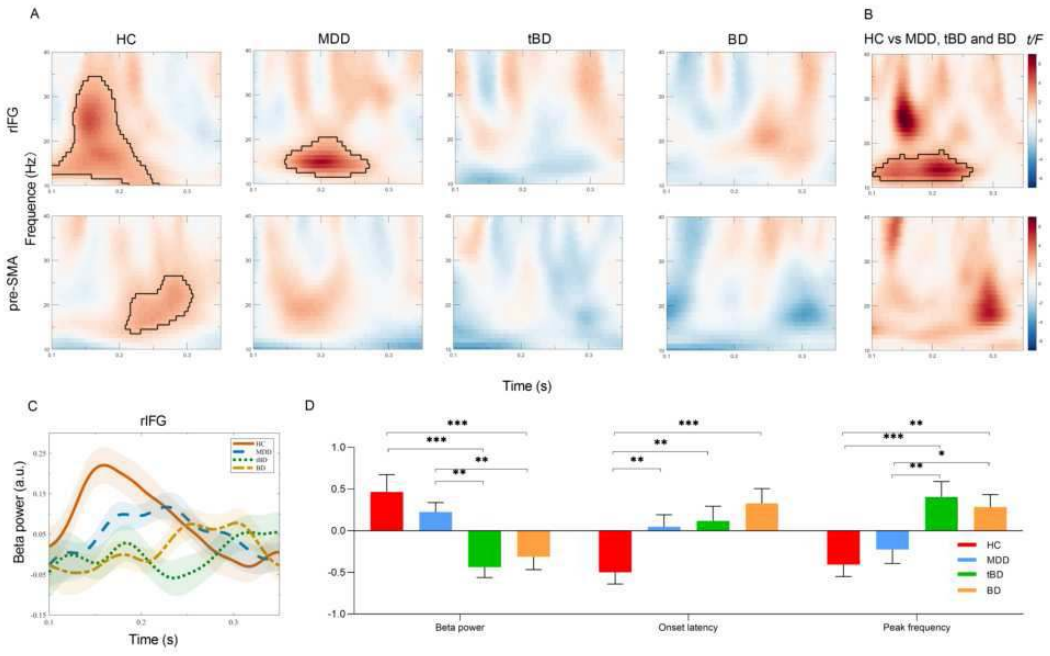

Conclusions: The inefficiency of the prefrontal control network is a shared mechanism of response inhibition impairment in mood disorders, while the abnormal activity of rIFG is more special to BD. Our findings demonstrate that neuronal responses during response inhibition could serve as a diagnostic biomarker for BD in early stage.

Poster No 606

Prediction of longitudinal anxiety in adolescents using mixed effects random forest regression

Paola Odriozola[1], Amanda Baker[1], Claire Waller[1], Nancy Le[1], Katie Bessette[1], Lucina Uddin[2], Tara Peris[1], Adriana Galván[1]

[1]UCLA, Los Angeles, CA, [2]Department of Psychiatry and Biobehavioral Sciences, University of California, Los Angeles, Los Angeles, CA

Introduction: Adolescence is a peak time for the onset of psychiatric disorders, with anxiety disorders being the most common, affecting as many as 1 in 3 youths (Beesdo et al., 2009; Kessler et al., 2005; Merikangas & Swanson, 2010). Despite its significant costs, understanding of factors that shape the persistence/remittance of anxiety over time remains limited. Using machine learning methods with multivariate longitudinal behavioral, clinical, and fMRI data from early to mid-adolescents, we took a data-driven approach to investigate whether it was possible to predict whose anxiety will worsen, remain the same, or remit years later. We hypothesized that mixed effects random forest regression would enable prediction of anxiety outcomes with high precision, and that the functional connectivity of brain regions previously shown to be implicated in anxiety (e.g., amygdala, hippocampus, ventral striatum, anterior insula (AI), anterior cingulate cortex (ACC), and ventromedial prefrontal cortex(vmPFC)) would be of highest importance in predicting anxiety outcomes.

Methods: 132 adolescent participants (61 F : 71 M; 11.4 +/-1.5 years at time 1) completed the Development of Anxiety in Youth Study (Galván & Peris, 2020), a prospective longitudinal study that occurred annually for 3 years. Participants completed a resting state fMRI scan, the Screen for Child Anxiety Related Disorders (SCARED) child and parent report questionnaires (Birmaher et al., 1997), and demographic questionnaires at each visit. We used the AAL3 atlas (Rolls et al., 2020) to parcellate the brain, and computed the functional connectivity between each parcel to generate a correlation matrix using AFNI FATCAT (Taylor & Saad, 2013). We then submitted scaled demographic, behavioral, and functional connectivity data to a stochastic mixed effects random forest regression analysis (sMERF) implemented in R using the LongituRF package (Capitaine et al., 2021). This package combines the feature selection aspects of random forests with an extension to include mixed-effects models to account for repeated measures for high-dimensional longitudinal data. We used a standard Ornstein-Uhlenbeck process which allows the covariance structure to vary over time (Capitaine et al., 2021). We used 80% of the data for training, and the other 20% for testing the model. The model contained 13,538 predictors which included functional connectivity values (functional connectivity of all AAL3 parcels), and demographic variables (i.e., age, sex at birth, race, ethnicity, family income, IQ, etc.) and the outcome of interest was child-reported SCARED total score. Prediction errors were calculated as root mean square error with 25 training/test set random splits.

Results: Prediction of future anxiety symptoms using sMERF yielded a root mean square error of 0.966. The top 5 variables that yielded the highest importance in the random forest model included (in order of relative importance): functional connectivity of the left gyrus rectus to left nucleus accumbens (Nacc), right crus I of cerebellar hemisphere to left locus coeruleus, right crus I of cerebellar hemisphere to left pregenual ACC, left temporal pole (middle temporal gyrus) to right Nacc, and lobule I and II of vermis to left lateral posterior thalamus.

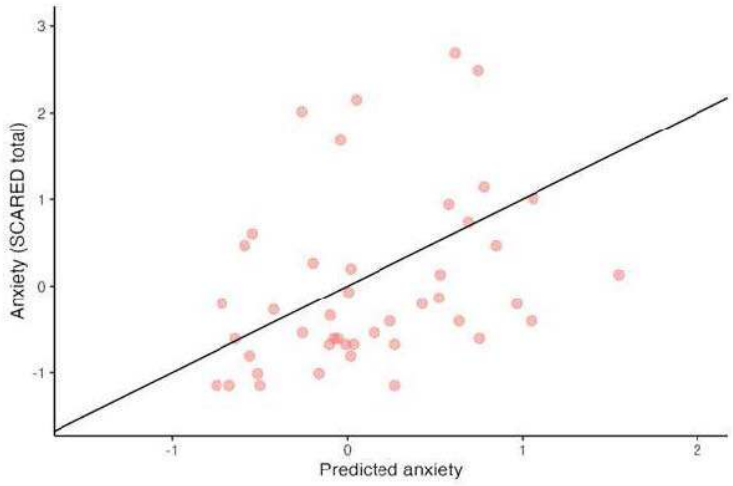

Figure 1. Predicted anxiety scores (scaled) of unseen test dataset in sMERF model by observed anxiety scores (scaled total scores from child-reported SCARED questionnaire). Perfect positive correlation line included for reference.

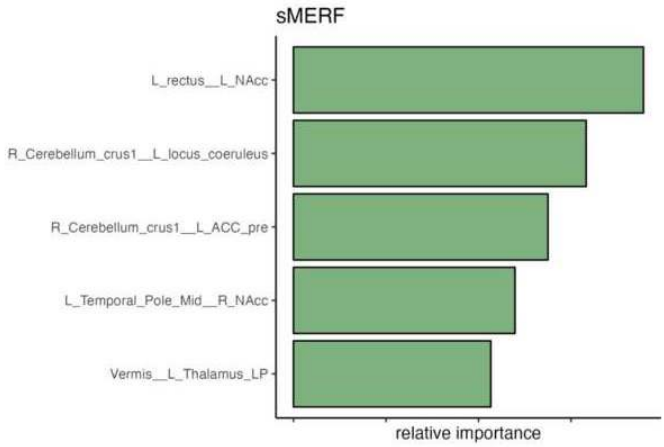

Figure 2. Resulting relative importance of top 5 variables in sMERF model. Variables were sorted by relative importance weights (mean standard error) that resulted from the sMERF model on the unseen test dataset.

Conclusions: Anxiety disorders often emerge during childhood and adolescence, yet not all youth benefit sufficiently from current evidence-based treatments and long-term outcomes are variable (Bai et al., 2023). Results from the present study suggest that resting functional connectivity between regions regions often overlooked in studies of anxiety- such as the Nacc, ACC, and cerebellum- may play a larger role in predicting anxiety outcomes. Increasing our understanding of factors that predict future anxiety outcomes across development is crucial for identifying optimal windows for prevention or intervention and specifying new targets for intervention for youth struggling with anxiety.

References

1. Bai, S. (2023). Anxiety symptom trajectories from treatment to 5- to 12-year follow-up across childhood and adolescence. Journal of Child Psychology and Psychiatry, and Allied Disciplines, 64(9), 1336–1345. https://doi.org/10.1111/jcpp.13796
2. Beesdo, K. (2009). Anxiety and Anxiety Disorders in Children and Adolescents: Developmental Issues and Implications for DSM-V. The Psychiatric Clinics of North America, 32(3), 483–524. https://doi.org/10.1016/j.psc.2009.06.002
3. Birmaher, B. (1997). The Screen for Child Anxiety Related Emotional Disorders (SCARED): Scale Construction and Psychometric Characteristics. Journal of the American Academy of Child & Adolescent Psychiatry, 36(4), 545–553. https://doi.org/10.1097/00004583-199704000-00018
4. Capitaine, L. (2021). Random forests for high-dimensional longitudinal data. Statistical Methods in Medical Research, 30(1), 166–184. https://doi.org/10.1177/0962280220946080
5. Galván, A. (2020). The Development of Anxiety in Youth Study (DAYS): A Prospective Study of Trajectories of Brain Maturation among Youth at Risk for Anxiety †. Journal of Psychiatry and Brain Science, 4(3). https://doi.org/10.20900/jpbs.20200025
6. Kessler, R. C. (2005). Prevalence and treatment of mental disorders, 1990 to 2003. N Engl J Med, 352(24), 2515–2523. https://doi.org/10.1056/NEJMsa043266
7. Merikangas, K. R. (2010). Comorbidity in anxiety disorders. Curr Top Behav Neurosci, 2, 37–59.
8. Rolls, E. T. (2020). Automated anatomical labelling atlas 3. NeuroImage, 206, 116189. https://doi.org/10.1016/j.neuroimage.2019.116189
9. Taylor, P. A. (2013). FATCAT: (An Efficient) Functional and Tractographic Connectivity Analysis Toolbox. Brain Connectivity, 3(5), 523–535. https://doi.org/10.1089/brain.2013.0154

Poster No 607

Using an Anticipatory Shock Stress-induction fMRI Task to Challenge Mood-Related Stress-Circuitry

Mark Kvarta[1], Akram Yusuf[2], Josh Chiappelli[2], L. Elliot Hong[3], Carlos Zarate[1]

[1]National Institute of Mental Health/NIH, Bethesda, MD, [2]University of Maryland Baltimore, Baltimore, MD, [3]University of Texas Houston, Houston, TX

Introduction: How stress across the lifespan impacts brain circuitry to contribute to psychiatric symptoms remains unclear. Brain areas responsible for processing stress have been implicated in depression including limbic areas like the hippocampus and reward areas. Stress-based tasks may be key to understanding how past and current stress experience intersect with symptoms in relevant brain regions. We hypothesized lifetime stress-induced perturbation of stress-sensitive cortico-limbic brain areas leads to altered activation in response to subsequent stressful situations, underlying altered stress responsivity in major depressive disorder (MDD) and contributing to symptoms.

Methods: The ankle shock threat (AST) paradigm is analogous to classic behavioral stress tasks in animals using foot shock and unpredictability, while human fMRI compatible and ethical. For this pilot, we recruited 26 patients with MDD (19/26 female)

and 30 psychiatrically healthy adult controls (HC, 17/30 female). Major life stress (Childhood Trauma Questionnaire-CTQ) and recent stress (past 30 days) was recorded (Perceived Stress Scale-PSS). State (current) and trait (longitudinal) depressive symptoms were measured (Maryland State and Trait Depression Scale). Imaging was completed using a 3-T Siemens Prisma scanner and 64-channel coil, with an electrode attached to one ankle of each participant. A pre-determined intensity of shock was applied for 0.1s intermittently during the task (similar to a static shock, Transcutaneous Aversive Stimulator, Coulborne Instruments). There were 3 conditions: (1) "shock" in which a several shocks are delivered while a color signal on screen indicate shocks are likely; (2) "threat" in which the same color is present but no shock is given; and (3) "safe" with safety signal present. All preprocessing included slice timing correction and volume co-registration. Images were linearly detrended, normalized into MNI standard space, and spatially smoothed (FWHM=8mm) using SPM12. First level models were developed for each subject with all volumes in a single analysis regressing the conditions. The contrast of interest was "threat"–"safe" to study threat processing but without the interference of actual shock. Regression analyses were completed in SPSS (IBM). All experimental protocols approved by the University of Maryland Baltimore IRB.

Results: Nominally significant group differences were found in multiple regions from the threat-safe contrast ($p<0.05$) in previous analyses. Two regions with significant patient-control differences were selected for this pilot depression study due to roles in stress processing and symptomatology: right hippocampus and ventral anterior cingulate. In controls, state and trait depression scores were highly correlated with each other ($r=+0.67$, $p<0.001$), and both correlated with recent stress PSS (state $r=0.62$ $p<0.001$; trait $r=0.46$ $p=0.015$). In MDD, PSS was associated with only state ($r=0.66$, $p<0.001$), but not trait depression. CTQ predicted trait depression ($r=0.59$, $p=0.02$), but not state depression ($p=0.5$). In the AST, PSS correlated negatively with R Hippocampal activation ($r=-0.45$, $p=0.026$), while CTQ was negatively associated with vACC activation ($r=-0.64$, $p=0.01$). There were no significant stress-activation associations in controls, revealing a differential relationship in stress activation and regulation.

Conclusions: We observed relationships between current stress and depressive symptoms, but differing associations between historical stress and stress task-related brain activity in MDD. Activity in this task revealed lifetime stress impact on vACC, key to reward processing and implicated in anhedonia, and recent stress impact on hippocampus, key to stress regulation and linked to MDD symptoms. These findings support a mechanism of altered stress vulnerability and stress processing in MDD, and provide support for stress-based tasks in disorders in which stress processing is dysregulated.

References

1. Kvarta MD*, Chiappelli J* et al. (2021), Aberrant Anterior Cingulate Processing of Anticipated Threat as a Mechanism for Psychosis. Psychiatry Res Neuroimaging Jul 30; 313: 111300.
2. Chiappelli J, et al. (2014), Assessment of trait and state aspects of depression in schizophrenia. Schizophrenia Bulletin. Jan;40(1):132-42.
3. McMenamin BW, et al. (2014), Network organization unfolds over time during periods of anxious anticipation. J Neurosci 34:11261–11273.

Poster No 608

Early-stage transdiagnostic prediction of functioning outcomes based on resting-state fMRI

Madalina-Octavia Buciuman[1], Paris Alexandros Lalousis[2], Shalaila Haas[3], Linda Antonucci[4], Lana Kambeitz-Ilankovic[5], Anne Ruef[6], Stefan Borgwardt[7], Joseph Kambeitz[8], Christos Pantelis[9], Rebecca Lencer[10], Alessandro Bertolino[11], Paolo Brambilla[12], Rachel Upthegrove[13], Stephen J. Wood[14], Peter Falkai[15], Anita Riecher-Rössler[16], Stephan Ruhrmann[5], Frauke Schultze-Lutter[17], Eva Meisenzahl[18], Jarmo Hietala[19], Raimo K. Salokangas[19], Dominic Dwyer[20], Nikolaos Koutsouleris[6]

[1]Department of Psychiatry and Psychotherapy, LMU University Hospital, LMU Munich, Munich, BAYERN, [2]Institute of Psychiatry, Psychology & Neuroscience, King's College London, London, United Kingdom, [3]Icahn School of Medicine at Mount Sinai, New York, NY, [4]University of Bari Aldo Moro, Milan, Italy, [5]University of Cologne, Cologne, Germany, [6]Department of Psychiatry and Psychotherapy, LMU University Hospital, LMU Munich, Munich, Bavaria, [7]Department of Psychiatry and Psychotherapy, University of Lübeck, Lübeck, Germany, [8]Department of Psychiatry and Psychotherapy, University of Cologne, Cologne, Bavaria, [9]Melbourne Neuropsychiatry Centre, Carlton, Victoria, [10]Institute for Translational Psychiatry, University Münster, Münster, Germany, [11]Department of Basic Medical Science, Neuroscience and Sense Organs, University of Bari Aldo Moro, Bari, Bari, [12]Department of Neurosciences and Mental Health, Fondazione IRCCS Ca' Granda Ospedale Maggiore Policli, Milan, Italy, [13]Institute of Mental Health, University of Birmingham, Birmingham, United Kingdom, [14]Centre for Youth Mental Health, University of Melbourne, Melbourne, Australia, [15]Department of Psychiatry and Psychotherapy, LMU University Hospital, LMU Munich, Munich, Germany, [16]Faculty of Medicine, University of Basel, Basel, Basel, [17]Heinrich-Heine University Düsseldorf, Düsseldorf, Germany, [18]Department of Psychiatry and Psychotherapy, Medical Faculty, Heinrich Heine University, Düsseldorf, Germany, [19]Department of Psychiatry, University of Turku, Turku, Finland, [20]Orygen, the National Centre of Excellence for Youth Mental Health, Melbourne, Victoria

Introduction: Impairments in daily functioning are prevalent in the early stages of psychosis and depression and are of increasing interest as clinical outcome metrics, due to their high impact on patients' quality of life. However, individualized risk stratification of functional outcomes is currently limited and would benefit from the exploration of novel methods and data modalities. In this context, group-level brain functional abnormalities have been extensively reported in psychotic and depressive disorders, but their value as early prognostic tools within the framework of precision psychiatry has been insufficiently explored. In the current work, we aimed to assess the value of the resting-state fractional amplitude of low frequency fluctuations (fALFF) as a longitudinal risk stratification tool of poor functioning in clinical high-risk for psychosis (CHR) and recent-onset depression (ROD).

Methods: A total number of 218 clinical high-risk (CHR) individuals and 197 recent-onset depression (ROD) patients coming from eight European sites within the multi-center European Personalised Prognostic Tools for Early Psychosis Management (PRONIA) study were used for the current analyses. Functional outcomes were measured using the Global Assessment of Functioning: Disability scale (Pedersen et al., 2007), with high functioning defined as more than 80 points on this scale. All machine learning analyses were conducted using an open source MATLAB-ased software (NeuroMiner 1.2, https://github.com/neurominer-git/NeuroMiner_1.2). We trained support vector machine classifiers within a leave-site-out nested cross-validated framework to predict functional outcomes at the 9-month follow-up, 18-month follow-up, as well as the persistence of high functioning from the 9-month to the 18-month follow-up based on multiband functional amplitude of low frequency fluctuations (fALFF). The fALFF data was computed for three different frequency sub-bands, in line with literature showing distinct sources and potential functional information captured at different frequencies (Yu et al., 2014; Wang et al., 2016): slow-5 (0.01 - 0.027 Hz), slow-4 (0.027 - 0.073), and slow-3 (0.073 – 0.0198 Hz). The statistical significance of the models' performance relative to chance level was assessed using 1000 permutation of the labels and the predictive features were visualized using sign-based consistency of feature weights (Gómez-Verdejo et al, 2019). Furthermore, we evaluated differences in accuracy between transdiagnostic and diagnosis-specific models (CHR vs ROD), associations of predictive patterns with broader clinical characteristics.

Results: Distributed fALFF increases/decreases were transdiagnostically predictive of functioning outcomes at the 9-month follow-up above chance level, with a maximal balanced accuracy obtained for the slow-5 frequency sub-band (Balanced accuracy = 63.4%, Sensitivity = 55.2%, Specificity = 71.6%, P<.001). For the 18-month follow-up time point, functioning outcomes were best predicted based on the activity in the slow-3 sub-band (Balanced accuracy = 63.8%, Sensitivity = 68.4%, Specificity = 59.2%). Lastly, the persistence of high functioning from the 9-month to the 18-month follow-up time point could be predicted by baseline fALFF data with higher accuracy than the individual time-points, based on both the slow-5 (Balanced accuracy = 67.8%, Sensitivity = 71.7%, Specificity = 64.0%) and slow-3 (Balanced accuracy = 69.7%, Sensitivity = 75.3%, Specificity = 64.0%) frequency sub-bands. Predictive patterns were predominantly spanned regions of the default-mode, frontoparietal and salience networks.

Conclusions: We provide first evidence for the relevance of rs-fMRI data as a transdiagnostic longitudinal biomarker of functioning outcomes in early psychotic and affective stages. These results could facilitate the development of multimodal risk stratification tools that incorporate functional brain biomarkers in the patient's prognostic assessment.

References

1. Pedersen, G., Hagtvet, K. A. & Karterud, S. Generalizability studies of the Global Assessment of Functioning–Split version. Compr. Psychiatry 48, 88–94 (2007).
2. Yu, R. et al. Frequency-specific alternations in the amplitude of low-frequency fluctuations in schizophrenia. Hum. Brain Mapp. 35, 627–637 (2014).
3. Wang, L. et al. Frequency-dependent changes in amplitude of low-frequency oscillations in depression: A resting-state fMRI study. Neurosci. Lett. 614, 105–111 (2016).
4. Gómez-Verdejo, V., Parrado-Hernández, E., & Tohka, J. (2019). Sign-consistency based variable importance for machine learning in brain imaging. Neuroinformatics, 17(4), 593-609.

Poster No 609

Revealing Hidden Patterns in Schizophrenia rs-fMRI via Novel Unsupervised Learning

Masoud Seraji[1], Charles Ellis[1], Mohammad Sendi[1], Vince Calhoun[1]

[1]*Center for Translational Research in Neuroimaging and Data Science (TReNDS), Atlanta, GA*

Introduction: Resting-state functional magnetic resonance imaging (rs-fMRI), especially with dynamic functional network connectivity (dFNC) analysis, has provided insights into neuropsychiatric disorders. In this field, clustering techniques are commonly used to identify dFNC states, uncovering connections between features and disorder pathology. However, in

multidimensional feature spaces, influential features may overshadow others relevant to the condition of interest. This is evident in schizophrenia (SZ), where whole brain dFNC analyses failed to detect SZ effects on the default mode network (DMN) [Sendi et al., 2020] that were later revealed in DMN-specific analyses [Sendi et al., 2021]. This raises questions about the potential for obscured effects in whole-DMN analyses. Our study aims to mitigate the potential obscuring influence of dominant features in clustering analyses by introducing a novel feature learning-based approach that identifies a maximally significant, minimally complex (MSMC) subset of DMN-related dFNC features associated with SZ.

Methods: Figure 1 shows our methodology, using the Functional Imaging Biomedical Informatics Research Network (FBIRN) dataset with 151 individuals with schizophrenia (SZs) and 160 healthy controls (HCs). Five initial mock scans were excluded before preprocessing. We employed statistical parametric mapping (SPM12) for motion correction and normalization to the echo-planar imaging template in the standard Montreal Neurological Imaging space (3x3x3 mm^3). The GIFT toolbox was then used to extract 7 independent components from the default mode detwork (DMN): three precuneus (PCu), two anterior cingulate cortex (ACC), and two posterior cingulate cortex (PCC) nodes. Subsequently, we applied a sliding tapered window to estimate dynamic functional network connectivity (dFNC) and extracted 21 connectivity features within the DMN. To identify an MSMC subset of features, we iteratively assigned samples to five clusters using k-means clustering with correlation distance, used Global Permutation Percent Change (G2PC) feature importance [Ellis et al., 2021] to identify and remove the most important feature, and repeated the process until correlation distance became inapplicable. We evaluated the impact of feature removal on the occupancy rate (OCR, i.e., the percentage of time each subject spent in each state), for SZs and HCs. Two-sample t-tests compared OCR differences between SZs and HCs at each iteration. Further analysis focused on the iteration with the most significant OCRs and the fewest features (i.e., the MSMC iteration).

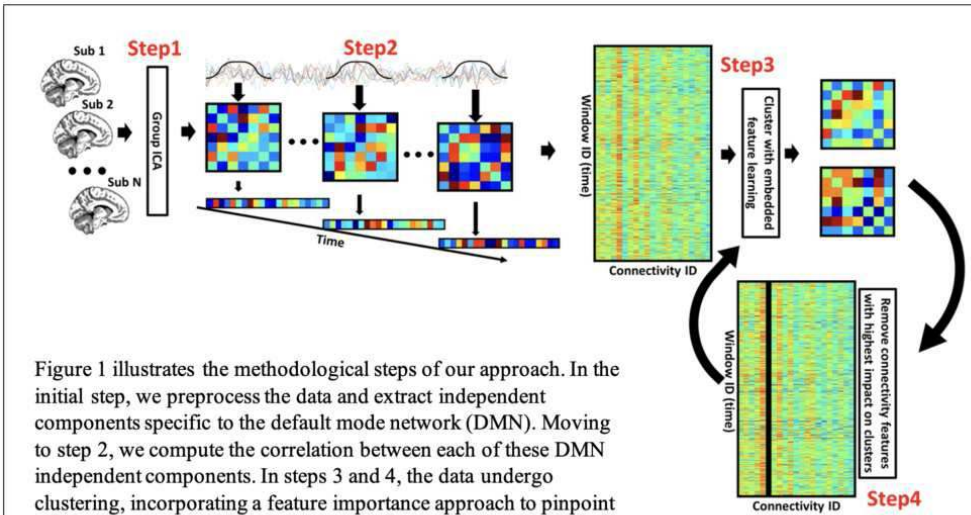

Figure 1 illustrates the methodological steps of our approach. In the initial step, we preprocess the data and extract independent components specific to the default mode network (DMN). Moving to step 2, we compute the correlation between each of these DMN independent components. In steps 3 and 4, the data undergo clustering, incorporating a feature importance approach to pinpoint crucial features. The process involves iteratively removing the most significant feature until only a small subset of features remain. This sequence of steps is repeated to systematically distill the relevant information.

Results: Figure 2 shows the OCR analysis, confirming our hypothesis that top features may overshadow more relevant dynamic features in SZ during clustering. Intra-PCC and intra-ACC features were removed, leaving some intra-PCN and inter-region features. SZ individuals primarily occupied states 0 and 4, characterized by high PCN/PCC correlation and moderate PCC1/ACC anticorrelation. In contrast, healthy controls (HCs) favored state 3, the least common state, marked by moderate to high PCN/PCC correlation and high PCC1/ACC correlation. Our PCN/PCC and PCC1/ACC findings fit with those of [Ellis et al., 2022] and [Ellis et al., 2023], respectively.

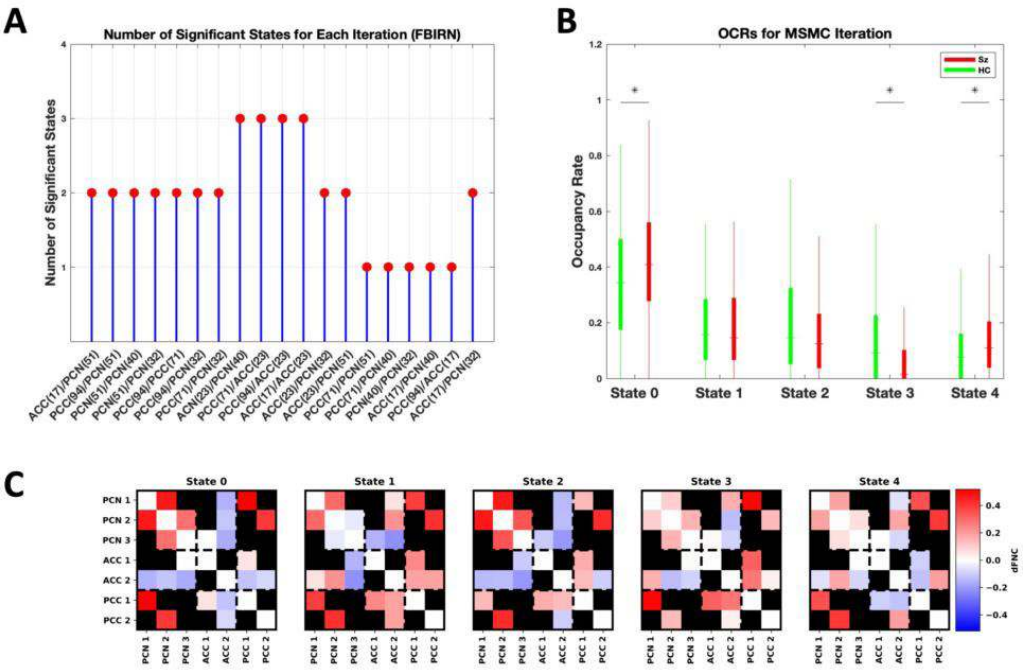

Figure 2 (A) Number of significant states based on the Occupancy Rate. The x-axes show from left to right the node removed at each iteration, and the y-axis shows the number of significant OCRs. (B) Occupancy Rates at the maximally significant minimally complex iteration, (i.e., iteration number 11, removal of ACC (17)/ACC (23)). Data for HCs and SZs are shown in green and red, respectively. Asterisks indicate that there is a difference between OCRs for SZs and HCs in a particular state. (C) The centroids of the MSMC iteration. The color black indicates that the corresponding feature was eliminated.

Conclusions: Prior research has indicated that conventional clustering methods used for identifying dFNC states might overlook crucial features associated with neuropsychiatric disorders. In this investigation, we introduced a novel methodology to explore this potential issue in the context of the DMN in SZ. Notably, we observed that the largest number of significant distinctions between individuals with SZ and HC only became apparent after eliminating several of the top features, thereby supporting the validity of our initial hypothesis. We anticipate that our innovative approach will enhance the comprehensive understanding of neuropsychiatric and neurological disorders in future studies.

References

1. Ellis CA, Sendi MSE, Geenjaar EPT, Plis SM, Miller RL, Calhoun VD (2021): Algorithm-Agnostic Explainability for Unsupervised Clustering. https://arxiv.org/abs/2105.08053v2.
2. Ellis CA, Miller R, Calhoun V. (2023): Explainable Fuzzy Clustering Framework Reveals Divergent Default Mode Network Connectivity Dynamics in Schizophrenia. bioRxiv.
3. Ellis CA, Sendi MSE, Miller R, Calhoun V (2022): An Unsupervised Feature Learning Approach for Elucidating Hidden Dynamics in rs-fMRI Functional Network Connectivity. IEEE Engineering in Medicine and Biology Conference 2022-July:4449-4452.
4. Sendi MSE, Zendehrouh E, Ellis CA, Liang Z, Fu Z, Mathalon DH, Ford JM, Preda A, van Erp TGM, Miller RL, Pearlson GD, Turner JA, Calhoun VD (2021): Aberrant Dynamic Functional Connectivity of Default Mode Network in Schizophrenia and Links to Symptom Severity. Front Neural Circuits 15:649417.
5. Sendi MSE, Zendehrouh E, Fu Z, Mahmoudi B, Miller RL, Calhoun VD (2020): A Machine Learning Model for Exploring Aberrant Functional Network Connectivity Transition in Schizophrenia. Proceedings of the IEEE Southwest Symposium on Image Analysis and Interpretation 2020-March:112–115.

Poster No 610

A whole-brain morphometry study of misophonia: comparing voxel-based and surface-based approaches

Nimesha Gerlus[1], Kevin LaBar[1], Andrada Neacsiu[2]

[1]Duke University, Durham, NC, [2]Duke University School of Medicine, Durham, NC

Introduction: Misophonia is a disorder of decreased tolerance to specific sounds and their associated stimuli, which often evoke negative emotional responses and distress. Research on misophonia's neural correlates is needed to inform the development of novel interventions. Previous MRI studies have used voxel-based morphometry (VBM) to compare individuals with misophonia to individuals with no psychiatric history. This study investigated whether individuals with misophonia display different morphometric characteristics compared to a group of clinical controls. We also examined whether the estimation of

group differences in whole-brain morphometry varies based on the utilization of surface-based morphometry (SBM) versus voxel-based techniques.

Methods: Participants were 27 adults with misophonia, and 27 adults with transdiagnostic emotion dysregulation and at least one DSM-V psychiatric disorder. All participants completed a T1-weighted MRI in a 3T scanner as part of a clinical neurostimulation trial. fMRIPrep was used to correct the bias field of the images. Freesurfer and FSL were respectively used for SBM and VBM analyses. General linear models were implemented to compare group differences in morphometry and controlled for the effects of estimated total intracranial volume. Vertex-wise and voxel-wise cluster-forming thresholds (p = 0.05) were established using permutation testing. All models were corrected for multiple comparisons at a cluster-wise threshold of pcorr = 0.05.

Results: Compared to clinical controls, individuals with misophonia display significantly increased volume of the right primary auditory cortex (5980 vertices, pcorr = 0.03) using SBM. The SBM method also revealed significantly larger surface area in the left paracentral lobule (11707 vertices, pcorr = 0.01) and the right rostral superior temporal gyrus (11304 vertices, pcorr = 0.04) in the misophonia group compared to the clinical control group. Individuals with misophonia displayed larger surface area in the right superior frontal gyrus (7482 vertices); however, this region did not survive the cluster-wise correction (pcorr = 0.08). No significant between-group differences in morphometry were observed using VBM.

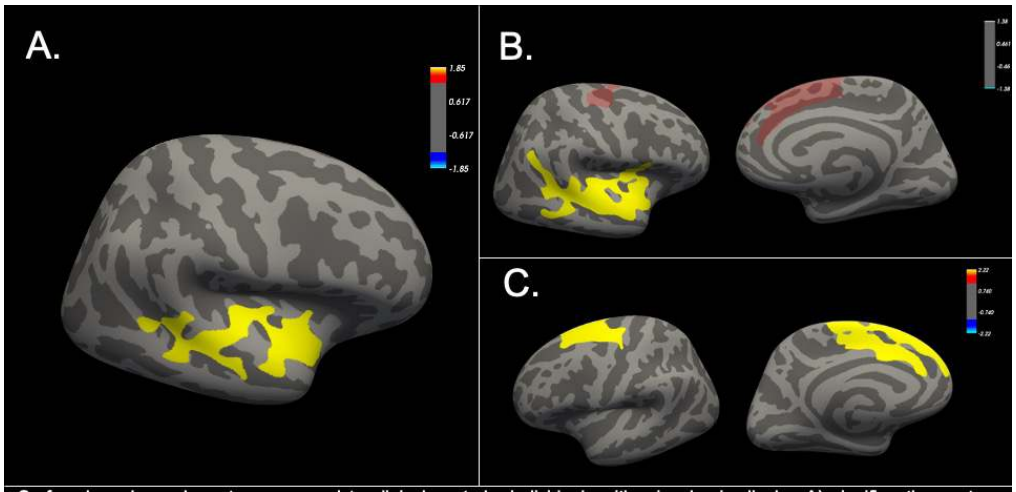

Surface-based morphometry: compared to clinical controls, individuals with misophonia display A) significantly greater volume of the right primary auditory cortex (p_{corr} = 0.03); B) significantly greater right rostral superior temporal gyrus surface area (p_{corr} = 0.04) and larger superior right frontal gyrus surface area (p_{corr} = 0.08); and C) significantly greater surface area of the left paracentral lobule (p_{corr} = 0.01).

Conclusions: Although emotional distress underlies the behavioral phenotype of both participant groups, only participants with misophonia experience emotional distress associated with misophonic trigger sounds. In these individuals, surface-based but not voxel-based morphometric techniques show perceptual regions with greater surface area and volume compared to clinical controls with transdiagnostic emotion dysregulation. Therefore, SBM may detect structural abnormalities in the misophonic brain with greater sensitivity than VBM. Specifically, increased right auditory cortex volume using SBM distinguishes misophonic participants from clinical control participants without auditory affective processing deficits. Future directions include using SBM to further characterize distinct structural features of misophonia by comparing morphometry to that of non-clinical controls, as well as examining whether identified morphometric features are associated with self-reported misophonic symptoms.

References

1. Swedo, S.E. (2020), 'Consensus definition of misophonia: a delphi study,' Frontiers in Neuroscience, vol. 16.
2. Eijsker, N. (2021), 'Structural and functional abnormalities in misophonia,' European Neuropsychopharmacology, vol. 52, pp. 62-71.

Poster No 611

Lesions that Cause Psychosis Map to a Common Brain Circuit Involving the Hippocampus

Andrew Pines[1], Summer Frandsen[1], William Drew[1], Garance Meyer[1], Calvin Howard[1], Stephan Palm[1], Frederic Schaper[1], Clemens Neudorfer[1], Andreas Horn[1], Shan Siddiqi[1]

[1]Brigham & Women's Hospital, Harvard Medical School, Boston, MA

Introduction: Schizophrenia is characterized by chronic symptoms of psychosis such as delusions, hallucinations, and thought disorder. Antipsychotic medications frequently cause intolerable side effects, and often do not fully resolve symptoms. To investigate alternative treatments, transcranial magnetic stimulation (TMS) has been studied to ameliorate psychotic symptoms. TMS trials for schizophrenia, however, have not consistently reduced psychotic symptoms. Defining the neuroanatomy that is causally implicated in psychotic symptoms could reveal a TMS target specific to schizophrenia.

Methods: We identified published cases of brain lesions associated with psychosis and screened them for causality. Functional and structural connectivity of each lesion was estimated using a human connectome database (n=1000). To determine connections common to lesions causing psychosis, we performed a sensitivity analysis by examining regions covered by a one-sample T-test and the overlap of the functional correlates of each lesion. We performed a specificity analysis using a Family-Wise-Error(FWE)-corrected voxel-wise two-sample t-test between the functional maps of lesions causing psychosis and control lesions that did not cause psychosis.

Results: 155 cases from the literature were determined to be causal of psychosis. Regions that were significant in a one-sample T-test (threshold T>7), functional overlap tests (50% overlap, T>7), and a two-sample T-test (pFWE<5 x 10-4) were the the hippocampus, ventral tegmental area, retrosplenial cortex, ventromedial prefrontal cortex, cerebbelar lobule IX, and the medial dorsal nuclei of the thalamus. The most sensitive and specific anatomy was the posterior subiculum of the hippocampus. We repeated the analyses after excluding lesions intersecting the hippocampus (n=52) and found similar functional connections across the whole brain with the same peak in the posterior hippocampus. In an independent cohort, lesions associated with psychosis-like symptoms exhibited significantly similar connectivity profiles to the psychosis network. Voxels in the ventromedial prefrontal cortex are highly correlated with the psychosis circuit and an appropriate target for TMS.

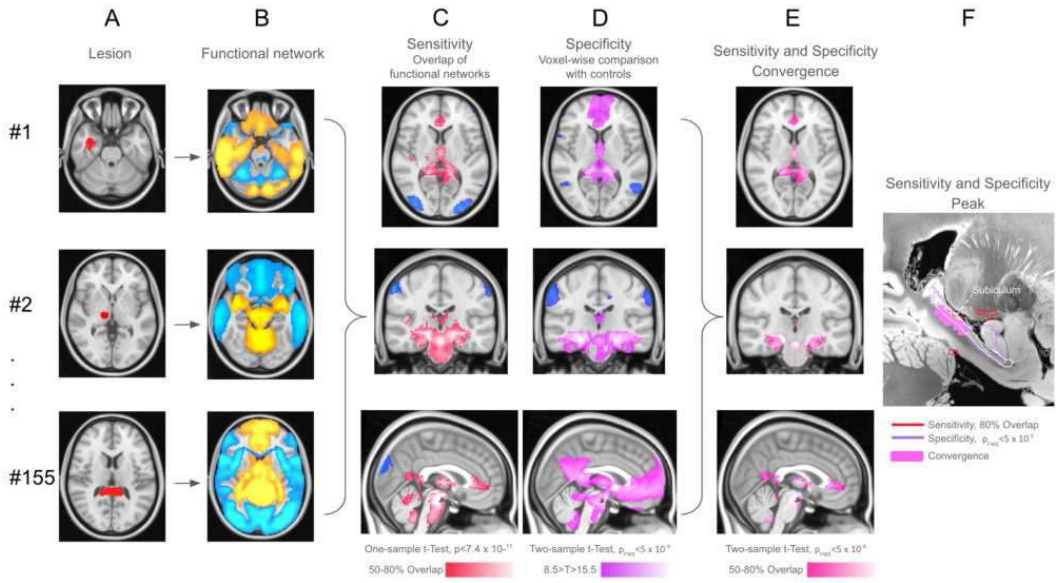

Conclusions: Lesions causing psychosis map to a common brain circuit. The posterior subiculum of the hippocampus is the most sensitive and specific area involved in this circuit. A region in this ventromedial prefrontal cortex is highly connected to this psychosis circuit and could serve as a TMS target for future studies.

Poster No 612

Is the neural oscillation in the pars opercularis of the rIFG related to antidepressant efficacy?

Tingting Xiong[1], Lingling Hua[1], Moxuan Song[2], Yingying Huang[1], Zhijian Yao[2], Qing Lu[3]

[1]Department of Psychiatry, the Affiliated Brain Hospital of Nanjing Medical University, Nanjing, Jiangsu, [2]The Affiliated Brain Hospital of Nanjing Medical University, Nanjing, Jiangsu, [3]Southeast University, Nanjing, Jiangsu

Introduction: In this study, we intend to explore the neuropathological mechanism of response inhibition deficit in depression by studying the local activity and whole-brain functional connectivity of beta frequency band in the pars opercularis of the right inferior frontal gyrus(rIFG) at the baseline period, to further investigate its association with the early efficacy of antidepressant drugs.

Methods: A total of 52 depressed patients and 26 healthy controls were included, All subjects completed a cranial magnetic resonance scan and magnetoencephalographic data acquisition under the Go/No-Go experimental paradigm at baseline. Meanwhile, a weekly assessment of the HAMD scale was performed to assess the efficacy without interfering with the patient's actual clinical treatment. The group of MDD patients was divided into Early responders and Early Nonresponders based on whether the reduction in total HAMD score at the end of 2-week treatment was ≥50%. Based on the AAL90 template, the pars opercularis of the rIFG was used as a seed point to establish functional connectivity with other brain regions in the whole brain. Also, Event-Related Desynchronization (ERD) in the beta frequency band of the pars opercularis of the rIFG of all subjects at baseline was compared between the three groups, In order to identify the differences and to analyze its correlation with the 2-week rate of reduction in the total HAMD score and each factor score, which was used to explore the best markers for differentiating the early efficacy of antidepressants.

Results: Functional connectivity in the beta band of the pars opercularis of the rIFG to other brain regions in the whole brain was reduced in the depressed group when compared to the healthy control group at baseline ($F = 5.093$, $P = 0.008$). whereas there was no significant difference in functional connectivity between Early responders and Early Nonresponders ($P > 0.05$); Compared with the healthy control group, Early responders and Nonresponders both showed a decrease in ERD of the beta frequency band in the pars opercularis of the rIFG during the baseline period ($P < 0.05$); Compared with Early responders, Early Nonresponders had a worse degree of desynchronization related to the pars opercularis of the rIFG ($P < 0.05$); The ERD in the beta frequency band during the baseline period was negatively correlated with the 2-week rate of reduction in the total HAMD score ($r = -0.364$, $P = 0.008$), Cognitive impairment factor($r = -0.365$, $P = 0.008$) and Block factor ($r = -0.441$, $P = 0.001$).

Conclusions: The pars opercularis of the rIFG in depressed patients suffers from both impaired function of its own and decreased synergism with other brain regions, which may be a pathophysiological mechanism for the response inhibition deficit in depression; the predictive value of functional connectivity between the pars opercularis of the rIFG and other brain regions for the Early efficacy evaluation still needs to be further explored; ERDs in the beta band of this region can be used as a biomarker related to the early efficacy of antidepressant drugs, which can provide a certain objective basis for whether cognitive deficits and psychomotor block symptoms can be effectively improved in patients with depression after 2 weeks.

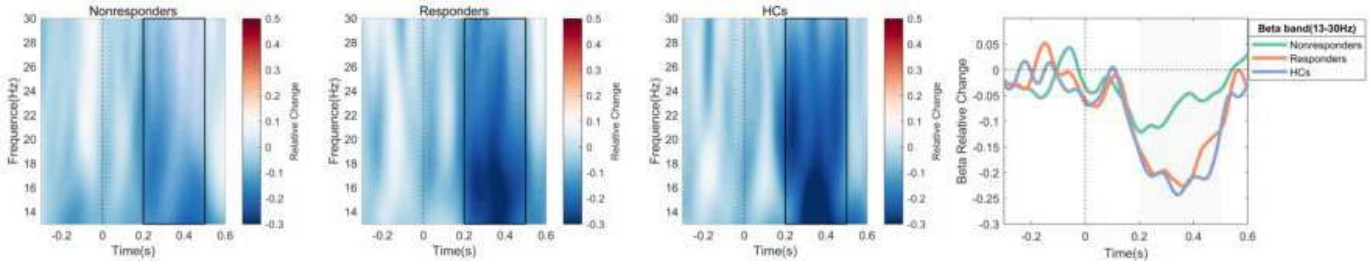

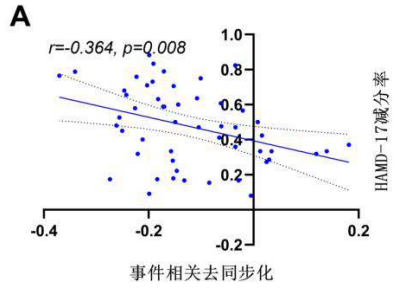

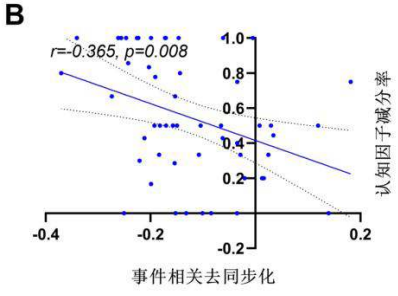

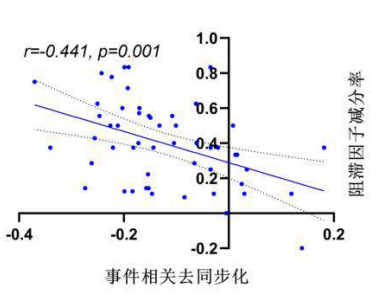

References
1. Aron, A. R., Robbins, T. W., & Poldrack, R. A. (2014). Inhibition and the right inferior frontal cortex: one decade on. Trends in cognitive sciences, 18(4), 177–185
2. Hack, L. M., Tozzi, L., Zenteno, S., Olmsted, A. M., Hilton, R., Jubeir, J., Korgaonkar, M. S., Schatzberg, A. F., Yesavage, J. A., O'Hara, R., & Williams, L. M. (2023). A Cognitive Biotype of Depression and Symptoms, Behavior Measures, Neural Circuits, and Differential Treatment Outcomes: A Prespecified Secondary Analysis of a Randomized Clinical Trial. JAMA network open, 6(6), e2318411
3. Schaum, M., Pinzuti, E., Sebastian, A., Lieb, K., Fries, P., Mobascher, A., Jung, P., Wibral, M., & Tüscher, O. (2021). Right inferior frontal gyrus implements motor inhibitory control via beta-band oscillations in humans. eLife, 10, e61679
4. Tozzi, L., Goldstein-Piekarski, A. N., Korgaonkar, M. S., & Williams, L. M. (2020). Connectivity of the Cognitive Control Network During Response Inhibition as a Predictive and Response Biomarker in Major Depression: Evidence From a Randomized Clinical Trial. Biological psychiatry, 87(5), 462–472
5. Vermeiden, M., Kamperman, A. M., Vulink, M. E., van den Broek, W. W., & Birkenhäger, T. K. (2015). Early improvement as a predictor of eventual antidepressant treatment response in severely depressed inpatients. Psychopharmacology, 232(8), 1347–1356
6. Li, F. F., Chen, X. L., Zhang, Y. T., Li, R. T., & Li, X. (2021). The role of prepotent response inhibition and interference control in depression. Cognitive neuropsychiatry, 26(6), 441–454

Poster No 613

A three-dimensional model of neural activity and phenomenal-behavioral patterns

Paola Magioncalda[1], Matteo Martino[1]

[1]*Taipei Medical University, Taipei, Taiwan*

Introduction: Understanding how phenomenal experience and behavior are related to neural activity represents an arduous challenge. As a potential approach to this issue, the complex subjective experience/behavior may be deconstructed into basic dimensions, such as psychomotricity, affectivity, and thought. This may help cluster and systematize heterogeneous constellations of phenomenal experiences and behaviors, along with related symptoms, into distinct elemental patterns. In turn, these dimensions might more precisely be mapped onto distinct and specific neural circuits and networks. Accordingly, the present work aims to propose a three-dimensional model of neural activity and phenomenal-behavioral patterns applicable to physiological and pathological conditions.

Methods: We reviewed the findings from a large number of functional neuroimaging studies on healthy subjects and neuropsychiatric disorders (including major depressive disorder, bipolar disorder, schizophrenia, attention-deficit/hyperactivity disorder, anxiety disorders, addictive disorders, Parkinson's disease, Tourette syndrome, Alzheimer's disease, and frontotemporal dementia) that report direct or indirect information on the relationship between brain functioning and the specific dimensions/symptomatology (including psychomotor hyperactivity, hyperkinesia, psychomotor retardation, hypokinesia, catatonia, anxiety, dysphoria, euphoria, panic, anhedonia, apathy, depersonalization, mind-wandering, repetitive thinking, hallucinations, delusions, attention deficit, cognitive deficit, and consciousness loss). Integrating this information and extending our previous work, we finally delineated a theoretically- and empirically-grounded model linking brain activity with phenomenal-behavioral patterns.

Results: In this model, neural activity is organized into distinct units in accordance with connectivity patterns and related input/output processing, manifesting in the different phenomenal-behavioral dimensions. (1) An external unit, which involves the sensorimotor circuit/brain's sensorimotor network and is connected with the external environment, processes external inputs/outputs, manifesting in the psychomotor dimension (processing of exteroception and somatomotor activity). External unit hyperactivity manifests in psychomotor excitation (hyperactivity/hyperkinesia/catatonia), while external unit hypoactivity manifests in psychomotor inhibition (retardation/hypokinesia/catatonia). (2) An internal unit, which involves the interoceptive-autonomic circuit/brain's salience network and is connected with the internal/body environment, processes internal inputs/outputs, manifesting in the affective dimension (processing of interoception and autonomic activity). Internal unit hyperactivity manifests in affective excitation (anxiety/dysphoria-euphoria/panic), while internal unit hypoactivity manifests in affective inhibition (anhedonia/apathy/depersonalization). (3) An associative unit, which involves the brain's associative areas/default-mode network and is connected with the external/internal units (but not with the environment), processes associative inputs/outputs, manifesting in the thought dimension (processing of ideas). Associative unit hyperactivity manifests in thought excitation (mind-wandering/repetitive thinking/psychosis), while associative unit hypoactivity manifests in thought inhibition (inattention/cognitive deficit/consciousness loss). Finally, these neural units interplay and dynamically combine into various neural states, resulting in the complex phenomenal experience and behavior.

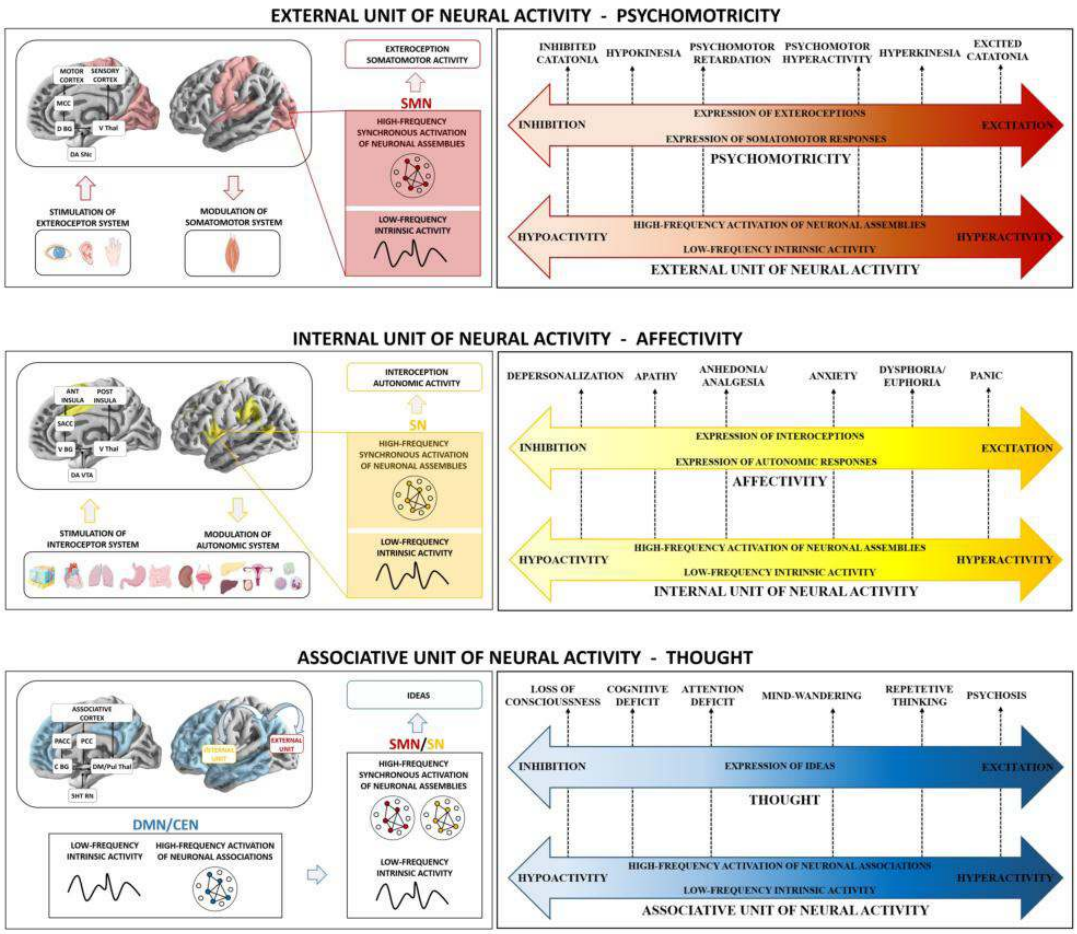

Conclusions: We propose a theoretical model of the relationship of neural activity with phenomenal experience and behavior along an external neural unit underlying psychomotricity, an internal neural unit underlying affectivity, and an associative neural unit underlying thought, representing the three fundamental and complementary dimensions of interaction between the organism and the environment.

References

1. Martino, M. and Magioncalda, P. (2023), 'A three-dimensional model of neural activity and phenomenal-behavioral patterns', Molecular Psychiatry, [accepted for publication]

Poster No 614

A novel psychotherapy based on traditional Chinese culture and its effectiveness on depression

Yifan Liao[1,2,3], Qinglin Gao[1,4], Tianjun Liu[5], Chaogan Yan[6]

[1]CAS Key Laboratory of Behavioral Science, Institute of Psychology, Beijing, China, [2]Department of Psychology, University of Chinese Academy of Sciences, Beijing, China, [3]International Big-Data Center for Depression Research, Institute of Psychology, CAS, Beijing, China, [4]International Big-Data Center for Depression Research, Institute of Psychology, CAS, Beijing, China, [5]MET Research Institute, Beijing, China, [6]Chinese Academy of Sciences, Beijing, China

Introduction: Moving to "Kong" Therapy (MKT) is a unique therapeutic approach rooted in traditional Chinese philosophy and medical theory, while retaining the structure of Western psychotherapies. The technique involves a simple 10-step framework (Fig.1) where therapists guide patients to visualize their target symptoms as symbolic objects and place them in a personalized "container". These symbols are then moved mentally across different distances until they gradually fade and disappear. The process helps to reduce the negative impact of the symptoms by leading the patient to a state of "Kong"- an infinite psychological space free of troubles (Tao, 2022). This innovative approach offers a promising alternative for treating various mental health conditions, including depression, anxiety, stress disorder, and chronic pain (Liu, 2019). Despite the remarkable clinical performance of MKT in Chinese medical practice, its effectiveness remains phenomenological, awaiting empirical

evidence and well-designed experiments to investigate the neurocognitive mechanisms underlying this novel therapeutic technique. In this study, we examined the effectiveness of MKT on major depressive disorder (MDD) using multiple methods, including resting-state fMRI (R-fMRI), questionnaires, and clinical interviews. We expect to reveal the therapeutic mechanisms of MKT and improve the clinical practice of MDD treatment.

Static Work (preparation process for the moving)

Steps	Operation	Objective/ Principles	Similar techniques in clinical practice
1.	**The Trio (Body, Breath, & mind) Relaxation Exercise**	Regulate the sympathetic and the parasympathetic nervous systems, increase mind-body awareness, calm the client, and get them prepared for the counseling	Mindfulness Meditation, Zen Relaxation, Respiratory Therapy, Somatic Experiencing Therapy (SE; Levine), Focusing Therapy (Gendingling)...
2.	**Select the target symptom**	Focus on the most problematic or urgent symptom of the client, identify the therapeutic target of the current session	Focusing Therapy, Imagery Communication Psychotherapy (ICP; Zhu), Active Imagination Technique (Jung), Gestalt Therapy...
3.	**Visualize and locate the target symptom ('symbol')**	abstract thinking → imagery thinking elusive symptoms → vivid image/object uncontrollable → operable, controllable	Focusing Therapy, Imagery Communication Psychotherapy (ICP; Zhu), Active Imagination Technique (Jung), Gestalt Therapy...
4.	**Visualize a Symbolic Container**	The container symbolizes the inner resources of the client	Focusing Therapy, Imagery Communication Psychotherapy (ICP; Zhu), Active Imagination Technique (Jung)...
5.	**Rate the impact of the symptom on a 0-10 Likert scale, draw the 'symbol' and 'Container' on the record paper A, and write down 3-5 features of them**	Evaluate the impact of the symptom, help the client to further concretize and visualize the symbolic object and the symbolic container	Expressive Arts Therapy, Focusing Therapy...

Dynamic Work (moving to the state of 'Kong')

Steps	Operation	Objective/ Principles	Similar techniques in clinical practice
6.	**Repeat the Trio (Body, Breath, & mind) Relaxation Exercise**	Deeper relaxation, bring the client back to a mindful state, prepare for the moving	Mindfulness Meditation, Respiratory Therapy, Somatic Experiencing Therapy (SE; Levine), Focusing Therapy (Gendingling)...
7.	**Place the symbolic object into the container, inspect and clean, and/or reinforce the packing**	Reconstruct the target symptom and invoke the client's inner resources, actively solve the problem in a symbolic (safer)way	Focusing Therapy, Imagery Communication Psychotherapy (ICP; Zhu), Active Imagination Technique, Gestalt Therapy...
8.	**Move the symbolic object into the psychological emptiness ('Kong')**	Self-distance through moving away, 'Kong' is a neutral state of equilibrium, neither positive nor negative, where there is no trouble	Focusing Therapy, Imagery Communication Psychotherapy (ICP; Zhu), symbolic therapy/ the active imagination technique (Jung), hypnosis..
9.	**Move the container back if the client would like to**	The symptom may change after the above operation- reconsolidation	Focusing Therapy, Imagery Communication Psychotherapy (ICP; Zhu), Active Imagination Technique, Gestalt Therapy...
10.	**Draw the 'symbol' and 'Container' on the record paper B if any changes happen, rate the impact of the target symptom again on a 0-10 Likert scale**	Re-evaluate the influence of the symptom, assess the therapeutic effects, and reflect on the counseling session	Expressive Arts Therapy, Focusing Therapy, Cognitive Behavioral Therapy...

Figure 1. The 10-step protocol of MKT. The MKT consists of two parts: the static work and the dynamic work. This chart illustrates the structural framework and the objective/principles of each operational step (referred to Tao et al., 2022). To better elucidate the logic and operation of MKT, some counseling techniques that share similar elements are listed in analogy with MKT.

Methods: Twenty-one MDD patients (15 females; mean age=26.5 years, range 21 to 34) were randomly assigned to an intervention group (received 8 weeks of MKT immediately after baseline, n=12) or a wait-list group (waited for 8 weeks before receiving the 8-week MKT, n=9). Participants completed clinical interviews, R-fMRI scans, and self-reported questionnaires (e.g., Beck Depression Inventory-II, BDI-II) before and after the MKT treatment. Depression and anxiety symptoms were assessed by experienced independent evaluators using the 17-item Hamilton Depression Scale (HAMD) and the Hamilton Anxiety Scale (HAMA). Brain imaging data were preprocessed with DPABISurf (Yan, 2021) before brain network construction with DPABINet (Yan, 2016). Paired-sample t-tests were conducted to examine the symptomatic, behavioral, and functional connectivity (FC) changes pre- and post-intervention of all participants.

Results: Our results revealed significant improvement in clinical symptoms among the participants after 8 weeks of MET, as demonstrated by a significant reduction in the HAMD score ($t=4.94$, $p<.001$), HAMA score ($t=3.89$, $p<.001$), BDI score ($t=4.01$, $p<.001$), and the Insomnia Severity Index (ISI) score ($t=3.81$, $p<0.01$). The patients also reported greater self-efficiency after MET, as evidenced by a significantly higher score ($t=-3.55$, $p<0.01$) on the General Self-Efficiency Scale (GSES) (Fig.2A). The functional network analysis revealed a significant decrease in FC across the whole brain posttreatment ($p< 0.001$, uncorrected). This tendency of reducing FC is similar to the effect of 8-week antidepressant treatment for MDD patients, as shown in our previous work (Li, 2022). Some increases were also observed in between-network FC for DMN-SC, DMN-LN, and within DMN (Fig.2B), suggesting that DMN may play a pivotal role in the therapeutic mechanism of MET on MDD treatment.

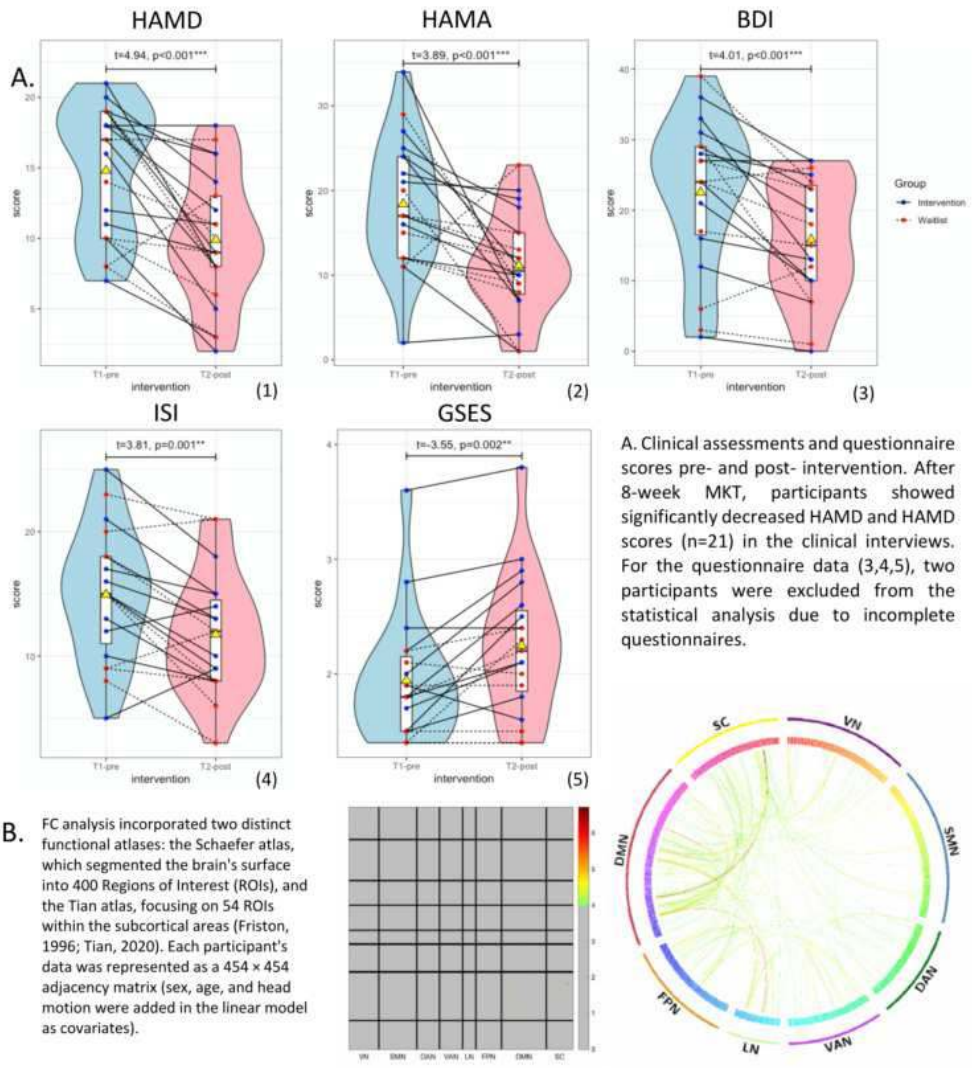

A. Clinical assessments and questionnaire scores pre- and post- intervention. After 8-week MKT, participants showed significantly decreased HAMD and HAMD scores (n=21) in the clinical interviews. For the questionnaire data (3,4,5), two participants were excluded from the statistical analysis due to incomplete questionnaires.

B. FC analysis incorporated two distinct functional atlases: the Schaefer atlas, which segmented the brain's surface into 400 Regions of Interest (ROIs), and the Tian atlas, focusing on 54 ROIs within the subcortical areas (Friston, 1996; Tian, 2020). Each participant's data was represented as a 454 × 454 adjacency matrix (sex, age, and head motion were added in the linear model as covariates).

B. Eight-week MKT reduced FC in MDD patients (n=21). (left) Edge-plot for the statistically significant changes in brain network. The color bar indicates T values; (right) Circos plot for the statistically significant changes in brain network. Green: decreased FC; orange: increased FC. *Uncorrected, P<0.001(two-tailed). DMN, default mode network; FPN, frontoparietal network; LN, limbic network; VAN, ventral attention network; DAN, dorsal attention network; SMN, somatosensory network; VN, visual network; SC, subcortical network.

Conclusions: In conclusion, the study initiatively provided empirical evidence for the effectiveness of MKT in treating MDD, showing significant improvements in clinical symptoms and changes in functional brain connectivity, particularly involving the DMN. Future research should focus on larger sample sizes, alternative neuroimaging methodologies (e.g., multi-modal imaging), and cross-cultural applicability to validate and generalize the findings. The findings of this study could open doors to cross-cultural collaborations and provide insights into the development of culturally sensitive and more effective mental health interventions.

References

1. Friston, K.J. (1996), 'Movement-related effects in fMRI time-series'. Magnetic resonance in medicine, vol. 35, no.3, pp. 346–355
2. Li, L. (2021), 'Eight-week antidepressant treatment reduces functional connectivity in first-episode drug-naïve patients with major depressive disorder', Human brain mapping, vol. 42, no. 8, pp. 2593–2605
3. Liu, T.J. (2019), 'Moving to Emptiness Therapy operation manual: A localized mind-body therapy technique', Chinese Medicine and Traditional Chinese Medicine Press
4. Tao, Y. (2022), 'The effectiveness of the Moving to Emptiness Technique on clients who need help during the COVID-19 Pandemic: A real-world study'. Frontiers in public health,
5. Tian, Y. (2020), 'Topographic organization of the human subcortex unveiled with functional connectivity gradients', Nature Neuroscience, vol. 23, no.11, pp. 1421-1432
6. Yan, C.G. (2021), 'DPABISurf: data processing & analysis for brain imaging on surface', Science Bulletin, vol. 66, no.24, pp. 2453-2455
7. Yan, C.G. (2016), 'DPABI: data processing & analysis for (resting-state) brain imaging'. Neuroinformatics, vol. 14, no. 3, pp.339-351

Poster No 615

Structural Covariance Network Topology in Individuals with Clinical High Risk for Psychosis

Siwei Liu[1], Paul Thompson[2], Dennis Hernaus[3], Maria Jalbrzikowski[4], Jimmy Lee[5], Juan Helen Zhou[1], ENIGMA Clinical High Risk for Psychosis Working Group[6]

[1]National University of Singapore, Singapore, Singapore, [2]Imaging Genetics Center, Keck School of Medicine of University of Southern California, Los Angeles, CA, [3]Maastricht University, Maastricht, Limburg, [4]Boston Children's Hospital, Boston, MA, [5]Department of Psychosis, Institute of Mental Health, Singapore, Singapore, [6]USC's Mark and Mary Stevens Neuroimaging and Informatics Institute, Southern California, CA

Introduction: There are widespread, subtle brain structural abnormalities in individuals at Clinical High Risk (CHR) for developing psychosis [Yung et al., 1996]. While the network approach was proposed to explain deficit propagation in schizophrenia [Chopra et al., 2021; Chopra et al., 2023; Shafiei et al., 2020], studies describing the grey matter structural network properties in CHR [Das et al., 2018] are scarce and suffer from small sample sizes, leaving gaps in understanding brain networks underlying disease progression and symptom development.

Methods: Here, we sought to test whether global and network-level structural covariance topographical properties differed between a) CHR and healthy controls, b) CHR who transitioned to psychosis (CHR-T) and those who did not (CHR-NT), and c) CHR subtypes. We further hypothesized that less efficient structural covariance topology would be related to more severe symptoms. Cross-sectional structural scans of 2864 individuals (1842 CHR and 1417 controls) from 31 Enhancing NeuroImaging Genetics through Meta-Analysis (ENIGMA) consortium [Baldwin et al., 2022; Haas et al., 2023; Jalbrzikowski et al., 2021] sites were included.

Results: At the global level, CHR individuals exhibited lower structural covariance (false discovery rate corrected p value $q<0.001$) and less optimal structural network configuration than controls, including lower global efficiency ($q=0.013$), local efficiency ($q=0.001$), and clustering coefficient ($q=0.025$). At the network level, the system segregation indexes (i.e., network distinctiveness) of distinct frontotemporal surface area networks were higher in CHR-T than CHR-NT and controls (all $q<0.013$). The system segregation index of frontal cortical thickness network was lower in CHR-T than CHR-NT ($q=0.012$) and controls ($q=0.065$). Furthermore, frontal networks also showed unique associations with positive symptoms in CHR-NT (surface area $q=0.008$) and negative symptoms in CHR-T (thickness $q=0.063$).

Conclusions: Our findings provide new insights in network-level alterations in CHR, and how such alterations may contribute to symptoms and, ultimately, conversion. Taken together, network topology offers a valuable perspective on pathology across different stages of illness in early psychosis.

References

1. Baldwin H (2022): Neuroanatomical heterogeneity and homogeneity in individuals at clinical high risk for psychosis. Translational Psychiatry 12:1–11.
2. Chopra S (2021): Differentiating the effect of antipsychotic medication and illness on brain volume reductions in first-episode psychosis: A Longitudinal, Randomised, Triple-blind, Placebo-controlled MRI Study. Neuropsychopharmacology 46:1494–1501.
3. Chopra S (2023): Network-Based Spreading of Gray Matter Changes Across Different Stages of Psychosis. JAMA Psychiatry. https://doi.org/10.1001/jamapsychiatry.2023.3293.
4. Das T (2018): Disorganized Gyrification Network Properties During the Transition to Psychosis. JAMA Psychiatry 75:613–622.
5. Haas SS (2018): Disorganized Gyrification Network Properties During the Transition to Psychosis. JAMA Psychiatry 75:613–622.

Poster No 616

Reactive astrocytes in the medial orbitofrontal cortex and cognitive functions in schizophrenia

Sunah Choi[1], Minah Kim[2], Sang Soo Cho[1], Woori Choi[1], Harin Oh[1], Jongrak Kim[1], Jungha Lee[1], Su-Jin An[1], Jun Seo Hwang[1], Yun-Sang Lee[3], In Chan Song[4], Sun-Young Moon[5], Silvia Kyungjin Lho[6], Jun Soo Kwon[1]

[1]Department of Brain and Cognitive Sciences, Seoul National University College of Natural Sciences, Seoul, Seoul, [2]Department of Neuropsychiatry, Seoul National University Hospital, Seoul, Seoul, [3]Department of Nuclear Medicine, Seoul National University College of Medicine, Seoul, Seoul, [4]Department of Radiology, Seoul National University College of Medicine, Seoul, Seoul, [5]Department of Public Health Medical Services, Seoul National University Bundang Hospital, Seoul, Seoul, [6]Seoul Metropolitan Government-Seoul National University Boramae Medical Center, Seoul, Seoul

Introduction: The underlying mechanism of negative and cognitive symptoms remains poorly understood in schizophrenia. Studies suggested alterations in the medial orbitofrontal cortex (mOFC) and abnormal astrocytes in the etiology of the symptoms (Schobel et al. 2009; Meyer et al. 2011; Shukla et al. 2019). However, there is inconsistency in in vivo results using

previous imaging targets (Meyer et al. 2020). Reactive astrocytes increase monoamine oxidase B (MAO-B) expression, and MAO-B binding positron emission tomography (PET) enables the in vivo imaging of astrocyte reactivity (Ng et al. 2017; Nisha Aji et al. 2023). We aimed to investigate the association between negative and cognitive symptoms and reactive astrocytes in the mOFC in schizophrenia patients using MAO-B binding PET.

Methods: We analyzed MAO-B binding [18F]THK5351 PET data from 33 schizophrenia patients and 35 age- and sex-matched healthy controls. We examined group differences in standardized uptake value ratio (SUVr) in the mOFC and their correlation with Positive and Negative Syndrome Scale (PANSS) negative symptom scores and Wisconsin Card Sorting Test (WCST) performance scores.

Results: We found higher SUVr in the bilateral mOFC in schizophrenia patients compared to healthy controls (left, $t = -2.01$, $p = 0.048$; right, $t = -2.04$, $p = 0.045$). There were negative correlations between SUVr and WCST scores (left, $r = -0.33$, $p = 0.006$; right, $r = -0.26$, $p = 0.032$). The correlation between SUVr and PANSS negative symptom scores was not significant.

Conclusions: Our findings support an association between reactive astrocytes in the mOFC and cognitive functioning including executive function in schizophrenia. This study suggests a potential biomarker for the neurobiological mechanism of cognitive symptoms in schizophrenia.

References

1. Meyer JH, Cervenka S, Kim M-J, et al (2020) Neuroinflammation in psychiatric disorders: PET imaging and promising new targets. The Lancet Psychiatry 7:1064–1074
2. Meyer U, Schwarz MJ, Müller N (2011) Inflammatory processes in schizophrenia: a promising neuroimmunological target for the treatment of negative/cognitive symptoms and beyond. Pharmacol Ther 132:96–110
3. Ng KP, Pascoal TA, Mathotaarachchi S, et al (2017) Monoamine oxidase B inhibitor, selegiline, reduces 18F-THK5351 uptake in the human brain. Alzheimers Res Ther 9:1–9
4. Nisha Aji K, Meyer JH, Rusjan PM, Mizrahi R (2023) Monoamine Oxidase B (MAO-B): A Target for Rational Drug Development in Schizophrenia Using PET Imaging as an Example. In: Drug Development in Psychiatry. Springer, pp 335–362
5. Schobel SA, Kelly MA, Corcoran CM, et al (2009) Anterior hippocampal and orbitofrontal cortical structural brain abnormalities in association with cognitive deficits in schizophrenia. Schizophr Res 114:110–118
6. Shukla DK, Chiappelli JJ, Sampath H, et al (2019) Aberrant frontostriatal connectivity in negative symptoms of schizophrenia. Schizophr Bull 45:1051–1059

Poster No 617

Aberrant Amygdala Gamma Responses to Unconscious Emotion Processing in MDD: An MEG study

Yishan Du[1], Lingling Hua[1], Zhijian Yao[2], Qing Lu[3], Moxuan Song[2], Tingting Xiong[1], Shui Tian[4], Zhilu Chen[5], Hao Tang[1]

[1]Department of Psychiatry, the Affiliated Brain Hospital of Nanjing Medical University, Nanjing, Jiangsu, [2]The Affiliated Brain Hospital of Nanjing Medical University, Nanjing, Jiangsu, [3]Southeast University, Nanjing, Jiangsu, [4]Nanjing Medical University, Nanjing, Jiangsu, [5]the Affiliated Nanjing Brain Hospital of Nanjing Medical University, Nanjing, Jiangsu

Introduction: Major depressive disorder (MDD) is associated with behavioral and neurobiological evidences of negative bias in unconscious emotional processing. However, little is known about the time course of amygdala gamma frequency band. The current study aimed to explore the unconscious processing of emotional facial expressions in the gamma band of amygdala in MDD patients by magnetoencephalography.

Methods: The time course of amygdala in gamma-band time processing of subliminal sad faces were recorded in 30 medication-free MDD patients and 26 healthy controls (HC) in a backward masking task. Then the relationship between amygdala activation and positive and negative emotions were calculated.

Results: Detection accuracy was at chance level for both groups, suggesting that the process was performed in the absence of conscious awareness of the emotional stimuli. In response to subthreshold negative emotional facial stimuli, cluster permutation test results revealed significant differences in energy activation of the left amygdala cluster between the MDD group and the HC group within the 50-250 ms time window and the high gamma frequency (cluster, P= 0.006). Specifically, the MDD group exhibited enhanced activation in the left amygdala compared to the HC group (P= 0.001), and this activation was found to be negatively correlated with positive emotions (r= -0.352, P= 0.009).

Conclusions: Our data suggested that negative processing bias exists on the unconscious level in individuals with MDD. particularly manifesting as increased activation in the left amygdala during a 50-250 ms time window with high gamma frequency, which can be used as a marker for diagnosis of MDD.

References
1. Zhang, D. (2016), 'Deficits of unconscious emotional processing in patients with major depression: An ERP study'. Journal of affective disorders,199, 13–20.
2. Diano, M. (2017). Amygdala Response to Emotional Stimuli without Awareness: Facts and Interpretations. Frontiers in psychology, 7, 2029.

Poster No 618

Interactive effect of adversity and irritability on brain volume in children

Camille Archer[1], Hee Jung Jeong[1], Gabrielle Reimann[1], Everett Durham[1], Shuti Wang[1], Antonia Kaczkurkin[1]

[1]Vanderbilt University, Nashville, TN

Introduction: Developmental psychopathology emphasizes the transactional nature of psychobiological vulnerabilities (e.g., irritability) and environmental challenges (e.g., adverse events) in predicting mental health outcomes. However, few studies have examined the pathophysiology of irritability, including potential neurostructural risk factors. The purpose of the current study was to examine the interactive effect of adverse events and irritability on regional gray matter volumes (GMV) over time in a large sample of children.

Methods: Participants included 9- to 10-year-old children (N=11,131) from the longitudinal Adolescent Brain Cognitive Development Study. Sum scores of both irritability and adverse events were created from clinical questionnaire data, and we examined whether their interaction predicted gray matter volume in 68 cortical and 19 subcortical regions using linear mixed effects modeling. GMV was collected at baseline and the second-year follow-up.

Results: Results showed that the interaction of greater irritability and adverse events predicted faster brain volume reductions in several regions, including the left paracentral lobe, left pars orbitalis, and right middle and superior temporal gyri (p-values ≤ .05). In other words, those with high levels of adversity and high levels of irritability showed steeper declines in volume.

Conclusions: There is a lack of research examining the neurostructural correlates of irritability in youth, while accounting for environmental context. Here we demonstrate that a unique combination of adversity and high irritability predicts faster brain volume reduction in children, demonstrating that irritability in the context of adversity may represent a unique neurostructural risk factor. While declines in GMV during childhood and early adolescence are normative, this study suggests that the combination of high adversity and irritability is associated with accelerated maturation, which may be a short-term adaptive response to high levels of stress. This highlights the need for more research on examining the pathophysiology of irritability in relation to environmental factors.

Poster No 619

Imbalanced functional architecture of anterior cingulate cortex subregions in unmedicated depression

Zilin Zhou[1], Yingxue Gao[1], Lingxiao Cao[1], Weijie Bao[1], Xinyue Hu[1], Hailong Li[1], Lianqing Zhang[1], Weihong Kuang[2], Qiyong Gong[1,3], Xiaoqi Huang[1]

[1]Huaxi MR Research Center (HMRRC), Department of Radiology, West China Hospital of Sichuan University, Chengdu, Sichuan, [2]Mental Health Center, Department of Psychiatry, West China Hospital of Sichuan University, Chengdu, Sichuan, [3]Department of Radiology, West China Xiamen Hospital of Sichuan University, Xiamen, Fujian

Introduction: Dysconnectivity of anterior cingulate cortex (ACC), a functionally heterogenous region along its ventral-dorsal continuum (Dixon et al., 2017), fulfills a crucial role in major depressive disorder (MDD) (Mulders et al., 2015; Pizzagalli & Roberts, 2022). Most studies on functional connectivity of ACC subregional networks relied on a priori coordinates or anatomical atlas, which may not be optimally aligned with current functional data, potentially introducing bias. The well-developed data-driven connectivity-based parcellation technique (CBP) (Eickhoff et al., 2018) enables a more accurate representation of functional subregions within the ACC by leveraging their functional connectivity properties. Our research utilized ACC subdivisions derived from CBP to precisely delineate the fine-grained ACC subregional functional connectivity alterations in MDD.

Methods: We enrolled 168 unmedicated patients with first-episode MDD and 128 healthy controls (HC) matched for age, sex and education level. All subjects were scanned using 3T Siemens MRI scanner with an 8-channel phased-array head coil. Resting-state functional MRI and T1-weighted anatomical images were preprocessed through a standardized pipeline in DPABI. The CBPtools (Reuter et al., 2020) implemented in Python3.7 was employed to segment the entire ACC per

hemisphere from automated anatomical labeling atlas (AAL2) into distinct subdivisions based on their resting-state functional connectivity (rsFC) with the rest of whole brain. Briefly, k-means clustering was applied to assign the ACC voxels into clusters with similar connectivity profiles at individual level, and group-level clustering incorporated relabeling individual clusters and computing mode of subject-wise relabeled clustering. Optimal cluster number was determined by Silhouette, Calinski-Harabasz and Davies-Bouldin indices. The rsFC maps of each ACC subregion were generated for all participants. Diagnosis-by-subregion flexible-factorial analysis of variance was performed to evaluate group differences in ACC subregional rsFC patterns, controlling for age, sex and head motion, followed by post-hoc analysis using the simple effects test in SPSS24.0. Moreover, relationships between the rsFC alterations with illness duration and symptom severity in MDD group were explored via partial correlation, with age, sex and head motion as covariates.

Results: Demographic and clinical information of all participants was detailed in Table 1. Two subdivisions of ACC per hemisphere, ventral ACC (vACC) and dorsal ACC (dACC), were identified according to all clustering quality metrics (Fig.1a/b). The ACC subregions obtained by CBP showed a similar spatial extent to those outlined in AAL3 (Fig.1c), and distinct rsFC patterns of vACC and dACC across all subjects were illustrated in Fig.1d. Flexible-factorial analysis of variance revealed a significant diagnosis-by-subregion interaction in the bilateral posterior cingulate cortex (PCC), manifested by a significant hypoconnectivity of vACC and bilateral PCC and a tendency for hyperconnectivity of dACC and bilateral PCC in MDD relative to HC (Fig.2a). Notably, we observed positive correlations between rsFC of bilateral dACC and bilateral PCC with suicide risk, and between rsFC of right vACC and bilateral PCC with illness insight (Fig.2b). Main effect of diagnosis showed an enhancement in rsFC of left ACC and right orbitofrontal cortex and of right ACC and right opercular part of inferior frontal gyrus in MDD compared to HC (Fig.2a).

Table 1 Demographic and clinical information

	MDD (N=168)	HC (N=128)	P values
Age (years)	30.98±10.75	32.92±10.41	0.119[a]
Sex (female/male)	107/61	74/54	0.304[b]
Educational level			0.532[c]
University and higher	109	83	
High school	28	10	
Middle school	24	24	
Primary school and lower	7	11	
First-episode illness duration	25.76±26.40	-	
Non-comorbidity (%)	154 (91.67%)	-	
HAMD total scores	25.49±5.36	-	
HAMA total scores	24.14±8.22	-	

Note: [a]Two-sample t test, [b]chi-square test, [c]Mann-Whitney U test.
Abbreviation: HAMD, Hamilton Depression Rating Scale; HAMA, Hamilton Anxiety Rating Scale; MDD, major depressive disorder; HC, healthy control.

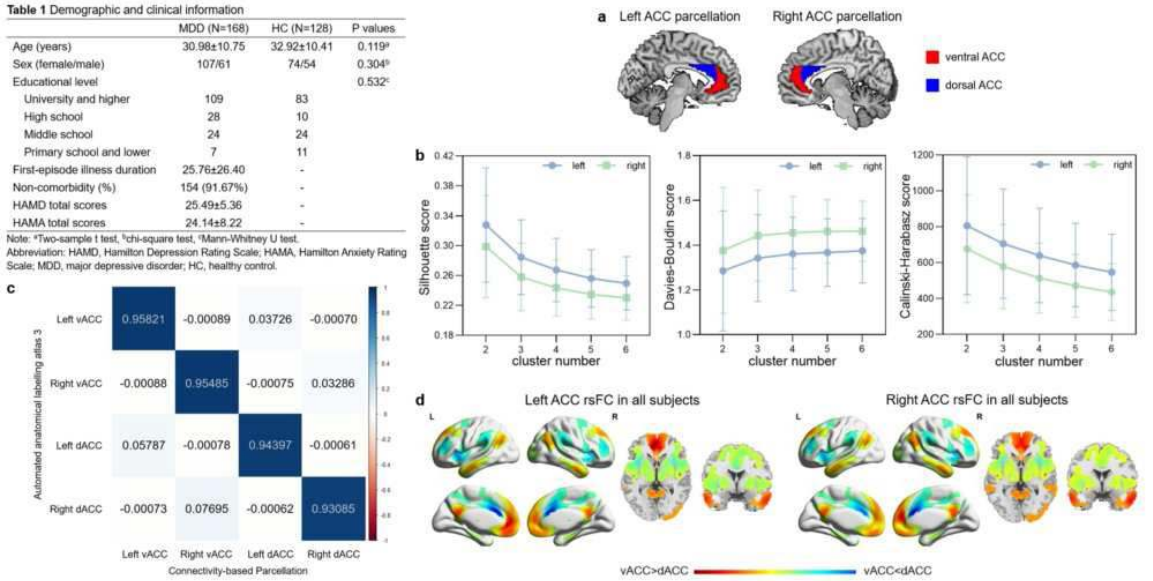

Figure1 (a). Two subdivisions of ACC per hemisphere identified using connectivity-based parcellation (CBP). **(b)**. Internal validity indicators for all parcellations (k=2, 3, 4, 5, 6) of the ACC per hemisphere. Higher Silhouette index (left) and Calinski–Harabasz index (right), while lower Davies–Bouldin index (middle), indicate a better fit. All indicators suggested two-cluster solution as the optimal parcellation. **(c)**. Spatial correlation between the vACC/dACC clusters derived from CBP and those defined in AAL3 (combined subgenual and pregenual ACC as the vACC). **(d)**. Distinct rsFC patterns of vACC and dACC in all subjects. Abbreviations: ACC, anterior cingulate cortex; vACC, ventral ACC; dACC, dorsal ACC; rsFC, resting-state functional connectivity.

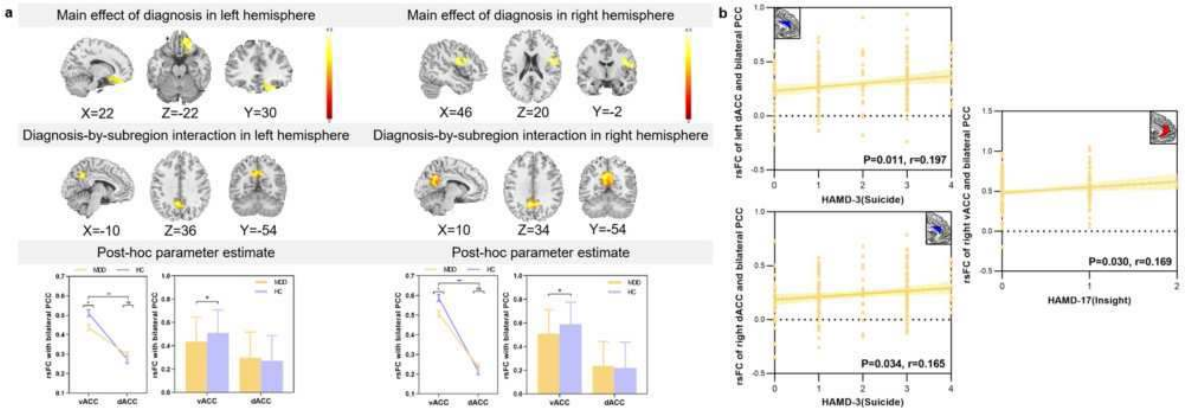

Figure2 (a). Alterations in rsFC of ACC subregions in MDD relative to HC, including main effect of diagnosis (upper), diagnosis-by-subregion interation (middle), and post-hoc simple effect analysis (buttom). *P<0.05, **P<0.001, Bonferroni corrected. **(b)**. Correlations between the rsFC alterations of vACC/dACC and PCC with the symptom severity, with a significant threshold of P<0.05 uncorrected. Abbreviations: ACC, anterior cingulate cortex; vACC, ventral ACC; dACC, dorsal ACC; PCC, posterior cingulate cortex; rsFC, resting-state functional connectivity.

Conclusions: A bipartite ventral-dorsal ACC subdivision was identified using data-driven CBP, consistent with the Rolls et al. (2019). We further discovered an imbalanced connectivity pattern between ACC subregions and bilateral PCC in patients with MDD, which was potentially related to illness insight and suicide risk. Our findings underscore functional heterogeneity of the ACC along its ventral-dorsal axis and provide valuable insights into the fine-grained ACC subregional dysfunctions in MDD.

References

1. Dixon, M. L., Thiruchselvam, R., Todd, R., & Christoff, K. (2017, Oct). Emotion and the prefrontal cortex: An integrative review. Psychol Bull, 143(10), 1033-1081.
2. Eickhoff, S. B., Yeo, B. T. T., & Genon, S. (2018, Nov). Imaging-based parcellations of the human brain. Nat Rev Neurosci, 19(11), 672-686.
3. Mulders, P. C., van Eijndhoven, P. F., Schene, A. H., Beckmann, C. F., & Tendolkar, I. (2015, Sep). Resting-state functional connectivity in major depressive disorder: A review. Neurosci Biobehav Rev, 56, 330-344.
4. Pizzagalli, D. A., & Roberts, A. C. (2022, Jan). Prefrontal cortex and depression. Neuropsychopharmacology, 47(1), 225-246.
5. Reuter, N., Genon, S., Kharabian Masouleh, S., Hoffstaedter, F., Liu, X., Kalenscher, T., Eickhoff, S. B., & Patil, K. R. (2020, May). CBPtools: a Python package for regional connectivity-based parcellation. Brain Struct Funct, 225(4), 1261-1275.
6. Rolls, E. T., Cheng, W., Gong, W., Qiu, J., Zhou, C., Zhang, J., Lv, W., Ruan, H., Wei, D., Cheng, K., Meng, J., Xie, P., & Feng, J. (2019, Jul 22). Functional Connectivity of the Anterior Cingulate Cortex in Depression and in Health. Cereb Cortex, 29(8), 3617-3630.

Poster No 620

Temporal Dynamics of EEG microstates in Elderly Depression and the Comorbidity of Parkinsonism

Yen-Liang Liu[1], Chiu-Jung Huang[1], Wei-Chung Mao[2], Tung-Ping Su[2], Li-Fen Chen[1,3]

[1]Institute of Brain Science, National Yang Ming Chiao Tung University, Taipei, Taiwan, [2]Department of Psychiatry, Cheng Hsin General Hospital, Taipei, Taiwan, [3]Brain Research Center, National Yang Ming Chiao Tung University, Taipei, Taiwan

Introduction: Major depressive disorder (MDD) is a common psychiatric disorder among elderly individuals, with a global prevalence of 31.74% (Zenebe et al., 2021). Late-life depression increases the likelihood of developing neurodegenerative disorders such as Parkinson's disease (PD) (Leentjens et al., 2003). Notably, a recent study indicates that diagnosing prodromal PD in elderly individuals with MDD is challenging because of the resemblance of explicit syndromes between "pseudo-parkinsonism" of depression and PD (Weiss & Pontone, 2019). EEG microstates have been proposed to reveal the spatiotemporal dynamics of large-scale brain networks and applied to identify abnormalities in patients with MDD (Murphy et al., 2020) and PD (Pal et al., 2021). In this study, we utilized EEG microstate analysis to investigate alternation of neural networks in patients with comorbidity of MDD and neurodegenerative disorders. Our objective is to explore the discrimination of dynamic patterns of neural networks between MDD and MDD with Parkinsonism (MDD-PD) patients.

Methods: We enrolled 14 patients with MDD, 7 patients with MDD-PD, and 14 healthy elderly individuals. The specific uptake ratio of TRODAT in the striatum of MDD-PD patients was below 0.8. Four-minute resting-state EEG signals with eyes-closed were recorded using a 32-channel cap (Easycap, Herrsching, Germany) and preprocessed by noise removal of eye blinks and electrocardiogram artifacts. The noise-free EEG data were then analyzed using MICROSTATELAB toolbox in EEGLAB (Nagabhushan Kalburgi et al., 2023) to extract five microstate template components for each group. Four parameters of each microstate, including mean duration, frequency of occurrence, time coverage, and transition probability (Murphy et al., 2020), were estimated for each individual. To examine the group differences in these microstate parameters, we conducted a one-way ANOVA with Bonferroni correction to adjust the p-value in the post hoc testing.

Results: The topographies of the microstates template components were similar between groups (Figure 1a). When compared to the healthy controls, the MDD group exhibited a significantly shorter duration in the microstates A ($p = 0.002$), C ($p = 0.008$), D ($p = 0.01$), and E ($p = 0.014$), as well as higher occurrence in microstates A ($p = 0.017$), B ($p = 0.013$), D ($p = 0.005$), and E ($p = 0.006$) (Figure 1b,1c). There were no significant differences in microstate coverage between groups (Figure 1d). Figure 2 depicts the probability of microstate transition within and between groups. Specific transition preferences in the MDD group (A to E, B to E, and D to C) were significantly different from the control group (Figure 2b). Furthermore, MDD-PD patients also demonstrated a higher transition probability from microstate D to C ($p = 0.005$) than MDD patients. There were no significant differences between the MDD-PD and control groups.

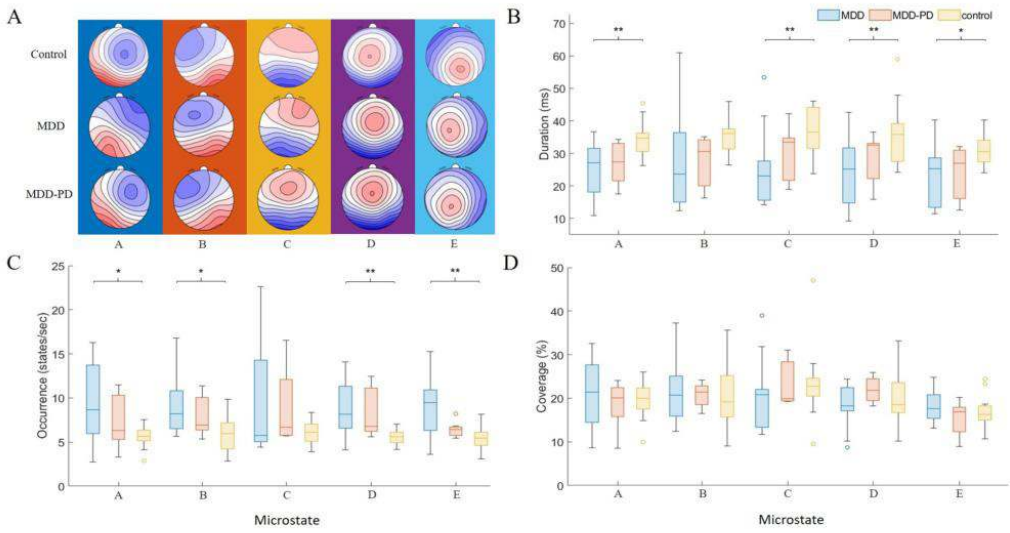

Figure 1. Boxplots showing the temporal parameters of each microstate in each of the three groups. Blue is the MDD group, red is the MDD-PD group, and yellow is the control group. *p < 0.05, **p < 0.01 Bonferroni correction following one-way ANOVA.

A

Control

From \ To	A	B	C	D	E
A		0.0222	0.0105	-0.0032	-0.0295
B	0.0062		0.0069	-0.0242	0.0109
C	-0.0029	0.0033		0.0262	-0.0265
D	-0.0028	-0.0204	0.0265		-0.0039
E	-0.0167	0.0223	0.0052	-0.0104	

MDD

From \ To	A	B	C	D	E
A		0.0214	-0.0111	-0.0111	0.0009
B	-0.0039		0.0429	0.0008	-0.0402
C	0.0275	0.0029		-0.0083	-0.0222
D	-0.0087	0.0230	-0.0393		0.0254
E	-0.0157	-0.0186	0.0307	-0.0105	

MDD-PD

From \ To	A	B	C	D	E
A		0.0261	0.0053	-0.0114	-0.0201
B	0.0056		0.0109	0.0209	-0.0375
C	-0.0197	0.0087		0.0139	-0.0025
D	-0.0197	0.0032	0.0174		-0.0008
E	-0.0068	-0.0291	0.0254	0.0103	

B

Control vs MDD

From \ To	A	B	C	D	E
A		0.0008	0.0216	0.0079	-0.0304
B	0.0101		-0.0360	-0.0250	0.0511
C	-0.0304	0.0004		0.0345	-0.0043
D	0.0059	-0.0434	0.0658		-0.0293
E	-0.0010	0.0409	-0.0255	-0.0001	

Control vs MDD-PD

From \ To	A	B	C	D	E
A		-0.0039	0.0052	0.0082	-0.0094
B	0.0006		-0.0040	-0.0451	0.0484
C	0.0168	-0.0054		0.0123	-0.0240
D	0.0169	-0.0236	0.0091		-0.0031
E	-0.0099	0.0514	-0.0202	-0.0207	

MDD vs MDD-PD

From \ To	A	B	C	D	E
A		-0.0047	-0.0164	0.0003	0.0210
B	-0.0095		0.0320	-0.0201	-0.0027
C	0.0472	-0.0058		-0.0222	-0.0197
D	0.0110	0.0198	-0.0567		0.0262
E	-0.0089	0.0105	0.0053	-0.0208	

Figure 2. (a) Matrix value showing the observed transition probabilities minus the expected one in each group. Colored boxes indicate statistically significant differences as calculated by paired-sample t-test. (b) Comparisons of the difference of observed minus expected transitions between groups. Colored boxes indicate statistically significant differences as calculated by ANOVA with Bonferroni correction ($p < 0.05$).

Conclusions: Our results reveal increased temporal dynamics in MDD group, which is consistent with previous report that excessive temporal variations in MDD reflect abnormal communications between large-scale brain networks (Long et al., 2020). Within the context of rapid network alterations, transition from microstate D to C could not only represent potential features for late-life depression but also provide insights for early detection of MDD patients with comorbidity of Parkinsonism. There was no significant difference in microstate between the MDD-PD and control groups due to the limited sample size in the MDD-PD population. In conclusion, microstate analysis could serve as an adjunctive tool to uncover different dynamic pattern in MDD and PD.

References

1. Leentjens, A. F. (2003), 'Higher incidence of depression preceding the onset of Parkinson's disease: a register study', Movement Disorders, 18(4), 414-418.
2. Long, Y. (2020), 'Altered resting-state dynamic functional brain networks in major depressive disorder: Findings from the REST-meta-MDD consortium', NeuroImage: Clinical, 26, 102163.
3. Murphy, M. (2020), 'Abnormalities in electroencephalographic microstates are state and trait markers of major depressive disorder', Neuropsychopharmacology, 45(12), 2030-2037.
4. Nagabhushan Kalburgi, S. (2023), 'MICROSTATELAB: The EEGLAB Toolbox for Resting-State Microstate Analysis', Brain Topography, 1-25.
5. Pal, A. (2021), 'Study of EEG microstates in Parkinson's disease: a potential biomarker?', Cognitive Neurodynamics, 15(3), 463-471.
6. Weiss, H. D. (2019), '"Pseudo-syndromes" associated with Parkinson disease, dementia, apathy, anxiety, and depression', Neurology Clinical Practice, 9(4), 354-359.
7. Zenebe, Y. (2021), 'Prevalence and determinants of depression among old age: a systematic review and meta-analysis', Annals General Psychiatry, 20(1), 55.

Poster No 621

Common and unique alterations of functional connectivity and topology in affective disorder

Hao Sun[1], Rui Yan[2], Xiaoqin Wang[3], Lingling Hua[4], Zhilu Chen[5], Yinghong Huang[6], Yishan Du[4], Yingying Huang[4], Moxuan Song[6], Na Shen[7], Qing Lu[8], Zhijian Yao[1]

[1]Nanjing Brain Hospital, Clinical Teaching Hospital of Medical School, Nanjing University, Nanjing, Jiangsu, [2]Department of Psychiatry, The Affiliated Brain Hospital of Nanjing Medical University, Nanjing, Jiangsu, [3]Nanjing medical university, Nanjing, Jiangsu, [4]Department of Psychiatry, the Affiliated Brain Hospital of Nanjing Medical University, Nanjing, Jiangsu, [5]the Affiliated Nanjing Brain Hospital of Nanjing Medical University, Nanjing, Jiangsu, [6]The Affiliated Brain Hospital of Nanjing Medical University, Nanjing, Jiangsu, [7]Nanjing Brain Hospital, Clinical Teaching Hospital of Medical School, Nanjing, Jiangsu, [8]Southeast University, Nanjing, Jiangsu

Introduction: Unipolar disorder (UD) and bipolar disorder (BD) are supposed to be whole-brain diseases with some shared clinical and neuropathology characteristics. It is important to study the neural mechanisms that distinguish between the two diseases. This study aims to explore the different neural mechanisms of functional connectivity and topology properties between BD and UD.

Methods: In this study, 265 patients with UD, 181 patients with BD, and 204 healthy controls completed Hamilton Depression Scale (HAMD) assessment and resting-state functional magnetic resonance imaging (rfMRI) scans. Functional connectivity of BD, UD and HC were compared. On the basis of the network alterations shared by BD and UD, the topological pattern of the two groups were analysed.

Results: Both BD and UD showed decreased FC in the whole-brain, mainly involving VN, SMN and DMN. Topological attribute analyses are carried out on nodes of SMN, DMN and VN. Results suggesting that both BD ($t=-2.093$, $p=0.037$) and UD ($t=-2.406$, $p=0.017$) showed a decrease in Cp. While only the BD group showed a decrease in Lp ($t = -2.888$, $p = 0.004$) and an increase in Eglob ($t = 3.402$, $p < 0.001$).

Conclusions: Our findings suggest that both BD and UD are disease with a wide range abnormal brain networks, mainly associated with VN, SMN and DMN. Unique topological characteristics alterations were only found in BD, which may provide possible characteristic markers to distinguish the two disorders.

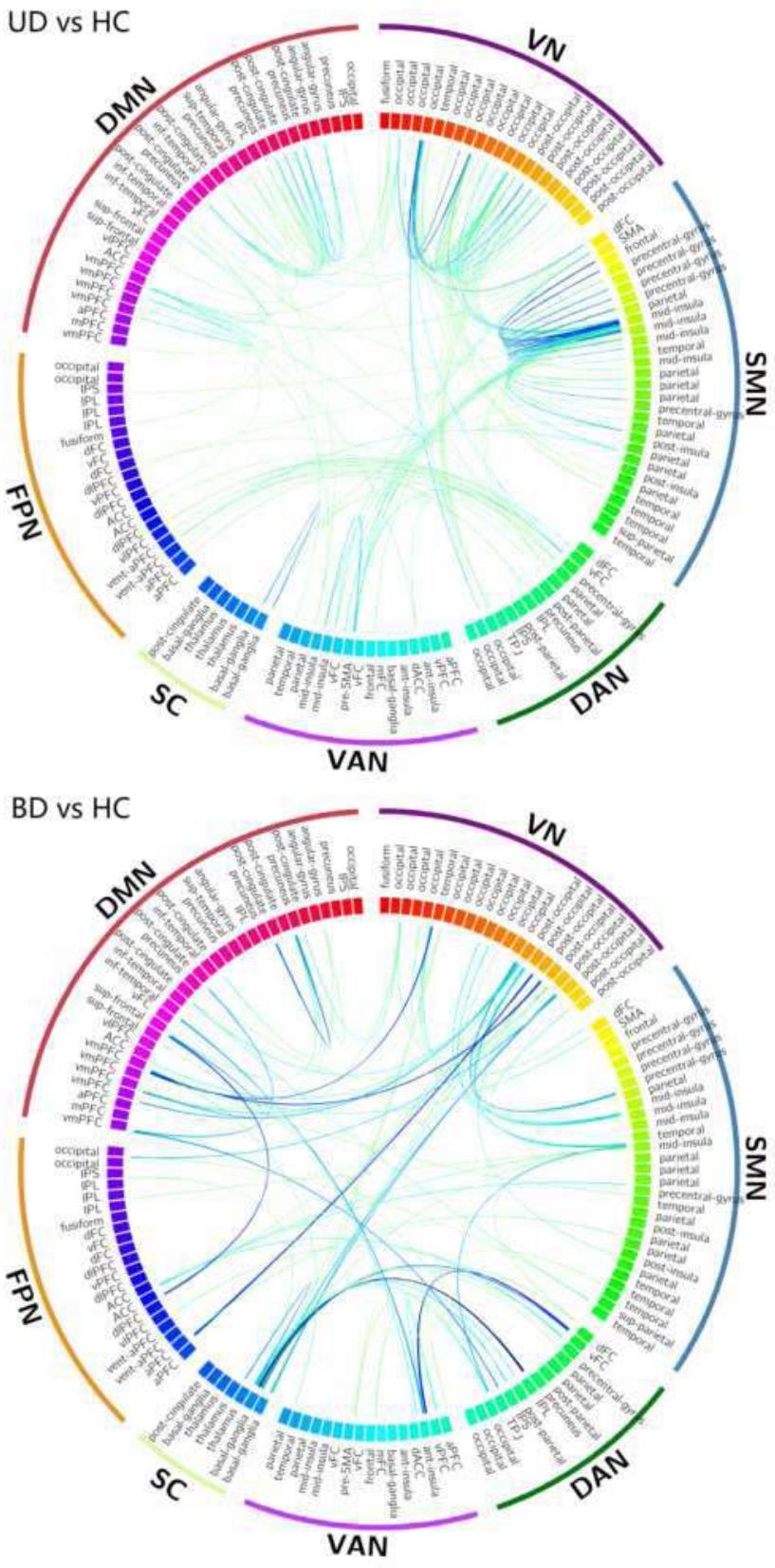

References

1. Yu, Ai-Hong et al. “Common and unique alterations of functional connectivity in major depressive disorder and bipolar disorder.” Bipolar disorders vol. 25,4 (2023): 289-300.

Poster No 622

Abnormal Structural Covariance Network in Major Depressive Disorder

Changmin Chen[1], Zhao Qing[1]

[1]*Southeast University, Nanjing, JiangSu*

Introduction: Major depressive disorder (MDD) is a prevalent mental disorder that can lead to disability. Structural magnetic resonance imaging (sMRI) has been widely employed to investigate structural changes in the brains of individuals with MDD. Structural covariance networks (SCN) can provide information on structural changes in the brain at the network level in addition to localized brain morphology changes. However, SCN rely on the correlation among individuals, requiring a larger sample size to obtain more reliable results. This study will use a recently established large-sample multi-center brain imaging database to explore SCN alterations in MDD.

Methods: A total of 798 T1-weighted MRI images from patients with MDD and 974 T1-weighted MRI images from health controls (HCs) from 24 sites of the REST-meta-MDD consortium were utilized after quality control. In the data analysis, voxel-based morphometry was first performed for all the images to generate a voxel-wise gray matter (GM) volume map for each subject. Then with the preprocessed GM images, we carried out the source-based morphometry processing using the GIFT toolbox. We extracted 20 components and labeled them as components A to component T. The scores for each component across subjects represent individual differences in the volume of this component. Therefore, two-sample t-tests with age, gender, education, and sites as covariates were used to examine whether there were significant group differences in each component between the MDD and NC groups. Results were corrected with the false discovery rate (FDR) method at $p < 0.05$. Subsequently, we calculated the SCN based on the SBM components. For each of the MDD and NC groups, Pearson' correlation analyses were performed on the individual scores between each pair of the 20 components, using age, gender, education, and sites as covariates. Interaction analyses were then utilized to assess whether the correlations were significantly different between the MDD and NC groups, the significance level was set at $p < 0.01$. Finally, we used the Network-based statistic (NBS) of correction to select the SCN networks that were significant between the MDD and NC groups, the significance level was set at $p < 0.05$.

Results: As shown in Figure 1, SBM decomposed all the variance of the GM volumes across subjects in our data into 20 components (components A-T). The results of two-sample t-tests after FDR correction ($p < 0.05$) revealed that 3 of the 20 components showed significant group differences between the MDD and NC groups: J ($p = 0.003$), R ($p = 0.003$), T ($p < 0.0001$). As illustrated in Figure 2, the SCNs of 11 pairs of components showed significant differences between the two groups. The red lines represent the structural covariance in MDD greater than that in NC, while the blue lines indicate the opposite.

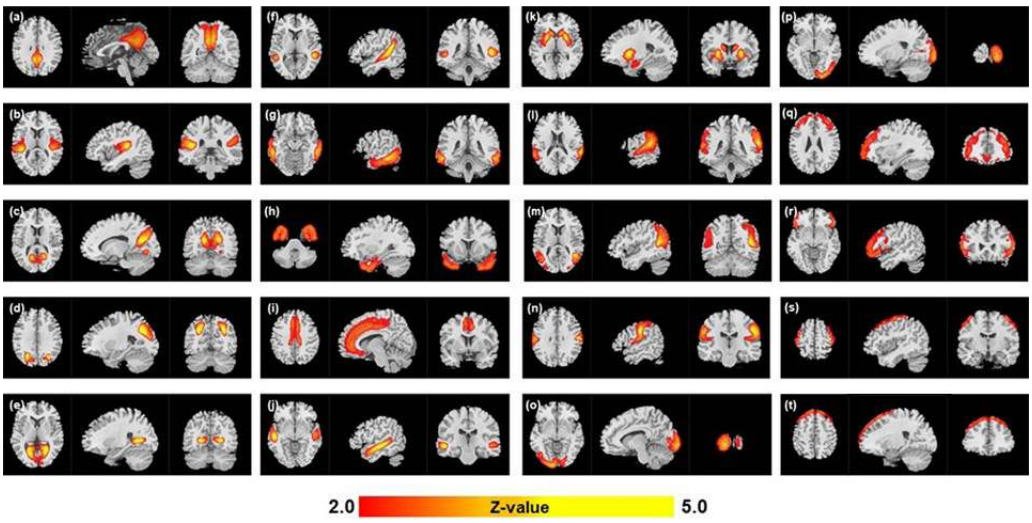

FIGURE 1. Source-based morphometry (SBM) component spatial maps. SBM estimated 20 structural covariance components (A–T) from 1772 subjects, including those with MDD and NCs. Coronal, sagittal, and axial views of the spatial map for each component are shown here. Images are the z statistics (from red to yellow, 2.0 to 5.0) overlaid on the high-resolution structural template.

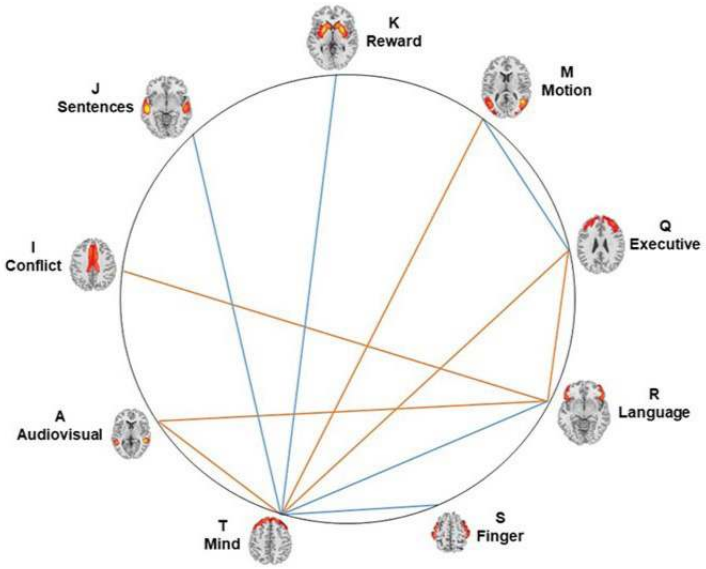

FIGURE 2. All the component pairs that had significant group differences in structural covariance. The red lines represent the structural covariance in MDD greater than that in NC, while the blue lines indicate the opposite. The text next to each component number is the function for which the spatial distribution map of this component yields the highest correlation in Neurosynth.

Conclusions: We identified 20 covariant brain components, with three components exhibiting significant differences between the MDD and HC groups. Our findings also suggest that the structural covariance network is altered in patients with MDD, and that there are both enhancements and attenuations in this alteration. Additionally, the prefrontal lobe is a key brain region in this alteration, which is consistent with existing studies.

References

1. Ancelin, M. L. (2019), 'Lifetime major depression and grey-matter volume', Journal of psychiatry & neuroscience: JPN, vol. 44, no. 1, pp. 45-53
2. Enneking, V. (2020), 'Brain structural effects of treatments for depression and biomarkers of response: a systematic review of neuroimaging studies', Psychological medicine, vol. 50, no. 2, pp. 87-209
3. Yan, C. G. (2019), 'Reduced default mode network functional connectivity in patients with recurrent major depressive disorder', Proceedings of the National Academy of Sciences of the United States of America, vol. 116, no. 18, pp. 9078-9083
4. Zalesky, A. (2010), 'Network-based statistic: identifying differences in brain networks', NeuroImage, vol. 53, no. 4, pp. 1197-1207

Poster No 623

Brain Controllability Analysis of Neuropsychiatric Symptoms Associated with Cognitive Impairment

Jared Cammon[1], Thiago Macedo e Cordeiro[2], Antonio Teixeira Jr[3], Yingchun Zhang[1]

[1]University of Houston, Houston, TX, [2]UTHealth Houston, Houston, TX, [3]UTHealth Houston, Houston, TX

Introduction: Alzheimer's disease (AD) is the most common cause of dementia, representing 60% to 80% of cases in the U.S. (2023 Alzheimer's disease facts and figures). Biomarkers are increasingly important as tools which can be utilized to identify Mild Cognitive Impairment (MCI), the prodromal stage of AD, and measure its progression into dementia stage. Neuropsychiatric Symptoms (NPS) occur in up to 85% of adults with MCI and have been shown to be diagnostic and prognostic indicators of AD (Martin et al., 2020,; Gallagher et al., 2017). Brain controllability analysis has recently been used to characterize the neural dynamics underlying neurocognitive deficits in the brain (Fang et al., 2021) and may serve as a more quantitative measurement of NPS, compared to qualitative clinical assessments. The goal of this research was to investigate the association between brain controllability and NPS in MCI, to determine if controllability analysis could serve as a biomarker for MCI.

Methods: Data from 19 MCI subjects and 15 Cognitive Normal (CN) subjects were selected from Phase ADNI2 of the Alzheimer's Disease Neuroimaging Initiative (ADNI) dataset. All MCI subjects experienced NPS, evidenced by a Neuropsychiatric Inventory Questionnaire (NPI-Q) total score of at least 5. Diffusion Tensor Imaging (DTI) data was preprocessed and reconstructed in DSI Studio and anatomical scans were parcellated according to the Brainnetome Atlas, featuring 210 cortical brain regions of interest. Tractography was then performed and utilized to create a structural connectivity matrix, from which the modal controllability of each region of interest was calculated and ranked according to

previous research (Fang et al., 2022). Region of interest controllability rankings were grouped based on anatomical location to obtain the structural controllability of large brain networks including the Default Mode Network (DMN), Central Executive Network (CEN), and Salience Network (SN). These brain networks make up the triple network model, which posits that all or some of these three networks are affected variably in psychiatric disorders (Menon et al., 2019). Controllability of these large brain networks was then compared to NPI-Q total scores and the spearman correlation was calculated to determine the degree and direction of association.

Results: Figure 1 shows a trend of increasing modal controllability with increasing NPI Score for the CEN. Spearman correlation between the large brain networks and NPI scores revealed a significant and strong positive correlation between CEN and NPS (P=.01, rs=.77). Though the SN had a moderate negative correlation with NPS, it was not significant (P=.17, rs=-.48). The DMN had the weakest correlation which was also not significant (P=.97, rs=.02).

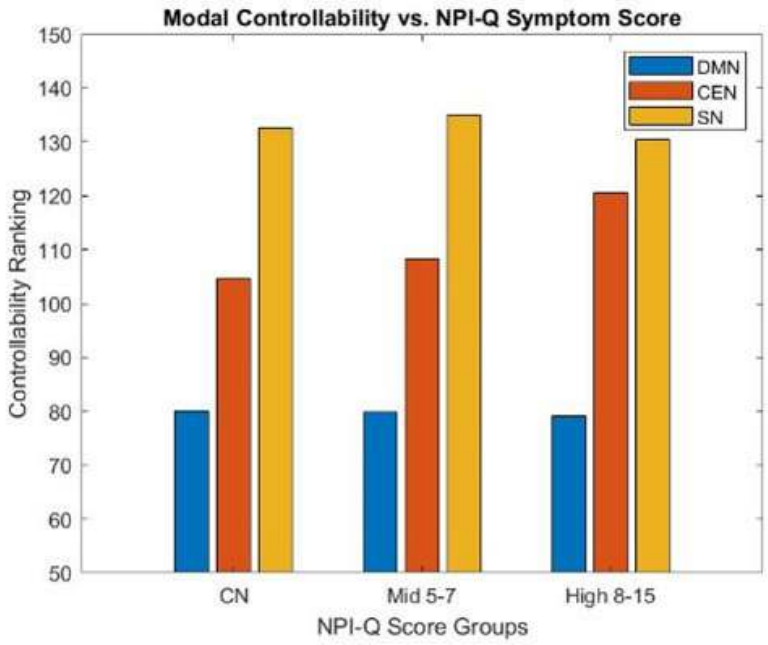

Conclusions: Controllability analysis shows promise as a potential biomarker for NPS in MCI, which are known to be prognostic and diagnostic indicators of the progression of AD. Particularly, CEN modal controllability shows a strong correlation with NPS severity. Areas of high modal controllability map to networks like the CEN, which is involved with executive functions and cognitive control (Gu et al., 2015). Controllability analysis is therefore a likely tool which can be used to help understand underlying impairments associated with NPS in MCI. A larger number of subjects and a multimodal approach, incorporating functional controllability as well, may provide a clearer picture as to the use of controllability analysis as a biomarker for NPS in MCI.

References

1. 2023 Alzheimer's disease facts and figures. (2023). Alzheimer's & dementia : the journal of the Alzheimer's Association, 19(4), 1598–1695. https://doi.org/10.1002/alz.13016
2. Martin, E., & Velayudhan, L. (2020). Neuropsychiatric Symptoms in Mild Cognitive Impairment: A Literature Review. Dementia and geriatric cognitive disorders, 49(2), 146–155. https://doi.org/10.1159/000507078
3. Gallagher, D., Fischer, C. E., & Iaboni, A. (2017). Neuropsychiatric Symptoms in Mild Cognitive Impairment. Canadian journal of psychiatry. Revue canadienne de psychiatrie, 62(3), 161–169. https://doi.org/10.1177/0706743716648296
4. Fang, F., Gao, Y., Schulz, P. E., Selvaraj, S., & Zhang, Y. (2021). Brain controllability distinctiveness between depression and cognitive impairment. Journal of Affective Disorders, 294, 847-856.
5. Fang, F., Godlewska, B., Cho, R. Y., Savitz, S. I., Selvaraj, S., & Zhang, Y. (2022). Personalizing repetitive transcranial magnetic stimulation for precision depression treatment based on functional brain network controllability and optimal control analysis. NeuroImage, 260, 119465.
6. Menon B. (2019). Towards a new model of understanding - The triple network, psychopathology and the structure of the mind. Medical hypotheses, 133, 109385. https://doi.org/10.1016/j.mehy.2019.109385
7. Gu, S., Pasqualetti, F., Cieslak, M., Telesford, Q. K., Yu, A. B., Kahn, A. E., Medaglia, J. D., Vettel, J. M., Miller, M. B., Grafton, S. T., & Bassett, D. S. (2015). Controllability of structural brain networks. Nature communications, 6, 8414. https://doi.org/10.1038/ncomms9414

Poster No 624

Biomarkers of Multiple Psychiatric Disorders Based on Consistency of Brain Structure and Function

Yuejia Zhong[1,2], Na Luo[1], Tianzi Jiang[1,2,3,4,5]

[1]Brainnetome Center, Institute of Automation, Chinese Academy of Sciences, Beijing, China, [2]School of Artificial Intelligence, University of Chinese Academy of Sciences, Beijing, China, [3]Center for Excellence in Brain Science and Intelligence Technology, Institute of Automation, Chinese, Beijing, China, [4]Research Center for Augmented Intelligence, Zhejiang Lab, Hangzhou, China, [5]Xiaoxiang Institute for Brain Health and Yongzhou Central Hospital, Yongzhou, China

Introduction: It has been widely substantiated that the functional architectures of the brain topographically correspond to specific structural patterns within particular networks (Greicius et al. 2009). This is manifested by a hierarchical organization of structure-function (S-F) relationships across specific networks in the brain, where the structure of primary sensory regions exhibits high coupling with function while higher-order association areas display reduced coupling (Wu et al. 2020). This systematic pattern follows the cerebral cortex's functional and cellular hierarchical structure (Gu et al. 2021). Subsequent studies have further demonstrated a hierarchical structure between structure and function from the perspective of spatial consistency and provided 45 pairs of S-F component maps based on a dataset comprising 15,000+ normal samples (Luo et al. 2020). Similarly, from a hierarchical perspective, differences in psychiatric disorders can be elucidated. Research suggests that the potential vulnerability of less constrained higher-order association areas might be a contributing factor to mental illnesses, potentially serving as an underlying cause (Sha et al. 2019). This finding underscores the importance of considering the hierarchical structure of the brain when studying psychiatric disorders. In this study, we therefore employed S-F component maps to explore biomarkers of multiple psychiatric disorders.

Methods: The data for this study were randomly selected from inpatient participants within the UK Biobank (UKB) (Sudlow et al. 2015), comprising 20 individuals each diagnosed with bipolar disorder (BD), major depressive disorder (MDD), and schizophrenia (SCZ). The structural and functional data were obtained from T1-weighted structural imaging and resting-state functional Magnetic Resonance Imaging (rs-fMRI), respectively. The preprocessing pipeline was consistent with the procedures used in the UK Biobank. Based on the S-F correspondence template (Luo et al. 2020), we extracted individual-level independent components (ICs) for each participant. The individual-level structural ICs were derived from structural templates and individual gray matter volume (GMV). The individual-level functional ICs were reconstructed from rs-fMRI data using Group Information Guided Independent Component Analysis (GIG-ICA) (Du et al. 2013) and functional templates. Next, we measured the consistency between structure and function by calculating the Pearson correlation coefficients between individual-level structural ICs and functional ICs. Finally, we assessed differences in S-F spatial coherence among different disorders using ANOVA followed by post-hoc comparisons.

Results: The results showed that there were significant inter-group differences in the four pairs of S-F coherence components (Figure 1), which were distributed in the bilateral precentral lobule, hippocampus, cerebellum, and middle temporal gyrus (Figure 2). The differential components between MDD and SCZ are distributed in the bilateral precentral lobule ($P < 0.05$), hippocampus ($P < 0.0001$), cerebellum ($P < 0.0001$), and middle temporal gyrus ($P < 0.001$), with differential components between MDD and BD predominantly located in the cerebellum ($P < 0.01$). Meanwhile, differential components between SCZ and BD are primarily found in the hippocampus ($P < 0.0001$) and middle temporal gyrus ($P < 0.05$).

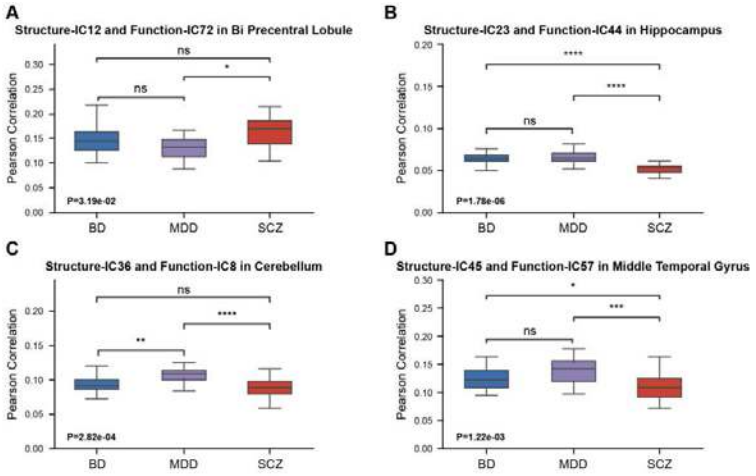

Figure 1 Quantitative comparison of S-F coherence among BD, MDD and SCZ. Four pairs of S-F coherence components exhibit significant inter-group differences among multiple psychiatric disorders.

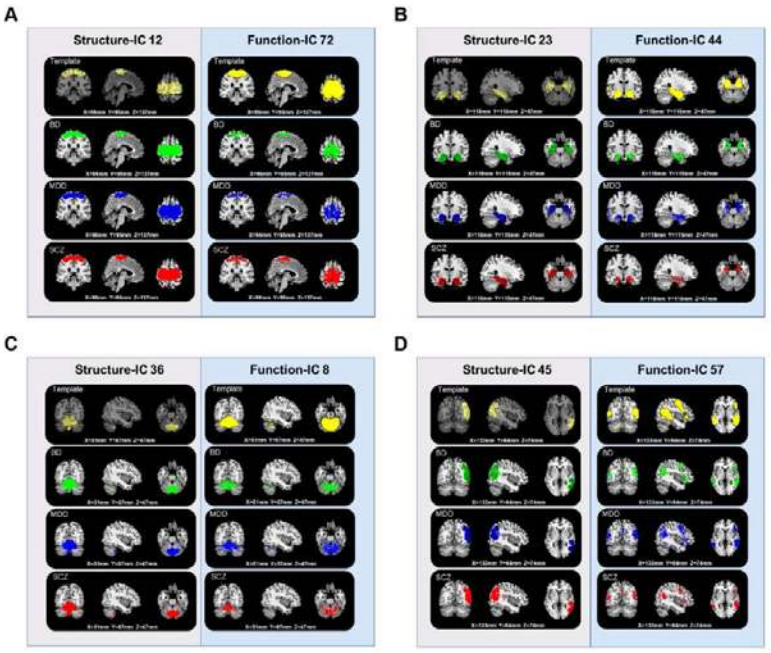

Figure 2 Qualitative comparison and spatial distribution of S-F coherence among BD, MDD and SCZ.

Conclusions: These findings have important implications for our understanding of the neural correlates of different psychiatric disorders and may provide valuable insights into potential treatment targets. Moreover, S-F coherence components with significant differences can serve as biomarkers for disorder diagnosis. Based on this, multi-disorder classifiers can be designed targeting the fused features to aid in disorder diagnosis.

References

1. Du, Y. (2013), 'Group information guided ICA for fMRI data analysis', Neuroimage, vol. 69, no. pp. 157-197.
2. Greicius, M. D. (2009), 'Resting-state functional connectivity reflects structural connectivity in the default mode network', Cerebral Cortex, vol. 19, no. 1, pp. 72-78.
3. Gu, Z. (2021), 'Heritability and interindividual variability of regional structure-function coupling', Nature Communications, vol. 12, no. 1, pp. 4894.
4. Luo, N. (2020), 'Structural Brain Architectures Match Intrinsic Functional Networks and Vary across Domains: A Study from 15 000+ Individuals', Cerebral Cortex, vol. 30, no. 10, pp. 5460-5470.
5. Sha, Z. (2019), 'Common Dysfunction of Large-Scale Neurocognitive Networks Across Psychiatric Disorders', Biological Psychiatry, vol. 85, no. 5, pp. 379-388.
6. Sudlow, C. (2015), 'UK biobank: an open access resource for identifying the causes of a wide range of complex diseases of middle and old age', PLoS Medicine, vol. 12, no. 3, pp. e1001779.
7. Wu, D. (2020), 'Hierarchy of Connectivity-Function Relationship of the Human Cortex Revealed through Predicting Activity across Functional Domains', Cerebral Cortex, vol. 30, no. 8, pp. 4607-4616.

Poster No 625

Neural circuits underlying emotion dysregulation in bulimia nervosa

Kaixi Zhang[1], Zhen Yuan[1,2], Zhiying Zhao[1,3]

[1]Centre for Cognitive and Brain Sciences, University of Macau, Taipa, Macau, [2]Faculty of Health Sciences, University of Macau, Taipa, Macau, [3]Yale School of Medicine, Department of Radiology & Biomedical Imaging, New Haven, CT, USA

Introduction: Up to 1% of young women around the world suffer from bulimia nervosa (BN) which is characterized by binge eating and inappropriate compensatory behavior (Mohajan & Mohajan, 2023). The etiology of BN is complex, and the neurobiological mechanisms underlying BN symptomology remain poorly understood. Similar to anorexia nervosa (Seidel et al., 2018), another type of eating disorder, individuals with BN display difficulties in emotion regulation. There are some studies suggest that deficits in utilizing adaptive emotion regulation strategies, such as cognitive reappraisal in both phenotypes (Dikmeer, Ersöz Alan, & Foto Özdemir, 2023). Such deficits in emotion regulation are linked to BN symptomatology (Azzi et al., 2023). However, in contrast to AN, no neuroimaging studies have examined the neural mechanisms of emotion dysregulation in BN. In this cross-sectional fMRI study, we compared the brain activation levels in core emotion regulation pathways between individuals with subclinical BN (sBN) and healthy controls with no eating disorder symptoms.

Methods: The current study recruited subclinical BN (sBN) female (n=22) and healthy control (HC) female participants (n=17) aged from 18 to 27 from the University of Macau, China. These young college students were screened and grouped based on the SCOFF questionnaire [] and interviews conducted based on DSM-5 criteria for BN. All participants were instructed to maintain a minimum fasting period of 12 hours prior to the experiment. They were allowed to drink water but were required to refrain from eating any food or consuming any other beverages. All experimental procedures were conducted in the morning. The emotion regulation task used in this study was adapted from Phan et al., (Phan et al., 2005) which consisted of four conditions: View Neutral, View Negative, Regulate Reappraisal and Regulate Suppression. The latter two were representative emotion regulation strategies. All the picture stimuli used in the study were selected from the International Affective Picture System based on their valence and arousal. Participants rated their level of negative emotion elicited by the images on a scale of 1-5 after viewing the pictures or emotion regulation. Generalized linear models were used to analyze and extract the activity levels from bilateral dorsolateral prefrontal cortex (dlPFC) and bilateral amygdala during the task using the beta-estimates extracted from these regions-of-interest (ROIs).

Results: In both groups, the negative emotion rating was lower in the View Neutral condition than the View Negative condition. However, there was no significant group differences in the emotion ratings when comparing the same conditions ($p>0.05$). Independent-sample t-test revealed significant differences between the groups in the right amygdala ($t = -2.567$, $p = 0.014$) with the sBN showing lower responsiveness to negative stimuli in this region compared to HC participants. Repeated-measures ANOVA revealed a significant emotion regulation strategy (regulateReappraisal, regulateSuppression) * Group (sBN, HC) interaction in bilateral amygdala (Left: F1,n = 4.630, $p = 0.038$, Right: df=1, $F = 4.495$, $p = 0.041$). Post-hoc analysis revealed that HC group decreased the bilateral amygdala activation level during suppression of the emotion (Suppression condition) to a larger extent comparing to the sBN (Left: $t = -2.836$ $p = 0.007$, Right: $t = -2.329$ $p = 0.025$), indicating failures in regulating negative emotion by the sBN group.

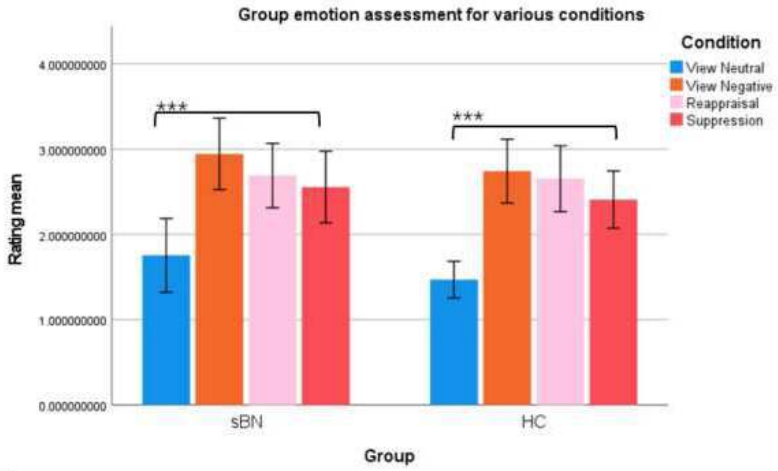

Figure 1.
In both groups, the negative emotion rating was lower in the View Neutral condition than the View Negative condition. However, there was no significant group differences in the emotion ratings when comparing the same conditions ($p>0.05$).

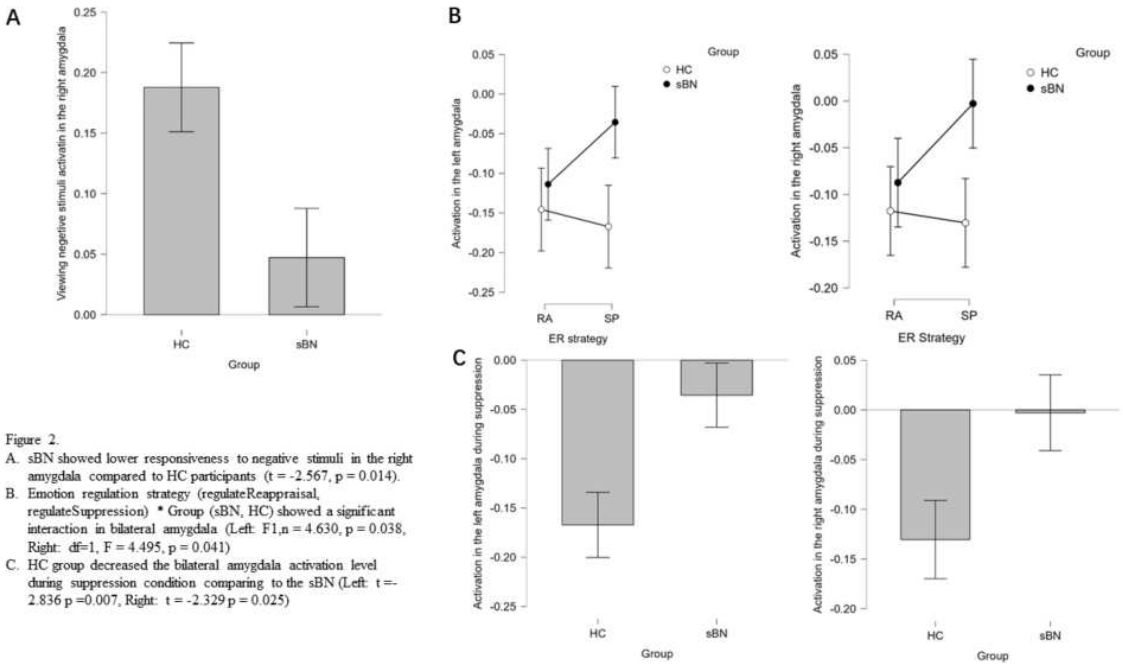

Figure 2.
A. sBN showed lower responsiveness to negative stimuli in the right amygdala compared to HC participants (t = -2.567, p = 0.014).
B. Emotion regulation strategy (regulateReappraisal, regulateSuppression) * Group (sBN, HC) showed a significant interaction in bilateral amygdala (Left: F1,n = 4.630, p = 0.038, Right: df=1, F = 4.495, p = 0.041)
C. HC group decreased the bilateral amygdala activation level during suppression condition comparing to the sBN (Left: t =-2.836 p =0.007, Right: t = -2.329 p = 0.025)

Conclusions: Our results suggest that individuals with BN symptoms (although not meeting the diagnostic criteria) are accompanied by reduced sensitivity to negative stimuli in the limbic pathway. Moreover, they were less efficient in down-regulating amygdala activity when using the maladaptive emotion regulation strategy compared to healthy. Giving the previously reported preference in using maladaptive strategies (Aldao et al., 2010), this finding shed light on the emotion deficits in the BN population.

References

1. Aldao, A., (2010). Emotion-regulation strategies across psychopathology: A meta-analytic review. Clinical psychology review, 30(2), 217-237.
2. Azzi, R., (2023). The association between mental health and Bulimia Nervosa among a sample of Lebanese young adults: the indirect effect of difficulties in emotion regulation. BMC Psychiatry, 23(1), 335.
3. Dikmeer, N., (2023). The role of mindfulness on the psychological aspects of anorexia nervosa. Clinical Child Psychology and Psychiatry, 13591045231190675.
4. Mohajan, D., (2023). Bulimia Nervosa: A Psychiatric Problem of Disorder. Innovation in Science and Technology, 2(3), 26-32.
5. Phan, K. L., (2005). Neural substrates for voluntary suppression of negative affect: a functional magnetic resonance imaging study. Biological psychiatry, 57(3), 210-219.
6. Seidel, M., (2018). Processing and regulation of negative emotions in anorexia nervosa: An fMRI study. NeuroImage: Clinical, 18, 1-8.

Poster No 626

Structural cerebellar connectivity in schizophrenia: Support for the cognitive dysmetria theory

Teresa Gomez[1], Sivan Jossinger[2], John Kruper[1], Adam Richie-Halford[3], Michal Ben-Schachar[2], Jason Yeatman[3], Ariel Rokem[1]

[1]University of Washington, Seattle, WA, [2]Bar-Ilan University, Ramat Gan, Israel, [3]Stanford University, Stanford, CA

Introduction: The cognitive dysmetria theory of schizophrenia (SZ) posits that the core cognitive deficits arise from dysfunctions of cortical-thalamic-cerebellar (CTC) circuits[1]. This theory has received empirical support from fMRI studies, which found increased connectivity in CTC in individuals with SZ[2]. In the present study, we focused on properties of the white matter tissue of the superior cerebellar peduncles (SCPs), a key component of the CTC circuit.

Methods: We analyzed diffusion MRI (dMRI) data from the UCLA Consortium for Neuropsychiatric Phenomics LA5c Study[3]. The sample includes 272 subjects (ages: 21-50): 49 with SZ, 49 with bipolar disorder, 41 with ADHD, and 123 healthy controls (HC). DMRI data were collected with 2 mm isotropic resolution and 1,000 s/mm2 b-value in 64 directions. The data were processed using QSIPrep. The SCPs were identified in each individual using pyAFQ (https://yeatmanlab.github.io/pyAFQ/) and anatomical criteria that capture the known decussation of this bundle[4] (Figure 1). Because the sample contains data of varying quality and the cerebellum was not always covered, visual QC of each subject's SCP was conducted by two observers (TG and AR, blind to group). A subject's data were included only if both observers considered SCP delineation to be in the correct anatomical location and with the expected decussation. This included 46 SZ, 39 bipolar, 35 ADHD, and 94 HC. Samples of

matched case/control were constructed from by simultaneously matching on age, sex and data quality (quantified as raw neighbor correlations). We focused on tract profiles of the mean diffusivity (MD) and fractional anisotropy (FA) calculated with DTI. Statistical differences were evaluated using tractable (https://yeatmanlab.github.io/tractable/), which models the tract profiles using generalized additive models (GAMs), accounting for the shape of the tract profiles along with variability among participants[5]. Model covariates included age, sex, and raw neighbor correlations.

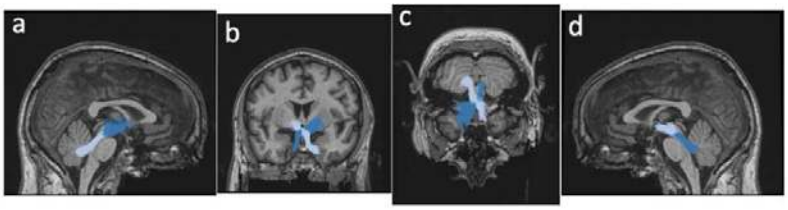

Figure 1: The left (dark blue) and right (light blue) SCP bundles visualized in an individual with SZ, with sagittal (a, d), coronal (b) and axial (c) anatomical views of the T1-weighted scan of this individual.

Results: Statistically significant differences were found in MD tract profiles of the left SCP, where individuals with SZ had lower MD than the matched controls ($p<0.05$; Figure 2). No other significant differences were found. In particular, individuals with ADHD and bipolar were no different from matched controls in SCP tissue properties.

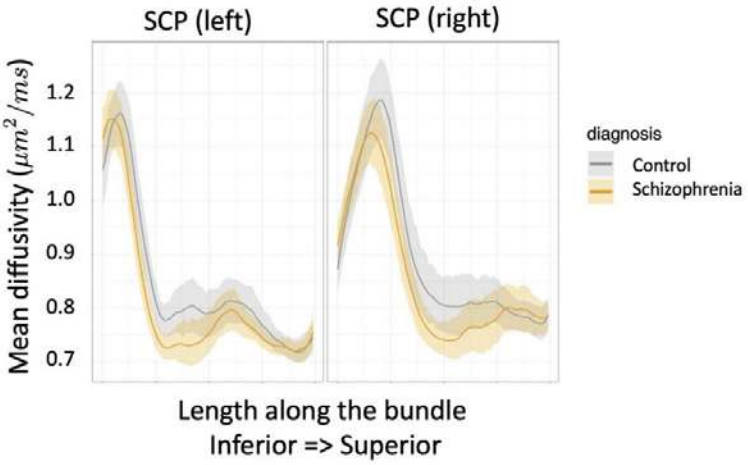

Figure 2: Mean tract profiles of MD in individuals with SZ (orange) and controls (gray) along the length of the SCP bundles, with bootstrapped 95% confidence intervals. The MD difference is statistically significant in the left hemisphere, but not in the right hemisphere.

Conclusions: Previous literature has associated schizophrenia with global abnormalities in diffusion measures, primarily measured as a reduction in FA[6]. Here, we found relatively decreased MD in the SCP, a component of the CTC. Lower MD could indicate increased myelination in SZ and therefore increased connectivity. increased density and directional coherence (but not axonal diameter) may also have similar effects on MD. Thus, these results may be in line with previous fMRI results that found increased functional connectivity in the CTC in individuals with SZ[2], and further supports the cognitive dysmetria theory of SZ.

References

1. N. C. Andreasen, S. Paradiso, D. S. O'Leary, "Cognitive dysmetria" as an integrative theory of schizophrenia: a dysfunction in cortical-subcortical-cerebellar circuitry? Schizophr. Bull. 24, 203–218 (1998).
2. H. Cao, et al., Cerebello-thalamo-cortical hyperconnectivity as a state-independent functional neural signature for psychosis prediction and characterization. Nat. Commun. 9, 3836 (2018).
3. K. J. Gorgolewski, J. Durnez, R. A. Poldrack, Preprocessed Consortium for Neuropsychiatric Phenomics dataset. F1000Res. 6, 1262 (2017).
4. S. Jossinger, M. Yablonski, O. Amir, M. Ben-Shachar, The contributions of the cerebellar peduncles and the frontal aslant tract in mediating speech fluency. Neurobiol. Lang. (Camb.), 1–40 (2023).
5. Nathan M. Muncy, Adam Kimbler, Ariana M. Hedges-Muncy, Dana L. McMakin, Aaron T. Mattfeld (2022),
6. General additive models address statistical issues in diffusion MRI: An example with clinically anxious adolescents,
7. NeuroImage: Clinical, 33: 102937
8. Kubicki, M., McCarley, R., Westin, C. F., Park, H. J., Maier, S., Kikinis, R., Jolesz, F. A., & Shenton, M. E. (2007). A review of diffusion tensor imaging studies in schizophrenia. Journal of psychiatric research, 41(1-2), 15-30. https://doi.org/10.1016/j.jpsychires.2005.05.005

Poster No 627

Insular Gray Matter Volume Explains Substance-Related Problems Beyond the Degree of Substance Use

Malin Hildebrandt[1], Nele Sauer[1], Raoul Wuellhorst[1], Tanja Endrass[1]

[1]TUD Dresden University of Technology, Dresden, Saxony

Introduction: Individuals with substance use disorders (SUD) show altered frontal, striatal, and insular gray matter volumes (GMV) compared to healthy controls. These groups differ in both the degree of substance use (quantity and frequency of use) and substance-related problems, the symptoms of SUD. Hence, the association of gray matter volumes with SUD may reflect either a specific link to substance-related problems, indicating SUD risk, or result from an underlying association with the degree of substance use. To test this, we applied a dimensional approach examining the incremental association of putative SUD risk factors with substance-related problems beyond the degree of substance use (Hildebrandt et al., 2023). Here, we examined GMV in five preregistered regions of interest for which we expected significant associations between GMV and substance-related problems when controlling for the degree of use.

Methods: Methods and hypotheses were preregistered (https://osf.io/9b35a). Using voxel-based morphometry, we analyzed structural MRI data of 134 (poly-)substance users (54 female). Participants additionally completed extensive measures of past year substance use and substance-related problems following the DSM-5 SUD diagnostic criteria with an additional severity rating for each symptom (Diagnostic and statistical manual of mental disorders: DSM-5, 2013). We performed linear regressions of GMV in five a priori regions of interest (bilateral ACC, left anterior and posterior insula, right posterior insula, bilateral dorsal striatum) on substance-related problems, the degree of substance use, as well as on substance-related problems controlled for the degree of use. Resulting p-values were Bonferroni-Holm corrected for the number of ROIs.

Results: While reduced GMV predicted substance-related problems in the left anterior insula (AI; $p = .046$, $\beta = -.15$) and the bilateral anterior cingulate (ACC; $p = .006$, $\beta = -.18$), this association only remained significant when controlling for the degree of use in the left AI ($p = .023$, $\beta = -.18$). GMV reductions in the ACC were associated with the degree of use ($p = .025$, $\beta = -.15$), explaining the bivariate association with substance-related problems. Associations with the other regions were not significant.

Conclusions: Reduced GMV in the ACC may reflect either substance effects on the brain, or risk for a high degree of substance use. In contrast, reduced GMV in the left AI may reflect specific SUD risk, potentially mediated by altered AI functionality relevant for SUD including incentive motivational, control, and interoceptive processes (Naqvi et al., 2014). Our results substantiate the role of a dimensional approach controlling for the degree of substance use for studying specific links to substance-related problems.

References

1. Diagnostic and statistical manual of mental disorders: DSM-5. (2013). American Psychiatric Association.
2. Hildebrandt, M. K. (2023). 'Dissociating the link of neural correlates of inhibition to the degree of substance use and substance-related problems: A preregistered, multimodal, combined cross-sectional and longitudinal study.' Biological Psychiatry, vol. 94, no.11, pp. 898-905
3. Naqvi, N. H. (2014). 'The insula: a critical neural substrate for craving and drug seeking under conflict and risk.' Annals of the New York Academy of Sciences, vol. 1316, no. 1, pp. 53-70

Poster No 628

Acute Neurostructural Effects of Escitalopram in Adolescents with Generalized Anxiety Disorder

Lu Lu[1], Jeffrey Mills[2], Heidi Schroeder[3], Kim Cecil[4], Qiyong Gong[1], Jeffrey Strawn[3]

[1]Huaxi MR Research Center (HMRRC), Department of Radiology, West China Hospital of Sichuan University, Chengdu, Sichuan, [2]Department of Economics, Lindner College of Business, University of Cincinnati, Cincinnati, OH, [3]Department of Psychiatry & Behavioral Neuroscience, College of Medicine, University of Cincinnati, Cincinnati, OH, [4]Department of Radiology, College of Medicine, University of Cincinnati, Cincinnati, OH

Introduction: Selective serotonin reuptake inhibitors (SSRIs) are effective in treating adolescents with anxiety disorders, including generalized anxiety disorder (GAD), but require weeks to produce clinical improvement (Strawn, Lu et al. 2021). Thus, it is important to reveal its underlying neuromechanism and find biomarkers that could predict its treatment response in the early course. Previous studies has investigated acute neurofunctional effects of SSRIs in adolescents with GAD, and indicated that SSRIs altered connectivity in amygdala-frontal circuit during rest and emotion processing (Lu, Mills et al. 2021, Lu, Li

et al. 2022). However, few studies has examined the acute neurostructural effects of SSRIs, and the relationship between neurostructural changes and symptom improvement in adolescents with GAD.

Methods: In the context of an 8-week, double-blind, placebo-controlled trial of escitalopram in adolescents with GAD, we enrolled 51 adolescents (aged 12–17 years) with a Pediatric Anxiety Rating Scale (PARS) score ≥15, and a Clinical Global Impression (CGI-Severity) score ≥4. From these, forty-one patients with eligible MR data were included in this study. Patients receiving escitalopram (n=20) and placebo (n=21) did not differ in age, gender, IQ, comorbidity, baseline anxiety severity, intracranial volume, cortical thickness, or amygdala volume at baseline (Figure 1). High-resolution anatomical images were acquired on a 3-Tesla scanner with a 32-channel phased-array head coil at baseline and 2 weeks after initial treatment. The T1-weighted images were preprocessed and analyzed with FreeSurfer longitudinal pipeline. The escitalopram effect on neurostructure was measured with percent change in cortical thickness and amygdala volume over the first 2 weeks of the trial (percent change = [week 2 – week 0]/2*week 0) with two stage model, and age, sex and intracranial volume as covariates. To further explore escitalopram effect on brain structural covariance, volume of 68 cortical regions (Desikan-Killiany atlas) and 14 subcortical nuclei in each patient at week 0 and 2 were extracted to construct the individual differential structural covariance network (IDSCN) for each patient (Liu, Palaniyappan et al. 2021). The network-based-statistic software was used to compare the IDSCN between patients receiving escitalopram and placebo (5000 iterations, $p<0.05$). The mixed effects model in R was used to examine the relationship between brain morphometric changes in the first 2 weeks and the trajectory of anxiety improvement using week 0, 1, 2, 4, 6 and 8 PARS scores in patients receiving escitalopram.

Results: Escitalopram-treated adolescents relative to placebo had increased percent change in cortical thickness in bilateral insula (left insula: cluster size=851mm2; Talairach coordinate: x=-33.8, y=12.6, z=-2.9; right insula: cluster size=1048mm2; Talairach coordinate: x=34, y=16.4, z=-4.3; Monte Carlo corrected) (Figure 2A). Escitalopram comparing to placebo increased the percent change in volume in left basal nucleus and right lateral nucleus, and decreased the percent change in volume in right coricoamygdoid transition (Figure 1). Escitalopram-treated adolescents also had a decreased structural covariance network compared to patients received placebo, which comprised 12 connectivity among 13 regions (Figure 2B). The rate of thickness change in left insula (β=-13.72, p=0.043), right insula (β=-15.58, p=0.0002), and the rate of volume change in right corticoamygdoid transition (β=-0.60, p=0.0002) was associated with trajectory of anxiety improvement in escitalopram group.

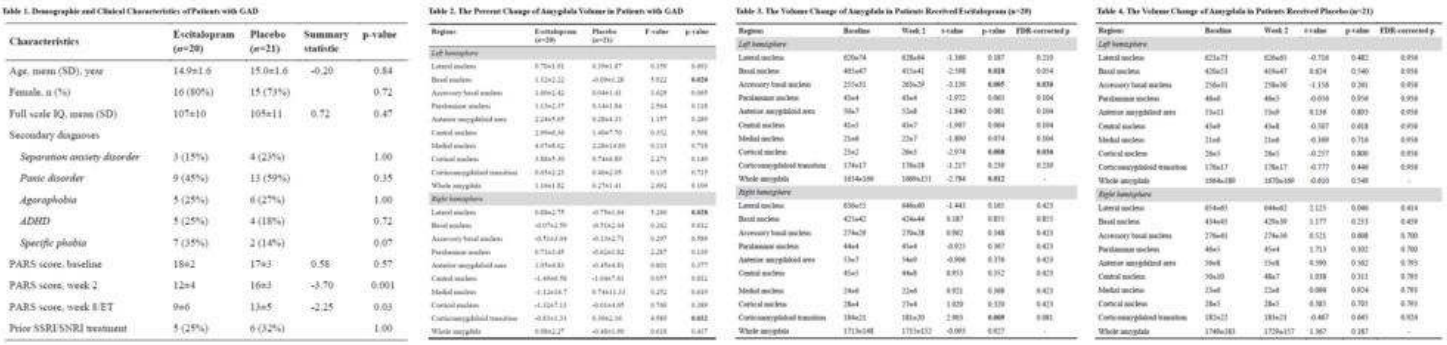

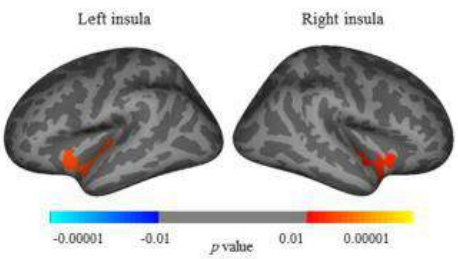

Figure 2A. The increased percent change in cortical thickness in adolescents who received escitalopram comparing to those who received placebo.

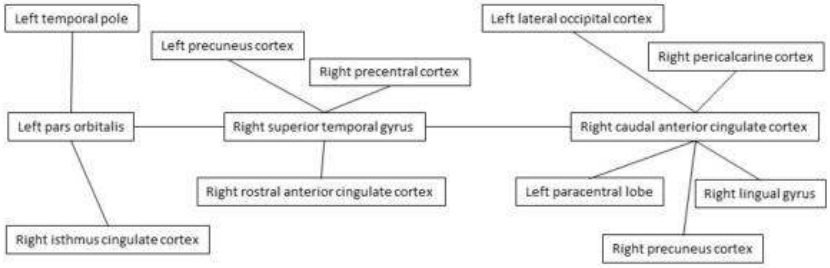

Figure 2B. A schematic diagram shown adolescents received escitalopram had a single network with decreased structural covariance comparing to adolescents received placebo.

Conclusions: Acute treatment with escitalopram altered the rate of neurostructural changes in insula and amygdala, and disrupted the structural covariance among regions associated with default mode, visual, and somatomotor networks. Moreover, these neurostructural changes-within two weeks of starting escitalopram-may represent biomarkers of treatment response.

References

1. Liu, Z. W., L. Palaniyappan, X. R. Wu, K. Zhang, J. N. Du, Q. Zhao, C. Xie, Y. Y. Tang, W. J. Su, Y. R. Wei, K. K. Xue, S. Q. Han, S. J. Tsai, C. P. Lin, J. L. Cheng, C. B. Li, J. J. Wang, B. J. Sahakian, T. W. Robbins, J. Zhang and J. F. Feng (2021). "Resolving heterogeneity in schizophrenia through a novel systems approach to brain structure: individualized structural covariance network analysis." Molecular Psychiatry 26(12): 7719-7731.
2. Lu, L., H. L. Li, W. T. Baumel, J. A. Mills, K. M. Cecil, H. K. Schroeder, S. A. Mossman, X. Q. Huang, Q. Y. Gong, J. A. Sweeney and J. R. Strawn (2022). "Acute neurofunctional effects of escitalopram during emotional processing in pediatric anxiety: a double-blind, placebo-controlled trial." Neuropsychopharmacology 47(5): 1081-1087.
3. Lu, L., A. J. Mills, H. L. Li, K. H. Schroeder, A. S. Mossman, T. S. Varney, M. K. Cecil, X. Q. Huang, Q. Y. Gong, B. L. Ramsey, P. M. DelBello, A. J. Sweeney and R. J. Strawn (2021). "Acute Neurofunctional Effects of Escitalopram in Pediatric Anxiety: A Double-Blind, Placebo-Controlled Trial." Journal of the American Academy of Child and Adolescent Psychiatry 60(10): 1309-1318.
4. Strawn, J. R., L. Lu, T. S. Peris, A. Levine and J. T. Walkup (2021). "Research Review: Pediatric anxiety disorders - what have we learnt in the last 10 years?" Journal of Child Psychology and Psychiatry 62(2): 114-139.

Poster No 629

Polygenic risk for stress-related disease correlates with fMRI stress task pulse rate recovery

Mira Erhart[1], Dorothee Poehlchen[2], Darina Czamara[1], Julia Fietz[1], Natan Yusupov[1], Anne Kühnel[3], Tanja Brückl[1], BeCOME study team[1], Michael Czisch[1], Elisabeth Binder[1], Philipp Sämann[1], Victor Spoormaker[1]

[1]Max-Planck-Institute of Psychiatry, Munich, Bavaria, [2]Max-Plack-Institute of Psychiatry, Munich, Bavaria, [3]University of Bonn, Bonn, Nordrhein-Westfalen

Introduction: Abnormal responses to acute stress are one of the key elements in the research of stress-related disorders (van Oort et al., 2020; White et al., 2014; Zorn et al., 2017). However, these disorders are multicausal and influenced by long-term predispositions such as stress exposure and genetic variants, too (Dalvie et al., 2021). In previous work, we showed that the incorporation of individual pulse rate (PR) traces in the fMRI analysis accounted for the highly individual and dynamic stress response and revealed – among others – limbic structures and the insula to be involved in the stress response (Figure 1A). We aimed to reproduce and extend our previous findings to a larger sample including 104 additional patients to examine the robustness of the correlation between individual PR patterns and limbic activity. Moreover, we aimed to evaluate the correlations between individual PR from this stress-task, polygenic risk scores (PRS) and stress exposure.

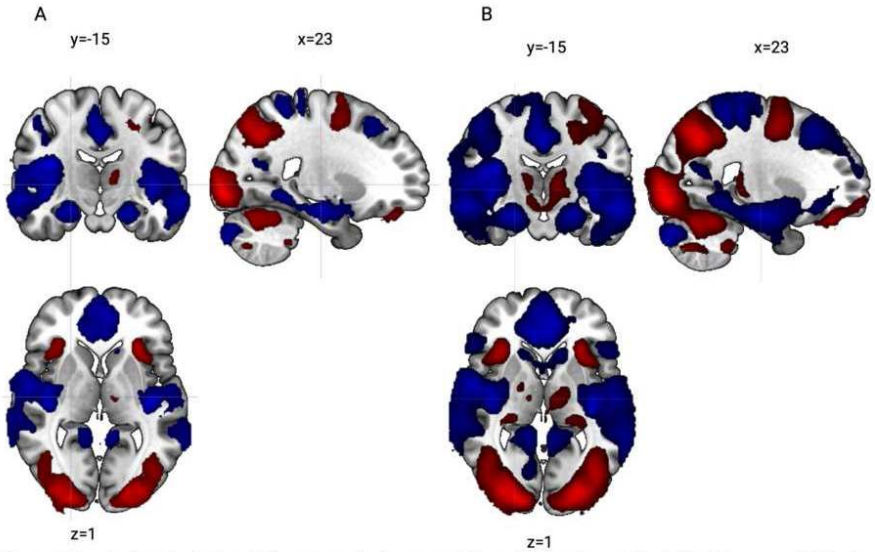

Figure 1: Results from the [+1] and [-1] contrasts for the parametric modulator of mean blockwise PR across all 15 task blocks. A: map for healthy controls (n=83) and B: map for merged sample (n=187). Red=positive correlation with PR, blue=negative correlation; Voxels are thresholded at $p_{voxel.FWE} < .05$ & k>25 voxel.

Methods: 266 participants from a transdiagnostic study including healthy controls and subjects with disorders such as depression or anxiety (Brückl et al., 2020) (female=128, mean age=34.8years, standard deviation=11.6) underwent the imaging stress test (IST) during fMRI including simultaneous pulse plethysmography. In three different phases (PreStress, Stress, PostStress) participants were asked to solve mental arithmetic tasks. Each phase consists of 5 mini-blocks [60s active calculus, 40s rest], with additional psychosocial stress applied during the 2nd phase. Postprocessing was conducted exactly as in our previous work (Erhart et al., submitted manuscript). In brief, the fMRI volumes were slice-time corrected, realigned to the mean, and normalized using the DARTEL technique. Denoising followed a 2-step-residualization, first against motion and

differential motion, after which time courses from white matter and cerebrospinal fluid masks were extracted and forwarded to a CompCor correction. Finally, images were smoothed (Gaussian, FWHM 6 mm isometric). The first level model was set up in the GLM framework of SPM with a single regressor capturing the 15 active blocks with mean individual PR per block as a parametric modulator. Random effect second-level analyses comprised a one-sample t-test of the estimates of the parametric modulator for the complete sample. Maps were thresholded at pvoxel.FWE-corrected <0.05, with a cluster extent >25. For correlations with lifetime stress and PRS proportional PR downswings were calculated by normalizing the mean change in PR from the Stress to the PostStress phase by the mean change from the PreStress to the Stress phase (upswing). PRS for major depressive disorder (MDD) (Howard, 2019) and post-traumatic stress disorder (PTBS) (Stein, 2021) were calculated using PRSice 2.3.5 software and thresholded at p<5e-05. Higher values indicate greater polygenic risk. Lifetime stress was assessed with the Munich Life Event List (Maier-Diewald, 1983). Higher values represent greater lifetime stress.

Results: We reproduced our main findings in the extended sample (Figure 1). Participants with a higher polygenic risk for MDD showed lower downswings after the stress phase (r=-.2, p=.003, Figure 2). Furthermore, negative correlations were observed between PR downswings and the polygenic risk for PTSD and two of its symptom subscales (sum: r=-.15, p=.001, hyperarousal: r=-.08, p=.003, avoidance: r=-.16, p=.001). Higher lifetime work distress was associated with decreased downswings after the stress phase in the IST (r=-.12, p=0.03).

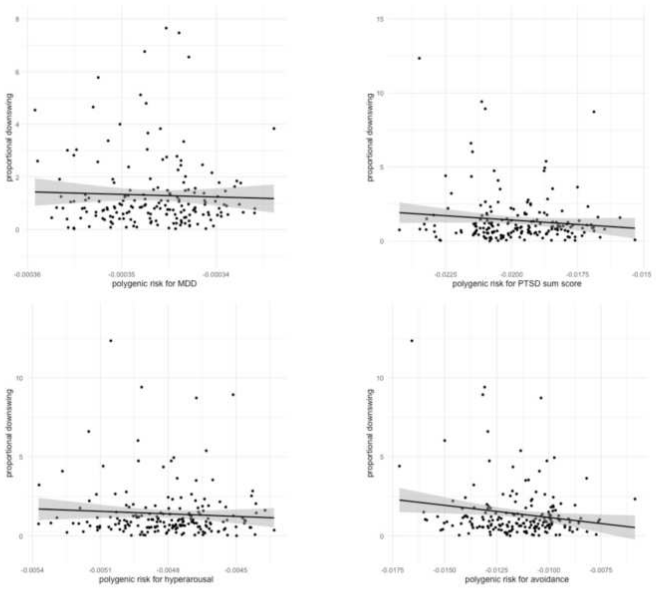

Figure 2. Correlation of polygenic risk scores for MDD and PTSD (and subscales) with proportional PR downswing. Negative correlations were observed for all scores. Correction for multiple comparisons was done with the calculated number of effective tests (R package poolr).

Conclusions: We could reproduce our previous finding of individual pulse rate markers in response to an intense psychosocial stress test being correlated with fMRI BOLD levels in the insula and amygdala/hippocampus, among other regions. We report in addition, that individual pulse rate recovery in turn is correlated with polygenic risk scores for depression and PTSD connecting an acute stress marker with more long-term risk factors for psychopathology.

References

1. Brückl, T. M., Spoormaker, V. I., Samann, P. G., Brem, A. K., Henco, L., Czamara, D., Elbau, I., Grandi, N. C., Jollans, L., Kuhnel, A., Leuchs, L., Pohlchen, D., Schneider, M., Tontsch, A., Keck, M. E., Schilbach, L., Czisch, M., Lucae, S., Erhardt, A., & Binder, E. B. (2020). The biological classification of mental disorders (BeCOME) study: a protocol for an observational deep-phenotyping study for the identification of biological subtypes. BMC Psychiatry, 20(1), 213. https://doi.org/10.1186/s12888-020-02541-z
2. Dalvie, S., Chatzinakos, C., Al Zoubi, O., Georgiadis, F., workgroup, P.-P. S. B., Lancashire, L., & Daskalakis, N. P. (2021). From genetics to systems biology of stress-related mental disorders. Neurobiol Stress, 15, 100393. https://doi.org/10.1016/j.ynstr.2021.100393
3. Howard, D. M., Adams, M. J., Clarke, T. K., Hafferty, J. D., Gibson, J., Shirali, M., ... & McIntosh, A. M. (2019). Genome-wide meta-analysis of depression identifies 102 independent variants and highlights the importance of the prefrontal brain regions. Nature Neuroscience, 22(23).
4. Maier-Diewald, W. W., H.U.; Werner-Eilert, K. (1983). Die Münchner Ereignisliste (MEL) - Anwendungsmanual. Munich: Max Planck Institute of Psychiatry.
5. Stein, M. B., Levey, D. F., Cheng, Z., Wendt, F. R., Harrington, K., Pathak, G. A., ... & Gelernter, J. . (2021). Genome-wide association analyses of post-traumatic stress disorder and its symptom subdomains in the Million Veteran Program. Nature genetics, 53(2).
6. van Oort, J., Kohn, N., Vrijsen, J. N., Collard, R., Duyser, F. A., Brolsma, S. C. A., Fernandez, G.,

7. Schene, A. H., Tendolkar, I., & van Eijndhoven, P. F. (2020). Absence of default mode downregulation in response to a mild psychological stressor marks stress-vulnerability across diverse psychiatric disorders. Neuroimage Clin, 25, 102176. https://doi.org/10.1016/j.nicl.2020.102176
8. White, S. W., Mazefsky, C. A., Dichter, G. S., Chiu, P. H., Richey, J. A., & Ollendick, T. H. (2014). Social-cognitive, physiological, and neural mechanisms underlying emotion regulation impairments: understanding anxiety in autism spectrum disorder. Int J Dev Neurosci, 39, 22-36. https://doi.org/10.1016/j.ijdevneu.2014.05.012
9. Zorn, J. V., Schur, R. R., Boks, M. P., Kahn, R. S., Joels, M., & Vinkers, C. H. (2017). Cortisol stress reactivity across psychiatric disorders: A systematic review and meta-analysis. Psychoneuroendocrinology, 77, 25-36. https://doi.org/10.1016/j.psyneuen.2016.11.036

Poster No 630

Functional Connectome Gradient Features in Rumination States and Major Depression Disorder

Zheng-Jia-Yi Hu[1], Chao-Gan Yan[1]

[1]*Institute of Psychology, Chinese Academy of Sciences, Beijing, Beijing*

Introduction: Major depression disorder (MDD) is a common mental illness with high rates of relapse, disability and suicide. The default mode network (DMN) plays an important role in exploring the brain mechanism in depression through fMRI. In recent years, researchers have found that rumination is often regarded as a psychological expression of DMN abnormalities in patients with depression (Kaiser et al., 2015). Lately, a popular approach to define the brain as a set of continuous scores along multiple axes is called functional connectome gradient (Vos de Wael et al., 2020). Previous study (Margulies et al., 2016) identified the first two gradients as the primary-transmodal gradient and the visual-sensorimotor gradient. Here is a universally proven result that the patients with MDD showed a narrower range of gradient scores, and regionally, the MDD group showed lower gradient scores mostly in the DMN than healthy controls (Xia et al., 2020). Therefore, this study aims to investigate cortical gradient features in healthy people and depression patients.

Methods: The discovery sample includes task-state fMRI data from 41 young healthy adults, which were collected in a previously published study. (Chen et al., 2020). The discovery set, which included 41 healthy control participants (HCs) and 45 MDD patients, was recruited from Guangji Hospital in Suzhou, China. The procedure was approved by the Ethics Committee of Institute of Psychology. The details of experimental design and MRI data analysis were introduced in the previous paper (Chen et al., 2020). Following the data preprocessing, the time series of the region of interest (ROIs) defined by Schaefer2018_400Parcels were extracted to yield a functional connectivity matrix for each participant. The BrainSpace toolbox based on Matlab (Vos de Wael et al., 2020) was utilized to calculate gradient values. Paired t-tests were then used to explore the significant variations between different states after false discovery rate (FDR) corrections. And the gradient metrics like explanation ratio, range, variance, and dispersion were also computed to explore global differences. For the validation states, after calculating the gradient matrix, a two-way mixed-effects ANOVA was conducted, incorporating a two-level fixed within-subject factor (rumination vs. distraction) and a two-level random between-subject factor (MDD patients vs. HCs).

Results: Consistent with previous findings, all the results showed the primary-transmodal gradient and the visual-sensorimotor gradient (Fig1.A). In brief, focused on the results of the first gradient, the results indicated that the rumination state had significantly lower range and variation than distraction state in individual sites (Fig2). As for the validation dataset, a significant condition effect of gradient variance was observed. From a regional perspective, compared with the distraction state, the rumination state presented lower gradient score in visual cortex and the posterior cingulate cortex within the DMN, with higher gradient score in the prefrontal cortical areas within the DMN and the frontoparietal network (FPN) (Fig1.B). Paired t-tests in validation data proved the variation of DMN and FPN. We used these two brain regions as masks for conducting the mixed-effect analysis on the validation dataset. There was not any significant interaction effect after the FDR correlation. However, before the correlation, the results indicate that the group and the different rumination states have interaction effect in DMN and frontoparietal network (Fig1.C).

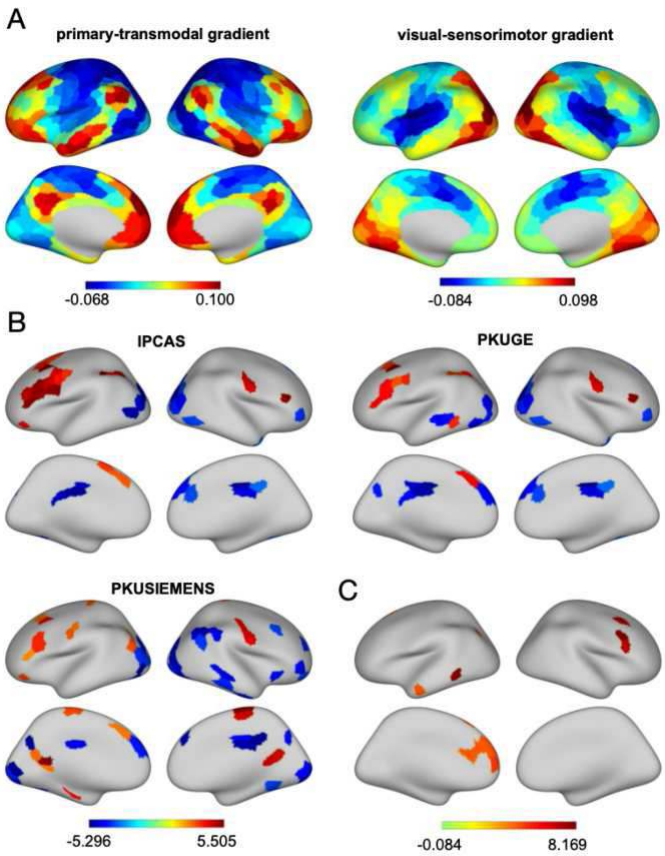

Figure 1. Gradient values and gradient differences between groups. (A) Primary-transmodal gradient and visual-sensorimotor gradient of rumination state at the IPCAS site. (B) Gradient differences in rumination state and distraction state across sites. (C) Clusters with significant interaction effects in the validation data set.

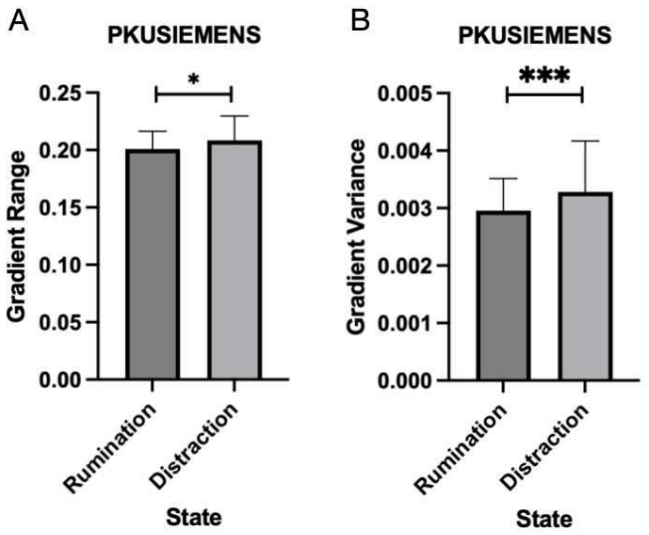

Figure 2. Global gradient difference. (A) Gradient range difference in PKUSIEMENS site. (B) Gradient variance difference in PKUSIEMENS site.

Conclusions: In the present study, both healthy subjects and MDD patients maintained the first and second gradients of the primary-transmodel in both rumination and distraction states. Rumination had a narrower gradient range and a lower gradient value in the DMN than distraction. However, unlike previous studies, we also found a rising gradient value in specific regions of the DMN in MDD patients and rumination states, which is worth exploring.

References

1. Chen, X., Chen, N.-X., Shen, Y.-Q., Li, H.-X., Li, L., Lu, B., Zhu, Z.-C., Fan, Z., & Yan, C.-G. (2020). The subsystem mechanism of default mode network underlying rumination: A reproducible neuroimaging study. NeuroImage, 221, 117185. https://doi.org/10.1016/j.neuroimage.2020.117185
2. Kaiser, R. H., Andrews-Hanna, J. R., Wager, T. D., & Pizzagalli, D. A. (2015). Large-scale network dysfunction in major depressive disorder. JAMA Psychiatry, 72(6), 603. https://doi.org/10.1001/jamapsychiatry.2015.0071
3. Margulies, D. S., Ghosh, S. S., Goulas, A., Falkiewicz, M., Huntenburg, J. M., Langs, G., Bezgin, G., Eickhoff, S. B., Castellanos, F. X., Petrides, M., Jefferies, E., & Smallwood, J. (2016). Situating the default-mode network along a principal gradient of macroscale cortical organization. Proceedings of the National Academy of Sciences, 113(44), 12574–12579. https://doi.org/10.1073/pnas.1608282113
4. Vos de Wael, R., Benkarim, O., Paquola, C., Lariviere, S., Royer, J., Tavakol, S., Xu, T., Hong, S.-J., Langs, G., Valk, S., Misic, B., Milham, M., Margulies, D., Smallwood, J., & Bernhardt, B. C. (2020). BrainSpace: A toolbox for the analysis of macroscale gradients in neuroimaging and Connectomics datasets. Communications Biology, 3(1). https://doi.org/10.1038/s42003-020-0794-7
5. Xia, M., Liu, J., Mechelli, A., Sun, X., Ma, Q., Wang, X., Wei, D., Chen, Y., Liu, B., Huang, C.-C., Zheng, Y., Wu, Y., Chen, T., Cheng, Y., Xu, X., Gong, Q., Si, T., Qiu, S., Lin, C.-P., … He, Y. (2020). Connectome Gradient Dysfunction in Major Depression and Its Association with Gene Expression Profiles. https://doi.org/10.1101/2020.10.24.352153

Poster No 632

Attentional bias to facial emotion expressions in nonsuicidal self-injury: an fMRI study

HaYoung Kim[1], Seokwon Choi[1], Hyeri Moon[1], HaYoung Bae[1], Jaeoh Lee[1], Yeojin Choi[1], Ji-Won Hur[1]

[1]Korea University, Seoul, Korea, Republic of

Introduction: Nonsuicidal self-injury (NSSI) is the deliberate infliction of damage to one's own body tissues without suicidal intent. Difficulties in emotional regulation have been identified as critical psychopathologies that contribute to the initiation and maintenance of NSSI. In this study, we sought to investigate the attentional bias towards negative emotional stimuli and its underlying neural correlates in NSSI. Attentional bias towards negative emotions is known to intensify negative affectivity in individuals with clinical symptoms such as suicide ideation, anxiety, and borderline personality disorder. We hypothesized that individuals with NSSI would have increased neural responses to negative facial emotions that might be related to their clinical symptoms.

Methods: We recruited 25 individuals with a history of NSSI and 14 sex- and handedness-matched controls. All participants completed the emotional dot-probe task. In the emotional dot-probe task, a facial emotion stimulus and a neutral face stimulus simultaneously on the screen. The stimuli disappeared immediately, and a target dot appeared on the left or right of the screen. Participants were then asked to indicate the location of the disappeared dot by pressing either the first (i.e., left) or second (i.e., right) button. The emotional stimuli consisted of negative facial emotion expressions (i.e., anger and disgust) and neutral facial expressions from 14 different actors (7 males, 7 females) using the Extended ChaeLee Korean Facial Expressions of Emotions (ChaeLee-E). This emotional dot-probe task included two conditions. In the congruent condition, the dot probe was presented at the exact location where the emotional stimuli appeared. In the incongruent condition, the dot probe was presented at the opposite location of the emotional stimuli. The CONN toolbox was used for the fMRI data preprocessing. We also used Statistical Parametric Mapping 12 to analyze the BOLD signal changes and SPSS version 27 to conduct correlation analyses between neural activities and clinical measures in NSSI.

Results: Individuals engaging in NSSI showed increased neural activation in the left medial frontal lobe and Heschl's gyri in the incongruent condition (incongruent > congruent) compared to controls. More specifically? In particular? individuals with NSSI also showed hyperactivity in the left opercular and triangular regions of the inferior frontal gyrus (IFG) in the anger condition (anger > neutral) and disgust condition (disgust > neutral), respectively. Greater levels of anxiety as measured by the General Anxiety Disorder-7 and impulsive behaviors as measured by the UPPS-P Impulsive Behavior Scale in the NSSI group were significantly correlated with the enhanced left medial frontal lobe activation in the incongruent condition. In addition, higher levels of guilt as measured by the Test of Self-Conscious Affect (TOSCA-3S) and perfectionism as measured by the Multidimensional Perfectionism Scale (MPS) in NSSI were both correlated with hyperactivity of the left opercular region of the IFG, and perfectionism was further correlated with the hyperactivity of the triangular regions of the IFG.

Conclusions: This study is the first to address the neural mechanisms of attentional bias in individuals engaging in NSSI. Our fMRI study revealed the attentional bias to the negative facial emotion expressions in individuals with NSSI and its underlying neural activity, which was related with anxiety, impulsive behaviors, guilt, and perfectionism. These identified neural mechanisms allow us further to understand the biased emotional processing in individuals with NSSI and provide rationale for developing interventions to target their attentional bias toward negative stimuli better.

References
1. Bantin, T. (2016). What does the facial dot-probe task tell us about attentional processes in social anxiety? A systematic review. Journal of behavior therapy and experimental psychiatry, 50, 40-51.
2. Hornung, J. (2019). Exploring the fMRI based neural correlates of the dot probe task and its modulation by sex and body odor. Psychoneuroendocrinology, 99, 87-96.
3. Kaiser, D. (2020). Patients with borderline personality disorder and comorbid PTSD show biased attention for threat in the facial dot-probe task. Journal of behavior therapy and experimental psychiatry, 67, 101437.
4. Lin, L.(2023). Attentional bias to emotional facial expressions in undergraduates with suicidal ideation: an ERP study. Archives of suicide research, 27(3), 938-955.
5. Nock, M. (2009). Nonsuicidal self-injury: Definition and classification.
6. Price, R. (2014). Looking under the hood of the dot-probe task: An fMRI study in anxious youth. Depression and anxiety, 31(3), 178-187.

Poster No 633

Association between body image disturbance and amygdala in healthy Japanese adolescent females: rest

Kaie Habata[1], Daichi Shiotsu[2], Kotaro Kowada[2], Taku Kamiya[2], Takuya Makino[3], Riku Sanada[2], Masatoshi Yamashita[4], Yoshifumi Mizuno[4], Hidehiko Okazawa[5], Bae Jihyun[6], Jung Minyoung[6], Hirotaka Kosaka[7]

[1]Department of Neuropsychiatry, University of Fukui, Eiheiji, Fukui, Japan, [2]Department of Neuropsychiatry, University of Fukui, Eiheiji, Fukui, [3]Department of Neuropsychiatry, University of Fukui, Eiheiji, Fukui, [4]Research Center for Child Mental Development, University of Fukui, Eiheiji, Fukui, [5]Biomedical Imaging Research Center, University of Fukui, Eiheiji, Fukui, [6]Cognitive Science Research Group, Korea Brain Research Institute, Daegu, Daegu, [7]University of Fukui, Fukui, NA

Introduction: The amygdala is thought to be associated with the perception of self body image. Recent studies have indicated that the amygdala is functutionally abnormal in patients with eating disorders, such as anorexia nervosa (AN), which involves body image disturbance (Burkert et al., 2019). We hypothesized that the amygdala would be associated with body image disturbance, and we explored the correlation between resting-state neural activity in each limbic region, including the amygdala, and subjective evaluations of body image.

Methods: Thirty adolescent healthy females were included in this study. Participants also provided subjective self-ratings of body image using the Basic Olomouc Body Rating (BOBR) scale (Šrámková et al., 2015), consisting of ten body image silhouettes representing different BMI (Body Mass Index) values. The degree of body image distortion was determined by calculating the difference between the participant's actual image and ideal image corresponding to their subjective self-selected body image silhouette. 3-Tesla MRI scans were performed, and functional connectivity analyses, seed to voxel analysis were carried out using the CONN-fMRI functional connectivity toolbox. Limbic regions (thalamus, caudate, putamen, pallidum, hippocampus, amygdala, accumbens nucleus) were selected as seed.

Results: Negative correlations with the degree of body image gap were shown for the connectivity with the right amygdala and temporal pole gyrus ($p<0.00001$).

Conclusions: Activation of the amygdala has been shown to play an important role in the emotional body evaluation of AN patients when they see distorted images of their own bodies (Seeger et al., 2002). In this study, we evaluated he relationship between body image gap and resting-state brain connectivity in limbic regions. The relationship between body image gap and amygdala activity reflected distorted perception of body image, suggesting that the amygdala may play an important role in body image even in healthy subjects.

References
1. Burkert. (2019), 'Body image disturbances, fear and associations with the amygdala in anorexia nervosa', Wien. Klin. Wochenschr., vol. 131, no. 3-4, pp. 61-67
2. Seeger. (2002), 'Body image distortion reveals amygdala activation in patients with anorexia nervosa -- a functional magnetic resonance imaging study', Neurosci, vol. 326, no. 1, pp. 25-28

Poster No 634

Disrupted thalamic FC explained the altered level of consciousness induced by ketamine

Tara Chand[1], Meng Li[2], Yuan Cao[3], Zümrüt Duygu Sen[4], Lena Danyeli[5], Nooshin Javaheripour[5], Vinod Kumar[6], Martin Walter[5]

[1]Jindal Institute of Behavioural Sciences, O. P. Jindal Global University, Sonipat, Haryana, India, [2]Jena University Hospital, Jena, Germany, [3]Jena University Hospital, Jena, Turingia, [4]Department of Psychiatry and Psychotherapy, Jena University Hospital, Jena, Thuringen, [5]Department of Psychiatry and Psychotherapy, Jena University Hospital, Jena, Thuringia, [6]MPI for Biological Cybernetics, Tübingen, Baden Württemberg

Introduction: The therapeutic potential of a single subanesthetic dose of ketamine in various mental illnesses, particularly treatment-resistant depression (TRD), has gained significant attention in the past decade (Kryst et al 2020). Beyond the rapid onset of therapeutic efficacy, ketamine administration can induce altered states of consciousness, which is known as dissociative states, encompassing disorientation, confusion, sensory perception changes (such as visual or auditory hallucinations), and feelings of detachment. The vital role of the thalamus in the ketamine-induced loss and return of consciousness, as well as altered states of consciousness, has been broadly reported (Krystal et al. 1994). Although the regional effect of ketamine on thalamic nuclei has been reported (Ferrer et al 1973; Rogers et al 2004), to date, it remains unclear how changes in the thalamo-cortical interactions lead to ketamine-induced dissociative states on the level of thalamus functional anatomy. This study aimed to investigate resting-state functional connectivity changes within the thalamus functional anatomy (Kumar et al., 2017) and their relation to ketamine-induced dissociative states.

Methods: In a randomized, double-blind, placebo-controlled, crossover study, thirty-five healthy males (mean age ± standard deviation (SD) = 25.08 ± 4.18 years) underwent 7T high-field functional MRI scans before and one day after ketamine or placebo infusions. fMRI data was acquired using echo-planar imaging (EPI) sequence with the following parameters: TE = 25 ms, TR = 1500 ms, flip angle = 70°, FoV = 212 mm, 60 slices, isotropic voxel size = 2 mm3, multi-band acceleration factor = 3, grappa acceleration factor PE = 2. The data underwent preprocessing using fMRIPrep, and rsFC was calculated using parcels from the functional anatomy atlas of the human thalamus (Kumar et al., 2017). To examine ketamine's effect on seed-based rsFC in the different parcels of the thalamus functional anatomy, a within-subject flexible factorial ANOVA was performed for each functional parcel separately in SPM, assessing the main effects of session (baseline vs. infusion), treatment (placebo vs. ketamine), and their interaction. Additionally, rsFC values from significant clusters were correlated with subjective consciousness levels measured by the score of Oceanic Boundlessness score (OB) from the five-dimensional altered states of consciousness.

Results: Within-subject flexible factorial ANOVA revealed a significant treatment * session interaction (clusterwise FWE-corrected at $p < 0.05$) in the FC of four thalamic parcel (bilateral 08, left 02, and 15) to the medial/inferior frontal gyrus (Figure 01; pFWE-cluster corrected, initial height threshold $p < 0.001$). The FC of left 15 and right 08 to the right-medial frontal gyrus during infusion showed significant negative correlations [left 15 ($r = -38$, $p = 0.27$), and right 08 ($r = -42$, $p = 0.013$)] with subjective consciousness measured by the OB score (Figure 02).

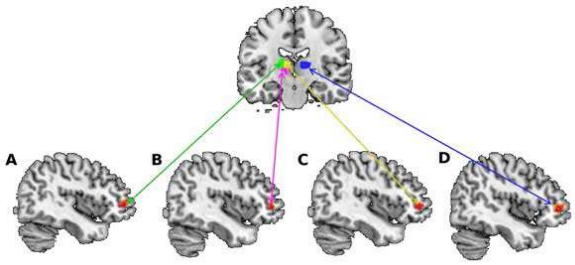

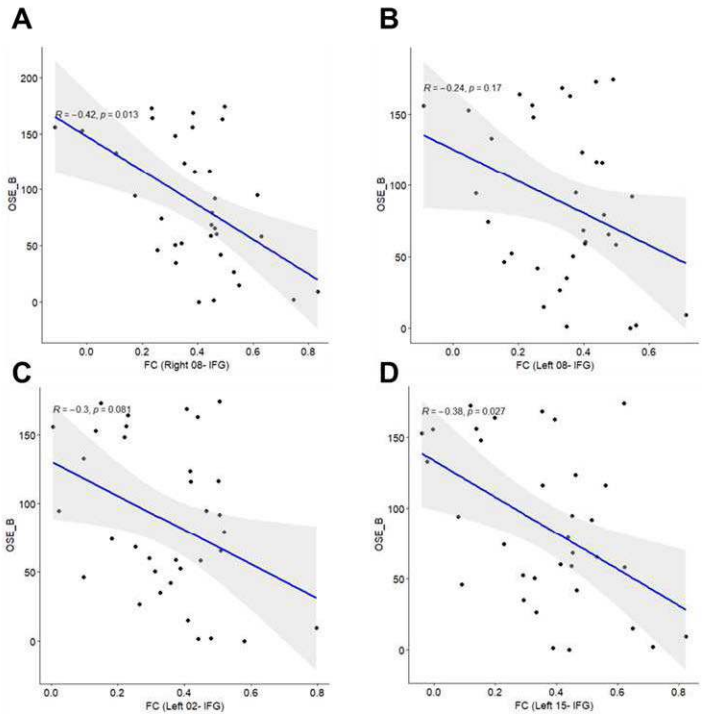

Conclusions: The ketamine show the changes in the thalamo-cortical functional connectivity between the specific thalamus nuclei (VA, Pul, VL, CL, VPL) with medial/inferior frontal gyrus, and right-medial frontal gyrus. Whereas the ketamine-impacted nuclei associate with the arousal, awareness, sensory, and visual processing (Kumar et.al. 2017, 2022). The CL is an intralaminar nucleus, enables rapid interactions between brainstem and cortex, and has been implicated in the arousal, awareness, and disorders of consciousness (Kumar et.al. 2017). Thalamic nuclei and their involvement in cortico-striatal-thalamo-cortical loops and their changes might be the essential component in ketamine-induced altering consciousness due to their role in salience processing and cortex gating.

References

1. Ferrer-Allado, T., Brechner, V. L., Dymond, A., Cozen, H. & Crandall, P. (1973) Ketamine-induced Electroconvulsive Phenomena in the Human Limbic and Thalamic Regions. Anesthesiology 38, 333–344 .
2. Kryst, J. et al. (2020) Efficacy of single and repeated administration of ketamine in unipolar and bipolar depression: A meta-analysis of randomized clinical trials. Pharmacol. Rep. 72, 543–562 .
3. Krystal, J. et al. (1994) Subanesthetic effects of the noncompetitive NMDA antagonist, ketamine, in humans. Psychotomimetic, perceptual, cognitive, and neuroendocrine responses. Archives of general psychiatry
4. Kumar, V.; van Oort, E.; Scheffler, K.; Beckmann, C.; Grodd, W.:(2017) Functional Anatomy of the Human Thalamus at Rest. NeuroImage 147, pp. 678 - 691
5. Rogers, R., Wise, R. G., Painter, D. J., Longe, S. E. & Tracey, I. (2004) An Investigation to Dissociate the Analgesic and Anesthetic Properties of Ketamine Using Functional Magnetic Resonance Imaging. Anesthesiology 100, 292–301
6. Kumar, V.J., Beckmann, C.F., Scheffler, K. et al.(2022) Relay and higher-order thalamic nuclei show an intertwined functional association with cortical-networks. Commun Biol 5, 1187 .

Poster No 635

Exercise Ameliorates Depressive Status through the Interaction between Motor and Reward Regions

Shiqi Di[1,2], Na Luo[1], Weiyang Shi[1], Tianzi Jiang[1,2,3,4,5]

[1]Brainnetome Center, Institute of Automation, Chinese Academy of Sciences, Beijing, China, [2]School of Artificial Intelligence, University of Chinese Academy of Sciences, Beijing, China, [3]Center for Excellence in Brain Science and Intelligence Technology, Institute of Automation, Chinese Academy of Sciences, Beijing, China, [4]Research Center for Augmented Intelligence, Zhejiang Lab, Hangzhou, China, [5]Xiaoxiang Institute for Brain Health and Yongzhou Central Hospital, Yongzhou, China

Introduction: Major depressive disorder (MDD) is a widespread mental disorder globally (Smith 2014), characterized by persistent feelings of low mood and anhedonia. Physical activity has been demonstrated as an effective non-pharmacological intervention for depression (D'Angelantonio et al. 2022). However, little attention has been paid to the underlying

neuroimaging mechanisms linking exercise and depression, as well as the microscale molecular basis underlying the macroscale imaging mechanisms. In this study, we therefore conduct a multiscale analysis to systematically investigate how physical activity modulates brain structure and its biological influence, thus leaving a positive impact on improving depressive status.

Methods: The MDD-1 dataset was obtained from the UK Biobank (https://www.ukbiobank.ac.uk/), including 1,027 subjects with 492 MDDs and 535 healthy controls (HCs). The dMRI preprocessing was conducted by the UK Biobank team (Miller et al. 2016). After that, we performed PROBTRACKx and established structural connectivity (SC) at the brain region level based on the Brainnetome Atlas (Fan et al. 2016). Partial least squares (PLS) regression was utilized to explore the significant link between SC pattern and physical activity score. The identified imaging pattern was then generalized to three independent datasets also with depressive symptoms (MDD-2, bipolar disorder (BD) and schizophrenia (SCZ) datasets) to explore the stability and specificity of the findings (Luo et al. 2018). Afterwards, the neuromaps toolbox (Markello et al. 2022) was applied to interpret the biological ontologies of the identified SC pattern. Finally, the Allen Human Brain Atlas dataset (Arnatkeviciute et al. 2019) and other genome databases (Zhou et al. 2019, Seidlitz et al. 2020) were adopted to explore its underlying genetic basis, pathways and cell types. The analysis pipeline was depicted in Figure 1.

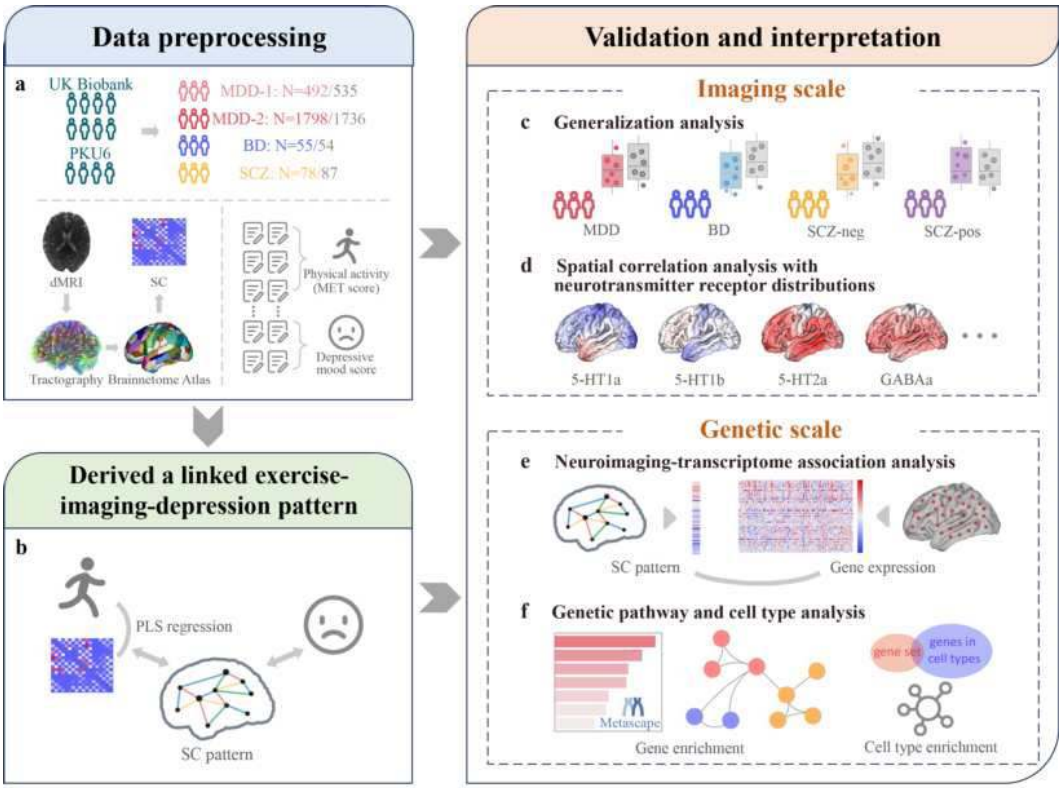

Figure 1. Overview of the analysis pipeline. a, Data preprocessing. **b,** Derived a linked exercise-imaging-depression pattern. Based on MDD-1 dataset, we identified a SC pattern that significantly associated with physical activity. **c,** Generalization analysis to another three independent datasets. **d,** Spatial correlation analysis with neurotransmitter receptor distributions. **e,** Neuroimaging-transcriptome association analysis. We explored the genetic underpinnings of the identified SC pattern by integrating neuroimaging and transcriptome features. **f,** Genetic pathway and cell type analysis. Gene enrichment and cell type analysis were performed based on the set of contributing genes.

Results: 1. A linked imaging-exercise pattern ($r = 0.67$, $p = 1.2e\text{-}134$) was identified to be both significantly correlated with depressive mood ($p = 6.0e\text{-}18$) and group discriminative ($p = 2.1e\text{-}4$) between MDDs and HCs. The structural connections with significant contributions were primarily located between the motor-related regions and reward-related regions (Figure 2). 2. When generalizing the SC pattern to three independent datasets, all datasets except for schizophrenia with positive symptoms presented a significant group difference ($p = 1.5e\text{-}2$ for another MDD dataset, $p = 7.4e\text{-}4$ for bipolar disorder, $p = 1.6e\text{-}4$ for schizophrenia with negative symptoms), suggesting that the identified SC pattern is generalizable to mental disorders involving depressive mood. 3. Based on the neurotransmitter receptor maps parcellated with the Brainnetome Atlas, the SC pattern exhibited spatial correlations with distributions of several neurotransmitter receptors, such as serotonin receptor 5-HT1a, 5-HT2a, and GABA receptor GABAa (FDR-corrected $p < 0.01$). 4. A further imaging-genetic analysis revealed a gene

list involving a total of 2,385 significant genes (|Z|>3), which decodes many depression-related genes like CRY1, VAMP2, ADCY9, and PTX3. These genes further enriched pathways like synaptic signaling, ion transport and astrocytes cell type, and diseases including “mood disorders”.

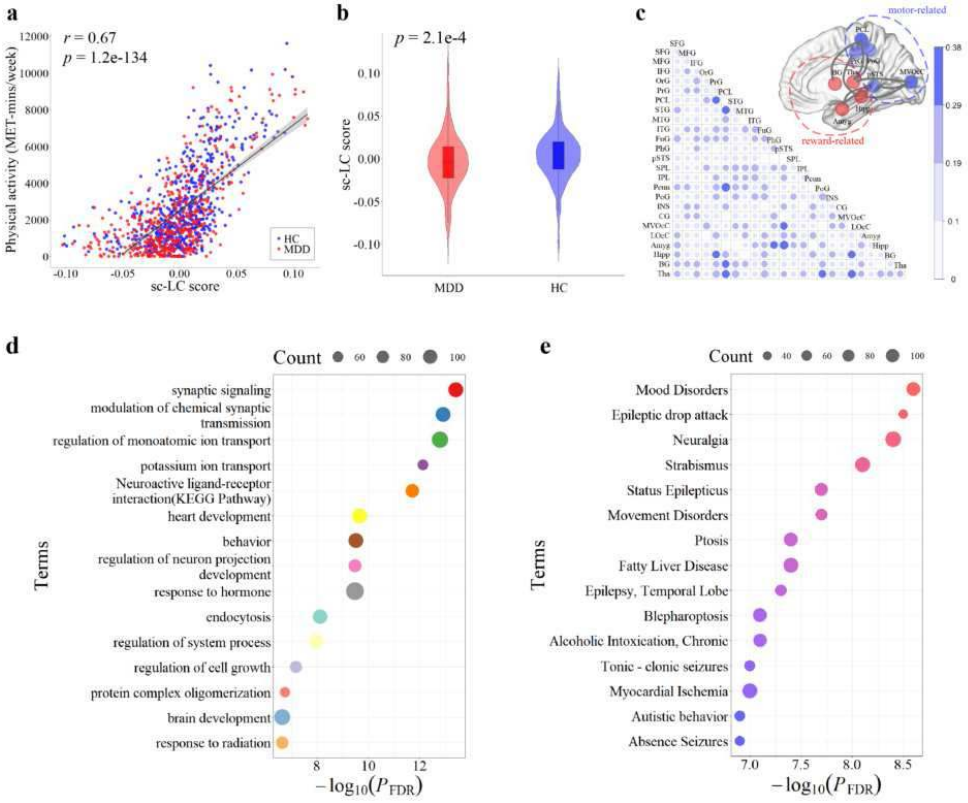

Figure 2. A linked imaging-exercise pattern and its genetic basis. a, Correlation between the sc-LC score (a weighted linear combination of 30,135 whole-brain structural connections) and physical activity (MET score) based on the MDD-1 dataset. **b,** Two-sample two-tailed t-test of sc-LC score between the MDDs and the HCs. **c,** Average contribution weights calculated based on reliable connections retained by Z scores of the sc-LC. **d,** The top 15 representative enriched terms of GO biological processes and KEGG pathway across g-LC gene list. **e,** The top 15 representative terms enriched in DisGeNET for g-LC gene list.

Conclusions: In conclusion, our findings emphasized the pivotal role of the interaction between the motor-related and reward-related networks underlying the ameliorative influence of physical activity on depressive mood. The interaction is further linked with serotonin and GABA receptors, and regulated through synaptic signaling, ion transport and astrocytes cell type. These findings engender a comprehensive comprehension of the multifaceted mechanisms behind the ameliorative effects, and concurrently furnish potential targets for therapeutic interventions of depression.

References

1. Arnatkeviciute, A. (2019), ‘A practical guide to linking brain-wide gene expression and neuroimaging data’, Neuroimage, vol. 189, no. pp. 353-367.
2. D’Angelantonio, M. (2022), ‘Physical exercise, depression, and anxiety in 2190 affective disorder subjects’, Journal of Affective Disorders, vol. 309, no. pp. 172-177.
3. Fan, L. (2016), ‘The Human Brainnetome Atlas: A New Brain Atlas Based on Connectional Architecture’, Cerebral Cortex, vol. 26, no. 8, pp. 3508-3526.
4. Luo, N. (2018), ‘A Schizophrenia-Related Genetic-Brain-Cognition Pathway Revealed in a Large Chinese Population’, EBioMedicine, vol. 37, no. pp. 471-482.
5. Markello, R. D. (2022), ‘neuromaps: structural and functional interpretation of brain maps’, Nature Methods, vol. 19, no. 11, pp. 1472-1479.
6. Miller, K. L. (2016), ‘Multimodal population brain imaging in the UK Biobank prospective epidemiological study’, Nature Neuroscience, vol. 19, no. 11, pp. 1523-1536.
7. Seidlitz, J. (2020), ‘Transcriptomic and cellular decoding of regional brain vulnerability to neurogenetic disorders’, Nature Communications, vol. 11, no. 1, pp. 3358.
8. Smith, K. (2014), ‘Mental health: a world of depression’, Nature, vol. 515, no. 7526, pp. 181.
9. Zhou, Y. (2019), ‘Metascape provides a biologist-oriented resource for the analysis of systems-level datasets’, Nature Communications, vol. 10, no. 1, pp. 1523.

Poster No 636

Altered Neural Activities to Approach-Avoidance Tendencies in Nonsuicidal Self-Injury

Seokwon Choi[1], HaYoung Kim[1], Hyeri Moon[1], HaYoung Bae[1], Jaeoh Lee[1], Yeojin Choi[1], Ji-Won Hur[1]

[1]Korea University, Seoul, Korea, Republic of

Introduction: Emotion regulation problems have been one of the core psychopathology of nonsuicidal self-injury (NSSI), the deliberate and direct damage to one's tissue without any suicidal intent. This study aimed to investigate the automatic behavioral tendencies of individuals with NSSI in response to positive and negative emotional stimuli. Approaching positive and avoiding negative stimuli are behavioral strategies that allow organisms to adapt. Moreover, given that rashly engaging in automatic behavioral tendencies might interfere with the optimal functions and social relationships of individuals, the ability to regulate the automatic reactions intentionally is considered a significant factor in mental health for individuals. To date, limited research has examined the automatic behavioral tendencies of NSSI groups in response to specific stimuli; therefore, the present fMRI study sought to investigate behavioral and neurophysiological patterns associated with approach-avoidance tendencies in individuals with NSSI.

Methods: We recruited 21 individuals with a history of NSSI within the past year and 17 sex-, age-, and handedness-matched controls. All participants completed the Approach-Avoidance Task (AAT) during fMRI scans. Participants were instructed to approach or avoid positive or negative emotional stimuli displayed in the center of the screen by pulling or pushing the joystick as quickly as possible. The AAT task consists of congruent and incongruent conditions, counterbalanced by switching between blocks. In the congruent condition, participants moved the joystick toward their own body when the positive stimuli appeared and away when fearful stimuli were presented. In the incongruent condition, participants pushed the joystick away from their body in response to positive stimuli and pulled it toward fearful stimuli. All stimuli used in the current study were drawn from the International Affective Picture System (IAPS) database and were validated in the community sample. Neuroimaging data were acquired in a 3T Siemens VIDA scanner with a 64-channel head coil. The fMRI data were preprocessed using the CONN toolbox in Statistical Parametric Mapping 12 (SPM12). Additional correlation analyses between the neural activities and clinical symptoms were performed using SPSS version 25.

Results: There were no significant differences in error rates between the NSSI and control groups. Reaction times tended to be longer in the NSSI group, but this finding did not reach statistical significance. During the presentation of negative emotional stimuli, individuals with NSSI showed increased neural activation in the left inferior temporal gyrus compared to the controls, which correlated with depression symptoms as measured by the Patient Health Questionnaire-9 (PHQ-9; $r = 0.49$, $p < .05$). In addition, for both positive and negative emotional stimuli, those with NSSI exhibited hyperactivation in the right fusiform gyrus, left and right superior parietal gyrus, and right postcentral cortex in the congruent condition. Individuals with NSSI also showed enhanced activation in the bilateral medial frontal gyrus, left superior anterior cingulate cortex, and left insula in the incongruent condition. Furthermore, impulsive behavior as measured by the UPPS-P Impulsive Behavior Scale was negatively correlated in both the right fusiform gyrus ($r = -0.482$, $p < .05$) and left superior anterior cingulate cortex($r = -0.491$, $p < .05$) within the NSSI group.

Conclusions: We found the brain regions involved in emotion processing individuals with NSSI were overrecruited during the deliberate regulation of automatic responses to emotional stimuli. Our findings provide the first neural evidence for the possibility that automatic behavioral tendencies play a key role in the mechanisms of emotion dysregulation in individuals with NSSI.

References

1. Bresin, K. (2020). Toward a unifying theory of dysregulated behaviors. Clinical psychology review, 80, 101885.
2. Lee, S. E., Yim, M., & Hur, J. W. (2022). Beneath the surface: clinical and psychosocial correlates of posting nonsuicidal self-injury content online among female young adults. Computers in Human Behavior, 132, 107262.
3. Nock, M. K., & Favazza, A. R. (2009). Nonsuicidal self-injury: Definition and classification
4. Paschke, L. M., Dörfel, D., Steimke, R., Trempler, I., Magrabi, A., Ludwig, V. U., ... & Walter, H. (2016). Individual differences in self-reported self-control predict successful emotion regulation. Social cognitive and affective neuroscience, 11(8), 1193-1204.
5. Plener, P. L., Bubalo, N., Fladung, A. K., Ludolph, A. G., & Lulé, D. (2012). Prone to excitement: Adolescent females with non-suicidal self-injury (NSSI) show altered cortical pattern to emotional and NSS-related material. Psychiatry Research: Neuroimaging, 203(2-3), 146-152.
6. Struijs, S. Y., Lamers, F., Vroling, M. S., Roelofs, K., Spinhoven, P., & Penninx, B. W. (2017). Approach and avoidance tendencies in depression and anxiety disorders. Psychiatry research, 256, 475-481.
7. Tatnell, R., Tatnell, R., & Hasking, P. A. (2015). Emotion regulation, the anterior cingulate cortex and non-suicidal self-injury. Culture and Cognition: A Collection of Critical Essays. Bern: Peter Lang, 163-78.
8. Hofmann, W., Friese, M., & Strack, F. (2009). Impulse and self-control from a dual-systems perspective. Perspectives on psychological science, 4(2), 162-176.

Poster No 637

Structural covariance networks in adolescents at familial high risk for schizophrenia or bipolar

Anna Plachti[1,2,3], William Baare[1], Enedino Hernandez-Torres[1], Kit Larsen[1], Anne Elgaard Thorup[4,5,6], Merete Nordentoft[4,5], Hartwig Siebner[1,7,8], Kathrine Skak Madsen[1]

[1]Danish Research Centre for Magnetic Resonance (DRCMR), Copenhagen, Denmark, [2]. Institute of Neuroscience and Medicine (INM-7), Research Centre Jülich, Jülich, Germany, [3]Institute of Systems Neuroscience, Medical Faculty and University Hospital Düsseldorf, Heinrich-Hein, Düsseldorf, Germany, [4]Faculty of Health and Medical Sciences, University of Copenhagen, Copenhagen, Denmark, Copenhagen, Denmark, [5]The Lundbeck Foundation Initiative for Integrative Psychiatry Research (iPSYCH), Aarhus, Denmark, [6]Mental Health Services in the Capital Region of Denmark, Child and Adolescent Mental Health Center, Copenhagen, Denmark, [7]Department of Neurology, Copenhagen University Hospital Bispebjerg and Frederiksberg, Copenhagen, Denmark, [8]Department of Clinical Medicine, Faculty of Health and Medical Sciences, University of Copenhagen, Copenhagen, Denmark

Introduction: Offspring of parents with schizophrenia (SCZ) or bipolar disorder (BD) have an increased risk of developing a psychiatric disorder themselves. Structural covariance (SC) patterns, i.e., patterns of morphological covariation across brain regions, is a valuable tool to examine neurodevelopmental structural abnormalities. In this cross-sectional study, we investigated whether SC networks of 12-year-old adolescents from the Danish High Risk and Resilience Study - VIA11, at familial high risk for SCZ (FHR-SCZ) or BD (FHR-BD), differed from population-based controls (PBC) or were reminiscent of disease-related atrophy maps from the ENIGMA consortium.

Methods: We investigated 278 adolescents (age mean=12.11, SD=0.28, N=140 females) at FHR-SCZ (N=101) or FHR-BD (N=64) and PBC (N=113), scanned at two sites. T1-weighted MRI images were parcellated using the Desikan atlas (Freesurfer 7.1). We regressed out age, sex, age-by-sex, ICV, handedness, and total Euler number from every brain parcel using a generalized additive model. Bootstrapping and distance correlation provided the most reliable and consistent whole-brain Pearson's residuals-based SC networks, for cortical thickness, surface area, and volume calculated for each group. Correlation coefficients were Fischer's r-to-z transformed. Network-Based Statistics (family-wise error rate $p < 0.001$), tested for potential differences in SC networks between groups. To get a better understanding of whether FHR groups already displayed anatomical topographic features of SCZ or BD, we further performed hub centrality analyses (difference between the sum of all weighted cortico-cortical covariations of the risk group minus controls) and epicenter mapping using the ENIGMA toolbox and atrophy maps (spatial spin permutation tests 10 000 iterations, $p < 0.05$). Findings were only reported if they were significant and convergent across both sites.

Results: The group of FHR-SCZ showed reduced and increased SC networks between frontal (left caudal middle frontal and lateral orbitofrontal), parietal (left inferior parietal, left precuneus) and temporal (left transverse temporal, left fusiform) cortical regions (Fig.1). The FHR-BD group showed a related deviating SC network with reduced covariation between frontal (right caudal middle frontal), parietal (left inferior parietal), temporal (left banks of the superior temporal sulcus, left fusiform), and occipital (right lateral occipital gyrus) cortices, and less prominent increased covariations (Fig.1). The hub centrality map of the FHR-SCZ group correlated significantly with BD-adults' thickness atrophy map ($r = 0.44$, $p < 0.001$, $p_{corr} = 0.015$) indicating similarity at the macro level. Potential epicenters in the group of FHR-SCZ adolescents were found for medial (thickness: $r = -.34$, $p < 0.05$) and lateral orbitofrontal cortex (thickness: $r=-.14$, surface area: $r=-.14$ $p < 0.05$) when comparing to BD adolescents' and adults' atrophy maps of thickness and surface area.

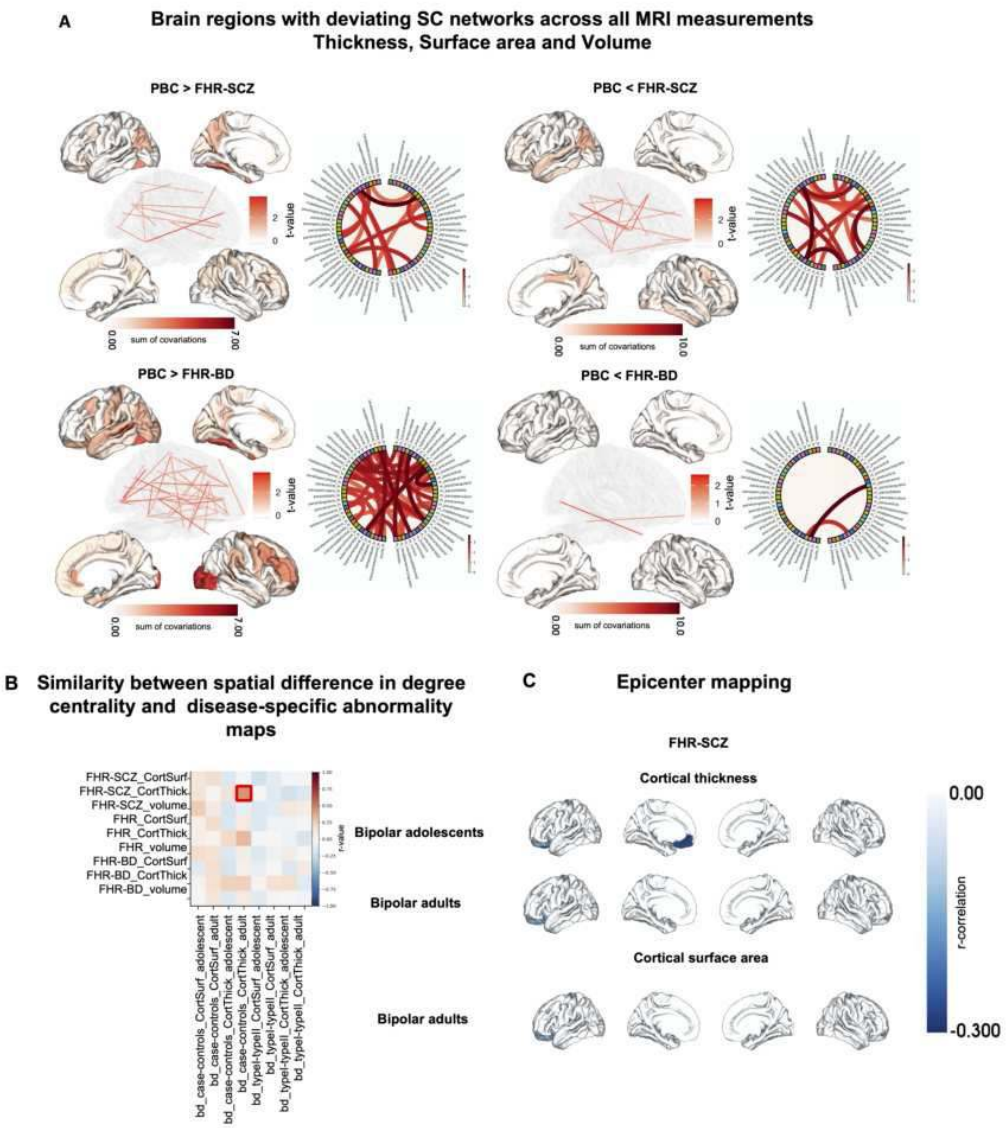

Conclusions: The differences in SC networks of FHR adolescents compared to PBC, suggested the involvement of multiple networks, including those related to executive control, socioemotional salience, default mode, and auditory-visual processing. Reduced SC networks in FHR-SCZ may indicate difficulties in multisensory integration such as visual and auditory processing and visuomotor integration (Teixeira et al., 2014). FHR-BD displayed reduced SC for posterior brain regions potentially related to social cognition (Adolphs, 2003; Hein & Knight, 2008). The caudal middle and orbitofrontal cortices, involved in mood, emotion, reward and decision-making, stood out across the analyses. Interestingly, dysfunction of these regions has been related to e.g. SCZ, depression, BD and obsessive-compulsive disorder (McTeague et al., 2020; Rolls et al., 2020). Longitudinal follow-up of the VIA participants will allow us to establish the developmental nature of observed differences that are predictive of future disease expression.

References

1. Adolphs, R. (2003, 2003/03/01). Cognitive neuroscience of human social behaviour. Nature Reviews Neuroscience, 4(3), 165-178. https://doi.org/10.1038/nrn1056
2. Hein, G., & Knight, R. T. (2008, Dec). Superior temporal sulcus--It's my area: or is it? J Cogn Neurosci, 20(12), 2125-2136. https://doi.org/10.1162/jocn.2008.20148
3. McTeague, L. M., Rosenberg, B. M., Lopez, J. W., Carreon, D. M., Huemer, J., Jiang, Y., Chick, C. F., Eickhoff, S. B., & Etkin, A. (2020, May 1). Identification of Common Neural Circuit Disruptions in Emotional Processing Across Psychiatric Disorders. Am J Psychiatry, 177(5), 411-421. https://doi.org/10.1176/appi.ajp.2019.18111271
4. Rolls, E. T., Cheng, W., & Feng, J. (2020). The orbitofrontal cortex: reward, emotion and depression. Brain Communications, 2(2). https://doi.org/10.1093/braincomms/fcaa196
5. Teixeira, S., Machado, S., Velasques, B., Sanfim, A., Minc, D., Peressutti, C., Bittencourt, J., Budde, H., Cagy, M., Anghinah, R., Basile, L. F., Piedade, R., Ribeiro, P., Diniz, C., Cartier, C., Gongora, M., Silva, F., Manaia, F., & Silva, J. G. (2014). Integrative parietal cortex processes: Neurological and psychiatric aspects. Journal of the Neurological Sciences, 338(1), 12-22. https://doi.org/10.1016/j.jns.2013.12.025

Poster No 638

Aberrant local brain oscillations in the clinical high risk for psychosis – a TMS-EEG study

Nadja Zimmermann[1,2,3], Miriam Stüble[1,3], Arndt-Lukas Klaassen[1], Chantal Michel[1], Michael Kaess[1,4], Jochen Kindler[1], Yosuke Morishima[2]

[1]University Hospital of Child and Adolescent Psychiatry and Psychotherapy, University of Bern, Bern, Switzerland, [2]Translational Research Center, University Hospital of Psychiatry, University of Bern, Bern, Switzerland, [3]Graduate School for Health Sciences, University of Bern, Bern, Switzerland, [4]Department of Child and Adolescent Psychiatry, Center for Psychosocial Medicine, University Hospital Heidelberg, Heidelberg, Germany

Introduction: A clinical high-risk (CHR) state for psychosis describes a possibly prepsychotic state, marked by prodromal symptoms such as impairment of cognition, affect, and social behaviour (Fusar-Poli, 2013). Such a state usually precedes the onset of Schizophrenia and other psychotic disorders by several years, but only a fraction of patients classified as CHR convert to a first episode psychosis (De Pablo, 2021). Dysconnection of brain networks has been recognized to lie at the base of psychotic disorders, causing a failure of functional integration on a synaptic level as well as in long-range connectivity. This could be a possible cause for psychotic symptoms as well as cognitive deficits observed in psychotic disorders (Stephan, 2009). Dysconnectivity in psychotic spectrum disorders has been predominantly observed in prefrontal areas, which is already evident in the CHR state (Pettersson-Yeo, 2011) but possibly to a lesser degree (Crossley, 2009). The concurrent use of transcranial magnetic stimulation (TMS) and electroencephalography (EEG) provides opportunities to measure the temporal order of activations of connected cortical areas and their causal interactions in regards to excitatory or inhibitory functioning (Hallett, 2017). While there is evidence of abnormal signal propagation (Frantseva, 2014) and abnormal synchronized neural oscillations (Ferrarelli, 2008) in schizophrenic patients measured by TMS-EEG, there is a lack of studies investigating these parameters in a CHR population. Therefore, in the current study, we utilized TMS-EEG to study abnormal neural oscillations in CHR.

Methods: Patients and healthy controls (HC) completed a psychopathological and neuropsychological assessment as well as an MRI and TMS-EEG session. In the individual structural MRIs, the left dorsolateral prefrontal cortex (lDLPFC) and left posterior parietal cortex (lPPC) were marked and subsequently used with a neuronavigational device to mark stimulation target sites on the EEG cap. At each site, single-pulse TMS was applied at both sub- and suprathreshold intensities of the individual motor threshold and TMS-evoked activity was measured simultaneously with a 64 channel EEG. The acquired EEG data was pre-processed in MATLAB, using the EEGLAB and tmseeg toolbox and subsequently analysed with custom scripts. Time-frequency information was extracted by performing Morlet-Wavelet convolution.

Results: The preliminary analyses of TMS-evoked spectral activity included 29 patients and 29 HC. For the HC group, lDLPFC TMS evoked gamma and beta activities at the site of stimulation and theta activity in a more central area. While the general spatiotemporal pattern of TMS-evoked spectral activity of the patient group looked similar to the HC, activity in all frequency bands was reduced compared to the HC. When stimulating the lPPC, the HC group showed a similar pattern to lDLPFC TMS evoked activity, but evoked theta activity was significantly lower when compared to lDLPFC stimulation. For patients, the asymmetry of theta activity was not present.

Conclusions: In the current study, we found an asymmetry in TMS-evoked theta activity between lDLPFC and lPPC, consistent with the typical anatomical asymmetry observed between feedforward and feedback networks (Chen, 2009). In contrast, this asymmetry was not present in the patient group. Theta-band oscillatory activity plays a key role in long-range communication between brain networks (Von Stein, 2000) suggesting that TMS-induced theta activity could represent feed-forward and feed-backward propagation. Our results suggest that patients with CHR have an impairment of the backpropagation of long-range transmission within brain networks.

References

1. Chen, C.C. (2009). 'Forward and backward connections in the brain: a DCM study of functional asymmetries', Neuroimage, vol. 45, no. 2, pp. 453-462.
2. Crossley, N.A. (2009). 'Superior temporal lobe dysfunction and frontotemporal dysconnectivity in subjects at risk of psychosis and in first-episode psychosis', Human brain mapping, vol. 30, no. 12, pp. 4129-4137.
3. De Pablo, G.S. (2021). 'Probability of transition to psychosis in individuals at clinical high risk: an updated meta-analysis', JAMA psychiatry, vol. 78, no. 9, pp. 970-978.
4. Ferrarelli, F. (2008). 'Reduced evoked gamma oscillations in the frontal cortex in schizophrenia patients: a TMS/EEG study', American Journal of Psychiatry, vol. 165, no. 8, pp. 996-1005.
5. Frantseva, M. (2014). 'Disrupted cortical conductivity in schizophrenia: TMS–EEG study', Cerebral Cortex, vol. 24, no. 1, pp. 211-221.
6. Fusar-Poli, P. (2013). 'The psychosis high-risk state: a comprehensive state-of-the-art review', JAMA psychiatry, vol. 70, no. 1, pp.107-120.
7. Hallett, M. (2017). 'Contribution of transcranial magnetic stimulation to assessment of brain connectivity and networks', Clinical Neurophysiology, vol. 128, no. 11, pp. 2125-2139.

8. Pettersson-Yeo, W. (2011). 'Dysconnectivity in schizophrenia: where are we now?', Neuroscience & Biobehavioral Reviews, vol. 35, no. 5, pp. 1110-1124.
9. Stephan, K.E. (2009). 'Dysconnection in schizophrenia: from abnormal synaptic plasticity to failures of self-monitoring', Schizophrenia bulletin, vol. 35, no. 3, pp. 509-527.
10. Von Stein, A. (2000). 'Different frequencies for different scales of cortical integration: from local gamma to long range alpha/theta synchronization', International journal of psychophysiology, vol. 38, no. 3, pp. 301-313.

Poster No 639

Temporal Pole, 'Impending Understanding' Aspect of Aberrant Salience, and Delusion

Jun Miyata[1], Yukako Nakagami[2], Shuraku Son[2], Yujiro Yoshihara[2], Toshiya Murai[2], Hidehiko Takahashi[3]

[1]Aichi Mecical University, Nagoya, Aichi, [2]Kyoto University, Kyoto, Kyoto, [3]Tokyo Medical and Dental University, Tokyo, Tokyo

Introduction: The aberrant salience hypothesis (Kapur, 2003) is a dominant pathophysiological hypothesis of schizophrenia, which postulates that a hyper-dopaminergic state in the midbrain-striatum causes heightened attribution of salience to ordinary stimuli, leading to the formation of delusion and hallucination. However, the exact neurobiological mechanisms of aberrant salience and delusion are unclear. Using resting-state functional magnetic resonance imaging (MRI) and the Aberrant Salience Inventory (ASI, Cicero et al., 2010), our previous study revealed region-specific functional connectivity between abnormal salience and the brain (manuscript in preparation by Nakagami et al.). In this study, we investigated the structural connectivity between gray matter and aberrant salience and its relevance to delusion severity.

Methods: We recruited 41 patients with schizophrenia and 67 healthy controls. We measured the intensity of subjective aberrant salience experience by using ASI, which consists of 29 items, and calculated scores of five subscales (increased significance, senses sharpening, impending understanding, heightened emotionality, and heightened cognition). We also rated delusional ideation from normal to pathological level by using the Peters et al Delusions Inventory-21 (Peters et al, 2004), and calculated the total score. T1-weighted MRI imaging data were acquired on a 3T scanner and were processed using a voxel-based morphometry pipeline, including segmentation, standardization, nonlinear-only Jacobian correction, and smoothing. Independent component analysis was applied to the resulting gray matter segment images, identifying 10 structural covariance networks (SCN) and calculating each subject's loading on these networks. Using these loadings as dependent variables, we performed multiple regression analyses with diagnosis, age, gender, and five subscales of ASI as explanatory variables, testing 1) the interaction between diagnosis and ASI and 2) the main effect of ASI. The significance level was set at $p < 0.05$ (FWE-corrected for network number, contrast number, and subscale number). When we found significant results we then explored their correlation with the PDI total score. This study received approval from the Kyoto University Medical Ethics Committee, and participants provided written and verbal consent after receiving an explanation of the research.

Results: We observed a significant interaction between diagnosis and the "Impending Understanding" subscale of ASI for an SCN involving bilateral temporal poles, amygdala, and hippocampus ($p < 0.018$, FWE). Post-hoc analysis revealed a negative slope in healthy controls and a positive slope in patients. This subscale was associated with the PDI total score for the whole sample ($r = 0.495$, $p < 0.001$) and for healthy people ($r = 0.586$, $p < 0.001$), but not for patients ($r = 0.241$, $p = 0.145$).

Conclusions: The association between the "Impending Understanding" subscale, which reflects a sense of profound meaning in familiar things, and the temporal pole, a neural correlate of semantic representation, supports the region-specificity of abnormal salience experiences. This association may also indicate the importance of aberrant salience for delusion formation.

References

1. Cicero DC et al. The Aberrant Salience Inventory: A new measure of psychosis proneness. Psychological Assessment. 2010;22(3):688–701
2. Kapur S. Psychosis as a State of Aberrant Salience: A Framework Linking Biology, Phenomenology, and Pharmacology in Schizophrenia. Am J Psychiatry. 2003;160(1):13–23.
3. Hafkemeijer A et al. Associations between age and gray matter volume in anatomical brain networks in middle-aged to older adults. Aging Cell. 2014;13(6):1068–74.
4. Peters E et al, Measuring Delusional Ideation: The 21-Item Peters et al. Delusions Inventory (PDI). Schizophr Bull,2004,30,1005-1022.

Poster No 640

Mindful-state Connectivity of Anterior Cingulate Cortex

Annika Rosenthal[1], Lorenz Mathewson[2], Michael Marxen[3], Nina Romanczuk Seiferth[4], Anne Beck[2]

[1]Charité - Universitätsmedizin, Berlin, Berlin, [2]Health and Medical University Potsdam, Potsdam, Brandenburg, [3]Technische Universität Dresden, Dresden, Saxony, [4]Medical School Berlin, Berlin, Berlin

Introduction: Mindfulness-based interventions (MBIs) have shown efficacy in the treatment of various psychiatric disorders such as alcohol use disorder (AUD) (Li et al., 2017). Among others, this efficacy has been shown to be linked to alterations in functional connectivity of the anterior cingulate cortex (ACC) (Sezer et al., 2022). We therefore aimed at investigating the impact of a brief mindfulness intervention on this region's functional connectivity and to compare healthy controls with mildly to moderately affected patients with AUD.

Methods: Participants with AUD (n=24) as well as healthy controls (n=18) were examined with functional magnetic resonance imaging (fMRI). Via an active noise canceling headphone system, participants were instructed to follow a guided mindfulness practice or listen to an audio of nature sounds. Data was analysed using the Matlab-based CONN toolbox. Seed-based connectivity maps and ROI-to-ROI connectivity matrices were generated to analyse the functional connectivity patterns of the anterior cingulate cortex (ACC) with 164 network and Harvard-Oxford atlas regions. Second level analysis investigated the effect of group (AUD versus healthy controls), condition (mindfulness versus nature sounds) and their interaction on these connectivity patterns.

Results: We found no functional connectivity differences between AUD and healthy controls. However, seed-based analysis showed increased functional connectivity of the ACC with clusters comprised of executive brain regions including bilateral superior frontal gyrus (0.009 p-FDR), bilateral frontal pole (right 0.02 p-FDR, left 0.03 p-FDR) and right middle frontal gyrus (0.009 p-FDR) during mindfulness practice compared to the nature sounds condition (see figure 1). We found no interaction effect of group and condition on functional connectivity strength.

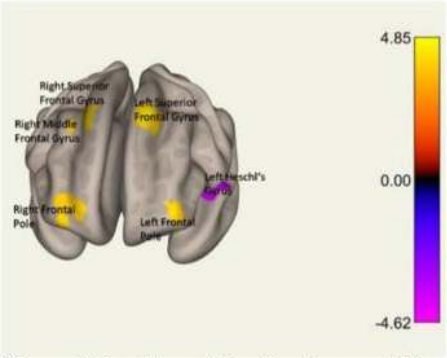

Figure 1 *Seed-based functional connectivity of the ACC comparing Mindfulness Practice>Nature Sounds conditions. During the mindfulness practice, subjects show an increased ACC functional connectivity to brain regions implicated in cognitive control. In addition, comparatively decreased functional connectivity between ACC and left Heschl's gyrus was found.*

Conclusions: Although no group or interaction effects were observed, the ACC displayed enhanced connectivity with a network implicated in cognitive control function. These findings align with studies demonstrating increased prefrontal control network activation due to MBIs (Tang et al., 2015). Despite potential limitations, such as a small sample size, our results suggest that mindfulness practice may enhance cognitive control function by increasing ACC – prefrontal cortex network connectivity, providing insights into the mechanism of MBIs in treating AUD.

References

1. Li, W., Howard, M. O., Garland, E. L., McGovern, P., & Lazar, M. (2017). Mindfulness treatment for substance misuse: A systematic review and meta-analysis. Journal of substance abuse treatment, 75, 62-96.
2. Sezer, I., Pizzagalli, D. A., & Sacchet, M. D. (2022). Resting-state fMRI functional connectivity and mindfulness in clinical and non-clinical contexts: A review and synthesis. Neuroscience and biobehavioral reviews, 135, 104583.
3. Tang, Y. Y., Hölzel, B. K., & Posner, M. I. (2015). The neuroscience of mindfulness meditation. Nature reviews neuroscience, 16(4), 213-225.

Poster No 641

Longitudinal associations between depression symptoms and brain structure in youth

Eira Aksnes[1], Dani Beck[2], Niamh MacSweeney[3], Marieke Bos[4], Lia Ferschmann[1], Linn Norbom[1], Valerie Karl[1], Lars Westlye[5], Christian Tamnes[1]

[1]University of Oslo, Oslo, Norway, [2]Diakonhjemmet Hospital, Oslo, Oslo, [3]University of Oslo/Diakonhjemmet Hospital, Oslo, Oslo, [4]Leiden University, Leiden, Netherlands, [5]Norwegian Centre for Mental Disorders Research (NORMENT), Oslo University Hospital, Oslo, Norway

Introduction: Emotional disorders have become the largest disease burden in adolescence during the last 10 years, especially in girls[1]. Adolescent-onset Major Depressive Disorder (MDD) is associated with a host of psychiatric and somatic comorbidities. Structural magnetic resonance imaging (sMRI) studies have sought to understand the neurobiological underpinnings of MDD, but findings have been inconsistent[2]. Compared to case-control studies of MDD, symptom-based investigations can capture the heterogenous nature of MDD[3]. Previous studies have reported associations between specific MDD symptoms and distinct brain structural features in adults[4,5]. However, this research is limited by cross-sectional designs, small sample sizes and few studies to date have focused on adolescent samples[5]. To this end, we investigate the association between dimensional aspects of depressive symptomatology and regional cortical thickness (CT) and hippocampal (HC) volume in youth using a large longitudinal sample. Based on previous work, we hypothesized that lower CT in the insula, medial orbitofrontal cortex (mOFC), cingulate (CI), fusiform gyrus (FG), and HC would be associated with specific symptoms of depression, and that these effects would exacerbate over time.

Methods: We used longitudinal symptom and sMRI data from the Adolescent Brain Cognitive Development (ABCD) Study. Data was extracted from three timepoints. Due to limited data availability, we used a subset of the ABCD youths who had data at the third wave, in addition to the first and/or second wave. Our final sample included 2892 children and adolescents (53 % male, mean age=12.11, SD=1.82). To match core MDD symptoms in DSM-5, we chose four items (sad, interest loss, worthless and low energy) derived from the parent-reported Child Behavioral Checklist (CBCL). Building on previous studies on MDD case-control differences4,5, we based our a priori MRI metrics and regions of interest on brain associations showing the largest bilateral effects6,7: CT in the CI, insula, mOFC, and FG, as well as HC volume. We harmonized imaging data across scanners using the long.combat R package, averaged left and right hemispheres, and residualized HC volume by intracranial volume. To test for associations between specific depressive symptoms and select brain measures, we estimated a panel graphical vector-autoregression network model using the psychonetrics package. This model estimates both between-person and within-person (contemporaneous and temporal) dynamics over time. Bootstrapping was applied to check for network stability. An Individual Network Invariance Test (INIT) was estimated to investigate potential differences between male and female networks.

Results: Both the saturated and pruned models showed good fit (TLI=.94/.96, CFI=.96, RMSEA=.042/.036). In the temporal network, we found positive associations between HC and CI in the brain domain, with auto-regressions for the HC, mOFC and insula. For symptoms, worthless was associated with sad, sad was associated with interest loss, and interest loss and low energy predicted each other over time. Auto-regressions were present for all symptoms except feeling worthless. The contemporaneous network showed associations between all symptoms, and all brain regions were associated apart from the HC. The between-persons network showed positive associations between low energy and sad, sad and worthless, and positive associations between all cortical areas, as well as the insula and HC. There was a negative association between HC and mOFC. Lastly there were no associations between brain-symptom domains in any of the three networks (Figure 1). The INIT did not identify significant sex differences.

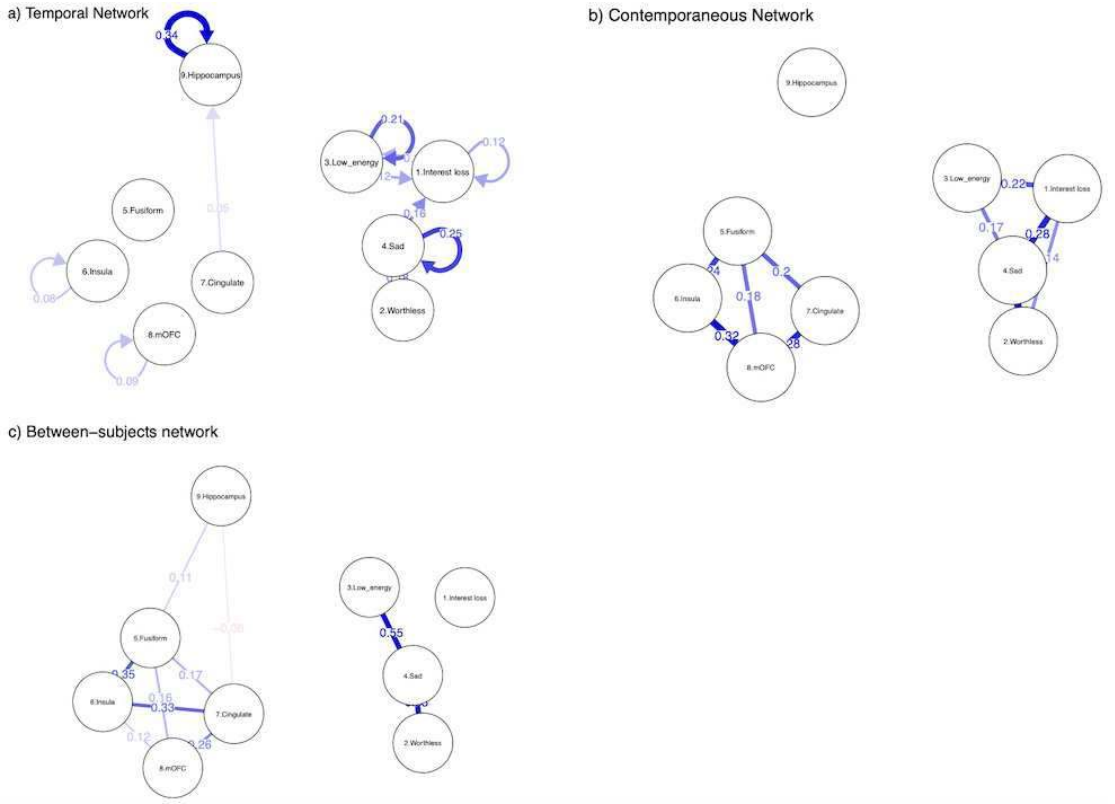

Figure 1: Within-person temporal and contemporaneous brain-symptoms networks based on panel GVAR model. Note: The temporal associations (panel A) represent directed partial correlations.

Conclusions: In the first three wave large-scale longitudinal study investigating brain-symptom relations in youth, we found no significant associations between select brain regions and depression symptoms. Further analysis will use self-report measures, which may be a preferred measure for depressive symptoms.

References

1. Thapar, A., Eyre, O., Patel, V. & Brent, D. Depression in young people. The Lancet 400, 617–631 (2022).
2. Toenders, Y. J. et al. Neuroimaging predictors of onset and course of depression in childhood and adolescence: A systematic review of longitudinal studies. Dev. Cogn. Neurosci. 39, 100700 (2019).
3. Fried, E. I., Flake, J. K. & Robinaugh, D. J. Revisiting the theoretical and methodological foundations of depression measurement. Nat. Rev. Psychol. 1, 358–368 (2022).
4. Hilland, E. et al. Exploring the links between specific depression symptoms and brain structure: A network study. Psychiatry Clin. Neurosci. 74, 220–221 (2020).
5. Freichel, R. et al. Unravelling Robust Brain-Behavior Links of Depressive Symptoms Through Granular Network Models: Understanding Heterogeneity and Clinical Implications. http://medrxiv.org/lookup/doi/10.1101/2023.09.13.23295278 (2023) doi:10.1101/2023.09.13.23295278.
6. Schmaal, L. et al. Subcortical brain alterations in major depressive disorder: findings from the ENIGMA Major Depressive Disorder working group. Mol. Psychiatry 21, 806–812 (2016).
7. Schmaal, L. et al. Cortical abnormalities in adults and adolescents with major depression based on brain scans from 20 cohorts worldwide in the ENIGMA Major Depressive Disorder Working Group. Mol. Psychiatry 22, 900–909 (2017).

Poster No 642

Functional Connectivity Differences in Nonsuicidal Self-injury with and without Depression

Hyeri Moon[1], Jinhee Kim[1], Ji-Won Hur[1]

[1]Korea University, Seoul, Korea, Republic of

Introduction: Nonsuicidal self-injury (NSSI), which refers to intentional and direct physical self-harm without any suicidal intent, is highly comorbid with affective disorders, most notably major depressive disorder (MDD) (Kiekens et al., 2018a; 2018b). Due to the complex intertwining of these two clinical conditions, there has been an ongoing effort to identify neurobiological features of NSSI that may distinguish it from MDD. However, to date, only a limited number of neuroimaging studies have examined MDD and NSSI together (Huang et al., 2021; Kang et al., 2022), and furthermore, only studies have focused on

NSSI behaviors in individuals with MDD. More research is needed on the neurological characteristics of individuals engaging in NSSI with and without MDD. Here, we used resting-state functional magnetic resonance imaging to examine intrinsic neuronal differences between NSSI with and without MDD and how they contribute to the clinical characteristics of these two populations.

Methods: A total of 91 individuals with NSSI (36 with MDD, 55 without MDD) and 84 controls underwent a 6-min resting-state fMRI scanning (Siemens 3T Trio Scanner from two sites) and completed the 36-item Difficulties in Emotion Regulation Scale (DERS) to assess emotion dysregulation. Image preprocessing was performed using the CONN's default pipeline, which includes motion correction, slice timing correction, EPI normalization to EPI template, and spatial smoothing with a 6mm^3 Gaussian kernel. With the preprocessed rs-fMRI data, 27 resting-state independent components were obtained using group spatial independent component analysis (Allen et al., 2011), as implemented in the GIFT toolbox (Calhoun, 2004). The identified independent components were categorized into sub-cortical network, visual network (VN), auditory network, somatosensory network (SMN), default mode network (DMN), cognitive-executive networks (CN). The functional connectivity (FC) matrices were calculated as the Fisher z-transformed temporal correlations between independent components and were then entered into an ANCOVA, accounting for group factor and DERS scores as covariates, with gender, age, and handedness included as nuisance covariates.

Results: The NSSI with MDD group, compared to the NSSI without MDD group, showed decreased CN functional connectivity between the frontal pole and supplementary motor cortex. Importantly, significant interactions between the NSSI group and DERS interactions were observed. The NSSI with MDD group had higher FC between the bilateral precentral gyrus (SMN) - ventromedial prefrontal cortex (DMN) and the medial temporal lobe (VN) - ventrolateral prefrontal cortex (CN) was positively correlated with emotion dysregulation. In contrast, the NSSI without MDD group showed a negative correlation between the FCs between these regions and emotion dysregulation. In addition, within the NSSI with MDD group, the decreased FC between the precentral gyrus (SMN) - bilateral fusiform gyrus (VN), the bilateral intracalcarine cortex (VN) - bilateral fusiform gyrus (VN), and the medial temporal lobe (VN) - precuneus (DMN), and the increased FC between these regions within the NSSI with MDD group were each related with emotional dysregulation.

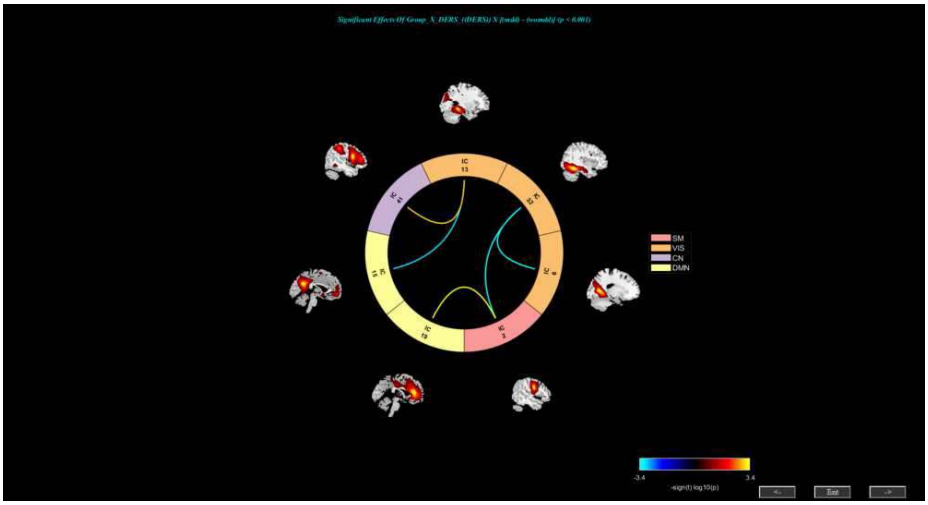

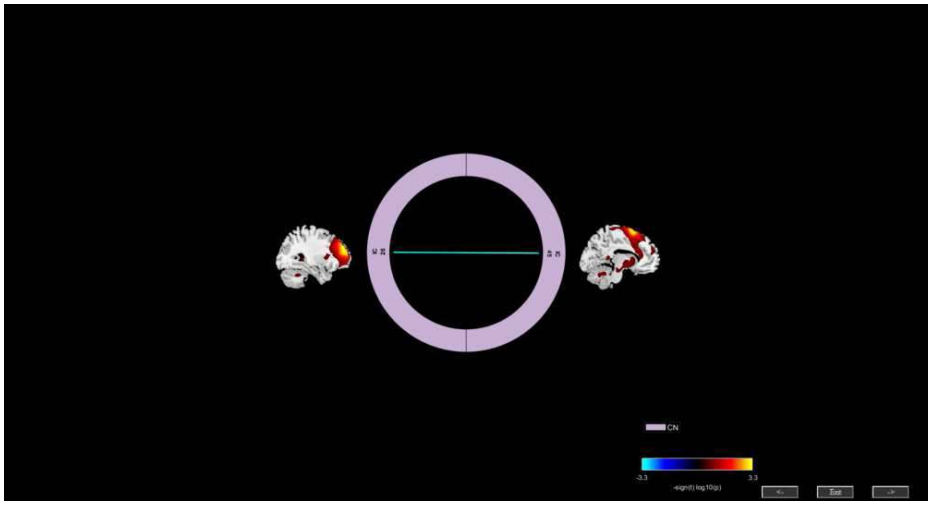

Conclusions: We found that the NSSI with MDD group showed differential resting-state functional connectivity compared to the NSSI without MDD group. These neurobiological distinctions differentiate NSSI subgroups, highlighting the need for targeted clinical interventions and personalized treatment.

References

1. Allen, E. A., Erhardt, E. B., Damaraju, E., Gruner, W., Segall, J. M., Silva, R. F., Havlicek, M., Rachakonda, S., Fries, J., & Kalyanam, R. (2011), 'A baseline for the multivariate comparison of resting-state networks', Frontiers in Systems Neuroscience, vol. 5, no. 2. http://www.ncbi.nlm.nih.gov/pmc/articles/PMC3051178/pdf/fnsys-05-00002.pdf
2. Calhoun, V. D. (2004), 'Group ICA of fMRI toolbox (GIFT)', Online at http://icatb.sourceforge.net.
3. Huang, Q., Xiao, M., Ai, M., Chen, J., Wang, W., Hu, L., ... & Kuang, L. (2021), 'Disruption of neural activity and functional connectivity in adolescents with major depressive disorder who engage in non-suicidal self-injury: a resting-state fMRI study', Frontiers in psychiatry, vol. 12, no. 571532.
4. Kang, L., Wang, W., Zhang, N., Nie, Z., Gong, Q., Yao, L., ... & Liu, Z. (2022), 'Superior temporal gyrus and cerebellar loops predict nonsuicidal self-injury in major depressive disorder patients by multimodal neuroimaging', Translational psychiatry, vol. 12(1), no. 474.
5. Kiekens, G., Hasking, P., Boyes, M., Claes, L., Mortier, P., Auerbach, R. P., ... & Bruffaerts, R. (2018a), 'The associations between non-suicidal self-injury and first onset suicidal thoughts and behaviors', Journal of affective disorders, vol. 239, pp. 171-179.
6. Kiekens, G., Hasking, P., Claes, L., Mortier, P., Auerbach, R. P., Boyes, M., ... & Bruffaerts, R. (2018b), 'The DSM-5 nonsuicidal self-injury disorder among incoming college students: Prevalence and associations with 12-month mental disorders and suicidal thoughts and behaviors', Depression and anxiety, vol. 35, no.7, pp. 629-637.

Poster No 644

Exploring the Role of vmPFC in Smoking Behavior: A Functional Connectivity Analysis

Chen Zheng[1], Tianye Jia[1]

[1]Fudan University, Shanghai, China

Introduction: Nicotine addiction is a major public health concern, significantly contributing to global mortality and economic impacts. Our recent study demonstrated that reduction in gray matter volume (GMV) in the left ventromedial prefrontal cortex (vmPFC) may causally influence rule-breaking behavior, leading to smoking initiation, while changes in the right vmPFC's GMV may modulate the hedonic effects of substance use, reinforcing and maintaining future use[1]. The current work delves into the functional mechanisms of the vmPFC in smoking behavior.

Methods: Data of Caucasian adults (age 24, n=1023) from the IMAGEN project were employed[2]. Smoking behavior was measured by the ESPAD survey. Participants with scores greater than 0 for item 'occasions of lifetime smoking' were considered smokers.The monetary incentive delay (MID) task was adopted[3], from which the big win vs. no win contrast were used for functional connectivity (FC) analysis using the CONN toolbox[4]. Hierarchical clustering were conducted with Ward's method to identify subregions in vmPFC among all participants. Two sample t-test were conducted to investigate the regions with different FC between smokers and non-smokers.

Results: Analysis of voxel-to-voxel FC within smoking-related areas identified by changes of GMV (Fig.1a-b) suggested the existence of subregions. Employing hierarchical clustering, we delineated 5 subregions (Fig. 1d) arranged from left to right as L1, R1, R2, L2, and R3 in the dendrogram (Fig.1c). L1 exhibited widespread negative FC, while L2 and R3 showed similar, vmPFC-focused patterns. Our findings highlight a significant inverse relationship between inter-hemispheric FC and the subjects' smoking history. Specifically, the analysis revealed the duration of daily smoking was inversely correlated with FC: between L1 and R1 ($r=-0.15$, $p=0.018$, Fig.1e), and between L2 and R3 ($r=-0.18$, $p=0.005$, Fig.1f). And the duration of smoking correlated negatively with FC: between L2 and R2 ($r=-0.09$, $p=0.036$, Fig.1g) and L2 and R3 ($r=-0.08$, $p=0.049$, Fig.1h). Within the subregions, L1 exhibited pronounced negative FC with key brain regions associated with inhibition control, namely the dorsolateral prefrontal cortex (DLPFC), the anterior cingulate cortex, and the lateral orbitofrontal cortex. Case-control analysis between smokers and non-smokers revealed that L1 in smokers displayed significantly enhanced FC with the right DLPFC (Fig.2a). Notably, this increased FC was positively correlated with smoking frequency ($r=0.08$, $p=0.01$, Fig.2b) and the duration of smoking ($r=0.07$, $p=0.034$, Fig.2c).

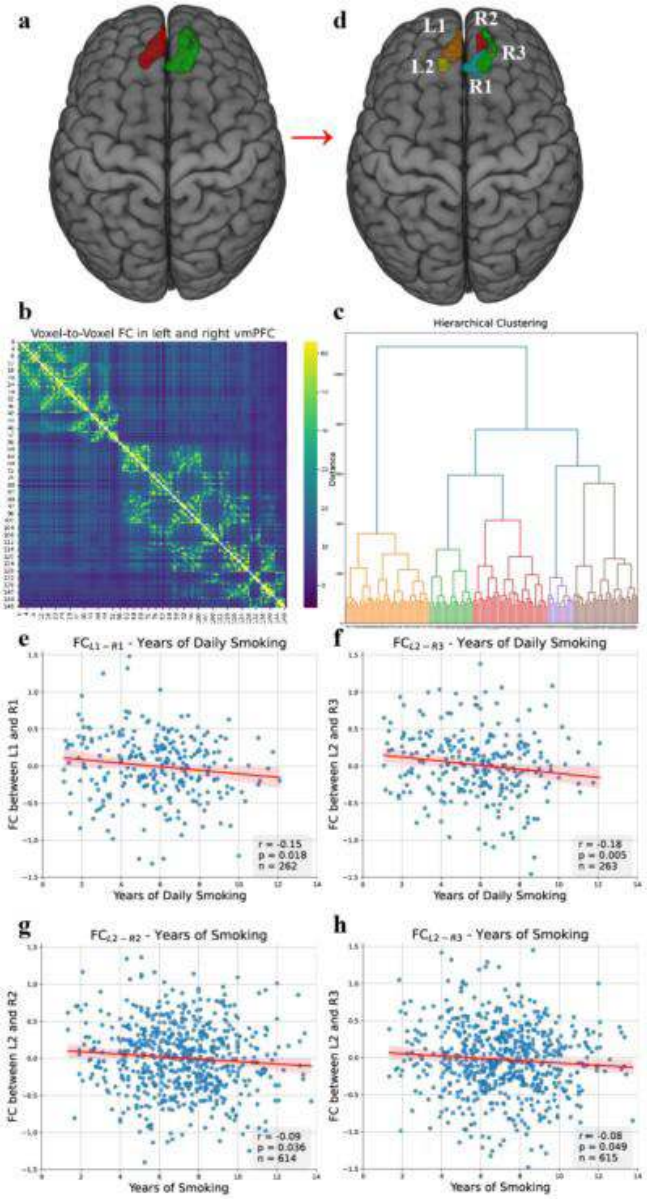

Figure 1: Characterization of vmPFC Subregions and Their Association with Smoking Behavior. (a) Left and right vmPFC related to smoking behavior indentified by changes in GMV. (b) Voxel-to-voxel FC within the vmPFC. (c) Dendrogram from hierarchical clustering applying Ward's method, illustrating the stratification into vmPFC subregions. (d) Functional subregions of vmPFC. (e-h) Correlations between inter-hemispheric subregional FC and smoking history.

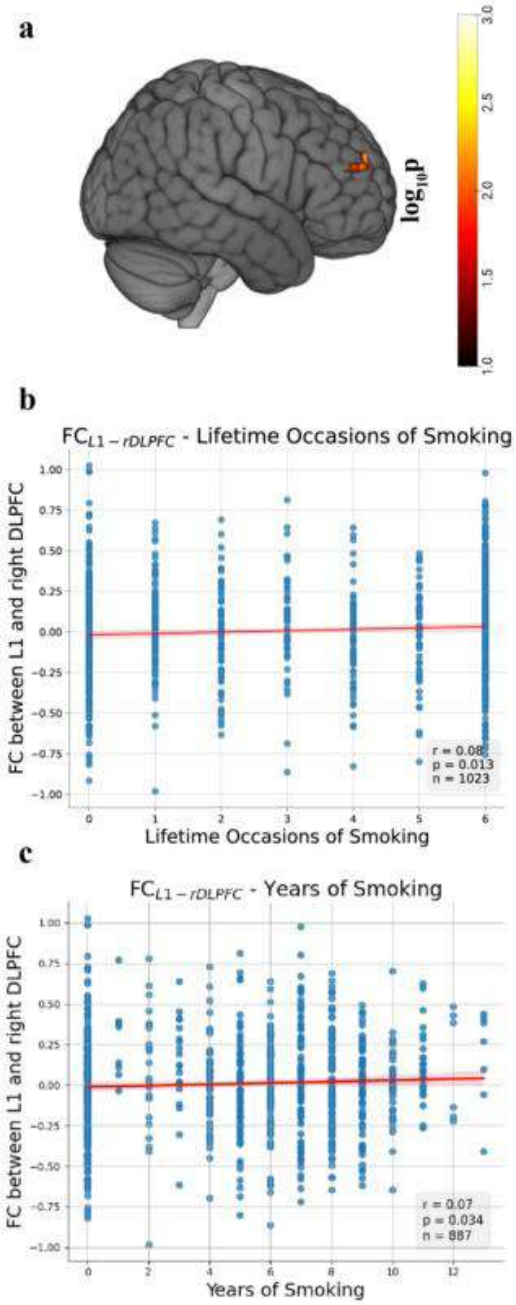

Figure 2: FC between subregion L1 and right DLPFC and its correlation with smoking behavior. (a) Right DLPFC exhibiting significantly stronger FC with L1. (b-c) Correlations between FC between L1 and right DLPFC and smoking behavior.

Conclusions: Our study extends previous research on GMV changes in the vmPFC by elucidating its functional mechanisms in relation to smoking behavior. We identified 5 functional subregions within the vmPFC, displaying distinct FC patterns. FC patterns among the subregions are significantly correlated with individuals' smoking histories, underscoring a potential neurobiological link between vmPFC activity and smoking behavior. The delineation of subregions represents a novel contribution to the field, providing a foundation for more nuanced investigations into the role of vmPFC in smoking. Notably, the FC between L1 and the right DLPFC correlated significantly with smoking history, highlighting a potentially critical pathway involving vmPFC, associated with evaluation processes, and the DLPFC, linked to inhibition control, in the context of smoking behavior. The identification of this pathway not only advances our understanding of the neurobiological mechanism of smoking but also opens new avenues for targeted research and interventions aimed at addressing nicotine addiction.

References
1. Xiang, S. (2023), 'Association between vmPFC Gray Matter Volume and Smoking Initiation in Adolescents', Nature Communications, vol. 14, no. 1, p. 4684.
2. Schumann, G. (2010), 'The IMAGEN Study: Reinforcement-related Behaviour in Normal Brain Function and Psychopathology', Molecular Psychiatry, vol. 15, no. 12, p. 1128-1139.
3. Knutson, B. (2001), 'Dissociation of Reward Anticipation and Outcome with Event-related fMRI', Neuroreport, vol. 12, no. 17, p. 3683-3687.
4. Susan, WG. (2012), 'CONN: a Functional Connectivity Toolbox for Correlated and Anticorrelated Brain Networks', Brain Connectivity vol. 2, no. 3, p. 125-141.

Poster No 645

Insula functional connectivity in obsessive-compulsive disorder: subregions and gradients

Lingxiao Cao[1], Hailong Li[1], Jiaxin Jiang[2], Bin Li[2], Shuangwei Chai[1], Huan Zhou[1], Qiyong Gong[1], Xiaoqi Huang[1]

[1]Department of Radiology and Huaxi MR Research Center, West China Hospital, Sichuan University, Chengdu, China, [2]Mental Health Center, West China Hospital of Sichuan University, Chengdu, China

Introduction: The insula is gaining increasing attention in neurocircuitry models of obsessive-compulsive disorder (OCD) (Shephard E, 2021). Most previous neuroimaging studies investigating insula functional connectivity (FC) in OCD have treated insula as a single, homogeneous region (Zhou Z, 2022), and thus any potential variation in connectivity across the topography of insula may be overlooked. The connectional variation can be characterized using two models: 1) discrete clusters (subregions) and 2) continua of variation (gradients), which have been applied to examine insula FC architecture in other psychiatric disorders (Tian Y, 2019), with few investigations in OCD yet. This study aimed to examine insula FC architecture in OCD with a novel clustering-based technique and gradient-based approach.

Methods: A total of 92 medication-free OCD patients and 90 age- and sex-matched healthy controls (HC) (Table 1) were scanned using 3T GE MRI. Subregions were generated using CBPtools (Reuter N, 2020). Specifically, k-means clustering was used to each subject's insula-to-whole-brain FC matrix to assign each insula voxel to a cluster, effectively grouping similar voxels based on their FC patterns. Then, the individual clusterings were relabeled and the mode of each insula voxel was computed, serving as the group-level clustering results. Diagnosis-by-subregion interaction effects were examined, with age, sex and mean FD as covariates. The FC values were extracted from the clusters showing significance for further post hoc analysis using simple effects test. Gradient mapping was generated using BrainSpace (Vos de Wael R, 2020). Specifically, only the top 10% connections of each insula voxel were used to calculate the cosine similarity. The similarity matrix was scaled into a normalized angle matrix and further fed into the diffusion map embedding algorithm. The global-level gradient distribution was compared using Mann-Whitney U test. Three global metrics, including gradient explanation ratio, range, and variation, were calculated, and compared by a GLM model with age, sex, and mean FD as covariates.

Results: Compared with HC, OCD patients showed enhanced insula FC with supplementary motor area (SMA), precuneus, cerebellum and inferior parietal lobule (Figure 1A). The insula was parcellated into two subregions corresponding to anterior insula and posterior insula (Figure 1B). We found significant diagnosis-by-subregion interaction in SMA, precentral gyrus (PCG), middle frontal gyrus (MFG) and dorsomedial prefrontal cortex (dmPFC) (Figure 1C). Relative to HC, the anterior subregion in OCD related to increased connectivity strength with the SMA, PCG and MFG, whereas the posterior subregion showed decreased connectivity strength with the dmPFC (Figure 1D). The spatial patterns of the group-averaged principle gradient maps of the insula were organized along a gradual anterior/posterior axis. A visual inspection of the histogram demonstrated that the extremes of the gradient were contracted in OCD relative to HC (Figure 2A), though the between-group comparisons in the cumulative distribution were not significant. The gradient of the left insula in OCD explained less variance than that in HC ($P = 0.026$, Figure 2B). Moreover, the OCD patients showed a narrower range of scores ($P = 0.040$, Figure 2C) and less spatial variation ($P = 0.042$, Figure 2D) in the left insula.

Table 1 Demographic and clinical characteristics

	OCD (n=92)	HC (n=90)	Comparison
Age, years	29.42 (8.67)	28.34 (10.85)	p=0.460
Sex (M/F)	57/35	55/35	p=0.907
Age of onset, years	22.03 (7.08)	-	-
Duration, years	7.39 (5.54)	-	-
YBOCS			
Total score	21.39 (5.51)	-	-
Obsession score	13.01 (5.09)	-	-
Compulsion score	8.38 (5.33)	-	-
HAMA	9.12 (4.67)	-	-
HAMD	9.03 (5.24)	-	-

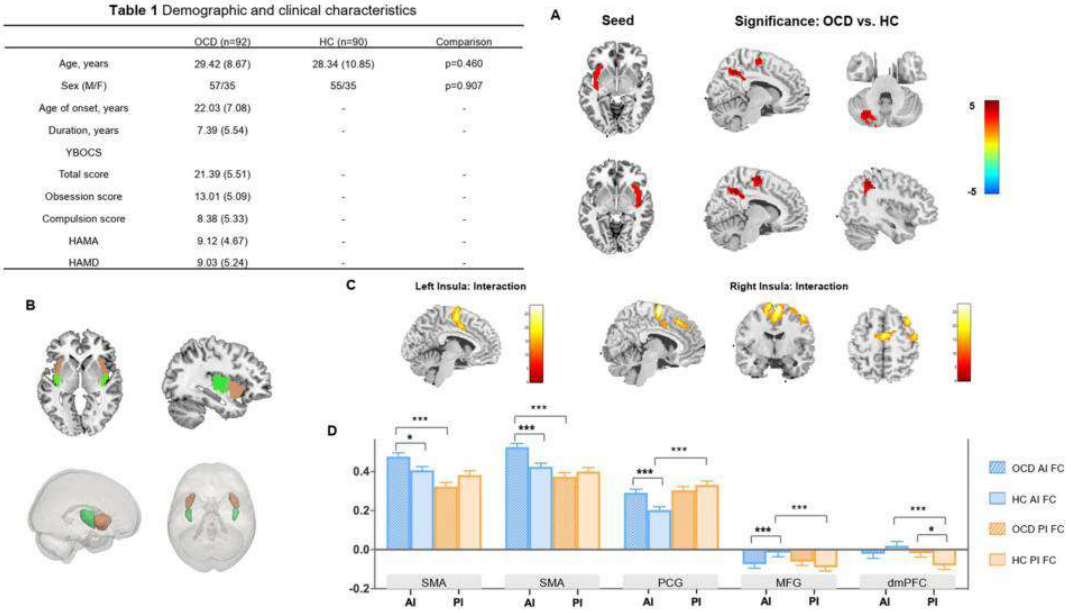

Figure 1 (A) Main effect of diagnosis (OCD vs. HC) on insula functional connectivity (Left insula: upper panel, Right insula : lower panel). **(B)** The two cluster solution derived by clustering-based technique that corresponds to anterior insula and posterior insula. **(C)** Significant interaction effects between diagnosis and subregion. **(D)** Results of post hoc analysis. Significance is indicated for *p < .05, **p < .01, ***p < .005.

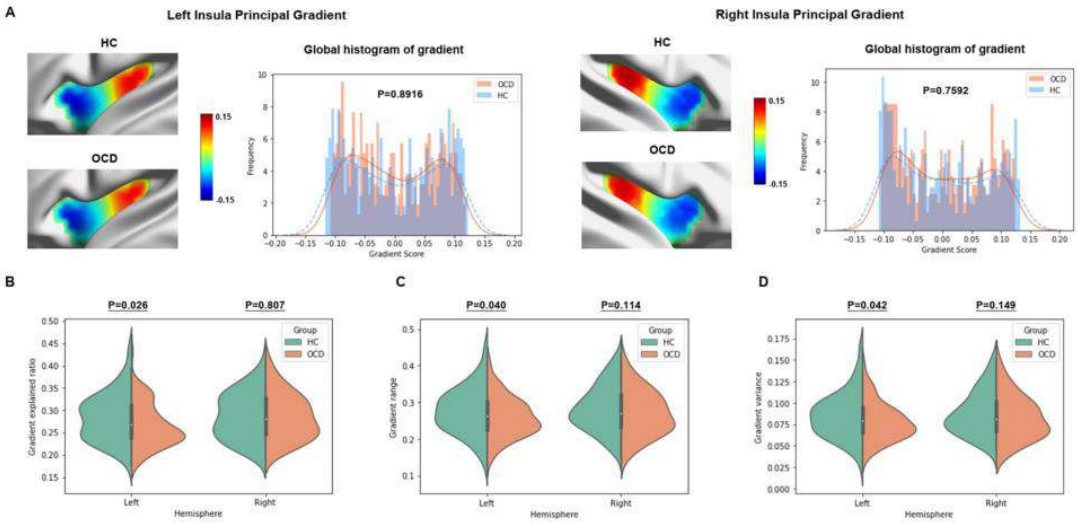

Figure 2 (A) The group-averaged maps of principal gradient in OCD and HC, and the global histogram of gradient showing the extremes of the anterior/posterior gradient were contracted in OCD relative to HC. **(B)** Case-control differences in the gradient explained ratio of the principal gradient. **(C)** Case-control differences in the gradient range. **(D)** Case-control differences in the gradient variance.

Conclusions: We comprehensively characterized insula FC architecture using discrete subregions as well as continual gradients in OCD. We found unbalanced insula subregional FC alterations in OCD patients with increased FC strength in the anterior subregion while decreased FC strength in the posterior subregion. We also found OCD patients exhibited global topographic alterations in the principal anterior-posterior gradient of the left insula. These results highlight the disrupted FC architecture of the insula in OCD, providing insights into the neurobiological underpinnings of OCD.

References

1. Reuter, N. (2020), 'CBPtools: a Python package for regional connectivity-based parcellation', Brain structure & function, vol. 225, no. 4, pp. 1261-1275.
2. Shephard, E. (2021), 'Toward a neurocircuit-based taxonomy to guide treatment of obsessive-compulsive disorder', Molecular psychiatry, vol. 26, no. 9, pp. 4583-4604.
3. Tian, Y. (2019), 'Insula Functional Connectivity in Schizophrenia: Subregions, Gradients, and Symptoms', Biological psychiatry. Cognitive neuroscience and neuroimaging, vol. 4, no. 4, pp. 399-408.
4. Vos de Wael, R. (2020), ' BrainSpace: a toolbox for the analysis of macroscale gradients in neuroimaging and connectomics datasets ', Communications biology, vol. 3, no. 1, pp. 103.
5. Zhou, Z. (2022), 'Abnormal resting-state functional connectivity of the insula in medication-free patients with obsessive-compulsive disorder', BMC Psychiatry, vol. 22, no. 1, pp. 742.

Poster No 646

Network localization of gray matter atrophy in addiction

Min Wang[1], Zhoukang Wu[1], Liangjiecheng Huang[1], Xiaochu Zhang[1], Xiaosong He[1]

[1]*University of Science and Technology of China, Hefei, Anhui*

Introduction: Imaging meta-analyses of addiction have summarized symptom-brain region correspondence patterns, revealing diagnosis-specific and transdiagnostic effects[1]. However, group average differences are not representative of individual cases[2]. There are both clinical and neuroanatomical variabilities at the single-subject level in addiction, complicating it challenging to develop neuroimaging biomarkers to track disease severity, progression, and treatment response. Here we demonstrate through normative model[3] and lesion network mapping[4] techniques that regional gray matter atrophy patterns across patients with addiction are highly heterogeneous, yet these deviations can be embedded in common functional circuits and networks.

Methods: T1-weighted data from 333 patients with substance use disorder and 957 healthy controls (HC) were collected from 3 public databases[5]. Voxel-based morphometry analyses via CAT12 were conducted to segment these images into gray matter, white matter, and cerebrospinal fluid. We used age, gender, intracranial volume, and site effect as covariates to build a voxel-wise normative model for the gray matter volume (GMV) of HC. Normative model can be used to define a normative range of variation against which new individuals are compared. Applying the model to each patient's data, we can generate a personalized whole-brain voxel-wise GMV deviation map. We identified all voxels with GMV deviation score < -2 as regions with extreme atrophy for each patient, corresponding to a 2 standard deviations below the mean GMV of HC, controlling for covariates. We overlaid binarized atrophy maps from all patients to identify regions consistently showing atrophy in the highest number of patients. Next, an "atrophy functional connectivity (FC) network" was derived for each patient, defined as brain network functionally connected to aforementioned atrophic regions. Using the binarized atrophy regions as seed, FC with the rest of the brain was calculated using the GSP1000 resting functional dataset[6]. For the 1000 FC maps generated for each atrophy seed for each patient, a one-sample t test was used to infer regions that were significantly connected to the seed atrophy region via FC and to obtain an FWE-corrected atrophy FC network map. Finally, we calculated the overlap ratio of these atrophic FC networks.

Results: We first verified that the age distributions and model fitting parameters in Fig1.A supported our hypothesis that the HC's demographic information can predict GMV well. We then overlapped the binary atrophy masks across all patients and within each subgroup of substance addiction. Surprisingly, regardless of drug type, only 10%-20% of patients showed consistent atrophy at same locations, suggest that at individual level, voxels exceeding -2 deviations distributed heterogeneously across each patient cohort (Fig1.B). In contrast, traditional group-level statistical inferences on the whole-brain deviation maps can still identify prominent gray matter atrophy pattens both across and within each subgroup (Fig1.C). By examining the overlay map of atrophy FC network we found that, although the locations of extreme atrophy were heterogeneous among patients, in fact, the atrophic structures of more than 60% of patients are functionally embedded into a homogeneous network, involving medial prefrontal cortex, middle/posterior cingulate cortex, and occipital lobe (Fig2.A). Importantly, this atrophic FC network was stable across all three drug subtypes (Fig2.B).

Fig.1 Regional heterogeneity of GMV deviations in addiction

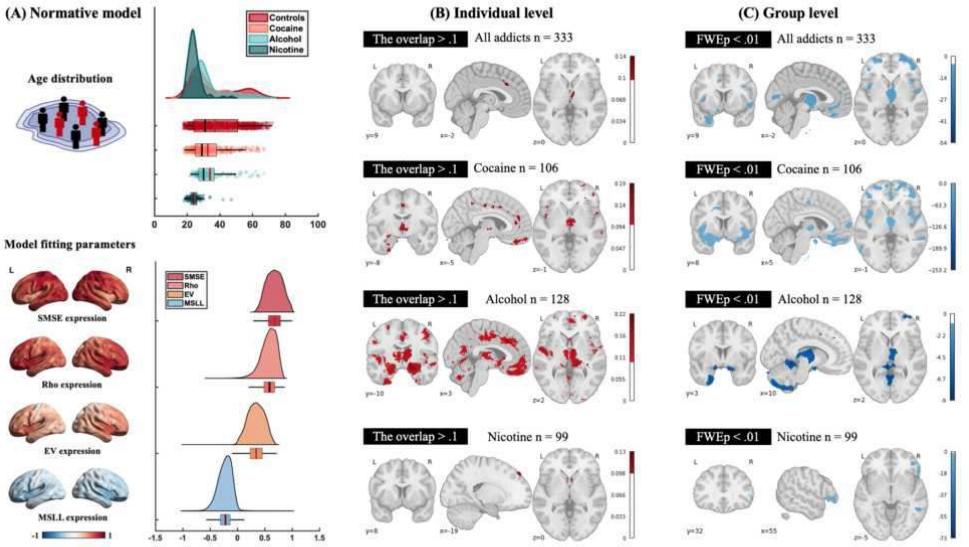

(A) Age distributions and NM fitting parameters. Higher explained variance (EXPV) & correlation between true/predicted responses (Rho), lower standardized mean squared error (SMSE), and more negative mean standardized log loss (MSLL) correspond to better model fit. (B) Percentage of subject-level atrophy maps (<-2) overlapping in same location. (C) Group-level T-map corrected by FWE.

Fig.2 Atrophy network mapping in addiction

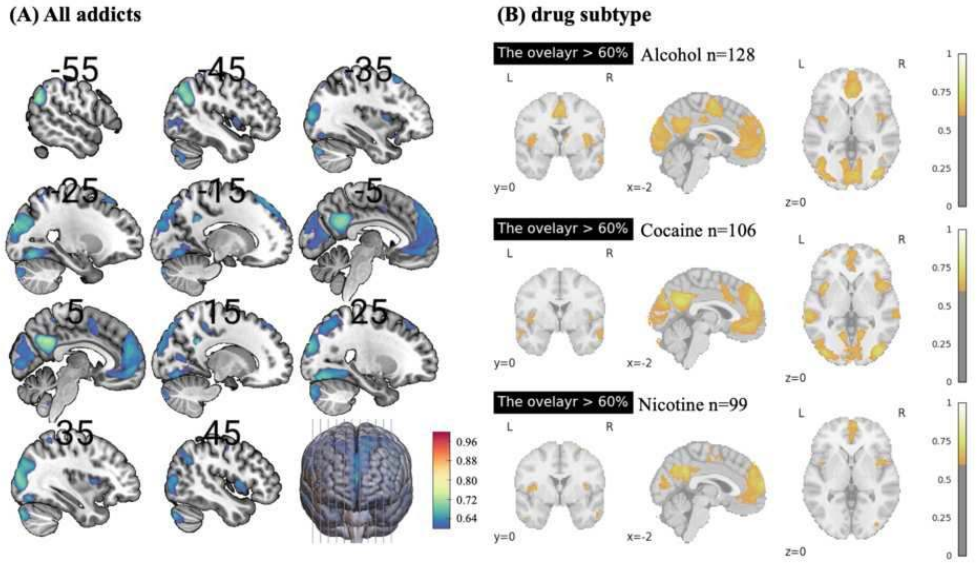

(A) The overlap percentage of the effect size of zFC in addicts. (B) The overlap percentage of the effect size of zFC for patients with alcohol/cocaine/nicotine use disorder.

Conclusions: Although high heterogeneity of GMV deviations is a general characteristic of addiction, these deviations are often coupled to common functional circuits and networks, offering a putative neural substrate for phenotypic similarities among individuals assigned the same diagnosis. Specifically, the common involvement of default mode network across subtype may shed light on the understanding of the progress of structural atrophy in patients with addition.

References

1. Luscher, C., Robbins, T. W. & Everitt, B. J. The transition to compulsion in addiction. Nat. Rev. Neurosci. 21, 247-263, (2020).
2. Wolfers, T. et al. Mapping the heterogeneous phenotype of schizophrenia and bipolar disorder using normative models. JAMA Psychiat 75, 1146–1155 (2018).
3. Rutherford, S. et al. The normative modeling framework for computational psychiatry. Nat. Protoc. 17, 1711-1734 (2022).
4. Aaron, MT. et al. Network localization of clinical, cognitive, and neuropsychiatric symptoms in Alzheimer's disease. Brain. 143(4), 1249-1260 (2020).
5. Wei, D. et al. Structural and functional brain scans from the cross-sectional Southwest University adult lifespan dataset. Sci Data 5, 180134 (2018).
6. Holmes AJ. et al. Brain Genomics Superstruct Project initial data release with structural, functional, and behavioral measures. Sci Data 2: 1–16 (2015).

Poster No 647

Deficits of Right Cortico-striatal Pathway predicts Internet Addiction Severity

Hui Zhou[1], Liangyu Gong[1], Conghui Su[1], Fengji Geng[1], Yuzheng Hu[2]

[1]Zhejiang University, Hangzhou, Zhejiang Province, [2]Zhejiang University, Hangzhou, Zhejiang

Introduction: Internet addiction (IA) is a new form of behavioral addiction, leading to anxiety, depression, and detrimental impacts on mental well-being, ultimately influencing students' academic performance (Lebni et al. 2020). Previous studies have identified dysfunctional prefrontal-striatum circuits in both substance use disorders (Hu et al. 2019) and internet gaming disorder (Gong et al. 2022), however, the underlying structural substrates remain elusive. Here we adopted voxel-based morphometry (VBM) and diffusion tensor imaging (DTI) techniques to investigate whether structural deficits of cortico-striatal pathway could predict severity of IA.

Methods: Ninety-six undergraduates from Zhejiang University participated in this study (age = 20.59± 2.27, 57 males). The severity of IA was assessed using the Internet Addiction Test (IAT) and DSM-5 criteria, while the level of self-control was assessed by Self-control scale. To explore the relationship between brain structure and IA severity, we first performed multiple linear regression analysis on gray matter volume and IAT scores, adjusting for intracranial volume, depression, anxiety scores, age, and gender. The gray matter volume of the region displaying a significant result was extracted for further correlation with DSM, and self-control scores. The region exhibiting a significant result in the multiple regression, specifically the dorsal anterior cingulate cortex (dACC, see below), and bilateral ventral striatum were chosen as seeds for tractography. Fractional anisotropy (FA), and radial diffusivity (RD) values from identified white matter pathways were extracted for correlation with severity of IA and self-control scores. In addition, the identified white matter pathway masks were mirrored by x-axis, and the FA and RD values were extracted from the flipped mask and correlated with severity of IA, and self-control. This step aimed to rule out the possibility that the laterality of results was induced by different voxels involved. Further mediation analysis was conducted to reveal the relationship between FA, severity of IA, and self-control.

Results: Multiple regression analysis showed a cluster located at dACC (cluster size: 908) was found negatively correlated with IAT score (Figure 1A, B). The gray matter volume of dACC was negatively correlated with DSM (r = -0.264, p =0.011), but not with self-control (r = 0.15, p = 0.167). The DTI tractography analysis identified white matter connections between dACC and rVS, lVS, respectively (Figure 2A). The results showed the FA and RD values of rVS-dACC white matter connection was negatively (r = -0.27, p = 0.011) and positively (r = 0.25, p = 0.020) correlated with IAT scores, respectively (Figure 2B). As for self-control, a significantly positive correlation was found with FA of rVS-dACC pathway (Figure 2B; r = 0.22, p = 0.036). No significant correlation was found between white matter indexes of lVS-dACC and IAT or self-control (pmin = 0.537). White matter indexes of the flipped rVS-dACC pathway did not correlate with IAT or self-control scores (pmin = 0.264), whereas the FA and RD of flipped lVS-dACC pathway was negatively and positively correlated with IAT (Figure 2C; r = -0.37, p < 0.001; r = 0.34, p = 0.001), respectively, and the FA of flipped lVS-dACC pathway was positively correlated with self-control scores (Figure 2C; r = 0.22, p = 0.037). Further mediation analyses showed that self-control completely mediated the relationship between FA of rVS-dACC and IAT. Specifically, a significant total effect of FA of rVS-dACC on IAT was identified (c = -67.24, p = 0.012). The mediation effect of self-control was significant (a*b = -26.67, CI [-52.08, -4.12]), and the direct effect of FA of rVS-dACC on IAT was not significant (c' = -40.57, p = 0.088).

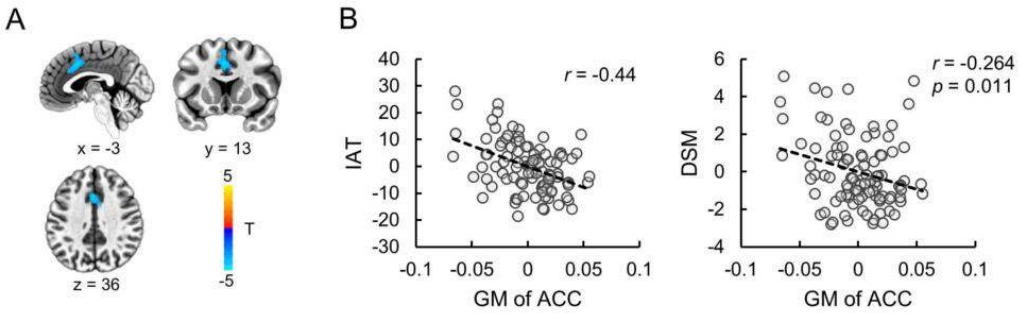

Figure 1.VBM results. (A) Multiple regression indicated the gray matter volume of dACC was negatively correlated with IAT scores after controlling for total intracranial volume, depression, anxiety scores and age as well as gender. (B) Partial correlation scatter plot of dACC gray matter volume and IAT, DSM scores. Abbreviations: GM, gray matter volume; dACC, dorsal anterior cingulate cortex. Abbreviations: IAT, internet addiction test.

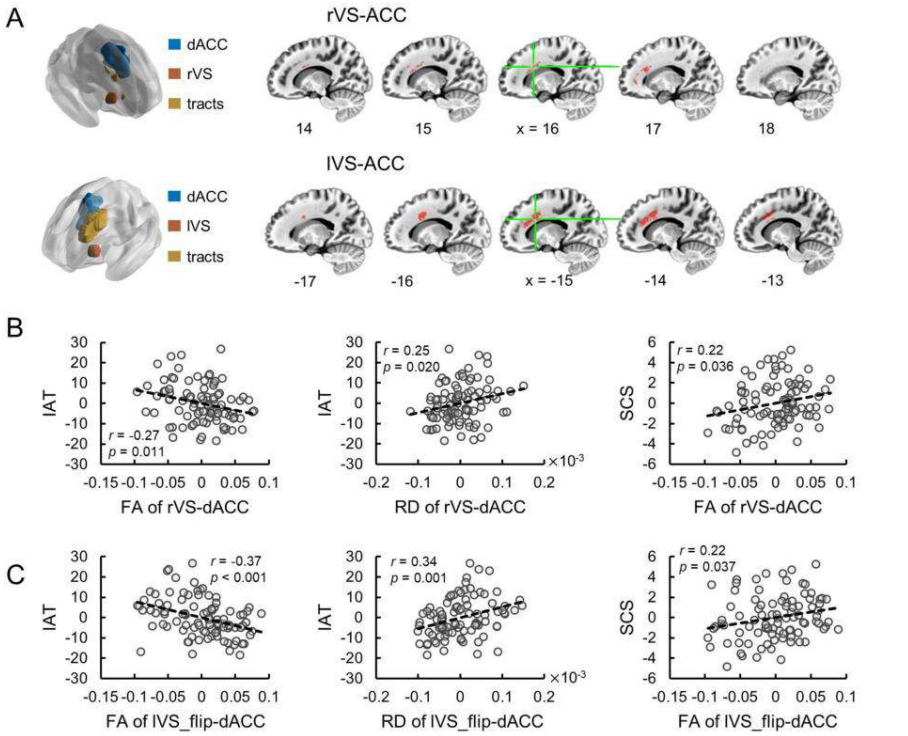

Figure 2. DTI results. (A) Bilateral VS-dACC white matter pathways identified by tractography. (B) Correlations between white matter indexes of rVS-dACC pathway and IAT, self-control scores. (C) Correlations between white matter indexes of flipped lVS-dACC pathway and IAT, self-control scores. Abbreviations: rVS, right ventral striatum; lVS, left ventral striatum; ACC, anterior cingulate cortex; IAT, internet addiction test; SCS, self-control score.

Conclusions: These results indicated that rVS-dACC pathway serves as the common substrate of self-control and IA, and the deficit of this pathway may lead to IA through insufficient involvement of self-control.

References

1. Gong, L. (2022). "Self-control impacts symptoms defining Internet gaming disorder through dorsal anterior cingulate–ventral striatal pathway." Addiction Biology 27(5).
2. Hu, Y. (2019). "Compulsive drug use is associated with imbalance of orbitofrontal- and prelimbic-striatal circuits in punishment-resistant individuals." Proc Natl Acad Sci U S A 116(18): 9066-9071.
3. Lebni, J. Y. (2020). "A study of internet addiction and its effects on mental health: A study based on Iranian University Students." Journal of Education and Health Promotion 9.

Poster No 648

Alpha Peak Frequency Shift as an Alternative Cognitive Marker for Depression

Sangwon Yu[1], Minsok Koo[1], Sang Ah Lee[1]

[1]Seoul National University, Gwanak-gu, Seoul

Introduction: Various oscillatory activities in the brain have been studied as neural markers for affective disorders[1]. A considerable number of studies have reported an alteration of alpha waves (8~13 Hz) in depression, but a change in its peak frequency has not been explored in full, particularly in relation to cognition. Increased alpha peak frequency is associated with relaxation, resilience, and mood[2,3,4]. At the same time, some argue that a gradual decrease of alpha frequency from posterior to anterior regions represents cortical hierarchies that form a frequency gradient that enables cortical traveling waves involved in cognition[5,6,7]. This study investigates the link between the dynamics of alpha peak frequency and depression symptoms in subclinical adults, shedding new light on the neural basis of the interaction between depressive symptoms and cognitive impairments.

Methods: We recorded rest-state EEG signals from 38 participants (female = 20, age range = 20-32) for five minutes, and while they performed an emotional scene-based memory task. During the encoding phase, 144 images of positive, negative, or

neutral events (48 images for each condition) were presented in pseudorandom order. Following the stimulus presentation, participants rated the valence (i.e., how positive or negative) and arousal (i.e., how exciting or calming) of each scene on a scale from 1–9. After the entire encoding phase, participants performed a scene recognition test. Alpha peak frequency was calculated with a Fitting Oscillations and One Over F (FOOOF) algorithm, dissociating the periodic components of the EEG power spectrum from the aperiodic component.

Results: During rest, we found significant increases of alpha peak frequency in the frontal regions for the depressed group compared to the non-depressed group ($F(1,36) = 1.00$, $p<0.0001$). This result was replicated across in an openneuro public dataset of 122 participants (female = 47, age range = 18-20, $F(1,120) = 7.30$, $p<0.0001$).The topographic patterns, showing an alpha peak frequency decrease from posterior to anterior regions, were similar between our lab's dataset and the public dataset. These resting-state findings largely replicate previous MEG experiments[5] and extend them to scalp EEG. Furthermore, during the encoding of emotional scenes, the depressed group showed no change (from pre- to post-stimulus periods) in alpha peak frequency in the frontal regions when presented with emotional scenes ($F(1,16) = 0.15$, $p>0.5$). In contrast, the non-depressed group showed a significantly decreased frontal alpha frequency while viewing scenes ($F(1,18) = 5.06$, $p<0.05$). We tested for a possible functional correlation between valence ratings and frontal peak frequency change during the encoding phase and found that an increase in the peak frequency in the depressed group was correlated with their rating of emotional scenes as less emotional, according to their valence and arousal ratings ($r=-0.55$, $p<0.05$). These results may indicate the need for greater frontal regulation of emotional scene content that also disrupts the posterior to anterior gradient for perceptual information processing.

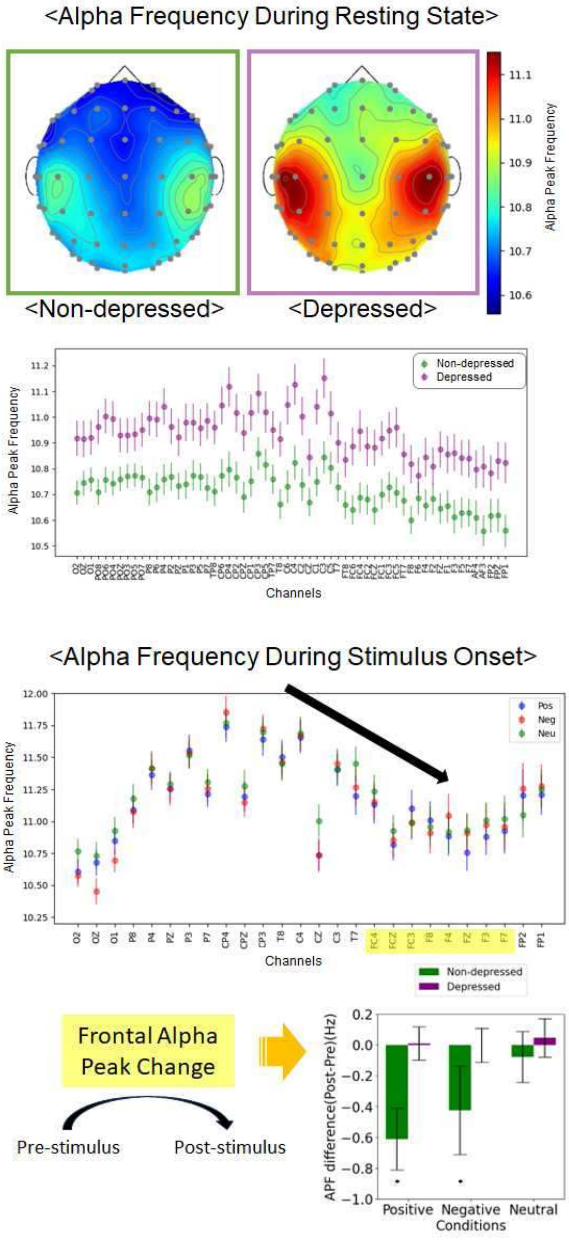

Conclusions: We propose that an alpha peak shift may reflect a neural change in individuals with symptoms of depression, and that the upward shift in alpha frequency may be indicative of abnormal neurocognitive function. One possible mechanism that may explain the increase, rather than decrease, of alpha peak frequency upon emotional stimulus is a potential emotional regulatory mechanism that perturbs the frequency gradient that promotes information flow from the posterior visual regions to the frontal regions of the cortex. Further studies are needed to test this hypothesis in detail.

References

1. de Aguiar Neto, F. S. and J. L. G. Rosa (2019). Depression biomarkers using non-invasive EEG: A review. Neuroscience & Biobehavioral Reviews 105, 83-93.
2. Kostyunina, M.B., Kulikov, M.A. (1996). Frequency characteristics of EEG spectra in the emotions. Neurosci Behav Physiol 26, 340–343 .
3. Lechinger, J., Bothe, K., Pichler, G. et al. (2013). CRS-R score in disorders of consciousness is strongly related to spectral EEG at rest. J Neurol 260, 2348–2356.
4. Mierau, A., et al. (2017). State-dependent alpha peak frequency shifts: Experimental evidence, potential mechanisms and functional implications. Neuroscience 360, 146-154.
5. Mahjoory, K., et al. (2020). The frequency gradient of human resting-state brain oscillations follows cortical hierarchies. eLife 9.
6. Zanos TP, elt al. (2015). A sensorimotor role for traveling waves in primate visual cortex. Neuron 85(3), 615-27.
7. Zhang, H., et al. (2018). Theta and alpha oscillations are traveling waves in the human neocortex. Neuron 98(6), 1269-1281.

Poster No 649

Brain age to identify structural alterations in schizophrenia unrelated with aging

Alejandro Roig-Herrero[1], Rafael Navarro-González[1], Álvaro Planchuelo-Gómez[1], Santiago Aja-Fernández[1], Juan Calabia del Campo[2], Vicente Molina-Rodríguez[1], Rodrigo De Luis-García[1]

[1]Universidad de Valladolid, Valladolid, Valladolid, [2]Hospital Clínico Universitario de Valladolid, Valladolid, Valladolid

Introduction: Neuroimaging has consistently revealed significant changes in the brain structure of schizophrenia patients. Some of these changes seem to be present even before illness onset[1,2], while others become more pronounced years after disease onset[3]. In the brain age paradigm, a machine learning model is trained to predict a person's age based on brain imaging data. The difference between the predicted age and the actual chronological age, known as the brain age gap, is considered a marker of brain health[4]. Since increased brain age has been consistently found in schizophrenia across several studies[5,6], a fundamental question naturally arises: are changes in the gray matter in schizophrenia the result of an accelerated brain aging process, or are they (at least in part) the result of a fundamentally different process? Our aim is to shed light on this question.

Methods: 67 chronic schizophrenia patients (30 females) and 97 healthy controls (43 females) underwent brain MRI acquisition including T1-weighted images using a Philips Achieva 3T MRI unit (Philips Healthcare, Best, the Netherlands) with a 32-channel head coil in the MRI facility at the Universidad de Valladolid (Spain). Acquisition parameters are available elsewhere[7]. Following the image acquisition, FastSurfer was employed to extract a total of 1,479 features[8]. Fastsurfer uses Deep Learning to perform brain segmentation based on the Desikan-Killiany atlas[9]. In this study 289 were considered, describing the volume of cortical and subcortical gray matter regions and white matter regions from the atlas, as well as the surface, thickness and curvature of the cortical regions. In parallel, a brain age prediction model was trained from 2,771 structural T1w MRI scans from different studies and databases. Details about this brain age model are available elsewhere[10]. The Shapiro-Wilk test and Levene's test for equality of variances were used to assess normality and homogeneity of variances in age and total intracranial volume. To test for significant differences, a t-test was used if the null hypothesis in the Shapiro-Wilk and Levene tests was not rejected; otherwise, the Wilcoxon rank-sum test was employed. To test for sex-related significant differences, a Fisher exact test was used. Brain age differences between groups were assessed with an analysis of covariance (ANCOVA), including age, total intracranial volume and sex as covariates. With regard to the 289 morphological features described before, an ANCOVA was performed, with age, total intracranial volume and sex as covariates. Next, the same analysis was repeated, but considering the estimated brain age as covariate instead of the chronological age. Bonferroni correction was applied for multiple comparisons after setting the level of statistical significance at $P<0.05$.

Results: No differences were found in age, intracranial volume or sex between the two groups. An increased brain age gap was found in the schizophrenia group with respect to healthy controls (7.4 years ± 9.8 vs -1.3 years ± 8.7, $P<10\text{-}8$, see Figure 1A). Figure 1B graphically compares the p-values obtained using both corrections. When correcting for chronological age, statistically significant differences were found in 31 imaging features ($P<0.000173$), generally indicating lower volume and cortical thickness across widespread brain regions. However, when correcting for brain age, significant differences were found in only three imaging features (see Figure 2).

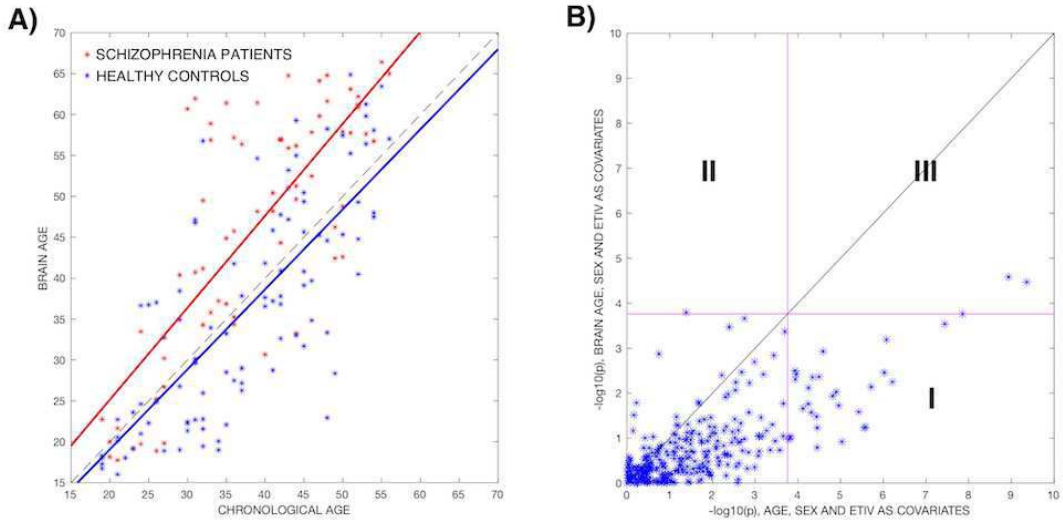

Figure 1: A) Scatter plot showing brain predicted age versus chronological age for schizophrenia patients (red) and healthy controls (blue). B) Scatter plot with p-values for each imaging feature obtained using ANCOVA with age, sex and estimated intracranial volume (eTIV) as covariables vs the same but using estimated brain age instead of chronological age. A negative logarithmic scale is employed, and Bonferroni threshold is depicted in magenta. Comparisons for most features show increased p-values when corrected for brain age (i.e. they are below the black line), which suggest some involvement of brain aging in that particular feature. Sector I comprises comparisons that are statistically significant when correcting for chronological age but not for brain age. Sector II comprises comparisons that are statistically significant when correcting for brain age but not for chronological age, and Sector III shows comparisons that are statistically significant for both corrections.

Features with significant differences (p<0.000173)				
Sex, eTIV and age as covariates			**Sex, eTIV and brain age as covariates**	
Feature	p-value	Cohen's d	Feature	p-value
		0.17	Volume_mm3_Left_Putamen	0.0002
Volume_mm3_Left_Accumbens_area	$<10^{-4}$	-0.53		
Volume_mm3_Right_Hippocampus	0.0001	-0.50		
ThickAvg_lh_fusiform	$<10^{-4}$	-0.89		
GrayVol_lh_lateralorbitofrontal	$<10^{-4}$	-0.64		
GrayVol_lh_lingual	$<10^{-4}$	-0.56		
ThickAvg_lh_middletemporal	$<10^{-4}$	-0.64		
SurfArea_lh_parahippocampal	0.0001	-0.56		
GrayVol_lh_parahippocampal	$<10^{-4}$	-0.74		
ThickAvg_lh_parsopercularis	$<10^{-4}$	-0.70		
GrayVol_lh_parstriangularis	0.0001	-0.55		
GrayVol_lh_postcentral	$<10^{-4}$	-0.54		
GrayVol_lh_rostralmiddlefrontal	$<10^{-4}$	-0.54		
GrayVol_lh_superiortemporal	$<10^{-4}$	-0.56		
ThickAvg_lh_superiortemporal	$<10^{-4}$	-0.91		
ThickAvg_rh_fusiform	$<10^{-4}$	-0.77		
ThickAvg_rh_inferiortemporal	0.0001	-0.64		
GrayVol_rh_lingual	$<10^{-4}$	-0.56		
ThickAvg_rh_lingual	$<10^{-4}$	-0.65		
GrayVol_rh_middletemporal	0.0001	-0.46		
ThickAvg_rh_middletemporal	$<10^{-4}$	-0.76		
GrayVol_rh_parahippocampal	$<10^{-4}$	-0.85	GrayVol_rh_parahippocampal	$<10^{-4}$
ThickAvg_rh_parahippocampal	$<10^{-4}$	-0.70		
ThickAvg_rh_parsopercularis	0.0002	-0.58		
GrayVol_rh_parstriangularis	0.0001	-0.58		
ThickAvg_rh_posteriorcingulate	$<10^{-4}$	-0.64		
GrayVol_rh_rostralanteriorcingulate	0.0001	-0.52		
ThickAvg_rh_superiortemporal	$<10^{-4}$	-0.97	ThickAvg_rh_superiortemporal	$<10^{-4}$
ThickAvg_rh_transversetemporal	0.0001	-0.66		
lhCortexVol	$<10^{-4}$	-0.47		
rhCortexVol	$<10^{-4}$	-0.47		
TotalGrayVol	$<10^{-4}$	-0.42		

Figure 2: Comparison of statistically significant results obtained correcting for chronological age and correcting for brain age. Positive Cohen's d values indicate increased feature value in the schizophrenia group, and viceversa.

Conclusions: Our results suggest that most structural variations in schizophrenia patients correlate with increased brain aging, yet a subset of these differences appears unrelated to that process. Focusing on these distinct changes is vital for comprehending the schizophrenia brain, offering potential insights into subgroups, treatment effects or prognostic indicators.

References

1. Bois, C. et al. (2015), 'Structural magnetic resonance imaging markers of susceptibility and transition to schizophrenia: a review of familial and clinical high risk population studies', Journal of Psychopharmacology, 29(2), 144-154.
2. Fusar-Poli, P. et al. (2014), 'Neuroanatomical markers of genetic liability to psychosis and first episode psychosis: a voxelwise meta-analytical comparison', The World Journal of Biological Psychiatry, 15(3), 219-228.
3. Olabi, B. et al. (2011), 'Are there progressive brain changes in schizophrenia? A meta-analysis of structural magnetic resonance imaging studies', Biological Psychiatry, 70(1), 88-96.
4. Franke, K. et al. (2010), 'Estimating the age of healthy subjects from T1-weighted MRI scans using kernel methods: exploring the influence of various parameters', Neuroimage, 50(3), 883-892.
5. Koutsouleris, N. et al. (2014), 'Accelerated brain aging in schizophrenia and beyond: a neuroanatomical marker of psychiatric disorders', Schizophrenia Bulletin, 40(5), 1140-1153.
6. Constantinides, C. et al. (2023), 'Brain ageing in schizophrenia: evidence from 26 international cohorts via the ENIGMA Schizophrenia consortium', Molecular Psychiatry, 28(3), 1201-1209.
7. Lubeiro, A. et al. (2017), 'Biological and cognitive correlates of cortical curvature in schizophrenia', Psychiatry Research: Neuroimaging, 270, 68-75.
8. Henschel, L. et al. (2020), 'Fastsurfer-a fast and accurate deep learning based neuroimaging pipeline', NeuroImage, 219, 117012.
9. Desikan, R. S. et al. (2006), 'An automated labeling system for subdividing the human cerebral cortex on MRI scans into gyral based regions of interest'. Neuroimage, 31(3), 968-980.
10. Navarro-González, R. et al. (2023), 'Increased MRI-based Brain Age in chronic migraine patients', The Journal of Headache and Pain, 24(1), 133.

Poster No 650

Decreased functional connectivity in bipolar disorder: a whole-brain connectome analysis using NBS

Chun-Hung Yeh[1], Matteo Martino[2], Hsiang-Yuan Lin[3], Rung-Yu Tseng[1], Benedetta Conio[4], Paola Magioncalda[5]

[1]Department of Medical Imaging and Radiological Sciences, Chang Gung University, Taoyuan, Taiwan, [2]Graduate Institute of Mind, Brain, and Consciousness, Taipei Medical University, Taipei, Taiwan, [3]Centre for Addiction and Mental Health, Department of Psychiatry, University of Toronto, Toronto, Canada, [4]University of Genoa, Genoa, Italy, [5]International Master/Ph.D. Program in Medicine, College of Medicine, Taipei Medical University, Taipei, Taiwan

Introduction: Bipolar Disorder (BD) is a major psychiatric disorder and is clinically defined by the occurrence of active phases of illness, mania and depression, alternated to asymptomatic periods of euthymia[1]. The manic and depressive states show opposite symptomatology across the psychomotor, affective, and thought dimensions. At a biological level, these distinct symptomatologic profiles may depend on distinct patterns of alterations in the functional architecture of intrinsic brain activity. This study aimed to characterize such differences in the functional connectome using Network-Based Statistic (NBS)[2] analysis in BD during mania, depression, and euthymia, comparing these states to a healthy control group.

Methods: We recruited 58 patients with BD, either in manic (n=17), depressive (n=24), or euthymic (n=17) states, along with 118 age-matched healthy controls (HC). Resting-state functional MRI (rs-fMRI) data of 6 minutes were acquired on a 1.5T GE MRI scanner using a gradient-echo EPI sequence with TR/TE=2000/30 ms and voxel size=3.75×3.75×5mm3. The preprocessing of rs-fMRI data was conducted using DPABISurf[3] based on the fMRIprep[4]. ICA-AROMA[5] and aCompCor[6] were used to denoise the data. applied to Functional connectomes were then generated based on z-transformed Pearson's correlation of functional time series across pair-wise brain regions, which were defined using Schaefer's cortical atlas (100 regions)[7], Tien's subcortical parcellation (50 regions)[8], and SUIT's cerebellum atlas (34 regions)[9] in this study. Functional connectomes were analyzed using NBS[2] to identify between-group disparity. Firstly, we compared the whole BD group to HC, and then separately compared the manic, depressive, and euthymic BD to HC.

Results: As shown in Figure 1, the whole BD group was characterized by a widespread decrease in functional connectivity of the somatosensory network, visual network, salience network, dorsal attention network, frontoparietal network, default-mode network, and subcortical structures, mostly involving the inter-network connections. Considering the different phases of BD separately, Figure 2 shows that such widespread decrease in functional connectivity was associated with depression and euthymia, where the latter shows the most extensive reduction of network connectivity (Figure 2, lower row). Conversely, no significant changes in functional connectivity were associated with mania.

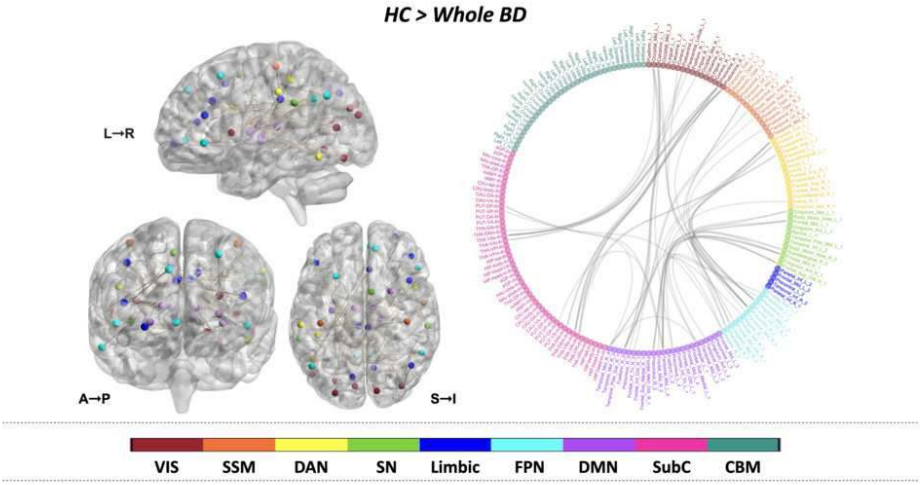

Figure 1: The comparison of functional connectivity between the healthy control (HC) group and the entire BD cohort. The results obtained from NBS are presented in three orthogonal views (left–right; anterior–posterior; inferior–superior) on the left and displayed using a 2D circular plot on the right. Brain regions are assigned to the functional networks as defined in [7]. Acronyms: VIS: visual; SSM: sensorimotor; DAN: dorsal attention; SN: salience network; FPN: frontoparietal; DMN: default mode network; SubC: subcortical; CBM: cerebellum.

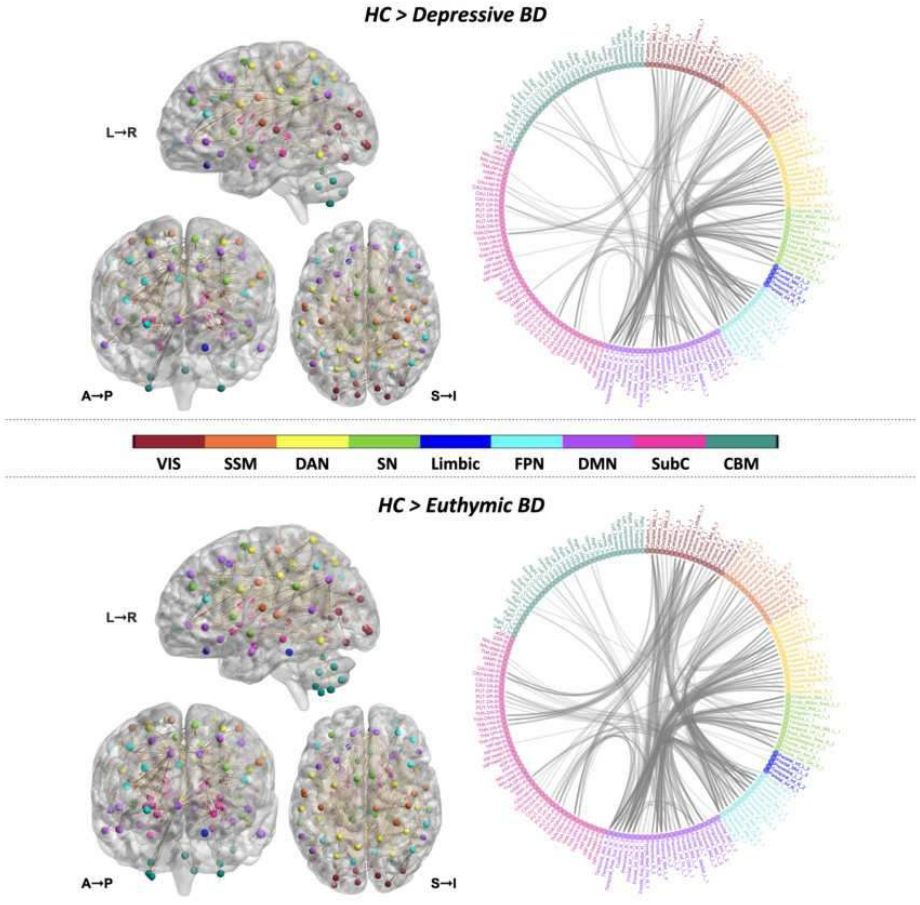

Figure 2: The comparison of functional connectivity between the healthy control (HC) group and the depressive BD (upper row) / euthymic BD (lower row). The results obtained from NBS are presented in three orthogonal views (left–right; anterior–posterior; inferior–superior) on the left and displayed using a 2D circular plot on the right. Brain regions are assigned to the functional networks as defined in [7]. Acronyms: VIS: visual; SSM: sensorimotor; DAN: dorsal attention; SN: salience network; FPN: frontoparietal; DMN: default mode network; SubC: subcortical; CBM: cerebellum.

Conclusions: Euthymia, marking the baseline and (mostly) asymptomatic state of BD, showed a general decrease in brain functional network connections. The active phases of illness showed distinct patterns of functional connectivity. Depression showed similar alterations to euthymia, whereas mania might be associated with a relative increase in functional connections with respect to the euthymic baseline. In conclusion, the results from this work showed that BD is associated with a functional reconfiguration of the architecture of intrinsic brain activity.

References
1. A.P.A., Diagnostic and Statistical Manual for Mental Disorders. 5th ed. (DSM-5). Washington: American Psychiatric Association. 2013.
2. Zalesky, A., A. Fornito, and E.T. Bullmore, Network-based statistic: Identifying differences in brain networks. NeuroImage, 2010. 53(4): p. 1197-1207.
3. Yan, C.-G., X.-D. Wang, and B. Lu, DPABISurf: data processing & analysis for brain imaging on surface. Science Bulletin, 2021. 66(24): p. 2453-2455.
4. Esteban, O., et al., fMRIPrep: a robust preprocessing pipeline for functional MRI. Nature Methods, 2019. 16(1): p. 111-116.
5. Pruim, R.H.R., et al., ICA-AROMA: A robust ICA-based strategy for removing motion artifacts from fMRI data. NeuroImage, 2015. 112: p. 267-277.
6. Behzadi, Y., et al., A component based noise correction method (CompCor) for BOLD and perfusion based fMRI. NeuroImage, 2007. 37(1): p. 90-101.
7. Schaefer, A., et al., Local-Global Parcellation of the Human Cerebral Cortex from Intrinsic Functional Connectivity MRI. Cerebral Cortex, 2017. 28(9): p. 3095-3114.
8. Tian, Y., et al., Topographic organization of the human subcortex unveiled with functional connectivity gradients. Nature Neuroscience, 2020. 23(11): p. 1421-1432.
9. Diedrichsen, J., et al., Imaging the deep cerebellar nuclei: A probabilistic atlas and normalization procedure. NeuroImage, 2011. 54(3): p. 1786-1794.
10. Yeo, B.T.T., et al., The organization of the human cerebral cortex estimated by intrinsic functional connectivity. Journal of Neurophysiology, 2011. 106(3): p. 1125-1165.

Poster No 652

Ontogenetic role for Broca's area in schizophrenic auditory hallucinations? A sulcal pits analysis

Pilar Salgado-Pineda[1], Lucila Barbosa[2], Joan Soler-Vidal[1], Cristian Caride-Padilla[3], Paola Fuentes-Claramonte[1], María Ángeles García-León[1], Noemi Hostalet[2], Mar Fatjó-Vilas[1], Yasser Alemán-Gómez[4], Laura Bucur[2], Andriana Karuk[2], Nuria Ramiro[3], Antonio Arévalo[5], Llanos Torres[6], Carmen Corte[6], Begoña Hoyos[7], Nuria Jaurrieta[5], Salvador Sarró[1], Raymond Salvador[1], Peter McKenna[1], Edith Pomarol-Clotet[1]

[1]FIDMAG Hermanas Hospitalarias Research Foundation-CIBERSAM-ISCIII, Sant Boi de Llobregat, Barcelona, [2]FIDMAG-Hermanas Hospitalarias Research Foundation, Sant Boi de Llobregat, Barcelona, [3]Hospital Sant Rafael, Barcelona, Barcelona, [4]Department of Radiology, Lausanne University Hospital and University of Lausanne (CHUV-UNIL), Lausanne, Switzerland, [5]Hospital Sagrat Cor, Martorell, Barcelona, [6]CSMA Vila de Gràcia-Cibeles, Barcelona, Barcelona, [7]CSMA Benito Menni Granollers, Granollers, Barcelona

Introduction: Auditory verbal hallucinations (AVH) are an important symptom of schizophrenia, but their biological basis is not well understood. Traditional structural neuroimaging studies have implicated the superior and middle temporal cortex, as well as the insula; however, results vary among studies (Palaniyaappan et al., 2012; Modinos et al., 2013; Barber et al., 2018). A more recent approach has suggested reduction in paracingulate gyrus length as a neurodevelopmental distinction between patients with and without AVH, yet this finding remains inconclusive (Garrison et al., 2015; Ćurčić-Blake et al., 2023). Another method for investigating neurodevelopmentally stable correlates of AVH involves the analysis of sulcal pits, an index of early cortical folding, which is assumed to be under tight genetic (Im et al., 2019, Auzias et al., 2015). In the present study, we utilized sulcal pit analysis to examine for presumptively neurodevelopmentally stable brain regions in schizophrenia patients with and without AVH.

Methods: Twenty-one patients experiencing continuous or near-continuous AVH (AVH-frequent) were compared with twenty-two well-matched patients who had never experienced AVH (AVH-never) regarding for number and depth of sulcal pits. Both patient groups were also compared to 58 healthy controls (HC) matched in terms of sex, age, and premorbid IQ. All subjects underwent scanning in a 3T MRI scanner to acquire high-resolution T1-weighted images, from which individual sulcal pit maps were extracted. For each group comparison, a specific group density map was constructed and divided into areas referred to as "areals" (Figure 1). Only areals in which 20 percent or more of the subjects exhibited one or more sulcal pits were included in the analysis.

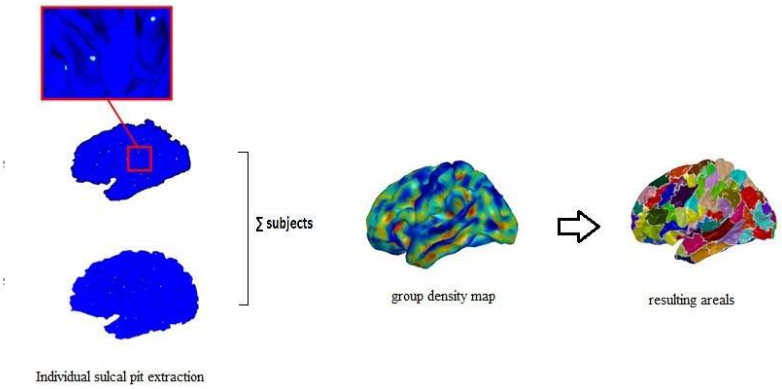

Results: : Compared to the AVH-never patients, the AVH-frequent patients had fewer sulcal pits within an areal in the left/ middle inferior frontal cortex, overlapping substantially with Broca's area (Figure 2). The AVH-frequent patients also showed a trend towards a smaller mean depth of sulcal pits compared to the HC in an areal roughly corresponding to the right homologue of Broca's area.

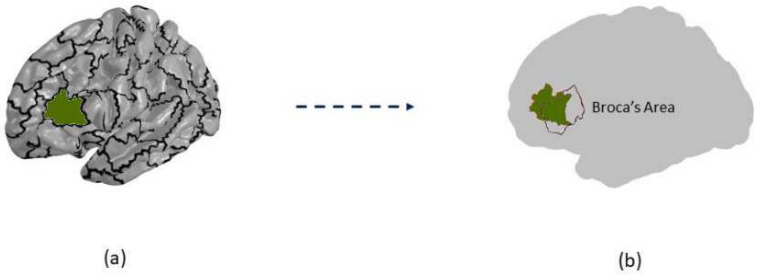

Conclusions: A smaller number of sulcal pits in AVH-frequent compared to AVH-never patients in a region co-extensive with Broca's area is consistent with the crucial role that Broca's area plays in speech production and its implications in functional neuroimaging investigations of AVH. Since sulcal pits represent anatomical landmarks that may be more closely related to brain function than other cortical measures(Im et al., 2019), our findings hint at an ontogenetic relevance for Broca's area in AVH in schizophrenia.

References

1. Palaniyaappan et al.(2012) Structural correlates of auditory hallucinations in schizophrenia: A meta-analysis. Schizophr Res 137, 169–173
2. Modinos et al.(2013) Neuroanatomy of auditory verbal hallucinations in schizophrenia: A quantitative meta-analysis of voxel-based morphometry studies. Cortex 49, 1046–1055
3. Barber et al. (2018) A review of functional and structural neuroimaging studies to investigate the inner speech model of auditory verbal hallucinations in schizophrenia. Transl Psychiatry 11, 582
4. Garrison et al. (2015) Paracingulate sulcus morphology is associated with hallucinations in the human brain. Nat Commun 6, 8956
5. Ćurčić-Blake et al. (2023) Paracingulate Sulcus Length and Cortical Thickness in Schizophrenia Patients With and Without a Lifetime History of Auditory Hallucinations. Schizophr Bull 49, S48–S57
6. Im et al. (2019) Sulcal pits and patterns in developing human brains. NeuroImage 185, 881–890
7. Auzias et al. (2015) Deep sulcal landmarks: Algorithmic and conceptual improvements in the definition and extraction of sulcal pits. NeuroImage 111, 12–25

Poster No 653

Exploring the Functional Connectivity of Insula Subregions in Children with Depression

Jiyoung Park[1,2], Euisun Kim[3,2], Maengkeun Oh[2], Yelim Lee[3,2], Sole Yoo[1,2], Jiho Min[4,2], WooYong Lee[3,2], Hae-Jeong Park[2,1,3,5]

[1]Department of Cognitive Science, Yonsei University, Seoul, Korea, Republic of, [2]Department of Nuclear Medicine, Severance Hospital, Yonsei University College of Medicine, Seoul, Korea, Republic of, [3]Graduate School of Medical Science, Brain Korea 21 Project, Yonsei University College of Medicine, Seoul, Korea, Republic of, [4]College of Humanities, Kyunghee University, Seoul, Republic of Korea, Seoul, Korea, Republic of, [5]Center for Systems and Translational Brain Sciences, Institute of Human Complexity and Systems Science, Yonsei University, Seoul, Korea, Republic of

Introduction: The insula integrates bottom-up and top-down information in emotional and cognitive processing, with networks centered on the anterior insula contributing to the integration of descending and ascending information in these processes.

Additionally, the ventral and dorsal anterior insula are associated with interoceptive self-awareness, and cognitive processing, while the posterior insula is known for processing interoceptive and exteroceptive sensations or sensory information. Each of these insula regions is implicated in the dysfunction of emotion regulation and interoceptive self-awareness in depression. However, specific functional abnormalities in the insula related to depression remain less elucidated. Therefore, this study aims to systematically investigate the functional connectivity of subregions of the insula, namely the dorsal anterior area (dAI), ventral anterior area (vAI), and posterior insula (PI), with other regions of the brain in children with depression.

Methods: The current study utilized data sourced from the Healthy Brain Network biobank (HBN) Study (ver.10.0 release) and the Adolescent Brain and Cognitive Development (ABCD) Study (ver. 4.0 release). The participants included 55 individuals diagnosed with Major Depressive Disorder (MDD), 15 with Persistent Depressive Disorder (PDD), and 70 healthy controls. Children aged 9 to 13 years were recruited from throughout the United States. The resting-state functional magnetic resonance imaging (rsfMRI) data underwent preprocessing with SPM12 and analysis using the CONN functional connectivity toolbox (Version 21a). A seed-based approach was employed to detect distinct functional connectivity patterns involving the three subregions of the insula in children with MDD and PDD. The region of interest (ROI) masks was selected: the left ventral anterior insula (-33, 13, -7), the right ventral anterior insula (32, 10 -6), the left dorsal anterior insula (-38, 6, 2), the right dorsal anterior insula (35, 7, 3), the left posterior insula (-38, -6, 5), the right posterior insula (35, -11, 6).

Results: Children with MDD exhibited heightened connectivity between the left vAI and the lateral occipital cortex compared to the control group, along with elevated connectivity between the right dAI and the cerebellum. Additionally, increased connectivity was observed between the left dAI and the precuneous cortex, cingulate gyrus, and cerebellum, while showing diminished connectivity with the brain stem. In the case of children with PDD, heightened connectivity was observed between the left vAI and the precuneous cortex, cingulate gyrus compared to the control group. Furthermore, increased connectivity was noted between the left PI and the angular gyrus, supramarginal gyrus in the PDD group.

Conclusions: Through this study, we observe enhanced neural connectivity in specific brain regions across MDD and PDD, previously distinguished by different diagnoses. Firstly, the left vAI, known to be associated with emotional processing, and the precuneus cortex, linked to self-referential thinking, exhibited heightened connectivity. Such elevated connectivity between these brain regions may be related to the specific symptoms of self-focused thinking and emotions observed in both MDD and PDD. Additionally, the heightened connectivity between left dAI and cerebellum in MDD children suggests difficulties in emotional regulation. On the other hand, the low connectivity between left dAI and brain stem implies challenges in physiological regulation, particularly in interactions with the autonomic nervous system. This may indicate difficulties in self-awareness and emotional processing in the context of MDD. These findings contribute to a deeper understanding of the neurobiological underpinnings of depression in the pediatric population indicating specific alterations in insula connectivity may play a significant role in the manifestation of depressive symptoms during childhood.

References

1. Avery, J. A. (2014). 'Major depressive disorder is associated with abnormal interoceptive activity and functional connectivity in the insula', Biological psychiatry, vol. 76, no. 3, pp. 258-266
2. Deen, B. (2011). 'Three systems of insular functional connectivity identified with cluster analysis', Cerebral cortex, vo. 21, no. 7, pp. 1498-1506
3. Iwabuchi, S. J.(2014). 'Alterations in effective connectivity anchored on the insula in major depressive disorder', European Neuropsychopharmacology, vol. 24, no.11, pp. 1784-1792
4. Marchitelli, R. (2022). 'Dynamic functional connectivity in adolescence-onset major depression: Relationships with severity and symptom dimensions', Biological Psychiatry: Cognitive Neuroscience and Neuroimaging, vol. 7, no. 4, pp. 385-396
5. Nieto-Castanon, A. (2020). 'Functional Connectivity measures. In Handbook of functional connectivity Magnetic Resonance Imaging methods in CONN', Hilbert Press, pp. 26–62
6. Penny, W. D. (2011). 'Statistical parametric mapping: the analysis of functional brain images', Elsevier.

Poster No 654

Longitudinal Inference of Multimodal Cortical and Hippocampal Connectivity in Psychosis Subtypes

Jana Totzek[1,2], Mallar Chakravarty[1,2], Ridha Joober[1,2], Ashok Malla[1,2], Jai Shah[1,2], Alexandra Young[3], Martin Lepage[1,2], Katie Lavigne[1,2]

[1]McGill University, Montreal, Quebec, [2]Douglas Research Centre, Montreal, Canada, [3]University College London, London, London

Introduction: The hippocampus is the neural correlate which shows the largest reduction in volume in psychosis (van Erp et al., 2016), while reductions in morphometric hippocampal-cortical connectivity predict negative symptoms as mediated by verbal memory (Makowski et al., 2020). Machine-learning approaches suggest that there are two distinct subtypes of neural

atrophy in psychosis, of which one begins in the hippocampus (Jiang et al., 2023). To date it remains open when multimodal hippocampal connectivity deviates in relation to other cortical modules across subtypes of psychosis.

Methods: We measured morphometric and resting-state functional connectivity. To derive morphometric connectivity, we sampled data from 175 patients with first episode (FEP) and enduring psychosis, and 117 non-clinical controls. 18 hippocampal and adjacent white matter volumes were derived through MAGeT (Pipitone et al., 2014), while cortical thickness was extracted through CIVET 2.1.1 (Ad-Dab'bagh et al., 2006), and parcellated into 62 DKT regions (Klein & Tourville, 2012). Structural covariance matrices were derived for patients and controls separately, and subject-specific structural covariance matrices through the jackknife bias estimation procedure (Ajnakina et al., 2021). The hippocampal regions were grouped into a hippocampal module while the cortical regions were grouped into the 7 Yeo modules (Makowski et al., 2020; Yeo et al., 2011), and we estimated the graph-theoretical participation coefficient as a measure of intermodular connectivity (Rubinov & Sporns, 2010). To derive resting-state functional connectivity, we sampled data from 66 FEP patients, and 51 controls. We used the CONN toolbox to extract functional correlation matrices between the 18 hippocampal MAGeT-regions and 46 cortical regions of the Harvard-Oxford atlas. The hippocampal regions were grouped into a hippocampal module and the 46 cortical regions were grouped into the Yeo modules to derive participation coefficients. We used the average participation coefficients of all 8 morphometric and 8 functional modules as input for two separate Subtype and Stage Inference (SuStaIn) analyses (Young, 2018). SuStaIn is a machine-learning algorithm which merges disease progression modeling and clustering, allowing us to derive connectivity progression patterns across psychosis subtypes.

Results: Following 10-fold cross-validation, SuStaIn resulted in two models with three subtypes each. In the morphometric and functional analyses, Subtype 0 included individuals with normal-range connectivity on all markers. In the morphometric analysis, Subtype 1 progressed from decreased somatomotor network connectivity to decreased dorsal attention (DAN), frontoparietal (FPN), visual, salience, and hippocampal network connectivity, followed by increased limbic and default mode network (DMN) connectivity, while Subtype 2 progressed from increased DMN and limbic network connectivity to decreased hippocampal, salience, DAN, FPN, visual, and somatomotor network connectivity. Different patterns emerged in the functional SuStaIn analysis. Subtype 1 progressed from decreased FPN, limbic, visual, DMN, and hippocampal network connectivity toward increased DAN, somatomotor, and salience network connectivity, while Subtype 2 progressed from increased somatomotor, salience, and DAN connectivity toward decreased hippocampal, DMN, visual, limbic, and FPN connectivity.

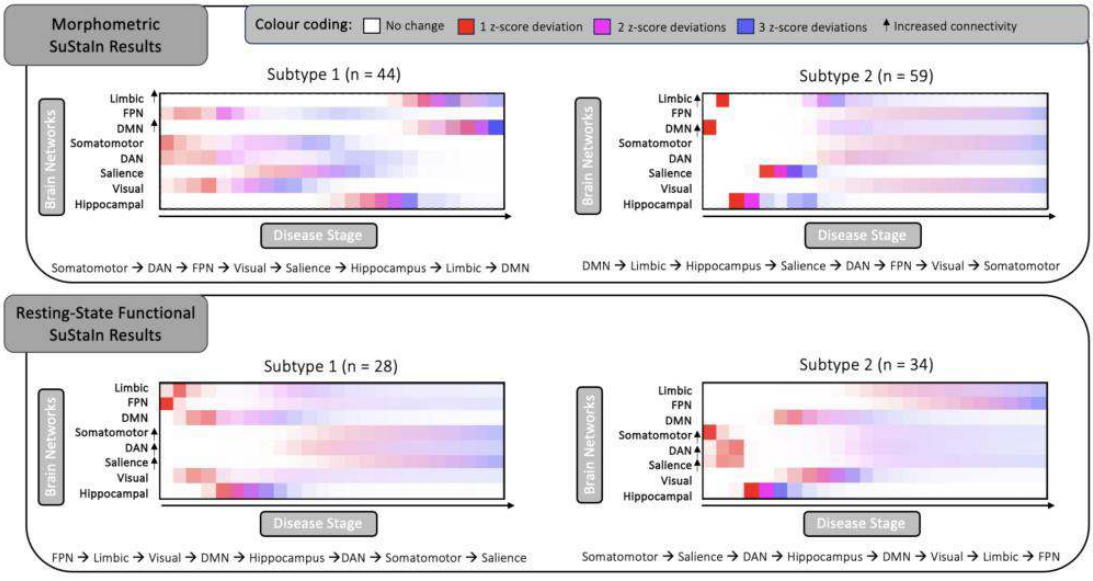

Note. FPN = Frontoparietal Network, DMN = Default Mode Network, DAN = Dorsal Attention Network

Conclusions: We found that hippocampal connectivity was the first to decrease after an increase in cortical connectivity across modalities. Our results are consistent with Jiang et al. (2023) and extend these findings into the field of multimodal connectivity, while underlining the role of bidirectional modeling in psychosis. Future work should address the relationship between the identified subtypes and clinical features of psychosis to evaluate the clinical utility of SuStaIn in using these neural progression patterns as a potential predictor of clinical outcomes.

References

1. Ad-Dab'bagh, Y. (2006). The CIVET image-processing environment: a fully automated comprehensive pipeline for anatomical neuroimaging research. Paper presented at the Proceedings of the 12th annual meeting of the organization for human brain mapping.
2. Ajnakina, O. (2021). Structural covariance of cortical gyrification at illness onset in treatment resistance: a longitudinal study of first-episode psychoses. Schizophrenia bulletin, 47(6), 1729-1739.

3. Jiang, Y. (2023). Neuroimaging biomarkers define neurophysiological subtypes with distinct trajectories in schizophrenia. Nature Mental Health, 1(3), 186-199.
4. Klein, A. (2012). 101 labeled brain images and a consistent human cortical labeling protocol. Frontiers in neuroscience, 6, 171.
5. Makowski, C. (2020). Altered hippocampal centrality and dynamic anatomical covariance of intracortical microstructure in first episode psychosis. Hippocampus, 30(10), 1058-1072.
6. Pipitone, J. (2014). Multi-atlas segmentation of the whole hippocampus and subfields using multiple automatically generated templates. Neuroimage, 101, 494-512.
7. Rubinov, M. (2010). Complex network measures of brain connectivity: uses and interpretations. Neuroimage, 52(3), 1059-1069.
8. van Erp, T.G. (2016). Subcortical brain volume abnormalities in 2028 individuals with schizophrenia and 2540 healthy controls via the ENIGMA consortium. Molecular psychiatry, 21(4), 547-553.
9. Yeo, B.T. (2011). The organization of the human cerebral cortex estimated by intrinsic functional connectivity. Journal of neurophysiology.
10. Young, A.L. (2018). Uncovering the heterogeneity and temporal complexity of neurodegenerative diseases with Subtype and Stage Inference. Nature communication

Poster No 655

FMRI multitask deep phenotyping: subject-specific deviation analysed across contrasts and tasks

Philipp Sämann[1], BeCOME study team[1], Michael Czisch[1]

[1]Max Planck Institute of Psychiatry, Munich, Germany

Introduction: Task fMRI is considered powerful to capture individual and task specific brain states and by this phenotype neuropsychiatric conditions. In the BeCOME study that is in part aligned to the RDoC classification principles we are currently deep-phenotyping subjects in a spectrum from super-healthy to moderate to severe anxiety and depression disorders [REF]. One major component of the neurobiological measurements is a task-fMRI battery distributed over two fMRI session on separate days (see methods). The major challenge lies in breaking down the fMRI task data to meaningful, condense information substrate that captures inter-individual variability on one hand, but allows for interpretation of the feature space. Here we pursue an BOLD activation based approach and similarity analyses between subjects to rank them, depending on 'atypicality' within the sample, both using separate key contrasts of the task model, the entire task, or all tasks. Our main questions are: (1) How independent is the information from different tasks and task contrasts when it comes to subject ranking along these axes? (2) How important is BOLD amplitude infomation gained from deactivations (also referred to as task-negative networks)?

Methods: In the BeCOME study we include healthy subjects and subjects with current or past disorders of the anxiety/depression spectrum. A data freeze was made July 2023 which left us with 238 subjects of which a homogeneous set of the following four tasks was available. TASKS. (i) N-Back task (with contrasts NB2<>NB0, NB2<>NB1, NB2<>NB1 and NB<>fixation), (ii) Reward anticipation task (money gain, verbal feedback, control; with contrasts money<>control, verbal<>control and money<>verbal), (iii) Hariri emotional faces matching task (with contrasts: all faces<>geometry, negative<>geometry, negative<>neutral) and (iv) Time Estimation Task with three feedback types (with contrasts correct<>false, correct<>uncertain and false<>uncertain). fMRI ANALYSIS: State-of-the-art preprocessing with slice timing correction, motion correction, spatial normalisation (DARTEL), physiological noise correction using CompCor, classical general linear models to estimate regressor influences and to generate individual contrast maps, SECOND LEVEL ANALYSIS AND ROI DEFINITION: ROIs were positioned in centers of group activation and deactivation maps; a 7x7x7 voxel box was weighted with the group T statistics. A total of 24 contrasts for the four tasks was defined, with 39 (N-back), 31 (Reward), 33 (Hariri) and 22 (TET) ROIs, and contrast values extracted from 238 subjects, resulting in 24 specific poly-regional BOLD response vectors per subject. CALCULATION OF INDIVIDUAL RANK: Per contrast (and later per task and across all tasks) we calculated the simple Eucledian distance which can be understood as a measure of (statistical) atypicality or abnormality.

Results: Key contrasts were inspected to detect preprocessing or modelling errors. Figure 1 exemplifies the positioning of a total of 13 ROIs (9 in the positive, 4 in the negative contrast of the NB2<>NB0 condition. Comparing the cross-correlation of the 24 ED vectors among eachother (Figure 2A-C) we found that (1) there is dissimilarity between the tasks compared against within-task, (2) a checkerboard-like structure indicating the independence of task-positive and task-negative subject ranking, (3) highest values for faces<>geometry against negative<>geometry (expected as most faces had a negative valence). In addition, the N-Back and Reward task were rather similar whereas the Hariri task was moderately related to N-Back and Reward, but unrelated to TET.

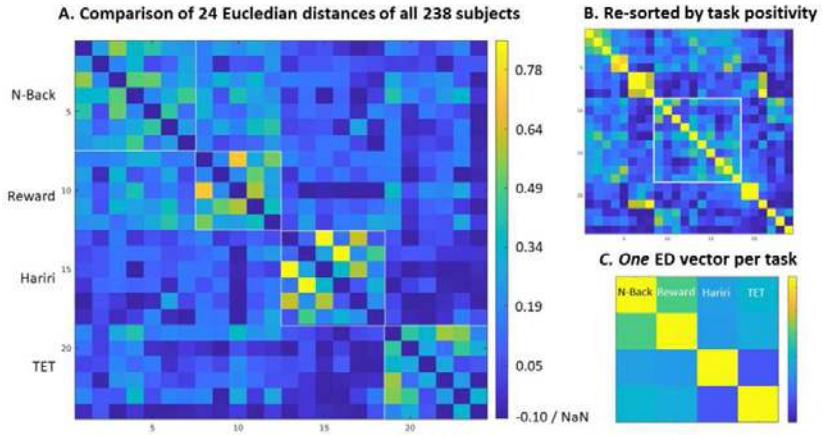

Conclusions: Calculating the Eucledian distance of a subject in relation to a group is a useful tool to investigate, if features generated from task-based fMRI are independent or redundant. Task-negative responses (typical default mode regions) seem to carry an independent information, possibly with task-specificity.

References

1. Brückl T, Spoormaker V, Sämann PG et al. (2020) 'The biological classification of mental disorders (BeCOME) study: a protocol for an observational deep-phenotyping study for the identification of biological subtypes.' BMC Psychiatry, vol 20, no 213
2. Chen J, Rashid B, Yu Q, Liu J, Lin D, Du Y, Sui J, Calhoun VD (2018), 'Variability in Resting State Network and Functional Network Connectivity Associated With Schizophrenia Genetic Risk: A Pilot Study'. Front Neurosci vol 12, no 114.

Poster No 656

Oxytocin alters fMRI intersubject correlation in psychotic disorders during emotional video watching

Vasco Diogo[1,2], Diana Prata[3,4]

[1]CIS-Iscte, Iscte-Instituto Universitário de Lisboa, Lisboa, Lisboa, [2]Instituto de Biofísica e Engenharia Biomédica - Faculdade de Ciências da Universidade de Lisboa, Lisboa, Portugal, [3]Instituto de Biofísica e Engenharia Biomédica - Faculdade de Ciências da Universidade de Lisboa, Lisboa, Lisboa, [4]Institute of Psychiatry, Psychology & Neuroscience King's College London, London, United Kingdom

Introduction: Psychotic disorders are characterized by deficits in social cognition, for which there are limited effective treatments. Oxytocin (OT), a neuropeptide involved in social cognition, has shown potential for clinical benefits in patients with psychotic disorders. Our recent study aimed to explore the effects of intranasal OT administration on the brain activity in patients with psychotic disorders during a naturalistic social cognition task.

Methods: Using functional magnetic resonance imaging (fMRI), we investigated the brain activity of 37 men with psychotic disorders randomly assigned to receive intranasal OT or a placebo, while 20 healthy men received a placebo (PBO). Participants viewed 16 40-second long video clips during the imaging session. Region of interest were defined using the AAL 2 parcellation and the Yeo 7 network parcellation. Data was analyzed using inter-subject correlation (ISC) within a Bayesian

multilevel framework. (Chen et. al, 2020) ISC was calculated between each pair of subjects belonging to the same group (within-group ISC) and compared across groups.

Results: Emotional videos elicited ISC in Visual and Dorsal Attention Networks in each and every group. Results demonstrated that patients who received the placebo showed decreased ISC in the Dorsal Attention and Visual networks compared to healthy controls. In contrast, patients who received OT did not show significant ISC differences compared to controls. Regarding AAL2 brain regions, patients receiving placebo showed decreased ISC in 28 regions and increased ISC in 7 regions when compared with healthy controls. The largest effect was observed in the left inferior occipital gyrus (z-score=-0.20, meaning HC were more synchronized than patients) Meanwhile, patients receiving OT showed decreased ISC in only 13 regions, and decreased ISC in 12 regions, with the largest estimate (z-score), being -0.09,in the right middle occipital gyrus.

Conclusions: These findings suggest that intranasal OT administration can normalize the inter-subject correlation of brain activity in patients with psychotic disorders across resting state networks. These findings also confirm that ISC is altered in patients with psychosis, with ISC being lower or higher in patients depending on the brain region. Intranasal OT administration is shown to normalize these alterations across multiple brain regions, decreasing or increasing ISC depending on the disfunction, and never exacerbating it. Sharing these findings is crucial as it provides insights into the neurobiological mechanisms underlying social cognition deficits in psychotic disorders and highlights the potential of OT as a therapeutic intervention for enhancing social cognition. These findings contribute to the development of more effective treatment strategies and improving the quality of life for individuals with psychotic disorders.

References

1. Gang C. (2020), 'Untangling the relatedness among correlations, part III: Inter-subject correlation analysis through Bayesian multilevel modeling for naturalistic scanning', NeuroImage, vol. 216, 116474

Poster No 657

Unravelling MDD brain circuits and clinical subtypes: A crossmodal ALE meta-analysis of 395 studies

Mónica Sobral[1,2], Raquel Guiomar[1], Manya Rezaeian[3], Maria Vasileiadi[4], Sara Cruz[5,6], Francisca Pacheco[1], Vera Mateus[1], Roser Palau-Costafreda[7,8], Johanna Pozo-Neira[9], Ana Weidenauer[10], Helena Moreira[1], Martin Tik[11], Ana Ganho-Ávila[1], Anna-Lisa Schuler[12]

[1]Center for Research in Neuropsychology and Cognitive Behavioral Intervention, Coimbra, Portugal, [2]Developmental Disorders Program and Mackenzie Center for Research in Childhood and Adolescence, São Paulo, Brazil, [3]Counseling Center of Tehran University, Tehran, Iran, [4]Medical University of Vienna, Vienna, Vienna, [5]The Psychology for Positive Development Research Centre, Lusiada University, Porto, Portugal, [6]Department of Psychology, School of Philosophy, Psychology & Language Sciences, University of Edinburgh, Edinburgh, United Kingdom, [7]ESIMar (Mar Nursing School), Parc de Salut Mar, Universitat Pompeu Fabra-affiliated, Barcelona, Spain, [8]SDHEd (Social Determinants and Health Education Research Group), IMIM (Hospital del Mar Medical Research Institute), Barcelona, Spain, [9]Institute of Neuroscience, Universidad Católica de Cuenca, Cuenca, Ecuador, [10]Medical University of Vienna, Vienna, Austria, [11]High Field MR Center, Center for Medical Physics and Biomedical Engineering, Medical University of Vienna, Vienna, Austria, [12]Max Planck Institute for Human Cognitive and Brain Sciences, Leipzig, Saxony

Introduction: The understanding and treatment of major depressive disorder (MDD) have faced challenges due to its heterogeneous clinical presentation and variable treatment outcomes, highlighting that there may exist multiple forms of depression[1]. Advancements in neuroimaging have revealed disrupted affective and neurocognitive brain circuitry, offering potential insights into symptom diversity through distinct circuit-based biotypes (e.g., clustering patients based on shared brain dysregulation signatures[1,2]. This emerging approach aims to target specific circuits associated with distinct symptom clusters, such as dysphoric and anxiosomatic, offering a promising avenue for more effective and personalised treatment strategies[3,4]. In this meta-analytical study, objectives were two-fold: first, to determine if the same brain pattern observed in MDD populations applies to one known subtype, those experiencing depressive symptoms during the peripartum period (PPD). Second, considering network effects that potentially support specific symptoms.

Methods: To accomplish this, we conducted a systematic literature search in PubMed, Embase and PsychINFO to identify peer-reviewed original studies in English across brain imaging modalities (functional and structural magnetic resonance imaging [MRI], diffusion tensor Imaging [DTI], positron emission tomography [PET], near-infrared spectroscopy [NIRS] and magnetic resonance spectroscopy [MRS]). Flow-chart of literature selection is depicted in Figure 1. We then performed a cross-modal coordinate-based meta-analysis using activation likelihood estimation (ALE) to combine peak coordinates from

included studies, using GingerALE (cluster-level inference of p<0.05, with 10000 thresholding permutations) for MDD, PPD and MDD female only subtypes, respectively.

Results: A total of 6624 MDD reports were screened for inclusion. Of these, 369 (11378 participants) were included for the MDD cluster meta-analysis. Regarding subgroup meta-analysis, we included 20 studies with only female MDD participants (318 participants). For the PPD subgroup, 592 reports were screened and 26 studies included (581 participants). Several clusters related to emotional and cognitive processing were found to be disrupted in the MDD full sample, namely right vmPFC, bilateral amygdala, left putamen and right insula (Figure 1). While for MDD female and PPD there was an overlap in the right amygdala, the right putamen and left DLPFC was stronger involved in PPD and the left VMPFC and DLPFC in MDD female (Figure 2). Furthermore, while PPD encompassed similar components as the anxiosomatic depression network, suggested by Cash et al. (4), there was no clear overlap suggesting involvement of other networks. Performing seed-based connectivity analysis from the right amygdala seed in PPD reveals involvement of somatomotor, temporal and prefrontal areas (Figure 2).

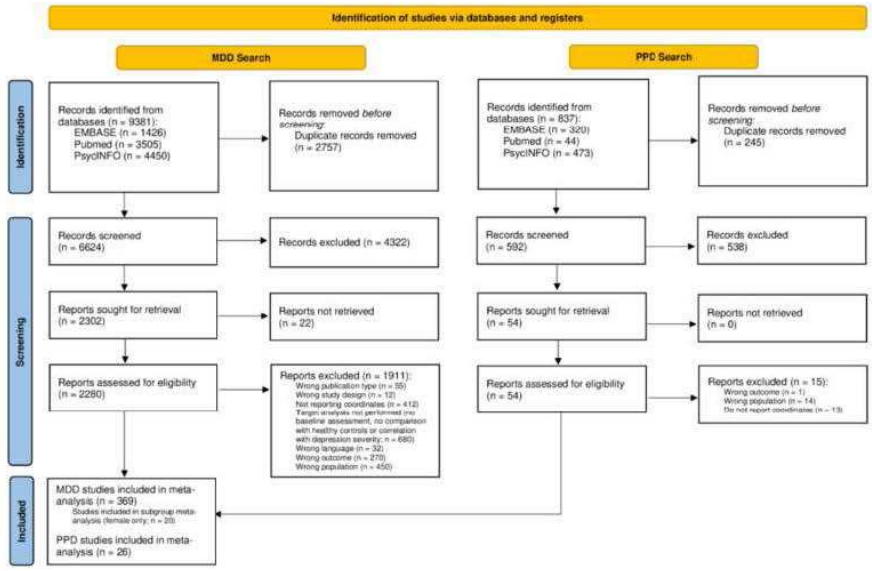

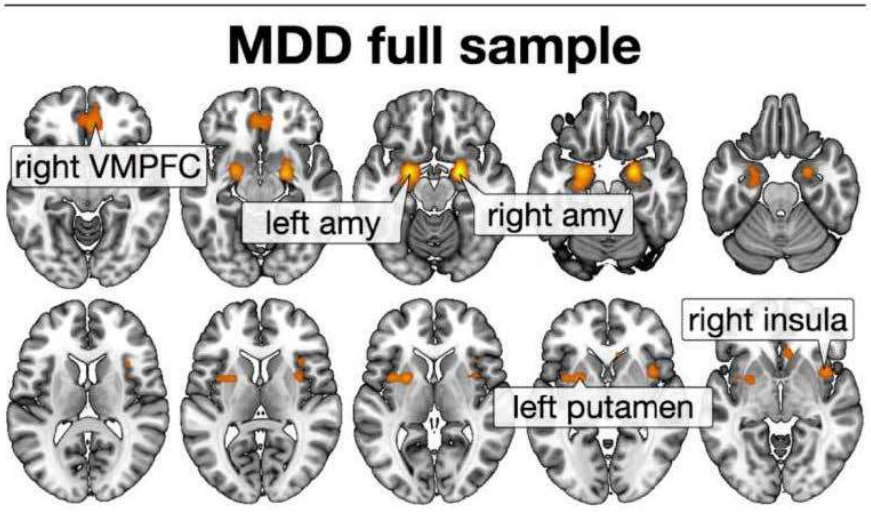

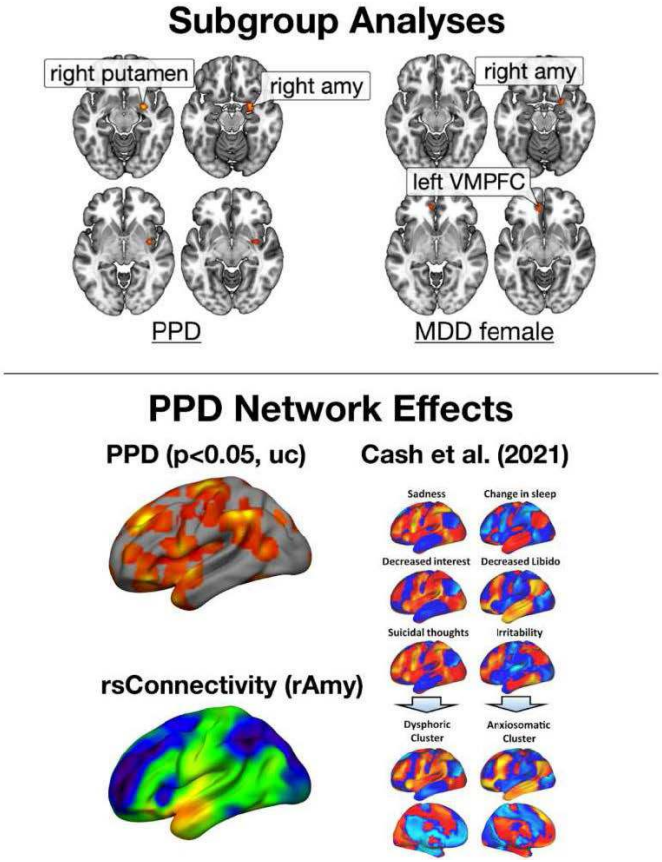

Conclusions: Current classification systems (e.g., 13 subtypes based on symptoms, such as atypical and melancholic) aimed to personalise treatment but fail to improve treatment outcomes (2). The distinct brain patterns differentiating general MDD from PPD sustain the need for tailored treatment approaches that consider MDD subtypes on a fine-grained level. Specifically, better targeting approaches of MDD subtypes might improve non-pharmacological approaches, such as TMS (3,4), considering as well the significance of sex/gender as a biomarker shaping the effects of therapeutic response (5).

References

1. Drysdale, A. T., Grosenick, L., Downar, J., Dunlop, K., Mansouri, F., Meng, Y., Fetcho, R. N., Zebley, B., Oathes, D. J., Etkin, A., Schatzberg, A. F., Sudheimer, K., Keller, J., Mayberg, H. S., Gunning, F. M., Alexopoulos, G. S., Fox, M. D., Pascual-Leone, A., Voss, H. U., Casey, B. J., … Liston, C. (2017), 'Resting-state connectivity biomarkers define neurophysiological subtypes of depression', Nature Medicine, vol. 23, no. 1, pp 28–38. https://doi.org/10.1038/nm.4246
2. Nestor, S. M., & Blumberger, D. M. (2020), 'Mapping symptom clusters to circuits: Toward personalizing TMS targets to improve treatment outcomes in depression', The American Journal of Psychiatry, vol. 177, no. 5, pp 373–375. https://doi.org/10.1176/appi.ajp.2020.20030271
3. Siddiqi, S. H., Taylor, S. F., Cooke, D., Pascual-Leone, A., George, M. S., & Fox, M. D. (2020), 'Distinct symptom-specific treatment targets for circuit-based neuromodulation', The American Journal of Psychiatry, vol. 17, no. 5, pp 435–446. https://doi.org/10.1176/appi.ajp.2019.19090915
4. Cash, R. F. H., Weigand, A., Zalesky, A., Siddiqi, S. H., Downar, J., Fitzgerald, P. B., & Fox, M. D. (2021), 'Using brain imaging to improve spatial targeting of transcranial magnetic stimulation for depression', Biological Psychiatry, vol. 90, no. 10, pp. 689–700. https://doi.org/10.1016/j.biopsych.2020.05.033
5. Hanlon, C. A., & McCalley, D. M. (2022), 'Sex/gender as a factor that influences transcranial magnetic stimulation treatment outcome: Three potential biological explanations', Frontiers in Psychiatry', vol. 13, 869070. https://doi.org/10.3389/fpsyt.2022.869070

Poster No 658

Distinct therapeutics of depression work on a common brain network

Wenqiang Xu[1], Gong-Jun Ji[2], Kai Wang[2], Yinian Yang[2]

[1]Anhui Medical University, Hefei, Anhui, [2]Anhui Medical University, Hefei, Anhui Province

Introduction: Understanding the neural mechanisms underlying depression remission is crucial for developing effective treatments. Here we tested whether brain regions longitudinally changed with antidepressive therapies were neuroanatomically heterogeneous but are part of a specific depression remission network.

Methods: We systematically searched the longitudinal studies of antidepressive therapies to identify brain regions of treatment-induced GMV increases in depression patients. Utilizing the study-derived coordinates, a novel remission network mapping (RNM) approach, incorporating sensitivity, specificity and conjunction analyses, was employed to delineate the depression remission network (DRN). This approach was conducted using the normative connectome data of 652 Asian participants (validated in a data of 1000 Western participants). Multiple datasets were used to validate this DRN, and show its clinical implication. Group- and individual-level validation datasets. We systematically searched longitudinal studies reporting cortical thickness (CT) increases after treatment. The reported coordinates were collected as group-level validation data. Individual-level validation was performed on two independent longitudinal datasets of depression patients treated by ECT (including USTC and AHMU cohorts) and one control group (patients with Parkinson's disease treated with rTMS). To further validate our DRN in the context of clinical therapies, we tested whether the DRN is spatially overlapped with common targets of deep brain stimulation (DBS) (11 sites in Burke, M.J., et al., 2022, Molecular Psychiatry) and target atlas of repetitive transcranial magnetic stimulation (rTMS) (Siddiqi, S.H., et al., 2020, The American Journal of Psychiatry) for depression. The statistical significance of was tested by permutation tests. Finally, the DRN was used to explain the outcome variability of rTMS treatment for depression patients (n=24). Specifically, the DRN was binarized to identify positive regions as a seedmap. We test whether the average changes of functional connectivity strength within seedmap mask were correlated to the Hamilton Depression Scale-17 (HAMD-17) improvement rates using partial Pearson correlation, controlling for age, gender, education, HAMA, HAMD-17, and disease duration

Results: Total of 17 depression experiments including 581 participants were included in this study. The included treatment modalities comprise pharmacotherapy, electroconvulsive therapy (ECT), psychotherapy, and magnetic seizure therapy.The RNM analysis identified bilateral amygdala and parahippocampal gyrus as hub regions of the DRN (Figure 1). The group-level validation analysis indicated the DRN showing stronger functional connectivity to brain regions with CT changes in depression than non-depressed patients (P=0.0073; figure 2A). The individual-level validation analysis indicated the DRN showing stronger spatial correlation with remission networks of individual depression patient (USTC cohort P<0.0001; AHMU cohort P=0.0006; figure 2B) than controls. The real DBS targets of depression showed greater functional connectivity to the DRN than random targets (P=0.0015, 10,000 permutation tests; figure 2C). The DRN is similar to the TMS targeting atlas previously reported (spatial similarity r=0.721, permutation test P=0.004, 10,000 permutation tests; figure 2D) uisng Neuromaps toolbox. Finally, we demonstrated that the amelioration of depression symptom is positively associated with the functional connectivity increase within the DRN (r=0.603, P=0.008; figure 2E). No significant correlation was found for non-depression symptoms.

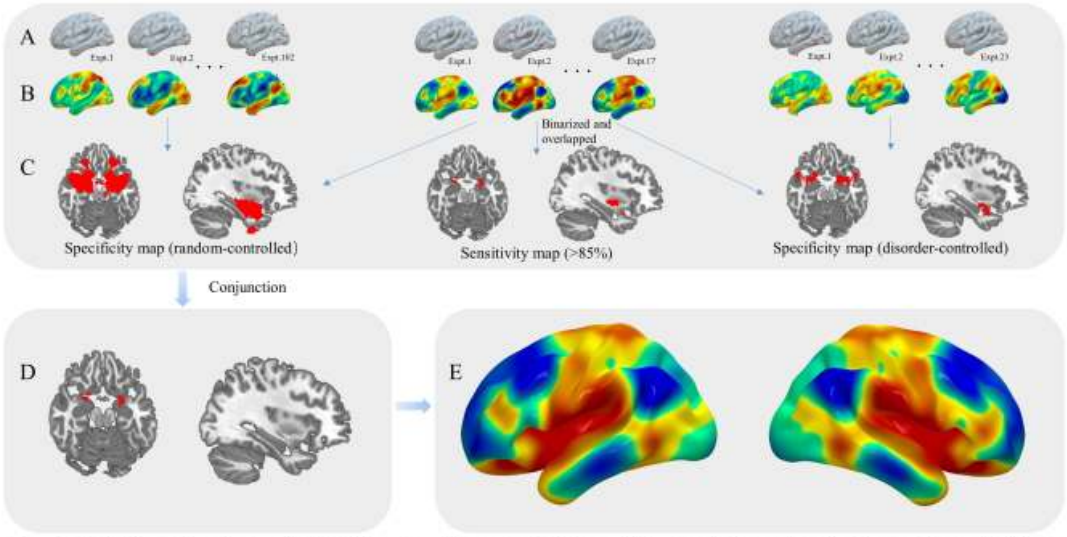

Figure 1.Remission network mapping (RNM) approach is comprised of sensitivity specificity and conjunction analyses. (A) Spheres 6 mm in diameter were first created centered at each extracted coordinate and multiple coordinates from one experiment were added together to generate an experiment-specific combined seed. **(B)** Functional connectivity of each seed location to the rest of the brain was computed using the normative connectome data of 652 Asian participants (voxel-wised Family-wise error [FWE]-corrected $P<0.01$). **(C) Generation of Sensitivity map.** experiment-level remission networks were then binarized with a threshold of $t > 5.1$ (corresponding to a voxel-wise FWE-corrected $P< 0.01$) and added together to identify remission network overlap map. **Generation of Specificity maps.** The experiment-level remission networks were compared with two control groups, a group of random networks computed using the same method as the experiment-level remission networks of depression, but the seed spheres were randomly redistributed in the gray matter and a group of nondepressed subjects derived from longitudinal treatment findings (cluster-level FWE-corrected $P < 0.05$) **(D)** Conjunction analysis was performed to identify the region that were both sensitive (i.e., connected to >85% of depression remission regions) and specific (voxels surviving all two specificity tests). The hub region of depression remission are located in the bilateral amygdala and the parahippocampal gyrus. **(E)** Using the normative connectome data, we examined the whole-brain functional connectivity of this hub regions. generating a depression remission network. This network incorporates longitudinal antidepressive therapy findings associated with depression remission while avoiding locations that are not.

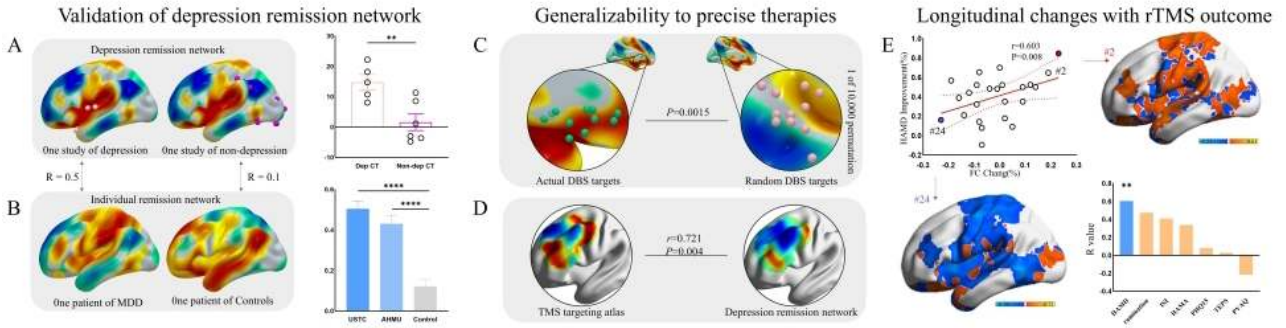

Figure 2. Validation and clinical implication of depression remission network. (A) Group-level validation. We separately extracted the t-value of the experiment-specific combined seeds of depressed cortical thickness (CT) and nondepressed CT from the depression remission network. The group-level validation analysis indicated depressed CT exhibited a higher correlation strength with depression remission network than nondepressed CT (P=0.0073). **(B) Individual-level validation.** The individual-level validation revealed that the individual remission networks of both USTC and AHMU cohorts exhibit significantly spatial correlation to depression remission network than controls (USTC cohort $P < 0.0001$; AHMU cohort P=0.0006). **(C) DBS treatment**, we identified 11 targets with evidence of efficacy in treating depression, which all fell within our depression remission network. we created 11 sham targets 10,000 times as a control group according spatial distribution of successful DBS targets. As hypothesized, the successful DBS targets showed significantly greater functional connectivity to the depression remission network than sham targets(P=0.0027, 10,000 permutation test). **(D) TMS treatment**, we identified a predecessors' TMS targeting atlas that have successfully been validated to treat depression and compared it with our own TMS targeting atlas via neuromaps, a toolbox for accessing, transforming and analyzing structural and functional brain annotations. This analysis concluded that our own TMS targeting atlas was similar to predecessors' TMS targeting atlas (spatial similarity r=0.721 and P=0.004, 10,000 permutation test). **(E)** Finally, we demonstrated that the average changes of functional connectivity strength within depression remission network were positively correlated with the HAMD-17 score improvement rates after rTMS treatment when controlling for age, gender, education, HAMA, HAMD-17, and disease duration (partial correlation r=0.603, P=0.008). No significant correlation was found for non-depression symptoms.

Conclusions: Distinct clinical therapies may work on a common brain network that underlying the remission of depression patients.

References

1. Burke, M.J. (2022) 'Placebo effects and neuromodulation for depression: a meta-analysis and evaluation of shared mechanisms', Molecular Psychiatry,
2. Siddiqi, S.H. (2020), 'Distinct Symptom-Specific Treatment Targets for Circuit-Based Neuromodulation', The American Journal of Psychiatry

Poster No 659

Dynamic Fusion of SNP and FNC in UK Biobank Reveals Static and Time-varying Manifolds

Jiayu Chen[1], Armin Iraji[2], Zening Fu[3], Pablo Andrés-Camazón[4], Bishal Thapaliya[1], Jingyu Liu[1], Vince Calhoun[5]

[1]GSU, Atlanta, GA, [2]Georgia State University, Atlanta, GA, [3]Tri-institutional Center for Translational Research in Neuroimaging and Data Science (TReNDS) Georgi, Atlanta, GA, [4]Hospital General Universitario Gregorio Marañón, Madrid, Spain, [5]GSU/GATech/Emory, Decatur, GA

Introduction: Psychiatric disorders are highly heritable[1] and genetic factors likely exert influence on clinical manifestations by affecting the brain[2]. Despite holding promise for individualized treatment, characterizing genetic and neurobiological profiles and their interrelationships has proven a big challenge for complex brain disorders, given the polygenic nature and modest effect sizes[3]. The current work proposes a novel dynamic fusion framework to perform multiple single nucleotide polymorphisms (SNPs) - dynamic functional network connectivity (dFNC) fusions to evaluate static and time-varying manifolds. We showcased how the proposed framework, coupled with the large UK Biobank (UKB) and aggregated schizophrenia (SZ) cohorts, offered additional insights into how genetic risk links to SZ-related dysconnectivity.

Methods: We used the QC'ed SNPs and resting fMRI (rsfMRI) data of 32,861 non-related European ancestry individuals of UKB (47% males, aged 45-81). The PGC 287 loci4 pruned at r2 < 0.2 yielded 12,946 SZ-risk SNPs. The rsfMRI data were processed using the fully automated NeuroMark pipeline[5]. The Neuromark_fMRI_1.0 network template served as a reference in a spatial-constrained independent component analysis[6] to derive 53 intrinsic connectivity networks (ICNs), based on which windowed FNC (wFNC) was estimated[7]. K-means clustering on wFNCs identified four dynamic states using the elbow criterion. Next, the state-specific dFNC was computed as the mean of wFNCs assigned to that state for each subject. Joint ICA8 was then applied to the concatenated SZ-risk SNPs and each of the four state-specific dFNC matrices (32,861 × 14,324) resulting in four parallel fusions of 35 joint SNP-dFNC components. Joint components were validated for relevance to SZ by projecting their dFNC parts to the state-specific dFNC features derived in the same way in an aggregated SZ cohort consisting of 1,237 individuals (43% SZ, 60% males, aged 16-79). A two-sample t-test identified SZ-discriminating dFNC components (FDR p < 0.05). For each component, we evaluated its modality-specific similarity with those of other three fusions, with low similarity indicating high

state-specificity, and hence high dynamism. For validated SZ-relevant components, we identified the top SNPs and dFNC features (|z-score|>3). Gene Ontology pathway analysis was conducted on the annotated genes of top SNPs for enriched biological processes. The top dFNC features (i.e., connectivity edges) were interpreted based on the anatomical labels of the involved ICNs.

Results: A wide range of dynamism was noted for both SNP and dFNC modality across four parallel fusions (Fig. 1a-1b). A total of 53 joint components were validated as SZ-relevant, which did not appear to be biased towards high or low dynamism. Fig. 1c-1f present component 9 of SNP-dFNCstate1 fusion (State1_jICA9) and State3_jICA7 as an example of intermediate similarity. Both dFNC components highlighted thalamus-seeded connections, and their SNP components shared 37% of the annotated genes, both enriched for cell projection organization. In contrast, Fig. 1g-1h shows State1_jICA4 as an example of low similarity. Its SNP component was enriched for cell projection also, despite not being correlated with State1_jICA9. Its dFNC component highlighted insula-seeded connections.

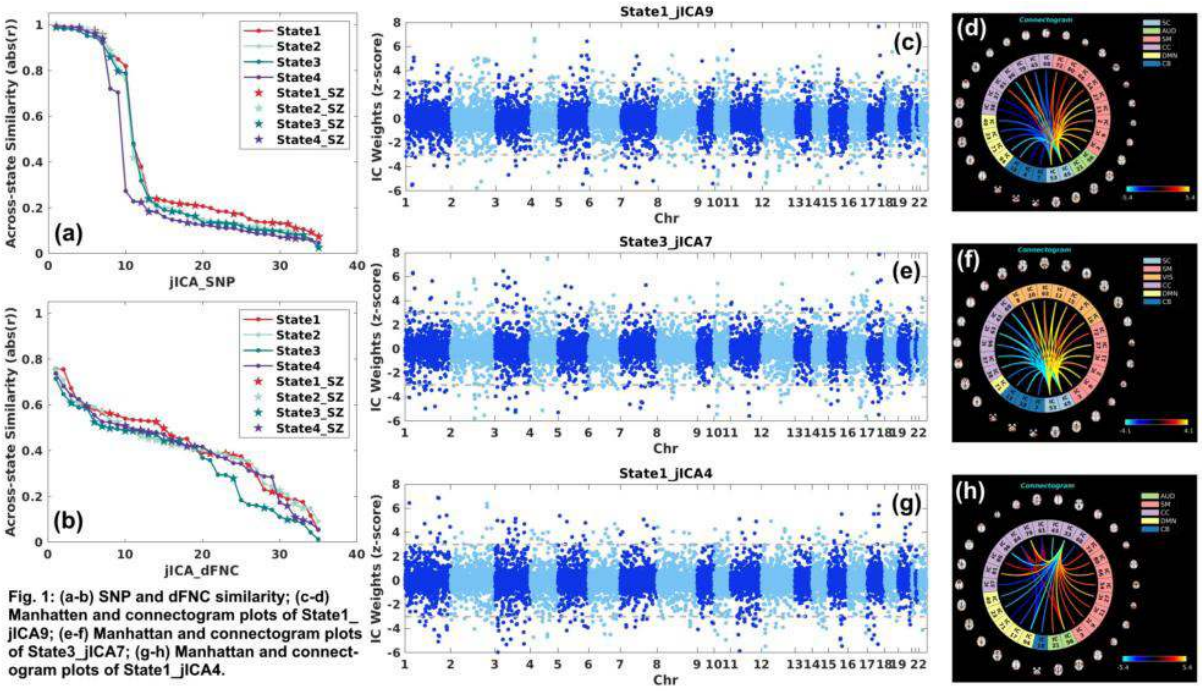

Fig. 1: (a-b) SNP and dFNC similarity; (c-d) Manhatten and connectogram plots of State1_jICA9; (e-f) Manhattan and connectogram plots of State3_jICA7; (g-h) Manhattan and connectogram plots of State1_jICA4.

Conclusions: Thalamus and insula dysconnectivity are well documented in SZ9,10. Cell projection organization results in the arrangement of constituent parts, disassembly of a prolongation, or process extending from a cell, e.g., a flagellum or axon. Notably, the State1_jICA4 SNPs, which might be elicited only upon dynamic fusion with dFNC given its high dynamism, might be complementary to State1_jICA9 to provide a more complete picture of the genomic factor conferring risk to SZ by affecting cell projection. This presents the benefit of the proposed dynamic fusion to expand the SNP data for time-varying manifolds that may provide additional insights into the underlying biology.

References

1. Sullivan PF, Kendler KS, Neale MC. Schizophrenia as a complex trait - Evidence from a meta-analysis of twin studies. Arch Gen Psychiat. Dec 2003;60(12):1187-1192. doi:DOI 10.1001/archpsyc.60.12.1187
2. McCutcheon RA, Marques TR, Howes OD. Schizophrenia—an overview. JAMA psychiatry. 2020;77(2):201-210.
3. Chen J, Liu J, Calhoun VD. Translational potential of neuroimaging genomic analyses to diagnosis and treatment in mental disorders. P Ieee. 2019;107(5):912-927.
4. Trubetskoy V, Pardinas AF, Qi T, et al. Mapping genomic loci implicates genes and synaptic biology in schizophrenia. Nature. Apr 2022;604(7906):502-508. doi:10.1038/s41586-022-04434-5
5. Du Y, Fu Z, Sui J, et al. NeuroMark: An automated and adaptive ICA based pipeline to identify reproducible fMRI markers of brain disorders. NeuroImage: Clinical. 2020;28:102375.
6. Du YH, Fan Y. Group information guided ICA for fMRI data analysis. Neuroimage. Apr 1 2013;69:157-197. doi:10.1016/j.neuroimage.2012.11.008
7. Allen EA, Damaraju E, Plis SM, Erhardt EB, Eichele T, Calhoun VD. Tracking Whole-Brain Connectivity Dynamics in the Resting State. Cerebral Cortex. Mar 2014;24(3):663-676. doi:10.1093/cercor/bhs352
8. Calhoun V, Silva R, Liu J. Identification of multimodal MRI and EEG biomarkers using joint-ICA and divergence criteria. IEEE; 2007:151-156.
9. Giraldo-Chica M, Rogers BP, Damon SM, Landman BA, Woodward ND. Prefrontal-thalamic anatomical connectivity and executive cognitive function in schizophrenia. Biological psychiatry. 2018;83(6):509-517.
10. White TP, Joseph V, Francis ST, Liddle PF. Aberrant salience network (bilateral insula and anterior cingulate cortex) connectivity during information processing in schizophrenia. Schizophrenia research. 2010;123(2-3):105-115.

Poster No 660

Neural dynamics of reinforcement learning in OCD: a functional connectivity study

Teresa Sousa[1,2,3], Ana Araújo[1,2,4,5,3], Catarina Duarte[1,2], Ana Telma Pereira[4,1], António Macedo[5,4,1], Miguel Castelo-Branco[1,2,6]

[1]Coimbra Institute for Biomedical Imaging and Translational Research (CIBIT), University of Coimbra, Coimbra, Portugal, [2]Institute for Nuclear Sciences Applied to Health (ICNAS), University of Coimbra, Coimbra, Portugal, [3]Shared co-first authorship, ., [4]Institute of Psychological Medicine, Faculty of Medicine, University of Coimbra, Coimbra, Portugal, [5]Department of Psychiatry, Coimbra Hospital and University Centre, Coimbra, Portugal, [6]Faculty of Medicine, University of Coimbra, Coimbra, Portugal

Introduction: Obsessive-compulsive disorder (OCD) is a common and potentially debilitating condition that affects approximately one person out of 40 at some point during their lifetime. It causes significant distress and can also lead to substantial disability by disrupting various aspects of daily life, including occupation and social activities[1]. Recent computational models[2,3] have suggested that individuals with OCD implicitly reinforce maladaptive behaviors. These models propose an explanation for the repetitive cycle of obsessions and compulsions, which are core features of OCD symptoms, within a framework of reinforcement learning. However, they have yet to be tested at the neuronal level. The aim of this study was to examine brain connectivity related to inhibitory learning using an actor-critic architecture. We hypothesized that patients with OCD would exhibit altered connectivity between the critic, the reward system, and the associated regulating networks.

Methods: Functional magnetic resonance imaging (fMRI) data were collected from 40 adult males, consisting of 19 OCD patients and 21 age-matched healthy subjects, during a Stop-Signal Task (SST). The analysis followed the actor-critic model[4], wherein the dopaminergic midbrain regions-the ventral tegmental area (VTA) and the substantia nigra (SN)-were considered as the critics, while the dorsal striatum served as the actor[5]. Functional connectivity was evaluated within the actor-critic network nodes using ROI-to-ROI correlation analysis. Additionally, seed-to-voxel correlation analysis was conducted to assess connectivity between each of these regions and all other brain regions. These connectivity analyses were performed in two ways: first, comparing the patient and control group, and second, dividing the patients into two subgroups based on their stop-signal reaction time (SSRT). The division was made into groups with SSRTs either lower or higher than the average, indicating different levels of inhibitory control.

Results: We did not find any functional connectivity differences between individuals with OCD and control subjects concerning the actor-critic regions. However, our seed-to-voxel analysis revealed reduced connectivity between the critic and several regions associated with error monitoring and cognitive control in OCD. Specifically, the VTA showed decreased connectivity with the angular gyrus/supramarginal gyrus and the superior frontal gyrus/frontal pole, while the SN exhibited decreased connectivity with the central opercular cortex/insular cortex and the anterior and posterior cingulate gyrus. When considering the actor regions (putamen or caudate) as seed regions, we did not observe any functional connectivity differences between individuals with OCD and healthy subjects. Notably, such decrease in functional connectivity between SN/VTA and error monitoring and cognitive control regions was particularly evident when comparing individuals with OCD and controls possessing high inhibitory control. When comparing patients and controls with low inhibitory control, we only found decreased connectivity between the SN and the occipital pole.

Conclusions: These findings suggest that comparing patients and controls with similar behavioral strategies (such as high inhibitory control) better emphasizes the distinct neural dynamics of OCD patients during inhibitory control. Furthermore, the decreased functional connectivity patterns identified in OCD may contribute to explaining the hyperactivity of error monitoring and reward regions in this clinical group[6]. The poor integration of both systems, mediated by network nodes acting as critics, might lead to an overload when each system operates independently. This insight could be valuable in understanding the etiological processes contributing to OCD, as it indicates potential alterations in the dynamics of the neural circuitry associated with reinforcement learning.

References

1. Robbins et al., 2019. Obsessive-Compulsive Disorder: Puzzles and Prospects. Neuron 102 (1): 27–47.
2. Sakai et al., 2022, Memory trace imbalance in reinforcement and punishment systems can reinforce implicit choices leading to obsessive-compulsive behavior. Cell Reports 40, 111275.
3. Zhongqiang et al., 2023 Impairment of arbitration between model-based and model-free reinforcement learning in obsessive–compulsive disorder. Front. Psychiatry 14:1162800.
4. Barto, A. G., 1995. Adaptive critics and the basal ganglia. In J. C. Houk, J. L. Davis, & D. G. Beiser (Eds.), Models of information processing in the basal ganglia (pp. 215–232). The MIT Press.
5. Lindsey, J.W., & Litwin-Kumar, A., 2022. Action-modulated midbrain dopamine activity arises from distributed control policies. ArXiv, abs/2207.00636.

6. Hampshire et al., 2020. Inhibition-Related Cortical Hypoconnectivity as a Candidate Vulnerability Marker for Obsessive-Compulsive Disorder, Biological Psychiatry: Cognitive Neuroscience and Neuroimaging 5 (2): 222-230.

Poster No 661

SPECT brain networks and their functional connectivity in schizophrenia patients vs controls

Amritha Harikumar[1,2], Maria Misiura[1,2], Daniel Amen[3,4], David Keator[5,6,7], Vince Calhoun[8,9]

[1]TReNDS Center, Atlanta, GA, [2] Georgia State University, N/A, [3]Change Your Brain Change Your Life Foundation, Costa Mesa, CA, [4] Amen Clinics Inc., N/A, [5]Psychiatry and Human Behavior, University of California, Irvine, CA, [6]Amen Clinics Inc., Costa Mesa, CA, [7]Change Your Brain Change Your Life Foundation, Costa Mesa, CA, [8]GSU/GATech/Emory, Decatur, GA, [9]Georgia State University, Atlanta, GA

Introduction: In the last decade, single photon emission computerized tomography (SPECT) scans have emerged as a useful imaging modality. Much like fMRI, the proliferation of SPECT imaging has led to applying this modality to various clinical populations, with advantages including the powerful ability to detect patterns of cerebral blood flow (CBF) that may be indicative of disrupted brain activity. Additionally, unlike fMRI, SPECT imaging has been proven to be a cost effective and easy imaging method to utilize for clinical populations. To date, little work has focused on data-driven analysis of SPECT data. Here we utilize SPECT data to compare group differences in patients with schizophrenia and healthy controls using fully automated, spatially constrained ICA (i.e., the Neuromark pipeline). We evaluate both the spatial regions as well as the whole brain SPECT connectome (assessed as covariation among subjects) to evaluate the neuroimaging links to schizophrenia.

Methods: 76 healthy controls, and 138 schizophrenia patient SPECT images were acquired from the Amen Clinic (https://www.amenclinics.com/), along with diagnostic information. Each patient participated in two SPECT brain scans, acquired during rest and while performing a Conners Continuous Performance Test (Conners Continuous Performance Test, CCPT-II, Multi-Health Systems, Toronto, Ontario) (Conners and Staff n.d.) across eleven clinical imaging sites. SPECT scans were acquired using Picker (Philips) Prism XP 3000 triple-headed gamma cameras with low energy high resolution fan beam collimators. Data acquisition yielded 120 images per scan with each image separated by three degrees, spanning 360 degrees. The resulting reconstructed image matrices were 128x128x78 with voxel sizes of 2.5mm^3. Scans were MNI space registered and raw count values were scaled by the maximum voxel. Preprocessed SPECT data were analyzed via spatially constrained ICA using the Neuromark ICA template. The template included 53 components reproduced from two large scale human fMRI datasets. The components are delineated into various domains including the subcortical (SC), auditory (AUD), visual (VIS), sensorimotor (SM), cognitive control (CC), default mode network (DMN), and cerebellar (CB) component regions. Following the analysis, pairwise correlations between the loading parameters for the SPECT components were analyzed for within and between group differences. Additionally, two sample t-tests on loading parameter values between both groups were performed to identify group differences.

Results: Results revealed significant differences between healthy controls and patient SPECT data. Out of the 53 components, 21 were found to show significant differences.

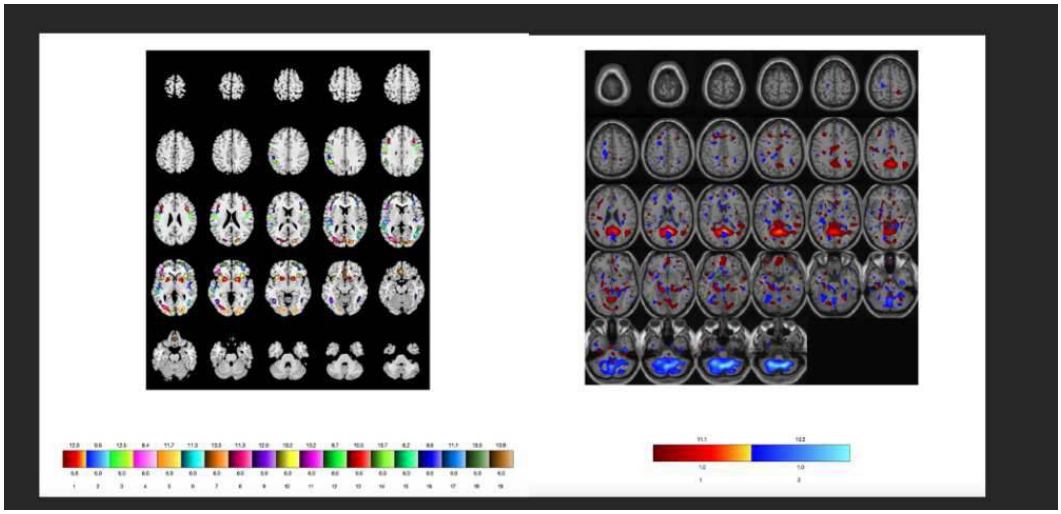

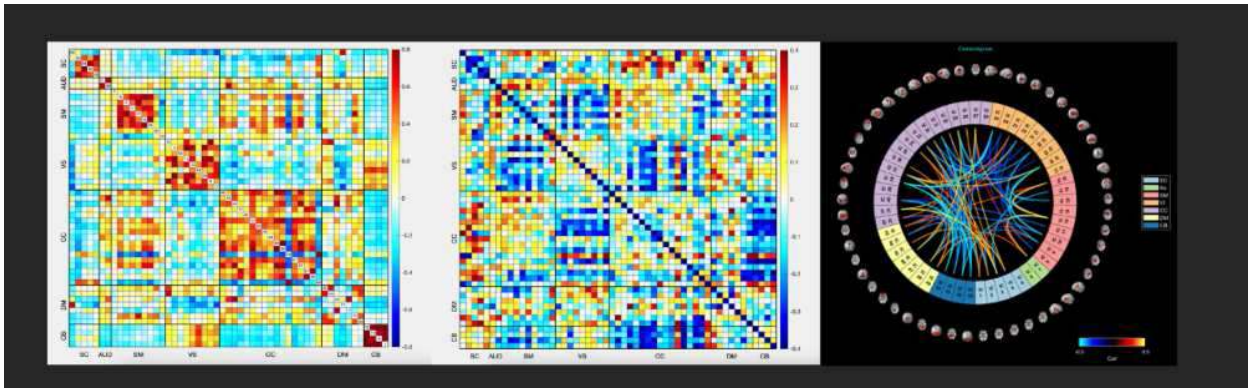

Conclusions: Analyzing SPECT data using ICA revealed multiple significant group differences in HC vs SZ. This poses interesting clinical questions related to possible disruptions in schizophrenia, particularly in the superior temporal gyrus, default mode network, and subcortical networks. These results shed further light on patterns of functional dysconnectivity identified in various studies relating disruption in these networks correlated with positive and negative symptoms in schizophrenia. Taken together with clinical data, we hope to further analyze the SPECT data to see how group differences emerge across a variety of neuropsychiatric disorders. Doing so will allow us to see if disrupted brain activity through analyzing components pose a similar pattern across disorders.

References

1. Amen, D. G. (2021). A new way forward: how brain SPECT imaging can improve outcomes and transform mental health care into brain health care. Frontiers in Psychiatry, 12, 2053.
2. Du, Y. (2020). NeuroMark: An automated and adaptive ICA based pipeline to identify reproducible fMRI markers of brain disorders. NeuroImage: Clinical, 28, 102375.
3. Kalyoncu, A (2021). The Emerging Role of SPECT Functional Neuroimaging in Schizophrenia and Depression. Frontiers in Psychiatry, 12, 716600.
4. Harikumar A. (2023). Revisiting Functional Dysconnectivity: a Review of Three Model Frameworks in Schizophrenia. Curr Neurol Neurosci Rep. 2023 Nov 24. doi: 10.1007/s11910-023-01325-8. Epub ahead of print. PMID: 37999830.

Poster No 662

The Effect of Weight Loss on Brain Age in Schizophrenia

Vittal Korann[1], Nicolette Stogios[2], Bjørn Ebdrup[3], Margaret Hahn[2], Mahavir Agarwal[2]

[1]University of Toronto, Toronto, ontario, [2]University of Toronto, Toronto, Ontario, [3]University of Copenhagen, Copenhagen, Copenhagen

Introduction: Individuals with schizophrenia (SCZ) often have metabolic comorbidities, such as type 2 diabetes, and experience a reduced life expectancy due to cardiovascular diseases. Obesity, a common comorbidity in SCZ, can negatively affect brain health. However, there is limited understanding of how metabolic disorders impact brain structure in individuals with SCZ, and the effects of weight changes following pharmacological interventions have not been explored. In this study, we will investigate changes in brain morphology, specifically brain-age, in overweight or obese individuals with or without diabetes who have been diagnosed with SCZ. Our primary objective will be to assess these changes before and after a 12-week period of pharmacological treatment targeting metabolic dysfunction. We hypothesized that 1) a change in BMI will be positively associated with the change in brain age between baseline and endpoint; 2) there will be no significant difference in the strength of the correlation between the medication and placebo groups. As exploratory analyses, we also looked at the association between brain age and cognition and metabolic parameters.

Methods: This analysis includes 48 participants, aged 18 to 65, from three double-blind studies investigating interventions for antipsychotic-induced metabolic dysfunction: TAO study (NCT01794429, 9 on medication and 8 on placebo), Metformin for prediabetes/diabetes study (NCT02167620, 11 on medication and 8 on placebo), and Topiramate in clozapine study (NCT02808533, 12 on medication). In brief, inclusion criteria include patients with a diagnosis of schizophrenia, schizoaffective disorder, or bipolar disorder, metabolic comorbidity of prediabetes or type 2 diabetes, and BMI of above 25 kg/m2. We collected brain structural MRI, metabolic measures, cognition data, and body mass index at baseline and week 12. We utilized a convolution neural network-based classifier that was trained and tested to estimate the brain age of each participant using high-quality brain anatomical T1 image. The study aims to examine the changes in BMI and estimated brain age scores using baseline and endpoint data.

Results: The BMI alteration demonstrated statistical significance within the whole sample ($p < 0.001$), as well as in both the medication ($p = 0.005$) and placebo groups ($p = 0.008$). Likewise, significant changes were found only in total and HDL (high-density lipoprotein) cholesterol levels across all three groups in terms of metabolic parameters. However, none of the groups exhibited any substantial changes in psychopathological scores or cognitive data between the baseline and endpoint assessments. Multiple regression analysis revealed a positive correlation between BMI change and alterations in brain age for the whole sample (beta = 0.263; t = 1.85; p = 0.05) and the medicated group (beta = 0.372; t = 2.12; p = 0.04), but not in the placebo group (beta = -0.106; t = -0.40; p = 0.69). However, no significant difference in the correlation strength was observed between the medication and placebo groups (p = 0.12). Furthermore, there was no significant association between changes in brain age and metabolic indicators such as total and HDL cholesterol. Lastly, no significant correlation was found between brain age and cognition.

Conclusions: In conclusion, our study showed a link between brain health (as assessed by delta brain age) and significant weight loss by anti-diabetic medication in patients with SCZ and comorbid obesity. These findings imply that large and extended weight loss, together with general improvements in cardiometabolic alterations, can prevent obesity-related abnormalities in brain health.

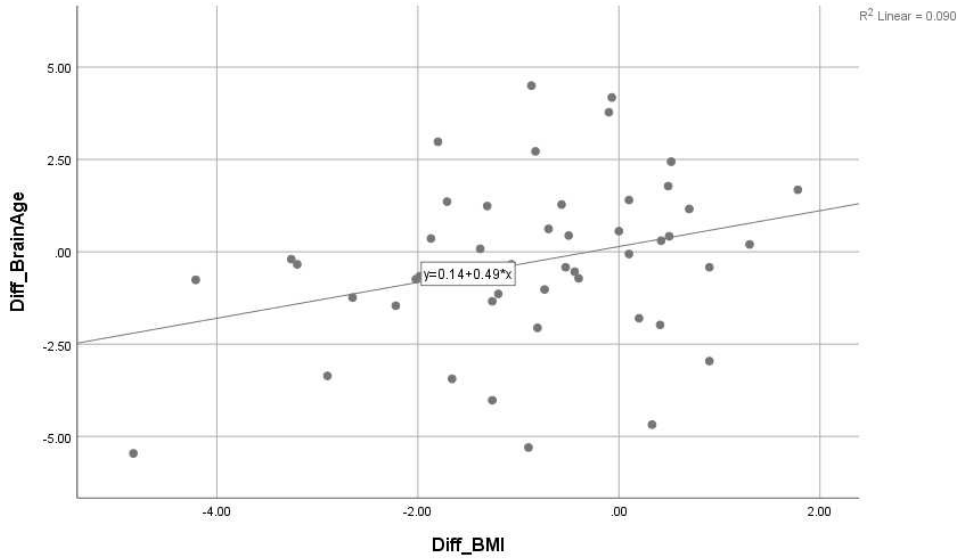

References

1. Bora E. (2017), The relationship between cognitive impairment in schizophrenia and metabolic syndrome: a systematic review and meta-analysis. Psychol Med. 2017;47(6):1030–1040.
2. Kolenic M. (2018), Obesity, dyslipidemia and brain age in first-episode psychosis. J Psychiatr Res. 2018;99:151–158.
3. Masouleh, S.K. (2016), Higher body mass index in older adults is associated with lower gray matter volume: implications for memory performance. Neurobiol. Aging 40, 1–10.
4. McWhinney S. (2021), Obesity as a Risk Factor for Accelerated Brain Ageing in First-Episode Psychosis-A Longitudinal Study. Schizophr Bull. 2021 Oct 21;47(6):1772-1781.
5. Mitchell AJ. (2013), Prevalence of metabolic syndrome and metabolic abnormalities in schizophrenia and related disorders—a systematic review and meta-analysis. Schizophr Bull. 2013b;39(2):306–318.
6. Rajkumar AP. (2017), Endogenous and Antipsychotic-Related Risks for Diabetes Mellitus in Young People With Schizophrenia: A Danish Population-Based Cohort Study. American Journal of Psychiatry. 2017;174:686-694.
7. Ronan, L. (2016). Obesity associated with increased brain age from midlife. Neurobiol. Aging 47, 63–70.
8. Vancampfort D. (2015), Risk of metabolic syndrome and its components in people with schizophrenia and related psychotic disorders, bipolar disorder and major depressive disorder: a systematic review and metaanalysis. World Psychiatry. 2015;14(3):339–347.
9. Wood DA. (2022), Accurate brain-age models for routine clinical MRI examinations. Neuroimage. 2022 Apr 1;249:118871.
10. Zeighami Y. (2022), Impact of weight loss on brain age: Improved brain health following bariatric surgery. Neuroimage. 2022 Oct 1; 259:119415.

Poster No 663

Differential Functional Connectivity of Insula Subdivisions in Pediatric Anxiety Disorders

Euisun Kim[1,2], Jiyoung Park[3,2], Yelim Lee[1,2], Maengkeun Oh[2], Sole Yoo[3,2], WooYong Lee[1,2], Jiho Min[4,2], Hae-Jeong Park[2,5,1,3]

[1]Graduate School of Medical Science, Brain Korea 21 Project, Yonsei University College of Medicine, Seoul, Korea, Republic of, [2]Department of Nuclear Medicine, Severance Hospital, Yonsei University College of Medicine, Seoul, Korea, Republic of, [3]Department of Cognitive Science, Yonsei University, Seoul, Korea, Republic of, [4]Kyung Hee University, Seoul, Korea, Republic of, [5]Center for Systems and Translational Brain Sciences, Institute of Human Complexity and Systems Scien, Seoul, Korea, Republic of

Introduction: The insula, classically associated with interoception, plays a crucial role beyond bodily awareness. Malfunctions in interoceptive processes, notably in anxiety disorders, distorts emotional experiences. This intricate relationship between insula function and emotional well-being emphasizes the necessity for thorough neural exploration. While existing research has primarily concentrated on the insula as a whole, we take a novel approach by examining the subdivisions of the insula-specifically, the ventral anterior insula (vAI), dorsal anterior insula (dAI), and posterior insula (PI). This exploration is grounded in recent findings indicating diverse structural and functional characteristics among these subdivisions. We hypothesize that, due to their distinct functional roles, the three insula subdivisions may exhibit different functional connectivity patterns in both generalized anxiety disorder (GAD) and social anxiety disorder (SAD) patients when compared to their healthy counterparts. By using the Healthy Brain Network (HBN) Biobank Data (Release 10.0) and the Adolescent Brain and Cognitive Development (ABCD) study data (Release 4.0), our objective is to contribute to a deeper understanding of the neural underpinnings of anxiety disorders.

Methods: We use resting-state functional magnetic resonance(rsfMRI) imaging data of 76 children with GAD, 37 children with SAD and 106 healthy children from the HBN Biobank and ABCD data. The age of the children included in our dataset was from 9 to 12 years old. To explore the functional connectivity patterns of the insula subdivisions, we performed Seed-to-Voxel analyses for the bilateral ventral anterior insula (vAI), the dorsal anterior insula (dAI), and the posterior insula (PI) across the three groups. Age and sex of participants in each group were controlled for as covariates. We conducted conventional preprocessing steps using SPM12 and analyzed seed-to-voxel functional connectivity and graph analysis using the CONN toolbox (version 21.a).

Results: Individuals with GAD showed the increased functional connectivity between the right posterior insula (rPI) and the left temporal superior lobules, suggesting heightened engagement in sensory and cognitive processes. Additionally, enhanced rPI connectivity with the right Rolandic operculum, known as the sensory system for gustatory and visceral sensation, pointed to potential involvement in altered sensory perception in GAD patients. The left ventral anterior insula (lvAI) in GAD patients displayed heightened connectivity with the right hippocampus, implicated in interoceptive processing, while connectivity with the right middle temporal gyrus, involved in multimodal sensory integration, decreased. Additionally, GAD patients showed increased connectivity between the left posterior insula (lPI) and the left inferior frontal gyrus, associated with language processing. In SAD patients, the right dorsal anterior insula (rdAI) exhibited heightened connectivity with the right precuneus, linked to emotional state evaluation. The left dorsal anterior insula (ldAI) in SAD patients demonstrated increased connectivity with the left precentral gyrus, associated with motor function. When comparing GAD and SAD, GAD patients displayed heightened connectivity between lvAI and regions related to gustatory and visceral sensation, along with decreased connectivity with the left cerebellum.

Conclusions: Our investigation of insula subdivisions in pediatric anxiety disorders revealed distinctive functional connectivity patterns. GAD patients exhibited heightened connectivity between the right posterior insula and sensory-cognitive regions, indicating increased engagement. In contrast, SAD patients displayed connectivity changes in emotion and motor-related areas. This study underscores the significance of investigating insula subdivisions, providing valuable insights into the nuanced neural underpinnings of anxiety.

References

1. Uddin LQ. (2017) 'Structure and Function of the Human Insula.' Journal of Clinical Neurophysiology, vol. 34, no. 4, pp. 300-306.
2. Kolesar, T. A. (2019). 'Systematic review and meta-analyses of neural structural and functional differences in generalized anxiety disorder and healthy controls using magnetic resonance imaging', NeuroImage: Clinical, vol. 24, pp. 102016
3. Steinhäuser, J. L. (2023). 'Reduced vmPFC-insula functional connectivity in generalized anxiety disorder: a Bayesian confirmation study', Scientific Reports, vol. 13, no. 1, pp. 9626
4. Fermin, A. S. (2022). 'An insula hierarchical network architecture for active interoceptive inference', Royal Society Open Science, vole. 9, no. 6, pp. 220226
5. Nieto-Castanon, A. (2020). 'Functional Connectivity measures. In Handbook of functional connectivity Magnetic Resonance Imaging methods in CONN', Hilbert Press, pp. 26–62

6. Alexander, L. (2017), 'An open resource for transdiagnostic research in pediatric mental health and learning disorders', Scientific Data, vol. 4, pp. 170181

Poster No 664

Inflammation Links to Functional Connectivity and White Matter Changes in Chronic Depression

Jungho Cha[1], Divyaansh Raj[2], Ki Sueng Choi[1], Justin Rajendra[3], Boadie Dunlop[4], Edward Craighead[4], Helen Mayberg[1]

[1]Icahn School of Medicine at Mount Sinai, New York, NY, [2]Johns Hopkins University of School of Medicine, Baltimore, MD, [3]National Institutes of Health, Bethesda, MD, [4]Emory University School of Medicine, Atlanta, GA

Introduction: There is increasing evidence for the role of inflammation in major depressive disorder (MDD)[1]. Notably, disease chronicity has garnered attention as a predictor of poor long-term outcomes[2]. However, a comprehensive understanding of the complex relationship between inflammation, changes in functional connectivity, and white matter (WM) microstructure in patients with chronic depression remains unclear.

Methods: 344 never treated MDD patients from the Emory PReDICT study a randomized controlled study of CBT and medication to biomarkers for never-treated MDD patients[3], 209 had usable DWI scans, and 132 had usable fMRI scans. We assessed inflammatory status by measuring CRP levels in blood samples. Chronicity was categorized based on current depression episodes lasting over 2 years. Imaging processing was performed using FMRIB Software Library (FSL)[4] and Analysis of Functional NeuroImages (AFNI)[5]. We conducted Tract-Based Spatial Statistics (TBSS) analyses[6] using fractional anisotropy (FA) values and explored whole-brain resting-state functional connectivity (RSFC) using seed regions from four brain networks, including default mode network (DMN), salience network (SN), affective network (AN), and control network (CN). To examine the impact of CRP levels on FA or RSFC and how these relationships differ between chronic and non-chronic patients, linear regression models with interaction terms for CRP and patient chronicity were utilized for FA and RSFC analyses, respectively. Significance was set at FWE-corrected $p < 0.05$. Correlation analyses were conducted to assess the connection between effects on gray matter and white matter. Furthermore, mediation analyses were conducted to explore the potential mediation relationships among CRP, RSFC, and FA, investigating the effects of CRP on RSFC and the role of FA changes in mediating this association.

Results: Significant interaction effects (chronicity x CRP) were observed for FA in the external capsule area including association pathway and cingulum tracts (Fig1 A). Additionally, significant interaction effects were noted in the RSFC between the posterior cingulate cortex (PCC) and dorsal anterior cingulate cortex (dACC) (i.e. within the DMN) (Fig1 B) and between the anterior insula (ant.INS) and anterior paracingulate (i.e. within the SN) (Fig1 C). Specifically, higher CRP levels were associated with lower FA values and increased FC patterns in chronic depression patients. Notably, these relationships were not observed in the nonchronic depression group. Furthermore, mediation analyses showed both direct and FA-mediated effects of CRP on the ant.INS-paracingulate RSFC (Figure 2A). Additionally, PCC-dACC RSFC was negatively correlated with FA across all patients, but there were no mediation effects (Figure 2B).

Figure 1. Interaction effect between Chronicity and CRP

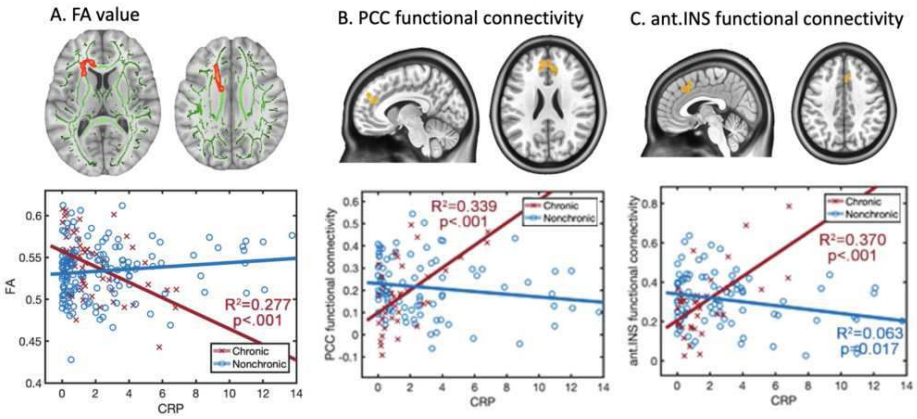

Figure2. Correlation and mediation analyses to explore the impact of CRP on RSFC and FA changes

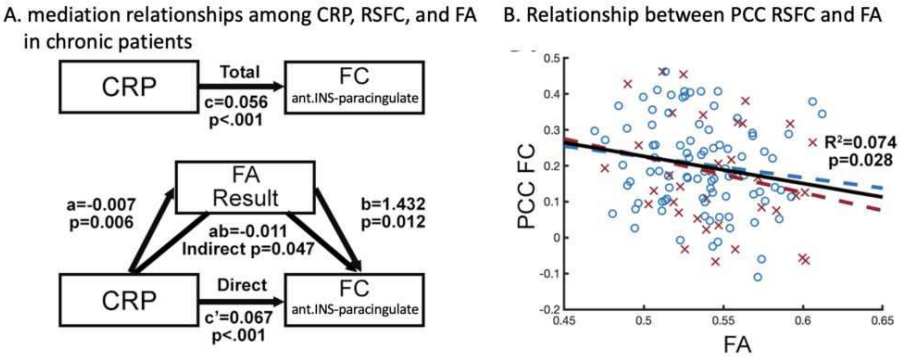

Conclusions: Our findings showed that CRP was associated with decreased FA and increased RSFC, specifically in chronic MDD patients. The relationship between PCC RSFC and FA was observed across all patient groups, indicating a common phenomenon shared among all depressed patients. Moreover, mediation analyses indicated both direct and FA-mediated effects of CRP on ant.INS-paracingulate RSFC in chronic patients. The result suggests that alterations in white matter microstructure may, at least partially, explain the relationship between CRP levels and changes in RSFC in this specific region and the direction of changes suggesting a specific compensatory change in function in the salience network in MDD.

References

1. Kraynak TE, Marsland AL, Wager TD, Gianaros PJ. Functional neuroanatomy of peripheral inflammatory physiology: A meta-analysis of human neuroimaging studies. Neurosci Biobehav Rev. 2018;94:76-92.
2. van Eeden WA, van Hemert AM, Carlier IVE, Penninx BW, Spinhoven P, Giltay EJ. Neuroticism and chronicity as predictors of 9-year course of individual depressive symptoms. J Affect Disord. 2019;252:484-92.
3. Dunlop BW, Binder EB, Cubells JF, Goodman MM, Kelley ME, Kinkead B, et al. Predictors of remission in depression to individual and combined treatments (PReDICT): study protocol for a randomized controlled trial. Trials. 2012;13:106.
4. Smith SM, Jenkinson M, Woolrich MW, Beckmann CF, Behrens TE, Johansen-Berg H, et al. Advances in functional and structural MR image analysis and implementation as FSL. Neuroimage. 2004;23 Suppl 1:S208-19.
5. Cox RW. AFNI: software for analysis and visualization of functional magnetic resonance neuroimages. Comput Biomed Res. 1996;29(3):162-73.
6. Smith SM, Jenkinson M, Johansen-Berg H, Rueckert D, Nichols TE, Mackay CE, et al. Tract-based spatial statistics: voxelwise analysis of multi-subject diffusion data. Neuroimage. 2006;31(4):1487-505.

Poster No 665

Cortical Thickness and Clinical Profile in Never Medicated Individuals with Psychosis

Luis Rivera-Chavez[1], Triana Tello-Gerez[1], Matthew Danyluik[2], Pablo Leon-Ortiz[1], Yohan Yee[2], Francisco Reyes-Madrigal[1], Mallar Chakravarty[2], Camilo de la Fuente-Sandoval[1]

[1]Laboratory of Experimental Psychiatry, National Institute of Neurology and Neurosurgery, Mexico City, Mexico, [2]Cerebral Imaging Centre, Douglas Mental Health University Institute, McGill University, Montreal, Quebec

Introduction: Reduced cortical thickness (CT) is well documented in schizophrenia and has been reported to progress throughout the course of illness. While previously established that a longer duration of untreated psychosis (DUP) is a predictor of poor clinical outcome, the field still lacks information on structural brain abnormalities in medication naive subjects with particular long DUP. In the present study we present a unique sample of never medicated first episode of psychosis patients (FEP) with a wide range of DUP.

Methods: FEP patients that had never been medicated with antipsychotics, along with healthy controls, were recruited at the National Institute of Neurology and Neurosurgery of Mexico. Clinical evaluation at recruitment included the MATRICS Consensus Cognitive Battery (MCCB). Magnetic resonance studies were performed on two scanners: some participants were scanned in a 3T GE whole-body scanner (Signa Excite HDxt) with a high-resolution 8-channel head coil, using a T1-weighted spoiled gradient-echo 3-dimensional axial acquisition (SPGR, echo time [TE] = 5.7ms, repetition time [TR] = 13.4ms, inversion time [IT] = 450ms, flip angle = 20°, field of view [FOV] = 25.6cm, ≥256 × ≥256 matrix, slice thickness ≤ 1.2mm), oriented above and parallel to the anterior-posterior commissure line. The other participants were scanned on a 3 T Siemens scanner (Magnetom Skyra), using a 20-channel phased array transmit/receive-head coil, using a high-resolution T1-weighted three-dimensional magnetization-prepared rapid acquisition with gradient echo (MPRAGE; TE = 5 ms, TR = 12 ms, IT = 450 ms, flip

angle = 20^0, FOV = 25.6 cm, 256x256 matrix, 186 slices, slice thickness = 1 mm), oriented above and parallel to the anterior commissure-posterior commissure line. T1-weighted images were preprocessed with bpipe pipeline (http://github.com/CobraLab/minc-bpipe-library/), which includes bias field correction, neck cropping, and Brain Extraction based on nonlocal Segmentation Technique (BEaST). CT analysis was done with CIVET processing pipeline (version 2.1.1; Montreal Neurological Institute). To remove unwanted scan variability due to scanner, CovBat harmonization was performed on data before analysis. To compare CT measures between groups, vertex-wise CT diagnosis contrast analyses were conducted, while accounting for age and sex in a linear model. For spatial distribution visualization, t-values were projected into a brain map of the participants' average surface with false discovery rates (FDR) thresholds set at 5-10%. Means of CT were used in linear models to compare groups and explore for possible correlations with demographic and clinical variables.

Results: Fifty-six FEP patients (DUP mean[range] in weeks = 145.79[1-1300]) and 52 healthy controls completed all clinical evaluations and MRI scanning (GE scanner n=47, Siemens scanner n=61). Obtained CT mean was lower in FEP than in controls (t=2.56, df=93, p=0.01). Regions with most differences in CT were found at the right and left occipital lobe, postcentral gyrus of the left parietal lobe, superior gyrus of the left temporal lobe, and the right uncus (Figure). The linear model obtained with mean CT confirmed a group effect, besides an effect due to age and sex (groupFEP t-value=-2.468, p=0.01; age t-value=-5.63, p<0.01; sexmale t-value=2.41, p=0.02). No significant associations were found in linear models of mean CT with cognitive domains values in either group. However, trends were observed for social cognition in the control group (t-value=1.92, p=0.06).

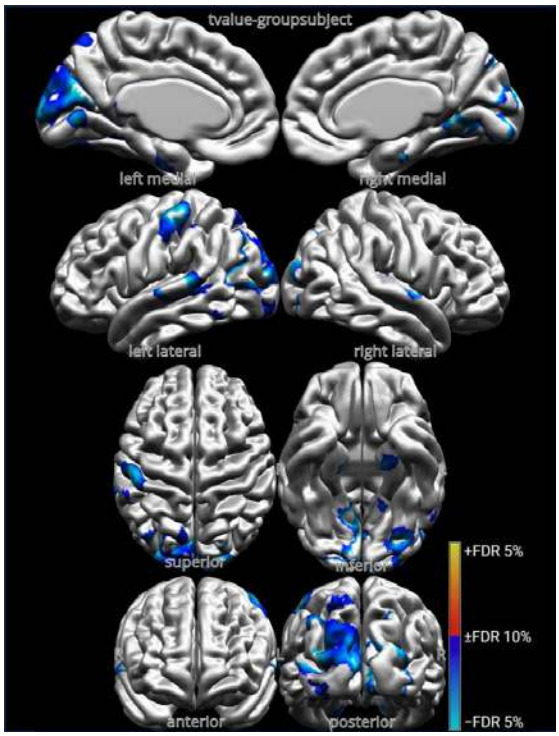

Conclusions: Present findings are in line with previous studies reporting decreased CT in patients with psychosis compared to controls. Dissimilar to published results on the matter, differences localized to the frontal lobe were not found. This could potentially be explained by the variability induced by the uncommonly prolonged DUP of the never medicated FEP group. Further studies are necessary to corroborate and expand findings in individuals with long DUP.

References

1. Ad-Dab'bagh, Y. (2006), 'The CIVET Image-Processing Environment: a Fully Automated Comprehensive Pipeline for Anatomical Neuroimaging Research', Proceedings of the 12th Annual Meeting of the Organization for Human Brain Mapping, Florence, Italy.
2. Andreasen, N.C. (2011), 'Progressive Brain Change in Schizophrenia: A Prospective Longitudinal Study of First-Episode Schizophrenia', Biological Psychiatry, vol. 70, no.7, pp. 672-679.
3. Chen, A.A. (2022), 'Mitigating Site Effects in Covariance for Machine Learning in Neuroimaging Data', Human Brain Mapping, vol. 43 no. 4, pp. 1179-1195.
4. Lerch, J.P. (2005), 'Cortical Thickness Analysis Examined Through Power Analysis and a Population Simulation', NeuroImage vol. 24, no. 1, pp. 163–173.
5. Liu, X. (2014), 'A Combined DTI and Structural MRI Study in Medicated-Naïve Chronic Schizophrenia', Magnetic Resonance Imaging, vol. 32, no. 1, pp. 1-8.
6. van Haren, N.E. (2011), 'Changes in Cortical Thickness During the Course of Illness in Schizophrenia', Archives of General Psychiatry, vol. 68, no. 9, pp. 871-880.
7. Zhang, W. (2015), 'Brain Structural Abnormalities in a Group of Never-Medicated Patients With Long-Term Schizophrenia', American Journal of Psychiatry, vol. 172, no. 10, pp. 995-1003.

Poster No 666

General Neural Correlates of Executive Impairment in Childhood Psychopathology

Adam Kaminski[1], Hua Xie[2], Brylee Hawkins[1], Laura Campos[2], Madison Berl[2], Lauren Kenworthy[2], Chandan Vaidya[1]

[1]Georgetown University, Washington, DC, [2]Children's National Hospital, Washington, DC

Introduction: Childhood psychopathology is a worsening public health crisis leading to negative life outcomes, including self-harm and suicide. A latent general factor of psychopathology, termed "p-factor", has gained traction given high rates of comorbidity and shared variance in symptoms, and there is debate about its functional underpinnings. Difficulty in controlling impulsivity and distractibility, termed executive control, as early as 3 years old predicts p-factor (Moffitt et al., 2011), which has led to the hypothesis that it reflects executive impairment. Here, we test this hypothesis by predicting that p-factor is related to dysfunction in functional connectivity (FC) network integration during the execution of demanding tasks, a theorized general feature of executive control (Menon & D'Esposito, 2022). We tested this prediction with a two-pronged approach, first identifying "hub" regions defined by high FC network integration across 3 executive control tasks and testing the strength of their between-network connections; and second, identifying regions most predictive of task performance defined by connectome-based predictive modeling (CPM) and testing their FC network integration. This strategy enabled us to first test association to p-factor of network integration broadly, and then to focus on regions specifically related to task behavior.

Methods: We included 204 children [53 F/149 M/2 NC; mean age (SD)=11 years (1.7)] with varied diagnoses (e.g., attention deficit disorder [n=80]; autism spectrum disorders [n=91]). Principal component analysis on parent-reported Child Behavior Checklist was used to define p-factor. For participants with high quality fMRI data on 3 tasks (n=79), tapping interference suppression and flexibility, working memory, and response inhibition, we examined FC connectomes reflecting a general executive control state (TR=2000ms, TE=30ms, 256x256mm FOV, 64x64 acquisition matrix, 90-degree flip angle; preprocessing with fMRIprep 22.0.1 [Esteban et al., 2019]). First, we selected regions in the top 5% for FC network integration, operationalized with the graph theory metric participation coefficient, in the group average connectome. We then took the weighted sum of FC for only between-network connections of these "hub" regions and tested for association with p-factor in a multiple linear regression. Second, we applied CPM to identify connections predictive of a latent general factor of in-scanner task performance. We then measured FC network integration, again operationalized with participation coefficient, of regions in the top 5% for predictive connections and tested for association with p-factor in a multiple linear regression.

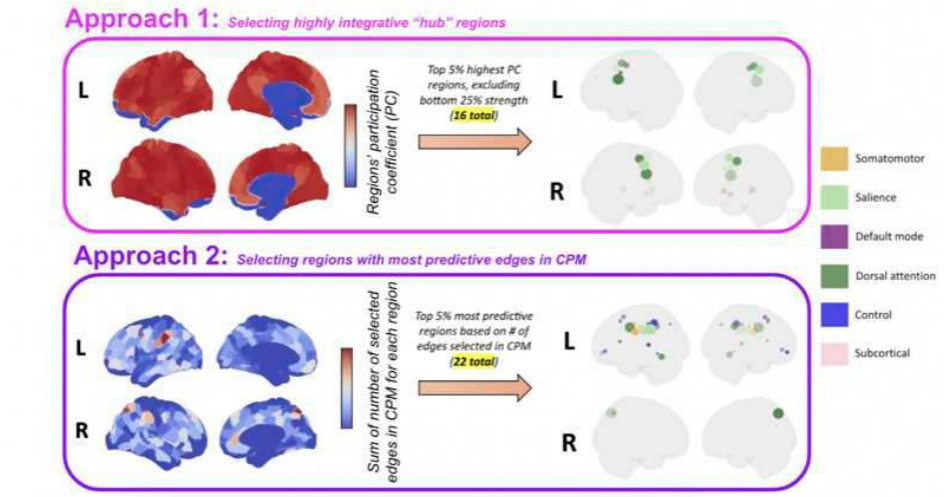

Fig 1. Two complementary approaches for selecting brain regions. Parcels from the Schaefer 400 parcellation (excluding limbic network) as well as the Harvard-Oxford subcortical atlas were used. In the first approach, parcels were selected if their participation coefficient, following iterative thresholding of the group average functional connectivity matrix from highest 20% to 5% of values, was in the top 5% of participation coefficients (n=16 regions). In the second approach, parcels were selected if the sum of their edges selected following connectome-based predictive modeling (CPM) was in the top 5% of summed edges (n=22 regions). CPM was implemented to predict a general dimension of task impairment.

Results: Our first approach yielded 16 regions in the top 5% for participation coefficient, highlighting executive networks as well as subcortical areas, and implicating motor control. Strength of between-network FC of two regions significantly predicted lower p-factor: right posterior middle (R^2=0.37, $F(16,62)$=2.25; B=-0.0041, $p<0.05$) and superior (B=-0.0047, $p<0.05$) frontal gyrus. Our second approach yielded 22 regions in the top 5% for predictive connections in the CPM. We repeated CPM 1,000 times with 10-fold cross validation (mean r=0.25, permutation p=0.02). Connections selected a maximum of 10,000 times

(10 folds * 1,000 repetitions) were predictive of task impairment (r=-0.5, p<0.001), highlighting executive networks as well as the default mode network. Participation coefficient of one region in left posterior superior frontal gyrus significantly predicted lower p-factor (R2=0.26, F(22,56)=0.87; B=-0.49, p<0.05).

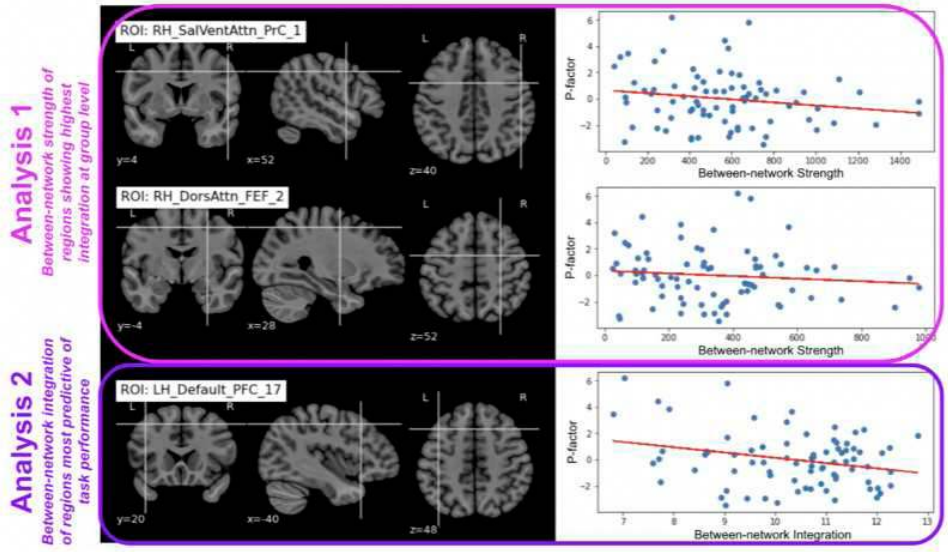

Fig 2. Results from two multiple linear regression models testing association with p-factor. Regions shown are those which significantly predicted reduced p-factor. For analysis 1, reduced p-factor was associated with increased strength of between-network functional connectivity of two right hemisphere executive/motor control areas. For analysis 2, reduced p-factor was associated with increased between-network integration of a left hemisphere executive/motor control area.

Conclusions: Between-network connectivity of portions of bilateral dorsolateral prefrontal cortex, associated with executive and motor control, explained individual variance in p-factor in two complementary analyses. Identification of such a neurobehavioral mechanism underlying p-factor may lead to novel intervention targets.

References

1. Esteban, O. (2019), 'fMRIPrep: a robust preprocessing pipeline for functional MRI', Nature methods, 16(1), 111-116
2. Menon, V., & D'Esposito, M. (2022), 'The role of PFC networks in cognitive control and executive function', Neuropsychopharmacology, 47(1), 90-103
3. Moffitt T.E., (2011), 'A gradient of childhood self-control predicts health, wealth, and public safety', Proceedings of the National Academy of Sciences, 108: 2693–2698

Poster No 667

Closed-Loop Self-Neuromodulation of the Amygdala Involves Co-Modulation of the Posterior Insula

Guy Gurevitch[1,2], Naomi Fine[1,3], Ayelet Or-Borichev[1,2], Tom Fruchtman-Steinbok[1,3], Talma Hendler[1,2,3,4]

[1]Sagol Brain Institute, Tel Aviv Sourasky Medical Center, Tel Aviv, Israel, [2]Department of Physiology and Pharmacology, Faculty of Medicine, Tel Aviv University, Tel Aviv, Israel, [3]School of Psychological Sciences, Tel Aviv University, Tel Aviv, Israel, [4]Sagol School of Neuroscience, Tel Aviv University, Tel Aviv, Israel

Introduction: Self-neuromodulation (also known as NeuroFeedback; NF) is a form of Brain Computer Interface through which individuals learn to modulate their own neural activity, by receiving reinforcing feedback regarding desired changes in neural activity patterns. Previous works have repeatedly shown individual variability in the ability to successfully modulate neural signals (Haugg et al., 2021) and the involvement of widespread brain networks other than the neural target during modulation (Emmert et al., 2016; Goldway et al., 2022). It remains an open question whether this variability stems from the direct accessibility to the target modulation or from co-modulation in other regions. To test these options, we combined data from multiple cohorts targeting Amygdala down-modulation using a validated fMRI informed EEG model (termed Electrical Finger Print; EFP, Keynan et al., 2019).

Methods: 125 patients diagnosed with either post-traumatic stress disorder (n=84) or Fibromyalgia (n=41) participated in clinical studies comprising 6-10 sessions of Amygdala driven-EFP (Amyg-EFP) training (Fruchtman-Steinbok et al., 2021; Fine et al., 2023). We assessed Pre- and post-training modulation with real-time fMRI-NF. Successful modulators in the fMRI-NF were defined by a negative mean BOLD estimate during regulation compared to a passive watch period in each session. The

fMRI data were preprocessed with fmriprep (Esteban et al., 2019) and further analyzed with SPM12 to demonstrate activation patterns in successful and unsuccessful modulators before and after NF training. Extra-target activation ROIs were selected and defined based on whole brain maps of the same contrast shown in previous results (Goldway et al., 2022) - See Figure 1 numbered circles - 1) Posterior insula; 2) Hippocampus; 3) Posterior cingulate cortex; 4) Medial prefrontal cortex. These activation clusters were extracted bilaterally from the first-level maps of each subjects and further assessed in a univariate ANOVA for group and session differences. Finally, a mediation analysis was used to depict the relationship between the fmri-NF target modulation and Amyg-EFP training through extra-target co-modulation.

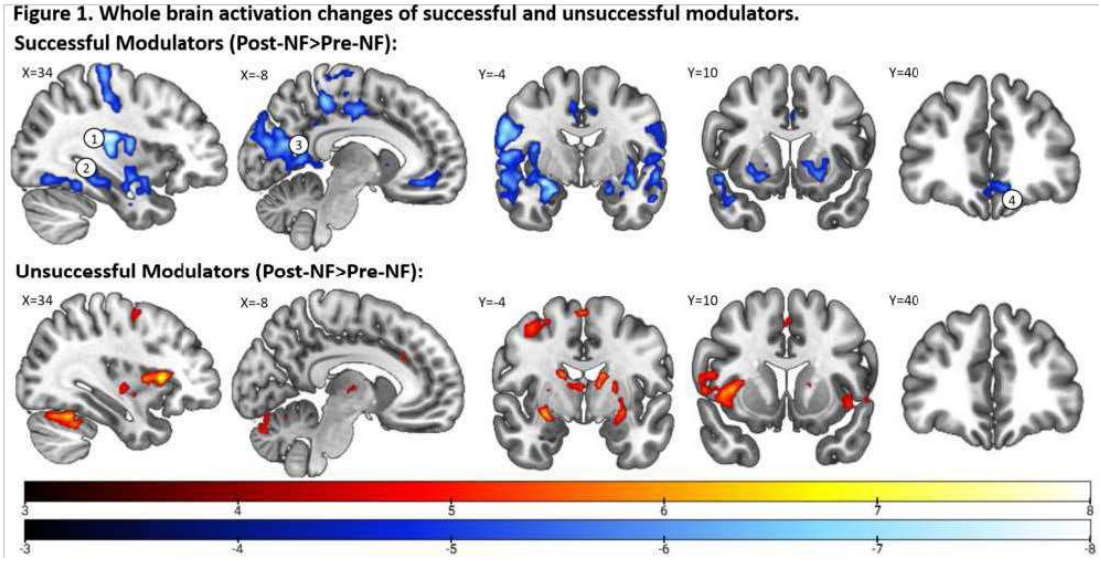

Results: Similar to previous works in healthy participants, we found distinct activation patterns for Amygdala down-modulation in successful compared to unsuccessful modulators across sessions. During the post-NF session relative to pre-NF, successful modulators showed enhanced distributed deactivations, while unsuccessful modulators showed enhanced distributed activations. Images were assessed for cluster-wise significance at p(FDR)<0.05; cluster defining threshold p<0.0001. (Fig 1). ROI analysis revealed a significant Group x Session x Condition interaction in the bilateral posterior insula (Fig 2A, F=9.224; p<0.012, corrected for multiple comparisons), showing that only successful modulators down-modulate this region during regulation compared to watch, and do so more after NF training with the Amyg-EFP probe (T=5.79, p<0.0001). Introducing a mediation model, we show that the association between Amyg-EFP modulation and Amygdala activation change is mediated by activation change in the posterior Insula (Fig 2B, Indirect path, Sobel Z=2.32; p<0.026).

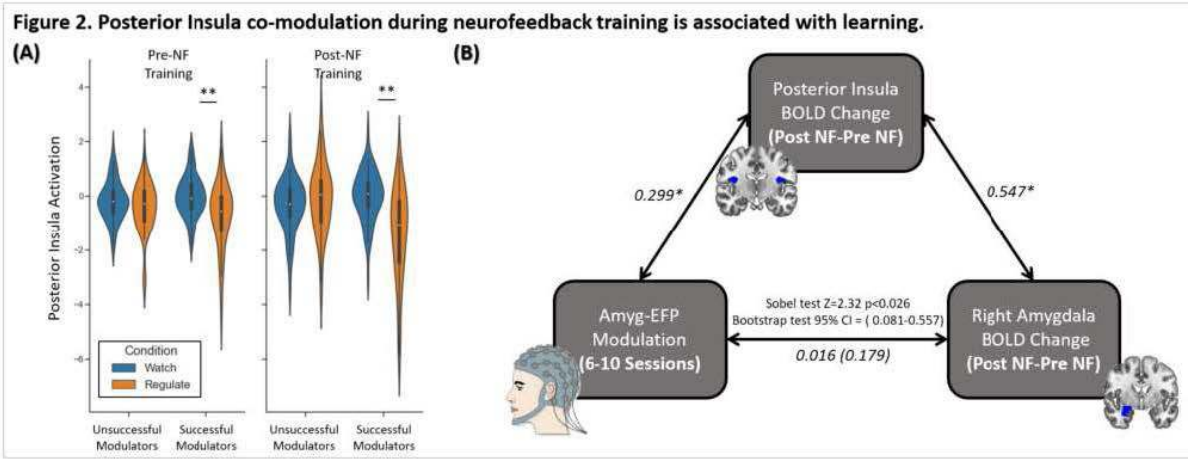

Conclusions: Our results demonstrate different network patterns activated during successful and unsuccessful down-modulation of the amygdala during NF training. Examining neural changes following multi-session training emphasizes the posterior insula as a region directly involved in learning to self-modulate the amygdala. Further research may support an understanding of the causal dynamics of such successful modulation. Altogether contribution of beyond-the-target regions for NF success, could be utilized in the future for guiding personalized NF training design in neuropsychiatry.

References
1. Emmert K. (2016) Meta-analysis of real-time fMRI neurofeedback studies using individual participant data: How is brain regulation mediated? NeuroImage 124:806–812.
2. Esteban O. (2019) fMRIPrep: a robust preprocessing pipeline for functional MRI. Nat Methods 16:111–116.
3. Fine N.B. (2023) Amygdala-related EEG NEURO-FEEDBACK as an add-on Therapy for treatment-resistant Childhood Sexual Abuse PTSD : Feasibility Study. Psychiatry Clin Neurosci:pcn.13591.
4. Fruchtman-Steinbok T. (2021) Amygdala electrical-finger-print (AmygEFP) NeuroFeedback guided by individually-tailored Trauma script for post-traumatic stress disorder: Proof-of-concept. NeuroImage: Clinical 32:102859.
5. Goldway N. (2022) Feasibility and utility of amygdala neurofeedback. Neuroscience & Biobehavioral Reviews 138:104694.
6. Haugg A. (2021) Predictors of real-time fMRI neurofeedback performance and improvement – A machine learning mega-analysis. NeuroImage 237:118207.
7. Keynan J.N. (2019) Electrical fingerprint of the amygdala guides neurofeedback training for stress resilience. Nature Human Behaviour 3:63–73.

Poster No 668

Changes in Default Mode Network connectivity following sleep deprivation in patients with depression

Artemis Zavaliangos-Petropulu[1], Noor Al-Sharif[1], Paloma Pfeiffer[2], Brandon Taraku[1], Ashish Sahib[1], Amber Leaver[3], Randall Espinoza[4], Katherine Narr[1,5]

[1]Department of Neurology, Geffen School of Medicine at the University of California, Los Angeles, CA, [2]Department of Neurology, Geffen School of Medicine at the University of California, Los Angeles, CA, [3]Department of Radiology, Northwestern University, Chicago, IL, [4]Jane and Terry Semel Institute for Neuroscience and Human Behavior, Department of Psychiatry and Bio, Los Angeles, CA, [5]Jane and Terry Semel Institute for Neuroscience and Human Behavior, Department of Psychiatry and Biobehavioral Sciences, Los Angeles, CA

Introduction: The mechanism driving the strong but transient antidepressant effects of total sleep deprivation (TSD) in patients with major depressive disorder (MDD) remains unclear (Ioannou et al., 2021). There is some evidence that suggests TSD impacts the default mode network (DMN) in both healthy controls (HC)(Lunsford-Avery et al., 2020) and MDD populations(Bosch et al., 2013). The DMN appears central to depression pathophysiology(Brakowski et al., 2017), and is often found to be hyperactive(Kaiser et al., 2015). Here, we examined how 24 hours of TSD modulates DMN connectivity in patients with MDD and HC. We hypothesized that changes in the DMN may contribute to the antidepressant effects of TSD.

Methods: Participants included N=60 individuals with MDD (age=32.6±11.6, 45% female) and N=54 HC (age=32.2±12.0, 43% female). All patients and a subset of HC (N=15, age=30±12.5, 40% female) participated in a monitored 24-hour sleep deprivation session at the UCLA Clinical and Translational Research Center. Brain imaging and mood assessments (Hamilton Depression Rating Scale; HDRS(Hamilton 1960)) were collected at baseline and 24 hours later (Figure 1a). T1- and T2-weighted images (voxel size(VS)=0.8mm3) and resting state fMRI (VS=2mm3), acquired on a Siemens 3T Prisma using Human Connectome Project (HCP) sequences, were preprocessed with the HCP minimal preprocessing pipeline(Glasser et al., 2013). Post-processing included ICA + FIX(Salimi-Khorshidi et al., 2014) and MSMALL alignment(Robinson et al., 2018). fMRI data was parcellated using the Schaefer 100 Yeo 17 Network atlas(Schaefer et al., 2018) to generate z-scored correlation matrices. Changes in HDRS and global signal average (GSA) were assessed using paired t-tests. Analyses were restricted to connectivity within-DMN nodes. Mixed effect models tested the effect of 1) time and 2) time*diagnosis, covarying for age, sex, and GSA. Linear regression models tested for 1) associations between change in connectivity and change in HDRS in patients and controls separately and 2) baseline differences between patients and controls, adjusting for age, sex, and GSA. All analyses were FDR corrected.

Results: HDRS significantly improved in MDD ($t=10.3$, $p=2.2e-16$), but not in HC ($p>0.05$)(Figure 1b). GSA significantly changed over time for both MDD ($t=5.1$, $p=3.89e-6$) and HC ($t=3.3$, $p=0.005$)(Figure 1c). Trending ($p<0.05$) changes after TSD showed 4 connections increasing and 32 decreasing in MDD, 2 increasing and 8 decreasing in HC, and an interaction between time*diagnosis for 15 connections, though these did not pass FDR correction. However, significant associations were observed between improvements in HDRS and increases in right hemisphere retrosplenial cortex (RSP)-medial PFC ($t=4.1$, $p=0.0002$) and right-medial PFC to left-RSP ($t=3.9$, $p=0.0003$) connectivity in MDD (Figure 2a-c). In HC, trending ($p<0.05$) negative correlations between change in connectivity and HDRS were identified between left ventral PFC with the right inferior parietal lobe and right RSP with one positive correlation between left hemisphere RSP to Precuneus (Figure 2d-f). At baseline, MDD patients showed 35 connections (including RSP-medial PFC) with trending ($p<0.05$) greater connectivity compared to HC (Figure 2g-h).

Conclusions: MDD patients showed significantly improved depressive symptoms following TSD, while mood remained stable in HCs. TSD induced significant changes in DMN resting state functional connectivity in both patients and HC. These

findings are in line with previous reports suggesting TSD modulates the DMN(Lunsford-Avery et al. 2020; Bosch et al. 2013). Changes in RSP-medial PFC, which differed by diagnosis at baseline, were exclusively correlated with improvements in mood in patients. Thus, core nodes of the DMN may be relevant to the antidepressant effects of TSD. Further research in larger samples is necessary to confirm these findings.

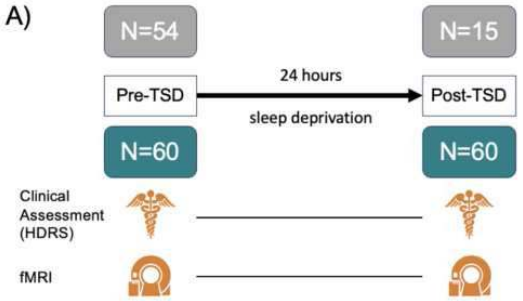

Figure 1. A) Description of study design. B) Following 24 hours of total sleep deprivation, significant changes were observed in mood as measured by the Hamilton Depression Rating Scale (HDRS: higher values = less depressive symptoms). C) Significant changes in global signal average (GSA) were observed in both patients and healthy controls following TSD. ***p=2.2e-16, ** p≤0.005

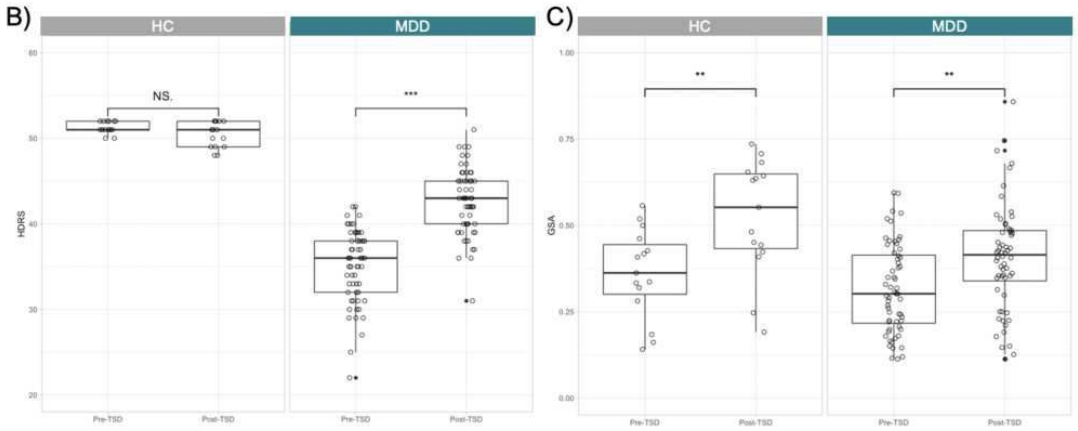

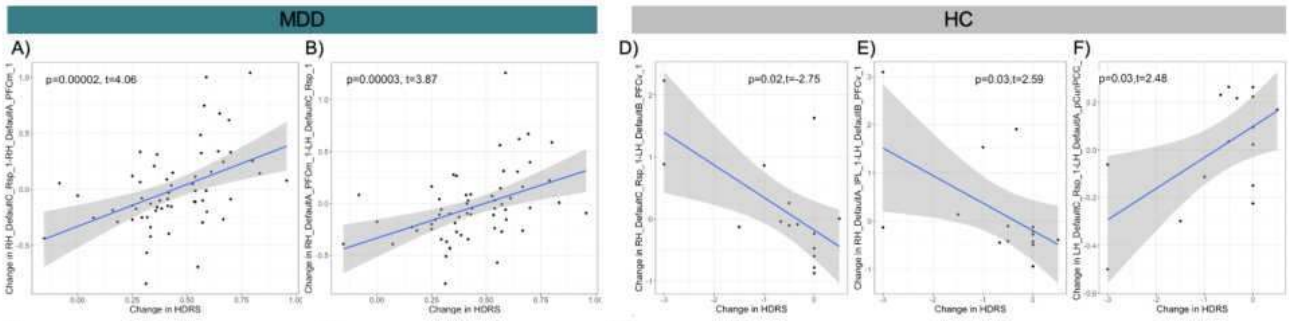

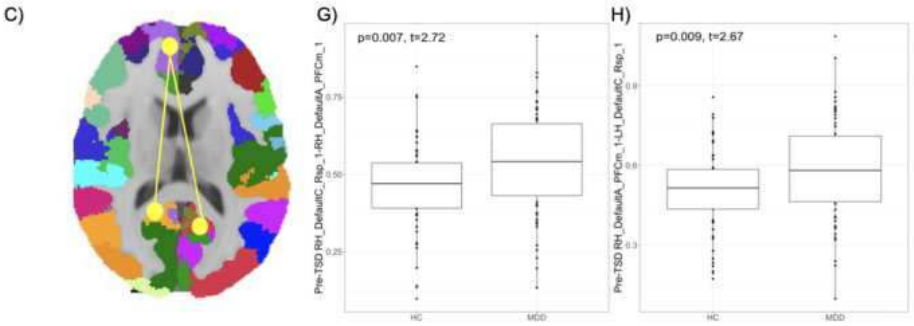

Figure 2. FDR corrected significant correlations with improvements in HDRS were observed between A) right hemisphere retrosplenial cortex (RSP)-medial PFC and B) right-medial PFC to left-RSP in MDD patients. C) These significant network connections are mapped onto the Schaefer atlas. In HC, trending ($p<0.05$) negative correlations between change in connectivity and HDRS were identified between D) left ventral PFC with the right RSP and E) left ventral PFC with the right inferior parietal lobe, and F) one positive correlation between left hemisphere RSP to Precuneus. Pre TSD, MDD patients showed trending ($p<0.05$) stronger connectivity between the G) right hemisphere retrosplenial cortex (RSP)-medial PFC and the H) right-medial PFC to left-RSP when compared to HC at baseline.

References

1. Bosch, O. G., et al (2013). Sleep deprivation increases dorsal nexus connectivity to the dorsolateral prefrontal cortex in humans. Proceedings of the National Academy of Sciences of the United States of America, 110(48), 19597–19602.
2. Brakowski, J., et al (2017). Resting state brain network function in major depression - Depression symptomatology, antidepressant treatment effects, future research. Journal of Psychiatric Research, 92, 147–159.
3. Glasser, M. F., et al (2013). The minimal preprocessing pipelines for the Human Connectome Project. NeuroImage, 80, 105–124.
4. Ioannou, M., et al (2021). Sleep deprivation as treatment for depression: Systematic review and meta-analysis. Acta Psychiatrica Scandinavica, 143(1), 22–35.

5. Kaiser, R. H., et al (2015). Large-Scale Network Dysfunction in Major Depressive Disorder: A Meta-analysis of Resting-State Functional Connectivity. JAMA Psychiatry, 72(6), 603–611.
6. Lunsford-Avery, et al (2020). Sleep/Wake Regularity Associated with Default Mode Network Structure among Healthy Adolescents and Young Adults. Scientific Reports, 10(1), 509.
7. Robinson, E. C., et al (2018). Multimodal surface matching with higher-order smoothness constraints. NeuroImage, 167, 453–465.
8. Salimi-Khorshidi, G., et al (2014). Automatic denoising of functional MRI data: combining independent component analysis and hierarchical fusion of classifiers. NeuroImage, 90, 449–468.
9. Schaefer, A., et al (2018). Local-Global Parcellation of the Human Cerebral Cortex from Intrinsic Functional Connectivity MRI. Cerebral Cortex, 28(9), 3095–3114.

Poster No 669

Differences in White Matter Associated with Relapse in Patients with Major Depressive Disorder

Jack Gomberg[1], Jungho Cha[1], Boadie Dunlop[2], Edward Craighead[2], Helen Mayberg[1], Ki Sueng Choi[1]

[1]Icahn School of Medicine at Mount Sinai, New York, NY, [2]Emory University, Atlanta, GA

Introduction: Episodes of recurrence in major depressive disorder (MDD) are common.[1] However, predictors of recurrence are not well established. Previous studies have found that differential functional connectivity (FC) in the salience and affective networks show promise for predicting symptom recurrence in previously remitted MDD patients.[2] Structural changes underlying these functional differences are unknown and may offer further predictors for recurrence.[3] Using diffusion-weighted imaging (DWI) and clinical data from the 21-month follow-up phase for remitters in the Predictors of Remission in Depression to Individual and Combined Treatments (PReDICT) trial, we evaluated if differences in white matter (WM) could identify patients who would experience recurrence.[4] We hypothesized that abnormal WM integrity would be found in the tracts between the right SCC and insula, given previous FC findings.

Methods: Of the 344 patients randomized to 12 weeks of CBT, SSRI, or SNRI in PReDICT, 60 patients had usable DWI imaging at both baseline and 12 weeks and achieved remission. Of these 60 patients, 14 were assigned to cognitive behavioral therapy (CBT), 22 to duloxetine, and 24 to citalopram. 8 experienced recurrences during the follow-up phase 24 months from the study baseline. Of these 8 patients, 2 had been assigned to CBT, 4 to duloxetine, and 2 to citalopram. MRI scans were obtained during the week prior to treatment randomization and 1-5 days prior to the week 12 visit. A Whole brain fractional anisotropy (FA) map was calculated for each subject using the Fdt FMRIB toolbox. Tract-Based Spatial Statistics (TBSS) analysis was performed for statistical comparison across outcome groups. A two-sample t-test with 5000 permutations was performed using a randomise toolbox in the FA maps of week 12 and the FA changes between baseline and 12 weeks of treatment. We used a significance threshold of family-wise error (FWE) corrected $\alpha < 0.05$.

Results: In the FWE corrected t-test, there was a significant difference in the change in FA in regions along the right corticospinal tract, superior longitudinal, and frontal-occipital fasciculi. Relapsed patients show significant FA reduction between baseline and week 12 (mean=-0.0259, SE 0.0144, p=0.002) in these white matter tracts, while non-relapse show no changes. There was no significant difference between relapsed and non-relapsed patients in week 12 alone.

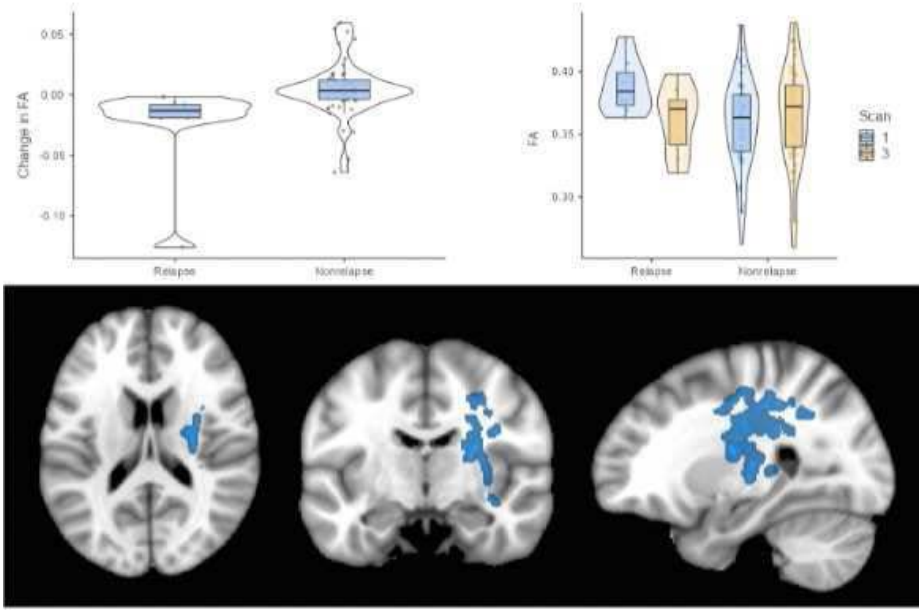

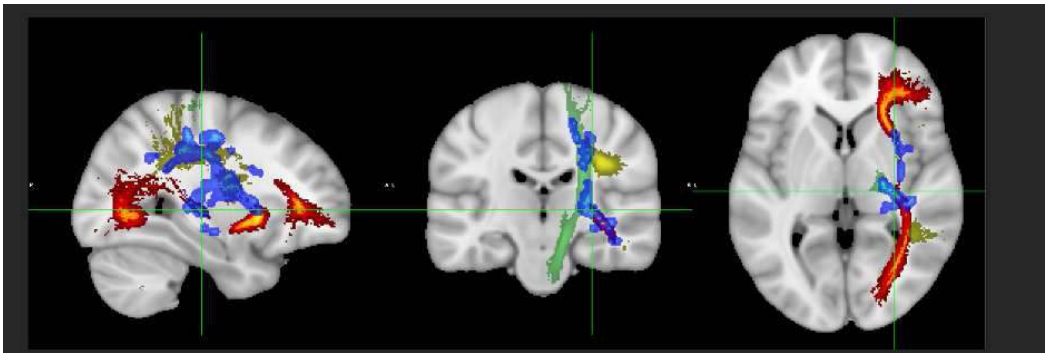

Figure 2: Overlay of findings with MNI white matter tracts

Blue is the region of interest showing significant difference between the change in relapsed patients and the change in non-relapsed patients over 12 weeks. Green = corticospinal tract, yellow = superior longitudinal fasciculus, and red = inferior fronto-occipital fasciculus.

Conclusions: These findings suggest that WM changes during treatment are important for relapse, not white matter integrity at the point of remission. This provides insight for the role of white matter in MDD treatment and relapse.

References

1. Bockting CL, Hollon SD, Jarrett RB, Kuyken W, Dobson K. A lifetime approach to major depressive disorder: The contributions of psychological interventions in preventing relapse and recurrence. Clin Psychol Rev. 2015;41:16-26. doi:10.1016/j.cpr.2015.02.003
2. Dunlop BW, Cha J, Choi KS, Nemeroff CB, Craighead WE, Mayberg HS. Functional connectivity of salience and affective networks among remitted depressed patients predicts episode recurrence. Neuropsychopharmacology. 2023;48(13):1901-1909. doi:10.1038/s41386-023-01653-w
3. Kennis M, Gerritsen L, van Dalen M, Williams A, Cuijpers P, Bockting C. Prospective biomarkers of major depressive disorder: a systematic review and meta-analysis. Mol Psychiatry. 2020;25(2):321-338. doi:10.1038/s41380-019-0585-z
4. Dunlop BW, Binder EB, Cubells JF, et al. Predictors of remission in depression to individual and combined treatments (PReDICT): study protocol for a randomized controlled trial. Trials. 2012;13:106. doi:10.1186/1745-6215-13-106

Poster No 670

Increased prefrontal activation to misophonic triggers in misophonia

Jasmine Tan[1,2], Sergio Osorio[1,2], Grace Levine[1,2], Seppo Ahlfors[3,2], Julie Arenberg[4], Tal Kenet[1,2]

[1]Department of Neurology, Harvard Medical School, Massachusetts General Hospital, Boston, MA, [2]Athinoula A. Martinos Center for Biomedical Imaging, Massachusetts General Hospital, Boston, MA, [3]Department of Radiology, Harvard Medical School, Massachusetts General Hospital, Boston, MA, [4]Department of Audiology, Harvard Medical School, Mass. Eye and Ear, Boston, MA

Introduction: Misophonia is a disorder of abnormal emotional reactions to specific sensory stimuli, and in particular auditory stimuli. Such stimuli, known as misophonic "triggers", are often sounds made by the body, like chewing or breathing, and may seem innocuous but can elicit anger, disgust, stress and anxiety for people suffering from misophonia (Vitoratou et al., 2021). Misophonic triggers have been shown to activate the salience network in people with misophonia (Kumar et al., 2017; Schröder et al., 2019), yet relatively little is known about the cortical underpinnings of misophonia. In this study, we used magnetoencephalography (MEG) to measure activation during an auditory spatial attention task.

Methods: Participants performed a classic auditory oddball paradigm while attending to the cued ear, and were instructed to ignore sounds in the non-cued ear. The sounds in the non-cued ear consisted of the same standard tones as in the cued ear, and two categories of deviant tones. One category consisted of novel stimuli such as claps or clinks that were rated as benign by participants ("distractors"), while the other category consisted of sounds that were selected to trigger misophonia in each individual participant, such as chewing ("triggers"). We hypothesized that while all deviant sounds in the un-cued ear will elicit involuntary "bottom-up" attention, the misophonia-specific trigger sounds will also lead to cortical activation related to emotional reactions not experienced by non-misophonic distractor sounds. Participants with self-reported misophonia were assessed by an audiologist to rule out other primary auditory processing disorders, and were included only if they met the misophonia criteria on the misophonia specific S-Five Questionnaire, which measures number of misophonic triggers and intensity of reaction to these triggers (Vitoratou et al., 2021). Thus far, MEG data has been acquired from 5 (out of a target of 40) misophonia participants (mean age = 24.2, SD = 4.27) and 2 healthy controls (mean age = 25.11, SD = 2,23). Individual

cortical surfaces were obtained from structural T1 MRI images, and BEM head models were computed. We used sLORETA-MNE source modelling to extract responses in source (cortical) space for each participant. Visual inspection of source space activations showed that peak activation to the misophonic trigger sounds followed an initial activation in response to the sound, which was not condition specific, and localized to the anterior regions of the prefrontal cortex (PFC), with some participants showing peak activation in the orbitofrontal cortex and others showing peak activation in the inferior frontal gyrus (IFG). After plotting grand-averaged source activations, the time window of 380-480ms after stimulus onset showed the largest difference in activation between the distractors and triggers conditions. sLORETA activation in this time window was then averaged to be compared across condition and group.

Results: In misophonic participants, the mean activation to misophonic triggers in the prefrontal ROIs was higher (in arbitrary units, mean = 22.7, SD = 7.12) than the mean activation to distractors that were not triggers (mean = 17.6, SD = 4.16). The two matched controls did not show any notable difference in mean activation to the misophonic triggers (mean = 12.4, SD = 3.52) versus the non-misophonic distractors (mean = 16.1, SD = 1.30).

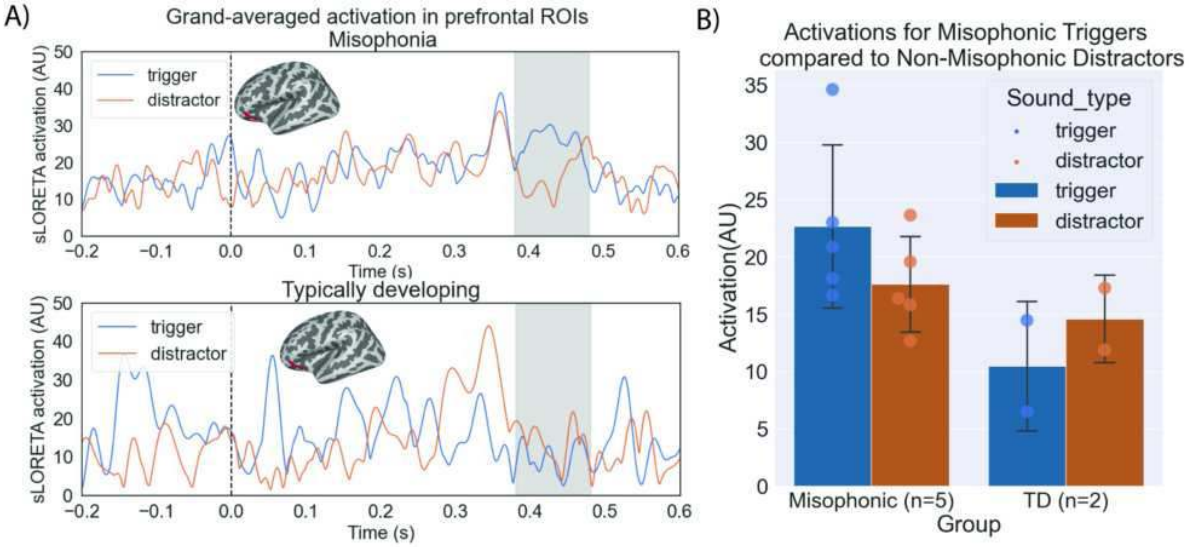

Fig 1. A) Grand averaged source-space activations from prefrontal regions of interest show that participants with misophonia have increased activity to the misophonic triggers compared to a non-misophonic distractors from 380-480ms after stimulus onset. Shaded region shows the time window of largest difference between conditions after initial activation. B) Bar plot for source-space activations averaged within the same time window of interest, compared across conditions, between participants with misophonia and healthy control participants. Whiskers show standard deviation of amplitudes.

Conclusions: These findings add support for the involvement of the prefrontal regions in the neural basis of misophonia. While the orbitofrontal cortex has been posited to relate to a failure of emotional reappraisal (Cerliani & Rouw, 2020), the left inferior frontal gyrus has yet to be linked to misophonia (Neacsiu et al., 2022). The left IFG has been linked to interpersonal emotion regulation, which may be relevant to the social aspect of being distressed by sounds made by others (Grecucci et al., 2013).

References

1. Cerliani, L. (2020). Increased orbitofrontal connectivity in misophonia. BioRXiv.
2. Grecucci, A.(2013). Reappraising social emotions: The role of inferior frontal gyrus, temporo-parietal junction and insula in interpersonal emotion regulation. Frontiers in Human Neuroscience, 7(SEP), 52765.
3. Kumar, S. (2017). The Brain Basis for Misophonia. Current Biology, 27(4), 527–533.
4. Neacsiu, A. D. (2022). The neurobiology of misophonia and implications for novel, neuroscience-driven interventions. Frontiers in Neuroscience, 16(July), 1–23.
5. Schröder, A. (2019). Misophonia is associated with altered brain activity in the auditory cortex and salience network. Scientific Reports, 9(1).
6. Vitoratou, S. (2021). Listening to People with Misophonia: Exploring the Multiple Dimensions of Sound Intolerance Using a New Psychometric Tool, the S-Five, in a Large Sample of Individuals Identifying with the Condition. Psych 2021, Vol. 3, Pages 639-662, 3(4), 639–662.

Poster No 671

Greater white matter hyperintensity volume as a predictor of late-life depression relapse

Leigh Pearcy[1], Helmet Karim[1], Meryl Butters[1], Layla Banihashemi[1], Robert Krafty[2], Brian Boyd[3], Sarah Szymkowicz[3], Jason Hassenstab[4], Bennett Landman[5], Olusola Ajilore[6], Warren Taylor[3], Carmen Andreescu[1]

[1]University of Pittsburgh, Pittsburgh, PA, [2]Emory University, Atlanta, GA, [3]Vanderbilt University, Nashville, TN, [4]Washington University in St. Louis, St. Louis, MO, [5]Vanderbilt University Medical Center, Nashville, TN, [6]University of Illinois at Chicago, Chicago, IL

Introduction: White matter hyperintensities (WMHs) are lesions characterized by increased signal intensity on MRI. They are strongly associated with age, making them common among older adults. WMHs are prevalent in late-life depression (LLD) and are associated with poorer treatment response. Little is known regarding the role of WMH in LLD relapse risk, with some data describing higher WMH in LLD relapsed participants (Taylor et al., 2003). In this study, we investigated group differences in WMH volume between never depressed older adults and older adults with remitted depression who have or have not relapsed.

Methods: We assessed WMHs in 145 participants using 3T MRI FLAIR across a multi-site study. We recruited 43 participants with no history of depression (Control) and 102 depressed participants (LLD) who received treatment and were remitted at time of MRI. Of those who were remitted, 21 relapsed within 8 months of the start of the study (LLD relapsed); the rest remained in remission for at least 8 months (LLD remitted). We used regression to compare WMH volumes between groups based on relapse status, while adjusting for intracranial volume and demographic features including age, sex, race, education, and study site.

Results: The LLD group (n=102) had greater WMH than the control group (n=43) when adjusting for intracranial volume ($F(1,139) = 4.66$, $P= 0.03$). Compared to control participants, the LLD relapsed group (n=21) showed greater WMH ($F(1,133)=4.94$, $P=0.03$) while the LLD remitted group (n=81) had similar WMH even after adjusting for demographic features.

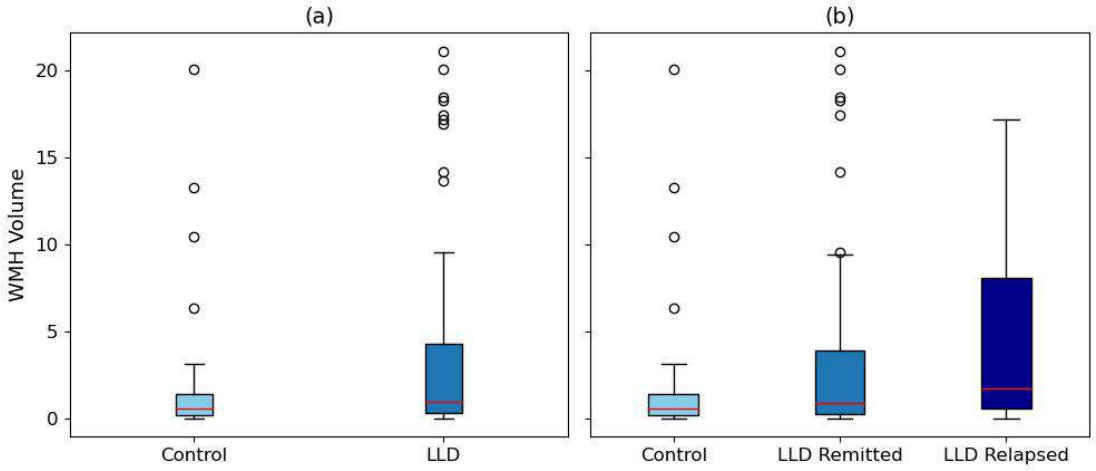

Fig 1. We report the mean (SD) WMH for each group, where (a) Control: 1.9 (3.87); LLD: 3.4 (5.14); (b) Remitted: 3.06 (5.01); Relapsed: 4.66 (5.54). Note the control group is identical in Figures (a) and (b).

Conclusions: Our results showed that compared to the control group, participants with LLD who relapsed had larger WMHs while those who stayed in remission showed no statistical difference in WMH volume, suggesting that individuals who relapse have greater WMH burden than otherwise healthy individuals. This supports the vascular depression hypothesis that individuals with greater WMH burden have worse disease courses, including higher rates of relapse.

References

1. Taylor, Warren D., et al. (2003), "White matter hyperintensity progression and late-life depression outcomes." Archives of General Psychiatry, vol. 60, no. 11, pp. 1090-1096.

Poster No 672

DMN hyperconnectivity and structure in the clinical high-risk stage of schizophrenia

Chelsea Ajunwa[1], Jiahe Zhang[2], Guusje Collin[3,4,5], William Stone[6], Jijun Wang[7], Yingying Tang[7], Tianhong Zhang[8], Martha Shenton[9,10,11], Margaret Niznikiewicz[12], Susan Whitfield Gabrieli[13,14]

[1]Northeastern University, Cambridge, MA, [2]Northeastern University, Boston, MA, [3]Radboudumc Department of Psychiatry, Nijmegen, Netherlands, [4]Donders Institute for Brain, Cognition and Behaviour, Nijmegen, Netherlands, [5]McGovern Institute for Brain Research, Cambridge, MA, [6]Beth Israel Deaconess Medical Center, Boston, MA, [7]Shanghai Mental Health Center, Shanghai Jiaotong University School of Medicine, Shanghai, Shanghai, [8]Shanghai Mental Health Center, Shanghai, China, [9]Brigham and Women's Hospital, Boston, MA, [10]Research and Development, VA Boston Healthcare System, Brockton, MA, [11]Department of Radiology, Brigham and Women's Hospital, Harvard Medical School, Boston, MA, [12]Department of Psychiatry, VA Boston Healthcare System, Brockton, MA, [13]Department of Psychology, Northeastern University and Department of Psychiatry, MGH, Boston, MA, [14]McGovern Institute for Brain Research, Massachusetts Institute of Technology, Cambridge, MA

Introduction: Schizophrenia is characterized by a diverse set of symptoms including hallucinations, delusions, social withdrawal, and impaired cognition (Tandon et al., 2009). Some of these deficits begin prior to the onset of illness, in the prodromal, or Clinical High Risk (CHR) stage, which typically occurs in adolescence or young adulthood (Cannon, 2015; Cornblatt et al., 1999; Yung & McGorry, 1996). Both hyperactivity and hyperconnectivity of the default-mode network (DMN) have been observed in early schizophrenia (Buckner, 2013; Whitfield-Gabrieli et al., 2009). Structural abnormalities have also been observed in the disorder, especially in temporal regions, and are associated with auditory hallucinations (Shenton et al., 2001). However, the extent to which abnormal connectivity and structure are present in the CHR stage, prior to illness onset, is unknown.

Methods: As part of the Shanghai At-Risk for Psychosis (SHARP) program, resting-state fMRI data were collected from 251 young adults (158 CHR and 93 healthy controls, M = 18.72, SD = 4.68, 129 male). Preprocessing and analysis were performed using the CONN toolbox. We examined functional connectivity of the DMN by performing a whole-brain seed-to-voxel analysis. A 10mm sphere centered at MNI coordinates (-3, 44, -2), in the medial prefrontal cortex (MPFC), was used as the seed. We examined cortical thickness across the whole brain using FreeSurfer. For each parcel, a t-test was performed to compare the average cortical thickness between CHR and healthy controls (HC). Parcels were defined by the Destrieux cortical atlas. Clinical and behavioral measures were also collected. A validated Chinese version of the Structural Interview for Prodromal Symptoms (SIPS) was administered, along with the Hamilton Anxiety Rating Scale (HAM-A) and Hamilton Depression Rating Scale (HAM-D).

Results: Compared to controls, CHRs exhibited significantly greater functional connectivity between the MPFC and 1) the PCC, another key DMN node, and 2) the auditory cortex (middle temporal gyrus and superior temporal gyrus). Furthermore, these two patterns of hyperconnectivity were associated with distinct symptom clusters. MPFC-PCC connectivity was significantly correlated with measures of anxiety and depression (r=0.19, p=0.01), while MPFC-auditory connectivity was significantly correlated with SIPS, a measure of prodromal symptom severity (r=0.26, p=0.0006). After FDR correction for multiple comparisons and correction for mean cortical thickness, CHRs exhibited decreased cortical thickness in a number of areas including the anterior cingulate cortex (p=0.02) and the dorsal PCC (p=0.02). They also exhibited decreased cortical thickness in the middle temporal gyrus (p=0.003) and superior temporal sulcus (p=0.006), two auditory regions.

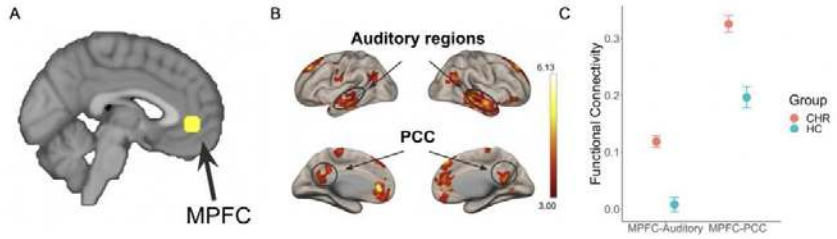

Figure 1. MPFC hyperconnectivity in CHR. **A)** We used a 8mm spherical seed in the MPFC[24]. **B)** Whole-brain search revealed hyperconnectivity between the MPFC seed and several regions, including auditory cortices and the posterior cingulate cortex (p <.001, uncorrected). **C)** Group-level summary statistics for MPFC-auditory and MPFC-PCC functional connectivity are displayed in magenta for CHR and in cyan for HC. Error bars indicate 1 standard error of the mean.

Conclusions: These results demonstrate that two dissociable patterns of DMN hyperconnectivity precede the onset of schizophrenia and may play a mechanistic role in the pathophysiology of the disease. Furthermore, cortical thickness is decreased in regions hyperconnected to the DMN, which suggests that there is a relationship between hyperconnectivity and structure in the CHR stage of schizophrenia. These findings also provide evidence for the resting-state hypothesis of auditory hallucinations, which states that auditory hallucinations are the result of an abnormal relationship between anterior DMN regions like the MPFC and auditory regions like the superior temporal gyrus and medial temporal gyrus (Northoff & Qin, 2011).

References

1. Buckner, R. L. (2013). The brain's default network: Origins and implications for the study of psychosis. Dialogues in Clinical Neuroscience, 15(3), 351–358.
2. Cannon, T. D. (2015). How Schizophrenia Develops: Cognitive and Brain Mechanisms Underlying Onset of Psychosis. Trends in Cognitive Sciences, 19(12), 744–756. https://doi.org/10.1016/j.tics.2015.09.009
3. Cornblatt, B., Obuchowski, M., Roberts, S., Pollack, S., & Erlenmeyer–Kimling, L. (1999). Cognitive and behavioral precursors of schizophrenia. Development and Psychopathology, 11(3), 487–508. https://doi.org/10.1017/S0954579499002175
4. Northoff, G., & Qin, P. (2011). How can the brain's resting state activity generate hallucinations? A 'resting state hypothesis' of auditory verbal hallucinations. Schizophrenia Research, 127(1), 202–214. https://doi.org/10.1016/j.schres.2010.11.009
5. Shenton, M. E., Dickey, C. C., Frumin, M., & McCarley, R. W. (2001). A review of MRI findings in schizophrenia. Schizophrenia Research, 49(1–2), 1–52.
6. Tandon, R., Nasrallah, H. A., & Keshavan, M. S. (2009). Schizophrenia, "just the facts" 4. Clinical features and conceptualization. Schizophrenia Research, 110(1), 1–23. https://doi.org/10.1016/j.schres.2009.03.005
7. Whitfield-Gabrieli, S., Thermenos, H. W., Milanovic, S., Tsuang, M. T., Faraone, S. V., McCarley, R. W., Shenton, M. E., Green, A. I., Nieto-Castanon, A., LaViolette, P., Wojcik, J., Gabrieli, J. D. E., & Seidman, L. J. (2009). Hyperactivity and hyperconnectivity of the default network in schizophrenia and in first-degree relatives of persons with schizophrenia. Proceedings of the National Academy of Sciences of the United States of America, 106(4), 1279–1284. https://doi.org/10.1073/pnas.0809141106
8. Yung, A. R., & McGorry, P. D. (1996). The Prodromal Phase of First-episode Psychosis: Past and Current Conceptualizations. Schizophrenia Bulletin, 22(2), 353–370. https://doi.org/10.1093/schbul/22.2.353

Poster No 673

Structural Brain Connectome Landscape of Mood and Anxiety Disorders

Yael Jacob[1], Laurel Morris[1], Priti Balchandani[1], James Murrough[1]

[1]Icahn School of Medicine at Mount Sinai, New York, NY

Introduction: Mood and anxiety disorders such as major depressive disorder (MDD), general anxiety disorders (Anx) and post-traumatic stress disorder (PTSD) exhibit high comorbidity and overlapping symptoms making diagnosis, research, and treatment challenging (Gorman 1996). Accumulating evidence suggests that psychiatric disorders manifest as aberrant communication between and within functional networks (Menon 2011). A network perspective may explain high comorbidity and varying treatment efficacy. Graph theory methods offer a flexible way to model whole-brain connectivity (i.e. 'connectome') (Sporns 2011). Common disturbances to key network features (e.g. 'modularity' and 'integration') are found in various disorders, possibly indicating shared mechanisms among seemingly disparate disorders. This theory, known as the 'connectome landscape of dysconnectivity' (van den Heuvel and Sporns 2019) (Fig.1), suggests a two-dimensional coordinate system framed by the principal features of modularity and integration. In this framework, optimal organization is achieved when there is a balance between whole-brain connectivity and modular organization, where efficient global communication is optimized. Disease processes are theorized to shift a connectome away from the optimal balance. However, this has not been empirically demonstrated as most networks are studied only one disorder at a time.

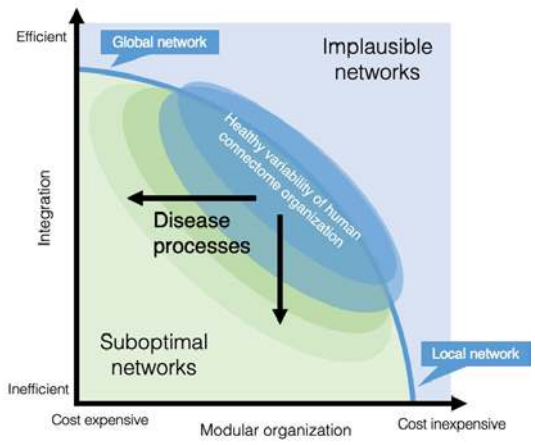

Methods: Data were acquired on a Siemens Magnetom 7T MRI scanner. All subjects (HC=36, MDD=20, Anx=18, and PTSD=11) underwent anatomical T1-weighted and diffusion-weighted imaging (DWI). DWI images were preprocessed using MRtrix3. Each subject's anatomical image was segmented into Desikan-Killiany Atlas (Desikan, Segonne et al. 2006) using FreeSurfer.v.6.0 and coregistered into DWI space to construct the connectome. The segmented 84 regions of interest (ROIs) represent the nodes and edges are defined by streamline count between any pairwise ROIs derived from probabilistic tractography. To construct the connectome landscape, we used the Brain Connectivity Toolbox (Rubinov and Sporns 2010), for each subject we calculated: 1) modularity- the number of edges that fall within the clusters in the network minus the expected number of edges if distributed randomly (Newman 2004); and 2) global efficiency- the average inverse shortest path length (minimum number of edges that must be traversed to go from one node to another) (Latora and Marchiori 2001). We then assessed the normal distribution within the connectome landscape by applying curve fitting analysis on all HC. The goodness of fit from the fitted curve was determined for each group by its summed square of residuals (SSE) (deviations predicted from actual) and root mean square error (RMSE). Global modularity-to-efficiency ratios were also calculated and linear models were used to compare each group's ratios to HC while controlling for age and gender.

Results: The optimal HC balance was estimated with a fitting curve (power 2) (Fig.2A). The goodness of fit to the curve of Anx (SSE=0.41, RMSE = 0.15) and PTSD (SSE=6.51, RMSE = 0.77), showed higher SSE and RMSE values indicating poorer goodness of fit compared to the MDD (SSE=0.18, RMSE = 0.094). In addition, the modularity-to-efficiency ratios of the Anx and PTSD groups were found to be significantly higher than HC (t=2.27, p=0.028 and t=2.93, p=0.0054, respectively) (Fig.2B). The PTSD group modularity-to-efficiency ratio was also significantly higher than MDD (t=2.16, p=0.041) (Fig.2B).

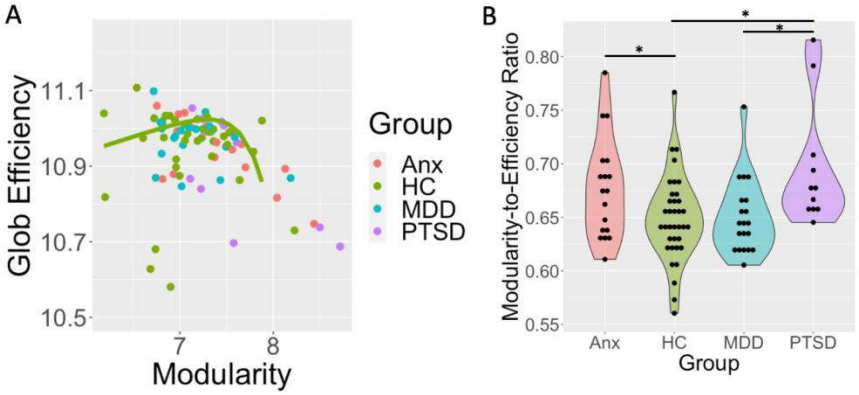

Conclusions: Our results show that MDD patients exhibit the same balance between efficiency and modularity as HC. However, individuals with Anxiety and PTSD demonstrate a tip in the balance, towards higher modular organization and lower network efficiency. These results demonstrate the ability of the connectome landscape framework to uncover unique network organization features related to anxiety, indicating that anxiety manifests as more global brain dysconnectivity.

References

1. Desikan, R. S., F. Segonne, B. Fischl, B. T. Quinn, B. C. Dickerson, D. Blacker, R. L. Buckner, A. M. Dale, R. P. Maguire, B. T. Hyman, M. S. Albert and R. J. Killiany (2006). "An automated labeling system for subdividing the human cerebral cortex on MRI scans into gyral based regions of interest." Neuroimage 31(3): 968-980.
2. Gorman, J. M. (1996). "Comorbid depression and anxiety spectrum disorders." Depression and Anxiety 4(4): 160-168.
3. Latora, V. and M. Marchiori (2001). "Efficient behavior of small-world networks." Physical review letters 87(19): 198701.
4. Menon, V. (2011). "Large-scale brain networks and psychopathology: a unifying triple network model." Trends in cognitive sciences 15(10): 483-506.
5. Newman, M. E. (2004). "Fast algorithm for detecting community structure in networks." Physical review E 69(6): 066133.
6. Rubinov, M. and O. Sporns (2010). "Complex network measures of brain connectivity: uses and interpretations." Neuroimage 52(3): 1059-1069.
7. Sporns, O. (2011). Networks of the Brain, MIT press.
8. van den Heuvel, M. P. and O. Sporns (2019). "A cross-disorder connectome landscape of brain dysconnectivity." Nature Reviews Neuroscience 20(7): 435-446.

Poster No 674

Investigating the effects of real-time biofeedback using 7-Tesla MRI for depression

Laurel Morris[1], James Murrough[2]

[1]Icahn School of Medicine at Mount Sinai, New York, NY, [2]Mt Sinai Icahn School of Medicine, Boston, MA

Introduction: Major Depressive Disorder (MDD) is a significant public health problem, but current treatments fail at relieving symptoms for many patients. Motivational deficits are a core feature of depression and are mediated by dopaminergic projections from the ventral tegmental area (VTA), a tiny midbrain region that has been largely inaccessible with traditional 3-Tesla MRI.

Methods: We have developed an ultra-high field 7-Tesla real-time biofeedback (RT-BF) protocol for VTA activity self-regulation, via a randomized, sham-controlled trial. To date, N=42 (MDD=20, HC=22) have been randomized to Active or Sham VTA biofeedback and have completed all measures. The 7T-MRI session includes a baseline, three rounds of training, and a transfer-test run. During training runs, participants use various abstract cognitive strategies to generate a heightened state of motivation (motivate trials). Participants in the Active group observe their own VTA activity, whereas participants in the Sham (control) group are yoked to a prior participant's activity. Separate repeated measures ANOVA were used to examine the effects of time (pre, post), intervention (Active, Sham), and group (depression, control) on self-reported transient depression (profile of mood states) and VTA activation (motivate>rest).

Results: There was a significant main effect of group ($F(1,38)=59.5$, $p<0.001$), and a group*time interaction effect ($F(1,38)=5.1$, $p=0.030$) on transient depression; where MDD participants showed a larger reduction in depression over time compared to controls. There was also an interaction between group*time intervention ($F(1,38)=4.9$, $p=0.032$), where MDD participants in the Active arm showed a larger reduction in depressed scores compared to the Sham arm, while control subjects showed negligible changes. For VTA activity regulation during biofeedback training, there were trends towards main effects of time ($F(1,30)=3.5$, $p=0.071$) and a group*time interaction ($F(1,30)=3.4$, $p=0.073$), whereby VTA activation increased over time, and MDD seemed to show the highest VTA activation at the end of training. All up-to-date results will be presented.

Conclusions: Early findings suggest the efficacy of 7T RT-BF in regulating VTA activity to improve mood in individuals with MDD.

Poster No 675

Brain-behaviour relationships in population-based and clinically-ascertained samples

Hajer Nakua[1], Lee Propp[1], Anne-Claude Bedard[1], Marcos Sanches[2], Stephanie Ameis[3], Brendan Andrade[2]

[1]University of Toronto, Toronto, Ontario, [2]Centre for Addiction and Mental Health, Toronto, Ontario, [3]Centre for Addiction and Mental Health, Toronto, Ontario

Introduction: Elevated externalizing behaviours in childhood predict development of various mental health disorders in adolescence (Copeland et al., 2009). Typically, children exhibiting elevated externalizing symptoms also show emotion dysregulation and callous-unemotional (CU) traits. These three dimensions may confer to varying risk trajectories of developing an externalizing disorder. Understanding whether these dimensions feature shared or distinct neurobiological correlates can complement the exploration of risk trajectories by providing insight on brain-based predictors of clinical and treatment outcomes. Here, we examined whether baseline brain structure in frontolimbic/striatal regions would be related to externalizing symptoms, emotion dysregulation, and CU traits in a population-based sample. We then determined whether brain structure of these regions would be predictive of improved conduct problems following a 15-week psychosocial treatment intervention in a separate pilot sample of children with externalizing disorders.

Methods: We fit separate linear mixed-effect models in two datasets to examine the relationship between baseline brain structure (parcellated from the Desikan-Killiany Atlas; Desikan et al., 2006) and externalizing psychopathology dimensions over time. Using the Adolescent Brain Cognitive Development (ABCD) Study (n=10,534,ages=9-11;Casey et al., 2018), we examined cross-sectional and longitudinal relationships between frontolimbic/striatal structures and externalizing symptoms, emotion dysregulation, and/or CU traits using various clinical measures to index these dimensions. Fixed effect covariates included sex, age, medication status, and household income. Random effects included family ID (for multiple siblings enrolled), site, and participant ID (for longitudinal models). Then, in a pilot sample of children with externalizing disorders(n=17,ages=9-12), we examined whether pre-treatment brain structure of frontal regions identified in ABCD were linked to reductions in conduct problems (derived from Strengths and Difficulties Questionnaire; SDQ) following psychosocial treatment. Fixed effect covariates included time, emotion dysregulation, ROI thickness, the interaction between these three variables, as well as conduct problems. Random effects included participant IDs. We corrected for multiple comparisons across analyses.

Results: In ABCD, higher baseline CU traits were significantly associated with increased baseline cortical thickness in the right rostral middle frontal gyrus (B=0.027,p=0.03) and the left and right pars orbitalis

(left:B=0.033,pcor=0.009;right:B=0.027,p=0.03). Greater baseline emotion dysregulation was significantly associated with baseline lower subcortical volume in the left caudate (B=-0.026,p=0.02), right amygdala (B=-0.027,p=0.02), left and right nucleus accumbens (left:B=-0.024, p=0.02;right:B=-0.037,p<0.001). Lower baseline cortical thickness in the left pars triangularis (F(2, 20576)=6.94,p=0.014) and left rostral middle frontal gyrus (F(2, 20619)=6.33,p=0.014) moderated the trajectory of externalizing symptoms over time. In the pilot study, greater thickness in the left insula and right rostral anterior cingulate cortex was associated with reduced conduct problems following treatment (B=1.01-3.88,p<0.01).

Conclusions: Our first analysis revealed that while the frontolimbic/striatal networks are implicated in externalizing psychopathology across a pediatric population-based sample, each dimension and the time-point being measured may influence the pattern and trajectory of brain-behaviour relationships found. Our second analysis revealed that frontal cortical regions may be predictive of treatment outcome in children with externalizing disorders. Although the two analyses identified different regions within the frontal cortical network, the overall results of this study shows that regions in this network may be implicated in externalizing psychopathology across different pediatric samples.

References

1. Casey BJ. (2018). The Adolescent Brain Cognitive Development (ABCD) study: Imaging acquisition across 21 sites. Dev Cogn Neurosci, 32:43-54.
2. Copeland WE. (2009). Childhood and adolescent psychiatric disorders as predictors of young adult disorders. Arch Gen Psychiatry, 66(7):764-772.
3. Desikan RS. (2006). An automated labeling system for subdividing the human cerebral cortex on MRI scans into gyral based regions of interest. Neuroimage, 31(3):968-980.

Poster No 676

Childhood Psychological Abuse and Adult Brain Function in a Large Psychiatric Cohort

David Keator[1,2,3], Frank Salgado[3], Prakruthi Praveen[3], Sydnyy Murray[3], Daniel Amen[4,5]

[1]University of California, Irvine, Irvine, CA, [2]Change Your Brain, Change Your Life Foundation, Costa Mesa, CA, [3]Amen Clinics, Costa Mesa, CA, [4]Change Your Brain Change Your Life Foundation, Costa Mesa, CA, [5] Amen Clinics Inc., N/A

Introduction: Childhood trauma such as psychological abuse (i.e. emotional abuse and neglect) has been associated with temporal lobe dysfunction[1,2] and increased frequency of mental health disorders in adulthood[3]. Here we study a large adult clinical population and evaluate the relationship between those who report psychological abuse in childhood as measured with the adverse childhood experiences assessment, adult brain function, and behavior.

Methods: Brain SPECT images were collected on 7,275 patients (mean age= 40.9 +/- 16.3 years; F/M= 3754/3521; mean number of diagnoses=2.4 +/-1.6) during a Connor 's Continuous Performance Test. Each participant received an age/weight-appropriate dose of technetium-99m hexamethylpropyleneamine oxime (Tc-99m HMPAO) intravenously in a dimly lit room and were scanned 30-45 minutes after injection using a InterMedical MultiCam 3000eco triple-headed gamma camera. SPECT data was processed, and attenuation correction performed using general linear (Chang) methods. The SPECT images were spatially registered to the Montreal Neurological Institute (MNI) space with the SPM12 Statistical Parametric Mapping tool. A voxel-based `one-sample t-test model was used to evaluate differences in cerebral perfusion among those reporting psychological abuse compared to those who did not, including age, sex, scan location, and number of comorbid diagnoses as covariates. Total Brain[4] behavioral assessments were available on 2,848 of the patients (mean age=40.3 +/- 14.9 years; F/M= 1146/1098; mean number of diagnoses=2.8 +/- 2.1).

Results: We found significant increases across bilateral temporal lobe regions and temporo-parietal regions along with decreases in anterior cingulate and bilateral lentiform nucleus, among others, in SPECT-derived brain perfusion of those reporting psychological abuse (Figure 1; Table 1). Statistically, most results did not survive multiple comparison corrections and had small effect sizes (Cohen's D). For the behavioral data, we found decreases in the patients with psychological abuse in the feeling domain score, averaging over stress control, anxiety control, and depressive mood control (t(1,2846)=-8.04; p<6.39e-16) and immediate memory from the verbal recognition task (t(12846)=-1.75; p<0.04). The superior temporal lobe has been associated with language (left) and spatial awareness (right)[5]; whereas, the medial aspects have been associated with declarative memory, novelty recognition, and detection[6,7]. The temporo-parietal junction is involved in multisensory integration, social cognition, and stimulus-driven attention functions[8], aberrant function being implicated in depression[9]. The anterior cingulate, has been associated with motivation, context-dependent behaviors, cognitive control, and conflict processing[10,11] and along with the precuneus, forms part of the default mode network (DMN). The putamen has been associated with learning and motor control, speech articulation, reward, cognitive function, and addiction[12]. Further, substance abuse has been associated with decreased left putamen activation[13] and so has major depressive disorder in response

to reward cues[14], both of which we found to have reduced function in those reporting psychological abuse. Taking the neuroimaging results together with the behavioral results, the reduction in feeling domain scores may be related to decreased function in the putamen and anterior cingulate, whereas, the reduction in verbal memory, associated with the increased temporal regions.

Figure 1: Correlations between ACE subtype scores and SPECT perfusion across three probability thresholds: p<0.01 unc., p<0.001unc., p<0.05 FWE.

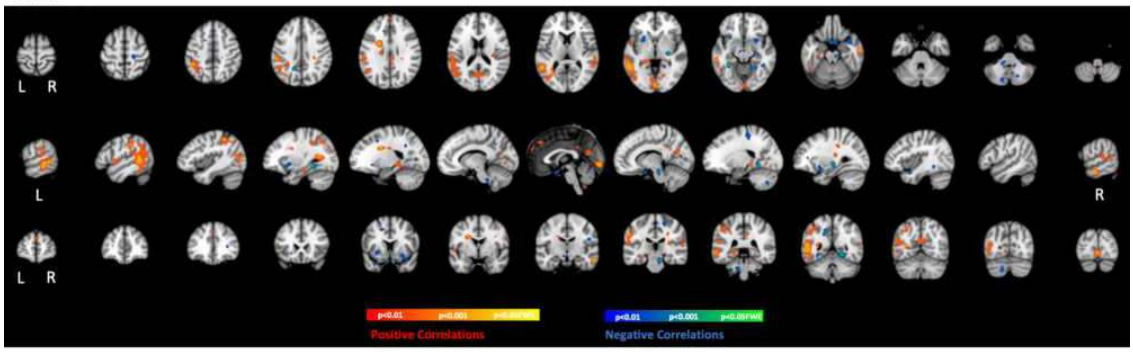

Table1: Regions of peak statistical value in the temporal lobe by type of abuse. Columns include MNI coordinates in millimeters, region name, p-value uncorrected (unc.) or family-wise error corrected (fwe.), and Cohen's D effect size.

Coordinate (x,y,z)	Region	Direction	T (1,7259)	P-value	Cohen's D
60 -28 10	Temporal Sup. R	Positive	2.96	.01 unc.	0.07
58 -12 -20	Temporal Inf. L	Positive	3.68	.001 unc.	0.09
-54 -48 14	Temporal Sup. L	Positive	3.57	.001 unc.	0.08
-56 -50 0	Temporal Mid. L	Positive	4.29	.001 unc.	0.10
-54 -30 34	Parietal Inf. L	Positive	3.64	.001 unc.	0.09
-26 10 -4	Lentiform Nucleus / Putamen L	Negative	3.08	.001 unc.	0.07
26 8 -10	Lentiform Nucleus / Putamen R	Negative	3.22	.001 unc.	0.08
-32 -44 -10	Fusiform L	Negative	4.61	.05 fwe.	0.11
-12 30 26	Anterior Cingulate L	Negative	2.84	.01 unc.	0.07
-16 -52 40	Precuneus L	Negative	3.65	.001 unc.	0.09
20 -26 58	Precentral Gyrus (BA 4)	Negative	2.92	.01 unc.	0.07

Conclusions: In this study we found psychological abuse in childhood to be associated with increases in temporal networks and decreases in basal ganglia and default mode network regions. In future work we will evaluate differences in psychological abuse by the sex assigned at birth and understand how other forms of childhood abuse (e.g. sexual abuse, violence, etc.), as measured with the ACE assessment, are associated with brain function and behavior.

References

1. Tozzi, L. et al. Interactive impact of childhood maltreatment, depression, and age on cortical brain structure: mega-analytic findings from a large multi-site cohort. Psychol. Med. 50, 1020–1031 (2020).
2. Teicher, M. H. & Samson, J. A. Annual Research Review: Enduring neurobiological effects of childhood abuse and neglect. J. Child Psychol. Psychiatry 57, 241–266 (2016).
3. Lippard, E. T. C. & Nemeroff, C. B. The Devastating Clinical Consequences of Child Abuse and Neglect: Increased Disease Vulnerability and Poor Treatment Response in Mood Disorders. Am. J. Psychiatry 180, 548–564 (2023).
4. Total Brain mental health and brain performance self-monitoring and self-care platform. Total Brain https://www.totalbrain.com/ (2020).
5. Karnath, H. O. New insights into the functions of the superior temporal cortex. Nat. Rev. Neurosci. 2, 568–576 (2001).
6. Squire, L. R., Stark, C. E. L. & Clark, R. E. The medial temporal lobe. Annu. Rev. Neurosci. 27, 279–306 (2004).
7. Shen, W., Yuan, Y., Liu, C. & Luo, J. The roles of the temporal lobe in creative insight: an integrated review. Think. Reason. 23, 321–375 (2017).
8. Eddy, C. M. The junction between self and other? Temporo-parietal dysfunction in neuropsychiatry. Neuropsychologia 89, 465–477 (2016).
9. Penner, J. et al. Temporoparietal Junction Functional Connectivity in Early Schizophrenia and Major Depressive Disorder. Chronic Stress (Thousand Oaks) 2, 2470547018815232 (2018).
10. Devinsky, O., Morrell, M. J. & Vogt, B. A. Contributions of anterior cingulate cortex to behaviour. Brain 118 (Pt 1), 279–306 (1995).
11. Braver, T. S., Barch, D. M., Gray, J. R., Molfese, D. L. & Snyder, A. Anterior cingulate cortex and response conflict: effects of frequency, inhibition and errors. Cereb. Cortex 11, 825–836 (2001).
12. Ghandili, M. & Munakomi, S. Neuroanatomy, Putamen. in StatPearls (StatPearls Publishing, 2023).
13. Heitzeg, M. M., Cope, L. M., Martz, M. E. & Hardee, J. E. Neuroimaging Risk Markers for Substance Abuse: Recent Findings on Inhibitory Control and Reward System Functioning. Curr Addict Rep 2, 91–103 (2015).
14. Pizzagalli, D. A. et al. Reduced caudate and nucleus accumbens response to rewards in unmedicated individuals with major depressive disorder. Am. J. Psychiatry 166, 702–710 (2009).

Poster No 677

The effect of transcranial photobiomodulation on local and distal brain activity in depression

Naomi Gaggi[1], Katherine Collins[2], Aura Hurtado[3], Xiaotong Song[4], Zamfira Parincu[2], Kathryn Evans[5], Julie Clancy[3], Anna Peterson[4], Paolo Cassano[6], Dan Iosifescu[4]

[1]New York University, Rockaway Park, NY, [2]Nathan S. Kline Institute, Orangeburg, NY, [3]Massachussets General Hospital, Boston, MA, [4]New York University, New York, NY, [5]Nathan S. Kline Institute, Orangeberg, NY, [6]Massachusetts General Hospital, Boston, MA

Introduction: Individuals with major depressive disorder (MDD) have shown to have aberrant neuronal activity, or fractional amplitude of low frequency fluctuations (fALFF), in the frontal region of the brain[1]. fALFF is a noninvasive neuroimaging measure of regional, voxel-wise, spontaneous fluctuations of the fMRI BOLD signal, which reflects variations in intrinsic brain activity[2]. Transcranial photobiomodulation (tPBM) is a novel, noninvasive, and non-pharmacological treatment that uses red and/or near infrared light to penetrate the cortex and is believed to alter cerebral blood flow and enhance cognition. In this preliminary study, we aimed to explore the local (i.e., directly irradiated) and distal (i.e., global) effects of tPBM on fALFF, which may serve as an modifiable target, in MDD.

Methods: We examined the change in fALFF in frontal regions directly irradiated by tPBM and distal regions not directly irradiated by tPBM. The 10 participants included in the analysis had mean age of 36 years, 70% female, 90% non-hispanic/latino, and were diagnosed with MDD. Then, they underwent three sequential resting state MRI scans (3T Siemens Trio & 12 channel head coil). Multi-echo echo planar imaging (EPI) was acquired pre-tPBM (baseline), during tPBM, and immediately post-tPBM. EPI parameters were: TR=2.5s; TE=12.8,32.33,51.04 ms; slice thickness 2.5 mm. Continuous wave tPBM was delivered via laser probes (808 nm) placed over the forehead bilaterally. Specific standard EEG electrode positions were directly irradiated (F4, F3, Fp2, Fp1, Fz, Fpz). fMRI data were pre-processed using afni_proc.py[3] customized for multi-echo EPI and FreeSurfer[4] was used to pre-process the structural T1. fALFF was calculated using afni 3dRSFC[5] and was extracted from regions of interest (ROI) using Marsbar[6]. The ROIs were created as 5 mm spheres centered on the cortical MRI coordinates of the bilateral irradiated regions[7]. All statistical tests were computed in R studio (R Core Team).

Results: In our preliminary analysis, we found that there was a non-significant, slight decrease of global mean fALFF from pre-tPBM (mean = .99) to during tPBM (mean = .94; t= 1.50, p=.17), which then increased post-tPBM towards baseline levels (mean = .96; t=-2.134, p =.062 (uncorrected)) assessed using paired samples t-tests. The increase from during tPBM to post-tPBM was trending towards significance. Similarly, we found local fALFF effects in regions directly irradiated by tPBM followed the same pattern as the global trends. However, we found that there was only a significant change from baseline to during tPBM in the F4, approximated to the be the right dorsolateral prefrontal cortex (dlPFC; t=2.27, p=.04 (uncorrected), Cohen's d=.91). No other regions showed significant differences when comparing the pre and during (F3: t=.14, p=.28, FP1: t=1.34, p= .21, FP2: t=.49, p=.64, FPZ: t=-.36, p=.73, FZ: t=1.04, p=.33), and the pre and post conditions (F3: t=.23, p=.83, F4: t=.16, p=.88, FP1: t=.40, p=.70, FP2: t=.34, p=.74, FPZ: t=-.60, p=.56, FZ: t=.33, p=.75).

Conclusions: Despite a small sample size, the effect size of the change during the pre to during tPBM condition in F4/dlPFC was large. It is well-demonstrated that the right dlPFC hyperactivity is related to depression severity in MDD[8] and responds to other forms of neuromodulation (i.e., transcranial magnetic stimulation)[9]. These preliminary results indicate that hyperactive regions may be targets for modulation using tPBM in MDD. These results also suggest that fALFF could be useful in exploring diverse tPBM parameters to further enhance target engagement in the MDD population.

References

1. Su L, Cai Y, Xu Y, Dutt A, Shi S, Bramon E. Cerebral metabolism in major depressive disorder: a voxel-based meta-analysis of positron emission tomography studies. BMC Psychiatry. 2014 Nov 19;14:321. doi: 10.1186/s12888-014-0321-9. PMID: 25407081; PMCID: PMC4240898.
2. Zou QH, Zhu CZ, Yang Y, Zuo XN, Long XY, Cao QJ, Wang YF, Zang YF. An improved approach to detection of amplitude of low-frequency fluctuation (ALFF) for resting-state fMRI: fractional ALFF. J Neurosci Methods. 2008 Jul 15;172(1):137-41. doi: 10.1016/j.jneumeth.2008.04.012. Epub 2008 Apr 22. PMID: 18501969; PMCID: PMC3902859.
3. Cox RW. AFNI: software for analysis and visualization of functional magnetic resonance neuroimages. Comput Biomed Res. 1996 Jun;29(3):162-73. doi: 10.1006/cbmr.1996.0014. PMID: 8812068.
4. Fischl B. FreeSurfer. Neuroimage. 2012 Aug 15;62(2):774-81. doi: 10.1016/j.neuroimage.2012.01.021. Epub 2012 Jan 10. PMID: 22248573; PMCID: PMC3685476.
5. Taylor PA, Saad ZS (2013). FATCAT: (An Efficient) Functional And Tractographic Connectivity Analysis Toolbox. Brain Connectivity 3(5):523-535.
6. Brett, M., Anton, J. L., Valabregue, R., & Poline, J. B. (2002, June). Region of interest analysis using an SPM toolbox. In 8th international conference on functional mapping of the human brain (Vol. 16, No. 2, p. 497).

7. Okamoto M, Dan H, Sakamoto K, Takeo K, Shimizu K, Kohno S, Oda I, Isobe S, Suzuki T, Kohyama K, Dan I. Three-dimensional probabilistic anatomical cranio-cerebral correlation via the international 10-20 system oriented for transcranial functional brain mapping. Neuroimage. 2004 Jan;21(1):99-111. doi: 10.1016/j.neuroimage.2003.08.026. PMID: 14741647.
8. Grimm, S., Beck, J., Schuepbach, D., Hell, D., Boesiger, P., Bermpohl, F., ... & Northoff, G. (2008). Imbalance between left and right dorsolateral prefrontal cortex in major depression is linked to negative emotional judgment: an fMRI study in severe major depressive disorder. Biological psychiatry, 63(4), 369-376.
9. Caparelli EC, Abulseoud OA, Gu H, Zhai T, Schleyer B, Yang Y. Low frequency repetitive transcranial magnetic stimulation to the right dorsolateral prefrontal cortex engages thalamus, striatum, and the default mode network. Front Neurosci. 2022 Sep 30;16:997259. doi: 10.3389/fnins.2022.997259. PMID: 36248660; PMCID: PMC9565480.

Poster No 678

Alterations of functional connectivity within the DMN of military Veterans with suicidal behavior

Jadwiga Rogowska[1], Perry Renshaw[1,2,3], Deborah Yurgelun-Todd[1,2,3], Erin McGlade[1,2,3]

[1]Diagnostic Neuroimaging Lab, University of Utah, Salt Lake City, UT, [2]Huntsman Mental Health Institute, University of Utah, Salt Lake City, UT, [3]MIRECC, Department of Veterans Affairs, Salt Lake City, UT

Introduction: In recent years, there has been an increased focus on suicide prevention for the American Veteran population[1-2]. Although a range of studies has been undertaken to identify potential risk factors, self-directed violence remains difficult to predict[3-4]. Anomalous functioning of the default mode network (DMN) has been associated with impairment in an individual's ability to monitor and inhibit behavior, and therefore may lead to the initiation of high-risk behavior such as suicide[5]. However, functional connectivity of DMN, especially among suicidal veterans, is not well documented. Therefore, the aim of the current study was to use resting state functional magnetic resonance imaging (rsFMRI) and functional connectivity (FC) of the DMN to identify and visualize brain changes in Veterans with suicide attempts as well as those with a history limited to suicidal ideation.

Methods: Seventy-eight Veterans (62 males, 16 females; mean age: 36.6) completed the demographic and clinical measures and an 8-min resting state fMRI on a 3T scanner. Participants included a suicidal ideation (SI) group (N= 30), a suicide attempt (SA) group (N=22) and a healthy control (HC) group, consisting of Veterans without a history of suicidal ideation or attempts (N=26). Participants completed the Columbia-Suicide Severity Rating Scale (C-SSRS). Image data were motion corrected, normalized and smoothed using DPARSFA and SPM8[6]. To further reduce motion-related artifacts, the data were "scrubbed"[7]. The FC maps were computed by using a standard seed-based whole brain correlation method with posterior cingulate cortex (PCC) as a seed region. One-sample t-tests were done to determine brain regions showing significant functional connectivity in the DMN ($p<.005$, FDRcorr). Factorial analyses controlling for both age and sex were performed for the three groups (HC, SI, SA) with group as an effect. Post-hoc analyses were then performed between participant groups ($p<0.05$, FWEcorr, $k>200$).

Results: The SA data as compared with HC data showed stronger DMN connectivity to the calcarine, cerebellum, right regions of superior occipital, lingual, fusiform, cuneus and inferior occipital ($k=708$, $p=0.003$), and right regions of insula, supramarginal, inferior frontal, precentral, postcentral, putamen and rolandic operand ($k=429$, $p=0.038$) (Fig. 1). In addition, SA group as compared with the SI group, demonstrated stronger DMN connectivity to the left precentral, postcentral, middle cingulate, inferior and middle temporal, insula and left and right precuneus ($k=1254$, $p<0.0001$), as well as to the right regions of precentral, insula, hippocampus, caudate and palladium ($k=499$, $p=0.015$) and superior and orbital frontal regions ($k=418$, $p=0.027$) (Fig. 2). All other group comparisons for DMN connectivity did not show any statistically significant differences.

Conclusions: There is a growing interest in understanding suicidal behavior using resting state connectivity [8-10]. Our results indicate that the DMN is hyperconnected to multiple brain areas in Veterans with suicide ideation and suicide attempts, reflecting highly synchronized brain circuitry at rest. Differences in connectivity between the SA and SI and between the SA and HC groups were identified and suggest that suicidal behavior in Veterans may be uniquely related to abnormal functional connectivity in the default mode network. These differences could be a potential biomarker in suicide behavior prediction as well as focal targets for intervention. Additional studies controlling for severity of behaviors, psychiatric diagnosis and medication are needed to further clarify brain changes related to suicide behaviors.

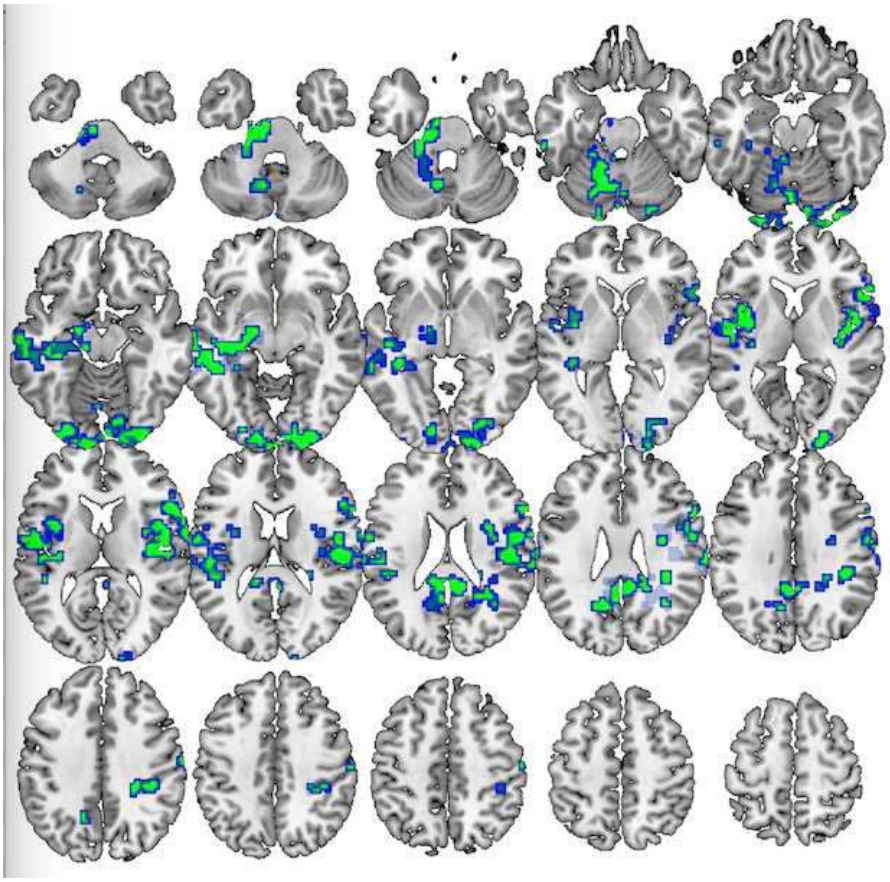

Figure 1. Functional connectivity in DMN demonstrates greater activation in SA relative to HC ($p<0.05$ and cluster size $k>200$).

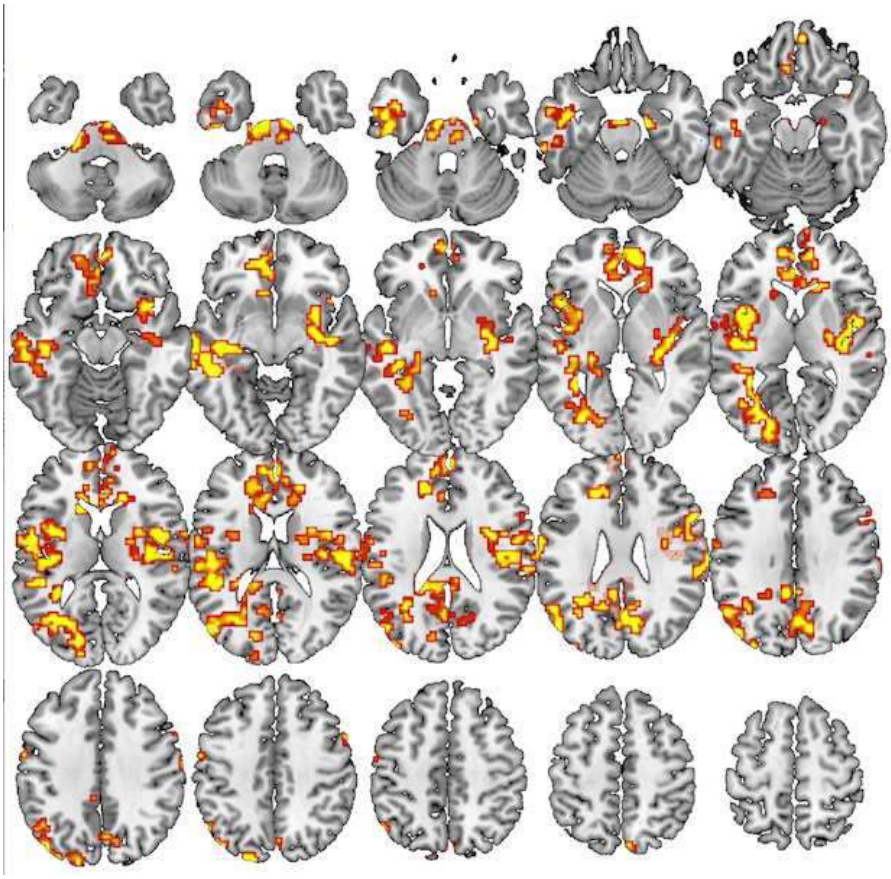

Figure 2. Functional connectivity DMN demonstrates greater activation in SA relative to SI ($p<0.05$ and cluster size $k>200$).

References
1. Kaplan, M.S. (2007), 'Suicide among male veterans: a prospective population-based study', J Epidemiol Community Health, vol. 61, pp. 619-24.
2. Pompili, M. (2013), 'Posttraumatic stress disorder and suicide risk among veterans: a literature review', The Journal of Nervous and Mental Disease, vol. 201, pp. 802-812.
3. Deshpande, G. (2016), 'A Neural Basis for the Acquired Capability for Suicide', Frontiers in Psychiatry, vol. 7, article 125.
4. van Heeringen, K. (2014). 'The neurobiology of suicide', Lancet, Jun; 1(1), pp. 63-72.
5. Stange, J.P. (2020), 'Using resting-state intrinsic network connectivity to identify suicide risk in mood disorders', Psychol Med, 50(14), pp. 2324-2334.
6. Chao-Gan, Y. (2010), 'DPARSF: A MATLAB toolbox for "pipeline" data analysis of resting-state fMRI', Frontiers in Systems Neuroscience, vol. 4, art. 13, pp. 1-7.
7. Power, J.D. (2012), 'Spurious but systematic correlations in functional connectivity MRI networks arise from subject motion', Neuroimage, vol 59, pp. 2142–2154.
8. Namaky, N. (2023), 'Suicidal thoughts and behaviours among military veterans: protocol for a prospective, observational, neuroimaging study', BMJ Open, 13(8):e070654.
9. Serafini, G. (2016), 'Understanding suicidal behavior: the contribution of recent resting-state fMRI techniques', Front Psychiatry, vol. 7, article 69, pp. 1-4.
10. Philippi, C.L. (2021), 'Distinct patterns of resting-state connectivity in U.S. service members with mild traumatic brain injury versus posttraumatic stress disorder', Brain Imaging Behav, 15(5), pp. 2616-2626

Poster No 679

Eating Disorder Diagnosis Moderates Pathological Exercise and White Matter Volume Relationship

Elana Kotler[1], Anastasia Haidar[2], Amanda Lyall[2], Ziyu Zhao[3], Adrienne Romer[4], Felicia Petterway[3], Lauren Lindman[3], Jason Scott[4], Meghan Slattery[3], Nour Shamseddine[2], Tara Kyaw[3], Caroline Judson[4], David Alperovitz[4], Judith Halperin[4], Kristin Javaras[4], Esther Dechant[4], Elizabeth Lawson[3], Jennifer Thomas[3], Marek Kubicki[2], Madhusmita Misra[3], Kamryn Eddy[3], Lauren Breithaupt[5]

[1]Massachusetts General Hospital, Lynnfield, MA, [2]Brigham and Women's Hospital, Boston, MA, [3]Massachusetts General Hospital, Boston, MA, [4]McLean Hospital, Belmont, MA, [5]Harvard Medical School, Boston, MA

Introduction: Both animal and human studies suggest that more frequent physical activity can promote brain health1. Observational studies consistently conclude that higher levels of physical activity are associated with global elevations of gray matter volume(GMV) and white matter volume(WMV). However, physical activity among individuals with restrictive eating disorders such as anorexia nervosa(AN) and atypical AN(At-AN) is a pathological component. While food restriction is the primary driver of weight loss in both AN and At-AN, pathological exercise compounds the effect of food restriction. Levels of pathological exercise are often similar between individuals with AN and At-AN, representing a symptom consistently associated with worse treatment outcomes4. Recent literature has shown that individuals diagnosed with AN have reduced GMV/WMV in the brain, which is driven by severe low-weight status5. Based on these findings, we hypothesized that the number of pathological exercise hours would positively predict GMV/WMV in At-AN. However, due to the consistent GMV loss reported in AN that is driven by low-weight status, we predicted exercise hours would negatively predict GMV/WMV in AN.

Methods: This study utilized structural MRI data from 54 females(14-35y, avg = 22.6y). Consistent with the image-processing pipeline at the Psychiatry Neuroimaging Laboratory8, MRI images were axis-aligned, centered, and visually quality checked prior to a high-definition brain extraction tool9 to omit non-brain tissue. Automatically generated masks were processed through Freesurfer(v7.1.0) using the Desikan-Killiany atlas10. Individuals were diagnosed with a current diagnosis of AN, AN in partial recovery(AN-prec), or At-AN based. In addition, individuals were characterized based on lifetime eating disorder history, classifying individuals into either lifetime AN or lifetime At-AN. Total exercise hours were defined by the number of hours spent exercising over the past 3 months.We investigated the within-group effect of exercise hours on GMV/WMV, between-diagnostic-group differences(AN, AN-prec, At-AN; lifetime AN, lifetime At-AN) in total GMV/WMV, and how diagnosis moderates the GMV/WMV-exercise relationship. Group differences between GMV, WMV, and exercise hours were assessed using linear mixed effect models while covarying for age, BMI z-scores, and head size. The relationship between GMV/WMV, exercise hours, and diagnostic group was evaluated using a linear model with diagnosis as the moderator.

Results: We found that within-group effects of exercise hours on total GMV and WMV were absent, as were between-group (AN vs. AN-prec vs. At-AN; lifetime AN vs lifetime At-AN) effects on GMV/WMV. Our analysis showed that both current and lifetime diagnoses moderated the WMV and exercise hours relationship(current: ß = 601, t = 2.4, p = 0.02; lifetime: ß = 662, t = 2.8, p = 0.008). Individuals with current(Figure 1) and lifetime(Figure 2) At-AN who exercised for a greater number of hours demonstrated greater WMV. WMV in current AN, current AN-prec, and lifetime AN remained suppressed in the context of greater exercise hours, likely due to the diagnosis' low-weight requirement.

Conclusions: Our preliminary results suggest that exercise does not impact GMV in AN or At-AN. However, they do illustrate that exercise hours may positively impact WMV but only in the context of At-AN. Future research is necessary to distinguish both eating disorder groups from a healthy control group and whether specific types of exercise influence the WMV/GMV-exercise relationship. Prospective developments could include investigating weight trajectories to determine if there is a weight range at which exercise is beneficial for the brain.

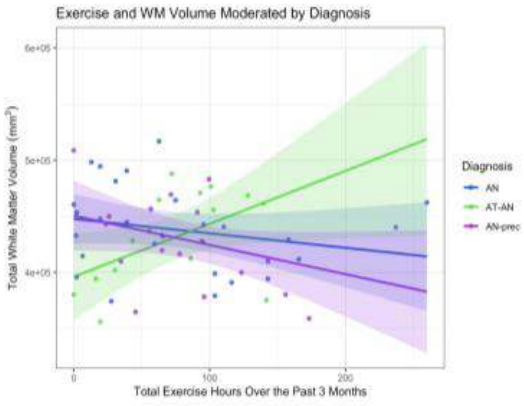

Figure 1. WMV is significantly higher among individuals with current At-AN who exercise more hours. However, individuals with current AN who exercise more hours have smaller global WMV.

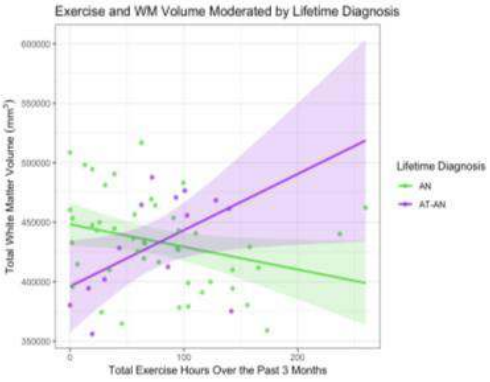

Figure 2. WMV is significantly higher among individuals with lifetime At-AN who exercise more hours. However, individuals with lifetime AN who exercise more hours have smaller global WMV.

References

1. Erickson KI, Leckie RL, Weinstein AM. Physical activity, fitness, and gray matter volume. Neurobiol Aging. 2014 Sep;35 Suppl 2:S20-8. doi: 10.1016/j.neurobiolaging.2014.03.034. Epub 2014 May 14. PMID: 24952993; PMCID: PMC4094356.
2. Gorrell S, Flatt RE, Bulik CM, Le Grange D. Psychosocial etiology of maladaptive exercise and its role in eating disorders: A systematic review. Int J Eat Disord. 2021 Aug;54(8):1358-1376. doi: 10.1002/eat.23524. Epub 2021 May 4. PMID: 33942917; PMCID: PMC8811798.
3. Dalle Grave, R. (2008, November). Excessive and compulsive exercise in eating disorders: Prevalence, associated features, and management. International Journal of Eating Disorders, 28(Vol. 28).
4. Fuglset, T.S., Endestad, T., Hilland, E. et al. Brain volumes and regional cortical thickness in young females with anorexia nervosa. BMC Psychiatry 16, 404 (2016). https://doi.org/10.1186/s12888-016-1126-9
5. https://github.com/pnlbwh/pnlutil
6. Isensee, F. et al. Automated brain extraction of multisequence MRI using artificial neural networks. Hum. Brain Mapp. 40, 4952–4964 (2019).
7. Fedorov, A. et al. 3D Slicer as an image computing platform for the Quantitative Imaging Network. Magn. Reson. Imaging 30, 1323–1341 (2012).

Poster No 680

Anatomical brain MRI markers of Suicidality in Bipolar Disorder Using Deep Learning

Melanie Garcia[1], Joan Camprodon[1], Benjamin Wade[2]

[1]Harvard Medical School, Massachusetts General Hospital, Charlestown, MA, [2]Massachusetts General Hospital, Somerville, MA

Introduction: Bipolar Disorder (BD) is characterized by extreme mood swings, including episodes of depression and mania, and is associated with an increased risk of suicidal ideation (SI) and psychological anxiety. Characterizing neural biomarkers of such symptoms in BD is crucial for prevention and early intervention. Artificial Intelligence (AI) methods may significantly improve the detection of biomarkers of depression symptoms in BD and offer new insights into complex mental health issues[1]. Here, we developed Deep Learning models to detect depression symptoms in BD patients through structural Magnetic Resonance Imaging (sMRI) scans. To this end, we utilized an open-source dataset from the "UCLA Consortium for Neuropsychiatric Phenomics LA5c Study,"[2,3]. The code of this project will be openly available on GitHub.

Methods: We used an open-source dataset available as ds000030 on OpenNeuro. This study employed anatomical data preprocessed with fmriprep[4] in native space, preserving maximum information as compared to registration to template space. Our approach involved training a 3D Convolutional Neural Network (CNN) with a DenseNet architecture[5]. The target variables for the model were derived from the Hamilton Depression Rating Scale (HAM-D), including for instance the presence or absence of depression and SI. Each model was trained with Adam optimizer and Cross-entropy loss. To interpret the model's predictions, we implemented a pipeline that included guided grad-CAM[6] and the HighRes3DNet[7] algorithms. This approach identified specific brain anatomical regions on sMRI scans that were important in predicting the presence of SI.

Results: From the dataset, we selected 41 subjects with BD, ensuring the inclusion of good quality scans and complete HAM-D scores. The sample comprised 22 males and 19 females, with a mean age of 34.7 years (standard deviation = 8.9). The dataset was divided into training (25 subjects), validation (5 subjects), and testing sets (15 subjects). Certain HAM-D subscales were underrepresented (small sample size) and could not be used. Others led to overfitting as target variables as the number of modalities was too high compared to sample size. Here, we focus on results on presence/absence of depression, of SI, and levels of psychological anxiety. Model accuracy is detailed on Figure 1. The most effective model in the prediction exhibited an accuracy of 52% in training, and 100% in both validation and testing sets. Despite low training accuracy - possibly due to cross-entropy loss penalization of low confidence predictions or to BD representation imbalance across datasets - the high performance on both validation and testing sets is promising, suggesting that the model may have successfully identified relevant patterns of neuroanatomy predictive of SI. Notably, the model identified biologically plausible brain regions, all in the right hemisphere, that were predictive of suicidal thoughts. In more than 80% of cases, these areas included the parietal operculum, planum temporale, transverse temporal gyrus, superior temporal gyrus, supramarginal gyrus, central operculum, middle temporal gyrus, posterior insula, and temporal white matter. Figure 2 represents these regions. The regions identified as important are well-aligned with pevious reports[8]. Future work will directly investigate this set of regions and their association with depressive symptoms in BD. These results could improve the diagnosis and early detection of SI in BD, leading to timely interventions that save lives and enable healthcare providers to tailor treatment plans more effectively.

Target	Absence/Presence of Depression	Absence/Presence of Suicidal Thoughts	Psychological anxiety level
Target type	Binary (0/1), HAM-D total score ≥ 10	Binary (0/1), HAM-D_3 score ≥ 10	Multiclass {0;1;2;3}, HAM-D_10 integer scores
Best model details	lr=10^{-2}, epoch 20	lr=10^{-4}, epoch 32	lr=10^{-4}, epoch 6
Train accuracy	60%	52%	28%
Validation accuracy	60%	100%	40%
Test accuracy	81,8%	100%	27,2%
Train accuracy per label	[81,3%; 22,2%]	[42,9%; 55,6%]	[0%; 71,4%; 16,7%; 11,1%; 0%]
Validation accuracy per label	[100%; 33,3%]	[100%; 100%]	[0%; 100%; NA; NA; 0%]
Test accuracy per label	[100%; 60%]	[100%; 100%]	[0%; 100%; 33,3%; 33,3%, 0%]

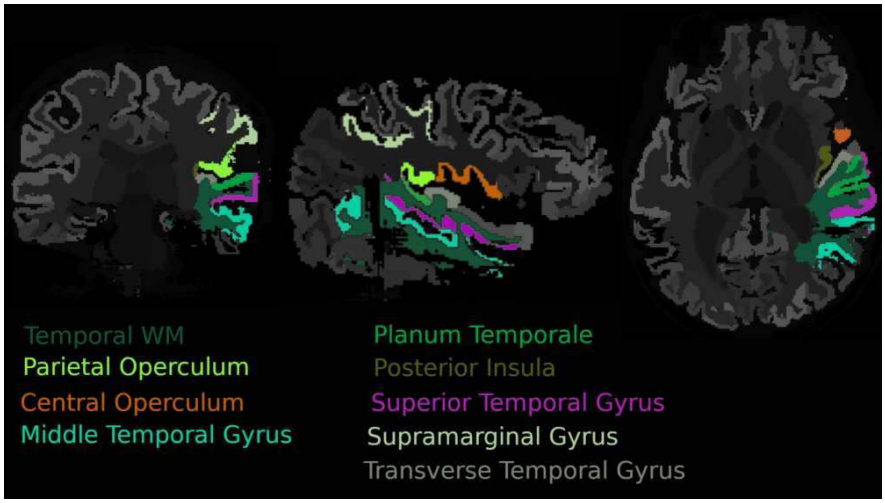

Conclusions: This study highlights how psychiatric research can leverage AI, particularly in identifying brain regions associated with suicidal thoughts in BD. These findings align with existing research and open avenues for more focused treatment approaches. Future work will include performing experiments on larger datasets and coupling sMRI with fMRI information.

References

1. Su, C., Xu, Z., Pathak, J., & Wang, F. (2020). Deep learning in mental health outcome research: A scoping review. Translational Psychiatry, 10(1), Article 1. https://doi.org/10.1038/s41398-020-0780-3
2. Preprocessed Consortium for Neuropsychiatric Phenomics dataset—PMC. (n.d.). Retrieved 13 November 2023, from https://www-ncbi-nlm-nih-gov.elib.tcd.ie/pmc/articles/PMC5664981/
3. Poldrack, R. A., Congdon, E., Triplett, W., Gorgolewski, K. J., Karlsgodt, K. H., Mumford, J. A., Sabb, F. W., Freimer, N. B., London, E. D., Cannon, T. D., & Bilder, R. M. (2016). A phenome-wide examination of neural and cognitive function. Scientific Data, 3(1), 160110. https://doi.org/10.1038/sdata.2016.110
4. Esteban, O., Markiewicz, C. J., Blair, R. W., Moodie, C. A., Isik, A. I., Erramuzpe, A., Kent, J. D., Goncalves, M., DuPre, E., Snyder, M., Oya, H., Ghosh, S. S., Wright, J., Durnez, J., Poldrack, R. A., & Gorgolewski, K. J. (2019). fMRIPrep: A robust preprocessing pipeline for functional MRI. Nature Methods, 16(1), Article 1. https://doi.org/10.1038/s41592-018-0235-4
5. Huang, G., Liu, Z., van der Maaten, L., & Weinberger, K. Q. (2017). Densely Connected Convolutional Networks. 4700–4708. https://openaccess.thecvf.com/content_cvpr_2017/html/Huang_Densely_Connected_Convolutional_CVPR_2017_paper.html
6. Selvaraju, R. R., Cogswell, M., Das, A., Vedantam, R., Parikh, D., & Batra, D. (2019). Grad-CAM: Visual Explanations from Deep Networks via Gradient-based Localization. arXiv:1610.02391 [Cs]. https://doi.org/10.1007/s11263-019-01228-7
7. Li, W., Wang, G., Fidon, L., Ourselin, S., Cardoso, M. J., & Vercauteren, T. (2017). On the Compactness, Efficiency, and Representation of 3D Convolutional Networks: Brain Parcellation as a Pretext Task. In M. Niethammer, M. Styner, S. Aylward, H. Zhu, I. Oguz, P.-T. Yap, & D. Shen (Eds.), Information Processing in Medical Imaging (pp. 348–360). Springer International Publishing. https://doi.org/10.1007/978-3-319-59050-9_28
8. Ellard, K. K., Zimmerman, J. P., Kaur, N., Van Dijk, K. R. A., Roffman, J. L., Nierenberg, A. A., Dougherty, D. D., Deckersbach, T., & Camprodon, J. A. (2018). Functional Connectivity Between Anterior Insula and Key Nodes of Frontoparietal Executive Control and Salience Networks Distinguish Bipolar Depression From Unipolar Depression and Healthy Control Subjects. Biological Psychiatry: Cognitive Neuroscience and Neuroimaging, 3(5), 473–484. https://doi.org/10.1016/j.bpsc.2018.01.013

Poster No 681

Autonomic Imbalance across the Brain-Heart Axis in Children with Autism

Jellina Prinsen[1], Nicky Daniels[2], Matthijs Moerkerke[1], Jean Steyaert[1], Bart Boets[1], Kaat Alaerts[1]

[1]KU Leuven, Leuven, [2]KU Leuven, Leuven,

Introduction: Because of its negative link to stress and anxiety, as well as its positive link to a wide range of positive psychological outcomes, heart rate variability (HRV) is increasingly considered as a marker of mental health and homeostasis (Schaffer & Ginsberg, 2017). In healthy adult subjects, HRV has also been shown to covary with changes in connectivity between brain regions of the central autonomic network (CAN), demonstrating a functional integration between cardiac and neural systems for maintaining and regulating homeostasis (Thayer et al., 2012). The high-frequency component of HRV (HF-HRV) in particular, exclusively denoting parasympathetic ("vagal") outflow, is associated with increased functional coupling between the medial prefrontal cortex (mPFC) and amygdala, thought to reflect a prefrontal top-down inhibition of amygdala-centered circuits. In children with ASD, extremely high prevalence rates of anxiety and autonomic stress are noted (Arora et al., 2021). Furthermore, hyperarousal at the level of the heart, caused by vagal withdrawal during prolonged stress

is often reported (Cheng et al., 2020), yet its extent, functional relevance and the role of the CAN network herein remain undetermined. Here, we aim to investigate the occurrence of cardiac autonomic (im)balance as well as associated differences in intrinsic CAN connectivity in 59 school-aged children with ASD (8-12 y/o) compared to 39 age- and IQ-matched typically developing (TD) children.

Methods: Cardiac monitoring was performed during concurrent resting-state 3T fMRI neuroimaging while at rest. We focused on the HF-HRV component - defined within the 0.24-1.04 Hz) frequency band in children - as an index of cardiac vagal tone. Besides addressing functional connectivity between core CAN brain regions (bilateral amygdala, mPFC, anterior cingulate cortex (ACC)), spectral dynamic causal modelling (spDCM) was adopted to specifically delineate effective connectivity between these region. As such, we can explicitly model the influence that one region (mPFC) exerts over another (amygdala) within a network model of causal neural dynamics. Parametric empirical Bayes (PEB) procedures were used to test how individual (within-subject) neural connections within the CAN relate to different between-subjects effects (group, HF-HRV%, parent-reported SRS scores).

Results: At the group level, we show similar band power in the HF-HRV frequency band in children with and without ASD, denoting similar levels of cardiac vagal tone during rest. Yet lower parasympathetic outflow at the level of the heart was found in ASD children with more severe ASD symptomatology, indicative of vagal withdrawal and higher autonomic arousal in these children. No group differences in CAN functional connectivity could be detected, but the effective connectivity analyses demonstrated increased excitatory feed-forward connections between bilateral amygdala and ACC in ASD children, combined with active inhibition of the mPFC by the amygdalae. Neuro-cardiac integration between functional amygdala-mPFC connectivity and HF-HRV was only shown in TD ($r = -.36$, $p = .03$), but not in ASD children (all $p > .38$). The spDCM analysis in combination with PEB estimation did show however that with increasing HF-HRV band power, the role of the mPFC becomes more prominent and exerts an inhibition over the amygdala, as proposed by the theory of neuro-cardiac integration (Thayer et al., 2012).

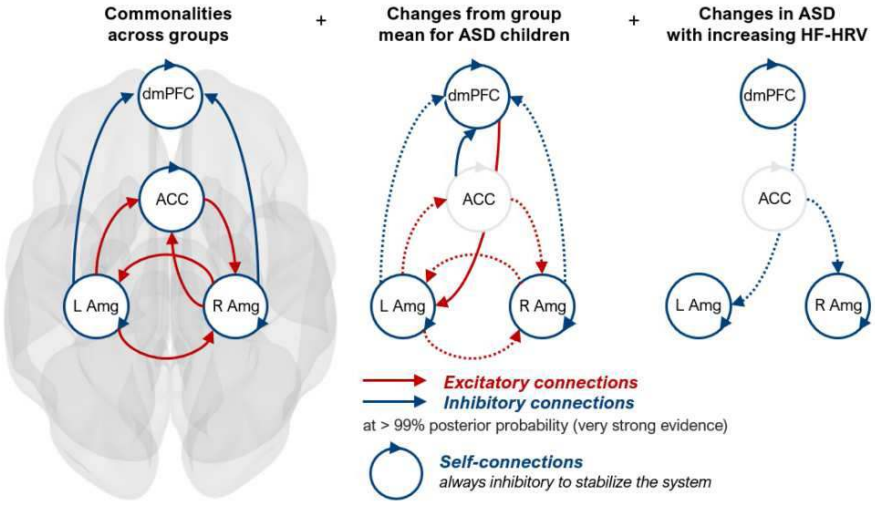

Conclusions: Despite no overall differences in cardiac vagal tone between TD vs. ASD children, the effective connectivity analyses demonstrated increased excitatory feed-forward amygdala-centered connections within the CAN network in children with ASD. Most importantly, higher cardiac vagal tone was related to lower ASD symptomatology and a more prominent top-down inhibition from the mPFC over the amygdala, providing further evidence for a functionally integrative brain-heart system that can be addressed as a marker of disrupted homeostasis in children ASD.

References

1. Arora et al. (2021). Is autonomic function during resting-state atypical in Autism: A systematic review of evidence. Neuroscience & Biobehavioral Reviews, 125, 417–441.
2. Cheng et al. (2020). Heart rate variability in individuals with autism spectrum disorders: A meta-analysis. Neuroscience & Biobehavioral Reviews, 118, 463–471.
3. Patriquin et al. (2019). Autonomic response in autism spectrum disorder: Relationship to social and cognitive functioning. Biological Psychology, 145, 185–197.
4. Shaffer & Ginsberg (2017). An Overview of Heart Rate Variability Metrics and Norms. Frontiers in Public Health, 5.
5. Thayer et al. (2012). A meta-analysis of heart rate variability and neuroimaging studies: Implications for heart rate variability as a marker of stress and health. Neuroscience and Biobehavioral Reviews, 36(2), 747–756.

Poster No 682

Bridging Psychiatric Nosology and Neuroimaging: Factor Analysis Yields Alignment

Frederick Goodson-Gregg[1], Jonathan Towne[2], Annie Dang[2], Larry Price[3], Peter Fox[4]

[1]University of Texas Health Science Center San Antonio, San Antonio, TX, [2]UT Health San Antonio, San Antonio, TX, [3]Texas State, San Marcos, TX, [4]The University of Texas Health Science Center at San Antonio, San Antonio, TX

Introduction: Mental illness is an enormous and growing public health burden. Due to decades of slow progress in mental health research, the National Institute of Mental Health has developed strategies to promote groundbreaking research. Two pillars of this strategy are 1) leveraging advances in human neuroimaging – especially connectomics – to improve our understanding of these disorders, 2) promoting alternative taxonomies of mental disorders, to better classify psychiatric patients. Psychometric meta-analyses have made substantial progress applying factor analysis to develop alternative taxonomies, together informing the creation of the Hierarchical Taxonomy of Psychopathology (HiTOP), a data-driven nosology of mental disorders, which has solicited neurobiological evidence in support of its theoretic constructs. This analysis addresses the hypothesis that neurobiology and psychopathology exhibit comparable data structures that can be exploited to bridge symptoms with brain networks and inform data-driven mental disorder taxonomies. This analysis relies on neuroimaging meta-analytic methods, applying both structural voxel-based morphometry (VBM) and functional voxel-based physiology (VBP) BrainMap databases to compute neurobiological "signatures" of mental disorders capable of quantifying similarity between disorders, subsequently enabling factor analysis and direct comparison of findings to psychiatric nosology data. Thus, this approach allows comparison of large and separate literatures, informing the validity of psychiatric nosology.

Methods: BrainMap structural (VBM) and functional (VBP) databases of group-wise, published, case-control contrasts were utilized to identify studies for the following psychiatric disorders: Alcohol Use Disorder (2,480 subjects), Anorexia Nervosa/ Bulimia Nervosa (1,511 subjects), Antisocial Personality Disorder (2,488 subjects), Generalized Anxiety Disorder (1,762 subjects), Major Depressive Disorder (10,286 subjects), Obsessive Compulsive Disorder (1,866 subjects), Psychosis (1,756 subjects), Post-Traumatic Stress Disorder (4,442 subjects). Structural and functional data were pooled together for each psychiatric disorder. The ALE algorithm (GingerALE 3.0.2) was subsequently applied to each disorder to compute a 3D map of ALE values reflecting the likelihood of disorder pathology at each coordinate. FSL was then utilized to calculate spatial similarity (spatial cross correlations) in a pairwise fashion between each psychiatric disorder. Factor analysis was then utilized to assess the validity of both the Internalizing and Externalizing psychometric construct. Results from this analysis were aligned to previous psychiatric meta-analytic data for direct comparison.

Results: Factor loadings are strongly aligned for Internalizing and Externalizing disorders between symptom score derived data (Figure 1B) (Ringwald), and neuroimaging derived data (Figure 1D). Factor loadings above 0.3 are typically considered meaningful, excluding only Generalized Anxiety Disorder (GAD) (0.284) and Antisocial Personality Disorder (0.290) from meeting this criterion (Figure 1D).

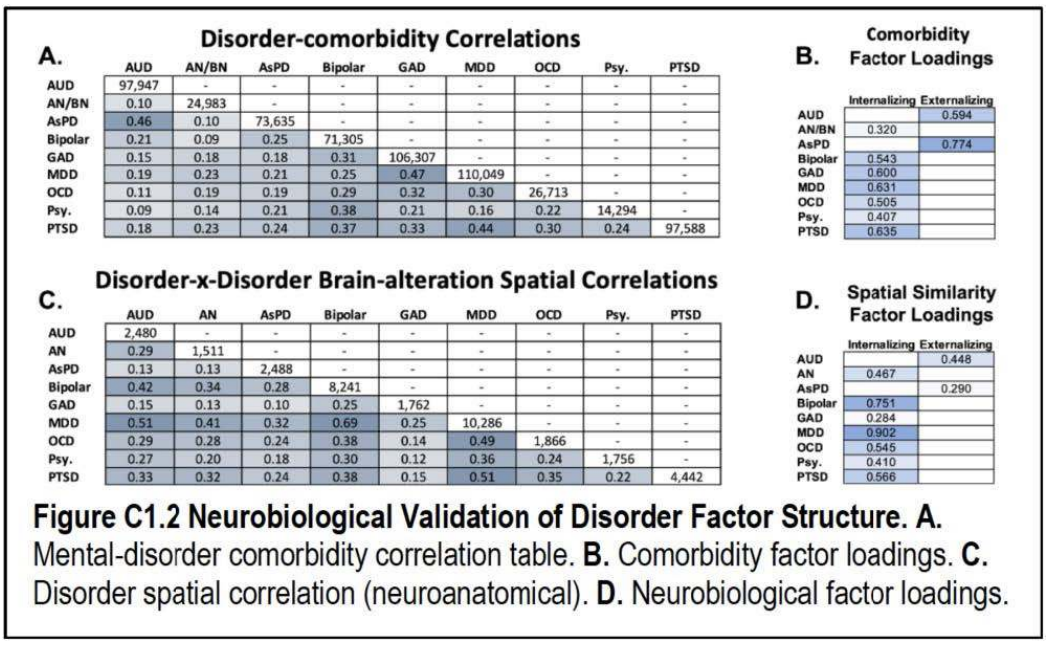

A. Disorder-comorbidity Correlations

	AUD	AN/BN	AsPD	Bipolar	GAD	MDD	OCD	Psy.	PTSD
AUD	97,947	-	-	-	-	-	-	-	-
AN/BN	0.10	24,983	-	-	-	-	-	-	-
AsPD	0.46	0.10	73,635	-	-	-	-	-	-
Bipolar	0.21	0.09	0.25	71,305	-	-	-	-	-
GAD	0.15	0.18	0.18	0.31	106,307	-	-	-	-
MDD	0.19	0.23	0.21	0.25	0.47	110,049	-	-	-
OCD	0.11	0.19	0.19	0.29	0.32	0.30	26,713	-	-
Psy.	0.09	0.14	0.21	0.38	0.21	0.16	0.22	14,294	-
PTSD	0.18	0.23	0.24	0.37	0.33	0.44	0.30	0.24	97,588

B. Comorbidity Factor Loadings

	Internalizing	Externalizing
AUD		0.594
AN/BN	0.320	
AsPD		0.774
Bipolar	0.543	
GAD	0.600	
MDD	0.631	
OCD	0.505	
Psy.	0.407	
PTSD	0.635	

C. Disorder-x-Disorder Brain-alteration Spatial Correlations

	AUD	AN	AsPD	Bipolar	GAD	MDD	OCD	Psy.	PTSD
AUD	2,480	-	-	-	-	-	-	-	-
AN	0.29	1,511	-	-	-	-	-	-	-
AsPD	0.13	0.13	2,488	-	-	-	-	-	-
Bipolar	0.42	0.34	0.28	8,241	-	-	-	-	-
GAD	0.15	0.13	0.10	0.25	1,762	-	-	-	-
MDD	0.51	0.41	0.32	0.69	0.25	10,286	-	-	-
OCD	0.29	0.28	0.24	0.38	0.14	0.49	1,866	-	-
Psy.	0.27	0.20	0.18	0.30	0.12	0.36	0.24	1,756	-
PTSD	0.33	0.32	0.24	0.38	0.15	0.51	0.35	0.22	4,442

D. Spatial Similarity Factor Loadings

	Internalizing	Externalizing
AUD		0.448
AN	0.467	
AsPD		0.290
Bipolar	0.751	
GAD	0.284	
MDD	0.902	
OCD	0.545	
Psy.	0.410	
PTSD	0.566	

Figure C1.2 Neurobiological Validation of Disorder Factor Structure. A. Mental-disorder comorbidity correlation table. **B.** Comorbidity factor loadings. **C.** Disorder spatial correlation (neuroanatomical). **D.** Neurobiological factor loadings.

Conclusions: This analysis provides neurobiological evidence supporting the alignment between clinical psychiatric nosology of mental disorders and neurobiologically derived disorder relationships and factor loadings. This analysis supports the validity of the HiTOP Internalizing psychometric construct by revealing neurobiologically driven factor loadings for several Internalizing disorders. This research identifies a promising approach to align symptom driven psychiatric literature and neuroimaging literature, which may serve to deepen our understanding of the etiology and diagnostic boundaries of these conditions, the alignment of psychiatric symptoms and neurobiology, and ultimately the quality of care received for patients with mental illness. Efforts are underway to extend this approach to additional disorders and psychiatric constructs beyond Internalizing and Externalizing.

References

1. Ringwald, W. R., Forbes, M. K., & Wright, A. G. C. (2023). Meta-analysis of structural evidence for the Hierarchical Taxonomy of Psychopathology (HiTOP) model. Psychological Medicine, 53(2), 533–546. https://doi.org/10.1017/S0033291721001902

Poster No 683

MPFC Metabolites and Their Association with Resting-State EEG in Schizophrenia Spectrum Disorder

Genc Hasanaj[1], Berkhan Karsli[2], Verena Meisinger[3], Marcel Kallweit[4], Gizem Vural[5], Lukas Röll[4], Julian Melcher[6], Boris Papazov[7], Joanna Moussiopoulou[8], Vladislav Yakimov[4], Elias Wagner[4], Florian Raabe[9], Daniel Keeser[10]

[1]Ludwig Maximillian University, Munich, Germany, [2]Ludwig Maximilian University, Munich, Bavaria, [3]Ludwig Maximilian University, Munich, Germany, [4]LMU University Hospital, Munich, Germany, [5]LMU Klinikum, Munich, Other, [6]LMU Klinikum, Munich, Bavaria, [7]LMU Munich, München, Bayern, [8]LMU Klinikum, München, Germany, [9]Department of Psychiatry and Psychotherapy, Ludwig-Maximilian University, Munich, Germany, [10]Department of Psychiatry and Psychotherapy, University Hospital LMU, Munich, Germany

Introduction: Aberrant modulatory effects and concentration of metabolites in the Medial Prefrontal Cortex (mPFC) have been the focus of recent research (Dixon et al., 2022), especially in the context of schizophrenia spectrum disorders (SSD). To date, evidence for the modulatory role of metabolites on directly measured neuronal mass activity in the brain is lacking. In this study, we investigated the possible role of gamma-aminobutyric acid (GABA) and Glutamine+Glutamate (Glx) in modulating resting-state EEG (rsEEG) activity for both healthy controls (HC) and patients with SSD. With this study, we aim to investigate the direct relationship between metabolite activity and rsEEG oscillations in sensor and source space to gain more mechanistic insights between these modalities and thus provide a basis for clinical translation.

Methods: Data from 63 patients with SSD and 62 HC was collected at the University Hospital LMU . Participants underwent multimodal MRI using a 3T MRI scanner, focusing on Single Voxel Spectroscopy at the mPFC (voxel size 20x20x20 mm3). Osprey and LC-Model were used to process the MRS data. Exclusions based on Cramer-Rao lower bounds (>50% SD), and later removal of outliers (2.5 SD above and below the median), the further analysis included 44 SSDs and 52 HCs. The rsEEG was recorded with 32 electrodes according to the international 10/20 system and included 5 minutes each with eyes open (EO) and eyes closed (EC). Data were preprocessed within an ICA preprocessing pipeline adapted and customized from (Adams et al., 2022). The source localized EEG activity of the mPFC ROI was extracted and the Power Spectrum Density was calculated within this source localized activity. Multiple linear regression using patient group as a covariate and Pearson correlation techniques were applied to estimate oscillatory activity from metabolites.

Results: Comparison between SSD and HC group showed no significant difference in metabolite concentration (Glx, GABA; $p > .05$). For the EC condition, the interaction of Glx and Group was significantly associated with Theta ($\beta = 0.0012$, $t = 3.07$, $p = 0.003$), Beta ($\beta = 0.0009$, $t = 1.99$, $p = 0.050$), and Total Absolute Power ($\beta = 0.0037$, $t = 2.22$, $p = 0.029$). Specifically, Glx correlated with Theta ($r = 0.51$, $p < 0.001$), Beta ($r = 0.43$, $p = 0.004$), and Total Absolute Power ($r = 0.45$, $p = 0.002$) in the SSD group, but no correlation was found for the HC group. For the EO condition, the Glx and Group interaction significantly predicted Theta ($\beta = 0.0007$, $t = 2.41$, $p = 0.018$). As with the EC condition, Glx correlated significantly with Theta activity in the SSD ($r = 0.47$, $p = 0.001$) but not in the HC group.

Conclusions: This study shows a distinct pattern of association between metabolite levels and canonical frequency band powers in the different resting states of the patient group. The interaction of Glx and Group was significantly associated with Theta, Beta, and Total Absolute Power during the EC condition. Additionally, Glx correlated with these power values, while no such correlation was found in the HC group. Similarly, for the EO condition, the interaction of Glx and Group was also significantly associated with Theta activity, with a correlation observed in the SSD but not in the HC group. The results suggest differences in the relationship between glutamatergic activity and brain oscillations between the SSD and HC groups, particularly in the EC and EO conditions. There are contradictory results in the literature regarding the differences

in metabolite levels in different patient groups and under different conditions (Dixon et al., 2022). The absence of significant group difference could be the possible normalization effect of antipsychotic medication in the SSD group (Kegeles et al., 2012). Due to the heterogeneity within the SSD group and the lack of concurrent MRS and EEG acquisition, which may introduce variability (Al-Iedani et al., 2018) and affect generalizability, these results must be interpreted with caution.

References

1. Adams, R. A. (2022). Computational Modeling of Electroencephalography and Functional Magnetic Resonance Imaging Paradigms Indicates a Consistent Loss of Pyramidal Cell Synaptic Gain in Schizophrenia. Biological Psychiatry, 91(2), 202–215.
2. Al-Iedani (2018). Diurnal stability and long-term repeatability of neurometabolites using single voxel 1H magnetic resonance spectroscopy. European Journal of Radiology, 108, 107–113.
3. Dixon, (2022). Frontal neural metabolite changes in schizophrenia and their association with cognitive control: A systematic review. Neuroscience and Biobehavioral Reviews, 132, 224–247.
4. Kegeles, (2012). Elevated prefrontal cortex γ-aminobutyric acid and glutamate-glutamine levels in schizophrenia measured in vivo with proton magnetic resonance spectroscopy. Archives of General Psychiatry, 69(5), 449.

Poster No 684

White Matter Integrity and Verbal Memory After a First Episode of Psychosis: A Longitudinal Study

Joseph Ghanem[1], Jana Totzek[1], Charlie Henri-Bellemare[1], Ethan Draper[2], Delphine Raucher-Chéné[2], Gregory Kiar[3], Raihaan Patel[4], Mallar Chakravarty[5], Jai Shah[1], Ridha Joober[1], Ashok Malla[1], Martin Lepage[1], Katie Lavigne[1]

[1]McGill University, Montreal, Quebec, [2]McGill University, Montreal, QC, [3]Child Mind Institute, Montreal, Quebec, [4]Department of Psychiatry, University of Oxford, Oxford, Oxfordshire, [5]Brain Imaging Centre, Douglas Research Centre, Montreal, Quebec

Introduction: Studies of white matter differences in psychotic disorders have reported lower fractional anisotropy (FA) in individuals with schizophrenia relative to controls[1,2], but the evidence in First Episode Psychosis (FEP) samples remains controversial. Many cross-sectional FEP studies observed no group differences in FA[3,4], whereas the few available longitudinal studies observed a reduction in FA in certain regions relative to controls[5,6]. Importantly, these studies were limited by short follow-up periods (6 and 12 weeks, respectively), and did not investigate the relationship between changes in FA and verbal memory, the cognitive domain most impaired in FEP. However, some cross-sectional examinations found positive correlations between verbal memory and FA in the anterior limb of the internal capsule[7] and the cingulum[8]. In the present study, we aimed to examine, over 15 months, longitudinal changes in FA and their association with changes in verbal memory in a large sample of individuals with a FEP.

Methods: Eighty Individuals with a FEP aged 18-35 were recruited from the 2-year Prevention and Early Intervention for Psychosis Program (PEPP) located in the catchment area of Southwest Montreal. Following clinical stabilization, they were scanned and assessed within the first 3 months of admission to PEPP and at months 6, 12, and 18. Fifty-five healthy controls were similarly scanned four times over 18 months. Verbal memory was assessed using the logical memory subtest of the Wechsler Memory Scale shortly prior to the scan at every timepoint. Two successive whole-brain diffusion-weighted images were acquired using a single-shot EPI sequence parallel to the anterior-posterior commissural plane. Preprocessing of diffusion images was performed using the FMRIB software library tools[9]. Subsequent diffusion image processing was performed using MRtrix 3.[10]. Tract-based spatial statistics were generated using the procedure outlined by the ENIGMA consortium-DTI group where each subject's FA map was skeletonized and used to extract the average FA per white matter region using the JHU-White matter parcellation. Group differences in FA and verbal memory over time were examined using linear mixed-effects models with age, sex, and years of education as covariates. Tests were corrected for multiple comparisons and considered significant at a 5% false discovery rate.

Results: At baseline, the FEP group was 63% male and 37% female, and the healthy control group was 66% male and 34% female. Individuals with a FEP had fewer years of education ($t(133)=3.90$, $p<.001$), and lower IQ relative to controls ($t(133)= 3.66$, $p<.001$). There was a significant main effect of time on FA in the left cingulum ($P_{corrected}= .022$), the right internal capsule ($P_{corrected}= .024$), the right posterior limb of the internal capsule ($P_{corrected}= .009$), and the right inferior fronto-occipital fasciculus ($P_{corrected}=0.041$). However, there was no significant group difference between FEP and controls in FA, and no significant interaction of group and time. Similarly, there was no significant main effect of verbal memory on FA, and no interaction between group, time, and verbal memory on FA.

Conclusions: In this longitudinal study, we observed a general change in FA over time in some white matter regions. FEP and controls did not significantly differ in FA, and there was no relationship between change in FA and in verbal memory over time. Our results are consistent with previous work that found no differences in FA between FEP and controls early in the course of illness. It is possible that early exposure to antipsychotic medication may have attenuated any observable differences, or that

group differences are small in the early stages of psychosis but progressively evolve over longer time periods. Future studies should follow individuals with a FEP for longer timeframes and integrate different measures of diffusion to capture a more comprehensive picture of white matter changes over time.

References

1. Kelly S (2018). Widespread white matter microstructural differences in schizophrenia across 4322 individuals: results from the ENIGMA Schizophrenia DTI Working Group. Molecular psychiatry, 23(5):1261-1269.
2. Fitzsimmons J (2009). Diffusion tractography of the fornix in schizophrenia. Schizophrenia research, 107(1):39-46.
3. Kim NS (2021). White matter correlates of theory of mind in patients with first-episode psychosis. Frontiers in Psychiatry, 12:617683.
4. Lee D (2012). White matter tract abnormalities in first-episode psychosis. Schizophrenia research, 141(1):29-34.
5. Wang Q (2013). White-matter microstructure in previously drug-naive patients with schizophrenia after 6 weeks of treatment. Psychological medicine, 43(11):2301-2309.
6. Szeszko PR (2014). White matter changes associated with antipsychotic treatment in first-episode psychosis. Neuropsychopharmacology, 39(6):1324-1331.
7. Levitt JJ (2012). Fractional anisotropy and radial diffusivity: diffusion measures of white matter abnormalities in the anterior limb of the internal capsule in schizophrenia. Schizophrenia research 136(1-3):55-62.
8. Ezzati A (2016). Hippocampal volume and cingulum bundle fractional anisotropy are independently associated with verbal memory in older adults. Brain imaging and behavior, 10:652-659.
9. Smith SM (2004). Advances in functional and structural MR image analysis and implementation as FSL. Neuroimage, 23:S208-S219.
10. Tournier (2019). MRtrix3: A fast, flexible and open software framework for medical image processing and visualisation. Neuroimage, 202:116137.

Poster No 685

EEG Network in Low-Beta as Biomarkers for Distinguishing PTSD, Panic, and Other Anxiety Disorders

Minhee Kim[1], Deung-Hyun Kang[2], Soo-Hee Choi[1]

[1]Department of Psychiatry, Seoul National University Hospital, Seoul, Korea, Republic of, [2]Department of Psychiatry, SMG-SNU BoramaeMedical Center Seoul, Seoul, Korea, Republic of

Introduction: Anxiety disorder is one of the highest rates of comorbidity in patients with posttraumatic stress disorder (PTSD) (Brady et al., 2000). And these disorders are similar in having anxiety related symptoms. PTSD patients with anxiety disorder showed decreased psychosocial function than the PTSD only patients (Ginzburg et al., 2010). Thus, for its proper diagnosis and treatment, it is important to discover what is different and same between PTSD and anxiety disorders. EEG connectivity network could reflect individuals' mental states and has beneficial to employing in clinical settings (Choi et al., 2021). In previous studies, disrupted brain network was discovered in PTSD (Shim et al., 2017). However, there's only few studies about brain network on anxiety disorder except social anxiety. Hence, in the present study, we aimed to investigate whether the brain network from resting-state EEG could distinguish PTSD, panic disorder, and other anxiety disorders on which frequency band.

Methods: Patients with PTSD (N=30), panic disorder (N=32), and other anxiety disorders (N=30) were recruited. Resting-state EEGs were recorded for 20 minutes with eyes closed. The data were pre-processed as following: band-pass filtering at 0.1-50Hz, average referencing, artifact rejection by visual inspection and ICA. Phase-locking values (PLVs) were calculated between each pair of channels and averaged for each frequency band (delta: 0.5-4Hz; theta: 4-8Hz; alpha: 8-12Hz; low-beta: 12-22Hz; high-beta: 22-30Hz; gamma: 30-50Hz). For further graph theoretical analysis, connectivity matrices were constructed using PLV values. In network analysis, global network indices including strength (STR), path length (PL), clustering coefficient (CC), and efficiency (EFF) were evaluated and averaged across participants for each disorder group. We conducted one-way ANOVAs to find significant group differences with each global network index as dependent variable, and post-hoc t-tests on significant network indices.

Results: The one-way ANOVA revealed that there was a significant difference in patient groups on low-beta band for all network indices: STR ($F(2, 89)=3.05$, $p<.05$), PL ($F(2, 89)=.52$, $p<.05$), CC ($F(2, 89)=.008$, $p<.05$), and EFF ($F(2, 89)=2.97$, $p=.057$) with trend level. Thus, in further t-tests, we analyzed group differences for these four network indices on low-beta band. Post-hoc t-tests between PTSD and anxiety disorder groups showed that the anxiety disorder was greater than the PTSD for the STR ($t(58)=2.34$, $p=.02$), CC ($t(58)=2.28$, $p=.03$), and EFF ($t(58)=2.30$, $p=.03$), and the PTSD was greater for the PL ($t(58)=2.35$, $p=.02$). Likewise, the same t-tests between panic and anxiety disorder groups showed that the anxiety disorder was greater than the panic disorder for the STR ($t(60)=2.11$, $p=.04$), CC ($t(60)=2.14$, $p=.04$), and EFF ($t(60)=2.02$, $p=.048$), and the panic disorder was greater for the PL ($t(60)=2.51$, $p=.02$). And there was no significant difference between for any network index between the PTSD and panic disorder groups.

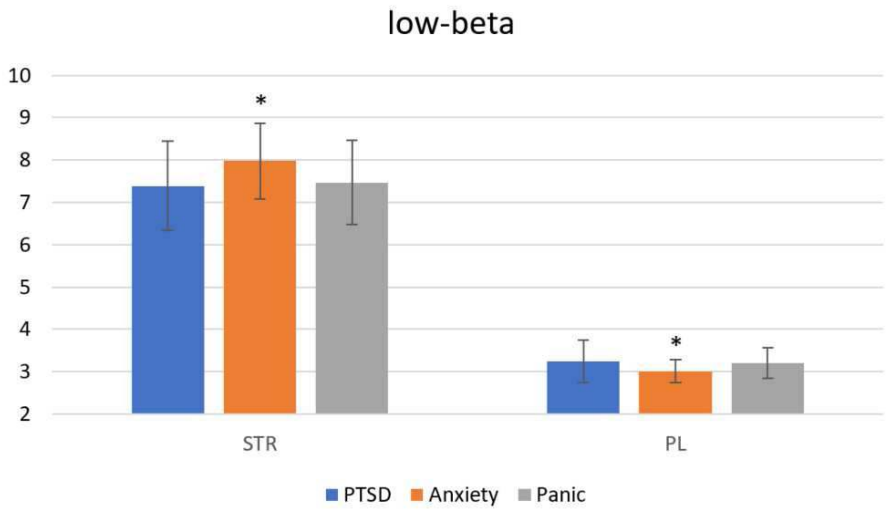

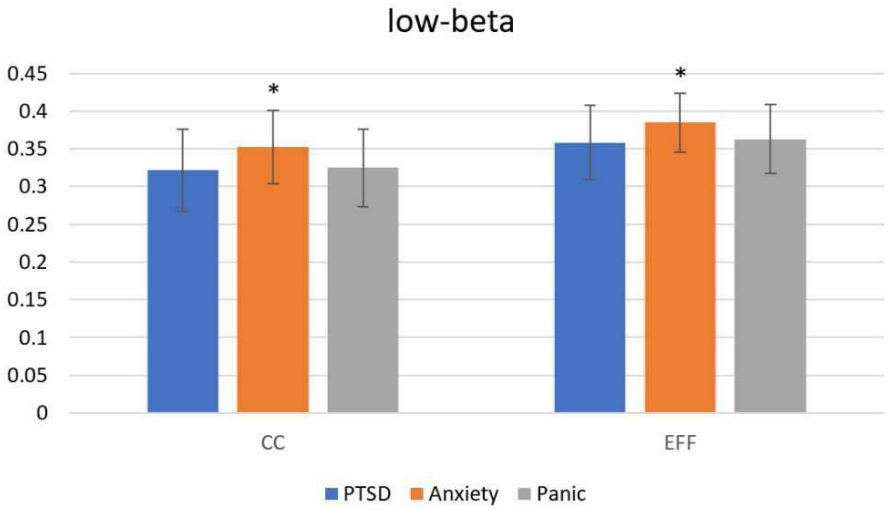

Conclusions: In this resting-state EEG study, we revealed that the brain network STR, CC, and EFF on low-beta band were greater, and PL was lesser on the patients with other anxiety disorders than the patients with PTSD and panic disorder. Given that the larger values of STR, CC, and EFF, and the lower value of PL reflect relative effective brain functional network, these results imply that in the other anxiety disorders their brain functional connectivity might be relatively closer to normal, compared to PTSD or panic disorder. In the previous study, patients with PTSD showed the lesser STR, CC, and EFF, and the greater PL on delta, theta, and low-beta band than control (Shim et al., 2017). And in the present study, we only found significant differences between patient groups on the low-beta band. This means that the brain network indices on the low-beta band could be biomarkers for discriminating the other anxiety disorders from the PTSD and panic disorder.

References

1. Brady, K. T., Killeen, T. K., Brewerton, T., & Lucerini, S. (2000), 'Comorbidity of psychiatric disorders and posttraumatic stress disorder', Journal of clinical psychiatry, 61, 22-32.
2. Choi, K. M., Kim, J. Y., Kim, Y. W., Han, J. W., Im, C. H., & Lee, S. H. (2021), 'Comparative analysis of default mode networks in major psychiatric disorders using resting-state EEG', Scientific reports, 11(1), 22007.
3. Ginzburg, K., Ein-Dor, T., & Solomon, Z. (2010), 'Comorbidity of posttraumatic stress disorder, anxiety and depression: a 20-year longitudinal study of war veterans', Journal of affective disorders, 123(1-3), 249-257.
4. Shim, M., Im, C. H., & Lee, S. H. (2017), 'Disrupted cortical brain network in post-traumatic stress disorder patients: a resting-state electroencephalographic study', Translational psychiatry, 7(9), e1231-e1231.

Poster No 686

Irregular Changes in Network Topology During Monotonic Learning in Health and Schizophrenia

Clifford Abel II[1], John Kopchick[2], Dhruval Bhatt[3], Hady Saad[3], Patricia Thomas[2], Dalal Khatib[2], Usha Rajan[2], Caroline Zajac-Benitez[3], Luay Haddad[2], Alireza Amirsadri[2], Jeffrey Stanley[2], Vaibhav Diwadkar[3]

[1]Wayne State University, Translational Neuroscience Program, Department of Psychiatry, Detroit, MI, [2]Wayne State University, Department of Psychiatry, Detroit, MI, [3]Wayne State University, Detroit, MI

Introduction: Task-based neuroimaging has recapitulated relationships between behavioral proficiency and brain imaging measures in specific examples such as retrieval success or retention (Barnett et al., 2023) but the issue is more complicated in for performance dynamics over time. In associative learning tasks, retrieval proficiency increases (as associations are consolidated), and has been associated with changes in effective connectivity that are disordered in schizophrenia (Banyai et al., 2011). However, these relationships have not been examined under the simple principle of monotonicity prevalent in human psychology (Grice et al., 2023). Thus, while performance improves in a weakly monotonic way (i.e., each iteration is greater or equal to the previous one), do connectomic changes reflect such monotonicity? Here, we implement this question as follows: 1) fMRI data were collected while healthy controls (HC) and patients with schizophrenia (SCZ) learned object location associations (resulting in negatively accelerated learning)(Hasan et al., 2023); 2) Network profiles across task conditions were summarized using the graph theoretic measure Betweenness Centrality (BC) that estimates the “hubness” of a region (node); 3) Finally, BC dynamics were tested for weak monotonicity. We demonstrate that at best, connectomic changes have obscure relationships with behavioral proficiency over time. ...

Methods: Participants (n=88, SCZ=49, Ages:18-45) gave informed consent to participate in fMRI acquisition (Siemens Verio 3T) while learning associations between memoranda (objects and locations) over eight epochs. Each epoch contained four conditions: Encoding, Post-Encoding Rest, Retrieval, Post-Retrieval Rest. For each participant, in all conditions and epochs, the functional connectome across 246 functionally defined nodes (Fan et al., 2016) was estimated using zero-lag functional connectivity. From each undirected graph, each node’s BC was estimated and rank ordered (BCRO).

Results: Both HC and SCZ showed increasing task proficiency over the eight epochs (Fig. 1a), but a higher proportion of SCZ did so non-monotonically (Fig. 1b, $p < 0.05$). Linear regression estimation of the relationship between epoch and BCRO for each node in each group/condition identified nodes displaying significant effects (pFDR<.01) but none of these nodes showed weak-monotonicity ($p < 0.05$). We therefore considered the subject-level within condition nodal variation in BCRO across the epochs. Separately for HC and SCZ, agglomerative clustering using the Ward method was applied across subjects to give five clusters of regions displaying similar variation (Fig 2).

Conclusions: Our failure to recapitulate the performance dynamics (weakly monotonic) in the connectomic dynamics (devoid of monotonicity) is a successful dissociation of behavior and the underlying brain activation; consistent behavioral dynamics are generated from highly variable connectomic fluctuations. A proper investigation of these connectomic dynamics must therefore treat the nodal BCRO variability as part of learning. Exploratory analyses suggest more a more heterogeneous distribution of clusters throughout the HC brain than the SCZ brain (Fig. 2). Banyai, M., Diwadkar, V., Erdi, P., 2011. Model-based dynamical analysis of functional disconnection in schizophrenia. NeuroImage 58(3), 870-877. Barnett, Alexander J. et al. (2023) “Hippocampal-cortical interactions during event boundaries support retention of complex narrative events.” Neuron, S0896-6273(23)00766-3 Fan, L. et al. (2016) The Human Brainnetome Atlas: A new brain atlas based on connectional architecture. Cerebral cortex, 26(8), 3508–3526 Grice, Matt et al. (2023) “The psychological scaffolding of arithmetic.” Psychological review, 10.1037/rev0000431 Hasan, S. et al. (2023) Learning without contingencies: A loss of synergy between memory and reward circuits in schizophrenia. Schizophrenia research 258, 21-35

Fig. 1

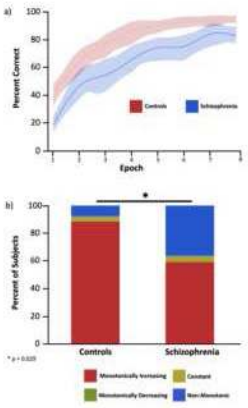

Fig. 2

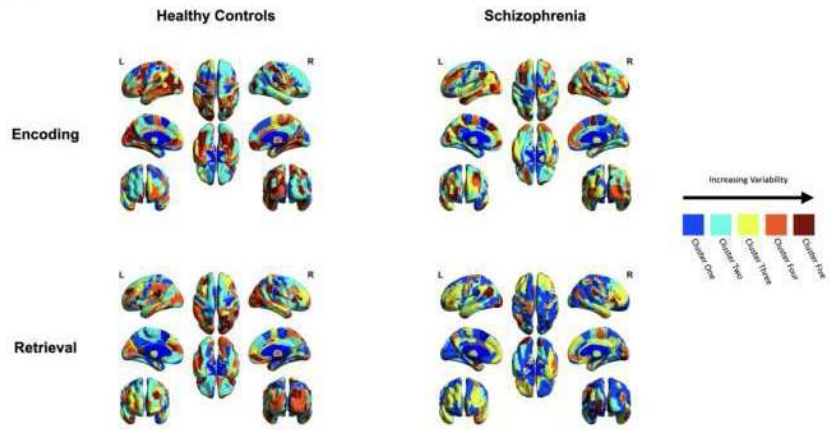

References

1. Banyai, M., Diwadkar, V., Erdi, P., 2011. Model-based dynamical analysis of functional disconnection in schizophrenia. NeuroImage 58(3), 870-877.
2. Barnett, Alexander J. et al. (2023) "Hippocampal-cortical interactions during event boundaries support retention of complex narrative events." Neuron, S0896-6273(23)00766-3
3. Fan, L. et al. (2016) The Human Brainnetome Atlas: A new brain atlas based on connectional architecture. Cerebral cortex, 26(8), 3508–3526
4. Grice, Matt et al. (2023) "The psychological scaffolding of arithmetic." Psychological review, 10.1037/rev0000431
5. Hasan, S. et al. (2023) Learning without contingencies: A loss of synergy between memory and reward circuits in schizophrenia. Schizophrenia research 258, 21-35

Poster No 687

The effect of ibudilast on functional connectivity in methamphetamine use disorder

Milky Kohno[1], Laura Dennis[2], Jazryn Nagum[3], tianna huss[3], Alea Sonnon[3], Sophia Swain[3], Joyce Zafaralla[3], Wesley Ng[3], Wililam Hoffman[2]

[1]Portland VA Health Care System, Portland, OR, [2]Portland VA Health Care System, PORTLAND, OR, [3]Oregon Health and Science University, Portland, OR

Introduction: Methamphetamine (MA) exposure has long-lasting neurotoxic effects, and evidence for MA-induced neuroinflammation comes from both clinical and preclinical studies. Animal models show that MA exposure leads to morphological changes that are consistent with reactive gliosis and increases the expression of factors associated with immune response activation, including pro-inflammatory cytokines released by activated glia cells. There is strong evidence that inflammatory biomarkers target the striatum and dysregulate dopamine signaling thereby contributing to dopamine-related behavioral deficits. Recently, animal models have shown a link between markers of inflammation and brain function; such that, administration of inflammatory cytokines alters the activation of reward-related brain regions and modifies the response to hedonic reward. These findings compliment neuroimaging results from humans showing a link between inflammation and striatal dysfunction. Taken together, these studies suggest that reducing inflammation is a reasonable therapeutic target and has the potential to accelerate effective strategies for stimulant-use disorders that present with inflammatory brain markers and abnormal brain function. This randomized placebo-controlled study of ibudilast, a nonselective phosphodiesterase (PDE) inhibitor tested whether reducing inflammation improved brain function in individuals diagnosed with a methamphetamine use disorder.

Methods: Thirteen participants with MA use disorder completed a double-blind randomized placebo-controlled trial of ibudilast. Neuroimaging measures, neurocognitive testing, and measures of drug use and craving was collected before and after the 6-week trial. Resting-state data was collected on a 3T Siemens TIM Trio. Standard preprocessing steps were applied. Seed-based analysis was performed using regions of interest of the right dorsolateral prefrontal cortex (DLPFC) and striatum. Two-way repeated measures ANOVA on parameter estimates between DLFPC and nucleus accumbens were examined in SPSS 22.

Results: Preliminary results indiciate a significant time by treatment interaction on RSFC, where the ibudilast group show greater change in the functional connectivity between the right DLPFC and nucleus accumbens. Increases in the connectivity

between the right DLPFC and striatum were correlated with reduction in MA use in the ibudilast group but not in the control group.

Conclusions: The results suggest that ibudilast alters brain connectivity, as indicated by significant time by treatment interaction on right DLPFC to ventral striatum connectivity. The results suggest that a downregulation of inflammation may positively effect corticostriatal connectivity to reduce drug use. Although preliminary, results provide a scientific basis for additional testing of ibudilast as a potential adjunct to treatment for MA dependence and other drug-use disorders

References

1. See poster for references

Poster No 688

Distinct and Shared Large-Scale Functional Network Dysconnectivity of BD II and MDD

Jia-En Jhou[1], Yen-Ling Chen[1], Ya-Mei Bai[2], Mu-Hong Chen[2], Pei-Chi Tu[3]

[1]Department of Occupational Therapy, I-Shou University, Kaohsiung, Taiwan, [2]Division of Psychiatry, Faculty of Medicine, National Yang-Ming University, Taipei, Taiwan, [3]Institute of Philosophy of Mind and Cognition, National Yang-Ming University, Taipei, Taiwan

Introduction: Bipolar II disorder (BD II) and major depressive disorder (MDD) have similar depressive episode characteristics. It is difficult to distinguish the two diseases during a depressive episode, and misdiagnosis can have harmful consequences. Although the depressive episode in BD II and MDD may appear similar, changes in specific brain networks could be significant. Moreover, the aid of neurobiological markers can improve understanding of BD II and MDD neuropathology. Therefore, this study aims to explore the differences and similarities in large-scale functional network connectivity between BD II and MDD, providing potential neurobiological indicators to assist in diagnosing these two disorders and understanding their neuropathology.

Methods: Resting-state functional MRI (rs-fMRI) data were collected from 59 BD II patients, 114 MDD patients, and 117 age- and sex-matched healthy control (HC). After preprocessing the rs-fMRI data, large-scale functional network connectivity was analyzed according to Shen's whole-brain functional-connectivity-based atlas to parcellate the brain into 268 regions. These regions were then categorized into eight networks: the medial frontal network (MFN), frontoparietal network (FPN), default mode network (DMN), subcortical and cerebellar (SC) regions, motor network (MON), visual I network (VisI), visual II network (VisII), and visual association network (VA). The differences in large-scale functional network connectivity among these three groups were examined using ANOVA. Moreover, the symptoms and functions of the patients with BD II and MDD were clinically assessed using the Hamilton Depression Rating Scale (HAM-D), Hamilton Anxiety Rating Scale (HAM-A), and Personal and Social Performance (PSP) Scale. Then, the correlation between network dysconnectivity and the symptoms and functions was investigated using Pearson correlation.

Results: There were 74 significant network dysconnectivity among the three groups with false discovery rate correction ($q < 0.01$, adjusted by age and sex). Compared to MDD and HC, all of these dysconnectivity had greater differences between BD II and HC. Furthermore, both BD II and MDD showed hyperconnectivity in MON to FPN, MON to MFN, MON to SC, and MFN to SC; both BD II and MDD showed hypoconnectivity in SC to FPN, SC to VisI, VA to SC, MON to MON, MON to DMN, and SC to SC. Moreover, BD II revealed hypoconnectivity in VisI to MON, VisII to MON, and SC to VisII, but MDD showed hyperconnectivity. BD II revealed hyperconnectivity in VisII to FPN and VisI to FPN, but MDD showed hypoconnectivity. In addition, BD II presented a significantly moderate correlation between SC to FPN connectivity and PSP, HAMA, and HAMD ($\rho = 0.43$, -0.49, and -0.49, respectively), but no correlation in MDD.

Conclusions: BD II showed greater network dysconnectivity in the distinct and shared network dysconnectivity in BD II and MDD than MDD, especially the VisI/VisII and MON or FPN connectivity. The network connectivity may be used as neurobiological markers for patients with BD II when differentiating from MDD. Furthermore, the network dysconnectivity of BD II may be involved in the representation of symptoms and functions but not those of MDD.

References

1. Dudek, D., et al. (2013), 'Diagnostic conversions from major depressive disorder into bipolar disorder in an outpatient setting: results of a retrospective chart review', Journal of Affective Disorder, vol. 144, no. 1-2, pp. 112-115
2. Ellard, K.K., et al. (2018), 'Functional connectivity between anterior insula and key nodes of frontoparietal executive control and salience networks distinguish bipolar depression from unipolar depression and healthy control subjects', Biological Psychiatry: Cognitive Neuroscience and Neuroimaging, vol. 3, no. 5, pp. 473-484

3. Gong, J., et al. (2020), 'Common and distinct patterns of intrinsic brain activity alterations in major depression and bipolar disorder: voxel-based meta-analysis', Translational Psychiatry, vol. 10, no. 1, pp. 353
4. Goya-Maldonado, R., et al. (2016), 'Differentiating unipolar and bipolar depression by alterations in large-scale brain networks', Human Brain Mapping, vol. 37, no. 2, pp. 808-818
5. Han, K.M., et al. (2019), 'Differentiating between bipolar and unipolar depression in functional and structural MRI studies', Progress in Neuro-Psychopharmacology and Biological Psychiatry, vol. 9, pp. 20-27

Poster No 689

Neural Correlates of PTSD Symptoms and Disturbances of Self-Organization in North Korean Refugees

Manjae Kwon[1], Jooyeon Im[2], Sang Hui Chu[3], Woo-Young Ahn[2], Young-Chul Jung[1]

[1]Department of Psychiatry, Severance Hospital, Yonsei University College of Medicine, Seoul, Republic of Korea, [2]Department of Psychology, Seoul National University, Seoul, Republic of Korea, [3]Department of Nursing, Yonsei University College of Nursing, Seoul, Republic of Korea

Introduction: Among refugee populations, both posttraumatic stress disorder (PTSD) and complex PTSD are highly prevalent, yet the neural mechanisms underlying posttraumatic stress symptoms and disturbances of self-organization (DSO) in these groups remain largely unexplored. Identifying the neural correlates of these symptoms in refugees could not only aid in clinical evaluation of individuals at high risk for PTSD but also contribute to a deeper understanding of the disorder.

Methods: We analyzed the whole-brain resting-state functional connectivity data using connectome-based predictive modeling (CPM) to predict the level of posttraumatic stress symptoms and DSO in 47 North Korean female refugees diagnosed with either PTSD or complex PTSD (PTSD group), as well as 47 North Korean female refugees who experienced trauma but did not develop PTSD or complex PTSD (non-PTSD group). CPM with leave-one-out cross validation was conducted, and posttraumatic stress symptoms and DSO were assessed using the International Trauma Questionnaire (ITQ).

Results: In the PTSD group, CPM successfully predicted individual levels of posttraumatic stress symptoms in the negative model of functional network connectivity ($r = 0.28$, $P = 0.05$), primarily involving the limbic, cerebellum, and parietal areas. However, the positive model did not show significant predictive power ($r = 0.16$, $P = 0.27$). Similarly, in the non-PTSD group, the negative model ($r = 0.29$, $P = 0.04$), but not the positive model ($r = -0.07$, $P = 0.62$), had significant prediction power for PTSD symptoms. While the limbic and cerebellum were shared features contributing to the prediction, the functional connectivity within and between the prefrontal cortex was a unique feature in the non-PTSD group. Moreover, only in the PTSD group, CPM predicted DSO in the positive model ($r = 0.36$, $P = 0.01$), primarily encompassing the limbic, cerebellar, and prefrontal areas, while the negative model did not show a meaningful prediction.

Conclusions: Our findings underscore the pivotal roles of functional connectivity within and between the limbic system, cerebellum, parietal areas, and prefrontal cortex in predicting posttraumatic stress symptoms and DSO. This study sheds light on the shared and unique brain-based features associated with these symptoms in refugee populations.

Poster No 690

Brain age estimation in subjects with anxiety/depression reliant on occipital cortex

Owen Vega[1], Nahian Chowdhury[1], Nikhil Chaudhari[2,1], Anar Amgalan[1], Andrei Irimia[2,3,1]

[1]Ethel Percy Andrus Gerontology Center, Leonard Davis School of Gerontology, University of Southern California, Los Angeles, USA, [2]Department of Biomedical Engineering, Viterbi School of Engineering, University of Southern California, Los Angeles, USA, [3]Department of Quantitative and Computational Biology, Dana and David Dornsife College of Letters, Arts and Sciences, University of Southern California, Los Angeles, USA

Introduction: Depression is a highly prevalent psychiatric disorder. It is the 19th most common disease in the world and the most diagnosed psychiatric disorder in adults - 1 in 5 people in the U.S. in any 6-month period suffers from depression. Depression can persist throughout life, with a 14.9-16.2% lifelong prevalence in the U.S. adult population (Kessler et al., 2015) (Richards, 2011). It can be fatal, as it increases suicide risk by 20.9-27 times, and it is a risk factor for cardiac disease (Lépine & Briley, 2011). Depression is also co-morbid with anxiety, another common psychiatric disorder. 85% of people with depression have anxiety, and 90% of people with anxiety have depression. Difficulties arise as both illnesses require different treatments (Tiller, 2013). Furthermore, the burden and prevalence of both anxiety and depression have increased following the 2020 COVID pandemic (COVID-19 Mental Disorders Collaborators, 2021). As anxiety and depression are both potentially lifelong disorders, age has been seen as a factor regarding both disorders (Gao et al., 2023). The interactions between aging and

anxiety or depression remain understudied. Our lab has developed a convolutional neural network that predicts a person's age from their T1-weighted magnetic resonance imaging (MRI) volume. The model outputs saliency maps that capture the contribution of each brain voxel to the age prediction. Here we investigate the interaction of anxiety and depression with aging by comparing patterns of saliency between subjects with these disorders and healthy controls.

Methods: Subject MRIs were obtained from the UK Biobank (UKBB). UKBB codes F32-33 and F40-43 were used to select subjects with primary or secondary diagnoses of depression and anxiety. Subjects with both anxiety and depression were excluded from the study. Subjects without MRI and subjects who had already been used to train the age prediction model were also excluded. Sets of healthy control subjects were age-, sex-, and sample size-matched to each case group. As such, the data was separated into four groups: anxiety (N=700), anxiety-control (N=700), depression (N=940), and depression-control (N=940). Age prediction and saliency map generation were performed for each subject using the trained model. Each subject's saliency map was normalized using min-max scaling and projected onto a shared cortical surface space. Saliency maps were averaged within-group across subjects. Maps of group differences were acquired by subtracting the mean saliency of each control cohort by the mean saliency of the corresponding case cohort and dividing the difference by the average saliency of the case group. All difference plots were smoothed using FreeSurfer 'fs_smooth.m' function with 5 iterations. Figures were plotted using MATLAB.

Results: Saliency differences were largely symmetrical across hemispheres in both the control/anxiety (Fig. 1) and control/depression (Fig. 2) comparisons. Both anxiety and depression groups showed roughly 6% higher saliency than controls in occipital regions. Meanwhile, controls exhibited ~6% higher saliency in pre/postcentral gyri and in the central sulcus.

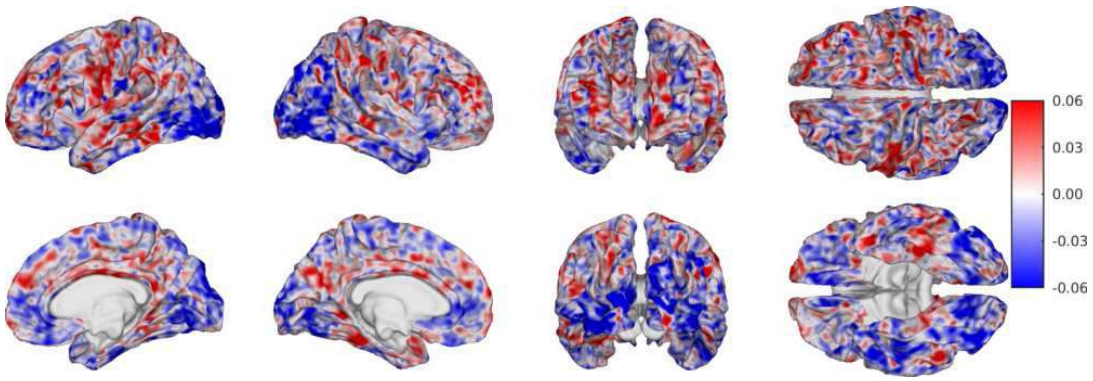

Figure 1. Saliency differences between anxiety group and anxiety-control group. Red indicates higher saliency in control group, while Blue indicates higher saliency in patients.

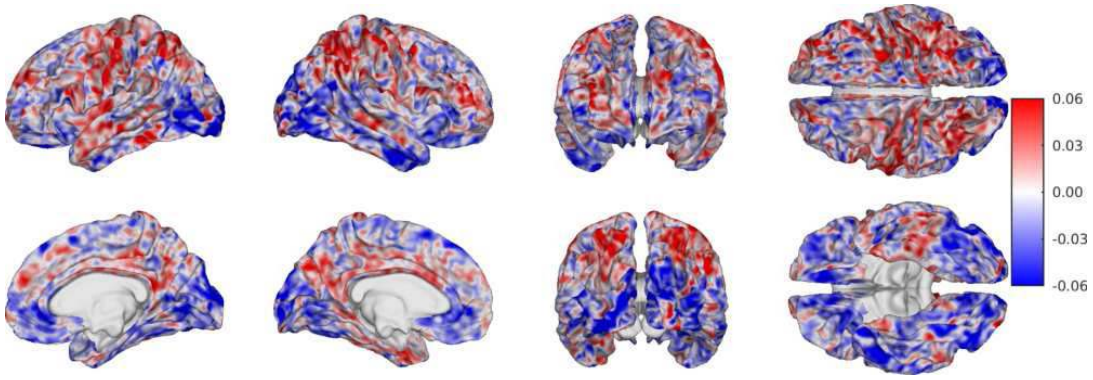

Figure 2. Saliency differences between depression group and depression-control group. Red indicates higher saliency in control group, while Blue indicates higher saliency in patients.

Conclusions: The two maps of saliency differences exhibit spatial overlap, suggesting that anxiety and depression influence the aging process in similar ways. Previous research has highlighted the occipital lobe as an affected area in anxiety/depression. Increased saliency at the occipital lobe in anxiety/depression subjects may relate to decreased function, which has been observed bilaterally in the occipital lobe in both task-based (Li et al., 2013) and resting-state fMRI (Peng et al., 2011) studies. A CT study also demonstrated early atrophy of the occipital lobe in subjects with depression (Tanaka et al., 1982). Grey matter volume in the right occipital region was found to be negatively correlated with anxious traits (Yin et al., 2016). Further research on how anxiety and depression influence the aging of the occipital lobe is recommended.

References
1. COVID-19 Mental Disorders Collaborators (2021). 'Global prevalence and burden of depressive and anxiety disorders in 204 countries and territories in 2020 due to the COVID-19 pandemic'. Lancet (London, England), vol. 398, no. 10312, pp. 1700–1712.
2. Gao, X. (2023). 'Accelerated biological aging and risk of depression and anxiety: evidence from 424,299 UK Biobank participants'. Nature Communications, vol. 14, no. 1, pp. 2277.
3. Kessler, R. C. (2015). 'Anxious and non-anxious major depressive disorder in the World Health Organization World Mental Health Surveys'. Epidemiology and Psychiatric Sciences, vol. 24, no. 3, pp. 210–226.
4. Lépine, J. P. (2011). 'The increasing burden of depression'. Neuropsychiatric Disease and Treatment, vol. 7, no. Suppl 1, pp. 3–7.
5. Li, J. (2013). 'Abnormal activation of the occipital lobes during emotion picture processing in major depressive disorder patients'. Neural regeneration research, vol. 8, no. 18, pp. 1693–1701.
6. Peng, D. H. (2011). 'Decreased regional homogeneity in major depression as revealed by resting-state functional magnetic resonance imaging'. Chinese Medical Journal, vol. 124, no. 3, pp. 369–373.
7. Richards D. (2011). 'Prevalence and clinical course of depression: a review'. Clinical Psychology Review, vol. 31, no. 7, pp. 1117–1125.
8. Tanaka, Y. (1982). 'Computerized tomography of the brain in manic-depressive patients--a controlled study'. Folia Psychiatrica et Neurologica Japonica, vol. 36, no. 2, pp. 137–143.
9. Tiller J. W. (2013). 'Depression and anxiety'. The Medical Journal of Australia, vol. 199, no. S6, pp. S28–S31.
10. Yin, P. (2016). 'The brain structure and spontaneous activity baseline of the behavioral bias in trait anxiety'. Behavioural Brain Research, vol. 312, pp. 355–361.

Poster No 691

Neurobehavioral responses to legal cannabis advertisements in youth and adults

Justine Chen[1], Nathan Chabin[2], Ruizhe Zhang[1], Jalen Grayson[1], Alisa Padon[3], Lynn Silver[3], Dara Ghahremani[1]

[1]UCLA, Los Angeles, CA, [2]Pitzer College, Pomona, CA, [3]Public Health Institute, Oakland, CA

Introduction: Exposure to marketing for legal substances has a significant impact on subsequent substance use, with underage youth especially susceptible to influence. Guidelines for regulating cannabis advertisements are needed to protect underage youth in locations where cannabis is legal. Identifying key features appealing to youth is an important step in specifying guidelines. The Content Appealing to Youth (CAY) index, developed for alcohol and tobacco ads (Padon et al., 2017, 2018), indicated key features that are appealing to youth. We sought to modify the CAY index for cannabis and to evaluate it for neural responses and self-reported liking of cannabis ads and use, with a broad goal of providing evidence to inform cannabis marketing policy. We hypothesized that, compared to adults, youth would show greater differentiation in neural responses to ads with high vs. low CAY indices in regions responsive to reward and arousal (e.g., ventral striatum and amygdala, respectively).

Methods: After modifying the CAY index using surveys and focus groups, we presented cannabis ads to youth and adults (N=63; 35 female; age range: 16-36 years old; M=24.4, SD=6.3) during fMRI scanning. We prepared non-cannabis control ads that closely matched cannabis ads on appearance. After each ad presentation (20 s), participants rated how much they liked the ad before presentation of the next trial (30 cannabis trials, 30 control trials; mixed event-related/blocked design). After the scan, participants viewed each cannabis ad again and indicated how much it made them want to use cannabis. Twenty-three of 37 participants scanned used cannabis regularly (>3x/week). We first compared brain responses to cannabis and control ads to determine brain activation specific to cannabis content. Then, we compared responses to cannabis ads with low and high CAY content across age. We focused on the ventral striatum and amygdala as a priori regions of interest, but exploratory whole-brain analyses were also conducted. We also examined correlations of brain activation with ad liking and wanting to use cannabis. Preprocessing and whole-brain voxel-wise univariate statistics were conducted (FSL, voxel height: Z>3.1, cluster: P<0.05; FLAME1, outlier removal).

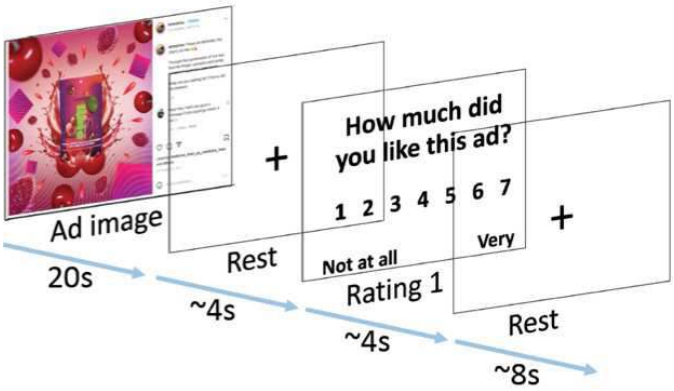

Figure 1. Task trial structure.

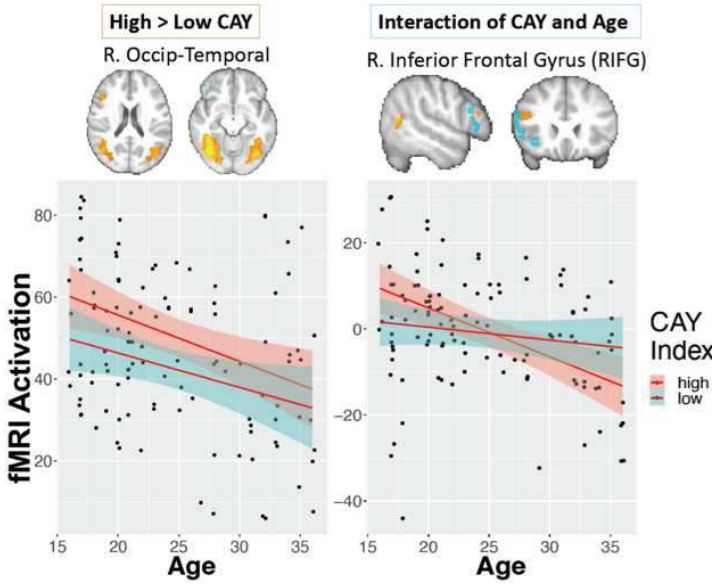

Figure 2. Whole-brain voxel-wise results. (Scatter plots of extracted parameter estimates are shown to illustrate distribution of data points and direction of interaction effects).

Results: Across age, high CAY ads elicited greater liking and the desire to use cannabis vs. low CAY ads (Ps<0.0001). Compared to control ads, cannabis ads elicited greater activation in the amygdala and ventral striatum (Ps<0.0001) as well as the precuneus and posterior cingulate in whole-brain analyses. Amygdala and ventral striatum did not differentiate between high and low CAY ads, but whole-brain analyses showed that bilateral occipito-temporal activation did, with activation positively correlated with wanting to use cannabis. The right inferior frontal gyrus (RIFG) showed a negative relationship between age and RIFG for high CAY ads and no relationship for low CAY ads (significant interaction). No effects of regular cannabis use were found in any analyses.

Conclusions: These preliminary results indicate that both youth and adults like ads with content previously shown to be appealing to youth, and both are also more likely to want to use cannabis after viewing an ad that they like. Amygdala and ventral striatum are sensitive to whether ads contain cannabis or not, but do not distinguish by content appealing to youth. Thus, high youth appeal may not be explained by reward and arousal mechanisms (as indexed by these brain regions). Occipito-temporal CAY-sensitivity may be a result of attention-related gain in higher order visual areas in response to high CAY ads. RIFG appears to be sensitive to high/low appeal differentially in youth and adults, suggesting a potential role of cognitive control when youth view appealing cannabis ads. Concerning policy implications, our results suggest that ads with features that are high on the CAY index should be restricted to media to which youth will be minimally exposed.

References

1. Padon AA, Maloney EK, Cappella JN. Youth-Targeted E-cigarette Marketing in the US. Tobacco regulatory science. 2017;3(1):95-101. Epub 2017/01/14. doi: 10.18001/trs.3.1.9.
2. Padon AA, Rimal RN, DeJong W, Siegel M, Jernigan D. Assessing Youth-Appealing Content in Alcohol Advertisements: Application of a Content Appealing to Youth (CAY) Index. Health communication. 2018;33(2):164-73. Epub 2016/12/17. doi: 10.1080/10410236.2016.1250331.

Poster No 692

Cerebellar volume in substance use disorders: a mega-analysis by the ENIGMA addiction working group

Jalil Rasgado Toledo[1], Alfonso Fajardo-Valdez[2], Ian Harding[3], Scott Mackey[4], Hugh Garavan[5], Eduardo Garza-Villarreal[1]

[1]Universidad Nacional Autónoma de México, Queretaro, Mexico, [2]McGill University, Montreal, Quebec, [3]Monash University, Melbourne, Australia, [4]The University of Vermont, Burlington, VT, [5]University of Vermont, Burlington, VT

Introduction: The cerebellum contributes in among a wide variety of higher-order processes, including rewarding and emotional functions (Zhang et al. 2023) and evidence suggests the involvement of the cerebellum in substance use disorders (SUDs) and addiction. A recent meta-analysis showed addiction to any substance was related to low brain volume in cerebellar white matter, while long-term use was related to high brain volume in cerebellar gray matter (Pando-Naude et al. 2021). In this study, we wanted to determine the brain volume of the cerebellum and subdivisions in different SUDs using a mega-analysis.

Methods: We used MRI T1w sequences from 3,172 individuals with SUDs (AUD n = 914, ATS n = 111, CANN n = 405, COH = 30, NIC n = 577, OPI n = 58, Controls n = 1,028) across 60 sites from the ENIGMA-addiction working group. After QC, we tested 2 methods: 1) a deep-learning-based approach for automatic cerebellar parcellation (ACAPULCO) using an anatomical atlas (Han et al. 2020) and 2) the spatially unbiased infratentorial template (SUIT) toolbox (Diedrichsen 2006) for voxel-based morphometry (VBM). To study functionally defined ROIs we also obtained the mean volume for 10 cerebellar regions from the Multi-Domain Task Battery atlas (MDTB) (King et al. 2019) using the SUIT toolbox. We then independently compared the ACAPULCO and MDTB volumes and the SUIT-VBM between groups (patients vs controls) in general and with Subtance subgroups with a permutation Welch Two Sample t-tests analysis. Each test was controlled for age, sex, intracranial volume, and site. The Benjamini-Hochberg procedure was used to control for multiple comparisons (p-FDR < 0.05).

Results: We found significant volume differences between SUDs and controls, which varied between types of substances. We found that SUD subjects displayed differences mainly in subregions 1, 4, 6, 9 and 10. In particular, the greatest effects appeared to be related to nicotine use disorder, with volume differences in almost all subregions, followed by amphetamine and alcohol. Subregions with the most group differences were 1 and 2. All group comparisons showed low to medium effect sizes. A set of affected regions were related depending on the substance, but some subregions of regions 1 and 4 according to the MDTB atlas, were found to have higher changes.

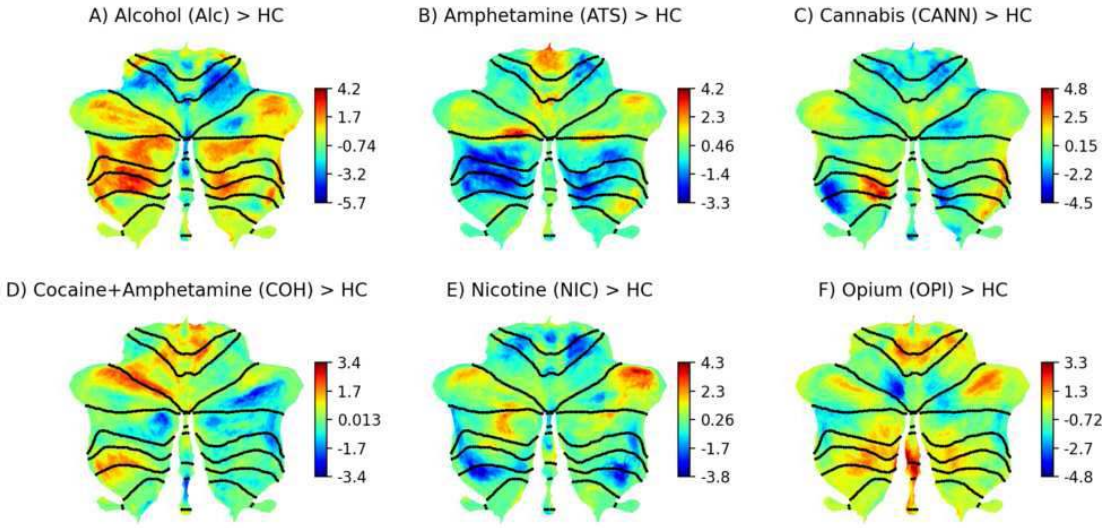

Voxel-base morphometry results of the comparison between each substance with controls. Color bars indicate tvalues.

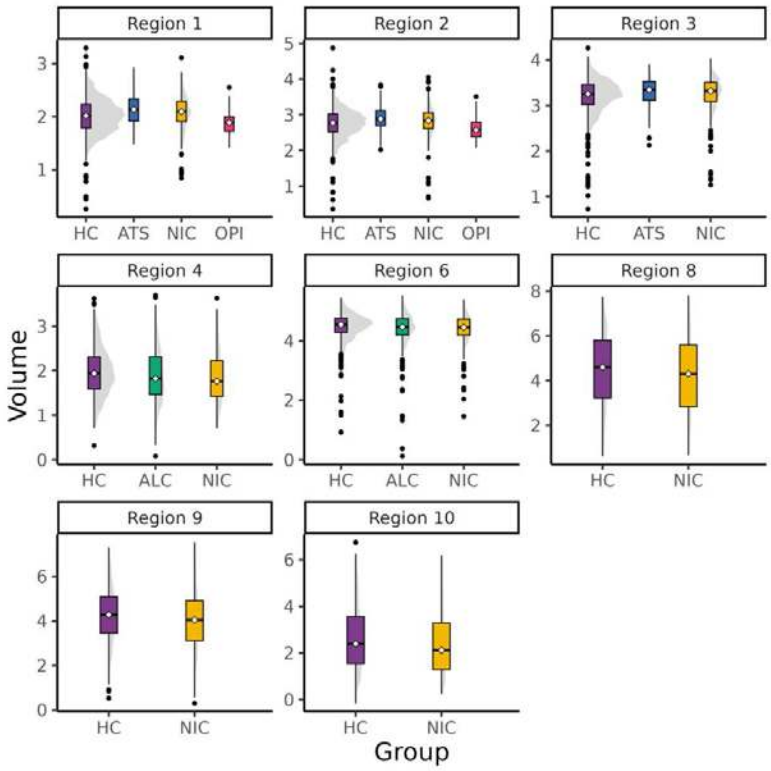

Significant volumes differences of each region of Multi-Domain Task Battery atlas (MDTB) between substance use disorder groups compared with controls.

Conclusions: Our results suggest that specific cerebellum regions are affected in SUDs, and some regions are affected in all SUDS, while other regions are only affected by substance. Regional variations may be associated with interference resolution, motor planning, active maintenance, and verbal comprehension, according to the MDTB atlas results.

References

1. Diedrichsen, J. (2006). A spatially unbiased atlas template of the human cerebellum. NeuroImage, 33(1), 127–138.
2. Han, S., Carass, A., He, Y., & Prince, J. L. (2020). Automatic cerebellum anatomical parcellation using U-Net with locally constrained optimization. NeuroImage, 218, 116819.
3. King, M., Hernandez-Castillo, C. R., Poldrack, R. A., Ivry, R. B., & Diedrichsen, J. (2019). Functional boundaries in the human cerebellum revealed by a multi-domain task battery. Nature Neuroscience, 22(8), 1371–1378.
4. Pando-Naude, V., Toxto, S., Fernandez-Lozano, S., Parsons, C. E., Alcauter, S., & Garza-Villarreal, E. A. (2021). Gray and white matter morphology in substance use disorders: a neuroimaging systematic review and meta-analysis. Translational Psychiatry, 11(1), 29.
5. Zhang, P., Duan, L., Ou, Y., Ling, Q., Cao, L., Qian, H., Zhang, J., Wang, J., & Yuan, X. (2023). The cerebellum and cognitive neural networks. Frontiers in Human Neuroscience, 17, 1197459.

Poster No 693

Lasting effects of electroconvulsive therapy on default mode network connectivity in depression

Noor Al-Sharif[1], Artemis Zavaliangos-Petropulu[1], Brandon Taraku[1], Randall Espinoza[2], Katherine Narr[1]

[1]Ahmanson-Lovelace Brain Mapping Center, Department of Neurology, Los Angeles, CA, [2]Jane and Terry Semel Institute for Neuroscience and Human Behavior, Los Angeles, CA

Introduction: Electroconvulsive therapy (ECT) is an effective treatment for individuals with major depressive disorder (MDD), particularly those whose symptoms have failed to respond to first-line antidepressant treatments(Li et al., 2020). Such individuals are categorized as having treatment resistant depression (TRD)(Rush et al., 2019). The precise mechanisms underlying the antidepressant efficacy of ECT remain unclear, however, the application of resting-state functional magnetic resonance imaging (fMRI) shows potential for identifying its therapeutic effects. Prior studies suggest that ECT disrupts functional connectivity within the default mode network (DMN)(Sinha et al., 2020), a large-scale network involved in introspection frequently found to be overactive in patients with depression(Kaiser et al., 2015). In this study, we compared pre-treatment within-DMN connectivity in patients with TRD and HC, and investigated long term changes in these networks after ECT treatment.

Methods: Participants included N=42 patients (age=39.8±14.8, 27 female) with TRD (defined as no response to at least two antidepressant treatments) and N=54 HC (age=32.2±12.0, 31 female). All TRD patients underwent ECT at UCLA Resnick Neuropsychiatric Hospital. Mood assessments (Hamilton Depression Rating Scale; HDRS(Hamilton, 1960)) and resting-state fMRI were collected at baseline (pre-treatment) and at follow-up (3 months post treatment). Human Connectome Project (HCP) protocol was used on a 3T Siemens Prisma to collect structural MRI (T1 and T2, voxel size (VS)=0.8mm3) and resting-state fMRI (VS=2mm3). Data were preprocessed with the HCP minimal preprocessing pipeline(Glasser et al., 2013), ICA + FIX(Salimi-Khorshidi et al., 2014), and MSMALL alignment(Robinson et al., 2018). The Schaefer 100 Yeo 17 Network atlas(Schaefer et al., 2018) was used to parcellate fMRI data to generate z-scored correlation matrices. Only within-DMN nodes were analyzed. A paired t-test was used to test for changes in HDRS. Linear regression was used to compare within-DMN connectivity between HC and TRD patients at baseline, adjusting for age, sex, and global signal average (GSA) as fixed effects, correcting for multiple comparisons with FDR. In a follow-up analysis, a mixed effect model tested for changes in connectivity after ECT, adjusting for age, sex, and GSA. We also performed a linear regression testing for associations between change in HDRS and change in connectivity, adjusting for age, sex, and GSA and correcting for multiple comparisons with FDR.

Results: Patients showed significant improvements in HDRS post-ECT (p-value=6.223e-05, t-value=5.1). When comparing baseline HC to TRD, 190 nodes showed significant differences in resting state connectivity, with 121 presenting greater connectivity and 69 presenting less connectivity. Of the nodes that differed by diagnosis, 27 significantly changed following ECT (p-value<0.05), with 15 nodes normalizing towards connectivity levels observed in HC. Changes in HDRS scores showed trending associations (p-value<0.05) to change in connectivity patterns in 112 nodes (17 increasing, 95 decreasing), but did not pass FDR.

Conclusions: In this study, we showed mood symptoms significantly improved in patients with TRD after 3 months following ECT. Pre-treatment, patients with TRD showed distinct connectivity patterns within the DMN compared to HC. Several nodes that were hyperactive at baseline in TRD normalized in the direction of HC at follow up, 3 months post-ECT treatment. Trending associations between improvements in mood and changes in connectivity were observed. Overall, these findings suggest that the antidepressant mechanisms of ECT may act long-term on the aberrant DMN in patients with TRD.

References

1. Glasser, M. F., et al. (2013). The minimal preprocessing pipelines for the Human Connectome Project. NeuroImage, 80, 105–124.
2. Hamilton, M. (1960). A rating scale for depression. Journal of Neurology, Neurosurgery, and Psychiatry, 23, 56–62.
3. Kaiser, R. H., et al (2015). Large-Scale Network Dysfunction in Major Depressive Disorder: A Meta-analysis of Resting-State Functional Connectivity. JAMA Psychiatry, 72(6), 603–611.
4. Li, M., et al (2020). Effects of Electroconvulsive Therapy on Depression and Its Potential Mechanism. Frontiers in Psychology, 11, 80.
5. Robinson, E. C., et al (2018). Multimodal surface matching with higher-order smoothness constraints. NeuroImage, 167, 453–465.
6. Rush, A. J., Aaronson, S. T., & Demyttenaere, K. (2019). Difficult-to-treat depression: A clinical and research roadmap for when remission is elusive. The Australian and New Zealand Journal of Psychiatry, 53(2), 109–118.
7. Salimi-Khorshidi, G., et al (2014). Automatic denoising of functional MRI data: combining independent component analysis and hierarchical fusion of classifiers. NeuroImage, 90, 449–468.
8. Schaefer, A., et a (2018). Local-Global Parcellation of the Human Cerebral Cortex from Intrinsic Functional Connectivity MRI. Cerebral Cortex, 28(9), 3095–3114.
9. Sinha, P., et al (2020). Resting State Functional Connectivity of Brain With Electroconvulsive Therapy in Depression: Meta-Analysis to Understand Its Mechanisms. Frontiers in Human Neuroscience, 14, 616054.

Poster No 694

Computational modeling reveals the altered brain dynamics of association cortex in schizophrenia

Yawei Ma[1], Weiyang Shi[1], Tianzi Jiang[1]

[1]Brainnetome Center, Institute of Automation, Chinese Academy of Sciences, Beijing, Beijing

Introduction: Schizophrenia (SCZ) is a mental disorder of altered brain connectivity, which is conceptualized as “dysconnectivity” and can relate to either a hypo- or hyper-integrative/connective condition between different brain areas (Bassett et al. 2012) . Astride the development of neuroimaging, the “dysconnectivity” hypothesis of SCZ has been gathering progressive support. Studies have so far demonstrated the extensive and repeatable deficiencies in integrative and connective competence of SCZ (Moran et al. 2013). What remains unclear, however, is how the biophysical properties of intrinsic dynamic have altered in SCZ, resulting in the “dysconnectivity” pattern. Substantial evidence demonstrated that computational models have provided a novel perspective for studying brain diseases through the relationship between brain structure, function, and dynamics (Misic et al. 2015) . Therefore, the purpose of this study was to utilize computational models to explore how brain dynamics varied in SCZ.

Methods: To elucidate the alterations of brain dynamics in SCZ, a total of 143 individuals (SCZ/HC = 67/76, from the 6th Hospital of Peking University) with high quality T1-weight data, resting-state fMRI data, diffusion weighted imaging data, complete PANSS score information were retained for subsequent analysis. The preprocessing protocol was common and the same as previous study (Li et al. 2020). Here, parametric mean field model (pMFM) (Deco et al. 2013, Kong et al. 2021) was utilized to study the biophysical mechanism changes within and between the brain regions in SCZ. Briefly, heterogeneity parameters (recurrent connection, noise amplitude and subcortical input current) combining myelinization profile and first functional gradient profile (Demirtas et al. 2019, Bazinet et al. 2023), and global coupling were optimized by fitting empirical functional connectivity and dynamic functional connectivity. We conducted 30 times of 75% resampling without replacement for the two groups respectively, and obtained 30 group-level optimal biophysical parameters, which could be compared in each brain region. Additionally, the spatial correlation between the maps of altered biophysical parameters and receptors was analyzed. Regional-based myelination, first functional gradient and receptors from neuromaps (Markello et al. 2022) and regional-based parameters of pMFM were acquired based on the Brainnetome Atlas (Fan et al. 2016).

Results: Specific forms of biophysical alterations have been found in SCZ. The correlation between empirical and computational model stimulated functional connectivity reached 0.41 both for HC and SCZ, and the Kolmogorov–Smirnov (KS) distance of dynamic functional distribution was less than 0.2 (Figure 1). Moreover, global coupling increases significantly in SCZ ($t = -4.59$, $p < .0001$), and significantly increase recurrent connection but decrease subcortical input of association cortex in SCZ according to the computational model (Figure 2). The two altered biophysical maps are inversely correlated ($r = -0.58$, $p < .0001$), and these alterations have a significant spatial correlation ($p < 0.05$, spin test) with the maps of MOR (mu-opioid receptor), 5-HT2a (serotonin receptor), mGluR5 (glutamate receptor), VAChT (acetylcholine transporter), D2 (dopamine receptor), NET (norepinephrine transporter).

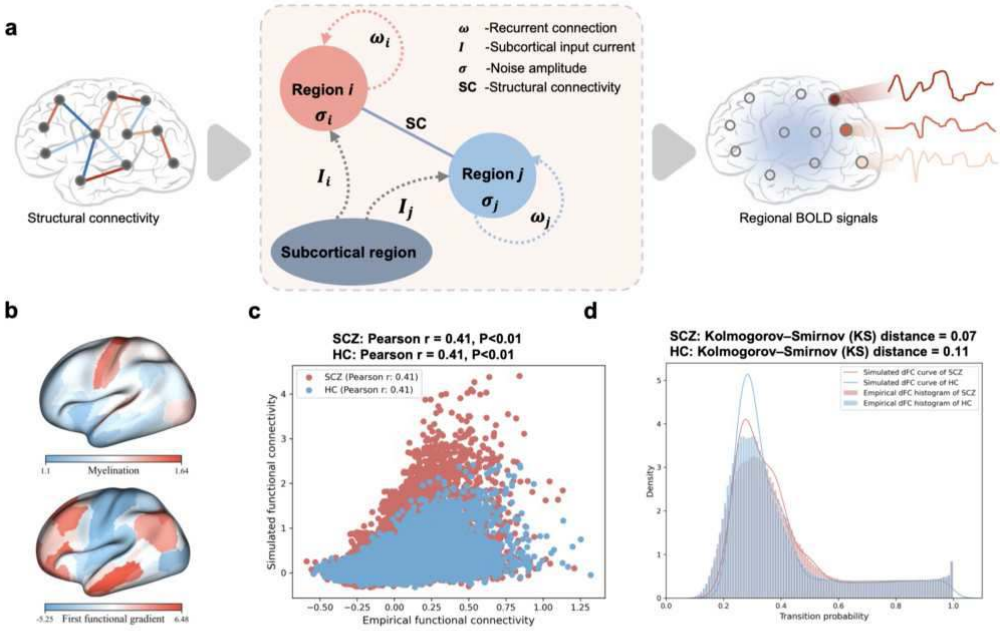

Figure 1. The framework of whole-brain computational model. (a) Structural connectivity were obtained by DWI after averaging across subjects. A computational model was then constructed using a set of stochastic differential equations coupled according to the connectivity matrix to produce regional bold signals. **(b)** The heterogeneous parameters were constraint by myelination and first functional gradient. The model spatiotemporal patterns to the ones observed in empirical data were compared to valid the model. In this case, the empirical functional connectivity **(c)** and dynamics **(d)** were measured using BOLD signals.

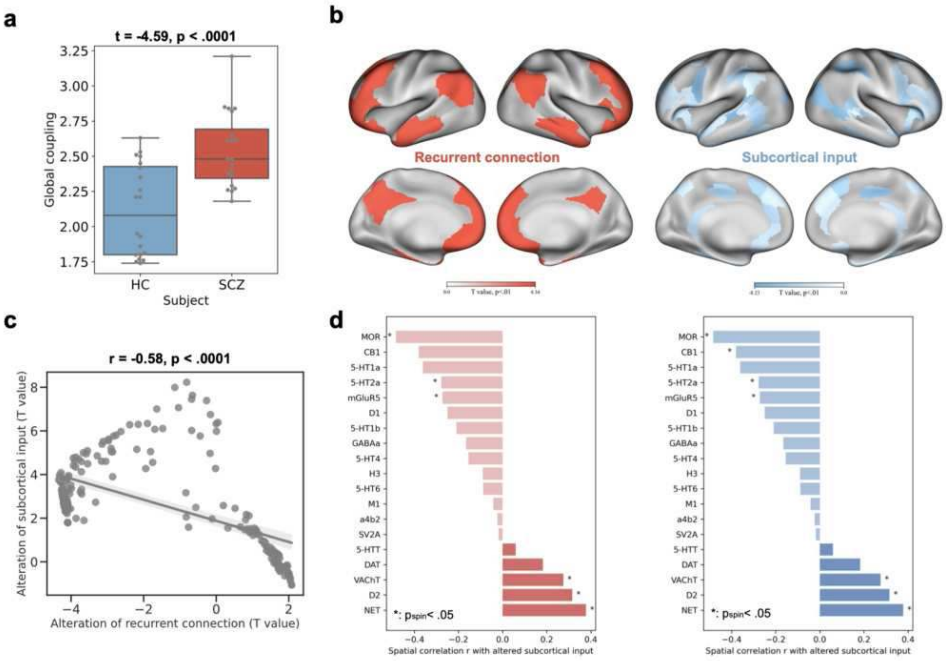

Figure 2. Biophysical alteration in SCZ. (a) Boxplot of global coupling in SCZ and HC. **(b)** Maps of altered recurrent connection and altered subcortical input. **(c)** Scatterplot and fitted curve of the relationship between altered recurrent connection and altered subcortical input. **(d)** Bar diagram of the spatial correlation between altered biophysical maps and receptor maps.

Conclusions: Collectively, the biophysical changes of SCZ derived from the whole brain computational model were significantly distributed in the association cortex, and these alterations have significant spatial correlation with the distribution of multiple receptors in the brain. This finding shed light on the regional biophysical alterations of brain activity in SCZ and provide a new perspective for understanding the brain dynamical changes in SCZ.

References

1. Bassett, D. S. (2012), 'Altered resting state complexity in schizophrenia', Neuroimage, vol. 59, no. 3, pp. 2196-2207.
2. Bazinet, V. (2023), 'Towards a biologically annotated brain connectome', Nature Reviews: Neuroscience, vol. 24, no. 12, pp. 747-760.
3. Deco, G. (2013), 'Resting-state functional connectivity emerges from structurally and dynamically shaped slow linear fluctuations', Journal of Neuroscience, vol. 33, no. 27, pp. 11239-11252.
4. Demirtas, M. (2019), 'Hierarchical Heterogeneity across Human Cortex Shapes Large-Scale Neural Dynamics', Neuron, vol. 101, no. 6, pp. 1181-1194 e1113.
5. Fan, L. (2016), 'The Human Brainnetome Atlas: A New Brain Atlas Based on Connectional Architecture', Cerebral Cortex, vol. 26, no. 8, pp. 3508-3526.
6. Kong, X. (2021), 'Sensory-motor cortices shape functional connectivity dynamics in the human brain', Nature Communications, vol. 12, no. 1, pp. 6373.
7. Li, A. (2020), 'A neuroimaging biomarker for striatal dysfunction in schizophrenia', Nature Medicine, vol. 26, no. 4, pp. 558-565.
8. Markello, R. D. (2022), 'neuromaps: structural and functional interpretation of brain maps', Nature Methods, vol. 19, no. 11, pp. 1472-1479.
9. Misic, B. (2015), 'Cooperative and Competitive Spreading Dynamics on the Human Connectome', Neuron, vol. 86, no. 6, pp. 1518-1529.
10. Moran, L. V. (2013), 'Disruption of anterior insula modulation of large-scale brain networks in schizophrenia', Biological Psychiatry, vol. 74, no. 6, pp. 467-474.

Poster No 695

Explore the brain connectivity of panic disorder patients based on the graph theoretical approach

Hye Jin Hong[1], Ji Seon Ahn[2,3,4], Jin Young Park[2,3,4], Jee Hang Lee[1,5]

[1]Department of AI & Informatics, Sangmyung University, Seoul, Korea, Republic of, [2]Department of Psychiatry, Yonsei University College of Medicine, Yongin Severance Hospital, Yongin, Korea, Republic of, [3]Institute of Behavioral Science in Medicine, Yonsei University College of Medicine, Seoul, Korea, Republic of, [4]Center for Digital Health, Yongin Severance Hospital, Yonsei University Health System, Yongin, Korea, Republic of, [5]Department of Human-Centered AI, Sangmyung University, Seoul, Korea, Republic of

Introduction: It is widely accepted that the brain structure and functions of patients with panic disorder (PD) are different from those of healthy controls (HCs) (Imperatori et al., 2019). In this study, we would like to explore the discrepancy of brain

connectivity between patients with panic disorder and healthy control based on the graph theoretical approach using EEG. To that end, we analyzed EEG data during both resting state (RS) and mental arithmetic (MA) tasks to explore the topological characteristics of the brain associated with information processing difficulties, particularly cognitive challenges observed in individuals with panic disorder. To construct functional networks within the individuals with PD and HC, we adopted a network perspective, treating the brain as a complex network. Employing a graph theoretical approach, a widely recognized means for assessing information communication in the human brain, we aimed to unveil topological alterations indicative of panic disorder-related changes in information processing dynamics.

Methods: In this study, 34 participants were included as a PD patients group, who had been diagnosed with PD. To recruit them, we retrospectively analyzed medical records and EEG data from patients who sought treatment for anxiety at a psychiatric outpatient clinic between Mar. 1, 2020 and Sep. 30, 2023. Paired with the PD group, we recruited the additional 34 healthy controls matched with respect to age and gender distribution (IRB reference number 9-2022-0199, Feb. 20, 2023). The experiment consisted of two sessions. In the first, participants were asked to keep their eyes closed for five minutes (we called the resting state; RS). Next, participants were asked to perform the mental arithmetic task for five minutes while keeping eyes closed (we called the mental arithmetic;MA). EEG data were recorded in both sessions. We used the graph-theoretical approach, specifically, computed Phase Locking Value (PLV) (Lachaux et al., 1999) among all pairs of EEG channels. It quantifies the degree of phase synchronization between two narrow-band signals (Aydore et al., 2013). We then constructed the brain network using the PLV matrices whose values were above 25 percentile. For each of the reconstructed graphs, two indices were computed: (i) Global Efficiency (GE) (Latora & Marchiori, 2001); (ii) Local Efficiency (LE) (Latora & Marchiori, 2001).

Results: Comparing the two graph network measures for all frequency bands between PD and HC in a RS, GE of the theta, beta, and gamma band was significantly higher in the HC group than that in the PD group while no significant results were found in the rest (Figure 1A-left). On the other hand, for LE, no significant results were found in all frequency bands (Figure 1A-right). Next, we compared GE and LE while participants performed the MA task. Notably, the result showed that GE of all frequency bands in the HC group was significantly higher than that in the PD group (Figure 1B-left) while there was no significance in LE (Figure 1B-right). Next, we tested the interaction effect of the task (RS, MA). In other words, we examined the changes in GE and LE of the two HC and PD groups in response to the changes in the task conditions, from RS to MA. It was clear that in the alpha band, HC's GE was significantly increased while PD's GE was significantly diminished ($p < 0.01$) (Figure 1C-Alpha). In addition, PD's GE in the beta band was significantly decreased while there were no changes in HC's GE (Figure 1C-Beta). With regards to LE, both HC and PD showed no effect in all bands (Figure 1D).

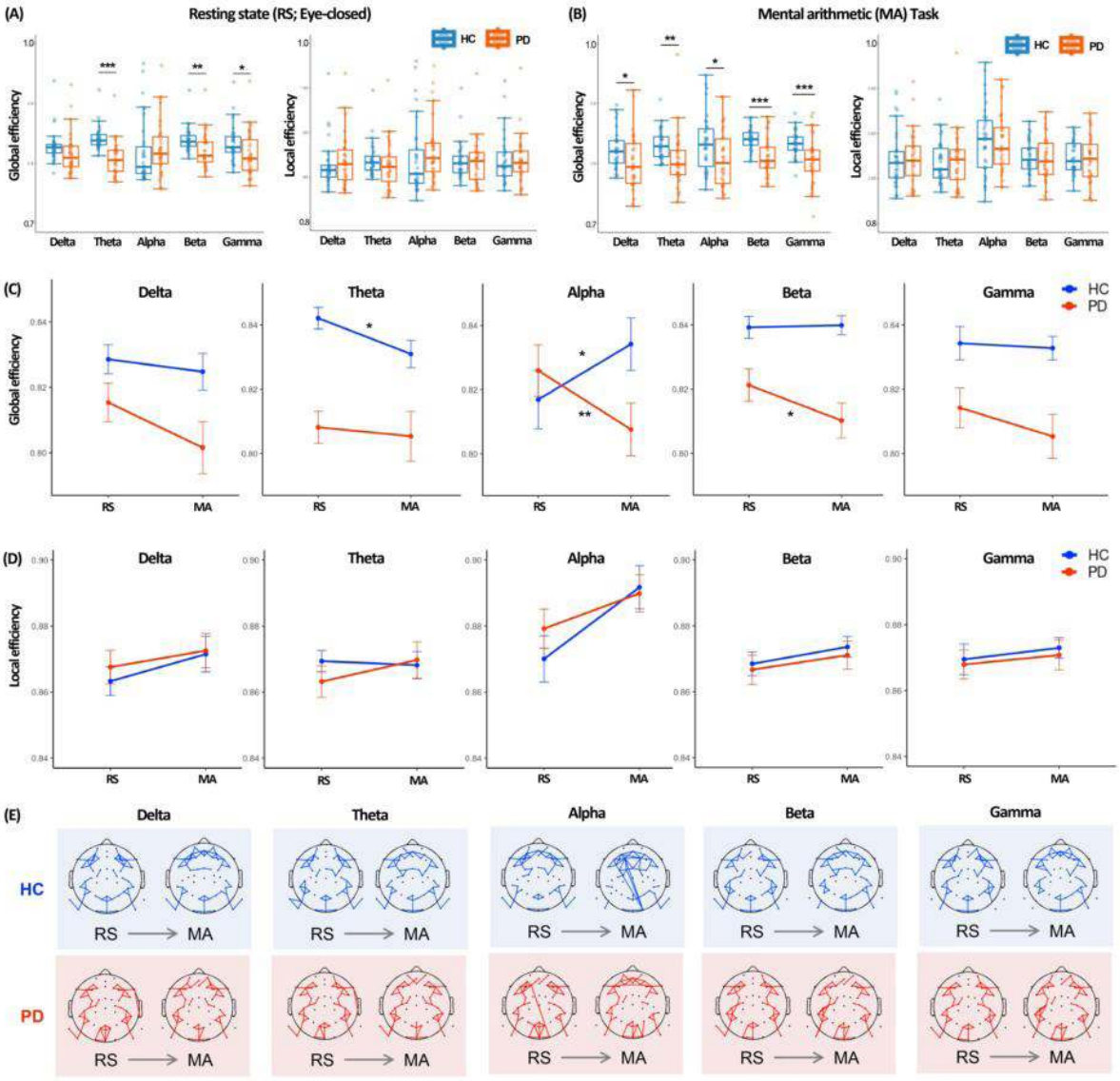

Figure 1. Graph theoretical analyses of EEG from patients with panic disorder (PD) and healthy control (HC) in the two different task conditions (Resting state;RS, and Mental arithmetic task; MA). (A) Global- (left) and Local efficiency (right) of PD and HC in the RS condition. The x- and y-axis refer to the frequency band and the efficiency, respectively. (paired sample t-test, *: $p < 0.05$, **: $p < 0.01$, ***: $p < 0.001$). **(B)** Global- (left) and Local efficiency (right) of PD and HC in the MA condition. The x- and y-axis refer to the frequency band and the efficiency, respectively. (paired sample t-test, *: $p < 0.05$, **: $p < 0.01$, ***: $p < 0.001$). **(C)** Changes in GE in response to changes in the task condition across all frequency bands. The x- and y-axis refer to the task condition and GE, respectively. The error bar is the standard error of the mean (paired sample t-test, *: $p < 0.05$, **: $p < 0.01$). **(D)** Changes in LE in response to changes in the task condition across all frequency bands. The x- and y-axis refer to the task condition and LE, respectively. The error bar is the standard error of the mean (paired sample t-test). **(E)** Topoplot representing the brain network connectivity of HC and PD between the task conditions across all frequency bands.

Conclusions: These results suggest that the PD group showed reduced GE in brain networks in all frequency bands compared to the HC group in general. This gives an indication that overall information processing efficiency is likely to be decreased in PD as the connectivity of brain networks decreases. We will further examine the role of each band in the connectivity of PD.

References

1. Aydore, S. (2013), 'A note on the phase locking value and its properties', Neuroimage, 74, pp. 231-244.
2. Howard, M. W. (2003), 'Gamma oscillations correlate with working memory load in humans', Cerebral cortex, 13(12), pp. 1369-1374.
3. Imperatori, C. (2019), 'Default mode network alterations in individuals with high-trait-anxiety: an EEG functional connectivity study', Journal of Affective Disorders, 246, pp. 611-618.
4. Ismail, L. E. (2020), 'A graph theory-based modeling of functional brain connectivity based on eeg: A systematic review in the context of neuroergonomics', IEEE Access, 8, 155103-155135.
5. Klimesch, W. (2012), 'Alpha-band oscillations, attention, and controlled access to stored information', Trends in cognitive sciences, 16(12), pp. 606-617.
6. Lachaux, J. P. (1999), 'Measuring phase synchrony in brain signals', Human brain mapping, 8(4), pp. 194-208.
7. Latora, V. (2001), 'Efficient behavior of small-world networks. Physical review letters', 87(19), 198701.
8. Spitzer, B., & Haegens, S. (2017), 'Beyond the status quo: a role for beta oscillations in endogenous content (re) activation', eneuro, 4(4).

Poster No 696

Auditory Thalamocortical Resting-State Hyperconnectivity in Schizophrenia

John Williams[1], Zu Zheng[2], Philip Tubiolo[3], Roberto Gil[1], Greg Perlman[1], Jodi Weinstein[1], Natalka Haubold[1], Eilon Silver-Frankel[1], Mark Slifstein[1], Guillermo Horga[4], Anissa Abi-Dargham[1], Jared Van Snellenberg[1]

[1]Renaissance School of Medicine at Stony Brook University, Stony Brook, NY, [2]SUNY Downstate Health Sciences University, Brooklyn, NY, [3]Stony Brook University, Stony Brook, NY, [4]New York State Psychiatric Institute, New York, NY

Introduction: Auditory hallucinations, and positive symptoms broadly, are a core component of schizophrenia (SCZ) and psychosis generally, yet their etiology remains unknown. Findings of aberrant thalamocortical resting-state (RS) functional connectivity (RSFC) have been mixed, though convergently showing hyperconnectivity between thalamus and somatosensory cortex. However, limitations in demarcating medial geniculate nucleus (MGN) from other thalamic nuclei suggests that the degree to which these results represent abnormalities within the auditory processing pathway is unclear. Here, we aim to specifically measure RSFC between auditory thalamus (MGN) and auditory cortex (AC) in unmedicated patients with SCZ (PSZ) and healthy control participants (HC), using a sensory thalamic localizer (TL) fMRI task in tandem with resting-state fMRI data acquired from the same subjects.

Methods: 53 PSZ and 45 HC completed study procedures. PSZ were medication-free for at least 3 weeks for reasons unrelated to this study . Symptom severity was assessed using the Positive and Negative Syndrome Scale (PANSS). Participants completed 4 runs each of resting-state fMRI and the TL fMRI task. Data were preprocessed using HCP minimal preprocessing pipeline 4.2.0. During the TL task, alternating auditory and visual stimuli were displayed, with task details shown in Figure 1. TL task data was analyzed by first identifying AC and visual cortex (VC) in each hemisphere. Participant-level Auditory − Visual contrast images were generated using SPM12. In each hemisphere, a single, contiguous cluster was generated within an AC mask and VC mask from among the top and bottom 10% of contrast values, respectively, and bilateral mean AC and VC time series were extracted. Hemispheric auditory and visual thalamic search region (TSR) masks were generated for each subject. Connectivity between each voxel's time series and mean AC and VC time series were calculated, to produce TSR-AC and TSR-VC connectivity maps, which were then thresholded based on the size of the TSR. The largest contiguous cluster remaining within each hemi-thalamus TSR-AC was identified as MGN. For each RS run of each participant, average time series were extracted from hemispheric MGN and LGN ROIs. RSFC correlations with both ipsilateral and contralateral AC were estimated for each hemispheric MGN, and then averaged across hemispheres and runs. Group differences in MGN-AC connectivity were assessed using an unequal variances t-test. Associations between MGN-AC connectivity and positive symptoms were primarily assessed across groups using a GLM with an intercept, and predictors for diagnosis (PSZ), lifetime medication exposure (dichotomous), and PANSS Positive scores. Follow-up analyses were conducted to assess the specificity of this associations by using this GLM with additional predictors for scores from the PANSS Negative and General Psychopathology Scales.

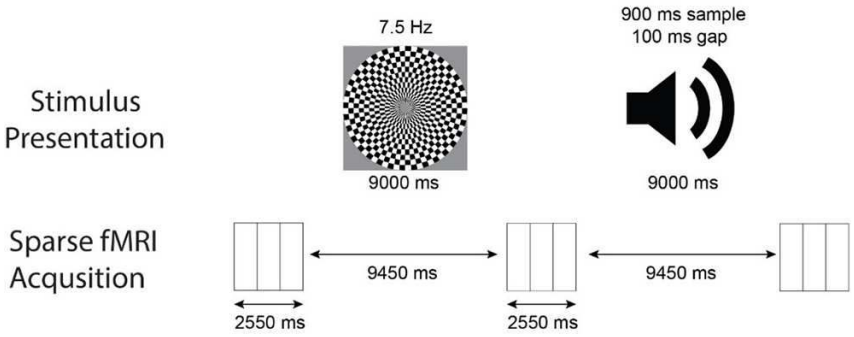

Figure 1. Schematic diagram of the sensory thalamic localizer (TL) task. Data are acquired using sparse temporal acquisition, such that no BOLD data are acquired during the presentation of stimuli. During each trial, a cluster of 3 volumes of BOLD data is acquired, starting 225 ms after stimulation ends. Visual stimulation is presented in the form of a 7.5 Hz alternating black-and-white checkerboard around a central fixation cross. Auditory stimulation is presented as 900 ms snippets of the song Transmission94 by Bonobo, normalized by mean amplitude, and separated from one another by 100 ms of silence. The duration of each trial is 12 seconds.

Results: Relative to HC, MGN-AC connectivity was significantly greater in PSZ (x-HC=0.0539, x-PSZ=0.0898, p=0.0332). MGN-AC connectivity was positively associated with PANSS Positive scores (β=0.0310, p=0.0229), but not diagnosis or medication exposure, across groups. When evaluated within PSZ separately, MGN-AC connectivity was associated with PANSS Positive scores (β=0.0276, p=0.0365). In a follow-up analysis including regressors for other symptom categories using the PANSS

Negative and General Psychopathology Scales in addition to diagnosis and medication exposure, MGN-AC connectivity was again associated with PANSS Positive scores (β=0.0395, p=0.0310), but no other predictors.

Conclusions: We used a dual fMRI paradigm in order to: 1) functionally localize AC and MGN, and 2) measure RSFC between these regions, in unmedicated PSZ and HC. We found that PSZ display significant hyperconnectivity between MGN and AC, and that this hyperconnectivity additionally predicts the severity of positive symptoms of psychosis dimensionally across groups.

References

1. Anticevic, A., K. Haut, J. D. Murray, G. Repovs, G. J. Yang, C. Diehl, S. C. McEwen, C. E. Bearden, J. Addington, B. Goodyear, K. S. Cadenhead, H. Mirzakhanian, B. A. Cornblatt, D. Olvet, D. H. Mathalon, T. H. McGlashan, D. O. Perkins, A. Belger, L. J. Seidman, M. T. Tsuang, T. G. van Erp, E. F. Walker, S. Hamann, S. W. Woods, M. Qiu and T. D. Cannon (2015). "Association of Thalamic Dysconnectivity and Conversion to Psychosis in Youth and Young Adults at Elevated Clinical Risk." JAMA Psychiatry 72(9): 882-891.
2. Anticevic, A., M. W. Cole, G. Repovs, J. D. Murray, M. S. Brumbaugh, A. M. Winkler, A. Savic, J. H. Krystal, G. D. Pearlson and D. C. Glahn (2014). "Characterizing thalamo-cortical disturbances in schizophrenia and bipolar illness." Cereb Cortex 24(12): 3116-3130.
3. Giraldo-Chica, M. and N. D. Woodward (2017). "Review of thalamocortical resting-state fMRI studies in schizophrenia." Schizophr Res 180: 58-63.
4. Fischl, B. (2012). "FreeSurfer." Neuroimage 62(2): 774-781.
5. Friston, K. J., J. Ashburner, S. Kiebel, T. Nichols and W. D. Penny (2007). Statistical parametric mapping : the analysis of funtional brain images. Amsterdam ; Boston, Elsevier/Academic Press,: 1 online resource (vii, 647 pages).
6. Glasser, M. F., S. N. Sotiropoulos, J. A. Wilson, T. S. Coalson, B. Fischl, J. L. Andersson, J. Xu, S. Jbabdi, M. Webster, J. R. Polimeni, D. C. Van Essen, M. Jenkinson and W. U.-M. H. Consortium (2013). "The minimal preprocessing pipelines for the Human Connectome Project." Neuroimage 80: 105-124.
7. Iglesias, J. E., R. Insausti, G. Lerma-Usabiaga, M. Bocchetta, K. Van Leemput, D. N. Greve, A. van der Kouwe, I. Alzheimer's Disease Neuroimaging, B. Fischl, C. Caballero-Gaudes and P.
8. M. Paz-Alonso (2018). "A probabilistic atlas of the human thalamic nuclei combining ex vivo MRI and histology." Neuroimage 183: 314-326.
9. Jiang, F., G. C. Stecker and I. Fine (2013). "Functional localization of the auditory thalamus in individual human subjects." Neuroimage 78: 295-304.
10. Kastner, S., D. H. O'Connor, M. M. Fukui, H. M. Fehd, U. Herwig and M. A. Pinsk (2004). "Functional imaging of the human lateral geniculate nucleus and pulvinar." J Neurophysiol 91(1): 438-448.
11. Kay, S. R., L. A. Opler and J. P. Lindenmayer (1989). "The Positive and Negative Syndrome Scale (PANSS): rationale and standardisation." Br J Psychiatry Suppl(7): 59-67.

Poster No 697

How to Transform AI Prototypes into Functional Healthcare Applications for Diagnostic Assistance?

Martin Dyrba[1], Devesh Singh[1], Doreen Goerss[2], Olga Klein[1], Marc-André Weber[3], Stefan Teipel[4]

[1]German Center for Neurodegenerative Diseases (DZNE), Rostock, Germany, [2]Rostock University Medical Center, Rostock, Germany, [3]Institute of Diagnostic and Interventional Radiology, Pediatric Radiology and Neuroradiology, Rostock, Germany, [4]Rostock University Medical Center & German Center for Neurodegenerative Diseases (DZNE), Rostock, Germany

Introduction: As the number of elderly people is rapidly increasing, we are facing a higher demand of diagnostic services, for example to detect neurodegenerative diseases. At the same time, the number of medical centers and experts remains almost constant, which poses a challenge. Tools for diagnostic assistance are urgently needed to improve the efficiency of healthcare. In three externally funded projects, we investigate aspects and strategies of how artificial intelligence (AI) prototype systems can be translated into functional healthcare applications.

Methods: In the ongoing project "ExplAInation" funded by the German research foundation (DFG), we have developed a deep learning framework that generates visual and textual explanations to improve the comprehensibility and interpretability of such models (Dyrba et al. 2021). A prototype system that supports the evaluation of MRI scans for the diagnosis of dementia is currently being evaluated. Within the project "Clinical AI-based Diagnostics" (CAIDX), funded by the European Interreg Baltic Sea Region program, we are investigating barriers and best practice recommendations for the integration of AI prototypes or commercial tools in hospitals. To this end, we have conducted initial interviews with various stakeholders from companies, developers, hospital administration, and clinical users. In the complementary project "TESIComp", funded by the Federal Ministry of Education and Research (BMBF), we are investigating ethical and social aspects of diagnostic AI tools. For the dementia use case, we interviewed patients, caregivers, and doctors from a memory clinic and will conduct focus groups and an observational study to examine how these tools may change the patient-physician relationship.

Results: We developed a deep learning application for the detection of dementia atrophy patterns in brain MRI scans (Fig.1). Derived relevance maps and textual summary reports highlight diagnostically important atrophy patterns for further evaluation by the physicians. Preliminary results from interviews with clinicians showed an explicit desire for AI tools in order

to reduce the workload by taking over repetitive tasks. Clinicians stated a reliable performance of results, and robust and efficient usability as prerequisites for regular use. The focus groups and observational study will elucidate future changes and challenges in the doctor's role and responsibilities and highlight ethical and social considerations with respect to the use of AI tools in clinical practice.

Conclusions: In "Healthcare 3.0", the digital transformation will change current diagnostic procedures and roles. Our activities focus on the stakeholders involved as well as on the regulatory aspects and implementation strategies to better steer this process. In CAIDX, we will develop best-practice guidelines for the overarching process of integrating AI tools in the hospital. In TESIComp, we will help to assess the future influence of AI-based approaches in clinical practice and will provide empirically informed ethical recommendations.

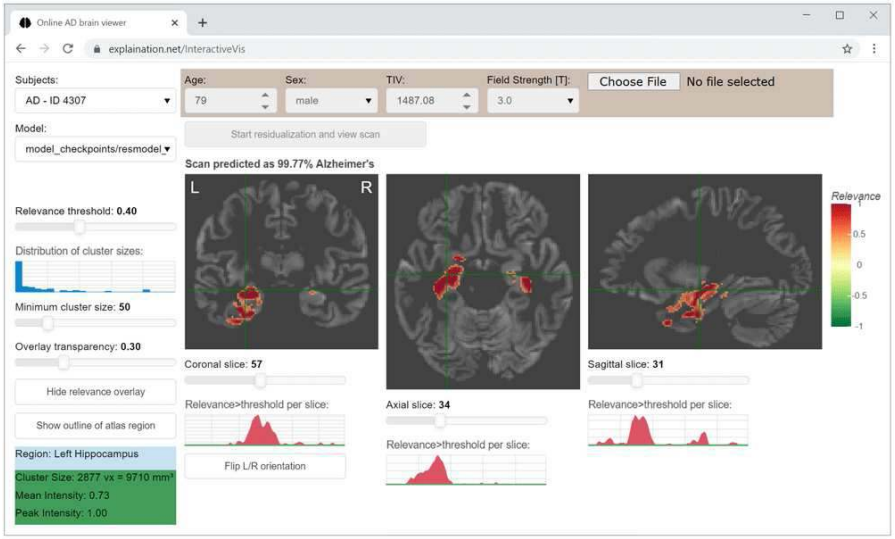

Figure 1: Interactive visualization app for the deep learning evaluation of MRI scans to highlight atrophy patterns of Alzheimer's disease. The app enables intuitive inspection and parameterization of the derived relevance maps. This app will serve as prototype and demonstrator for the collaboration research activities.

References

1. Dyrba M, Hanzig M, et al. (2021). 'Improving 3D convolutional neural network comprehensibility via interactive visualization of relevance maps: evaluation in Alzheimer's disease'. Alzheimers Res Ther 13:191. https://doi.org/10.1186/s13195-021-00924-2

Poster No 698

Societal Impacts of Neurofeedback and Relevant Regulatory Frameworks in the United States

Fiona Furnari[1], Haesoo Park[2], Gideon Yaffe[1], Michelle Hampson[2]

[1]Yale Law School, New Haven, CT, [2]Yale University School of Medicine, New Haven, CT

Introduction: Today, we are witnessing rapid advancement of brain imaging technologies, not only in terms of their precision and our ability to characterize brain activities but also their accessibility. Now, one can easily order a device online that can track their brain activity as they go about their day, with the hope of making better decisions about their lives. But as with any technology, the development of brain imaging technologies and their utilization in our society will involve agents with their own economic and political motives, raising concerns regarding abuse of the technology. One brain imaging technology of particular concern is neurofeedback, a brain training technique based on feedback learning. Neurofeedback has the potential to relieve symptoms for various clinical populations and improve mental functions for healthy populations. However, recent studies suggest that it also has the potential to be abused. Studies have demonstrated that it can change people's facial preferences and mental associations covertly, rendering it a potentially dangerous tool for manipulating people's decision-making processes. While neurofeedback technology continues to evolve and become more accessible, it is important to examine, evaluate, and extend as needed, the legal framework for regulating its influence. Here, we describe a collaboration between neurofeedback researchers from Yale School of Medicine and members of the Yale Law School that aimed to begin this effort.[1]

Methods: 1. Literature review of neurofeedback experiments that clarify the potential of neurofeedback for manipulating the decision-making processes of individuals. 2. Examine existing legal frameworks in the United States to identify possible avenues for regulating neurofeedback influence. 3. Consider what is needed, both scientifically, and in terms of political action, to guide the development of effective regulation that protects society without infringing unnecessarily on individual freedoms.

Results: 1. Neurofeedback learning has three key characteristics that are relevant to this discussion. One, neurofeedback can target and manipulate specific mental functions. Two, neurofeedback influence can be achieved covertly or without the awareness of those who are affected. Three, research has shown neurofeedback influence to persist, inducing long-lasting effects on people. Beyond these three characteristics, we also discuss how neurofeedback technologies are evolving to become more accessible to a broader audience. 2. Disclaimer requirements in the political sphere, unfair and deceptive trade practice statutes, and undue influence laws are possible starting points for regulating neurofeedback influence. However, existing legal frameworks have problematic limitations, including a dependence on difficult judgements regarding when the influence of the technology becomes unacceptable. 3. To guide judgements regarding the influence of neurofeedback, we propose experiments to explore how critical parameters of neurofeedback design affect the magnitude of its influence. We also highlight the need for a more flexible and rapid system of regulatory development to address the social impacts of modern technology.

Conclusions: Neurofeedback advancements are just one part of a much larger technological shift in neuro-technologies. Coupled with advancements in AI and exponentially growing accessibility to personal data, neuro-technologies will likely see rapid transformations in the coming years. We conclude that current regulatory frameworks are likely insufficient for protecting the public and that responding reactively to changes will not be sufficient. Technological transformations are ever more rapid, and their consequences are often irreversible. We must begin conversations now and educate the public regarding novel neuro-technologies, risks to their cognitive liberty in the face of these technologies, and gaps in the existing regulatory frameworks that may prove problematic.

References

1. Furnari, F. (2023), 'Neurofeedback: Potential for Abuse and Regulatory Frameworks in the United States', Philosophical Transactions of the Royal Society B, (under review)

Poster No 699

ACC oscillations reflect scientific conceptual change at different levels of cognitive conflict

Chuan-Cheng Shih[1], Hsiao-Ching She[1], Meng-Jun Chen[1], Li-Yu Huang[2], Wen-Chi Chou[2], Tzyy-Ping Jung[3]

[1]National Yang Ming Chiao Tung University, Hsinchu City, Taiwan, [2]National Changhua University of Education, Changhua, Taiwan, [3]University of California, San Diego, La Jolla, CA

Introduction: Research has shown that students harbor misconceptions that are difficult and highly resistant to change despite receiving formal science education (Osborne & Cosgrove, 1983; Carey, 1986). Scientific conceptual change involves transforming and restructuring alternative conceptions into scientific conceptions which has is the top issue in science education since past decades. It has been proposed in many studies that creating cognitive conflict plays a key role in triggering conceptual change (Strike and Posner,1985; She, 2002, 2004). Several studies have also found that the scientific concepts encompass more underlying concepts, which makes conceptual change difficult (She, 2002, 2004). Botvinick et al. (1999) suggested that ACC activity is more significant during trials with high rather than low levels of conflict. Krug and Carter (2010) suggested that the ACC detects response conflict during correct high-conflict and error trials. She et al. (2023) reported the ACC was more active when retrieving of correct scientific concepts than incorrect ones (She et al., 2023). Other studies have found that parietal alpha are crucial for successful memory encoding and retrieving scientific concepts (Liang et al., 2020; Tsai et al., 2019). The present study investigates whether conceptual change is more difficult for high conflict tasks than low conflict tasks. Additionally, we investigated whether successful conceptual changes would lead to greater ACC theta and parietal alpha activity than low-conflict tasks.

Methods: Fifty eight participants (41male and 17 female, 22-26 years of age) were recruited to participate in the scientific conceptual change tasks with the use of high density EEG (64 channels). The 40 scientific question items, 22 were low conflict and 18 were high conflict task. Figure 1 depicted the protocol of a single trial of high and low conflict of scientific concepts which consisted of six stages, question presentation, prediction making, confidence rating, experiment video watching, conflict rating, and thinking and explaining. Each trial lasted for an average of 85.5 s, total are 90 minutes. We used Neuroscan SynAmps2 amplifier (Neuroscan, El Paso, TX, USA) equipped with 66 electrodes mounted on an elastic cap to record

participants' EEG. We analyzed the data using custom MATLAB scripts built on the open-source EEGLAB toolbox (Delorme & Makeig, 2004) (http://sccn.ucsd.edu/eeglab).

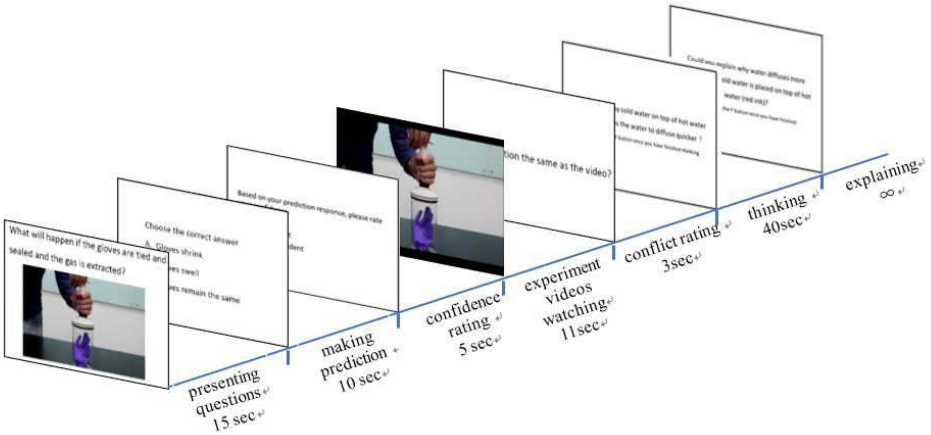

Results: Results indicated that low conflict task had significantly higher conceptual change accuracy ($F = 50.44$, $p < 0.001$) than to the high conflict task during scientific conceptual change process. The level of conflict reporting by students are significantly higher for high conflict than low conflict tasks ($F=170.67$, $p < 0.001$). When conceptual change was successfully achieved, high conflict tasks displayed significantly higher ACC oscillations across stages than low conflict tasks (Figure 2). While conceptual change failed, the oscillation power of ACC did not differ significantly between low- and high-conflict tasks (Figure 3). Low conflict tasks exhibited slightly higher parietal alpha suppression than high conflict tasks, but no statistically significant differences were observed. The regression also indicated that oscillation power of ACC at the video watching and thinking and explanation stage can predict the success of conceptual change.

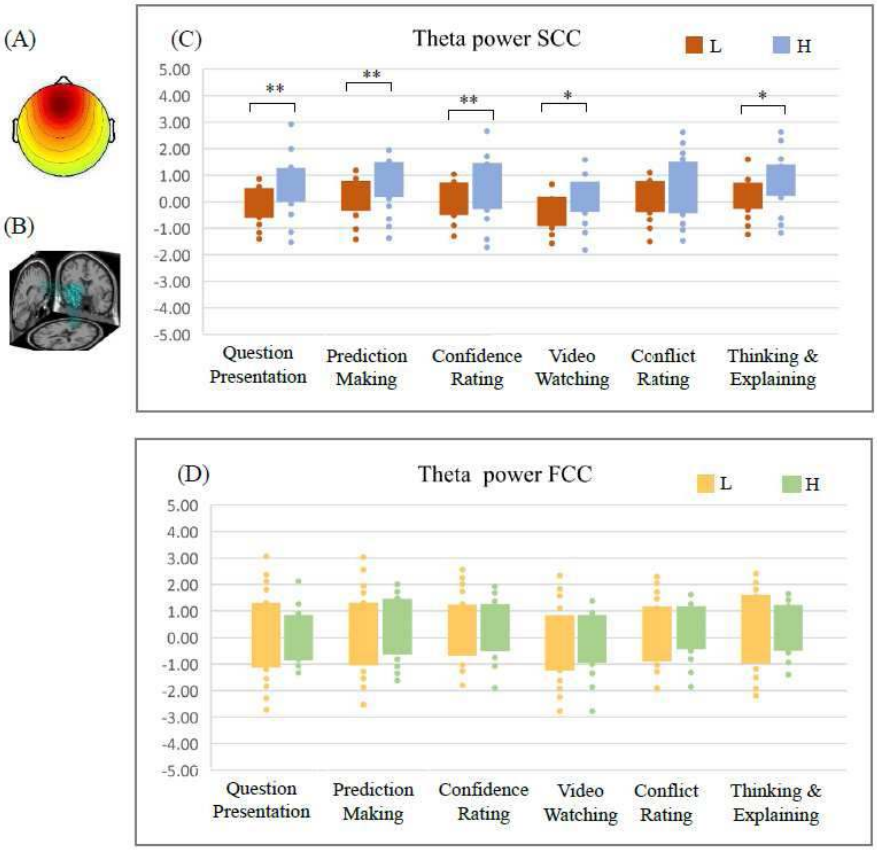

Figure 2. A comparison of high (H) and low (L) conflict scientific tasks showed ACC theta mean power in six stages. (A) scalp map (B) dipole density (C) successful conceptual change (SCC) (D) failure conceptual change (FCC)

Conclusions: Conceptual change accuracy was significantly higher for low conflict tasks than for high conflict tasks, confirming previous suggestions that high conflict tasks subsume scientific concepts, thus making conceptual change difficult. Moreover, high conflict tasks evoke significantly higher ACC oscillation power than low conflict tasks only when conceptual change is successfully achieved.

References

1. Botvinick, M.M., Nystrom, L.E., Fissell, K.L., Carter, C. S., Cohen, J. D. (1999), 'Conflict monitoring versus selection-for-action in anterior cingulate cortex', Nature, vol. 402, no. 6758, pp. 179-181.
2. Carey, S. (1986), 'Cognitive science and science education', American Psychologist, vol. 41, no. 10, pp. 1123–1130.
3. Krug, M.K., & Carter, C.S. (2010), 'Anterior cingulate cortex contributions to cognitive and emotional processing: a general purpose mechanism for cognitive control and self-control'. In V. A. Harden, G. B. Risse (Eds) Self-control in Society, Mind and Brain (pp.3-27). Oxford: Oxford University Press.
4. Liang, C.P., She, H.C., Huang, L.Y., Chou, W.C., Chen, S.C. & Jung, T.P. (2020), 'Human Brain Dynamics Reflect the Correctness and Presentation Modality of Physics Concept Memory Retrieval', Frontiers in Human Neuroscience, doi.org/10.3389/fnhum. 2020.00331
5. Osborne, R.J., & Cosgrove, M.M. (1983), 'Children's conceptions of the changes of state of water', Journal of Research in Science Teaching, vol. 20, no. 9, pp. 825–838.
6. She, H.C. (2004), 'Fostering "Radical" conceptual change through Dual Situated Learning Model', Journal of Research in Science Teaching, vol. 41, no. 2, 142-164.
7. She, H.C. (2002), 'Concepts of higher hierarchical level required more dual situational learning events for conceptual change: A study of students' conceptual changes on air pressure and buoyancy', International Journal of Science Education, vol. 24, no. 9, 981-996.
8. She, H.C., Huang, L.Y, & Duann, J.R. (2023), 'A Shared Hippocampal Network in Retrieving Science-related Semantic Memories', International Journal of Neural Systems. doi: 10.1142 /S012906572350034X
9. Strike, K.A., & Posner, G.J. (1985), A conceptual change view of learning and understanding. In L. H. T. West, & A. L. Pines (Eds.), Cognitive structure and-conceptual change. New York: Academic Press.
10. Tsai, P.Y., She, H.C., Chen, S.C., Huang, L.Y., Chou, W.C., Duann, J.R., Jung, T.P. (2019), 'Eye Fixation-related Fronto-parietal Neural Network Correlates of Memory Retrieval', International Journal of Psychophysiology, vol. 138, 57-70.

Poster No 700

The triple nexus in the brain: corpus callosum, brain asymmetry and cognition

Chenghui Zhang[1], Yilamujiang Abuduaini[1], Bolong Wang[1], Xiangzhen Kong[1,2,3]

[1]Department of Psychology and Behavioral Sciences, Zhejiang University, Hangzhou 310058, China, [2]Department of Psychiatry of Sir Run Run Shaw Hospital, Zhejiang University School of Medicine, Hangzhou 310016, China, [3]The State Key Lab of Brain-Machine Intelligence, Zhejiang University, Hangzhou 310058, China

Introduction: The corpus callosum (CC), a remarkable structure in the human brain, serves as a vital bridge of communication between the left and right hemispheres. Two theories exist regarding its specific functions (Güntürkün et al. 2020). One theory suggests that the CC serves to inhibit neural activity in the nondominant hemisphere to enhance hemispheric specialization, while the other suggests that it serves to facilitate and enhance interhemispheric interaction. Some studies have suggested that the CC may serve both inhibitory and excitatory functions, depending on the specific neural circuits involved (Van et al. 2011). The present study aims to investigate the large-scale associations between the CC and hemispheric structural asymmetries, and the potential roles in cognitive function.

Methods: Data (N = 40070; 46-82 years old) were obtained from the UK Biobank as part of research application of 75807. These data included fractional anisotropy (FA) of the three CC segments: genu, body, and splenium, morphometric measures (cortical thickness [CT], surface area [SA], and gray matter volume [GMV]) of the 62 cortical regions (31 per hemisphere), and behavioral data of cognitive functions. First, we ran a canonical correlation analysis (CCA) to investigate the multivariate association between the CC segments and the asymmetries of cortical regions. We split the total samples into two datasets for showing the reliability of the CCA results: Dataset #1 with 26955 participants whose cognitive function data were available; Dataset #2 with the remaining 13115 participants whose cognitive function data were not available in the database. Three pairs of components were obtained for each analysis. Next, we explored the functional correlates of these components using a linear regression. The general cognitive ability was included as the independent variable in the regression, which was derived from the first principal component of the principal component analysis of the 10 variables of cognitive functions. Variables including sex, age, imaging assessment center, and others were included as covariates. Finally, we examined the mediation model with the general cognitive ability as the dependent variable, the CC components as the mediator, and hemispheric asymmetry components as independent variable.

Results: Three pairs of components were derived from each CCA of the CC and hemispheric asymmetry features, and similar results, particularly for the first component, were obtained in the two independent datasets (Fig. 1). Each component showed

various correlations with the cognitive functions (Fig. 2). While the mediation effects were significant in most cases, we found that the mediation effect with the first pair of components from the CCA were the most pronounced (p = 6.7x10-16) (Fig. 2).

Conclusions: Our results provided robust evidence for the link between the CC and hemispheric asymmetry based on the large-scale datasets. The mediation analyses further support the role of the interhemispheric communications on the indirect link between hemispheric asymmetries and cognitive function. It provides a new perspective for revealing the mechanisms between corpus callosum, brain asymmetry, and cognition.

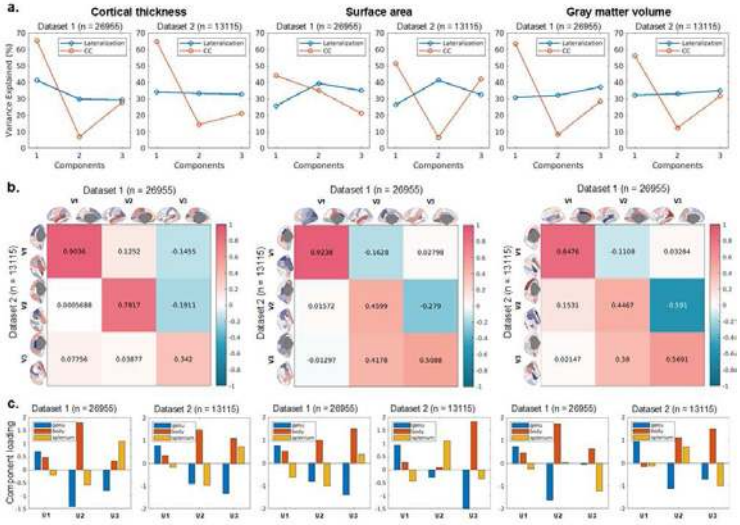

Fig 1. Canonical correlation analysis (CCA) of the CC segments and hemispheric asymmetries. **a**. The variability explained by each principal component. **b**. Component loadings of each cortical region (V1, V2, V3) derived from the CCA, and the similarity results of the component loadings between the two CCA which were based on two independent datasets. **c**. The component loadings of each CC segment (U1, U2, U3) derived from the CCA.

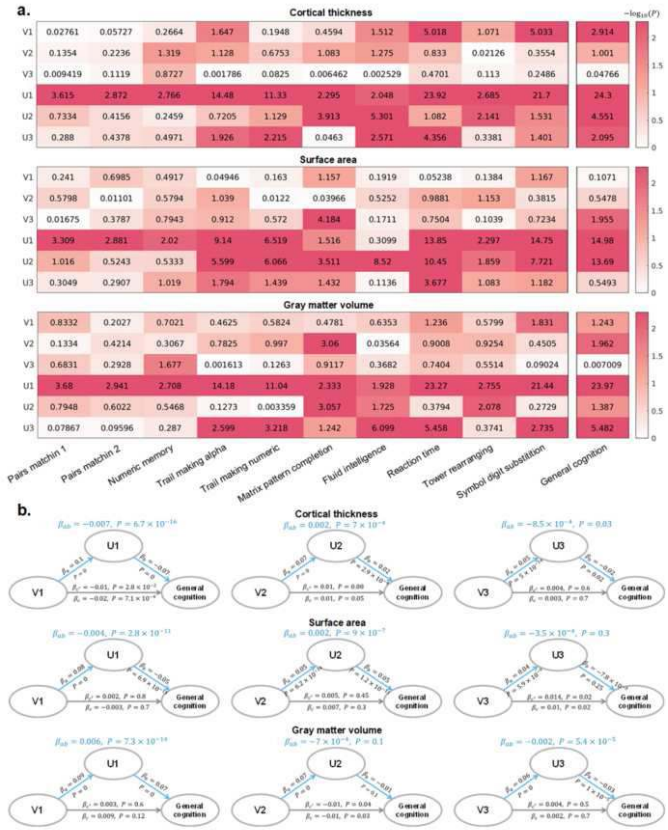

Fig 2. The associations between of cognitive functions and the principal components of the CC and cortical asymmetries. **a**. The pair-wise association between cognitive functions and the CCA components. **b**. The mediation model results of the CCA components and general cognitive ability. V1/V2/V3 indicates the principal components of the cortical asymmetries derived from the CCA; U1/U2/U3 indicates the principal components of the CC segments.

References
1. Güntürkün O.(2020), 'Brain Lateralization: A Comparative Perspective', Physiological reviews, 100(3), 1019-1063.
2. van der Knaap LJ, 'How does the corpus callosum mediate interhemispheric transfer? A review.', Behavioural brain research, 223(1), 211-221.

Poster No 701

Temporal associations with financial adversity on subcortical volume and BMI amongst youth in ABCD

Shana Adise[1], Christopher Machle[1], Kevin Myers[2], Jonatan Ottino-Gonzalez[1], Michael Goran[1], Elizabeth Sowell[1]

[1]CHLA, Los Angeles, CA, [2]Bucknell, Lewisburg, PA

Introduction: In animal and human models, stress has been negatively associated with brain development, which in turn has adverse health effects. Yet, disentangling the effects of stress on the brain and adverse health outcomes is complex. Chronic stress alters the normal neurobiological response and increases obesity risk due to its association with triggering food intake, while weight gain has been associated with altered neurodevelopment. Ample evidence for lasting impacts of early-life stress, but qualitatively different stressors may have unique influence at different points in development. Therefore, in the current study we focus on one particular stressor – financial adversity – and its association with developing adolescent brain structure as a risk factor for obesity. Importantly, our sample focused on youth who initially were of a healthy weight to allow for insight into how these associations may relate to progression of weight gain.

Methods: Data were gathered from a subset of healthy weight youth enrolled in the Adolescent Brain Cognitive Development Study (nT0=3606 [59% male, 71.3% White; 15.6% Latino, aged 9/10-years-old]; nT2=2395 [51% male; 71.9% White; 16% Latino, aged 11/12-years-old] no siblings). Estimates of subcortical volume (16 regions of interest [ROI] were obtained from T1w images parcellated with the Desikan FreeSurfer atlas. Financial adversity was assessed at T0 and T2, using a caregiver-reported 7-item binary response questionnaire that asks questions on perceived inability to pay for basic life necessities. A summary score was utilized in the analyses (0=no financial adversity; 7=extreme financial adversity). Body mass index (BMI) was assessed from height and weight by a trained researcher. Multiple crossed random-effects (scanner model, subject) mixed models were conducted in Python to examine three-way interactions between Financial Adversity*ROI*Time (modeled continuously as days since the baseline visit on BMI while controlling for income-to-needs ratio, the caregiver's highest education, puberty, and intracranial volume. Sex showed no effects on weight gain ($p>0.8$), so it was removed from the model. Sensitivity analyses were conducted to determine if there were sex-specific differences in developmental trajectories of Financial Adversity*ROI*Time on BMI. Analyses were corrected using the Benjamini-Hochberg approach.

Results: All youth were of a healthy weight at baseline, but by T2 13.3% of youth (n=319) transitioned to have overweight/obesity. Results of the mixed model revealed significant negative interactions between ROI*Time*Financial Adversity in the bilateral caudate, nucleus accumbens and right pallidum ($p< 0.05$, FDR corrected). In other words, in comparison to baseline, by T2, youth who experienced any financial adversity demonstrated a stronger negative relationship between subcortical volume and BMI compared to youth who did not experience financial adversity. Sensitivity analyses that examine whether these patterns differed by sex, showed no sex-specificity.

Conclusions: The relationship between subcortical volume and BMI across time depends on financial adversity as at 9/10-years-old (i.e., baseline), these relationships were non-existent. This suggests the possibility that duration of financial adversity affect the brain and health outcomes more than severity. Moreover, findings suggest a critical window between 9-12-years-old for prevention and intervention efforts that may wish to focus on mitigating detrimental effects of stress on the brain and health outcomes. Future studies are needed to assess whether these relationships are related to other health outcomes commonly associated with financial adversity, such as increased impulsive behavior and mental health problems.

Poster No 702

Dynamic Functional Connectivity of Brain Networks during Acute Stress Regulates Stress Resilience

Juan Yang[1]

[1]Southwest University, Chongqing, Chongqing

Introduction: Stress resilience has been largely regarded as a process in which individuals actively cope with and recover from stress. Over the past decade, the emergence of large-scale brain networks has provided a new perspective for the study

of the neural mechanisms of stress. However, it remains unclear how stress resilience is supported by inter-network functional connectivity (FC) and whether such FCs undergoes time-dependent dynamic changes during stress induction.

Methods: To bridge this knowledge gap, seventy-seven participants (age, 17–22 years, 37 women) were recruited for a ScanSTRESS brain imaging study. We initially adopt a static perspective, using changes in FC that obtained from stress vs. control condition during the entire stress induction phase as a static indicator. Further, we analyze changes in FC between different stress runs as an index of temporal dynamics. Meanwhile, participants' salivary cortisol levels during stress were collected and analyzed as an index of stress resilience. In addition, participants' trait resilience was measured by the sensitivity of behavioral activation system (BAS).

Results: We found that, for the static index, enhanced FC between the salience network (SN), default mode network (DMN) and limbic network (LBN) during acute stress could negatively signal stress resilience. For the temporal dynamics index, FC among the dorsal attention network (DAN), central executive network (CEN) and visual network (VN) decreased significantly during repeated stress induction. Moreover, the decline of FC positively signaled a rapid salivary cortisol recovery, and this relationship only exist in people with high BAS.

Conclusions: In all, this study, for the first time, concurrently investigates the neural mechanisms of stress resilience from both static and dynamic perspectives and elucidates the relationship among dynamic neural activity, stress resilience, and trait resilience within a unified framework.

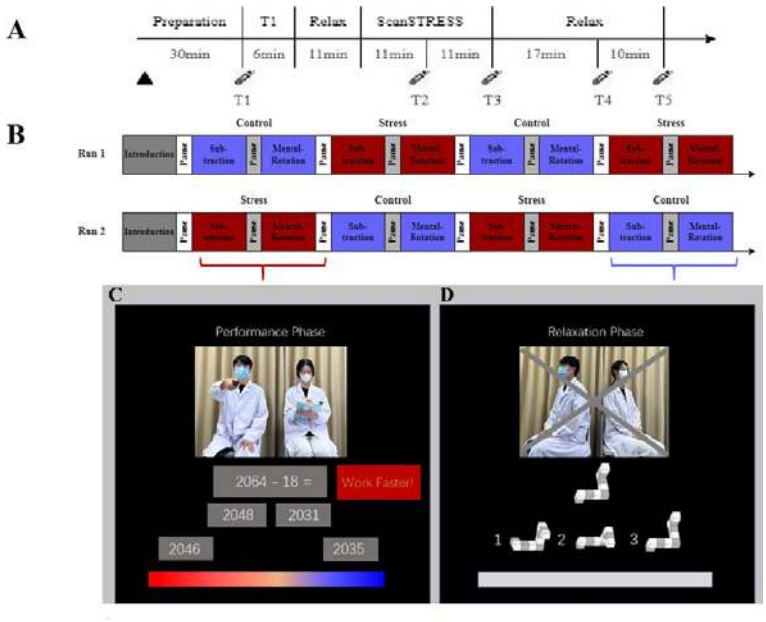

Figure 1. Experimental procedure (A), scanning runs (B), stress condition (C) and control condition (D) in the ScanSTRESS paradigm

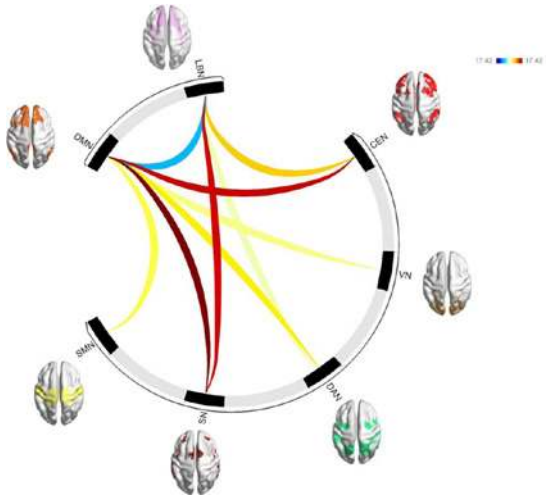

Figure 3 (A) FC of brain networks induced by acute stress (stress vs. control). Depicted lines indicate pairs of ROIs that demonstrate increased FC (red lines) and decreased FC (the blue line).

References

1. Abaied, J. L., & Emond, C. (2013). Parent Psychological Control and Responses to Interpersonal Stress in Emerging Adulthood. Emerging Adulthood, 1(4), 258-270. doi:10.1177/2167696813485737
2. Arnsten, A. F. T. (2009). Stress signalling pathways that impair prefrontal cortex structure and function. Nature Reviews Neuroscience, 10(6), 410-422. Retrieved from ://WOS:000266199300009. doi:10.1038/nrn2648
3. Broeders, T. A. A., Schoonheim, M. M., Vink, M., Douw, L., Geurts, J. J. G., van Leeuwen, J. M. C., & Vinkers, C. H. (2021). Dorsal attention network centrality increases during recovery from acute stress exposure. Neuroimage Clin, 31, 102721. Retrieved from https://www.ncbi.nlm.nih.gov/pubmed/34134017. doi:10.1016/j.nicl.2021.102721
4. Burke, H. M., Davis, M. C., Otte, C., & Mohr, D. C. (2005). Depression and cortisol responses to psychological stress: a meta-analysis. Psychoneuroendocrinology, 30(9), 846-856. Retrieved from https://www.ncbi.nlm.nih.gov/pubmed/15961250. doi:10.1016/j.psyneuen.2005.02.010
5. Carver, C. S., & White, T. L. (1994). Behavioral inhibition, behavioral activation, and affective responses to impending reward and punishment: the BIS/BAS scales. Journal of Personality and Social Psychology, 67(2), 319.
6. Casada, J. H., & Roache, J. D. (2005). Behavioral inhibition and activation in posttraumatic stress disorder. J Nerv Ment Dis, 193(2), 102-109. Retrieved from https://www.ncbi.nlm.nih.gov/pubmed/15684912. doi:10.1097/01.nmd.0000152809.20938.37
7. Del Giudice, M., Ellis, B. J., & Shirtcliff, E. A. (2011). The Adaptive Calibration Model of stress responsivity. Neurosci Biobehav Rev, 35(7), 1562-1592. Retrieved from https://www.ncbi.nlm.nih.gov/pubmed/21145350. doi:10.1016/j.neubiorev.2010.11.007
8. Feder, A., Fred-Torres, S., Southwick, S. M., & Charney, D. S. (2019). The Biology of Human Resilience: Opportunities for Enhancing Resilience Across the Life Span. Biological Psychiatry, 86(6), 443-453. Retrieved from ://WOS:000482590500005. doi:10.1016/j.biopsych.2019.07.012
9. Fergus, S., & Zimmerman, M. A. (2005). Adolescent resilience: a framework for understanding healthy development in the face of risk. Annu Rev Public Health, 26, 399-419. Retrieved from https://www.ncbi.nlm.nih.gov/pubmed/15760295. doi:10.1146/annurev.publhealth.26.021304.144357

Poster No 703

Reward driven proactive control of emotional conflict

Sukalyan Deb[1], Srikanth Padmala[2]

[1]Indian institute Of Science, Bangalore, Karnataka, [2]Indian Institute Of Science, Bangalore, Karnataka

Introduction: Deficits in the cognitive control of salient emotional distractions have been implicated in several mental health disorders (Etkin et al., 2007). However, the majority of the past work has focused on the cognitive control of non-emotional distractors. For instance, it has been reported that the enhancement of proactive control in the presence of reward incentives resulted in the reduction of non-emotional conflict both at the level of brain and behavior (Padmala & Pessoa, 2011; Soutschek et al., 2015). Very little is known regarding whether and how reward motivation can modulate emotional conflict, which involves competition between salient task-relevant vs. task-irrelevant affective information (Etkin et al., 2006). This is important to study as resolving emotional (compared to non-emotional) conflict might involve distinct neural substrates involving the rostral anterior cingulate cortex and the amygdala (Egner et al., 2008). To address this gap, we employed functional MRI to investigate the effects of reward motivation on emotional conflict processing in the human brain.

Methods: In a 3T MRI scanner, healthy adult human volunteers (N=39; 15 males) performed an emotional face-word conflict task (Etkin et al., 2006). To manipulate motivation, each trial started with the presentation of a reward or no-reward cue, signaling an opportunity to win a performance-based bonus monetary reward or not (Fig. 1). After a variable interval, an emotional face-plus-word display was shown during the task phase. Participants were instructed to categorize the facial emotion expression while ignoring the overlaid word, which was emotionally congruent or incongruent with the facial expression (Fig. 1). In the reward cue condition, participants received a bonus reward of Rs 2 per trial for every fast and accurate response. In the no-reward cue condition, participants did not receive any bonus reward. Our paradigm resulted in a 2 Reward (reward, no-reward) x 2 Congruency (congruent, incongruent) within-subject factorial design at the task phase.

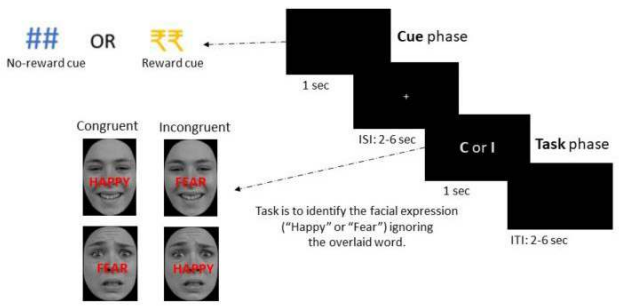

Figure 1: Task paradigm. After the presentation of a no-reward ("##") or a reward ("₹₹") cue, participants were instructed to identify the facial emotional expression ignoring the overlaid word. C: Congruent; I: Incongruent; ISI: inter-stimulus interval; ITI: inter-trial interval

Results: The 2x2 rmANOVA on the behavioral accuracy data revealed the main effects of Reward and Congruency along with a significant Reward x Congruency interaction. Specifically, the emotional conflict effect (i.e., incongruent vs. congruent) was reduced in the reward relative to the no-reward condition. The rmANOVA on the Reaction time data revealed only the main effects of Reward and Congruency without a significant interaction. In the fMRI data, we found increased activation during the processing of reward (vs. no-reward) cues in the ventral striatum and attentional regions, such as the intra-parietal sulcus (IPS). During the emotional conflict task phase, paralleling the behavioral interaction pattern, fMRI responses exhibited a significant Reward x Congruency interaction in the Amygdala (detected in the ROI analysis) and the Supplementary motor area (Figure 2). Finally, reward (vs. no-reward) cue-related activation across participants in the IPS predicted the behavioral accuracy interaction scores at the subsequent task phase.

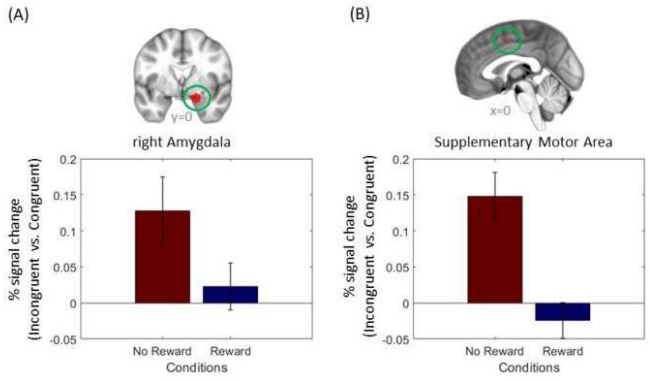

Figure 2: Emotional Conflict (i.e., Incongruent *minus* Congruent) related activity at the task phase during reward and no-reward conditions.

Conclusions: The results so far suggest that a network of brain regions, including sub-cortical reward-related and cortical attentional regions, were recruited during reward anticipation, suggesting enhancement of preparatory control mechanisms. The enhanced reward-driven preparatory control helped to deal better with the emotional conflict at the subsequent task phase, reflected in the interaction patterns observed in the behavioral accuracy and amygdala responses. Notably, the enhanced preparatory activity during the processing of reward (vs. no-reward) cues predicted the behavioral interaction pattern at the subsequent task phase. Overall, these findings advance our understanding of how reward motivation influences emotional conflict processing in the healthy human brain, with implications for mental health disorders, including anxiety.

References

1. Egner, T., (2008), 'Dissociable neural systems resolve conflict from emotional versus nonemotional distracters'. Cerebral cortex, 18(6), 1475-1484.
2. Etkin, A., (2006), 'Resolving emotional conflict: a role for the rostral anterior cingulate cortex in modulating activity in the amygdala'. Neuron, 51(6), 871-882.
3. Etkin, A., (2007), 'Functional neuroimaging of anxiety: a meta-analysis of emotional processing in PTSD, social anxiety disorder, and specific phobia'. American journal of Psychiatry, 164(10), 1476-1488.
4. Padmala, S., (2011), 'Reward reduces conflict by enhancing attentional control and biasing visual cortical processing'. Journal of cognitive neuroscience, 23(11), 3419-3432.
5. Soutschek, A., (2015), 'Dissociable effects of motivation and expectancy on conflict processing: An fMRI study'. Journal of Cognitive Neuroscience, 27(2), 409-423.

Poster No 704

Short-term restriction of physical and social activities effects on brain structure and connectivity

Yajuan Zhang[1], Lianghu Guo[1], Zhuoyang Gu[1], Siyan Han[1], Han Zhang[1,2]

[1]School of Biomedical Engineering, ShanghaiTech University, Shanghai, China, [2]Shanghai Clinical Research and Trial Center, Shanghai, China

Introduction: The prolonged exposure to enclosed environments during the COVID-19 pandemic has raised concerns about its potential impact on physical and mental well-being (Aknin et al., 2022; Chu et al., 2020). Recent systematic review highlights that the fear of infections and the enforcement of strict social distancing measures contribute to intensified negative emotions, impairing cognitive and mental functioning (Ganesan et al., 2021; Leaune et al., 2020). Moreover, physical inactivity (i.e., sedentary behavior) and lacking social interactions during the pandemic significantly increase the risk of health issues. Neuroimaging studies have indicated the plasticity of the adult brain, showing that environmental factors can alter the brain (Malhi & Mann, 2018). Therefore, there is a growing concern regarding the potential manifestation of structural and functional

changes in the brain resulting from short-term restriction of physical and social activities. The lockdown during COVID-19 pandemic offers a unique opportunity to evaluate such an impact on the brain in young adult.

Methods: Twenty healthy college students (ages 18-27) underwent an initial MRI scan (Scan1) before the lockdown. Three months later, they experienced a lockdown with restricted physical and social activities (strict quarantine protocol, staying in confined dormitory conditions, for a minimum of two months). After two months of lockdown, 29 participants (comprising 14 original and 15 new participants) were immediately recruited for a second MRI scan (Scan2). Four months after the lockdown measures were lifted, 27 out of the 29 participants underwent a third follow-up MRI scan (Scan3). Anatomical T1w images (TR/TE=7.4/3.4ms, FOV=256×240 mm2, Slice thickness=0.8mm, slice number=208) and the FMRI data (TR/TE=800/35ms, FOV=209×209mm2, slices number=72, slice thickness=1.8 mm, 450 volumes) were acquired with a 3.0T scanner (uMR890, United Imaging). The AAL2 (Rolls et al., 2015) atlas was used to calculate region-averaged gray matter volume (GMV). FMRI preprocessing involves motion correction, distortion correction, ICA denoising, and temporal band-pass filtering. Pearson correlation (fisher z-transformed) coefficients of the regional mean time series of all possible pairs of brain regions acts as the network links. Longitudinal comparisons were conducted among the three groups using paired t-tests to examine changes in GMV. For whole-brain pairwise FC, nonlinear mixed-effects models were used to outline the longitudinal trajectories of the whole-brain FC architecture.

Results: Compared to the pre-lockdown scan, notable reductions in GMV were observed in the right rectus and cuneus right after the lockdown. Four months after the lockdown, additional brain regions exhibited significant volumetric decrease (Fig 1, P < 0.05, FDR corrected). For FC changes, significant U-shaped trajectories of the FC links between the default mode network (DMN) and somatomotor network (SMN) were found (Fig 2A). Specifically, the FC between DMN and SMN and those within SMN were significantly decreased right after lockdown and then nearly recovered after four months post-lockdown (Fig 2B, P < 0.01, FDR corrected).

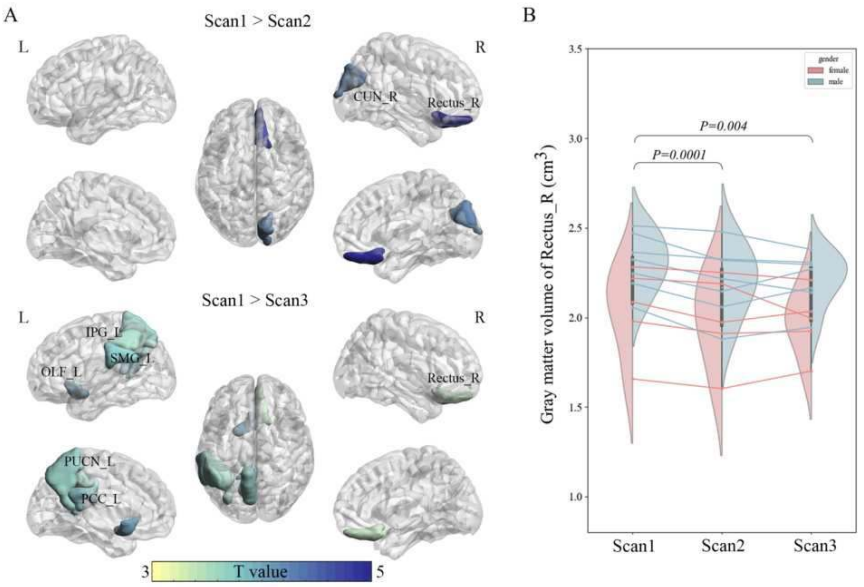

Fig 1 Group differences of gray matter volume. (A) Regions with significant differences in gray matter volume between before lockdown and right after lockdown (upper) and between before lockdown and four-month after lockdown (paired t-test, $P < 0.05$, FDR correction). (B) Longitudinal alteration in the gray matter volume in right rectus between groups. There were a significant decreased GMV in during lockdown and after lockdown compared to before lockdown (Scan1 > Scan2 : $P = 0.0001$; Scan1 > Scan3 : $P = 0.004$; paired t-test).

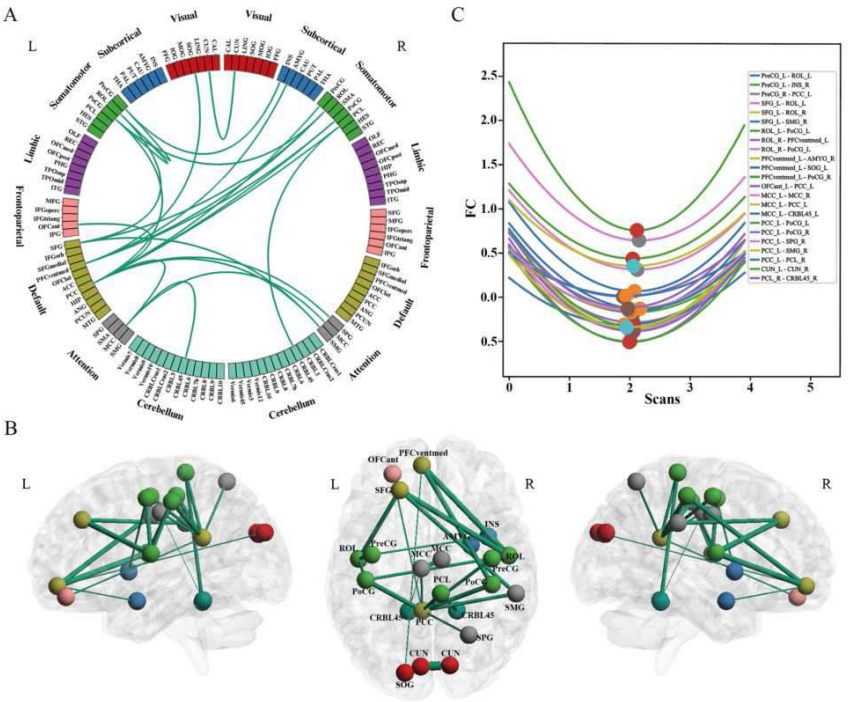

Fig 2 Longitudinal trajectories of FC across all brain regions. (A) and (B) The significant trajectories in the FC fit curves ($P < 0.01$, FDR-corrected). (C) These fit curves show that the FC decreased from pre-lockdown to right after lockdown and then increased from right after lockdown to post-lockdown. The color of the circle and node denotes the 120 different AAL2 regions. The edge width in (B) represents the quadratic term of the fitted curves.

Conclusions: This study examines the impact of a short-term restriction of physical and social activities on the brain morphology and function in young adults, demonstrating a significant macroscopic effect on the brain possibly due to such an event. The brain plasticity regarding the functional connectivity is especially interesting, suggesting a huge recover potential of human brain connectome. However, the gradual progression of brain structural changes warrants further investigation with longer follow-up periods. Current findings may provide valuable insights into understanding the impact of prolonged isolation and reduced physical/social activities on human brain. Our findings also shed light on the rehabilitation mechanism and potential intervention for patients under the same physical/social conditions.

References

1. Aknin, L. B. (2022). Policy stringency and mental health during the COVID-19 pandemic: a longitudinal analysis of data from 15 countries. Lancet Public Health, 7(5), e417-e426.
2. Chu, I. Y. (2020). Social consequences of mass quarantine during epidemics: a systematic review with implications for the COVID-19 response. J Travel Med, 27(7).
3. Ganesan, B. (2021). Impact of Coronavirus Disease 2019 (COVID-19) Outbreak Quarantine, Isolation, and Lockdown Policies on Mental Health and Suicide. Front Psychiatry, 12, 565190.
4. Leaune, E. (2020). Suicidal behaviors and ideation during emerging viral disease outbreaks before the COVID-19 pandemic: a systematic rapid review. Preventive medicine, 141, 106264.
5. Malhi, G. S. (2018). Depression. Lancet, 392(10161), 2299-2312.
6. Rolls, E. T. (2015). Implementation of a new parcellation of the orbitofrontal cortex in the automated anatomical labeling atlas. Neuroimage, 122, 1-5.
7. Acknowledgement
8. This work is partially supported by the STI 2030—Major Project (2022ZD0209000, 2021ZD0200516), Shanghai Pilot Program for Basic Research—Chinese Academy of Science, Shanghai Branch (JCYJ-SHFY-2022-014), Open Research Fund Program of National Innovation Center for Advanced Medical Devices (NMED2021ZD-01-001), Shenzhen Science and Technology Program (No. KCXFZ20211020163408012), and Shanghai Pujiang Program (No. 21PJ1421400).

Poster No 705

Parieto-striatal activation predicts stress reactivity in anxious individuals during COVID-19

Shu-Hui Lee[1], Tai-Li Chou[2]

[1]Center for General Education, National Tsing Hua University, Hsinchu, Taiwan, [2]Department of Psychology, National Taiwan University, Taipei, Taiwan

Introduction: The COVID-19 pandemic had adversely affected individuals' mental health, yet it is unknown how and to what extent the psychological outcomes of this stressful event are influenced by individual traits in a long-term basis. Factors such as anxiety traits and attentional bias toward unpleasant stimuli has been suggested as crucial pathogenetic indicators in individual variations in susceptibility to stress (Cannito et al., 2020; Somma et al., 2021). However, the neurocognitive mechanism of this reactivity toward pandemic-related information under prolonged uncertainty remains unclear in anxious individuals during the pandemic. Thus, this functional magnetic resonance imaging study aimed to determine the relationship between attentional bias toward pandemic-related stimuli and perceived stress in anxious adults across two visits during COVID-19.

Methods: The sample consisted of 31 high trait anxious (HTA, 16 men, 15 women) participants and 31 low trait anxious (LTA, 17 men, 14 women) participants. They were followed up with a one-year interval. Participants were asked to perform a counting Stroop task preceded by pandemic-related or neutral pictures during scans before and after the pandemic. Attentional bias was indexed using the contrast of pandemic-related Stroop versus neutral Stroop. We conducted two series of analyses. First, we employed a 2 group (HTA, LTA) by 2 visit (time 1, time 2) ANOVA. Second, simple regression analyses were used to determine whether brain activity of emotional Stroop task at time 1 (T1) was predictive of time 2 (T2) minus time 1 (T1) perceived stress for each group.

Results: First, a group-by-visit interaction indicated that the magnitude of T2-T1 time difference was greater for LTA than HTA participants in the precuneus, caudate, and rostral anterior cingulate cortex (rACC), reflecting greater difficulties for HTA participants to resolve emotional interference. Second, in response to the epidemic versus neutral stimuli, caudate activation was predictive of changes in perceived stress for HTA, but not for LTA participants. In contrast, precuneus activation was predictive of changes in perceived stress for LTA, but not for HTA participants. However, no significant results were found for regression analyses using the rACC as the predictor.

Conclusions: Regarding that parieto-striatal regions are responsible for the emotional modulation, abnormalities in these regions may indicate poor attentional allocation to unpleasant signals related to COVID-19 information for HTA individuals. Overall, the sustained attention of threatening information makes individuals with higher level of anxiety more vulnerable to increased exposure of stress during the pandemic. Our longitudinal findings provide further understanding of the relationships between stress and anxious traits.

References

1. Cannito, L., Di Crosta, A., Palumbo, R., Ceccato, I., Anzani, S., La Malva, P., ... & Di Domenico, A. (2020). Health anxiety and attentional bias toward virus-related stimuli during the COVID-19 pandemic. Scientific Reports, 10(1), 16476.
2. Somma, F., Bartolomeo, P., Vallone, F., Argiuolo, A., Cerrato, A., Miglino, O., ... & Gigliotta, O. (2021). Further to the left: Stress-induced increase of spatial pseudoneglect during the COVID-19 lockdown. Frontiers in psychology, 12, 573846.

Poster No 706

Neural correlates of optimism and pessimism in healthy adolescents

Tara Samson[1], Benjamin Sipes[1], Angela Jakary[1], Tiffany Ngan[1], Yi Li[1], Eva Henje[2], Tony Yang[1], Olga Tymofiyeva[1]

[1]University of California, San Francisco, San Francisco, CA, [2]University of Umeå, Umeå, n/a

Introduction: Adolescents face a mounting struggle against depression, with 5 million adolescents in the US experiencing at least one major depressive episode in the past year and relapse rates around 50%[2,5]. Notably, dispositional optimism has a demonstrated strong negative association with adolescent depression with research suggesting optimism and depression may even arise from shared neural correlates in the amygdala and anterior cingulate cortex (ACC)[9,10]. Prior work also links optimism with neural correlates in the putamen and ventromedial prefrontal cortex (vmPFC)[3,4,7]. Clarifying the neural underpinnings of optimism and pessimism could reveal how these traits render adolescents especially protected from or vulnerable to depression[1,10]. We aim to (1) replicate the correlation between optimism and depressive symptoms in adolescents, extending the link to pessimism as well, (2) identify neural correlates of optimism and pessimism, and (3) propose a neural circuit underlying these traits in healthy adolescents.

Methods: 117 healthy adolescents (15.9±1.3 yrs, 51 females) underwent a 3T MRI scan that included a T1-weighted sequence and a diffusion-weighted sequence with 55 directions reconstructed using High Angular Resolution Diffusion-Weighted Imaging (HARDI). Node strength was calculated as the sum of the connections from each region of interest to all other brain regions weighted by the average fractional anisotropy (FA) along the tractography streamlines (Figure 1)[8]. All participants self-reported on the Revised Life Orientation Test (LOT-R) and the Reynolds Adolescent Depression Scale-2nd edition (RADS-2). Our analyses focused on key regions of interest– the amygdala, ACC, putamen, and vmPFC. Note that the

vmPFC corresponded to the medial orbitofrontal cortex (mOFC) in the AAL atlas in our study. We did not correct for multiple comparisons due to the exploratory nature of this analysis.

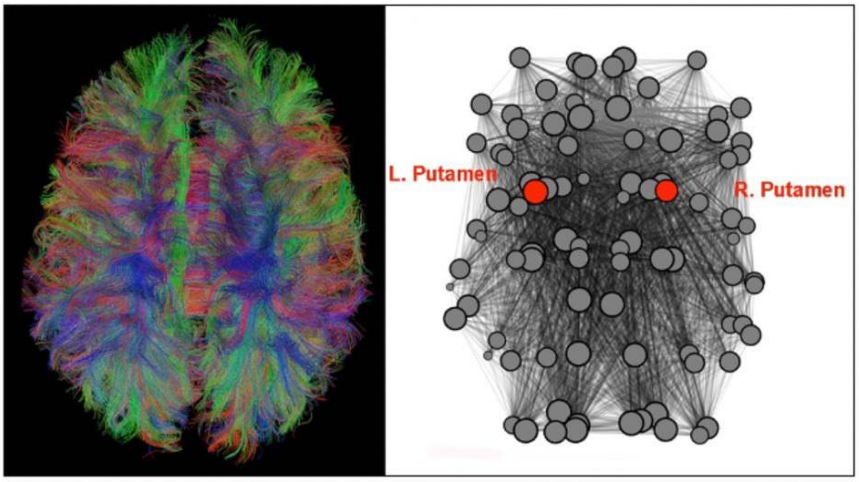

Figure 1. DTI-based whole-brain tractogram in a healthy adolescent (left image); the corresponding graph depicting the connectome with putamen nodes highlighted in red (right image)

Results: First, we confirmed a negative correlation between the level of self-reported depressive symptoms (RADS-2 T-score) and self-reported dispositional optimism (LOT-R) (r=-0.473; p<.001, Figure 2). We also found a positive correlation between depressive symptoms and dispositional pessimism (LOT-R) (r=0.450; p<.001). Secondly, we found significant correlations between optimism scores and the structural node strength of the bilateral putamen (r=0.188; p=.045) and bilateral amygdala (r=0.209; p=.025). There was also a significant correlation between pessimism scores and the structural node strength of the bilateral vmPFC (r=-0.208; p=.027). We did not find any significant correlations with ACC node strength.

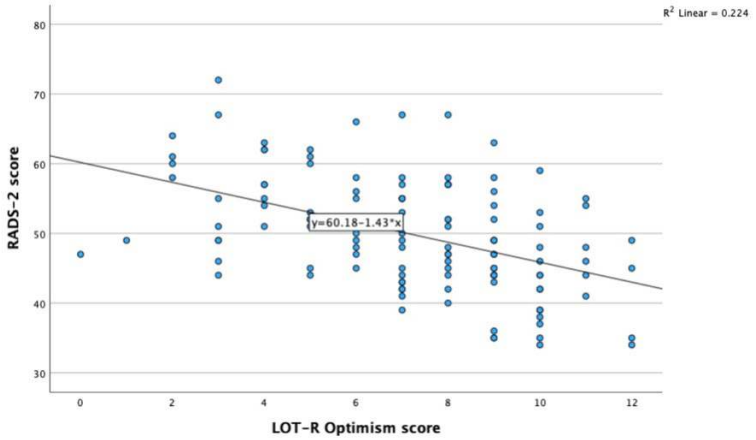

Figure 2. Data points represent each participant's depressive symptoms (RADS-2) and optimism (LOT-R) scores with a best-fit line demonstrating the negative correlation between these variables

Conclusions: Our findings reinforce that dispositional optimism and pessimism are associated with depressive symptoms in healthy adolescents. Based on the significant associations between our regions of interest– the putamen, amygdala, and vmPFC– and optimism and pessimism scores, we theorize that the amygdalofugal pathway may contribute to optimistic and pessimistic tendencies in youth. The amygdalofugal pathway is a main efferent from the amygdala which links emotional motivations and drives arising in the limbic system (amygdala) to reward-driven actions in the striatum (putamen) and reward learning and memory in the medial frontal cortex (vmPFC).[11]. It follows that this system could also influence dispositional optimism and pessimism as forms of future reward prediction. Future studies could advance this theory by investigating the associations between optimism and pessimism scores and the functional connectivity of the amygdalofugal pathway. Importantly, optimism is not a fixed trait. Treatments like cognitive behavioral group therapy can increase optimism in people with depression[6]. We hope that by deepening our understanding of the neural underpinnings of optimism and pessimism, we will discover better ways to foster optimism and protect against depression in vulnerable adolescents.

References
1. Ames, M. E. (2013), 'The protective role of optimism and self-esteem on depressive symptom pathways among canadian aboriginal youth,' Journal of Youth and Adolescence, vol. 44, no. 1, pp. 142-154
2. Curry, J. (2011), 'Recovery and recurrence following treatment for adolescent major depression,' Archives of General Psychiatry, vol. 68, no. 3, pp. 263-269
3. Erthal, F. (2021), 'Unveiling the neural underpinnings of optimism: A systematic review,' Cognitive, Affective, & Behavioral Neuroscience, vol. 21, no. 5, pp. 895-916
4. Lai, H. (2020), 'Neurostructural correlates of optimism: Gray matter density in the putamen predicts dispositional optimism in late adolescence,' Human Brain Mapping, vol. 41, no. 6, pp. 1459-1471
5. 'Major depression,' (2023), National Institutes of Mental Health
6. Moloud, R. (2022), 'Cognitive-behavioral group therapy in major depressive disorder with focus on self-esteem and optimism: an interventional study,' BMC Psychiatry, vol. 22, no. 299
7. Ran, Q. (2017), 'The association between resting functional connectivity and dispositional optimism,' PLOS ONE, vol. 12, no. 7, pp. e0180334
8. Rubinov, M. (2010), 'Complex network measures of brain connectivity: uses and interpretations', NeuroImage, vol. 52, no. 3, pp. 1059-1069
9. Sharot, T. (2007), 'Neural mechanisms mediating optimism bias,' Nature, vol. 450, no. 7166, pp. 102-105
10. Uribe, F. A. R. (2021), 'Association between the dispositional optimism and depression in young people: a systematic review and meta-analysis', Psicologia, reflexao e critica : revista semestral do Departamento de Psicologia da UFRGS, vol. 34, no. 1, pp. 37
11. Wright, A. (2020), 'Chapter 6: Limbic system: Amygdala,' Neuroscience Online–UTHealth McGovern Medical School

Poster No 707

Emotion Dynamics in Reciprocity:Deciphering the Role of Prosocial Emotions in Social Decision-making

Jaewon Kim[1], Su Hyun Bong[1], Dayoung Yoon[1], Bumseok Jeong[1]

[1]Korea Advanced Institute of Science and Technology, Daejeon, Daejeon

Introduction: Social decision-making is frequently investigated using an ultimatum game (UG). When responder rejects, none of the players receive the reward; hence, the proposer should act more prosocially. Recently, predictive emotions, in the form of the emotion prediction error (EPE), were also reported to predict the choices of UG responders (Heffner, Son et al. 2021): Participants demand more prosocial interaction by punishing their partners when they receive smaller rewards or feel less pleased and more emotionally aroused than expected. Therefore, emotions in response to a proposer's offer could be better explored using basic and prosocial affect dimensions. By adopting a dynamics approach and unsupervised neural network classification algorithm, we aim to investigate trajectory of responders' predictive emotions and social decision-making during UG. We predict that there will be groups that show distinct pattern of social decision-making, as well as related experiences of reward expectation, predictive emotions.

Methods: A total of 476 participants participated in an ultimatum game (UG). The rewards in each block were pseudo-randomised values with three fairness level. During each trial, partcipants responded expected amount of offer, decisions to either accept or reject, and emotions before and after offer. K-means clustering was applied to the entire time series of participants' expected reward and reward acceptance, rather than individual time points. To identify groups of distinct emotion trajectories with fairness level changes, we applied t-distributed stochastic neighbor embedding (t-SNE) and a deep neural network unsupervised classifier. Then UMAP dimensionality reduction algorithm was applied to the time series of expected and experienced emotions for visualization (Figure). The kernel density estimation plot was visualised separately for each emotion group.

Results: Clustering of the participants based on the trajectories of their expected reward, reward acceptance, and expected and experienced emotions resulted in solutions with equal numbers of components. Clustering for all components resulted in solutions wherein the cluster centroids showed three distinct stationary trajectories with consistently low, middle, and high values and one distinct dynamic trajectory that chased the actual reward. UMAP embedding results were plotted, and each emotion group's kernel density estimation plot was overlaid separately (Figure). The results supported our hypothesis that individuals will be grouped into those with distinct pattern of reward expectation, social decision, and emotion experience.

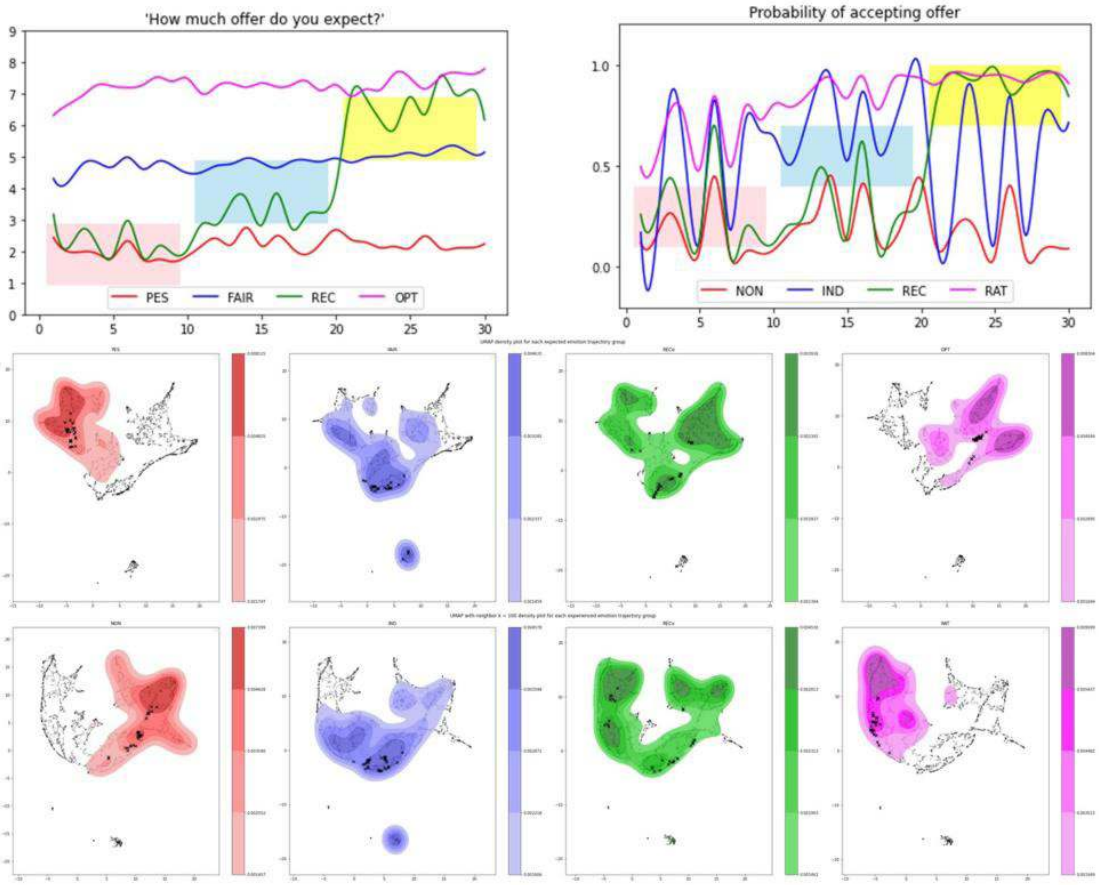

Conclusions: We identified inherent subsets of participants who show distinct temporal pattern of reward expectation, social decision making, and emotion experiences and propose a novel algorithm that can identify these clusters.

References

1. Heffner, J., J.-Y. Son and O. FeldmanHall (2021). "Emotion prediction errors guide socially adaptive behaviour." Nature human behaviour 5(10): 1391-1401.
2. Russell, J. A. and A. Mehrabian (1977). "Evidence for a three-factor theory of emotions." Journal of research in Personality 11(3): 273-294.
3. Tangney, J. P., J. Stuewig and D. J. Mashek (2007). "Moral emotions and moral behavior." Annu. Rev. Psychol. 58: 345-372.

Poster No 708

Exploring consistent neural representation of valence in watching and recalling

Hyeonjung Kim[1], Jongwan Kim[2]

[1]Jeonbuk National University, Jeonju-si, Jeollabuk-do, [2]Jeonbuk National University, Jeon-su si, Jeollabuk-do

Introduction: The valence is one of core affect dimensions, describing negative and positive feelings along a bipolar dimension (Russell, 1980). The debate surrounding valence pertains to whether affective representation is consistent or specific across different sensory modality (Barrett & Bliss-Moreau, 2009). The debate has led to two hypotheses, modality-general (consistent representations across modalities) and modality-specific (unique representations for each of modalities). Our study aimed to investigate the brain regions supporting the modality-general hypothesis by using a recall paradigm. Although recall often evoked similar emotions to prior experiences (Tulving, 2002), it does not always rely on external stimuli. Thus, we aimed to confirm whether valence representations were consistent across modalities.

Methods: 2.1. Data and experimental design In this study, we re-analyzed two shared datasets. Chen et al. (2017) collected fMRI data from 17 participants while they watched the first episode of BBC Sherlock and then later orally recalled it during fMRI measurement. The episode was divided into 48 scenes for both the watching and recall sessions. In Kim et al. (2020), the same stimuli were divided into 621 segments, with 125 participants rating affective responses on a 9×9 grid with valence (X-axis) and arousal (Y-axis) dimensions. We reorganized these two datasets for this study. We excluded fMRI data of both watching and recall sessions if the scene was not successfully recalled. The valence rating of a specific scene was calculated

by averaging the valence ratings of multiple segments within that scene. 2.2 Searchlight analysis To explore the regions showing modality-general representation, we conducted the searchlight analysis using 5×5×5 cubic neighboring voxels with cross-participant cross-modal regression-based decoding (Fig 1). The process involved assigning 16 participants to the training set and left-one participant to the testing set, with these sets representing different modality conditions. Multiple regression was then conducted with the training set, using voxel data and valence ratings. We multiplied each regression coefficient by each voxel of the testing set, yielding predicted valence ratings associated with scenes. The Pearson correlation between predicted valence ratings and participant valence ratings was used as the prediction accuracy. This procedure was repeated by swapping the modality condition of testing and training sets, and the two modality maps were averaged to form the consistency brain map. This procedure was repeated 17 times to assign each participant in the testing set once. The brain maps were used for a one-sample t-test (uncorrected α=.001), using statistical parametric mapping 12 (SPM12). To test significance, 1,000 permutations were conducted (α=.05).

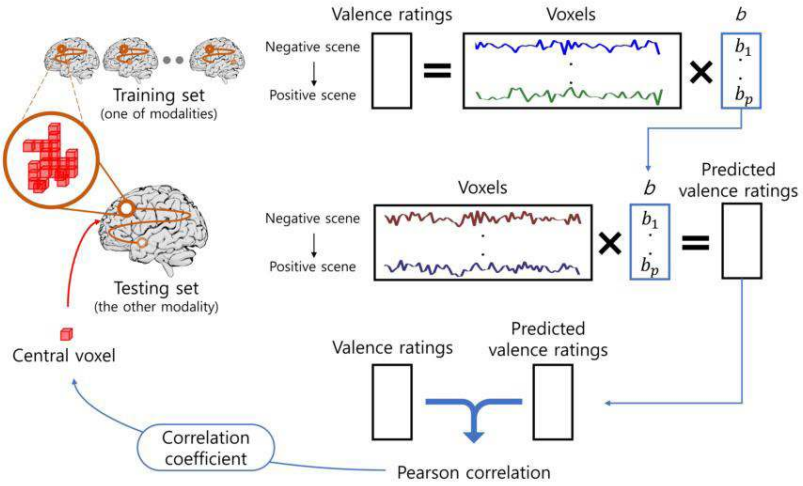

Results: We only used the fMRI data for scenes which participants successfully recalled, with each participant recalling a different number of scenes (M=34, range=24 to 46), and valence ratings for scenes were unbiased toward one direction of valence (average valence ratings' range=-2.98 to 1.08). To identify the regions representing consistent valence representation across modalities, we conducted a searchlight analysis with permutation test. The result revealed the right middle temporal gyrus (MTG), right inferior temporal gyrus (ITG), and left ITG/fusiform gyrus (ps<.05, cluster size>174, Figure 2).

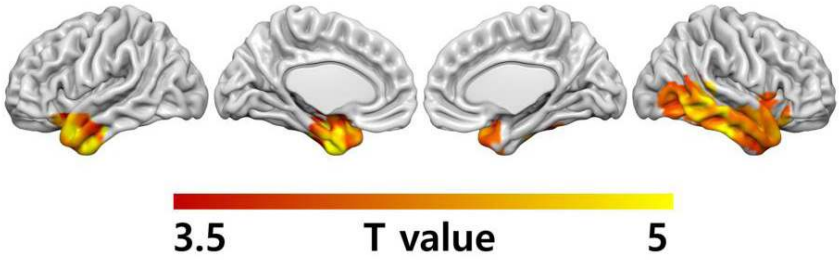

Conclusions: This study, considering the consistency across people, aimed to confirm whether affective representations in a watching and recall were consistent. The result revealed modality-general representation in three brain regions, known to be associated with high-level visual processing (e.g. face processing), recall, and emotion. Particularly, ITG engages in recalling visual elements. These brain regions showed consistent affective representations across watching and recall, providing support for the modality-general hypothesis of emotion.

References

1. Barrett, L. F. (2009). 'Affect as a Psychological Primitive'. Advances in experimental social psychology, 41, 167-218.
2. Chen, J. (2017). 'Shared memories reveal shared structure in neural activity across individuals'. Nature neuroscience, 20(1), 115-125.
3. Kim, J. (2020). 'A study in affect: Predicting valence from fMRI data'. Neuropsychologia, 143, 107473.
4. Russell, J. A. (1980). 'A circumplex model of affect'. Journal of Personality and Social Psychology, 39(6), 1161-1178.
5. Tulving. (2002). 'Episodic Memory: From Mind to Brain'. Annual review of psychology, 53(1), 1-25.

Poster No 709

Switching and Coordination of Survival Actions in the Human Hypothalamus

Jaejoong Kim[1], Dean Mobbs[2]

[1]University of Minnesota, Saint Paul, MN, [2]California Institute of Technology, Pasadena, CA

Introduction: Comparative research suggests that the hypothalamus is critical in switching between survival states such as a switching between hunting and escaping. However, it is unclear if this is the case in humans due to the lack of naturalistic experimental paradigms that can investigate this question and the difficulty of investigating hypothalamic neural signals.

Methods: Here, we introduce a gamified experimental paradigm where volunteers switch between hunting and escape in response to encounters with a continuously-moving virtual predator and prey. Given the small size and low tissue contrast of the hypothalamus, we used deep learning-based segmentation to identify individual-specific hypothalamus and its subnuclei as well as imaging sequence optimized for hypothalamic signal acquisition. Computational modeling of continuous hunting and escaping behaviors was done to identify the latent process of generating these survival behaviors. Multi-voxel pattern analysis (MVPA), as well as the Multi-voxel connectivity analysis, was performed to investigate region-level encoding and network-level encoding of switching between hunting and escaping behavior in the hypothalamus. Finally, model-based functional MRI analysis was applied to investigate how the hypothalamic switching signal is associated with the optimal survival movement generation process.

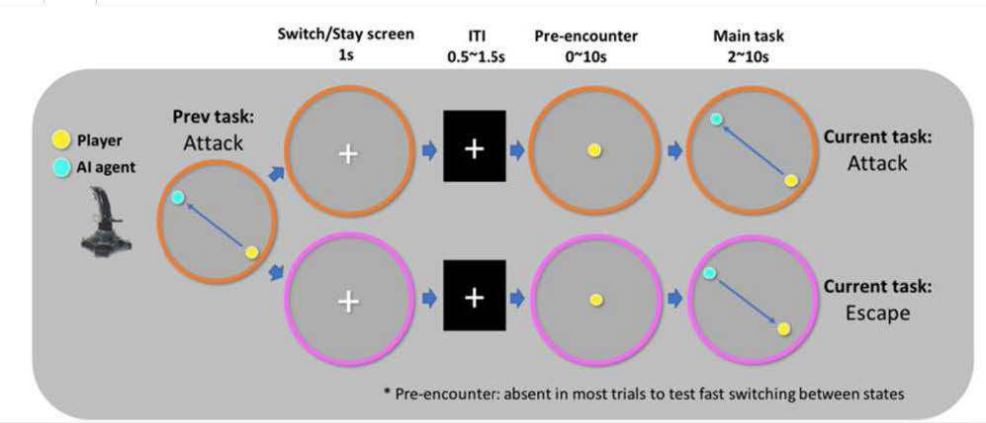

Results: Across two experiments, the winning model of the Bayesian model comparison showed that an agent utilizes an internal model of moving virtual prey or predator to guide an appropriate movement decision during both hunting and escaping behavior. Decoding of model parameter space showed that internal movement generation processes were highly specific to each task ($p<0.001$ in t-test against chance level). In experiment 2, multi-voxel pattern analyses showed that the hypothalamus, hippocampus and periaqueductal gray encode switching of survival states while not encoding simple motor switching outside of the survival context (all $p<0.05$ in t-test against chance level). Furthermore, multi-voxel connectivity analyses revealed a network including the hypothalamus as encoding survival switching and how the hypothalamus is connected to other regions in this network (network-based statistic; $p<0.001$). Finally, model-based fMRI analyses showed that a strong hypothalamic multi-voxel switching signal is predictive of optimal behavioral coordination after switching, especially when this signal was synchronized with multi-voxel switching signals in the amygdala (mixed-effect linear regression; $p<0.001$).

Conclusions: These findings extend understanding of the human hypothalamus from a region that regulates our internal bodily states to a region that switches survival states and coordinates strategic survival behaviors.

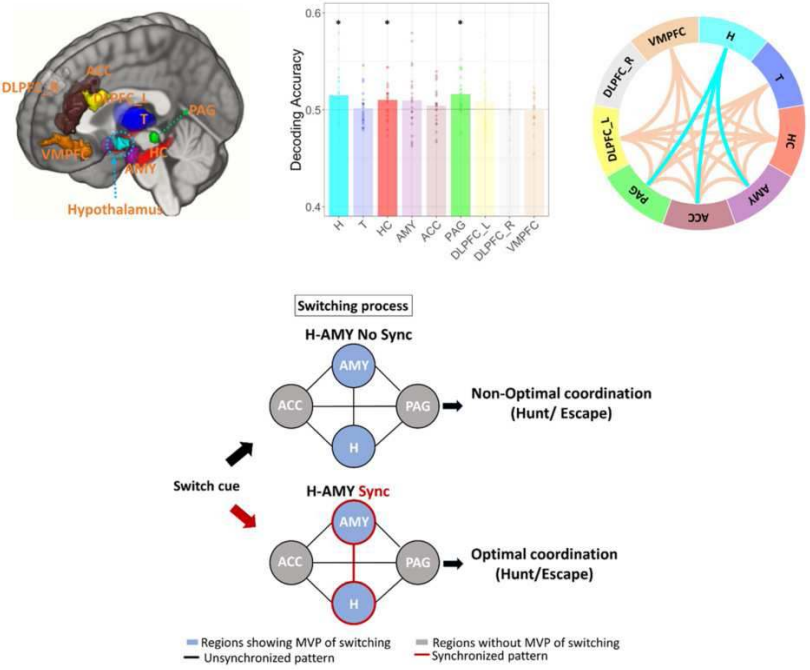

References

1. Mobbs, D. (2020). Space, Time, and Fear: Survival Computations along Defensive Circuits. Trends in Cognitive Sciences 24, 228–241. 10.1016/j.tics.2019.12.016.
2. Li, Y. (2018). Hypothalamic Circuits for Predation and Evasion. Neuron 97, 911-924.e5. 10.1016/j.neuron.2018.01.005.

Poster No 710

Deconstructing the brain bases of emotion regulation: A Bayes factor system-identification approach

Ke Bo[1], Thomas Kraynak[2], Mijin Kwon[1], Michael Sun[1], Peter Gianaros[2], Tor Wager[1]

[1]Dartmouth College, Hanover, NH, [2]University of Pittsburgh, Pittsburgh, PA

Introduction: Emotion regulation is fundamental to physical and mental health. Reappraisal is a particular emotion regulation tactic that involves reinterpreting the meaning of events to alter emotional responses to them. Reappraisal and emotion-generation processes may interact non-additively, and some brain regions may be uniquely or jointly involved in both emotion regulation and generation. At present, however, it is not clear whether some regions are uniquely engaged by reappraisal or emotion-generation states, which precludes developing brain measures of these processes. Here, we applied a systems identification approach to two large community samples (n=182 and 178), who viewed and reappraised aversive images from the International Affective Picture System (IAPS) during fMRI scanning. We aimed to identify brain regions that correspond to four potential system components: (1) 'Reappraisal only' regions responding only to reappraisal demand, not negative images; (2) 'Common appraisal' regions activated by negative images and further increased during reappraisal; (3) 'Non-modifiable emotion generation' regions activated by negative images but unaffected by reappraisal; and (4) 'Modifiable emotion generation' regions activated by negative images and reduced by reappraisal.

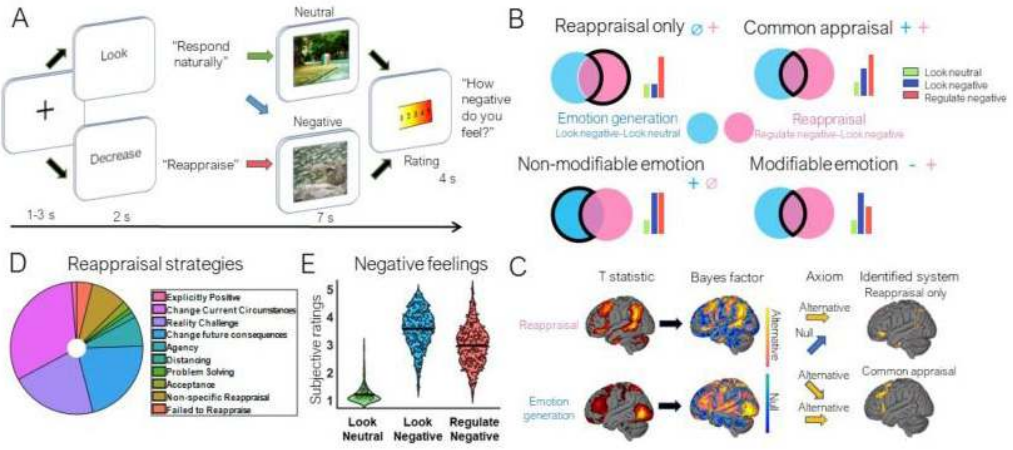

A.Task paradigm. B.Concepts of system components. C. Visualization of axiomatic methods. D. Specific reappraisal strategies in current study. E. Subjective negative rating of each condition

Methods: We established an axiomatic method based on a Bayes Factor approach to identify specific voxels for each system component. This involved an exhaustive search of whole brain voxels. For a voxel to be classified into a particular system component, it must satisfy predefined axioms. These axioms are established based on the observed activation and null effects across two contrasts: [Look Negative – Look Neutral] and [Reappraise – Look Negative]. Bayes Factors are applied to quantify the evidence for and against activation or null effects. We calculated them using the JZS prior, based on T statistics and degrees of freedom. The spatial similarity of the identified system components was compared with a series of neural transmitter receptor density maps. These analyses aim to understand the neural chemical associations of these system components

Results: Our data identified regions consistently associated with each component across both datasets. 'Reappraisal only' regions included anterior prefrontal cortex, temporal-parietal junction and temporal pole. 'Common appraisal' regions (the component with the largest number of associated brain voxels) included fronto-parietal regions, nucleus accumbens, and medial prefrontal cortex. Among emotion generation regions, most subcortical regions were not modified by reappraisal, including amygdala, brainstem, PAG, parabrachial complex, and thalamus, while visual and attention-related regions were modifiable by reappraisal. Brain activities in 'Reappraisal only', 'Common appraisal' and 'Modifiable emotion generation' regions correlated with successful regulation of negative emotions. These regions also coincided spatially with serotonin, GABA, and glutamate receptor-dense regions.

Conclusions: Our findings indicate that the brain regions engaged by reappraisal highly overlap with regions that may generate emotion, but some activations patterns were spatially selective for reappraisal. Automatic appraisal was observed to be supported by subcortical structures and are not influenced by reappraisal, while regions pertaining to sensory representation were the main regulatory targets.

References

1. Morawetz, Carmen, et al. "Multiple large-scale neural networks underlying emotion regulation." Neuroscience & Biobehavioral Reviews 116 (2020): 382-395.
2. Rouder, Jeffrey N., et al. "Bayesian t tests for accepting and rejecting the null hypothesis." Psychonomic bulletin & review 16 (2009): 225-237.
3. Hansen, Justine Y., et al. "Mapping neurotransmitter systems to the structural and functional organization of the human neocortex." Nature neuroscience 25.11 (2022): 1569-1581.

Poster No 711

An fMRI Study of Sex Differences in Relation to Aggression in Humor Styles

Yu-Chen Chan[1], Chia-Yueh Chang[2], Hao Chang[2]

[1]National Tsing Hua University, Hsinchu, Taiwan, [2]National Taiwan Normal University, Taipei, Taiwan

Introduction: An increasing amount of research focuses on how different sexes perceive humor involving aggression. The results are nuanced, implying divisions among various forms of aggression, and the underlying neural mechanisms and

behaviors are still fully characterized (Chan, 2016). The Humor Styles Questionnaire (HSQ) has been used in many studies. However, in this study, the HSQ was replaced with a two-panel cartoon, the first of which was set up to establish the situation (setup stage) and the second of which offered an unexpected and humorous resolution (punch line stage) (Chan et al., 2023).

Methods: Participant A total of 94 participants were recruited-47 men and 47 women, all right-handed and ages 20 to 35. The Research Ethics Committee of National Tsing Hua University approved all experimental procedures. Stimuli Each stimulus consisted of two stages: a setup and a punch line. The setup was to generate expectations, while the punch line violated the expectations established by the setup (Chan et al., 2023)-a total of 40 two-stage aggressive humor styles and 20 two-stage non-humor (i.e., baseline). Experimental paradigm The fMRI paradigm employed in this investigation was event-related. Pre-scan (practice), in-scan (fMRI scanning), and post-scan (debriefing) phases were carried out by the participants. The participants were initially presented with a fixation for every trial. They provided the setup and punch line. The participants used the response pad to rate the level of funniness (from 1 to 4). Four runs in all, given in a counterbalanced order for each participant, were conducted. Each participant's fMRI session lasted for about 45 minutes. Image acquisition A Siemens Magnetom Prisma 3 T scanner was used to collect the MRI data. The E-Prime 3 program was used to display the visual stimuli. Multiband interleaved echo-planar imaging (EPI) with an acceleration factor of three was used to acquire functional images. The pulse sequence used was TR = 1000 ms, TE = 30 ms, FA = 60, number of slices = 39, and voxel size = 3.43mm×3.43mm×3.40 mm. Image analysis We used an event-related analysis procedure to enter each participant's preprocessed data into a general linear model (GLM). For each participant, the contrasts and conjunction analyses were p-valued (family-wise error) at a significance level of .05.

Results: During humor comprehension (incongruity-resolution) of the aggressive humor style, women showed greater activation than men in the bilateral posterior superior temporal gyri (pSTG), left inferior frontal gyrus (IFG), and bilateral inferior parietal gyri (dorsal attention network). However, men demonstrated greater activation than women in the bilateral IFG and right temporoparietal junction (TPJ, ventral attention network). During humor appreciation (amusement or mirth) of the aggressive humor style, women displayed greater activation than men in the left substantial nigra of the midbrain, while men exhibited greater activation than women in the anterior insula (salience network) and orbitofrontal cortex (OFC). The results of conjunction analysis showed women and men greater activation in the left amygdala, midbrain, OFC, anterior insula, and TPJ during humor appreciation.

Conclusions: Previous research on "general humor" revealed that women displayed more activity in the amygdala, midbrain, insula, and OFC during humor appreciation (e.g., Chan, 2016). Nonetheless, the present study focused on the "aggressive humor style," the findings indicated that sex differences existed in how aggressive humor was appreciated. Whereas women displayed more activation in the limbic network (such as the midbrain), men demonstrated more robust activation in the salience network (such as the anterior insula).

References

1. Chan, Y. C. (2016). Neural correlates of sex/gender differences in humor processing for different joke types. Frontiers in Psychology, 7, 536.
2. Chan, Y. C., Zeitlen, D. C., & Beaty, R. E. (2023). Amygdala-frontoparietal effective connectivity in creativity and humor processing. Human Brain Mapping, 44(6), 2585-2606.

Poster No 712

Sex differences in resting-state fMRI functional connectivity by the perspective of humor processing

Chia-Yueh Chang[1], Yu-Chen Chan[2], Hsueh-Chih Chen[1]

[1]National Taiwan Normal University, Taipei, Taiwan, [2]National Tsing Hua University, Hsinchu, Taiwan

Introduction: Little research has delved into the relationship between functional connectivity (FC) during resting-state and the sense of humor and whether this connection varies between sexes. A review of previous studies has explored the neural mechanisms involved in humor processing[1,2,3,4] and humor processing across diverse groups, considering factors like sex[4]. These studies have uncovered sex variations in the cognitive and emotional aspects of humor processing[4]. The findings suggest that, compared to men, women exhibit heightened activation in humor appreciation, resulting in increased amusement and more extensive cognitive inferences in response to jokes. Conversely, men show greater activation levels in humor comprehension, indicating a more integrated cognitive processing of humor. This study aims to investigate whether there are sex differences in FC during the resting-state and to explore the association between FC and the sense of humor.

Methods: Participants A total of 56 (26 men, mean age = 23.54 ± 4.94 and 30 women, mean age = 23.67 ± 3.46) healthy right-handed with normal or corrected-to-normal vision and no history of psychiatric or neurological diseases participated in this

study. The study was approved by the Research Ethics Committee of National Taiwan University. rsfMRI data acquisition The resting-state fMRI (rsfMRI) scans were performed using a 3T Siemens Magnetom Prisma scanner (Erlangen, Germany) and a standard 20-channel head coil and underwent a rsfMRI scan of 12 minutes. Functional images using the following acquisition parameters: TR = 2s, TE = 26ms, FA = 90°, number of slices = 40, and voxel size = 3.4 mm×3.4mm×3.4 mm. The image data were preprocessed following the procedures implemented in the CONN toolbox. Data analysis The images were processed through whole-brain analysis with the CONN toolbox, and FC was measured using the seed-based correlation method. The study uses CONN's default seeds that exert a complete brain parcellation encompassing 106 cortical and subcortical areas from the FSL Harvard-Oxford Atlas, 26 cerebellar areas of the AAL atlas, and 32 additional areas corresponding to main networks, default mode (DMN), salience, dorsal attention, fronto-parietal, and language. Multidimensional Sense of Humor Scale The present study utilized the Multidimensional Sense of Humor Scale[5]. It comprises six subscales, totaling 54 items, namely "humor comprehension," "humor creation," "using humor in the social context," "humor coping," "attitude toward humor," and "tendency to laugh." Scoring is conducted on a Likert five-point scale, with a higher total score indicating a greater sense of humor.

Results: The results showed sex differences in FC associated with a sense of humor (Figure 1). Compared with women, men's greater FC between the right inferior frontal gyrus and the supramarginal gyrus was associated with a higher attitude toward humor; the greater FC between the right middle temporal gyrus and the precuneus cortex was associated with higher humor coping; and the greater FC between the right IFG of the language network and the right frontal pole was associated with higher humor coping. On the other hand, women with stronger FC between the temporal pole and right angular gyrus were associated with higher use and sense of humor in social contexts.

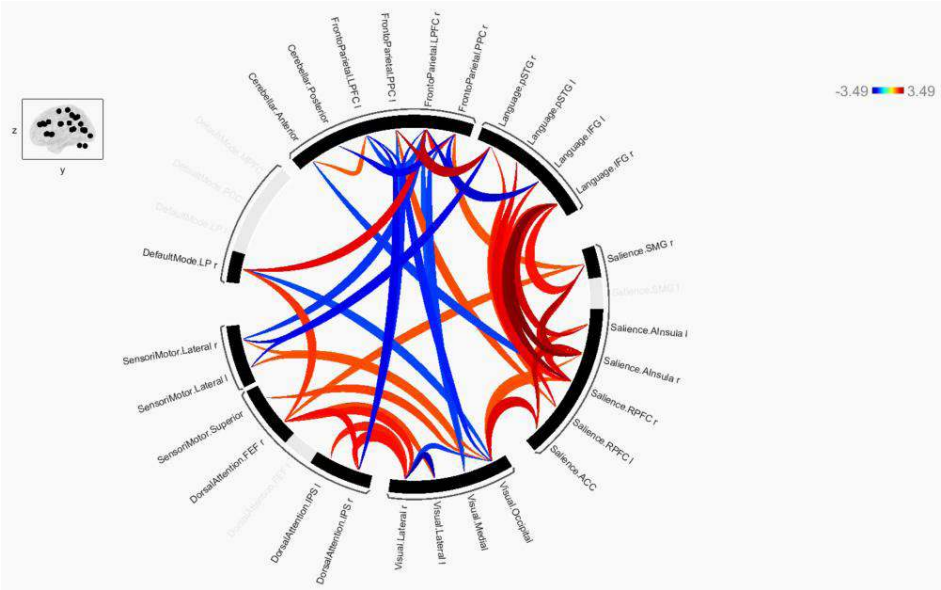

The sex differences in the functional connectivity (men > women)

Conclusions: The results of FC revealed sex differences consistent with previous research, highlighting that women exhibited more robust connectivity in humor appreciation, whereas men demonstrated more vital connectivity in humor comprehension[4]. Interestingly, this study found that when men displayed higher levels of humor coping, the FC between the rMTG and precuneus and the right IFG and right frontal pole in the language networks were stronger. Meanwhile, when women had a higher sense of humor and the ability to use humor in social contexts, the FC between rTP and rAG was stronger.

References

1. Chan, Y.-C., Chou, T.-L., Chen, H.-C., & Liang, K.-C. (2012). Segregating the comprehension and elaboration processing of verbal jokes: An fMRI study. NeuroImage, 61(4), 899-906. https://doi.org/10.1016/j.neuroimage.2012.03.052
2. Chan, Y.-C., Chou, T.-L., Chen, H.-C., Yeh, Y.-C., Lavallee, J. P., Liang, K.-C., & Chang, K.-E. (2013). Towards a neural circuit model of verbal humor processing: An fMRI study of the neural substrates of incongruity detection and resolution. NeuroImage, 66(1), 169-176. https://doi.org/10.1016/j.neuroimage.2012.10.019
3. Chang, C.-Y., Chan, Y.-C., & Chen, H.-C. (2023). Verification of the Four-Stage Model of Humor Processing: Evidence from an fMRI Study by Three-Element Verbal Jokes. Brain Sciences, 13(3), 417. https://doi.org/10.3390/brainsci13030417
4. Chan, Y.-C. (2016). Neural Correlates of Sex/Gender Differences in Humor Processing for Different Joke Types. Frontiers in Psychology, 7, 536. https://doi.org/10.3389/fpsyg.2016.00536
5. Chen, S.-J., & Chen, H.-C. (2005) Development of the Multidimensional Sense of Humor Scale. Research in Applied Psychology, (26), 167-187.

Poster No 713

Separable and overlapping functional connectome architecture for impulsivity and anxiety

E-Young Chung[1,2], M. Justin Kim[1,2]

[1]Sungkyunkwan University, Seoul 03063, Korea, Republic of, [2]Center for Neuroscience Imaging Research, Institute for Basic Science, Suwon 16419, Korea, Republic of

Introduction: The connection between impulsivity and anxiety remains elusive, with some studies suggesting independence, while others propose a negative association between the two psychological traits. While impulsivity is characterized by exhibiting rapid and unplanned reactions to stimuli and acting without forethought, anxiety is characterized by hyper-control, excessive anxious apprehension about potential outcomes, seemingly incongruent with one another. However, there exists a subset of individuals exhibiting both traits, suggesting a complex interplay between impulsivity and anxiety. This study aims to explore whole brain functional connectivity differences underlying impulsivity and anxiety, and to investigate whether individuals who possess both high impulsivity and anxiety might exhibit specific functional network patterns. Identifying such patterns could help elucidate the nature of the association between impulsivity and anxiety and shed further light on the unique characteristics of their shared state.

Methods: A total of 162 functional connectomes were built using resting state functional magnetic resonance imaging (fMRI) data from the Leipzig Study for Mind-Body Emotion Interactions dataset. We classified the “High Impulsivity (HI)” group (i.e., within the top 55% for impulsivity & outside the top 55% for anxiety) and the “High Anxiety (HA)” group (i.e., within the top 55% for trait anxiety & outside the top 55% for impulsivity) based on self-reported measures of each trait. Among these participants, those who had both high impulsivity and anxiety scores (i.e., within the top 55% for both measures) were categorized as the “High Impulsivity & High Anxiety (HIHA)” group. Then, to define ‘impulsivity > anxiety’ and ‘anxiety > impulsivity’ networks, we conducted two-sample t-tests with leave-one-out cross validation performed on each edge within the functional connectome between the HI group and HA group. Additionally, to identify HIHA specific networks by comparing them with the HI and HA groups, a one-way ANOVA was conducted for each edge in the functional connectomes to explore network differences between three groups (HI/HA/HIHA) with a significance threshold of $P < 0.01$. Additionally, to validate the ‘shared-specific’ network, two-sample t-tests were conducted within these networks to compare the HIHA group with the HI and HA groups.

Results: Two-sample t-tests yielded statistically significant differences in the overall strength of ‘impulsivity > anxiety’ and ‘anxiety > impulsivity’ networks ($t(116) = 6.494$, $p < 0.001$). Specifically, the HI group exhibited heightened functional connectivity in the cerebellum and basal ganglia, both of which are associated with motor control. Conversely, the HA group displayed increased functional connectivity between the frontoparietal network (FP) and the default mode network (DMN), and the FP and the medial frontal network (MF), both of which are known to be involved in emotion dysregulation. On the other hand, the HIHA group showed significantly decreased the FP-cerebellar network strength compared to the HI group ($t(85) = -4.410$, $p < 0.001$) as well as the HA group ($t(84) = -4.778$, $p < 0.001$). No differences in the strength of this shared network were observed between the HI and HA groups ($p = 0.584$). The HIHA group demonstrated the weakest functional network strength in the FP-cerebellar network, suggesting that insufficient regulation of the FP may have contributed to the inability to control both impulsive and anxious traits.

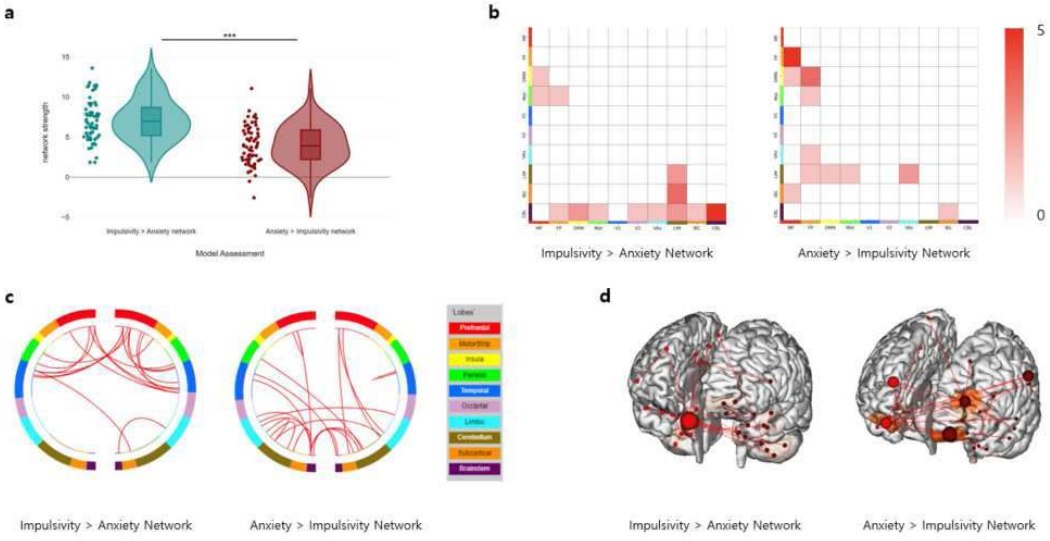

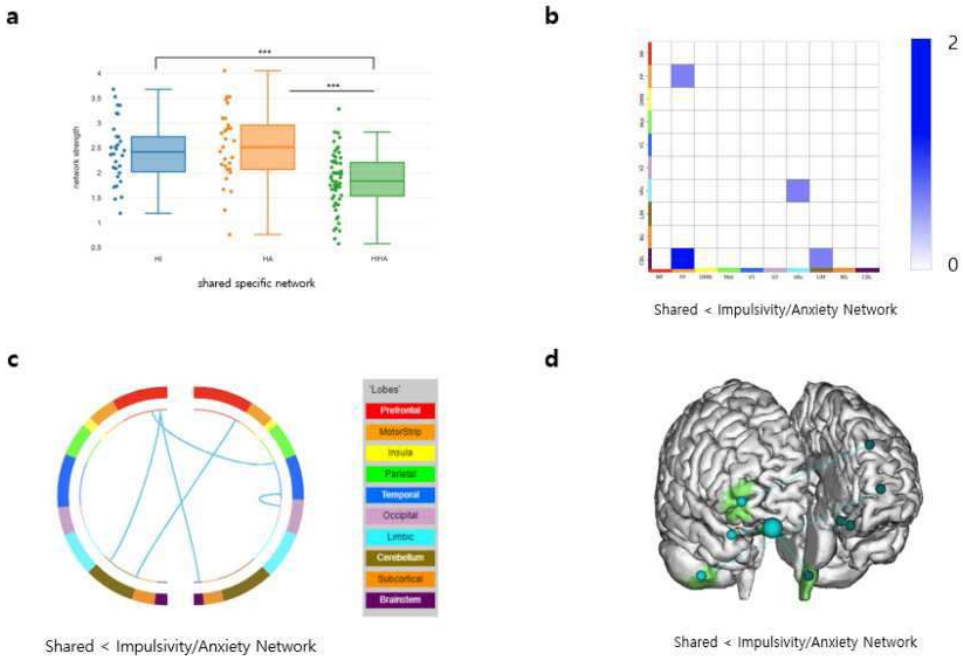

Conclusions: Individuals characterized by either only high impulsivity or high anxiety demonstrated distinct functional networks. Furthermore, we found that individuals who possess both traits exhibit unique functional connectivity patterns of their own, providing preliminary evidence for a neural characteristic of those who are able to conduct impulsive decision-making behavior in the presence of high anxiety.

References

1. Barratt, E. S. (1983). The biological basis of impulsiveness: The significance of timing and rhythm disorders. Personality and individual differences, 4(4), 387-391.
2. Bellani, M., Hatch, J. P., Nicoletti, M. A., Ertola, A. E., Zunta-Soares, G., Swann, A. C., ... & Soares, J. C. (2012). Does anxiety increase impulsivity in patients with bipolar disorder or major depressive disorder?. Journal of psychiatric research, 46(5), 616-621.
3. Brown, G. W., Harris, T. O., & Eales, M. J. (1996). Social factors and comorbidity of depressive and anxiety disorders. The British Journal of Psychiatry, 168(S30), 50-57.
4. Del Carlo, A., Benvenuti, M., Fornaro, M., Toni, C., Rizzato, S., Swann, A. C., ... & Perugi, G. (2012). Different measures of impulsivity in patients with anxiety disorders: a case control study. Psychiatry research, 197(3), 231-236.
5. Caci, H., Askenazy, F., Frequelin, N., Nadalet, L., Myquel, M., Staccini, P., ... & Boyer, P. (1998). Validation of the Impulsivity Rating Scale and relationship with anxiety in healthy French adolescents. International Journal of Methods in Psychiatric Research, 7(3), 128-135.
6. Gray, J. A. (1970). The psychophysiological basis of introversion-extraversion. Behaviour research and therapy, 8(3), 249-266.
7. Moeller, F. G., Barratt, E. S., Dougherty, D. M., Schmitz, J. M., & Swann, A. C. (2001). Psychiatric aspects of impulsivity. American journal of psychiatry, 158(11), 1783-1793.
8. Summerfeldt, L. J., Hood, K., Antony, M. M., Richter, M. A., & Swinson, R. P. (2004). Impulsivity in obsessive-compulsive disorder: comparisons with other anxiety disorders and within tic-related subgroups. Personality and Individual Differences, 36(3), 539-553.
9. Taylor, C. T., Hirshfeld-Becker, D. R., Ostacher, M. J., Chow, C. W., LeBeau, R. T., Pollack, M. H., ... & Simon, N. M. (2008). Anxiety is associated with impulsivity in bipolar disorder. Journal of anxiety disorders, 22(5), 868-876.
10. Zinbarg, R. E., & Barlow, D. H. (1996). Structure of anxiety and the anxiety disorders: a hierarchical model. Journal of abnormal psychology, 105(2), 181.

Poster No 714

Music-induced metabolic changes measured with functional PET/MRI

Vesa Putkinen[1]

[1]*University of Turku, Turku, US and Canada only*

Introduction: Music is as a common source of pleasure for most people, and activates the same hedonic brain circuitry supporting pleasure derived from other rewarding experiences. Yet, little is known about the brain metabolic demands induced by pleasurable music-listening. Here, we utilize simultaneous functional [18F]FDG-PET and functional magnetic resonance imaging (fMRI) to measure concurrent changes in brain glucose metabolism and hemodynamic activity during

music-induced pleasure. Unlike PET imaging with the traditional bolus administration of the tracer, fPET employs constant FDG infusion and allows the quantification of task-specific changes in glucose metabolism in a single scan.

Methods: Twenty-seven subjects underwent a 90-min simultaneous PET-MRI recording. Twenty percent of the tracer was administered in a bolus followed by a constant infusion across the entire scan. The experiment included two 10-min blocks of self-selected pleasurable music and two 10-min blocks neutral auditory stimulation. During the blocks, 45-sec sound stimulation (music or control stimuli) altered with 15-sec silent periods. For the PET data, voxel-vise time activity curves were modeled with a general linear model (GLM) with task-specific regressors for the Music and Control conditions and a regressor for baseline metabolism. The fMRI data were modelled with a GLM with boxcar regressors (silence vs. sound stimulation) for the music and control blocks.

Results: Pleasurable music listening increased FDG uptake in the auditory cortex, right inferior frontal gyrus, the pre- and post-central gyri, and in limbic regions such as the nucleus accumbens. The fMRI results replicated these findings showing increased in haemodynamic activity in the auditory, motor and limbic regions during pleasurable music.

Conclusions: Our results indicate that pleasurable music induces heightened energy consumption in the sensory, motor and emotion circuits of the brain. The results confirm the feasibility of simultaneous fPET-fMRI in studying the metabolic and haemodynamic changes associated with music-induced pleasure. The imaging modalities provided both converging and unique information about the neural underpinning of music-induced pleasure. Simultaneous fPET-fMRI presents novel possibilities for functional brain imaging of human emotions.

References

1. Hahn, A., Gryglewski, G., Nics, L., Hienert, M., Rischka, L., Vraka, C., Sigurdardottir, H., Vanicek, T., James, G. M., Seiger, R., Kautzky, A., Silberbauer, L., Wadsak, W., Mitterhauser, M., Hacker, M., Kasper, S., & Lanzenberger, R. (2016). Quantification of Task-Specific Glucose Metabolism with Constant Infusion of 18F-FDG. Journal of Nuclear Medicine, 57(12), 1933–1940. https://doi.org/10.2967/jnumed.116.176156
2. Koelsch, S. (2014). Brain correlates of music-evoked emotions. Nature Reviews. Neuroscience, 15(3), 170–180. https://doi.org/10.1038/nrn3666

Poster No 715

Resting-state Functional Connectivity Differences in the Gelotophobes and Non-Gelotophobes

Hao Chang[1], Hsueh-Chih Chen[1], Yu-Chen Chan[2]

[1]National Taiwan Normal University, Taipei, Taiwan, [2]National Tsing Hua University, Hsinchu, Taiwan

Introduction: Humor plays an important role in the construction and maintenance of interpersonal relations. However, humor could be interpreted differently from various perspectives. Non-gelotophobes (normal people) regard humor as a form of kidding, while gelotophobes view humor as an insult. Previous studies have indicated that non-gelotophobes had greater activation in the ventral mesocorticolimbic system, whereas gelotophobes had greater activation in the dorsal corticostriatal system, which was related to top-down cognitive control of emotion (Chan, 2016). Although some task-driven fMRI studies have studied the neural variances between gelotophobes and non-gelotophobes, little attention has been placed on the resting-state (rs-)fMRI. It is worthwhile to investigate the resting-state neural differences between gelotophobia and gelotophilia. In this study, we evaluated the default mode network (DMN; precuneus and medial prefrontal cortex, mPFC), executive control network (ECN; inferior frontal gyrus, IFG), and salience network (SN; amygdala and cingulate cortex).

Methods: Participants Ninety-three right-handed and neurologically normal participants (47 male, mean age 24.47 ± 3.51 years) were recruited in this study. The study was approved by the Research Ethics Committee of National Tsing Hua University. Materials All participants were assessed using the PhoPhiKat-TC Scale (Chen et al., 2011), which is a reliable and valid tool employed to evaluate the participants' gelotophobia, gelotophilia, and katagelasticism. Participants were divided into two groups based on the PhoPhiKat-TC Scale results, consisting of 37 gelotophobes and 56 non-gelotophobes. MRI data acquisition Resting-state blood oxygen level-dependent (BOLD) signals were acquired for 6 minutes using a specific imaging sequence (TR=1s, TE=30ms) on the 3-Tesla Siemens Magnetom Prisma scanner equipped with a 20-channel head coil. During the scan session, participants were asked to lie motionless and passively view a fixation dot. Data analysis To examine functional connectivity in brain regions of rs-fMRI relevant to gelotophobia and non-gelotophobia, voxel-based correlational analyses were performed using the Functional Connectivity (CONN) toolbox of SPM 12. According to previous studies, we focused on the precuneus, mPFC, IFG, amygdala, insula, PCC and dlPFC. Region of interest (ROI)-based correlations were also conducted using these areas as seeds.

Results: The results revealed stronger connections in the midbrain and the precuneus gyrus among non-gelotophobes. Previous studies have suggested that the precuneus is involved in processing self-relevant information, while the dorsal midbrain is more activated when considering a high-self concept. Additionally, the midbrain is associated with cognitive control and reward networks. Non-gelotophobes also displayed stronger connections in the accumbens, a key brain region in the reward network, and the ACC, which is integral to the reward circuit. In contrast to non-gelotophobes, participants with gelotophobia showed stronger connections in the ACC of the SN and precuneus. Based on previous research, the connectivity in the ACC and the precuneus was stronger, indicating a lower GABA concentration in the ACC. Gelotophobes also exhibited stronger connections in the PCC of the DMN and IFG. Previous studies have indicated that the DMN networks are related to human cognition and memory processing. Notably, the results demonstrated stronger connectivity in the amygdala and the frontal pole, suggesting the need for further investigation.

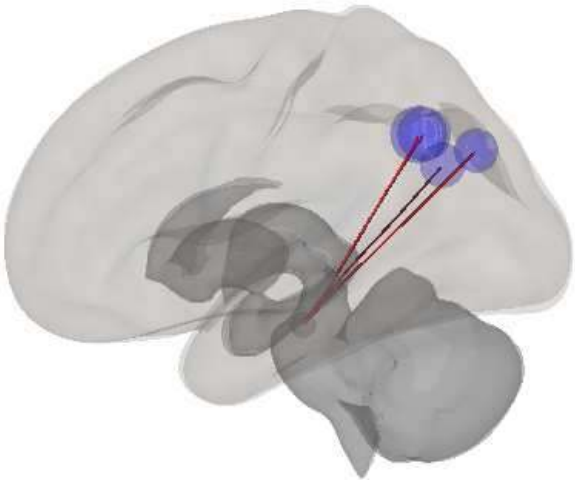

Figure 1. Functional connectivety in the Midbrain and Precuneus Gyrus (Non-gelotophobes > Gelotophobes)

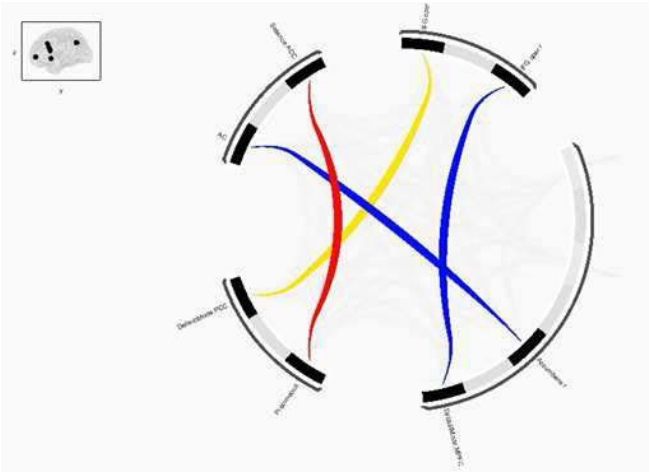

Figure 2. Functional connectivety in the Salience and DMN networks (Gelotophobes > Non-gelotophobes)

Conclusions: These findings provided evidence that resting-state functional connectivity differs between gelotophobes and non-gelotophobes. The brain areas related to cognition were more activated in the gelotophobes, while the reward circuits were more activated in the non-gelotophobes. In summary, the current study explored the neural patterns of individuals with different perspectives on humor.

References

1. Chan, Y. C. (2016). Neural correlates of deficits in humor appreciation in gelotophobics. Scientific Reports, 6(1), 34580.
2. Chen, H. C., Chan, Y. C., Ruch, W., & Proyer, R. T. (2011). Evaluating the reliability and validity of a traditional Chinese version of the PhoPhiKat-45. Psychological Testing, 58(1), 119-145.

Poster No 716

Unravelling sex-specific neural patterns associated with negative emotions

Tajwar Sultana[1], Dua Ijaz[1], Fareha Asif Khan[1], Maryam Misaal[1], Elvisha Dhamala[2], Adeel Razi[3]

[1]NED University of Engineering and Technology, Karachi, Sindh, [2]Feinstein Institutes for Medical Research, Glen Oaks, NY, [3]Monash University, Melbourne, Australia

Introduction: Do the male and female brains have different connectivity patterns for emotions? This question is of importance because sex is a crucial aspect of human identity and has been the subject of numerous studies and research over the past years[1]. Negative emotions are feelings that are generally unpleasant and associated with unpleasant experiences, such as sadness, anger, fear, disgust, and frustration. Various studies have explored sex differences in response to negative emotion regulation, reactivity, experiences, and perception[2–5]. Ignoring these distinctive outcomes between males and females may result in unsuccessful interventions and therapies for internalizing disorders such as anxiety and depression. Although there has been extensive research on sex differences in emotions[1–3], there is no previous work on investigating the sex differences in resting-state brain effective connectivity, specifically related to basic negative emotion. In this study, we expand upon the previous studies and investigate the underlying neural mechanisms of emotional trait-like personality in male and female using resting-state fMRI.

Methods: Our dataset consists of 1079 preprocessed resting-state fMRI scans from Human Connectome Project (HCP) that was acquired using 3T MRI scanner and their emotional assessment using NIH toolbox emotion battery. Some of the subjects, as has also been previously reported[6], showed the minimum scores within each emotion group ratings resulting in a bimodal distribution. The cause of this anomaly remains unknown. We removed those 176 subjects and ended up with 410 male and 493 female subjects. These subjects were divided into two groups (of males and females) which were subdivided according to their score levels (high, moderate, and low) for each emotion category (anger-affect, fear-affect, and sadness). The ROIs were taken from three well-known resting-state networks that have a high significance in emotional processing namely default mode, executive, and salience networks. The selected regions in each brain network are 1) default mode network: posterior cingulate cortex (PCC), medial prefrontal cortex (mPFC) and bilateral hippocampus (lHP and rHP); 2) salience network: dorsal anterior cingulate cortex (dACC), bilateral anterior insula (lAI and rAI) and bilateral amygdala (lAMG and rAMG) and; 3) executive network: bilateral dorsal lateral prefrontal cortex (lDLPFC and rDLPFC). A fully connected spectral dynamic causal model over 11 ROIs was estimated for each subject[7,8]. Then in the group-level analysis, using parametric empirical Bayes (PEB)[9,10], associations were found between estimated model parameters and self-reported scores in which estimated effective connectivity for each subject was taken to group-level to estimate group effects.

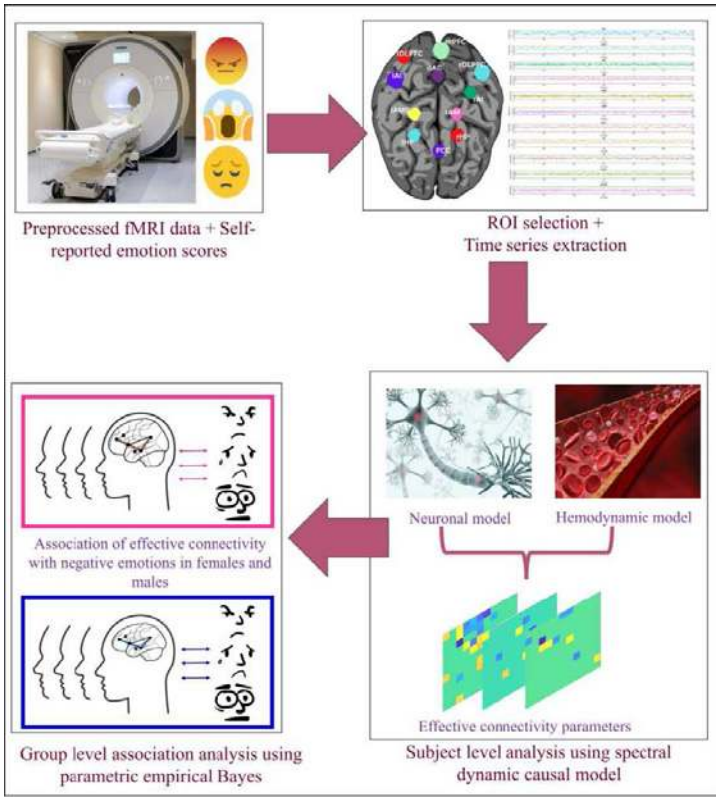

Results: We only report our group level PEB results with strong evidence that is at a posterior probability > 0.95. Our results have shown strongest negative association of self-connection of hippocampus with each of the heightened negative emotions in females. In males, our study revealed the associations of the self-connection of dACC, inhibitory connection from right amygdala to dACC and inhibitory connection from dACC to left hippocampus with high fear-affect, anger-affect and sadness respectively.

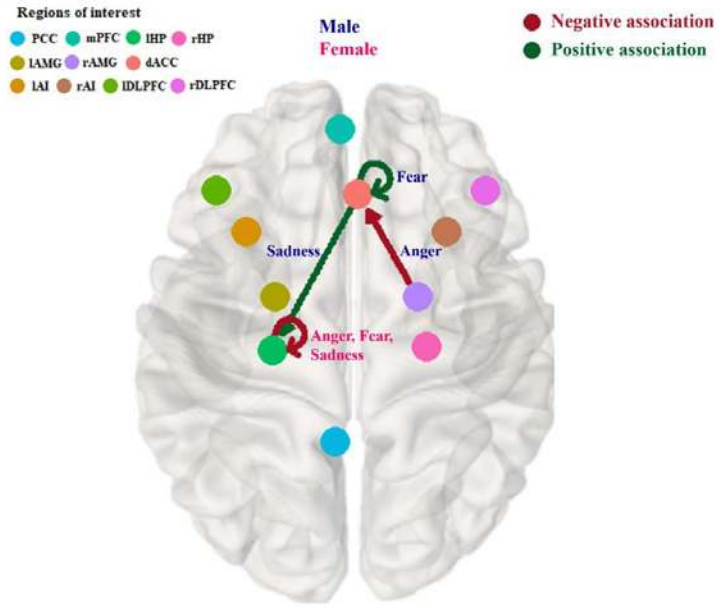

We only show the top most associations of effective connectivity with self-reported basic negative emotions, in both male and female groups. Green and red lines show positive and negative associations.

Conclusions: Our research provide evidence that the attitude towards basic negative emotions has different underlying neural mechanism in males and females. The key results signify the prominent roles of dACC and left hippocampus in heightened negative emotions of anger, fear and sadness in male and female respectively. Our investigation suggests that targeting these specific brain areas for sex-specific therapies and interventions for psychopathology treatment may result in better health outcomes.

References

1. Bouziane, Ismail, et al. (2022) “Enhanced Top-down Sensorimotor Processing in Somatic Anxiety.” Translational Psychiatry, vol. 12, no. 1, Nature Publishing Group
2. Deng, Yaling, et al. (2016) “Gender Differences in Emotional Response: Inconsistency between Experience and Expressivity.” PloS One, vol. 11, no. 6, PLoS One
3. Domes, Gregor, et al. (2010) “The Neural Correlates of Sex Differences in Emotional Reactivity and Emotion Regulation.” Human Brain Mapping, vol. 31, no. 5, Hum Brain Mapp
4. Fischer, Agneta H., et al. (2018) “Gender Differences in Emotion Perception and Self-Reported Emotional Intelligence: A Test of the Emotion Sensitivity Hypothesis.” PloS One, vol. 13, no. 1, PLoS One
5. Friston, Karl J, et al. (2014) “A DCM for Resting State FMRI.” NeuroImage, vol. 94, pp. 396–407
6. Friston, Karl J., et al. (2016) “Bayesian Model Reduction and Empirical Bayes for Group (DCM) Studies.” NeuroImage, vol. 128, Academic Press Inc., pp. 413–31
7. Razi, Adeel, et al. (2015) “Construct Validation of a DCM for Resting State FMRI.” NeuroImage, vol. 106, Academic Press Inc., pp. 1–14,
8. Stoica, T., et al. (2021) “Gender Differences in Functional Connectivity during Emotion Regulation.” Neuropsychologia, vol. 156, Neuropsychologia
9. Whittle, Sarah, et al. (2011) “Sex Differences in the Neural Correlates of Emotion: Evidence from Neuroimaging.” Biological Psychology, vol. 87, no. 3, pp. 319–33
10. Zeidman, Peter, et al. (2019) “A Guide to Group Effective Connectivity Analysis, Part 2: Second Level Analysis with PEB.” NeuroImage, vol. 200, Academic Press Inc., pp. 12–25,

Poster No 717

Limbic Network Response to Anti-Vaping Messages Predicts Reduced Vaping in Young Adult Vapers

Jiaying Liu[1,2,3], Jessica Fabbricatore[2], Joshua McMains[3], Allison Worsdale[2], Erin Jones[3], Yidi Wang[1], Jason Cheng[4], Lawrence Sweet[3]

[1]Department of Communication, University of California Santa Barbara, Santa Barbara, CA, [2]Department of Communication Studies, University of Georgia, Athens, GA, [3]Department of Psychology, University of Georgia, Athens, GA, [4]Queen Margaret's School, Duncan, British Columbia

Introduction: Vaping is the most common method of tobacco use among young adults (YA) in the US (Cornelius et al., 2020). Vaped substances are often flavored, palatable and misperceived as safe (Romijnders et al., 2018). Anti-vaping public service announcements (PSAs) utilizing cognitive, emotional, and social appeals to discourage vaping have been adopted as a crucial part of tobacco control efforts (Tan et al., 2018). However, evidence regarding the neurobehavioral mechanism and utility of each message type is sparse. This study employed functional MRI (fMRI) to determine whether neural responses to anti-vaping PSAs in limbic and perceptual networks predict YA vaping frequency 1-month later, and to examine how different types of message appeals may influence these expected effects.

Methods: 49 YA non-smokers who vaped >15 of the past 30 days completed an fMRI PSA reactivity paradigm that included series of anti-vaping messages with cognitive, emotional, and social appeals (Figure 1). Messages were presented in a counterbalanced block design during two imaging runs, with each appeal type appearing in six 30s blocks of 10s PSAs. Six 20s blocks of scrambled control images were also displayed. Vaping severity was assessed via 4 weekly self-report timeline follow-back surveys (Pedersen et al., 2012). Echoplanar data were acquired using a GE 3T MRI with 2s temporal and 3.5mm3 spatial resolution. Data processing included slice-time correction, registration, outlier/motion censoring, removal of linear drift, a 5mm blur, and stereotaxic standardization. Effects per brain voxel were quantified with general linear modeling of the fMRI signal using the time course of each message type as regressors and observed movement as covariates. Hypotheses were tested in regression analyses predicting 1-month vaping frequencies, from mean fMRI responses in 12 regions of interest (ROIs) in limbic and visual perception networks, known to be associated with the efficacy of health messaging on tobacco use behaviors (Shi et al., 2023).

Figure 1

Example Cognitive, Emotional and Social PSAs and a Scrambled Control Image

(a) Cognitive PSA (b) Emotional PSA (c) Social PSA (d) Scrambled Control

Results: 12 of 14 a priori ROIs exhibited significant response to any of the PSA types (one sample t-test vs. 0; $p<.05$) and were therefore used in hypothesis testing. Table 1 shows these 12 a priori ROIs nested within the two networks. Stronger activation responses to PSAs in the limbic network were significantly associated with lower vaping frequencies during the following month ($\beta=-.43$, $p=.008$). Neural activity in the visual perception network was not linked to vaping outcomes ($\beta=-.19$, $p=.258$). Significant limbic network effects were then examined by PSA type. A significant moderation effect of message type was observed such that increased limbic network activity during exposure to cognitive ($\beta=-.48$, $p=.002$) and social ($\beta=-.46$, $p=.004$), but not emotional PSAs ($\beta=-.23$, $p=.178$), was associated with reduced vaping severity one month later.

Table 1
A Priori Regions of Interest and Coordinates

Regions of Interest	x	y	z
Limbic Subnetwork			
Left hippocampus	20	12	-7
Left amygdala	23	5	-15
Left insula	34	9	-2
Right hippocampus/amygdala	-23	9	-12
Unimodal and Multimodal Perception Subnetwork			
Left middle occipital gyrus	35	69	1
Left inferior occipital gyrus	43	76	0
Left fusiform gyrus	33	78	-11
Left inferior temporal gyrus	39	47	-6
Left middle temporal gyrus	48	69	9
Right inferior occipital/temporal gyrus	-46	72	1
Right fusiform gyrus	-41	53	-11
Right calcarine sulcus	-10	88	5

Note. RAI Talairach x, y, z coordinates. Each ROI is defined by a radius of 5mm around the specified coordinates.

Conclusions: Results suggest that anti-vaping messages elicit significant responses in limbic and visual perceptual networks, and that the intensity of limbic response specifically predicts subsequent vaping frequency. This predictive utility is driven by responses to cognitive and social, but not emotional messages in limbic nodes associated with emotion, episodic learning, and memory. This counter-intuitive finding suggests that emotional responses to cognitive and social appeals, but not to emotional appeals, may serve as useful neuromarkers of vaping outcomes. Cognitive and social messages may prove most effective in predicting reductions in vaping when they provoke deeper processing via greater individual interpretations of emotional salience. In contrast, lower predictive utility of emotional PSAs might be due to provocation of counter arguing. These findings highlight the potential of fMRI to identify neuromarkers of vaping severity, providing insights for prioritizing message appeals in anti-vaping educational campaigns targeting YAs.

References

1. Cornelius, M.E. et al. (2020), 'Tobacco product use among adults — United States, 2019', Morbidity and Mortality Weekly Report, vol. 69, no. 46, pp. 1736–1742.
2. Pedersen, E.R. et al. (2012), 'Concurrent validity of an online version of the timeline follow-back assessment', Psychology of addictive behaviors: Journal of the Society of Psychologists in Addictive Behaviors, vol. 26, no. 3, pp. 672–677.
3. Romijnders, K.A.G.J. et al. (2018), 'Perceptions and reasons regarding e-cigarette use among users and non-users: A narrative literature review', International Journal of Environmental Research and Public Health, vol. 15, no. 6, pp. 1190.
4. Shi, Z., et al. (2023). 'Effects of emotional arousal on the neural impact and behavioral efficacy of cigarette graphic warning labels', Addiction, vol. 118, no. 5, pp. 914–924.
5. Tan, A. S. L. et al. (2018), 'Effects of exposure to anti-vaping public service announcements among current smokers and dual users of cigarettes and electronic nicotine delivery systems', Drug and Alcohol Dependence, vol. 188, pp. 251–258.

Poster No 718

Neuroforecasting online engagement with nature images

Tara Srirangarajan[1], Nik Sawe[1], Tierney Thys[2], Cynthia Wu[1], Brian Knutson[1]

[1]Stanford University, Stanford, CA, [2]California Academy of Sciences, San Francisco, CA

Introduction: Visual images can facilitate online engagement and support for endangered species, but the mechanisms supporting their impact remains unclear. By combining behavior, neuroimaging, and surveys, we sought to examine how images depicting endangered species encourage engagement on a popular social media platform (i.e., Instagram.com). Specifically, we leveraged a neuroforecasting approach by using brain activity prior to choice not only to predict subsequent choice in individuals, but also to forecast aggregate choice in other groups[1]. Prior research has shown that group neural activity can forecast aggregate demand in different markets ranging from music sales[2] to the effectiveness of health advertising campaigns[3]. A consistent set of brain regions whose activity has been associated with affect and motivation have been implicated in previous neuroforecasting literature. According to an Affect-Integration-Motivation (or AIM) framework, Nucleus Accumbens (or NAcc) activity is associated with gain anticipation and predicts approach behavior, Anterior Insula (or AIns) activity is associated with loss anticipation and predicts avoidance behavior, and Medial PreFrontal Cortex (or MPFC)

activity is associated with value integration and identity and predicts approach behavior[4]. We predicted that activity in these regions (i.e., +NAcc, –AIns, +MPFC) would predict individual engagement with nature images, and that group activity in a subset of these regions might also forecast aggregate engagement.

Methods: 37 healthy right-handed English-speaking adults with pre-existing Instagram accounts participated in the neuroimaging study. FMRI data were acquired using a 3.0 T General Electric MRI scanner equipped with a 32-channel head coil at the Stanford Center for Cognitive and Neurobiological Imaging. During FMRI scanning, participants viewed 56 photographs selected from the Instagram feed of a prominent environmentally-focused publication (i.e., National Geographic Magazine). Photos sampled wildlife images selected from a pool of 888 total images posted over the span of three months. 14 images were preselected from each quartile of engagement (e.g., the most and least popular quarter of photos). Trials first included presentation of an image (4 sec), next a question about liking (2 sec), followed by a choice prompt (Y/N counterbalanced left/right; 4 sec), then a question about donation (2 sec) followed by a choice prompt (Y/N counterbalanced left/right; 4 sec), and finally a variable intertrial interval indicated by a central fixation cross (2-6 sec). To maintain incentive compatibility, one liking decision and one donation decision were randomly selected to count as binding at the conclusion of the experiment. For anatomically-targeted data analyses, neural Volumes Of Interest (VOIs) were specified in regions highlighted in the AIM framework (4). Specifically, spherical Volumes Of Interest (VOIs; 8 mm in diameter) were centered on bilateral foci in the Nucleus Accumbens (NAcc; TC: ±10, 12, –2), Anterior Insula (AIns; TC: ±34, 24, –4), and Medial PreFrontal Cortex (MPFC; TC: ±4, 45, 0). Activity within each VOI was averaged across voxels and then averaged bilaterally to derive activity time courses.

Results: As predicted, findings indicated that activity in brain circuits associated with anticipatory affect (i.e., the NAcc and MPFC) predicted individual liking and donations (NAcc: $Z=2.11$, $p < 0.001$; MPFC: $Z=5.21$, $p < 0.001$). Group brain activity in an integrative part of this circuit (MPFC) also forecast engagement on Instagram ($t=2.55$, $p < 0.001$) (Figure 1).

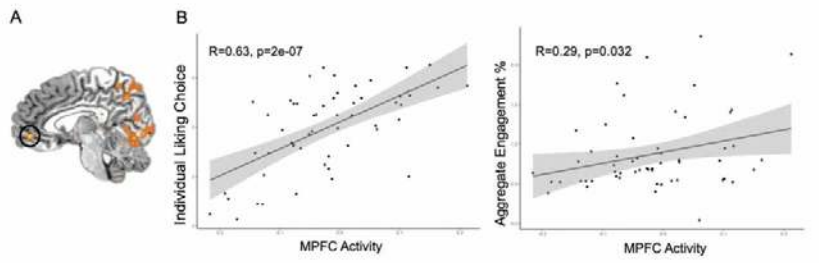

Figure 1: MPFC activity associated with individual liking choice as well as ranked aggregate liking of nature images. A. Whole-brain activation map indicating regions associated with processing images eliciting higher versus lower engagement ($p < 0.001$). Superimposed black circle indicates predefined MPFC VOI based on meta-analytic foci (from Neurosynth.org). B. Pairwise correlations of MPFC activity with individual liking choice (middle panel) and online aggregate liking (right panel).

Conclusions: To examine how images of endangered species elicit engagement, we combined behavioral probes, a neuroimaging experiment, and representative surveys. These findings not only extend neuroforecasting to online engagement with images of endangered species, but also offer the possibility that neural data might reveal which image features drive online engagement.

References

1. Knutson, B. (2018), 'Neuroforecasting Aggregate Choice,' Current Directions Psychological Science 27(2), 110-115.
2. Berns, G. S. (2012), 'A neural predictor of cultural popularity,' Journal of Consumer Psychology 22, 154–160.
3. Falk, E. B. (2012), 'From Neural Responses to Population Behavior: Neural Focus Group Predicts Population-Level Media Effects,' Psychological Science 23, 439–45.
4. Samanez-Larkin, G. R. (2015), 'Decision making in the ageing brain: changes in affective and motivational circuits,' Nature Reviews Neuroscience, 16(5), 278–289.

Poster No 719

Impact of Emotional Regulation on Well-being and Its Association with Brain Volume

Brenda Arce[1], Maribel Delgado[1], Azalea Aguilar[2]

[1]Universidad Nacional Autónoma de México, Querétaro, México, [2]Universidad Nacional Autónoma de México, México, México

Introduction: Emotional regulation (ER) involves perceiving, understanding, and managing emotions (Navarro et al., 2018). The strategies for emotional regulation that have received greater empirical support are Cognitive Reappraisal (CR) and Expressive Suppression (ES) (Gross, 1998; Navarro et al., 2018). CR modifies the emotion by reinterpreting situations to alter its emotional impact (Gross, 1998; John & Gross, 2007); its frequent use is associated with better interpersonal functioning, enhanced psychological well-being, and reduced symptoms of depression in healthy individuals (Gross & John, 2003; Goldin et al., 2019). In contrast, ES focuses on inhibiting emotional expression (John & Gross, 2007; Navarro et al., 2018); is negatively associated with well-being and positively associated with anxiety, and depressive symptoms (Gross, 2002; Goldin et al., 2008). Structural neuroimaging studies have shown findings regarding the differential use of ER strategies, specifically usage of ES shows variations in gray matter volume in the ventromedial and dorsomedial PFC, dorsal anterior cingulate cortex, superior frontal gyrus and insula (Welborn et al., 2009; Hermann et al., 2014; Moore et al., 2016). Whereas CR shows variations in the superior frontal cortex, ventromedial PFC, dorsal anterior cingulate and amygdala (Welborn et al., 2009; Hermann et al., 2014; Moore et al., 2016). These findings suggest that both RE strategies are differentially associated with emotional well-being and that their frequent use generates variations in the volume of gray matter; however, whole-brain structural studies are needed based on individual differences in the use of RE strategies.

Methods: Objective Explore the relationship between brain volumes in emotion regulation strategies structures and emotional well-being, considering individual differences in CR and ES. Participants 53 healthy volunteers (20 male) between 24-41 years old (M =27.18, SD =3.10), native Spanish speakers, right-handed, and without neurological or psychiatric disorders. Measures Emotional regulation strategies: the Spanish adaptation of the Emotion Regulation Questionnaire (ERQ). Emotional well-being variables: the Spanish adaptation of the Beck's Depression Inventory (BDI-IA), the Mexican version of the State-Trait Anxiety Inventory (STAI), the Mexican version of the Perceived Stress Scale (PSS-14) and the spanish version of the Interpersonal Reactivity Index (IRI) divided into four independent dimensions: Fantasy (FS), Perspective Taking (PT), Empathic Concern (EC) and Personal Distress (PD). MRI acquisition and analysis The anatomical scans were acquired using a 3 Tesla whole-body scanner (Philips, Amsterdam, Netherlands) and a Sense-Head-32 channel coil. Structural images were acquired using a T1-weighted 3D turbo field echo (TFE) sequence consisting of 176 sagittal slices (TR=8.3 ms, TE= 3.9 ms, flip angle: 8°, FoV: 256 256 mm, voxel size: 1 x 1 x 1 mm). Acquisition time: 6 minutes. Preprocessing and structure volumes were generated using vol2Brain pipeline v.2.0. [https://volbrain.net].

Results: Negative correlations between CR and anxiety, depression, and stress (Figure 1a). Positive correlations between ES and depression, anxiety, distress, and stress. Grouping based on CR and ES scores revealed higher stress in the low CR group and higher stress, anxiety, depression, and distress in the high ES group (Figure 1b). Brain volume analysis showed positive correlations between state anxiety and specific frontal brain regions and hippocampus, PT and specific frontal regions and cingulate, and FS and specific frontal brain regions, all for the high ES group. Multiple linear regressions indicated predictive relationships between ES strategy groups, emotional well-being, and brain volume (Figure 2a and 2b).

a

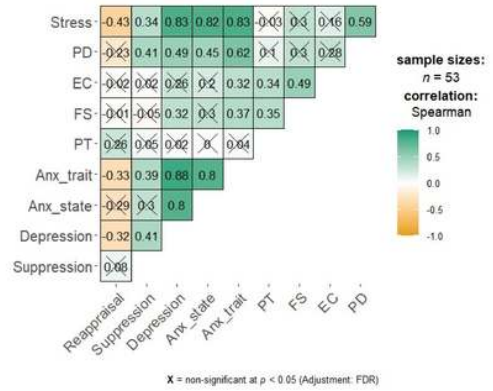

b

	Cognitive Reappraisal			Expressive Suppression		
	high	low		high	low	
	n=29	n=24		n=26	n=27	
	Median (IQR)	Median (IQR)	p Value	Median (IQR)	Median (IQR)	p Value
Depression	7 (16)	12 (15.5)	N.S.	17.5 (16.5)	6 (9.5)	<0.001
Stait Anxiety	38 (19)	43 (23.75)	N.S.	45.5 (18.75)	33 (16)	<0.01
Trait Anxiety	44 (18)	50.5 (16.25)	N.S.	52.5 (11.75)	38 (19)	<0.001
Stress	18 (17)	31.5 (16.75)	<0.01	29.5 (14.25)	17 (18.5)	<0.01
PT	18 (4)	15 (6.25)	N.S.	18 (7.25)	16 (4)	N.S.
FS	14 (4)	13.5 (6.25)	N.S.	13 (5.75)	14 (4.5)	N.S.
EC	15 (5)	14 (3)	N.S.	15.5 (3.75)	14 (5)	N.S.
PD	11 (5)	13 (6.75)	N.S.	14.5 (5.5)	11 (6)	<0.01

Figure 1. In a. Correlation analysis between emotional regulation strategies and emotional well-being variables. Significant negative correlations between CR and depression, trait anxiety, and stress. Significant positive correlations between SE and depression, trait anxiety, stress and PD. Non-significant correlations are marked with an 'x'. FDR adjusted p-value (0.05). **In b.** Between-group comparisons of high and low CR and SE scores. The p value was adjusted using the Holm method. Significant differences between high and low CR and stress for the low CR group. Significant differences between high and low SE and almost all the emotional well-being variables, except in PT, FS and EC for the high SE group.

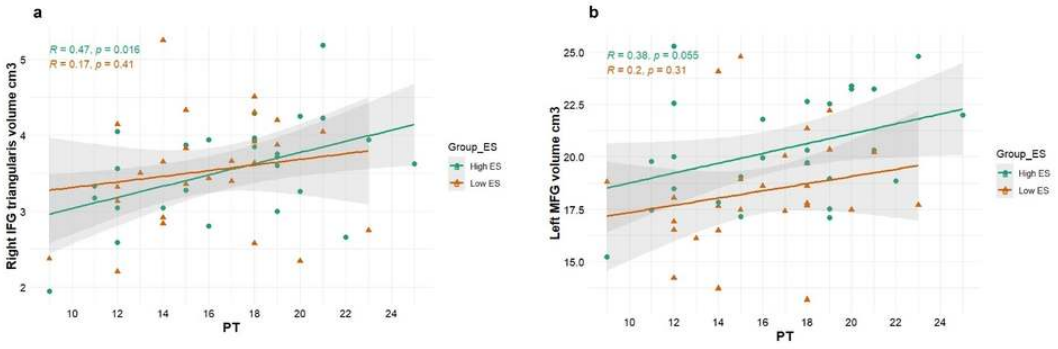

Figure 2. In a. Multiple linear regressions between PT scores and the volume of the right IFG opercularis in relation to high and low SE groups. Higher PT scores predict an increase in the volume of the right IFG opercularis (F= 10.32, R= 0.26, p<0.001) in the high SE group. **In b.** Multiple linear regressions between PT scores and the volume of the left MFG in relation to high and low SE groups. Higher PT scores predict an increase in the volume of the left MFG (F= 6.35, R= 0.17, p<0.01) in the high SE group.

Conclusions: The results of this study emphasize the importance of the differential role of the ES strategy and its relationship on emotional well-being and brain volume.

References

1. Goldin, P. R. (2008), 'The neural bases of emotion regulation: reappraisal and suppression of negative emotion', Biological psychiatry, 63(6), 577–586. https://doi.org/10.1016/j.biopsych.2007.05.031
2. Goldin, P. R. (2019), 'Acceptance versus reappraisal: Behavioral, autonomic, and neural effects', Cognitive, affective & behavioral neuroscience, 19(4), 927–944. https://doi.org/10.3758/s13415-019-00690-7
3. Gross, J. J. (1998), 'The Emerging Field of Emotion Regulation: An Integrative Review', Review of General Psychology, 2(3), 271-299. https://doi.org/10.1037/1089-2680.2.3.271
4. Gross J. J. (2002), 'Emotion regulation: affective, cognitive, and social consequences', Psychophysiology, 39(3), 281–291. https://doi.org/10.1017/s0048577201393198
5. Gross, J. J. (2003), 'Individual differences in two emotion regulation processes: implications for affect, relationships, and well-being', Journal of personality and social psychology, 85(2), 348–362. https://doi.org/10.1037/0022-3514.85.2.348
6. Hermann, A. (2014), 'Brain structural basis of cognitive reappraisal and expressive suppression', Social cognitive and affective neuroscience, 9(9), 1435–1442. https://doi.org/10.1093/scan/nst130
7. John, O. P. (2007), 'Individual Differences in Emotion Regulation', In J. J. Gross (Ed.), Handbook of emotion regulation (pp. 351–372). The Guilford Press.
8. Moore, M. (2016), 'Localized or diffuse: the link between prefrontal cortex volume and cognitive reappraisal', Social cognitive and affective neuroscience, 11(8), 1317–1325. https://doi.org/10.1093/scan/nsw043
9. Navarro, J. (2018), 'Validación psicométrica del Cuestionario de Regulación Emocional (ERQ-CA) en población adolescente Española [Psychometric validation of the Emotional Regulation Questionnaire (ERQ-CA) in adolescent population]', Revista de Psicología Clínica con Niños y Adolescentes, 5(1), 9–15. https://doi.org/10.21134/rpcna.2018.05.1.1
10. Welborn, B. L., Papademetris, X., Reis, D. L., Rajeevan, N., Bloise, S. M., & Gray, J. R. (2009), 'Variation in orbitofrontal cortex volume: relation to sex, emotion regulation and affect'. Social cognitive and affective neuroscience, 4(4), 328–339. https://doi.org/10.1093/scan/nsp028

Poster No 720

Subcortical emotion-related circuitry serves as brain-based classifier of math anxiety in children

Yi-Cheng Cho[1], Chan-Tat Ng[1], Ting-Ting Chang[1,2]

[1]Department of Psychology, National Chengchi University, Taipei City, Taiwan, [2]Research Center for Mind, Brain, and Learning, National Chengchi University, Taipei City, Taiwan

Introduction: Math anxiety (MA) has been shown to severely impact children's mathematical performance. While prior research identified brain regions associated of math and emotion like intraparietal sulcus, amygdala, and insula (Lyons and Beilock, 2012, Young et al., 2012, Pletzer et al., 2015), understanding of the functional circuits underlying MA remains scarce. This study leveraged data-driven machine learning to fully capture the potential whole-brain resting-state functional connectivity (FC) features associated with MA.

Methods: We recruited 133 participants aged 7 to 19 years (M = 10.40, SD = 0.45; 76 females and 57 males) in this study, categorized as high and low MA based on mean MA scores from the Chinese-adapted Child Math Anxiety Questionnaire (CMAQ; Ng et al., 2022). Participants underwent a series of cognitive assessments, including Block Design, Vocabulary,

and Digit Span subtests from the WISC-IV, along with an arithmetic fluency test (Chang et al., 2018) (Fig. 1A). During the MRI session, participants underwent an eye-closed resting-state functional scans (Fig. 1B). The functional imaging data were preprocessed using SPM12, and whole-brain resting-state FC measures were computed across 166 brain regions of interest (ROIs) based on the automated anatomical labeled (AAL3) atlas, resulting in 13,695 ROI-to-ROI FC measures (Fig. 1C). Feature selection was then conducted in two stages: initially through Pearson correlation to identify FC measures that were linearly correlated to MA (with a significance threshold of $p < .001$), followed by mutual information techniques (Vergara & Estévez, 2014) for feature refinement, narrowing to the top 40 most informative features. Two distinct features sets were established: brain-only features comprised only of FC measures and brain-and-cognition features which included both FC measures and cognitive scores. These features were then used respectively in a random-forest machine learning model with 5-fold cross validation for MA classification. The model trained on 80% of the data, reserving 20% for validation and feature importance analyses (Fig. 1D).

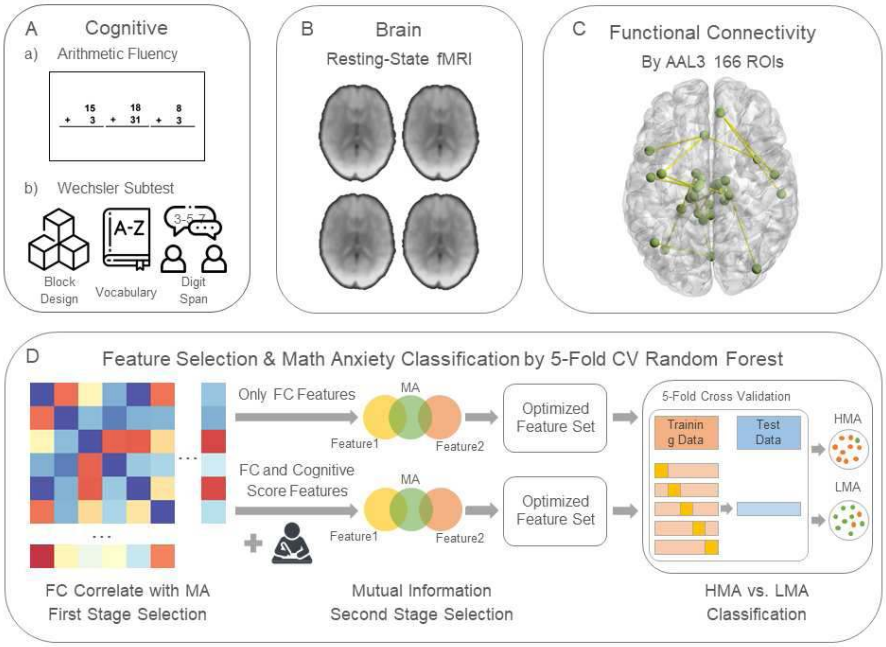

Figure 1. Pipeline of the current study for math anxiety (MA) classification using cognitive and resting-state functional connectivity (FC) measures. (A) Cognitive assessments comprised of arithmetic fluency test and WISC-IV subtests. **(B)** Collection of resting-state MRI data with participants' eyes closed. **(C)** ROI-to-ROI functional connectivity analysis based on 166 brain regions using the AAL3 atlas for whole-brain parcellation. **(D)** Two-stage feature selection process utilizing Pearson correlation to initially identify FC measures correlated with MA at $p < .001$, followed by mutual information for feature refinement, resulting in two optimized features sets: one incorporating only brain FC measures, and the other combining these with cognitive measures. MA classification (high or low MA) performed using a 5-fold cross-validated random forest model with the two optimized feature sets, respectively.

Results: The initial stage of feature selection found 197 FC measures significantly correlating with MA. These measures were primarily associated with connections within or between subcortical regions (94.9% of the significant connections), predominately the thalamus and cerebellum. Following the application of mutual information techniques, we distilled these measures down to two optimized sets of 40 features each for the subsequent MA classification. Both brain-only and brain-and-cognition models demonstrated high MA classification accuracy scores (81.5% and 85.2%, respectively) (Fig. 2). Further feature importance analyses highlighted the pivotal role of subcortical connections, especially those involving the thalamus (20 out of 40 features) and cerebellum (12 out of 40 features). Additionally, we identified connections between subcortical and cortical regions, especially those implicated in emotional processing (such as the anterior cingulate cortex and insula) and the default mode network (including the angular gyrus and posterior cingulate cortex, mean |SHAP| value exceeds 0.1). While the inclusion of cognitive abilities in the brain-and-cognition model, notably the subtraction component of arithmetic fluency, enhanced model accuracy, the predominant contributors to the classification success were connectivity measures.

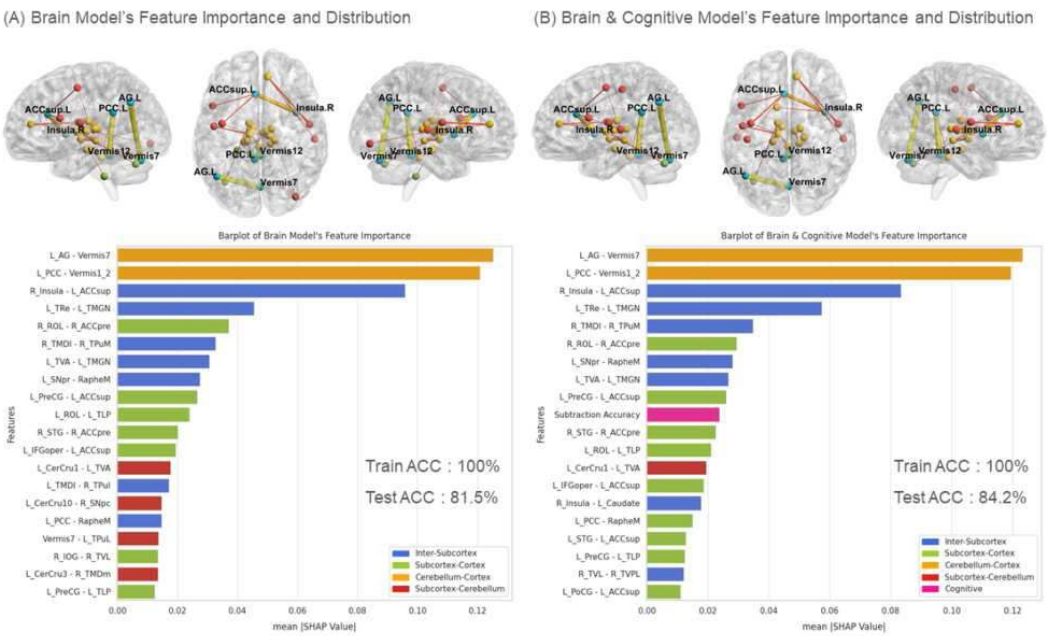

Figure 2. Performance and feature importance analyses of the 5-fold cross-validated random forest classifiers. Anatomical locations (top panel) and feature importance values (bottom panel) of the connectivity or cognitive measures among the top 20 important features in (A) the brain-only model and (B) brain-and-cognition model.

Conclusions: Using a data-driven machine learning approach, our study highlights the pivotal contributions of subcortical regions for MA. Particularly, we demonstrated that subcortical connections involving thalamus and cerebellum, rather than within-cortical connection or cognitive ability, were among the top contributors in MA classification. This integrated approach deepens our understanding of math anxiety's multifaceted nature, providing potential subcortical brain-based biomarkers for MA identification and remediation.

References

1. Chang, T. T., Lee, P. H., & Metcalfe, A. W. (2018). Intrinsic insula network engagement underlying children's reading and arithmetic skills. NeuroImage, 167, 162-177.
2. Lyons, I. M., & Beilock, S. L. (2012). Mathematics anxiety: Separating the math from the anxiety. Cerebral cortex, 22(9), 2102-2110.
3. Ng, C. T., Chen, Y. H., Wu, C. J., & Chang, T. T. (2022). Evaluation of math anxiety and its remediation through a digital training program in mathematics for first and second graders. Brain and behavior, 12(5), e2557.
4. Pletzer, B., Kronbichler, M., Nuerk, H. C., & Kerschbaum, H. H. (2015). Mathematics anxiety reduces default mode network deactivation in response to numerical tasks. Frontiers in human neuroscience, 9, 202.
5. Vergara, J. R., & Estévez, P. A. (2014). A review of feature selection methods based on mutual information. Neural computing and applications, 24, 175-186.
6. Young, C. B., Wu, S. S., & Menon, V. (2012). The neurodevelopmental basis of math anxiety. Psychological science, 23(5), 492-501.

Poster No 721

Brain Circuits During Arithmetic Are Predictive of Real-Time Trial-Based Math Anxiety Measurement

Chan-Tat Ng[1], Yi-Cheng Cho[1], Xin-Yu Chen[1], Ting-Ting Chang[1,2]

[1]Department of Psychology, National Chengchi University, Taipei, Taiwan, [2]Research Center for Mind, Brain, and Learning, National Chengchi University, Taipei, Taiwan

Introduction: Math anxiety (MA) poses a global educational challenge, affecting learners of different ages (Barroso et al., 2021). While neuroimaging studies have provided insights into brain mechanisms of MA, they often focused on trait anxiety measure outside the scanner. This study addresses this gap by investigating the neural predictors associated with real-time MA during math problem-solving in adults using functional MRI and machine-learning techniques.

Methods: Fig 1 depicts the overall methodology. We recruited 43 adults (M = 22.6, SD = 2.12; 26 females) in this study. During fMRI scanning, participants performed math problems of varying complexity (Lyons et al., 2012), and real-time MA was evaluated via post-trial ratings, averaging standardized differences in emotional responses and perceived difficulty between complex and simple problems. Generalized Anxiety Disorder-7, Chinese-adapted Math Anxiety Questionnaire for Adults (MAQA; Szczygiel, 2022), WAIS-IV working memory, and arithmetic fluency (Chang et al., 2018) were assessed in separate

sessions and used as control variables. Brain activity was analyzed using SPM12's general linear model. After a standard preprocessing pipeline, voxel-wise t-maps contrasting complex and simple problems were generated for each participant. Whole-brain group-level regression was performed to explore the differences in the relative brain activity between median-split groups based on real-time MA, identifying activations at a voxel-wise threshold of $p < .001$ and a cluster threshold of $p < .01$. Further analyses were conducted based on 21 predefined regions of interest (ROIs), identified via Neurosynth's term-based meta-analysis. We extracted clusters based on search terms "anxiety", "arithmetic", and "DMN" (default mode network), with a cluster size of $k >= 50$. LASSO regression with a logistic function was conducted 1000 times with 10-fold cross-validation for feature selection, identifying the most relevant ROIs based on a 75% frequency threshold of nonzero selection. Moderation analyses within the selected ROIs were conducted to assess the impact of MA on the brain-performance relationship.

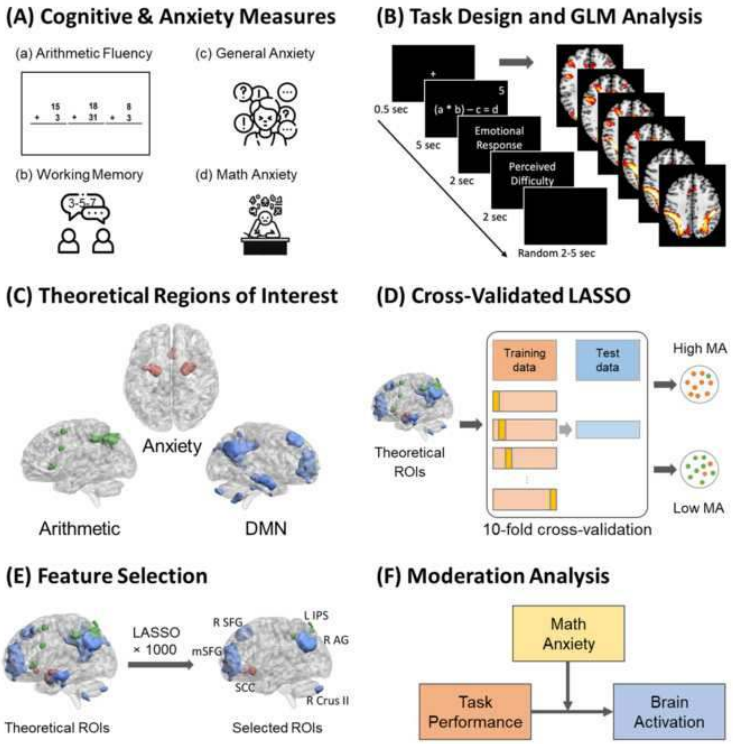

Fig 1. Methodological framework for assessing real-time math anxiety (MA). (A) Cognitive and anxiety assessments, including arithmetic fluency, working memory, general anxiety, and math anxiety. **(B)** The math problem-solving task used in this study, along with the collection of emotional response and perceived difficulty ratings during fMRI scanning. **(C)** Theoretical regions of interest (ROIs) were identified through Neurosynth using search terms "anxiety", "arithmetic", and "DMN" (default mode network). **(D)** Implementation of a 10-fold cross-validated LASSO regression to classify real-time MA based on the theoretical ROIs, aiming for feature selection. **(E)** Selection of consistently contributing features from 1000 iterations of cross-validated LASSO, with a 75% frequency threshold for nonzero selection. **(F)** Moderation analysis investigating the impact of real-time MA on the association between task performance and brain activation within the LASSO-selected ROIs.

Results: Spearman correlation analyses revealed that real-time MA was moderately correlated with MAQA ($r = .438$, $p = .005$) and task error rate ($r = .321$, $p = .043$), controlling for other variables. Whole-brain analyses revealed that participants with higher real-time MA showed increased brain activity within the medial superior frontal gyrus (mSFG) and left middle frontal gyrus (MFG; Fig 2A). ROI analyses identified 6 brain regions as stably contributing to the cross-validated LASSO model: the right intraparietal sulcus (IPS) from the arithmetic network, the subcallosal cortex (SCC) from the anxiety network, and the left angular gyrus (AG), mSFG, right SFG, and right crus II from the DMN (Fig 2B). All these predictors showed positive relative beta coefficients, except for IPS being negative (Fig 2C). Critically, interactive effects between relative task error rate and MA group on relative brain activity were observed in the SCC ($p = .016$) and right SFG ($p = .005$) after accounting for the control variables (Fig 2D). Particularly, marginally significant connections between brain and behavior were observed in the low-level MA group ($p = .080$ and $.081$, respectively) but not in the high-level MA group ($p > .10$).

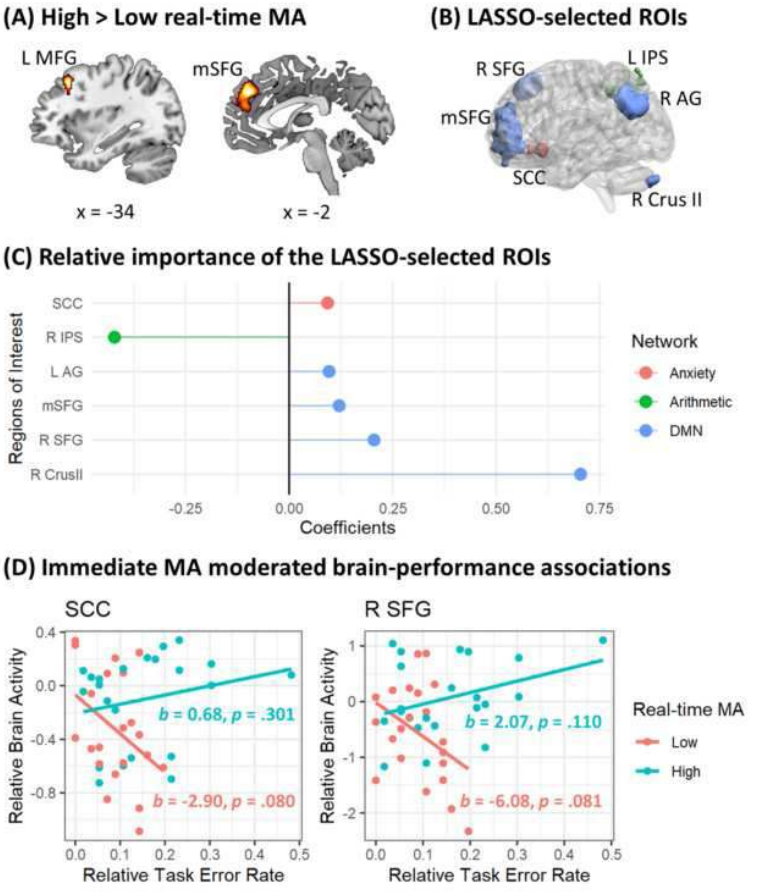

Fig 2. Neural activity and feature selection in relation to real-time trial-based math anxiety (MA). (A) Whole-brain analysis indicates increased activity in the left MFG and mSFG among participants with high real-time MA compared to those with low real-time MA. **(B)** Among the 21 pre-defined regions of interest (ROIs) within the anxiety, arithmetic, and default mode (DMN) networks, six regions – SCC, L IPS, R SFG, mSFG, R AG, and R Crus II – showed stable contribution across 1000 iterations in a 10-fold cross-validated LASSO model. **(C)** Depiction of average beta coefficients for the LASSO-selected ROIs, demonstrating the direction and relative magnitude of their contribution. Positive coefficients suggested that increased activity was associated with high real-time MA, and negative coefficients indicated the opposite. **(D)** Scatterplots show interaction effects between the relative task error rate and brain activity in the SCC and right SFG across high and low MA groups. L/R, left/right; m, medial; MFG, middle frontal gyrus; SFG, superior frontal gyrus; SCC, subcallosal cortex; IPS, intraparietal sulcus; AG, angular gyrus.

Conclusions: This study advances our understanding of the neural correlates of real-time MA, highlighting its impact on task performance and brain activity within relevant networks. The whole-brain analysis and LASSO feature selection together demonstrated real-time MA to be associated with heightened activity within the DMN and prefrontal cortex, as well as reduced activity in right IPS. Notably, real-time MA also moderated the connection between brain activation and task performance during math problem-solving. These findings provide valuable perspectives for strategies targeting MA and potential applications in educational contexts.

References

1. Barroso, C. (2021), 'A meta-analysis of the relation between math anxiety and math achievement', Psychological Bulletin, vol. 147, no. 2, pp. 134-168.
2. Chang, T.-T. (2018), 'Intrinsic insula network engagement underlying children's reading and arithmetic skills', NeuroImage, vol. 167, pp. 162-177.
3. Lyons, I.M. (2012), 'When math hurts: Math anxiety predicts pain network activation in anticipation of doing math', PLoS One, vol. 7, no. 10, Article e48076.
4. Szczygiel, M. (2022), 'Not only reliability!: The importance of the ecological validity of the math anxiety questionnaire for adults', European Journal of Psychological Assessment, vol. 38, no. 2, pp. 78-90.

Poster No 722

Exploring the Brain, Emotion, and Personality with Video Games - An appraisal perspective

Mi Xue Tan[1], Joana Leitao[1], Dimitri Van De Ville[2], Patrik Vuilleumier[3]

[1]University of Geneva, Geneva, Geneva, [2]École Polytechnique Fédérale de Lausanne, Lausanne, Switzerland, [3]University of Geneva, Geneva, Switzerland

Introduction: The nature of emotions and their neural underpinnings remain debated. Here we study whether appraisal theories the component process model may account for the differentiation of emotional states and their functional organisation in the brain. This theory proposes that events are perceived and evaluated according to distinct cognitive dimensions (appraisals) that are key to eliciting the range of emotions we experience. Appraisals trigger changes in behaviour, physiology, and brain activity patterns. Building on a previous study, we manipulated the appraisal of goal obstructiveness during a first-person video game.

Methods: We developed a stealth game to manipulate appraisals in a systematic yet immersive way. The interactive nature of video games heightens self-relevance through goal-directed action, evoking strong emotions. The goal of the game was to maximise points and avoid enemies in a virtual labyrinth. Goal obstructiveness was manipulated at two levels by varying the number of enemies. 55 participants performed this game while undergoing fMRI (3T Siemens, GE-EPI, TE=31ms, 54 axial slices, TR=720ms, MB factor=4). Behavioural measures i.e. sum of inverse distance to all enemies and player's projected distance were extracted as an indirect measure of goal obstructiveness.The fMRI data were preprocessed using fMRIPrep. Participants completed personality questionnaires, including the Beck Depression Inventory (BDI). We conducted Partial Least Square Correlation (PLSC) analyses to establish links between personality questionnaires and functional connectivity. Functional connectivity matrices were constructed for each level of each behavioural measure. Personality questionnaires with more than three unadjusted raw scores underwent dimensionality reduction. General Linear Model (GLM) with parametric modulators allowed us to examine brain activation patterns associated with changes in behaviour. The modulated regressor served as the psychological regressor in subsequent Psychophysiological Interaction (PPI) analysis. Functional images were parcellated to derive 400 cortical regions using the Schaefer atlas and 19 subcortical regions from the Human Connectome Project - MultiModal Parcellation atlas. Each of these regions were used as a seed, with each of the remaining regions as targets.

Results: The PLSC analyses revealed one latent component identified as significant (Figure 1b) through permutation testing, explaining 50% of the covariance. Notably, BDI scores emerged as the most significant contributor to personality score loadings within this latent component. Activity in the insula, locus coeruleus, periaqueductal grey, and the dorsal attention network typically linked to avoidance, panicking, freezing, and heightened attention were modulated by the sum of the inverse distance to the enemies; whereas brain regions linked to the reward system such as the ventral and dorsal striatum and the medial prefrontal cortex were modulated by the player's projected distance. The PPI analysis related to the distance to enemies revealed an enhanced connectivity between the prefrontal cortex and the somatomotor cortex.The orbitofrontal cortex, typically involved in processing emotional valence, coactivated with the frontoparietal areas in the dorsal and ventral attention networks. PPI results related to the player's distance show increased connectivity of somatomotor and visual areas with prefrontal cortex; while the precuneus, associated with self-referential processing, had heightened connectivity with the visual and dorsal attention networks.

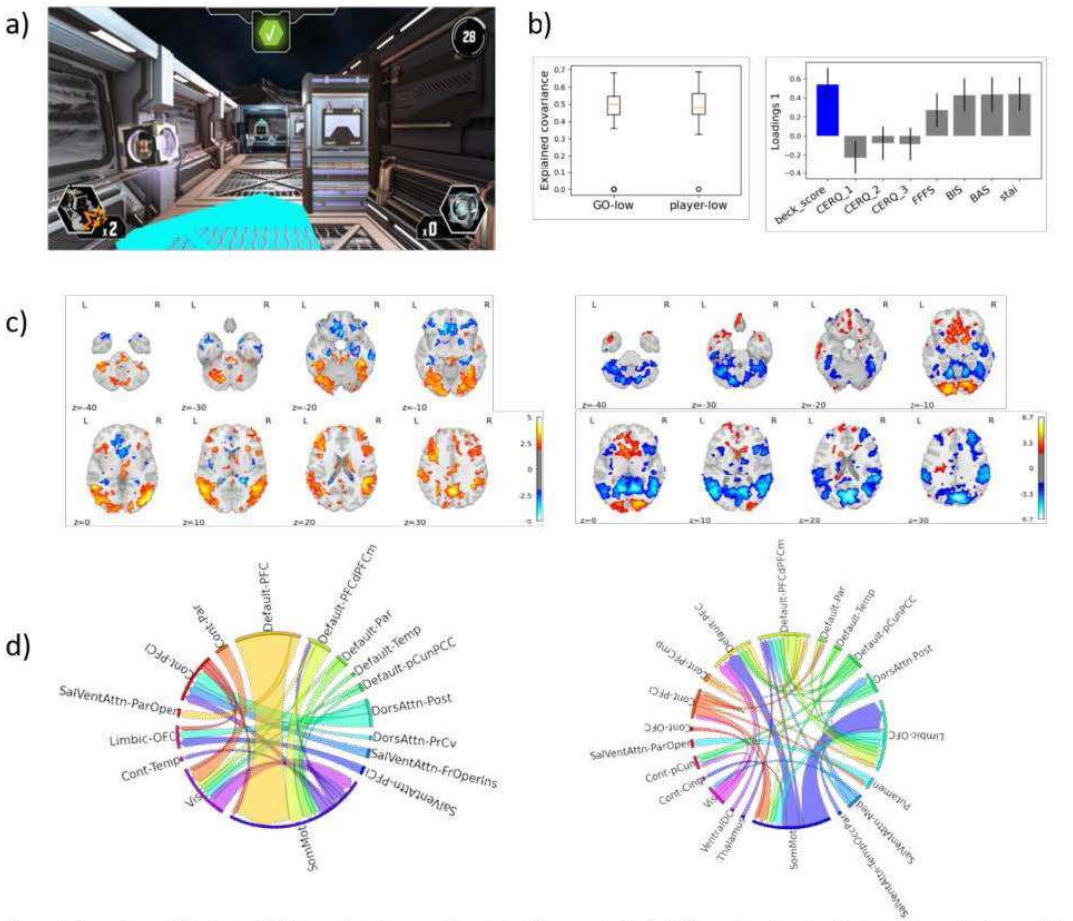

Figure 1. Experimental design and fMRI results. a) Screenshot of the video game. Each trial lasted for 30s, in which participants had to avoid enemies by hiding behind the walls and move forwards to collect points. b) Explained covariance by the significant latent component and the representative loadings of this component. c) Second-level GLM modulated by the sum of inverse distance to all enemies (left); and player's projected distance (right) corrected at $p < 0.05$ (FPR). d) Whole brain psychophysiological analysis (PPI). Here the top 50 PPI weights are shown for illustration purposes.

Conclusions: The development of our video game allowed systematic and controlled manipulations of appraisals with interactive and first-person experience. A complex interaction between multiple brain networks was observed, whose interconnectivity mediates the integration of cognitive and emotional information in response to self-relevant events, with differential expression associated with individual affective traits.

References

1. Scherer, K. R. (2009). The dynamic architecture of emotion: Evidence for the component process model. Cognition and Emotion, 23(7), 1307–1351. https://doi.org/10.1080/02699930902928969
2. Leitão J, Meuleman B, Van De Ville D, Vuilleumier P. Computational imaging during video game playing shows dynamic synchronization of cortical and subcortical networks of emotions. PLoS Biol. 2020 Nov 12;18(11):e3000900. doi: 10.1371/journal.pbio.3000900. PMID: 33180768; PMCID: PMC7685507.

Poster No 723

Happiness matters: distributed brain patterns underlie different positive emotions in OFC

Alessandra Pizzuti[1], Sebastian Dresbach[1], Assunta Ciarlo[2], Michael Luehrs[2], Rainer Goebel[1]

[1]Department of Cognitive Neuroscience, Faculty of Psychology and Neuroscience, Maastricht, Netherland, [2]Brain Innovation B.V., Maastricht, Limburg

Introduction: Positive psychology is a promising branch in the field of psychology and the distinction of positive emotions receives increasing attention. Theoretical frameworks have proposed a "family tree" of 9 positive emotions that developed during evolution[1]. However, the neuroscientific basis of these emotions is poorly understood[2,3,4]. To shed light on this issue, a crucial aspect is to effectively elicit specific positive emotions. Unfortunately, using stock-photos has led to variable results[5]. Therefore, we utilized a novel, individualized approach to collect and rate positive emotions of memories. These memories

were then used in fMRI experiments to investigate neural representations of positive emotions in healthy volunteers. Our insights may offer a promising path towards a biomarker of subjective wellbeing.

Methods: 11 healthy volunteers participated in the experiment. Crucially, participants used the "Matter"-App[6] to collect images that could be associated with individual memories and rate to which degree each of 9 positive emotions (Fig1A) was present. Firstly, participants collected 3 peak-memories per emotion from their lives. Peak memories were used as reference for newly collected memories. Secondly, they recorded positive memories for 6 weeks to reach a minimum of 110 memories in total. From these memories, we selected a subset of 72 that best distributed the occurrence of each emotion. During the fMRI experiment, individual images from this set were presented for 5s while participants vividly recall the memory and the emotional content associated with it. After 5s, the image was replaced by a gray fixation dot with a yellow border while participants continue reliving the emotional memory for 15 seconds without the image cue (while keeping fixation on the dot). Individual trials were separated by 20s of rest periods indicated by the disappearance of the yellow border of the fixation dot. The setup ensured that the participants' images were not seen by the experimenters. Whole brain (f)MRI data (see Fig1B) was collected on a classical 7T Siemens Magnetom Plus scanner at Scannexus (Maastricht, NL) at 1.8 iso mm resolution and TR=1s. Data was analyzed as follows: slice time correction, motion correction[8], geometric distortion correction[9], high-pass filtering with 5 cycles[8]. FMRI data were co-registered to anatomical images using the boundary-based registration and registered to the MNI space in[8]. Finally, we computed a parametric general linear model (GLM) by using subjective ratings from the Matter App.

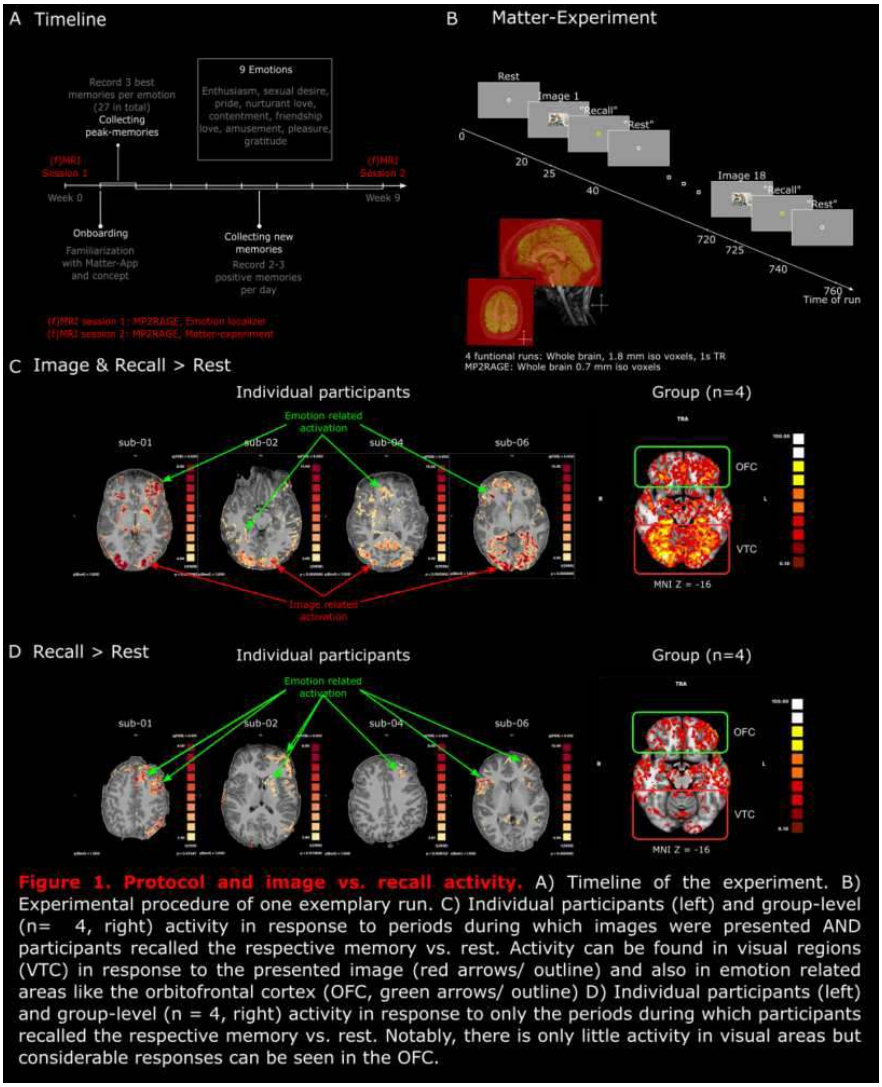

Figure 1. Protocol and image vs. recall activity. A) Timeline of the experiment. B) Experimental procedure of one exemplary run. C) Individual participants (left) and group-level (n= 4, right) activity in response to periods during which images were presented AND participants recalled the respective memory vs. rest. Activity can be found in visual regions (VTC) in response to the presented image (red arrows/ outline) and also in emotion related areas like the orbitofrontal cortex (OFC, green arrows/ outline) D) Individual participants (left) and group-level (n = 4, right) activity in response to only the periods during which participants recalled the respective memory vs. rest. Notably, there is only little activity in visual areas but considerable responses can be seen in the OFC.

Results: Our results from 4 participants show that viewing the images and "recalling" the associated positive memories elicited strong activity in both visual processing areas (VTC) and in emotion-related regions (Fig1C) such as orbital frontal cortex (OFC). Notably, the responses to only the recall phase show little visual activity, but still emotion related activations, as expected (Fig1D). These results indicate that participants engaged in the task and were able to recall the emotions. Fig2 shows the group-level responses to four individual emotions. Remaining emotions were not clearly differentiated. Averaging

across subjects can indeed suppress emotion-specific patterns due to individual variation in distributed patterns. Our future efforts will involve the use of a multivariate pattern analysis that might be more effective in differentiating individual neural correlates of emotions.

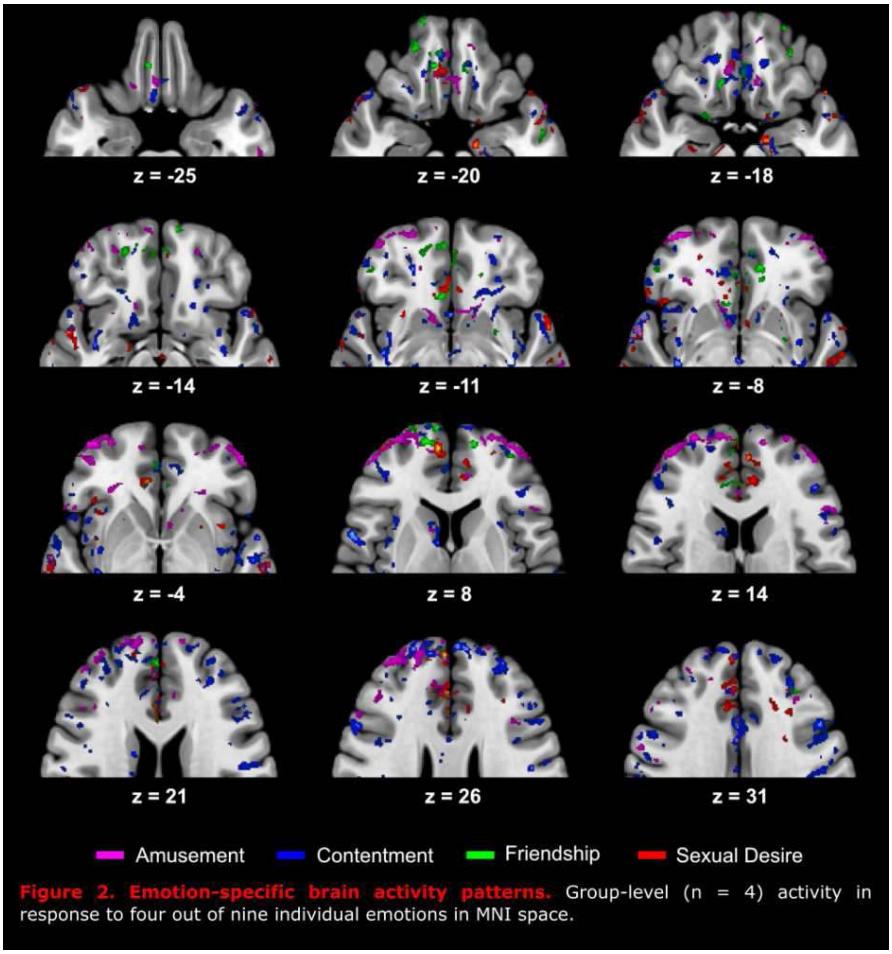

Figure 2. Emotion-specific brain activity patterns. Group-level (n = 4) activity in response to four out of nine individual emotions in MNI space.

Conclusions: With our novel approach which uses personal memories for eliciting positive emotions in a fMRI environment, we were able to show distinct responses to individual positive emotions in our cohort. This opens the door for in-depth investigations of positive emotions as the experimenter can rely on the participants information about what they felt in the scanner. Furthermore, this approach may aid patients to engage in positive memories during clinical neurofeedback studies using emotion regulation training for depression treatment[7].

References

1. Shiota, M. N., Campos, B., Oveis, C., Hertenstein, M. J., Simon-Thomas, E., & Keltner, D. (2017). Beyond happiness: Building a science of discrete positive emotions. American Psychologist, 72(7), 617.
2. Turnbull, O. H., & Salas, C. E. (2021). The Neuropsychology of Emotion and Emotion Regulation: The Role of Laterality and Hierarchy. Brain Sciences, 11(8), 1075. MDPI AG. Retrieved from http://dx.doi.org/10.3390/brainsci11081075
3. Ralph Adolphs, How should neuroscience study emotions? by distinguishing emotion states, concepts, and experiences, Social Cognitive and Affective Neuroscience, Volume 12, Issue 1, January 2017, Pages 24–31, https://doi.org/10.1093/scan/nsw153
4. Celeghin A, Diano MBagnis A, Viola M, Tamietto M (2017) Basic Emotions in Human Neuroscience: Neuroimaging and Beyond. Front. Psychol., 24 August 2017
5. Wei M, Roodenrys S, Miller L, Barkus E. Complex Scenes From the International Affective Picture System (IAPS). Exp Psychol. 2020 May;67(3):194-201. doi: 10.1027/1618-3169/a000488. PMID: 32900297; PMCID: PMC8210657.
6. Matter Neuroscience (2023) Matter - Science and Happiness (Version 1.0) [Mobile app] Apple TestFlight. URL
7. Mehler DMA, Sokunbi MO, Habes I, Barawi K, Subramanian L, Range M, Evans J, Hood K, Lührs M, Keedwell P, Goebel R, Linden DEJ. (2019). Targeting the affective brain - a randomized controlled trial of real-time fMRI neurofeedback in patients with depression. Neuropsychopharmacology, 43(13):2578-2585.
8. Goebel, R. (2012) 'BrainVoyager - Past, present, future', NeuroImage, 62(2), pp. 748–756. doi: 10.1016/j.neuroimage.2012.01.083.
9. Smith, S. M. et al. (2004) 'Advances in functional and structural MR image analysis and implementation as FSL', in NeuroImage. doi: 10.1016/j.neuroimage.2004.07.051.

Poster No 724

Modulation of affected emotions using binaural beats: Simultaneous EEG-fMRI study

Changha Lee[1], Jae-eon Kang[1], Jong-Hwan Lee[1]

[1]Department of Brain and Cognitive Engineering, Korea University, Seoul, Korea, Republic of

Introduction: Future mobility would prioritize passengers' comfort via potential mood modulation during the transportation[1]. Understanding the non-invasive regulation of affective moods and employing appropriate stimuli is crucial, considering the subjective nature of affective moods. In this context, binaural beats have potential owing to cost-effectiveness for mood modulation[2,3]. Several studies suggest white noise enhances the multisensory signal recognition[4]. Certain combinations of binaural beats and vehicle noises would influence the mood states of the passengers. This study investigates how combining binaural beats with vehicle noises affects passenger mood. We aim to identify candidate binaural beats from an experiment with emotional stimuli and vehicle noises and to provide evidence of modulated brain activity using simultaneous EEG and fMRI data.

Methods: Seventeen participants (mean age ± SD: 24.6 ± 2.7 years; 16 males) completed six runs of simultaneous EEG-fMRI recordings, each with eight sound trials. Various beats (400/7Hz binaural, 400/10Hz binaural, 400Hz monaural) and car sounds (Normal, Powerful) served as background sounds. Each 6-second sound trial followed a pseudo-randomized order. Eight sound stimuli from the International Affective Digital Sound (IADS) dataset were chosen based on prior experiments, with two sounds from each valence and arousal quadrant[5]. Participants rated valence and arousal on a 1-9 scale after each trial[6]. Two participants with excessive head movement were excluded from further analysis. fMRI data were preprocessed using SPM8 software with the standard preprocessing pipeline. Then, the ArtRepair toolbox was used to correct any potential interpolation errors from the realignment of large motions and for de-spiking. A general linear model (GLM) was applied to the fMRI data using each trial as a regressor. The resulting beta maps were used as input for the two-way ANOVA (beats x vehicle noises). EEG data were collected using an MR-compatible 31-channel cap following the international 10-20 system. Preprocessing in EEGLAB included gradient artifact removal, ballistocardiogram removal, down-sampling to 110Hz, and independent component analysis (ICA). Manually removing noise-related components from each subject, the data were segmented from -0.3s to 6s relative to the sound onset and baseline-corrected using the pre-stimulus interval. Dipole locations of the components were estimated using the DIPFIT toolbox and clustered across subjects based on dipole location, spectrum, and topography. A two-way ANOVA (beats x vehicle noises) on the cluster's component alpha activity identified significant ($p<0.05$) time points indicating emotional modulations for each sound stimulus.

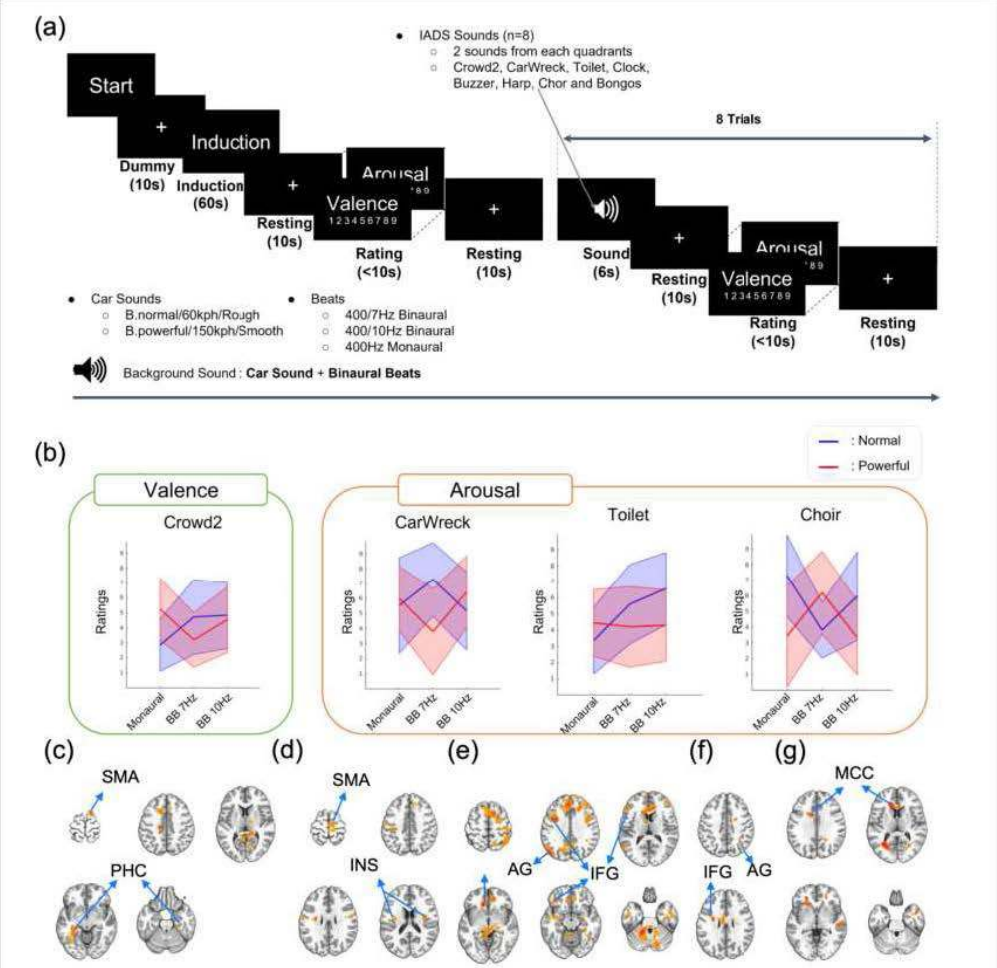

Figure 1. Experimental paradigm and results from behavior and fMRI data. (a) The simultaneous EEG-fMRI paradigm consisted of a binaural beat induction phase and sound stimulation phase followed by valence/arousal ratings. (b) Two-way ANOVA results of the subjective ratings. These four IADS stimuli showed significant interactions ($p < 0.05$). (c)–(g) fMRI analysis results from the four identified IADS sound stimuli. (a)–(d) shows significant ($p_{corrected} < 0.05$) interactions from 'Crowd2', 'CarWreck', 'Toilet', and 'Choir' respectively. (e) The main effect of the car from 'Choir'. PHC, parahippocampus; IFG, inferior frontal gyrus; ACC, anterior cingulate cortex; SMA, supplementary motor area; AG, angular gyrus; INS, insular.

Results: Four of the eight sounds revealed significant ($p<0.05$) interactions between the binaural beats and vehicle noises. The sound 'Choir' showed significant interactions and yielded a significant ($p<0.05$) main effect of the car sound. From fMRI results, the representative clusters from the interactions of binaural beats and vehicle noises included the parahippocampus, inferior frontal gyrus, anterior cingulate cortex, supplementary motor area, angular gyrus, and insular. The EEG results indicated the entrainment of alpha-band-based binaural beats, with significant alpha-band activity elicited during the specific sound stimulus.

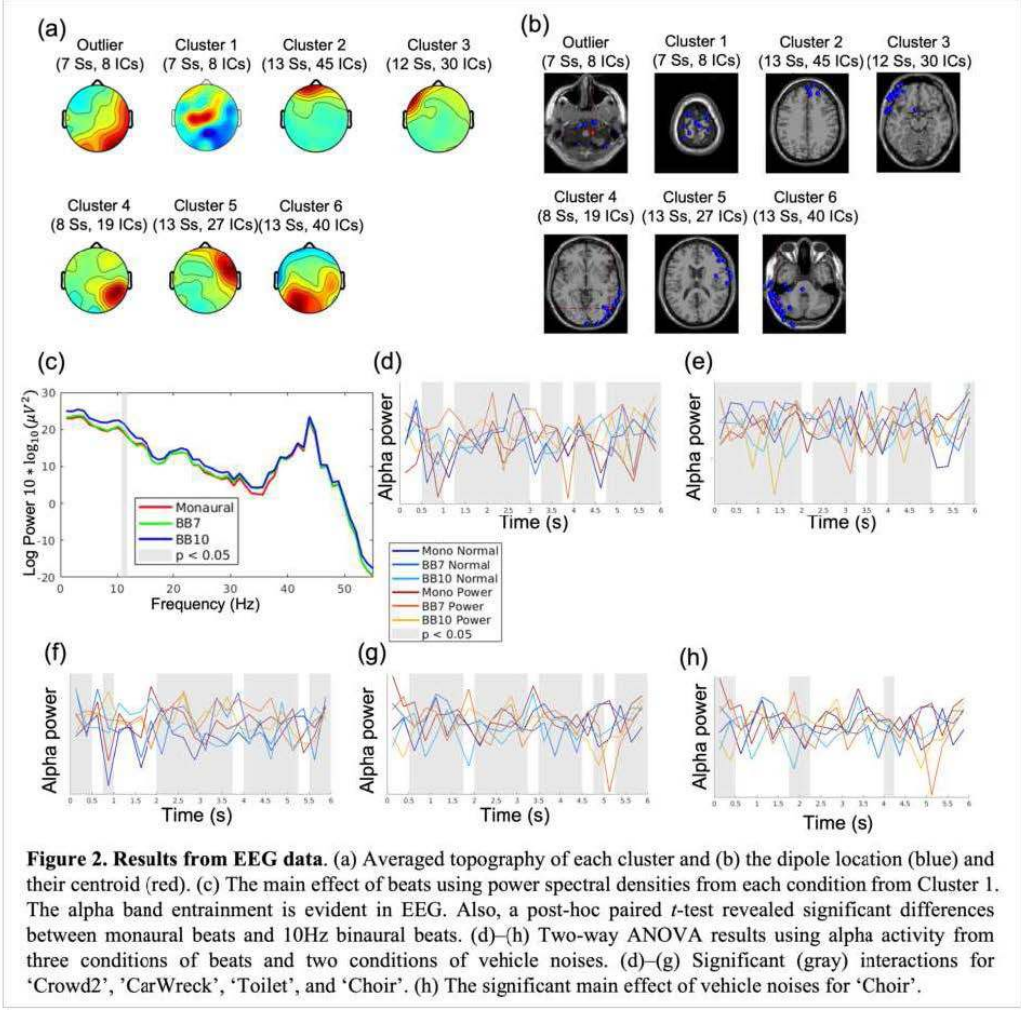

Figure 2. Results from EEG data. (a) Averaged topography of each cluster and (b) the dipole location (blue) and their centroid (red). (c) The main effect of beats using power spectral densities from each condition from Cluster 1. The alpha band entrainment is evident in EEG. Also, a post-hoc paired *t*-test revealed significant differences between monaural beats and 10Hz binaural beats. (d)–(h) Two-way ANOVA results using alpha activity from three conditions of beats and two conditions of vehicle noises. (d)–(g) Significant (gray) interactions for 'Crowd2', 'CarWreck', 'Toilet', and 'Choir'. (h) The significant main effect of vehicle noises for 'Choir'.

Conclusions: We demonstrated the feasibility of alpha band-based binaural beats in background vehicle noises for potential mood alteration from behavioral data and entrainment of brain activity. The modulation of mood status was found in four out of eight IADS stimuli with significant interactions of the binaural beats and the vehicle noises. The spatial patterns from fMRI supported these findings by revealing brain regions in the emotion regulation network[7–9]. The entrainment of the alpha band-based binaural beats was also shown from EEG, in which significant brain activity was induced from the alpha band[10].

References

1. Quek B-K, Ibanez-Guzman J and Lim K-W 2006 A survivability framework for the development of autonomous unmanned systems 2006 9th International Conference on Control, Automation, Robotics and Vision (IEEE) pp 1–6
2. Lane J D, Kasian S J, Owens J E and Marsh G R 1998 Binaural Auditory Beats Affect Vigilance Performance and Mood Physiology & Behavior 63 249–52
3. Jirakittayakorn N and Wongsawat Y 2017 Brain responses to 40-Hz binaural beat and effects on emotion and memory International Journal of Psychophysiology 120 96–107
4. Söderlund G B, Sikström S, Loftesnes J M and Sonuga-Barke E J 2010 The effects of background white noise on memory performance in inattentive school children Behavioral and Brain Functions 6 55
5. Stevenson R A and James T W 2008 Affective auditory stimuli: Characterization of the International Affective Digitized Sounds (IADS) by discrete emotional categories Behavior research methods 40 315–21
6. Kim H-C, Bandettini P A and Lee J-H 2019 Deep neural network predicts emotional responses of the human brain from functional magnetic resonance imaging NeuroImage 186 607–27
7. Onton J and Makeig S 2006 Information-based modeling of event-related brain dynamics Progress in brain research 159 99–120
8. Anon The neural bases of emotion regulation | Nature Reviews Neuroscience
9. Kohn N, Eickhoff S B, Scheller M, Laird A R, Fox P T and Habel U 2014 Neural network of cognitive emotion regulation — An ALE meta-analysis and MACM analysis NeuroImage 87 345–55
10. On F R, Jailani R, Norhazman H and Zaini N M 2013 Binaural beat effect on brainwaves based on EEG 2013 IEEE 9th International Colloquium on Signal Processing and its Applications 2013 IEEE 9th International Colloquium on Signal Processing and its Applications pp 339–43

11. Acknowledgment: This work was supported by the National Research Foundation (NRF) grant (NRF-2021M3E5D2A01022515, No. RS-2023-00218987) and the Electronics and Telecommunications Research Institute (ETRI) grant [23ZS1100, Core Technology Research for Self-Improving Integrated Artificial Intelligence System] funded by the Korea government (MSIT).

Poster No 725

The Maturation of Functional Network Connectivity Supporting Emotion Regulation before Adolescence

Ekomobong Eyoh[1,2], Kody DeGolier[2], Elina Thomas[3], Trevor Day[1], Maryam Mahmoudi[2,4], Katharina Pittner[5], Martin Bauer[5], Fiona O'Donovan[5], Claudia Buss[5], Eric Feczko[2,6], Joel Nigg[7], Jed Elison[1,2], Damien Fair[1,2,6], Alice Graham[7], Oscar Miranda Dominguez[2,6]

[1]Institute of Child Development, University of Minnesota, Minneapolis, MN, [2]Masonic Institute for the Developing Brain, University of Minnesota, Minneapolis, MN, [3]Earlham College, Richmond, IN, [4]Department of Pediatrics, University of Minnesota, Minneapolis, MN, [5]Charité – Universitätsmedizin Berlin, Berlin, Germany, [6]Department of Pediatrics, University of Minnesota Medical School, Minneapolis, MN, [7]Oregon Health and Science University, Portland, OR

Introduction: Emotion regulation (ER) has been proposed as a transdiagnostic factor in the development of psychopathology and neurodevelopmental disorders (Aldao et al., 2016). The development of individual ER has been hypothesized to begin with co-regulation of stress between parents and infants which transitions into more self-mediated top-down control from frontal regions on subcortical regions in adolescence (Gee et al., 2014; Silvers, 2022). Understanding dynamic changes in ER and its supporting brain circuitry will yield insight into the typical development of this construct and help identify critical periods when perturbations in typical maturation are associated with increased risk for psychopathology and neurodevelopmental disorders. We hypothesize that left amygdala connectivity to other cortical and subcortical regions of the brain will be differentially associated with ER at different developmental stages.

Methods: We used high-quality data from a large sample representative of the US population (the Adolescent Brain Cognitive Development, ABCD, study, N=6900, age 9-11) to derive reproducible brain-behavior associations related to ER (Byington et al., 2023). Resulting models were used to calculate brain scores of ER in independent samples with individuals of different ages. To do this, we used subjects from the Baby Connectome Project (BCP) and infants from a study at the University of California – Irvine (UCI). First, the resting state functional connectivity of 6900 subjects from ABCD was parcellated according to the regions of interest (ROIs) designated by Gordon et al. (2016). Then, the correlation of the left amygdala with each other brain cortical and subcortical region was calculated. The resulting 351 connections were grouped into 14 networks as defined in Fig. 1A. ß-weights were generated by modeling the CBCL internalizing raw score as the weighted contribution of each connection when controlling for collection site, gender, race, and ethnicity (Figure 1B). The ß-weights were used to calculate polyneuro risk scores (PNRS, predicted scores of behavior given left amygdala connectivity) by network in 90 18-60-month-olds in the BCP and 54 1-month-olds in the UCI study. In addition, we calculated PNRSes for the ABCD sample using a split half approach, where one half of the ABCD subjects were used as the training sample to generate PNRSes in the other half and vice versa. Differences in brain scores by network and across age were tested via repeated measures ANOVA using aggregated data from all three samples. Additionally, the interaction between network and age was tested to determine whether means were changing over time within each network. Median PNRSes per network by cohort were calculated and ranked from lowest to highest to map the change in the association between amygdala connectivity to networks and ER. Lower scores indicate better ER and higher scores indicate more ER difficulties.

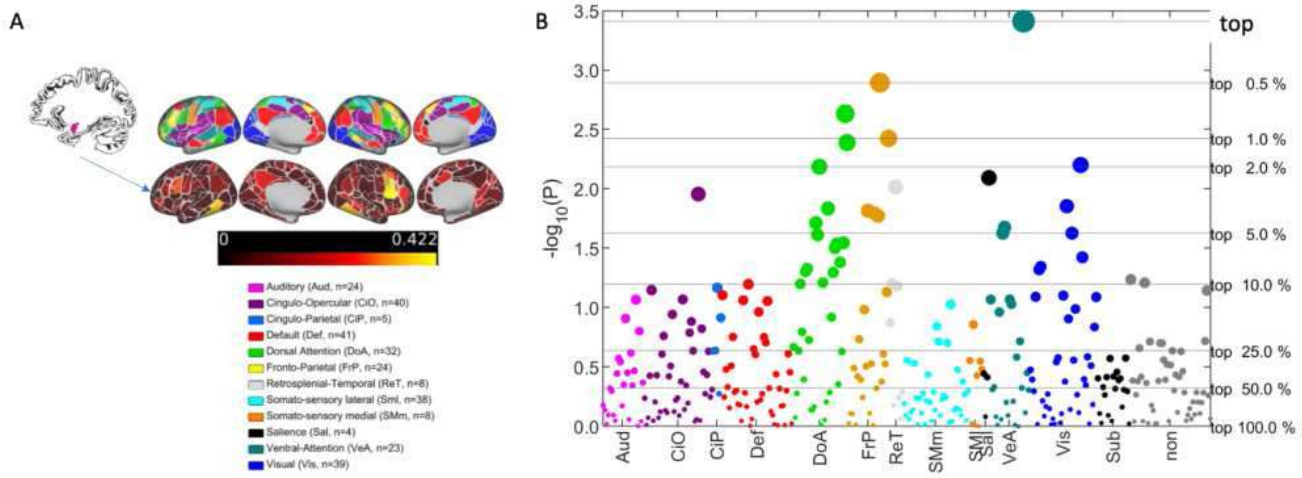

Results: Results of the ANOVA indicate that there is a significant difference in means by network ($F = 43.184$, $p = <0.001$) and an interaction between age and network ($F = 29.151$, $p<0.001$). Thus, network PNRS means are different from one another,

and mean scores differ by network across age. Large changes in rank occurred in the ReT (UCI: 10, BCP: 12, ABCD: 2) and Sal (UCI: 13, BCP: 13, ABCD: 4). Generally, scores across networks become more negative over time, indicating that amygdala connectivity to other regions results in better regulation as children get older. This was not the case for all networks as amygdala connectivity to the cingulo-parietal network was consistently indicative of higher emotion dysregulation. These transitions are denoted in Figure 2 (top panels).

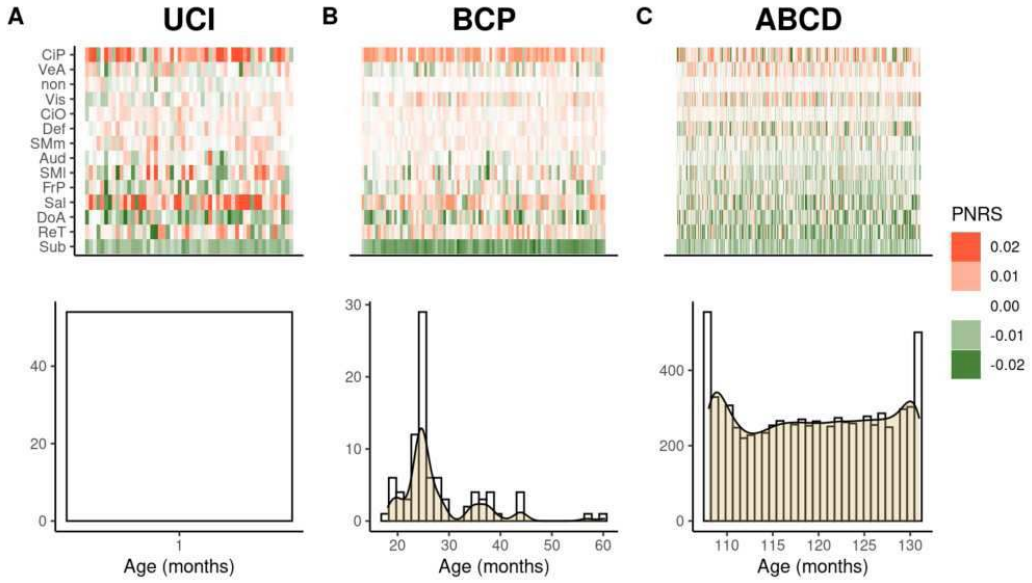

Conclusions: The results yield evidence that changes in network connectivity to the left amygdala are associated with changes in ER across infancy to early adolescence. Further inquiry into the ways in which the Sal and ReT networks differentially modulate ER across childhood is needed.

References

1. Aldao, A. (2016), 'Emotion regulation as a transdiagnostic factor in the development of internalizing and externalizing psychopathology: Current and future directions', Development and Psychopathology, vol. 28, no. 4pt1, pp. 927–946
2. Byington, N. (2023), 'Polyneuro risk scores capture widely distributed connectivity patterns of cognition', Developmental Cognitive Neuroscience, vol. 60, 101231.
3. Gee, D. G. (2014), 'Maternal Buffering of Human Amygdala-Prefrontal Circuitry During Childhood but Not During Adolescence', Psychological Science, vol. 25, no. 11, pp. 2067–2078
4. Gordon, E. M. (2016), 'Generation and Evaluation of a Cortical Area Parcellation from Resting-State Correlations', Cerebral Cortex, vol. 26, no. 1, pp. 288–303
5. Silvers, J. A. (2022), 'Adolescence as a pivotal period for emotion regulation development. Current Opinion in Psychology', vol. 44, pp. 258–263

Poster No 726

Facial Video-Based Remote Eye Movement Detection using Electrooculography and Deep Neural Network

Jin Soo Jeon[1], Jong-Hwan Lee[1]

[1]Department of Brain and Cognitive Engineering, Korea University, Seoul, Korea, Republic of

Introduction: Blink duration and rate have been widely recognized as consistent and reliable parameters for assessing drowsiness and arousal[1]. Electrooculography (EOG) has precisely measured eye movement features, such as eyeblink rate, closing phase, opening phase, and blink duration[2]. Despite the established validity and reliability of the EOG signal in capturing eye movements, the necessity of electrode attachment near eyeballs for EOG measurement significantly limits its utility. Consequently, our study addresses this limitation by leveraging facial videos and deep neural network (DNN).

Methods: We employed the facial video and EOG data available in the DEAP dataset[3], a widely recognized multimodal dataset for human emotion analysis. To ensure synchronization with the video recordings at 50 frames per second, we downsampled the EOG signal to 50Hz. Subsequently, we re-referenced the vertical EOG signal to its corresponding electrode and applied bandpass filtering in the range 0.01–25Hz. Epochs were extracted from –5s to 60s with baseline removal using –5s to 0s signals. We utilized the discrete wavelet transform method[4] to mitigate baseline drift and further reduced residual noise

via a moving median filter[5]. For blink peak detection from the preprocessed EOG, we implemented min-max scaling within subjects and employed a local maxima algorithm[4]. Blink phase detection, pinpointing the precise time points for initial closure, complete closure, and reopening of eyes were obtained using the derivative value of the vertical EOG signal[6]. We categorized target labels for all video frames into three distinct states of eye movements (i.e., normal, closing, and opening) based on the blink phase detection from EOG. A Pearson's correlation analysis using the identified EOG labels and self-reports from subjects was conducted to evaluate the validity of the extracted labels. We trained a DNN model using recorded facial videos for eye movement detection. Our DNN model consists of (a) an Inception-ResNetV1 module to extract hierarchical visual features from each video frame, (b) a Long Short-Term Memory (LSTM) module to analyze the sequence of video frames, and (c) fully connected layers for the classification of the target labels (Fig. 2a). The performance of the model was evaluated on both the DEAP dataset and the DROZY database[7] based on the five-folds cross-validation (CV). The face region was detected and cropped by the OpenCV face detection model[8]. Six consecutive video frames were used as DNN input and model parameters were optimized using a random search method[9].

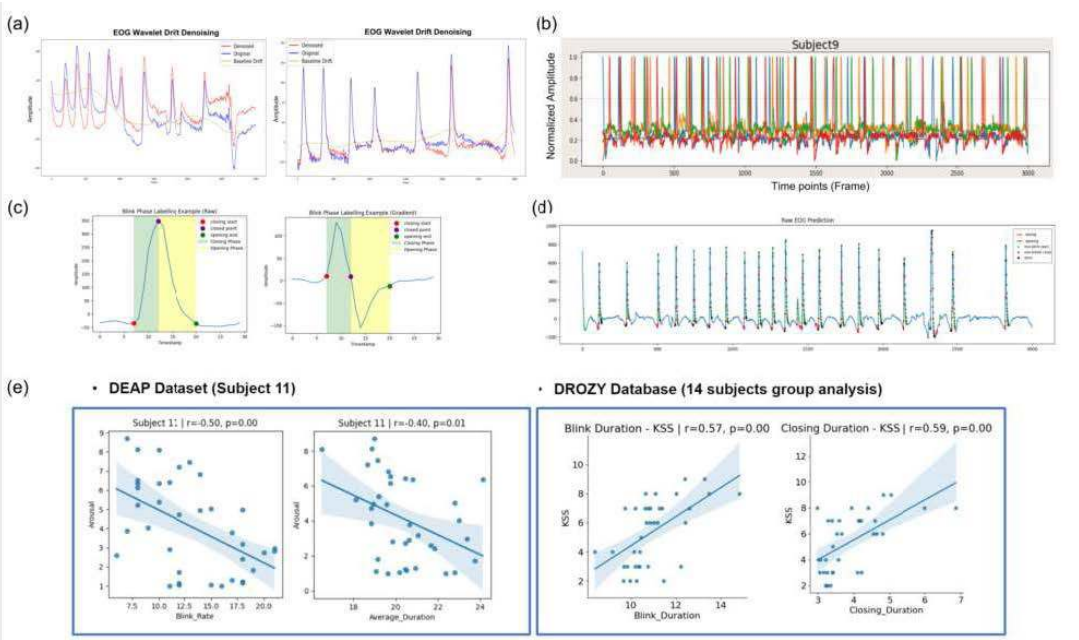

Figure 1. (a) Examples of discrete wavelet transform-based baseline drift removal. (b) Example of preprocessed EOG signal. (c) Example of blink phase labeling. (d) Detected eye blink states from EOG signal. (e) Correlation between blink-related features and arousal.

Results: Our adopted EOG preprocessing pipeline effectively denoised EOG signals while maintaining important temporal features of eye movements (Fig. 1a-d). Among the 16 subjects in the DEAP dataset with valid EOG signals, seven showed a meaningful negative correlation between blink duration and arousal (Fig. 1e). From the DROZY Database, data from all 14 subjects revealed a substantially high correlation of 0.59 ($p < 0.01$) between blink duration and Karolinska Sleepiness Scale Score. Our trained DNN yielded a 98.2% average test accuracy across the 5-fold CV using the DEAP dataset. The proposed DNN effectively predicted eye movements in facial videos, demonstrating that the average duration error, compared to the EOG label, was approximately 60ms (3 frames) with a minimal delay of 40ms (2 frames) (Fig. 2c).

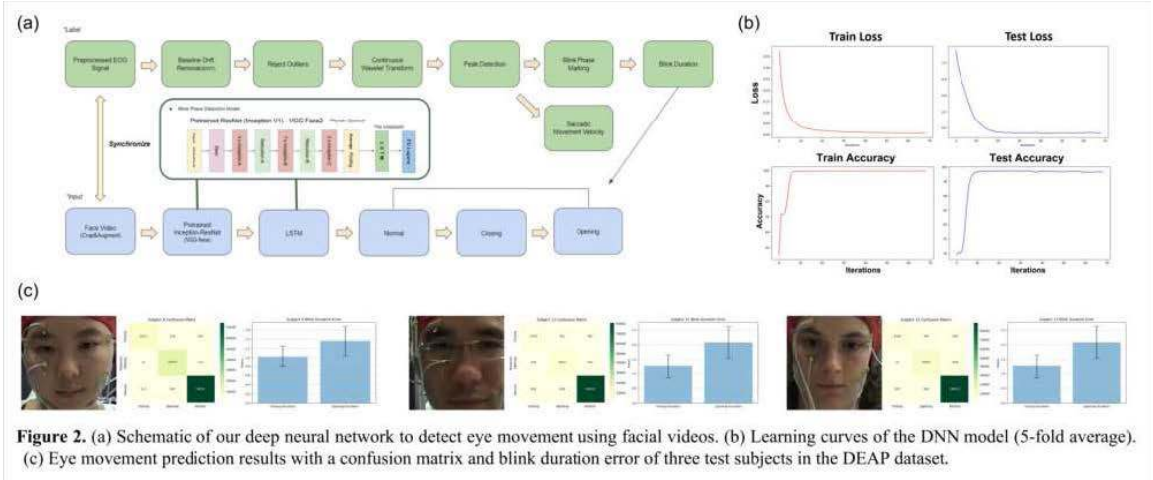

Figure 2. (a) Schematic of our deep neural network to detect eye movement using facial videos. (b) Learning curves of the DNN model (5-fold average). (c) Eye movement prediction results with a confusion matrix and blink duration error of three test subjects in the DEAP dataset.

Conclusions: We developed a DNN model to extract vertical eye blink movements from facial videos robustly. Notably, our facial video-based blink detection model often outperformed the EOG label in predicting the observable eye movement. This would be because the EOG, which captures electric signals originating from inner muscle movement, may inherently introduce minor differences from overt eye movements. The estimated eye blink movements can potentially estimate affective states and arousal, including drowsiness, remotely using a camera without EOG electrodes.

References

1. Damousis, I., Cester, I., Nikolaou, S., & Tzovaras, D. (2007). Physiological indicators based sleep onset prediction for the avoidance of driving accidents. 2007 29th Annual International Conference of the IEEE Engineering in Medicine and Biology Society, 6699–6704.
2. Cori, J. M., Anderson, C., Shekari Soleimanloo, S., Jackson, M. L., & Howard, M. E. (2019). Narrative review: Do spontaneous eye blink parameters provide a useful assessment of state drowsiness? Sleep Medicine Reviews, 45, 95–104.
3. Koelstra S, Muhl C, Soleymani M, Lee J-S, Yazdani A, Ebrahimi T, Pun T, Nijholt A and Patras I (2011) Deap: A database for emotion analysis; using physiological signals IEEE Trans. Affect. Comput. 3 18–31
4. Ebrahim, P. (2016). Driver drowsiness monitoring using eye movement features derived from electrooculography
5. Bulling, A., Ward, J. A., Gellersen, H., & Tröster, G. (2010). Eye movement analysis for activity recognition using electrooculography. IEEE transactions on pattern analysis and machine intelligence, 33(4), 741-753.
6. Abbas, S. N., & Abo-Zahhad, M. (2017). Eye Blinking EOG Signals as Biometrics. In R. Jiang, S. Al-maadeed, A. Bouridane, Prof. D. Crookes, & A. Beghdadi (Editor), Biometric Security and Privacy: Opportunities & Challenges in The Big Data Era (pp 121–140). Springer International Publishing.
7. Massoz, Q., Langohr, T., François, C., & Verly, J. G. (2016, March). The ULg multimodality drowsiness database (called DROZY) and examples of use. In 2016 IEEE Winter Conference on Applications of Computer Vision (WACV) (pp. 1-7).
8. Khan, M., Chakraborty, S., Astya, R., & Khepra, S. (2019, October). Face detection and recognition using OpenCV. In 2019 International Conference on Computing, Communication, and Intelligent Systems (ICCCIS) (pp. 116-119). IEEE.
9. Bergstra, J., & Bengio, Y. (2012). Random search for hyper-parameter optimization. Journal of machine learning research, 13(2).
10. Acknowledgment: This work was supported by the National Research Foundation (NRF) grant funded by the Korea government (MSIT) (NRF-2021M3E5D2A01022515, No. RS-2023-00218987), and in part by the Electronics and Telecommunications Research Institute (ETRI) grant funded by the Korean government [23ZS1100, Core Technology Research for Self-Improving Integrated Artificial Intelligence System].

Poster No 727

Mapping idiographic affective appraisals to brain activity using semantic embeddings

Luke Chang[1], Eshin Jolly[1], Nir Jacoby[1], Younji Choi[1], Tor Wager[1], Jeremy Manning[1]

[1]Dartmouth College, Hanover, NH

Introduction: Emotions are coordinated, multi-system responses to events and situations relevant to survival and well-being. These responses emerge from appraisals of personal meaning that reference one's goals, memories, internal body states, and beliefs about the world [Ashar et al., 2017]. Dysregulation of emotions is central to many brain and body-related disorders, making it of paramount importance to understand the neurobiological mechanisms that govern emotional experiences. In our prior work, we have observed that the ventromedial prefrontal cortex (vmPFC) involved in processing these affective appraisals appears to be highly idiosyncratic across individuals [Chang et al., 2021]. While discrete patterns of activity within the vmPFC appear to broadly correspond to affective experiences across participants, it remains an open question as to how the vmPFC generates specific appraisals [Roy et al., 2012]. In this study, we develop a novel computational framework to measure an individual's idiosyncratic appraisals that arise in the context of naturalistic movie viewing that combines collaborative filtering with recent advances in natural language processing.

Methods: Participants (N=122) watched 8 emotionally engaging emotional stories while undergoing fMRI. After participants completed their scanning session, they were presented with a transcript of each story and were asked to mark on the document to indicate what they were thinking about for any time point they could remember. We embedded each thought into a 384-dimensional semantic space using a BERT Sentence Transformer [Reimers and Gurevych, 2019] (Figure 1A). Then for every single embedding dimension, we performed collaborative filtering with a 20-second boxcar kernel to create a dense participant-by-time-by-embedding dimension tensor using the Neighbors toolbox [Jolly et al., 2022] (Figure 1B). For each participant, we used distance correlations [Székely et al., 2007] to map the time-varying multivariate semantic embeddings of their appraisals to their multivariate brain activity separately for each region from a k=50 whole brain parcellation [de la Vega et al., 2016]. We performed a sign permutation test over participants and corrected for multiple comparisons using FDR $q < 0.05$.

Results: Overall, we found strong associations between participants' idiosyncratic appraisals and dynamic fluctuations in the vmPFC, dmPFC, ventral striatum, amygdala, thalamus, and visual cortex. These results demonstrate that the vmPFC plays a critical role in generating affective meaning based on subjective interpretations of unfolding narrative events.

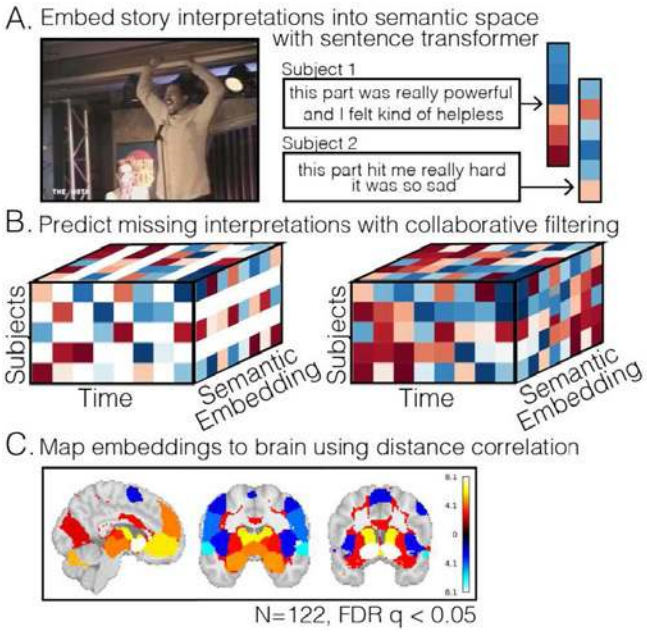

Conclusions: This study provides a proof of concept of how subjective interpretations of a single individual can be measured and mapped onto brain activity. Similar to work studying how the vmPFC generates idiosyncratic value in the field of decision neuroscience [Plassmann et al., 2007], we find strong evidence that individuals' unique interpretations of the unfolding narratives is encoded in the vmPFC. This finding is particularly striking given that participants Our results have significant implications for translational work for characterizing how patients suffering from psychiatric symptoms may be experiencing mood dysregulation based on maladaptive appraisals of the world.

References

1. Ashar YK, Chang LJ, Wager TD (2017): Brain Mechanisms of the Placebo Effect: An Affective Appraisal Account. Annu Rev Clin Psychol 13:73–98.
2. Chang LJ, Jolly E, Cheong JH, Rapuano KM, Greenstein N, Chen P-HA, Manning JR (2021): Endogenous variation in ventromedial prefrontal cortex state dynamics during naturalistic viewing reflects affective experience. Sci Adv 7. http://dx.doi.org/10.1126/sciadv.abf7129.
3. Jolly E, Farrens M, Greenstein N, Eisenbarth H, Reddan MC, Andrews E, Wager TD, Chang LJ (2022): Recovering Individual Emotional States from Sparse Ratings Using Collaborative Filtering. Affect Sci 3:799–817.
4. Plassmann H, O'Doherty J, Rangel A (2007): Orbitofrontal cortex encodes willingness to pay in everyday economic transactions. J Neurosci 27:9984–9988.
5. Reimers N, Gurevych I (2019): Sentence-BERT: Sentence embeddings using Siamese BERT-networks. arXiv [cs.CL]. arXiv. https://github.com/UKPLab/.
6. Roy M, Shohamy D, Wager TD (2012): Ventromedial prefrontal-subcortical systems and the generation of affective meaning. Trends Cogn Sci 16:147–156.
7. Székely GJ, Rizzo ML, Bakirov NK (2007): Measuring and testing dependence by correlation of distances. Ann Stat 35:2769–2794.
8. de la Vega A, Chang LJ, Banich MT, Wager TD, Yarkoni T (2016): Large-Scale Meta-Analysis of Human Medial Frontal Cortex Reveals Tripartite Functional Organization. J Neurosci 36:6553–6562.

Poster No 728

Individual differences in shame- and guilt-proneness and its relationship with autistic trait

Isaac IP[1], Hey Tou Chiu[1], Savio Wong[1]

[1]The Chinese University of Hong Kong, Shatin, Hong Kong

Introduction: Shame and guilt are self-conscious emotions (SCEs) that serve to motivate us to act in accordance with social norms and personal standards (Else-Quest et al., 2012). These SCEs promote the attainment of social goals and motivate behaviors that promote social acceptance (Tracy & Robins, 2004). Shame is generated by attributing a failure or transgression to the global self and is coupled with motivation tendency to avoid or withdraw. In contrast, guilt is behavior specific and is associated with motivation tendency to repair. While guilt after a transgression can help maintain social relationships, too much of shame or a lack of guilt could inhibit prosocial behaviors and formation of close social relationships (Tangney & Dearing, 2002). In this study, we examine the neural basis of individual differences in shame- and guilt-proneness and its relationship with autistic trait in neurotypical (NT) individuals using resting-state fMRI. Previous studies have showed that

autism can be treated as a set of continuous traits that extend into the general population (Sucksmith et al., 2011). These include a set of subclinical behaviors and characteristic that are qualitatively similar to autism. Individuals with autism or high in autistic traits showed a different tendency to experience shame and guilt than NT individuals. Davidson et al. (2017) reported that those who scored higher in autism traits had higher shame-proneness but lower guilt-proneness than those who scored lower in autism traits.

Methods: Forty-five participants (20 females, age: M = 22.0, SD = 3.88) completed a resting state fMRI scan as part of a larger study. Written informed consent was obtained from all participants. Autistic trait was assessed with the Broad Autism Phenotype Questionnaire (BAPQ; Hurley et al., 2007) which measures personality and language characteristics, that are subclinical and qualitatively similar to the defining features of autism. Proneness to shame and guilt were measured by the Test of Self-Conscious Affect 3 (TOSCA-3; Tangney & Dearing, 2004). Scanning was performed using a Siemens Prisma 3T MR scanner. Five minutes of resting state BOLD function scans and a MPRAGE image were acquired for each participant. Preprocessing of the imaging data was performed using the CONN toolbox with the default preprocessing pipeline for volume-based analyses. To identify ROIs, Intrinsic Connectivity Contrast (ICC) maps were computed to assess hypothesis-free whole-brain connectivity for each voxel in the brain. The 1st-level analysis yields a map for each participant where a higher value represents the strength of connectivity of that voxel with the rest of the brain and thus a network measure of node centrality. Two separate 2nd-level GLM that includes proneness to shame and guilt, with BAPQ as a covariate were used to delineate ROIs where their node centrality would be associated with individual differences in autistic traits and proneness to shame and guilt. The obtained ROIs were used for follow-up seed-based connectivity (SBC) analyses to probe further into their functional connectivity (FC) with specific brain regions.

Results: The correlation analysis showed that higher scores in BAPQ were associated with higher levels of shame-proneness, $r = .47$, $p < .001$ but lower levels of guilt-proneness, $r = -.34$, $p = .013$. The right frontal pole (rFP) is identified in the ICC analysis as the seed of the following SBC analysis in which BAPQ scores were found to associate with the FC at ACC, PCC, right superior frontal gyrus (rSFG), and left posterior mid temporal gyrus. Mediation analyses showed that the positive association between autistic traits and shame-proneness is mediated by the FC between rFP and ACC, PCC, and rSFG while the negative association with guilt-proneness is mediated by the FC between rFP and rSFG.

Conclusions: Our results show that autistic traits had indirect effects on shame- and guilt-proneness through the FC between rFP and midline cortical structures (ACC and PCC).

References

1. Davidson, D. (2017), Proneness to Self-Conscious Emotions in Adults With and Without Autism Traits. Journal of Autism and Developmental Disorders, 47(11), 3392–3404.
2. Else-Quest, N. (2012), Gender Differences in Self-Conscious Emotional Experience: A Meta-Analysis. Psychological Bulletin, 138, 947–981.
3. Hurley, R. S. (2007). The broad autism phenotype questionnaire. Journal of autism and developmental disorders, 37, 1679-1690.
4. Sucksmith, E. (2011). Autistic traits below the clinical threshold: re-examining the broader autism phenotype in the 21st century. Neuropsychology review, 21, 360-389.
5. Tangney, J. P., & Dearing, R. L. (2004). Shame and guilt (Paperback ed. 2004). Guilford Press.
6. Tracy, J. L., (2004) "Putting the Self Into Self-Conscious Emotions: A Theoretical Model." Psychological Inquiry, 15(2), 103–125.

Poster No 729

Trait Impulsivity and Frontal Lobe Response to Anti-Vaping Messaging Predict Reduced Craving

Somin Kim[1], Jiaying Liu[1,2,3], Jessica Fabbricatore[3], Joshua McMains[1], Allison Worsdale[3], Colleen Markey[1], Michelle Perez[1], Lawrence Sweet[1]

[1]Department of Psychology, University of Georgia, Athens, GA, [2]University of California Santa Barbara, Santa Barbara, CA, [3]Department of Communication Studies, University of Georgia, Athens, GA

Introduction: With the rise in vaping among young adults in the US, the search for effective methods to reduce vaping has become a new challenge and priority in public health (Dai & Leventhal, 2019). Impulsivity, a major risk factor for early tobacco use is often associated with vaping and cognitive control difficulties (Fernie et al., 2013; Leshem, 2016) However, little is known about how individual differences in levels of impulsivity affect processing of anti-vaping public service announcements (PSAs) at the neural level. This study examines whether and how frontal cortex activation and its interaction with impulsivity predict craving reduction after exposure to anti-vaping PSAs with emotional, cognitive and social appeals.

Methods: Functional MRI (fMRI) data were obtained from 51 young adult nonsmokers who vaped on more than 15 out of the past 30 days (Mean age = 20 yrs; 45 women). A PSA fMRI paradigm was presented where anti-vaping messages, featuring

cognitive, emotional, and social appeals, were shown for 30sec each, repeated 6 times across two imagine runs in pseudo-random order. Six 20sec blocks of a scrambled control image were also included. A GE 3T MRI scanner acquired data with a temporal resolution of 2s and a spatial resolution of 3.5mm^3. Preprocessing steps included slice-time correction, registration, censoring, removal of linear drift, smoothing and stereotaxic standardization. The preprocessed fMRI signals of each task condition were further analyzed using a general linear model to compute effects per brain voxel. We selected the bilateral inferior, middle, and superior frontal gyri as a priori regions of interest to explore frontal activation. Participants' desire to vape was assessed after the presentation of visual vaping cues and PSAs. Reduction in craving was operationalized as the difference between these ratings. Impulsivity scores were measured using the UPPS-P Impulsive Behavior Scale (Whiteside et al., 2001). Multiple regression models were used to examine the effect of frontal response and impulsivity on reduced craving.

Results: Among the six frontal regions, lower activation of right inferior frontal gyrus (IFG) showed a marginal statistical significance, predicting a greater reduction in response to emotionally appealing anti-vaping messages (βrIFG=-.29, p=.066). The interaction effect between the right IFG activity and impulsivity significantly predicted craving reduction (βrIFG*impulsivity=2.08, p=.011; Figure 1). In individuals with low impulsivity, a less activated right IFG significantly predicted a greater reduction in craving. Right IFG response to PSAs with social appeals was not related to reduced craving (β rIFG=-.12, p=.462), while the interaction effect was significant (βrIFG*impulsivity=1.81, p=.037). Neither the main effect (βrIFG=-.10, p=.527) nor the interaction effect (βrIFG*impulsivity=1.43, p=.112) was significant during exposure to cognitive appeals.

Table 1

The moderating effect of impulsivity between the right IFG and reduced craving in three anti-vaping messages

	Emotional appeal				Cognitive appeal				Social appeal			
	β	*p*	*β*	*p*	*β*	*p*	*β*	*p*	*β*	*p*	*β*	*p*
Right IFG	-.29	.066	-2.32	**.005**	-.10	.527	-1.51	.094	-.12	.462	-1.90	.029
Impulsivity	.08	.575	.11	.428	.05	.734	.03	.838	.04	.805	.26	.800
Right IFG x impulsivity			2.08	**.011**			1.43	.112			1.81	**.037**
R^2	.09		.22		.012		.07		.02		.11	
F	2.21		4.04		.26		1.06		.33		1.79	
p	.12		**.01**		.772		.38		.72		.16	

Note. β = standardized coefficients. IFG: inferior frontal gyrus.

Figure 1

The Effect of right IFG Activation on the reduced amount of craving after watching emotionally appealing messages by different impulsivity level

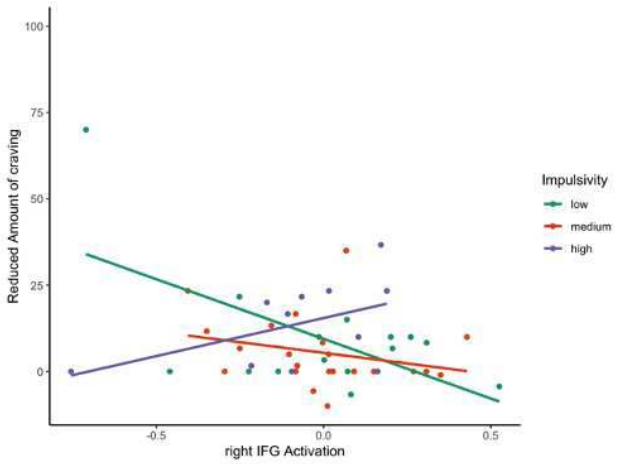

Conclusions: Finding suggests that greater engagement of cognitive control function, involving the right IFG, is associated with more effective anti-vaping messages, especially in less impulsive individuals. While increased involvement in cognitive processes could potentially be helpful for criticizing or rejecting PSA messages, such cognitive capacity might not be sufficient in individuals with high impulsivity. This relationship was the most significant in the context of anti-vaping messages with emotional appeals, suggesting that heightened cognitive thinking could override the effects of emotional messages. Given that different levels of impulsivity lead to varying levels of cognitive processing when viewing anti-vaping messages, it is important to consider the impulsive traits of the potential audience when devising anti-vaping public service announcements.

References
1. Dai, H., & Leventhal, A.M. (2019), 'Prevalence of e-Cigarette use among adults in the United States, 2014-2018', JAMA, vol. 322, no. 18, pp. 1824-1827.
2. Fernie, G., Peeter, M., Gullo, M.J., Christiansen, P., Cole, J.C., Sunmnall, H., & Field, M. (2013), 'Multiple behavioural impulsivity tasks predict prospective alcohol involvement in adolescents', Addiction, vol. 108, no. 11, pp. 1916-1923.
3. Leshem, R. (2016), 'Relationships between trait impulsivity and cognitive control: the effect of attention switching on response inhibition and conflict resolution', Cognitive Processing, vol. 17, no. 1, pp. 89-103.
4. Whiteside, S.P., & Lynam, D.R. (2001), 'The Five Factor Model and impulsivity: using a structural model of personality to understand impulsivity', Personality and Individual Differences, vol. 30, no. 4, pp. 669-689.

Poster No 730

Functional and anatomical profiles of functionally selective and integrative zones in the insula

Mijin Kwon[1], Lukas Van Oudenhove[2], Philip Kragel[3], Tor Wager[1], Affective Neuroimaging Consortium[1]

[1]Dartmouth College, Hanover, NH, [2]KU Leuven, Leuven, Belgium, [3]Emory University, Atlanta, GA

Introduction: A central question in cognitive neuroscience is understanding how the brain constructs unified perceptual experiences by integrating interoceptive, emotional and exteroceptive signals across modalities. The insular cortex has been proposed as a critical hub, with the anterior insula hypothesized as an integrative zone synthesizing diverse functional modalities. However, the insula also contains specialized areas (e.g., the posterior insula for pain) demonstrating significant functional specificity. Reconciling functional specialization and integration has been hindered by limitations in spatial specificity and small samples in prior research. Here, leveraging Bayes factor analysis of aggregated task fMRI data (N = 540 participant-level maps; 36 studies) across pain, appetitive processes, aversive processes, and cognitive control domains, we examine the balance of functional integration and modular specialization in the human insular cortex. We ask: 1) Are there discrete functionally selective zones alongside a domain-general hub? 2) What microscale and macroscale functional and anatomical features enable this complex organization?

Methods: We first aggregated 540 participant-level contrast images from 36 task-based fMRI studies systematically sampling from each domain (each with 3 subdomains, 3 independent studies within each subdomain, and 15 participants equally sampled from each study) (Figure 1). The current study was conducted as part of a collaborative research effort, Affective Neuroimaging Consortium[1]. We then applied a Bayes factor framework testing voxelwise activation selectivity for each domain versus domain-general convergence by assessing evidence for and against activation. This identified voxels activated exclusively by one domain or across all domains. We characterized the functional and anatomical properties enabling selectivity and integration: 1) Neurosynth decoding of represented functions, 2) cytoarchitectonic mapping, 3) neurotransmitter receptor density profiling, and 4) whole-brain co-activation.

Results: Bayes factor analysis revealed domain-selective zones exhibiting selectivity pain (mid-posterior insula), appetitive processes (mid-insula), aversive processes (ventral anterior insula), and cognitive control (dorsal anterior/mid-insula) alongside a distinct domain-general hub in the dorsal anterior insula, showing overall activations across all domains (Fig. 1). Each domain-selective and domain-general zones showed distinct patterns in functional decoding, cytoarchitectonic mapping, neurotransmitter receptor density profile, and coactivation with other brain areas. For example, the pain-selective zone showed: 1) highest association with pain-related topics such as "pain", "somatosensory stimulation" (functional decoding); 2) highest overlap with the granular-dysgranular cytoarchitectonic cluster that is well positioned to receive main somatosensory inputs (cytoarchitectonic mapping); 3) relatively higher association with glutamate, GABA, and opioids (neurotransmitter receptor density profile); 4) connections with a pain processing network including somatosensory, cingulate, and medial prefrontal cortex (Fig. 2).

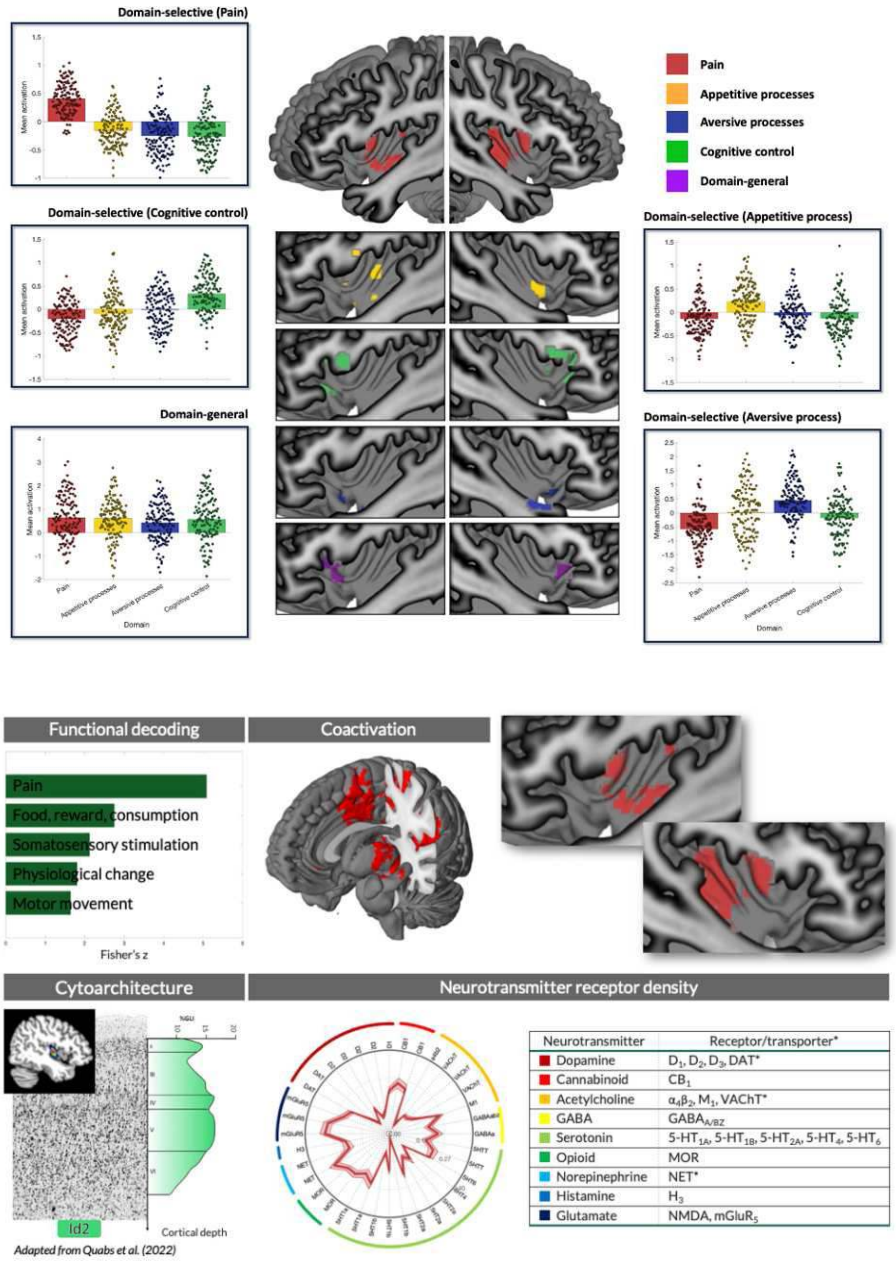

Conclusions: In summary, leveraging a Bayesian framework, large-scale multi-study dataset, and multi-level functional and anatomical profiling, our study provides comprehensive mapping of insular functional topology. The results validate discrete domain-selective modules alongside a distinct domain-general hub in the insula. By situating these functional zones within specific microscale and macroscale anatomical contexts, we reveal neurobiological mechanisms enabling both domain-specific representation and multi-modal integration.

References

1. Chang, L. J., Yarkoni, T., Khaw, M. W., & Sanfey, A. G. (2013). "Decoding the Role of the Insula in Human Cognition: Functional Parcellation and Large-Scale Reverse Inference". Cerebral Cortex, 23(3), 739–749.
2. Craig, A. D. (2009). "How do you feel — now? The anterior insula and human awareness". Nature Reviews Neuroscience, 10(1), 59–70.
3. Glasser, M. F., Coalson, T. S., Robinson, E. C., Hacker, C. D., Harwell, J., Yacoub, E., Ugurbil, K., Andersson, J., Beckmann, C. F., Jenkinson, M., Smith, S. M., & Van Essen, D. C. (2016). "A multi-modal parcellation of human cerebral cortex". Nature, 536(7615), 171–178.
4. Kelly, C., Toro, R., Di Martino, A., Cox, C. L., Bellec, P., Castellanos, F. X., & Milham, M. P. (2012). "A convergent functional architecture of the insula emerges across imaging modalities". NeuroImage, 61(4), 1129–1142.
5. Kragel, P. A., Kano, M., Van Oudenhove, L., Ly, H. G., Dupont, P., Rubio, A., Delon-Martin, C., Bonaz, B. L., Manuck, S. B., Gianaros, P. J., Ceko, M., Reynolds Losin, E. A., Woo, C.-W., Nichols, T. E., & Wager, T. D. (2018). "Generalizable representations of pain, cognitive control, and negative emotion in medial frontal cortex". Nature Neuroscience, 21(2), 283–289.
6. Kurth, F., Zilles, K., Fox, P. T., Laird, A. R., & Eickhoff, S. B. (2010). "A link between the systems: Functional differentiation and integration within the human insula revealed by meta-analysis". Brain Structure and Function, 214(5), 519–534.

7. Mazzola, L., Royet, J.-P., Catenoix, H., Montavont, A., Isnard, J., & Mauguière, F. (2017). "Gustatory and olfactory responses to stimulation of the human insula". Annals of Neurology, 82(3), 360–370.
8. Quabs, J., Caspers, S., Schöne, C., Mohlberg, H., Bludau, S., Dickscheid, T., & Amunts, K. (2022). Cytoarchitecture, probability maps and segregation of the human insula. NeuroImage, 260, 119453.
9. Rouder, J. N., Speckman, P. L., Sun, D., Morey, R. D., & Iverson, G. (2009). "Bayesian t tests for accepting and rejecting the null hypothesis". Psychonomic Bulletin & Review, 16(2), 225–237.
10. Uddin, L. Q., Nomi, J. S., Hebert-Seropian, B., Ghaziri, J., & Boucher, O. (2017). "Structure and function of the human insula". Journal of Clinical Neurophysiology, 34(4), 300–306.
11. Wager, T. D., & Barrett, L. F. (2017). From affect to control: Functional specialization of the insula in motivation and regulation. BioRxiv, 102368.

Poster No 731

A Neurofeedback Booster for Emotion Regulation Therapy: A Randomized Controlled Trial

Miroslava Jindrova[1], Christian Schmahl[1], Christian Paret[1]

[1]*Central Institute for Mental Health, Mannheim, Germany*

Introduction: Borderline Personality Disorder (BPD) patients show hyper-response of the amygdala to emotional stimuli and decreased habituation. Moreover, the hyper-reactivity of the amygdala is linked to decreased activity in the dorsolateral prefrontal cortex. This is strongly implicated with emotion dysregulation as one of the key symptoms of BPD, causing individual suffering and leading to social turbulence. Dialectical Behavioral Therapy (DBT) is an evidence-based treatment leading to reduced amygdala activity and enhanced fronto-limbic connectivity. However, more than half of BPD patients do not respond. Real-time fMRI amygdala-neurofeedback (amy-NF) targets the amygdala-hyperactivity and weak top-down control of the amygdala by the prefrontal cortex. During amy-NF, patients learn to voluntarily decrease amygdala activation in response to real-time visual feedback when viewing affective stimuli. This study investigated if amy-NF can augment the effects of DBT in people with BPD. Outcome measures included affective instability in daily life, amygdala reactivity, and self-reported BPD symptomatology.

Methods: Patients demonstrating ongoing high levels of BPD symptomatology after six weeks of DBT were invited to participate in the study with random assignment to either neurofeedback (N=23) or treatment as usual (N=13). fMRI amy-NF training involved three sessions scheduled in a two-week period. Outcomes are measured before the intervention, immediately after the intervention, and at 3 and 6-month follow-up timepoints. At the first three timepoints, affective instability was monitored using Ecological Momentary Assessment over 4 days in hourly intervals. Affect instability was investigated by calculating the mean square successive difference. Amygdala reactivity was assessed using an established fMRI task. BPD symptoms were assessed using the BSL-23 and other self-report questionnaires at all four timepoints. The change in outcome measures was compared between the two groups. N=12 dropped out before the second timepoint and were thus excluded from the subsequent analysis. Drop-outs were mostly caused by therapy discontinuation. The final sample size was N=15 in the neurofeedback group and N=9 in the treatment as usual. The trial is registered at clinicaltrials.gov (NCT04333888).

Results: The mean negative affect decreased with time in both groups. We observed a significant time effect, $F(1.61, 30.54) = 8.94$, $p < 0.01$, but no significant group or group x time interaction effect. No significant differences between the groups were observed in the mean positive affect and the instability of positive and negative affect. Decrease in amygdala reactivity was observed in both groups with more stable effect in the neurofeedback group at the 3-month follow-up. However, none of these effects were significant, $F(2, 30) = 0.49$, $p > 0.05$. BPD symptomatology measured by BSL-23 showed reduced problems after the therapy in both groups. However, the symptoms increased at the 3-month and 6-month follow-ups, and no effect of neurofeedback was observed. The time effect was significant, $F(2.17, 28.15) = 11.92$, $p < 0.001$.

Conclusions: This study couldn't prove neurofeedback to be an effective booster for BPD therapy. This was mainly caused by a small sample size and insufficient statistical power to uncover moderate or small effects. Future studies should be planned with sufficient time and financial support to enable reaching the recruitment goals. The results confirm the current knowledge that DBT is an effective treatment for BPD, but also indicate the need to strenghten the retention of the effects after the therapy.

References

1. Schulze, L. et al. (2016), 'Neural Correlates of Disturbed Emotion Processing in Borderline Personality Disorder: A Multimodal Meta-Analysis', Biological Psychiatry 79, 97–106
2. Goodman, M. et al. (2014), 'Dialectical behavior therapy alters emotion regulation and amygdala activity in patients with borderline personality disorder', Journal of Psychiatric Research, 57, 108–116
3. Paret, C. et al. (2016), 'Alterations of amygdala-prefrontal connectivity with real-time fMRI neurofeedback in BPD patients', Social Cognitive and Affective Neuroscience, 11, 952–960

Poster No 732

Neural correlates of expectation vs. expectation violation in delayed fear extinction learning

Isabelle Ridderbusch[1], Adrian Wroblewski[1], Yunbo Yang[2], Hans-Ulrich Wittchen[3], Andre Pittig[4], Andreas Ströhle[5], Jennifer Mumm[6], Alfons Hamm[7], Jan Richter[2], Maike Hollandt[7], Christoph Szeska[8], Martin Lotze[7], Volker Arolt[9], Udo Dannlowski[9], Katja Koelkebeck[10], Dirk Adolph[11], Jürgen Margraf[11], Silvia Schneider[11], Jan Cwik[12], Jürgen Deckert[13], Katharina Domschke[14], Martin Herrmann[13], Ulrike Lueken[15], Ricarda Evens[15], Constantin Rothkopf[16], Winfried Rief[1], Tilo Kircher[1], Benjamin Straube[1]

[1]University of Marburg, Marburg, Germany, [2]University of Hildesheim, Hildesheim, Germany, [3]University of Dresden, Dresden, Germany, [4]University of Goettingen, Goettingen, Germany, [5]Charité Berlin, Berlin, Germany, [6]Freie Universität Berlin, Berlin, Germany, [7]University of Greifswald, Greifswald, Germany, [8]University of Potsdam, Potsdam, Germany, [9]University of Münster, Münster, Germany, [10]University of Duisburg-Essen, Essen, Germany, [11]University of Bochum, Bochum, Germany, [12]University of Cologne, Cologne, Germany, [13]University of Würzburg, Würzburg, Germany, [14]University of Freiburg, Freiburg, Germany, [15]Humboldt Universität zu Berlin, Berlin, Germany, [16]University of Darmstadt, Darmstadt, Germany

Introduction: Fear extinction is learning that a prior threat signal no longer indicates danger. An essential aspect of extinction learning is the violation of an expected outcome, in the context of fear specifically the expectation of an upcoming aversive event. This is experimentally operationalized via extinction training: a CS+ (conditioned stimulus, previously paired with an aversive stimulus) is repeatedly presented without an US (unconditioned aversive stimulus). A meta-analysis on neural correlates of fear extinction showed consistent brain activation in the cingulate cortex and insula in the overall CS+>CS- comparison in healthy subjects (HS)[1]. However, fMRI studies typically do not distinguish between expectation (EXP) and its violation (VIO) during CS-presentations. To close this knowledge gap, here we analyzed the beginning of CS-presentation (where the EXP of US/no US is set), separate from the timepoint at which the US would be present during conditioning (VIO) to investigate the following questions: 1) How does neural activation differ between the EXP of a potential aversive event and the VIO of this expectation? 2) Is there an interaction between CS-type and EXP vs. VIO?

Methods: We used an optimized protocol of delayed extinction training[2]: For fear conditioning, one of two neutral visual stimuli (CS+) was followed (5 seconds after stimulus start) by an aversive electric US (electric stimulus, 60% reinforcement rate) while the other stimulus (CS-) was never paired with the US. The US was applied by an MRI compatible electrodermal electrode attached to the inside of the non-dominant forearm. 24h later, uninstructed extinction over 20 trials was tested during functional magnetic resonance imaging (fMRI). Time courses of subjects' brain activity were acquired using 3-Tesla MR scanners equipped with a 12-channel head matrix receive coils. Functional images were obtained using a T2-weighted gradient-echo echo-planar imaging (EPI) sequence sensitive for the BOLD contrast (TE=30ms, TR=2s, flip angle 90°, matrix size 64×64 voxels, voxel size 3.6×3.6×4.0mm, slice thickness 4mm, inter-slice gap 0.4mm, field of view (FOV)=230mm, 33 slices, ascending phase encoding direction)[3]. A Family-wise error (FWE) correction was used. Quality controlled data-sets of n=103 HS from five sites in Germany were included.

Results: 1) Differential activation between the overall EXP and VIO during the full course of the experiment was found: activation in the MCC and anterior insula was higher during EXP, in the basal ganglia (nucleus caudate, putamen, pallidum), thalamus, middle frontal and temporal cortices activation was higher during VIO. 2) An Interaction between stimulus type (CS+ vs. CS-) and the EXP vs. VIO phase of the stimulus presentations was found in the inferior frontal gyrus, supramarginal gyrus and cerebellum, suggesting that EXP and VIO provide complementary information about neural processing of fear and safety signals. Separate post-hoc analyses for EXP and VIO respectively on CS-type associated differences revealed higher activation in the middle cingulate cortex, nucleus caudate and in the anterior insula towards CS+ than towards CS- during EXP, whereas in the paracentral lobule it was higher towards CS . During VIO, activation in the basal ganglia, the anterior cingulate cortex, the inferior frontal cortex including the anterior insula and in temporal areas and the cerebellum was higher towards CS+ than towards CS-, whereas in the medial orbitofrontal cortex and gyrus rectus it was higher towards CS-.

Conclusions: Our findings suggest that the differentiation between EXP an VIO phase of CS-presentation provides useful additional information about extinction learning processes on the neural level. This finer strategy of analysis holds the potential to possibly better detect and understand altered processes in patients with anxiety disorders compared to HS in future analyses.

References

1. Fullana, M.A., Albajes, A. et al. (2018), 'Fear extinction in the human brain: a meta-analysis of fMRI studies in healthy participants', Neurosci. Biobehav. Rev., vol. 88, pp. 16-25.
2. Hollandt, M., Wroblewski, A., et al. (2020), 'Facilitating translational science in anxiety disorders by adjusting extinction training in the laboratory to exposure-based therapy procedures', Transl. Psychiatry, vol. 10, p. 110.
3. Ridderbusch, I. C., Wroblewski, A., et al. (2021), 'Neural adaptation of cingulate and insular activity during delayed fear extinction: A replicable pattern across assessment sites and repeated measurements', NeuroImage, vol. 237, pp. 118157.

Poster No 733

An fMRI study on over-generalization of social fear in patients with potential traumatic event

Minji Kim[1], Dasom Lee[2], Soo-Hee Choi[3]

[1]Seoul National University College of Medicine, Seoul, Seoul, [2]Seoul National University Hospital, Seoul, Seoul, [3]Department of Psychiatry, Seoul National University Hospital, Seoul, Korea, Republic of

Introduction: While most individuals experience at least one potentially traumatic event (PTE), only around 20% develop posttraumatic stress disorder (PTSD). The key to understanding the pathophysiology of PTSD lies in the abnormal fear conditioning and over-generalization, where fear responses extend to stimuli similar to the original threat. Although there is a wealth of research on fear learning in PTSD, studies addressing abnormal fear in patients experiencing chronic pain after PTE are lacking. Given the challenges in daily functioning and social interaction faced by these patients, further investigations into fear generalization in social context in this population are needed.

Methods: A fear conditioning paradigm (Fig.1.a) was assessed during fMRI scanning in 22 healthy controls (HC) and 22 chronic pain patients with PTE. In acquisition, participants were presented with photographs of female faces, some of which were repeatedly paired with an aversive unconditioned stimulus (US) consisting of an angry expression and contemptuous comments (CS+), or with a neutral expression and comments (CS-) (Fig.1.b). In generalization, eight morphed faces of CS in each continuum served as generalized stimuli (GSs, Fig.1.c). Participants were instructed to rate their perceived level of risk (US expectancy). To investigate the neural activity in the generalization phase, functional regions-of-interest (fROIs) were selected based on the acquisition phase results (CS+ > CS-, Fig.2.a). These fROIs include the inferior frontal gyrus (IFG), inferior parietal lobule (IPL), insula, middle/inferior temporal gyrus, supplementary motor area, fusiform gyrus, thalamus, rostral anterior cingulate cortex (ACC), and amygdala. Ventromedial prefrontal cortex (vmPFC) and the adjacent rectal gyrus were also included, following relevant findings (Lissek et al., 2014). Statistical analysis involved a 2 × 6 repeated-measures ANOVA. Posttraumatic Diagnostic Scale was included as a covariate to account for group differences based on PTE exposure, irrespective of PTSD onset. One patient was excluded due to excessive head motion (> 0.5mm).

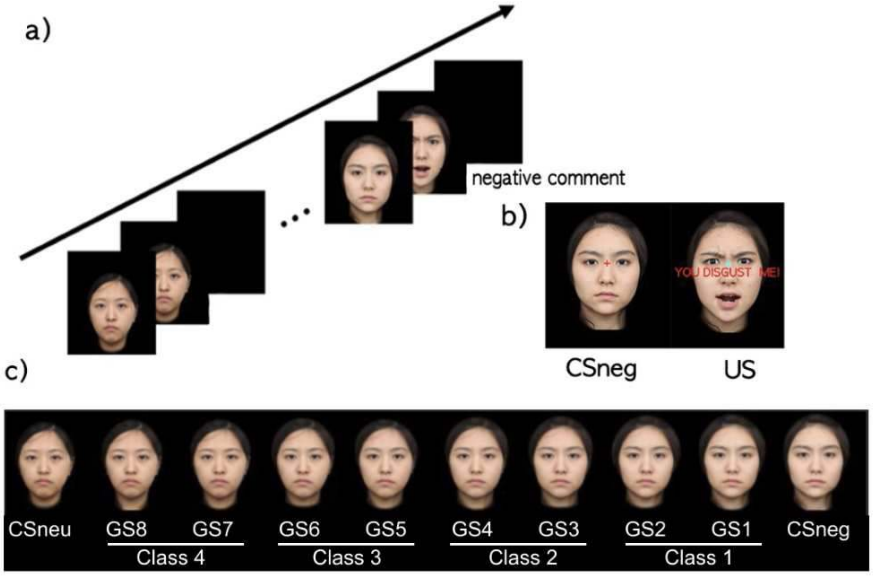

Fig. 1. Fear generalisation task design.

Results: Behavioral results indicated higher US expectancy in PTE than HC during the generalization. While reaction time showed no group differences, post-hoc tests indicated that, unlike HC, PTE hesitated significantly longer for ambiguous stimuli (C2, C3) than for CS-. Imaging results revealed three distinct patterns. Firstly, in regions associated with fear inhibition including vmPFC, the two groups showed opposite pattern [Stimulus * Group: left, F=6.585, p=.003, right, F=5.931, p=.005] (Fig.2.b). Unlike HC, the PTE group exhibited persistent deactivation even for stimuli closer to CS-, implying challenges in fear inhibition processing. Secondly, in areas related to fear excitation (right IPL), PTE exhibited significantly higher excitation compared to the control group for C1 [Group: F=5.970, p=.019] (Fig.2.c). Lastly, PTE exhibited increased activity in thalamus in response to ambiguous GSs (C2, C3) [Stimulus * Group: left, F=2.159, p=.060, right, F=2.689, p=.034] (Fig.2.d), reflecting enhanced early perceptual processing of potential threat in patients.

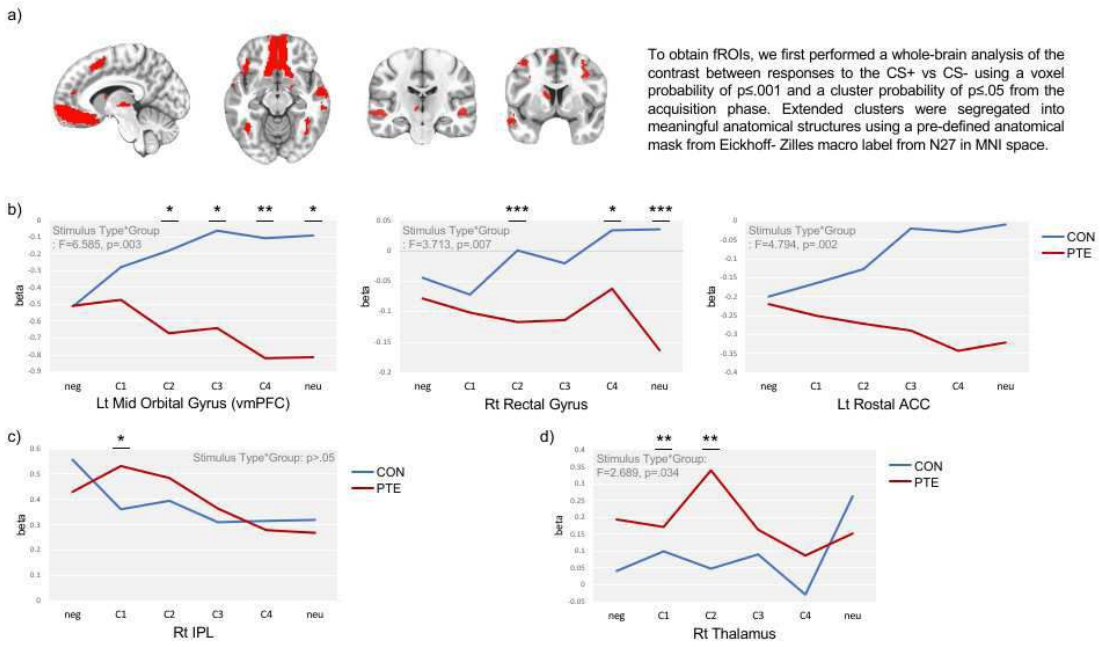

Fig. 2. Functional regions of interest used to analyse and results

Conclusions: Patients with PTE exhibited abnormal neural activity in regions involved in emotional regulation and early evaluation of potential threats, which may contribute to aberrant fear responses in this population.

References

1. Lissek, S. (2014), 'Neural substrates of classically conditioned fear-generalization in humans: a parametric fMRI study', Social cognitive and affective neuroscience, vol. 9, no. 8, pp. 1134-1142.
2. Webler, R. D. (2021), 'The neurobiology of human fear generalization: meta-analysis and working neural model', Neuroscience & Biobehavioral Reviews, vol. 128, pp. 421-436.

Poster No 734

Induced emotional state modulates aperiodic activity of the amygdala

Haeorum Park[1], Carl Hacker[1], Hohyun Cho[1], Eric Leuthardt[1], Peter Brunner[1], Jon Willie[1]

[1]*Washington University School of Medicine in St. Louis, St. Louis, MO*

Introduction: Mood disorders, leading to diminished motivation and, in extreme cases, suicidal behavior, saw a dramatic increase of over 25% during the COVID-19 pandemic. While the underlying mechanisms have been extensively explored through neuroimaging techniques such as EEG, MRI, and MRS, electrophysiological biomarkers of mood, directly recorded from cortical and subcortical regions, remain largely unexplored. Recent studies suggest that the 1/f slope in the frontal lobe's power spectrum is a significant indicator of depression severity. However, the role of aperiodic exponents representing the 1/f slope, particularly in the amygdala, a crucial center for emotional processing, is not well understood. This study aims to shed light on the amygdala's electrophysiological responses in emotionally induced states, potentially contributing to a deeper understanding of mood disorder pathophysiology.

Methods: In this study, we elicited emotional responses to 20-40-second long videos while simultaneously recording local field potentials in 16 patients with intractable epilepsy who underwent intracranial monitoring prior to resective brain surgery. These videos were previously evaluated by Samide et al. (2020), and rated for emotional valence and arousal by 100 healthy subjects. After viewing each video, we asked our intracranially monitored subjects how watching this video made them feel. Subjects responded on a Likert scale ranging from one (unpleasant) to nine (pleasant). In our post-hoc analysis, for each subject, we determined the correlation between the aperiodic exponents of the power spectrum (i.e., the 1/f slope) and normative valence/arousal (from 100 health subjects), as well as subject-specific Likert scale ratings (from our 16 subjects). To determine the aperiodic component, we applied the FOOOF algorithm to the neural signals within the canonical beta and gamma bands (i.e., 12-50 Hz frequency range). To account for the inherently negative nature of the 1/f slope, we used the absolute value of this slope for a more intuitive representation of steeper exponents. We conducted a region-wise statistical

analysis to compare the aperiodic slopes between high (1st quantile) and low (4th quantile) mood states. Subjects without amygdala electrode contact were excluded from our analysis.

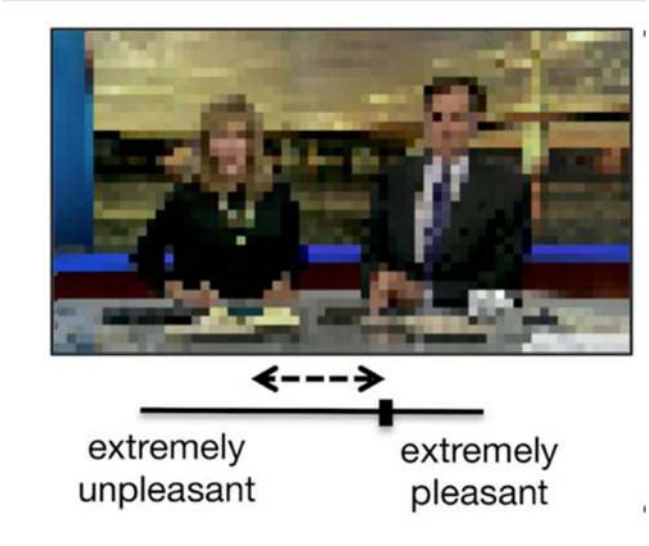

Results: We found a significant positive correlation between the 1/f slope and normative valence of the videos (r=0.619, p<0.001) and a significant negative correlation between the 1/f slope and normative arousal (r=-0.448, p<0.001). The subjects rated the videos on a sigmoid-shaped psychometric curve, confirming the tendency to perceive positively valenced stimuli as pleasant and negatively valenced stimuli as unpleasant (refer to Fig 2). Within the amygdala, the majority of electrodes (60%) showed a statistically significant negative correlation between the aperiodic exponent and mood ratings, indicating that a flattened 1/f slope in the power spectrum was associated with positive emotions. This negative correlation was statistically significant in both one-sample and paired-sample hypothesis testing (p=0.003), with less than 20% of electrodes exhibiting a statistically significant positive correlation.

Conclusions: Prior research indicates that low and high-power activity in the prefrontal cortex is inversely correlated with depression severity, suggesting that the aperiodic exponent may vary with mood states. Building on this, our study explores emotional states induced by video stimuli, proposing a link between power and aperiodic slope that represents emotional fluctuations. We observed that positive emotional states induce flatter power spectra within the amygdala, underscoring its critical role as an emotional hub. Our observation aligns with the canonical understanding of the aperiodic exponent of the power spectrum, highlighting the significance of the amygdala's aperiodic electrophysiological activity in emotional processing.

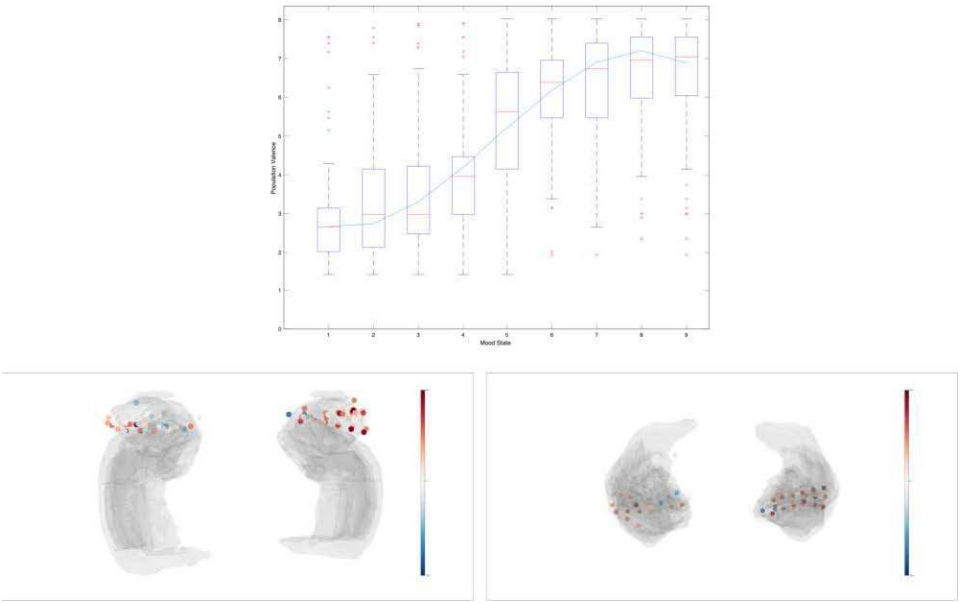

Fig 2. Boxplot of emotional states and valence. Amygdala electrodes placements.

References
1. Samide R. (2020). 'A database of news videos for investigating the dynamics of emotion and memory', Behavior Research Methods, 52, 1469-1479.
2. Xiao, J. (2023). 'Decoding depression severity from intracranial neural activity'. Biological Psychiatry.

Poster No 735

Neural Correlates of Eye-Gaze Perception as a function of Autism Trait Severity in Adults

Shadi Bagherzadeh Azbari[1], Changsong Zhou[2], Andrea Hildebrandt[3], Gilbert Ka Bo Lau[4], Werner Sommer[5], Ming Ann LUI[4]

[1]Charité – Universitätsmedizin Berlin, Berlin, Germany, [2]Hong Kong Baptist University, Kowloon, Hong Kong, [3]University of Oldenburg, Oldenburg, Germany, [4]Hong Kong Baptist University, Kowloon, Hong Kong, [5]Humboldt-Universität Zu Berlin, Berlin, Germany

Introduction: Humans as social species intensely use facial expressions and eye gaze for transmitting social signals. Individuals with Autism Spectrum Disorder (ASD) exhibit atypical face processing, including atypical attention to eye gaze and emotional expression identification.

Methods: We investigated how gaze and expression perception, assessed by event-related brain potentials (ERPs) depends on autism trait severity. ERPs were recorded from 46 EEG channels in 150 young adults - diagnosed with the autism spectrum- to the presentation of pictures of faces with emotional expressions, which had to be judged for gaze changes.

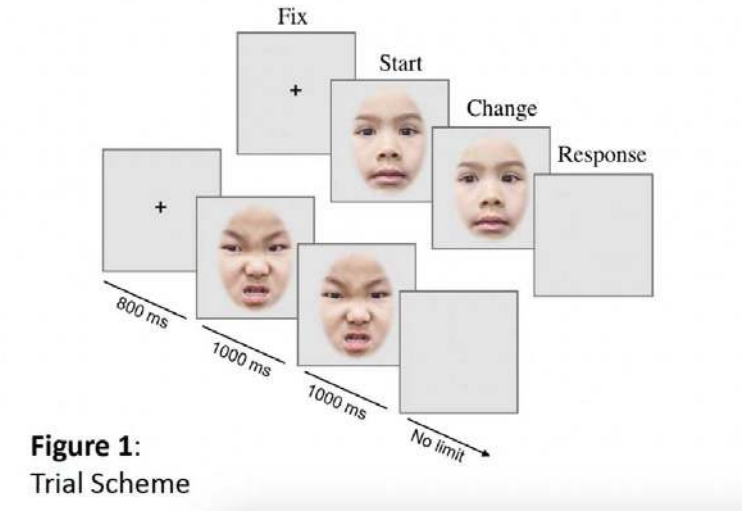

Figure 1:
Trial Scheme

Results: The mean age of the participants was 21.27 years (SD: 3.23, Range [19:23], and 58% of them were female. In line with previous studies, N170 amplitudes were larger to averted than to direct gaze. This effect was negatively correlated with the participant's scores of the Autism Diagnostic Observation Schedule (ADOS) total score scale. The early posterior negativity (EPN) was also interpreted as a signal of enhanced attention to angry emotion relative to neutral facial expressions.

Conclusions: The study suggests decreased sensitivity in the eye contact detection system for individuals with high autism traits.

References
1. Bagherzadeh-Azbari S, Lau GKB, Ouyang G, Zhou C, Hildebrandt A, Sommer W and Lui M (2023) Neural Correlates of Eye-Gaze Perception as a function of Autism Trait Severity in Adults. (in prepration)

Poster No 736

Neural Mechanisms Underlying Improving Health Behavior with Cognitive Training under Stress

Qianqian Ju[1,2], Yujia Peng[1,2,3,4], Yiqun Gan[1,2]

[1]Peking University, Beijing, China, [2]School of Psychological and Cognitive Sciences, Beijing Key Laboratory of Behavior and Mental Health, Beijing, China, [3]Institute for Artificial Intelligence, Peking University, Beijing, China, [4], Beijing, China, [4]National Key Laboratory of General Artificial Intelligence, BIGAI, Beijing, China

Introduction: Individuals under stress are likely to overeat high-calorie food. ROC (Regulation of Craving) intervention can reduce the intake of unhealthy high-calorie food. However, the neural mechanism of inhibitory control of food stimuli underlying ROC intervention in exposure to stress remains unclear. The current study aims to investigate the effect of ROC on diet behavior and whether the impact of stress on food could be alleviated to form healthier diet behavior. We further examine neural mechanisms of how ROC can effectively improve food choices and promote dietary health by influencing inhibition control through EEG.

Methods: A total of 24 human subjects (13 females) participated in the EEG experiment of high/low-calorie food-related inhibitory control. The study adopted a 2 * (intervention group: ROC vs. control, between-subject) * 2 (stress group: stress vs. no-stress, between-subject) * 2 (task type: high-calorie vs. low-calorie task, within-group) mixed experimental design. We used the Revised Trier Social Stress Task (TSST) to manipulate acute stress. Inhibitory control was measured through the classic Go/No-go task in an EEG setting (Figure 1). Event-related potentials (ERPs) between stress and no stress among intervention and control groups were analyzed.

Results: Five data were removed due to failing to finish the experiment. Behavior results showed that ROC intervention significantly increased inhibitory control performances (i.e., larger ACC, smaller RT) under stress conditions in low-calorie tasks. ERP results on N2 revealed a significant three-way interaction between intervention, stress, and task (Figure 2). Specifically, under the stress-invoked condition, a significant two-way interaction showed that ROC yielded a greater reduction of no-go N2 amplitude in frontal/frontal-central in high-calorie tasks compared to low-calorie tasks. Meanwhile, under the no-stress condition, the ROC intervention group yielded an overall reduction of N2 amplitude for both high- and low-calorie tasks compared to the control group.

Conclusions: The current study demonstrated the negative impact of stress on food-related inhibition control, that a greater effort of inhibition was needed when facing high-calorie food in exposure to stress. We also confirmed a positive effect of ROC intervention for improving inhibition control under both stress and no-stress conditions, especially for high-calorie food, which may contribute to forming healthier diet behavior under stressful situations.

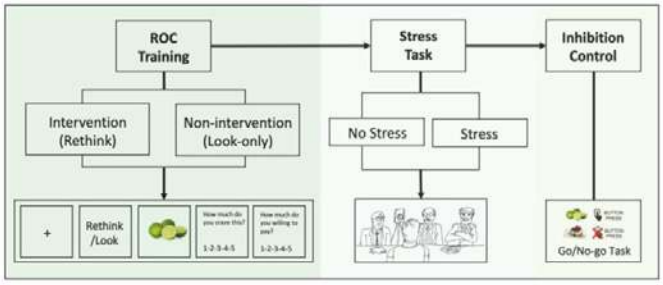

Figure 1. Experiment procedure

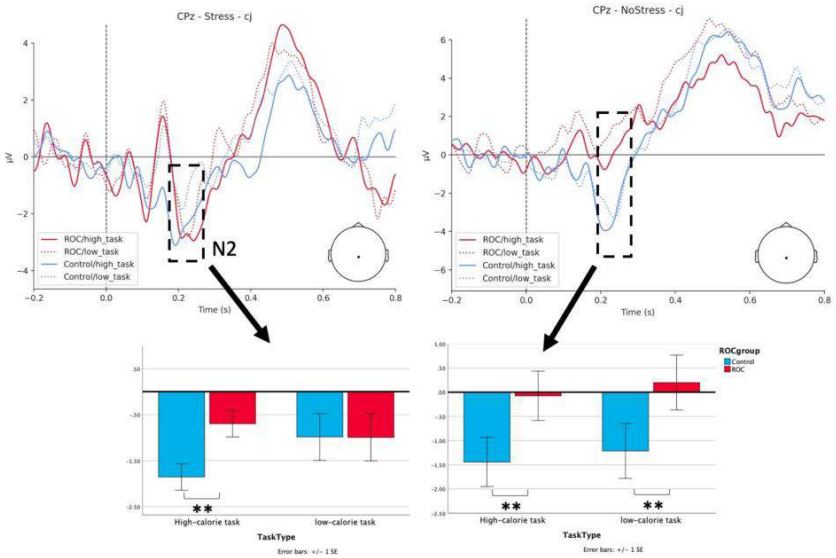

Figure 2. The interaction of stress, intervention and task type on P2 in food no-go task
Notes. ERP was averaged from electrode sites of frontal, frontal-central, central , central-parietal and parietal (only show CPz here), cj = correct rejection, error bars was ±1 SE.

References

1. Boswell, R. G., Sun, W., Suzuki, S., & Kober, H. . (2018). Training in cognitive strategies reduces eating and improves food choice. Proceedings of the National Academy of Sciences.
2. Boswell, R. G., & Kober, H. . (2016). Food cue reactivity and craving predict eating and weight gain: a meta-analytic review. Obesity Reviews, 17(2), 159-117.
3. Chen B.B., Shi Z., Sun S. (2017). Life history strategy as a mediator between childhood environmental unpredictability and adulthood personality. Personality and Individual Differences, 111, 215-219
4. Harris, Alison, Hare, Todd, Rangel, & Antonio. (2013). Temporally dissociable mechanisms of self-control: early attentional filtering versus late value modulation. Journal of Neuroscience(33), 18917–18931.
5. Hill, D. C., Moss, R. H., Sykes-Muskett, B., Conner, M., & O'Connor, D. B. (2018). Stress and eating behaviors in children and adolescents: Systematic review and meta-analysis. Appetite, 123, 14-22. https://doi.org/10.1016/j.appet.2017.11.109
6. Tomiyama, A. J. (2019). Stress and Obesity. Annual review of psychology, 70(1), 703-718. https://doi.org/10.1146/annurev-psych-010418-102936
7. Wilson, G. T., Grilo, C. M., & Vitousek, K. M. . (2007). Psychological treatment of eating disorders. American Psychologist, 62(3), 199-216.
8. Zhou, Y., Liu, Y., Du, J., & Chen, H. (2018). Effects of food exposure on food-related inhibitory control in restrained eaters: An ERP study. Neuroscience Letters, 672(13), 130-135. https://doi.org/10.1016/j.neulet.2018.02.048

Poster No 737

Physiological and neural responses to witnessing animal suffering and connection

Byeol Kim Lux[1], Melanie Kos[2], David Ward[1], Tor Wager[1]

[1]Dartmouth College, Hanover, NH, [2]Temple University, Philadelphia, PA

Introduction: Witnessing suffering can be a potent stressor. Nonhuman animals exhibit inflammatory responses and depressive behavior when exposed to counterparts' suffering (Sial et al., 2015). In humans, observing pain activates brain regions associated with physical pain (Krishnan et al., 2016). Despite this, the psychological and physiological costs of causing distress to animals and the benefits of fostering compassion remain largely unexplored. This study aims to uncover neurobiological responses to witnessing animals' suffering and connection, using diverse modalities, including 3T fMRI and physiological measures (N = 88). This poster explores the variations in heartbeat and skin conductance during the viewing of animal videos and the associated brain representations linked to autonomous activity. These results indicate the activation of the sympathetic nervous system, eliciting fight-or-flight responses triggered by the perceived threat of witnessing suffering.

Methods: The fMRI experiment was conducted over two-day sessions. During the fMRI scans, participants viewed a 30-minute aversive video depicting animal treatment in the food industry, such as slaughterhouses, or a positive video showing the intelligence of farm animals engaging in games and forming meaningful connections with humans. They viewed either of the two types of video in each session, and the order of videos was counterbalanced. Following the movie runs, a 10-minute resting state fMRI run was conducted. Additionally, we measured heart rate and skin conductance during the MR scans.

Results: To examine the impact on heartbeat and skin conductance during the viewing of two distinct videos, we compared interbeat-interval (IBI) and skin conductance. We found a significant decrease in IBI, signifying an increased heart rate (Figure 1; paired t-test, $t = 2.026$, $p = 0.046$, $df = 84$), and a significant higher in skin conductance level (SCL) ($t = -3.757$, $p < 0.001$, $df = 50$) when participants viewed negative clips versus positive ones. Moreover, the skin conductance response (SCR) exhibited a higher standard deviation during the negative session compared to the positive one ($t = -3.232$, $p = 0.002$, $df = 50$). These observed rapid heartbeats and increased skin conductance levels indicate an activated sympathetic nervous system and escalated physiological arousal in response to negative stimuli. The greater variability of skin conductance implies that they experienced more momentary arousal fluctuations. Subsequently, we explored whether the physiological responses persisted during the resting state after the movie-watching. Notably, the significantly lower IBI endured in the resting state even after exposure to the negative clips ($t = 2.955$, $p = 0.004$, $df = 85$). Transitioning to an examination of brain representations linked to autonomous activity, we analyzed activation patterns during video viewing, focusing on associations with IBI and SCL. We found that increased activity in specific areas–the pre-supplementary motor area, ventral anterior insula (valns), and posterior orbitofrontal cortex (pOFC)–when heart rate was higher during the negative session compared to the positive one (Figure 2, False Discovery Rates corrected $q < 0.05$). Notably, prior research has associated the valns and pOFC with interoceptive awareness and emotional processing, providing context for our observed neural responses (Craig, 2009, Kringelbach, 2005).

Figure 1. Physiological responses to witnessing animal suffering and connections

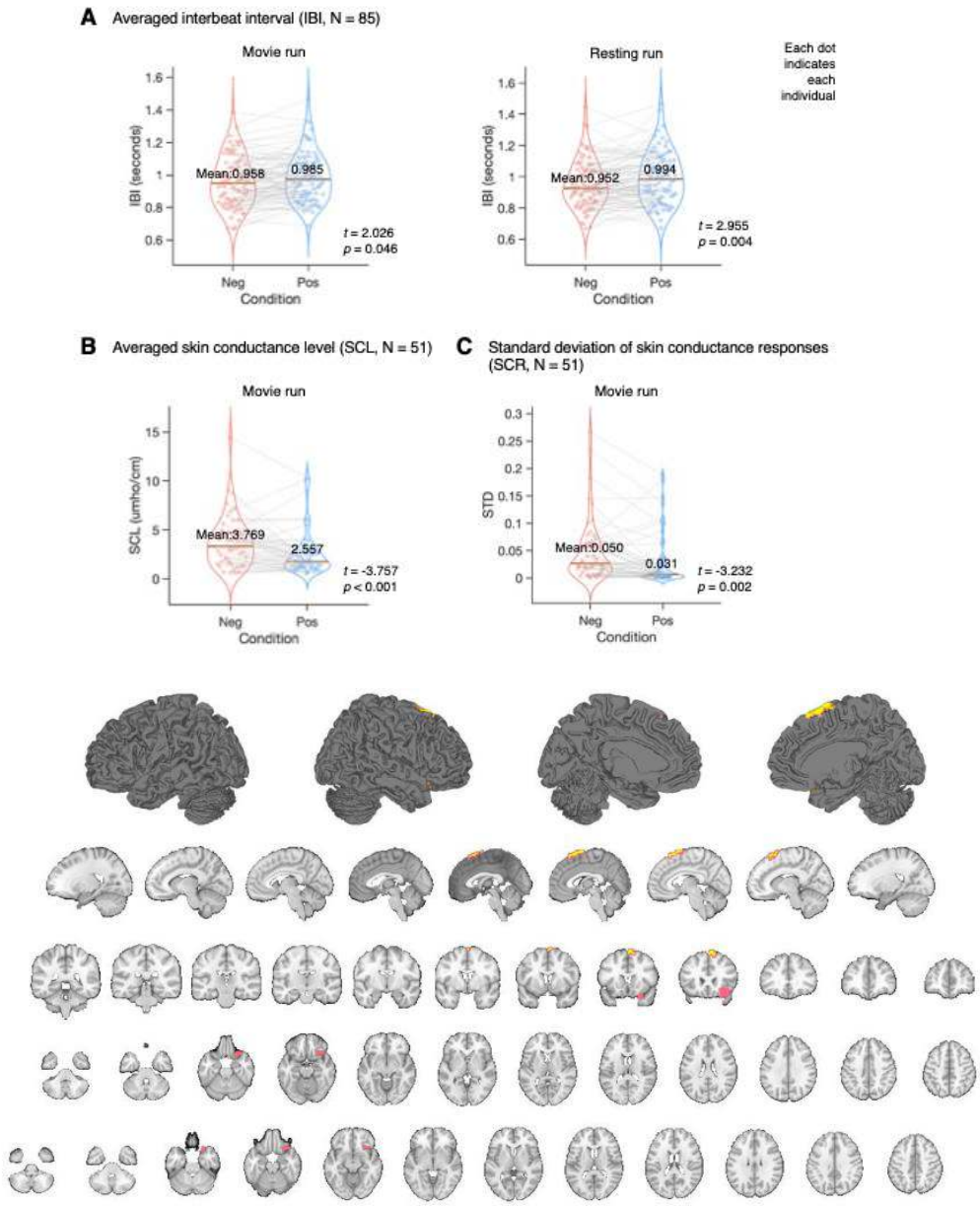

Conclusions: The physiological arousal induced by negative movie viewing, coupled with the continual elevated heart rate, persisted even after the viewing. These findings suggest that participants underwent stress-inducing arousal while viewing animal suffering. Also, we identified the neural representations linked to the heightened heart rate during negative movie watching compared to positive movie watching. These results mark an initial step in uncovering the impact of witnessing animal suffering and animal connection on our body and brain.

References

1. Avants, B. B. (2008). Symmetric diffeomorphic image registration with cross-correlation: evaluating automated labeling of elderly and neurodegenerative brain. Medical image analysis, 12(1), 26-41.
2. Boyacioğlu, R. Improved sensitivity and specificity for resting state and task fMRI with multiband multi-echo EPI compared to multi-echo EPI at 7 T. Neuroimage, 119, 352-361.
3. DuPre, E. (2021). TE-dependent analysis of multi-echo fMRI with* tedana. Journal of Open Source Software, 6(66), 3669.
4. Esteban, O. (2019). fMRIPrep: a robust preprocessing pipeline for functional MRI. Nature methods, 16(1), 111-116.
5. Krishnan, A. (2016). Somatic and vicarious pain are represented by dissociable multivariate brain patterns. elife, 5, e15166.
6. Sial, O. K. (2016). Vicarious social defeat stress: Bridging the gap between physical and emotional stress. Journal of neuroscience methods, 258, 94-103.
7. Steel, A. (2022). Evaluating the efficacy of multi-echo ICA denoising on model-based fMRI. Neuroimage, 264, 119723.

Poster No 738

Brain network associated with interpersonal static touch

Ryo Kitada[1], Hiroaki Kawamichi[2], Yuki Hamano[3,4], Eri Nakagawa[5], Sho Sugawara[6], Norihiro Sadato[7,8]

[1]Graduate School of Intercultural Studies, Kobe University, Kobe, Hyogo, [2]Gunma University, Maebashi, Japan, [3]Waseda University, Tokyo, Japan, [4]the Japan Society for the Promotion of Science, Tokyo, Japan, [5]Shizuoka University, Hamamatsu, Japan, [6]Tokyo Metropolitan Institute of Medical Sciences, Tokyo, Tokyo, [7]Ritsumeikan University, Kyoto, Kyoto, [8]National Institute for Physiological Sciences, Okazaki, Japan

Introduction: Hand is the most touchable body part in social interaction and stationary hand contact between socially-close persons can alleviate distress. Neuroimaging studies have revealed the involvement of limbic structure and somatosensory cortices in affective processing of interpersonal touch. However, because these studies focused on the effect of stroking hairy skin, the brain network for interpersonal touch on the glabrous skin is scarcely understood. Here, we conducted an fMRI study to examine neural correlates of interpersonal touch by manipulating the touched body part and social closeness of the toucher.

Methods: We used two 3-T whole-body MRI scanners (Verio; Siemens) with a multiband EPI sequence: gradient-echo EPI, TR = 1,000 ms, multiband factor = 6, echo time (TE) = 35 ms, flip angle = 65°, 60 axial slices of 2-mm thickness with a 25% slice gap, and in-plane resolution = 2.0 × 2.0 mm2. Seventeen pairs of volunteers participated in the study (16 female friends and 18 male-female couples). We tested two types of stimuli: human hand and cosmetic brush. We manipulated the human hand stimulation with the two factors: the body area of the stimulation (hand and forearm) and the social closeness of the person who the subject believed touched their body (close person or stranger). Brush stimulation was used to serve as control of tactile input for interpersonal touch and to examine activity sensitive to slow brushing that is associated with peripheral C tactile fibers in the forearm. The brush stimulation was also manipulated with the two factors: the location of the stimulation (hand and forearm) and brushing speed (3 levels). In each trial, the participant's right hand (palm side of the hand) and arm were stimulated by either brush or other's hand (finger pads). After 5-s stimulation, the participants used their left thumb to control the three buttons to answer their feelings using the visual-analogue scale (VAS). We preprocessed fMRI data and conducted mass-univariate analyses using SPM12. In the mass-univariate analysis, the statistical threshold for the spatial extent test on the clusters was set at $p < 0.05$, family-wise error (FWE) corrected for multiple comparisons over the whole brain. The height (cluster-forming) threshold was set at $p < 0.001$ (uncorrected). We used CoSMoMVPA toolbox to perform the multi-voxel pattern analysis (MVPA).

Results: Univariate analyses: As compared to brush stimulation, the contact by other revealed regions of significant activation including the medial prefrontal cortex, posterior cingulate cortex, and temporal-parietal junction. We evaluated the effect of social closeness to the toucher on brain activity by comparing the close-person's touch with the stranger's touch. The close-person effect was found in the anterior cingulate cortex (ACC), bilateral ventromedial prefrontal cortex (vmPFC), middle occipital gyrus (MOG), and inferior temporal gyrus regardless of the body part. This close-person effect was stronger for hand than forearm in multiple brain regions such as ACC, anterior insula and nucleus accumbens (NAcc). MVPA Permutation tests on orbitofrontal cortex (OFC), ACC, NAcc, postcentral gyrus (PostCG) and parietal operculum (PO)/insula (with Bonferroni correction) showed significant results on all regions for interpersonal hand touch (p values < 0.05). The effect for other's contact to the arm was observed in all regions except for PO/insula (p values < 0.05). Paired t tests (with Bonferroni correction) showed that accuracy was greater for the hand than the forearm in the postCG, PO/Insula and ACC in the contact by others (p values < 0.001).

Conclusions: These results suggest that ACC, vmPFC, and MOG constitute nodes of a network for the social-closeness effect, regardless of the body part. Furthermore, the anterior insula and NAcc may be additional nodes to cause the emotional effect unique to interpersonal hand touch.

Poster No 739

Decoding emotional signals: intersubject correlation exploration of naturalistic stimuli

Junhyeok Jang[1], Jongwan Kim[2]

[1]Jeonbuk National University, Jeonju-si, Jeollabuk-do, [2]Jeonbuk National University, Jeon-su si, Jeollabuk-do

Introduction: Valence, which characterizes the positivity or negativity of emotions, profoundly influences our perceptions of the world (Barrett et al., 2004). Functional magnetic resonance imaging (fMRI) studies have revealed the neural basis of

valence processing by analyzing brain activity during emotional processing (Baucom et al., 2012; Kim et al., 2017). However, conventional fMRI approaches faced challenges when examining neural activation patterns induced by naturalistic stimuli. Intersubject correlation (ISC) addresses these limitations in traditional fMRI analysis methods (Hasson et al., 2004). This technique quantifies neural synchrony between regions or voxels across participants, assuming that specific stimuli inducing behavioral or psychological changes will result in synchronized neural activation patterns (Nastase et al., 2019). ISC excels in capturing complex activation patterns over time, reducing issues of multiple comparisons and overfitting (Hejnar et al., 2007). In this study, we analyzed fMRI data in response to naturalistic emotional stimuli to identify regions with high interparticipant synchrony of affect changes using ISC.

Methods: In this study, we reanalyzed datasets from two sources: Chen et al. (2017) and Kim et al. (2020). Chen et al. (2017) involved 17 participants (12 males, 10 females, aged 18-26, mean age 20.8; 5 participants' data excluded) who watched "Sherlock" episode 1 during fMRI scans. Kim et al. (2020) collected emotion ratings from 125 undergraduate students (34 males, 91 females, mean age 20.38) who watched the same episode. Kim et al. (2020) preprocessed and aligned the fMRI data with segment and emotion rating times using TR multiples. We used 621 valence data and segments, excluding arousal ratings, to examine neural responses to valence changes. We used the searchlight analysis method (Kriegeskorte et al., 2006), offering greater flexibility than traditional whole-brain analyses. This method systematically moved a spherical or cubic "searchlight" through the brain volume, recording values in all voxels to create a comprehensive map. ISC was used to identify synchronized neural activation patterns during emotional changes. Data from 17 participants were divided into a target participant (S_i) and the remaining participants (S_(n-1)), and voxel activation levels were extracted within a searchlight cube for ISC evaluation (Figure 1 A). ISC quantifies the correlation between the brain activity patterns of each S_i and averaged S_(n-1) at each segment (Figure1. B, C). Subsequently, we calculated correlation coefficients between the ISC values and valence ratings (Figure1. D). This process was repeated for all 17 participants, yielding 17 ISC-valence correlation brain maps. Following individual analyses, a group level analysis was conducted to examine the ISC-valence correlation patterns across all participants. To determine cluster size, a permutation test with 100 iterations was conducted to establish a null distribution, setting the significance threshold at α = .05.

Results: The searchlight analysis method based on ISC was performed to identify brain regions where neural activation synchrony increased as valence increased. The permutation test identified a critical significance threshold of a cluster size of 145 at the p=.05 percentile of the cluster size distribution. The left superior parietal gyrus (SPG) (MNI coordinates x= -39, y= -45, z= 60; cluster size 169; peaked t value= 5.93) exhibited increased synchronization of neural activation as valence levels rose (Figure 2.).

Conclusions: In our study, we examined the consistency of neural activation synchrony across participants within specific brain regions associated with valence. The searchlight analysis unveiled an increase in neural synchrony in the SPG in response to emotional changes, suggesting a potential link to participants' emotional processing and social interaction processes (van der Velde et al., 2014).

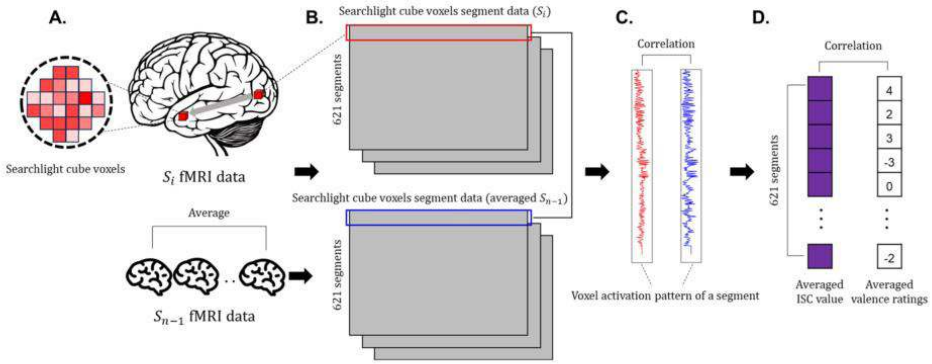

Figure 1. Illustration of the procedure for calculating the ISC-valence ratings correlation coefficient for searchlight cube

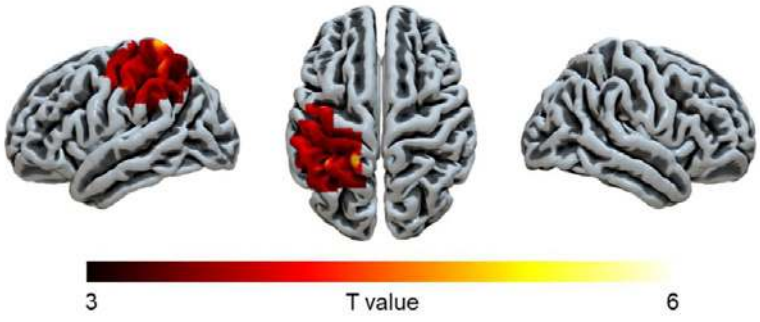

Figure 1. Illustration for of the results of searchlight analysis

References

1. Barrett, L. F., Quigley, K. S., Bliss-Moreau, E., & Aronson, K. R. (2004). Interoceptive sensitivity and self-reports of emotional experience. J Pers Soc Psychol, 87(5), 684-697. https://doi.org/10.1037/0022-3514.87.5.684
2. Baucom, L. B., Wedell, D. H., Wang, J., Blitzer, D. N., & Shinkareva, S. V. (2012). Decoding the neural representation of affective states. NeuroImage, 59(1), 718-727. https://doi.org/10.1016/j.neuroimage.2011.07.037
3. Chen, J., Leong, Y. C., Honey, C. J., Yong, C. H., Norman, K. A., & Hasson, U. (2017). Shared memories reveal shared structure in neural activity across individuals. Nat Neurosci, 20(1), 115-125. https://doi.org/10.1038/nn.4450
4. Hasson, U., Nir, Y., Levy, I., Fuhrmann, G., & Malach, R. (2004). Intersubject synchronization of cortical activity during natural vision. Science, 303(5664), 1634-1640. https://doi.org/10.1126/science.1089506
5. Hejnar, M. P., Kiehl, K. A., & Calhoun, V. D. (2007). Interparticipant correlations: a model free FMRI analysis technique. Hum Brain Mapp, 28(9), 860-867. https://doi.org/10.1002/hbm.20321
6. Kim, J., Shinkareva, S. V., & Wedell, D. H. (2017). Representations of modality-general valence for videos and music derived from fMRI data. NeuroImage, 148, 42-54. https://doi.org/10.1016/j.neuroimage.2017.01.002
7. Kim, J., Weber, C. E., Gao, C., Schulteis, S., Wedell, D. H., & Shinkareva, S. V. (2020). A study in affect: Predicting valence from fMRI data. Neuropsychologia, 143, 107473. https://doi.org/10.1016/j.neuropsychologia.2020.107473
8. Kriegeskorte, N., Goebel, R., & Bandettini, P. (2006). Information-based functional brain mapping. Proceedings of the National Academy of Sciences, 103(10), 3863-3868. https://doi.org/doi:10.1073/pnas.0600244103
9. Nastase, S. A., Gazzola, V., Hasson, U., & Keysers, C. (2019). Measuring shared responses across subjects using intersubject correlation. Soc Cogn Affect Neurosci, 14(6), 667-685. https://doi.org/10.1093/scan/nsz037
10. van der Velde, J., Gromann, P. M., Swart, M., Wiersma, D., de Haan, L., Bruggeman, R., Krabbendam, L., & Aleman, A. (2014). Alexithymia influences brain activation during emotion perception but not regulation. Social Cognitive and Affective Neuroscience, 10(2), 285-293. https://doi.org/10.1093/scan/nsu056

Poster No 740

Sex differences in the effects of anxiety on behavioral and regional responses to negative emotions

Hak Kei Wong[1], Shefali Chaudhary[2], Yu Chen[2], Sheng Zhang[2], Chiang-Shan Li[2]

[1]University College London, London, London, [2]Yale University School of Medicine, New Haven, CT

Introduction: Men and women are known to show differences in the incidence and clinical manifestations of mood and anxiety disorders[1]. The lifetime and 12-months male to female prevalence ratios of anxiety disorder were 1:1.7 and 1:1.8, respectively, with women having higher rates of lifetime diagnosis of most anxiety disorders[2]. Further, women with a lifetime diagnosis of an anxiety disorder were more likely than men to be also diagnosed with another anxiety disorder and major depressive disorder[2]. Many imaging studies have investigated the neural correlates of sex differences in emotion processing. However, it remains unclear how anxiety might impact behavioral and neural responses during emotion processing differently in men and women.

Methods: We recruited 119 healthy adults and assessed their levels of anxiety using State-Trait Anxiety Inventory (STAI) State score. With functional magnetic resonance imaging (fMRI), we examined regional responses to negative vs. neutral (Neg-Neu) picture matching in the Hariri task[3]. Clinical and behavioral data were analyzed using regression and repeated-measures analysis of covariance with age as a covariate, and fMRI data were analyzed using a full-factorial model with sex as a factor and age as a covariate and evaluated with a corrected threshold, according to current reporting standards. We performed the regression analyses on STAI score for men and women together as well as separately. For behavioral and neural outcomes identified in men or women alone, we performed slope tests in confirming sex differences. Finally, we performed mediation analyses to investigate the inter-relationship amongst anxiety, neural correlates of anxiety, and performance metrics from the Hariri task.

Results: Men and women did not differ in STAI score (p = 0.137), or accuracy rate or reaction time (RT) (Neg-Neu) (both p's > 0.060). However, STAI scores correlated positively with RT (Neg-Neu) in women but not in men (r = 0.48, p<0.001 and r = -0.05, p = 0.699, respectively; Figure 1). Further, a slope test revealed significant sex differences in regression slope of RT (Neg-Neu) vs. STAI score (z = -3.21, p = 0.001). At voxel p<0.001 uncorrected and cluster p<0.05 FWE-corrected, men and women did not show significant differences in regional responses to Neg. vs. Neu trials. However, in regression analyses, STAI score correlated positively with lingual gyrus (LG) and negatively with medial prefrontal cortex (mPFC, Figure 2) and superior frontal gyrus (SFG) activity during Neg vs. Neu trials in women. The parameter estimates (β's) of mPFC also correlated with RT (Neg-Neu) in women but not in men. Generalized psychophysiological interaction (gPPI) analysis in women revealed mPFC connectivity with the right inferior frontal gyrus, right SFG, and left parahippocampal gyrus during Neg vs. Neu trials in positive correlation with both STAI score and RT (Neg-Neu). In a mediation analysis, mPFC gPPI but not mPFC activity mediated the association between STAI scores and RT (Neg-Neu).

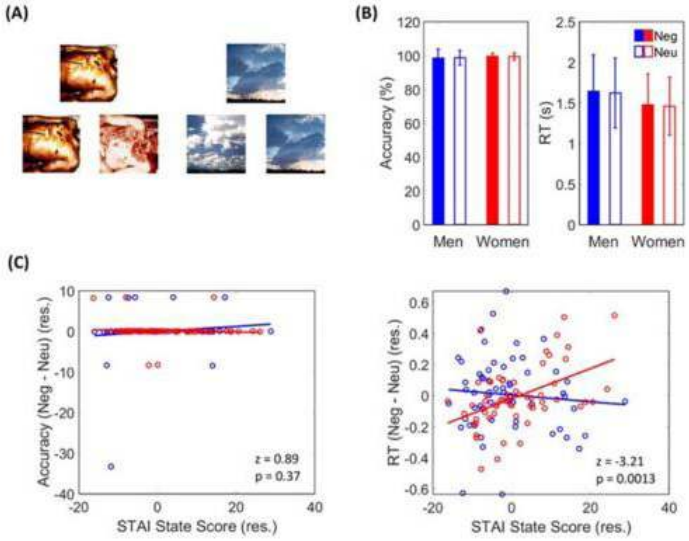

Figure 1. Behavioral task and performance. **(A)** Example images used in the matching task. **(B)** Accuracy rate and reaction time (RT) plotted separately for men and women. **(C)** Correlation of difference in accuracy rate and of RT between negative and neutral blocks with anxiety scores. Note: Data points representing men and women are shown in blue and red, respectively.

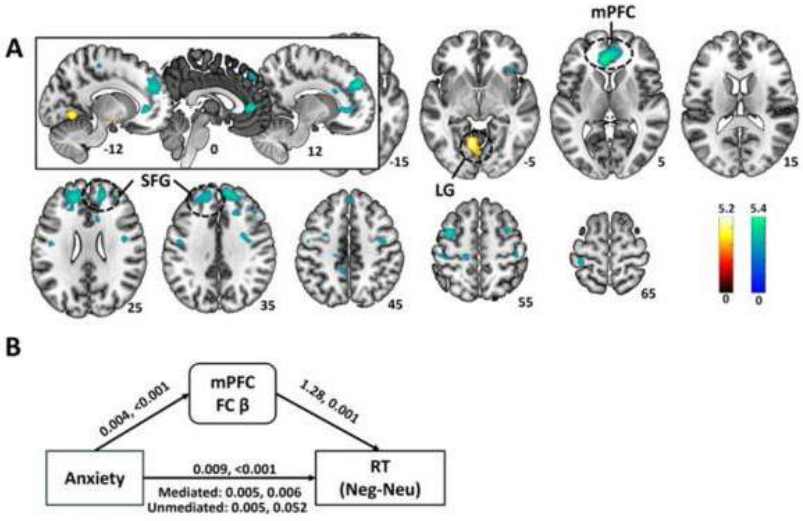

Figure 2. (A) Whole-brain regression of the contrast "Neg – Neu" against STAI state score with age as a covariate in women, evaluated at p<0.001, uncorrected. Color bars show voxel T values, with warm and cool color each for positive and negative correlation. LG: lingual gyrus; mPFC: medial prefrontal cortex; SFG: superior frontal gyrus. The inset in showed the mPFC cluster in sagittal sections. **(B)** Mediation model of mPFC β/mPFC FC β, anxiety, RT (Neg-Neu), with age as covariate. Note: the path statistics represent the coefficient and p value; mPFC: middle prefrontal cortex, FC: functional connectivity, β: parameter estimate, RT: reaction time.

Conclusions: These findings are consistent with the most recent meta-analyses reporting no significant sex differences in regional responses to negative emotions. On the other hand, women and men demonstrated significant differences in the impact of individual anxiety on behavioral outcomes and neural correlates in identifying negative emotions. In women, those with higher levels of anxiety showed prolonged RT and diminished mPFC activation in matching negative vs. neutral images. With anxiety affecting the behavioral and neural responses to negative emotions in women but not in men and considering the known roles of the mPFC in emotion regulation[4], we discussed heightened sensitivity and regulatory demands during negative emotion processing as neurobehavioral markers of anxiety in women.

References

1. Altemus, M., Sarvaiya, N. and Neill Epperson, C. (2014) 'Sex differences in anxiety and depression clinical perspectives.', Frontiers in neuroendocrinology, 35(3), pp. 320–330. doi: 10.1016/j.yfrne.2014.05.004.
2. McLean, C. P. et al. (2011) 'Gender differences in anxiety disorders: prevalence, course of illness, comorbidity and burden of illness.', Journal of psychiatric research, 45(8), pp. 1027–1035. doi: 10.1016/j.jpsychires.2011.03.006.
3. Hariri AR, Tessitore A, Mattay VS, Fera F, Weinberger DR, 2002. The amygdala response to emotional stimuli: a comparison of faces and scenes. Neuroimage 17, 317–323. doi: 10.1006/nimg.2002.1179.
4. Etkin, A. and Wager, T. D. (2007) 'Functional neuroimaging of anxiety: a meta-analysis of emotional processing in PTSD, social anxiety disorder, and specific phobia.', The American journal of psychiatry, 164(10), pp. 1476–1488. doi: 10.1176/appi.ajp.2007.07030504.

Poster No 741

Common and distinct neural representations of interoceptive attention and emotion regulation

Xiaoqin Wang[1], Huang Wang[1], Li He[2]

[1]Zhejiang Normal University, Jinhua, Zhejiang, [2]Beijing Normal University, Beijing, Beijing, Beijing

Introduction: Interoceptive attention denotes an individual's observation of visceral signals, such as respiration, cardiac activity, and hunger. A fundamental prerequisite for the effective emotion regulation (ER) is the awareness of emotional states, which intricately linked with the interoceptive attention. Previous studies suggested that reappraisal, an established ER strategy involving the reevaluation and reframing of the meaning attributed to situation or experience was facilitated by interoception. A recent meta-analysis study using univariate activation has suggested that the neural substrates of interoceptive attention and cognitive reappraisal involve common and distinct brain regions. However, to our knowledge, there is no neuroimaging evidence based on intra-individual fMRI data to indicate whether interoceptive attention and cognitive reappraisal share neural representation patterns. Additionally, cardiac and respiratory system as typical interoceptive attention, exhibit complex characteristics and hierarchically integrate within discrete regions of the central nervous system. Therefore, it is important to test whether interoceptive attention of cardiac and respiratory system involve dissociable global neural representation patterns, and independently links to the cognitive reappraisal.

Methods: Participants (N = 160, 109 females; mean age = 20.3 years; SD = 2.63) completed both the cognitive reappraisal task (CRT) and the interoceptive attention task (IAT) while inside the MRI scanner. To explore the activated brain regions during the interoceptive attention and reappraisal, we conducted univariate activation analyses. For CRT, we defined a contrast (DecreaseNeg > WatchNeg) to examine the brain activation during reappraisal. For IAT, we set up contrasts for respiratory interoception (respiration > sound), cardiac interoception (heartbeat > sound), and an integrated state of interoceptive attention ([respiration + heartbeat] > sound). Subsequently, we performed a conjunction analysis to identify overlapping regions for the cognitive reappraisal and the integrated interoceptive attention condition. To investigate voxel-wise similarities in the representational patterns of cognitive reappraisal and interoceptive attention, the representational similarity analyses (RSA) were conducted within each overlapped ROIs. In addition, we conducted searchlight analyses across the whole brain to confirm and extend the results from the ROI analysis.

Results: The results revealed that commonly activated regions for reappraisal and interoceptive attention were including the bilateral MFG, the bilateral dorsal agranular insula/ IFG, the right IPL/Angular cortex and MTG, and Medial Frontal Gyrus/ SMA/ ACC (see Figure 1). Using these overlapping regions as ROIs, RSA results indicated that all ROIs excluding left insula were shared similar representational patterns between cognitive reappraisal and interoceptive attention. Importantly, both searchlight and RSA results consistently indicated that the Medial Frontal Gyrus robustly represented similar neural activity patterns during integrated interoceptive attention and reappraisal, as well as during the cardiac interoceptive and reappraisal. However, the neural representational similarities for the respiratory interoception and reappraisal were uniquely located in the Angular Cortex (see Figure 2).

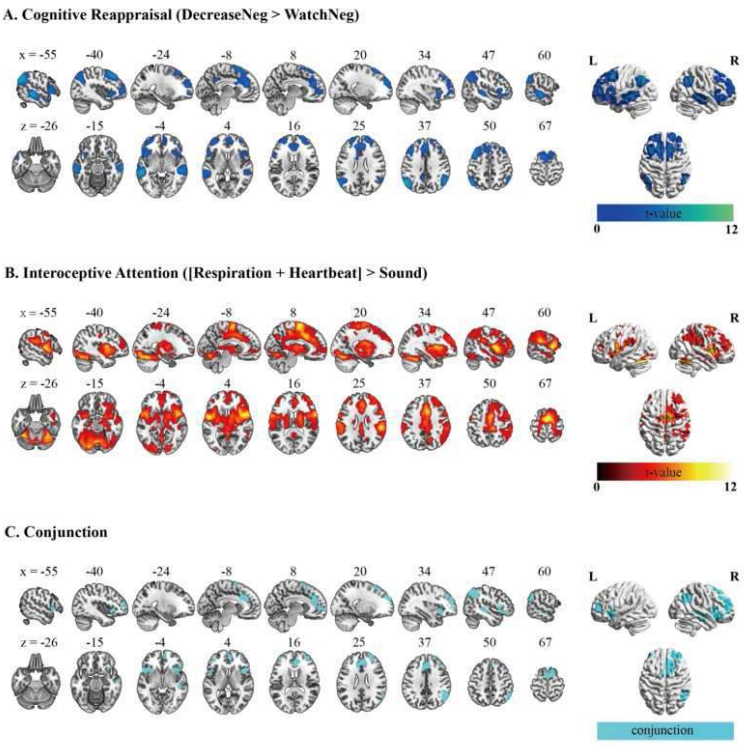

Figure 1. Results of univariate fMRI analyses for neural activity associated with reappraisal and interoceptive attention, as well as the overlapping regions between them. **A** illustrates the activation clusters associated with cognitive reappraisal, encompassing the bilateral Angular, bilateral MTG, left MFG, MCG, as well as the right IFG. **B** depicts the activation clusters related to interoceptive attention, covering the bilateral SMA and left MFG. **C** shows the overlapping regions between cognitive reappraisal and interoceptive attention, including the bilateral IFG, bilateral Insula, bilateral MFG, right MTG, as well as Superior and Medial Frontal Gyrus. All images were thresholded using a voxel-wise threshold of $p < .001$ (uncorrected) and a cluster-wise threshold of $p < .05$ FWE corrected. Additionally, the conjunction map was presented with a cluster-size threshold of 30 voxels.

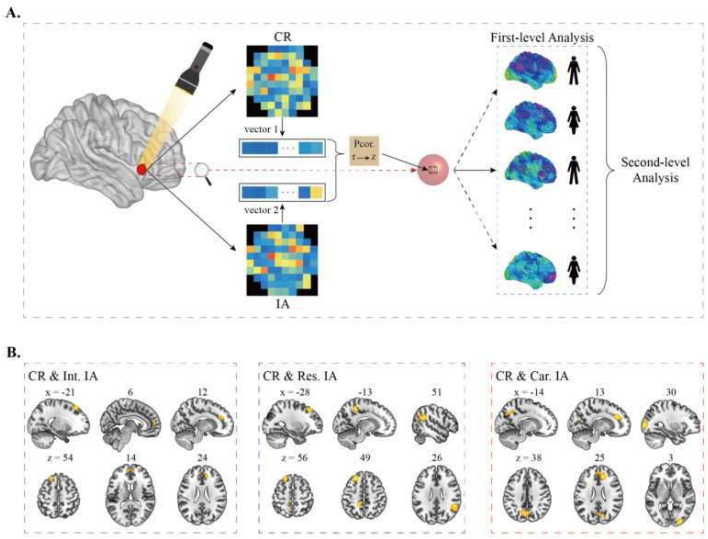

Figure 2. The Schematic overview and results of searchlight RSA. Abbreviation: CR, cognitive reappraisal; IA, interoceptive attention; Pcor., Pearson's correlations; Int., integrated; Res., respiratory; Car., cardiac. **A** depicts the schematic overview of the searchlight RSA. During this analysis, we defined a sphere with a 4 mm radius centered around each voxel in the brain. Within each sphere, parameter estimates for each condition (CR and IA) were extracted and organized into two vectors. Pearson's correlations between these two vectors were calculated and then performed Fisher transformation. The transformed values were assigned to the center voxel of the sphere. Following the completion of the first-level pattern analysis, the resulting representation similarity map was smoothed with a 2 mm FWHM Gaussian kernel and entered into the second-level analysis for group statistics. **B** displayed the results map of the searchlight RSA. The map underwent correction for multiple comparisons using a cluster-level FDR correction with a significance threshold set at $p < .05$, and a primary voxel-level threshold of $p < .001$. For cognitive reappraisal and integrated interoceptive attention, we observed significant representation similarity in the bilateral Medial Frontal Gyrus, left SFG, and the right ACC. In the comparison between cognitive reappraisal and respiratory interoceptive attention, significant representation similarity was found in the left SFG, MFG, MCG, and Precuneus, as well as the right Supramarginal Gyrus and Angular. Additionally, for cognitive reappraisal and cardiac interoceptive attention, significant representation similarity was identified in the bilateral Precuneus, left Middle Occipital Gyrus (MOG), right Medial Frontal Gyrus, and ACC.

Conclusions: Across univariate and multivariate analyses, we revealed that interoceptive attention and cognitive reappraisal shared neural representation patterns. Distinct neural representation patterns were observed between reappraisal and two interoceptive systems (respiratory and cardiac attention). These overlapping regions, including the right anterior insula, medial frontal gyrus, and Angular Cortex, suggested that the processing of the integration of visceral signals and emotional awareness, plays a crucial role in the intricate relationships between interoceptive attention and reappraisal.

References
1. Khalsa, et al. Interoception and Mental Health: A Roadmap. Biol. Psychiatry Cogn. Neurosci. Neuroimaging 3, 501–513 (2018).
2. Critchley, H. D. & Garfinkel, S. N. Interoception and emotion. Curr. Opin. Psychol. 17, 7–14 (2017).
3. Tan, Y., Wang, X., Blain, S. D., Jia, L. & Qiu, J. Interoceptive attention facilitates emotion regulation strategy use. Int. J. Clin. Heal. Psychol. 23, 100336 (2023).
4. Füstös, J., Gramann, K., Herbert, B. M. & Pollatos, O. On the embodiment of emotion regulation: Interoceptive awareness facilitates reappraisal. Soc. Cogn. Affect. Neurosci. 8, 911–917 (2013).
5. Tan, Y., Yan, R., Gao, Y., Zhang, M. & Northoff, G. Spatial-topographic nestedness of interoceptive regions within the networks of decision making and emotion regulation: Combining ALE meta-analysis and MACM analysis. Neuroimage 260, 119500 (2022).
6. Engelen, T., Solcà, M. & Tallon-baudry, C. Interoceptive rhythms in the brain. Nat. Neurosci. Rev. 26, (2023).

Poster No 742

An fMRI-based neuromarker for anxious anticipation of threat under uncertainty

Benjamin Becker[1], Feng Zhou[2], Xiqin Liu[3]

[1]The University of Hong Kong, Hong Kong, Hong Kong, [2]Southwest University, Chongqing, China, [3]Sichuan University, Chengdu, China

Introduction: Uncertainty about potential future threats and the associated anxious anticipation represents a key neurocognitive mechanism of anxiety. While anxiety serves an important adaptive function and allows to avoid or cope with potential danger excessive anxious anticipation under uncertainty represents a key symptom of anxiety disorders. Despite a number or previous fMRI studies that combined threat anticipation paradigms with conventional fMRI a comprehensive and accurate architecture for the subjective experience of anxious anticipation has not been established.

Methods: The present study developed a novel uncertain shock paradigm that allowed a precise modulation of the level of momentary anxious arousal during fMRI and capitalized on recent progress in multivariate predictive modelling. The decoder was developed and tested in a series of task-based fMRI studies including training, test and generalization datasets. A series of further fMRI studies as well as analyses utilizing publicly available datasets was employed to further demonstrate the robustness and specificity of the neurofunctional signature.

Results: The 'shock uncertainty-induced threat anticipation signature' (SUITAS) was predictive of the level of uncertainty-induced experience of anxious arousal on the population and individual level. The signature showed a robust prediction in the training sample (n = 44) as well as the validation sample (n = 30) and an independent prospective generalization data-set (n = 50). The SUITAS was not – or less – sensitive to associated processes such as pain, anticipation, as well as unspecific negative emotional and autonomic arousal. Further comparison with established decoders for fear (Zhou et al., 2021) and negative affect (Chang et al., 2015) underscore that anxious anticipation relies on distributed neural representation that is (partly) distinct from the representations of these processes.

Conclusions: The sensitive, generalizable, and specific neuromarker for subjective anxious arousal experienced during uncertain threat anticipation may facilitate model development and clinical translation (Liu et al., 2023).

References
1. Chang LJ, Gianaros PJ, Manuck SB, Krishnan A, Wager TD (2015) 'A sensitive and specific neural signature for picture-induced negative affect. PLoS Biology, vol. 13: 1-28
2. Liu X, Jiao G, Zhou F, Kendrick KM, Yao D, Xiang S, Jia T, Zhang X, Zhang J, Feng J, Becker B (2023) 'A neural signature for the subjective experience of threat anticipation under uncertainty'. BioRxiv.org; doi: 10.1101/2023.09.20.558716
3. Zhou F, Zhao W, Qi Z, Geng Y, Yao S, Kendrick KM, Wager TD, Becker B (2021) 'A distributed fMRI-based neuromarker for the subjective experience of fear', Nature Communications, vol. 12:6643

Poster No 744

Resilience-driven neural synchrony during naturalistic movie watching: an ultra-high field fMRI stud

Shuer Ye[1], Leona Bätz[1], Avneesh Jain[1], Alireza Salami[2], Maryam Ziaei[1]

[1]Norwegian University of Science and Technology, Trondheim, Norway, [2]Karolinska Institutet & Umeå University, Stockholm, Stockholm

Introduction: In today's world, frequent traumatic events pose a significant challenge to psychological well-being. This underscore the crucial role of psychological resilience, which is the capacity to effectively navigate and cope with adversity. Resilience empowers individuals to perceive and regulate emotions adaptively, offering a safeguard against detrimental consequences (Denckla et al., 2020; Kalisch et al., 2017). Accumulating evidence suggests that neural variations in brain regions involved in emotion regulation and salience detection may serve as neural markers of resilience (Norbury et al., 2023) and personality traits, such as intolerance to uncertainty (IU) may modulate our ability to maintain resilience (Sahib et al., 2023). Movie fMRI offers an ecologically valid opportunity to study resilience in a real-world context (Eickhoff et al., 2020). When individuals watch movies, synchronized brain activities occur, providing opportunities to detect similarities in neural responses (Baek et al., 2022). Currently, our understanding of how resilience gates the way we perceive and process real-life emotional stimuli is limited. This study is the first to explore the influence of resilience on individuals' neural responses to external naturalistic stimuli. Moreover, we further explore the modulation effect of IU, a personality trait that may shape our perception and serve as a risk factor of mood disorder, on the association between resilience and brain synchrony.

Methods: We presented two movies, one with negative and one with neutral emotional valence to 62 healthy (Mean age of 25.68 ± 4.30 years, 29 females) adults while undergoing brain MRI scans (Figure 1). The resilience scores and IU scores were collected via self-report questionnaires. Inter-subject correlation and inter-subject representational similarity analysis were combined (Chen et al., 2020; Finn et al., 2020) to investigate the association between resilience level and brain-to-brain synchrony while watching movies. Binarized resilience scores (pairs with high or low scores) and resilience similarity (estimated using the Anna Karenina model, which defines similarities based on the lower score in a pair, suggesting that individuals with high resilience scores are similar, whereas those with low scores are more idiosyncratic, i.e., Figure 2C) were calculated. Linear mixed-effect models were applied to predict neural synchrony. Moreover, IU was incorporated into the model to examine its modulatory effect.

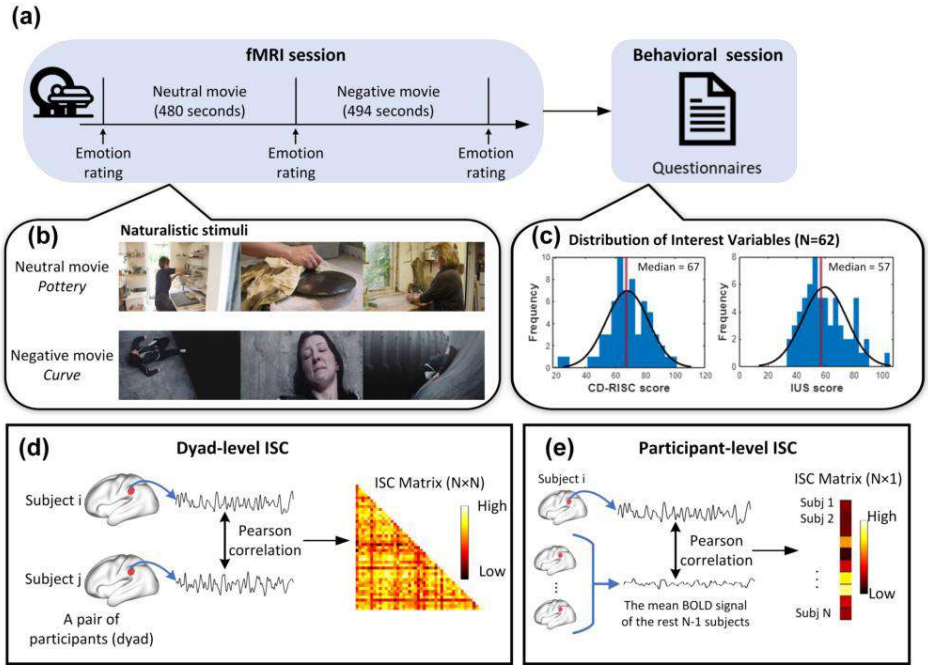

Results: Resilience-driven neural synchrony was found in a wider set of regions including the default mode (DMN), control, and dorsal attentional networks, in response to the negative movie compared to the neutral one (Fig. 2b). High-resilience individuals had similar neural activities to their peers, whereas low-resilience individuals showed more variable neural activities (Figure 2d). Additionally, the modulation effect of IU found in that increased IU enhanced the resilience-driven brain synchrony within the DMN when processing negative movie but not in the neutral one.

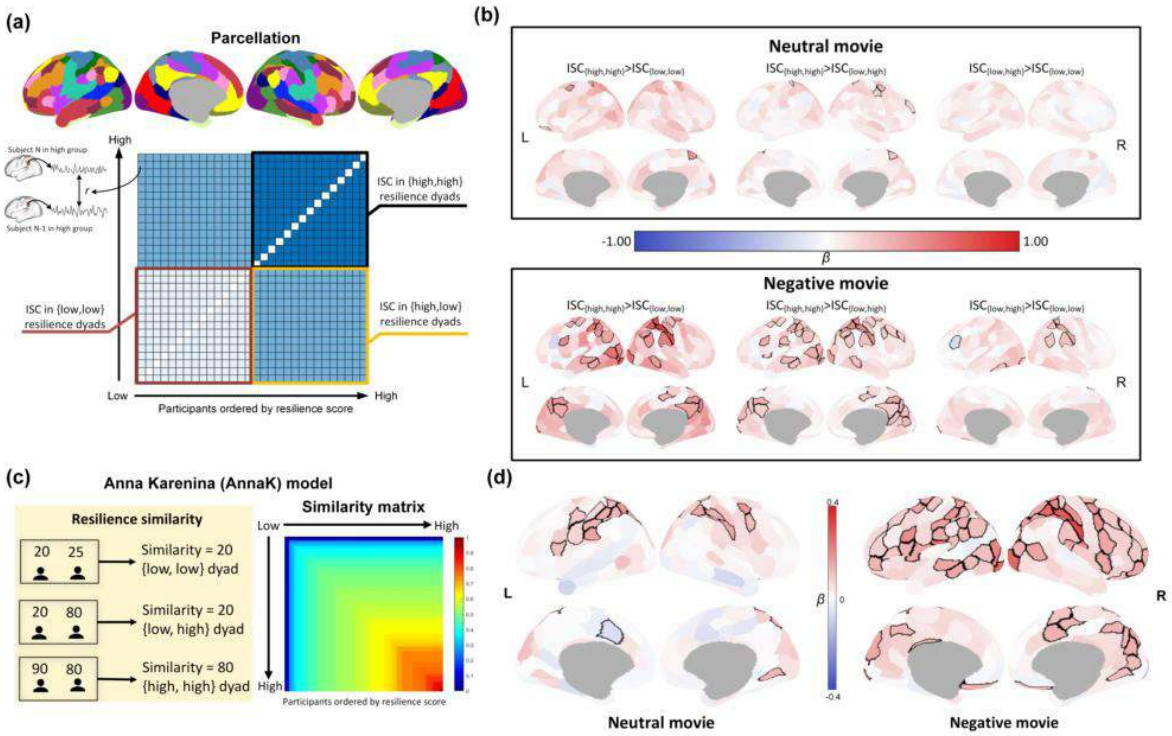

Conclusions: Our results corroborate the Anna Karenina model in which it suggests that "all happy families are alike, and all unhappy families are different in their own way". Our findings indicate consistent neural responses among resilient individuals that signify their aligned adaptive emotional processing, which fosters social understanding and connections, ultimately serving as a protecting factor against adversity. Conversely, the variability in neural responses among low-resilience individuals indicates vulnerability to adverse psychological outcomes, potentially associated with maladaptive emotional responses and regulation. Our findings provide novel insights into the mechanisms of resilience, suggesting that maintaining similar selective attention, inhibitory control, and social cognitive functioning in an adaptive way may be the core feature of resilient individuals.

References

1. Baek, E. C., Hyon, R., López, K., Finn, E. S., Porter, M. A., & Parkinson, C. (2022). In-degree centrality in a social network is linked to coordinated neural activity. Nature Communications, 13(1), Article 1. https://doi.org/10.1038/s41467-022-28432-3
2. Chen, G., Taylor, P. A., Qu, X., Molfese, P. J., Bandettini, P. A., Cox, R. W., & Finn, E. S. (2020). Untangling the relatedness among correlations, part III: Inter-subject correlation analysis through Bayesian multilevel modeling for naturalistic scanning. NeuroImage, 216, 116474. https://doi.org/10.1016/j.neuroimage.2019.116474
3. Denckla, C. A., Cicchetti, D., Kubzansky, L. D., Seedat, S., Teicher, M. H., Williams, D. R., & Koenen, K. C. (2020). Psychological resilience: An update on definitions, a critical appraisal, and research recommendations. European Journal of Psychotraumatology, 11(1), 1822064. https://doi.org/10.1080/20008198.2020.1822064
4. Eickhoff, S. B., Milham, M., & Vanderwal, T. (2020). Towards clinical applications of movie fMRI. NeuroImage, 217, 116860. https://doi.org/10.1016/j.neuroimage.2020.116860
5. Finn, E. S., Glerean, E., Khojandi, A. Y., Nielson, D., Molfese, P. J., Handwerker, D. A., & Bandettini, P. A. (2020). Idiosynchrony: From shared responses to individual differences during naturalistic neuroimaging. NeuroImage, 215, 116828. https://doi.org/10.1016/j.neuroimage.2020.116828
6. Kalisch, R., Baker, D. G., Basten, U., Boks, M. P., Bonanno, G. A., Brummelman, E., Chmitorz, A., Fernàndez, G., Fiebach, C. J., Galatzer-Levy, I., Geuze, E., Groppa, S., Helmreich, I., Hendler, T., Hermans, E. J., Jovanovic, T., Kubiak, T., Lieb, K., Lutz, B., … Kleim, B. (2017). The resilience framework as a strategy to combat stress-related disorders. Nature Human Behaviour, 1(11), Article 11. https://doi.org/10.1038/s41562-017-0200-8
7. Norbury A., Seeley S. H., Perez-Rodriguez M. M., & Feder A. (2023). Functional neuroimaging of resilience to trauma: Convergent evidence and challenges for future research. Psychological Medicine, 53(8), 3293–3305. https://doi.org/10.1017/S0033291723001162
8. Sahib, A., Chen, J., Cárdenas, D., & Calear, A. L. (2023). Intolerance of uncertainty and emotion regulation: A meta-analytic and systematic review. Clinical Psychology Review, 101, 102270. https://doi.org/10.1016/j.cpr.2023.102270

Poster No 745

Neural Mechanisms Behind the Effects of Tactile False Feedback on Emotion Perception

Joel Patchitt[1], Hugo Critchley[1], Mark Miller[2], Manos Tsakiris[3], Sarah Garfinkel[4], Andy Clark[5]

[1]Brighton and Sussex Medical School, Brighton, East Sussex, [2]University of Edinburgh, Edinburgh, The City of Edinburgh, [3]Royal Holloway, Egham, Surrey, [4]University College London, London, Greater London, [5]University of Sussex, Brighton, East Sussex

Introduction: Bi-directional mismatches between perceived and veridical physiological signals during false physiological feedback (FFB) exerts subtle effects on ambiguous emotional judgements (Valins, 1966; Gray et al., 2007). The determinants of these effects are proposed to be reliant on the conscious appraisal of interoceptive information (Crucian et al., 2000; Gray et al., 2007). Most paradigms use auditory FFB, finding increases in emotional intensity ratings, irrespective of FFB direction (Valins, 1966; Gray., et al, 2007), with right anterior insula (rAI) serving as a mismatch comparator (Critchley., et al, 2004; Gray et al., 2007). Few paradigms have looked at the effects of tactile FFB, which could be interpreted as a more veridical sensation of HR. We hypothesized that tactile FFB would be interpreted as a veridical physiological signal, with increased FFB activating the rAI and other socio-emotional regions, resulting in bi-directional effects on emotional face ratings.

Methods: During fMRI BOLD acquisition using a Siemens 3T scanner, 41 participants performed a simple emotional intensity rating task in which 80 faces (positive/negative) biased towards neutral were shown and repeated for four conditions of vibro-tactile FFB stimulation on the right wrist (Higher than HR, lower than HR, same HR, No FFB). Conditions changed and repeated every five trials totalling 20 seconds per block. A linear mixed model analysis (LMM) was conducted on the behavioural data: Condition (Higher, Lower, Null), Valance (Positive, Negative) and Trial[1-5]. Data was pre-processed using fMRIPrep and analysed in FSL. Contrasts were run for A) feedback of any type vs no feedback B) Higher FFB vs Lower FFB C) Interaction between FFB (Higher, Lower) and Valance (Positive v Negative).

Results: We found a three way interaction between Condition, Valance and Trial $F(2) = 49.792$, $p = <0.001$ (see fig 1). Bonferroni corrected Post hoc LMM revealed an interaction between Valance and Trial in the Higher $F(1) = 62.185$, $p = <0.00$ and Lower $F(1) = 39.375$, $p = <0.001$ conditions but not for Null $F(1) = 0.14$, $p = .708$. Correlations were found for: Contrast A in the left dorsal pre-motor cortex (lPMd), bilateral OP1, right dorsal posterior insula (rPId) and right primary sensorimotor cortex/corticospinal tract (rSMI), Contrast B in the rPId, middle (rMId) and anterior insula (rAId), right pars opercularis (rPOp) and pars orbitalis (rPOr), right superior temporal gyrus (rSTGs), inferior supramarginal gyrus (rSMGs) and bilateral occipital fusiform gyrus (OFG) and Contrast C in the left OP1.

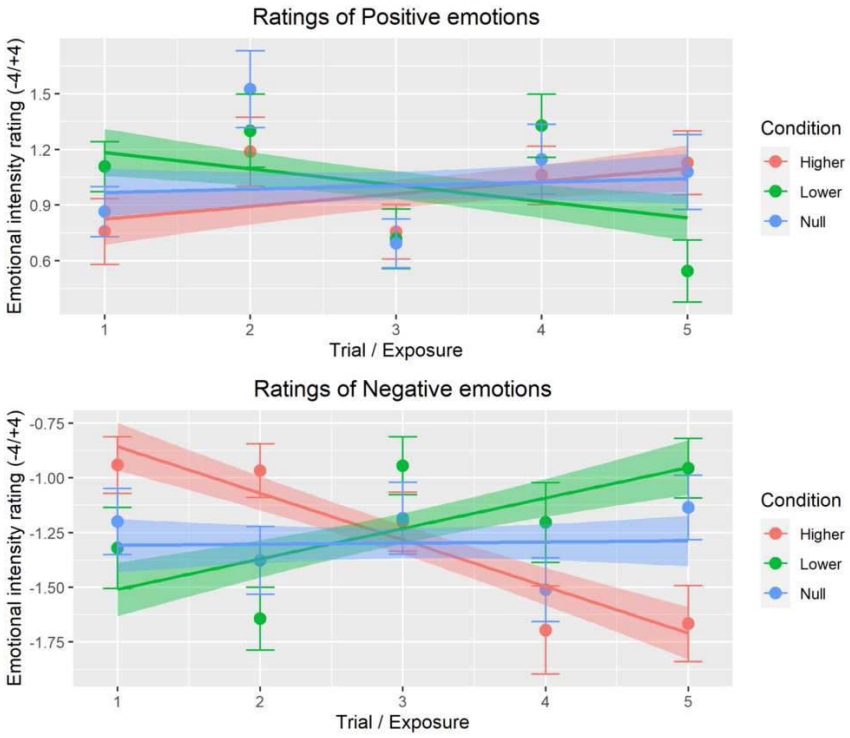

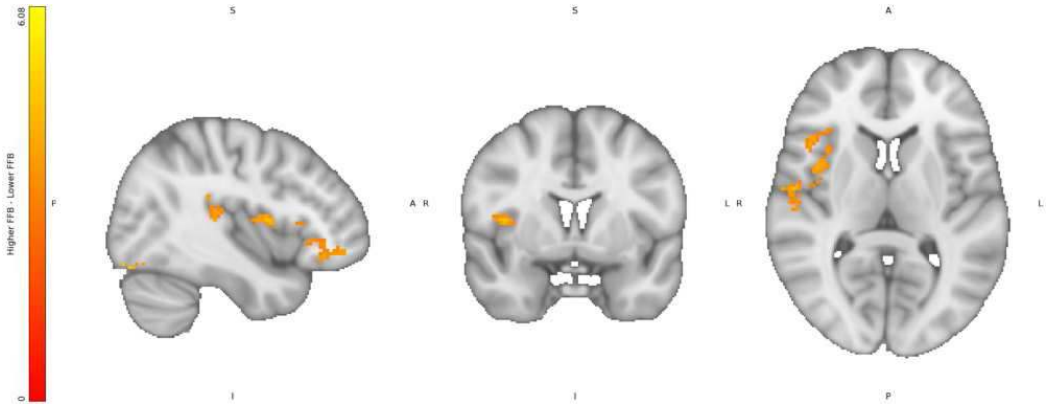

Conclusions: Behavioural results suggest a bi-directional exposure effect of FFB on subjective intensity ratings of emotionally ambiguous faces. This mimics the effect of arousal on emotional decision making, suggesting that tactile FFB is treated as a veridical interoceptive afferent. Bilateral OP1 and rPId suggest that FFB signals are ascending via c-type fibres as part of an affective touch pathway (Morrison et al., 2016), upon which a body ownership vs threat to peri-personal space decision is made in the lPMv (Bekrater-Bodmann et al., 2011). Activation within regions relating to body ownership (rPId, rMId, lPMv) suggest that FFB is integrated as a bodily owned percept (Tsakiris et al., 2007), potentially suppressing defensive reflexes via transcallosal pathways between the lPMv and rSMI (Bestmann et al., 2007). Activations across rAId and other regions in Contrast C suggest an effect of FFB across a socio-emotional network related to interoceptively induced changes emotion perception (Xu et al., 2021). Interaction between FFB and emotion in the contralateral OP1 suggests multimodal integration of sensory stimuli affecting prior bias in perceptual decision making (Preuschoff et al., 2010). This data highlights the potential of tactile feedback at biasing emotionally charged perceptual decisions and provides insight into the neural mechanisms by which interoceptive channels exert this bias.

References

1. Bekrater-Bodmann, R., Foell, J., & Kamping, S. (2011). The importance of ventral premotor cortex for body ownership processing. Journal of Neuroscience, 31(26), 9443–9444. https://doi.org/10.1523/jneurosci.2302-11.2011
2. Bestmann, S., Swayne, O., Blankenburg, F., Ruff, C. C., Haggard, P., Weiskopf, N., Josephs, O., Driver, J., Rothwell, J. C., & Ward, N. S. (2007). Dorsal premotor cortex exerts state-dependent causal influences on activity in contralateral primary motor and dorsal premotor cortex. Cerebral Cortex, 18(6), 1281–1291. https://doi.org/10.1093/cercor/bhm159
3. Critchley, H. D., Wiens, S., Rotshtein, P., Öhman, A., & Dolan, R. J. (2004). Neural systems supporting interoceptive awareness. Nature Neuroscience, 7(2), Article 2. https://doi.org/10.1038/nn1176
4. Crucian, G. P., Hughes, J. D., Barrett, A. M., Williamson, D. J. G., Bauer, R. M., Bowers, D., & Heilman, K. M. (2000). Emotional and Physiological Responses to False Feedback* *This paper was presented in part at the 27th annual meeting of the International Neuropsychological Society, Boston, MA, February, 1999. Cortex, 36(5), 623–647. https://doi.org/10.1016/S0010-9452(08)70542-2
5. Gray, M. A., Harrison, N. A., Wiens, S., & Critchley, H. D. (2007). Modulation of Emotional Appraisal by False Physiological Feedback during fMRI. PLOS ONE, 2(6), e546. https://doi.org/10.1371/journal.pone.0000546
6. Morrison, I. (2016). Ale Meta-analysis reveals dissociable networks for affective and discriminative aspects of touch. Human Brain Mapping, 37(4), 1308–1320. https://doi.org/10.1002/hbm.23103
7. Preuschhof, C., Schubert, T., Villringer, A., & Heekeren, H. R. (2010). Prior information biases stimulus representations during vibrotactile decision making. Journal of Cognitive Neuroscience, 22(5), 875–887. https://doi.org/10.1162/jocn.2009.21260
8. Tsakiris, M., Hesse, M. D., Boy, C., Haggard, P., & Fink, G. R. (2006). Neural signatures of body ownership: A sensory network for bodily self-consciousness. Cerebral Cortex, 17(10), 2235–2244. https://doi.org/10.1093/cercor/bhl131
9. Valins, S. (1966). Cognitive effects of false heart-rate feedback. Journal of Personality and Social Psychology, 4(4), 400. https://doi.org/10.1037/h0023791
10. Xu, P., Peng, S., Luo, Y., & Gong, G. (2021). Facial expression recognition: A meta-analytic review of theoretical models and neuroimaging evidence. Neuroscience & Biobehavioral Reviews, 127, 820–836. https://doi.org/10.1016/j.neubiorev.2021.05.023

Poster No 746

Task induced dynamics of human bed nucleus of stria terminalis from direct neuronal recordings

Saurabh Sonkusare[1], Yingying Zhang[2], Qiong Ding[3], Yashu Feng[4], Linbin Wang[2], Violeta Casero[3], Shikun Zhan[4], Dianyou Li[4], Bomin Sun[4], Valerie Voon[3]

[1]Department of Psychiatry, University of Cambridge, Cambridge, United Kingdom, [2]Institute of Science and Technology for Brain-Inspired Intelligence, Fudan University, Shanghai, Chi, Shanghai, China, [3]Department of Psychiatry, University of Cambridge, Cambridge, United Kingdom, Cambridge, United Kingdom, [4]Ruijin Hospital, Shanghai Jiao Tong University School of Medicine, Shanghai, China, Shanghai, China

Introduction: The bed nucleus of the stria terminalis (BNST), a part of 'extended amygdala'[1], is densely connected with limbic structures, hypothalamic and brainstem nuclei. It plays a critical role in emotional processing especially fear, anxiety[2] and prosocial behaviour[3] with its dysfunction implicated in many psychiatric illnesses including major depression[4]. Yet, its functional dynamics remain poorly characterised in humans.

Methods: We acquired neuronal recordings from BNST from a cohort of 23 patients (Figure 1A) with treatment resistant depression undergoing deep brain stimulation (DBS) in a clinical trial. We employed two tasks (Figure 1B): 1) empathy for pain (painful and non-painful pictures), 2) affect task (positive and negative pictures). We first characterised task induced spectral dynamics and used permutation testing to assess condition differences. Time-frequency clusters showing condition differences were then tested for their association with depression and anxiety scores.

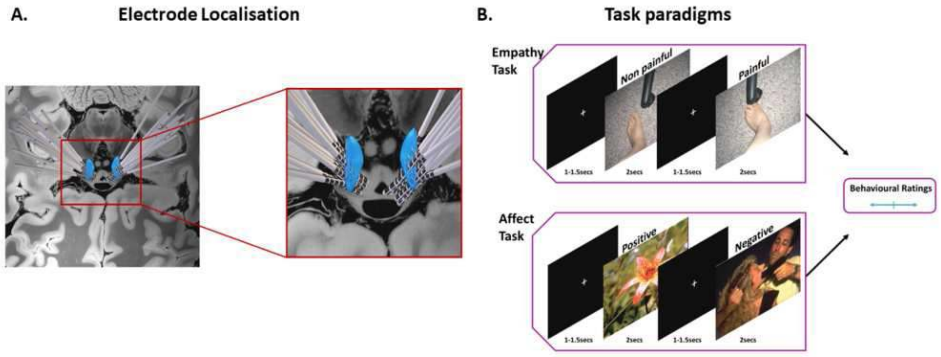

Results: Behavioural ratings showed differences in painful and non-painful pictures (p<.001, Figure 2A i). Broad frequency range induced activity was seen for the empathy for pain task with condition differences in the alpha and theta frequency range activity which was greater in the painful condition (p<.001, Figure 2A ii, iii). Crucially, alpha activity correlated with baseline anxiety (r=.51, p¬FDR<.05) and depression scores (r= .55, p¬FDR<.05) and remarkably also predicted reduction in anxiety symptoms at 3-month follow up (r= .53, p¬FDR<.05). Behavioural ratings showed differences in positive and negative valence pictures (p<.011, Figure 2B i). For the affect task, early theta range (0-250 ms) activity was significantly greater for negative pictures (p<.001, Figure 2B ii, iii) and which correlated with baseline anxiety (r = .50, p¬FDR<.05) and depression scores(r= .52, p¬FDR<.05).

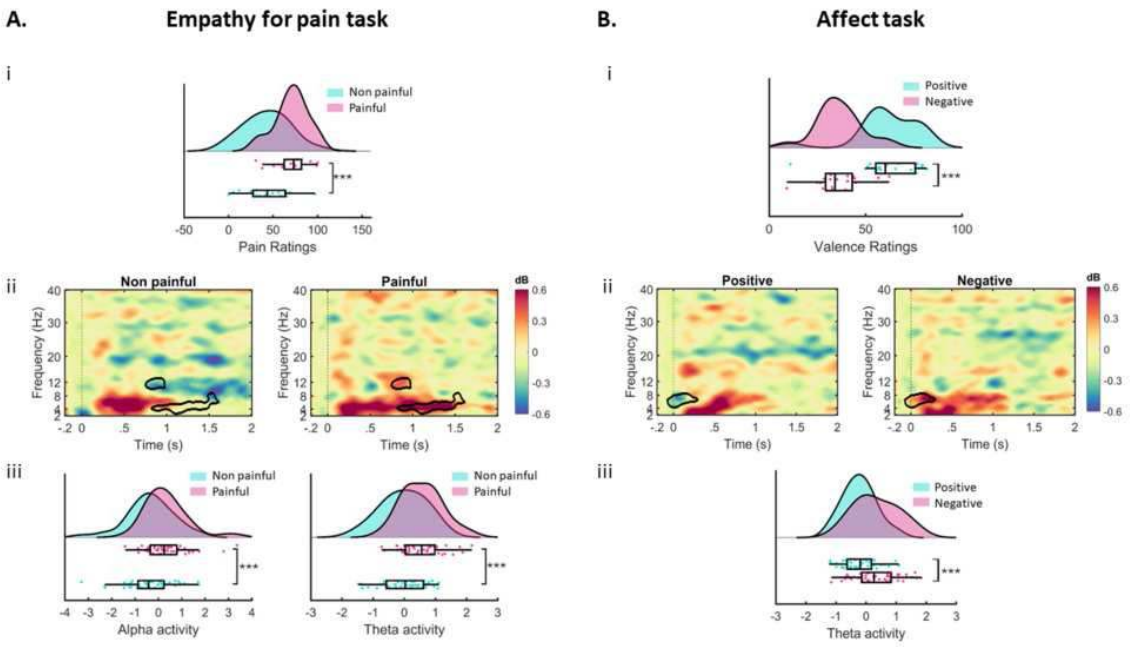

Conclusions: In a unique and rare invasive neurosurgical dataset, we investigated direct neural recordings from human BNST in two task paradigms of empathy for pain and affect picture viewing. We characterised the spectral dynamics of task-evoked activity demonstrating condition differences in the theta-alpha frequency range. Specifically, late alpha and theta activity in the empathy for pain paradigm was increased in the painful condition whilst greater early onset theta activity differentiated the negative stimuli from positive stimuli. Finally, alpha activity for empathy for the pain paradigm and theta for the affect paradigm were correlated with anxiety and depression severity with the alpha activity for empathy predicting anxiety outcomes at

3-month follow-up. Our study thus adds important informative knowledge about the functional and clinical significance of BNST essential for translational research in DBS field. These spectral characteristics can be targeted as a potential biomarker for depression and anxiety severity and predictors of therapeutic outcome.

References

1. Fox, A. S. and A. J. Shackman (2019). "The central extended amygdala in fear and anxiety: Closing the gap between mechanistic and neuroimaging research." Neuroscience letters 693: 58-67.
2. Lee, Y. and M. Davis (1997). "Role of the hippocampus, the bed nucleus of the stria terminalis, and the amygdala in the excitatory effect of corticotropin-releasing hormone on the acoustic startle reflex." Journal of neuroscience 17(16): 6434-6446
3. Vekaria, K. M., K. O'Connell, S. A. Rhoads, K. M. Brethel-Haurwitz, E. M. Cardinale, E. L. Robertson, B. Walitt, J. W. VanMeter and A. A. Marsh (2020). "Activation in bed nucleus of the stria terminalis (BNST) corresponds to everyday helping." Cortex 127: 67-77
4. Lozano, A. M., N. Lipsman, H. Bergman, P. Brown, S. Chabardes, J. W. Chang, K. Matthews, C. C. McIntyre, T. E. Schlaepfer and M. Schulder (2019). "Deep brain stimulation: current challenges and future directions." Nature Reviews Neurology 15(3): 148-160

Poster No 747

Context modulates Perceived Empathy in Human-Voice Agent Interactions

Hurshitha Vasudevan[1], Bhoomika Kar[2]

[1]Center of Behavioural and Cognitive Sciences, University of Allahabad, Prayagraj, Uttar Pradesh, [2]Center of Behavioural and Cognitive Sciences, University of Allahabad, Uttar Pradesh,India., Prayagraj, Uttar Pradesh

Introduction: Perceived empathy is the ability of humans to form an embodied representation of another human being's emotional state while simultaneously being aware of the causal mechanism that induced that emotional state[1]. The present study aimed to investigate perceived empathy expressed in a human-voice agent interaction using the 'computers as social actors' (CASA) paradigm where computers are treated as social agents by the human[2]. The CASA paradigm can also be extended to voice agents[3]. We hypothesized that empathy shown by voice agents and humans is perceived similarly in a human- voice-agent interaction and shows similar brain activation in empathy regions. Considering that human-voice agent interactions occur across different social contexts, we also hypothesized that behavioral responses given by the participants and the brain activations while participants passively view the videos, context would modulate the level of empathy perceived in a Human-Voice agent empathetic interaction.

Methods: Sixteen video stimuli 1-4 minutes each were developed across four contexts (Figure 1). The videos were rated by 31 participants and the contexts (visit to a nutritionist and plan a trip) with high mean ratings for dialogue/context comprehension were selected for the fMRI experiment. 23 Participants were scanned in a 3 Tesla fmri scanner (TR = 2780 ms, TE = 22 ms, FOV = 250 mm^3, 52 slices with a voxel size of 2.5 x 2.5 x 3.0 mm3) while they viewed eight videos pertaining to visit to a nutritionist and plan a trip context across four empathy conditions. After every video participants rated perceived empathy for the human- voice agent interaction on a 4 point Likert Scale.

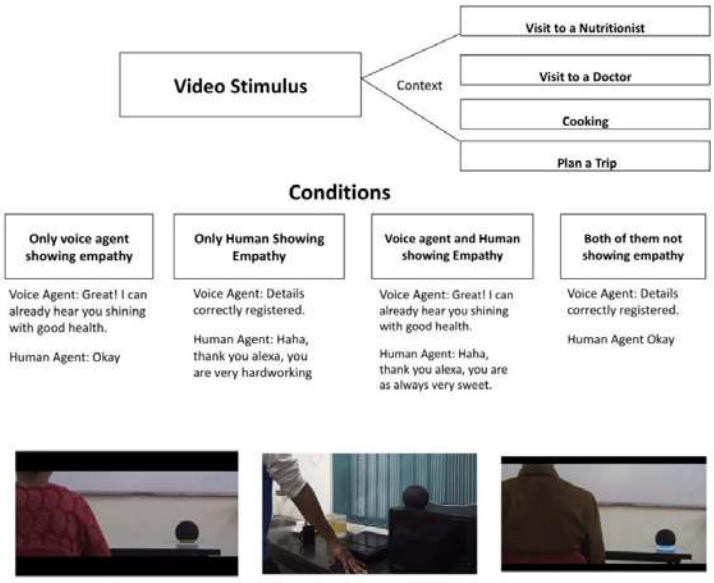

Figure 1: Video Stimulus Development

Results: Participants' ratings were analysed and a 2 (context) x 4 (empathy conditions) repeated measures ANOVA revealed a significant effect of perceived empathy when human/voice /both agents showed empathy ($p < .05$) and the effect of context ($p < .05$), when voice/both agents showed empathy. The BOLD response was acquired during video viewing and analyzed using the General Linear Model with SPM12 ($p < 0.05$, FWE Corrected). The effect of empathy showed significant activations in superior temporal gyrus (STG) associated with cognitive empathy and perspective taking. The interaction between context and empathy for human and Voice agent showed activations in the left STG. The contrast human showing empathy > voice agent showing empathy in visit to a nutritionist context showed activation in Posterior Insula associated with affective empathy and left cingulate gyrus associated with cognitive empathy in plan a trip context. Region of Interest ($p < 0.05$, uncorrected) based functional connectivity analysis in CONN (Figure 2) showed that right STG and anterior cingulate cortex associated with cognitive empathy were positively correlated. Activation in STG and anterior insula positively correlated when human showed empathy and negatively correlated when the voice agent showed empathy in the visit to a nutritionist context. Increased connectivity between anterior insula and STG was observed when the voice agent showed empathy in the Plan a trip context which was not significant in the case of human actor. Thus neural correlates coding for empathy varied as a function of context for both the agents. Increased positive correlation between right insula and STG for both agents suggests the interaction between affective and cognitive empathy.

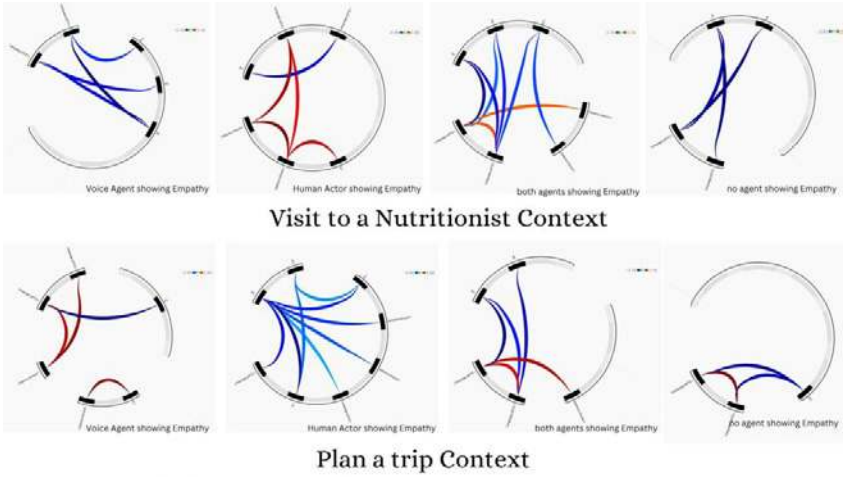

Figure 2: Functional connectivity Region of Interest analysis across 4 conditions in 2 contexts

Conclusions: Empathy is perceived from a voice agent in a human-voice agent interaction supported by behavioral and fMRI results. The fMRI results highlight the role of context modulating perceived empathy in human-voice agent interactions coded by regions associated with cognitive and affective empathy i.e. Superior Temporal gyrus, Insula and Cingulate Cortex reflected in condition-specific contrasts and connectivity results. The finding highlights the significance of explicit empathetic cues in the voice and scripts for effective Human-Voice agent Interaction.

References

1. Gonzalez-Liencres C, Shamay-Tsoory SG, Brüne M. (2013). Towards a neuroscience of empathy: ontogeny, phylogeny, brain mechanisms, context, and psychopathology. Neuroscience Biobehavioural Review, 37(8), 1537-1548.
2. Nass, Clifford, Steuer, Jonathan, & Siminoff, Ellen. (1994). Computers are social actors. Proceedings of the Conference on Human Factors in Computing Systems, 204.
3. Gambino, A., Fox, J., & Ratan, R. A. (2020). Building a stronger CASA: Extending the computers are social actors paradigm. Human-Machine Communication, 1, 71–85.

Poster No 748

Consistent representation of affective states between movie watching and recall using hyperalignment

Jongwan Kim[1], Chaery Park[2]

[1]Jeonbuk National University, Jeonju-si, Jeollabuk-do, [2]Jeonbuk National University, Jeonju-Si, North Jeolla

Introduction: Recalling past experiences rekindles emotions similar to the original events, facilitated by memory reconstruction during recall. It serves as a potent method for inducing emotions in experimental studies, with physiological responses indicating similar reactivation of positive and negative emotions. The key distinction between experiences and recall lies in external stimuli during the former and reliance on internal representation during the latter. Recall involves integrating internal information from previous experiences, differing systematically from how information is processed

during experiences. Neurological evidence supports distinct neural activation patterns during recall, suggesting its different functioning from experiences, even though it may evoke similar emotions. The aim of this study is to identify common affective representations when experiencing emotions and recalling.

Methods: We reanalyzed the fMRI data from Chen et al. (2017) that investigated the representation of shared memories across individuals. In this study, 17 participants watched an episode of the Sherlock in two fMRI sessions. We also used the behavioral data from Kim et al. (2020), where they presented the same stimuli and asked participants to rate affective responses on valence and arousal dimensions. After preprocessing of fMRI data, we applied hyperalignment (Haxby et al., 2020). Hyperalignment is a method to capture shared information by projecting pattern vectors of neural responses into a common information space. Affine transformations are computed to optimize alignment between trajectories, preserving the geometry of dissimilarities between pattern vectors. This method is known to be advantageous, particularly when individuals exhibit different neuroanatomical structures even when representing a common construct, which benefits cross-participant analyses. We performed hyperalignment between watching and recall datasets for each participant. Initially, we computed a common template between the watching and recall datasets using Procrustes rotation and subsequently aligned each pattern to this common template, generating a new common template. Finally, we aligned each dataset to the mean alignment from the previous iteration. We repeated this procedure for all participants. We conducted regression-based decoding to confirm if affective states of signed and unsigned valence and arousal can be predicted between watching and recall datasets. The training set was either watching or recall dataset while the testing set was the left one, and then computed regression-based decoding. This procedure was repeated for all subjects. A permutation test was performed for significance testing.

Results: The results revealed significant accuracy in correctly predicting arousal, $p<.001$. However, predictions of signed and unsigned valence were not significant, $ps>.05$. We performed repeated measures analyses of variance to compare scene-to-recall and recall-to-scene decoding types and three types of affect (arousal, signed, and unsigned valence). Two decoding types were not significantly different, $p=.936$, whereas the effect of affect was significant, $p=.009$. A trend analysis revealed that the linear contrast (signed vs. unsigned valence) was not significant, $p=.141$, while the quadratic contrast (signed and unsigned valence vs. arousal) was significant, $p=.015$.

Conclusions: This study investigated how affective states elicited by naturalistic stimuli are represented in the brain. Specifically, we explored if signed and unsigned valence and arousal can be predicted based on neural responses. The hyperalignment technique (Haxby et al., 2020) was employed to transform movie watching and recall datasets into the shared information space. We were able to predict arousal based on neural responses at the whole brain level and representation of arousal is consistent between movie watching and recall.

References

1. Chen, J., Leong, Y. C., Honey, C. J., Yong, C. H., Norman, K. A., & Hasson, U. (2017). Shared memories reveal shared structure in neural activity across individuals. Nature Neuroscience, 20(1), 115–125. https://doi.org/10.1038/nn.4450
2. Haxby, J. V, Guntupalli, J. S., Nastase, S. A., & Feilong, M. (2020). Hyperalignment: Modeling shared information encoded in idiosyncratic cortical topographies. Elife, 9, e56601.
3. Kim, J., Weber, C. E., Gao, C., Schulteis, S., Wedell, D. H., & Shinkareva, S. V. (2020). A study in affect: Predicting valence from fMRI data. Neuropsychologia, 143, 107473. https://doi.org/10.1016/j.neuropsychologia.2020.107473

Poster No 749

Rotten to the core–a neural signature of subjective core disgust generalizes to sociomoral contexts

Xianyang Gan[1,2], Feng Zhou[3], Ting Xu[1,2], Xiaobo Liu[4], Ran Zhang[1,2], Zihao Zheng[1,2], Xi Yang[5], Xinqi Zhou[6], Fangwen Yu[1,2], Jialin Li[7], Ruifang Cui[1,2], Lan Wang[1,2], Jiajin Yuan[6], Dezhong Yao[1,2], Benjamin Becker[1,2,8,9]

[1]Sichuan Provincial People's Hospital, University of Electronic Science and Technology of China, Chengdu, China, [2]The Clinical Hospital of Chengdu Brain Science Institute, MOE Key Lab for Neuroinformation, Chengdu, China, [3]Faculty of Psychology, Southwest University, Chongqing, China, [4]McConnell Brain Imaging Centre, Montreal Neurological Institute, McGill University, Montreal, Canada, [5]Faculty of Health, Medicine and Life Sciences, Maastricht University, Maastricht, Netherlands, [6]Institute of Brain and Psychological Sciences, Sichuan Normal University, Chengdu, China, [7]Max Planck School of Cognition, Leipzig, Germany, [8]State Key Laboratory for Brain and Cognitive Sciences, The University of Hong Kong, Hong Kong, China, [9]Department of Psychology, The University of Hong Kong, Hong Kong, China

Introduction: Recent affective and clinical neuroscience perspectives propose a paradigm shift towards subjective and conscious emotional experiences (Kyzar et al, 2023; LeDoux et al., 2017; Wager et al., 2018; Zhou et al., 2021). However, neurobiological models that accurately describe the respective neural representations are scarce. Disgust originates in the hard-wired mammalian distaste reflex, but in humans its conscious emotional experience is strongly shaped by subjective

appraisal and may extend to sociomoral contexts. Here, we combined functional MRI with recent methodological advances in multivariate pattern analytic neural decoding techniques to develop an accurate and generalizable whole-brain signature predictive of momentary self-reported subjective disgust experience, and in turn utilize the neural disgust signature to test the evolutionary perspective on disgust.

Methods: First, consistent with methods evaluated in previous studies developing neuroaffective decoders (Chang et al., 2015; Zhou et al., 2021), we employed a linear support vector regression model to identify a whole-brain signature of fMRI activation predictive of self-reported disgust experience elicited by core disgust stimuli using data from a discovery cohort (n=78). The performance of the resultant visually induced disgust signature (VIDS) was then evaluated across multiple core disgust datasets: the discovery (10×10-fold cross-validation), validation (n=30), and generalization (n=26) cohorts. Next, we determined which brain regions and systems contribute to the whole-brain disgust prediction through a bootstrap test (Kohoutová et al., 2020) and the computation of model encoding maps (Haufe et al., 2014), and we further tested whether isolated regions or networks traditionally involved in disgust such as the insula or default mode network were sufficient to predict subjective disgust experience. Moreover, functional decoding analysis based on Neurosynth was also conducted to evaluate the neurobiological validity of the developed VIDS. We next systematically examined the functional specificity of the VIDS by conducting predictive comparisons with established decoders for subjective fear (VIFS; Zhou et al., 2021) and negative affect (PINES; Chang et al., 2015), respectively. Finally, we tested the evolutionary perspective on disgust by applying the decoders in fMRI experiments on gustatory distaste (n=30) and sociomoral disgust (fairness norm violations; n=43).

Results: The results showed that the developed VIDS (Fig. 1a) accurately predicted momentary self-reported subjective disgust across three core disgust datasets (Fig. 1b,c,d), such that the averaged within-subject correlation between predicted and true disgust ratings was ≥0.88 in all cases and classification accuracies between different disgust levels were high (≥76%). The conscious experience of disgust is represented in distributed subcortical and cortical systems (Fig. 1e), and the contribution of insula (Fig. 1f) and large-scale networks (Fig. 1g) show lower predictive accuracy compared to the VIDS. More interestingly, the functional decoding analysis supported the disgust signature as a biologically plausible disgust model (Fig. 1h). The three affective decoders most accurately predicted the respective target experience, and the VIDS moreover outperformed the VIFS and PINES in predicting disgust experience in response to both gustatory distaste and sociomoral disgust (unfair offers) as revealed by both prediction accuracy and effect size (for more details see Gan et al., 2023).

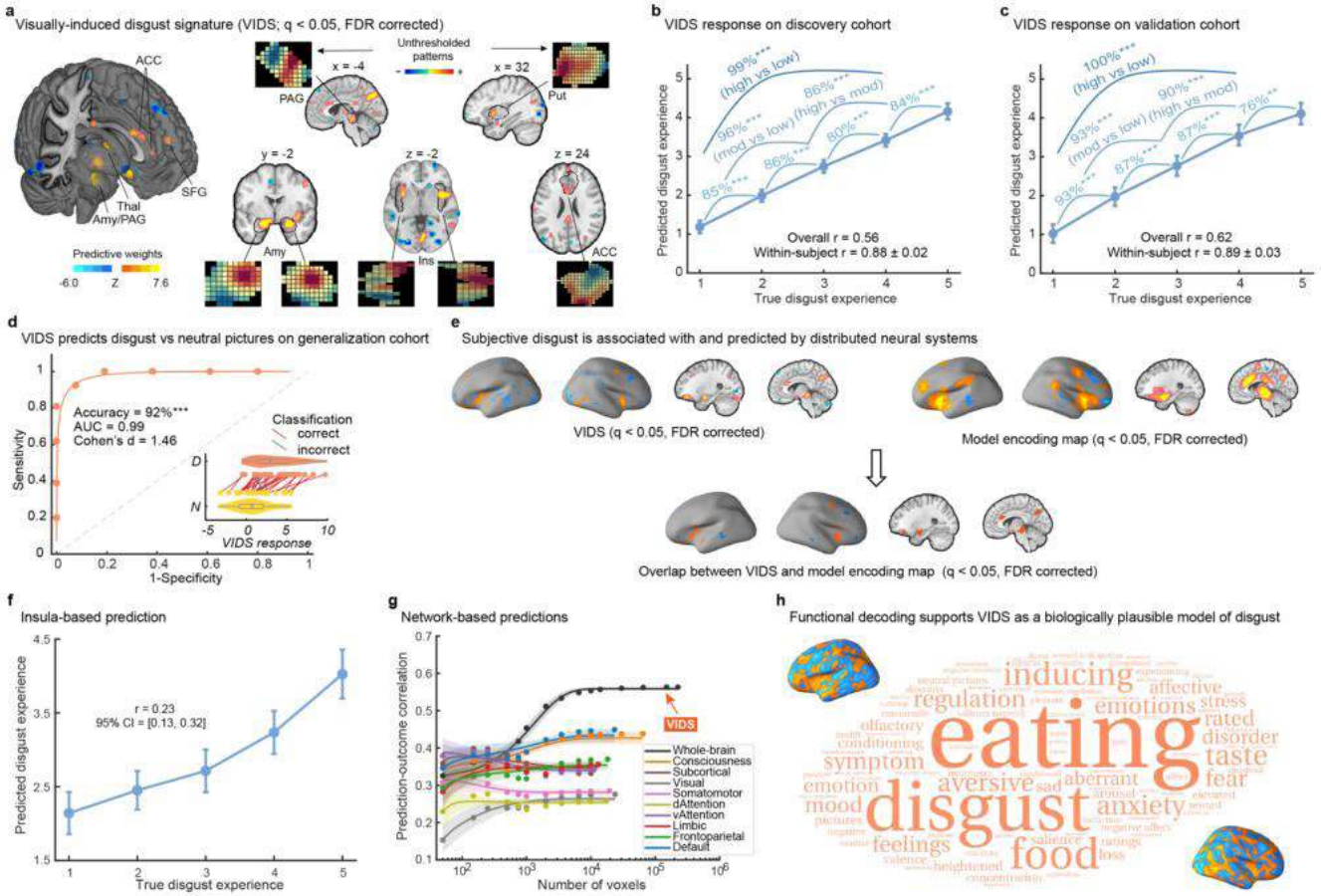

Fig. 1. Visually-induced disgust signature (VIDS). **a**, The spatial topography of the unthresholded patterns in some anatomical regions of interest (ROIs). This panel illustrates the VIDS pattern thresholded using a 10,000-sample bootstrap procedure at q<0.05, FDR corrected. Inserts show the spatial topography of the unthresholded patterns in some anatomical ROIs. **b**,**c**, Predicted disgust experience (subjective ratings; mean±SE) compared to actual disgust ratings in the cross-validated discovery cohort (n=78) and the independent validation cohort (n=30), respectively. Accuracy provided for forced-choice comparisons. P values based on two-sided independent binomial tests. r indicates Pearson correlation coefficient between predicted and true ratings. Error bar indicates standard error of the mean. **d**, Generalization of the VIDS in an independent dataset (using two-alternative forced-choice to classify disgust vs neutral stimuli). The figure shows the receiver-operating characteristics (ROC), and the inlet shows the VIDS response for different conditions (D=disgust; N=neutral). Each line connecting dots represents paired data from the same participant (red/blue=correct/incorrect classification). P value was based on a binomial test, two-sided. **e**, subjective disgust experience is associated with and predicted by distributed brain regions. **f**, Cross-validated predictions from insula-based prediction analysis. Error bar indicates standard error of the mean. **g**, Subjective experience of disgust is distributed across multiple systems. Model performance was evaluated as increasing numbers of voxels (x-axis) were selected to predict subjective disgust in different regions of interest including the entire brain (black), consciousness network (light orange), subcortical network (brown), or individual large-scale cerebral networks (other colored lines). The y-axis denotes the cross-validated prediction-outcome correlation. Colored dots indicate the mean correlation coefficients, solid lines indicate the mean parametric fit, shaded regions indicate standard deviation. **h**, Neurosynth functional decoding of the unthresholded VIDS. Here, the 100 most strongly correlated terms were displayed, with a larger font size indicating a larger Pearson correlation coefficient. ACC=anterior cingulate cortex, Amy=amygdala, AUC=area under the curve, Ins=insula, PAG=periaqueductal gray, Put=putamen, SFG=superior frontal gyrus, Thal=thalamus.

Conclusions: The present study developed a sensitive neural signature for subjective disgust experience, which robustly generalizes across core disgust, gustatory distaste, and sociomoral contexts. The neural basis of subjective disgust is encoded in multiple distributed brain systems rather than isolated brain regions. We provide an accurate fMRI-signature for disgust with a high potential to resolve ongoing evolutionary debates.

References

1. Chang, L. J., Gianaros, P. J., Manuck, S. B., Krishnan, A., & Wager, T. D. (2015), 'A sensitive and specific neural signature for picture-induced negative affect', PLoS Biology, vol. 13, no. 6, pp. e1002180.
2. Gan, X., Zhou, F., Xu, T., Liu, X., Zhang, R., Zheng, Z., . . . Becker, B. (2023), 'Rotten to the core – a neurofunctional signature of subjective core disgust generalizes to socio-moral contexts', bioRxiv.
3. Haufe, S., Meinecke, F., Görgen, K., Dähne, S., Haynes, J.-D., Blankertz, B., & Bießmann, F. (2014), 'On the interpretation of weight vectors of linear models in multivariate neuroimaging', Neuroimage, vol. 87, pp. 96-110.
4. Kohoutová, L., Heo, J., Cha, S., Lee, S., Moon, T., Wager, T. D., & Woo, C.-W. (2020), 'Toward a unified framework for interpreting machine-learning models in neuroimaging', Nature Protocols, vol. 15, no. 4, pp. 1399-1435.
5. Kyzar, E. J., & Denfield, G. H. (2023), 'Taking subjectivity seriously: towards a unification of phenomenology, psychiatry, and neuroscience', Molecular Psychiatry, vol. 28, no. 1, pp. 10-16.
6. LeDoux, J. E., & Brown, R. (2017), 'A higher-order theory of emotional consciousness', Proceedings of the National Academy of Sciences of the United States of America, vol. 114, no.10, pp. E2016-E2025.
7. Wager, T. D., Krishnan, A., & Hitchcock, E. (2018), 'How are emotions organized in the brain?', In A. S. Fox, R. C. Lapate, A. J. Shackman, & R. J. Davidson (Eds.), The nature of emotion. Fundamental questions (pp. 112-118). New York, NY: Oxford University Press.
8. Zhou, F., Zhao, W., Qi, Z., Geng, Y., Yao, S., Kendrick, K. M., . . . Becker, B. (2021), 'A distributed fMRI-based signature for the subjective experience of fear', Nature Communications, vol. 12, no. 1, pp. 6643.

Poster No 750

Frontal beta activity as a marker for depression-related negativity bias in emotional association

Minsok Koo[1], Sang Ah Lee[2]

[1]Seoul National University, Seoul, Seoul, [2]Seoul National University, Gwanak-gu, Seoul

Introduction: In our daily lives, we often experience multiple emotionally significant events, occurring in the same place or context. Evidence suggests that our emotional responses are bound to these spatial contexts in memory, and that these associated emotions often resurface when we revisit these locations. Disproportionate recall of negative over positive emotions in mixed emotional memories could indicate a person's susceptibility to affective disorders such as depression. Higher activation in the prefrontal cortex, especially in the medial regions, is associated with decision-making in ambiguous emotional situations[4]. There are several well-known EEG markers for emotion-processing in the frontal lobe, with some studies highlighting the importance of beta oscillations[2], while others reporting effects in the theta and alpha bands[5]. Our study aims to examine the neural underpinnings of emotional association with a spatial context (scene), using scalp EEG, and to investigate how this emotional memory and its neural correlates are related to individual levels of depression.

Methods: 20 healthy participants(mean age: 28.9) were recruited for the experiment and were asked to complete the Beck Depression Index-II(BDI-II) to measure their depression-like symptoms. During the encoding part of the task, a neutral background scene was presented, followed by two separate emotional scenarios on top of the same scene in subsequent order. Each of the two emotional images was either negative(N), positive(P), or neutral(Neu), and participants were asked to provide valence ratings from a scale of -3 to +3. During the retrieval part of the task, previously shown neutral background scenes,without the foreground emotional images, were presented, and participants were asked to rate the emotional valence associated with each scene.

Results: We first examined if the final image reinstated the intended emotion and how depression levels affected valence ratings. A repeated-measures ANOVA revealed significant within-subject differences among valence ratings across the emotion conditions (mixed (N-P, P-N pairs), neutral (Neu-Neu), negative (N-N), positive (P-P) conditions) ($F(3,51)=6.494, p<0.01$) and between-subject effects of depression ($F(1,17)=10.314, p<0.01$). Depression scores negatively correlated with valence ratings in mixed($r=-.555, p<0.05$), neutral($r=-.713, p<0.001$), and positive($r=-.502, p<0.05$) conditions, but not in negative($r=.259, p>0.1$) ones, indicating a consistent rating of negativity across all subjects in fully negative conditions. The interaction between Emotion Condition and Depression was only marginally significant ($F(3,51)=2.497, p=0.079$). We tested the hypothesis of possibility of greater frontal lobe engagement in mixed emotions by analyzing scalp EEG data during final retrieval and found a positive correlation between depression scores and frontal beta power in the mixed($r=.523, p<0.05$), N-N($r=.475, p<0.05$), and P-P($r=.480, p<0.05$) conditions. To investigate whether differences in frontal beta activity serve as a marker for severity of depression symptoms, which consequently impacts one's memory of associated emotion, we performed a mediation analysis and found that depression scores significantly affected frontal beta activity, influencing valence ratings of scenes associated with mixed emotions ($z=-2.07, p<0.05$).

Conclusions: Our study reveals that frontal beta activity signals depression-linked changes in regulating and remembering context-bound emotions, especially in scenes associated with mixed emotions. One of the key brain regions for mediating ambiguous emotion is the ventromedial prefrontal cortex. According to EEG source localization studies, frontal beta during emotional processing may indicate vmPFC activation reinstating of the negative scenarios over positive ones. This contributes to our understanding of how depression affects emotional processing and memory, and opens up possibilities for research and clinical interventions targeting these neural pathways.

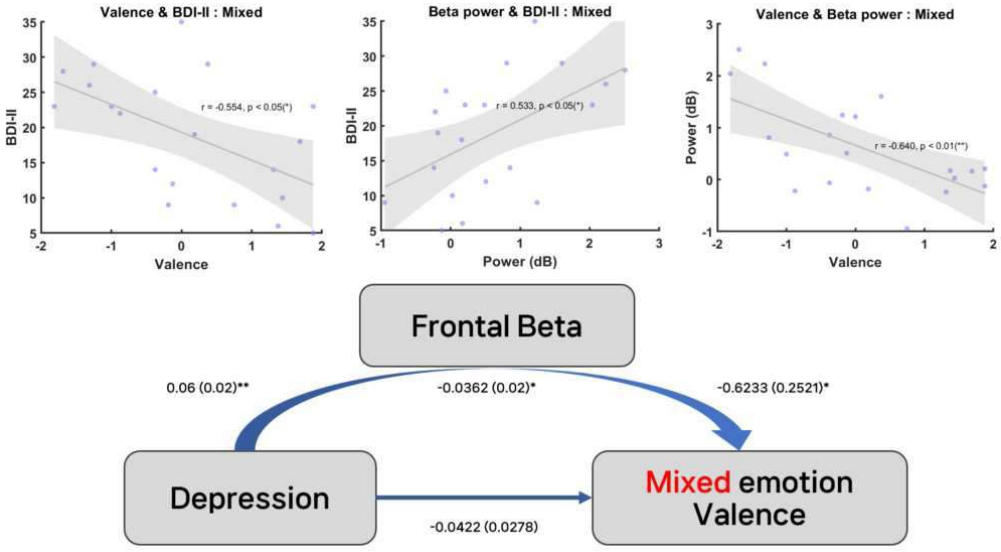

References

1. Alexander, L., Wood(2023). The ventromedial prefrontal cortex and emotion regulation: lost in translation?. The Journal of Physiology, 601(1), 37-50.
2. Güntekin, B(2010). Event-related beta oscillations are affected by emotional eliciting stimuli. Neuroscience letters, 483(3), 173-178.
3. Kaping, D. (2011). Specific contributions of ventromedial, anterior cingulate, and lateral prefrontal cortex for attentional selection and stimulus valuation. PLoS biology, 9(12), e1001224.
4. Lipsman (2014). Beta coherence within human ventromedial prefrontal cortex precedes affective value choices. Neuroimage, 85, 769-778.
5. Reznik (2018). Frontal asymmetry as a mediator and moderator of emotion: An updated review. Psychophysiology, 55(1), e12965.

Poster No 751

Five weeks of Heart Rate Variability Biofeedback Improves Emotion in Older Adults: An fMRI Study

Huan Zhang[1], Chunling Zhang[1], Chaoliang Sun[1], Yongfu Hao[1], Zhang Yu[1]

[1]Zhejiang Lab, Hangzhou, Zhejiang

Introduction: Heart rate variability (HRV) biofeedback improves clinical symptoms relating to anxiety and depression[1]. However, how HRV regulates brain circuits underlying emotional processing is unknown. We used emotional regulation task and resting-state fMRI data to evaluate HRV-induced changes in brain activation and connectivity patterns. Our results suggest that HRV biofeedback up-regulates emotion pathways in the brain, including amygdala, prefrontal and parietal cortex, and down-regulates depression and anxiety scores in behaviours.

Methods: The behaviour and fMRI data were downloaded from the HRV biofeedback project (https://openneuro.org/datasets/ds003823/versions/1.3.3). Among which, 23 old participants (6 male, age: 55-80 years) with complete Emotion Regulation Task (10 min) and Resting-state (7 min) fMRI data were included in this study. All subjects underwent a 5-week HRV biofeedback experiment[2]. Structural and functional MRI data were acquired using a 3T Siemens MAGNETOM Trio MRI scanner. Before and after HRV regulation, all subjects the completed the questionnaires for depression (Center for Epidemiological Studies Depression Scale (CES-D)) and anxiety (TAI). We used fMRIPrep (https://fmriprep.org/en/stable/) for data pre-processing and nilearn (https://nilearn.github.io/stable/index.html) for analysis of brain activation and functional connectivity. Specifically, we used general linear model (GLM) to evaluate the changes in brain activation for the contrasts of “diminish>view”, “intensify>view” and “intensify>diminish” during the emotion regulation task. We choose the left amygdala as the seed to calculate the whole-brain functional connectivity.

Results: Participants showed a significant decrease in depression (CES-D scale, T-score=-2.24, p=0.0356), and a trend of decreasing in anxiety scores (TAI: T-score=-1.54, p=0.135) after HRV biofeedback, and a significant effect of intensifying their emotions during the regulation task (T=2.26, p=0.029) (Figure 1a). In the emotion regulation task (Figure 1c), we found strong activation for right superior and middle temporal gyrus (STG, MTG), bilateral inferior frontal gyrus (IFG) and putamen for the contrast of “diminish>view”, left superior and middle frontal gyrus (SFG, MFG), IFG, STG and right parahippocampal gyrus (PHG) for the contrast of “intensify >view”, and left MFG,SFG, inferior parietal lobe (IPL), putamen, precentral gyrus

and thalamus for the contrast of “intensify > diminish”. Moreover, we detected significant associations between the intensify-related IFG activity with CES-D score (r=-0.41, p=0.04), and between the diminish-related PHG activity with TAI (r=-0.049, p=0.016) after HRV biofeedback. Additionally, we observed a significant increase in the functional connectivity (Figure 2a) between left amygdala with the widespread emotion circuits including left IFG, MFG, supplementary motor area (SMA), anterior cingulate gyrus (ACC), IPL, STG, MTG and insula. Remarkably, the functional connectivity of left-amygdala was significantly associated with the CES-D scale in MFG (r=-0.48, p=0.019), IFG (r=-0.54, p=0.007), IPL (r=-0.43, p=0.041), and insula (r=-0.57, p=0.004) after HRV biofeedback.

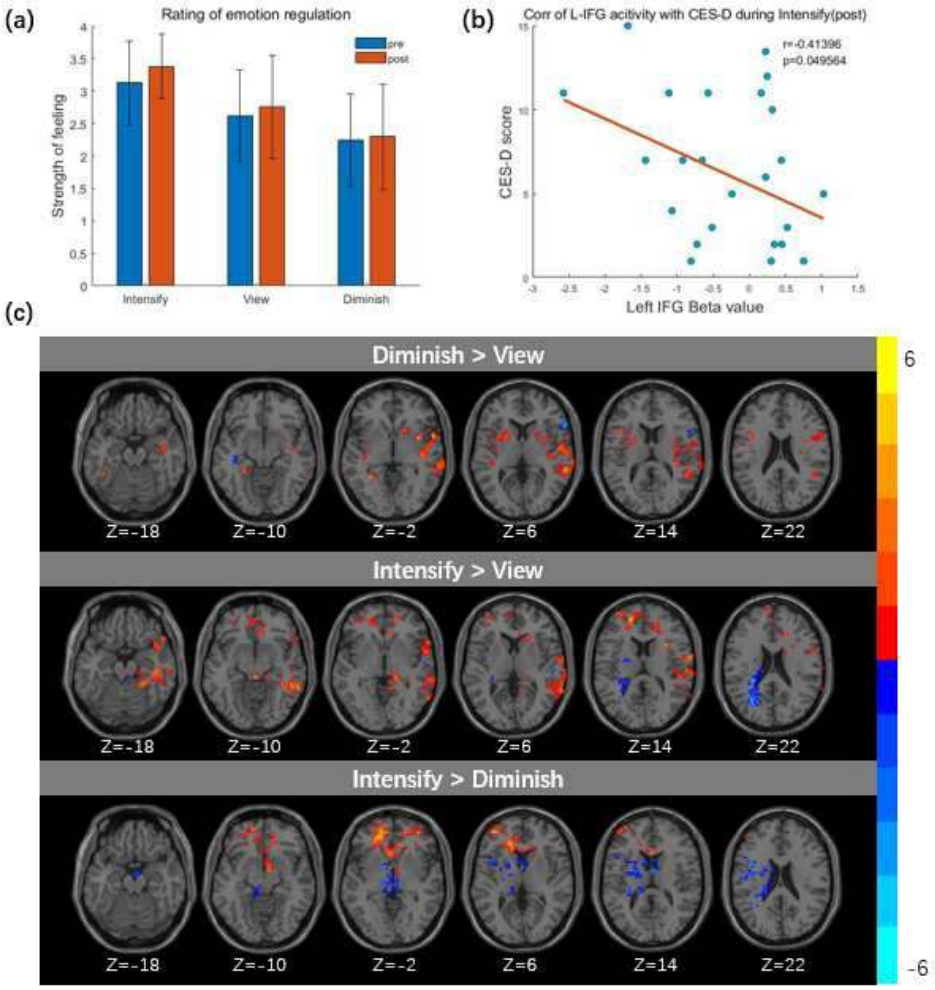

Fig. 1. (a) Rating of feelings during emotion regulation task. (b) Association between left IFG activity (Intensify condition of emotion regulation task) with CES-D score after HRV biofeedback. (c) HRV-induced changes of brain activations during the emotion regulation task (GRF correction, p<0.05).

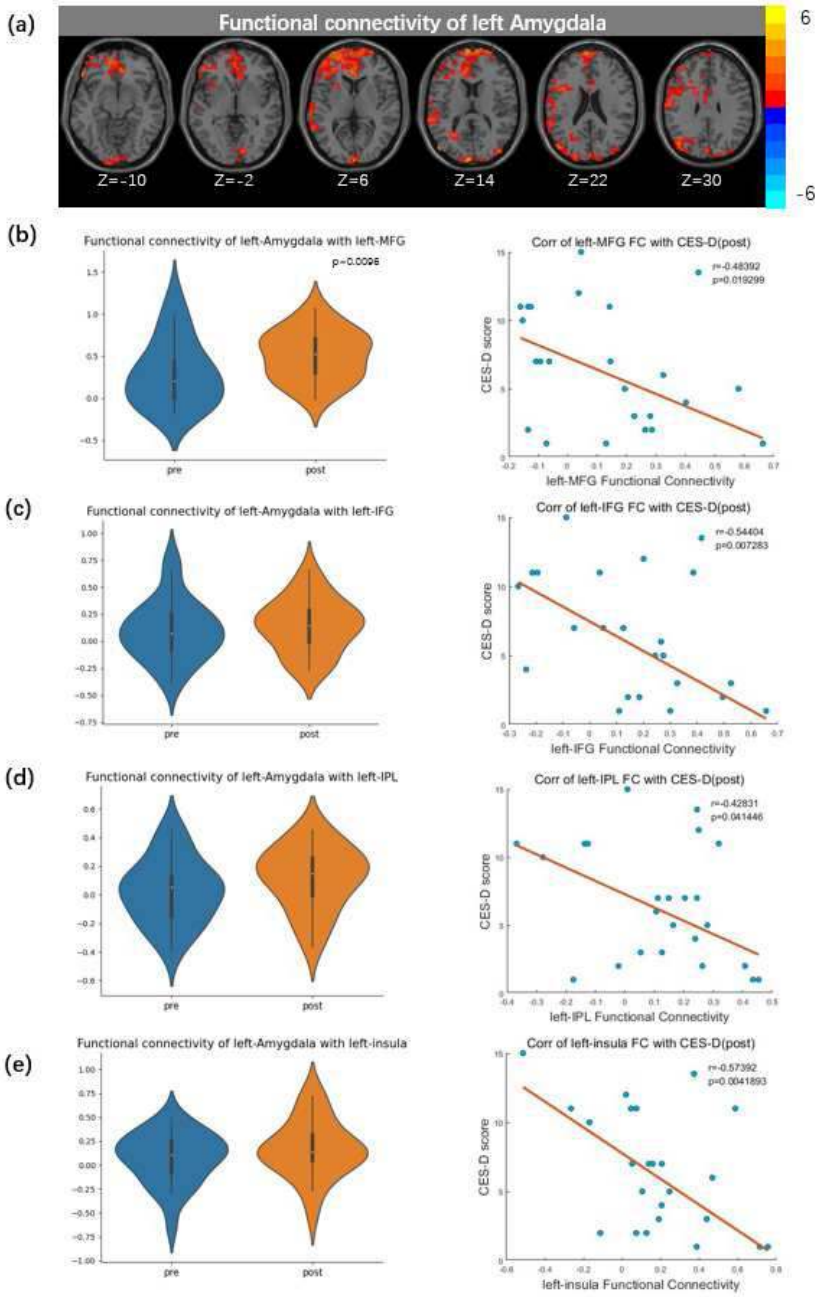

Fig. 2. (a) HRV-induced changes in the functional connectivity of left amygdala (GRF correction, $p<0.05$). We found significant associations between amygdala connectivity and the CES-D scale after HRV biofeedback in the regions of left-MFG (b), left-IFG (c), left-IPL (d) and left-insula (e).

Conclusions: In this study, we investigated brain and behavioural changes due to a 5-week HRV biofeedback. Our results demonstrated a critical role of prefrontal cortex in up-regulating emotions, and PHG in down-regulating emotions. Both of which are associated with the decrease of depression and anxiety symptoms after HRV biofeedback. We also found an increase in prefrontal-amygdala connectivity and its association with decreased depression scores due to the HRV biofeedback. In summary, our study suggests a potential treatment of HRV biofeedback as emotion regulation and depression.

References

1. Lehrer, Paul, et al. "Heart rate variability biofeedback improves emotional and physical health and performance: A systematic review and meta analysis." Applied psychophysiology and biofeedback 45 (2020): 109-129.
2. Yoo, Hyun Joo, et al. "Multimodal neuroimaging data from a 5-week heart rate variability biofeedback randomized clinical trial." Scientific Data 10.1 (2023): 503.

Poster No 752

Brain activation, age, gender, and mood disorder effects on facial emotion processing

Rebecca Easter[1], Emily Briceño[2], Lisa Rapport[3], Erin Kaufman[4], Mindy Westlund Schreiner[5], Melvin McInnis[2], Scott Langenecker[6]

[1]Johns Hopkins University, Baltimore, MD, [2]University of Michigan, Ann Arbor, MI, [3]Wayne State University, Detroit, MI, [4]University of Utah, Salt Lake City, UT, UT, [5]University of Utah, Salt Lake City, UT, [6]Ohio State University, Columbus, OH

Introduction: Facial emotion processing (FEP) is a complex and rapid set of interwoven and competing cognitive processes that involves attention, perception, evaluation, production of one's own emotion response to the stimulus, and regulation of that response. An intricate network of subcortical-cortical pathways is involved in supporting these processes. A predominately ventral brain system is implicated in stimulus appraisal and affective response production, whereas a predominately dorsal brain system underlies affect regulation and related behavior. These two systems interact with and modulate one another to effectively manage behavioral responses (Phillips et al., 2003; Langenecker et al., 2014). Age and gender have been connected to FEP, wherein younger adults and women demonstrate better FEP than older adults and men respectively (Briceño et al., 2015; Wright et al., 2009). Additionally, FEP has been implicated in mood disorders, such that individuals with major depressive disorder (MDD: Krause, Linardatos, Fresco, & Moore, 2021) or bipolar disorder (BD: Vederman et al., 2011) demonstrate deficits in FEP compared to healthy controls (HC). The goal of this study is to examine age, gender, and clinical effects of FEP in a large sample of HC and individuals with MDD or BD. We also aimed to identify key activation areas in the brain during FEP.

Methods: 1200 individuals (45% female; HC = 370, MDD = 318, BD = 516) completed a diagnostic interview and the Facial Emotion Perception Test (FEPT) at two sites. At one site, 39 individuals completed FEPT during functional MRI using a FE Signa 3T scanner. The fMRI series consisted of 30 contiguous oblique-axial sections 4mm thick using a forward/reverse spiral sequence. FEPT is a computerized test of FEP that involves rapid presentation of faces of happiness, sadness, anger, fear, or neutrality followed by a forced-choice selection. The test also includes a forced-choice identification of animals task. We conducted regressions to examine the effects of age, gender, and clinical status on facial emotion processing accuracy, reaction time (RT), and efficiency (accuracy – RT). To investigate brain activation, comparisons were made between activation during the affective and animal FEPT tasks. Regression models were utilized to examine the relationships between age, gender, FEP, and brain activation within HC.

Results: Education and age both predicted FEP, such that individuals with higher education and/or younger age presented with higher accuracy overall. Additionally, individuals with both MDD and BD performed worse than HC. Moreover, women, younger adults, and HC individuals had significantly faster reaction times and efficiency than men, older adults, and those with MDD and BD respectively. Within HC, individuals demonstrated predominant activation in bilateral inferior and middle frontal gyri, bilateral amygdala and anterior hippocampus, and bilateral cuneus during the FEP task compared to the animal identification one. An effect of age on brain activation was also detected, such that older individuals demonstrated reduced activation in some areas, including in left middle insular and dorsal caudate and precuneus.

Conclusions: Our findings replicate previous studies that age and gender are associated with FEP, such that women and younger individuals performed faster and more efficiently. Younger age and more education were also associated with higher accuracy. We also replicated the finding that individuals with MDD or BD demonstrate worse FEP than HC. Furthermore, we identified key areas of activation during FEP, including bilateral inferior and middle frontal gyri, amygdala, hippocampus, and cuneus. We only found a few activation differences in fusiform face areas, the left fusiform/parahippocampal gyrus. With increasing age, there was left lateralized decreases in activation in insula, precuneus, and dorsal caudate. Overall these results suggest that clinical and sociodemographic factors impact brain activation and FEP.

References

1. Phillips, M.L. (2003) Neurobiology of emotion perception I: The neural basis of normal emotion perception. Biol Psychiatry, 54(5), 504-514.
2. Langenecker, S.A. (2014). Current neural and behavioral dimensional constructs across mood disorders. Current Behavioral Neuroscience Reports, 1, 114-153.
3. Briceño, E.M. (2015). Age and gender modulate the neural circuitry supporting facial emotion processing in adults with major depressive disorder. Am J Geriatr Psychiatry, 23(3), 304-313.
4. Wright, S.L. (2009) Gender-specific disruptions in emotion processing in younger adults with depression. Depression Anxiety, 26(2), 182-189.
5. Krause, F.C. (2021). Facial emotion recognition in major depressive disorder: A meta-analytic review. Journal of Affective Disorders, 293, 320-328.
6. Vederman, A.C. (2012) Modality-specific alterations in the perception of emotional stimuli in Bipolar Disorder compared to Healthy Controls and Major Depressive Disorder. Cortex, 48(8), 1027-1034.

Poster No 753

Exploring Neural Responses to Six Naturalistic emotional videos: An fMRI study using CMU-MOSEI data

Jin-Su Kim[1], Hyun-Chul Kim[1]

[1]Kyungpook National University, Daegu, Korea, Republic of

Introduction: The CMU Multimodal Opinion Sentiment and Emotion Intensity (CMU-MOSEI) dataset consists of a diverse collection of opinion video clips, each labeled subjective emotion and sentiment intensity[1]. It is a collection of thousands of annotated YouTube clips expressing diverse opinions. Integrating functional magnetic resonance imaging (fMRI) with this dataset would offer a new way to explore neural reactions to emotion and sentiment during naturalistic stimuli. This study aimed to investigate the neural responses during emotional processing while exposed to CMU-MOSEI's multimodal stimuli, followed by an evaluation of the emotional responses elicited by the stimuli.

Methods: We selected 120 video clips from each of six emotional categories (anger, disgust, fear, happiness, sadness, and disgust) in the CMU-MOSEI dataset, each lasting 45–75 seconds. During fMRI data acquisition, ten right-handed healthy participants (age = 24.6 ± 2.6; 4 males, 6 females) watched these clips and rated their emotions on a nine-point SAM scale[2] for arousal, dominance, and valence. To compare emotion levels in the valence-arousal space[3], the rated individual scores were normalized using the z-score method across all clips for each SAM and the averages were computed across subjects. Raw fMRI data were preprocessed using a standard pipeline, and physiological noise from the white matter and cerebral spinal fluid was removed using the Anatomical Component-based correction (AcompCor) method with the Analysis of Functional Neuroimages software[5]. Subsequently, using general linear model (GLM) the preprocessed fMRI data were analyzed at the individual level to estimate whole-brain activations from the naturalistic video stimuli. The estimated beta-value maps from GLM were used for one-way ANOVA (within-factor = emotion).

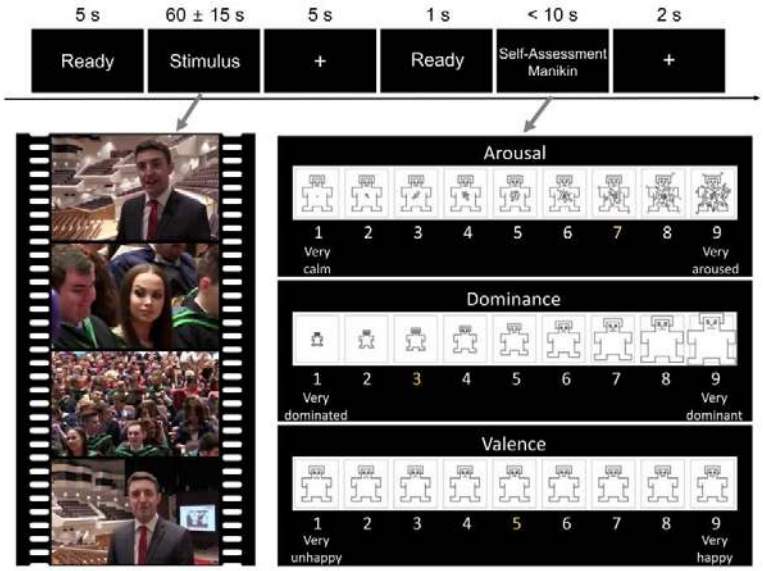

Figure 1. The illustration of a trial of a task paradigm. Stimuli and Self-Assessment Manikin (SAM) sections are presented after a 5-second and 1-second ready sign, respectively. A video clip lasts 45-75 seconds, followed by rating scores for three kinds of emotions. Three screens collecting SAM scores for arousal, dominance, and valence which are presented in a random order. The number in yellow indicates the score where the current cursor is located.

Results: We observed that the rated scores for each of the emotional categories are distributed close to the area reported in previous studies within the valence-arousal space[3,4]. In particular, previous studies have consistently reported that happiness corresponds to a high valence and high arousal area (Fig. 2a). In this study, subjects rated high emotional scores for both valence and arousal when watching happiness-associated video clips. Figure 2b shows the ANOVA results that the superior medial gyrus, the medial frontal gyrus and insula revealed positive activations for all contrast maps while regions tied to emotional processing, such as the hippocampus, the olfactory cortex, and the middle temporal gyrus showed negative activation.

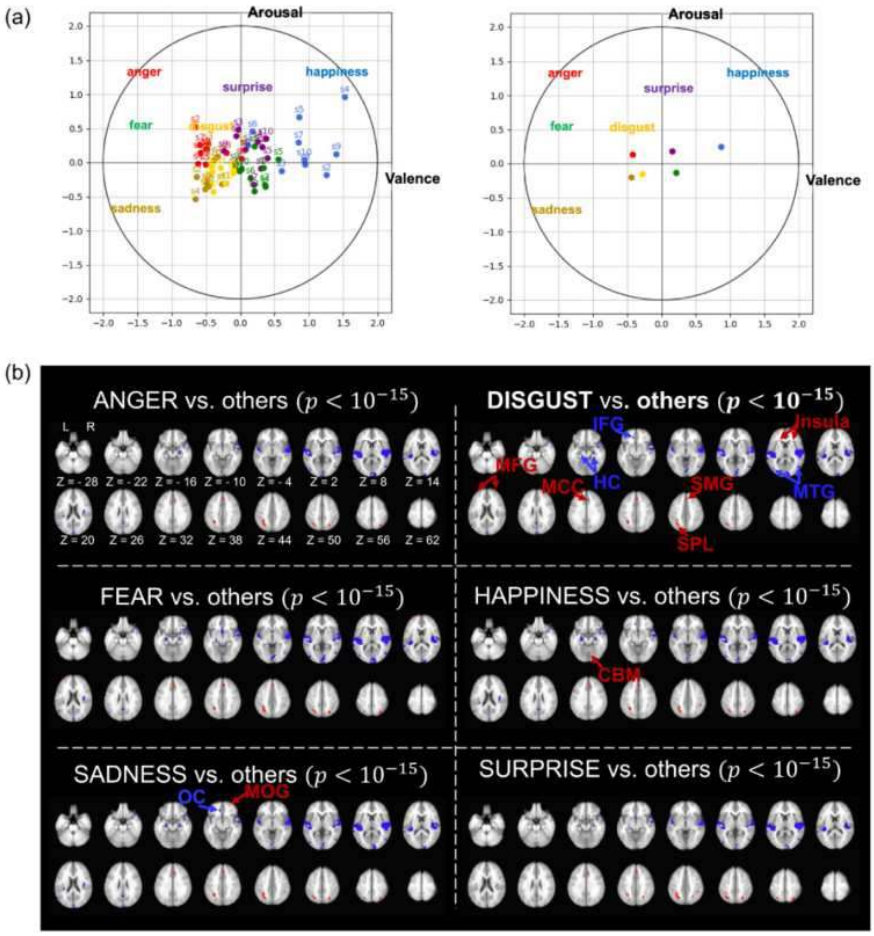

Figure 2. (a) Emotional response on Valence-Arousal space. The left figure shows z-scored SAM responses across all clips for a subject, while right one shows the averaged across all subjects. (b) one-way analysis of variance (ANOVA, within factor: emotion) result. Texts in red and blue color indicate positive and negative activations respectively. L, left; R, right; CBM, cerebellum; HC, hippocampus; IFG, inferior frontal gyrus; MCC, middle cingulate cortex; MFG, middle frontal gyrus; MOG, middle orbital gyrus; MTG, middle temporal gyrus; OC, olfactory cortex; SMG, superior medial gyrus; SPL, superior parietal lobule.

Conclusions: We found that video clips from the CMU-MOSEI dataset could elicit changes in emotional and neural responses. For further investigations, the three-dimensional emotion space (including dominance) should be compared to the distribution of rated scores. Additionally, extracted features from deep neural networks, such as convolutional neural networks, should be investigated to ensure consistency with the statistical analysis.

References

1. Acknowledgement: This work was supported by the National Research Foundation of Korea(NRF) grant funded by the Korea government(MSIT) (No. RS-2022-00166735 & No. RS-2023-00218987).
2. Zadeh, A. B., Liang, P. P., Poria, S., Cambria, E., & Morency, L. P. (2018, July). Multimodal language analysis in the wild: Cmu-mosei dataset and interpretable dynamic fusion graph. In Proceedings of the 56th Annual Meeting of the Association for Computational Linguistics (Volume 1: Long Papers) (pp. 2236-2246).
3. Bradley, M. M., & Lang, P. J. (1994). Measuring emotion: the self-assessment manikin and the semantic differential. Journal of behavior therapy and experimental psychiatry, 25(1), 49-59.
4. Russell, J. A., Lewicka, M., & Niit, T. (1989). A cross-cultural study of a circumplex model of affect. Journal of personality and social psychology, 57(5), 848.
5. Bhattacharjee, Ananya, et al. “On the Performance Analysis of APIs Recognizing Emotions from Video Images of Facial Expressions.”2018 17th IEEE International Conference on Machine Learning and Applications (ICMLA). IEEE, 2018.
6. Cox, R. W. (1996). AFNI: software for analysis and visualization of functional magnetic resonance neuroimages. Computers and Biomedical research, 29(3), 162-173.
7. Kim, H. C., Bandettini, P. A., & Lee, J. H. (2019). Deep neural network predicts emotional responses of the human brain from functional magnetic resonance imaging. NeuroImage, 186, 607-627.

Poster No 754

Awe is represented as an ambivalent experience in the human behavior and cortex

Jinwoo Yi[1], Danny Han[2], Jiook Cha[1,2,3,4]

[1]Department of Brain and Cognitive Sciences, Seoul National University, Seoul, Korea, Republic of, [2]Interdisciplinary Program of Artificial Intelligence, Seoul National University, Seoul, Korea, Republic of, [3]Department of Psychology, Seoul National University, Seoul, Korea, Republic of, [4]Graduate School of Data Science, Seoul National University, Seoul, Korea, Republic of

Introduction: Awe encompasses a complex emotional experience, transitioning from the initial negative feelings elicited by immense objects to subsequent positive ones (Keltner & Haidt, 2003). Nevertheless, the ambivalent nature of awe was not fully investigated due to its incompatibility with the prevailing framework of affective science (e.g., the constructionist approach). To address this knowledge gap, we delved into the following questions: (1) Does self-reported ambivalent states during awe experience better explain variances in awe intensity than simple positive/negative ratings? (2) Is the ambivalent state of awe also represented in the neural space as a distinctive valence state? We hypothesized that the self-reported ambivalence would predict awe intensity more accurately than positive/negative ratings. We also posited an existence of neural representation specific to ambivalent state during awe experiences.

Methods: We recorded a 19-channel electroencephalogram (EEG) while participants (N = 43) watched four 360° video stimuli: three awe-conditioned and one control. In each trial, they watched a clip and continuously rated subjective valence (i.e., positive, negative, neutral, and mixed) via key press. After the trial, they reported Awe Experience Scale (AWE-S) (Yaden et al., 2019), Evaluative Space Grid for valence (Larsen et al., 2009), and Likert-scaled arousal and motion sickness items. First, we examined which ratings significantly predicted AWE-S and how precisely they do so through a linear mixed model ('behavioral analysis'). Second, by applying contrastive learning specialized for time series data (CEBRA)(Schneider, Lee & Mathis, 2023), we constructed latent neural spaces that embed key-pressed valence labels in a within-subject design. To test whether each valence state could be distinctively clustered in the neural space, we calculated silhouette scores for subject's each trial and performed 1,000 permutation tests to assess their significance ('clustering analysis'). Third, we decoded the keypress valence labels using EEG time series to evaluate idiosyncrasy of neural representations linked to each valence state. We fitted a kNN classifier, the simplest model that does not require any training, with the out-of-bag samples from clustering analysis to predict key-pressed valence label in within-individual approach. We calculated the weighted F1 score using each sample's last 15% time-series as test set. To compare the performance with random chance, we also computed a weighted F1 score with a permuted dataset ('decoding analysis').

Results: In behavioral analysis, we found that only the intensity of positivity ($\beta = .094$, $p = .035$) and ambivalence ($\beta = .220$, $p = .001$) rated in Evaluative Space Grid and "mixed" keypress duration ($\beta = .565$, $p = .039$) were significantly associated with the AWE-S scores when controlling for random effects of participants and clips. A linear mixed model with these three predictors explained 69.7% of the variance of AWE-S scores. From the clustering analysis, we discovered that each valence state was clearly congregated except for one participant (averaged silhouette score = .871). In the decoding analysis, we observed that participants' self-reported valence label was predicted with the neural embeddings at each time point above the random chance (averaged test F1 score = .332).

Conclusions: Our results imply that, at the behavioral level, awe is encoded as an ambivalent experience rather than a positive or negative one. We also found that ambivalent states during awe experience exhibit distinct neural representations, just as positive/negative states do. Although some unsolved questions remain (e.g., identifying the brain regions mainly engaging in ambivalent states, building EEG-valence decoder with better performance), these findings support ambivalent properties of awe and suggest reconsidering ambivalent state as a meaningful unit of neuronal representation of valence.

References

1. Keltner, D., & Haidt, J. (2003). Approaching awe, a moral, spiritual, and aesthetic emotion. Cognition and emotion, 17(2), 297-314.
2. Yaden, D. B., Kaufman, S. B., Hyde, E., Chirico, A., Gaggioli, A., Zhang, J. W., & Keltner, D. (2019). The development of the Awe Experience Scale (AWE-S): A multifactorial measure for a complex emotion. The journal of positive psychology, 14(4), 474-488.
3. Larsen, J. T., Norris, C. J., McGraw, A. P., Hawkley, L. C., & Cacioppo, J. T. (2009). The evaluative space grid: a single-item measure of positivity and negativity. Cognition and Emotion, 23(3), 453-480.
4. Schneider, S., Lee, J. H., & Mathis, M. W. (2023). Learnable latent embeddings for joint behavioural and neural analysis. Nature, 1-9.

Poster No 755

Voluntary modulation of mental effort affects the attentional retraction induced by angry faces

Daniela Ballotta[1], Riccardo Maramotti[1], Eleonora Borelli[1], Fausta Lui[1], Giuseppe Pagnoni[1]

[1]University of Modena & Reggio Emilia, Modena, Italy

Introduction: Several studies have shown that approach and avoidance arm movements are facilitated by positive and negative emotional stimuli, respectively (Fox et al., 2001). We have previously found that negative stimuli affect attentional allocation in a paradoxical way, whereby the initial transient phase of attentional capture by the negative stimulus is quickly followed by a withdrawal of the attentional spotlight away from it and towards the observer (Ballotta et al., submitted). Here we used an fMRI paradigm to investigate whether an additional voluntary investment of cognitive effort could offset this automatic attentional retraction induced by angry faces.

Methods: 28 healthy female subjects (age 21.4 ± 2.2 years) took part in the study. An angry (neg) or a happy (pos) face from a set of 72 items (Lundwist et al., 1998) was displayed on the back wall of a virtual corridor. Volunteers were asked to respond as fast as possible to a target stimulus (a red sphere) appearing 350 ms after the face and perceptually closer either to the observer (observer-close, OC) or to the face stimulus (stimulus-close, SC), while gaze had to be maintained on the face stimulus (Figure 1). Crucially, participants were asked to execute the task either "with maximum exertion" (EXR) or "as relaxed as possible" (RLX) in different blocks of trials. Functional data were acquired with a 3T scanner and an EPI sequence (TR=1500 ms; 320 volumes x 4 sessions; 47 axial slices; 3x3x2.7mm voxels; 0.3mm gap). For both EXR and RLX blocks, we modelled the effect of valence and target location on reaction times (RTs) using a shifted log-normal distribution, whose parameters were estimated with a Bayesian approach. Functional data of each participant were preprocessed and analysed using AFNI. A mixed-effects group analysis was performed, yielding whole-brain t-maps, which were thresholded at a family-wise alpha<0.05. In this presentation, we will focus mainly on the interaction effect of target location and invested effort for negative faces, on both RTs and imaging data.

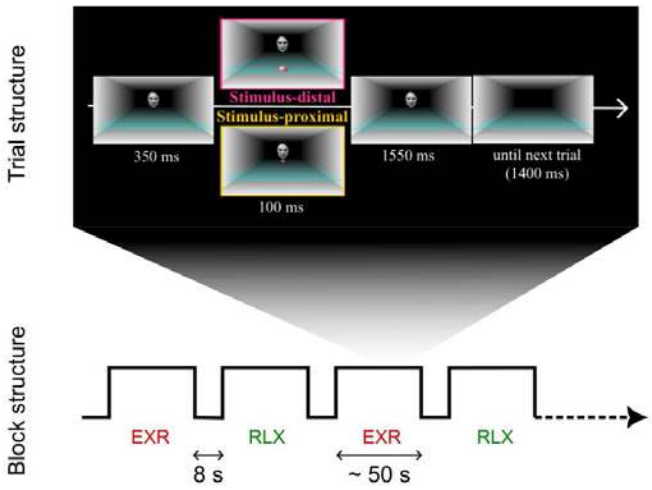

FIGURE 1 Block and trial structure of the stimulus presentation sequence. There were 8 blocks per imaging run (4 runs total), with 14 trials each.

Results: RTs were significantly faster in the EXR condition (mean = 232.3 ms), compared to the RLX one (mean = 269.2 ms). An interaction effect of valence and target position was observed for the RLX condition, but not for the EXR one. This result was led by a reduction in the RT difference between the OC and SC conditions for negative faces in the EXR (mean effect = 9.1 ms, SEM = 8.2 ms) compared to the RLX condition (mean effect = 18.2 ms, SEM = 11.8 ms) (Figure 2, left side). The corresponding contrast, (OC-SC)/EXR > (OC-SC)/RLX for negative faces, revealed significant clusters of activation in the bilateral fusiform face complex (FFC), V2 and V3, bilateral intraparietal sulcus (IPS), bilateral inferior frontal gyrus/anterior insula (IFG/AI), and pre-supplementary motor area (pre-SMA; Figure 2, right side).

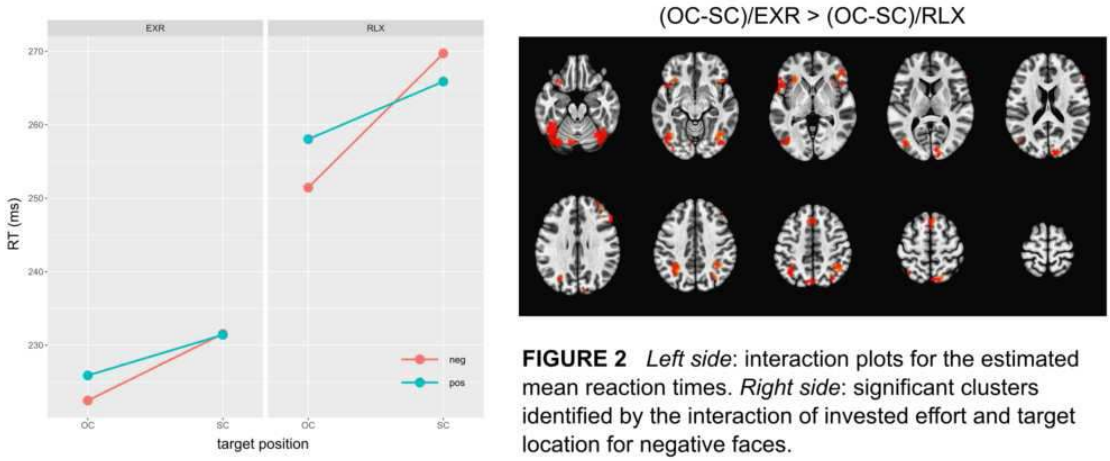

FIGURE 2 *Left side*: interaction plots for the estimated mean reaction times. *Right side*: significant clusters identified by the interaction of invested effort and target location for negative faces.

Conclusions: The reduced RTs difference between the negative OC and SC conditions, for EXR compared to RLX, suggests that the automatic attentional retraction induced by angry faces may be weakened by the voluntary investment of additional mental effort. The neural substrates of this effect include attentional (pre-SMA, IPS), face (FFC), and salience (IFG/AI) processing areas.

References

1. Fox, E. et al. (2001). Do threatening stimuli draw or hold visual attention in subclinical anxiety? Journal of Experimental Psychology: General, 130(4), 681.
2. Ballotta, D. et al. How angry faces scare away attention: a behavioral and fMRI study. Submitted.
3. Lundwist, D. et al. (1998). The Karolinska Directed Emotional Faces-KDEF [CD-ROM]. Department of Clinical Neuroscience, Psychology section, Karolinska Institutet, Stockholm, Sweden.

Poster No 756

Double Dissociation Facial Expression Perception - Evidence from a (N=108) human lesion-based study

Prabhakar AT[1], Allison McKendrick[2], Olivia Carter[3], Marta Garrido[4]

[1]Christian Medical College, Vellore, Tamil Nadu, [2]Division of Optometry, School of Allied Health, University of Western Australia, Perth, Western Australia, [3]Melbourne School of Psychological Sciences, Melbourne, Victoria, [4]The University of Melbourne, Melbourne, Australia

Introduction: The ability to perceive and recognize faces is an essential aspect of social interaction in humans. Two functionally distinct cortical pathways process different aspects of facial information. The ventral pathway, which includes the occipital face area (OFA) and the fusiform face area (FFA), preferentially responds to invariant facial features while a lateral pathway, that involves the posterior superior temporal sulcus (pSTS) responds to the changeable facial aspects, such as emotional expressions and eye-gaze direction. By studying patients with focal brain lesions we aimed to demonstrate a double dissociation between the dynamic and static facial recognition.

Methods: Patients (N=108) with focal brain lesions to the occipital, temporal and parietal cortices were recruited for this study. All participants completed behavioural tasks to assess the recognition of static and dynamic facial emotional expressions. The static stimuli included forty color photographs of faces of different ethnicity, expressing the four basic feelings happy, sad, angry, and fearful, as well as no emotion expression. The dynamic stimuli consisted of 1.5 s movie clips of digitally generated avatars expressing happy, sad, anger, surprise, disgust, or fearful expressions. Structural MRI scans were reviewed, and the lesions were mapped to the template brain manually. Then, using ROI analysis and a multivariate lesion symptom mapping method based on Support vector regression (SVR-LSM), lesion symptom mapping (based on T1), lesion network mapping (based on resting-state fMRI) and lesion disconnectome mapping (based on DWI) were performed to study the relationship between the lesion and the impairment in the behavioural scores.

Results: The ROI analysis showed, that the patients with isolated right FFA lesions had significantly lower scores on static emotion recognition and patients with isolated lesions in right STS had significantly lower scores on dynamic emotion recognition ($p < 0.001$). We saw a double dissociation between STS and FFA in their association with static and dynamic emotion recognition, respectively. The STS-lesioned group had significantly higher scores on dynamic emotions compared to the FFA group ($p < .001$), while the FFA-lesioned group had significantly higher scores on static emotions compared to

the STS group ($p < .001$). The SVR-LSM analysis showed that dynamic emotion recognition was associated with a significant cluster localized along the right superior temporal sulcus involving pSTS ROI. Static emotion recognition was associated two significant clusters in bilateral inferotemporal, and occipital cortices involving the fusiform and the lingual gyri and included the FFA ROI.

Conclusions: Using the method of double dissociation, we have been able to demonstrate the existence of two independent face cortical pathways: one for static faces projecting along the ventral surface including the OFA and FFA, and the other for dynamic faces projecting along the lateral surface involving pSTS. We add causal evidence to the claim that the pSTS plays an important role in the processing of dynamic facial expressions. Critically, we show for the first time that perception of dynamic and static facial emotion expressions are processed via dissociable cortical pathways.

References

1. Arcaro, M. J., Mautz, T., Berezovskii, V. K., & Livingstone, M. S. (2020). Anatomical correlates of face patches in macaque inferotemporal cortex. Proceedings of the National Academy of Sciences, 117(51), 32667–32678. https://doi.org/10.1073/pnas.2018780117
2. Choi, S.-H., Jeong, G., Kim, Y.-B., & Cho, Z.-H. (2020). Proposal for human visual pathway in the extrastriate cortex by fiber tracking method using diffusion-weighted MRI. NeuroImage, 220, 117145. https://doi.org/10.1016/j.neuroimage.2020.117145
3. Pitcher, D., Pilkington, A., Rauth, L., Baker, C., Kravitz, D. J., & Ungerleider, L. G. (2020). The Human Posterior Superior Temporal Sulcus Samples Visual Space Differently From Other Face-Selective Regions. Cerebral Cortex (New York, NY), 30(2), 778–785. https://doi.org/10.1093/cercor/bhz125
4. Pitcher, D., & Ungerleider, L. G. (2021). Evidence for a Third Visual Pathway Specialized for Social Perception. Trends in Cognitive Sciences, 25(2), 100–110. https://doi.org/10.1016/j.tics.2020.11.006
5. Weiner, K. S., & Gomez, J. (2021). Third Visual Pathway, Anatomy, and Cognition across Species. Trends in Cognitive Sciences, 25(7), 548–549. https://doi.org/10.1016/j.tics.2021.04.002

Poster No 757

Effects of executive function difficulty on brain responses to infant crying

Daiki Hiraoka[1,2], Shannon Powers[1], Genevieve Patterson[1], Jenna Chin[1], Yun Xie[1], Tom Yeh[3], Pilyoung Kim[1]

[1]University of Denver, Denver, CO, [2]University of Fukui, Fukui, Japan, [3]University of Colorado - Boulder, Boulder, CO

Introduction: Infant crying is a primal signal that motivates caregiving behavior while often triggering negative emotions, necessitating emotional regulation. Executive function comprises top-down cognitive processes, including the regulation of behaviors and emotions (Diamond, 2013; Gyurak et al., 2012). Parents with higher executive function exhibit greater sensitivity with their infants (Harris et al., 2021). Additionally, executive function-mediated difficulties in emotional regulation have been linked to increased child abuse risk (Crouch et al., 2018), suggesting that executive function could underpin the cognitive basis for appropriate caregiving by regulating neural processing of infant signal. This study seeks to investigate the association between the multifaceted aspects of executive function and brain activity in response to infant crying.

Methods: Participants in this study were 87 postpartum birthing parents who underwent the fMRI task. These individuals also completed the Behavior Rating Inventory of Executive Function - Adult Version (BRIEF-A) during their late pregnancy. The average age of participants at the time of the MRI was 28.89 years (SD = 5.62), and the scans were conducted on average 1.35 months postpartum (SD = 0.96). In the Infant Cry task, participants heard four sound types: their own infant's cry, another infant's cry, white noise matched to their infant's cry, and white noise matched to the other infant's cry. Each was played five times for 20 seconds, totaling 20 sounds with 8-12 second intervals. The BRIEF-A assesses difficulties with daily executive functioning (Roth et al., 2005). The BRIEF-A comprises 75 items across 9 clinical scales. In this research, the scales were aggregated into four higher-order factors: the Behavioral Regulation, the Emotional Regulation, the External Metacognition, and the Internal Metacognition. fMRI data were preprocessed and analyzed utilizing the fMRI prep and AFNI software. Covariates included age, months postpartum, and the average income-to-needs ratio during pregnancy. Corrections for multiple comparisons were applied across the whole brain, with a cluster extent threshold of $k \geq 16$ at a height threshold of $p < .001$, as determined by 3dClustSim.

Results: Across all subscales, clusters including the right superior temporal gyrus (R STG) were significant in the interactions with sound (cry vs. white noise) condition (Figure 1 and 2A), indicating that birthing parents with greater executive dysfunction exhibited increased brain activity during the crying condition. For all subscales except the Behavioral Regulation, clusters involving the right middle temporal gyrus (R MTG) showed a similar pattern (Figure 1 and 2B). Conversely, the Behavioral Regulation demonstrated an inverse interaction effect in clusters including the right middle frontal gyrus (R MFG) during the crying condition (Figure 1 and 2C).

Figure 1: Significant clusters for the interaction of sound type (infant cry and white noise) with executive dysfunction across BRIEF-A subscales. STG = superior temporal gyrus, MFG = middle frontal gyrus, MTG = middle temporal gyrus.

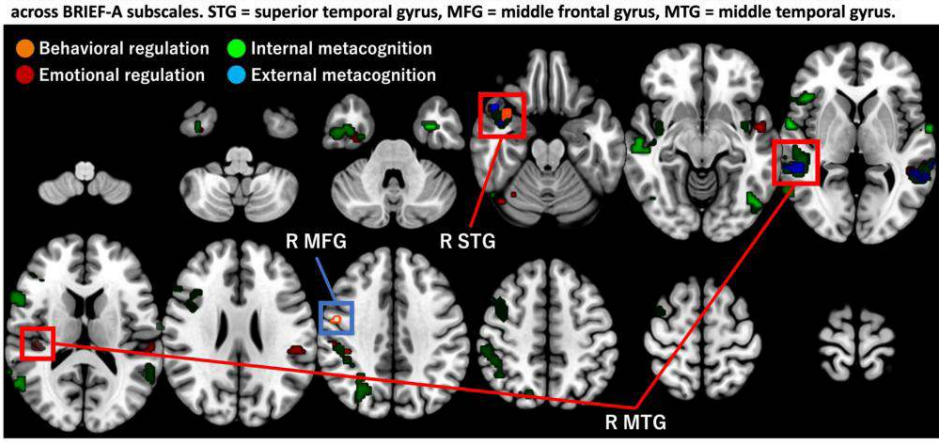

Figure 2: A) Scatter plots for the common significant activation in the right superior temporal gyrus (R STG) across all BRIEF-A subscales. B) Scatter plots for the common significant activation in the right middle temporal gyrus (R MTG) across emotion regulation difficulties, external metacognition difficulties, and internal metacognition difficulties. C) Scatter plot showing the unique negative correlation between the right middle frontal gyrus (R MFG) and the behavioral regulation difficulties.

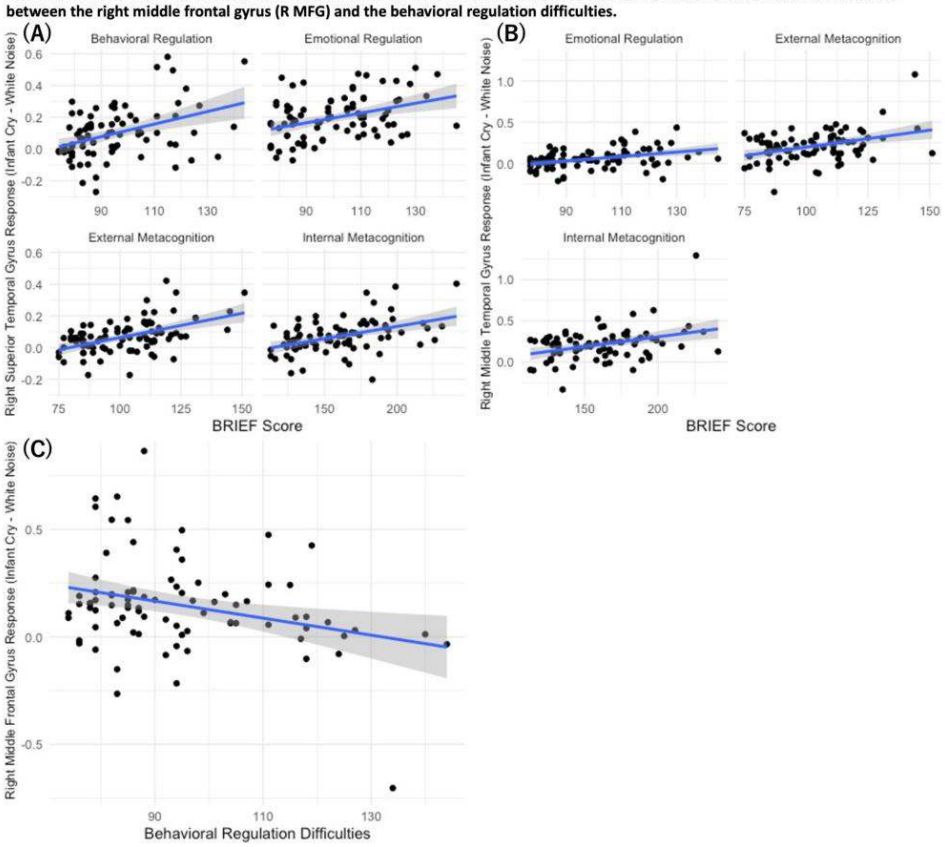

Conclusions: STG and MTG are crucial for processing infant cries (Witteman et al., 2019), and central to mentalizing and intentional empathy (de Greck et al., 2012; Feldman, 2015). Higher behavioral inhibition was associated with increased activity in the STG when responding to infant cries (Montoya et al., 2012). Our finding suggests that parents with executive dysfunctions might need greater activation in these areas to compensate for impaired mentalizing for the crying infant. In contrast, the MFG, which is involved in emotional regulation (Feldman, 2015), showed reduced activation in parents with more significant behavioral regulation difficulties. This reduction might reflect an impaired capacity to control the distress caused by infant cries. The MFG response to crying is influenced by perceived stress and lower income (Kim et al., 2016), which points to the potential for future research to explore the moderating or mediating effects of executive function in this relationship between socioeconomic disadvantages and the MFG's response to infant crying.

References

1. Crouch, J. L. (2018), 'Do emotion regulation difficulties explain the association between executive functions and child physical abuse risk?', Child Abuse & Neglect, vol. 80, pp. 99–107

2. de Greck. (2012), 'Neural substrates underlying intentional empathy', Social Cognitive and Affective Neuroscience, vol. 7, no. 2, pp. 135–144
3. Diamond, A. (2013), 'Executive functions', Annual Review of Psychology, vol. 64, pp. 135–168
4. Feldman, R. (2015), 'The adaptive human parental brain: Implications for children's social development', Trends in Neurosciences, vol. 38, no. 6, pp. 387–399.
5. Gyurak, A. (2012), 'Executive functions and the down-regulation and up-regulation of emotion', Cognition and Emotion, vol. 26, no. 1, pp. 103–118
6. Harris, M. (2021), 'Maternal adverse childhood experiences, executive function & emotional availability in mother-child dyads', Child Abuse & Neglect, vol. 111, 104830.
7. Kim, P. (2016), 'Socioeconomic disadvantages and neural sensitivity to infant cry: Role of maternal distress', Social Cognitive and Affective Neuroscience, vol. 11, no. 10, pp. 1597–1607
8. Montoya, J. L. (2012), 'Regional brain responses in nulliparous women to emotional infant stimuli', PloS One, vol. 7, no. 5, e36270
9. Roth, R. M. (2005), 'Behavior Rating Inventory of Executive Function - Adult Version (BRIEF-A)', Archives of Clinical Neuropsychology: The Official Journal of the National Academy of Neuropsychologists, vol. 20, no. 7
10. Witteman, J. (2019), 'Towards a neural model of infant cry perception', Neuroscience and Biobehavioral Reviews, vol. 99, pp. 23–32

Poster No 758

Dissecting the Roles of Medial Cingulate Cortex and Anterior Insula in Clinician Empathy

Maryam Amini[1], Nikta Khalilkhani[2], Theoni Varoudaki[3], Morgan Gianola[4], Elizabeth Losin[2]

[1]Penn State University, University Park - State College, PA, [2]Penn State University, State College, PA, [3]Penn State Univeristy, State College, PA, [4]University of Miami, Coral Gables, FL

Introduction: Empathy is a complex construct with significant implications for clinical decision-making. Understanding its neural basis, particularly during pain evaluation and treatment, is crucial for improving clinical practice (Decety & Jackson, 2004). Although several brain areas have been suggested to play an important role in pain empathy, this conclusion has primarily been drawn from studies outside of a clinical context. Two of these brain areas are the anterior midcingulate cortex (aMCC), thought to be more involved in cognitive aspects of empathy, and the Anterior Insula (AI), which is believed to play a role in more reactive affect sharing (Gu et al. 2010; Timmers et al., 2018). Our study's examination of the role of these regions in a simulated clinical context aims to enhance understanding of their roles in clinical pain empathy and decision making. This approach may ultimately contribute to translating the broader findings of social neuroscience into practical clinical applications, enriching our comprehension of how empathy's neural dynamics operate in different contexts.

Methods: 67 medical students (34 females) participated in a series of simulated pain management appointments while undergoing fMRI. The pain management task involved virtual appointments with 36 mock patients with diverse demographics. Each session began with a medical vignette describing the patient's injury, followed by a series of brief videos depicting pain behaviors in response to evoked pain stimulation, meant to simulate a clinical examination. Medical students, acting as clinicians, were then tasked with evaluating pain levels and rating how likely they would be to prescribe an analgesic. For the present analysis we employed a multivariate method known as Stochastic Search Variable Selection (SSVS) (Bainter et al. 2020) to examine which subset of the 28 questions from a well-validated measure of empathy, the interpersonal reactivity intex (IRI) most effectively predicted neural activity in the AI and aMCC regions of interest (ROIs) while clinicians were observing the patient pain videos. The IRI is a measure of dispositional empathy with subscales representing personal distress, empathic concern, fantasy, and perspective taking (Davis, 1983). These ROIs were identified based on their established association with empathy for pain in a landmark meta-analysis conducted by Lamm et al. (2011).

Results: We identified specific items within the IRI that were significant predictors of activity in the aMCC and the AI among clinicians observing patients in pain. We found that IRI question 8 from the Perspective Taking sub-scale, which assessed clinicians' ability to consider diverse perspectives during conflicts, emerged as a significant positive predictor of increased activity in the aMCC. In contrast, IRI question 27 from the Personal Distress Scale, which measures the intensity of emotional distress experienced when encountering someone in an emergency situation, was found to positively predict increased neural activity in both the aMCC and the AI.

Conclusions: Our findings are consistent with previous studies of empathy outside of clinical contexts in suggesting that the AI is generally associated with affective responses to pain whereas the aMCC is also involved in goal specific aspects of pain evaluation. Future analyses will test to what degree these regions are involved in patient pain assessment and treatment decisions. These insights may ultimately aid in developing more effective and context-sensitive pain management strategies, which have the potential to significantly improve patient outcomes.

References

1. Bainter, S. A., McCauley, T. G., Wager, T., & Losin, E. A. R. (2020). Improving practices for selecting a subset of important predictors in psychology: An application to predicting pain. Advances in Methods in Psychological Science, 3(1), 66-80. https://doi.org/10.1177/2515245919885617
2. Davis, M. H. (1983). Measuring individual differences in empathy: Evidence for a multidimensional approach. Journal of Personality and Social Psychology, 44(1), 113–126. https://doi.org/10.1037/0022-3514.44.1.113
3. Decety J, Jackson PL. The functional architecture of human empathy. Behav Cogn Neurosci Rev. 2004 Jun;3(2):71-100. doi: 10.1177/1534582304267187. PMID: 15537986.
4. Gu, X., Liu, X., Guise, K. G., Naidich, T. P., Hof, P. R., & Fan, J. (2010). Functional dissociation of the frontoinsular and anterior cingulate cortices in empathy for pain. Journal of Neuroscience, 30(10), 3739–3744. https://doi.org/10.1523/JNEUROSCI.4844-09.2010
5. Halpern J. What is clinical empathy? J Gen Intern Med. 2003 Aug;18(8):670-4. doi: 10.1046/j.1525-1497.2003.21017.x. PMID: 12911651; PMCID: PMC1494899.
6. Timmers I, Park AL, Fischer MD, Kronman CA, Heathcote LC, Hernandez JM, Simons LE. Is Empathy for Pain Unique in Its Neural Correlates? A Meta-Analysis of Neuroimaging Studies of Empathy. Front Behav Neurosci. 2018 Nov 27;12:289. doi: 10.3389/fnbeh.2018.00289. PMID: 30542272; PMCID: PMC6277791.

Poster No 759

Perceived Effectiveness of Cognitive and Emotional Messages in the Limbic and Perception Networks

Colleen Markey[1], Jiaying Liu[2], Joshua McMains[1], Jessica Fabbricatore[1], Allison Worsdale[3], Somin Kim[4], Michelle Perez[1], Lawrence Sweet[5]

[1]University of Georgia, Athens, GA, [2]University of California Santa Barbara, Santa Barbara, CA, [3]Department of Communication Studies, University of Georgia, Athens, GA, [4]University of Georgia, Athen, GA, [5]Department of Psychology, University of Georgia, Athens, GA

Introduction: The prevalence of vaping is rapidly increasing in the U.S., especially among young adults (Sanders-Jackson et al., 2019). Anti-vaping public service announcements (PSAs) may prevent vaping among susceptible youth (Tan et al., 2018). Understanding how individuals respond to these PSAs is also paramount to minimizing their exposure to nicotine and harmful toxins (Selya, A., et al. (2023). This study utilized functional MRI (fMRI) to determine whether young adult neural responses to cognitive and emotional appeals in the limbic and visual perception networks are linked to perceived message effectiveness.

Methods: A group of 43 young adult non-smokers, who vaped more than 15 of the last 30 days, took part in a PSA fMRI paradigm. The study included sequences of messages designed to discourage vaping through cognitive and emotional appeals. Vaping appeals were presented in a pseudo-randomized block design during two imaging runs. Each appeal type appeared in six 30s blocks comprised of three 10s PSAs. Scrambled control images were displayed in six 20s blocks. Perceived effectiveness was assessed via self-report following fMRI. Echoplanar data were acquired using a GE 3T MRI with 2s temporal and 3.5mm3 spatial resolution. Data processing included slice-time correction, registration, outlier/motion censoring, removal of linear drift, a 5mm blur, and stereotaxic standardization. Effects per brain voxel were quantified with general linear modeling of the fMRI signal using the time course of each message type as regressors and observed movement as covariates. Hypotheses were tested using correlations between mean fMRI responses in 12 regions of interest (ROIs) in the limbic and visual perception networks and perceived effectiveness across cognitive and emotional appeal PSAs.

Results: 14 a priori ROIs were examined. Two did not display a significant response to any of the PSAs (one sample t-test vs. 0; $p<.05$) and were eliminated from further analyses. The remaining 12 ROIs were segmented into two networks; limbic and visual perception. ROIs and results of statistical tests are listed in Table 1. Perceived effectiveness of cognitive appeals was significantly correlated positively with the visual perceptual, but not the limbic network; while perceived effectiveness of emotional appeals was significantly associated positively with the limbic, but not the visual perceptual network. The perceptual network effect was evident in significant positive correlations in all of its component nodes (i.e., left fusiform gyrus, inferior occipital gyrus, inferior temporal gyrus, and the right inferior occipital gyrus) and the limbic network effect was evident in all of its component nodes (i.e., left hippocampus and insula). Mean perceived effectiveness for cognitive appeal PSAs was 2.84 out of 5 (SD =.69) and emotional appeal PSAs was 2.63 out of 5 (SD =.68).

Table 1. Associations between brain response by network and perceived efficacy.

	Cognitive Appeals		*Emotional Appeals*	
	r-value	*p-value*	*r-value*	*p-value*
Visual Perceptual Network	**.317**	**.038**	.062	.688
Left Fusiform Gyrus	**.330**	**.031**	.035	.820
Left Inferior Occipital Gyrus	**.321**	**.036**	.054	.723
Left Inferior Temporal Gyrus	**.304**	**.048**	.164	.288
Left Middle Temporal Gyrus	**.349**	**.022**	.048	.756
Right Inferior Occipital Gyrus	**.426**	**.004**	.124	.421
Limbic Network	.171	.273	**.368**	**.014**
Left Hippocampus	.284	.065	**.370**	**<.01**
Left Insula	.019	.902	**.298**	**.007**

Conclusions: Results suggest a double dissociation such that anti-vaping PSAs with cognitive appeals elicit significant responses specifically in the visual perceptual network, while emotional appeals elicit significant responses specifically in the limbic network. Cognitive appeals are often aligned with cold processing, which involves critically evaluating factual information and assessing long-term consequences associated with vaping. Both of which may contribute to vaping cessation. Emotional appeals are often affiliated with hot processing, for which individuals rely on their emotions to make decisions. This might help convey the potential harms of vaping by creating a strong emotional response that supports the decision to quit. We conclude that greater activity in the limbic and visual perceptual networks serve as specific neuromarkers that suggest increased engagement in the PSAs and therefore, greater efficacy. Understanding these hot and cold processes may be useful in curating effective anti-vaping messages targeted at young adults.

Figure 1. Examples of anti-vaping public service announcements by appeal type.

(a) Emotional Appeal PSA

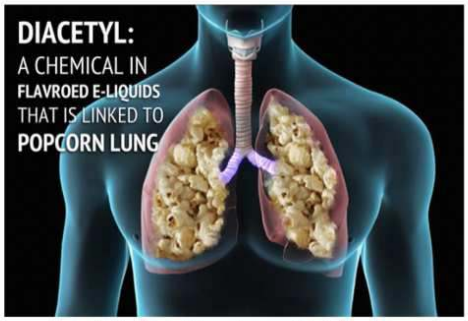

(b) Cognitive Appeal PSA

References

1. Sanders-Jackson, A., et al. (2019). Testing the effect of vapor in ENDS public service announcements on current smokers and ENDS users' psychophysiological responses and smoking and vaping urge. Journal of Health Communication, 24(4), 413–421.
2. Selya, A., et al. (2023). What substances are adolescents vaping? Estimating nicotine-specific and cannabis-specific vaping from us national youth surveys. Substance Use & Misuse.
3. Tan, A. S. L. et al. (2018), 'Effects of exposure to anti-vaping public service announcements among current smokers and dual users of cigarettes and electronic nicotine delivery systems', Drug and Alcohol Dependence, vol. 188, pp. 251–258.

Poster No 760

Late pregnancy oxytocin levels predict lower brain responses to infant cues at one-month postpartum

Yun Xie[1], Shannon Powers[1], Rebekah Tribble[1], Orna Zagoory[2], Ruth Feldman[2], Tom Yeh[3], Pilyoung Kim[1]

[1]University of Denver, Denver, CO, [2]Reichman University, Herzliya, Tel Aviv, [3]University of Colorado - Boulder, Boulder, CO

Introduction: Oxytocin (OT) is widely theorized to be a hormone that is closely related to modalities of mammal affiliative behaviors (Ross & Young, 2009). The majority of studies found that OT exposure was related to more optimal affiliative behaviors including more sensitive parenting and elevated neural responses to infant cues (Levine et al., 2007; Riem et al., 2011). Another line of research indicated that OT was related to higher parenting stress and negative perinatal experiences, which were related to less sensitive parenting (Feldman et al., 2011; Prevost et al., 2014). The current study aimed to answer

the question of how OT levels during late pregnancy predicted birthing parents' parenting and their neural responses to infant cry postnatally.

Methods: 61 pregnant individuals provided saliva OT samples during their late pregnancies. The samples were collected 40 minutes and 78 minutes after visit start time. Log-transformations of means of OT levels were conducted to improve normality. After parity, birthing-parents (M±SD age=30.07±5.47 years, M±SD postpartum days=35.67±17.38) completed the infant cry task listening to different sounds in a Magnetic Resonance Imaging (MRI) scanner. The infant cry task was consisted of 2 functional runs and 4 task conditions (own infant cry, own infant cry matched noise, control infant cry, and control infant matched noise) of 20-second stimulus blocks (Swain et al., 2008). Each run contained 5 trials per condition separated by fixations with randomized duration (M=10s, range=8-12s). At around the same time postpartum, 10-minute videos was recorded during natural parent-infant interactions; trained researchers coded the interaction using the Emotional Availability scale (EA, Biringen, 2008). The EA scale yielded 4 adult subscales including Sensitivity, Structuring, Non-intrusiveness, and Non-hostility. Preprocessing of functional MRI data was conducted using fMRI prep (version 22.0.02, (Esteban et al., 2019) and Analysis of Functional Neuroimages software (AFNI, version 23.0.02, (Cox, 1996). At group level, a whole-brain linear mixed effect model was conducted using 3dLME in AFNI (R. W. Cox, 1996). Between-subject log-transformed OT and within-subject variables (sound: cry vs. noise; identity: own vs. control) were entered in the model, controlling for postpartum months and sample collection time. Significant voxels within the whole brain were corrected for multiple comparisons with a cluster extended threshold of k≥16 with a height threshold of p<.001, equivalent to a whole brain corrected false positive probability of p<.05. This threshold was calculated with the 3dClustSim package with spatial autocorrelation function (ACF) option.

Results: We observed significant negative relationship between prenatal OT level and parental sensitivity controlling for sample collection time (β=-.76, p<.05). fMRI results indicated that higher prenatal OT levels were associated with dampened neural response to infant cry in the right Inferior Frontal gyrus (BA47; x,y,z=30,28,-7; k=25; r=-.32; p<.05; Figure 1) and the right Precentral gyrus (BA9; x,y,z=39, 3, 39;k=24; r=-.38; p<.01; Figure 2). However, prenatal OT was not related to postnatal brain activations to white noise. Exploratory analysis revealed that higher brain activation to infant cry in the right Inferior Frontal Gyrus (r(59)=.35, p<.05), and the right Prefrontal Gyrus (r(59)=.32, p<.05) was related to higher parental sensitivity.

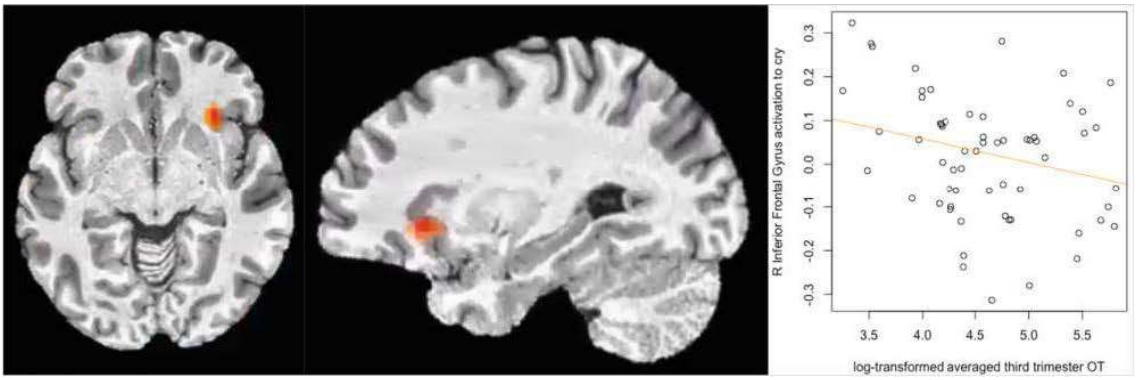

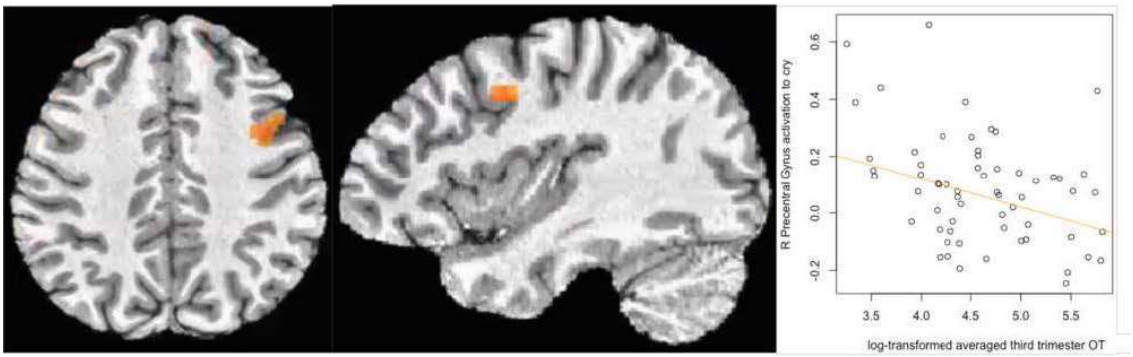

Conclusions: Our results implicated that the neural plasticity of the caregiving network during pregnancy and early postpartum was related to the function of the neuroendocrine OT system. Higher OT during late pregnancy predicted birthing-parents' dampened neural response to infant cry. These dampened responses were further related to lower parental sensitivity during a parent-infant interaction. OT might be an indicator of stress during the perinatal period in the current sample.

References

1. Biringen, Z. (2008). The Emotional Availability (EA) scales and EA zones evaluation: Infancy/early childhood version; middle childhood/ youth versions; therapist/interventionist/professional manual; couple relationship manual (4th ed.).
2. Cox, R. W. (1996). AFNI: Software for Analysis and Visualization of Functional Magnetic Resonance Neuroimages. Computers and Biomedical Research, 29(3), 162–173. https://doi.org/10.1006/cbmr.1996.0014
3. Esteban, O., Markiewicz, C. J., Blair, R. W., Moodie, C. A., Isik, A. I., Erramuzpe, A., Kent, J. D., Goncalves, M., DuPre, E., Snyder, M., Oya, H., Ghosh, S. S., Wright, J., Durnez, J., Poldrack, R. A., & Gorgolewski, K. J. (2019). fMRIPrep: A robust preprocessing pipeline for functional MRI. Nature Methods, 16(1), 111–116. https://doi.org/10.1038/s41592-018-0235-4
4. Feldman, R., Gordon, I., & Zagoory-Sharon, O. (2011). Maternal and paternal plasma, salivary, and urinary oxytocin and parent–infant synchrony: Considering stress and affiliation components of human bonding. Developmental Science, 14(4), 752–761. https://doi.org/10.1111/j.1467-7687.2010.01021.x
5. Levine, A., Zagoory-Sharon, O., Feldman, R., & Weller, A. (2007). Oxytocin during pregnancy and early postpartum: Individual patterns and maternal-fetal attachment. Peptides, 28(6), 1162–1169. https://doi.org/10.1016/j.peptides.2007.04.016
6. Prevost, M., Zelkowitz, P., Tulandi, T., Hayton, B., Feeley, N., Carter, C. S., Joseph, L., Pournajafi-Nazarloo, H., Yong Ping, E., Abenhaim, H., & Gold, I. (2014). Oxytocin in Pregnancy and the Postpartum: Relations to Labor and Its Management. Frontiers in Public Health, 2. https://doi.org/10.3389/fpubh.2014.00001
7. Riem, M. M. E., Bakermans-Kranenburg, M. J., Pieper, S., Tops, M., Boksem, M. A. S., Vermeiren, R. R. J. M., van IJzendoorn, M. H., & Rombouts, S. A. R. B. (2011). Oxytocin Modulates Amygdala, Insula, and Inferior Frontal Gyrus Responses to Infant Crying: A Randomized Controlled Trial. Biological Psychiatry, 70(3), 291–297. https://doi.org/10.1016/j.biopsych.2011.02.006
8. Ross, H. E., & Young, L. J. (2009). Oxytocin and the neural mechanisms regulating social cognition and affiliative behavior. Frontiers in Neuroendocrinology, 30(4), 534–547. https://doi.org/10.1016/j.yfrne.2009.05.004
9. Swain, J. E., Tasgin, E., Mayes, L. C., Feldman, R., Constable, R. T., & Leckman, J. F. (2008). Maternal brain response to own baby-cry is affected by cesarean section delivery. Journal of Child Psychology and Psychiatry, 49(10), 1042–1052.

Poster No 761

Decoding laughter: MEG insights on auditory perception of volitional and spontaneous vocalizations

Clara El Khantour[1], Anne-Lise Saive[2], Yann Harel[1], Jens Kreitewolf[3], Arthur Dehgan[1], Sophie Scott[4], Guillaume Dumas[5], Karim Jerbi[6]

[1]University of Montreal, Montreal, Quebec, [2]Institut de recherche Paul Bocuse, Écully, Auvergne-Rhône-Alpes, [3]McGill University, Montreal, Quebec, [4]University College London, London, London, [5]CHUSJ Research Center, University of Montreal, Montreal, Quebec, [6]Computational and Cognitive Neuroscience Lab, Department of Psychology, University of Montreal, Montreal, Quebec

Introduction: Laughter is a non-verbal emotional vocalization we use in our everyday life. Its complexe nuances allows it to serve various purposes including spontaneous emotional expression (spontaneous laughter) and communication during social interaction (voluntary laughter) (Scott et al., 2014). Using fMRI, distinct brain regions have been found to be involved during the perception of distinct types of laughter (McGettigan et al., 2015): Regions typically involved in auditory processing are more activated when hearing spontaneous laughter while greater activations were found in regions implicated in mentalizing in the case of volitional laughter. EEG investigations have reported differences in the N100 and P200 ERP components between volitional and spontaneous laughter (Kosilo et al., 2021). Another study has identified differences also in later stages (Late Positive Component; Conde et al., 2022). Although encouraging, there are still many open questions when it comes to the neural processing patterns of this vocalization. This current project investigates the neural correlates of the perception and discrimination of laughter in healthy individuals through the application of magnetoencephalography (MEG).

Methods: The brain activity of 32 healthy subjects was recorded in MEG (CTF-MEG, 270 channels) during two tasks, a passive listening condition and an active task consisting of classifying the type of laughter heard. The MEG data were preprocessed using the MNE-BIDS-PIPELINE (Gramfort et al., 2014) on 27 subjects (5 subjects rejected due to technical problems during recording). In total, 3 stimulus categories were employed: laughter stimuli, comprising 25 volitional and 25 spontaneous instances, and two sets of control stimuli. The duration of the stimuli was between 1.5 and 3 sec. Evoked related potentials (ERPs) were obtained by averaging epochs (-0.5s to 1.5s) for each task and conditions respectively. We applied a non-parametric cluster-level paired t-test for spatio-temporal data to compare the ERPs between our conditions.

Results: At the behavioral level, the discrimination rate of laughter types was 74.05%. Reaction times were faster for correct responses compared to incorrect response. No significant differences were found for discrimination rate nor the reaction between volition and spontaneous laughter. As for the ERPs, the comparison between social and spontaneous laughter revealed 2 clusters in both tasks. In the passive task, one cluster was found in the right frontal channels (786-868ms) and another one in the left parietal area (801-833ms). For the active task, a similar cluster in the right frontal sensors (898-956ms) was detected as well as one in the right occipital (772-829ms).

Conclusions: Taken together, our findings suggest that discriminating spontaneous and voluntary laughter may be mediated by a component in the late stage of auditory integration. This implies that late processes play a role in distinguishing between volitional and spontaneous laughter, complementing prior research on the topic (Conde et al., 2022) that underscores the necessity of high-level cognitive processes in the discrimination of laughter. Ongoing work involves determining the spatial and spectral dynamics of the neuro-magnetic processes at play during laughter perception

References

1. Conde, T., A. I. Correia, M. S. Roberto, S. K. Scott, C. F. Lima and A. P. Pinheiro (2022). "The time course of emotional authenticity detection in nonverbal vocalizations." Cortex 151: 116-132.
2. Gramfort, A., M. Luessi, E. Larson, D. A. Engemann, D. Strohmeier, C. Brodbeck, L. Parkkonen and M. S. Hämäläinen (2014). "MNE software for processing MEG and EEG data." Neuroimage 86: 446-460.
3. Kosilo, M., M. Costa, H. E. Nuttall, H. Ferreira, S. Scott, S. Menéres, J. Pestana, R. Jerónimo and D. Prata (2021). "The neural basis of authenticity recognition in laughter and crying." Scientific Reports 11(1): 23750.
4. McGettigan, C., E. Walsh, R. Jessop, Z. K. Agnew, D. A. Sauter, J. E. Warren and S. K. Scott (2015). "Individual differences in laughter perception reveal roles for mentalizing and sensorimotor systems in the evaluation of emotional authenticity." Cereb Cortex 25(1): 246-257.
5. Scott, S. K., N. Lavan, S. Chen and C. McGettigan (2014). "The social life of laughter." Trends Cogn Sci 18(12): 618-620.
6. Sivasathiaseelan, H., C. R. Marshall, E. Benhamou, J. E. P. van Leeuwen, R. L. Bond, L. L. Russell, C. Greaves, K. M. Moore, C. J. D. Hardy, C. Frost, J. D. Rohrer, S. K. Scott and J. D. Warren (2021). "Laughter as a paradigm of socio-emotional signal processing in dementia." Cortex 142: 186-203.

Poster No 762

Training Increases Reward Learning and Decreases Depression Symptoms Across Repeated Sessions

Shivani Goyal[1,2], John Wang[1], Vanessa Brown[3], Jacob Lee[1], Nanda Sankarasubramanian[1], Brooks Casas[1,2], Pearl Chiu[1,2]

[1]Fralin Biomedical Research Institute at Virginia Tech Carilion, Roanoke, VA, [2]Department of Psychology, Virginia Tech, Blacksburg, VA, [3]Department of Psychiatry, University of Pittsburg, Pittsburg, PA

Introduction: Disrupted neural and behavioral indices of reward learning have been suggested to play a mechanistic role in depression[1,2]. If this mechanism were supported, we would expect improving reward learning to decrease depression symptoms across time. Here, we address this question with a longitudinal design, investigating if repeated sessions of behavioral training change reward learning and decrease depression symptoms across time.

Methods: Participants: We recruited 929 online participants from Amazon's Mechanical Turk platform and 40 in-person participants from regions of southwest Virginia to complete our longitudinal study. Behavioral Training: Participants completed a probabilistic reward learning task with repeated queries about a feature of the task environment (learning queries; Figure 1a) or control queries. Learning queries trained participants on one of four computational-based learning targets known to affect reinforcement learning (Figure 1b). For up to 12 total study visits, participants repeated the task and completed a depression symptom questionnaire two to three times per week. Depression questionnaire scores at baseline were used to split participants into no-depression and depression subgroups, where individuals in the depression subgroup met threshold for at least mild depression severity. Computational Modeling and Symptom Analysis: A Q-learning model was fit to behavioral responses using hierarchical Bayesian estimation to provide estimates of reward sensitivity and learning rate for each participant on each visit. Reward sensitivity captured participants' value dissociation between high versus low outcome values, while learning rate informed how much participants learned from previously experienced outcomes. Mixed linear models assessed relationships between learning parameters, depression symptoms, and study progression. fMRI Analysis: Participants that completed the study in-person underwent functional magnetic resonance imaging in a 3T Siemens Prisma Fit on the first and last study visits. Preprocessing of echo-planar images included slice timing correction, realignment, co-registration to a T1 structural image, normalization, and smoothing with a 6x6x6 mm kernel in SPM12. On the individual level, hemodynamic responses to outcome events were assessed. General linear models were used to perform individual and group level analyses.

Results: Across time, learning queries increased reward sensitivities in no-depression participants ($\beta = 0.036$, $p =< 0.001$, 95% CI (0.022, 0.049)). In contrast, control queries did not change reward sensitivities in no-depression participants across time (($\beta = 0.016$, $p = 0.303$, 95% CI (-0.015, 0.048)). Of the learning queries, those targeting value comparison processes improved depression symptoms ($\beta = -0.509$, $p = 0.015$, 95% CI (-0.912, -0.106)) and increased reward sensitivities across time ($\beta = 0.052$, $p =< 0.001$, 95% CI (0.030, 0.075)) in depression participants. Increased reward sensitivities related to decreased depression symptoms across time in these participants ($\beta = -2.905$, $p = 0.002$, 95% CI (-4.75, -1.114)). In the neuroimaging sample, regardless of time, individuals receiving value comparison queries showed increased outcome activity in the left nucleus accumbens, medial orbitofrontal cortex, and right caudate compared to those who received control queries (Figure 2).

Conclusions: Behavioral reward learning was improved through repeated sessions of targeted training for participants with a range of clinical symptoms. Improved behavioral reward learning was associated with improved clinical symptoms with time. Neural results showed increased outcome activity in reward circuitry brain regions with targeted training. These results support disrupted reward learning as a mechanism in depression and suggest the potential of behavioral training to target neurobehavioral deficits in reward learning and evoke symptom change.

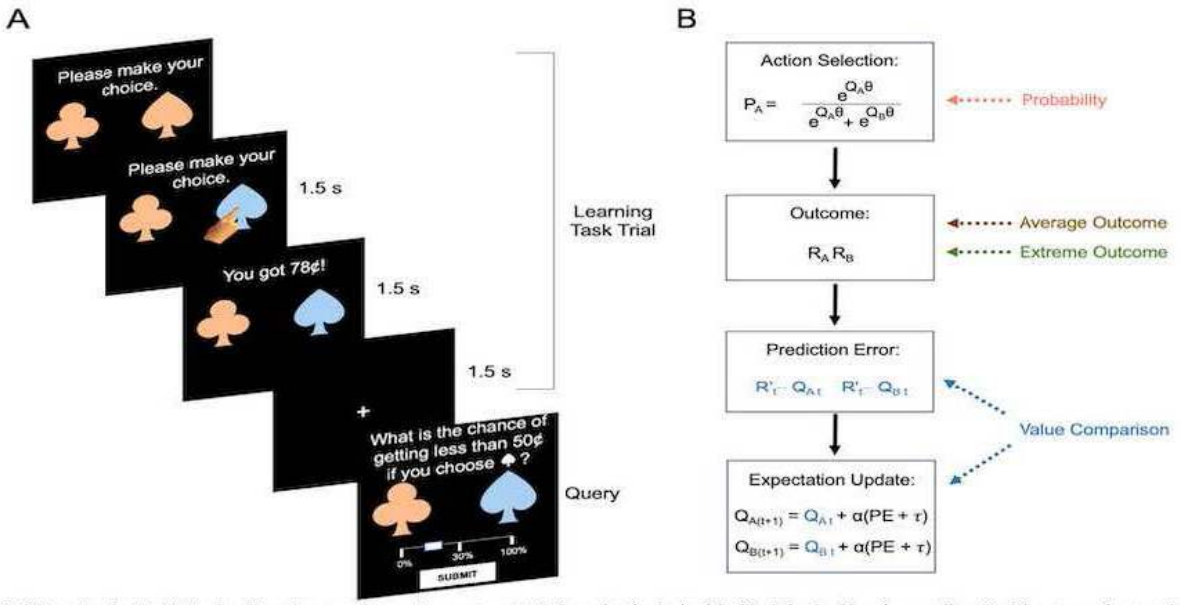

Figure 1. Schematic of guided behavioral learning paradigm and query targets. A) Example of a single trial of the behavioral learning paradigm. Participants were instructed to select one of two presented stimulus options. Upon selection, their selected choice turned blue for 1.5 seconds, and the outcome value was presented for 1.5 seconds. Participants were queried about a specific task component (e.g., the chance of getting less than $0.50 for the last chosen option) every third trial. Participants in a given query arm were presented with the same query for all study visits.
B) Learning targets for query arms. Learning query arms targeted one of four learning components commonly associated with reinforcement learning. Probability queries targeted action selection, while average outcome and extreme outcome queries targeted outcome components. Average and extreme outcome queries differed by directing participant attention to either the average outcome for a stimulus (average outcome queries) or to the highest or lowest outcome for a stimulus (extreme outcome queries). Queries targeting value comparison focused on comparison processes, shown in blue, involved in the prediction error and expectation update processes.

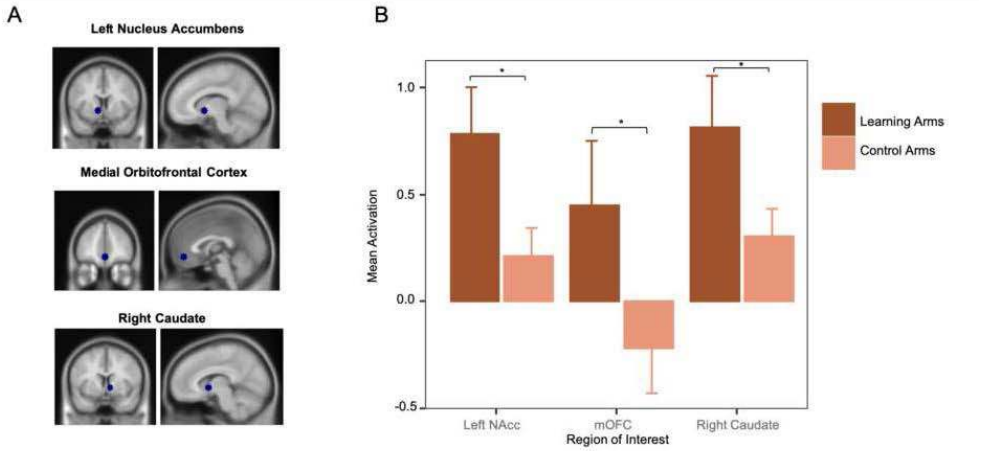

Figure 2. Neural activity associated with outcome events for learning and control arms. A) Regions of interest (ROIs) for outcome events of the probabilistic reward learning task. ROIs were selected from peak coordinates from meta-analyses of blood-oxygen level dependent responses for outcome events in reward learning tasks [3,4]. B) Comparison of mean ROI values across visits for participants in learning arms vs. control arms. Bars indicate standard error. *p<0.05.

References

1. Halahakoon, D. C., Kieslich, K., O'Driscoll, C., Nair, A., Lewis, G., & Roiser, J. P. (2020), 'Reward-Processing Behavior in Depressed Participants Relative to Healthy Volunteers: A Systematic Review and Meta-analysis', JAMA Psychiatry, vol. 77, no. 12, pp. 1286–1295.
2. Pike, A. C., & Robinson, O. J. (2022), 'Reinforcement Learning in Patients With Mood and Anxiety Disorders vs Control Individuals: A Systematic Review and Meta-analysis', JAMA Psychiatry, vol. 79, no. 4, pp. 313–322.
3. Liu, X., Hairston, J., Schrier, M., & Fan, J. (2011), 'Common and distinct networks underlying reward valence and processing stages: a meta-analysis of functional neuroimaging studies', Neuroscience and biobehavioral reviews, vol. 35, no. 5, pp. 1219–1236.
4. Diekhof, E. K., Kaps, L., Falkai, P., & Gruber, O. (2012), 'The role of the human ventral striatum and the medial orbitofrontal cortex in the representation of reward magnitude - an activation likelihood estimation meta-analysis of neuroimaging studies of passive reward expectancy and outcome processing', Neuropsychologia, vol. 50, no.7, pp. 1252–1266.

Poster No 763

Neurocomputational Dynamics of Pain Value-Based Decision Making

Léane Beaulieu-Laliberté[1], Mathieu Roy[2], Michel-Pierre Coll[1]

[1]Laval University, Québec, Quebec, [2]McGill University, Montreal, Quebec

Introduction: While pain is generally to be avoided, there are times when it is necessary to endure pain to achieve a goal, a reward or a more valuable outcome. Assigning too high a value to pain can lead to avoiding beneficial experiences (Crombez et al., 2012), while completely ignoring pain lead to in reckless behaviours. In a recent study, we used functional magnetic resonance imaging to understand how the brain independently represents the value of potential future pain in an economic context (Coll et al., 2022). However, the techniques used in this study don't allow for determining how the representation of pain evolves over time and is dynamically compared to potential rewards. Identifying the dynamic aspects of brain activity during decision-making in the presence of pain is crucial for a better understanding of the mechanisms involved in this process. Here, we aimed to investigate how the brain dynamically represents the prospect of pain in economic contexts and how this representation is integrated with external rewards to guide behaviour.

Methods: Fifty healthy adults (27 females, mean age = 24.72 +/- 4.14) took part in an EEG experiment (64 channels, Brain Vision Acticap). In the first phase, participants passively observed cues indicating that they would receive one of five levels of pain (from threshold to tolerance) or one of five monetary rewards (1-5 $CAD) before receiving a painful electric shock or feedback indicating monetary gain. This passive phase was used to measure brain activity during the anticipation of pain and monetary reward in isolation (Figure 1A). In the second phase (Figure 1B), participants had to decide at each trial to accept or reject offers combining different levels of pain and money. If they accepted the offer, they immediately received a painful stimulation and the amount of money was added to their potential earnings for the task. If they refused the offer, they did not receive any pain or opportunity to receive the money. We preprocessed EEG data using a standard approach, including bandpass filtering, removal of bad channels, artifactual independent components and trials with high amplitude jumps. We first performed event-related potential analyses to confirm differential responses to cues indicating different levels of upcoming pain and money in the passive phase. We then followed with decoding analyses in sensor space that were used to create classifiers capable of discriminating between the anticipation of pain and money during the passive phase for each participant. We then applied these classifiers to EEG activity during decisions to attempt to predict whether participants would accept or reject offers.

Results: Behavioural results replicate previous studies using a similar approach (Coll et al., 2022, Slimani et al., 2022) and show that participants' decisions and deliberation times were significantly impacted by both pain and money levels offered (Figure 1C). Event-related potential analyses confirmed that cues indicating different levels of pain and money led to a differential response emerging around 400 ms after cue onset (Figure 2A and 2B). EEG decoding analyses in sensor space showed that classifiers trained to discriminate cues indicating upcoming pain or money could accurately classify pain and money cues in the passive phase (accuracy: 0.69 +/- 0.1, $p < 0.001$). These classifiers were also able to predict participants' decisions to approach or avoid pain in exchange for a reward (balanced accuracy: 0.54 +/- 0.09, $p = 0.03$), suggesting that the representation of pain and rewards are involved in the decision to approach and avoid pain.

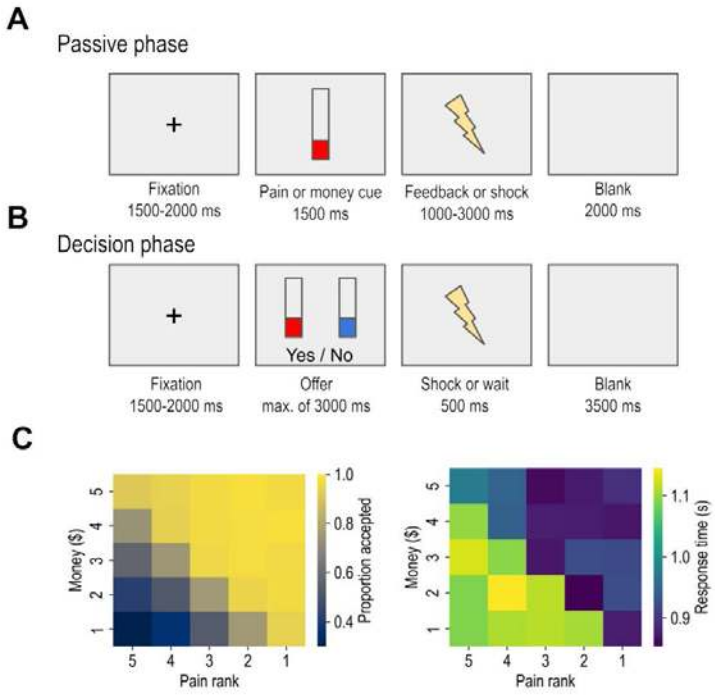

Figure 1. (A) Schematic illustration of an experimental trial for the passive phase and **(B)** the decision phase of the experimental paradigm. **(C)** Behavioural results showing the average proportion of offers accepted (left) and the response time (right) during the decision phase for each combination of pain levels and monetary amount.

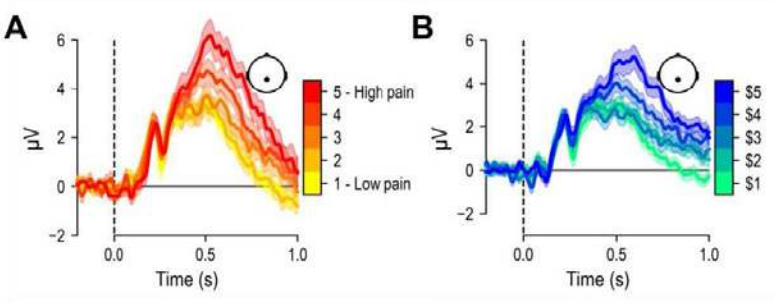

Figure 2. (A) Event-related potentials in response to cues indicating different levels of upcoming pain (left) or **(B)** monetary reward (right) at location CPz. The shading shows +/- 1 standard error of the mean.

Conclusions: Our results show that the representation of pain and reward anticipation can be decoded from EEG data and used to predict choices during approach/avoidance decisions. This study will contribute to our understanding of the brain mechanisms involved in decision-making about potential future pain and to our comprehension of disorders marked by inadequate avoidance of pain.

References

1. Coll, M. P. & al. (2022), 'The neural signature of the decision value of future pain', Proceedings of the National Academy of Sciences of the United States of America, vol.119, no. 23, e2119931119.
2. Crombez, G. & al. (2012), 'Fear-avoidance model of chronic pain: the next generation', Clinical Journal of Pain. vol. 28, no.6, pp. 475-83.
3. Slimani, H. & al. (2022), 'The aversive value of pain in human decision-making', European journal of pain, vol. 26, no.3, pp 668–679.

Poster No 764

Enhanced Activation in the Left Anterior Insula Induced by Reward Cues

Yasunori Kotani[1], Yoshimi Ohgami[1], Hajime Kageyama[2], Nobukiyo Yoshida[3], Hiroyuki Akai[2], Akira Kunimatsu[4], Shigeru Kiryu[5], Yusuke Inoue[6]

[1]Tokyo Institute of Technology, Meguro, Tokyo, [2]The University of Tokyo, Minato, Tokyo, [3]Niigata University of Health and Welfare, Niigata, Niigata, [4]International University of Health and Welfare, Minato, Tokyo, [5]International University of Health and Welfare, Narita, Chiba, [6]Kitasato University, Sagamihara, Kanagawa

Introduction: The stimulus-preceding negativity (SPN) is an event-related potential reflecting anticipation of a salient stimulus. Previous studies propose the anterior insula (aINS) as a source of the SPN. A shared characteristic of the SPN and aINS is the right hemisphere dominance. However, some reports indicate that the right hemisphere dominance of the SPN diminishes when recorded before a reward-related stimulus due to increased left hemisphere activity triggered by reward (Ohgami et al., 2006). If the aINS is the source of the SPN, activation in the left aINS should be increased by a reward-related stimulus, and the aINS should exhibit no hemisphere difference. In the present fMRI study, we investigated whether the right hemisphere dominance of the aINS would be diminished by the presentation of a reward-related stimulus. Additionally, we manipulated the content of the reward-related stimulus (reward cue and reward outcome). The reward cue informed participants about the possibility of receiving a monetary reward, initiating the reward anticipation process. The reward outcome stimulus provided information about the actual amount of monetary reward received, triggering the reward consumption process. There is a possibility that the right hemisphere dominance of the aINS could change between the cue and the outcome because the two stimuli elicit distinct brain activation patterns (Zen et al., 2022). We assume that the right hemisphere dominance of the aINS could be diminished by the reward cue because the aINS is involved in anticipation of salient stimuli (Ohgami et al., 2023).

Methods: Participants included 31 healthy adults. They performed a time estimation task, where they were instructed to press a button when they believed that a specified time (3, 5, or 7 seconds) had passed. Following the button press, a reward cue stimulus (Cue) was presented, indicating whether they could receive a monetary reward (RW condition) or not (NR condition) in the current trial. A few seconds after the Cue, a reward outcome stimulus (Outcome) displayed the amount of reward received (100 JPY in the RW and 0 JPY in the NR). Regressors were set at onsets of cue and outcome stimuli, and four fMRI images at the Cue and the Outcome in the two conditions were generated (RW/Cue, NR/Cue, RW/Outcome, and NR/Outcome). Beta values were extracted from the left and right aINS, and the values in the four images were separately subjected to repeated-measures analyses of variance (ANOVA) with Hemisphere (left/right) as a factor to assess the right hemisphere dominance of the aINS.

Results: Significant activations were observed in the bilateral aINS in the RW/Cue, NR/Cue, and RW/Outcome. In the NR/Outcome, only the activation in the right aINS reached significance. ANOVAs indicated no right hemisphere dominance in the RW/Cue, while significant right hemisphere dominance was observed in the other three conditions (NR/Cue, RW/Outcome, and NR/Outcome). We also compared the beta value in the left aINS between the RW/Cue and NR/Cue. The analysis revealed that the left aINS in the RW/Cue showed greater activation than in the NR/Cue.

Conclusions: The approach-withdrawal theory (Davidson & Irwin, 1999) suggests that positive information is predominantly processed in the left hemisphere, while negative information is predominantly processed in the right hemisphere. This could explain the increased activation in the left aINS in response to reward information. The present study demonstrates that the activation in the left aINS was heightened by the reward cue stimulus, which provides information about a potential future monetary reward. The aINS functions as a gatekeeper of information flow, and this region initiates activation before salient stimuli (Ohgami et al., 2023). The preparatory activation in the aINS may explain why increased activation in the left aINS was observed at the reward anticipation stage rather than at the reward consumption stage.

References

1. Davidson, R. J., & Irwin, W., The functional neuroanatomy of emotion and affective style. Trends in Cognitive Sciences, 3, 11–21, 1999
2. Yasunori Kotani, Yoshimi Ohgami, Takayuki Ishiwata, Jun-ichiro Arai, Shigeru Kiryu, and Yusuke Inoue, Source analysis of stimulus-preceding negativity constrained by functional magnetic resonance imaging, Biological Psychology, 111, 53-64, 2015
3. Yoshimi Ohgami, Yasunori Kotani, Tetsuji Tsukamoto, Kazufumi Omura, Yusuke Inoue, Yasutsugu Aihara, and Minoru Nakayama, Effects of monetary reward and punishment on stimulus-preceding negativity, Psychophysiology, 43, 227-236, 2006
4. Yoshimi Ohgami, Yasunori Kotani, Nobukiyo Yoshida, Hiroyuki Akai, Akira Kunimatsu, Shigeru Kiryu, Yusuke Inoue, The contralateral effects of anticipated stimuli on brain activity measured by ERP and fMRI, Psychophysiology, 60(3), e14189, 2023
5. Zeng, J., Yan, J., Cao, H., Su, Y., Song, Y., Luo, Y., & Yang, X. (2022). Neural substrates of reward anticipation and outcome in schizophrenia: a meta-analysis of fMRI findings in the monetary incentive delay task. Translational psychiatry, 12(1), 448. https://doi.org/10.1038/s41398-022-02201-8

Poster No 765

Saliency of Instructive Stimulus Affects the Activation of the Anterior Insula

Yoshimi Ohgami[1], Yasunori Kotani[1], Hajime Kageyama[2], Nobukiyo Yoshida[3], Hiroyuki Akai[2], Shigeru Kiryu[4], Yusuke Inoue[5]

[1]Tokyo Institute of Technology, Meguro, Tokyo, [2]The University of Tokyo, Minato, Tokyo, [3]Niigata University of Health and Welfare, Niigata, Niigata, [4]International University of Health and Welfare, Narita, Chiba, [5]Kitasato University, Sagamihara, Kanagawa

Introduction: The stimulus-preceding negativity (SPN) is an event-related potential that reflects anticipatory attention. Many studies have suggested that the anterior insula (aINS) could be a source of the SPN. One of the features of the SPN is that it can be recorded before a feedback stimulus conveying information about the correctness of the response, while it cannot be recorded before an instruction stimulus that conveys information about how to perform the task. A possible explanation for the lack of SPN before an instruction stimulus is the saliency theory (Kotani et al., 2017). This theory posits that instruction stimuli are less salient compared to feedback stimuli, and reduced saliency could lead to the absence of SPN. If the saliency theory is correct, the aINS that is a core hub of the salience network should not be activated before instruction stimuli, and the region should be activated when the saliency of instruction stimulus is enhanced. In the present fMRI study, we manipulated the saliency of the instruction stimulus by adding reward information (reward and no-reward conditions) to investigate if the aINS activation was affected by the saliency of instruction stimuli.

Methods: Participants were 26 healthy adults who performed a time estimation task. In the task, there were two trial types: an instruction (Inst) trial and a feedback (FB) trial. The Inst trial was always followed by the FB trial. In the Inst trial, the visual stimulus showed an instruction about the second that should be estimated in the following FB trial (3, 5, or 7 seconds) as well as the amount of possible reward for the following feedback trial (reward condition: 10, 100, or 1000; no-reward condition: 0 Japanese yen). In the subsequent FB trial, the FB stimulus was presented after the button press with time estimate to inform participants about the correctness of their time estimate (the button press was too early, correct, or too late) and the amount of reward. In the reward condition (RW), participants received the reward for a correct response, and they did not receive any reward in the no-reward condition (NR). The experiment was conducted inside a 3-Tesla magnetic resonance scanner, and four contrast images: (1) Inst/RW, (2) Inst/NR, (3) FB/RW, and (4) FB/NR were constructed at the group level. Beta values reflecting the level of activation in the left and right aINS were extracted from the four contrast images, and these values were subjected to a repeated-measures analysis of variance (ANOVA) with hemisphere (left/right), reward (reward/no-reward), and stimulus (instruction/feedback) as factors. Subjective ratings on the saliency of the instruction stimuli were also collected to estimate the saliency of Inst stimuli.

Results: Significant activations in the left and right aINS were found in three of the four contrast images, except for the Inst/NR contrast. The ANOVA on beta values of the aINS revealed that the beta values in the left aINS were increased in the RW than in the NR for instruction and feedback stimuli. Regarding the right hemisphere dominance before the instruction stimulus, the beta value of the aINS showed right hemisphere dominance in the Inst/RW, while there was no hemisphere difference in the Inst/NR. The subjective rating on instruction stimuli showed that the saliency of Inst/RW was larger than that in the Inst/NR.

Conclusions: As we hypothesized, the aINS was not activated before instruction stimuli. On the other hand, the aINS was activated when the saliency of instruction stimulus was increased. Previous studies show that the salience network of the brain exhibits right hemisphere dominance. In the present study, beta values in the aINS in the Inst/RW also showed right hemisphere dominance. These results support the saliency theory of SPN, and suggest that the saliency of the stimuli could affect the activation of the aINS that is a source of the SPN.

References

1. Yasunori Kotani, Yoshimi Ohgami, Takayuki Ishiwata, Jun-ichiro Arai, Shigeru Kiryu, and Yusuke Inoue, Source analysis of stimulus-preceding negativity constrained by functional magnetic resonance imaging, Biological Psychology, 111, 53-64, 2015
2. Yoshimi Ohgami, Yasunori Kotani, Nobukiyo Yoshida, Hiroyuki Akai, Akira Kunimatsu, Shigeru Kiryu, Yusuke Inoue, The contralateral effects of anticipated stimuli on brain activity measured by ERP and fMRI, Psychophysiology, 60(3), e14189, 2023
3. Yoshimi Ohgami, Yasunori Kotani, Tetsuji Tsukamoto, Kazufumi Omura, Yusuke Inoue, Yasutsugu Aihara, and Minoru Nakayama, Effects of monetary reward and punishment on stimulus-preceding negativity, Psychophysiology, 43, 227-236, 2006

Poster No 766

Anterior Insula Processes a Subjective Salience Prediction Error

Jae-Chang Kim[1], Lydia Hellrung[1], Stephan Nebe[1], Philippe Tobler[1]

[1]*University of Zurich, Zurich Switzerland*

Introduction: The process of learning is not solely affected by the degree to which outcomes are better or worse than predicted (signed value prediction error; Rescorla and Wagner, 1972; Sutton and Barto, 1998), but also by the level of surprise they elicit, irrespective of their direction (unsigned value prediction error; Mackintosh, 1975; Pearce and Hall, 1980). Surprise is salient and the insula has been associated with salience processing. However, it remains unclear how exactly the insula processes a formal salience prediction error. We studied the insulas role in processing salience prediction errors using a novel Pavlovian conditioning paradigm involving appetitive, aversive, and neutral stimuli as reinforcers.

Methods: We studied 41 participants (22.4 ± 0.43 years, mean ± SEM; 19 women) across three lab sessions, including a taste screening session and two main task sessions within an MRI scanner. During screening, we matched two appetitive and two aversive tastes in unsigned subjective value. Distilled water with the main ionic components of saliva served as neutral liquid. Participants evaluated these liquids by bidding (Becker-DeGroot-Marschak auction; Becker, DeGroot, & Marschak, 1964) and rating (general labelled magnitude scale; Barrett & Simmons, 2015; Bartoshuk et al., 2004). In the main task, we used Pavlovian associations (pre-trained during the screening session; Figure a) between visual cues and one of the three outcomes (appetitive, aversive, or neutral). Outcome probability varied across cues (p=0, 0.5, 1). We estimated general linear models that assessed both objective (defined by cues and outcomes) and subjective (based on individual cue and outcome ratings) salience prediction errors. Furthermore, we differentiated the insula's response to appetitive, aversive, and neutral modalities, investigating whether subjective salience prediction error activity reflected general processing of surprise or was specific to outcome kind.

Results: A non-parametric analysis revealed a significant objective salience prediction error signal for valenced outcomes (i.e., appetitive and aversive; Figure b) but not for non-valenced liquids (i.e., neutral) within the insula at the time of the outcome ($p<0.05$, FWE-whole brain voxel-level corrected). A parametric approach replicated these results and revealed both objective and subjective salience prediction error signals in the anterior insula (Figure c). Direct comparisons showed a significantly stronger association of insula activity with subjective than objective salience prediction errors at the time of the outcome ($p<0.05$, FWE-whole brain voxel-level corrected; Figure c, top, right side). Moreover, subjective salience prediction errors activated the anterior insula also at the time of the cue (Figure c, bottom, left side). As one would expect based on discounting, this signal was significantly weaker than the signal at the time of the outcome (Figure c, bottom, right side). Finally, separate analyses for the different modalities (i.e., appetitive, aversive, neutral, and no outcome) revealed subjective salience prediction error signals for all modalities in the anterior insula at the time of the outcome ($p<0.05$, FWE-whole brain voxel-level corrected; Figure d, top). By contrast, at the time of the cue, a subjective salience prediction error occurred only for cues predicting aversive outcomes (Figure d, bottom), compatible with weaker discounting of aversive than appetitive or neutral outcomes.

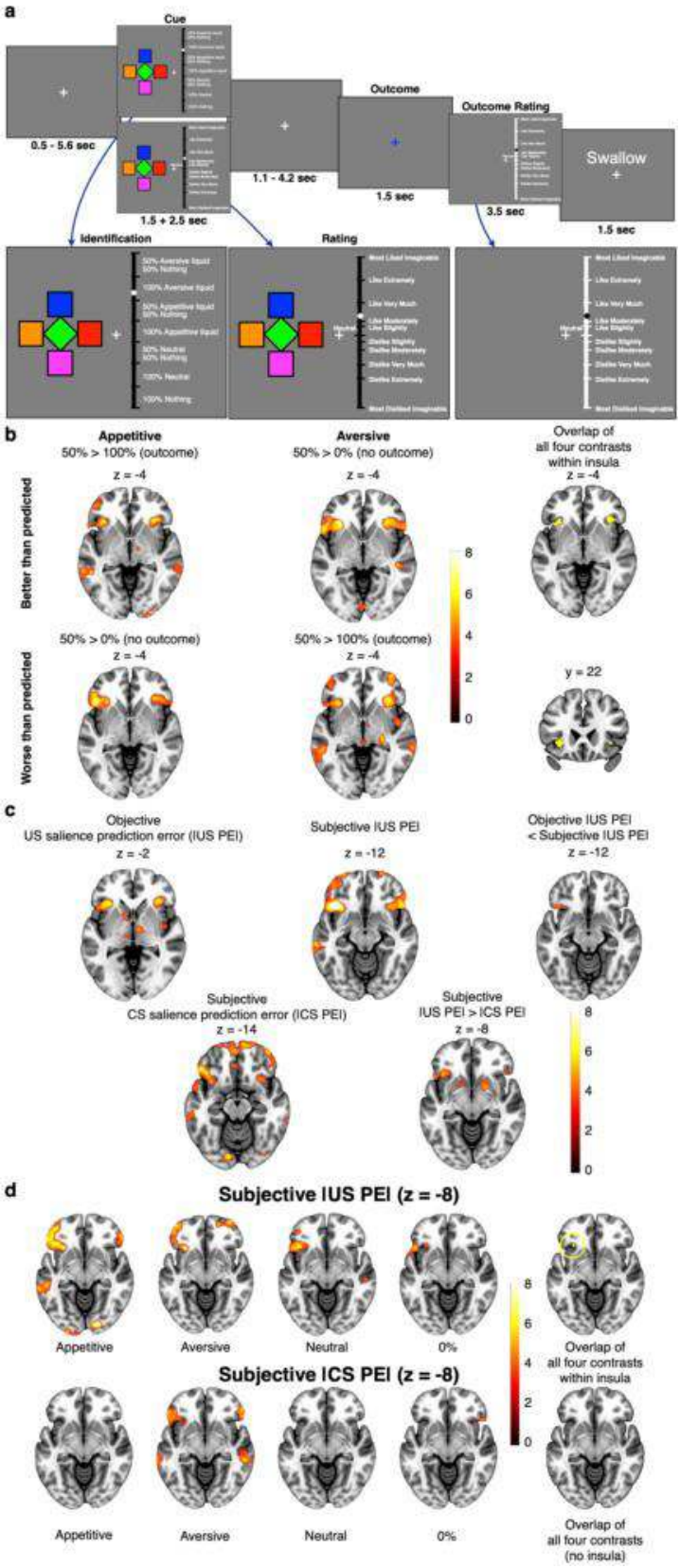

Conclusions: Our findings demonstrate that the insula actively processes subjective salience prediction errors. These subjective salience prediction error signals appear to be more modality-general at the time of the outcome than at the time of the cue. By extension, the anterior insula appears to compute salience prediction error for aversive stimuli with a different time constant than for non-aversive stimuli, which could explain why some studies view it as a region primarily interested in the aversive domain.

References

1. Recorla, R. A., & Wagner, A. R. (1972). A Theory of Pavlovian Conditioning: Variations in the Effectiveness of Reinforcement and Nonreinforcement. In A. H. Black, & W. F. Prokasy (Eds.), Classical Conditioning II: Current Research and Theory (pp. 64-99). New York: Appleton- Century-Crofts.
2. Sutton, R. S., & Barto, A. G. (1998). Reinforcement Learning: An introduction.
3. Cambridge, MA: MIT Press.
4. Mackintosh, N. J. (1975). A theory of attention: Variations in the associability of stimuli with reinforcement. Psychological Review, 82(4), 276-298.
5. Pearce, J. M., & Hall, G. (1980). A model for Pavlovian learning: Variations in the effectiveness of conditioned but not of unconditioned stimuli. Psychological Review, 87(6), 532-552.
6. Becker, G. M., DeGroot, M. H., & Marschak, J. (1964). Measuring utility by a single-response sequential method. Behav Sci, 9(3), 226-232.
7. Barrett, L. F., & Simmons, W. K. (2015). Interoceptive predictions in the brain. Nature reviews neuroscience, 16(7), 419-429.
8. Bartoshuk, L. M., Duffy, V. B., Chapo, A. K., Fast, K., Yiee, J. H., Hoffman, H. J. et al. (2004). From psychophysics to the clinic: missteps and advances. Food Quality and Preference, 15(7-8), 617-632.

Poster No 767

Delay gratification ability biases motivation for delayed rewards via cortico-striatal network

Yang Xu[1], Yachao Rong[1], Ping Wei[1]

[1]School of Psychology, Capital Normal University, Beijing, China

Introduction: Pursuing rewards is essential for human survival and reproduction, prompting individuals to adjust behaviors in their pursuit. However, when the expected delivery of rewards is delayed, task performance declines with blunted neural activities[1], posing a real-world challenge. As the Expected Value of Control (EVC) theory[2] predicts, the discounted value of delayed-reward (DR) compared to immediate-reward (IR) may lead to declined performance for DR. Individual's delay gratification tendency plays a key role in forming the value of DR vs. IR. While existing research has pinpointed this possibility, the underlying neural mechanisms are not revealed[3]. In this study, we aim to employ fMRI to elucidate the neural mechanisms underlying the impact of delay gratification on pursuing delayed rewards.

Methods: 50 participants (48 remained after exclusion, 19 female, M=23) were recruited to finish a modified Monetary Incentive Delay (MID) task in fMRI scanner, and to complete a delay discounting task (DDT) post-scan. In the MID task, participants were required to discriminate the color of a circle after a reward cue indicating potential reward (IR, DR, or no-reward). Then, the response-contingent feedback was displayed to indicate the reward outcome. The monetary reward gained in the IR condition was cashed out immediately after the experiment, while the reward gained in the DR condition was paid out three months later. After that, participants finished a DDT whose data were fit using a hyperbolic discounting model, serving as a measure of delay gratification ability (i.e., logk). For the neural data, our focus centered on the reward anticipation phase of contrast IR vs. DR within three a priori defined regions of interest (ROIs): the ventral striatum (VS), dorsal anterior cingulate cortex (dACC), and anterior insula (AI). Brain-behavior correlations and mediation analysis were conducted to unveil whether these regions underpin the process of biasing motivation differentially for IR and DR, driven by delay gratification. Additionally, dynamic causal modeling (DCM) was employed to elucidate how these ROIs interacted to transform cue value into motivation for getting corresponding rewards. Finally, multivariate pattern analysis (MVPA), including classification and support vector regression (SVR), and inter-subject representational analysis (IS-RSA) were conducted to provide complementary evidence regarding how delay gratification ability biases motivation for DR vs. IR.

Results: The reaction times revealed a hierarchical pattern (IR < DR < NR). Brain-behavior correlation and mediation analyses revealed that VS, dACC, and AI mediated the link between delay gratification and RT (DR vs. IR). DCM analysis further identified a model with full recurrent connectivities between these ROIs, with inputs originating in AI. Notably, contrasting IR vs. DR in cue-related inputs correlated with activities in these ROIs, as well as with RTs and marginally with logk. MVPA demonstrated that neural patterns within these ROIs could decode IR vs. DR reward anticipation, with decoding accuracy of dACC and AI varying based on logk. Lastly, using SVR and IS-RSA, we found VS carried over the information of individual logk. Taken together, delay gratification modified the neural activities within the cortico-striatal network, thereby biasing the motivation in pursuit of DR as compared to IR.

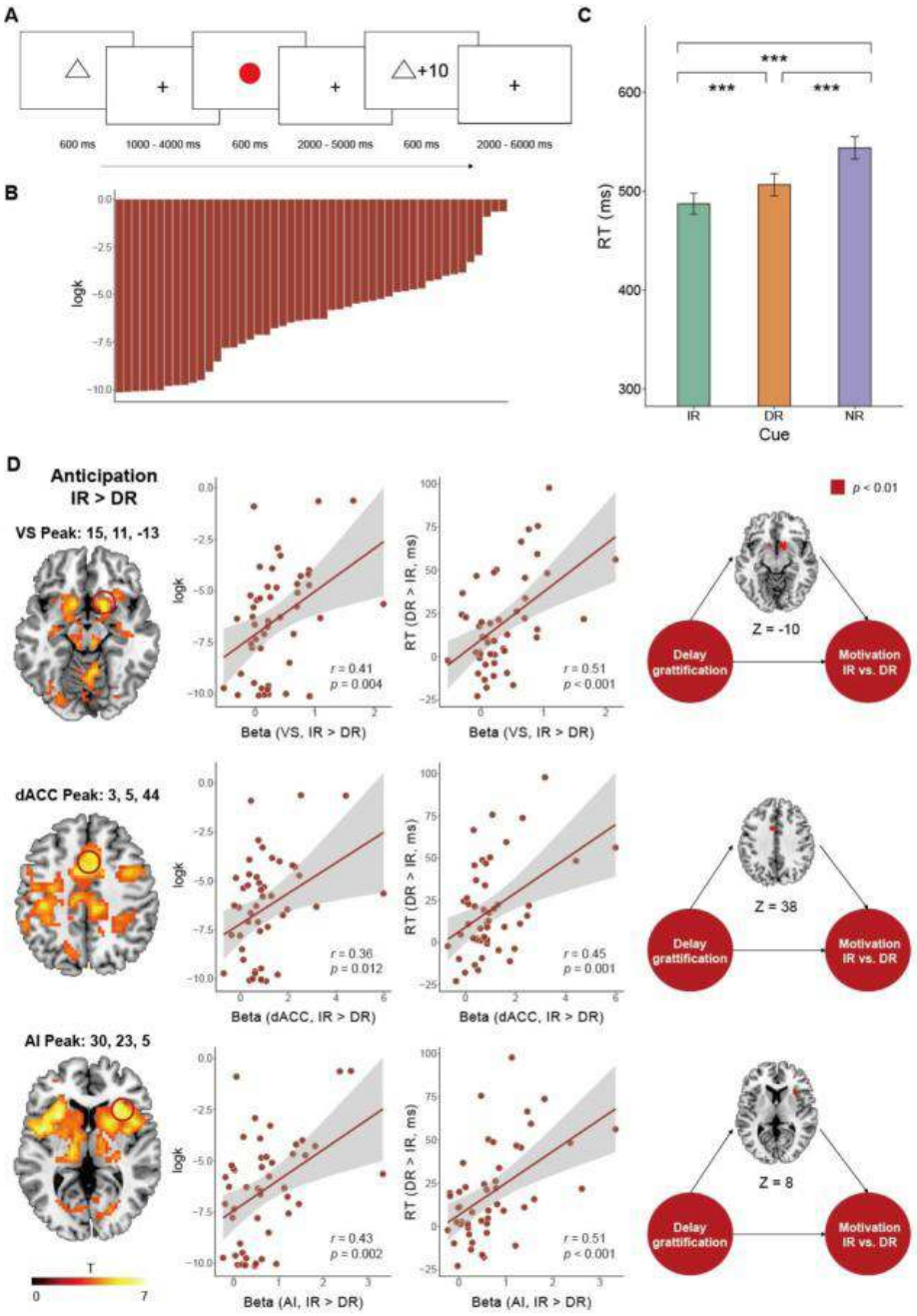

Figure 1. Trial structure, behavioral results, and neural activities in VS, dACC, and AI. A. Task structure for MID task. B. Model parameters characterizing delay gratification fitted from hyperbolic discounting model. C. RTs for the MID task. D. During reward anticipation, the contrast of IR > DR revealed significant activation in VS, dACC and AI, and the contrast activities not only correlated with logk and RT differences, but also served as mediators between them. VS = ventral striatum. dACC = dorsal anterior cingulate cortex, AI = anterior insula, IR = immediate-reward, DR = delayed-reward, NR = no-reward, MID = monetary incentive delay task, RT = reaction time.

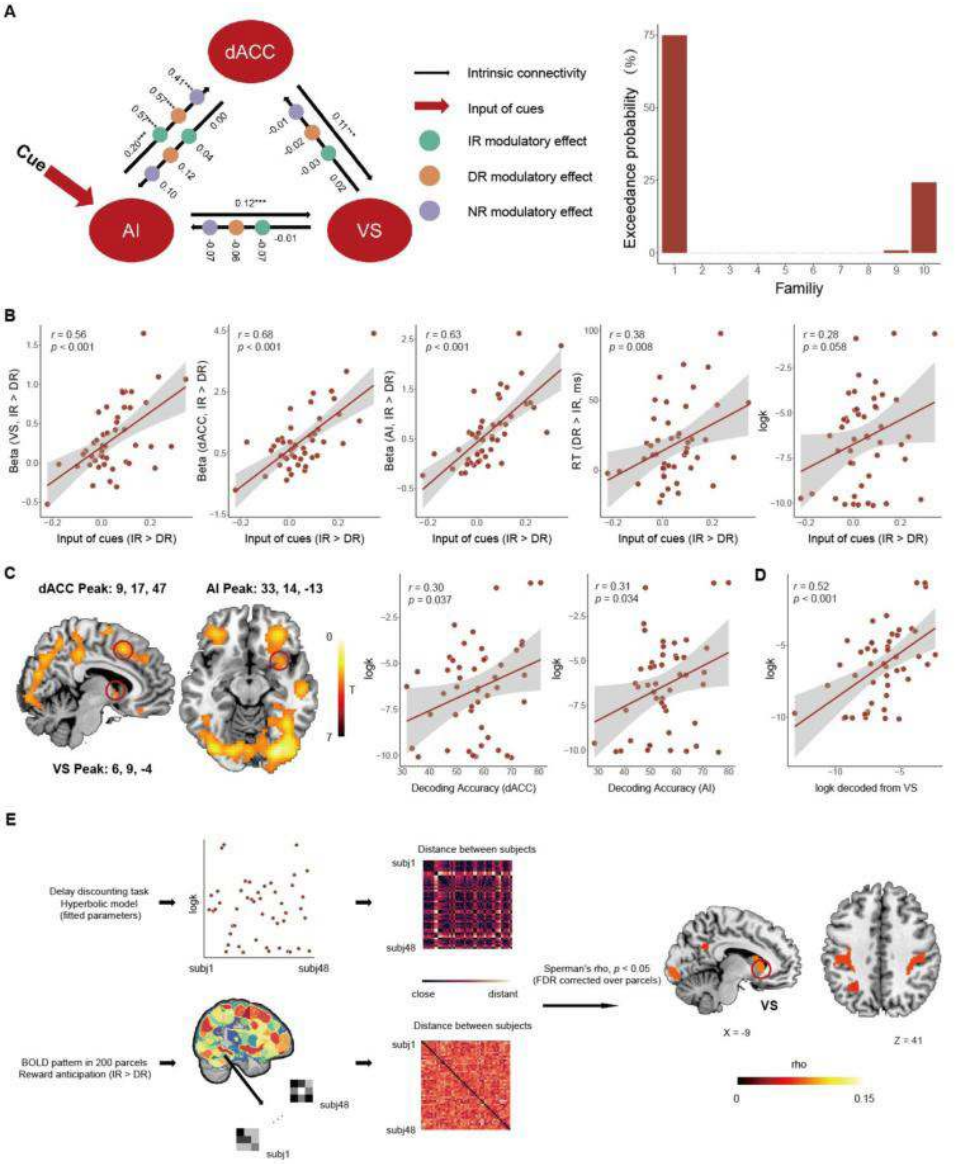

Figure2. DCM and multivariate analysis results. A. A full-connected family performed best under Bayesian Model Selection. B. The model input effects of IR vs. DR correlated with neural activities of VS, dACC, AI, and RT, as well as logk (marginally). C. The neural pattern of VS, dACC and AI can discriminate the anticipation of IR vs. DR above chance, and the decoding accuracy of dACC and AI correlated with logk. D. The individual logk can be decoded from neural pattern of VS during anticipation of IR vs. DR. E. Inter-subject representational analysis revealed that participants with more similar logk had a more similar neural patterns within VS during the anticipation of IR vs. DR. DCM = dynamic causal modeling, VS = ventral striatum, dACC = dorsal cingulate cortex, AI = anterior insula, IR = immediate-reward, DR = delayed-reward, FDR = false discovery rate.

Conclusions: Motivation in pursuit of delayed rewards is decreased as compared to immediate reward. Individual's delay gratification ability determines value representation for delayed reward compared to immediate reward, and biases motivation for such rewards through the cortico-striatal network. These findings not only contribute to our understanding of the impact of delayed-reward delivery on motivation but also extends the EVC theory to cases where reward delivery is delayed.

References

1. Rong, Y. (2022). "Expectations of immediate and delayed reward differentially affect cognitive task performance." NeuroImage 262: 119582.
2. Shenhav, A. (2013). "The Expected Value of Control: An Integrative Theory of Anterior Cingulate Cortex Function." Neuron 79(2): 217-240.
3. Lee, N. C. (2012). "Academic motivation mediates the influence of temporal discounting on academic achievement during adolescence." Trends in Neuroscience and Education 1(1): 43-48.

Poster No 768

Social jetlag and habitual short sleep duration affect neural reward function

Shuo Wang[1], Yun Tian[1], Ruyue Xie[1], Hanfei Chen[1], DeXu Yin[1], Huimin Duan[1], Xu Lei[1]

[1]*Southwest University, Chongqing, China*

Introduction: Although social jetlag was indeed found to affect reward function in previous studies, these studies often confounded the effects of social jetlag (SJL) and habitual short sleep duration on reward dysfunction. Therefore, the present study focused on the different effects of social jetlag and habitual short sleep duration on reward function.

Methods: Sixty-three college students were enrolled in 4 study groups according to the presence of SJL and habitual short sleep duration (2 groups with SJL with or without habitual short sleep duration and 2 groups without SJL without habitual short sleep duration). They completed a functional magnetic resonance imaging scan using a gambling risk task and self-reported questionnaires. Region-interest analyses focused on the medial prefrontal cortex (mPFC) and striatum both of which are implicated reward function. Analyses adjusted gender, age, Body mass index (BMI) and chronotype scores.

Results: In the reward anticipation phase, between-group differences were found only in the whole-brain action analysis, and no intergroup differences were found in the two regions of interest (GRF correction, the cluster-level: $P < 0.05$; two-tailed, with voxel level $P < 0.005$). Post hoc analyses showed that the habitual short sleep duration group exhibited significantly increased activation in the right superior occipital gyrus and right middle occipital gyrus compared to the control group (Figure 1A). Compared to the control group, the social jetlag group showed significantly increased activation in the right superior occipital gyrus, right middle occipital gyrus, and right superior parietal gyrus (Figure 1B). The difference in activation between the control group and the habitual short sleep duration co-social jetlag group was not significant. Compared to both the habitual short sleep duration and social jetlag groups, the habitual short sleep duration co-social jetlag group exhibited significant reductions in activation in the left dorsolateral prefrontal cortex, left medial frontal gyrus, and left orbital part of the middle frontal gyrus (Figure 1C).

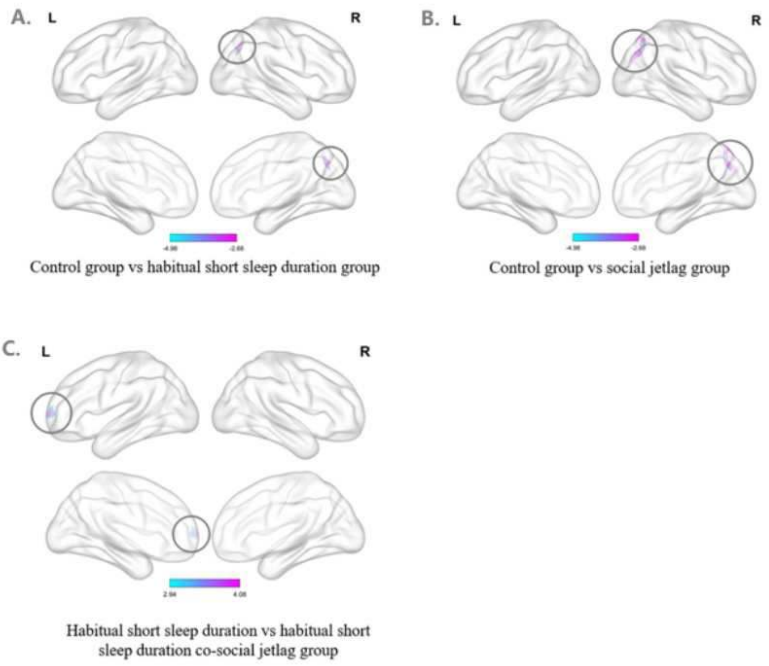

Conclusions: In addition to habitual short sleep duration and social jetlag, the habitual short sleep duration co-social jetlag can lead to mood changes and change in reward and punishment sensitivity, and these changes in cognitive function may be due to impaired neural reward function. Further neuroimaging results corroborate this finding.

References

1. Baranger, D. A. A., Lindenmuth, M., Nance, M., Guyer, A. E., Keenan, K., Hipwell, A. E., . . . Forbes, E. E. (2021). The longitudinal stability of fMRI activation during reward processing in adolescents and young adults. Neuroimage, 232.
2. Curtis, B. J., Williams, P. G., & Anderson, J. S. (2019). Neural reward processing in self-reported short sleepers: examination of gambling task brain activation in the Human Connectome Project database. Sleep, 42(9).
3. Hasler, B. P., Casement, M. D., Sitnick, S. L., Shaw, D. S., & Forbes, E. E. (2017). Eveningness among late adolescent males predicts neural reactivity to reward and alcohol dependence 2 years later. Behavioural Brain Research, 327, 112-120.

4. Hasler, B. P., Graves, J. L., Soehner, A. M., Wallace, M. L., & Clark, D. B. (2022). Preliminary Evidence That Circadian Alignment Predicts Neural Response to Monetary Reward in Late Adolescent Drinkers. Frontiers in Neuroscience, 16.
5. Hasler, B. P., Sitnick, S. L., Shaw, D. S., & Forbes, E. E. (2013). An altered neural response to reward may contribute to alcohol problems among late adolescents with an evening chronotype. Psychiatry Research: Neuroimaging, 214(3), 357-364.
6. Nechifor, R. E., Ciobanu, D., Vonica, C. L., Popita, C., Roman, G., Bala, C., . . . Rusu, A. (2020). Social jetlag and sleep deprivation are associated with altered activity in the reward-related brain areas: an exploratory resting-state fMRI study. Sleep Medicine, 72, 12-19.

Poster No 769

Data-driven Evaluation of Brain Network Engagement with Reward Task Gain Anticipation

Su Hyoun Park[1,2], Andrew Michael[3], Anne Baker[1,2], Carina Lei[1,2], Katherine Martucci[1,2,3]

[1]Department of Anesthesiology, Human Affect and Pain Neuroscience Laboratory, Duke University School, Durham, NC, [2]Center for Translational Pain Medicine, Duke University Medical Center, Durham, NC, [3]Duke Institute for Brain Sciences, Duke University, Durham, NC

Introduction: Reward motivation is essential in shaping human behavior and cognition[1]. Brain reward systems are critical in modulating pain experiences[2,3,4] and consistently appear to be dysregulated among individuals with chronic pain conditions such as fibromyalgia[5,6,7,8]. Fibromyalgia is characterized by widespread musculoskeletal pain, fatigue, cognitive problems, and mood-related symptoms. To gain a more comprehensive understanding of how brain reward circuits are altered in chronic pain, we used Independent Component Analysis (ICA) to investigate how brain networks contribute to altered reward processing in fibromyalgia.

Methods: From female individuals with fibromyalgia (N=24) and female healthy controls (N=24), we acquired fMRI data while participants performed a monetary incentive delay (MID) reward task. A group ICA (GICA) was performed on the functional data for the two MID task scans using GIFT v4.0 software. GICA computes brain functional networks and their timecourses in a data-driven manner. The denoised preprocessed functional data were provided as input into the GICA toolbox. The fMRI data were decomposed into 30 functional networks and were visually inspected. Networks of interest were selected based on their relevance to reward processing and included the left motor network, basal-ganglia network, and value-driven attention network. These functional networks were selected prior to conducting ICA. To measure patients vs. healthy control group differences, we evaluated each functional network's temporal correlation with the gain anticipation task timecourse. First, we modeled the gain anticipation timecourse based on the task's timing. Using the FMRIB Software Library[9], we constructed the task timecourse model by convolving the timecourse of gain anticipation with the hemodynamic response function. Then, we evaluated the correlation between the gain anticipation timecourse vs. each ICA-derived network timecourse. At this step, we regressed out six motion parameters (three translation and three rotation) from each participant's functional network timecourse. The resulting correlation coefficients indicated the degree of similarity between each ICA network's timecourse and the gain anticipation timecourse at the individual level. These correlation coefficients were then Fisher's r-to-z transformed before group analyses. We repeated this process for all participants. Finally, we performed the group comparison of correlation coefficients between patients vs. healthy controls (Figure 1).

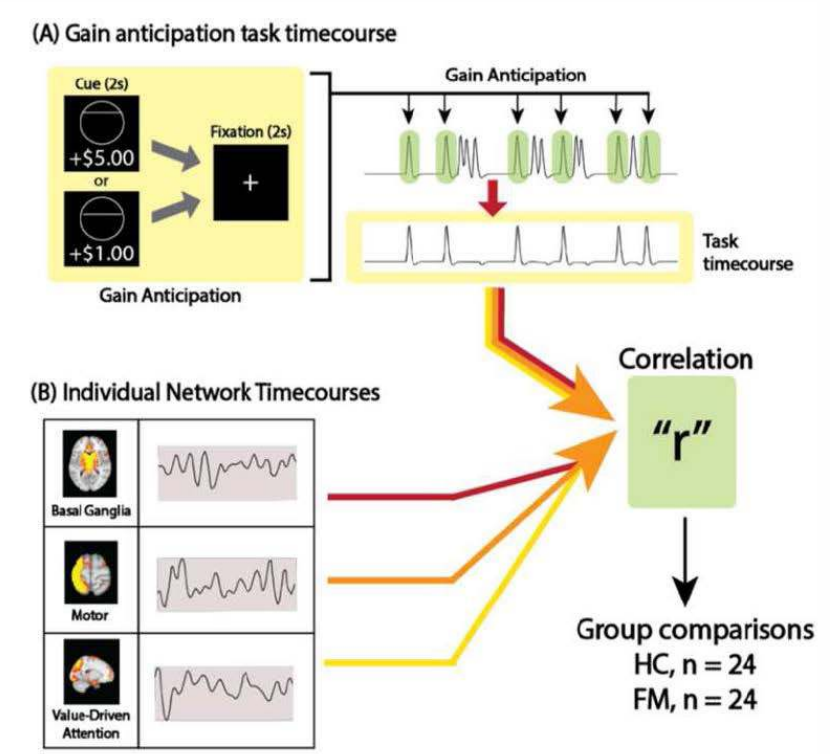

Figure 1. Example pipelines for the analyses of functional network engagement during gain anticipation. (A) Gain anticipation task timecourses were constructed by convolving the timecourse of MID task gain anticipation with the hemodynamic response function. (B) Functional ICA network timecourses were identified from the ICA analysis. Correlations coefficients between the gain anticipation task timecourse (A) vs. each of the 3 network timecourses (B) were evaluated for the main analysis at the individual-level. Then, individual participants' correlation values were averaged per group and compared across groups to evaluate group differences. Abbreviation: FM, fibromyalgia; HC, healthy control; ICA, independent component analysis; MID, monetary incentive delay; r, Pearson correlation coefficient.

Results: Compared to controls, the fibromyalgia cohort demonstrated significantly stronger correlation between the left motor network timecourse and the task-timecourse, indicating the left motor network was more engaged with gain anticipation in fibromyalgia. In an exploratory analysis, we compared motor network engagement during early vs. late phases of gain anticipation. Across both cohorts, greater motor network engagement (i.e., stronger correlation between network timecourse and task-timecourse) occurred during the late timepoint, which reflected enhanced motor preparation immediately prior to target response. Consistent with the main results, patients exhibited greater engagement of the motor network during both early and late phases as compared with healthy controls (Figure 2). Visual-attention and basal ganglia networks revealed similar engagement in the task across groups. As indicated by post-hoc analyses, motor network engagement was positively related to anxiety ($r = 0.434$, $p = 0.043$) and negatively related to reward responsiveness ($r = -0.429$, $p = 0.036$).

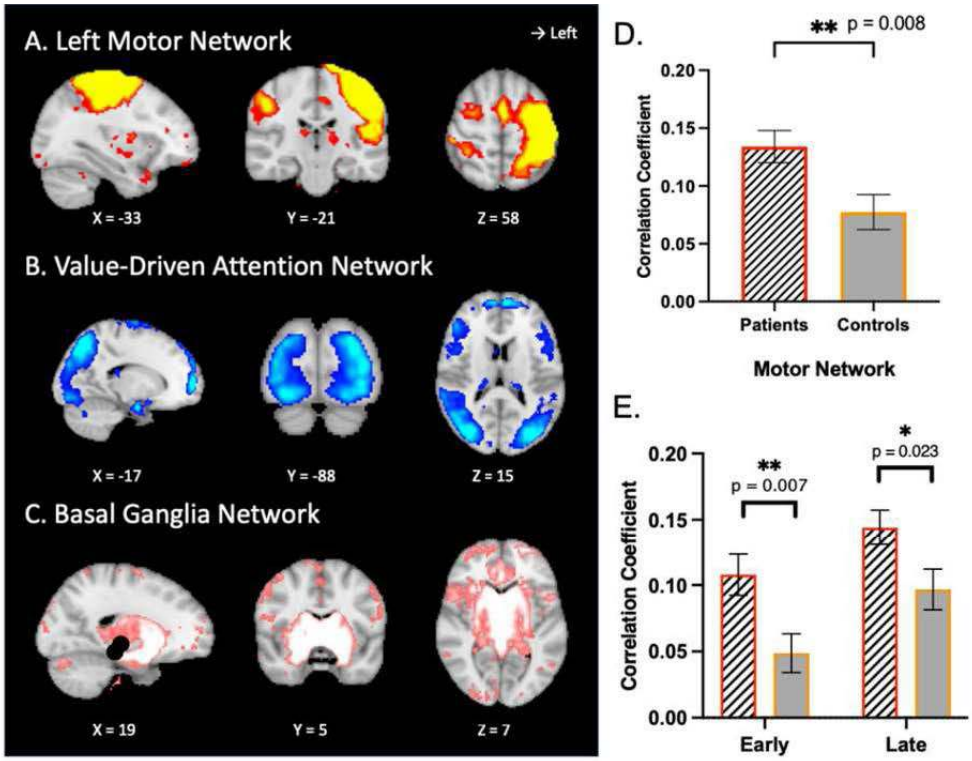

Figure 2. ICA-Identified functional networks matching pre-selected networks of interest and correlations between gain anticipation timecourse vs. network timecourses. Functional networks are shown at peak activation with MNI coordinates. (A) The left motor network included the left superior and middle frontal gyrus and the left pre- and post-central gyrus. (B) The value-driven attention network included the early visual cortex, lateral occipital cortex, intraparietal sulcus, and caudate tail. (C) The basal-ganglia network included a large portion of subcortical brain regions such as the NAcc, thalamus, caudate, pallidum, hippocampus, amygdala, and putamen. (D) Correlation between gain anticipation task presentation and activation in left motor network. (E) Group differences in functional network – gain anticipation correlation coefficients during early vs. late phases in left motor network. Patients showed stronger correlations with the task timecourse than controls at both early and late phases of gain anticipation. In addition, the correlations were stronger during the late phase in both groups. Abbreviation: ICA, Independent Component Analysis; MNI, Montreal Neurological Institute; NAcc, nucleus accumbens.

Conclusions: In summary, by using a novel data-driven ICA approach to analyze task-based fMRI data, we identified enhanced reward-task related engagement of the motor network in fibromyalgia. This study provided broader insights to how brain networks are altered during performance of a reward task in chronic pain.

References

1. Banich, M. T., & Floresco, S. (2019). Reward systems, cognition, and emotion: Introduction to the special issue. Cognitive, Affective, & Behavioral Neuroscience, 19(3), 409–414. https://doi.org/10.3758/s13415-019-00725-z
2. Becerra, L., Breiter, H. C., Wise, R., Gonzalez, R. G., & Borsook, D. (2001). Reward circuitry activation by noxious thermal stimuli. Neuron, 32(5), 927–946. https://doi.org/10.1016/s0896-6273(01)00533-5
3. Becerra, L., & Borsook, D. (2008). Signal valence in the nucleus accumbens to pain onset and offset. European Journal of Pain (London, England), 12(7), 866–869. https://doi.org/10.1016/j.ejpain.2007.12.007
4. DosSantos, M. F., Moura, B. de S., & DaSilva, A. F. (2017). Reward Circuitry Plasticity in Pain Perception and Modulation. Frontiers in Pharmacology, 8, 790. https://doi.org/10.3389/fphar.2017.00790
5. Berger, S. E., Baria, A. T., Baliki, M. N., Mansour, A., Herrmann, K. M., Torbey, S., Huang, L., Parks, E. L., Schnizter, T. J., & Apkarian, A. V. (2014). Risky monetary behavior in chronic back pain is associated with altered modular connectivity of the nucleus accumbens. BMC Research Notes, 7, 739. https://doi.org/10.1186/1756-0500-7-739
6. Martucci, K. T., Borg, N., MacNiven, K. H., Knutson, B., & Mackey, S. C. (2018). Altered prefrontal correlates of monetary anticipation and outcome in chronic pain. Pain, 159(8), 1494–1507. https://doi.org/10.1097/j.pain.0000000000001232
7. Martucci, K. T., MacNiven, K. H., Borg, N., Knutson, B., & Mackey, S. C. (2019). Apparent Effects of Opioid Use on Neural Responses to Reward in Chronic Pain. Scientific Reports, 9(1), 9633. https://doi.org/10.1038/s41598-019-45961-y
8. Park, S. H., Deng, E. Z., Baker, A. K., MacNiven, K. H., Knutson, B., & Martucci, K. T. (2022). Replication of neural responses to monetary incentives and exploration of reward-influenced network connectivity in fibromyalgia. Neuroimage: Reports, 2(4), 100147.
9. Jenkinson, M., Beckmann, C. F., Behrens, T. E., Woolrich, M. W., & Smith, S. M. (2012). Fsl. Neuroimage, 62(2), 782–790.

Poster No 770

Towards a Neurobehavioral Phenotype of Human Hedonic Capacity

Ryan Yan[1], Leili Mortazavi[1], Brian Knutson[2], Hongye Li[3]

[1]Stanford University, Stanford, CA, [2]Stanford University, Palto Alto, CA, [3]University of California, Los Angeles, Los Angeles, CA

Introduction: Hedonic capacity, or the ability to experience pleasure, has been identified as an important mental health symptom profile (Cuthbert & Insel, 2013; Insel et al., 2010). Reduced hedonic capacity is a key symptom in various psychiatric disorders including depression and schizophrenia. Neuroimaging studies have linked self-reported hedonic capacity to reduced subcortical activity (especially in the ventral striatum) during reward processing, particularly during reward anticipation (Green et al., 2019; Wacker et al., 2009; Wu et al., 2014). Many of these studies, however, were conducted on depressed patients. Additionally, research has not clarified whether blunted ventral striatal responses to reward are specifically associated with self-reported reward anticipation versus consumption.

Methods: In a pre-registered study, we will recruit 60 healthy participants in total. This abstract presents preliminary results based on N = 41 quality-assured participants collected to date. Participants completed two reward processing tasks while being scanned with functional Magnetic Resonance Imaging (fMRI at 3T GE, TE = 25 ms, TR = 2000 ms, flip = 70°, 28 slices) – the Monetary Incentive Delay (MID) task (Knutson et al., 2001), and a skewed gambling task (Wu et al., 2011). In MID task trials, participants see a cue indicating potential monetary gain or loss ($5, $1 or $0 gain or loss), then responded to a rapidly presented target after waiting a variable delay, to try to acquire gains or avoid losses. In skewed gambling task trials (Leong et al., 2016), participants saw a risky option and a safe option, chose between them, and were notified of the outcome. Thus, both tasks included anticipation phase and outcome phases. High resolution images (1.5 mm isotropic) were acquired with manually-prescribed partial coverage of mesolimbic projections spanning the midbrain and the dorsal striatum. Self-reported hedonic capacity was measured by the Temporal Experience of Pleasure Scale (TEPS), which contains an anticipatory component (TEPS-ANT) and a consummatory component (TEPS-CON). Functional neuroimaging data was preprocessed using a standard protocol with AFNI (Srirangarajan et al., 2021) and co-registered to MNI space using FSL. The time course data and regression coefficients for anticipation and outcome periods were extracted for mesolimbic projection regions (including the Nucleus Accumbens (NAcc) of the ventral striatum).

Results: Healthy participants with higher hedonic capacity (as indexed by a higher TEPS score) tended to respond faster to obtain monetary rewards (β = -0.27, p = .055). This pattern appeared to generalize over all cue types, not just the high reward incentive responses. Averaged peak NAcc signal during high reward (+$5) anticipation was also associated with higher TEPS-ANT (β = 0.31, p = .045), but not with TEPS-CON (β = 0.03, p = .839). This association of TEPS-ANT with neural activity was specific to the +$5 anticipatory activity, since neither NAcc nor MPFC response to +$5 outcome was associated with the TEPS score. Further, observed results trended towards generalizing to the skewed gambling task. While +$5 cue anticipatory NAcc activity in the MID task was not significantly associated with NAcc activity during anticipation of gamble acceptance (β = 0.15, p = .169), NAcc activity in anticipation of gamble outcomes was indeed associated with overall TEPS score (β = 0.32, p = .036). Unlike the MID task, this association was not specific to TEPS-ANT (β = 0.20, p = .198).

Conclusions: In a preliminary analysis, self-reported variation in hedonic capacity was associated with NAcc activity during reward anticipation in healthy humans. This association may generalize to another incentivized task with an anticipatory phase. These preliminary findings are consistent with the idea that hedonic capacity is an affective trait which can vary across healthy and clinical samples.

References

1. Cuthbert, B. N., & Insel, T. R. (2013). Toward the future of psychiatric diagnosis: The seven pillars of RDoC. BMC Medicine, 11(1), 126. https://doi.org/10.1186/1741-7015-11-126
2. Green, I. W., Pizzagalli, D. A., Admon, R., & Kumar, P. (2019). Anhedonia modulates the effects of positive mood induction on reward-related brain activation. Neuroimage, 193, 115–125.
3. Insel, T., Cuthbert, B., Garvey, M., Heinssen, R., Pine, D. S., Quinn, K., Sanislow, C., & Wang, P. (2010). Research domain criteria (RDoC): Toward a new classification framework for research on mental disorders. Am Psychiatric Assoc.
4. Srirangarajan, T., Mortazavi, L., Bortolini, T., Moll, J., & Knutson, B. (2021). Multi-band FMRI compromises detection of mesolimbic reward responses. NeuroImage, 244, 118617.
5. Wacker, J., Dillon, D. G., & Pizzagalli, D. A. (2009). The role of the nucleus accumbens and rostral anterior cingulate cortex in anhedonia: Integration of resting EEG, fMRI, and volumetric techniques. Neuroimage, 46(1), 327–337.
6. Wu, C. C., Samanez-Larkin, G. R., Katovich, K., & Knutson, B. (2014). Affective traits link to reliable neural markers of incentive anticipation. NeuroImage, 84, 279–289.

Poster No 771

Punishment interferes reward learning through altering exploration behavior: an fMRI study in humans

Wen-Wei Lin[1,2], Ming-Tsung Tseng[3]

[1]National Taiwan University, Taipei, Taiwan, [2]Graduate Institute of Brain and Mind Sciences, Taipei, Taiwan, [3]Graduate Institute of Brain and Mind Sciences, Taipei, TAIWAN

Introduction: Reward and punishment act as important factors that modulate human behavior through learning to maximize the former, and minimizing the latter. Although much is known about how reward and punishment contribute to guiding our behavior independently, how these two types of learning interact with each other and the underlying mechanism remain largely unclear. By simultaneously associating an overlapped option with rewarding and punishing outcomes in an instrumental learning task, we aim to investigate the interaction between reward learning and punishment learning.

Methods: We scanned 30 healthy subjects using 3 Tesla functional magnetic resonance imaging (fMRI) while they performed a probabilistic instrumental learning task with binary choices. The learning task included both reward learning and punishment learning at the same time with a choice option overlapping in both learnings. We used monetary reward as reward stimuli, and monetary loss or electrical painful stimulation as punishment stimuli. The subjects were instructed to try their best to maximize reward and avoid receiving punishment during the learning task.

Results: We found that only the performance (i.e., the correct rate) of reward learning was interfered by punishment learning, but not vice versa, when the overlapped option was in both learnings. Further, the performance of the interfered reward learning correlated with participants' exploration behavior, which could be explained by an increase in BOLD signals within exploration-related brain regions.

Conclusions: In conclusion, our study suggests a behavioral interference effect of punishment learning on reward learning, which may be linked to participant's altered exploration behavior. From a neural aspect, increased BOLD signals in exploration-related brain regions provides insights into the asymmetry in the interaction between reward learning and punishment learning.

References

1. Palminteri, S., Khamassi, M., Joffily, M., & Coricelli, G. (2015). 'Contextual modulation of value signals in reward and punishment learning', Nature Communications 6, 8096.

Poster No 773

Noise in neural value signals links preference variability, choice stochasticity and confidence

Raphael Le Bouc[1], Gilles de Hollander[1], Marcus Grueschow[1], Rafael Polania[2], Christian Ruff[1]

[1]UZH, Zürich, Switzerland, [2]ETH, Zürich, Switzerland

Introduction: The capacity to evaluate and choose the most rewarding options in the environment is crucial for survival. However, humans show surprising variability in their preferences, confidence and choices regarding rewards, a phenomenon that lacks a comprehensive mechanistic explanation. This variability is classically attributed to the presence of random noise in behavioural measures or in the neural processes underlying behaviour. However, the specific neural computations affected by this noise remain uncertain.

Methods: Here we provide evidence that variability in value-based decision-making arises in part from the idiosyncratic precision with which the value of each reward option is encoded in the brain. We demonstrate this using behavioural tasks that measure the individual variability in the subjective value participants assign to food items, their confidence in the expressed value, and their stochasticity in two-option choices. We then relate these measures to the precision of probabilistic neural value representations decoded using functional magnetic resonance imaging and a population receptive field model combined with a Bayesian decoder.

Results: Reward items with more precise value representations in ventromedial prefrontal cortex were evaluated more reliably, with higher confidence, and were chosen more consistently.

Conclusions: Thus, our findings offer a unified explanation for the imprecision observed in decision-making behaviours, which reflects not only random neural noise but a more fundamental property, the precision with which the brain encodes reward value.

Poster No 774

Tracking neural representations of cues and contexts during fear acquisition and extinction

Antoine Bouyeure[1], Marie-Christin Fellner[1], Nikolai Axmacher[1]

[1]Department of Neuropsychology, Faculty of Psychology, Ruhr University Bochum, Bochum, North-Rhine Westphalia, Germany

Introduction: Neural representations of fear-conditioned stimuli change dynamically during fear and extinction learning, reflecting the way the brain learns valence[1,2]. However, little is known regarding how the neural representations of contexts change through distinct fear learning phases. We tracked changes in the neural representations of cues and contexts using an fMRI fear learning paradigm including four successive learning phases: an initial fear acquisition phase (FA1), a second fear acquisition phase with full reversal of contingencies (FA2), and two fear extinction phases, in which new contexts (FE1), or contexts previously shown during fear acquisition (FE2), were presented.

Methods: 30 participants took part in a two-days fMRI fear learning task. FA1 and FA2 were conducted during the first day, FE1 and FE2 during the second day (Figure 1a). In each phase, cues (pictures of electric items) were embedded into contexts (neutral videos of scenes) such that the valence of the cues was orthogonal to the contexts. During FA1 and FA2, the US was a mild electric shock. No US was administered during FE1 and FE2. During FA1, participants saw 8 cues 16 times each in random order. Four cues were CS+ (50% reinforcement) and 4 were CS-. Contexts consisted in a set of 4 videos ("Contexts A"). FA2 consisted in a full reversal of contingencies: 2 cues remained CS+ (CS++ cues), 2 previous CS- cues became CS+ (CS-+), 2 previous CS+ cues were extinguished (CS+-), and 2 previous CS- cues remained CS- (CS--). Contexts consisted in a new set of 4 videos ("Contexts B"). In both FE1 and FE2, none of the cues were followed by a US. In FE1, a set of new videos were shown as contexts ("Contexts C"), while in FE2, Contexts A and Contexts B were presented. ROIs were obtained from freesurfer segmentations. Neural pattern similarity was estimated on the beta-series of trial-specific activation maps obtained with a Least Square Separate approach[3], yielding trial-by-trial neural similarity matrices for each ROI. These were used to estimate measures of within- and between-cue similarity, and within- and between-context similarity. Additionally, context specificity was estimated through the within-context vs. between-context similarity difference, with lower values indicating higher generalization.

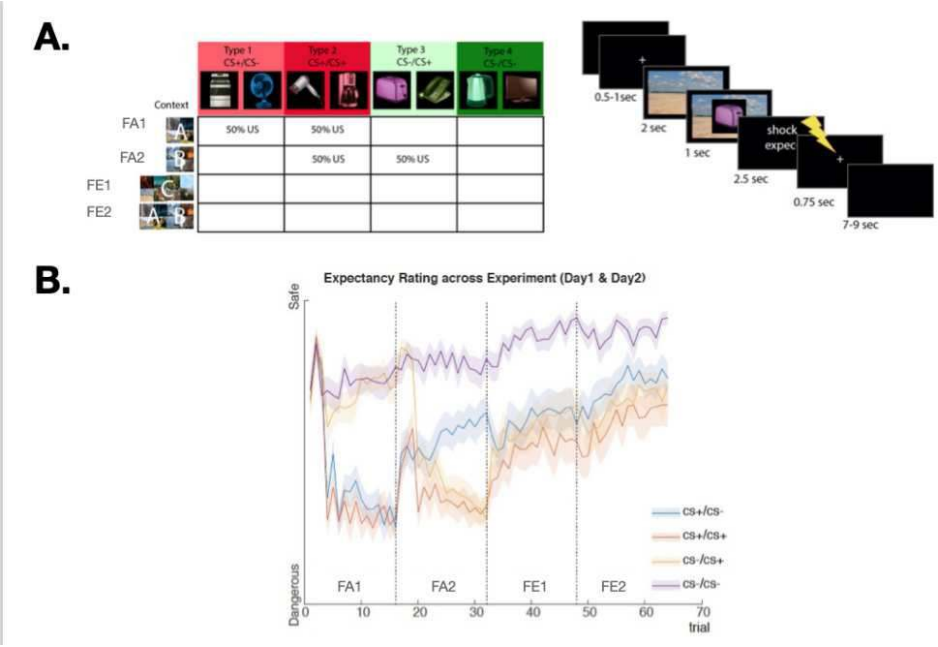

Results: Behaviorally, participants learned quickly the valence of the cues during each phase (Figure 1b). RSA showed ROI-specific changes of within-cue and between-cue similarity during the successive learning phases. Compared to FA1, within- and between-cue neural similarity of the now extinguished cue (CS+-) decreased during FA2 while similarity for the now punished cue (CS-+) increased in middle temporal and prefrontal ROIs (Figure 2a). In these same ROIs, neural similarity in the fear extinction phases compared to the fear acquisition phases decreased for all cues except the ones that were never punished (CS--). For context representations, we found higher context specificity in FA1 compared to FA2 and FE1 in the occipital lobe and superior prefrontal cortex (Figure 2b). Moreover, across all ROIs, the more the similarity of cues diminished from fear acquisition to fear extinction with old context (but not new contexts), the more context generalization was found during fear extinction with old contexts (but not new contexts) ($p<0.001$).

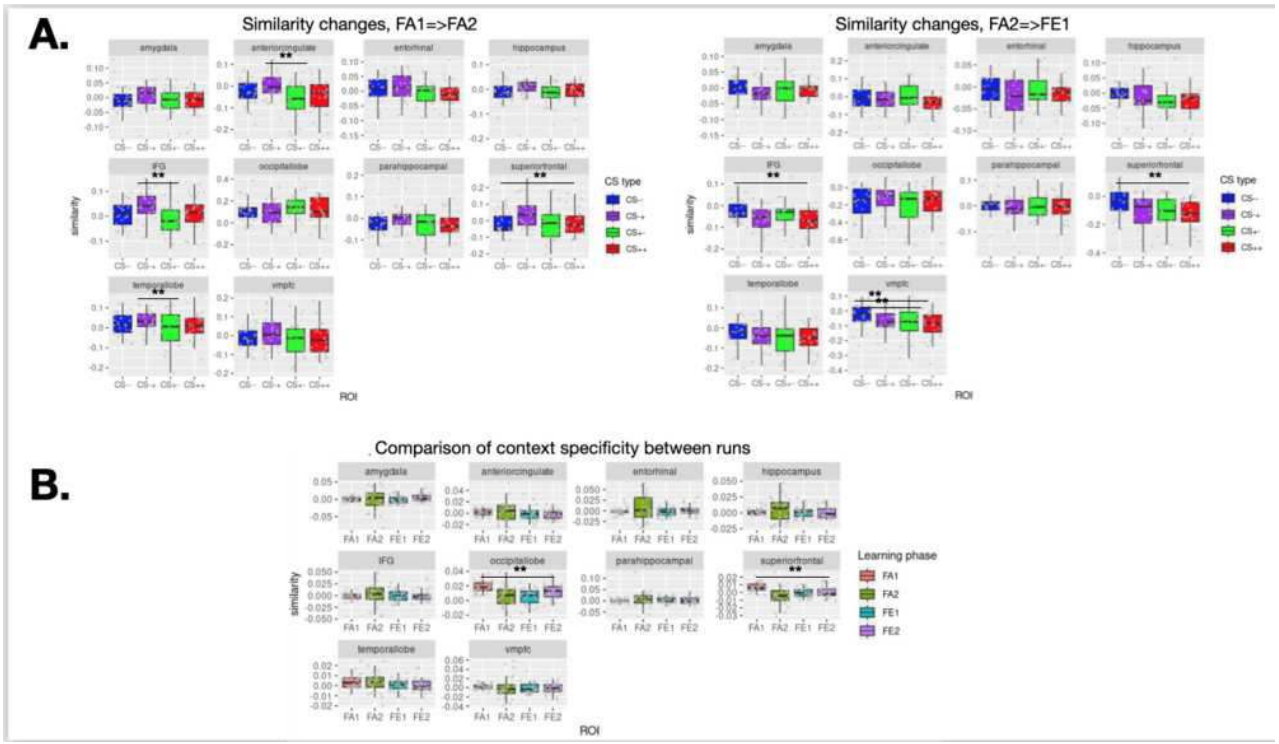

Conclusions: Neural representations of cue valence are shaped dynamically across learning phases, reflecting valence changes. Higher context specificity was found during initial fear acquisition. However, the more the neural pattern similarity of cues diminished during extinction with previous contexts compared to acquisition, the more context generalization was present during fear extinction with previous context. Context generalization mechanisms that depend on context familiarity could thus contribute to successful fear extinction.

References

1. Visser, R. M., Scholte, H. S., & Kindt, M. (2011). Associative learning increases trial-by-trial similarity of BOLD-MRI patterns. Journal of Neuroscience, 31(33), 12021-12028.
2. Visser, R. M., Scholte, H. S., Beemsterboer, T., & Kindt, M. (2013). Neural pattern similarity predicts long-term fear memory. Nature neuroscience, 16(4), 388-390.
3. Hunar Abdulrahman and Richard N Henson (2016). Effect of trial-to-trial variability on optimal event-related fmri design: implications for beta-series correlation and multi-voxel pattern analysis. NeuroImage, 125:756–766.

Poster No 775

Hemodynamic latency reflects dopamine physiology in humans

Ian Ballard[1], Ioannis Pappas[2], Daniella Furmann[3], Anne Berry[4], Robert White III[5], Andrew Kayser[6], William Jagust[7], Mark D'esposito[3]

[1]University of California, Riverside, Riverside, CA, [2]Keck School of Medicine, University of Southern California, Los Angeles, CA, [3]University of California, Berkeley, CA, [4]Brandeis University, Waltham, MA, [5]Washington University in Saint Louis, Saint Louis, MO, [6]University of California, San Francisco, San Francisco, CA, [7]University of California, Berkeley, Berkeley, CA

Introduction: Dopamine and vasculature are closely associated as dopaminergic neurons innervate microvessels, and dopamine agonists can elicit cerebrovascular dilations (Edvinsson et al., 1985). However, the relationship between dopamine physiology and hemodynamics in humans is unclear. Given the involvement of dopamine in both healthy cognition and in neurological and psychiatric disorders, it is important to identify additional methods for assessing dopamine function. There has been growing interest in using the variability in the latency of the hemodynamic response to assess underlying physiology in the brain (Tong et al., 2019). We report convergent results across multiple datasets and modalities that the influence of dopamine on vascular dilation is in reflected in hemodynamic latencies within the striatum.

Methods: PET/fMRI/dopamine/genetics study This dataset has been described elsewhere (Furman JOCN 2021, Furman, Pappas 2022). Participants were recruited based on genetic polymorphisms associated with cortical (COMT Val158Met) and striatal (Taq1A) DA system function. Eligible participants were scheduled for three pharmacological study sessions on

different days in a double-blind, placebo-controlled design (bromocriptine (1.25 mg), tolcapone (200 mg) or placebo). Subjects performed three 10-minute sessions of task-fMRI in each session. In a separate session, subjects underwent PET imaging to obtain estimates of dopamine synthesis capacity (Ki) using 6-[18F]fluoro-l-m-tyrosine ([18F]FMT;) and baseline D2/3 receptor-binding potential using [11C]raclopride (Berry et al., 2018). Our dataset, after exclusions, comprised 52 individuals. Cocaine dataset For the analysis of cocaine use disorder, we analyzed a publicly available OpenNeuro Dataset ds003346 (Garza-Villarreal et al., 2021). The researchers collected anatomical T1w scans and 10 minutes of resting state fMRI from cocaine use disorder patients (CUD) and non-CUD controls as part of the Mexican MRI dataset of patients with cocaine use disorder (SUDMEX CONN). After exclusions, we analyzed 40 CUD subjects and 39 healthy controls. Hemodynamic lags To extract hemodynamic lags we used the package optimized open source implementation of the RIPTiDe processing stream (https://github.com/bbfrederick/rapidtide). The fMRI time course for each voxel is cross-correlated with a global time course, and the optimal delay of this cross-correlation is derived (Tong et al., 2019), defining hemodynamic latency.

Results: We found that hemodynamic lags varied across the striatum, demarcating the boundary of the nucleus accumbens (Figure 1). Proximity to major arteries did not drive this effect. Additionally, we found that dopamine synthesis capacity in the nucleus accumbens was associated with reduced hemodynamic lags, indicating that higher dopamine tone results in faster hemodynamics. We found variability in the DRD2 gene was associated with differences in hemodynamic lags in the striatum (Figure 2). Moreover, bromocriptine, a D2 antagonist, influenced hemodynamic lags differentially based on genotype. We found a similar relationship between D2-receptor density and hemodynamic lags. These results are consistent with an inverted-U relationship between D2 activation and hemodynamic latency (Edvinsson et al., 1985). We found that subjects with cocaine use disorder had significantly slower hemodynamic latency throughout the striatum. This finding was not observed in the sensory cortex, which receives little dopamine innervation. Multivariate analyses revealed that increased hemodynamic latency in the anterior striatum differentiated between cocaine use disorder patients and controls.

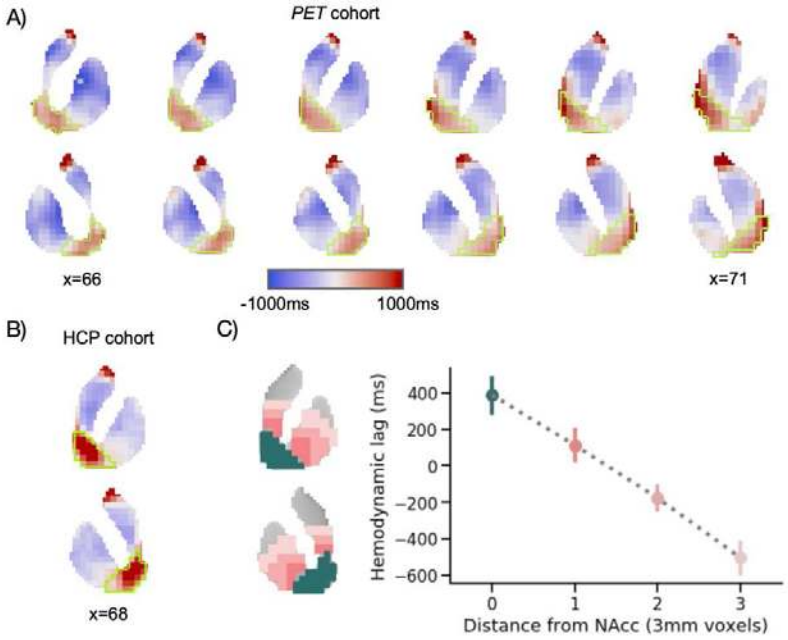

Figure 1: Hemodynamic lags trace nucleus accumbens boundary. A) Hemodynamic lags overlaid on coronal slices of the striatum, spanning from posterior to anterior, from our fMRI dataset. The anatomical outline of the nucleus accumbens is depicted in green. Hemodynamic lags derived from fMRI data trace the boundary of of the accumbens B) This same pattern is replicated in the HCP dataset. C) Quantification of lag as a function of distance from anatomical nucleus accumbens in our fMRI dataset.

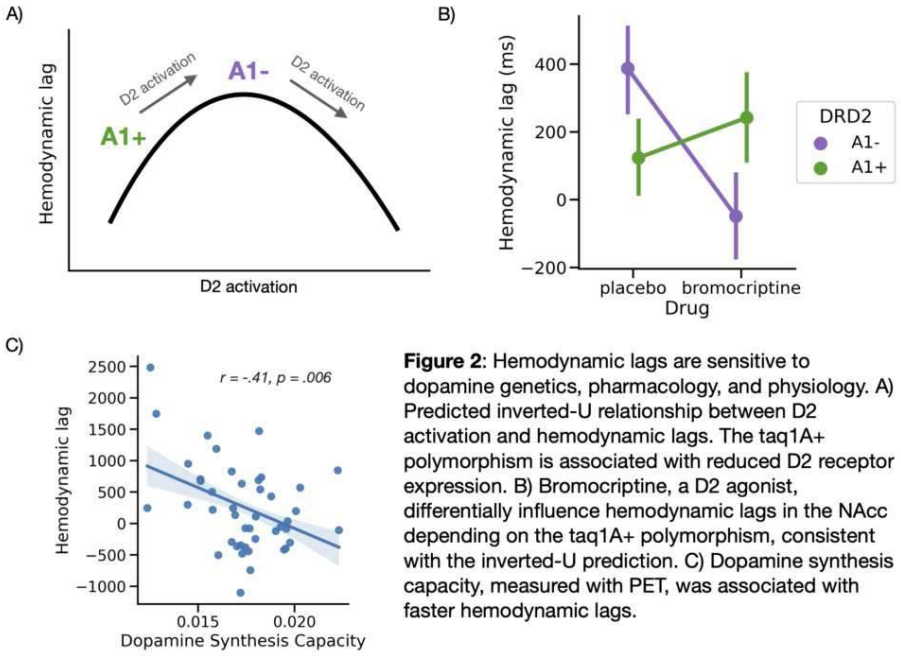

Figure 2: Hemodynamic lags are sensitive to dopamine genetics, pharmacology, and physiology. A) Predicted inverted-U relationship between D2 activation and hemodynamic lags. The taq1A+ polymorphism is associated with reduced D2 receptor expression. B) Bromocriptine, a D2 agonist, differentially influence hemodynamic lags in the NAcc depending on the taq1A+ polymorphism, consistent with the inverted-U prediction. C) Dopamine synthesis capacity, measured with PET, was associated with faster hemodynamic lags.

Conclusions: We found convergent evidence that dopamine release in the nucleus accumbens influences hemodynamic latencies. Moreover, these results raise the possibility that hemodynamic lags may provide a novel proxy measure of dopaminergic tone in humans.

References

1. Edvinsson et al., (1985), Vasomotor responses of cerebral arterioles in situ to putative dopamine receptor agonists. Br J Pharmacol. 1985 Jun; 85(2): 403–410.
2. Tong, Y., et al (2019). Low Frequency Systemic Hemodynamic "Noise" in Resting State BOLD fMRI: Characteristics, Causes, Implications, Mitigation Strategies, and Applications. Frontiers in Neuroscience, 13.
3. Furman, D. J., et. al. (2021). Enhancing dopamine tone modulates global and local cortical perfusion as a function of COMT val158met genotype. NeuroImage, 242, 118472.
4. Furman, D. J., et. al (2020). Effects of Dopaminergic Drugs on Cognitive Control Processes Vary by Genotype. Journal of Cognitive Neuroscience, 32(5), 804–821.
5. Eduardo A. Garza-Villarreal et. al (2021). SUDMEX_CONN: The Mexican dataset of cocaine use disorder patients. OpenNeuro.
6. Berry, A. S., et. al. (2017). Dopamine Synthesis Capacity is Associated with D2/3 Receptor Binding but Not Dopamine Release. Neuropsychopharmacology 43(6), 1201–1211.

Poster No 776

Hippocampal novelty signals dynamically predict goal-relevant VTA activation

Blake Elliott[1], Vishnu Murty[2]

[1]Temple University, Philadelphia, PA, [2]Temple University, Philadelphia, PA

Introduction: Novelty is an important learning signal that is known to invigorate goal-oriented behavior via engagement of the mesolimbic dopamine (DA) system. Structurally, an afferent circuit with the hippocampus (HPC) is crucial for regulating sustained signaling of VTA DA neurons (Lisman & Grace, 2005). Specifically, animal research shows that HPC novelty signals lead to increased sustained mesolimbic engagement, which in turn magnifies phasic VTA responses to goal-relevant targets. However, the extent of these interactions during active human behavior remains unclear.

Methods: We employed a novel analysis of fMRI data from human subjects (n=91) performing a target-detection task intermixed with familiar and novel pictures. Hierarchical linear regressions examined goal-relevant VTA activation and HPC-VTA regulation during novelty.

Results: We found that activation to novel events in the HPC dynamically predicted subsequent goal-relevant activation in the VTA ($\beta = 0.042$, $p<0.05$). Notably, as predicted by animal models, this relationship did not hold true for striatal novelty signals ($\beta = 0.017$, $p=0.25$).

Conclusions: These findings support models of goal-oriented behavior in which HPC regulatory systems in response to novelty invigorate VTA responsivity. Future work will integrate how prefrontal responses may interact with VTA-HPC circuitry to result in diminished goal-oriented behavior.

References

1. Lisman, J. E. (2005). The hippocampal-VTA loop: controlling the entry of information into long-term memory. Neuron, 46(5), 703-713.

Poster No 777

Association between cortical dopamine receptor patterns and valuative network functional responses

Niall Duncan[1], Melanie Sun[2]

[1]Taipei Medical University, Taiwan, Taipei, [2]Taipei Medical University, Taipei, Taipei City

Introduction: The dopamine system is integral to how we learn from experiences in the world. It appears to respond to events that provide positive or negative consequences to update internal models that then inform future behavioural decisions. Studying this system in humans is challenging though, as there are limited non-invasive options available for characterising it (Sands et al., 2023). One technique that can give insight is PET imaging using ligands that bind to dopamine receptors. A limitation of this approach is that it primarily gives static estimates of receptor distributions. Integration of these with functional imaging techniques is therefore required. In this work we aimed to relate dopamine receptor (D1 and D2) distributions with fMRI responses from a task in which participants had to make choices that resulted in them either winning or losing money.

Methods: Openly available maps of D1 and D2 receptor distributions were used (Hansen et al., 2022), with D1 receptors being the primary target. D1 receptors were imaged with SCH23390. A group map was made by averaging across the 13 participants. D2 receptors were imaged with FLB457, with a group map being made in the same manner (n = 55). Serotonin receptor maps (5-HT1A and 5-HT2A) were also analysed as controls. Task fMRI data was also taken from an open dataset (Botvinik-Nezer et al., 2019). In this, participants did a gambling task where they could either win or lose a certain amount of money. In one group (n = 54), the win and loss amounts were the same ("equal range") whilst in the other potential winnings were larger than losses ("equal indifference"). Task data were analysed with a standard GLM approach to produce activation maps for gains and losses. These activation maps were then correlated with receptor maps through spin permutation.

Results: The fMRI task produced distinct activation maps for the two groups (Figure 1A). Gain activation in the "equal indifference" group was centred around the vmPFC whilst activations in the "equal range" group were seen in more lateral prefrontal regions. Loss trials showed responses centred more around the midcingulate in both groups. D1 receptors alone were correlated with task responses during winning trials in the "equal indifference" group (Figure 1B). No associations were found with responses in the "equal gain" group. Taking the "equal indifference" gain maps, the specificity of the relationship with D1 receptors was then investigated. No relationship was found with the D2 receptor distribution. A potential correlation with 5-HT2A receptors was identified but this did not survive correction for multiple comparisons (Figure 1C).

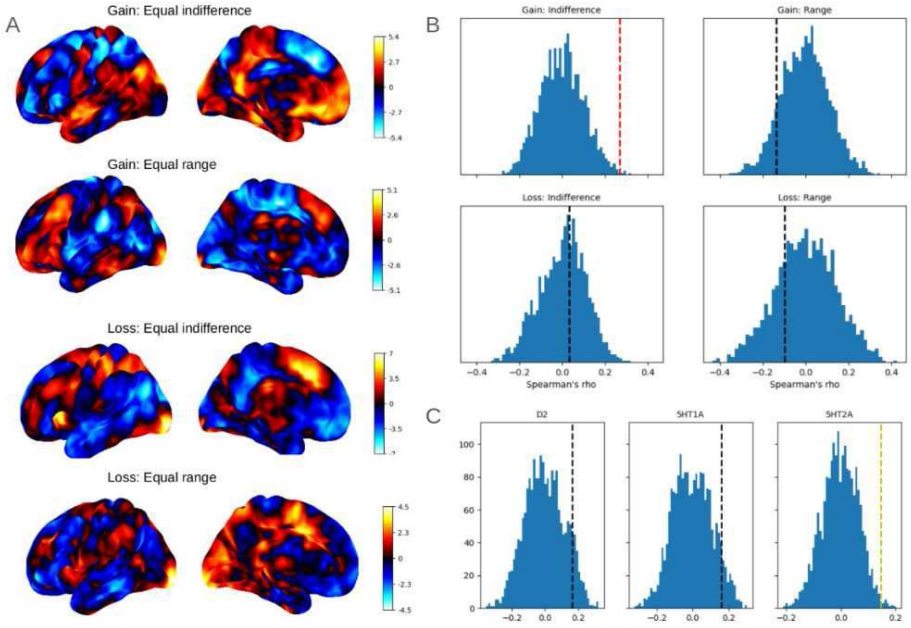

Conclusions: These results suggest that cortical D1 receptors specifically are involved in modulating local responses to positive valuations. This appears only to be true, though, when there is a difference in valuation to be attached to two options as there was no relationship with activity patterns in response to equal win/loss outcome values. This points to a role for cortical D1 receptors in modulating local neural network dynamics to facilitate decision making in contexts where a choice for potentially advantageous outcomes are present and when that predicted outcome is delivered. This may fit with the more general view of the dopamine system's involvement in outcome prediction and the updating of internal models based upon mismatch signals (Dabney et al., 2020). This would provide useful additional information from humans in vivo that builds upon that obtained from non-human primates.

References

1. Botvinik-Nezer, R., Iwanir, R., Holzmeister, F., Huber, J., Johannesson, M., Kirchler, M., Dreber, A., Camerer, C.F., Poldrack, R.A., Schonberg, T., 2019. fMRI data of mixed gambles from the Neuroimaging Analysis Replication and Prediction Study. Sci. Data 6, 106. https://doi.org/10.1038/s41597-019-0113-7
2. Dabney, W., Kurth-Nelson, Z., Uchida, N., Starkweather, C.K., Hassabis, D., Munos, R., Botvinick, M., 2020. A distributional code for value in dopamine-based reinforcement learning. Nature 577, 671–675. https://doi.org/10.1038/s41586-019-1924-6
3. Hansen, J.Y., Shafiei, G., Markello, R.D., Smart, K., Cox, S.M.L., Nørgaard, M., Beliveau, V., Wu, Y., Gallezot, J.-D., Aumont, É., Servaes, S., Scala, S.G., DuBois, J.M., Wainstein, G., Bezgin, G., Funck, T., Schmitz, T.W., Spreng, R.N., Galovic, M., Koepp, M.J., Duncan, J.S., Coles, J.P., Fryer, T.D., Aigbirhio, F.I., McGinnity, C.J., Hammers, A., Soucy, J.-P., Baillet, S., Guimond, S., Hietala, J., Bedard, M.-A., Leyton, M., Kobayashi, E., Rosa-Neto, P., Ganz, M., Knudsen, G.M., Palomero-Gallagher, N., Shine, J.M., Carson, R.E., Tuominen, L., Dagher, A., Misic, B., 2022. Mapping neurotransmitter systems to the structural and functional organization of the human neocortex. Nat. Neurosci. 25, 1569–1581. https://doi.org/10.1038/s41593-022-01186-3
4. Sands, L.P., Jiang, A., Liebenow, B., DiMarco, E., Laxton, A.W., Tatter, S.B., Montague, P.R., Kishida, K.T., 2023. Subsecond fluctuations in extracellular dopamine encode reward and punishment prediction errors in humans. Sci. Adv. 9, eadi4927. https://doi.org/10.1126/sciadv.adi4927

Poster No 778

Intracranial neurophysiological mechanisms underlying rumination

Xiao Chen[1], Zhen Fan[2], Dong Chen[3], Liang Wang[3], Liang Chen[4], Chao-Gan Yan[1]

[1]Institute of Psychology, Chinese Academy of Sciences, Beijing, Beijing, [2]Department of Neurosurgery of Huashan Hospital, Shanghai, Shanghai, [3]Institute of Psychology, Chinese Academy of Sciencess, Beijing, Beijing, [4]Huashan Hospital of Fudan University, Shanghai, Shanghai

Introduction: Rumination is uncontrollable, self-reflective, and repetitive thinking about the distress and its possible causes and consequences (Watkins & Roberts, 2020). A wealth of studies has linked it to major depressive disorder (MDD) and indicated its pivotal role in the psychopathology of MDD (Lyubomirsky et al., 2015). Accordingly, a better understanding of its neural basis may pave the way for the next-generation treatment of MDD. Existing evidence from studies using functional magnetic resonance imaging (fMRI) has shown that brain regions of the default mode network (DMN) are involved in active rumination (Zhou et al., 2020). Our previous study further highlighted the enhanced functional connectivity between two subsystems of DMN (i.e., core subsystem and medial temporal lobe (MTL) subsystem) in the neural mechanism underlying the rumination (Chen et al., 2020). To date, no research has investigated the electrophysiological organization underlying the existing functional neuroimaging evidence. Here, leveraging the intracranial electroencephalogram (iEEG) recordings from a group of patients with epilepsy engaging in an active rumination state, we intended to delineate the electrophysiological features of two key nodes from the core subsystem (precuneus) and the MTL subsystem (parahippocampal gyrus). We hypothesized that these two regions would show different electrophysiological activity patterns during rumination as compared to the control condition.

Methods: Twenty patients with intractable epilepsy participated in this study. They had been surgically implanted with stereotactic electrodes as part of their pre-surgical assessment of seizure focus. All electrodes' placements were decided based on clinical evaluation for surgery. Participants provided written consent to participate in research and the research protocol was approved by the local Institutional Review Board. Participants were asked to finish a rumination state task. Recordings were performed at the Huashan Hospital using a standard clinical system (EEG-1200C, Nihon Kohden, Irvine, CA) with 2000 Hz sampling rate. We performed electrode localization with FieldTrip version 20221210 (Stolk et al., 2018) run in the MATLAB R2023b (The MathWorks Inc., Natick, MA, US) platform. A power spectrum was obtained by performing five-cycle Morlet wavelets at 76 logarithmically spaced frequencies ranging from 0 to 150 Hz. The log power values were then Z-scored at the channel level over all the interested conditions (rumination and distraction). Finally, the mean powers of 6 different frequency bands (delta, 1-4 Hz; theta, 4-8 Hz; alpha, 8-12 Hz; beta, 12-30 Hz; low gamma, 30-70 Hz; and high gamma, 70-

150Hz) were obtained by averaging all Z-standardized power value time-series across all corresponding frequencies. A paired t-test was performed on the subject-level mean power values.

Results: A one-way anova revealed a significant condition effect (F(4, 76) = 12.08, p < 0.001, eta2 = 0.32). Post hoc comparisons showed that participants' emotional levels after the sad memory condition were significantly lower than those before and after the resting state. Emotional levels after the rumination condition were lower than those after the distraction condition (Figure 1). We observed a decreased low gamma and high gamma band power in the parahippocampal gyrus (low gamma: t = -2.48, p = 0.02; high gamma: t = -2.66, p = 0.02). On the contrary, enhanced delta (t = 3.81, p = 0.001), theta (t = 3.20, p = 0.02), and alpha (t = 2.70, p = 0.03) band powers were revealed in the precuneus (Figure 2).

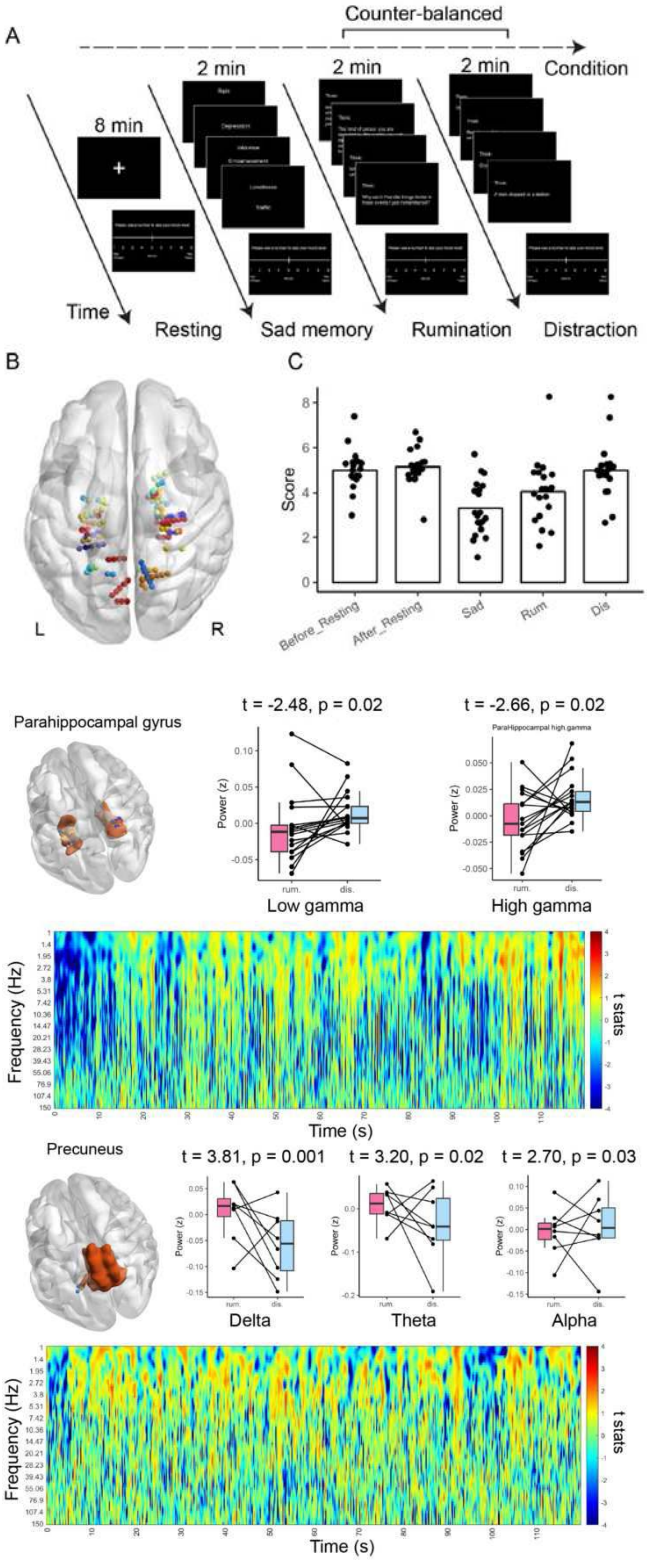

Conclusions: We found dissociated power changes in the precuneus and parahippocampal gyrus during a continuous rumination state as compared to the control condition. Our results unveiled the electrophysiological mechanism underlying the functional coupling between the core and MTL subsystems of DMN during an active rumination state.

References

1. Chen, X., Chen, N. X., Shen, Y. Q., Li, H. X., Li, L., Lu, B., Zhu, Z. C., Fan, Z., & Yan, C. G. (2020). The subsystem mechanism of default mode network underlying rumination: A reproducible neuroimaging study. Neuroimage, 221, 117185. https://doi.org/10.1016/j.neuroimage.2020.117185
2. Lyubomirsky, S., Layous, K., Chancellor, J., & Nelson, S. K. (2015). Thinking about rumination: the scholarly contributions and intellectual legacy of Susan Nolen-Hoeksema. Annu Rev Clin Psychol, 11, 1-22. https://doi.org/10.1146/annurev-clinpsy-032814-112733
3. Stolk, A., Griffin, S., van der Meij, R., Dewar, C., Saez, I., Lin, J. J., Piantoni, G., Schoffelen, J. M.,
4. Knight, R. T., & Oostenveld, R. (2018). Integrated analysis of anatomical and electrophysiological human intracranial data. Nat Protoc, 13(7), 1699-1723. https://doi.org/10.1038/s41596-018-0009-6
5. Watkins, E. R., & Roberts, H. (2020). Reflecting on rumination: Consequences, causes, mechanisms and treatment of rumination. Behav Res Ther, 127, 103573. https://doi.org/10.1016/j.brat.2020.103573
6. Zhou, H. X., Chen, X., Shen, Y. Q., Li, L., Chen, N. X., Zhu, Z. C., Castellanos, F. X., & Yan, C. G. (2020). Rumination and the default mode network: Meta-analysis of brain imaging studies and implications for depression. Neuroimage, 206, 116287. https://doi.org/10.1016/j.neuroimage.2019.116287

Poster No 779

Neural connectivity associated with Psychological Well-Being in older Koreans

Hankyeong Lee[1], Sung-Ha Lee[2], Yoosik Youm[3], Jeanyung Chey[1]

[1]Seoul National University, Seoul, Korea, [2]Center for Happiness Studies, Seoul National University, Seoul, Korea, [3]Department of Sociology, Yonsei University, Seoul, Korea

Introduction: The psychological well-being (PWB) has been reported to be associated with physical (e.g., proinflammatory markers, mortality) and cognitive health in older adults. However, research on the neural underpinnings of the PWB remains notably insufficient. Here, we examined whether PWB in older Koreans exhibits a protective effect on cognitive and daily functions. Also, we explored the question of what brain functional connectivity serves as the mechanism underlying PWB.

Methods: 1. Participants: 128 individuals (aged 65 and above) were recruited residing in rural areas of South Korea in 2018, without a history of psychiatric or neurological conditions, and capable of undergoing a series of neuropsychological assessments. Among them, 65 individuals with feasible MRI scans were subjected to analysis. Furthermore, 107 and 65 participants from the initial cohort underwent additional longitudinal neurocognitive assessments in 2021 and 2023, respectively. 2. Measurement - Memory assessment: Using the Elderly Memory Scale (EMS), the working memory index was calculated through a composite of digit span and spatial span tests (forward and backward). - Daily Functioning: Instrumental activities of daily living (IADL) was inspected using an 11-item questionnaire. - Psychological well-being: Psychological Well-Being scale (PWB) was measured using Ryff's (1995) Psychological Well-Being Scale, consisting of 18 items. 3. Resting State Functional Connectivity: Resting-state fMRI was acquired using a 3T Siemens scanner with parameters including TR=2000ms, TE=30ms, FOV=240mm, and voxel size=3.0 x 3.0 x 3.0mm. Connectivity analysis, including preprocessing, was conducted using the CONN toolbox 22.a (Whitfield-Gabrieli & Nieto-Castanon, 2012). 4. ROI definition and group difference: To set the seed for PWB, we selected regions of interest (ROIs) deemed relevant to reward and threat based on prior studies (Reward: Left VMPFC, Left DMPFC, Left VLPFC, Left and Right Ventral Striatum; Threat: Left and Right Amygdala). Seed-to-voxel analysis was performed using these ROIs. Employing a median-split approach to categorize PWB high and low groups, we identified regions showing significant differences between the two groups. Z-transformed Fisher's correlation coefficients were extracted for subsequent regression analysis. 5. Statistical analysis: Using SPSS 26, Linear regression analyses were conducted. All analyses controlled for age, gender, and education, considering PWB showed significat correlations with these variables.

Results: 1. PWB was significantly associated with better Working Memory (β=0.279, p=0.015) and less longitudinal decline in IADL (β =0.311, p=0.031) after controlling for age, gender, and educational attainment. 2. Lower PWB was significantly associated with increased connectivity between threat-related regions and proximal, emotion related areas. Specifically, as PWB decreased, there is an increase in connectivity between the left amygdala and right planum temporal (β=-0.490, p<.001), left precentral gyrus (β =-0.343, p=.014), and right precentral gyrus (β=-0.353, p=.008). Similarly, the right amygdala and left postcentral gyrus (β=-0.349, p=.012), right precentral gyrus (β=-0.352, p=.010), and right postcentral gyrus (β=-0.317, p=.025) showed increased connectivity as PWB decreases. Conversely, as PWB decreases, connectivity between the right amygdala and right frontal pole (β=0.465, p=.001), right anterior paracingulate gyrus (β=0.312, p=.023), and right angular gyrus (β=0.447, p=.001) exhibited a decreasing pattern.

Conclusions: 1. Psychological Well-Being was systematically related with cognitive and daily living functioning of older adults. 2. Lower Psychological Well-Being may be associated with heightened sensitivity to threat stimuli, as indicated by increased connectivity between the amygdala and proximal emotion-related regions, along with decreased connectivity between the amygdala and distal regions associated with integrative and adaptive functioning.

References

1. Ryff, C. D., & Keyes, C. L. M. (1995). The structure of psychological well-being revisited. Journal of personality and social psychology, 69(4), 719.
2. Chey, J. Y. (2007). Elderly memory disorder scale. Seoul, Hakjisa.
3. Eisenberger, N. I., & Cole, S. W. (2012). Social neuroscience and health: neurophysiological mechanisms linking social ties with physical health. Nature neuroscience, 15(5), 669-674.
4. Whitfield-Gabrieli, S., & Nieto-Castanon, A. (2012). Conn: a functional connectivity toolbox for correlated and anticorrelated brain networks. Brain connectivity, 2(3), 125-141.

Poster No 780

Social Rejection affects Self-Evaluation of Incompetence: an fMRI Study

Yi Ding[1,2,3], Kentaro Oba[1], Ryo Ishibashi[1,4], Shinsuke Suzuki[5], Motoaki Sugiura[1,6]

[1]Institute of Development, Aging and Cancer, Tohoku University, Sendai, Japan, [2]Graduate School of Medicine, Tohoku University, Sendai, Japan, [3]Japan Society for the Promotion of Science, Sendai, Japan, [4]Center for Information and Neural Networks, National Institute of Information and Communications Technology, Osaka, Japan, [5]Department of Finance, Faculty of Business and Economics, The University of Melbourne, Melbourne, Australia, [6]International Research Institute of Disaster Science, Tohoku University, Sendai, Japan

Introduction: Although people tend to perceive themselves in a positive light, previous research has found that people evaluate their morality positively and their competence negatively[1,2]. Furthermore, negative self-evaluation occurs in both positive and negative conditions, which are associated with different motivations. Positive valence is linked to the self-enhancement motive and negative valence is linked to the self-protection motive. According to sociometric theory[3], social rejection drives people to alter their behavior to avoid being excluded by others. Thus, negative self-evaluation may derive from different interpersonal strategies aimed at avoiding social rejection. Neuroimaging findings revealed activation in the lateral prefrontal cortex including the inferior frontal gyrus (IFG), a region associated with cognitive control, during the self-referential process[4]. These findings may indicate that people may control their evaluation of competence and it is potentially linked to sense of social rejection. However, the relationship between brain activation during the self-referential process in different domains and the sense of rejection remains unclear. In this study, we aimed to investigate the relationships between the neural mechanism of the self-referential process in different domains and the sense of rejection. We hypothesized that during the self-referential process, activation of IFG in the competence condition instead of moral conditions would be associated with sense of social rejection, as a previous study found negative self-evaluation in competence domains[1]. We also expected that these associations may vary across positive and negative conditions.

Methods: We recruited forty-five healthy young adults (32 males; mean age = 21.60 ± 1.79). Participants were asked to complete both self- and other-evaluation using the same 80 adjectives. The adjectives were from four domains encompassing social values (morality and competence) and valences (positive and negative)[1]. To measure individual differences in social rejection, participants completed the Sense of Rejection scale after scanning. We used SPM12 in MATLAB to implement the preprocessing and 2-level analysis. In the first-level analysis, we modeled events of interest for the self and other evaluations as “Moral-Positive”, “Moral-Negative”, “Competent-Positive”, and “Competent-Negative”, respectively. The missing trials were modeled as events of no interest, and six estimated motion regressors were added to the model. For each modeled event of interest, we created the self > other contrast for each participant and entered it into a second-level group analysis. We performed four whole-brain correlations to identify brain regions involved in the self-referential process in the four conditions associated with sense of rejection. We used $P < 0.001$ as the initial uncorrected threshold and set the threshold to FWE-corrected $P < 0.05$ using cluster size.

Results: The results showed that sense of rejection was positively correlated with brain activation in the inferior frontal gyrus (IFG) during self-referential processing ([self>other]) when evaluating negative competence words. A previous study suggested that IFG might indicate an inhibition response to undesirable information[5]. Thus, those who felt more social rejection were more likely to inhibit their evaluation response during the self-referential process of negative competence words.

Conclusions: These results suggest that, in the context of self-protective motives, people may inhibit their intuitive responses when evaluating competence, and that such inhibited responses may be influenced by social exclusion. These findings

contribute to our understanding of the cognitive control process, which is associated with social rejection, occurring in negative self-evaluation. Moreover, it may imply the function of negative self-evaluation in interpersonal relationships.

References
1. Ding Y, Sugiura M (2021): Unique Prevalence of the Better-than-average Effect in the Moral Domain under Self-protection among Young Japanese Adults. PsyArXiv. https://psyarxiv.com/cw7bp/.
2. Yamagishi T, Hashimoto H, Cook KS, Kiyonari T, Shinada M, Mifune N, Inukai K, Takagishi H, Horita Y, Li Y (2012): Modesty in self-presentation: A comparison between the USA and Japan. Asian J Soc Psychol 15:60–68.
3. Leary MR, Tambor ES, Terdal SK, Downs DL (1995): Self-esteem as an interpersonal monitor: The sociometer hypothesis. J Pers Soc Psychol 68:518–530.
4. Sugiura M (2017): The Self-Trait Evaluation Task: Exodus from the Cortical Midline Structure Dogma. In: Tsukiura, T, Umeda, S, editors. Memory in a Social Context: Brain, Mind, and Society. Tokyo: Springer Japan. pp 119–145.
5. Sharot T, Kanai R, Marston D, Korn CW, Rees G, Dolan RJ (2012): Selectively altering belief formation in the human brain. Proc Natl Acad Sci USA 109:17058.

Poster No 781

Neural Signatures of Individual Differences in the Influence of Interoceptive Signals on Preference

Yuri Kim[1], Jinhee Kim[1], Hackjin Kim[1]

[1]Korea University, Seoul, Korea, Republic of

Introduction: Interoception, the ability to sense visceral signals, plays a pivotal role in recognizing oneself as an integrated individual, working in conjunction with exteroception. Previous research has shown that individual differences in interoception influence various psychological functions, including preference decisions. This study aims to identify the neural mechanisms involved in individual differences in the influence of interoceptive signals on preference and perceptual decisions.

Methods: Participants were instructed to choose between two movie titles based on either subjective preferences (preference condition) or the luminance of the characters written (luminance condition) during fMRI scanning. In each task condition, half of the trials were the congruent condition, where the more preferred movie had higher luminance, while the remaining trials were the incongruent condition, where the less preferred movie had higher luminance. The loss of efficiency in incongruent compared to the congruent condition during luminance task was used to assess the interference of stimulus-related external and self-related internal information, respectively. Interoceptive sensitivity was measured through the heartbeat counting task and self-reported survey.

Results: Repeated-measures analysis of variance on inverse efficiency scores (response time/accuracy) revealed a significant congruency effect (CE) in both task conditions, indicating that incongruency between preference and luminance information led to a loss of decision-making efficiency. Individuals with lower CE in the luminance task showed higher interoceptive awareness in both subjective and objective measures. Conjunction and contrast analysis of neural features at the preference and luminance decision onsets revealed that individuals with larger CE in the luminance task tend to involve the Superior Parietal Lobule (SPL), post- and precentral gyrus during both preference and luminance decisions. In contrast, individuals with lower CE in the luminance task showed higher activation at the rostromedial PFC (rmPFC) region during preference decisions compared to perceptual decisions.

Conclusions: This study suggests that individuals with less accurate interoceptive awareness engage a valuation mechanism that relies on external sensory information for both preference and non-preference decisions. In contrast, individuals with more accurate interoceptive awareness predominantly use an internal sensory information-based valuation mechanism, with a focus on the rmPFC, particularly when making preference decisions.

Acknowledgements
This research was supported by the Bio & Medical Technology Development Program of the National Research Foundation (NRF) funded by the Korean government (MSIT) (No. 2021M3E5D2A01022483; No. 2022M3E5E8018285) and the National Research Foundation of Korea (NRF) grant funded by the Korea government (MSIT) (No. RS-2023-00218987).

Poster No 782

Mapping the pre-reflective experience of "self" to the brain – an fMRI study

Maria Chiara Piani[1,2], Thomas Koenig[2], Martin Jandl[2], Julie Nordgaard[3], Yosuke Morishima[2]

[1]Graduate School of Health Sciences, University of Bern, Bern, Switzerland, [2]Translational Research Center, University Hospital of Psychiatry, University of Bern, Bern, Switzerland, [3]Department of Clinical Medicine, University of Copenhagen, Copenhagen, Denmark

Introduction: Selfhood is fundamental in human consciousness and has been divided into two main components: pre-reflective and reflective. Disorders at the pre-reflective level have been empirically demonstrated to constitute a psychopathological feature of schizophrenia spectrum disorders (Henriksen, 2021). Imaging studies have focused on reflective processes and point to the involvement of cortical midline structures (CMS) and default mode network (DMN). Additionally, some of the structures involved in reflective self-experience may also play a role in pre-reflective, particularly the medial prefrontal cortex (mPFC) (Northoff, 2006). With our study, we further investigated the neural correlates of the pre-reflective and reflective self-experience with a lexical task in functional magnetic resonance imaging (fMRI) in a sample of healthy adult volunteers.

Methods: The experimental protocol consisted of a trait-judgment task and a control task modified from Esslen et al. (2008). In the main task, participants expressed yes/no judgments on three-word phrases referring to themselves or someone they knew well. In the control task, used to assess a task specificity of results, participants made a yes/no decision about the color concordance between the words. In both tasks, a jitter was applied between pronouns and adjectives to separate activity associated with the pre-reflective component from the reflective component, and additional pronouns alone were randomly interspersed and displayed for 0.5 sec. The total duration of each task was 15 min. In the experiment, the pre-reflective component was hypothesized to occur at the level of pronouns, primarily first-person, while the reflective at the level of adjectives. The study sample included 32 healthy adult individuals (21F, 11M; mean age 24.4 ± 4.0 years). The structural and functional image acquisition was performed with a 7T MAGNETOM Terra Siemens scanner equipped with a 64-channel head coil. The MRI data were processed with SPM12 (Friston, 2003) and CAT12 (Gaser, 2016). In the first-level analyses, task conditions (self-pronoun, other-pronoun, self-adjective, other-adjective) were modeled. The subsequent group-level, random-effect analysis considered pronouns and adjectives, including self vs. other and other vs. self conditions, separately for the two tasks.

Results: In the trait-judgment task, at the level of pronouns, the analysis did not yield any significant difference between self and other-references. At the level of adjectives, we found a significantly higher activation in self- than in other-reference in the left frontpolar cortex (coordinates x, y, z: -26 60 20) and paracingulate cortex (-2 48 2), and in the right pre-supplementary motor area (pre-SMA) (4 20 60) ($p<0.001$, cluster family-wise error (cFWE) corrected). In contrast, we did not observe any significant difference in any of the conditions in the control task.

Conclusions: We can conclude that the fMRI modality is best suited to investigate self-reflective processes. Overall, the regions involved in self-reference in adjectives overlapped with brain areas involved in self-referential mentation (Northoff, 2006). Additionally, the control task has proven the specificity of our findings.

References

1. Esslen M. (2008), 'Pre-reflective and reflective self-reference: a spatiotemporal EEG analysis', NeuroImage, vol. 42, no. 1, pp. 437-49
2. Friston K. (2003), 'Statistical Parametric Mapping', Neuroscience Databases, vol. 85, pp. 237–250
3. Gaser C. (2016), 'Alzheimer"s Disease Neuroimaging Initiative. A Computational Anatomy Toolbox for the Analysis of Structural MRI Data', bioRxiv
4. Henriksen M. G. (2021), 'Self-disorders and psychopathology: a systematic review', The Lancet Psychiatry, vol. 8, no. 11, pp. 1001-1012
5. Northoff, G. (2006), 'Self-referential processing in our brain—A meta-analysis of imaging studies on the self', NeuroImage, vol. 31, no. 1, pp. 440–457

Poster No 783

Linking Hormonal Shifts during Pill Use Changes with Female Functional Brain Architecture and Mood

Ann-Christin Kimmig[1], Patrick Friedrich[2], Bernhard Drotleff[3], Michael Lämmerhofer[3], Inger Sundström Poromaa[4], Susanne Weis[2], Birgit Derntl[1]

[1]Department of Psychiatry and Psychotherapy, University of Tübingen, Tübingen, Germany, [2]Institute of Neuroscience and Medicine (INM-7), Research Centre Jülich, Jülich, Germany, [3]Institute of Pharmaceutical Sciences, University of Tübingen, Tübingen, Germany, [4]Department of Women's and Children's Health, University of Uppsala, Uppsala, Sweden

Introduction: The use of oral contraceptives (OC) has been associated with changes in functional brain architecture and socio-affective processes, specifically mood, with potential implications for mental well-being. OC-related depressive side-effects are expected to occur in a small subsample of hormone-susceptible OC users[1]. Nevertheless, flattening of positive mood was associated with the initiation of OCs in a longitudinal study[2]. Moreover, a recent placebo-controlled trial showed that OC use was linked to changes in functional brain connectivity, which were consistently associated with the OC-related emergence of adverse mood side-effects[3]. It has been suggested that OC intake could induce a hyper-progestogenic functional brain state[4]. However, previous studies have often been constrained by cross-sectional designs or failed to account for synthetic sex hormone concentrations. The aim of this study is to explore in a longitudinal design the association of changing hormone profiles with functional brain architecture in healthy young women and mood-related measures.

Methods: To this end, we conducted two fMRI scans on 88 young healthy women, with an interval of three to eight months between scans. The participants were categorized into four groups: 26 natural cycling women during menses, 26 long-term OC users in the active intake phase, 25 OC discontinuers, and 11 OC starters before and after discontinuation or initiation, respectively. We collected 3T anatomical (MP2Rage) and resting-state data, along with blood hormone samples and self-reported mood measures (including Beck's Depression Inventory and the Positive and Negative Affect Schedule). The resting-state and anatomical data underwent pre-processing with fMRIPrep, which included slice time correction and normalization to the MNI152Lin6Asym template. For the analysis of parcel-wise resting-state activity, BOLD timeseries were extracted from the 268 nodes of the Shen atlas, and a noise correction for white matter and cerebrospinal fluid was applied. The first eigenvariate of the activity time course per node was then computed. Pairwise Pearson correlations were calculated for each node with all other nodes and standardized. In addition to mean-based analyses of changes in hormone concentrations and mood-related measures, we employed inter-subject representational similarity analyses (IS-RSA) to explore relationships between interindividual variability across different measurement levels, including changes of hormone concentrations, resting-state functional connectivity (RSFC), and mood-related measures.

Results: Changes of RSFC in frontal, subcortical and cerebellar regions resembled the change patterns in progestogen levels (progesterone and progestin). Particularly noteworthy were the RSFC change patterns observed for the superior orbitofrontal gyrus (sOFG), which also corresponded with the change patterns of positive mood. Women who had more similar changes in progestogen concentrations, therefore, were also more similar regarding changes in sOFG RSFC and positive mood. Despite finding no correlation in the change patterns of depressive symptoms or negative affect with sex hormones or RSFC, the mean for depressive symptoms significantly decreased following the discontinuation of OCs.

Conclusions: In conclusion, changes in functional brain architecture and positive mood seem to be associated with shifts in progestogen profiles rather than estrogen concentrations, posing the sOFG as a possible neural correlate of OC-related changes in positive mood. Additionally, our findings support the notion that women who encounter adverse mood effects are more likely to stop using OCs, potentially contributing to their underrepresentation in research studies and causing an underestimation of the number of women dealing with mental health issues related to OC use. We thank the DFG, the German Academic Scholarship Foundation and the G.-A.-Lienert foundation for their financial support.

References

1. De Wit, A. E. (2021), 'Hormonal contraceptive use and depressive symptoms: systematic review and network meta-analysis of randomised trials', BJPsych Open, vol. 7, no. 4, e110
2. Lisofsky, N. (2016). 'Hormonal contraceptive use is associated with neural and affective changes in healthy young women', NeuroImage, vol. 134, pp. 597-606
3. Hidalgo-Lopez, E. (2023). 'Triple network model of brain connectivity changes related to adverse mood effects in an oral contraceptive placebo-controlled trial', Translational Psychiatry, vol. 13, no. 209
4. Casto, K. (2022), 'Hormone-based models for comparing menstrual cycle and hormonal contraceptive effects on human resting-state functional connectivity', Frontiers of Neuroendocrinology, vol. 67, 101036

Poster No 784

Decoding self-related networks in colour judgement task

Tzu-Yu Hsu[1]

[1]*Taipei Medical University, Taipei City, Taiwan*

Introduction: Self-related brain networks have been linked to cortical midline structure through self-oriented tasks involving self-referential stimuli such as one's name or autobiographical images. These were also highlighted with an alternative self-oriented task that utilises non-self-referential colour stimuli along with simple preference (self-related) or similarity (non-self) choices. However, this original study had limited statistical power due to the low sample size. To address this, we conducted a

replication study using an adapted version of the colour preference task with a larger sample size. Additionally, we used MVPA decoding techniques to determine which regions of the task-induced network can best differentiate between self-referential and non-self-referential task conditions.

Methods: 60 right handed, non-medicated, young adults (age, mean = 27.8, SD = 4.90) recruited from the student body of Taipei Medical University and locals residents through referral. T1 and T2* weighted images were collected with a Siemens Prisma 3T scanner and 64-channel head coil at National Taiwan University. Colour preference task consisted of three blocks, each contained a semi-random sequence of 70-trial colour choice trials. Data were preprocessed with fMRIPrep, followed by GLM analysis and permutation tests in FSL. Decoding analyses were conducted with custom scripts implemented with Python toolboxes.

Results: Self-related response results provided robust findings, demonstrating that midline structure brain regions and DLPFC activity are higher in the preference condition than in the similarity condition. Intriguingly, several brain regions in basal ganglia showed higher activation in the similarity condition in comparison to the preference condition. In our decoding analysis,we observed frontal and parietal networks has above chance decoding accuracy.

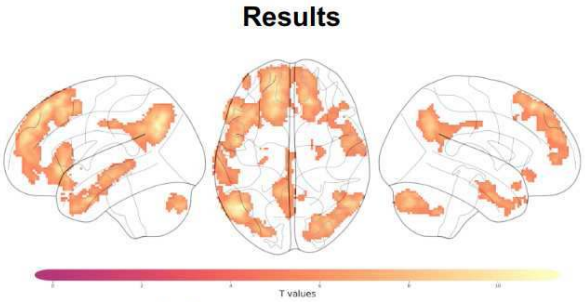

Figure 2A. Contrast preference > similarity

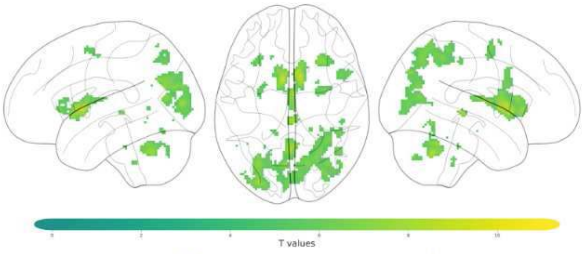

Figure 2B. Contrast similarity > preference

Conclusions: The task requirement in colour judgement task can probe the self-related networks. More importantly, frontal and parietal regions of this network plays a critical role in differentiate self-related and non-self-related processes. This provided evidence may contribute to the understanding of neural correlated of self consciousness.

References

1. Northoff G, Bermpohl F. (2004). 'Cortical midline structures and the self'. Trends Cogn Sci. 8(3), 102-7.
2. Qin P, Northoff G. (2011). 'How is our self related to midline regions and the default-mode network?' Neuroimage. 57(3), 1221-33.

Poster No 785

Human pheromones: How female body odors affect women's reactions to other women's faces

Elena Losse[1], Maya Armin[1], Susanne Nehls[1], Thilo Kellermann[1], Ute Habel[1], Natalia Chechko[1]

[1]RWTH University Hospital Aachen, Aachen, North Rhine-Westphalia

Introduction: In the animal kingdom, females signal their fertility via body odor changes depending on their reproductive and hormonal state. Growing evidence suggests similar mechanisms in humans. For women, olfactory signals contribute to intrasexual competition, enabling them to discriminate between other women's reproductive states via the scent. This evaluation appears to be additionally guided by the reproductive status of the evaluating woman. The aim of this study is to investigate whether and to what extent pheromones modulate human social communication and particularly, how women's menstrual cycle stages interact with this effect.

Methods: Axillary odor samples were collected from 12 women during ovulation and menstruation (mean age= 23.67 SD = 3.92) and 12 women in the first trimester of pregnancy (mean age = 28.33 SD = 3.28). 16 healthy, heterosexual, and single female participants (mean age = 22.69 SD = 2.73) participated in a functional MRI experiment twice, once while menstruating and once while ovulating. They were presented with female faces in combination with the body odors obtained during menstruation (ME), ovulation (OV) and pregnancy (PRG) as well as in combination with odorless air (no-odor condition; NO). Using a whole-brain analyses, differences in neural activity patterns were examined between the 4 odor conditions and across the two different menstrual cycle stages of the fMRI participants (cluster-forming threshold at voxel-level p <.001 uncorrected).

Results: The results revealed distinct activation patterns depending on the body odors as well as the participants' menstrual cycle stages. In ovulating participants, OV > NO and NO > PRG led to increased activation in the bilateral postcentral gyrus, superior parietal gyrus, precuneus, and the right paracentral lobule. In menstruating participants, ME led to increased activation in the right fusiform gyrus, parahippocampal gyrus and cerebellum (crus 4 and 5) when compared to NO, and in the bilateral anterior cingulum, right superior medial frontal gyrus and medial orbitofrontal gyrus when compared to PRG. Comparing activation differences between the two cycle stages of the participants revealed increased activity for ovulating compared to menstruating women for OV > ME in the right temporal lobe and right fusiform gyrus; when contrasting PRG > ME in the bilateral medial orbitofrontal gyrus, bilateral anterior cingulate cortex and bilateral superior medial frontal gyrus; and both, ME + OV > PRG, in the left inferior parietal lobule, supramarginal gyrus and postcentral gyrus.

Conclusions: A particular stage in a woman's menstrual cycle appears to be accompanied by a heightened sensitivity toward body odors of the same cycle stage, influencing the processing of other sensory input, e.g. faces. Ovulating women show increased sensory processing and integration, and a heightened attention toward the presented visual stimuli when exposed to other ovulating women's scent. This indicates that fertile women might detect potential sexual competitors via their odor which, from an evolutionary perspective, could benefit them in the intrasexual competition by allowing a closer assessment of a rival. Menstruating women contrarily, when presented with the body odor of likewise menstruating women, displayed higher sensitivity toward emotional facial cues and more complex emotional processing such as empathy. As this fertility phase presents no necessity for intrasexual competition, no evolutionary advantage would stem from increased critical evaluation of the counterpart. Rather, evoked feelings of empathy and sensitivity toward the facial signalling of affective states might even foster social cooperation. In general, ovulating women exhibited higher sensitivity via stronger activation patterns than menstruating women in response to the body odors of other women. In line with the aforementioned, this underlines the heightened relevance of detecting other women's cycle stage via the body odor for fertile women.

References

1. Derntl, B. & Hack, R. & Kryspin-Exner, I. & Habel, U. (2012). Association of menstrual cycle phase with the core component of empathy. Hormones and behavior. 63. 10.1016/j.yhbeh.2012.10.009.
2. Fisher, M. L. (2004). Female intrasexual competition decreases female facial attractiveness. Proceedings of the Royal Society of London. Series B: Biological Sciences. Royal Society. https://doi.org/10.1098/rsbl.2004.0160
3. Hahn, A. C., Fisher, C. I., Cobey, K. D., DeBruine, L. M., & Jones, B. C. (2016). A longitudinal analysis of women's salivary testosterone and intrasexual competitiveness. Psychoneuroendocrinology, 64, 117-122.
4. Kuukasjarvi S., Eriksson C.J.P., Koskela E., Mappes T., Nissinen K., Rantala M.J. (2004). Attractiveness of women's body odors over the menstrual cycle: the role of oral contraceptives and receiver sex. Behavioral Ecology, 15(4), 579–584. https://doi.org/10.1093/beheco/arh050
5. Paciello M., Fida R., Cerniglia L., Tramontano C., Cole E. (2013). High cost helping scenario: The role of empathy, prosocial reasoning and moral disengagement on helping behavior. Personality and Individual Differences, 55(1), 3–7.

Poster No 786

Unveiling White Matter Abnormalities in PTSD after Sexual Assault with Advanced Deep Neural Network

Seoyoung Lim[1], Jiook Cha[2]

[1]Seoul National University, Department of Brain and Cognitive Science, Seoul, Korea, [2]Seoul National University, Department of Psychology, Seoul, Korea

Introduction: Experiencing sexual assault can significantly increase the likelihood of developing posttraumatic stress disorder (PTSD). As delineated by the American Psychiatric Association in 2013, these manifestations can encompass PTSD symptoms such as recurrently reliving the distressing event, proactively evading its reminders, undergoing negative alterations in emotions and cognition. This study aimed to investigate the relationship between sexual assault and psychological trauma load and alterations in white matter intensity among sexual assault survivors particularly focusing on two distinct timeframes : initially at one month and subsequently after undergoing treatment, at a six-month period post-assault. Beyond statistical

based neuroimaging technique, this study leveraged deep learning transfer techniques informed by big data, alongside explainable artificial intelligence, to decode the intricate patterns of brain alterations in sexually abused adolescent girls.

Methods: In the initial phase of our study, we navigated the complex relationship between childhood trauma load, brain white matter features, and the onset of Post-Traumatic Stress Disorder (PTSD) symptoms in sexual assault survivors using regression analysis. Subsequently, our focus shifted towards scrutinizing the mediating role of white matter integrity in the progression of PTSD symptoms, particularly investigating how alterations in white matter might act as a neurological pathway translating sexual abuse trauma into PTSD symptomatology. We conducted a detailed examination across two different timeframes: one and six months following the sexual assault. To address the challenges presented by the small sample size and the previous variability in neuroimaging techniques, we leveraged a deep neural network approach; we utilized a pre-trained model developed with the Adolescent Brain Cognitive Development (ABCD) data similar to this PTSD study, transferring weights to a smaller dataset from sexual abuse survivors.

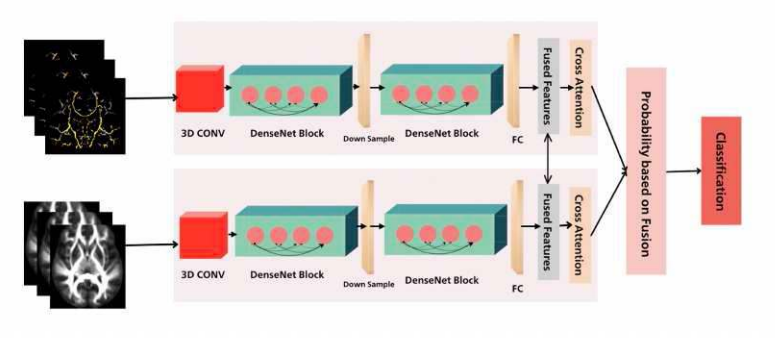

Figure 12: Overall Architecture of Cross-Attention Multimodal CNN

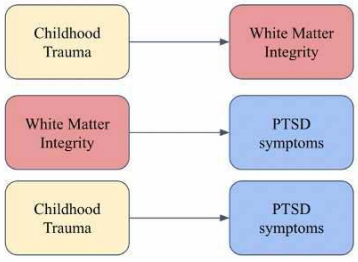

Figure 3-a

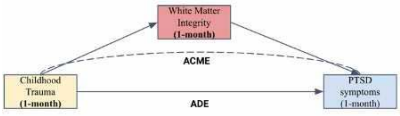

Figure 3 b

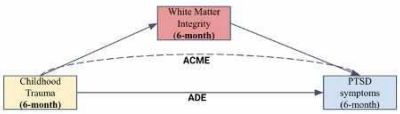

Figure 3 c

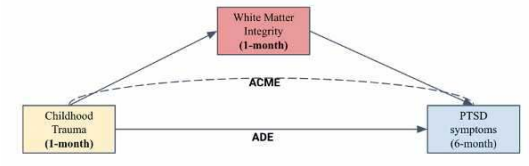

Figure 3 d

Results: In exploring the neural ramifications of childhood sexual abuse and its trajectory of PTSD, our study highlighted that Childhood Trauma Questionnaire (CTQ) sexual abuse scores markedly influenced Fractional Anistropy (FA) in the Corticospinal Tract,independent of age and sex considerations. At the 1-month follow-up, only the direct effects of sexual abuse on the brain were evident without extending to PTSD symptom, however only the Corticospinal Tract have the indirect effect on 6-month

PTSD symptom score as evidenced by an Average Causal Mediation Effect (ACME) of 0.040 (P-value <0.05,FDR corrected) and an Average Direct Effect (ADE) of 0.028 (P-value <0.05, FDR corrected). Furthermore, by the 6-month longitudinal assessment post-treatment, it was the emotional abuse that demonstrated effect on the Cingulum area, with an ACME of 0.048 (P-value <0.05, FDR corrected) and an ADE of 0.056 (FDR corrected). Further, using ABCD dataset, we developed a white matter specific deep neural network tailored to sexual abuse. The application of this model through transfer learning to the affected adolescent girls yielded a higher performance with an AUC exceeding the baseline by over 30%. Lastly, through explainable artificial intelligence, we confirmed the importance of the Corticospinal tract and cingulum regions in the model's learning process.

Conclusions: This study elucidated the impact of childhood trauma on brain structure and function. Focusing on children who have endured sexual abuse – a subset of trauma with distinct characteristics – our analyses have probed the specificity of such experiences on white matter alterations. Consequently, this study has demonstrated neuropathological changes associated with sexual abuse in adolescents.

References

1. Lim, S.*, Kim, B., Lee, S., Carolini, A., Cha, J. (In preparation). "Unveiling White Matter Abnormalities in PTSD after Sexual Assault with DTI and Advanced Deep Neural Network"

Poster No 787

Hemodynamic and electrophysiological responses of the human amygdala during face imitation

Tetsuya Iidaka[1], Satoshi Maesawa[1], Noriaki Kanayama[2], Makoto Miyakoshi[3], Tomotaka Ishizaki[1], Ryuta Saito[1]

[1]Nagoya University, Nagoya, Aichi, [2]AIST, Tsukuba, Ibaraki, [3]Cincinnati Children's Hospital Medical Center, Cincinnati, OH

Introduction: Mimicry of facial expressions is associated with emotional and social characteristics of human behavior; however, the precise mechanism underlying face imitation remains elusive. In the present study, we investigated neural activity in the human amygdala during an imitation task in which the imitation phase was temporally separated from the facial expression observation phase. We measured hemodynamic responses using fMRI in healthy participants and electrophysiological responses using intracranial electroencephalogram (iEEG) in patients with epilepsy.

Methods: The face imitation task involved 40 colored movies in which actors portrayed several different expressions (Fujimura and Umemura, 2018). The expressions were angry (negative), joyful (positive), and one with closing-eyes (neutral). Participants were instructed to pay attention to each of the facial expressions (movie task). After 2 seconds, a silhouette of the face and a question mark were simultaneously shown to the participants, who were instructed to imitate the expression of the actor that appeared immediately before (imitation task). Eighteen healthy individuals (14 females; mean age 21.6 years) participated in the fMRI experiment. The brains of the participants were scanned during the task using a 3T MRI system (Siemens Verio), with a multiband echo-planar imaging (EPI) acquisition (multiband factor = 3, TR = 1.0 s, TE = 30 ms) (Moeller et al., 2010; Xu et al., 2013). The fMRI data was preprocessed using SPM12 according to a standard protocol. Group level analysis was conducted using one-sample t-test to investigate differences between the expressions with a statistical threshold of p = 0.001, uncorrected for the peak level. Six male patients (mean age; 28.2 years) with medically refractory epilepsy participated in the iEEG experiment. The iEEG was recorded using a NicoletOne system (Gadelius Medical) with a sampling rate of 1024 Hz. In total, 13 and 17 electrodes inserted in the left and right amygdala, respectively in the 6 epilepsy patients. The iEEG data were processed using EEGLAB. The iEEG data were sorted according to negative, positive, and neutral conditions, and time-frequency analysis was subsequently performed. The difference of power in the high gamma band range (80-240Hz) between the conditions was investigated. The statistical threshold was set at $p < 0.05$ after false discovery rate (FDR) correction for multiple comparisons. In this report, only the results of the imitation task are presented for the both fMRI and iEEG experiments.

Results: In the fMRI experiment, the amygdala, in both the left and right hemispheres, was significantly more active in both the negative and positive conditions than in the neutral condition (Fig. 1). There was no significant difference in the degree of amygdala activation between the negative and positive conditions. The results of the iEEG time-frequency analysis showed that the negative condition had a significantly greater activity than the neutral condition in both the left and right amygdalae. Conversely, the positive condition showed greater activity than the neutral condition only in the right amygdala (Fig. 2). The differences in high gamma band activity were found in 500 ms after stimulus onset.

Conclusions: A similarity was found between the results of the fMRI experiment and those from the iEEG experiment; both showed that mimicry of facial expressions activated the amygdala significantly more under emotional conditions than under

non-emotional conditions. Time-frequency analysis of the iEEG data revealed that activity in response to mimicry was in the high gamma band range and the late time window. Since the facial image was not presented to the participants during the task, it is suggested that tactile information due to facial movement are conveyed to the amygdala. This information may be combined in the amygdalar nuclei with information from other modalities to initiate or modulate affective processing in humans.

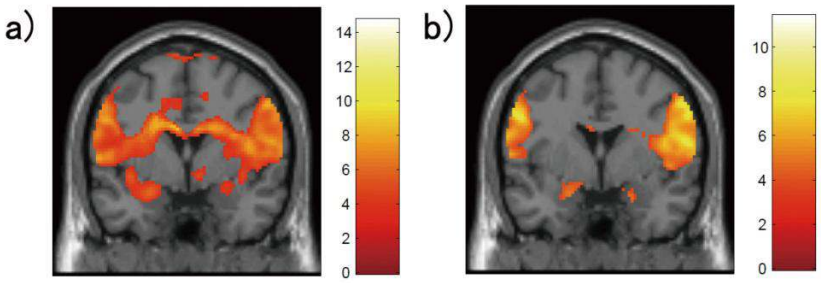

The results of fMRI experiment. a) The subtraction between the negative versus neutral condition. b) The subtraction between the positive versus neutral condition. The coronal slices are at y = 0 mm. Color bars indicate T value. The left side of the figure is the left side of the brain.

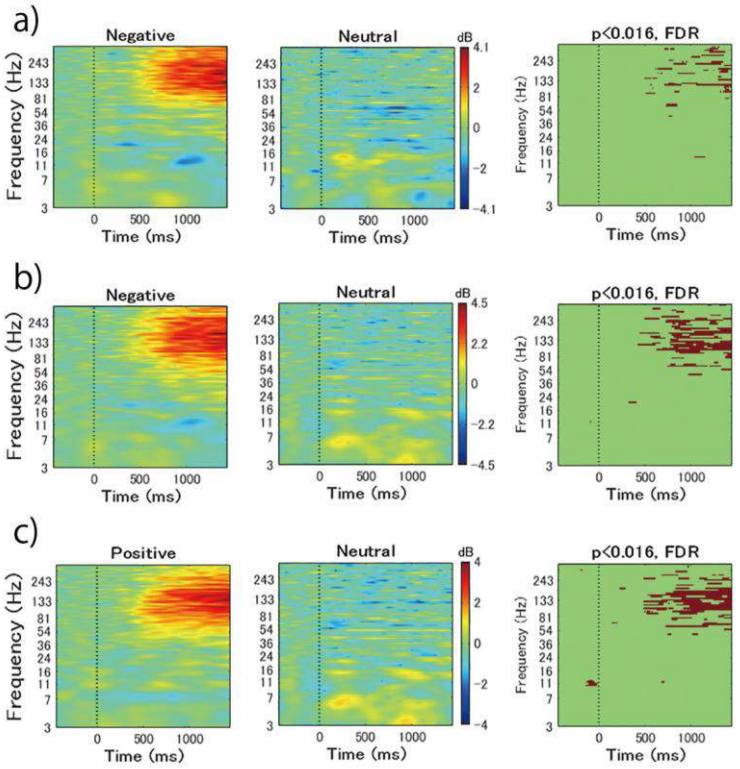

The results from pairwise t-tests of the time-frequency analysis between the conditions. The column on the right indicates the statistical results. (a) negative versus neutral condition in the left amygdala, (b) negative versus neutral condition in the right amygdala, (c) positive versus neutral condition in the right amygdala. Other comparisons did not survive the statistical threshold.

References

1. Fujimura, T., Umemura, H. (2018) 'Development and validation of a facial expression database based on the dimensional and categorical model of emotions' Cognition and Emotion, 32, pp. 1663-1670.
2. Moeller, S., Yacoub, E., Olman, C. A., Auerbach, E., Strupp, J., Harel, N., Ugurbil, K. (2010) 'Multiband multislice GE-EPI at 7 tesla, with 16-fold acceleration using partial parallel imaging with application to high spatial and temporal whole-brain fMRI' Magnetic Resonance in Medicine 63, pp. 1144-1153.
3. Xu, J., Moeller, S., Auerbach, E. J., Strupp, J., Smith, S. M., Feinberg, D. A., Yacoub, E., Ugurbil, K. (2013) 'Evaluation of slice accelerations using multiband echo planar imaging at 3 T' Neuroimage 83, pp. 991-1001.
4. SPM12, https://www.fil.ion.ucl.ac.uk/spm
5. EEGLAB, ver. 2019.0 https://sccn.ucsd.edu/eeglab/

Poster No 788

Elevated Frontal Brain Activity in Social Cognition - A Risk Marker of Bipolar Disorder?

Dahna Choi[1], Katharina Förster[1], Malin Hildebrandt[2], Lara Maliske[1], Konrad Lehmann[1], Philipp Kanske[1], Emanuel Jauk[3]

[1]Clinical Psychology and Behavioral Neuroscience, Technische Universität Dresden, Dresden, Germany, [2]Addiction Research, Technische Universität Dresden, Dresden, Germany, [3]Medical Psychology and Psychotherapy, Medical University of Graz, Graz, Austria

Introduction: The identification of endophenotypes is of great importance for characterizing individuals at risk for psychiatric disorders. Especially in the case of bipolar disorders (BD), these research endeavors are imperative considering that the frequently delayed diagnoses and longer illness durations are associated with symptom exacerbation and lower recovery rates. In the present study, we investigated the role of social affect and -cognition as potential endophenotypes of BD. To this end, in a community sample (N = 140), we tested our preregistered hypotheses (https://osf.io/kh2tv) on associations between hypomanic personality traits as a marker of BD risk and behavioral and neural measures of empathy and ToM from an fMRI paradigm (EmpaToM). In consideration of indications from previous studies, we hypothesized behavioral empathy and task-based neural activity in empathy-related ROIs to be positively associated with hypomanic personality traits, and behavioral ToM performance and task-based neural activity in ToM-related ROIs to be negatively associated with hypomanic personality traits.

Methods: Data were acquired in the scope of a larger study (Hildebrandt et al., 2021; Jauk et al., in press). As a measure of social affect and -cognition, we used the EmpaToM, a naturalistic fMRI paradigm assessing behavioral and neural correlates of empathy and ToM (Kanske et al., 2015). For assessing hypomanic personality traits, data from the the Hypomanic Personality Scale (HPS) were analyzed. Exploratory whole-brain analyses as well as more targeted ROI analyses were performed. Based on findings from previous neuroimaging research (Kanske et al., 2015; Miskowiak et al., 2017; Schurz et al., 2021), bilateral inferior frontal gyri pars orbitalis (IFG), bilateral angular gyri, precuneus, and left cerebellum were selected as empathy-ROIs, while ToM-ROIs comprised bilateral triangular parts of the IFG, left posterior cingulate gyrus, two areas in the middle temporal gyrus, right cerebellum, and bilateral superior medial frontal cortices (mPFC). Additional whole brain analyses were calculated at a voxel-level threshold of $p < .001$ (uncorrected) with a cluster threshold of $k > 10$ contiguous voxels. For all linear regression and t-test analyses in R, a standard threshold of $p < .05$ (uncorrected) was taken as the inference criterion for hypothesis testing. Analyses were conducted by means of multiple linear regressions, testing for associations between the HPS and the respective dependent variables. In each regression model, study participants' sex and age were added as control covariates into the model.

Results: Linear regression analyses revealed a significant effect of the HPS on ToM-related neural activity in the right mPFC ($\beta = .171$, $p = .046$). In the scope of exploratory whole-brain-analyses, results indicate further ToM-related neural activity to be positively associated with the HPS, mainly located in a cluster in the rostral anterior cingulate cortex (ACC, $x = 3$, $y = 33$, $z = 6$; $k = 31$, voxel level: $p < .001$). Analyses on behavioral ToM yielded no significant results regarding the effect of the HPS on behavioral ToM performance ($p = .582$). There were no significant results on the effect of the HPS on behavioral nor neural correlates of empathy (all $p > .05$).

Conclusions: Based on our study findings, we suggest elevated mPFC and ACC activity in association with BD risk to conceivably indicate additional resources that are activated in situations demanding socio-cognitive functioning. We encourage further research endeavors to investigate socio-affective and -cognitive mechanisms in differentially characterized BD-risk populations. Prospectively, our study contributes to driving towards a more comprehensive and potentially neurobiologically grounded phenotype of BD risk for a more differential understanding of risk and resilience mechanisms.

References

1. Hildebrandt, M.K., et al. (2021), 'Brain Activation during Social Cognition Predicts Everyday Perspective-Taking: A Combined fMRI and Ecological Momentary Assessment Study of the Social Brain', NeuroImage, vol. 227
2. Jauk, E., et al. (in press), 'Psychological and Neural Correlates of Social Affect and Cognition in Narcissism: a Multimethod Study of Self-Reported Traits, Experiential States, and Behavioral and Brain Indicators'
3. Kanske, P., et al. (2015), 'Dissecting the Social Brain: Introducing the EmpaToM to Reveal Distinct Neural Networks and Brain–Behavior Relations for Empathy and Theory of Mind' NeuroImage, vol. 122, pp. 6–19
4. Miskowiak, K.W., et al. (2017), 'The Search for Neuroimaging and Cognitive Endophenotypes: A Critical Systematic Review of Studies Involving Unaffected First-Degree Relatives of Individuals with Bipolar Disorder', Neuroscience & Biobehavioral Reviews, vol. 73, pp. 1–22.
5. Schurz, M., et al. (2021), 'Toward a Hierarchical Model of Social Cognition: A Neuroimaging Meta-Analysis and Integrative Review of Empathy and Theory of Mind', Psychological Bulletin, vol. 147, no. 3, pp. 293–327

Poster No 789

Agency to Choose Social Information Enhances Peer Influence in Adolescent Risky Decision-making

Shuhan Wang[1,2], John Wang[1], Natalie Melville[1], Mark Orloff[3], Matthew Caton[1], Pearl Chiu[1,2], Brooks Casas[1,2]

[1]Fralin Biomedical Research Institute at Virginia Tech Carilion, Roanoke, VA, [2]Department of Psychology, Virginia Tech, Roanoke, VA, [3]Center for Mind and Brain, University of California, Davis, CA

Introduction: Adolescence is a unique developmental stage often identified with more engagement in risky behaviors. While evidence suggests that peer influence contributes to the spread of risk-taking among adolescents[2], little attention has been paid to how adolescents receive peer influence impacts their behavior. Given prior work showing that in non-social contexts, information acquired under agency becomes more valuable[3], we examine in adolescents whether autonomously chosen (i.e., under agency) or passively provided social information potentially leads to different extents of peer influence and attendant neural responses.

Methods: Participants: 46 adolescents were recruited in this study around Roanoke, Virginia. After applying exclusion criteria, we analyzed data from 37 participants (22 females; age = 13.24 ± 0.44). Experimental Design: We used a risky decision-making paradigm[1] in which participants made sequential choices between a safer and a riskier monetary gamble, either after seeing the choices of others (Info trial) or alone (Solo trial). On Info trials, participants were shown the choices of two anonymous social peers before they made their own choices. On Solo trials, participants made choices without viewing social others' choices. To evaluate the effects of agency on peer influence, these trials were shown under 'Choice' or 'No-Choice' conditions. In the 'Choice' condition, participants decided whether or not to view others' choices, and in the 'No-Choice' condition, a computer algorithm pseudorandomly selected whether social information was displayed. Computational Modeling: To quantify the impact of social information on adolescent risky choices, we adapted a behavioral economic utility model with parameters capturing the value of social information (other-conferred-utility), risk preference, inverse temperature, and the effect of agency on each of these. All parameters were fit using hierarchical Bayesian inference. Alternative models were compared using leave-one-out cross-validation estimation. fMRI Analysis: Functional and structural brain images were acquired in a 3T Siemens Prisma during the task. The echo-planar images were preprocessed using Statistical Parametric Mapping 12, using a standard preprocessing pipeline. Separate design matrices were constructed to evaluate the BOLD signal when viewing social others' choices on Info trials.

Results: Adolescent choices are influenced by social others, as evidenced by greater than chance selection of the options chosen by social others (t(36) = 2.05, p = .047 for No-choice condition, t(36) = 3.34, p = .002 for Choice condition). Modeling results reveal that larger utility is conferred to the gambles chosen by social others in the Choice condition than in the No-choice condition (t(36) = 2.61, p = .013), indicating an increased value of social information under agency. Furthermore, vmPFC response tracks the utility of this social information (r = .37, p = .029 for No-choice condition; r = .37, p = .027 for Choice condition; Figure 1A). Participants with greater change in the utility of social information also show greater change in the activation of vmPFC across conditions (t(17) = 2.68, p = .016; Figure 1B). dACC is less activated in the Choice relative to the No-Choice condition when viewing social information (peak-level pFWE =.004; Figure 1C).

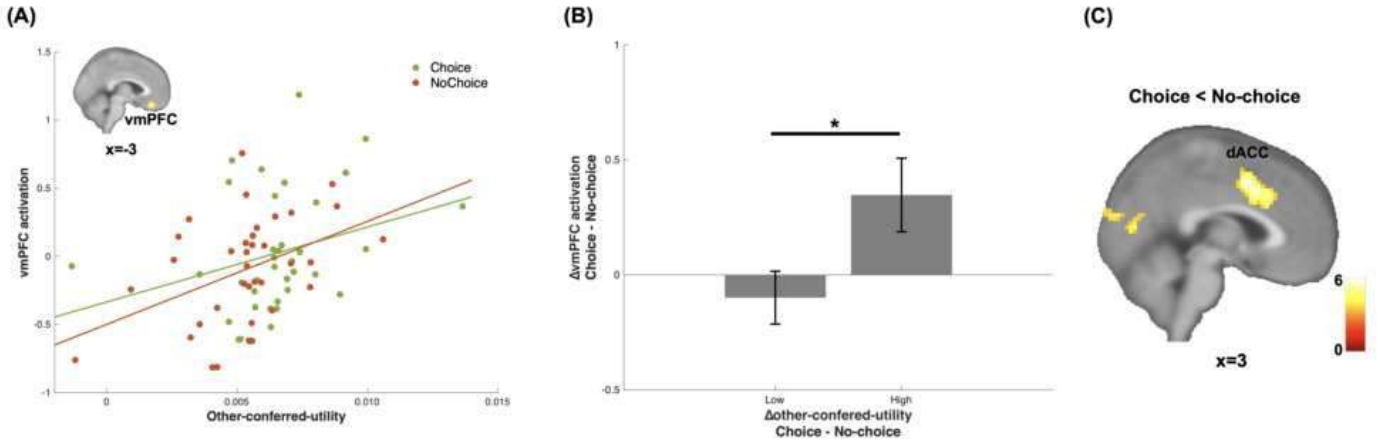

Figure 1. (A) Other-conferred-utility is significantly correlated with the activation of vmPFC when viewing social others' choices in both conditions, indicating a unified valuation system of social information. Region of interest used for vmPFC is shown on the top left penal. **(B)** Participants with greater change in other-conferred-utility ($OCU_{Choice} - OCU_{No\text{-}choice}$) also had significantly greater change in vmPFC activation ($vmPFC_{Choice} - vmPFC_{No\text{-}choice}$) across conditions, verifying the value of social information is encoded in vmPFC. Error bars represent s.e.m. *p<.05. **(C)** Whole brain analysis revealed a significantly less activation in dACC in Choice condition when viewing social others' choices. This is potentially related to the resolved conflict between multiple sources contributing to risky choice, since they choose the social information autonomously. Displayed at p<.001 uncorrected, k > 20 voxels, dACC is significant at p<.05 FWE.

Conclusions: These results support the hypothesis that in adolescents, social information acquired under agency is associated with greater value than the same information acquired passively. This increased value is associated with enhanced peer influence on choices about risky options. Regardless of agency condition, we observe valuation signals in vmPFC that encode the utility of social information. Acquiring social information with agency leads to decreased activation in the dACC, suggesting less decision conflict when adolescents make choices with agency to view social information.

References
1. Chung, D. (2015). Social signals of safety and risk confer utility and have asymmetric effects on observers' choices. Nature neuroscience, 18(6), 912-916.
2. Ciranka, S. (2019). Social influence in adolescent decision-making: A formal framework. Frontiers in psychology, 10, 1915.
3. Leotti, L. A. (2011). The inherent reward of choice. Psychological science, 22(10), 1310-1318.

Poster No 790

Empathising-systemising along the unimodal-transmodal axis

Marcin Radecki[1,2], Amin Saberi[3,4,5], Bin Wan[3,4], Dorothea Floris[6,7,8], Richard Bethlehem[9], Meng-Chuan Lai[2,10,11], Michael Lombardo[12], Luca Cecchetti[1], Simon Baron-Cohen[2], Sofie Valk[3,4,5]

[1]Social and Affective Neuroscience Group, IMT School for Advanced Studies Lucca, Lucca, Italy, [2]Autism Research Centre, Department of Psychiatry, University of Cambridge, Cambridge, United Kingdom, [3]Otto Hahn Group Cognitive Neurogenetics, Max Planck Institute for Human Cognitive and Brain Sciences, Leipzig, Germany, [4]Institute of Neuroscience and Medicine (INM-7: Brain and Behaviour), Research Centre Jülich, Jülich, Germany, [5]Institute of Systems Neuroscience, Heinrich Heine University Düsseldorf, Düsseldorf, Germany, [6]Methods of Plasticity Research, Department of Psychology, University of Zürich, Zürich, Switzerland, [7]Donders Institute for Brain, Cognition and Behaviour, Radboud University, Nijmegen, Netherlands, [8]Department of Cognitive Neuroscience, Radboud University Medical Center, Nijmegen, Netherlands, [9]Department of Psychology, University of Cambridge, Cambridge, United Kingdom, [10]The Margaret and Wallace McCain Centre for Child, Youth & Family Mental Health and Azrieli Adult Neurodevelopmental Centre, Campbell Family Mental Health Research Institute, Centre for Addiction and Mental Health, Toronto, ON, Canada, [11]Department of Psychiatry, Temerty Faculty of Medicine, University of Toronto, Toronto, ON, Canada, [12]Laboratory for Autism and Neurodevelopmental Disorders, Istituto Italiano di Tecnologia, Rovereto, Italy

Introduction: The unimodal-transmodal gradient of functional organisation (G1)[1] was shown to differentially situate meta-analytic activations underlying cognitive and affective empathy – understanding others' mental states and responding to them with an appropriate emotion, respectively[2]. Leveraging this empathic distinction, we hypothesised that G1 reflects the "D-score" – the drive to systemise (understand and build systems) relative to empathise, as proposed by the Empathising-Systemising (E-S) theory[3].

Methods: We included 100 typical adults (Mage = 29 ± 7 years, range = 18-48; 43 F) with two 3T multi-band resting-state acquisitions[4]. For each participant, two 32k-fsLR time series were parcellated using multimodal solutions[5] (Fig. 1A), functional-connectivity (rsFC) matrices were averaged, and 10 gradients were extracted via diffusion-map embedding with normative HCP gradients (N = 207[6]) as the reference (Fig. 1B) in a Procrustes alignment[7] (Fig. 1C). G1 loadings were averaged within: two meta-analytically thresholded empathy clusters (Cognitive and Affective)[2]; four novel empathy clusters building on these (Fig. 1E); and seven canonical rsFC networks[8] (Fig. 1D). The D-score was the difference between standardised scores on the 40-item Empathy Quotient (EQ) and 75-item Systemising Quotient-R (SQ)[9]. From each score, we subtracted the mean and divided the outcome by the maximum possible score, such that D-score = S – E (i.e. the higher the D-score, the stronger the drive to systemise relative to empathise). Based on the D-score percentiles, we identified those of Type E ("empathisers"; 0-35th), Type B ("balanced"; 35-65th), and Type S ("systemisers"; 65-100th) [9, 10]. The EQ and SQ had good-to-excellent internal consistency (Cronbach's α = 0.89 and 0.92) and explained 40 and 28% of the variance in the D-score, respectively.

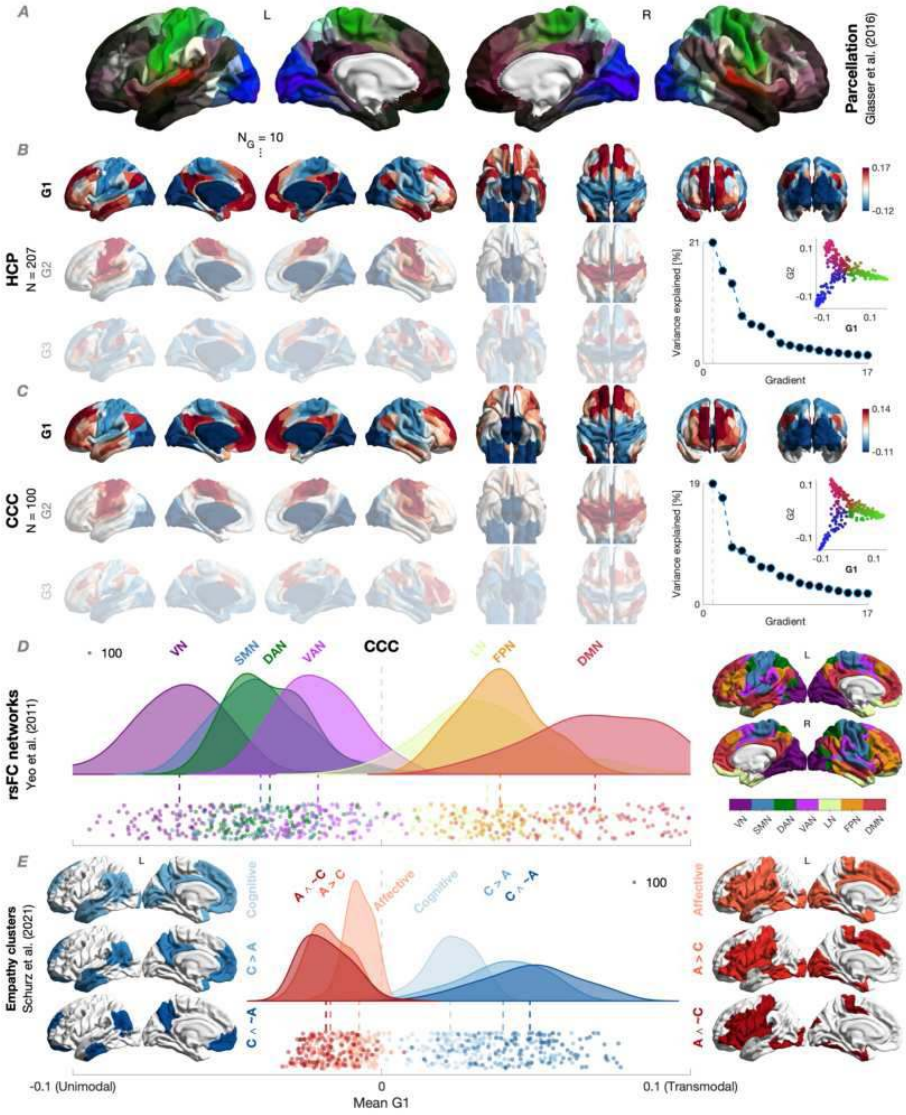

Results: First, we tested whether mean G1 loadings within four empathy clusters (Fig. 2A) had an effect on the D-score, controlling for age and sex in a robust linear regression. A > C G1 had a positive effect on the D-score following Bonferroni correction (βZ = 0.25 [95% CI: 0.06, 0.44], PBon = 0.039, adj. R2 = 0.16) (Fig. 2B). Next, we tested whether these clusters differed by E-S type. Similarly, A > C G1 differed by E-S type following Bonferroni correction (F[2, 95] = 6.02, PBon = 0.014, adj. R2 = 0.24), becoming progressively transmodal from Type E to Type S – although these two groups differed on every cluster (Fig. 2C). Next, we tested the effect of G1 loading within each parcel on the D-score. No parcel survived FDR correction (all PsFDR ≥ 0.660) (Fig. 2D). Finally, we spatially correlated these standardised D-score betas with two raw empathy maps and two thresholded empathy clusters excluding null parcels (Fig. 2E). Following 1,000 spin permutations, the D-score map correlated negatively with the Cognitive cluster (Spearman's ρ = -0.50, Pspin = 0.001, Nparcel = 158), such that a stronger meta-analytic loading of the parcel reflected its stronger unimodal relationship with the D-score. Conversely, the D-score map correlated positively with the Affective map (Spearman's ρ = 0.34, Pspin = 0.017, Nparcel = 360), such that a stronger meta-analytic loading of the parcel reflected its stronger transmodal relationship with the D-score (Fig. 2F).

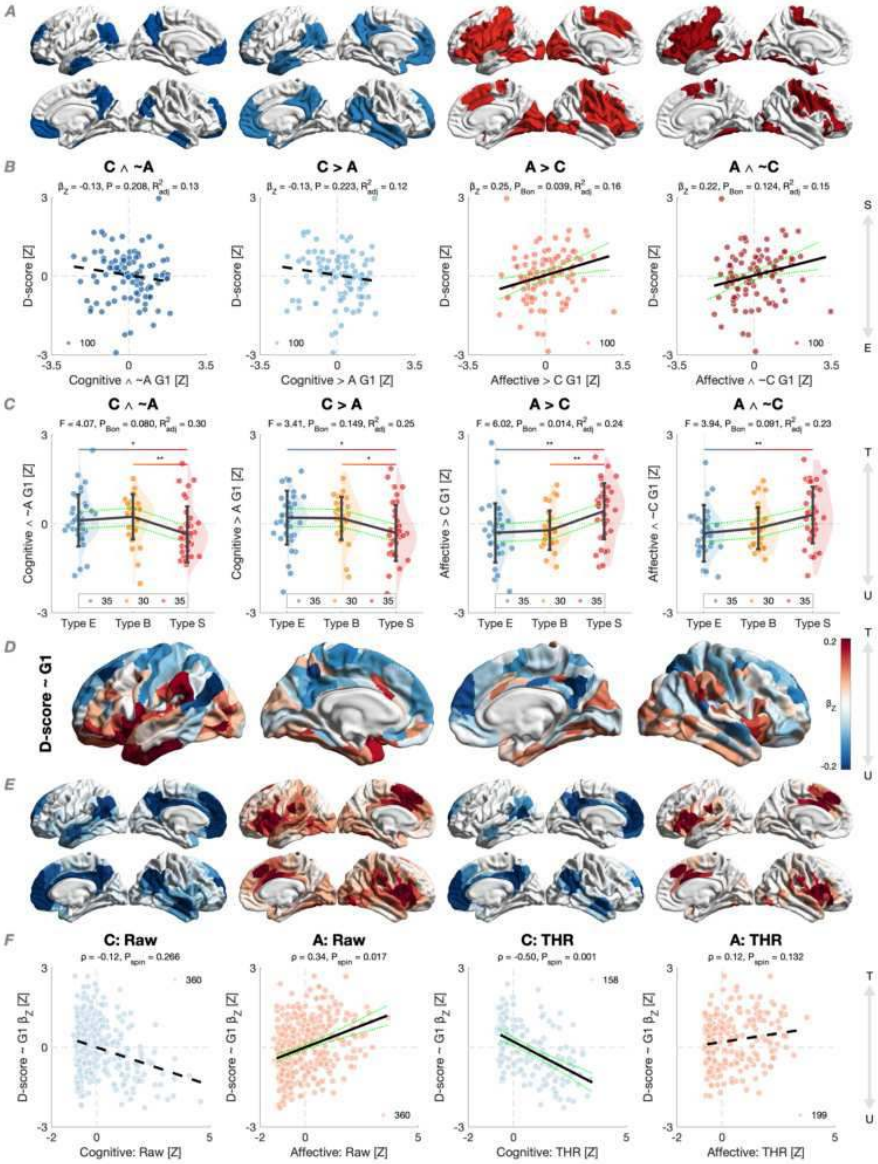

Conclusions: A > C G1 correlated positively with the D-score and differed by E-S type; a stronger transmodal loading within this cluster reflected a stronger drive to systemise relative to empathise. As reflected in G1 across the cortex, the D-score showed opposite relationships with meta-analytic cognitive and affective empathy, further suggesting the importance of this distinction for the D-score in the brain. We will probe these findings using independent data and in a neurodevelopmental condition well-characterised in relation to E-S – autism [3, 9, 10].

References

1. Margulies, D. S. et al. (2016). Situating the default-mode network along a principal gradient of macroscale cortical organization. Proceedings of the National Academy of Sciences of the United States of America, 113(44), 12574–12579. https://doi.org/10.1073/pnas.1608282113
2. Schurz, M. et al. (2021). Toward a hierarchical model of social cognition: A neuroimaging meta-analysis and integrative review of empathy and theory of mind. Psychological Bulletin, 147(3), 293–327. http://doi.org/10.1037/bul0000303
3. Baron-Cohen, S. (2002). The extreme male brain theory of autism. Trends in Cognitive Sciences, 6(6), 248–254. https://doi.org/10.1016/s1364-6613(02)01904-6
4. Kliemann, D. et al. (2022). Caltech Conte Center, a multimodal data resource for exploring social cognition and decision-making. Scientific Data, 9(1), 138. https://doi.org/10.1038/s41597-022-01171-2
5. Glasser, M. F. et al. (2016). A multi-modal parcellation of human cerebral cortex. Nature, 536(7615), 171–178. https://doi.org/10.1038/nature18933
6. Larivière, S. et al. (2021). The ENIGMA Toolbox: Multiscale neural contextualization of multisite neuroimaging datasets. Nature Methods, 18(7), 698–700. https://doi.org/10.1038/s41592-021-01186-4
7. Vos de Wael, R. et al. (2020). BrainSpace: A toolbox for the analysis of macroscale gradients in neuroimaging and connectomics datasets. Communications Biology, 3(1), 103. https://doi.org/10.1038/s42003-020-0794-7
8. Yeo, B. T. T. et al. (2011). The organization of the human cerebral cortex estimated by intrinsic functional connectivity. Journal of Neurophysiology, 106(3), 1125–1165. https://doi.org/10.1152/jn.00338.2011

9. Wheelwright, S. et al. (2006). Predicting Autism Spectrum Quotient (AQ) from the Systemizing Quotient-Revised (SQ-R) and Empathy Quotient (EQ). Brain Research, 1079(1), 47–56. https://doi.org/10.1016/j.brainres.2006.01.012
10. Greenberg, D. M. et al. (2018). Testing the Empathizing-Systemizing theory of sex differences and the Extreme Male Brain theory of autism in half a million people. Proceedings of the National Academy of Sciences of the United States of America, 115(48), 12152–12157. https://doi.org/10.1073/pnas.1811032115

Poster No 791

The Value Expectation Bias in Test Anxiety Individuals: Test Specificity or Threat Generality?

Yuhong Ou[1], Renlai Zhou[1]

[1]Nanjing University, Nanjing, Jiangsu

Introduction: The value expectation (reward or punishment) of outcomes based on experience and current information (Inzlicht et al., 2018) decides whether to do and how much effort to put into performing the current task (Shenhav et al., 2013). Individuals with test anxiety have difficulty inhibiting test-related and test-unrelated threat stimuli (Zhang et al., 2019; Wei et al., 2021). We suggested that the excessive negative value expectation for threat stimuli played an important role. Thus, the current study investigated the value expectation towards test-related and test-unrelated threat stimuli in test anxiety individuals.

Methods: 27 high test anxiety individuals (HTA) (15 females) and 29 low test anxiety individuals (LTA) (22 females) were invited. The improved simple gambling task was employed. In this experiment, the two options were cards with test-related or test-unrelated threat words on the one side and cards with test-unrelated neutral words on the other side. The participants were informed that they had to try their best to explore the pattern between the option and feedback and obtain more benefits. The probability of both positive and negative feedback occurring was 50%. An electroencephalogram (EEG) was recorded continuously using a 64 Ag-AgCl electrodes elastic cap. EEGLAB (Version 13.0.0.1b) was used for off-line analysis. The FRN, △FRN(230-330ms), and P3 (340-440ms) components induced by feedback were analyzed. Letswave7 was used for time-frequency analysis. The ERD (300-500ms) in the theta (4-7Hz) band and the ERS (200-400ms) in the beta (13-18Hz) band were analyzed.

Results: FRN: The interaction among stimulus attribute, feedback type, and test anxiety was significant, $F(3,162)= 7.209$, $p<.001$. In the HTA group, both the test-related and test-unrelated threat stimuli induced a greater positive FRN amplitude than the corresponding neutral conditions following positive feedback. Conversely, the FRN amplitude induced by negative feedback was more negative in the test-related and test-unrelated threat conditions compared to the corresponding neutral conditions. No differences were observed in the LTA group. Moreover, the FRN amplitude induced by negative feedback following test-related and test-unrelated threat stimuli was significantly more negative in the HTA group than in the LTA group. △FRN: The interaction between stimulus attribute and test anxiety was significant, $F(2,108)= 3.532$, $p<.05$. A more negative FRN difference was induced by the test-related and test-unrelated threat stimuli in the HTA group. No differences were observed in the LTA group. In addition, the HTA group showed a more negative FRN difference wave than the LTA group in the test-related condition. P3: No significant interaction was found. Theta: No significant interaction was found. Beta: The interaction among stimulus attribute, feedback type, and test anxiety was significant, $F(3,162)= 2.904$, $p<.05$. In the LTA group, under the positive feedback condition, the ERD power after the neutral stimuli in the test-unrelated condition was stronger than those in the test-related condition. In the HTA group, under the negative feedback condition, the ERD power after test-related stimuli was stronger than those after test-unrelated stimuli; The ERD power after test-unrelated stimuli was weaker than those after the neutral stimuli. Additionally, it was found that the ERD power induced by negative feedback after test-unrelated stimuli was weaker in the HTA group than in the LTA group.

Conclusions: Firstly, individuals with HTA showed weaker reward sensitivity and stronger punishment sensitivity towards both test-related and unrelated threat stimuli, which indicated the individuals with HTA had a negative value expectation for threat stimuli. Secondly, the individuals with HTA had a more negative value expectation for test-related stimuli.

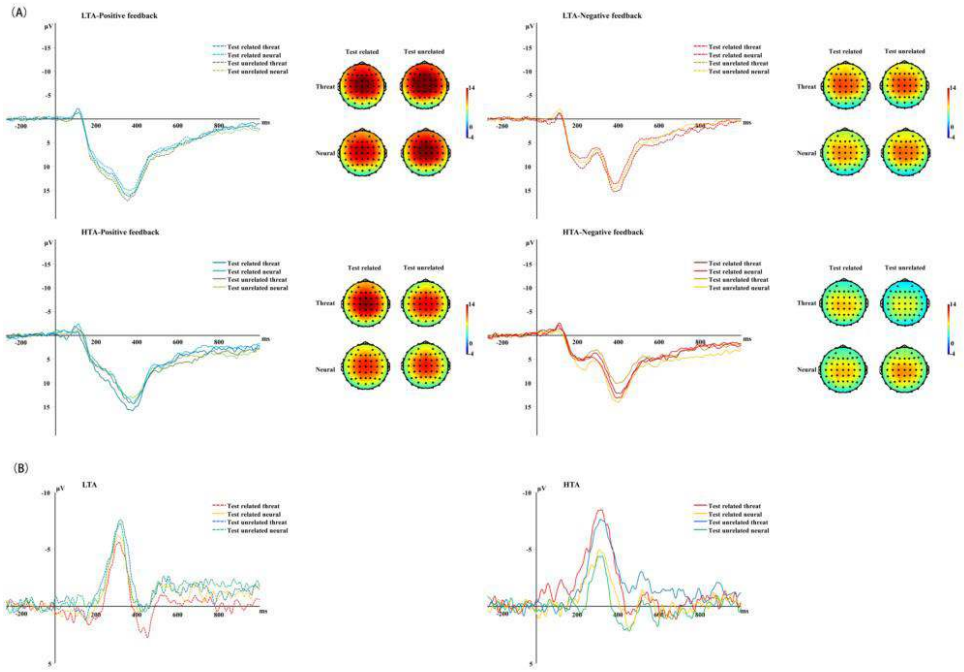

Figure 1. ERP results. (A) The average FRN at Fz and its topographical distribution for all conditions. (B) The average FRN difference wave at Fz for all conditions.

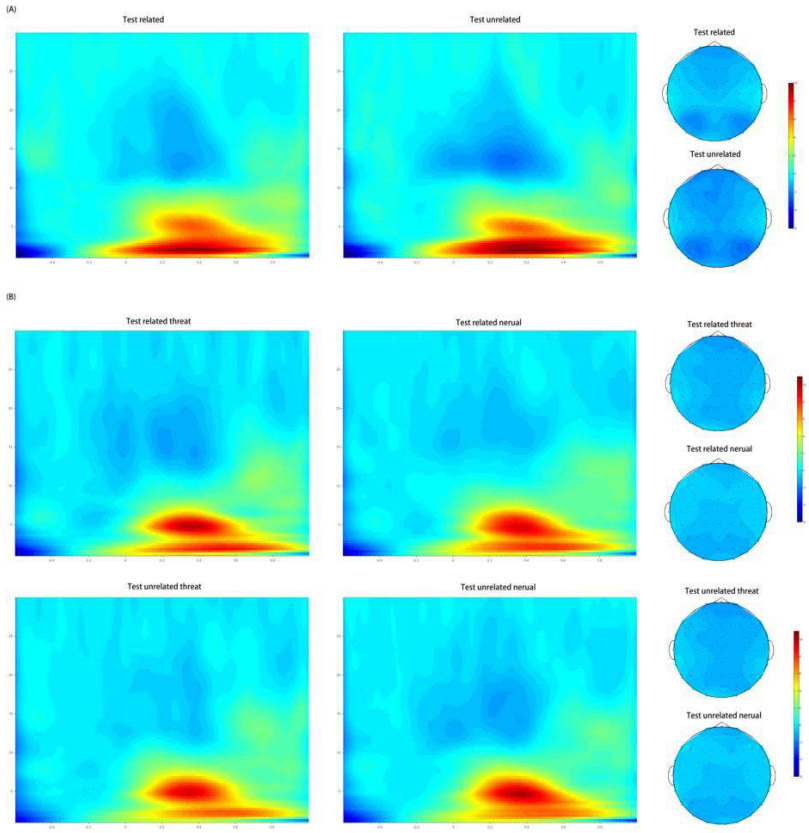

Figure 2. ERSP results in the beta band. (A) LTA: The ERD (power) at Fz for the neutral stimuli in the test-related and test-unrelated conditions under the positive feedback condition. (B) HTA: The ERD

Poster No 792

Perceiving social interactions implicitly engages typical theory of mind areas

Zizhuang Miao[1], Heejung Jung[1], Philip Kragel[2], Patrick Sadil[3], Martin Lindquist[3], Tor Wager[1]

[1]Dartmouth College, Hanover, NH, [2]Emory University, Atlanta, GA, [3]Johns Hopkins University, Baltimore, MD

Introduction: Experimental paradigms investigating the neural correlates of social interaction perception and theory of mind (ToM) have often confounded the two. For instance, animations of geometric shapes have been taken as instances of both types of process (e.g., Moessnang et al., 2016; Varrier & Finn, 2022), and the false belief stories designed to study theory of mind (Saxe & Kanwisher, 2003) include significantly more social interactions than control stories. These confounds possibly contributed to large variations across studies (e.g., Schurz et al., 2014) and obscured our understanding of the neural correlates of social interaction perception and ToM. Here, we directly compared the neural correlates of perceiving social interactions and demand on ToM during naturalistic narrative perception within a single study.

Methods: Ninety-three healthy adults listened to ("Audio") or read ("Text") narratives (each 2-4 minutes long) during fMRI scanning. Each narrative includes a mix of social interactions and nonsocial scenarios, along with a blend of characters' actions and mental activities. Social interaction scenarios explicitly involved interpersonal communication or shared activity (e.g., "he told her to take care"), whereas nonsocial scenarios involved only one person or lacked interactions (e.g., "they were friends for years"). Descriptions of characters' mental activities, marked by verbs such as "thought", "felt", and "knew", placed explicit demands on participants' ToM. We coded social interactions and explicit ToM demands on a clause-by-clause basis. The codings were relatively independent ($r = -0.08$ and -0.25 under the Text and Audio conditions, respectively, all variance inflation factors < 1.1), which enables modeling them in one regression model.

Results: Across the Audio and Text conditions, group-level univariate activations of social interactions (SInt) and ToM were both significant in left temporoparietal junction (TPJ), left superior temporal sulcus (STS), bilateral precuneus (PC), and left dorsomedial prefrontal cortex (dmPFC) (false discovery rate (FDR) corrected, $q < .01$). Contrasting SInt and ToM indicated that SInt more strongly activated bilateral TPJ, left STS, and right dmPFC (FDR $q < .01$). We compared the SInt - ToM contrast maps with three a priori term maps from Neurosynth.org (Yarkoni et al., 2011), namely "tom", "mentalizing", and "social interaction", and found significant correlations with "tom" ($r = .18$, $p < .001$) and "mentalizing" maps ($r = .12$, $p < .001$) but not the "social interaction" map ($r = .03$, $p = .26$). Further, two ToM regions of interest (ROI) were defined as where z values in the "tom" and "mentalizing" map are > 3, and the average activation of SInt in both ROIs was significantly larger than ToM ($t(92) = 3.49$, $p < .001$; $t(92) = 2.31$, $p = .023$).

Conclusions: Consistent with previous studies, we found TPJ, STS, precuneus, and dmPFC responded to both social interaction perception and explicit demands of theory of mind. More importantly, minimal social interaction perception – listening to or reading stories in which two or more characters directly interacted – induced activity in classic ToM-related regions and more similar spatial patterns with prototypical ToM-related activation maps. Within those regions, the effects of social interaction perception were stronger than the effects of listening to or reading narratives that explicitly referred to characters' mental activities. This suggests that, even in the absence of explicit demands of ToM, participants were implicitly more inclined to engage the typical brain areas activated by previous ToM tasks when social interactions were present. Our findings underscore the necessity for improved experimental designs to better distinguish between social interaction perception and theory of mind, thereby advancing our knowledge of their neural correlates.

References

1. Moessnang, C. (2016), 'Specificity, reliability and sensitivity of social brain responses during spontaneous mentalizing', Social Cognitive and Affective Neuroscience, vol. 11, no. 6, pp. 1687–1697
2. Saxe, R. (2003), 'People thinking about thinking people. The role of the temporo-parietal junction in "theory of mind."', NeuroImage, vol. 19, no. 4, pp. 1835–1842
3. Schurz, M. (2014), 'Fractionating theory of mind: a meta-analysis of functional brain imaging studies', Neuroscience and Biobehavioral Reviews, vol. 42, pp. 9–34
4. Varrier, R. S. (2022), 'Seeing social: A neural signature for conscious perception of social interactions', The Journal of Neuroscience: The Official Journal of the Society for Neuroscience, vol. 42, no. 49, pp. 9211-9226
5. Yarkoni, T. (2011), 'Large-scale automated synthesis of human functional neuroimaging data', Nature Methods, vol. 8, no. 8, pp. 665–670

Poster No 793

Neural signatures of emotional inference and experience align during social consensus

Marianne Reddan[1], Desmond Ong[2], Tor Wager[3], Sonny Mattek[4], Isabella Kahhale[5], Jamil Zaki[6]

[1]Albert Einstein College of Medicine, The Bronx, NY, [2]University of Texas at Austin, Austin, TX, [3]Dartmouth College, Hanover, NH, [4]University of Oregon, Eugene, OR, [5]University of Pittsburgh, Pittsburgh, PA, [6]Stanford University, Stanford, CA

Introduction: Humans seamlessly transform dynamic social signals into inferences about the internal states of the people around them. The neural processes that lead to conscious inference are computationally complex and require integration across multiple sources of information such as an observer's internal homeostatic state, their past experiences, expectations, and social schemas[1,2]. Neuroimaging studies have implicated the medial prefrontal cortex, temporoparietal junction, and precuneus[3,4] in socioemotional inference; however, integrated models of how multiple brain regions interact to form an inference are lacking. Furthermore, prior research sometimes equates the signaller's intended emotion with the observer's inference. Here we seek to (1) disentangle the neural processes underlying the perception of signal intent from inference, and (2) test how concordance between these processes is related to inference accuracy.

Methods: We collected fMRI data from participants (N = 100) as they watched 24 videos of social targets describing real-life emotional stories of both positive and negative valence. Participants rated the emotional intensity of people (targets) describing significant life events. Targets rated themselves on the same scale to indicate the intended "ground truth" emotional intensity of their videos. We used LASSO-PCR, a multivariate regression technique, to train two models of observer brain activity via leave-one-subject-out cross-validation (Fig 1). 8 video trials comprised the training set, while the remaining 12 trials comprised the held-out validation set. Videos were selected from the Stanford Emotional Narratives Dataset (SENDv1)[5]. After we identified these two unique components that underlie socioemotional processing, we sought to test how they interact in relation to an individual person's empathic accuracy. To do this, we applied the "ground truth" and inference models to participant-level brain activity when participants made inaccurate inferences (low empathic accuracy) and accurate inferences (high empathic accuracy; Fig 2A). Then we correlated the predictions of the two models across all participants.

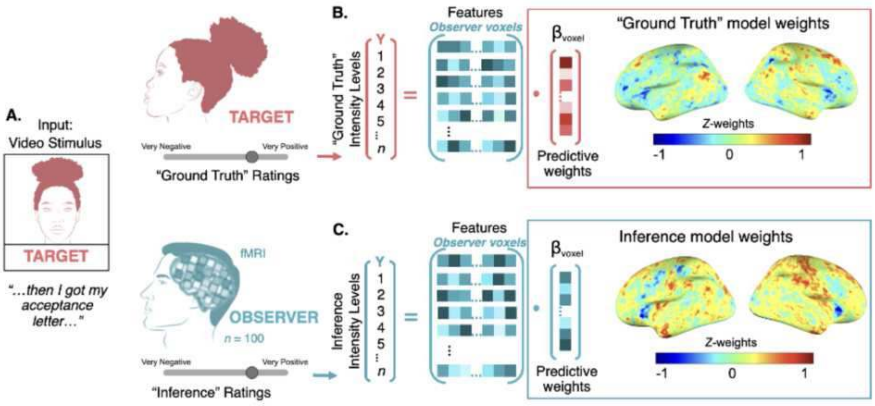

Figure 1. Training the neural models of "ground truth" and inference

A. Paradigm schematic. Observers viewed videos in the MRI and rated what they thought the target felt, moment-by-moment. "Ground truth" and inference ratings were subsequently transformed into five (valence independent) levels of intensity. **B-C. Model Training.** Two models were trained from the same video stimuli: One aimed to characterize the "ground truth," and the other aimed to characterize the observer's inferences. First, brain activity for each intensity level, within each participant, was averaged into a single beta map (these voxels comprised the model's features). Next, a multivariate LASSO-PCR model was trained to predict both "ground truth" and inference intensity levels (Y = 1 to 5, 5 being the highest intensity) from the corresponding whole brain beta maps (features). Models were trained using LOO-CV. Plotted on the surface maps are the unthresholded predictive *Z*-weights for each model.

Results: Both the "ground truth" emotional state of the target (r = 0.50, 5,000 bootstrap samples, P < 0.0001), and an observer's inference about the target (r = 0.53, 5,000 bootstrap samples, P < 0.0001) could be predicted from the observer's brain activity. These neural patterns predictive of "ground truth" and inference are dissociable (cosine similarity = 0.29). The alignment between the two models was significantly greater during high accuracy performance than low accuracy performance (z = -2.71, P = 0.003; Fig 2B). We verified this effect in the validation trials (low empathic accuracy alignment r = 0.58, P < 0.0001; high empathic accuracy alignment r = 0.79, P < 0.0001; two-tailed z-test of the correlation difference z = 2.83, P = 0.005; Fig 2C).

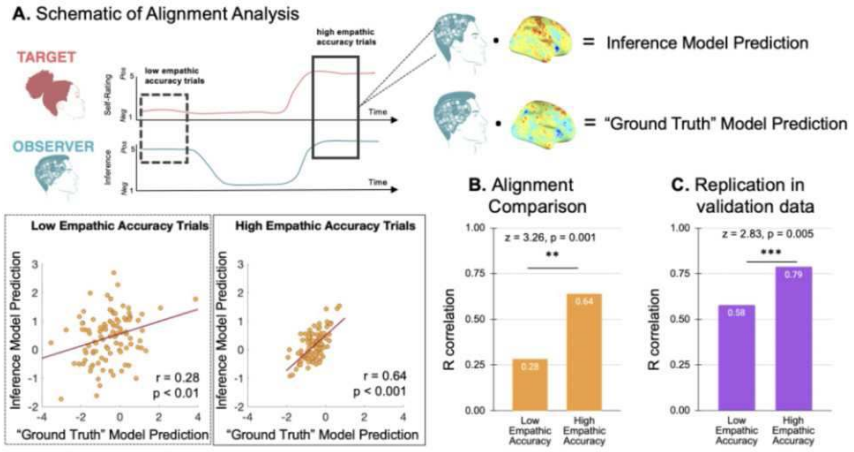

Figure 2. Increased alignment between the "ground truth" and inference models is related to empathic accuracy

A. Schematic of alignment analysis. First, we took the dot-product between each model and individual subject's (N = 100) maps of empathic accuracy at two levels: low and high accuracy, and then added in the models' intercepts. **B. Alignment comparison.** To test how the alignment of the "ground truth" and inference patterns are related to empathic accuracy, we correlated each model's predictions across all participants. When participants are inaccurate, there is more variance across the predictions of the "ground truth" and inference models, and therefore they are weakly correlated ($r = 0.28$, $P < 0.01$). However, when participants are accurate, the models predictions are better correlated ($r = 0.64$, $P < 0.001$). Alignment between the two models was significantly greater during high accuracy performance than low accuracy performance ($z = -2.71$, $P = 0.003$). **C. Replication in validation data.** We verified this effect in the validation trials (two-tailed z-test of the correlation difference $z = 2.83$, $P = 0.005$).

Conclusions: Using naturalistic socioemotional stimuli and machine learning, we developed reliable brain signatures that predict what an observer thinks about a target, what the target thinks about themselves, and investigated the correspondence between them. Interestingly, we found that greater concordance between the latent representation of the target's intended signal intensity and the observer's inference indicates greater empathic accuracy. These results give insight into the neural processes that transform social signals into conscious inference during social interactions. Future work will apply these signatures in clinical data to better our understanding of socioemotional dysfunction in people with mood disorders.

References

1. Chang, L. J., Jolly, E., Cheong, J. H., Rapuano, K. M., Greenstein, N., Chen, P.-H. A., & Manning, J. R. (2021). Endogenous variation in ventromedial prefrontal cortex state dynamics during naturalistic viewing reflects affective experience. Science Advances, 7(17), eabf7129. https://doi.org/10.1126/sciadv.abf7129
2. Pugh, Z. H., Choo, S., Leshin, J. C., Lindquist, K. A., & Nam, C. S. (2022). Emotion depends on context, culture and their interaction: Evidence from effective connectivity. Social Cognitive and Affective Neuroscience, 17(2), 206–217. https://doi.org/10.1093/scan/nsab092
3. Zaki, J., Weber, J., Bolger, N., & Ochsner, K. (2009). The neural bases of empathic accuracy. Proceedings of the National Academy of Sciences, 106(27), 11382–11387. https://doi.org/10.1073/pnas.0902666106
4. Skerry, A. E., & Saxe, R. (2014). A Common Neural Code for Perceived and Inferred Emotion. The Journal of Neuroscience, 34(48), 15997–16008. https://doi.org/10.1523/JNEUROSCI.1676-14.2014
5. Ong, D. C., Wu, Z., Zhi-Xuan, T.,Reddan, M., Kahhale, I., Mattek, A., & Zaki, J, (2021),
6. 'Modeling emotion in complex stories: the Stanford Emotional Narratives Dataset,' IEEE Transactions on Affective Computing, vol. 12, no. 3, pp. 579-594

Poster No 794

Prefrontal and Parietal Cortices Engagement in Cognitive Maps for Social Navigation

Taihan Chen[1], Xinrui Li[2], Xia Liu[1], Runchen Gan[3], Yidan Qiu[2], Ruiwang Huang[4]

[1]South China Normal University, Guangzhou, China, [2]South China Normal University, Guangzhou, Guangdong, [3]South China Normal Unversity, Guangzhou, Guangdong, [4]School of Psychology, Key Laboratory of Brain, South China Normal University, Guangzhou, Guangdong

Introduction: A cognitive map is an internal representation of the relationships between entities to support flexible prediction and decision[1]. Previous studies found that the hippocampus, entorhinal cortex, prefrontal cortex are key regions in cognitive mapping. The hippocampus and entorhinal cortex encode spatial information, and the prefrontal cortex drives the hippocampus to update cognitive maps for efficient navigation[2,3]. These maps are not limited to spatial navigation but extend to abstract social space, facilitating the understanding of social relationships and aiding in making informed social interaction

decisions[4,5,6]. However, it remains unclear how cognitive maps are transformed across the hippocampal-prefrontal circuits to represent the abstract information, and previous studies also found that brain regions such as the inferior parietal cortex and posterior cingulate cortex function in social navigation [5, 6, 7, 8]. Thus, we re-analyzed the task-fMRI data [9, 10], which were obtained from subjects performing a naturalistic, role-playing task, which was adopted by following Tavares et al.[6], to study the neural mechanisms underlying the representation of cognitive maps in social space.

Methods: Participants. We recruited 40 adult healthy participants (17M/23F, age = 20.4 ± 1.5 years) from the campus of South China Normal University (SCNU). The fMRI datasets from 2 subjects were excluded for excessive head movement. The study was approved by the IRB of SCNU. Data acquisition and preprocessing. The MRI data was acquired on a 3T Siemens Trio MRI scanner equipped with a 32-channel phased-array head coil. Both the anatomical and functional MRI data were preprocessed with fMRIPrep (Ver 23.1.4). The obtained images were first smoothed with a 5-mm FWHM Gaussian kernel, and then were filtered with a high-pass filtering (with a cutoff period of 100s) to eliminate the low-frequency artifacts. Experimental design and procedures. Figs. 1a and 1b show that the participants interacted with five main characters by choosing one of two given options. Each participant went through 3 trials (narrative condition, optional condition, and baseline) in each of the social interaction blocks during the scanning. We recorded the trajectory of main characters and calculated the vector length (v), vector angle (θ), vector length variation (Δv), and vector angular variation (Δθ) according to the equations in Fig. 1b. Whole-brain GLM analysis. We performed two univariate GLM analyses for the fMRI data by using FEAT/FSL. Both GLM analyses include three main regressors (narrative condition, optional condition, and baseline) and six head movement regressors. We set Δv as another regressor in GLM1 and set Δθ in GLM2 to estimate the corresponding brain activation, respectively.

Results: Fig. 1c shows the Δv related significant activation in the right medial prefrontal cortex (mPFC), right orbitofrontal cortex (OFC) and bilateral inferior parietal cortex (IPC). Fig. 1d shows the Δθ related significant activation in the right cingulate cortex, right OFC, and right IPC. The detail information of these clusters is listed in Table 1.

Conclusions: We found that the PFC and IPC were involved in encoding the variation of vector parameters. These results indicated that these two regions may be correlated to the process of encoding the variations in social relationship, and implied that hippocampal-prefrontal circuits may encode social information into cognitive maps. Further studies are required to confirm and expand upon our initial observations.

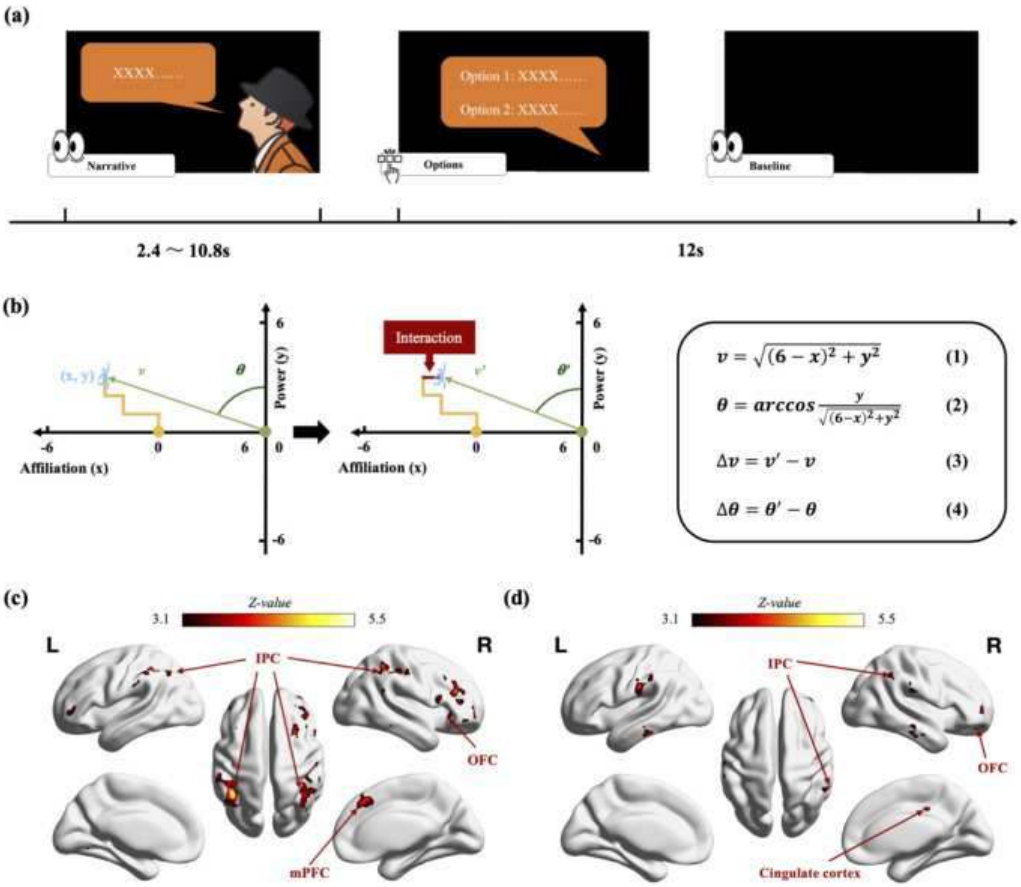

Figure 1. Experimental design and brain regions showing significant neural activity response to the performance.

(a) Illustration of the experimental procedures. In the narrative trials, the participants watched slides that provided background information about the story or the words of a fictitious character in a bubble. In the optional trials, the participant made a decision in a bubble followed by a black screen. A black screen slide was analyzed as the baseline.

(b) The trajectory and coordinates of characters and equations to calculate regressors in GLM analyses. In this 2D social space (left), x-axis represents affiliation dimension and y-axis represents power. The vector, extending from the participant's theoretical position (6, 0) to the character's location (x, y) during social interaction process (orange trajectory), quantifies the social relationship between the participant and the given character. Vector length (v) and angle (θ) represent the social distance and the power dimension normalized by affiliation, respectively. Vector length variation (Δv) and vector angular variation ($\Delta\theta$) represent social decision-making, quantifying route planning, search, and direction shifts. These measures are calculated according to eqs. (1 - 4) as shown in the black box (right).

(c) Brain clusters (mPFC, OFC, and IPC) corresponding to significant differences in activation for the contrast of the vector length variation (Δv) versus baseline.

(d) Brain clusters (cingulate cortex, OFC, and IPC) corresponding to significant differences in activation for the contrast of the vector angular variation ($\Delta\theta$) versus baseline.

Table 1. Brain clusters corresponding to significant difference in activation for the contrasts of the vector length variation versus baseline as well as the vector angular variation versus baseline. (Gaussian random field (GRF) correction, voxel level $p < 0.001$ and cluster-level $p < 0.05$).

Location of the peak voxel	Cluster size (voxels)	Peak coordinate in the MNI space			*Z*-value
		x	y	z	
Vector length variation (Δv) > baseline					
Frontal_Inf_Tri_R	1, 626	48	36	26	5.43***
Parietal_Inf_R	1, 607	40	-46	50	5.36***
Frontal_Sup_Medial_R	460	8	32	42	4.65***
Frontal_Inf_Orb_R	146	32	28	-6	4.34***
Temporal_Inf_R	104	52	-32	-28	4.26**
Frontal_Inf_Orb_R	72	50	46	-4	3.79*
Temporal_Sup_R	68	58	-48	22	3.63*
Parietal_Inf_L	1, 083	-40	-52	44	5.08***
Cerebellum_Crus1_L	414	-14	-72	-28	4.58***
Frontal_Mid_L	245	-46	52	2	5.23***
Frontal_Mid_L	108	-36	22	50	3.92**
Insula_L	103	-28	26	-8	4.03**
Vector angular variation ($\Delta\theta$) > baseline					
SupraMarginal_R	179	62	-28	50	4.49***
Temporal_Inf_R	136	56	-20	-26	3.98***
Frontal_Mid_R	122	36	56	4	3.98**
Parietal_Inf_R	121	54	-48	44	3.91**
Cingulum_Mid_R	91	6	-28	38	4.03*
Frontal_Mid_Orb_R	72	28	54	-14	3.74*
SupraMarginal_R	71	58	-24	24	3.79*
Postcentral_L	246	-62	-20	28	4.61***
Temporal_Inf_L	74	-58	-26	-24	4.06*

Note. MNI: Montreal Neurological Institute, *Sup*: superior, *Inf*: inferior, *Mid*: middle, *Tri*: triangularis, *Orb*: orbital, *L* (*R*): left (right) hemisphere.

*$p < .05$. **$p < .01$. ***$p < .001$.

References

1. Behrens, T. E., Muller, T. H., Whittington, J. C., Mark, S., Baram, A. B., Stachenfeld, K. L., & Kurth-Nelson, Z. (2018). What is a cognitive map? Organizing knowledge for flexible behavior. Neuron, 100(2), 490-509.
2. Epstein, R. A., Patai, E. Z., Julian, J. B., & Spiers, H. J. (2017). The cognitive map in humans: spatial navigation and beyond. Nature Neuroscience, 20(11), 1504-1513.
3. Patai, E. Z., & Spiers, H. J. (2021). The versatile wayfinder: Prefrontal contributions to spatial navigation. Trends in Cognitive Sciences, 25(6), 520–533.
4. Park, S. A., Miller, D. S., & Boorman, E. D. (2021). Inferences on a multidimensional social hierarchy use a grid-like code. Nature Neuroscience, 24(9), 1292-1301.
5. Schafer, M., & Schiller, D. (2018). Navigating social space. Neuron, 100(2), 476-489.
6. Tavares, R. M., Mendelsohn, A., Grossman, Y., Williams, C. H., Shapiro, M., Trope, Y., & Schiller, D. (2015). A map for social navigation in the human brain. Neuron, 87(1), 231-243.
7. Park, S. A., Miller, D. S., Nili, H., Ranganath, C., & Boorman, E. D. (2020). Map making: constructing, combining, and inferring on abstract cognitive maps. Neuron, 107(6), 1226-1238.
8. Park, S. A., Miller, D. S., & Boorman, E. D. (2021). Inferences on a multidimensional social hierarchy use a grid-like code. Nature Neuroscience, 24(9), 1292-1301.
9. Zhang, L., Chen, P., Schafer, M., Zheng, S., Chen, L., Wang, S., Liang, Q., Qi, Q., Zhang, Y., & Huang, R. (2022). A specific brain network for a social map in the human brain. Scientific Reports, 12(1), 1773.
10. Wu, X., Zhang, L., Liu, B., Liao, J., Qiu, Y., & Huang, R. (2023). Social navigation modulates the anterior and posterior hippocampal circuits in the resting brain. Brain Structure and Function, 228(3-4), 799-813.

Poster No 795

Redefining Me to We: How Psychedelics Reshape Social Boundaries

Pablo Mallaroni[1], Samuel Ereira[2], Katrin Preller[3], Natasha Mason[1], Johannes Ramaekers[1]

[1]Maastricht University, Maastricht, Limburg, [2]Queen Mary University of London, London, [3]University of Zurich, Zurich, Switzerland

Introduction: Meaningful social interactions hinge on our ability to flexibly intuit others' beliefs, a capacity rooted in the brain's ability to encode and simulate others' neural belief patterns. Self-other distinction is thus central to social cognition, and its impairment is a transdiagnostic marker of neuropsychiatric disorders. Psychedelics are suggested to ameliorate socio-cognitive functioning by impairing self-referential awareness and heightening social connectedness (Preller and Vollenweider 2019). While this self-other mergence may stem from a 5-HT2A-mediated perturbation of 'social' brain regions such as the medial prefrontal cortex (mPFC), it is unknown how this is enacted at a neurocomputational level (Stoliker, Egan et al. 2022). We hypothesise serotonergic psychedelics elicit persisting changes to self-other mergeance by impeding belief attribution in a manner that is predictable by acute changes in functional connectivity.

Methods: Here, we fitted agent-specific reinforcement learning models to data from 21 healthy participants collected in a probabilistic false-belief task (p-FBT) + 24 hours following the administration of 15mg of psilocybin and 20 mg 2C-B in a within-subjects, placebo-controlled trial. The p-FBT requires participants to assess the probability of an event while also estimating a third-party's perspective on the same event (Ereira, Hauser et al. 2020). Importantly, participants are aware that the third-party might have access to information that differs from their own. By fitting Rescorla–Wagner learning models to subject reports, we defined leakage' parameters between belief updates for Self and Other, hypothesising greater leakage to cause beliefs for Self and Other to covary. To understand how acute perturbations in mPFC connectivity may drive aberrant belief updating, we leveraged corresponding 7T resting-state fMRI data collected 90 min after administration. Regions of interest (ROIs) were extracted from a extended theory of mind (ToM) network comprising the mPFC defined by a reverse inference Neurosynth approach (Yarkoni, Poldrack et al. 2011) and were denoised by regressing six head-motion, cerebrospinal fluid, and white matter parameters. Low-frequency signal drifts were filtered using a 128-s high-pass filter. To assess how causal changes may influence our leakage parameter we employed spectral dynamic causal modelling (sDCM), which fits the complex cross-spectral density using a (parameterized) power-law model of endogenous neuronal fluctuations (Daunizeau, David and Stephan 2011). This consequently provides the effective connectivity (EC) between regions, as well as the amplitude of endogenous neuronal fluctuations within each region. Second-level analyses on the extracted ROI EC values were performed using the Parametric Empirical Bayes Method (Morris 1983).

Results: We find that an egocentric model parameter, quantifying the extent to which observations available to the Self erroneously update estimates of the Other's belief, is significantly reduced following the administration of a psychedelic ($F(63)=7.44$, $p=0.008$) First-level fMRI analyses derived four empirical ToM ROIs correspondent to the mPFC, Precuneous, L/R Temporal Parietal Junction (TPJ), which exceeded a DCM explained variance of 50%. ROIs exhibited widespread changes in connectivity in a manner that was interrelated with social cognition outcomes.

Conclusions: Overall, our findings suggest psychedelics foster a less self-centred perspective of others' beliefs, further implicating the 5-HT2A receptor in social learning and offering potential mechanisms for symptomatic relief.

References

1. Daunizeau, J., O. David and K. E. Stephan (2011). "Dynamic causal modelling: a critical review of the biophysical and statistical foundations." Neuroimage 58(2): 312-322.
2. Ereira, S., T. U. Hauser, R. Moran, G. W. Story, R. J. Dolan and Z. Kurth-Nelson (2020). "Social training reconfigures prediction errors to shape Self-Other boundaries." Nature Communications 11(1): 3030.
3. Morris, C. N. (1983). "Parametric Empirical Bayes Inference: Theory and Applications." Journal of the American Statistical Association 78(381): 47-55.
4. Preller, K. H. and F. X. Vollenweider (2019). "Modulation of Social Cognition via Hallucinogens and "Entactogens"." Front Psychiatry 10: 881.
5. Stoliker, D., G. F. Egan, K. J. Friston and A. Razi (2022). "Neural Mechanisms and Psychology of Psychedelic Ego Dissolution." Pharmacological Reviews 74(4): 876-917.
6. Yarkoni, T., R. A. Poldrack, T. E. Nichols, D. C. Van Essen and T. D. Wager (2011). "Large-scale automated synthesis of human functional neuroimaging data." Nat Methods 8(8): 665-670.

Poster No 796

A meta-analysis of fMRI studies on in-group and out-group categorization

Kelly Sng[1,2], Xavier Lim[2], SH Annabel Chen[2,3,4,5], Gianluca Esposito[6]

[1]Neuroscience, Interdisciplinary Graduate Programme, Nanyang Technological University, Singapore, Singapore, [2]Psychology Program, School of Social Sciences, Nanyang Technological University, Singapore, Singapore, [3]Centre for Research and Development in Learning (CRADLE), Nanyang Technological University, Singapore, Singapore, [4]Lee Kong Chian School of Medicine, Nanyang Technological University, Singapore, Singapore, [5]Office of Educational Research, National Institute of Education, Singapore, Singapore, [6]Department of Psychology and Cognitive Science, University of Trento, Rovereto, Italy

Introduction: Different social groups exhibit varying degrees of closeness to the self, with some memberships readily discernible based on appearance (e.g., ethnicity) while others (e.g., nationality) necessitate higher-level cognitive processing. Although different group memberships could elicit distinct neural networks, most neuroimaging meta-analyses examining functional networks on in-out-group biases do not make such distinctions Similarly, differential functional activation may exist for bias toward the in- over the out-group (IG>OG) and out- over the in-group (OG>IG) across different tasks, depending on the modality involved. The activation likelihood estimation (ALE) has 2 aims: (1) summarise the cortical networks for overall IG>OG and OG>IG processing, and (2) provide additional information on ethnicity as group membership, and empathy processing.

Methods: A systematic review (PRISMA guidelines) was performed on PubMed and Scopus on fMRI studies (Figure 1). Inclusion criteria: task-fMRI studies, whole-brain analyses in a standard stereotaxic space, involved healthy adults, and published in English. The overall IG>OG processing included 64 studies (106 contrasts, 493 foci), and overall OG>IG processing included 34 studies (59 contrasts, 347 foci). Group membership classification found 37 Ethnicity studies on in-group bias (IG>OG; 58 contrasts, 268 foci). fMRI task types found 29 studies in Empathy processing on in-group bias (IG>OG; 49 contrasts, 249 foci). All other group memberships and fMRI task-types did not have enough studies for adequate power to conduct the ALE analyses. Meta-analyses were performed using GingerALE. An uncorrected threshold of p<.005, 200mm3 was used to minimise false negative findings (Saarinen et al., 2021).

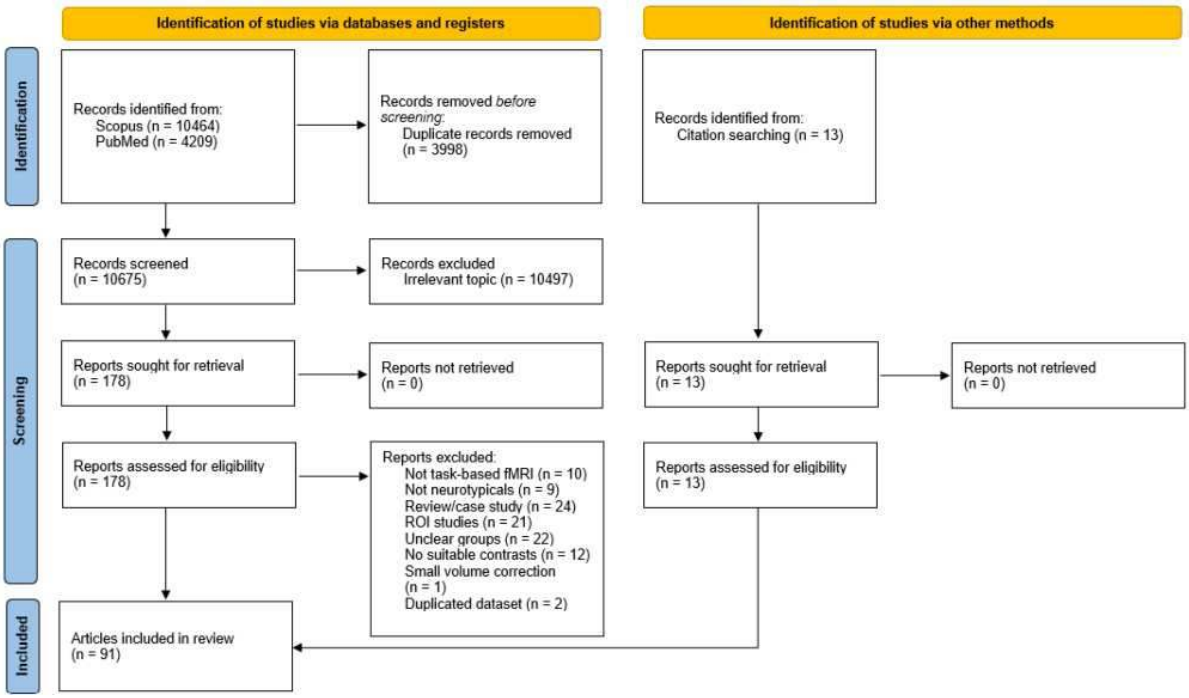

Results: ALE analysis for IG>OG processing revealed 24 significant clusters (Figure 2a), with the largest (3480mm3) located in the left insula, inferior frontal gyrus, and uncus. OG>IG processing revealed 30 significant clusters (Figure 2b), with the largest (2000mm3) located in the bilateral presupplementary motor area. Analysis for Ethnicity (IG>OG) revealed 31 significant clusters (Figure 2c), with the largest (1680mm3) located in the right middle occipital gyrus, middle temporal gyrus, inferior occipital gyrus, and fusiform. Analysis of the task type, Empathy Processing (IG>OG) revealed 23 significant clusters (Figure 2d), with the largest (2648mm3) located in the right postcentral gyrus and posterior cingulate gyrus.

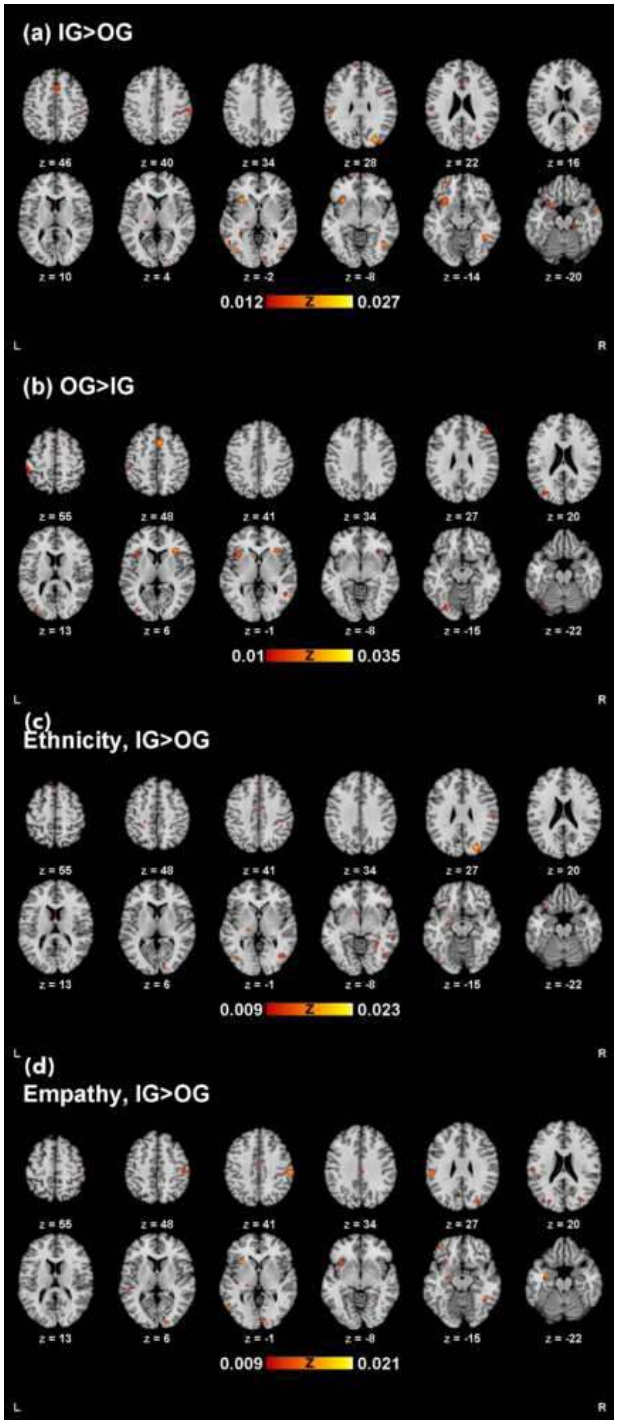

Conclusions: Overall IG>OG processing engaged left insula and inferior frontal gyrus, both of which are activated when the self is involved (Northoff & Bermpohl, 2004), in line with the idea that the in-group is closely related to the self (Smith & Henry, 1996). Our meta-analysis showed more recruitment of self-related areas in in-group bias as expected. The bilateral presupplementary motor area, implicated in cognitive control (Hertrich, 2016) was observed in overall OG>IG processing, suggesting that in-group processing may be more automatic whereas more cognitive resources are required for out-group processing. Occipital involvement for Ethnicity group processing is consistent with a review (Bagnis et al., 2020) reporting recruitment of these regions for racial traits perception. As occipital regions are linked with facial representation and encoding of invariant visual traits like ethnicity, heightened activation seen in IG>OG contrast could imply greater focus on individual distinctions within the in-group. Our observation of the engagement of postcentral gyrus and posterior cingulate in Empathy Processing aligns with prior literature associating these areas with empathy's sensory and affective facets, respectively (Singer et al., 2004; Völlm et al., 2006). This stronger empathic response appears evident for the in-group than the out-group as expected. The findings add to our understanding of the neuro-networks involved in in-group/out-group processes.

References
1. Bagnis, A. (2020), 'Functional neuroanatomy of racial categorization from visual perception: a meta-analytic study', Neuroimage, 217, 116939.
2. Hertrich, I. (2016), 'The role of the supplementary motor area for speech and language processing', Neuroscience & Biobehavioral Reviews, 68, 602-610.
3. Northoff, G. (2004), 'Cortical midline structures and the self', Trends in Cognitive Sciences, 8(3), 102-107.
4. Saarinen, A. (2021), 'Neural basis of in-group bias and prejudices: A systematic meta-analysis', Neuroscience and biobehavioral reviews, 131, 1214–1227.
5. Singer, T. (2004), 'Empathy for pain involves the affective but not sensory components of pain', Science, 303(5661), 1157-1162.
6. Smith, E. R. (1996), 'An in-group becomes part of the self: Response time evidence', Personality and Social Psychology Bulletin, 22(6), 635-642.
7. Völlm, B. A. (2006), 'Neuronal correlates of theory of mind and empathy: a functional magnetic resonance imaging study in a nonverbal task', Neuroimage, 29(1), 90-98.

Poster No 797

Moral behavior and brain mechanisms in commanders and intermediaries

Kalliopi Ioumpa[1], Emilie Caspar[2], Valeria Gazzola[3], Christian Keysers[3]

[1]Ghent University, Ghent, Belgium, [2]Ghent University, Ghent, Belgium, [3]The Netherlands Institute for Neuroscience, KNAW Research Institute, Amsterdam, Amsterdam

Introduction: Fractioning operations between several individuals along a hierarchical chain is commonly found in the way organizations function. A superior communicates a plan and a subordinate executes it. The superior then has responsibility for the decision but is distanced from the outcomes, while the subordinate experiences authorship over the action but reduced responsibility for its outcomes (Bandura, 2006). As the superiors are often following instructions themselves, they also end up in intermediary roles. Experimental research has shown that this fractioning allows diffusing responsibility between components of the chain, which can disinhibit the commission of actions that harm others (Kilham & Mann, 1974; Milgram, 1974). However, the neural mechanisms by which being in the intermediary or commanding position disinhibit harming others remains largely unknown. Here we conducted two studies, one using fMRI and one using EEG, to investigate how commanding or being in an intermediary position impacts the sense of agency and the processing of victim's pain. In the age of military drones, we also explored whether commanding a human or robot agent influences these processes. Finally we compared these results with results obtained from a study on agents, directly harming a victim (Caspar & Ioumpa et al., 2020).

Methods: Forty participants were tested in the fMRI study (13males; 25.05 y±3.6SD) using a 3-Tesla Philips Ingenia CX system. Forty-eight participants were tested in the EEG study (24males; 23.9 y±3.9SD) with a 64-channel electrode cap. In both studies, participants were recruited in pairs and respectively played the role of the person giving orders or the role of the 'victim'. When they were giving orders, participants had to give an order to an agent to send or not to send a real, mildly painful electric shock to the 'victim' in exchange for a small monetary gain. In that position, participants were either free to decide which order to send to the agents (were 'commanders') or were given an order by the experimenter that they had to transmit to the agent (were 'intermediaries'). When participants were in the commander position, we also modulated the entity executing their orders: they were either giving orders to another human or to a non-humanoid robot. Sense of agency was additionally measured in the EEG study through the intentional binding effect (Moore & Haggard, 2010). Participants had to estimate the duration of the time interval between pressing the button to transmit an order to the agent and its consequence (shock or no shock) and shorter time estimates indicate a stronger sense of agency.

Results: EEG results showed that the neural response over P3, which is sensitive to the observation of pain in others (Coll, 2018), was higher when the executing agent was a robot compared to a human. Source reconstruction of the EEG signal revealed that this effect was mediated by areas including the insula and ACC. The sense of agency did not differ between commanders and intermediaries, no matter if the executing agent was a robot or a human. fMRI results comparing commanders and agents, revealed that activation in social cognition and empathy-related brain regions as IFG, IPL and SII was equally low when witnessing a victim receiving a painful shock when participants were commander or intermediary transmitting an order, and both were lower compared to being the agent directly delivering the shock to harm the victim.

Conclusions: Summarizing, being a commander or intermediary seemed to reduce processing the pain of the victim compared to being the agent directly administering the pain. Commanding a human agent led to reduced responsibility and activation compared to commanding a robot agent but there were no differences in the sense of agency levels. These results shed some more light on how hierarchical situations can facilitate the commission of actions that harm others as responsibility and empathy are reduced and split across multiple individuals.

References
1. Bandura, A. (2006). Toward a Psychology of Human Agency. Perspectives on Psychological Science, 1(2), 164–180.
2. Caspar, E. A. & Ioumpa, K. (2020). Obeying orders reduces vicarious brain activation towards victims' pain. NeuroImage, 222, 117251.
3. Coll, M. P. (2018). Meta-analysis of ERP investigations of pain empathy underlines methodological issues in ERP research. Social cognitive and affective neuroscience, 13(10), 1003-1017.
4. Kilham, W., & Mann, L. (1974). Level of destructive obedience as a function of transmitter and executant roles in the Milgram obedience paradigm. Journal of Personality and Social Psychology, 29(5), 696–702.
5. Milgram, S. (1974). The Dilemma of Obedience. The Phi Delta Kappan, 55(9), 603–606.

Poster No 798

Is Empathy a Risky Strength?

Annika Konrad[1,2], Katharina Förster[1], Jason Stretton[2], Tim Dalgleish[2], Anne Böckler-Raettig[3], Fynn-Mathis Trautwein[4], Tania Singer[5], Philipp Kanske[1]

[1]Clinical Psychology and Behavioral Neuroscience, Technische Universität Dresden, Dresden, Germany, [2]MRC Cognition and Brain Sciences Unit, University of Cambridge, Cambridge, United Kingdom, [3]Department of Psychology, Julius-Maximilians-Universität Würzburg, Würzburg, Germany, [4]Department of Psychosomatic Medicine and Psychotherapy, University Medical Center Freiburg, Freiburg, Germany, [5]Social Neuroscience Lab, Max Planck Society, Berlin, Germany

Introduction: Internalizing symptoms such as elevated stress and sustained negative affect can be important warning signs for developing mental disorders. A recent theoretical framework suggests a complex interplay of empathy, Theory of Mind (ToM), and negative thinking processes as a crucial risk combination for internalizing symptoms (Tone & Tully, 2014). Therefore, this study utilizes neural, behavioral, and self-report data to examine how the interplay between empathy, ToM, and negative thinking processes relates to stress and negative affect.

Methods: We reanalyzed the baseline data of N = 302 healthy participants (57% female, age: M = 40.52, SD = 9.30) who participated in a large-scale mental training study, the ReSource project (Singer et al., 2016). Recruitment followed a multi-step procedure, including screening, interviews, and questionnaires. Empathy and ToM were assessed via self-report and a validated fMRI paradigm featuring naturalistic video stimuli and specific questions (EmpaToM task, Kanske et al., 2015). Contrasts of interest were emotional > neutral videos and ToM > nonToM (factual reasoning) videos and questions. Additional self-report scales were employed to measure internalizing symptoms (perceived stress, negative affect) and negative thinking processes (rumination and self-blame). We conducted multiple linear and nonlinear regression analyses to investigate whether negative thinking processes moderate the effects of self-reported and behaviorally assessed empathy and ToM on internalizing symptoms. Second, we used flexible factorial models on the whole brain level to probe whether empathy- and ToM-related brain activations differ depending on individual stress and negative affect levels. The contrast of interest was the interaction between the respective covariates (stress or negative affect) and the empathy or ToM factor. Last, to examine whether negative thinking processes moderate the effects of empathy- and ToM-related brain activity on internalizing symptoms, we extracted brain activation of pre-defined regions of interest and used the respective estimates in linear and nonlinear regression analyses.

Results: The regression models using self-report and behavioral empathy- and ToM-related measures revealed that people with lower self-reported ToM and higher empathic distress may be at risk for more internalizing symptoms. There were no quadratic associations between (self-reported or behavioral) empathy or ToM, negative thinking processes, and internalizing symptoms (all ps > .05). Also, the flexible factorial models on the whole brain level showed that none of the activation patterns for the interactions survived the correction threshold. However, quadratic associations of empathy- and ToM-related brain activation with internalizing symptoms depended on negative thinking processes, suggesting differential effects of cognitive and affective functioning on internalizing symptoms (see Figure 1). Specifically, we found that low and high empathy- and compassion-related insula activity, in interaction with rumination, was associated with more stress. Moreover, low and high ToM-related activity in the middle temporal gyrus was associated with more negative affect, but only in those with lower rumination.

Figure 1
Brain activation derived from the (A) emotional > neutral contrast; (B) ToM > nonToM contrast during the video epoch, and the (C) ToM > nonToM contrast during the question epoch

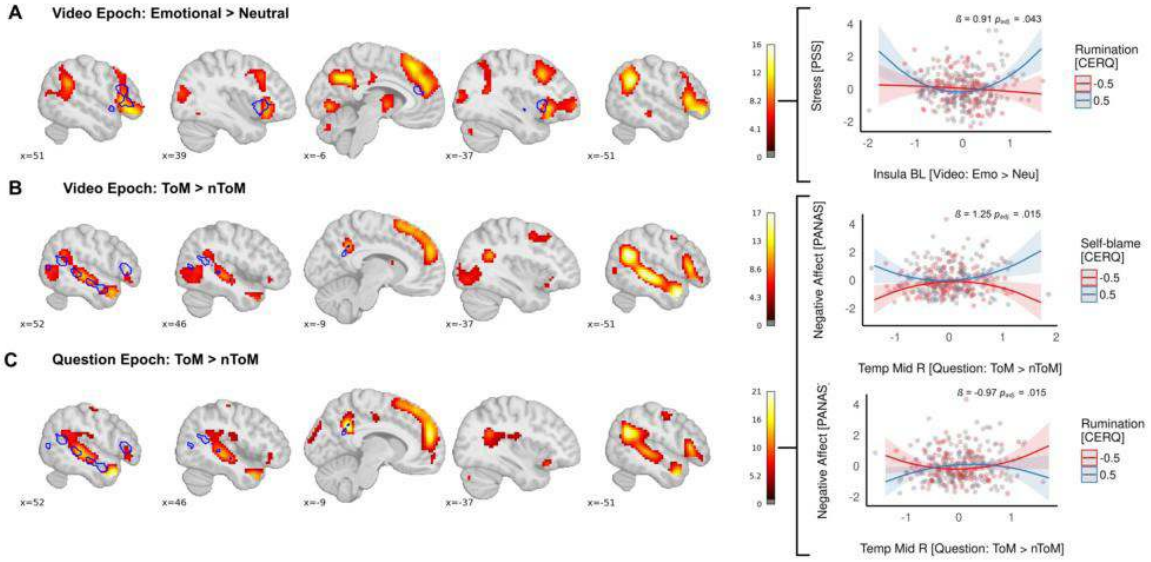

Conclusions: Using a multi-method approach, this study contributes to current research by illuminating the complex risk combinations of cognitive and affective functioning that are relevant to internalizing symptoms. People with lower self-reported ToM and higher empathic distress may be at risk for more internalizing symptoms. Quadratic associations of empathy- and ToM-related brain activation with internalizing symptoms depended on negative thinking processes, suggesting differential effects of cognitive and affective functioning on internalizing symptoms. These risk combinations may be of interest for future interventions.

References

1. Kanske, P. (2015), 'Dissecting the social brain: Introducing the EmpaToM to Reveal Distinct Neural Networks and Brain-Behavior Relations for Empathy and Theory of Mind', NeuroImage, vol. 122, pp. 6–19
2. Singer, T. (2016), 'The ReSource Project. Background, Design, Samples, and Measurements', Max Planck Institute for Human Cognitive and Brain Sciences
3. Tone, E.B. (2014), 'Empathy as a Risky Strength: A Multilevel Examination of Empathy and Risk for Internalizing Disorders', Development and Psychopathology, vol. 26, pp. 1547–1565

Poster No 799

Comparative Analysis of Social Brain Network Structures in Criminal Offenders

Mikhail Votinov[1], Irina Knyazeva[2], Lena Hofhansel[3], Ute Habel[3]

[1]Institute of Neuroscience and Medicine (INM-10), Research Centre Jülich, Jülich, Germany, [2]N.P. Bechtereva Institute of Human Brain, Saint Petersburg, Russian Federation, [3]Department of Psychiatry, Psychotherapy and Psychosomatics, RWTH Aachen University Hospital, Aachen, Germany

Introduction: Evidence suggests that individuals engaged in criminal behavior may exhibit deficits in social cognition, manifesting as challenges in recognizing social cues and potential deficiencies in empathy and theory of mind (Mariano, M et al., 2017; Newbury-Helps, J., 2017). Our recent fMRI study revealed that offenders, being more sensitive to personal insults, exhibited heightened implicit aggression and decreased connectivity in cognitive control networks, including the dorsomedial prefrontal cortex, precuneus, and middle/superior temporal regions (Hofhansel, L et al., 2022). To corroborate these findings and enhance our understanding of disparities in cortical communication between brain regions involved in social processes among criminal offenders and the noncriminal population, we conducted resting-state MRI measurements combined with topological brain network analysis. Utilizing the social brain atlas, we anticipated observing differences primarily in limbic and high-level clusters.

Methods: In our resting-state (rsMRI) study, we included 27 male violent offenders (OFF), convicted of at least one violent crime, and a matched noncriminal control group (HC). The study utilized a 3T scanner, and rsMRI data were acquired using EPI with parameters: 240 volumes; TR = 2300 ms; TE = 29 ms, lasting for 9 minutes. The fMRI data underwent preprocessing

with the fmriprep tool (Esteban et al., 2019). Postprocessing for network analysis involved smoothing with a 6 mm kernel, regression of head motion parameters, mean WM and CFS signal, and high-pass filtering. Using the social brain atlas (Alcalá-López et al., 2018), representing 36 brain regions highly involved in social processes, we computed a connectivity matrix for each subject. A t-test contrasting the two groups for each pairwise connection was performed, with any edge having a t-value exceeding 2.9 considered as a set of suprathreshold links for the network-based statistic (NBS) approach (Zalesky, 2010). NBS simulations were conducted with the Brain Connectivity Toolbox for Python. To better understand group differences identified by NBS, we employed a graph analysis approach. Computed measures included the shortest path length (SPL), centrality, clustering coefficient, and node efficiency (Liu, Jin, et al., 2017). Binary graphs from correlation matrices were generated with thresholds spaced from 0 to 0.6, using NetworkX in Python.

Results: The NBS revealed a subnetwork with 9 regions connected by 16 links and a separate subnetwork with a single link, significantly different for the OFF group. In the first cluster, all edges except one involved the left supramarginal gyrus (lSMG) region. The second cluster had a single link between the anterior midcingulate cortex and precuneus. Prominent group differences emerged in node-based network measures for lSMG and precuneus regions. Specifically, the shortest path length (SPL), representing the average path length between a predefined node and all others, showed higher values for the OFF group compared to HC for both lSMG and precuneus regions across all applied thresholds. The shortest path is crucial for efficient information transmission in a brain network, enabling faster information transfer and reducing overall brain consumption. Simultaneously, the Betweenness Centrality, quantifying the number of times a node acts as a bridge along the shortest path between two other nodes, was lower for both regions in the OFF group.

Conclusions: Our results revealed distinctions in the topological network organization of temporal and parietal regions for the OFF group compared to the HC. These regions are associated with cognitive processes such as self-referential thinking, mentalizing, and perspective-taking. This aligns with our earlier task-based findings and could elucidate a deficiency in social cognition among criminal offenders.

References

1. Mariano, M., Pino, M. C., Peretti, S., Valenti, M., & Mazza, M. (2017). Understanding criminal behavior: Empathic impairment in criminal offenders. Social Neuroscience, 12(4), 379-385.
2. Newbury-Helps, J., Feigenbaum, J., & Fonagy, P. (2017). Offenders with antisocial personality disorder display more impairments in mentalizing. Journal of personality disorders, 31(2), 232-255.
3. Hofhansel, L., Weidler, C., Clemens, B., Habel, U., & Votinov, M. (2022). Personal insult disrupts regulatory brain networks in violent offenders. Cerebral Cortex.
4. Alcalá-López, D., Smallwood, J., Jefferies, E., Van Overwalle, F., Vogeley, K., Mars, R. B., ... & Bzdok, D. (2018). Computing the social brain connectome across systems and states. Cerebral cortex, 28(7), 2207-2232.
5. Parkes, L., Fulcher, B., Yücel, M., & Fornito, A. (2018). An evaluation of the efficacy, reliability, and sensitivity of motion correction strategies for resting-state functional MRI. Neuroimage, 171, 415-436.
6. Esteban, O., Markiewicz, C. J., Blair, R. W., Moodie, C. A., Isik, A. I., Erramuzpe, A., ... & Gorgolewski, K. J. (2019). fMRIPrep: a robust preprocessing pipeline for functional MRI. Nature methods, 16(1), 111-116.
7. Zalesky, Andrew, Alex Fornito, and Edward T. Bullmore. “Network-based statistic: identifying differences in brain networks.” Neuroimage 53.4 (2010): 1197-1207.
8. Liu, Jin, et al. “Complex brain network analysis and its applications to brain disorders: a survey.” Complexity 2017 (2017).
9. Liu, J., Li, M., Pan, Y., Lan, W., Zheng, R., Wu, F. X., & Wang, J. (2017). Complex brain network analysis and its applications to brain disorders: a survey. Complexity, 2017.

Poster No 800

Functional Recruitment of the Cerebellum Supports the Emergence of Theory of Mind in Early Childhood

Aikaterina Manoli[1,2,3,4], Charlotte Grosse Wiesmann[2], Sofie Valk[2,3,5]

[1]International Max Planck Research School on Cognitive Neuroimaging, Leipzig, Germany, [2]Max Planck Institute for Human Cognitive and Brain Sciences, Leipzig, Germany, [3]Institute of Neuroscience and Medicine, Brain & Behavior (INM-7), Research Centre Jülich, Jülich, Germany, [4]Faculty of Medicine, Leipzig University, Leipzig, Germany, [5]Institute of Systems Neuroscience, Medical Faculty, Heinrich Heine University Düsseldorf, Düsseldorf, Germany

Introduction: Although traditionally associated with motor processing, accumulating evidence suggests that the cerebellum is heavily implicated in social cognition, including Theory of Mind (ToM), i.e., the ability to infer the mental states of others (Frith & Frith, 2006). However, the role of the cerebellum in ToM development remains elusive, despite clinical evidence linking early-life cerebellar injury to dramatic and long-lasting social cognitive deficits (Olson et al., 2023). Here, we investigated the contribution of the cerebellum to the emergence of ToM in young children in the context of local functional activations and functional connectivity to the cerebral cortex. We expected to observe differences in the functional involvement

of the cerebellum between children who have and have not yet developed ToM abilities, as well as between childhood and adulthood.

Methods: We leveraged open functional MRI and behavioral data of typically developing children (N=41; age range: 3-12 years) and adults (N=78) who watched an in-scanner ToM movie (Kliemann et al., 2022; Richardson et al., 2018). Children's ToM abilities were measured with an out-of-scanner task requiring them to point out others' false beliefs. Prior to analyses, the cerebellum was isolated and normalized to the Spatially Unbiased Infratentorial Template (SUIT; Diedrichsen, 2006). Functional images were masked with the cerebellar isolation mask, only retaining signals originating from the cerebellum. We used contrast analyses to identify cerebellar functional clusters in response to ToM movie events in children with ToM abilities (N=22), children without ToM abilities (N=19), and adults, while controlling for general executive functions (i.e., response inhibition and intelligence). Cerebellar activation clusters were used in seed-to-voxel correlation analyses to compare cerebro-cerebellar connectivity between the three groups. Lastly, we used dynamic causal modelling (DCM) to examine the directionality of cerebro-cerebellar connections during ToM processing. We specified full bilinear deterministic DCMs between seeds in the cerebellum and the cerebral ToM network (Schurz et al., 2014), based on ToM movie activation clusters. This way, we allowed for all possible forward and backward connections to be estimated. We then constructed a group-level parametric empirical Bayes (PEB) model which allowed us to examine individual differences in connectivity (e.g., ToM abilities) by including them as covariates in our models (Friston et al., 2015).

Results: Children with ToM abilities demonstrated activation clusters in the posterior cerebellum (Crura I-II), which were consistent with activations in adults, but absent in children without ToM abilities (Fig. 1A). Seed-to-voxel correlations revealed a functional reorganization of the cerebellum as a function of ToM abilities, shifting from non-ToM network connections with the right Crus I towards connections between the ToM network and the right Crus II as children developed ToM abilities (Fig. 1B). Lastly, DCM analyses identified forward connections from the posterior cerebellum to the ToM network in children with ToM abilities, whereas adults primarily demonstrated inverse connections from the ToM network to the posterior cerebellum (Fig. 2).

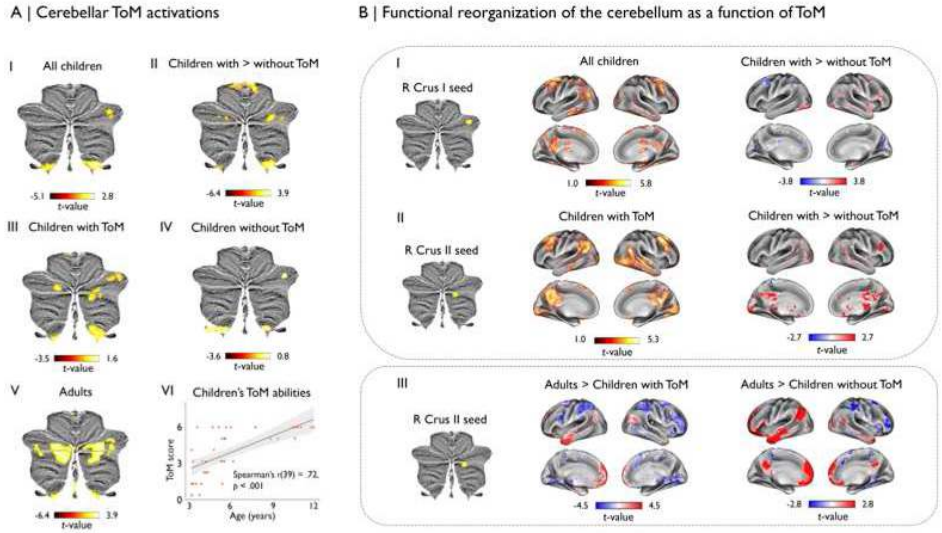

Figure 1. Functional involvement of the cerebellum in early-life ToM emergence. A | Functional clusters of cerebellar activations in the ToM task condition, following false discovery rate (FDR) correction ($q < .05$). **I, III-V)** Group-level one-sample *t*-tests of single-subject ToM > bodily transformation movie scene contrasts in all children (I), children with ToM (III), children without ToM (IV), and adults (V). **II)** General linear model of differences between children with and without ToM with ToM task performance (0-6) as a ratio predictor. **VI)** Distribution of children's ToM abilities based on an out-of-scanner ToM task. Children with a score of 4 or higher were considered to have ToM abilities. **B** | Seed-to-voxel connectivity between cerebellar activation clusters and the cerebral cortex, following FDR correction ($q < .05$). **I)** Left: Group-level one-sample *t*-test of connectivity of right (R) Crus I, a common cluster found in children with and without ToM abilities (see A|I), and the cerebral cortex in the whole sample of children. Right: Group-level independent-sample *t*-test of connectivity differences between children with and without ToM abilities for R Crus I. **II)** Left: Group-level one-sample *t*-test of connectivity of right (R) Crus II, a cluster found in children with ToM abilities (see A|III), and the cerebral cortex in children with ToM. Right: Group-level independent-sample *t*-test of connectivity differences between children with and without ToM abilities for R Crus II. **III)** Left: Group-level independent-sample *t*-test of connectivity differences between children with ToM abilities and adults for R Crus II, a common cluster between children with ToM abilities and adults (see A|III & V). Right: Group-level independent-sample *t*-test of connectivity differences between children without ToM abilities and adults for R Crus II.

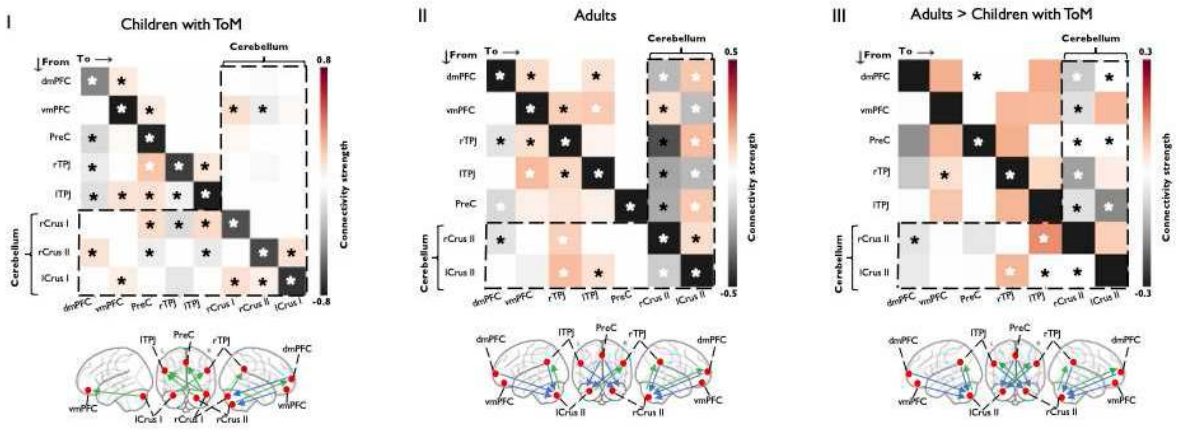

Figure 2. Dynamic causal modelling (DCM) of the cerebellum and the cerebral ToM network in children with ToM abilities and adults. I) Fixed (endogenous) connections in children with ToM abilities using group-based ROIs from a group-level one-sample *t*-test (see Fig. 1A|III). **II)** Fixed (endogenous) connections in adults using group-based ROIs from a group-level one-sample *t*-test (see Fig. 1A|V). **III)** Fixed (endogenous) connectivity differences in children with ToM abilities and adults using common group-based ROIs from a group-level one-sample *t*-test (see Fig. 1A|V)and group type (adult, child) as a covariate. Green arrows in the glass brains represent connections from the cerebellum to the cerebral cortex. Blue arrows represent connections from the cerebral cortex to the cerebellum. * = Bayesian posterior probability > .95. Abbreviations: dmPFC=dorsomedial prefrontal cortex; vmPFC=ventromedial prefrontal cortex; PreC=precuneus; r/lTPJ=right/left temporoparietal junction.

Conclusions: We showed functional involvement of the posterior cerebellum in early-life ToM emergence, with growing connections to the cerebral ToM network as a function of ToM abilities. Interestingly, we found inverse cerebro-cerebellar connectivity patterns in children with ToM abilities and adults, with greater dependence on connections from cerebellar Crura I-II to the cerebral ToM network early in life. This could suggest a crucial role of the posterior cerebellum in the initial construction of ToM schemas. Future research should investigate how the development of the posterior cerebellum might contribute to social cognitive deficits in neurodevelopmental disorders, such as autism.

References

1. Diedrichsen, J. (2006). 'A Spatially Unbiased Atlas Template of the Human Cerebellum', NeuroImage, vol. 33, pp. 127–138.
2. Friston, K. (2015). 'Empirical Bayes for DCM: A Group Inversion Scheme', Frontiers in Systems Neuroscience, vol. 9, pp. 164.
3. Frith, C. D. (2006). 'The Neural Basis of Mentalizing' Neuron, vol. 50, no. 4, pp. 531–534.
4. Kliemann, D. (2022). 'Caltech Conte Center, a Multimodal Data Resource for Exploring Social Cognition and Decision-Making' Scientific Data, vol. 9, no. 1.
5. Olson, I. R. (2023). 'Little Brain, Little Minds: The Big Role of the Cerebellum in Social Development', Developmental Cognitive Neuroscience, vol. 60, pp. 101238.
6. Richardson, H. (2018). 'Development of the Social Brain from Age Three to Twelve Years', Nature Communications, vol. 9, no. 1.
7. Schurz, M. (2014). 'Fractionating Theory of Mind: A Meta-Analysis of Functional Brain Imaging Studies', Neuroscience & Biobehavioral Reviews, vol. 42, pp. 9–34.

Poster No 801

Prenatal exposure to socioeconomic adversity and functional connectivity during an infant cry task

Pilyoung Kim[1], Nolan Brady[2], Shannon Powers[1], Genevieve Patterson[1], Seungwook Lee[3], Tom Yeh[3], Alexander Dufford[4]

[1]University of Denver, Denver, CO, [2]University of Colorado Boulder, Boulder, CO, [3]University of Colorado - Boulder, Boulder, CO, [4]Oregon Health & Science University, Portland, OR

Introduction: Pregnancy triggers dynamic changes in the parental brain's structure and function (Martínez-García, Paternina-Die et al. 2021). Severe stress during this time, such as from poverty, can disrupt these changes and affect postpartum brain and behavioral responses to offspring (Kim 2021). Our previous research demonstrated that postpartum poverty was associated with reduced brain responses to infant cries in the prefrontal and temporal brain regions (Kim, Capistrano et al. 2016). The current study investigates whether poverty during pregnancy prospectively influences parental brain functional connectivity in response to infant cries. We utilize connectome-based predictive modeling (CPM) and hypothesize that prenatal exposure to poverty would be associated with altered functional connectivity when birthing parents listen to infant cues.

Methods: 80 pregnant individuals (age M=29.5 years) were recruited at 14 weeks of pregnancy. Exposure to poverty was assessed throughout the pregnancy (14 weeks, 22 weeks, and 32 weeks pregnancy, and 2-4 weeks postpartum). In 4-6 weeks postpartum, a fMRI session was conducted. The participants had a diverse socioeconomic and racial/ethnic background (37.5% low-income; 66.3% Caucasian, 28.7% Hispanic). Exposure to poverty was assessed based on an income-to-needs ratio

(INR), calculated by dividing total family income by the poverty threshold specified by the U.S. Census Bureau. The range of the average prenatal INR was 0.28 to 11.62, with a standard deviation of 2.47, and 37.5% of the sample lived in poverty or near poverty (income-to-needs ratio ≤ 2). The Infant Cry task was organized into two functional runs, in which blocks of cry stimuli and control sounds lasted 20 s. Each run contained blocks of four sound stimuli-(A) own infant cry, (B) control infant cry, (D) own infant cry matched noise and (D) control infant cry matched noise. In the CPM analysis, we focused on own infant cry condition. The study utilized fMRIPrep for preprocessing and Connectome-Based Predictive Modeling (CPM) (Shen, Finn et al. 2017) to examine how stress exposure (i.e. lower prenatal INR) impacts functional connectivity. CPM involved: 1) using linear regression for feature selection to link connectome edges to stress exposure in the training data, 2) summarizing features by summing the strength of selected edges per participant, and 3) creating a model to associate the summary values with stress exposure. The model was used to test connectome-wide associations in both the positive and negative directions. The study used a feature selection threshold of p<.001, adjusting for participant age, frame-wise displacement, postpartum months, and parity, and internal model validation using 10-fold cross-validation.

Results: The overall CPM model revealed that patterns of brain-wide connectivity were associated with INR (combined positive and negative networks: r=0.325, RMSE = 2.35, p=0.001 via permutation testing) (Fig. 1A). High degree nodes for the positive associative network included a right temporoparietal junction (BA39) node with connections to prefrontal, temporal-parietal, and sensorimotor nodes (Fig. 1B; Fig. 2C). High degree nodes for the negative associative network included a bilateral premotor cortex (BA6) node with connections to limbic, temporal-parietal, and occipital nodes (Fig. 1B; Fig. 2C).

Figure 1. Brain-wide functional connectivity correlates with the income-to-needs ratio (INR). (A) Panel A depicts a plot comparing the actual (x-axis) to the forecasted (y-axis) INR using Connectome-Based Predictive Modeling (CPM). A histogram represents the distribution of Pearson correlation coefficient (r) values across 1000 iterations with randomly shuffled INR, which is used to calculate nonparametric P values. (B) Panel B shows a visual representation of node degree, indicating the number of predictive connections per node, for both the positive and negative networks. Nodes with a higher degree, meaning more significant edges, are shown in darker colors and contribute more in the CPM model.

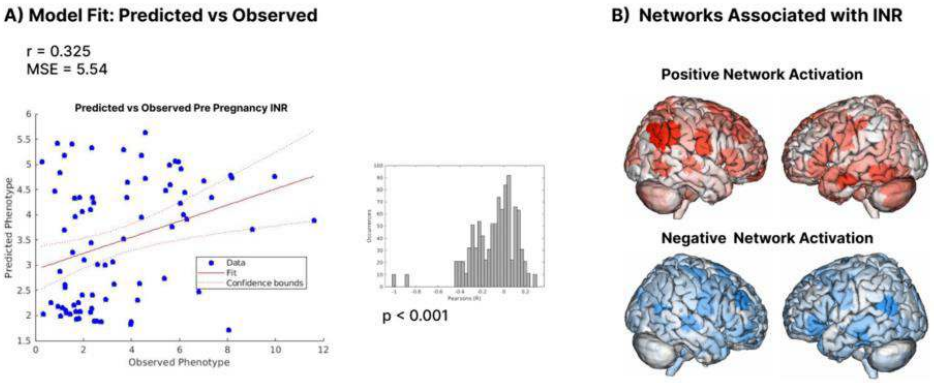

Figure 2. (A) Connectivity within and between networks for the combined, positive, and negative networks. The cells illustrate the total number of connecting edges for nodes within and between each network, with darker shades indicating more edges. (B) Brain regions in an anatomical sequence, with longer lines denoting more extensive connections. To visualize these networks and highlight the most significant edges for the CPM model, edges from nodes with a degree of 15 or more (left), 20 or more (middle), and 25 or more (right) are presented. (C) The positive (red) and negative (blue) networks as predicted by the INR. In positive networks, a higher INR is associated with stronger edge weights (increased functional connectivity). Conversely, in negative networks, a higher INR is linked to lower functional connectivity among significant edges). Nodes with a greater number of significant edges are marked with larger spheres, while nodes with fewer significant edges are indicated by smaller spheres.

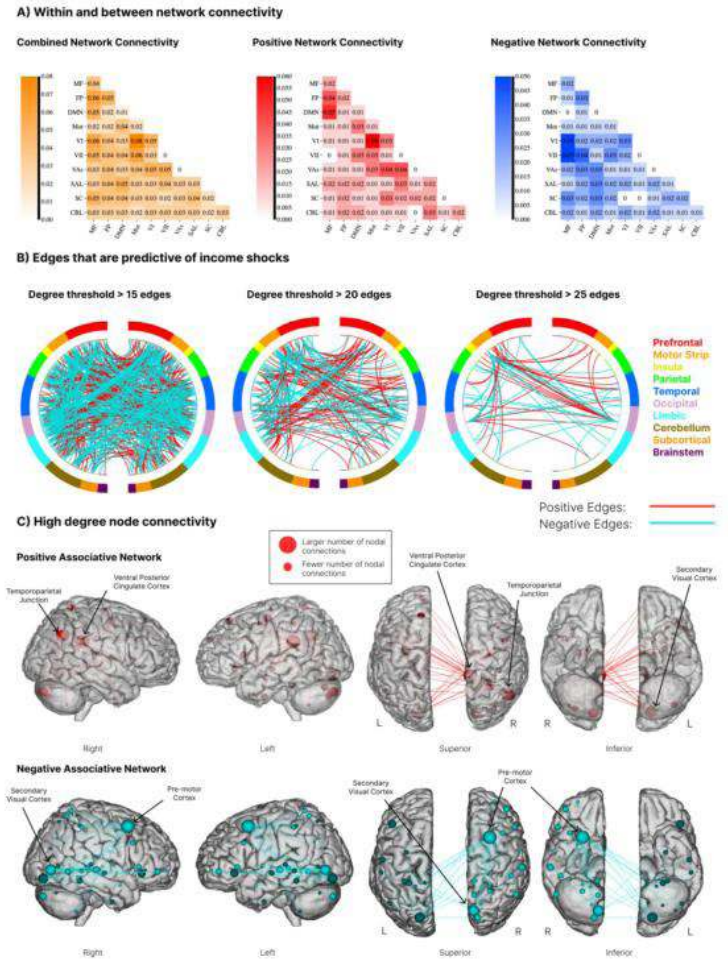

Conclusions: This study demonstrates a prospective link between prenatal poverty exposure and brain connectivity in new birthing parents while they listening to their baby's cry. Higher INR, indicating less exposure to poverty, was associated with greater connectivity in the right temporoparietal junction-a critical area for cognitive empathy linked to sensitive parenting. Conversely, lower INR, indicative of greater exposure to poverty, was linked to increased connectivity in the bilateral premotor cortex, a connectivity pattern observed in new parents with heightened anxiety from stress exposure.

References

1. Kim, P. (2021). "How stress can influence brain adaptations to motherhood." Frontiers in Neuroendocrinology 60: 100875.
2. Kim, P., C. Capistrano and C. Congleton (2016). "Socioeconomic disadvantages and neural sensitivity to infant cry: role of maternal distress." Social cognitive and affective neuroscience 11(10): 1597-1607.
3. Martínez-García, M., M. Paternina-Die, M. Desco, O. Vilarroya and S. Carmona (2021). "Characterizing the brain structural adaptations across the motherhood transition." Frontiers in global women's health: 76.
4. Shen, X., E. S. Finn, D. Scheinost, M. D. Rosenberg, M. M. Chun, X. Papademetris and R. T. Constable (2017). "Using connectome-based predictive modeling to predict individual behavior from brain connectivity." Nat Protoc 12(3): 506-518.

Poster No 802

Robust Multivariate Assessment of Empathic Function without Empathy Tasks

Leonardo Christov-Moore[1], Nicco Reggente[1]

[1]*Institute for Advanced Consciousness Studies, Santa Monica, CA*

Introduction: Deficits in empathic function have deleterious effects on individual, relational and community function, encouraging isolation, increasing the risk of unemployment and homelessness, and impacting long-term health outcomes. Assessing empathic function in vulnerable neurodivergent or nonverbal populations using self-reports and in-scanner tasks is frequently unfeasible. Encouraging evidence suggests that characteristic interactions between brain networks underlying empathy are observable at rest. Leveraging this to assess empathic function without self-reports or in-scanner tasks could be invaluable for clinical practice. We tested whether machine learning-aided analysis (LASSO) of resting fMRI data could predict subdimensions of empathy (empathic concern, personal distress, and perspective-taking) in 74 healthy participants.

Methods: Participants: 74 equivalently recruited participants aged 18-26 (38 female) scanned at the Ahmanson-Lovelace Brain Mapping Center at UCLA on a Siemens Trio 3T between 1/12/2015 and 6/22/2016. Eligibility criteria included: right handed, no prior or concurrent diagnosis of any neurological, psychiatric, or developmental disorders, and no history of drug or alcohol abuse. Procedure :Participants filled out the Interpersonal Reactivity Index (IRI), to assess three subdimensions of empathy: Empathic Concern: sympathetic reactions to the distress of others; Perspective Taking: the tendency to take other's perspective; Personal Distress: aversive reactions to the distress of others. Resting state data was acquired via a series of MRI scans conducted in a Siemens Trio 3T scanner housed in the Ahmanson-Lovelace Brain Mapping Center at UCLA. Participants passively observed a white fixation cross on a black screen. Images were acquired over 36 axial slices covering the whole cerebral volume using an echo planar T2*-weighted gradient echo sequence. A T1-weighted volume was also acquired. Following motion correction, high-pass filtering (.01Hz) and smoothing (6mm FHWM). Preprocessed data was subjected to probabilistic ICA in MELODIC. Noise components were identified and removed. Functional data was coregistered to standard space (MNI 152 template) via nonlinear registration (FNIRT). We created resonance network and control network with 22 ROIs within the Seitzman atlas. Using mean time-courses from each ROI, correlation matrices were created for each participant. We leveraged a LASSO regression model built on N-10 participants' feature sets for each IRI subscale. The model's intercept and outcome beta values were used as coefficients for each left-out subject's feature set-obtaining a predicted subscale measure for that individual. After N folds, we correlated the predicted values with the actual values, yielding Pearson's R– a measure of our model's ability to capture variance across participants. We repeated this cross-validation 50 times, then averaged R values to converge on a true test statistic estimate. To correct for multiple comparisons, matrices of p-values were created using a Benjamini-Hochberg approach in R and corrected p-values were considered significant at the 5% positive tail. To enhance replicability, we also applied Bonferroni correction and generally treated this as 'full' significance.

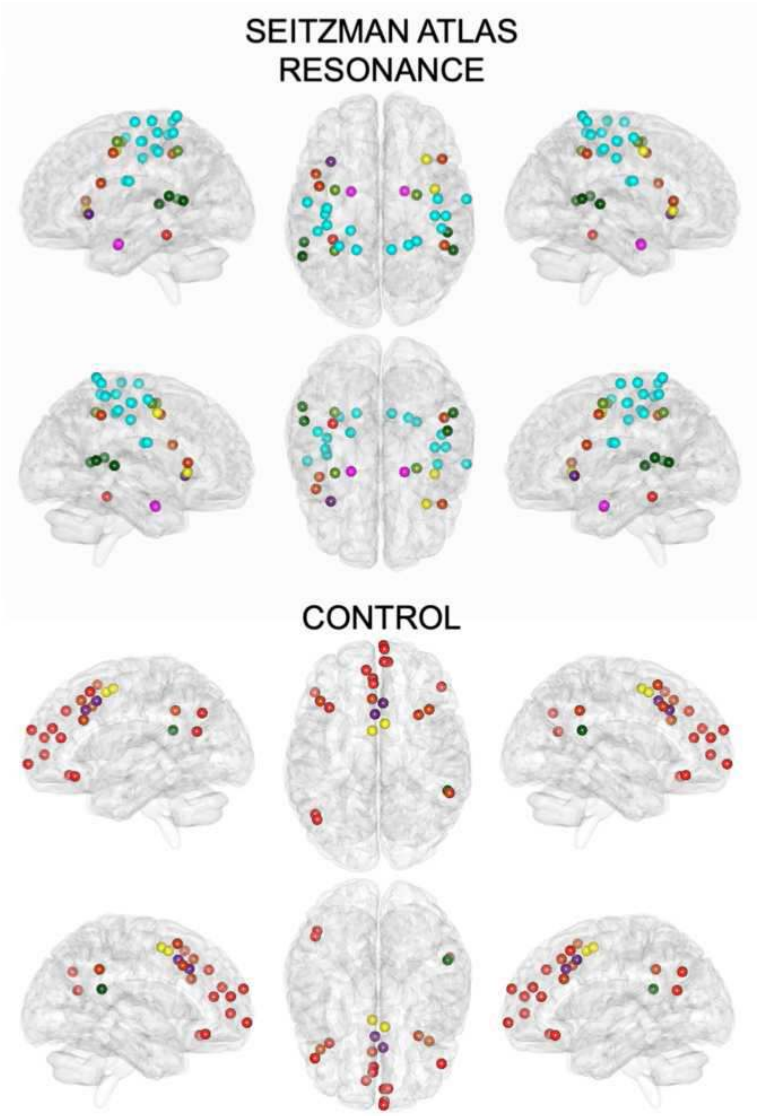

Results: rsFC within a priori networks predicted empathic concern and perspective-taking. Empathic concern was predicted by a far wider array of systems than personal distress and perspective-taking: out of 12 individual and 14 combined networks tested, empathic concern was significantly predicted by 7 individual and 8 combined networks. In contrast, Personal Distress was predicted by 1 individual and 2 combined, and Perspective-Taking by 2 individual and 4 combined, respectively.

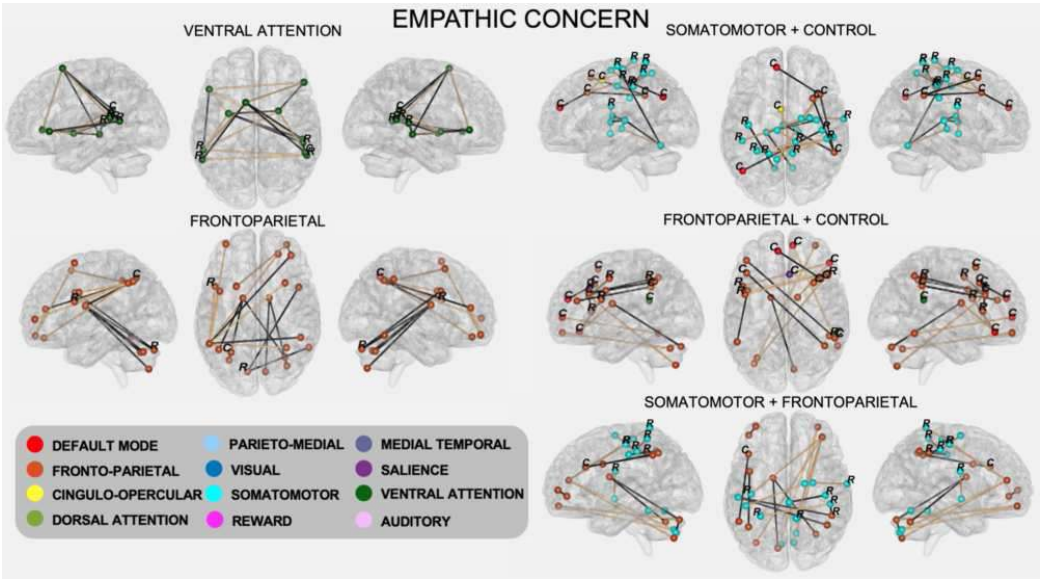

Conclusions: Trait empathy can be robustly predicted from resting brain activity, with possible applications for diagnosis in vulnerable populations.

References
1. Christov-Moore, L., Reggente, N., Feusner, J., Iacoboni, M. (2020) Predicting Empathy from Resting Connectivity: A Multivariate Approach. Frontiers in Integrative Neuroscience. 14(February):1-3

Poster No 803

Neurobehavioral impacts of a social observer on risky decision-making in cigarette smokers

HeeYoung Seon[1], Cheolin Yoo[2], Dongil Chung[1]

[1]Ulsan National Institution of Science and Technology, Ulsan, Republic of Korea, [2]Ulsan University Hospital, University of Ulsan College of Medicine, Ulsan, Republic of Korea

Introduction: Smoking is a health risk behavior that is sensitive to social contexts. One of the primary reasons for initiating smoking is social influence, while social support groups are proposed as an effective way to maintain abstinence. However, it has not been systematically investigated about how smokers, individuals who are known for their biased preference towards the health risk behavior of smoking, respond to such social influences. Here, we tested two possible factors that may lead smokers to act riskily under social contexts. Specifically, we examined i) whether smokers perceive themselves as similar to others who engage in risky behaviors, and ii) whether smokers exhibit altered sensitivity to the influence of risky others.

Methods: To investigate individuals' risky behavior in a social context, a three-phased gambling task was employed. The current task included 30 never-smokers (all male, age=53±4.82) and 42 ever-smokers (all male, age=55.79±6.54, smoking period = 10.69±6.32 years). After a brief phase where we assessed individuals' risk preferences, participants learned about the risk preferences of two social partners; unbeknownst to participants, one was risk-averse and the other was risk-seeking. At the end of this phase, individuals answered questions regarding their impressions of each partner (e.g., similarity). During the last phase, participants were asked to choose between one risky gamble and one safe (guaranteed) gamble. On some trials, they were instructed that either the risk-averse or risk-seeking partner would observe their choices. Throughout the task, electroencephalogram (EEG) data were recorded to explore the neural mechanisms underlying decisions under social influence.

Results: First, we confirmed that never- and ever smokers showed comparable risk preferences (t(70)=-0.24, P=0.81) and learning accuracies (partner: F(1)=0.42, P=0.52, group: F(1)=0.087, P=0.77, interaction: F(2)=0.97, P=0.33). In the self-report questionnaire that followed the learning phase, ever-smokers tended to report that they considered the risk-seeking partner to be more similar to themselves than risk-averse partner (t(41)=-1.88, P=0.068, never-smoker: t(29)=0.23, P=0.82). Moreover, the proportion of participants who perceived the risk-seeking partner to be more similar to them was higher in ever-smokers than in never-smokers (chi-square=7.145, P=0.0075). In contrast to the common expectation about smokers, ever-smokers chose the risky option significantly less under the risk-averse partner's observation compared to their choice under no observation (t(41)=-2.73, P=0.0094), while such social influence was not observed under the risk-seeking partner's observation (t(41)=-0.76, P=0.45). This was paralleled by distinct ERP patterns in ever-smokers. Specifically, ever-smokers only exhibited exaggerated P300 amplitude for the risk-averse partner's observation compared with that for no observation trials (averse: t(40)=-2.11, P=0.043; seeking: t(40)=-0.35, P=0.73), which was not the case in never-smokers (averse: t(27)=-2.62, P=0.015; seeking: t(27)=-2.90, P=0.008).

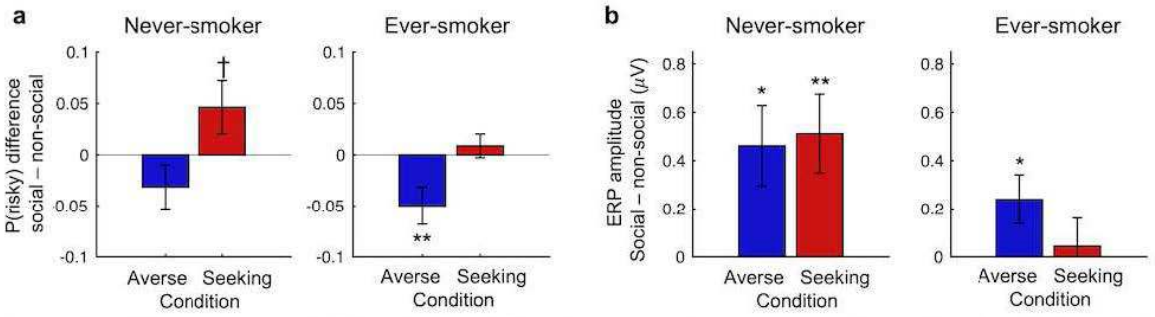

Figure 1. a. Differences in probability of risky choices between social and non-social conditions. b. P300 amplitude differences between social condition and non-social condition. The left graph shows the P300 amplitudes for never-smokers. The left graphs of a and b display the differences in the probability of risky choices for never-smoker. The right graph shows these differences for ever-smokers. The blue bar indicates the risk-averse condition, and the red bar indicates the risk-seeking condition.

Conclusions: This study examined how smokers process social information in the context of risky decision-making. Our findings suggest that smokers may possess a biased belief in their similarity to others who engage in risky behaviors, affecting their decision-making in social contexts. Moreover, choices and the corresponding EEG data under social observation suggest that ever-smokers do not perceive the observation of the risk-seeking partner differently from a non-social situation. This research contributes to understanding how smokers are influenced by social context and may help develop effective social strategies for smoking cessation.

References

1. Delorme A & Makeig S (2004) EEGLAB: an open-source toolbox for analysis of single-trial EEG dynamics, Journal of Neuroscience Methods 134:9-21.

Poster No 804

Decision-making for others' time and money

Sunmin Kim[1], Dongil Chung[1]

[1]Department of Biomedical Engineering, Ulsan National Institute of Science and Technology, Ulsan, Republic of Korea

Introduction: People often make choices on behalf of others, such as decisions related to investments or scheduling. However, it remains unknown how individuals decide for others without knowing others' preferences. Here, we used a computational modeling approach and functional near-infrared spectroscopy (fNIRS) to investigate how individuals make gamble choices for both themselves and anonymous others. Given that individuals' choices vary depending on the reward domains (e.g., money, time), we hypothesized that individuals' decisions for others may also be dissociable between choices for different reward domains. When making choices for others, decision-makers may either use inferred preferences of others based on their beliefs or be insensitive about others' earnings and make random choices. We hypothesized that individuals who empathize more with others would be less likely to make random choices, but make choices based on a certain preference they set as decision strategy for others.

Methods: We used a lottery game in which participants made choices between a safe lottery (a guaranteed payoff) and a risky lottery (a 25, 50, or 75% chance of receiving a higher payoff or no payoff). Participants made choices regarding time (waiting time) and money (bonus) lotteries for themselves and a randomly chosen partner, respectively in both gain- and loss-only frames (i.e., 'Self-Time', 'Partner-Time', 'Self-Money', 'Partner-Money' conditions). To characterize individuals' behavioral patterns in each condition, we analyzed the response times taken to make choices and also estimated individual-level risk preference, loss aversion, and sensitivity to value differences based on a power-utility function. In addition, we measured hemodynamic changes in the prefrontal region during the task and calculated mean activation levels of oxygenated hemoglobin (HbO) signal for Self and Partner conditions. At the end of the task, participants completed a Questionnaire of Cognitive and Affective Empathy (QCAE), which we used to investigate the association between individuals' empathic trait and their behavioral patterns in choices for others.

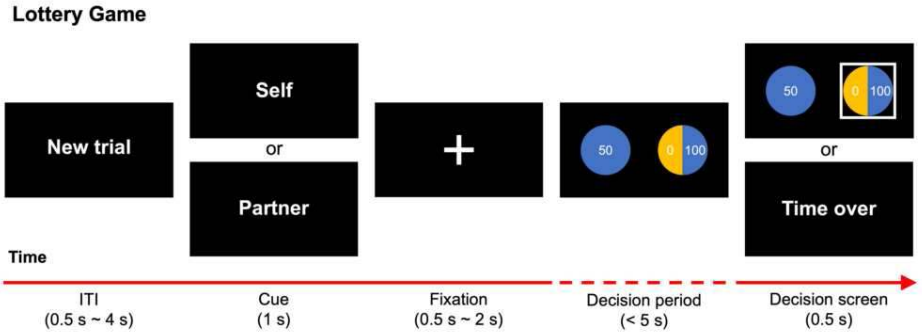

Figure 1. Experimental paradigm. On each trial, a cue 'Self' or 'Partner' was displayed indicating for whom they had to make the choice. During the decision period, participants were asked to choose between one safe lottery and one risky lottery. Participants made a series of these choices regarding time and money domains. The order of the reward domains was counterbalanced across participants.

Results: Participants showed a longer response time (RT) to make decisions for themselves compared with decisions for their partner ($F(1,37) = 9.66$, $p = 0.004$), and a longer RT when deciding between lotteries with monetary payoffs than that with time payoffs ($F(1,37) = 6.72$, $p = 0.014$). At the presentation of the cue indicating for whom they are making the choice, individuals who showed a larger RT difference between decisions for others and that for themselves showed a higher HbO signal in the frontopolar region on the decisions for others compared with the choices for themselves, and vice versa. Estimated behavioral

characteristics revealed that individuals were in general more loss-averse when deciding about time payoffs than monetary payoffs, and that they had higher value sensitivity (i.e., making more consistent choices) in Partner-Money than in Partner-Time condition. Individuals' empathy score was positively correlated with their value sensitivities (Partner-Time: $r = 0.42$, $p = 0.008$; Partner-Money: $r = 0.56$, $p < 0.001$), estimated from the decisions made for their partner.

Conclusions: In the current study, participants showed different choice patterns between decisions for others compared with that for themselves. Differences in RT and HbO signal suggest that decisions for oneself are made more deliberatively and with more mental efforts. When making choices that may lead to others' monetary earnings (or losses), individuals make more consistent choices than the case when others' time is at stake. Furthermore, individuals who empathize more with others indeed made more consistent choices, which is consistent with our interpretation regarding diminished deliberation in decisions for others. Together, our results suggest that social context affects individuals' decisions under risk in different domains.

References

1. Fareri, D. S. (2022), 'Choosing for others changes dissociable computational mechanisms underpinning risky decision-making', Scientific Reports, vol. 12, no. 1, 14361
2. Festjens, A. (2015), 'Time-based versus money-based decision making under risk: An experimental investigation', Journal of Economic Psychology, vol. 50, pp. 52-72
3. Polman, E. (2010), 'Information distortion in self-other decision making', Journal of Experimental Social Psychology, vol. 46, no. 2, pp. 432-435
4. Stone, E. R. (2013), 'I can take the risk, but you should be safe: Self-other differences in situations involving physical safety', Judgment and Decision making, vol. 8, no. 3, pp. 250-267
5. Tak, S. (2016), 'Sensor space group analysis for fNIRS data', Journal of neuroscience methods, vol. 264, pp. 103-112
6. Zhang, X. (2017), 'Decisions for others are less risk-averse in the gain frame and less risk-seeking in the loss frame than decisions for the self', Frontiers in psychology, vol. 8, 1601

Poster No 805

Neural structures for ingroup bias and its malleability

Pyungwon Kang[1], Yurong Sun[2], JuYoung Kim[3], Hackjin Kim[3], Sunhae Sul[4], Grit Hein[5], Philippe Tobler[6]

[1]University of Zurich, Zürich, Switzerland, Other, [2]East China Normal university, Shanhai, China, [3]Korea University, Seoul, Korea, Republic of, [4]Pusan National University, Pusan, Pusan, [5]University of Würzburg, Würzburg, Germany, [6]University of Zurich, Zurich, Switzerland

Introduction: Ingroup bias is the tendency to favor ingroup members over outgroup members. It is pervasive in humans and contributes to inter-group conflict based on nationality or race (Bernhard, Fischbacher, & Fehr, 2006; Brewer, 1979, 1999). Although many neuroimaging studies investigated brain correlates of ingroup bias, most of them focused on differences in neural activity elicited by ingroup versus outgroup conditions (Han, 2018; Molenberg 2013). Thus, it remained largely unknown whether differences in neural structures underpin differences in ingroup bias. Here, we investigated the grey-matter volume of brain areas associated with implicit (implicit association test) and explicit (donation) measures of ingroup bias as well as their change over time.

Methods: We combined two studies, performed with two different types of outgroups in South Korea, and measured the bias of South Koreans against individuals from outside South Korea. More specifically, in both studies, participants (Study 1: n=70, 35 female, age: 25.75±3.86 years; Study 2: n=108, 52 female, age: 23.44±2.24 years) decided whether to incur a monetary cost to donate to charities benefitting the ingroup (Study 1 and 2: South-Koreans) or outgroup (Study 1: North Koreans; Study 2: Southeast Asians in South Korea) and performed an implicit association task (Greenwald et al. 1998) towards ingroup and outgroup members with positive and negative words. We examined whether the association between the volume of cortical and subcortical brain regions and behavior were specific for the type of ingroup bias measure and/or for the type of outgroup or whether a brain region commonly associated with multiple ingroup bias behavior. In addition, to investigate structural commonalities related to the change of implicit and explicit biases in different types of behaviors as well as different intergroup settings, we measured the same types of behaviors (IAT and donation) before and after indirect exposure to outgroup-related information through a political event (Study 1 : inter Korea summit which occurred only for the second time within 70 years at the time of the first measurement) and to video-clips featuring interviews with outgroup members conducted in Korean (Study 2).

Results: We found that the grey-matter volume of a cluster in the putamen ($Z=3.76$, small volume corrected $p < 0.05$) was positively correlated with greater donation to charities benefitting the ingroup. In contrast, the volume of clusters in ventromedial prefrontal cortex ($Z =4.74$, whole brain corrected $p < 0.001$) and inferior temporal lobe ($Z = 3.86$, whole brain

corrected p < 0.001) correlated positively and primarily with stronger implicit bias (i.e. D score) favoring the ingroup, indicating that the grey-matter volume and ingroup bias relations are more task specific. In addition, grey-matter volume in a dorsal anterior cingulate cortex (dACC) cluster correlated with the change of the ingroup biases in both implicit and explicit biases in the two studies (IAT: Z= 3.93, whole brain corrected FWE p <0.05, donation : Z = 3.09, small volume corrected FWE p <0.05) indicating that the dACC may contribute to the change of ingroup bias in a broad sense. Age, total intracranial volume, and the experiment types were controlled in all analyses.

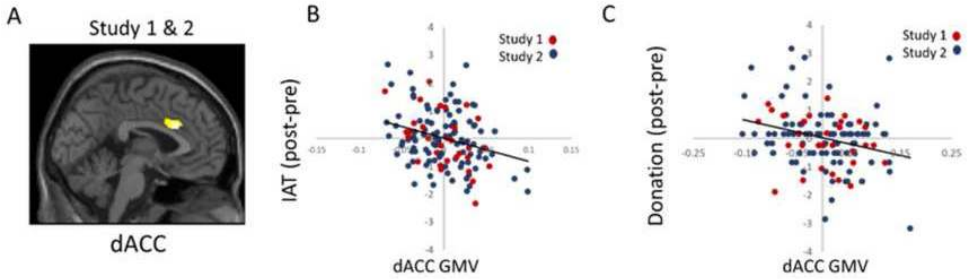

Figure 1. A) dACC cluster correlated with the improvement of ingroup bias after the intervention. Scatter plot of the IAT difference (B) and donation (C) between after and before the intervention in both Study 1 and 2.

Conclusions: Both the strength of the ingroup bias and its malleability appear to be related to differences in neuroarchitecture, in-keeping with the notion that brain-based interventions can reduce the bias.

References

1. Bernhard, H. (2006). Parochial altruism in humans. Nature, 442(7105), 912-915.
2. Brewer, M. B. (1979). In-group bias in the minimal intergroup situation: A cognitive-motivational analysis. Psychological bulletin, 86(2), 307.
3. Brewer, M. B. (1999). The psychology of prejudice: Ingroup love and outgroup hate? Journal of social issues, 55(3), 429-444.
4. Greenwald, A. G (1998). Measuring Individual Differences in Implicit Cognition : The Implicit Association Test, Journal of Personality and Social Psychology, 74(6), 1464–1480.
5. Han, S. (2018).Neurocognitive basis of racial ingroup bias in empathy. Trends in cognitive sciences, 22(5), 400-421
6. Molenberghs, P. (2013). The neuroscience of in-group bias. Neuroscience & Biobehavioral Reviews, 37(8), 1530-1536.

Poster No 806

Map-like and graph-like representations of social knowledge in the hippocampus

DASOM KWON[1,2], Luke Chang[3], Eshin Jolly[3], WON MOK SHIM[1,2]

[1]Sungkyunkwan University, Suwon-si, Korea, Republic of, [2]Center for Neuroscience Imaging Research, Suwon-si, Korea, Republic of, [3]Dartmouth College, Hanover, NH

Introduction: Humans and animals utilize knowledge structures based on either map-like or graph-like representations to facilitate adaptive behaviors[1,2]. Two essential types of information crucial for social interactions, personality traits of each individual and relationships among them, can be organized into distinct structures[3,4]. Personality traits can be structured like a map, indicated by coordinates, while relationships follow a graph-based structure, represented by connections and distance. The hippocampus has been previously proposed as a central hub for structuring relational knowledge[1,2,5,6]. In this study, we examine how the hippocampus organizes these diverse types of social knowledge, each characterized by distinct representational structures, for the same group of social agents in naturalistic settings.

Methods: We collected high spatial resolution (1.5mm isotropic voxels) 7T fMRI data while participants (N = 24) watched first-person movies and played a social interaction game within a custom-built Minecraft environment. They also assessed seven personality traits (dominance, warmth, extroversion, competence, trustworthiness, neuroticism, and agreeableness) and two relationships traits (closeness and trust) of characters, including themselves, across three consecutive episodes of a narrative story during fMRI scanning. In the Minecraft virtual world, participants interacted with six characters, each with distinct personality traits, making social decisions in the conversational context (as in the narrative script). To examine the neural representation of knowledge structures related to both social traits, we employed a representational similarity analysis[7]. Neural representational dissimilarity matrices (RDM) were generated from the rating task using beta coefficients from the general linear model (GLM), encompassing both personality traits and relationship distances.

Results: First, participants exhibited a clear understanding of the intended personality (r = .62, s. d. across participants = .07) and relationship traits (r = .56, s. d. = .12) among characters, including themselves, as designed in our study. The rank correlation between the neural RDMs and social knowledge RDMs across three episodes revealed that the hippocampus represents both map-like knowledge of personality traits (anterior hippocampus: t(23) = 5.02, p < .001; posterior hippocampus: t(23) = 3.47, p = .002) and graph-like knowledge of relationships (anterior hippocampus: t(23) = 2.06, p = .051; posterior hippocampus: t(23) = 3.45, p = .002). Furthermore, hippocampal structures associated with personality and relationship traits were extracted from the parametric GLM using distance metrics in each knowledge structure. In the first episode, these structures were positively correlated (t(23) = 2.97, p = .007), consistent with behavioral data, indicating that initially, characters perceived as similar in personality were also thought to have closer relationships. However, this pattern did not persist through the second and third episodes (the second episode: t(23) = 1.03, p = .314; the third episode: t(23) = 1.33, p = .196), suggesting separate computational processes for the two distinct knowledge structures.

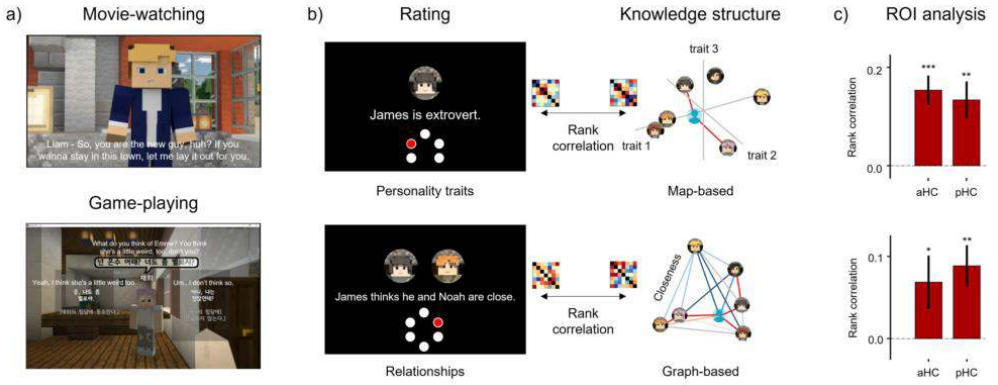

Figure 1. Experimental design, knowledge structure, and fMRI results of the ROI analysis, a) Participants watched a first-person movie and played a social interaction game within a Minecraft environment across three episodes. b) Following a series of social events in movies and games, participants rated the personality traits and directional relationships of characters. Using these ratings and pre-built social narratives, we generated two knowledge structures: a map-based structure for personality traits and a graph-based structure for social relationships. Rank correlations between the two knowledge structures and the corresponding neural RDMs from the hippocampus were computed. c) ROI analysis revealed that both the anterior and posterior hippocampus organized both types of knowledge structures. ∗: p < .05, ∗∗: p < .01, ∗∗∗: p < .001

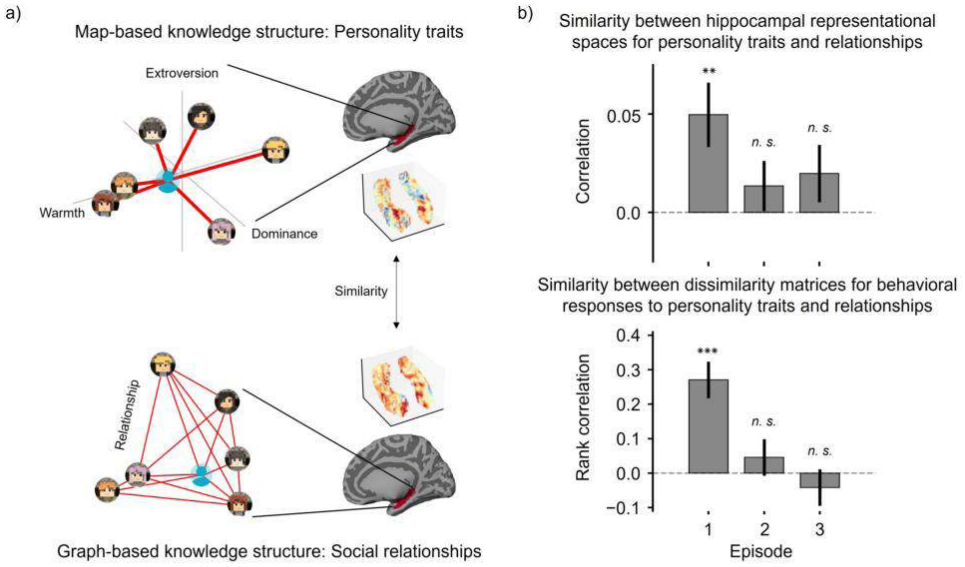

Figure 2. The knowledge structures in the hippocampus. a) Using parametric GLM, we extracted beta coefficients maps for distance metrics in each knowledge structure and computed Pearson correlations between the two hippocampal structures. b) A positive correlation was observed in the first episode, but it was not evident in the second and third episodes. Participants assessed that characters with similar personalities were close in the first episode (t(23) = 6.17, p < .001) but not in the second and third episode (ps > .336). ∗: p < .05, ∗∗: p < .01

Conclusions: Our social environment inherently encompasses diverse forms of relational knowledge that facilitate the formation of either map or graph representations. In this study, we demonstrated the role of the hippocampus in representing both map-like and graph-like knowledge structures for the same group of social agents. Our findings suggest distinct mechanisms in the hippocampus for structuring these two different knowledge structures, raising further research questions of how the hippocampus constructs these types of knowledge structures during ongoing social experiences.

References
1. Behrens, T. E. J., Muller, T. H., Whittington, J. C. R., Mark, S., Baram, A. B., Stachenfeld, K. L., & Kurth-Nelson, Z. (2018). What Is a Cognitive Map? Organizing Knowledge for Flexible Behavior. Neuron, 100(2), 490–509.
2. Peer, M., Brunec, I. K., Newcombe, N. S., & Epstein, R. A. (2021). Structuring Knowledge with Cognitive Maps and Cognitive Graphs. Trends in Cognitive Sciences, 25(1), 37–54.
3. Hassabis, D., Spreng, R. N., Rusu, A. A., Robbins, C. A., Mar, R. A., & Schacter, D. L. (2014). Imagine all the people: how the brain creates and uses personality models to predict behavior. Cerebral Cortex, 24(8), 1979–1987.
4. Kwon, D., Jolly, E., Chang, L. J., & Shim, W. M. (2023). Neural representation of dynamic social interaction. Manuscript in preparation.
5. Tolman, E.C. (1948). Cognitive maps in rats and men. Psychological Review. 55, 189–208.
6. Whittington, J. C. R., McCaffary, D., Bakermans, J. J. W., & Behrens, T. E. J. (2022). How to build a cognitive map. Nature Neuroscience, 25(10), 1257–1272.
7. Kriegeskorte, N., Mur, M., & Bandettini, P. (2008). Representational similarity analysis - connecting the branches of systems neuroscience. Frontiers in Systems Neuroscience, 2, 4.

Poster No 807

Oxytocin's role on the central and autonomic neurophysiological correlates of salience attribution

Gonçalo Cosme[1], Diana Prata[2]

[1]Instituto de Biofísica e Engenharia Biomédica, Lisbon, AK, [2]Instituto de Biofísica e Engenharia Biomédica, Lisboa, AK

Introduction: Well-adapted cooperative behaviours are crucial for our species survival. Behaviours like resource sharing, group defense, social bonding, and support between peers have been associated with the neuropeptide oxytocin which is now known to be a key neuromodulator of social cognition in humans. Evidence suggests the involvement of the oxytocinergic system in the etiology of mental disorders, particularly those characterized by social deficits, for which intranasal oxytocin administration may represent a promising therapeutic solution. However, a large body of evidence have failed to converge in support of oxytocin's foremost hypothesis that oxytocin acts as a pure facilitator of pro-social behaviour. Currently, one leading hypothesis posits oxytocin to increase salience towards social relevant/rewarding stimuli (Shamay-Tsoory and Abu-Akel, 2016), yet the social specificity of the hypothesis has been questioned by others (Quintana and Guastella, 2020). In this study we tested this hypothesis by recording central (eye-gaze) and autonomic (pupil size) neurophysiological correlates of salience attribution during two paradigms: free-video watching of social interactions, to probe oxytocin's salience attribution in varying levels of arousal and valence; and the social salience attribution test, where the social and reward value of stimuli were orthogonalized, to probe the social specificity of oxytocin's salience attribution.

Methods: We carried the study with 62 healthy male participants in a double-blind, placebo-controlled, between-subjects design with intranasal administration of oxytocin. In the first paradigm participants free viewed 16 short clips of social interactions varying in arousal (high vs. low) and valence (positive vs. negative). Four short clips of landscapes were used as a non-social and neutral condition. From participants' eye gaze we computed a spatio-temporal salience score (Traver et al., 2021) across each clip, for each drug group. On the other hand, the social salience attribution test (Roiser et al., 2009) was reinforcement learning paradigm where stimuli varied in social (faces or fruits; task-irrelevant) and color (red or blue; task-relevant) dimensions, and participants were monetarily incentivized to learn which type of stimuli were more rewarding.

Results: During video watching, intranasal oxytocin increased, compared to placebo, the spatio-temporal salience score for 19 out of 20 clips. On average, the high arousing negative clips elicited the highest mean scores and as expected, the neutral condition, the lowest. Salience scores did not differ between drug groups for high vs. low arousing clips. During the social salience attribution test, we found a significant drug by socialness interaction on pupil size where oxytocin increased pupil dilation for social vs non-social stimuli, during stimuli onset. We also found a significant drug by reinforcement probability interaction where oxytocin increased pupil dilation for rewarding vs non-rewarding stimuli, but close to feedback. Crucially, there was no socialness by reinforcement probability interaction effect on pupil size, validating our orthogonalization.

Conclusions: Taken together, these results support the social salience hypothesis of oxytocin given we found evidence, from two distinct paradigms, that oxytocin increased the salience towards social stimuli, measured by neurophysiological correlates of central and autonomic activity in eye gaze and pupil size. Specifically, from the free viewing paradigm, we found specificity of salience attribution to negatively valenced stimuli in line with previous studies indicating consistently that oxytocin reduces amygdala activation to fearful stimuli (Labuschagne et al., 2010). From the social salience attribution test we found specificity of salience attribution to both rewarding and social, but in different moments of the task, nonetheless supporting a suggested oxytocin and dopamine interplay (Shamay-Tsoory and Abu-Akel, 2016). This work was supported by: FCT UIDB/00645/2020.

References
1. Shamay-Tsoory, S.G. (2016) 'The Social Salience Hypothesis of Oxytocin', Biological Psychiatry 79(3), pp. 194–202.
2. Quintana, D.S. (2020) 'An Allostatic Theory of Oxytocin'. Trends in Cognitive Sciences 24(7), pp. 515–528.

3. Traver, V.J. (2021) 'Glimpse: A Gaze-Based Measure of Temporal Salience'. Sensors 21(9), pp. 3099.
4. Roiser, J.P. (2009) 'Do patients with schizophrenia exhibit aberrant salience?' Psychological Medicine 39(2), pp. 199.
5. Labuschagne, I (2010) 'Oxytocin Attenuates Amygdala Reactivity to Fear in Generalized Social Anxiety Disorder', Neuropsychopharmacology 35(12), pp. 2403–2413.

Poster No 808

Temporal Dynamics of Oxytocin in Aging: Putting the Tri-Phasic Model into the Test

Didem Pehlivanoglu[1], Alayna Shoenfelt[1], Tian Lin[1], Marilyn Horta[1], Eliany Perez[1], Adam Woods[1], David Feifel[2], Natalie Ebner[1]

[1]University of Florida, Gainesville, FL, [2]UC San Diego, La Jolla, CA

Introduction: Intranasal oxytocin (OT), which circumvents the blood-brain barrier possibly via olfactory nerve pathways (Quintana et al., 2018), is a non-invasive route of exogenous OT delivery to the human brain for studying social cognition (Horta et al., 2021). Given the evidence on age-related decline in plasma OT levels (Elabd et al., 2014) combined with reduced face recognition ability in aging (Grainger et al., 2017), it is possible that intranasal administration of OT may enhance older adults' attention to faces. To test this idea, the current study leveraged the Tri-Phasic Model of Oxytocin (TRIO; Pehlivanoglu et al., 2020), which proposes that OT modulates attention in the brain across three processing stages. Specifically, in the perception stage, OT enhances initial attention irrespective of stimuli characteristics. In the selection stage, OT increases selective attention to in-group related stimuli. In the evaluation stage, OT enhances sustained attention to positively valenced out-group related stimuli. In the present study, by employing event-related potentials (ERPs) in a sample of older adults, we expected that intranasal OT (vs. P) would result in: larger N170 amplitudes for faces in the perception stage (Hypothesis 1); greater N2 for in-group (older) than out-group (young) faces in the selection stage (Hypothesis 2); and larger LPP for happy out-group (young) than angry and/or in-group (older) faces in the evaluation stage (Hypothesis 3).

Methods: The data comprised 60 healthy older participants (Mean Age = 72.02 years, SD = 6.64, Range = 57-95 years, 50% OT), who were randomly assigned to either the OT or P condition in a double-blind fashion for intranasal self-administration of four weeks 24 IUs twice daily. Before and after the intervention, participants completed a behavioral task during which they were asked to view 72 face images (Ebner et al., 2010) that systematically varied in face age (young vs older) and emotion (happy vs. angry) for 2 seconds, which was followed by rating the trustworthiness of each face. Throughout the task, ERPs were recorded from 32-channel active electrodes (Ag/Ag-Cl; international 10–20 system; actiCHamp, Brain Products). Data were re-referenced to the average of the mastoid electrodes offline and digitally bandpass filtered using a 2nd order infinite impulse response (IIR) Butterworth filter (half-amplitude cutoffs at 0.01 and 100 Hz, 12 dB/octave roll-off). All data processing was performed in MATLAB using the EEGLAB (Delorme & Makeig, 2004) and the ERPLAB (Lopez-Calderon & Luck, 2014) toolboxes. Further statistical testing of the hypotheses was conducted by performing mixed ANOVA models.

Results: First, in line with Hypothesis 1, the main effect of Drug was statistically significant ($t(58) = 1.82$, $p = .04$) as reflected by larger N170 amplitude for faces in the OT (vs. P) group during the 150-200 ms time window at parietal electrode sites (Figure1). Second, the Drug x Face Age interaction was not statistically significant during the 290-350 ms time window at frontocentral electrode sites ($F(1, 58) = 0.25$, $p = .62$), thus not supporting Hypothesis 2. Third, the Drug x Face Age x Face Emotion interaction was statistically significant during the 650-850 ms time window at frontotemporal electrode sites ($F(1, 58) = 4.65$, $p = .03$). That is, OT (vs. P) enhanced overall processing of faces in aging with this enhancement among older adults more pronounced for in-group happy faces than in-group angry or out-group faces, partially supporting Hypothesis 3 (Figure 2).

Figure 1

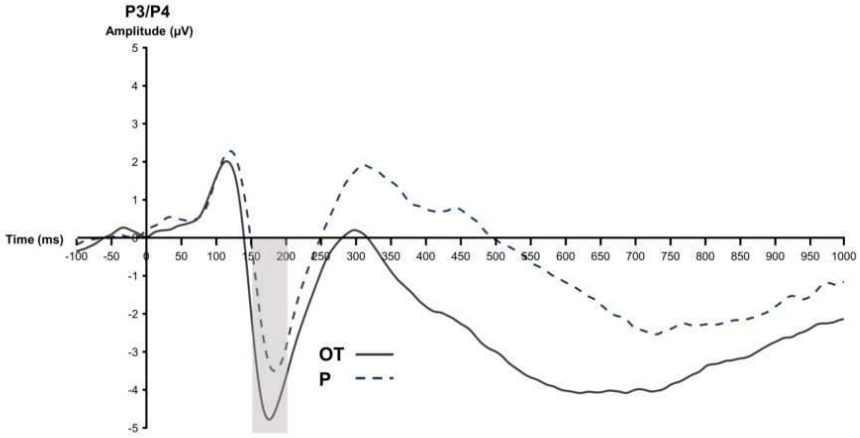

Note: OT = oxytocin; P = placebo. The highlighted gray area indicates the N170 component.

Figure 2

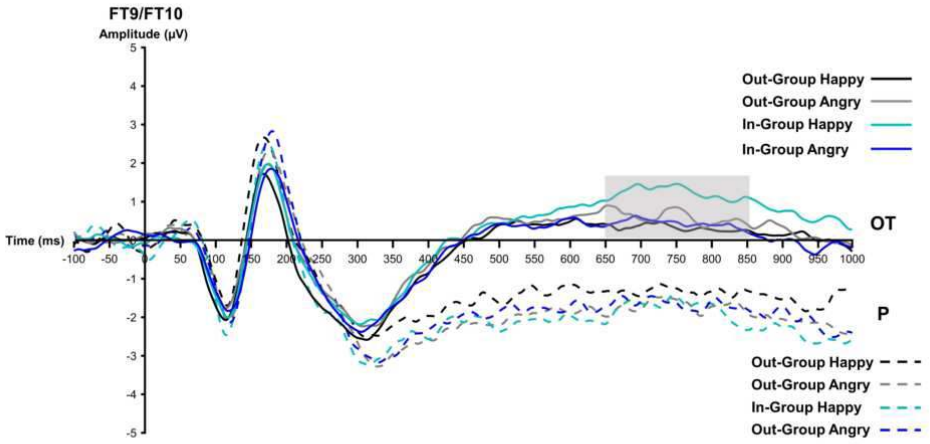

Note: OT = oxytocin; P = placebo. The highlighted gray area indicates the LPP component.

Conclusions: These findings largely align with the TRIO model, in that OT enhanced initial perceived salience of faces during the perception stage as well as sustained attention to salient information in the evaluation stage. Future work will need to determine the impact of task-inherent characteristics (e.g., still vs. dynamic faces) as well as participants' sex and level of socioemotional functioning on OT-related ERP effects in older adults.

References

1. Ebner, Natalie C., Michaela Riediger, and Ulman Lindenberger. "FACES—A database of facial expressions in young, middle-aged, and older women and men: Development and validation." Behavior Research Methods 42 (2010): 351-362.
2. Elabd, Christian, Wendy Cousin, Pavan Upadhyayula, Robert Y. Chen, Marc S. Chooljian, Ju Li, Sunny Kung, Kevin P. Jiang, and Irina M. Conboy. "Oxytocin is an age-specific circulating hormone that is necessary for muscle maintenance and regeneration." Nature Communications 5, no. 1 (2014): 4082.
3. Delorme, Arnaud, and Scott Makeig. "EEGLAB: an open source toolbox for analysis of single-trial EEG dynamics including independent component analysis." Journal of Neuroscience Methods 134, no. 1 (2004): 9-21.
4. Grainger, Sarah A., Julie D. Henry, Louise H. Phillips, Eric J. Vanman, and Roy Allen. "Age deficits in facial affect recognition: The influence of dynamic cues." Journals of Gerontology Series B: Psychological Sciences and Social Sciences 72, no. 4 (2017): 622-632.
5. Horta, Marilyn, Kathryn Kaylor, David Feifel, and Natalie C. Ebner. "Chronic oxytocin administration as a tool for investigation and treatment: A cross-disciplinary systematic review." Neuroscience & Biobehavioral Reviews, 108 (2020): 1-23.
6. Lopez-Calderon, Javier, and Steven J. Luck. "ERPLAB: an open-source toolbox for the analysis of event-related potentials." Frontiers in Human Neuroscience 8 (2014): 213.
7. Pehlivanoglu, Didem, Elisha Myers, and Natalie C. Ebner. "Tri-Phasic Model of Oxytocin (TRIO): a systematic conceptual review of oxytocin-related ERP research." Biological Psychology 154 (2020): 107917.
8. Quintana, Daniel S., Knut T. Smerud, Ole A. Andreassen, and Per G. Djupesland. "Evidence for intranasal oxytocin delivery to the brain: recent advances and future perspectives." Therapeutic Delivery 9, no. 7 (2018): 515-525.

Poster No 809

Disentangling the functional relationship between neural networks of social cognition

Lara Maliske[1], Matthias Schurz[2], Philipp Kanske[3]

[1]Technische Universität Dresden, Dresden, Saxony, [2]Institute of Psychology and Digital Science Center, University of Innsbruck, Innsbruck, Tyrol, [3]Clinical Psychology and Behavioral Neuroscience, Technische Universität Dresden, Dresden, Germany

Introduction: Recent advances in the study of empathy and Theory of Mind (ToM) demonstrate the need to investigate the two in interaction: naturalistic settings often blur the distinction between affect and cognition and demand the simultaneous processing of such different stimulus dimensions. Here, we followed up on the results of a recent coordinate-based meta-analysis and hierarchical clustering analysis (Schurz et al., 2021), as well as a follow-up meta-analytic connectivity modeling analysis (Maliske et al., 2023) that described a hierarchical model of social affect and cognition, as well as how neural representations of empathy and ToM were enabled through network co-activation and connectivity. Specifically, we further investigated the relationship between social affective, cognitive, and complex social neural activation maps by projecting them along a principal gradient of macroscale cortical organization (Margulies et al., 2016), and comparing them to other neural activation patterns related to social cognition.

Methods: We re-analyzed data from a meta-analysis and agglomerative hierarchical clustering (Schurz et al., 2021) including 188 studies from the empathy and ToM literature across 11 more narrow tasks groups, that were clustered into three overarching clusters of neural activation related to social affect and cognition (cognitive, intermediate, affective cluster). Furthermore, we re-analyzed data from a follow-up meta-analytic connectivity modeling study (Maliske et al., 2023) including 140 studies associated with the right anterior cingulate cortex, right posterior cingulate cortex, left temporoparietal junction, and left anterior insula. To project the meta-analytic (co-activation) maps onto a principal gradient of macroscale organization, as well as more narrow task groups, we determined overlap between neural activation maps using a variant of the dice score (indicating the percentage of voxels in i1 that overlap with i2). Specifically, we calculated the overlap between meta-analytic (co-activation) maps and a) continuous changes in the functional spectrum described by the principal gradient (in increments of 5%), as well as b) more narrow task groups related to social affect and cognition (see Schurz et al., 2021).

Results: Meta-analytic (co-activation) maps related to social affect and cognition (affective and cognitive cluster, respectively) were positioned at separable locations along the principle gradient, while meta-analytic (co-activation) maps related to complex social cognition (intermediate cluster) tended to overlap with the locations of both the affective (located towards the sensory/ unimodal part of the gradient, 30-55th percentile) and the cognitive cluster (located towards the transmodal end of the gradient, 80-95th percentile. In terms of overlap with specific tasks, the cognitive cluster showed most pronounced overlap with the false belief task (e.g., Saxe & Kanwisher, 2002; overlap ranging from 81-95%). Neural (co-)activation patterns related to social affect and complex social cognition (affective and intermediate cluster, respectively) showed overlap with diverse task profiles, although some trends emerged (e.g., a larger overlap of affective cluster and observing pain, as well as reading the mind in the eyes meta-analytic maps).

Conclusions: Re-analysis of coordinate-based meta-analyses and meta-analytic connectivity modeling allowed us to further probe the relationship between neural activation patterns related to social affect, cognition, as well as complex social tasks. More precisely, in contrasts to the notion of independence of empathy and ToM-related neural networks, the results presented here indicate that complex social tasks (intermediate cluster) rely on cross-network interaction (network integration), and their neural activation are similar to a neural activation patterns related to a range of different tasks measuring empathy and ToM.

References

1. Schurz, M. (2021). 'Towards a Hierarchical Model of Social Cognition: A Neuroimaging Meta-Analysis and Integrative Review of Empathy and Theory of Mind', Psychological Bulletin, vol. 147, no. 3, pp. 293-327.
2. Maliske, L. (2023). 'Interactions within the social brain: Co-activation and connectivity among networks enabling empathy and Theory of Mind', Neuroscience & Biobehavioral Reviews, vol. 147, article 105080, pp. 1-13.
3. Margulies, D. (2016). 'Situating the default-mode network along a principal gradient of macroscale cortical organization', Proceedings of the National Academy of Sciences, vol. 113, no. 44, pp. 12574-12579.
4. Saxe, A. (2003). 'People thinking about thinking people. The role of the temporo-parietal junction in "theory of mind"', NeuroImage, vol. 19, pp. 1835-1842.

Poster No 810

Person memory is supported by the neural reinstatement of social interactions

Eshin Jolly[1], Sushmita Sadhukha[1], Maryam Iqbal[1], Luke Chang[1]

[1]Dartmouth College, Hanover, NH

Introduction: How does remembering other people comport with our understanding of episodic memory? One possibility based on prior work in social cognition is that we remember people as a function of their intrinsic attributes (e.g. personality traits) (Uleman & Kressel, 2013). Another possibility based on event-segmentation theory is that people are simply contained with the broader events that we use to segment our experiences (Zacks, 2020). More recent work has demonstrated that relationships between people drive how we represent and remember others (Jolly et al., 2023). We compared these possibilities using naturalistic neuroimaging to estimate a measure of neural reinstatement by having participants watch a rich character drama and later recall what they could about each character in an unconstrained manner.

Methods: Participants (N=36) watched the first four episodes of the television show Friday Night Lights, and later performed a naturalistic character recall task in which they recounted aloud what they could remember about each main character for two minutes while undergoing fMRI. Average memory patterns were estimated for each recalled character separately for each participant in 268 parcellated regions of interest (Shen et al., 2013) using a general linear model (GLM). Three estimates of neural reinstatement were computed by comparing the spatial similarity of each memory pattern to brain activity during episode watching for: (a) general narrative events involving a character; (b) specific moments in time when a character could be seen or heard; (c) even more specific moments when a character having a social interaction. Reinstatement effects were compared within each participant using a multi-level model to identify what regions showed preferential reinstatement of social interactions when remembering each character (Fig 1). To link reinstatement activity to memory content, we further identified any regions in which the magnitude of neural reinstatement for specific social interactions predicted the probability of participant's remembering that specific relationship when recalling a character (Fig 2). All analyses were performed using permutation testing and corrected for multiple comparisons across ROIs using FDR $q < 0.05$.

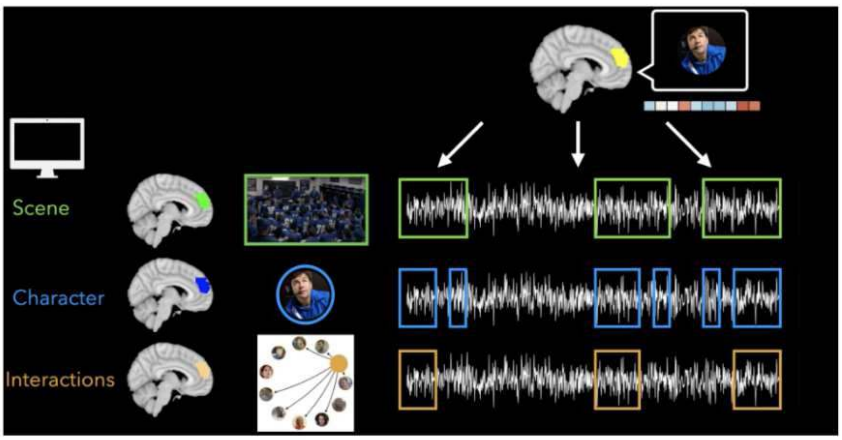

Figure 1 | Computing neural reinstatement Neural patterns during memory recall of specific characters were compared to patterns of activity during episode watching for the: (green) contiguous scenes and events in which a character was involved; (blue) the collection of moments a character was present; (orange) and the specific moments of time when a character interacted with others. Reinstatement effects were compared within participants using a multi-level linear contrast to discover regions that preferentially reinstated interactions (Fig 2A).

Results: Overall, several notable regions within both the social brain (dmPFC, pSTS, ATL) and episodic memory (PMC, hippocampus) networks showed preferential reinstatement for social interactions relative to general character information or events that involved a character. Within these identified regions, a single node within the right pSTS predicted the probability of participants recalling specific relationships as a function of reinstatement magnitude for observing those particular relationships.

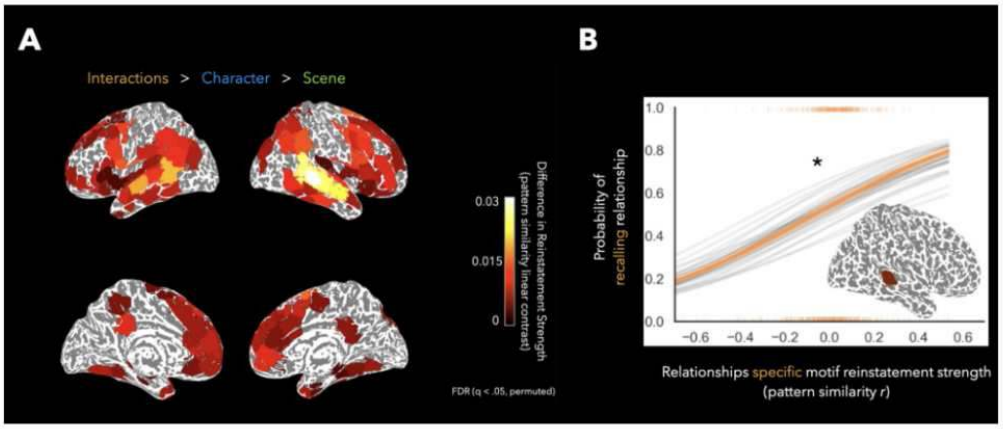

Figure 2 | Comparing reinstatement types (A) Regions that preferentially reinstated interactions when recalling memories of specific characters. No regions survived the reverse contrast or other comparisons **(B)** Only a node within the right pSTS predicted the probability of recalling *specific* relationships based on the magnitude of reinstatement

Conclusions: This study provides neural evidence that social memory for individuals consists of the information we learn about how they interact with others. This provides a mechanism for why we represent and remember people through their relationships with others (Jolly et al., 2023) rather than intrinsic attributes like traits (Uleman & Kressel, 2013) or more general narrative events (Zacks, 2020). These findings also provide convergent evidence for recent work demonstrating that social interaction features can predict time-series activity in the pSTS when recalling general narrative information (Masson et al., 2022). This raises the possibility the pSTS in particular may play a role in memory beyond social perception (Pitcher & Ungerleider, 2021) by specifically reinstating social interaction information that we acquire.

References

1. Jolly, E., Sadhukha, S., Iqbal, M., Molani, Z., Walsh, T. M., Manning, J. R., & Chang, L. J. (2023). People are represented and remembered through their relationships with others. Psyarxiv.
2. Masson, H. L., Chen, J., & Isik, L. (2022). A shared neural code for social interaction encoding and memory in the human superior temporal sulcus. In bioRxiv (p. 2022.10.03.510639). https://doi.org/10.1101/2022.10.03.510639
3. Pitcher, D., & Ungerleider, L. G. (2021). Evidence for a Third Visual Pathway Specialized for Social Perception. Trends in Cognitive Sciences, 25(2), 100–110.
4. Shen, X., Tokoglu, F., Papademetris, X., & Constable, R. T. (2013). Groupwise whole-brain parcellation from resting-state fMRI data for network node identification. NeuroImage, 82, 403–415.
5. Uleman, J. S., & Kressel, L. M. (2013). A brief history of theory and research on impression formation. Oxford Handbook of Social Cognition, 53–73.
6. Zacks, J. M. (2020). Event Perception and Memory. Annual Review of Psychology, 71, 165–191.

Poster No 811

Inferring Affective States of Others Within Dynamic Social Interactions

Jisu Ro[1], Luke Chang[2], Ye Eun Seo[3], Won Mok Shim[4]

[1]Sungkyunkwan University, Gangseo-gu, Seoul, [2]Dartmouth College, Hanover, NH, [3]Kaist, Yuseong-gu, Daejeon, [4]CNIR/SKKU, Suwon-si, Kyonggi-do

Introduction: A key aspect of social cognition is inferring how another person is feeling. These inferences can be influenced by prior emotional states (Thornton et al, 2017), as well as by interactions with others (Houlihan et al, 2023). Although recent studies have attempted to characterize the predictive process of social cognition by examining prediction errors through simplified social actions within structured experimental context (Park et al, 2020), they have often dismissed the intricate nature of social interaction in a real life environment (Zaki et al, 2009). Therefore, in this study, we aim to elucidate how our social brain integrates social context information to dynamically update subjective predictions of others' state during naturalistic social interaction.

Methods: We developed several computational models outlining how participants might be generating their predictions of each characters' affective state for each scene. The reduced model recursively updates based on the valence prediction error (valence PE) - the difference between the observed and predicted valence ratings for a specific character. The full model further incorporates aspects of the social interaction - specifically the difference or mismatch between the two character's

social intentions. We performed nested model comparisons to assess which model provided the best account of participant's valence rating data. To explore the neural dynamics of predictive computations, we collected brain imaging data with an independent group of participants (n=37) while they watched the movie inside the scanner without any task (3T, voxel size =3mm^3, TR =1s). We correlated the voxel-wise activity with each model component to investigate distinct neural responses associated with the predictive processes during social interaction.

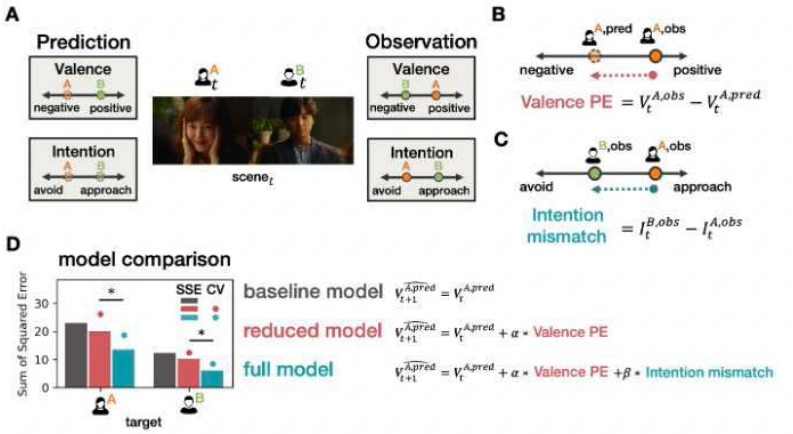

Fig 1. Modeling the predictions about other's valence. **A. Prediction task structure**. For each segmented scene of a character, independent groups of participants rated the predicted and observed valence or social intention inferred by the actions before and after viewing the scene. **B. Valence prediction error**; calculated by the difference between the predicted and the observed valence ratings. This was taken by our models to account for updates towards the observation from the previous estimates. **C. Intention mismatch**; calculated by the difference in social intention ranging from avoiding to approaching. **D. model comparison**. We conducted the nested model comparisons.The "baseline model" indicates that subsequent predictions are fully based on its previous estimates measured by the behavioral rating. The reduced model only integrates the valence PE into the current state prediction, whereas the full model employs both the valence PE and intention mismatch. * indicates p<.05.

Results: For both characters in the movie, the full model incorporating the intention mismatch significantly outperformed the reduced model in explaining how participants' inferred each character's affective state. Univariate analysis revealed that the unsigned valence PE explains the striatal activity whereas its signed version elicited greater responses in the right temporal parietal junction (rTPJ). In contrast, the effect of intention mismatch was observed in the superior and middle temporal gyrus (STG, MTG) which expanded to more high-order cortical regions such as the angular gyrus (AG) and post cingulate cortex (PCC).

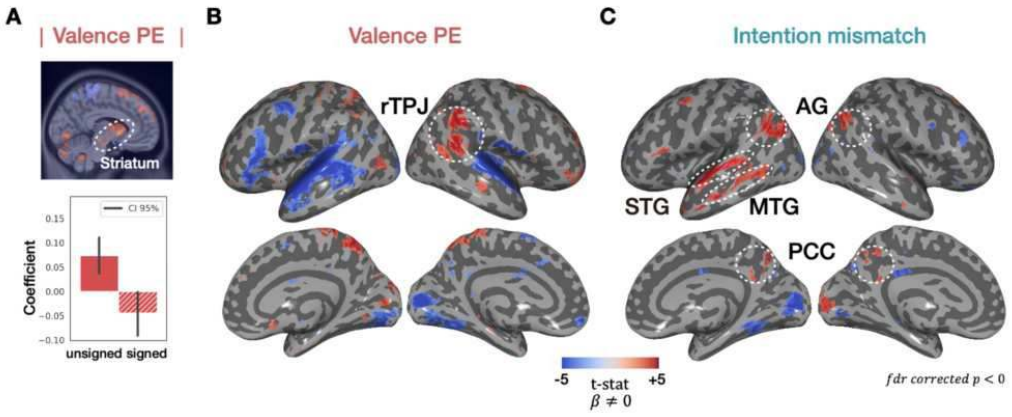

Fig 2. Neural correlates of the valence PE and intention mismatch

Conclusions: Our findings suggest that our social brain processes naturalistic social interactions in a predictive fashion. Participants appear to update their prediction about another person's affective state for each state based on prediction error. However, participants also appeared to simulate the consequences of the other social agent's intended action to generate more accurate predictions about how they might feel. These two distinct inference processes appear to be

processed in distinct regions of the brain. Updating predictions based on overall errors is processed in the social cognition regions including the right TPJ, while tracking mismatches in intentions within the interaction appears to recruit the STG, MTG, AG and PCC. Together, this work provides a substantial advance towards understanding the complex psychological and neural processes that sustain our remarkable ability to infer another person's emotional state embedded in dynamic social interaction.

References

1. Houlihan, S. D., Kleiman-Weiner, M., Hewitt, L. B., Tenenbaum, J. B., & Saxe, R. (2023). Emotion prediction as computation over a generative theory of mind. Philosophical Transactions of the Royal Society A, 381(2251), 20220047.
2. Park, B., Fareri, D., Delgado, M., & Young, L. (2021). The role of right temporoparietal junction in processing social prediction error across relationship contexts. Social Cognitive and Affective Neuroscience, 16(8), 772-781.
3. Thornton, M. A., & Tamir, D. I. (2017). Mental models accurately predict emotion transitions. Proceedings of the National Academy of Sciences, 114(23), 5982-5987.
4. Zaki, J., & Ochsner, K. (2009). The need for a cognitive neuroscience of naturalistic social cognition. Annals of the New York Academy of Sciences, 1167(1), 16-30.
5. , Jong Gwan Kim (ATNINE FILM, 2016)

Poster No 812

Neural Markers of Clinicians' empathy for Patients' Pain Predict Pain Assessment and Treatment

Elizabeth Losin[1], Nikta Khalilkhani[2], Theoni Varoudaki[3], Morgan Gianola[4]

[1]The Pennsylvania State University, State College, PA, [2]Penn State University, State College, PA, [3]Penn State Univeristy, State College, PA, [4]University of Miami, Coral Gables, FL

Introduction: Unequal prescribing of opioid and non-opioid analgesics among demographic groups contributes to two major health disparities in the United States. Overprescribing of opioid analgesics to treat both acute and chronic nonmalignant pain, especially in non-Hispanic whites, has fueled an epidemic of opioid abuse. Underprescribing of opioid and non-opioid analgesics in minorities and women reduces the effectiveness of pain management in these groups. Existing literature suggests one possible mechanisms underlying analgesic prescribing disparities is that clinicians may experience less shared pain as indexed by reduced activation of pain-related neural systems (e.g. anterior cingulate, anterior insula), when observing the pain of demographic outgroup vs ingroup patients resulting in reduced analgesic prescription to these patients (i.e., the vicarious pain hypothesis). Ultimately, understanding the sociocultural, psychological, and neurobiological mechanisms underlying these disparities may help us train clinicians in ways that reduce them.

Methods: In order to test possible mechanisms underlying pain assessment and treatment disparities we had N=67 (34 f) medical students complete a virtual pain management task while undergoing fMRI. Each clinician saw a diverse group of 36 mock patients with acute musculoskeletal pain from a recent injury. During each simulated pain management appointment clinicians 1) saw a medical vignette with patient information, 2) saw a video depicting the patient in pain meant to simulate the clinical examination, and 3) rated how much pain they thought the patient was experiencing and how likely they would be to prescribe an analgesic. In order to test for the best predictors of clinician's accuracy in their assessment of patients' pain (defined as the difference between the clinician and patients' pain intensity rating) and in their assessment of the patient's need for treatment (defined as the difference between the clinicians' likelihood of prescribing an analgesic and the patients' ratings of their pain unpleasantness) we performed an exploratory analysis using Stochastic Search Variable Selection. In this analysis, brain predictors included average brain activity of clinicians when reading patient medical vignettes and observing their pain expressions in two a priori regions of interest related to pain empathy from a previous meta-analysis as well as a mask of regions associated with empathy from an automated meta-analysis using Neurosynth. We also included a suite of other predictors related to both the clinician (e.g. clinician's year of medical training, and clinician's responses to an empathy questionnaire) and the mock patient (e.g. the intensity of the patient's pain facial expression).

Results: We found that the clinician's reported level of trait empathic concern and brain activity within the Neurosynth empathy mask when observing patients in pain positively predicted the accuracy with which the clinician assessed the patients pain. We also found that the clinician's reported level of trait empathic concern and perspective taking and the clinician's perception of the patient's higher attractiveness and higher socioeconomic status positively predicted the accuracy of their assessment of the patient's need for treatment.

Conclusions: Our findings are consistent with the vicarious pain hypothesis and suggest that the degree to which clinicians empathize with and vicariously share the pain of their patients (as indexed by pain-related brain activation) increases a clinician's ability to accurately assess their patient's pain. Given that a wealth of literature in social neuroscience demonstrates

that people display a reduction in brain markers of pain empathy for targets they perceive to be outgroup members, all of these findings are plausible mechanisms of widespread pain assessment and treatment disparities.

Poster No 813

Neural predictors of interpersonal trust across cultures

Huan Wang[1], Christy Wang[1], Brian Knutson[1], Jeanne Tsai[1]

[1]Stanford University, Palto Alto, CA

Introduction: Trust based on prior interaction has been associated with increased activity in mesolimbic regions including the Medial PreFrontal Cortex (MPFC) and Nucleus Accumbens (NAcc; Rilling et al., 2002; Bellucci et al., 2017), and linked to pursuit of cooperation and gains (Samanez-Larkin & Knutson, 2015). Distrust of strangers, however, has been associated with increased Anterior Insula (AIns) activity, and linked to avoidance of social betrayal (Aimone et al., 2014) and losses (Samanez-Larkin & Knutson, 2015). Therefore, prior information about interaction partners offers reputational information that can facilitate cooperation and trust, even in different cultures (Delgado et al., 2005; Bente et al., 2014). Behavioral research suggests, however, that different cultures may have different default expectations of trustworthiness. Specifically, European Americans may trust strangers more than East Asians (Buchan et al., 2002; Kiyonari et al., 2006). We aimed to investigate whether individuals from these cultures would show different trust defaults as well as neural predictors of choices to trust strangers.

Methods: We assessed brain activity using Functional Magnetic Resonance Imaging (FMRI) in 25 healthy European American and 27 Chinese adults as they played 72 trials of a single-shot Trust Game (Glaeser et al. 2000). On each trial, subjects saw a picture of a partner's face (4s), followed by information about the previous reciprocation history of that partner (i.e., the percentage of previous players who rated the partner as trustworthy; 4s), and finally a spatially counterbalanced prompt to indicate how much they chose to invest in the partner (between $0 to $6 endowment in an increment of $2; 4s), which served as a proxy for trust. To ensure incentive compatibility, subjects were notified that one randomly-chosen trial would be chosen to count as binding after scanning.

Results: As predicted, European Americans chose to invest more often than Chinese ($F = 20.10$, $p < .001$), consistent with a higher default expectation of trust among European Americans. Neural activity was extracted from three Volumes Of Interest (VOIs; i.e., NAcc, AIns, and MPFC) immediately before subjects chose whether to invest in partners. Multivariate mixed-effect logistic regressions used this brain data to predict choices on each trial. Analyses revealed a culture by AIns interaction ($t = -2.30$, $p = .022$), in which AIns activity negatively predicted choices to invest for European Americans ($B = -.56$, $p = .007$). Analyses also revealed culture by NAcc ($t = -2.93$, $p = .003$) and culture by MPFC ($t = -2.18$, $p = .029$) interactions, in which activity in these regions positively predicted choices to invest for Chinese (MPFC: $B = .32$, $p < .001$; NAcc: $B = .36$, $p = .047$). VOI analyses using the same brain data further demonstrated that low reputation partners increased AIns activity more for European Americans than for Chinese ($F = 3.51$, $p = .03$; $t = 2.69$, $p = .01$), whereas high reputation partners increased NAcc activity more for Chinese than for European Americans ($F = 4.95$, $p = .001$; $t = 2.73$, $p = .009$).

Conclusions: Together, these findings suggest that cultural values can shape the default level of trust, which may then interact with a partner's reputation to determine cultural predictors of trust. On the one hand, European Americans with high trust default expectations distrusted disreputable partners, which was predicted by higher AIns activity. On the other hand, Chinese with low trust default expectations trusted reputable partners, which was predicted by increased NAcc and MPFC activity. Together, these findings suggest that culture may modulate motivations to trust – a lesson with potential implications for improving cross-cultural communication and cooperation.

References

1. Rilling, J. K., Gutman, D. A., Zeh, T. R., Pagnoni, G., Berns, G. S., & Kilts, C. D. (2002). A neural basis for social cooperation. Neuron, 35(2), 395-405.
2. Bellucci, G., Chernyak, S. V., Goodyear, K., Eickhoff, S. B., & Krueger, F. (2017). Neural signatures of trust in reciprocity: A coordinate-based meta-analysis. Human brain mapping, 38(3), 1233-1248.
3. Aimone, J. A., Houser, D., & Weber, B. (2014). Neural signatures of betrayal aversion: an fMRI study of trust. Proceedings of the Royal Society B: Biological Sciences, 281(1782), 20132127.
4. Samanez-Larkin, G. R., & Knutson, B. (2015). Decision making in the ageing brain: changes in affective and motivational circuits. Nature Reviews Neuroscience, 16(5), 278-289.
5. Delgado, M. R., Frank, R. H., & Phelps, E. A. (2005). Perceptions of moral character modulate the neural systems of reward during the trust game. Nature neuroscience, 8(11), 1611-1618.
6. Bente, G., Dratsch, T., Kaspar, K., Häßler, T., Bungard, O., & Al-Issa, A. (2014). Cultures of trust: Effects of avatar faces and reputation scores on German and Arab players in an online trust-game. PloS one, 9(6), e98297.

7. Buchan, N. R., Croson, R. T., & Dawes, R. M. (2002). Swift neighbors and persistent strangers: A cross-cultural investigation of trust and reciprocity in social exchange. American journal of sociology, 108(1), 168-206.
8. Kiyonari, T., Yamagishi, T., Cook, K. S., & Cheshire, C. (2006). Does trust beget trustworthiness? Trust and trustworthiness in two games and two cultures: A research note. Social psychology quarterly, 69(3), 270-283.
9. Glaeser, E. L., Laibson, D. I., Scheinkman, J. A., & Soutter, C. L. (2000). Measuring trust. The quarterly journal of economics, 115(3), 811-846.

Poster No 814

Implicit robot bias: differential amygdala activation to subthreshold and suprathreshold robots

Zhengde Wei[1], Ying Chen[1], Xiaochu Zhang[1]

[1]University of Science and Technology of China, Hefei, Anhui

Introduction: As robots increasingly become part of our daily lives, understanding human-robot interactions is imperative[1-2]. An increasing body of studies have addressed this issue of evaluations of robots with self-reports; yet evidence for evaluations of robots has been inconsistent, ranging from enthusiasm to anxiety and fear of robots[3-5]. A potentially more direct and useful approach for understanding the fundamental processes underlying controlled and automatic evaluations of robots is to probe brain response to different perception levels of robot-related stimuli.

Methods: In Experiment 1, we recruited 66 participants and asked them to complete an attitude toward robots questionnaire and an implicit association test (IAT; Figure 1a) with image stimuli of humanoid robots and Caucasian individuals. In Experiment 2, we scanned 59 participants with functional magnetic resonance imaging (fMRI) while they completed a backward masking task, in which they viewed suprathreshold (duration: 200 ms) and subthreshold (duration: 17 ms) presentations of humanoid robot and Caucasian stimuli. In Experiment 3, Out of the 59 participants in fMRI experiment above, 23 participants proceeded to complete a positive evaluative conditioning task. Afterwards, they repeated the backward masking task while undergoing fMRI scanning.

Results: Self-reports and behavioral measures demonstrated a discrepancy between explicit positive and implicit negative attitudes toward robots (Figure 1b-c). Consistent with negative implicit attitudes, fMRI during a backward masking task showed heightened responses in the left amygdala to subthreshold (implicit) as opposed to suprathreshold (explicit) robot images (Figure 2a-c). Importantly, by pairing robot images with positive stimuli, we were able to reduce negative implicit attitudes, which corresponded with attenuated amygdala response to subthreshold robot images (Figure 2d-f).

Conclusions: Our studies offer compelling evidence for distinct patterns of amygdala activation between controlled and automatic processing of robots. This sheds light on how people evaluate and interact with robots that are increasingly entering our social environment. The future of social robots is undeniably exciting, and insights from neuropsychology research will guide the future direction of robot development and bring us closer to interacting with social robots.

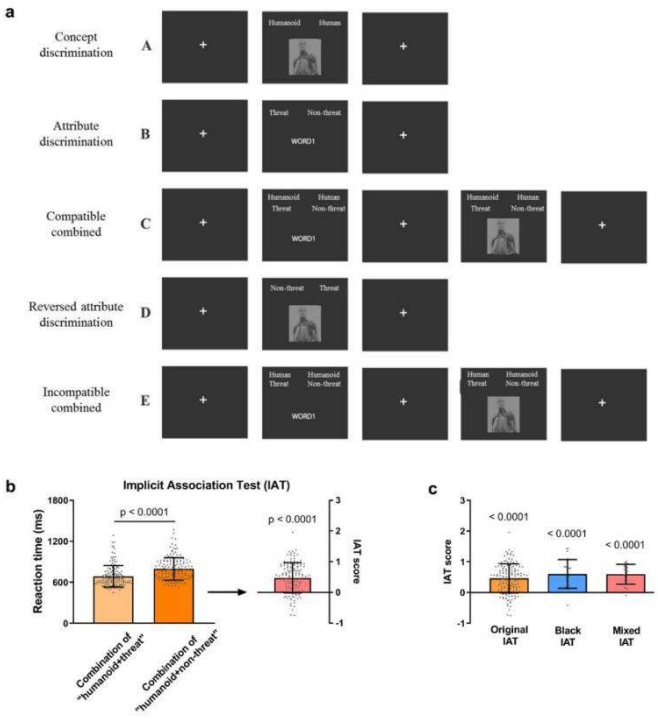

Figure 1. Implicit association test and its results. (a) Procedure of the Robot-Caucasian implicit association test. (b) Negative implicit attitudes toward humanoid robots. In the Robot-Caucasian implicit association test (IAT), participants responded faster to the combination of "humanoid + threat" than to the combination of "humanoid + nonthreat", and the computed IAT scores (effect size) were significant. (c) Participants displayed larger IAT scores in the Robot-Caucasian, Black, and Mixed IATs. Plotted data represent the mean ± SD across participants.

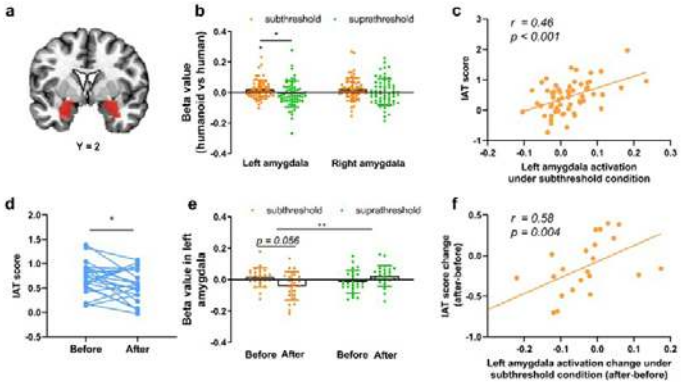

Figure 2. Humanoid robot image-related amygdala activity and amygdala activity changes. (a) The region of interest for the bilateral amygdala. (b) Although no amygdala activity differences were detected for suprathresholdly presented humanoid robot vs. human images, greater left amygdala activity was induced by humanoid robot images than by images of humans under subthreshold presentation. (c) A greater IAT score was associated with greater left amygdala activity under subthreshold conditions. (d) Significantly smaller IAT scores were found after modulation than those before modulation, indicating that participants' negative implicit attitude toward humanoid robots was successfully weakened. (e) The left amygdala activity differences of humanoid robot vs. human images did change under subthreshold presentation after successfully weakening the negative implicit attitudes toward humanoid robots. (f) There was a significant correlation between IAT score changes and activation changes in the left amygdala under subthreshold presentation. * $p < 0.05$, ** $p < 0.01$, *** $p < 0.001$. For b and e, plotted data represent the mean ± SD across participants. IAT = implicit association test.

References

1. Yang, G.-Z. et al. The grand challenges of Science Robotics. Sci Robot 3, eaar7650 (2018).
2. Bossi, F. et al. The human brain reveals resting state activity patterns that are predictive of biases in attitudes toward robots. Sci Robot 5, eabb6652 (2020).
3. Naneva, S., Sarda Gou, M., Webb, T. L. & Prescott, T. J. A Systematic Review of Attitudes, Anxiety, Acceptance, and Trust Towards Social Robots. Int J of Soc Robotics 12, 1179–1201 (2020).
4. Latikka, R., Savela, N., Koivula, A. & Oksanen, A. Attitudes Toward Robots as Equipment and Coworkers and the Impact of Robot Autonomy Level. Int J of Soc Robotics 13, 1747–1759 (2021).
5. Graaf, M. M. A. de, Allouch, S. B. & Lutfi, S. What are people's associations of domestic robots?: Comparing implicit and explicit measures. in (2016). doi:10.1109/ROMAN.2016.7745242.

Poster No 815

Wavelet analysis of fMRI hyperscanning reveals that social interaction affects inter-brain coherence

Rik Sijben[1], Robert Friedmann[1], Rea Rodriguez-Raecke[1]

[1]Brain Imaging Facility, Interdisciplinary Center for Clinical Research, RWTH Aachen University, Aachen, Germany

Introduction: Social cooperation relies on the interaction between individuals who acknowledge each other's identity. Data obtained from a single participant, responding to an often faked social situation, is limited in reflecting cognitive processing of such interaction. Using functional Near Infrared Spectroscopy (fNIRS) hyperscanning, previous studies (Cheng et al., 2015; Cui et al., 2012; Reindl et al., 2018) have shown that neuronal activation of the superior frontal cortex of dyads synchronizes during certain cooperative tasks. In the current study we expand on these findings using an fMRI based hyperscanning platform.

Methods: By synchronizing two MRI scanners using a locally hosted virtual server (Fig.1) we measured whole brain neural activation while participants performed several cooperative or competitive tasks. Similar to previous studies, competitive behavior was achieved by instructing the participants (n=60) to provide a keyboard response to a visual stimulus faster than their counterpart. Cooperative behavior was achieved by instructing participants to try and respond simultaneously instead. The social aspect was enhanced in a communication task which allowed the dyads to communicate prior to each trial, using noise cancelling MRI headphones. Additionally, participants performed control tasks by themselves or passively watched the task being performed. Neural signals were extracted from 400 regions of interest (ROI); task-specific synchronization between participants was analyzed through wavelet coherence using an analytic Morlet wavelet. This approach yields time-varying, frequency specific coherence values, enabling more nuanced interpretations of neural synchronization. Initial coherence calculations were performed on 75 scales ranging from 3.9 mHz to 0.29 Hz; the frequency band of interest was empirically defined based on the task related peak found in coherence values, averaging over all dyads, ROIs, and time-points (Fig. 2). This yielded a period range from 6.5 to 12.3 seconds, resembling the frequency of the trials. Task-based coherence was corrected for by calculating coherence in 29 additional permutations. For each iteration an artificial dyad was generated. Any coherence between these signals is considered a task effect and was subtracted from the real data. Repeated measures ANOVAs were run for each ROI, comparing corrected coherence values between conditions. Post-hoc tests were performed for ROIs which yielded significant (FDR corrected) F values.

Results: Pairwise comparisons showed significantly (FDR corrected) different coherence patterns. During cooperation, dyads showed increased coherence in occipital fusiform and paracingulate regions, indicating an increased object related focus. Comparing competition to cooperation surprisingly revealed coherence in anterior cingulate cortex and temporal pole, indicating an increased social cognitive component during competitive tasks. Finally, communication showed coherence in several bilateral temporal ROIs. As coherence values were corrected for task effects, this difference suggests that active communication, rather than just auditory perception, played an important role here.

Conclusions: This study established an fMRI hyperscanning platform at our institute. Additionally, we showed the feasibility of wavelet coherence-based analysis of paired fMRI data. This approach offers several benefits: First, this approach can reveal phase-lagged coherence, often lost in different approaches. Second, it enables the analysis of different frequency bands. And third, it is optimized for the analysis of time varying signals. Using whole brain fMRI we expanded the finding of previous fNIRS studies showing that interaction related coherence occurs in multiple regions across the cortex and depends on more than cooperation alone. We believe that the current task serves as an ideal baseline to further unravel the concept of interbrain synchronization and to interpret its meaning.

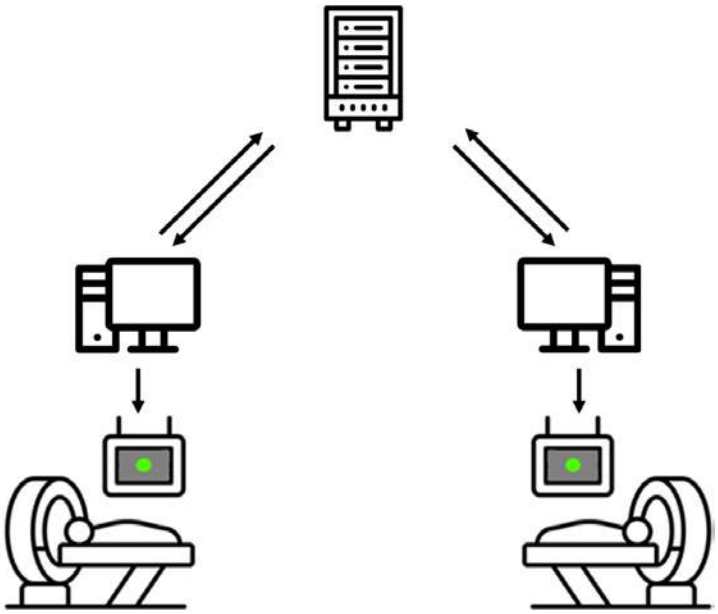

Fig. 1 Technical setup of fMRI hyperscanning platform. Clients communicate with a local server to synchronize two MRI scanners.

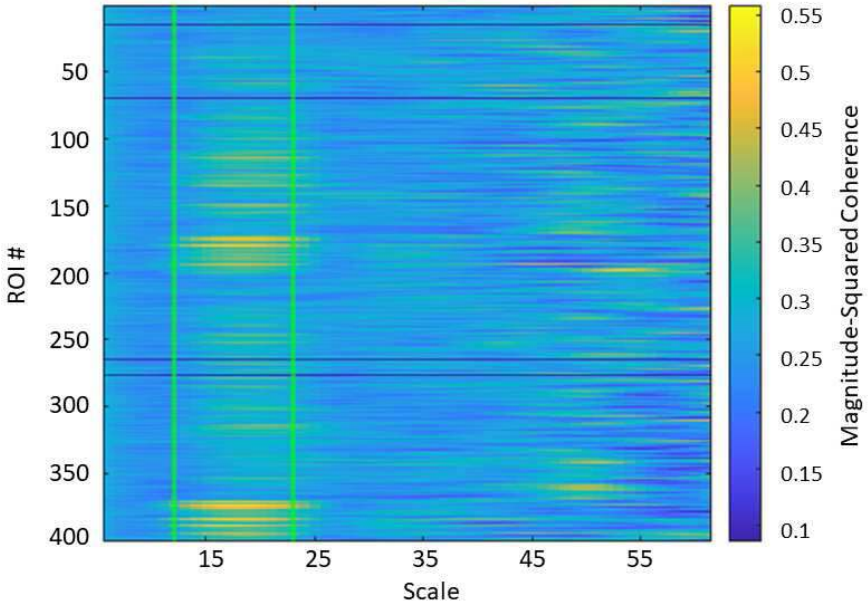

Fig. 2 Frequency range (indicated by green bars) is selected based on task related coherence of averaged data.

References

1. Cheng, X. (2015), 'Synchronous brain activity during cooperative exchange depends on gender of partner: A fNIRS-based hyperscanning study: Synchronous Brain Activities', Human Brain Mapping, vol. 36, no. 6, pp. 2039–2048
2. Cui, X. (2012), 'NIRS-based hyperscanning reveals increased interpersonal coherence in superior frontal cortex during cooperation', NeuroImage, vol. 59, no. 3, pp. 2430–2437
3. Reindl, V. (2018), 'Brain-to-brain synchrony in parent-child dyads and the relationship with emotion regulation revealed by fNIRS-based hyperscanning', NeuroImage, vol. 178, pp. 493–502

Poster No 816

Neurocomputational Components of Trust

Xiaoyan WU[1], Niklas Bürgi[2], Gökhan Aydogan[2], Chao Liu[3], Christian Ruff[2]

[1]Beijing Normal University, Beijing, GU, [2]University of Zurich, Zurich, Zurich, [3]Beijing Normal University, Beijing, Beijing

Introduction: Objective: People often assess others' trustworthiness based on past interactions, but existing research has typically focused only on single aspects of such experiences. What is lacking is a comprehensive model of how people decide to trust based on different aspects of past social interactions. Here we introduce such an experimental and modelling framework, which systematically evaluates how individuals decide to trust based on three key social experiences: Generosity, favoritism, and reward. This framework may be useful for studying individual differences and pathologies of trust.

Methods: Methods: Investors and trustees played a modified trust game preceded by various rounds of laboratory interactions. The investors first had to complete various political and personal questionnaires that allowed us to build real social profiles of them. After 3-5 days, the trustees were shown pairs of the investors' social profiles and had to allocate varying amounts of money between them. After another 3-5 days, the investors were asked to play a trust game with the trustees during the scanning. In each round, investors were asked make the investment decision after they were showed the trustee's generosity (how much they shared with both investors), favoritism (how much they allocated to the investor), and reward (the final amount the investor received) in past interaction. In various classes of computational models, we investigated how the resulting trust decisions depended on these three types of social experiences, over and above general social preferences and betrayal aversion.

Results: Results: Participants increased their investment with larger rewards (linear mixed-effects model, $p<0.001$) and generosity ($p<0.001$). An interaction of generosity × favoritism ($p<0.001$) indicated specific trust if generous trustees previously favored the investor. Computational modeling showed that participants' decisions are best described by a model with social preferences and betrayal aversion. Subjective value from the betrayal aversion model is primarily represented in the dlPFC, Parietal Cortex, NAcc, and Precuneus (left panel). Generosity and Favoritism are differentially represented when making trust decisions. While Generosity is primarily represented in the left TPJ and right dlPFC, Favoritism, in addition to these regions, is also represented in reward areas such as the ventral striatum and anterior insula.

Conclusions: Conclusion: People systematically evaluate and infer the social characteristics of others from previous interactions and use this information to guide their future behavior. Our new model formalizes how these past experiences overcome betrayal aversion to facilitate trust. The model predictions are validated by brain imaging to show that different past experiences are represented in distinct brain networks. Our paradigm and model extend the understanding of the cognitive components underlying trust and may inform interventions aimed at fostering trust in interpersonal interactions. The experimental and modelling approach may be useful for studying pathological alterations of trust in patient populations.

References

1. Bradshaw, A. R., & McGettigan, C. (2021). Instrumental learning in social interactions: Trait learning from faces and voices. Quarterly Journal of Experimental Psychology, 74(8), 1344-1359.
2. Hackel, L. M., Doll, B. B., & Amodio, D. M. (2015). Instrumental learning of traits versus rewards: dissociable neural correlates and effects on choice. Nature Neuroscience, 18(9), 1233-1235.

Poster No 817

The Neural Mechanisms of Naturalistic Interactive Cultural Learning

Siyuan Zhou[1], Xinran Xu[2], Xiangyu He[2], Chunming Lu[2]

[1]Sichuan Normal University, Chengdu, PR China, [2]Beijing Normal University, Beijing, PR China

Introduction: In the era of globalization, people frequently encounter information from other cultures either directly through social interactions or indirectly through social media. In such cases, our cultural mindset is subtly shifted, a process known as cultural learning (Herrmann et al., 2007; Tomasello et al., 1993). Previous research has revealed that individuals can acquire the representations of other cultures, thereby aligning their neurocognitive process more closely with other cultures (Kitayama et al., 2017; Kitayama et al., 2011). However, few studies have investigated this issue in a direct social interaction context, leaving the cognitive process behind naturalistic culture learning and the underlying neural bases unknown.

Methods: Thirty-one Chinese learners were paired with 31 American instructors to form the cultural learning group, while 35 Chinese learners were paired with 35 Chinese instructors to form the control group. All participants were proficient in Chinese and had limited intercultural experience. This study focuses exclusively on the Chinese learners in both groups. The cultural mindset of instructors was assessed using the Analytical-Holistic Scale (AHS, Nisbett et al., 2005) before the experiment. The formal experiment was comprised of three phases (Fig. 1A). Firstly, each learner engaged in a 20-minute discussion on a culture-related topic and then rated the quality of communication. Secondly, all learners independently viewed a 7-minute ambiguous animated video in the Heider & Simmel style, which narrates through the movement of geometric shapes (Fig. 1B, Nguyen et al., 2019). Functional near-infrared spectroscopy (fNIRS) data were collected during this phase. Immediately

after video viewing, all learners were asked to freely recall the video contents based on their understanding (Fig. 1C). First, we estimated the hemodynamic response to the geometric video by calculating the inter-subject correlation (ISC) across learners in each group separately. Then, we examined the cultural learning effect by comparing the ISC between two groups. Third, to verify that the ISC change in the cultural learning group was derived from a shift in the learner's cultural mindset, we conducted an inter-subject representational similarity analysis (IS-RSA) on the hemodynamic response to the video and the recall text embedding using the Universal Sentence Embedding (USE) model (Fig. 2B). Finally, to explore whether the shift in the learner's cultural mindset was the result of interactive cultural learning, a modulation model on the instructor's cultural mindset (American AHS scores), the communication quality, and the cultural learning effect in the brain (learner's ISC) were built (Fig. 2D).

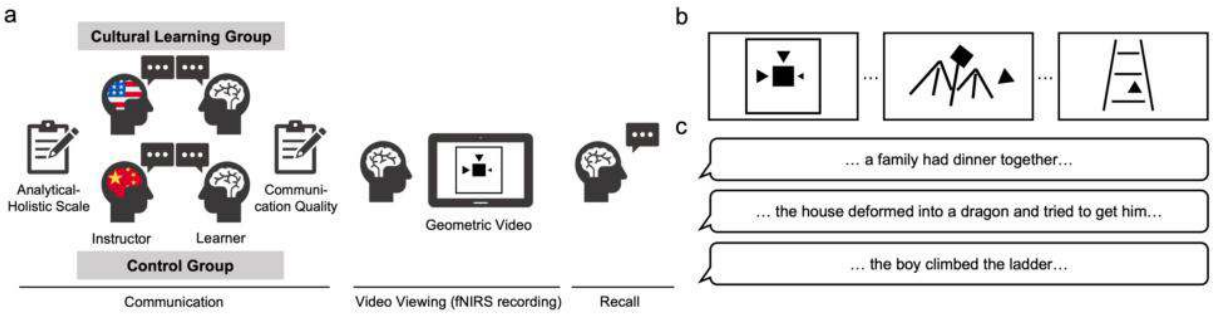

Results: As illustrated in Figure 2A, when viewing the geometric video, the ISC in the left posterior middle temporal gyrus (pMTG) of Chinese learners who interacted with American instructors was reduced compared to those who interacted with Chinese instructors. The IS-RSA results showed that a similar brain response pattern to videos in the pMTG was associated with a similar cognitive processing pattern, which suggested the reduced brain response in the pMTG of the cultural learning group was related to the shift of cultural mindset (Fig. 2C). Finally, the modulation analysis revealed that the transformation of cultural mindset from American instructors to Chinese learners was modulated by the learner's communication quality (Fig. 2E).

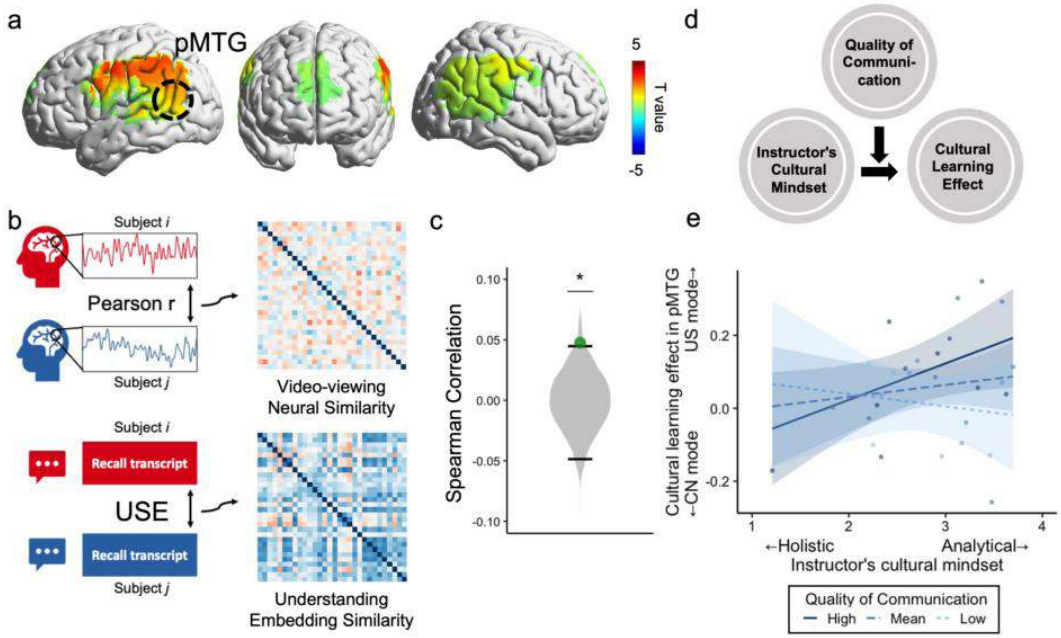

Conclusions: The current study provides novel evidence that the cultural mindset could be transformed through naturalistic social interaction whereby a cultural learning process occurs. Specifically, after social interaction with American instructors, Chinese learners exhibited a notable shift from the Chinese holistic mindset to the American analytical mindset, which was associated with a change in brain responses in left pMTG. Additionally, this shift in cultural mindset was modulated by the learner's communication quality.

References
1. Finn, E. S.(2020). Idiosynchrony: From shared responses to individual differences during naturalistic neuroimaging. NeuroImage, 215(April), 116828.
2. Hasson, U.(2004). Intersubject synchronization of cortical activity during natural vision. Science, 303(5664), 1634–1640.
3. Herrmann, E.(2007). Humans Have Evolved Specialized Skills of Social Cognition: The Cultural Intelligence Hypothesis. Science, 317(5843), 1360–1366.
4. Kitayama, S.(2017). Culture embrained: Going beyond the nature-nurture dichotomy. Perspectives on Psychological Science, 12(5), 841–854.
5. Kitayama, S.(2011). Culture, mind, and the brain: Current evidence and future directions. Annual Review of Psychology, 62, 419–449.
6. Nguyen, M.(2019). Shared understanding of narratives is correlated with shared neural responses. NeuroImage, 184(August 2018), 161–170.
7. Nisbett, R. E.(2005). The influence of culture: Holistic versus analytic perception. Trends in Cognitive Sciences, 9(10), 467–473.
8. Tomasello, M.(1993). Cultural learning. Behavioral and Brain Sciences, 16(3), 495–552.

Poster No 818

A dynamic functional network connectivity study on social emotion regulation

Jiazheng Wang[1], Bharat Biswal[2]

[1]University of Electronic Science and Technology of China, Chengdu, Sichuan, [2]New Jersey Institute of Technology, Newark, NJ

Introduction: Social emotion regulation (SER) is a critical ability for recovering from negative emotions during social interaction (Butler, 2011; Dixon-Gordon, Bernecker, & Christensen, 2015). For instance, a hug from a friend could warm our heart, particularly when we are feeling down. More importantly, SER is beneficial for individual in establishing well-conditioned social relationships, and contributing to prosocial behavior (Hofmann, 2014). Crucially, disturbance in SER is a vital hallmarks of various disorders, such as depression and borderline personality (Zaki, 2020). The neural substrates of SER emphasize that empathy network, cognitive control work and affective generation network sustain the employment of IER processing (Morawetz, Berboth, & Bode, 2021). However, it remains unclear how the functional connectivity, as well as its temporal variations among these network during the entire SER process. The present study aims to verify the static and dynamic functional connectivity of SER related network during the entire SER processing.

Methods: The present study utilized an SER task mode-fMRI and a sliding windows approach to examine both the static and dynamic functional network connectivity of SER processing. 55 healthy participants were recruited for the present SER study. The task was utilized a classical SER task, which includes two conditions: SER condition and Watch condition (Xie et al. 2016). During the SER condition, a short video clip by the experimenter was presented to guide the subjects how to down-regulate their negative emotions. The Watch condition needs the subjects experience their negative emotions, as the base-line for IER processing (figure 1). Firstly, the group independent component analysis (GICA) was conducted to identify the independent components (ICs) during the SER processing, and the peak coordinate of each IC was utilized as SER spatial map for further analysis (Klugah-Brown et al., 2019). Then, the static and dynamic functional network connectivity utilized Pearson's correlation based on the ICs in ROI wise. The sliding window length in 30TR and steps of 1TR, and the windows × IC × IC matrix was obtained for dynamic SER processing (Hutchison, Womelsdorf, Gati, Everling, & Menon, 2013). After that, we used the K-mean to classify the dynamic functional connectivity and the betweenness centrality to extract crucial hubs during the SER processing.

Results: The GICA results yielded 30 distinct ICs, which were subsequently mapped onto SER-related functional networks based on their corresponding peak coordinates. The static functional connectivity results showed strong positive correlations within visual network, empathy network, affective generation network and cognitive control network (Figure 2). The dynamic activity across in SER process exhibited 4 distinct states (Figure 3). The empathy network occurs across all the 4 brain states. Additionally, a 'top-down' pattern is observed between the connectivity of the cognitive control network and the affective generation network during the cognitive control stage and affective response modulation stage.

Conclusions: By employing sliding window approaches, this study has broadened the scope of emotion regulation research, showcasing distinct functional network connectivity states during the dynamic processing of SER. Four unique brain states were identified, each associated with a domain network profiling the dynamic cognitive processing throughout the SER stage. It's shedding light on the cognitive and neural mechanisms underlying this intricate process.

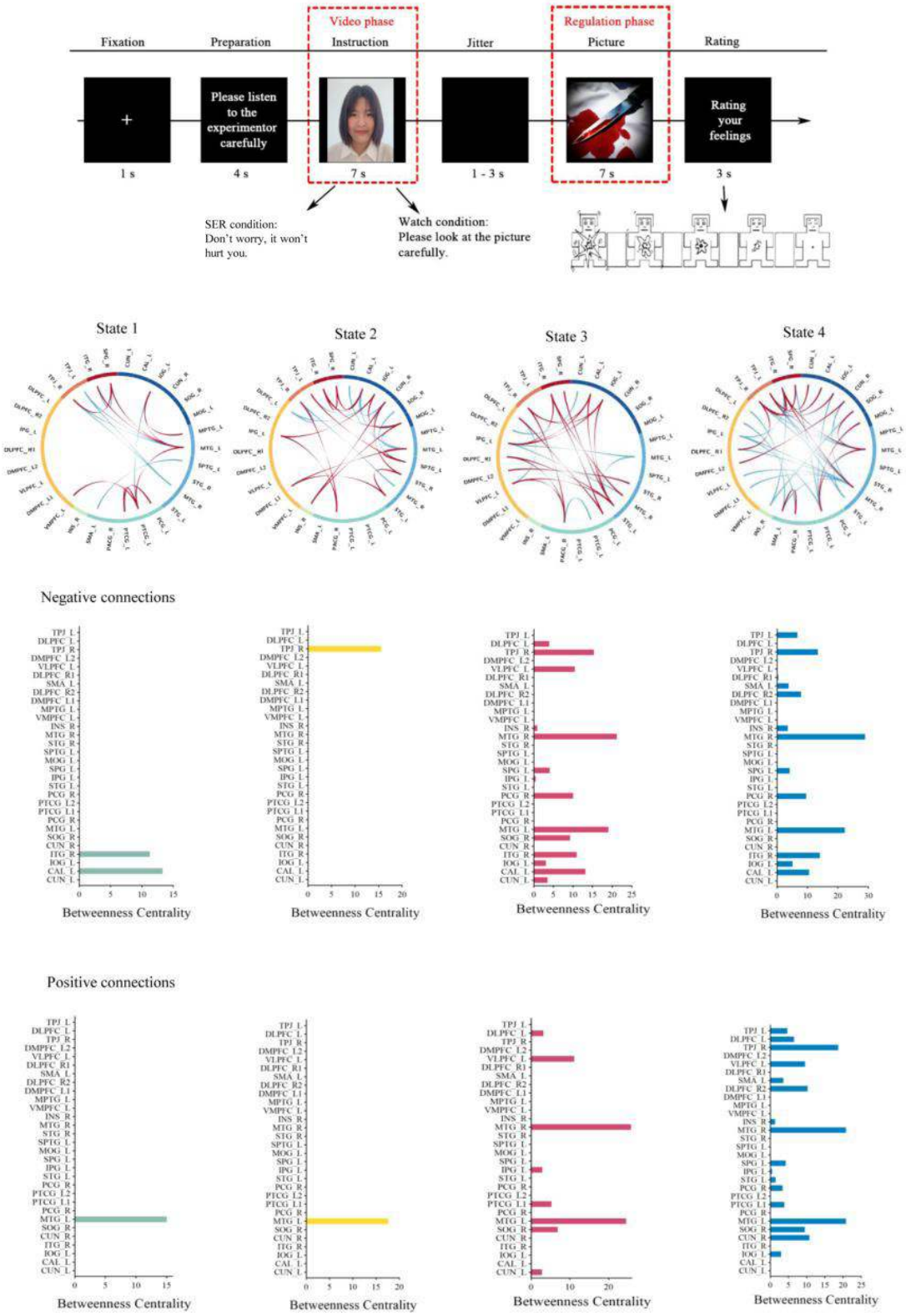

References

1. Butler, E. A. (2011). Temporal interpersonal emotion systems: The "TIES" that form relationships. Personality and Social Psychology Review, 15(4), 367-393. DOI: 10.1177/1088868311411164
2. Dixon-Gordon, K. L., Bernecker, S. L., & Christensen, K. (2015). Recent innovations in the field of interpersonal emotion regulation. Current Opinion in Psychology, 3, 36-42. DOI: http://dx.doi.org/doi:10.1016/j.copsyc.2015.02.001
3. Hofmann, S. G. (2014). Interpersonal emotion regulation model of mood and anxiety disorders. Cognitive therapy and research, 38, 483-492. DOI 10.1007/s10608-014-9620-1

4. Hutchison, R. M., Womelsdorf, T., Gati, J. S., Everling, S., & Menon, R. S. (2013). Resting-state networks show dynamic functional connectivity in awake humans and anesthetized macaques. Human brain mapping, 34(9), 2154-2177. DOI: 10.1002/hbm.22058
5. Klugah-Brown, B., Luo, C., He, H., Jiang, S., Armah, G. K., Wu, Y., . . . Yao, D. (2019). Altered dynamic functional network connectivity in frontal lobe epilepsy. Brain topography, 32, 394-404. DOI: https://doi.org/10.1007/s10548-018-0678-z
6. Morawetz, C., Berboth, S., & Bode, S. (2021). With a little help from my friends: The effect of social proximity on emotion regulation-related brain activity. Neuroimage, 230, 117817. DOI: 10.1016/j.neuroimage.2021.117817
7. Xie X, Mulej Bratec S, Schmid G, Meng C, Doll A, Wohlschläger A, Finke K, Förstl H, Zimmer C, Pekrun R, et al. How do you make me feel better? Social cognitive emotion regulation and the default mode network. NeuroImage. 2016:134:270–280
8. Zaki, J. (2020). Integrating empathy and interpersonal emotion regulation. Annual review of psychology, 71, 517-540. DOI: 10.1146/annurev-psych-010419-050830

Poster No 819

More Than Close Friends: Higher Emotional Coordination in Romantic Relationships

Yijun Chen[1], Zhengde Wei[1], Xiaochu Zhang[1]

[1]*University of Science and Technology of China, Hefei, Anhui*

Introduction: Emotions are fundamental to social interaction and deeply intertwined with interpersonal dynamics (Nummenmaa et al., 2012), especially in romantic relationships, which are characterized by their deep emotional bonds (Hazan & Shaver, 1987). Previous hyperscanning studies often entail interactive processes that are intricately intertwined with emotions (Barrett et al., 2007; Parkinson & Simons, 2009), posing a challenge to disentangle whether the observed neural synchronization reflects the emotions during the interaction or is intrinsic to the interaction itself. Moreover, studies have shown a strong association between relationship quality and emotional coordination (Larson & Almeida, 1999; Randall et al., 2013), thus warranting additional research in the romantic context.

Methods: The final statistics include a total of 25 pairs of heterosexual couples (mean age = 22.90, SD = 3.20) and 25 pairs of heterosexual friends (mean age = 21.86, SD = 2.61). Heterosexual couples in relationships lasting less than 3 months or more than 36 months were excluded. All participants took part in EEG hyperscanning in dyads. In a designated setting (see Figure 1), participants engaged in a silent joint video-viewing task presented by E-prime 2.0 synchronously. The task comprised 2 blocks, each containing 6 randomly ordered videos. We selected two suitable videos for each of the six emotions: happiness, joy, anger, sadness, fear, and disgust. All 12 videos had durations ranging from 50 seconds to 250 seconds. EEG data were collected using the EEG hyperscanning device provided by Neuracle (http://www.neuracle.cn/). Two 64-channel caps with electrodes arranged according to the international 10-20 system were employed to simultaneously record EEG signals at a sampling rate of 1000 Hz. We utilized the phase lag index (PLI) and the power spectral density (PSD) to quantify neural synchronization and individual activation. Correlation analysis, mediation analysis, and support vector machine analysis were employed to clarify the underlying mechanisms.

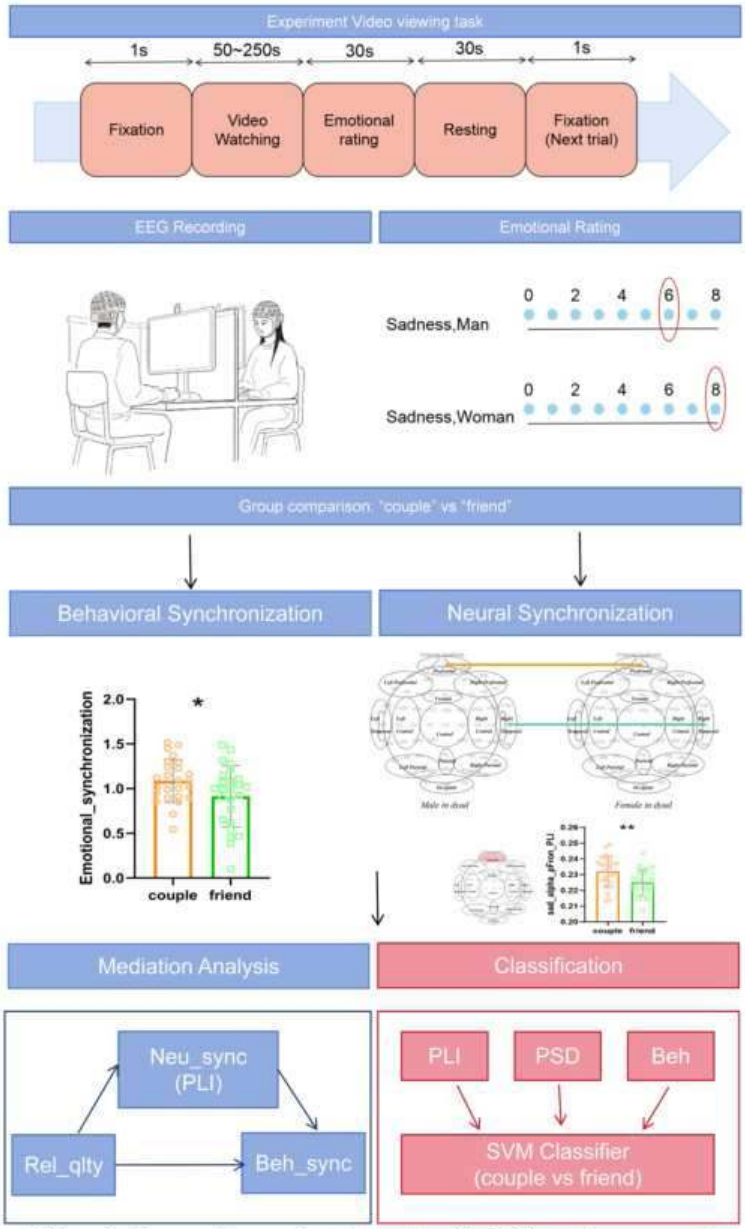

Figure 1: Schematic diagram of the experimental procedure. The EEG recordings were continuously obtained throughout the entire process. Participants were asked to rate the intensity of each of the six emotions on a scale of 0-8 after each video watching. The analysis method is shown in the figure, and we found higher behavioral synchronization and higher alpha prefrontal PLI in couples. Another neural difference appeared in the right temporal lobe, where the beta PLI in couples was significantly smaller than in friends.We conducted mediation analysis and found a partial mediation among relationship quality, prefrontal PLI, and behavioral synchronization. Finally, we used the SVM classifications to further clarify the two types of relationship and got the best model when we only used prefrontal PLI as the feature.

Results: Our results indicated that couples had significantly higher emotional behavioral synchronization and higher alpha PLI in the prefrontal cortex than friends (Figure 1). Pearson correlation analysis found that relationship quality was significantly correlated with both emotional behavioral synchronization and neural synchronization in the couple group rather than in the friend group (Figure 2a-f). Among these three variables, we observed partial mediation in couples (path: relationship quality[X] ➔ neural synchronization[M] ➔ behavioral synchronization[Y]), suggesting a compensatory mechanism among them. Moreover, we calculated the PSD in the prefrontal cortex of the alpha band and found a significant interaction effect of “gender*group” (Figure 2h). Couples showed gender differences in PSD and these activation were significantly associated with differences in relationship quality in males (Figure 2i,j). These differences help distinguish the two types of relationships, and the best classification performance was achieved by utilizing only alpha PLI between the PFCs of the dyads (Figure 2k-m).

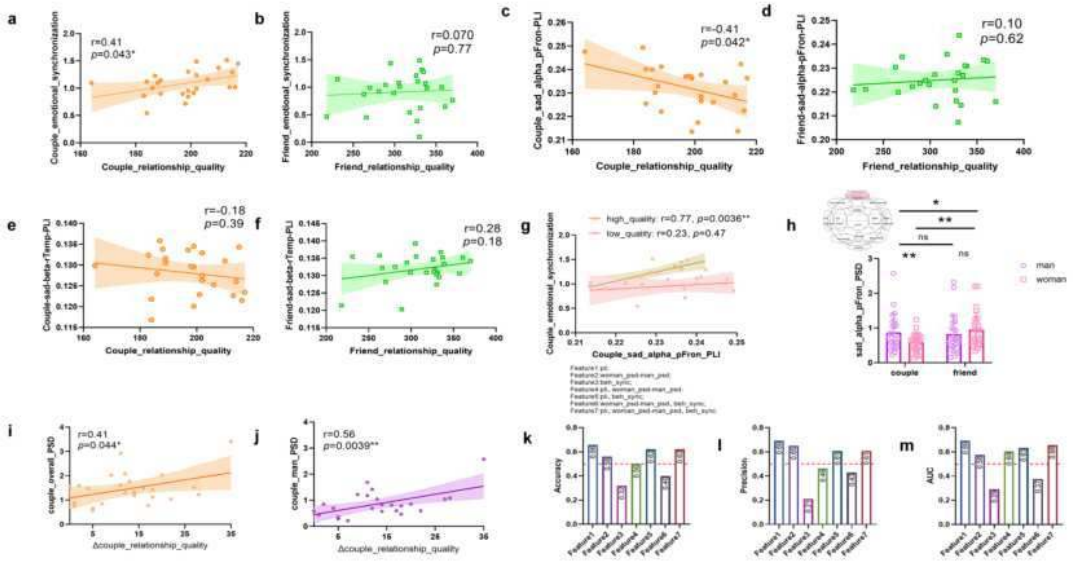

Figure 2. The main results. We first calculated the correlation between the behavioral synchronization and relationship quality, and we found that relationship quality only significantly correlates with behavior synchronization in couples (a), not in freinds (b). Then, we calculated the correlation between the relationship quality and the neural synchronization in the two significant different regions. Relationship quality only significantly correlates with PLI in couples' prefronatl cortex (c), not in other situations (d-f). To clarify the role of relationship quality, we divided the couples into two groups based on medium quality. We found that the correlations between neural synchronization and behavioral synchronization were only significant in the high-quality group, not the low-quality group(g). Combining partial mediation relationships among these three factors, this suggests that low-quality couples exhibit compensatory increases in brain activity. Regarding individual activation, we observed significant gender differences within couples, whereas no differences were found among friends (h), and the ANOVA analysis indicated a significant interaction between group and gender. We also discovered that male activation (j) and overall activation(i) within couples exhibited a significant positive correlation with individual assessments of relationship

Conclusions: We examined differences in emotional experiences, both in neural and behavioral performance, between heterosexual couples and heterosexual friends from a dyad synchronization perspective without direct interaction. Our results reveal that in romantic relationships, there is a deeper emotional connection and a significant correlation with relationship quality. Couples use brain synchronization to overcome relationship challenges and exert influence on gender-based differences in brain activity, distinguishing them from friends. Overall, our study sheds light on the neural mechanisms underlying emotional coordination within romantic contexts, offering the potential to strengthen emotional bonds and enhance relationship quality between partners.

References

1. Barrett, L. F. (2007). 'The Experience of Emotion', Annual Review of Psychology, vol. 58, no. 1, pp. 373–403
2. Hazan, C. (1987). 'Romantic love conceptualized as an attachment process', Journal of Personality and Social Psychology, vol. 52, no. 3, pp. 511–524
3. Larson, R. W. (1999). 'Emotional Transmission in the Daily Lives of Families: A New Paradigm for Studying Family Process', Journal of Marriage and Family, vol. 61, no. 1, pp. 5–20
4. Nummenmaa, L. (2012). 'Emotions promote social interaction by synchronizing brain activity across individuals', Proceedings of the National Academy of Sciences, vol. 109, no. 24, pp. 9599–9604
5. Parkinson, B. (2009). 'Affecting Others: Social Appraisal and Emotion Contagion in Everyday Decision Making', Personality and Social Psychology Bulletin, vol. 35, no. 8, pp. 1071–1084
6. Randall, A. K. (2013). 'Cooperating with your romantic partner: Associations with interpersonal emotion coordination', Journal of Social and Personal Relationships, vol. 30, no. 8,pp. 1072–1095

Poster No 820

Learning from ingroup experiences changes intergroup impressions

Yuqing Zhou[1], Björn Lindström[2], Alexander Soutschek[3], Pyungwon Kang[4], Philippe Tobler[4], Grit Hein[5]

[1]Chinese academy of Sciences, Beijing, Beijing, [2]Karolinska Institutet, Stockholm, Sweden, [3]Ludwig Maximilian University, Munich, Germany, [4]University of Zurich, Zurich, Switzerland, [5]University of Würzburg, Würzburg, Germany

Introduction: In multicultural societies, people encounter individuals from their own social group (ingroup members) and from different social groups (outgroup members), and form impressions towards these ingroup and outgroup individuals. As impressions predict behaviors, it is important to understand the mechanisms that shape impressions in intergroup contexts. One basic mechanism that shapes impressions is learning. According to learning theory, positive experiences with a person establish positive associations towards this individual, while negative experiences have the opposite effect, driven by unpredicted positive or negative experiences that elicit prediction errors. Importantly, in complex social environments, individuals learn from intermixed experiences with both ingroup and outgroup members. However, it remains unclear how

such ingroup and outgroup experiences dynamically shape neural learning processes and learning-related changes in impressions towards in- and outgroups. To address this question, we designed an experiment in which identical experiences with the in- and outgroup could dynamically affect the impressions towards both groups.

Methods: 30 healthy swiss males volunteered to take part in this fMRI study. Participants were about to receive shock in each trial while the individual from the ingroup or the outgroup ostensibly could give up money to save the participant from pain. At the beginning of each trial, the participants rated their closeness toward the ingroup and outgroup on separate rating scales that were presented in randomized order. Next, participants rated their expectancy of receiving shock, followed by the symbol that represented the ostensible decision of the other person. In reality, participants were relieved from pain in 75% both from ingroup and outgroup individuals. Before and after learning, we used an impression scale to assess participants' impressions towards ingroup (Swiss) and outgroup (Middle Eastern) individuals. We modeled participants' trial-by-trial expectancy ratings using a standard Rescorla-Wagner (Rescorla & Wagner, 1972) reinforcement learning (RL) algorithm. We then fitted the trial-by-trial closeness ratings regarding the ingroup or outgroup as a linear function of previous prediction errors derived from the reinforcement learning models.

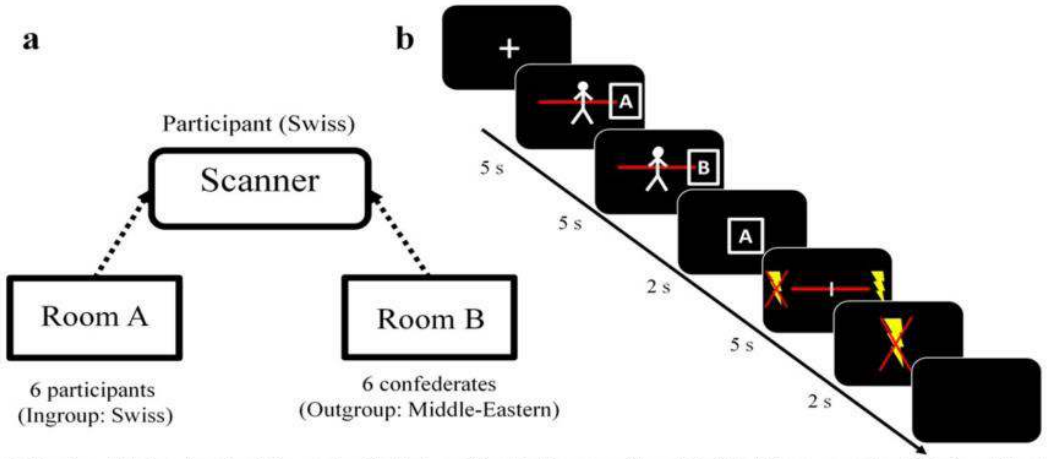

Figure 1. Experimental task. a, Experimental procedure. The Swiss participant in the scanner interacted with both ingroup members (6 Swiss participants, in this example seated in Room A) and outgroup members (6 Middle Eastern confederates, in this example seated in Room B) during the experiment. The assignment of room type (A or B) to social groups (ingroup or outgroup) was counterbalanced across participants. b, Example trial sequence. At the beginning of each trial, the participants rated their closeness toward the ingroup and outgroup on separate rating scales that were presented in randomized order. To do so, they moved a manikin representing themselves toward or away from the room in which ingroup or outgroup members were seated. The next screen revealed the room in which the person that could influence the participant's experience of electric shock was located (e.g., Room "A," which in this example represented the ingroup). Next, participants rated their expectancy of receiving shock, followed by the symbol that represented the ostensible decision of the other person (a crossed-out lightning bolt representing the decision to give up money to save the participant from shocks and a lightning bolt representing the decision to keep the money, resulting in pain for the participant). The experienced outcome (painful shock or no shock) was delivered during the final blank screen.

$$\Delta\ Closeness_i(t) = W_i \sum_{j=1}^{t} \gamma^{t-j}\, \delta_{ij}$$

W: The extent to which prediction errors influence closeness updates.
γ: The discounting parameters.
δ: Prediction errors.
i: ingroup/outgroup.
j: trial index.

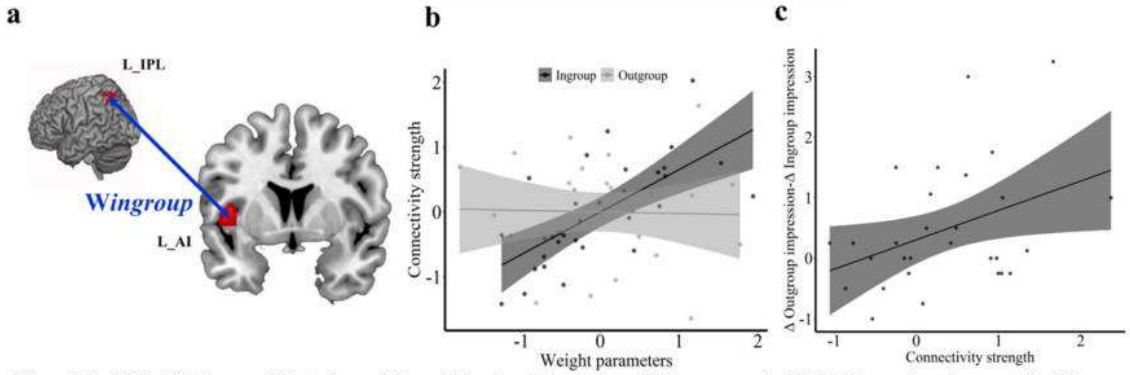

Figure 2. Left IPL-left AI connectivity influenced by weights given to ingroup prediction errors and related to impression change. a, The $W_{ingroup}$ parameter (extracted from the closeness model shown above) modulated the coupling between left IPL and left AI during ingroup feedback revelation. Significant clusters were identified by SVC-FWE in the entire neural network that was involved in the processing of negative prediction errors. The association between weight parameters and left IPL to left AI coupling was significantly stronger when receiving feedback from the ingroup compared with the outgroup. c, The connectivity strength between left IPL and left AI when receiving ingroup feedback correlated with the decline in ingroup favoritism in impression ratings. Display threshold at $p < 0.001$. Error bars indicate SEM.

Results: We first found a significant group × time interaction ($\chi2(1) = 7.34$, $p = 0.007$) in impression rating, showing the reduction of ingroup favoritism in the course of learning. Next, we built up computational models to test how ingroup and outgroup prediction errors affected trial-by-trial changes in ingroup and outgroup closeness ratings. In our models, we assumed that changes in closeness to group i (i.e., the ingroup or the outgroup) were a linear function of the time-discounted sum of previous prediction errors to outcomes from i. Having built up the respective models that capture the change of closeness towards the in- and the outgroup, we extracted the model parameters and associated the parameters with the change of intergroup impressions. The results revealed that the reduction of the ingroup bias in impression ratings was uniquely predicted by the weight given to ingroup prediction errors ($\beta = 0.74$, $SE = 0.29$, $t = 2.56$, $p = 0.017$). Importantly, the more strongly an individual weighted ingroup prediction errors, the more pronounced the reduction of ingroup bias in impression ratings was. Neurally, the individual weight for ingroup prediction errors was related to the coupling between the left inferior parietal lobule (IPL), the region specifically encoding the negative prediction errors from the ingroup members, and the left anterior insula (AI), which, in turn, predicted learning-related changes in intergroup impressions.

Conclusions: Our findings provide computational and neural evidence for ingroup-focused theories, highlighting the importance of ingroup experiences in shaping social impressions in intergroup settings.

References

1. Amodio, D. M., & Cikara, M. (2021). The social neuroscience of prejudice. Annu. Rev. Psychol., 72, 439-469
2. Rescorla, R. A., & Wagner, A. R. (1972). A theory of Pavlovian conditioning: Variations in the effectiveness of reinforcement and nonreinforcement. In A. H. Black & W. F. Prokasy (Eds.), Classical Conditioning II: Current Research and Theory (pp. 64-99). Appleton-Century-Crofts
3. Hein, G., Engelmann, J. B., Vollberg, M. C., & Tobler, P. N. (2016). How learning shapes the empathic brain. Proc. Natl Acad. Sci. USA, 113, 80-85

Poster No 821

Forecasting intergroup contest outcome with inter-brain neural synchronization

Xiaochun Han[1], Jiaxin Yang[2], Yina Ma[2,3]

[1]Faculty of Psychology, Beijing Normal University, Beijing, China, [2]State Key Laboratory of Cognitive Neuroscience and Learning, Beijing Normal University, Beijing, China, [3]Chinese Institute for Brain Research, Beijing, China

Introduction: Forecasting the outcome of intergroup contests is of great interest in human society, from sports betting to warfare victor prediction. However, accurately predicting the outcome of intergroup contests remains challenging, even for experts (Bunker & Susnjak, 2022). Therefore, the development of an accurate predictive model for intergroup contests holds both theoretical and practical significance. By leveraging the strengths of simultaneous neural recording of individuals engaged in real-time intergroup contests (Yang et al., 2020) and advanced machine-learning techniques (Kohoutová et al., 2020), the current study aims to investigate whether and if so, how a neural predictive model based on intra- and/or inter-brain activity can effectively forecast the outcome of intergroup contests.

Methods: We adopted a previously established intergroup contest game paradigm in the laboratory consisting of three attackers and three defenders and simultaneously recorded the brain activities of six participants using functional near-infrared spectroscopy (fNIRS) (Figure 1A&B). The fNIRS channels were positioned over the right temporal-parietal junction and the dorsolateral prefrontal cortex (Yang et al., 2020; Zhang et al., 2023). To forecast the contest outcome, we extracted the activities of the two brain regions during the decision-making phase of the contests, including two sets of intra-brain neural activities, i.e., activation level and functional connectivity, and two sets of inter-brain neural synchronization, i.e., neural synchronization between individuals within the group and between groups (Figure 1C). We developed the predictive neural model in the Discovery cohort (N = 30 sessions, with 6 participants in each session) using a support vector machine algorithm with a radial basis kernel (Figure 1D, Patle et al., 2013). Then, we examined the key brain features in forecasting contest outcomes. Lastly, we examined the neural model's generalizability in an independent Testing cohort (N = 36 sessions).

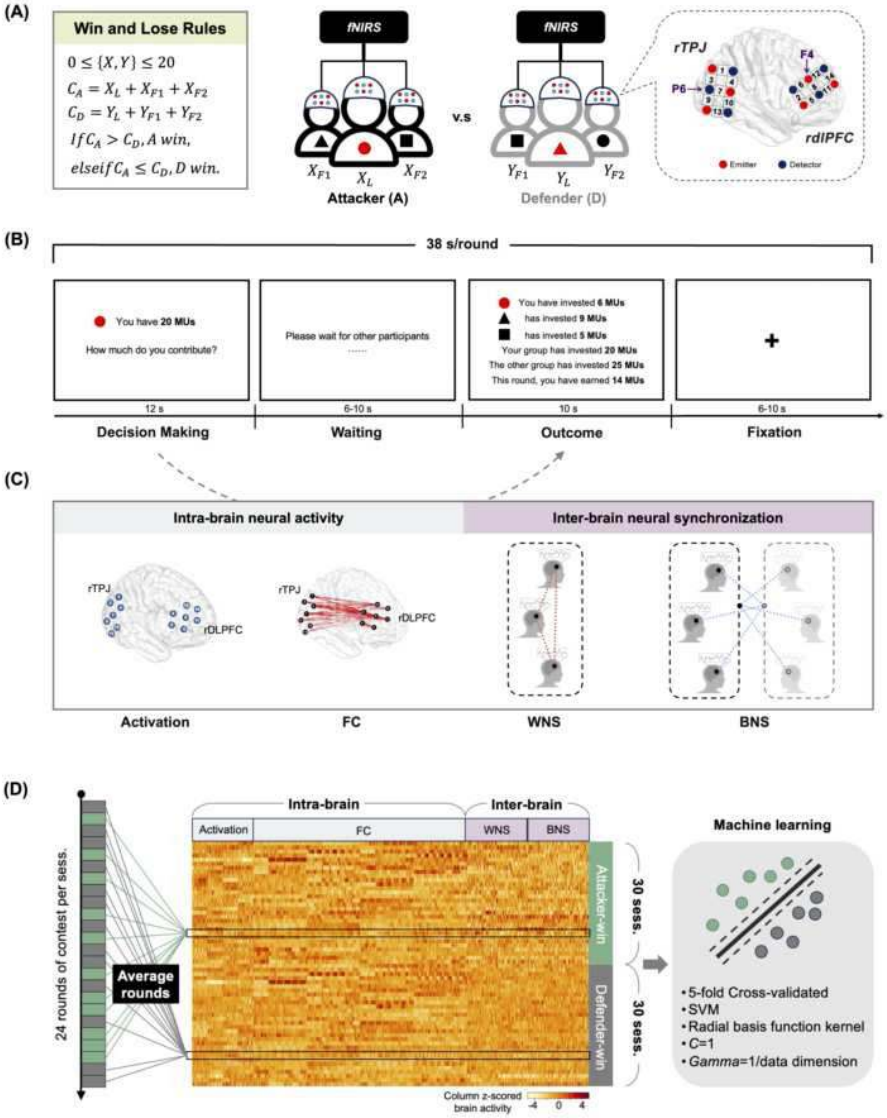

Figure 1. Experimental settings and brain features. (A) Participants were invited to the laboratory in groups of six strangers and randomly assigned to either a 3-person attacker or a 3-person defender group. A group leader was elected for each 3-person group before engaging in 24 rounds of the intergroup contest, during which two identical fNIRS systems simultaneously collected imaging data from all six participants. On each of 24 consecutive contest rounds, both the leader (signaled in a red mark) and followers in the attacker (defender) group contribute X (Y) out of their personal endowments 20 MUs to the group pool ($C_A = [X_L + X_{F1} + X_{F2}]$; $C_D = [Y_L + Y_{F1} + Y_{F2}]$). Contributions were non-recoverable. When $C_A > C_D$, the attacker group won and took away defender group D's all non-invested resources (i.e., 60 - C_D). When $C_A \le C_D$, the defender group D won, and all members of both groups kept their remaining endowment (i.e., 20- {X, Y}). **(B)** The timeline of one contest round. Each contest round involved a decision-making phase where participants had 12 seconds to decide on their contribution. The contest outcome screen of 10 seconds then displayed the contribution of each ingroup member, the total contributions made by both groups, as well as the participant's payoff. **(C)** To forecast the contest outcomes, we extracted four sets of brain activity data during the decision-making phase for each individual per round, including individual brain activation, individual functional connectivity (FC), within-group neural synchronization (WNS), and between-group neural synchronization (BNS). **(D)** Neural features of the decision-making phase, including brain activation, FC, WNS, and BNS, were averaged across rounds where either attacker or defender won the contests. These neural features were then used to predict the outcomes of attacker-win vs. defender-win using a support vector machine with a radial basis function kernel and default parameters. To prevent overfitting, we assessed the predictive accuracy of the neural model with a five-fold cross-validation procedure.

Results: The predictive model developed in the Discovery cohort using both intra- and inter-brain neural activities achieved an accuracy of 76.18% ($p < 0.0002$; Figure 2A&B). We further compared the contributions of intra- and inter-brain features in predicting contest outcomes. Interestingly, only inter-brain neural synchronizations made significant contributions to prediction accuracy, indicated by substantial decreases in prediction accuracy when shuffling these feature sets (decreased acc = 9.92% and 12.17%, pFWE = 0.02 and 0.01, respectively for within- and between-group neural synchronization). Moreover, we showed that the model utilizing only inter-brain neural synchronizations achieved an increased predictive accuracy of 92.12% (pFWE < 0.0004; Figure 2C&D). However, when relying solely on intra-brain neural activities, the model exhibited limited ability to forecast the contest winner (acc = 58.23%, pFWE = 0.068; Figure 2E&F). Consequently, we opted to employ the predictive model exclusively based on inter-brain neural synchronization for contest outcome forecasting, which we termed the Predictive Neuromarker of Intergroup Contest Outcome. The feature importance analysis for each of the neuromarker's features showed that the inter-brain neural synchronizations of the attacker group played a predominant role in predicting the outcome of intergroup contests. Lastly, we applied the neural model to an independent Testing cohort and revealed a high accuracy of 81.94% ($p < 0.0002$) in the generalization test.

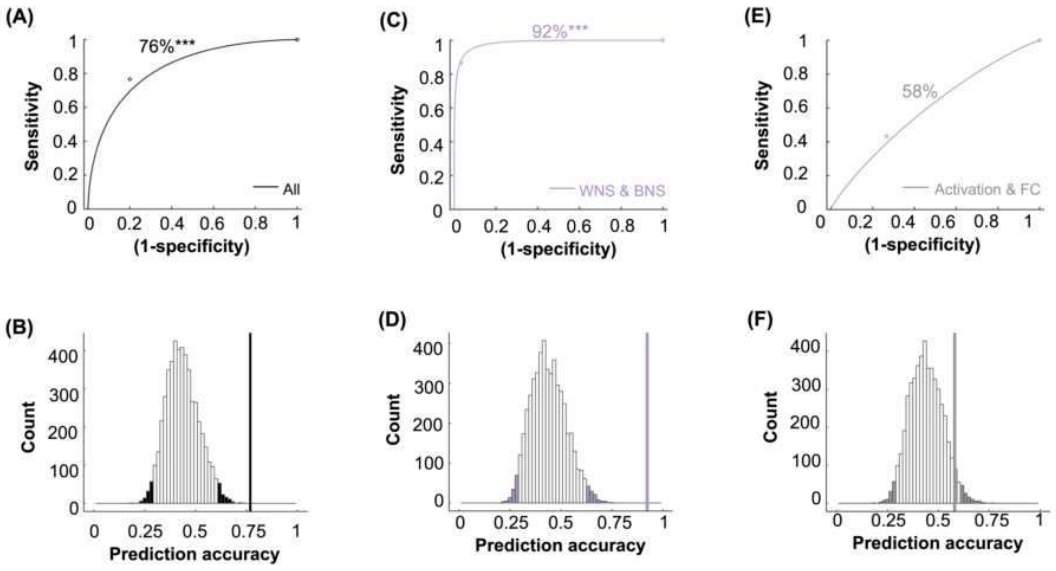

Figure 2. Accurate neural prediction of intergroup contest outcome. (A/B) The receiver-operating-characteristic plot **(A)** and a permutation test **(B)** for predicting attacker-win vs. defender-win using all four sets of brain features (i.e., individual brain activity, FC, WNS, and BNS). **(C-F)** The ROC plots and permutation tests for predicting attacker-win vs. defender-win separately using either BNS and WNS (**C**, purple line; **D**) or individual activation and FC (**E**, grey line; **F**). For panels **B**, **D**, and **F**, the null distributions are plotted with values larger than 95% confidence interval colored, while a vertical line indicates the observed accuracy measures. ***$p_{FWE} < 0.0004$.

Conclusions: The current work has developed a neural predictive model that incorporates both within- and between-group inter-brain neural synchronization, enabling accurate prediction of the winner of intergroup contests. These findings shed light on the development of sophisticated neural models for complex social interactions by considering the dynamic interaction of brain activities between different individuals.

References

1. Bunker, R., & Susnjak, T. (2022), 'The application of machine learning techniques for predicting match results in team sport: A review', Journal of Artificial Intelligence Research, vol. 73, pp. 1285-1322.
2. Kohoutová, L., Heo, J., Cha, S., Lee, S., Moon, T., Wager, T. D., & Woo, C. W. (2020), 'Toward a unified framework for interpreting machine-learning models in neuroimaging', Nature protocols, vol. 15, no. 4, pp. 1399-1435.
3. Patle, A., & Chouhan, D. S. (2013), 'SVM kernel functions for classification', International conference on advances in technology and engineering, pp. 1-9.
4. Yang, J., Zhang, H., Ni, J., De Dreu, C. K., & Ma, Y. (2020), 'Within-group synchronization in the prefrontal cortex associates with intergroup conflict', Nature neuroscience, vol. 23, no. 6, pp. 754-760.
5. Zhang, H., Yang, J., Ni, J., De Dreu, C. K., & Ma, Y. (2023), 'Leader–follower behavioural coordination and neural synchronization during intergroup conflict', Nature Human Behaviour, pp. 1-13.

Poster No 822

Beyond Temporal Alignment: Enhanced Spatial Pattern Similarity When Sharing Concrete Information

Yulei Shen[1], Takahiko Koike[2], Shohei Tsuchimoto[3], Ayumi Yoshioka[4], Kanae Ogasawara[2], Norihiro Sadato[5], Hiroki Tanabe[1]

[1]Department of Cognitive & Psychological Sciences, Graduate School of Informatics, Nagoya University, Nagoya, Aichi, [2]Inter-Brain Dynamics Collaboration Unit, RIKEN Center for Brain Science, Tokyo, Tokyo, [3]Division of Neural Dynamics, NIPS, Okazaki, Aichi, [4]Section of Brain Function Information, National Institute for Physiological Sciences, Okazaki, Aichi, [5]Ritsumeikan University, Kyoto, Kyoto

Introduction: We often transform the things we see into spoken information, and convert the spoken words we hear into vivid images in our minds. To investigate the neural mechanisms of this process, we conducted a hyperscan fMRI experiment. Unlike previous hyperscan fMRI studies[1,3], this study delved into a more nuanced aspect: the shared neural spatial representation of tangible information. While the information sender's perception of the target appears to be a direct representation, the receiver obtained information that has been transformed by the sender, thereby forming an indirect representation of the target. It also depends on the amount of information. We hypothesized that the neural representations

of the receiver become more closely aligned with those of the sender when the transmitted content is large. To address this hypothesis, we computed the similarity of spatial patterns between interacting pairs.

Methods: Forty-six subjects participated in the experiment. They were randomly assigned to same-sex dyads. We designed a novel "introduction-response" hyperscan task. In this task, a participant (sender) was asked to view a face picture and then to verbally introduce this picture to a partner (receiver) within 16s based on the hints; the receiver was asked to imagine the picture within 6s after hearing the description. Each participant was pseudo-randomly assigned to act as sender and receiver. To examine whether the effect of mental imagery would be further affected by the amount of information, the sender was given either two (low vividness) or five hints (high vividness) by the experimenter to describe a face picture. MRI time-series data were acquired using two MRI scanners (Magnetom Verio 3T, Siemens) with standard 32-channel phased array coils. Functional images were acquired using T2*-weighted, gradient- EPI with the multiband sequence (TR 1,000 ms, voxel size 2 × 2 × 2mm3). Anatomical images were acquired using a T1-weighted MP-RAGE sequence (voxel size 0.8 × 0.8 × 0.8 mm3). Image preprocessing was performed by FSL. To find the brain regions that showed high spatial pattern similarity between sender and receiver, the preprocessed whole-brain data were parcellated into 400 nodes using the Schaefer 400 parcels atlas[2]. We then calculated the average intensity for each voxel of the sender's time-series data during the speaking period, and those of the receiver's during the imagery periods. For each node, the all included voxel data from both sender and receiver were spatially aligned and Pearson's correlation was calculated in each trial per condition. Leave-one-trial-out iterations within each condition were employed for the validation of similarity matrices. These correlation coefficients were Fisher's z transformed. We then constructed similarity difference matrices between high and low vividness of face information by subtraction. Bootstrapping with 3000 iterations was used to generate a null distribution for these similarity difference matrices. We applied FDR correction for multiple comparisons.

Results: When sharing more vivid face information, statistically significant higher pairwise spatial pattern similarity between speak phase of sender and imagery phase of receiver was found in the visual system (bilateral V1, V2 and V3, right FG), frontal-parietal cortex (Bilateral FP, IFG, SFG, MFG and preSMA; left precentral, SPL, IPS and IPL; right FOC), DMN (ACC and ParaCC), and right insular and hippocampus (Fig. 1, $p < 0.05$ post-FDR correction).

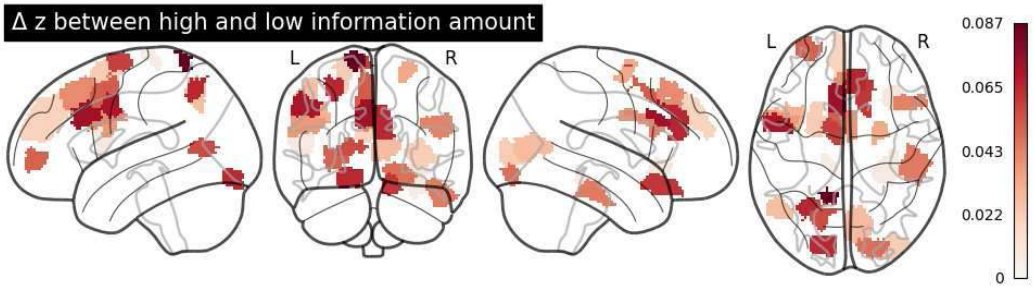

Conclusions: The present study has shown that, even in the absence of physical time point alignment, the spatial patterns of neural activity representing the same target information become increasingly similar between interacting pairs as the information becomes more specific in the real-time interaction. This similarity was reflected in a wide range of areas, including visual cortex, semantic processing network, visual imagery network, and the default mode network.

References

1. Koike, Takahiko, et al. "Role of the right anterior insular cortex in joint attention-related identification with a partner." Social cognitive and affective neuroscience 14.10 (2019): 1131-1145.
2. Schaefer, Alexander, et al. "Local-global parcellation of the human cerebral cortex from intrinsic functional connectivity MRI." Cerebral cortex 28.9 (2018): 3095-3114.
3. Yoshioka, Ayumi, et al. "Neural substrates of shared visual experiences: a hyperscanning fMRI study." Social Cognitive and Affective Neuroscience 16.12 (2021): 1264-1275.

Poster No 823

Dyadic similarity in social value orientation modulates hyper-brain connectivity in interaction

Hanxuan Zhao[1], Sihua Xu[2]

[1]Shanghai International Studies University, Shanghai, China, [2]School of Business and Management, Shanghai International Studies University, Shanghai, China

Introduction: As the inherent inclination towards distributing resources between oneself and others in situations of interdependence, the social value orientation (SVO) has been viewed as the crucial personality in the social interaction(Zhao et al., 2023). However, whether dyadic similarity in SVO would affect the real-time interpersonal interaction and the underlying intra-brain and inter-brain mechanism still remained unknown.

Methods: With the functional near-infrared spectroscopy (fNIRS) – based hyperscanning technique, the present study examined the hyper-brain functional connectivity pattern underlying the effect of the dyadic similarity in SVO on the interpersonal interaction during the button pressing task(Cui et al., 2012). Using the Social Value Orientation (SVO) slider measure, we recruited 88 participants forming 44 dyad (22 prosocial-prosocial dyads, 22 proself-proself dyads). The cooperation index and the competition index in the i trial were respectively denoted as follows. Competition Index= |RT_(1,i)-RT_(2,i) |×(RT_(1,i)+RT_(2,i)) Cooperation Index= |RT_(1,i)-RT_(2,i) | / (RT_(1,i)+RT_(2,i)) Adopting the prefrontal cortex (PFC) as the targeted brain region, the intra-brain functional connectivity (FC) and the inter-brain synchronization (INS) among different regions of interest (ROIs) were assessed using the cross-correlation between oxyhemoglobin (HbO) concentration time series according to the existing studies.

Results: Our behavioral results reported that the competition index in the proself-proself (SS) group was significantly lower than that in the prosocial-prosocial (CC) group ($t[42] = -2.21$, $p < 0.05$), demonstrating more intense competition in the SS group. It was also found that the cooperation index in the proself-proself (SS) group was significantly higher than that in the prosocial-prosocial (CC) group ($t[42] = 2.82$, $p < 0.01$), demonstrating more cooperative performance in the CC group. Our intra-brain functional connectivity results reported significant interaction effect of BLOCK × SVO SIMILARITY in the FC between left superior frontal gyrus (lSFG) and right frontopolar cortex (rFPC) ($F[1, 42] = 14.26$, FDR-corrected $p < 0.05$). In the SS group, the FC of lSFG – rFPC in the cooperation block were significantly higher than that in the competition block. In the CC group, the FC of lSFG – rFPC in the competition block was significantly higher than that in the cooperation block. Our inter-brain synchronization results showed significant interaction effect of BLOCK × SVO SIMILARITY in the FC between right frontopolar cortex (rFPC) and left middle frontal gyrus (lMFG) ($F[1, 42] = 13.58$, FDR-corrected $p < 0.05$). In the SS group, the FC of rFPC – lMFG in the competition block were significantly higher than that in the cooperation block. In the CC group, the FC of rFPC – lMFG in the cooperation block was significantly higher than that in the competition block.

Conclusions: Taken together, the present study uncovered the distinct hyper-brain functional connectivity patterns underlying the effect of the dyadic similarity in SVO on the interpersonal cooperation and competition.

References

1. Cui, X.(2012),'NIRS-based hyperscanning reveals increased interpersonal coherence in superior frontal cortex during cooperation', Neuroimage, vol.59,no.3, pp. 2430-2437
2. Zhao, H.X. (2023),'Distinct inter-brain synchronization patterns underlying group decision-making under uncertainty with partners in different interpersonal relationships', Neuroimage, vol. 272, pp.120043

Poster No 824

The Relationship Between Family Personality & Neural Synchrony in Parent-Child Dyads: A fNIRS Study

Khalil Thompson[1], Clayton Schneider[1], Emily Furtado[2], Shreeja Vachhani[3], Soo Ju[4], Shri Jeyaram[1], Bedilia Mata-Centeno[5], Joscelin Rocha-Hidalgo[6], Koraly Perez-Edgar[6], Susan Perlman[7]

[1]Washington University in St. Louis, St. Louis, MO, [2]University of Minnesota, Minneapolis, MN, [3]University of Michigan, Ann Arbor, MI, [4]University of Pennsylvania, Philadelphia, PA, [5]Macalester University, Saint Paul, MN, [6]Pennsylvania State University, State College, PA, [7]Washington University- St. Louis, Saint Louis, MO

Introduction: Many theories in personality and temperament characterize the development of dispositional attributes of the individual. However, from birth, the development of children's temperament occurs within a dynamic, interactive environment, initially with parents or caregivers. While these dynamics are frequently examined at the self-report and/or behavioral level, these approaches only provide a limited degree of insight into interaction. Uncovering the neural underpinnings driving family functioning in interactive contexts would provide an additional layer of information that could illuminate key facets of early childhood brain development. Interpersonal dynamics are best explored using second-person neuroscientific approaches, such as hyperscanning, which attempts to model the temporal synchrony in brain activity between two social partners during interaction. Our study was designed to investigate personality in the context of family interaction and illuminate the underlying neurobiological mechanisms of the expression of family personality using a two-person neuroimaging modality.

Methods: We explored the relationship between family functionality and parent-child neural synchrony in 105 dyads (mean age 5 years 4 months; range 46–95 months). We employed functional near-infrared spectroscopy (fNIRS) hyperscanning

to measure neural synchrony while dyads completed the Disruptive Behavior Diagnostic Observation Schedule: Biological Synchrony (DB-DOS) task. This interactive paradigm measures dyadic, interdependent responses from parents and children across different social contexts: 1) a pre-play "Baseline" period; 2) a "Stress" period in which a challenging, time-limited interactive puzzle task serves as a mild stressor; and 3) a post-play "Recovery" period. Family functioning was operationalized through parent responses to The Family Adaptability and Cohesion Scale IV (FACES-IV) questionnaire, which creates two orthogonal dimension scores: "cohesion", or emotional bonding between family members, and "flexibility", or the quality and expression of leadership and organization, role relationship, and relationship rules and negotiations. Pearson's correlations and hierarchical regression models were conducted to determine the association between cohesion and flexibility scores and neural synchrony in 3 regions of interest (ROIs): 1) the frontal cortex 2) the temporoparietal junction (TPJ) and 3) both regions together.

Results: Findings from permutation testing indicated that real dyad synchrony was significantly greater than false dyad synchrony during all conditions, demonstrating the construct of neural synchrony during interaction beyond that of similar experience. Synchrony during the stress context was significantly greater than synchrony during both the baseline and recovery contexts. However, there was no significant difference in synchrony between the pre-play and post-play contexts. Hierarchical regression models demonstrated a significant positive relationship between family flexibility and neural synchrony in the frontal cortex during the stress condition ($B = .341$, $t = 3.21$, $p = .002$), but this effect was not found for family cohesion ($B = -.149$, $t = -1.38$, $p = .170$). There were no significant results in the TPJ or across both ROIs.

Conclusions: Family flexibility, defined as the capacity to shift and negotiates roles and rules within the family unit, was significantly related to frontal cortex neural synchrony during a mildly stressful collaborative task. We posit that the parent's propensity to support their children's ideas during problem solving and allow them moments to take a leadership role in decision-making may positively influence the dyads cooperation and continued social engagement during frustrating situations. This is one of the first studies to utilize a two-person imaging modality to explore the role of family structure and interaction dynamics on the interbrain synchrony between parents and their children.

References

1. Czeszumski, A., Eustergerling, S., Lang, A., Menrath, D., Gerstenberger, M., Schuberth, S., Schreiber, F., Rendon, Z. Z., & König, P. (2020). Hyperscanning: A valid method to study neural inter-brain underpinnings of social interaction. Frontiers in Human Neuroscience, 14, 39.
2. Gramfort, A., Luessi, M., Larson, E., Engemann, D., Strohmeier, D., Brodbeck, C., Goj, R., Jas, M., Brooks, T., Parkkonen, L., & Hämäläinen, M. (2013). MEG and EEG data analysis with MNE-Python. Frontiers in Neuroscience, 7. https://www.frontiersin.org/articles/10.3389/fnins.2013.00267
3. Olson, D. H., Waldvogel, L., & Schlieff, M. (2019). Circumplex model of marital and family systems: An update. Journal of Family Theory & Review, 11(2), 199–211.
4. Perlman, S. B., Lunkenheimer, E., Panlilio, C., & Pérez-Edgar, K. (2022). Parent-to-Child Anxiety Transmission Through Dyadic Social Dynamics: A Dynamic Developmental Model. Clinical Child and Family Psychology Review, 25(1), 110–129. https://doi.org/10.1007/s10567-022-00391-7
5. Pincus, A. L., Hopwood, C. J., & Wright, A. G. (2020). The Interpersonal Situation. The Oxford Handbook of Psychological Situations, 124.
6. Quiñones-Camacho, L. E., Fishburn, F. A., Camacho, M. C., Hlutkowsky, C. O., Huppert, T. J., Wakschlag, L. S., & Perlman, S. B. (2020). Parent–child neural synchrony: A novel approach to elucidating dyadic correlates of preschool irritability. Journal of Child Psychology and Psychiatry, 61(11), 1213–1223.
7. Redcay, E., & Schilbach, L. (2019). Using second-person neuroscience to elucidate the mechanisms of social interaction. Nature Reviews Neuroscience, 20(8), Article 8. https://doi.org/10.1038/s41583-019-0179-4
8. Wakschlag, L. S., Briggs-gowan, M. J., Hill, C., Danis, B., Leventhal, B. L., Keenan, K., Egger, H. L., Cicchetti, D., Burns, J., & Carter, A. S. (2008). Observational Assessment of Preschool Disruptive Behavior, Part II: Validity of the Disruptive Behavior Diagnostic Observation Schedule (DB-DOS). Journal of the American Academy of Child & Adolescent Psychiatry, 47(6), 632–641. https://doi.org/10.1097/CHI.0b013e31816c5c10

Poster No 825

Interplay of Brain Maturation, social development in the Context of Puberty Age and Mental Health

Niousha Dehestani[1], Tim Silk[2], Sarah Whittle[3]

[1]Deakin University, Centre for Social and Early Emotional Development, School of Psychology, Faculty, Melbourne, Victoria, [2]Deakin University, Melbourne, Victoria, [3]University of Melbourne, Melbourne, Victoria

Introduction: Adolescents, deeply involved in school and peer interactions, navigate the intricate interplay of social development. Untangling the dynamics between social development, brain maturation, and the collective influence of puberty is crucial for understanding the nuanced implications for mental health during this crucial developmental period. This study investigates the interplay between brain maturation and social development, examining the mechanisms linking puberty to mental health issues and exploring the collective impact of these factors on adolescent well-being.

Methods: Leveraging data from 10,983 participants aged 9 to 14 from the community-setting, multicenter Adolescent Brain Cognitive Development (ABCD) study. Individuals were assessed for a range of the contributions of peer and school networks on variations of the brain imaging outcomes. Using canonical correlation analysis and multivariate methods, our study aimed to reveal nuanced associations. A specific emphasis was placed on investigating the mediating role of canonical variables derived from brain imaging and social developmental scales in establishing links between puberty age which reflects pubertal timing and mental health. To evaluate puberty, we used the pubertal developmental scale. One participant was selected from each family, and assessed at multiple time points, including baseline, and during the first, second, third, and fourth-year follow-ups. We employed a multimodal imaging approach, including T1-weighted (T1w) scans, resting-state functional magnetic resonance imaging (rs-fMRI), and microstructure analysis of diffusion tensor imaging (DTI), encompassing fractional anisotropy (FA) and mean diffusivity (MD). Additionally, we utilized a social development scale comprising peer behavior, network, experience, school environment, disengagement, and involvement during the second-year follow-up. Furthermore, psychopathology symptoms were assessed at baseline and during the first, second, third, and fourth follow-ups using internalizing and externalizing dimension scores derived from the parent-reported Child Behavior Checklist.

Results: A cohort of 6,788 individuals (47.6% female) underwent Canonical Correlation Analysis (CCA) with brain maturation and social development scales during the second-year follow-up. Structural T1w evaluations revealed three components of specific brain patterns respectively associated with age ($r = 0.71$, $p < 0.001$), sex ($r = 0.36$, $p < 0.001$), and peer influence ($r = 0.31$, $p < 0.001$). Assessing rs-fMRI and the social developmental scale, two components emerged, one of them linking school/peer network with age ($r = 0.60$, $p < 0.001$) and the second component relating the negative effect of peers' behavior on functional connectivity ($r = 0.30$, $p < 0.001$). Notably, no components related to peers or school were found in association with FA or MD. Additionally, a significant association was identified between a positive puberty age gap and canonical variables from peer networks in T1w, as well as peer/school networks in rs-fMRI. Furthermore, the peer network in T1w was found to mediate the association between puberty age and externalizing problems and there was no mediation role for internalizing problems.

Conclusions: The impact of the social developmental scale on both the structural and functional aspects of the brain is substantial. Understanding the collective effect of social development scales provides insights into the interplay between puberty as a biological mechanism and leads to externalizing symptoms. Notably, school and peer influence emerge as significant factors during adolescence, underscoring their importance as potential targets for future interventions and treatment programs. Addressing these influential profiles has the potential to enhance outcomes related to social development and mental health across the developmental spectrum.

References

1. Dehestani, Niousha, et al. "Developmental brain changes during puberty and associations with mental health problems." Developmental Cognitive Neuroscience 60 (2023): 101227.
2. Dehestani, N., Vijayakumar, N., Ball, G., Mansour L, S., Whittle, S., & Silk, T. J. (2022). "Puberty age gap": A new method of pubertal timing and its association with psychopathology. medRxiv, 2022-05.
3. Ekstrand, B. (2015). What it takes to keep children in school: a research review. Educational Review, 67(4), 459-482.
4. van Hoorn, J., Fuligni, A. J., Crone, E. A., & Galvan, A. (2016). Peer influence effects on risk-taking and prosocial decision-making in adolescence: Insights from neuroimaging studies. Current Opinion in Behavioral Sciences, 10, 59-64.
5. Vijayakumar, N., Youssef, G., Bereznicki, H., Dehestani, N., Silk, T., & Whittle, S. (2022). The social determinants of mental health problems in adolescents experiencing off-time puberty.

Poster No 826

Activity in empathy-related brain regions predicts clinicians' pain treatment decisions

Nikta Khalilkhani[1], Theoni Varoudaki[2], Morgan Gianola[3], Elizabeth Losin[4]

[1]Pennsylvania State University, State college, PA, [2]Penn State Univeristy, State College, PA, [3]University of Miami, Coral Gables, FL, [4]Penn State University, State College, PA

Introduction: Pain is a global public health problem, disproportionately affecting individuals from marginalized groups, women, and older adults. Both undertreatment and overtreatment of pain contribute to adverse downstream effects, such as ineffective pain management, unnecessary exposure to opioids, and health disparities. Understanding underlying mechanisms of pain assessment and treatment decisions is essential to developing intervention aimed at improving pain management. Despite evidence that pain management decisions are influenced by many factors beyond patient reported pain, the neurobehavioural process underlying these decisions are poorly understood. Here we focused on the role of the clinician's cognition and brain activity during the clinical assessment and pain management decisions. We hypothesize that the

greater a clinician's pain-related empathic brain activity is when seeing their patient in pain the more accurate they will be at assessing that patient's pain and need for treatment.

Methods: To test this hypothesis we recruited N=67 (34 f) medical students and had them complete a virtual pain management task while undergoing fMRI. Each clinician interacted with a diverse group of 36 mock patients. Each simulated clinical interaction consisted of 4 sections: 1) a medical vignette with mock patient injury information, 2) pain behavior videos meant to simulate the clinical exam: 3 x 4-second clips of previous research participants responding to evoked pain, and 3-4) pain and treatment rating, where clinicians rated how much pain they thought the patient was in and the likelihood they would prescribe any analgesic. To investigate clinician's brain activity related to pain empathy we chose an a priori brain mask consisting of regions related to empathy from a Neurosynth automated meta-analysis. To test which (if any) aspects of empathy these brain regions were related to in our sample of clinicians, we ran an exploratory analysis using Stochastic Search Variable Selection. We predicted average brain activity within the Neurosynth empathy mask using all 28 of the questions in the Interpersonal Reactivity Index (IRI), a well-validated empathy questionnaire. We then included IRI questions that had a maximum inclusion probability above 0.5 in a multiple regression to test their relationship with average activity within the empathy mask.

Results: We found that clinicians who reported having higher empathic concern for others' misfortune, had significantly higher activity within the empathy brain mask while observing patients in pain, suggesting brain activity within this Neurosynth mask was indeed related to trait empathy in our sample of clinicians. We found that average activity within the Neurosynth empathy mask predicted the accuracy of both clinicians' assessment of patients' pain (defined as the difference between the clinician and patients' pain intensity rating) and their assessment of the patient's need for treatment (defined as the difference between the clinicians' likelihood of prescribing an analgesic and the patients' ratings of their pain unpleasantness).

Conclusions: Our findings suggest that clinicians with higher neural responses associated with pain empathy when viewing their patients in pain may be able to more accurately perceive the pain of their patient, and, more importantly, may be able to more effectively assess the patient's need for treatment. More broadly, our findings suggest that medical training that teaches clinicians to empathize more with their patient's pain, rather than detach from it as is often found to occur across the course of medical training and practice, could improve the efficacy of pain management.

References

1. Esteban, O., Blair, R., Markiewicz, C. J., Berleant, S. L., Moodie, C., Ma, F., Isik, A. I., Erramuzpe, A., Goncalves, M., Poldrack, R. A., & Gorgolewski, K. J. (2017). poldracklab/fmriprep: 1.0.0-rc5. [Software]. Zenodo. https://doi.org/10.5281/zenodo.996169
2. Gorgolewski, Krzysztof J. ; Esteban, Oscar ; Burns, Christopher ; Ziegler, Erik ; Pinsard, Basile ; Madison, Cindee ; Waskom, Michael ; Ellis, David Gage ; Clark, Dav ; Dayan, Michael ; Manhães-Savio, Alexandre ; Notter, Michael Philipp ; Johnson, Hans ; Dewey, Blake E ; Halchenko, Yaroslav O. ; Hamalainen, Carlo ; Keshavan, Anisha ; Clark, Daniel ; Huntenburg, Julia M. ; Hanke, Michael ; Nichols, B. Nolan ; Wassermann, Demian ; Eshaghi, Arman ; Markiewicz, Christopher ; Varoquaux, Gael ; Acland, Benjamin ; Forbes, Jessica ; Rokem, Ariel ; Kong, Xiang-Zhen ; Gramfort, Alexandre ; Kleesiek, Jens ; Schaefer, Alexander ; Sikka, Sharad ; Perez-Guevara, Martin Felipe ; Glatard, Tristan ; Iqbal, Shariq ; Liu, Siqi ; Welch, David ; Sharp, Paul ; Warner, Joshua ; Kastman, Erik ; Lampe, Leonie ; Perkins, L. Nathan ; Craddock, R. Cameron ; Küttner, René ; Bielievtsov, Dmytro ; Geisler, Daniel ; Gerhard, Stephan ; Liem, Franziskus ; Linkersdörfer, Janosch ; Margulies, Daniel S. ; Andberg, Sami Kristian ; Stadler, Jörg ; Steele, Christopher John ; Broderick, William ; Cooper, Gavin ; Floren, Andrew ; Huang, Lijie ; Gonzalez, Ivan ; McNamee, Daniel ; Papadopoulos Orfanos, Dimitri ; Pellman, John ; Triplett, William ; Ghosh, Satrajit (2016). Nipype: a flexible, lightweight and extensible neuroimaging data processing framework in Python. 0.12.0-rc1. Zenodo. 10.5281/zenodo.50186
3. Nilearn contributors. (n.d.). Nilearn [Software]. Retrieved from https://github.com/nilearn/nilearn

Poster No 827

Hormesis-enhanced interoceptive refocusing (HEIR): An intervention linking the periphery and center

Otto Muzik[1], Timothy Mann[2], John Kopchick[2], Mario Yacou[2], Asadur Chowdury[2], Jamie Vadgama[2], Daniel Bonello[2], Vaibhav Diwadkar[2]

[1]Wayne State University, Department of Pediatrics, Detroit, MI, [2]Wayne State University, Department of Psychiatry, Detroit, MI

Introduction: Several behavioral techniques have sought to combine hormetic stressors with meditation. In our recent work, we have studied a specific example of Hormesis-Enhanced Interoceptive Refocusing (HEIR): the technique activates cold-stress driven sympathetic responses in combination with controlled hypocapnia, that are both yoked to interoceptive refocusing. In trained experts, HEIR leads to increased brain activity in regions associated with interoceptive control as well as in autonomic brainstem areas implicated in stress-induced analgesia[1]. These effects suggest that HEIR may drive the release of endogenous cannabinoids in both the periphery and the CNS. Such release may induce feelings of euphoria, anxiolysis and a general sense of well-being. These hypotheses motivated our current multi-modal imaging study in novice volunteers. Following a 6-week training regime, we quantified HEIR-induced longitudinal changes using PET and fMRI.

Methods: fMRI was used to investigate acute changes in brain sub-network activity in response to a sympathetic challenge, and PET/CT imaging was used with the [18F]FMPEP-d2 tracer (an inverse agonist of the CB1 receptor). Both PET/CT and fMRI data were acquired before and after the 6-week HEIR intervention. A homogenous group (age: 24-26y) group of novice healthy male volunteers participated (only males were recruited given previous studies demonstrating gender differences in brain CB1 receptor binding[2]). Participants were evaluated using the SCID, YMRS and Hamilton Depression Rating Scale (HAM-D17), and were free of current medical and psychiatric illness. The 6-week guided HEIR intervention consisted of six weekly sessions that included forceful breathing, meditation and sustained cold exposure (up-to head immersion in ice bath). Between the weekly sessions, participants maintained a daily record of their self-guided conduct of a daily 10-min deep breathing/meditation session and a cold shower. To assess the effects of repeated cold exposure on the regulation of interoceptive function by cognitive networks, a previously developed fMRI paradigm was applied designed to generate periods of mild hypothermia interspersed by periods of return to basal core body temperature[3]. Functional connectivity (FC) analyses were performed to assess connectomic changes in an a priori a set of brain regions associated with homeostasis, interoception and executive control.

Results: Psychiatric assessments did not identify any psychiatric symptoms in the participants. Global and regional analyses of the PET data revealed that HEIR drive substantial increases in CB1 receptor binding across the brain. This was especially notable in regions associated with executive, interoceptive and homeostatic functions including the ACC, OFC, AIC and the brainstem (Figure 1A). Notably, HEIR-driven increases in global CB1 receptor binding were significantly associated with improvements in sub-threshold depressive symptoms (Figure 1B), suggesting a compelling impact of HEIR on changing the brain's underlying biology and the relationship between these changes and mood. HEIR also drove increased fMRI responses in the bilateral AIC and the bilateral OFC (Figure 2A), suggesting greater regional engagement evoked by sympathetic responses. Finally, FC analysis demonstrated increased connectivity between executive and interoceptive regions (Figure 2B), suggestive of improved regulation of interoceptive function.

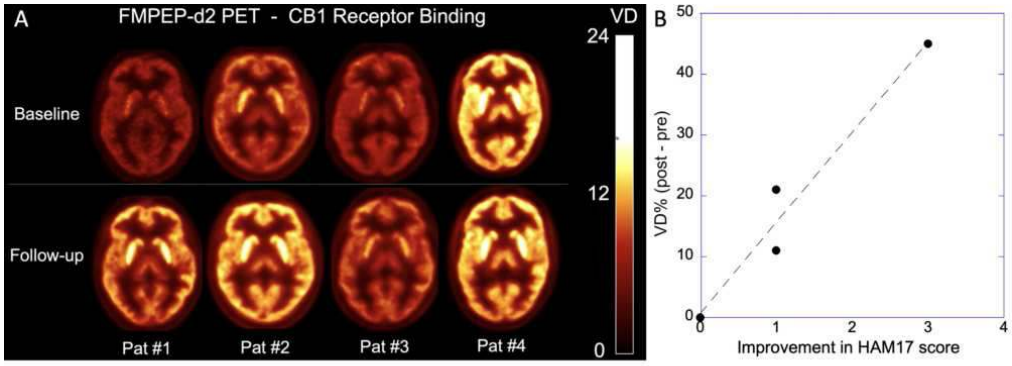

Figure 1. (A) Baseline (top row) and follow-up (bottom row) [F18]FMPEP-d2 PET images for each of the four participant. As can be seen, substantially increased global brain CB1 VD values were observed in three of the four participants. Overall, average VD values were about 20% higher following the HEIR intervention in the cortex and bilateral caudate, with smaller increases (~5%) determined in white matter. **(B)** Correlation between the increase in whole brain VD following the HEIR intervention and the HAM17 score. The graph indicates that improvement (decrease) in the total HAM17 score was associated with a significant increase in CB1 VD (r^2=.95, F=42.25, p<0.02), small sample size notwithstanding.

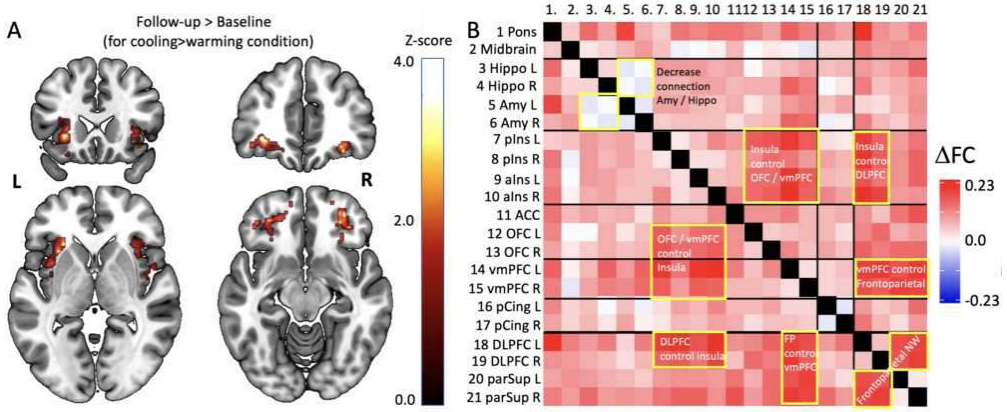

Figure 2. (A) Post HEIR intervention, exposure to whole body cold stress evoked increased responses in the bilateral anterior insula and the bilateral orbitofrontal cortex. **(B)** Adjacency matrix depicting the increase in functional connectivity (ΔFC) between brain nodes. The matrix indicates increased connectivity between central executive regions (DLPFC) and interoceptive brain areas (anterior/posterior Insula) as well as between nodes of the DMN (vmPFC, OFC) and the insula post HEIR intervention. These results suggest improved regulation of interoceptive function by cognitive networks as a result of the intervention.

Conclusions: The practice of HEIR appears to drive phasic changes in brain cannabinoid receptor signaling and functional brain activity (evoked by sympathetic nervous responses to whole-body cooling)4. These data suggest that HEIR exerts beneficial effects by evoking a balanced interaction between autonomic responses to controlled stress (exerted in the periphery) and ancillary psychological processes that are evoked in response to the activation of such autonomic processes (at the center).

References

1. Muzik O, Reilly KT, Diwadkar VA. 2018. "Brain over body"-A study on the willful regulation of autonomic function during cold exposure. Neuroimage 172: 632-641.
2. Laurikainen H, Tuominen L, Tikka M, Merisaari H, Armio RL, Sormunen E, Borgan F, Veronese M, Howes O, Haaparanta-Solin M, Solin O, Hietala J; METSY group. 2019. Sex difference in brain CB1 receptor availability in man. Neuroimage 184: 834-842.
3. Muzik O, Diwadkar VA. 2016. In vivo correlates of thermoregulatory defense in humans: Temporal course of sub-cortical and cortical responses assessed with fMRI. Hum Brain Mapp 37(9): 3188-202
4. Muzik, O., Baajour, S., Chowdury, A., Diwadkar, V.A., 2022. Effective connectivity of brain networks controlling human thermoregulation. Brain Struct Funct 227 (1), 299-312.

Poster No 828

Functional brain networks are uniquely associated with sex and gender in children

Elvisha Dhamala[1], Dani Bassett[2], B. T. Thomas Yeo[3], Avram Holmes[4]

[1]Feinstein Institutes for Medical Research, Glen Oaks, NY, [2]UPenn, Philadelphia, PA, [3]National University of Singapore, Singapore, Singapore, [4]Department of Psychiatry, Brain Health Institute, Rutgers University, Piscataway, NJ

Introduction: A fundamental aspect of our human experience is our sex and gender, how we perceive them, and how they are perceived by others. Sex and gender can explain our behavior and influence our health and disease throughout the lifespan. Women, people assigned female at birth, and sex/gender minorities have historically been excluded from biomedical research[1]. Consequently, this group of individuals is more likely to be underdiagnosed or misdiagnosed for common brain disorders (e.g., ADHD), and suffer adverse effects from treatment interventions (e.g., medications). An understanding of the functional brain correlates of sex and gender is essential for the study of brain disorders that exhibit sex differences.

Methods: Here, we used neuroimaging data from the Adolescent Brain Cognitive Development (ABCD) Study[2] (4757 children, 2351 females, 9-10 years old) at baseline, and self- and parent- reported gender data at the 1-year follow-up time point to quantify the functional correlates of sex and gender. First, we evaluated sex differences in self- and parent- reported gender data. Next, we use cross-validated linear ridge regression models[3] to establish associations between functional connectivity and sex and gender. Sex-independent (models trained on all individuals) and sex-specific (models trained specifically within each sex) approaches were used to quantify the functional correlates of gender. Finally, we evaluated whether shared or distinct functional networks were associated with sex and gender using the Haufe-transformed[4] feature weights extracted from the regression models.

Results: Self- and parent- reported gender scores were more similar in children assigned female at birth (AFAB) than in children assigned male at birth (AMAB), and AMAB children exhibited greater sex congruence than AFAB children for both self- and parent- report scores (Fig. 1A). Across all individuals, functional connectivity was significantly associated with sex, self-reported gender, and parent-reported gender (Fig. 1B). Within each sex, functional connectivity was not associated with self-reported gender, but was significantly associated with parent-reported gender in both AFAB and AMAB children (Fig. 1C). For the sex-independent models, functional connections associated with sex largely overlapped with those associated with gender, suggesting that models trained to capture variability in gender are capturing variability related to sex, and vice versa (Fig. 2A). For the sex-specific models, functional connections associated with sex were distinct from the functional connections associated with gender in AFAB and AMAB children (Fig. 2A). Functional correlates of sex were largely found in the somatomotor, visual, control and limbic networks, while the functional correlates of gender were more dispersed throughout the cortical networks (Fig. 2B). In AFAB children, functional correlates of gender largely involved connections within and between temporal parietal, limbic, dorsal/ventral attention, and somatomotor networks. In AMAB children, functional correlates of gender additionally included connections within and between default mode and visual networks.

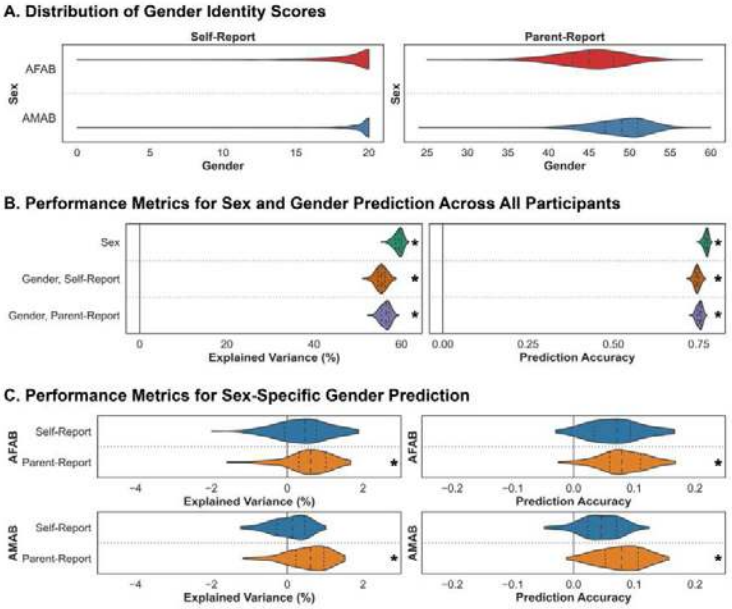

Figure 1: Functional connectivity is associated with assigned sex and gender.
(A) Violin plots display the distribution of the self- and parent- reported gender expression scores for AFAB (red) and AMAB (blue) children. (B) Explained variance (%) and prediction accuracy (correlation between true and predicted values) obtained from the models trained to predict sex. Black asterisks (*) indicate that the model performed significantly better than the null models ($p<0.05$). Results are shown for both the true (green) and the null (orange) predictions. (C) Explained variance (%) and prediction accuracy (correlation between true and predicted values) obtained from the models trained to predict self- and parent- reported gender expression. Black asterisks (*) denote that the model performed significantly better than the null models (corrected $p<0.05$). For all violin plots, the shape indicates the entire distribution of values; the dashed lines indicate the median; and the dotted lines indicate the interquartile range. AFAB – assigned female at birth; AMAB – assigned male at birth.

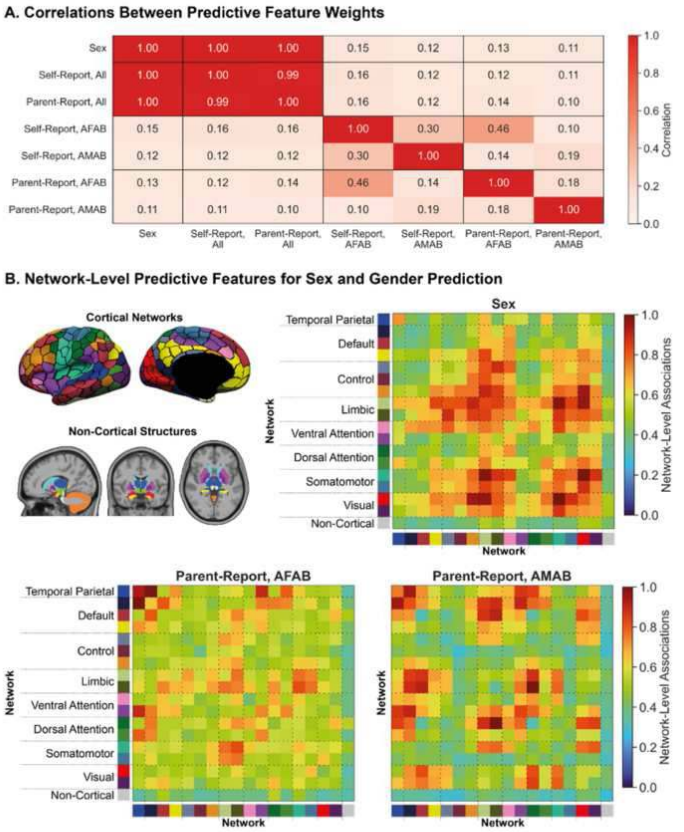

Figure 2: Distinct functional networks are associated with assigned sex and gender.
(A) Correlation coefficient between Haufe-transformed absolute pairwise regional feature weights from distinct models trained to predict assigned sex and gender expression. Models trained to predict gender were either trained across all participants (All), only in AFAB children (AFAB), or only in AMAB children (AMAB). Warmer colors indicate a stronger correlation between the feature weights. (B) Regional pairwise feature weights were summarized to a network-level by mapping the Schaefer 400 cortical parcels to 17 large-scale cortical networks and assigning the non-cortical regions to a single non-cortical network (top left). Associations between functional network connectivity and sex (top right) and parent-reported gender expression (bottom) are shown as per the colormap, where warmer colors indicate stronger correlations and cooler colors indicate weaker correlations. AFAB – assigned female at birth; AMAB – assigned male at birth.

Conclusions: Sex and gender differences in biology and behavior are tied to health outcomes throughout the lifespan. An understanding of the neurobiological underpinnings of sex and gender is crucial for the subsequent identification of how sex and gender influence health and illness and the development of sex-specific and gender-oriented diagnostic and prognostic tools. Here, we demonstrate that functional connectivity is associated with sex and parent-reported gender, and that sex and gender uniquely map onto functional brain networks in AFAB and AMAB children. As such, sex and gender must both be studied concurrently to fully capture the differences and similarities that exist between males and females, between boys and girls, and between other genders.

References

1. Taylor, C.M., L. Pritschet, and E.G. Jacobs, The scientific body of knowledge–Whose body does it serve? A spotlight on oral contraceptives and women's health factors in neuroimaging. Frontiers in neuroendocrinology, 2021. 60: p. 100874.
2. Casey, B.J., et al., The Adolescent Brain Cognitive Development (ABCD) study: Imaging acquisition across 21 sites. Dev Cogn Neurosci, 2018. 32: p. 43-54.
3. Dhamala, E., B.T. Yeo, and A.J. Holmes, Methodological Considerations for Brain-Based Predictive Modelling in Psychiatry. Biological Psychiatry, 2022.
4. Haufe, S., et al., On the interpretation of weight vectors of linear models in multivariate neuroimaging. Neuroimage, 2014. 87: p. 96-110.

Poster No 829

Altered Brain Synergistic and Redundant Interactions in Individuals with Antisocial Behavior

Weixiong Jiang[1], Shuaiqi Li[1], Hong Wu[2], Lin Li[1], Yulong Xia[1], Shoujun Huang[1], Feng Gao[3], Jing Yuan[1], Xiaoping Ouyang[4]

[1]College of Mathematical Medicine, Zhejiang Normal University, Jinhua, Zhejiang, [2]School of Marxism, Hunan First Normal University, Changsha, Hunan, [3]School of Electronic Information, Hunan First Normal University, Changsha, Hunan, [4]State Key Laboratory of Fluid Power & Mechatronic Systems, Zhejiang University, Hangzhou, Zhejiang

Introduction: The public health concern surrounding antisocial behavior (ASB) is profound, due to its extensive impact on society (Romeo 2006). Previous research has established a relationship between ASB and abnormalities in brain regions and functional connectivity (Jiang 2021; Mackey 2017), but detailed analyses of brain interaction remain scarce. Recent advancements have focused on nuanced constituents of brain activity, such as the decomposition of brain region interactions into synergistic and redundant components (Mediano 2021). This differentiation has revealed that synergistic interactions are prevalent in higher-order networks, while redundant interactions in sensorimotor ones (Luppi 2022). Our study aims to investigate the distinctions of these information components between individuals with ASB and those without, thus enhancing our understanding of ASB-associated brain dynamics.

Methods: We recruited 49 volunteers (22.38 ± 3.25) from the School for Youth Offenders of Hunan Province, including 33 ASB subjects and 16 normal controls (NC). Resting-state fMRI data were preprocessed and parcellated into 268 regions of interest. Using the novel Integrated Information Decomposition (ΦID) method, we dissected brain interactions between each pair of brain regions into 16 distinct interactive elements (Mediano 2021), focusing on redundant (information that overlaps in two regions) and synergistic information (information that emerges when both regions are considered together, not by either region alone) (Luppi 2022). We constructed two connection matrices per subject: one for synergistic interaction and the other for redundant interaction. To investigate the characteristics of each component, we assessed ASB-related alterations in these interactions at both regional and network levels. Additionally, we complemented the analysis with network regional measures, including the betweenness centrality to assess the significance of a region and the clustering coefficient to gauge the tendency of nodes to cluster together (Rubinov 2010).

Results: ASB subjects showed significant reductions in synergistic interactions, particularly in the left ventral and inferior frontal areas, right superior frontal regions, bilateral temporal, right parietal including precuneus areas, bilateral subcortical (insula, cingulum, and hippocampus), and occipital visual regions (Fig. 1A). In particular, the visual association network showed significant decreases (P=0.0126), a trend that was consistent across other networks (Fig. 1B). Redundant interactions also predominantly decreased in ASB subjects, particularly in the bilateral inferior temporal to temporal pole, bilateral inferior prefrontal areas, left middle cingulum, insula, and inferior parietal areas (Fig. 1C). While subnetwork analysis did not show significant differences, a generalized decline in redundant interactions was detected (Fig. 1D). Network metrics indicated altered patterns in both synergistic (Fig. 2A, B) and redundant (Fig. 2C, D) interactions in ASB individuals, characterized by a predominance of decreased betweenness centrality in synergistic interactions and clustering coefficient in redundant interactions. Conversely, the clustering coefficient in synergistic interactions and the betweenness centrality in redundant interactions showed variable changes across different brain regions.

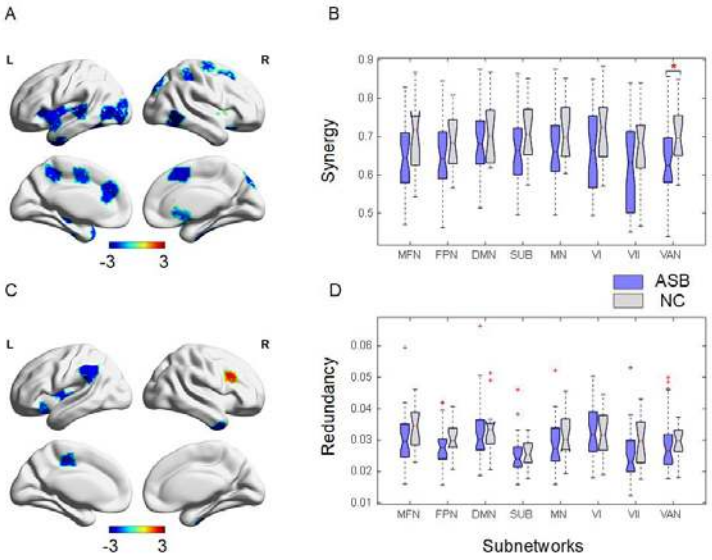

Figure 1. Significant differences in synergistic (A) and redundant (C) interactions in ASB subjects compared to normal controls, accompanied by subnetwork analysis for synergistic (B) and redundant (D) interactions. MFN: medial frontal network; FPN: frontoparietal network; DMN: default mode network; SUB: subcortical-cerebellum network; MN: motor network; VI: visual I network ; VII: visual II network; VAN: visual association network.The colorbar indicates the t-values of two-sample t-test. *: P<0.05.

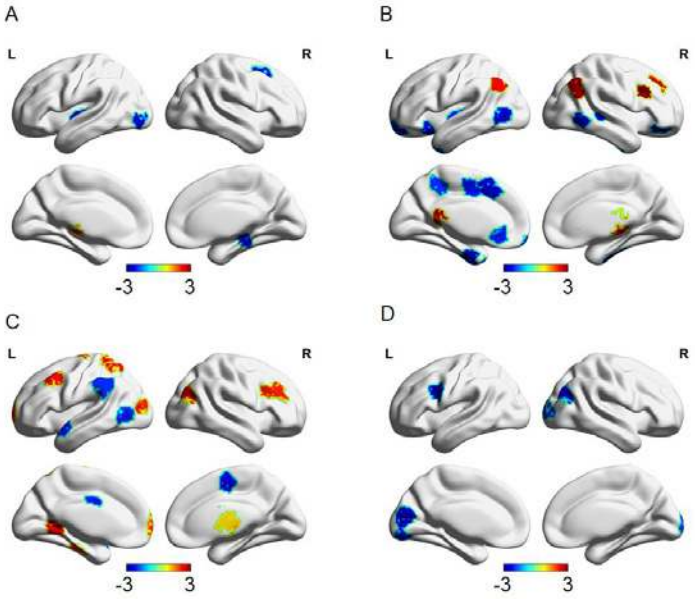

Figure 2. Significant regions of betweenness centrality (A, C) and clustering coefficient (B, D) when comparing ASB subjects to normal control at a sparsity level of 10%. (A) and (B) are for synergistic interaction, while (C) and (D) for redundant interaction.The colorbar indicates the t-values of two-sample t-test. ASB: antisocial behavior.

Conclusions: Our findings revealed significant reductions in both synergistic and redundant interactions in ASB subjects, suggesting impairments in functional brain connectivity. The pronounced decrease in synergy within the visual association network indicates potential disruptions in higher-order visual processing capabilities in individuals with ASB. Changes in network metrics further underscore the altered interaction patterns, signifying the intricate nature of the neural mechanisms involved in ASB. These insights offer a novel perspective into the neural underpinnings of ASB through the lens of synergistic and redundant brain interactions.

References

1. Jiang, W. (2021), 'Dynamic neural circuit disruptions associated with antisocial behaviors', Human Brain Mapping, vol. 42, no. 2, pp.329-344.
2. Luppi, A.I. (2022), 'A synergistic core for human brain evolution and cognition', Nat Neurosci, vol. 25, no. 6, pp. 771-782.
3. Mackey, S. (2017), 'Brain Regions Related to Impulsivity Mediate the Effects of Early Adversity on Antisocial Behavior', Biol Psychiatry, vol. 82, no. 4, pp.275-282.

4. Mediano, P.A. (2021), 'Towards an extended taxonomy of information dynamics via Integrated Information Decomposition', arXiv preprint arXiv:2109.13186.
5. Piras, I.S. (2023), 'A preliminary transcriptomic analysis of the orbitofrontal cortex of antisocial individuals', CNS Neuroscience & Therapeutics.
6. Romeo, R. (2006), 'Economic cost of severe antisocial behaviour in children-and who pays it', BJPsych, vol. 188, no. 6, pp.547-553.
7. Rubinov, M.(2010), 'Complex network measures of brain connectivity: uses and interpretations', Neuroimage, vol. 52, no. 3, pp.1059-1069.

Poster No 830

Neural Mechanisms of Mental Illness Knowledge Acquisition via 1st Person Perspective Virtual Reality

Wey Guan Lem[1], Kelssy Hitomi dos Santos Kawata[1], Koki Ono[1], Hiroshi Oyama[1]

[1]The University of Tokyo, Japan, Tokyo

Introduction: The public stigma of mental illness is the general public's negative misconceptions about people with mental illness[1,2]. Public stigma regarding mental illness significantly impacts individuals with such conditions, often leading to detrimental outcomes like employment disparities[3] and inhibited treatment-seeking behaviors[4]. First-person perspective (1PP) immersive virtual reality (IVR) anti-stigma intervention has emerged as a method to improve knowledge of mental illness knowledge[5,6]. However, the neural correlates of individual difference in mental illness knowledge acquisition using 1PP IVR anti-stigma intervention and the effectiveness of stigma reduction has not yet been studied. This study explores the neurobiological underpinnings of how individual differences in mental illness knowledge acquisition manifest following a 1PP IVR anti-stigma intervention and the effectiveness of this intervention to the stigma reduction.

Methods: Using a randomized cross-over trial, 32 right-handed native Japanese (14 female; M = 24.00, SD = 6.10 years) were randomized into either the IVR-control group or control-IVR group. As for the intervention, the IVR group used a 1PP Immersive Virtual Reality Anti-stigma (IVRAS) application via head-mounted display (HMD), while participants in the control group watched the same content of the 1PP IVRAS application through a computer screen. In the 1PP IVRAS application, participants took on the role of a person with mental illness in 1PP and experienced stigma from colleagues and support from family. Pre- and post-intervention assessments included standardized measures for mental illness knowledge (MIDUS) and public stigma (RIBS-J), and functional magnetic resonance imaging (fMRI) scanning. During the fMRI scanning, all participants were asked to listen to the main auditory content of the 1PP IVRAS application while wearing a sleeping mask to minimize the visual effects generated on removing the HMD after using the IVR application. For the behavioural data, the two-way Repeated Measures ANOVA and Friedman tests were conducted for MIDUS and RIBS-J, respectively, with time as a within-participant factor (pre- vs. post-intervention) and intervention type as the between-participant factor (IVR vs. control). Regression analysis on the absolute changes in the MIDUS scores, mental illness knowledge acquisition brain activity was examined for each group. The voxel-wise statistics used an uncorrected p-value of <0.005 for the cluster-forming threshold and at a threshold of family-wise error (FWE)-corrected p-value of <0.05 for cluster extent. The protocol received approval from the Research Ethics Committee of the Faculty of Medicine and Graduate School of Medicine of the University of Tokyo (2019099NI).

Results: Both the 1PP IVR and control groups showed improvement in mental illness knowledge acquisition score, but only the 1PP IVR group showed reduced public stigma score towards people with mental illness. Furthermore, distinct brain activation was identified for both groups. Mental illness knowledge acquisition using the 1PP IVRAS application was associated with right superior frontal gyrus (SFG) activation, a critical brain region for empathic concern when mentalizing about another person's illness[7]. In contrast, control group showed right anterior insula activation previously implicated in empathic distress about people with mental illness[8].

Conclusions: Our findings indicate that 1PP IVRAS application specifically enhance mental illness knowledge retention and decrease public stigma by changing brain regions associated with empathic understanding. This suggests the potential of 1PP IVR in educational strategies for stigma reduction. By identifying the SFG's role in stigma intervention, this study opens avenues for targeted brain-based stigma mitigation approaches and underscores the importance of 1PP IVRAS in empathy-driven learning on stigma.

References

1. Corrigan PW, Bink AB: The Stigma of Mental Illness. In: Encyclopedia of Mental Health. Volume 4, edn. Edited by Friedman HS. Cambridge: Academic Press; 2016: 230-234.
2. Link BG, Phelan JC, Bresnahan M, Stueve A, Pescosolido BA: Public conceptions of mental illness: labels, causes, dangerousness, and social distance. Am J Public Health 1999, 89(9):1328-1333.
3. Hampson ME, Watt BD, Hicks RE: Impacts of stigma and discrimination in the workplace on people living with psychosis. BMC Psychiatry 2020, 20(1):1-11.

4. Schnyder N, Panczak R, Groth N, Schultze-Lutter F: Association between mental health-related stigma and active help-seeking: systematic review and meta-analysis. Br J Psychiatry 2017, 210(4):261-268.
5. Hadjipanayi C, Michael-Grigoriou D: Arousing a wide range of emotions within educational virtual reality simulation about major depressive disorder affects knowledge retention. Virtual Reality 2021, 26(1):343-359.
6. Formosa NJ, Morrison BW, Hill G, Stone D: Testing the efficacy of a virtual reality-based simulation in enhancing users' knowledge, attitudes, and empathy relating to psychosis. Australian Journal of Psychology 2020, 70(1):57-65.
7. Shin WG, Woo CW, Jung WH, Kim H, Lee TY, Decety J, Kwon JS: The Neurobehavioral Mechanisms Underlying Attitudes Toward People With Mental or Physical Illness. Front Behav Neurosci 2020, 14:1-12.
8. Decety J, Lamm C: Empathy versus Personal Distress: Recent Evidence from Social Neuroscience. In: The Social Neuroscience of Empathy. edn.; 2009: 199-214.

Poster No 831

Brain morphology and early substance use in adolescence: a large prospective cohort study

Olga Boer[1], Ingmar Franken[2], Ryan Muetzel[3], Janna Cousijn[4], Hanan El Marroun[2]

[1]Erasmus University Rotterdam / Erasmus Medical Center, Rotterdam, South-Holland, [2]Erasmus University Rotterdam, Rotterdam, South-Holland, [3]Erasmus Medical Center, Rotterdam, Zuid Holland, [4]Erasmus University Rotterdam, Rotterdam, Zuid-Holland

Introduction: Substance use during adolescence, especially when initiated early, has been associated with substance use disorders (SUD) later in life (Huggett et al., 2019; Trujillo et al., 2019). When investigating the neurobiological underpinnings of this association, it is crucial to disentangle the causes from consequences of substance use. As such, identifying pre-existing brain variations allows us to pinpoint brain areas that might be specifically vulnerable to the effects of substance use. While the existing literature has identified pre-existing brain variations as vulnerability markers for substance use initiation (Boer et al., 2022), the role of timing of early initiation is yet unclear. Furthermore, previous studies often relied on small samples, which could lead to inflated effect sizes and false-positive findings. Therefore, the current study employed a population-based prospective study cohort, the Generation R Study (Kooijman et al., 2016), to investigate the association between brain morphology in late childhood (age 10) and very early alcohol and tobacco initiation (age < 13) in adolescence.

Methods: Brain morphology (gray matter volume, cortical thickness and surface area) in children was assessed two times using magnetic resonance imaging (MRI), around age 10 and age 14. At age 14, participants reported on alcohol and tobacco use initiation. To examine pre-existing brain differences in very early substance use initiators, we used logistic regression to examine the longitudinal association between brain morphology of regions of interest (ROIs) around age 10 and reported initiation (yes/no) of alcohol/tobacco use before the age of 13 (N = 2218). Then, to determine whether any pre-existing differences were not present at age 10, but emerged between the two neuroimaging waves, we examined the cross-sectional association between brain morphology of the ROIs around age 14, and alcohol/tobacco use initiation before age 13 (N = 1817). Separately, we examined both the longitudinal and cross-sectional associations with a surface-based approach (without predefined ROIs) using the R package QDECR (Lamballais & Muetzel, 2021). Sensitivity analyses included rerunning analyses after applying inverse probability weighting, and stratifying the samples by sex. Models were adjusted for age at neuroimaging, sex, maternal ethnicity and education, household income, prenatal alcohol/tobacco exposure, parental psychopathology and history of SUD, and child non-verbal IQ. Missing data on confounders was imputed using multiple imputation by chained equations (van Buuren & Groothuis-Oudshoorn, 2011) and a false discovery rate correction was applied to control for type I errors (Benjamini & Hochberg, 1995).

Results: No associations were found between brain morphology at both research waves and early alcohol/tobacco use initiation (age < 13), neither in the ROI nor the surface-based analyses. Sex-specific analyses revealed a cross-sectional association between smaller thalamic volume at age 14 and early initiated tobacco use in girls (OR = .26, CI[.11 - .58], p = .001, pFDR = .03), possibly reflecting the emergence of sex-specific pre-existing neural variations between age 10 and 14.

Conclusions: The present study could not find robust brain morphometry measures of very early (age < 13) alcohol/tobacco initiation in a large population-based sample of young adolescents. This finding is important for interpreting existing research on neurobiological consequences of substance use in the general population. Furthermore, a sex-specific finding for smaller thalamic volume hinted towards differential substance use vulnerability in girls, considering the assumed role of the thalamus in SUD development (Huang et al., 2018). Future longitudinal studies are needed to specify whether these findings can be extended to later initiation and continuation of alcohol and tobacco use in later stages of adolescence.

References

1. Benjamini, Y., & Hochberg, Y. (1995). Controlling the False Discovery Rate: A Practical and Powerful Approach to Multiple Testing [https://doi.org/10.1111/j.2517-6161.1995.tb02031.x]. Journal of the Royal Statistical Society: Series B (Methodological), 57(1), 289-300. https://doi.org/https://doi.org/10.1111/j.2517-6161.1995.tb02031.x
2. Boer, O. D., El Marroun, H., & Franken, I. H. A. (2022). Brain Morphology Predictors of Alcohol, Tobacco, and Cannabis Use in Adolescence: A Systematic Review. Brain Res, 148020. https://doi.org/S0006-8993(22)00244-X
3. Huang, A. S., Mitchell, J. A., Haber, S. N., Alia-Klein, N., & Goldstein, R. Z. (2018). The thalamus in drug addiction: from rodents to humans. Philos Trans R Soc Lond B Biol Sci, 373(1742). https://doi.org/rstb.2017.0028
4. Huggett, S. B., Keyes, M., Iacono, W. G., McGue, M., Corley, R. P., Hewitt, J. K., & Stallings, M. C. (2019). Age of initiation and transition times to tobacco dependence: Early onset and rapid escalated use increase risk for dependence severity. Drug Alcohol Depend, 202, 104-110. https://doi.org/S0376-8716(19)30199-1
5. Kooijman, M. N., Kruithof, C. J., van Duijn, C. M., Duijts, L., Franco, O. H., van, I. M. H., de Jongste, J. C., Klaver, C. C., van der Lugt, A., Mackenbach, J. P., Moll, H. A., Peeters, R. P., Raat, H., Rings, E. H., Rivadeneira, F., van der Schroeff, M. P., Steegers, E. A., Tiemeier, H., Uitterlinden, A. G., . . . Jaddoe, V. W. (2016). The Generation R Study: design and cohort update 2017. Eur J Epidemiol, 31(12), 1243-1264. https://doi.org/10.1007/s10654-016-0224-9
6. Lamballais, S., & Muetzel, R. L. (2021). QDECR: A Flexible, Extensible Vertex-Wise Analysis Framework in R. Front Neuroinform, 15, 561689. https://doi.org/10.3389/fninf.2021.561689
7. Trujillo, C. A., Obando, D., & Trujillo, A. (2019). An examination of the association between early initiation of substance use and interrelated multilevel risk and protective factors among adolescents. PLoS One, 14(12), e0225384. https://doi.org/PONE-D-19-16848
8. van Buuren, S., & Groothuis-Oudshoorn, K. (2011). mice: Multivariate Imputation by Chained Equations in R. Journal of Statistical Software, 45(3), 1 - 67. https://doi.org/10.18637/jss.v045.i03

Poster No 832

The interaction of oxytocin and nicotine addiction on psychosocial stress: an fMRI study

Jiecheng Ren[1], Zhengde Wei[1], Xiaochu Zhang[1]

[1]University of Science and Technology of China, Hefei, Anhui

Introduction: The anxiolytic effect of oxytocin (OXT) on psychosocial stress has been well documented (Heinrichs M., 2003). However, there is still a need for further in-depth research to fully understand the mechanisms of OXT's effect on psychosocial stress (Takayanagi Y., 2021). Various factors, such as nicotine addiction, can interact with OXT's anxiolytic effect (Chen, F.S., 2011). Investigating the effects and interaction of OXT and nicotine addiction is essential in determining the effectiveness of OXT intervention for psychosocial stress, particularly for smokers. We assumed that functions of the overlapping brain areas of OXT's anxiolytic effect and nicotine addiction are essential for the effects and interaction of OXT and nicotine addiction.

Methods: Firstly, after intranasal administration of randomized OXT or placebo (saline), a group of healthy participants (n=27) and a group of smokers (n=26) completed the Montreal Imaging Stress Task (MIST) in an MRI scanner (Figure 1A, C, D). Secondly, a group of smokers (n=22) was recruited to complete a transcranial direct current stimulation (tDCS) experiment (Figure 1B), in which anodal tDCS was applied on subjects' anterior right superior temporal gyrus (rSTG). In both experiment, subjective stress ratings, salivary cortisol samples and the amount of daily cigarette consumption were obtained from each participant.

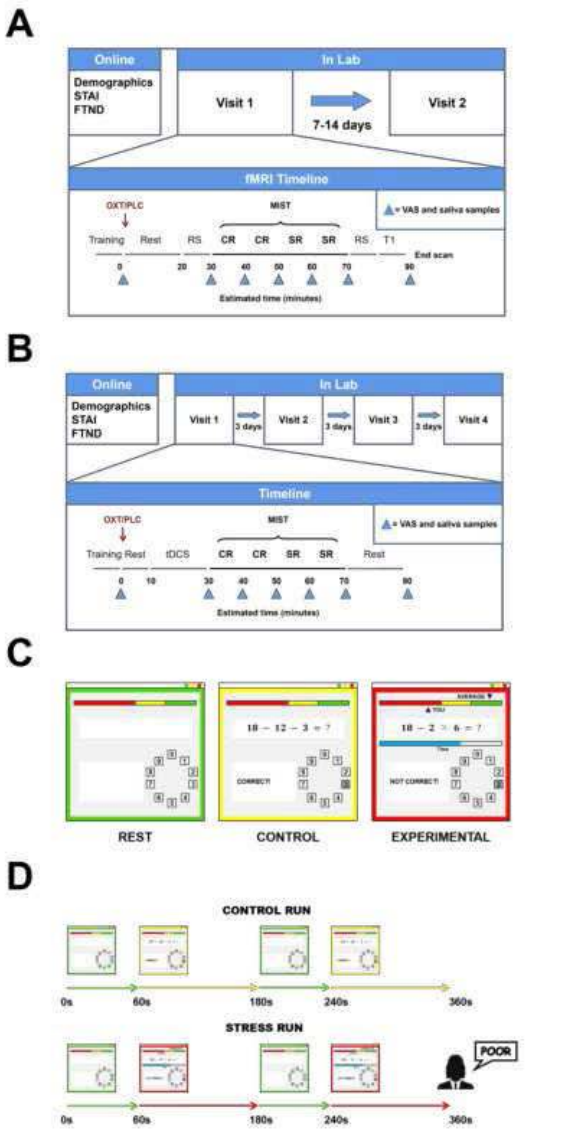

Figure 1. Schematic diagram of the first fMRI experiment (A) and second tDCS experiment (B). The estimated time points of VAS, salivary sample collection and each MIST run are shown. The user interface of the Rest, Control and Experimental conditions of the MIST. (C) Each run consisted of two sets of the 60 s rest condition followed by 120 s math problem-solving condition. (D) STAI: state-trait anxiety inventory; FTND: Fagerstrom Test of Nicotine Dependence; MIST: Montreal Imaging Stress Task; VAS: visual analog scale; RS: resting-state; CR: control run; SR: stress run; OXT: oxytocin; PLC: placebo; tDCS: transcranial direct current stimulation.

Results: In first fMRI experiment, analysis of variance (ANOVA) revealed an interaction of OXT and nicotine addiction on subjective stress (Figure 2A). In smokers, OXT failed to suppress the elevation of subjective stress and craving ratings after psychosocial stress (Figure 2A, C), but successfully suppressed salivary cortisol level (Figure 2B). A voxel-wise ANOVA of fMRI data identified an interaction between OXT and nicotine addiction in the anterior right superior temporal gyrus (rSTG), medial frontal gyrus, right lentiform nucleus / inferior frontal gyrus, and right parahippocampal gyrus (Figure 2D). Among these regions, changes in anterior rSTG activity were found inversely associated with daily cigarette consumption after administration of PLC in smokers (Figure 2E), along with a correlation between activations of anterior rSTG and salivary cortisol (Figure 2F). We also found an interaction between OXT and nicotine addiction in anterior rSTG's functional connectivity with right middle frontal gyrus (Figure 2G). Correlation between this functional connectivity and subjective psychosocial stress was also found abnormal in smokers, in which nicotine addiction reversed the direction of the correlation, even after OXT administration (Figure 2H, I). In second tDCS experiment, we found that after tDCS on anterior rSTG, OXT was able to successfully suppress the elevation of subjective stress and craving ratings after psychosocial stress (Figure 2J, K, L).

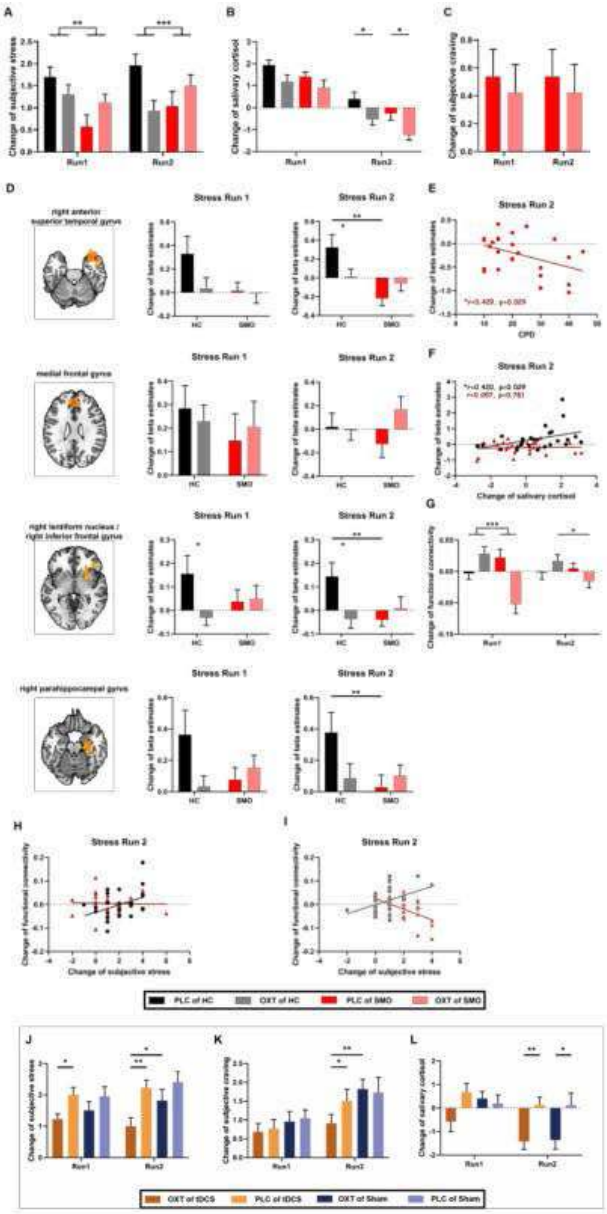

Figure 1. Changes in subjective stress ratings (A), salivary cortisol levels (B) and subjective craving ratings (C) in first fMRI experiment. Neural activity during psychosocial stress in four brain areas revealed interaction of oxytocin and nicotine addiction (D). The changes in beta estimates of the anterior rSTG in stress run 2 were inversely correlated with an index of nicotine addiction after PLC administration (E). In the HC group, changes in beta estimates of the anterior rSTG were positively associated with changes in salivary cortisol after the administration of PLC in stress run 2 (F). Changes in functional connectivity between the anterior rSTG and right middle frontal gyrus (rMFG) in stress runs 1 and 2. (G) nicotine addiction reversed the direction of the correlation between this functional connectivity and changes of subjective stress ratings, even after OXT administration (H, I). Changes in subjective stress ratings (J), subjective craving ratings (K) and salivary cortisol level (L) in stress run 1 and stress run 2 in the tDCS experiment. HC: healthy participants group; SMO: smokers group; PLC: placebo; OXT: oxytocin; *p<0.05, **p<0.01; ***p<0.001.

Conclusions: In summary, our study provides novel behavioral and neural information on the effects and interaction of OXT and nicotine addiction on psychosocial stress. Our findings suggest that nicotine addiction blocks OXT's anxiolytic effect on psychosocial stress, which is related to abnormalities in the anterior right superior temporal gyrus, and its functional connectivity with right middle frontal gyrus. These findings will support further development on oxytocin's intervention of psychosocial stress in nicotine addiction, and provides essential information for indicating OXT's effectiveness.

References

1. Chen, F.S. (2011), 'Common oxytocin receptor gene (OXTR) polymorphism and social support interact to reduce stress in humans', Proceedings of the National Academy of Sciences of the United States of America, vol. 108, pp. 19937-42.
2. Heinrichs, M. (2003), 'Social support and oxytocin interact to suppress cortisol and subjective responses to psychosocial stress', Biological Psychiatry, vol. 54, pp. 1389–98.
3. Takayanagi, Y. (2021), 'Roles of Oxytocin in Stress Responses, Allostasis and Resilience', International Journal of Molecular Sciences, vol. 23, pp. 150.

Poster No 833

Conducting tourism research based on RSA: A case study on brand extension problem

Hang Yuan[1], Siyang Luo[1]

[1]*Department of Psychology, Sun Yat-sen University, Guangzhou, Guangdong*

Introduction: Tourism neuroscience primarily employs neuroscience technologies to explore individuals' behavior and neural activities in specific scenarios(Li et al., 2023). As an interdisciplinary field, it lacks integration of results from multimodal data. This research introduces representation similarity analysis (RSA) to studying tourism issues (Haxby et al., 2014). Using the example of brand extension, we demonstrate how to construct similarity models and conduct cross-modal comparisons. Brand extension refers to a strategy wherein a brand with a certain level of recognition is applied to new products, aiming to reduce the market risks(Tauber, 1981). The evaluation of extension products determines whether it can achieve success in the market. Oxytocin, as a crucial hormone may enhance individuals' sensitivity to social cues(Groppe et al., 2013) and facilitate the recognition of social stimuli(Winslow & Insel, 2002). In this case, we conducted an experiment based on EEG and employed the RSA method to explore the potential mechanisms through which oxytocin influences consumers' attitudes toward brand extension products.

Methods: This study recruited 52 male participants (M = 20.13, SD = 2.296). A 2 (treatment: oxytocin(OT), placebo(PL)) × 2 (brand type: domestic, foreign) × 3 (perceived fitness: high, moderate, low) mixed-design was employed. During the experiment, participants were instructed to rate the fitness between brands and their extension products. Based on preprocessed EEG data, representational dissimilarity matrixes (RDM) of different modalities were constructed, and the similarity between cross-modal matrices was compared. First, to examine the impact of oxytocin on neural activity patterns, the consistency of neural activity patterns within each group was calculated (Figure 1A). Second, to explore the influence of OT intervention on the relationship between neural activity patterns and conceptual models as well as behavioral patterns, behavior models were constructed based on participants' ratings of fitness. Theoretical models were built based on the similarity levels across stimuli. RDMs of neural activity were constructed over time points. Subsequently, the Mantel test (Mantel, 1967) was conducted at each time point to compare the similarity of RDMs.

Results: The t-test was employed to compare the differences in the neural activity similarities(r) between subjects in the OT and the PL group at each time point. The results revealed that within the 480~580 ms, participants in the OT group exhibited significantly higher consistency in neural activity patterns than PL group (Fig.1B). Cross-modal comparisons between neural activity and behavioral RDMs for both the OT and PL groups indicated significant similarity between neural patterns and behavioral performance across multiple time windows (Fig.2B, D). It indicated that the relational patterns of neural activity were consistent with the patterns of behavioral performance. Furthermore, comparisons between neural activity RDM and conceptual RDM revealed that, in the OT group, within the time windows of 420~460ms and 590~650ms, participants exhibited significantly similar neural representation patterns in the occipito-temporal clusters to the conceptual model (Fig. 2C). In contrast, in the PL group, participants did not show significant similarity (Fig. 2E). These findings suggested that OT intervention enhances participants' neural representation of different types of stimuli.

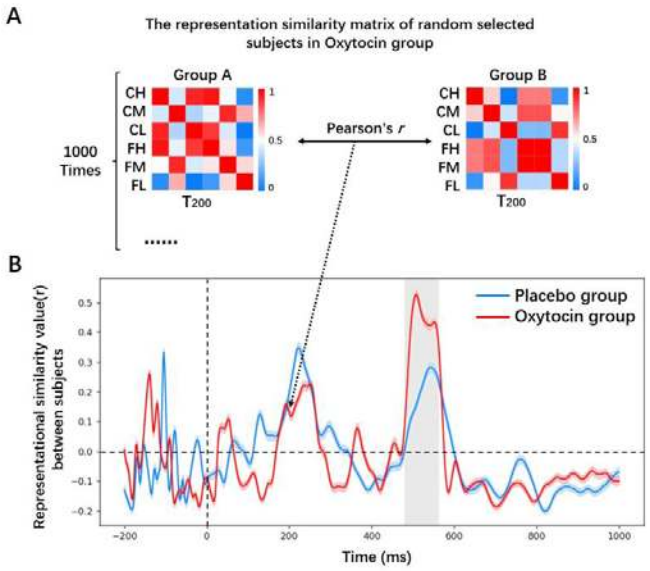

Figure 1: (A) Schematic representation of within-group representational similarity of OT groups: Firstly, at each time point (depicted as the 200th time point in the figure), each group was randomly sampled 1000 times. In each sampling, subjects were randomly divided into two groups of equal size, and a sliding time window of 40ms was used to construct neural activity RDM for the two groups of subjects in the fronto-central (FCz, Cz, CPz, C1, C2) clusters induced by different types of stimuli (domestic brand-high fitness(CH), domestic brand -moderate(CM), domestic brand-low fitness(CL), foreign brand-high fitness(FH), foreign brand -moderate(FM), foreign brand-low fitness(FL),). Subsequently, Mantel tests were employed to obtain 1000 within-group representational similarity values (r) for OT groups at each time point. **(B)** Changes in within-group consistency of neural activity patterns for OT group (red solid line) and PL group (blue solid line). The shaded area around the solid line represents the 95% confidence interval, and the gray rectangle highlights the time windows with significant differences in the consistency of neural activity patterns between the two groups.

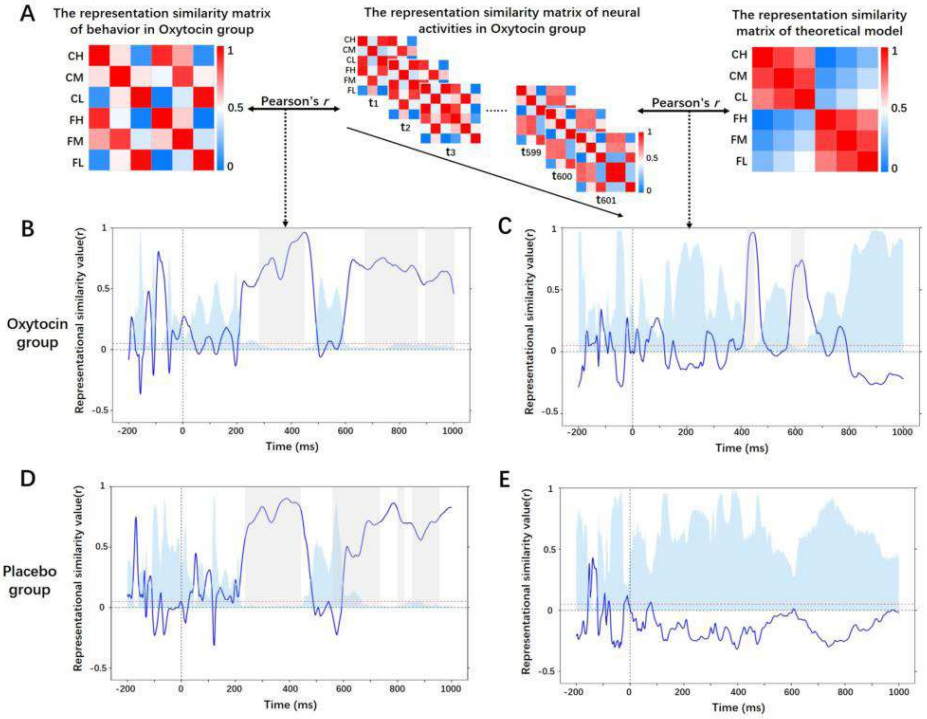

Figure 2: (A) RDM of behavioral data for participants in the OT group (left), time-point-wise neural activity RDMs (middle), and theoretical RDM (right); Time-point-wise representational similarity values (r) between neural activity RDM and behavioral RDM in the OT group**(B)** and PL group **(D)**; Time-point-wise representational similarity values (r) between neural activity RDM and theoretical RDM for participants in the OT group **(C)** and PL group **(E)**.

Conclusions: This study introduced the RSA analysis method into tourism neuroscience and conducted cross-modal analyses from a pattern perspective. Using the example of brand extension, we found that oxytocin not only enhances participants' neural representations of different extended brands but also promotes the consistency of their response patterns. In summary, conducting tourism studies using the RSA method can help us delve more profoundly into scientific questions in the field of tourism from a pattern perspective.

References
1. Groppe, S. E. (2013), 'Oxytocin influences processing of socially relevant cues in the ventral tegmental area of the human brain', Biological Psychiatry, 74(3), 172-179.
2. Haxby, J. V. (2014), 'Decoding neural representational spaces using multivariate pattern analysis', Annual Review of Neuroscience, 37, 435-456.
3. Li, S. (2023), 'A review of research into neuroscience in tourism: Launching the annals of tourism research curated collection on neuroscience in tourism', Annals of Tourism Research, 101, 103615.
4. Mantel, N. (1967). 'The detection of disease clustering and a generalized regression approach', Cancer Research, 27(2), 209-220.
5. Tauber, E. M. (1981). 'Brand franchise extension: New product benefits from existing Brand Names', Business Horizons, 24(2), 36-41.
6. Winslow, J. T. (2002), 'The social deficits of the oxytocin knockout mouse', Neuropeptides, 36(2-3), 221-229.

Poster No 834

The Oxytocin Receptor Gene (OXTR) Dependent Intranasal Oxytocin Effect on Neural Responses to Trust

Qin Duan[1], Siyang Luo[1], Shihui Han[2]

[1]Department of Psychology, Sun Yat-sen University, GuangZhou, China, [2]Department of Psychology, Peking University, Bejing, China

Introduction: Trust and betrayal of trust are general in social interaction. Oxytocin (OT) has been proved to be closely related to trust (Kosfeld et al., 2005; Nave, Camerer, & McCullough, 2015). The effect of OT on trust adaptation after betrayal of trust was associated with decrease activation in the amygdala, the midbrain regions, and the dorsal striatum, which indicated that OT influence trust adaptation by reducing fear processing and feedback learning (Baumgartner et al., 2008; Ide et al., 2018). Furthermore, the impact of oxytocin on trust may be influenced by variations in the oxytocin receptor gene (OXTR). Research suggests that certain polymorphisms of the OXTR gene may be linked to variations in social behavior, emotional cognition, and perceptions of trust (Kogan et al., 2011; Chen et al., 2020). To investigate the OXTR dependent intranasal oxytocin effect on neural mechanism underlying trust and trust adaptation after betrayal, the current research applied a double-blind economic trust experiment by using intranasal OT and functional magnetic resonance imaging (fMRI).

Methods: A total of 120 healthy university students (all male, age = 21.12±2.20 years) participated in this study, comprising 64 A/A individuals and 56 G/G individuals. At the experiment's outset, participants were randomly assigned to either the oxytocin group or the placebo group. After treated with intranasal oxytocin or placebo, participants were positioned in the scanner and required to finish the economic trust task. The fMRI experiment comprised 8 sessions, each featuring 8 trials. We employed reinforcement learning models to analyze behavioral data, determining the rate at which each participant adapted to targets deemed trustworthy and untrustworthy. Then, we constructed GLMs to investigate the neural activity responses to trustworthy and untrustworthy target peoples. Dynamic causal models (DCM) were applied to investigate the effect of OT and OXTR on neural responses to trust adaptation.

Results: Behavioral results revealed that A/A participants treated with oxytocin increase their trust in trustworthy condition, while decrease their trust in untrustworthy condition. Conversely, G/G participants treated with oxytocin decrease their trust in trustworthy condition, while increase their trust in untrustworthy condition. The reinforcement learning model showed that trust adaptation was based on the difference between the invested amount and the feedback outcome. The whole-brain analysis examined patterns of trust adaptation-related neural activity responses to trustworthy people and untrustworthy people in the two genotype groups following either oxytocin or placebo treatment. The difference in trust adaptation is associated with the specific activation pattern in the anterior cingulate cortex and dorsal medial prefrontal cortex (Fig1). Comparing to interacting with trustworthy target people, subjects in OT group showed stronger activation in ACC and DMPFC when interacting with untrustworthy target people. However, this effect was not found in subjects in placebo group. Dynamic casual modeling (DCM) further revealed distinct connectivity patterns during trust decision between different OXTR genotype group and treatment group.

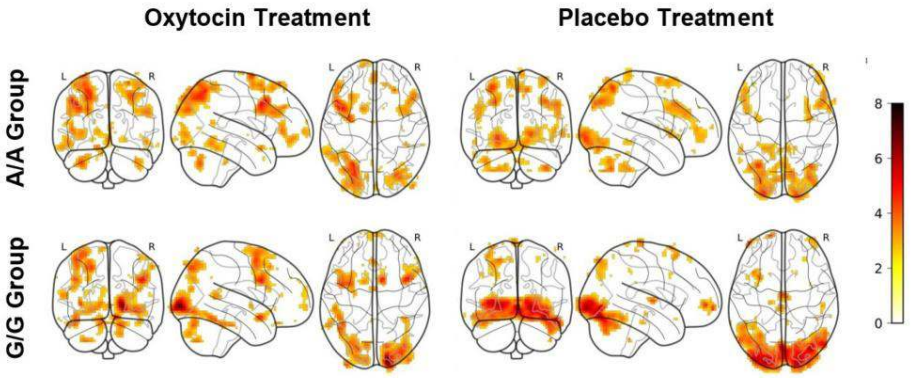

Figure 1. The results of the whole-brain analysis are depicted in four activation maps. On the left side, the top map represents the A/A genotype group's neural response related to trust adaptation under oxytocin treatment, while the bottom map depicts the G/G group's neural response under same treatment. On the right side, the top map illustrates the A/A genotype group's neural response related to trust adaptation under placebo treatment, and the bottom map portray the G/G group's neural response related to trust adaptation under placebo treatment.

Conclusions: The current study underscores the significant role of OT and OXTR in shaping trust dynamics in social interactions. We observed that OT treatment consistently maintained trust, contrasting with the placebo group's varied trust responses. Brain activity in the ACC and DMPFC, alongside distinct neural connectivity patterns, underlines this genotype-dependent trust adaptation. This highlights the intricate interplay of genetics and neurobiology in shaping social trust behaviors.

References

1. Baumgartner, T. (2008), 'Oxytocin shapes the neural circuitry of trust and trust adaptation in humans', Neuron, vol. 58, no. 4, pp. 639-650. https://doi.org/10.1016/j.neuron.2008.04.009
2. Chen, X. (2020), 'OXTR methylation modulates exogenous oxytocin effects on human brain activity during social interaction', Genes, Brain and Behavior, vol. 19, no. 1, e12555. https://doi.org/10.1111/gbb.12555
3. Ide, J. S. (2018), 'Oxytocin attenuates trust as a subset of more general reinforcement learning, with altered reward circuit functional connectivity in males', Neuroimage, no. 174, pp. 35-43. https://doi.org/10.1016/j.neuroimage.2018.02.035
4. Kogan, A. (2011), 'Thin-slicing study of the oxytocin receptor (OXTR) gene and the evaluation and expression of the prosocial disposition', Proceedings of the National Academy of Sciences, vol. 108, no. 48, pp. 19189-19192. https://doi.org/10.1073/pnas.1112658108
5. Kosfeld, M. (2005), 'Oxytocin increases trust in humans', Nature, vol. 435, no. 7042, pp. 673-676. https://doi.org/10.1038/nature03701
6. Nave, G. (2015), 'Does oxytocin increase trust in humans? A critical review of research', Perspectives on Psychological Science, vol. 10, no. 6, pp. 772-789. https://doi.org/10.1177/1745691615600138

Poster No 835

Interpersonal Support, Functional Brain Architecture, and Internalizing Symptoms during Adolescence

Sunghyun Hong[1], Cleanthis Michael[1], Felicia Hardi[1], Scott Tillem[1], Jeanne Brooks-Gunn[2], Vonnie McLoyd[1], Colter Mitchell[1], Luke Hyde[1], Christopher Monk[1]

[1]University of Michigan, Ann Arbor, MI, [2]Columbia University, New York, NY

Introduction: Interpersonal support is the perceived ability to receive desired support through social connections. Interpersonal support buffers against the negative effects of stress and contributes to overall psychological well-being. While there is preliminary work linking interpersonal support to the functional activation of various brain regions, it is unknown how interpersonal support relates to the overall functional organization of the brain. This study investigated the association between interpersonal support and functional brain organization in adolescence and how these networks are related to internalizing symptoms, which become more prevalent during this developmental period.

Methods: The study included 173 adolescents from the Future of Families and Child Wellbeing Study, a population-based study. Interpersonal support was measured using the Interpersonal Support Evaluation List, while depressive and anxiety symptoms were assessed using the Center for Epidemiologic Studies Depression Scale and Brief Symptom Inventory 18. We measured functional brain architecture by integrating resting-state and task-based scans (with task effects regressed out), generating 20+ minutes of 'pseudo-rest' fMRI data to enhance metric reliability. Weighted, undirected graphs were constructed to examine three whole-brain level metrics: global efficiency (integration), modularity (segregation), and small-world propensity (segregation-integration balance). Several demographic covariates (e.g., sex, household income, and

puberty status) and head motion during scanning were included. Multiple path analyses were conducted. First, we examined the association between youth interpersonal support and network metrics while controlling for covariates. Subsequently, we investigated associations between network metrics and depression, as well as network metrics and anxiety, while controlling for covariates. In an exploratory analysis, a single model included interpersonal support, depression, anxiety, and covariates as predictors of network metrics, considering the influences of current depressive and anxiety symptoms on perceived support. False discovery rate correction was applied, and Full Information Maximum Likelihood was used to handle missing data.

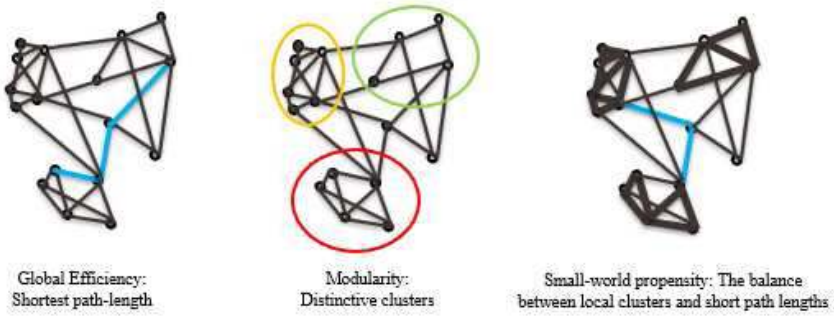

Graph Analysis Network Metrics. Weighted, undirected graphs were constructed to examine three whole-brain level metrics—global efficiency (integration), modularity (segregation), and small-world propensity (segregation-integration balance). The figure provides a visual representation of each metric.

Results: Higher youth interpersonal support was associated with reduced global efficiency (β=-0.178, padj=0.026) and small-world propensity (β=-0.225, padj=0.009), with no association found for modularity (β=-0.048, padj=0.496). Reduced global efficiency and small-world propensity were linked to decreased levels of anxiety (β=0.202, padj=0.018; β=0.261, padj=0.003). Small-world propensity was also associated with decreased levels of depression (β=0.256, padj=0.003). Additionally, the relationship between interpersonal support and global efficiency (β=-0.168, padj=0.042), as well as small-world propensity (β=-0.186, padj=0.042), remained significant even after adjusting for depression, anxiety, and covariates.

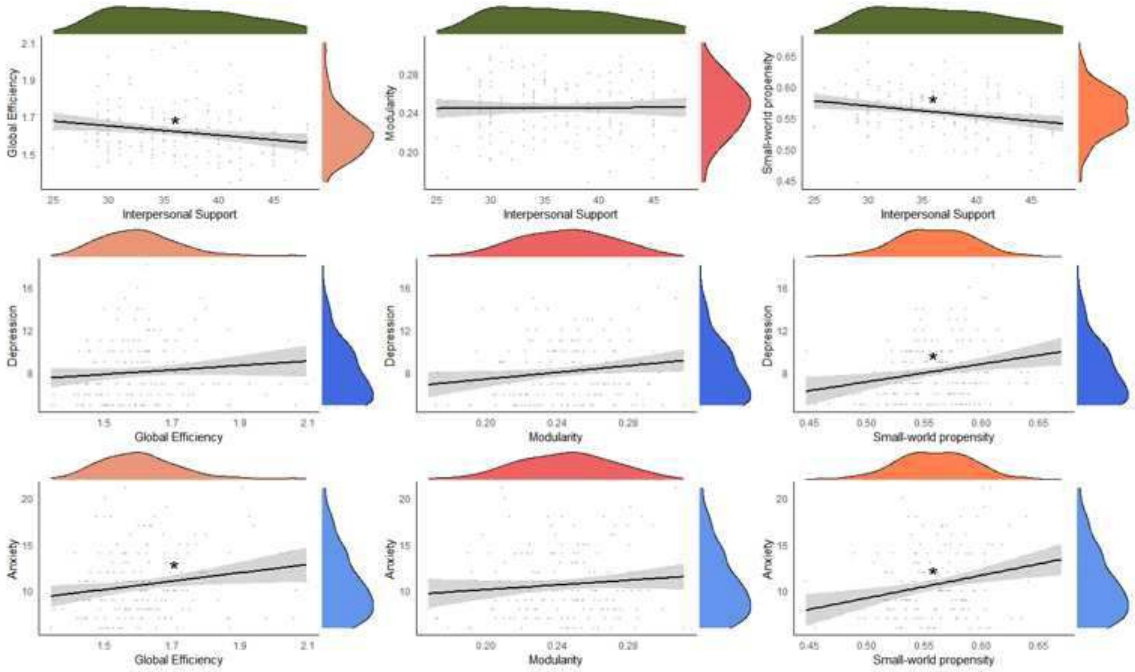

Associations between interpersonal support and network metrics, as well as between network metrics and internalizing symptoms. Significant associations are marked with asterisks. The distributions for each variable are presented above the graph.

Conclusions: A higher level of interpersonal support was associated with lower global efficiency and small-world propensity, suggesting less efficient information flow and a less optimal balance between integration and segregation. These topological alterations were, in turn, linked to lower anxiety (for both global efficiency and small-world propensity) and depression (for small-world propensity only). These findings suggest that interpersonal support-linked neural changes may be adaptive for mental health in youth. While our cross-sectional analyses cannot directly address developmental pace, the results

suggest that having a higher level of interpersonal support may be associated with a more protracted pace of functional neurodevelopment. We are currently following up with participants at age 22 to assess the longitudinal implications of our findings on changes in social conditions, network metrics, and psychological well-being during their transition to young adulthood.

References

1. Bassett, D. S. (2017). Network neuroscience. Nature neuroscience, 20(3), 353-364.
2. Cho, J. W. (2021). Impact of concatenating fMRI data on reliability for functional connectomics. Neuroimage, 226, 117549.
3. Cohen, S. (1985) Stress, social support, and the buffering hypothesis. Psychological Bulletin, 98(2), 310-357,
4. Fair D.A. (2007) A method for using blocked and event-related fMRI data to study "resting state" functional connectivity. NeuroImage. 35 (1) 396-405.
5. Gong, Q. (2015). Depression, neuroimaging and connectomics: a selective overview. Biological Psychiatry, 77(3), 223-235.
6. Gunnar, M. R. (2015) Parental buffering of fear and stress neurobiology: Reviewing parallels across rodent, monkey, and human models. Social neuroscience, 10(5), 474–478.
7. Holz, N. E. (2020) Resilience and the brain: a key role for regulatory circuits linked to social stress and support. Molecular psychiatry, 25(2), 379-396.
8. Kraus, B. T. (2021). Network variants are similar between task and rest states. Neuroimage, 229, 117743.
9. Power, J. D. (2010) The development of human functional brain networks. Neuron, 67(5), 735-748.

Poster No 836

Neurobiological Consequences of Racism: Exploring Accelerated Brain Aging in Black Americans

Gabriella Alvarez[1]

[1]*University of Pittsburgh, Pittsburgh, PA*

Introduction: As individuals age, the human brain undergoes structural changes, such as volume reductions and cortical thinning (de Lange et al., 2020). These alterations are linked to cognitive decline and an increased risk of neurodegenerative disorders. While senescent brain deterioration is recognized, there is considerable variation in neurobiological aging trajectories among older populations, prompting neuroimaging studies to explore potential markers for brain aging. In the context of racial disparities observed in brain-related diseases, especially Alzheimer's in Black populations (Babulal et al., 2018), researchers suggest that socioeconomic status (SES) may underlie racial differences in brain aging. However, the potential role of racism, a unique societal stressor experienced by marginalized populations, in influencing neurobiological aging remains underexplored. This study addresses this gap by investigating links between racism exposure and brain aging in Black Americans, examining predicted brain age as a biomarker. Leveraging brain-age estimation methods, we explore associations while controlling for relevant covariates.

Methods: Seventy-two Black American participants from the Midlife in the United States (MIDUS) dataset underwent a multi-stage assessment, completing discrimination exposure questionnaires and MRI scans. Discrimination exposure was measured comprehensively, and a composite score was derived. MRI scans occurred 9 months to 20 years post-questionnaire, providing high-resolution images for brain age estimation using the BrainageR package. Regression analyses explored the association between discrimination exposure and brain age, controlling for age, SES, and gender. The study also examined robustness to confounders and the impact of the time between survey and MRI on the discrimination exposure and brain age gap association.

Results: Participant's ages ranged from 26.66-75.33 years (M=54.42, SD=12.53). Analyses revealed a significant main effect of discrimination exposure on brain age (b=4.59, SE=1.476, p=0.003), indicating that discrimination exposure was associated with accelerated brain age. This effect remained statistically significant after controlling for chronological age, SES, and gender. Gender differences revealed decelerated brain age in Black women (b=-5.836, SE=1.705, p=0.001). The time elapsed between survey completion and MRI scan significantly moderated the association between discrimination exposure and brain age gap (b=-1.957, SE=6.227, p=0.003). Specifically, simple slope analyses revealed a positive association between discrimination exposure and accelerated brain age among participants with a shorter lag between survey and MRI completion (b=4.73, se=1.70, p=0.01) while those with a longer lag demonstrated decelerated brain aging (b=-5.72 years, se=2.20, p=0.01). Associations between discrimination exposure and brain age remained robust even after accounting for potential confounders related to discrimination and aging, including symptoms of depression, anxiety, education, income, and neuroticism. Interestingly, neuroticism demonstrated a unique and negative association with brain age in this sample such that greater levels of neuroticism were associated with decelerated brain age (b=-1.957, se=3.67, p=0.001).

Conclusions: This study provides compelling evidence of an association between discrimination exposure and accelerated brain aging in Black Americans. The temporal dynamics unveiled in our analysis, introduces a novel dimension to the

understanding of this relationship. This temporal sensitivity suggests that the impact of discrimination on brain aging may not be static and may evolve over time, demanding a nuanced examination of the temporal aspects in future investigations. Future research should explore the intricate interplay of sociodemographic, psychosocial, and neurobiological factors to inform targeted interventions for mitigating discrimination's adverse effects on brain health in vulnerable populations.

References

1. Babulal, G. M., Quiroz, Y. T., Albensi, B. C., Arenaza-Urquijo, E. M., Astell, A., Babiloni, C., ... & O'Bryant, S. (2018). Perspectives on ethnic and racial disparities in alzheimer's disease and related dementias: update and areas of immediate need. Alzheimer's &Amp; Dementia, 15(2), 292-312. https://doi.org/10.1016/j.jalz.2018.09.009
2. Cole JH, Poudel RPK, Tsagkrasoulis D, Caan MWA, Steves C, Spector TD et al. Predicting brain age with deep learning from raw imaging data results in a reliable and heritable biomarker. NeuroImage 2017; 163C: 115-124.
3. de Lange, A. G., Anatürk, M., Suri, S., Kaufmann, T., Cole, J. H., Griffanti, L., Zsoldos, E., Jensen, D. E. A., Filippini, N., Singh-Manoux, A., Kivimäki, M., Westlye, L. T., & Ebmeier, K. P. (2020). Multimodal brain-age prediction and cardiovascular risk: The Whitehall II MRI sub-study. NeuroImage, 222, 117292. https://doi.org/10.1016/j.neuroimage.2020.117292
4. Franke, K. and Gaser, C. (2019). Ten years of brainage as a neuroimaging biomarker of brain aging: what insights have we gained?. Frontiers in Neurology, 10. https://doi.org/10.3389/fneur.2019.00789

Poster No 837

Neural Correlates of the Behavioral Immune System: An fMRI Study

Jeyoon Choi[1], Motoaki Sugiura[2]

[1]Tohoku University, Sendai, Miyagi, [2]Institute of Development, Aging and Cancer, Tohoku University, Sendai, Miyagi

Introduction: The Behavioral Immune System hypothesis posits that evolutionary pressures to avoid infections have profoundly influenced human behavior, particularly in shaping social dynamics. Prior research has explored the connections between disease threat perceptions and collectivistic social attitudes, delving into the behavioral aspects of fear and collectivism in response to health threats, as well as the impact of cultural collectivism on pandemic responses[1-4]. However, the exploration of these relationships has largely been confined to the behavioral level, leaving a significant gap in our understanding of the neural mechanisms at play. Specifically, how the brain processes pre-existing collectivist orientations and their adaptations in response to perceived infection threats is yet to be fully elucidated. Our study, utilizing functional Magnetic Resonance Imaging (fMRI), aimed to explore two key aspects: (1) investigating how pre-existing collectivist orientations are reflected in brain responses to infection-related stimuli; and (2) examining specific brain areas in relation to changes in collectivism as a result of exposure to these stimuli.

Methods: Our research focused on two primary objectives. The first was to map brain activation patterns in participants with varying degrees of collectivist orientations when presented with infection-related stimuli. The second objective was to track alterations in brain activity correlating with changes in collectivist attitudes following exposure to these stimuli. We recruited 55 participants to explore the neural correlates of collectivism in response to perceived infection threats. During the MRI task, participants were exposed to 'infection' and 'neutral' images, designed to elicit infection-related emotional responses and serve as controls, respectively. Each participant underwent two sessions, each consisting of 20 trials, where they rated their emotional reactions-disgust, fear, and infection concern-using a 4-point Likert scale. We also administered questionnaires to measure "Perceived Vulnerability to Disease"[5] and "Horizontal-Vertical Collectivism and Individualism"[6] before and after the MRI sessions.

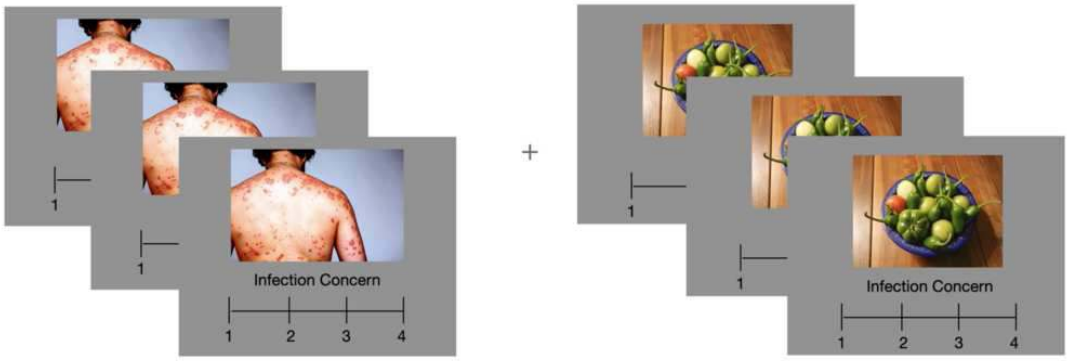

Figure 1. Example of the fMRI task

Results: In our fMRI analysis, we identified specific neural responses aligned with our research objectives. Addressing the first research purpose, we discovered a negative correlation between participants' pre-task collectivism scores and neural activity

in key areas: notably, the right inferior frontal gyrus and insula. This suggests that individuals with higher collectivism scores exhibit distinct neural patterns when processing infection-related stimuli. For the second research purpose, we observed that changes in collectivism scores corresponded with significant alterations in brain activity. These changes were particularly evident in the calcarine, cuneus, and right fusiform area, indicating a neural basis for the adaptation of collectivist orientations in response to perceived infection threats.

Conclusions: This study illuminates the neural underpinnings of the behavioral immune system, particularly highlighting how collectivism influences brain responses to infection threats. Our findings indicate that higher collectivist orientations are associated with reduced neural activity in the right inferior frontal gyrus and insula, suggesting an inhibitory cognitive and emotional response to health threat. Furthermore, shifts in collectivism scores were linked to changes in neural activity within the calcarine, cuneus, and right fusiform area, suggesting an adaptive neural mechanism in response to infection threats, potentially involving visual-emotional integration. These insights are pivotal for understanding the neural basis of cultural orientations like collectivism and their impact on health-related decision-making. Future research should delve into how these neural responses translate into behavioral outcomes and their long-term effects on health behavior in various cultural setting.

References

1. Benjamin J. M et al., (2023), 'What Activates the Behavioral Immune System During a Global Pandemic? Testing the Disgust Calibration Hypothesis.', Evolutionary Psychological Science volume 9, pages 356–371
2. Fukukawa, Y. et al., (2014), 'Development of a Japanese version of the Perceived Vulnerability to Disease Scale.', The Japanese Journal of Psychology, 85(2), 188–195.
3. Triandis, H.C., & Gelfand, M.J. (1998). 'Converging measurement of horizontal and vertical individualism and collectivism.', Journal of Personality and Social Psychology, 74(1), 118-128.
4. Thornhill, R. et al., (2014), 'The parasite-stress theory of sociality, the behavioral immune system, and human social and cognitive uniqueness.', Evolution and Human Behavior, 35(5), 376-388.
5. Tybur, J.M. et al., (2020), 'Preregistered Direct Replication of 'Sick Body, Vigilant Mind: The Biological Immune System Activates the Behavioral Immune System'.', Psychological Science, 31(10), 1241–1253.
6. Schaller, M. & Justin H, P. (2011), 'The Behavioral Immune System (and Why It Matters).', Current Directions in Psychological Science, 20(2), 99-103.

Poster No 838

Neural representations in MPFC and Insula encode individual differences in preference estimation

Hyeran Kang[1], Kun Il Kim[1], Jinhee Kim[1], Hackjin Kim[1]

[1]Korea University, Seoul, Korea, Republic of

Introduction: In human society, successful social interactions hinge on appropriate reactions achieved through accurate estimation of other's perspectives, often necessitating the consideration of contextual information. The study delves into the neural mechanism underpinning this cognitive capacity, employing a preference estimation task.

Methods: Task-based functional MRI data were collected using the 3T Siemens Trio scanner while 38 healthy female participants performed the preference estimating task. In this task, participants, upon seeing the target's face, were tasked with predicting the extent to which the target would prefer a given item. Preference estimation accuracy is quantified by the percentage of correct guesses, aligning with the target's preferences on a 4-point Likert scale. In the first-level, preprocessed functional images were modeled using a general linear model, incorporating the self-trial and the target-trial at the face and item phase. In the group-level, we adapted both univariate and multivariate approach to reveal the neural activity as well as the neural representation associated with the individual difference in preference estimation. In univariate approach, to identify brain regions associated with individual preference estimation accuracy, we performed a linear regression analysis with individual accuracy score as covariates. In multivariate approach, to identify brain regions associated with variability in preference estimation accuracy, we performed inter-subject representational similarity analysis (IS-RSA).

Results: Univariate findings reveal the involvement of subregions of the medial prefrontal cortex (mPFC) in precisely assessing others' preferences. Multivariate results, utilizing inter-subject representational similarity analysis (IS-RSA), demonstrate that the multi-voxel patterns in the pregenual anterior cingulate cortex (pgACC) and the anterior insula (AI) predict individual variability in preference estimation accuracy. This implies that the diverse behavioral patterns among participants in inferring others' preferences were mirrored in the multivariate neural representations in these areas, both of which are strongly associated with individual differences in interoception and context-dependent ambiguous facial emotion estimation.

Conclusions: The present study suggests that the mPFC and AI play a pivotal role in accurately estimating others' preferences with minimal information. The application of multivariate pattern analysis unveils insights beyond the scope of traditional approaches, shedding light on the intricate neural processes involved in this social cognitive task.

Acknowledgements
This research was supported by the Bio & Medical Technology Development Program of the National Research Foundation (NRF) funded by the Korean government (MSIT) (No. 2022M3E5E8018285; No. RS-2023-00218987).

Poster No 839

How does a 4-day working week change default mode network connectivity?

Magdalena Pfaff[1], Joanna McLaren[21], Sinéad Moore[1], Chris Racey[1], Samira Bouyagoub[2], Daniel Campbell-Meiklejohn[1], Sarah Garfinkel[3], Charlotte Rae[1]

[1]University of Sussex, Brighton, Sussex, [2]Brighton and Sussex Medical School, Brighton, Sussex, [3]University College London, London, Greater London

Introduction: The Default Mode Network (DMN) is associated with daydreaming, meditation, thoughts related to the self, or episodic memories related to the self (Vessel, et al., 2013) and is comprised of dorsal medial prefrontal cortex, the medial and lateral parietal, and the lateral temporal cortices (Raichle, et al., 2015). Connectivity within the DMN is influenced by many factors, such as sleep, exercise, mental health, stress, or lifestyle (Krause, et al., 2017, Schiller, et al., 2018) which are often affected by occupational demands such as working hours and the maintenance of a work/life balance (Holt-Gosselin et al., 2021). This research investigated how working patterns influence the connectivity of the DMN during resting state, by studying full-time employees switching from a 5-day working week to a 4-day working week, with no loss of salary. We hypothesised that reducing time at work would increase connectivity within the DMN, given previous research finding that lifestyle can change resting-state networks.

Methods: In this study, 35 participants shifted from a 5-day to a 4-day work week whilst retaining their salary. The participants were scanned with a 3T Siemens Prisma, using Human Connectome Project (HCP) resting-state fMRI acquisition protocols (15 minutes total fMRI duration) at baseline (while still working 5 days), and then again after a 12-week trial of working 4 days a week. Additional scans were collected using HCP protocols (T1, T2, task fMRI), which were used for HCP multi-modal preprocessing. Data were preprocessed using HCP multi-modal pipelines, with further normalization of the fMRI timeseries to MNI space, for further statistical analysis in the CONN toolbox. Using region of interest (ROI) to ROI analysis, we investigated the changes in DMN connectivity pre- compared to post-4-day work week trial, using the dorsal Default Mode Network template provided by Shirer et al (2012).

Results: DMN connectivity showed no significant difference between pre- and post-4-day work week trial, $T(34)= -1.87$, $p = 0.070$ for global efficiency and 0.051 for local efficiency. However, a trend towards stronger DMN connectivity was observed post 4-day week, compared to the 5-day week.

Conclusions: Time spent at work may influence brain connectivity, potentially underpinning changes to wellbeing and performance at work (Collewet, & Sauermann, 2017), but we did not observe significant effects of a 4-day week on the DMN, in our present sample. Research shows that stress levels significantly reduce in a 4-day week (Schiller, et al., 2018). Experiencing more stress is associated with higher cortisol levels, which substantially lowers DMN connectivity (Zeev-Wolf, et al., 2019). Sleep has also been found to improve in a 4-day work week (Schiller, et al., 2018) and to alter DMN connectivity, where sleep deprivation leads to reduced DMN connectivity (Krause, et al., 2017). Thus, via different mechanisms, DMN connectivity could increase in a 4-day week. While not significant here, we can see a clear trend. Recruitment is continuing to investigate how sub-groups may respond differently to the work time reduction.

References

1. Collewet, M., & Sauermann, J. (2017). Working hours and productivity. Labour economics, 47, 96-106. https://doi.org/10.1016/j.labeco.2017.03.006
2. Holt-Gosselin, B., Keller, A., Chesnut, M., & Williams, L. (2021). Default Mode Network Moderates the Relationship Between Lifestyle Changes and Natural Improvements in Clinical Symptoms Over Time in Untreated Participants. Biological Psychiatry, 89(9), S111. https://doi.org/10.1016/j.biopsych.2021.02.287
3. Krause, A. J., Simon, E. B., Mander, B. A., Greer, S. M., Saletin, J. M., Goldstein-Piekarski, A. N., & Walker, M. P. (2017). The sleep-deprived human brain. Nature Reviews Neuroscience, 18(7), 404-418. https://doi.org/10.1038/nrn.2017.55
4. Raichle, M. E. (2015). The brain's default mode network. Annual review of neuroscience, 38, 433-447. https://doi.org/10.1146/annurev-neuro-071013-014030
5. Schiller, H., Lekander, M., Rajaleid, K., Hellgren, C., Åkerstedt, T., Barck-Holst, P., & Kecklund, G. (2018). Total workload and recovery in relation to worktime reduction: a randomised controlled intervention study with time-use data. Occupational and environmental medicine, 75(3), 218-226. http://dx.doi.org/10.1136/oemed-2017-104592
6. Soares, J. M., Marques, P., Magalhaes, R., Santos, N. C., & Sousa, N. (2017). The association between stress and mood across the adult lifespan on default mode network. Brain Structure and Function, 222, 101-112. https://doi.org/10.1007/s00429-016-1203-3

7. Vessel, E. A., Starr, G. G., & Rubin, N. (2013). Art reaches within: aesthetic experience, the self and the default mode network. Frontiers in neuroscience, 7, 258. https://doi.org/10.3389/fnins.2013.00258
8. Zeev-Wolf, M., Levy, J., Goldstein, A., Zagoory-Sharon, O., & Feldman, R. (2019). Chronic early stress impairs default mode network connectivity in preadolescents and their mothers. Biological Psychiatry: Cognitive Neuroscience and Neuroimaging, 4(1), 72-80. https://doi.org/10.1016/j.bpsc.2018.09.009

Poster No 841

Rehumanizing the dehumanized: Neural responses for the unhoused using dimension-based rehumanization

Akila Kadambi[1,2,3], Sofronia Ringold[1,3], Aditya Jayashankar[1,3], Nandita Raman[1,3], Shruti Kamath[1,3], Srini Narayanan[4], Antonio Damasio[1], Jonas Kaplan[1], Lisa Aziz-Zadeh[1,3]

[1]Brain and Creativity Institute, University of Southern California, Los Angeles, CA, [2]Psychiatry and Biobehavioral Sciences, UCLA, Los Angeles, CA, [3]USC Mrs. T.H. Chan Division of Occupational Science, Los Angeles, CA, [4]Google DeepMind, Zurich

Introduction: Despite our need for societal inclusion and empathy, dehumanization is an affliction of society that undermines humanity. Functional neuroimaging (fMRI) studies show that unhoused individuals are prevalently dehumanized (Tan & Harris, 2021). Viewing pictures of unhoused individuals evokes neural activity commonly associated with disgust and reduced mentalizing (Harris & Fiske, 2006). In contrast, observing high status groups (e.g., white, middle class) evokes neural activity associated with positive humanized feelings, including increased activity in mentalizing and somatomotor regions relative to viewing unhoused individuals (Harris & Fiske, 2009). Whether it is possible to re-engage neural circuits to rehumanize the unhoused, and what dimensions may be particularly relevant, remains unknown. To this aim, we conducted an fMRI study to rehumanize perceptions of unhoused individuals, aimed at revealing informative dimensions for rehumanization and their neural correlates.

Methods: 34 American participants (Mage = 21.81 ± 3.34; range: 18 - 33) from the Los Angeles area participated in the study. fMRI data was collected on a 3T Siemens MAGNETOM Prisma scanner in a block design across 3 runs. Standard preprocessing was applied using FSL software library. In the first run, participants viewed pictures of unhoused and high status groups to collect baseline neural responses to each group. In the next run, different dimensions of rehumanization were measured across 6 blocks, repeated 3 times. In each block, participants viewed a picture of an unhoused individual and read text associated with the following dimensions: (1) self-similarity (e.g., “they like Beyonce” [tailored to participant responses collected prior to the scan]); (2) universalism (e.g., “they’re someone’s sister”); (3) motor simulation (e.g., “imagine them running”); (4) warmth (e.g., “they smile often”); (5) competence (e.g., “expert chess player”). All dimensions were compared to control blocks in which participants responded whether a dot was present on the photograph of the unhoused person. In the last run, participants viewed new pictures of unhoused and high status individuals.

Results: Using general linear modeling implemented in FSL FEAT, we compared changes in baseline neural activity between pre- and post- rehumanization runs for each group (cluster corrected, $Z > 2.3$, $p < .01$). While we found no change in neural activity for high status groups, for unhoused individuals after rehumanization, we found increased activity in regions associated with increased humanization, spanning bilateral somatomotor cortex, parietal operculum, inferior parietal lobe, and middle temporal gyri (MTG), relative to baseline. No significant activity was found in the reverse direction (pre>post rehumanization). Additionally, we found robust activity for self-similarity, universalism, motor simulation, and competence dimensions versus the control block. Self-similarity elicited bilateral activity across the entire mentalizing network: ventral and dorsomedial prefrontal cortices (vmPFC, dmPFC), anterior cingulate cortices, temporal pole, precuneus, parahippocampal gyri, hippocampi (HC), MTG, and sparse activity in the occipital pole and lateral occipital cortices. Similar activity was found for universalism across mentalizing regions, spanning the mPFC and left MTG. For motor simulation, activity was localized primarily to left somatomotor regions spanning the supplementary motor area, as well as a few clusters in the vmPFC and bilateral HC. Activity for competence was found in bilateral mentalizing regions including the vmPFC, MTG, HC, central operculum, and the right precentral gyrus.

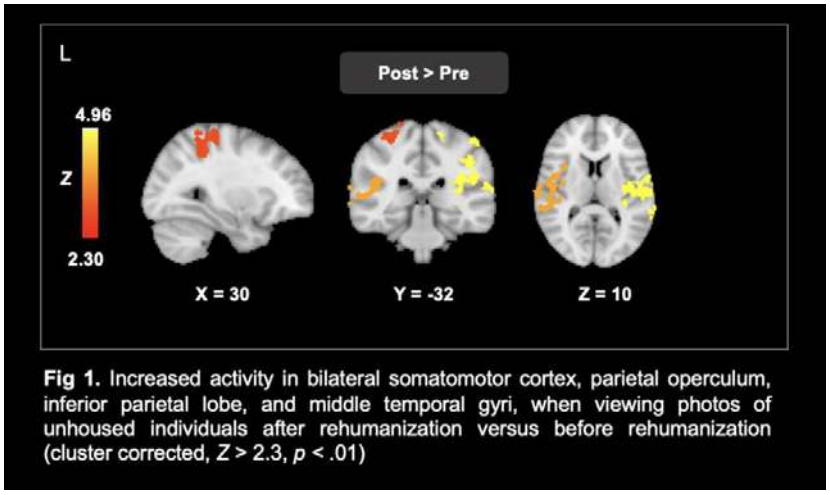

Fig 1. Increased activity in bilateral somatomotor cortex, parietal operculum, inferior parietal lobe, and middle temporal gyri, when viewing photos of unhoused individuals after rehumanization versus before rehumanization (cluster corrected, $Z > 2.3$, $p < .01$)

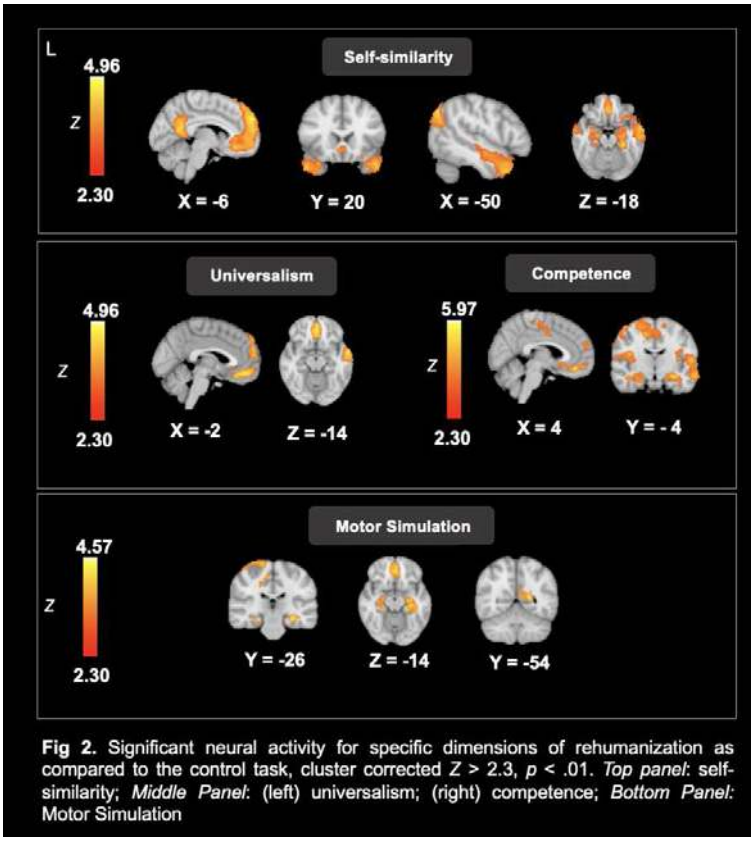

Fig 2. Significant neural activity for specific dimensions of rehumanization as compared to the control task, cluster corrected $Z > 2.3$, $p < .01$. *Top panel*: self-similarity; *Middle Panel*: (left) universalism; (right) competence; *Bottom Panel:* Motor Simulation

Conclusions: Together, the results suggest that neural activity for dehumanized groups can be positively altered following a rehumanization intervention. Self-similarity, universalism, competence, and motor simulation appear to be promising dimensions for rehumanization.

References

1. Harris, L. T (2006). Dehumanizing the lowest of the low: Neuroimaging responses to extreme out-groups. Psychological science, 17(10), 847-853.
2. Harris, L. T (2009). Social neuroscience evidence for dehumanised perception. European review of social psychology, 20(1), 192-231.
3. Tan, N (2021). The Neuroscience Underlying Dehumanised Perception Towards People Who Are Homeless. In Proceedings of the British Academy. Oxford University Press.

Poster No 842

An fMRI Examination of Ballet Dance Styles using Intersubject Correlation (ISC) and a Motion Index

Frank Pollick[1], Naree Kim[2], Donald Glowinski[3], Jukka-Pekka Kauppi[4], Antonio Camurri[5], Jussi Tohka[4], Seon Hee Jang[2]

[1]University of Glasgow, Glasgow, UK, [2]Sejong University, Seoul, Republic of Korea, [3]University of Geneva, Geneva, Switzerland, [4]University of Eastern Finland, Kuopio, Finland, [5]University of Genoa, Genoa, Italy

Introduction: While much is known about the neural basis of action perception, less is known about the processing of more complex aspects of action interpretation. Actions can be performed in different styles and these stylistic differences can convey meaning (Pollick et al. 2001; Chen, Pollick, and Lu 2023). Ballet provides an example of a corpus of actions that can be performed according to different stylistic guidelines (Jang and Pollick 2011). In this research we used fMRI to investigate brain responses to viewing short segments of ballet performed in classical, romantic and modern ballet styles. Dance theory would suggest that these different styles would produce different subjective impressions. Specifically, classical ballet emphasises form while romantic ballet emphasises emotion and embodiment. We were interested in whether differences in brain processing would be obtained.

Methods: Dance stimuli were black and white videos without audio of 3 ballet dances with the face blurred out, each 90 second in duration performed by the same skilled ballerina, starting and ending in the same posture. For each clip a measure of the Motion Index of the dancer (Noble et al. 2014; Lillywhite et al. 2022) was calculated. The three dance pieces were chosen on the basis that each should be representative of its genre and included Odette's solo in Act II of Swan Lake for Classical ballet, the female solo dance from Agon for Modern ballet, and Giselle's solo dance in Act II of Giselle for Romantic ballet. These three dances were termed Classical, Modern and Romantic. Eighteen dance-naïve individuals (8 males, 10 females) participated in the study and viewed all three ballet dance videos while being scanned. Presentation order of the clips was counterbalanced across participants. Brain data were acquired during stimulus presentation using a 3T Tim Trio Siemens scanner with a TR of two seconds, resulting in 45 volumes of each dance used in subsequent analyses. Preprocessing included 3D motion correction, high pass filtering set to one cycle, and normalization of the data into Talairach space. Data analysis was performed using BrainVoyager and the ISC Toolbox (Kauppi, Pajula, and Tohka 2014; Hasson et al. 2004). Analyses included calculation of ISC maps, and comparison of ISC maps as well as examination of the Motion Index as a predictor in the general linear model (Noble et al. 2014).

Results: ISC analysis was performed on each dance clip individually, and all dances revealed ISC in occipital, temporal and parietal areas, while only Romantic and Classical dance clips revealed ISC in frontal cortex. The greatest volume of ISC was found for the Romantic dance clip, and this was due primarily to greater ISC in a large occipitotemporal cluster as well as several clusters in frontal cortex. Statistical comparison of ISC maps (Herbec et al. 2015) revealed several differences. Notably, Classical dance obtained greater ISC than Romantic in lingual gyrus while Romantic dance had greater ISC than Classical in cuneus, precuneus and inferior parietal cortex. Results from using the Motion Index as a predictor showed an overlapping region for all three dances in bilateral occipitotemporal cortex, as well as activity in fusiform gyrus for Classical dance and lingual gyrus for Modern dance.

Conclusions: Results showed that for the prototypical ballet dance segments chosen, there were differences between styles found in both ISC maps and Motion Index results. Broadly speaking, and with a focus on Classical and Romantic dance, these results speak toward greater processing of the Classical ballet segment in ventral regions and greater processing of the Romantic ballet segment in dorsal regions. These results provide a first indication that the neural processing of different dance styles can be identified and could form a basis for aesthetic interpretation. Generalising these results past dance reveals the potential to design brain response to viewed movement that could be useful in rehabilitation.

References

1. Chen, Yi-Chia, Frank Pollick, and Hongjing Lu. 2023. 'Aesthetic Preferences for Prototypical Movements in Human Actions'. Cognitive Research: Principles and Implications 8 (1): 55. https://doi.org/10.1186/s41235-023-00510-0.
2. Hasson, Uri, Yuval Nir, Ifat Levy, Galit Fuhrmann, and Rafael Malach. 2004. 'Intersubject Synchronization of Cortical Activity During Natural Vision'. Science 303 (5664): 1634–40. https://doi.org/10.1126/science.1089506.
3. Herbec, Aleksandra, Jukka-Pekka Kauppi, Corinne Jola, Jussi Tohka, and Frank E. Pollick. 2015. 'Differences in fMRI Intersubject Correlation While Viewing Unedited and Edited Videos of Dance Performance'. Cortex 71 (October): 341–48. https://doi.org/10.1016/j.cortex.2015.06.026.
4. Jang, Seon Hee, and Frank E Pollick. 2011. 'Experience Influences Brain Mechanisms of Watching Dance'. Dance Research 29 (supplement): 352–77. https://doi.org/10.3366/drs.2011.0024.
5. Kauppi, Jukka-Pekka, Juha Pajula, and Jussi Tohka. 2014. 'A Versatile Software Package for Inter-Subject Correlation Based Analyses of fMRI'. Frontiers in Neuroinformatics 8. https://www.frontiersin.org/articles/10.3389/fninf.2014.00002.

6. Lillywhite, Amanda, Dewy Nijhof, Donald Glowinski, Bruno L. Giordano, Antonio Camurri, Ian Cross, and Frank E. Pollick. 2022. 'A Functional Magnetic Resonance Imaging Examination of Audiovisual Observation of a Point-Light String Quartet Using Intersubject Correlation and Physical Feature Analysis'. Frontiers in Neuroscience 16 (September): 921489. https://doi.org/10.3389/fnins.2022.921489.
7. Noble, Katie, Donald Glowinski, Helen Murphy, Corinne Jola, Phil McAleer, Nikhil Darshane, Kedzie Penfield, Sandhiya Kalyanasundaram, Antonio Camurri, and Frank E. Pollick. 2014. 'Event Segmentation and Biological Motion Perception in Watching Dance'. Art & Perception 2 (1–2): 59–74. https://doi.org/10.1163/22134913-00002011.
8. Pollick, Frank E, Helena M Paterson, Armin Bruderlin, and Anthony J Sanford. 2001. 'Perceiving Affect from Arm Movement'. Cognition 82 (2): B51–61. https://doi.org/10.1016/S0010-0277(01)00147-0.

Poster No 843

Confound regression models for intersubject correlation analysis with naturalistic stimuli

Samuel Nastase[1], Uri Hasson[1]

[1]*Princeton University, Princeton, NJ*

Introduction: Intersubject correlation (ISC) analysis has become a workhorse method for measuring shared, stimulus-evoked neural activity in naturalistic paradigms (Hasson et al., 2004; Nastase et al., 2019). In ISC analysis, we use one subject's (or the average of many subjects') brain activity to model another subject's brain activity. This approach effectively isolates synchronized, stimulus-evoked responses and filters out idiosyncratic signals like head motion. How are ISC analyses affected by nuisance signals like head motion and physiological noise? Inspired by related efforts in the resting-state functional connectivity literature (e.g. Ciric et al., 2017; Parkes et al., 2018), we evaluate a variety of confound regression models for mitigating head motion and physiological noise.

Methods: To robustly evaluate different confound models, we used a large sample from the "Narratives" dataset (Nastase et al., 2021): fMRI data for 284 subjects listening to subsets of seven different naturalistic, spoken stories. We used fMRIPrep to minimally preprocess the data and extract a variety of different confound variables (Esteban et al., 2019). For simplicity, we limit our initial analyses to the average time series in early auditory cortex (EAC), which exhibits strong ISC in subjects listening to natural spoken language. We evaluated 20 different confound models ranging from no confound variables (model 0) to models comprising different combinations of head motion (HM), global signal (GS), white matter (WM) and cerebrospinal fluid (CSF) signals, spike censoring, as well as aCompCor and tCompCor components. We evaluated the confound models in two ways: (1) how does confound regression affect ISC in EAC? and (2) how does confound regression affect correlation between ISC and subject-level framewise displacement (FD)?

Model	Confound variables	#
model 0	no confound variables	0
model 1	6 HM	6
model 2	12 HM derivatives	12
model 3	24 HM expansion	24
model 4	1 FD	1
model 5	1 WM, 1 CSF	2
model 6	1 GS	1
model 7	6 HM, 1 WM, 1 CSF	8
model 8	6 HM, 1 WM, 1 CSF, 1 GS	9
model 9	24 HM, 4 WM, 4 CSF expansions	32
model 10	24 HM, 4 WM, 4 CSF, 4 GS expansions	36
model 11	6 tCompCor	6
model 12	10 aCompCor	10
model 13	6 HM, 10 aCompCor	16
model 14	12 HM derivatives, 10 aCompCor	22
model 15	24 HM expansion, 10 aCompCor	34
model 16	24 HM, 4 GS expansions, 10 aCompCor	38
model 17	6 HM, 10 aCompCor, 1 FD	17
model 18	12 HM, 10 aCompCor, 1 FD	23
model 19	6 HM, *k* spike regression	$6 + k$
model 20	24 HM, 4 WM, 4 CSF, 4 GSR expansions, *k* spike regression	$32 + k$

Table 1. Confound regression models. Confound model labels are listed with the corresponding confound variables and the total number of model parameters.

Results: Overall, ISCs were fairly robust across confound models. No confound models reduced ISC, whereas several models increased ISC. Models containing HM, signals from WM/CSF, and GS performed comparably well. We observed that ISCs were negatively correlated with head motion (r = -.183 for model 0): that is, subjects with larger overall head motion had lower ISCs. Several models provide a good compromise: for example, the relatively simple model 13, comprising 6 head motion parameters and 5 aCompCor components from WM and CSF, both significantly improved ISC (from r = .356 to r = .474; t = 22.705, p < .001, FDR) and reduced the negative correlation between ISC and FD (from r = -.258 to r = -.146). We observed qualitatively similar results for other language ROIs (e.g. IFG).

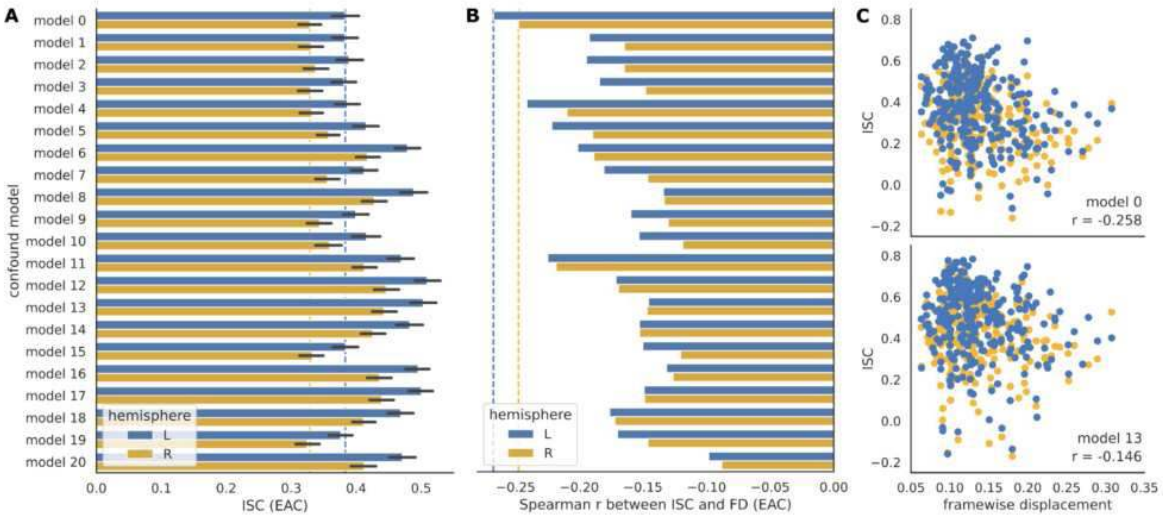

Figure 1. Evaluating confound regression models for ISC analysis. All models were applied to the average time series in left (L) and right (R) hemisphere early auditory cortex (EAC). (**A**) ISC in L (blue) and R (yellow) EAC for all confound models. Vertical dotted lines correspond to the baseline *model 0*, which contains no confound variables. (**B**) Spearman correlation between ISC in EAC and subject-level head motion quantified with framewise displacement (FD) across 284 subjects. (**C**) Correlation between ISC in L (blue) and R (yellow) EAC (*y*-axis) and FD (*x*-axis) across subjects for two example models: *model 0* and *model 13*.

Conclusions: Overall, ISC is fairly robust to head motion. While head motion can artificially inflate e.g. estimates of functional connectivity, ISC analysis is negatively correlated with head motion (more head motion yields lower ISCs). Several relatively simple confound models both improve ISC and mitigate the negative correlation between ISC and head motion.

References

1. Ciric, R. (2017), 'Benchmarking of participant-level confound regression strategies for the control of motion artifact in studies of functional connectivity', NeuroImage, vol. 154, pp. 174–187.
2. Esteban, O. (2019), 'fMRIPrep: a robust preprocessing pipeline for functional MRI', Nature Methods, vol. 16, pp. 111–116.
3. Hasson, U. (2004), 'Intersubject synchronization of cortical activity during natural vision', Science, vol. 303, no. 5664, pp. 1634–1640.
4. Nastase, S. A. (2019), 'Measuring shared responses across subjects using intersubject correlation', Social Cognitive and Affective Neuroscience, vol. 14, no. 6, pp. 667–685.
5. Nastase, S. A. (2021), 'The "Narratives" fMRI dataset for evaluating models of naturalistic language comprehension', Scientific Data, vol. 8, p. 250.
6. Parkes, L. (2018), 'An evaluation of the efficacy, reliability, and sensitivity of motion correction strategies for resting-state functional MRI', NeuroImage, vol. 171, pp. 415–436.

Poster No 844

Daily Family Assistance and Behavioral and Neural Associations of Giving to Others

Jasmine Hernandez[1], Maira Karan[1], Lee Lazar[1], Naomi Eisenberger[1], Adriana Galván[1], Andrew Fuligni[1]

[1]*UCLA, Los Angeles, CA*

Introduction: Family assistance is an essential aspect of family relationships across cultures and contexts exemplified by caring for siblings, running errands, and providing emotional and financial support (Telzer et al., 2010). Family assistance is associated with positive aspects of psychological well-being and giving towards others (Armstrong-Carter & Telzer, 2021). A few studies have suggested an increased differentiation of giving more to familiar others, including the family, than strangers in adolescence (Karan et al., 2022, van de Groep et al., 2022). It is possible that daily family assistance promotes giving

behavior towards the family and that youth who report more daily family assistance exhibit increased giving towards family in comparison to others. At the neural level, giving resources to family at a loss to oneself has been linked with neural activation in regions implicated in cognitive control, social cognition, and reward processing, which undergo significant change during adolescence (Karan et al. 2022). The current study examined the extent to which daily family assistance is associated with adolescents giving resources to others – family, friends, and strangers – at a cost to themselves while imaging brain activation in key regions associated with prosocial behavior in a fMRI scanner. We hypothesized that daily family assistance will be associated with more giving towards caregivers at a cost to oneself in comparison to giving to others, and concomitant neural activation in regions associated with cognitive control, social cognition, and reward processing.

Methods: Data are drawn from the first wave of a longitudinal study of 185 adolescents (Mage = 11.8 years, Range = 9-15 years, 47.8% Female) designed to assess the association between daily family assistance and giving towards family using behavioral and neural data. Participants completed a fMRI decision-making task in which they had the opportunity to give money to caregivers, friends, and strangers. Participants also completed daily diary checklists for 7 days, reporting whether they provided family assistance (i.e., cooking, cleaning, running errands, taking care of siblings) and the amount of time they spent doing so. We used a linear mixed effects model to assess whether giving behavior (denoted by percentage of accepted costly giving trials) varied according to average daily family assistance acts by target (caregiver, friend, stranger). Targets were defined as the within-subject effect and costly giving behavior as the between-subject effect. We then employed bivariate associations between ROIs implicated in cognitive control (dlPFC, vlPFC), social cognition (TPJ), and reward processing (VS, VTA), and average daily family assistance acts.

Results: Results from the linear mixed effects model are presented in Table 1. We found that adolescents who engage in more family assistance acts each day were less likely to give to strangers (b = -0.02, p < .0.04), showing a preference for family and friends (see Figure 1). Further, daily family assistance was unassociated with activation in selected ROIs associated with cognitive control, social cognition, and reward processing.

	Effects of Assistance per Day and Target on Costly Giving Behavior		
Predictors	*Estimates*	*CI*	*p*
(Intercept)	0.54	0.47 – 0.62	**<0.001**
Friend	-0.07	-0.14 – -0.01	**0.015**
Stranger	-0.09	-0.15 – -0.03	**0.005**
Assistance per Day	-0.01	-0.03 – 0.01	0.277
Friend x Assistance per day	0.00	-0.01 – 0.02	0.599
Stranger x Assistance per Day	-0.02	-0.04 – -0.00	**0.039**

Table 1. Linear Mixed Effects Model

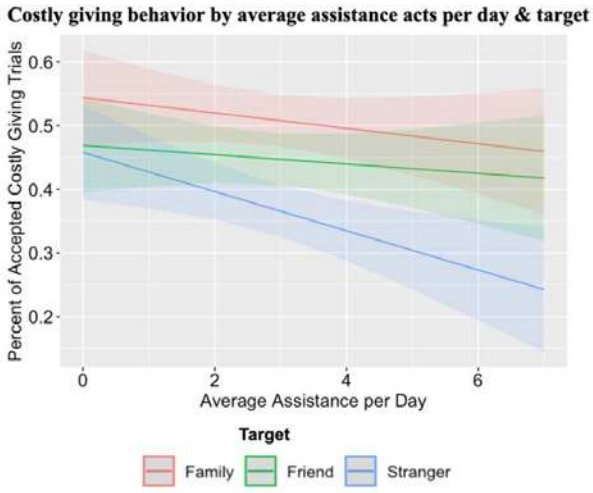

Figure 1. Adolescents who engage in more family assistance acts each day were less likely to give to strangers, showing a preference for family and friends.

Conclusions: We found that daily family assistance acts in adolescence was linked with less giving behavior towards strangers and a greater preference for giving to family and friends, suggesting that this may reflect an in-group bias associated with less prosocial behavior towards unknown others. Although the bivariate associations between the ROI mean activation levels and daily family assistance acts do not reveal significant associations, this suggests the links between daily family assistance and giving towards others may be more complex during adolescence. These results highlight the importance of considering a more nuanced understanding (e.g., functional connectivity between ROIs) of the association between daily family assistance and neural processing while giving to others.

References

1. Armstrong-Carter, E. (2021). Family Assistance Spills Over Into Prosocial Behaviors Toward Friends and Positive Academic Behaviors. Journal of Research on Adolescence, 31(4), 1188–1201. https://doi.org/10.1111/jora.12629
2. Karan, M. (2022). Giving to others and neural processing during adolescence. Developmental Cognitive Neuroscience, 56, 101128. https://doi.org/10.1016/j.dcn.2022.101128
3. Telzer, E. H. (2010). Gaining while giving: An fMRI study of the rewards of family assistance among White and Latino youth. Social Neuroscience, 5(5–6), 508–518. https://doi.org/10.1080/17470911003687913
4. van de Groep, S. (2022). Growing in generosity? The effects of giving magnitude, target, and audience on the neural signature of giving in adolescence. Developmental Cognitive Neuroscience, 54, 101084. https://doi.org/10.1016/j.dcn.2022.101084

Poster No 845

Interoceptive abilities and neural dynamics related to moral intuition aligned with group consensus

JuYoung Kim[1], Hackjin Kim[1]

[1]Korea University, Seoul, Korea, Republic of

Introduction: Moral decision-making is often intuitive, where individuals align their choices with societal norms. Adhering to this sense of moral duty may reduce metabolic costs (Theriault et al., 2021), ultimately enhancing survival. Interoception, the sense of the body's internal state, is crucial in allostatic processes of the brain. However, empirical examination regarding the connection between moral decision-making and an individual's awareness of introspective interoceptive signals has been lacking. Our hypothesis posits that individuals with higher interoceptive sensitivity are more likely to align with prevailing moral norms. Conforming to societal expectations may enhance the predictability of one's social environment, reducing the need for others to revise their expectations of the conformer's intentions or behavior, and ultimately decreasing metabolic expenditure. Consequently, higher interoceptive sensitivity is expected to correlate with a greater propensity to adhere to prevailing moral standards.

Methods: For the online moral dilemma task, 48 scenarios were translated into Korean and assessed for clarity and difficulty by 14 native Korean university students. Participants, acting as protagonists, made binary utilitarian or deontological choices and rated decision difficulty on a Likert scale. Group consensus moral decisions per scenario were determined by majority choice (52 or more participants) and as a continuous ratio of utilitarian decisions. Individual moral tendencies towards group consensus were calculated based on the group consensus moral decisions. Moral similarity was calculated as the ratio of individual's moral decisions matching the group consensus moral decisions, and moral distance was calculated as the Euclidean distance between participants' choices and the group's utilitarian decision ratio. Functional connectivity analysis and a Hidden Markov model explored resting state neural dynamics related to moral alignment with the group. The whole brain functional connectivity of the anterior insula, a region critically involved in processing interoceptive information (Kleckner et al., 2017), was assessed. For the Hidden Markov model, the time series of the brain areas included in the classic resting-state networks that are involved in interoceptive processing and social decision-making were used as input and the model with the optimal number of hidden states was selected based on BIC scores. The fractional occupancy of each state was calculated and correlated with the participants' moral distance measure. The functions of the hidden states were inferred through meta-analytic functional decoding using the Neurosynth database.

Results: Participants consistently aligned their moral decisions with group consensus in both Study 1($M = .790$, $SD = .054$, $t(73) = 46.165$, $p < .001$) and Study 2 ($M = .718$, $SD = .130$, $t(29) = 9.177$, $p < .001$). In Study 1, subjective interoceptive awareness positively correlated with moral similarity ($r(74) = .237$, $p = .042$) and negatively with moral distance from group consensus ($r(74) = -.240$, $p = .039$), the two measures of moral alignment with the group. In Study 2, interoceptive accuracy, assessed through the heartbeat detection task, correlated with moral similarity ($r(30) = .422$, $p = .020$) and moral distance ($r(30) = -.436$, $p = .016$). The strength in the functional connectivity between the anterior insula and the precuneus (MNI: $x = 4$, $y = -52$, $z = 30$, p-FDR $= .017$) was negatively correlated with the moral distance measure. Also, the fractional occupancy of the hidden brain state characterized by lowered activity in the precuneus and the medial prefrontal cortex positively correlated with moral distance ($r(74) = .329$, $p = .004$).

Conclusions: In summary, this study provides empirical support for the crucial role of interoception in shaping and implementing intuitive moral decisions aligned with group consensus, along with the neural dynamics associated with this tendency.

References

1. Kleckner, I. R. (2017). Evidence for a large-scale brain system supporting allostasis and interoception in humans. Nature human behaviour, 1(5), 0069.
2. Theriault, J. E. (2021). The sense of should: A biologically-based framework for modeling social pressure. Physics of Life Reviews, 36, 100-136.

Poster No 846

The Genetic Architecture of the Morphometry of the Human Corpus Callosum

Ravi Bhatt[1], Shruti Gadewar[1], Ankush Shetty[1], Iyad Ba Gari[1], Elizabeth Haddad[1], Shayan Javid[1], Abhinaav Ramesh[1], Elnaz Nourollahimoghadam[1], Alyssa Zhu[1], Christaan de Leeuw[2], Paul Thompson[1], Sarah Medland[3], Neda Jahanshad[1]

[1]University of Southern California, Marina Del Rey, CA, [2]VU University, Amsterdam, Amsterdam, [3]QIMR Berghofer Medical Research Institute, Brisbane, N/A

Introduction: The corpus callosum (CC) is the largest interhemispheric white matter tract in the human brain. It's essential for coordinating sensorimotor responses, performing associative/executive functions, and representing information in multiple dimensions. Morphometric CC alterations are associated with neurodevelopmental and neuropsychiatric disorders, and structural variations are highly heritable. Understanding genetic and molecular mechanisms shaping CC morphometry is vital for improved comprehension of factors influencing CC development and targeted therapies.

Methods: We developed a tool, Segment, Measure & Auto QC the midsagittal Corpus Callosum (SMACC)[1] to: (a) extract the midsagittal CC (midCC) from 3D structural brain MRI; and (b) quantify its area and thickness (TH) in the UK Biobank (45-82 years old) and ABCD (8-13 years old) study (N=46,685 individuals of European ancestry). To investigate biological pathways influencing midCC morphology, genome-wide analysis was conducted on midCC area and mean TH, and the Witelson scheme parcellations[2]. Meta-analysis was conducted using METAL[3]. Single nucleotide polymorphism (SNP) based heritability (h2SNP) estimates were completed using the genomic-relatedness-based restricted maximum-likelihood approach in GCTA[4] and LDSC[5]. h2SNP of variants in specific tissues and cell types were computed using LDSC-SEG[6]. Genetic risk loci (GRL) were mapped to genes using FUMA[7]. Pathway enrichment, gene-property, and gene-set analyses were completed in MAGMA[8]. Transcriptome-wide associations (TWAS) were completed using expression quantitative trait loci (eQTL) and splicing QTL (sQTL) from GTEx8[9] using LAVA-TWAS[10]. We used LDSC to examine global genetic correlations (rGs) across cerebral cortex regions[11] and with neuropsychiatric disorders. LAVA[12] assessed local rGs on all protein-coding genes. Causal genetic liability between CC metrics, and cerebral cortex regions and neuropsychiatric traits was assessed via Mendelian randomization (GSMR)[13].

Results: We identified 28 and 9 GRL associated with midCC area and TH (Fig 1), respectively. There were 5 GRL positionally mapped to genes (IQCJ-SHIP1, FIP1L1, HBEGF, CDKN2B-AS1, FAM107B) that overlapped across area and TH. Common SNPs explained 16% of the variability in both area (SE = 0.03) and thickness (SE = 0.02). Gene-based associations identified 30 and 34 genes for area and TH, respectively; five were overlapping. Findings implicated mechanisms such as axon guidance, and action potential conduction via organizing molecular complexes at nodes of Ranvier and axon initial segments. Regionally, there were between 7-23 GRL for area, and 2-9 GRL for TH. GRL for area overlapped across Witelson parcellations in a rostral-caudal gradient. This implicated the Wnt signaling pathway and neuron migration regulation. FOXO3 overlap along posterior body and isthmus area, h2SNP enrichment in immune cells, and TWAS associations of ATP13A2 expression in fibroblasts implicate immune-mediated mechanisms responsible for posterior CC thinning. h2SNP enrichment of TH was observed in the fetal brain and cortex-derived neurospheres in chromatin, supported by gene sets involved in histone regulation and acetylation. CC area and TH showed rGs with surface area and cortical TH of regions in the cingulate, parietal and occipital lobes of the cortex. GSMR showed causal effects of midCC metrics on cortical structure, but not vice versa (Fig 2). Negative rGs were observed with ADHD and bipolar disorder (BD). Posterior body TH and BD had positive rG along the 20q13.33 cytogenetic band. GSMR highlighted causal associations of BD on CC metrics, but not vice versa.

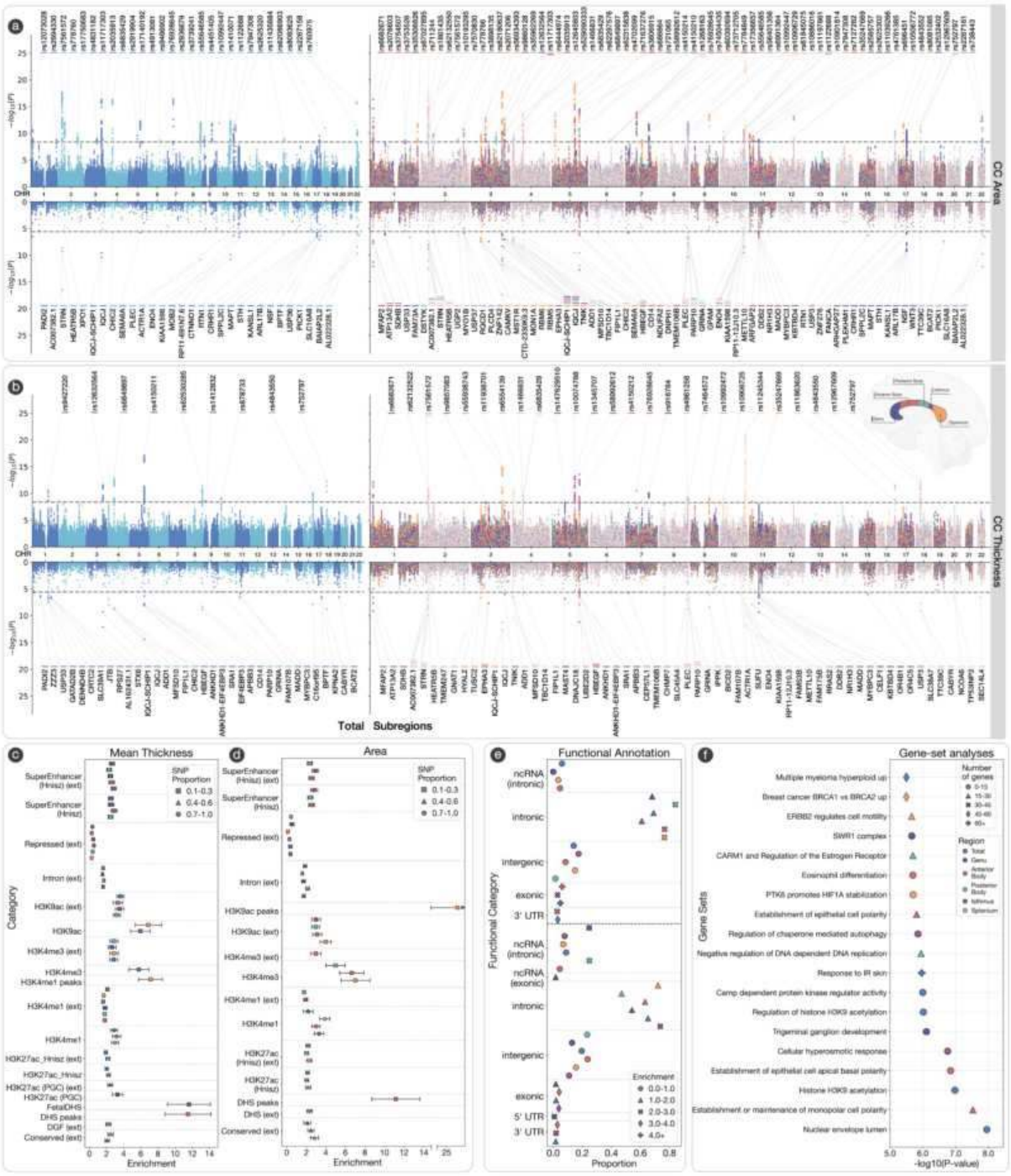

Figure 1: **GWAS meta-analysis of corpus callosum shape.** (A) Miami plot for SNPs (top) and genes (bottom) based on MAGMA gene analysis for total area and (B) total mean thickness. (C) Proportion of GWAS SNPs in each functional category from ANNOVAR across each CC phenotype. (D) Significant enrichment of SNP heritability in 53 annotation categories computed via LD score regression across each CC phenotype. (E) Significant MSigDB 7.0 gene sets from the MAGMA gene-set analysis after Bonferroni correction across each CC phenotype.

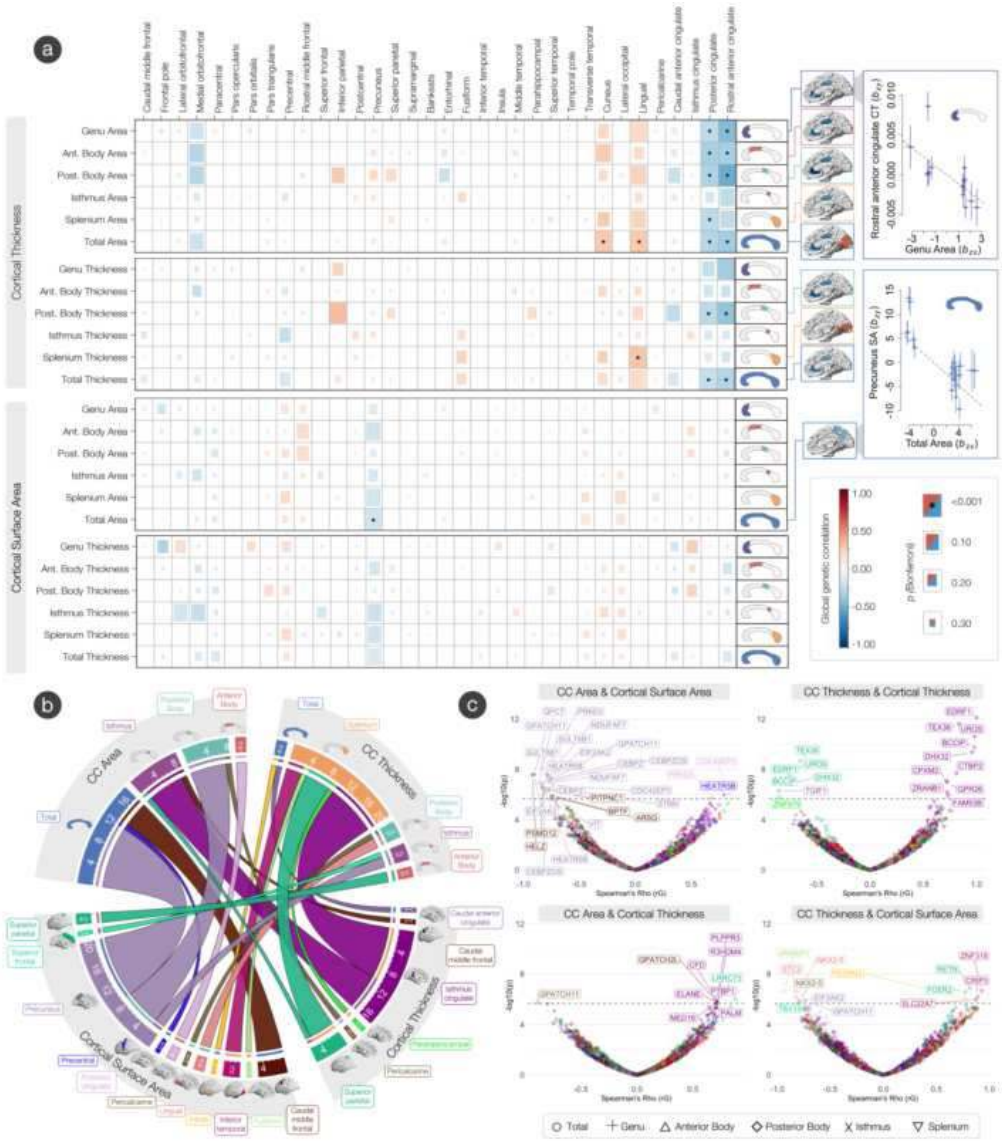

Figure 2: **The genetic overlap of the corpus callosum and cerebral cortex.** (A) Global genetic correlations (LDSC - rG) between CC phenotypes and cerebral cortex phenotypes. The Bonferroni significance threshold was set at $p = 3.1 \times 10^{-5}$. Surface area and cortical thickness of significant cortical regions with each CC phenotype are displayed on brain plots. Of the significant global genetic correlations, significant Mendelian randomization (GSMR) results are displayed, representing the unidirectional effect of CC phenotypes on cortical phenotypes free of non-genetic confounders. (B) Chord plot displays the number of significant bivariate local genetic correlations (LAVA) between CC and cortical phenotypes. Underlined numbers represent the total number of genes shared with that phenotype. (C) Volcano plots showing degree (-log10 *p*-values) and direction (rG) of local genetic correlations (LAVA) between cortical and CC phenotypes. Colors represent cortical regions labeled on the chord plot in section B. Significant genes (Bonferroni significance threshold was set at $p = 2.23 \times 10^{-6}$) across all phenotypes are labeled.

Conclusions: This work identifies genome-wide significant loci of morphometry of total and parcellations of the corpus callosum, convergence on biological functions, tissues and cell types, as well as the genetic overlap with the cerebral cortex and neuropsychiatric conditions.

References

1. Gadewar, S.P., Nourollahimoghadam, E., Bhatt, R.R., Ramesh, A., Javid, S., Gari, I.B., Zhu, A.H., Thomopoulos, S., Thompson, P.M., and Jahanshad, N. (2023). A Comprehensive Corpus Callosum Segmentation Tool for Detecting Callosal Abnormalities and Genetic Associations from Multi Contrast MRIs. ArXiv.
2. Witelson, S.F. (1989). Hand and sex differences in the isthmus and genu of the human corpus callosum. A postmortem morphological study. Brain 112 (Pt 3), 799–835.
3. Willer, C.J., Li, Y., and Abecasis, G.R. (2010). METAL: fast and efficient meta-analysis of genomewide association scans. Bioinformatics 26, 2190–2191.
4. Yang, J., Lee, S.H., Goddard, M.E., and Visscher, P.M. (2011). GCTA: a tool for genome-wide complex trait analysis. Am. J. Hum. Genet. 88, 76–82.
5. Bulik-Sullivan, B., Loh, P.R., Finucane, H.K., Ripke, S., Yang, J., Patterson, N., Daly, M.J., Price, A.L., Neale, B.M., Corvin, A., et al. (2015). LD score regression distinguishes confounding from polygenicity in genome-wide association studies. Nat. Genet. 47, 291–295.

6. Finucane, H.K., Reshef, Y.A., Anttila, V., Slowikowski, K., Gusev, A., Byrnes, A., Gazal, S., Loh, P.-R., Lareau, C., Shoresh, N., et al. (2018). Heritability enrichment of specifically expressed genes identifies disease-relevant tissues and cell types. Nat. Genet. 50, 621–629.
7. Watanabe, K., Taskesen, E., Van Bochoven, A., and Posthuma, D. (2017). Functional mapping and annotation of genetic associations with FUMA. Nat. Commun. 8, 1–10.
8. de Leeuw, C.A., Mooij, J.M., Heskes, T., and Posthuma, D. (2015). MAGMA: generalized gene-set analysis of GWAS data. PLoS Comput. Biol. 11, e1004219.
9. GTEx Consortium (2020). The GTEx Consortium atlas of genetic regulatory effects across human tissues. Science 369, 1318–1330.
10. de Leeuw, C., Werme, J., Savage, J.E., Peyrot, W.J., and Posthuma, D. (2023). On the interpretation of transcriptome-wide association studies. PLoS Genet. 19, e1010921.
11. Grasby, K.L., Jahanshad, N., Painter, J.N., Colodro-Conde, L., Bralten, J., Hibar, D.P., Lind, P.A., Pizzagalli, F., Ching, C.R.K., McMahon, M.A.B., et al. (2020). The genetic architecture of the human cerebral cortex. Science 367. 10.1126/science.aay6690.
12. Werme, J., van der Sluis, S., Posthuma, D., and de Leeuw, C.A. (2022). An integrated framework for local genetic correlation analysis. Nat. Genet. 54, 274–282.
13. Zhu, Z., Zheng, Z., Zhang, F., Wu, Y., Trzaskowski, M., Maier, R., Robinson, M.R., McGrath, J.J., Visscher,

Poster No 847

International genomic analysis of intracranial and subcortical brain volumes in 70,000 individuals

Luis M. Garcia Marin[1], Adrian Campos[2], Santiago Diaz-Torres[1], Jill Rabinowitz[3], Brittany Mitchell[1], Katrina Grasby[1], Jackson Thorp[1], ENIGMA consortium[4], CHARGE consortium[5], M Arfan Ikram[6], Sudha Seshadri[7], Paul Thompson[4], Claudia Satizabal[7], Sarah Medland[1], Miguel Renteria[1]

[1]Mental Health & Neuroscience Program, QIMR Berghofer Medical Research Institute, Brisbane, QLD, [2]Regeneron Genetics Centre, Tarrytown, NY, [3]Department of Psychiatry, Robert Wood Johnson Medical School, Rutgers University, Piscataway, NJ, [4]Imaging Genetics Center, Mark and Mary Stevens Neuroimaging and Informatics Institute, Marina del Rey, CA, [5]Baylor College of Medicine Human Genome Sequencing Center, Houston, TX, [6]Department of Epidemiology, Erasmus MC University Medical Center, Rotterdam, Netherlands, [7]Glenn Biggs Institute for Alzheimer's and Neurodegenerative diseases, San Antonio, TX

Introduction: Several studies have documented individual differences in subcortical brain structures and intracranial volume in most major neurological diseases, from Alzheimer's and Parkinson's disease to psychiatric and developmental brain disorders. However, there is a growing need to uncover genetic variants that provide insights into the mechanistic pathways responsible for variation in the volumes of subcortical brain structures.

Methods: We performed genome-wide association studies (GWAS) meta-analyses of intracranial and nine subcortical brain volumes, namely the brainstem, caudate nucleus, putamen, hippocampus, globus pallidus, thalamus, ventral diencephalon, nucleus accumbens, and amygdala in more than 70,000 participants of European ancestry from the ENIGMA, CHARGE, UK Biobank and ABCD cohorts. Then, we investigated the genetic overlap among these brain volumes using linkage disequilibrium score regression, bivariate MiXeR, and genomic structural equation modeling analyses. We also conducted functional annotation and gene prioritisation analyses via gene-based tests, eQTL mapping, and the integration of single-cell RNA sequencing data with GWAS summary statistics. Moreover, we evaluated the predictive utility of polygenic scores for these brain volumes in a diverse ancestral population using data from the ABCD study, a population-based study of preadolescent youth that includes individuals of diverse ancestral backgrounds. Finally, we investigated the overlap and potential causal genetic effects between the observed brain-associated genomic loci and genomic markers implicated in major neurological and psychiatric diseases, yielding structure-specific genetic associations with major brain diseases.

Results: Our results implicated more than 245 independent genetic variants associated with intracranial volume or the volumes of the brainstem, caudate nucleus, putamen, hippocampus, globus pallidus, thalamus, nucleus accumbens, amygdala and, for the first time, the ventral diencephalon. Of these 245 independent genetic variants, 216 have not been reported in previous studies. We observed 20 genes expressed in specific neural cell types across different differentiation time points that influence intracranial and subcortical brain volumes and are involved in autophagy, immune and inflammatory response, organelle biogenesis and maintenance, apoptosis, or the aetiology of neurodegenerative disorders. In addition, we observed genetic overlap and putative causal genetic effects of intracranial and subcortical brain volumes with neuropsychiatric conditions, including Parkinson's disease, ADHD, and insomnia. Polygenic scores for intracranial and subcortical volumes showed predictive ability for their corresponding phenotypic measurements in the ABCD cohort, a diverse ancestral population of children.

Conclusions: In the present study, we conducted a worldwide study of 49 study samples from 19 countries and led the largest international genetic analysis of human subcortical brain volumes and intracranial volume to date. We provide evidence for the polygenic architecture of intracranial and subcortical brain volumes, present novel findings regarding the relevance of ventral

diencephalon volume for the first time, and show that distinct genetic variants have a specific effect on the variation of a single brain volume. Our results point towards the generalisability of intracranial and subcortical brain volumes polygenic scores to both European and non-European ancestry individuals, suggesting a shared genetic basis of these brain volumes across diverse ancestral groups. Overall, our findings advance the understanding of the brain's complex and polygenic architecture and implicate multiple gene expression patterns and molecular pathways in human brain structure, suggesting that several genetic variants of small effect size are likely to be involved in the development of specific brain volumes.

References

1. Adams, H. H. et al. Novel genetic loci underlying human intracranial volume identified through genome-wide association. Nat. Neurosci. 19, (2016).
2. Hibar, D. P. et al. Novel genetic loci associated with hippocampal volume. Nat. Commun. 8, 13624 (2017).
3. Rentería, M. E. et al. Genetic architecture of subcortical brain regions: common and region-specific genetic contributions. Genes Brain Behav. 13, 821–830 (2014).
4. Satizabal, C. L. et al. Genetic architecture of subcortical brain structures in 38,851 individuals. Nat. Genet. 51, 1624–1636 (2019).
5. Stein, J. L. et al. Identification of common variants associated with human hippocampal and intracranial volumes. Nat. Genet. 44, 552–561 (2012).
6. Thompson, P. M. et al. ENIGMA and global neuroscience: A decade of large-scale studies of the brain in health and disease across more than 40 countries. Transl. Psychiatry 10, 1–28 (2020).
7. Walton, E. et al. Exploration of Shared Genetic Architecture Between Subcortical Brain Volumes and Anorexia Nervosa. Mol. Neurobiol. 56, (2019).

Poster No 848

Phenotypic and Genetic Relationship between Brain Structure and Endogenous Sex-hormone Levels in UKB

Xochitl Diaz[1], Santiago Daiz-Torres[2], Xikun Han[3], Adrian Campos[4], Stuart MacGregor[3], Jue Ong[3], Miguel Renteria[5]

[1]Queenslan Institute of Medical Research, Brisbane, Queensland, [2]QIMR Berghofer Medical Research Institute, Brisbane, QLD, [3]Queenslan Institute of Medical Research, Brisbane, QLD, [4]Regeneron Genetics Centre, Tarrytown, NY, [5]Mental Health & Neuroscience Program, QIMR Berghofer Medical Research Institute, Brisbane, AK

Introduction: Sex hormones, including testosterone and sex hormone-binding-globulin (SHBG), are steroid hormones that play vital roles in sexual development, reproduction, and general health. Deficiencies have been linked to many age-related disorders such as cardiovascular disease, Parkinson's disease, Alzheimer's disease and diabetes. In the present study, we leveraged structural neuroimaging and serum biochemistry data from up to 17,000 middle-aged participants in the UK Biobank. We interrogated sex-stratified cohorts to comprehensively map the phenotypic and genetic relationships between endogenous sex hormone levels and 74 brain morphometry phenotypes. We hypothesised that, for specific regions in the brain, differences in endogenous sex-hormone levels might contribute to variation in brain structure irrespective of sex and that the presence of sex differences on the genetic basis of brain structure may, in part, be explained by the sex-specific genetic influence of endogenous sex hormones.

Methods: We screened all trait-pair associations between sex hormone level and brain morphometry phenotype. Our analysis can be summarised into three main steps: Step 1: We performed cross-sectional multivariable linear regression analyses to evaluate the observational sex-specific association between neuroimaging phenotypes and endogenous sex hormone levels. Step 2: We use a linear mixed model association implemented in BOLT-LMM and perform GWAS for each rank-transformed neuro-imaging phenotype by sex. Then, we estimated the genetic correlation (Gr) between sex hormone levels and brain morphology in both sexes via LD-score regression. Step 3: Finally, we followed up correlated trait pairs with genetic causality analyses (e.g., Mendelian randomisation) to test for evidence of a potential causal (i.e., directional) relationship.

Results: Observational findings: We identified 15 associations between brain morphology traits and SHBG, with 13 associations shown in women and two associations in men. Notably, the surface area of the supramarginal gyrus was associated with differences in endogenous SHBG levels in both sexes. There were strong associations between testosterone phenotypes and thickness of paracentral and precentral (p=1e-4). Genetic correlations: Except for six, all brain morphology traits had an estimated Gr above 0.8 between males and females, suggesting limited evidence for a sex difference in the genetic architecture of neuroimaging traits. Gr between brain morphology and sex hormone levels were modest (ranging from -0.13 to 0.16)[Figure 1]. Across both sexes, 6 out of 7 subcortical volume phenotypes were genetically correlated with SHBG levels: pallidum, thalamus, accumbens, caudate, amygdala and hippocampus. The surface area of the isthmus cingulate gyrus showed the strongest evidence of being genetically correlated with both freeT and totalT in females. Some brain traits were genetically associated with testosterone levels in the opposite direction, including the supramarginal and superior temporal

gyri thickness. Causal inference: Only the MR association between SHBG and the caudate nucleus volume in women and the association between SHBG and thickness of the pericalcarine in women showed consistent effect sizes across our association analyses. The strongest MR association was observed for genetically predicted SHBG on the subcortical volume of the putamen, although the phenotypic association was negligibly small.

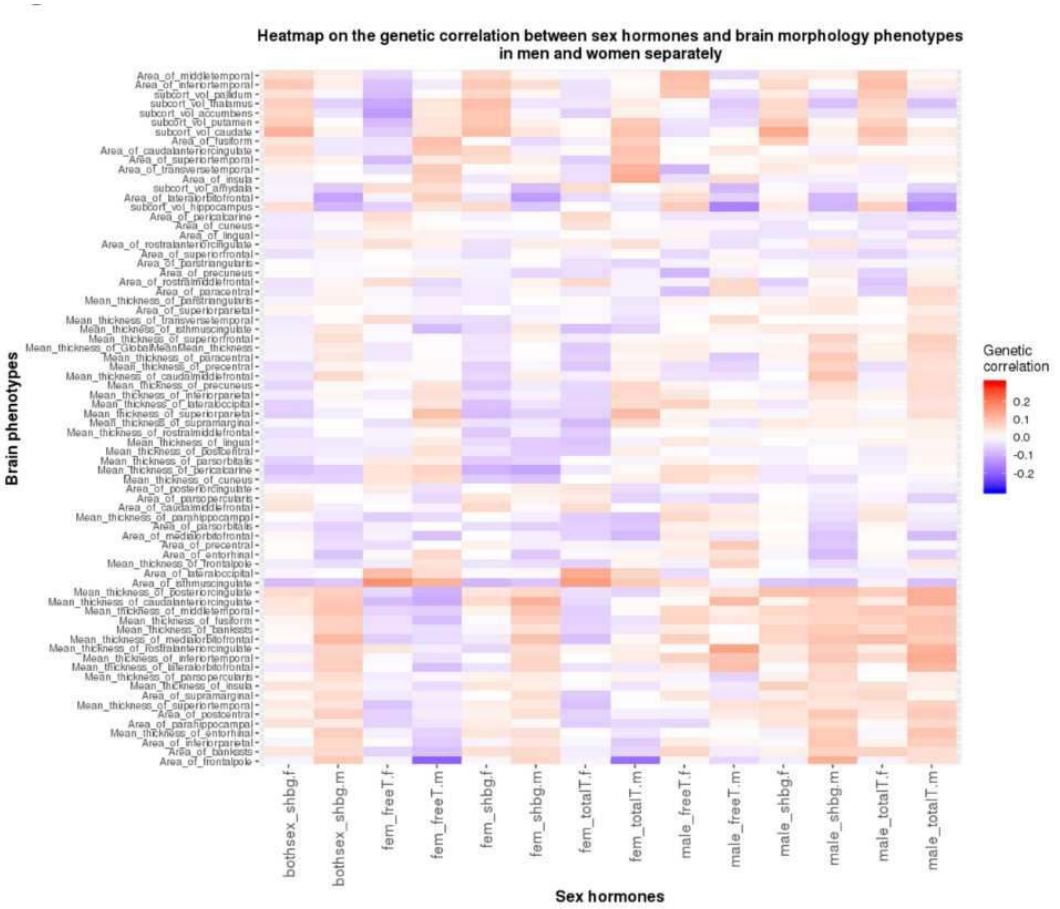

Figure 1. Sex-stratified Gr estimates between endogenous sex hormones and brain morphology phenotypes.

Conclusions: Although the robust phenotypic and genetic relationship between SHBG and cortical thickness in women confirms findings from previous studies, several novel findings, such as those between testosterone and the surface area of the lateral orbitofrontal cortex, warrant independent validation. While we show that the pattern of Gr between sex hormones and morphology phenotypes might differ by sex, evidence of genetic causality between the two remains limited.

References

1. McEwen BS, Milner TA. Understanding the broad influence of sex hormones and sex differences in the brain. J Neurosci Res. (2017) https://doi.org/10.1002/jnr.23809.
2. Di Zhao, Eliseo Guallar, Pamela Ouyang, Vinita Subramanya, Dhananjay Vaidya, Chiadi E. Ndumele, Joao A. Lima, Matthew A. Allison, Sanjiv J. Shah, Alain G. Bertoni, Matthew J. Budoff, Wendy S. Post, Erin D. Michos. Endogenous Sex Hormones and Incident Cardiovascular Disease in Post-Menopausal Women, Journal of the American College of Cardiology (2018) https://doi.org/10.1016/j.jacc.2018.01.083.
3. Kim C, Halter JB. Endogenous sex hormones, metabolic syndrome, and diabetes in men and women. Curr Cardiol Rep. (2014) https://doi.org/10.1007/s11886-014-0467-6.
4. Gegenhuber, B., Wu, M.V., Bronstein, R. et al. Gene regulation by gonadal hormone receptors underlies brain sex differences. Nature (2022) https://doi.org/10.1038/s41586-022-04686-1
5. Bruce S. McEwen, Teresa A. Milner. Understanding the Broad Influence of Sex Hormones and Sex Differences in the Brain. J Neurosci Res. (2017) https://doi.org/10.1002/jnr.23809
6. Shansky RM, Hamo C, Hof PR, Lou W, McEwen BS, Morrison JH. Estrogen promotes stress sensitivity in a prefrontal cortex-amygdala pathway. Cereb Cortex. (2010) https://doi.org/10.1093/cercor/bhq003.
7. Lise Eliot, Adnan Ahmed, Hiba Khan, Julie Patel. Dump the “dimorphism”: Comprehensive synthesis of human brain studies reveals few male-female differences beyond size. Neuroscience & Biobehavioral Reviews (2021) doi: https://doi.org/10.1016/j.neubiorev.2021.02.026
8. Bianco A, Antonacci Y, Liguori M. Sex and Gender Differences in Neurodegenerative Diseases: Challenges for Therapeutic Opportunities. International Journal of Molecular Sciences. (2023) https://doi.org/10.3390/ijms24076354
9. Stuart J Ritchie, Simon R Cox, Xueyi Shen, Michael V Lombardo, Lianne M Reus, Clara Alloza, Mathew A Harris, Helen L Alderson, Stuart Hunter, Emma Neilson, David C M Liewald, Bonnie Auyeung, Heather C Whalley, Stephen M Lawrie, Catharine R Gale, Mark E Bastin, Andrew M McIntosh, Ian J Deary, Sex Differences in the Adult Human Brain: Evidence from 5216 UK Biobank Participants, Cerebral Cortex, Volume

Poster No 849

Revisiting Spatial Patterns in Gene-Brain Associations: Insights from the Allen Human Brain Atlas

Chien Ming Lo[1], Niall Duncan[2]

[1]Taipei Medical University, Taipei, Taiwan, [2]Taipei Medical University, Taiwan, Taipei

Introduction: The Allen Human Brain Atlas has been a significant tool in neuroscience, facilitating investigations into the brain's organizational principles. Studies have focused on correlated gene expression patterns and their relation to brain features, necessitating spatial correlations and specialized significance testing on the cortical sheet.

Methods: We collected regional microarray expression data from six post-mortem brains provided by the Allen Human Brain Atlas. The data underwent preprocessing using the abagen toolbox and was then mapped onto the Schaefer-400 atlas. We used several categorical gene sets and implemented PCA to identify main spatial patterns in gene expression variations across the cortex. Our analysis also included a non-linear dimensionality reduction technique and the creation of a transcriptomic null distribution through nonparametric permutation.

Results: The first principal components of transcriptomic covariances revealed a consistent spatial pattern across gene sets, including 'unspecific' and 'specific' sets. The brain-specific PC1 showed a strong association with the T1w/T2w map, challenging the assumption that dominant spatial patterns in AHBA data are exclusive to specific gene sets. Furthermore, our analysis indicated that the observed spatial patterns are not solely due to specific gene sets but might be a more generalized characteristic of the brain's transcriptomic organization.

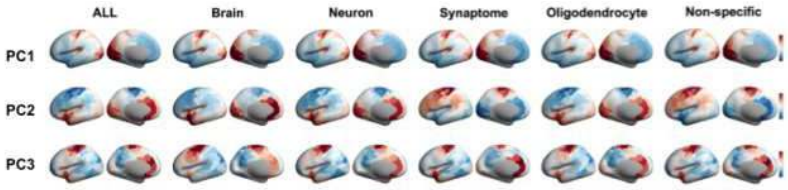

Figure 1: Principal Components of Regional Transcriptomic Similarity Across Different Gene Sets. This figure illustrates the first three Principal Components (PC) representing regional transcriptomic similarity indexed by covariance matrix across six different gene sets on Schaefer 400 parcelation scheme. Notably, the first PC, which explains the majority of the variance (mean: 59%), appears to exhibit a universal spatial pattern regardless of the specific gene sets. All values are standardized (z-scored) and color-coded with limits set to two standard deviations (σ).

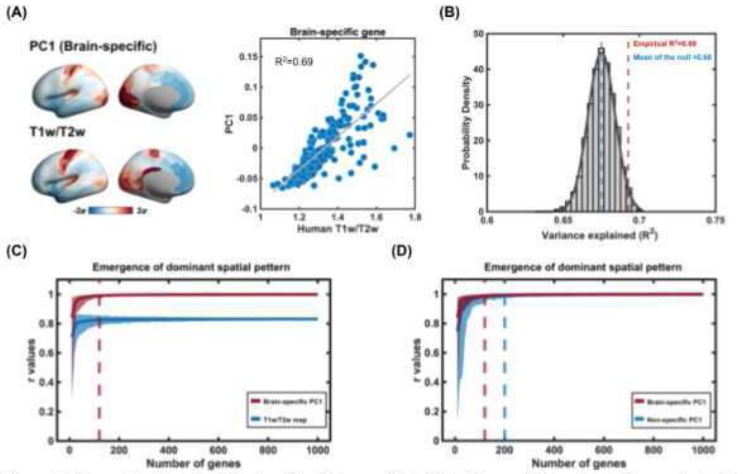

Figure 2: Re-evaluating the Relationship Between T1w/T2w Map and Dominant Transcriptomic Spatial Pattern Using Null Gene Distribution (A) The left column demonstrates the replicable spatial pattern of PC1 derived from the brain-specific gene set, akin to the human T1w/T2w map. Both maps are standardized in σ units. The scatter plot on the right illustrates a strong correlation between these two maps (R^2=0.69, P<0.001, Spearman rank correlation) as previous studies shown. **(B)** We establish a null distribution by correlating the human T1w/T2w map with PC1 derived from 5000 permutations of 1899 genes sampled from all gene sets. The mean R^2 of the null distribution is 0.68 (blue dashed line), while the empirical R^2 is 0.69 (red dashed line), ranking at 97.5%. **(C)** We examine the emergence of the dominant spatial pattern. The x-axis represents the number of genes included in re-calculating PC1 (ranging from 10 to 1000 in intervals of 10). Each gene subset is bootstrapped 500 times to estimate a 95% confidence interval (CI). The red solid line represents the average correlation values (r) between the Brain-specific PC1 and subsets of PC1, with the shaded line indicating the 95% CI. The red dashed vertical line indicates the point at which an r value of 0.99 is reached (N=120). The blue solid line depicts the average r values between the T1w/T2w map and subsets of PC1, with the shaded line indicating the 95% CI. **(D)** Similar to (C), this figure explores whether the emergence pattern differs between gene sets, specifically Brain-specific (in red) and Non-specific (in blue). The dashed vertical line indicates the point at which an r value of 0.99 is achieved (N=120 for Brain-specific and N=200 for Non-specific).

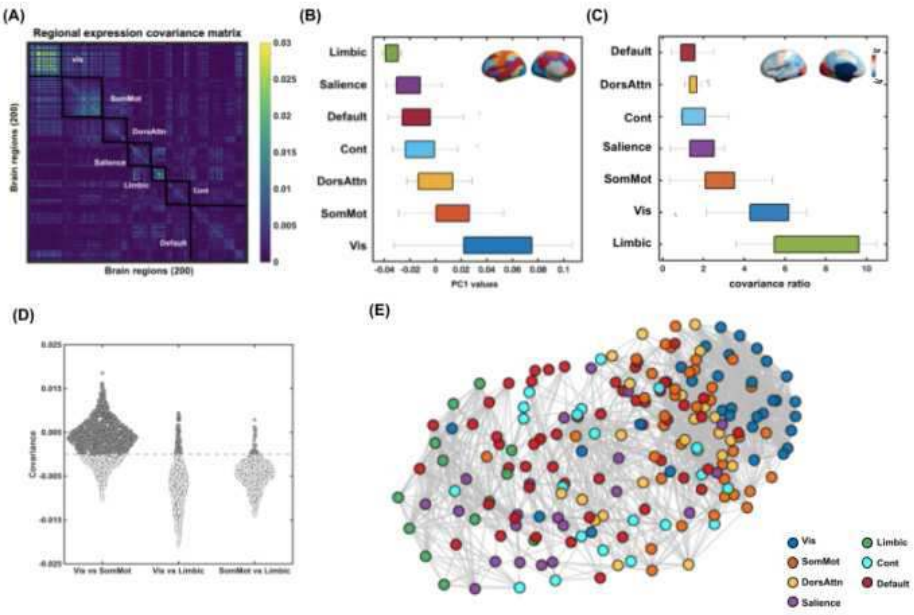

Figure 3: Exploring Transcriptomic Covariance Patterns Across Functional Networks (A) The regional transcriptomic covariance matrix outlined by Yeo-7 functional network boundaries, with acronyms provided for reference. Key networks include Vis (Visual), SomMot (Somatomotor), DorsAttn (Dorsal Attention), Salience (Salience and Ventral Attention), Cont (Control), Limbic (Limbic), and Default (Default Mode). **(B)** Boxplot representation of PC1 values, organized and sorted by functional networks. The distribution highlights that Vis and SomMot networks are at one end of the axis, while the Limbic network is at the other. Cortical map of network assignments are color-coded in the top-right corner of the plot. **(C)** Boxplot illustrating the inter-/intra-covariance ratio, sorted by functional networks. Vis, SomMot, and Limbic networks exhibit significantly higher intra-network transcriptomic similarity compared to inter-network relationships ($F(6, 65.32) = 46.05$, $p < 0.001$). The index is visualized on the cortical surface and displayed in standard deviation (σ) units in the top-right corner of the plot. **(D)** The inter-network covariance comparison between Vis, SomMot, and Limbic networks. Values above zero are presented in gray. Notably, the Limbic network exhibits lower inter-network covariances between both Vis and SomMot networks. **(E)** An force-directed graph representation of the transcriptomic covariance matrix (top 90%) using the compound spring embedder (CoSE) algorithm in Cytoscape (public available at https://cytoscape.org/download.html). This visualization method reveals network relationships within the expression similarity. Notably, it reinforces the close association between the Vis and SomMot networks, while also illustrating that the Limbic network appears relatively distant, despite its high covariance pattern.

Conclusions: Our findings challenge prevailing assumptions about the specificity of gene-brain property associations and suggest a more generalized transcriptomic spatial pattern. The unique covariance characteristics within specific functional networks, particularly the Visual, Somatomotor, and Limbic networks, appear to influence these spatial transcriptomic patterns. This study prompts a critical reevaluation of methodologies and assumptions in understanding gene-brain associations, offering new insights into the complex relationships governing brain organization and gene expression patterns.

References

1. Burt, J.B. et al. (2018), 'Hierarchy of Transcriptomic Specialization across Human Cortex Captured by Structural Neuroimaging Topography', Nature Neuroscience, vol. 21, no. 9, pp. 1251-1259.
2. Arnatkevičiūtė, A., Fulcher, B.D., & Fornito, A. (2019), 'A Practical Guide to Linking Brain-wide Gene Expression and Neuroimaging Data', Neuroimage, vol. 189, pp. 353-367.
3. Richiardi, J. et al. (2015), 'Correlated Gene Expression Supports Synchronous Activity in Brain Networks', Science, vol. 348, no. 6240, pp. 1241-1244.
4. Schaefer, A. et al. (2018), 'Local-Global Parcellation of the Human Cerebral Cortex from Intrinsic Functional Connectivity MRI', Cerebral Cortex, vol. 28, no. 9, pp. 3095-3114.
5. Glasser, M.F. (2016), 'A Multi-modal Parcellation of Human Cerebral Cortex', Nature, vol. 536, no. 7615, pp. 171-178.

Poster No 850

APOE-stratified genome-wide association meta-analysis for accelerated brain age in Korean population

Bo-Hyun Kim[1], Kwangsik Nho[2], Yen-Ning Huang[3], Shannon Risacher[2], Junpyo Kim[4], Dahyun Yi[5], Min Soo Byun[6], Hee Jin Kim[7], Hong-Hee Won[8], Andrew Saykin[2], Dong Young Lee[5], Sangwon Seo[4]

[1]Samsung Medical Center, Seoul, Seoul, [2]Indiana University School of Medicine, Indianapolis, IN, [3]Department of Radiology and Imaging Sciences, Indiana University School of Medicine, Indianapolis, IN, [4]Samsung medical center, Seoul, None, [5]Seoul National University, Seoul, Korea, Republic of, [6]Seoul National University College of Medicine, Seoul, Korea, Republic of, [7]Samsung Medical Center, Sungkyunkwan University School of Medicine, Seoul, Seoul, [8]SAIHST, Sungkyunkwan University, Samsung Medical Center, Seoul, Seoul

Introduction: Aging and APOE4 are key risk factors for Alzheimer's disease (AD) and have significant structural impacts on the brain. Machine learning approaches have been developed to estimate the biological age of the brain from MRI scans. Here, we performed APOE4-stratified genome-wide association (GWAS) meta-analysis of accelerated brain aging in two independent Korean AD cohorts.

Methods: Participants included 1,738 Korean older adults from two independent cohorts that consisted of preclinical and clinical stages of AD (n=1,209 from the K-ROAD cohort (Korea-Registries to Overcome and Accelerate Dementia Research Project) and n=529 from the KBASE cohort (Korean Brain Aging Study for the Early Diagnosis and Prediction of Alzheimer's Disease)). Brain age was estimated from structural MRI scans using brainageR. Brain age acceleration (predicted brain age - chronological age) was calculated for each participant. GWAS for brain age acceleration were performed using PLINK after accounting for age, sex, APOE4 carrier status, and diagnosis. In addition, APOE4-stratified (APOE4 carrier and non-carrier) GWAS meta-analyses for brain age acceleration were also performed. Meta-analysis was performed using METAL, followed by transcriptomic analysis. Polygenic risk scores for brain age acceleration were calculated with PRS-CS using GWAS meta-analysis summary statistics, followed by molecular imaging analysis.

Results: GWAS meta-analysis using all individuals identified six intronic SNPs in the LRBA (Lipopolysaccharide responsive Beige-like Anchor) locus on chromosome 4 as significantly associated with brain age acceleration with the most significant signal at rs7699001 (Fig. 1; $p < 5 \times 10\text{-}8$). APOE4-stratified GWAS meta-analysis identified two intergenic SNPs in the MYRFL (Myelin Regulatory Factor Like) locus on chromosome 12 as significantly associated with brain age acceleration with the most significant signal at rs789331 (Fig. 1; $p=1.4 \times 10\text{-}8$) in the APOE4 non-carrier group. rs789331 in the MYRFL locus showed a significant interaction (Fig. 2; $p=5.7 \times 10\text{-}5$) with APOE4 in the K-ROAD cohort and a marginal interaction effect (Fig. 2; $p=8.2 \times 10\text{-}2$) in the KBASE cohort. LRBA is highly expressed in the brain, especially in microglia. The LRBA and MYRFL genes were differentially expressed in AD compared to cognitively normal older adults. rs7699001 and rs789331 were associated with expression levels of the LRBA and MYRFL genes, respectively, in tissue from several organs including brain. rs7690001 in the LRBA locus has been reported to be associated with inferior parietal cortical thickness in non-Hispanic whites ($p= 5 \times 10\text{-}3$). rs789331 in the MYRFL locus was significantly associated with hippocampal volume ($p=1.2 \times 10\text{-}2$). Polygenic risk scores of brain age acceleration in the K- ROAD cohort were significantly associated with amyloid-β deposition measured from amyloid PET scans ($p=2.7 \times 10\text{-}4$).

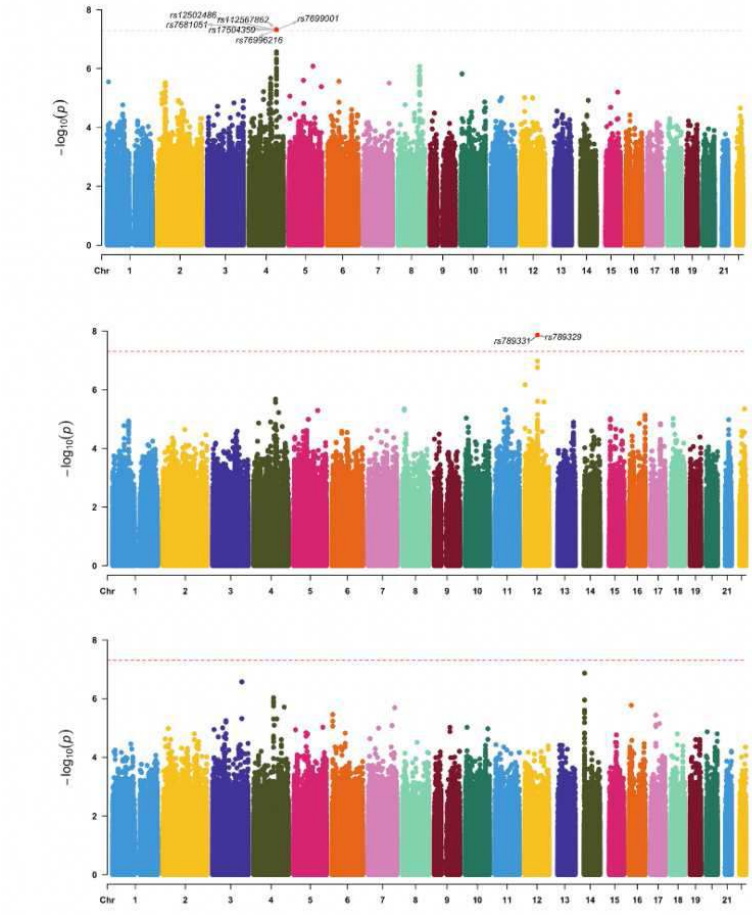

Fig.1 Manhattan plots of GWAS results (top), in APOE ε 4 negative (middle), and APOE ε 4 positive (bottom) groups.

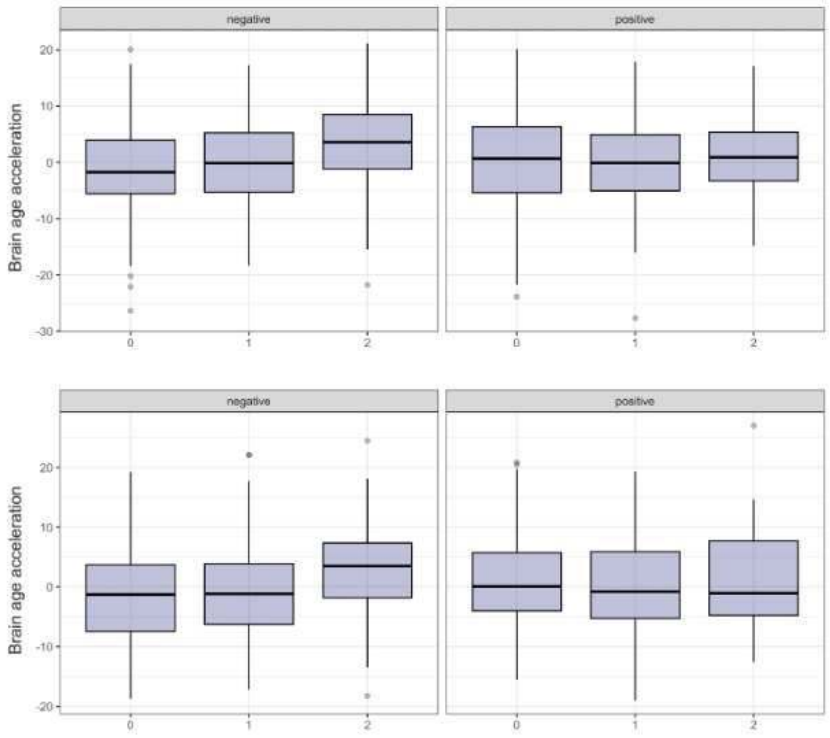

Fig 2 Box plots of association between genotypes of rs789331 and brain age acceleration in K-ROAD cohort (top) and KBASE cohort (bottom).

Conclusions: LRBA and MYRFL are novel genetic risk factors for brain aging in the Korean population with relevance for AD. The microglial LRBA protein may be involved in phagocytosis, which has been implicated in aging processes and AD progression. The myelin regulatory factor is an important transcriptional factor for the central nervous system myelination. Replication in other populations and mechanistic follow-up studies are warranted.

References
1. Ge, Tian, et al. "Polygenic prediction via Bayesian regression and continuous shrinkage priors." Nature communications 10.1 (2019): 1776.
2. Cole JH, Ritchie SJ, Bastin ME, Valdes Hernandez MC, Munoz Maniega S, Royle N et al. Brain age predicts mortality. Molecular psychiatry 2018; 23: 1385-1392.
3. Willer, Cristen J., Yun Li, and Gonçalo R. Abecasis. "METAL: fast and efficient meta-analysis of genomewide association scans." Bioinformatics 26.17 (2010): 2190-2191.
4. Emery, Ben, et al. "Myelin gene regulatory factor is a critical transcriptional regulator required for CNS myelination." Cell 138.1 (2009): 172-185.

Poster No 851

Mendelian randomization shows unidirectionality from amyloid-β to tau in Alzheimer's disease

Hyunwoo Lee[1], Junpyo Kim[1], Han-na Kim[2], Bo-Hyun Kim[3], Sangwon Seo[1]

[1]Samsung medical center, Seoul, Korea, Republic of, [2]Biomedical Statistics Center, Research Institute for Future Medicine, Samsung Medical Center, Seoul, Korea, Republic of, [3]Samsung Medical Center, Seoul, Seoul

Introduction: According to the amyloid cascade hypothesis in Alzheimer's disease (AD), the accumulation of amyloid-β (Aβ) is crucial in initiating a chain of subsequent events that includes tau aggregation, neuronal death, and cognitive impairment. While previous studies have shown that abnormalities in amyloid biomarkers precede the changes in tau biomarkers, asserting causality based on temporal relationships alone can be debatable. Mendelian randomization (MR) has been proven to be a powerful approach for clarifying causal relationships using genetic variants as instrumental variables. (IVs). In this study, we performed a two-sample bidirectional MR study to dissect the potential causal association of Aβ and tau, leveraging summary statistics data from genome-wide association studies (GWASs).

Methods: The two-sample MR study was conducted using GWAS summary statistics regarding amyloid PET and tau PET. For the exposure data set, summary statistics of amyloid PET were generated from 13 cohorts, including 11,816 non-Hispanic whites (NHWs) participants. The tau PET GWAS summary statistics were derived from a meta-analysis combining seven GWAS data sets of 1,449 NHW ancestry individuals. We used the inverse-variance weighted (IVW) method as the primary MR analysis, and MR-Egger regression, weighted median, and mode-based analyses were additionally performed to test the robustness of our study. One-sample MR analysis was also performed to reinforce and verify the experimental results of two-sample MR using autopsy data from the Religious Orders Study/Memory and Aging Project cohort. The exposure and outcome variables for the one-sample MR were neuritic plaque burden and neurofibrillary tangle burden determined by neuropathological examination, respectively.

Results: In total, 20 SNPs identified in amyloid GWAS that were available in the tau PET GWAS summary dataset were included in our two-sample MR analysis. MR results showed a significant causal association between amyloid and tau (IVW method OR 1.77(1.56-2.01), p =7.28×10-19), and MR-Egger regression, weighted median, and mode-based analyses showed consistent results. Neither the heterogeneity test for the IVW method (p=0.32) nor the MR-PRESSO global test for horizontal pleiotropy was statistically significant(p=0.38), indicating no heterogeneity or pleiotropy. MR using tau PET as an exposure and amyloid PET as an outcome showed that the causal association was insignificant (p=0.35). Also, the one-sample MR analysis showed the presence of casual direction from neuritic plaque to neurofibrillary tangle ($p < 2\times10^{-16}$), and a weak instrument test identified that PRS is eligible as IV.

Conclusions: MR is a powerful tool for improving causal inference when GWAS summary statistics data are available for exposure and outcome. While the direction of causation between amyloid and tau has been inferred based on the temporal relationship of the biomarkers, our results strengthen evidence for the presence and the direction of causal association.

References
1. Long JM. 'Alzheimer Disease: An Update on Pathobiology and Treatment Strategies'. Cell. 2019;179(2):312-39.
2. Musiek ES,. 'Three dimensions of the amyloid hypothesis: time, space and 'wingmen''. Nat Neurosci. 2015;18(6):800-6.
3. Gouveia Roque C. 'CREB3L2-ATF4 heterodimerization defines a transcriptional hub of Alzheimer's disease gene expression linked to neuropathology'. Sci Adv. 2023;9(9):eadd2671.
4. Ali M. 'Large multi-ethnic genetic analyses of amyloid imaging identify new genes for Alzheimer disease'. Acta Neuropathol Commun. 2023;11(1):68.

5. Nho K. 'Novel CYP1B1-RMDN2 Alzheimer's disease locus identified by genome-wide association analysis of cerebral tau deposition on PET'. medRxiv. 2023.
6. Bennett DA. 'Apolipoprotein E epsilon4 allele, AD pathology, and the clinical expression of Alzheimer's disease'. Neurology. 2003;60(2):246-52.
7. Burgess S. 'Mendelian randomization analysis with multiple genetic variants using summarized data'. Genet Epidemiol. 2013;37(7):658-65.
8. Bowden J. 'Mendelian randomization with invalid instruments: effect estimation and bias detection through Egger regression'. Int J Epidemiol. 2015;44(2):512-25.
9. Bowden J. 'Consistent Estimation in Mendelian Randomization with Some Invalid Instruments Using a Weighted Median Estimator'. Genet Epidemiol. 2016;40(4):304-14.
10. Hartwig FP. 'Robust inference in summary data Mendelian randomization via the zero modal pleiotropy assumption'. Int J Epidemiol. 2017;46(6):1985-98.
11. Hemani G. 'The MR-Base platform supports systematic causal inference across the human phenome'. elife. 2018;7:e34408.

Poster No 852

Hippocampal subfield atrophy in high genetic risk for AD:Unraveling sex- and AD stage-specific rates

Tavia Evans[1], Natalia Vilor-Tejedor[2], Albert Rodrigo[2], Patricia Genius[2], Blanca Rodríguez-Fernández[2], Federica Anastasi[2], Arcadi Navarro[2], Juan Domingo Gispert[2], Hieab Adams[3]

[1]Erasmus mc, Rotterdam, Zuid Holland, [2]Barcelonaβeta Brain Research Center, Barcelona, Catalonia, [3]Department of Genetics, Radboud University, Nijmegen, Gelderland

Introduction: Neuropathological studies have shown that hippocampal atrophy is affected in cognitive aging and Alzheimer's disease (AD) (Brickman, 2011; Evans, 2018). Moreover, current evidence suggests that hippocampal subfields have partially different genetic architecture and may improve the sensitivity of the detection of AD (Liu, 2015). In this study, we aimed at evaluating whether hippocampal subfield trajectories exhibit variations across different stages of AD, as well as to evaluate whether there is a sex-related impact on the rate of hippocampal volume decline. Additionally, we investigated whether genetic predisposition to AD contributes to the accelerated rate of hippocampal volume atrophy across AD stages and sex, and how this contribution is specifically driven by variants located in the APOE gene.

Methods: The study comprised 562 participants from the Alzheimer's Disease Neuroimaging Initiative (ADNI-1) cohort (75.2 yo; 42.3% women), with complete demographic, genetic, and 1.5T magnetic resonance imaging scans at baseline and every 6 months for a total of 96 months (Controls (amyloid negative), CUN= 161; mild cognitive impairment, MCIN = 260, AD patients, ADN = 141). Hippocampal subfields were extracted using the longitudinal processing method within FreeSurfer (version 6.0). Genetic predisposition to AD was assessed through polygenic scoring using PRSice version 2, with and without considering the APOE region (chr19:45,409,011-45,412,650; GRCh37/hg19). Linear mixed-effect models with random- time slope and intercept for individuals were used to investigate the association between genetic predisposition to AD and hippocampal subfields volumetric trajectories over time. Models were adjusted by age, sex, AD disease status (CU, MCI, AD), years of education and total hippocampal volume. Disease and sex status-specific trajectories dependent on genetic predisposition to AD were assessed by including an interaction term.

Results: We observed significant reduction in hippocampal subfields volumes over time, showing more pronounced atrophy among participants with MCI and AD compared to CN [Figure 1A]. In addition, high genetic predisposition to AD was associated with accelerated atrophy rates in the CA1, hippocampal tail, molecular layer, presubiculum, subiculum, as well as the overall hippocampal region [Figure 1B]. Disease-dependent models showed that MCI participants at high genetic predisposition to AD exhibited a more severe atrophy rate in the hippocampal tail, molecular layer, presubiculum, subiculum, and the overall hippocampus compared to those with a lower genetic predisposition [Figure 2A]. Sex-related differences were also observed, with women at high genetic predisposition showing more pronounced atrophy in the fimbria and hippocampal fissure regions [Figure 2B]. All effects ceased to be significant when the variants in the APOE gene region were not considered. Additional analyses evaluating the effect of functional genetic variants of the APOE gene revealed that the effects were mainly driven by brain hippocampal eQTLs of the APOE gene (e.g. rs75627662).

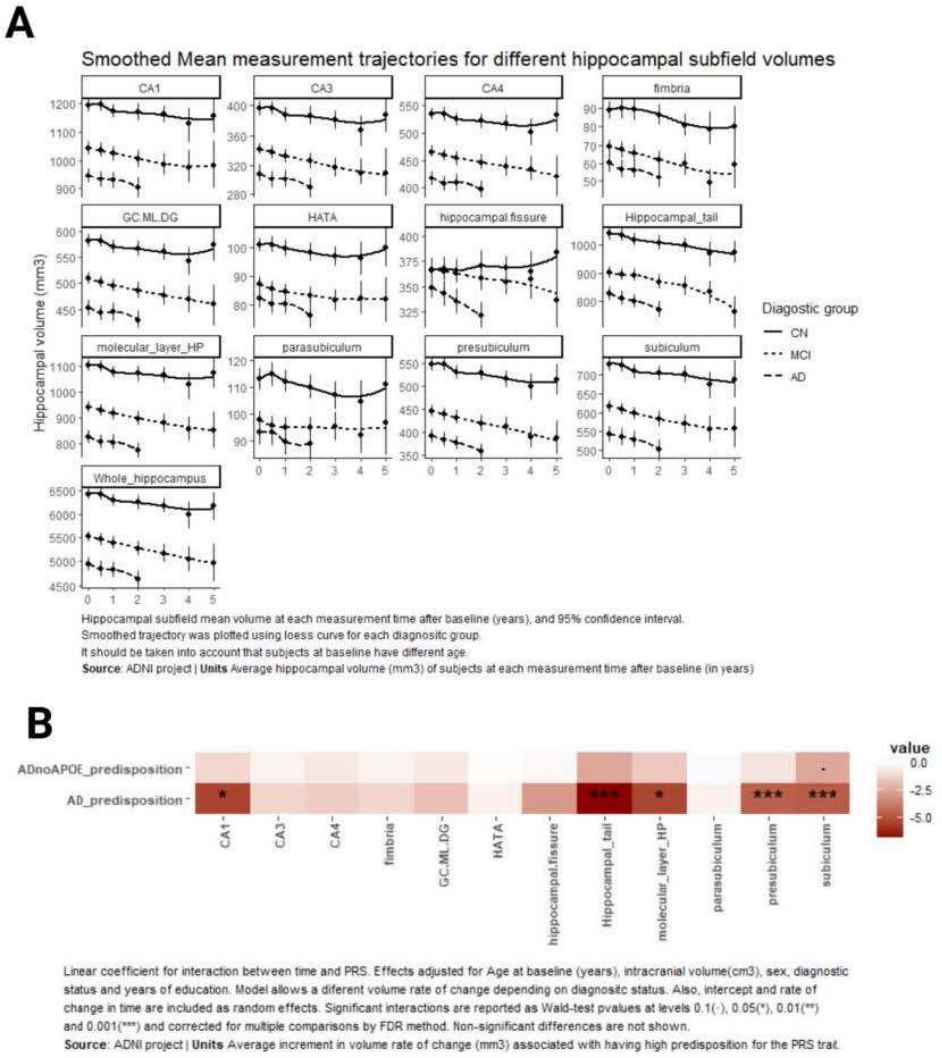

Figure 1. A) Smoothed Mean Hippocampal Subfields Trajectories by Diagnostic Group. B) Association between genetic predisposition to Alzheimer's disease and hippocampal subfields trajectories.

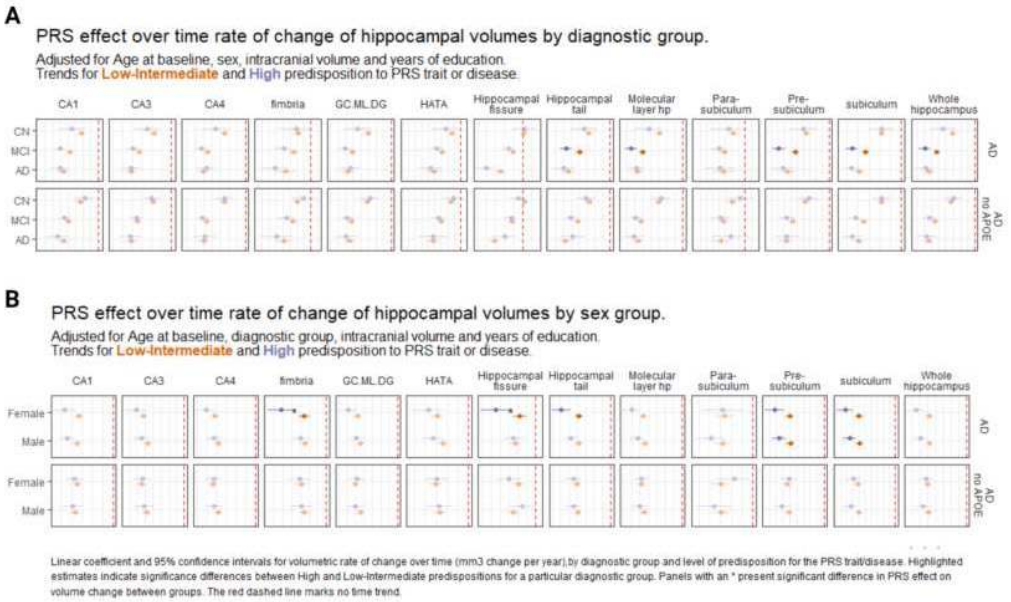

Figure 2. Influences of genetic predisposition to Alzheimer's disease on hippocampal subfields volumetric changes over time. A) By diagnostic group (AD, MCI, CN). B) By sex (Female, Male).

Conclusions: Our findings emphasized the importance of considering both hippocampal subfields and genetic predisposition to AD, specifically APOE variants, and their interactions in understanding AD progression and sex-specific trajectories. Moreover, our results suggested different patterns of atrophy between CN (amyloid negative individuals) and MCI and AD patients (amyloid positive individuals), suggesting differences related to aging versus AD pathophysiology in hippocampal subfields trajectories. The findings provide valuable insights for refining early detection strategies and targeted intervention approaches for more effective AD management.

References

1. Brickman AM (2011), Hippocampal subregions differentially associate with standardized memory tests. Hippocampus. 21(9):923-8.
2. Evans TE (2018), Subregional volumes of the hippocampus in relation to cognitive function and risk of dementia. Neuroimage. 1;178:129-35.
3. Liu, Y (2015). APOE genotype and neuroimaging markers of Alzheimer's disease: systematic review and meta-analysis. Journal of Neurology, Neurosurgery & Psychiatry, 86(2), 127-134.

Poster No 853

Unraveling Glioblastoma Diversity: Insights into Methylation Subtypes and Spatial Relationships

Martha Foltyn-Dumitru[1], Haidar Alzaid[1], Felix Sahm[1], Wolfgang Wick[1], Martin Bendszus[1], Philipp Vollmuth[1], Marianne Schell[1]

[1]Heidelberg University Hospital, Heidelberg, Germany

Introduction: Gliomas, particularly Isocitrate Dehydrogenase (IDH) wild-type variants, represent a formidable challenge in neuro-oncology due to their intrinsic heterogeneity (Parker et al., 2015). As our understanding of glioma subtypes evolves, integrating advanced imaging modalities and molecular profiling becomes imperative for unraveling the complex interplay between tumor genetics and neuroanatomy. This retrospective study elucidates the intricate relationships between specific brain regions and molecular subtypes in glioblastomas.

Methods: A cohort of 441 consecutive patients with IDH-wild-type glioma, diagnosed between 2009 and 2020, underwent preoperative MRI at Heidelberg University Hospital. The imaging protocol encompassed T1-weighted images, 2D FLAIR, and T2-weighted images. Molecular analysis determined IDH status and subclassification via DNA methylation profiling (Capper et al., 2018). Initially, brain extraction and tumor segmentation utilized HD-GLIO, a deep learning-based approach, further validated by a neuroradiology resident (Isensee et al., 2019; Kickingereder et al., 2019). Subsequently, all T1-weighted images were registered to the FSL 1mm MNI template using a modified version of the fsl_anat function, employing both linear and non-linear registration with additional tumor area masking. The resulting transformation mask was applied to the tumor masks. For the third step, support vector regression-based lesion-symptom mapping (SVR-LSM) was employed to detect distinct brain regions associated with methylation subtypes (DeMarco & Turkeltaub, 2018; Zhang et al., 2014). Lesion maps were resampled to $2mm^3$, data were corrected for lesion volume, and beta maps were thresholded at $p < 0.005$ based on 10,000 permutations, with a minimum cluster size of >100 voxels.

Results: Out of the initially screened 441 patients, 423 (95.9%) met inclusion criteria, with six patients lacking voxels meeting the minimum lesion cutoff (n=10), and the rest excluded due to missing high-resolution T1w images. Following DNA methylation profiling, patients were classified into methylation subclasses. Predominantly, RTK II was observed (n=172, 40.7%), followed by MES (n=142, 33.6%), RTK I (n=75, 17.7%), and others (n=34, 8%). SVR-LSM unveiled distinct brain regions for different methylation subtypes. MES revealed a left-hemispheric cluster (superior temporal gyrus, posterior temporal lobe, insula cortex, posterior limb of internal capsule). RTK I showed two clusters in the right superior and middle frontal brain parenchyma. RTK II showed three clusters in the left hemisphere, two in the frontal lobe (including the inferior frontal gyrus) and one in the parietal lobe (supramarginal and angular gyrus). See Figures 1 and Table 1.

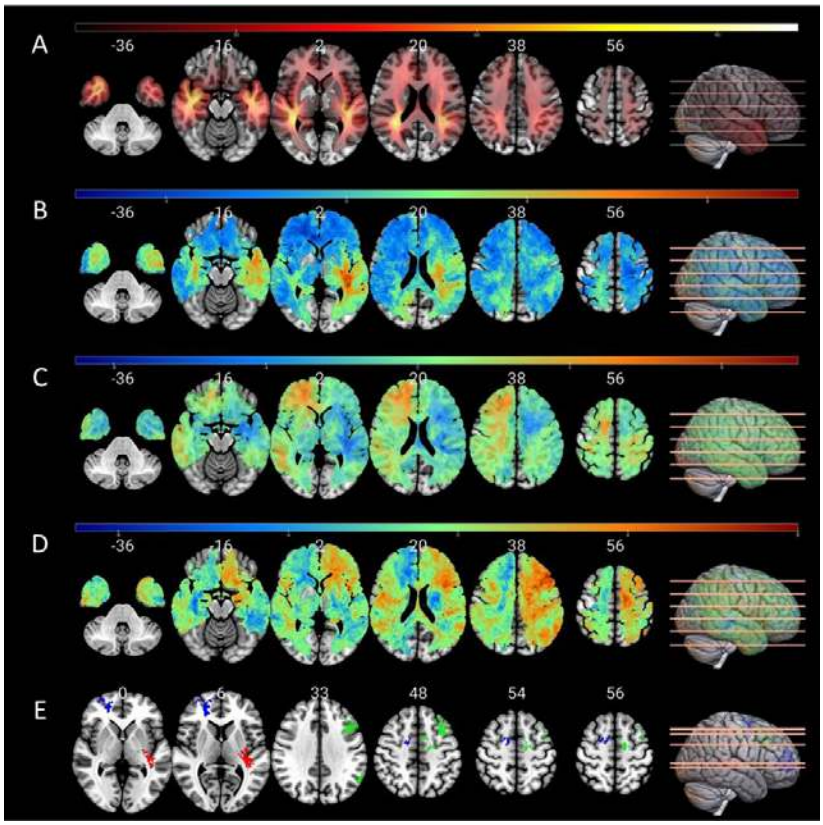

Figure1. A) Overlay of all tumor masks. Unthresholded beta maps for the distinct methylation subclasses, B) MES, C) RTK I, and D) RTK II. E) Final clusters: red MES, blue RTK I, and green RTK II.

Parameter	MES	RTK I	RTK II	p-value
Clinical				
Number of patients	142	75	172	NA
Age in years [mean ±std]	61±12	63±11	64±11	0.37
Gender[% female]	49	33	47	0.06
Survival in months [mean ±std]	16±16	16±19	16±13	0.44
Volume [in mm³]				
Whole tumor [mean ±std cm³]	87±60	89±61	82±59	0.65
Edema [mean ±std cm³]	63±48	56±44	54±40	0.30
Contrast enhancement [mean ±std cm³]	17±18	23±22	20±20	0.09
Necrosis [mean ±std cm³]	7.2±11	11±15	8.2±12	0.09
VLSM cluster				
N of clusters	1	1	1	NA
Volume in mm³	3080	3072	6320	
Peak MNI coordinates (x,y,z)	-38, -34, 0	21, 59, 0	-45, 12, 34	
N of clusters		2	2	NA
Volume in mm³		1680	1976	
Peak MNI coordinates (x,y,z)		11, -2, 66	-7, -2, 60	
N of clusters			3	NA
Volume in mm³			800	
Peak MNI coordinates (x,y,z)			-63, -48, 30	

Table 1. Overview of methylation subclasses.

Conclusions: This study bridged the gap between molecular heterogeneity and spatial characteristics in glioblastomas through SVR-LSM, elucidating complex relationships. It unveiled associations between molecular subtypes of glioblastomas and their spatial characteristics. The significance of the work was underscored by the integration of multi-modal approaches, offering a comprehensive understanding of glioma heterogeneity. These insights not only unraveled the intricate landscape of glioma biology but also held promise for guiding future research and informing clinical applications.

References

1. Chavez, L., Reuss, D. E., Kratz, A., Wefers, A. K., Huang, K., Pajtler, K. W., Schweizer, L., Stichel, D., Olar, A., Engel, N. W., Lindenberg, K., . . . Pfister, S. M. (2018). DNA methylation-based classification of central nervous system tumours. Nature, 555(7697), 469-474. https://doi.org/10.1038/nature26000
2. DeMarco, A. T., & Turkeltaub, P. E. (2018). A multivariate lesion symptom mapping toolbox and examination of lesion-volume biases and correction methods in lesion-symptom mapping. Hum Brain Mapp, 39(11), 4169-4182. https://doi.org/10.1002/hbm.24289
3. Isensee, F., Schell, M., Pflueger, I., Brugnara, G., Bonekamp, D., Neuberger, U., Wick, A., Schlemmer, H. P., Heiland, S., Wick, W., Bendszus, M., Maier-Hein, K. H., & Kickingereder, P. (2019). Automated brain extraction of multisequence MRI using artificial neural networks. Hum Brain Mapp, 40(17), 4952-4964. https://doi.org/10.1002/hbm.24750
4. Kickingereder, P., Isensee, F., Tursunova, I., Petersen, J., Neuberger, U., Bonekamp, D., Brugnara, G., Schell, M., Kessler, T., Foltyn, M., Harting, I., Sahm, F., Prager, M., Nowosielski, M., Wick, A., Nolden, M., Radbruch, A., Debus, J., Schlemmer, H. P., . . . Maier-Hein, K. H. (2019). Automated quantitative tumour response assessment of MRI in neuro-oncology with artificial neural networks: a multicentre, retrospective study. Lancet Oncol, 20(5), 728-740. https://doi.org/10.1016/s1470-2045(19)30098-1
5. Parker, N. R., Khong, P., Parkinson, J. F., Howell, V. M., & Wheeler, H. R. (2015). Molecular heterogeneity in glioblastoma: potential clinical implications. Front Oncol, 5, 55. https://doi.org/10.3389/fonc.2015.00055
6. Zhang, Y., Kimberg, D. Y., Coslett, H. B., Schwartz, M. F., & Wang, Z. (2014). Multivariate lesion-symptom mapping using support vector regression. Hum Brain Mapp, 35(12), 5861-5876. https://doi.org/10.1002/hbm.22590

Poster No 854

Plasma proteomics identifies proteins and pathways associated with incident depression

Jujiao Kang[1], Liu Yang[1], Tianye Jia[1], Jintai Yu[1], Wei Cheng[1], Jianfeng Feng[2]

[1]Fudan University, Shanghai, Shanghai, [2]Institute of Science and Technology for Brain inspired Intelligence, Shanghai, Shanghai

Introduction: Depression, a growing global concern with a prevalence surpassing 5%(Collins, Patel et al. 2011), gravely impairs the wellbeing and quality of life of affected individuals and posing substantial societal burdens(Herrman, Patel et al. 2022). The limited success in achieving consistent remission is intricately linked to our incomplete understanding of its pathogenesis(Yuan, Yang et al. 2023). Unraveling these elusive mechanisms is paramount, setting the stage for more effective therapeutic interventions. While several studies have delved into the association between plasma proteins and depression(Zhang, Guo et al. 2022), their insights, albeit valuable, are constrained by small sample sizes or limited proteomic scope. Thus, it is crucial to explore the profiling protein dysregulations prior to depression onset using large biobanks. Besides, given that depression arises from a sophisticated interplay of biological and environmental elements(Yuan, Yang et al. 2023), examining these proteins within diverse biological and environmental factors and understanding their linked pathways is essential.

Methods: Utilizing the prospective UKB cohort, we assessed associations between 1448 baseline plasma protein levels and incident depression among 45,505 participants. We initially employed survival analysis to profile proteomic concentrations associated with incident depression. Accordingly, we related these depression-linked proteins to neuroimaging data, genetic indicators, and environmental variables, and subsequently characterized the biological pathways. To underscore the clinical implications, we applied MR to establish causal links, spotlighting potential therapeutic targets. Overall, we aim to identify risk signatures, decipher underlying pathogenesis, and inform tailored therapeutic.

Results: We examined the association between plasma protein level and incident depression using the cox proportional hazard model and identified 212 proteins significantly associated with incident depression (Fig. 1A). Notably, growth/differentiation factor 15 (GDF15); tumor necrosis factor receptor superfamily member 10B (TNFRSF10B); neurofilament light polypeptide (NEFL); urokinase plasminogen activator surface receptor (PLAUR); and insulin-like growth factor-binding protein 4 (IGFBP4) had the most significant associations. (Fig. 1B). Overall, 206 of the 212 depression-associated proteins showed cross-sectional associations with baseline PHQ4 scores after Bonferroni correction (Fig. 1C). After further adjustment for the PHQ4 score, 95 of the 212 proteins remained significantly associated with the incident depression (Fig. 1D). We examined the associations between the 95 identified depression-associated proteins and brain structures. After FDR correction, 43 of the 95 proteins showed at least one association with the four global brain structures (Fig. 2A). We also identified 43 proteins that exhibited significant associations with at least one brain regional measure. Several brain regions implicated in depression, including left middle temporal gyrus, left medial orbitofrontal gyrus, bilateral hippocampus, bilateral thalamus, were associated with at least 3 proteins (Fig. 2B). In addition, bilateral posterior thalamic radiation, bilateral anterior thalamic radiation, left cingulate gyrus part of cingulum, were associated with at least 3 proteins (Fig. 2C). Furthermore, these protein alterations showed stronger correlations with stress-related events than genetic factors. Pathway analysis highlighted the central role of the immune response and TNF emerged as a key hub in the protein-protein expression network. BTN3A2 was identified as having a causal association with depression.

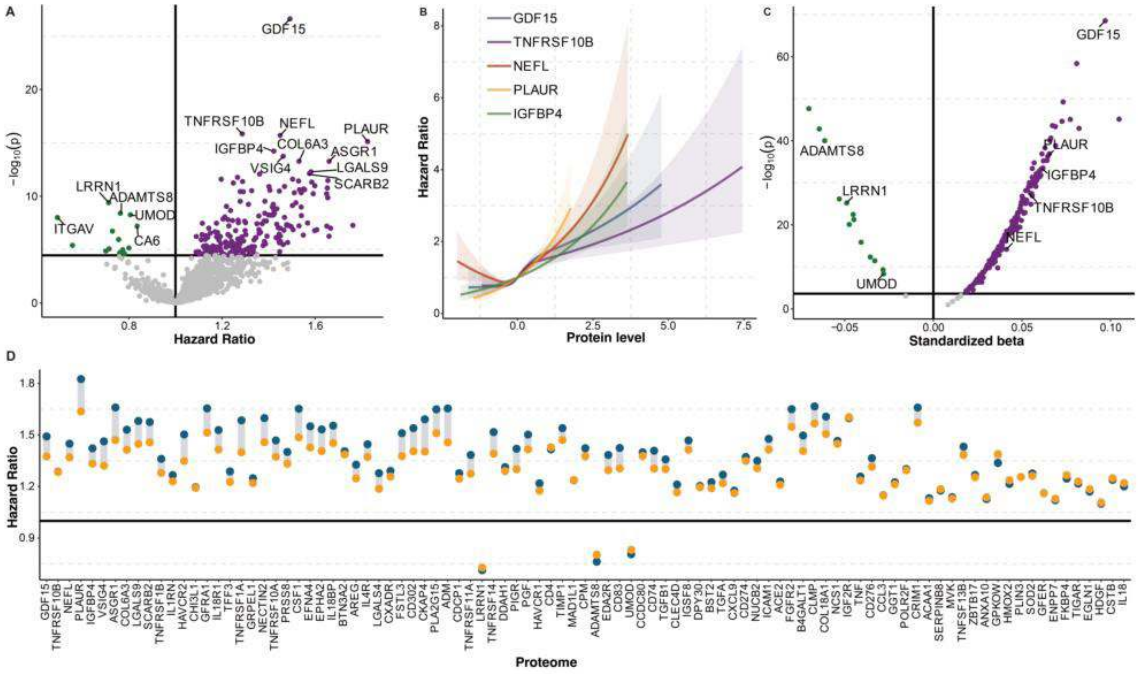

Figure 1: Proteome-wide associations with incident depression.

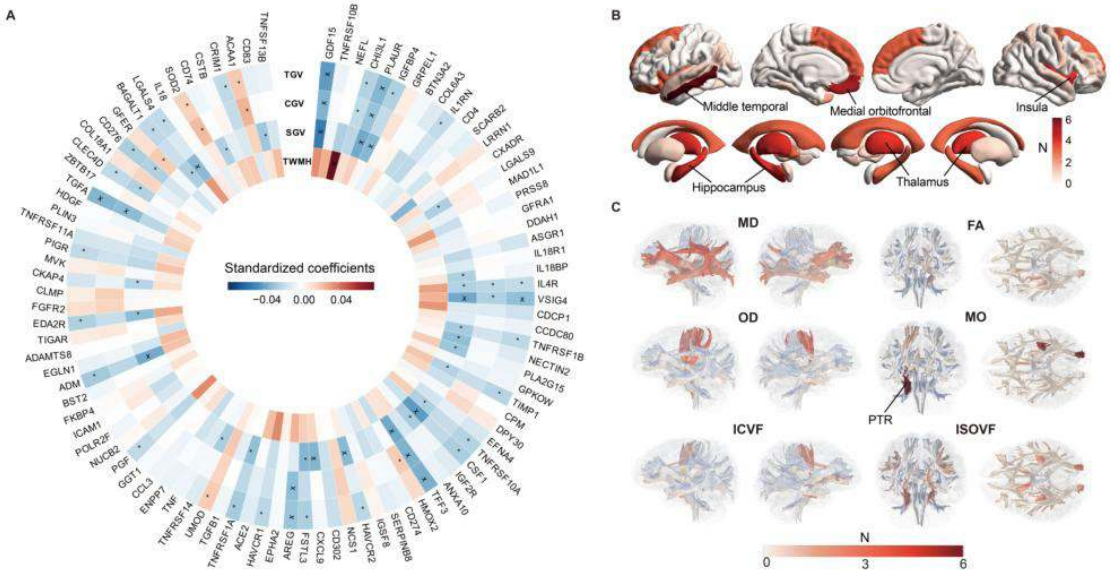

Figure 2: Association of depression-associated proteins with brain structure.

Conclusions: Our findings bridge critical knowledge gaps, emphasizing the potential of proteomic markers in both predicting and possibly mitigating depression's onset, setting the stage for more personalized and effective therapeutic strategies.

References

1. Akil, H., et al. (2018). "Treatment resistant depression: A multi-scale, systems biology approach." Neurosci Biobehav Rev 84: 272-288.
2. Choi, H., et al. (2021). "Serum proteomic analysis of major depressive disorder patients and their remission status: Novel biomarker set of zinc-alpha-2-glycoprotein and keratin type II cytoskeletal 1." Int J Biol Macromol 183: 2001-2008.
3. Collins, P. Y., et al. (2011). "Grand challenges in global mental health." Nature 475(7354): 27-30.
4. Herrman, H., et al. (2022). "Time for united action on depression: a Lancet-World Psychiatric Association Commission." Lancet 399(10328): 957-1022.
5. Li, S., et al. (2021). "Multiregional profiling of the brain transmembrane proteome uncovers novel regulators of depression." Sci Adv 7(30).
6. Malhi, G. S. and J. J. Mann (2018). "Depression." Lancet 392(10161): 2299-2312.
7. Marx, W., et al. (2023). "Major depressive disorder." Nat Rev Dis Primers 9(1): 44.
8. Shin, D., et al. (2022). "Integrating proteomic and clinical data to discriminate major psychiatric disorders: Applications for major depressive disorder, bipolar disorder, and schizophrenia." Clin Transl Med 12(6): e929.
9. Thase, M. E. and T. L. Schwartz (2015). "Choosing medications for treatment-resistant depression based on mechanism of action." J Clin Psychiatry 76(6): 720-727; quiz 727.

10. Yuan, M., et al. (2023). “Epigenetic regulation in major depression and other stress-related disorders: molecular mechanisms, clinical relevance and therapeutic potential.” Signal Transduct Target Ther 8(1): 309.
11. Zhang, M. M., et al. (2022). “IL-1R/C3aR signaling regulates synaptic pruning in the prefrontal cortex of depression.” Cell Biosci 12(1): 90.
12. Zhdanava, M., et al. (2021). “The Prevalence and National Burden of Treatment-Resistant Depression and Major Depressive Disorder in the United States.” J Clin Psychiatry 82(2).

Poster No 855

GWAS of EEG oscillations unveils genetic pleiotropy between brain structure, function, and behavior

Philippe Jawinski[1], Jacquelyn Meyers[2], José Morosoli Garcia[3], Sarah Medland[4], ENIGMA-EEG Consortium[5], Paul Thompson[6], Dirk Smit[7]

[1]Humboldt-Universität zu Berlin, Berlin, Germany, [2]Downstate Health Sciences University, Brooklyn, NY, [3]QIMR Berghofer Medical Research Institute, Herston, Australia, [4]QIMR Berghofer Medical Research Institute, Brisbane, Australia, [5]Cross-Instutional, Worldwide, [6]University of Southern California, Los Angeles, CA, [7]University of Amsterdam, Amsterdam, Noord-Holland

Introduction: Oscillations in neuronal brain activity play a crucial role in information processing and have been studied extensively as biological markers of human behavior and psychopathology[1]. A century ago, in 1924, Hans Berger’s discovery marked the inception of a transformative era in neuroscience, leading to crucial advancements in our understanding of brain function and the corresponding behavioral phenomena[2]. Twin studies have demonstrated that individual differences in EEG oscillations are strongly driven by genetic factors[3]. However, our understanding of their molecular genetic architecture is still very limited. Here, we conducted a genome-wide association study (GWAS) of resting-state EEG oscillations to discover associated genomic loci and to examine the pleiotropic relationships with other complex traits, i.e., the links with brain structure and mental illness.

Methods: We conducted to our best knowledge the largest GWAS of resting-state EEG to date, combining data from 9 cohorts with a total N = 14,361 participants. EEGs were recorded during a three- to five-minute eyes-closed resting-state condition. We used harmonized analysis protocols to examine the power of the EEG frequency bands alpha, beta, delta, theta, and broadband at the vertex site, as well as alpha power and alpha peak frequency at occipital leads. GWAS analyses were run in RAREMETALWORKER[4] followed by cross-cohort meta-analysis in METAL[5]. We used LD score regression[6] and pleioFDR[7] to investigate a shared genetic basis with other complex traits, including MRI-derived brain structure variables[8] and psychiatric disorders[9]. Variant discoveries were annotated using positional and functional mapping strategies based on RefSeq[10], GTEx[11], and other omics databases. Finally, we estimated the degree of polygenicity of EEG oscillations via genetic effect size distribution analyses implemented in GENESIS[12].

Results: SNP-based heritability estimates ranged from 14-27% (SE: 3.7%). We discovered two genome-wide significant loci: an intergenic region at 13q12.3 (p = 6.6e-09), and a known schizophrenia risk locus in an intron of FANCA at 16q24.3 (p = 1.4e-08). Both loci were associated with alpha peak frequency. We identified 32 additional likely associated loci by leveraging pleiotropy with psychiatric traits such as schizophrenia, major depression, and bipolar disorder. Of these loci, 27 have a nearest gene that is protein-coding, and 24 are known GTEx expression quantitative trait loci (eQTLs). Using genetic correlations, we demonstrate a shared genetic basis between EEG power and MRI-derived cerebral white matter volume (rG = -0.33, p = 3.0e-07) and cortical surface area (rG = 0.26, p = 2.0e-04), with the top regional associations implicating the orbitofrontal, anterior cingulate, and precuneus surface area. Genetic correlations also indicated an overlap with generalized epilepsy, neuroticism, and loneliness. Polygenicity analyses revealed an estimated number of ~5.5k (SE: 2.7k) underlying variants contributing to the SNP-based heritability of EEG oscillations, which is lower when compared to estimates derived for height (12.5k; SE: 1.3k) and neuroticism (1.62k; SE: 2.2k).

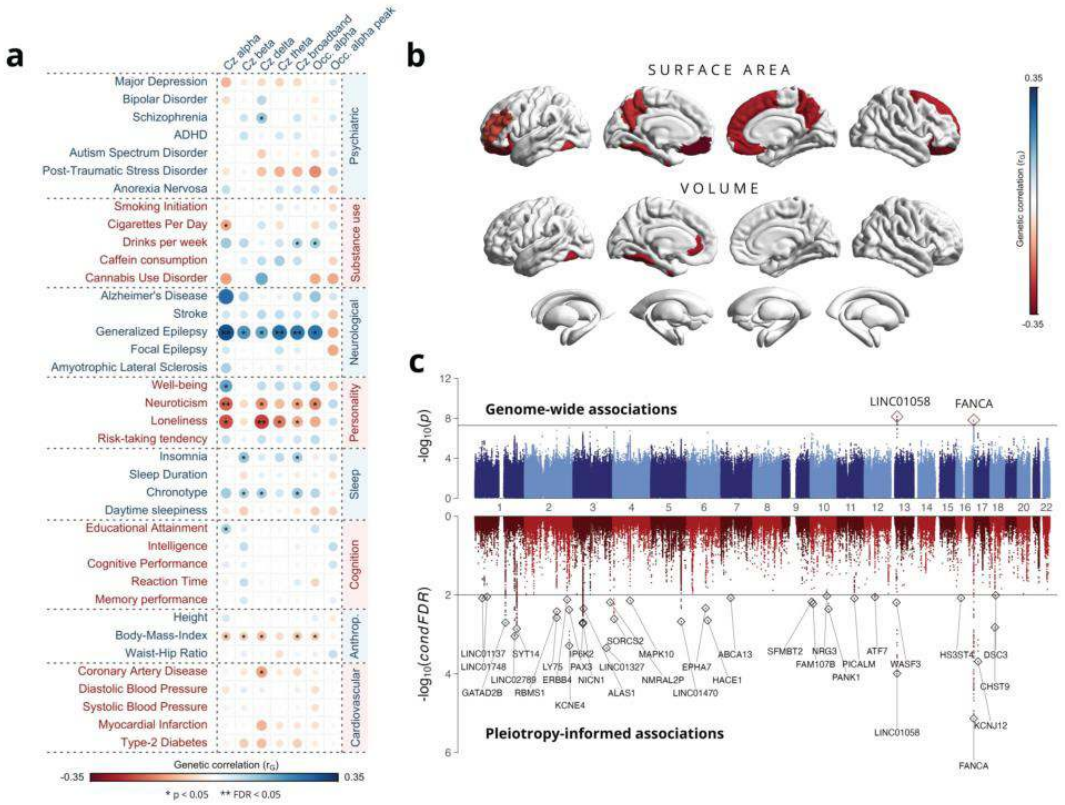

Fig. 1 Genetic associations for resting-state EEG oscillations in N = 14,361 individuals. **a** Genetic correlations between seven EEG variables (alpha, beta, delta, theta, and broadband power at Cz; alpha power and alpha peak frequency at occipital leads) and 38 selected traits from different health domains. **b** Significant genetic correlations between EEG broadband power and MRI-derived regional brain volume and surface area (FreeSurfer aparc and ase goutput). **c** Miami plot showing variant base pair positions along the chromosomes on the x-axis and p values from genome-wide associations (top) and conditional FDR values from pleiotropy-informed analyses (bottom) on the y-axis (-log10 scale). Results were merged across EEG variables (using the lowest p and FDR value per variant). Solid horizontal lines indicate the thresholds of significance (top: p = 5e-8; bottom: FDR < 0.01). Index variations are highlighted by diamonds and were annotated with the nearest gene identified through positional mapping.

Conclusions: Our results suggest that common genetic variation substantially affects EEG oscillations, with a genetic architecture that overlaps those of brain structure variables. In addition, our results provide support for genetic pleiotropy with psychiatric and neurological traits. Genetic effect size distribution analyses unveiled a relatively low degree of polygenicity, indicating a rapid increase of discoveries in future studies with larger sample sizes. In sum, our study supports twin studies on the strong heritability of brain oscillations, identifies novel gene loci, and reveals evidence for pleiotropic associations between MRI-derived brain variables, brain electrophysiology, and neurological and psychiatric disorders.

References

1. Newson et al. (2018). EEG Frequency Bands in Psychiatric Disorders: A Review of Resting State Studies. Front. Hum. Neurosci. 12, 521.
2. Salisbury et al. (2023): 100th year anniversary of the discovery of electroencephalography. Clin. EEG Neurosci. 15500594231217520 (2023).
3. van Beijsterveldt et al. (2002). Twin and family studies of the human electroencephalogram: a review and a meta-analysis. Biol. Psychol. 61, 111–138.
4. Willer et al. (2010). METAL: fast and efficient meta-analysis of genomewide association scans. Bioinformatics 26, 2190–2191.
5. Feng et al. (2014). RAREMETAL: fast and powerful meta-analysis for rare variants. Bioinformatics 30, 2828–2829.
6. Bulik-Sullivan et al. (2015) An atlas of genetic correlations across human diseases and traits. Nat. Genet. 47, 1236–1241.
7. Andreassen et al. (2013) Improved detection of common variants associated with schizophrenia and bipolar disorder using pleiotropy-informed conditional false discovery rate. PLoS Genet. 9, e1003455.
8. Smith et al. (2021) An expanded set of genome-wide association studies of brain imaging phenotypes in UK Biobank. Nat. Neurosci. 24, 737–745.
9. Sullivan et al. (2017) Psychiatric Genomics: An Update and an Agenda. Am. J. Psychiatry 175, 15–27.
10. O'Leary et al. (2016) Reference sequence (RefSeq) database at NCBI: current status, taxonomic expansion, and functional annotation. Nucleic Acids Res. 44, D733-45.
11. Aguet et al. (2017) Genetic effects on gene expression across human tissues. Nature 550, 204–213.
12. Zhang et al. (2018). Estimation of complex effect-size distributions using summary-level statistics from genome-wide association studies across 32 complex traits. Nat. Genet. 50, 1318–1326.

Poster No 856

Rare variant genetic architecture of human cortical organization

Kuldeep Kumar[1], Sayeh Kazem[1], Zhijie Liao[1], Jakub Kopal[2], Guillaume Huguet[3], Thomas Renne[1], Martineau Jean-Louis[3], Zhe Xie[1], Zohra Saci[3], Laura Almasy[4], David Glahn[5], Tomas Paus[6], Guillaume Dumas[1], Carrie Bearden[7], Paul Thompson[8], Richard Bethlehem[9], Varun Warrier[10], Sébastien Jacquemont[3]

[1]CHUSJ Research Center, University of Montreal, Montreal, Quebec, [2]McGill University, Montreal, Quebec, [3]CHU Saint-Justine, Montreal, QC, [4]Perelman School of Medicine, University of Pennsylvania, Philadelphia, PA, [5]Department of Psychiatry, Harvard Medical School, Boston, MA, [6]Université de Montréal, Montreal, Quebec, [7]University of California at Los Angeles, Los Angeles, CA, [8]Imaging Genetics Center, Keck School of Medicine of University of Southern California, Los Angeles, CA, [9]Autism Research Centre, Department of Psychiatry, University of Cambridge, Cambridge, United Kingdom, [10]University of Cambridge, Cambridge, Cambridgeshire

Introduction: The development and organization of the human cortex are highly heritable [Hibar (2015), Elliott (2018), Grasby (2020)]. Genome-wide association studies (GWAS) have identified common variants influencing the global and regional cortical phenotypes derived using magnetic resonance imaging (MRI) [Grasby (2020), Smith (2021), Warrier (2023)]. Studies focusing on a very small set of rare variants, previously associated with neuropsychiatric disorders, have shown large effects on cortical structures [Modenato (2021)]. However, genome-wide studies have not been conducted and the rare variant architecture of the cerebral cortex remains unknown. Here we aimed to map the effects of rare variants, genome-wide, on twelve MRI-derived phenotypes, measured globally and regionally, in general population cohorts. We also compared the phenotype burden genetic correlations with common variant genetic correlations to gain insights into the relationship between common and rare variant architectures.

Methods: We analyzed structural and diffusion MRI-derived phenotypes and all copy-number-variants (CNV) >50 kilobases from 40,000 UK Biobank participants [Smith (2021), Moreau (2023)] and 8,000 ABCD participants [Hagler (2019)]. Our analysis focused on seven macrostructural measures derived from T1w MRI: cortical thickness (CT), surface area (SA), volume (Vol), folding index, intrinsic curvature index, mean curvature (MC), and Gaussian curvature; and five microstructural measures derived from diffusion MRI: fractional anisotropy, mean diffusivity (MD), isotropic volume fraction (ISOVF), intracellular volume fraction, and orientation diffusion index [Warrier (2023)]. Since the current sample size remains underpowered to detect gene-level or variant-level associations for most rare variants, we used a functional burden association test. The latter aggregates the variants that disrupt genes involved in a given biological function in each individual. Genes were assigned to biological functions using previously published cell-type marker genes [Wagstyl (2022)], Gene Ontology terms, and spatial transcriptomics [Hawrylycz (2012)]. The burden association analysis is a linear model that estimates the mean effect size on MRI phenotypes of genes within each gene-set (and corresponding biological function) of interest. Analyses are performed, for deletions and duplications separately, and are adjusted for age, sex, site, and ancestry. We estimated burden genetic correlations between pairs of MRI phenotypes and between variant-types by correlating the effect sizes across all biological functions by adapting a previously published approach [Weiner (2023)].

Results: Out of 24,768 burden associations (12 phenotypes x 1032 gene sets x 2 variant type), 437 showed FDR significance. Vol, SA, and CT showed the strongest association with gene dosage, while ISOVF, MD, and MC showed much weaker associations. The CNV burden genetic correlations were positive and negative across 58% and 42% pairs of traits, respectively. These CNV burden genetic correlations were concordant with those previously published using common-variants ($r=0.84$, $p<1e-4$). The effect sizes of deletions and duplications were negatively correlated for the majority of phenotypes, suggesting that deletions and duplications show preferential effects across MRI traits and biological functions. Analyses at the regional level showed significant associations across many functional gene sets. The CNV burden genetic correlations across brain regions were concordant with those previously reported for common variants.

Conclusions: Our study revealed that the common and rare variant architectures of human cortical MRI phenotypes are concordant, with most MRI phenotypes preferentially sensitive to either deletions or duplications. Because deletions and duplications have large negative and positive effects on gene expression (respectively), our analysis provides insight into the effects of changes in transcription on MRI phenotypes.

References

1. Hibar, D.P., (2015). "Common genetic variants influence human subcortical brain structures." Nature 520.7546: 224-229.
2. Elliott, L.T., (2018). "Genome-wide association studies of brain imaging phenotypes in UK Biobank." Nature 562.7726: 210-216.
3. Modenato, C., (2021): "Lessons learned from neuroimaging studies of copy number variants: a systematic review." Biological Psychiatry 90.9: 596-610.
4. Grasby, K.L., (2020). "The genetic architecture of the human cerebral cortex." Science 367.6484: eaay6690.

5. Smith, S.M., (2021). “An expanded set of genome-wide association studies of brain imaging phenotypes in UK Biobank.” Nature Neuroscience 24.5: 737-745.
6. Warrier, V. (2023) “Genetic insights into human cortical organization and development through genome-wide analyses of 2,347 neuroimaging phenotypes.” Nature Genetics 55.9: 1483-1493.
7. Weiner, D.J., (2023). “Polygenic architecture of rare coding variation across 394,783 exomes.” Nature 614.7948: 492-499.
8. Moreau, C.A., (2023). “Genetic heterogeneity shapes brain connectivity in psychiatry.” Biological Psychiatry 93.1: 45-58.
9. Hawrylycz, M., (2012). “An anatomically comprehensive atlas of the adult human brain transcriptome.” Nature 489, 391–399.
10. Wagstyl, K., (2022). “Transcriptional cartography integrates multiscale biology of the human cortex.” bioRxiv : 2022-06.
11. Hagler, D.J., (2019). “Image processing and analysis methods for the Adolescent Brain Cognitive Development Study.” NeuroImage 202: 116091.

Poster No 857

Multitrait GWAS Analysis with Brain Morphometry Uncovers New Parkinson’s Disease Risk Loci

Natalia Ogonowski[1,2], Santiago Diaz-Torres[1,2], Luis M. Garcia Marin[1,2], Xochitl Diaz[1], Zuriel Ceja[1,3], Miguel Renteria[1,2]

[1]Mental Health & Neuroscience Program, QIMR Berghofer Medical Research Institute, Brisbane, QLD, Australia, [2]School of Biomedical Sciences, Faculty of Medicine, The University of Queensland, Brisbane, QLD, Australia, [3]School of Biomedical Sciences, The University of Queensland, Brisbane, QLD, Australia

Introduction: Parkinson’s disease (PD) is the second most common neurodegenerative disorder, characterised by motor symptoms (resting tremor, rigidity, and bradykinesia), as well as non-motor symptoms, such as cognitive impairment and sleep disturbances. Its etiology is multifactorial, encompassing genetic, environmental, and age-related factors. Despite recent progress in elucidating the genetic aetiology of PD, considerable gaps remain in understanding the genetic architecture of the disease. Further investigation into the genetic underpinnings of PD could significantly advance our comprehension of its biological mechanisms. In this study, we used summary statistics from genome-wide association studies (GWAS) of brain morphometry and PD to increase our knowledge about the genetic basis of PD.

Methods: We performed a meta-analysis of GWAS for PD using summary statistics from the Nalls et al. 2019 and FinnGen release 9, followed by a Multi-Trait Analysis of GWAS (mTAG) between PD and neuroimaging phenotypes (intracranial volume and the volumes of the accumbens, brainstem, caudate, pallidum, putamen, thalamus, and ventral diencephalon), yielding a combined effective sample size of 62,294 PD cases and 1,938,001 controls. Our results identified genetic variants associated with PD. We also conducted conditional and joint analyses to identify the genetic variants that best account for heritable variation. Finally, we performed functional annotation and pathway analyses to gain insights into the biological mechanisms underlying the observed associations.

Results: Our study identified 206 independent genome-wide significant risk signals across 83 genomic regions, of which 99 were novel. Gene-based association tests revealed 226 genes associated with PD. Additionally, we identified three biological pathways involved in the development of PD: regulation of axon extension in axon guidance, signalling to p38 via RIT and RIN, and genes down-regulated in hypertrophic hearts (due to the expression of a constitutively active form of PPP3CA) that are predicted to be targets of the miR-1 microRNA.

Conclusions: Our findings advance the understanding of the genetic basis of PD by combining genetic results from neuroimaging traits. Additionally, prioritising genes involved in PD aetiology provides new avenues to understand biological mechanisms associated with PD risk and offers new avenues for treatment development.

References

1. Nalls MA, et al (2019). ‘Identification of novel risk loci, causal insights, and heritable risk for Parkinson’s disease: a meta-analysis of genome-wide association studies’. Lancet Neurol, 18(12):1091-1102.
2. Turley P, et al (2018). ‘Multi-trait analysis of genome-wide association summary statistics using MTAG’. Nat Genet, 50(2):229-237.
3. Xu H, et al (2023). ‘Identifying genetic loci and phenomic associations of substance use traits: A multi-trait analysis of GWAS (MTAG) study’. Addiction,18(10):1942-1952.

Poster No 858

Shared Genetic Aetiology of Suicide Attempt with Intracranial and Subcortical Brain Structures

Zuriel Ceja[1], Luis M. Garcia Marin[1], Jill Rabinowitz[2], Miguel Renteria[3]

[1]QIMR Berghofer Medical Research Institute, Brisbane, QLD, [2]Department of Mental Health Johns Hopkins Bloomberg School of Public Health, Baltimore, MD, [3]Mental Health & Neuroscience Program, QIMR Berghofer Medical Research Institute, Brisbane, AK

Introduction: Introduction: Suicide accounts for one in every 100 deaths in the world, and it is the fourth leading death cause for individuals aged between 15 and 29. Genetic studies have identified several genomic regions associated with suicide attempt (SA) risk. These putative risk genes are related to multiple domains, including epigenetics and cellular stress response, and are expressed in the brain and pituitary gland tissues. Understanding the complex biological basis of SA risk might enable the development of targeted interventions and improve public health strategies. This study leverages GWAS summary-based data to estimate genetic correlations between SA and brain morphometry measurements, aiming to produce novel insights into potential causal relationships.

Methods: Methods: We used GWAS summary statistics comprising 43,871 SA cases and 915,025 controls; participants included individuals of European ancestry from The International Suicide Genetics Consortium (ISGC) and The Million Veteran Program (MVP). We then examined genetic correlations between SA and intracranial volume (ICV) and nine subcortical brain volumes (i.e. caudate nucleus, hippocampus, brainstem, ventral diencephalon, thalamus, globus pallidus, putamen, nucleus accumbens, and amygdala). We used LD score regression (LDSC) and GWAS-pairwise (GWAS-PW) to identify shared genomic features to elucidate their interplay with SA. Lastly, we performed functional annotation and gene-based association analyses to gain insights into the biological mechanisms underlying the observer associations.

Results: Results: We identified significant genetic correlations between SA and specific brain regions. After adjusting for multiple testing, only the genetic correlation between SA and intracranial volume (ICV) was significant (rG = -0.10, p-value = 0.0019). GWAS-Pairwise identified ten genomic segments involving SA and at least one of the eight brain structures via the same genetic variants. The thalamus shared the largest number of shared segments (7 segments), followed by the putamen (2 segments) and caudate (1 segment). Lastly we performed functional annotation observing the enrichment of 7 genes (BTN3A2, HIST1H1B, HIST1H2BL, HIST1H2BN, HIST1H2AJ, HIST1H4L, and OR2B2) in the thalamus followed by the putamen and caudate, each sharing 2 (PPP4R1 and DCC) and 1 (DCC) enriched genes respectively with SA.

Conclusions: Conclusion: Our findings provide additional evidence for a genetic link between SA and intracranial volume (ICV). We found a negative correlation, meaning a reduced ICV may be associated with an increased risk of SA. This finding offers novel insights into the potential for genetic factors to concurrently influence brain structural changes and SA risk.

References

1. Turecki, G. et al. Suicide and suicide risk. Nat Rev Dis Primers 5, 74 (2019).
2. Shepard, D. S., Gurewich, D., Lwin, A. K., Reed, G. A., Jr & Silverman, M. M. Suicide and Suicidal Attempts in the United States: Costs and Policy Implications. Suicide Life Threat. Behav. 46, 352–362 (2016).
3. Domínguez-Baleón, C., Gutiérrez-Mondragón, L. F., Campos-González, A. I. & Rentería, M. E. Neuroimaging Studies of Suicidal Behavior and Non-suicidal Self-Injury in Psychiatric Patients: A Systematic Review. Front. Psychiatry 9, 500 (2018).
4. Auerbach, R. P., Pagliaccio, D., Allison, G. O., Alqueza, K. L. & Alonso, M. F. Neural Correlates Associated With Suicide and Nonsuicidal Self-injury in Youth. Biol. Psychiatry 89, 119–133 (2021).
5. Campos, A. I. et al. Brain Correlates of Suicide Attempt in 18,925 Participants Across 18 International Cohorts. Biol. Psychiatry 90, 243–252 (2021).
6. Desmyter, S., van Heeringen, C. & Audenaert, K. Structural and functional neuroimaging studies of the suicidal brain. Prog. Neuropsychopharmacol. Biol. Psychiatry 35, 796–808 (2011).
7. Roy, A., Segal, N. L., Centerwall, B. S. & Robinette, C. D. Suicide in twins. Arch. Gen. Psychiatry 48, 29–32 (1991).
8. Mann, J. J. et al. Candidate endophenotypes for genetic studies of suicidal behavior. Biol. Psychiatry 65, 556–563 (2009).
9. Edwards, A. C. et al. On the Genetic and Environmental Relationship Between Suicide Attempt and Death by Suicide. Am. J. Psychiatry 178, 1060–1069 (2021).
10. Caspi, A. et al. Influence of life stress on depression: moderation by a polymorphism in the 5-HTT gene. Science 301, 386–389 (2003).
11. Willour, V. L. et al. A genome-wide association study of attempted suicide. Mol. Psychiatry 17, 433–444 (2012).
12. Docherty, A. R. et al. Genome-wide association study meta-analysis of suicide attempt in 43,871 cases identifies twelve genome-wide significant loci. medRxiv 2022.07.03.22277199 (2022) doi:10.1101/2022.07.03.22277199.
13. Mullins, N., International Suicide Genetics Consortium & Million Veteran Program. Genome-Wide Association Study of Over 40,000 Cases Within the International Suicide Genetics Consortium. Biol. Psychiatry 91, S29 (2022).
14. Li, Q. S. et al. Genome-wide association study meta-analysis of suicide death and suicidal behavior. Mol. Psychiat

Poster No 859

Mendelian Randomization Studies of Adolescent Brain Morphometry and Parkinson's Disease

Lang Liu[1], Konstantin Senkevich[2], Alain Dagher[3], Ziv Gan-Or[1]

[1]McGill University, Montreal, QC, [2]McGill University, Montreal, Quebec, [3]Montreal Neurological Institute and Hospital, McGill University, Montreal, QC

Introduction: Significant genetic correlations have been found between Parkinson's disease (PD) and volumes of multiple subcortical structures, including the putamen and brainstem (García-Marín et al., 2023). And a putative causal relationship has been suggested between larger putamen and increased risk of PD by conducting Mendelian randomization (MR). The previous research focuses on adult and elderly populations. There is currently limited research on the long-term impact of adolescent brain development on the risk of PD. In rare instance, Parkinson's-like symptoms can be found in adolescence and such early-onset parkinsonism in adolescence is genetically heterogeneous (Morales-Briceño et al., 2020). And the detected genetic mutations are sometimes associated with altered brain imaging phenotypes. It remains unclear whether the variability observed in brain structure during adolescence is associated with vulnerability to PD. Therefore, we aim to identify if there is an early genetic predisposition to PD by influencing the brain developmental changes in the adolescent stage.

Methods: The Adolescent Brain Cognitive Development (ABCD) Study release 4.0 was used as the main cohort in this project (Casey et al., 2018). After performing quality control and following exclusion criteria: non-European ancestry, mismatch between genetic and self-reported sex as well as relation to another participant closer than cousin, there were 4696 participants remaining in the analysis. Genome wide association studies (GWAS) were conducted on imaging-derived phenotypes (thickness, surface area and volume) from 25 subcortical regions. Age, sex and the first 10 genetic principal components were included as covariates. Heritability and genetic correlation were calculated using LDSC (linkage disequilibrium score regression) (Bulik-Sullivan et al., 2015). The power to detect genetic association can indeed be limited when conducting GWAS on a relatively small sample size. And genetic correlation across the various brain regions have been reported for cortical thickness, cortical surface and subcortical volume (Eyler et al., 2010; Hofer et al., 2020). Thus, a tool called multi-trait analysis of GWAS (MTAG) was implemented to leverage the genetic correlation between traits to boost the power of GWAS (Turley et al., 2018). There are two major confounding factors in Mendelian randomization: pleiotropy and sample structure . To account for these two confounding factors, we implemented a unified approached named MR Accounting for Pleiotropy and Sample Structure (MR-APSS). The p-value threshold for instrument variable in the MR was set at 5e-05 as the default threshold. P values of the resulting causal effect derived from MR-APSS were corrected by the false discovery rate approach.

Results: There was no significant causal effect detected by MR-APSS between subcortical volume and PD, as described in Figure 1.

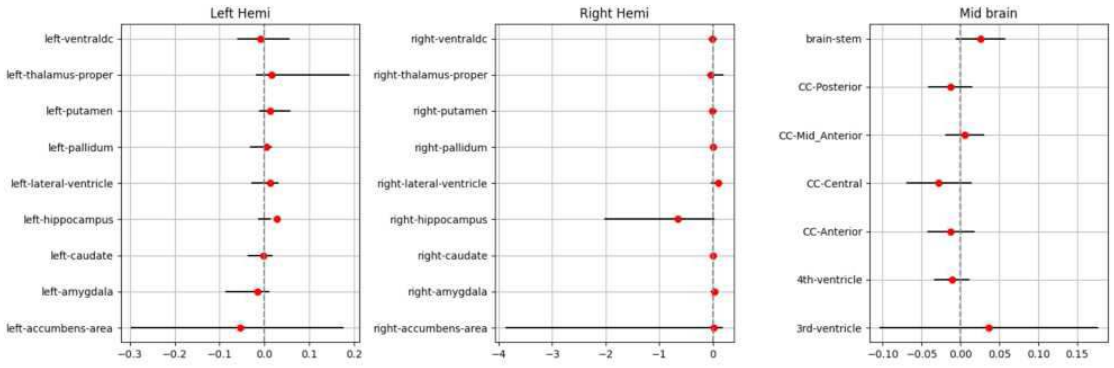

Figure 1. the causal effects of subcortical volume on Parkinson' s disease, derived from Mendelian randomization – Accounting for Pleiotropy and Sample Structure (MR-APSS).

Conclusions: In the adolescent stage, change in the subcortical structures may not causally affect the risk of developing PD in the later stage of lifetime. And GWAS was derived from participants with age ranging from 9 to 10 years old. The genetic predisposition to PD in brain developmental changes at age of 9-10 might be not displayed. It is also possible that our MR analysis was restricted by the statistical power of GWAS since the cohort had a relatively small sample size. Next steps will be incorporating scanning data from multiple visits together to increase the sample size and therefore increase the statistical power of our analysis.

References
1. Bulik-Sullivan, B.(2015). An atlas of genetic correlations across human diseases and traits. Nature Genetics, 47(11), Article 11.
2. Casey, B. J.(2018). The Adolescent Brain Cognitive Development (ABCD) study: Imaging acquisition across 21 sites. Developmental Cognitive Neuroscience, 32, 43–54.
3. Eyler, L. T.(2010). Genetic patterns of correlation among subcortical volumes in humans: Results from a magnetic resonance imaging twin study. Human Brain Mapping, 32(4), 641–653.
4. García-Marín, L. M. (2023). Shared molecular genetic factors influence subcortical brain morphometry and Parkinson's disease risk. Npj Parkinson's Disease, 9(1), Article 1. https://doi.org/10.1038/s41531-023-00515-y
5. Hemani, G. (2018). Evaluating the potential role of pleiotropy in Mendelian randomization studies. Human Molecular Genetics, 27(R2), R195–R208.
6. Hofer, E. (2020). Genetic correlations and genome-wide associations of cortical structure in general population samples of 22,824 adults. Nature Communications, 11(1), Article 1. https://doi.org/10.1038/s41467-020-18367-y
7. Kang, H. M. (2010). Variance component model to account for sample structure in genome-wide association studies. Nature Genetics, 42(4), Article 4.
8. Morales-Briceño, H. (2020). Clinical and neuroimaging phenotypes of genetic parkinsonism from infancy to adolescence. Brain, 143(3), 751–770.
9. Sanderson, E.(2021). The use of negative control outcomes in Mendelian randomization to detect potential population stratification. International Journal of Epidemiology, 50(4), 1350–1361.
10. Turley, P. (2018). Multi-trait analysis of genome-wide association summary statistics using MTAG. Nature Genetics, 50(2), Article 2.

Poster No 860

Transcriptional substrates underlying the maintenance of the brain network in human adult

Changshuo Wang[1,2,3], Kristofferm Madsen[4,5], Yuan Zhou[1,6,7], Tianzi Jiang[3,8,9,10,11]

[1]CAS Key Laboratory of Behavioral Science, Institute of Psychology, Chinese Academy of Sciences, Beijing 100101, China, [2]Sino-Danish Center, University of Chinese Academy of Sciences, Beijing 100190, China, [3]Brainnetome Center, Institute of Automation, Chinese Academy of Sciences, Beijing 100190, China, [4]Department of Applied Mathematics and Computer Science, Technical University of Denmark, Kongens Lyngby, Denmark, [5]Danish Research Centre for Magnetic Resonance, Copenhagen University Hospital Amager and Hvidovre, Copenhagen, Denmark, [6]Department of Psychology, University of Chinese Academy of Sciences, Beijing 100049, China, [7]The National Clinical Research Center for Mental Disorders & Beijing Key Laboratory of Mental Disorders, Beijing 100120, China, [8]School of Artificial Intelligence, University of Chinese Academy of Sciences, Beijing 100190, China, [9]Center for Excellence in Brain Science and Intelligence Technology, Institute of Automation, Chinese Academy of Sciences, Beijing 100190, China, [10]Research Center for Augmented Intelligence, Artificial Intelligence Research Institute, Zhejiang Lab, Hangzhou, Zhejiang Province 311100, China, [11]Xiaoxiang Institute for Brain Health and Yongzhou Central Hospital, Yongzhou, Hunan Province 425000, China

Introduction: Billions of neurons and their synaptic connections constitute the human brain, forming a complex structural network supporting a variety of behaviors and cognitive functions (Lynn and Bassett 2019). In the adult stage, the brain's network rarely undergoes changes, and even after brain injury, some connections would be repaired to maintain the function of the entire brain network under the regulation of gene activities (Osmanlıoğlu et al. 2020; Low and Cheng 2006). Considering the between-individual conserved topology of brain network, there should be some transcriptional molecules responsible for such maintenance of specific network structure, that is, the robustness and stability of adult brain. In this study, the joint analysis is performed on structural connectivity (SC) and transcriptome data to investigate the transcriptional substrates underlying the maintenance of adult brain network.

Methods: Based on Human Brainnetome Atlas (HBA), the probabilistic fiber tracking algorithm is performed on the neuroimage data: Human Connectome Project (HCP) S500 dataset, to obtain the region-level SC map. And the whole-brain transcriptome data is extracted from six postmortem brains, provided by the Allen Human Brain Atlas (AHBA) (Hawrylycz et al. 2015). Then, a partial least square regression (PLSR) model is built to project the SC matrix and region-gene transcriptome matrix into the latent space, to study the distribution of the SC-transcriptome gradients across the brain. Genes are ranked according to the PLSR loadings, and high ranked genes are identified as the important genes. The whole framework of the PLSR analysis has been illustrated in the Figure 1. Finally, several enrichment analyses are performed to annotate the key genes selected, including the temporal-specific expression analysis, gene ontology (GO) and disease ontology (DO). The spin test is performed to test the significance of PLSR model to exclude the effect of spatial autocorrelation(Alexander-Bloch et al. 2018). The gene selection process is validified by the bootstrapping resampling to test whether the gene loading is significant above chance. The result of gene enrichment analysis has been corrected for the multiple comparison using Benjamini-Hochberg (BH) method.

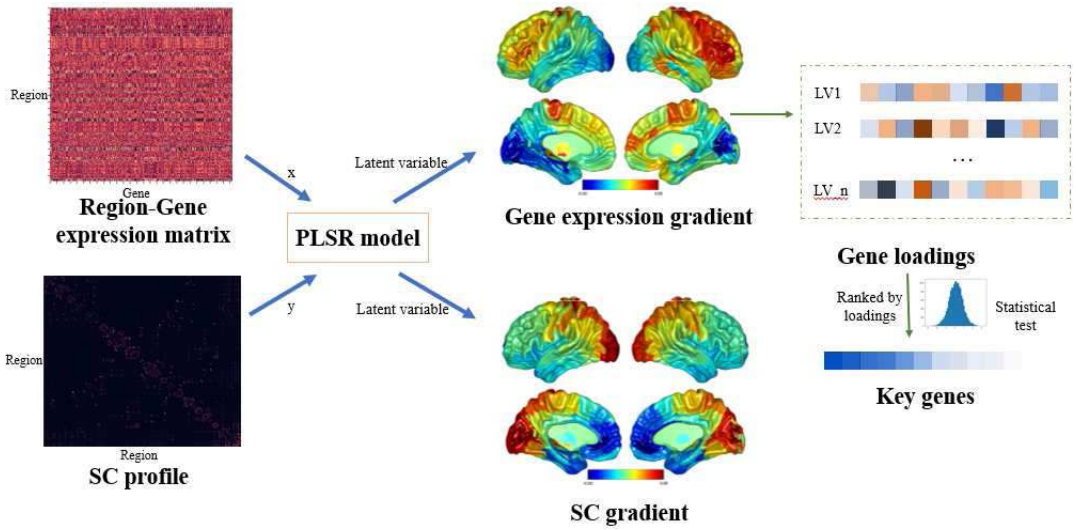

Figure 1. The framework for the PLSR analysis

Results: The PLSR analysis between SC and gene expression reveals two consistent gradients along the early development axes: the rostral-caudal axis and the medial-lateral axis. Based on PLSR loadings, the key genes for each gradient are identified as two group: positive loading group and negative loading group. Several well-known morphogen-related genes are identified as key genes, such as PAX6, WNT family and NOTCH family genes. According to functional annotation, both gene sets are related with the development of the nervous system. More interestingly, the positive loading genes and negative loading genes exhibit a clear chronological order on the temporal specific expression. The disease ontology associates the key genes with the development-related diseases, including the epilepsy, intellectual disability, and autism spectral disorder.

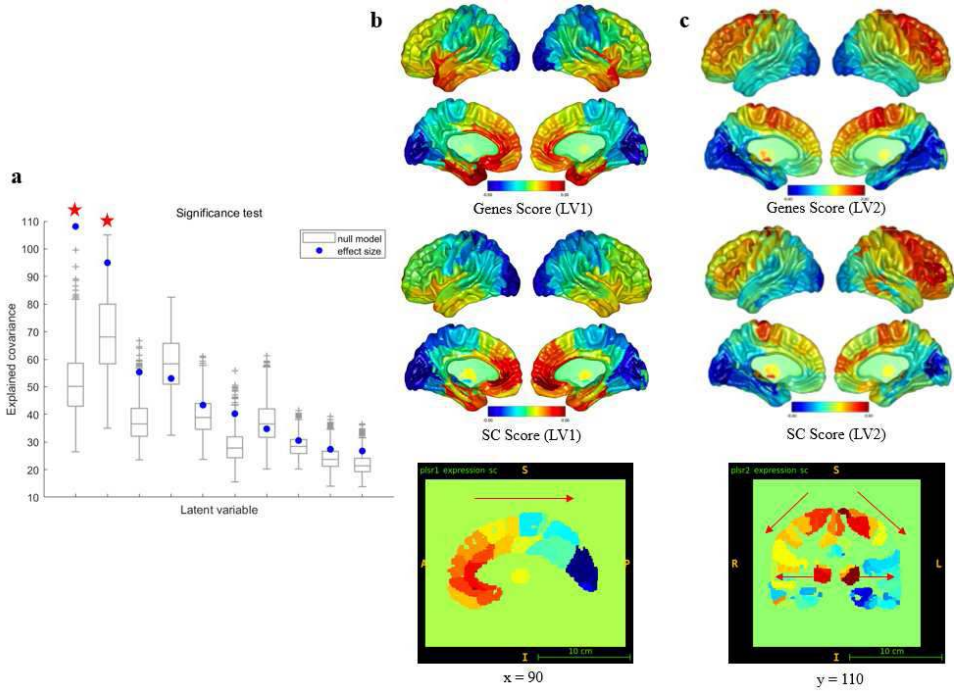

Figure 2. The performance of the PLSR model

Conclusions: In this study, we jointly analyze the transcriptome data and the SC profile to understand the molecular basis underlying the maintenance of brain network in human adult. The topology of adult brain network is significantly fitted by the whole-brain transcriptional expression matrix via a PLSR model. Also, two development-related molecular gradients are found highly correlated with the adult SC network and several transcriptional molecules are found accounting for the whole-brain SC formation. The key genes selected are found associated with the development process and some development-related diseases. Overall, this study provides a clear insight into the coupling between brain network structure and transcriptional activity, and further expand our understanding on how the gene activities support the structure and functions of the brain network.

References
1. Alexander-Bloch, Aaron F., Haochang Shou, Siyuan Liu, Theodore D. Satterthwaite, David C. Glahn, Russell T. Shinohara, Simon N. Vandekar, and Armin Raznahan. 2018. 'On Testing for Spatial Correspondence between Maps of Human Brain Structure and Function'. NeuroImage 178 (September): 540–51. https://doi.org/10.1016/j.neuroimage.2018.05.070.
2. Hawrylycz, Michael, Jeremy A Miller, Vilas Menon, David Feng, Tim Dolbeare, Angela L Guillozet-Bongaarts, Anil G Jegga, et al. 2015. 'Canonical Genetic Signatures of the Adult Human Brain'. Nature Neuroscience 18 (12): 1832–44. https://doi.org/10.1038/nn.4171.
3. Low, Lawrence K, and Hwai-Jong Cheng. 2006. 'Axon Pruning: An Essential Step Underlying the Developmental Plasticity of Neuronal Connections'. Philosophical Transactions of the Royal Society B: Biological Sciences 361 (1473): 1531–44. https://doi.org/10.1098/rstb.2006.1883.
4. Lynn, Christopher W., and Danielle S. Bassett. 2019. 'The Physics of Brain Network Structure, Function and Control'. Nature Reviews Physics 1 (5): 318–32. https://doi.org/10.1038/s42254-019-0040-8.
5. Osmanlıoğlu, Yusuf, Jacob A Alappatt, Drew Parker, and Ragini Verma. 2020. 'Connectomic Consistency: A Systematic Stability Analysis of Structural and Functional Connectivity'. Journal of Neural Engineering 17 (4): 045004. https://doi.org/10.1088/1741-2552/ab947b.

Poster No 861

The Genetics of Structural Similarity Networks in the Brain

Isaac Sebenius[1], Varun Warrier[2], Richard Bethlehem[3], Eva Stauffer[2], Richard Dear[2], Sarah Morgan[1], Edward Bullmore[4]

[1]Cambridge University, Cambridge, Cambridgeshire, [2]University of Cambridge, Cambridge, Cambridgeshire, [3]Autism Research Centre, Department of Psychiatry, University of Cambridge, Cambridge, United Kingdom, [4]University of Cambridge, Cambridge, United Kingdom

Introduction: Recent imaging-genetics research has demonstrated that heritable MRI-derived brain structural features show important genetic overlaps with brain function and psychopathology[1,2,3]. Yet, while the brain forms a genetically-coordinated network, existing work on the genetics of brain structure has focused on structural features at the global or regional level. As such, the genetics of network-based measures of brain structure remain largely unknown. In this work, we conducted hundreds of genome-wide association studies (GWAS) to comprehensively characterize the genetics of structural similarity networks in the brain. Specifically, using N>30,000 subjects from the UK Biobank, we studied the genetics of Morphometric INverse Divergence (MIND), a robust and biologically-validated method to construct structural similarity networks from MRI[4]. We identified 109 independent genomic regions associated with MIND, many of which were not associated with the structural feature from which the networks were derived. We observed positive genetic correlations between MIND network edges and the corresponding edges from functional connectivity (FC) networks, offering new evidence for a shared genetic basis for brain structure and function. Moreover, we identified putative causal relationships between MIND and functional connectivity that were specific to the association cortex. Finally, we observed evidence for local genetic correlations between MIND network connectivity and schizophrenia, identifying specific genes such as CACNA1c that may disproportionately contribute to the shared genetic basis of brain connectivity and mental illness.

Methods: MIND networks based on neurite density index (NDI) were constructed for 31,365 subjects of European ancestry in the UK Biobank using a coarse-grained version of the HCP parcellation with 276 network edges (Fig. 1a)[4]. Using the process described in[1], we conducted a GWAS on each of these MIND network edges and the corresponding edges from FC networks. Genetic correlations were calculated using LDSC and HDL[5,6]. Mendelian randomization was performed using MRAPSS[7]. Local genetic correlations were performed with SUPERGNOVA[8].

Results: 109 independent genomic regions were associated with at least one of the 276 MIND network edges at an experiment-wide significance threshold ($P < 1.8e\text{-}10$, Fig. 1b). Using pairwise LDSC and Louvain clustering, we identified three genetically-defined clusters of MIND network edges corresponding to distinct anatomy and functional processes: edges corresponding to 1) visual cortex, 2) paralimbic cortex, and 3) association and somatomotor cortex (Fig. 2a). We observed a shared genetic signal between brain structure and function; 87% of network edges showed positive genetic correlations between MIND and functional connectivity (FC), and over one-third of these relationships were statistically significant after FDR-correction (Fig. 2b). As shown in Fig. 2c, these structure-function genetic correlations were strongest in clusters 2 and 3. Using Mendelian randomization, we observed a putative causal relationship ($\beta = 0.18$, $P = 0.0002$) between MIND and FC specific to connectivity in cluster 3 (Fig. 2d). We observed 81 genomic regions with significant local genetic correlations between MIND and schizophrenia (Fig. 2e). Many genomic regions showed local genetic effects in discordant directions, suggesting that global genetic correlations may not capture the full extent of the genetic relationship between brain network connectivity and SCZ. The region that most strongly contributed to MIND connectivity and SCZ fell within chromosome 12p13.33 and contained a single gene, CACNA1c, which encodes a calcium channel subunit and has been robustly associated with SCZ[9].

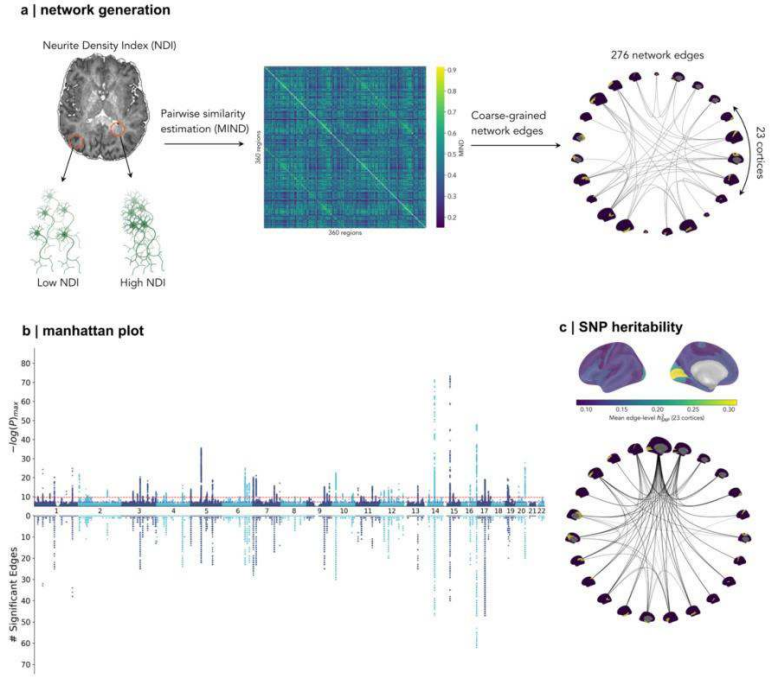

Fig. 1 MIND network generation and genetic associations. A) The process for generating MIND networks with 276 edges (corresponding to 23 cortical areas) based on a coarse-grained version of the 360-region HCP parcellation. Neurite density index (NDI) estimates the local density of axons and dendrites; it was selected as the sole input feature to MIND calculation given its interpretable relationship to microstructural composition and strong prior evidence of psychiatric relevance [3,4]. B) Miami plot summarizing genomic associations with MIND across all 276 studied network edges. The top panel indicates the most significant association of each variant across all edges. The purple line indicates genome-wide significance ($P < 5e-08$), and the red line indicates experiment-wide significance ($P < 5e-08$, FDR-corrected). The bottom panel indicates the number of network edges at which each variant achieves experiment-wide (FDR corrected) significance. C) The heritability of MIND network edges, illustrated as (top panel) the average heritability of edges at each of the 23 cortical areas or (bottom panel) the top 20% most heritable MIND network edges, with the thickness of each connection proportional to its heritability. As shown, SNP-based heritability was highest in the visual cortex.

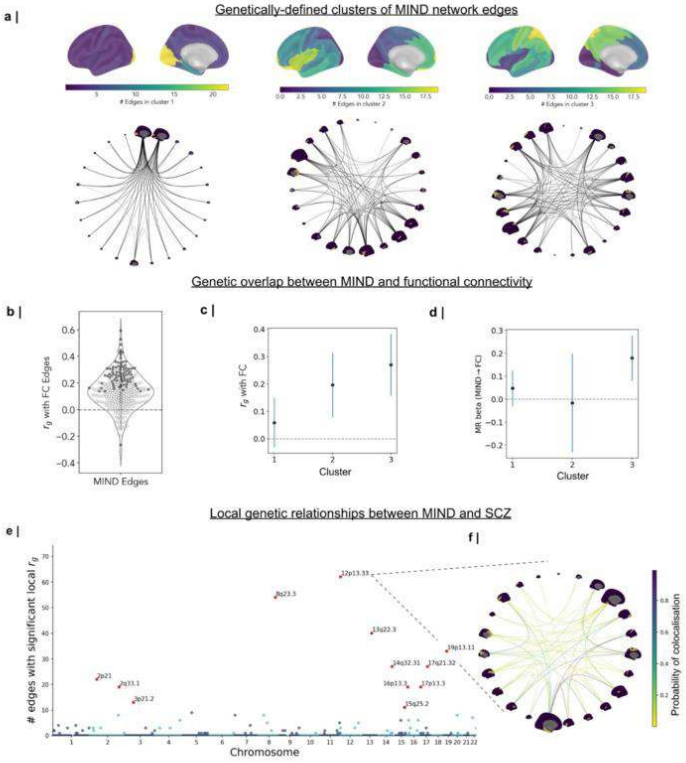

Fig. 2 Genetic insights of MIND network phenotypes. A) The anatomical locations of three genetically-defined clusters of MIND network edges, defined using Louvain clustering on an edge-by-edge similarity matrix computed by pairwise genetic correlations. Upper panels indicate the number of connections in each cluster belonging to each cortical region, and the bottom circos plots visualize the specific connections included in each cluster. The size of each node is proportional to the number of edges connected to each region. B) The distribution of genetic correlations between the 276 MIND network edges and their corresponding edges from functional connectivity (FC) networks. Filled-in points indicate the 83 genetic correlations (31%) that are statistically significant after FDR correction at $P < 0.05$. For visualization, two extreme outlying points are omitted. C)-D) The genetic correlations (C) and forward MR causal effect estimates (D) for MIND and FC based on connectivity within each of the three modules defined in part (A). Error bars indicate 95% confidence intervals. E) Manhattan plot indicating the number of MIND edges at which each of 2252 quasi-independent genomic regions showed significant local genetic correlations with SCZ. The label of each point refers to the most proximal chromosomal band. F) The anatomical locations of the 62 MIND edges with significant local correlations with a genomic region on 12p13.33 exclusively containing the gene *CACNA1c*. Edge colors represent the colocalization probabilities between MIND and SCZ, determined by Hyprcoloc [10].

Conclusions: Through genome-wide analysis of MIND network phenotypes, we offer novel evidence for shared genetics underlying structural similarity networks, functional connectivity, and schizophrenia.

References
1. Warrier, V. et al. Genetic insights into human cortical organization and development through genome-wide analyses of 2,347 neuroimaging phenotypes. Nat Genet. 55, 1483–1493 (2023).
2. Stauffer, EM. et al. The genetic relationships between brain structure and schizophrenia. Nat Commun 14, 7820 (2023). https://doi.org/10.1038/s41467-023-43567-7
3. Zhao, B., Li, T., Smith, S.M. et al. Common variants contribute to intrinsic human brain functional networks. Nat Genet 54, 508–517 (2022). https://doi.org/10.1038/s41588-022-01039-6
4. Sebenius, I. et al. Robust estimation of cortical similarity networks from brain MRI. Nat Neurosci 26, 1461–1471 (2023). https://doi.org/10.1038/s41593-023-01376-7
5. Bulik-Sullivan, B., Loh, PR., Finucane, H. et al. LD Score regression distinguishes confounding from polygenicity in genome-wide association studies. Nat Genet 47, 291–295 (2015). https://doi.org/10.1038/ng.3211
6. Ning, Z., Pawitan, Y. & Shen, X. High-definition likelihood inference of genetic correlations across human complex traits. Nat Genet 52, 859–864 (2020). https://doi.org/10.1038/s41588-020-0653-y
7. Hu X, et al. Mendelian randomization for causal inference accounting for pleiotropy and sample structure using genome-wide summary statistics. PNAS 2022 Jul 12;119(28):e2106858119. doi: 10.1073/pnas.2106858119. Epub 2022 Jul 5.
8. Zhang, Y., Lu, Q., Ye, Y. et al. SUPERGNOVA: local genetic correlation analysis reveals heterogeneous etiologic sharing of complex traits. Genome Biol 22, 262 (2021). https://doi.org/10.1186/s13059-021-02478-w
9. Moon, A L, et al. CACNA1C: Association With Psychiatric Disorders, Behavior, and Neurogenesis, Schizophrenia Bulletin, Volume 44, Issue 5, September 2018, Pages 958–965, https://doi.org/10.1093/schbul/sby096
10. Foley, C.N., Staley, J.R., Breen, P.G. et al. A fast and efficient colocalization algorithm for identifying shared genetic risk factors across multiple traits. Nat Commun 12, 764 (2021). https://doi.org/10.1038/s41467-020-20885-8

Poster No 862

Validation of polygenic scores for longitudinal changes in brain structures

Jalmar Teeuw[1], Rachel Brouwer[2], Shotaro Hato[1], Sonja de Zwarte[1], Sophia Thomopoulos[3], Neda Jahanshad[3], Paul Thompson[3], Hilleke Hulshoff Pol[4]

[1]Department of Psychiatry, University Medical Center Utrecht, Utrecht, Netherlands, [2]Department of Complex Trait Genetics, Center for Neurogenomics and Cognitive Research, Amsterdam, Netherlands, [3]Keck School of Medicine, University of Southern California, Los Angeles, California, United States, [4]Department of Experimental Psychology, Helmholtz Institute, Utrecht University, Utrecht, Netherlands

Introduction: Longitudinal changes in brain structure are phenotypically and genetically related to neuropsychiatric disorders, and may be predictive of the onset for some (Brans et al., 2008; van Haren et al., 2008; Teeuw et al, 2021). Recently, we reported on genetic variants driving brain development and brain aging in a genome-wide association study (GWAS) of changes in multiple brain volumes measured by longitudinal magnetic resonance imaging (MRI) from the ENIGMA consortium (Brouwer et al., 2022). Here we report on the validity and predictive value of polygenic scores (PGS) derived from this study.

Methods: We validated PGS derived from the GWAS in three cohorts: ABCD (N=2523; ages 9–11 years; Barch et al., 2018), UK Biobank (N=2536; ages 46–80 years; Sudlow et al., 2015), and UMCU (N=322; ages 10–65 years; 21% patients with schizophrenia and bipolar disorder). Change rates for 15 brain structures were obtained from longitudinal MRI using FreeSurfer (Fischl, 2012). Genotyped DNA was processed into PGS using PRSice-2 and PRScs (Choi and O'Reilly, 2019; Ge et al., 2019). The GWAS analysis was repeated three times leaving out each of the cohorts in turn to avoid overlap between the discovery and application sample while minimizing the impact on the power of the GWAS. Associations between PGS and rate of brain changes were determined by linear mixed effects model to derive percentage of variance of brain volume change explained by the PGS (ΔR^2). Models were adjusted for sex, age, overall head size, and population stratification.

Results: PGSs were significantly and largely positively associated with their respective changes in ABCD (ΔR^2 up to 0.45%; pmin=6.60E-04), UK Biobank (ΔR^2 up to 0.40%; pmin=1.35E-03), and UMCU (ΔR^2 up to 1.65%; pmin=7.43E-03) (Figure 1). The PGS for longitudinal change rate in lateral ventricles and putamen volume were consistently found across all three cohorts. Higher PGS for lateral ventricles was associated with accelerated increase in volume of the lateral ventricles in ABCD (β=+0.068, p=6.60E–04), UK Biobank (β=+0.044, p=1.24E–02), and UMCU cohorts (β=+0.137, p=7.43E–03) across the lifespan. In contrast, the association of the putamen inverts from a negative association – i.e, higher PGS predicted lower rate of change/decrease in volume of the putamen – in the childhood and adolescent ABCD cohort (β=–0.045, p=2.70E–02), to a positive association in the on average older participants in UK Biobank (β=+0.063, p=1.35E–03) and UMCU cohorts (β=+0.115, p=3.67E–02). Further investigation is needed to determine if PGS that are significant in a cohort-specific manner indicate possible associations with brain development and aging across the lifespan or disease-specific associations. Although results

between the PRSice-2 and PRScs method are similar in the larger ABCD (ICC(1)=+0.593, p=6.47E−03) and UK Biobank cohort (ICC(1)=+0.525, p=1.61E−02), there is still considerable variation between the two methods in the UMCU cohorts (ICC(1)=−0.252, p=0.829 [n.s.]). Despite previous reports (Ni et al., 2021), the modern PRScs method did not always outperform the traditional clumping and threshold approach from PRSice-2 in this study.

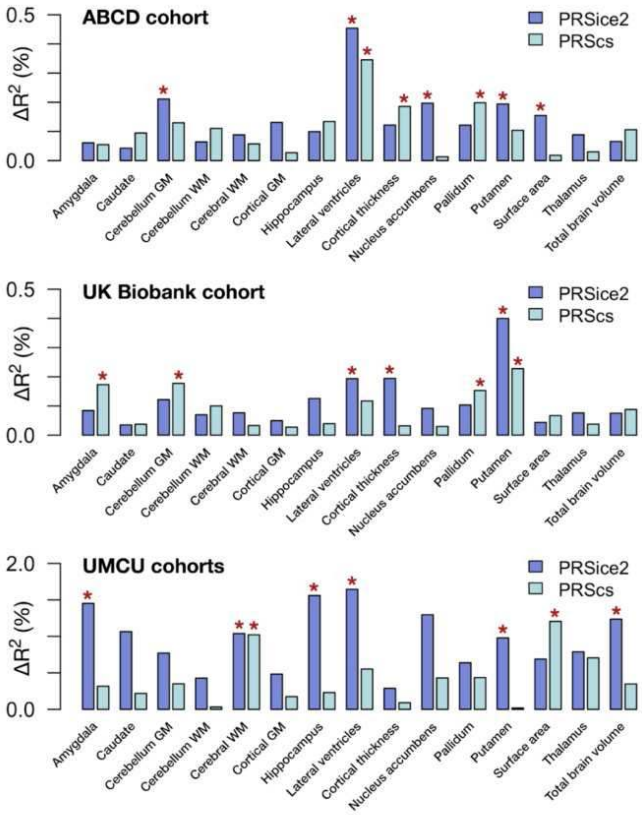

Figure 1. Predictive value of the PGS for longitudinal changes in brain structures in the ABCD, UK Biobank, and UMCU cohorts. Asterisk (*) marks PGS with significant predictive value (p<0.05).

Conclusions: Polygenic scores for longitudinal changes in brain structures have now been validated and can be used to assess associations with other traits, such as (risk for) neuropsychiatric disorders and cognitive functioning.

References

1. Brans, R.G.H., van Haren, N.E.M., van Baal, G.C.M., Schnack, H.G., Kahn, R.S., Hulshoff Pol, H.E. (2008). 'Heritability of changes in brain volume over time in twin pairs discordant for schizophrenia'. Arch. Gen. Psychiatry vol. 65, pp. 1259–1268
2. Brouwer, R.M., Klein, M., Grasby, K.L., Schnack, H.G., Jahanshad, N., Teeuw, J., Thomopoulos, S.I., Sprooten, E., ..., Thompson, P.M., Hulshoff Pol, H.E. (2022). 'Genetic variants associated with longitudinal changes in brain structure across the lifespan'. Nat. Neurosci. vol. 25, pp. 421–432
3. Choi, S.W., O'Reilly, P.F. (2019). 'PRSice-2: Polygenic Risk Score software for biobank-scale data'. Gigascience, giz082
4. Fischl, B. (2012). 'FreeSurfer'. Neuroimage vol. 62, pp. 774–781
5. Ge, T., Chen, C.-Y., Ni, Y., Feng, Y.-C.A., Smoller, J.W. (2019). 'Polygenic prediction via Bayesian regression and continuous shrinkage priors'. Nat. Commun. vol. 10, pp. 1776
6. Karcher, N.R., Barch, D.M. (2021). 'The ABCD study: understanding the development of risk for mental and physical health outcomes'. Neuropsychopharmacology vol. 46, pp. 131–142
7. Ni, G., Zeng, J., Revez, J.A., Wang, Y., Zheng, Z., Ge, T., Restuadi, R., Kiewa, J., Nyholt, D.R., Coleman, J.R.I., Smoller, J.W., Schizophrenia Working Group of the Psychiatric Genomics Consortium, Major Depressive Disorder Working Group of the Psychiatric Genomics Consortium, Yang, J., Visscher, P.M., Wray, N.R., 2021. A Comparison of Ten Polygenic Score Methods for Psychiatric Disorders Applied Across Multiple Cohorts. Biol. Psychiatry vol. 90, pp. 611–620
8. Sudlow, C., Gallacher, J., Allen, N., Beral, V., Burton, P., Danesh, J., Downey, P., Elliott, P., Green, J., Landray, M., Liu, B., Matthews, P., Ong, G., Pell, J., Silman, A., Young, A., Sprosen, T., Peakman, T., Collins, R. (2015). 'UK biobank: an open access resource for identifying the causes of a wide range of complex diseases of middle and old age'. PLoS Med., e1001779
9. Teeuw, J., Ori, A.P.S., Brouwer, R.M., de Zwarte, S.M.C., Schnack, H.G., Hulshoff Pol, H.E., Ophoff, R.A. (2021). 'Accelerated aging in the brain, epigenetic aging in blood, and polygenic risk for schizophrenia'. Schizophr. Res. vol. 231, pp. 189–197
10. van Haren, N.E.M., Hulshoff Pol, H.E., Schnack, H.G., Cahn, W., Brans, R., Carati, I., Rais, M.,
11. Kahn, R.S. (2008). 'Progressive brain volume loss in schizophrenia over the course of the illness: evidence of maturational abnormalities in early adulthood'. Biol. Psychiatry vol. 63, pp. 106–113

Poster No 863

Association between brain structure and risk SNPs for depression in adolescence

Jingyu Liu[1], Chan Aek Panichvatana[2], Vince Calhoun[3]

[1]GSU, Atlanta, GA, [2]Georgia State University, Atlanta, GA, [3]GSU/GATech/Emory, Decatur, GA

Introduction: The global rising prevalence of depressive and anxiety symptoms in children and adolescents posts a pressing issue for public health and warrants special attention of the research community. Multiple factors, ranging from genetic vulnerabilities to environmental stressors, influence the risk for these mental disorders. This study aims to investigate how risk genetic mutations of major depression associate with brain structural variations during the key developmental phase. To leverage big data collected across cohorts in different countries, we have implemented a decentralized data-analyses algorithm, decentralized parallel independent component analysis (dpICA). dpICA enables analyzing MRI images and single nucleotide polymorphism (SNP) data located at different centers, without sharing the raw data, and computing statistical models and identifying the associations between genetic and brain structure.

Methods: We have investigated data from three cohorts: Adolescent Brain and Cognitive Development Study (USA, age of 9-10), Consortium on Vulnerability to Externalizing Disorders and Addictions (India, age of 6-17) and IMAGEN (Europe, age of 14). Risk SNPs were selected based on a recent genome-wide association study of major depression. We chose SNPs associated with major depression with $p < 1e\text{-}3$, and passing quality control and pruning, leading to 1664 risk SNPs for further analyses. T1 weighted MRI images from all three cohorts went through a SPM12 standard pipeline to derive gray matter images normalized into MNI space. Finally gray matter and SNPs from 6209 independent participants of ABCD cohort, 1526 participants of IMAGEN, and 571 participants of cVEDA were analyzed through dpICA. Briefly, data from each cohort were first reduced through principal component analysis (PCA), and only limited number of PCs with large variances were passed to one global site, At the global site, PCs from three sites were concatenated and further merged through another PCA. Then, three global PCs of SNP data associated significantly with race were removed. The rest of global PCs of SNP data and global PCs of MRI data were analyzed with parallel ICA, which extracts independent gray matter components and SNP components, and iteratively maximizes the correlation between participants' loadings of SNP and gray matter components.

Results: Among 25 gray matter components and 27 SNP components, one SNP component was identified to be significantly associated with one gray matter component with the overall correlation $r = 0.06$ ($p<1e\text{-}6$), and correlations in each cohort were 0.07, 0.11 and 0.17 for ABCD, IMAGEN and cVEDA respectively. There are 19 main contribution SNPs, with the highest contributing SNPs being rs2782446 and rs8002150 in chromosome 13 noncoding regions. The associated brain regions are from superior parietal, precuneus, posterior cingulate, lingual gyrus and cerebellum.

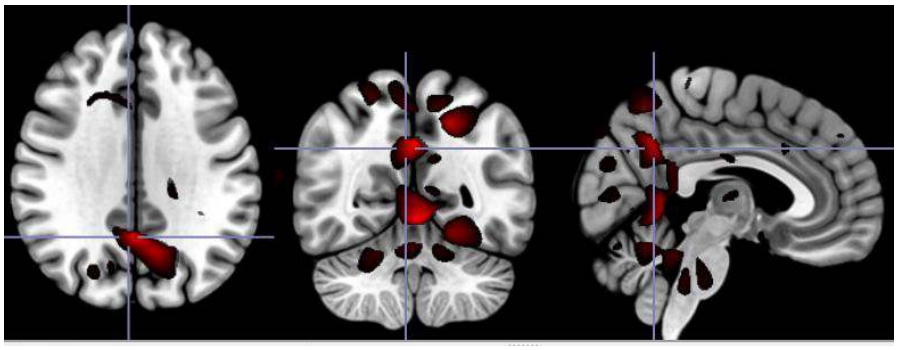

Fig. Gray matter component associated with SNPs

Conclusions: Our pilot analyses indicate that SNPs with risk for major depression, mainly adult depression, have showed associations with gray matter variation during children and adolescent development phase, even though the effect size is small. Further stability and generalizability of our finding needs to be performed.

References

1. Howard DM, (2019) 'Genome-wide meta-analysis of depression identifies 102 independent variants and highlights the importance of the prefrontal brain regions.' Nature Neuroscience. 22(3):343-352
2. Zhang, Y. (2020), 'The Consortium on Vulnerability to Externalizing Disorders and Addictions (c-VEDA): an accelerated longitudinal cohort of children and adolescents in India.' Molecular Psychiatry 25, 1618–1630
3. Maricic, L.(2020), 'The IMAGEN study: a decade of imaging genetics in adolescents.' Molecular Psychiatry 25, 2648–2671
4. Volkow ND, (2018), 'The conception of the ABCD study: From substance use to a broad NIH collaboration. Developmental Cognitive Neuroscience, 32, 4-7,
5. Panichvatana, C.A.,(2023),'Decentralized Parallel Independent Component Analysis for Multimodal, Multisite Data,' IEEE Annu Int Conf IEEE Eng Med Biol Soc.

Poster No 864

RAMP: A pipeline for brain-wide genome-wide association studies based on the ENIGMA protocols

Lea Waller[1], Micael Andersson[2,3], Gina-Isabelle Henze[1], Ilya Veer[4], Paul Thompson[5], Sarah Medland[6], Susanne Erk[7], Henrik Walter[1]

[1]Department of Psychiatry and Neurosciences CCM, Charité Universitätsmedizin Berlin, Berlin, Germany, [2]Department of Integrative Medical Biology (IMB), Faculty of Medicine, Umeå University, Umeå, Sweden, [3]Umeå Centre for Functional Brain Imaging (UFBI), Faculty of Medicine, Umeå University, Umeå, Sweden, [4]Department of Developmental Psychology, University of Amsterdam, Amsterdam, Netherlands, [5]Imaging Genetics Center, University of Southern California, Marina Del Rey, CA, USA, [6]QIMR Berghofer Medical Research Institute, Herston, QLD, Australia, [7]Charité Universitätsmedizin Berlin, Berlin, Germany

Introduction: Imaging genetics provides a uniquely powerful view into molecular genetic mechanisms influencing human behavior in relation to the brain (Hariri and Weinberger 2003). It also enables a number of downstream analyses, such as the ability to derive polygenic scores. These can be used in predictive modeling as well as the study of heritability and genetic correlations. The ENIGMA consortium has performed a number of large-scale imaging genetics studies, generating mechanistic insight into brain structure and function (Thompson et al. 2020). Although detailed protocols are publicly available, running them for hundreds of phenotypes creates computational challenges. To make these protocols more accessible for large-scale studies, we have developed containers for key steps and re-implemented parts in highly performant Python code. The result is a processing pipeline named RAMP (Rapid Associations for Many Phenotypes) that can calculate genome-wide association statistics across a large number of brain phenotypes.

Methods: The ENIGMA genetics protocols (available at https://enigma.ini.usc.edu/wp-content/uploads/2020/02/ENIGMA-1KGP_p3v5-Cookbook_20170713.pdf) begin with multidimensional scaling and quality control of the raw genetic data. This is followed by imputation using the Michigan Imputation Server. For users who cannot upload their data to the server, we have also embedded the Imputation Server into a container that can be run in Docker or Singularity and works by starting a temporary Apache Hadoop instance on the local machine. After phenotype extraction and imputation, we have provided a script to stratify the samples into ancestry groups, if required (Figure 1b). This command can also aid in matching subject IDs between the imaging and the genetics data files. Finally, we have provided a high-performance command to calculate genome-wide association statistics that can handle missing values (Figure 1c). It is a re-implementation of RAREMETALWORKER (Feng et al. 2014), allowing the inclusion of both related and unrelated samples. A core goal was ensuring interoperability with the existing ENIGMA HALFpipe processing pipeline for functional MRI data (Waller et al. 2022), which is based on fMRIPrep (Esteban et al. 2019). To this end, we have added a command to extract functional and structural brain phenotypes from previously calculated imaging files (Figure 1a).

A) Create `phenotypes.tsv` and `covariates.tsv` files in the output directory based on BIDS-formatted input images and brain atlases

Command line syntax	Explanation

`singularity run \`
`  --contain --bind /mnt --bind /tmp \`
`  /mnt/containers/halfpipe-latest.sif \`
	Configure container runtime

`--num-threads 16 \`	Configure HALFpipe
`group-level \`	

`--input-directory \`
`  /mnt/data/berlin/derivatives/halfpipe \`
`  /mnt/data/paris/derivatives/halfpipe \`
	Select directories

`--output-directory /mnt/data/gwas \`	
`--exclude task rest \`	Subset inputs
`--include task nback \`	
`--rename task mid reward \`	Harmonize naming
`--rename taskcontrast 0BackVs2Back wmLoadVsControl \`	
`--qc-exclude-file /mnt/data/halfpipe/exclude.json \`	Exclude bad scans
`--fd-mean-cutoff 0.5 \`	
`--fd-perc-cutoff 10 \`	
`--aggregate run \`	Merge multiple scans
`--aggregate ses \`	
`--spreadsheet /mnt/data/participants.tsv \`	Specify covariates
`--id-column id \`	
`--continuous-variable age \`	
`--categorical-variable sex --levels female male \`	
`--derived-variable age_squared "age**2" \`	Create additional covariates
`--derived-variable sex_by_age "(sex == 'male') * age" \`	
`--derived-variable sex_by_age_squared \` `  "(sex == 'male') * (age ** 2)" \`	

`--imaging-variable fd_mean fd_perc \`
`  mean_gm_tsnr aroma_noise_frac \`
`  total_intracranial_volume \`
`  jacobian_mean jacobian_variance \`
	Add quality metrics as covariates or phenotypes

`--export-variable fd_mean fd_perc \`
`  mean_gm_tsnr aroma_noise_frac \`
`  total_intracranial_volume \`
`  jacobian_mean jacobian_variance \`	

`--export-atlas atlas-Brainnetome z \`
`  /mnt/data/atlases/atlas-Brainnetome_dseg.nii.gz \`
`  /mnt/data/atlases/atlas-Brainnetome_dseg.tsv`
	Specify brain atlas

B) Stratify phenotypes by ancestry group and age group to generate `stratified_phenotypes.tsv` and `stratified_covariates.tsv`

Command line syntax	Explanation

`singularity exec \`
`  --contain --bind /mnt --bind /tmp \`
`  /mnt/containers/ramp.sif \`
	Configure container runtime

`stratify \`	

`--phenotypes phenotypes.tsv \`
`--covariates covariates.tsv \`
`--output-directory /mnt/data/gwas \`
	Specify inputs and outputs

`--mds HM3_b37mds2R.mds.csv \`
`--component-count 4 \`
`--add-components-to-covariates \`
	Specify components for ancestry classification

`--by-super-population \`
`--by age \`
`--group childAndAdolescent 5 18 \`
`--group adult 18 inf \`
`--minimum-sample-size 50`
	Configure how the dataset should be split

C) Calculate genome-wide association statistics

Command line syntax	Explanation

`singularity exec \`
`  --contain --bind /mnt --bind /tmp \`
`  /mnt/containers/ramp.sif \`
	Configure container runtime

`score \`
`--num-threads 4 \`
`--mem-gb 16 \`
	Specify inputs and outputs

`--vcf chr*.dose.vcf.gz \`
`--phenotypes stratified_phenotypes.tsv \`
`--covariates stratified_covariates.tsv \`
`--output-directory /mnt/data/gwas \`
	Specify components for ancestry classification

`--kinship-minor-allele-frequency-cutoff 0.05 \`
`--kinship-r-squared-cutoff 0 \`
`--score-minor-allele-frequency-cutoff 0.005 \`
`--score-r-squared-cutoff 0.5`
	Configure post-imputation filters

Results: RAMP has been tested in diverse environments, including laptops, workstations and high-performance compute clusters. It requires at least 16 GB of memory and can process hundreds of phenotypes in only a few days. These genetic associations are compressed efficiently, requiring about 250 megabytes of storage space per phenotype. We have developed integration tests relying on simulated phenotypes and real genetics data from the OpenSNP dataset (Greshake et al. 2014). The integration tests ensure that the program runs correctly and generates results consistent with RAREMETALWORKER. These are run after any change to the code, ensuring that errors affecting correctness will be caught early.

Conclusions: We have released RAMP at https://github.com/HippocampusGirl/RAMP under an open source license. RAMP makes a major contribution toward enabling genome-wide association studies for larger numbers of brain imaging phenotypes.

References

1. Esteban, Oscar, Christopher J. Markiewicz, Ross W. Blair, Craig A. Moodie, A. Ilkay Isik, Asier Erramuzpe, James D. Kent, et al. 2019. "fMRIPrep: A Robust Preprocessing Pipeline for Functional MRI." Nature Methods 16 (1): 111–16. https://doi.org/10.1038/s41592-018-0235-4.
2. Feng, Shuang, Dajiang Liu, Xiaowei Zhan, Mary Kate Wing, and Gonçalo R. Abecasis. 2014. "RAREMETAL: Fast and Powerful Meta-Analysis for Rare Variants." Bioinformatics 30 (19): 2828–29. https://doi.org/10.1093/bioinformatics/btu367.
3. Greshake, Bastian, Philipp E. Bayer, Helge Rausch, and Julia Reda. 2014. "openSNP–A Crowdsourced Web Resource for Personal Genomics." Edited by Tricia A. Thornton-Wells. PLoS ONE 9 (3): e89204. https://doi.org/10.1371/journal.pone.0089204.
4. Hariri, Ahmad R, and Daniel R Weinberger. 2003. "Imaging Genomics." British Medical Bulletin 65 (1): 259–70. https://doi.org/10.1093/bmb/65.1.259.
5. Thompson, Paul M., Neda Jahanshad, Christopher R. K. Ching, Lauren E. Salminen, Sophia I. Thomopoulos, Joanna Bright, Bernhard T. Baune, et al. 2020. "ENIGMA and Global Neuroscience: A Decade of Large-Scale Studies of the Brain in Health and Disease across More than 40 Countries." Translational Psychiatry 10 (1): 1–28. https://doi.org/10.1038/s41398-020-0705-1.
6. Waller, Lea, Susanne Erk, Elena Pozzi, Yara J. Toenders, Courtney C. Haswell, Marc Büttner, Paul M. Thompson, et al. 2022. "ENIGMA HALFpipe: Interactive, Reproducible, and Efficient Analysis for Resting-State and Task-Based fMRI Data." Human Brain Mapping 43 (9): 2727–42. https://doi.org/10.1002/hbm.25829.

Poster No 865

Unraveling the Link between CNVs, General Cognition, and Individual Neuroimaging Deviaton Scores

Charlotte Fraza[1], Andre Marquand[2], Rune Boen[3], Ida Sønderby[3]

[1]Donders Institute for Brain, Cognition and Behaviour, Nijmegen, gelderland, [2]Radboud University Nijmegen, Nijmegen, Gelderland, [3]Oslo University Hospital, Oslo, Norway

Introduction: Copy number variations (CNVs) are genetic variants that involve a deletion or a duplication of a larger segment of the genome. Certain CNVs yield a higher risk of developing neurodevelopmental and psychiatric disorders, but with considerable differences in outcome between carriers (Malhotra & Sebat, 2012; Modenato et al., 2021; Sanders et al., 2019). Understanding their individual-level effects on the brain and behavior is pivotal for unraveling their intricate contributions to cognition and mental health. While conventional studies often contrast cases from controls, this is limited to groups that have sufficient sample sizes and thus often excludes mapping of the rare, pathogenic CNVs with high impact. Normative modeling offers a solution by quantifying individual deviations from reference populations which may aid in decoding complex brain disorders (Marquand et al., 2016, 2019). This study employs normative modeling to explore the personalized impacts of pathogenic CNVs on brain function and behavior, highlighting the 1q21.1 distal deletion and duplication. By linking brain deviation scores from a reference model to cognition and investigating shared alterations among individuals with similar CNVs, this research gives insights into the nuanced role of CNVs in shaping personalized brain deviation maps.

Methods: An overview of our analytic workflow is presented in Fig. 1. In brief, we fitted normative models for several image derived phenotypes (IDPs), derived from three primary imaging modalities: structural, functional, and diffusion MR data, and the Jacobian determinants to create a comprehensive exploration of the effect of CNVs on the brain. We selected specific CNVs that have previously been proposed to be pathogenic and that have been associated with a decrease in cognition (Kendall et al., 2017, 2019). Fig. 1A visually outlines our study workflow: i. We mapped participants with pathogenic CNVs, such that they can be placed in our test set. ii. We created the normative models for each individual IDP taking into account several covariates, such as age and sex. iii. We counted the number of extreme deviations for each participant and map where participants with a pathogenic CNV lie on this distribution. iv. We correlated the extreme z-scores with cognition.

Results: We delved into individual brain deviation scores associated with specific CNVs, with a special emphasis on 1q21.1 distal deletion and duplication, see figure 2. We counted extreme deviations ($|Z|>2$) and provided maps of deviation scores that highlighted regions with pronounced alterations. Our analysis revealed that individuals with 1q21.1del displayed more positive deviations indicating more volume expansions, while those with 1q21.1dup exhibited more negative deviations indicating more volume contractions. We conducted a joint analysis to uncover common and divergent deviation scores in specific brain regions, and this approach proved applicable to various other pathogenic CNVs. Furthermore, we explored the relationship between brain deviation scores and cognitive deficits. Our hypothesis posited that certain CNVs might impact cognition, especially in the absence of protective factors. Our Pearson correlation analysis indicated that a higher number of extreme negative deviations was associated with a lower general cognitive ability, while no significant correlation was observed for extreme positive deviations.

Conclusions: Our study emphasizes the importance of individual-level analysis over traditional case-control thinking within pathogenic CNV research and neuroimaging. We advocate for an "individual patient first" approach in psychiatry, acknowledging the diversity and comorbidities in mental disorders and their underlying causal pathways. We believe

comprehensive normative models can capture the inherent heterogeneity present in participants with pathogenic CNVs, and the effects of these CNVs on brain morphology, providing a valuable perspective for future research.

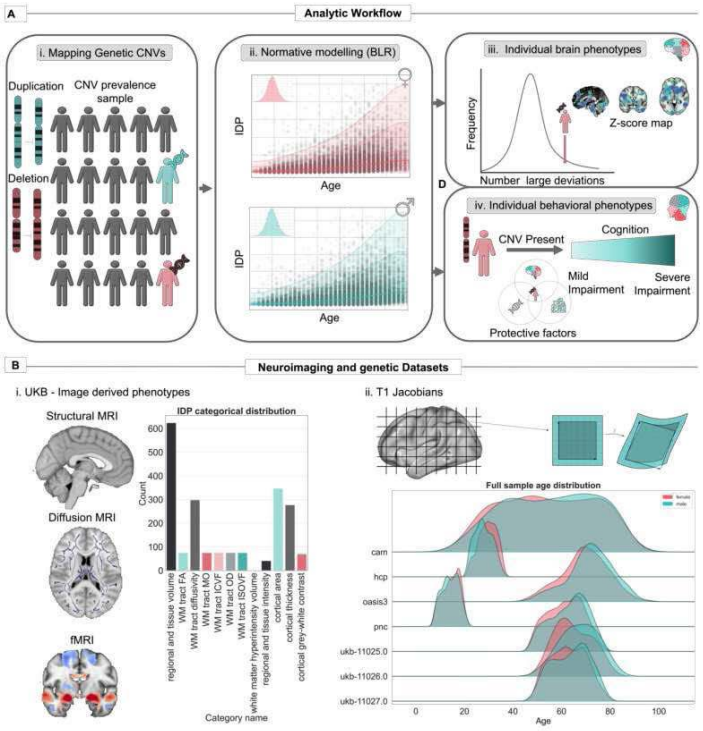

Fig. 1 | Overview of study design and data resources. A, Schematic overview of the study workflow and hypothesis. First, we quantify the number of participants with pathogenic CNVs, previously linked to neurodevelopmental and psychiatric disorders. Then we create normative models for the IDPs and the voxel-wise Jacobians. Afterward, we calculate the number of large deviation scores (|Z|>2). We plot the number of large deviation scores for individuals with pathogenic CNVs compared to the rest of the population. Finally, we correlate the extreme brain deviation scores and general cognitive ability. CNV, Copy Number Variant; IDP, image derived phenotype; BLR, Bayesian Linear Regression. B, Overview of the neuroimaging datasets used in this study. i. Distribution of the IDPs present in the UK biobank dataset, derived from functional, structural, and diffusion tensor imaging. ii. Distributions of the data from seven sites used in the Jacobian normative model, split by sex. In total, we use 44,456 participants in the IDP study, and 19,620 visually quality controlled participants in the Jacobian-voxel-based study.

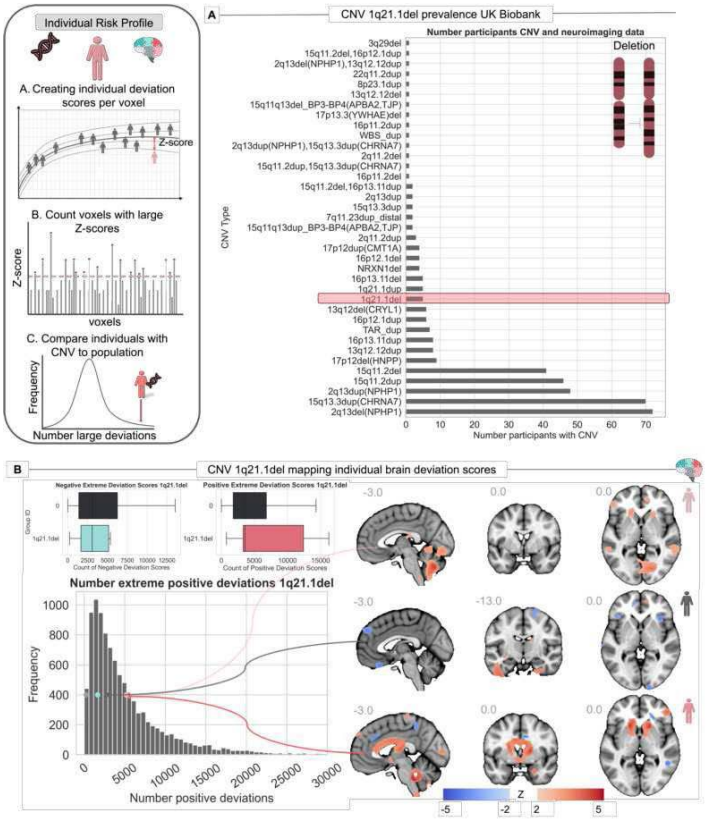

Fig. 2 | Individual Risk Profiles 1q21.1 deletion. A, Showing the prevalence of 1q21.1del in the UK Biobank. **B**, Displaying the counts of extreme positive and negative deviation scores (|Z|>2) among participants with a 1q21.1 deletion in contrast to participants without a pathogenic CNV. Left: Dots show each individual 1q21.1 deletion carrier's position in the distribution. Right: Displaying the profile of three selected 1q21.1 distal deletion CNV carriers.

References

1. Holz, Nathalie E., Mariam Zabihi, Seyed Mostafa Kia, Maximillian Monninger, Pascal-M. Aggensteiner, Sebastian Siehl, Dorothea L. Floris, et al. 2023. 'A Stable and Replicable Neural Signature of Lifespan Adversity in the Adult Brain'. Nature Neuroscience, August, 1–10. https://doi.org/10.1038/s41593-023-01410-8.
2. Kendall, Kimberley M., Matthew Bracher-Smith, Harry Fitzpatrick, Amy Lynham, Elliott Rees, Valentina Escott-Price, Michael J. Owen, Michael C. O'Donovan, James T. R. Walters, and George Kirov. 2019. 'Cognitive Performance and Functional Outcomes of Carriers of Pathogenic Copy Number Variants: Analysis of the UK Biobank'. The British Journal of Psychiatry 214 (5): 297–304. https://doi.org/10.1192/bjp.2018.301.
3. Kendall, Kimberley M., Elliott Rees, Valentina Escott-Price, Mark Einon, Rhys Thomas, Jonathan Hewitt, Michael C. O'Donovan, Michael J. Owen, James T. R. Walters, and George Kirov. 2017. 'Cognitive Performance Among Carriers of Pathogenic Copy Number Variants: Analysis of 152,000 UK Biobank Subjects'. Biological Psychiatry, Neurodevelopmental Alterations: Mechanisms and Consequences, 82 (2): 103–10. https://doi.org/10.1016/j.biopsych.2016.08.014.
4. Malhotra, Dheeraj, and Jonathan Sebat. 2012. 'CNVs: Harbingers of a Rare Variant Revolution in Psychiatric Genetics'. Cell 148 (6): 1223–41. https://doi.org/10.1016/j.cell.2012.02.039.
5. Marquand, Andre F., Seyed Mostafa Kia, Mariam Zabihi, Thomas Wolfers, Jan K. Buitelaar, and Christian F. Beckmann. 2019. 'Conceptualizing Mental Disorders as Deviations from Normative Functioning'. Molecular Psychiatry 24 (10): 1415–24. https://doi.org/10.1038/s41380-019-0441-1.
6. Marquand, Andre F., Iead Rezek, Jan Buitelaar, and Christian F. Beckmann. 2016. 'Understanding Heterogeneity in Clinical Cohorts Using Normative Models: Beyond Case-Control Studies'. Biological Psychiatry 80 (7): 552–61. https://doi.org/10.1016/j.biopsych.2015.12.023.
7. Modenato, Claudia, Sandra Martin-Brevet, Clara A. Moreau, Borja Rodriguez-Herreros, Kuldeep Kumar, Bogdan Draganski, Ida E. Sønderby, and Sébastien Jacquemont. 2021. 'Lessons Learned From Neuroimaging Studies of Copy Number Variants: A Systematic Review'. Biological Psychiatry, Rare and Common Genetic Variance and Psychosis, 90 (9).
8. Rutherford, Saige, Charlotte Fraza, Richard Dinga, Seyed Mostafa Kia, Thomas Wolfers, Mariam Zabihi, Pierre Berthet, et al. 2022. 'Charting Brain Growth and Aging at High Spatial Precision'

Poster No 866

Mapping Mutual Information of Neuroimages and Allelic Variants Unveils Determinants of Brain Aging

Nicholas Kim[1], Anar Amgalan[1], Nahian Chowdhury[1], Nikhil Chaudhari[1], Phoebe Imms[1], Paul Thompson[2], Andrei Irimia[1]

[1]University of Southern California, Los Angeles, CA, [2]Imaging Genetics Center, Keck School of Medicine of University of Southern California, Los Angeles, CA

Introduction: Single-nucleotide polymorphisms (SNPs) are genetic variations with effects on brain aging. Mapping their influence on brain structure can elucidate the genetic correlates of neurological/psychiatric disorders. However, most genome-wide association studies use linear measures of dependents which ignore the nonlinear dependence of phenotype on genotype. In this study, we used mutual information (MI), an information-theoretic measure of reciprocal (nonlinear) dependence between two variables, to map how SNPs act nonlinearly on cortical morphology.

Methods: In 6,000 UK Biobank participants (including 3,209 females) aged 54 to 84, we extracted mean T1-weighted MRI intensities at each cortical location. Intensities were projected onto a reference atlas to accommodate variations in brain morphology. We mapped the MI between MRI intensity and 706,000 SNP variants to quantify the dose-response relationship between (A) SNP variant number and (B) the location-dependent MRI intensity of the cerebral cortex. A cortical map of MI with MRI intensity was generated for each SNP. The mean MI of each map was used to rank SNPs according to genetic influence. Maps were normalized by calculating z-scores at each cortical location using the distribution of SNP MIs at that specific location.

Results: Cortical MI maps reveal novel genetic influences on brain structure that involve neurocognitive and psychiatric conditions. SNPs found to act most strongly on cortical structure involved the introns of PRPF31 (previously linked to smaller brain volume), NHSl1 (cortical surface area), and LINC00299 (microglia; activity in early neurodegeneration). KIF6, linked to attention-deficit/hyperactivity disorder (ADHD), ranks among the SNPs with strongest effect on MRI intensity. Prefrontal cortex mediates behavioral inhibition frequently affected in ADHD. As depicted in Figure 1, the number of KIF6 alleles has significantly higher MI ($p < 0.05$) with MRI intensity than the average SNP in this lobe, specifically in the right ventrolateral region. Such influence is notably pronounced in features of the prefrontal cortex in the right hemisphere, a notable lateralization effect consistent with findings in prior studies (Arnsten, 2009). The APOE allele, the strongest genetic risk factor for Alzheimer's disease (AD), ranks among the top 0.1% of SNPs acting on MRI intensity. As shown in Figure 2, the number of APOE-ε4 alleles has significantly higher MI ($p < 0.05$) with MRI intensity in the medial parietal lobe, temporal lobes, and left inferior occipital lobe, three brain regions responsible for long-term memory recall, language processing, and visual perception (Ackerman, 1992). These findings reflect AD symptoms, which include memory loss, impaired verbal fluency, and reduced peripheral vision (Weintraub et al., 2012). Other findings reveal similar relationships between SNPs

involved in neurological/psychiatric conditions and brain structure. Results were reproduced in a larger sample of 43,000 UKBB participants.

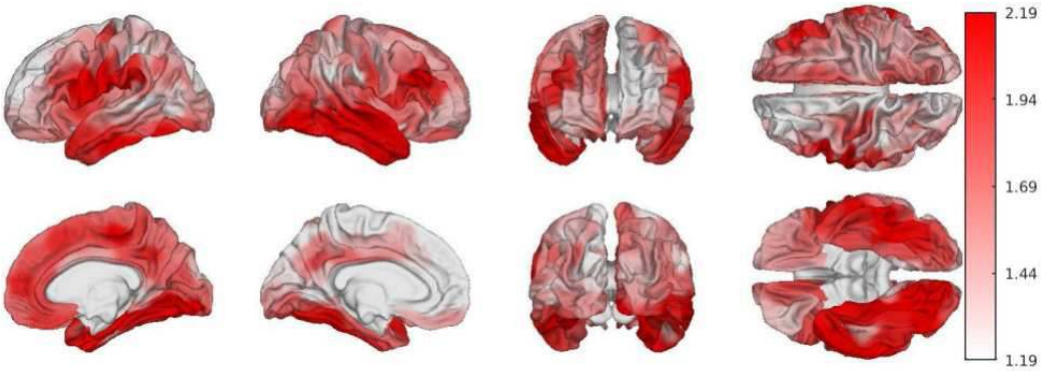

Figure 1. Canonical views of the normalized MI between the KIF6 SNP and participant MRIs. $Z = (x - \mu) / \sigma$. μ and σ are the average and standard deviation, respectively, of the MI with MRI intensity for 7,600 SNPs across the genome. Darker red indicates high MI, while lighter red indicates the reverse.

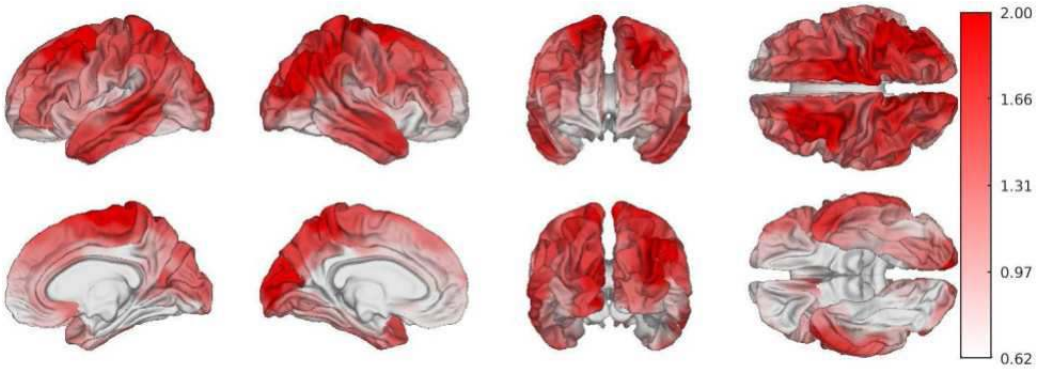

Figure 2. Same as **Figure 1**, but for the normalized MI between the APOE-ε4 SNP and participant MRIs.

Conclusions: Our findings suggest that mapping MI between MRI intensities and SNPs can reveal the genetic influences of SNPs on brain structure in health and in neurological/psychiatric disease.

References

1. Ackerman, S. (1992), 'Major Structures and Functions of the Brain', In Discovering the Brain. National Academies Press (US)
2. Arnsten, A. F. T. (2009), 'The Emerging Neurobiology of Attention Deficit Hyperactivity Disorder: The Key Role of the Prefrontal Association Cortex', The Journal of Pediatrics, vol. 154, no. 5, I-S43
3. Weintraub, S. (2012), 'The Neuropsychological Profile of Alzheimer Disease', Cold Spring Harbor Perspectives in Medicine, vol. 2, no. 4, a006171

Poster No 867

Alzheimer's disease Genetic Pathways Impact on Imaging Endophenotypes In Non-Demented Individuals

Luigi Lorenzini[1], Lyduine Collij[1], Niccoló Tesi[1], Natalia Vilor-Tejedor[2], Silvia Ingala[1], Betty Tijms[1], Andre Altmann[3], Frederik Barkhof[4]

[1]Amsterdam UMC, Amsterdam, Netherlands, [2]BarcelonaBeta Brain Research Center, Barcelona, CT, [3]UCL, London, I am not in the U.S. or Canada, [4]Amsterdam University Medical Centre, Amsterdam, Noord-Holland

Introduction: Little is known about the genetic factors and the downstream molecular pathways determining individual variability in imaging biomarkers associated with Alzheimer's disease (AD). We studied polygenic risk scores (PRS) and pathway-specific PRS in relationship with AD fluid and imaging biomarkers, in non-demented individuals from the European Prevention of Alzheimer's Dementia (EPAD) cohort.

Methods: EPAD inclusion criteria were age>50 and Clinical Dementia Rating≤0.5. AD-PRS was determined based on 85 previously identified loci, including and excluding APOE (PRSAPOE, PRSnoAPOE). Using gene-variant and variant-pathway

mapping, six pathway-specific PRSnoAPOE were identified, representative of 1) immune-activation, 2) signal-transduction, 3) inflammatory-response, 4) migration, 5) amyloid-production, and 6) clearance (Figure 1). Linear models were used to assess the relationship of the global and pathway PRS with fluid AD biomarkers, including Aβ1-42, p-Tau181, and t-tau; and several imaging biomarkers, including hippocampal volume, global and lobar white matter hyperintensities (WMH) volumes, fractional anisotropy (FA) in 14 regions of interest from diffusion tensor imaging, and 10 resting-state network connectivity from functional MRI. Models were adjusted for age, sex, site, and multiple comparisons.

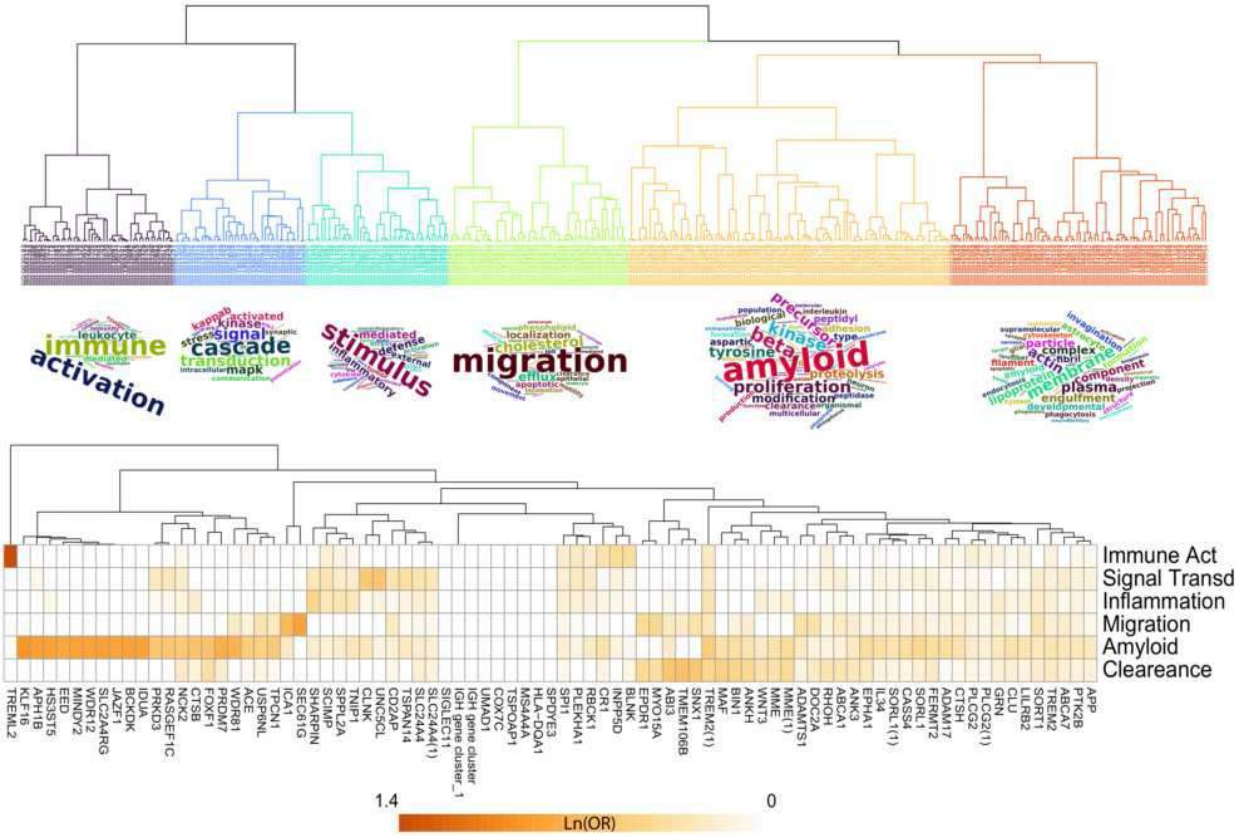

Figure 1. Results of the pathway analysis.

Results: 1738 participants met the inclusion criteria for this study. Mean age was 65.72 + 7.31 years, and 767 were males. Overall, participants were cognitively unimpaired, and only the 27.4% had a CDR=0.5 (very mild impairment). All pathway-PRSs were associated with CSF Aβ1-42 (all FDR adjusted p<0.05), except for the migration pathway that showed a trend-level association only (FDR adjusted p=0.08). All pathway-PRSs were also significantly associated with CSF p-Tau181 even when correcting for CSF Aβ1-42 (all FDR adjusted p<0.05), except for the inflammation pathway that showed a trend-level association (FDR adjusted p=0.08). Association of pathway-PRS with quantitative imaging biomarkers are shown in Figure 2. Lower hippocampal volumes showed a mild association with higher pathway-PRSs of migration and clearance, which did not survive multiple testing corrections. For white matter hyperintensities (WMH) volumes, higher clearance pathway-PRS was associated with higher WMH volumes in most regions. The effect was most pronounced in global, frontal, and temporal periventricular, and parietal deep white matter. Only the migration pathway was related to increases in FA in the splenium, body, and genu of the corpus callosum. Lower FC within the ventral default mode network (DMN) was associated with higher scores in the pathway-PRS of signal transduction.

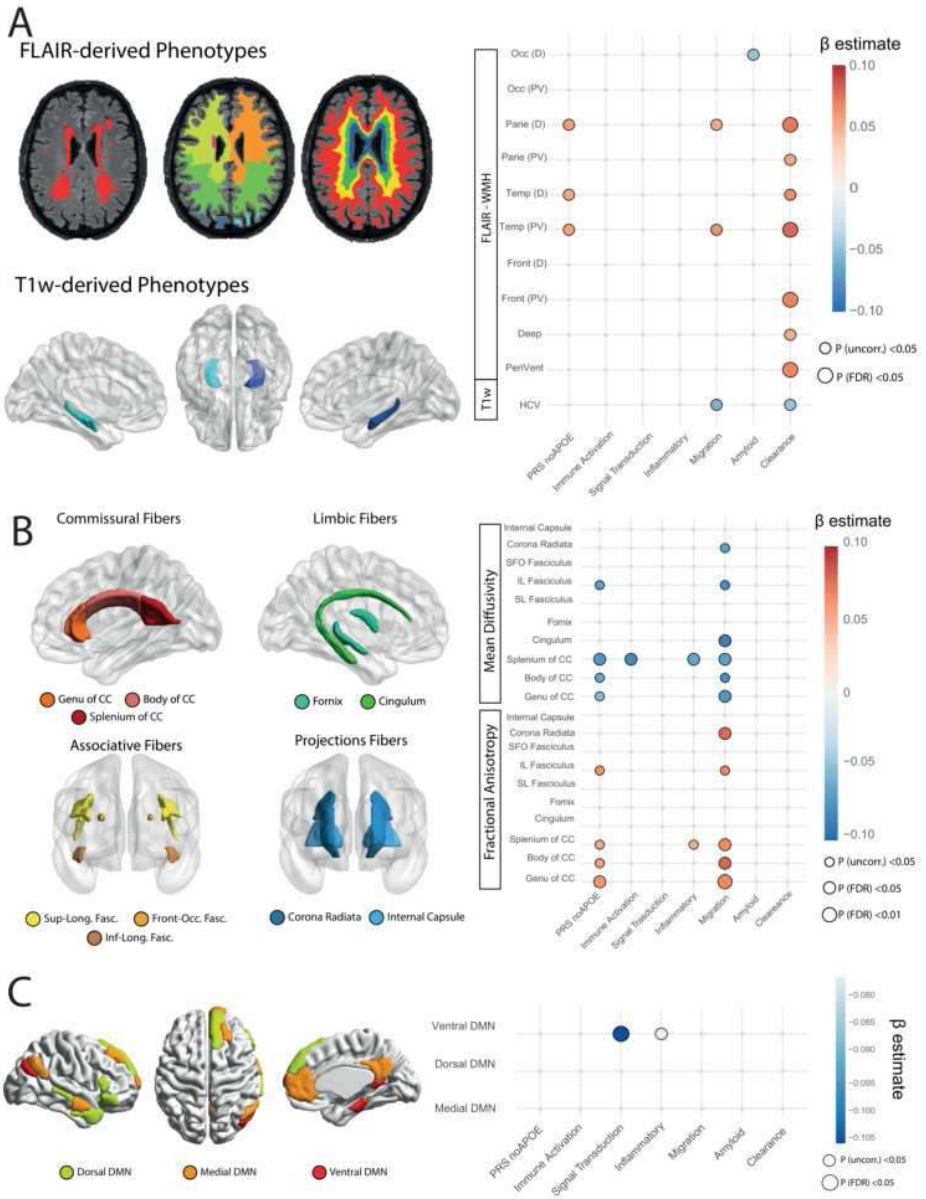

Figure 2. Association of pathways with quantitative multimodal imaging-derived phenotypes.

Conclusions: We show that genetic risk beyond APOE facilitates the manifestation of AD related pathologies, and that risk in distinct pathways may contribute to differential neuropathological fingerprints. We demonstrate that clearance and migration pathways were associated with neuroimaging measures of white matter integrity, while FC alterations were mostly determined by genetic risk in variants related to synaptic communication and plasticity.

Poster No 868

Multiphenotype analysis revealed novel hippocampal signatures associated with genetic AD risk

Natalia Vilor-Tejedor[1], Patricia Genius[1], Blanca Rodríguez-Fernández[1], Tavia Evans[2], Carolina Minguillon[1], Manel Esteller[3], Arcadi Navarro[1], Hieab Adams[4], Juan Domingo Gispert[1]

[1]BarcelonaBeta Brain Research Center, Barcelona, Catalonia, [2]Erasmus University Medical Center, Rotterdam, Zuid Holland, [3]Josep Carreras Leukaemia Research Institute, Barcelona, Catalonia, [4]Department of Genetics, Radboud University, Nimejgen, Holland

Introduction: Brain imaging genetic studies investigate genetic influences on brain structure and function by integrating neuroimaging-based features and genetic data. While many studies focus on individual genetic correlations with single

brain measurements, the field emphasizes the necessity of multivariate methods. We conducted a detailed analysis of how genetic predisposition to Alzheimer's disease (AD) influences multivariate hippocampal subfields modeling. We compared the results with those from univariate analyses underscoring the significance of multivariate methodologies in unraveling genetic influences of hippocampal structures.

Methods: A total of 1,411 cognitively unimpaired participants from the ALFA study (55.8yo in average; 62.4% women), with available information on both genetics and magnetic resonance imaging were included. Volumes for 8 hippocampal subfields were quantified from ultra-high resolution dual-echo Inversion-Recovery MRI scans covering the hippocampal formation and acquired in the direction of the planum temporale with the following parameters: Voxel Size = 0.4 x 0.4 x 2.0 mm; field of view: 230 x 184 x 78 mm; TR: 3000/8000 ms; TE = 26 ms; Refocusing Angle = 120° using Automatic Segmentation of Hippocampal Subfields (ASHS). Briefly, ASHS involves deformable registration of the T1- and T2-weighted images, multi-atlas joint label fusion, and voxelwise learning-based error correction. This process is employed to transfer anatomical labels from a collection of manually labeled training images to an unlabeled imageGenetic predisposition to AD was estimated by calculating polygenic risk scores using PRSice version 2. Canonical Correlation Analysis (CCA) and Compositional Data Analysis (CODA) were applied for identifying joint patterns of variation in hippocampal subfields volumetric changes influenced by genetic predisposition to AD. CCA enables the identification of hippocampal subfields simultaneously associated with a higher genetic predisposition to AD. CODA identified an optimal multivariate hippocampal structural signature involving the joint modulation of hippocampal subfields associated with higher genetic predisposition to AD.

Results: CCA revealed that higher volumes of CA1, GC-ML-DG, and CA3 were simultaneously associated with higher genetic predisposition to AD. Applying CODA, the optimal hippocampal signature associated with higher genetic predisposition to AD was defined by the joint modulation of CA3, CA1 as well as CA4, hippocampal fissure, and hippocampal tail. Finally, when evaluating univariate effects no significant results were found after multiple comparison correction.

Conclusions: The study underscores the importance of employing multivariate methodologies in investigating genetic influences on hippocampal structures, particularly in the context of AD. Overall, our study contributes valuable insights to the field of brain imaging genetics, emphasizing the better performance of multivariate analyses in unraveling the complex interplay between genetics and brain hippocampal volumes in the context of AD.

Poster No 869

FEMA-GWAS: mixed-effects algorithms for discovery of genome-wide non-linear SNP-by-age interactions

Pravesh Parekh[1], Nadine Parker[1], Diana Smith[2], Diliana Pecheva[2], Carolina Makowski[2], Evgeniia Frei[1], Gleda Kutrolli[1], Hao Wang[2], Dennis van der Meer[1,3], Alexey Shadrin[1], Thomas Nichols[4], Oleksandr Frei[1], Anders Dale[2], Ole Andreassen[1]

[1]University of Oslo, Oslo, Norway, [2]University of California San Diego, San Diego, CA, [3]Maastricht University, Maastricht, Netherlands, [4]University of Oxford, Oxford, United Kingdom

Introduction: Coupling longitudinal neuroimaging and genetics data can be useful in discovering the genetic associations underlying neurodevelopment, brain maturation, and neurodegeneration. These discoveries can then be linked to disease but are computationally intensive and almost impractical at the voxel- or element-level. In this work, we present a novel mixed-effects framework for performing longitudinal genome-wide association studies (GWAS), as well as discovery of non-linear interactions of single nucleotide polymorphisms (SNPs) or other genetic variants with age/time.

Methods: The longitudinal nature of the data and family structure (in studies like the ABCD Study) requires a mixed effect model, so we use a mixed modeling framework where the SNPs are the fixed effects, modeled individually, in addition to other nuisance effects. Considering the dimensionality of whole-brain neuroimaging data as well as the number of SNPs typically modeled in the GWAS framework (>1 million), it is computationally extremely laborious to use currently available mixed modeling frameworks. Therefore, we leverage our recently developed fast and efficient mixed-effects algorithm (FEMA) framework, which is a computationally efficient solution for performing whole-brain mixed modeling. For FEMA-GWAS with non-linear interactions, our approach is as follows (see Figure 1 for an overview): 1) using FEMA, estimate the effect of the fixed covariates on the imaging variables (phenotypes) as well as the variance parameters for the random effects. 2) Use a two-stage estimation approach that is equivalent to the conventional approach (Frisch-Waugh theorem) where we pre-residualize the genotype as well as the imaging variables for the effects of these covariates. This simplifies the estimation problem to estimating the effect of the residualized SNPs on the residualized phenotype. 3) For non-linear interactions, use natural cubic splines with user-defined knots – these basis functions are used for expanding the (main) effect of SNP. 4) Finally, we use generalized least squares (re-using the estimated variance parameters from the first step) to estimate the parameters for this

expanded set of predictors. As an additional feature, we allow these expanded set of predictors to interact with dummy-coded sex variable, thereby separately estimating the effects of the SNP-by-age interactions for males and females.

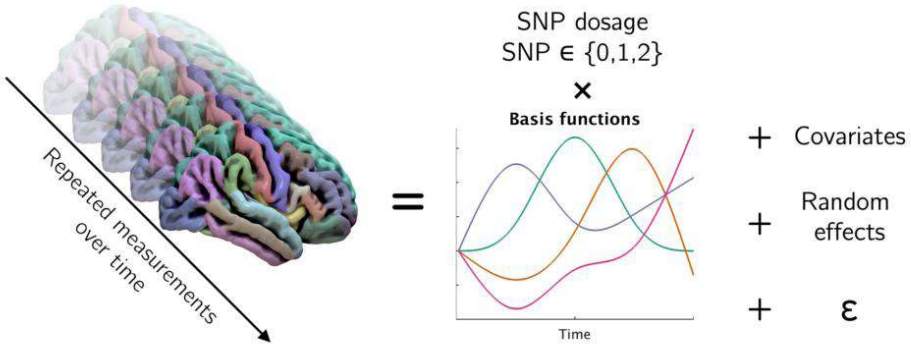

Schematic of FEMA-GWAS modeling: For repeated measures imaging data (region of interest, voxel-wise, vertex-wise, or connectome-wide), we model the effect of single nucleotide polymorphisms (SNPs). For non-linear interactions with age/time, we create basis functions using natural cubic splines – each SNP interacts with these basis functions to create an expanded set of predictors. We estimate the effect of these expanded set of predictors on the imaging variable while accounting for various covariates of no interest as well as other sources of variance, specified as random effects.

Results: The main result is the development of FEMA-GWAS, a novel MATLAB-based software that allows computationally efficient discovery of SNP-by-age interaction across the entire genome for a large number of imaging variables. Using simulations, we show that FEMA-GWAS has i) well-controlled type I error; and provides: ii) equivalent estimates to standard mixed effects implementation, and iii) accurate parameter recovery for various interaction terms. As a practical use-case, we present results for non-linear interaction of SNP and age for cortical thickness using samples from the longitudinal ABCD Study.

Conclusions: We have developed a software that enables users to perform longitudinal GWAS and discover the non-linear interactions of SNPs with age/time. FEMA-GWAS is specifically designed with the needs of the neuroimaging community in mind, easily scaling to a large number of outcome variables. Our work will enable users to perform these analyses at multiple levels of granularity – region of interest, voxel-wise, vertex-wise, and connectome-wide. We expect FEMA-GWAS to have wide-ranging impact – from applications in discovery of SNPs which drive the rate of change of imaging variables to establishing genetically adjusted normative models of brain phenotypes. FEMA is available to the public at: https://github.com/cmig-research-group/cmig_tools and FEMA-GWAS will be available as part of the same package soon.

References

1. Parekh, P., Fan, C.C., Frei, O., Palmer, C.E., Smith, D.M., Makowski, C., Iversen, J.R., Pecheva, D., Holland, D., Loughnan, R., Nedelec, P., Thompson, W.K., Hagler, D.J., Andreassen, O.A., Jernigan, T.L., Nichols, T.E., Dale, A.M., 2023. FEMA: Fast and efficient mixed-effects algorithm for large sample whole-brain imaging data. https://doi.org/10.1101/2021.10.27.466202

Poster No 870

Genome-wide Pleiotropy Analyses between Chronic Physical Conditions and Brain Disorders

Yujie Zhao[1], Wei Cheng[1]

[1]Fudan University, Shanghai

Introduction: Comorbidity between chronic physical conditions and brain disorders is highly prevalent, driven prominently by the shared genetic architecture. Yet, the extent to which shared genetics contribute to these complex comorbidities remains unclear. To elucidate the shared genetic etiologies between chronic and brain diseases, and to reveal the effect of polygenic risk architecture on the risk of comorbidity.

Methods: Leveraging the published large-scale genome-wide association studies (GWAS), we first performed cross-trait genetic correlation analyses between 9 chronic physical conditions and 15 brain disorders. Genome-wide pleiotropic association analyses sequentially detected pleiotropic single nucleotide polymorphisms (SNPs), loci, and genes, and

enrichment analyses elucidated the potential shared neurobiological pathways. Bidirectional Mendelian Randomization (MR) analyses were utilized to identify the causality across these pairwise diseases. Survival analyses using diagnostic outcomes from UK Biobank (UKB) and polygenic risk scores (PRSs) evaluated whether PRS for one disease predicts the risk of comorbidity with another disorder.

Results: Incorporating the GWAS data involving 9 chronic physical conditions and 15 brain disorders, we uncovered substantial genetic correlations among 35 out of 135 pairwise diseases. Pleiotropic analyses revealed 3,448 significant pleiotropic SNPs across these 35 pairwise diseases, mapped to 250 pleiotropic loci, with 63 loci showing evidence of colocalization. Gene-based association analyses pinpointed 167 unique pleiotropic genes, notably enriched in brain structural tissues, including the hippocampus, amygdala, and anterior cingulate cortex, as well as neuronal development phenotypes and protein synthesis pathways. In disease-level analyses, cross-trait MR analyses illustrated bidirectional causality in 4 disease pairs and 25 associations with unidirectional causality. Survival analyses identified extensive results on PRS-based risk prediction for developing comorbidity, across 2 chronic physical conditions (CHD and T2D) and 8 brain disorders (ALD, ANX, AD, BP, MDD, MS, PTSD, and SCZ), and demonstrated increased polygenic level of one disease would escalate the risk of comorbidity with another disease in pairs by up to six-fold.

Conclusions: These findings uncovered a comprehensive landscape of shared genomic variants, loci, genes, and neurobiological pathways between these two categories of diseases, providing a foundation for developing precision medicine approaches from a polygenic perspective.

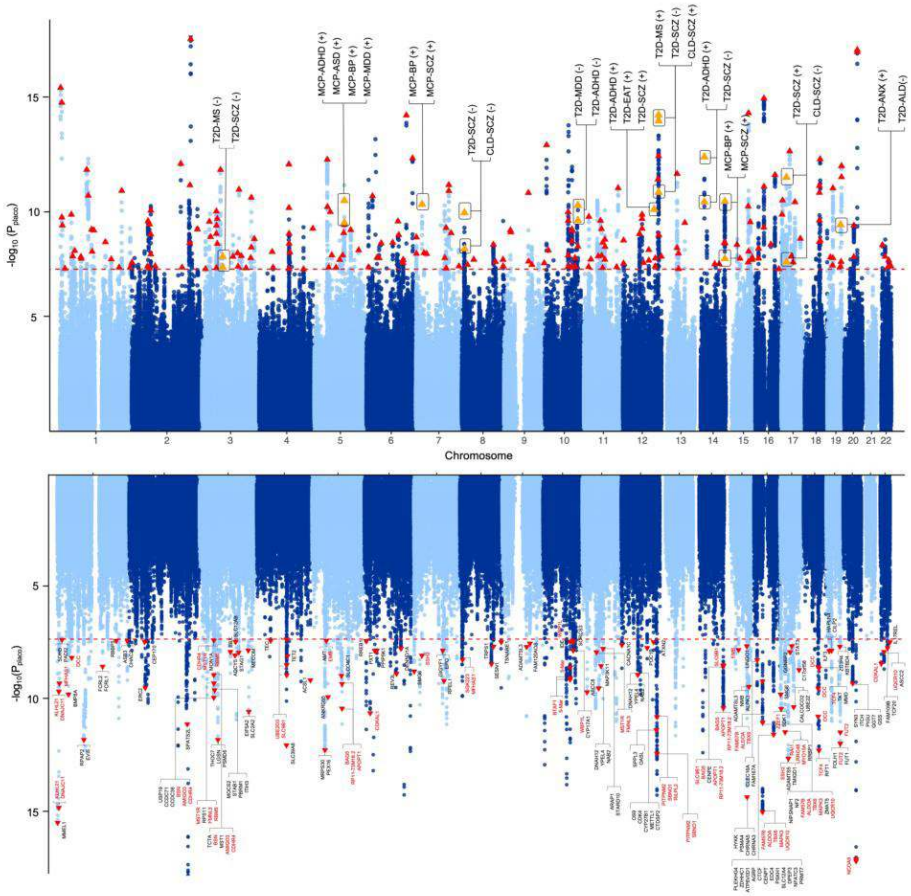

Fig. 1 Manhattan plots of pleiotropic analysis and genome-wide gene-based association analysis

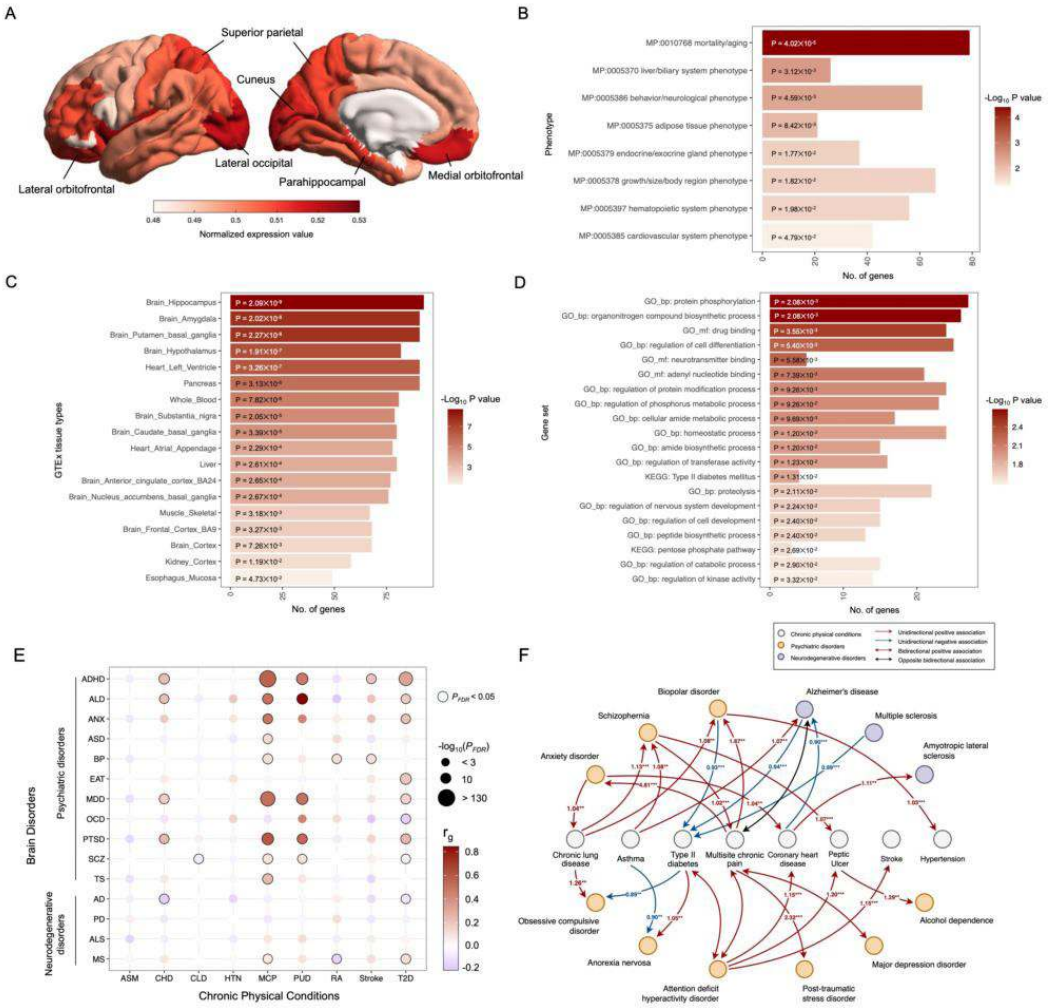

Fig. 2. Gene-level and disease-level analyses

References

1. Cross-Disorder Group of the Psychiatric Genomics Consortium. (2013), 'Genetic relationship between five psychiatric disorders estimated from genome-wide SNPs', Nature Genetics, vol.45, pp. 984–994.

Poster No 871

Heritability of Moment-to-Moment Neural Variability During Emotion Recognition

Tugce Yildiz-Ahola[1], Fredrik Åhs[2], Jörgen Rosén[1,2], Granit Kastrati[1], Tomas Furmark[3], Douglas Garrett[4,5], Kristoffer Månsson[1,6]

[1]Department of Clinical Neuroscience, Karolinska Institutet, Stockholm, Sweden, [2]Department of Psychology and Social Work, Mid Sweden University, Östersund, Sweden, [3]Department of Psychology, Emotion Psychology, Uppsala University, Uppsala, Sweden, [4]Center for Lifespan Psychology, Max Plank Institute for Human Development, Berlin, Germany, [5]Max Planck, UCL Centre for Computational Psychiatry and Ageing Research, Berlin, Germany, [6]Department of Clinical Psychology and Psychotherapy, Babeș-Bolyai University, Cluj-Napoca, Romania

Introduction: Heritability, the extent to which differences in traits can be attributed to genetic factors, plays a fundamental role in shaping brain function. In functional magnetic resonance imaging (fMRI), the average blood-oxygen-level-dependent (BOLD) signal across time/trials (i.e., MEANBOLD remains the typical approach in task-based fMRI studies. This model disregards variability from trial to trial as unwanted noise. In contrast, a growing body of evidence has shown that moment-to-moment variability in the BOLD signal (e.g., standard deviation of the BOLD response; SDBOLD) represents a viable measure of brain function. For instance, neural variability to socio-emotional faces has shown both high test-retest reliability, and sensitivity to inter-individual differences (Månsson et al. 2022). Further, identifying facial emotions is an inherent human skill and crucial for social interactions. Even though the ability to recognize emotions in faces is facilitated by a fundamental neural circuit (Haxby, Hoffman, and Gobbini 2002), the genetic contribution to this ability is overlooked. Therefore, this study explores

genetic influence on socio-emotional moment-to-moment neural variability during emotion recognition while going beyond traditional measures.

Methods: To investigate the heritability of BOLD-fMRI signals during an emotion recognition task, we employed a classical twin design with 144 pairs (69 monozygotic (MZ) and 75 dizygotic (DZ); N=288). Participants performed an emotion recognition task while scanned with MRI (3T General Electric), consisting of 4 emotional face and 5 geometrical shape matching blocks. The MR scanning parameters were set with a repetition time (TR) of 2.4 seconds, resulting in a total of 160 volumes. The heritability of brain signals was estimated using the fast and non-iterative APACE (Accelerated Permutation Inference for ACE model) method, which calculates the influence of additive genetics (A), shared environment (C), and unique environment (E) on phenotypic variance. Age and sex were included as covariates to control for their potential effects. Heritability (h2) is the measure of the proportion of phenotypic variance that is attributable to additive genetics and is obtained through statistical methods embedded in APACE. Statistical comparisons were performed voxel-wise (whole-brain) in MZ and DZ twin pairs. Significant clusters of heritability were defined with a whole-brain cluster-wise Family-Wise Error (FWE) correction threshold with alpha set at $P < 0.05$.

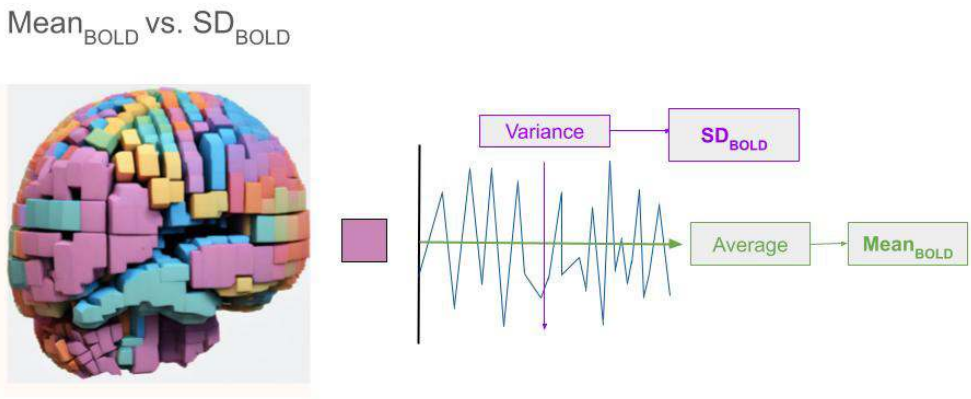

The figure depicts brain activation patterns during an emotion recognition task, illustrating two distinct metrics for each voxel. MeanBOLD (average blood-oxygen-level-dependent signal across multiple time points) and provides a measure of the average brain activity during a particular condition (e.g., task or rest), while SDBOLD (standard deviation of the BOLD response) captures moment-to-moment neural variability around the mean and represents dynamic changes in brain activity during a condition.

Results: The heritability (voxel-wise, averaged h2 across the whole-brain) of emotion recognition neural variability (SDBOLD) was statistically significant (h2 = 0.25, 95% CI 0.12, 0.39; permuted P = 0.029) and more than twice as high relative to the non-significant heritability of MEANBOLD emotion recognition (h2 = 0.10, 95% CI 0.05, 0.16; permuted P = 0.240). FWE corrected, significant clusters of SDBOLD emotion recognition heritability included the occipital lingual gyrus (h2 = 0.69), anterior cingulate cortex (h2= 0.61), parahippocampal gyrus (h2= 0.56), and thalamus (h2 = 0.62).

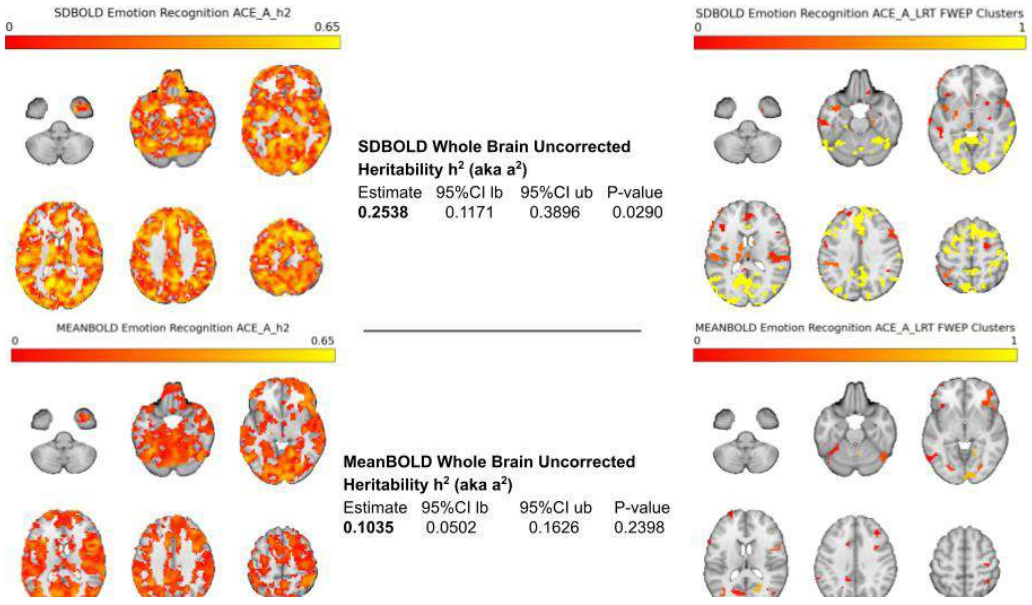

Conclusions: Our study demonstrates that moment-to-moment neural variability during an emotion recognition task is more heritable than average neural responses, highlighting the importance of variability in brain activity in heritability estimates. Our findings revealed significant clusters of heritability for SDBOLD in specific brain regions implicated in emotional face processing. These include the anterior cingulate gyrus and the parahippocampal gyrus that are activated during emotional face recognition (Xu et al. 2021) (Zhao et al. 2017), and the thalamus with its damage leading to an impairment in facial emotion recognition (Cheung et al. 2006). These identified clusters provide valuable insights into the genetic influences on moment-to-moment variability during the task of emotional face recognition. SDBOLD could be a new and more powerful signature of how genetics influence brain function.

References

1. Cheung, Crystal C. Y., Tatia M. C. Lee, James T. H. Yip, Kristin E. King, and Leonard S. W. Li. 2006. "The Differential Effects of Thalamus and Basal Ganglia on Facial Emotion Recognition." Brain and Cognition 61 (3): 262–68.
2. Haxby, James V., Elizabeth A. Hoffman, and M. Ida Gobbini. 2002. "Human Neural Systems for Face Recognition and Social Communication." Biological Psychiatry 51 (1): 59–67.
3. Månsson, Kristoffer N. T., Leonhard Waschke, Amirhossein Manzouri, Tomas Furmark, Håkan Fischer, and Douglas D. Garrett. 2022. "Moment-to-Moment Brain Signal Variability Reliably Predicts Psychiatric Treatment Outcome." Biological Psychiatry 91 (7): 658–66.
4. Xu, Pengfei, Shaoling Peng, Yue-Jia Luo, and Gaolang Gong. 2021. "Facial Expression Recognition: A Meta-Analytic Review of Theoretical Models and Neuroimaging Evidence." Neuroscience and Biobehavioral Reviews 127 (August): 820–36.
5. Zhao, Ke, Jia Zhao, Ming Zhang, Qian Cui, and Xiaolan Fu. 2017. "Neural Responses to Rapid Facial Expressions of Fear and Surprise." Frontiers in Psychology 8 (May): 761.

Poster No 872

Heritability of the Heschl Gyrus morphology

Gerson Robles Rodríguez[1], Diego Ramírez Gónzalez[1], Talía Román López[1], Ian Espinosa Méndez[1,2], Maria Guadalupe Garcia-Gomar[3], César Domínguez Frausto[1], Alejandra Ruiz Contreras[4], Alejandra Medina Rivera[5], Miguel Renteria[6], Sarael Alcauter[1]

[1]Instituto de Neurobiología, Universidad Nacional Autónoma de México., Querétaro, México., [2]Escuela Nacional de Estudios Superiores, Universidad Nacional Autónoma de México., Querétaro, México., [3]Harvard Medical School, Boston, MA, [4]Facultad de Psicología, Universidad Nacional Autónoma de México, Ciudad de México, México., [5]Laboratorio Internacional de Investigación sobre el Genoma Humano, Universidad Nacional Autónoma de, Querétaro, México, [6]QIMR Berghofer Medical Research Institute, Brisbane, AK

Introduction: The auditory cortex is situated in the temporal lobe, specifically within Heschl's gyrus (HG). The morphology of the HG exhibits high variability among hemispheres and individuals. Anatomical variations include both unique and duplicated HG. Duplicates are classified as a HG with an intermediate sulcus dividing half of the gyrus (Common Steam Duplication), and complete duplications where two gyri are formed (Complete Posterior Duplication; Moerel et al., 2014). These variations have been linked to diverse abilities, including musical and linguistic skills, cognition, and conditions such as schizophrenia and bipolar disorder (Takahashi et al., 2021). However, little is known about the relevance of genetic factors in the shape of the HG. Heritability quantifies the proportion of the variance that is attributed to genetic factors, and can be estimated by twin studies, comparing the traits in monozygotic twins (MZ, 100% shared DNA) and dizygotic twins (DZ, 50% shared DNA). Heritability may vary among populations, particularly in genetically admixed populations like the Mexican population. This study aims to estimate the heritability of the HG morphology.

Methods: High-resolution T1w images from 188 twins (124 MZ, 64 DZ) from the Mexican Twin Registry underwent preprocessing and parcellation using FreeSurfer's recon-all pipeline. Later, TASH, a toolbox that utilizes the output from FreeSurfer, was used to segment the HG in a detailed and automated manner, obtaining measurements of cortical thickness, surface area, and gray matter volume; subsequently, the MCAI toolbox was employed for the automated assessment of anatomical variations (Dalboni da Rocha et al., 2020; 2023). Heritability was assessed for the 3 morphological characteristics in both hemispheres using the ACE model, which estimates the proportion of variance attributable to additive genetic factors (A), common environmental (C) and non-shared environmental factors (E; Posthuma, 2009). Concordance rates (CR), which indicate the probability that both twins in a pair share a specific characteristic or condition (Mcgue, 1992), were evaluated for the anatomical variation assessment.

Results: The ACE model showed that for thickness, the left HG exhibited a heritability (genetic influence, a^2) of 0.56 and individual environmental influence (e^2) at 0.43. The right HG showed a^2 at 0.47 and e^2 at 0.52. Regarding surface area, the left HG showed a^2 at 0.10, shared environment influence (c^2) at 0.24, and e^2 at 0.65. For the right HG, a^2 was 0, c^2 was 0, and e^2 was 1. For volume, the left HG a^2 at 0.27, c^2 at 0.03, and e^2 at 0.69. The right HG exhibited a^2 at 0, c^2 at 0.24, and e^2 at 0.75. Regarding CR, MZ twins had 27 concordant pairs and 35 discordant pairs, resulting in a CR of 0.5. DZ twins had 19

concordant pairs and 26 discordant pairs, yielding a CR of 0.6, indicating a greater environmental influence regarding the HG anatomical variations.

Conclusions: Cortical thickness emerged as the most heritable feature, with non-shared environmental factors predominantly influencing surface area and volume-contrary to existing literature suggesting significant genetic influences on surface area (Schmitt et al., 2020). Regional variability in the heritability of cortical thickness within the temporal lobes (Rimol et al, 2010) may explain the high heritability observed in the specific area of the HG. Surface area and volume correlated with HG duplication patterns, contributing to the high levels of e^2 for these characteristics and for CR. The study suggests that non-shared environmental factors play a more significant role than genetic factors in explaining anatomical variations and morphological characteristics of the HG.

References

1. Dalboni da Rocha, J. L., Kepinska, O., Schneider, P., Benner, J., Degano, G., Schneider, L., & Golestani, N. (2023). Multivariate Concavity Amplitude Index (MCAI) for characterizing Heschl ' s gyrus shape. 272(September 2022). https://doi.org/10.1016/j.neuroimage.2023.120052
2. Dalboni da Rocha, J. L., Schneider, P., Benner, J., Santoro, R., Atanasova, T., Van De Ville, D., & Golestani, N. (2020). TASH: Toolbox for the Automated Segmentation of Heschl's gyrus. Scientific Reports, 10(1), 1–15. https://doi.org/10.1038/s41598-020-60609-y
3. Moerel, M., De Martino, F., & Formisano, E. (2014). An anatomical and functional topography of human auditory cortical areas. Frontiers in Neuroscience, 8(8 JUL), 1–14. https://doi.org/10.3389/fnins.2014.00225
4. Neuschwander, P., Hänggi, J., Zekveld, A. A., & Meyer, M. (2019). Cortical thickness of left Heschl's gyrus correlates with hearing acuity in adults – A surface-based morphometry study. Hearing Research, 384. https://doi.org/10.1016/j.heares.2019.107823
5. Posthuma, D. (2009). Handbook of Behvior Genetics (Y.-K. Kim (ed.); Vol. 01). Springer International Publishing. https://doi.org/https://doi.org/10.1007/978-0-387-76727-7_4
6. Rimol, L. M., Panizzon, M. S., Fennema-Notestine, C., Eyler, L. T., Fischl, B., Franz, C. E., Hagler, D. J., Lyons, M. J., Neale, M. C., Pacheco, J., Perry, M. E., Schmitt, J. E., Grant, M. D., Seidman, L. J., Thermenos, H. W., Tsuang, M. T., Eisen, S. A., Kremen, W. S., & Dale, A. M. (2010). Cortical Thickness Is Influenced by Regionally Specific Genetic Factors. Biological Psychiatry, 67(5), 493–499. https://doi.org/10.1016/j.biopsych.2009.09.032
7. Schmitt, J. E., Raznahan, A., Liu, S., & Neale, M. C. (2020). The genetics of cortical myelination in young adults and its relationships to cerebral surface area, cortical thickness, and intelligence: A magnetic resonance imaging study of twins and families: Genetics of Cortical Myelination, Area, Thickness, and Int. NeuroImage, 206(May 2019), 116319. https://doi.org/10.1016/j.neuroimage.2019.116319
8. Takahashi, T., Sasabayashi, D., Takayanagi, Y., Furuichi, A., Kido, M., Nakamura, M., Pham, T. V., Kobayashi, H., Noguchi, K., & Suzuki, M. (2021). Altere

Poster No 873

Generating Gene Embedding for Early Diagnosis of Alzheimer's Disease

Kyeongho Kim[1], YeonJu Park[1], Jong-Min Lee[2]

[1]Department of Artificial Intelligence, Hanyang University, Seoul, Republic of Korea, [2]Department of Electronic Engineering, Hanyang University, Seoul, Republic of Korea

Introduction: Alzheimer's disease (AD) is characterized by memory dysfunction and language disorders in patients. The elevated prevalence of AD in individuals aged 65 and older has raised significant concerns among the elderly. With the global aging of the population, it is predicted that the number of Alzheimer's patients will increase approximately triple in 2050[1]. Consequently, there has been recent extensive research leading to the development of new drugs for AD. Currently developed drugs play a role in slowing down the progression of diseases rather than restoring the state of health[2]. Therefore, it is necessary to utilize medication as early as possible through early diagnosis of AD to slow down the progression of the disease. Early diagnosis of AD techniques mainly use neuroimaging data. However, there are limitations in the accuracy when early diagnosis of AD based on neuroimaging data. Recognizing that the estimated heritability of AD is 60%-80%[3], it is expected that genetic data will play an important role in early diagnosis. But current methods like minor allele counting and one-hot vectors are simplistic to explain complex genetic data. So We generate gene embedding through deep learning from the input of genes used in early diagnosis of AD.

Methods: In this study, 623 individuals from Alzheimer's Disease Neuroimaging Initiative (ADNI) dataset with available Single Nucleotide Polymorphism (SNP) information are utilized. This cohort includes 285 AD and 338 cognitively normal (NC). We use the top 10 genes closely associated with AD. SNPs are represented in diploid with two complete sets of chromosomes, one from each parent. However, Natural Language Processing (NLP) models typically take single sentences as inputs. Therefore, we transformed diploid into single sentences form. SNPs composed of four alphabet letters (i.e., A, C, G and T) can be paired up into ten different alphabet letters, excluding the repetitive ones. We use the k-mer method to tokenize SNPs as one word. We make use of Bidirectional Encoder Representations from Transformers (BERT) to create meaningful embedding vectors for k-mer tokens. BERT employs two unsupervised learning tasks (Masked Language Model (MLM) and Next Sentence Prediction

(NSP)) for training. However, we only used MLM because our model only takes information about a person as input. 15% of the input tokens were randomly masked in each subject's SNPs. BERT learns to predict the correct token through the hidden vector of mask token. To create gene embeddings, the embedded k-mer tokens are fed into Long Short-Term Memory (LSTM) as input. LSTM is employed to classify 10 genes. The process involves taking a single gene's nucleotide sequence as input, passing it through BERT, resulting in 120-dimensional embedding values for each token. These embeddings are then fed into LSTM sequentially. We leverage the final output value, capturing the meaning of the entire nucleotide sequence, to create a 120-dimensional embedding for the gene's sequence.

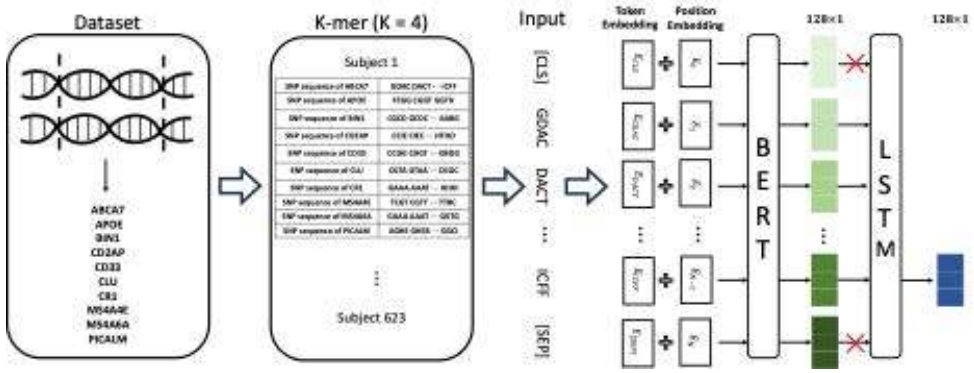

Fig. Overall structure of the model

Results: To train LSTM, learning was conducted using 5000 gene data, and evaluation is carried out using 1230 gene data. We obtained the results through cross-entropy with the outcomes of a model predicting 10 types of gene. Figure 2 shows t-SNE and confusion matrix representing the classification results of 10 types of genes. Classification average results of 10 types of genes is 69.2%. Additionally, to investigate whether the gene embeddings influence early diagnosis of AD, we conduct early AD diagnosis using T1-weighted images and gene embedding.

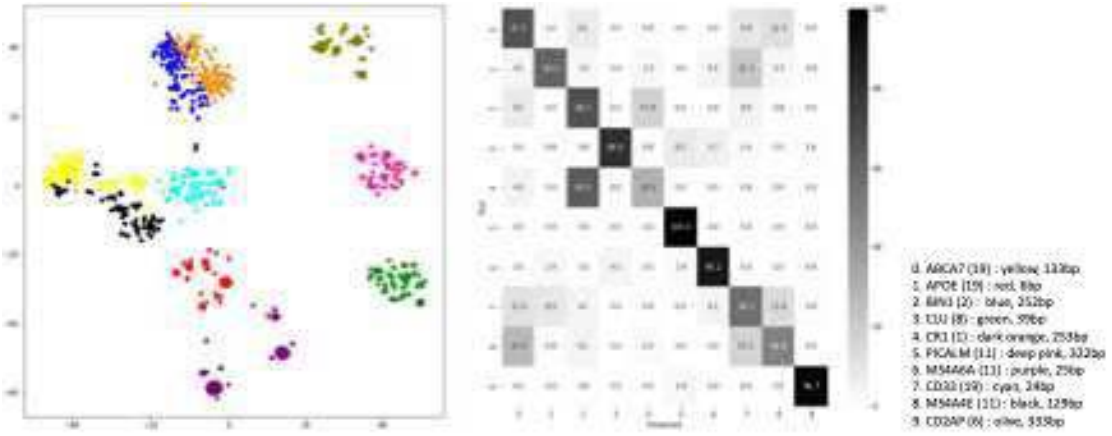

Fig. t-SNE and confusion matrix representing the classification results of 10 types of genes

Conclusions: In this study, we utilize BERT and LSTM for the training of gene embedding. After which we conducted early AD diagnosis using T1-weighted images and gene embeddings. In future work, early diagnosis of AD will be conducted using not only T1-weighted images and gene embedding but also other types of data.

References

1. Hao, Xiaoke, et al. "Multi-modal Self-paced Locality Preserving Learning for Diagnosis of Alzheimer's Disease." IEEE Transactions on Cognitive and Developmental Systems (2022).
2. Sims, John R., et al. "Donanemab in early symptomatic Alzheimer disease: the TRAILBLAZER-ALZ 2 randomized clinical trial." Jama 330.6 (2023): 512-527.
3. Lagisetty, Yashwanth, et al. "Identification of risk genes for Alzheimer's disease by gene embedding." Cell genomics 2.9 (2022).
4. Ji, Yanrong, et al. "DNABERT: pre-trained Bidirectional Encoder Representations from Transformers model for DNA-language in genome." Bioinformatics 37.15 (2021): 2112-2120.
5. Cahyawijaya, Samuel, et al. "SNP2Vec: Scalable Self-Supervised Pre-Training for Genome-Wide Association Study." Proceedings of the 21st Workshop on Biomedical Language Processing. 2022.
6. Kenton, Jacob Devlin Ming-Wei Chang, and Lee Kristina Toutanova. "Bert: Pre-training of deep bidirectional transformers for language understanding." Proceedings of naacL-HLT. Vol. 1. 2019.
7. Hochreiter, Sepp, and Jürgen Schmidhuber. "Long short-term memory." Neural computation 9.8 (1997): 1735-1780.

Poster No 874

Assessment of subthreshold group differences in rs-fMRI by higher criticism: adult phenylketonuria

Benedikt Sundermann[1,2,3], Reinhold Feldmann[4], Christian Mathys[1,3,5], Johanna Rau[4], Stefan Garde[6], Anke McLeod[1], Josef Weglage[6], Bettina Pfleiderer[7]

[1]Evangelisches Krankenhaus Oldenburg, Medical Campus University of Oldenburg, Oldenburg, Germany, [2]University of Münster, Münster, Germany, [3]Research Center Neurosensory Science, University of Oldenburg, Oldenburg, Germany, [4]University Hospital Münster, Münster, Germany, [5]University of Düsseldorf, Düsseldorf, Germany, [6]University Hospital Münster, Münster, Germany, Münster, Germany, [7]University of Münster, Münster, Germany, Münster, Germany

Introduction: Phenylketonuria (PKU) is an inherited metabolic disorder affecting neurocognitive development (van Spronsen et al., 2021). Despite early treatment adults with PKU exhibit minor cognitive impairments (Romani et al., 2022). Knowledge about the integrity of brain networks and their functional connectivity (FC) in PKU measured by resting-state functional magnetic resonance imaging (rs-fMRI) is limited, including initial evidence of altered default mode network (DMN) and prefrontral cortex FC (De Giorgi et al., 2023). The rarity of PKU limits fMRI sample sizes. A multi-scale testing approach using "higher criticism" (HC), a technique to detect rare and weak effects in high-dimensional data (Donoho & Jin, 2015), at the level of sub-networks could recently provide evidence of group differences widely distributed across cognition-related networks in fetal alcohol syndrome, which conventional mass-univariate testing failed to detect (Sundermann et al., 2023). The purpose of this analysis was therefore to assess the ability of this HC-based approach to detect FC alterations in cognitive networks in adults with PKU.

Methods: Patients with PKU (n = 11, age: 27.2 ± 3.7 years, all female) and healthy controls (n = 11, age: 25.9 ± 3.8 years, all female) were included. MRI data acquisition at 3 Tesla: 9:45 min rs-fMRI (234 volumes, repetition time: 2500 ms, echo time: 35 ms, spatial resolution 3.6 x 3.6 x 3.6 mm), 3D T1 (inversion-prepared turbo field echo). Preprocessing with denoising was based on fmriprep (Esteban et al., 2019). FC was calculated as linear correlation between 243 atlas regions in 10 cognition-related sub-networks (Schaefer et al., 2018). Subsequent modelling was based on multiple linear regression models comparing FC between groups (one test per pair of regions, including age and head motion as covariates). Resulting main effects of group were subjected to HC-based multiscale testing, first determining whether there is any alteration of FC in PKU in the full cognitive connectome, and subsequently resolving these findings to the level of either FC within each network or between-network connectivity (Sundermann et al., 2023). HC statistics test a joint hypothesis of an excess of low p-values in such multiple primary tests as evidence of non-zero effects (Donoho & Jin, 2015). Finally, individual connections were assessed using conventional mass-univariate testing with multiple comparison correction.

Results: Global analysis (HC, omnibus test): FC among cognition-related brain regions was significantly altered in PKU compared with controls. Within-network analysis (HC): Significant group effects in the all 4 attention-related networks (dorsal and ventral/salience), and 2 out of 3 DMN sub-networks. No group effects in the fronto-parietal control network (3 sub-networks). Between-network analysis (HC): No significant group effects. Conventional mass-univariate analysis of single connections: No significant group effects (global multiple comparison correction).

Conclusions: Group differences in the DMN are in line with limited previous research on functional networks in PKU (De Giorgi et al., 2023). Alterations within attention-related systems are compatible with the clinical phenotype (i.e. including attentional deficits) previously observed in this adult age group (Romani et al., 2022). Contrary to findings of frontal-lobe associated performance deficits typically reported in children (Diamond, 2007), we did not observe group differences in the fronto-parietal control network, which is in line with the notion that these deficits might become less important when PKU patients reach adulthood (Weglage et al., 1999). Despite the relatively small sample, this HC-based analysis could detect group effects at the network level, which were missed by a conventional mass-univariate analysis. Thus, HC-based global hypothesis testing might be an informative complementary analysis approach in rs-fMRI studies of rare disorders.

References

1. De Giorgi, A., Nardecchia, F., Manti, F., Campistol, J. and Leuzzi, V. 2023. 'Neuroimaging in early-treated phenylketonuria patients and clinical outcome: A systematic review', Mol Genet Metab, vol. 139, pp. 107588
2. Diamond, A. 2007. 'Consequences of variations in genes that affect dopamine in prefrontal cortex', Cereb Cortex, vol. 17, no Suppl 1, pp. i161-70.
3. Donoho, David, and Jiashun Jin. 2015. 'Higher Criticism for Large-Scale Inference, Especially for Rare and Weak Effects', Statistical Science, vol 30, pp. 1-25.
4. Esteban, O., Markiewicz, C. J., Blair, R. W., Moodie, C. A., Isik, A. I., Erramuzpe, A., Kent, J. D., Goncalves, M., DuPre, E., Snyder, M., Oya, H., Ghosh, S.S., Wright, J., Durnez, J., Poldrack, R.A. and Gorgolewski K. J. 2019. 'fMRIPrep: a robust preprocessing pipeline for functional MRI', Nat Methods, vol. 16, pp. 111-16.
5. Romani, C., Olson, A., Aitkenhead, L., Baker, L., Patel, D., Spronsen, F. V., MacDonald, A., Wegberg, A.V., and Huijbregts, S. 2022. 'Meta-analyses of cognitive functions in early-treated adults with phenylketonuria', Neurosci Biobehav Rev, vol. 143, pp. 104925.

6. Schaefer, A., Kong, R., Gordon, E. M., Laumann, T. O., Zuo, X.N., Holmes, A.J., Eickhoff, S.B. and Yeo, B.T.T. 2018. 'Local-Global Parcellation of the Human Cerebral Cortex from Intrinsic Functional Connectivity MRI', Cereb Cortex, vol. 28, pp. 3095-114.
7. Sundermann, B., Feldmann, R., Mathys, C., Rau, J.M.H., Garde, S., Braje, A., Weglage, J. and Pfleiderer, B. 2023. 'Functional connectivity of cognition-related brain networks in adults with fetal alcohol syndrome', medRxiv. DOI: 10.1101/2023.05.18.23289319
8. van Spronsen, F. J., Blau, N., Harding, C., Burlina, A., Longo, N. and Bosch, A.M. 2021. 'Phenylketonuria', Nat Rev Dis Primers, vol. 7, pp. 36.
9. Weglage, J., Pietsch, M., Denecke, J., Sprinz, A., Feldmann, R., Grenzebach, M., and Ullrich, K. 1999. 'Regression of neuropsychological deficits in early-treated phenylketonurics during adolescence', J Inherit Metab Dis, vol. 22, pp. 693-705.

Poster No 875

Development of regional cortical GM and WM volumes in utero in fetuses with Trisomy 21

Abi Fukami - Gartner[1], Alena Uus[1], Vanessa Kyriakopoulou[1], Helena Sousa[1], Roos Bos[1], Daniel Cromb[1], Megan Hall[1], Joseph Hajnal[1], Maria Deprez[1], Jana Hutter[1], Lisa Story[1], Jonathan O'Muircheartaigh[1], Mary Rutherford[1]

[1]Centre for the Developing Brain, King's College London, London, United Kingdom

Introduction: Trisomy 21 (T21, i.e., Down syndrome) is the most common cause of intellectual disability with a known genetic aetiology affecting approximately 1 in 1000 live births (De Graaf 2021). Most individuals with T21 are classified as having mild to moderate intellectual disability, although a wide and largely unexplained range of neurodevelopmental outcomes are observed (Chapman 2000). There is still a gap in knowledge about detailed structural brain development in utero in T21. We have recently published a comprehensive volumetric phenotyping of the neonatal brain in T21 (Fukami-Gartner, 2023). Here, we investigate the timing and differences in the development of regional cortical grey matter (GM) and white matter (WM) volumes in utero in fetuses with T21.

Methods: Typically developing controls (TDC) were comprised of n=397 fetal participants (gestational age, GA, range=19.86 to 38.29 weeks) from 3 studies: the 'developing Human Connectome Project' (dHCP, REC 14/LO/1169, n=257); the 'Placental Imaging Project' (PiP, REC 16/LO/1573, n=78); and, the 'individualised risk prediction [..] in pregnancies that deliver preterm' study (PRESTO, REC 21/SS/0082, n=62). T2-weighted (T2w) MRI were acquired on a 3T Philips Achieva system at TE=250ms (for dHCP) or TE=180ms (for PiP and PRESTO) as detailed in (Uus 2023). 25 fetuses with confirmed T21 (GA=24.00 to 35.71) from the 'early brain imaging in DS' (eBiDS, REC 19/LO/0667) were imaged with the above protocols at either TE=180ms (n=20) or 250ms (n=5). All T2w images were motion-corrected and 3D SVR reconstructed to 0.5mm isotropic pixel resolution. Total tissue volume, total cortical GM and WM were initially segmented using the BOUNTI pipeline (Uus 2023). These were sub-divided into frontal, parietal, occipital, temporal, insular and cingulate regions in atlas space (Fig 1A) and propagated into subjects using classical registration methods. Non-linear regressions of volumes against GA were fitted and compared using the extra-sum-of-squares F-test in Graphpad Prism v9.0.

Results: Total tissue volume had a significantly different non-linear fit from 24 to 36 weeks GA for fetuses with T21 (F-test, pFDR < 0.0001) with reduced volumes particularly after 30 GA. As such, total GM volume and total WM volume (both pFDR < 0.0001) also showed significantly different non-linear fits throughout gestation. Total WM volumes were more markedly reduced than total GM volumes after 30 GA in T21 (Fig.1B). A breakdown into frontal, parietal, occipital and temporal segments provided details of regional volumetric differences between T21 and TDC. Frontal and occipital GM had a significantly different non-linear fit (both pFDR < 0.0001) with reduced volumes in T21, whilst parietal (pFDR = 0.42) and temporal GM volumes (pFDR = 0.18) did not show any difference in non-linear fit across gestation. All WM regional volumes had a significantly different non-linear fit (all pFDR < 0.0001) with reduced volumes in T21. Volumetric reductions after 30 GA were more marked in frontal, occipital and temporal WM than in parietal WM (Fig.2A-B).

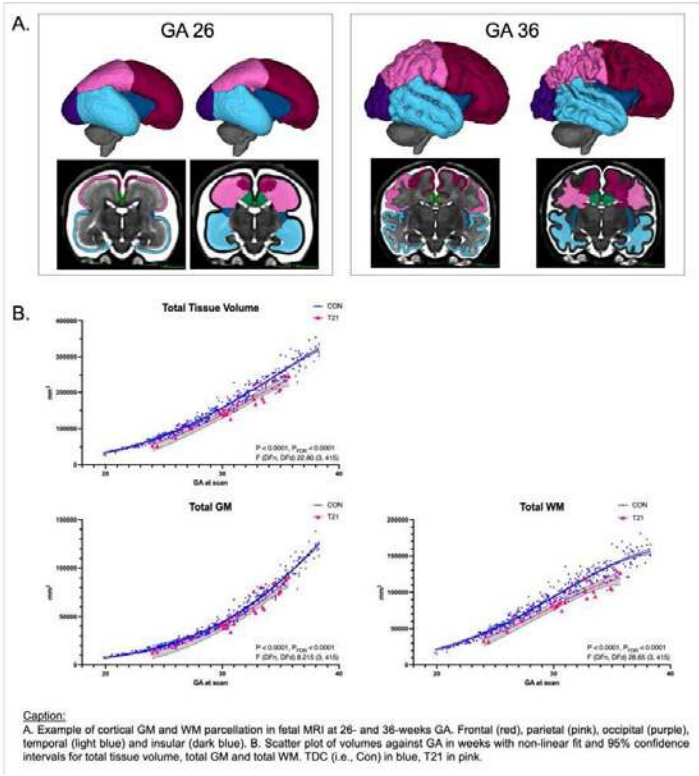

Caption:
A. Example of cortical GM and WM parcellation in fetal MRI at 26- and 36-weeks GA. Frontal (red), parietal (pink), occipital (purple), temporal (light blue) and insular (dark blue). B. Scatter plot of volumes against GA in weeks with non-linear fit and 95% confidence intervals for total tissue volume, total GM and total WM. TDC (i.e., Con) in blue, T21 in pink.

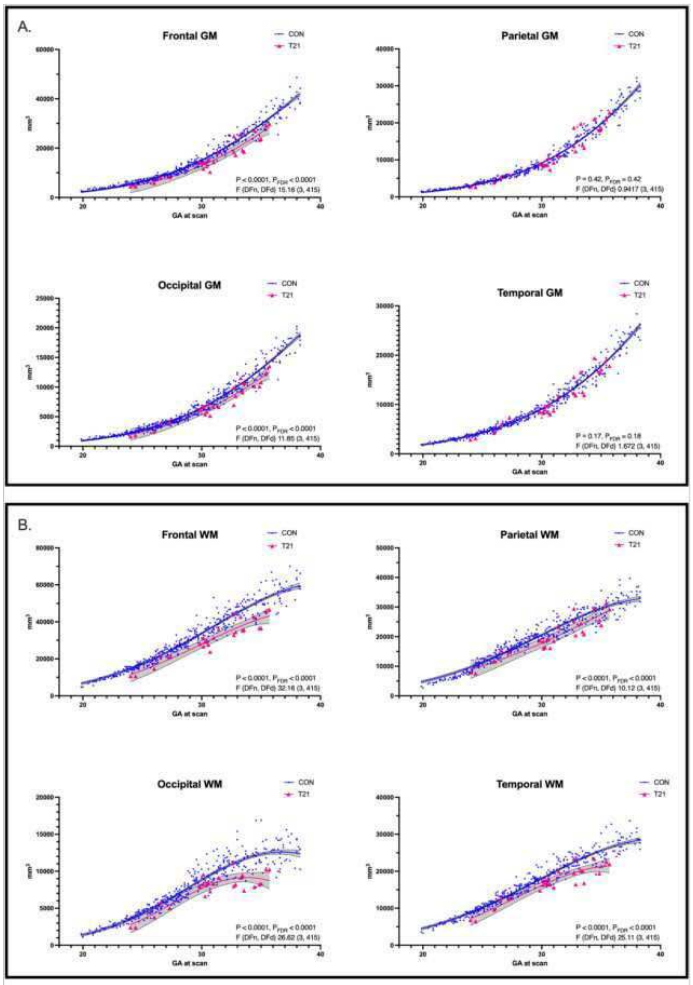

Caption:
Scatter plot of volumes against GA in weeks with non-linear fit and 95% confidence intervals for A. cortical GM regions and B. WM regions. TDC (i.e., Con) in blue, T21 in pink.

Conclusions: To the best of our knowledge, the detailed development of regional cortical GM and WM volumes has never been studied in utero in T21 (Hamner 2018, Tarui 2020). With regards to cortical GM, this analysis showed that frontal and occipital GM volumes deviated from TDC, with particularly reduced volumes after 30 GA, whilst parietal and temporal GM volumes did not show any significant difference across gestation. All WM regions deviated from TDC, although parietal WM volumes did not have a marked reduction in volume after 30 GA, as per other WM regions. This analysis corroborates our findings in neonates with T21 following delivery (Fukami-Gartner 2023) and further elucidates the timings of volumetric deviations in utero. These volumetric results may be associated with brachycephaly, as identified in unpublished craniofacial biometry in this cohort, and evidenced in ex vivo fetal examinations (Guihard-Costa 2006).

References

1. Chapman RS. 2000. Behavioral phenotype of individuals with Down syndrome. Ment Retard Dev Disabil Res Rev. 6:84–95.
2. de Graaf G. 2021. Estimation of the number of people with Down syndrome in Europe. Eur J Hum Genet. 29:402–410.
3. Fukami-Gartner A. 2023. Comprehensive volumetric phenotyping of the neonatal brain in Down syndrome. Cereb Cortex. 33:8921–8941.
4. Guihard-Costa AM. 2006. Biometry of face and brain in fetuses with trisomy 21. Pediatr Res. 59:33–38.
5. Hamner T. 2018. Pediatric Brain Development in Down Syndrome: A Field in Its Infancy. J Int Neuropsychol Soc. 24:966–976.
6. Tarui T. 2020. Quantitative MRI Analyses of Regional Brain Growth in Living Fetuses with Down Syndrome. Cereb Cortex. 30:382–390.
7. Uus AU. 2023. BOUNTI: Brain vOlumetry and aUtomated parcellatioN for 3D feTal MRI. Elife. 12:RP88818.

Poster No 876

Structural Connectivity Differences In White Matter Tracts Of Nerve Growth Factor Mutation Carriers

Arnas Tamasauskas[1], Andrew Marshall[1], Irene Perini[2], India Morrison[2]

[1]University of Liverpool, Liverpool, Merseyside, [2]Linköping University, Linköping, Linköping

Introduction: The research of pain and nociceptive reactions of people with Nerve Growth Factor (NGF) mutations has revealed congenitally reduced density of C-nociceptor afferent fibres in the peripheral nerve system, but the impact of these gene mutations on whole brain connectivity has not yet been explored.

Methods: This study utilised Diffusion Tensor Imaging (DTI) and T1-weighted scans of a group of 11 R221W heterozygous carriers, who have impaired pain and temperature perception, and 11 gender-, age-, and education-matched healthy controls. DTI scans were acquired using single phase encoding. For preprocessing, Synb0, was utilised to synthesize reverse phase encoding from T1 scans. Whole-brain Voxel-based Tract-Based Spatial Statistics (TBSS) and Fixel-based group comparison analyses were performed to examine different metrics of white-matter structure and integrity. More specifically, TBSS investigated: fractional anisotropy (FA), mean diffusivity (MD), and Radial Diffusivity (RD), while Fixel-based statistics were used to analyse: microstructural fibre density (FD), fibre cross-section (FC), and combined fibre density and cross-section metric (FDC). Significance thresholding ($p<0.05$) was applied to Fixel FD, FC and FDC metrics, which were then registered to a John Hopkins University (JHU) ICBM-DTI-81 white-matter labels atlas using FSL Linear Image Registration Tool. Additionally, these tracts were converted to Voxels and used for Region of Interest (ROI) specified Probabilistic Second-order Integration over Fibre Orientation Distributions (iFOD2).

Results: TBSS analysis showed no significant differences between the R221W carrier group and healthy controls in FA, MD or RD. Fixel-based group comparison between R221W carriers and healthy controls showed significant FD and FDC reductions in specific white matter tracts in midbrain and pons ($p < 0.05$) (Figure 1), but no significant differences in FC. JHU atlas-based White-matter investigations provided specificity in identifying tracts with significantly reduced FD and FDC of R221W carrier group as compared to healthy controls. These affected tracts were: the middle cerebellar peduncle, corticospinal tract, medial lemniscus, and inferior and superior cerebellar peduncles. Some minimal but significant ($p<0.005$) FD and FDC differences were seen in: corona radiata, as well as slight FD differences in external capsule, and slight FDC differences in internal capsule and uncinate fasciculus. Voxel-based iFOD2 analysis supported significant difference findings in FD and FDC populations in the midbrain, pons, cerebellum, and parts of temporal and occipital cortices. ($p < 0.05$) (Figure 2).

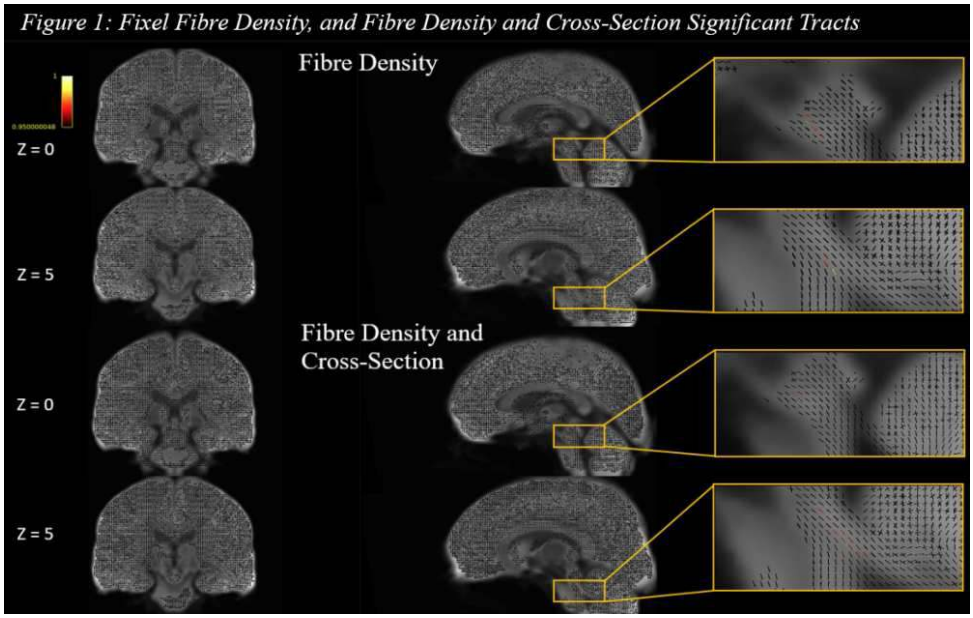

Figure 1: Fixel Fibre Density, and Fibre Density and Cross-Section Significant Tracts

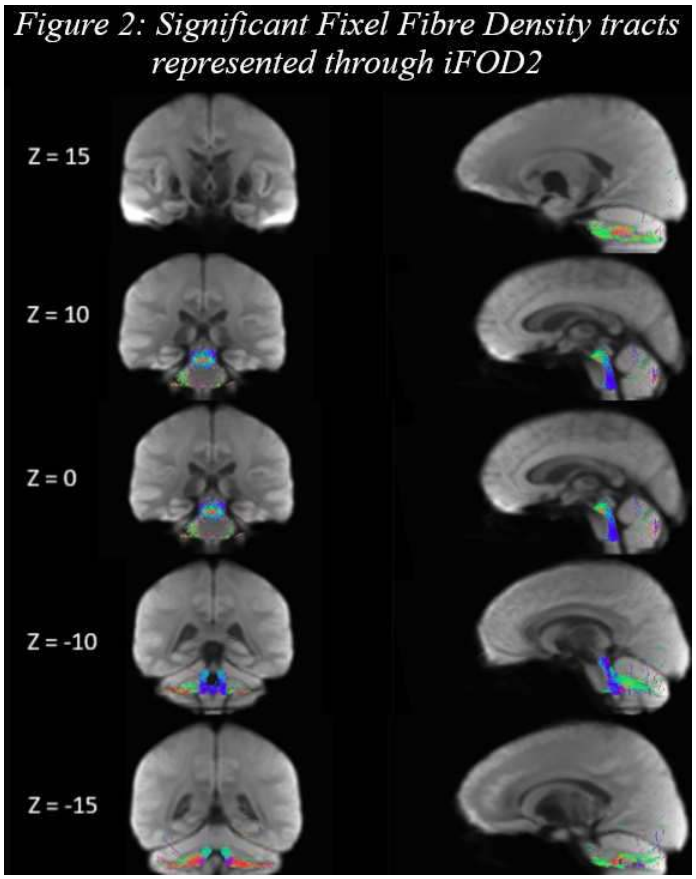

Figure 2: Significant Fixel Fibre Density tracts represented through iFOD2

Conclusions: While Voxel-based statistics did not indicate any significant structural white matter differences, Fixel-based FD and FDC findings suggest reduced intra-axonal volume in the spinothalamic and corticothalamic tracts of R221W carriers. This would indicate that the reduction of C-nociceptor afferent nerve density of R221W carriers is not constrained to the periphery, but is also present in parts of the brain. Particularly, brainstem pathways to the cerebellum and deep brain structures appear to have the most fibre density and cross-section reduction. However, the differences are not constrained to the brainstem as some differences are present in tracts located in occipital and temporal lobes. Fixel-based analyses provided a more detailed investigation of fibre orientations than TBSS, but iFOD2 provided additional support for significant difference findings in fibre density and cross-section when converted to voxel-based metrics. Further ROI TBSS, Fixel-based and Voxel-based analyses are needed to investigate the differences in intra-axonal volume and crossing-fibres of specific brain regions.

References

1. Perini, I., Ceko, M., Cerliani, L., van Ettinger-Veenstra, H., Minde, J., & Morrison, I. (2020). Mutation carriers with reduced C-afferent density reveal cortical dynamics of pain–action relationship during acute pain. Cerebral Cortex, 30(9), 4858-4870.
2. Schilling, K. G., Blaber, J., Hansen, C., Cai, L., Rogers, B., Anderson, A. W., ... & Landman, B. A. (2020). Distortion correction of diffusion weighted MRI without reverse phase-encoding scans or field-maps. PLoS One, 15(7), e0236418.
3. Schilling, K. G., Blaber, J., Huo, Y., Newton, A., Hansen, C., Nath, V., ... & Landman, B. A. (2019). Synthesized b0 for diffusion distortion correction (Synb0-DisCo). Magnetic resonance imaging, 64, 62-70.
4. Smith, S. M., Jenkinson, M., Johansen-Berg, H., Rueckert, D., Nichols, T. E., Mackay, C. E., ... & Behrens, T. E. (2006). Tract-based spatial statistics: voxelwise analysis of multi-subject diffusion data. Neuroimage, 31(4), 1487-1505.
5. Raffelt, D. A., Tournier, J. D., Smith, R. E., Vaughan, D. N., Jackson, G., Ridgway, G. R., & Connelly, A. (2017). Investigating white matter fibre density and morphology using fixel-based analysis. Neuroimage, 144, 58-73.
6. Mori, S., Wakana, S., Van Zijl, P. C., & Nagae-Poetscher, L. M. (2005). MRI atlas of human white matter. Elsevier.
7. Jenkinson, M., & Smith, S. (2001). A global optimisation method for robust affine registration of brain images. Medical image analysis, 5(2), 143-156.
8. Jenkinson, M., Bannister, P., Brady, M., & Smith, S. (2002). Improved optimization for the robust and accurate linear registration and motion correction of brain images. Neuroimage, 17(2), 825-841.
9. Tournier, J. Donald, Fernando Calamante, and Alan Connelly. "Improved probabilistic streamlines tractography by 2nd order integration over fibre orientation distributions." Proceedings of the international society for magnetic resonance in medicine. Vol. 1670. John Wiley & Sons, Inc, New Jersey, 2010.

Poster No 877

Unveiling White Matter Changes in NOTCH3 Variant Carriers: A Fixel-Based Analysis of Diffusion MRI

Fan Huang[1,2], Shi-Ming Wang[1,3], Hung-Chieh Chen[4,5], Yi-Ming Chen[4,6,7,8], Hsu-Wen Huang[9], Chih-Mao Huang[1,10], Wei-Ju Lee[4,6,11,12]

[1]Department of Biological Science and Technology, National Yang Ming Chiao Tung University, Hsinchu, Taiwan, [2]Interdisciplinary neuroscience PhD program, National Yang Ming Chiao Tung University, Hsinchu, Taiwan, [3]Department of Computer Science, National Yang Ming Chiao Tung University, Hsinchu, Taiwan, [4]Faculty of Medicine, National Yang Ming Chiao Tung University, Taipei, Taiwan, [5]Division of Neuroradiology, Department of Radiology, Taichung Veterans General Hospital, Taichung, Taiwan, [6]Department of Post-Baccalaureate Medicine, College of Medicine, National Chung Hsing University, Taichung, Taiwan, [7]Department of Medical Research, Taichung Veterans General Hospital, Taichung, Taiwan, [8]Precision Medicine Research Center, College of Medicine, National Chung Hsing University, Taichung, Taiwan, [9]National Center for Geriatrics and Welfare Research, National Health Research Institutes, Miaoli, Taiwan, [10]Institute of Brain Science, National Yang Ming Chiao Tung University, Hsinchu, Taiwan, [11]Neurological Institute and Dementia Center, Taichung Veterans General Hospital, Taichung, Taiwan, [12]Brain Research Center, National Yang Ming Chiao Tung University, Taipei, Taiwan

Introduction: Cerebral autosomal dominant arteriopathy with subcortical infarcts and leukoencephalopathy (CADASIL) is the most prevalent monogenetic disease that causes cerebral small vessel disease and stroke. It is caused by mutations in the NOTCH3 gene[1]. Approximately 70% of cases of CADASIL are attributed to the NOTCH3 p.R544C mutation, located within the EGFR domains 13/14 in the Taiwanese population[2]. Recent studies have indicated that the NOTCH3 p.R544C mutation constitutes a significant risk factor for ischemic stroke[3,4] and frequently goes undiagnosed due to its relatively less severe phenotype, A hallmark neural feature of CADASIL is the manifestation of widespread cerebral white matter (WM) lesions, suggesting that multiple WM microstructural density and connectivity may be susceptible to the effects of CADASIL. In this Diffusion MRI study, we employed fixel-based analysis (FBA)[5] to investigate cerebral white-matter alterations in carriers of the NOTCH3 R544C mutation. FBA is the advanced diffusion imaging analysis and enables the acquisition of intricate details regarding fiber density, crossing, and morphology. By using the FBA, we aim to uncover the specific impact of the Notch3 R544C mutation on the microstructural integrity of cerebral white matter.

Methods: T1-weighted images and multi-shell diffusion-weighted imaging (DWI) were collected on 69 carriers of the NOTCH3 R544C mutation (mean age = 56.8 years; 35 females) and 39 healthy controls (mean age = 54.7 years; 20 females). The images were acquired using a GE Healthcare SIGNA™ 1.5T MRI scanner. T1-weighted images: TR/TE=2154ms/3.1ms, with voxel size of 0.5 mm×0.5mm×1mm. The inversion time was set at 797ms and the flip angle of 12°. The DWI: TR/TE = 7600ms/76.9ms; voxel size = 1×1×0.5 mm3; b-values of 0 and 1000 s/mm^2 in 30 diffusion directions per shell. Intracranial volume was quantified from T1-weighted images using FSL's Brain Extraction Tool (BET). FBA was conducted utilizing MRtrix3, adhering to the recommended pipeline[5], with MP-PCA denoising, Gibbs ringing artifact removal, correction for motion and distortion, and bias field correction. The distribution of fiber orientations within each voxel was estimated through multi-tissue constrained spherical deconvolution. A study-specific template was generated via spatial normalization across all subjects, employing FOD-based registration. Within each voxel, we quantified fixel-specific measures as follows: fiber density (FD), fiber bundle cross-section (FC), and fiber density and cross-section (FDC). White matter differences between groups were assessed using voxel-wise paired t-tests, adjusting for global intracranial volume, age, and gender. Connectivity-based fixel enhancement[6]

for multiple comparison correction was applied (p< 0.05). Tract correspondences were identified using tract segmentations acquired from TractSeg[7].

Results: Fig.1 indicates that after adjusting for age, gender, and ICV, carriers with R544C mutation exhibit widespread white matter changes across FD, FC, and FDC compared to healthy controls. FBA revealed carriers had lower FD across several white matter tracts than healthy controls, with significant cluster located fibers within anterior and superior thalamic radiation, fronto-pontine tract, striato-fronto-orbital, and superior cerebellar peduncle. Moreover, d lower FDC was observed in the carriers when compared with healthy participants in the bilateral corticospinal tract, parieto-occipital pontine, superior cerebellar peduncle, superior thalamic radiation, striato-precentral, and thalamo-centered tracts.

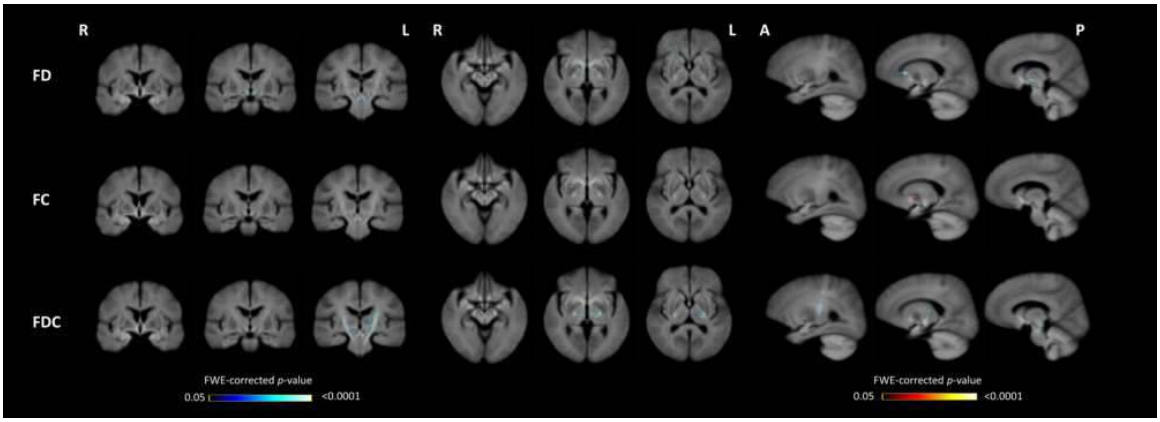

Fixel based analysis results demonstrating statistically significant differences in diffusion metrics between groups (FWE-corrected p < 0.05).

Conclusions: FBA results showed specific effects of NOTCH3 R544C mutation on white matter. NOTCH3 R544C carriers exhibit notable white matter alterations, characterized by reduced FD and FDC but increased FC in specific tracts. These findings provide insight into the microstructural changes of NOTCH3 mutations and pathological trajectory of CADASIL.

References

1. Joutel, A., et al., Notch3 mutations in CADASIL, a hereditary adult-onset condition causing stroke and dementia. Nature, 1996. 383(6602): p. 707-710.
2. Liao, Y.-C., et al., Characterization of CADASIL among the Han Chinese in Taiwan: distinct genotypic and phenotypic profiles. PloS one, 2015. 10(8): p. e0136501.
3. Tang, S.C., et al., Prevalence and clinical characteristics of stroke patients with p. R544C NOTCH3 mutation in Taiwan. Annals of clinical and translational neurology, 2019. 6(1): p. 121-128.
4. Lee, Y.-C., et al., NOTCH3 cysteine-altering variant is an important risk factor for stroke in the Taiwanese population. Neurology, 2020. 94(1): p. e87-e96.
5. Raffelt, D.A., et al., Investigating white matter fibre density and morphology using fixel-based analysis. Neuroimage, 2017. 144: p. 58-73.
6. Raffelt, D.A., et al., Connectivity-based fixel enhancement: Whole-brain statistical analysis of diffusion MRI measures in the presence of crossing fibres. Neuroimage, 2015. 117: p. 40-55.
7. Wasserthal, J., P. Neher, and K.H. Maier-Hein, TractSeg-Fast and accurate white matter tract segmentation. NeuroImage, 2018. 183: p. 239-253.

Poster No 878

Williams Syndrome Hemideletion and GTF2I Sequence Variation Relate to Insula Structure and Function

Michael Gregory[1], Mbemba Jabbi[2], Shane Kippenhan[1], Tiffany Nash[1], Madeline Garvey[1], Carolyn Mervis[3], Daniel Eisenberg[1], Shau-Ming Wei[1], Philip Kohn[1], Bhaskar Kolachana[1], Peter Schmidt[1], Karen Berman[1]

[1]NIMH, National Institutes of Health, Bethesda, MD, [2]University of Texas, Austin, TX, [3]University of Louisville, Louisville, KY

Introduction: The insula, located deep within the lateral sulcus, subserves a multitude of neurofunctional domains including sensorimotor, chemosensory, cognition, and socio-emotional processing (1). Anterior portions of the insula mediate socio-emotional processes, including empathy, social cognition, emotional experience, and simulating others' mental states (2). Williams syndrome (WS), a rare neurodevelopmental disorder caused by hemideletion of ~26 genes at the 7q11.23 chromosomal locus, offers a valuable opportunity to understand how genetic changes affect brain development and translate into complex behaviors because both the genetics and neurobehavioral phenotypes are well-circumscribed and well-defined. The neurobehavioral profile of WS includes increased sociability, overfriendliness, and empathy (3), characteristics that have

been related to structural and functional changes of the anterior insula (Ai) (4). Additionally, GTF2I, a gene in the 7q11.23 WS Critical Region (WSCR), has also been linked to the WS social phenotype (4,5,6). Here, we test whether Ai structure and function are altered in children and adolescents with WS, and if so, which, if any, WSCR genes are associated with Ai structure by conducting a region-wide association study ("mini-GWAS") restricted to just the WSCR. Further, as GTF2I has been linked to brain myelination (7), we specifically examined whether development of myelin underlying the insular cortex was related to GTF2I variation.

Methods: First, we compared Ai gray matter volume (GMV) from longitudinal scans of 30 children and adolescents with WS (79 visits, age=12.6±4.7 years, 10 males) to 74 typically developing individuals ([TDs]; 197 visits, age=12.4±3.3 years, 27 males) using linear mixed-effects modeling, controlling for age and sex. Next, we compared Ai regional cerebral blood flow (rCBF) derived with ASL MRI of 13 individuals with WS (18 visits, age=15.1±5.5 years, 1 male) and 25 TDs (44 visits, age=15.3±5.5 years, 2 males) using linear mixed-effects modeling, controlling for age and sex. Then, to investigate the genetic underpinnings of insular structure, we tested whether GMV of the Ai was related to genetic variation in the WSCR in 222 healthy adults using a mini-GWAS of just this genetic region, and we sought replication of the findings in a second, independent sample of 265 healthy adults from the Human Connectome Project (HCP). Finally, using longitudinal mcDESPOT imaging of myelin water fraction (MWF) from 134 TDs (423 visits, age=12.9±2.9 years, 68 males), we tested whether genetic variation predicting GTF2I cortical expression was related to the development of MWF with mixed-effect spline modeling. Imaging analyses were FDR-corrected for multiple comparisons, and mini-GWAS analyses were Bonferroni-corrected for the number of LD-independent signals in the WSCR.

Results: GMV of two distinct portions of the bilateral Ai were altered in children with WS: a superior portion with less GMV and an inferior area with greater GMV (both p-FDR<0.001). rCBF of bilateral Ai clusters that overlapped the areas of decreased GMV was significantly lower in individuals with WS (both p-FDR<0.01). In the discovery group of healthy adults, Ai GMV related to SNPs spanning the initiation site of GTF2I (peak SNP p=4.37x10-4), a finding replicated in the HCP sample (peak SNP p=1.3x10-3). Finally, GTF2I expression scores related to development of MWF in the bilateral anterior temporal lobe white matter directly projecting to Ai: individuals predisposed to greater GTF2I expression had increased myelin as they approached adulthood (p<0.001).

Conclusions: These results provide evidence of a GTF2I-related neurogenetic mechanism important in insular cortex structural and functional organization. Given the associations of GTF2I with the social phenotype of WS and with myelination, our results linking Ai structure, function, and myelination with GTF2I variation underscore a critical role in the behavioral and brain alterations of WS.

References

1. Uddin L. (2017), Structure and function of the human insula. J Clin Neurophysiol. 34(4): 300–306.
2. Lamm C. (2010), The role of anterior insular cortex in social emotions. Brain Struct Funct. 214(5-6):579-91.
3. Mervis CB. (2000), Williams syndrome: cognition, personality, and adaptive behavior. Ment Retard Dev Disabil Res Rev. 6(2):148-58.
4. Jabbi M. (2012), The Williams syndrome chromosome 7q11.23 hemideletion confers hypersocial, anxious personality coupled with altered insula structure and function. Proc Natl Acad Sci. 109(14):E860-6.
5. Jarvinen A. (2013), The Social Phenotype of Williams Syndrome. Curr Opin Neurobiol. 23(3): 414–422.
6. Crespi B. (2014), Cognitive-behavioral phenotypes of Williams syndrome are associated with genetic variation in the GTF2I gene, in a healthy population. BMC Neurosci. 15:127.
7. Barak B. (2019), Neuronal deletion of Gtf2i, associated with Williams syndrome, causes behavioral and myelin alterations rescuable by a remyelinating drug. Nat Neurosci. 22(5):700-708.

Poster No 879

Brain volumetric study of patients with Crouzon and Apert syndromes

Ombline Delassus[1,2,3], Lucas Chollet[1,3], Adèle Rohée-Traoré[3], Quentin Beaufort[4], Antonio Messina[4], Maxime Taverne[3], Giovanna Paternoster[5,6], Nathalie Boddaert[4], Jeanne Amiel[1], Jean-François Mangin[2], Roman Hossein Khonsari[7,6,3], David Germanaud[8,9,10]

[1]Imagine Institute, Paris, France, [2]Université Paris-Saclay, CEA, CNRS, Neurospin, Gif-sur-Yvette, France, [3]Necker-Enfants Malades Hospital, Craniofacial Growth and Form Lab, Paris, France, [4]Necker-Enfants Malades Hospital, Department of Radiology, Paris, France, [5]Necker-Enfants Malades Hospital, Department of Pediatric Neurosurgery, Paris, France, [6]Université Paris Cité, Paris, France, [7]Necker-Enfants Malades Hospital, Department of Maxillofacial Surgery and Plastic Surgery, Paris, France, [8]CEA Paris-Saclay, Institut Frederic Joliot, NeuroSpin, UNIACT, Gif-sur-Yvette, France, [9]Université Paris Cité, Inserm, NeuroDiderot, inDEV, Paris, France, [10]Service de génétique (CRMR DI-TND), AP-HP Hôpital Robert-Debré, Paris, France

Introduction: Craniostenosis is a cranial malformation caused by premature closure of some sutures[Mathijssen] that may be syndromic origin, such as in the rare Crouzon (CS) and Apert (AS) syndromes (1/50 000-1/65 000 birth resp.[Levesque, Hilton]),

caused by FGFR-2 mutations[Hilton], a gene involved in cranial and brain development. The neurological involvement is a complex clinical issue, but few quantitative studies have been carried out so far on the brain anatomy alone. We have taken advantage of a unique monocentric tertiary expertise on craniostenosis to propose a first quantitative insight into the large intracranial compartments and the global brain gyrification.

Methods: Genotyped patients imaged before surgery and typically developing controls, aged 1.5 to 18 years (y/o), were recruited from the clinical series of the Necker-Enfants Malades hospital between 2010 and 2023. 3D T1-weighted MRI were performed at 1.5T or 3T on 3 different scanners (4 different IR-prep ultrafast GE sequences) and resampled to exact millimetric isotropic resolution. Exclusion criteria were MRI insufficient resolution/quality and report of factors potentially damaging for brain development. The MRI dataset included 14 preoperative patients with CS (1,5-16y/o, avg 4.14y/o, 7 males), 3 with AS, and 75 controls (2-18y/o, avg 10y/o, 36 males). Four out-center patients with AS were added (final range 3-21y/o, avg 13y/o, 7 AS, 3 males) for secondary analyses. The data were automatically segmented with volBrain[Manjón] (Fig.1) and Morphologist (BrainVISA)[Fischer] to provide the volume of different large intracranial compartments and the hemispheric cortical and hull surfaces to compute the global gyrification index. Statistical analyses included OLS Multiple Linear Regression (age, gender, sequence and group effect), and a normative analysis based on growth modeling in controls (von Bertalanffy model) to provide 10th, 50th and 90th percentile (perc.) and test whether there was an excess of patients under or over these normative perc.

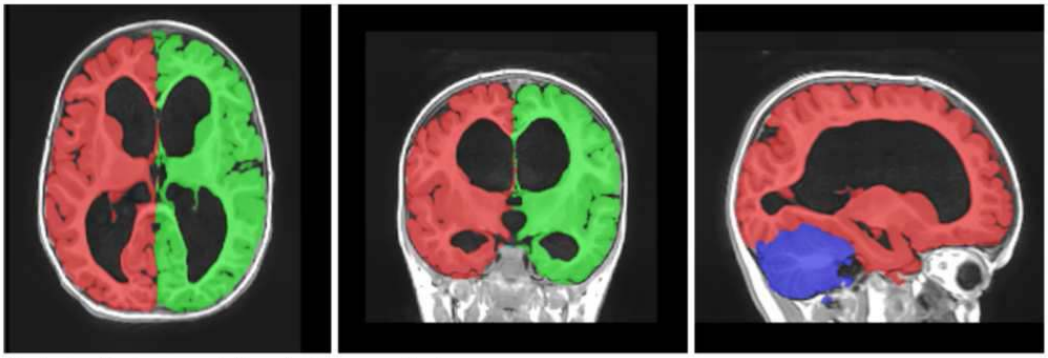

Fig.1 : A volBrain segmentation of a Crouzon patient

Results: In the 1,5 to 7y/o range, multiple linear regression found a difference between CS and control groups only for the lateral ventricle volume. Intracranial, cerebral and cerebellar volumes were mainly affected by patient age($p<0.028$), as was brainstem also impacted by gender. The MRI sequence had an impact on white matter and CSF volumes($p<0.032$). Normative analysis based on growth modeling in controls showed no excess of patients with CS outside the 10th and 90th perc. except for the lateral ventricles volume (2 patients below the 10th, 4 for the 10th to the 50th, 2 for the 50th to the 90th and 6 above the 90th, $p<0.01$) (Fig.2). In AS patients, normative analyses showed intracranial and cerebellar volumes were higher than controls (5 patients above the 90th perc., $p<0.006$). For CSF and lateral ventricles, 6 patients were above the 90th of controls model($p=0.001$), and 4 for the grey matter($p=0.02$). For gyrification, all variables but the disease one had a significant influence in the multiple linear regression within the 1,5-7y/o range. However, in the normative analysis, 10 CS and 6 AS patients were for the 10th to the 90th perc. for both hemispheres and total gyrification, consistent with no major gyrification impact of the disease.

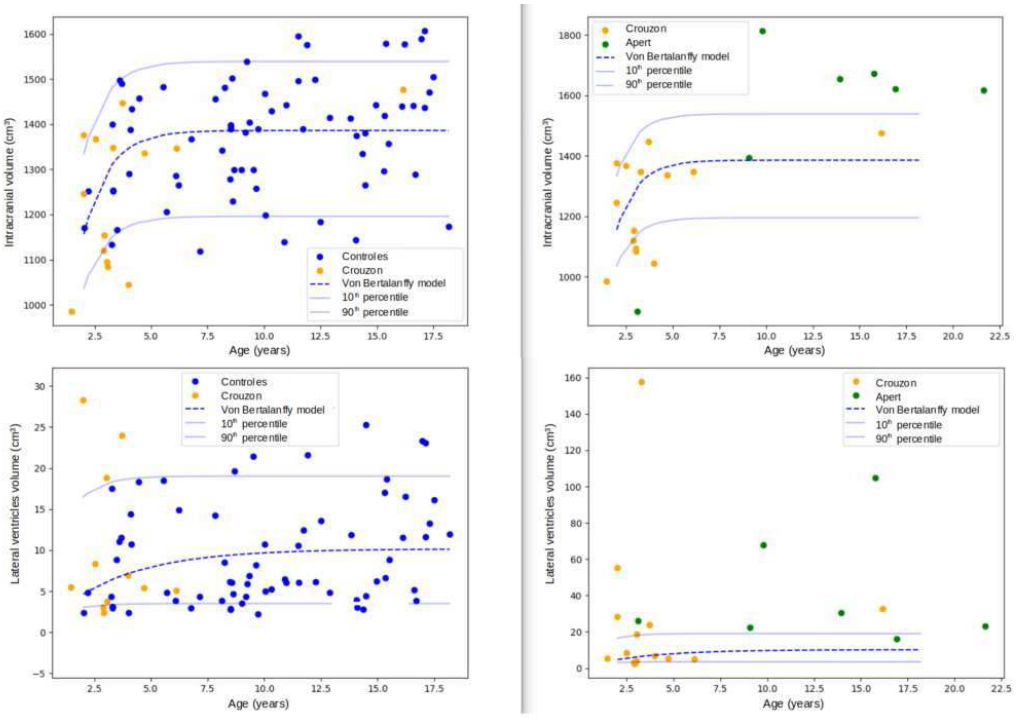

Fig.2 : Normative analysis based on growth modeling in controls of intracranial volume and lateral ventricles and volumes of Crouzon and Apert patients.

Conclusions: We propose a first comparison to typically developing controls of the volumes of the large compartment of the brain and its global gyrification in patients with AS or CS. Our CS patients showed volumes similar to controls except for larger lateral ventricles. However, our AS patients had much larger cerebral and cerebellar volumes than controls, aside with ventricular volume enlargement. Moreover, global gyration remained in the normal range in our 2 patient groups. Although relatively small and heterogeneous, our dataset remains rare and will enable us to further analyze brain anatomy in these two very rare conditions and provide insight into the poorly understood, but important, brain developmental involvement.

References

1. Fischer, C. (2012), 'Morphologist 2012: the new morphological pipeline of BrainVISA', Proceedings of the 18th HBM Scientific Meeting NeuroImage
2. Hilton, C. (2017m), 'An Exploration of the Cognitive, Physical and Psychosocial Development of Children with Apert Syndrome', International Journal of Disability, Development and Education, vol. 64, no. 2, pp. 198–210
3. Levesque, D. (2019), 'Hydrocéphalie obstructive et syndrome de Crouzon', Journal Français d'Ophtalmologie, vol. 42, no. 4, pp. e165–e168
4. Manjón, J.V. (2016), 'volBrain: An Online MRI Brain Volumetry System', Frontiers in Neuroinformatics, vol. 10
5. Mathijssen, I.M.J. (2015s), 'Guideline for Care of Patients With the Diagnoses of Craniosynostosis : Working Group on Craniosynostosis', Journal of Craniofacial Surgery, vol. 6, no. 26, pp. 1735–1807

Poster No 880

Impact of Copy Number Variation of the 7q11.23 Williams Syndrome Critical Region on Brain Structure

Madeline Garvey[1], Tiffany Nash[2], Shane Kippenhan[3], Philip Kohn[2], Carolyn Mervis[4], Daniel Eisenberg[2], Anne Ilsley[5], Anna Kelemen[5], Megan Spurney[6], Ariana Chavannes[5], Michael Gregory[7], Karen Berman[2]

[1]NIMH/University of Cambridge, Washington, DC, [2]NIMH, National Institutes of Health, Bethesda, MD, [3]NIH, Bethesda, MD, [4]University of Louisville, Louisville, KY, [5]National Institute of Mental Health, Bethesda, MD, [6]Section on Functional Imaging Methods, NIMH, Bethesda, MD, [7]NIMH, Bethesda, MD

Introduction: Copy number variations (CNVs), where the number of copies of one or more genes varies from the expected two copies, can result from deletions or duplications of segments of DNA.(7) One particularly interesting example of such a CNV occurs at chromosomal locus 7q11.23, where hemideletion of ~26 genes results in Williams syndrome (WS) and duplication of these same genes results in 7q11.23 duplication syndrome (Dup7). Because the affected 7q11.23 DNA segment is flanked by low copy DNA repeats, >90% of these deletions or duplications span the same ~1.5 megabase region.[1] Cognitively, people with WS often have mild to moderate intellectual disability, pronounced deficits in visuospatial abilities, and relative strength in overall language skills;[2] whereas people with Dup7 typically have low-average intellectual ability, relatively preserved

visuospatial abilities, and language delays.[3,6] Additionally, while individuals with WS are often described as "hypersocial," people with Dup7 have significant social anxiety and shyness.[6] Because both the genetics and neurobehavioral phenotypes of these two conditions are well-circumscribed and well-defined, they offer a privileged setting to explore how genetic changes affect brain development and translate into complex behaviors. Previous neuroimaging literature has consistently shown that individuals with WS have smaller brains with regionally decreased volume of parieto-occipital areas and relatively increased cerebellar volume,[5] but neuroimaging studies of individuals with Dup7 have been relatively sparse, with data primarily from case series. Some of these case series have shown increased ventricle size, increased total brain volume, and decreased corpus callosal volume,[4] but quantitative, group-level studies directly comparing people with WS and Dup7 are lacking. Here, we investigated the effect of 7q11.23 CNVs on macrostructural brain volume measures to better define the brain phenotypes of these disorders and to test for gene-dosage effects.

Methods: Children and adolescents with WS and Dup7, along with age- and sex-matched typically developing individuals (TDs), participated in the NIMH Intramural Research Program Study of Brain Development in 7q11.23 CNVs. Three T1-weighted Multi Echo MPRAGE scans were collected for each participant. Scans were averaged together and processed with Freesurfer version 7.1.1 to determine volumetric measures in each person's native brain space. Linear regressions in SPSS tested for relations between 7q11.23 copy number (WS=1 copy, TD=2 copies, Dup7=3 copies), and total brain volume (TBV), relative gray matter, cortical gray, subcortical gray, white matter, ventricular, and cerebellar volumes, with each analysis controlling for age and sex. Participants included 30 individuals with WS (age=12.5±3.9, 9 males), 92 TD individuals (age=13.1±3.2, 34 males), and 16 individuals with Dup7 (age=14.5±2.3, 8 males).

Results: Gene dosage was related to TBV in a step-wise manner, with children with Dup7 having the largest brains and those with WS having the smallest ($p<0.001$). Given that TBV differed as a function of 7q11.23 copy number, subsequent analyses controlled for TBV to test for relative volume differences. Relative ventricular volume, relative total white matter volume, and relative subcortical gray matter volume all varied by copy number in a step-wise, increasing manner (Dup7>TD>WS, $p<0.001$). Conversely, relative total gray matter volume, relative cortical gray volume, and relative cerebellar volume all significantly varied by copy number in a step-wise, decreasing manner (WS>TD>Dup7, $p<0.001$).

Conclusions: These results document the effects of 7q11.23 copy number variation on macrostructural brain measures. The step-wise nature of these findings with copy number offer insights into genetic mechanisms driving neural development. Future work will attempt to uncover the contributions of specific genes to these phenotypes and will explore associations with regional brain measures.

References

1. Kozel, B. A. (2021), 'Williams syndrome,' Nature Reviews Disease Primers 7, 42. https://doi.org:10.1038/s41572-021-00276-z
2. Mervis C.B. (2000), 'The Williams syndrome cognitive profile,' Brain and Cognition, 44(3):604-28. DOI: 10.1006/brcg.2000.1232.
3. Mervis C.B. (2015), 'Children with 7q11.23 duplication syndrome: Psychological characteristics,' American Journal of Medical Genetics Part A;167(7):1436-50. DOI: 10.1002/ajmg.a.37071.
4. Morris C.A. (2015), '7q11.23 duplication syndrome: Physical characteristics and natural history,' American Journal of Medical Genetics Part A;167A(12):2916-35. DOI: 10.1002/ajmg.a.37340.
5. Thom R.P. (2023), 'Neuroimaging research in Williams syndrome: Beginning to bridge the gap with clinical care,' Neuroscience and Biobehavioral Reviews;153:105364. DOI: 10.1016/j.neubiorev.2023.105364.
6. Velleman S.L. (2011), 'Children with 7q11.23 duplication syndrome: Speech, language, cognitive, and behavioral characteristics and their implications for intervention,' Perspectives on Language Learning and Education, 18(3):108-116. DOI: 10.1044/lle18.3.108.
7. Stankiewicz P. (2010), 'Structural variation in the human genome and its role in disease,' Annual Review of Medicine;61:437-55. DOI: 10.1146/annurev-med-100708-204735.

Poster No 881

Automated Segmentation and Volumetric Analysis of the Subplate in Fetuses with Down Syndrome

Helena Sousa[1], Abi Fukami - Gartner[2], Alena Uus[2], Vanessa Kyriakopoulou[3], Jonathan O'Muircheartaigh[1], Joseph Hajnal[4], Megan Hall[1], Jana Hutter[1], Lisa Story[1], Donald Tournier[4], Alexander Hammers[1], Mary Rutherford[1], Maria Deprez[5]

[1]King's College London, London, London, [2]King's College London, London, Other, [3]King's College London, London, United Kingdom, [4]King's College London, London, England, [5]King's College London, London, N/A

Introduction: Down syndrome (DS) is the most common cause of intellectual disability with a known genetic aetiology affecting approximately 1 in 1000 live births[1]. There is a gap in knowledge about structural brain development in utero in DS. In particular, the growth trajectory of the subplate (SP), a transient compartment of the fetal brain, has never been defined in fetuses with DS. Here, we performed automatic segmentation of the SP in T2-weighted (T2w) fetal brain MRI, using a novel

deep learning solution[2], to assess any differences in SP volumes across gestational age (GA) in fetuses with DS compared to appropriate controls.

Methods: T2w fetal MRI were acquired on a 3T Philips Achieva system for 376 control subjects (21 to 36 weeks GA) from 3 studies: 257 subjects from the developing Human Connectome Project (dHCP, REC 14/LO/1169, with TE=250ms); 78 subjects from the Placental Imaging Project (PiP, REC 16/LO/1573, TE=180ms); and 33 subjects from the individualised risk prediction of adverse neonatal outcome in pregnancies that deliver preterm study (PRESTO, REC 21/SS/0082, with TE=180ms). 25 fetuses from the early brain imaging in DS study (eBiDS, REC 19/LO/0667), (24 to 36 weeks GA) were scanned at either TE=180 ms (20 subjects) or 250ms (5 subjects). All T2w scans were motion-corrected and 3D SVR reconstructed to 0.5mm isotropic resolution, as per[3]. The SP (and total WM) were segmented using an automated Attention-Unet model trained as per[2]. Non-linear regressions of volumes against GA were fitted and compared using the extra-sum-of-squares F-test in Graphpad Prism v9.0.

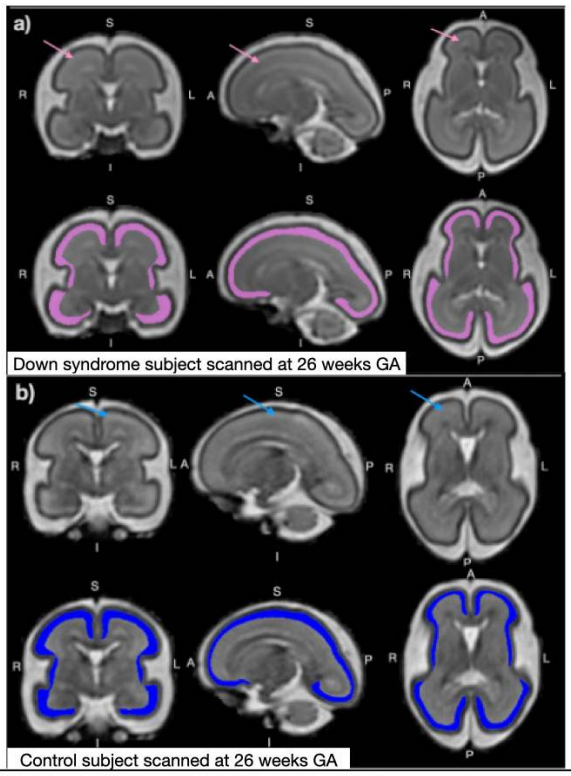

Figure 1: a) Axial, Sagittal and Coronal planes of fetal brain MRI from a Down Syndrome subject scanned at 26 weeks of GA and **b)** of a control subject at same GA. Regions where the subplate layer is visible is indicated on the top row (pink/blue arrows) and segmentations obtained from the model described in **[2]** are shown in bottom row.

Results: Figure 2a illustrates the exponential growth of total WM volume across gestation in both DS and control groups, although DS had a significantly different fit (p value < 0.0001) and reduced WM volumes. The SP (a sub-segment of total WM) showed growth from approximately 21 to 30 GA, followed by a plateau until 36 GA. The DS group showed a similar trend although the non-linear fit was significantly different (p value < 0.0001) with markedly reduced SP volumes. The SP volumes relative to total WM (Fig 2c) showed a linear decrease as the SP gradually resolved across gestation. The DS group showed a similar trend although linear fit was significantly different (p value < 0.0001) with reduced relative SP volumes. Visual assessment of the morphology of SP in both populations show an initial thick and continuous layer at early GA (21-26 weeks) followed by a gradual dissolution in sulcal pits as cortical gyrification progresses along GA.

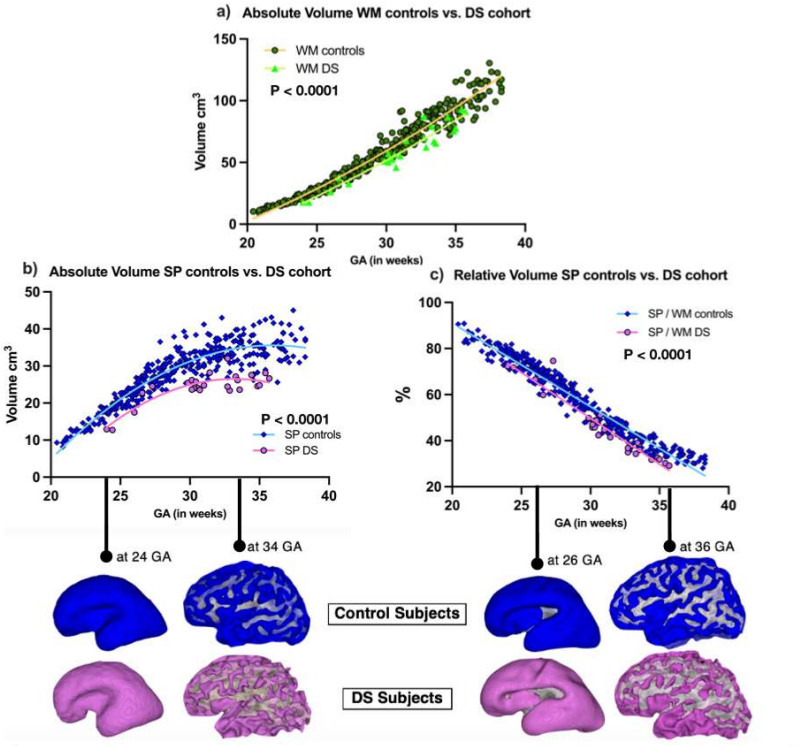

Figure 2: a) Absolute WM volumes and **b)** absolute SP volumes across GA for control and DS groups fitted with a non-linear growth curve and P-value for F-test; **c)** SP volumes relative to total WM volume across GA fitted with a linear regression showing a decrease in relative SP volume. 3D renderings of SP segmentations for controls and DS subjects at 24, 26, 34 and 36 weeks of GA are also illustrated in **b)** and **c)**.

Conclusions: To the best of our knowledge the evolution of SP volumes has never been assessed in utero in fetuses with DS. This analysis showed that absolute SP volumes were markedly reduced across gestation from 24 to 36 weeks in DS. SP volumes also represented a smaller proportion of total WM across gestation in DS. It has been shown that there is altered cortical folding in fetuses with DS[4]. Thus, in future, it would be interesting to associate SP volumes with metrics related to cortical folding. Finally, this finding is in line with volumetry in neonates with DS, whereby relative regional WM volumes were significantly reduced[5].

References

1. de Graaf, G., Buckley, F., & Skotko, B. G. (2021). Estimation of the number of people with Down syndrome in Europe. European journal of human genetics : EJHG, 29(3), 402–410. https://doi.org/10.1038/s41431-020-00748-y
2. Sousa, H.S. et al. (2023). A Deep Learning Approach for Segmenting the Subplate and Proliferative Zones in Fetal Brain MRI. In: Link-Sourani, D., Abaci Turk, E., Macgowan, C., Hutter, J., Melbourne, A., Licandro, R. (eds) Perinatal, Preterm and Paediatric Image Analysis. PIPPI 2023. Lecture Notes in Computer Science, vol 14246. Springer, Cham. https://doi.org/10.1007/978-3-031-45544-5_2
3. Uus, A. U., Kyriakopoulou, V., Makropoulos, A., Fukami-Gartner, A., Cromb, D., Davidson, A., Cordero-Grande, L., Price, A. N., Grigorescu, I., Williams, L. Z. J., Robinson, E. C., Lloyd, D., Pushparajah, K., Story, L., Hutter, J., Counsell, S. J., Edwards, A. D., Rutherford, M. A., Hajnal, J. V., & Deprez, M. (2023). BOUNTI: Brain vOlumetry and aUtomated parcellatioN for 3D feTal MRI. bioRxiv : the preprint server for biology, 2023.04.18.537347. https://doi.org/10.1101/2023.04.18.537347
4. Yun, H. J., Perez, J. D. R., Sosa, P., Valdés, J. A., Madan, N., Kitano, R., Akiyama, S., Skotko, B. G., Feldman, H. A., Bianchi, D. W., Grant, P. E., Tarui, T., & Im, K. (2020). Regional Alterations in Cortical Sulcal Depth in Living Fetuses with Down Syndrome. Cerebral Cortex, 31(2), 757–767. https://doi.org/10.1093/cercor/bhaa255
5. Fukami-Gartner, A., Baburamani, A. A., Dimitrova, R., Patkee, P. A., Ojinaga-Alfageme, O., Bonthrone, A. F., Cromb, D., Uus, A. U., Counsell, S. J., Hajnal, J. V., O'Muircheartaigh, J., & Rutherford, M. A. (2023). Comprehensive volumetric phenotyping of the neonatal brain in Down syndrome. Cerebral Cortex, 33(14), 8921–8941. https://doi.org/10.1093/cercor/bhad171

Poster No 882

Reduced Contralateral Cerebello-Cortical Functional Connectivity in 22q11.2 Deletion Syndrome

Hoki Fung[1], Charles Schleifer[1], Leila Kushan[1], Elizabeth Bondy[1], Carrie Bearden[1,2]

[1]Department of Psychiatry and Biobehavioral Sciences, University of California, Los Angeles, Los Angeles, CA, [2]Department of Psychology, University of California, Los Angeles, Los Angeles, CA

Introduction: 22q11.2 Deletion Syndrome (22qDel) is a genetic disorder resulting from a microdeletion on the long arm of chromosome 22. It occurs in approximately 1 in 4000 live births, and is associated with a wide range of clinical manifestations including heart defects, immune dysfunction, and developmental delay. It is also linked to elevated risks for neurodevelopmental and neuropsychiatric disorders including schizophrenia, autism spectrum disorder, and attention-deficit/hyperactivity disorder[1]. 22qDel is highly pleiotropic, offering a valuable framework for elucidating the links between genes, brain development, and transdiagnostic psychiatric phenotypes[2]. Previous studies have reported structural and functional alterations in cortical and subcortical regions, as well as their associations with cognitive deficits and neuropsychiatric symptoms in 22qDel[3-6]. However, the cerebellum - a region traditionally associated with motor control but increasingly recognized for its involvement in higher cognitive functions - remains an understudied neuroendophenotype in 22qDel research[7]. This study sought to address this gap by examining network-specific resting-state cerebello-cortical functional connectivity (FC) in individuals with 22qDel.

Methods: Resting-state functional magnetic resonance imaging (rs-fMRI) and high-resolution T1-weighted structural images were acquired on two scanners (Siemens 3T MAGNETOM Trio and Prisma) in 77 participants with 22qDel (M=17.1y, SD=8.26y; 59.7% F) and 74 demographically comparable typically developing (TD) control participants (M=14.7y, SD=6.76y; 54.0% F). The images were preprocessed using the Quantitative Neuroimaging Environment & Toolbox with the Human Connectome Project minimal preprocessing pipeline. Additional processing of the rs-fMRI data included bandpass filtering, motion scrubbing, and spatial smoothing. The whole brain, including the cerebellum, was parcellated into 718 parcels using the Cole-Anticevic brain-wide network partition[8], where each parcel was assigned to one of the 12 large-scale brain networks (Figure 1). Network cerebello-cortical FC was calculated as the Fisher z-transformed pairwise Pearson correlation between the cortical and cerebellar parcels from the frontoparietal cognitive control (FPN), default-mode (DMN), and dorsal attention (DAN) networks. Differences in FC between the control and 22qDel groups were investigated using linear regression models. All models included age, sex, and scanner as covariates, and the results were corrected with a false-discovery rate threshold of q<.05.

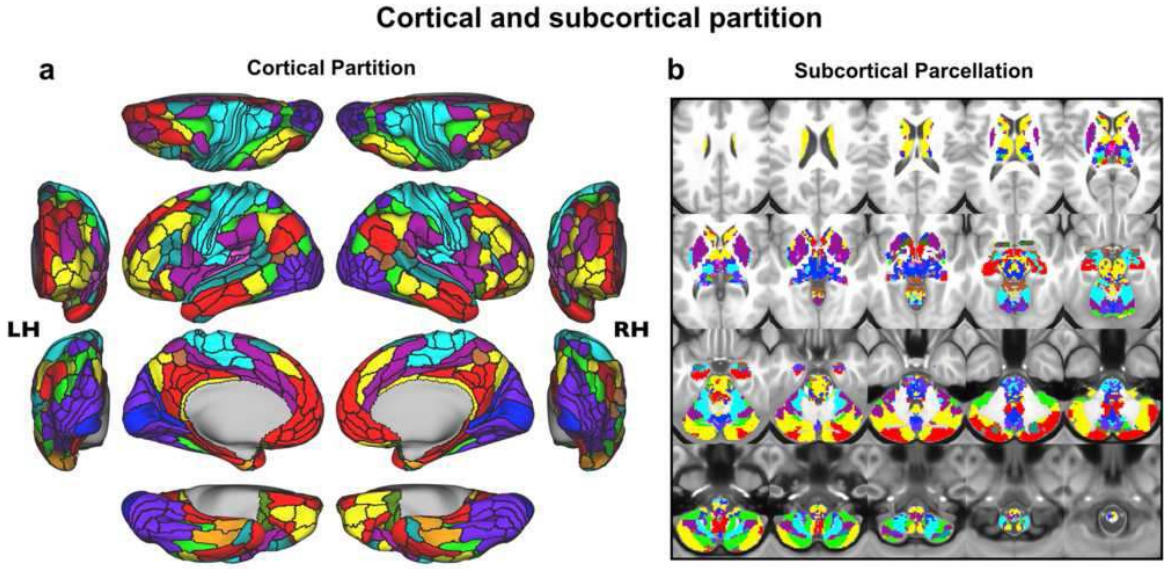

Fig 1. Cole-Anticevic brain-wide network partition (CAB-NP). Extracted from Figure 1 in Ji et al., 2019[8].

Results: In comparison to TD controls, 22qDel exhibited significantly reduced FC in three distinct cerebello-cortical pairs (FDR q<.05; see Figure 2). Specifically: 1. Dorsal-Attention-R-Cerebellum and Dorsal-Attention-L-Cortex (β = - .25, p = .002, 95% CI [-0.40, -0.10]), 2. Frontoparietal-L-Cerebellum and Frontoparietal-R-Cortex (β = - .25, p = .002, 95% CI [-0.40, -0.10]), and 3. Default-R-Cerebellum and Frontoparietal-L-Cortex (β = - .23, p = .004, 95% CI [-0.23, -0.07]).

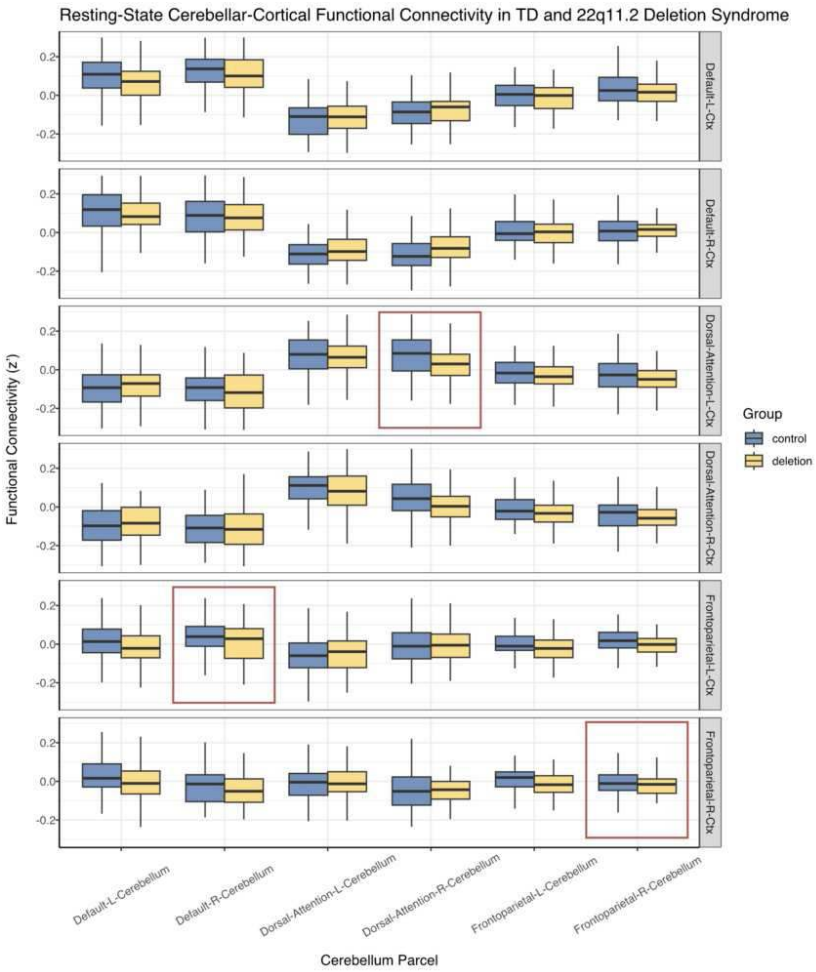

Fig 2. Cerebellar-Cortical FC in TD and 22q11.2 Deletion Syndrome. Red bounding box indicates the z' difference between TD controls and 22qDel is significant at FDR q<.05.

Conclusions: To our knowledge, this study is the first to examine cerebello-cortical FC in individuals with 22qDel. Using a novel functional parcellation approach, our study revealed disruptions in network-specific FC between the cerebellum and cortex in individuals with 22qDel. Specifically, three cerebello-cortical pairs from the DAN, FPN, and DMN exhibited significantly reduced FC in 22qDel relative to controls. Notably, all three pairs displayed a contralateral pattern. While anatomical and tractography studies [9-10] have previously established that structural cerebello-cortical connections are contralateral, the implications for functional connectivity remain unclear. This prompts further exploration into the concept of laterality in cerebello-cortical FC research and an investigation into how disruptions in contralateral connectivity may be linked to cognitive outcomes and psychiatric symptoms in 22qDel.

References

1. Cortés-Martín, J. (2022). Deletion syndrome 22q11. 2: a systematic review. Children, 9(8), 1168.
2. Jonas, R. K. (2014). The 22q11. 2 deletion syndrome as a window into complex neuropsychiatric disorders over the lifespan. Biological psychiatry, 75(5), 351-360.
3. Lin, A. (2017). Mapping 22q11. 2 gene dosage effects on brain morphometry. Journal of Neuroscience, 37(26), 6183-6199.
4. Ching, C. R. (2020). Mapping subcortical brain alterations in 22q11. 2 deletion syndrome: Effects of deletion size and convergence with idiopathic neuropsychiatric illness. American Journal of Psychiatry, 177(7), 589-600.
5. Schleifer, C. (2019). Dissociable disruptions in thalamic and hippocampal resting-state functional connectivity in youth with 22q11. 2 deletions. Journal of Neuroscience, 39(7), 1301-1319.
6. Lin, A. (2020). Reciprocal copy number variations at 22q11. 2 produce distinct and convergent neurobehavioral impairments relevant for schizophrenia and autism spectrum disorder. Biological psychiatry, 88(3), 260-272.
7. Schmitt, J. E. (2021). A comprehensive analysis of cerebellar volumes in the 22q11. 2 Deletion Syndrome. Biological Psychiatry: Cognitive Neuroscience and Neuroimaging.
8. Ji, J. L. (2019). Mapping the human brain's cortical-subcortical functional network organization. Neuroimage, 185, 35-57.
9. Palesi, F. (2017). Contralateral cortico-ponto-cerebellar pathways reconstruction in humans in vivo: implications for reciprocal cerebro-cerebellar structural connectivity in motor and non-motor areas. Scientific reports, 7(1), 12841.
10. Palesi, F. (2015). Contralateral cerebello-thalamo-cortical pathways with prominent involvement of associative areas in humans in vivo. Brain Structure and Function, 220, 3369-3384.

Poster No 883

An emerging cascade? Identifying a downstream target of TBX1 for oligodendrogenesis and myelination

Anne Wells[1], Takeshi Hiramoto[1], Shuken Boku[2], Gina Kang[1], Noboru Hiroi[1]

[1]UT Health San Antonio, San Antonio, TX, [2]Kumamoto University, Kumamoto, Japan

Introduction: Cognitive deficits are debilitating impairments seen across neuropsychiatric disorders, some of which are thought to arise from aberrant structural processes. Copy number variations (CNVs), like 22q11.2 hemizygous deletion, are relatively large genetic deletions or duplications that result in a wide spectrum of neuropsychiatric symptoms with cognitive deficits in humans. Our mouse model of the heterozygous deletion of Tbx1, a transcription factor gene encoded within a 1.5 Mb commonly deleted segment of the 22q11.2 locus, resulted in cognitive speed deficits in acquiring the Morris Water Maze and Attentional Set Shifting tasks in adult mice, as well as myelin deficits specific to the fimbria (Hiramoto et al., 2022; Mol Psych). We also demonstrated that, when Tbx1 heterozygosity was initiated in post-embryonic stem cells by tamoxifen given at postnatal day 1 to day 5 in nestinCreERTM;Tbx1flox/+ (cTbx1+/-P1-P5) mice, they exhibited a slow speed to complete spontaneous alternation in a T-maze without slow motor movement; when Tbx1 heterozygosity was initiated by tamoxifen at postnatal day 21 to day 25, there was no effect. As Tbx1 is enriched in post-embryonic stem cells and in zone of postnatal neurogenesis (e.g., subventricular zone [SVZ]), we hypothesize that Tbx1 plays a critical role in the proliferation and maintenance of stem cells in the SVZ, which may be critical to the myelination of the fimbria (Hiramoto et al., 2011; Human Mol Genet.), via a downstream target.

Methods: To test this hypothesis, we performed a ChIP-seq analysis and identified several hundred binding targets of TBX1 within promotors or enhancer sites of protein-coding genes. We then sought a rationale for selection of a downstream target of interest by cross referencing our ChIP-seq results across databases of genes implicated in adult neurogenesis, cerebral dysmyelination, and neurodevelopmental disorders in human patients. We then harvested neural progenitor cells (NPCs) from the subventricular zone of postnatal mice (P2) and cultured them as neurospheres under proliferative conditions. Using this paradigm, we demonstrate that FOXG1 colocalizes with TBX1 in proliferating NPCs in vitro. We then sought to determine the extent to which TBX1 functionally directs FoxG1 expression under proliferating conditions in NPCs using a siRNA technique, which prevents Tbx1 mRNA from undergoing translation.

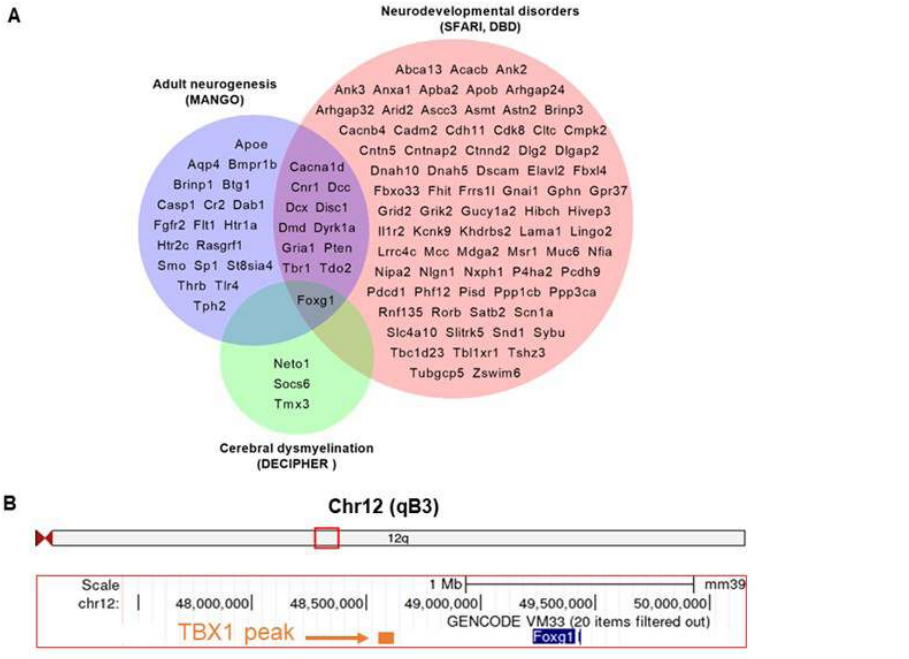

Fig A1. ChIP-Seq cross-referenced with genomic data from human patients reveals *FoxG1* as likely target of TBX1 in cerebral dysmyelination. (A) TBX1 binds to loci near or at genes implicated in adult neurogenesis (blue circle), autism and neurodevelopmental disorders (pink circle), and cerebral dysmyelination (green circle). Mammalian Adult Neurogenesis Gene Ontology (MANGO), SFARI and Geisinger Developmental Brain Disorder Database), and DECIPHER v11.15 were used. (B) Our ChiP-Seq revealed a peak binding site of TBX1 near a likely enhancer site for *FoxG1* (UCSC Genome Browser on Mouse [GRCmm39]). Adapted from *Hiramoto et al. (2021)* preprint, BioRxiv.

Results: This study revealed FoxG1 as a downstream target of TBX1 implicated among a small subset of genes. Thus, we sought to test the plausibility of a TBX1-FoxG1 interaction within the SVZ and fimbria in vivo. Here, we demonstrate that in

postnatal C57BL6/J mice (P4), FOXG1 colocalizes with TBX1 and is expressed in subpopulations of both stem cells (SOX2+), neural stem cells (DCX+) and oligodendrocyte precursor cells (NG2+) in the SVZ (N = 4). Moreover, in the fimbria and cells surrounding the fimbria, including the laterally adjacent posterior subventricular zone (pSVZ), FOXG1 colocalizes with TBX1 in postnatal mice, as well as SOX2+ cells. However, FOXG1 colocalizes with NG2+ oligodendrocyte precursor cells only in the pSVZ and cells just outside of the fimbria, but not within the fimbria proper (N = 4). Thus, we hypothesized that TBX1-FoxG1 interactions in NG2+ cells were more essential in proliferating cells, rather than functionally myelinating cells. Using our siRNA technique, which prevents Tbx1 mRNA from undergoing translation, we have thus far successfully silenced Tbx1 mRNA through our siRNA technique against robust controls for maintenance (e.g., 18s, Pkg1, Atpb5) and cell cycle (e.g., Cyc1) markers.

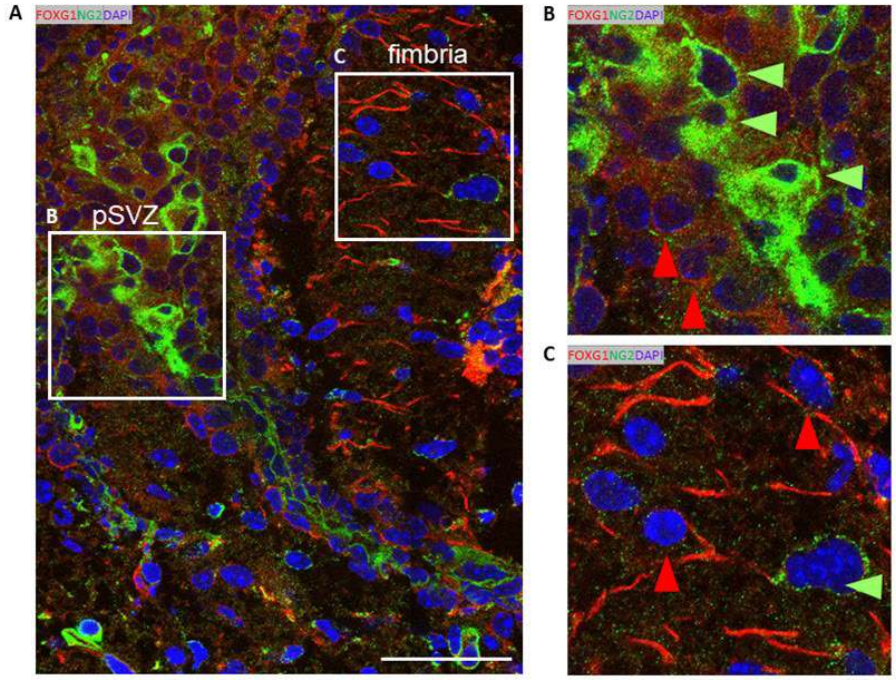

Fig A2. FOXG1 colocalizes with NG2 in the subventricular zone in cells that have yet to enter the fimbria proper. (A) Representative confocal images of NG2, an essential marker of oligodendrocyte precursor cells, and FOXG1 from the posterior subventricular zone (pSVZ) and within the fimbria proper (N = 4; 63x objective, 20 μm). (B) Enlarged view of NG2 and FOXG1 colocalize primarily in pSVZ and ventrally-adjacent cells to the fimbria. (C) In contrast, enlarged view of distinct FOXG1 labeling pattern within fimbria proper without NG2 colocalization.

Conclusions: Taken together, our data suggests that TBX1 in differentiated stem cell populations may be required for the normal development oligodendrocyte precursor cells via FoxG1. A transcription factor signaling axis specific to postnatal oligodendrocyte precursor cells in mice may explain the specificity of Tbx1+/- in the dysmyelination of the fimbria and slowed cognitive speed.

References

1. Hiramoto, T., et al. (2011), 'Tbx1: identification of a 22q11.2 gene as a risk factor for autism spectrum disorder in a mouse model', Human Molecular Genetics, 20(24), 4775–4785.
2. Hiramoto, T., et al. (2022). 'Tbx1, a gene encoded in 22q11.2 copy number variant, is a link between alterations in fimbria myelination and cognitive speed in mice', Molecular Psychiatry 2022 27:2, 27(2), 929–938.

Poster No 884

Compressed representation of brain genetic transcription

James Ruffle[1], Henry Watkins[1], Robert Gray[1], Harpreet Hyare[1], Michel Thiebaut de Schotten[2], Parashkev Nachev[1]

[1]UCL Queen Square Institute of Neurology, London, UK, [2]Groupe d'Imagerie Neurofonctionnelle, Institut des Maladies Neurodégénératives- UMR 5293, CNRS, CEA, Bordeaux, France

Introduction: The architecture of the brain is too complex to be intuitively surveyable without the use of compressed representations that project its variation into a compact, navigable space. The task is especially challenging with high-dimensional data, such as gene expression, where the joint complexity of anatomical and transcriptional patterns demands maximum compression. Established practice is to use standard principal component analysis (PCA), whose computational felicity is offset by limited expressivity, especially at great compression ratios.

Methods: Employing whole-brain, voxel-wise Allen Brain Atlas transcription data, here we systematically compare compressed representations based on the most widely supported linear and non-linear methods-PCA, kernel PCA, non-negative matrix factorization (NMF), t-stochastic neighbour embedding (t-SNE), uniform manifold approximation and projection (UMAP), and deep auto-encoding-quantifying reconstruction fidelity, anatomical coherence, and predictive utility with respect to signalling, microstructural, and metabolic targets.

Results: Qualitatively, PCA, kPCA, and NMF yielded less structured representations than t-SNE, UMAP, or the auto-encoder. Projection of each component into brain anatomical space revealed patterns varying in their anatomical coherence. PCA, kPCA, and NMF broadly differentiated between cerebellum and the rest of the brain in the first component, and (weakly for NMF) between surface and deeper regions in the second, without any regional specificity. T-SNE highlighted a dorsoventral gradient across the whole brain in the first component and a rostrocaudal one in the second. UMAP yielded a more finely granular structure, but exhibited abrupt regional variations of doubtful anatomical fidelity. The auto-encoder representation captured multiple scales of spatial organisation in an anatomically plausible manner, distributed across the two components. Testing on held-out data, we evaluated the models' ability to reconstruct the source from representations of varying dimensionality and input image resolution. For all input resolutions and representational dimensionalities, the auto-encoder achieved the best root-mean- squared-error (RMSE) (ANOVA $p<0.0001$) (Figure 1). Inspection of each 2D representation annotated by each feature revealed varying degrees of qualitative coherence (Figure 2). The most expressive representations-UMAP, t-SNE, and auto-encoding-yielded the most structured apparent relationships, with auto-encoding in particular revealing multiple scales of related organization. The auto-encoder achieved the best average RMSE and R2 on the held-out test set across all experiments (mean RMSE 0.1295, mean R2 0.3563). A one-way ANOVA found a significant difference in model performance across representational methods ($p<0.0001$). Tukey post-hoc comparison showed the auto-encoder, UMAP, and t-SNE all yielded significantly superior performance (by R2) than PCA, kPCA, and NMF (all $p<0.0001$). There was no significant difference between auto-encoder, UMAP, and t- SNE performance ($p=0.866$ or higher), or between PCA, kPCA, and NMF ($p=0.555$ or higher).

Conclusions: We show that deep auto-encoders yield superior representations across all metrics of performance and target domains, supporting their use as the reference standard for representing transcription patterns in the human brain.

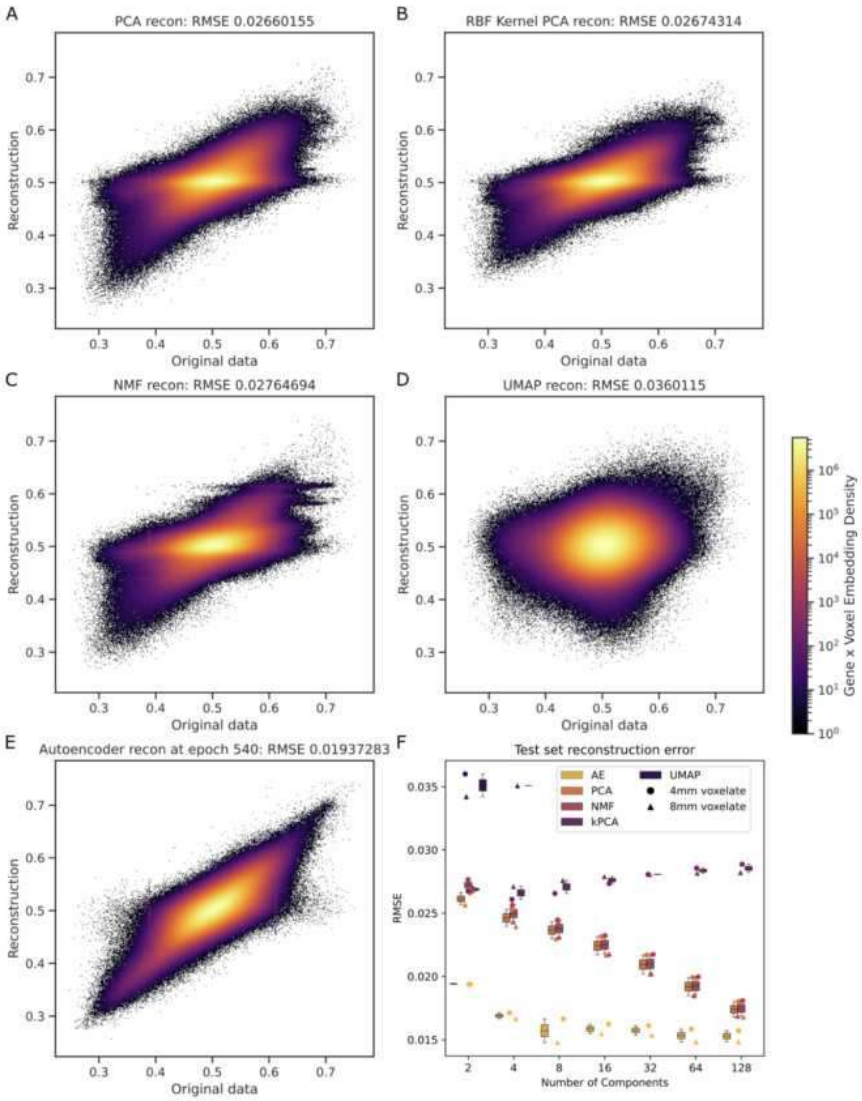

Figure 1. Test set reconstruction model performance. Reconstruction errors for A) PCA, B) kPCA, C) NMF, D) UMAP, and E) auto-encoder (AE), showing original data values on the x-axis, and reconstructed predictions on the y-axis. F) Box and whisker plot with superimposed individual points depicts reconstruction performance (by RMSE) across all component size and voxel resolutions. Note, reconstruction of the original data is not possible for t-SNE owing to the nature of the algorithm, and for UMAP was computationally feasible only with 2 components at 4mm³ and 8mm³ resolutions, and 4 components at 8mm³ resolution (see discussion of technical obstacles here[26]. Note clear superiority of auto-encoding across all resolutions and dimensionalities.

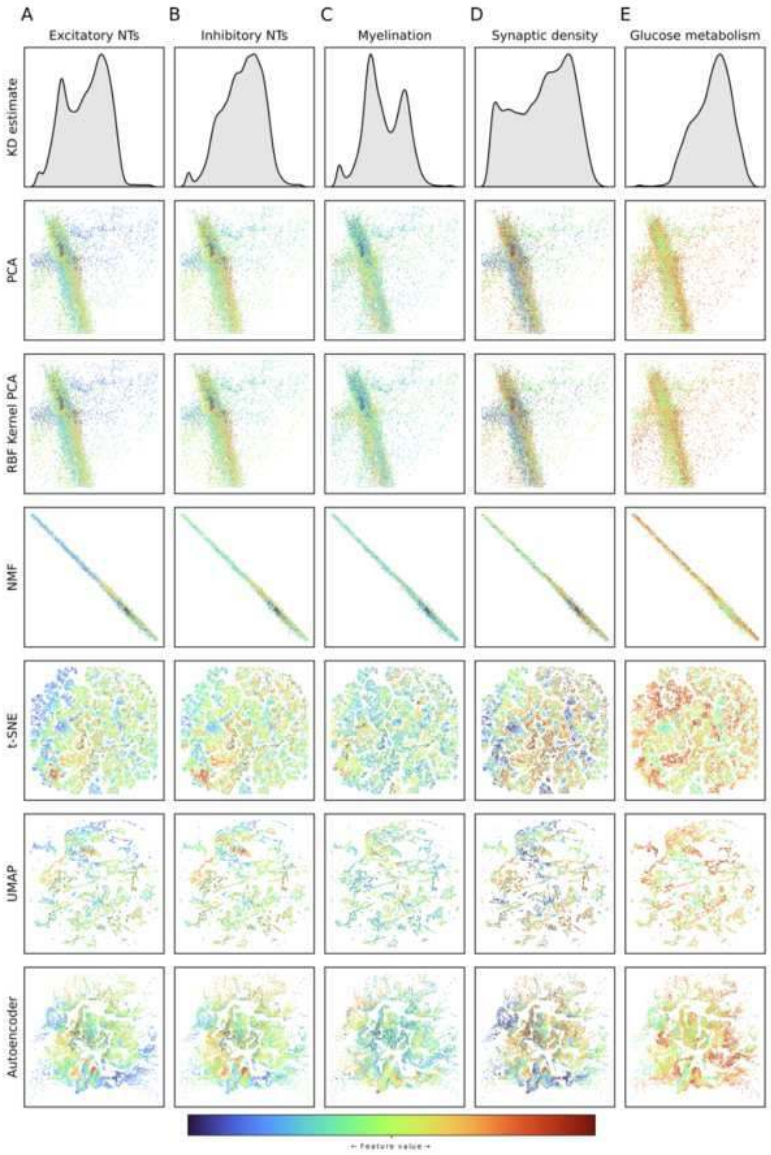

Figure 2. Feature annotation maps revealing the relationship between 2D transcriptional representations (rows) and brain signalling, microstructural, and metabolic characteristics (columns). Plots of each voxel from each representation are coloured by the feature value from the corresponding map, expressed in arbitrary units: A) excitatory neurotransmitters (NTs), B) inhibitory neurotransmitters, C) myelination, D) synaptic density, and E) glucose metabolism. The first row shows a kernel density (KD) estimate of each feature distribution.

References
1. XGBoost - https://xgboost.readthedocs.io
2. PyTorch - https://pytorch.org
3. scikit-learn - https://scikit-learn.org/stable/
4. UMAP - https://umap-learn.readthedocs.io/en/latest/

Poster No 885

Transcriptomic gradient of the human hippocampus: A vertex-wise atlas of post-mortem gene expression

Alexander Ngo[1], Jordan DeKraker[1], Sara Larivière[2], Lang Liu[3], Jessica Royer[1], Raúl Rodriguez-Cruces[1], Jacob Vogel[4], Ziv Gan-Or[3], Alan Evans[1], Boris Bernhardt[1]

[1]Montreal Neurological Institute and Hospital, Montreal, QC, [2]Brigham and Women's Hospital, Boston, MA, [3]McGill University, Montreal, QC, [4]Lund University, Lund

Introduction: The hippocampus is involved in multiple aspects of brain function and dysfunction. Unravelling its complex organization requires the integration of multiscale data, linking molecular features to macroscale hierarchies. Gene expression is a fundamental molecular phenotype, and its profiling can provide a reference description of how microstructural features are distributed across the brain. Post-mortem gene expression samples, however, are often spatially discontinuous and biased towards coarse brain parcellations, thus potentially overlooking fine-grained information. Here, we charted gene expression patterns within the hippocampus with unprecedented resolution, providing a unified atlas of the hippocampal transcriptome and relating our findings to its functional and structural hierarchies.

Methods: Allen Human Brain Atlas. We used the structural T1w magnetic resonance imaging (MRI) and microarray expression data of six deceased human donors (five males, mean ± SD age = 42.5 ± 13.4 years) from the Allen Human Brain Atlas-a brain-wide atlas comprised of bulk transcriptomic measures from over 20,000 genes sampled across 3,702 spatially distinct tissue samples[1]. Vertex-wise mapping of hippocampal gene expression. Donor-specific hippocampal surfaces were generated from individual structural scans using HippUnfold-an automated pipeline for hippocampal unfolding, subfield segmentation, and novel surface-based hippocampal registration[2,3]. In parallel, we preprocessed the microarray expression data through intensity-based filtering of microarray probes, selection of a representative probe for each gene across both hemispheres, normalization, and aggregation across donors[4]. Tissue sampled within the hippocampus (n=125) were mapped to subject-specific hippocampal surfaces. We interpolated expression values across the hippocampus, weighted by the geodesic distance of a given vertex to its nearest sampled neighbour. Continuous donor-specific transcriptomic maps were averaged to generate a single expression map for each gene (Fig 1A). Code and data availability. All code to preprocess imaging, microarray data, and hippocampal transcriptomic maps will be made available as part of the HippoMaps-a toolbox for multiscale and multimodal contextualization of the hippocampus (https://github.com/MICA-MNI/hippomaps).

Results: We generated an atlas of vertex-wise maps of hippocampal expression for 13,561 genes. Dimensionality reduction using principal component analysis on the concatenated expression maps of all genes identified a main transcriptomic axis that explained 17.5% of the variance and differentiated anterior from posterior regions (Fig 1B), as previously observed in volumetric analyses[5]. Gene ontology enrichment analysis of the most influential genes (top 5% of PC1 loadings) revealed a consistent set of biological processes related to synapse organization, axonal growth, development, and behaviour (all pFDR < 0.05; Fig 2A). We further generated histology- and MRI-derived profiles of the hippocampus, revealing its structural and functional organization, and assessed their spatial correlation to the genetic gradient identified herein using autocorrelation preserving null models[6]. These multimodal comparisons revealed significant and specific spatial association between the predominant gene expression and the resting-state functional gradients (r=0.88, pspin<0.001; Fig 2B).

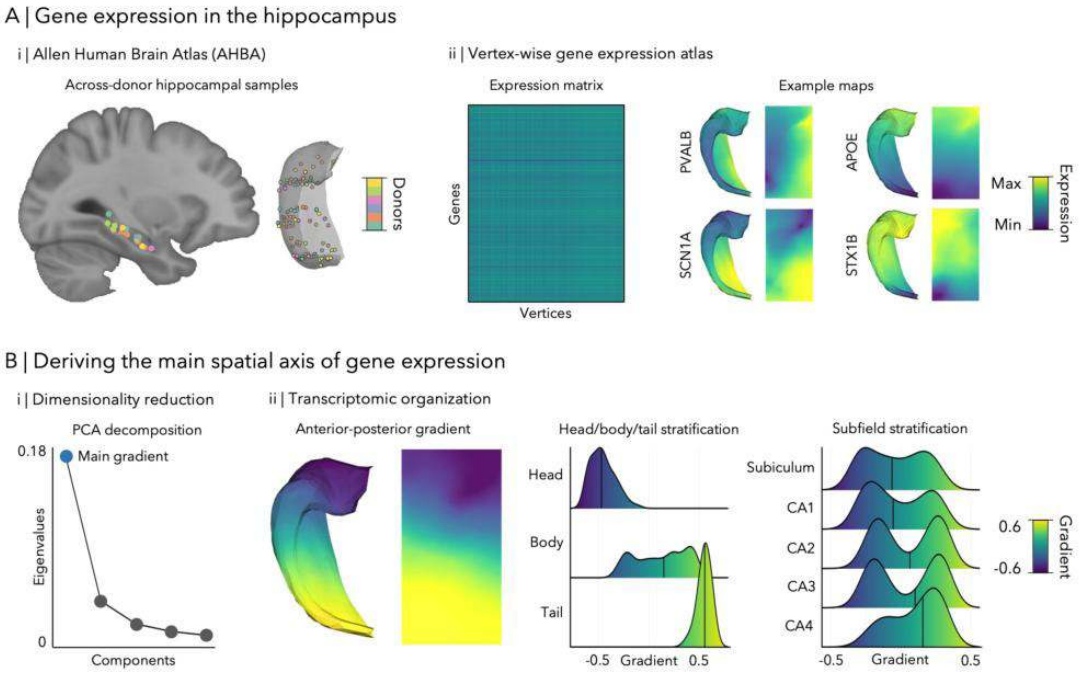

Figure 1 | Gene expression within the hippocampus. (A) Spatially discontinuous *post-mortem* microarray samples from Allen Human Brain Atlas (AHBA) were projected and interpolated along MRI-derived hippocampal surfaces to generate continuous maps of gene expression. **(B)** Principal component analysis (PCA) applied to the concatenated expression maps revealed a predominant anterior-to-posterior gradient. Stratification of gradient scores revealed distinct profiles following the head/body/tail rather than subfield divisions of the hippocampus.

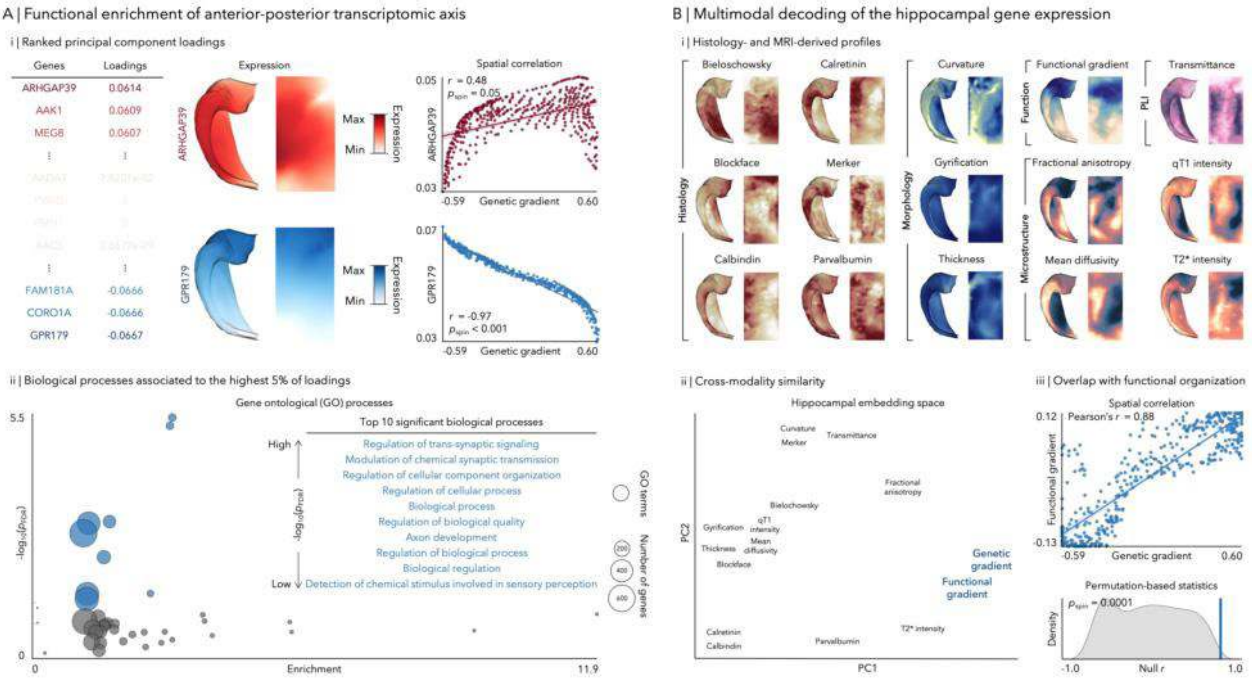

Figure 2 | Decoding the anterior-posterior axis of gene expression. (A) Gene ontology (GO) enrichment analysis of most influential genes (top 5% of principal component loadings) showed multiple biological processes including synapse organisation, axonal development, and behaviour. The ten most significant GO terms are highlighted in blue. **(B)** Histological and MRI-derived features from BigBrain Project[a] (merker), AHEAD[b] (bieloschowsky, blockface, calbindin, calretinin, Parvalbumin) and MICA-MICs[c] (curvature, fractional anisotropy, functional gradient, gyrification, mean diffusivity, qT1 intensity, thickness). Cross-modality correlation analyses revealed strongest correspondence between functional and transcriptomic organization within the hippocampus. [a]Amunts K et al., 2012, *Science*, 340:1472-1475, [b]Alkemade A et al. 2020, *Neuroimage*, 221:117200, [c]Royer J et al., 2022, *Sci Data*, 9(1):569.

Conclusions: Capitalizing on recent imaging-transcriptomic initiatives, we generated vertex-wise maps of hippocampal gene expression from six post-mortem human brains, that mainly followed an anterior-posterior gradient. The presence of fundamental transcriptomic distinctions within the hippocampus may be associated with varying cognitive and functional roles along its longitudinal axis. Taken together, this continuous atlas may advance our understanding of human brain organization and offers a bridge to link multiple neural scales across the hippocampus, both in health and disease.

References

1. Alexander-Bloch, A.F. (2018), 'On testing for spatial correspondence between maps of human brain structure and function', Neuroimage, vol. 178, pp. 540-551
2. Arnatkeviciute, A. (2019), ' A practical guide to linking brain-wide gene expression and neuroimaging data', Neuroimage, vol. 189, pp. 353-367
3. DeKraker, J. (2022), 'Automated hippocampal unfolding for morphometry and subfield segmentation with HippUnfold', eLife, vol. 11, e77945
4. DeKraker, J. (2023), 'Evaluation of surface-based hippocampal registration using ground-truth subfield definitions', eLife, vol 12, RP88404
5. Hawrylycz, M.J. (2012), ' An anatomically comprehensive atlas of the adult human brain transcriptome', Nature, vol. 489, pp. 391-399
6. Vogel, J.W. (2020), 'A molecular gradient along the longitudinal axis of the human hippocampus informs large-scale behavioral systems', Nature Communications, vol. 11, pp. 960

Poster No 886

The link between volumetric changes associated with early life stress and neuromodulator expression

Megan Sheppard[1], Niall Duncan[2], Marta Litwinczuk[1], Rebecca Elliott[1], Elizabeth McManus-Day[1], Eduardo Garza-Villarreal[3], Nils Muhlert[1]

[1]University of Manchester, Manchester, UK, [2]Taipei Medical University, Taiwan, Taipei, [3]Universidad Nacional Autónoma de México, Mexico City, Mexico

Introduction: An individual's early life experiences play a key role in the development of the brain as plasticity is disrupted in those who have experienced early life stress (ELS) (Teicher et al., 2016). Specifically, grey matter volumes throughout the brain are known to change following ELS including in regions such as the prefrontal cortex, amygdala, and the caudate nucleus (Lee et al., 2011; DeBellis & Zisk, 2014). The function of neurotransmitters and neuroendocrine responses are thought to be dysregulated in those who have experienced ELS, specifically impacting catecholamines (Somaini et al., 2011). However, it is unclear whether this change is specific to catecholamine dysregulation or whether this relationship is also true for the

wider group of neuromodulators. Therefore, this study aimed to investigate a potential relationship between volumetric changes associated with ELS and genetic expression of the four key neuromodulators: dopamine, serotonin, acetylcholine, and noradrenaline.

Methods: Data from the UK Biobank (2022 release) were used in this analysis. Participants with any previous neurological illness or injury were excluded. Two groups were defined by their responses to questions assessing the individual's environment growing up including any instances of abuse and neglect. This constituted the ELS measure, with those who scored highly comprising the high ELS group with scores ranging from 7-20. The second group had no previous experience of ELS. For demographics, see Table 1. A voxel-based morphometry (VBM) model was conducted to identify regions that display volumetric grey matter changes associated with ELS whilst controlling for age and sex to prevent potential confounds. The Allen Human Brain Atlas gene expression maps for each neuromodulator subunit (serotonin, noradrenaline, acetylcholine, and dopamine) were then correlated against any morphometric changes identified in the VBM.

Table 1. Demographics of the sample

	Overall	High ELS	No ELS
N	715	350	365
Age	53.67 (±7.50)	53.25 (±7.62)	54.06 (±7.41)
Sex			
Male	202	85	117
Female	513	265	248

Results: Results: Six regions displayed volumetric increases associated with ELS after controlling for false positives using false discovery rate (FDR) correction. These regions include the inferior occipital lobe, inferior temporal lobe, cerebellum, an anterior portion of the superior frontal gyrus and the putamen. Two further regions displayed volumetric decreases associated with ELS: a more dorsal aspect of the superior frontal gyrus and the cingulate. The gene expression maps of all neuromodulator subunits significantly ($p < 0.001$) negatively correlated with the volumetric increases identified in the VBM associated with ELS. However, only a select number of subunits correlate with the identified ELS-associated volumetric decreases ($p < 0.05$). These include four serotonin subunits (5HT1B, 5HT1D, 5HT2C and 5HT3A), three cholinergic subunits (CHRNA2, CHRNA3 and CHRNA6), two dopaminergic receptors (D2 and D3) and two noradrenergic receptors (ADRA2B and ADRB3). These subunits all positively correlated with the volumetric decreases except for the serotonin receptor 5HT2C which significantly ($p<0.001$) negatively correlated with these ELS associated volumetric reductions.

Conclusions: Our findings suggest that there are distinct morphometric alterations associated with early life stress. The volumetric increases associated with ELS are related to expression of all neuromodulator subunits, whereas there is a more specific relationship between neuromodulators and reductions in grey matter volume associated with ELS. Future research will use rodent models aim to further define this relationship by investigating the relationship between potential volumetric changes in targeted brain regions associated with the acute stress response (for example, the amygdala) and genetic expression of these key neuromodulators.

References

1. DeBellis, M. D., & Zisk, A. (2014). The biological effects of childhood trauma. Child and Adolescent Psychiatric Clinics of North America, 23(2), 185–222. https://doi.org/10.1016/j.chc.2014.01.002
2. Lee, H.-Y., Tae, W. S., Yoon, H.-K., Lee, B.-T., Paik, J.-W., Son, K.-R., Oh, Y.-W., Lee, M.-S., & Ham, B.-J. (2011). Demonstration of decreased gray matter concentration in the midbrain encompassing the dorsal raphe nucleus and the limbic subcortical regions in major depressive disorder: An optimized voxel-based morphometry study. Journal of Affective Disorders, 133(1–2), 128–136. https://doi.org/10.1016/j.jad.2011.04.006
3. Somaini, L. et al. (2011) 'Adverse childhood experiences (ACES), genetic polymorphisms and neurochemical correlates in experimentation with psychotropic drugs among adolescents', Neuroscience & Biobehavioral Reviews, 35(8), pp. 1771–1778. doi: 10.1016/j.neubiorev.2010.11.008.
4. Teicher, M. H., Samson, J. A., Anderson, C. M., & Ohashi, K. (2016). The effects of childhood maltreatment on brain structure, function, and connectivity. Nature Reviews Neuroscience, 17(10), 652–666. https://doi.org/10.1038/nrn.2016.111

Poster No 887

Macaque cell type and gene expression correlates of neuroanatomy

Burke Rosen[1], Takuya Hayashi[2], David van Essen[1], Matthew Glasser[1]

[1]Washington University in St. Louis, St. Louis, MO, [2]RIKEN Center for Biocystems Dynamics Research, Kobe, Hyogo

Introduction: The morphology and physiology of every cell is largely determined by the relative transcription levels of its genes. Earlier cortical transcriptomic studies using bulk tissue assays found that the first principal component (PC1) of brain-enriched gene expression predicts the cortical T1w/T2w ratio, an indicator of myelin content[1] and hierarchical relationships[2], and a subset of these genes moderately predict human vs chimpanzee evolutionary expansion of cortex[3]. However, these studies did not identify cell types. Cell type composition is potentially more informative than aggregate expression because species differences in expression are sometimes constrained to specific cell types[4], the patterns of expression can be spatially opposed in different types[5], and because cells' gestalt transcription is statistically more robust than individual gene expression. A recent spatial transcriptomic survey of the entire macaque cortex[6] examined anterior-posterior (A-P) gradients of cell type composition but these data were not compared to cortical thickness, myelin, or evolutionary expansion. We performed these comparisons by mapping areal transcription[6] to the cortical surface.

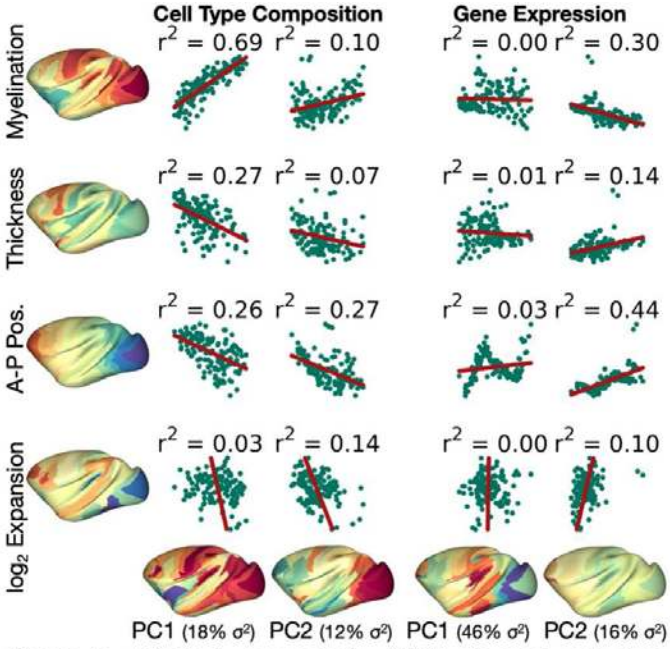

Figure 1. Principal components (PCs) of areal cell type composition and gene expression vs neuroanatomical brain measures. PCs and measures are displayed on inflated template macaque surface. Each green marker represents a parcel. Red traces show least-squares linear fits.

Methods: Individual macaque cortical surfaces were reconstructed from T1 and T2 weighted MR Images[7]. Group average (n=32) surfaces and maps of cortical myelin and thickness were obtained. As described in a companion poster, human vs macaque evolutionary expansion was estimated. Cells in[6] are localized to the volumetric D99_v2 atlas[8]. We projected the atlas to the surface with Connectome Workbench[9]. For each parcel, the expression profile of all cells was averaged to yield a pseudo-bulk parcel x gene matrix (131x15929). Counts of cells were tallied to create a parcel x cell type matrix (131x258). First, in an exploratory analysis following[2], expression and composition PCs explaining the most variance across parcels were compared to brain measures. To determine which genes and cell types are most predictive of each brain measure, we fit elastic net regularized generalized linear models (GLMs)[10] by cross-validation.

Results: PC1 of areal cell type composition explains considerable variance in myelin (69%), thickness (27%), and A-P position (26%) across parcels, whereas PC1 of pseudo-bulk gene expression explains only 0%, 1%, and 3%, respectively (Fig. 1). PC2 of expression was more predictive than cell type of the examined brain measures, though less predictive than cell type PC1. Expansion was not well captured by either factorization. Elastic net GLMs identified a subset of cell type or gene predictors that explain a large degree of variance in brain measures (Fig. 2). Models of cell type composition explain 95%, 84%, 96%, and 74% of variance in myelin, thickness, A-P position, and expansion vs 94%, 89%, 98%, and 40%, for expression. L2 and L4 glutamatergic neurons are prominent among predictors of cortical thickness, and evolutionary expansion, respectively. RELN-expressing inhibitory neurons are prominent predictors of cortical thickness.

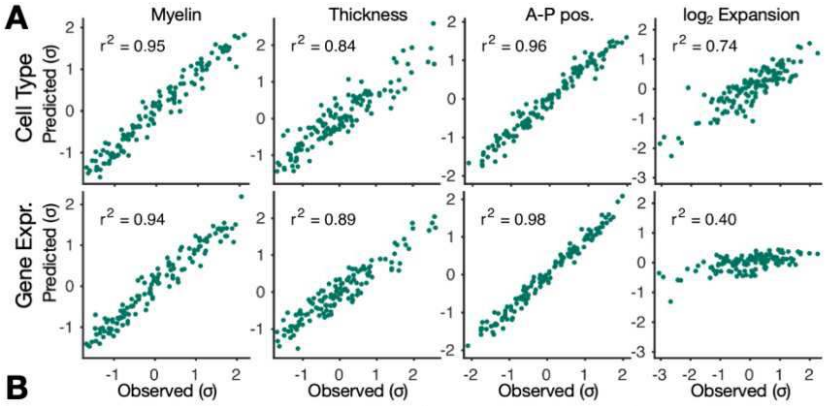

B

Myelin			Thickness			A-P pos.			log$_2$ Expansion		
Cell Type	Class	Coef	Cell Type	Class	Coef	Cell Type	Class	Coef	Cell Type	Class	Coef
PVLAB.24	GABA	0.20	L2.5	glu.	-0.23	L4/5/6.10	glu.	0.10	L3/4.11	glu.	-0.19
L2.3	glu.	0.16	L2.9	glu.	0.15	PV_CHC.1	GABA	0.08	L4.9	glu.	-0.18
VIP.7	GABA	-0.10	L4/5.3	glu.	0.15	VIP_RELN.7	GABA	-0.08	L4/5/6.10	glu.	0.15
ASC.2	non-nrn.	-0.08	RELN.3	GABA	0.13	RELN.9	GABA	0.07	PV_CHC.4	GABA	-0.13
L3/4.11	glu.	0.07	MG.1	non-nrn.	0.12	RELN.6	GABA	0.07	L4/5/6.3	glu.	-0.13
VIP_RELN.9	GABA	0.07	L4/5.16	glu.	0.12	SST.3	GABA	-0.06	L3/4.2	glu.	0.11
PVALB.8	GABA	0.06	L2.1	glu.	0.11	L2.2	glu.	0.06	L6.2	glu.	-0.10
L2/3.8	glu.	0.06	RELN.10	GABA	0.10	L6.6	glu.	0.05	PVALB.21	GABA	-0.10
VIP_RELN.8	GABA	0.05	L2/3.7	glu.	0.10	OLG.11	non-nrn.	-0.05	ASC.1	non-nrn.	-0.10
L4/5.8	glu.	0.05	SST.29	GABA	-0.09	PVALB.8	GABA	-0.05	L4/5.18	glu.	-0.09

C

# Non-null Model Predictors		
	Cell Type	Gene Expr.
Myelin	43	83
Thickness	36	63
A-P Pos.	75	84
Expansion	52	10

Figure 2. Elastic net GLMs. **A.** Model predictions vs observations. Each marker is a parcel. Variance explained is inset. **B.** Most predictive cell types for each brain measure. Labeled cell classes include glutamatergic and GABA-ergic neurons, as well as and non-neuronal cells. **C.** Total number of non-null predictors selected in each model.

Conclusions: The predictive power of cell type composition PC1 with respect to myelination is greater than previously reported for human bulk gene expression[2] and any pseudo-bulk gene expression PC, consistent with the hypothesis that cell type is more informative that individual gene expression. The elastic net GLM analysis is more ambiguous; the cell type GLM captures more variation in expansion but selects more predictors. Intriguingly, L4 pyramidal neurons, whose abundance was previously hypothesized to be associated with primate evolutionarily divergence[6], feature prominently and type L4.9 is a primate-specific neuron[6]. While macaque transcription was less able to explain evolutionary expansion than other brain measures, this is not unexpected as much of the variability in expansion is presumably results from human transcription[4]. Future interspecies comparisons are needed.

References

1. Glasser MF, Van Essen DC. Mapping Human Cortical Areas In Vivo Based on Myelin Content as Revealed by T1- and T2-Weighted MRI. Journal of Neuroscience. 2011;31(32):11597–11616.
2. Burt JB, Demirtaş M, Eckner WJ, Navejar NM, Ji JL, Martin WJ, Bernacchia A, Anticevic A, Murray JD. Hierarchy of transcriptomic specialization across human cortex captured by structural neuroimaging topography. Nature Neuroscience. 2018;21(September).
3. Wei Y, de Lange SC, Scholtens LH, Watanabe K, Ardesch DJ, Jansen PR, Savage JE, Li L, Preuss TM, Rilling JK. Genetic mapping and evolutionary analysis of human-expanded cognitive networks. Nature Communications. 2019;10(1):4839.
4. Jorstad NL, Song JHT, Exposito-Alonso D, Suresh H, Castro-Pacheco N, Krienen FM, Yanny AM, Close J, Gelfand E, Long B, et al. Comparative transcriptomics reveals human-specific cortical features. Science. 2023;382(6667).
5. Jorstad NL, Close J, Johansen N, Yanny AM, Barkan ER, Travaglini KJ, Bertagnolli D, Campos J, Casper T, Crichton K. Transcriptomic cytoarchitecture reveals principles of human neocortex organization. Science. 2023;382(6667):eadf6812.
6. Chen A, Sun Y, Lei Y, Li C, Liao S, Meng J, Bai Y, Liu Z, Liang Z, Zhu Z, et al. Single-cell spatial transcriptome reveals cell-type organization in the macaque cortex. Cell. 2023;186(17):3726-3743.e24.
7. Hayashi T, Hou Y, Glasser MF, Autio JA, Knoblauch K, Inoue-Murayama M, Coalson T, Yacoub E, Smith S, Kennedy H, et al. The nonhuman primate neuroimaging and neuroanatomy project. NeuroImage. 2021;229:117726.
8. Saleem KS, Avram A V, Glen D, Yen CC-C, Frank QY, Komlosh M, Basser PJ. High-resolution mapping and digital atlas of subcortical regions in the macaque monkey based on matched MAP-MRI and histology. Neuroimage. 2021;245:118759.
9. Glasser MF, Sotiropoulos SN, Wilson JA, Coalson TS, Fischl B, Andersson JL, Xu J, Jbabdi S, Webster M, Polimeni JR. The minimal preprocessing pipelines for the Human Connectome Project. Neuroimage. 2013;80:105–124.
10. Zou H, Hastie T. Regularization and variable selection via the elastic net. Journal of the Royal Statistical Society Series B: Statistical Methodology. 2005;67(2):301–320.

Poster No 888

Energy Profiles of Neurons and Glial Cells in the Human Brain

Laura Fraticelli[1], Gabriel Castrillón[2], Valentin Riedl[3]

[1]Klinikum rechts der Isar der Technischen Universität München, Munich, Bavaria, [2]Friedrich-Alexander University, Erlangen, Germany, [3]Technical University of Munich, Erlangen, Germany

Introduction: Brain cells exhibit divergent metabolic profiles that have been mainly studied in animal models and in-vitro. Neurons are recognized as oxidative cells, and astrocytes (Ast) are glycolytic. Lipid and fatty acid (FA) oxidation occurs primarily in glial cells (Ast, microglia (Mic) and oligodendrocytes (OLs)) and is pivotal for normal brain function. Furthermore, Mic are metabolically versatile as the brain's resident immune cells and OLs are essential for the myelination of axons. These preferential cell profiles have not been validated in the human brain. Metabolic differences within the cell types emerge predominantly from differential gene expressions. Transcriptomic data of post-mortem brains from the Allen Human Brain Atlas (AHBA) enabled us to investigate the expression patterns of metabolism and cell type-related genes in cortical and subcortical areas of the human brain.

Methods: The spatial microarray data from the AHBA was processed through abagen to study the energy profiles of neurons and glial cells. Left hemisphere data was assigned to the HCPex parcellation, an extended version of the HCP-MMP1, including subcortical areas. Microarray data was normalized and aggregated across donors' brains to generate expression maps of 15637 genes across 203 regions. Cell types and metabolic pathways were represented by the expression of distinct gene sets. Pathways of interest were glycolysis (Gly), oxidative phosphorylation (OxPhos), FA metabolism, reactive oxygen species (ROS), peroxisome (Per) and myelin-related (My) genes. Cell-type markers were extracted from Seidlitz et al. 2020. The median expression of cell-type and metabolic gene sets was plotted according to the 203 HCPex areas. Spearman correlation was calculated between cell-type and metabolic expression maps and tested for significance through t-tests. P-values were Bonferroni adjusted.

Results: The median of cell-type and metabolic expression maps revealed alternating expression patterns in cortical and subcortical areas. In subcortical areas, the expression of excitatory and inhibitory neurons (ExNeu and InhNeu) decreased substantially, while Ast, OL and Mic increased. Similar to the glial expression maps, Fa, Per and My increased subcortically. Gly and OxPhos genes are stably expressed across cortex and subcortex. We found divergent correlation patterns in cortical versus subcortical areas. In cortical areas, ExNeu correlated positively with Gly, OxPhos, and ROS. Both ExNeu and InhNeu correlated negatively with My. Ast correlated positively with Gly, FA, Per and My. Mic showed positive correlations with Gly, ROS, FA, Per and My, while OLs correlated with Per and My. In subcortical areas merely Mic and OLs showed significant correlations with metabolic gene sets. Mic correlated positively with Ox, ROS, FA, My and OLs with Gly, Ox, FA, Per, and My.

Conclusions: Studies on the human brain focus predominantly on the cerebral cortex, even though the subcortex is pivotal for cognitive functions. The HCPex enabled us to follow expression patterns of cell- and metabolism-specific genes across cortical and subcortical areas. Glia to neuron ratio is higher in subcortical regions, which is reflected in decreased neuronal and increased glial marker expression in subcortical areas. Glia-related metabolic pathways increased concordantly. Our correlation analysis underpinned that excitatory neurotransmission consumes majority of the brain's energy. Gly, OxPhos and ROS correlated with ExNeu but not InhNeu. Glial cells are mainly responsible for FA and lipid metabolism, with FA oxidation primarily occurring in astrocytes. Peroxisomes are essential for FA α-oxidation and the biosynthesis of myelin sheath lipids. Accordingly, we find correlations between glial cells, FA, and Per. Intriguingly, neuronal and glial cells display diverging correlation patterns in subcortical areas highlighting distinct cellular and metabolic organization in the human cortex and subcortex.

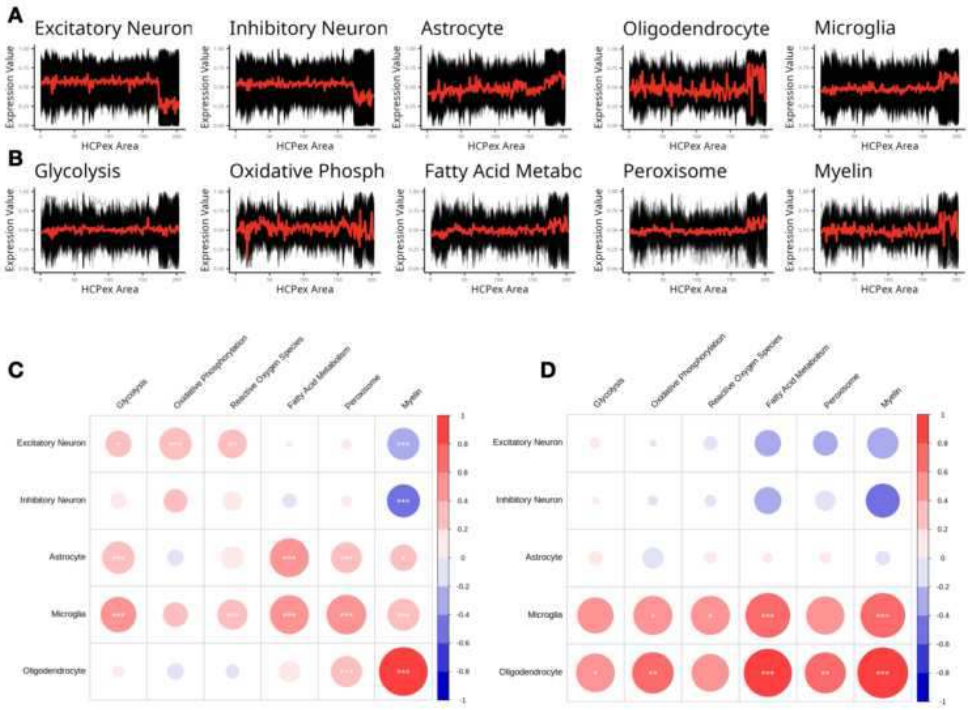

Figure 1: Transcriptomic data reveals distinct expression patterns of celltype marker and metabolic genes across cortical and subcortical regions of the human brain. AHBA microarray data from six post-mortem brains was assigned to the HCPex parcellation through the python package abagen. Expression of genes corresponding to specific celltypes and metabolic pathways were extracted and their expression patterns across cortical and subcortical areas analysed. Expression of genes across 203 HCPex regions corresponding to **A** celltypes and **B** metabolic pathways. Median expression of genes across ROIs is depicted in red. While neuronal expression decreases in subcortical areas, the expression of glial and glial-related metabolic genes (FA, Per and My) increases in subcortical areas. Gly and OxPhos appear stable across cortical and subcortical structures. Spearman correlation between median celltype and metabolic pathway expression maps was calculated across **C** cortical and **D** subcortical areas. In cortical areas, ExNeu correlated positively with Gly, OxPhos, and ROS. Both ExNeu and InhNeu correlated negatively with My. No significant correlation between both ExNeu and InhNeu and predominantly glial pathways (FA, Per) was detected. Contrary, Ast did not correlate significantly with OxPhos and ROS but with Gly, FA, Per and My. Mic showed positive correlations with Gly, ROS, FA, Per and My, while OLs correlated with Per and My. In subcortical areas merely Mic and OLs showed significant correlations with metabolic gene sets. Mic correlated positively with Ox, ROS, FA, My and OLs with Gly, Ox, FA, Per, and My. Spearman correlations (R) were calculated in R. The correlations were tested for significance by the application of t-tests and the computed p-values were adjusted through Bonferroni correction (n=60). ***p < 0.001, **p < 0.01, *p < 0.05. Abbreviations: ExNeu: excitatory neuron, InhNeu: inhibitory neuron, Ast: astrocyte, Mic: microglia, OL: oligodendrocytes, FA: fatty acid, Gly: glycolysis, My: myelin, OxPhos: oxidative phosphorylation, Per: peroxisome, ROS: reactive oxygen species, ROI: region of interest.

References

1. Dienel, G. A. (2019). Brain glucose metabolism: integration of energetics with function. Physiological reviews, 99(1), 949-1045.
2. Markello, R. D., (2021). Standardizing workflows in imaging transcriptomics with the abagen toolbox. elife, 10, e72129.
3. Arnatkevičiūtė, A., (2019). A practical guide to linking brain-wide gene expression and neuroimaging data. Neuroimage, 189, 353-367.
4. Hawrylycz, M. J., (2012). An anatomically comprehensive atlas of the adult human brain transcriptome. Nature, 489(7416), 391-399.
5. Huang, C. C., (2022). An extended Human Connectome Project multimodal parcellation atlas of the human cortex and subcortical areas. Brain Structure and Function, 227(3), 763-778.
6. Seidlitz, J.,(2020). Transcriptomic and cellular decoding of regional brain vulnerability to neurogenetic disorders. Nature communications, 11(1), 3358.
7. Azevedo, F. A., (2009). Equal numbers of neuronal and nonneuronal cells make the human brain an isometrically scaled-up primate brain. Journal of Comparative Neurology, 513(5), 532-541.
8. Barber, C. N., (2019). Lipid metabolism crosstalk in the brain: glia and neurons. Frontiers in cellular neuroscience, 13, 212.
9. Garcia Corrales, A. V.,(2021). Fatty acid synthesis in glial cells of the CNS. International Journal of Molecular Sciences, 22(15), 8159.
10. Bell, P. T.,(2016). Subcortical contributions to large-scale network communication. Neuroscience & Biobehavioral Reviews, 71, 313-322.

Poster No 889

Topological properties of brain functional networks are associated with individual risk tolerance

Wi Hoon Jung[1]

[1]*Gachon University, Seongnam-si, Gyeonggi-do*

Introduction: Risk tolerance refers to the extent to which an individual is willing to take risks to achieve greater expected returns. Individual differences in the risk tolerance are associated with real-life outcomes, such as financial choices and health behaviors (Krain et al., 2008). In the brain, these individual differences are functionally associated with areas belonging to the valuation and salience networks (such as the medial prefrontal cortex, ventral striatum, anterior insula, and anterior cingulate cortex) and areas that process emotions (such as amygdala) (Levy et al., 2010; De Martino et al., 2010; Knutson and Huettel, 2015; Jung et al., 2018). However, it remains unknown how individual risk tolerance is associated with whole-brain functional network topological properties. Thus, this study investigates whether the topological properties of individual brain functional networks are associated with individual risk tolerance using resting-state fMRI data in conjunction with a graph theoretical analysis approach (Rubinov and Sporns, 2010).

Methods: A total of 67 healthy young adults were included in the analysis (37 males/30 females; age = 24.00±1.41 years; risk tolerance = 0.60±0.25). While performing the risk preference task, participants were asked to make a series of 120 choices between a smaller-but-certain reward and a larger-but-risky rewards (Glimcher, 2008; Levy et al., 2010; Jung et al., 2018). The smaller-but-certain reward was fixed at a 100% chance of 10,000 Korean won (KRW, approximately USD 8~9) and the larger-but-risky rewards ranged from KRW 11,000 to KRW 63,000 and their probability varied from 13% to 98%. Individual behavioral data were fitted using a logistic regression function with maximum likelihood estimate to capture the probability of choosing the larger-but-risky reward as a stochastic function of the difference in subjective value (SV) between the two options. To estimate risk tolerance, the SV was followed by the function form of expected utility. A detail description of the risk tolerance estimation method can be found elsewhere (Jung et al., 2018). After preprocessing the resting-fMRI data, brain areas (i.e., nodes) for these data were divided using the atlas with 160 areas functionally defined by Dosenbach et al. (2010). Next, Pearson correlation coefficients (i.e., edges) between a pair of these divided areas were calculated to construct a functional brain network for each participant. Then, several global topological properties were estimated with different sparsity thresholds ($0.10 < S < 0.40$), including small-world parameters (i.e., clustering coefficient, characteristic path length, small-worldness, global efficiency, and local efficiency), and a regional topological property, including betweenness centrality. Finally, Spearman's rank correlation analyses were performed to examine the association between (log-transformed) individual risk tolerance and each of the network topological properties.

Results: Individual risk tolerance was positively associated with global topological properties, including the normalized clustering coefficient, related to the degree of information segregation (r-value = 0.29, p-value = 0.02), and small-worldness, related to the balance between information segregation and integration in a network (r-value = 0.27, p-value = 0.03). We also found that individuals with higher risk tolerance exhibited greater centrality in the ventromedial prefrontal cortex (vmPFC), associated with the subjective value of the given options (r-value = 0.35, p-value = 0.01).

Conclusions: Consistent with previous studies, we confirmed that the whole-brain functional network had a small-world architecture. These results extend our understanding of how individual differences in risk tolerance are associated with functional brain organization, particularly regarding the balance between segregation and integration in functional networks, and highlight the important role of the connections of the vmPFC as the hub.

References

1. De Martino, B., Kumaran, D., Seymour, B., and Dolan, R.J. (2006), 'Frames, biases, and rational decision-making in the human brain', Science, vol. 313, pp. 684-687.
2. Dosenbach, N.U., Nardos, B., Cohen, A.L., Fair, D.A., Power, J.D., Church, J.A., et al. (2010), 'Prediction of individual brain maturity using fMRI', Science, vol. 329, no. 5997, pp. 1358-1361.
3. Glimcher, P.W. (2008), 'Understanding risk: a guide for the perplexed', Cognitive Affective & Behavioral Neuroscience, vol. 8, pp. 348-354.
4. Jung, W.H., Lee, S., Lerman, C., Kable, J.W. (2018), 'Amygdala Functional and Structural Connectivity Predicts Individual Risk Tolerance', Neuron, vol. 98, no. 2, pp. 394-404.e4.
5. Knutson, B., Huettel, S.A. (2015), 'The risk matrix', Current Opinion in Behavioral Sciences, vol. 5, pp.141-146.
6. Krain, A.L., Gotimer, K., Hefton, S., Ernst, M., Castellanos, F.X., Pine, D.S., and Milham, M.P. (2008), 'A functional magnetic resonance imaging investigation of uncertainty in adolescents with anxiety disorders', Biological Psychiatry, vol. 63, pp. 563-568.
7. Levy, I., Snell, J., Nelson, A.J., Rustichini, A., Glimcher, P.W. (2010), 'Neural representation of subjective value under risk and ambiguity', Journal of Neurophysiology, vol. 103, pp. 1036-1047.
8. Rubinov, M., and Sporns, O. (2010), 'Complex network measures of brain connectivity: uses and interpretations', Neuroimage, vol. 52, pp. 1059-1069.

Poster No 890

Mapping fMRI responses to combinations of foods in the human brain

Hui-Kuan Chung[1], Philippe Tobler[2]

[1]University of Zurich, Zurich, Zurich, [2]University of Zurich, Zurich, Switzerland

Introduction: Overweight is on the rise world-wide. One possibly contributing factor is that the pleasure derived from specific food combinations leads to more consumption than when the constituents are consumed separately. The classic pairing of beer and chips serves as a prime example. People often find it more satisfying to enjoy chips with beer than consuming them separately. These food combinations are known as complementary goods, where indulging in one often triggers the desire for the other. In contrast, substitute goods are interchangeable to some degree, like regular beer and low-calorie beer, and providing one typically reduces desire for the other. These phenomena underscore the importance of investigating the valuation process for combinations of goods, but we know still relatively little about the conditional valuation of the different relationships between foods. The present study investigates these relationships at both the behavioral and the neural level.

Methods: Thirty-eight healthy volunteers (22 women; BMI range = 18.79-26.47), participated in this study. Participants provided willingness to pay (WTP) bids for the same food items, sometimes in isolation (single condition) and sometimes in combination with other foods (paired condition) inside the MRI scanner. In the paired condition, participants were given a free food on top of the food item they were bidding for. This novel design allowed us to investigate how WTP differed between single and paired conditions (ΔWTP= WTPaired - WTPsingle) while controlling for the intrinsic value of the food item. We predicted that the valuation of a particular food item would change as a function of which other items it was paired with. To identify the brain regions decoding different food relationships, we conducted a multi-voxel pattern analysis (MVPA) on the fMRI data. In the MVPA analysis. Specifically, the support vector machine classifier was trained to distinguish between high (i.e., complementary goods) versus low (i.e., substituting goods) ΔWTP. Additionally, the identified region was used as a seed region in a psychophysiological interaction (PPI) analysis, with high versus low ΔWTP serving as the psychological factor.

Results: As predicted, ΔWTP increased when the combined foods were rated as more complementary but decreased when combined foods were rated as more substituting. These findings indicate that complementary and substituting relations between foods differentially affect valuation. Moreover, regression analyses revealed a positive relationship between increased combined valuation of an item and the self-reported frequency with which participants consumed the two items together. Neurally, we observed that the occipital lobe, cerebellum, and hippocampus were involved in processing the value change related to combining foods (ΔWTP; whole-brain FWE <0.05). Furthermore, the hippocampus exhibited stronger functional connectivity with the putamen when foods were more complementary compared to when they were more substituting (whole-brain uncorrected <0.001).

Conclusions: Together, our behavioral and neural findings are compatible with the notion that memory contributes to the enhancement of value when goods are more complementary. By recognizing the role of memory in processing the valuation of combined foods, it paves the way for interventions aimed at promoting balanced and nutritious eating habits.

References

1. Suzuki, Shinsuke et al (2017), 'Elucidating the underlying components of food valuation in the human orbitofrontal cortex.', Nature neuroscience vol. 20, no. 12, 1780-1786.

Poster No 892

Neural encoding of rapidly adapting risk preferences

Simon Steinkamp[1], David Meder[1], Oliver Hulme[1,2,3]

[1]Danish Research Centre for Magnetic Resonance, Copenhagen University Hospital - Amager and Hvidovre, Copenhagen, Denmark, [2]London Mathematical Laboratory, London, United Kingdom, [3]Department of Psychology, University of Copenhagen, Copenhagen, Denmark

Introduction: Economic decision-making theories assume that risk preferences are trait-like, variable over people, but stable over the lifetime. A recent theory inspired by physics predicts that risk preferences should be determined by the type of environmental dynamics that people face (Peters, 2019). Meder et al. (2021) provided behavioral evidence for this theory, showing that participants were more risk-averse when deciding between multiplicative as opposed to additive gambles. In the study, participants first completed a learning task in which the value of nine images was implicitly learned from their effects on wealth. Participants then decided between gambles comprised of these images. In one session the effect of the images

was additive (fixed changes), in the other multiplicative (% changes of current wealth). Here, we analyze fMRI data collected with the behavioral data in Meder et al. (2021), aiming to infer how risk preferences are encoded in the brain, and whether they reflect the changes that were observed behaviorally. We do this, by fitting reward learning models to the learning task that use either changes of the linear or log-transformed wealth trajectories (Fig. 1B) as a reward signal, thus integrating models of risk taking into reinforcement learning models.

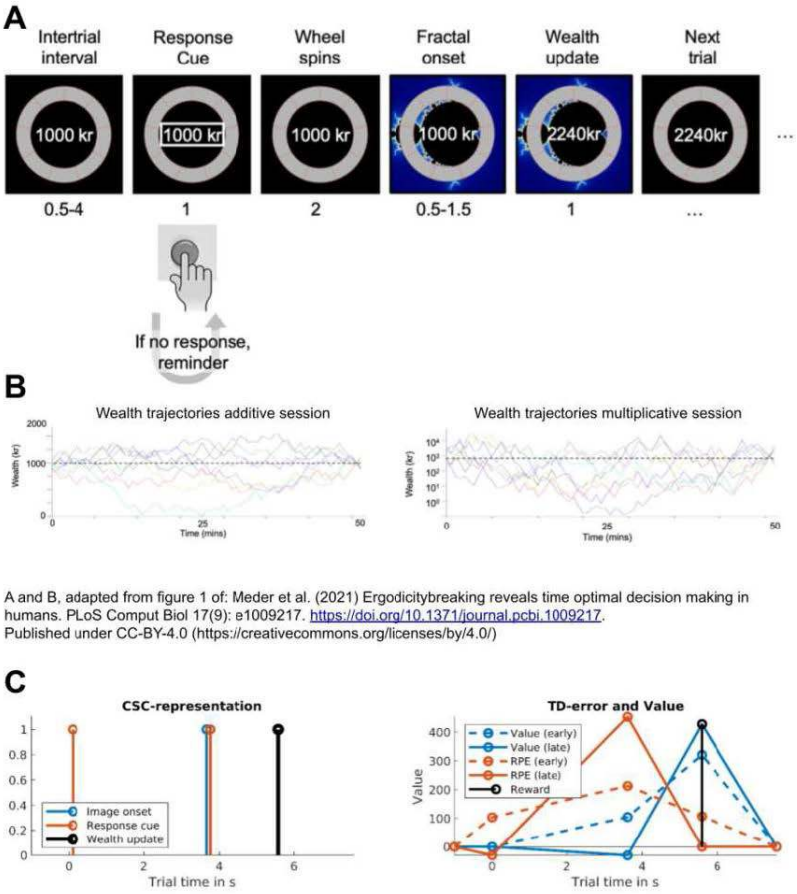

A and B, adapted from figure 1 of: Meder et al. (2021) Ergodicitybreaking reveals time optimal decision making in humans. PLoS Comput Biol 17(9): e1009217. https://doi.org/10.1371/journal.pcbi.1009217.
Published under CC-BY-4.0 (https://creativecommons.org/licenses/by/4.0/)

Methods: We analyzed fMRI data from 14 participants (n=19, 5 excluded) from Meder et al. (2021), who completed the learning task. Each session had two runs of 168 trials each, resulting in up to 60 min of fMRI data per session. To estimate the reward prediction errors (RPE) in the experiment we used two types of TD-learning models. One used linear wealth changes as the reward signal (TDlin), the other used changes in logarithmic wealth (TDlog). For each trial, the RPE was estimated at the onset of the response cue, the image, and the wealth update (Fig. 1A&C). The RPE signal was then used as a parametric modulator in first-level GLMs. First, we tested TDlin vs TDlog within each session, by comparing the cross-validated log model evidence of the GLMs using the MACS toolbox for SPM (Soch & Allefeld, 2018). We also looked at the group effect of the parametric modulator for TDlin in the additive and TDlog in the multiplicative session. We also tested changes in risk preferences directly, by including both sessions in first-level GLMs. GLM one had parametric modulators of TDlin for the additive session and TDlog for the multiplicative session; GLMs two and three used TDlin or TDlog for both sessions. We used the difference of the Bayesian information criterion to compare the models on the group level.

Results: We found group-level evidence for the main effect of linear RPE under the additive condition in striatal regions, while evidence for the main effect of logarithmic RPE was revealed in VMPFC in the multiplicative condition (both $p < 0.001$, unc., Fig. 2A). When evaluating shifts in risk preferences (Fig. 2B&C), we found that VMPFC has strong evidence for the TDlin model over the TDlog model under additive conditions, and strong evidence for the TDlog model over the TDlin model under multiplicative conditions. This observed pattern of activity appears to correspond to the RPE encoding that one would expect given the behaviorally observed changes in risk preferences.

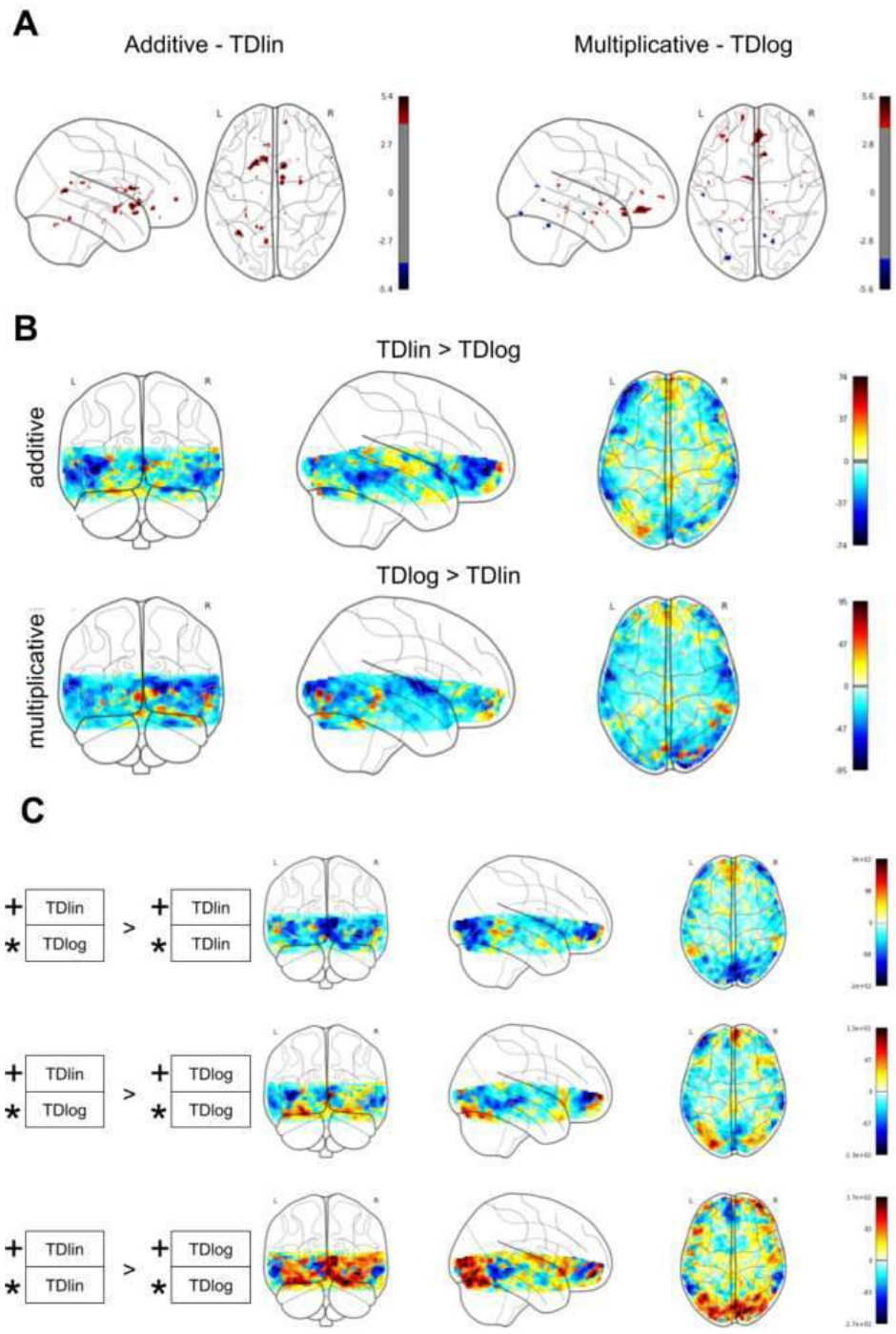

Conclusions: Our preliminary results suggest that VMPFC shows an RPE signal that is sensitive to the dynamics of the environment, indicating that reward encoding changes from a linear utility function in an additive environment to a logarithmic utility function in a multiplicative one. The weak main effect of RPE, however, suggests that our TD-model may not be optimal. Considering the behavioral results of Meder et al. (2021), it is also likely, that while participants gravitated towards logarithmic or linear risk-preferences, there is both substantial individual variability, and a bias towards risk aversion, which may also impact the model fit. In later analysis, we will attempt to directly map individual risk preferences onto brain data.

References

1. Meder D., Rabe F., Morville T., Madsen K.H., Koudahl M.T., et al. (2021) Ergodicity-breaking reveals time optimal decision making in humans. PLOS Computational Biology 17(9): e1009217. https://doi.org/10.1371/journal.pcbi.1009217
2. Peters, O. (2019). The ergodicity problem in economics. Nature Physics, 15(12), 1216–1221. https://doi.org/10.1038/s41567-019-0732-0
3. Soch, J., & Allefeld, C. (2018). MACS – a new SPM toolbox for model assessment, comparison and selection. In Journal of Neuroscience Methods (Vol. 306, pp. 19–31). Elsevier BV. https://doi.org/10.1016/j.jneumeth.2018.05.017

Poster No 893

Pain Now! The dmPFC Reflects Pain Preferences for Inter-Temporal Choices

Taryn Berman[1], Sean Devine[1], Éliane Rochelet[1], Ross Otto[1], Mathieu Roy[1]

[1]*McGill University, Montreal, Quebec*

Introduction: Accepting pain is counterintuitive, yet individuals willfully accept immediate discomfort to gain long-term benefits. Studies using hypothetical pain or short temporal delays suggest that people may prefer future pain to avoid immediate pain (Harris, 2012), while others propose that people prefer immediate pain to get it over with (Berns et al., 2006; Story et al., 2013). Improving upon previous literature, our study sought to investigate how inter-temporal choices for pain are made and the underlying brain mechanisms involved.

Methods: Fifty-eight Participants (F = 43, Mean Age = 21.00 ± 2.72) first underwent a sensory calibration procedure to assess their pain tolerance. Next, they performed an inter-temporal choice task in an fMRI, wherein they selected between two choices which differed in pain intensity (i.e., 60%, 70%, 80%, or 90% of their pain tolerance) and delay (i.e., pain now vs. 15s, 30s, 1-hour, or 1-month). Importantly, all participants were required to return after one-month to receive the delayed pain chosen.

Results: We found that subjects preferred more pain in order to experience it sooner ($t(57) = 10.635$, $p < .001$, $M = .655$ (95% CI = [.626, .684]), $d = 1.399$). Using multilevel modeling, we found that delay ($\gamma = 1.253$, $p < .001$) and pain intensity ($\gamma = 13.270$, $p < .001$) for each offer predict pain now decisions. Computational modeling results revealed that delayed pain is perceived and "valued" as being worse than immediate pain. Brain imaging analyses revealed that worse pain offers – those of higher pain intensity and longer delay which are lower in subjective value – were associated with clusters of activation in regions of the dorsomedial prefrontal cortex (dmPFC). We also observed that two distinct neural systems were associated with short (i.e., 15s and 30s) and long (i.e., 1-hour and 1-month) delays. Short delays saw activation in regions connected with pain perception and anticipation (i.e., anterior cingulate cortex and anterior insula; Ploghaus et al., 1999), while longer delays were related to imagining the future (i.e., superior parietal lobule, dmPFC, dorsolateral PFC, precuneus, and posterior cingulate cortex; Addis et al., 2007; Schacter et al., 2012). All fMRI data was two-tailed FDR corrected ($q < .05$).

Conclusions: Overall, our results suggest that people would rather accept more immediate pain than wait for less. Neural activations in the dmPFC suggest that this region integrates stimulus magnitude and delay and produces a value for a given future event. Activity associated with delay indicates that, as delay increases, there is an increasing focus on imagining the future delay rather than pain intensity. This study has important implications for interventions aimed to reduce detrimental biases that lead to added suffering.

References

1. Addis, D. R., Cheng, T., P. Roberts, R., & Schacter, D. L. (2011), 'Hippocampal contributions to the episodic simulation of specific and general future events', Hippocampus, vol. 21, no. 10, pp. 1045–1052.
2. Berns, G. S., Chappelow, J., Cekic, M., Zink, C. F., Pagnoni, G., & Martin-Skurski, M. E. (2006). 'Neurobiological substrates of dread', Science, vol. 312, no. 5774, pp. 754–758.
3. Harris, C. R. (2012). 'Feelings of Dread and Intertemporal Choice', Journal of Behavioral Decision Making, vol 25, pp. 13–28.
4. Ploghaus, A., Tracey, I., Gati, J. S., Clare, S., Menon, R. S., Matthews, P. M., & Rawlins, J. N. P. (1999). 'Dissociating pain from its anticipation in the human brain', Science, vol. 284, no. 5422, pp. 1979–1981.
5. Schacter, D. L., Addis, D. R., Hassabis, D., Martin, V. C., Spreng, R. N., & Szpunar, K. K. (2012). 'The Future of Memory: Remembering, Imagining, and the Brain', Neuron, vol 76, no. 4, pp. 677–694.
6. Story, G. W., Vlaev, I., Seymour, B., Winston, J. S., Darzi, A., & Dolan, R. J. (2013). 'Dread and the Disvalue of Future Pain', PLoS Computational Biology, vol. 9, no. 11, pp. 1-18.

Poster No 894

Test-retest reliability of decisions under risk: Evidence from two behavioral and EEG experiments

Jia Jin[1], Qin Xiao[1], Qiang Shen[1]

[1]*Shanghai International Studies University, Shanghai, China*

Introduction: Decisions involving risk are ubiquitous, and understanding how individuals manage risk is crucial in everyday life (Korucuoglu et al., 2020). Consequently, accurately measuring individuals' risk-taking propensities and the stability of these preferences over time has become increasingly important in recent years. However, few studies have systematically examined the reliability of EEG responses during risk-taking activities, and the potential of EEG to act as a predictor of behavior remains elusive.

Methods: In this study, we recruited a sample of 41 healthy participants to undertake the same experimental tasks involving risk twice over a short-term interval of 7-14 days. Thirty-six subjects successfully completed both sessions. In each session, we simultaneously recorded their behavioral and EEG data for two risk-related tasks, which included a classical 5-25 monetary gambling task (Task 1) and a mixed gambling task (Task 2). We performed Intraclass Correlation Coefficient (ICC) analyses on both the behavioral and EEG data to assess the test-retest reliability.

Results: In the 5-25 monetary gambling task, participants generally tended to choose options with larger outcomes, a tendency that became especially prominent after experiencing a large loss in a prior trial. This behavioral pattern was reflected by a good ICC index of 0.677. Regarding the Event-Related Potential (ERP) data, we observed a prominent Feedback-Related Negativity (FRN) amplitude and an attenuated P300 amplitude in loss conditions, compared to gain conditions. Moreover, our analyses revealed fair reliability for FRN (0.440-0.599), while the reliability for P300 was relatively poor (0.258-0.617). Notably, single-trial EEG analyses suggested that these feedback-sensitive FRN and P300 could predict risk propensity in subsequent trials, a finding that remained robust in the retest phase. In the mixed gambling task, subjects consistently demonstrated a preference for riskier choices, with no significant loss aversion detected in either session. While there was a general tendency to accept gambling opportunities, their inclination to do so was modest, yet exhibited good reliability across sessions (ICC = 0.701). EEG patterns were consistent with those observed in Experiment 1. The trial-wise analysis further supported these findings; specifically, outcomes eliciting increased FRN and decreased P300 amplitudes were linked to the magnitude of feedback. Additionally, more pronounced fluctuations in both FRN and P300 were observed when the Expected Value (EV) was negative, indicating a stronger neural response to anticipated losses. The reliabilities of FRN (0.707-0.719) and P300 (0.624-0.654) in response to gains and losses were good. Notably, the individual-level analysis suggested that the feedback-sensitive P300 amplitude in the 5-25 gambling task could predict the risk preference displayed in the mixed gambling task.

Conclusions: The study concludes that subjects' propensities for risk-taking remained consistent, even following a one to two-week break. The good ICC for both FRN and P300 amplitudes, in addition to their significant correlation with risk preference behaviors, suggests the potential of these electrophysiological markers to characterize risk preferences. Thus, these measures may serve as viable biomarkers to distinguish individual variations in risk preferences, applicable in both controlled laboratory conditions and real-world environments.

References

1. Korucuoglu, O. (2020), 'Test-retest reliability of fMRI-measured brain activity during decision making under risk', Neuroimage, vol. 214, no. 116759.

Poster No 895

Cortico-striatal connectivity relates to the malleability of intertemporal decisions

Yueting Su[1], Xinyu Liang[1], Deniz Vatansever[1]

[1]Fudan University, Shanghai, Shanghai

Introduction: Human decisions often involve the evaluation of outcomes at multiple timescales. Individual variation in such intertemporal decisions is suggested to rely on a cortico-striatal circuitry, which is predictive of both impulsivity and mental health symptoms[1]. However, emerging evidence also indicate a level of malleability of intertemporal choices via behavioural nudges[2], which may be reflected by interindividual differences in the macro-scale connectivity architecture of the human brain. Here, introducing pre-selected "default choice" options in an intertemporal choice paradigm, we first identify striatal regions engaged in intertemporal decisions and computationally model participants' propensity to be influenced by behavioural nudges. In a subsequent connectivity analysis at rest, we provide brain-behaviour links between individual's decision bias, connectivity profiles and ADHD symptoms.

Methods: Using an HCP-style data acquisition protocol[3], a group of 41 healthy participants (mean = 24.25 years, SD = 2.49, F/M ratio = 29/12) were scanned at 3T MRI, both at rest (AP/PA) and while performing two runs of a Nudged-Intertemporal Choice (NIT) paradigm (Fig. 1a). In the NIT task, participants were asked to make intertemporal monetary decisions between an immediate and a delayed reward option across 96 trials that included both easy and hard options. Importantly, a proportion of choices were nudged using a pre-selected "default choice" option. To assess the influence of default nudges on each individual's decision starting point (i.e. bias "z" parameter), task response data was modelled with a hierarchical Bayesian parameter estimation of the drift diffusion model[4]. Imaging data was minimally preprocessed using Qunex containerized versions of the HCP preprocessing pipelines[5]. The task fMRI data was then statistically modelled using FSL FEAT routines to contrast Intertemporal Choice versus Control conditions, corrected for individual discount rates. Significant regions of interest

from the NIT task fMRI results were used as seeds to quantify whole-brain functional connectivity via Pearson correlation. Adult ADHD Self-Report Scale (ASRS)[6] symptom scores, NIT task decision bias scores and connectivity estimates were used to assess brain-behaviour relationships. Statistical significance was estimated using non-parametric permutation testing via PALM (FDRp < .05).

Results: Behaviourally, computational modelling of NIT task responses indicated a significant effect of default nudges on the decision starting point, specifically within hard trials (p < .05) (Fig. 1b). At the neural level, the contrast of ITC > Control, revealed greater activity centered on a set of brain regions commonly associated with monetary decisions including the bilateral ventral striatum, medial prefrontal, orbitofrontal, and anterior cingulate cortices (Fig. 2a). Activated regions in the bilateral ventral striatum (VS) were selected as seed regions of interest in a subsequent resting state functional connectivity analysis, to reveal the neural circuitry associated with intertemporal decisions. The analysis showed strong VS connectivity with regions within the default mode and frontoparietal control networks (Fig. 2b). Notably, connectivity of VS to the right medial prefrontal cortex (mPFC), a region within the default mode network, positively correlated with decision bias (r = 0.59, p < .001) and was negatively linked to ASRS Inattentive sub-scores (r = .36, p = .02) (Fig. 2c).

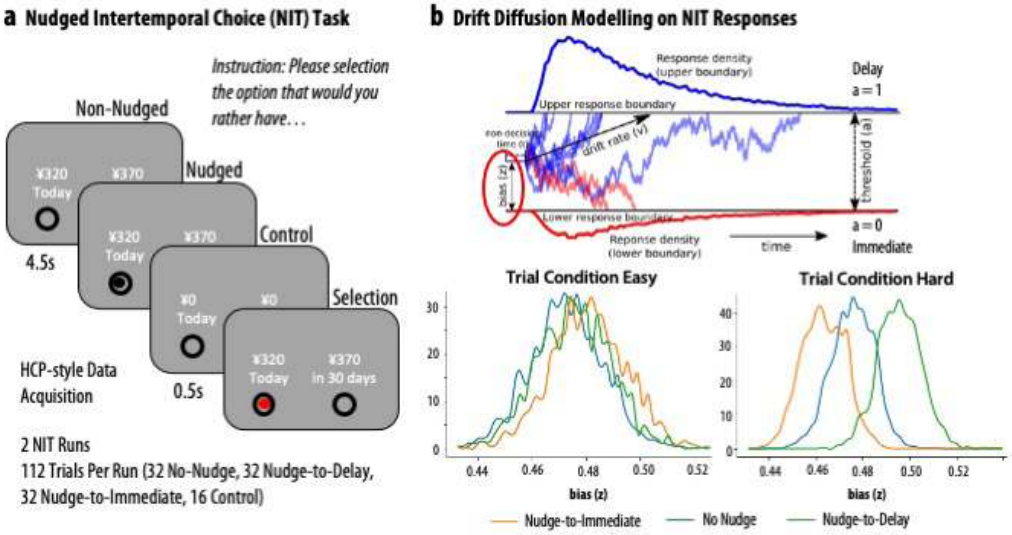

Figure 1. Influence of default nudges on intertemporal decision behavior. a. The classic intertemporal choice (ITC) paradigm was modified to introduce "default nudges" i.e. pre-selection for both smaller-immediate and larger-delayed options. Across all 112 trials, participants were given 4.5 s to make a response and their selection was highlighted with a red radio button (0.5 s). **b.** A hierarchical Bayesian drift diffusion model estimation was applied across three nudge conditions (No-Nudge, Nudge-to-Immediate, Nudge-to-Delay), separately for easy and hard trials. The decision bias (z), defined as the starting point of the binary decision-making process, was shown to be shifted by "default nudges" along the nudge direction, specifically within the hard trials (Condition Hard: Nudge-to-Immediate > No Nudge: p = 0.14, No Nudge > Nudge-to-Delay: p = 0.05, Nudge-to-Immediate > Nudge-to-Delay: p = 0.005).

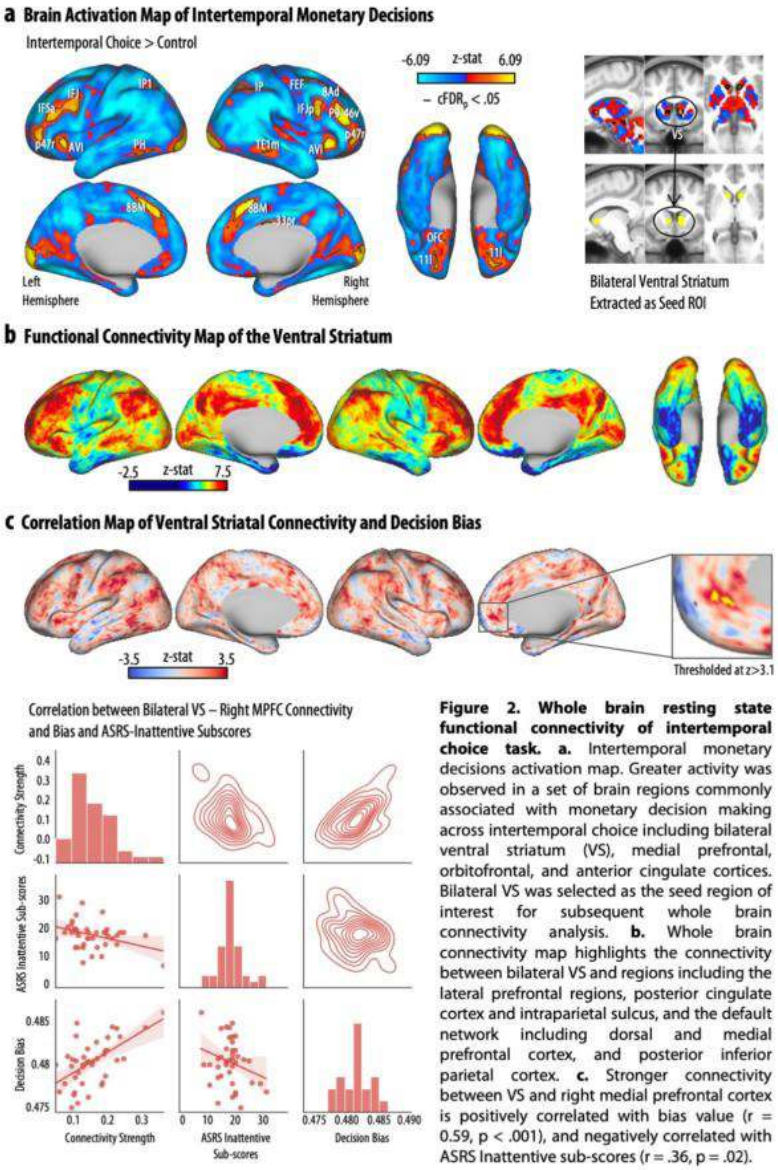

Figure 2. Whole brain resting state functional connectivity of intertemporal choice task. a. Intertemporal monetary decisions activation map. Greater activity was observed in a set of brain regions commonly associated with monetary decision making across intertemporal choice including bilateral ventral striatum (VS), medial prefrontal, orbitofrontal, and anterior cingulate cortices. Bilateral VS was selected as the seed region of interest for subsequent whole brain connectivity analysis. **b.** Whole brain connectivity map highlights the connectivity between bilateral VS and regions including the lateral prefrontal regions, posterior cingulate cortex and intraparietal sulcus, and the default network including dorsal and medial prefrontal cortex, and posterior inferior parietal cortex. **c.** Stronger connectivity between VS and right medial prefrontal cortex is positively correlated with bias value ($r = 0.59$, $p < .001$), and negatively correlated with ASRS Inattentive sub-scores ($r = .36$, $p = .02$).

Conclusions: Collectively, our results indicate that default nudges constitute an effective behavioral strategy to alter individual's intertemporal decisions. In this context, a ventral striatal – medial prefrontal cortex circuitry is highlighted to play a vital role, providing mechanistic insight on the behavioral nudging of intertemporal decisions and revealing a potential neural target for future interventions in the treatment of impulsivity disorders.

References

1. Bos, W. van den, Rodriguez, C. A., Schweitzer, J. B., & McClure, S. M. (2014), 'Connectivity Strength of Dissociable Striatal Tracts Predict Individual Differences in Temporal Discounting', Journal of Neuroscience, vol. 34, no. 31, pp. 10298–10310.
2. Lempert K., Phelps E. (2016), 'The malleability of intertemporal choice', Trends in Cognitive Sciences, vol. 20, no. 1, pp. 64-74.
3. Glasser, M. F., Smith, S. M., Marcus, D. S., Andersson, J. L. R., Auerbach, E. J., Behrens, T. E. J., Coalson, T. S., Harms, M. P., Jenkinson, M., Moeller, S., Robinson, E. C., Sotiropoulos, S. N., Xu, J., Yacoub, E., Ugurbil, K., & Van Essen, D. C. (2016), 'The Human Connectome Project's neuroimaging approach', Nature Neuroscience, vol. 19, no. 9, pp. 1175–1187.
4. Wiecki, T., Sofer, I., & Frank, M. (2013), 'HDDM: Hierarchical Bayesian estimation of the Drift-Diffusion Model in Python', Frontiers in Neuroinformatics, vol. 7.
5. Ji, J. L., Demšar, J., Fonteneau, C., Tamayo, Z., Pan, L., Kraljič, A., Matkovič, A., Purg, N., Helmer, M., Warrington, S., Winkler, A., Zerbi, V., Coalson, T. S., Glasser, M. F., Harms, M. P., Sotiropoulos, S. N., Murray, J. D., Anticevic, A., & Repovš, G. (2023), 'QuNex—An integrative platform for reproducible neuroimaging analytics', Frontiers in Neuroinformatics, vol. 17.
6. Kessler, R. C., Adler, L., Ames, M., Demler, O., Faraone, S., Hiripi, E., Howes, M. J., Jin, R., Scnik, K., Spencer, T., Ustun, T. B., & Walters, E. E. (2005), 'The World Health Organization adult ADHD self-report scale (ASRS)', Psychological Medicine, vol. 35, no. 2, pp. 245-256.

Poster No 896

Relationship of striatal and anterior insula activity with real-life investment success

Stephan Nebe[1,2], Nick Sidorenko[1,2], Alexandra Bagaïni[1,3], Steve Heinke[3], Silvia Maier[2], Alexandre Ziegler[4], Isabella Kooij[2], Kevin Trutmann[3], Thorsten Hens[4], Jörg Rieskamp[3,5], Rui Mata[3,6,5], Philippe Tobler[2,5]

*[1]Shared First-Authorship, *, [2]Department of Economics, University of Zurich, Zurich, Switzerland, [3]Department of Psychology, University of Basel, Basel, Switzerland, [4]Department of Banking and Finance, University of Zurich, Zurich, Switzerland, [5]Shared Senior-Authorship, *, [6]Max Planck Institute for Human Development, Berlin, Germany*

Introduction: As the proportion of households with stock ownership has increased over the past decades, more and more individual investors make their own investment decisions. Poor financial decisions can lead to financial insecurity, stress, and declining mental health, raising the question how more successful investors differ from less successful ones. As part of a pre-registered study on the foundations of successful financial decision making (Heinke et al., 2021), we used a newly developed investment task (Figure 1) to examine individual differences in neural markers of value and risk sensitivity and their correlation with investors' trading behavior and performance. Previous research has implicated the ventral striatum and the anterior insula in the representation of outcomes (rewards and punishments) and risk, respectively, in a neural network associated with value-based decision making. Therefore, we focused on the contribution of these two regions of interest (ROI) in our fMRI analyses.

Methods: 154 participants with a mean age of 39 years (SD=12; 9% female) participated in the MRI arm of the study. In the task, they had to repeatedly make decisions between a risky option, which was presented to them by showing the average expected outcome magnitude and volatility, and a safe option that included no risk but also had a lower outcome magnitude. Computational models of expected value, expected utility, prospect theory, and mean-variance-skewness were fitted to the behavioral data to further explore the behavioral task data. Meta-analytically generated masks of the ventral striatum and anterior insula were used as ROI for fMRI analyses of outcome value and risk, respectively.

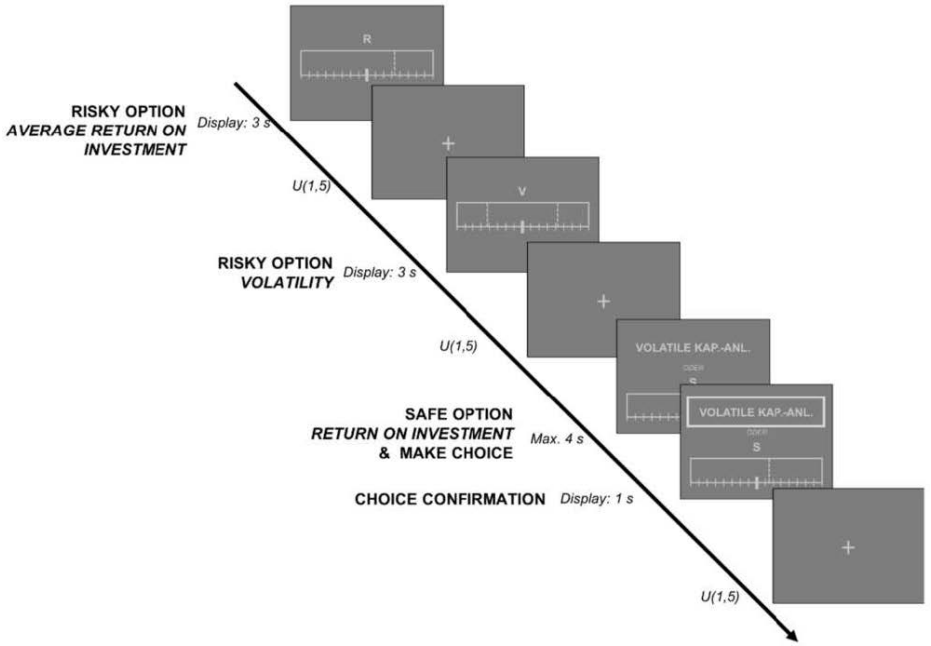

Figure 1. Trial sequence of the Investment task. Participants saw the magnitude of the risky outcome ("average return of investment") followed by the expected volatility of returns in half of the trials. In the other half, the two pieces of information were presented in reversed order to control for sequence effects. Then, participants saw the magnitude of a certain outcome ("safe option") and had to decide between the risky and safe option.

Results: A simple expected value model with no distortions of outcome value or risk showed the best fit to the behavioral data at the group level. The other three models performed comparably but required more free parameters. Note that our convenience sample consisted predominantly of active retail investors, which could explain why a simple expected value model best fitted the behavioral task data. ROI analyses testing associations between outcome magnitude and BOLD signals in the ventral striatum and between risk and BOLD signals in the anterior insula revealed weak associations. Specification curve analyses (SCA) predicting real-life trading behaviors and outcomes did not show substantial associations with individually extracted, aggregated BOLD signals from either ROI. To further investigate the relationship between activity in the predefined ROIs and key real-life trading measures, we conducted exploratory analyses. By directly contrasting BOLD

responses to outcome magnitude and risk, we aimed to identify neural activity that was more specifically associated with reward over risk and vice versa. Activations obtained with these contrasts were then extracted from ventral striatum and anterior insula for each contrast. We performed the same SCA to test the association of these exploratory neural indicators with portfolio risk, return, and performance. Activity in this striatum ROI not only showed a preferential relationship to reward over risk, but activity in voxels identified with this contrast was also significantly associated with portfolio return and variance (Figure 2).

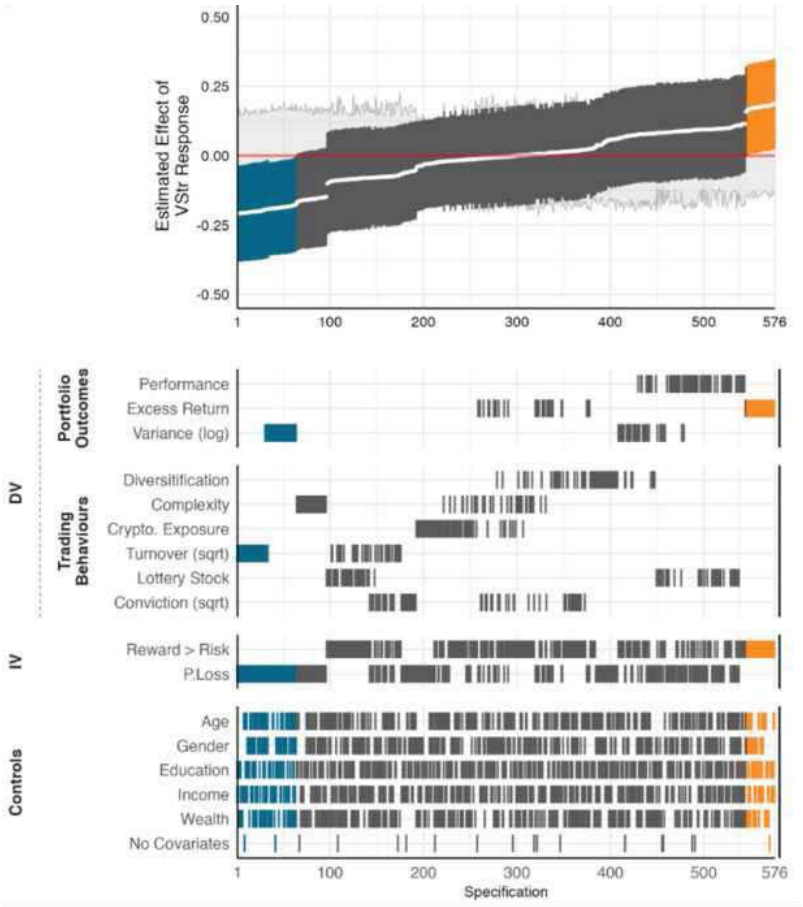

Figure 2. Results of the specification curve analysis. Reward sensitivity in the ventral striatum (VStr)was used as regressor together with the common set of covariates (i.e., age, gender, age of portfolio, wealth, income, and education; all variables were standardized). The bottom graph indicates which dependent and independent variables entered each of the model specifications. The upper graph shows the association between the independent variable of interest and the dependent variables across all implemented model specifications (sorted by effect size). The dots show the estimated effect sizes, and the vertical lines depict the 95% confidence intervals. The light gray band in the background shows the distribution of effect sizes to be expected under the null hypothesis of no effect. Blue and orange signify negative and positive effects on the dependent variable, respectively.

Conclusions: Our pre-registered analyses provided little explanatory power for real-life trading behaviors and outcomes. However, additional exploratory analyses within the same ROIs showed that ventral striatal BOLD signals with preferential relation to outcome magnitude over risk are positively associated with trading outcomes in real-life financial decisions. Thus, neural outcome sensitivity in a core region of the brain valuation system explains investment success in part. This study is to our knowledge the first demonstration that BOLD responses to outcome magnitude have predictive power for real-life trading behavior.

References

1. Heinke, S. et al., 'The Foundations of Successful Financial Decision Making.' OSF, Jun. 15, 2021. https://osf.io/w84fr

Poster No 897

Ventromedial cortex in a gambling task. Effective connectivity responses to the outcome feedback

Miroslaw Wyczesany[1], Thomas Kroker[2], Anna Lesniewska[1], Maimu Rehbein[2], Kati Roesmann[3], Ida Wessing[2], Markus Junghöfer[2]

[1]Jagiellonian University, Krakow, PL, [2]University of Münster, Münster, DE, [3]University of Siegen, Siegen, DE

Introduction: In our previous study, we were able to show that cognitive biases that are associated with decision-making (the framing effect or the gambler's fallacy) can be reduced by the offline transcranial magnetic stimulation of the ventromedial prefrontal cortex (vmPFC) in a gambling task (Kroker et al. 2022). To get better insight into the role of this structure in rational decision-making, we carried out an effective connectivity analysis of MEG responses to feedback that informs participants of gains or losses. To manipulate the activity of the vmPFC, we performed off-line transcranial magnetic stimulation of this area.

Methods: 37 subjects (age 19-29 yrs, mean 23.4; 17 women, 20 men). Each of them took part in two counterbalanced offline TMS sessions, held on different days (excitatory EX or inhibitory IN. A gambling task with a choice of either holding or losing a known sum of money or gambling for a potential higher gain was described in (Kroker et al. 2023). We analyzed 1.5-second epochs of brain responses to feedback information that marked WIN or LOSE trials. MEG signals were collected using a 275 whole-head sensor system (CTF Systems; first-order axial gradiometers). Preprocessing was based on the procedure in (Mantini et al. 2011) and further extended in (Spadone et al. 2021) using the Atlantis Connectivity Toolbox (https://atlantis.psychologia.uj.edu.pl). The signal was filtered (2–48 Hz) and screened for bad channels and artifacts. Then ICA was run, followed by automatic classification of brain and non-brain components. Brain components were then localized with the Minimum Norm Method using their weight matrices. The preselected ROIs were as follows: perigenual vmPFC (pgVM; 0 37 -13), lateral orbitofrontal cortex (L/R latOFC'; -33 32 -19 / 34 32 -19), dorsolateral PFC (L/R DL; -39 34 37 / 32 50 26), dorsal anterior cingulate (dACC'; 4 24 34), anterior insula (L/R aIns; 36 20 0 / -34 20 2), temporal pole (L/R TmpPole; -45 6 -45 / 45 16 -45). ROI signals were reconstructed a sum of IC signals in the ROI locations subjected to PCA to yield a scalar value. The resulting signals were corrected for source leakage (Colclough et al. 2015). Finally, the directional connectivity was estimated in the beta and gamma bands using the non-normalized directed transfer function in the theta, alpha and beta bands (Kaminski, Blinowska, 1991)).

Results: The main effect of session revealed a massive increase of network activity (EX>IN) of the vmPFC, OFC, DL and aIns regions. The vmPFC mostly increased its inflow, while the DL areas their outflows. Also, heightened outflows from bilateral aIns towards bilateral TmpPole were visible. The main effects of outcome was mainly seen as an increased signaling from the pgVM to the ROFC and the RTmpPole in response to LOSS feedback. Interaction effects included increased flow from the pgVM to the RaIns after the EX stimulation for GAIN feedback. Another interaction observed was a strengthened connectivity from both pgVM and RDL towards LDL after the EX stimulation in response to LOSS cues.

Conclusions: The observed effects accompany behavioral changes seen as improved rationality of choices after pgVM excitatory stimulation. The impact of stimulation on the configuration of outflows and inflows indicates the cascade of information flow between involved nodes when processing decision feedback. Two functionally separate networks can be distinguished based on connectivity data, the first one including vmPFC, OFC, and DL areas, and the second one including bilateral aIns and TmpPole regions. The observed interaction of stimulation and feedback information can be considered a neural substrate of increased sensitivity to loss signals after pgVM excitation, which may guide more efficient preparation of behavioral plans important for decision-making.

References

1. Colclough GL, Brookes MJ, Smith SM, Woolrich MW. (2015). 'A symmetric multivariate leakage correction for MEG connectomes'. NeuroImage. vol. 117, pp. 439–448
2. Kamiński MJ, Blinowska KJ. (1991). 'A new method of the description of the information flow in the brain structures'. Biological Cybernetics. vol. 65(, no. 3, pp. 203–210.
3. Kroker T, Wyczesany M, Rehbein MA, Roesmann K, Wessing I, Junghöfer M. (2022). 'Noninvasive stimulation of the ventromedial prefrontal cortex modulates rationality of human decision-making'. Scientific Reports. vol. 12, no 1, pp. 20213.
4. Kroker T, Wyczesany M, Rehbein MA, Roesmann K, Wessing I, Wiegand A, et al. (2023). 'Excitatory stimulation of the ventromedial prefrontal cortex reduces cognitive gambling biases via improved feedback learning'. Scientific Reports. vol. 13, no 1, pp. 17984.
5. Mantini D, Penna SD, Marzetti L, de Pasquale F, Pizzella V, Corbetta M, et al. (2011). 'A Signal-Processing Pipeline for Magnetoencephalography Resting-State Networks. Brain Connectivity' Brain Connectivity vol. 1, no. 1, pp. 49–59.
6. Spadone S, Wyczesany M, Della Penna S, Corbetta M, Capotosto P. 'Directed flow of beta band communication during reorienting of attention within the dorsal attention network'. Brain connectivity. vol. 11, no. 9, pp. 717–72

Poster No 898

Identifying the Outliers: Insights from the Reanalysis of Tom et al.(2007) and Botvinik-Nezer (2020)

Chun-Chia Kung[1], Hanshin Jo[1], Le-Si Wang[1]

[1]National Cheng Kung University, Tainan, Taiwan

Introduction: One of the prominent news of the year 2020's fMRI circle (2019~20) was the NARPS project (and the 2020 Nature paper), inviting 71 labs to co-analyze the same dataset (ds001734), as a registered replication of the original Tom et al. (2007 Science) study (ds005). The results, as was revealed in the Nature2020 paper, were a startling discrepancy: only 1 out of the 9 registered hypotheses was supported by the majority of the analysis teams. While the Nature2020 paper focused on the influences of the varieties of preprocessing pipelines among labs, the reasons for the discrepant fMRI results were still unclear. To find out, in the course of three fMRI graduate courses (2019 Spring, 2020 Fall, and 2023 Summer), the teacher and the students co-analyzed two then-released fMRI raw data from openneuro.org (ds005 and ds001734), with identical analysis pipelines, to dig further into this puzzle.

Methods: The fMRI preprocessings were done with spm12, and the parametric modulation (both positive and negative) of group-wise GLM was applied by neuroelf under Matlab.

Results: We successfully replicated two studies with comparable results (qualitative evaluation). Furthermore, the number-matched comparisons (e.g., randomly picking 16 out of the odd-numbered 54 subjects, and comparing with the Tom07 N=16, for 1000 times), also showed that the 4 hypothesized ROIs (Caudate, Insula, Amygdala, and mPFC) were mostly different. Along with the final leave-one-subject-out cross-validation ROI multi-voxel pattern analysis (MVPA), which showed only 6-9 subjects that were more different from the remaining 10-7 subjects.

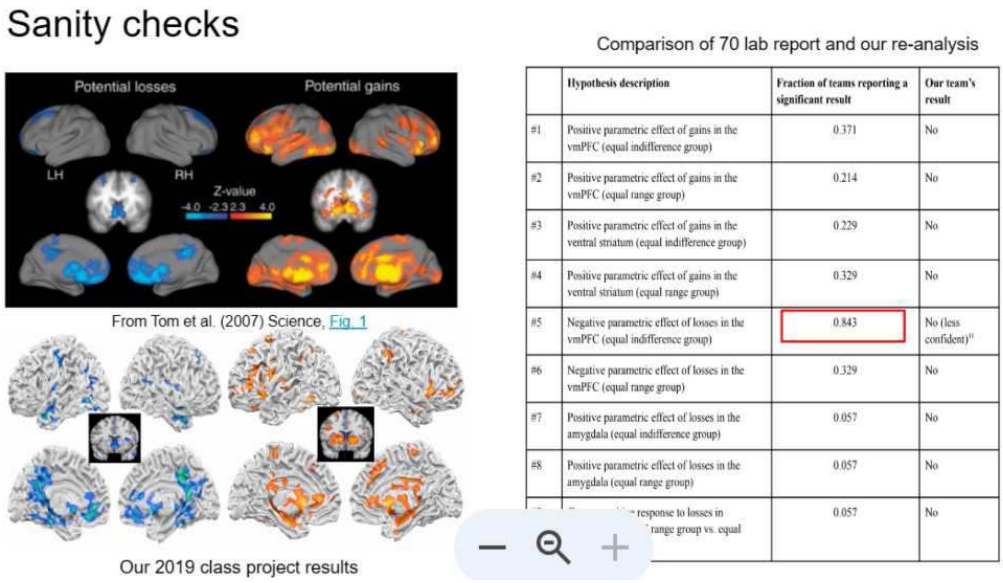

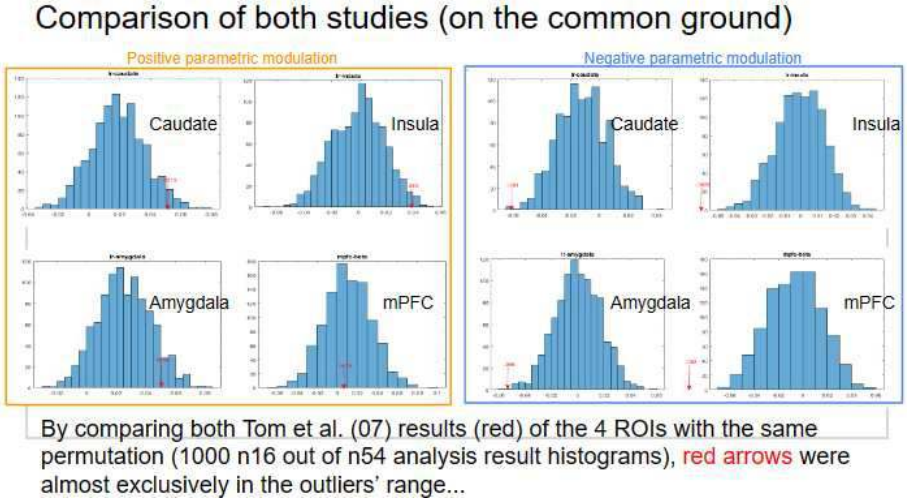

Conclusions: It was probably not the analysis package difference, nor were all the 16 UCLA subjects, as the primary reason for the resulting discrepancy. Rather, it was due more to a few outliers that resulted in the main difference. Taken together, these findings lend further support to the 'law of small numbers': that extreme results are more likely to happen in small-sample studies.

References

1. Tom, S. M., Craig R. Fox, Christopher T, and R. A. Poldrack. 2007. "The Neural Basis of Loss Aversion in Decision-Making under Risk." Science 315 (5811): 515–18.
2. Botvinik-Nezer, R, Holzmeister, F., Camerer, C. F., Dreber, A., Huber, J. Johannesson, M. Kirchler, M., et al. 2020. "Variability in the Analysis of a Single Neuroimaging Dataset by Many Teams." Nature 582 (7810): 84–88.

Poster No 899

Neural Mechanisms Underlying Enhanced Episodic Memory for Drug Associations in Smokers

Jeung-Hyun Lee[1], Maria Jieun Hwang[1], Sang Ah Lee[2], Woo-Young Ahn[1]

[1]Seoul National University, Seoul, Korea, Republic of, [2]Seoul National University, Gwanak-gu, Seoul

Introduction: Episodic memory plays a crucial role in drug-associated decisions (Bornstein & Pickard, 2020; Goldfarb et al., 2020). Drug experiences, including spatial context and emotions linked to drug consumption are encoded and retrieved to induce craving and impulse to smoke. While literature suggests that it is a major contributor to relapse in smokers (Janes et al., 2015), the link between retrieval of drug-associated memories and smoking choice remains unclear. The current study aimed to (1) test if smokers show enhanced memory accuracy for smoking-related associations and (2) investigate the neural correlates of the link.

Methods: Forty-three smokers participated in the protocol of visiting the lab for two consecutive days (Lee et al., 2023). On Day 1, participants formed associations between visual stimuli of smoking/neutral items and sceneries. On Day 2 (24 hours later), participants were exposed to an acute laboratory-based stressor (socially evaluated cold pressor test, SECPT, Schwabe & Wolf, 2013) or a matched control condition. Then, participants recognized a specific item given its associated place and rated preference of all the stimuli during fMRI scanning. We distinguished the accuracy of memory into specific (i.e., precisely correct) or gist (i.e., lure items with similar content) categories. Three participants did not take part in the fMRI scanning due to claustrophobic symptoms, 5 participants were rejected due to excessive head motion, and 8 participants were removed from the analysis due to technical issues. In total, 27 participants (Stress group=17, Control group=10) were included in the following analyses.

Results: Behavior analysis confirmed that smokers showed a significantly better performance in memory retrieval of smoking-related associations, compared to neutral associations ($F(1, 94)=4.68$, $p=0.03$, Figure A). The insula and the left dorsomedial prefrontal cortex (dmPFC) were activated during memory retrieval with the [smoking vs neutral] contrast ($p<0.001$, uncorrected, Figure B, left). The precuneus was activated during preference rating with the [smoking vs neutral] contrast ($p<0.001$, uncorrected, Figure B, right). Here, the beta values from the precuneus were positively correlated with correct retrieval of smoking associations and the mean confidence level (Figure C).

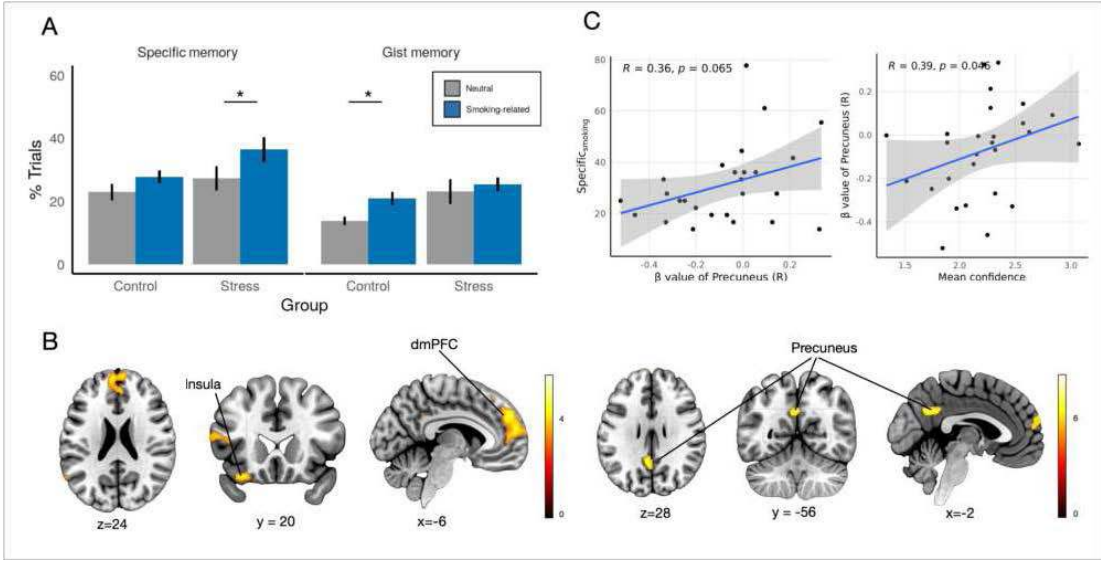

Conclusions: The findings demonstrate that smokers exhibit enhanced episodic memory performance for smoking-related associations. Moreover, fMRI results suggest that regions involved in valuation (e.g., the mPFC and the insula) and self-referential processing (e.g., the precuneus) play a key role in retrieving smoking-related associations.

References

1. Bornstein AM, Pickard H. (2020), "Chasing the first high": memory sampling in drug choice, Neuropsychopharmacology. 45(6), pp. 907–915.
2. Goldfarb EV, Fogelman N, Sinha R. (2020), Memory biases in alcohol use disorder: enhanced memory for contexts associated with alcohol prospectively predicts alcohol use outcomes. Neuropsychopharmacology. 45(8), pp. 1297–1305.
3. Janes AC, Ross RS, Farmer S, et al. (2015). Memory retrieval of smoking-related images induce greater insula activation as revealed by an fMRI-based delayed matching to sample task. Addiction Biology, 20(2), pp. 349–356.
4. Lee JH, Kang S, Maier SU, Lee SA, Goldfarb EV, Ahn WY. (2023). Acute Stress Enhances Memory and Preference for Smoking-Related Associations in Smokers, Nicotine & Tobacco Research.
5. Schwabe L, Wolf OT. (2013). Stress and multiple memory systems: from "thinking" to "doing", Trends in Cognitive Science, 17(2), pp. 60–68.

Poster No 900

Differential Roles of Intraparietal Sulcus and pre-Supplementary Motor Area in Intertemporal Choice

Gizem Vural[1,2], Natasha Katruss[3], Alexander Soutschek[4]

[1]LMU Klinikum, Munich, Other, [2]General and Experimental Psychology Ludwig-Maximilians-University, Munich, Germany, [3]Department of Psychology/Neuro-Cognitive Psychology of the Ludwig-Maximilians-Universität München, Munich, Germany, [4]Ludwig Maximilian University, Munich, Germany

Introduction: The ability to delay gratification in intertemporal decision-making involves complex neural mechanisms that have not been fully elucidated. While most previous research focused on the role of the prefrontal control network for intertemporal decisions, our study investigated the roles of the pre-supplementary motor area (pre-SMA) and the posterior parietal cortex (PPC), two regions that were neglected by past research, for the decision process. Specifically, we used time-locked transcranial magnetic stimulation (TMS) in combination with a process model of intertemporal decision making (drift diffusion model, DDM) to investigate the contributions of the pre-SMA and the PPC to early versus late components of the choice process.

Methods: The study enrolled 32 participants (mean age: 26, including 16 females) in a within-subject design, involving two experimental conditions as early and late phase of TMS along with no stimulation condition as a control. Before the experimental session, a Siemens Prisma 3-Tesla MRI scanner (Siemens AG, Munich, Germany) was used to acquire structural scans for identifying the targeted brain regions. The Brainsight neuronavigation software (Rogue Research Inc.) was then utilized to position the PowerMAG ppTMS stimulator, which is equipped with a flat, figure-eight PowerMAG double coil PMD70 (2 x 70mm diameter) (MAG & More). To manipulate early components of the decision process, early TMS was administered 100 ms after stimulus presentation. In contrast, late TMS was tailored to each participant's median decision times from previous decisions to target the evidence accumulation process. This approach allows for a precise examination of the early and late components of decision-making processes in the pre-SMA and PPC during the intertemporal decision-making task. In the decision task, participants made choices between smaller-sooner (SS) and larger-later (LL) monetary rewards delivered after varying temporal delays.

Results: Analyses of the binary choice data (without considering the choice process) revealed a weaker preference for LL over SS rewards (stronger temporal discounting) following late-phase TMS of the pre-SMA. In contrast, early pre-SMA TMS reduced choice consistency rather than temporal discounting per se. However, these standard analyses do not provide insights into which subcomponents of the decision process underlie the observed TMS effects. An analysis of the decision process with a hierarchical DDM indicated that early pre-SMA TMS reduced the influence of reward magnitudes on evidence accumulation. This informs the findings from the choice consistency analyses by suggesting that less consistent choices in the early pre-SMA TMS condition result from a weaker representation of rewards in the decision-making process. Disruption of the PPC via both early and late TMS induced a tendency towards quicker, less cautious decision-making, implying a rise in rapid and impulsive choices compared to the control condition. Notably, the PPC stimulation did not significantly alter reward or delay drift rates, indicating its limited impact on the evidence accumulation process.

Conclusions: The application of TMS to the pre-SMA disrupted both the preference for delayed rewards and choice consistency, leading to more impulsive decision-making favoring immediate gratification. The lower choice consistency can be explained by altered reward valuation during evidence accumulation. Conversely, PPC stimulation appears to affect the speed of decision-making without compromising the evidence accumulation process or altering the initial decision-making

bias. Together, these findings contribute to our understanding of the neurobiological underpinnings of decision-making, highlighting the distinct roles of the pre-SMA and PPC in mediating the trade-off between immediate and delayed rewards.

References
1. Soutschek, A. (2023), "Toward a unifying account of dopamine's role in cost-benefit decision making", Biological Psychiatry Global Open Science, 3(2), 179-186.

Poster No 901

Neural Activation Differences Relative to Nursing Experience during Multitasking: A VR-fMRI Study

Koki Ono[1], Kelssy Hitomi dos Santos Kawata[1], Wey Guan Lem[1], Shoichiro Amari[1], Mihoko Sasaka[2], Kimikazu Kashiwagi[3], Hiroshi Oyama[1]

[1]The University of Tokyo, Tokyo, Japan, [2]Tokyo Ariake University of Medical and Health Sciences, Tokyo, Japan, [3]National College of Nursing, Japan, Tokyo, Japan

Introduction: Novice nurses frequently encounter difficulties in multitasking due to the discrepancy between the educational training they received as students and the reality of practical clinical setting demands[1]. Previous neuroscience studies in related medical fields, such as surgery, have found that as a surgeon's technical skills increase, there is decreased brain activity in the anterior cingulate cortex (ACC)[2]. The ACC is broadly divided into areas involved in behavior monitoring and behavioral regulation, social cognition, and emotion, particularly in humans. The multitasking capability of nurses in clinical settings may be associated with the behavioral monitoring and behavioral regulation functions of the ACC. While it is established that clinical experience enhances a nurse's multitasking capability[3], the specific neural mechanisms that support a nurse's capacity to understand the situation and prioritize actions remain unclear. We hypothesized that the ACC, which monitors the consequences of actions and mediates subsequent changes in behavior[4], would respond to multitasking within a simulated Immersive Virtual Reality (IVR) clinical setting differently for nursing students compared to experienced nurses.

Methods: The study involved 15 final-year nursing students without clinical experience and 11 experienced nurses with a minimum of five years working in clinical practice. Participants engaged in a First-Person Perspective (1PP) IVR multitasking scenario designed to simulate a high-pressure nursing environment which required understanding the situation and prioritizing actions. The 1PP IVR multitasking experience tasked nurses with simultaneously addressing a patient's call for assistance and observing another patient displaying signs of distress. Participants had to understand the context and choose among three decision options with varying degrees of appropriateness and were scored accordingly (maximum score = 2). A Wilcoxon rank-sum test was performed to compare the difference in the 1PP IVR multitasking experience scores between nursing students and experienced nurses. The participants' brain activity was measured via functional magnetic resonance imaging (fMRI) before and after the 1PP IVR multitasking scenario. During the fMRI scanning, participants were instructed to listen to the auditory content of the 1PP IVR multitasking scenario to mentally re-engage their understanding and decision-making process of the multitasking task they experienced earlier. Participants were required to verbally provide their response as to which decision option they thought to be most appropriate while in the fMRI. Neural activation was examined using one-sample t-tests (post > baseline), with age, sex, and intelligence quotient via the Japanese Adult Reading Test score as covariates, applying an uncorrected p-value of < 0.005 for the cluster-forming threshold and a FWE-corrected threshold p-value of < 0.05 for cluster extent. Ethical approval was obtained from The University of Tokyo Research Ethics Committee (2019107NI).

Results: No significant difference in the 1PP IVR multitasking scenario score was observed between the nursing students (mean = 1.27, SD = 0.59) and experienced nurses (mean = 1.55, SD = 0.52). However, although both groups may have reached the same decision option, fMRI results showed that a significant activation was observed in the right ACC only for nursing students. As activity in the ACC is known to increase with uncertainty during evidence accumulation[5], these results suggest that nursing students experienced and utilized a different control demand strategy during the multitasking scenario compared to experienced nurses.

Conclusions: These insights into the neural basis of clinical multitasking may contribute to the development of targeted educational interventions aimed at bridging the gap between theoretical knowledge and practical clinical skills for nurses.
This work was supported by JSPS KAKENHI Grant Number JP20H00558.

References
1. Imai, T. (2021), 'Factors That Lead to Errors While Multitasking in Newly Graduated Nurses Simultaneously Caring for More Than One Patient: Analyzing the Interview Data of Newly Graduated Nurses Using the KJ Method', Journal of Japan Society of Nursing Research, vol. 44, no. 2, pp. 195–209

2. Leff, D. R. (2008), 'Could Variations in Technical Skills Acquisition in Surgery Be Explained by Differences in Cortical Plasticity?', Annals of Surgery, vol. 247, no. 3, pp. 540–543
3. Hoffman, K. A. (2009), 'A comparison of novice and expert nurses' cue collection during clinical decision-making: Verbal protocol analysis', International Journal of Nursing Studies, vol. 46, no. 10, pp. 1335–1344
4. Allman, J. M. (2001), 'The Anterior Cingulate Cortex', Annals of the New York Academy of Sciences, vol. 935, no. 1, pp. 107–117
5. Stern, E. R. (2010), 'Updating Beliefs for a Decision: Neural Correlates of Uncertainty and Underconfidence', Journal of Neuroscience, vol. 30, no. 23, pp. 8032–8041

Poster No 902

Towards interoception as a transdiagnostic biomarker of health-harming disorders

Micah Allen[1], Francesca Fardo[2], Leah Banellis[3], Malthe Brændholt[3], Niia Nikolova[3]

[1]Aarhus University, Lystrup, Denmark, [2]Aarhus University, Aarhus, Denmark, [3]Aarhus University, Aarhus, DK

Introduction: Interoception, the process of sensing, monitoring, and regulating our internal, homeostatic rhythms, is experiencing a renaissance in neuroscience. Recent advancements in systems neuroscience and neurobiology are uncovering specific, and at times surprising, mechanisms of brain-body interaction. For instance, we've discovered that multi-organ interoceptive axes influence a broad range of brain processes, from global neural oscillations to domain-specific computations. However, our progress in integrating these insights has been hampered by methodological constraints in measuring interoception in humans. To address this, we've developed various computational and psychophysical tools to assess interoception across gastric, cardiac, and respiratory axes. In my talk, I'll share findings from our Visceral Mind Project, a comprehensive dataset of 530 participants, encompassing brain, body, mental health, and psychophysiological measures.

Methods: In my presentation, I will present data from the Visceral Mind Project (VMP), a large-scale brain biobank with 530 participants, collected in Aarhus, Denmark. The VMP dataset offers comprehensive profiles that index various cognitive domains, with a special focus on computational indices of multi-modal predictive processing, affect, and interoception. It includes extensive mental health symptom inventories, lifestyle and well-being assessments, alongside numerous cognitive tasks paired with physiological measures such as respiration, pulse, and ECG. The brain imaging component of the VMP is particularly rich, featuring quantitative MRI maps that detail cortical myelination and iron concentration using R2*, MT, and R1 mapping. Functional MRI and MEG data is also included, covering resting state, task-based, and naturalistic movie-watching conditions, complemented by a range of physiological measures such as electrogastrography, respiration, electrodermal response, pupillometry, and blood inflammatory markers. Additionally, we have gathered detailed interoceptive sensitivity and metacognition profiles for all participants using our validated Bayesian psychophysical approach.

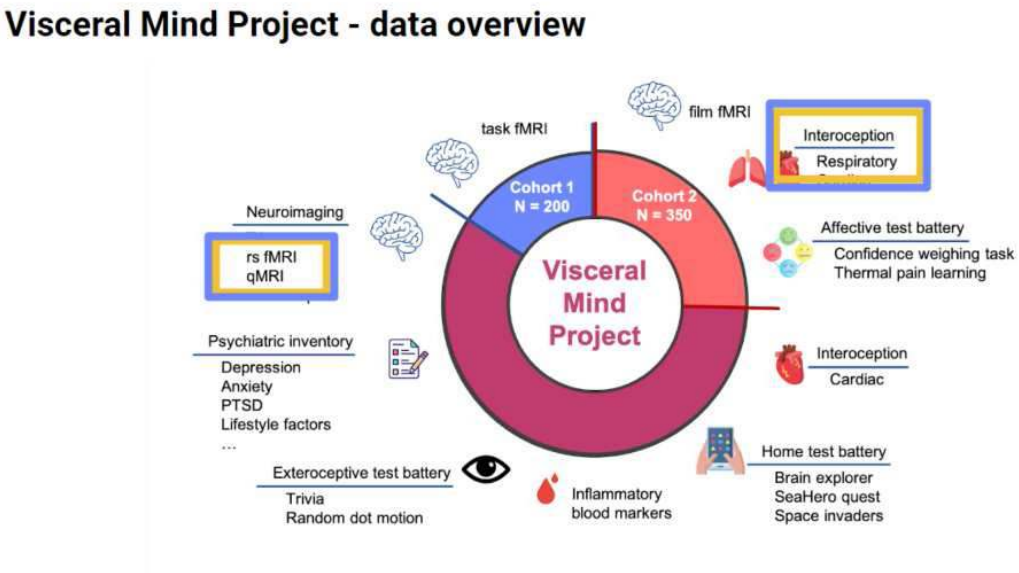

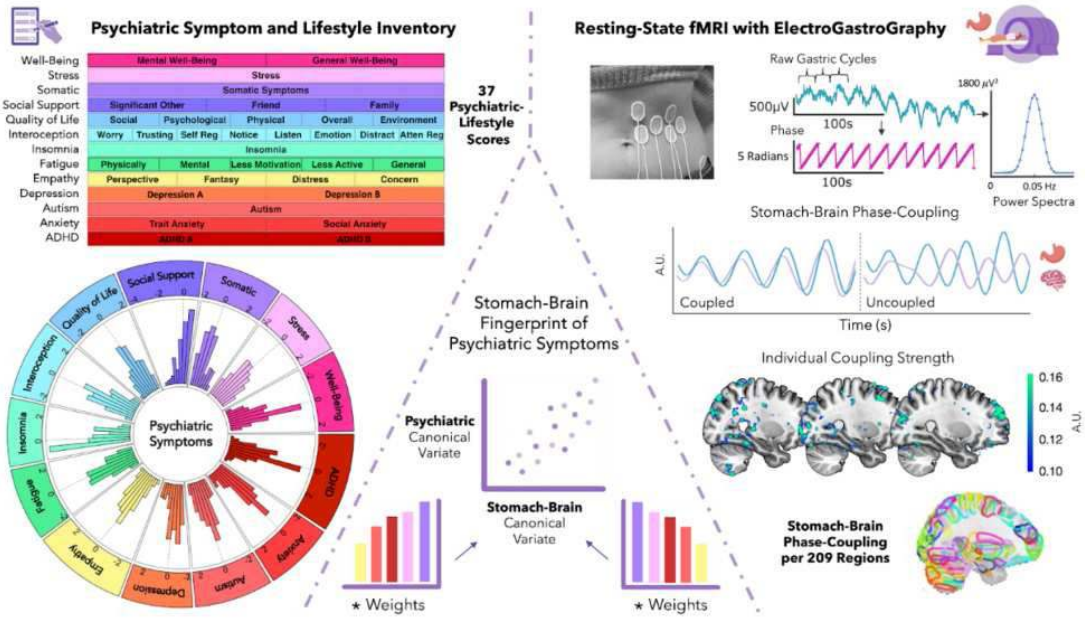

Results: My presentation will explore three sets of results derived from the VMP dataset: 1. Cortical Markers of Respiratory Interoception and Metacognition: Here, we've used whole-brain voxel-based quantification techniques to identify brain-behavior biomarkers associated with respiratory interoception. This involves mapping out the cortical areas that are active in sensing and understanding the body's respiratory signals and their role in cognitive processes. 2. Psychiatric Symptom Fingerprints in the Stomach-Brain Axes: We've employed cross-validated canonical correlation analyses to pinpoint a robust biomarker of stomach-brain coupling. This biomarker is significant for its ability to index mental health symptoms, offering new insights into the complex relationship between gastrointestinal processes and psychiatric conditions. 3. Computational Modelling of Respiratory-Brain Interactions: Using hierarchical drift diffusion modelling, we've explored how respiratory rhythms influence neural gain during perceptual processing. This approach sheds light on the intricate ways respiratory patterns can impact brain function, particularly in the context of perception. .

Conclusions: The VMP represents a major milestone in the cognitive and computational neuroscience of interoception and brain-body interaction. The project has enabled us to develop a variety of open-source tools for quantifying these domains, and offers the community with both a unique data library and set of tools for engaging with it. Our findings underscore the importance of brain-body interaction for mental and health-harming disorders and points towards new computational theories of interoception.

References

1. Allen, M. (2020). Unravelling the Neurobiology of Interoceptive Inference. Trends in Cognitive Sciences.
2. Allen, M. (2023). The Tell-Tale Heart: Interoceptive Precision and Ecological Fear Experiences. PsyArXiv. https://doi.org/10.31234/osf.io/ngamx
3. Allen, M., Levy, A., Parr, T., & Friston, K. J. (2022). In the Body's Eye: The computational anatomy of interoceptive inference. PLOS Computational Biology, 18(9), e1010490. https://doi.org/10.1371/journal.pcbi.1010490
4. Allen, M., Varga, S., & Heck, D. H. (2022). Respiratory rhythms of the predictive mind. Psychological Review. https://doi.org/10.1037/rev0000391
5. Legrand, N., & Allen, M. (2022). Systole: A python package for cardiac signal synchrony and analysis. Journal of Open Source Software, 7(69), 3832.
6. Legrand, N., Nikolova, N., Correa, C., Brændholt, M., Stuckert, A., Kildahl, N., Vejlø, M., Fardo, F., & Allen, M. (2022). The heart rate discrimination task: A psychophysical method to estimate the accuracy and precision of interoceptive beliefs. Biological Psychology, 168, 108239. https://doi.org/10.1016/j.biopsycho.2021.108239
7. Luettich, A., Sievers, C., Alfaro Almagro, F., Allen, M., Jbabdi, S., Smith, S. M., & Pattinson, K. T. S. (2023). Functional connectivity between interoceptive brain regions is associated with distinct health-related domains: A population-based neuroimaging study. Human Brain Mapping, 44(8), 3210–3221. https://doi.org/10.1002/hbm.26275
8. Nikolova, N., Harrison, O., Toohey, S., Brændholt, M., Legrand, N., Correa, C., Vejlø, M., Jensen, M. S., Fardo, F., & Allen, M. (2022). The respiratory resistance sensitivity task: An automated method for quantifying respiratory interoception and metacognition. Biological Psychology, 170, 108325. https://doi.org/10.1016/j.biopsycho.2022.108325
9. Schoeller, F., Horowitz, A., Maes, P., Jain, A., Reggente, N., Christov-Moore, L., Trousselard, M., Klein, A., Barca, L., Pezzulo, G., Allen, M., Adrien, V., Miller, M., Salomon, R., Riva, G., DiLernia, D., Tsakiris, M., Verdonk, C., Chalah, M. A., ... Friston, K. (2022). Interoceptive technologies for clinical neuroscience. PsyArXiv. https://doi.org/10.31234/osf.io/sqr6z

Poster No 903

Neural predictors of risky choice replicate and generalize within and beyond the laboratory

Leili Mortazavi[1], Charlene Wu[2], Elnaz Ghasemi[1], Brian Knutson[3]

[1]Stanford University, Stanford, CA, [2]Toyota Research Institute, Palo Alto, CA, [3]Stanford University, Palto Alto, CA

Introduction: Neuroimaging researchers can currently use neural activity to predict risky choice in humans but consensus on underlying mechanisms has remained elusive (Knutson & Huettel, 2015). Recently, the replicability and generalizability of neuroimaging findings have additionally been questioned (Marek et al., 2022). Thus, identifying and optimizing neural predictors of risky choice requires verifying integrity of both neural and behavioral measures. Risky gambles minimally require balancing potential positive against negative uncertain outcomes. Dissociation of anticipatory choice processes from sensory input and motor output might identify the most generalizable predictors of risky choice. Thus, we combined a temporally staged task with converging analyses to localize neural predictors of risky choice in humans in three steps. First, we applied Volume-Of-Interest (VOI) and whole-brain analyses to functional MRI data in an original dataset, followed by replication in an independent sample and generalization to two additional samples using a different task. Second, we tested whether identified neural predictors could be dissociated from sensory and motor correlates of risky choice. Third, we investigated whether neural predictors of risky choice could predict individual differences in risk preferences within and beyond the laboratory.

Methods: In the original sample (N=75; age: 26±7; 25 female), healthy subjects chose between gambles and a safe option while being scanned with FMRI (optimized for detection of subcortical activity; Srirangarajan et al., 2021). Multivariate prediction of trial-by-trial risky choice was derived from pre-choice activity (2s) in three predicted VOIs (i.e., in the Nucleus Accumbens (NAcc), Anterior Insula (AIns) and Medial PreFrontal Cortex (MPFC)) or across the whole brain using Support Vector Machines with Recursive Feature Elimination (SVM-RFE). Each analysis was first conducted on the original dataset. After optimizing processing steps and model parameters, identical preprocessing and modeling procedures were applied to raw data from previously published samples using the same task (N=32; age: 52±20; 17 female; Leong et al., 2016) or a different risky choice task (N=15; Tom et al., 2007; N=108; Botvinik-Nezer et al., 2020).

Results: Across four samples (total N=230) and two tasks, NAcc pre-choice activity robustly predicted risk-seeking choices but AIns activity predicted risk-averse choices. These predictive patterns recurred in both VOI-based and whole-brain analyses. As predicted, analysis of the original sample with SVM-RFE recovered features consistent with a triple dissociation (Figure 1a-b), in which visual cortex activity classified spatial position of the risky gamble, mesolimbic activity classified upcoming risky choice, and motor cortex activity classified laterality of the button press response (Figure 1c). Across individuals, NAcc activity did not correlate with risk preferences (Rho=−0.11, p=.36) but MPFC activity was associated with risk seeking (Rho=0.39, p=.0008), and AIns activity was associated with risk aversion (Rho=−0.24, p=.034). Further, individual differences in AIns activity during presentation of negatively-skewed gambles was associated with less real-world debt (Rho=−0.39, p=.034).

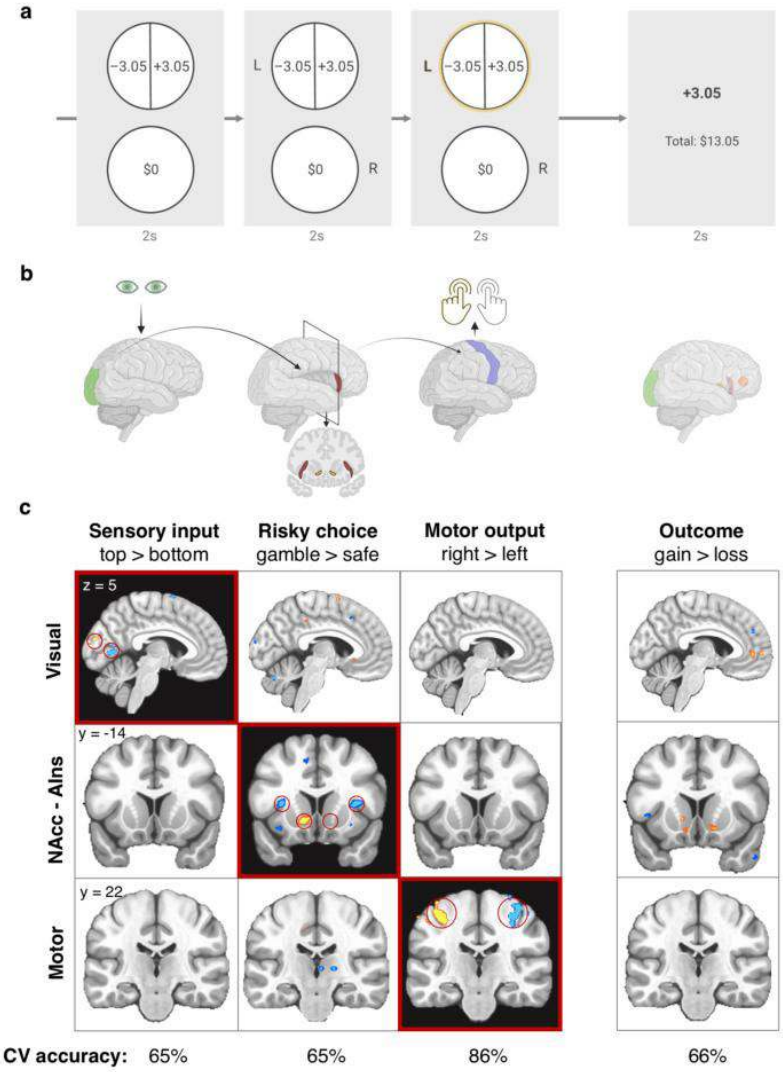

Figure 1. Triple dissociation demonstrating the specificity of neural predictors of risky choice from sensorimotor correlates involving option visualization and choice execution.

Conclusions: This work demonstrates not only that neural predictors of risky choice can be dissociated from sensorimotor components, but also that these predictors replicate across samples, generalize to other similar risky choice tasks, and hold some validity for explaining risk preferences both within and beyond the laboratory. Theoretically, the findings help resolve a persistent neuroeconomic question by indicating that two opposing anticipatory affective signals drive risk seeking versus risk avoidance. Practically, the findings also highlight a generalizable set of features for predicting risky choice in humans, and for causally manipulating neural targets in other species.

References

1. Botvinik-Nezer, R., Holzmeister, F., Camerer, C. F., Dreber, A., Huber, J., Johannesson, M., Kirchler, M., Iwanir, R., Mumford, J. A., Adcock, R. A., Avesani, P., Baczkowski, B. M., Bajracharya, A., Bakst, L., Ball, S., Barilari, M., Bault, N., Beaton, D., Beitner, J., … Schonberg, T. (2020). Variability in the analysis of a single neuroimaging dataset by many teams. Nature, 582(7810), Article 7810. https://doi.org/10.1038/s41586-020-2314-9
2. Knutson, B., & Huettel, S. A. (2015). The risk matrix. Current Opinion in Behavioral Sciences, 5, 141–146. https://doi.org/10.1016/j.cobeha.2015.10.012
3. Leong, J. K., Pestilli, F., Wu, C. C., Samanez-Larkin, G. R., & Knutson, B. (2016). White-Matter Tract Connecting Anterior Insula to Nucleus Accumbens Correlates with Reduced Preference for Positively Skewed Gambles. Neuron, 89(1), 63–69. https://doi.org/10.1016/j.neuron.2015.12.015
4. Marek, S., Tervo-Clemmens, B., Calabro, F. J., Montez, D. F., Kay, B. P., Hatoum, A. S., Donohue, M. R., Foran, W., Miller, R. L., Hendrickson, T. J., Malone, S. M., Kandala, S., Feczko, E., Miranda-Dominguez, O., Graham, A. M., Earl, E. A., Perrone, A. J., Cordova, M., Doyle, O., … Dosenbach, N. U. F. (2022). Reproducible brain-wide association studies require thousands of individuals. Nature, 603(7902), Article 7902. https://doi.org/10.1038/s41586-022-04492-9
5. Srirangarajan*, T., Mortazavi*, L., Bortolini, T., Moll, J., & Knutson, B. (2021). Multi-band FMRI compromises detection of mesolimbic reward responses. NeuroImage, 244, 118617. https://doi.org/10.1016/j.neuroimage.2021.118617
6. Tom, S. M., Fox, C. R., Trepel, C., & Poldrack, R. A. (2007). The Neural Basis of Loss Aversion in Decision-Making Under Risk. Science, 315(5811), 515–518. https://doi.org/10.1126/science.1134239

Poster No 904

Single-Trial EEG Analysis of Age-Related Differences in Model-Based Learning

Yangchu Huang[1], Shanshan Zhen[1]

[1]*Department of Social and Behavioural Sciences, City University of Hong Kong, Hong Kong, China*

Introduction: Planning in a mental model of the world to guide goal-directed decisions can be computationally demanding (Kool et al., 2018). Due to the limited cognitive resources, older adults tend to rely more on habitual, model-free learning systems than younger adults (Eppinger et al., 2013). Recent studies suggest that this tendency may stem from age-related deficits in representing a cognitive map (Bolenz et al., 2019; Ruel et al., 2023), the foundation of model-based learning systems (Vikbladh et al., 2019). However, since previous studies used practice and detailed instructions to help participants understand the task structure, it remains unclear whether older adults have difficulty constructing a cognitive map from scratch. Here, we investigate the reinforcement learning (RL) process of both older and younger adults, aiming to explore whether there are age-related differences in model-based learning, specifically in how the probabilistic task structure is acquired and the corresponding neural representation.

Methods: 57 younger adults (from 18 to 31, M=21.46, SD=2.62) and 62 older adults (from 61 to 83, M=68.94, SD=5.06) performed a sequential two-choice Markov decision task (Fig. 1A, adapted from Gläscher et al., 2010). Among them, concurrent EEG data were recorded from 38 younger adults and 39 older adults. The experiment comprised three sessions (lower panel of Fig. 1A). Both Session 1 and Session 3 consisted of 80 trials each. We first analyzed second-stage reaction times (RT) to examine whether participants acquired the knowledge of state transitions in Session 1 and 3. Longer reaction times following rare transitions (0.3) in contrast to common transitions (0.7) imply that participants have acquired state knowledge (Seow et al., 2021). To unfold the learning process, we fitted the choice data of both Session 1 and 3 to the modified HYBRID model built upon prior work (Gläscher et al., 2010; Oguchi et al., 2023) using a hierarchical Bayesian approach. The current model described the mix of model-free and model-based learning using separate model-based weight parameters, w1 for the first half (1-40 trials) and w2 for the second half (41-80 trials) of Session 3. The model also included model-based and model-free learning rate parameters, deciding the learning speed of model-based and model-free learning. Inverse temperature parameters were defined to control the degree of exploitation. To investigate the underlying neural dynamics, we performed multiple linear regression of single-trial EEG data. The stimuli-locked ERP was expected to covary with trial-by-trial state prediction error (SPE) signals derived from the HYBRID model. In Session 1, we only considered SPE as the predictor, whereas in Session 3, we included both reward prediction error (RPE) signals and SPE.

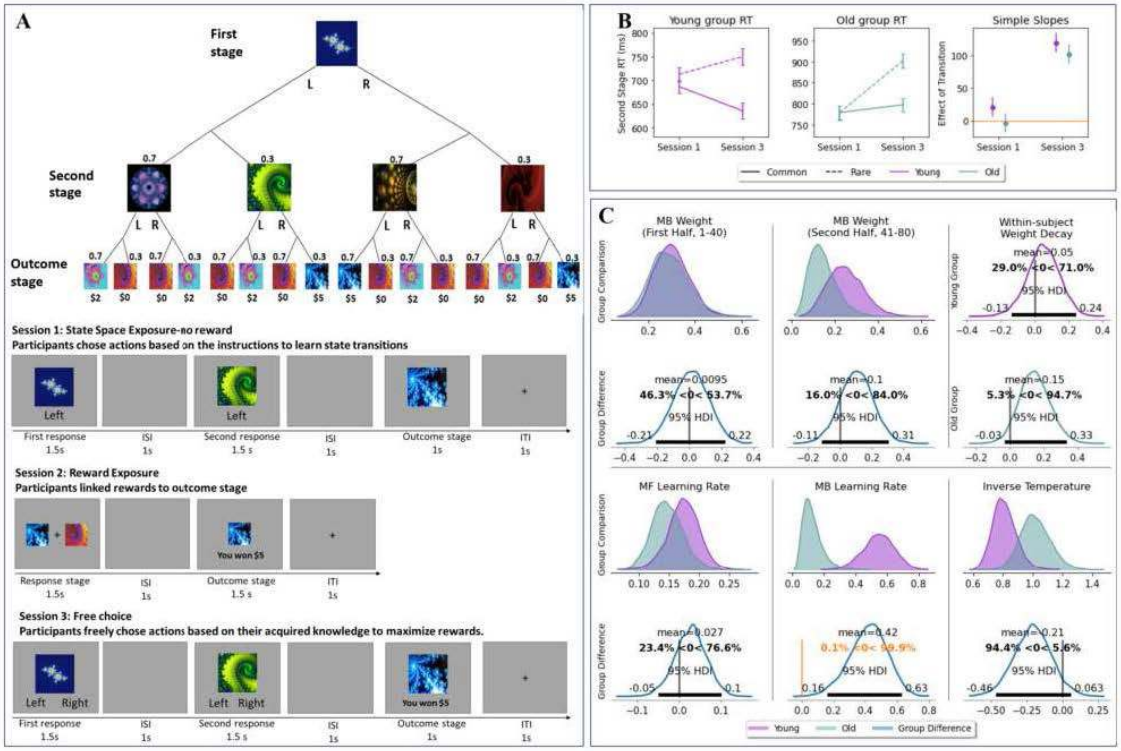

Fig. 1: A. The task structure (upper panel) and experimental procedure (lower panel). B. Analysis of secondstage reaction times. C. Computational modelling results.

Results: A hierarchical Bayesian linear regression on second-stage RT revealed no evidence for the transition effect in Session 1 for Old group, but a strong effect for Young group (Fig. 1B), meaning Young group acquired state transition knowledge faster than Old group. Similarly, computational modelling results indicated that younger adults showed faster model-based learning than older adults (MB learning rate in the lower panel of Fig. 1C). The single-trial EEG regression results exhibited congruent patterns with the observed behavioural results. In Session 1, only Young group's second-stage stimuli-locked ERP covaried with trial-by-trial SPE, whereas Old group's ERP didn't show significant results (Fig. 2A). In Session 3, both groups' second stage (Fig. 2B) and outcome stage (Fig. 2C) ERP showed sensitivity to SPE.

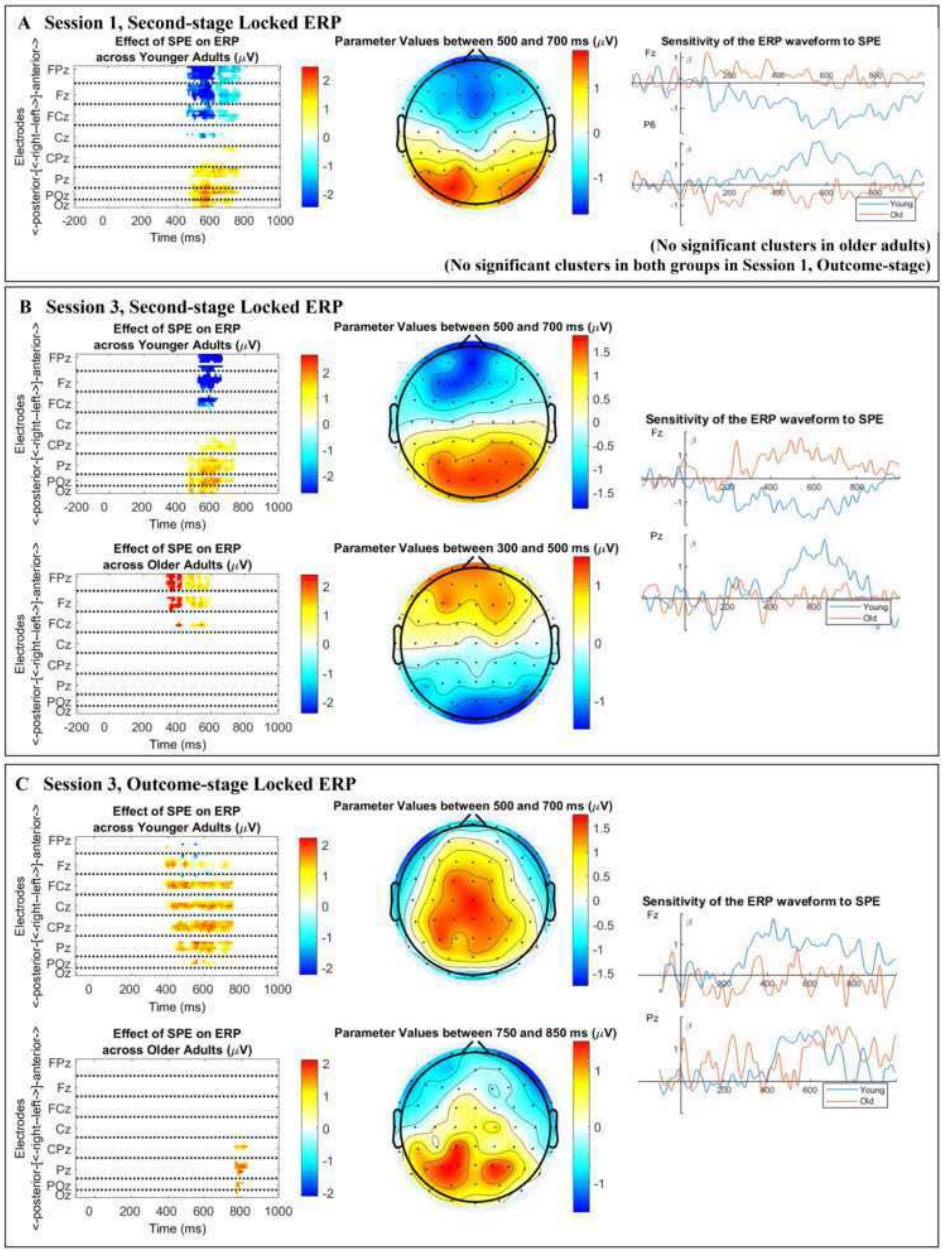

Fig. 2: Single-trial EEG analysis results.

Conclusions: This research demonstrates that while older adults may display slower model-based learning compared to younger adults, they are still capable of acquiring knowledge of task structures. Through model-based single-trial EEG analyses, we identified distinctive EEG signal characteristics linked to the probabilistic updates of state transition knowledge.

References

1. Bolenz, F., Kool, W., Reiter, A. M., & Eppinger, B. (2019). Metacontrol of decision-making strategies in human aging. Elife, 8, e49154.
2. Eppinger, B., Walter, M., Heekeren, H. R., & Li, S. C. (2013). Of goals and habits: age-related and individual differences in goal-directed decision-making. Frontiers in neuroscience, 7, 253.
3. Gläscher, J., Daw, N., Dayan, P., & O'Doherty, J. P. (2010). States versus rewards: dissociable neural prediction error signals underlying model-based and model-free reinforcement learning. Neuron, 66(4), 585-595.

4. Kool, W., Gershman, S. J., & Cushman, F. A. (2018). Planning complexity registers as a cost in metacontrol. Journal of cognitive neuroscience, 30(10), 1391-1404.
5. Oguchi, M., Li, Y., Matsumoto, Y., Kiyonari, T., Yamamoto, K., Sugiura, S., & Sakagami, M. (2023). Proselfs depend more on model-based than model-free learning in a non-social probabilistic state-transition task. Scientific Reports, 13(1), 1419.
6. Ruel, A., Bolenz, F., Li, S. C., Fischer, A., & Eppinger, B. (2023). Neural evidence for age-related deficits in the representation of state spaces. Cerebral Cortex, 33(5), 1768-1781.
7. Seow, T. X., Benoit, E., Dempsey, C., Jennings, M., Maxwell, A., O'Connell, R., & Gillan, C. M. (2021). Model-based planning deficits in compulsivity are linked to faulty neural representations of task structure. Journal of Neuroscience, 41(30), 6539-6550.
8. Vikbladh, O. M., Meager, M. R., King, J., Blackmon, K., Devinsky, O., Shohamy, D., ... & Daw, N. D. (2019). Hippocampal contributions to model-based planning and spatial memory. Neuron, 102(3), 683-693.

Poster No 905

Temporal credit assignment in alcohol use disorder

Jiwon Park[1], Manjae Kwon[2,3], Young-Chul Jung[2,3], Dongil Chung[1]

[1]Department of Biomedical Engineering, Ulsan National Institute of Science and Technology, Ulsan, Korea, Republic of, [2]Department of Psychiatry, Severance Hospital, Yonsei University College of Medicine, Seoul, Korea, Republic of, [3]Institute of Behavioral Science in Medicine, Yonsei University College of Medicine, Seoul, Korea, Republic of

Introduction: Decisions made in the present usually result in immediate outcomes. However, the timing of the consequences of our choices can sometimes be uncertain. For instance, diseases may develop much later as a result of unhealthy eating habits. Given such temporal uncertainty, having the ability to correctly attribute outcomes to a specific choice made in the past is crucial for making decisions that have long-term benefits, such as in matters related to health. Previous studies suggested that individuals with substance use disorder (SUD) may have a diminished ability to learn from experience and show shortsighted behavioral patterns. However, it is still unclear if there is a specific association between individual's substance use and their comprehension of causal relationships between action and outcomes. In this study, we hypothesize that individuals with alcohol use disorder (AUD) may have a biased tendency to attribute reward outcomes, or omission of rewards, more to recent choices than to those made in the distant past.

Methods: 60 participants were recruited for the current study. Participants were initially screened with Alcohol Use Disorder Identification Test (AUDIT), and were further interviewed by a board-certified psychiatrist to determine their categorization based on the Diagnostic and Statistical Manual of Mental Disorders, Fifth Edition (DSM-5) criteria for alcohol use disorder. 29 individuals were categorized as the AUD group and 31 individuals were categorized as the healthy control (HC) group. Participants were asked to make a series of choices between two options where the reward contingency associated with each option could only be learned through experience. Most importantly, reward outcomes were temporally delayed, such that individuals were informed about the consequence of each choice only after an uncertain delay, sampled from a Poisson distribution. After each choice, the reward outcomes delayed to the corresponding trial were summed and displayed on the screen. All participants underwent functional neuroimaging during the task, and upon completion, they reported their beliefs about the immediate and long-term effects of drinking on a 21-point scale (-10: very negative; +10: very positive). To investigate how individuals attributed rewards across their choices in past trials, we conducted linear regression analyses, with individuals' choices as dependent variables and three sets of potential causal choice-outcome associations (immediate, 1-back, and 2-back) as independent variables.

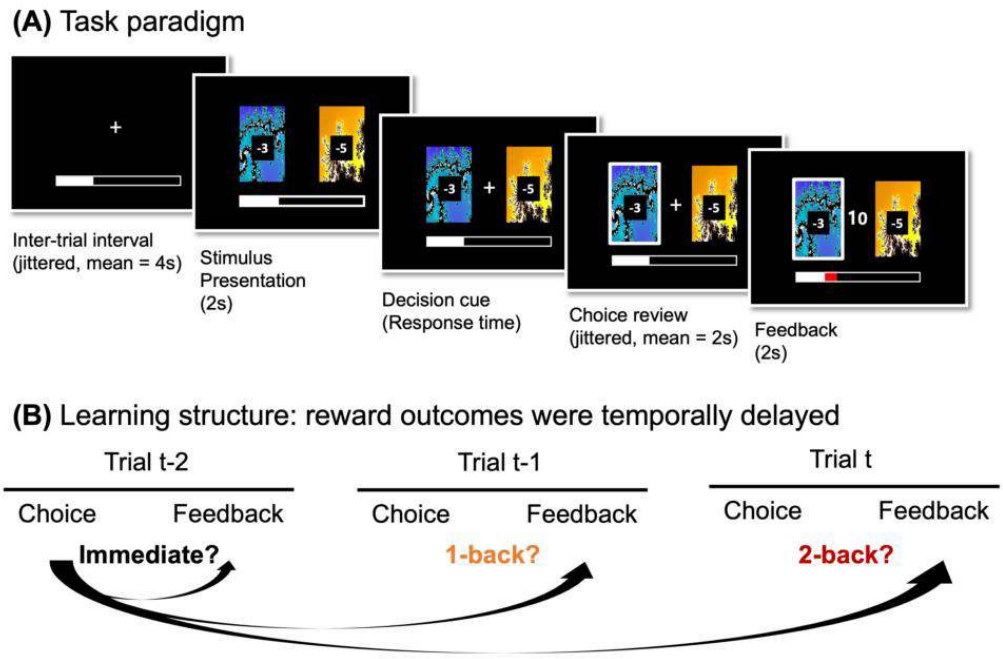

Figure 1. Experimental paradigm. (A) Participants were asked to make a series of choices between two options where reward contingencies associated with each option were not explicitly revealed. A cost for choosing each option independent of its reward contingency was presented on top of the option. **(B)** Reward outcomes were temporally delayed, such that individuals were informed about the consequence of each choice only after an uncertain delay. **(A,B)** At the end of each trial, the reward outcomes delayed to the corresponding trial were summed and displayed on the screen.

Results: In the HC group, regression coefficients for the associations between choices and delayed outcomes (1- and 2- back) surpassed those between choices and immediate outcomes. Notably, the effects of 2-back associations were significantly larger than those of the immediate or 1-back associations. On the other hand, the AUD group did not exhibit a similar emphasis on long-term associations over the immediate ones. Specifically, the effects of 1- and 2- back associations between choices and delayed outcomes were significantly diminished in the AUD group compared to the HC group. Self-reports showed that, regardless of AUD diagnosis, both groups believed the immediate outcome of drinking to be positive, whereas they believed the long-term outcome of drinking to be negative.

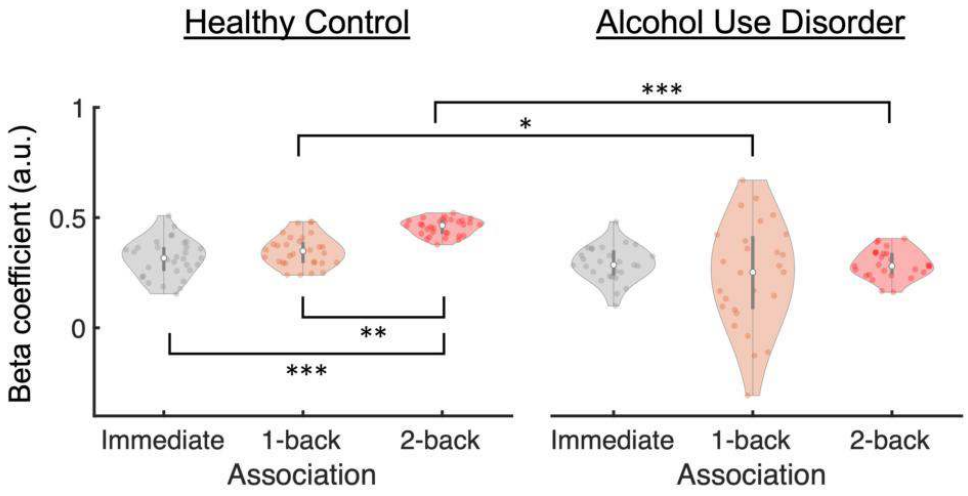

Figure 2. In the HC group, regression coefficients for the associations between choices and delayed outcomes surpassed those between choices and immediate outcomes. Particularly, the effects of 2-back associations were significantly larger than those of the immediate or 1-back associations. On the other hand, the AUD group did not exhibit a similar emphasis on long-term associations over the immediate ones. Specifically, the effects of 1- and 2-back associations between choices and delayed outcomes were significantly diminished in the AUD group compared to the HC group. Unfilled circle indicates mean value of each beta coefficient distribution, and each filled dot represents individuals; *P < 0.05, **P < 0.01, ***P < 0.001.

Conclusions: The regression results suggest that healthy individuals incorporate the long-term consequences of their choices in learning, while this pattern was diminished in individuals with alcohol use disorder. Task-independent self-reports

suggest that individuals' alcohol using behavior cannot be accounted for by their biased beliefs about health risks associated with alcohol. Together, our data show that alcohol use disorder is associated with individuals' biased tendency to attribute outcomes to recent choices, and suggest that such biases in temporal credit attribution may underlie their habitual and excessive alcohol use behavior.

References

1. Dick, Danielle M., et al. "Understanding the construct of impulsivity and its relationship to alcohol use disorders." Addiction biology 15.2 (2010): 217-226.
2. Jocham, Gerhard, et al. "Reward-guided learning with and without causal attribution." Neuron 90.1 (2016): 177-190.
3. Galandra, Caterina, et al. "Impaired learning from regret and disappointment in alcohol use disorder." Scientific Reports 10.1 (2020): 12104.
4. Galandra, Caterina, et al. "Impaired learning from regret and disappointment in alcohol use disorder." Scientific Reports 10.1 (2020): 12104.

Poster No 906

Two-step value normalization explains process of re-estimation of option triggered by sold-out event

Minho Hwang[1], Dongil Chung[2]

[1]Ulsan National Institution of Science and Technology, Ulsan, Ulsan, [2]UNIST, Ulsan, NA

Introduction: Choices are often influenced by the context that changes over time. For instance, changes in an item's availability (e.g., an item being sold-out) affect subsequent purchasing choices. Previous studies reported that the presence of an unavailable option leads to more random choices, even when it is unrelated to the choice[1]. Value normalization theories, which propose that the neural encoding of the value for each option is normalized by the total value of all available options, accounted for such impacts of the choice-irrelevant option[2]. However, it is still unknown whether choices under context changes can be explained by the same value normalization mechanism. Here, we proposed a Two-step value normalization model (TSVN) that offers a potential explanation for the impacts of changes in the available options, using a context-adaptive value normalization process. Furthermore, we tested whether the normalized values estimated from our proposed model were represented in neural and physiological data.

Methods: In the current study, 36 participants (male/female = 20/16, age = 21.15 ± 3.11) were recruited and asked to make a series of gamble choices while their gaze information, pupil dilation, and electroencephalogram (EEG) data were recorded. During the gambling task, three gamble options were presented at the beginning of each choice trial. On some trials, one of the three options became unavailable ('Sold-out' trials) before the presentation of the choice cue, prompting participants to make their decisions from the remaining two options. On some other trials, only two options were displayed from which individuals were asked to choose ('Two-option' trials). Our TSVN model proposes that the sold-out of one option triggers the 2nd-step normalization, which only takes into account the 1st-step values of the two remaining options. Pupil dilation was calculated based on the diameter of the pupil during gaze at option. The average amplitude of EEG signals during each option presentation epoch was used to calculate the event-related potential (ERP) and, event-related spectral perturbation (ERSP) was computed for each frequency band to measure oscillatory responses induced by the sold-out cues.

Results: To test the impacts of the sold-out, individuals' choices were compared between Sold-out and Two-option trials. Linear regression analysis revealed that the proportion of individuals' choices unpredicted by their risk preference (independently measured from a typical 2AFC gambling task) increased as a function of the sum of all three options' values (ß = -0.99, $p < 0.001$). In a formal model-comparison against other normalization models, our TSVN model best explained individuals' choices both with and without the occurrence of sold-out options. The TSVN predicts that the value of each option can change after the revelation of its unavailability, and pupil dilation data supported this prediction. Specifically, 1st-step value differences were only significantly represented before the sold-out, while 2nd-step value differences were only represented after the sold-out. EEG data also showed evidence of the TSVN. Specifically, the amplitudes of P300 and late positive deflection (LPD) in the parietal region were positively associated with the value of the sold-out option. Furthermore, spectral strength of the gamma band oscillation in the frontal region was negatively associated with the 2nd-step value differences.

Conclusions: Our data confirms that the change of option availability significantly affects individuals' choices. Consistent with the value normalization theories, the extent to which individuals change their choices at sold-out was associated with the sum of all options' values. More importantly, both pupil and EEG data reflected value information aligning with predictions made by our TSVN model. Together, the current study provides a neurophysiological account explaining how the context change during choice valuation affects individuals' decision process.

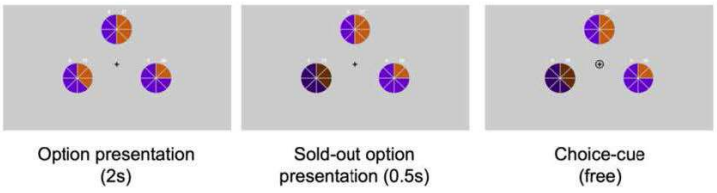

Figure 1. **Task design.** Participants were presented with three gamble options, but on some trials, one of the three options was indicated as unavailable.

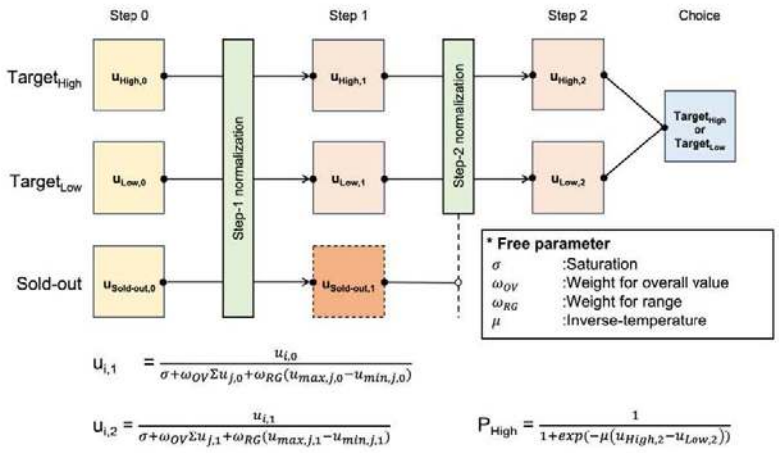

Figure 2. **Two-step normalization model.** Two-step value normalization model. At the sold-out of an option, the model proposes that the 2nd-step value normalization occurs between the two remaining available options.

References

1. Itthipuripat, S., Cha, K., Rangsipat, N., & Serences, J. T. (2015). Value-based attentional capture influences context-dependent decision-making. Journal of Neurophysiology, 114(1), 560-569.
2. Louie, K., Khaw, M. W., & Glimcher, P. W. (2013). Normalization is a general neural mechanism for context-dependent decision making. Proceedings of the National Academy of Sciences, 110(15), 6139-6144.

Poster No 907

TMS-fMRI evidence that magnitude representations in IPS causally drive risky choice

Marius Moisa[1], Gilles de Hollander[2], Christian Ruff[3]

[1]University of Zurich, Zürich, Zurich, [2]UZH, Zürich, Switzerland, [3]University of Zurich, Zurich, Zurich

Introduction: Risk appetite refers to the extent to which decision-makers are willing to choose options that increase potential returns at the cost of a higher variance of those returns. A recent study showed that individuals with a noisier approximate number sense (ANS) are less consistent in making risky choices and, notably, tend to be more risk-averse. This result highlights a crucial influence of perceptual processes on apparent risk appetite that defies mainstream economic theory(1). Here, we aimed to elucidate the causal relevance of the parietal ANS by perturbing it using theta-burst TMS2 over intraparietal cortex (IPS).

Methods: 78 participants performed a risky choice task while undergoing fMRI, choosing between a sure option with a fixed payout and a risky option with a 55% probability of a larger payout. We estimated a numerical population receptive field model (nPRF) in parietal cortex (1, 3) quantifying which voxels in IPS are reliably tuned to a preferred numerosity (Fig. 2A). Thirty-five participants showed reliable numerosity fields, no random behavior, and no adverse effects to TMS. These subjects underwent 2 more sessions, where rTMS was applied either over their individual nPRF cluster in IPS, or over vertex, immediately before performing risky choices.

Results: We observed no difference in the raw risky choice proportion between the IPS and vertex stimulation conditions (Fig. 1A). However, when we split choices by the order in which the risky and safe options were presented, IPS stimulation increased the proportion of risky choices where the safe option was presented first from 56.3% to 61.6% ($F(1, 34)=5.00$, $p=0.032$, Fig. 1B). Choice proportions can be modulated by both a shift in preference or in the noisiness of the response. To differentiate between these two accounts, we also modeled choice data using a psychometric model, yielding for each subject both (1) an indifference point (a measure of risk appetite) and (2) a slope (a measure of choice consistency) (Fig. 1C). This analysis shows that subjects after IPS stimulation are generally more risk-seeking (pmcmc=0.022) and marginally more noisy (pmcmc=0.066). Crucially, we show that both effects are driven by the trials on which the safe options were presented first. That is, only in trials where the safe option was presented first, both risk appetite (pmcmc=0.001) and choice consistency (pmcmc=0.013) were significantly decreased by IPS stimulation. The interaction effect between presentation order and stimulation condition was significant for both risk appetite (pmcmc=0.002) and choice consistency (pmcmc=0.0338). A Bayesian model of risky choice can explain the interaction between order and TMS stimulation as an increase in noise for small, but not larger payoff magnitudes after TMS. This is consistent with the large majority of nPRFs in parietal cortex having preferred numerosities that are relatively low compared to the risky payoff magnitudes. We also probed the effect of TMS on neural magnitude representations in IPS. We found significantly lower nPRF amplitudes after IPS stimulation ($t(33) = 2.71$, $p=0.011$) compared to vertex stimulation (Fig. 2B), but no difference in the average preferred numerosity ($t(33) = 1.32$, $p=0.19$) or the dispersion of the nPRFs ($t(33) = 0.82$, $p=0.418$). This highlights a specific effect of TMS on the amplitude of the nPRF. Accordingly, an inverted nPRF model showed higher decoding accuracy in the vertex vs the IPS condition (mean $r=0.142$ versus $r=0.092$, $F(1,34) = 4.99$, $p=0.032$, Fig. 2C), consistent with the noisier behavior of the subjects.

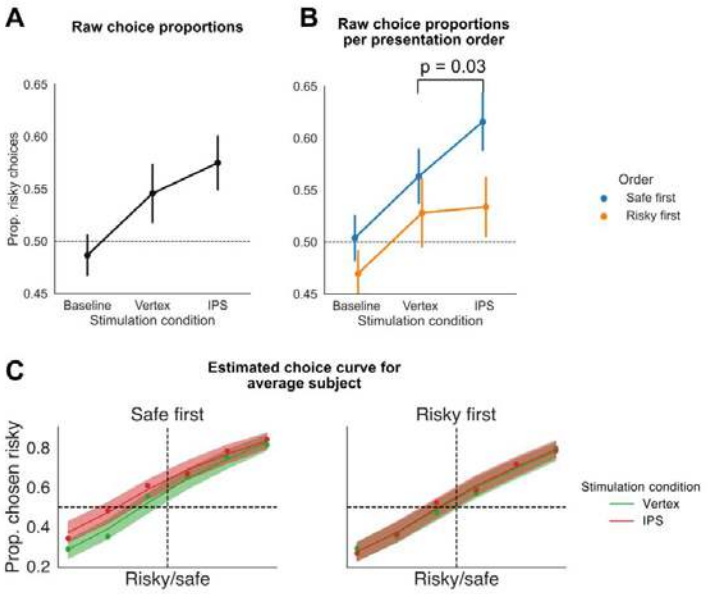

Figure 1: Behavioral results. A) Raw proportion of risky choices was numerically but not significantly, larger after IPS stimulation. B) When safe options were presented first, subjects were more likely to choose the risky option after TMS stimulation. C) Posterior predictive plots of the psychometric model. Note how, when safe options came first, subjects both became both more risk seeking (indifference point shifts leftwards) and less consistent (slope of curve is shallower).

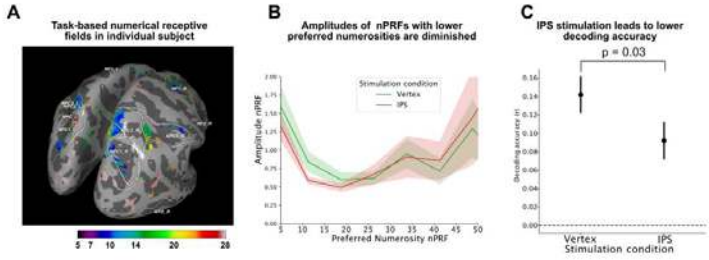

Figure 2: Neural results. A) Numerical receptive fields for a representative subject. It shows how most non-linearly tuned regions are within the IPS and their preferred numerosity is generally below 20. B) The amplitudes of nPRFS tended to be lower after IPS stimulation. In particular for numerical receptive fields with relatively low preferred numerosity. C) Accordingly, decoding of presented numerosity on unseen data was less accurate after IPS stimulation.

Conclusions: We provide evidence for a crucial causal role of neural magnitude representations in the IPS in risky choices. The results corroborate a neurocognitive account of risk aversion where risk preferences are determined by noisy, biased perception of magnitudes. This highlights the relevance of 'low-level' perceptual processes and their neurocognitive substrates for economic choice theory.

References

1. M. Barreto-Garcia & G. de Hollander, et al. Individual risk attitudes arise from noise in neurocognitive magnitude representations, Nature Human Behaviour, 2023
2. Y. Huang et al. Theta burst stimulation of the human motor cortex, Neuron, 2005
3. B. Harvey & S. Duomolin, Can responses to basic non-numerical visual features explain neural numerosity responses?, Neuroimage, 2017

Poster No 908

Stress changes risk-taking by altering Bayesian magnitude coding in the parietal cortex

Maike Renkert[1], Gilles de Hollander[2], Gökhan Aydogan[1], Saurabh Bedi[3], Christian Ruff[1]

[1]University of Zurich, Zurich, Zurich, [2]UZH, Zürich, Switzerland, [3]Department of Neuroeconomics, University Zurich, Zurich, Switzerland

Introduction: Acute stress is an inevitable aspect of life, with long-lasting consequences for physical and financial well-being (DeLongis et al 1988). Previous research documents a link between acute stress and altered risk preferences (Buckert et al. 2014), with suggestions that stress may contribute to the perpetuation of poverty (Haushofer & Fehr 2014). However, despite ample research, little is known about the neurocognitive processes that translate stress into altered risky decision-making. Here, we shed light on these processes in an experimental study of risky choices under laboratory-induced stress. We employed a perceptual account of risky choice, assuming that decision-makers make financial decisions based on noisy and biased perceptual representations of payoffs (Khaw et al., 2020; Garcia et al. 2023). This allowed us to decompose stress-induced shifts in risk preferences to latent Bayesian perceptual processes, specifically to either noisier sensory representation or altered beliefs. Importantly, those cognitive variables have neural surrogates that relate to how numerosities are represented in the parietal magnitude processing system that can be derived from fMRI data.

Methods: Participants (n=50) performed a risky gamble task in a first baseline fMRI session, before being randomly assigned to either a stress or control group. For the risks task, each payoff is presented separately as cloud of coins to enable (numerical) population receptive field mapping later on. To induce stress in the second fMRI session, we interleaved the risk task with an adapted version of the well-established MIST with additional social evaluative threat. Cortisol levels from saliva samples across 6 timepoints were collected to obtain a physiological measure of stress (overview of study design in fig.1). Behavior was analysed with a cognitive model that assumes Bayesian perception of payoffs (noisy logarithmic coding model - NLC). Crucially, this enables disentanglement of noise and bias from decisions, which we could relate to neural measures in the next step. For that, we used an encoding/decoding framework that builds on the idea of neural populations that are tuned to numerosity, so-called numerical population receptive fields (nPRFs), which lie predominantly in the intra-parietal sulcus (IPS; example in fig. 2). Here, the precision with which one can decode the number from neural data given the model parameters relates to the noise with which numbers are represented in the parietal magnitude processing system. Bias, in turn, was measured as a shift in neural coding, quantifying how much neural population representations of numerosities change in a specific direction for one subject between sessions.

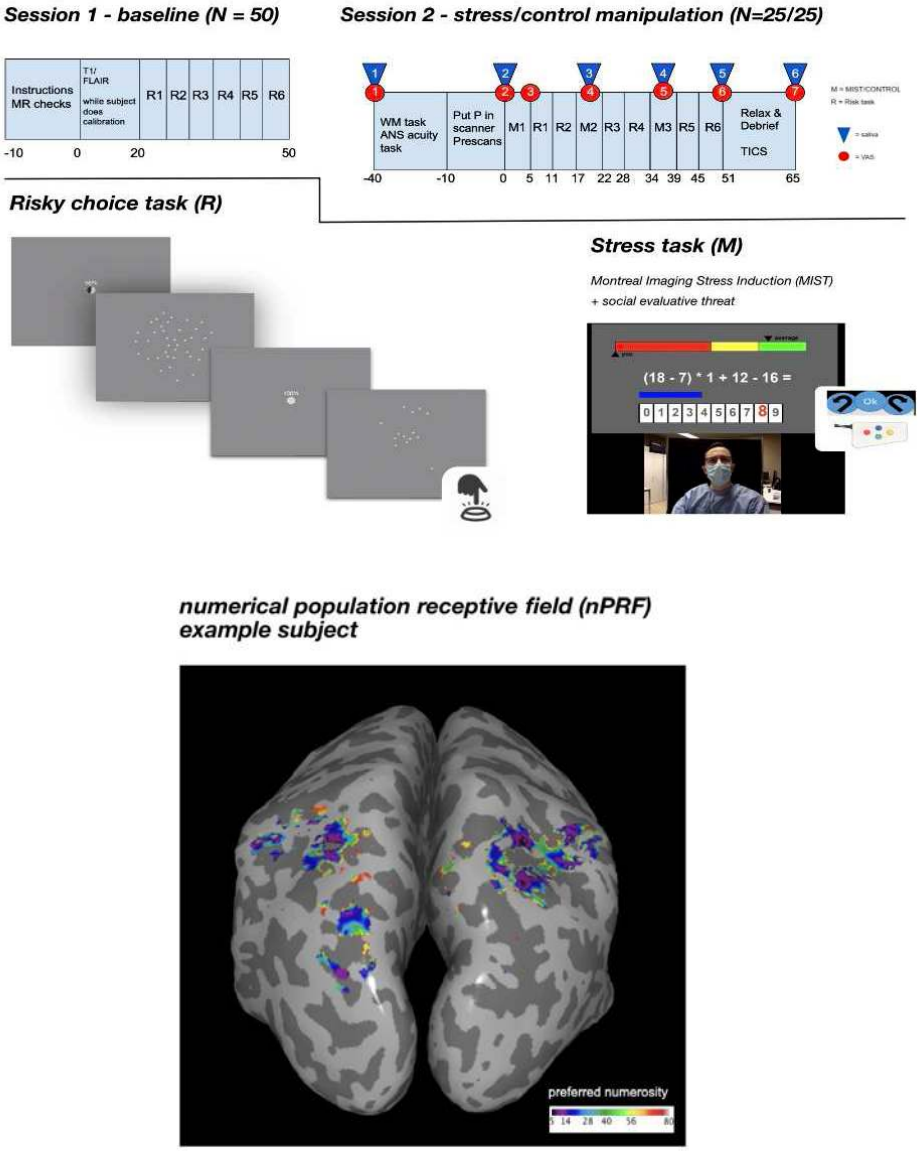

Results: The stress induction was successful, as cortisol levels were significantly higher in the stress group compared to the control group ($p<0.001$). Stress led to a systematic shift in risk preferences, with more risk-seeking behavior under stress ($p=0.03$). Inspection of model parameters revealed that the shift in risk preference under stress was induced by more optimistic (and mostly more realistic) prior beliefs about the magnitude of the risky payoffs ($p<0.01$). By contrast, the noisiness of the inferred payoff representations was unaltered. Neural results aligned with this, as there was a large shift of neural coding only for the stressed group (two sample T-Test on group specific shifts: $p=0.002$) but no change in neural precision. The shift in neural coding correlated with the shift in risky prior ($r=0.31, p=0.034$) and each of them with the individual cortisol response.

Conclusions: In conclusion, our Bayesian perceptual approach together with nPRF modelling allowed us to provide a mechanistic perspective on the cognitive and neural processes driving the effect of stress on risky choice. Our results indicate that stress does not lead to noisier processing of information, but to shifts in prior beliefs and, correspondigly, the underlying neural representations of numerosities.

References

1. DeLongis et al (1988), 'The impact of daily stress on health and mood: psychological and social resources as mediators', J Pers Soc Psychol. 1988 Mar;54(3):486-95. doi: 10.1037//0022-3514.54.3.486.
2. Buckert et al. (2014), 'Acute stress affects risk taking but not ambiguity aversion', Front Neurosci. 2014; 8: 82
3. Haushofer & Fehr (2014), 'On the psychology of poverty', Science, 2014 May 23;344(6186):862-7
4. Khaw et al., (2020), 'Cognitive imprecision and small-stakes risk aversion', The Review of Economic Studies, Volume 88, Issue 4, July 2021, Pages 1979–2013
5. Garcia et al. (2023), 'Individual risk attitudes arise from noise in neurocognitive magnitude representations', Nat Hum Behav. 2023 Sep;7(9):1551-1567

Poster No 909

Grid-like representation in value-based decision-making

Mark Orloff[1], Seongmin Park[2], Jake Blumwald[1], Philippe Domenech[3], Erie Boorman[1]

[1]UC Davis, Davis, CA, [2]CNRS, Lyon, Auvergne-Rhône-Alpes, [3]Paris Brain Institute, Paris, France

Introduction: Reward is encoded in the 'brain valuation system (BVS),' comprised of regions such as: dorsomedial prefrontal cortex (dmPFC)[1], posterior cingulate cortex (PCC)[2] and ventromedial prefrontal cortex (vmPFC)[3,4]. This value coding has been shown to reflect subjective value-how rewarding something is based on an individual's preference[2,5,6]. However, how a given rewarding option gets transformed into a subjective value (SV) signal is unclear. One candidate for how this transformation could theoretically happen is via the brain's cognitive mapping system. A grid code, originally identified for its role in representing an animal's position and enabling path integration in physical space[7], encodes an individual's location in abstract task space (i.e., a non-physical 2D relational space)[8]. These grid-like signals have been found in entorhinal cortex (EC) and mPFC. Further work in rodents has shown that grid cell firing can be distorted with environmental deformations[9]. Here, we ask if humans use a grid-like representation to efficiently represent a 2D SV space and to infer decision vectors for risky decisions in this space.

Methods: Participants (N = 35) were asked to make binary choices between two sequentially shown shape options drawn from two sets of shapes that vary along two continuous dimensions (such as width and orientation) corresponding to reward amount ($) and probability (%), respectively, while undergoing fMRI. We utilized the Cumulative Prospect Theory model to calculate the SV of each participant's choices[10]. We use two separate GLMs to test if BOLD activity is associated with 1) SV signal and 2) subjectively-weighted hexagonal modulation, characteristic of a grid-like representation. Specifically, we tested the following regressors in separate GLMs at the time that the second shape was shown: SVshape = A^ρ × e^[-(-log (P))^α] SV difference: Schosen - Sunchosen, where SVshape represents the SV of a shape, A represents the reward amount, P represents the probability of winning the reward, ρ represents an individual's risk preference, and α represents an individual's probability weighting; and hexagonal modulation of the decision vector over the attribute space (as predicted by grid cell firing fields): cos(6θ), where θ represents the angle of the decision vector between the first and second shapes for each binary choice in a 2D SV space of subjective amount, norm^{0,1}(A^ρ), and subjective probability, norm^{0,1}(e^[-(-log (P))^α]), where norm^{0,1}(·) scales the values from 0 to 1. Threshold free cluster enhancement (TFCE) was used, with small-volume (S-V) correction in hypothesized regions-of-interest.

Results: We identified a subjective value comparison effect at decision time in PCC and vmPFC (PTFCE-S-V < 0.05), and an inverse effect in dmPFC, lateral prefrontal cortex (lPFC), and anterior insula (AI; PTFCE < 0.05)[2]. We also find a grid-like representation of decision vectors between options through an individual's distorted subjective value space in bilateral EC (PTFCE-S-V < 0.05), and, marginally, in mPFC (PTFCE-S-V = 0.07). This representation is specific to a six-fold periodicity (as opposed to 4-, 5-, 7-, or 8-fold control periodicities). Finally, we show that the strength of activation for subjective value difference in PCC and grid-like representation in bilateral EC is correlated across participants, controlling for decision consistency (inverse temperature).

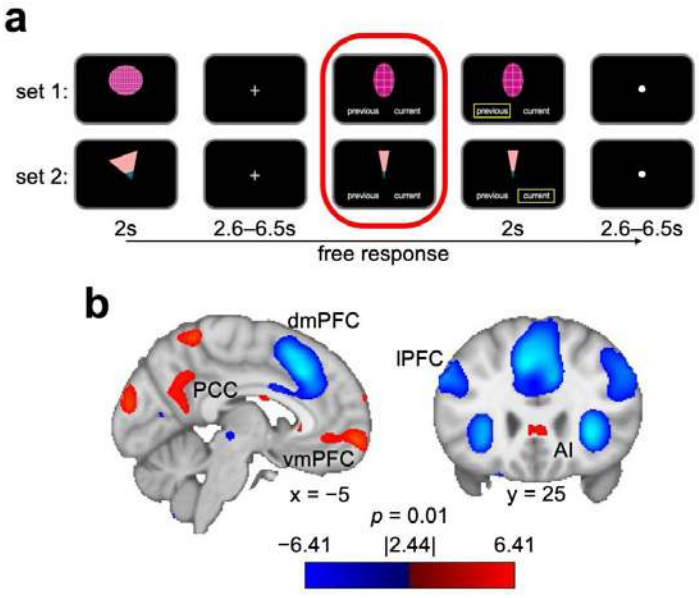

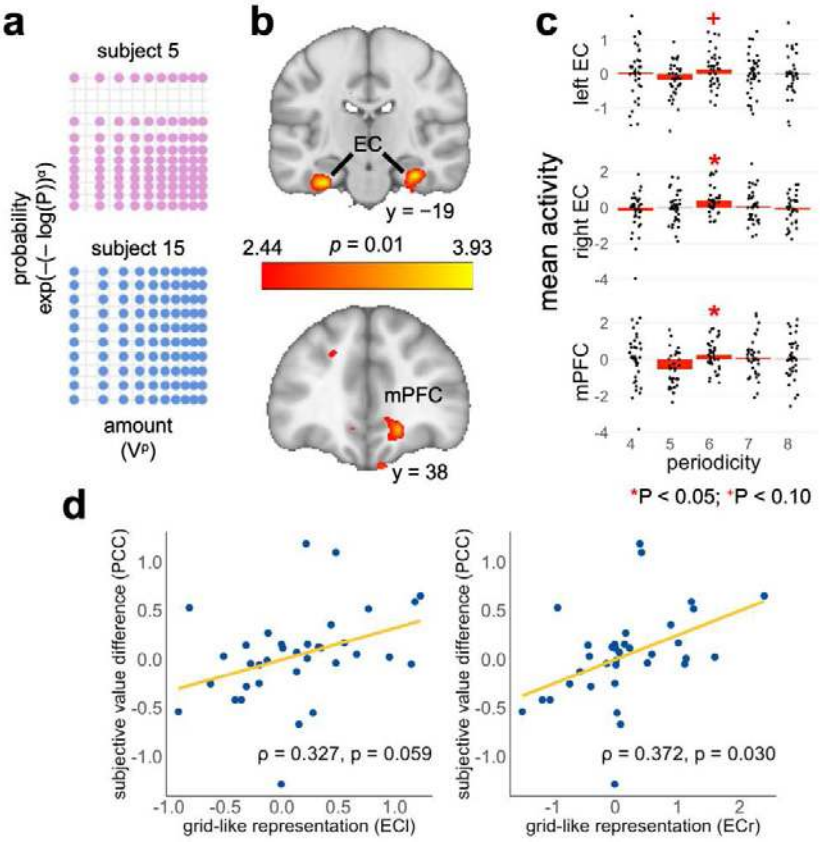

Conclusions: In this study, we demonstrated that a grid-like representation of decision vectors in an SV space was utilized during risky choice. To our knowledge, this is the first demonstration of a grid-like representation of decision-vectors in a subjective 'value' space of probability and reward amount. Further, effects in the BVS and grid-like representation system were correlated, providing evidence that these systems are working collectively.

References

1. Kennerley SW, Behrens TEJ, Wallis JD. Double dissociation of value computations in orbitofrontal and anterior cingulate neurons. Nat Neurosci. 2011;14: 1581–1589. doi:10.1038/nn.2961
2. Bartra O, McGuire JT, Kable JW. The valuation system: A coordinate-based meta-analysis of BOLD fMRI experiments examining neural correlates of subjective value. NeuroImage. 2013;76: 412–427. doi:10.1016/j.neuroimage.2013.02.063
3. Lebreton M, Jorge S, Michel V, Thirion B, Pessiglione M. An Automatic Valuation System in the Human Brain: Evidence from Functional Neuroimaging. Neuron. 2009;64: 431–439. doi:10.1016/j.neuron.2009.09.040
4. Chib VS, Rangel A, Shimojo S, O'Doherty JP. Evidence for a Common Representation of Decision Values for Dissimilar Goods in Human Ventromedial Prefrontal Cortex. J Neurosci. 2009;29: 12315–12320. doi:10.1523/jneurosci.2575-09.2009
5. Padoa-Schioppa C, Assad JA. Neurons in the orbitofrontal cortex encode economic value. Nature. 2006;441: 223. doi:10.1038/nature04676
6. Boorman ED, Behrens TEJ, Woolrich MW, Rushworth MFS. How Green Is the Grass on the Other Side? Frontopolar Cortex and the Evidence in Favor of Alternative Courses of Action. Neuron. 2009;62: 733–743. doi:10.1016/j.neuron.2009.05.014
7. Hafting T, Fyhn M, Molden S, Moser M-B, Moser EI. Microstructure of a spatial map in the entorhinal cortex. Nature. 2005;436: 801–806. doi:10.1038/nature03721
8. Park SA, Miller DS, Boorman ED. Inferences on a multidimensional social hierarchy use a grid-like code. Nat Neurosci. 2021;24: 1292–1301. doi:10.1038/s41593-021-00916-3
9. Keinath AT, Epstein RA, Balasubramanian V. Environmental deformations dynamically shift the grid cell spatial metric. eLife. 2018;7: e38169. doi:10.7554/elife.38169
10. Tversky A, Kahneman D. Advances in prospect theory: Cumulative representation of uncertainty. J Risk Uncertain. 1992;5: 297–323. doi:10.1007/bf00122574

Poster No 910

Cortical Microstructural Integrity is Associated with Decision-Making Biases in Older Adulthood

Patrick Hewan[1], Alfie Wearn[2], Roel van Dooren[3], Lindsay Wyatt[1], Ilana Leppert[4], Giulia Baracchini[5], Colleen Hughes[2], Jennifer Tremblay-Mercier[6], Elisabeth Sylvain[6], Judes Poirier[6], Sylvia Villeneuve[7], Christine Tardif[4], R. Nathan Spreng[8], Gary Turner[1]

[1]York University, Toronto, Ontario, [2]McGill University, Montreal, Québec, [3]Institutes of Psychology & Brain and Cognition, Leiden University, The Netherlands, Leiden, South Holland, [4]McConnell Brain Imaging Centre, Montreal Neurological Institute and Hospital, Montreal, Quebec, [5]Montreal Neurological Institute and Hospital, Montreal, Quebec, [6]Douglas Mental Health University Institute, Montreal, Québec, [7]Brain Imaging Centre, Douglas Institute Research Centre, Montreal, Qc, [8]Montreal Neurological Institute, McGill University, Montreal, Quebec

Introduction: The exploration-exploitation (EE) trade-off is a decision-making process that relies on cortical regions involved in reward processing and monitoring, and their integration with subcortical nuclei involved in attention and learning1. In recent work, we used quantitative MRI (qMRI) to examine the microstructural integrity of the locus coeruleus (LC), a core subcortical node in the EE circuit, and showed that this brain measure robustly predicts performance on a foraging-based measure of EE2. Here, we investigated whether a similar relationship exists across cortical regions implicated in EE, examining cellular microstructure as related to foraging performance in medial orbitofrontal cortex (mOFC), rostral middle frontal gyrus (rMFG), frontopolar cortex (FPC), and dorsal anterior cingulate cortex (dACC)-core cortical regions identified in a recent meta-analysis from our lab3 and related theoretical models1,4. We predicted that lower integrity would be associated with sub-optimal decision-making performance, marked by an exploitation-bias in older adulthood5.

Methods: PARTICIPANTS: 132 cognitively healthy older adults (mean age 70s, 68% female) from the PREVENT-AD cohort6. BEHAVIORAL TASK7: A computerized foraging task. Participants control an avatar and forage for points within 5 minutes. NEUROIMAGING PROTOCOL: MRI scans were acquired on a 3T Siemens PrismaFit including: T1w MPRAGE (1mm isotropic, TR/TE/TI=2300/2.96/900ms, FA=9°); Three multi-echo sequences (1mm isotropic, total TA=17:30) with predominant weighting for: T1 (TR=18ms, 6 echoes, TE=2.16-14.81ms, FA 20°), magnetization transfer (MT) (TR=27ms, 6 echoes, TE=2.04-14.89ms, FA 6°, MT pulse FA 540°, 2.2kHz off-resonance, 12.8ms) and proton density (TR=27ms, 8 echoes, TE=2.04-22.20ms, echo-spacing=2.57ms, FA 6°). IMAGE PROCESSING: MTsat maps were calculated using the hMRI toolbox8. Cortical ROIs were defined using the Desikan-Killiany atlas9. ANALYSIS: Marginal value theorem determined optimal foraging performance on a group level10. Partial correlations were conducted between core regions, a cortical control region not predicted to be associated with EE, and foraging performance. Partial correlations controlled for age, gender, education, brain volume, cortical thickness in each ROI, and MTsat in the corpus callosum to control for generalized age-related changes in MTsat.

Results: MTsat values in the mOFC, rMFG, and FPC were significantly correlated with task performance (mOFC: $pr(126) = 0.19$, $p < 0.05$; rMFG: $pr(126) = 0.25$, $p < 0.01$, FPC: $pr(126) = 0.19$, $p < 0.05$ while dACC was not significant ($pr(126) = 0.14$, $p = 0.13$). Additionally, there was no correlation between MTsat and foraging performance in the lateral occipital cortex (LO; $pr(126) = 0.07$, $p= 0.4$), a region we predicted not to be associated with foraging performance.

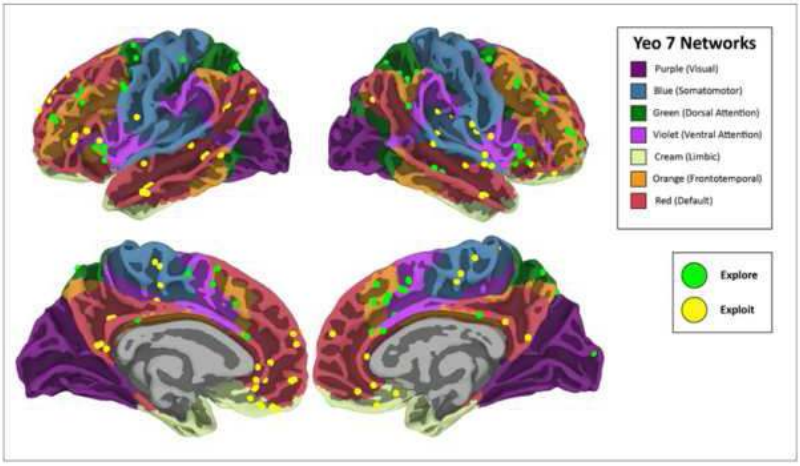

Figure 1. Meta-analysis results depicting regions active during exploration-exploitation based choice. Identified 'core' regions include mOFC, FPC, rMFG, and dACC[1].

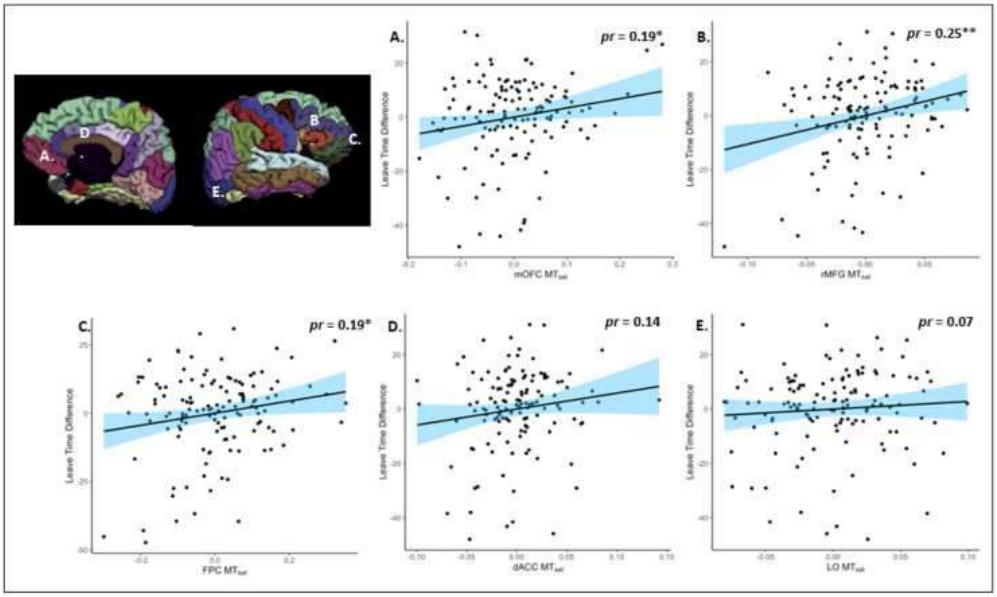

Figure 2. Top left panel shows the ROIs used based on the Desikan-Killiany atlas[9]. Panels A-E: Correlation plots for MTsat residuals (after controlling for variables of non-interest) in EE regions (A-D) and a cortical control region (LO, Panel E) with exploration vs. exploitation (LTD). LTD values above 0 indicate an exploration bias while values below 0 indicate an exploitation bias. mOFC = medial orbitofrontal cortex, rMFG = rostral middle frontal gyrus, FPC = frontopolar cortex, dACC = dorsal anterior cingulate cortex, LO = lateral occipital cortex. *p<0.05, **p<0.01

Conclusions: We examined whether the integrity of core cortical regions previously implicated in EE decision-making is associated with performance on a foraging task. As predicted, qMRI-derived MTsat values were significantly and positively correlated with EE decision-making in the mOFC, rMFG, and FPC, with a similar trend observed for dACC, all core EE decision-making nodes. In contrast, MTsat in the LO, a cortical control region not previously implicated in EE, was not related to EE performance. Specifically, lower MTsat values in EE regions were associated with increased exploitation, replicating a recent finding in LC2. Critically, no behavioural associations were observed with grey matter volume in these EE regions, nor when controlling for volumes in our correlation models with MTsat. MTsat as measured by qMRI is a promising marker of the integrity of this cortico-subcortical circuit, providing a novel lens on the neural mechanisms underlying changes in decision-making performance, and the emergence of a exploitation bias in later life5.

References

1. Cohen, J. D. (2007). Should I stay or should I go? How the human brain manages the trade-off between exploitation and exploration. Philos.Trans.R.Soc.Lond.B. 362, 933-942.
2. Turner, R. G. (2023). Lower microstructural integrity of locus coeruleus is associated with an exploitative decision-making bias in older adults. Submitted.
3. Wyatt, L. (2023). Exploration versus exploitation decisions in the human brain: A systematic review of functional neuroimaging and neuropsychological studies. Neuropsychologia (In Press). https://doi.org/10.1016/j.neuropsychologia.2023.108740
4. Aston-Jones, G. (2005). Adaptive gain and the role of the locus coeruleus-norepinephrine system in optimal performance. Journal of Computational Neurology. 493, 99-110.
5. Spreng, R. N. (2021). From exploration to exploitation: a shifting mental mode in late life development. Trends in cognitive sciences 25, 1058-1071
6. Tremblay-Mercier, J. (2021) Open science datasets from PREVENT-AD, a longitudinal cohort of presymptomatic Alzheimer's disease. NeuroImage. Clinical 31, 102733
7. van Dooren, R. (2021). The exploration-exploitation trade-off in a foraging task is affected by mood-related arousal and valence. Cogn Affect Behav Neurosci 21, 549-560
8. Tabelow, K. (2019). hMRI - A toolbox for quantitative MRI in neuroscience and clinical research. NeuroImage 194, 191-210.
9. Desikan, S. R. (2006). An automated labeling system for subdividing the human cerebral cortex on MRI scans into gyral based regions of interest. NeuroImage. 31, 968-980
10. Charnov, E. L. (1976). Optimal foraging, the marginal value theorem. Theories in Population Biology. 9, 129-136.

Poster No 912

When the target is a moving target: Practical issues in using task fMRI for rTMS targeting

Lysianne Beynel[1], Bruce Luber[1], Hannah Gura[2], Zeynab Rezaee[1], Ekaete Ekpo[1], Zhi Deng[1], Janet Joseph[3], Paul Taylor[1], Sarah Lisanby[1]

[1]National Institute of Health, Bethesda, MD, [2]University of Pennsylvania, Philadelphia, PA, [3]Brown University, Providence, RI

Introduction: Individualized task-based fMRI is often used to define rTMS targets. However, determining the optimal number of trials to attain sufficient statistical power while balancing the effects of practice, learning, and fatigue remains a challenge. This choice can substantially impact target selection and thus, rTMS effects. In this study, participants performed a numerical Stroop task (NST). In each trial, a pair of numbers, one larger in font size than the other, was displayed and participants were asked to select the number with the higher numerical value. Trials were randomly and evenly distributed across two conditions: Congruent (the visually larger number was numerically larger), and Incongruent (the visually larger number was numerically smaller). rTMS was applied to the spot within the right intraparietal sulcus (IPS) showing the strongest activation in the Incongruent > Congruent contrast across all blocks. No significant rTMS effect was observed on task performance. To evaluate whether the lack of effect could be due to a change in activation across blocks (resulting from practice, learning, and/or fatigue), we investigated how activations differed between the first and last pairs of blocks.

Methods: Nineteen healthy adults (14 female, 5 male; mean age 39 ± 14 years old) were enrolled, and then practiced a block of 48 trials of the NST. They then performed four more blocks of 48 trials each while in the scanner. fMRI data were analyzed with AFNI (3). First, @SSwarper was used (4) for skull stripping and alignment of the anatomical image from native to MNI space. Then afni.proc.py was used to setup a full pipeline for the fMRI analysis. The hemodynamic response was modeled with a gamma function using the onset of the Congruent and Incongruent trials. In this first follow-up analysis, the Incongruent > Congruent contrast for all trials was computed. In a second analysis, activations in the Incongruent > Congruent contrast were compared between the first and second halves of the acquisition.

Results: The analysis of all trials revealed moderate activation in the left IPS (t > 2.10, 23 voxels), along with some larger clusters in subcortical structures, including the bilateral corpus callosum, and the left cingulate cortex, known to be involved in conflict monitoring (1). Noticeable changes were found in activation pattern when comparing the first and last pairs of NST blocks. The comparison between the Incongruent > Congruent contrast obtained for the last blocks vs. the first ones revealed a strong negative cluster (t > 2.16, p < 0.05, 1827 voxels, Figure 1a) largely spanning the bilateral IPS. Interestingly, we also observed a small positive cluster in the left dorsolateral prefrontal cortex. IPS activations observed in the first blocks (Figure 1b) totally disappeared in the last blocks (Figure 1c). At the behavioral level, accuracy remained quite high and constant across all blocks while reaction time continued to improve (Figure 2), suggesting that fatigue did not play a role and that in fact task efficiency continued to become optimized.

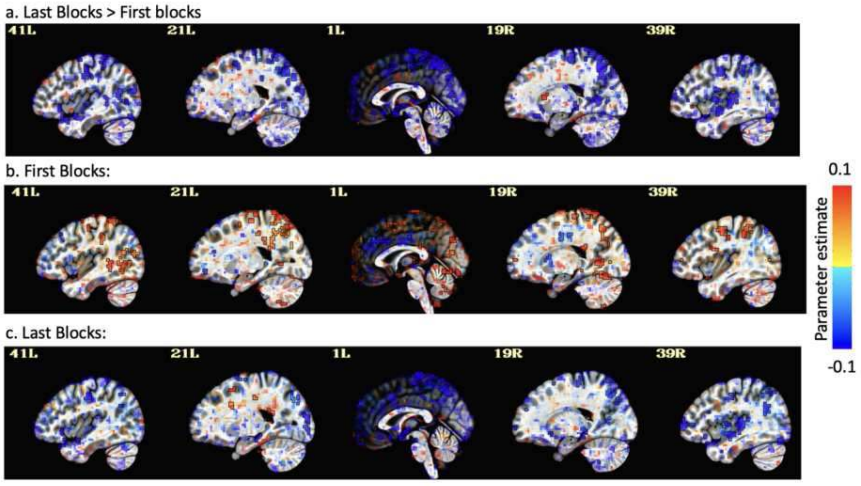

Figure 1. Colors show the value of the effect estimate in the Incongruent > Congruent contrast (hot colors for positive activations, and cold for negative activations) in: a) Last blocks > First blocks, b) the First blocks only, and c) the Last blocks only. Each voxel is thresholded by its t-stat values and the transparent thresholding was applied (5) (Threshold: t = 2.16, bi-sided; p < .05) on a sagittal view.

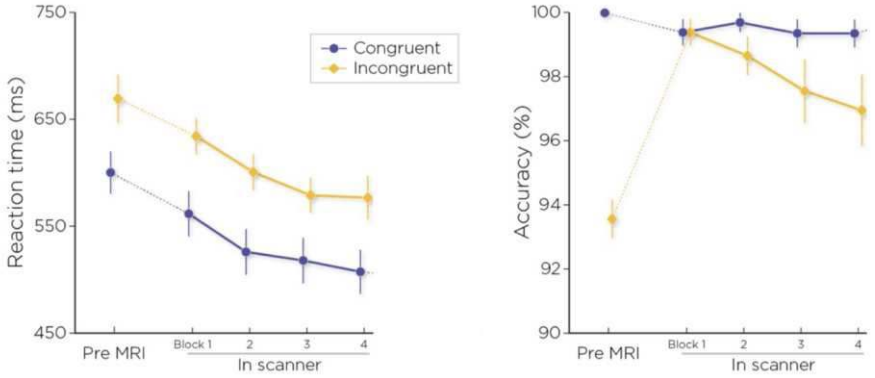

Figure 2. Behavioral performance (reaction time and accuracy) for Congruent and Incongruent trials of the numerical Stroop task.

Conclusions: While more trials should provide more power (2) for rTMS target selection, this analysis indicated that the observed measures in the last blocks differed from those earlier and highly impacted the overall activation estimations. Since behavioral performance kept improving, a likely interpretation is of a learning effect during which one (or both) of two changes occurred: either the IPS was highly involved in the earlier learning stages of the task and became less necessary with practice, with possible shifts to other regions; or the number of IPS neurons necessary for task performance decreased with the optimization caused by practice, with subsequent diminishment of signal. This suggests that defining a rTMS target requires a better understanding of the local and network changes associated with task practice and learning effects to estimate the best parameters.

References

1. Botvinick, M. M. (2001), Conflict monitoring and cognitive control. Psychological review, vol. 108, no. 3, pp. 624
2. Chen, G. (2022). Hyperbolic trade-off: the importance of balancing trial and subject sample sizes in neuroimaging. NeuroImage vol. 247, no.118786.
3. Cox, R.W. (1996), AFNI: software for analysis and visualization of functional magnetic resonance neuroimages. Computers and Biomedical Research, vol. 29, no. 3, pp.162-173.
4. Saad, Z.S. (2009). A new method for improving functional-to-structural MRI alignment using local Pearson correlation. Neuroimage, vol. 44, no. 3, pp. 839–848.
5. Taylor, P. A. (2023). Highlight Results, Don't Hide Them: Enhance interpretation, reduce biases and improve reproducibility. NeuroImage, vol. 274, pp.120138.

Poster No 913

Predictive validity of within and cross brain EEG connectivity indices of infant executive function

Lorena Santamaria[1], Stanimira Georgieva[1], Elizabeth Shephard[2], Anthonieta Looman[2], Daniel Fatori[2], Guilherme Polanczyk[2], Victoria Leong[1,3]

[1]Psychology, Nanyang Technological University, Singapore, Singapore, [2]Department of Psychiatry, Faculdade de Medicina, Universidade de São Paulo, Sao Paulo, Brazil, [3]Department of Pediatrics, Cambridge University, Cambridge, United Kingdom

Introduction: Executive functions (EFs) are core cognitive control skills that predict life success. These skills begin developing during the early years to allow children to sustain attention and resist distraction (inhibitory control), hold and manipulate information in mind (memory updating) and shift attention and strategies to adapt to changing demands (cognitive flexibility) (Fiske and Holmboe 2019; Lehto et al. 2003). EF development occurs within the context of positive social interactions and variations in the quality of parent-child interaction impact EF development. However, little is known about the intra- and interpersonal neural mechanisms (and their relative importance) in mediating influences of parent-child social interaction on early developing executive function skills. Here, we take adopt a computational machine learning approach to objectively contrast the feature importance of within and cross brain connectivity metrics on prediction of infant attention set-shifting performance (a precursor of cognitive flexibility). Importantly, we assess the reproducibility and generalisability of these neural indices by testing their predictive performance (1) within two different countries (each sampled separately) and (2) across countries (a stronger test of generalisation).

Methods: A total of N=96 mother-infant dyads participated in this study across two countries, Brazil (N=57) and Singapore (N=39). Infants were aged, in days, 426±141.65 (SG) and 363±69.38 (BR) respectively. Infant and maternal brain activity were concurrently recorded via electroencephalography (EEG) whilst they performed an object play task to assess parental

scaffolding of infant attention set-shifting (Tan and Leong 2023). Neural connectivity metrics (wPLI,(Vinck et al. 2011)) were computed using within-infant, within-mother and dyadic (mother-infant) EEG data. Identical pre-processing pipelines were used for all neural datasets (within and cross-brain). Graph theory-based metrics were calculated using three different thresholds (10%,15%,20%) to avoid possible bias(Bassett and Sporns 2017). Feature selection was performed using Mutual Information (MI) scoring to determine the best subset of "elite" neural features (pooling across within-infant, within-mother and dyadic indices) to enter into the predictive models. Understanding MI between two variables as a measure of the reduction in uncertainty for one variable given a known value of the other one. Two machine learning models (one linear and one non-linear) were implemented to predict infant shifting performance (2-class median split) using the elite neural indices(Nocedal and Wright 2006; Hastie et al. 2009). Model performance was evaluated using a leave-one-out cross-validation technique.

Results: Overall, model classification performance achieved up to 86.2% accuracy within country, and 74.9% in the combined cross-country transfer scenario. Importantly, MI feature selection revealed that dyadic (mother-infant) metrics were the most important predictors of infant shifting in the cross-country transfer scenario, followed by maternal and infant brain metrics (see Fig 1A). This advantage for dyadic metrics was observed across both types of models (linear and non-linear), as well as across all three threshold values used. The higher MI total score of the dyadic feature indicates a stronger connection between these features and infant EF performance.

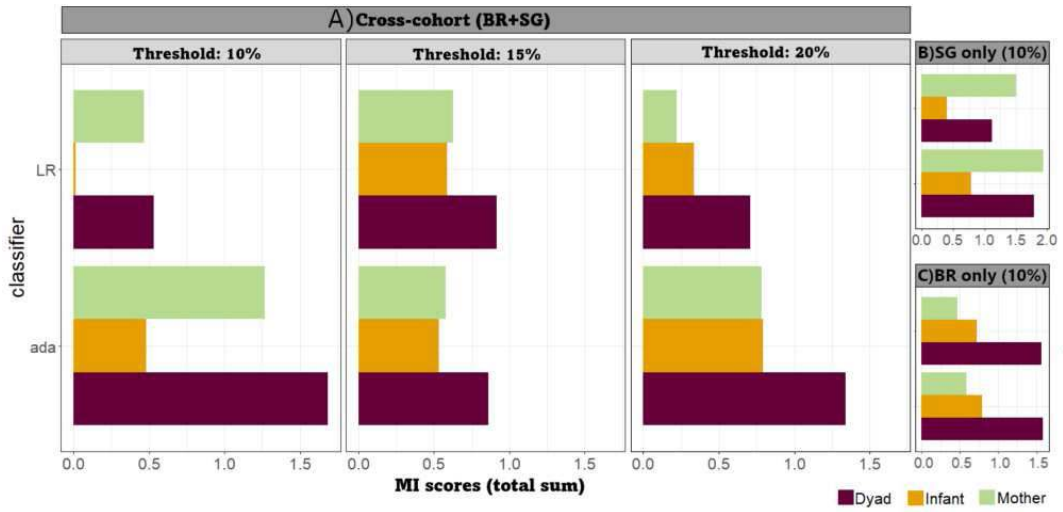

Figure 1. Summary of the MI scores by member: dyad (red), infant (yellow) and mother (green).

Conclusions: Our results suggest that during early life, dyadic measures of parent-infant neural connectivity may provide robust and generalisable indices for the prediction of developing cognition, particularly emerging executive function skills. This empirical validation is an important first step toward developing reliable screening tools for early assessment of EF and its disorders.

References

1. (Fiske et al. 2019; Lehto et al. 2003)
2. (Tan et al. 2023)
3. (Vinck et al. 2011)
4. (Bassett et al. 2017)
5. (Nocedal et al. 2006; Hastie et al. 2009)

Poster No 914

Decoding the Neural Architecture of Compositional Meaning Generalization

Xiaochen Zheng[1], Mona Garvert[2], Hanneke den Ouden[1], Lisa Horstman[3], David Richter[4], Roshan Cools[3]

[1]Donders Institute for Brain, Cognition and Behaviour, Nijmegen, Netherlands, [2]Julius-Maximilians-Universität Würzburg, Würzburg, Germany, [3]Radboud University Medical Center, Nijmegen, Netherlands, [4]Vrije Universiteit Amsterdam, Amsterdam, Netherlands

Introduction: The ability to generalize previously learned knowledge to novel situations is essential for adaptive behavior. We are very good at combining "building blocks" for inferring the meaning of novel compositional words. For example, when encountering the word "un-reject-able-ish" for the first time, one can easily infer its meaning by integrating knowledge

of its constituent parts based on abstract structural rules (such as the sequential order of word parts). In this study, we investigate the neural mechanisms of the ability to infer novel compositional word meanings. Specifically, we aimed to assess whether compositional inference in language recruits a medial prefrontal-hippocampal network that is also recruited by compositional action planning, compositional vision and constructive relational memory (Baram et al., 2021; Barron et al., 2020; Schwartenbeck et al., 2023).

Methods: In a pre-registered fMRI study (aspredicted.org/mk5i2.pdf), we taught 43 participants the meanings of artificial compositional words consisting of known stems ("good") and novel affixes ("kla") (Figure 1A). The meaning of the compositional words depended on the position of the novel affix ("goodkla = bad", "kladog = puppy"). We then asked them to infer the meaning of novel compositional words ("richkla =?", "klarich =?") that were either congruent or incongruent with the established rule ("klarich" is incongruent because a small version of "rich" does not exist). In the scanner, participants performed a semantic priming task in which the novel words served as either congruent ("richkla") or incongruent primes ("klarich") and their synonyms ("poor") served as targets. After the scanning session, they were asked to indicate (i) whether these novel words held any meaning and, (ii) if so, what they meant. Analyses of fMRI data focused on the inferential computation as a function of univariate repetition suppression (Barron et al., 2016) and multivariate representational similarity (RSA, Kriegeskorte et al., 2018).

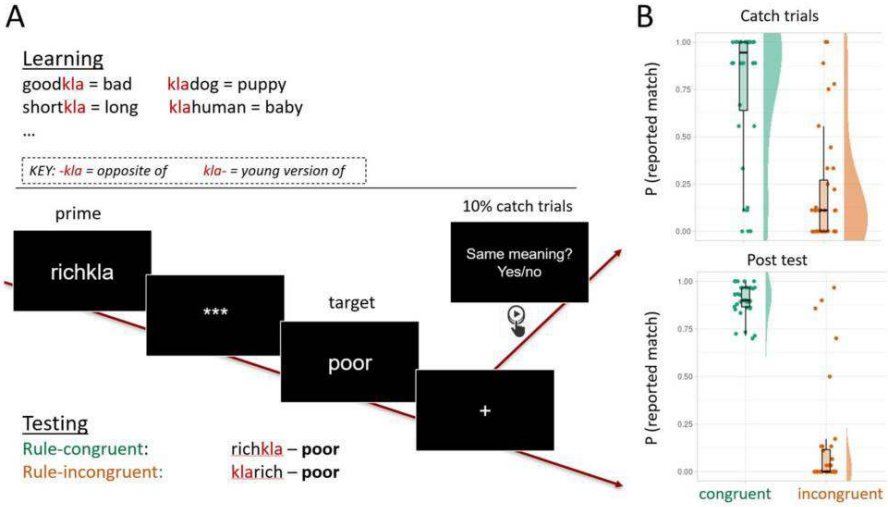

Figure 1. Experimental paradigm and behavioral results. (A) Top: participants learned artificial compositional words consisting of known stems and novel affixes, without being explicitly taught the rules. Bottom: In the scanner, participants were asked to infer the meaning of novel compositional words that were either congruent or incongruent with the learned rules. (B) behavioral response on whether the novel compositional words (prime) matches the target words, as a function of conditions (top: catch trials during the fMRI session; bottom: posttest after the fMRI session).

Results: Our results demonstrated that participants were able to generate novel compositional meanings on the fly, successfully inferring meanings of congruent versus incongruent words (Figure 1B). Univariate analysis of congruent versus incongruent prime-related fMRI activity revealed a broad frontal-parietal network, including the hippocampus, a brain area commonly associated with the generalization process of structural relationships (Figure 2A, top panel). Analysis at target words revealed greater repetition suppression when primed with congruent than incongruent words in the left inferior frontal gyrus, which suggests that novel meanings are presented in this linguistic "building" hub (Figure 2A, bottom panel). Furthermore, multivariate RSA revealed that, excitingly, this representation was already decodable at the time of prime (Figure 2B, "meaning representation"). Intriguingly, RSA also revealed representations of the newly derived abstract rules in a bilateral frontoparietal network (Figure 2B, "rule representation"), also commonly implicated in the representation of task state spaces and abstract rules in working memory for goal-directed action planning.

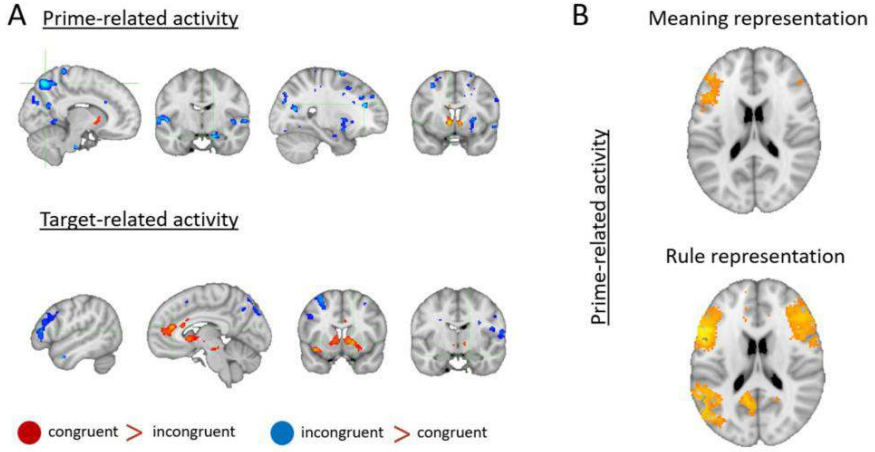

Figure 2. Univariate and multivariate representational similarity analysis of fMRI data. (A) univariate analysis of congruent versus incongruent prime-related BOLD activity (top panel) and target-related activity (ie. repetition suppression, bottom panel). (B) multivariate representational similarity analysis of prime-related activity (top: whole brain searchlight outcome based on a model representing target word meanings; bottom: whole brain searchlight outcome based on a model representing affix rules). All plots thresholded at $p < .001$ (uncorrected).

Conclusions: The compositional nature of language enables us to freely combine morphemes into words, words into sentences, and to convey an infinite array of thoughts and ideas. Using an artificial language learning paradigm, we show that participants are able to generalize recently learned structural rules to infer novel meanings on the fly. This compositional process in language engages a domain-general control network, while newly inferred meanings are represented in more language-specific regions (Hagoort, 2005). Our results demonstrate that our ability to generate novel compositional meaning representations for language recruits abstract rule representations in a frontoparietal network that also represents abstract task representations for generative action selection (Vaidya & Badre, 2022).

References

1. Baram, A. B., Muller, T. H., Nili, H., Garvert, M. M., & Behrens, T. E. J. (2021). Entorhinal and ventromedial prefrontal cortices abstract and generalize the structure of reinforcement learning problems. Neuron, 109(4), 713-723.
2. Barron, H. C., Garvert, M. M., & Behrens, T. E. (2016). Repetition suppression: a means to index neural representations using BOLD?. Philosophical Transactions of the Royal Society B: Biological Sciences, 371(1705), 20150355.
3. Barron, H. C., Reeve, H. M., Koolschijn, R. S., Perestenko, P. V., Shpektor, A., Nili, H., ... & Dupret, D. (2020). Neuronal computation underlying inferential reasoning in humans and mice. Cell, 183(1), 228-243.
4. Hagoort, P. (2005). On Broca, brain, and binding: a new framework. Trends in Cognitive Sciences, 9(9), 416-423.
5. Kriegeskorte, N., Mur, M., & Bandettini, P. A. (2008). Representational similarity analysis-connecting the branches of systems neuroscience. Frontiers in Systems Neuroscience, 4.
6. Schwartenbeck, P., Baram, A., Liu, Y., Mark, S., Muller, T., Dolan, R., ... & Behrens, T. (2023). Generative replay underlies compositional inference in the hippocampal-prefrontal circuit. Cell, 186(22), 4885-4897.
7. Vaidya, A. R., & Badre, D. (2022). Abstract task representations for inference and control. Trends in Cognitive Sciences, 26(6), 484-498.

Poster No 915

A 7T fMRI Pilot Study on Colorectal Cancer-Related Cognitive Impairment

Sharon Chao[1], Nathan Nguyen[1], Tara Riddle[2], Debapriya Dutta[2], Ashley Hill[2], Robert Yu[2], Suparna Mantha[2], Kendrith Rowland[2], Zhaoyue Shi[2]

[1]Carle Illinois College of Medicine, Urbana, IL, [2]Carle Foundation Hospital, Urbana, IL

Introduction: Cognitive impairment affecting executive functions such as information processing speed and working memory has been observed in colorectal cancer patients following diagnosis with no significantly added effects of adjuvant therapy.[1,2] Colorectal cancer-related cognitive impairment (CRCI) has already been studied in the literature using cognitive assessments such as objective neuropsychological testing and subjective self-reported questionnaires.[1,2,3] However, little is known regarding the neural mechanism of colorectal CRCI which makes the development of evidence-based therapies currently unattainable. This study aims to utilize 7T magnetic resonance imaging (MRI) to (1) compare the resting state functional connectivities (rsFC) between early-stage colorectal cancer survivors and healthy controls (HCs), and (2) identify specific brain regions and networks that are associated with CRCI by examining relationships between rsFC node strength and cognitive assessment scores.

Methods: Ten participants included five colorectal cancer survivors (stage I or II, aged 66.2 ± 6.9 years) who had surgery without adjuvant therapy within six months and five age/sex/education matched HCs (aged 64.4 ± 5.4 years). Each underwent cognitive assessments and MRI on the same day. All participants had no prior malignancy or history of neurological disorders. Cognitive assessments included objective neuropsychological tests such as the Trail Making Test (TMT), Hopkins Verbal Learning Test (HVLT), and Controlled Oral Word Association Test (COWAT), as well as subjective self-reported questionnaires including the Functional Assessment of Cancer Therapy-Cognitive Function (FACT-Cog), Beck Depression Inventory (BDI), and State-Trait Anxiety Inventory (STAI). MRI was performed on a Siemens MAGNETOM Terra 7T scanner. MRI acquisition protocol consisted of a T1-weighted MP2RAGE (TR = 4530 ms, TE = 2.32 ms, 0.7 mm3 isotropic) and T2*-weighted BOLD fMRI (TR = 1000 ms, TE = 25 ms, 1.6 mm3 isotropic, 485 volumes). Standard preprocessing steps included distortion correction, motion correction, removal of physiological noise, temporal filtering (0.01-0.1 Hz), spatial smoothing (5mm FWHM Gaussian kernel), and spatial normalization to the MNI152 template (2 x 2 x 2 mm3). Regions of interest (ROIs) within the central executive network (CEN) and default mode network (DMN) as provided in Atlas55+ were selected for further analysis.[4] The average time series for each ROI was calculated across all voxels within that ROI. rsFC node strength was calculated as the average Pearson's correlation coefficient among the time series of a given ROI and the time series of all other ROIs in the network.

Results: The survivor group had significantly higher perceived cognitive impairment ($p<0.05$) and lower information processing speed ($p<0.05$) compared to HCs, as assessed by the FACT-Cog and TMT-A, respectively. There were no significant differences in the HVLT, COWAT, BDI or STAI scores between the two groups. Additionally, the survivor group showed significantly reduced rsFCs in the medial prefrontal cortex (mPFC), anterior cingulate cortex (ACC), and precuneus within the DMN (Fig. 1A), as well as significantly reduced rsFCs in the left middle frontal gyrus (MFG), left inferior parietal gyrus (IPG), and right superior parietal gyrus (SPG) within the CEN compared to HCs (Fig. 1B). Furthermore, among all participants, the rsFC node strengths of the mPFC and ACC were linearly correlated with perceived cognitive impairment scores, and the rsFC node strengths of the SPG and IPG were linearly correlated with TMT-A scaled scores (Fig. 2).

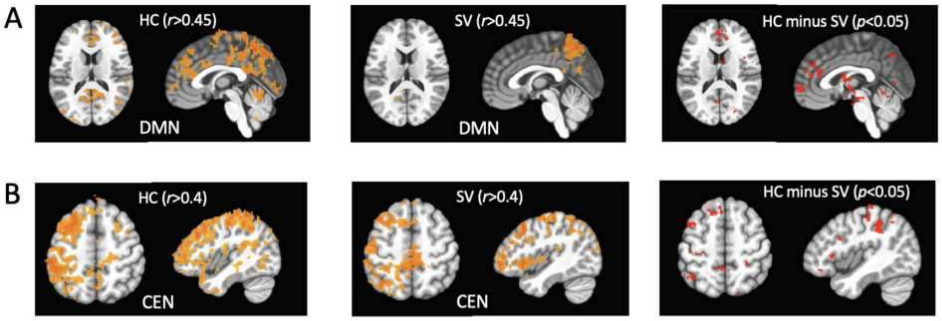

Figure 1. RSFC maps of HCs versus colorectal cancer survivors (SV) for the: **(A)** DMN using the right precuneus as the ROI. The SV group showed significantly lower rsFC among the mPFC, ACC, and precuneus ($p<0.05$). **(B)** CEN using the left MFG as the ROI. The SV group showed significantly lower FC in the left MFG, left IPG, and right SPG ($p<0.05$).

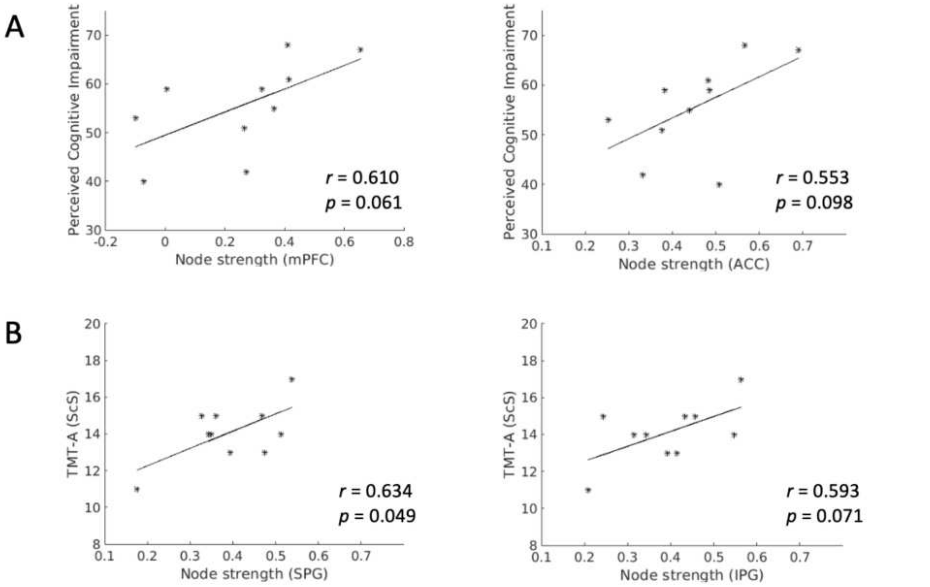

Figure 2. Brain-behavior relationships used to identify brain regions associated with colorectal CRCI. **(A)** Linear relationship between perceived cognitive impairment scores and rsFC node strengths in mPFC and ACC. Perceived cognitive impairment score was calculated from FACT-Cog, such that a higher score corresponded to less perceived cognitive impairment. **(B)** Linear relationship between TMT-A (scaled score) and rsFC node strengths in the right SPF and left IPG.

Conclusions: This ongoing study identified altered brain regions and networks in early-stage colorectal cancer survivors that may be associated with CRCI. Further data collection is currently underway. Findings will help provide biological targets for developing pharmacological or neuro-cognitive interventions for treating colorectal CRCI.

References

1. Vardy, Janette L., et al. "Cognitive function in patients with colorectal cancer who do and do not receive chemotherapy: a prospective, longitudinal, controlled study." Journal of Clinical Oncology 33.34 (2015): 4085.
2. Visovatti, Moira A., et al. "Assessment of cognitive impairment and complaints in individuals with colorectal cancer." Oncology nursing forum. Vol. 43. No. 2. NIH Public Access, 2016.
3. Vardy, J., et al. "Cognitive function and fatigue after diagnosis of colorectal cancer." Annals of oncology 25.12 (2014): 2404-2412.
4. Doucet, Gaelle E., et al. "Atlas55+: brain functional atlas of resting-state networks for late adulthood." Cerebral Cortex 31.3 (2021): 1719-1731.

Poster No 916

Neural Correlates of Impaired Cognitive Control in Individuals with Methamphetamine Dependence

Ani Zerekidze[1], Meng Li[1], Nooshin Javaheripour[2], Laura Huff[1], Thomas Weiss[3], Martin Walter[2], Gerd Wagner[1]

[1]Jena University Hospital, Jena, Thuringia, [2]Jena University Hospital, Jena, Germany, [3]Friedrich Schiller University, Jena, Thuringia

Introduction: The abuse of methamphetamine (crystal meth) has markedly increased in the last decades (UNODC 2022), which gave rise to the discussion about its harmful effects on the brain function because of its strong and direct impact on the central nervous system. Because of these wide-ranging neurochemical effects of methamphetamine intake, chronic abuse of crystal meth has been related to alteration in several cognitive domains (Homer et al. 2008; Chang et al. 2002; Salo et al. 2002; Potvin et al. 2018). Impaired cognitive and behavioral control has often been observed in people who use methamphetamine. A meta-analysis of 18 studies summarized that individuals with methamphetamine use disorders showed medium size deficits in cognitive control functions involving response inhibition and problem-solving (Scott et al. 2007). The findings of abnormal cognitive control functions coincides well with the clinical observations (Monterosso et al. 2005; Rubenis et al. 2018). However, a comprehensive understanding of the neural substrates underlying these impairments is still lacking. The goal of the present study was to study the neural correlates of impaired cognitive control in individuals with methamphetamine dependence. As the cognitive control was associated with activation in dorsolateral prefrontal cortex,

anterior cingulate cortex, and striatal regions, we expected to find a reduced blood oxygenation level dependent signal in these brain regions in individuals with MA dependence, particularly in the incongruent condition of Stroop test. We also expected to find an association between altered brain activation and impaired behavioral performance in the task.

Methods: Eighteen individuals with methamphetamine dependence and twenty-one healthy controls were investigated by the manual version of the Stroop task (Wagner et al. 2015) in an event-related fMRI design. All imaging data were collected on a 3 T whole body system equipped with a 64-element head matrix coil (MAGNETOM PRISMA FIT, Siemens Healthineers, Erlangen, Germany). Firstly, a structural T1 image was acquired followed by the Stroop test, presented in the MR scanner to measure activation patterns in dorsolateral prefrontal cortex, anterior cingulate cortex, and striatal regions with respect to the degree of cognitive control during a Stroop task. Impulsivity was assessed by a German version of the impulsive behavior scale (Schmidt, Gay, and Van der Linden 2008), exploring four dimensions of impulsivity: lack of premeditation, urgency, sensation seeking, and lack of perseverance.

Results: Patients were found to have significantly poorer overall accuracy in the Stroop task and higher self-rated impulsivity. Comparing brain activations during the task, decreased activation in the dorsolateral prefrontal cortex, anterior midcingulate cortex, and dorsal striatum was observed in individuals with methamphetamine dependence, compared to healthy controls. Altered functional magnetic resonance imaging signal in dorsolateral prefrontal cortex and anterior midcingulate cortex significantly correlated with impaired behavioral task performance in individuals with methamphetamine dependence. Furthermore, significantly lower and pronounced brain activations in the methamphetamine group were additionally detected in several sensory cortical regions, i.e., in the visual, auditory, and somatosensory cortices. The results of the current study provide evidence for the negative impact of chronic crystal meth consumption on the proper functioning of the fronto-cingulate and striatal brain regions, presumably underlying the often-observed deficits in executive functions in individuals with methamphetamine use disorder.

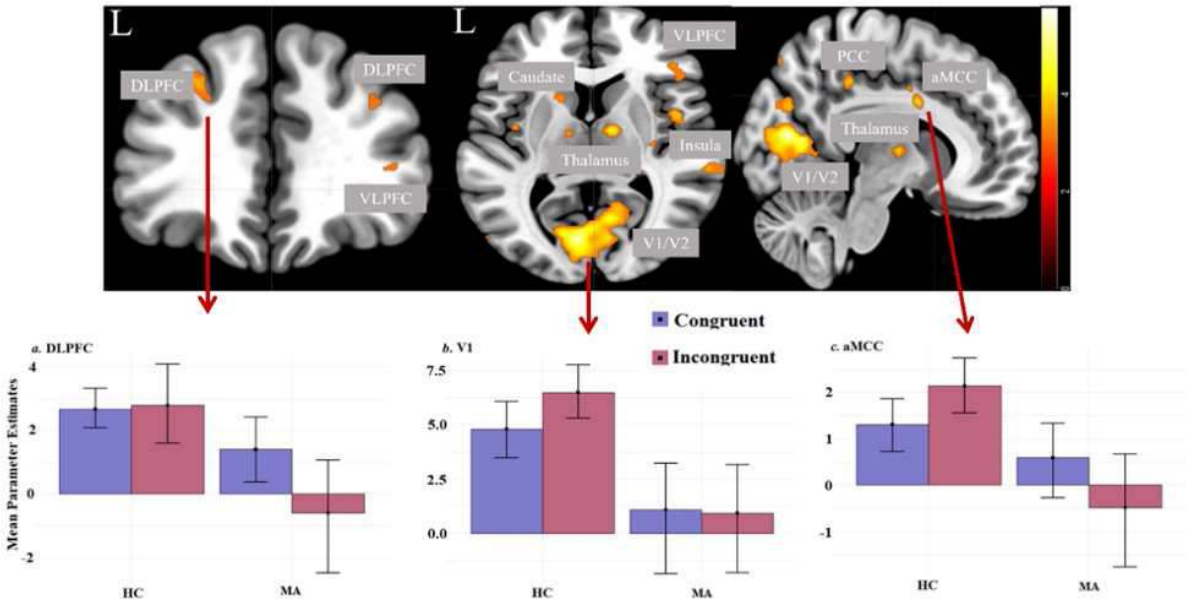

Significant group differences in brain activation during the incongruent Stroop task condition voxel-level: $p < 0.001$ uncorr., cluster-level: corrected according to expected voxels per cluster ≥ 16)

Conclusions: In this study, we observed decreased brain activation during the Stroop task performance in the fronto-cingulate and striatal regions, but also, as a new finding, in several sensory cortical regions in methamphetamine abusers relative to healthy controls.

References

1. Chang, L., et al. (2002). "Perfusion MRI and computerized cognitive test abnormalities in abstinent methamphetamine users." Psychiatry Res, vol. 114(2), pp. 65-79.
2. Homer, B. D., et al. (2008). "Methamphetamine abuse and impairment of social functioning: a review of the underlying neurophysiological causes and behavioral implications." Psychol Bull, vol. 134(2), pp. 301-310.
3. Monterosso, J. R., et al. (2005). "Deficits in response inhibition associated with chronic methamphetamine abuse." Drug Alcohol Depend, vol. 79(2), pp. 273-277.
4. Potvin, S., et al. (2018). "Cognitive deficits in individuals with methamphetamine use disorder: A meta-analysis." Addict Behav, vol. 80, pp. 154-160.

5. Rubenis, A. J., et al. (2018). “Impulsivity predicts poorer improvement in quality of life during early treatment for people with methamphetamine dependence.” Addiction, vol. 113(4), pp. 668-676.
6. Salo, R., et al. (2002). “Preliminary evidence of reduced cognitive inhibition in methamphetamine-dependent individuals.” Psychiatry Res, vol. 111(1), pp. 65-74.
7. Schmidt, R. E., et al. (2008). “Facets of impulsivity are differentially linked to insomnia: evidence from an exploratory study.” Behav Sleep Med, vol. 6(3), pp.178-192.
8. Scott, J. C., et al. (2007). “Neurocognitive effects of methamphetamine: a critical review and meta-analysis.” Neuropsychol Rev, vol. 17(3), pp. 275-297.
9. UNODC (2022). World Drug Report 2022. Drug Market Trends, United Nations Publication. 4.
10. Wagner, G., et al. (2015). “Structural and functional dysconnectivity of the fronto-thalamic system in schizophrenia: a DCM-DTI study.” Cortex, vol. 66, pp. 35-45.

Poster No 917

The Role of VLPFC in the Link Between Low Self-Efficacy and Self-Protective Behavior

Jinhee Kim[1], Hackjin Kim[1]

[1]Korea University, Seoul, Republic of Korea

Introduction: Self-efficacy, defined as individual’s belief in their ability to achieve goals (Bandura, 2014), is recognized as a protective factor for mental health (Schönfeld et al., 2016). While empirical evidence suggests its role as a buffer against others’ opinions, its underlying neural mechanism remains unknown.

Methods: This study involved 36 participants undergoing functional magnetic resonance imaging (fMRI) during a reciprocal artwork evaluation task (Yoon et al., 2018). Each trial of the task included two phases: receiving an evaluation of one’s own artwork from a partner and evaluating the same partner’s artwork. Task-based fMRI data were collected using a 3-Tesla Siemens Tim Trio MRI scanner (the multi-band accelerated EPI sequence with factor 4, TR/TE = 1200/33.2 ms, 60 2.5-mm3 slices, approx. 20 min duration). Images were pre-processed using SPM 12, which included slice timing correction, realignment, co-registration normalization, and spatial smoothing with a 6 mm Gaussian kernel. A reinforcement learning model was used to analyze choice behavior influenced by social evaluative feedback. This model was used to estimate learning rates, trial-by-trial self-protection values, and signed prediction errors (PE), with the latter two being used as parametric modulators in the first-level general linear model analyses. Participants’ self-efficacy trait was assessed using the general self-efficacy scale, and a whole-brain correlation analysis was conducted between neural parameters (i.e., PE and self-protection value) and the self-efficacy scores. Intersubject representational similarity analysis (IS-RSA) was used to explore multivariate neural representations of PE and self-protection value in relation to self-efficacy.

Results: Behavioral results indicated that lower self-efficacy was associated with higher learning rates for negative evaluative feedback. The right ventrolateral prefrontal cortex (VLPFC) encoded PE at the feedback receipt phase, and this encoding was linked to individual differences in self-efficacy. Specifically, individuals with high self-efficacy exhibited increased VLPFC activity in response to unpredicted positive feedback, whereas those with low self-efficacy showed increased activity for unpredicted negative feedback. Furthermore, IS-RSA revealed that individual variability in self-efficacy was reflected in the neural representation of bilateral VLPFC encoding PE.

Conclusions: In summary, these findings suggest that the VLPFC, implicated in emotional regulation, track different aspects of social feedback depending on individual differences in self-efficacy. This provides a neural explanation for the self-protective bias observed in individuals with lower self-efficacy in response to negative social feedback.

Acknowledgements
This research was supported by Basic Science Research Program through the National Research Foundation of Korea (NRF) funded by the Ministry of Education (2020R1I1A1A01070413), Bio & Medical Technology Development Program of the National Research Foundation (NRF) funded by the Korean government (MSIT) (NRF-2021M3A9E4080780), and a Korea University Grant.

References

1. Bandura, A. (2014). Self-efficacy mechanism in psychobiologic functioning. Self-Efficacy, Taylor & Francis: 355-394.
2. Schönfeld, P., et al. (2016). “The effects of daily stress on positive and negative mental health: Mediation through self-efficacy.” Int J Clin Health Psychol 16(1): 1-10.
3. Yoon, L., et al. (2018). “Development of MPFC function mediates shifts in self-protective behavior provoked by social feedback.” Nat Commun 9(1): 3086.

Poster No 918

Varying task demands show that social perception is distributed over both cortical surface and depth

Logan Dowdle[1], Luca Vizioli[1], Essa Yacoub[1], Geoff Ghose[1]

[1]*Center for Magnetic Resonance Research, Minneapolis, MN*

Introduction: Human faces are a remarkable visual stimulus, in that subtle changes in perceived features supports a powerful information classification system. For example, social categories, such emotive state, are of obvious and immediate behavioral relevance but characterized by modest changes in visual input. Previous research has identified a clear network of brain regions that favor faces relative to other stimulus categories (Haxby et al., 2001; Kanwisher and Yovel, 2006), however, how faces are actually processed to extract social meaning remains unknown. Previous work from our group suggests that the use of face-stimulus relevant tasks, opposed to somewhat generic tests of memory such as N-back, may be necessary to characterize these complex networks (Dowdle et al., 2021). Here we extend these previous findings under a social perception framework, and acquire neuroimaging data at fine spatial and fast temporal scales.

Methods: Nine participants completed a non-social color task and two social tasks: perception of gender and perception of expression. Across two separate visits we obtained separate high spatial (fine session; 0.8mm isotropic) and high temporal (fast session; 0.5s) resolution 7 Tesla BOLD images. Participants viewed partially degraded faces (1s on, 2 to 6s ISI) and made 2AFC choices (male/female; happy/neutral, blue/red border). Stimuli and timing were identical across tasks. NORDIC denoising (Vizioli et al., 2021) was applied to maximize SNR. Responses to each stimulus class and task-specific hemodynamic responses were estimated using a finite impulse response (FIR) model. Activations were examined under the typical univariate framework as well as a cross-validated multivariate pattern analysis (MVPA) searchlight approach to determine cortical areas that contain information sufficient to distinguish the tasks. This searchlight was employed across the entire cortical surface for the fast session (averaging over depths), as well as for 3 unique cortical depths within the fine spatial session. Typical face regions of interest (ROIs) were derived using a separate face localizer task, completed for both sessions. (Stigliani et al., 2015).

Results: In univariate analyses (Fig 1A), the non-social task showed significantly weaker responses ($p<0.05$, corrected) in the fusiform face and occipital face areas (FFA; OFA) compared to social tasks (Fig 1B). However, no significant differences were found between the two social perception tasks (Fig 1C). For the whole-brain searchlight, we reproduced univariate findings and were able to decode non-social versus social in typical face ROIs. In addition, we also observe significant ($pFWE<0.05$, permutation corrected) decoding between the 2 social tasks, notably outside of typical ROIs, spread across the cortical surface (Fig 2). Zooming in to the ventral temporal cortex, we find that decoding between the social tasks differs across cortical depths – with evidence that in the anterior temporal cortex the outer depths contain more information to separate social tasks, while for the posterior regions, this decoding is more successful in the inner depths.

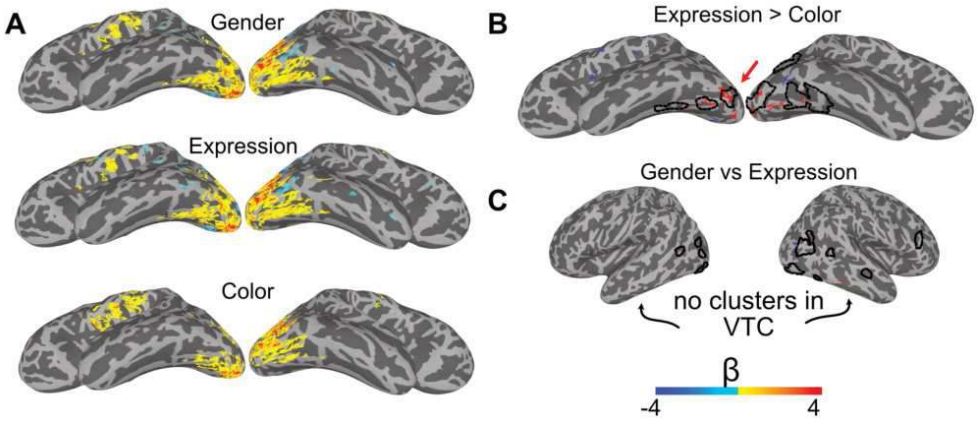

Fig 1. A) Similar responses in Tasks, B) Differences between social vs. non social. C) No sign. differences observed between 2 social tasks. Black outlines show typical ROIs.

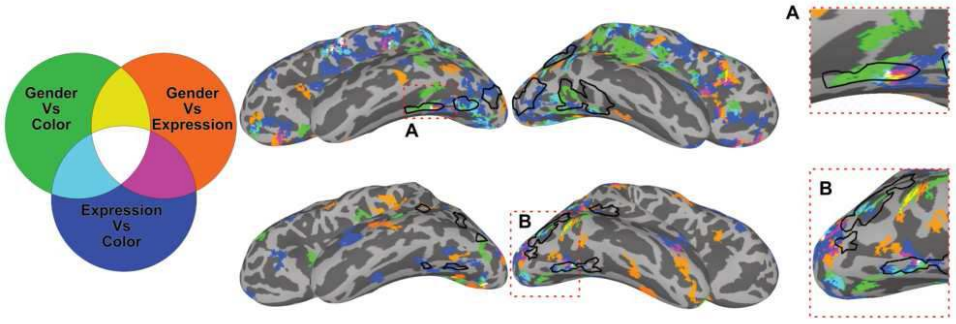

Fig 2. Color denotes successful decoding between single or multiple task pairs with clusters pFWE<0.05. A) Subpopulations of decoding accuracy. B) Social task decoding outside typical ROIs.

Conclusions: Through the lens of socially relevant task demands and high spatial and temporal resolution brain imaging we observe signals that: 1) are manipulated by task demands, 2) show information content outside of typical face areas, 3) may not be resolvable with typical acquisition strategies and 4) are relevant to naturalistic processes. Our depth dependent findings suggest that, for the ventral temporal cortex, averaging over depths may obscure information. Collectively these results underscore fMRI's ability to capture dynamic changes across multiple scales based on moment-to-moment perceptual demands.

References

1. Dowdle, L.T. (2021), Clarifying the role of higher-level cortices in resolving perceptual ambiguity using ultra high field fMRI. NeuroImage 227, 117654. https://doi.org/10.1016/j.neuroimage.2020.117654
2. Haxby, J.V. (2001), Distributed and overlapping representations of faces and objects in ventral temporal cortex. Science 293, 2425–2430. https://doi.org/10.1126/science.1063736
3. Kanwisher, N. (2006), The fusiform face area: a cortical region specialized for the perception of faces. Philosophical Transactions of the Royal Society B Biol. Sci. 361, 2109–2128. https://doi.org/10.1098/rstb.2006.1934
4. Stigliani, A. (2015), Temporal Processing Capacity in High-Level Visual Cortex Is Domain Specific. Journal of Neuroscience. 35, 12412–12424. https://doi.org/10.1523/JNEUROSCI.4822-14.2015
5. Vizioli, L., (2021), Lowering the thermal noise barrier in functional brain mapping with magnetic resonance imaging. Nature Communication 12, 5181. https://doi.org/10.1038/s41467-021-25431-8
6. Supported by National Institutes of Health RF1 MH117015

Poster No 919

Connectome-based predictive models of cognitive control based on volumetric versus grayordinate data

Shijie Qu[1], Kwangsun Yoo[2], Marvin Chun[1]

[1]Yale University, New Haven, CT, [2]Sungkyunkwan University, Seoul, Korea, Republic of

Introduction: Connectome-based predictive modeling (CPM, Finn et al., 2015; Shen et al., 2017) can predict individual cognitive differences based on variations in brain connectomes. Here, we develop resting-state connectome models to predict different aspects of cognitive control (Miyake et al., 2000). In doing so, we also compared models based on volumetric vs. grayordinate data, and we found grayordinate models to be more predictive of behavior and more generalizable across tasks.

Methods: For this study, we used neuroimaging data from the latest release of the WU-Minn Human Connectome Project (HCP) dataset (Van Essen et al., 2013), which contains data from approximately 1200 healthy adults, including neuroimaging and behavioral measurements. We focused on resting-state fMRI data and cognitive control-related behavioral measurements. The resting-state fMRI data comes from the first session, consisting of two 15-minute runs. The volumetric data were minimally preprocessed using the default pipeline, as illustrated in (Glasser et al., 2013). We further regressed out the motion parameters, white matter, cerebrospinal fluid signals, global signals, as well as linear trends. The grayordinate data, provided by HCP, preserves only gray matter signals, and represents cortical areas using 2-D vertices instead of 3-D voxels. The data were preprocessed using the pipelines described in Smith et al. (2013), which additionally use the ICA-FIX method to denoise the data. Since ICA-FIX already handled motion regression and linear detrending, here we only further regressed out white matter signals, cerebrospinal fluid signals, and global signals for grayordinate data. When generating the functional connectivity matrices, we used the Shen268 (Shen et al., 2013) atlas for volumetric data and the Cole-Anticevic atlas (Ji et al.,

2019) for grayordinate data. For behavioral data, we included corresponding measurements for out-of-scanner list sorting, card sorting, and flanker tasks-three established tasks that respectively tap into three cognitive-control-related components: working memory update, set switching, and response inhibition (Miyake et al., 2000). Between each combination of data format and behavioral measurement, we trained a CPM model with 10-fold cross-validation and repeated the procedure 1000 times to obtain reliable estimates of CPM performance. Pearson correlation coefficients are calculated to represent model predictive performance.

Results: Connectome-based predictive models based on volumetric data or grayordinate data significantly predicted individual differences in the tasks they were trained on (all p's < .05, all r's > .12). Grayordinate-data models significantly ($p < .05$) outperformed volumetric-data models for list sort and card sort within-task testing (tasks used for model training with 10-fold cross-validation) and for all cross-task testing (tasks not used for model training), even after controlling for the number of edges used for model testing. Lastly, anatomical analyses of the predictive edges revealed that the models trained on grayordinate data captured a denser group within and between frontal-parietal, cingulo-opercular, and default networks. Conversely, models trained on volumetric data covered a broader range of edges, including additional motor and visual networks.

Conclusions: Overall, we identified several differences in the application of grayordinate versus volumetric fMRI data in CPM analysis of cognitive control. Further analyses are needed to understand the reasons for these differences and their implications for dissociating components of cognitive control and their underlying neural networks.

References

1. Finn, E. S. (2015). 'Functional connectome fingerprinting: identifying individuals using patterns of brain connectivity', Nature neuroscience, vol. 18, no. 11, pp. 1664–1671
2. Glasser, M. F. (2013), 'The minimal preprocessing pipelines for the Human Connectome Project', NeuroImage, vol. 80, pp. 105–124
3. Ji, J. L. (2019), 'Mapping the human brain's cortical-subcortical functional network organization', NeuroImage, vol. 185, pp. 35–57
4. Miyake, A. (2000), 'The unity and diversity of executive functions and their contributions to complex "Frontal Lobe" tasks: a latent variable analysis', Cognitive psychology, vol 41, no. 1, pp. 49–100
5. Shen, X. (2013), 'Groupwise whole-brain parcellation from resting-state fMRI data for network node identification', NeuroImage, vol. 82, pp. 403–415
6. Shen, X. (2017), 'Using connectome-based predictive modeling to predict individual behavior from brain connectivity', Nature protocols, vol. 12, no. 3, pp. 506–518
7. Smith, S. M. (2013), 'Resting-state fMRI in the Human Connectome Project', NeuroImage, vol. 80, pp. 144–168
8. Van Essen, D. C. (2013), 'The WU-Minn Human Connectome Project: an overview', NeuroImage, vol. 80, pp. 62–79

Poster No 920

Common and Distinct Brain Correlates of Cognitive Flexibility Tasks: Quantitative fMRI Meta-analyses

Zhanna Chuikova[1], Andrei Filatov[1], Andrei Faber[1], Marie Arsalidou[2]

[1]HSE University, Moscow, Russian Federation, [2]York University, Toronto, Canada

Introduction: Cognitive flexibility is the ability to switch between different tasks, ideas or strategies (Miyake et al., 2000). Although the Wisconsin card sorting test (WCST) and the task switching paradigm (TSP; Shallice, 2008) are popular in assessing cognitive flexibility, the WCST relies on rule discovery whereas for the TSP the rule is known. Meta-analyses of functional magnetic resonance imaging (fMRI) studies examined brain responses to these tasks and identified a set of areas including frontoparietal cortices (Rodríguez-Nieto et al., 2022; Zhang et al., 2021). Critically, no study to date has directly contrasted WCST and TSP. We examine for the first time common and distinct concordance in brain responses between the WCST and the TSP, as well as between TSP's subtypes using quantitative meta-analyses.

Methods: Literature searches were conducted in PubMed and Web of Science databases using the following search string: ("cognitive flexibility" OR "set-shifting" OR "task-switching") AND (fMRI). The search yielded a total 3973 results, out of which 67 articles met the eligibility criteria. There were 15 WCST (25 experiments) and 52 TSP articles (69 experiments). Among TSP articles there were 18 contained attribute switching (24 experiments), 20 with operation switch (20 experiments), and 13 with response rule switching (13 experiments). Activation likelihood estimation (ALE; version 3.0.2) was used for quantitative evaluation of brain activation patterns (Eickhoff et al., 2009). Statistical maps of individual analyses were thresholded at $p < .05$ using a cluster-level family-wise error correction for multiple comparisons, and a cluster-forming threshold at $p < .001$. Contrast and conjunction analyses were thresholded at $p < .01$ uncorrected (10,000 permutations, 200 mm^3 minimum volume).

Results: The WCST shows concordance in frontoparietal and cingulo-opercular areas, namely in inferior (BA 47) and medial frontal gyri (BA 8) in both hemispheres, left insular, left inferior parietal lobule, and right thalamus. Regarding the TSP, areas with the highest likelihood of being detected are left medial frontal gyrus (BA 8), left inferior parietal lobule (BA 40), and

left middle frontal gyrus (BA 9) which are part of the first three largest clusters. Conjunction analysis revealed common concordance for the WCST and the TSP in left lateralized frontoparietal areas with a single exception for the claustrum, which was bilateral. Contrast analysis showed that the WCST was associated with increased engagement in multiple cortical and subcortical regions in both hemispheres. We highlight the implication of frontopolar areas (Brodmann Area 10), fusiform gyri, insular cortex, thalamus and caudate nucleus. TSP's specific activation was found only in the left cingulate gyrus. No significant differences in concordance were observed among the three task switching paradigm types.

Conclusions: Both tasks implicate frontoparietal and cingulo-opercular locations mainly in the left hemisphere. These regions are implicated in all sorts of executive functions such as working memory, inhibition and switching that are necessary for flexible thinking. Importantly, the WCST showed increased concordance mainly in frontopolar regions and subcortical areas in both hemispheres, which may be associated with the increased demands required for sorting rule discovery. The lack of distinctions we observe among the three TSP types of switching supports that the general cognitive task demands are comparable (i.e., not significantly different). Our meta-analysis revealed that frontoparietal brain regions associated with task-switching appear to be largely comparable across diverse task contexts and are not significantly influenced by them. We propose a neuroanatomical map of cognitive flexibility in stereotaxic space (Figure 1). This map will be useful for future studies that examine cognitive flexibility in samples with and without neurodevelopmental disorders.

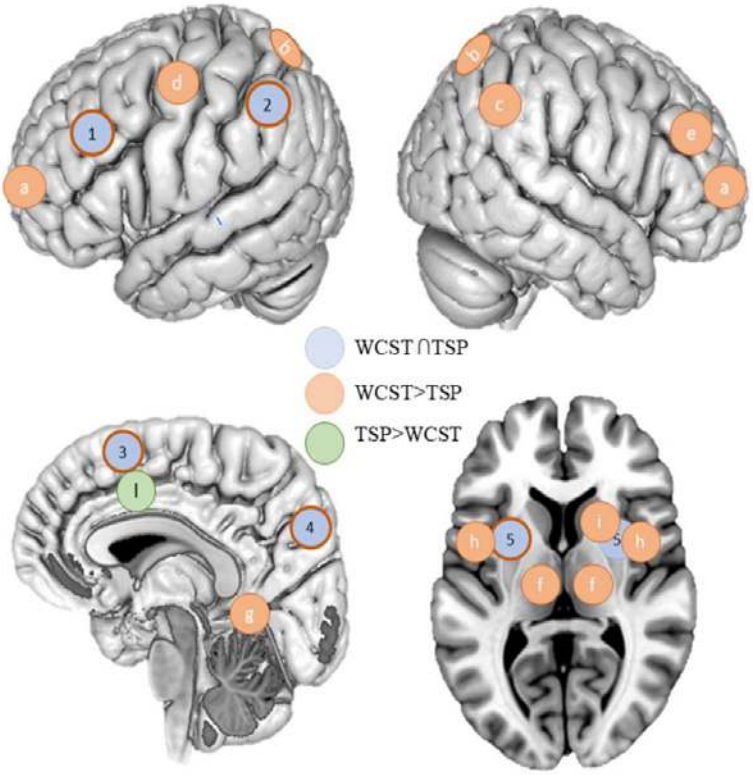

Figure 1. Common and distinct areas for the WCST and the TSP

References

1. Eickhoff, S. B. (2009), 'Coordinate-based activation likelihood estimation meta-analysis of neuroimaging data: A random-effects approach based on empirical estimates of spatial uncertainty', Human Brain Mapping, vol. 30, no. 9, pp. 2907–2926
2. Miyake, A. (2000), 'The Unity and Diversity of Executive Functions and Their Contributions to Complex "Frontal Lobe" Tasks: A Latent Variable Analysis', Cognitive Psychology, vol. 41, no. 1, pp. 49–100
3. Rodríguez-Nieto, G. (2022), 'Inhibition, Shifting and Updating: Inter and intra-domain commonalities and differences from an executive functions activation likelihood estimation meta-analysis', NeuroImage, vol. 264
4. Shallice, T. (2008), 'Mapping task switching in frontal cortex through neuropsychological group studies', Frontiers in Neuroscience, vol. 2, no. 1, pp. 79–85
5. Zhang, Z. (2021), 'Neural substrates of the executive function construct, age-related changes, and task materials in adolescents and adults: ALE meta-analyses of 408 fMRI studies', Developmental Science, vol. 24, no. 6.

Poster No 921

Eyetracking & DeepLearning Model for Executive Function during Visual Encoding in Psychosis and OCD

Jungha Lee[1], Minah Kim[2], Soo Yong Lee[3], Minji Ha[1], Inkyung Park[4], Youngeun Cho[5], Moonyoung Jang[2], Sunghyun Park[2]

[1]Seoul National University, Seoul, Seoul, [2]Department of Neuropsychiatry, Seoul National University Hospital, Seoul, Seoul, [3]KAIST, Daejeon, Daejeon, [4]Seoul National University, Seoul, -, [5]Seoul National University, Seoul, Seoul

Introduction: Executive function and visuospatial memory are often impaired in patients with psychosis and obsessive-compulsive disorder (OCD), and other various psychiatric and neurological disorders. To directly and rapidly assess such deficits linking them to underlying brain dysfunctions, a biomarker-based assessment is needed, with potential applications to a wider range of disorders. This study aimed to develop a foundational eye-tracking-based deep learning model using the Rey-Osterrieth Complex Figure Test (RCFT) to assess executive function during visuospatial memory encoding. Initially devised from patients with early psychosis, OCD, and healthy controls (HCs), with potential for expansion to other psychiatric and neurological disorders.

Methods: Eye-tracking was conducted in 56 patients with first-episode psychosis (FEP), 26 subjects at clinical high risk for psychosis (CHR), 70 OCD patients, and 125 HCs during a 3-minute RCFT figure memorization. The fixation points, where the eyes focus on specific areas, were converted into scanpath images, training Convolutional Neural Networks (CNN) to extract visuospatial eye movement patterns alongside conventional RCFT organization scores for executive function and immediate recall scores for visuospatial memory. The raw fixation points were also used to train Long-Short-Term-Memory (LSTM) to extract sequential eye movement patterns, using the same conventional RCFT scores.

Results: The CNN model accurately predicted executive function (F1 score: 95.65%) and visual memory (F1 score: 92.5%) for superior and impaired levels. The LSTM model accurately predicted executive function (F1 score: 81.19%) and visual memory (F1 score: 94.06%) for superior and impaired levels in early psychosis and OCD, regardless of their disease diagnosis.

Conclusions: These findings suggest that the eye-tracking and deep learning based RCFT model can provide a more direct and rapid assessment tool for executive function in visuospatial memory encoding, with potential future applications to other psychiatric and neurological disorders.

References

1. Kim, M.-S., Namgoong, Y., & Youn, T. (2008). Effect of organizational strategy on visual memory in patients with schizophrenia. Psychiatry and Clinical Neurosciences, 62(4), 427–434. https://doi.org/10.1111/j.1440-1819.2008.01821.x
2. Savage, C. R., Baer, L., Keuthen, N. J., Brown, H. D., Rauch, S. L., & Jenike, M. A. (1999). Organizational strategies mediate nonverbal memory impairment in obsessive–compulsive disorder. Biological Psychiatry, 45(7), 905–916. https://doi.org/10.1016/s0006-3223(98)00278-9
3. Seidman, L. J., Lanca, M., Kremen, W. S., Faraone, S. V., & Tsuang, M. T. (2003). Organizational and visual memory deficits in schizophrenia and bipolar psychoses using the Rey-osterrieth complex figure: Effects of duration of illness. Journal of Clinical and Experimental Neuropsychology, 25(7), 949–964. https://doi.org/10.1076/jcen.25.7.949.16482
4. Rey, A. (1941). L'examen psychologique dans les cas d'encéphalopathie traumatique. (Les problems.) [The psychological examination in cases of traumatic encepholopathy. Problems]. Archives de Psychologie, 28, 215–285.

Poster No 922

Neural mechanisms of craving and buying behahior in subclinical compulsive shoppers: a 3T fMRI study

ChengHsiang Tsai[1], Tsai-Jing Yang[2], Jen-Ruey Hsueh[3], Chun-Chia Kung[1], Huiyi Luo[4]

[1]National Cheng Kung University, Tainan, Taiwan, [2]National Cheng Kung University(NCKU), Tainan, Taiwan, [3]I-Shou University, Kaohsiung, Taiwan, [4]National Chung-Hsing University, Taichung, Taiwan

Introduction: Compulsive shopping is a prevalent societal ailment in modern society, with an estimated prevalence rate of 8~10%. In behavioral research, there has been a clear definition of compulsive buying (CB) disorder. Previous studies in neuroeconomics have also identified the brain regions involved in human decision-making during shopping. However, neuroimaging research on the neural mechanisms of CB populations seems very limited. Therefore, this study uses functional magnetic resonance imaging (fMRI) to compare the neural underpinnings associated with craving and purchasing behavior in individuals with subclinical compulsive shopping tendencies vs. normal controls.

Methods: This study firstly used two screening instruments to identify general shoppers (i.e., control group) and compulsive shoppers (i.e., experimental group, also called subclinical CBers). Faber and O'Guinn (1992) developed their compulsive-

buying scale (CBS) and the scale has been used widely in consumer research. However, only using CBS might underestimate the ratio of compulsive buying. Therefore, we include the Richmond Compulsive Buying Scale (RCB) and the scale was developed based on the theoretical classification of CB as an obsessive–compulsive spectrum disorder (Ridgway et al., 2008). After recruiting participants, we conducted an fMRI experiment on each valid respondent. In the fMRI session, participants completed two shopping tasks. The first task required participants to rate their cravings for each product (with relevant descriptions) within 20 seconds (on a scale of 1 to 4 and indicating low to high craving). The second task mimicked the experimental design of Knuton et al. (2007), in which participants viewed the product image for 4 seconds, followed by 4 seconds of added product price, then 4 seconds to decide whether to purchase the product or not, and ended with a variable fixation period of 4 to 8 seconds until the subsequent trial.

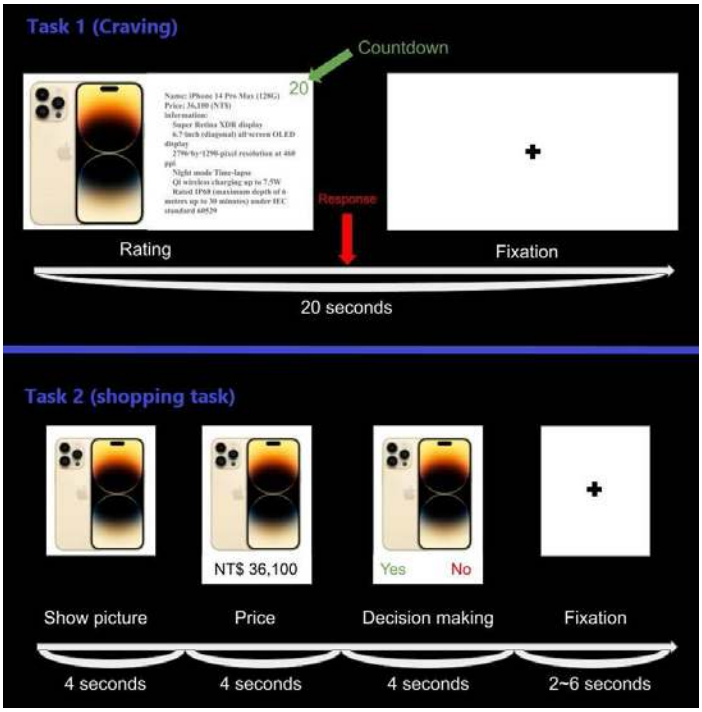

Results: In total, 115 participants were recruited from a number of general internet discussion forums, and community sites (e.g., Dcard, PTT Bulletin Board System). After two screening instruments (CBS and RCB), we recruited six subclinical CBers and four no CBers. Then, the study utilized General Linear Model (GLM) analysis to compare the differences in brain activation between the control and experimental groups. In the first task, it was observed that the activation in the posterior cingulate cortex (PCC) significantly increased when the CB group viewed high-craving (rated 4) compared to low-craving products (rated 1). This phenomenon was not observed in the control group. In other words, PCC seems to play a crucial role in reward-related behaviors and decision-making of CB participants. In the second task, the CB group exhibited higher nucleus accumbens (NAcc) activities in the “buy vs. not-buy” contrast, while the control group showed the opposite (i.e., higher NAcc in the not-buy condition). Furthermore, the same group (CB VS. control) x condition (buy vs. not-buy) interaction effect was observed again in the medial prefrontal cortex (MPFC). Additionally, the control group’s anterior insula (aINS) showed lower negative responses in the buy (relative to not-buy) condition, similar to what Knutson et al. have shown. The CB participants’ aINS, in contrast, did not show a significant difference between buy and not-buy conditions.

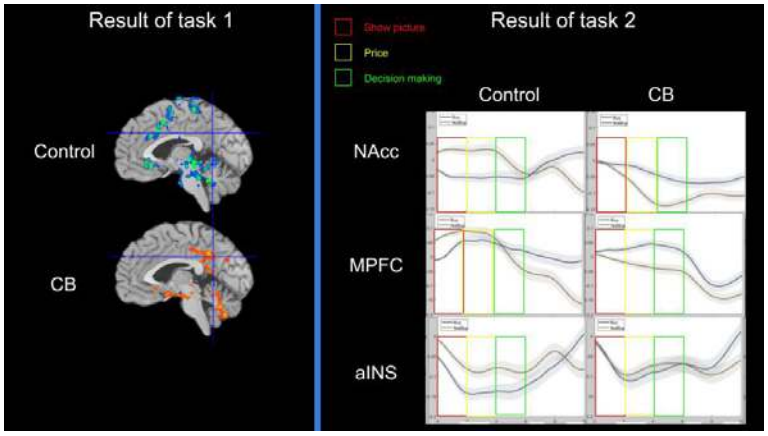

Conclusions: In two fMRI tasks, this study revealed differential neural activation patterns between CB vs. normal control participants. In task 1 (craving task), PCC seems to be the critical site differentiating the two groups. In task 2, CB participants also showed opposite-to-control-group patterns in all the shopping-related regions (NAcc, MPFC, and aINS). Together, these results not only add to the literature on the neurological mechanisms of CB but also could be taken as the target regions for related treatments, such as neurofeedback training.

References

1. Knutson B, Rick S, Wimmer GE, Prelec D, Loewenstein G. (2007). Neural predictors of purchases. Neuron. 53:147–56. https://doi.org/10.1016/j.neuron.2006.11.010.

Poster No 923

Task and stimulus coding in the multiple-demand network

Sneha Shashidhara[1], Moataz Assem[2], John Duncan[3]

[1]Ashoka University, Sonipat, Haryana, [2]MRC Cognition and Brain Sciences Unit, University of Cambridge, Cambridge, Cambridgeshire, [3]MRC Cognition and Brain Sciences Unit, Cambridge, Cambridgeshire

Introduction: In the human brain, "multiple-demand" or MD regions are characterised by increased activity associated with many different kinds of cognitive demand (Duncan & Owen, 2000; Duncan et al., 2020), with core components in lateral frontal, dorsomedial frontal and lateral parietal cortex, and multivariate activity patterns that discriminate the contents of many cognitive activities. Using data from 449 participants in the Human Connectome Project (HCP) (Glasser et al., 2016), Assem et al., 2020 found overlapping activity for three types of cognitive demand was strongest in a set of 10 core regions per hemisphere, distributed over the lateral frontal, dorsomedial frontal, insular and lateral parietal cortex MD. Frontal single neuron data show strong selectivity for cognitive operation but weaker selectivity for the stimulus on which this operation is conducted. They also show mixed selectivity; activity depends on the conjunction of multiple task features, such as a particular stimulus object presented at a particular place in a memory list or a particular move planned at a specific position in a sequence (Warden & Miller, 2010; Mushiake et al., 2006; Sigala et al., 2008). Here, we searched for similar properties in fMRI data from core MD regions.

Methods: Using the advanced fMRI methods of the Human Connectome Project (HCP) and their 360-region cortical parcellation, we conducted a study with 50 human subjects, 37 of whom were included in the analysis. The study consisted of three visual executive tasks intermixed within a scanning run and four scanning runs. Tasks were: n-back working memory (WM), task-switching, and stop-signal, variations of which have previously been shown to recruit the MD network (Fedorenko et al., 2013). The eight blocks of each task consisted of four hard and four easy blocks, two of each using faces and two buildings. We obtained the multivoxel activation pattern for each participant in each of the 360 cortical parcels, and averaged them across cortical networks of core MD and 12 resting-state networks (Ji et al., 2019). To measure dissimilarity between activation patterns we used linear discriminant contrast (LDC) (Nili et al., 2014; Carlin & Kriegeskorte, 2017). We calculated three means for each parcel from the full matrix of LDC distances. STDS was calculated as the mean distance between the face and building blocks in the same task, averaged across tasks. DTSS was calculated as the mean distance between tasks holding stimulus category constant, e.g., n-back face and task switch face averaged across all task pairs and face and building blocks. DTDS was calculated as the mean distance between conditions differing in task and stimulus category, averaged across six such distances. The nonlinearity index was calculated as (STDS+DTSS)-DTDS.

Results: Stimulus discrimination was strongest in a large region of the early and higher visual cortex. Weak discrimination in core MD regions was accompanied by somewhat stronger discrimination close by in the lateral parietal and frontal cortex, in two bands of regions ventral to the MD core. For DTSS, in contrast, discrimination was strong in the MD core and adjacent regions. For DTDS, as expected, discrimination was widespread, reflecting the union of patterns for STDS and DTSS.

Conclusions: Core MD had one of the highest non-linearity indices in the brain, albeit a small index. There was scant evidence for mixed selectivity; throughout the brain, discriminations of task and stimulus combined almost linearly. In MD regions, human fMRI data recapitulate some but not all aspects of electrophysiological data from nonhuman primates.

References

1. Assem, M. (2020). A Domain-General Cognitive Core Defined in Multimodally Parcellated Human Cortex. Cerebral Cortex, 30, 4361–4380
2. Carlin, J. D. (2017). Adjudicating between face-coding models with individual-face fMRI responses. PLOS Computational Biology, 13(7), e1005604.
3. Duncan, J. (2020). Integrated Intelligence from Distributed Brain Activity. In Trends in Cognitive Sciences (Vol. 24, Issue 10, pp. 838–852)
4. Duncan, J. (2000). Common regions of the human frontal lobe recruited by diverse cognitive demands. Trends in Neurosciences, 23(10), 475–483.
5. Fedorenko, E. (2013). Broad domain generality in focal regions of frontal and parietal cortex. Proc. NatL Acad. Sci. USA, 110(41), 16616–16621.
6. Glasser, M. F. (2016). A multi-modal parcellation of human cerebral cortex. Nature, 536, 171–178.
7. Ji, J. L. (2019). Mapping the human brain's cortical-subcortical functional network organization. NeuroImage, 185, 35–57.
8. Mushiake, H. (2006). Activity in the Lateral Prefrontal Cortex Reflects Multiple Steps of Future Events in Action Plans. Neuron, 50(4), 631–641.
9. Nili, H. (2014). A Toolbox for Representational Similarity Analysis. PLoS Computational Biology, 10(4), e1003553.
10. Sigala, N. (2008). Hierarchical coding for sequential task events in the monkey prefrontal cortex. Proc. NatL Acad. Sci. USA, 105(33), 11969–11974.
11. Warden, M. R. (2010). Task-Dependent Changes in Short-Term Memory in the Prefrontal Cortex. Journal of Neuroscience, 30(47), 15801–15810.

Poster No 924

Ultrashort echo time brain imaging links myelin content to cognitive flexibility

Liz Lee[1], Chie Takahashi[1], Katharina Zühlsdorff[1], Onur Ozyurt[1], Diana Rotaru[1], Zhen Jiang[2], Humberto Monsivais[2], Guy B. Williams[1], Uzay Emir[2], Zoe Kourtzi[1]

[1]University of Cambridge, Cambridge, United Kingdom, [2]Purdue University, West Lafayette, Indiana

Introduction: Flexibly adapting to new situations and changes in dynamic environments is a key ability known as cognitive flexibility (Kupis and Uddin, 2023). Cognitive flexibility is typically studied using tasks that require switching between rules (e.g. Wisconsin Card Sorting Test, WCST; probabilistic reversal learning, PRL). Previous work has implicated dorsolateral prefrontal cortex (DLPFC) (Kim et al., 2011) and hippocampus (Rubin et al., 2014) in adopting new probabilistic rules and forming relational memory representations, respectively. Most brain imaging studies of cognitive flexibility have focused on functional activity and connectivity as measured by fMRI. However, the role of myelination - the process of forming myelin to enhance neural information transmission - in cognitive flexibility remains largely unknown. Here, we test the role of myelination in DLPFC and hippocampus in cognitive flexibility. We employ cutting-edge ultrashort echo time (UTE) and ultrashort echo time magnetization transfer (UTE-MT) sequences to extract magnetisation transfer ratio (MTR). MTR is known to significantly correlate with myelin content as measured by histopathology (Guglielmetti et al., 2020). Yet, conventional MRI measures of myelination are confounded by iron concentration. Due to the specific chemical environment of the bilayer-bound protons, 80% of the myelin lipid 1H protons have T2* values well below 1 ms (Baadsvik et al., 2023). As their signal decays too fast to be captured by conventional MRI techniques with TEs in milliseconds or longer in "multiple gradient/spin echo imaging", UTE provides a promising method for direct measurement of myelin (Wilhelm et al., 2012).

Methods: Fifty-four participants (26 female, age 43±6.6) from NIHR BioResource completed one behavioral and one MRI session. In the behavioural session, we measured cognitive flexibility using WCST and PRL tasks. In the MRI session (3T), we used UTE to estimate iron concentration (Shen et al., 2023) and UTE-MT to estimate (Guglielmetti et al., 2020). Image reconstruction was performed with ESPIRiT calibration using the Berkeley Advanced Reconstruction Toolbox and non-uniform fast Fourier transform. Image preprocessing was performed with FSL (coregistration,brain extraction), AFNI (bias correction), and SPM (Figure 1). We extracted ROI-based MTR and iron concentrations (Brainnetome atlas) (Fan et al., 2016) in DLPFC (Brodmann areas 8, 9, 46) (Sanches et al., 2009) and hippocampus. For iron concentration we regressed out age and sex. To control for iron contribution to myelin content, we regressed out iron concentration in addition to age, sex.

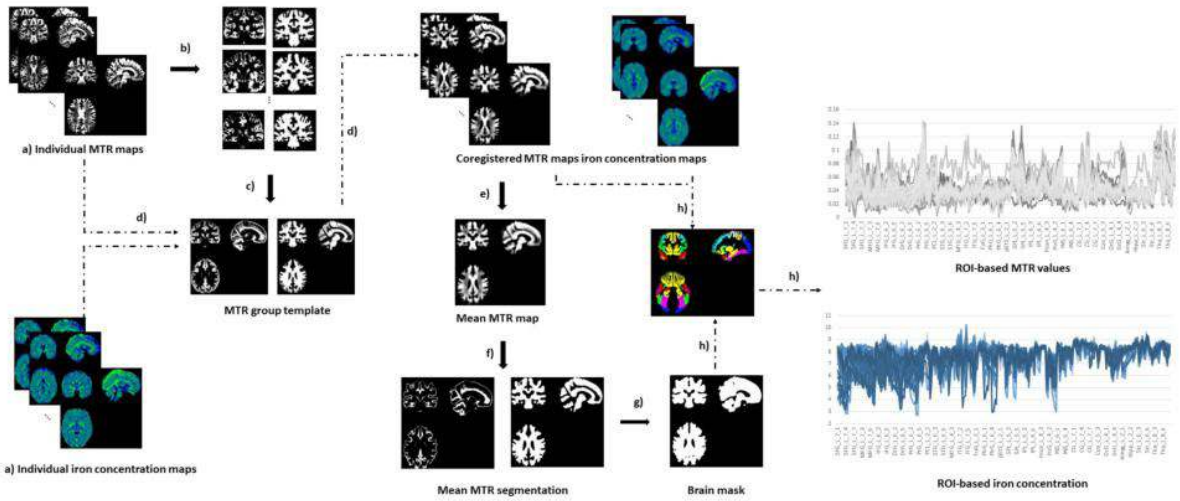

Figure 1. Pipeline for MTR and iron concentration extractingpreprocessing pipeline. a) MTR and iron concentration maps for individual participants were reconstructed and coregistered to MNI space. **b)** Segmenting MTR maps for individual participants. **c)** MTR group template with grey matter and white matter segmented from step a. **d)** Coregistering individual MTR maps and iron concentration maps to the group template. **e)** Extracting MTR map by averaging coregistered MTR maps across participants . **f)** Segementing mean MTR map to extract grey matter and white matter. **g)** Creating a brain mask with grey matter and white matter. **h)** Adjusting Brainnetome atlas with the study brain mask and extracting ROI-based MTR values and iron concentrations.

Results: We observed a significant negative correlation of myelin content in DLPFC with PRL perseverative errors (Figure 2A; r = -0.30, p = .046). In contrast, iron concentration in DLPFC did not correlate significantly with perseverative errors (r = -0.18, p = .232), suggesting that higher myelin content - rather than iron concentration - in DLPFC is associated with stronger flexibility in adopting new rules. Further, we observed a significant positive correlation of myelin content in the hippocampus with WCST perseverative errors (Figure 2B; r = 0.28, p = .042). In contrast, iron concentration in the hippocampus negatively correlated with WCST perseverative errors (r = -0.28, p = .041). Note that correlations of MTR without regressing out iron with perseverative errors were not significant (PRL, DLPFC, r = -0.19, p = .209; WCST, hippocampus, r = 0.265, p = .053), consistent with a confounding effect of iron in myelin measurements.

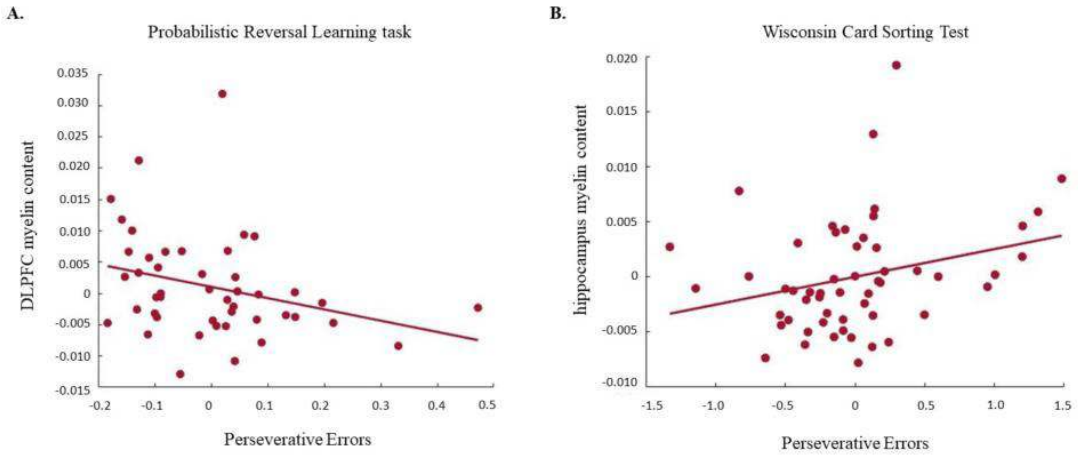

Figure 2. Myelin content after regressing out iron from MTR correlates with behavioral performance. A) Negative correlation between DLPFC myelin content and perseverative error in Probabilistic Reversal Learning task (p = 0.046, r = -0.30). **B)** Positive correlation between hippocampus myelin content and perseverative error in Wisconsin Card Sorting Test (p = 0.042, r = 0.28).

Conclusions: Our results suggest that myelin content in the frontal and hippocampal regions relates to our ability to learn new rules in the context of cognitive flexibility tasks. Employing UTE and UTE-MT sequences, we control for the confounding effect of iron concentration in MTR measurements, providing new insights into the role of myelin in adaptive behaviour and cognitive flexibility.

References
1. Baadsvik, E. L. et al. (2023). Quantitative magnetic resonance mapping of the myelin bilayer reflects pathology in multiple sclerosis brain tissue. Science Advances, 9(32), eadi0611.
2. Fan, L. et al. (2016) 'The Human Brainnetome Atlas: A New Brain Atlas Based on Connectional Architecture', Cerebral Cortex, 26(8), pp. 3508–3526.
3. Guglielmetti, C. et al. (2020) 'Longitudinal evaluation of demyelinated lesions in a multiple sclerosis model using ultrashort echo time magnetization transfer (UTE-MT) imaging', NeuroImage, 208, p. 116415.
4. Kim, C. et al. (2011) 'Common and Distinct Mechanisms of Cognitive Flexibility in Prefrontal Cortex', The Journal of Neuroscience, 31(13), pp. 4771–4779.
5. Kupis, L.B. and Uddin, L.Q. (2023) 'Developmental Neuroimaging of Cognitive Flexibility: Update and Future Directions', Annual Review of Developmental Psychology, 5(1).
6. Rubin, R.D. et al. (2014) 'The role of the hippocampus in flexible cognition and social behavior', Frontiers in Human Neuroscience, 8.
7. Sanches, M. et al. (2009) 'An MRI-based approach for the measurement of the dorsolateral prefrontal cortex in humans', Psychiatry Research: Neuroimaging, 173(2), pp. 150–154.
8. Shen, X. et al. (2023) 'Ultra-short T 2 components imaging of the whole brain using 3D dual-echo UTE MRI with rosette k-space pattern', Magnetic Resonance in Medicine, 89(2), pp. 508–521.
9. Wilhelm, M. J. et al. (2012). Direct magnetic resonance detection of myelin and prospects for quantitative imaging of myelin density. Proceedings of the National Academy of Sciences, 109(24), 9605-9610.

Poster No 925

Individuals with overweight and obesity fail to suppress food-related memories? An fMRI study

Yuan Gao[1], Xiao Gao[2]

[1]Department of Psychology and Behavioral Sciences, Zhejiang University, Hangzhou, [2]Faculty of Psychology, Southwest University, Chongqing

Introduction: As per the World Health Organization (WHO), obesity has now reached epidemic proportions and it is estimated that by 2030 over one billion adults worldwide will be obese. Obesity is associated with a higher frequency of food cravings. Here, we propose a new hypothesis that individuals with overweight or obesity may encounter difficulties in halting their contemplation of sensory memories when tempting thoughts intrude, which underscores the challenges they face in managing their cravings and dietary choices.

Methods: This study included 36 young female students, with 18 having healthy BMI and 18 being overweight/obese. Participants completed questionnaires, provided ratings of food stimuli perceptual reward value, and performed the food Think/No-Think task in an fMRI session. MRI data were collected on a Siemens Trio 3.0T scanner. BOLD images were acquired with EPI sequence during the Think/No-Think phase. FMRI data preprocessing and analysis were conducted using SPM12. Comparisons were made between Think and No-Think conditions. Seed regions of interest included inhibitory control areas of dorsolateral prefrontal cortex, inferior frontal gyrus, and middle frontal gyrus. Memory areas included bilateral hippocampus, parahippocampal gyrus and fusiform gyrus. Accuracy of recalling the cued food and its location in the test phase was scored and entered into repeated-measures ANOVAs with conditions as within-subject variables and BMI group as between-subject variables. ROI analysis was conducted on fMRI data. Functional connectivity analysis was performed using generalized psychophysiological interaction models to estimate task-dependent connectivity between seeded frontal control regions and memory areas while controlling for task activation.

Results: The healthy BMI group showed the typical pattern of greater recall accuracy for Think relative to No-Think items, demonstrating successful memory suppression. However, the overweight/obese group failed to show significant differences between Think and No-Think accuracy. The inferior frontal gyrus was most activated in healthy BMI controls during No-Think trials, while dorsolateral prefrontal cortex dominated in overweight/obese. Overweight/obese had significantly greater activation in the right hippocampus dentate gyrus during No-Think trials compared to controls. Functional connectivity results demonstrated connections between prefrontal inhibitory control seeds and memory areas in both groups, but there were qualitative differences. In healthy controls, multiple control regions including IFG, MFG and dlPFC all showed negative connectivity with hippocampus and other memory areas, indicating coordinated inhibitory signaling. Greater negative connectivity was associated with lower No-Think recall. In contrast, overweight/obese had positive connectivity between dlPFC and hippocampus, and behavior correlations showed this related to higher No-Think recall, indicating failed inhibition. Overweight/obese also differed by having connectivity between IFG and reward areas rather than memory regions.

Conclusions: Individuals with overweight/obesity demonstrated deficits in food-related memory suppression, alongside altered prefrontal activation and fronto-hippocampal connectivity patterns indicating impaired inhibitory control mechanisms. This expands existing evidence for inhibitory control impairments in overweight/obesity into the domain of memory suppression.

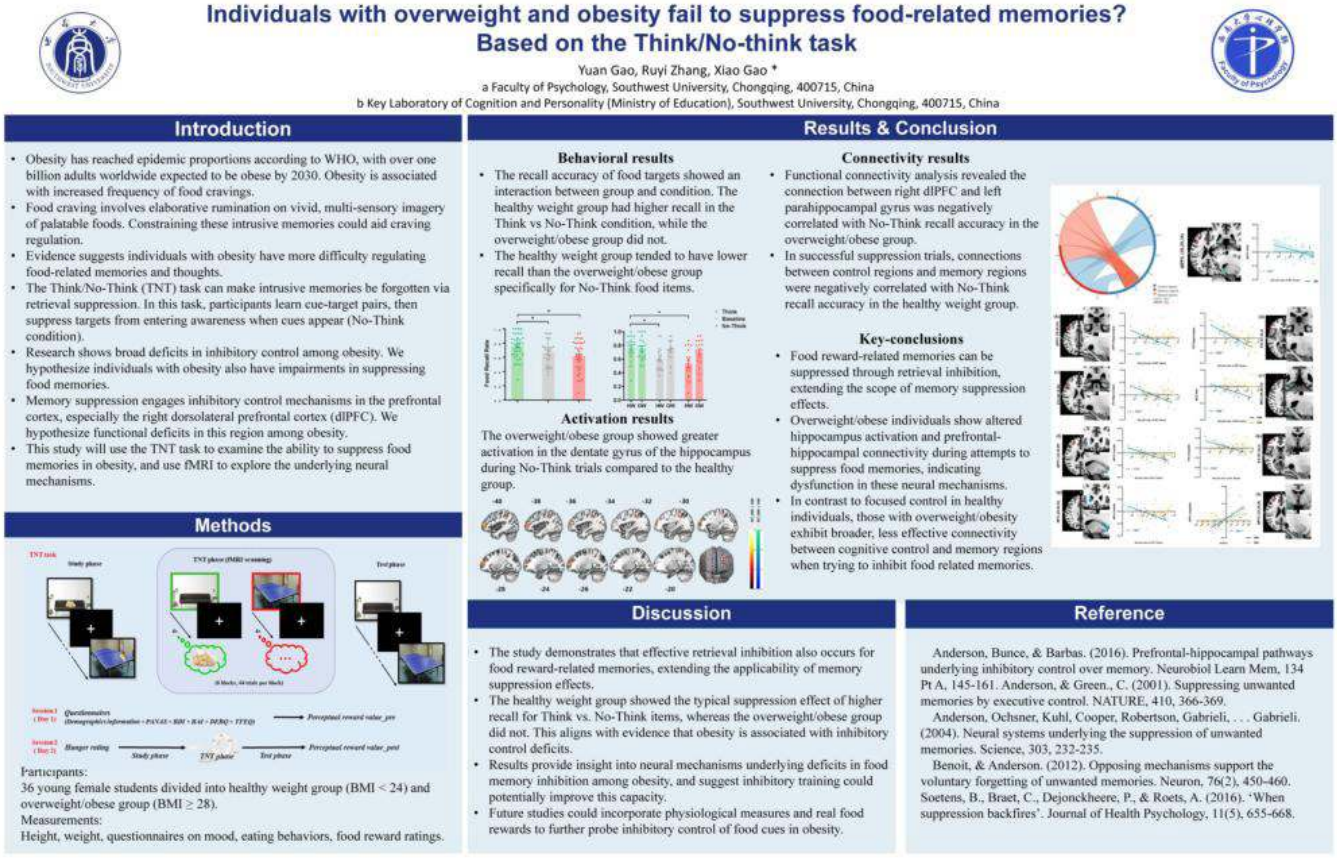

References

1. Anderson, Bunce, & Barbas. (2016). Prefrontal-hippocampal pathways underlying inhibitory control over memory. Neurobiol Learn Mem, 134 Pt A, 145-161. doi:10.1016/j.nlm.2015.11.008
2. Anderson, & Green., C. (2001). Suppressing unwanted memories by executive control. NATURE, 410, 366-369.
3. Anderson, Ochsner, Kuhl, Cooper, Robertson, Gabrieli, . . . Gabrieli. (2004). Neural systems underlying the suppression of unwanted memories. Science, 303, 232-235.
4. Benoit, & Anderson. (2012). Opposing mechanisms support the voluntary forgetting of unwanted memories. Neuron, 76(2), 450-460. doi:10.1016/j.neuron.2012.07.025
5. Schmitz, T. W., Correia, M. M., Ferreira, C. S., Prescot, A. P., & Anderson, M. C. (2017). Hippocampal gaba enables inhibitory control over unwanted thoughts. Nat Commun, 8(1), 1311. doi:10.1038/s41467-017-00956-z
6. Soetens, B., & Braet, C. (2007). Information processing of food cues in overweight and normal weight adolescents. British Journal of Health Psychology, 12(2), 285-304. doi:10.1348/135910706x107604
7. Soetens, B., Braet, C., Dejonckheere, P., & Roets, A. (2016). 'When suppression backfires'. Journal of Health Psychology, 11(5), 655-668. doi:10.1177/1359105306066615

Poster No 926

White Matter Connectivity and Executive Functions in Youth: Insights from Fixel-based analysis

Xin-Yu Chen[1], Rung-Yu Tseng[2], Chun-Hung Yeh[2], Ting-Ting Chang[1,3]

[1]Department of Psychology, National Chengchi University, Taipei City, Taiwan, [2]Department of Medical Imaging and Radiological Sciences, Taoyuan City, Taiwan, [3]Research Center for Mind, Brain, and Learning, National Chengchi University, Taipei City, Taiwan

Introduction: Executive functions (EFs), such as inhibition, working memory, and shifting (Miyake, 2000), are crucial in children and adolescents' learning, with their development tied to neural network connectivity (see Goddings et al., 2021 for a review). Despite the known impact of white matter integrity on EFs in aging (Vernooij et al., 2009), its role in the cognitive development of younger individuals is less certain and yields mixed results (e.g., Ursache et al., 2016; Liston et al., 2006). Additionally, traditional neuroimaging methods like diffusion tensor imaging (DTI) face challenges in depicting complex neural structures. Our study addresses the limitations by using advanced fixel-based analysis (FBA) framework (Raffelt et al., 2017), providing a deeper understanding of how white matter fiber properties correlate with EFs during critical school years.

Methods: A total of 48 children (F/M=33/15; age=7.87±0.47 years, range=7.07–8.75 years) and 34 adolescents (F/M=18/16; age=14.94±1.93 years, range=12.33–18.89) underwent diffusion MRI scans and assessments of EFs, specifically inhibition and working memory. The Flanker task and Wechsler's Digit Span Backwards subtest were used for these assessments, respectively. Whole-brain fixel-based analysis was conducted to investigate categorical differences (children vs. adolescents) in white matter micro-/macrostructure and the associations between white matter structure and EFs. These analyses involved assessing FBA metrics including fiber density (FD), fiber cross-section (FC), and the combined index (FDC). Statistical significance for all analyses was determined at a per-fixel P-FWE threshold of < 0.05.

Results: Inter-group comparisons: Compared to adolescents, children showed higher FD/FC/FDC in the bilateral posterior limb of internal capsule, higher FD/FDC in the bilateral fornix and bilateral external capsule, higher FC/FDC in the left anterior corona radiata (ACR), higher FD in the crus I and bilateral superior cerebellar peduncle, along with higher FC in the left cingulum (Fig. 1A). Conversely, there were some white matter tracts where children showed lower FBA metrics than adolescents, including lower FD/FC/FDC in the left superior corona radiata (SCR) and corpus callosum (CC), lower FD/FDC in the right superior longitudinal fasciculus (SLF), lower FC/FDC in the bilateral corona radiata (CR) and bilateral corticospinal tracts (CST), as well as lower FDC in the left SLF (Fig. 1B). Working memory: FD/FDC in the left SLF, along with FDC in the CC and posterior thalamic radiation showed age group-by-working memory interactions (Fig. 2A). Within the children group, negative correlations between working memory capacity and FD/FC/FDC were found in CC. Additionally, working memory negatively correlated with FD/FDC in anterior commissure and posterior limb of internal capsule, with FC/FDC in fornix and left cerebral peduncle, and with FDC in the right CR (Fig. 2B). For the adolescent group, no significant associations were observed between working memory and fixel metrics. Inhibition: There were no significant interactions between age groups or correlations between inhibition and fixel metrics in either children or adolescents.

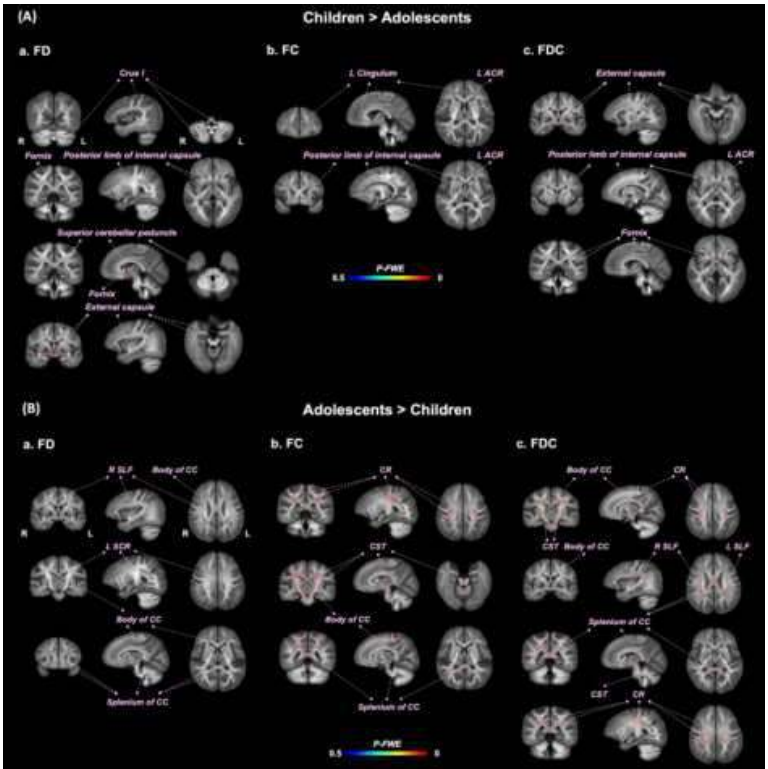

Fig. 1 Results of categorical comparisons from the FBA. White matter tract segments that have significant group differences in FD, FC, and FDC metrics are exhibited and colored by the *P-FWE* value. (A) Children > Adolescents. (B) Adolescents > Children. Abbreviations: *R* Right, *L* Left.

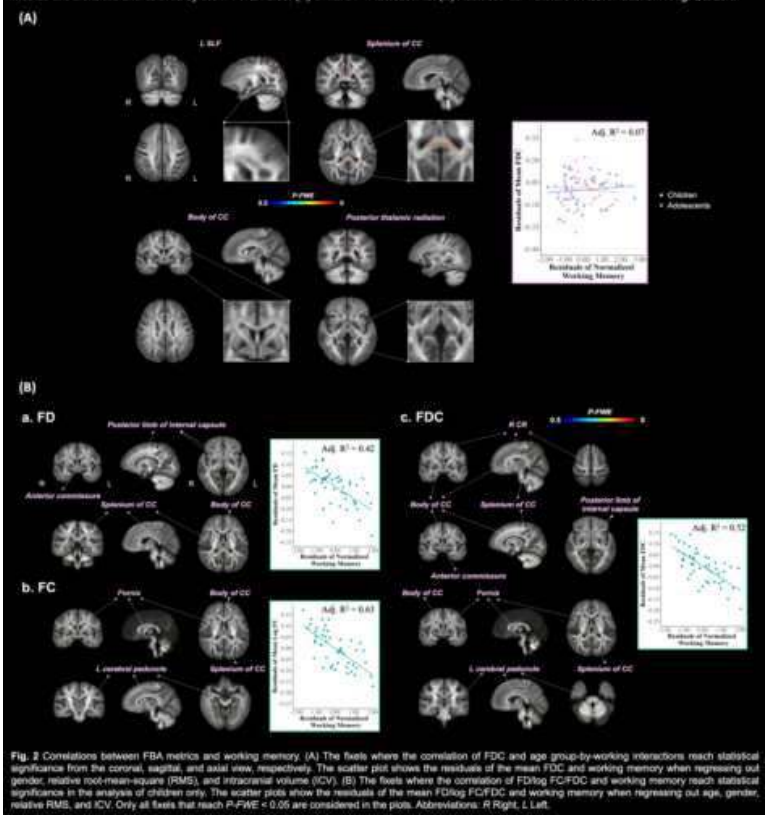

Fig. 2 Correlations between FBA metrics and working memory. (A) The fixels where the correlation of FDC and age group-by-working interactions reach statistical significance from the coronal, sagittal, and axial view, respectively. The scatter plot shows the residuals of the mean FDC and working memory when regressing out gender, relative root-mean-square (RMS), and intracranial volume (ICV). (B) The fixels where the correlation of FD/log FC/FDC and working memory reach statistical significance in the analysis of children only. The scatter plots show the residuals of the mean FD/log FC/FDC and working memory when regressing out age, gender, relative RMS, and ICV. Only all fixels that reach *P-FWE* < 0.05 are considered in the plots. Abbreviations: *R* Right, *L* Left.

Conclusions: Our study reveals a distinct developmental pattern in fiber tracts, highlighting changes in white matter micro-/macrostructure related to EFs. In children, there is a negative correlation between working memory and fronto-parietal (Krogsrud et al., 2018) and occipito-temporal tracts, indicative of increased neural efficiency potentially due to synaptic pruning and myelination. Conversely, in adolescents, the lack of significant correlations suggests a stabilization of mature neural pathways. The absence of correlations between inhibition and white matter in both age groups may stem from the rapid and diverse development of inhibition (Huizinga et al., 2006). These findings provide insights into the evolving relationship between brain connectivity and EFs across developmental stages.

References
1. Goddings, A.L. (2021), 'Development of white matter microstructure and executive functions during childhood and adolescence: a review of diffusion MRI studies', Developmental Cognitive Neuroscience, vol. 51
2. Huizinga, M. (2006), 'Age-related change in executive function: developmental trends and a latent variable analysis', Neuropsychologia, vol. 44, no. 11, pp. 2017-2036
3. Krogsrud, S.K. (2018), 'Development of white matter microstructure in relation to verbal and visuospatial working memory-A longitudinal study', PloS One, vol. 13, no. 4
4. Liston, C. (2006), 'Frontostriatal microstructure modulates efficient recruitment of cognitive control', Cerebral cortex (New York, N.Y. : 1991), vol. 16, no. 4, pp. 553-560
5. Miyake, A. (2000), 'The unity and diversity of executive functions and their contributions to complex "Frontal Lobe" tasks: a latent variable analysis', Cognitive psychology, vol. 41, no. 1, pp. 49-100
6. Raffelt, D.A. (2017), 'Investigating white matter fibre density and morphology using fixel-based analysis', NeuroImage, vol. 144, Pt A, pp. 58-73
7. Ursache, A. (2016), 'Socioeconomic status, white matter, and executive function in children', Brain and Behavior, vol. 6, no. 10
8. Vernooij, M.W. (2009), 'White matter microstructural integrity and cognitive function in a general elderly population', Archives of general psychiatry, vol. 66, no. 5, pp. 545-553

Poster No 927

Neural Signatures of Predictive Processing under Central vs Peripheral Noradrenergic Blockade

Ashley Tyrer[1], Micah Allen[2]

[1]Aarhus University, Aarhus, Aarhus C, [2]Aarhus University, Lystrup, Denmark

Introduction: While considerable research has been conducted regarding the effects of noradrenergic manipulations on uncertainty and prediction, little is known about the differential effects on cognitive functioning of central vs peripheral noradrenergic blockade, and how such manipulations may impact the processing of uncertainty in contrasting ways – particularly in the context of magnetoencephalography (MEG). Further, little is known about how such manipulations may affect brain-body interactions in response to uncertainty and prediction error. Here, we employed task-based MEG, pharmacological manipulation and pupillometry in a double-blinded, placebo-controlled, within-subject context to investigate how the processing of uncertainty and prediction may be influenced by central vs peripheral beta-adrenoceptor antagonism in 50 young healthy participants. We aimed to elucidate the neural and embodied signatures of (unexpected) uncertainty, and how these may be altered by changes in central or peripheral noradrenaline. Therefore, we expected participants across both conditions to exhibit slower learning rates and belief updating, reduced internal model flexibility, and stronger weighting of prior beliefs in decision-making, in line with previous analyses. In addition to examining neural activity in response to uncertainty, we also examined a variety of physiological responses such as cardiac and respiratory signals to probe how brain-body responses to uncertainty are altered in central and peripheral noradrenaline manipulation.

Methods: Fifty young healthy participants attended three separate study visits each in this double-blinded, placebo-controlled, within-subject study, where each study visit consisted of a single acute drug administration (40 mg propranolol, 10 mg bisoprolol, or a matched placebo) followed by simultaneous MEG imaging, physiological recordings and pupillometry, during which participants completed a perceptual reversal learning task. This task consisted of a revised version of the common probabilistic associative learning task with the addition of confidence ratings at the end of each trial and was preceded by individual staircasing of visual stimuli, i.e., emotional faces. Further, following the MEG scan participants completed 60 minutes of cognitive tasks on a computer outside the scanner. Participants completed brief testing measures of their interoceptive sensitivity, in both the cardiac and respiratory domain, namely the Heart Rate Discrimination task (HRD) and the Respiratory Resistance Sensitivity Task (RRST).

Results: We found a significantly attenuated neural response to task-related prediction error in the propranolol condition compared with the placebo condition. We also found that greater metacognitive ability was reflected in greater task prediction accuracy and found this to be improved under propranolol, in line with previous work. We also noted a reduced attentional response to stimuli and a blunted response to prediction errors under propranolol but not bisoprolol. This speaks to the centrally mediated nature of saliency detection, and therefore enabled us to better tease apart the neural representations of emotional stimuli in the bisoprolol condition. Additionally, through the use of Active Inference modelling of behavioural responses we generated subject-specific conditional estimates of internal model volatility under each drug condition. Further, under bisoprolol, we found a significantly reduced cardiac response to uncertainty compared with the placebo condition.

Conclusions: Overall, we show here that neural activations in task-relevant brain regions associated with uncertainty and predictive processing, such as the anterior cingulate cortex, are altered in response to belief updating and model volatility,

differentially for central vs peripheral noradrenergic manipulation. We also demonstrate subject-specific neural and behavioural profiles of internal model volatility and predictive processing in response to uncertainty.

References
1. Aston-Jones, G. 2005. 'An integrative theory of locus coeruleus-norepinephrine function: adaptive gain and optimal performance', Annual Review of Neuroscience, 28: 403-50.
2. Brodde, O. E. 2008. 'Beta-1 and beta-2 adrenoceptor polymorphisms: functional importance, impact on cardiovascular diseases and drug responses', Pharmacology and Therapeutics, 117: 1-29.
3. Lawson, R. P. 2017. 'Adults with autism overestimate the volatility of the sensory environment', Nature Neuroscience, 20: 1293-99.
4. Legrand, N. 2022. 'The heart rate discrimination task: A psychophysical method to estimate the accuracy and precision of interoceptive beliefs', Biological Psychology, 168: 108239.
5. Nikolova, N. 2022. 'The respiratory resistance sensitivity task: An automated method for quantifying respiratory interoception and metacognition', Biological Psychology, 170: 108325.
6. Sales, A. C. 2019. 'Locus Coeruleus tracking of prediction errors optimises cognitive flexibility: An Active Inference model', PLoS Computational Biology, 15: e1006267.

Poster No 928

DMN activation at task-switches reflects mental task set structure

Ashley Zhou[1], Daniel Mitchell[2], John Duncan[3]

[1]University of Cambridge, Cambridge, Cambridgeshire, [2]MRC Cognition and Brain Sciences Unit, University of Cambridge, Cambridge, Cambridgeshire, [3]MRC Cognition and Brain Sciences Unit, Cambridge, Cambridgeshire

Introduction: Recent findings challenge views of the DMN as a purely task-negative or self-oriented network, by showing increased DMN activity during demanding external task-switches between cognitive domains, versus within-domain switches or task repeats (Crittenden et al., 2015; Smith et al., 2018). In this fMRI study, we examine how the DMN's response to task switches depends on current task set complexity, task expectancy, and instructional order. Results showed that while DMN activation at task switches was unaffected by either the number of currently relevant tasks, or task expectancy, it depended on the order in which groups of tasks had been learnt. This suggests sensitivity to an intrinsic task-set hierarchy, and a role in complex cognitive control processes. Results may also explain inconsistent observations of DMN activation across task-switch studies.

Methods: 36 healthy participants (13 male), aged 18-45, were tested. For each of four task domains (lexical, semantic, faces, shapes), two different tasks were cued by colored frames. Participants learned task-color pairs in two groups of two domains, and performed them in the scanner in the same groups (four 2-domain runs) or all intermixed (two 4-domain runs). Per trial, a colored frame cued a binary judgement on a central stimulus. The task sequence defined equal numbers of different transition types (e.g. task repeat, within-domain switch, between-domain switch). Task expectancy (variable by switch type, balanced per switch type) was varied across runs, crossed with domain number. Data were acquired on a 3T Siemens Prisma MRI scanner, using T2*-weighted EPI (TR 1.2 s, TE 30 ms, flip angle 67°, 3×3x3 mm voxels, multiband factor 2). Pre-processing (using SPM12 and AutomaticAnalysis; Cusack et al., 2015) applied spatial realignment, slice-time correction, co-registration, and normalization to the MNI template, with no spatial smoothing. A GLM was created by convolving the response periods of all trials per condition with the canonical HRF. Conditions counterbalanced each combination of switch type (task repeat, within-domain switch, between-domain switch, between-group-switch, restart, rest), number of active task domains (2 or 4), task expectancy (variable, balanced), and task group (learnt 1st or 2nd). Movement parameters and block means were added as covariates. Analysis focused on mean signal from a Core DMN ROI.

Results: Mean reaction time (RT) was 1.1 s. Expected switch costs were seen, with RT of switch trials (mean across switch types) slower than for task repeats (t35 =10.1, p<0.01, BF>2x10^10). Activity in Core DMN was significantly higher for averaged switch trials compared to task repeats (t35 =6.47, p<0.01, BF>4x10^5). Two-way ANOVA with factors of switch type (within-domain, between-domain) and number of domains (2, 4) showed a significant effect of switch type (F(1,35) =19.6, p<0.01, BF=270) but no effect of domain number (F(1,35)=1.15, p=0.29, BF=0.36) or interaction (F(1,35)=1.08, p=0.31, BF=0.35). Similarly, a two-way ANOVA with switch type and task expectancy as factors found no effect of task expectancy (F(1,35)=1.16, p=0.29, BF=0.36) or interaction (F(1,35) =0.65, p=0.43, BF=0.29). However, a two-way ANOVA with factors of switch type and instructed order found a significant interaction, with higher activity for between-domain switches of later-learned domains (F(1,35)=5.42, p=0.03, BF=2.17), but no main effect of instructional order (F(1,35)=0.02, p=0.89, BF=0.22).

Conclusions: We investigated influences on DMN activation at task switches. Results suggest that DMN activity is sensitive to task structure complexity, but depends on learning order rather than the number of currently relevant tasks or particular task expectancies. As later-learned tasks increase complexity of the task set, DMN shows a different response profile across

task transitions. Results speculatively suggest that a capacity-limited, two-level, hierarchical task model underlies DMN involvement in task transitions.

References
1. Cusack, R., Vicente-Grabovetsky, A., Mitchell, D. J., Wild, C. J., Auer, T., Linke, A. C., & Peelle, J. E. (2015). Automatic analysis (aa): Efficient neuroimaging workflows and parallel processing using Matlab and XML. Frontiers in Neuroinformatics, 8. https://www.frontiersin.org/articles/10.3389/fninf.2014.00090
2. Crittenden, B. M., Mitchell, D. J., & Duncan, J. (2015). Recruitment of the default mode network during a demanding act of executive control. eLife, 4, e06481–e06481. https://doi.org/10.7554/eLife.06481
3. Smith, V., Mitchell, D. J., & Duncan, J. (2018). Role of the Default Mode Network in Cognitive Transitions. Cerebral Cortex (New York, N.Y. 1991), 28(10), 3685–3696. https://doi.org/10.1093/cercor/bhy167

Poster No 929

A behaviorally-relevant multiple-demand operating system underlying diverse cognitive tasks

Weidong Cai[1], Jalil Taghia[2], Vinod Menon[1]

[1]Stanford University, Palo Alto, CA, [2]Uppsala University, Uppsala, Sweden

Introduction: The human brain is a flexible, yet stable, system that allows rapid and adaptive allocation of cognitive resources to meet moment-by-moment changes in task demands (Braun et al., 2015; Shine et al., 2016; Taghia, et al., 2018). A converging body of evidence now points to a core set of distributed brain areas that are consistently engaged during diverse cognitive tasks (Cai et al., 2019; Dosenbach et al., 2006; Duncan, 2010). This commonality naturally raises the critical and challenging question of how the same brain areas might underlie cognition across multiple task domains. Addressing this question has the potential to uncover mechanisms underlying a multiple-demand, domain-general, functional system underlying cognition and identify transdiagnostic features of cognitive dysfunction in psychiatric and neurological disorders. Here we use a state space hidden Markov model and novel computational analyses to address this challenge. We identify common brain states that are dynamically engaged across seven different cognitive paradigms, across multiple participant cohorts, and demonstrate their behavioral relevance.

Methods: We leveraged a total of seven different fMRI experiments across a wide range of cognitive domains, including n-back working memory, continuous performance, cued task switching, Sternberg working memory, Stroop, and Stop-signal tasks, and relational processing tasks (Braver et al., 2021; Van Essen et al., 2012). The Bayesian switching dynamical systems state space (BSDS) algorithm was used to identify brain states in each task and examine their correspondence with brain states in a canonical n-back working memory reference task (Taghia, et al., 2018). The latent brain state was determined by unique patterns of activity and functional connectivity between key nodes of the salience, central executive, and default mode networks. Using the n-back working memory as a reference task, we asked whether task-optimal latent brain states that occur during the high cognitive load condition in the n-back task are also engaged during each of the other seven cognitive tasks. Our choice of the working memory task was motivated both by the fact that it is widely used to probe cognitive function and dysfunction, and by our identification of optimal and non-optimal brain states associated with cognitive performance and decision-making (Taghia et al., 2018). State temporal closeness, which measures the similarity of two latent brain states' temporal profiles, and state space closeness which measures the similarity of two latent brain states' space feature profiles, were developed to match latent brain states between different studies. Whether a latent brain state in an independent task matches an optimal working memory task brain state was determined by how close they were in their space and temporal parameters.

Results: BSDS uncovered a number of latent brain states in each study. State temporal closeness and state space closeness measures consistently identified a shared dynamic latent brain state engaged across diverse experiments and four data cohorts (Figure 1). Importantly, despite significant differences in experimental paradigms, data acquisition protocols, and participant cohorts, the temporal properties of brain states predicted cognitive task performance in each of the tasks ($ps<0.05$, Figure 2). Moreover, the occurrence rates of the shared latent state also predicted behavioral performance ($ps<0.05$). Furthermore, weak engagement of the shared brain state was related to inattention symptoms ($r=0.38$, $p=0.01$), suggesting that our generative model is also relevant for investigations of psychopathology.

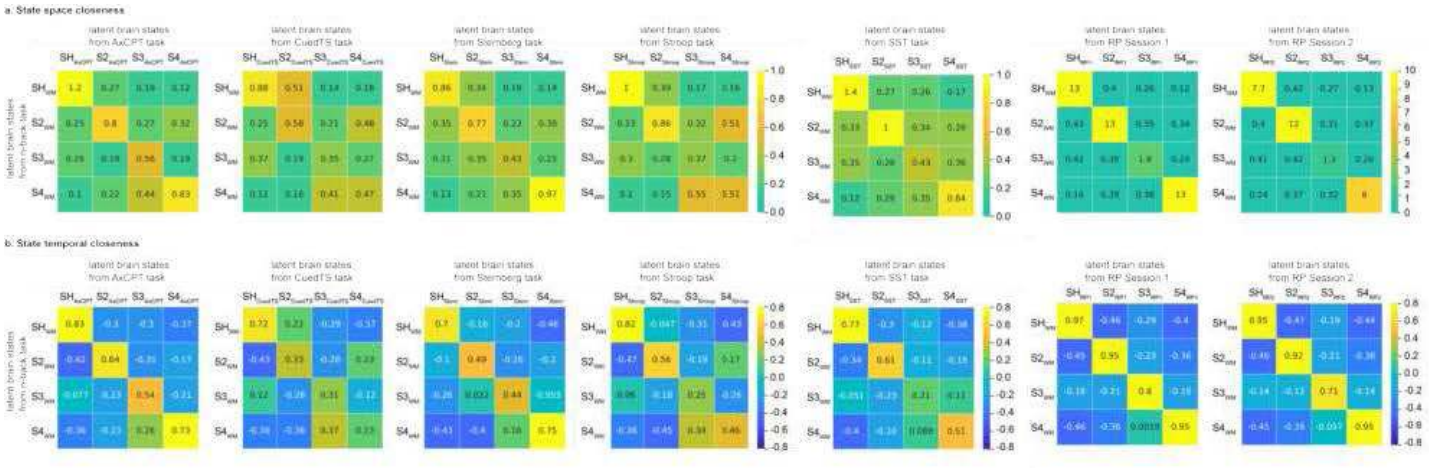

Figure 1. State Matching between cognitive tasks.

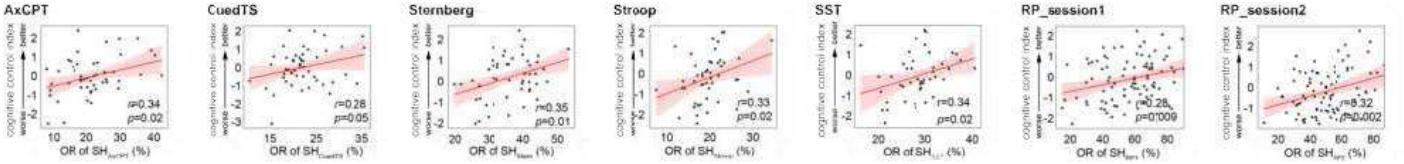

Figure 2. Occupancy rate (OR) of the shared latent brain state is associated with cognitive performance in each task.

Conclusions: Our findings uncover a general dynamic brain state that is preferentially engaged during cognition, and demonstrates that functional circuits associated with the multiple-demand system can adaptively contribute to a wide range of cognitive functions.

References

1. Braun U, et al. Dynamic reconfiguration of frontal brain networks during executive cognition in humans. Proceedings of the National Academy of Sciences of the United States of America 112, 11678-11683 (2015).
2. Braver TS, Kizhner A, Tang R, Freund MC, Etzel JA. The dual mechanisms of cognitive control (DMCC) project. Journal of Cognitive Neuroscience 33, 1990-2015 (2021).
3. Cai W, et al. Hyperdirect insula-basal-ganglia pathway and adult-like maturity of global brain responses predict inhibitory control in children. Nat Commun 10, 4798 (2019).
4. Dosenbach NU, et al. A core system for the implementation of task sets. Neuron 50, 799-812 (2006).
5. Duncan J. The multiple-demand (MD) system of the primate brain: mental programs for intelligent behaviour. Trends in cognitive sciences 14, 172-179 (2010).
6. Shine JM, et al. The Dynamics of Functional Brain Networks: Integrated Network States during Cognitive Task Performance. Neuron 92, 544-554 (2016).
7. Taghia J, et al. Uncovering hidden brain state dynamics that regulate performance and decision-making during cognition. Nat Commun 9, (2018).
8. Van Essen DC, et al. The Human Connectome Project: a data acquisition perspective. NeuroImage 62, 2222-2231 (2012).

Poster No 930

Cue switching but not task switching drives fronto-parietal activity in cued task switching paradigm

Patrick Bissett[1], Sunjae Shim[1], Jaime Ali Rios[1], Jeanette Mumford[2], Russell Poldrack[1]

[1]Stanford University, Stanford, CA, [2]Stanford University, Madison, WI

Introduction: Task switching incurs behavioral costs, and in the lab it is commonly measured with the cued task switch task, which involves cueing the subject to one of two tasks (e.g., magnitude judgment vs. odd-even judgment, see Figure 1), followed by a speeded response to a probe. Task switch cost is commonly ascribed to reconfiguring a task set, which is an "appropriate configuration of mental resources" (Monsell, 2003). A theoretical alternative is that the process of encoding a new cue drives the task switch cost, perhaps from cue repetition benefits (Logan & Bundesen, 2003). Task-set reconfiguration can be distinguished from cue-related theories by introducing two cues per task (e.g., magnitude & high/low, odd/even & parity), which allows separation of the cost of switching tasks (measured by task switch - cue switch) from switching cues (measured by cue switch - cue stay). Task set reconfiguration theories predicting large task switch cost with little or no cue switch cost, and cue-related theories predict large cue switch cost with little or no task switch cost. When separated

behaviorally, cue switch costs are often significant and large, and sometimes there are no additional task switch costs (Logan & Bundesen, 2003; Mayr & Kliegl, 2003). Task switch fMRI studies commonly find a fronto-parietal network (Ruge et al., 2013), but the literature is dominated by tasks with 1 cue per task that cannot distinguish cue-switch and task switch activity. In the few fMRI studies with 2 cues per task, fronto-parietal activity was found in the task switch contrast but not the cue switch contrast (De Baene & Brass, 2011), consistent with this activity instantiating task set reconfiguration. However, this work did not account for RT differences between conditions (Mumford et al., 2023), which may be driving spurious contrast differences. In two independent datasets with two cues per task, while accounting for reaction time confounds, we evaluate whether the fronto-parietal fMRI network observed in task switching is responsive to cue switching or task switching.

Methods: Dataset 1 (Bissett et al., 2023): 88 fMRI participants completed cued task switching with multiband 8, TR = 0.68s, and 2.2mm iso voxels. Dataset 2: 18 fMRI participants each completed 5 sessions of cued task switching with multi-band 3, 3 echoes, TR = 1.49s, and 2.8mm iso voxels. Data were quality assured using MRIQC (Esteban et al., 2017) and pre-processed using Tedana (only Dataset 2; DuPre, Salo et al., 2021) and fMRIPrep (Esteban et al., 2019). First-level models were built that coded for the key conditions and reaction time (Mumford et al., 2023). For Dataset 2, fixed effects maps were created averaging across all 5 sessions. Statistical maps were created with Randomise TFCE values above 0.95 (equivalent to $p < 0.05$) with 5000 permutations. Conjunction maps are the binarized, voxel-wise intersection of the positive voxels in the TFCE maps.

Figure 1. Cued Task Switching Task: Participants were instructed to make a choice response to a probe number presented after a cue. Probes could be 1, 2, 3, 4, 6, 7, 8, and 9. 1a) In dataset 1, if the cue was Magnitude or High-Low, the participants were instructed to respond whether the number was larger or smaller than 5; if the cue was Color or Orange-Blue, the participants were instructed to respond whether the color of the number was orange or blue. The cue was presented for either 100ms or 900ms and these two durations were combined in the results. 1b) Dataset 2 had a similar design, except the color task was replaced with an odd-even judgment with cues "Parity" and "Odd-Even". The cue was presented for 150ms.

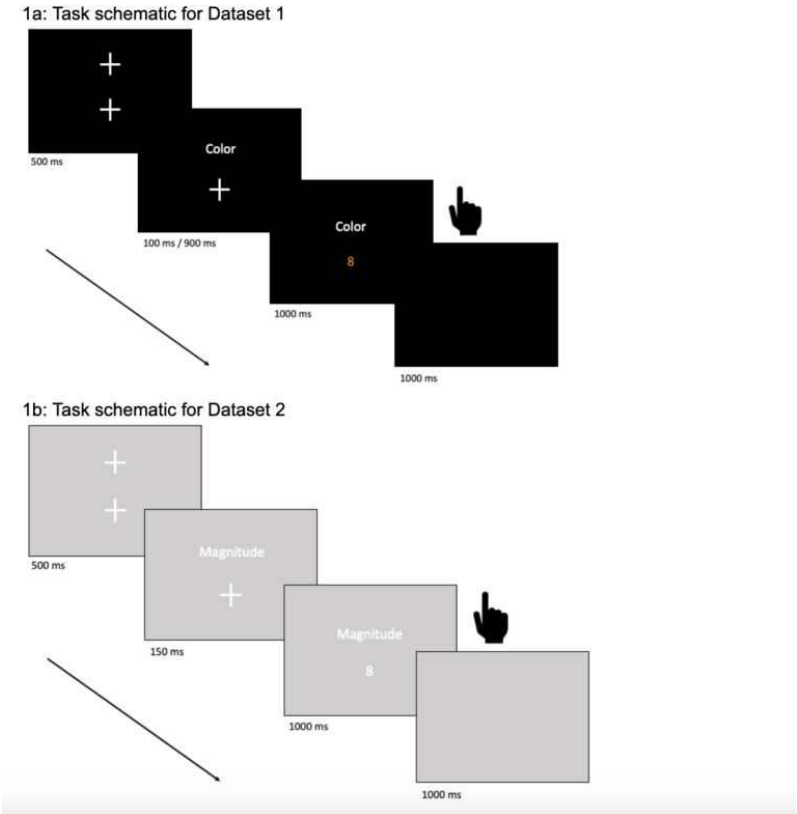

Results: We observed significant RT cue switch costs in dataset 1 (M=38ms) and dataset 2 (M=63ms) as well as task switch costs in dataset 1 (M = 25ms) and dataset 2 (M = 22ms) (Four one-sample t-tests vs. 0 each had p's<.001). Paired-sample, two-tailed t-tests showed that cue switch costs were significantly larger than task switch costs in dataset 2 (p<.001) but not dataset 1 (p=.19). In our conjunction maps, we found left lateralized dlPFC and parietal activity in the cue switch contrast (Figure 2) but no activity in task switch contrast (not shown).

Figure 2. Conjunction activity of cue switch contrast (cue switch - cue stay). Conjunction maps revealing the overlap of the thresholded positive TFCE corrected activation present in both Dataset 1 and Dataset 2. We focus on conjunction maps to ensure activity patterns are replicable across two independent samples. Figure 2a shows representative axial slices of the conjunction contrast and 2b projects the same contrast onto the surface using nilearn's plot_img_on_surf with threshold = .5. We do not present the task switch contrast (task switch - cue switch) activity because there were no voxels that were active in both datasets for this contrast.

2a.

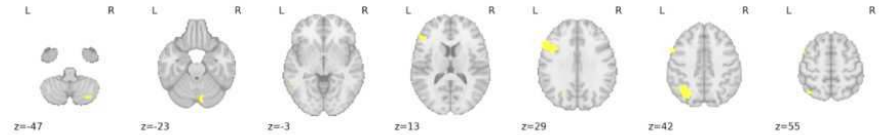

2b.

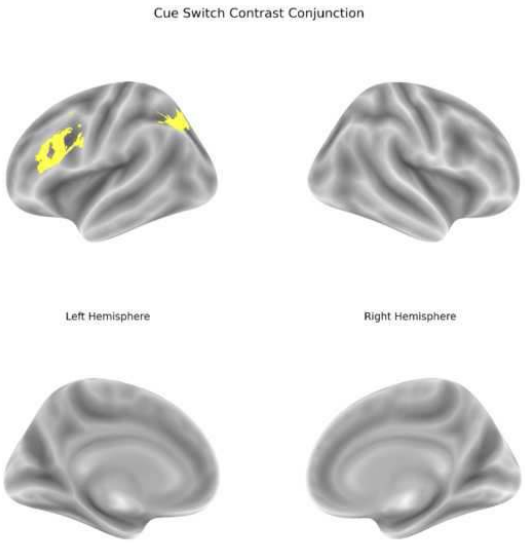

Conclusions: We show the commonly observed fronto-parietal network in cued task switching is not the result of switching tasks, but is instead capturing a more general process of encoding a new cue. This challenges the widespread linking proposition between frontal-parietal activity in task switching and the endogenous act of control of "task set reconfiguration", and is more consistent with cue-repetition benefits (Logan & Bundesen, 2003), perhaps from stimulus priming.

References

1. Bissett, P. G., Eisenberg, I. W., Shim, S., Rios, J. A. H., Jones, H. M., Hagen, M. P., Enkavi, A. Z., Li, J. K., Mumford, J. A., MacKinnon, D. P., Marsch, L. A., & Poldrack. R. A. (2023). Cognitive tasks, anatomical MRI, and functional MRI data evaluating the construct of self-regulation. https://www.biorxiv.org/content/10.1101/2023.09.27.559869v1
2. De Baene, W., & Brass, M. (2011). Cue-switch effects do not rely on the same neural systems as task-switch effects. Cognitive, Affective, and Behavioral Neuroscience, 11, 600-607.
3. Du Pre, E., Salo, T., Ahmed, Z., Bandettini, P. A., Bottenhorn, K. L., Caballero-Gauden, C., ..., & Handwerker, D. A. (2021). TE-dependent analysis of multi-echo fMRI with tedana. The Journal of Open Source Software, 6(66), 3669.
4. Esteban, O., Birman, D., Schaer, M., Koyejo, O. O., Poldrack, R. A., & Gorgolewski, K. J. (2017). MRIQC: Advancing the automatic prediction of image quality in MRI from unseen sites. PloS one, 12, e0184661.
5. Esteban O., Markiewicz C. J., Blair R. W., Moodie C. A., Isik A. I., Erramuzpe A., ... Gorgolewski K. J. (2019). fMRIPrep: a robust preprocessing pipeline for functional MRI. Nature Methods, 16, 111-116.
6. Logan, G. D., & Bundesen, C. (2003). Clever homunculus: Is there an endogenous act of control in the explicit task-cuing procedure? Journal of Experimental Psychology: Human Perception and Performance, 29(3), 575–599.
7. Mayr, U., & Kliegl, R. (2003). Differential effects of cue changes and task changes on task-set selection costs. Journal of Experimental Psychology: Learning, Memory, and Cognition, 29(3), 362-372.
8. Monsell, S. (2003). Task switching. Trends in Cognitive Sciences, 7(3), 134-140.
9. Mumford, J. A., Bissett, P. G., Jones, H. M., Shim, S., Rios, J. A. H., & Poldrack, R. A. (2023). The response time paradox in functional magnetic resonance imaging analyses. Nature Human Behaviour,
10. Ruge, H., Jamadar, S., Zimmerman, U., & Karayanidis, F. (2013). The many faces of preparatory control in task switching: Reviewing a decade of fMRI research. Human Brain Mapping, 34, 12-35.

Poster No 931

Mapping task measures to latent constructs: An expert survey of the NIMH RDoC cognitive domain

Patrick Bissett[1], Logan Bennett[1], Jaime Ali Rios[1], Sunjae Shim[1], Paul McKee[2], Christopher Iyer[1], Nilam Ram[1], Russell Poldrack[1]

[1]Stanford University, Stanford, CA, [2]Duke University, Durham, NC

Introduction: The National Institute of Mental Health (NIMH) Research Domain Criteria (RDoC; Insel et al., 2010) reconceptualizes mental health research by shifting focus from symptom-based diagnostic categories to a set of cross-disorder dimensional domains. The cognitive systems domain of the RDoC matrix includes three constructs: attention, cognitive control, and working memory. As shown in Figure 1, these constructs are indicated by more specific subconstructs (third row of Figure 1, subsequently we use "construct" to indicate construct or subconstruct), which are measured by specific tasks. However, because tasks are not observed manifest variables on their own, an additional layer of information is needed to engage with and evaluate the proposed relations among cognitive constructs. In particular, the constructs must be mapped to specific measurements that quantify individuals' behavior in the tasks. To do so, we enlisted a group of experts to stipulate links between RDoC constructs and specific measures obtained from common cognitive tasks.

Figure 1. RDoC Cognitive Systems tree diagram. Top-down tree diagram of the RDoC's Cognitive Systems domain (top level), the three constructs that are the focus of this study (second level, attention, cognitive control, and working memory), subconstructs (third level), and the 11 tasks that were evaluated in this study (bottom level). Arrows indicate the links that are currently stipulated in the RDoC matrix (https://www.nimh.nih.gov/research/research-funded-by-nimh/rdoc/constructs/rdoc-matrix).

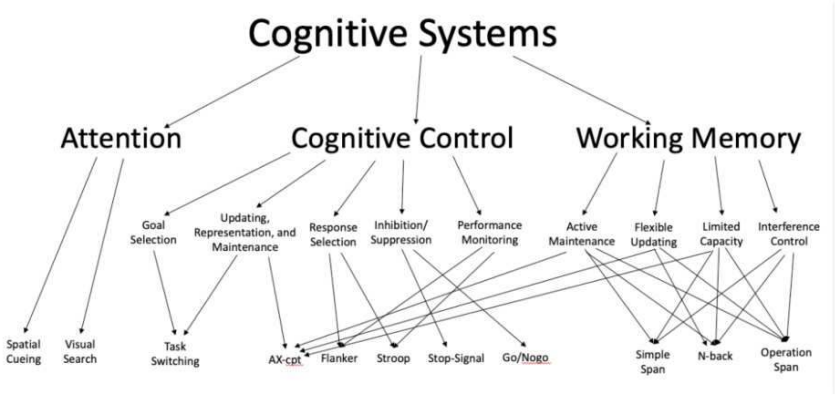

Methods: We used a two-step survey to identify researchers with expertise in cognitive tasks and obtain their expert opinions on the construct–measure mappings. First, we distributed an online screener to experts identified through PubMed searches for relevant keywords, focusing on corresponding authors of publications with the highest citation counts. Then, we shared the screener link on Twitter/X, leveraging our online social networks to reach a broader audience. The screener requested age, academic training, contact information, and which tasks they published two or more scientific articles on. If respondents had published two or more articles on a given task, provided an academic email address, and had begun a PhD in a related field, they received a second survey for that task. The second survey included a brief description of each task and a list of primary task measures that we identified. Respondents stipulated which RDoC constructs are operationalized by each measure, selecting none, one, or more than one construct as a multi-choice response.

Results: From the 689 responses received to the initial screener, we identified and obtained survey responses from 34 respondents who were experts in and completed surveys about one or more tasks. For each task, we obtained, on average, 10.7 experts' mappings between the task measures and constructs. To operationalize consensus, we binarized the data using a threshold that >=50% of the experts stipulated a construct-to-measure link. Figure 2 displays these binarized results, with constructs as columns and measures as rows. Here we highlight some key results. Different measures within a given task were often mapped onto different cognitive constructs, confirming the need to stipulate the relationship between measures and constructs (and not just tasks and constructs, as in the current RDoC matrix). Attention was stipulated in an overwhelming majority of all measures across tasks (81%), consistent with attention being a key construct across various measures of cognitive control (Posner & Boies, 1971). Conversely, some constructs were very sparsely linked to measures (e.g., only two measures were linked to the interference control), suggesting narrow operationalization and/or experts' disagreement.

Figure 2. Expert survey consensus results. Figure 2 presents the constructs (columns) that >=50% of the expert respondents mapped onto a given measurement (rows) in black. The task that the measure was extracted from is in the far left column.

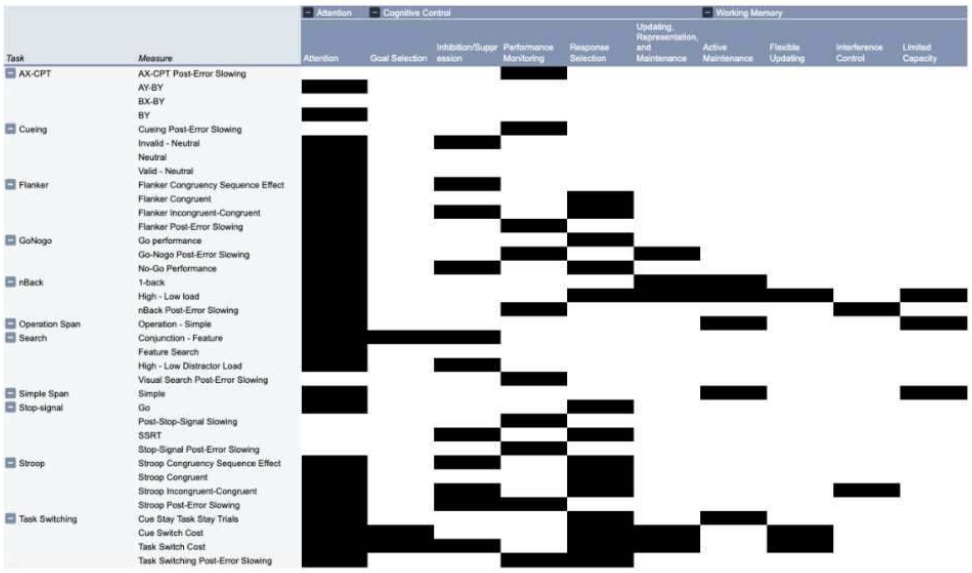

Conclusions: In this work, we surveyed domain experts to obtain consensus opinions on how the RDoC cognitive constructs are linked to observable task measures. This is the first step in an NIH-funded study in which our group aims to validate the neural circuits underlying key cognitive constructs. These expert survey results provide the basis for a model of the current state-of-the-field, to be related to neural circuits in a new dense neuroimaging sample (N=65, 15-hours of MRI each) based upon these same tasks. This MRI acquisition will test if expert beliefs are validated in relationships between the tasks' underlying neural circuits.

References

1. Insel, T., Cuthbert, B., Garvey, M., Heinssen, R., Pine, D. S., Quinn, K., Sanislow, C., & Wang, P. (2010). Research Domain Criteria (RDoC): Toward a new classification framework for research on mental disorders. The American Journal of Psychiatry, 167, 7.
2. Poldrack, R. A., Kittur, A., Kalar, D., Miller, E., Seppa, C., Gil, Y., Parker, D. S., Sabb, F. W., & Bilder, R. M. (2011). The cognitive atlas: toward a knowledge foundation for cognitive neuroscience. Frontiers in Neuroinformatics, 5, 17.
3. Posner, M. I., & Boies, S. J. (1971). Components of attention. Psychological Review, 78(5), 391-408.

Poster No 932

Linking cognitive load with mental fatigue: a resting-state functional connectivity approach

John Read[1], Camille Guillemin[1], Maëlle Charonitis[1], Nikita Beliy[1], Florence Requier[1], Mohamed Bahri[1], Laurent Lamalle[2], Mikhail Zubkov[1], Pierre Maquet[1], Christophe Phillips[1], Gilles Vandewalle[2], Fabienne Collette[1]

[1]University of Liège, Liège, Belgium, [2]Sleep and Chronobiology Lab, GIGA-Institute, CRC-In Vivo Imaging Unit, University of Liège, Liège, Belgium

Introduction: Technological advance drastically changed our working life, leading to significant increases in work demand and effort requirement (Hockey, 2013). Eventually, higher cognitive load comes with higher mental fatigue (MF) and its negative impact on human performance (Borragán et al., 2017). Along with behavioral paradigms also came an explosion of imaging studies seeking to unravel the neural bases of the disease of modern age. While their results are often discrepant, it has been suggested that some MF effects on the brain are task-related (Ioannucci et al., 2023). In the meantime, increased activity in the Default Mode Network (DMN) has also been observed, which was interpreted as compensatory mechanisms occurring when the effort needed increases with time on task (Gergelyfi et al., 2021). Fortunately, MF experience tends to attenuate while resting (Gilsoul et al., 2021). However, recent work proposed that fatigue after-effect on short timescales could be separated into two components (Matthews et al., 2023; Müller et al., 2021): one that is recoverable with rest and another that is not. In fact, few studies showed that changes in neural functioning could persist at rest after MF induction (Esposito et al., 2014;

Gergelyfi et al., 2021). Our goal was to investigate if induction of MF with administration of a task requiring high cognitive load could lead to subtle alterations in the functional connectivity at rest in two networks of interest, DMN and task-related.

Methods: A sample of 19 healthy volunteers (age: 31.42y ± 5.76y; 14 women) realized a 3-session fatiguing protocol (see Fig1 for the detailed protocol). With this paradigm, we induced MF by varying the cognitive load in two conditions of the Time Load Dual Back task (TLDB, Borragán et al., 2017): the Low or the High Cognitive Load (LCL and HCL, respectively). Following both TLDB experimental conditions, participants underwent a 3T resting-state fMRI acquisition of 7 minutes (TR = 1170 ms; voxel size 3x3x3 mm^3). They were asked to keep their eyes open and stare at a white fixation cross. Respiration and pulse signals were recorded during fMRI time series in order to correct for physiological noise in the signal. So far, we conducted exploratory resting-state functional connectivity (rs-FC) analyses – in the HCL condition only – using CONN22.a. More precisely, ROI-to-ROI connectivity matrices were estimated characterizing the rs-FC between each pair of regions among the Control Executive Networks (CEN) as well as the DMN (Schaefer et al., 2018). Group-level analyses were performed using General Linear Models with random-effects across subjects and sample covariance estimation across age and sex. Finally, network-level inferences were based on nonparametric statistics from Network Based Statistics analyses (Zalesky et al., 2010).

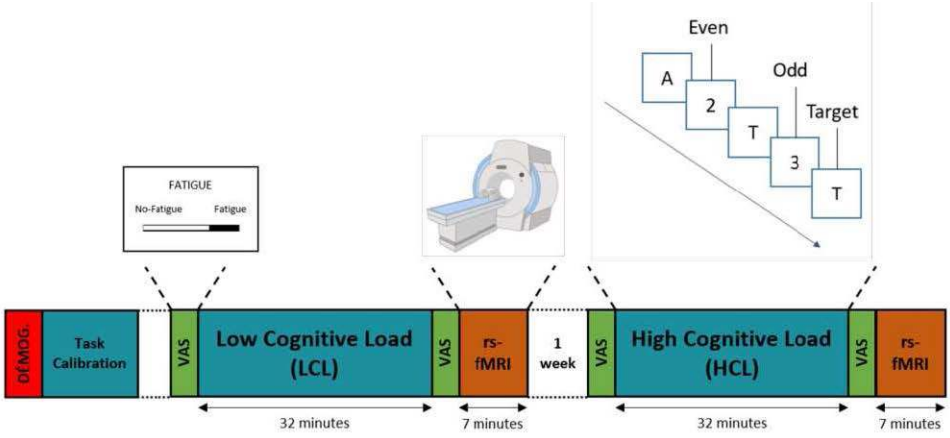

Figure 1 | Fatigue induction protocol.

Participants came three times to the lab. The first session was dedicated to demographical data collection and task training. The second and third sessions were similar except that the task difficulty was different between two sessions (fatiguing HCL or non-fatiguing LCL) which were counterbalanced for each participant. Participants had to rate their level of state fatigue by the mean of Visual Analog Scale before and after the task then performed an NBack task (not shown) followed by a 7 minutes resting-state fMRI.

Results: We extracted connectograms from our two networks of interest at a corrected threshold of p-FDR < 0.001 after the HCL condition (Fig2). Regarding the DMN, preliminary results showed high inter-hemispheric functional connectivity between the precuneus posterior cingulate cortices as well as anti-correlation between the right precuneus and the left prefrontal cortex. Moreover, we observed high connectivity between the left prefrontal cortex and the right dorso-medial prefrontal cortex. Regarding the CEN, we observed an overall high connectivity inside the network, with high inter-hemispheric connectivity for the cingulate and lateral prefrontal cortices.

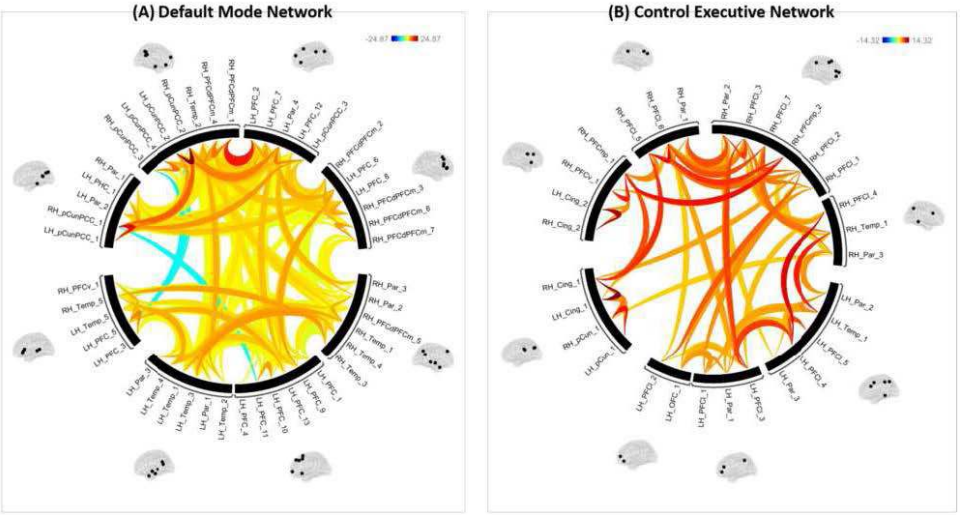

Figure 2| Connectivity inside our two networks of interest after the High Cognitive Load condition.

Links between ROI represent significant functional connections (*t*-statistics). Positive *t*-value (warm colors) indicate positive correlation while negative *t*-value (cold colors) indicate negative correlation. **(A)** Pattern of connectivity inside the Default Mode Network mainly shows high inter-hemispheric connectivity between the precuneus posterior cingulate cortices. **(B)** Pattern of connectivity inside the Control Executive Network mainly shows high overall connectivity in the task-related network.

Conclusions: For the HCL condition inducing high MF level, our results suggest 1) high patterns of rs-FC in the CEN with a tendency to look like small world topology; 2) high inter-hemispheric connectivity between precuneal DMN areas. Further statistical analyses remain to be done to show if these patterns persist when the cognitive load is low (LCL condition). Besides, future analyses should also focus on detailed network properties.

References

1. Borragán, G., Slama, H., Bartolomei, M., & Peigneux, P. (2017). 'Cognitive fatigue: A Time-based Resource-sharing account'. Cortex, vol. 89, pp. 71–84. https://doi.org/10.1016/j.cortex.2017.01.023
2. Esposito, F., Otto, T., Zijlstra, F. R. H., & Goebel, R. (2014). 'Spatially Distributed Effects of Mental Exhaustion on Resting-State FMRI Networks'. PLoS ONE, vol. 9, no. 4, e94222. https://doi.org/10.1371/journal.pone.0094222
3. Gergelyfi, M., Sanz-Arigita, E. J., Solopchuk, O., Dricot, L., Jacob, B., & Zénon, A. (2021). 'Mental fatigue correlates with depression of task-related network and augmented DMN activity but spares the reward circuit'. NeuroImage, vol. 243, 118532. https://doi.org/10.1016/j.neuroimage.2021.118532
4. Gilsoul, J., Libertiaux, V., & Collette, F. (2021). 'Cognitive fatigue in young, middle-aged, and older: Breaks as a way to recover'. Applied Psychology, pp. 1–33. https://doi.org/10.1111/apps.12358
5. Hockey, R. (2013). 'The psychology of fatigue: Work, effort and control'. Cambridge University Press.
6. Ioannucci, S., Chirokoff, V., Dilharreguy, B., Ozenne, V., Chanraud, S., & Zénon, A. (2023). 'Neural fatigue by passive induction: Repeated stimulus exposure results in cognitive fatigue and altered representations in task-relevant networks'. Communications Biology, vol. 6, no. 1, pp. 142. https://doi.org/10.1038/s42003-023-04527-5
7. Matthews, J., Pisauro, M. A., Jurgelis, M., Müller, T., Vassena, E., Chong, T. T.-J., & Apps, M. A. J. (2023). 'Computational mechanisms underlying the dynamics of physical and cognitive fatigue'. Cognition, vol. 240, 105603. https://doi.org/10.1016/j.cognition.2023.105603
8. Müller, T., Klein-Flügge, M. C., Manohar, S. G., Husain, M., & Apps, M. A. J. (2021). 'Neural and computational mechanisms of momentary fatigue and persistence in effort-based choice'. Nature Communications, vol. 12, no. 1, 4593. https://doi.org/10.1038/s41467-021-24927-7
9. Schaefer, A., Kong, R., Gordon, E. M., Laumann, T. O., Zuo, X.-N., Holmes, A. J., Eickhoff, S. B., & Yeo, B. T. T. (2018). 'Local-Global Parcellation of the Human Cerebral Cortex from Intrinsic Functional Connectivity MRI'. Cerebral Cortex, vol. 28, no. 9, pp. 3095–3114. https://doi.org/10.1093/cercor/bhx179
10. Zalesky, A., Fornito, A., & Bullmore, E. T. (2010). 'Network-based statistic: Identifying differences in brain networks'. NeuroImage, vol. 53, no. 4, pp. 1197–1207. https://doi.org/10.1016/j.neuroimage.2010.06.041

Poster No 933

Exploring the relationship between resting fMRI and proactive interference in ageing

Pernilla Andersson[1], Martien Schrooten[1], Jonas Persson[2]

[1]Örebro university, Örebro, Sweden, [2]Karolinska Institutet, Stockholm, Sweden

Introduction: Proactive interference (PI) occurs when old information interferes with newly acquired information and has been suggested as a major source of forgetting in working memory (Oberauer, 2008). Research shows that the ability to overcome PI declines with increasing age (Loosli, 2014; Samrani, 2021). Evidence suggests that a network consisting of the inferior

frontal gyrus (IFG), the striatum, and the anterior cingulum underlie the ability to resolve PI in working memory (Persson, 2013; Samrani, 2019). However, the mechanisms underlying age-related decline in this ability are not yet fully understood. In this study, we investigated, in an adult lifespan sample (N = 239), how resting state functional connectivity (rsFC) relates to the ability to resolve PI in working memory, using seed-based(bilateral IFG) analysis as a function of aging.

Methods: The study sample consisted of 132 younger/ middle-aged (25-64 years) and 107 older (65-80 years) adult participants at baseline, and 93 younger/ middle-aged and 63 older adults at follow-up. All included participants were cognitively healthy (MMSE above 24 and no neurological condition) across the two timepoints. PI was assessed using a modified N-back task, designed to induce interference. This version of the task includes non-familiar no-trials (new), target yes-trials, and familiar no-trials (lures). PI scores reflect the combined relative proportional difference in RT and accuracy between new trials and lure trials. FMRI data were processed and analyzed using CONN (v.22a). Preprocessing followed the standard pipeline in CONN. Seed-based analyses were conducted (bilateral IFG) to investigate the effects of age, PI, and age group × PI interaction, respectively, on rsFC strength. All analyses were conducted cross-sectionally and longitudinally.

Results: Cross-sectional analyses revealed a significant, positive cluster related to PI across the whole sample centered in the right putamen. Additionally, age group × PI interactions identified three clusters These clusters were centered in the right inferior occipital cortex (rIOC; 5420 voxels; MNI: +50 -82 -02), the right precentral gyrus (rPCG; 2809 voxels; MNI: +34 -12 +66), and the right caudate (rC; 1974 voxels; MNI: +16 +22 +02), respectively. Interestingly, more PI was associated with more rsFC between the IFG and the rIOC and rPCG clusters in older adults but with less rsFC in younger/middle-aged adults. Similarly, more PI correlated with less rsFC between the IFG and the rC cluster in older but more rsFC in younger/middle-aged adults. Longitudinal analyses did not reveal any significant clusters.

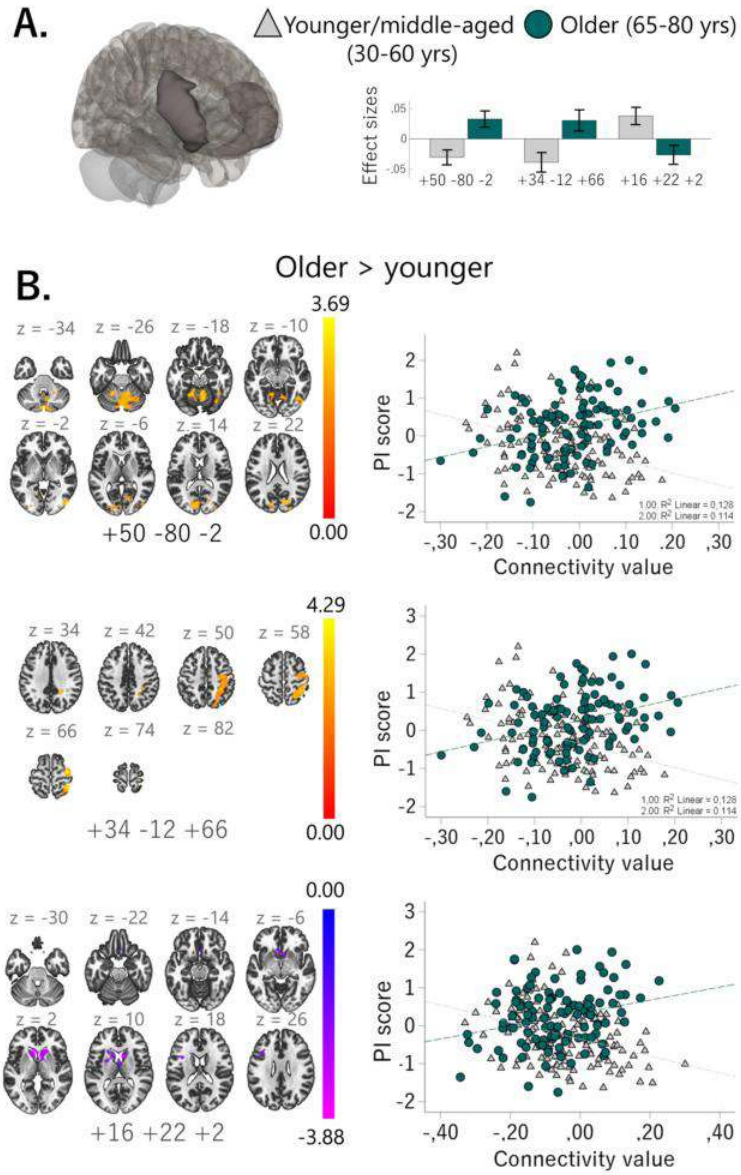

Conclusions: The present results demonstrate an association between IFG rsFC and PI. The association between more PI and more IFG – rPCG rsFC may be related to age-related overactivation in this region during cognitive control processing in working memory updating, which is related to worse performance (Qin, 2020). Previous studies have also found that connections between the ventrolateral prefrontal cortex (located on the IFG) and the caudate is important in working memory updating and that older adults show reduced coupling between these regions together with reduced performance (Podell, 2012). This connection may reflect inhibitory control processing involved in successfully resolving PI during working memory updating. The observed association between more PI and less IFG – rC rsFC in the present study may, thus, reflect reduced inhibitory control. While the rIOC has primarily been associated with visual working memory, especially concerning faces, this cluster was very large and also included large portions of the cerebellum. The cerebellum has been suggested to contribute to verbal working memory by predicting future material in the phonological loop (Sheu, 2019). Taken together, the results contribute to the understanding of decreased control of PI in aging by showing that rsFC is differentially associated with PI in older as compared with younger/middle-aged adults.

References

1. Loosli, S. V. (2014). 'Developmental change in proactive interference across the life span: evidence from two working memory tasks'. Developmental Psychology, 50(4), 1060-1072.
2. Oberauer, K.(2008). 'Forgetting in immediate serial recall: decay, temporal distinctiveness, or interference?', Psychological review, 115(3), 544–576. https://doi.org/10.1037/0033-295X.115.3.544
3. Persson, J. (2013). 'Imaging Fatigue of Interference Control Reveals the Neural Basis of Executive Resource Depletion', Journal of Cognitive Neuroscience, 25(3), 338-351.
4. Podell, J. E., (2012) 'Neurophysiological correlates of age-related changes in working memory updating', Neuroimage. 2012 Sep;62(3):2151-60. doi: 10.1016/j.neuroimage.2012.05.066.
5. Samrani, G. (2019). 'Interference Control in Working Memory Is Associated with Ventrolateral Prefrontal Cortex Volume', Journal of Cognitive Neuroscience, 31(10), 1491-1505.
6. Samrani, G. (2021). 'Proactive interference in working memory is related to adult age and cognitive factors: cross-sectional and longitudinal evidence from the Betula study', Neuropsychology, Development and Cognition. Section B Aging, Neuropsychology and Cognition, 28(1), 108-127.
7. Sheu, Y. S., (2019). 'Disruption of Cerebellar Prediction in Verbal Working Memory', Frontiers in human neuroscience, 13, 61. https://doi.org/10.3389/fnhum.2019.00061
8. Qin, S. (2020). 'Age-related differences in brain activation during working memory updating: An fMRI study', Neuropsychologia, 138, 107335. https://doi.org/10.1016/j.neuropsychologia.2020.107335

Poster No 934

Predicting metacognitive abilities across sensory modalities with functional networks

Katarzyna Hat[1], Paola Galdi[2], Kristian Sandberg[3], Michał Wierzchoń[4]

[1]Consciousness Lab, Psychology Institute, & Centre for Brain Research, Jagiellonian University, Kraków, Lesser Poland, [2]School of Informatics, University of Edinburgh, Edinburgh, United Kingdom, [3]Center of Functionally Integrative Neuroscience, Aarhus University, Aarhus, Denmark, [4]Consciousness Lab, Psychology Institute, & Centre for Brain Research, Jagiellonian University, Kraków, Poland

Introduction: Metacognition is a person's ability to correctly assess and control their cognitive processes. One of the leading debates in metacognition research is whether it is a domain-general or a domain-specific process (Rouault et al., 2018). Here, we investigate metacognition in different sensory modalities with resting-state networks.

Methods: Behavioural data: 4 homologous perceptual tasks were administered outside the scanner in 4 sensory modalities: vision, audition, nociception and touch. Each task consisted of 2 alternative forced choice tasks followed by confidence judgement on a 10%-step size scale from 50% (guessing) to 100% (fully confident). Data was analysed with the Signal Detection Framework using the bhsdtr2 package (Paulewicz & Blaut, 2020), and a type-2 d' (metacognitive sensitivity - meta-d') was estimated (Maniscalco & Lau, 2012). Resting-state fMRI: 302 participants underwent resting-state fMRI recording on a Siemens Skyra 3T (eyes open with fixation cross; TR=801ms, voxel size=2,5mm isotropic, 18min of acquisition). Data were preprocessed with fMRIPrep 21.0.2 and rsDenoise (github) following Finn et al. (2015), excluding Global Signal Regression. Functional connectivity: Denoised data were parcellated into 400 cortical parcels from Schaefer et al. (2018), 17 subcortical parcels defined as in the HCP CIFTI files (Glasser et al., 2013), and 28 cerebellar parcels using the SUIT atlas (Diedrichsen et al., 2009). Average time series were extracted from parcels to estimate functional connectivity as pairwise Pearson's correlation. Predictive framework: Functional connections were used to predict the meta-d' scores using elastic net linear regression and nested cross-validation. We included data from 193 subjects in visual, 182 in auditory, 135 in tactile and 161 in nociceptive task. We run predictions using all connections (whole-brain) and different combinations of artificial lesions, following Dubois et al. (2018), to measure the impact of specific resting-state networks on prediction. We used the 17 Yeo networks (2011)

plus the cerebellum and subcortical regions as additional networks, for a total of 19 networks. We used 'all but 1' and 'all but 2' networks lesions (i.e. using only 1 or 2 networks for prediction). We measured Pearson's correlation between predicted and actual meta-d' scores and controlled for false discovery rate (FDR) with the Benjamini-Hochberg procedure, setting the significance level at α=0.05.

Results: We found significant results for both types of lesions but not for whole-brain predictions. For brevity, we focus only on 'all but 2 networks' lesions. The functional connections selected as most predictive for each task are shown in Figure 1. All pairs of networks that produced significant predictions are listed in Table 1 together with the correlation scores and associated q-values (p-values after FDR correction). Most of the pairs are specific to a given modality but some pairs of networks appear in multiple modalities, and some networks by themself are prominent in all or most modalities.

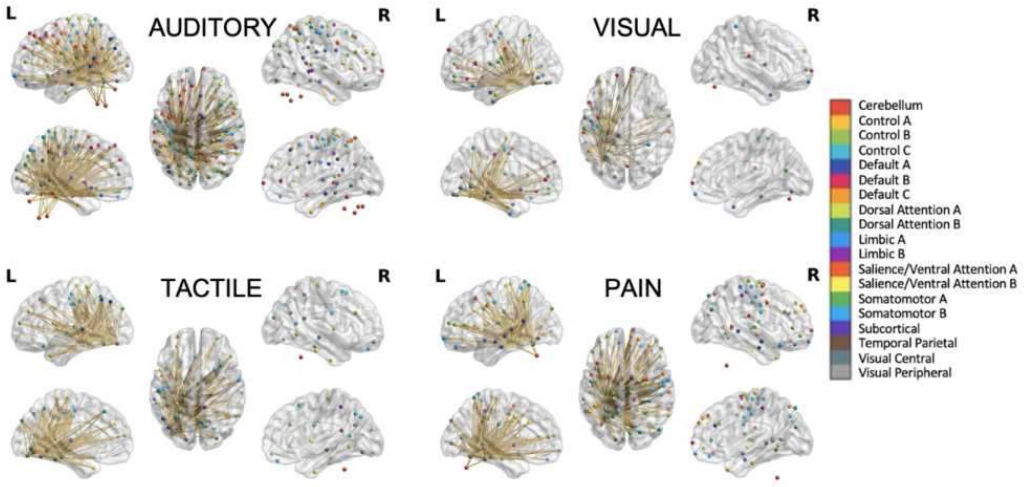

Figure 1. Predictive edges for each modality obtained with 'all but 2 networks' lesions with 19 networks

Table 1. Predictive pairs of networks per modality with q-values.

Auditory: • central visual and default B networks: rho=0.247,p=0.00697 • somatomotor B and dorsal attention B networks: rho=0.222,p=0.01704 • somatomotor B and ventral attention A networks: rho=0.215,p=0.02220 • somatomotor B and ventral attention B networks: rho=0.214,p=0.02263 • somatomotor B and default B networks: rho=0.268,p=0.00274 • dorsal attention A and dorsal attention B networks: rho=0.208,p=0.02777 • dorsal attention A and control C networks: rho=0.200,p=0.03559 • dorsal attention A and default A networks: rho=0.229,p=0.01355 • dorsal attention B and ventral attention B networks: rho=0.379,p=0.00000 • dorsal attention B and limbic B networks: rho=0.209,p=0.02656 • dorsal attention B and limbic A networks: rho=0.291,p=0.00097 • dorsal attention B and default B networks: rho=0.195,p=0.04121 • ventral attention B and control C networks: rho=0.244,p=0.00783 • ventral attention B and default B networks: rho=0.208,p=0.02777 • ventral attention B and temporal parietal networks: rho=0.237,p=0.01025 • control A and control C networks: rho=0.291,p=0.00097 • control A and default A networks rho=0.208,p=0.02764
Visual: • central visual and peripheral visual networks: rho=0.214,p=0.01853 • central visual and limbic B networks: rho=0.222,p=0.01383 • central visual and limbic A networks: rho=0.334,p=0.00000 • central visual and control A networks: rho=0.250,p=0.00444 • central visual and default C networks: rho=0.299,p=0.00034 • peripheral visual and ventral attention B networks: rho=0.263,p=0.00255 • peripheral visual and control A networks: rho=0.335,p=0.00000 • dorsal attention A and dorsal attention B networks: rho=0.223,p=0.01306 • ventral attention B and temporal parietal networks: rho=0.192,p=0.03803 • limbic B and control C networks: rho=0.195,p=0.03544
Tactile: • somatomotor A and somatomotor B networks: rho=0.276,p=0.00978 • somatomotor A and limbic A networks: rho=0.285,p=0.00719 • somatomotor B and default B networks: rho=0.226,p=0.04158 • ventral attention B and default B networks: rho=0.222,p=0.04506 • control A and default B networks: rho=0.249,p=0.02219
Nociceptive: • peripheral visual and default B networks: rho=0.237,p=0.01697 • somatomotor B and control A networks: rho=0.212,p=0.03585 • dorsal attention B and default B networks: rho=0.294,p=0.00187 • ventral attention A and default A networks: rho=0.228,p=0.02233 • ventral attention A and default B networks: rho=0.213,p=0.03544 • ventral attention B and default B networks: rho=0.225,p=0.02407

Conclusions: Our analysis suggests that metacognition can be studied with a 'lesion' approach, while the mechanism is not robust enough to be detected in the whole brain analysis, at least with the current sample. We found each modality portrays a different set of predictive pairs of networks, suggesting at least some part of processing to be domain-specific. However, we also found candidates for metacognitive hubs, especially control A and ventral attention B networks, which are present in results for all modalities. Also default B, somatomotor B and dorsal attention B have the potential to participate in more general processes of metacognition, with the first two not present only in visual modality, and default B participating in multiple pairings. Given the data acquisition was run with eyes open and fixation cross, stronger activation of visual regions could potentially impact the predictivity of metacognitive abilities in this modality.

References

1. Diedrichsen, J. (2009). A probabilistic MR atlas of the human cerebellum. neuroimage, 46(1), 39-46.
2. Dubois, J. (2018). A distributed brain network predicts general intelligence from resting-state human neuroimaging data. Philosophical Transactions of the Royal Society B: Biological Sciences, 373(1756), 20170284.
3. Finn, E. S. (2015). Functional connectome fingerprinting: identifying individuals using patterns of brain connectivity. Nature neuroscience, 18(11), 1664–1671.
4. Glasser, M. F. (2013). The minimal preprocessing pipelines for the Human Connectome Project. NeuroImage, 80, 105–124.
5. Maniscalco, B. (2012). A signal detection theoretic approach for estimating metacognitive sensitivity from confidence ratings. Consciousness and cognition, 21(1), 422–430. https://doi.org/10.1016/j.concog.2011.09.021.
6. Paulewicz, B. (2020). The bhsdtr package: A general-purpose method of Bayesian inference for signal detection theory models. Behavior Research Methods, 52(5), 2122–2141.
7. Rouault, M. (2018). Human metacognition across domains: insights from individual differences and neuroimaging. Personality neuroscience, 1, e17. https://doi.org/10.1017/pen.2018.16.
8. rsDenoise: https://github.com/adolphslab/rsDenoise
9. Schaefer, A. (2018). Local-Global Parcellation of the Human Cerebral Cortex from Intrinsic Functional Connectivity MRI. Cerebral cortex (New York, N.Y. : 1991), 28(9), 3095–3114.
10. Yeo, B. T. (2011). The organization of the human cerebral cortex estimated by intrinsic functional connectivity. Journal of neurophysiology, 106(3), 1125–1165.

Poster No 935

Tuned responses to visual short-term memory load in a fronto-parietal topographic map hierarchy

Ben Harvey[1], Martijn van Ackooij[2], Joeri van Helden[3], Evi Hendrikx[2], Nathan van der Stoep[2], Surya Gayet[2], Jacob Paul[4]

[1]Utrecht University, Utrecht, Nederland, [2]Utrecht University, Utrecht, Utrecht, [3]University of Birmingham, Birmingham, West Midlands, [4]University of Melbourne, Melbourne, Victoria

Introduction: Visual short-term memory (VSTM) is essential for tasks in which visual information must be briefly remembered. Behavioral studies often focus on quantifying the amount or complexity of information that participants can remember (i.e., how much can be remembered). This reflects performance in executive tasks. Conversely, neuroimaging studies have investigated how the memory content is represented in the brain (i.e., what is remembered). This reflects properties of the stimulus. Here, we asked how the brain's responses change with executive task demands, specifically the quantity of visual information that is remembered (i.e., VSTM load). As more information must be remembered to perform tasks accurately, we must allocate more cognitive and neural resources. It may follow that neural response amplitudes in brain areas supporting these executive tasks would monotonically increase with VSTM load. On the other hand, sensory processing is distributed across neural populations using tuned neural responses, organized in hierarchical networks of topographic maps. Here we asked whether these same principles apply to executive processes like task demands.

Methods: We designed a task that keeps visual stimulation as similar as possible while varying VSTM load, specifically the number of unique orientations that had to be remembered (Figure 1A-B). During ultra-high field (7T) fMRI, we gradually changed the VSTM load (Figure 1C, top). This elicited remarkably different profiles at nearby recording sites (voxels) (Figures 1C, 1D & 2A). We compared these responses to the predictions of (linear and logarithmic) monotonic and tuned neural response functions of VSTM load. We then analyzed how the parameters of the best fitting response functions differed within and between responsive areas.

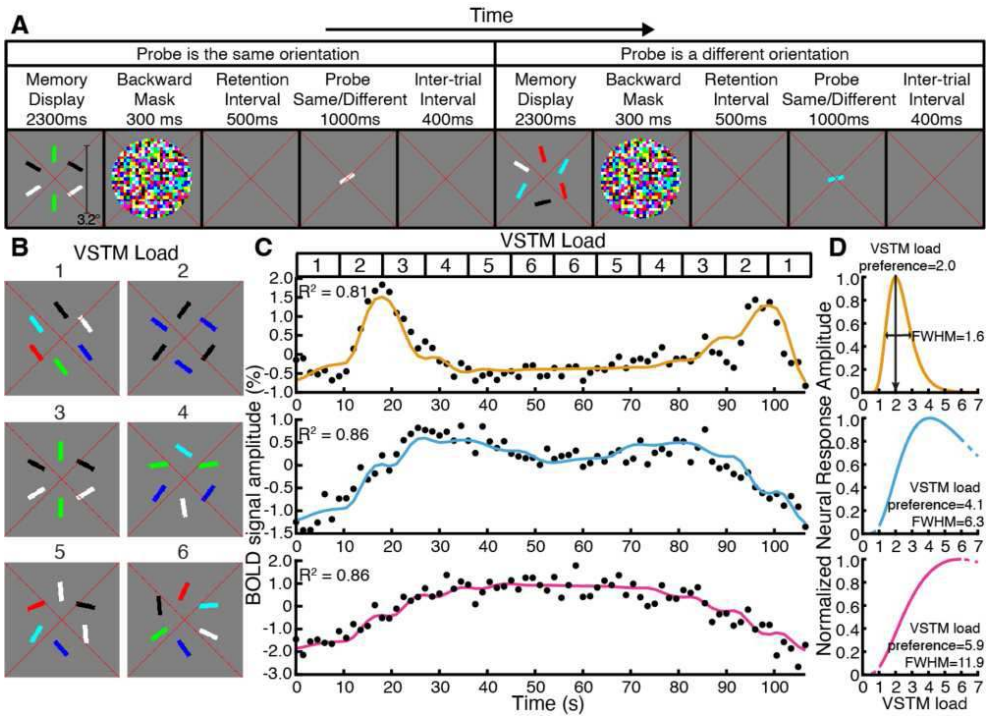

Results: The model which best described the observed responses consisted of a logarithmic Gaussian function with two free parameters (Figure 1D): VSTM load preference and tuning width (the range of VSTM loads producing a response). These models explained the different responses of different voxels (Figure 1C) using different parameters of VSTM load-tuned response functions (Figure 1D). Projecting the VSTM load preference of each voxel onto each participant's cortical surface revealed topographic maps organized by the VSTM load preferences of their constituent neural populations (Figure 2A). We defined maps of VSTM load preferences by identifying regions where preferences consistently and progressively increased from low to high VSTM loads in all participants. We identified 11 maps in each hemisphere, located in regions that are implicated in visual processing (lateral and dorsal occipital areas, superior parietal lobule, postcentral and precentral sulci), control of spatial attention (superior parietal lobule, intraparietal sulcus, postcentral and precentral sulci) and executive control (precentral sulcus, middle frontal gyrus). VSTM load preferences were significantly correlated with cortical distance across the map in 109 out of 132 maps (Figure 2B). We also found systematic differences in responses to VSTM load between maps. The mean VSTM load preferences of the voxels in each map increased from posterior to anterior maps. Furthermore, responses in superior parietal cortices were clearer and subtended a larger cortical area then elsewhere. VSTM load preferences were not correlated with visual field position or numerosity preferences. The responses were absent if participants viewed the same stimuli without performing the task.

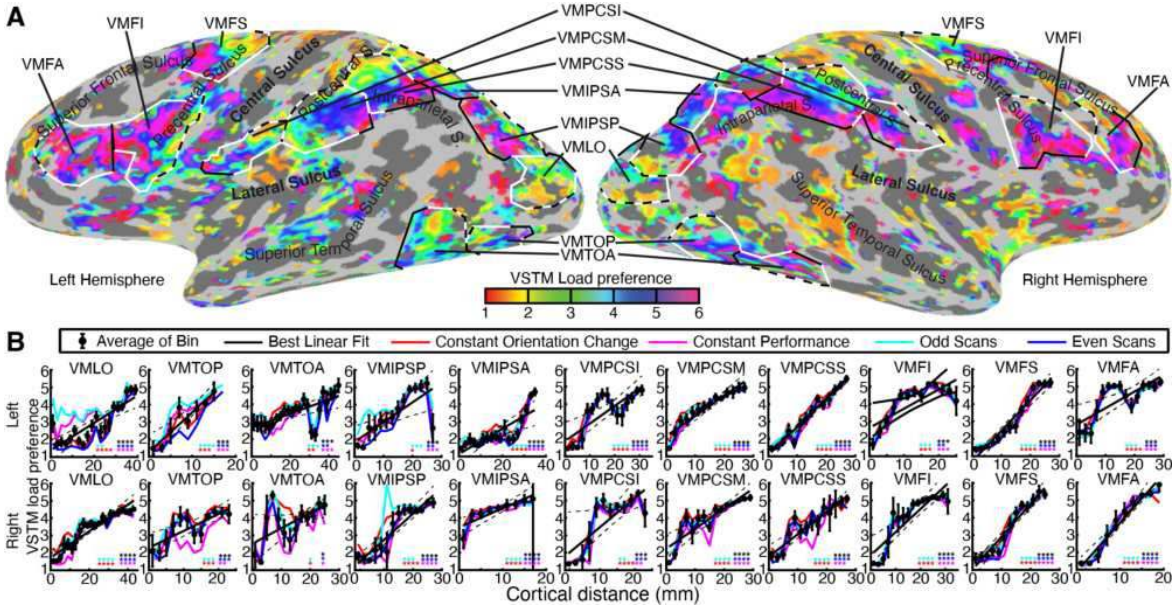

Conclusions: Our results show that tuned, topographically organized, and hierarchically processed neural responses distribute complex tasks across neural populations throughout the brain. Therefore, these neural encoding schemes, common in sensory processing, generalize to complex higher-order executive functions. As a result of this generalization, established methods to investigate sensory neural tuning can reveal new mechanisms of underlying executive processes.

References

1. Alvarez, G.A., and Cavanagh, P. (2004). The capacity of visual short-term memory is set both by visual information load and by number of objects. Psychological science 15, 106–111.
2. Dijkstra, N., Bosch, S.E., and van Gerven, M.A.J. (2019). Shared Neural Mechanisms of Visual Perception and Imagery. Trends Cogn Sci 23, 423–434.
3. Tsouli, A., Harvey, B.M., Hofstetter, S., Cai, Y., van der Smagt, M.J., te Pas, S.F., and Dumoulin, S.O. (2022). The role of neural tuning in quantity perception. Trends in Cognitive Sciences. 10, 1016
4. Harvey, B.M., Klein, B.P., Petridou, N., and Dumoulin, S.O. (2013). Topographic Representation of Numerosity in the Human Parietal Cortex. Science. 341, 1123–1126.

Poster No 936

Catecholamine-Driven Low-Dimensional Brain Dynamics and Cognitive Task Performance

Gabriel Wainstein[1], Christopher Whyte[1], Eli Müller[1], Daniella Furmann[2], Mark D'esposito[2], Sharon Naismith[1], James Shine[3]

[1]University of Sydney, Sydney, NSW, [2]University of California, Berkeley, CA, [3]University of Sydney, Sydney, NA

Introduction: Cognitive flexibility underlies our ability to adapt to new and unexpected conditions in our environment. Genetic variations, such as the COMT Val158Met polymorphism, are known to influence this executive function. This study investigates the effects of the COMT genotype and the administration of tolcapone, a COMT inhibitor, on cognitive flexibility, utilizing fMRI and novel large-scale dynamic system analysis to explore underlying neural mechanisms (shine et al,. 2016; Munn et all., 2021).

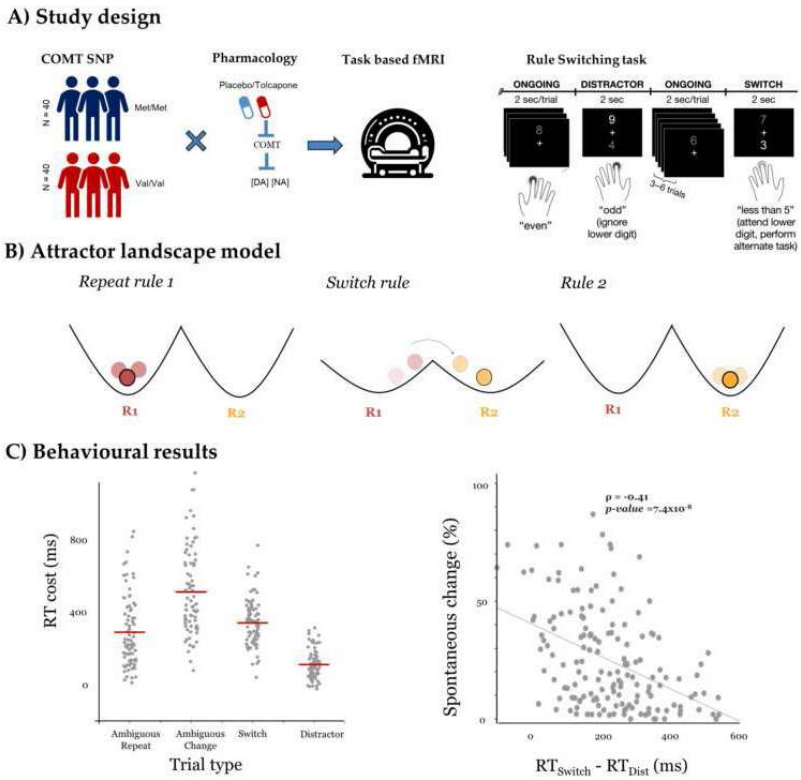

Figure 1: Experimental design and behavioural results. A) Study Design: Eighty participants were stratified into two groups based on the catechol-O-methyltransferase (COMT) single nucleotide polymorphism (SNP). Each group underwent a double-blind pharmacological trial, receiving either placebo or tolcapone—a COMT inhibitor. Participants performed a cognitive task requiring rule switching to assess the effects of COMT inhibition on cognitive flexibility. B) Attractor Landscape Model: This schematic represents the cognitive state of participants during the task under two rule conditions (R1 and R2). The ball symbolizes the participant's current state, which varies depending on the rule being applied. The model illustrates the cognitive transition between rules, simulating the mental shift required during the task. C) Left - Reaction Time (RT) Results: The scatter plot displays the RTs for the four task conditions (Ambiguous, Ambiguous-Switch, Switch, Distractor) across the trial types. Right - Switching Cost Analysis: This plot correlates the difference in RT between the Switch and Distractor conditions against the propensity to switch to Rule 2 during ambiguous trials. The slope indicates the relationship between their bias/position on the landscape (spontaneous switch) and the time required to switch.

Methods: Eighty participants were genotyped for the COMT Val158Met polymorphism and randomly assigned to receive either tolcapone or a placebo in a double-blind trial. Participants engaged in a cognitive task requiring rule switching, designed to probe cognitive flexibility. We conducted functional connectivity analysis to define large-scale network modules and network integration, principal component regression to identify networks involved in task execution, and energy landscape representations to visualize state transitions during task performance.

Results: Functional connectivity analysis revealed significant modularity influenced by COMT genotype and drug interaction, with tolcapone markedly affecting Val allele carriers (Figure 2 A-C). Principal component regression highlighted distinct involvement of control and default mode networks (PC2) and the engagement of dorsal attention networks (PC3) in task execution (Figure 2D). Energy landscapes showed that higher network integration, as induced by tolcapone in Val carriers, corresponded to reduced switch costs, indicative of more efficient cognitive state transitions (Figure 2E).

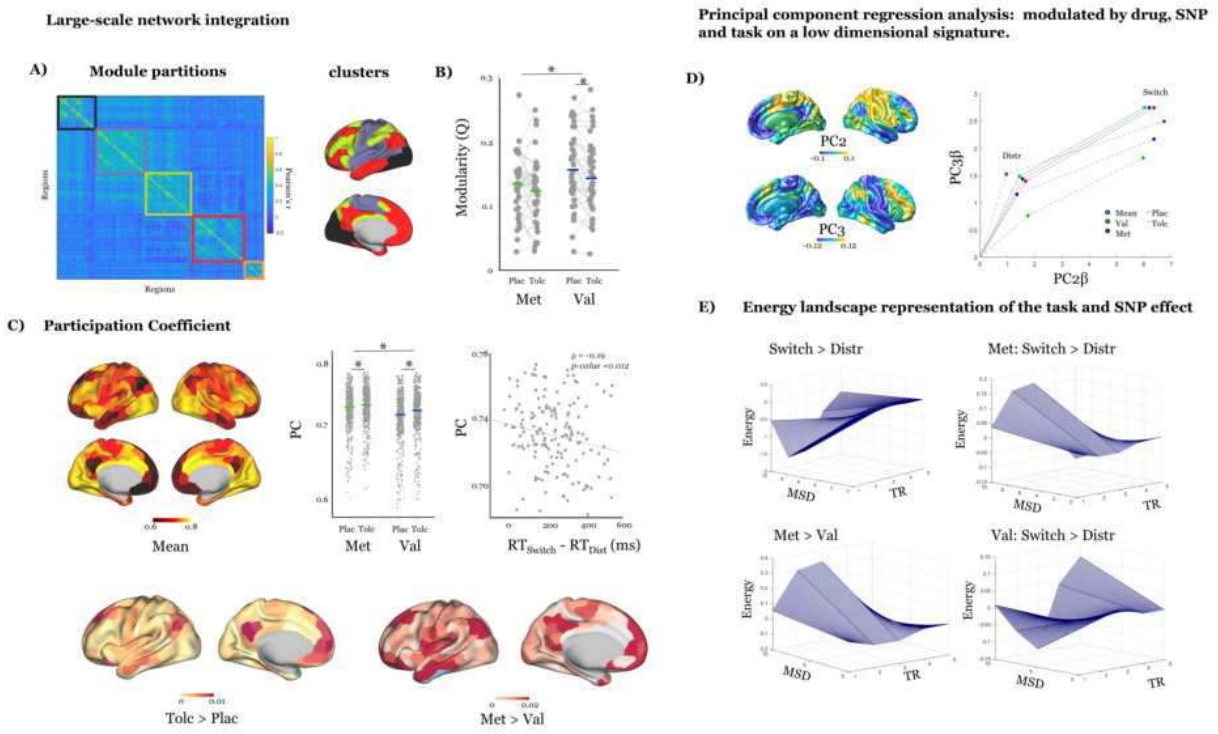

Figure 2: large-scale fMRI analysis: A) Module Partitions and Functional Connectivity matrix among brain regions, with modules identified via Louvain analysis. The accompanying brain maps highlight the modular structure within the brain's network. B) Modularity Index: The scatter plot at the top right quantifies the modularity index, which measures the strength of division of a network into modules. The analysis reveals that tolcapone administration significantly affects the modularity in participants with the Val allele. C) Participation Coefficient Analysis: The middle panels depict the participation coefficient of brain regions, a metric of network integration. An overall trend toward increased integration across all regions is observed. The bottom right scatter plot shows a correlation between this increased integration and switch cost, indicating that higher network integration is associated with lower switch cost, thus affecting cognitive task performance. The contrasts below the participation coefficient maps (Tolc > Plac and Met > Val) visually represent areas of increased integration under the influence of tolcapone and genetic variation. D) Principal Component Regression Analysis - This section displays the results of a principal component regression analysis, elucidating the brain's low-dimensional reconfiguration during task-specific events, namely distractor and switching. The brain maps highlight the loading of the first three principal components (PC2 and PC3) across the cortex, differentiating between control networks versus the default mode network (PC2), and the dorsal attention network (PC3). The scatter plot to the right illustrates the impact of each principal component on the task's evoked responses, with separate trajectories observed for each genetic group under the influence of the drug (blue = group mean; red = Met/Met group; green = Val/Val group; dashed line is tolcapone effect). E) Energy Landscape Representation - The four 3D plots provide an energy landscape view of the task-evoked neural states. Each plot corresponds to a different condition or genetic variant and shows the directional change toward a lower energy state during the task. The plots 'Switch > Distr', 'Met: Switch > Distr', 'Met > Val', and 'Val: Switch > Distr' represent the dynamic shifts within the neural substrate as a function of task demands and genetic predisposition, influenced by the pharmacological modulation.

Conclusions: Our findings suggest that the COMT Val158Met polymorphism and pharmacological intervention with tolcapone synergistically modulate cognitive flexibility. The enhanced network integration and reduced switch costs in Val carriers treated with tolcapone point to a genotype-specific enhancement of cognitive flexibility. These insights and framework advance our understanding of the neurogenetic basis of executive functions and have potential implications for personalized interventions in disorders characterized by impaired cognitive flexibility.

References

1. Munn, B. R., Müller, E. J., Wainstein, G., & Shine, J. M. (2021). The ascending arousal system shapes neural dynamics to mediate awareness of cognitive states. Nature communications, 12(1), 6016.
2. Shine, J. M., Bissett, P. G., Bell, P. T., Koyejo, O., Balsters, J. H., Gorgolewski, K. J., ... & Poldrack, R. A. (2016). The dynamics of functional brain networks: integrated network states during cognitive task performance. Neuron, 92(2), 544-554.

Poster No 937

The neural processing of cognitive control deters substance use through altruism

Jungmeen Kim-Spoon[1], Ya-Yun Chen[1], Tae-Ho Lee[1], Morgan Lindenmuth[1], Claudia Clinchard[1], Jacob Lee[2], Brooks Casas[2]

[1]Virginia Tech, Blacksburg, VA, [2]Fralin Biomedical Research Institute, Roanoke, VA

Introduction: According to the neuromaturational models of risk taking (Casey et al., 2008; Steinberg, 2008), the cognitive control neural systems (involved in maintaining future goals and inhibiting prepotent responses) are important predictors of adolescent health risk behaviors such as substance use (Kim-Spoon et al., 2017). Yet, no study has examined whether developmental changes in cognitive control (task-based) functional connectivity predict substance use. The first aim of this study is to conduct longitudinal analyses examining changes in functional connectivity during adolescence related to substance use in young adulthood. In the field of addiction research, Volkow et al. (2011) proposed that social reward can deter substance use working as a powerful reinforcer to compete with high-reward value of substances. The second aim of this study is to conduct longitudinal mediation analyses in which cognitive control predicts substance use through altruism prosocialness, following the neurocognitive social transactional model of vulnerability (McCrory et al., 2022).

Methods: Participants: Eighty-five healthy adolescents (42 males; 43 females) aged 13-14 (M = 14.02, SD = 0.56 at Time 1) were assessed approximately annually across 7 time points (i.e., mean ages 14 to 20 years). Measures: At Times 1-5, cognitive control-related neural processing was assessed by blood-oxygen-level-dependent responses during the Multi-Source Interference Task (MSIT; Bush et al., 2003). At Times 5-7, substance use was assessed by frequency of cigarette, alcohol, and marijuana use. At Time 6, altruism was assessed using the altruism scale representing other-oriented values (Büssing et al., 2012). Experimental paradigm: In the MSIT, on each trial, the participant was presented with three digits and asked to identify the digit that was different from the others by pressing the button corresponding to the digit. For trials in the neutral condition, the target's identity was congruent with the target's relative position on the screen, but in the interference condition, the target's identity did not match its relative position. Four blocks of 24 interference trials and 4 blocks of 24 neutral trials were interleaved with an interstimulus interval of 1.75 seconds. Imaging analysis: 3.4x3.4x4mm EPI images were realigned to the first volume then normalized to the MNI 3mm standard template and smoothed at 6mm using SPM8. For each participant, all stimuli onsets were modeled through convolution with a canonical hemodynamic response function.

Results: We examined patterns of connectivity difference between interference and neutral conditions during the MSIT by using the generalized psychophysiological interaction analysis (gPPI). By defining the seed region as the dorsal anterior cingulate cortex (dACC), the dACC-dlPFC change from age 14 to 17 predicted substance use (maximum average scores of cigarette, alcohol, and marijuana use) during ages 18-20 (r = -.41, see Figure 1). We also found that more positive dACC-dlPFC connectivity predicted higher altruism one year later between ages 18 and 19 (r = .45, see Figure 2). Finally, our data indicated significant mediation effects of altruism: greater dACC-dlPFC connectivity during cognitive control at age 18 predicted higher altruism at age 19, which in turn predicted lower substance use at age 20 (95%CI [-.297; -.032] for cigarette/tobacco use; 95%CI [-.282; -.013] for marijuana use).

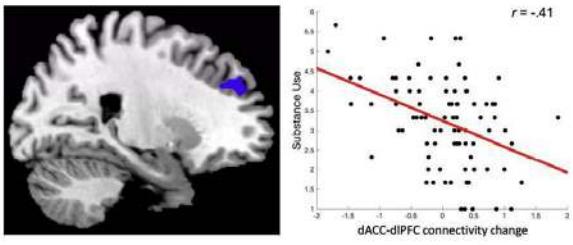

Figure 1. Decreased dACC-dlPFC connectivity during cognitive control from age 13 to 17 predicts higher substance use (i.e., mean of cigarette, alcohol, and marijuana use) across ages 18-20 (shown at $p < .001$ uncorrected).

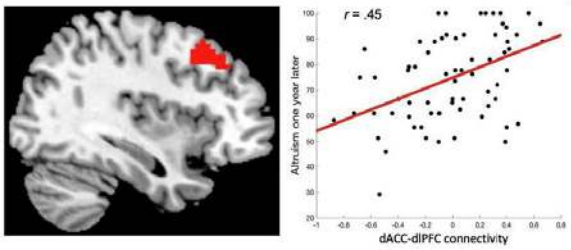

Figure 2. Higher dACC-dlPFC connectivity during cognitive control predicts higher altruism one year later (shown at $p < .005$ uncorrected).

Conclusions: We found evidence that developmental changes in cognitive control brain functioning during adolescence predicts substance use during young adulthood. Further, our mediation analysis suggests that neural processing of cognitive control is linked to later substance use through altruism, highlighting the important role of social functioning in linking neurocognitive functioning and health outcomes. The current study enhances our understanding of the neurobiological and social factors jointly contribute to the development of substance use.

References

1. Bush, G., Shin, L. M., Holmes, J., Rosen, B. R., & Vogt, B. A. (2003). The Multi-Source Interference Task: Validation study with fMRI in individual subjects. Molecular Psychiatry, 8(1), 60-70. https://doi.org/10.1038/sj.mp.4001217
2. Büssing, A., Reiser, F., Michalsen, A. & Baumann, K. (2012). Engagement of patients with chronic diseases in spiritual and secular forms of practice: Results with the shortened SpREUK-P SF17 questionnaire. Integrative Medicine: A Clinician's Journal, 11, 28–38. https://doi.org/10.1186/1477-7525-3-53
3. Casey, B. J., Getz, S. & Galvan, A. (2008). The adolescent brain. Developmental Review, 28(1), 62-77. https://doi.org/10.1016/j.dr.2007.08.003
4. Kim-Spoon, J., Kahn, R. E., Lauharatanahirun, N., Deater-Deckard, K., Bickel, W. K., Chiu, P. H., & King-Casas, B. (2017). Executive functioning and substance use in adolescence: Neurobiological and behavioral perspectives. Neuropsychologia, 100, 79-92. https://doi.org/10.1016/j.neuropsychologia.2017.04.020
5. McCrory, E., Foulkes, L., & Viding, E. (2022). Social thinning and stress generation after childhood maltreatment: A neurocognitive social transactional model of psychiatric vulnerability. The Lancet Psychiatry. https://doi.org/10.1016/S2215-0366(22)00202-4
6. Steinberg, L. (2008). A social neuroscience perspective on adolescent risk-taking. Developmental Review, 28(1), 78-106. https://doi.org/10.1016/j.dr.2007.08.002
7. Volkow, Nora D., Baler, Ruben D. & Goldstein, Rita Z. (2011). Addiction: Pulling at the neural threads of social behaviors. Neuron, 69(4), 599-602. https://doi.org/10.1016/j.neuron.2011.01.027

Poster No 938

Dual-task interference in fibromyalgia: behavioral and neural data

Francisco Mercado[1], David Ferrera[1], Paloma Barjola[1], Alberto Carpio[1], Roberto Fernandes[1], María Carmen Martín-Buro[1]

[1]Universidad Rey Juan Carlos, Madrid, Madrid

Introduction: Cognitive dysfunction is currently recognized as one of the most disabling symptoms in fibromyalgia, surpassing even the impact of pain itself. Evidence from neuropsychological investigations indicates that this dysfunction becomes more pronounced during high-demand executive function tasks, suggesting an abnormal functioning within the cerebral cortices of the frontal-parietal network. Specifically, individuals with fibromyalgia report difficulties when daily activities require them to handle multiple sources of information simultaneously, as these stimuli compete for the same processing resources. Given that cognitive processing involves rapid stages encompassing various mental operations, electroencephalographic activity was recorded and analyzed through event-related potentials.

Methods: Forty-three right-handed women participated in the experiment, including nineteen fibromyalgia patients and twenty-four healthy subjects, with ages ranging from 33 to 66 years. The psychological refractory period (PRP) paradigm was employed in the experimental setting to study dual-task interference, analyzing both behavioral and neural responses. In each trial, two different visual stimuli (S1 and S2) were presented, each requiring independent responses. S1 comprised two types of geometric figures (a blue square or a red square), while S2 was either the letter 'O' or the letter 'X'. This dual-task paradigm, adapted from Luck (1998), involved stimuli presented against a black background for 100 ms, with the stimulus onset asynchrony (SOA) manipulated across three conditions (100, 250, or 400 ms). This manipulation resulted in three task conditions, with shorter SOAs producing more intense interference in response selection and increasing the reaction time to S2 associated with stimulus categorization. The amplitude of the P3 component, known for modulating its amplitude when processing resources need to be shared between tasks was analyzed. Thus, the probability of S2 occurrence was manipulated with frequent (75%) and infrequent (25%) alternatives.

Results: Behavioral analyses revealed a main effect of SOA, indicating that shorter SOAs (100 ms) led to higher response times than longer SOA conditions (250 and 400 ms). Additionally, fibromyalgia patients exhibited longer reaction times compared to healthy subjects. At the neural level, the P3 wave's amplitude at parietal sites significantly increased at shorter SOAs for patients with fibromyalgia compared to healthy subjects. The augmented response times in fibromyalgia patients suggested a reduction in the availability of cognitive resources for identifying and categorizing S2. However, the increase of P3 amplitude at short SOAs in fibromyalgia patients likely indicated an inefficient use of cognitive resources when they faced with the need to share them between two sources of stimulation, even during seemingly simple tasks involving stimulus categorization.

Conclusions: The findings suggest that experimental conditions involving a high demand for cognitive resources (dual tasks with short SOAs) can reveal cognitive dysfunctions in fibromyalgia. Nevertheless, further research is necessary to fully comprehend and define dysfunctional cognition in fibromyalgia. This research was supported by the Ministerio de Ciencia e Innovación of Spain (MICINN; grant PID2020-115463RB-I00).

References

1. Luck, S. J. (1998). Sources of dual-task interference: Evidence from human electrophysiology. Psychological Science. 9 (3), 223-227.
2. Dick, B. D.; Verrier, M. J.; Harker, K. T. & Rashiq, S. (2008). Disruption of cognitive function in Fibromyalgia Syndrome. Pain. 139, 610-616.
3. Samartin-Veiga N, González-Villar AJ, Carrillo de la Peña MT (2019). Neural correlates of cognitive dysfunction in fibromyalgia patients: Reduced brain electrical activity during the execution of a cognitive control task. Neuroimage Clin. 23:101817
4. Seo J, Kim S-H, Kim Y-T, et al. (2012). Working memory impairment in fibromyalgia patients associated with altered frontoparietal memory network. PLoS One;7(6):e37808.
5. Mercado, F; Ferrera, D; Fernandes-Magalhaes, R; Peláez, I; Barjola, P. (2021). Altered sub-processes of working memory in fibromyalgia patients: An ERP study using N-back task. Pain Medicine. 23(3):475-487

Poster No 939

Uncertainty about Action Choices: Human Reach Target Selection using Conflicting Sensory Signals

Niloofar Gharesi[1], John Kalaska[2], Sylvain Baillet[3]

[1]McGill University, Montréal, Quebec, [2]Université de Montréal, Montreal, Quebec, [3]Montreal Neurological Institute, Montreal, Quebec

Introduction: Daily decisions often involve conflicting sensory inputs, requiring the choice of one action from multiple alternatives. The dorsal premotor cortex (PMd) plays a crucial role in guiding voluntary arm movements, serving as a convergence point for sensory instructional and action-related information. Neural activity in the PMd is strongly modulated by sensory inputs that support different motor responses and in constructing representations of potential arm movement choices[1]. Moreover, PMd activity exhibits correlations with high-level abstract concepts related to actions even before these actions are fully specified, such as the overarching goal of future actions or a visuomotor task rule[2,3]. It can also express learned stimulus–response associations during mental rehearsal without the occurrence of actual movements[4,5]. Kalaska and colleagues conducted several studies on the involvement of PMd in reaching decisions in tasks requiring subjects to discern the dominant color of a multi-colored checkerboard Decision Cue (DC) to choose between two color-coded targets. The strength of DC evidence was manipulated by varying the proportion of small squares of the two choice colors. In the Targets First (TF) task, the two-colored targets appeared first in each trial, followed by the DC after a delay. The TF task revealed that PMd neural activity in monkeys correlated with strength of DC evidence and the direction of the selected target but was poorly modulated by the color of the evidence itself[6]. However, functional interpretation of the observed PMd neural responses in this task was confounded by the fact that the onset of the DC could simultaneously initiate both perceptual deliberation and action selection processes. The Checkerboard First (CF) task addresses this limitation. In the CF task, the DC appears before the two-colored targets, enabling participants to make a categorical perceptual decision about the dominant DC color independently of how the decision would be reported[7]. In monkeys, PMd is active during action selection but does not participate in the perceptual components of the decision-making process[8]. PMd units exhibit strongly-modulated activity only when complete information about the stimulus–response associations determining action choices is accessible. PMd activity predominantly reflects the chosen reach direction, the strength of evidence supporting those actions, and the temporal dynamics of the action decisions, but not the dominant color of the DC evidence.

Methods: We employed similar tasks while human subjects underwent magnetoencephalography (MEG) recordings. Subjects performed a TFD and CFD task with an enforced delay interval after each of the two instructional cues appeared. The number of Cyan or Orange squares supporting the correct color/target choice was kept constant in each DC, and we varied the amount of conflicting evidence for the wrong choice. Specifically, the number of DC squares of each color in a trial could be 64/1, 64/32, 64/48, 64/56, 64/60, or 64/62 of either C/O or O/C, resulting in a set of 12 distinct DCs. A differential auditory tone at the end of each trial provided the subjects with knowledge of results (KR; correct or incorrect target choice).

Results: We found the classic pattern of progressive beta-band power suppression over PMd during each instructed-delay epoch of the trial, followed by a rebound after chosen movement onset. The strength of suppression was strongest during second delay epoch of both the TFD and CFD tasks, when full information about response choices was available. The rate of beta suppression during that second delay epoch was also modulated by the strength of DC evidence in both tasks, but not by the dominant color.

Conclusions: Importantly, the auditory KR tones evoked a beta suppression/rebound that was modulated by the DC evidence strength on which the subjects made their decision in each trial, which is a potential neural correlate of a response prediction error signal in PMd.

References

1. Cisek, P., & Kalaska, J. F. (2005). Neural correlates of reaching decisions in dorsal premotor cortex: specification of multiple direction choices and final selection of action. Neuron, 45(5), 801-814.
2. Buch, E. R., Brasted, P. J., & Wise, S. P. (2006). Comparison of population activity in the dorsal premotor cortex and putamen during the learning of arbitrary visuomotor mappings. Experimental brain research, 169, 69-84.
3. Wallis, J. D., & Miller, E. K. (2003). From rule to response: neuronal processes in the premotor and prefrontal cortex. Journal of neurophysiology, 90(3), 1790-1806.
4. Cisek, P., & Kalaska, J. F. (2004). Neural correlates of mental rehearsal in dorsal premotor cortex. Nature, 431(7011), 993-996.
5. Gharesi, N., Luneau, L., Kalaska, J. F., & Baillet, S. (2023). Evaluation of abstract rule-based associations in the human premotor cortex during passive observation. bioRxiv.
6. Coallier, É., Michelet, T., & Kalaska, J. F. (2015). Dorsal premotor cortex: neural correlates of reach target decisions based on a color-location matching rule and conflicting sensory evidence. Journal of neurophysiology, 113(10), 3543-3573.
7. Coallier, É., & Kalaska, J. F. (2014). Reach target selection in humans using ambiguous decision cues containing variable amounts of conflicting sensory evidence supporting each target choice. Journal of neurophysiology, 112(11), 2916-2938.
8. Wang, M., Montanède, C., Chandrasekaran, C., Peixoto, D., Shenoy, K. V., & Kalaska, J. F. (2019). Macaque dorsal premotor cortex exhibits decision-related activity only when specific stimulus–response associations are known. Nature communications, 10(1), 1793.

Poster No 940

Arrangement of specialized and general control regions in the LPFC evaluated using precision fMRI

Zach Ladwig[1], Nathan Labora[2], Megan Dorn[1], Joanna Hernandez[1], Rodrigo Braga[1], Caterina Gratton[2]

[1]Northwestern University, Chicago, IL, [2]Florida State University, Tallahassee, FL

Introduction: There is debate regarding whether regions of the human lateral prefrontal cortex support specific cognitive functions or respond to many diverse demands (Duncan & Owen 2000). Recent evidence from several single-subject precision fMRI studies suggest that there are LPFC regions which respond to specific domains (e.g., language, theory of mind, episodic projection, auditory processing, visual processing) and distinct but nearby general control regions which respond to many cognitive demands (Fedorenko et al., 2011, DiNicola et al., 2020, Noyce et al., 2017, Assem et al., 2020). However, these sets of regions have been identified in different individuals using different paradigms, so an open question is how these regions are arranged relative to each other within single individuals. To address this question, we deeply sampled a small number of individuals using a comprehensive task-based fMRI battery in order to understand the relative arrangement of specialized and general control regions in the LPFC.

Methods: A preliminary dataset of two highly sampled subjects (2F) was used for these analyses, each with 13-15 hours of task fMRI. Tasks included sentence processing, episodic projection, theory of mind, and a wide variety of cognitive control tasks targeting working memory, attention, and inhibition. Between 45 and 90 minutes of data were collected per task. Each of these tasks were taken from or adapted directly from the precision fMRI literature. MRI data underwent structural and functional preprocessing including motion correction, distortion correction, registration, normalization, projection to the surface, and spatial smoothing. Contrast maps were generated for each subject using a task-specific, block design GLM. In these two subjects, we completed a split-half analysis for each task and found that with sufficient data (typically 30 minutes per contrast), it was possible to obtain reliable subject-specific activation maps that reliably located fine-scale organizational patterns.

Results: We found that task contrasts targeting distinct high-level cognitive functions (language, cognitive control, episodic projection, and theory of mind) activated distributed sets of distinct but nearby regions throughout the brain and including the lateral prefrontal cortex. That is, language task contrasts activated a distributed set of regions different from those activated during theory of mind task contrasts, etc. This was shown first by using split-half analysis to define thresholded task-specific ROIs in one half of the data and quantifying relative activation to various cognitive demands in the second half (Figure 1). This was also shown by visualizing the overlap (or lack thereof) of thresholded contrast maps on the surface (Figure 2). In both subjects, we saw separation between cognitive domains in the LPFC as well as other brain regions. In addition, we found in both subjects that there were “general control” regions activated by many cognitive control contrasts that were also non-overlapping with but nearby to the domain-specialized regions. In several cases, regions with distinct functional profiles lay side-by-side in an interdigitated fashion. There was one exception - language and auditory processing demands activated overlapping regions in both subjects.

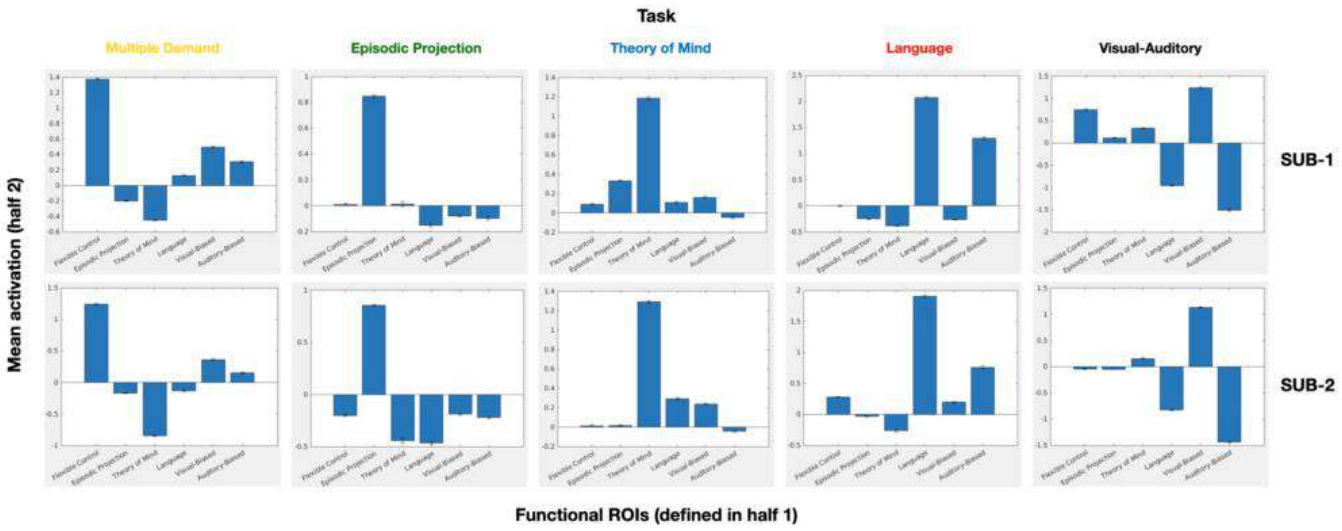

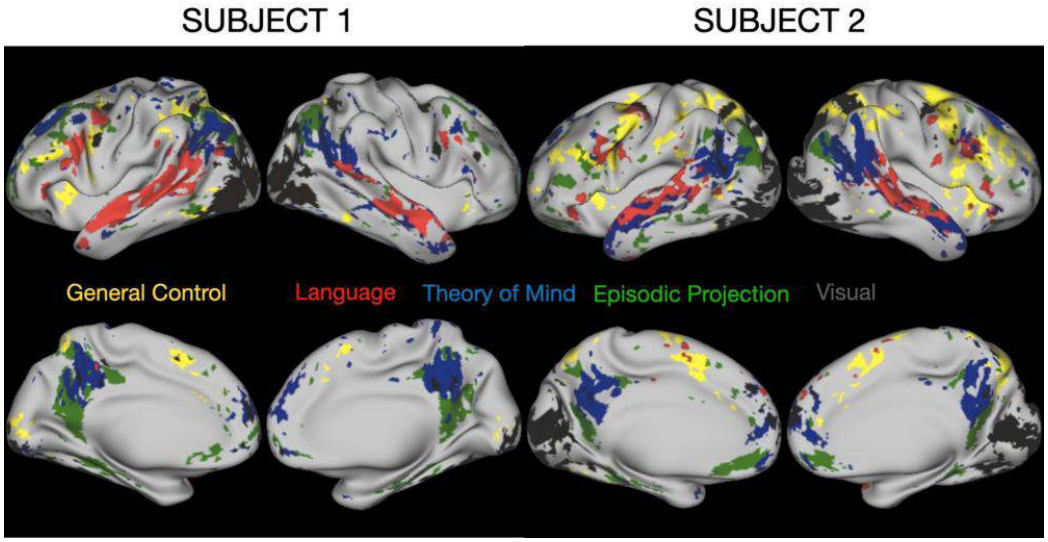

Conclusions: These results support the view that high-level functions are supported by distinct sets of distributed regions which are interdigitated with one another throughout the cortex, rather than by large swaths of multifunctional cortex or slowly changing cortical gradients. Further, they support the idea that there are regions which respond to diverse cognitive control demands and these too are distributed throughout the cortex and interdigitated with specialized regions. We plan to extend this work to include more subjects, more cognitive domains, and the consideration of large-scale functional networks defined by functional connectivity.

References

1. Duncan, J. & Owen, A. M. (2000) Common regions of the human frontal lobe recruited by diverse cognitive demands. Trends Neurosci. 23, 475–483
2. Fedorenko, E., Behr, M. K. & Kanwisher, N. (2011) Functional specificity for high-level linguistic processing in the human brain. Proc. Natl. Acad. Sci. U. S. A. 108, 16428–16433
3. DiNicola, L. M., Braga, R. M. & Buckner, R. L. (2020) Parallel distributed networks dissociate episodic and social functions within the individual. J. Neurophysiol. 123, 1144–1179
4. Noyce, A. L., Cestero, N., Michalka, S. W., Shinn-Cunningham, B. G. & Somers, D. C. (2017) Sensory-Biased and Multiple-Demand Processing in Human Lateral Frontal Cortex. J. Neurosci. 37, 8755–8766
5. Assem, M., Glasser, M. F., Van Essen, D. C. & Duncan, J. A (2020) Domain-General Cognitive Core Defined in Multimodally Parcellated Human Cortex. Cereb. Cortex 30, 4361–4380

Poster No 941

Neural representation dynamics reveal computational principles of cognitive task learning

Ravi Mill[1], Michael Cole[1]

[1]*Rutgers University-Newark, Newark, NJ*

Introduction: Learning cognitive tasks is a ubiquitous feature of everyday life, yet the neural basis for this essential human skill remains unclear. During learning, neural task representations must be rapidly constructed for novel task performance, then optimized for robust practiced task performance. The present study interrogated changes to neural representational geometry that underpin this transition from novel to practiced task performance. We integrated computational ideas from multiple neuroscientific sub-fields (long-term memory, contextual decision-making and cognitive control) to test a task learning framework underpinned by subcortical-cortical representational dynamics (Figure 1). The core hypothesis of this framework is that practice involves a shift in the brain from compositional representations (task-general activity patterns that can be flexibly reused across tasks) to conjunctive representations (task-specific activity patterns specialized for the current task).

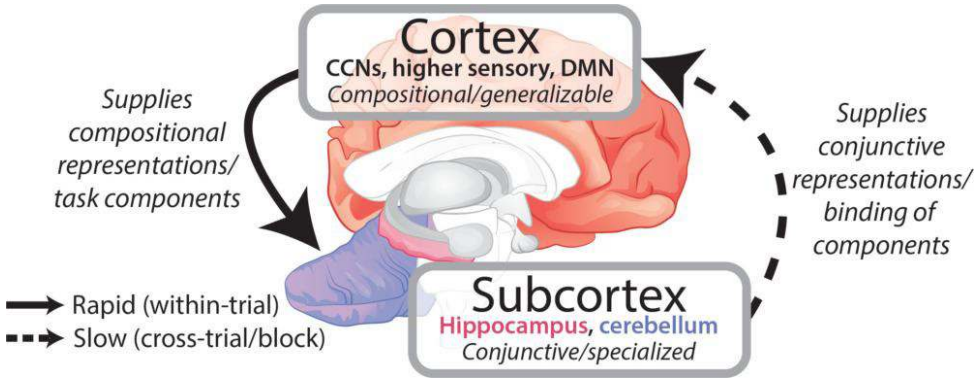

Fig 1. Hypothesized cortical-subcortical dynamics underlying the transition from compositional to conjunctive neural representations over task learning.

Methods: Multiband functional MRI (fMRI) data were recorded from 44 healthy young adults (age mean=22.25, age range=18-36; 23 female) as they performed 2 sessions of our newly developed concrete permuted rule operations (C-PRO2) paradigm. This allows for the presentation of 64 distinct multi-sensory tasks, based on permutations of individual logic, sensory and motor rules (Figure 2). In the first session (Practice), subjects practiced a subset of 4 tasks repeatedly. In the second session (Test), these practiced tasks were intermixed with the remaining 60 novel tasks. The design therefore enabled fMRI recording as multiple complex tasks were performed from first novel presentation through repeated practice. The resulting fMRI data underwent preprocessing (Glasser et al., 2013) and general linear modeling to estimate task activations for cortical vertices and subcortical voxels. A functional atlas (Glasser et al., 2016; Ji, Spronk et al., 2019) was used to affiliate these vertices/voxels to regions and large-scale functional networks, which was key for our multivariate analyses.

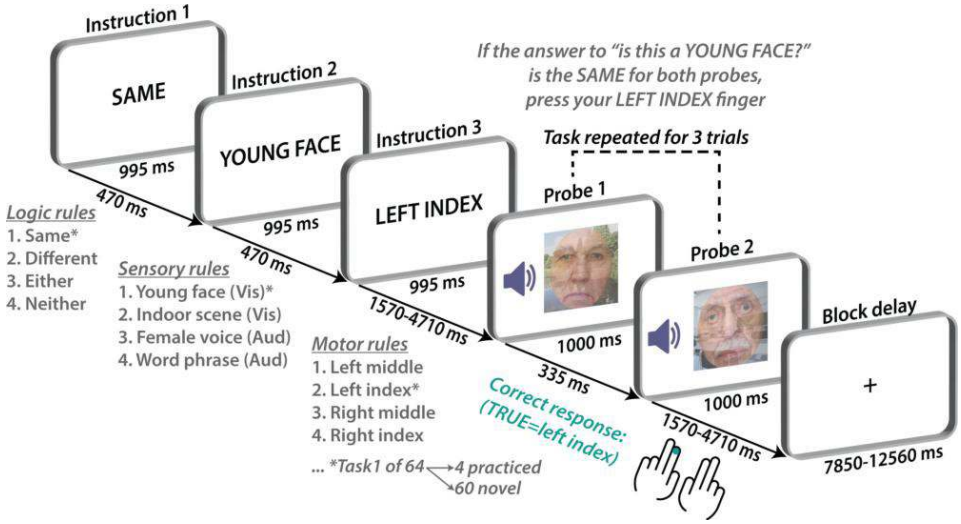

Fig 2. C-PRO2 task design. Depicted is one example task trial and accompanying correct response. This format was preserved for all 64 tasks, across practiced/novel tasks and Practice/Test sessions.

Results: We firstly observed behavioral evidence of learning, in the form of improvements to accuracy and reaction time as tasks were repeatedly practiced. We then developed analytic methods inspired by multivariate pattern analysis and machine learning to interrogate changes to neural representational geometry that underpinned these behavioral practice effects. Specifically, novel tasks presented in the held-out Test session were used to build neural templates of individual (i.e. compositional) rule types, and their non-linear interaction (i.e. conjunction). These were fit simultaneously via multiple linear regression to each of the practiced tasks in the Practice session, so as to dynamically quantify the strength of rule compositions and rule conjunctions over task learning. The results substantiated the hypothesized dynamic shift from compositional to conjunctive representations with repeated task practice. Further, we found that conjunctions originated in subcortex (hippocampus and cerebellum) and slowly spread to cortex. Critically, it was the strengthening of conjunctive representations in cortex that was uniquely associated with signatures of effective task practice (improved behavior and reduced task interference).

Conclusions: Our findings reveal a precise neural mechanism underlying changes to neural representational geometry that occur over learning: increasing non-linear conjunction (binding) of task rule elements. This extends computational concepts from long-term memory (O'Reilly & Rudy, 2001) and contextual decision-making (Kikumoto & Mayr, 2020) to the domain of cognitive task learning. The formation of cortical conjunctive representations hence serves as a computational mechanism of effective task practice, reflecting cortical-subcortical dynamics that optimize task representations in the human brain.

References

1. Glasser, M. F., Coalson, T. S., Robinson, E. C., Hacker, C. D., Harwell, J., Yacoub, E., Ugurbil, K., Andersson, J., Beckmann, C. F., Jenkinson, M., Smith, S. M., & Van Essen, D. C. (2016). A multi-modal parcellation of human cerebral cortex. Nature, 536(7615), 171–178. https://doi.org/10.1038/nature18933
2. Glasser, M. F., Sotiropoulos, S. N., Wilson, J. A., Coalson, T. S., Fischl, B., Andersson, J. L., Xu, J., Jbabdi, S., Webster, M., Polimeni, J. R., Van Essen, D. C., Jenkinson, M., & WU-Minn HCP Consortium. (2013). The minimal preprocessing pipelines for the Human Connectome Project. Neuroimage, 80, 105–124. https://doi.org/10.1016/j.neuroimage.2013.04.127
3. Ji, J. L., Spronk, M., Kulkarni, K., Repovš, G., Anticevic, A., & Cole, M. W. (2019). Mapping the human brain's cortical-subcortical functional network organization. NeuroImage, 185, 35–57. https://doi.org/10.1016/j.neuroimage.2018.10.006
4. Kikumoto, A., & Mayr, U. (2020). Conjunctive representations that integrate stimuli, responses, and rules are critical for action selection. Proceedings of the National Academy of Sciences, 117(19), 10603–10608. https://doi.org/10.1073/pnas.1922166117
5. O'Reilly, R. C., & Rudy, J. W. (2001). Conjunctive representations in learning and memory: Principles of cortical and hippocampal function. Psychological Review, 108(2), 311–345. https://doi.org/10.1037/0033-295X.108.2.311

Poster No 942

Mapping the developmental course of the multispectral dynamics serving executive functioning

Jake Son[1], Caroline Howard[2], Elizabeth Santos[3], Abraham Killanin[1], Mikki Schantell[1], Thomas Ward[1], Grace Ende[1], Danielle Rice[1], Anna Coutant[1], Giorgia Picci[1], Tony Wilson[1]

[1]Institute for Human Neuroscience, Boys Town, NE, [2]Duke University, Durham, NC, [3]St. Mary's University, San Antonio, TX

Introduction: Executive functioning refers to the processes that allow one to monitor environmental cues and flexibly adapt behavior to facilitate the attainment of specific tasks. Selective attention provides the scaffolding necessary for the acquisition and refinement of executive function and is known to emerge in early childhood with a protracted developmental trajectory. Alterations in selective attention have been tied to numerous forms of psychopathology, including ADHD, anxiety, and depression[1-3]. A better understanding how executive functions emerge in typically developing youth will provide critical insights into the neurobiological correlates of executive dysregulation, which presents transdiagnostically across mental health disorders. Herein, we investigate age-related changes in the neural oscillatory dynamics serving executive function in a sample of youth using magnetoencephalographic (MEG) imaging.

Methods: MEG data were collected from 78 children and adolescents (ages 11-16; Mean = 12.78; SD = 1.17; 43 males) using a 306-sensor MEGIN Neo MEG system (Helsinki, Finland) equipped with 306 sensors (204 planar-gradiometers, 102 magnetometers) using a 1 kHz sampling rate and an acquisition bandwidth of 0.1-330Hz in a two-layer magnetically shielded room. During MEG, participants completed a 15-minute executive function task designed to probe perceptual decision-making. At the beginning of each trial, participants were presented with a centrally-presented fixation cross, followed by the presentation of a set of three images. The "target" object was presented above the fixation crosshair, while the two remaining objects were presented below the fixation. Participants were instructed to respond whether the left object (1, index finger) or right object (2, middle finger) matched the target in either shape or pattern. A total of 200 pseudorandomized trials were completed by each participant. Structural co-registration, preprocessing, and sensor/source-level analyses have been described in greater detail in previously reported pipelines[4-5]. Briefly, artifact-free epochs of MEG data were transformed into

the time-frequency domain and evaluated for clusters of time-frequency bins that differed from the baseline, using a stringent two-stage statistical approach. Significant responses at the sensor level were source imaged using the dynamic imaging of coherent sources (DICS) beamformer, using task and baseline periods of equal duration and bandwidth[6]. These images were subject to whole-brain correlation analyses with age to determine brain regions that were developmentally sensitive in the context of the executive functioning task.

Results: Sensor-level analyses revealed significant alpha (12 – 18 Hz, 1350 – 1750 ms) and gamma (72 – 90 Hz, 100 – 250 ms) oscillatory responses during the executive functioning task across all trials and participants. These time-frequency windows were imaged in each participant and the voxel-wise whole-brain images were then correlated with age per response. In the alpha band, the anterior cingulate cortex (ACC) and dorsolateral prefrontal cortex (dlPFC) were significantly correlated with age ($p < .005$), such that weaker oscillations (i.e., less negative relative to baseline) were observed in older participants. In the gamma band, activity within the left prefrontal cortex, supramarginal gyrus, and superior parietal cortex decreased with age ($p < .005$).

Conclusions: The present work demonstrates the developmental sensitivity of the neural dynamics underlying executive function in brain regions serving higher-order cognition (i.e., ACC, PFC). These regions are known to be critical components of intrinsic connectivity networks (e.g., salience / frontoparietal networks) that change significantly throughout development[7-8]. These findings also contribute to the growing literature examining the spectral, temporal, and regional specificity of neurodevelopmental effects during a critical window in an executive functioning task.

References

1. Martel, M. M., Pan, P. M., Hoffmann, M. S., Gadelha, A., do Rosário, M. C., Mari, J. J., Manfro, G. G., Miguel, E. C., Paus, T., Bressan, R. A., Rohde, L. A., & Salum, G. A. (2017). A general psychopathology factor (P factor) in children: Structural model analysis and external validation through familial risk and child global executive function. Journal of Abnormal Psychology, 126(1), 137–148.
2. Mogg, K., Salum, G. A., Bradley, B. P., Gadelha, A., Pan, P., Alvarenga, P., Rohde, L. A., Pine, D. S., & Manfro, G. G. (2015). Attention network functioning in children with anxiety disorders, attention-deficit/hyperactivity disorder and non-clinical anxiety. Psychological Medicine, 45(12), 2633–2646.
3. Rock, P. L., Roiser, J. P., Riedel, W. J., & Blackwell, A. D. (2014). Cognitive impairment in depression: a systematic review and meta-analysis. Psychological Medicine, 44(10), 2029–2040.
4. Schantell, M., Taylor, B. K., Spooner, R. K., May, P. E., O'Neill, J., Morsey, B. M., Wang, T., Ideker, T., Bares, S. H., Fox, H. S., & Wilson, T. W. (2022). Epigenetic aging is associated with aberrant neural oscillatory dynamics serving visuospatial processing in people with HIV. Aging, 14(24), 9818–9831.
5. Wiesman, A. I., & Wilson, T. W. (2020). Attention modulates the gating of primary somatosensory oscillations. NeuroImage, 211, 116610.
6. Gross, J., Kujala, J., Hamalainen, M., Timmermann, L., Schnitzler, A., & Salmelin, R. (2001). Dynamic imaging of coherent sources: Studying neural interactions in the human brain. Proceedings of the National Academy of Sciences of the United States of America, 98(2), 694–699.
7. Menon, V. (2011). Large-scale brain networks and psychopathology: a unifying triple network model. Trends in Cognitive Sciences, 15(10), 483–506.
8. Uddin, L. Q., Supekar, K., & Menon, V. (2010). Typical and atypical development of functional human brain networks: insights from resting-state FMRI. Frontiers in Systems Neuroscience, 4, 21.

Poster No 943

Shared and unique multimodal profiles of individual variation in executive function and intelligence

Andrew Reineberg[1]

[1]University of Pittsburgh, Pittsburgh, PA

Introduction: Individual differences in higher-level cognition are important for success in school, the workplace, relationships, and maintenance of physical health (Diamond et al., 2013). Two cognitive constructs, executive function (EF) and intelligence, are phenotypically and genetically correlated (Friedman et al., 2008). However, correlations between these constructs are not one. Recent evidence shows EF may be a unique predictor of psychopathology outcomes such as major depression while intelligence may be a unique predictor of educational attainment outcomes (Hatoum et al., 2023). The pattern of brain structure and function that underlies these cognitive constructs are an important intermediate phenotype between genes and outcomes such as psychopathology and educational attainment. The goal of the current study is to determine how the brain-based predictive signal for EF and intelligence are similar and different. To do so, we used an established predictive modelling framework (Shen et al., 2015) extended to include all imaging modalities and cognitive measures available in the UK Biobank dataset (Sudlow et al., 2015).

Methods: The current study is an analysis of behavioral, resting-state fMRI, anatomical MRI, and diffusion MRI data of 38,100 participants from the UK Biobank. EF and intelligence scores were calculated for each participant via a factor analysis of behavioral data collected at three time points: initial recruitment, an at-home follow-up analysis, and at time of brain scan.

Imaging data analysis pipelines have been described previously in Miller et al. (2016). Brain measures from each modality - 25 global cortical and subcortical volume measures, 48 diffusion tracts, and 441 functional connections – were reduced to factors using ICA and entered in ridge regression models with 10% held out for later validation testing. One ridge regression model was run for each of the intelligence and executive function behavioral factor scores. All analyses controlled for age, motion during the resting scan, income, gender, and socioeconomic status. Only participants within three standard deviations of the mean motion during resting scan were analyzed. Final sample size included in models was n = 28674 individuals with all imaging modalities and behavior (Mage = 61.29, sdage = 7.09).

Results: Ridge regression models predicted 25.8% of variance in the EF and 17.6% of variance in intelligence in the hold-out sample. See Figure 1 for a visual representation of the brain components that most contributed to these predictions. For the sake of interpretation, brain factors are described as a summary of the individual phenotypes with the highest loadings on the factor. Overall, the signals were mostly overlapping with only a few notable differentiating phenotypes. Of 514 total brain phenotypes, 205 and 188 were substantial contributors to prediction of EF and intelligence, respectively. 157 features were shared predictors of both phenotypes, predominantly global brain volume measures and functional connectivity between higher order association areas such as parts of the dorsal attention, frontoparietal, and default networks. Features uniquely associated EF were global grey matter and cerebrospinal fluid volumes; mean fractional anisotropy of pontine crossing tract and tapetum; and 42 functional connectivity features. Features uniquely associated with intelligence were 32 functional connectivity features.

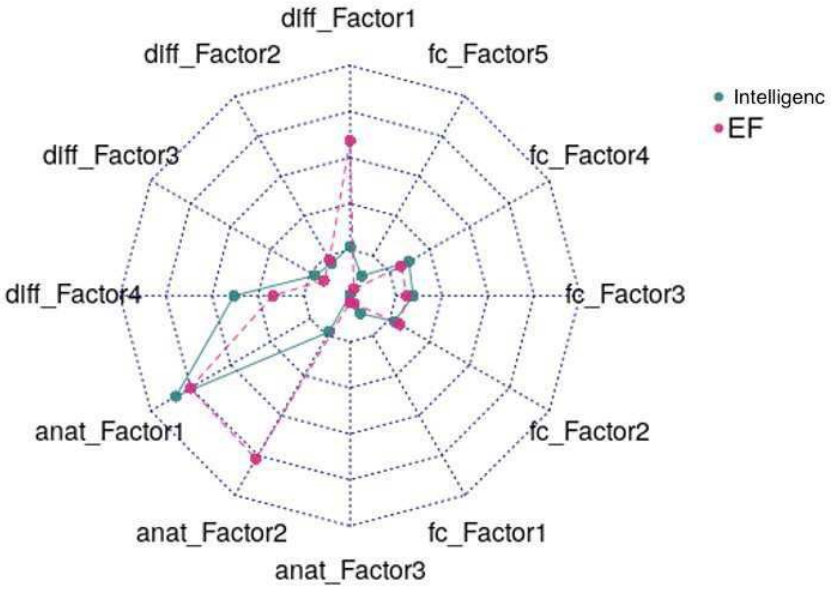

Factor loadings. Strength of association between each brain modality factor and executive function (EF) or intelligence is visualized as distance from center. Larger distances = higher loading.

Conclusions: Although EF and intelligence are highly correlated both behaviorally and generically, this correlation is not perfect. Brain signals associated with the unshared variance between these two cognitive constructs could be important intermediate phenotypes between genes and psychopathology. Our results suggest global grey matter volume measures, two white matter tracts, and a subset of the functional connectome are uniquely associated with EF and thus are candidate endophenotypes for psychopathology.

References

1. Diamond, Adele. (2013) “Executive Functions.” Annual Review of Psychology 64, 135–68. https://doi.org/10.1146/annurev-psych-113011-143750.
2. Friedman, Naomi P, Akira Miyake, Susan E Young, John C Defries, Robin P Corley, and John K Hewitt. “Individual Differences in Executive Functions Are Almost Entirely Genetic in Origin.” Journal of Experimental Psychology. General 137, no. 2 (May 2008): 201–25. https://doi.org/10.1037/0096-3445.137.2.201.
3. Hatoum et al., “Genome-Wide Association Study Shows That Executive Functioning Is Influenced by GABAergic Processes and Is a Neurocognitive Genetic Correlate of Psychiatric Disorders.”
4. Miller, K. L., Alfaro-almagro, F., Bangerter, N. K., Thomas, D. L., Yacoub, E., Xu, J., ... Smith, S. M. (2016). Multimodal population brain imaging in the UK Biobank prospective epidemiological study. Nature Neuroscience, 19(11), 1523–1541. http://doi.org/10.1038/nn.4393
5. Shen et al., “Using Connectome-Based Predictive Modeling to Predict Individual Behavior from Brain Connectivity.”
6. Sudlow, Cathie, John Gallacher, Naomi Allen, Valerie Beral, Paul Burton, John Danesh, Paul Downey, et al. “UK Biobank: An Open Access Resource for Identifying the Causes of a Wide Range of Complex Diseases of Middle and Old Age.” PLOS Medicine 12, no. 3 (March 31, 2015): e1001779. https://doi.org/10.1371/journal.pmed.1001779.

Poster No 944

Mild videogaming is associated with enhanced cognitive performance and mental health in children

Bader Chaarani[1]

[1]*University Of Vermont, Burlington, VT*

Introduction: It is estimated that by the end of 2023 there will be over three billion active videogamers (VGs) worldwide 1. According to a recent American Psychological Association survey, more than 90% of children in the U.S. play videogames 2, a significant increase from an estimated 70% of children VGs in 2013, when the American Academy of Pediatrics (AAP) recommended limiting entertainment screen-use to <2h/day (AAP, 2013). While prior research links videogaming with adverse cognitive, behavioral and mental health outcomes in children, these studies were conducted in relatively small datasets, limiting their power to investigate videogaming exposure hours including the specific <2h/day AAP recommendation. We have recently shown 3, using the large Adolescent Brain Cognitive Development (ABCD) study® dataset, that videogaming for ≥3h/day is associated with enhanced cognitive performance in children but also higher attention problems, depression, and attention-deficit/hyperactivity disorder scores, albeit well below clinical thresholds, compared to non-videogamers (NVGs). To investigate these effects in children who spend less time videogaming, we compared mental health and cognitive measures as well as BOLD signal during a working memory N-Back fMRI task in the ABCD Study, defining samples of 9- and 10-year-old children who play <1h/day, 1-2h/day, 2-3h/day and ≥3h/day and NVGs (0h/day).

Methods: Participants completed a screen time survey asking how much time they "Play video games on a computer, console, phone or other device (Xbox, PlayStation, iPad)?". Videogaming hours were self-reported for a typical weekday and weekend day, from which videogaming hours/day were derived. Outcomes of interest included mental health scores from the Child Behavior Checklist (CBCL), cognitive scores from the NIH Toolbox® cognition battery, in addition to working memory performance and region-based cortical BOLD signal from the N-back fMRI task (available for approximately half the sample). These outcomes were compared across the groups using linear mixed models with, age, sex, race/ethnicity, combined parental income, TV watching, parental monitoring, and sibling status as nuisance covariates, and scanner site as a random effect. FDR-corrected p values<.05 were considered significant.

Results: VGs who play <1h/day (N=5824) and 2-3h/day (N=1024) did not have higher CBCL measures (uncorrected-p>0.055) compared to NVGs (N=1711), while VGs who play >3h/day (N=1233) had higher scores than all groups on attention, depression and ADHD (Figure 1). Mild and moderate VGs (<3h/day) were the best performers on the NIH toolbox cognitive tasks compared to NVGs, scoring significantly better on pattern recognition and Flanker tasks, and having higher fluid and total IQ scores. Importantly, 1h/day VGs scored higher than all groups on card sorting and picture memory tests, had the highest IQ scores and lower externalizing, depression and conduct disorder scores compared to NVGs. Lastly, all VGs groups (<1h/day: N=4306; 1-2h/day: N=1631; 2-3h/day: N=711; 3h+/day: N=750) performed significantly better on the N-back task and showed higher neural activation on the 2-back vs. fixation contrast compared to NVG (N=1278) in bilateral precuneus and the right precentral gyrus (Figure 2).

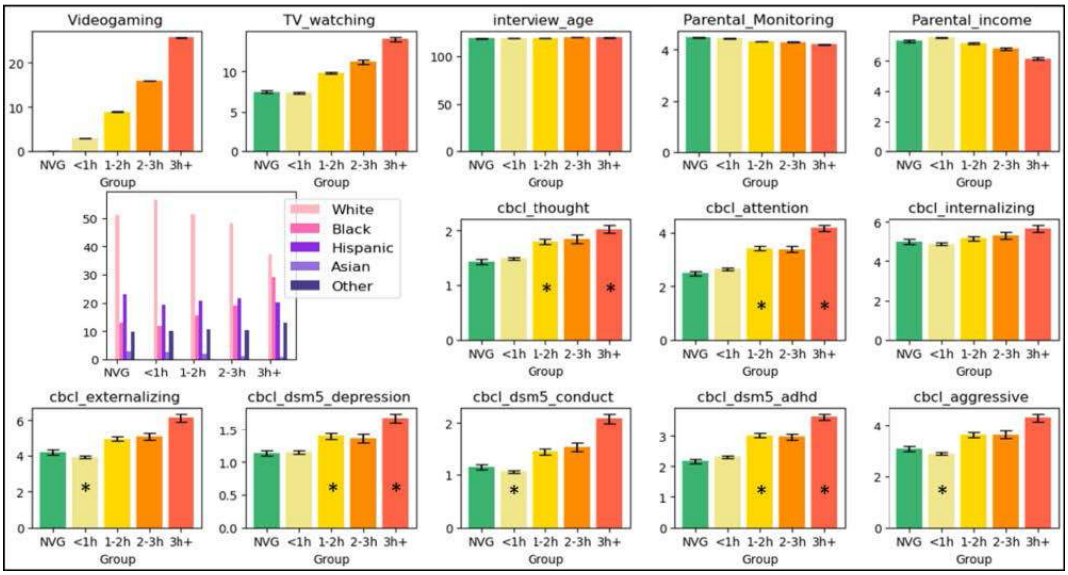

Figure 1. Demographics and CBCL measures across non-videogamers (NVG) and all videogamer groups. Asterisks indicate significant differences between NVG and videogamers with FDR-corrected p<.05.

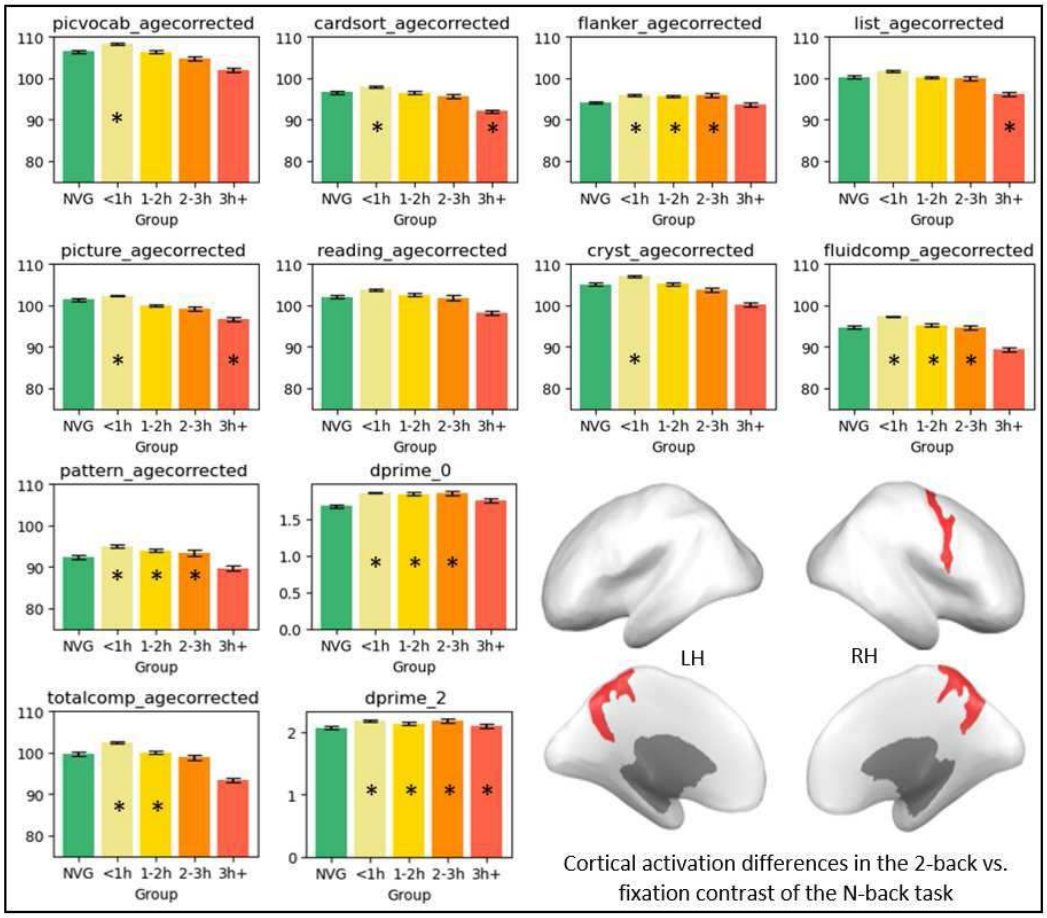

Figure 2. Cognitive and behavioral measures and BOLD comparisons between non-videogamers (NVG) and all videogamer (VGs) groups. Asterisks and red clusters: significant differences between NVG and VGs.

Conclusions: The present findings strongly support the AAP recommendations and further show that 1h/day or less of videogaming is associated with better cognitive performance and mental health in children. The enhanced performance on the N-back task, coupled with higher neural activation in cortical brain regions playing a critical role in working memory and visuospatial attention, support the hypothesis that these areas exhibit a practice effect associated with the cognitively demanding videogaming.

References

1. Newzoo Global Games Market Report 2020 | Light Version. Newzoo https://newzoo.com/resources/trend-reports/newzoo-global-games-market-report-2020-light-version.
2. Resolution on Violent Video Games. American Psychological Association (APA). February 2020 Revision.
3. Chaarani, B. et al. Association of Video Gaming With Cognitive Performance Among Children. JAMA Network Open 5, e2235721 (2022).

Poster No 945

Neurocognitive Effects of Mobile Cognitive Bias Modification Games on Smokers

Shin Ah Kim[1], Seowoo Kim[1], Ji-Hye Lim[2], Won-Jun Suh[2], Hyun-Chul Kim[2]

[1]Delvine, Inc., Seoul, South Korea, [2]Kyungpook National University, Daegu, South Korea

Introduction: More than half of individuals who have quit smoking ultimately revert back to being smokers within a week[1]. It is known that smokers' cognitive biases toward stimuli, including attentional bias (AT), approach bias (ApB), and impulsive response (IR), play a key role in relapses among smokers[2,3]. Prior research has demonstrated that cognitive bias modification training (CBM) has the potential to rectify these biases and aid individuals in quitting smoking[4,5]. Nevertheless, CBM may appear less attractive because of its repeated nature, resulting in the withdrawal of participants. In order to tackle this problem, a few studies have implemented gamification CBM in mobile applications (apps) and assessed its efficacy[6]. Nevertheless, there is limited knowledge regarding the impact of the use of CBM apps on implicit attitudes and neural

activation in response to smoking-related stimuli. Furthermore, although the importance of the intention to stop smoking in the interventions has been recognized[7], it remains unexplored whether this intention significantly impacts the efficacy of CBM apps. Therefore, we aimed to examine the efficacy of our newly developed CBM app, which includes games designed to address AB, ApB, and IR, and the impact of this app on implicit attitudes and brain activation in response to smoking-related stimuli. In addition, we investigated whether the intention to quit smoking influences the neurocognitive effects of the CBM intervention.

Methods: A total of 52 male heavy smokers participated in the study. Prior to the experiment, their intention to quit smoking was evaluated, and all individuals scored above 5 on the contemplation ladder. They were randomly assigned to use either a mobile application including a smoking diary and educational materials (no game group, NG), or one that included additional CBM games (game group, OG). Over two weeks, participants utilized their designated application on a daily basis. Before and after the intervention period, they performed a personalized Implicit Association Test (p-IAT) designed to evaluate implicit attitudes toward smoking cues. Their daily smoking behavior was collected from the smoking diary implemented in the app. Lastly, we recorded Event-Related Brain Potentials (ERPs) in response to smoking-related stimuli compared to neutral stimuli and measured the amplitude of the late positive potential (LPP).

Results: The participants were split into two groups according to their contemplation ladder scores: moderate intention group (MI) and high intention group (HI). Behaviorally, a three-way repeated measures analysis of variance (rmANOVA) with Time (pre, post), Intention (MI, HI), and Intervention (OG, NG) on both the p-IAT, and daily smoking revealed significant interactions. Post-hoc analysis indicated that OG showed a greater decrease in p-IAT score compared to NG. However, this effect was only observed in the HI. Similarly, OG demonstrated a more substantial decrease in daily smoking, but this effect was observed only in the HI. In addition, the same rmANOVA on the LPP in response to smoking-related stimuli also revealed significant interaction. OG showed a greater LPP toward smoking-related stimuli compared to neutral stimuli. which was only observed in the HI.

Conclusions: The findings indicated that the CBM games can change the implicit attitudes toward smoking in a negative way, decrease daily smoking, and increase brain activation associated with negative emotional arousal in response to smoking-related stimuli. Notably, the impact of the intervention is influenced by the individual's intention to quit smoking. Hence, our mobile CBM games appear to be efficacious in aiding smokers to quit smoking, particularly when they have a strong determination to quit.

References

1. Herd, N., Borland, R., & Hyland, A. (2009). Predictors of smoking relapse by duration of abstinence: findings from the International Tobacco Control (ITC) Four Country Survey. Addiction, 104(12), 2088-2099.
2. Powell, J., Dawkins, L., West, R., Powell, J., & Pickering, A. (2010). Relapse to smoking during unaided cessation: clinical, cognitive, and motivational predictors. Psychopharmacology, 212, 537-549.
3. Wiers, C. E., Kühn, S., Javadi, A. H., Korucuoglu, O., Wiers, R. W., Walter, H., ... & Bermpohl, F. (2013). Automatic approach bias towards smoking cues is present in smokers but not in ex-smokers. Psychopharmacology, 229, 187-197.
4. Kerst, W. F., & Waters, A. J. (2014). Attentional retraining administered in the field reduces smokers' attentional bias and craving. Health Psychology, 33(10), 1232.
5. Elfeddali, I., de Vries, H., Bolman, C., Pronk, T., & Wiers, R. W. (2016). A randomized controlled trial of Web-based Attentional Bias
6. Modification to help smokers quit. Health Psychology, 35(8), 870.
7. Scholten, H., Luijten, M., & Granic, I. (2019). A randomized controlled trial to test the effectiveness of a peer-based social mobile game intervention to reduce smoking in youth. Development and psychopathology, 31(5), 1923-1943.6.
8. Wu, L., Sun, S., He, Y., & Zeng, J. (2015). Effect of smoking reduction therapy on smoking cessation for smokers without an intention to quit: an updated systematic review and meta-analysis of randomized controlled trials. International journal of environmental research and public health, 12(9), 10235-10253.

Poster No 946

Dynamic brain activity during creative storytelling

Xitong Liang[1], Mingnan Cai[2], Gaohan Jing[2], Chengming Zhang[2], Li Liu[2]

[1]State Key Laboratory of Cognitive Neuroscience and Learning, Beijing Normal University, Beijing, Beijing, [2]State Key Laboratory of Cognitive Neuroscience and Learning, Beijing Normal University, Beijing, Beijing

Introduction: Creative storytelling is an extraordinary human ability that requires both various cognitive processes and transitions between them. Despite that previous research has examined the relationship between creative thinking and diverse cognitive processes (Beaty et al., 2015; Nijstad et al., 2010; Kleinmintz et al., 2019), the intricate dynamic interplay between these mechanisms, particularly in the realm of creative storytelling, remains elusive. Consequently, the purpose of this study is to unravel the flexible dynamic brain activity underlying creative storytelling through fMRI data from 41 college

students. Through a method of dynamic functional connectivity, we identified dynamic brain activity that played a crucial role in the conception and articulation of creative stories.

Methods: In this study, a total of 47 normal adult college students aged 18-26 were recruited as participants. Following exclusion of participants with excessive head movement and program errors during the experiment, the analysis involved data from a total of 41 participants. Each participant was required to perform a creative storytelling task and an uncreative storytelling task during fMRI scans, which was designed to improve upon a task developed by Howard-Jones et al. (Howard-Jones et al., 2005). The raw data was preprocessed using fmriprep (Esteban et al., 2018), which included registration, artifact correction, MNI spatial standardization, motion parameter estimation, and spatial smoothing. Head movement was removed using the ICA-AROMA of FSL (Pruim et al., 2015). Two participants excluded due to movements greater than 3mm. In the present study, we employed the Schaefer brain atlas to divide the brain into 100 distinct regions based on the Yeo17 network (Schaefer et al., 2018). Subsequently, we performed dynamic functional connectivity analyses under both creative and uncreative story conditions. Following this, we utilized clustering analysis to discern any significant variations between task and control conditions.

Results: The brain networks demonstrating significant differences between the conception of creative and uncreative stories in dynamic functional connectivity, primarily in default mode networks, control networks, and other networks. Similarly, the distinction between narrating creative stories and narrating uncreative story conditions was assessed. The exploration disclosed that the dynamic functional link mode of the whole brain network during telling creative stories demonstrated a notable boost, compared to telling uncreative stories. For a more comprehensive understanding of these results, please refer to Figure 1.

Conclusions: In conclusion, we have employed a dynamic functional connectivity method to investigate the dynamic patterns of the brain during the creative storytelling process. Results revealed that the dynamic connection mode between the default mode network, control network, and other networks significantly escalated during the creative story conception process. In addition, the dynamic functional connection mode of the whole brain network demonstrated a significant increase during the creative story narration phase. Based on prior studies, the dynamic functional connection between the default mode network and the control network may be related to the evaluation of creativity (Beaty et al., 2015; Kleinmintz et al., 2019). The dynamic functional connection mode of the whole brain network may symbolize a state of free association (Lord, et al., 2019), which is more prevalent during the creative generation phase. These findings underline the importance of generating and evaluating ideas for crafting creative stories. Thus, creative thinking may be characterized by dynamic transition and cycling among multiple cognitive processes. Our study sheds new light on the dynamic transition patterns of the brain during the creative story conception and narration process.

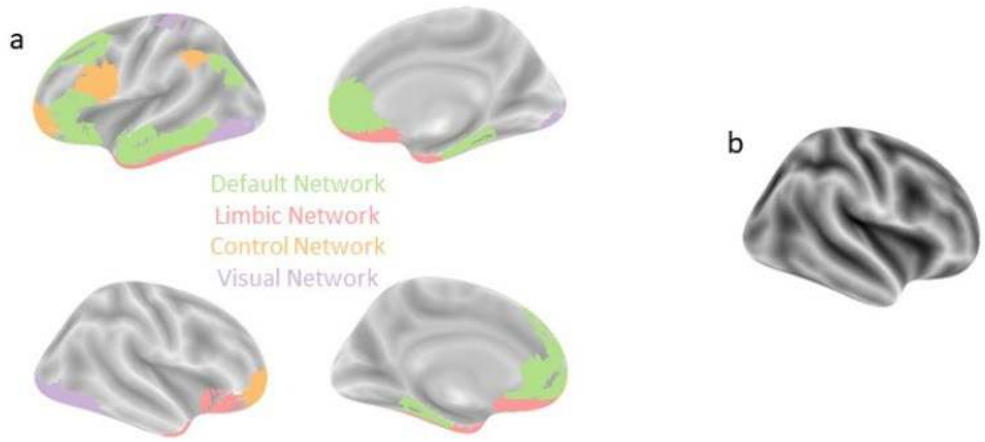

Figure 1. a) Brain networks with significant differences in dynamic functional connectivity during the process of conceptualizing creative stories are mainly composed of default mode networks, control networks, visual networks and limbic networks. **b)** Brain networks with significant differences in dynamic functional connectivity during the process of telling creative stories involve the whole brain network.

References

1. Beaty, R. E., Benedek, M., Kaufman, S. B., & Silvia, P. J. (2015), 'Default and Executive Network Coupling Supports Creative Idea Production'. Scientific reports, 5, 10964.
2. Nijstad, B.A., De Dreu, C.K.W., Rietzschel, E.F., Baas, M., (2010), 'The dual pathway to creativity model: creative ideation as a function of flexibility and persistence.' European Review of Social Psychology. 21, 34–77.
3. Kleinmintz O.M., Ivancovsky T., Shamay-Tsoory S.G. (2019), 'The twofold model of creativity: the neural underpinnings of the generation and evaluation of creative ideas.' Current Opinion in Behavioral Sciences, 27, 131-138.
4. Howard-Jones, P. A., Blakemore, S. J., Samuel, E. A., Summers, I. R., & Claxton, G. (2005). 'Semantic divergence and creative story generation: an fMRI investigation. Brain research.' Cognitive brain research, 25(1), 240–250.
5. Esteban, O., Markiewicz, C. J., Blair, R. W., Moodie, C. A., Isik, A. I., Erramuzpe, A., Kent, J. D., Goncalves, M., DuPre, E., Snyder, M., Oya, H., Ghosh, S. S., Wright, J., Durnez, J., Poldrack, R. A., & Gorgolewski, K. J. (2019). 'fMRIPrep: a robust preprocessing pipeline for functional MRI.' Nature methods, 16(1), 111–116.
6. Pruim, R. H. R., Mennes, M., van Rooij, D., Llera, A., Buitelaar, J. K., & Beckmann, C. F. (2015). 'ICA-AROMA: A robust ICA-based strategy for removing motion artifacts from fMRI data.' NeuroImage, 112, 267–277.
7. Schaefer, A., Kong, R., Gordon, E. M., Laumann, T. O., Zuo, X. N., Holmes, A. J., Eickhoff, S. B., & Yeo, B. T. T. (2018). 'Local-Global Parcellation of the Human Cerebral Cortex from Intrinsic Functional Connectivity MRI.' Cerebral cortex (New York, N.Y. : 1991), 28(9), 3095–3114.
8. Lord, L. D., Expert, P., Atasoy, S., Roseman, L., Rapuano, K., Lambiotte, R., Nutt, D. J., Deco, G., Carhart-Harris, R. L., Kringelbach, M. L., & Cabral, J. (2019). 'Dynamical exploration of the repertoire of brain networks at rest is modulated by psilocybin.' NeuroImage, 199, 127–142.

Poster No 947

An fMRI study on neural basis of occluded image interpretation under different mental workloads

Bao Li[1], Li Tong[1], Chi Zhang[1], Panpan Chen[1], Hui Gao[1], Long Cao[1]

[1]PLA Strategic Support Force Information Engineering University, Zhengzhou, Henan Province

Introduction: When images become occluded, the visual system receives reduced information input, which increases the difficulty of recognizing objects (Rajaei et al., 2019). Nevertheless, experts in visual imaging are able to accurately interpret images with limited visual information, and this skill plays an important role in daily life (Bain, Wareing and Henderson, 2017). This study aims to investigate the neural mechanisms underlying the interpretation of occluded image under different mental workloads using functional magnetic resonance imaging (fMRI) techniques.

Methods: A total of 64 participants (32 females) were enlisted for this study, and their behavioral and fMRI data were collected during the image interpretation task. To explore the cognitive ability for interpreting images under varying mental workloads, we designed three levels of image occlusion tasks (10%, 70%, and 90% occlusion) to elicit different levels of workload (low, mid and high workload) (refer to Figure 1A) (Li et al., 2023). Each participant completed 2 runs, and each run consisting of 30 blocks, and each task in 10 randomly selected blocks (Figure 1B). The experiment entailed a simple binary decision from the participants, who were tasked with determining whether the viewed image depicted aircraft A or B (Figure 1C). We conducted a first-level Generalized Linear Model (GLM) analysis to assess variations in brain activation among all participants under different levels of mental workload (Monti, 2011). Utilizing the behavior data, we categorized all participants into two groups based on their performance: a high-ability group and a low-ability group. Subsequently, a second-level GLM analysis was performed to explore the differences in brain activity between the two groups during task execution. A significance threshold for the statistical results was set at $p<0.05$, corrected by FDR (Benjamini and Hochberg, 1995).

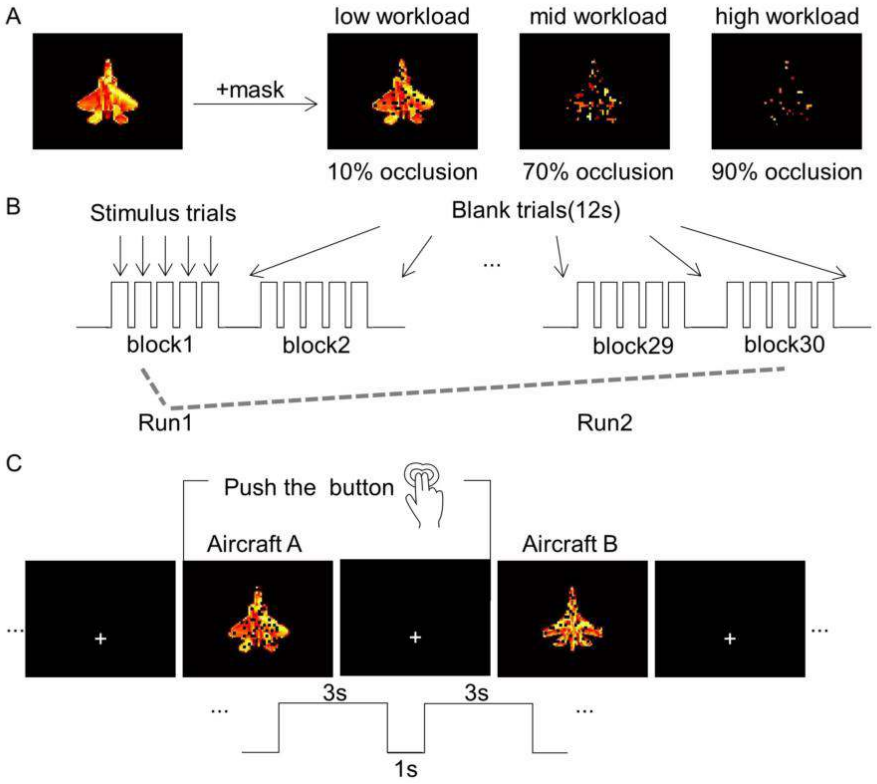

Figure 1. The fMRI experimental paradigm. (A) Occlusion Image Set. (B) The whole process of MRI scans. (C) Task operations in each trail.

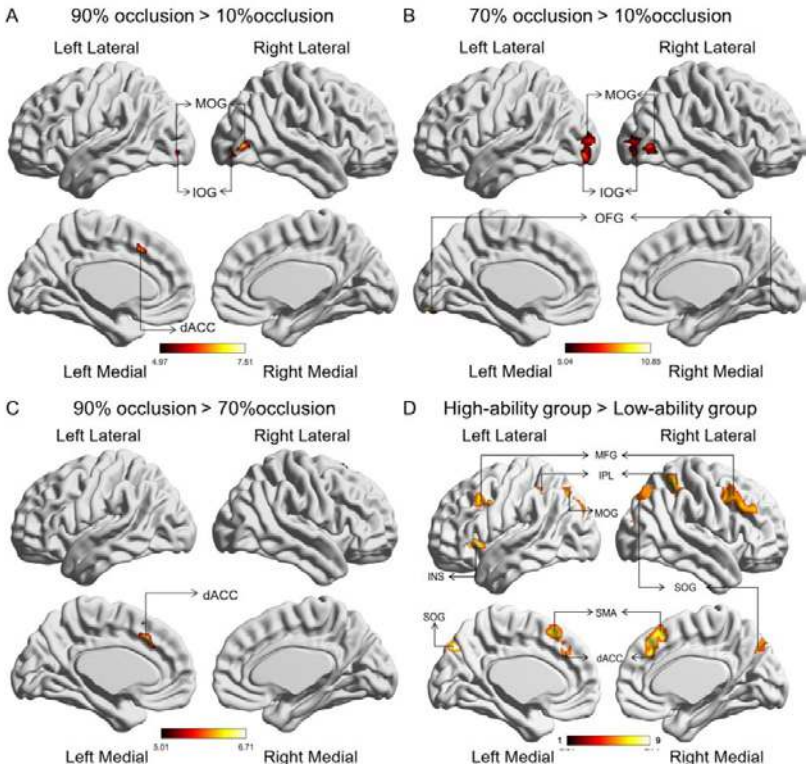

Figure 2. The GLM analysis results. (A-C) Brain activation maps in comparison between tasks with different occlusion levels. (D) Brain activation maps in comparison between the the two groups.

Results: The first-level GLM analysis indicated that tasks with higher mental workloads were associated with increased activation in the dorsal anterior cingulate cortex (dACC), inferior occipital gyrus (IOG), middle occipital gyrus (MOG) and occipital fusiform gyrus (OFG) (Figures 2A-B). Notably, dACC activation continued to strengthen as the workload level

escalated from mid to high (Figure 2C). The second-level GLM analysis revealed that the high-ability group exhibited higher activation in the dACC, supplementary motor area (SMA), middle frontal gyrus (MFG), superior occipital gyrus (SOG), MOG, inferior parietal lobe (IPL) and insula when performing the image recognition task (Figure 2D).

Conclusions: Our study uncovered the critical involvement of the dorsal anterior cingulate cortex (dACC) and occipital gyrus in performing image interpretation tasks under high mental workload. Comparisons across different ability groups further demonstrated that increased activation in the dACC, occipital gyrus, and insula was associated with superior image interpretation abilities. In conclusion, these findings enhance our understanding of the neural mechanisms involved in the interpretation of occluded images under different mental workloads.

References

1. Bain, P., Wareing, A. and Henderson, I. (2017) 'A review of peer-assisted learning to deliver interprofessional supplementary image interpretation skills', Radiography, 23, pp. S64–S69. Available at: https://doi.org/10.1016/j.radi.2017.05.002.
2. Benjamini, Y. and Hochberg, Y. (1995) 'Controlling the False Discovery Rate: A Practical and Powerful Approach to Multiple Testing', Journal of the Royal Statistical Society: Series B (Methodological), 57(1), pp. 289–300. Available at: https://doi.org/10.1111/j.2517-6161.1995.tb02031.x.
3. Li, B. et al. (2023) 'Brain Functional Representation of Highly Occluded Object Recognition', Brain Sciences, 13(10), p. 1387. Available at: https://doi.org/10.3390/brainsci13101387.
4. Monti, M.M. (2011) 'Statistical Analysis of fMRI Time-Series: A Critical Review of the GLM Approach', Frontiers in Human Neuroscience, 5, p. 28. Available at: https://doi.org/10.3389/fnhum.2011.00028.
5. Rajaei, K. et al. (2019) 'Beyond core object recognition: Recurrent processes account for object recognition under occlusion', PLOS Computational Biology. Edited by L. Isik, 15(5), p. e1007001. Available at: https://doi.org/10.1371/journal.pcbi.1007001.

Poster No 948

Naturalistic "dark matter": Inter-subject correlations persist after regressing stimulus features

Thomas Botch[1], Hayoung Song[2], Tamara Vanderwal[3], Monica Rosenberg[2], Emily Finn[1]

[1]Dartmouth College, Hanover, NH, [2]University of Chicago, Chicago, IL, [3]Department of Psychiatry, University of British Columbia, Vancouver, BC

Introduction: Everyday experience is composed of rich, multimodal sensory information. The brain leverages certain features of incoming information to make meaning amidst this complexity. One analytic approach for capturing brain responses to incoming information is intersubject correlation (ISC), in which brain activity to a time-locked stimulus is correlated across people to isolate stimulus-driven responses[1,2]. Yet, while ISC can tell us how much brain activity is driven by a stimulus, it cannot tell us which specific features drive this activity. Prior work has related ISC to known stimulus features[1,3,4], essentially treating a naturalistic stimulus as equivalent to the sum of its parts. Here, we investigate the "dark matter" of ISC, or the shared signal remaining after modeling known features.

Methods: We used a published fMRI dataset[5] where subjects (N=43) watched four audiovisual movies (range: 7:27-12:27 min). We also used a subset of the Narratives dataset[6] with N=45 subjects that listened to four auditory stories (range: 6:40-13:57 min). First, we calculated "baseline" ISC using a voxel-wise, leave-one-subject-out approach. We identified voxels showing significant ISC using null distributions based on 1000 random time shifts. Then, across both datasets, we extracted 23 stimulus features (Fig. 1a) spanning auditory (e.g., loudness, speech), visual (e.g., luminance, faces), and language (e.g., concreteness) modalities. We also included the first-derivative of each feature to track both presence and changes in each feature. This resulted in 42 features for the audiovisual movies (auditory & visual features) and 18 features for the auditory stories (auditory & language features). We then used a general linear model (GLM) to model stimulus features in each subject's timeseries. Here, we also extracted the residual timeseries (the unmodeled signal) for each subject. Using the outputs of the GLM, we evaluated group-level univariate responses to each feature using a one-sample t-test ($q<0.001$) and calculated ISC over the residual timeseries ("residual" ISC). Lastly, we contrasted baseline and residual ISC values to assess the extent to which the regression removed variance in brain activity attributable to the stimulus.

Results: As expected, sensory features (e.g., loudness, luminance) elicited consistent responses within their corresponding sensory cortices: luminance in primary visual cortex and loudness in primary auditory cortex (Fig 1b/c; $q<0.001$). Interestingly, in the audiovisual movies, sensory features also drove responses in unrelated unimodal (e.g., luminance within auditory cortex) and association cortex. This suggests that the multimodal nature of the stimulus alters how and where features are represented. To address our primary question, we compared stimulus-driven signal (as indexed by ISC) before and after modeling known features. At baseline (before regression), there was widespread ISC ($p<0.05$) within both datasets. ISC was highest in primary sensory regions; specifically, auditory/visual cortices for audiovisual movies (Fig. 2a) and auditory regions for Narratives (Fig. 2b). Although the modeled features captured some explainable variance in brain activity, causing ISC

to decrease following regression, significant stimulus-driven signal remained across cortex. In fact, our model explained only a limited portion of the ISC signal – on average 10.1% (max 45.3%) in the Narratives dataset and 20% (max 61%) in the audiovisual movies – suggesting this shared signal may relate to unknown (or at least unmodeled) dimensions important for cognitive processing.

Conclusions: Findings indicate that the brain represents naturalistic stimuli as more than the sum of individual features. Although some stimulus-driven signal was removed by modeling 23 known features, the majority of this signal persisted. We suggest that there are potentially unknown/emergent features driving neural responses to naturalistic stimuli.

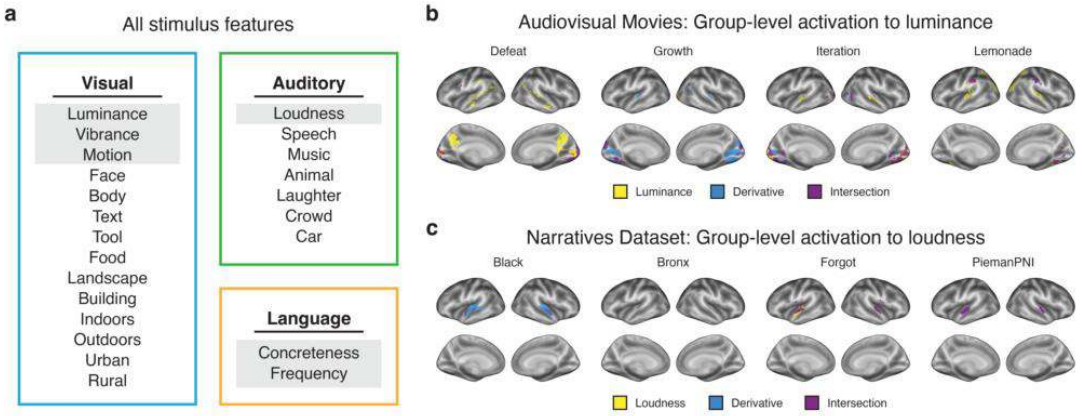

Figure 1. Modeling stimulus features. (a) We extracted a total of 23 stimulus features that spanned the visual, auditory, and language modalities (gray boxes denote continuous-valued features, while all other features are model-derived probabilities [ranging 0-1] for the presence of that feature at a given timepoint). We also calculated the derivative of each feature to model both the presence and change of each feature of interest. **(b/c)** Across both datasets, low-level stimulus features evoked significant, group-level responses within their respective sensory cortices (FDR $q < 0.001$). Each of the four panels depicts an individual stimulus (film [Audiovisual] or podcast [Narratives]).

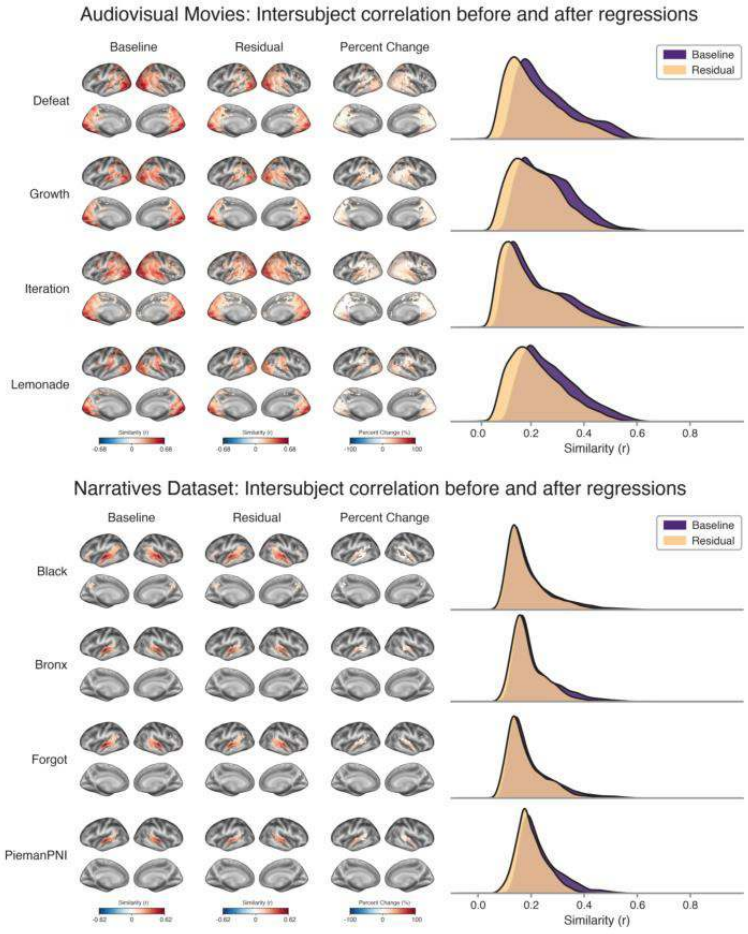

Figure 2. Effects of modeling stimulus features on intersubject correlation. We calculated the intersubject correlation before and after modeling stimulus-related features. **(a/b)** Across both datasets, ISC decreased most in primary sensory cortices (visual/auditory). Even so, a large amount of ISC remained despite regressing out these known stimulus-related features from neural responses (all ps < 0.05).

References
1. Hasson, U. et al., (2004). Intersubject Synchronization of Cortical Activity During Natural Vision. Science, 303(5664), 1634–1640.
2. Nastase, S. A., Gazzola, V., Hasson, U., & Keysers, C. (2019). Measuring shared responses across subjects using intersubject correlation. Social Cognitive and Affective Neuroscience, 14(6), 667–685.
3. Pajula, J., Kauppi, J.-P., & Tohka, J. (2012). Inter-Subject Correlation in fMRI: Method Validation against Stimulus-Model Based Analysis. PLoS ONE, 8(8), e41196.
4. Hasson, U., Malach, R., & Heeger, D. J. (2010). Reliability of cortical activity during natural stimulation. Trends in Cognitive Sciences, 14(1), 40–48.
5. Sava-Segal, C., Richards, C., Leung, M., & Finn, E. S. (2023). Individual differences in neural event segmentation of continuous experiences. Cerebral Cortex, 33(13), 8164–8178.
6. Nastase, S. A. et al. (2021), The "Narratives" fMRI dataset for evaluating models of naturalistic language comprehension. Sci. Data 8, 250.

Poster No 949

Study of color quality space at subvoxel fMRI resolution using the repetition-suppression approach

Ali Moharramipour[1], Hakwan Lau[1]

[1]Laboratory for Consciousness, CBS, RIKEN, Wako, Saitama

Introduction: The subjective quality of an experience is defined by its comparison to other experiences. It has been suggested that our brain contains neural representations of the so-called mental quality space in which distances between experiences in this space define how subjectively similar they are[1,2,3]. In the present study, we aimed to find the neural representations of the color quality space that shape our subjective color perceptions. We hypothesize finding the color space in not only the visual areas but also higher brain areas like the lateral prefrontal cortex (LPFC) since it is not only the physical attribute of the colors that form our color quality space but also their conscious perceptual contents. To this end, we recorded fMRI signals during a color viewing task designed to take advantage of the repetition-suppression (RS). With the right experimental design, RS can become a powerful tool to reveal the representational space of the neural populations within a single fMRI voxel[4], a finer resolution than the conventional fMRI approaches, like multivoxel pattern analysis[5]. It is noteworthy that the RS-fMRI approach has been employed before[6,7], but here, we used a block design to maximize its power. Moreover, we ran a simulation, a forward model from the neuronal to the fMRI level, to verify our RS method, address its limitations, and offer solutions.

Methods: 12 iso-luminant colors (Fig. 1B) were selected and used as 4 sets of 5 colors in the experiment. Four participants were recruited and scanned extensively (~5 hours) to achieve accurate results at individual levels. The color space for each participant was derived from a behavioral two-alternative forced choice color similarity judgment task (e.g., Fig. 2A). Fig. 1A shows our RS-fMRI task with stimulus blocks of flashing a single color or two alternating colors. If the representational space of an fMRI voxel matches with the color space, it is expected to observe higher suppression during alternating similar colors than dissimilar colors due to their higher overlapping neural representation. Taking this into account, we set up a general linear model analysis consisting of color-related regressors, a regressor picking up general suppressions, and another suppression-related regressor modulated by the behaviorally derived individual color space. The latter regressor, called dissimilarity modulation regressor, would identify the areas containing the color space.

Results: Fig. 2B shows the areas with significant dissimilarity modulations (neural representations with the color space) in one participant. The color space areas were consistently observed in the visual areas of V4 to V1, the posterior part of the parieto-occipital sulcus (POS), the parietal association cortex, and the LPFC. To our surprise, the majority of the color space vertices were located in the POS area (covering some of the peripheral visions and area V6) and then the area V4, which is known to hold color representations[8]. It is noteworthy that we rarely found any vertices with an inverted representation of the color space. Furthermore, the above-mentioned areas better represented the spaces of the sets with close colors (sets 2 and 4) than the sets with far colors (sets 1 and 3), except LPFC, which represented both equally well. This may suggest a higher multi-selectivity in the LPFC vertices than in the other areas. Lastly, our simulation verified our RS method and uncovered possible neuronal formation within a voxel with the color space representation.

Conclusions: We found the neural representation of the color quality space not only in the visual areas but also in higher brain areas using a novel RS-fMRI approach. This may indicate that conscious perception involves broad brain areas, including the LPFC, rather than being confined to a localized visual region. Moreover, the POS area emerged as the main hub with the color space representation despite often being overlooked in the existing literature on color perception.

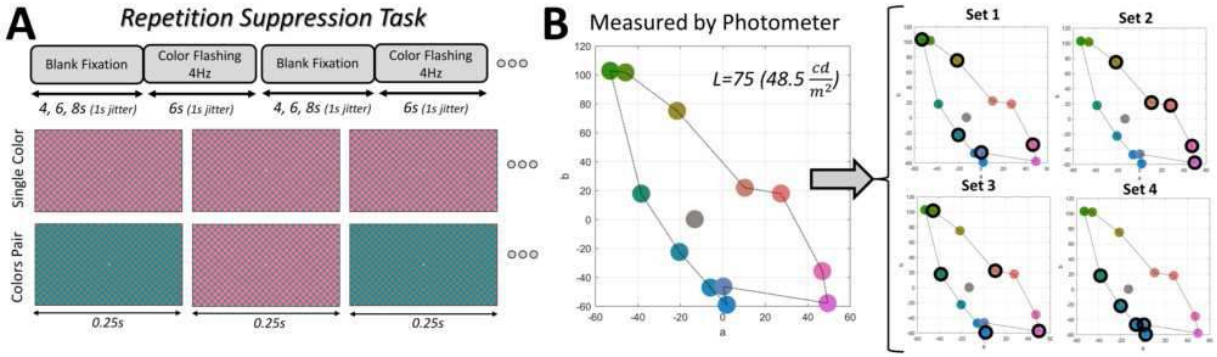

Fig. 1. (A) Schematic of our RS experimental design to find the voxels with neuronal representational space matching the individual's color space. Colors were presented in a checkerboard style, covering the entire screen in 6 seconds stimulus blocks separated by pseudorandom 4, 6, 8 seconds blank fixation blocks. There were two types of stimulus blocks, one with a single color and one with two alternating colors. In both types, pieces of checkerboard shift every 250 ms (i.e., 4 Hz), but in the latter type, the color alternates as well. Participants were instructed to hold fixation during the entire task. Furthermore, to make the task more engaging, they were instructed to press a key at the beginning and another key at the end of the stimulus block. (B) The iso-luminant colors used in the study. The shown Lab values of the colors are measured by a photometer. The 12 colors were broken down into 4 sets of 5 colors, and each set was used separately in the RS task. The shown iso-luminant gray color served as the background color and one of the pieces of the checkerboard in the RS task.

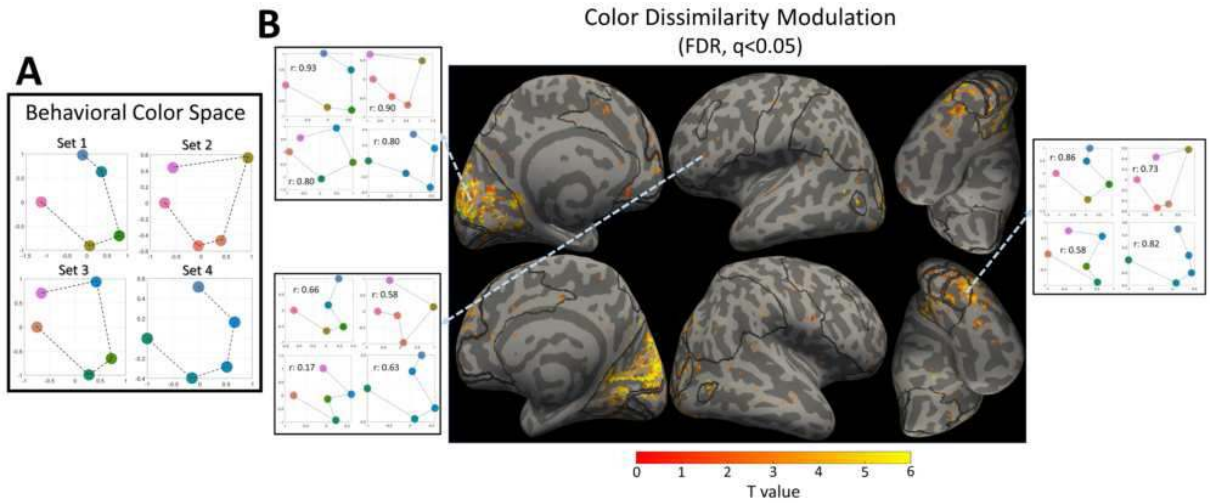

Fig. 2. (A) Color spaces in one of the participants derived from a behavioral color similarity judgment task. (B) The brain areas with significant (FDR, q<0.05) color dissimilarity modulation, the vertices whose representational space calculated from the RS task (Fig. 1A) significantly matched with the participant's color spaces derived behaviorally (Fig. 2A). The representational color spaces in some of the brain vertices are shown as an example in the subpanels. The r value represents the Pearson correlation between the example neuronal color space and the actual behavioral color space.

References

1. Clark, A. (2000). A theory of sentience. Clarendon press.
2. Rosenthal, D. (2010). How to think about mental qualities. Philosophical Issues, 20, 368-393.
3. Lau, H. (2022). The mnemonic basis of subjective experience. Nature Reviews Psychology, 1(8), 479-488.
4. Rigotti, M (2016). Estimating the dimensionality of neural responses with fMRI Repetition Suppression. arXiv preprint arXiv:1605.03952.
5. Lewis-Peacock, J. A. (2014). Multi-voxel pattern analysis of fMRI data. The cognitive neurosciences, 512, 911-920.
6. Barron, H. C. (2016). Repetition suppression: a means to index neural representations using BOLD?. Philosophical Transactions of the Royal Society B: Biological Sciences, 371(1705), 20150355.
7. Bhandari, A. (2019). Measuring prefrontal representational geometry: fMRI adaptation vs pattern analysis. In 2019 Conference on Cognitive Computational Neuroscience (pp. 2019-1162). CCN.
8. Brouwer, G. J. (2009). Decoding and reconstructing color from responses in human visual cortex. Journal of Neuroscience, 29(44), 13992-14003.

Poster No 950

Functional dissociations of the DMN reflect the type of representation and not perceptual engagement

Meichao Zhang[1], Katya Krieger-Redwood[2], Jonathan Smallwood[3], Elizabeth Jefferies[2]

[1]Institute of Psychology, Chinese Academy of Sciences, Beijing, China, [2]University of York, York, United Kingdom, [3]Department of Psychology, Queen's University, Ontario, Canada

Introduction: The default mode network (DMN) not only enables us to deploy representations from long-term memory to understand the significance of perceptual inputs like words and pictures (e.g., semantic cognition), but also supports internally

directed cognition decoupled from the external environment (e.g., in autobiographical memory and mind-wandering). These processes differ in both the need to interface with perceptible events and in the type of representation to be accessed. A challenge therefore is to understand whether functional subdivisions within DMN reflect the type of representation being accessed or perceptual engagement, since these aspects of tasks are often confounded in the literature.

Methods: To answer this question, we employed a within-subject 2 (Task: Semantic vs. Episodic) × 2 (Cognitive mode: Perceptually coupled vs. Decoupled) design. We performed functional magnetic resonance imaging (fMRI) as participants were asked to perform semantic and episodic tasks. For the semantic task, participants were required to either (1) judge whether a currently presented word was semantically related to a previous word (Semantic Coupled) or (2) generate word that was semantically related to a previous word (Semantic Decoupled); for the episodic task, they were required to either (3) recognise a learned word list (Episodic Coupled) or (4) recall a list of words in the absence of external input (Episodic Decoupled).

Results: • Distinct DMN regions responded selectively to semantic and episodic task states regardless of whether they were perceptually coupled or not (see Figure 1A-C). Dorsomedial DMN was associated with semantic cognition, while core DMN regions in medial parietal regions were recruited in both episodic tasks. • Both dorsomedial and core DMN exhibited stronger activation during perceptually coupled states (see Figure 1D-E), showing that DMN is not inherently biased towards internal aspects of cognition. • In addition, core DMN can change its patterns of functional connectivity with task-relevant regions to support different task states (see Figure 2).

Conclusions: In conclusion, DMN supports different types of memory-based representations that can be accessed from both sensory inputs and during internal thought.

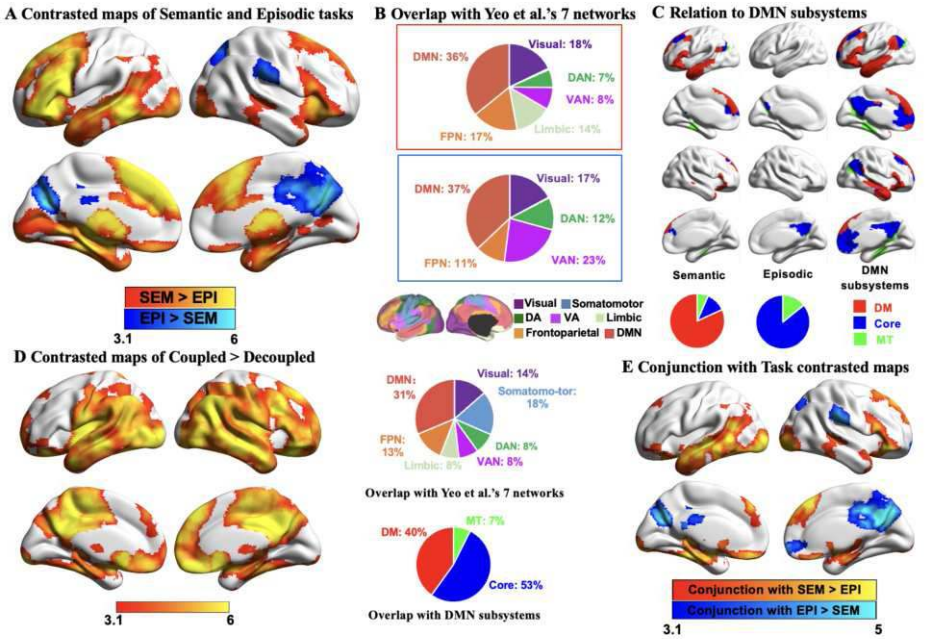

Figure 1. Effects of Task and Cognitive mode. **(A)** A comparison of regions showing significantly greater activity during semantic (*Semantic* > *Episodic*; red) or episodic tasks (*Episodic* > *Semantic*; blue). **(B)** Overlap of the observed patterns of activity with the large-scale networks defined by Yeo et al. (2011) in a 7-network parcellation of whole-brain intrinsic functional connectivity. The pie charts in boxes show the proportion of significant voxels associated with each task that fell within each network (Red box = *Semantic* > *Episodic;* Blue box = *Episodic* > *Semantic*). **(C)** Relationship between the patterns of observed activity during semantic and episodic tasks and their relationship to the subsystems of the DMN as described by Yeo et al. (2011). In this panel, regions in red fall within the dorsomedial (DM) subsystem, regions in blue fall within the core subsystem, and regions in green fall within the medial temporal (MT) subsystem. The pie charts show the proportion of significant voxels associated with each condition that fall within each subsystem. **(D)** A comparison of regions showing significantly greater activity during perceptually coupled state relative to decoupled state (*Coupled* > *Decoupled*). Overlap of the observed pattern of activity with the large-scale networks defined by Yeo et al. (2011). The pie charts show the proportion of significant voxels that fell within each network and that fall within each DMN subsystem. **(E)** A formal conjunction between these regions in (E) showing more activation during perceptually coupled state and those showing greater activity during semantic and episodic tasks (i.e., red and blue regions in Figure 1A showing main effect of task contrast). DA = Dorsal attention; VA = Ventral attention.

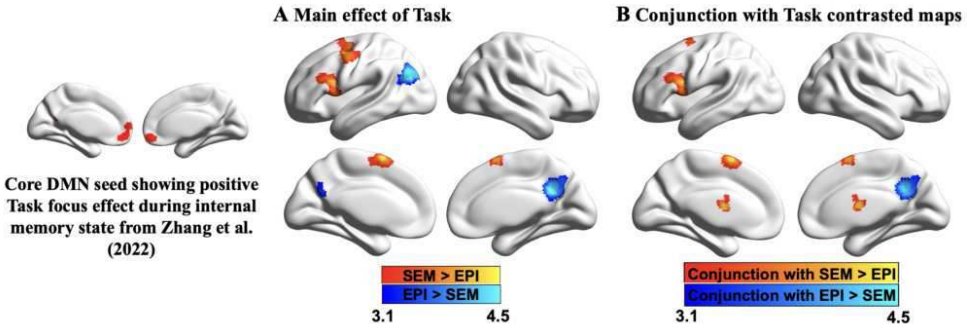

Figure 4. Results of task-based functional connectivity analyses. Analyses examining the functional coupling of core DMN associated with better memory performance during internal state (i.e., Personal memory recall; Zhang et al., *eLife*, 2022). Panel **(A)** shows the regions exhibiting stronger functional connectivity with core DMN seed during semantic (i.e., *Semantic* > *Episodic*; regions in red) and episodic tasks (i.e., *Episodic* > *Semantic*; regions in blue). Panel **(B)** shows the results of a formal conjunction between regions associated with greater activity during semantic versus episodic tasks, and regions showing stronger correlation during task with core DMN seed associated with better memory performance.

References

1. Lambon Ralph, M. A., Jefferies, E., Patterson, K., & Rogers, T. T. (2017). Nature Reviews Neuroscience, 18(1), 42-55.
2. Smallwood, J., Bernhardt, B. C., Leech, R., Bzdok, D., Jefferies, E., & Margulies, D. S. (2021). Nature Reviews Neuroscience, 22(8), 503-513.
3. Smallwood, J., Turnbull, A., Wang, H.-T., Ho, N. S., Poerio, G. L., Karapanagiotidis, T. ... Jefferies, E. (2021). Iscience, 102132.
4. Chiou, R., Humphreys, G. F., & Lambon Ralph, M. A. (2020). Cerebral Cortex, 30(10), 5484-5501.
5. Zhang, M., Bernhardt, B. C., Wang, X., Varga, D., Krieger-Redwood, K., Royer, J., Rodríguez-Cruces, R., de Wael, R. V., Margulies, D. S. ... Jefferies, E. (2022). Elife, 11, e74011.

Poster No 951

Neural Dynamics of Truth and Deception: Insights from Brain States

Yulong Xia[1], Weixiong Jiang[1], Enbo Hu[2], Gang Li[1], Shuaiqi Li[1], Lin Li[1], Jinhua xu[1], Shoujun Huang[1], Xiaoping Ouyang[3], Jing Yuan[1]

[1]College of Mathematical Medicine, Zhejiang Normal University, Jinhua, Zhejiang, [2]School of Electronic Information, Hunan First Normal University, Changsha, Hunan, [3]State Key Laboratory of Fluid Power & Mechatronic Systems, Zhejiang University, Hangzhou, Zhejiang

Introduction: Deception, a complex human behavior, requires advanced cognitive functions and activates specific brain regions, notably the prefrontal and anterior parietal cortex (Hakun 2020; Gao 2022). Recent dynamic exploration of brain states has revealed rapid changes triggered by external stimuli and cognitive demands (McCormick 2020). Analyzing brain states provides insight into both temporal and spatial dimensions of brain dynamics (Medaglia 2018). However, the nuanced dynamics of brain states related to deception remain elusive. In this study, we initially investigated representative brain states associated with lie-, inverse-, and truth-telling. Subsequently, we examined their dynamic attributes and spatial patterns to understand the cognitive processes underlying deception.

Methods: 53 young men (20.20 ± 1.56 ys) participated in this study and their fMRI data were acquired using task block experiments (Jiang 2015). Each subject was instructed to engage in truth-, inverse-, or lie-telling for each task block. The preprocessed fMRI data were parcellated into 232 regions of interest (ROIs) (Luppi 2022). Brain state was defined as the profiles of BOLD signals across all ROIs at a single time point. Using each brain state as a node and the inverse of the Euclidean distance between two nodes as the weight of an edge, we constructed a large temporal network (7632*7632). To mitigate threshold-related biases, we generated four weighted sparse networks at sparsity of 10%, 20%, 30% and 40%. The Louvain community clustering algorithm, with λ ranging from 0.8 to 3 in increments of 0.1, was applied to each network 100 times, and a consensus algorithm was used to derive representative states (Medaglia 2018). Dynamic attributes of the states were quantified through fractional occupancy (FO) and average dwell time (DT). FO represents the fraction of time spent in each state over each task duration of each subject (48 TRs) (Meer et al. 2020). Repeated ANOVA across all tasks and paired comparisons were conducted to discern changes in FO and DT ($P<0.05$, FWE corrected), identifying two states with significant differences between lie-telling and truth-telling. Further analyses of these two states were performed at the levels of the whole-brain and network to unravel their spatial and functional implications.

Results: The results unveiled six representative states when λ=1.6 and sparsity=20%, exhibiting similar states when λ ranged from 1.5 to 1.7 and sparsity varied from 10% to 30%. Two states exhibited significant difference in FO ($F=7.47$, $P=7.98E-04$;

F=11.99, P=1.43E-05, respectively) and DT (F=4.11, P=0.0182; F=3.22, P=0.0425) (Fig. 1). In the Lie-prefer State, lie-telling showed a larger FO (P=6.59E-04) and DT (P=0.0041) compared to the true-telling, indicating a more frequent and prolonged presence. In contrast, in the Truth-prefer State, true-telling demonstrated higher FO and DT (Fig. 1). The spatial characteristics of Truth-prefer State revealed elevated BOLD signals in the somatomotor areas (Fig. 2A), while the Lie-prefer State exhibited heightened BOLD signals in the frontal and parietal cortex (Fig. 2B). Subnetwork analysis disclosed significant increases in the frontoparietal network (FPN) (P=3.40E-50) and default mode network (DMN) (P=7.98E-21) when comparing the Lie-prefer State with the Truth-prefer State, along with significant decreases in five networks (Fig. 2C) (P<4.70E-05) and no significance in the limbic network (LIM) (P=0.1371).

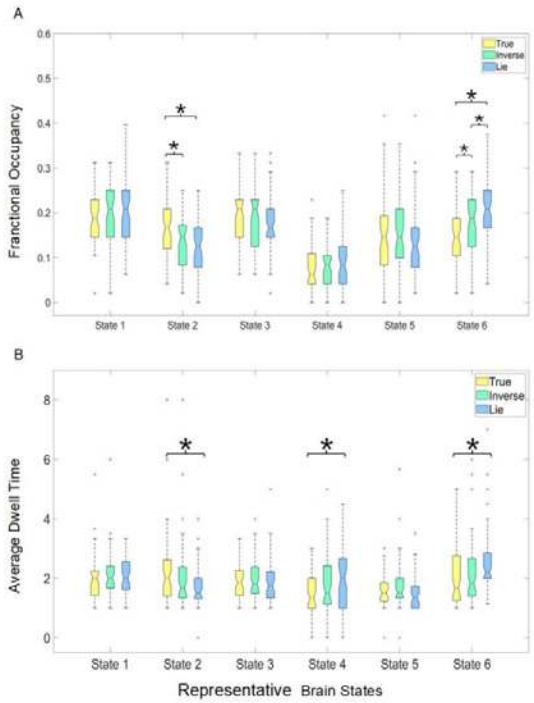

Figure 1. Franctional occupancy (A) and average dwell time (B) of six representative brain states corresponding to true-telling, inverse-telling, and lie-telling. The second idetified state was labeled as the Truth-prefer State, while the sixth state was designated as the Lie-prefer State. *: P < 0.05.

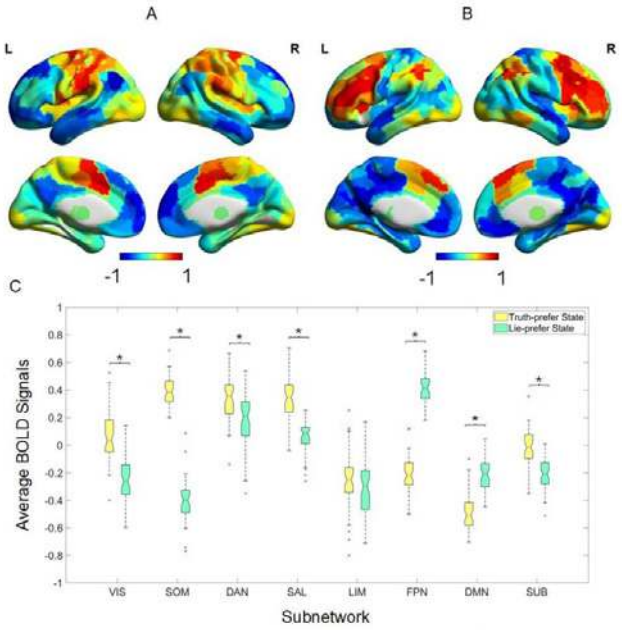

Figure 2. Spatial activation patterns of Truth-prefer State (A) and Lie-prefer State (B) accompanied by subnetwork analysis (C). VIS: visual network; SOM: somatomotor network; DAN: dorsal attention network; SAL: salience/ventral attention network; LIM: limbic network; FPN: frontoparietal network; DMN: default mode network; SUB: subcortical network. The colorbar indicates the average BOLD z-score across subjects. *: P<0.05.

Conclusions: This study revealed two brain states with different dynamic properties when lie-telling versus truth-telling. These states showed marked disparities in spatial patterns and network characteristics. The Lie-prefer State showed heightened cognitive involvement with increased activation in the FPN and DMN regions. These findings emphasize the difference of two key brain states during lie-related tasks, suggesting that their dynamic attributes may serve as biomarkers reflecting the varied cognitive involvement in such tasks.

References

1. Gao, J. (2022), 'Effective Connectivity in Cortical Networks During Deception: A Lie Detection Study Based on EEG', IEEE Journal of Biomedical and Health Informatics, vol. 26, no. 8, pp. 3755-3766.
2. Hakun, J.G. (2020), 'fMRI investigation of the cognitive structure of the Concealed Information Test', Neuroscience and Crime, pp. 59-67.
3. Jiang, W. (2015), 'Decoding the processing of lying using functional connectivity MRI', Behavioral and Brain Functions, vol. 11, no. 1, pp. 1–11.
4. Luppi, A. I. (2022), 'A synergistic core for human brain evolution and cognition', Nature Neuroscience, vol. 25, no. 6, pp. 771-782.
5. McCormick, D.A. (2020), 'Neuromodulation of brain state and behavior', Annual Review of Neuroscience, vol. 43, pp. 391-415.
6. Medaglia, J.D. (2018), 'Brain state expression and transitions are related to complex executive cognition in normative neurodevelopment', NeuroImage, vol. 166, pp. 293-306.
7. Meer, J.N. (2020), 'Movie viewing elicits rich and reliable brain state dynamics', Nature Communications, vol. 11, no. 1, pp. 5004.

Poster No 952

Brain network dynamics predict moments of surprise across contexts

Ziwei Zhang[1], Monica Rosenberg[1,2]

[1]Department of Psychology, The University of Chicago, Chicago, IL, [2]Neuroscience Institute, The University of Chicago, Chicago, IL

Introduction: We experience surprise, a transient process supported by distributed brain networks (Mazancieux et al., 2023), when reality conflicts with our expectations. Characterizing brain network dynamics allows us to discover commonalities between surprise in distinct contexts. We investigated network dynamics by computing two brain regions' moment-by-moment co-deflections, known as their co-fluctuation or edge time series (Faskowitz et al. 2020; Zamani Esfahlani et al., 2020) using fMRI. We propose an edge-fluctuation-based predictive model (EFPM) that predicts moment-to-moment changes in belief-inconsistent surprise across datasets.

Methods: We analyzed existing dataset collected as participants performed a task where they learned to predict the location of an upcoming object (N=32; McGuire et al., 2012; Kao et al., 2020). McGuire et al. (2012) developed a normative model tracking change point probability (changes in the mean of an occluded generative distribution of the object's location; CPP) and uncertainty (about the generative mean; RU). We operationalized surprise in this task as a composite measure of the two (CPP+RU*[1-CPP]). To identify functional brain networks whose strength predicted this measure, we calculated the edge time series (Faskowitz et al., 2020, Zamani Esfahlani, 2020) of all pairs of 268 brain regions in a functionally defined atlas as the product of their z-scored BOLD-signal time series. To build the EFPM, we used cross-validation to identify edges whose strength varied across trials with surprise (Fig. 1). In each training fold, we selected n-1 participants and calculated the partial Spearman correlation (rho) between their edge time series and their surprise time course, controlling for head motion. We selected edges significantly correlated with surprise across the group. In the held-out individual, we correlated the strength of these edges with the belief-inconsistent surprise. This process was repeated so that each individual was held out once. After training the surprise EFPM in the learning task, we tested whether it generalized to predict surprise in a naturalistic context in an independent dataset. We analyzed openly available fMRI data collected as novel participants watched NCAA basketball games (N=20; Antony et al., 2021). Antony et al. (2021) provided a measure of surprise from change in a team's win probability. We calculated moment-to-moment surprise EFPM summary score (Fig. 1) and ran a linear mixed effects model using this time course to predict belief-inconsistent surprise in the basketball videos, controlling for nuisance regressors (e.g., head motion).

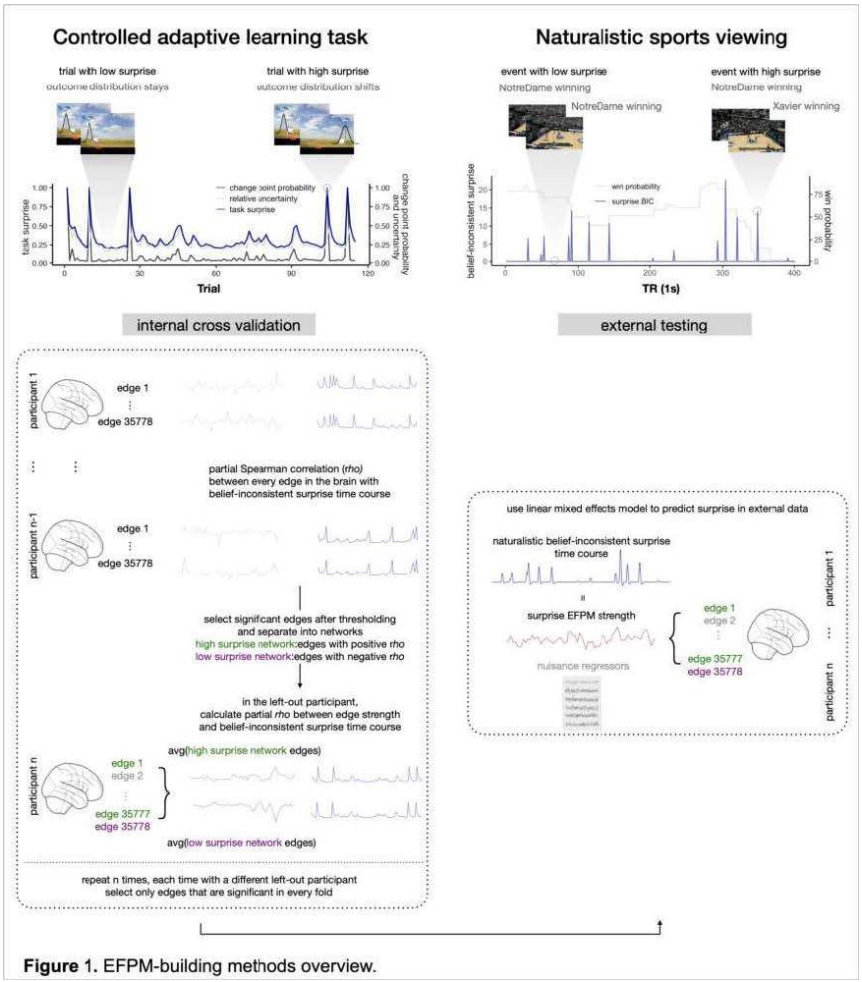

Figure 1. EFPM-building methods overview.

Results: EFPM successfully predicted task surprise in held-out individuals (Fig. 2). Edges positively correlated with surprise were stronger on trials with more unexpected outcomes (mean within-subject partial rho=0.09; p=0.001) whereas edges negatively correlated with surprise showed the opposite pattern (mean within-subject partial rho=-0.10; p=0.001). The surprise EFPM also predicted surprise in the NCAA basketball videos (ß=0.037, t(65136.852)=3.947, p=0.044), even when controlling for low-level factors (e.g., video luminance). Moreover, neither models built from BOLD activation nor from connectivity in canonical networks generalized across datasets to predict surprise. EFPMs built from other related behavioral measures also did not predict surprise out-of-sample.

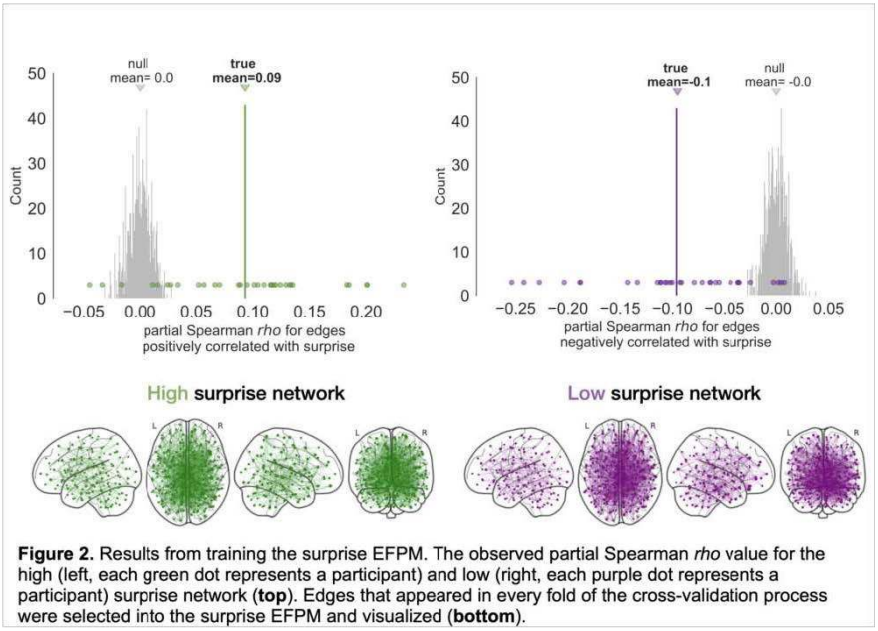

Figure 2. Results from training the surprise EFPM. The observed partial Spearman *rho* value for the high (left, each green dot represents a participant) and low (right, each purple dot represents a participant) surprise network (**top**). Edges that appeared in every fold of the cross-validation process were selected into the surprise EFPM and visualized (**bottom**).

Conclusions: We identified a brain network model, the surprise EFPM, that predicts surprise in controlled and naturalistic tasks from high-frequency edge dynamics. This model generalizes across contexts and uniquely predicts surprise, capturing expectation violations better than models built from other brain networks, fMRI measures, and behavioral metrics. Thus, the surprise EFPM captures common neural underpinnings of surprise experienced in distinct cognitive contexts in different groups of individuals.

References

1. Antony, J. W., Hartshorne, T. H., Pomeroy, K., Gureckis, T. M., Hasson, U., McDougle, S. D., & Norman, K. A. (2021). Behavioral, Physiological, and Neural Signatures of Surprise during Naturalistic Sports Viewing. Neuron, 109(2), 377-390.e7. https://doi.org/10.1016/j.neuron.2020.10.029
2. Faskowitz, J., Esfahlani, F. Z., Jo, Y., Sporns, O., & Betzel, R. F. (2020). Edge-centric functional network representations of human cerebral cortex reveal overlapping system-level architecture. Nature Neuroscience, 23(12), 1644–1654. https://doi.org/10.1038/s41593-020-00719-y
3. Kao, C.-H., Khambhati, A. N., Bassett, D. S., Nassar, M. R., McGuire, J. T., Gold, J. I., & Kable, J. W. (2020). Functional brain network reconfiguration during learning in a dynamic environment. Nature Communications, 11(1), Article 1. https://doi.org/10.1038/s41467-020-15442-2
4. Mazancieux, A., Mauconduit, F., Amadon, A., Willem de Gee, J., Donner, T. H., & Meyniel, F. (2023). Brainstem fMRI signaling of surprise across different types of deviant stimuli. Cell Reports, 42(11), 113405. https://doi.org/10.1016/j.celrep.2023.113405
5. McGuire, J. T., Nassar, M. R., Gold, J. I., & Kable, J. W. (2014). Functionally Dissociable Influences on Learning Rate in a Dynamic Environment. Neuron, 84(4), 870–881. https://doi.org/10.1016/j.neuron.2014.10.013
6. Zamani Esfahlani, F., Jo, Y., Faskowitz, J., Byrge, L., Kennedy, D. P., Sporns, O., & Betzel, R. F. (2020). High-amplitude cofluctuations in cortical activity drive functional connectivity. Proceedings of the National Academy of Sciences, 117(45), 28393–28401. https://doi.org/10.1073/pnas.2005531117

Poster No 953

Multimodal covariance network reflects individual cognitive flexibility

Lin Jiang[1], Guangying Wang[1], Runyang He[1], Dezhong Yao[1], Fali Li[1], Peng Xu[1]

[1]School of Life Science and Technology, University of Electronic Science and Technology of China, Chengdu, China

Introduction: Cognitive flexibility refers to the capacity to shift between patterns of mental function and relies on functional neural activity supported by inherent anatomical structures. However, the intrinsic structural-functional coordination subserving cognitive flexibility remains unrevealed. Herein, we quantitatively evaluate the structural-functional interactions within and across brain subsystems by multimodal covariance network (Jiang, et al. 2023), to uncover the coordinated structural-functional substrates supporting human cognitive flexibility at a large-scale level.

Methods: A total of 182 unmedicated healthy participants (63 females, aged 20 - 80 years) were enrolled with the approval of the ethics committee at the medical faculty of the University of Leipzig. All participants were instructed to perform the trail-making test, and the trail-making test B-A score was calculated to measure individual cognitive flexibility. Then, the large-scale multimodal covariance networks were constructed by combining electroencephalograph, structural, functional, and diffusion magnetic resonance imaging features that were divided into regions using the Desikan-Killiany atlas (Fig. 1). The relationships between multimodal covariance network and individual cognitive flexibility were probed by Pearson's correlation from three levels (i.e., network topology, whole-brain network properties, and subsystem properties). Finally, representative features were uncovered, with a prediction model being built by the stepwise multivariable linear regression, to help predict individual cognitive flexibility performance.

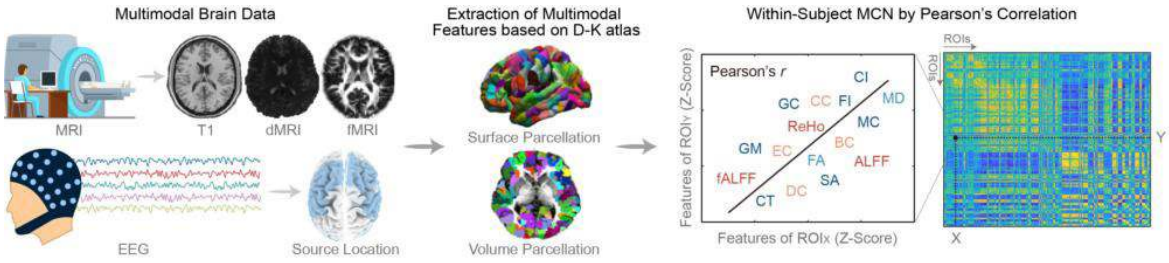

Fig. 1. Schematic illustration of multimodal covariance network construction. Multimodal covariance network is constructed based on fused functional and morphometric features that are parcellated by the Desikan-Killiany atlas.

Results: Results show that the intra-subsystem covariation of the somatomotor and visual network and inter-subsystem couplings spanning the somatomotor and visual/frontoparietal/default mode network are significantly related to individual cognitive flexibility (pFDR < 0.01, Fig. 2a). Meanwhile, significant correlations were observed between the cognitive flexibility

scores and both the whole-brain network properties (Fig. 2b) and subsystem properties (particularly the somatomotor and visual network; Fig. 2c). Based on these (sub)network properties, a stepwise multivariable linear regression model with the leave-one-out cross-validation approach was employed to achieve the prediction of the cognitive flexibility performance. We found that network properties significantly contribute to predicting cognitive flexibility ($r = 0.44$, $p < 0.001$). Additionally, the root mean square error was calculated as 19.18, indicating a satisfactory level of prediction accuracy.

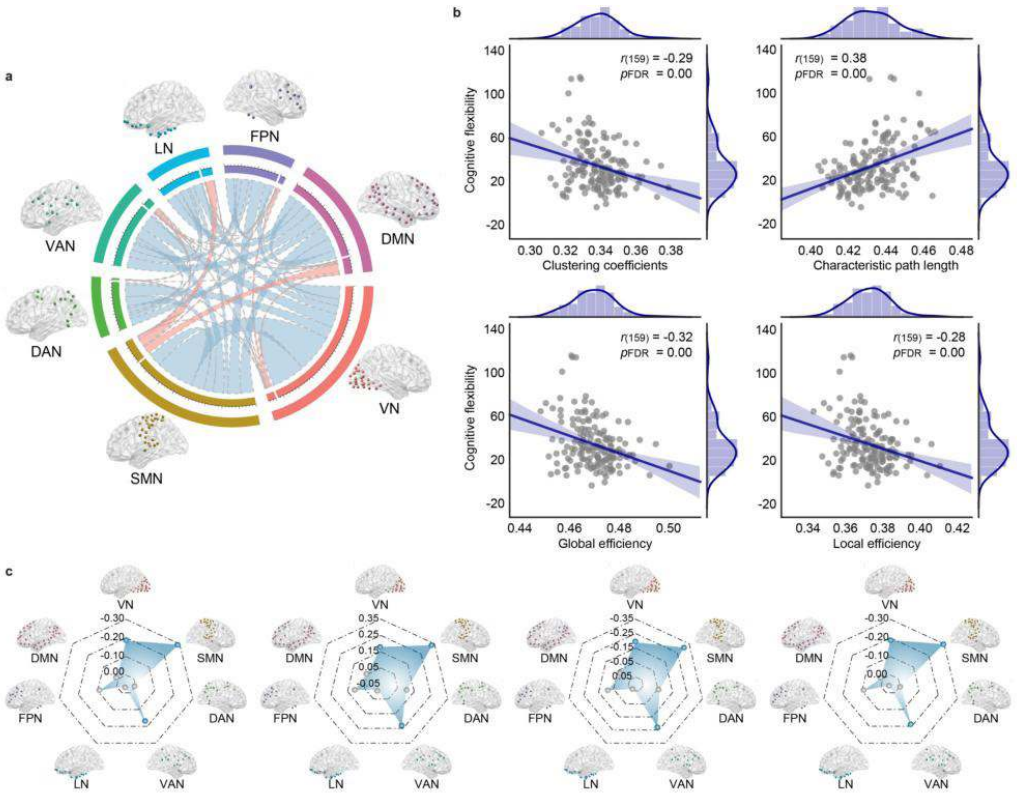

Fig. 2. Relationship between multimodal covariance network and individual cognitive flexibility. **a.** Network topologies significantly correlated with cognitive flexibility ($pFDR < 0.01$). The blue and red solid lines represent edges with significantly negative and positive correlations, respectively. **b.** Correlation between brain-wide network properties and cognitive flexibility. **c.** Correlation between subsystem properties and cognitive flexibility. The radar map shows the correlation coefficient between the properties of each subsystem and cognitive flexibility performance, and the blue circles denote subsystems with significantly positive or negative correlations ($pFDR < 0.01$).

Conclusions: Collectively, current discoveries enhanced our understanding of cognitive flexibility from the viewpoint of structural-functional interaction and will further derive useful physiological markers of cognitive functioning.

References

1. Jiang, L. (2023), 'Transcriptomic and Macroscopic Architectures of Multimodal Covariance Network Reveal Molecular-Structural-Functional Co-alterations', Research, vol. 6, pp. 0171

Poster No 954

Comparative study of EEG in groups of tantric and non-tantric practitioners. Preliminary results

Julia Boytsova[1], Ngawang Norbu[2], Lodoe Sangpo[3], Kokurina Elena[4], Kaplan Alexander[5], Zhironkina Julia[6], Telo Tulku Rinpoche[7], Kunga Lhundup[8], Lobsang Jangchup[9], Thupten Namdol[9], Jamyang Jamyang[8], Lharkyab Lharkyab[8], Stanzin Lhakpa[10], Yeshi Dorjee[3], Chhoktan Lama[3], Tanzin Mutup[11], Thupten Sherap[11], Lobsang Jinpa[11], Amchok Lobsang[12], Tanzin Chhonden[12], Tenzin Wangchuk[11], Lobsang Phuntsok[2], Jampa Thakchoe[2], Tashi Tashi[13], Tenzin Lhasa[14], Medvedev Svyatoslav[1]

[1]Institute of Biomedical Problems of the Russian Academy of Sciences, Moscow, Russia, [2]Sera Jey Monastic University, Bylakuppe, India, [3]Gaden Jangtse Monastic College, Mundgod, India, [4]Academician Natalya Bekhtereva Foundation, St. Petersburg, Russia, [5]Moscow State University, Moscow, Russia, [6]Save Tibet Foundation, Moscow, Russia, [7]Center for Tibetan Culture and Information, Moscow, Russia, [8]Drepung Gomang Monastic College, Mundgod, India, [9]Gyuto Tantric Monastery, Dharamsala, India, [10]Tashi Lhunpo Monastery, Bylakuppe, India, [11]Drepung Loseling Monastic College, Mundgod, India, [12]Gaden Shartse Monastic College, Mundgod, India, [13]Sera Jey Monastic University, Bylakuppe, India, [14]Gyudmed Tantric Monastery, Hunsur, India

Introduction: In the context of cognitive neuroscience, Buddhist meditations has been studied quite widely. But since the term "meditation" embraces many different practices, it leads to a wide variety of data. This is the reason why researchers try to classify meditations (Lutz et al., 2008, Travis et al., 2010). One approach to such classification is based on the autonomic nervous system activity and assumes that Buddhist tantric practices may differ from non-tantric meditations (Kozhevnikov 2019, Kozhevnikov et al., 2022). In Buddhism, meditations can be generally divided into two categories: 1) one-pointed concentration and 2) analytical meditation. Both skills are equally necessary to proceed to more advanced tantric practices that include elements of one-pointed and analytical meditations. Buddhist tantric meditations involve complex visualizations of Buddhist deities, their palaces, elements of "subtle anatomy" and transformative work with the "energies" of the human body. With the exception of some works (Benson et al., 1990, Lehmann et al., 2001, Kozhevnikov 2019, Kozhevnikov et al., 2022, DeLuca, Daly, 2023), Buddhist tantric meditations remain the least integrated into neuroscience research. We have the opportunity to study Buddhist meditations in the tantric monasteries of the Gelugpa tradition in India. We suggest that tantric and non-tantric meditations may have different effects on the brain activity of practitioners not only during meditation, but regular tantric practice can also lead to long-term changes that are different from those resulting from regular implementation of non-tantric types of meditation.

Methods: Practitioners from Buddhist monasteries in India of the Gelugpa tradition took part in the study. One group - 17 monks (age 52 ± 9 years, of which 5 monks participated in the study twice), performed tantric meditation during the study and as a regular practice (duration of regular practice was 16 ± 7 years). Another group of monks - 9 practitioners (age 54 ± 5 years, of which 3 monks participated in the study twice), performed non-tantric meditations: one-pointed concentration and analytical meditation on emptiness, impermanence or bodhicitta during the study, as well as a regular practice (duration 11 ± 7 years). EEG recording (from 19 electrodes) was carried out in a state of quiet wakefulness before meditation - EC (5-6 minutes), during meditation (20-30 minutes) and in a state of wakefulness after meditation – EC2 (5-6 minutes). EEG spectral analysis in 7 frequency bands was calculated for EEG signals in the gICA model. For statistical analysis of EEG-data t-statistics for independent samples was used.

Results: During EEG spectral analysis, we obtained the following preliminary results: (a) in the EC state (before meditation), the group of tantric practitioners differ from non-tantric group in less beta1- and beta2-power for gICs located in the central-frontal region and in the parietal-occipital regions, and tantric practitioners also had less alpha2-power for gICs located in the parieto-occipital regions, at the same time this group had more delta-power for gICs located in the frontal midline region; (b) during meditation we observed the same differences between groups, with the exception of an increase in delta-power in the frontal midline region; (c) in EC2 state (after meditation), the group of tantric practitioners still had less alpha2-, beta1- and beta2-powers, but only for gICs located in the parieto-occipital regions.

Conclusions: Our results showed that the groups of tantric and non-tantric practitioners differed not only during the meditation itself, but also in the non-meditative state both before and after meditation. This confirms that long-term meditation practice is associated with the neuroplasticity phenomena, and long-term changes may differ between tantric and non-tantric practitioners.

References

1. DeLuca J.W., et al. (2023), 'The inner alchemy of Buddhist tantric meditation: A QEEG case study using low resolution electromagnetic tomography (LORETA)'. Subtle Energies & Energy Medicine, vol. 13, no. 2., pp. 155-208.
2. Lutz, A., et al. (2008), 'Attention regulation and monitoring in meditation', Trends Cogn. Sci. vol. 12, pp. 163 – 169.
3. Travis F., et al. (2010), 'Focused attention, open monitoring and automatic self-transcending: Categories to organize meditations from Vedic, Buddhist and Chinese Traditions', Consciousness and Cognition, vol. 19, pp. 1110–1118.
4. Kozhevnikov M., et al. (2022), 'Beyond mindfulness: Arousal-driven modulation of attentional control during arousal-based practices', Current Research in Neurobiology, vol. 3, no. 100053. https://doi.org/10.1016/j.crneur.2022.10005
5. Kozhevnikov M. (2019), 'Enhancing Human Cognition Through Vajrayana Practices', Review J Relig Health, vol. 58, no. 3, pp. 737-747. doi: 10.1007/s10943-019-00776-z.
6. Benson H., et al. (1990), 'Three case reports of the metabolic and electroencephalographic changes during advanced Buddhist meditation techniques', Behav. Med., vol. 16, no. 2, pp. 90-95.
7. Lehmann D., et al. (2001), 'Brain Sources of EEG Gamma Frequency During Volitionally Meditation-Induced, Altered States of Consciousness, and Experience of the Self' Psychiatry Research: Neuroimaging Section, vol. 108, pp. 111-121.

Poster No 955

FMRI-based brain signature of divergent thinking

Cheng Liu[1], Kaixiang Zhuang[2], Xueyang Wang[1], Jiang Qiu[1]

[1]Southwest University, Chongqing, China, [2]The Institute of Science and Technology for Brain-inspired Intelligence (ISTBI), Shanghai, China

Introduction: Divergent thinking constitutes a vital component of creativity – a complex cognitive process that necessitates the collaborative engagement of multiple brain regions involved in distinct functions[1,2]. Prior studies employed connectivity measures at rest and have implicated the involvement of default, salience and executive systems[3]. However, the neural signature of divergent thinking during task performance remains elusive, requiring further characterization of this higher cognitive process. Here, we employed fMRI data from two large samples in conjunction with machine learning techniques to identify and delineate a neural marker capable of predicting divergent thinking ability both at the group and individual levels. We then further described this marker in the context of cortical connectivity gradients and meta-analytic decoding to unravel its architectural principals within the hierarchical organization of the human brain.

Methods: Across two study samples (n=55 and n=31), we acquired fMRI data while participants performed an AUT inside the scanner. In this task, participants were asked to generate either a “novel” or a “general” use example for an everyday object. Outside the scanner, participants were then asked to rate the originality of their responses on a 1-5 Likert scale. For data analysis, we used an MVPA-based neural decoding technique to identify a brain pattern that successfully classified the two conditions (subject-level beta map) with highest accuracy. To investigate the organizational principles of this neural signature, we then conducted a spatial correlation analysis between the brain pattern and cortical connectivity gradients, and used cognitive terms from the Neurosynth database for meta-analytic decoding. Finally, to assess the generalizability of our findings from group to individual-level, we tested the accuracy of the brain pattern in predicting originality ratings using relevance vector regression.

Results: To identify the multivariate patterns of fMRI activation, we applied linear SVMs to discriminate novel and general use conditions. The classification models have high accuracy that is 80%±3.8% on sample1 and 85%±4.6% on sample2. Notably, the weighted average of two models was calculated as the group-level neural signature of divergent thinking due to high correlation (Figure1A,r=0.838,p<0.001). Novel versus general use prediction weights were positive in bilateral DLPFC, bilateral DMPFC, left VLPFC, bilateral ACC, bilateral OFC, left AG, left MTG, and bilateral thalamus, right cerebellum, and negative in the right SPL, right precuneus, right ILOC (Figure1B). In this brain pattern, feature weights were mainly distributed across the default network and frontal-parietal control networks (Figure1C), associated with higher cognitive processes, such as judgment, retrieval, memory and semantic (Figure1D). More importantly, there was a high correlation between brain patterns and the principal connectivity gradient (r=0.60,p<0.0001), suggesting that regions closer to a segment of the default network may play an important role in divergent thinking (Figure1E). Finally, to validate the effectiveness of the brain pattern as biomarker for predicting divergent thinking, we applied RVR with single-trial beta maps (only novel use condition for each subject) as features to predict originality ratings. The distribution of the correlation (r) between the predicted and true value in 10×10-fold cv ranged from 0.21-0.39 on sample1 (Figure2A), and 0.09-0.17 on sample2 (Figure2B).

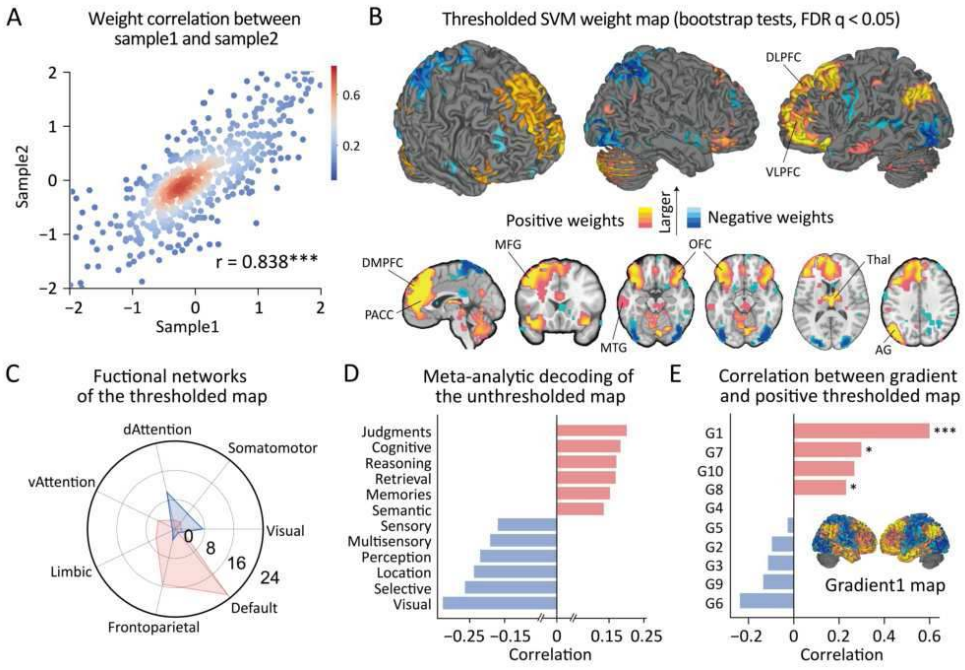

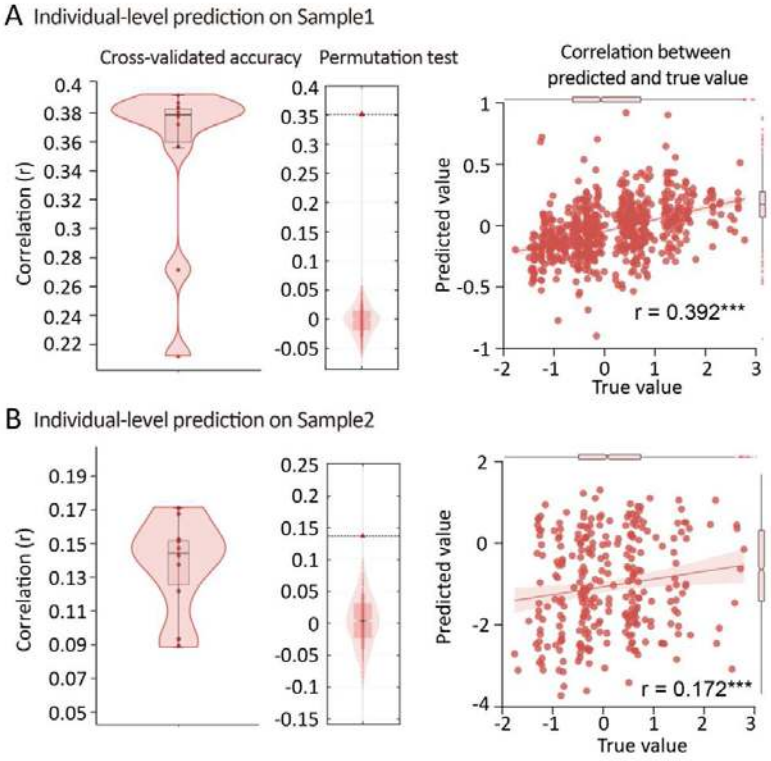

Conclusions: Our analysis has identified a comprehensive neural representation and organizational principle of divergent thinking. We show that divergent thinking is inextricably linked to a variety of higher cognitive processes and that its neural patterns are organized in the default and frontoparietal control networks in a manner that is consistent with the principal gradient of functional connectivity.

References

1. Benedek M. (2014), 'Intelligence, creativity, and cognitive control: The common and differential involvement of executive functions in intelligence and creativity', Intelligence, 46:73-83.
2. Kenett YN. (2018), 'Flexibility of thought in high creative individuals represented by percolation analysis', Proceedings of the National Academy of Sciences, 115(5):867-72.
3. Beaty RE. (2018), 'Robust prediction of individual creative ability from brain functional connectivity', Proceedings of the National Academy of Sciences, 115(5):1087-92.

Poster No 956

The Temporal Neural Dynamics of Math and Reading in the Adult Human Brain

Gizem Cetin[1,2], Mareike Grotheer[1,2], Daniel Kaiser[3,2]

[1]Department of Psychology, Philipps University Marburg, Marburg, Germany, [2]Center for Mind, Brain, and Behavior (CMBB), Marburg, Germany, [3]Mathematical Institute, Justus-Liebig University Gießen, Gießen, Germany

Introduction: Math and reading abilities play a fundamental role in our everyday life, influencing the well-being and career prospects of individuals. Neuroimaging studies have revealed that these skills rely on specialized brain networks spanning from the ventral temporal cortex to the frontal cortex (e.g., Grotheer et al., NComm, 2019). However, the precise temporal dynamics of information exchange within these networks remain unclear. To gain insights into the temporal dynamics of mathematical and reading processing in the brain, we evaluated neural responses during math and reading tasks in the EEG, using an established experimental design where both tasks are performed on the same visual stimuli.

Methods: At the onset of each trial, a cue was presented. Participants (N=30) then viewed four number-letter morph stimuli, each for 1 second, followed by a 2-second answer screen, during which they provided responses through button presses. Across different runs, participants performed three different tasks: reading, math, and a control task (color discrimination) (Fig. 1). Multivariate pattern analyses were conducted on EEG sensor data to evaluate the spatio-temporal dynamics of information flow during the tasks. Specifically, we tested when different groups of electrodes carry information about the participants' task, whether participants viewed more number- or letter-like morphs, and the resulting word or sum.

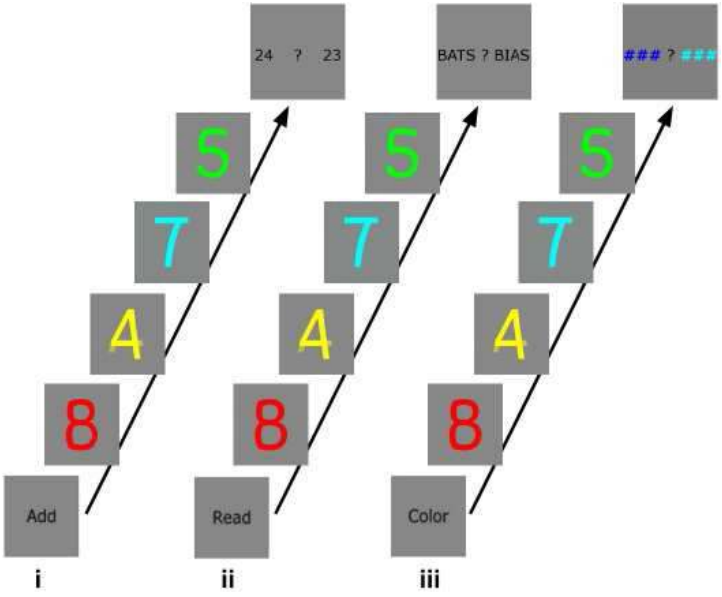

Fig 1. Experimental design. In a given trial, participants are prompted to perform (i) an adding task, (ii) a reading task, or (iii) a color task. At the end of the trial, participants indicate their answers with a button press.

Results: We found that the task participants were performing could first be decoded from electrodes in the frontal cortex and only later be decoded from electrodes in the occipito-temporal cortex. These temporal dynamics were similar across hemispheres, but decoding accuracy was overall higher in the left hemisphere. We could not decode the specific morph stimulus that the participants were looking at. Similarly, we could not significantly decode the resulting word/sum in either the math or the reading task.

Conclusions: We were able to decode the task participants were performing but not the visual stimulus they were seeing, which suggests that the performed task has a greater impact on neural responses than the visual stimuli. Further, our results suggest that information about current task demands can first be found in the frontal cortex and is subsequently fed back into the visual system to modulate processing in a task-specific way. This finding suggests that frontal control systems play a critical role in formatting visual representations of the same visual inputs for efficient use during math and reading tasks. Future research combining EEG and fMRI could resolve neural information flows during these essential tasks with even greater spatial precision.

References

1. Grotheer, M., Zhen, Z., Lerma-Usabiaga, G. et al. (2019), 'Separate lanes for adding and reading in the white matter highways of the human brain', Nature Communications, vol. 10, no. 1, 3675.

Poster No 957

Neural Signatures of Ongoing Thoughts During Rest

Jin Ke[1], Xiaochen Ding[1], Taylor Chamberlain[2], Anna Corriveau[1], Hayoung Song[1], Ziwei Zhang[1], Taysha Martinez[1], Laura Sams[1], Monica Rosenberg[1]

[1]The University of Chicago, Chicago, IL, [2]Columbia University, New York, NY

Introduction: While we rest, our mind often spontaneously wanders from ourselves to others, from the past to the future. These thoughts can be elicited by precipitating events and also emerge in the absence of direct external stimuli. Self-generated thoughts and feelings have been suggested to reflect personal traits[1] and provide behavioral markers for mental disorders[2]. Building on an emerging literature that utilizes neuroimaging[3] and natural language processing[4] to study the neural correlates and content of self-generated thoughts, here, we introduce an annotated resting-state fMRI paradigm for nuanced understandings of associations between unconstrained thoughts and brain dynamics. We use functional brain connectivity patterns[5] to track dimensions, topics, and linguistic sentiment of spontaneous thoughts.

Methods: Across two fMRI scan sessions, participants (N=50) completed four 10-min runs (32 rest periods total) of an annotated rest task in which they rested for 30s, verbally reported their ongoing thoughts for 10s, and rated their thoughts on 9 dimensions[6] using a slider bar (e.g., thinking about the future vs past). 5 thought topics (e.g., positive social memory) were extracted from the 9 dimensions using principal component analysis. We used a roBERTa-based model[7], a pre-trained

sentiment analysis model based on Twitter posts, to conduct sentiment analysis on the recording transcriptions to generate probabilities of the speech being negative or positive. A whole-brain functional connectivity (FC) pattern was generated for each 30s rest period using 268 functionally-defined ROIs[8]. We built support vector regression models with a leave-one-subject-out cross-validation approach to predict thought dimensions or topics (PCs) from FCs observed during the intermittent rest periods. These connectome-based models (CPMs)[9] were trained using data concatenated across all training subjects' rest periods and tested on each of the held-out subject's rest periods separately. Model performance was assessed by correlating predicted and observed values within subjects and comparing the mean within-subject correlation to a null distribution generated with permutation testing.

Results: Dimensions of ongoing thoughts correlated with each other as well as with speech sentiment decoded by linguistic analysis (Fig.1A). CPMs yielded above-chance predictive accuracy in predicting 5 out of 9 dimensions (Fig.2) and 4 out of 5 thought topics as well as positive (r=.047,p=.011) and negative (r=.049,p=.009) speech sentiment. Additionally, CPMs trained on positivity ratings predicted positive (r=.041,p=.030) and negative speech (r=-.106,p<.001) sentiment. Pairs of dimensions share significantly more overlapping edges than chance (Fig.1B). The number of shared edges predicts the absolute value of behavioral correlation between pairs of dimensions (Spearman's r=.591,p<.001). Further, whole-brain FC pattern similarity predicted thought similarity, such that rest periods with more similar FC patterns were accompanied by more similar self-reported ratings (mean within-subject correlation r= .089, p<.001).

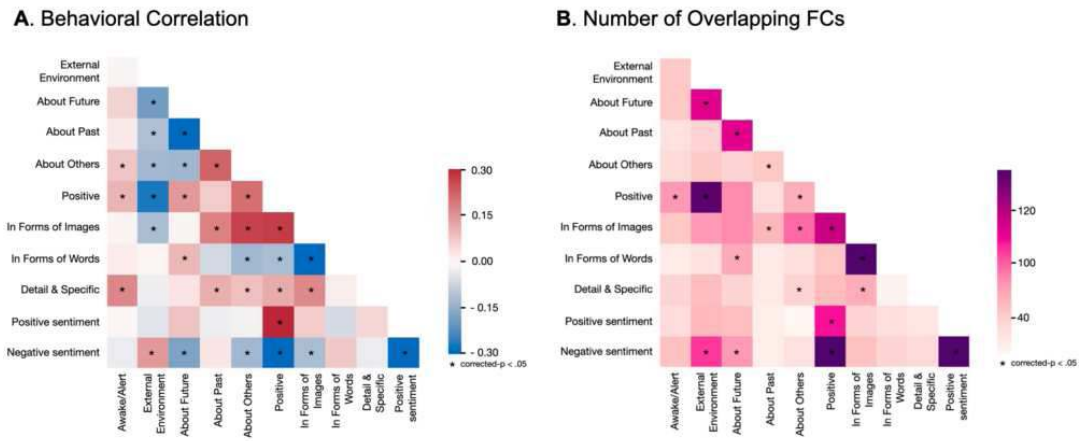

Figure 1. A. Behavioral similarity between pairs of thought dimensions and speech sentiment. B. Number of overlapping FCs between pairs of thought dimensions and speech sentiment.

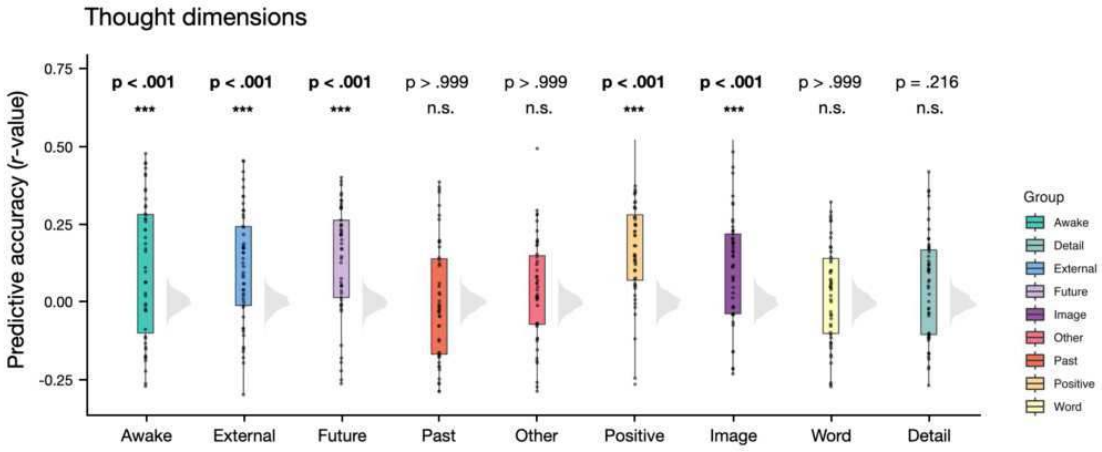

Figure 2. Functional connectivity during intermittent rest predicts dimensions of ongoing thoughts.

Conclusions: Functional brain correlations between regions observed during intermittent rest encode the self-reported dimensions and topics as well as linguistic sentiment of ongoing thoughts. FC networks predicting these dimensions overlap with each other, suggesting related dimensions of ongoing thoughts share underlying neural correlates. Further, thoughts arise in the brain as topics that are decodable from brain activity patterns. Additionally, sentiment analysis provides complementary tools to decode the emotional components of ongoing thoughts in a linguistic space beyond self-reported ratings.

References
1. Killingsworth, M. A. (2010). A wandering mind is an unhappy mind. Science, 330(6006), 932-932
2. Smallwood, J. (2007). Mind-wandering and dysphoria. Cognition and Emotion, 21(4), 816-842.
3. Karapanagiotidis, T. (2020). The psychological correlates of distinct neural states occurring during wakeful rest. Scientific reports, 10(1), 21121.
4. Li, H. (2021). Exploring self-generated thoughts in a resting state with natural language processing. Behavior Research Methods, 1-19.
5. Gonzalez-Castillo, J. (2015). Tracking ongoing cognition in individuals using brief, whole-brain functional connectivity patterns. Proceedings of the National Academy of Sciences, 112(28), 8762-8767.
6. Ho, N. S (2020). Facing up to the wandering mind: Patterns of off-task laboratory thought are associated with stronger neural recruitment of right fusiform cortex while processing facial stimuli. Neuroimage, 214, 116765.
7. Liu, Y. (2019). Roberta: A robustly optimized bert pretraining approach. arXiv preprint arXiv:1907.11692.
8. Shen, X. (2013). Groupwise whole-brain parcellation from resting-state fMRI data for network node identification. Neuroimage, 82, 403-415.
9. Shen, X. (2017). Using connectome-based predictive modeling to predict individual behavior from brain connectivity. nature protocols, 12(3), 506-518.

Poster No 958

Distinct representations of physical and perceived numerosity in convolutional neural networks

桂芬 苏[1,2], Yuxuan Cai[1,2], Delong Zhang[1,2]

[1]School of Psychology, South China Normal University, Guangzhou, Guangdong, China, [2]Guangdong Provincial Key Laboratory of Mental Health and Cognitive Science, South China Normal Unive, Guangzhou, Guangdong, China

Introduction: The “underestimation effect” on numerosity refers to the perceived phenomenon that a stimulus is subjectively perceived as less than its physical numerosity due to the configuration of the set, such as spatial adjacency, regular arrangement, and connectedness. However, it remains unclear whether the brain represents the physical and/or perceived numerosity. Recently, Kim et al. (2021) discovered spontaneous representation of numerosity in untrained convolutional neural networks (CNN) eliciting similar responses as numerosity-selective neurons in human brains. The CNN is believed to be analogous to the human brain, especially the ventral stream, given the hierarchical structure of information processing. Here, we employ CNN to explore the physical-perceived representations of numerosity and establish a link between the neural mechanism and behavior.

Methods: Stimulus materials: Two various types of stimuli, i.e., isolated dots (Fig. 1A) and connected dots (Fig. 1B), were employed in this study. To control the influence of different low-level features on the observed numerosity tuning in CNN, we categorized each lattice stimulus condition into three types: constant dot size, constant total area, constant convex hull but varying shapes in terms of stimuli. The numerosity included in each stimulus condition is as follows: 1, 2, 4...26, 28, 30 (with a gap of 2) (Fig. 1A). The stimuli are designed as images with the specific number of white dots distributed on a black background, with dimensions of 224*224 pixels or 227*227 pixels (depending on the properties of the neural network). Analysis: We input the isolated stimuli into the CNN, conducting a two-way ANOVA to identify neurons exhibiting numerosity-selective responses similar to the observations in the human brains, and analyze the preferred numerosity of these neurons. Then, we analyze whether these numerosity neurons exhibit similar response patterns to two different types of numerosity stimuli: isolated stimuli and connected stimuli. Specifically, we examine whether numerosity neurons demonstrate distinct response patterns to the two categories of numerosity stimuli that share the same physical quantity of dots (Fig2. A-B). Next, we identified numerosity-selective neurons and their preferred numerosities under the two conditions, respectively. We compared the preferred numerosity of identical neurons between two stimulus conditions (Fig2. C-D). We calculated the proportion of numerosity-selective neurons under connected stimulus conditions that exhibited a bias toward larger numerosity, serving as a quantitative measurement of the underestimation effect in the CNN (Fig2. C-D). Finally, we conducted validation analyses on multiple untrained and pretrained CNN (VGG16, VGG19, AlexNet).

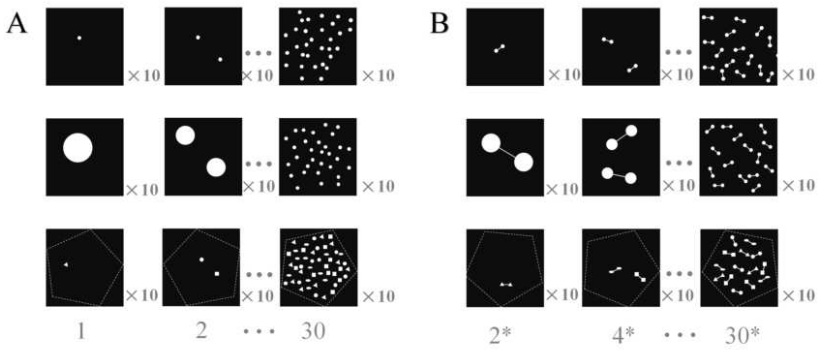

Fig. 1. Illustration of stimuli and experimental design. (A) Isolated stimuli. Each dot is presented in isolation without connections. Each column represents different numerosities, ranging from 1, 2, 4...26, 28, 30, in total of 16 numerosities. **(B) Connected stimuli.** Stimuli in which every two dots are connected by a line segment, and the center-to-center distance between two connected dots is four times the dots radius. Each column includes the physical numerosities of 2, 4, 6...26, 28, 30, in total of 15 numerosities. For both types of stimuli, each row represents a different condition: constant dot size, constant total area, constant convex hull but varying shapes in terms of stimuli. Each stimulus image is replicated 10 times with various random distribution of the dots each time.

Results: We found numerosity-selective neurons exhibit distinct response profiles between the isolated and connected stimuli (Fig2. A). More specifically, the preferred numerosity elicited by the connected stimuli appeared larger than those of the isolated stimuli (Fig2. C), indicating an underestimation effect on perceived numerosity compared to physical numerosity. Furthermore, we only observed these effects in the pretrained neural networks, but not in the untrained networks.

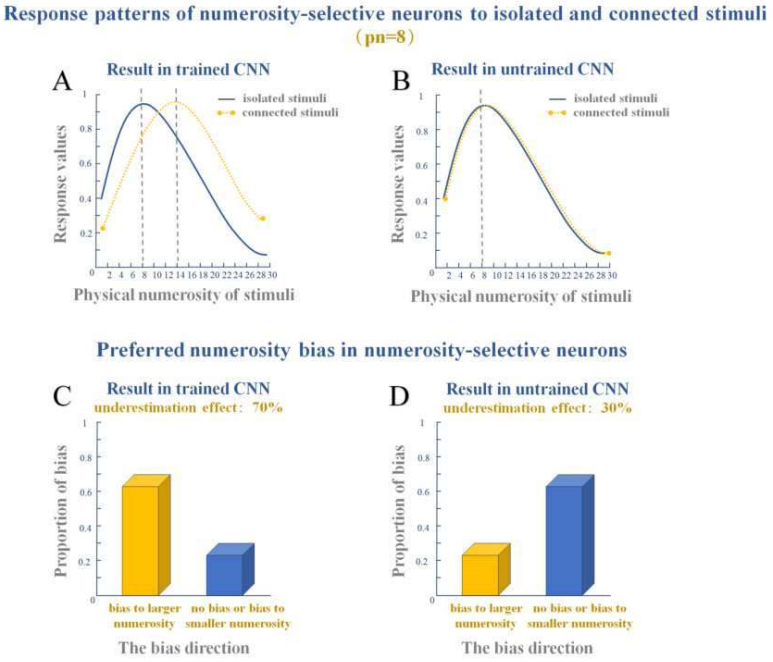

Fig. 2. Example responses of neurons preferring a numerosity (i.e., 8) to isolated or connected stimuli (A, B) and quantification of the underestimation effect (C, D) in pretrained and untrained networks, respectively. **(A)**Distinct responses to isolated and connected stimuli in trained network. Specifically, response to isolated stimuli (solid blue line) peaks at the same physical numerosity as the preferred numerosity (i.e. 8), whereas response to connected stimuli (dashed yellow line) reach the peak later at a larger physical numerosity (i.e. 14) which would perceived as less (i.e. 7), indicating an underestimation effect. **(B)** Nearly identical response to isolated and connected stimuli in untrained networks. Both responses peaks at the preferred numerosity, thus no underestimation effect was observed on connected stimuli. **(C)** In the trained networks, a large proportion of neurons shows numerosity preference bias towards larger physical numerosity under connected stimulus condition. **(D)** In the untrained networks, most of the neurons did not exhibit underestimation effects.

Conclusions: Our findings indicate that CNN represent the perceived numerosity of stimuli, and this effect is observed exclusively in pretrained neural networks. In other words, unlike untrained neural networks that automatically represent numerosity, the representation of perceived numerosity in pretrained neural networks relies on specific training weights. Our results provide neural computational evidence for the postnatal nature representation of perceived numerosity in human, suggesting that humans may have an innate foundational representation of numerosity, while more advanced and nuanced representations may require the involvement of postnatal visual experience.

References
1. Gwangsu Kim et al. (2021), 'Visual number sense in untrained deep neural networks'. Sci. Adv.7, eabd6127.
2. He L, Zhang J, Zhou T, Chen L. (2009), 'Connectedness affects dot numerosity judgment: Implications for configural processing', Psychonomic Bulletin & Review. 16(3). 509–517.
3. K. Nasr, P. Viswanathan, A. Nieder (2019), 'Number detectors spontaneously emerge in a deep neural network designed for visual object recognition'. Sci. Adv. 5, eaav7903.

Poster No 959

Neural Correlates of Psychological Flexibility

Verena Schuster[1,2], Christoph Vogelbacher[1,2], Marlon Westhoff[1], Stefan Hofmann[1,2]

[1]Department of Psychology, Philipps-University, Marburg, Germany, [2]Center for Mind, Brain and Behavior, Philipps-University, Marburg, Germany

Introduction: Psychological flexibility involves adapting to changing contexts, balancing competing desires, and being open to experiences while maintaining a commitment to one's values. It is an increasingly important but complex construct encompassing cognitive, emotional, and behavioral dimensions[1]. FMRI provides a powerful tool to explore the neural underpinnings of this flexibility by allowing researchers to observe brain activity in response to various stimuli and tasks. Reliable fMRI data is essential for accurately mapping the brain regions involved in psychological flexibility. Furthermore, consistent fMRI results are vital for replicating studies, a cornerstone of scientific research, ensuring that findings are not just artifacts but represent true brain function related to psychological flexibility. However, the replication crisis prompted a surge in robust methodologies to counter reliability challenges in neuroscientific research. Variations in operating systems[2], noise[3], and algorithm differences pose instability, impacting data acquisition and analyses[4,5]. The reliability of fMRI data is fundamental in advancing our understanding of psychological flexibility. This study explores an fMRI paradigm used by Benoit et al.[6], probing the neural correlates of suppressing future fears, a facet of psychological flexibility.

Methods: Fifty-nine healthy participants (42 women, 17 men) consented to the study, approved by the local Ethics Committee. MRI scans were conducted on a 3T Siemens Tim Trio scanner using a 32-channel head matrix Rx-coil. T2*-weighted echo-planar images were acquired, including five dummy volumes per run. The study replicated previous MR parameters, integrating newer techniques like multiband sequences for shorter TRs. Participants were tasked with either imagining or suppressing pre-identified future fears during the fMRI measurement using a pseudo-randomized block design. Detailed methodology is available in the referenced study[6]. The General Linear Model (GLM) was applied for analyzing fMRI data, with first-level analysis conducted using the Brain Imaging Data Structure (BIDS) model and the fitlins software on preprocessed data (using fmriprep). Movement parameters and the first six anatomical CompCor noise components were used as regressors alongside a high-pass filter (0.008 Hz) and 8 mm FWHM smoothing. Single-subject contrasts for imagine > suppress and vice versa were calculated. Second-level analysis utilized z-standardized contrasts for a one-sample T-test, with results thresholded at a false positive rate < .001. Cluster identification was achieved using the DIFUMO atlas, focusing on clusters of at least 15 voxels.

Results: Similar to the original study, the analysis revealed distinct brain activation patterns. For suppress > imagine, significant activity was noted in the inferior frontal gyrus, middle frontal gyrus, superior parietal lobule, and superior occipital sulcus. Conversely, imagine > suppress showed activation in the bilateral posterior cingulate cortex and ventromedial prefrontal cortex. Notably, hippocampal activation was absent, diverging from previous findings[6], suggesting alternative neural pathways in suppressing or imagining future fears.

Conclusions: The study successfully replicated core brain activations related to the suppression and imagination of future fears, utilizing updated and standardized data analysis methods. The lack of hippocampal activation might indicate a different neural mechanism at play in this specific psychological flexibility aspect, warranting further investigation. This paradigm is useful for studying psychological flexibility, a critical cognitive ability that enables adaptation to changing circumstances and emotional regulation. Understanding psychological flexibility is crucial for understanding mental health conditions and developing effective therapeutic interventions.

References
1. Kashdan TB. (2010), Psychological flexibility as a fundamental aspect of health. Clinical Psychology Review. Nov;30(7):865-78. doi: 10.1016/j.cpr.2010.03.001.
2. Glatard T. (2015), Reproducibility of neuroimaging analyses across operating systems. Frontiers in Neuroinformatics. Apr 24;9:12. doi: 10.3389/fninf.2015.00012. PMID: 25964757; PMCID: PMC4408913.
3. Lewis, L. (2017), Robustness and reliability of cortical surface reconstruction in CIVET and FreeSurfer. Annual Meeting of the Organization for Human Brain Mapping, Vancouver.

4. Bowring, A. (2019), Exploring the impact of analysis software on task fMRI results. Human Brain Mapping, 40(11), 3362–3384. https://doi.org/10.1002/hbm.24603
5. Klein, A. (2009), Evaluation of 14 nonlinear deformation algorithms applied to human brain MRI registration. NeuroImage, 46(3), 786–802. https://doi.org/10.1016/j.neuroimage.2008.12.037
6. Benoit, R. G.(2016), Reducing future fears by suppressing the brain mechanisms underlying episodic simulation. Proceedings of the National Academy of Sciences, 113(52), E8492–E8501. https://doi.org/10.1073/pnas.1606604114

Poster No 960

Brain responses to complex division problems in children, adolescents and adults

Asya Istomina[1], Andrei Faber[1], Maxim Ublinskiy[2], Andrei Manzhurtsev[2], Marie Arsalidou[3]

[1]HSE University, Moscow, Russian Federation, [2]Clinical and Research Institute of Emergency Pediatric Surgery and Trauma, Moscow, Russian Federation, [3]York University, Toronto, Ontario

Introduction: Complex computational mathematics plays a pivotal role as the foundation for numerous academic disciplines. Proficiency in mathematics frequently serves as a prerequisite for further education[1,2]. Division, among mathematical operations, is considered the most difficult and least explored. Functional magnetic resonance imaging (fMRI) studies consistently show that solving division problems elicits activation in fronto-parietal areas in adults[3,4]. However, results in children are less consistent, and to our knowledge, no study has examined division problem-solving involving 2-digit and 3-digit problems in children, adolescents, and adults.

Methods: Structural (TR = 2300 ms; matrix = 240 × 222, voxel size = 1.0 × 1.0 × 1.0 mm; FOV = 240 × 240 × 170 mm; TE = 3.9 ms; FA = 8°) and functional (TR = 2500 ms; TE = 35 ms; FOV = 230 × 230 × 150; 260 measurements per run; voxel size = 3.0 × 3.0 × 3.0 mm) brain data were collected from 20 children (9 female, aged 11–13 years), 20 adolescents (9 female, aged 14–16 years), and 20 adults (12 females, aged 18–29 years) using a Philips Achieva dStream 3.0T magnetic resonance scanner. Participants performed 2-digit and 3-digit division tasks in a block design, with each block lasting 32 seconds. They were instructed to provide as many correct answers as possible. All materials and procedures were approved by the local ethics committee. AFNI software (version AFNI for Mac OS versions 23.2.04;[5]) was utilized to preprocess and analyze the data. A high-resolution T1-weighted anatomical scan underwent nonlinear warp estimation using the 3dQwarp AFNI function[6]. Functional data underwent correction for differences in slice-time acquisition, head motion, linear trends, and low-frequency noise. These images were registered to each participant's T1-weighted anatomical warped image, normalized to the Montreal Neurological Institute (MNI) coordinate system, and spatially smoothed using an 8-mm Full Width at Half Maximum Gaussian smoothing kernel. Individual participants' whole-brain responses were modeled using a general linear model (GLM), with each experimental condition serving as a regressor. Individual parametric maps were then combined into a mixed-effects group GLM employing the 3dMEMA function in AFNI[7]. Statistical maps were corrected for multiple comparisons using a false discovery rate (FDR) q-value of 0.05.

Results: Behavioral scores revealed that children exhibited significantly lower accuracy and longer latencies compared to adolescents and adults. FMRI results indicated that solving difficult division problems elicited activity in both common and distinct regions across the age groups. Common areas included the middle and superior frontal gyri, bilateral supplementary motor areas, and the inferior parietal lobule, consistent with previous research on mathematical operations[8,9,10]. However, distinct areas in adults engaged the bilateral middle and superior temporal gyri, while in children and adolescents, temporal activation was observed in the left hemisphere. Activation in the left middle and superior temporal cortices was associated with storing arithmetic facts in long-term memory[11]. Left lateralized engagement of the insular cortex was observed in adolescents and adults but not in children.

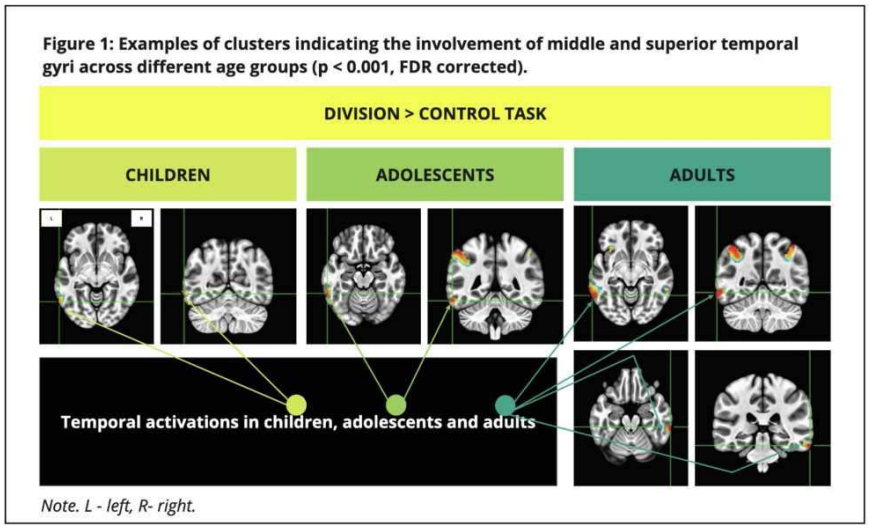

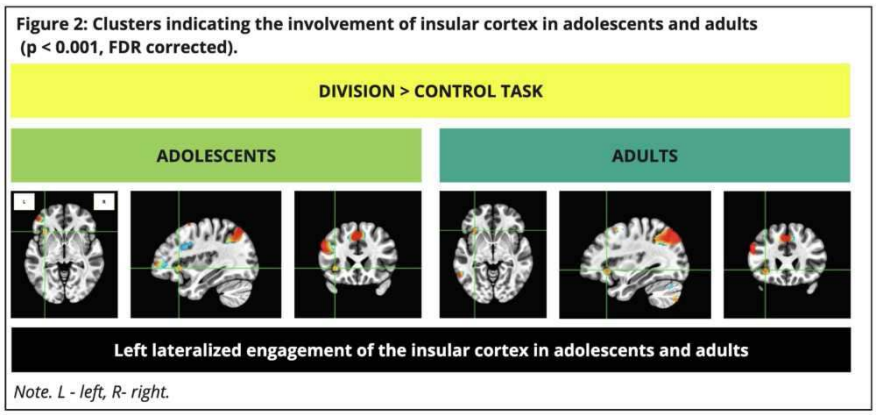

Conclusions: In conclusion, these findings suggest that cognitive strategies may not be fully developed in children. The agreement in brain areas among adults or between adults and adolescents, contrasted with their absence in children and adolescents, provides insights into neural processing during challenging mathematical tasks. These highlights reveal developmental distinctions in brain function and cognitive abilities across these age groups. This work was supported by operation grant from The Brain Program of the IDEAS Research Center.

References

1. Foley, A. E., Herts, J. B., Borgonovi, F., Guerriero, S., Levine, S. C., & Beilock, S. L. (2017). The math anxiety-performance link: A global phenomenon. Current directions in psychological science, 26(1), 52-58.
2. Klein, E., Zamarian, L., & Kaufmann, L. (2023). Challenges in Understanding Numerical Learning: Editorial for Brain Sciences Special Issue "Neurocognitive Signatures of Math (Learning) across the Lifespan and Their Interrelation with Other Aspects of Cognition and Emotion". Brain Sciences, 13(3), 420.
3. Fehr, T., Code, C., & Herrmann, M. (2007). Common brain regions underlying different arithmetic operations as revealed by conjunct fMRI–BOLD activation. Brain research, 1172, 93-102.
4. Wood, Guilherme, Hans-Christoph Nuerk, Korbinian Moeller, Barbara Geppert, Ralph Schnitker, Jochen Weber, and Klaus Willmes. "All for one but not one for all: How multiple number representations are recruited in one numerical task." Brain research 1187 (2008): 154-166.
5. Cox, R. W. (1996). AFNI: software for analysis and visualization of functional magnetic resonance neuroimages. Computers and Biomedical research, 29(3), 162-173.
6. Cox, R. W., & Glen, D. R. (2013). Nonlinear warping in AFNI. In Poster presented at the 19th Annual Meeting of the Organization for Human Brain Mapping.
7. Chen, G., Saad, Z. S., Nath, A. R., Beauchamp, M. S., & Cox, R. W. (2012). FMRI group analysis combining effect estimates and their variances. Neuroimage, 60(1), 747-765.
8. Arsalidou, M., & Taylor, M. J. (2011). Is 2+ 2= 4? Meta-analyses of brain areas needed for numbers and calculations. Neuroimage, 54(3), 2382-2393.
9. Arsalidou, M., Pawliw-Levac, M., Sadeghi, M., & Pascual-Leone, J. (2018). Brain areas associated with numbers and calculations in children: Meta-analyses of fMRI studies. Developmental cognitive neuroscience, 30, 239-250.
10. Hawes, Z., Sokolowski, H. M., Ononye, C. B., & Ansari, D. (2019). Neural underpinnings of numerical and spatial cognition: An fMRI meta-analysis of brain regions associated with symbolic number, arithmetic, and mental rotation. Neuroscience & Biobehavioral Reviews, 103, 316-336.
11. Prado, J., Mutreja, R., Zhang, H., Mehta, R., Desroches, A. S., Minas, J. E., & Booth, J. R. (2011). Distinct representations of subtraction and multiplication in the neural systems for numerosity and language. Human brain mapping, 32(11), 1932-1947.

Poster No 961

Brain mechanisms of ego- and allocentric representations in VR-based imagined and actual navigation

Jie Song[1], Emmanuel Badier[1], Ilaria Sani[1], Patrik Vuilleumier[1]

[1]*University of Geneva, Geneva, Switzerland*

Introduction: Every day we need to navigate and be aware of our location in space. Previous studies suggested that brain mechanisms of actual navigation operate using two different reference frames - egocentric (orienting based on a frame of reference centered on the self) and allocentric (orienting based on the spatial relationship between landmarks)[1]. However, it is still unclear whether and how we rely on different strategies in imagined navigation during route planning, and how brain mechanisms differ between imagined and actual navigation in virtual reality (VR) environments.

Methods: Participants: We recruited 19 healthy participants (7M/12F, age 23-30; 9 for behavior only; 10 for fMRI; inclusion criteria: no history of psychological or neurological disease and with normal or corrected vision; ethics approval # 2023-00325). fMRI: MRI data were obtained on a 3T Siemens Prisma MRI scanner with a 32-channel head coil. The functional data were obtained using GE-EPI sequence with TR=1300 ms, TE= 30 ms, FA = 64°, FoV=210 × 224 mm2, image matrix=84 × 84, slice thickness = 2.5 mm, voxel size = 2.5 mm, and 84 sagittal slices covering the whole brain. VR tasks: We leveraged two VR navigational tasks[2] with encoding, imagination, and retrieval phases to assess participants' ability to repeat/retrace a route in the same/reverse directions. In encoding phase, participants started from a black car and moved passively through 3 street intersections until a red telephone box (Fig. 1). Different intersections featured different houses. In imagination phase, participants were positioned at one intersection/car and asked to imagine the route to the phone box (repetition task) or at one intersection/phone box to imagine the route back to the car (retracing task). In retrieval phase, participants passively moved to one intersection where they chose to turn left, turn right, or proceed straight to reach their goal. After their response, participants were always moved to the correct direction and received feedback for wrong responses. Behavioral data were collected with (in scanner) and without the imagination phase. Data analysis: Behavioral data were analyzed in terms of accuracy and reaction times. Functional MRI data were preprocessed using fMRIprep 20.2.2 with slice-timing correction, co-registration, normalization, and 6 mm FWHM smoothing. We used a generalized linear model (GLM) to analyze main effects of egocentric (navigate from car/phone box) and allocentric (navigate from intermediate intersection) conditions, for both imagination (GLM1) and retrieval (GLM2) phases. Motion parameters, global signal, and top 10 anatomical components were included as nuisance variables. Group-level statistics were estimated from individual z maps.

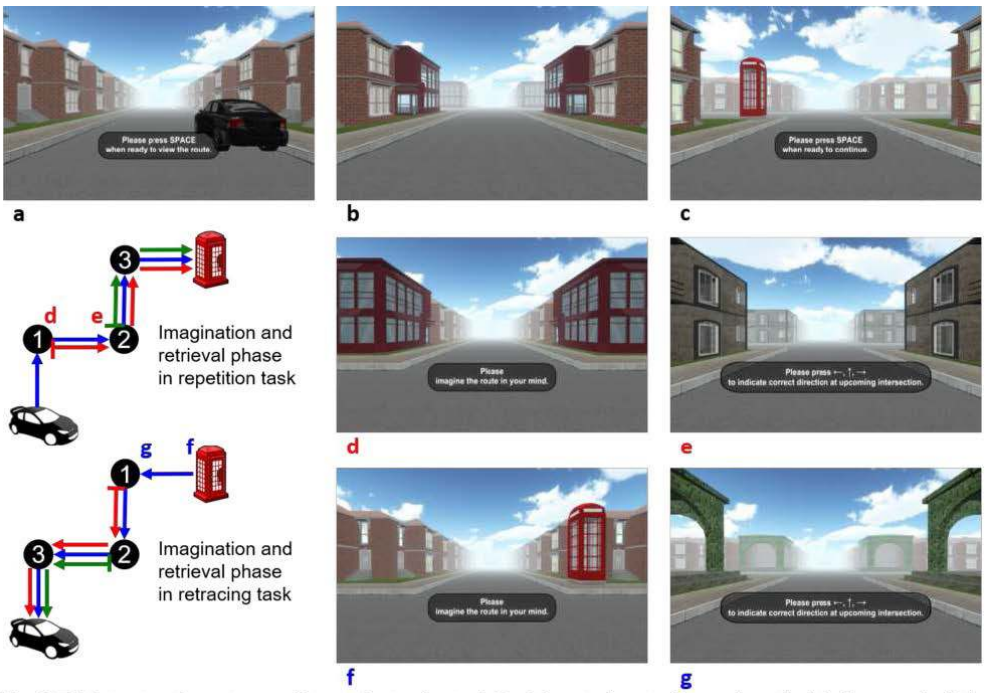

Fig. 1. Trial structure for route repetition and retracing task. Participants departed from where the black car parked (a) and passively moved to the upcoming intersection featured with four identical houses (b). They went through 3 intersections and saw a red phone box as a destination (c). Each intersection featured different houses within a single trial. They were then located at the start/end (f) (Car's position for the repetition task / Phone box's position for the retracing task) or one of the intersections (d) that face the next street of the route, and imagined moving from their current location to the goal (Phone box in the route repetition task / Car's position in route retracing task). In the retrieval phase, participants passively moved to the upcoming intersection (e & g) from the current location and indicated to turn left, turn right, or proceed straight to find the goal.

Results: Behavior: Orienting choice RTs were longer (indicating higher cognitive cost) on tasks without imagination phase (Fig. 2a) compared to tasks with imagination (Fig. 2b), which suggests participants benefited from imagined navigation. Interestingly, the farther from the navigation start (intersection 3 > 2 > 1), the longer were the RTs to identify the location and choose the direction (Fig. 2a). fMRI Results: During imagined navigation, brain activation was higher in parahippocampal gyrus (PHC), bilateral lingual gyrus, and retrosplenial cortex (RSC) in allocentric conditions, and higher in right superior parietal cortex (SPC) in egocentric conditions (Fig. 2c, GLM1). During actual navigation, activation was stronger in anterior and posterior cingulate gyrus in allocentric conditions, and in caudate and occipital cortex in egocentric conditions (Fig. 2d, GLM2).

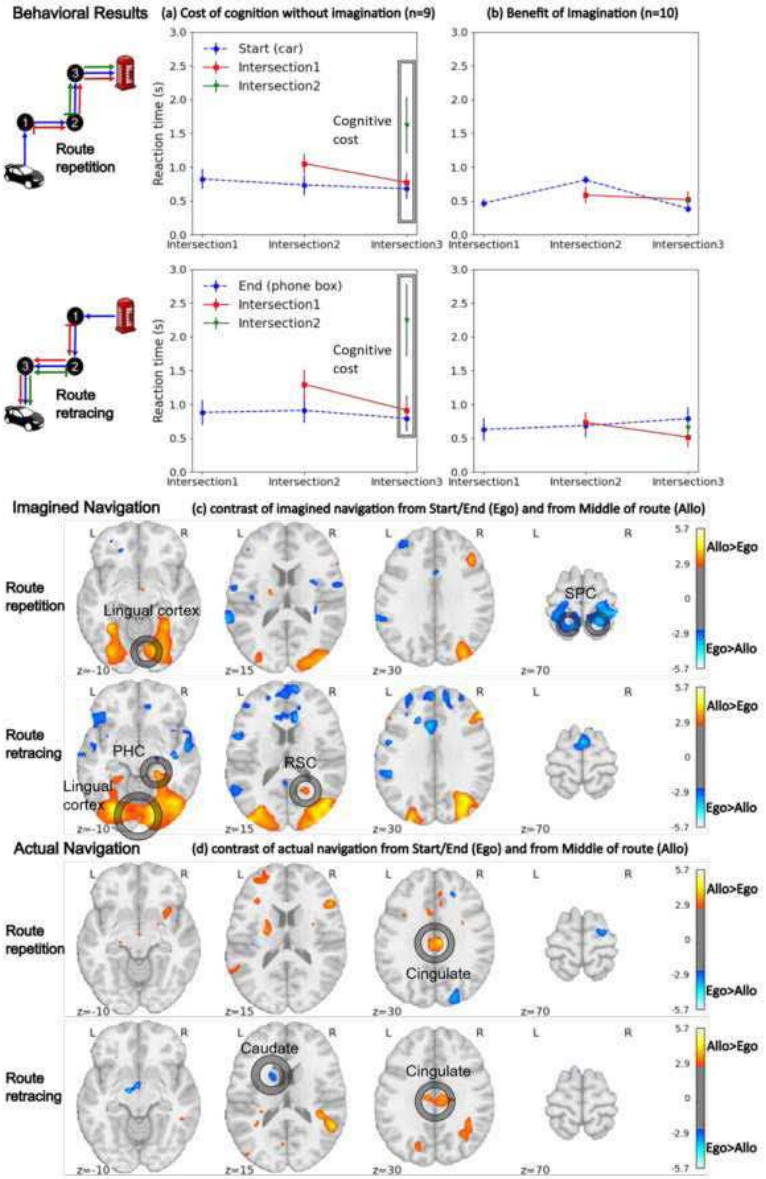

Fig. 2. (a) Average reaction time (RT) among all intersections on the task with imagination. Blue dots represented RT at each intersection in egocentric conditions (navigate from the car in the repetition task or phone box in the retracing task). The red square and green triangle represented RT of allocentric condition (navigate from the intermediate intersection). (b) Average RT among all intersections on the task without imagination. (c) Voxels responding to the main effect of egocentric and allocentric imagined navigation (p<0.005, uncorrected). (d) Voxels responding to the main effect of egocentric and allocentric actual navigation (p<0.005, uncorrected). SPC: superior parietal cortex; PHC: parahippocampal gyrus; RSC: retrosplenial cortex

Conclusions: Our findings suggest that planning a route to the goal in the imagination phase could benefit to actual navigation. Allocentric navigation mainly relied on PHC, RSC, lingual, and cingulate cortex, while egocentric mainly relied on SPC and caudate. Imagined and actual navigation using both ego and allocentric strategies may engage different brain mechanism.

References

1. Bottini, R. and C.F. Doeller (2020), 'Knowledge Across Reference Frames: Cognitive Maps and Image Spaces', Trends Cogn Sci, vol. 24, no. 8, pp. 606-619
2. Wiener, J.M., et al. (2020), 'A novel virtual-reality-based route-learning test suite: Assessing the effects of cognitive aging on navigation', Behav Res Methods, vol. 52, no. 2, pp. 630-640

Poster No 962

Effect of Food Diary on Dietary Intake and Correlation with Neural Substrate

Takuto Matsuhashi[1], Kenchi Hosokawa[1], Chihiro Hosoda[1]

[1]Tohoku University, Sendai, Miyagi

Introduction: Lifestyle-related diseases represent a significant health cost, highlighting the need to cultivate healthy behaviors, particularly during key developmental periods such as adolescence. This study examines the effectiveness of personalized feedback in promoting sustained healthy eating behaviors in university students, while investigating the role of the frontal pole cortex (FPC) in supporting behavior change and maintenance. Interventions were tailored to individual stages of change using daily food records and dietary analyses. The study aimed to determine whether the FPC is associated with sustained healthy behaviors in the future.

Methods: We recruited 50 participants (personalized feedback (PF) group: 25, age = 21.44 ± 1.81 years; control feedback group: 25, 21.68 ± 2.68 years). Participants underwent a 28-day intervention including dietary recording, mental health recording (anxiety: STAI), nutrient analysis, and received personalized or control feedback via email. Dietary intake was recorded via a web application and 13 nutrients were analyzed. The PF group received personalized feedback on dietary components and future health risks, whereas the CF group received general feedback on nutritional knowledge. All images acquired using Siemens Prisma (3.0 T) comprised T1w, T2w and diffusion weighted images, processed using HCP pipelines, FreeSurfer and FSL tools for cortical thickness, T1w/T2w ratio and FA data. Image statistics were performed using the PALM toolbox and FSL/Randomise for voxel-wise comparisons, corrected for age and sex. Cortical thickness, T1w/T2w ratio and FA values were extracted using frontal pole masks.

Results: The results showed significantly more food diary records in the PF group compared to the CF group across feedback cycles received ($p = .043$). Improvements in calcium, vitamin A, vitamin C and fibre intakes were observed in the PF group (ps $< .05$). Trait anxiety was significantly reduced in the PF group post-intervention compared to pre-intervention ($p < .001$). When the relationship between FPC and food diary records was examined, there was a positive correlation in the PF group between greater cortical thickness, T1w/T2w ratio, FA and food diary records (ps $< .05$).

Conclusions: Our investigation revealed positive associations between food diary records and cortical thickness, T1w/T2w ratio, and FA, suggesting a correlation between future-oriented behavior and brain structure.

References

1. Hosoda, C. (2020), 'Plastic frontal pole cortex structure related to individual persistence for goal achievement', Communications Biology, 3(1), 194.

Poster No 963

Laminar profiles of hippocampal subfields are differentially associated with navigation strategies

Khazar Ahmadi[1], David Stawarczyk[1], Viktor Pfaffenrot[2], Carlos Gomes[1], Sriranga Kashyap[3], Zita Patai[1], David Norris[4], Nikolai Axmacher[5]

[1]Department of Neuropsychology, Institute of Cognitive Neuroscience, Ruhr University Bochum, Bochum, North Rhine Westfalen, Germany, [2]Erwin L. Hahn Institute for Magnetic Resonance Imaging, University of Duisburg-Essen, Essen, North Rhine Westfalen, Germany, [3]Krembil Brain Institute, University Health Network, Toronto, Ontario, Canada, [4]Donders Institute for Brain Cognition and Behaviour, Radboud University, Nijmegen, Gelderland, Netherlands, [5]Department of Neuropsychology, Institute of Cognitive Neuroscience, Ruhr University Bochum, Bochum, North Rhine Westfalen,, Germany

Introduction: The Hippocampus (HP) is a critical region for core cognitive functions including memory and spatial navigation. Although these functions have been extensively studied at macroscale[1], the underlying circuit-level mechanisms are yet to be determined. Harnessing the current advancements in functional magnetic resonance imaging (fMRI) at submillimeter scale, we aimed to investigate the laminar organization of HP subfields during spatial navigation and their associations with distinct navigation strategies.

Methods: 39 healthy volunteers underwent a 2-session fMRI study using a 7T MAGNETOM-Terra scanner. During the first day, an anatomical image was acquired with 3D-MP2RAGE[2] sequence (isotropic spatial resolution of 0.75 mm3). This was followed by the acquisition of two fMRI runs using a 3D GRE-EPI sequence[3] with BOLD contrast (isotropic voxel size of 0.8 mm3, phase-encoding direction = A-P, TR = 2500 ms). On day 2, six additional fMRI runs were obtained. During each run, the participants navigated to six hidden objects randomly distributed in a virtual arena and completed 18 trials per run, each consisting of

a retrieval and a subsequent re-encoding phase (see Fig.1A). Following preprocessing of the fMRI data and subsequent alignment with the anatomical images, HP was segmented into subfields including cornu ammonis (CA 1-4), stratum radiatum/lacunosum-moleculare (SRLM) and dentate gyrus (see ref.4). Furthermore, three folded surfaces were generated using an equivolume model, representing inner/outer sections and mid-thickness of the HP gray matter (Fig.1B). These surfaces were then transformed into the space of the corresponding anatomical image and equidistantly sampled into 30 depth bins using an in-house MATLAB script. This allowed for extraction of the BOLD signal across the bins during the navigation phase, that were later grouped into the inner, middle and outer depths. We further assessed trial-specific performance, i.e., drop error (see Fig.1A). Afterwards, different navigation strategies were quantified with two metrics: straightness index (SI), and median deviation to the boundary (MDB; see Fig.2A). Subsequently, we performed linear mixed-effect models to assess the association of subregional laminar profiles with drop error and navigation strategies. The extraction of laminar profiles in subfields is still ongoing (N = 13 until now).

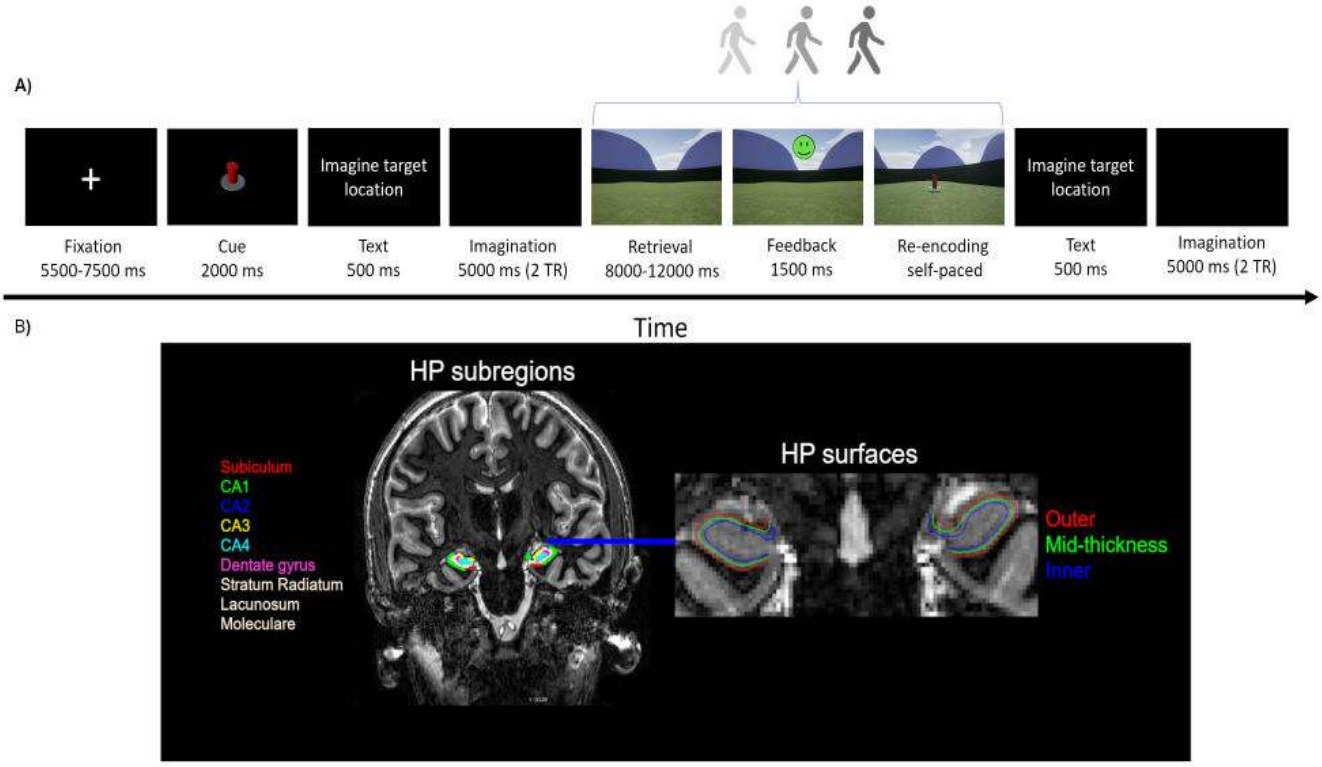

Figure 1. A) Overview of the paradigm. Each trial began with presentation of a fixation cross.This was followed by displaying an object (cue) which subjects had to place accurately in its correct location later in the retrieval phase. They were asked to imagine the target location, navigate, and drop the object. Feedback was provided based on drop error (Euclidian distance between drop location and the correct location of the object). The object was then shown at its correct location, and subjects re-encoded it by walking to that location. Trials ended by a second round of imagination. **B)** Hippocampal (HP) segmentation using Hippunfold package (see ref 4). The subregions are overlaid on a bias-field corrected and denoised short-inversion time (TI) image of the MP2RAGE sequence. Folded surfaces (right panel) are generated using an equivolume approach indicating inner and outer boundaries of the HP as well as mid-thickness of its grey matter.

Results: Drop error decreased across runs and trials, indicating a gradual improvement of the participants' behavioral performance (see Fig.2B). During the navigation phase, an inverse U-shaped pattern of the BOLD signal was observed throughout the layers of CA1 and the adjacent segment of SRLM whereas the laminar profile of CA3 demonstrated a largely monotonous decrease from inner to outer depths (Fig.2C). Further, higher drop error was associated with increased BOLD activity in inner, middle and outer depths of CA1, CA3 (β = 3.02, 4.46, p = 0.0002, 0 | β = 2.53, 4.96 p = 0.003, 0 | β = 1.77, 5.27, p = 0.04, < 0.0001, respectively) and the neighboring SRLM regions (β = 2.34, p = 0.002 SRLM-CA1; β = 3.75, p = 0.0001 SRLM-CA3). While SI was positively correlated with laminar activity only in the middle and outer layers of CA1 (β = 2.43, 3.59 p = 0.005, 0.0001, respectively), lower SI was associated with elevated BOLD signal across all three layers of CA3 (inner: β = -3.74, p = 0.0003, middle: β = -4.26, p = 0.0001, outer: β = -4.45, p = < 0.0001) and SRLM-CA3 (β = -2.99, p = 0.001). By contrast, an increase in MDB was accompanied by a higher BOLD signal specifically in CA3 (inner: β = 2.59, p = 0.01, middle: β = 2.67, p = 0.01, outer: β = 2.76, p = 0.007) and SRLM-CA3 (β = 2.66, p = 0.004).

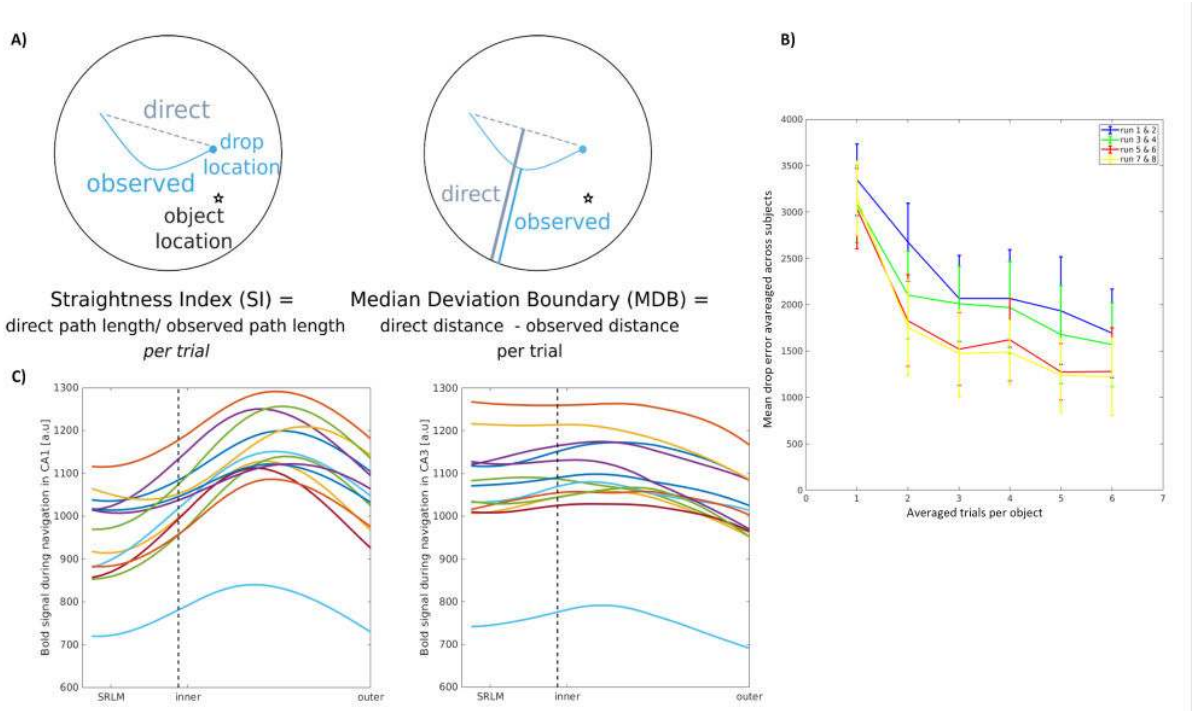

Figure2. A) Schematic illustration of different navigation strategies. Both metrics are calculated based on the observed path to the drop location of the object and an optimal path, had the subjects taken a direct path. For SI, a value close to 1 would indicate a straight path. For MDB, a positive value indicates that the observed path deviated more towards the boundary while a negative value is an indication of path deviation towards the center. **B)** Reduction of drop error across runs and participants. **C)** Laminar profile of the BOLD signal intensity during navigation phase across depths of CA1 (left) and CA3 (right), averaged across all functional runs per participant. While the signal in CA1 has an inverse U-shape profile across layers, it decreases largely monotonously towards the outer depth of CA3. The first 10 bins on the x-axis indicate the adjacent SRLM segment and the remaining 20 bins represent the sampling in CA1 and CA3 with bin 11 being the innermost and bin 30 the outer most depths, respectively.

Conclusions: Our preliminary results demonstrate the feasibility of laminar-resolution recordings in human HP. They suggest that distinct navigation strategies are differentially related to subregion-specific laminar profiles, and that higher BOLD responses in CA1 and CA3 are negatively related to navigation performance.

References

1. Julian, J. B. (2021). Remapping and realignment in the human hippocampal formation predict context-dependent spatial behavior. Nature neuroscience, 24(6), 863-872.
2. Marques, J. P. (2010). MP2RAGE, a self bias-field corrected sequence for improved segmentation and T1-mapping at high field. Neuroimage, 49(2), 1271-1281.
3. Stirnberg, R. (2021). Segmented K-space blipped-controlled aliasing in parallel imaging for high spatiotemporal resolution EPI. Magnetic resonance in medicine, 85(3), 1540-1551.
4. DeKraker, J. (2022). Automated hippocampal unfolding for morphometry and subfield segmentation with HippUnfold. Elife, 11, e77945.

Poster No 964

Multivariate neural pattern changes reflect within-subject shifts in subjective interpretations

Clara Sava-Segal[1], Tory Benson[1], Emily Finn[1]

[1]*Dartmouth College, Hanover, NH*

Introduction: Dynamically changing percepts can be reconstructed from multivariate neural representations[1]. This is usually studied with simple bistable stimuli in which people fluctuate between two mutually exclusive percepts. However, real-world ambiguities, like social contexts, tend to be more subjective, eliciting a wider range of spontaneous interpretations. Work with high-level, ambiguous stimuli (e.g., naturalistic narratives) shows that neural activity differs based on self-generated interpretations[2-4]. Thus, differences in neural activity are associated with differences in interpretations across subjects. However, it remains unknown if and where multivariate activity patterns change within subjects as individuals shift between interpretations of the same information. Given that we often encounter alternative explanations for the same event in social situations (e.g., a friend's opinion), we gave subjects an innovative, well-validated behavioral task that mimics ambiguous social scenarios. We tested the hypothesis that within-subject multivariate pattern shifts would predict self-reported shifts in subjective interpretations.

Methods: During fMRI scanning (3T, voxel size=2.7mm3, TR=1.057), subjects(n=10) performed a task where, on each trial, they were presented with ambiguous photographs and interpreted them. Next, on experimental trials only, they read another

possible interpretation sourced from a real subject (alternate interpretation). They then completed an appraisal task where they rated the likelihood of either just the self-generated interpretation (for control trials) or both the self-generated and the alternate interpretation (for experimental trials; Fig. 1). Scanning was conducted in an iterative design, where alternative interpretations were obtained from earlier subjects and selected in real-time, ensuring balanced distributions of 1)semantic distance between the self-generated and alternate interpretation, and 2)the identity of whom inputs were sourced from. Data collection is ongoing (target n=70). Voxels were grouped into 100 cortical nodes using the Schaefer parcellation[5]. An event-related general linear model GLM) approach was applied. Each event was modeled by the onset and offset of a given trial phase (e.g., initial or second viewing;Fig. 1) convolved with the hemodynamic response function, yielding a beta weight for each trial phase per voxel. We computed neural shifts as the cosine distance (1-r) between multivoxel patterns in a given node between the two viewing phases of a trial (Fig. 2a). To predict the effect of condition, a linear mixed effects model was run per parcellation node predicting neural shifts by condition. Separate linear models were fit per subject. Within experimental trials, a separate linear mixed effects model was used to identify the effect of neural shifts on behavioral shifts in interpretation ("reappraisal"). Beta estimates from these models are plotted. An uncorrected threshold of $p<.05$ was applied.

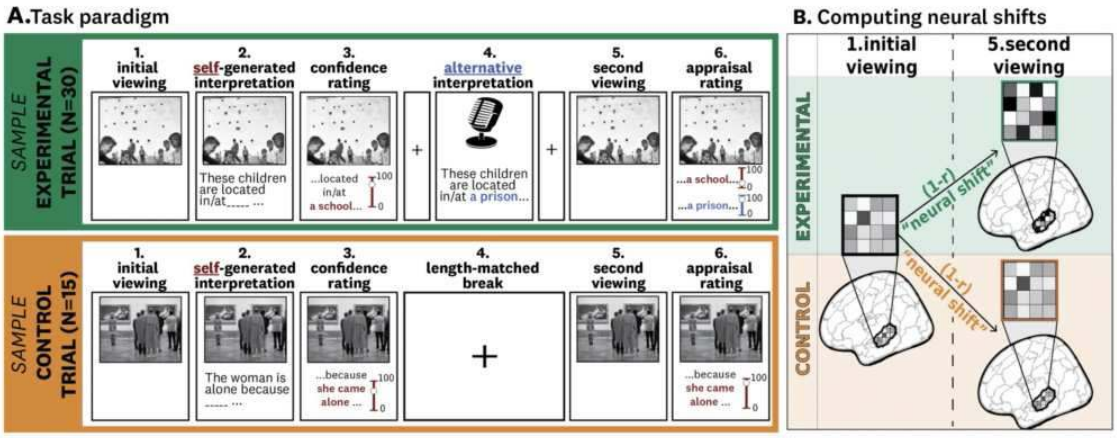

Figure 1.
A. *Task Paradigm.* Participants are presented with a different image on each trial. Differences between experimental and control trials are displayed. All interpretations are generated by filling in the blanks of a "MadLibs"-style passage with three blanks. Alternative interpretations follow the same format and are sourced from other participants. Data collection was conducted in an iterative design.
B. *Computing neural shifts.* Neural shifts were computed by getting the cosine distance between multivariate patterns when looking at the same stimulus across phases (within trial; phase 1 to phase 5). In control trials, this is a repetitive viewing. In experimental trials, this is after being exposed to an alternative interpretation.

Results: Compared to the control condition, the degree of neural shift between viewings of the same sensory input in the experimental condition increased on a cortical gradient, with the largest differences across nodes in the frontoparietal network (FPN) and the default mode network (DMN; Fig. 2a). This cortical gradient holds at the individual-subject level (Fig. 2a, right). This indicates that simply being presented with an alternative interpretation is enough to drive changes in multivariate activity to the same visual stimulus. Further, we see within a subset of regions, including regions in the DMN and FPN, neural shifts predict behaviorally reported reappraisal, suggesting that these regions are involved in the process of reframing the visual input to change how it is ultimately perceived.

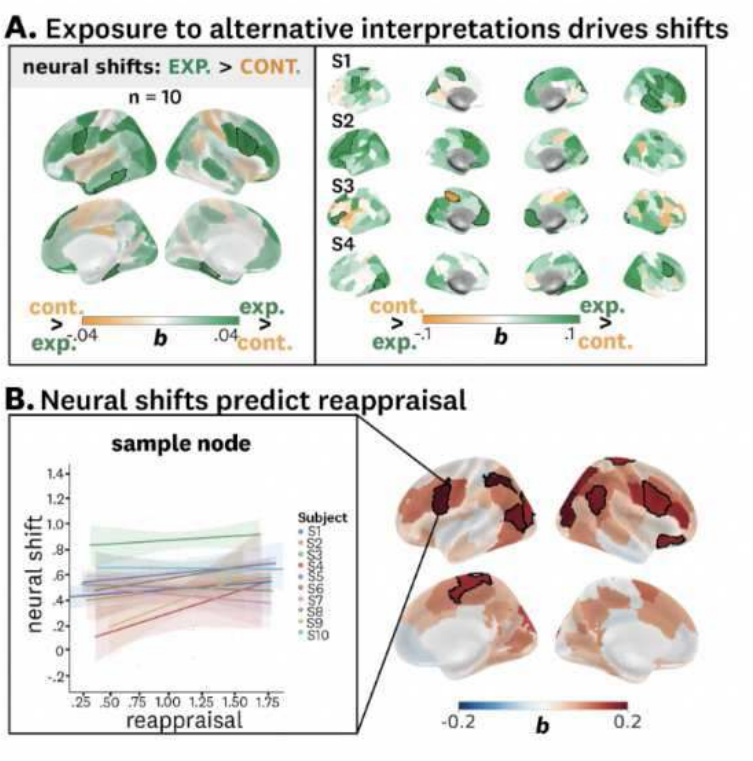

Figure 2:

A. *Exposure to an alternative interpretation.* (Left) Being exposed to an alternative interpretation evoked greater neural shifts across much of the brain (experimental > control trials; computed using the following linear mixed effects model: *neural shifts ~ condition (exp > contr.) + (1|subject) + (1|stimulus)*). Effect size increased along an anterior-to-posterior (sensory-to-association) gradient, with some of the largest shifts in prefrontal and anterior temporal areas. One model was fit per node. Beta estimates from each model are plotted on the corresponding node. (Right) This effect was visible at the single-subject level. The following linear models were run per subject: *neural shifts ~ condition*. Beta estimates from each model are plotted on the corresponding node. Contours reflect a threshold of p<.05.

B. *Neural shifts predict reappraisal.* Greater neural shifts predict the degree of reappraisal (i.e., self-reported behavioral shifts). This was computed with the following linear mixed effects model: *reappraisal ~ neural shift + (1|subject) + (1|stimulus)*. One model was run per node. Beta estimates from each model are plotted on the corresponding node. Inset: Sample node shows that while the magnitude differs at the individual subject level, the directionality generally holds. Reappraisal was calculated in the following manner: *reappraisal = confidence rating* (Fig. 1; phase 3) - *appraisal self* (phase 6) + *appraisal alternative* (phase 6).

Conclusions: Using a task with ambiguous social content, we identified that discernable multivariate pattern changes when processing the same sensory input can predict shifts in behavioral interpretation.

References

1. Wang, M., Arteaga, D. & He, B. J. Brain mechanisms for simple perception and bistable perception. Proceedings of the National Academy of Sciences 110, E3350–E3359 (2013).
2. Nguyen, M., Vanderwal, T. & Hasson, U. Shared understanding of narratives is correlated with shared neural responses. NeuroImage 184, 161–170 (2019).
3. Finn, E. S., Corlett, P. R., Chen, G., Bandettini, P. A. & Constable, R. T. Trait paranoia shapes inter-subject synchrony in brain activity during an ambiguous social narrative. Nat Commun 9, 2043 (2018).
4. Sava-Segal, C., Richards, C., Leung, M. & Finn, E. S. Individual differences in neural event segmentation of continuous experiences. Cerebral Cortex bhad106 (2023) doi:10.1093/cercor/bhad106.
5. Schaefer, A. et al. Local-Global Parcellation of the Human Cerebral Cortex from Intrinsic Functional Connectivity MRI. Cereb Cortex 28, 3095–3114 (2018).

Poster No 965

Improving Masticatory Behavior Enhances Brain Function: Two Randomized Controlled Studies

Ma. Therese Sta. Maria[1,2], Yoko Hasegawa[1], Shogo Yoshimura[1], Yukina Miyazaki[3], Tatsuya Suzuki[3], Kazuhiro Hori[1], Yumie Ono[4], Kensuke Yamamura[5], Takahiro Ono[6]

[1]Comprehensive Prosthodontics, Niigata University Graduate School of Medical and Dental Sciences, Niigata, Japan, [2]Department of Prosthodontics, College of Dentistry, Manila Central University, Caloocan, Philippines, [3]Electrical Engineering Program, Graduate School of Science and Technology, Meiji University, Kanagawa, Japan, [4]Department of Electronics and Bioinformatics, School of Science and Technology, Meiji University, Kanagawa, Japan, [5]Division of Oral Physiology, Niigata University Graduate School of Medical and Dental Sciences, Niigata, Japan, [6]Department of Geriatric Dentistry, School of Dentistry, Osaka Dental University, Osaka, Japan

Introduction: In recent years, researchers recommended the maintenance of masticatory function since it has been shown to prevent frailty and malnutrition, enhance brain activity, cognitive function, arousal, and alertness, preserving brain function. Studies also reported that using wearable chewing counter (bitescan, SHARP Co. Sakai, Japan) can alter daily chewing habits and improve masticatory behavior. Although chewing is known to improve cognitive function temporarily, the effect of daily increase in chewing on brain function is still unclear, and if it varies with the age of the subjects. Therefore, this study aimed to examine cortical activity and cognitive function changes by improving masticatory behavior using bitescan.

Methods: We enrolled 41 young adults aged 22-35 years old and 50 older adults over 65 years old, randomly allocated into intervention and control groups (Niigata University Ethics Review Committee Approval No: 2020-0478). Participants in intervention group were encouraged to increase the number of chewing strokes during each meal using bitescan for 30 days, while control group ate meals as usual without bitescan. The following were assessed at baseline and follow-up: masticatory behavior by measuring the number of chewing strokes during consumption of 100g rice balls while using bitescan, cognitive function using CogEvo app (Total Brain Care Inc., Kobe, Japan) to assess the level of orientation, attention, memory, planning, and spatial awareness; and performing Color Stroop and Two-back tasks to assess executive function, selective attention, and working memory. During the two cognitive tasks, cortical activity was evaluated by measuring the oxygenated hemoglobin (Oxy-Hb) concentration using functional Near-Infrared Spectroscopy (fNIRS) to identify which brain regions had significant hemodynamic changes. Two-way ANOVA and post hoc tests were used to evaluate whether improving masticatory behavior affected the cortical activity and cognitive function of the participants.

Results: Masticatory behavior significantly improved in intervention group of both ages with increased number of chewing strokes while consuming a 100g riceball at follow-up compared to the control group. This change was more significant in older adults, with higher number of chews ($p=0.017$) and longer chewing time ($p<0.001$). For cognitive function, intervention group of older adults significantly performed better than control group in memory tasks ($p=0.013$), while no significant differences were found in young adults. Intervention group of both ages also showed higher values at follow-up, but the effect of the intervention was not found. Hemodynamic changes in the Oxy-Hb concentration were seen at follow-up, with significantly decreased cortical activity observed in the premotor-motor ($p<0.001$), somatosensory ($p<0.001$), and dorsolateral prefrontal cortex (DLPFC) ($p<0.016$) of intervention group of older adults during the Color Stroop task even when intervention group of both ages had significantly higher scores and shorter reaction times, and in temporal association cortex of intervention group of both ages (young: $p=0.019$; old: $p=0.007$) and somatosensory cortex ($p=0.048$) of intervention group of older adults during the two-back task with significantly higher scores and shorter reaction times seen only in young adults. The results suggest that the use of bitescan successfully improved masticatory behavior, executive function, selective attention, and working memory, and enhanced the efficiency of DLPFC and temporal association cortex during Color Stroop and two-back tasks enabling the same tasks to be performed with less brain activity, indicating a neuroplastic change in the memory-related neural network.

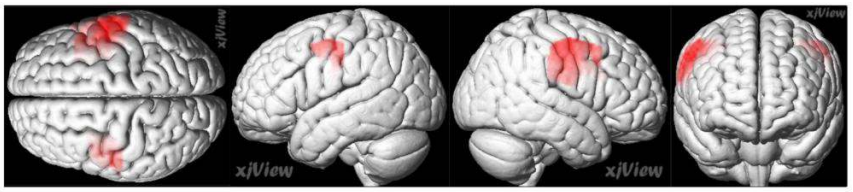

A. During Color Stroop Task

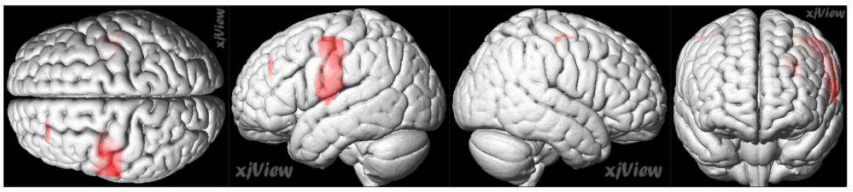

B. During Two-back Task

Conclusions: Our study suggests that the effect of intervention using bitescan promoted changes in masticatory behavior, and possibly enhanced brain function related to memory, which was especially pronounced in older adults.

References

1. Chang, F., H. Li, N. Li, S. Zhang, C. Liu, Q. Zhang and W. Cai (2022). "Functional near-infrared spectroscopy as a potential objective evaluation technique in neurocognitive disorders after traumatic brain injury." Frontiers in psychiatry 13: 903756.
2. Hori, K., F. Uehara, Y. Yamaga, S. Yoshimura, J. Okawa, M. Tanimura and T. Ono (2021). "Reliability of a novel wearable device to measure chewing frequency." J Prosthodont Res 65(3): 340-345.
3. Hori, S., K. Hori, S. Yoshimura, F. Uehara, N. Sato, Y. Hasegawa, K. Akazawa and T. Ono (2022). "Masticatory Behavior Change with a Wearable Chewing Counter: A Randomized Controlled Trial." J Dent Res: e-pub ahead of print.
4. Ichii, S., T. Nakamura, T. Kawarabayashi, M. Takatama, T. Ohgami, K. Ihara and M. Shoji (2020). "CogEvo, a cognitive function balancer, is a sensitive and easy psychiatric test battery for age-related cognitive decline." Geriatrics & Gerontology International 20(3): 248-255.
5. Lin, C.-S., S.-Y. Wu, C.-Y. Wu and H.-W. Ko (2016). "Gray matter volume and resting-state functional connectivity of the motor cortex-cerebellum network reflect the individual variation in masticatory performance in healthy elderly people." Frontiers in Aging Neuroscience 7: 247.
6. Sta. Maria, M. T., Y. Hasegawa, A. M. M. Khaing, S. Salazar and T. Ono (2023). "The relationships between mastication and cognitive function: A systematic review and meta-analysis." Japanese Dental Science Review 59: 375-388.
7. Uehara, F., K. Hori, Y. Hasegawa, S. Yoshimura, S. Hori, M. Kitamura, K. Akazawa and T. Ono (2022). "Impact of Masticatory Behaviors Measured With Wearable Device on Metabolic Syndrome: Cross-sectional Study." JMIR Mhealth Uhealth 10(3): e30789.
8. Yoshimura, S., K. Hori, F. Uehara, S. Hori, Y. Yamaga, Y. Hasegawa, K. Akazawa and T. Ono (2022). "Relationship between body mass index and masticatory factors evaluated with a wearable device." Sci Rep 12(1): 4117.

Poster No 966

The Role of the Hippocampus in Forecasting Future Rewards during Goal-Directed Behavior

Jiwoong Park[1,2,3], Won Mok Shim[1,2,3]

[1]Center for Neuroscience Imaging Research, Institute of Basic Science (IBS), Suwon, Korea, Republic of, [2]Department of Biomedical Engineering, Sungkyunkwan University (SKKU), Suwon, Korea, Republic of, [3]Department of Intelligent Precision Healthcare Convergence, Sungkyunkwan University (SKKU), Suwon, Korea, Republic of

Introduction: The hippocampus has been reported to exhibit sequential neural activities that correspond to locations before they are actually visited during episodic experiences, involving the anticipation of future events yet to occur (Dragoi and Tonegawa, 2011). This anticipatory process potentially facilitates the simulation of upcoming scenarios. Among the numerous potential future events, predicting a future reward is particularly crucial for learning and adaptive behaviors. A recent animal study demonstrated that alterations in reward structure induce remapping within the hippocampus (Krishnan et al., 2022), indicating the involvement of the hippocampus in reward processing. In this study, we hypothesized that the predictive response of the hippocampus would be engaged in anticipating future rewards during episodic experiences. Specifically, we aimed to investigate the role of the hippocampus in forecasting future events, especially those associated with acquiring rewards during goal-directed behavior in naturalistic settings.

Methods: As part of the 7T Naturalistic Perception, Action & Cognition (NatPAC) dataset, we introduced a novel Shepherding task that immerses participants in a 3D minecraft world where they engage with various biological entities in real-time by strategically planning and executing hierarchical actions tailored to a complex environment. The task requires herding sheep to a specified goal location while navigating challenges, such as avoiding puddles and evading a randomly spawning fox. To

enhance the realism of the shepherding dynamics, we incorporated the behavioral dynamics based on an ethological study of flock behavior (Strömbom et al., 2014). We collected both functional neuroimaging data and diverse behavioral gameplay data as participants actively engaged in this Minecraft-based interactive 3D video game (Fig. 1A). To examine the hippocampal response to potential rewards, we identified three distinct event types during gameplay: "No loss" and "Loss" events, depending on whether the sheep fell into puddles or not, and "Near loss" event if the sheep almost fell but ultimately avoided puddles (Fig. 1B). This approach allowed for a comparison of selective responses to predictable reward loss.

Results: Our results revealed an increased hippocampal response preceding reward loss compared to events where no loss occurred. Moreover, this heightened hippocampal response before reward loss was also observed in the near loss events, suggesting the potential predictive nature of these responses for losses, when participants anticipated loss based on the risk evaluated before the actual outcome (Fig. 1C, Top). In contrast, we observed that the nucleus accumbens (NAcc), a central hub of the reward system, selectively responded to actual reward loss but not to anticipated but unrealized reward loss (Fig. 1C, Bottom), indicating a dissociation between the hippocampus and NAcc in predictive reward processing.

Conclusions: Our results suggest that the hippocampus is involved in predictive responses associated with potential reward loss, highlighting its intricate role in anticipating future rewards during episodic experiences. In contrast to the hippocampus, the nucleus accumbens exclusively responds to actual reward loss, suggesting the distinct role of the hippocampus in predicting and encoding potential reward loss in naturalistic settings.

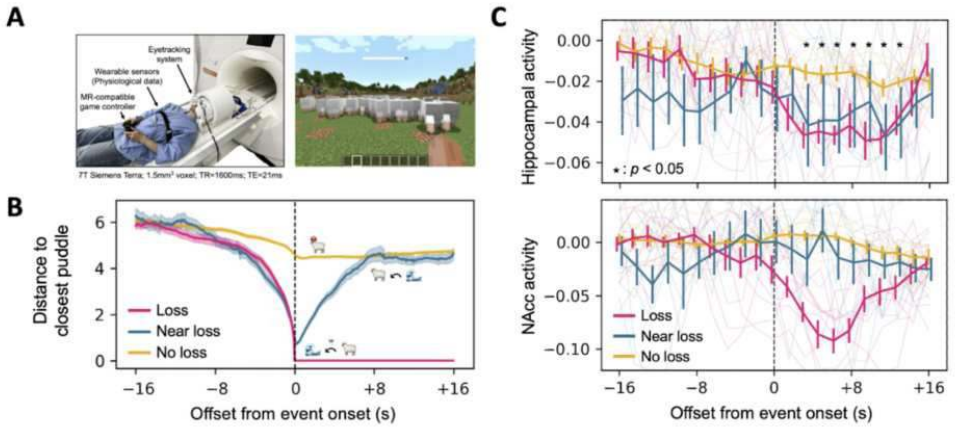

Figure 1. (A) Experimental paradigm: Participants played a custom-built Minecraft-based 3D interactive video game inside an MRI scanner. (B) Behavioral results: Data from three distinct type of reward-related events (i.e. Loss, Near loss, and No loss). (C) Neural responses of the hippocampus and the NAcc. The hippocampus demonstrated increased responses prior to potential reward loss, whereas the NAcc showed a response exclusively to actual reward loss. (B-C) Error bars represent ±1 standard error of mean across participants.

References

1. Dragoi, G. & Tonegawa, S. (2011) Preplay of future place cell sequences by hippocampal cellular assemblies. Nature 46 9, 397–40.
2. Krishnan, S., Heer, C., Cherian, C. et al. (2022) Reward expectation extinction restructures and degrades CA1 spatial maps through loss of a dopaminergic reward proximity signal. Nat Commun 13, 6662
3. Strömbom, D. et al. (2014) Solving the shepherding problem: heuristics for herding autonomous, interacting agents. J R oy Soc Interface 11, 20140719.

Poster No 967

Neural correlates of internal context transitions in continuous thoughts during free speaking

Kwon Heo[1], Dasom Kwon[1], Won Mok Shim[1]

[1]CNIR/SKKU, Suwon-si, Gyeonggi-do

Introduction: Continuous experiences of external input can be organized into discrete events, and the boundaries of these events elicit neural responses in the hippocampus[1]. Similar neural responses are also triggered during transitions in mental context when recalling movie narratives, indicating that neural dynamics may capture shifts in both external and internal situational contexts[4]. Analogous to context transitions in movie recall, changing topics during spontaneous thoughts coincides with shifts in mental states[7]. However, the neural mechanism underlying such shifts in internally generated context without

external input remains elusive. In this study, we examined the neural dynamics of topic transitions during free speaking by quantifying the degree of context changes in one's speech based on a language model.

Methods: During fMRI scan, independent groups of participants engaged in three speaking tasks: 1) freely expressing spontaneous thoughts (think-aloud, N = 63), 2) alternately discussing two pre-given topics at their own pace (topic-alternating, N = 53), and 3) recalling movies that they had watched (movie-recall, N = 24). Following the scan, participants received a transcript of their speech and retrospectively identified topic boundaries in think-aloud and topic-alternating tasks. For the movie-recall task, topic boundaries were labeled by the author, corresponding to movie event segmentation reported by independent annotators. To assess the degree of context transition of speech, we calculated next sentence prediction (NSP) scores using a pre-trained language model[2], indicating the likelihood of each spoken sentence given the preceding context. Additionally, we measured pause length (PL), the silent interval between spoken sentences to examine the impact of sensory and motor changes in speaking behaviors associated with topic transitions.

Results: We computed the linear regression coefficient (β) between the predicted single-event hemodynamic response at the end of each sentence and BOLD signals in 1000 brain parcels[6]. As the NSP scores and pause length were correlated in all speech tasks (think-aloud: $\rho = -0.22$, $p < 0.01$; topic-alternating: $\rho = -0.31$, $p < 0.01$; movie-recall: $\rho = -0.15$, $p < 0.01$), partial rank correlations were used to disentangle their individual effects. Specifically, we examined the relationship between β coefficients and NSP scores when controlling for pause length ($\rho\beta \cdot NSP \mid PL$) and vice versa ($\rho\beta \cdot PL \mid NSP$). In the control network, significant negative correlations were observed between the coefficients and NSP scores when controlling for pause length, indicating increased responses when the context changed. Conversely, in the same network, positive correlations between the coefficients and pause length were observed (see Fig 1). To examine the impact of context transitions estimated by the language model compared to topic transitions perceived by humans, we computed coefficients after topic boundaries indicated by human annotators in each speaking task. Consistent with the NSP results, the control network exhibited increased responses at the annotated topic boundaries compared to the midst of topics across all tasks. In contrast, the hippocampus showed increased responses at topic boundaries only during movie-recall.

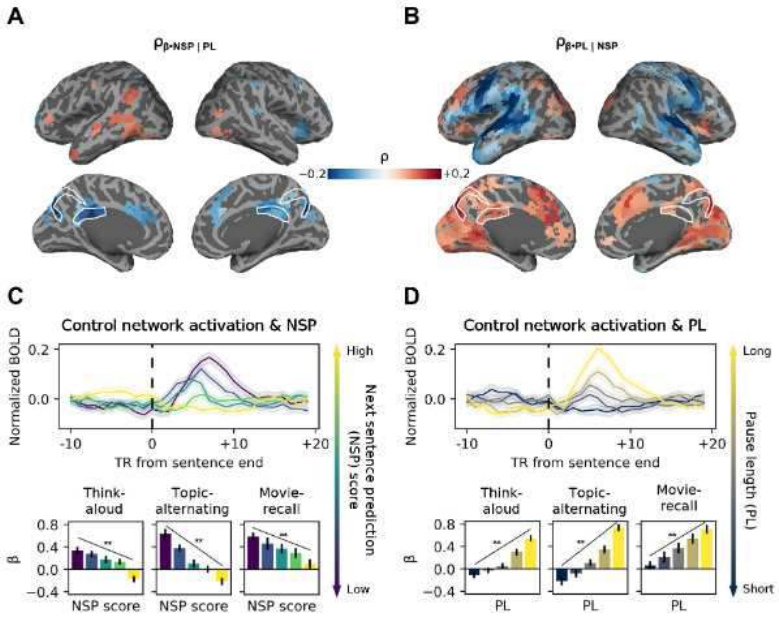

Figure 1. A) $\rho_{\beta \cdot NSP \mid PL}$, B) $\rho_{\beta \cdot PL \mid NSP}$. Parcels with significant ($p < 0.05$, FDR corrected) partial correlations during the topic-alternating task are highlighted, with the white line indicating the control network (ContC in Yeo's 17 networks [8]). C) (Upper) The NSP scores were divided into five equal-size bins based on participants' speech transcriptions. Lower NSP scores (purple to yellow) correspond to increased activity in the control network. (Lower) Significant linear correlations between the NSP scores and β were observed across all speaking tasks (** $p < 0.01$, FDR corrected). D) The same analysis was applied to PL, showing positive linear correlations in the control network across all speaking tasks (** $p < 0.01$, FDR corrected).

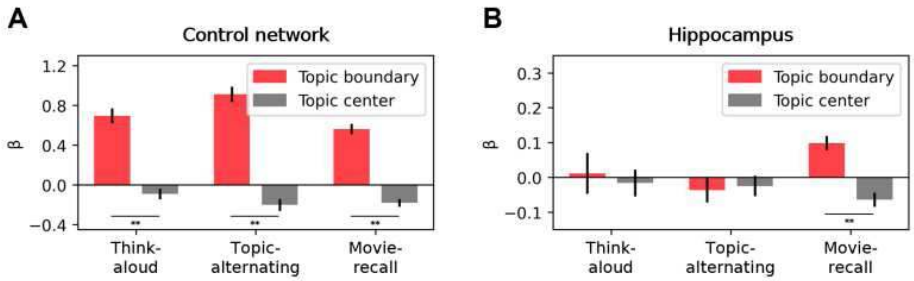

Figure 2. A) The control network exhibited stronger activation (β) at topic boundaries in all speaking tasks (** $p < 0.01$, FDR corrected). B) Hippocampal responses increased exclusively at topic boundaries in the movie-recall task.

Conclusions: In summary, our findings highlight the unique functional roles of the control network and the hippocampus in organizing internally generated thoughts. The results suggest that the control network contributes to cognitive processing associated with topic transitions during spontaneous thoughts, possibly by regulating introspective processes[3]. Conversely, the hippocampus is more involved in narrative retrieval, regardless of whether observing existing narratives or generating them internally. The distinct roles of these two brain regions may collectively involve a process of discretizing continuous experiences into meaningful chunks[5].

References

1. Brunec, I. K. (2018). Boundaries shape cognitive representations of spaces and events. Trends in cognitive sciences, 22(7), 637-650.
2. Devlin, J. (2018). Bert: Pre-training of deep bidirectional transformers for language understanding. arXiv preprint arXiv:1810.04805.
3. Dixon, M. L. (2018). Heterogeneity within the frontoparietal control network and its relationship to the default and dorsal attention networks. Proceedings of the National Academy of Sciences, 115(7), E1598-E1607.
4. Lee, H. (2022). A generalized cortical activity pattern at internally generated mental context boundaries during unguided narrative recall. Elife, 11, e73693.
5. Radvansky, G. A. (2017). Event boundaries in memory and cognition. Current opinion in behavioral sciences, 17, 133-140.
6. Schaefer, A. (2018). Local-global parcellation of the human cerebral cortex from intrinsic functional connectivity MRI. Cerebral cortex, 28(9), 3095-3114.
7. Sripada, C. (2020). Structure in the stream of consciousness: Evidence from a verbalized thought protocol and automated text analytic methods. Consciousness and Cognition, 85, 103007.
8. Yeo, B. T. (2011). The organization of the human cerebral cortex estimated by intrinsic functional connectivity. Journal of neurophysiology.

Poster No 968

Electrophysiological correlates of impending multitasking performance

Jee Eun Park[1,2,3,4,5], Wan-Yu Hsu[4,5], Kevin Jones[4,5], Elizabeth Johnson[6], Adam Gazzaley[4,5], Theodore Zanto[4,5]

[1]Department of Psychiatry, Seoul National University College of Medicine, Seoul, Korea, Republic of, [2]Department of Psychiatry, Seoul National University Hospital, Seoul, Korea, Republic of, [3]Medical Research Center, Institute of Human Behavioral Medicine, Seoul, Korea, Republic of, [4]Department of Neurology, University of California, San Francisco, San Francisco, CA, USA, [5]Neuroscape, University of California, San Francisco, San Francisco, CA, USA, [6]Departments of Medical Social Sciences, Pediatrics, and Psychology, Northwestern University, Evanston, IL, USA

Introduction: This study investigated brain activity related to the preparatory state for multitasking. We aimed to uncover electroencephalography (EEG) predictors of impending multitasking performance as indexed by response times. EEG data were analyzed while participants engaged in visuomotor tracking, in anticipation of (prior to) multitasking (visuomotor tracking + target discrimination). Data was also analyzed to assess the effects of longitudinal theta-band (6 Hz) transcranial alternating current stimulation (tACS) on the potential for these EEG measures to predict performance.

Methods: EEGs from 133 healthy adults (young, n=80; old, n=53) were obtained from three studies conducted by the same research group (Anguera et al., 2013; Hsu et al., 2017; Hsu et. al., 2019; Zanto et. al., 2021; Jones et al., 2022). Among them, 98 people participated in clinical trials to examine the effects of theta tACS on cognitive performance. All participants performed a game-based multitasking paradigm, Neuroracer, which consisted of repeated multitasking (visuomotor tracking + target discrimination) with adaptive difficulty. Only the participants who performed the tasks at least 20 trials were included in this study (mean = 47.94). The mean-centered response time (mcRT) of each performance per individual was calculated as the time difference from the individual's mean response time. Theta and beta oscillations were mainly examined as possible correlates

of the preparatory state for multitasking performance based on the results of these previous studies. For the first analysis, the response time (mcRT), age (young vs. old), and their interaction were included as fixed factors in a linear mixed model to predict one's theta and beta band power. For the second analysis, we added two more factors into the models, stimulation (tACS vs. control) and time (pre- vs. post-tACS), as well as their interactions. Post-hoc analyses focused on the mean difference in band power according to the binary response group: each response was categorized as fast or slow compared to the individual median response time.

Results: Theta power showed a significant association with response times (frontal theta, $F=20.642$, $p<0.001$; posterior theta, $F=19.750$, $p<0.001$). Furthermore, this relationship was affected by age group (mcRT x age interaction on frontal theta, $F=6.071$, $p=0.014$; posterior theta, $F=6.744$, $p=0.009$). Post-hoc analyses demonstrated that theta power and response time were more strongly associated in younger adults. When the effect of tACS application was included in the analysis, tACS had an influence on beta power during the preparatory state in accordance with individual response time (stimulation x time x mcRT interaction on frontal beta, $F=3.898$, $p=0.048$; posterior beta, $F=4.469$, $p=0.035$). This association was also affected by age (stimulation x time x mcRT interaction on frontal beta, $F=3.950$, $p=0.047$; posterior beta, $F=5.395$, $p=0.020$): in older adults, the effect of tACS on beta power was more associated with faster responses.

Conclusions: We investigated the association of EEG spectral power with individual multitasking performance. Theta power was related to a highly attentive state in multitasking performance, especially in younger adults. After applying tACS, increased beta power was associated with improved response times, which was most prominent in older adults. Together, these results identify EEG measures associated with the preparatory state of multitasking. Moreover, results showed that tACS can affect the preparatory state of multitasking, which may occur in frequencies outside the applied stimulation frequency.

References

1. Anguera JA, et al. (2013), 'Video game training enhances cognitive control in older adults', Nature, 5;501(7465):97-101
2. Hsu WY, et al. (2017), 'Enhancement of multitasking performance and neural oscillations by transcranial alternating current stimulation', PLoS One, 31;12(5):e0178579.
3. Hsu WY, et al. (2019) 'Parametric effects of transcranial alternating current stimulation on multitasking performance', Brain Stimulation,12(1):73-83.
4. Jones KT, et al. (2022) 'Structural and functional network mechanisms of rescuing cognitive control in aging', Neuroimage, 15;262:119547

Poster No 969

The distinct roles of bilateral inferior frontal gyrus during creative idea generation

Qunlin Chen[1], Ke Ding[2], Yoed N. Kenett[2], Jiang Qiu[1]

[1]Southwest University, Chongqing, China, [2]Israel Institute of Technology, Haifa, Israel

Introduction: Existing research and reviews on the neurocognitive mechanisms underlying creative thinking consistently point to the involvement of the inferior frontal gyrus (IFG) in various creative tasks. Neuroimaging studies have consistently shown recruitment of bilateral IFG during creative idea generation (Abraham et al., 2012; Becker et al., 2020; Benedek et al., 2014). This involvement is associated with the controlled memory retrieva, potentially boosting the retrieval of relatively weak semantic associations (Becker et al., 2020; Ralph et al., 2017). Converging evidence for the left IFG suggests its implication in a releasing effect during creative production. Patients with damage to the left IFG, for example, exhibit higher scores on divergent thinking tasks and intensified artistic creativity (Ovando-Tellez et al., 2019). A recent tDCS meta-analysis demonstrated a significant positive effect linked to excitatory stimulation of the right IFG through anodal tDCS, while an inhibitory effect was observed over the left IFG. According to the hemispheric balance hypothesis, inhibiting the left IFG leads to a preponderance of the right, facilitating the production of novel ideas. Despite growing evidence suggesting that bilateral IFG contributes to the originality of creative ideas during both the generation and evaluation phases, it remains unclear whether there is a differential functional role of the right and left IFG and how they are involved in creative idea generation.

Methods: In this study, we initially conducted two independent task-fMRI procedures involving single-response (Exp. 1, 28 subjects) and multi-response (Exp. 2, 32 subjects) alternative using tasks (AUT), respectively. In the AUT, subjects were asked to come up with one (Exp. 1) or four (Exp. 2) novel and unique uses for each concrete objects; for the control conditions, subjects were asked to think of one or our common and appropriate using for each concrete objects. Through these two experiments, we compared brain activation patterns and differences between the right and left IFG during novel idea generation. In the Exp. 3 (38 subjects), we utilized high-definition transcranial direct current (tDCS) stimulation to modulate the activity of both the right and left IFG, and further examined the changing pattern of idea generation measured by the serial order effect in the multi-response alternative task.

Results: Exp. 1 and Exp. 2 showed significantly greater activation in the left IFG compared to the right IFG in novel using condition, however, activation in the right IFG was more associated with high-quality originality ideas, whereas the left IFG was more associated with common-quality ideas. Exp. 3 showed that anodal tDCS over the right IFG increased response time (RT) for outputting novel ideas, whereas anodal tDCS in the left IFG decreased RT for outputting novel ideas.

Conclusions: These findings indicate that the left IFG contributes to the creative process through flexible semantic processing, leading to the generation of more novel ideas in the early stage. Conversely, the right IFG is involved in generating original ideas by inhibiting prepotent semantic associations, resulting in the production of unique ideas in the later stage. In summary, the right and left IFG contribute to the generation of creative ideas through slow and fast semantic retrieval processing, respectively.

References

1. Abraham, A., Pieritz, K., Thybusch, K., Rutter, B., Kröger, S., Schweckendiek, J., . . . Hermann, C. (2012). Creativity and the brain: uncovering the neural signature of conceptual expansion. Neuropsychologia, 50(8), 1906-1917.
2. Becker, M., Sommer, T., & Kühn, S. (2020). Inferior frontal gyrus involvement during search and solution in verbal creative problem solving: A parametric fMRI study. NeuroImage, 206, 116294.
3. Benedek, M., Jauk, E., Fink, A., Koschutnig, K., Reishofer, G., Ebner, F., & Neubauer, A. C. (2014). To create or to recall? Neural mechanisms underlying the generation of creative new ideas. NeuroImage, 88, 125-133.
4. Ovando-Tellez, M. P., Bieth, T., Bernard, M., & Volle, E. (2019). The contribution of the lesion approach to the neuroscience of creative cognition. Current Opinion in Behavioral Sciences, 27, 100-108.
5. Ralph, M. A. L., Jefferies, E., Patterson, K., & Rogers, T. T. (2017). The neural and computational bases of semantic cognition. Nature reviews neuroscience, 18(1), 42-55.

Poster No 970

Cognitive map-like representations of semantic structure during movie watching

Siyang Li[1,2], Weiyang Shi[3,1], Yongfu Hao[1], Xia Liang[2], Zhang Yu[1], Tianzi Jiang[3,1]

[1]Zhejiang Lab, Hangzhou, Zhejiang, China, [2]Harbin Institute of Technology, Harbin, Heilongjiang, China, [3]Brainnetome Center, Institute of Automation, Chinese Academy of Sciences, Beijing, China

Introduction: Neuroscience aims to unravel the link between cognition and neural activity, with a growing focus on how the brain represents naturalistic stimuli like movie-watching (Kringelbach, Perl et al. 2023). Studies shown that the brain segments continuous stimuli into discrete events and forms narrative graphs, impacting memory performance in behaviors (Lee and Chen 2022). However, the precise characterization and neural representations of such naturalistic information in the human brain remains unclear. This study investigates cognitive map-like brain representations during movie watching, based on the theory that the brain encodes and organizes experiences in a relational map (Tolman 1948, Behrens, Muller et al. 2018). In this study, we explored the cognitive map-like representations in the brain during movie watching and their convergence with the underlying semantic structure of movie lines.

Methods: We used the 7T movie-watching fMRI data acquired from the Human Connectome Project (HCP) dataset (Elam, Glasser et al. 2021). Building upon our prior research (Li et al., under revision), we identified brain states within cognitive-map networks (Figure 1). Initially, we computed the similarity matrix (W) for brain-state occurrences, followed by t-SNE for dimensional reduction and k-means for clustering analysis. Subsequently, we embedded all clusters of brain-state occurrences into a two-dimensional (2D) space. Next, we constructed a predictive map (M) of brain-state occurrences, employing the successor representation (SR) technique. Finally, we estimated the predictivity score based on the backward skewness of SR fields (i.e., columns of M). To validate the cognitive-map-like representation of naturalistic stimuli, we extracted the semantic features from each movie segment by applying the wave2vec model to movie lines. We then calculated the semantic similarity matrix (S) between segments. Subsequently, we assessed the association of these semantic similarities with the predictive map.

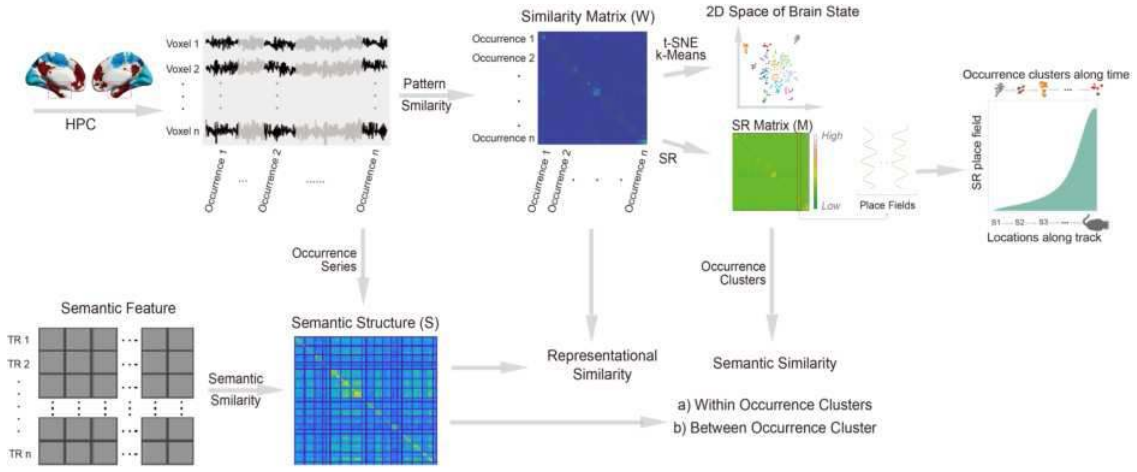

Figure 1. Analytical flowchart of the study.
Building upon our prior research (Li et al., under revision), we identified brain states within cognitive-map networks (Figure 1). Initially, we computed the similarity matrix (W) for brain-state occurrences, followed by t-SNE for dimensional reduction and k-means for clustering analysis. Subsequently, we embedded all clusters of brain-state occurrences into a two-dimensional (2D) space. Next, we constructed a predictive map (M) of brain-state occurrences, employing the successor representation (SR) technique. Finally, we estimated the predictivity score based on the backward skewness of SR fields (i.e., columns of M). To validate the cognitive-map-like representation of naturalistic stimuli, we extracted the semantic features from each movie segment by applying the wave2vec model to movie lines. We then calculated the semantic similarity matrix (S) between segments. Subsequently, we assessed the association of these semantic similarities with the predictive map.

Results: We identified two alternating brain states using movie-watching fMRI data (Figure 2). Among which, State1 predominantly involved DMN and hippocampus, while State2 exhibited strong activation in sensorimotor regions and hippocampus. Upon estimating the representation similarity between brain-state occurrences and semantic features, we observed significantly lower representational similarity in State1. Notably, during movie watching, this representational similarity exhibited an increase trend in State1, probably updating internal representations with information gained from the movie segment, but still lower than State2. When embedding the brain-state occurrences into a 2D state space, we found higher semantic similarity (shorter distance) within occurrence clusters than between clusters for both states, but with higher within-cluster similarity in State1. Subsequent SR modeling of State1 revealed typical 'place fields' of occurrence clusters, suggesting a cognitive-map-like representation. Notably, the predictivity score of SR fields (backward skewness of SR) was strongly covaried with individual vocabulary skills and verbal comprehension, evaluated by the Picture Vocabulary Test.

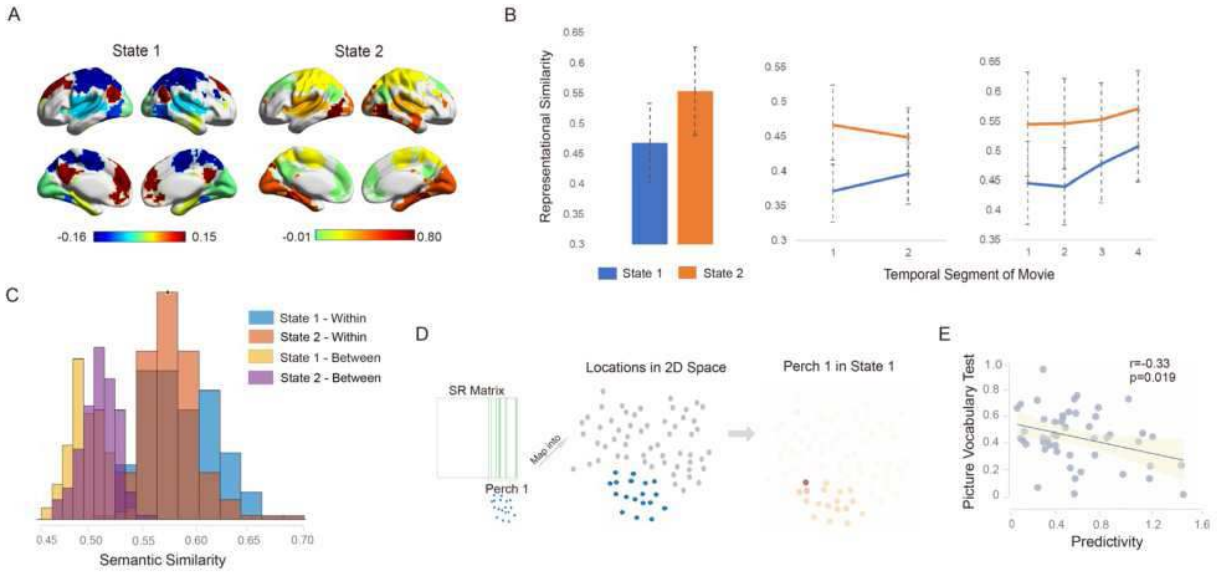

Figure 2. Cognitive map-like representations of semantic structure.
(A) Two alternating brain states cognitive-map networks identified using fMRI data during movie watching. State 1 (left) was dominated by DMN and hippocampus and State 2 (right) was dominated by sensorimotor regions and hippocampus. **(B)** Analyses in representation similarity between similarity matrix (W) and semantic similarity matrix (S). (left) Representation similarity was significantly smaller in State 1 than in State 2. (middle and right) Representation similarity exhibited significant increase only in State 1, when dividing the state series into 2 (middle) and 4 (right) segments. **(C)** Semantic similarity within occurrence clusters (blue and orange) was significantly stronger than that between clusters (yellow and purple), especially in State 1 (blue and yellow). **(D)** Visualization of the place field of an example perch in one subject. **(E)** Predictivity in State 1 was significantly correlated with individual performance in Picture Vocabulary Test. Significance was considered at $P < 0.05$.

Conclusions: Our study has identified two alternating brain states associated with internal and external focus during movie watching. State2 predominantly responds to sensory processing of external stimuli, while State1 integrates abstract relational representations of the movie segment into internal knowledge maps. This supports the cognitive map theory, wherein 'modules' within the semantic structure are represented as brain-state occurrence clusters, exhibiting characteristic 'place field' patterns. Notably, the predictivity score of SR fields was strongly associated with participants' verbal comprehension in

the Picture Vocabulary Test, suggesting an underlying semantic representation mechanism of natural stimuli during internal cognitive processing.

References
1. Behrens, T. E. J., T. H. Muller, J. C. R. Whittington, S. Mark, A. B. Baram, K. L. Stachenfeld and Z. Kurth-Nelson (2018). "What Is a Cognitive Map? Organizing Knowledge for Flexible Behavior." Neuron 100(2): 490-509.
2. Elam, J. S., M. F. Glasser, M. P. Harms, S. N. Sotiropoulos, J. L. R. Andersson, G. C. Burgess, S. W. Curtiss, R. Oostenveld, L. J. Larson-Prior, J. M. Schoffelen, M. R. Hodge, E. A. Cler, D. M. Marcus, D. M. Barch, E. Yacoub, S. M. Smith, K. Ugurbil and D. C. Van Essen (2021). "The Human Connectome Project: A retrospective." Neuroimage 244: 118543.
3. Kringelbach, M. L., Y. S. Perl, E. Tagliazucchi and G. Deco (2023). "Toward naturalistic neuroscience: Mechanisms underlying the flattening of brain hierarchy in movie-watching compared to rest and task." Sci Adv 9(2): eade6049.
4. Lee, H. and J. Chen (2022). "Predicting memory from the network structure of naturalistic events." Nat Commun 13(1): 4235.
5. Li S, et al. "Predictable navigation through spontaneous brain states with cognitive-map-like representations." Under revision.
6. Tolman, E. C. (1948). "Cognitive maps in rats and men." Psychol Rev 55(4): 189-208.

Poster No 971

Intelligence brain networks of early adolescent: Waxing and waning

Jiadong Yan[1], Yasser Iturria Medina[1], Gleb Bezgin[2], Alan Evans[3], Sherif Karama[4]

[1]McGill University, Montreal, Quebec, [2]Neuroinformatics for Personalized Medicine lab, Montreal Neurological Institute, McGill University, Montreal, Quebec, [3]McGill Centre for Integrative Neuroscience (MCIN), Montreal, Quebec, [4]Douglas Institute, McGill University, Montreal, Canada, Montreal, Quebec

Introduction: Mounting evidence has established a relationship between intelligence and whole-brain morphometric measures. Studies have indicated that individuals with thicker cortexes in specific brain regions tend to exhibit better performance in certain cognitive tasks. Additionally, subcortical volumes of specific structures have been associated with particular cognitive ability differences. During early adolescence, the brain undergoes significant changes, including variations in cortical thickness and subcortical volume. However, in this developmental stage, the direct relationship between the co-varying patterns of brain geospatial indicators and intelligence remains incompletely understood. To gain deeper insights into this complex association, it becomes essential to identify intelligence brain networks. These intelligence brain networks will provide a valuable understanding of intelligence development and its connection with brain topography. We employ a stable and interpretable machine learning model to fit a large dataset, thereby elucidating the relationship between intelligence development and the co-varying brain networks.

Methods: Data Preprocessing: The data we utilized is from the Adolescent Brain Cognitive Development (ABCD) dataset. We selected 7910 subjects of 9-14 years old which have both T1 data and cognitive data. According to age, we divided these samples into three groups (9-10, 11-12, and 13-14 years old). Cortical and subcortical surface morphometric measures were calculated with FreeSurfer 7.1.1. Cortical thickness was measured across 148 grey matter brain regions based on the Destrieux anatomical atlas. And subcortical volume measurements were made across 20 subcortical regions based on the ASEG atlas. Intelligence definition: We used all the available cognitive measurements in the ABCD dataset, such as vocabulary, attention, reading, and short delay recall. Then we performed a PCA on those measurements to obtain the first principal component (Fig. 1). This component is known to be a fair estimate of general intelligence. Interpretable Linear Regression Model: Our linear regression model has three improvements compared to the basic linear regression model (Fig. 1). First, it removes feature collinearity. Second, it adopts L1 regularization to select important features. Third, it utilizes gradient descent instead of least squares to get better predictions based on big data. We used this model to study the relationship between age and brain topography as well as between intelligence and brain geography.

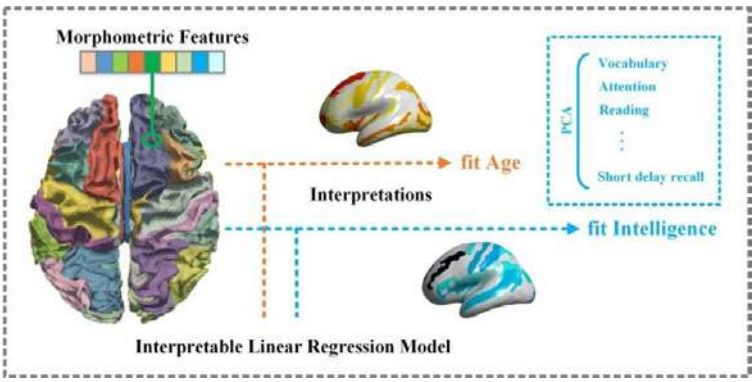

Results: Based on the Interpretable Linear Regression Model, we used brain topography data to predict age and intelligence. Both models work well (r>0.3, and pass permutation tests). Moreover, in order to identify important brain regions, we visualized the weights of the linear regression models (Fig. 2). We found that co-varying brain networks corresponding to age are similar to those corresponding to intelligence. And those co-varying brain networks are similar among different age periods.

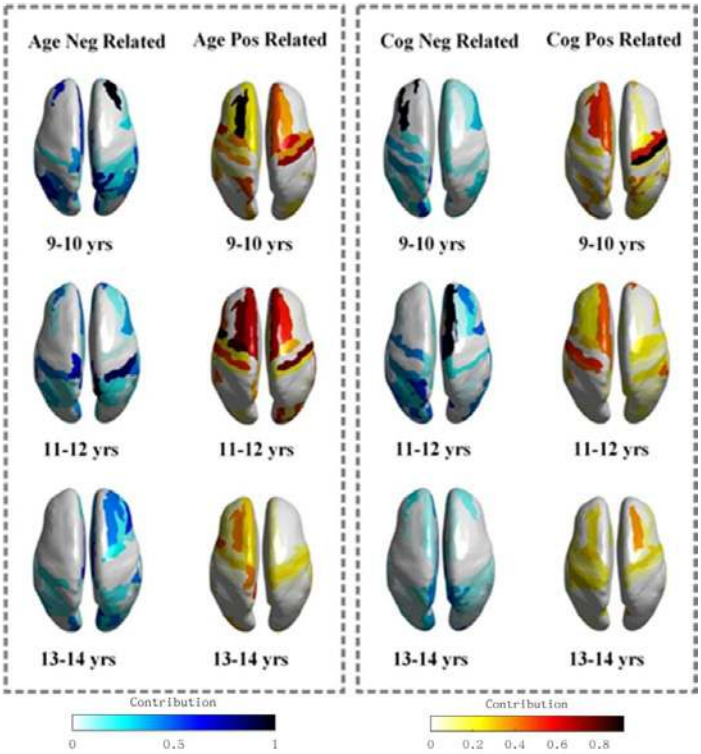

Conclusions: 1. There exists a significant linear relationship between age and brain topographical features, as well as between intelligence and brain geographical features. 2. Brain topographical networks associated with age closely resemble those linked to intelligence. Furthermore, their patterns exhibit considerable similarity across different age groups.

References

1. Sripada, C. et al. (2020), 'Prediction of neurocognition in youth from resting state fMRI', Molecular Psychiatry, vol. 25, no. 12, pp. 3413-3421.
2. Yan, J. et al. (2022), 'Modeling spatio-temporal patterns of holistic functional brain networks via multi-head guided attention graph neural networks (Multi-Head GAGNNs)', Medical Image Analysis, vol. 80, pp. 102518.
3. Tian, Y. et al. (2021), 'Machine learning prediction of cognition from functional connectivity: Are feature weights reliable?', NeuroImage, vol. 245, pp. 118648.

Poster No 972

Compositional representation of tasks in human multiple-demand cortex

Jinkang (Derrick) Xiang[1], Moataz Assem[2], Geoffrey Ngo[1], John Duncan[2], Marieke Mur[1,3,4]

[1]Western Institute of Neuroscience, University of Western Ontario, Canada, [2]MRC Cognition and Brain Sciences Unit, University of Cambridge, UK, [3]Department of Psychology, University of Western Ontario, Canada, [4]Department of Computer Science, University of Western Ontario, Canada

Introduction: The execution of complex cognitive tasks activates an extensive network of frontal and parietal regions, known as the multiple-demand (MD) system, whose distributed activity patterns carry information about the task (Cole et al., 2011; Duncan, 2010; Woolgar et al., 2011). However, the functional organization of task representation remains unclear. Do certain tasks elicit more similar activity patterns than others? If so, what drives the functional organization? Computational work suggests that tasks may be represented in a compositional fashion in prefrontal cortex, where the representation of a task can be expressed as the algebraic sum of vectors representing the underlying sensory, cognitive and motor processes (Yang et al., 2019). Empirical evidence for compositional coding is limited (Cole et al., 2011; Reverberi et al., 2012). It remains to be tested if this principle generalizes to tasks that require context-dependent decisions.

Methods: We approach these questions by conceptualizing tasks as combinations of features (Cole et al., 2011; Mante et al., 2013; Rigotti et al., 2013). The feature dimensions define a task space, and points in this task space correspond to multivariate activity patterns elicited by tasks composed of different combinations of features. We designed a delayed-match-to-sample experiment where the task space was spanned by two feature dimensions: attended sensory modality and match rule (Fig. 1A). We measured brain activity of 32 healthy young adults while they performed the tasks in a 3T fMRI scanner (2D echo-planar imaging, 46 slices, voxel size: 2.5 mm^3, TR: 1.53 s, TE: 30 ms). To compare the neural response elicited by different tasks, we estimated representational dissimilarity matrices (RDMs) using cross-validated Mahalanobis distances for each participant. To probe into the representational content of the data RDMs, we first created model RDMs based on single task features and their interactions. Next, we fitted the model RDMs to the data RDMs using linear combinations of task features, then additionally included their interactions, using non-negative weights (Jozwik et al., 2016). Model performance was evaluated by the cosine similarity between data RDMs and predicted RDMs (Diedrichsen et al., 2021). We compared performance across models for different regions of interest (Assem et al., 2020) (Fig. 1C). If adding interaction terms to the model does not improve performance, this provides evidence for compositional coding (Fig. 1E, F).

Results: Our tasks strongly engage the MD system and both the attended sensory modality and the match rule are decodable from cortical regions comprising the MD system (Fig. 1D). Attended sensory modality is more widely decodable than match rule, consistent with the presence of attentional effects in sensory regions. Furthermore, representations in the MD system and higher visual regions are better modeled by task dimensions than those in lower visual regions. Importantly, across regions of interest, the interaction between task dimensions does not explain the task representation over and above their linear combination (Fig. 1E, F). These results suggest that tasks are represented in the MD system in a compositional fashion.

Conclusions: The representation of tasks differs across the cortical hierarchy. Early processing regions show a representation that is more strongly dominated by attended sensory information and less by abstract task rules, while later processing regions such as the MD system show a representation that carries a broad array of task information. In addition, task representations can be modeled as a linear combination of the representations of task features, while their interactions do not contribute significantly, supporting the compositional coding strategy. Future work should test for compositional coding in a broader range of tasks and across spatial scales.

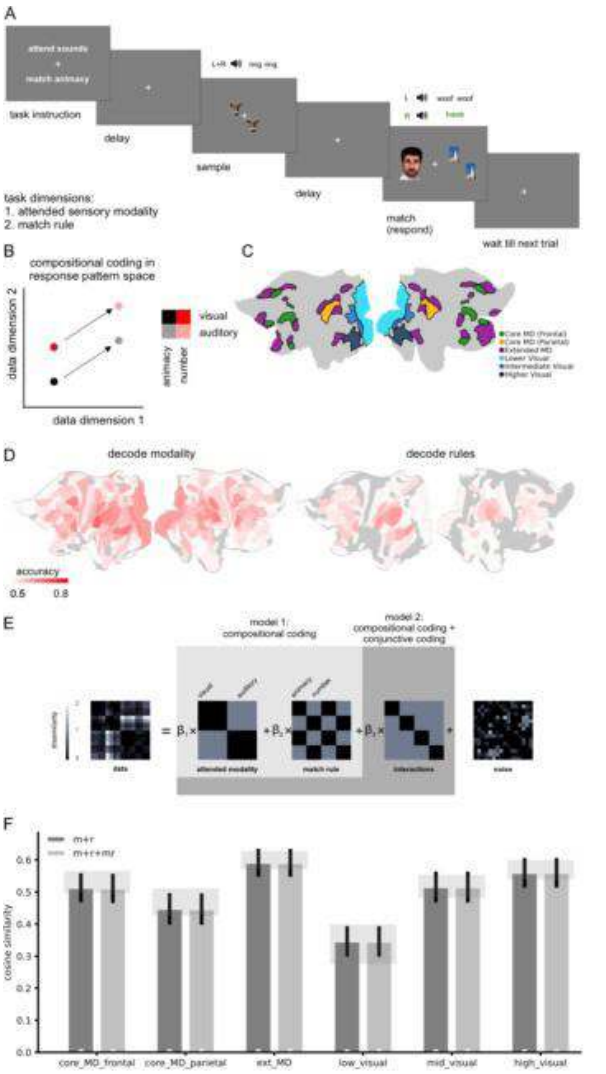

A. Delayed-match-to-sample task. The participants were asked to indicate the side (left or right) of the competing stimuli that matched the stimulus sampled in the same modality (visual or auditory) while applying the same rule (animacy or number). B. Schematic showing compositional coding where tasks can be represented as a sum of vectors representing attended sensory modality and match rule. C. Regions of interest (ROIs) (Assem et al., 2020). D. Multivoxel pattern decoding accuracies for attended sensory modality and match rule. Multivoxel patterns for each HCP parcel were extracted using t-values against baseline then fed into a Linear Discriminant Analysis classifier using leave-one-run-out cross-validation for individual participants. Decoding results were averaged across participants and thresholded using a one-sided t-test (against chance level, 0.5), corrected for multiple comparisons across all HCP parcels.E. Schematic showing how to model data RDMs using feature RDMs. F. Cross-validated RDM model performance across ROIs. Dark gray: model including RDMs for modality and rule only; light grey: model including RDMs for modality, rule, and their interaction. Error bars show standard error of the mean across bootstrap resampled participants. White half circles at the bottom indicate above-zero model performance (t-test, $p < 0.05$, uncorrected). Horizontal gray shaded areas show the noise ceiling. Neither model performed significantly worse than the lower bound of the noise ceiling across ROIs (t-test, uncorrected). Model performance did not significantly differ in any ROI (t-test, uncorrected).

References

1. Assem, M., Glasser, M. F., Van Essen, D. C., & Duncan, J. (2020). A Domain-General Cognitive Core Defined in Multimodally Parcellated Human Cortex. Cerebral Cortex, 30(8), 4361–4380. https://doi.org/10.1093/cercor/bhaa023
2. Cole, M. W., Etzel, J. A., Zacks, J. M., Schneider, W., & Braver, T. S. (2011). Rapid Transfer of Abstract Rules to Novel Contexts in Human Lateral Prefrontal Cortex. Frontiers in Human Neuroscience, 0. https://doi.org/10.3389/fnhum.2011.00142
3. Diedrichsen, J., Berlot, E., Mur, M., Schütt, H. H., Shahbazi, M., & Kriegeskorte, N. (2021). Comparing representational geometries using whitened unbiased-distance-matrix similarity (arXiv:2007.02789). arXiv. https://doi.org/10.48550/arXiv.2007.02789

4. Duncan, J. (2010). The multiple-demand (MD) system of the primate brain: Mental programs for intelligent behaviour. Trends in Cognitive Sciences, 14(4), 172–179. https://doi.org/10.1016/j.tics.2010.01.004
5. Jozwik, K. M., Kriegeskorte, N., & Mur, M. (2016). Visual features as stepping stones toward semantics: Explaining object similarity in IT and perception with non-negative least squares. Neuropsychologia, 83, 201–226. https://doi.org/10.1016/j.neuropsychologia.2015.10.023
6. Mante, V., Sussillo, D., Shenoy, K. V., & Newsome, W. T. (2013). Context-dependent computation by recurrent dynamics in prefrontal cortex. Nature, 503(7474), Article 7474. https://doi.org/10.1038/nature12742
7. Reverberi, C., Görgen, K., & Haynes, J.-D. (2012). Compositionality of Rule Representations in Human Prefrontal Cortex. Cerebral Cortex, 22(6), 1237–1246. https://doi.org/10.1093/cercor/bhr200
8. Rigotti, M., Barak, O., Warden, M. R., Wang, X.-J., Daw, N. D., Miller, E. K., & Fusi, S. (2013). The importance of mixed selectivity in complex cognitive tasks. Nature, 497(7451), Article 7451. https://doi.org/10.1038/nature12160
9. Woolgar, A., Thompson, R., Bor, D., & Duncan, J. (2011). Multi-voxel coding of stimuli, rules, and responses in human frontoparietal cortex. NeuroImage, 56(2), 744–752. https://doi.org/10.1016/j.neuroimage.2010.04.035
10. Yang, G. R., Joglekar, M. R., Song, H. F., Newsome, W. T., & Wang, X.-J. (2019). Task representations in neural networks trained to perform many cognitive tasks. Nature Neuroscience, 22(2), 297–306. https://doi.org/10.1038/s41593-018-0310-2

Poster No 973

The Meaning-Making Process of Visual Artworks Engages the Default Mode Network

Dominika Grygarova[1], Petr Adámek[1], Ladislav Kesner[1], Jiri Horacek[2]

[1]National Institute of Mental Health, Klecany, Czech Republic, [23]rt Medical faculty of Charles Univ., Prague, Praha

Introduction: While one may be immediately captivated by a visual artwork, the profound experience typically unfolds through an intentional process of meaning-making, extending over minutes, days, or even weeks and months. As Gadamer (1977) aptly notes, 'the artwork demands to be understood as what it 'means,' what it says.' Such insights align with contemporary neuro-cognitive models of art experience, emphasizing reflection and knowledge assimilation (Pelowski et al. 2017). Recent studies investigating neural processes in the comprehension of symbolic cultural forms, such as narratives in texts or movies (Simony et al. 2016), have highlighted the crucial role of the default mode network (DMN). However, no neuroimaging study has explored the impact of repeated encounters with artwork accompanied by intentional and effortful meaning-making activities. Our study aims to investigate the effects of intentional meaning-making of artworks through (1) self-driven reflection and (2) absorption of new information conveyed by texts.

Methods: We conducted an fMRI experiment (n=35) employing a novel experimental paradigm, prompting participants to engage in a repeated dialogue with artworks. Initially, participants were scanned while freely viewing 85 figural paintings with affective content. Post-scanning, they rated the images based on perceived affective impact, resulting in two personalized sets of stimuli for home study: 10 paintings strongly affecting them (SA) and 10 not affecting them (NA). Over two weeks, participants repeatedly observed these paintings, and (1) reflected on the personal meaning of half the paintings and (2) read art-historical commentaries on the other half. After this home intervention, participants underwent a second scanning session while viewing the same set of stimuli as in the first scanning. We conducted a whole-brain analysis using a full-factorial model. We considered as significant the results with semi-conservative cluster-level family-wise error (pFWE, $p \leq 0.05$) correction for all grey matter voxels.

Results: (1) In the second scanning, stimuli exposed to reflection intervention compared to stimuli without any intervention elicited increased activation in the precuneus, posterior cingulate cortex, inferior parietal lobule, as well as the medial and superior frontal cortex and orbitofrontal cortex. Additionally, large clusters of activations were observed in the left inferior frontal gyrus, left inferior temporal gyrus, and bilateral insula. (2) During the second scanning, stimuli exposed to the text-reading intervention, compared to stimuli without any intervention, exhibited a similar pattern of brain activations as the reflection intervention. Unlike reflection, text-reading intervention resulted in a strong left lateralization of the activation pattern and stronger activations in the left middle posterior temporal gyrus.

Conclusions: Both the reflective and information-absorption effects of intentional meaning-making processing of artworks reflected a combination of self-related and semantic processing. Regions implicated in the DMN, together with temporal regions connected to semantic processing, were identified in both forms of intervention. Our results support the conceptualization of the DMN as a "sense-making network", integrating external information with pre-existing intrinsic knowledge (Yeshurun et al., 2021).

References

1. Gadamer HG (1977). Philosophical Hermeneutics, University of California Press
2. Pelowski M, Markey PS, Forster M, Gerger G, Leder H. (2017). Move me, astonish me... delight my eyes and brain: The Vienna Integrated Model of top-down and bottom-up processes in Art Perception (VIMAP) and corresponding affective, evaluative, and neurophysiological correlates. Phys Life Rev 21, 80-125

3. Simony E, Honey C, Chen J, Lositsky O, Yeshurun Y, Wiesel A, Hasson U (2016). Dynamic reconfiguration of the default mode network during narrative comprehension. Nature Communications 7, 12141. 10.1038/ncomms12141
4. Yeshurun, Y., Nguyen, M, Hasson, U (2021). The default mode network: where the idiosyncratic self meets the shared social world. Nat Rev Neurosci 22, 181–192

Poster No 974

Neural representations of action-integrated reward in naturalistic foraging

Jaeyoung Jeon[1,2,3], Won Mok Shim[1,2,3], Seng Bum Yoo[1,2,3]

[1]Ctr. for Neurosci. Imaging Res., Inst. for Basic Sci. (IBS), Suwon, Korea, Republic of, [2]Dept. of Intelligent Precision Healthcare Convergence,Sungkyunkwan Univ., Suwon, Korea, Republic of, [3]Dept. of Biomed. Engin., Sungkyunkwan Univ., Suwon, Korea, Republic of

Introduction: Foraging is a continuous decision-making process aimed at maximizing long-term benefits. Such a process requires accurate beliefs about the spatial distribution of rewards, essential for constructing an efficient exploitation route. Furthermore, foraging behaviors can be understood in the context of evidence accumulation, where individuals strategically shift their preferences to accept or reject presented rewards, known as skipping behaviors (Hayden et al., 2018). However, previous studies that imitate foraging behaviors at an abstract level, such as patch-leaving, interpreted skipping behaviors predominantly in terms of reducing temporal cost (Constantino et al., 2015). Here, we introduced a two-step foraging task within an interactive 3D Minecraft-based platform, where participants are encouraged to exploit spatial regularities in a partially observable environment to maximize rewards.

Methods: We designed a spatial foraging task in a 3D-grid world featuring two different types and values of rewards (Fig. 1A). Participants were instructed to collect rewards as much as possible within a specified time, under a given type-to-value transition rule. Transition rules, determining the ratio between the requested types of harvested rewards (i.e. 1:1, 1:3), were implemented. The task consisted of two stages: 1) a regularity detection phase, during which participants reported whether each type of reward was spatially clustered (structured) or randomly distributed (random) (Fig. 1B), and 2) a reward collection phase, where participants either accepted or rejected offers at each step while navigating the environment based on their beliefs about the spatial regularity identified in the previous stage. Functional 7T MRI data (N=6, 12 maps) were collected after a practice session.

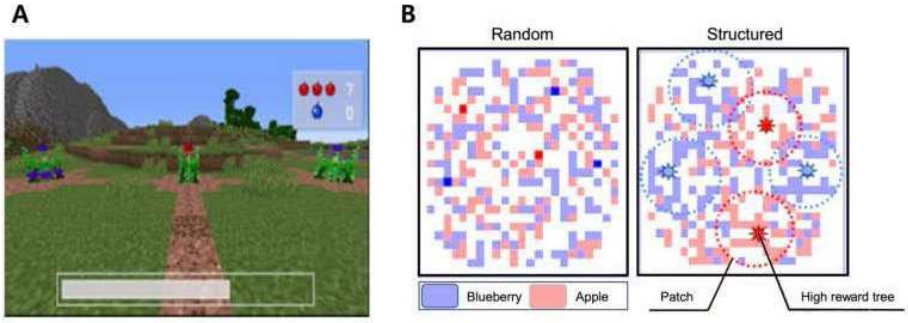

Figure 1: (A) An example of task view. (B) Examples of environment structures. In a random map, rewards were randomly distributed across the map regardless of their types and quantity. On the other hand, in a structured map, each type of reward was clustered at multiple locations.

Results: We first examined the effect of individuals' belief in spatial regularity on skipping frequency. Participants exhibited a significantly higher frequency of skipping behaviors in structured maps ($t(5) = 2.19$, $p < .05$) (Fig 2A), indicating their successful detection of reward clusters in structured maps. In addition, foraging scores were positively correlated (Pearson correlation coefficient, $r = 0.41$, $p < .05$) with skipping frequency (Fig 2B), emphasizing the role of skipping behavior as a key foraging strategy. Next, we examined neural activity in regions associated with reward processing in response to the presence of rewards and the selection of an action. Participants' actions as they approach the next reward position were categorized into three types: moving to a location without a reward (no reward), moving to a location with a reward but not collecting it later (skip), and moving to a location with a reward and collecting it (forage). We observed an increased BOLD response in the dACC when participants moved to a location with a present reward, regardless of whether they eventually harvested it or not, indicating its sensitivity to the observation of rewards (Fig 2C). In contrast, the vmPFC showed increased responses when a reward was foraged compared to when it was skipped, reflecting its involvement in anticipating significant future value linked to one's actions, rather than merely responding to the presence of a reward.

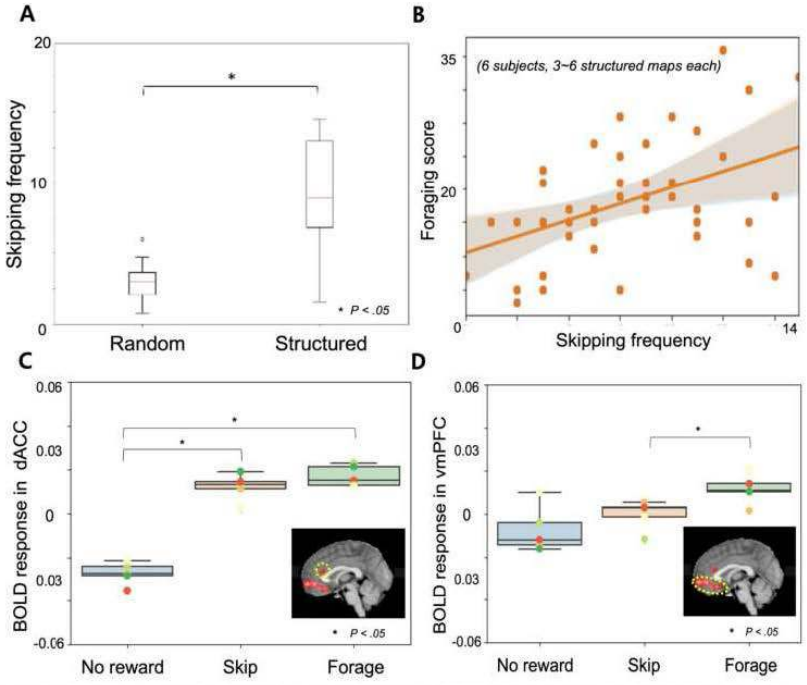

Figure 2: (A) Skipping frequency in random and structured maps. (B) Correlation between foraging scores and skipping frequency in the structured map condition. Higher frequency of skipping decisions were associated with increased foraging scores in structured maps. Each dot represents a session on an individual map. BOLD response in (C) dACC and (D) vmPFC during three different types of participants' actions.

Conclusions: Our results demonstrated that humans strategically adopt the skipping strategy to enhance foraging efficiency based on the expected spatial distribution of rewards. This behavioral pattern was associated with distinct neural activity in the reward circuit (Juechems et al., 2019), suggesting a unique role for the dACC and vmPFC in representing the presence of rewards and the reward value that integrates future decision-making related to action selection. The observed skipping behavior serves as evidence that human subjects actively leverage information about spatial regularities to formulate optimal foraging routes, highlighting the integration of beliefs about reward regularities in the external environment for long-term reward maximization.

References

1. Hayden, B. Y. (2018). Economic choice: the foraging perspective. Current Opinion in Behavioral Sciences, 24, 1-6.
2. Constantino, S. M. (2015). Learning the opportunity cost of time in a patch-foraging task. Cognitive, Affective, & Behavioral Neuroscience, 15, 837-853.
3. Juechems, K. (2019). A network for computing value equilibrium in the human medial prefrontal cortex. Neuron, 101(5), 977-987.

Poster No 975

Brain structural and functional features of individuals with higher controllability of motor imagery

Tomoyo Morita[1], Tomoya Furuta[2], Gen Miura[2], Park Jihoon[1], Eiichi Naito[1]

[1]National Institute of Information and Communications Technology, Osaka, Japan, [2]Osaka University, Osaka, Japan

Introduction: Motor imagery is a higher-order cognitive brain function that mentally simulates movements without performing the actual physical one (Jeannerod,1994). Although many studies have dealt with motor imagery, neural bases that determine individual differences in motor imagery ability are not well understood. In this study, using magnetic resonance imaging and controllability of motor imagery (CMI) test that can objectively evaluate individual ability to manipulate one's imaginary postures, we elucidated the structural and functional characteristics of the brain that determine individual differences in motor imagery ability.

Methods: 89 healthy right-handed young adults (53 men: mean age, 22.1 ± 1.7) participated in this study. To evaluate individual's ability to accurately manipulate motor imagery, we used CMI test (Nishida et al. 1986; Naito 1994), in which the participants internally generate, manipulate, and hold one's imaginary body postures from a first-person perspective in response to each of five consecutive verbal instructions regarding movements of body parts (left or right arms, left or

right legs, upper body, and head/neck). After the final instruction, participants were asked to perform the final posture by themselves. By evaluating the final posture, whether the participants could manipulate their motor imagery appropriately during the test can be assessed. A T1-weighted image was acquired, with a magnetization-prepared rapid gradient echo (MP-RAGE) sequence using a 3.0-Tesla MRI scanner (Trio Tim; SIEMENS, Germany) and a 32-channel array coil for each participant. We performed voxel-based morphometry (VBM) analysis to examine white and gray matter structures that expand in higher CMI test scorers. We also collected functional images using T2*-weighted gradient echo-planar imaging (EPI), with the same scanner while 33 of 89 participants performed a CMI task and a control task. We identified imagery-related activity during the CMI task when compared with the control task, and also examined brain regions where imagery-related functional coupling with seed regions changes in relation to the CMI test score across participants by conducting a generalized psychophysiological interaction analysis. The study protocol was approved by the Ethics Committee of the NICT. We explained the details of the present study to all participants before the experiment, and they then provided written informed consent. The study was conducted according to the principles and guidelines of the Declaration of Helsinki (1975).

Results: Individuals with higher CMI test scores showed bilateral expansion of white matter regions where the three branches of superior longitudinal fasciculus (SLF I, II, and III) are likely running (Figure 1). When compared with the control task, CMI task activated the bilateral dorsal premotor cortex (PMD) and superior parietal lobule (SPL) that are likely connected by the SLF I and II. Among these regions, the left PMD and/or the right SPL enhance functional coupling with the visual body, somatosensory, and motor/kinesthetic areas in the higher scorers (Figure 2).

Conclusions: This study introduced the CMI test that can objectively evaluate an individual's ability to manipulate one's imaginary postures and has elucidated structural and functional features characterizing the brains of individuals with higher controllability of motor imagery. Structurally, such individuals have expanded frontoparietal white matter that enables fast and rich neural processing of spatial/motor and corporeal information. Functionally, in their brains, the core network of mental simulation (superior frontoparietal network of PMD–SPL), particularly the left PMD and/or the right SPL, likely has top–down access to the visual body, somatosensory, and motor/kinesthetic areas and enhances functional coupling with these for sensory emulation (prediction). This study advanced the understanding of individual difference in motor imagery ability.

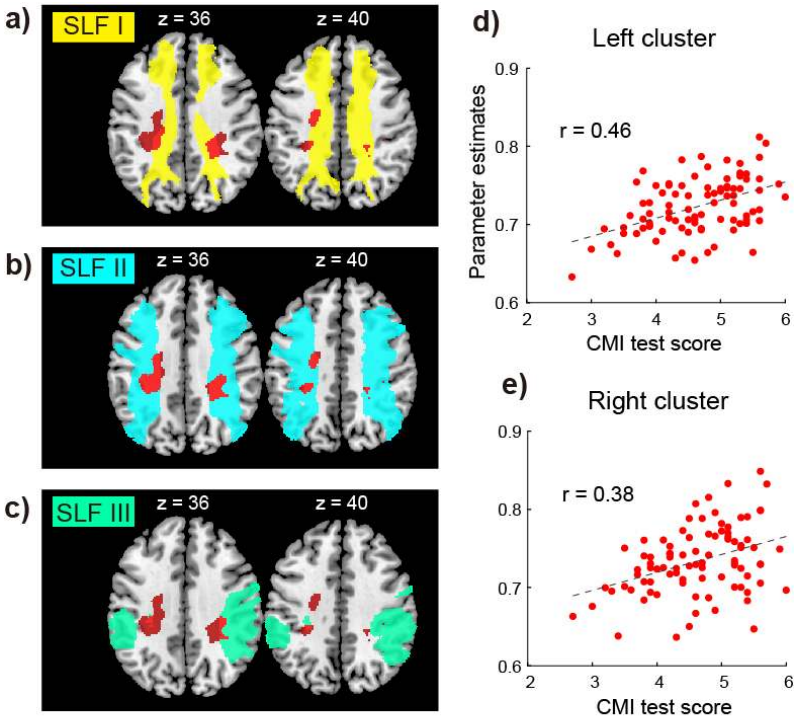

Figure 1 Results of VBM analysis

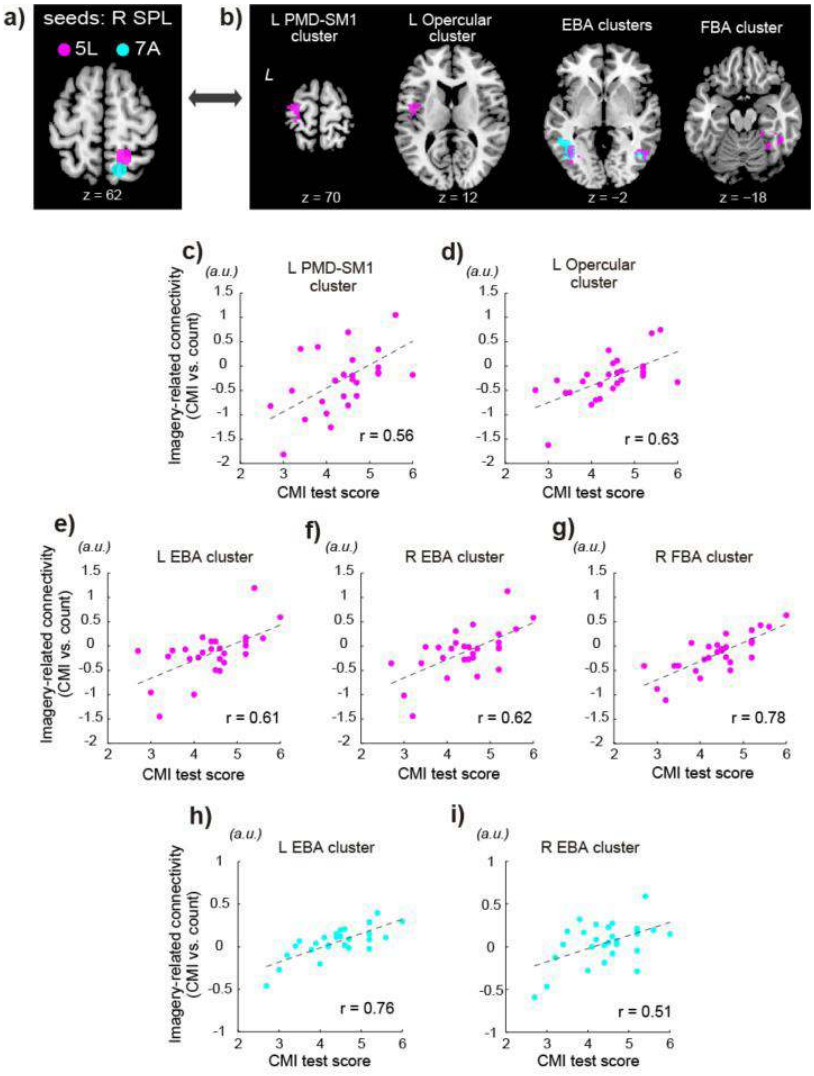

Figure 2 Results of functional connectivty analysis from the right SPL

References

1. Furuta, T. et al. (2023), 'Structural and functional features characterizing the brains of individuals with higher controllability of motor imagery' bioRxiv, https://www.biorxiv.org/content/10.1101/2023.10.11.560970v1.
2. Jeannerod, M. (1994), 'The representing brain: Neural correlates of motor intention and imagery', Behavioral and Brain Sciences, vol.17, pp.187-202.
3. Naito, E. (1984), 'Controllability of motor imagery and transformation of visual imagery', Perceptual and Motor Skills, vol. 78, pp.479-487.
4. Nishida, T. et al. (1986), 'A new test for controllability of motor imagery: The examination of its validity and reliability', Japan Journal of Physical Education, Health and Sport Sciences, vol. 31, pp.13-22.

Poster No 976

Reconstruction of melodies with relative pitch height decoding in music imagery:Electrocorticography

Jii Kwon[1], June Sic Kim[1], Chun Kee Chung[2]

[1]Seoul National University, Seoul, Republic of Korea, [2]Seoul National University Medical Research Center, Seoul, Republic of Korea

Introduction: Melody, consisting of a pitch series, is an essential element in music, essential in distinguishing music. Melody could be perceived by the pattern of interval distances between the tones (relative pitches), not by absolute pitches in most subjects. Here, we aimed to reconstruct an imagined melody by decoding the relative pitch heights during music imagery with electrocorticography (ECoG). Furthermore, we try to elucidate the major neural features contributing the classification accuracy.

Methods: Ten medically intractable epilepsy patients without professional musical backgrounds participated in the present study. Five well-known children's songs were used. We used a questionnaire to assess their familiarity with scores ranging from 1 to 5 for each song (1, least familiar; and 5, most familiar). Patients performed the task of listening, followed by imagery of certain melody parts. During the music imagery, we observed significantly increased high gamma activities in the temporal, the inferior frontal, and the sensorimotor cortices. Neural features activated during music imagery were used in decoding the relative pitch height (Do-Re-Mi-Fa-Sol-La) by Random Forest algorithms with the sequential forward floating selection (SFFS). To quantify the contribution of each feature in the classification accuracy, an increment value was calculated during SFFS. With decoding in order within one melody chunk, we reconstruct the imagined melody. Spearman's correlation coefficient was employed to evaluate reconstructed imagined melody with the original one.

Results: High frequency activities, including gamma and high gamma, from the left superior temporal gyrus (STG) and the right rostral middle frontal cortex (rostral MFC) significantly contributed to relative pitch decoding in music imagery. After then, we could reconstruct imagined melodies, with a mean Spearman's correlation coefficient of 0.58 ($p < 0.01$) with the original melodies. Lower familiarity scores are, lower is the correlation of reconstructed imagined melodies, and vice versa in higher familiarity for each of the 5 songs analyzed.

Conclusions: We successfully reconstructed imagined melodies of children's songs with ECoG. We demonstrated the feasibility of decoding relative pitch height in the single-note domain with significantly increased high-gamma responses during music imagery. Critically, we found that left STG and the right rostral MFC significantly contributed in decoding. The left STG, traditionally linked to auditory processing and pitch perception, is involved in music imagery, suggesting a shared neural substrate for music perception and imagery. Meanwhile, the right rostral MFC's contribution underlines an intricate interplay of auditory processing and executive functions, suggesting the cognitive complexity inherent in music imagery.

References

1. Badre, D. (2009). "Is the rostro-caudal axis of the frontal lobe hierarchical?" Nature Reviews Neuroscience 10(9): 659-669.
2. Gómez, E. (2003). Melody description and extraction in the context of music content processing. Journal of New Music Research, 32(1), 23-40.
3. Levitin, D. J. (2005). "Absolute pitch: perception, coding, and controversies." Trends in cognitive sciences 9(1): 26-33.
4. Patterson, R. D. (2002). "The processing of temporal pitch and melody information in auditory cortex." Neuron 36(4): 767-776.
5. Zatorre, R. J. (2005). "Mental concerts: musical imagery and auditory cortex." Neuron 47(1): 9-12.

Poster No 977

Decoding Number of Syllables from Human Intracranial Electroencephalography

Gyuwon Lee[1], Chun Kee Chung[1]

[1]*Seoul National University, Seoul, Korea, Republic of*

Introduction: Speech decoding is a prominent field in the human brain-computer interface (BCI) over the past decade. While successful decoding has been reported for attempted tasks, including overt speech and mimed speech, achieving intelligible sounds for imagined speech remains unsolved. This difficulty arises due to the absence of automatic feedback and the distinct neural substrates associated with attempted speech. To address this, we used a linguistic innate property, the number of syllables, to predict the imagined spoken word. In this study, we investigated the encoding features of the number of syllables in imagined speech and decoded based on the findings.

Methods: We recruited six patients with drug-resistant epilepsy underwent intracranial electroencephalography (iEEG) for clinical purpose. During a session, 108 words were presented to the patients, each displayed for 3 seconds with a preceding fixation slide lasting one second. These words were grouped into four classes based on the number of syllables (1, 2, 3, >4 syllables). Patients were instructed to mentally speak the presented word at any time, and simultaneous iEEG signals were recorded simultaneously. A deep learning classifier, comprising a single bidirectional gated recurrent unit (GRU) layer and one fully-connected layer, was used to predict the number of syllables. Each frequency band (delta: 1–4 Hz, theta: 4–8 Hz, alpha: 8–13 Hz, beta: 13–30 Hz, low gamma: 30–70 Hz, high gamma: 70–170 Hz) from the iEEG signals was selected as a model input sequentially. The input was bootstrapped 20 times to generate an accuracy distribution, and the significance of accuracy was assessed using surrogate data.

Results: The accuracy from surrogate data was notably high ($p<0.001$) at 32.19%, and features surpassing this threshold were considered significant. The envelope of the alpha wave showed the greatest number of significant features. These significant features were observed across diverse regions, including pSTG, vSMC, pMTG, medial occipital gyrus, and angular

gyrus. With these features, the decoding of the number of syllables achieved an accuracy exceeding 40% across the four specified classes.

Conclusions: In this study, we demonstrated the number of imagined syllables can be successfully decoded from iEEG signals. Moreover, we observed that the processing related to the number of imagined syllables occurs across various regions.

References

1. Meng, K. (2023) 'Continuous synthesis of artificial speech sounds from human cortical surface recordings during silent speech production', Journal of Neural Engineering, vol. 20, no. 4.
2. Metzger, S.L. (2023) 'A high-performance neuroprosthesis for speech decoding and avatar control', Nature, vol. 620, no. 7976, pp. 1037–1046

Poster No 978

Opposite gradients of mental imagery and perception in orbitofrontal and occipitotemporal cortex

Jianghao Liu[1], Laurent Cohen[1], Minye Zhan[2], Paolo Bartolomeo[1]

[1]Paris Brain Institute, Paris, France, [2]Neurospin, Gif-sur-Yvette, France

Introduction: Subjective visual experience can be shaped bottom-up by external reality or built top-down in visual mental imagery[1]. Specifically, we previously found that mental imagery of faces and colors recruits the relevant domain-preferring ventral occipito-temporal (VOTC) cortical patches[2]. We further discovered face- and color-preferring orbitofrontal cortex (OFC) patches in human participants, localized in a medial-lateral fashion similar to those of the VOTC[2].However, how does this OFC activity relate to VOTC activity? How do these patches sustain subjective visual experience through bottom-up and top-down processing? For example, individuals with congenital aphantasia show some visual cortex activation in the absence of subjective imagery experience. Does aphantasia impact neural activity in these patches?

Methods: We collected 7T fMRI data from 10 typical imagers and 10 aphantasic individuals while they performed mental imagery and perceptual tasks in five different domains of stimuli: faces, object colors, object shapes, words, and a map of France. After scanning, they also arranged experimental items either by semantic features, or by perceived visual features. In individual participants, we identified 4 VOTC face-preferring patches, 3 VOTC color-preferring patches, and 1 OFC patch each for face and color domains. Fig. 1A displays a representative typical imager. We investigated: activity magnitude, domain selectivity, neural representations (representational similarity analysis) compared to behavioral arrangements, and functional connectivity (psychophysiological interaction). We examined differences between patches through repeated-measures ANOVAs and conducted post-hoc gradient tests to identify prevailing trends across posterior to anterior patches, comparing their activity during imagery and perception, in typical imagers and in aphantasic individuals.

Results: OFC face-preferring patches were consistently located lateral to the OFC color-preferring patches (x-coordinates, Bayes factor = 12.68), similar to their spatial arrangement in VOTC. Across posterior to anterior VOTC and OFC patches during perception, activity amplitudes were highest at V1, decreased along the VOTC and OFC patches; during imagery however, the activity amplitude showed the opposite pattern, which increased from posterior to anterior patches. Functional connectivity also showed opposite flows between perception and imagery, with OFC patches serving as the apex of the top-down process. Although domain selectivity and the similarity of neural representations to behavioral arrangements increased from posterior to anterior patches, both during perception and imagery.Aphantasic individuals showed comparable activities in the VOTC patches but reduced OFC activities, including decreased visual color representation in OFC color patchs, reduced activity amplitude, and orbitofrontal-temporal connectivity in both modalities. See an illustrative figure of results in Fig.1B.

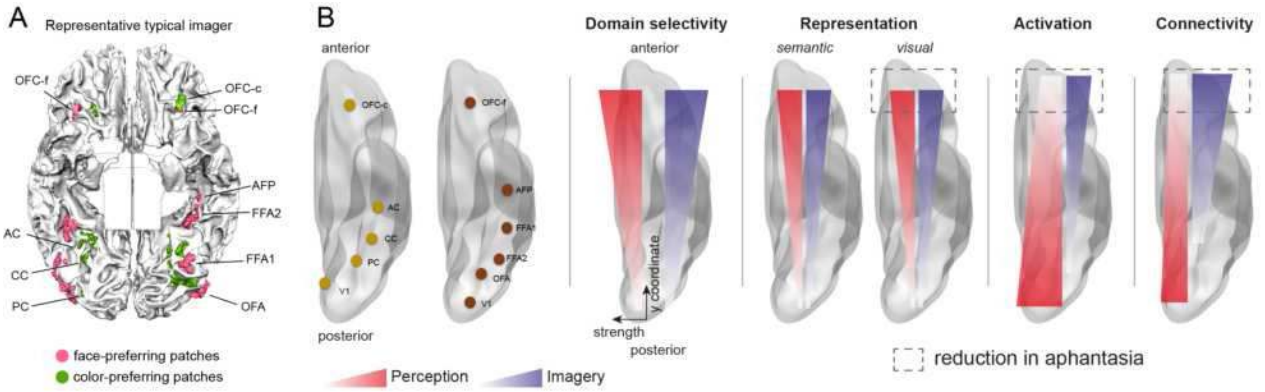

Fig. 1 (A) Face- and color-preferring patches in a representative typical imager. From posterior to anterior, face patches include: occipital face area (OFA), fusiform face area 1 (FFA1), fusiform face area 2 (FFA2), anterior face patch (AFP), orbitofrontal face (OFC-f) patches; color patches include: posterior color (PC), central color (CC), anterior color (AC), orbitofrontal color (OFC-c) patches.
(B) Illustration of gradients of representations and processes of face- and color-visual systems during imagery and perception.

Conclusions: During visual perception and visual mental imagery of faces and colors, activity of domain-preferring cortical patches is not uniform but follows functional gradients across the ventral visual cortex and OFC cortex. The newly discovered domain-preferring OFC patches seem to be located close to the apex of top-down processing in mental imagery. Aphantasic individuals showed decreased OFC activity in mental imagery, perhaps linked to impaired metacognitive monitoring or read-out activities (3). Thus, aphantasia is associated with different patterns of activity in the OFC cortex, but not in the high-level visual cortex.

References

1. Bartolomeo et al.(2024) 'Colors in the mind's eye', Cortex j.cortex.2023.10.002
2. Liu et al. bioRxiv (2023) 'Visual mental imagery in typical imagers and in aphantasia: A millimeter-scale 7-T fMRI study', 2023.2006.2014.544909
3. Liu & Bartolomeo (2023) 'Probing the unimaginable: The impact of aphantasia on distinct domains of visual mental imagery and visual perception' Cortex, 166, 338-347

Poster No 979

Hypnotic induction modulates both state and dynamics EEG measures during an imagination task

Ruxandra Tivadar[1], Nina Rimorini[1], Geoffroy Solelhac[1], Chantal Berna[1]

[1]Centre Hospitalier Universitaire Lausanne (CHUV), Lausanne, Switzerland

Introduction: Measures of neural information content have been shown to successfully quantify human awareness and consciousness levels (Carhart-Harris et al., 2014; Lau et al., 2022). Here, we viewed the EEG signal as a complex system and described characteristics of its state and dynamics (Khanna et al., 2015). We investigated whether measures of signal complexity (i.e. dynamics) can discriminate between neural activity during an imagination task following or not a hypnotic induction. Complexity has been shown to fluctuate with states of consciousness (Aamodt et al., 2021; Alnes et al., 2023; Schartner et al., 2015; Schartner et al., 2017), administration of psychedelic substances (Schartner et al., 2017), or tasks (Cnudde et al., 2023). Given evidence of variation of microstate characteristics with behavioural states (Lehmann et al., 2010), neuropsychiatric disorders (Pirondini et al., 2020) and interventions (Khanna et al., 2015), we also studied whether such changes were illustrated in topographical measures (i.e. the state) of brain activity, Finally, we correlated these measures. We hypothesized an increase in brain complexity during hypnosis, as compared to outside of hypnosis, given evidence that high entropy states might be rich in phenomenological experience (Carhart-Harris, 2018; Tagliazucchi et al., 2014). In addition, imagery during hypnosis is often experienced as being enhanced (Crawford et al., 1983), more intense and hallucinatory (Kunzendorf, 1986), and subjects reportedly shift to more holistic, imagery-oriented strategies during hypnosis (Crawford et al., 1983). We also expected changes in the duration of microstates during hypnosis, as transitions in functional brain states are thought to be mirrored in modulations in microstate characteristics (Lehmann et al., 2009).

Methods: We recorded 3 minutes of continuous 128-channel EEG in 4 volunteers (3 female, 1 male) while participants engaged in free imagination of a safe place outside of hypnosis and following a hypnotic induction. We focused our exploratory EEG analysis on global, reference-independent measures. We explored global broadband Lempel-Ziv complexity (LZc) over all 128 channels and over the full (1-40Hz) EEG signal as in (Alnes et al., 2023). LZc is a measure of signal diversity, or how regular a signal is across time. We also explored topographical microstates, which are defined as short periods of quasi-

stable distributions of electrical potentials (Lehmann et al., 2009), in the attempt to characterise the brain response during an imagination task in the Hypnosis and the No Hypnosis conditions.

Results: LZc. LZc was generally higher in Hypnosis (μ = 0.25) as compared to the No Hypnosis (μ = 0.22) condition (n.s., Figure 1). Microstates. Our screeplot indicated an elbow after 5 microstates. These 5 microstates explained 65% of the total variance across the EEG recordings in both conditions. The duration of each of the microstates was extracted, and plots suggest differences between the Hypnosis and No Hypnosis condition (not significant, n.s.). The duration of the 5th microstate showed a moderate (r = 0.53, n.s.) correlation with LZc overall.

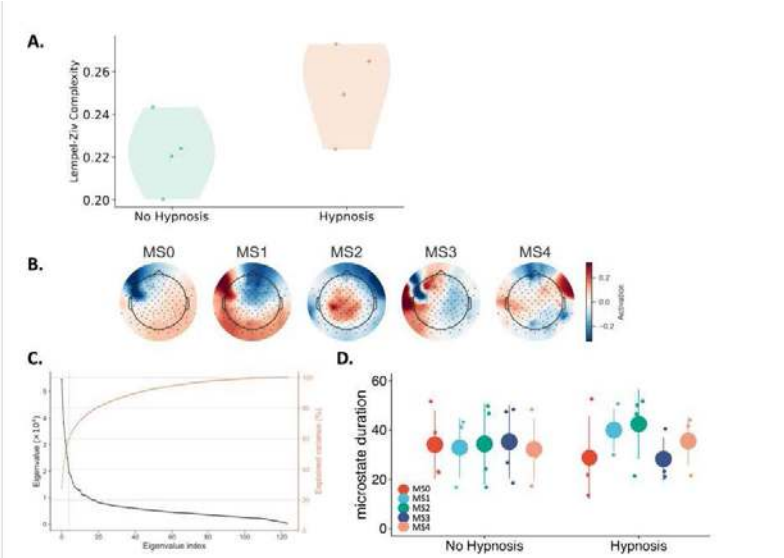

Figure 1. Complexity measures and microstate analysis for 4 subjects. **A.** Lempel-Ziv complexity values inside and outside of hypnosis. While green values are measurements derived from recordings of mental imagination outside of hypnosis, orange values represent measurements of the same task after a hypnotic induction. **B.** 5 Microstates best describe the combined EEG activity. The number of these microstates was chosen using a screeplot. **C.** The plot of the eigenvalues illustrates that the 5 microstates explain around 65% of the total variance. **D.** Mean duration of microstates inside and outside of hypnosis. Each coloured circle represents the mean duration of a microstate across participants. The extended lines illustrate the standard deviation and single points represent the actual measurements (1 point per subject).

Conclusions: Our results indicate trend-level changes in both complexity measures and microstate duration. Decreases in complexity were found during visualization as compared to a mind wandering task, indicating more focused attention (Walter & Hinterberger, 2022). On the contrary, increases in complexity measures during mind wandering are thought to reflect greater processing flexibility across functional configurations (Cnudde et al., 2023). These measures have the potential to inform us about the cortical mechanisms by which a hypnotic induction might induce changes in cognitive processing. With data collection ongoing until a target sample of N=50 is reached, these preliminary results will be strengthened and expanded upon.

References

1. Aamodt, A. (2021). EEG Signal Diversity Varies With Sleep Stage and Aspects of Dream Experience. Frontiers in Psychology, 12.
2. Alnes, S. (2023). Neural complexity and the spectral slope characterize auditory processing in wakefulness and sleep. Authorea Preprints.
3. Carhart-Harris, R.L. (2018). The entropic brain-revisited. Neuropharmacology, 142, 167–178.
4. Carhart-Harris, R.L. (2014). The entropic brain: a theory of conscious states informed by neuroimaging research with psychedelic drugs. Frontiers in Human Neuroscience, 20.
5. Cnudde, K. (2023). EEG complexity during mind wandering: A multiscale entropy investigation. Neuropsychologia, 180.
6. Crawford, J.H. (1983). Spatial memory processing: Enhancement during hypnosis. Theoretical and Clinical Applications, 209–216.
7. Khanna, A. (2015). Microstates in resting-state EEG: Current status and future directions. Neuroscience & Biobehavioral Reviews, 49, 105–113.
8. Kunzendorf, R.G. (1986). Hypnotic hallucinations as “unmonitored” images: An empirical study. Imagination, Cognition and Personality, 5(3), 255–270.
9. Lau, Z.J. (2022). Brain entropy, fractal dimensions and predictability: A review of complexity measures for EEG in healthy and neuropsychiatric populations. European Journal of Neuroscience, 56(7), 5047–5069.
10. Lehmann, D. (2009). EEG microstates. Scholarpedia, 4(3).
11. Lehmann, D. (2010). Core networks for visual-concrete and abstract thought content: a brain electric microstate analysis. Neuroimage, 49(1), 1073–1079.

12. Pirondini, E. (2020). Resting-state EEG topographies: Reliable and sensitive signatures of unilateral spatial neglect. NeuroImage: Clinical, 26.
13. Schartner, M.M. (2017). Increased spontaneous MEG signal diversity for psychoactive doses of ketamine, LSD and psilocybin.Scientific Reports, 7(1).
14. Schartner, M.M. (2017). Global and local complexity of intracranial EEG decreases during NREM sleep. Neuroscience of Consciousness, 2017(1).
15. Schartner, M.M. (2015). Complexity of multi-dimensional spontaneous EEG decreases during propofol induced general anaesthesia. PloS One, 10(8).
16. Tagliazucchi, E. (2014). Enhanced repertoire of brain dynamical states during the psychedelic experience. Human Brain Mapping, 35(11).
17. Walter, N. (2022). Determining states of consciousness in the electroencephalogram based on spectral, complexity, and criticality features. Neuroscience of Consciousness, 2022(1).

Poster No 980

Movies of our minds: Hierarchical neural patterns of event, scene, and object construction

Pitshaporn Leelaarporn[1], Julia Taube[1], Yilmaz Sagik[2], Cornelia McCormick[1]

[1]University Hospital Bonn, Bonn, NRW, [2]German Center for Neurodegenerative Diseases, Bonn, NRW

Introduction: Most of us can easily conjure up detail-rich mental events to envision future scenarios, remember past events or indulge in fictitious day-dreaming[1]. Neurally, these types of events are thought to rely on hierarchical neural structures involving the ventromedial prefrontal cortex (vmPFC), hippocampus, and visuoperceptual cortex (VC)[2,3]. In this hierarchy, we have proposed earlier that the vmPFC maybe the apex, initiating, and coordinating hippocampal scene construction processes to support the elaboration of vivid mental extended events[4,5]. We further proposed that the hippocampus constructs spatially coherent mental scenes[6,7] and directs activity in the VC which may be involved in assembling rich details needed to populate scenes within events[4]. Original data supporting this thesis are missing. Therefore, we contrast event, scene, and object imagery to expose the underlying neural hierarchy. Our hypothesis deems a hierarchy indicating that the vmPFC supports mental events greater than scenes and objects, the hippocampus supports event and scene imagery greater than object imagery, and that the VC supports all three constructions equally.

Methods: 20 healthy young right-handed individuals (age: 28 ± 3.49 years old, Males: 8, years of education: 19.4 ± 3.71 years) were recruited with informed consent to complete an experimental fMRI task consisting of four different types of word cues imagery: objects (e.g., espresso), scenes (e.g., mountain range), events (e.g., concert), and non-words (e.g., Tribuomnus). Participants were instructed to construct mental visuoperceptual images of each of the word cues, followed by their rating of their own ability to visualize. The MRI protocol included a whole-brain T1-weighted scan and task-based rapid whole-brain submillimeter functional MRI (fMRI) sequences, acquired using a MAGNETOM 7T Plus ultra-high field scanner (Siemens Healthineers, Germany). fMRI preprocessing was performed using SPM12 software package. Using a GLM model, we analyzed the imagery time (5 s) for each imagery type as mini-blocks. 1-sample t-contrasts were calculated and thresholded at $p<0.001$, unc.: 1. Events <> Scenes, 2. Scenes <> Objects, 3. Events > Non-words, 4. Scenes > Non-words, and 5. Objects > Non-words. Regions-of-interest (ROI) spheres with a diameter of 5 mm were created for the right vmPFC, hippocampus, and VC and % signal change was extracted using the contrasts 3, 4, and 5, and was then assessed using 1-way RM-ANOVA with Tukey's multiple comparison test.

Results: Figures 1 and 2 illustrate that the vmPFC showed stronger activation for event imagery than scene and object imagery, and the hippocampus showed stronger activation for both event and scene imagery in contrast to object imagery. Furthermore, the VC showed no preference for event, scene, or object imagery. Some other brain regions also exhibited preferential activation patterns which will be discussed in more detail later. Furthermore, effective connectivity models may provide more detailed insights into the hierarchical nature of these relationships. These results suggest that there is a hierarchy of neural structures supporting our ability to construct detail-rich extended mental events in front of our mind's eye, with the vmPFC being at the apex, initiating, and directing our minds' movies construction.

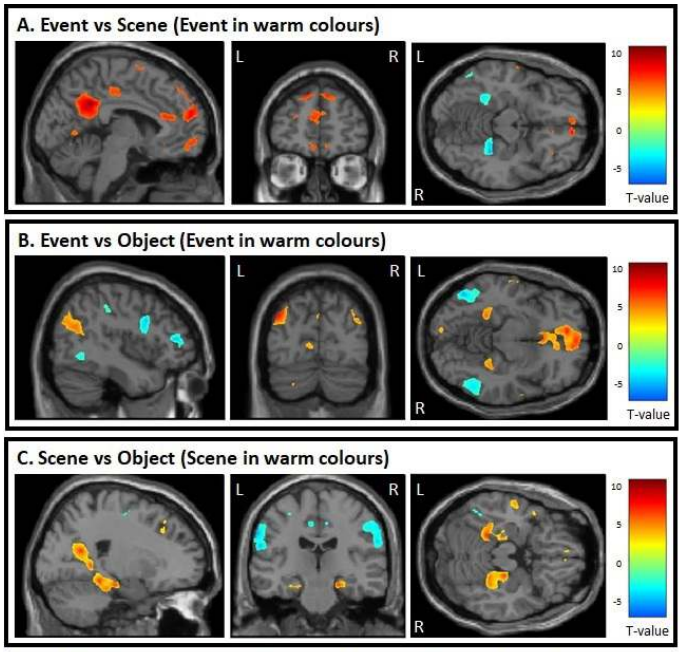

Figure 1. Whole-brain activations during mental imagery of Events vs Scenes, Events vs Objects, and Scenes vs Objects. *Greater activation in the vmPFC for Events than Scenes (A) and Events than Objects (B). In addition, greater activation in the hippocampus for Events vs Objects (B) and Scenes vs Objects (C).*

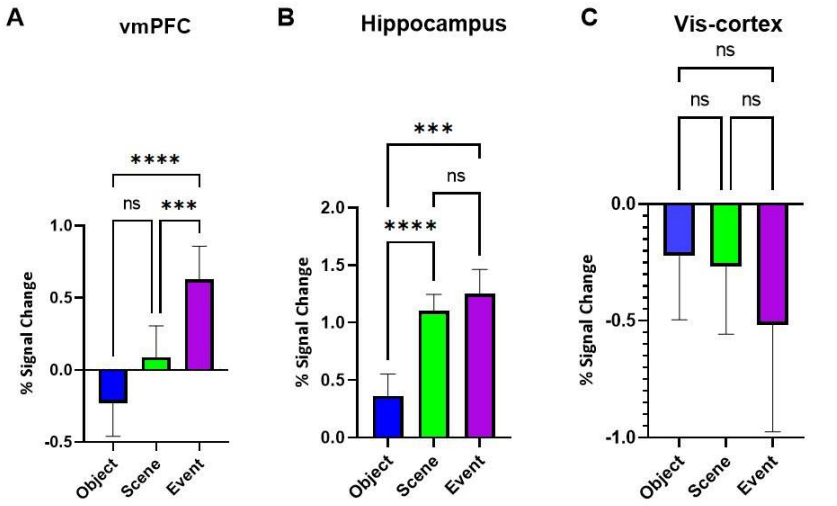

Figure 2. Comparisons of % signal change in the vmPFC (x = 10, y = 53.6, z = -12.4), hippocampus (x = 22.2, y = -22, z = -18), and visuoperceptual cortex (x = 45, y = -77, z = -10) for all three types of imagery (taken from the contrasts of Events, Scenes, and Objects against non-words). A. In the vmPFC, event construction showed stronger activation than scene and object construction. B. In the hippocampus, event and scene construction showed stronger activation than object construction. C. In the visuoperceptual cortex, all three imagery conditions showed equal activation.

Conclusions: Here, we set out to examine the specific contributions of the vmPFC, hippocampus, and VC to the construction of detail-rich mental extended events. We presented event-, scene-, and object-cues to participants during fMRI scanning and asked participants to imagine the displayed cues. With these tight contrasts, we found that the vmPFC preferentially supported event construction, whereas the hippocampus supported both event and scene construction. In addition, the VC supported all three types of mental imagery. These results provide the first evidence that these brain regions align on a hierarchy, potentially expanding the visual process stream up to the vmPFC.

References

1. Pearson, J. (2019). The human imagination: the cognitive neuroscience of visual mental imagery. Nature reviews neuroscience, 20(10), 624-634.
2. McCormick, C., St-Laurent, M., Ty, A., Valiante, T. A., & McAndrews, M. P. (2015). Functional and effective hippocampal–neocortical connectivity during construction and elaboration of autobiographical memory retrieval. Cerebral cortex, 25(5), 1297-1305.
3. Pearson, J., Naselaris, T., Holmes, E. A., & Kosslyn, S. M. (2015). Mental imagery: functional mechanisms and clinical applications. Trends in cognitive sciences, 19(10), 590-602.
4. McCormick, C., Ciaramelli, E., De Luca, F., & Maguire, E. A. (2018). Comparing and contrasting the cognitive effects of hippocampal and ventromedial prefrontal cortex damage: a review of human lesion studies. Neuroscience, 374, 295-318.

5. McCormick, C., Barry, D. N., Jafarian, A., Barnes, G. R., & Maguire, E. A. (2020). vmPFC drives hippocampal processing during autobiographical memory recall regardless of remoteness. Cerebral Cortex, 30(11), 5972-5987.
6. Dalton, M. A., Zeidman, P., McCormick, C., & Maguire, E. A. (2018). Differentiable processing of objects, associations, and scenes within the hippocampus. Journal of Neuroscience, 38(38), 8146-8159.
7. McCormick, C., Dalton, M. A., Zeidman, P., & Maguire, E. A. (2021). Characterising the hippocampal response to perception, construction and complexity. Cortex, 137, 1-17.

Poster No 981

Mapping body size estimation accuracy using a 3D avatar: an fMRI task proof of concept

Joel Diaz-Fong[1,2], Sameena Karsan[2], Madison Lewis[2,3], Zeina Beidas[2], Jamie Feusner[1,2]

[1]Institute of Medical Science, University of Toronto, Toronto, Canada, [2]Centre for Addiction and Mental Health, Toronto, Canada, [3]Department of Psychology, University of Toronto, Toronto, Canada

Introduction: Body image disturbance is a key characteristic of body dysmorphic disorder (BDD), an often-severe psychiatric disorder that affects 1 in 40 individuals (Phillips, 2004). Somatomap 3D is a digital avatar tool used to quantify body image disturbance through measuring body size estimation (BSE) accuracy. Somatomap 3D has been previously used to examine abnormalities in BSE accuracy among individuals with anorexia nervosa compared to healthy controls (Ralph-Nearman, 2021). However, its use during fMRI to probe body processing regions and networks involved in accurate internal representations of one's body has yet to be tested. Previous fMRI studies have established that tasks involving viewing body images result in brain activation in areas including the extrastriate body area (EBA; Downing, 2001), the fusiform body area (Peelen, 2005), somatosensory cortex (Saxe, 2006) and the temporoparietal junction (TPJ; Hamamoto, 2023). As an initial proof of concept, the current study examined brain activation related to BSE accuracy using Somatomap 3D in individuals with and without BDD. We hypothesized that body processing regions including the EBA, the fusiform body area, and the TPJ would be activated while completing the Somatomap task.

Methods: Participants were recruited from the Greater Toronto Area. Twenty unmedicated adults (18-38 years, 24.55±5.74; 80% female) with BDD (n=6), sub-clinical BDD (n=5), and healthy controls (n=9) were included in this preliminary analysis. During fMRI, participants used the Somatomap 3D tool to adjust 23 different body parts on the avatar to create, as accurately as possible, their current body's size and shape. Participants completed the task using an MR-compatible trackball. While completing the task, eye movements and mouse clicks were recorded and synchronized with the fMRI scan. Using mouse click timestamps, body size estimation was defined in the time-series as the periods when the participant was rotating the avatar or adjusting the avatar body size. The baseline contrast included intervening periods between these rotations/adjustments. As this preliminary sample was small, it did not permit subgroup analyses or comparisons; we thus modeled responses across the whole group. Single group average fMRI data analysis was carried out using FSL FEAT. Z (Gaussianized T/F) statistic image were thresholded using clusters determined by Z>3.1 and a corrected cluster significance threshold of P=0.05. Peak MNI coordinates were identified using the Harvard-Oxford atlas. To identify activation patterns that overlap with the specific regions of interest involved in body processing, Neurosynth masks using the term "body" were generated and compared to the cluster results.

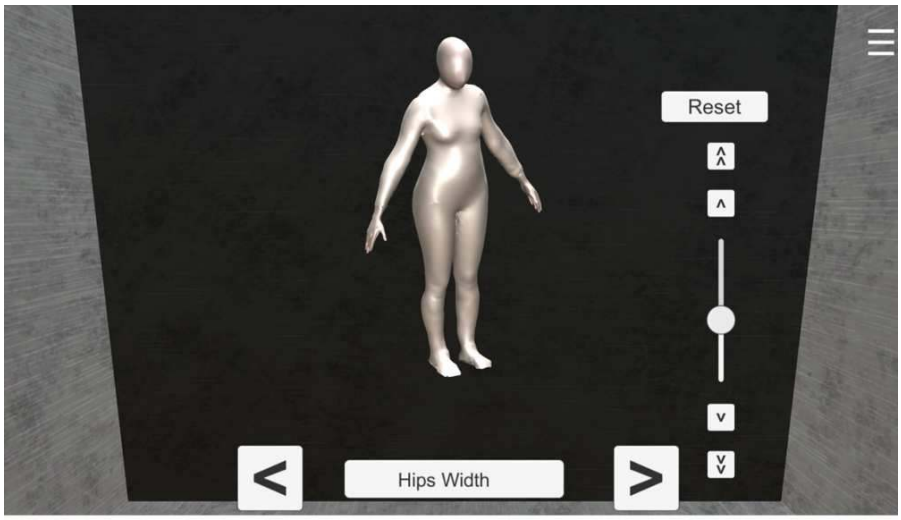

Figure 1. The Somatomap 3D tool includes 23 selectable body parts of which the size and shape can be adjusted with a slider. The avatar can be rotated and adjusted from all angle.

Results: Multiple statistically significant clusters were evident in the whole-brain, voxelwise analysis corresponding to the body part adjustment/rotation periods vs. baseline (Table 1). Specifically, the supramarginal gyrus and postcentral gyrus (right: voxels=3088, Z=5.82; left: voxels=302, Z=5.02), the precentral gyrus (right: voxels=1899, Z=6.05), the lateral occipital cortex (right: voxels=1811, Z=5.43; left: voxels=363, Z=5.46), the supplementary motor cortex (right: voxels=1048, Z=5.29), and the inferior frontal gyrus (right: voxels=417, Z=4.96). In addition, cluster activations overlapped with the EBA, fusiform body area, and insular cortex but not the TPJ.

Table 1: Group average clusters

Harvard-Oxford Atlas Regions	Voxels	*p*-value [-log10(*p*)]	Max Z value	MNI Coordinates (mm)		
				X	Y	Z
Supramarginal Gyrus, Postcentral Gyrus	3088	< .0001 [123]	5.82	52	-26	40
Precentral Gyrus, Inferior Frontal Gyrus	1899	< .0001 [88.1]	6.05	52	-26	18
Lateral Occipital Cortex	1811	< .0001 [85.3]	5.43	54	8	-2
Supplementary Motor Cortex	1048	< .0001 [58.5]	5.29	48	-68	62
Inferior Frontal Gyrus, Precentral Gyrus	417	< .0001 [30.6]	4.96	12	-8	2
Lateral Occipital Cortex, Middle Temporal Gyrus	363	< .0001 [27.7]	5.46	-52	12	2
Postcentral Gyrus, Supramarginal Gyrus	302	< .0001 [24.2]	5.02	-46	-68	40
Unknown	117	< .0001 [11.8]	3.99	-58	-26	22

Note: Only clusters >50 voxels are reported in this Table for visualization.

Conclusions: Although this preliminary sample size is modest, this proof-of-concept study suggests that BSE using Somatomap 3D is associated with brain activation patterns in known body processing regions such as the EBA, fusiform body area, insula, somatosensory, and inferior frontal brain regions. The study suggests Somatomap 3D is a task that may be used to examine neural mechanisms underlying BSE accuracy. As such, it may be useful to probe pathophysiological mechanisms associated with body image disturbance in those with body-image related disorders such as BDD and eating disorders.

References

1. Downing, P. E. (2001), 'A cortical area selective for visual processing of the human body', Science, vol. 293, no. 5539, pp. 2470–2473.
2. Hamamoto, Y. (2023), 'Neural mechanisms of perceptual and affective body-image disturbance during own-body and ideal-body estimation', Behavioural Brain Research, vol. 444, pp. 114349.
3. Peelen, M. V. (2005), 'Selectivity for the human body in the fusiform gyrus', Journal of Neurophysiology, vol. 93, no. 1, pp. 603–608.
4. Phillips K. A. (2004), 'Body dysmorphic disorder: recognizing and treating imagined ugliness', World Psychiatry, vol. 3, no. 1, pp. 12–17.
5. Ralph-Nearman, C. (2021), 'Visual mapping of body image disturbance in anorexia nervosa reveals objective markers of illness severity', Scientific Reports, vol. 11, no. 1, pp. 12262.
6. Saxe, R. (2006), 'My body or yours? The effect of visual perspective on cortical body representations', Cerebral cortex, vol. 16, no. 2, pp. 178–182.

Poster No 982

Representational Gradients of Musical Information and Evoked Emotions Revealed by CNN

Seung-Goo Kim[1], Tobias Overath[2], Daniela Sammler[1]

[1]Max Planck Institute for Empirical Aesthetics, Frankfurt am Main, Germany, [2]Duke University, Durham, NC

Introduction: Music often evokes strong emotions. Yet, how musical auditory representations are abstracted in the brain and how these different representations contribute to the emergence of felt emotions remains poorly understood. Recent work suggests that pretrained audio convolutional neural networks (CNNs) can capture information in real-world music that is relevant to felt emotions and neural activity in the medial prefrontal cortex (mPFC; Kim et al., 2023). Here, we explored (i) whether increasingly abstract representations of music in different layers of the CNN are encoded along a well-established

functional gradient-from unimodal sensory to transmodal associative regions (Margulies et al., 2016), and (ii) how layer-specific CNN embeddings predict human behavioral ratings of musical emotions.

Methods: We analyzed the fMRI dataset (openneuro-ds003085) of Sachs et al. (2020). During scanning, 37 participants listened to one 'happy' and two 'sad' instrumental musical pieces. After scanning, they re-listened and continuously rated their felt 'Emotionality' (how strongly happy or sad) and 'Enjoyment' in two separate sessions. Encoding models: Embeddings for sliding 1-sec spectrograms of the music were extracted from all 24 layers of a CNN (VGGish; Hershey et al., 2016). The first 50 principal components (PCs) of the high-dimensional embeddings at each layer (explaining 40-98% of the variance) were fed into ridge regression (Caucheteux et al., 2022) to predict group-averaged fMRI time series and emotion ratings. Cortical gradient mapping: For each voxel, we determined the best layer (argmax) and the centroid layer in the 24-layer profile of prediction accuracies. Volumetric data were projected onto FreeSurfer template surfaces, and their correspondence with the functional gradient of Margulies et al. (2016) was statistically tested using a geometrical permutation test (Alexander-Bloch et al., 2018). Layer-wise fMRI encoding patterns were further inspected in 4 regions-of-interest (ROIs) selected based on Kim et al. (2023): superior and middle temporal gyri (STG & MTG), inferior frontal gyrus (IFG), and mPFC (Destrieux et al., 2010).

Results: Fig 1a displays spatial patterns of the best layers over the whole cortex. Activity in auditory regions and association cortex was best explained by the superficial and deep layers, respectively. This gradient-like pattern was even more pronounced in a centroid layer mapping (Fig 1b). Both the best layer ($r = 0.23$, $P = 0.0001$) and the centroid layer ($r = 0.26$, $P = 0.0001$) maps showed significant correlations with the functional gradient map (Fig 1c). As a negative control, the best layer and centroid layer maps computed with negative lags showed no significant correspondence ($P > 0.16$, Fig 1d, e). Fig 2 illustrates layer-wise prediction accuracies of ROI-based fMRI signals and emotional ratings. Accuracies in STG and MTG peaked at superficial layers, while mPFC and IFG showed peaks at deeper layers (Fig 2a). Interestingly, 'Emotionality' was best explained by superficial and deep layers, while accuracy for 'Enjoyment' ratings peaked at intermediate layers (Fig 2b).

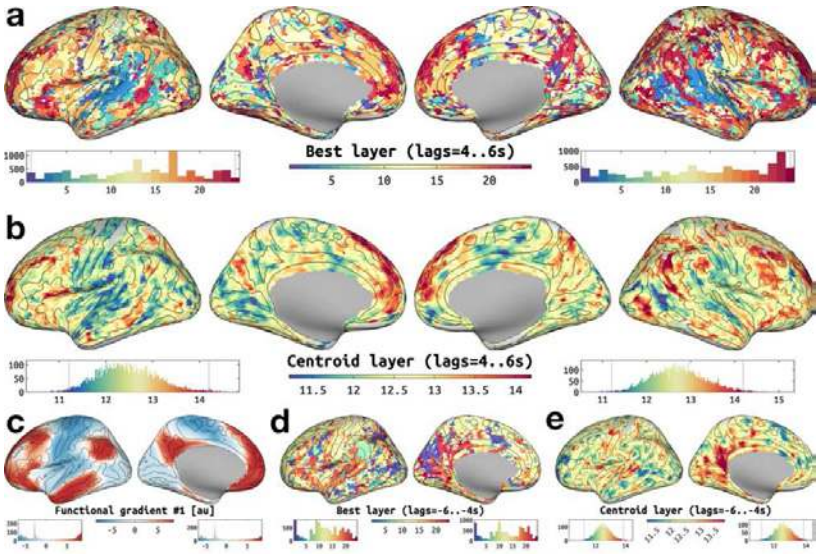

Fig 1. Spatial patterns of neural encoding of VGGish embeddings. (a) Best [i.e., argmax] layers with positive lags [4, 5, 6 s]. For each layer, high-dimensional embeddings [128 to 393k+ dimensions] were reduced to the first 50 principal components [explaining 40% to 98% of the variance depending on layers]. (b) Centroid layers with positive lags. (c) First functional gradient axis [Margulies et al., 2016; recreated from the template data included in BrainSpace v0.1.10]. Spatial correspondence between best/centroid layer maps and the functional gradient map was tested using "spin-test" (Alexander-Bloch et al., 2018) with 10,000 random rotations of spherical coordinates of the surface-mapped data. As a negative control, (d) best layers and (e) centroid layers were estimated with negative lags [-6, -5, -4 s].

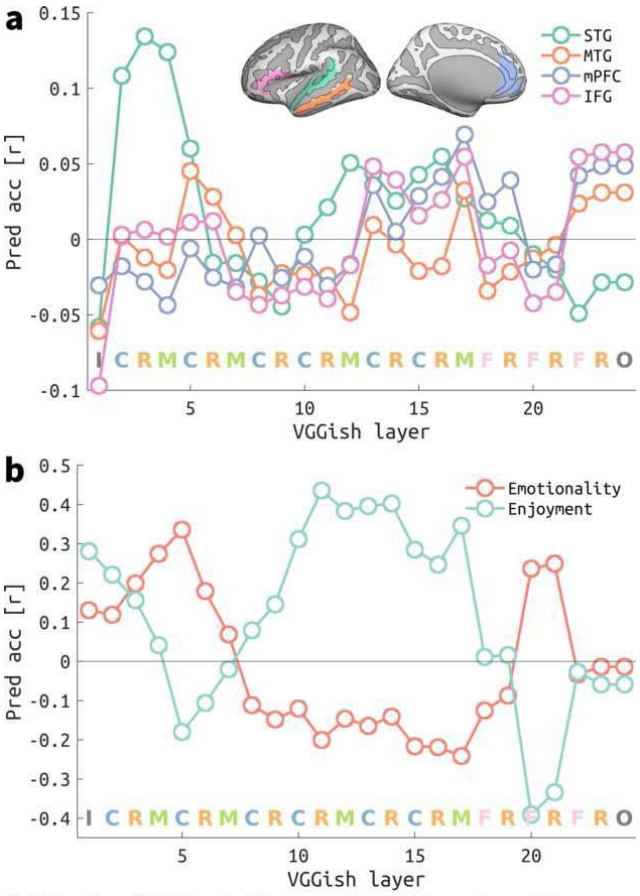

Fig 2. Encoding of VGGish embeddings across layers. (a) Layer-wise prediction accuracies (Pearson correlation) for each ROI [STG: superior temporal gyrus, MTG: middle temporal gyrus, mPFC: anterior cingulate gyrus and sulcus including mPFC, IFG: inferior frontal gyrus] are plotted over VGGish layers [I: input layer, C: convolution layer, R: rectified linear layer, M: max pooling layer, F: fully connected layer, O: output layer]. (b) Prediction accuracies for each emotional rating over layers.

Conclusions: The marked correspondence between the CNN layer-specific representational gradient of musical information and the intrinsic functional gradient (Margulies et al., 2016) suggests that the transformation of the auditory signal along the cortical hierarchy may involve an abstraction mechanism that behaves similarly to what the CNN implements, beyond the auditory systems (cf. Giordano et al., 2023). The distinct encoding patterns of the 'Emotionality' and 'Enjoyment' ratings across CNN layers suggest that basic and aesthetic emotional experiences may depend on different abstraction levels of the audio signal represented along the cortical gradient. Overall, the comparison of representational gradients of music in the brain and behavior may open new ways to better understand the multi-layered mechanisms of musical emotions (Juslin, 2013)

References

1. Alexander-Bloch, A. F., Shou, H., Liu, S., Satterthwaite, T. D., Glahn, D. C., Shinohara, R. T., Vandekar, S. N., & Raznahan, A. (2018). On testing for spatial correspondence between maps of human brain structure and function. Neuroimage, 178, 540-551. doi:10.1016/j.neuroimage.2018.05.070
2. Caucheteux, C., Gramfort, A. & King, JR. (2023) Evidence of a predictive coding hierarchy in the human brain listening to speech. Nature Human Behaviour, 7, 430–441. doi: 10.1038/s41562-022-01516-2
3. Giordano, B.L., Esposito, M., Valente, G. et al. (2023) Intermediate acoustic-to-semantic representations link behavioral and neural responses to natural sounds. Nature Neuroscience 26, 664–672. doi:10.1038/s41593-023-01285-9
4. Hershey, S., Chaudhuri, S., Ellis, D. P., Gemmeke, J. F., Jansen, A., Moore, R. C., ... & Wilson, K. (2017, March). CNN architectures for large-scale audio classification. In the Proceedings of 2017 IEEE international conference on acoustics, speech and signal processing (ICASSP), pp. 131-135.
5. Juslin, P. N. (2013). From everyday emotions to aesthetic emotions: Towards a unified theory of musical emotions. Physics of life reviews, 10(3), 235-266.
6. Kim SG., Overath T., Sammler D. (2023, August). Emotion-relevant Representations of Music Extracted by Convolutional Neural Networks Are Encoded in Medial Prefrontal Cortex. In the Proceedings of The Joint Conference of the 17th International Conference on Music Perception and Cognition (ICMPC) and the 7th Conference of the Asia-Pacific Society for the Cognitive Sciences of Music (APSCOM), Tokyo, Japan, pp. 398.
7. Margulies, D. S., Ghosh, S. S., Goulas, A., Falkiewicz, M., Huntenburg, J. M., Langs, G., Bezgin, G., Eickhoff, S. B., Castellanos, F. X., Petrides, M., Jefferies, E., & Smallwood, J. (2016). Situating the default-mode network along a principal gradient of macroscale cortical organization. Proceedings of the National Academy of Sciences, 113(44), 12574-12579. doi:10.1073/pnas.1608282113.
8. Sachs, M. E., Habibi, A., Damasio, A., & Kaplan, J. T. (2020). Dynamic intersubject neural synchronization reflects affective responses to sad music. NeuroImage, 218, 116512. doi:10.1016/j.neuroimage.2019.116512

Poster No 983

A multimodal dataset targeting music processing: neuroimaging, behavior & computational models

Peer Herholz[1], Karim Jerbi[2], Jean-Baptiste Poline[3]

[1]The Neuro (Montreal Neurological Institute-Hospital), McGill University, Montreal, QC, [2]Computational and Cognitive Neuroscience Lab, Department of Psychology, University of Montreal, Montreal, Quebec, [3]The Neuro (Montreal Neurological Institute-Hospital), McGill University, Montreal, Quebec

Introduction: Due to methodological advancements, the investigation of auditory perception and its neuronal and behavioral correlates has made tremendous progress in recent years. However, a vast amount of previous research work focused on auditory percepts across a broad range of sound categories[1,2], hence missing fine-grained within-category organization, which has been mainly explored for speech[3]. So far, only a very limited amount of studies concentrated on other categories, such as music, which, given its high diversity and dimensionality, poses as an ideal candidate to probe how perceived auditory signals are processed along the hierarchy of the auditory system, combining low level (acoustic) and high level (category/semantic) features in order to achieve behaviorally relevant percepts and how these could be explained by models of varying complexity and sources. The majority of these studies furthermore restricted themselves to a single data modality (e.g. fMRI, behavior or EEG) and did not share the data in a findable, accessible, interoperable and reusable (FAIR) manner.

Methods: Aiming to address this gap, we acquired a multimodal dataset targeting the processing of music, which will be openly shared with the community in a standardized and FAIR way. Divided into 5 sub-datasets, it entails sub-datasets spanning 1. fMRI (n=15), 2. EEG (n=12), 3. behavioral data (n=20), and 4. simple acoustic feature, as well as complex computational models that comprise low and high-level features of 5. independently validated (n=20) music stimuli from 20 genres. The genres and examples therein were selected based on prior research and music classification resources. In sub-datasets encompassing neuroimaging, stimuli were presented in a 1-hour long passive listening design, and across all datasets, participants performed a 1-hour behavioral multi-arrangement task. Additionally, a broad range of general demographic and auditory processing-related information was accessed per participant. All datasets will be provided in a version-controlled (via DataLad[4]) and standardized form (BIDS[5]), comprising abundant metadata and derivatives. The latter encompass quality control, preprocessing and statistical modelling to validate the datasets.

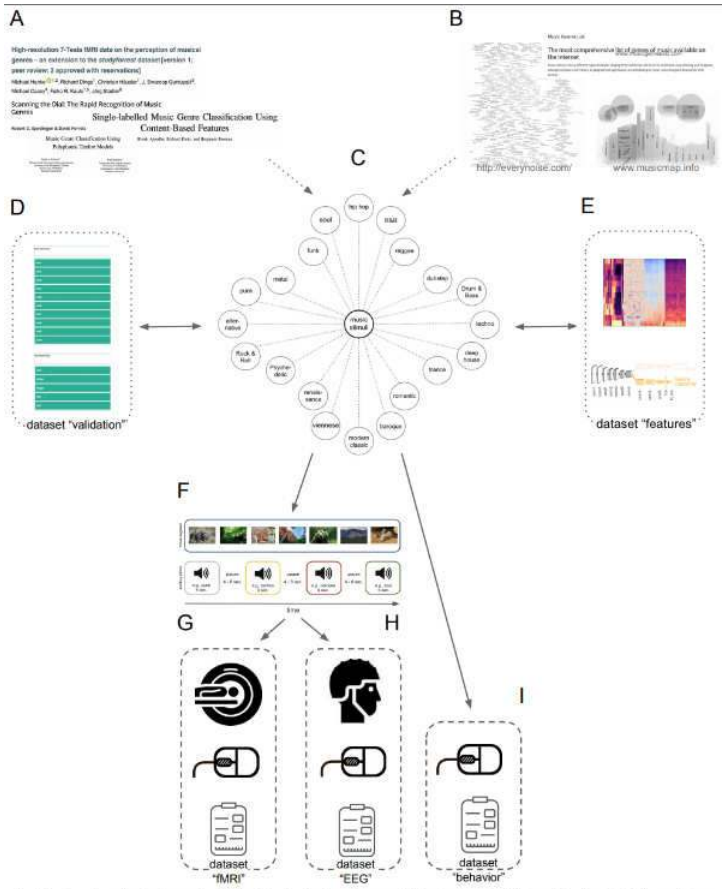

Fig. 1 Overview of experiment and procedure, including datasets. Based on prior research (A) and public music databases (B), a stimuli set of 20 genres (C) was created. Ten stimuli per subgenre were rated by an independent group of participants (D, n=20) and the those rated most representative of a given subgenre selected for the main study. From these stimuli a variety of low (acoustic) and high-level (artificial neural networks) features were extracted (E). Furthermore, the stimuli were used in a passive listening design (F) with brain and behavioral responses being recorded via fMRI (G, n=15) or EEG (H, n=12). Additionally, a dataset with only behavioral responses was acquired (I, n=20).

Results: Outcomes of the quality control and preprocessing steps indicated that the data was suitable for utilization as no significant artifacts but feasible signal-to-noise ratios were present in the neuroimaging data and the behavioral paradigm yielded reliable responses both within and across participants. Results from the statistical modeling indicated stable responses for all participants in all tested analysis approaches. Here, dataset validity was tested via two commonly applied analyses: stimulus-evoked responses (general linear models in fMRI and event-related potentials in EEG) and encoding models within which the different low and high-level features were employed as predictors. Both indicated spatial and temporal patterns in line with prior research, suggesting not only stimulus-related responses but also that the included features capture aspects of the stimuli that are appropriate for respective modeling approaches. In more detail, the stimuli evoked/the features predicted primary and non-primary regions of the auditory cortex bilaterally (in fMRI) and auditory processing-related ERP components such as P/N1 and P/N2 (in EEG). Moreover, simpler acoustic features predicted primary regions and earlier time points better and vice versa more complex computational models, non-primary regions and later time points.

Conclusions: The obtained datasets provide a FAIR and holistic resource for the multimodal investigation of auditory perception, specifically music processing. It allows to examine respective complex aspects through the integration of diverse data types, including fMRI, EEG, behavioral data and computational models. This furthermore entails its feasibility as a benchmark and validation dataset.

References

1. Sharda, M. (2012), Auditory perception of natural sound categories–an fMRI study. Neuroscience, 214, 49-58.
2. Giordano, B. L. (2013), Abstract encoding of auditory objects in cortical activity patterns. Cerebral cortex, 23(9), 2025-2037.
3. Preisig, B. C. (2022), Speech sound categorization: The contribution of non-auditory and auditory cortical regions. NeuroImage, 258, 119375.
4. Halchenko, Y. (2021), DataLad: distributed system for joint management of code, data, and their relationship. Journal of Open Source Software, 6(63).
5. Gorgolewski, K. J. (2016), The brain imaging data structure, a format for organizing and describing outputs of neuroimaging experiments. Scientific Data 3, 160044.

Poster No 984

Neuronal avalanches support cognitive processes during speech and music listening

Matteo Neri[1], Claudio Runfola[2], Noemie te Rietmolen[3], Pierpaolo Sorrentino[2], Daniele Schon[2], Benjamin Morillon[2], Giovanni Rabuffo[2]

[1]Aix Marseille Université, CNRS, INT, Institut de Neurosciences de la Timone, Marseille, France, [2]Aix Marseille Université, INSERM, INS, Institut de Neurosciences des Systèmes, Marseille, France, [3]Language and Computation in Neural Systems Group, Max Planck Institute for Psycholinguistics, Nijmegen, Netherlands

Introduction: Neuronal avalanches consist of collective network events propagating across the brain in short-lived and aperiodic instances[1]. These salient events have garnered a great interest in the study of cortical dynamics. They have been observed across different imaging modalities and scales, and have been used to successfully distinguish between healthy and pathological conditions or between resting wakefulness and sleep states[4]. While a growing body of literature investigated neuronal avalanches in task-free conditions, whether they index cognitive functions or purely reflect physiological states remains an open question. In this work we investigated neuronal avalanches to index cognition, analyzing an intracranial stereo electroencephalography (sEEG) dataset collected during speech and music listening (naturalistic stimuli of about 10 min. each) and resting state, in 19 epileptic patients.

Methods: Neuronal avalanches were estimated by binarizing the z-scored neural activity, estimated as high-frequency activity (80-120 Hz; obtained as in[6]; Fig. 1A left). We then defined the activity profile (AP) as the sum of the binarized data across channels (Fig. 1A right). To investigate whether avalanches occurred in a stimulus-driven manner, we assessed the extent to which neuronal avalanches were similarly distributed in time across participants listening to the same stimuli. To this end, we computed the average inter-subject correlation of the APs for each condition, assessed results significance with a null model based on random permutations of time steps and finally correlated the APs across participants in a time-resolved way, using a sliding window approach (Fig. 1B-C). To assess the engagement of different brain regions in speech and music listening, we compared the number of times a channel was above threshold during highly correlated time windows (red dots in Fig. 1C) with respect to rest (in Fig. 1D). To investigate how avalanches propagate in the different cognitive states, we computed the avalanche transition matrices (ATMs), which estimate the transition probability of an avalanche across any pair of channels (Fig 2A-B)[5]. We correlated the ATMs across conditions for each participant (Fig. 2C). To disentangle the contribution of local (intra-areal) and distributed (inter-areal) processes, we separated auditory (Heschl's gyrus, H) and non-auditory (noH) channels, and estimated ATMs within (H-H, noH-noH) and between (H-noH; noH-H) them (Fig. 2D).

Results: Firstly, we observed that avalanches relate to cognitive processes insofar as they are similarly distributed in time across patients while listening to speech and music, but not during rest (Fig. 1B). Secondly, we found that there are time windows in which avalanches are particularly coordinated across participants, and this is the case for both music and speech in partially overlapping but distinct distributed networks involving auditory and non-auditory regions (Fig. 1D). Then, we observed that ATMs tend to be overall more similar during music and rest, than speech (Fig. 2C). Furthermore this analysis revealed that the directed functional connections that differ the most across conditions (speech, music and resting state) are the ones between auditory and non auditory regions (Fig. 2D). This underlines the importance of feedforward and feedback mechanisms in shaping brain dynamics during speech and music perception.

Conclusions: With the present work we contribute to extend an approach based on neuronal avalanches, adopted in the past mainly in the study of resting state, to the investigation of cognitive functions, here speech and music[2]. Moreover, given the broad range of different contexts in which neuronal avalanches have been studied[3], our work provides the cognitive and system neuroscience communities with a set of theoretical and computational tools to investigate local and global properties of neural activity, with a particular focus on cognitive functions and naturalistic stimuli.

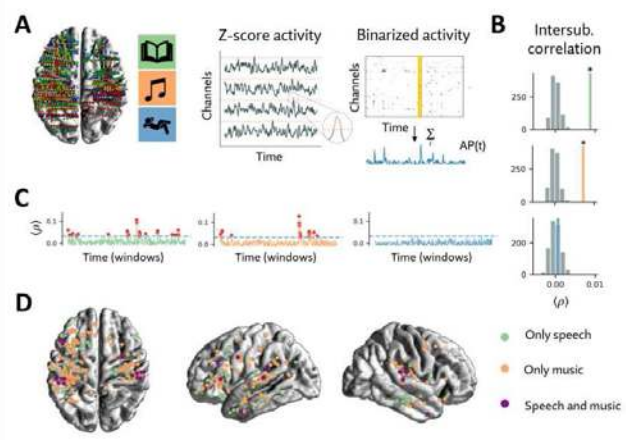

Figure 1. A) (left) Anatomical localization of the sEEG electrodes of our population, different colors correspond to different participants (N=19). **(right)** Binarization pipeline for the investigation of neuronal avalanches and the activity profile (AP) obtained as the sum across channels of the binarized matrix (channels x times). **B)** The null model distribution (gray) compared to the observed average intersubject correlation, green vertical line for speech, orange for music and blue for resting state. **C)** The evolution of the intersubject correlation in time windows of 1 second (50 time steps). **D)** The channels with a significantly high engagement (i.e. number of above threshold activity peaks during highly correlated time windows), with respect to a null model based on the resting state activity.

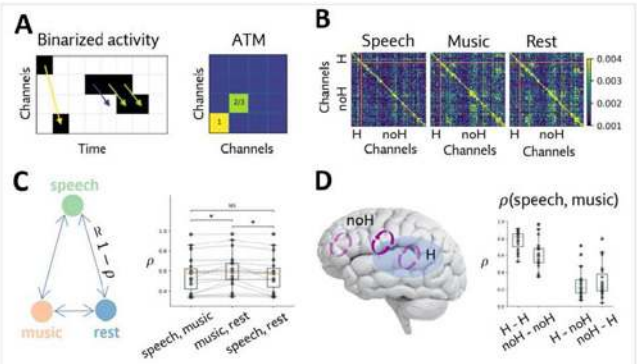

Figure 2. A) The pipeline to compute the activity transition matrix (ATM) and in **B)** an example: the ATM for speech, music and resting state of 1 participant. **C) (left)** A conceptual graph: the ATMs of music and rest are more correlated (represented closer to each other) than speech and music or speech and rest. **(right)** The distribution of correlation values (ρ) across participants, computed between ATMs of pairs of conditions. Solid/dashed gray lines: participants showing the expected/reversed effect. Wilcoxon test (*P < 0.01; NS non-significant). **D) (left)** A conceptual graph: the links between auditory (Heschl's gyrus, H) and non-auditory (noH) channels are the one differing the most between speech and music. **(right)** Distribution of correlation values across participants, computed between ATMs of speech and music (similar plots for the correlation between speech and rest or music and rest), H and noH channels were separated and ATMs were estimated within (H-H, noH-noH) and between (H-noH; noH-H) brain areas. The boxplots in panels **C-D** represent median and the interquartile range.

References
1. Beggs, J.M. (2003), 'Neuronal avalanches in neocortical circuits', The Journal of Neuroscience, 23(35):11167–77
2. Finn, E.S. (2021), 'Is it time to put rest to rest?', Trends in Cognitive Sciences (Regul Ed), 25(12):1021–32
3. Girardi-Schappo, M. (2021), 'Brain criticality beyond avalanches: open problems and how to approach them', Journal of Physics: Complexity, 2(3):031003
4. Priesemann, V. (2013), 'Neuronal avalanches differ from wakefulness to deep sleep-evidence from intracranial depth recordings in humans', PLOS Computational Biology, 9(3):e1002985
5. Sorrentino, P. (2021), 'The structural connectome constrains fast brain dynamics', eLife, 10
6. Te Rietmolen, N. (2022), 'Speech and music recruit frequency-specific distributed and overlapping cortical networks', BioRxiv

Poster No 985

High-frequency audibility affects alpha activity response to the perception of musical emotion

Jihyun Lee[1,2], Ji-Hye Han[1,2], Hyo-Jeong Lee[1,2,3]

[1]Laboratory of Brain & Cognitive Sciences for Convergence Medicine, Hallym University College of Medicine, Anyang, Gyeonggi-Do, Korea, Republic of, [2]Ear and Interaction Center, Doheun Institute for Digital Innovation in Medicine (D.I.D.I.M.), Hallym University Sacred Heart Hospital, Anyang, Gyeonggi-Do, Korea, Republic of, [3]Department of Otorhinolaryngology, Hallym University College of Medicine, ChunCheon, Kangwon-Do, Korea, Republic of

Introduction: People with hearing loss complain of listening to music (Caldwell et al., 2015; Hopyan et al., 2016), and it is even more challenging to perceive the emotions of music (Picou et al., 2018). Although a large body of studies are focused on the perception of musical emotions in people with hearing loss, the underlying cortical mechanisms for the perception of musical emotions in people with hearing loss are unclear. In this study, to investigate the effect of audibility, we measured cortical activity response to the emotional perception of music.

Methods: Normal hearing group (NHO) and simulated high- (NHH), and low- (NHL) frequency hearing loss groups were created by using original stimuli and applying low-, and high-pass filtering (1000 Hz cutoff) to musical stimuli, respectively. A total of 48 healthy participants were randomly assigned to three groups (16 people / group). Fifteen musical stimuli developed in our lab were used for the study. The pre-evaluated stimuli (Lee et al., 2023) were composed of five melodies, and each melody was expressed differently according to emotions including happiness, sadness, and neutrality. During 64-channel EEG recording, participants listened to the randomly presented stimuli binaurally via two speakers followed by ratings of arousal and valence (dimensional model) and selecting emotions (discrete model, thus named discrete). A total of 300 trials were conducted 20 times repeatedly for 15 stimuli.

Results: The NHL group had lower ratings for arousal than the NHH group and for valence than the NHH and NHO groups. To examine the effect of hearing loss, we performed a time-frequency analysis and dynamic imaging of coherent source (DICS) analysis comparing three groups. We also applied surface Laplacian spatial filtering to reduce volume conductivity before time-frequency analysis. We selected trials according to the rating criteria of arousal and valence (happy>7, sad<4, and 4<=neutral<=6) and the percent corrects of emotions. As a result, the topography of the NHL group showed higher alpha activity in parietal channels than the other two groups in all emotions for arousal, valence, and discrete. Therefore, we chose parietal channels to examine the differences of alpha activity among three groups in time-frequency analysis. There are non-significant differences among the three groups with cluster-based permutation tests nonetheless showing increased alpha activities in the NHL group. However, in the DICS analysis, the alpha activity of the NHL group was significantly higher than the NHH group in the right parietal and temporal areas after 2 seconds of stimulation onset in happy stimuli rating over the criteria of valence conditions.

Conclusions: The composer of these stimuli expressed sadness with a slow tempo. This might make it easy for all participants to distinguish sad stimuli, which could lead to non-changing alpha activity among groups. However, in the happy stimuli which were differentiated among groups, the results of DICS analysis suggest that high-frequency audibility rather than low-frequency audibility affects alpha activity response to the perceived emotion of music.

References
1. Caldwell, M., Rankin, S.K., Jiradejvong, P., Carver, C., Limb, C.J., 2015. Cochlear im- plant users rely on tempo rather than on pitch information during perception of musical emotion. Cochlear Implants Int. 16, S114–S120.
2. Hopyan, T., Manno III, F.A., Papsin, B.C., Gordon, K.A., 2016. Sad and happy emotion discrimination in music by children with cochlear implants. Child Neuropsychol. 22, 366–380.
3. Picou EM, Singh G, Goy H, Russo F, Hickson L, Oxenham AJ, et al. 2018 Hearing, emotion, amplification, research, and training workshop: current understanding of hearing loss and emotion perception and priorities for future research. Trends Hear, 22, 2331216518803215

4. Lee J, Han JH, Lee HJ 2023 Development of novel musical stimuli to investigate the perception of musical emotions in individuals with hearing loss. J Korean Med Sci, 27, 38(12): e82

Poster No 986

The genetic architecture of rhythm functional connectivity

Yasmina Mekki[1], Jennifer Below[1], Reyna Gordon[1]

[1]*Vanderbilt university medical center, Nashville, TN*

Introduction: Understanding genetically associated brain individual differences underlying the human capacity to perceive and synchronize to musical rhythm will provide insights into its neural mechanisms. Prior studies linked genetic variation to the ability to move in time with a musical beat and revealed a complex, and polygenic genetic architecture underlying human rhythm. At the brain level, its genetic architecture remains largely unknown. Neural activity measured during task performance is the standard approach to study rhythm processing. However, a growing body of evidence suggests that there is a close correspondence between resting state networks and known cognitive task activation maps (smith et al., 2009, Cole et al., 2014, Tavor et al., 2016). Our aim is to take advantage of resting-state functional MRI data to understand how the brain supports rhythm by unveiling the genetic factors that might contribute to it.

Methods: We used individuals from the UK Biobank cohort with both resting-state functional MRI and genotyping data. We excluded participants with unusual heterozygosity, high missingness, and sex mismatches. We further restricted our analyses to individuals with white British ancestry in order to avoid any possible confounding effects related to ancestry. This resulted in 31,768 individuals (mean age = 55.31, 16,507 females) passing the sample QC. Using PLINK v1.9, we excluded variants with minor allele frequency < 0.01, and imputation quality INFO scores < 0.8. Multiallelic variants were also removed. 53 Regions of interest (ROIs) were defined as the intersection between rhythm networks (informed by Kasdan et al. 2022) and the combination of parcellations from AICHA and Diedrichsen cerebellar atlases. We constructed a rhythm functional connectome for each individual using a shrunk estimate of partial correlation between each pair of the defined ROIs, resulting in 1,378 functional connectivities (FCs) for each individual. These FCs were pre-residualised controlling for covariates including sex, genotype array type, age, recruitment site, and first ten genetic principal components, then normalized using a rank-based inverse-normal transformation. We estimated the SNP-based heritability of the FCs using GCTA (v1.93.0beta) and performed a multivariate genome-wide association study (mGWAS) using MOSTest (Van der meer et al., 2020).

Results: SNP-based heritability analysis showed that 146 out of the 1,378 FCs are heritable (pFDR<0.05). We investigated which genetic variants contribute to the heritable rhythm-related FCs by performing a mGWAS. There were 22 significant loci (genomic threshold p<5e-8) associated with different aspects of the rhythm network. We investigated the shared genetic underlying both brain rhythm network mGWAS and behavioral rhythm GWAS (Niarchou et al., 2022) and found a significant genetic correlation (ρ=0.18, se=±0.05, p=1.93e-14). An extensive functional annotation performed highlighted a significant functional enrichment of genes involved in embryonic brain expression.

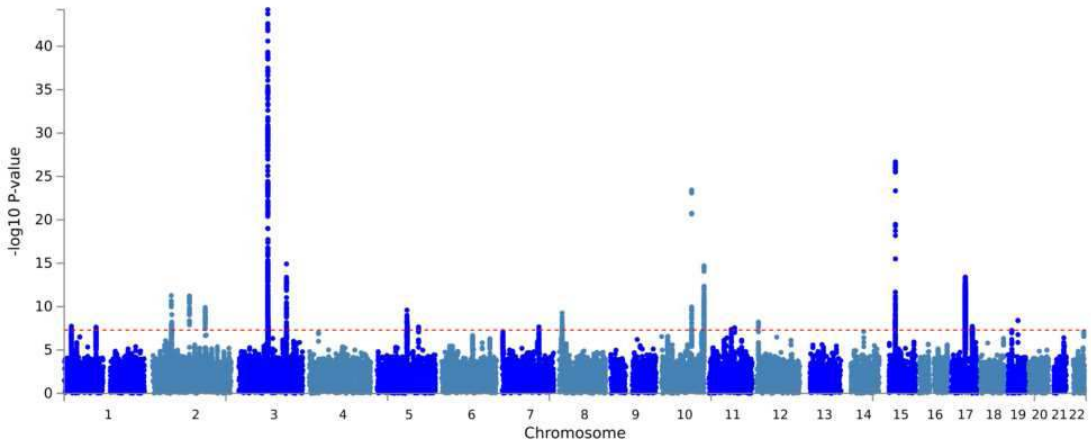

Conclusions: This preliminary work represents a step forward towards understanding how genes influence the neurofunctional basis of human rhythm skills, complementing behavioral results. By using resting-state fMRI data, we tried to contribute to alternative task-free approaches to study behavioral traits such as rhythm and its genetic underpinnings.

References
1. Smith, S. M., Fox, P. T., Miller, K. L., Glahn, D. C., Fox, P. M., Mackay, C. E., ... & Beckmann, C. F. (2009). Correspondence of the brain's functional architecture during activation and rest. Proceedings of the national academy of sciences, 106(31), 13040-13045.
2. Cole, M. W., Bassett, D. S., Power, J. D., Braver, T. S., & Petersen, S. E. (2014). Intrinsic and task-evoked network architectures of the human brain. Neuron, 83(1), 238-251.
3. Tavor, I., Jones, O. P., Mars, R. B., Smith, S. M., Behrens, T. E., & Jbabdi, S. (2016). Task-free MRI predicts individual differences in brain activity during task performance. Science, 352(6282), 216-220.
4. Kasdan, A. V., Burgess, A. N., Pizzagalli, F., Scartozzi, A., Chern, A., Kotz, S. A., ... & Gordon, R. L. (2022). Identifying a brain network for musical rhythm: A functional neuroimaging meta-analysis and systematic review. Neuroscience & Biobehavioral Reviews, 136, 104588.
5. van der Meer, D., Frei, O., Kaufmann, T., Shadrin, A. A., Devor, A., Smeland, O. B., ... & Dale, A.
6. M. (2020). Understanding the genetic determinants of the brain with MOSTest. Nature communications, 11(1), 3512.
7. Niarchou, M., Gustavson, D. E., Sathirapongsasuti, J. F., Anglada-Tort, M., Eising, E., Bell, E., ... & Gordon, R. L. (2022). Genome-wide association study of musical beat synchronization demonstrates high polygenicity. Nature Human Behaviour, 6(9), 1292-1309.

Poster No 987

Electrophysiological resting-state signatures link polygenic scores to general intelligence

Rebecca Engler[1], Dorothea Metzen[2], Stefan Arnau[3], Javier Schneider Penate[4], Christina Stammen[3], Jan Digutsch[5], Patrick Gajewski[3], Stephan Getzmann[3], Christoph Fraenz[3], Jörg Reinders[3], Fabian Streit[6], Sebastian Ocklenburg[7], Daniel Schneider[3], Michael Burke[3], Jan Hengstler[3], Carsten Watzl[3], Michael Nitsche[3], Robert Kumsta[8], Edmund Wascher[3], Erhan Genc[1]

[1]Leibniz Research Centre for Working Environment and Human Factors, Dortmund, Germany, [2]Klinische und Biologische Psychologie, Technische Universität Dortmund, Dortmund, Germany, [3]Leibniz Research Centre for Working Environment and Human Factors at the Technical University of Dor, Dortmund, Germany, [4]Department of Neuropsychology, Ruhr University Bochum, Bochum, Germany, [5]Institute of Behavioral Science and Technology, University of St. Gallen, St. Gallen, Switzerland, [6]Central Institute of Mental Health, Medical Faculty Mannheim, Mannheim, Germany, [7]Department of Psychology, Medical School Hamburg, Hamburg, Germany, [8]Department of Behavioural and Cognitive Sciences, Luxemburg, Luxembourg

Introduction: Interindividual differences in human intelligence, especially the neural underpinnings they arise from, have fascinated researchers for over a century. Intelligence is a highly polygenic trait and the most reasonable pathway from genetic disposition to intelligent thinking involves changes to specific brain properties as an intermediate step. The relationships between genes and intelligence as well as intelligence and various neural correlates have been studied for decades, albeit separately from another. Research investigating the entire pathway from genes via brain properties to intelligence remains scarce. In the recent past, it has been shown that the link between polygenic scores (PGS), a genetic summary measure, and general intelligence is to some extent mediated by the structural network connectivity of specific brain regions as derived from diffusion-weighted imaging. Another method of investigating the brain's connectome, often overlooked by intelligence researchers, is resting-state electroencephalography (rs-EEG). Here, we employed rs-EEG to investigate whether regional and global markers of network efficiency and clustering can serve as mediators of the biological-functional pathway via which genetic variants shape intelligence.

Methods: We computed PGS of intelligence in a large sample comprising 520 healthy individuals from the Dortmund Vital Study (ClinicalTrials.gov Identifier: NCT05155397). To investigate potential age differences, the data of young adults (< 40 years of age) and older adults (> 40 years of age) were analyzed separately. All participants completed a cognitive test battery and underwent rs-EEG recordings (eyes closed) on a 64-channel system before and after the test battery. Scores from the cognitive test battery were subjected to confirmatory factor analysis to obtain a general factor of intelligence (g). Resting-state EEG recordings were analyzed by means of graph theory to quantify the brain's functional connectivity across different frequencies (delta, theta, high alpha, low alpha, beta). We tested whether graph theoretical measures, such as efficiency and clustering, mediated the association between PGS and g by means of elastic-net regressions. This was done on a whole-brain level as well as for local brain regions, as derived from EEG source localization. Functional connectivity between brain regions was estimated in the form of spectral coherence. As the rs-EEG was recorded twice, approximately two hours apart from each other, we also computed the test-retest reliability of rs-EEG metrics.

Results: As expected, our results revealed an association between g and PGS of intelligence. The rs-EEG metrics showed good to excellent test-retest reliability across all frequencies and in both age groups. On the whole-brain level, we did not observe any associations between PGS, rs-EEG metrics, and g. On the level of single brain regions, we found rs-EEG metrics of specific frequency bands to be related to g. These associations were partly different for younger and older adults. In the younger adults, the association between PGS and g was mainly mediated by beta and theta band nodal efficiency as well as theta band local clustering in areas predominantly located in parieto-frontal regions. In older adults, the association between

PGS and intelligence was mainly mediated by low alpha and theta band nodal efficiency in areas predominantly located in parieto-visual regions.

Conclusions: This study represents a crucial first step in the endeavor of identifying the missing neural links in the pathway from genetic variability to cognitive performance. Our results indicate that the brain's short- and long-range information transfer is impacted by an individual's genetic predisposition, which in turn affects general intelligence. The observation that respective associations varied between young and older adults is highly relevant for attempts to mitigate age-related cognitive decline via techniques such as individualized brain stimulation.

References

1. Genç, E. et al. (2023), `Structural architecture and brain network efficiency links polygenic scores to intelligence`, Human Brain Mapping. 04 April, https://doi.org/10.1002/hbm.26286. Epub.

Poster No 988

What can errors in reasoning tell us about inductive biases in human abstract rule learning?

Caroline Ahn[1,2], Quan Do[1,3], Leah Bakst[4,2], Michael Pascale[4,2], Joseph McGuire[4,1,2], Michael Hasselmo[4,1,3], Chantal Stern[4,2,1]

[1]Graduate Program for Neuroscience, Boston University, Boston, MA, [2]Cognitive Neuroimaging Center, Boston University, Boston, MA, [3]Center for Systems Neuroscience, Boston University, Boston, MA, [4]Department of Psychological and Brain Sciences, Boston University, Boston, MA

Introduction: Humans can extract rules from limited examples and generalize them across contexts, an ability that is lacking in AI. We propose that selecting the right level of abstraction for rule representations is key to fast, flexible learning, and in humans this process is guided by inductive biases – our pre-existing assumptions about data structure and rule relations[1,2]. However, these biases can lead to errors in reasoning. It is unknown to what degree these inductive biases are shared across individuals, and whether they prioritize certain features over others during rule learning. We present our behavioral findings from a novel, visuospatial abstract rule learning task, the Cognitive Neuro Abstraction and Reasoning Corpus (CogNARC). Future fMRI work using this task is planned. CogNARC is an open-response task that tests few-shot learning and requires subjects to generate solutions on an interactive interface. The original task was introduced as a benchmark for AI abstraction and generalization, but has also been used to study human cognition[3,4,5]. CogNARC reasoning problems are varied in the types and numbers of rules that dictate input-output solutions. A single problem can contain multiple rules with complex conditional relations. Learned rules do not carry over across problems. Therefore, CogNARC is less forgiving to random guessing or brute force methods compared to other measures of abstract reasoning, which tend to be multiple-choice and can be extensively trained upon[6,7,8]. With CogNARC, we are able to identify where reasoning tends to fail by systematically probing different types of human errors.

Methods: We collected online behavioral data from 220 subjects (52.27% male) on Amazon Mechanical Turk. Subjects ranged in age from 20 to 35 years (M = 29.6, SD = 4.1). 75 problems were selected to represent a variety of rules and difficulty levels. Subjects were allowed up to 4 hours to complete all problems. Subjects learned input-output transformation rules from 2 – 6 example pairs, then applied the rules to a test input by drawing their own output on an editable grid. They were allowed up to 3 attempts per trial and were paid $5 for task completion, with a performance bonus of up to $15. To identify common errors, we transformed action sequences into graphical representations and applied hierarchical clustering algorithms to group solutions by shared strategies across subjects. We chose the graph analysis approach due to its efficiency in representing abstract concepts and quantifying their relationships[8,9].

Results: Our exploratory examination aimed to identify a qualitative interpretation for clusters that emerged from the data-driven graph analysis. Subjects' accuracy on the CogNARC task (M = 78.9%, SD = 19.4%) greatly outperformed AI programs (21% best accuracy[10]). While some erroneous solutions could be attributed to carelessness, motor error, or random guessing, most were conceptually close to the correct solution but arose from mis-learning of rule relations. These errors were more evident in complex problems that required learning of hierarchical rules across multiple feature dimensions. By studying these errors, we were able to infer inductive biases of subjects such as a tendency towards color-based over size- or pattern-based rules. In cases where multiple inductive biases were present, a hierarchy of these biases emerged.

Conclusions: The task design of CogNARC is well-suited for studying the formation and structure of abstract rule representations in humans. In particular, graphical analysis of action sequences allows for in-depth investigation into how common error patterns reflect underlying inductive biases which lead humans to assume rule relations for certain features and

ignore others. Future work will study cognitive processes during CogNARC with methods such as eye-tracking, EEG, or fMRI, with the aim of mapping the behavioral results from this study to the underlying brain activity.

References
1. Heit, E. (2000), 'Properties of Inductive Reasoning', Psychonomic Bulletin & Review, vol. 7, pp. 569-592.
2. Griffiths, T.L. (2010), 'Probabilistic Models of Cognition: Exploring Representations and Inductive Biases', Trends in Cognitive Sciences, vol. 14, no. 8, pp. 357-364.
3. Chollet, F. (2019), 'On the Measure of Intelligence', arXiv preprint arXiv:1911.01547.
4. Johnson, A. (2021), 'Fast and Flexible: Human Program Induction in Abstract Reasoning Tasks', arXiv preprint arXiv:2103.05823.
5. Acquaviva, S. (2022), 'Communicating Natural Programs to Humans and Machines', Advances in Neural Information Processing Systems, vol. 35, pp. 3731-3743.
6. Raven, J. (2003), 'Raven Progressive Matrices', In Handbook of Nonverbal Assessment (pp. 223-237). Boston, MA: Springer US.
7. Zerroug, A. (2022), 'A Benchmark for Compositional Visual Reasoning', Advances in Neural Information Processing Systems, vol. 35, pp. 29776-29788.
8. Odouard, V.V. (2022), 'Evaluating Understanding on Conceptual Abstraction Benchmarks', arXiv preprint arXiv:2206.14187.
9. Wille, R. (1997), 'Conceptual Graphs and Formal Concept Analysis', In Conceptual Structures: Fulfilling Peirce's Dream: Fifth International Conference on Conceptual Structures, ICCS'97 Seattle, Washington, USA, August 3–8, 1997 Proceedings 5 (pp. 290-303). Springer Berlin Heidelberg.
10. Zhu, G. (2016), 'Computing Semantic Similarity of Concepts in Knowledge Graphs', IEEE Transactions on Knowledge and Data Engineering, vol. 29, no. 1, pp. 72-85.

Poster No 989

Historical Feedback Representations in the Brain Robustly Guide Learning

Sangsoo Jin[1], Juhyeon Lee[1], Jong-Hwan Lee[1]

[1]Department of Brain and Cognitive Engineering, Korea University, Seoul, Korea, Republic of

Introduction: A developing child often needs to guess the internal structure of the environment only relying on received feedback[1]. Similarly, reinforcement learning models can construct representations of learning from the action-feedback loop without any instructions[2]. We identified robust neural representations during feedback-guided learning using a novel real-life task.

Methods: We developed a novel feedback-guided learning task called the Photographer paradigm[3] (Fig. 1a). Participants virtually explored five city scenes in random order and captured eight photographs for each city or run. They were instructed to capture scenes with the highest feedback score. Internally, the feedback scores were computed as conceptual similarities between captured scenes and the target context (shared across the cities) via a Contrastive Language-Image Pretraining (CLIP) model[4]. Neither the target context nor internal mechanics of feedback were instructed to participants. The fMRI data was collected using a 3-T Siemens Tim-Trio MRI scanner with a 12-channel head coil (TR = 2000 ms; TE = 30 ms; 3×3×4 mm3 voxel size). We independently analyzed[5] 32 participants as the Discovery (n = 16; acquired in 2022) and Validation (n = 16; acquired in 2023) groups. We first applied a standard preprocessing pipeline using fMRIPrep 23.0.2[6]. Run-wise GLMs were fitted using 3dDeconvolve to identify trial-wise Feedback betas while controlling the systematic effect of head motions. We investigated what kind of feedback information is robustly represented within each run using representational similarity analysis (RSA). Fig. 1b depicts model representation dissimilarity matrices (RDMs) with three levels of historical information. In counterpart, neural RDMs were defined from trial-wise Feedback betas within the 3-voxel radius searchlight spheres[7]. To focus on within-run learning components while minimizing systematic variations between runs, we performed RSA by each run separately and averaged run-wise RSA maps. Group inferences were conducted by a one-sample t-test for each historical model using 3dttest++. We identified robust RSA clusters (voxel-wise $p < 0.005$ and cluster-level $\alpha < 0.05$) that were significant in both the Discovery and Validation groups. We further hypothesized that the strength of the within-run feedback representation in a cluster may predict the level of within-run learning[8]. Linear mixed-effect models were fitted to estimate mean feedback scores of the current or following runs from the median RSA strength in each cluster.

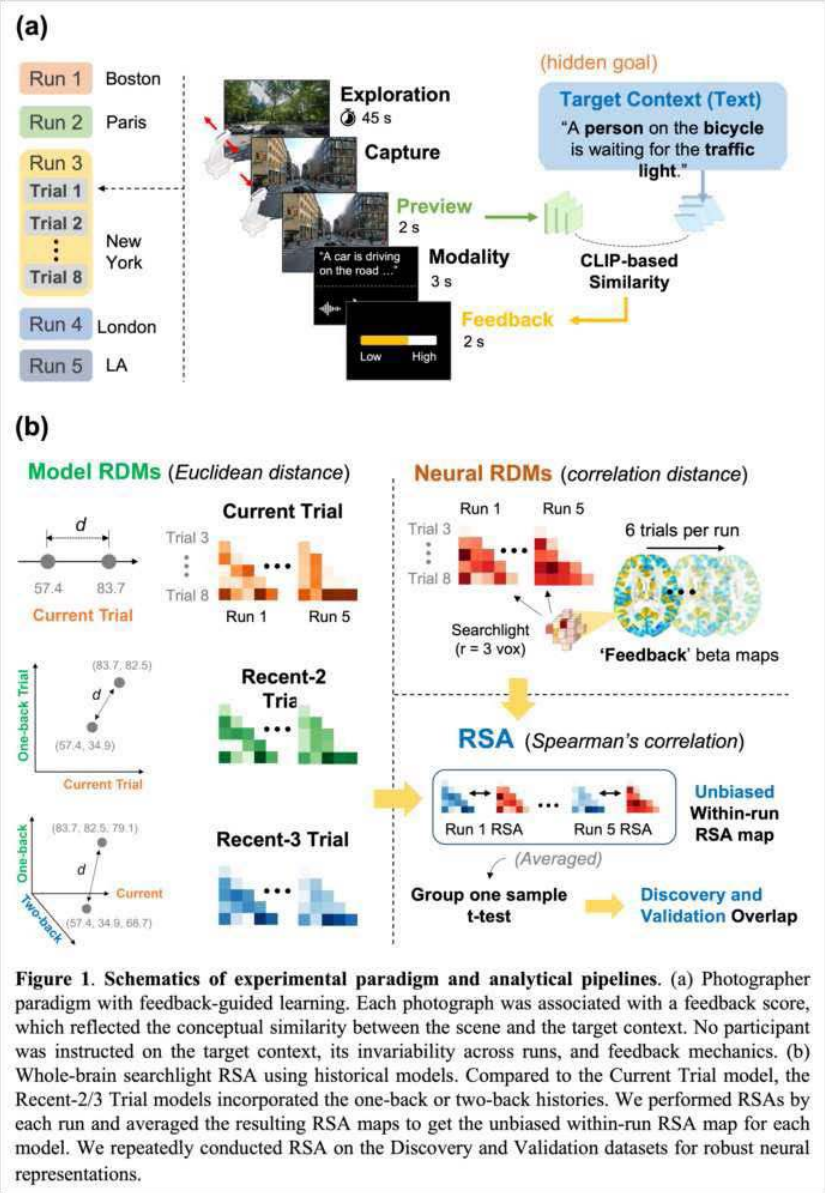

Figure 1. Schematics of experimental paradigm and analytical pipelines. (a) Photographer paradigm with feedback-guided learning. Each photograph was associated with a feedback score, which reflected the conceptual similarity between the scene and the target context. No participant was instructed on the target context, its invariability across runs, and feedback mechanics. (b) Whole-brain searchlight RSA using historical models. Compared to the Current Trial model, the Recent-2/3 Trial models incorporated the one-back or two-back histories. We performed RSAs by each run and averaged the resulting RSA maps to get the unbiased within-run RSA map for each model. We repeatedly conducted RSA on the Discovery and Validation datasets for robust neural representations.

Results: Fig. 2a-b represents the model RDMs and associated neural clusters that were significant across the Discovery and Validation groups. Only historical models (i.e., Recent-2/3 Trial) were robustly represented in two groups. Notably, the middle orbital gyrus (MOG) and inferior frontal gyrus encoded historical dynamics during feedback phases. The ventral striatum was associated with the Recent-3 Trial model, suggesting that the dopaminergic learning signal may incorporate the current, one-back, and two-back trials. We found an association between the neural-model coupling and the level of within-run learning. Fig 2c elucidates the RSA strength of the Recent-3 Trial model in the MOG area predicted the mean feedback score of the following run rather than the current run. This effect remains significant after controlling the previous mean feedback and variability of individuals and runs.

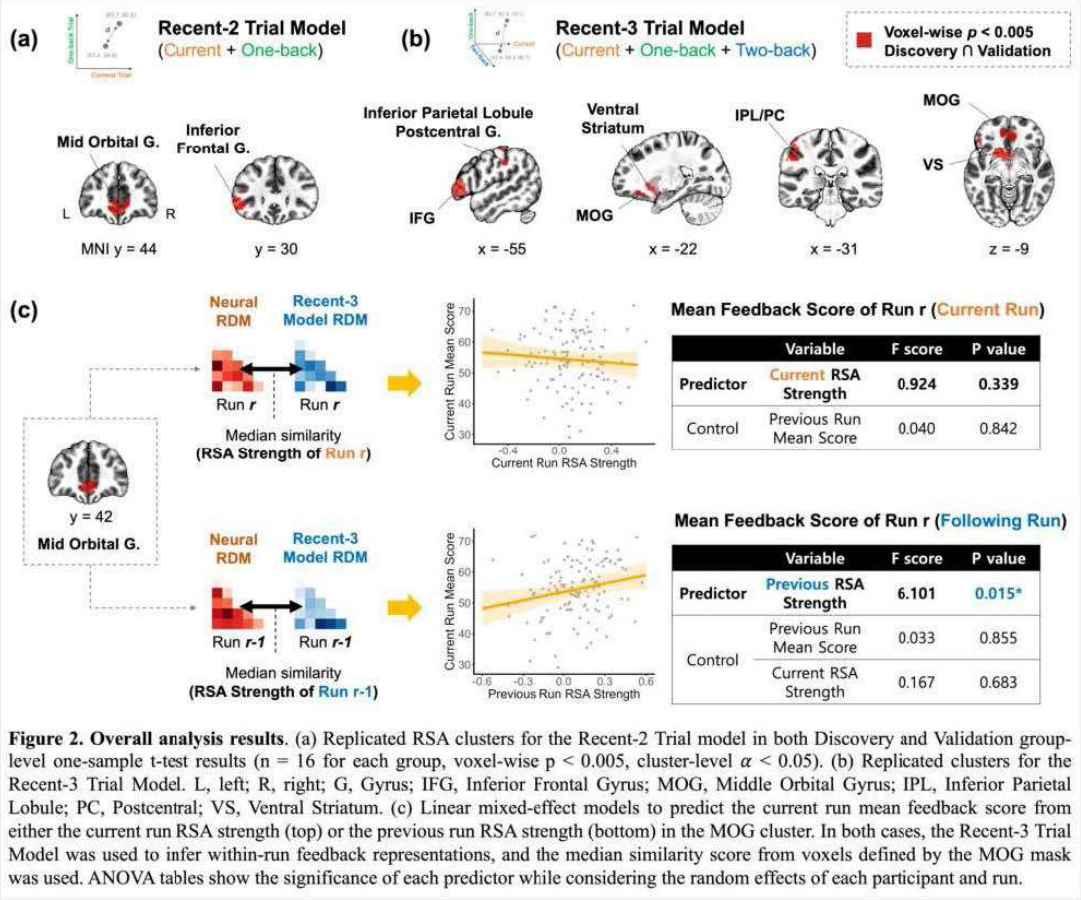

Figure 2. Overall analysis results. (a) Replicated RSA clusters for the Recent-2 Trial model in both Discovery and Validation group-level one-sample t-test results (n = 16 for each group, voxel-wise $p < 0.005$, cluster-level $\alpha < 0.05$). (b) Replicated clusters for the Recent-3 Trial Model. L, left; R, right; G, Gyrus; IFG, Inferior Frontal Gyrus; MOG, Middle Orbital Gyrus; IPL, Inferior Parietal Lobule; PC, Postcentral; VS, Ventral Striatum. (c) Linear mixed-effect models to predict the current run mean feedback score from either the current run RSA strength (top) or the previous run RSA strength (bottom) in the MOG cluster. In both cases, the Recent-3 Trial Model was used to infer within-run feedback representations, and the median similarity score from voxels defined by the MOG mask was used. ANOVA tables show the significance of each predictor while considering the random effects of each participant and run.

Conclusions: We identified historical feedback representations in the brain during real-life, feedback-guided learning. The ventromedial reward network[9] may encode the current feedback structure even when the goal is unknown, and the learned structure would help future learning. Our study may suggest critical neural signatures of feedback-guided learning that are generalizable for humans[6] and reinforcement learning models[10].

References

1. Nussenbaum K and Hartley C A 2019 Reinforcement learning across development: What insights can we draw from a decade of research? Dev. Cogn. Neurosci. 40 100733
2. Cross L, Cockburn J, Yue Y and O'Doherty J P 2021 Using deep reinforcement learning to reveal how the brain encodes abstract state-space representations in high-dimensional environments Neuron 109 724-738.e7
3. Jin S, Lee J and Lee J-H 2023 How to Be a Good Photographer: Multi-modal Learning In a Real-life Environment
4. Radford A, Kim J W, Hallacy C, Ramesh A, Goh G, Agarwal S, Sastry G, Askell A, Mishkin P, Clark J, Krueger G and Sutskever I 2021 Learning Transferable Visual Models From Natural Language Supervision (arXiv)
5. Kim H-C, Jang H and Lee J-H 2020 Test–retest reliability of spatial patterns from resting-state functional MRI using the restricted Boltzmann machine and hierarchically organized spatial patterns from the deep belief network J. Neurosci. Methods 330 108451
6. Esteban O, Markiewicz C J, Blair R W, Moodie C A, Isik A I, Erramuzpe A, Kent J D, Goncalves M, DuPre E, Snyder M, Oya H, Ghosh S S, Wright J, Durnez J, Poldrack R A and Gorgolewski K J 2019 fMRIPrep: a robust preprocessing pipeline for functional MRI Nat. Methods 16 111–6
7. Lee J, Jung M, Lustig N and Lee J-H 2023 Neural representations of the perception of handwritten digits and visual objects from a convolutional neural network compared to humans Hum. Brain Mapp. 44 2018–38
8. Kim D-Y, Jung E K, Zhang J, Lee S-Y and Lee J-H 2020 Functional magnetic resonance imaging multivoxel pattern analysis reveals neuronal substrates for collaboration and competition with myopic and predictive strategic reasoning Hum. Brain Mapp. 41 4314–31
9. Bartra O, McGuire J T and Kable J W 2013 The valuation system: A coordinate-based meta-analysis of BOLD fMRI experiments examining neural correlates of subjective value NeuroImage 76 412–27
10. Botvinick M, Ritter S, Wang J X, Kurth-Nelson Z, Blundell C and Hassabis D 2019 Reinforcement Learning, Fast and Slow Trends Cogn. Sci. 23 408–22

11. Acknowledgment: This work was supported by the National Research Foundation (NRF) grant funded by the Korea government (MSIT) (NRF-2021M3E5D2A01022515, No. RS-2023-00218987), and in part by the Electronics and Telecommunications Research Institute (ETRI) grant funded by the Korean government. [23ZS1100, Core Technology Research for Self-Improving Integrated Artificial Intelligence System].

Poster No 990

Phase alignment as a neural mechanism for crossmodal temporal prediction

Rebecca Burke[1], Jonathan Daume[2], Till Schneider[1], Andreas Engel[1]

[1]University Medical Center Hamburg-Eppendorf (UKE), Hamburg, Germany, [2]Cedars-Sinai Medical Center, Los Angeles, CA, USA

Introduction: Our representation of time is embedded within multisensory perception, such as sight, sound or touch (Buzsáki, 2017). However, despite being a crucial aspect of daily life, the neural dynamics of crossmodal temporal predictions remain elusive. The objective of this study was to investigate neural correlates of tactile-to-visual influences on temporal prediction using Magnetoencephalography (MEG). We hypothesized increased inter-trial phase consistency (ITPC) in the low-frequency delta range [0.5-3Hz], corresponding to the length of the temporal prediction intervals. Additionally, stronger ITPC values should correlate with a steeper slope of the psychometric function, indicating phase alignments as a likely cause for more consistent temporal predictions.

Methods: The study was conducted within one MEG session employing a modified version of the time prediction task by Roth (2013) and Daume (2021). Participants (N=23) observed a visual stimulus moving towards an occluder. Shortly before reaching the occluder, the visual stimulus faded in luminance to make the visual offset less informative. Instead, participants received a brief tactile stimulus to the ipsilateral hand at the timepoint of disappearance, generating a temporal expectation regarding its reappearance on the opposite side of the occluder. After variable time intervals, a visual stimulus reappeared, and participants had to indicate whether this was “too early” or “too late” compared to the movement before disappearance. A non-predictive control condition involved participants judging the variable luminance of the reappearing visual stimulus compared to its initial luminance in the beginning of the trial. The order of conditions was randomized, and feedback was provided at the end of each block. Psychometric curves were fitted to the behavioural data of each participant and condition, and MEG recordings were analysed using time-frequency representations obtained through wavelet convolution. To compare spectral power and ITPC estimates between conditions within frequency bands showing significant differences to the pre-stimulus baseline, we used cluster-based permutation statistics. Pearson’s correlations were employed to examine the relationship between ITPC or power estimates and the steepness of each participant’s psychometric function.

Results: ITPC analysis revealed strong increases in the delta range [0.5-3Hz] around stimulus disappearance and reappearance. Delta ITPC was significantly stronger during temporal prediction compared to the control condition (cluster-p=.02) in time bins around 200ms to 900ms after disappearance, indicated by cluster-based permutation analyses. This cluster included sensors from right temporal and frontal regions, contralaterally to the visuo-tactile stimulus presentation. Spectral power analysis also showed significant increases in the delta band around movement onset, disappearance, and reappearance compared to baseline. However, delta ITPC, but not delta power, correlated with the the steepness of the psychometric curve (r=0.47, p=.01). Notably, this correlation was not observed in the non-predictive control condition.

Conclusions: Our findings suggest that the increase in delta ITPC is likely due to a phase reset driven by the temporal prediction process rather than evoked neural activity. Furthermore, our results indicate that phase alignments occur during crossmodal visuo-tactile-to-visual temporal predictions, even with a combination of non-rhythmic and discrete stimulation. This highlights the broad applicability of phase resets as a mechanism for predicting timing across various types of stimuli. Overall, this study provides valuable insights into the neural mechanisms involved in anticipating upcoming crossmodal events by elucidating the role of phase alignments.

References

1. Buzsáki, G. (2017), ‘Space and Time in the Brain’. Science, vol. 358, no. 6362, pp. 482-485.
2. Daume, J. (2021), ‘Non-Rhythmic Temporal Prediction Involves Phase Resets of Low-Frequency Delta Oscillations’, NeuroImage, vol. 224, pp. 117376.
3. Roth, M. J. (2013), ‘The Cerebellum Optimizes Perceptual Predictions about External Sensory Events’, Current Biology, vol. 23, no. 10, pp. 930-935.

Poster No 991

Generic neural computational construct for instantaneous estimation: a pilot study

Lydia Yingzhe Li[1], Guang Ouyang[2]

[1]The University of Hong Kong, Hong Kong, Hong Kong, [2]The University of Hong Kong, Hong Kong, Hong Kong

Introduction: Instantaneous estimation of scale, spanning numerical, spatial, and temporal domains, stands as a fundamental skill crucial to our daily functioning. For instance, the split-second estimations involved in throwing a grenade--calculating target distance, grenade weight, and explosion timing-signify its vital role in decisive moments. This efficiency hints at a shared computational construct underlying these estimations, which is also supported by empirical evidence such as SNARC effect (Dehaene et al., 1993). However, a comprehensive investigation into a unified framework encompassing instantaneous estimations across various domains is lacking. Our study utilizes EEG's high temporal resolution to investigate these fast time scale cognitive processes. Both neural and behavioral indicators were collected to model the construct structure based on structure equation modelling. We aim to address two questions: 1. Are these estimations governed by unified brain computational mechanism? 2. If so, is it differentiable from other basic cognitive abilities such as working memory and mental speed?

Methods: We employed two distinct approaches based on five tasks: one examines the convergent validity by identifying shared construct across the three domains for instantaneous estimations, while the other examines the discriminant validity by comparing these constructs against working memory and mental speed (Figure 1). Numerical estimation: Subtask 1 involves judging "more" or "less" on two dot sets that slightly vary in total number. Subtask 2 (control task) presents two frames: the first replicates subtask 1, while the second might add or remove five dots from the first frame. Participants judged if the two frames are identical. Visual consistency between subtask 1 and 2 enables us to isolate ERP effect related to numerical estimation. Spatial estimation: Participants assessed whether a line passes through the center of a circle. Trials vary in difficulty based on the line-center distance. ERP differences between easy and hard conditions can be obtained to represent spatial estimation. Temporal estimation: Subtask 1 involved discriminating between sounds of slightly different durations. Subtask 2 (control task) presented the same sounds without prompting duration estimation. Auditory consistency between two subtasks allows us to isolate ERP effect related to temporal estimation. Working memory: Delayed match-to-sample paradigm was adopted. Participants identified if the three delayed comparison stimuli are identical with the target. We assessed the working memory load by comparing ERPs corresponding to the sample and comparison stimuli. Mental speed: This task measures how quickly participants respond to stimuli by pressing a button. We examined the N1 latency and used it as a neural indicator of perceptual mental speed.

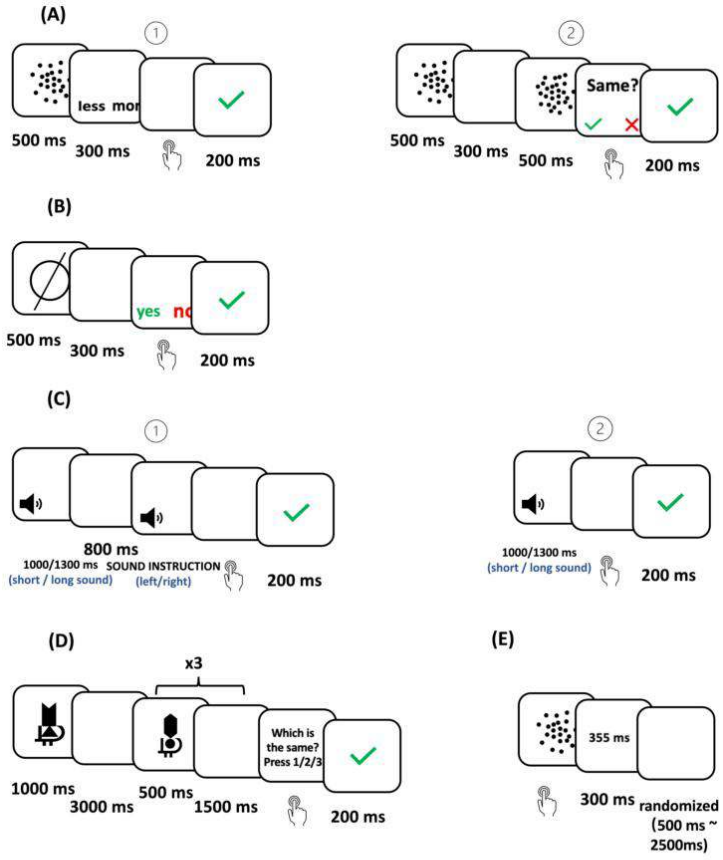

Figure 1. The schematic diagrams outlining one trial for each task (A-E): numerical estimation task, spatial estimation task, temporal estimation task, working memory task, and mental speed task.

Results: Based on 15 participants in the pilot study, we have successfully identified significant neural effects from all of tasks (except for the mental speed where only latency is needed. See the detailed effect patterns in Figure 2A-E). These neural effects were used to examine the inter-task relationships, shown in the correlation matrix in Figure 2F (together with the behavioral counterpart). The correlations between numerical, spatial, and temporal estimation largely aligned with our expectations. We have also conducted power analysis based on the correlation (Wang & Rhemtulla, 2020), which estimated a requirement of 200 participants. The structural relationships between the construct of instantaneous estimation and other basic abilities will be examined by SEM as shown in Figure 2G.

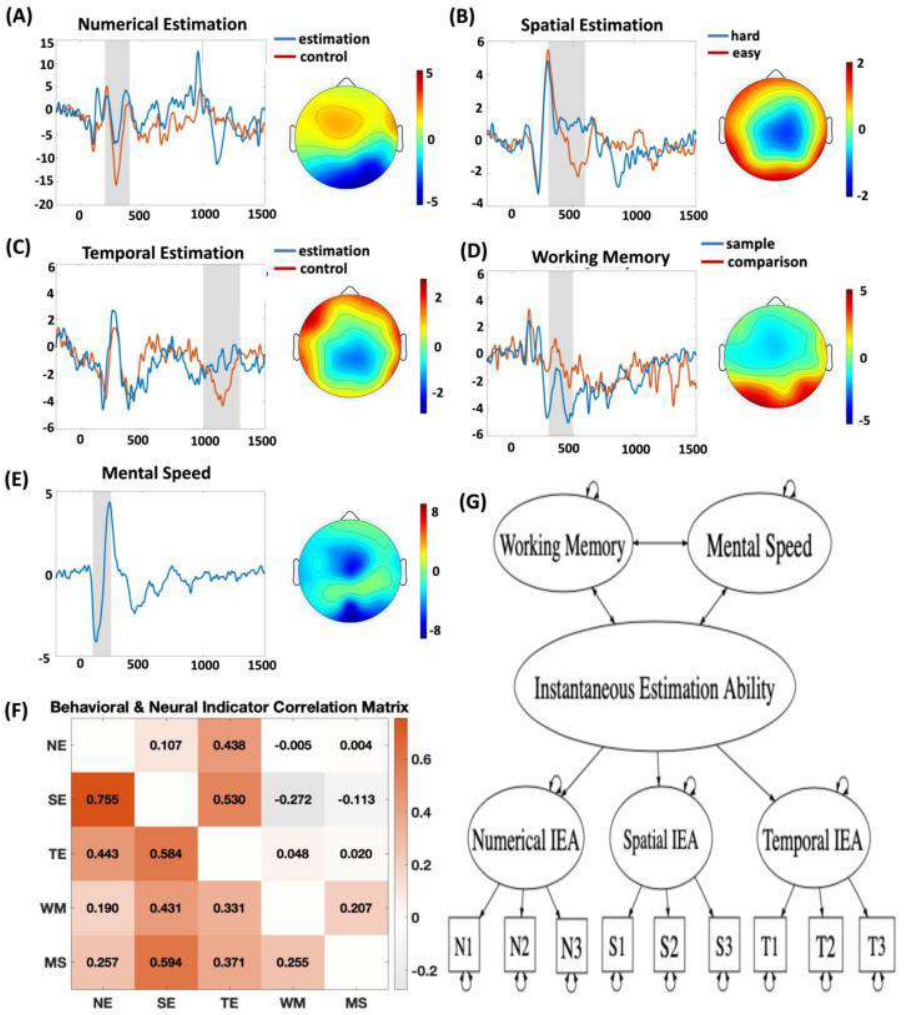

Figure 2. Neural Effects in different tasks. The ERP waveforms were generated by averaging data from electrodes showing the most pronounced effects. The scalp maps display ERP differences between conditions (with the exception of the **(E)** mental speed task, demonstrating the topography of N1 component), extracted from the time windows marked by the gray-shaded area. Details of ERP subtraction method to extract effects: **(A)** numerical estimation: estimation minus control; **(B)** spatial estimation: hard minus easy; **(C)** temporal estimation: estimation minus control; **(D)** working memory: sample minus comparison. **(F)** Correlation matrices of behavioral indicators (lower triangular) and neural indicators (upper triangular). **(G)** Conceptual structural equation model.

Conclusions: Our study on instantaneous estimation across domains unveils intricate task relationships. Initial findings show intriguing connections despite some divergence, highlighting the necessity for further investigation using a larger sample via structural equation modeling.

References

1. Dehaene, S., et al. (1993), 'The mental representation of parity and number magnitude', Journal of Experimental Psychology: General, vol. 122, no. 3, pp. 371–396, https://doi.org/10.1037/0096-3445.122.3.371
2. Wang, Y. A., et al. (2020), 'Power analysis for parameter estimation in structural equation modeling: A discussion and tutorial', Structural Equation Modeling: A Multidisciplinary Journal, vol. 27, no. 4, pp. 555-580.

Poster No 992

Dissociable Neuroanatomical Correlates of Spatial and Temporal Processing

Masakazu Sugimoto[1,2], Ikko Kimura[3], Masamichi Hayashi[1,2]

[1]Graduate School of Frontier Biosciences, Osaka University, Suita, Japan, [2]Center for Information and Neural Networks, Advanced ICT Research Institute, National Institute of Information and Communications Technology, Suita, Japan, [3]Laboratory for Brain Connectomics Imaging, RIKEN Center for Biosystems Dynamics Research, Kobe, Japan

Introduction: Processing time and space is critical for optimizing our perception and behavior in an ever-changing environment. The ability to process temporal and spatial information is highly variable across individuals. While both temporal and spatial processing are known to involve frontoparietal circuits (Hayashi et al., 2018; Sack et al., 2007), it is unclear whether an individual's ability to discriminate temporal and spatial information is reflected in brain structures. To identify the neuroanatomical correlates of temporal and spatial processing, here we investigated whether interindividual differences in duration and orientation estimation ability correlate with gray matter (GM) and white matter (WM) structures.

Methods: Thirty-seven right-handed adults participated in three experimental sessions. In the first session, we collected structural (T1-weighted, 0.8 mm isotropic) and diffusion MRI (69 directions, 1.7 mm isotropic, b = 0, 700 and 2000) data using 3T MRI. In the following two sessions, we tested participants' spatiotemporal processing ability by measuring duration and orientation discrimination thresholds using the one-up-three-down staircase method, two times per session. In the duration task, two visual stimuli (i.e., black disks) were presented sequentially and participants judged whether the second disk was presented for a shorter or longer duration than the first. In the orientation task, two Gabor patches were presented sequentially and participants judged whether the orientation of the second stimulus was rotated clockwise or counterclockwise with respect to the first. The mean of the last six reversal points obtained in each measurement, which lasted 270 s for the duration task and 215 s for the orientation task, was averaged over the two measurements. Individual thresholds were then determined by averaging the mean thresholds collected over the two experimental sessions. To identify the brain structures associated with the ability to process temporal and spatial information, we examined the correlations between individual differences in behavioral thresholds and regional GM volume and the two metrics of WM microstructural integrity, fractional anisotropy (FA) and mean diffusivity (MD), using SPM12 and FSL software.

Results: Our analyses revealed that individuals with greater GM volume in the right inferior frontal operculum, left middle frontal gyrus, and right inferior temporal gyrus were associated with better duration discrimination abilities, whereas no correlations were found for any metrics of WM structure. In contrast, larger GM volumes in the left lingual gyrus, smaller GM volumes in the right superior occipital gyrus, and crus1 in the bilateral cerebellum were associated with better orientation discrimination thresholds. In addition, larger MD values of the WM structure in the left superior longitudinal fasciculus and the inferior fronto-occipital fasciculus were also associated with better orientation discrimination thresholds. Given the previous study showing that the inferior front-occipital fasciculus connects the lingual gyrus with the inferior frontal gyrus (Palejwala et al., 2021), our results suggest that this pathway may be critical for orientation discrimination. FA values were not associated with interindividual differences in orientation discrimination performance.

Conclusions: Our study shows that individual differences in GM volume of frontal and temporal regions were associated with duration estimation performance. In contrast, GM volume of the occipital regions and bilateral cerebellum, as well as WM structures associated with left occipital-frontal pathways, were correlated with the ability to estimate orientation. In conclusion, our findings suggest that distinct GM and WM structures reflect interindividual differences in the ability to process temporal and spatial information.

References

1. Hayashi, M. J., van der Zwaag, W., Bueti, D., & Kanai, R. (2018). Representations of time in human frontoparietal cortex. Communications Biology, 1(1), 1–10.
2. Sack, A. T., Kohler, A., Bestmann, S., Linden, D. E. J., Dechent, P., Goebel, R., & Baudewig, J. (2007). Imaging the brain activity changes underlying impaired visuospatial judgments: Simultaneous fMRI, TMS, and behavioral studies. Cerebral Cortex, 17(12), 2841–2852.
3. Palejwala, A. H., Dadario, N. B., Young, I. M., O'Connor, K., Briggs, R. G., Conner, A. K., O'Donoghue, D. L., & Sughrue, M. E. (2021). Anatomy and White Matter Connections of the Lingual Gyrus and Cuneus. World Neurosurgery, 151, e426–e437.

Poster No 993

Time in action: action time estimation following unilateral brain damage

Valentina Pacella[1], Michele Scandola[2], Maria Bà[2], Maddalena Beccherle[2], Nicola Smania[2], Daniele Volpe[3], Elena Rossato[4], Valentina Moro[2]

[1]University School for Advanced Studies (IUSS-Pavia), Pavia, Pavia, [2]University of Verona, Verona, Verona, [3]Casa di Cura Villa Margherita via Costacolonna n 1 Arcugnano, Vicenza, Italy, Vicenza, Vicenza, [4]IRCSS Sacro Cuore Don Calabria, [37]024 Negrar, Verona, Italy, Verona, Verona

Introduction: Time perception is a multifaceted concept[1], and the neural mechanisms underlying it are not yet fully understood. Additionally, temporal perception can be influenced by physical attributes of the stimulus[2], such as its intensity or movement, further complicating the matter. While prior research has shown that time perception can be affected following a brain lesion[3,4], the specific roles of the left and right hemispheres are still largely unknown. In order to shed light on this topic, this study conducted two experiments to assess the temporal estimation abilities of 33 patients with unilateral brain lesions in response to multi-second actions and non-biological movements. Additionally, the study explores the potential modulatory effects of induced embodiment processes on temporal estimation.

Methods: The Action Time Estimation (ATE, Figure 1a) task was used to measure potential differences between left (N = 13), right brain damage (with (AHP, N = 7) and without (RBD, N = 13) anosognosia for hemiplegia) and control (N = 42) groups in estimating the temporal durations (3000, 4500, 6500 ms) of actions presented as a series of videos. These included the use of a tool (by the left or right hand) with actions seen from a first-person perspective. A control task showed a vertical movement of a circle toward a horizontal line (Movement-Time Estimation MTE, Figure 1c). Embodiment effects on time estimation were investigated via two additional tasks. In one, embodiment was inhibited by removing the hand from the videos, eliminating the presence of an effector (ATE-No Hand, Figure 1e). In the other the embodiment was artificially forced by the verbal instruction (E-ATE, Figure 1g). An explorative lesion analysis was conducted via linear regression to investigate the lesioned brain structure associated with estimation errors of movement without body.

Results: In ATE, the pairwise t-test comparison between the left patients (LBD) and controls' estimation errors showed significant underestimation in LBD of the durations of 4500 ms ($p = 0.02$) and 6500 ms ($p < 0.001$, Figure 1b). In MTE, the AHP and RBD groups overestimated only the 3000ms durations ($p = 0.035$, $p = 0.015$, Figure 1d) when compared to controls. In ATE-No Hand, RBD and AHP overestimated the shortest duration of 3000 ms ($p = 0.003$, $p = 0.004$, Figure 1f). LBD underestimated the 6500 ms actions ($p = 0.03$, Figure 1h). In E-ATE, the AHP and RBD groups significantly underestimate all the durations compared to the ATE task estimations. All findings were Bonferroni corrected for multiple comparisons. The lesion analysis revealed the involvement in estimation errors of MTE task the inferior parietal cortex, angular, supramarginal, postcentral and inferior frontal gyri, the rolandic operculum, and the insula (Figure 2).

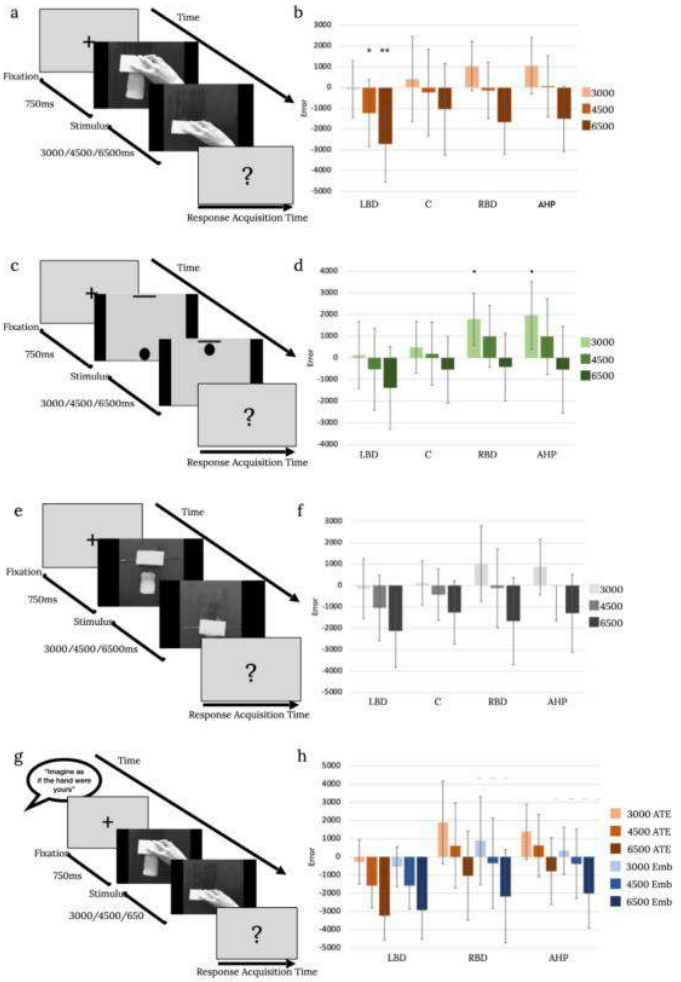

Figure 1. Experimental task representation and behavioural results. (a) Flow of events in the ATE task. (b) Error differences between controls and each patient group for the ATE task. (c) Flow of events in the MTE task. (d) Error differences between controls and each patient group for the MTE task. (e) Flow of events in the ATE-no hand task. (f) Error differences between controls and each patient group for the ATE-no hand task. (g) Flow of events in the E-ATE task. (h) Error differences between controls and each patient group for the E-ATE. For all tasks there were no response time constraints and response time acquisition lasted until the patient's response.*$p < 0.05$; **$p < 0.001$. Boxes represent the mean error of each group, for each duration; bars represent standard deviation. LBD, left brain-damaged patients; C, controls; RBD, right brain-damaged patients; AHP, anosognosia for hemiplegia patients.

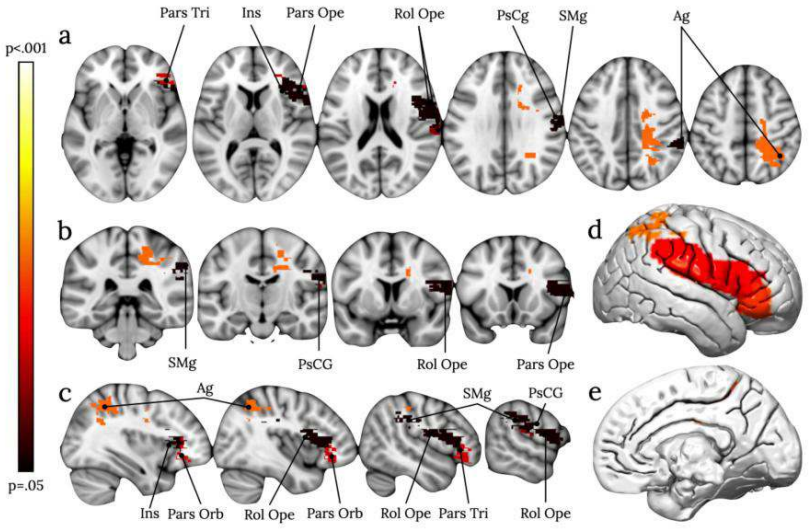

Figure 2. Lesion analysis results. (a) axial, (b) coronal, (c) sagittal, (d) lateral 3D, (e) ventral 3D views of the results of the lesion analysis computed on the errors of duration estimation in the MTE (3000 ms duration) for the RBD + AHP groups (9 patients in total). Voxels with $p < 0.05$ FDR-corrected are represented. Ag, angular gyrus; Ins, insular cortex; Pars Orb, pars orbitalis of the inferior frontal gyrus; Pars Ope, pars opercularis of the inferior frontal gyrus; Pars tri, pars triangularis of the inferior frontal gyrus; PsCg, postcentral gyrus; Rol Ope, rolandic operculum; SMg, supramarginal gyrus.

Conclusions: The study indicates a joint, complementary contribution of left and right hemispheres in temporal estimations of supra-second actions, referred both to different durations and to the presence of actions or no-biological movements. The two hemispheres respond in a different way for shorter (3000 ms) and longer (4500–6500) durations, with a role that might be prevalent for the right hemisphere in the former and for the left hemisphere for the latter. These differences do not refer exclusively to the duration but also to the presence or absence of actions. In fact, RBDs fail when there is a moving geometrical shape. Embodiment modulates temporal estimation of action only in right damaged patients who even accelerate (underestimation) the duration when they imagine the body part as their own.

References

1. Stevens MC, Kiehl KA, Pearlson G, Calhoun VD. Functional neural circuits for mental timekeeping. Hum. Brain Mapp. 2007;28:394–408.
2. Nather FC, Bueno JLO. Static images with different induced intensities of human body movements affect subjective time. Percept. Mot. Skills. 2011;113:157–170.
3. Basso G, Nichelli P, Frassinetti F, Di Pellegrino G. Time perception in a neglected space. NeuroReport. 1996;7:2111–2114.
4. Teghil A, Di Vita A, Pietranelli V, Matano A, Boccia M. Duration reproduction in regular and irregular contexts after unilateral brain damage: Evidence from voxel-based lesion-symptom mapping and atlas-based hodological analysis. Neuropsychologia. 2020;147:107577.

Poster No 994

Hippocampal iEEG Correlates of Memory Improvement across Repeated Spatial Navigation Experience

Sang-Eon Park[1], Sang Ah Lee[2]

[1]Seoul National University, Seoul, Korea, Republic of, [2]Seoul National University, Gwanak-gu, Seoul

Introduction: Underlying mechanisms of navigation-based hippocampal enhancement have been elusive due to the co-occurrence of other improvements in general cognitive functions. In addition, although hippocampal size has been correlated with spatial memory performance[4], previous studies using functional MRI presented confounding results of increased/decreased hippocampal activation as a result of spatial training[2,3]. Given the well-described function of hippocampal theta oscillations in spatial memory, measuring hippocampal intracranial EEG (iEEG) across repeated experience in a navigational task may reveal specific changes in hippocampal function associated with cognitive improvement. In this study, we investigated the possibility that hippocampal theta power may change over the course of multiple trials and sessions of a spatial navigation task with feedback on every trial. We also compared older and younger adults, in order to gain insight into age-related markers of memory improvement.

Methods: We used iEEG recordings across the whole hippocampus in 67 presurgical epilepsy patients (19 to 61 years of age) while they performed a computer-based spatial navigation task over 1 or 2 sessions (48 trials per session). One trial of the task included two encoding periods, during which participants were asked to memorize the location of the target object while they were passively driven to the target, and a retrieval phase requiring participants to find the hidden object by freely navigating the arena. Specifically, we isolated periodic narrowband power from the aperiodic component (1/f spectral slope) by applying the FOOOF (fitting oscillations & one-over f) algorithm[1]. A change in neural activity over the progress of repeated trials was measured by calculating the slope from a linear fitting between trial number and spectral features.

Results: We found a subset of participants whose performance gradually improved (slope>0) over the progress of the spatial navigation task (N=35 out of 67). The improvement was observed not only in the first session (48 trials, 12.5% increase) but also in the second session despite a smaller amount (6.5%). To look for the neural correlate of individual differences in performance changes (i.e. decline or improvement), we compared hippocampal aperiodic and periodic features (theta, alpha, beta, and gamma power) over trials. First, we found that all spectral features were engaged during spatial memory encoding, as their amplitude was time-locked to the navigation episode. Among these features, theta power was the only neural correlate of individual performance, as indicated by a marginally significant positive correlation across individuals ($r=0.297$, $p=0.059$). More importantly, theta power was a significant marker of individual memory improvement over the course of repeated trials ($r=0.377$, $p=0.026$), suggesting that enhanced theta power mediated the improvement in spatial memory. In addition, we found that a different pattern of spatial memory improvement was observed for the older and younger groups. In the match-view condition in which encoding and retrieval paths were oriented in the same direction, the older group (age>42) showed a significant improvement ($t(7)=3.019$, $p=0.019$). However, the young group showed an improvement in the view-independent condition in which the retrieval direction was opposite from the encoding ($t(9)=3.461$, $p=0.007$). A comparison of theta power change suggested that increased theta power during the retrieval may have played a crucial role in the old participants for improved view-based spatial memory (e.g. distal landmarks) ($r=0.656$, $p=0.055$).

Conclusions: Using hippocampal iEEG, we demonstrated that improvement in cognitive performance in a spatial navigation task was accompanied by an increase in theta power, the most well-known marker in the medial temporal lobe. These results show promise for a mechanistic explanation of the effectiveness of spatial navigation training for enhancing hippocampal functions.

References

1. Donoghue, T. (2020). Parameterizing neural power spectra into periodic and aperiodic components. Nature neuroscience, 23(12), 1655-1665.
2. Hötting, K. (2013). Effects of a cognitive training on spatial learning and associated functional brain activations. BMC neuroscience, 14, 1-16.
3. Sacco, K. (2022). A virtual navigation training promotes the remapping of space in allocentric coordinates: evidence from behavioral and neuroimaging data. Frontiers in Human Neuroscience, 16, 693968.
4. Wenger, E. (2012). Cortical thickness changes following spatial navigation training in adulthood and aging. Neuroimage, 59(4), 3389-3397.

Poster No 996

Arithmetic and Numerosity Networks from Childhood to Adulthood: A Neuroimaging Meta-analysis

Xavier Lim[1], SH Annabel Chen[1,2,3], Chiao-Yi Wu[4]

[1]Psychology, School of Social Sciences, Nanyang Technological University, Singapore, Singapore, [2]Centre for Research and Development in Learning, Nanyang Technological University, Singapore, Singapore, [3]Lee Kong Chian School of Medicine, Nanyang Technological University, Singapore, Singapore, [4]National Institute of Education, Nanyang Technological University, Singapore, Singapore

Introduction: Numbers permeate our lives from infancy to adulthood. Undoubtedly, the ability to recognize, manipulate, and relate quantities is a contemporary necessity. Numeracy comprises two major components (Butterworth, 2005): arithmetic (manipulating numbers and performing calculations, such as addition and multiplication) and numerosity (making semantic judgements about numbers without explicit manipulation). Considerable progress has been made in understanding the neural networks implicated in adult mathematical cognition, suggesting that bilateral frontal and parietal regions are involved in both arithmetic and numerosity (Hawes et al., 2019). However, there is less meta-analytic research on children and the developmental trajectory of numeracy (Peters & De Smedt, 2018). Therefore, we aimed to use a coordinate-based activation likelihood estimation (ALE) approach to investigate the shared and distinct neural networks implicated in numeracy for both adults and children.

Methods: Using the PRISMA framework (Page et al., 2021), we conducted searches of fMRI studies on arithmetic and numerical processing in PubMed, PsycINFO, Scopus, and Web of Science databases. Studies included in the meta-analysis (n = 141) involved active control contrasts, neurotypical children (< 18 years old) and/or adults (18-35 years old), and whole-brain results reported in MNI or Talairach coordinates. The dataset was categorized by task: arithmetic (studies: nChildren = 22, nAdults = 55; foci: nChildren = 331, nAdults = 1281) and numerosity (studies: nChildren = 25, nAdults = 63; foci: nChildren = 286, nAdults = 1105). GingerALE (v3.0.2; Eickhoff et al., 2009) was used to perform the following ALE meta-analyses: (1) conjunction of (adults ∩ children) for arithmetic and numerosity to identify shared networks; (2) contrasts between adults and children for arithmetic and numerosity to identify age-specific networks.

Results: We observed bilateral activations for numeracy in children (Fig. 1A) and adults (Fig. 1B). The conjunction analysis for arithmetic (Fig. 2A) revealed that both children and adults recruited the frontoparietal regions for arithmetic tasks, including the left inferior parietal lobule (IPL), bilateral precuneus (PCN) and precentral gyrus (PreCG), right superior parietal lobule (SPL) and superior frontal gyrus (SFG). For numerosity, only the right insula was observed. For the contrast analysis of arithmetic (Fig. 2B), we observed greater activations in the bilateral inferior frontal gyri (IFG), left insula, right medial frontal gyrus (MFG), and left cingulate gyrus in adults compared to children. For numerosity, adults showed greater activations in the bilateral SPL and right PCN compared to children. No significant activations were observed for the Children > Adults contrasts.

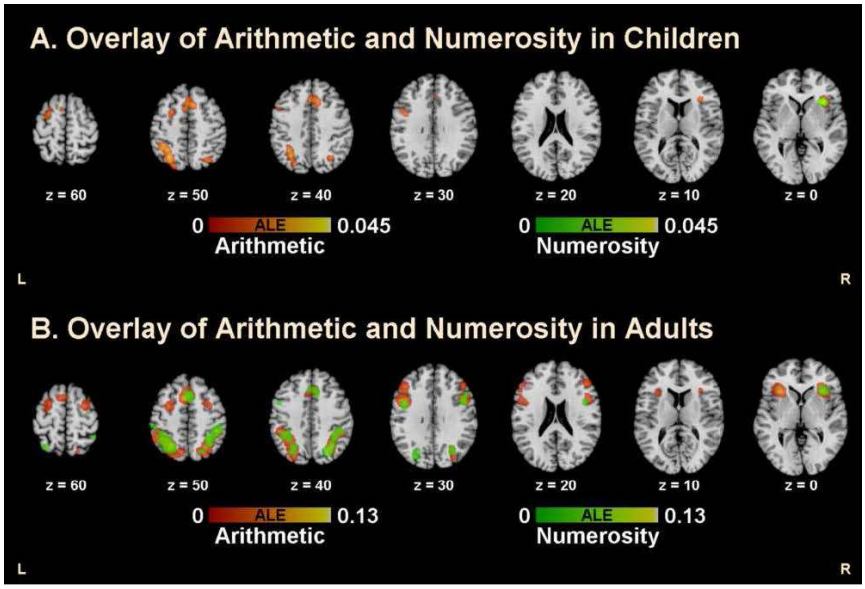

Fig. 1. ALE results for arithmetic (red) and numerosity (green) single-domain analyses for (A) children and (B) adults, thresholded at cluster-level $p < .01$ (FWE corrected). All results were overlaid onto the Colin27 T1 template.

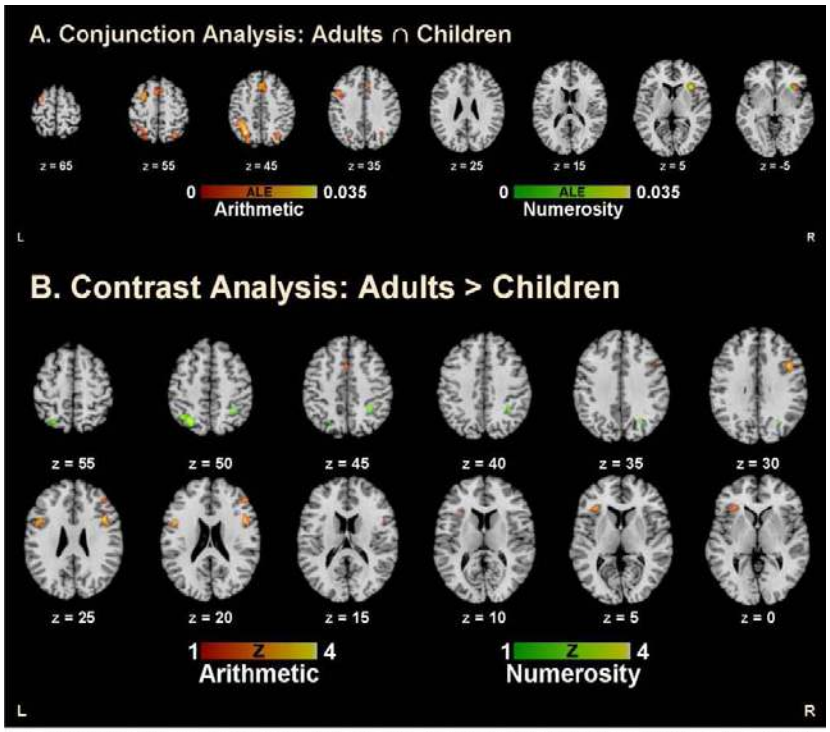

Fig. 2. (A) ALE results for conjunction analysis showing networks activated for both children and adults in arithmetic (red) and numerosity (green). (B) ALE results for contrast analysis showing regions with greater activations for adults than children in arithmetic task (red) and numerosity task (green). No greater activations were observed for children than adults. The analyses were thresholded at $p < .01$ (uncorrected) with 10,000 permutations and cluster size > 200mm^3. All results were overlaid onto the Colin27 T1 template.

Conclusions: We examined shared and distinct neural networks for arithmetic and numerosity in children and adults. Consistent with past research (Arsalidou et al., 2018; Houdé et al., 2010), frontoparietal regions were observed in mathematical processing. The activation of executive control networks (e.g., IFG, IPL) in arithmetic may reflect the active manipulation and maintenance of quantities, compared to semantic judgment in numerosity (Hinault & Lemaire, 2016). The results of contrast analyses revealed age-related differences in brain activations that might be associated with arithmetic and numerosity. In particular, greater activation for adults in the frontal regions and parietal regions might suggest increased specificity with age in calculation-based arithmetic and numerical processing, respectively (Hawes et al., 2019). Altogether, results from this study contribute to a nuanced neurodevelopmental understanding of numeracy and provide evidence for age-related differential activations in arithmetic and numerical processing, which may aid in intervention planning for math-related deficits (e.g., dyscalculia).

References
1. Arsalidou, M., (2018), 'Brain areas associated with numbers and calculations in children: Meta-analyses of fMRI studies', Developmental Cognitive Neuroscience, vol. 30, pp. 239-250.
2. Butterworth, B. (2005), 'The development of arithmetical abilities', Journal of Child Psychology and Psychiatry, vol. 46, no. 1, pp. 3-18.
3. Eickhoff, S. B. (2009), 'Coordinate-based activation likelihood estimation meta-analysis of neuroimaging data: A random-effects approach based on empirical estimates of spatial uncertainty', Human Brain Mapping, vol. 30, no. 9, pp. 2907-2926.
4. Hawes, Z., (2019), 'Neural underpinnings of numerical and spatial cognition: An fMRI meta-analysis of brain regions associated with symbolic number, arithmetic, and mental rotation', Neuroscience & Biobehavioral Reviews, vol. 103, pp. 316-336.
5. Hinault, T., (2016), 'Age-related changes in strategic variations during arithmetic problem solving: The role of executive control', Progress in Brain Research, vol. 227, pp. 257-276.
6. Houdé, O., (2010). 'Mapping numerical processing, reading, and executive functions in the developing brain: an fMRI meta-analysis of 52 studies including 842 children', Developmental Science, vol. 13, no. 6, pp. 876-885.
7. Page, M. J., (2021), 'The PRISMA 2020 statement: an updated guideline for reporting systematic reviews', International Journal of Surgery, vol. 88, pp. 105906.
8. Peters, L., (2018), 'Arithmetic in the developing brain: A review of brain imaging studies', Developmental Cognitive Neuroscience, vol. 30, pp. 265-279.

Poster No 997

Neural representations of new words: Does learning method matter?

Shuai Wang[1], Sophie Restoy[1], Julien Sein[2], Bruno Nazarian[2], Jean-luc Anton[2], Anne-Sophie Dubarry[3], Clément François[1], Felipe Pegado[4], Franck Lamberton[5], Chotiga Pattamadilok[1]

[1]Aix Marseille Univ, CNRS, LPL, Aix-en-Provence, France, [2]Aix Marseille Univ, CNRS, Centre IRM-INT@CERIMED, Institut des Neurosciences de la Timone; UMR 7289, Marseille, France, [3]Aix Marseille Univ, CNRS, LNC, Marseille, France, [4]Université Paris Cité; LaPsyDé; CNRS, Paris, France, [5]CERMEP; Imagerie du vivant, MRI Department and CNRS UMS3453, Lyon, France

Introduction: Learning new vocabulary is part of everyday life. Sometimes new words are learned orally with or without seeing speakers' articulatory gestures. Sometimes, they are learned by reading. Our previous behavioral study suggests that new words which were learned by different methods might be consolidated and stored in the mental lexicon differently (Pattamadilok et al., 2022), with bimodal learning methods leading to higher learning efficiency than unimodal. This difference in learning efficiency could be due to the nature of the underlying representations built up by the different learning methods. Here, we combined a learning paradigm and fMRI to investigate 1) whether new words which were learned by different methods evoked the same or different brain activity, and 2) which learning method led to the brain activity that was most similar to known words.

Methods: 25 native French speakers were recruited. They were asked to learn three sets of 15 new words associated with 15 unknown objects by three methods, i.e., auditory alone (Aud), auditory associated with spelling (Aud-Ort) and auditory associated with articulatory gestures (Aud-Artic), in a within-subject design. The fMRI acquisition was conducted in two sessions: Immediately after the learning phase and ~24hrs later. In each session, participants performed an auditory lexical decision task on five categories of spoken inputs: pseudoword, known word and new words learned by the three methods. FMRIPrep and AFNI were used for processing MRI data. To address the first question, a multivariate model with Stimulus and Session as factors was applied for the group analysis at the whole-brain level (3dMVM). Activation induced by spoken words learned by the three methods were compared. The commonality of activation was examined by a conjunction analysis performed on the contrasts between each of the three methods and pseudowords. Statistical tests were FWE corrected at $p < 0.05$ (voxel-level $p < 0.005$). To address the second question, activation similarity was estimated between the five categories on both days by computing Spearman correlation on T maps.

Results: On Day1, words learned by the Aud-Ort method led to higher activation in the left middle temporal gyrus (MTG), right ventromedial prefrontal cortex (vmPFC) and right cerebellum 8b, and words learned by the Aud-Artic method led to higher activation in the left MTG and left vmPFC, both compared to words learned by the Aud method. The comparison between the two bimodal learning methods showed higher activation in right rectal gyrus in the Aud-Artic method (Fig. 1A). Interestingly, these differences disappeared after the consolidation period of one night (Day2). On Day1, the conjunction analysis showed a common network involved for all types of new words in the left inferior parietal lobule (IPL), left angular gyrus and left fusiform gyrus, which are parts of the language system, left cuneus, precuneus and middle cingulate, which are involved in episodic memory, as well as right superior occipital gyrus and right cerebellum 7a. On Day2, the common network was reduced to the left IPL and anterior fusiform, suggesting that the areas related to episodic memory were disengaged while part of the language system was maintained (Fig. 1B). The similarity matrix (Fig 2) showed that, within the classic language network (Lipkin et al., 2022), all types of new words became more similar to known words from Day1 to Day2, reflecting the impact of new knowledge consolidation.

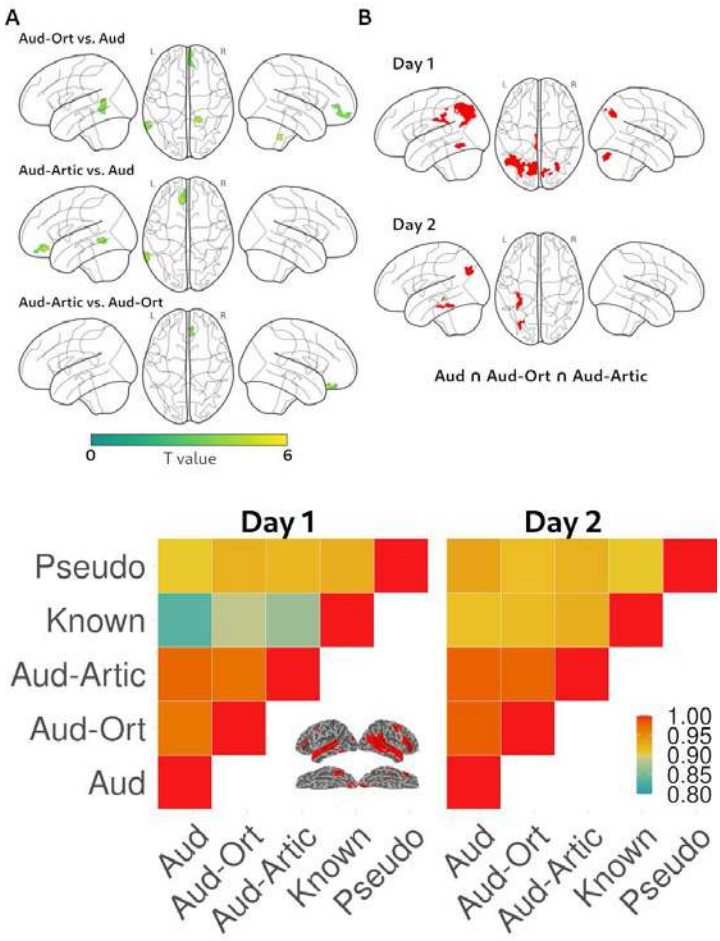

Conclusions: Our finding provides additional evidence supporting the Complementary Learning Systems model (Davis et al., 2009). The impact of learning modality was found at the initial stage of learning, i.e., when the newly learned information was still encoded in the episodic memory in a modality-specific manner. However, such impact disappeared once the knowledge had been consolidated and probably lexicalized.

References

1. Davis, M. H. (2009), A complementary systems account of word learning: Neural and behavioural evidence. Philosophical Transactions of the Royal Society B 364, 3773–3800
2. Lipkin, B. (2022), Probabilistic atlas for the language network based on precision fMRI data from >800 individuals. Scientific Data 9, 529
3. Pattamadilok, C. (2022), The contribution of visual articulatory gestures and orthography to speech processing: Evidence from novel word learning. Journal of Experimental Psychology: Learning, Memory, and Cognition, 48(10), 1542–1558

Poster No 998

Sign-language learning evokes linguistic-domain-specific functional alterations

Yael Coldham[1], Neta Haluts[1], Eden Elbaz[1], Tamar Ben David[1], Nell Racabi[1], Shachar Gal[1], Naama Friedmann[1], Ido Tavor[1]

[1]Tel Aviv University, Tel Aviv, Israel

Introduction:

Language processing is a complex neural mechanism encompassing various regions of the human brain. Previous studies have described language comprehension as a multi-stage framework with separate phonological, semantic, and syntactic components (Bibbs et al., 2000; Gvion & Friedmann, 2012), and specific brain regions have been associated with the different linguistic domains (Friederici, 2012). In the current study we investigate the functional changes evoked by learning a novel language in a new modality, and focus on the processing of each linguistic component of the newly-learned language. We hypothesize that learning-induced functional alterations will be unique per linguistic component, driving distinct activation patterns following learning.

Methods: Seventy-nine naive hearing participants (ages 21-37, 50 females) completed a comprehensive Israeli Sign Language (ISL) course. They underwent task-fMRI scans at two time-points, pre- and post-learning, in which they watched ISL content in four conditions: sentences, learned words, unlearned words and matched non-linguistic gestures. Syntax processing is expected to be involved in ISL sentences, semantics in sentences and learned words, phonology in all three linguistic components, and no linguistic components in non-linguistic gestures. Thus, contrasting neural activation in different conditions is expected to yield activation maps corresponding with the processing of specific linguistic components (e.g., the contrast sentences>learned words would correspond with syntactic processing). First-level analysis yielded contrast maps of all condition pairs, per participant per time-point. For each task contrast, a one-tailed paired t-test on the pre- and post-learning contrast maps was used to detect group-level regions of increased activity following sign-language learning ($p<0.05$, FDR corrected). Moreover, a searchlight representational similarity analysis (RSA, Fig.2A) (Kriegeskorte et al., 2008) was applied on the whole-brain BOLD signal in all task conditions post-learning, using CoSMo Multivariate Pattern Analysis (CoSMoMVPA; Oosterhof et al., 2016), to identify cortical regions associated with the three linguistic components. This analysis resulted in maps of brain regions significantly associated with syntactic, semantic and phonological processing (10,000 iterations permutation testing with threshold-free cluster enhancement, $p<0.001$ (Smith and Nichols, 2009; Stelzer et al., 2013)). A Dice coefficient was calculated between each pair of RSA-generated maps to assess the overlap between them. We additionally calculated a representational dissimilarity matrix (RDM) between the whole-brain BOLD signal, averaged across trials, of each pair of task conditions with the dissimilarity measure of 1-Pearson's r.

Results: We found increased ($p<0.05$, FDR corrected) group-level brain activity in all task contrasts (Fig.1), reflecting significant functional alterations following sign-language learning in the processing of all three linguistic components. Additionally, low Dice coefficients were found between the RSA-generated syntax and semantics maps (0.21), semantics and phonology maps (0.18) and syntax and phonology maps (0.04, Fig.2B), indicating minimal overlap between the neural regions engaged in the processing of the three linguistic domains post-learning. This is further supported by high dissimilarity scores between the whole-brain BOLD signal in different conditions, ranging from 1.18 to 1.94 (values of 0 mean perfect correlation, Fig.2C).

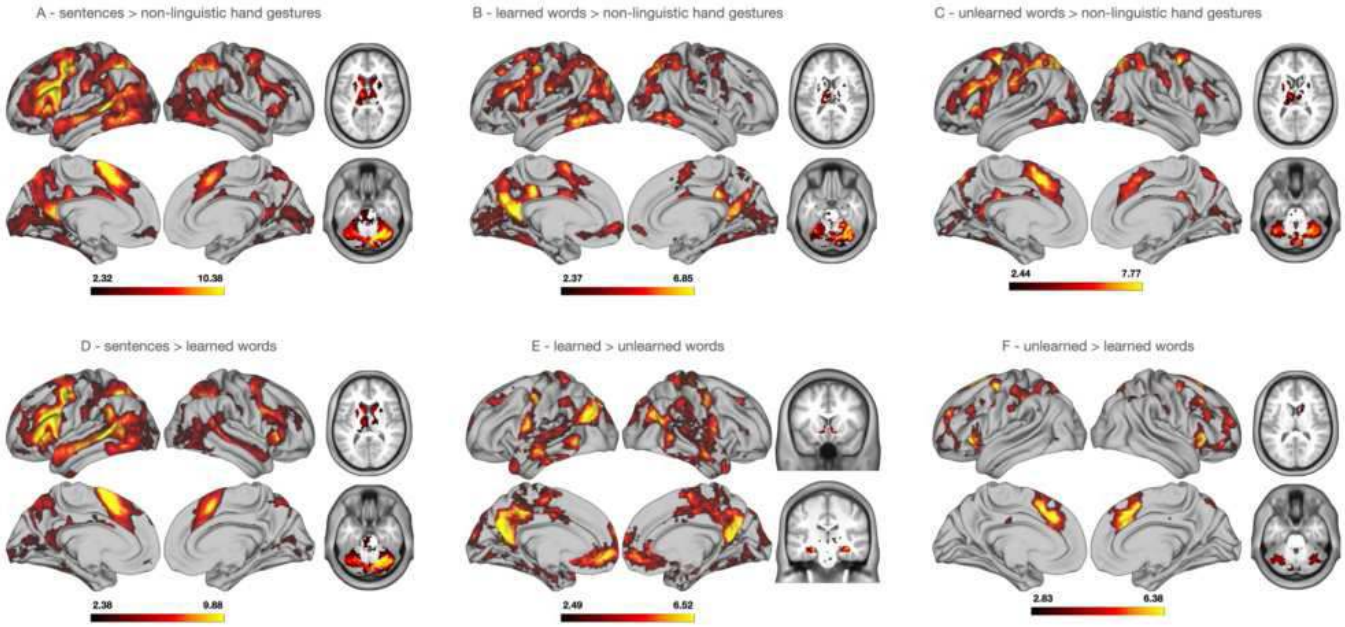

Figure 1. Changes in task-induced activation following sign-language learning Increased activation post- vs. pre- sign-language learning ($p<0.05$, FDR corrected for 91,282 comparisons) in the contrasts (A) sentences > non-linguistic hand gestures, (B) learned words > non-linguistic hand gestures, (C) unlearned words > non-linguistic hand gestures, (D) sentences > learned words, (E) learned > unlearned words, and (F) unlearned > learned words. Colorbars indicate Z-scores.

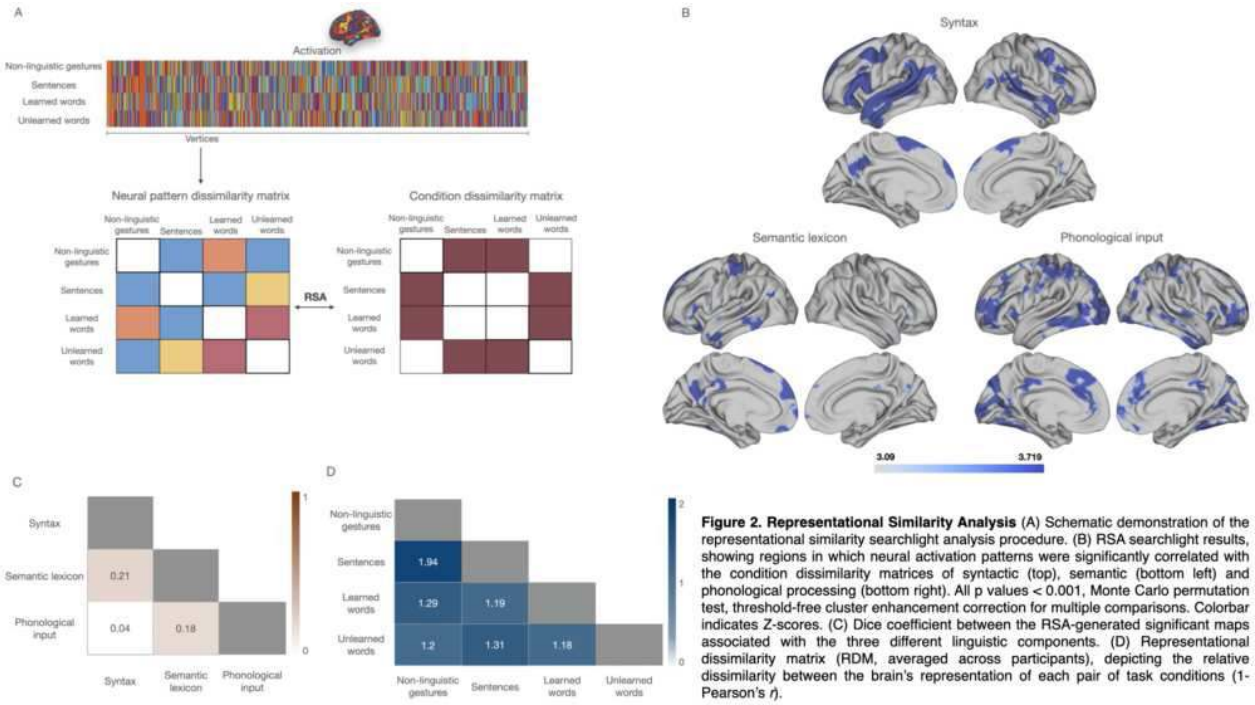

Figure 2. Representational Similarity Analysis (A) Schematic demonstration of the representational similarity searchlight analysis procedure. (B) RSA searchlight results, showing regions in which neural activation patterns were significantly correlated with the condition dissimilarity matrices of syntactic (top), semantic (bottom left) and phonological processing (bottom right). All p values < 0.001, Monte Carlo permutation test, threshold-free cluster enhancement correction for multiple comparisons. Colorbar indicates Z-scores. (C) Dice coefficient between the RSA-generated significant maps associated with the three different linguistic components. (D) Representational dissimilarity matrix (RDM, averaged across participants), depicting the relative dissimilarity between the brain's representation of each pair of task conditions (1-Pearson's *r*).

Conclusions: In the current work we show the dissimilarity between the functional alterations associated with syntactic, semantic and phonological processing in a newly-learned language of a novel modality. Based on the language comprehension framework, our findings support the attribution of unique neural representations to the different stages of language processing and demonstrate its manifestation within a learning process.

References

1. M.W. Woolrich, S. Jbabdi, B. Patenaude, M. Chappell, S. Makni, T. Behrens, C. Beckmann, M. Jenkinson, S.M. Smith.(2009) Bayesian analysis of neuroimaging data in FSL. NeuroImage, 45:S173-86
2. S.M. Smith, M. Jenkinson, M.W. Woolrich, C.F. Beckmann, T.E.J. Behrens, H. Johansen-Berg, P.R. Bannister, M. De Luca, I. Drobnjak, D.E. Flitney, R. Niazy, J. Saunders, J. Vickers, Y. Zhang, N. De Stefano, J.M. Brady, and P.M. Matthews. (2004). Advances in functional and structural MR image analysis and implementation as FSL. NeuroImage, 23(S1):208-19.
3. Fischl, B. (2012). FreeSurfer. NeuroImage, 62(2), 774–781.
4. Bibb, B., Nickels, L., & Coltheart, M. (2000). Impaired auditory lexical access and the effect of speech-reading. Asia Pacific Journal of Speech, Language and Hearing, 5(2), 129-135.
5. Gvion, A., & Friedmann, N. (2012). Phonological short-term memory in conduction aphasia. Aphasiology, 26(3-4), 579-614.
6. Friederici, A. D. (2012). The cortical language circuit: from auditory perception to sentence comprehension. Trends in cognitive sciences, 16(5), 262-268.
7. Kriegeskorte, N., Mur, M., & Bandettini, P. A. (2008). Representational similarity analysis-connecting the branches of systems neuroscience. Frontiers in systems neuroscience, 4.
8. Oosterhof, N. N., Connolly, A. C., & Haxby, J. V. (2016). CoSMoMVPA: multi-modal multivariate pattern analysis of neuroimaging data in Matlab/GNU Octave. Frontiers in neuroinformatics, 10, 27.
9. Smith, S. M., & Nichols, T. E. (2009). Threshold-free cluster enhancement: addressing problems of smoothing, threshold dependence and localisation in cluster inference. Neuroimage, 44(1), 83-98.
10. Stelzer, J., Chen, Y., & Turner, R. (2013). Statistical inference and multiple testing correction in classification-based multi-voxel pattern analysis (MVPA): random permutations and cluster size control. Neuroimage, 65, 69-82.

Poster No 999

Structural Neuroplasticity Induced by Language Learning in Older Adults

Ladan Ghazi Saidi[1,2], kiley Allgood[1], Lauren Secilmis[3], Annelie Persson[4], Lauren Rezac[5], Cary Savage[5,2], Douglas Schultz[5,2]

[1]University of Nebraska at Kearney, Kearney, NE, [2]Center for Brain Biology and Behavior, Lincoln, NE, [3]University of nebraska Lincoln, Lincoln, NE, [4]University of Nebraska in Omaha, Omaha, NE, [5]University of Nebraska Lincoln, Lincoln, NE

Introduction: Emerging evidence suggests that lifelong bilingualism may bolster cognitive reserve, enabling better maintenance of cognitive functioning in aging. Better cognitive reserve is evidenced by superior performance on cognitive tasks compared to monolingual peers as well as more efficient functional network and structural differences. However, the impact of acquiring a new language in later life on cognitive reserve and brain structure remains uncharted territory. Our

study aims to elucidate whether learning a new language in older adulthood contributes to cognitive reserve. Specifically, we focus on assessing structural brain changes, including volumetric alterations and cortical thickness variations, in older adults engaging in new language acquisition.

Methods: Our sample includes 41 healthy monolingual participants (60-80) living in a monolingual environment (Nebraska). Participants used an online language learning program to learn a language of their choice. The intervention (language learning) was for four months, 5 days a week, 90 minutes per day. Participants were monitored daily for their performance and retention. Participants were scanned before and after the language learning intervention using a whole-brain 3T Siemens Skyra MRI scanner equipped with a 32-channel head coil. T1-weighted MPRAGE were collected (TR/TE=2200/3.37 ms, inversion time=1110 ms, flip angle=7°, 1 mm3 voxels). Acquisition time was around 7 min. Cortical thickness across various brain regions was estimated with Freesurfer and the recon-all command with default settings and using the Destrieaux atlas. Cortical thickness was compared between pre and post intervention. Pre and post intervention values were compared using General Linear Model, Repeated Measures using IBM SPSS, version 29, and corrected for multiple comparisons with False Discovery Rate (FDR).

Results: Behavioral results suggest that all participants successfully learn their language of choice with an average performance score of 96% in the post intervention proficiency test. Pre-post-intervention cortical thickness was different in 49 brain areas in the left hemisphere and 22 brain areas in the right hemisphere including bilateral inferior, lateral and superior temporal gyri and sulci; bilateral insular cortex including superior and anterior circular insular sulci; bilateral occipito-temporal gyri; bilateral pre and post central sulci, bilateral inferior frontal sulci as well as the left cuneus and precuneus gyri, the left dorsal and ventral cingulate gyri and bilateral cingulate marginalis sulci; the left inferior and superior parietal gyri including the angular gyrus; the left inferior opercular and orbital gyri and orbital sulcus ($P<.001$). These brain areas are involved in different language and cognitive processes including attention processing, working memory and inhibitory control.

Conclusions: These results suggest that learning a new language in older adults for four months can induce structural neuroplasticity. These changes are especially noticeable in the left hemisphere with cortical thickness. These results may suggest that learning a new language in older adults has an effect on cortical morphology which may contribute to slowing cognitive decline. These results are promising, however, they should be interpreted by caution, given that this study lacks a control group.

References

1. Harvard University & Massachusetts General Hospital. (n.d.). FreeSurfer: Software Suite for Longitudinal and Cross-sectional Analysis. Retrieved from https://surfer.nmr.mgh.harvard.edu/
2. Garbin, G., Sanjuan, A., Forn, C., Bustamante, J. C., Rodríguez-Pujadas, A., Belloch, V., ... & Ávila, C. (2010). Bridging language and attention: Brain basis of the impact of bilingualism on cognitive control. NeuroImage, 53(4), 1272-1278.
3. Bak, T. H., Long, M. R., Vega-Mendoza, M., & Sorace, A. (2016). Novelty, challenge, and practice: the impact of intensive language learning on attentional functions. PloS one, 11(4), e0153485.
4. Bialystok, E. (2021). Bilingualism: Pathway to cognitive reserve. Trends in cognitive sciences, 25(5), 355-364.
5. Stern, Y., Arenaza-Urquijo, E. M., Bartrés-Faz, D., Belleville, S., Cantilon, M., Chetelat, G., ... & Okonkwo, O. (2018). Whitepaper: Defining and investigating CR, brain reserve, and brain maintenance. Alzheimer's & Dementia.
6. Klein, D., Mok, K., Chen, J. K., & Watkins, K. E. (2014). Age of language learning shapes brain structure: a cortical thickness study of bilingual and monolingual individuals. Brain and language, 131, 20-24.
7. Han, X., Jovicich, J., Salat, D., van der Kouwe, A., Quinn, B., Czanner, S., ... & Fischl, B. (2006). Reliability of MRI-derived measurements of human cerebral cortical thickness: the effects of field strength, scanner upgrade and manufacturer. Neuroimage, 32(1), 180-194.

Poster No 1000

Learning Effect Mediates Age-related Differences in Foreign Word Learning: An ERP Study

Yiyuan Chen[1], Wenwen Chen[2], Yan Huang[3], Hengyi Rao[4,5]

[1]Institute of Linguistics, Shanghai International Studies University, Shanghai, China, [2]Shanghai International Studies University, Shanghai, China, [3]School of Foreign Languages, East China University Science and Technology, Shanghai, China, [4]Center for Functional Neuroimaging, Department of Neurology, University of Pennsylvania, Philadelphia, PA, USA, [5]Chronobiology and Sleep Institute, Department of Psychiatry, University of Pennsylvania, Philadelphia, PA, United States

Introduction: Old language learners might be poorer learners, but the relationship between age and foreign language learning ability is far more complex. Previous studies have examined the neural mechanisms underlying the fast acquisition of foreign vocabulary and revealed dynamic changes in several event-related potential (ERP) components during novel word learning. However, few studies have discussed the role ERP components in the process of foreign language learning among different ages.

Methods: The present study used ERP and administered a paired-associate word learning task and a recall test in two sections to 55 healthy young, middle-aged, and older adults (21 males). During each section, participants were instructed to learn and memorize 60 pairs of English pseudowords with Chinese meanings over three rounds, followed by a pen-and-paper cued-recall test. While performing the word learning task, electroencephalography (EEG) was recorded.

Results: For the recall test, a decrease in performance was observed with increasing age. For the ERP record, N400 as a landmark ERP component for semantic accessibility, was found in both sections. Interestingly, the mediation analysis shows that N400 amplitude difference of two recall tests, partially mediated the age effect on word learning task. The regression coefficient of the N400 amplitude difference is 7.293 ($p < 0.05$) and statistically significant, showing that N400 amplitude difference positively influences recall test score.

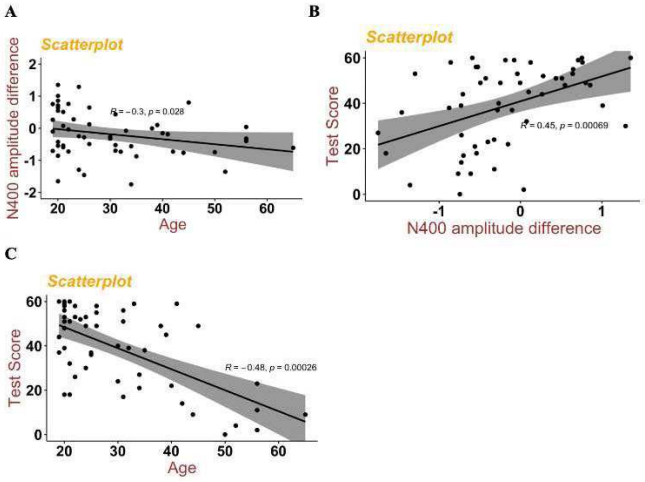

Figure.1. All three scatterplots clearly show the correlation between age and N400 amplitude difference (A), N400 amplitude difference and second recall test score (B), and age and second recall test.

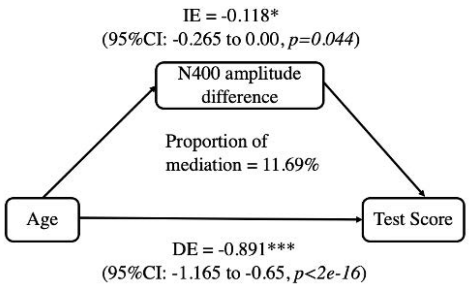

Figure.2. Between age and second score, IE means the indirect effect, DE means direct effect.

Conclusions: This finding shows the learning effect of N400 plays an important role in the construction of foreign word learning across different age groups. The word learning efficiency of young people is better than that of elderly. Future research should test the generalizability of the results in other aspects of language such as syntax.

References

1. Bakker, I. (2015). Tracking lexical consolidation with ERPs: Lexical and semantic-priming effects on N400 and LPC responses to newly-learned words. Neuropsychologia, 79, 33–41.
2. Balass, M. (2010). Word learning: An ERP investigation of word experience effects on recognition and word processing. Contemporary Educational Psychology, 35(2), 126–140.
3. Borovsky, A. (2012). Once is Enough: N400 Indexes Semantic Integration of Novel Word Meanings from a Single Exposure in Context. Language Learning and Development, 8(3), 278–302.
4. Huang, Y. (2023). Vigilant attention mediates the association between resting EEG alpha oscillations and word learning ability. NeuroImage, 281, 120369.
5. Kutas, M. (2011). Thirty Years and Counting: Finding Meaning in the N400 Component of the Event-Related Brain Potential (ERP). Annual Review of Psychology, 62(1), 621–647.
6. Li, S. (2021). The methodology of the research on language aptitude: A systematic review. Annual Review of Applied Linguistics, 41, 25–54.
7. Qi, Z. (2017). Native-language N400 and P600 predict dissociable language-learning abilities in adults. Neuropsychologia, 98, 177–191.
8. Yum, Y. N. (2014). An ERP study on initial second language vocabulary learning. Psychophysiology, 51(4), 364–373.
9. Zhang, J. (2023). Dynamic brain responses to Russian word acquisition among Chinese adult learners: An event-related potential study. Human Brain Mapping, 44(9), 3717–3729.

Poster No 1001

Brain connectivity dimensions modulate language processing with modality-specific mechanisms

Lidon Marin-Marin[1,2], Susanne Eisenhauer[1,2], Elizabeth Jefferies[1,2]

[1]University of York, York, United Kingdom, [2]York Neuroimaging Centre, York, United Kingdom

Introduction: Whole-brain patterns of functional connectivity are crucial for language processing. Decompositions of intrinsic connectivity have identified the dimensions of these patterns (called gradients) [Margulies et al., 2016]. The principal gradient represents the gradual shift from input-driven processes (sensory-motor) to more abstract ones (heteromodal). The second gradient represents the separation of visual from auditory and somatomotor regions. Finally, the third gradient describes a distinction between the default mode network and task-positive systems. The objective of our study was to investigate how these gradients influence brain activation during auditory and visual language processing, establishing whether these dimensions capturing the large-scale brain organisation of connectivity underlie similarities and differences across modalities.

Methods: 204 right-handed Dutch participants (100 males, mean age=22) in the MOUS ('Mother Of Unification Studies') dataset [Schoffelen et al., 2019] read or listened to sentences during fMRI. Data were pre-processed following a previous study analysing the visual task-fMRI data [Eisenhauer et al., 2023] using FSL. We used parameters of interest equivalent to those considered in that study to maintain results comparable between modalities: number of phonemes, phonological distance, word frequency, semantic similarity and position. GLMs in FSL were used to estimate the effects of each of the parameter on brain activation, averaged for 400 surface parcels [Schaefer et al., 2018]. Similarities between the visual and auditory maps were investigated by means of Pearson correlations using spin permutations to assess statistical significance and strength of correlations was compared. Each parameter's cortical map was related to the three gradients of connectivity using linear or quadratic models in R. The interaction between gradient and modality's effect on activation maps was also investigatedadding modality as an interaction term.

Results: Brain activation maps of semantic similarity were significantly and positively correlated between visual and auditory modalities (r=0.34, pspin<.002), while word length (letters/phonemes) (r=-0.21, pspin=.038) and orthographic/phonological distance (r=-0.25, pspin<.016) were negatively correlated (Fig.1). The strength of semantic similarity's correlation was significantly higher than the other two (z=6.41, p<.001; z=6.88, p<.001). We found a statistically significant interaction between the principal gradient and modality on brain activation maps in the following parameter pairs: word length (letters/phonemes) (pspin<.002) and orthographic/phonological distance (pspin<.002; Fig.2). The second gradient interacted significantly with modality in semantic similarity (pspin<.002) and orthographic/phonological distance (pspin=.018; Fig.2). Finally, we found a significant interaction between the third gradient and modality on word frequency (pspin<.002), and word length (pspin<.002; Fig.2).

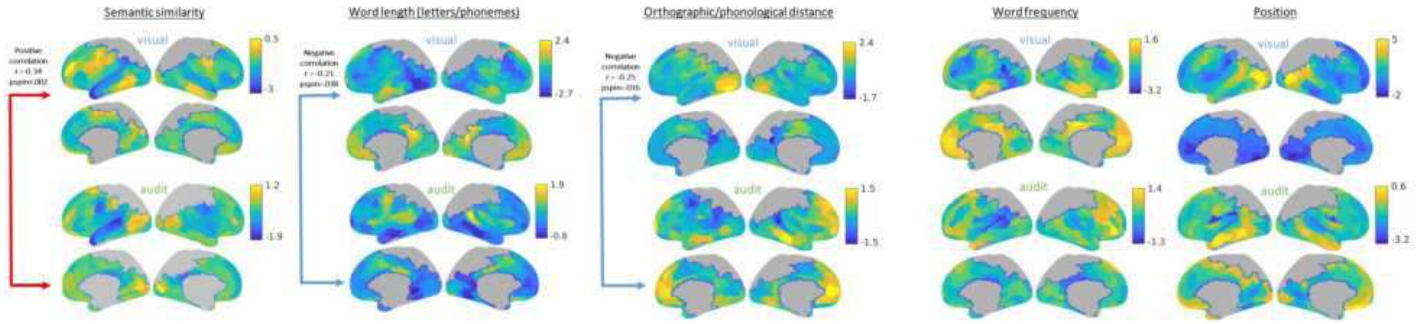

Figure 1. Visual and auditory activation maps of parameters of interest and significant correlations (spin permutation-corrected) between modalities. (High-res image available upon request)

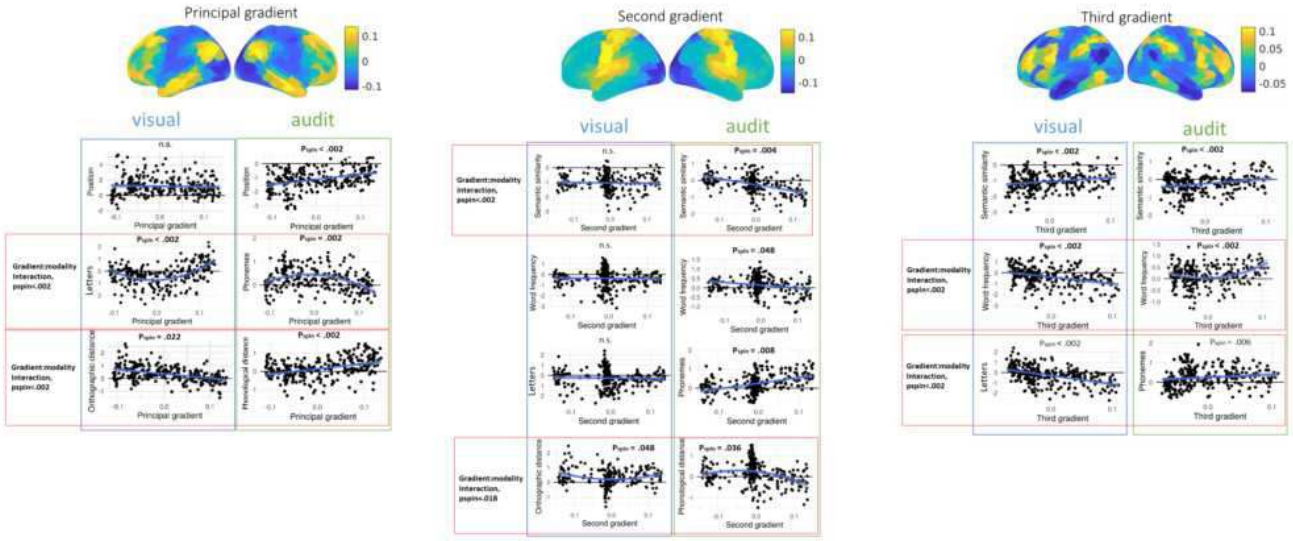

Figure 2. Gradient maps, relationships between activation maps of parameters of interest and gradients, and significant interactions between gradient and modality. (High-res available upon request).

Conclusions: Brain activation for semantic similarity was positively correlated between visual and auditory modalities, while visual/auditory variables showed a negative correlation between maps, and more differences in their relationship to gradients across modalities. This supports the idea of processing dissociation for sensory input and integration for more abstract representations. Differences between modalities in visual/auditory variables also relate to previous behavioural studies [Eisenhauer et al., 2023, Suárez et al., 2011, Baddeley et al., 1975; Jefferies et al., 2011], suggesting divergent difficulty mechanisms. In sum, the different effects of semantic, lexical and input-level linguistic variables are captured by connectivity gradients. All dimensions of connectivity exhibit different relationships to language processing depending on modality, which could be related to the transient nature of auditory processing, as compared to visual processing, more explicit and transparent.

References

1. Baddeley AD, Thomson N, Buchanan M (1975): Word length and the structure of short-term memory. Journal of Verbal Learning and Verbal Behavior 14:575–589.
2. Eisenhauer S, Alam TR del JG, Cornelissen PL, Smallwood J, Jefferies E (2023): Individual word representations dissociate from linguistic context along a cortical unimodal to heteromodal gradient. bioRxiv:2023.04.25.538257.
3. Jefferies E, Frankish C, Noble K (2011): Strong and long: Effects of word length on phonological binding in verbal short-term memory. Quarterly Journal of Experimental Psychology 64:241–260.
4. Margulies DS, Ghosh SS, Goulas A, Falkiewicz M, Huntenburg JM, Langs G, Bezgin G, Eickhoff SB, Castellanos FX, Petrides M, Jefferies E, Smallwood J (2016): Situating the default-mode network along a principal gradient of macroscale cortical organization. Proceedings of the National Academy of Sciences of the United States of America 113:12574–12579.
5. Schaefer A, Kong R, Gordon EM, Laumann TO, Zuo X-N, Holmes AJ, Eickhoff SB, Yeo BTT (2018): Local-Global Parcellation of the Human Cerebral Cortex from Intrinsic Functional Connectivity MRI. Cerebral Cortex (New York, NY) 28:3095.
6. Schoffelen JM, Oostenveld R, Lam NHL, Uddén J, Hultén A, Hagoort P (2019): A 204-subject multimodal neuroimaging dataset to study language processing. Scientific Data 2019 6:1 6:1–13.
7. Suárez L, Tan SH, Yap MJ, Goh WD (2011): Observing neighborhood effects without neighbors. Psychonomic Bulletin and Review 18:605–611.

Poster No 1002

Left inferior parietal lobe and auditory cortex jointly contribute to sound knowledge retrieval

Philipp Kuhnke[1,2], Johannah Voeller[2], Vincent Cheung[3], Ole Numssen[2], Konstantin Weise[2,4], Markus Kiefer[5], Gesa Hartwigsen[1,2]

[1]Leipzig University, Leipzig, Saxony, Germany, [2]Max Planck Institute for Human Cognitive and Brain Sciences, Leipzig, Saxony, Germany, [3]Sony Computer Science Laboratories, Tokyo, Japan, [4]Leipzig University of Applied Sciences, Faculty of Engineering, Leipzig, Saxony, Germany, [5]Ulm University, Ulm, Baden-Württemberg, Germany

Introduction: Conceptual knowledge is central to human cognition. Previous neuroimaging studies suggest that conceptual processing relies on the joint contribution of modality-specific perceptual-motor and multimodal brain regions (Kuhnke et al. 2023). In particular, the multimodal left inferior parietal lobe (IPL) coupled with auditory cortex during sound knowledge retrieval and with somatomotor cortex during action knowledge retrieval (Kuhnke et al. 2021). However, as neuroimaging

is correlational, it remains unknown whether the interaction between modality-specific and multimodal cortices is causally relevant for conceptually-guided behavior. To tackle this issue, we applied inhibitory transcranial magnetic stimulation (TMS) over modality-specific cortex (somatomotor, auditory, or sham), before 24 healthy participants received TMS over multimodal cortex (IPL, or sham) during action and sound judgment tasks on written words (Figure 1A).

Methods: To optimize the subject-specific coil position and intensity for each stimulation target, we performed a priori computational electric field (e-field) simulations (Figure 1B). Specifically, we determined the coil positions that maximize the e-field magnitude in each target, and matched the stimulation intensities to the subject-specific cortical stimulation thresholds (i.e. the e-field magnitude in primary motor cortex at resting motor threshold; Numssen, Kuhnke et al. 2023). Behavioral data were analyzed using a drift diffusion model (DDM), which models response times and accuracies collectively, accounting for potential speed–accuracy tradeoffs and response biases (Voss and Voss 2007). The DDM assumes that during binary decision processes, the subject accumulates evidence for a certain decision from a stimulus, beginning at a starting point (z), until a decision boundary (a = "yes", or 0 = "no") is reached (Figure 2A). The key parameter-of-interest is the drift rate (v), the average rate of evidence accumulation. Thus, after the DDM was fit to the data, we normalized the drift rates for all TMS conditions to sham stimulation and performed Bayesian Wilcoxon signed-rank tests on the sham-normalized drift rates. Finally, Bayesian linear regression tested for relationships between drift rates and e-field strength in each target.

Results: We found that combined stimulation of the left auditory cortex and IPL selectively impaired drift rates for sound judgments on low sound–low action words (Figure 2B). The data were >5 times more likely under the hypothesis that auditory + IPL TMS impaired sound judgments than under the null hypothesis of no TMS effect (BF10 = 5.316). Post-hoc paired comparisons provided evidence for anatomical specificity: Combined auditory + IPL TMS impaired sound judgments more strongly than auditory-only TMS (BF10 = 4.244), somatomotor + IPL TMS (BF10 = 1.854), somatomotor-only TMS (BF10 = 1.887), and IPL-only TMS (BF10 = 1.426). Moreover, we found evidence for task specificity: TMS over auditory cortex + IPL induced a stronger impairment of sound judgments than action judgments on the same words (BF10 = 1.499). Crucially, stronger stimulation of left auditory cortex was associated with worse performance on sound judgments under auditory + IPL TMS (Figure 2C; BFM = 4.189). No other condition showed convincing evidence for a TMS effect.

Conclusions: Our results indicate that the joint contribution of multimodal IPL and auditory cortex is causally relevant for sound knowledge retrieval: The functional relevance of left IPL depends on the integrity of the auditory cortex, and vice versa, as single perturbation of either region did not disrupt performance. However, our data do not provide evidence for a functional relevance of the joint contribution of multimodal IPL and somatomotor cortex to action knowledge retrieval. These findings suggest substantial robustness of the conceptual system to disruption, which could be further studied by combining non-invasive brain stimulation with neuroimaging.

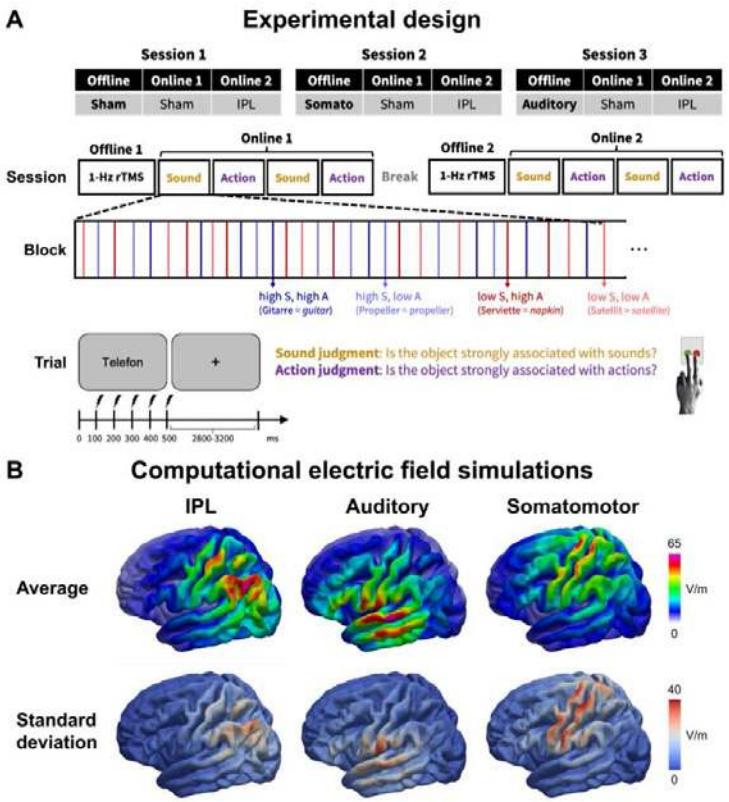

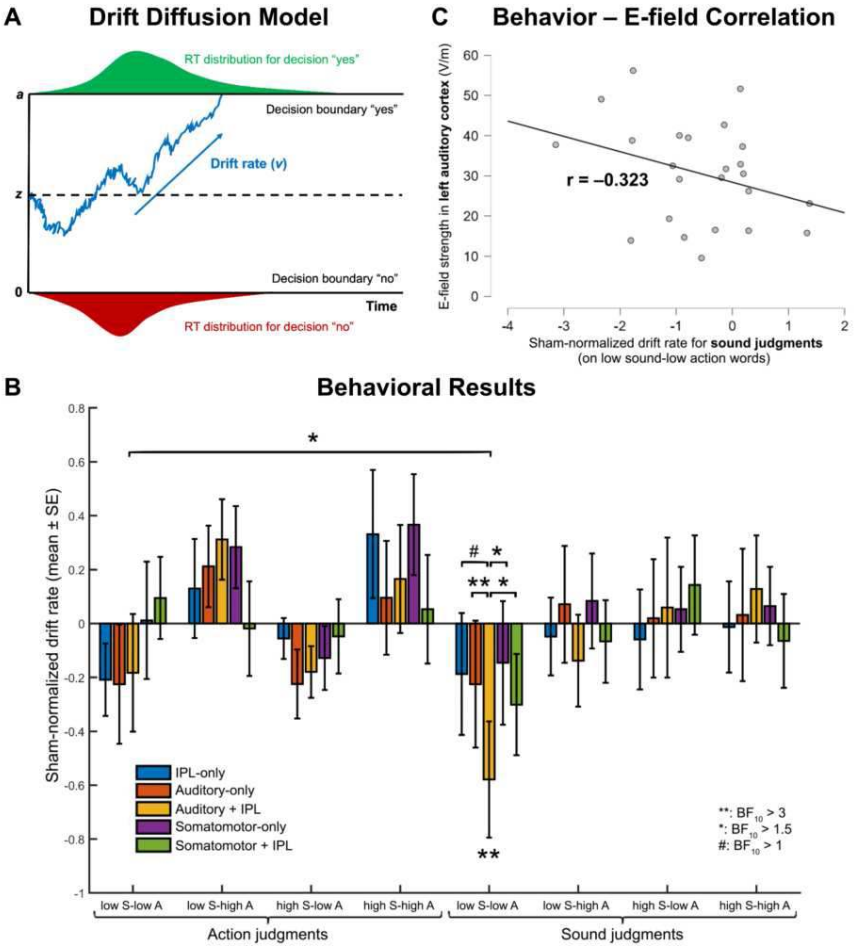

References

1. Kuhnke P, Beaupain MC, Arola J, Kiefer M, Hartwigsen, G (2023) Meta-analytic evidence for a novel hierarchical model of conceptual processing. Neurosci Biobehav Rev 144:104994. https://doi.org/10.1016/j.neubiorev.2022.104994
2. Kuhnke P, Kiefer M, Hartwigsen G (2021) Task-Dependent Functional and Effective Connectivity during Conceptual Processing. Cereb Cortex 31:3475–3493. https://doi.org/10.1093/cercor/bhab026
3. Numssen O, Kuhnke P, Weise K, Hartwigsen G (2023) Electrical field based dosing improves non-invasive brain stimulation. bioRxiv 1–25. https://doi.org/10.1101/2023.07.31.551253
4. Voss A, Voss J (2007) Fast-dm: A free program for efficient diffusion model analysis. Behav Res Methods 39:767–775. https://doi.org/10.3758/BF03192967

Poster No 1004

Evidence in dual pathway coding of speech with prediction errors

Baihan Lyu[1,2], Xiuyi Wang[2], Yi Du[1,2,3]

[1]Department of Psychology, University of Chinese Academy of Sciences, Beijing, China, [2]CAS Key Laboratory of Behavioral Science, Institute of Psychology, Chinese Academy of Sciences, Beijing, China, [3]Chinese Institute for Brain Research, Beijing, China

Introduction: The human brain integrates external information with predictions from long-term memory to facilitate language comprehension. Research has elucidated phonological and semantic representations in natural language processing contexts. However, the manner in which these representations are affected when predictions are violated remains elusive. This study delves into the neural representations of phonological and semantic information in two scenarios: when information is missing but can be predicted based on context and long-term memory, and when incongruent information is presented that contradicts both context and long-term memory. We aim to determine whether the same mechanisms or distinct pathways are involved in representing these divergent forms of information.

Methods: In an fMRI experiment, 29 native Chinese speakers (19 females; mean age = 21 years) were presented with Chinese idiomatic phrases, each comprising 4 characters (e.g., “羊入虎口” - “sheep enters tiger’s mouth”). We designed 3 conditions by

manipulating the final character (target) of each phrase. In the 'Expected' condition (EP), participants heard the correct phrase. In the 'Missing' condition (M), the target was omitted. In the 'Unexpected' condition (UP), an incorrect target was provided (see Fig. 1A for an example). Catch trials were included to maintain participant engagement, where participants indicated whether the previous target matched the current character on the screen (see Fig. 1B). We used a set of 18 phrases, with 3 phrases sharing the same target, resulting in 54 experimental trials and 12 catch trials per run. All items were presented once per run, with a total of 8 runs. We extracted the whole-brain activation beta map for each phrase using a general linear model. We conducted univariate analysis to compare the activation maps across conditions. To reveal regions representing phonological and semantic information in each condition, we conducted the representation similarity analysis (RSA) by fitting linguistic (phonological and semantic) representation distance matrices against the neural RDM through multiple regression. In the UP condition, we built two RDMs: one for the predicted but unpresented correct word, and the other for the perceived error word (see Fig. 1C).

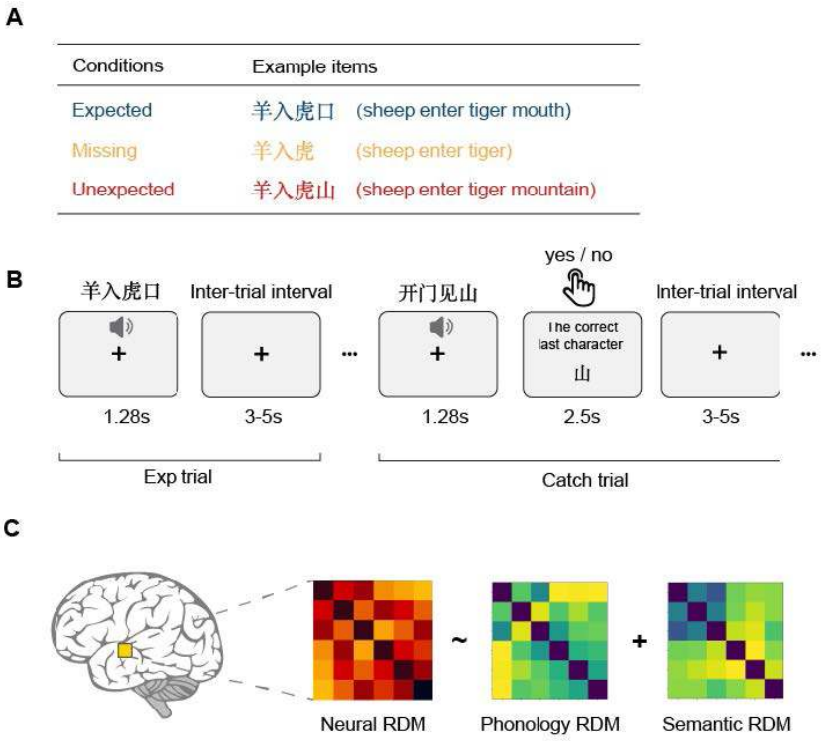

Figure 1. A-B) Illustration of the experimental design and the procedure for both experimental trials and catch trials. C) The multiple regression RSA. Neural RDM was constructed by calculating pairwise 1 - Spearman correlation coefficients between trials within each condition. Similarly, language RDMs were derived from extracted phonological and semantic features. Subsequently, we assessed the variance explained by each language RDM through multiple regression RSA.

Results: Greater activation was found in inferior frontal gyrus (IFG) pars opercularis and superior temporal gyrus (STG) in M than in EP, while auditory cortex and semantic memory regions (e.g., IFG pars triangularis, angular gyrus, middle temporal gyrus) showed the reverse pattern (Fig. 2A). Left frontal-temporal semantic regions exhibited greater semantic representations in M than in EP; conversely, the opposite pattern was observed in precentral gyrus (Fig.2B). Thus, understanding correct phrases relies on the long-term semantic memory system. However, when information is absent, the ventral temporal semantic pathway becomes crucial for information prediction and recovery. In UP, auditory, attention and general control systems showed greater activation than in EP, but no region showed the reverse pattern (Fig. 2A). The semantic representation of perceived words was observed in ventral pathway areas, including anterior STG and IFG. Conversely, the semantic representation of predicted words was found in precentral, inferior parietal area and posterior cingulate cortex (Fig. 2B). These suggest bottom-up semantic processing for actual words and top-down memory retrieval for predicted words when predictions are violated.

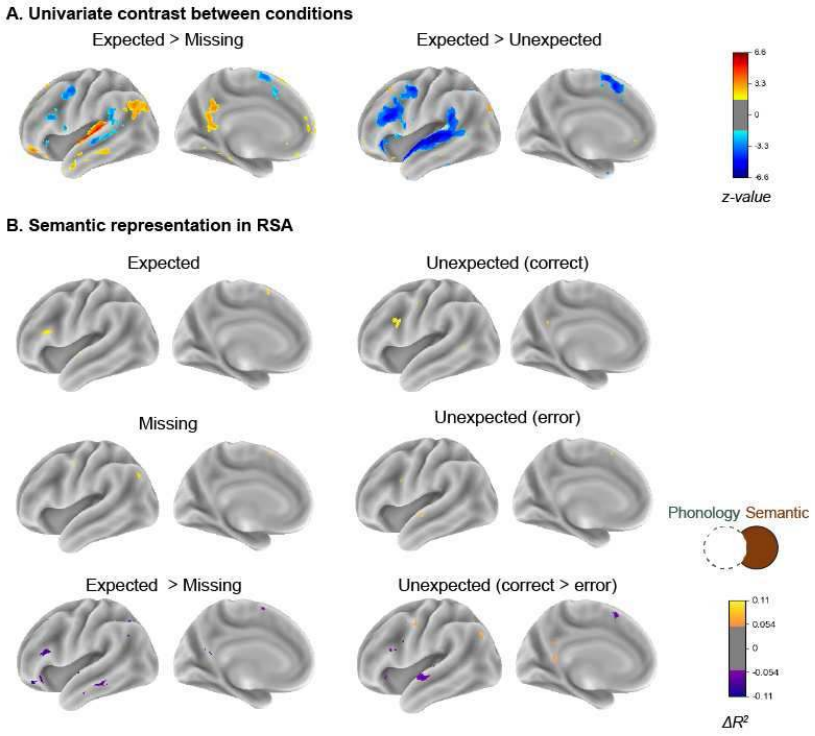

Figure 2. A) The activation patterns across conditions. B) The semantic representation in each condition and between conditions. To control for multiple comparisons, we applied FDR-correction at $p < 0.05$.

Conclusions: Our preliminary results identified distinct pathways for understanding normal phrases and predicting information from long-term memory to recover missing words. We also revealed separate pathways for representing semantic information related to perceived error words and predicted words. While we mainly observed distinct sensitivity to semantic representations, we will further explore in relation to phonological representations.

References

1. Esteban, O., Ciric, R., Finc, K., Blair, R. W., Markiewicz, C. J., Moodie, C. A., Kent, J. D., Goncalves, M., DuPre, E., Gomez, D. E. P., Ye, Z., Salo, T., Valabregue, R., Amlien, I. K., Liem, F.,
2. Jacoby, N., Stojić, H., Cieslak, M., Urchs, S., ... Gorgolewski, K. J. (2020). Analysis of task-based functional MRI data preprocessed with fMRIPrep. Nature Protocols, 15(7), Article 7. https://doi.org/10.1038/s41596-020-0327-3.
3. Prince, J. S., Charest, I., Kurzawski, J. W., Pyles, J. A., Tarr, M. J., & Kay, K. N. (2022). Improving the accuracy of single-trial fMRI response estimates using GLMsingle. eLife, 11, e77599. https://doi.org/10.7554/eLife.77599.

Poster No 1005

Neural representations of pain and sensory vocabulary: a 7T study of novel word acquisition

Natalia Egorova-Brumley[1], Marie Spehar[1]

[1]University of Melbourne, Melbourne, Australia

Introduction: The concepts represented by abstract words, such as pain, are fundamental to the human experience and therefore to communication. Investigations into how these words are learnt and mentally represented have been hindered by the subjectivity and variability of their meanings across individuals. Informed by the general theories of word learning (McClelland et al., 1995; Davis & Gaskell, 2009), we hypothesised that pain and sensory word neural representations would be both disembodied in heteromodal language cortices (Binder et al., 2009) and embodied in the physical experiences that comprise their meanings (Hauk et al., 2004).

Methods: The word learning paradigm utilising experimental pain methods in this study involved the presentation of written pseudowords with heat stimuli of varying intensities (painful, innocuous, and absent). It enabled the creation of abstract words with controlled sensory meanings. The acquisition of these words in 29 right-handed participants (10 male, mean age = 23.9 ± 4.3 years) was evaluated using semantic judgement tasks on 2 consecutive days, with task-fMRI used to examine their cortical representations after a night of sleep.

Results: All words were successfully learned, with the behavioural tasks revealing significantly better learning for words denoting painful compared sensory experiences. One day after learning, significant activation in the fusiform gyrus was observed in response to all pseudowords. Furthermore, activation for pain-related words was observed in areas commonly associated with tactile and painful stimulus perception.

Conclusions: In addition to demonstrating that word meanings can be acquired from sensory contexts, these results provide preliminary evidence of rapidly emerging distributions of cortical activation that are consistent with abstract word meanings being both disembodied and embodied in sensory experiences.

References

1. Binder, J. R., Desai, R. H., Graves, W. W., & Conant, L. L. (2009). Where is the semantic system? A critical review and meta-analysis of 120 functional neuroimaging studies. Cerebral Cortex, 19(12), 2767-2796. https://doi.org/10.1093/cercor/bhp055
2. Davis, M. H., & Gaskell, M. G. (2009). A complementary systems account of word learning: Neural and behavioural evidence. Philosophical Transactions of the Royal Society B: Biological Sciences, 364(1536), 3773-3800. https://doi.org/10.1098/rstb.2009.0111
3. Hauk, O., Johnsrude, I., & Pulvermüller, F. (2004). Somatotopic representation of action words in human motor and premotor cortex. Neuron, 41(2), 301-307. https://doi.org/10.1016/S0896-6273(03)00838-9
4. McClelland, J. L., McNaughton, B. L., & O'Reilly, R. C. (1995). Why there are complementary learning systems in the hippocampus and neocortex: Insights from the successes and failures of connectionist models of learning and memory. Psychological Review, 102(3), 419-457. https://doi.org/10.1037/0033-295X.102.3.419

Poster No 1006

Left-right asymmetrical contribution of the anterior temporal lobe in semantic processing

Tomoki Uno[1,2], Marc Teichmann[3], Kouji Takano[1], Kimihiro Nakamura[1]

[1]National Rehabilitation Center for Persons with Disabilities, Tokorozawa, Japan, [2]Japan Society for the Promotion of Sciences, Tokyo, Japan, [3]French National Reference Center for « Rare or Early-Onset Dementias », Pitié-Salpêtrière Hospital, Paris, France

Introduction: The anterior temporal lobe (ATL) in the left and right hemispheres have been shown to act as a "semantic hub" converging multimodal information (Rice et al., 2015; Lambon Ralph et al., 2017). However, the functional architecture of ATL remains elusive because there are two competing models regarding the hemispheric specialization in semantic processing. On the one hand, the "functional specialization model" assumes that left and right ATLs are specifically involved in verbal and nonverbal semantics, respectively (Mesulam et al., 2014). On the other hand, the "unitary model" posits that the left and right ATLs equally contribute to multimodal semantic processing (Lambon Ralph et al., 2017). Interestingly, each of the two different models has gained empirical support from previous studies using transcranial magnetic stimulation (TMS) (Pobric et al., 2010; Bonni et al., 2015). However, this inconsistency may be attributed to the use of demanding cognitive tasks (i.e., semantic association) of which strong strategic components can cancel out possible differences between verbal and non-verbal semantic processing. The purpose of the present study is to examine whether or not the left and right ATLs are functionally asymmetrical in semantic processing by using repetitive transcranial magnetic stimulation (TMS) with a semantic priming paradigm which taps more implicit and automatic aspects of semantic processing.

Methods: Eighteen native Japanese speakers participated in the present study (8 females, all right-handed). They made real vs. nonreal judgments about visually presented words (lexical decision (LD)) or objects (object decision (OD)), preceded by semantically related or unrelated primes with short stimulus onset asynchrony (300 ms). Low-frequency ('inhibitory') repetitive TMS was applied prior to the two tasks to the left ATL, the right ATL or the vertex (control).

Results: For vertex stimulation, we confirmed typical effects of semantic priming in both LD and OD, whereby participants responded faster when targets were preceded by semantically related primes than by unrelated primes. Critically, we observed that semantic priming in LD was eliminated by left ATL stimulation but not by right ATL stimulation, suggesting that verbal semantics is represented in the left ATL. By contrast, semantic priming in OD was impaired by both left and right ATL stimulation, suggesting that the retrieval/analysis of non-verbal semantic information relies on the functional coordination of the left and right ATLs.

Conclusions: The present TMS data indicate that the left ATL is specialized for verbal semantic processing. This hemispheric asymmetry may be formed via strong structural and functional connections between the ATL and other language areas in the dominant left hemisphere (e.g., left middle-temporal gyrus and inferior frontal gyrus). Our results also showed that non-verbal semantic information is distributed in both hemispheres, probably because semantic analysis of visual objects relies on both the lexicosemantic knowledge in the left hemisphere and the visual shape analysis predominant in the right hemisphere (Seimons et al., 2003). Therefore, the functional coupling between the left and right ATL may play a crucial role

in the interhemispheric integration of multimodal information during semantic processing. Taken together, these results partially support the hemispheric specialization model (Mesulam et al., 2014) and extend our understanding of the functional architecture in the anterior temporal semantic hub.

References

1. Bonni, S. (2015), 'Role of the anterior temporal lobes in semantic representations: Paradoxical results of a cTBS study', Neuropsychologia, vol. 76, pp. 163-169.
2. Lambon Ralph, M. A. (2017), 'The neural and computational bases of semantic cognition', Nature Reviews Neuroscience, vol. 18, no. 1, pp. 42-55.
3. Mesulam, M. M. (2014), 'Primary progressive aphasia and the evolving neurology of the language network', Nature Reviews Neurology, vol. 10, no. 10, pp. 554-569.
4. Pobric, G. (2010), 'Amodal semantic representations depend on both anterior temporal lobes: evidence from repetitive transcranial magnetic stimulation', Neuropsychologia, vol. 48, no. 5, pp. 1336-1342.
5. Rice, G. E. (2015), 'The roles of left versus right anterior temporal lobes in conceptual knowledge: An ALE meta-analysis of 97 functional neuroimaging studies,' Cerebral Cortex, vol. 25, no. 11, pp. 4374-4391.
6. Simons, J. S. (2003), 'Neural mechanisms of visual object priming: evidence for perceptual and semantic distinctions in fusiform cortex', Neuroimage, vol. 19, no. 3, pp. 613-626.

Poster No 1007

The dynamics of GABA and Glutamate in semantic control: a combined 7T fMRS and fMRI study

JeYoung Jung[1], Adam Berrington[2]

[1]University of Nottingham, Nottingham, Nottingham, [2]University of Nottingham, Nottingham, Please Select

Introduction: Semantic control involves the adaptable skill of entering and handling meaningful information, allowing individuals to concentrate on the pertinent facets of a concept in accordance with a given context or objective (Jefferies, 2013; Lambon Ralph et al., 2016). This encompasses the ability to enhance less prominent features or uncommon meanings of a word while suppressing more prominent but unrelated attributes. Additionally, it includes the aptitude to transition between tasks effortlessly and address conflicting meanings or uncertainties. While the inferior frontal gyrus (IFG) has been associated with semantic control (Thompson-Schill et al., 1997; Wagner et al., 2001), the neurochemical mechanism underlying this process remains unclear. Proton magnetic resonance spectroscopy (MRS) is a non-invasive, in vivo technique that measures neurometabolite levels in the brain, including the inhibitory neurotransmitter GABA and the excitatory neurotransmitter glutamate. Functional MRS (fMRS) acquires multiple spectra during a task, providing a dynamic measurement of neurometabolites changes in response to stimuli (Stanley and Raz, 2018). While the existing literature on fMRS is limited, there is evidence indicating remarkable sensitivity in detecting task-related dynamic changes in glutamate and GABA within functionally relevant areas of the brain (Stanley and Raz, 2018). Here, we employed a combination of 7T fMRS and fMRI to examine the dynamic changes in GABA and glutamate within the left IFG during semantic control processing.

Methods: Sixteen healthy English speakers (4 males, mean age = 23yrs old) participated in this study. Participants performed a semantic categorization task at two different difficulty levels (easy [ES] and hard [HS]) during fMRS and a semantic categorization task and a picture matching task as a control task during fMRI (Fig. 1A). fMRS started with the fixation (2mins) followed by a semantic task (6mins) and ended with the fixation (3mins) (Fig. 1A). During fMRS, we measured GABA and glutamate in the left IFG (Fig. 1B).

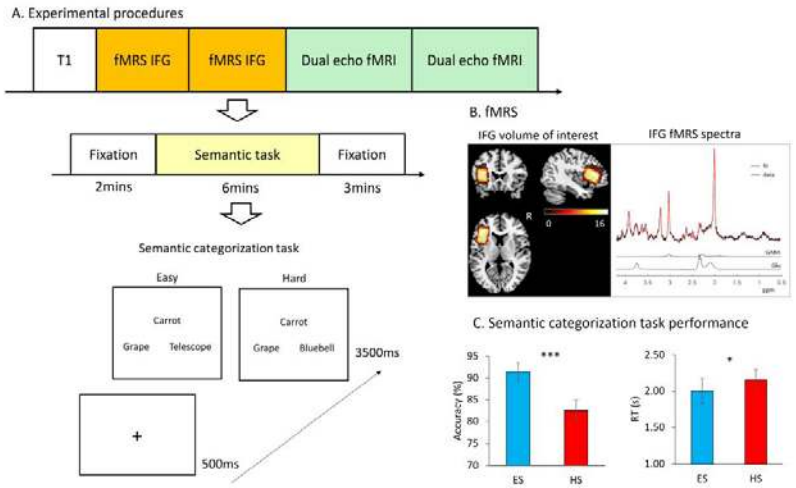

Results: Results showed that participants performed better in the easy task compared to the hard task, with higher accuracy and faster reaction times (Fig. 1C). We found that the levels of GABA and glutamate exhibited distinct patterns of changes corresponding to task difficulty. During the easy task, GABA concentrations in the IFG seemed to be stable, whereas during the demanding semantic control processing of the hard task, GABA levels increased (Fig. 2 Top). Contrary to GABA, glutamate was increased during the easy task and did not show any changes during the hard task (Fig. 2 Top). fMRI revealed increased regional activity in the IFG during the hard semantic task compared to the easy task (Fig.2 Bottom). Importantly, the task-modulated GABA changes were significantly correlated with task-induced regional activity in the IFG during the hard semantic task (Fig.2 Bottom). Furthermore, individual GABA levels were positively correlated with hard semantic task performance.

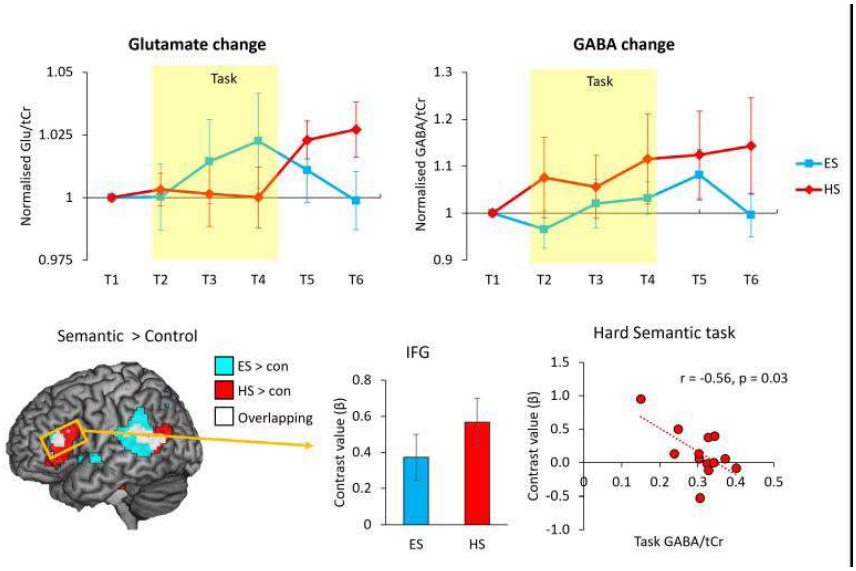

Conclusions: Our data suggests that semantic control processing modulates regional GABA and glutamate levels as well as fMRI activation in the IFG. GABAergic inhibition in the IFG seems to be important to shape task-induced regional activity and semantic control acuity.

References

1. Jefferies E (2013) The neural basis of semantic cognition: converging evidence from neuropsychology, neuroimaging and TMS. Cortex 49:611-625.
2. Lambon Ralph MA, et al. (2017) The neural and computational bases of semantic cognition. Nature Review Neuroscience 18 (1), 42-55
3. Stanley JA, et al. (2018) Functional Magnetic Resonance Spectroscopy: The "New" MRS for Cognitive Neuroscience and Psychiatry Research. Front Psychiatry 9:76.
4. Thompson-Schill SL, et al. (1997) Role of left inferior prefrontal cortex in retrieval of semantic knowledge: a reevaluation. Proceedings of the National Academy of Sciences 94:14792-14797.
5. Wagner AD, et al. (2001) Recovering meaning: left prefrontal cortex guides controlled semantic retrieval. Neuron 31:329-338.

Poster No 1008

Neurological Perspectives on Pragmatic Inference: Examining Conversational Sentences

Jiseon Baik[1], Sole Yoo[2,3], Euisun Kim[4,3], Jiyoung Park[2,3], Jiho Min[1], Hae-Jeong Park[2,3,4,5], Haeil Park[1]

[1]Kyung Hee University, Seoul, Korea, Republic of, [2]Department of Cognitive Science, Yonsei University, Seoul, Korea, Republic of, [3]Department of Nuclear Medicine, Severance Hospital, Yonsei University College of Medicine, Seoul, Korea, Republic of, [4]Department of Nuclear Medicine, Graduate School of Medical Science, BK 21 Project, Yonsei University, Seoul, Korea, Republic of, [5]Center for Systems and Translational Brain Sciences, Institute of Human Complexity and Systems Science, Yonsei University, Seoul, Korea, Republic of

Introduction: With the rise of social media, people have increasingly used emojis and small digital images, often featuring a face, as a means of communication. However, because of its nature, emojis can lack verbal meaning, which sometimes leads to confusion in our communication. Prior to the emergence of emoji, people used interjections such as "wow!" and "gross!" to express emotions, which are context-specific linguistic signs. By understanding the impact of these elements on language use and comprehension, we can enhance our understanding of the role of verbal cues in communication. In some ways, both expressions play a similar role in everyday conversations, and therefore, we aimed to investigate whether different brain regions are involved depending on the form of expression.

Methods: Thirty-three right-handed native English speakers (18 women) with normal vision and no neurological disorders participated in this imaging study. All participants provided written informed consent prior to participation. The study involved two sessions, each with 16 sentences, divided into four conditions: Type, Congruency, and Session. A total of 64 English sentence stimuli were used in this study. During the experiment, participants were asked to make judgments about each sentence, and the session lasted for approximately six minutes. The participants were scanned using a 3-T MRI system (Philips 3-T magnet) and functional imaging was performed to measure brain activation via the BOLD signal. For group-level inferences, a cluster-level criterion with a voxel-level threshold of $P < 0.005$ and a cluster size of >196 was used.

Results: The imaging experiment revealed significant differences in brain activation patterns between the various conditions. The contrast between 'Emoji' and 'Interjection' conditions demonstrated greater activation in the fusiform gyrus and right inferior frontal gyrus for 'Emoji,' while 'Interjection' showed greater activation in the left superior temporal gyrus (STG), right STG, middle temporal gyrus (MTG). The 'Incongruent' condition relative to 'Congruent' condition demonstrated greater activity in the regions associated with error detection, including the anterior cingulate cortex (ACC) and right inferior frontal gyrus (IFG). Additionally, the contrast between 'Session 2' and 'Session 1' indicated increased activation in the supramarginal gyrus, angular gyrus, and frontal operculum for 'Session 2'.

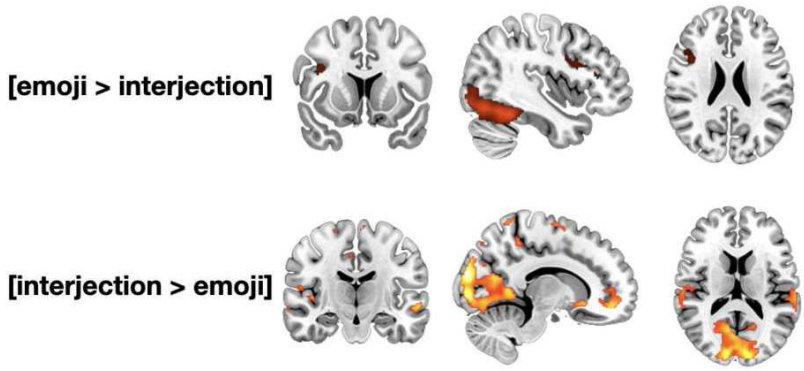

Fig. Activation regions for each contrast

Conclusions: The study found that activation in language-related areas and the superior temporal gyrus is associated with speech perception. Despite participants reading interjections instead of hearing them, activation in the speech perception areas was anticipated. In the emoji condition, activation in the fusiform gyrus (facial expressions) and right inferior frontal gyrus suggested that participants connected sentence meaning with emojis, potentially involving facial imagery. This aligns with the role of the right inferior frontal gyrus in syntactic reanalysis and linguistic judgement (Mack et al., 2013). In incongruent situations, participants tended to undergo reanalysis, whether the sentence ended with an emoji or an interjection. Increased complexity in mismatches prompts more inferences and context reinterpretation. Inhibitory control is crucial for resolving conflicts and suppressing automatic responses triggered by incongruent stimuli in mismatch tasks. Notably, 'Session 2' vs. 'Session 1' showed increased activation in the supramarginal gyrus, associated with social context, suggesting participants speculated about others' mental states during the experiment.

References

1. Chatzichristos, Christos.(2020), 'Emojis Influence Autobiographical Memory Retrieval from Reading Words: An fMRI-based study', PloS one, vol. 15, no. 7, e0234104.
2. Dietrich, Susanne.(2008), 'Understanding the Emotional Expression of Verbal Interjections: A functional MRI study', Neuroreport, vol. 19, no. 18, pp.1751-1755.
3. Mack, Jennifer E. (2013). 'Neural correlates of processing passive sentences'. Brain sciences vol. 3, no. 3, pp 1198-1214

Poster No 1009

Foreign language modulates brain activity and connectivity during emotional text reading

Tatiana Davydova[1], César Ávila[1], Lidón Marin Marin[1], María Baena Pérez[1], Eva Calderón Rubio[1], Víctor Costumero[1]

[1]*Jaume I University, Castellón de la Plana, Spain*

Introduction: Reduced emotional resonance during second language (L2) processing is a well-established phenomenon (Caldwell-Harris, 2014) that has been demonstrated across different research modalities, including skin conductance (Harris & Berko Gleason, 2003), pupillary response (Iacozza et al., 2017), electroencephlography (EEG) (Chen et al., 2015; Opitz &

Degner, 2012), and functional neuroimaging studies (Chen et al., 2015). However, most of the research has focused on single word processing, with only one neuroimaging study existing currently that studied L1/L2 emotional processing differences during silent reading of more complex verbal stimuli (Hsu et al., 2015). Thus, further research is needed to elucidate the neural mechanisms underlying differences in brain activity during emotional reading in L2. In this fMRI study, a group of unbalanced Spanish (L1)/ English (L2) bilinguals completed a bilingual silent reading task of negative, positive, and neutral texts selected from multiple fiction books. The analysis centered on studying the interaction effect of language and condition upon whole-brain activity, as well as on the functional connectivity patterns between the areas involved in semantic and emotional processing.

Methods: Twenty-four (24) unbalanced Spanish (L1) / English (L2) bilinguals were included in this study (11 females, mean age = 22.46, sd = ± 3.4). Assessment of English proficiency was carried out by way of the LexTALE vocabulary test (Lemhöfer & Broersma, 2012) with mean score = 69.95, (sd = ± 6.63). Each participant read a series of negative, positive, and neutral texts in their L1 and L2 during the scan. Structural 3D and functional EPI sequences were acquired on a 3T GE Signa-Architect scanner. Functional data was pre-processed according to the standard pipeline using SPM12 (Wellcome Trust Centre for Neuroimaging, London, UK). Group analyses centered on investigating the interaction effect between language and condition on neural activity and seed-to-seed functional connectivity between the areas involved in semantic (temporal lobe) and emotional (amygdala, hippocampus) processing.

Results: Our results showed a significant language/condition interaction on the activity of the left hippocampus during the processing of negative texts (P = .013, FWE cluster-corrected, with a height threshold of P < .001) driven by higher activity during the processing of negative texts in L1, as evidenced by post-hoc analysis. Furthermore, our seed-to-seed connectivity analysis showed significant language/condition interaction effect on the functional connectivity between the left middle temporal pole and the right nucleus accumbens (F = 4.99, P = .036) during the processing of positive texts and between the left superior temporal pole and the left amygdala (F = 6.09, P = .021) during the processing of negative texts.

Conclusions: Our results provide further evidence of attenuated emotional response in L2 as seen by the lower activity in the left hippocampus during the processing of negative texts in the second language. Furthermore, we found language and condition interaction effect on the functional connectivity between the semantic and emotional processing areas. During the processing of positive texts, this effect was seen in the connectivity between the left middle temporal pole and the nucleus accumbens, an area that plays an important role in the processing of rewards and has been reported to activate in response to positive verbal stimuli (Hamann & Mao, 2002), whereas with the negative texts, this effect was seen in the connectivity between the left superior temporal pole and the left amygdala, the region involved in the processing of negative verbal stimuli (Nakic et al., 2006).

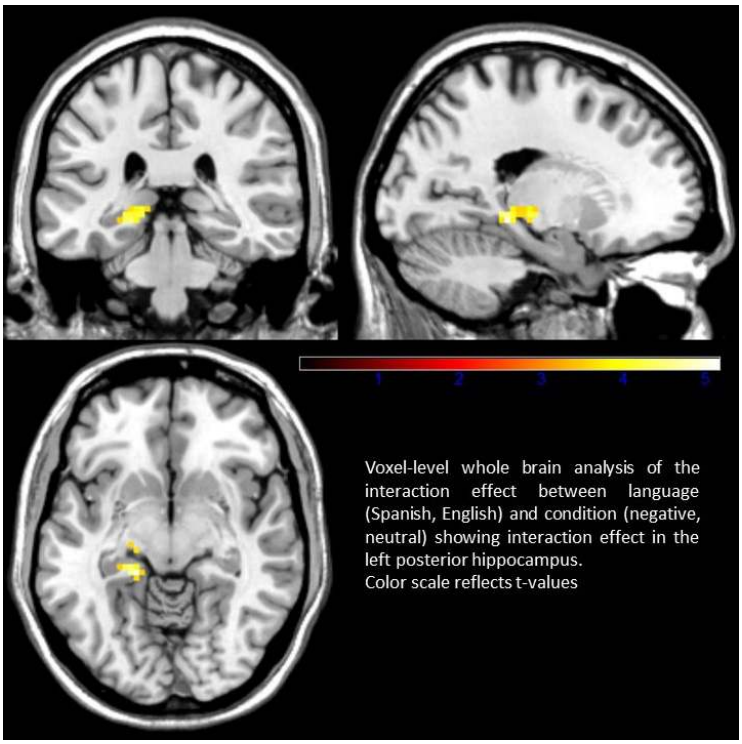

References

1. Caldwell-Harris, C. L. (2014). Emotionality differences between a native and foreign language: Theoretical implications. Frontiers in Psychology, 5(SEP). https://doi.org/10.3389/fpsyg.2014.01055
2. Chen, P., Lin, J., Chen, B., Lu, C., & Guo, T. (2015). Processing emotional words in two languages with one brain: ERP and fMRI evidence from Chinese-English bilinguals. Cortex, 71(June), 34–48. https://doi.org/10.1016/j.cortex.2015.06.002
3. Hamann, S., & Mao, H. (2002). Positive and negative emotional verbal stimuli elicit activity in the left amygdala. Neuroreport, 13(1), 15–19. https://doi.org/10.1097/00001756-200201210-00008
4. Harris, C. L., & Berko Gleason, J. (2003). Taboo words and reprimands elicit greater autonomic reactivity in a first language than in a second language. Applied Psycholinguistics, 24, 561–579. https://doi.org/10.1017.S0142716403000286
5. Hsu, C. T., Jacobs, A. M., & Conrad, M. (2015). Can Harry Potter still put a spell on us in a second language? An fMRI study on reading emotion-laden literature in late bilinguals. Cortex, 63, 282–295. https://doi.org/10.1016/j.cortex.2014.09.002
6. Iacozza, S., Costa, A., & Duñabeitia, J. A. (2017). What do your eyes reveal about your foreign language? Reading emotional sentences in a native and foreign language. PLoS ONE, 12(10). https://doi.org/10.1371/journal.pone.0186027
7. Lemhöfer, K., & Broersma, M. (2012). Introducing LexTALE: A quick and valid Lexical Test for Advanced Learners of English. Behavior Research Methods, 44(2), 325–343. https://doi.org/10.3758/s13428-011-0146-0
8. Nakic, M., Smith, B. W., Busis, S., Vythilingam, M., & Blair, R. J. R. (2006). The impact of affect and frequency on lexical decision: The role of the amygdala and inferior frontal cortex. NeuroImage, 31(4), 1752–1761. https://doi.org/10.1016/j.neuroimage.2006.02.022
9. Opitz, B., & Degner, J. (2012). Emotionality in a second language: It's a matter of time. Neuropsychologia, 50(8), 1961–1967. https://doi.org/10.1016/j.neuropsychologia.2012.04.021

Poster No 1010

Language Similarity of Bilingual's Languages Has an Effect on Their Language Processing

Juraj Jonáš[1], Jan Štrobl[1], Vlastimil Koudelka[1], Mabel Rodriguez[1]

[1]National Institute of Mental Health, Klecany, Česká republika

Introduction: Previous studies in bilingualism have focused on the factors, such as the age of second language acquisition, its attained proficiency level, the manner of acquisition, or relative dominance of one language over the other. Several studies suggest that language similarity may also significantly influence cognitive and language functioning. Behavioral studies suggest that language similarity has an effect on mechanisms of lexical and syntactical representation and selection (Cui, & Shen, 2016; Huang et al., 2019), selective attention (Olguin et al., 2019), and executive functions (Oschwald et al., 2018). There has been however lacking the studies which would look into processing on the neurophysiological level.

Methods: Participants: three groups of bilingual participants (N=23) were compared: 1. bilinguals with similar (mutually intelligible languages as reported by van Heuven et al., 2015) - Slovak and Czech languages; 2. bilinguals with different languages - Czech and German and 3. bilinguals with partly mutually intelligible languages - Czech and Russian. Language status of participants was measured with the Language History Questionnaire 2.0. Procedure: Two event-related potentials experiments have been conducted. Participants did both paradigms in both of their languages. Results of both languages were averaged. 1. N200 experiment consisted of go/no-go task, where participants were asked to react only to objects (visual) with feminine grammatical gender. In case of other grammatical gender they were supposed to withhold reaction. Incongruent stimuli were stimuli with different gram. gender in subject's both languages. Incongruent stimuli should elicit larger N200 wave. In general, bilinguals elicit larger N200 in incongruent verbal stimuli than monolinguals. N200 measures the cognitive inhibition. We expected different N200 effect (the difference between avarage reaction to congruent and incongruent stimuli) for each language group. 2. N400 experiment was based on Semantic violation task: Subjects were presented semantically correct or incorrect sentences. Participants were ask to react to the incorrect ones only. Semantically violated stimuli elicit larger amplitude in bilinguals than in monolinguals. We hypothesized that N400 ERP would differ in accordance to language similarity.

Results: Analysis: peaks of average congruent and incongruent wave were defined for each participant. These were subtracted, so te ERP effect was found. This was done for both, the N200 and N400 wave. N200 amplitude: Shapiro-Wilk test did not show normal distribution, so Kruskal-Wallis test was applied. Between groups no significant difference has been found. N200 latency: 2-factor mixed-design with a use of an M-estimator and bootstrap with Bonferoni correction for 2 tests had been used. No difference between groups was observed. N400 amplitude: Normal distribution and homogeneity of data had not been rejected (Shapiro-Wilk test, Leven test), 2-factor mixed ANOVA had been used. Significant differences between German and Russian group (p=0.0147) and also between German and Slovak group (p=0.0074) ahs been observed. N400 latency: 2-factor mixed-design (M-estimator and bootstrap) had been used. Significant difference in latency was observed between Russian and Slovak group (p=0,0006).

Conclusions: No effect of the language similarity on language processing, neither in terms of amplitude nor latency has been observed on N200 ERP. However, differences were observed in both N400 latency and amplitude. This difference however

might have been a result of different script (Russian use Azbuka, all other languages use Latin script). We conclude that early language processing (cognitive inhibition) is not affected by language similarity, but late processing is (semantic). Language similarity might be one of the factors behind a large inconsistency in bilingual research data.

References

1. Huang, J., Pickering, M. J., Chen, X., Cai, Z., Wang, S., & Branigan, H. P. (2019). Does language similarity affect representational integration?. Cognition, 185, 83-90.
2. Olguin, A., Cekic, M., Bekinschtein, T. A., Katsos, N., & Bozic, M. (2019). Bilingualism and language similarity modify the neural mechanisms of selective attention. Scientific reports, 9(1), 1-14.
3. Oschwald, J., Schättin, A., Von Bastian, C. C., & Souza, A. S. (2018). Bidialectalism and bilingualism: Exploring the role of language similarity as a link between linguistic ability and executive control. Frontiers in psychology, 9, 1997.
4. van Heuven, V. J., Gooskens, C. S., Bezooijen, R. V., & Navracsics J, B. S. (2015). Introducing Micrela: Predicting mutual intelligibility between closely related languages in Europe. In: Studies in Psycholinguistics, 127-145.

Poster No 1011

Organisation of structure-function coupling in the brain with respect to language laterality

Ieva Andrulyte[1], Christophe de Bezenac[1], Simon Keller[1]

[1]University of Liverpool, Liverpool, Merseyside

Introduction: Language is one of the most studied lateralised cognitive functions in the human brain, which functionally relies on the left hemisphere in most people. Nevertheless, the precise mechanisms through which a relatively stable white matter architecture is established to directly underpin language function in each individual remain uncertain. Previous studies utilised structural connectivity (SC) and functional connectivity (FC) coupling for individual fingerprinting and task decoding (Griffa et al., 2022), implying that the variability in brain entropy could serve as a distinguishing characteristic for individual brain identification. In this study, we investigated a large cohort (n=1006) of young, healthy individuals (ages 22 to 35) to look at each subject's SC-FC coupling and identify potential markers that could help to distinguish between different language laterality groups, defined as bilateral, left-, and right-language dominant.

Methods: Language laterality was predetermined using task fMRI for language comprehension via a story-math contrast (Binder et al., 2011). Functional connectivity was measured by extracting rsfMRI time-series data from 360 brain regions using HCP atlas parcellation (Glasser et al., 2016). Functional connections were defined as weighted direct edges, modelled using Pearson correlation coefficients, producing a correlation matrix representing interregional functional connectivity (Gu et al., 2022) (Fig. 1a). To enhance interpretability, negative values in each connectivity matrix were set to zero (Luppi and Stamatakis, 2021). Structural connectivity was determined using a whole-brain deterministic fibre tractography algorithm leveraging spin distribution functions (SDFs) (Yeh et al., 2010). Two types of structural connectivity matrices per subject were generated: using (1) the counts of connecting tracts (streamlines) and (2) quantitative anisotropy (QA) between each node (Panesar et al., 2018) (Fig. 1b). The HCP atlas was employed for brain parcellation, with two ROIs deemed connected only if a fibre originated from one ROI and terminated in the other. Structure-function coupling was defined as the Pearson correlation between non-zero elements of regional structural (number of fibres and QA) and functional (correlation coefficient of rsfMRI) connectivity profiles across the whole brain (Baum et al., 2020) (Fig. 1c). For each participant, regional connectivity profiles were represented as vectors of connectivity strength from a single network node to all other nodes (Zarkali et al., 2021). Statistical analyses of group differences used the permutation analysis of linear models (PALM) toolbox in FSL, with family-wise error correction of $p<0.05$ and inclusion of sex, age, and handedness as covariates of no interest (Winkler et al., 2014).

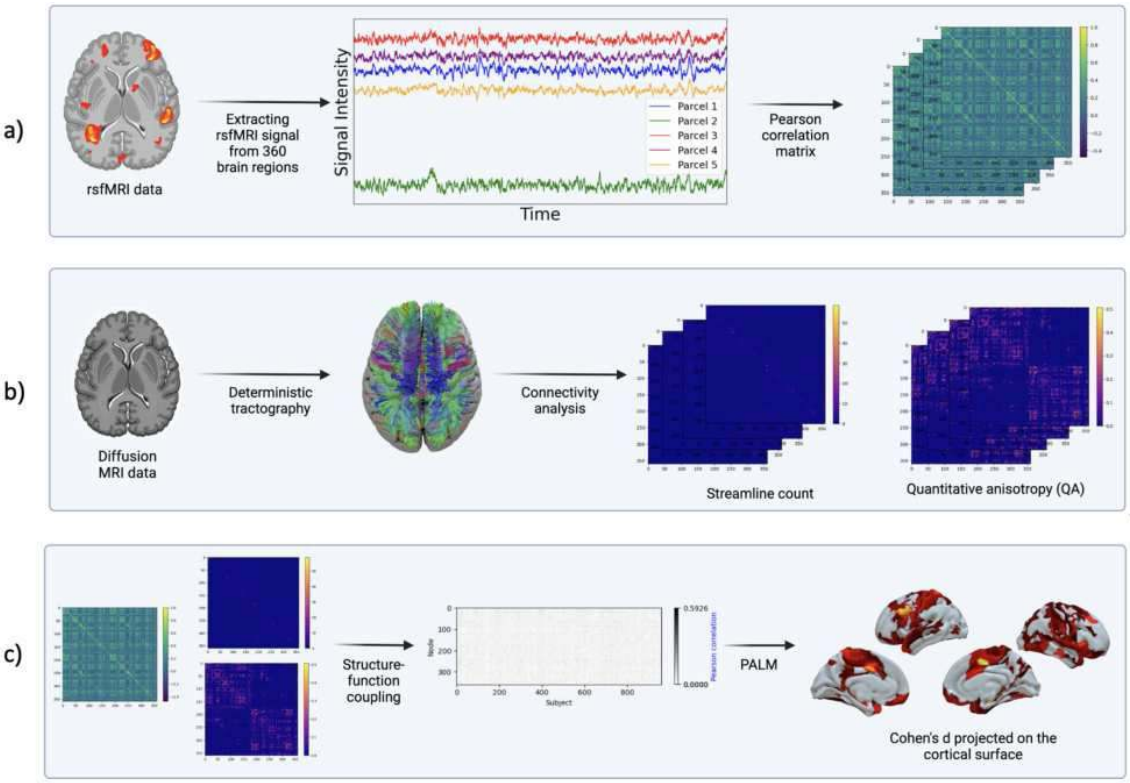

Results: The results revealed a significant positive correlation in SC-FC coupling in the left 8c (a part of the dorsolateral prefrontal cortex) and right ventral area 24d (a part of paracentral lobular and mid-cingulate) in individuals with left language dominance (LLD) and right language dominance (RLD) compared to bilateral individuals (pFDR<0.05) (Fig. 2). Notably, this effect was observed only at the microstructural diffusion level (QA). Individuals with RLD also exhibited a greater coupling in the right hippocampus compared to bilateral individuals, a pattern not observed in LLD individuals. Additionally, SC-FC coupling in the right middle and agranular insular area was significantly tighter in people with RLD compared to LLD (FDR<0.01; difference observed at the streamline count level).

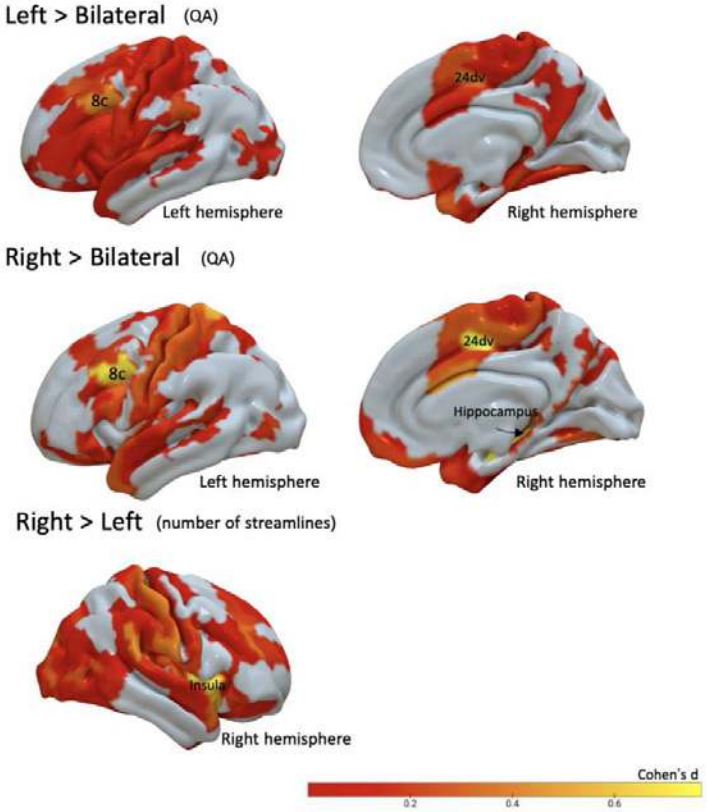

Conclusions: In summary, lateralised individuals exhibit greater SC-FC coupling, while bilateral individuals show no differences on the group level. This suggests a reliance on structure and less functional variability in lateralized individuals regarding language specialisation compared to their bilateral counterparts.

References

1. Baum, G. L. et al. (2020). Development of structure–function coupling in human brain networks during youth. Proceedings of the National Academy of Sciences, 117(1), 771-778.
2. Binder, J. R. et al. (2011). Mapping anterior temporal lobe language areas with fMRI: a multicenter normative study. Neuroimage, 54(2), 1465-1475.
3. Glasser, M. F. et al. (2013). The minimal preprocessing pipelines for the Human Connectome Project. Neuroimage, 80, 105-124.
4. Griffa, A. et al. (2022). Brain structure-function coupling provides signatures for task decoding and individual fingerprinting. NeuroImage, 250, 118970.
5. Luppi, A. I. & Stamatakis, E. A. (2021). Combining network topology and information theory to construct representative brain networks. Network Neuroscience, 5(1), 96-124.
6. Panesar, S. S. et al. (2018). A quantitative tractography study into the connectivity, segmentation, and laterality of the human inferior longitudinal fasciculus. Frontiers in neuroanatomy, 12, 47.
7. Winkler, A. M. et al. (2014). Permutation inference for the general linear model. Neuroimage, 92, 381-397.
8. Wirsich, J. et al. (2016). Whole-brain analytic measures of network communication reveal increased structure-function correlation in right temporal lobe epilepsy. NeuroImage: Clinical, 11, 707-718.
9. Yeh, F. C. et al. (2010). Generalized q-sampling imaging. IEEE transactions on medical imaging, 29(9), 1626-1635.
10. Zarkali, A. et al. (2021). Organisational and neuromodulatory underpinnings of structural-functional connectivity decoupling in patients with Parkinson's disease. Communications biology, 4(1), 86.

Poster No 1012

White matter correlations of sentence processing in individuals with post-stroke aphasia

Sabrina Beber[1,2], Ahmad Beyh[3], Chris Foulon[4], Piergiorgio Tomasi[5], Stefano Terruzzi[6], Jacopo Bonavita[5], Marco Tettamanti[7], Gabriele Miceli[6], Stephanie Forkel[8]

[1]Center for Mind/Brain Sciences (CIMeC), Rovereto, Trento, Italy, [2]Donders Institute for Brain Cognition Behaviour, Radboud University, Nijmegen, Gelderland, Netherlands, [3]Donders Institute – Radboud University, Nijmegen, Nijmegen, [4]Groupe d'Imagerie Neurofonctionnelle (GIN), Institut des Maladies Neurodegeneratives-UMR 5293, CNRS, Bordeaux, France, [5]Villa Rosa Rehabilitation Department, Azienda Provinciale Servizi Sanitari, Pergine Valsugana, Trento, Italy, [6]Center for Mind/Brain Sciences (CIMeC) – University of Trento, Rovereto, Trento, Italy, [7]University of Milano-Bicocca, Milano, Milano, [8]Donders Institute for Brain Cognition Behaviour, Radboud University, Nijmegen, Gelderland

Introduction: This research builds on lesion-symptom mapping analyses involving patients with aphasia (PWA) who exhibit comprehension deficits in reversible sentences due to temporo-parietal damage. Previous studies (e.g., Thothathiri et al., 2012) have predominantly focused on cortical analyses and thematic role reversal errors in sentence comprehension (e.g., understand 'that a boy is kissing a girl' hearing 'The boy is kissed by the girl'). However, we recognise the importance of investigating the impact of white matter lesions and morphosyntactic processes on sentence comprehension. Our study aims to explore whether the cortical neurofunctional correlates of sentence comprehension extend to the white matter, particularly in the context of thematic role assignment errors, while controlling for morphosyntactic difficulties.

Methods: 21 individuals with aphasia following left hemisphere stroke (13 males; age: 18-80 years; >6 years of education; Italian mother tongue; right-handed) and 50 matched healthy controls (28 males) participated in a sentence-picture matching task including thematic role and morphosyntactic foils. Structural and diffusion 3T-MRI (dir=64, b-value=2000, number of B0=12) data were acquired using a PRISMA scanner and underwent preprocessing. Lesions were manually delineated and normalised to the MNI152-1mm space using ANTs (http://stnava.github.io/ANTs/). The lesion-based probability of tract disconnections was assessed using Tractotron (Foulon et al., 2018) and statistically analysed alongside sentence performance using a Kruskal-Wallis test, with Mann-Whitney post-hoc analysis with Benjamini-Hochberg correction. Personalised tractography dissections were based on spherical deconvolution modelling (Dell'Acqua et al., 2010; 2013) and visualised using TrackVis (https://trackvis.org) based on manually defined regions of interest (Forkel et al., 2023). The volume (measured as voxels intersected by a streamline) of each dissected tract was subjected to partial correlation analysis with Bootstrapping, Bonferroni corrected, and associated with sentence performance.

Results: All PWA exhibited difficulties in sentence comprehension, as determined by the cut-off score from healthy controls. The probability of damage to the anterior segment of the arcuate fasciculus correlated with thematic role foils difficulties ($p<.05$, Benjamini-Hochberg corrected). No significant correlations were identified in the posterior segment of the arcuate fasciculus, frontal aslant tract, inferior fronto-occipital fasciculus, inferior longitudinal fasciculus, uncinate fasciculus and cortical-spinal tract. The long segment of the arcuate and the corpus callosum were disconnected in all PWA and, while

visualised, were not included in the analysis (Figure 1-Chart). The personalised tractography analysis revealed that the volume of all segments of the arcuate fasciculus was associated with reduced accuracy on thematic role foils (p<.005, Bonferroni corrected). When covarying for morphosyntactic foils, both the long and posterior segments exhibited correlations (p<.005, Bonferroni corrected) with diminished accuracy on thematic role foils. In contrast, no significant correlations were observed in the corpus callosum and corticospinal tract, which served as non-linguistic control tracts (Figure 1-Dissections).

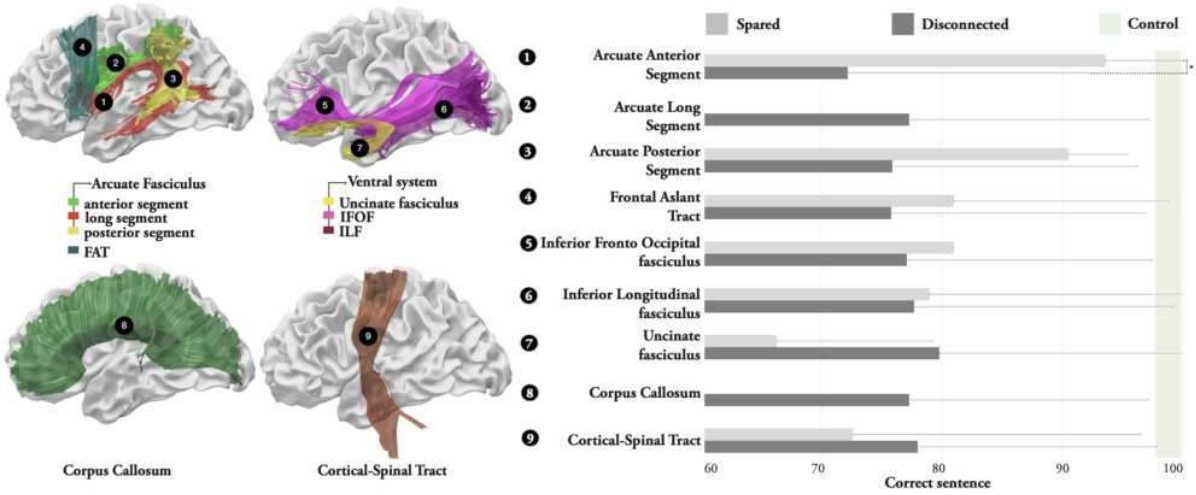

Figure 1 - **Dissections** (on the left) of the white matter tracts were analysed using two methods: lesion-based probability of tract disconnections and tractography analysis.
- **Chart** (on the right) showed the results of the lesion-based probability of tract disconnections associated with thematic role assignment. The Kruskal-Wallis test was used with Mann-Whitney post-hoc analysis, with p-value <.05 (Benjamini-Hochberg corrected). It presented the mean performance of patients with (dark grey) and without (light grey) disconnection, and the healthy control group (green, with control of intervals to 95% CIs).
* p <.05

Conclusions: The study of thematic role assignment difficulties revealed significant involvement of the arcuate fasciculus, complementing previous cortical-focused research. In the lesion-based probability analysis, a correlation was observed between damage to the anterior segment and thematic role assignment. In the tractography-based analysis, when controlled for performance on morphosyntactic foils, the long and posterior segments were significantly associated with thematic role assignment, aligning with previous lesion studies implicating temporo-parietal regions. Our findings highlight the crucial role of a fronto-temporo-parietal white matter network in sentence processing.

References

1. Avants, B.B. (2011), 'A reproducible evaluation of ANTs similarity metric performance in brain image registration', NeuroImage, 54(3), 2033–2044.
2. Avants, B.B. (2014), 'The Insight ToolKit image registration framework', Frontiers in Neuroinformatics, 8.
3. Forkel, S.J. 'Dissecting White Matter Pathways: A neuroanatomical approach. In Handbook of Diffusion MRI Tractography (Eds Leemands/ Dell'Acqua)', preprint.
4. Foulon, C. (2018), 'Advanced lesion symptom mapping analyses and implementation as BCBtoolkit', Gigascience, 7(3), giy004.
5. Thothathiri, M. (2012), 'The neural basis of reversible sentence comprehension: evidence from voxel-based lesion symptom mapping in aphasia', Journal of Cognitive Neuroscience, 24(1), 212-222.

Poster No 1014

Spatiotemporal contribution to semantic decoding before speech onset: Intracranial EEG study

Ye Jin Park[1], Jii Kwon[1], Chun Kee Chung[1]

[1]Seoul National University, Seoul, Seoul

Introduction: Speech processing involves auditory, semantic, and articulatory dimensions. Recent advancements in Brain-Computer Interface (BCI) systems have largely focused on auditory and articulatory information. However, this approach faces challenges when applied to individuals who lack articulatory capabilities. To address this gap, developing BCI systems that rely on semantic processing is needed. Since semantic processing needs time dependent processing in different brain areas, our study aims to elucidate these spatiotemporal contributions using intracranial EEGs.

Methods: Four epilepsy patients with intracranial electrodes implanted to speech relevant areas participated in this study. Subjects performed a Korean word reading task with intracranial EEGs recorded. The spoken words were categorized into

2 semantic groups, specifically body vs. non-body parts, or subject vs. predicate. Preprocessing included detrending and applying the Common Average Reference (CAR), followed by bandpass filtering in two frequency ranges: 70-110 Hz (HG1) and 130-170 Hz (HG2). Firstly, we selected features with significant differences between the two categories. We then employed various classification algorithms such as Linear Discriminant Analysis (LDA), Support Vector Machine (SVM), K-Nearest Neighbors (KNN), and Random Forest Classifier, to evaluate the decoding performance of semantic processing in successive 150ms epochs, from the presentation of a word to the onset of speech.

Results: In this study, there were notable differences in brain activity between two semantic categories. Spatially, there was an initial activation of frontal areas, including the left inferior frontal gyrus (IFG), followed by the temporal areas, such as the left primary auditory cortex and the superior temporal gyrus (STG), with the time approaching the speech onset. The highest accuracy, 88.9% (±9% SE) in the left IFG, was achieved in distinguishing between body parts and non-body parts, occurring 150-300ms after word presentation. Between subjects and predicates, the highest accuracy was 76.7% (±13% SE) in the left pars triangularis, pars orbitalis, and primary auditory cortex, 450 to 600ms post-word presentation.

Conclusions: In semantic processing, there were distinct temporal and spatial contributions. Our results are in line with the previous evoked response studies on N400 component in semantic processing, and previously identified speech related areas including the STG and the IFG. With decoding of spatiotemporal contribution, we could decode semantic processing, potentially extending the current limitation of speech BCI.

References

1. Brouwer, H., Crocker, M. W., Venhuizen, N. J., & Hoeks, J. C. (2016). A neurocomputational model of the N400 and the P600 in language processing. Cognitive Science, 41, 1318–1352. https://doi.org/10.1111/cogs.12461
2. Brown, C., & Hagoort, P. (1993). The processing nature of the N400: Evidence from masked priming. Journal of Cognitive Neuroscience, 5(1), 34–44. https://doi.org/10.1162/jocn.1993.5.1.34
3. Bhaya-Grossman, I., & Chang, E. F. (2022). Speech computations of the human superior temporal gyrus. Annual Review of Psychology, 73(1), 79–102. https://doi.org/10.1146/annurev-psych-022321-035256
4. Rabbani, Q., Milsap, G., & Crone, N. E. (2019). The potential for a speech brain–computer interface using chronic electrocorticography. Neurotherapeutics, 16(1), 144–165. https://doi.org/10.1007/s13311-018-00692-2

Poster No 1015

Mapping semantic representations of depression using simple lexical choices

Line Kruse[1], Roberta Rocca[2], Mikkel Wallentin[3]

[1]Aarhus University, Aarhus, Aarhus, [2]Aarhus University, Aarhus, Aarhus, [3]Aarhus University, Aarhus C, DK

Introduction: Depression is characterized as a disorder of self, involving maladaptive distortions in the experiential and narrative self (Newell et al., 2018; Davey & Harrison, 2022). Evidence indicate that differences in mental states are well reflected in both language use and processing and predict many psychiatric disorders, as well as personality and demographic traits (Behdarvandirad & Karami, 2022; Christian et al., 2021; Lai et al., 2021). Spatial demonstratives (in English “this” and “that”) are typically used to distinguish peri- and extrapersonal space and have been shown to engage brain regions associated with spatial information processing (Rocca et al., 2020). Recent work based on the Demonstrative Choice Task (DCT) showed that choice of demonstratives are not only indicative of distance in a physical space, but also of the experienced or emotional proximity to the self (Rocca & Wallentin, 2020). Capturing important dimensions concerning self-focused mental representations, the DCT may encode information relevant to inferring the presence of depression and may provide means to identify and study the structure of semantic representations underlying individual differences in depression and other disorders of self.

Methods: This work included two behavioral studies and an fMRI study using a 300-item DCT. Behavioral analyses were based on two independent samples of 775 and 879 participants, respectively. A PHQ9 sum score of 10 was used as threshold for partitioning participants into control and clinical group (Kroenke et al., 2001). Classification models were trained to predict outcome label (control or clinical) based on principal component representations of DCT responses. fMRI analyses included 69 participants of which 32 were diagnosed with clinical depression and 37 were healthy. Data were preprocessed using standard fMRIprep preprocessing pipelines (Esteban et al., 2019). First-level T-contrasts and second-level intercept models addressed neural differences between trials associated with a proximal compared to distal demonstrative choice. Voxel-wise encoding models using wordnet categories as feature space were computed to assess individual differences in neural representations of semantic features (Huth et al., 2012). Encoding models included L2-regularized linear regression models fit to each subject independently.

Results: Behavioral results showed that DCT based classification models predicted depression group significantly better than chance with F1-scores between 62% and 66% across samples. Semantic analyses showed that proximal responses for words scoring high on the features sadness, fear, disgust and anger predicted higher PHQ9 symptom scores, while the opposite was true for the features valence, joy and trust (Figure 1). fMRI analyses showed significantly increased activity in the left precuneus, p<.05 (Figure 2), for trials associated with proximal compared to distal demonstrative forms. Voxel-wise encoding models indicated individual differences in neural representations across semantic features related to depression symptom scores.

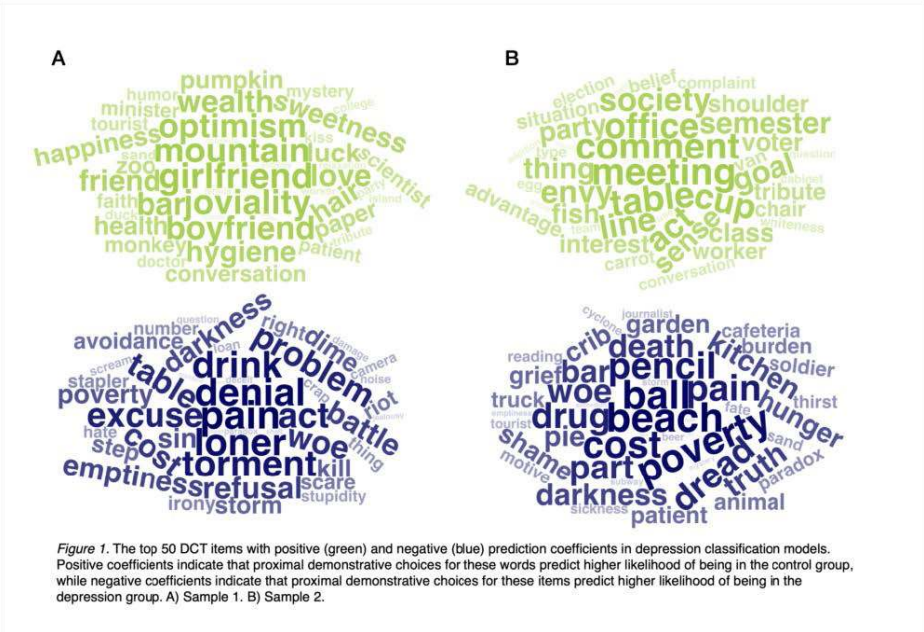

Figure 1. The top 50 DCT items with positive (green) and negative (blue) prediction coefficients in depression classification models. Positive coefficients indicate that proximal demonstrative choices for these words predict higher likelihood of being in the control group, while negative coefficients indicate that proximal demonstrative choices for these items predict higher likelihood of being in the depression group. A) Sample 1. B) Sample 2.

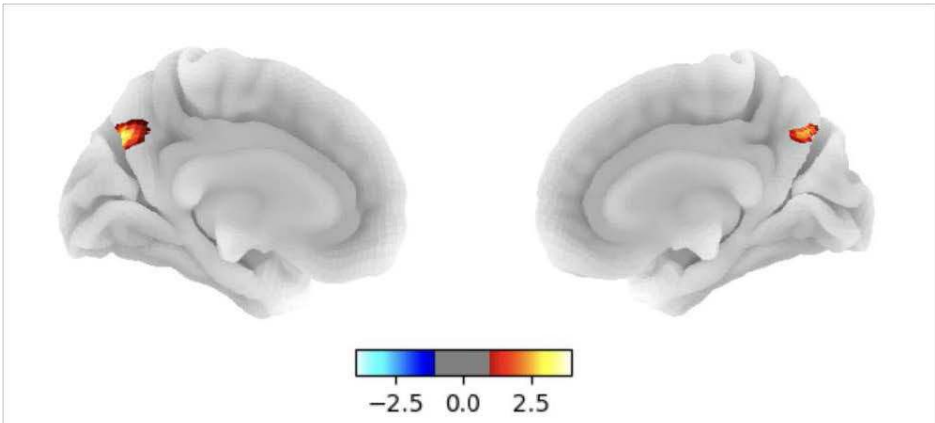

Figure 2. Group-level permutation test of significance (p<.05) for contrast proximal demonstrative choice trials > distal demonstrative choice trials. Significant cluster is observed in the left precuneus, MNI peak cooridnates [-4, -74, 37], cluster extent =43 voxels, volume=223.9 mm. Values are on the log-scale.

Conclusions: Results indicated that a simple lexical choice task reliably captured semantic characteristics of experiential states that are predictive of depression symptom severity and recover semantic effects of valence previously associated with depression. The paradigm engaged posterior parietal regions typically associated with spatial processing and a core node in the DMN, indicating that choice of proximal demonstratives on the DCT involves increased self-referential processing of DCT items. Assessing subject-specific semantic maps of neural representations across semantic features of DCT items support depression-related differences observed in the behavioral effects. Investigating and characterizing semantic representations underlying individual experiential states may contribute importantly to symptom profiling approaches and provide novel information on individual differences in depressive states.

References

1. Behdarvandirad, S., & Karami, H. (2022). Depression, neuroticism, extraversion and pronoun use in first and foreign languages following mood induction. Language Sciences, 94, 101503.
2. Christian, H., et al. (2021). Text based personality prediction from multiple social media data sources using pre-trained language model and model averaging. Journal of Big Data, 8(1), 68.

3. Davey, C. G., & Harrison, B. J. (2022). The self on its axis: A framework for understanding depression. Translational Psychiatry, 12(1), Article 1.
4. Esteban, O. et al. (2019). fMRIPrep: A robust preprocessing pipeline for functional MRI. Nature Methods, 16(1), Article 1.
5. Huth, A. G. et al. (2012). A Continuous Semantic Space Describes the Representation of Thousands of Object and Action Categories across the Human Brain. Neuron, 76(6), 1210–1224.
6. Kroenke, K. et al. (2001). The PHQ-9: Validity of a brief depression severity measure. Journal of General Internal Medicine, 16(9), 606–613.
7. Lai, Y. et al. (2021). Neural Demographic Prediction in Social Media with Deep Multi-view Multi-task Learning. In C. S. Jensen, E.-P. Lim, D.-N. Yang, W.-C. Lee, V. S. Tseng, V. Kalogeraki, J.-W. Huang, & C.-Y. Shen (Eds.), Database Systems for Advanced Applications (pp. 271–279). Springer International Publishing.
8. Newell, E. E. et al. (2018). You Sound So Down: Capturing Depressed Affect Through Depressed Language. Journal of Language and Social Psychology, 37(4), 451–474.
9. Rocca, R. et al. (2020). Language beyond the language system: Dorsal visuospatial pathways support processing of demonstratives and spatial language during naturalistic fast fMRI. NeuroImage, 216, 116128.
10. Rocca, R., & Wallentin, M. (2020). Demonstrative Reference and Semantic Space: A Large-Scale Demonstrative Choice Task Study. Frontiers in Psychology, 11.

Poster No 1016

Mapping higher-order language regions in the cerebellum with precision functional MRI

Joseph James Salvo[1], Nathan Anderson[1], Rodrigo Braga[1]

[1]Northwestern University, Chicago, IL

Introduction: The brain is populated by large-scale networks that interconnect regions in the cerebrum and cerebellum (Buckner et al. 2011; Xue et al. 2021). Supporting specialization at the level of the entire cerebral-cerebellar networks, estimates of language task-related activity reveal that perisylvian cerebral areas activate alongside cerebellar regions during linguistic tasks (Petersen et al., 1989; Ashida et a. 2019). Recently, within-individual estimates from resting-state functional connectivity have outlined a set of cerebellar regions that putatively belong to a distributed language network (Xue et al., 2021; King et al., 2019). Here, we tested the correspondence between these cerebellar language network regions and regions showing task-evoked responses during auditory and visual language tasks.

Methods: Extensive task and resting-state 3T fMRI data were collected from 8 neurotypical adults over the course of 8 sessions, using a multi-echo protocol. Participants were presented with written (total 40 min; Fedorenko et al., 2010) or spoken (total 48 min; Scott et al., 2017) sentences, as well as control (contrast) conditions including lists of written pronounceable pseudowords or distorted speech, respectively. Participants also provided 16 resting-state runs (total 112 min). Runs containing head motion were excluded if max framewise displacement (FD) > 0.4mm, and/or max absolute displacement > 2mm, or were visually checked for exclusion if max FD > 0.2 and/or max absolute displacement > 1mm. We verified that each run's field of view contained the full cerebellum. Included runs were aligned to a T1 template and projected to a standardized cerebral (Fischl et al., 1999) and cerebellar surface (Diedrichsen & Zotow, 2015). Functional connectivity was used to estimate the language network in the cerebrum based on Braga et al. (2020), using manually chosen seeds and data-driven clustering. Cerebellar vertices were assigned to networks defined on the cerebrum using a winner-take-all approach based on functional connectivity (Xue et al., 2022).

Results: Functional connectivity reliably defined multiple language network regions in the cerebellum. In some participants, these regions were right-lateralized (i.e., larger on the right hemisphere), while in others we observed bilateral regions. Across participants, we consistently observed 3-4 distinct regions in the posterior cerebellum, rather than one contiguous region. Despite individual differences, we in general observed correspondence between the functional connectivity estimates and task-related activity for both the auditory and visual language tasks. Finally, in between the distinct regions we observed other networks, suggesting fine-scale interdigitation between networks when individual-level anatomy is considered. Finally, mirroring our observations in the cortex, we observed that the auditory task led to more bilateral cerebellar activity in most participants, which could have been driven by recruitment of auditory processing regions.

Conclusions: The results suggest that resting-state functional connectivity-based estimates of the language network can delineate language-task-responsive regions of the cerebellum. Further, the results suggest that these language network regions respond similarly to spoken or written language. Ongoing work is exploring the relationship of these higher-order language regions with sensory input streams.

References

1. Ashida, R. (2019), 'Sensorimotor, language, and working memory representation within the human cerebellum', vol. 40, no. 16, pp. 4732-4747.

2. Buckner, R. (2011), 'The organization of the human cerebellum estimated by intrinsic functional connectivity', vol. 106, no. 5, pp. 2322-2345
3. Diedrichsen, J. (2015), 'Surface-Based Display of Volume-Averaged Cerebellar Imaging Data', vol. 10, no. 7, pp. e0133402
4. Fedorenko, E. (2010), 'New method for fMRI investigations of language: Defining ROIs functionally in individual subjects. Journal of Neurophysiology', vol. 104, no. 2, pp. 1177–1194
5. Fischl, B. (1999) 'Cortical surface-based analysis. II: Inflation, flattening, and a surface-based coordinate system', Neuroimage, vol. 9, no. 2, pp. 195-207
6. King, M. (2019), 'Functional boundaries in the human cerebellum revealed by a multi-domain task battery', Nature neuroscience, vol 22, no. 8, pp. 1371-1378
7. Petersen, S. (1989), 'Positron Emission Tomographic Studies of the Processing of Single Words', vol. 1, no. 2, pp. 153-170
8. Scott, J. (2017) 'A new fun and robust version of an fMRI localizer for the frontotemporal language system', Cognitive Neuroscience, vol. 8, no. 3, pp. 167-176
9. Xue, A. (2021), 'The detailed organization of the human cerebellum estimated by intrinsic functional connectivity within the individual', Journal of neurophysiology, vol 125, no. 2, pp. 358-384

Poster No 1017

Metaphor in Mind and Machine: Unraveling Conceptual Metaphors for NLP Applications

Hyeonseop Yoon[1], Shin-ae Yoon[2]

[1]Hankuk University of Foreign Studies, Seoul, WI, [2]Konkuk University, Seoul, WI

Introduction: This paper delves into the intricate realm of natural language understanding by comparing the cognitive processes of the human brain to state-of-the-art natural language processing (NLP) models, focusing on the comprehension of metaphorical phrases. Metaphor phrase, more commonly known as conceptual metaphor, refers to the understanding of one idea, or conceptual domain, in terms of another. Cognitive linguistics consider language processing as reflecting general aspect of cognition rather than adopting a modular view of mind[1,2] the meaning emerges from context, not a literal text itself. We understand language within context using conceptual metaphor[3]. From the tenet of conceptual metaphor, we seek to unravel the extent to which NLP models can replicate the human language processing, specifically in metaphor.

Methods: To achieve this, we took the data from Openneuro's pragmatic language for our NLU dataset[4]. The protocol is aimed to distinguish whether given linguistic expression is metaphorical, literal, or absurd or not. We re-analyzed the fMRI data involving 28 Spanish-speaking participants (22.78 ± 1.79, 13 men, 15 women). The experimental paradigm was divided into 2 runs. In each run, 40 experimental events were randomly presented (i.e., 20 literal phrases, 10 metaphorical phrases, 10 absurd phrases). Participants were asked to answer either YES or NO button attached on MRI, whether given linguistic stimuli are specific category followed by (i.e., literal, metaphorical, and absurd). Another experiment involved 43 subjects (26.22 ± 3.14 years, 21 men, 22 women) with linguistic stimuli consisting of 40 literal phrases, 20 metaphorical phrases, and 20 absurd phrases. In this experiment, they had to choose which category (literal, metaphoric, absurd) the given linguistic stimuli belong to. The hits for each trial was evaluated. Concurrently, we employed a range of NLP models, including BERT, GPT-NeoX, and LSTM, to scrutinize their performance in metaphor comprehension. Our analysis encompassed both behavioral and internal representation aspects. The Representational Similarity Analysis(RSA), which is a method comparing neural pattern with non-neural pattern by configurating representational dissimilarity matrixes (RDMs), was applied to both fMRI data and language models' hidden representation by each layers. We have designed neural RDM(N_v^s) using fMRI data within Pysearchlight (radius=6) at the voxel v of subject s, model RDM (M_l^k) using layer embedding at the layer l of model k. Across every voxel of whole brain, we have checked Spearman's rho, t-test[5].

Results: The results revealed that, as for behavioral accuracy, human accuracy of each categories (literal, metaphorical, absurd) are 93.62%, 92.75%, 90.91%, and the average LLM accuracy are 96.42, 94.42, 93.35 respectively. Latter rivaled or exceeded human performance in recognizing language stimuli. The results in the Representational Similarity Analysis (RSA) lay in the crux of our investigation, which unveiled intriguing patterns of neural similarity between the human brain and NLP models. RSA brain has the significant t-score, calculated by random permutation of 5000. Looking upon a brain map, notably, regions such as the early visual cortex (EVC), posterior cingulate cortex (PCC), inferior frontal gyrus (IFG), and middle temporal gyrus exhibited parallels with previous semantic-pragmatic fMRI research in metaphor processing.

Conclusions: In summary, our study offers a compelling exploration of the convergence and divergence between human cognition and artificial intelligence in metaphor comprehension. Future endeavors will need to be delved deeper into uncovering the hierarchical and mechanistic underpinnings of conceptual metaphors, which would shed light on the evolving landscape of NLP in cognitive linguistics. These findings are thought to illuminate the remarkable capabilities of NLP models in replicating certain aspects of human cognitive processes.

References
1. Feldman, J., & Narayanan, S. (2004). Embodied meaning in a neural theory of language. Brain and language, 89(2), 385-392.
2. Du Castel, B. (2015). Pattern activation/recognition theory of mind. Frontiers in computational neuroscience, 9, 90.
3. Lakoff, G., & Johnson, M. (2008). Metaphors we live by. University of Chicago press.
4. Rasgado-Toledo, J. and Lizcano-Cortés, F. and Olalde-Mathieu, V. and Zamora-Ursulo, M. and Licea-Haquet, G. and Carillo-Peña, A. and Navarrete, E. and Reyes-Aguilar, A.* and Giordano, M (2021). Pragmatic Language. OpenNeuro. [Dataset] doi: 10.18112/openneuro.ds003481.v1.0.3
5. Lee, J., Jung, M., Lustig, N., & Lee, J. H. (2023). Neural representations of the perception of handwritten digits and visual objects from a convolutional neural network compared to humans. Human Brain Mapping, 44(5), 2018-2038.

Poster No 1018

Neural Mechanism of Pain Assessment Bias among Monolingual and Multilingual Medical Trainees

Morgan Gianola[1], Elizabeth Losin[2], Theoni Varoudaki[2], Nikta Khalilkhani[2]

[1]University of Miami, Coral Gables, FL, [2]Penn State University, State College, PA

Introduction: Medical providers show bias in their prescribing of opioid analgesics for pain, overprescribing among white patients and undertreating pain among marginalized demographic groups (Santoro & Santoro, 2018; Keister et al., 2021). Moreover, low English proficiency patients tend to receive fewer pain assessments and lower pain evaluations than English proficient patients (Schwartz et al., 2022), and language concordant care has been associated with improvements across several health outcomes (Diamond et al., 2019). While differences in pain assessment and opioid prescribing across patients' language preferences have been noted (Schwartz et al., 2022), limited research has considered clinician language ability as a potentially relevant factor in pain assessment and opioid prescribing biases.

Methods: During fMRI scanning, 66 medical trainees (32 male) participated as clinicians in a series of simulated patient interactions and pain assessments. They viewed short videos of mock patients experiencing genuine evoked pain before estimating each patient's pain intensity and reporting their likelihood to prescribe an analgesic. All participants saw 36 patients (from a pool of 72) evenly divided across six demographic groups: male and female non-Hispanic black, Hispanic, and non-Hispanic white. Trainee participants' evaluations of patients' pain were compared against the mock patients' own ratings of their pain. Outcomes of pain evaluation accuracy and likelihood of analgesia prescribing were compared across monolingual (N=23) and multilingual (N=43, knowing two or more languages) participants with mixed effects multilevel models with random effects for participants. Fixed effect variables for patient demographics and their interaction with participant language ability were included in the models. Neuroimaging data were pre-processed and univariate GLM whole brain activity was compared across monolingual and multilingual participants using FSL version 6.0.6.5

Results: Monolingual trainees tended to underestimate black patients' pain as multilingual participants slightly overestimated pain in this group (B=0.78, t(109)=2.26, p=.026). Alternatively both mono- and multi-lingual trainees were fairly accurate in assessing non-Hispanic white patients' pain, resulting in a significant patient race by clinician language interaction (B= -0.62, t(2302)= -2.14, p=.032; Figure 1). These effects remain after controlling for the strength of patient's pain facial expressions. While pain overestimation positively predicted prescribing likelihood overall (B= 0.35, t(2337)= 22.96, p<.0001), both mono- and multi-lingual participants were less likely to prescribe analgesics to white (compared to black) patients (B= -0.41, t(2300)= -2.08, p=.037). When making treatment decisions for white patients, multilingual participants showed significantly greater activation in a cluster encompassing portions of left superior parietal and supramarginal gyrus (z=2.3, cluster corrected p<.05; Figure 2) compared to monolingual participants.

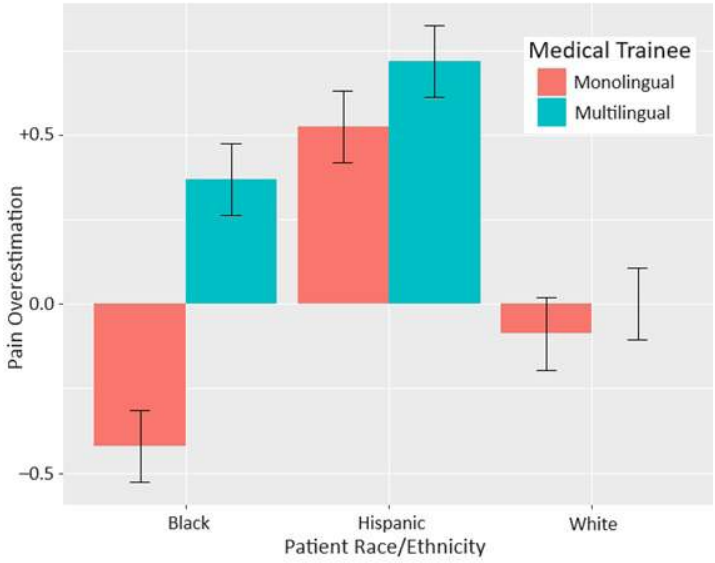

Figure 1: Pain evaluation accuracy of monolingual and multilingual medical trainees across different patient racial/ethnic groups.

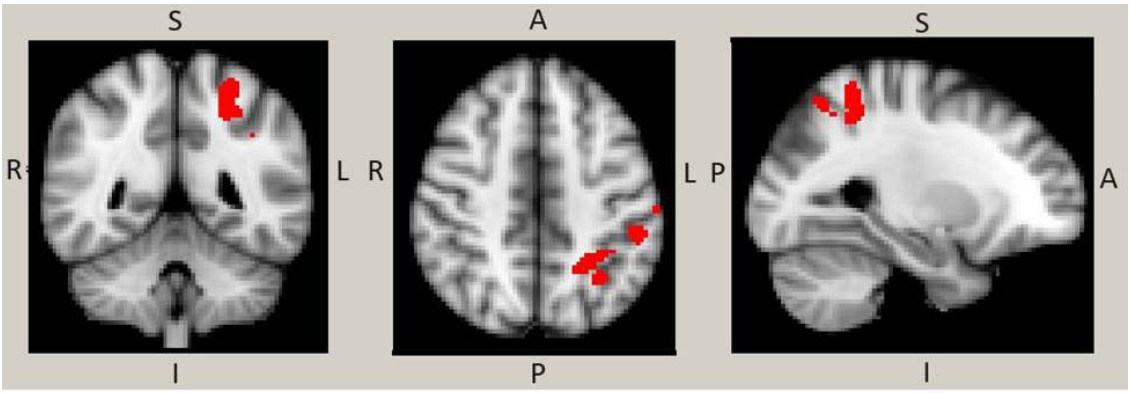

Figure 2: Cluster showing significantly higher activity among multilingual compared to monolingual medical trainees when determining likelihood to prescribe an analgesic medication to a white patient. This cluster includes portions of the supramarginal gyrus, superior parietal lobule, and postcentral gyrus. Coordinates in MNI Space: X= -26, Y=-48, Z=46

Conclusions: This research demonstrates that pain assessment accuracy and prescribing biases across patient demographics may differ between mono- and multi-lingual clinicians. However, assessment accuracy differences didn't necessarily alter prescribing behavior. This could suggest education around opioid abuse stereotypes among more recent trainee cohorts help alleviate previously observed prescribing biases (Morden et al., 2021). This racially and ethnically diverse sample of multilinguals showed greater activity in regions involved in valuation and social decision making (Ho et al., 2021) when deciding to treat white patients, potentially reflecting a wider range of factors being weighed, compared to monolinguals, reducing prescribing likelihood. These findings could relate to greater exposure to people from different demographic backgrounds among multilingual clinicians or wider bodies of information considered when making prescribing decisions.

References

1. Santoro, T. N., & Santoro, J. D. (2018). Racial bias in the US opioid epidemic: a review of the history of systemic bias and implications for care. Cureus, 10(12).
2. Keister, L. A., Stecher, C., Aronson, B., McConnell, W., Hustedt, J., & Moody, J. W. (2021). Provider bias in prescribing opioid analgesics: a study of electronic medical records at a hospital emergency department. BMC public health, 21(1), 1-9.
3. Diamond, L., Izquierdo, K., Canfield, D., Matsoukas, K., & Gany, F. (2019). A systematic review of the impact of patient–physician non-English language concordance on quality of care and outcomes. Journal of General Internal Medicine, 34, 1591-1606.
4. Schwartz, H., Menza, R., Lindquist, K., Mackersie, R., Fernández, A., Stein, D., & Bongiovanni, T. (2022). Limited English Proficiency Associated With Suboptimal Pain Assessment in Hospitalized Trauma Patients. Journal of Surgical Research, 278, 169-178.
5. Morden, N. E., Chyn, D., Wood, A., & Meara, E. (2021). Racial inequality in prescription opioid receipt—role of individual health systems. New England Journal of Medicine, 385(4), 342-351.
6. Ho, S. S., Gonzalez, R. D., Abelson, J. L., & Liberzon, I. (2012). Neurocircuits underlying cognition–emotion interaction in a social decision making context. NeuroImage, 63(2), 843-857.

Poster No 1019

High-Resolution Diffusion Tractography Reveals Structural Asymmetries in the Language Network

Lilit Dulyan[1], Cesare Bortolami[2], Michel Thiebaut de Schotten[3], Stephanie Forkel[4]

[1]Radboud University, Nijmegen, Netherlands, [2]University of Genoa, Genoa, Italy, [3]Groupe d'Imagerie Neurofonctionnelle, Institut des Maladies Neurodégénératives- UMR 5293, CNRS, CEA, Bordeaux, France, [4]Donders Institute for Brain Cognition Behaviour, Radboud University, Nijmegen, Gelderland

Introduction: The language connectome has evolved from the conventional arcuate fasciculus model to a complex and extensive network of white matter tracts that goes well beyond the traditional boundaries of Broca and Wernicke areas (Dick et al., 2014). These tracts have been described in both brain hemispheres, questioning the previously dominant perspective of language functional lateralisation solely in the left hemisphere. Relying on the most precise dataset currently openly available (7T HCP), we mapped the extended language network in the human brain to comprehensively capture its structural asymmetry and interindividual variability. The normative atlas will facilitate the study of the functional relevance of the pathways and shed light on brain recovery in the extended bilateral language network.

Methods: The study involved 172 healthy participants (29.5±3.6 years, 60.5% females) from the Human Connectome Project's (HCP) 7T diffusion-weighted imaging (DWI) datasets (Vu et al., 2015). Data underwent preprocessing using the HCP default pipeline (v3.19.0; Glasser et al., 2013), addressing field, motion, and geometric distortions with FSL's TOPUP and EDDY functions (Andersson & Sotiropoulos, 2016). Whole-brain fibre orientation distribution (FOD) estimation used StarTrack software (https://www.mr-startrack.com) in the native DWI space. Spherical deconvolutions employed a damped Richardson-Lucy algorithm (Dell'acqua et al., 2010; Dell'Acqua & Tournier, 2019) with a fixed fibre response ($\alpha = 1.5 \times 10{-}3\,mm2\,s{-}1$) and a geometric damping parameter, involving 200 iterations. For tractography, we set an absolute threshold (3x the spherical FOD of a grey matter isotropic voxel) and a relative threshold (8% of the maximum amplitude of the FOD; Thiebaut de Schotten et al., 2011). Streamline tractography used a modified Euler algorithm with a 35° angle threshold, 0.5 mm step size, and a 15 mm minimum streamline length (Dell'Acqua et al., 2013). The fixed absolute threshold, 0.0036, aligns with previous studies (Beyh et al., 2022; Thiebaut de Schotten et al., 2020), informed by post-mortem Klingler dissections. Structural connectome data was registered to the MNI space. Manual dissection of seven tracts in both hemispheres included FAT, IFOF, ILF, UF, and three AF segments. Microstructural indices (HMOA) and macro structural measurements (tract count, TC and volume, VC) were extracted for each tract. The lateralisation index (LI) was calculated as (right-left)/(right+left), with negative values indicating left lateralisation, positive values indicating right lateralisation, and an LI of 0 for bilateral distribution (Thiebaut de Schotten et al., 2011). One sample t-tests in R Studio compared each tract's LI to zero (Rstudio, 2020).

Results: The examination of seven tracts engaged during language processes unveils intriguing nuances. The long arcuate fasciculus and the ILF exhibit a pronounced inclination towards left lateralization (Figure 1). The IFOF and the FAT, manifest significant leftward asymmetry solely in the HMOA lateralization index ($t(171)=-8.34$, $p<.0008$ and $t(171)=-5.68$, $p<.0008$, respectively). The posterior arcuate fasciculus (AFp) emerges as the only bilateral tract, exhibiting symmetry in hemisphere-specific microstructure and volume (Figure 1). Conversely, the UF and the anterior arcuate fasciculus (AFa) demonstrate a predilection for right lateralisation.

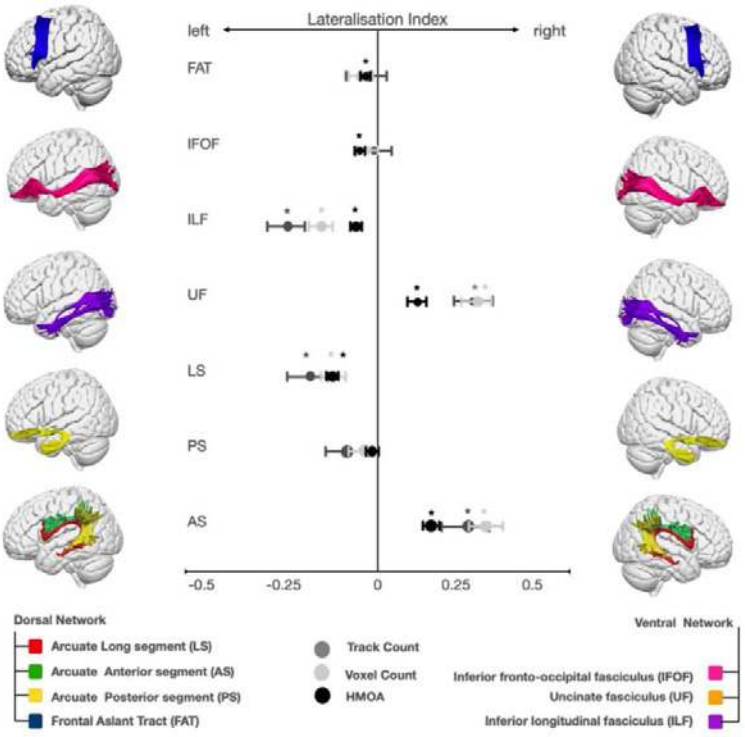

Figure 1. The normative structural asymmetry atlas of the key language-recruited tracts.

Conclusions: This atlas, covering tracts implicated in language processes, has considerable potential to improve the accuracy of localizing white matter lesions linked to language disorders. Illuminating the nuanced interplay of structural asymmetries within the language network, our findings provide a foundational understanding that could pave the way for more precise interventions and therapies in the field of language-related neurological conditions. All data will be openly available.

References

1. Andersson, J. L. R. et al. (2016). An integrated approach to correction for off-resonance effects and subject movement in diffusion MR imaging. NeuroImage, 125, 1063–1078.
2. Beyh, A. et al. (2022). The medial occipital longitudinal tract supports early stage encoding of visuospatial information. Communications Biology, 5(1), 318.
3. Dell'acqua, F. et al. (2010). A modified damped Richardson-Lucy algorithm to reduce isotropic background effects in spherical deconvolution. NeuroImage, 49(2), 1446–1458.
4. Dell'Acqua, F. et al. (2013). Can spherical deconvolution provide more information than fiber orientations? Hindrance modulated orientational anisotropy, a true-tract specific index to characterize white matter diffusion. Human Brain Mapping, 34(10), 2464–2483.
5. Dell'Acqua, F. et al. (2019). Modelling white matter with spherical deconvolution: How and why? NMR in Biomedicine, 32(4).
6. Dick, A. S. et al. (2014). The Language Connectome: New Pathways, New Concepts. The Neuroscientist, 20(5), 453–467.
7. Glasser, M. F. et al. (2013). The minimal preprocessing pipelines for the Human Connectome Project. NeuroImage, 80, 105–124. =
8. Rstudio, T. (2020). RStudio: Integrated Development for R. In Rstudio Team, PBC, Boston, MA URL http://www.rstudio.com/.
9. Thiebaut de Schotten, M. et al. (2011). Atlasing location, asymmetry and inter-subject variability of white matter tracts in the human brain with MR diffusion tractography. NeuroImage. https://doi.org/10.1016/j.neuroimage.2010.07.055
10. Thiebaut de Schotten, M. et al. (2020). Brain disconnections link structural connectivity with function and behaviour. Nature Communication

Poster No 1020

Structure-functional coupling at birth predicts cognitive and language function at 2 years of age

Yuehua Xu[1], Xuhong Liao[2], Tengda Zhao[1], Minhui Ouyang[3], Hao Huang[4], Yong He[2]

[1]State Key Laboratory of Cognitive Neuroscience and Learning, Beijing Normal University, Beijing, Beijing, [2]Beijing Normal University, Beijing, Beijing, [3]Children's Hospital of Philadelphia, Philadelphia, PA, [4]University of Pennsylvania, Philadelphia, PA

Introduction: Recent studies suggest that the functional interactions among regions are largely shaped by the underlying structural networks in the human brain[1]. The coupling between structural and functional networks increased with development, which was associated with executive performance in youth[2]. Of note, the human brain undergoes explosive

growth in both structure and function during infancy period, laying the critical foundations for cognitive and behavior development in later life[3]. However, it remains unclear how structural networks develop during the prenatal period to support functional activity and cognitive development in later life. Here, we employed multi-modal MRI data in 40 neonates aged around 32 to 41 postmenstrual weeks, to characterize the development of structural connectivity-functional connectivity (SC-FC) coupling during the third trimester, and whether the coupling is predictive for future cognition, language, and motor development.

Methods: Forty neonates (age at scan: 31.9-41.7wk; 29 males) were recruited and scanned with natural sleep using a Philips 3T MR Achieva scanner at Children's Medical Center at Dallas. In a follow-up, 26 infants underwent the Bayley-III test to evaluate the cognitive, language and motor development at age 2[4]. The MRI protocol contains anatomical T2 weighted, diffusion MRI (dMRI) and resting-state functional MRI (R-fMRI)[5,6]. The dMRI data were preprocessed with DTIStudio and Diffusion Toolkit and the deterministic fiber tractography was used for fiber tracking[6]. The R-fMRI data were preprocessed with SPM 12 and GRETNA[5]. After data preprocessing, we built the structural and functional network for each infant (Fig.1). The nodes of each subject were obtained by JHU neonate atlas[7]. The strength of structural connectivity was defined as the number of fibers connected two regions multiplied by the mean fractional anisotropy (FN*FA) across fibers. The strength of functional connectivity was estimated as the Pearson's correlation between two regions. Notably, we used the absolute Pearson's correlation coefficients to measure the coupling strength between nodal SC and FC. To further detect the age effects on the nodal SC-FC coupling, we used a general linear model in which gender, mean frame-wise displacement, postnatal age at scan and duration time between birth and scan were included as covariates. Finally, we performed a support vector regression approach and leave-one-out cross-validation to assess whether the SC-FC coupling at birth could predict cognitive, language, and motor skills at 2 years of age. To assess the prediction accuracy, we calculated the Pearson's correlation between the real score and the predicted score. The statistical significance of this prediction was evaluated by the permutation test (10,000 times).

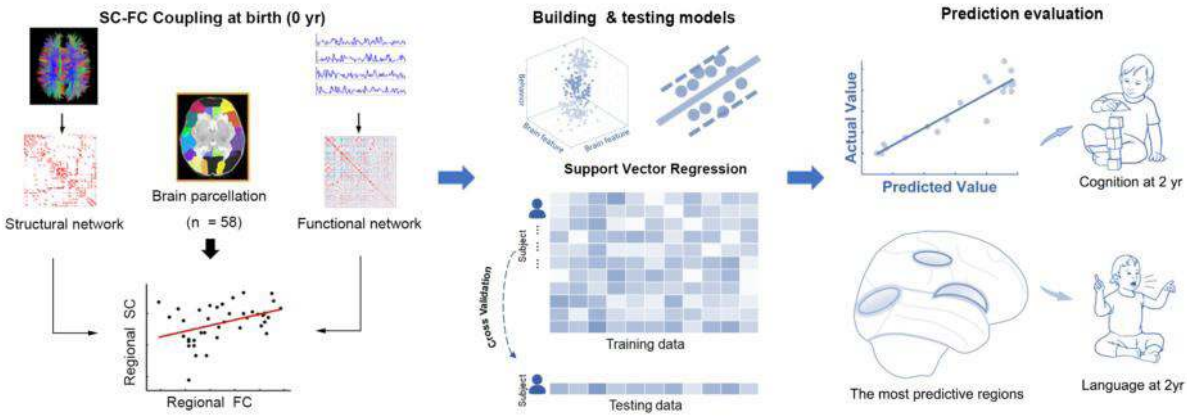

Figure 1. Flowchart of SC-FC coupling estimation and behavior prediction analysis. We used the SC-FC coupling at birth to predict cognitive and language abilities assessed with Bayley-III Scales at 2 years of age. The prediction workflow includes the following steps: (1) The SC-FC coupling was quantified as the Pearson's correlation values between structure connectivity and functional connectivity and input as feature vectors. (2) Prediction models were established and tested with support vector regression model and cross-validation. (3) Prediction accuracy was evaluated by correlation between predicted and actual scores. Feature contributions from brain regions in the model were quantified by normalized feature contribution weights. SC-FC, structural connectivity and functional connectivity.

Results: The fitted spatial patterns of SC-FC coupling from 32 to 41 weeks were displayed in Fig. 2A. We found that the SC-FC coupling exhibited heterogeneous spatial patterns across the entire brain, with higher strength in the association areas, whereas lower strength in the primary regions (Fig.2A). Brain regions with significant age-dependent increase were left angular gyrus and right middle fronto-orbital gyrus (Fig. 2B,C $p<0.05$, FDR correction). The support vector regression analysis revealed that the SC-FC coupling at birth could significantly predict the cognitive (Fig. 2D, $r=0.32$, $p=0.025$) and language (Fig. 2E, $r=0.56$, $p<0.001$) scores at 2 years of age. Notably, the contributing features were primarily distributed in the medial and lateral frontal regions, left precuneus, and right cingulate gyrus for cognitive prediction (Fig. 2D); and the left inferior frontal gyrus, insular, inferior occipital gyrus, and cingulate gyrus for language prediction (Fig. 2E).

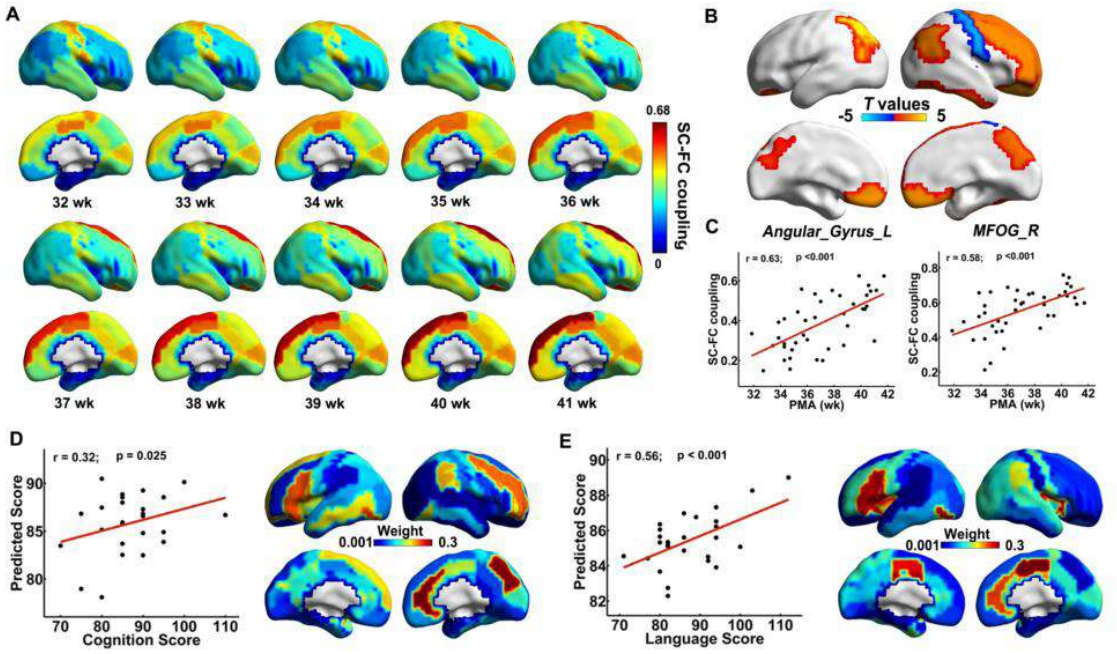

Figure 2. (A) Fitted spatial patterns of nodal SC-FC coupling corrected for gender, postnatal age at scan and the duration time between birth and scan. **(B)** Age effects on regional SC-FC coupling (p<0.05, without correction). **(C)** SC-FC couplings in left angular gyrus and right middle fronto-orbital gyrus significantly increased with age (p<0.05, with FDR correction). SVR model-based prediction of individual's cognition **(D)** and language **(E)** scores at 2 years of age. Individual SC-FC coupling maps at birth were input as features. Left panel, Pearson's correlation between the predicted scores and the real scores (r=0.32, p=0.025 for cognition; r=0.56, p<0.001 for language). Right panel, absolute weight of brain regions in the SVR model of the neurodevelopmental outcomes prediction. SC-FC, structural connectivity and functional connectivity; PMA (weeks), postmenstrual age in weeks; SVR, support vector regression.

Conclusions: Our findings highlight the development of brain SC-FC coupling during the third trimester, and provide new insights into the understanding of the brain and behavior relationships in early life.

References

1. Suarez, L.E., et al., Linking Structure and Function in Macroscale Brain Networks. Trends Cogn Sci, 2020. 24(4): p. 302-315.
2. Baum, G.L., et al., Development of structure-function coupling in human brain networks during youth. Proceedings of the National Academy of Sciences of the United States of America, 2020. 117(1): p. 771-778.
3. Cao, M., H. Huang, and Y. He, Developmental Connectomics from Infancy through Early Childhood. Trends Neurosci, 2017. 40(8): p. 494-506.
4. Bayley, N., Bayley Scales of Infant and Toddler Development– Third Edition. San Antonio, TX: Harcourt Assessment. 2006.
5. Xu, Y., et al., Development and Emergence of Individual Variability in the Functional Connectivity Architecture of the Preterm Human Brain. Cereb Cortex, 2019. 29(10): p. 4208-4222.
6. Zhao, T., et al., Structural network maturation of the preterm human brain. Neuroimage, 2019. 185: p. 699-710.
7. Oishi, K., et al., Multi-contrast human neonatal brain atlas: application to normal neonate development analysis. Neuroimage, 2011. 56(1): p. 8-20.

Poster No 1021

A Multimodal Exploration of Brain Activation for Language and Cognitive and Linguistic Skills

Irene Balboni[1,2,3], Alessandra Rampinini[3,2], Olga Kepinska[4,5], Raphael Berthele[1], Narly Golestani[4,5,3]

[1]Institute of Multilingualism, University of Fribourg, Fribourg, Switzerland, [2]National Centre for Competence in Research Evolving Language, Switzerland, Switzerland, [3]Department of Psychology, Faculty of Psychology and Educational Sciences, University of Geneva, Geneva, Switzerland, [4]Brain and Language Lab, Cognitive Science Hub, University of Vienna, Vienna, Austria, [5]Department of Behavioral and Cognitive Biology, Faculty of Life Sciences, University of Vienna, Vienna, Austria

Introduction: Language learning and use both require a complex set of skills ranging from auditory perception to higher-order syntactic processing. Abilities related to memory, pattern recognition, and motor control are all involved in language functions. The neural underpinnings of language abilities[1–3], language experience[4,5], as well as other language-relevant cognitive skills[6–8] have been established by a wealth of publications, and recent work emphasises the importance of multimodal and multivariate analyses of language learning profiles using not only language measures but also domain general cognitive ones[9]

The aim of the present work is to carry out a data-driven investigation of the key dimensions underlying language processing and learning, their subcomponents and their relationship with language-related brain activation.

Methods: We obtained behavioural and brain data from 136 participants with a broad multilingual background. A subsample (N=25) had previously been diagnosed with dyslexia. We included general cognitive measures such as fluid intelligence, attention, and memory as well as measures of arithmetic, musicality, and fine motor skills. All the participants were also assessed on language-specific tests, spanning from traditional language aptitude measures to tests used to diagnose dyslexia. The participants also completed questionnaires regarding motivation for language learning and experience, reading history, and musical training. For each participant, fMRI data were collected using a 3-Tesla Siemens Prisma scanner. Functional activation maps for language were obtained using an adapted version of the AliceLoc localiser from[10]. In the localiser, participants listened to 24 passages (18 s each) from the book 'Alice in Wonderland', read by a female native speaker of their first language (L1). The baseline condition consisted of 24 degraded versions of the passages (procedure from[10]). The above work has resulted in two types of data: behavioural data, comprising 36 variables derived from the most relevant scores on the tasks and questionnaires, and brain imaging data comprising voxel-wise brain activation for the L1. Partial Least Squares Correlation (PLS; Figure 1) was used to uncover the dimensions commonly underlying the two types of data (henceforth, 'data modalities'). This method allows to first identify the main dimensions explaining the variation within each type of data, and in a second step to uncover multivariate patterns underlying common features between the two data modalities.

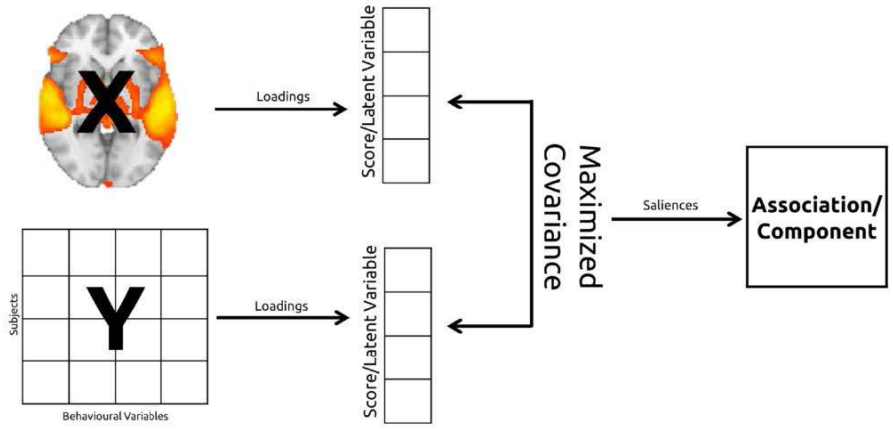

Figure 1. Schematic representation of the PLS analysis

Results: The PLS analysis revealed two significant components, together explaining 53% of the variance. The first component was positively correlated with performance on higher-level general cognitive measures as well as with language-specific tasks relying on executive functions. In the neural data, this component was associated with greater brain activation in predominantly bilateral cortical areas involved in higher-level cognitive and linguistic skills. The second component was negatively correlated with both lower- and higher-level linguistic tasks and with motor skills, and was positively correlated with greater activation in predominantly left-lateralised brain regions linked to lower-level phonetic and acoustic processing.

Conclusions: The present work reveals both associations and dissociations between key dimensions underlying language learning. Higher-level language-related skills and general cognition appear to be associated with activation in brain areas traditionally associated with higher level linguistic skills (i.e. semantic, syntactic processing, and sound-symbol association). We've also identified a complementary pattern of results in a component reflecting skills and brain areas related to lower-level acoustic, phonetic and motor domains.

References

1. Turker, S., Kuhnke, P., Eickhoff, S. B., Caspers, S., & Hartwigsen, G. (2023). Cortical, subcortical, and cerebellar contributions to language processing: A meta-analytic review of 403 neuroimaging experiments. Psychological Bulletin. https://doi.org/10.1037/BUL0000403
2. Hervais-Adelman, A. G., Moser-Mercer, B., & Golestani, N. (2011). Executive control of language in the bilingual brain: Integrating the evidence from neuroimaging to neuropsychology. Frontiers in Psychology, 2(SEP), 10307. https://doi.org/10.3389/FPSYG.2011.00234/BIBTEX
3. Turker, S., Seither-Preisler, A., & Reiterer, S. M. (2021). Examining Individual Differences in Language Learning: A Neurocognitive Model of Language Aptitude. Neurobiology of Language, 1–27. https://doi.org/10.1162/nol_a_00042
4. Hervais-Adelman, A., Egorova, N., & Golestani, N. (2018). Beyond bilingualism: multilingual experience correlates with caudate volume. Brain Structure and Function, 223(7), 3495–3502. https://doi.org/10.1007/s00429-018-1695-0
5. Jouravlev, O., Mineroff, Z., Blank, I. A., & Fedorenko, E. (2021). The Small and Efficient Language Network of Polyglots and Hyper-polyglots. Cerebral Cortex, 31(1), 62–76. https://doi.org/10.1093/cercor/bhaa205

6. Brissenden, J. A., & Somers, D. C. (2019). Cortico–cerebellar networks for visual attention and working memory. Current Opinion in Psychology, 29, 239–247. https://doi.org/10.1016/J.COPSYC.2019.05.003
7. Earle, F. S., Del Tufo, S. N., Evans, T. M., Lum, J. A. G., Cutting, L. E., & Ullman, M. T. (2020). Domain-General Learning and Memory Substrates of Reading Acquisition. Mind, Brain, and Education, 14(2), 176–186. https://doi.org/10.1111/MBE.12234
8. Zhang, R., Geng, X., & Lee, T. M. C. (2017). Large-scale functional neural network correlates of response inhibition: an fMRI meta-analysis. Brain Structure and Function, 222(9), 3973–3990. https://doi.org/10.1007/S00429-017-1443-X/FIGURES/4
9. Feng, G., Ou, J., Gan, Z., Jia, X., Meng, D., Wang, S., & Wong, P. C. M. (2021). Neural Fingerprints Underlying Individual Language Learning Profiles. Journal of Neuroscience, 41(35), 7372–7387. https://doi.org/10.1523/JNEUROSCI.0415-21.2021
10. Malik-Moraleda, S., Ayyash, D., Gallamp, J., Affourtit, J., Hoffmann, M., Mineroff, Z., Jouravlev, O., & Fedorenko, E. (2022). An investigation across 45 languages and 12 language families reveals a universal language network. Nature Neuroscience 2022, 1–6. https://doi.org/10.1038/s41593-022-01114-5

Poster No 1022

Unraveling the genetics underlying the language-related human brain white matter tracts

Yasmina Mekki[1]

[1]*Vanderbilt University Medical Center, Nashville, TN*

Introduction: Human brain development and language are closely connected (Kuhl, 2010). White matter connections play a critical role in shaping the brain organization and function as it supports the interactions between brain regions. Prior studies linked genetic variation to language revealed a complex, and polygenic genetic architecture (Eising et al., 2022, Mekki et al., 2022). Our aim is to investigate and elucidate the neurobiological underpinnings of human brain connection support of language.

Methods: We used individuals from the UK Biobank cohort with both diffusion MRI and genotyping data. We excluded participants with unusual heterozygosity, high missingness, and sex mismatches. We further restricted our analyses to individuals with white British ancestry in order to avoid any possible confounding effects related to ancestry. This resulted in 31,465 individuals passing the sample QC. Using PLINK, we excluded variants with minor allele frequency < 0.01, and imputation quality INFO scores < 0.8. Multiallelic variants were also removed. We considered 35 well-known language-related white matter tracts defined from the probabilistic atlas (Rojkova et al., 2016) and extracted a set of image derived phenotypes (IDPs). We estimated the SNP-based heritability of the IDPs using GCTA and performed a multivariate genome-wide association study using MOSTest (Van der meer et al., 2020). We controlled for covariates including age, sex, genotype array type, MRI assessment center and the first ten genetic principal components capturing population genetic diversity. We performed a rank-based inverse normalization to ensure that the distribution of the IDPs are normally distributed.

Results: 3.1. Language-related brain structural connectivities are heritable. All but the left Fronto Insular tract 4 phenotype showed significant SNP-based heritability (FDR-corrected $p<0.05$), ranging from 7.6% for the Left Frontal Inferior longitudinal fasciculus to 61.5% for the Corpus callosum. 3.2. Language-related brain structural connectivities are highly polygenic. There were 268 independent genome-wide significant loci associated with different aspects of language-related brain structural connectivities. Of 173 previously reported dyslexia-associated genes (Doust et al., 2022), 38 showed genome-wide significance. 3.3. Associated genetic mechanisms point to neurodevelopmental gene set. 75 biological systems were found significantly associated with human language-related brain structural connectivities. A significant functional enrichment of genes involved in different brain organizations, including the pathways of neurogenesis, neuronal differentiation, and embryonic brain expression were identified. 3.4. The neurobiological development of language-related human brain structural connectivities is active during the early to late prenatal period. We found relatively higher mRNA expression of human language structural connectivities associated genes during early-prenatal ($p=1.46e-5$), to late prenatal ($p=3.76e{-}8$), from 9 ($p=1.23e{-}6$) to 21 ($p=2.03e{-}6$) post conception week (FDR-corrected $p < 0.05$).

Conclusions: In this work, we investigated the genetic architecture of language-related brain white matter tracts using state of the art genomic strategies and highlighted new candidate genes. This preliminary work represents a step forward towards understanding how genes influence the language network brain structures, complementing behavioral and brain functional studies.

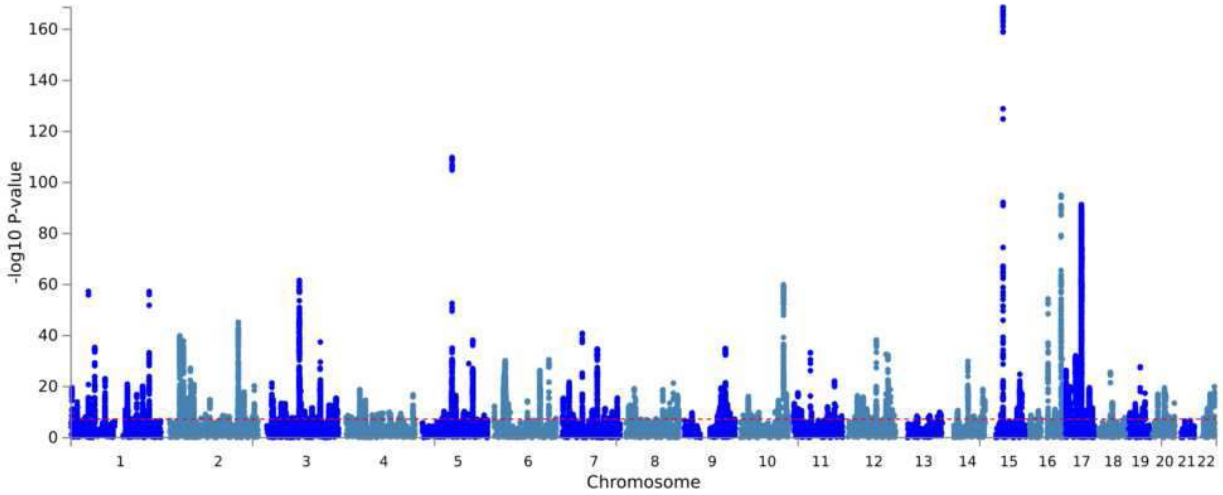

Multivariate GWAS Analysis of 314 Heritable Structural Connectivities in 31,465 Participants. The Red Dashed Line Indicates the Genome-Wide Significance Threshold (p=5e-8).

References

1. Kuhl, P. K. (2010). Brain mechanisms in early language acquisition. Neuron, 67(5), 713-727.
2. Eising, E., Mirza-Schreiber, N., De Zeeuw, E. L., Wang, C. A., Truong, D. T., Allegrini, A. G., ... & Fisher, S. E. (2022). Genome-wide analyses of individual differences in quantitatively assessed reading-and language-related skills in up to 34,000 people. Proceedings of the National Academy of Sciences, 119(35), e2202764119.
3. Mekki, Y., Guillemot, V., Lemaître, H., Carrión-Castillo, A., Forkel, S., Frouin, V., & Philippe, C. (2022). The genetic architecture of language functional connectivity. Neuroimage, 249, 118795.
4. Rojkova, K., Volle, E., Urbanski, M., Humbert, F., Dell'Acqua, F., & Thiebaut de Schotten, M. (2016). Atlasing the frontal lobe connections and their variability due to age and education: a spherical deconvolution tractography study. Brain Structure and Function, 221, 1751-1766.
5. Van der Meer, Dennis, et al. "Understanding the genetic determinants of the brain with MOSTest." Nature communications 11.1 (2020): 3512.
6. Doust, C., Fontanillas, P., Eising, E., Gordon, S. D., Wang, Z., Alagöz, G., ... & Luciano, M. (2022). Discovery of 42 genome-wide significant loci associated with dyslexia. Nature genetics, 54(11), 1621-1629.

Poster No 1023

Gray Matter Morphometry is Related to Reading Abilities, but not Meaningfully

Steven Meisler[1,2], John Gabrieli[2,3]

[1]Harvard University, Cambridge, MA, [2]Massachusetts Institute of Technology, Cambridge, MA, [3]McGovern Institute for Brain Research, Cambridge, MA

Introduction: Reading is a skill that must be explicitly learned, being introduced too recently to be a product of evolutionary pressure. Reading is almost universally taught to young children, whose brains tend to be more plastic, adapting in response to development and experience. However, despite the amount of research that has already been done investigating gray matter morphometric correlates of reading skills, there has been little convergence of results outside of a relationship between global brain volume and reading skills[1]. This calls into question whether individual differences in reading skill are reflected by MRI features of particular brain structures (such as left-hemisphere regions that support reading), which one would expect if brain plasticity is domain-specific. Beyond the possibility that there is not a relationship between local brain morphometry and reading skills, several factors could be contributing to prior inconsistent findings, including small sample sizes, various MRI acquisition and processing techniques, and different cohort-specific phenotype characteristics. All of these limitations can be addressed by using high-quality publicly-available data. We rigorously examined how gray matter morphometry relates to individual differences in reading skills across childhood and adolescence using the Healthy Brain Network dataset[2].

Methods: Our final cohort consisted of 1943 participants aged 5-21. Participants had quality-controlled T1-weighted (T1w) images and phenotypic data including the Tests of Word Reading Efficiency (TOWRE; n=1810) and the Wechsler Individual Achievement Test (WIAT; n=1835) to gauge reading scores. All T1w images were run through FreeSurfer's recon-all pipeline,

resulting in morphometric surface maps of gray matter volume (GMV), surface area (SA), and cortical thickness (CT). These maps were normalized to a standard "fsaverage" space, harmonized across sites using NeuroHarmonize[3], and finally parcellated using the Destrieux anatomical atlas. Intracranial volume (ICV) was also calculated and harmonized across sites. Using the R package mgcv, we ran generalized additive models (GAM) to test for correlations between region-wise morphometric measures and raw reading scores. Linear covariates included sex, image quality (coefficient of joint variation), and for some models intracranial volume (if the morphometric measure was GMV or SA). Age was included as a smooth regressor, given the wide age range of participants. Separate models were run to test for associations between ICV and reading scores.

Results: Several anatomical parcels across both hemispheres exhibited significant and positive associations between reading scores and both SA and GMV, ($p < 0.05$; FDR corrected across regions), but not CT (Figures 1 and 2). However, despite statistical significance, the effect sizes (unique adjusted R-squared coefficient attributed to the reading score in predicting the brain metric) were modest, never exceeding 0.01, and some effect sizes were negative. In models relating ICV to reading scores, there were similarly positive statistically significant associations ($p < 0.05$, even after controlling for non-verbal IQ), also with only modest effect sizes.

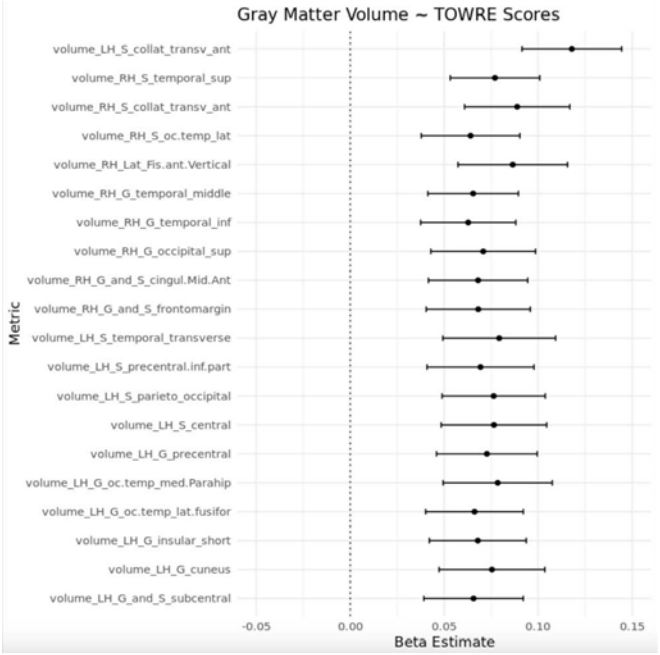

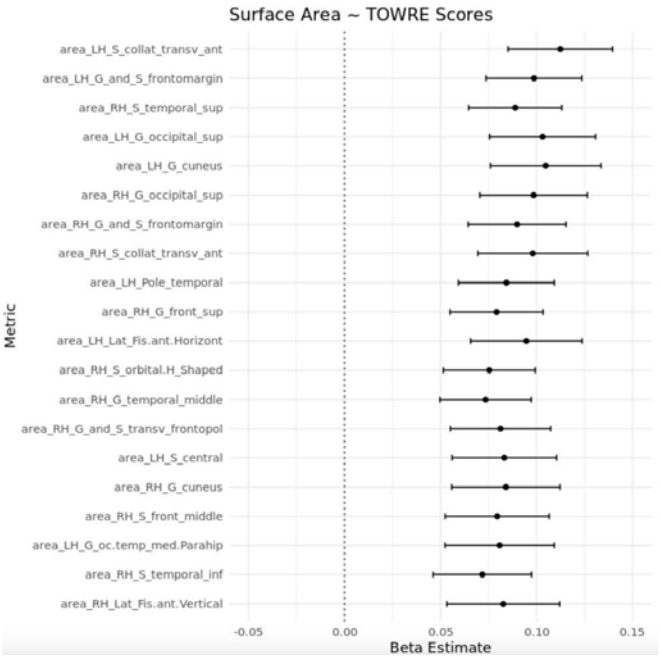

Conclusions: Despite statistical significant relationships between reading skills and brain morphometry on global and local scales, limited effect sizes confound interpretability of these associations. Our findings suggest variability in reading abilities may not meaningfully contribute to predicting brain morphometry when compared to other variables in the models. This study reinforces earlier findings indicating a statistical link between morphometry and reading performance[14], and advances this understanding by using a large quality-controlled sample of children and adolescents. However, these findings also underscore concerns of the limitations of cross-sectional MRI models in capturing brain-behavior relationships in reading.

References

1. Ramus, F. (2018), 'Neuroanatomy of developmental dyslexia: Pitfalls and promise', Neuroscience & Biobehavioral Reviews, vol. 84, pp. 434-452.
2. Alexander, L.M., Escalera, J., Ai, L., Andreotti, C., Febre, K., Mangone, A., Vega-Potler, N., Langer, N., Alexander, A., Kovacs, M. and Litke, S. (2017), 'An open resource for transdiagnostic research in pediatric mental health and learning disorders. Scientific data', vol. 4, no. 1, pp.1-26.
3. Pomponio, R., Erus, G., Habes, M., Doshi, J., Srinivasan, D., Mamourian, E., Bashyam, V., Nasrallah, I.M., Satterthwaite, T.D., Fan, Y. and Launer, L.J. (2020), 'Harmonization of large MRI datasets for the analysis of brain imaging patterns throughout the lifespan', NeuroImage, vol. 208, p.116450.
4. Carrión-Castillo A, Paz-Alonso PM, and Carreiras M. (2023), 'Brain structure, phenotypic and genetic correlates of reading performance', Nature Human Behaviour, vol. 7, pp. 1120–1134.

Poster No 1024

Neurostimulation improves phonological decoding in dyslexia

Sabrina Turker[1,2], Philipp Kuhnke[1,2], Vincent Cheung[3], Gesa Hartwigsen[1,2]

[1]Leipzig University, Leipzig, Germany, [2]Max Planck Institute for Human Cognitive and Brain Sciences, Leipzig, Germany, [3]Sony Computer Science Laboratories, Tokyo

Introduction: Literacy is key to social contacts, education, and employment, and significantly influences personal well-being and mental health (Huettig, 2015). This is detrimental for the at least two children in every classroom worldwide who have dyslexia, a learning disability affecting reading and writing (ICD-11: 6A03.04; WHO, 2019/21). From a cognitive perspective, dyslexia is mainly characterized by problems in phonological decoding and accessing the respective phonological representations of words (Ramus, 2006). One of the most consistently reported neural characteristics of dyslexia is hypoactivation of the left temporo-parietal cortex (TPC), an area referred to as the 'phonological decoding' center (Richlan, 2009). Neurostimulation constitutes a promising technique to alleviate reading deficits in dyslexia (Cancer, 2018; Turker, 2021) but stimulation-induced changes in activation and connectivity remain unclear.

Methods: In the present study, we combined offline facilitatory repetitive transcranial magnetic stimulation (TMS) with fMRI in a within-subject design. We applied sham and effective TMS over the left TPC of 26 adults with dyslexia (18-39 years) before they read simple (2 syllables, 4-6 letters) and complex (3-4 syllables, 10-14 letters) words and pseudowords aloud during fMRI. Our goal was to explore TMS-induced changes in reading performance, functional activation and connectivity. To do so, we performed linear mixed models for investigating behavioural improvements and combined univariate and multivariate analyses (Multivariate Pattern Analysis; Hebart, 2015) to explore changes in functional activation. Last, we used Dynamic Causal Modeling (Friston, 2003) to explore effective connectivity during reading within the classical reading network (left inferior frontal gyrus/IFG, left TPC and left ventral occipito-temporal cortex/vOTC) and an extended network comprising hypoactive regions in the respective sample.

Results: Behaviorally, the facilitation of the left TPC improved speech onsets for complex pseudowords and better performance was directly linked to functional coupling between the left IFG and the left vOTC. Whereas stimulation did not affect activation within the left TPC, it led to a lower recruitment of right-hemispheric areas for words and pseudowords, as well as to significantly altered neural interactions in the classical and extended reading network. In addition to a stronger recruitment of the ventral reading route (vOTC - IFG), stronger pseudoword-specific connectivity from the left supramarginal gyrus and lower inhibition from the right cerebellum on other reading areas seemed to be crucial for improving phonological decoding in dyslexia. Moreover, we found that only one subregion within the larger TPC region, the anterior SMG, showed deactivation for simple and complex pseudowords (see also Turker, 2023), suggesting that only this portion of the left TPC is causally involved in the phonological deficit in dyslexia.

Conclusions: We provide evidence for a crucial role of the left TPC for complex pseudoword reading and highlight the importance of network interactions within the core reading network and hypoactive brain areas in adults with dyslexia. Based on our findings on the importance of right-hemispheric regions both in terms of activation and connectivity, we conclude that

current models of reading in dyslexia might need an update to capture the variety of areas involved in reading processing in dyslexia and future research should more closely investigate the contributions of the right cerebellum to reading difficulties.

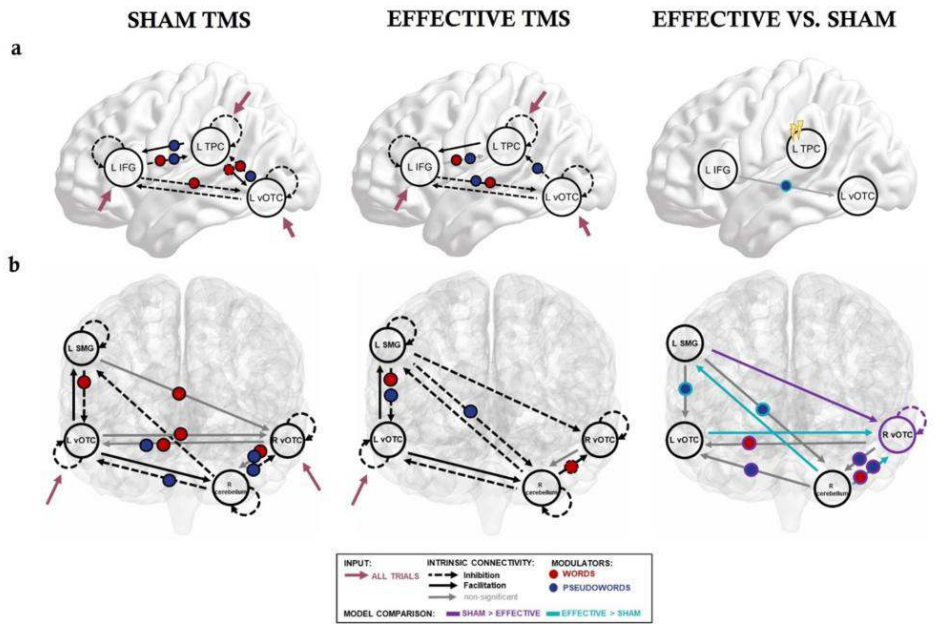

Fig. TMS-induced changes in network interactions in the classical (a) and extended reading network (b).

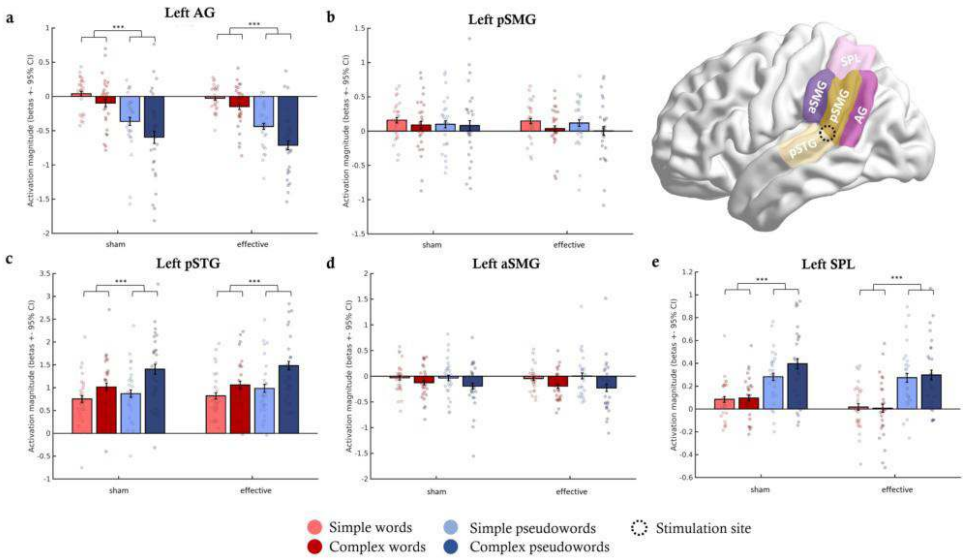

Fig. Contributions of subregions with the left TPC to word and pseudoword reading

References

1. Cancer, A. (2018), 'tDCS modulatory effect on reading processes: A review of studies on typical readers and individuals with dyslexia', Frontiers in Behavioral Neuroscience, vol. 12. https://doi.org/10.3389/fnbeh.2018.00162
2. Friston, K. (2003), 'Dynamic causal modelling', NeuroImage, vol. 19, no. 4, pp. 1273–1302. https://doi.org/10.1016/S1053-8119(03)00202-7
3. Hebart, M. (2015). 'The Decoding Toolbox (TDT): A versatile software package for multivariate analyses of functional imaging data', Frontiers in Neuroinformatics, vol. 8. https://www.frontiersin.org/articles/10.3389/fninf.2014.00088
4. Huettig, F. (2015), 'Literacy Influences Cognitive Abilities Far Beyond the Mastery of Written Language', LESLLA Symposium Proceedings, vol. 10, no.1, pp. 115–127. https://doi.org/10.5281/zenodo.8024395
5. Ramus, F. (2006), 'Weighing the evidence between competing theories of dyslexia'. Developmental Science, vol. 9, no. 3, pp. 265–269. https://doi.org/10.1111/j.1467-7687.2006.00488.x
6. Richlan, F. (2009), 'Functional abnormalities in the dyslexic brain: A quantitative meta-analysis of neuroimaging studies', Human Brain Mapping, vol. 30, no. 10, pp. 3299–3308. https://doi.org/10.1002/hbm.20752
7. Turker, S. (2022), 'The use of noninvasive brain stimulation techniques to improve reading difficulties in dyslexia: A systematic review', Human Brain Mapping, vol. 43, no. 3, pp. 1157–1173. https://doi.org/10.1002/hbm.25700
8. https://doi.org/10.1016/j.neuroimage.2023.120373
9. Turker, S. (2023), 'Disrupted network interactions serve as a neural marker of dyslexia', Communications Biology, vol. 6, no. 11114. https://doi.org/10.1038/s42003-023-05499-2
10. World Health Organization (2019/2021), 'International Classification of Diseases, Eleventh Revision (ICD-11)'. https://icd.who.int/

Poster No 1025

Targeted Reading Treatment Combined with Aerobic Exercise Improves Aphasia Outcomes

Olga Boukrina[1], Abubakar Yamin[2], Brian Sandroff[1], Elizabeth Madden[3], Yekyung Kong[4], William Graves[5]

[1]Kessler Foundation, West Orange, NJ, [2]Rutgers New Jersey Medical School, Newark, NJ, [3]Florida State University, Tallahassee, FL, [4]Kessler Institute for Rehabilitation, West Orange, NJ, [5]Rutgers, The State University of New Jersey, Newark, NJ

Introduction: An estimated 30% of stroke survivors worldwide experience aphasia[1,2], an acquired communication disorder, affecting multiple aspects of language, such as speaking, understanding, reading and writing[3]. Reading deficits in aphasia are common and severely limit one's autonomy and quality of life[2,4]. Our research aims to fill the gap in the current treatment approaches by focusing on cognitive and neural processes critical to reading. The study tested a personalized targeted intervention combining the beneficial impact of aerobic exercise training (AET) with an intensive phono-motor reading treatment (PMT)[5] aimed at rebuilding and strengthening damaged phonological neural networks involved in reading. Multiple studies have shown that cerebral blood flow (CBF) is decreased in the left hemisphere for weeks to months following stroke in areas that are not directly affected by an obvious structural lesion and this is correlated with language and reading impairments[6–8]. We tested the hypothesis that regular aerobic exercise improves brain circulation and promotes the acquisition, retention, and generalization of skills learned during reading therapy.

Methods: Seven individuals with chronic post-stroke aphasia (M age=57.8, SD=11.7, 2 women) participated in the study. Four participants completed 60 hours of PMT alone, while 3 participants received 22-60 hours of PMT preceded by 20 min of AET (stationary cycling at 60% heart rate range) and 10 min warm-up and cool-down. Treatment was delivered to both groups 5x/week for 2 hours/session. We assessed language and reading outcomes before and after the intervention and collected perfusion MRI data in the AET+PMT participants before, after 1 AET session, and after treatment. We also recorded fMRI brain activity during a reading task and at rest before and after treatment.

Results: Among participants who received combined AET+PMT, reading aloud accuracy improved by 15% (SD=14%, Cohen's d=0.70, medium effect size (ES)) for real words and by 25% (SD=25%, Cohen's d=.77, large ES) for novel nonwords. Nonwords measure participants' flexibility in converting letters into corresponding sounds and are especially difficult for participants with aphasia. Western Aphasia Battery(9) aphasia quotient (AQ) increased by an average of 6.4 points (SD=0.88), indicating a clinically significant improvement in aphasia severity(10). The PMT-only group improved by 5% (SD=7%, Cohen's d=.11, small ES) in word reading and by 22% (SD=17%, Cohen's d=.62, medium ES) in nonword reading. Only 2 out of 4 PMT-only participants showed improved WAB-AQ (M change=3.6, SD=0.35). For 2 AET+PMT participants who completed the full treatment (60h of PMT+20h of AET), global CBF increased, indicating that more oxygen and nutrients were delivered to the brain (see Fig.1). Dynamic resting state functional connectivity increased between visual and auditory and dorsal and ventral frontoparietal networks bilaterally (Fig.2). For the reading aloud fMRI task, we de-coupled brief word/nonword presentation from periods of overt speech. Following AET+PMT, activation during word/nonword viewing increased significantly in the right anterior temporal lobe, frontal pole, subcallosal cortex, posterior superior temporal gyrus, and bilateral lateral occipital cortex. Activation during speech periods increased in the left Heschl's gyrus (primary auditory cortex) and left sensorimotor cortex corresponding to face and hand areas.

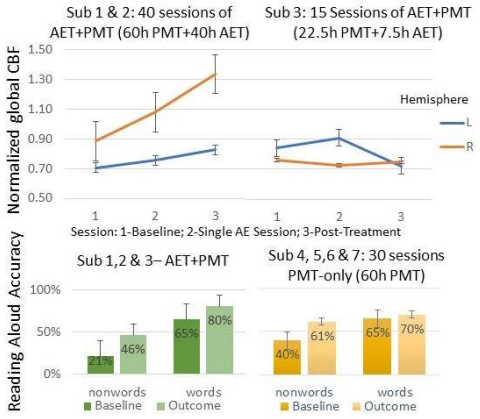

Fig.1. Hemispheric cerebral blood flow (CBF) at baseline, after 1 cycling session (AE-aerobic exercise), and after treatment. Reading aloud accuracy at baseline and after treatment for participants receiving Phono-Motor Therapy (PMT)+AE Treatment (AET) vs. PMT only. Sub 1 Male, 74; Sub 2 Male, 52; Sub 3 Female, 51, Sub 4&5 Male, 61, Sub 6 Male, 67, Sub 7 Female, 42.

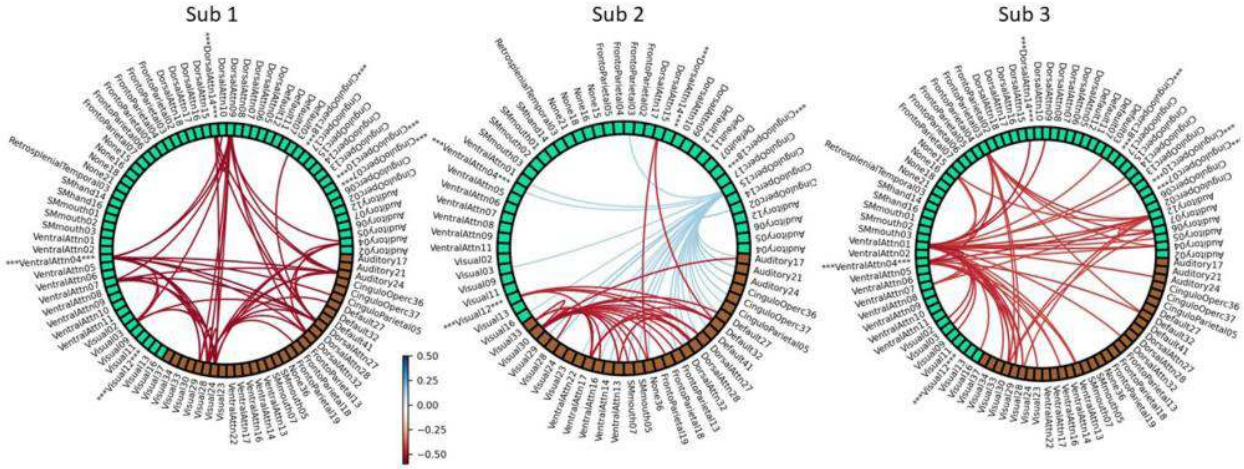

Fig.2. Geodesic dominant set clustering of the dynamic FC in 3 participants who completed AET+PMT treatment across a subset of the 94 Gordon atlas ROI that spatially overlap with a reading network mask derived from the Neurosynth database. The input dynamic rsFC matrices were constructed using Pearson correlation within a sliding window of 30 TRs (45 s) and a step size of 2 TRs (3 s). This resulted in 148 rsFC 94x94 matrices per participant describing the modulation of connectivity along the entire recorded sequence. The FC matrices were recoded as vectors representing distance from the centroids of the geodesic distance clusters and used in a classification scheme (Linear SVM & Lasso Regularized Logistic Regression). Top 1% of connections from the sensitivity analysis contrasting baseline vs. post-treatment connectivity are shown. ROI identified with *** include areas consistently implicated in reading, including left posterior fusiform, inferior temporal, middle temporal, supramarginal, and inferior frontal gyri. Color scheme: green – left hemisphere; orange – right hemisphere, red and blue connections represent connectivity increase and decrease, respectively. Note: S2 had a sizable left hemisphere lesion, thus most of the increased connectivity is in the right hemisphere.

Conclusions: Incorporating aerobic exercise into a targeted reading intervention led to a 19% improvement enhancement in nonword and 220% in word reading accuracy compared to reading therapy alone and resulted in greater overall improvement of aphasia severity. Neuroimaging data suggested that these gains were supported by increased global cerebral circulation, bilateral brain activation and dynamic functional connectivity. This study offers crucial early empirical evidence supporting the integration of AET with cognitive rehabilitation strategies.

References

1. Pedersen PM, Vinter K, Olsen TS. Aphasia after stroke: Type, severity and prognosis: The Copenhagen aphasia study. Cerebrovasc Dis. 2004;17(1):35–43.
2. Flowers HL, Skoretz SA, Silver FL, Rochon E, Fang J, Flamand-Roze C, et al. Poststroke Aphasia Frequency, Recovery, and Outcomes: A Systematic Review and Meta-Analysis. Arch Phys Med Rehabil [Internet]. 2016;97(12):2188-2201.e8. Available from: http://dx.doi.org/10.1016/j.apmr.2016.03.006
3. Brookshire CE, Willson JP, NAdeau SE, Gonzalez Rothi LJ, Kendall DL. Frequency, nature, and predictors of alexia in a convenience sample of individuals with chronic aphasia. Aphasiology. 2014 Aug 12;(August):1–17.
4. Koleck M, Gana K, Lucot C, Darrigrand B, Mazaux J-M, Glize B. Quality of life in aphasic patients 1 year after a first stroke. Qual Life Res. 2017 Jan;26(1):45–54.
5. Kendall DL, Oelke Moldestad M, Allen W, Torrence J, Nadeau SE. Phonomotor versus semantic feature analysis treatment for anomia in 58 persons with aphasia: A randomized controlled trial. J Speech, Lang Hear Res. 2019;62(12):4464–82.
6. Cloutman LL, Newhart M, Davis CL, Heidler-Gary J, Hillis AE. Neuroanatomical correlates of oral reading in actue left hemisphere stroke. Brain Lang. 2011;116(1):14–21.

7. Walenski M, Chen Y, Litcofsky KA, Caplan D, Kiran S, Rapp B, et al. Perilesional Perfusion in Chronic Stroke-Induced Aphasia and Its Response to Behavioral Treatment Interventions. Neurobiol Lang. 2022;3(2):345–63.
8. Boukrina O, Barrett AMM, Graves WWW. Cerebral perfusion of the left reading network predicts recovery of reading in subacute to chronic stroke. Hum Brain Mapp. 2019;40(18):1–14.
9. Kertesz A. Western Aphasia Battery Revised. San Antonio, TX: Pearson; 2007.
10. Gilmore N, Dwyer M, Kiran S. Benchmarks of Significant Change After Aphasia Rehabilitation. Arch Phys Med Rehabil. 2019;100(6):1131-1139.e87.

Poster No 1026

Neural systems for phonology differentially contribute to the act of writing

Mio Yokoi[1,2], Kouji Takano[1], Tomoki Uno[1,2], Kimihiro Nakamura[1]

[1]National Rehabilitation Center for Persons with Disabilities, Tokorozawa, Japan, [2]Japan Society for the Promotion of Science, Tokyo, Japan

Introduction: Phonological knowledge plays a pivotal role in most aspects of language processing, but it remains unclear whether it is required for writing. This is especially the case for phonologically opaque writing systems, e.g., Japanese logograms (kanji), where each character represents several different sounds. The present study used transcranial magnetic stimulation (TMS) to investigate whether left-hemisphere neural systems associated with phonology contribute to the act of writing.

Methods: Eighteen right-handed participants orally named target pictures ('naming') or wrote down their names ('writing') while they received single-pulse TMS at the ventral premotor cortex (PMv) associated with articulatory codes, supramarginal gyrus (SMG) associated with letter-to-sound translation or superior temporal gyrus (STG) associated with speech perception. Each target was preceded by a syllabic character (kana) prime which represented the initial syllable of the target name or a different syllable. We manipulated the phonological overlap between primes and targets and measured written or oral naming latency to assess the impact of TMS on phonological priming for each task for each site.

Results: In preliminary analyses, we found that TMS of SMG, but not that of PMv and STG, disrupted phonological priming during oral naming. By contrast, phonological priming was disrupted only by TMS of PMv during kana writing and by TMS of PMv and STG during kanji writing, respectively.

Conclusions: These findings suggest that neural systems for phonology contribute to word production differentially according to the functional demands of tasks and support the view that phonology plays a non-specific modulatory role to enhance neurocognitive systems involved in reading and writing.

Poster No 1027

An age-related posterior to anterior shift in brain alterations of the OT area in reading disability

Xiaohui Yan[1], Shilin Xu[2], Ziyi Wang[3], Fan Cao[4]

[1]The University of Hong Kong, Hong Kong, Hong Kong, [2]Department of Psychology, Sun Yat-sen University, Guangzhou, Guangdong, [3]Guangdong University of Foreign Studies, Guangzhou, Guangdong, [4]The University Of Hong Kong, Hong Kong, Hong Kong

Introduction: The left occipitotemporal areas (OT) play important roles in reading acquisition (Dehaene et al., 2010; Richlan, 2012) and development (Pleisch et al., 2019), which, however, consistently show abnormalities in individuals with reading disability (RD) (Richlan et al., 2011). Previous studies have examined developmental changes in the left OT region in typical readers; however, nothing is known about the developmental changes in this region in RD readers. Moreover, the specific functions of the left OT areas have also been a debate. Multivariate analysis might be more powerful than univariate methods in revealing the functions in which this region is involved. It is crucial to understand the development of the left OT region in individuals with RD, as well as the functions of this region.

Methods: In a cross-sectional study, we recruited 61 fifth-grade children (mean age: 11.07 years), 44 seventh-grade adolescents (mean age: 13.21 years), and 61 college students (mean age: 20.80 years) with and without RD. An auditory rhyming task was administered during the fMRI scanning. Both univariate and multivariate analysis were conducted.

Results: We found that individuals with RD performed worse than their age-controls in phonological awareness tests and the auditory rhyming task, which suggests persistent phonological deficits across ages. We also found persistent reduction of

brain activation in left OT regions in individuals with RD than age controls. However, the reduced brain activation shifted from the posterior OT region to the anterior OT region with increasing age. This was driven by the fact that only age controls but not individuals with RD showed a posterior-to-anterior shift in the left OT region. Representational similarity analysis (RSA) showed that the left OT region is involved in orthographic representation rather than phonological representation. We also found different developmental patterns in the left STG and right supramarginal gyrus in individuals with RD and age controls.

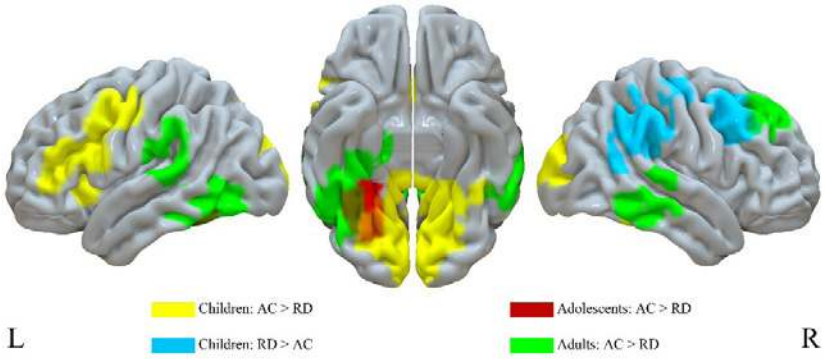

Figure 1. Simple main effect of RD in children, adolescents and adults.

Conclusions: We found persistent phonological deficits in individuals with RD across ages. In the brain, individuals with RD showed different developmental patterns from age controls, especially in the left OT region, where there is a lack of poster-to-anterior shift with age in individuals with RD. These findings provide important insights about brain mechanisms of RD from a developmental perspective.

References

1. Dehaene, S., Pegado, F., Braga, L. W., Ventura, P., Filho, G. N., Jobert, A., Dehaene-Lambertz, G., Kolinsky, R., Morais, J., & Cohen, L. (2010). How learning to read changes the cortical networks for vision and language. Science, 330(6009), 1359. doi:10.1126/science.1194140
2. Pleisch, G., Karipidis, II, Brauchli, C., Rothlisberger, M., Hofstetter, C., Stampfli, P., Walitza, S., & Brem, S. (2019). Emerging neural specialization of the ventral occipitotemporal cortex to characters through phonological association learning in preschool children. Neuroimage, 189, 813-831. doi:10.1016/j.neuroimage.2019.01.046
3. Richlan, F., Kronbichler, M., & Wimmer, H. (2011). Meta-analyzing brain dysfunctions in dyslexic children and adults. Neuroimage, 56(3), 1735-1742. doi:10.1016/j.neuroimage.2011.02.040
4. Richlan, F. (2012). Developmental dyslexia: dysfunction of a left hemisphere reading network. Frontiers in Human Neuroscience, 6, 120. doi:10.3389/fnhum.2012.00120

Poster No 1028

Longitudinal analysis of letter and speech sound association

Joanna Beck[1,2], Katarzyna Jednoróg[1]

[1]Laboratory of Neurobiology of Language, Nencki Institute of Experimental Biology PAS, Warsaw, Mazovia, [2]Bioimaging Research Center, Institute of Physiology and Pathology of Hearing, Warsaw, Poland

Introduction: The initial step in reading development involves acquiring letter-speech sound (LS) associations, with literature consensus on the left superior temporal cortex as the integration site in adults and children (e.g., Blau et al., 2009). This research focuses on understanding the brain development of LS integration in children. Polish children from kindergarten to 8th grade participated in a computer-based letter-to-phoneme game, which measured their reaction time and accuracy in judging whether the letters and speech sounds were identical. Data showed that children master accurate LS association within a year of reading instruction. However, they needed more time (around three years) to automatize this ability, as reflected by decreasing reaction times in the game. Longitudinal fMRI analysis (N = 67, age at TP1: mean = 6.93, TP3: mean = 8.92), in the prior study, revealed significant changes in brain activation during the first two years of education, indicating a shift in sensory areas activation. Brain activity decreased in response to unimodal speech sounds and letters but increased for multimodal LS pairs (Beck et al., under review).

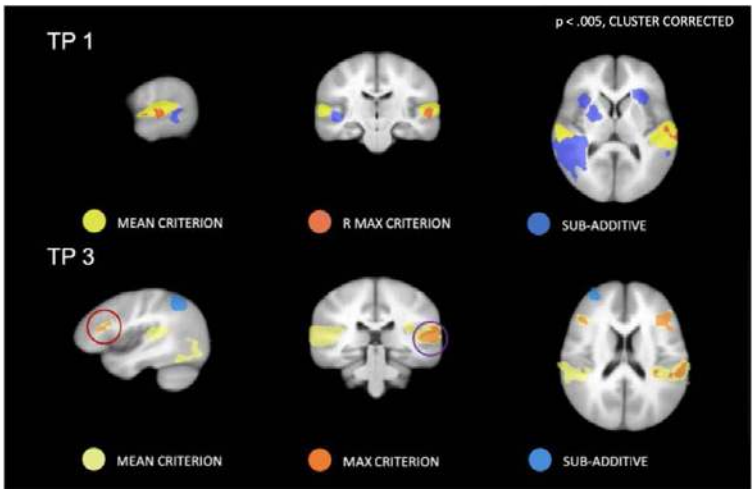

Fig. Lower level of letter and speech sound association at TP1 and TP3

Methods: Twenty-eight children from Beck et al. (under review) underwent an additional fMRI scan in the 8th grade (TP4: mean = 14.26). Using fMRI, brain activity was measured during the presentation of visual letters, speech sounds, congruent and incongruent LS pairs. Participants pressed a button for the word "cat," the picture of a cat, and the spoken word "/cat/." LS association was measured on two levels: A. Lower (basic sensory aspects) - multimodal enhancement - stronger response to multimodal congruent condition compared to unimodal conditions [i.e super-additive effect (congruent LS > letters + speech sounds), max criterion (congruent LS > letters) (congruent LS > speech sounds) or mean criterion (2 * congruent LS > letters + speech sounds)] or opposite effect, multimodal suppression (i.e sub-additive effect). B. Higher (orthographic and phonological): (in)congruency effect, i.e congruent vs. incongruent LS pairs Pre-processing and analyses were conducted using BrainVoyager 22.2.1 software, with results reported at $p < .005$ corrected for multiple comparisons at the cluster level.

Results: Extending prior analyses (Beck et al., under review), sensory areas exhibited decreased activity in response to unimodal speech sounds and letters, while multimodal LS pairs showed increased activity. Lower-level comparisons revealed engagement in the left inferior frontal gyrus and superior temporal gyrus for multisensory enhancement (super-additive effect). No significant differences were observed at the higher level of integration.

Fig. Lower level of letter and speech sound association at TP4

Conclusions: Contrary to expectations, the developmental trajectory of Polish children did not exhibit the anticipated congruency effect. While initial hypotheses suggested multisensory enhancement and (in)congruency effects as children automated this skill, our study only partially confirmed these expectations. Possible factors include insufficient number of participants, limited stimuli presentations, and potential fMRI paradigm influences. These results may also be linked to the unique timing of children's brain development, prompting further exploration of these factors and their implications.

References

1. Blau, V., van Atteveldt, N., Ekkebus, M., Goebel, R., & Blomert, L. (2009). Reduced neural integration of letters and speech sounds links phonological and reading deficits in adult dyslexia. Current Biology, 19(6), 503-508.
2. Blau, V., Reithler, J., van Atteveldt, N., Seitz, J., Gerretsen, P., Goebel, R., & Blomert, L. (2010). Deviant processing of letters and speech sounds as proximate cause of reading failure: a functional magnetic resonance imaging study of dyslexic children. Brain, 133(3), 868-879
3. Beck, J., Dzięgiel-Fivet, G., & Jednoróg, K. (2023). Similarities and differences in the neural correlates of letter and speech sound integration in blind and sighted readers. NeuroImage, 278, 120296.
4. Beck, J., Chyl, K., Dębska, A., Łuniewska, M., van Atteveldt, N., Jednoróg, K., (2023). Letter-speech sound integration in typical reading development during the first years of formal education (under review)
5. van Atteveldt, N. M., Formisano, E., Goebel, R., and Blomert, L. (2004). Integration of letters and speech sounds in the human brain. Neuron 43, 271–282. doi: 10.1016/j.neuron.2004.06.025

Poster No 1029

From Brain Patterns to Academic Success: Unveiling Multimodal Signatures in Reading and Mathematics

Ping Long[1], Rui Chen[1], Dongmei Zhi[1], Vince Calhoun[2], Sha Tao[1], Jing Sui[1]

[1]State Key Laboratory of Cognitive Neuroscience and Learning, Beijing Normal University, Beijing, China, [2]Tri-institutional Center for Translational Research in Neuroimaging and Data Science (TReNDS), Atlanta, Georgia, United States

Introduction: Children's reading and mathematics are two essential abilities that are critical to academic achievements and future career development. Existing neuroimaging research often concentrated on a single ability (reading or mathematical processing)[1,3], or compared them using one specific MRI modality[2,4,5]. However, the multimodal neuroimaging signatures significantly associated with reading and mathematics remained unexplored. Here, via a supervised three-way MRI fusion (fALFF, FA, and GMV), we identified the MRI signatures for comprehensive reading and mathematical processing for 562 children to reveal the common and unique underlying neurobiological basis. Moreover, the longitudinal predictability of the identified baseline MRI signatures for estimating 5 types of cognitive scores one year later (including attention, memory, reasoning, visual perception, and cognitive composite) was examined and validated.

Methods: This study recruited 562 typically developing children aged 9-11 years from two independent cohorts (N = 441 and N = 121) with MRI scans, academic attainment scores, and cognitive scores. Firstly, academic-guided fusion was performed in children from the PKU dataset. Specifically, reading and mathematics scores were used respectively as a reference to guide a three-way MRI feature fusion,i.e., fALFF, FA, and GMV, by multimodal canonical correlation analysis with reference plus joint independent component analysis (MCCAR + jICA)[6]. Then, structural similarity index measure (SSIM) was used to measure the degree of similarity for joint components between reading, math and cognitive domains for each modality. Next, the multimodal brain patterns obtained from PKU were used to predict five cognitive scores one year later with linear support vector regression (SVR) and validated in another cohort.

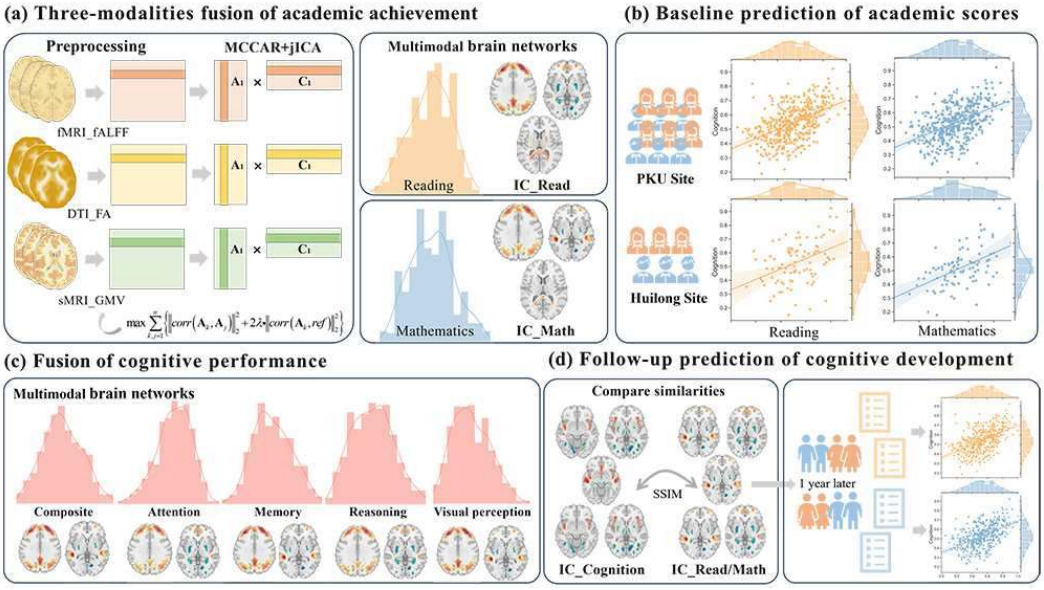

Figure 1. The analysis flowchart.

Results: Results highlighted the prefrontal regions and posterior default mode network as the most commonly prominent brain networks for academic achievements. The Broca's area and posterior cingulate cortex in fractional amplitude of low-frequency fluctuation, and anterior cingulate cortex in grey matter volume were more extensively involved in reading[12], while the middle temporal gyrus and angular gyrus in grey matter volume was specifically engaging in mathematics[345]. Moreover, academic achievements were both highly associated with reasoning, whereas mathematics was more extensively involved in visual perception than reading. Most importantly, the identified multimodal signatures can successfully predict children's current academic achievements and distinct cognitive domains at one year later, especially the highest predictive power of cognitive composite validated by another independent cohort ($r > 0.35$).

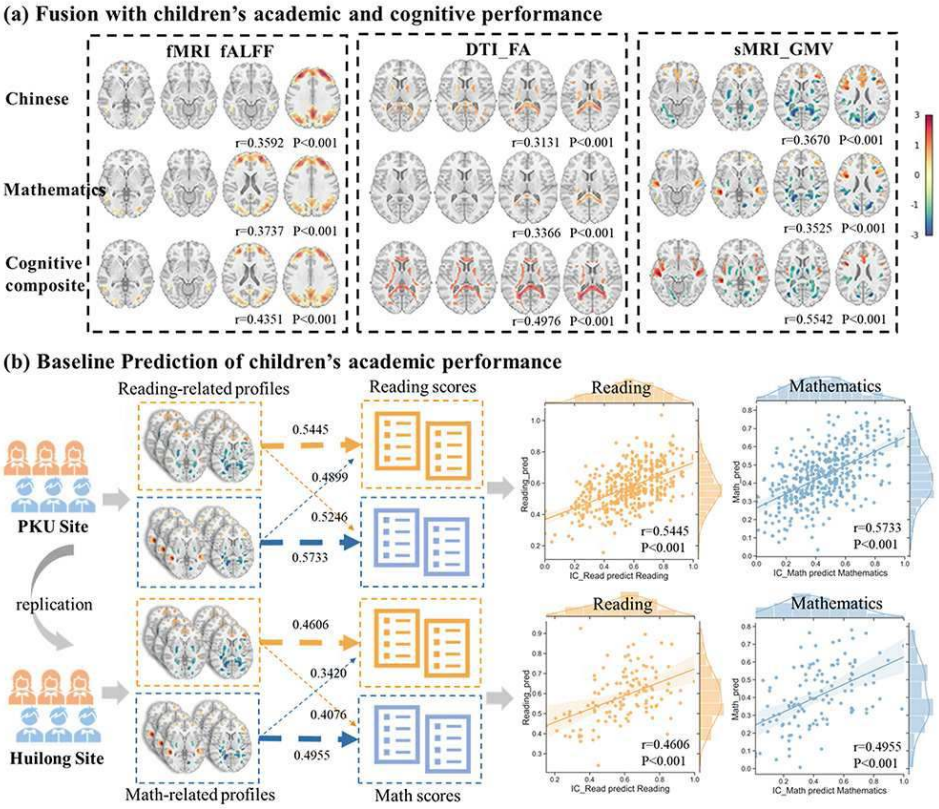

Figure 2. (a) Results of three-way fusion with children's academic and cognitive score.(b) Results of prediction based on the identified academic-associated brain networks.

Conclusions: In this study, we searched for the common and unique multimodal signatures between reading and mathematics, as well as their relationships with distinct cognitive domains by a supervised multimodal fusion. To the best of our knowledge, this is the first attempt to utilize reading and mathematics as references to guide the three-way multimodal MRI fusion, where the multimodal signatures can significantly predict one-year-later cognitive abilities, especially the cognitive composite, which were also validated in another independent cohort. Our findings contribute to a better understanding of the brain relationships between academic achievement and cognitive abilities, which would have important implications for the early detection of learning difficulties and the development of targeted interventions to support children's academic growth.

References

1. Evans, T. M. (2016), 'Functional neuroanatomy of arithmetic and word reading and its relationship to age', Neuroimage, vol. 143, pp. 304-315.
2. Huber, E. (2018), 'Rapid and widespread white matter plasticity during an intensive reading intervention', Nature Communications, vol. 9, no. 1, pp. 2260.
3. Kersey, A. J. (2019), 'Developing, mature, and unique functions of the child's brain in reading and mathematics', Developmental Cognitive Neuroscience, vol. 39, pp. 100684.
4. Peters, L. (2018), 'Arithmetic in the developing brain: A review of brain imaging studies', Developmental Cognitive Neuroscience, vol. 30, pp. 265-279.
5. Price, G. R. (2018), 'Prospective relations between resting-state connectivity of parietal subdivisions and arithmetic competence', Developmental Cognitive Neuroscience, vol. 30, pp. 280-290.
6. Qi, S. (2018), 'Multimodal Fusion with Reference: Searching for Joint Neuromarkers of Working Memory Deficits in Schizophrenia', IEEE Transactions on Medical Imaging, vol. 37 no. 1, pp. 93-105.

Poster No 1030

Enhancing Reading Rehabilitation in Subacute Stroke Using fMRI Neurofeedback

Olga Boukrina[1], Yekyung Kong[2], Pranav Reddy[1], Guang Yue[1], Yury Koush[3]

[1]Kessler Foundation, West Orange, NJ, USA, [2]Kessler Institute for Rehabilitation, West Orange, NJ, USA, [3]Skolkovo Institute of Technology, Moscow, Russian Federation

Introduction: Each year, 21-38% of the 13.7 million stroke survivors worldwide experience reading impairments as a result of an acquired communication disorder called aphasia[1–4]. For more than half of persons with aphasia, reading and language impairments become a chronic condition[5], preventing them from maintaining independent living, accessing information, and pursuing education or career opportunities. This means that a large proportion of stroke survivors with reading impairments have an incomplete response to rehabilitation. There is an urgent need for effective early interventions that can improve this statistic. We developed and tested a novel neurobehavioral reading intervention using fMRI neurofeedback (NFB). Stroke participants were given real-time NFB about their ongoing brain activity to help them in developing brain regulation strategies. We hypothesized that using NFB can increase neural activation of the affected neural circuits and thereby improve recovery of reading abilities.

Methods: Four individuals with subacute left hemisphere stroke (M age=63.5, SD=17, all men, M days post stroke =21.3, SD = 5.8, WAB[6] Aphasia Quotient (AQ)=73.38, SD=31.11) and 3 age-matched healthy controls (HCs) (M age=66, SD=6, all men) participated in the study. Participants underwent 3 NFB training scans, spaced one week apart, consisting of two 15-min runs. During the intervals between scans, they completed 10 30-min homework sessions to practice the strategies learned during NFB training. We measured the NFB signal, reading accuracy, reading comprehension using the RCBA[7], and aphasia severity using the WAB before and after training. During NFB training[8], participants imagined right hand finger movements, e.g. typing on a keyboard, tracing letters in a book, tapping on piano keys, or tapping each finger in sequence. Our goal was to activate the left Supramarginal Gyrus (SMG), known to support letter-to-sound conversion[9,10], as well as kinesthetic motor imagery and planning of finger movements(11,12). After the motor imagery block participants read aloud real and novel words (8 words presented for 1s+2s response period, jittered). The NFB signal was computed as the difference between the imagine and read blocks relative to a fixation baseline, scaled to 0-100. The sequence of blocks (baseline (21s), imagine (21s), read (24s)) was repeated 9 times per run and participants received intermittent feedback after each repeat.

Results: Two of 3 HCs and 3 of 4 patients showed increased NFB signal post- compared to pre-training, as measured using transfer runs without overt feedback to participants (Pre: M HC =41.39,SD=51.16; M Patients=7.07,SD=10.20; Post: M HC=63.63,SD=47.13, M Patients=8.24,SD=13.09). This indicates that following training activity in the left SMG increased during imagine and read blocks relative to baseline (Fig.1). Among stroke patients, reading accuracy increased by 4.5% (SD=6.4) for real words and by 13% (SD=10.42) for pseudowords. WAB AQ increased by 5.48 points (SD=4.25), indicating a clinically significant reduction in the overall aphasia severity. RCBA scores increased by 9.75 points (SD=6.29), indicating improved reading comprehension. Overall, participants rated their motivation and commitment to participate in the NFB training as high to very high, and the difficulty of the training as somewhat easy to neutral.

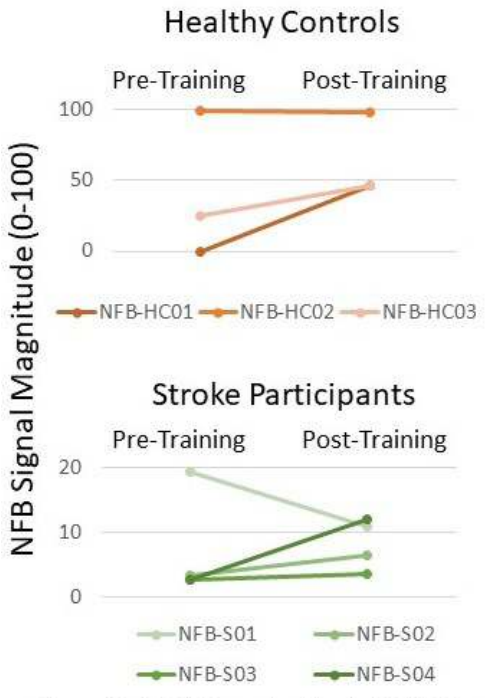

Figure 1. fMRI Neurofeedback (NFB) signal magnitude before vs. after NFB signal training.

Conclusions: To date, only 5 fMRI NFB stroke rehabilitation studies, including 2 on aphasia with 2-8 stroke participants each, have been published. Our study contributes to this limited body of research by showing the feasibility and potential of fMRI NFB in post-stroke reading rehabilitation. However, our initial results, limited by a male-only sample and the possibility of spontaneous recovery, should be interpreted cautiously. More robust conclusions await future studies incorporating a sham NFB control group. This research marks a preliminary step in developing biologically-informed interventions for reading deficits in aphasia.

References

1. Brookshire CE, Willson JP, NAdeau SE, Gonzalez Rothi LJ, Kendall DL. Frequency, nature, and predictors of alexia in a convenience sample of individuals with chronic aphasia. Aphasiology. 2014 Aug 12;(August):1–17.
2. Dickey L, Kagan A, Lindsay MP, Fang J, Rowland A, Black S. Incidence and profile of inpatient stroke-induced aphasia in Ontario, Canada. Arch Phys Med Rehabil. 2010 Feb;91(2):196–202.
3. Engelter ST, Gostynski M, Papa S, Frei M, Born C, Ajdacic-Gross V, et al. Epidemiology of aphasia attributable to first ischemic stroke: incidence, severity, fluency, etiology, and thrombolysis. Stroke. 2006 Jun;37(6):1379–84.
4. Berthier ML. Poststroke aphasia: Epidemiology, pathophysiology and treatment. Drugs and Aging. 2005;22(2):163–82.
5. Pedersen PM, Vinter K, Olsen TS. Aphasia after stroke: Type, severity and prognosis: The Copenhagen aphasia study. Cerebrovasc Dis. 2004;17(1):35–43.
6. Kertesz A. Western Aphasia Battery Revised. San Antonio, TX: Pearson; 2007.
7. La Pointe LL, Horner J. Reading Comprehension Battery for Aphasia. 2nd. Austin, TX: Pro-Ed; 1998.
8. Koush Y, Ashburner J, Prilepin E, Sladky R, Zeidman P, Bibikov S, et al. OpenNFT: An open-source Python/Matlab framework for real-time fMRI neurofeedback training based on activity, connectivity and multivariate pattern analysis. Neuroimage. 2017;156(June):489–503.
9. Cattinelli I, Borghese NA, Gallucci M, Paulesu E. Reading the reading brain: A new meta-analysis of functional imaging data on reading. J Neurolinguistics. 2013 Sep;26(1):214–38.
10. Stoeckel C, Gough PPM, Watkins KKE, Devlin JJT. Supramarginal gyrus involvement in visual word recognition. Cortex. 2009;45(9):1091–6.
11. Guillot A, Collet C, Nguyen VA, Malouin F, Richards C, Doyon J. Brain activity during visual versus kinesthetic imagery: An fMRI study. Hum Brain Mapp. 2009;30(7):2157–72.
12. Andres M, Pelgrims B, Olivier E, Vannuscorps G. The left supramarginal gyrus contributes to finger positioning for object use: a neuronavigated transcranial magnetic stimulation study. Eur J Neurosci. 2017 Dec;46(12):2835–43.

Poster No 1031

An fMRI Approach to Investigate Reading Deficits in Medulloblastoma Survivors

Josue Luiz Dalboni da Rocha[1], Ping Zou Stinnett[2], Matthew Scoggins[1], Heather Conklin[1], Amar Gajjar[1], Robert Ogg[1], Ranganatha Sitaram[1]

[1]St. Jude Children's Research Hospital, Memphis, TN, [2]St. Jude Children Research Hospital, Memphis, TN

Introduction: Medulloblastoma (MB), the most common childhood malignant brain tumor, has a 5-year survival rate near 80% with recent progress in treatment. However, survivors often encounter cognitive challenges, including reading deficits (Zou et al., 2016). These deficits may manifest as difficulties in core processes supporting fluent reading-phonological awareness and rapid visual naming (Stappen et al., 2018). This study reports an fMRI study in MB survivors using Rapid Automatized Naming (RAN) and Orthographic Processing of Letters (OPL) tasks to investigate skills supporting reading (Powell et al., 2014).

Methods: This study received ethical approval from the Institutional Review Board (IRB) and written informed consent was obtained from each participant. 50 MB survivors (mean age at fMRI = 14.4 years; SD = 4.1) and 96 healthy controls (mean age at fMRI = 14.3 years; SD = 5.1) participated in 3 visits for fMRI acquisition, spaced at 12-month intervals. For RAN, we examined the Blood Oxygenation Level Dependent (BOLD) differences between the conditions of naming letters and naming colors. For OPL, we evaluated BOLD differences between identifying matching pairs of letters versus lines (Powell et al., 2014). FMRI analysis utilized between-subject comparison based on a region-of-interest (ROI) activation score, in 3 key steps: 1) Within-Subject Analysis: Voxel-wise t-values were extracted for each subject by comparing two task conditions (i.e., for RAN: letter vs color; for OPL: letters vs lines). These t-values at each voxel were henceforth called voxel-wise activation scores. 2) ROI Averaging: Voxel-wise activation scores were averaged within predefined ROIs for each subject, resulting in a single activation score per ROI, henceforth called ROI activation score. The ROIs were 127 brain regions segmented from the Neuromorphometrics atlas (Tourville et al., 2010). 3) Between-Subject Analysis: An intersubject t-test was conducted to compare the ROI activation score. This step determined whether there were significant differences across subjects within each ROI, for the pair of task conditions in analysis.

Results: Medulloblastoma survivors exhibited an abnormality in BOLD response for letter versus color naming. This abnormality reached statistical significance (p-value < 0.05, Bonferroni corrected for 381 multiple comparisons) only during the third visit, predominantly observed in the right Fusiform Gyrus (p=0.02) and right Occipital Pole (p=0.04), as in Fig 1. On the

other hand, BOLD response abnormalities in medulloblastoma survivors for letter versus lines equal pair identification were statistically significant (p-value < 0.05, Bonferroni corrected for 127 multiple comparisons) in all visits. The top brain regions affected included right inferior occipital gyrus (p=6*10^-11), and bilateral angular gyrus [right (p=8*10^-7) and left (p=5*10^-6)], as in Fig 2.

Fig 1. Right Fusiform Gyrus and Right Occipital Pole: ROIs (in red) where abnormal BOLD response for letter versus color naming was observed.

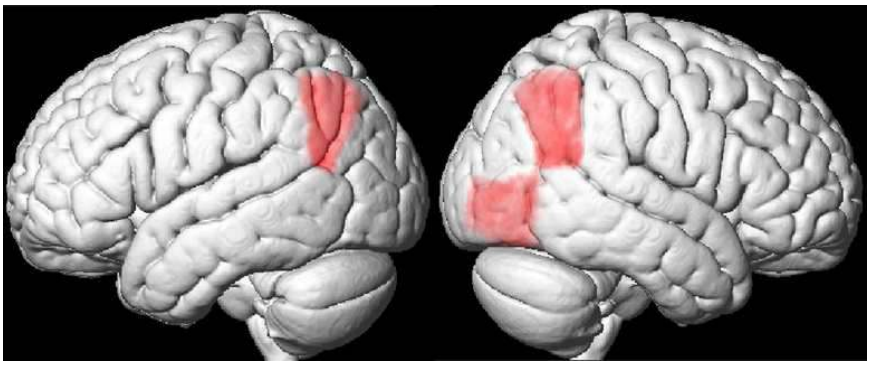

Fig 2. Left Angular Gyrus (left side), Right Angular Gyrus and Right Occipital Gyrus (right side): ROIs (in red) where abnormal BOLD response for letter versus lines was observed.

Conclusions: The processing of letters in RAN appears to be sensitive to phonological processing and is often compromised in children with reading disorders. Conversely, the RAN of colors tends to be impaired in children with attention disorders. The delayed onset abnormality in letter versus color naming emphasizes the importance of long-term monitoring and cognitive support for this population. Additionally, the early detection of abnormalities in letters versus lines suggests potential targets for intervention and rehabilitation. Our findings reveal distinct patterns of BOLD response abnormalities in medulloblastoma survivors, which may provide insights into the neural mechanisms underlying their reading deficits. These findings may signify early orthographic processing issues, hinting at the likelihood that younger children, who rely more on orthographic decoding than phonological skills, may manifest these impairments earlier. Understanding these neurofunctional changes may guide the development of tailored strategies to enhance the cognitive outcomes of medulloblastoma survivors.

References

1. Powell, D., et al. (2014), 'Deficits in Orthographic Knowledge in Children Poor at Rapid Automatized Naming (RAN) Tasks?', Scientific Studies of Reading, 18:3, 192-207, DOI: 10.1080/10888438.2013.862249
2. Stappen, C.V., et al. (2018), 'Phonological Awareness and Rapid Automatized Naming Are Independent Phonological Competencies With Specific Impacts on Word Reading and Spelling: An Intervention Study', Front. Psychol. 9:320. DOI: 10.3389/fpsyg.2018.00320
3. Tourville J., et al. (2010), 'Cortical Parcellation Protocol', http://neuromorphometrics.com/ParcellationProtocol_2010-04-05.PDF
4. Zou, P., et al. (2016), 'Functional MRI in medulloblastoma survivors supports prophylactic reading intervention during tumor treatment', Brain Imaging and Behavior 10, 258–271. https://doi.org/10.1007/s11682-015-9390-8

Poster No 1032

Brain Structural Connectivity and Pre-Reading Abilities in Children with Prenatal Alcohol Exposure

Mohammad Ghasoub[1], Meaghan Perdue[1], Xiangyu Long[1], Claire Donnici[1], Preeti Kar[1], Deborah Dewey[1], Ben Gibbard[1], Chris Tortorelli[1], Catherine Lebel[1]

[1]*University of Calgary, Calgary, Alberta*

Introduction: Worldwide, approximately 10% of people consume alcohol while pregnant. Children with prenatal alcohol exposure (PAE) can go on to develop cognitive deficits including reading disorders. PAE is also associated with a range of structural neural alterations, including abnormal white matter microstructure and altered connectivity. Alterations have been found in brain pathways associated with reading, but very few studies have directly examined the association between structural connectivity and early reading performance in children with PAE. Using graph theory analysis, we examined associations between structural network connectivity in areas of the brain associated with reading/pre-reading in young children, and the extent to which PAE moderates these associations.

Methods: 363 scans from 135 children (53 with PAE, 82 controls) collected longitudinally between ages 3-7 years were examined. Children from both groups completed pre-reading assessments including Phonological Processing and Speeded Naming and underwent a diffusion MRI scan on a GE 3T MR750w system with a 32-channel head coil at each time point. Diffusion tensor imaging (DTI) data were acquired using single-shot spin-echo, echo planar imaging (EPI) sequence of 1.6 × 1.6 × 2.2 mm resolution (resampled to 0.78 × 0.78 × 2.2 mm on scanner), TR = 6,750 ms; TE = 79 ms, 30 gradient encoding directions at b = 750 s/mm, and 5 baselines at b = 0 s/mm2 (4:03 minutes total). DTI preprocessing protocol included flipping/permuting images, as well as signal drift, Gibbs ringing, head motion, and eddy current distortion corrections. Diffusion tensor was calculated to delineate the FA values, and whole brain diffusion tractography was performed using seedpoint resolution = 2 × 2 × 2 mm3, seed fractional anisotropy (FA) threshold = 0.15, fiber length range = 50–500 mm, angle threshold = 30°, step size = 1. We defined a reading network consisting of 16 brain regions from both hemispheres known from prior work to be associated with reading (Figure 1). We used the mean FA extracted from the whole-brain tractography, and Automated Anatomical Atlas (AAL 90) to generate FA-weighted connectivity matrices. A 16x16 connectivity matrix of regions from both hemispheres as well as 8x8 connectivity matrices from each hemisphere were extracted for analysis. The following graph theory measures of network properties were calculated for each hemisphere and bilaterally using the Brain Connectivity Toolbox: global efficiency, local efficiency, clustering coefficient, and nodal degree. Linear mixed effects models were used to test the associations between graph theory measures and pre-reading assessments as well as the effect of PAE on these associations, accounting for age and sex (fixed effects), and repeated measures within subjects (random effect).

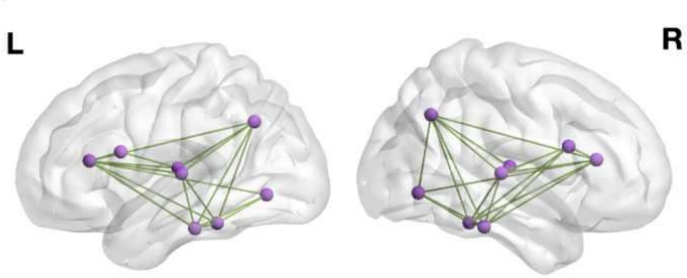

Figure 1. 16 Regions of interest (8 from each hemisphere) included in the network of interest: opercular part of the inferior frontal gyrus, the triangular part of the inferior frontal gyrus, the lingual gyrus, the fusiform gyrus, the angular gyrus, Heschl's gyrus, the superior temporal gyrus, and the inferior temporal gyrus.

Results: Children with PAE had significantly lower mean graph theory metrics than controls across all networks (Figure 2). They also had lower Phonological Processing and Speeded Naming scores ($p < 0.001$). PAE significantly moderated the associations between Phonological Processing and global efficiency in both the bilateral ($p = 0.005$) and left hemisphere ($p = 0.025$) networks, as well as nodal degree in the bilateral ($p = 0.005$) network. No significant associations were found for Speeded Naming.

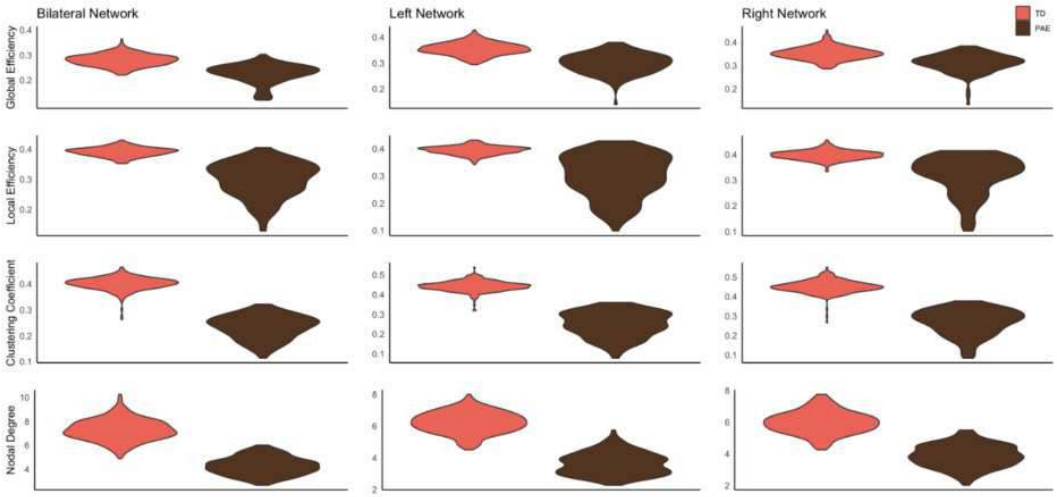

Figure 2. Violin plots displaying variations in mean scores of graph theory metrics between PAE and Control groups in bilateral brain network and each hemisphere. The violin plots are color-coded to represent the two groups, with the PAE group in brown and the control group in coral. TD children had significantly higher graph theory metrics than children with PAE across all networks and measures ($p < 0.05$).

Conclusions: Children with PAE had lower pre-reading skills as well as overall reduced structural connectivity properties compared to unexposed children. PAE moderated the associations between Phonological Processing and global efficiency and nodal degree, suggesting that PAE may influence information integration in the reading networks. It is notable that PAE influenced brain-pre-reading relationships in preschool aged children before the beginning of formal reading instructions at school. Further research is required to better understand this moderation effect and its implications for early interventions.

References

1. Hendricks, G., Malcolm-Smith, S., Adnams, C., Stein, D. J., & Donald, K. A. M. (2019). 'Effects of prenatal alcohol exposure on language, speech and communication outcomes: A review longitudinal studies'. Acta Neuropsychiatrica, 31(2), 74–83.
2. Kar, P., Reynolds, J. E., Grohs, M. N., Gibbard, W. B., McMorris, C., Tortorelli, C., & Lebel, C. (2021). 'White matter alterations in young children with prenatal alcohol exposure'. Developmental Neurobiology, 81(4), 400–410.
3. Lebel, C., Rasmussen, C., Wyper, K., Walker, L., Andrew, G., Yager, J., & Beaulieu, C. (2008). 'Brain Diffusion Abnormalities in Children With Fetal Alcohol Spectrum Disorder'. Alcoholism: Clinical and Experimental Research, 32(10), 1732–1740.
4. Long, X., Kar, P., Gibbard, B., Tortorelli, C., & Lebel, C. (2019). 'The brain's functional connectome in young children with prenatal alcohol exposure'. NeuroImage: Clinical, 24, 102082.
5. Long, X., & Lebel, C. (2022). 'Evaluation of Brain Alterations and Behavior in Children With Low Levels of Prenatal Alcohol Exposure'. JAMA Network Open, 5(4), e225972.
6. Long, X., Little, G., Beaulieu, C., & Lebel, C. (2018). 'Sensorimotor network alterations in children and youth with prenatal alcohol exposure.' Human Brain Mapping, 39(5), 2258–2268.
7. Long, X., Little, G., Treit, S., Beaulieu, C., Gong, G., & Lebel, C. (2020). 'Altered brain white matter connectome in children and adolescents with prenatal alcohol exposure'. Brain Structure and Function, 225(3), 1123–1133.
8. Roos, A., Fouche, J.-P., Ipser, J. C., Narr, K. L., Woods, R. P., Zar, H. J., Stein, D. J., & Donald, K. A. (2021). 'Structural and functional brain network alterations in prenatal alcohol exposed neonates'. Brain Imaging and Behavior, 15(2), 689–699.
9. Treit, S., Lebel, C., Baugh, L., Rasmussen, C., Andrew, G., & Beaulieu, C. (2013). 'Longitudinal MRI Reveals Altered Trajectory of Brain Development during Childhood and Adolescence in Fetal Alcohol Spectrum Disorders'. Journal of Neuroscience, 33(24), 10098–10109.

Poster No 1033

Brain response dynamics during novel script reading as compared to familiar script reading

Amelie Haugg[1,2], Nada Frei[1,2], Alexander Zeller[1], Chayenne Garcia[1], Vinzenz Schmid[1], Anna-Marie Conrad[1], Sara Steinegger[1], Martina Röthlisberger[1,2], Silvia Brem[1,3,2]

[1]University of Zurich, Zurich, Switzerland, [2]NCCR Evolving Language, Zurich, Switzerland, [3]Neuroscience Center Zurich, Zurich, Switzerland

Introduction: Learning to read is a complex cognitive process that requires the development of an extensive, specialized reading network (RN) in the brain[1]. This network's functional organization becomes increasingly refined and consolidated through continued practice[2]. In this study, we investigated how, in adults, different brain regions of this established RN respond to processing words in a recently learned artificial script (AS) compared to a native and highly familiar Latin script

(LS). Further, we analyzed the influence of attention and working memory on the reading process in the novel and well-established scripts.

Methods: 61 typical-reading, native German-speaking adults (24.10 years, 38 f) participated in the study and completed tests to assess working memory, attention, and reading fluency. In the MRI scanner (3T), participants trained 12 associations between letters written in the AS and phonemes of the German alphabet. Then, they performed a lexical decision task with words and pseudowords written in AS and LS (Figure 1). Finally, fluency in reading the newly learned AS was tested outside the scanner. fMRI data analyses with SPM12 included standard preprocessing and a general linear model with two regressors of interest (AS and LS). For ROI analyses, mean beta values were extracted from predefined brain regions of the RN. Finally, the activation time series of key brain regions were extracted using the eigenvalues of the signal.

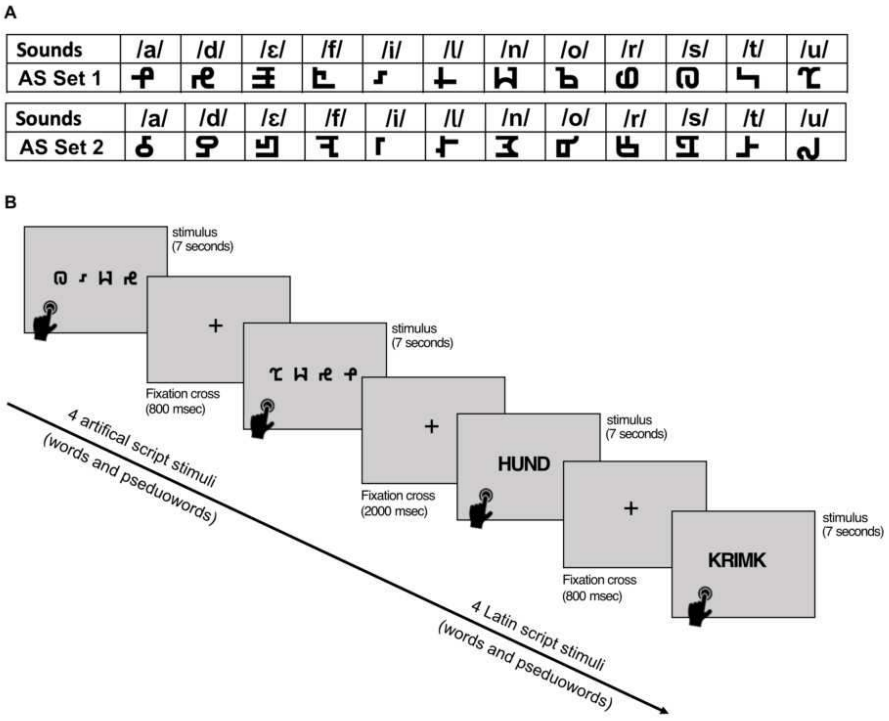

Figure 1. A. Artificial script characters. Each participant was trained to learn 12 letter speech sound associations between characters written in an artifical script (AS) and phonemes of the German alphabet. All participants were randomly assigned one of two AS sets. **B. Lexical decision task with lexical stimuli in artifical script and Latin script.** During the lexical decision task, participants were presented with blocks of words and pseudowords which were written either in artificial script or in Latin script. During each block, four stimuli were presented for 7 seconds each and participants were instructed to perform a button press to indicate whether a stimulus was a word or a pseudoword. Each block condition was repeated 10 times.

Results: Fluency in reading AS correlated more strongly with attention ($r(60)=0.56$, $p<0.001$) and working memory ($r(60)=0.38$, $p=0.003$) measures than LS reading fluency (attention: $r(60)=0.26$, $p=0.04$; difference: $z(60)=1.90$, $p=0.03$; working memory: $r(60)=0.10$, $p=0.46$; difference: $z(60)=1.63$, $p=0.05$), but AS and LS reading fluency were not correlated ($r(60)=0.04$, $p=0.77$). When comparing AS to LS reading during the lexical decision task, we observed activation (FWE-corrected $p<0.05$) in the multiple demand (MDN) network[3], the middle occipital gyrus, thalamus, ventral tegmental area (VTA), and in key regions of the RN such as the lexical and perceptual visual word form area[4] (VWFA; Figure 2A). Activation in the whole MDN was not correlated with attention ($r(60)=0.14$, $p=0.28$) or working memory ($r(60)=0.12$, $p=0.36$), while VWFA activity was associated with working memory (lexical VWFA: $r(60)=0.28$, $p=0.03$; perceptual VWFA: $r(60)=0.24$, $p=0.07$), but not with attention (lexical VWFA: $r(60)=0.177$, $p=0.17$; perceptual VWFA: $r(60)=0.11$, $p=0.39$). BOLD time courses of the MDN and VWFA showed rapid increases and decreases in activation during each LS stimulus presentation, but sustained activation throughout the entire AS condition (Figure 2B). Other key regions of the RN, such as the superior temporal gyrus (STG) and inferior frontal gyrus (IFG), demonstrated stimulus-driven increases and decreases for both AS and LS stimuli, while activation in non-reading-related brain regions such as the VTA appeared to not be driven by individual stimuli.

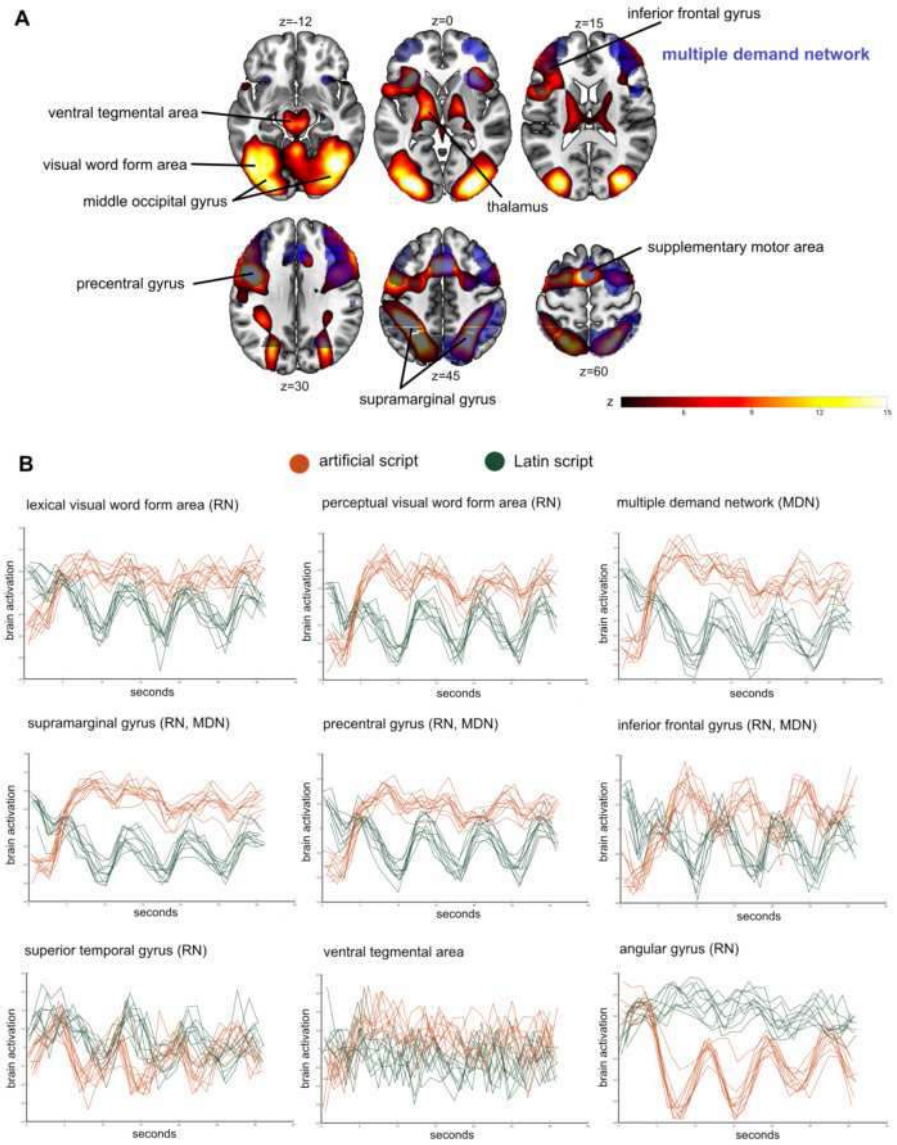

Figure 2. A. Brain activation during artifical script reading as compared to Latin script reading. We observed activation across large parts of the multiple demand network (MDN), the middle occipital gyrus and visual word form area, as well as the ventral tegmental area and thalamus. **B. Time courses during artifical script reading and Latin script reading.** Each line reflects brain signals averaged over all participants for one of 10 blocks per condition. Brain regions that are considered key areas of the reading network are marked with 'RN', brain regions that are considered key areas of the multiple demand network are marked with 'MDN'.

Conclusions: Our results show the influence of attention and working memory on reading performance in a recently learned script compared to a well-known script. This is consistent with the more pronounced activation of the MDN network during AS compared to LS processing, demonstrating the increase in cognitive effort during novel script reading. Subsequent time course analyses of AS and LS processing unveiled a pronounced difference in the dynamics of the BOLD response within key brain regions of the RN. While most brain regions demonstrated increased sustained activation during AS but not during LS reading, this was not the case for the STG, IFG, and angular gyrus. Further, our findings demonstrate that several brain regions not only exhibited distinct activation intensity but also a shift in the timing of peak activation between AS and LS reading, emphasizing the importance of considering temporal dynamics in neural processing when investigating lexical stimuli of different familiarity.

References

1. Kearns, D. M., Hancock, R., Hoeft, F., Pugh, K. R., & Frost, S. J. (2019). The neurobiology of dyslexia. Teaching Exceptional Children, 51(3), 175-188.
2. Turkeltaub, P. E., Gareau, L., Flowers, D. L., Zeffiro, T. A., & Eden, G. F. (2003). Development of neural mechanisms for reading. Nature neuroscience, 6(7), 767-773.
3. Duncan, J. (2010). The multiple-demand (MD) system of the primate brain: mental programs for intelligent behaviour. Trends in cognitive sciences, 14(4), 172-179.
4. Lerma-Usabiaga, G., Carreiras, M., & Paz-Alonso, P. M. (2018). Converging evidence for functional and structural segregation within the left ventral occipitotemporal cortex in reading. Proceedings of the National Academy of Sciences, 115(42), E9981-E9990.

Poster No 1034

Meta-Analytic Connectivity Modelling of Neural Networks for Reading and Math in Children

Chiao-Yi Wu[1], Xiaowen Lin[2], SH Annabel Chen[2,3,4]

[1]National Institute of Education, Nanyang Technological University, Singapore, Singapore, [2]Psychology, School of Social Sciences, Nanyang Technological University, Singapore, Singapore, [3]Centre for Research and Development in Learning, Nanyang Technological University, Singapore, Singapore, [4]Lee Kong Chian School of Medicine, Nanyang Technological University, Singapore, Singapore

Introduction: Literacy and numeracy are fundamental skills for the attainment of academic competence in school. Previous studies have suggested that reading and math involve both domain-specific and domain-general neurocognitive mechanisms (Ashkenazi et al., 2013). Executive function (EF) has been shown to be a domain-general ability that supports reading and math processing. While EF ability has been associated with literacy and numeracy (Willcutt et al., 2013), how it supports reading and math processing at the neurobiological level remains to be elucidated. In the current study, we performed coordinate-based activation likelihood estimation (ALE) meta-analysis and meta-analytic connectivity modelling (MACM) to examine functional connectivity between the domain-general and domain-specific networks between reading and math.

Methods: We followed the PRISMA framework (Page et al., 2021) to search for fMRI studies on reading and math in 5 databases. All selected studies (reading: 39 contrasts, 364 foci; math: 38 contrasts, 371 foci) involved typically developing children aged ≤ 13-year-old and reported MNI or Talairach coordinates from whole-brain analyses (Wu et al., 2021). The analysis procedures are summarized in Fig. 1. A conjunction and contrast ALE meta-analysis was conducted in GingerALE (v3.0.2; Eickhoff et al. 2009) to identify domain-general (reading ∩ math) and domain-specific (reading > math and math > reading) areas. Region-of-interest (ROI) masks were created as 6mm-spheres around the peak coordinates of the significant domain-general and domain-specific clusters, which were used as seeds for subsequent MACM analyses (Eickhoff et al., 2011). Searches with each ROI mask were performed in Sleuth (v3.0.4), and the outputs were submitted to single-dataset analyses in GingerALE. For network modelling (Meier et al., 2021), mean ALE values from all ROIs were extracted from the MACM result for each seed in Mango. The p values representing covariance statistics were checked for significance with Bonferroni correction. Functional decoding was analyzed on the domain-general ROIs using the behavioral and paradigm analysis plug-ins in Mango (Lancaster et al., 2012).

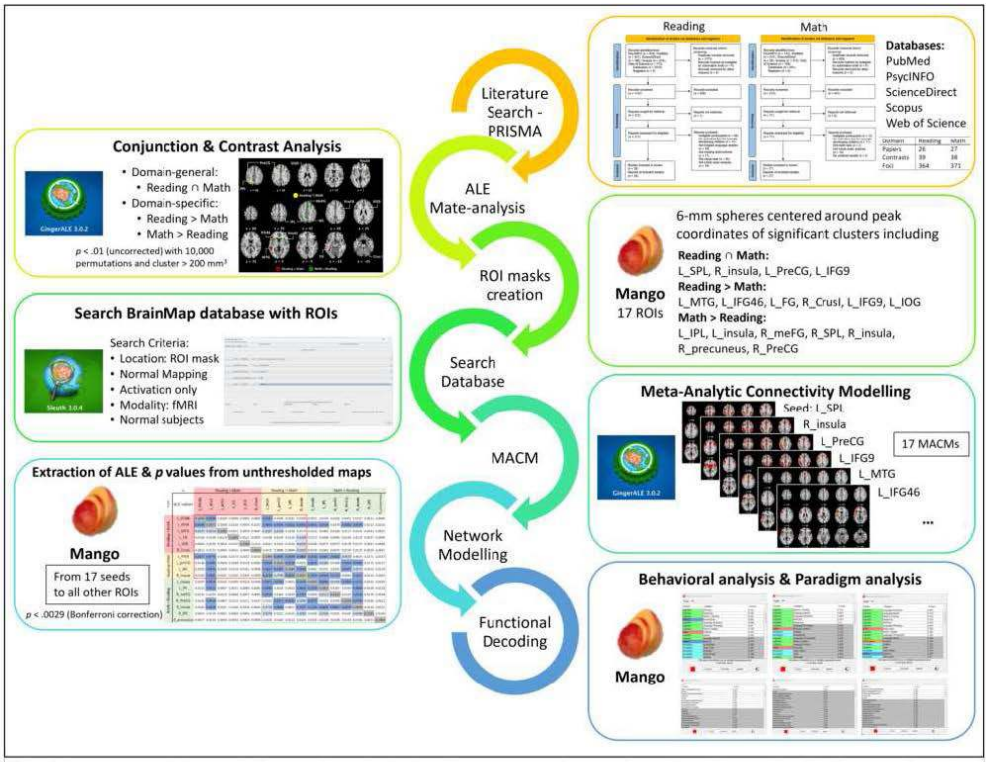

Fig. 1. A summary of the analysis procedures including literature search, coordinate-based activation likelihood estimation (ALE) meta-analysis, meta-analytic connectivity modelling (MACM), network modelling, and functional decoding.

Results: The conjunction analysis and the contrast analyses of reading > math and math > reading yielded 4, 6 and 7 clusters, respectively (Fig. 2A). Hence, MACM analyses were performed with 17 seed ROIs. The conjunction of reading ∩ math identified

4 areas which were associated with working memory domain and EF paradigms as revealed by functional decoding analysis ($z \geq 3$). Network modelling matrix showed that they were highly connected bidirectionally (Fig. 2B). Within the reading network, functional connectivity was found (1) from the reading-specific left middle temporal gyrus to the inferior frontal gyrus (IFG), (2) from reading-specific areas to domain-general areas, and (3) bidirectionally between the reading-specific left IFG (BA 9) and domain-general areas. For the math network, functional connectivity was found (1) bidirectionally between bilateral insulae and math-specific areas in the frontal and parietal lobes, (2) bidirectionally between math-specific and domain-general areas and (3) among math-specific areas.

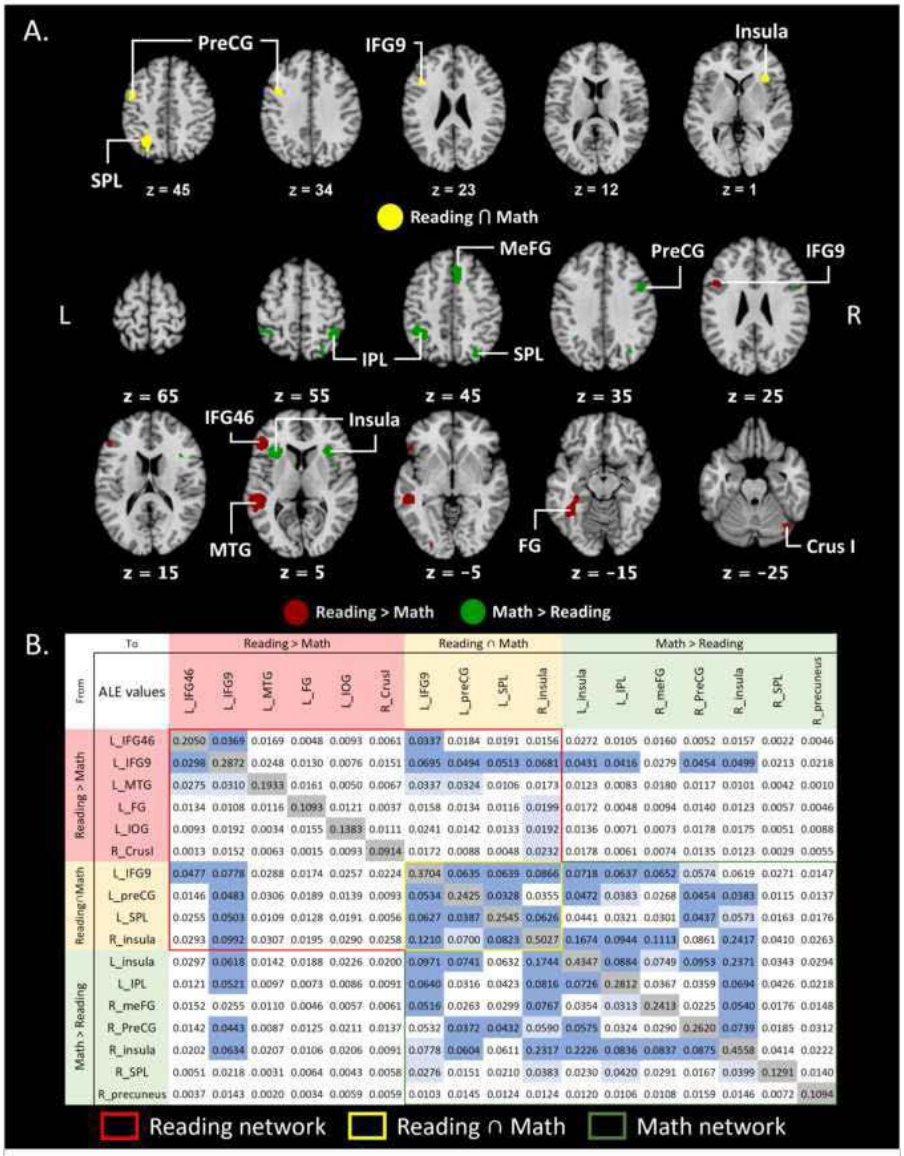

Fig. 2. (A) ALE results of the conjunction Reading ∩ Math (yellow), contrast of Reading > Math (red), and Math > Reading (green) overlaid onto the Colin27 T1 template, thresholded at $p < .01$ (uncorrected) with 10,000 permutations and cluster > 200 mm^3. (B) MACM matrix summarizing the connectivity in ALE values from seed regions (left column) to all ROIs. Significant connectivity ($p < .05/17 = .0029$, with Bonferroni correction) are highlighted in dark blue (bidirectional) and light blue (unidirectional). L: left; R: right; IFG46/9: inferior frontal gyrus (BA 46/9); MTG: middle temporal gyrus; FG: fusiform gyrus; IOG: inferior occipital gyrus; CrusI: cerebellar Crus I; preCG: precentral gyrus; IPL/SPL: inferior/superior parietal lobule; meFG: medial frontal gyrus.

Conclusions: This is the first study to examine functional connectivity in the domain-general and domain-specific networks between reading and math using a meta-analytic approach. The domain-general areas resembled the lateral frontoparietal network and the salience network (Uddin et al. 2019), which was behaviorally associated with working memory and functionally connected with reading- and math-specific areas. While the left IFG was the main hub connecting reading areas with domain-general areas in the reading network, highly bidirectional communications between math areas and domain-general areas were observed in the math network. Our results identified nodes and networks for future investigations on brain-behavior relationships to elucidate individual differences in reading and math skills.

References

1. Ashkenazi, S., (2013), 'Neurobiological Underpinnings of Math and Reading Learning Disabilities', Journal of Learning Disabilities, vol. 46, no. 6, pp. 549-569.
2. Eickhoff, S. B., (2009), 'Coordinate-based activation likelihood estimation meta-analysis of neuroimaging data: A random-effects approach based on empirical estimates of spatial uncertainty', Human Brain Mapping, vol. 30, no. 9, pp. 2907-2926.
3. Eickhoff, S. B., (2011), 'Co-activation patterns distinguish cortical modules, their connectivity and functional differentiation', Neuroimage, vol. 57, no. 3, pp. 938-949.
4. Lancaster, J., (2012), 'Automated regional behavioral analysis for human brain images', Frontiers in Neuroinformatics, vol. 6.
5. Meier, S. K., (2021), 'Meta-analytic connectivity modelling of deception-related brain regions', PLoS ONE, vol. 16, no. 8, pp. e0248909.
6. Page, M. J., (2021), 'The PRISMA 2020 statement: an updated guideline for reporting systematic reviews', BMJ, vol. 372, pp. n71.
7. Uddin, L. Q., (2019), 'Towards a Universal Taxonomy of Macro-scale Functional Human Brain Networks,' Brain Topography, vol. 32, no. 6, pp. 926-942.
8. Willcutt, E. G., (2013), 'Comorbidity Between Reading Disability and Math Disability: Concurrent Psychopathology, Functional Impairment, and Neuropsychological Functioning', Journal of Learning Disabilities, vol. 46, no. 6, pp. 500-516.
9. Wu, C.-Y., (2021), 'Meta-Analysis of Neural Networks for Reading, Math, and Working Memory in School-Age Children', poster presented at The 27th Annual Meeting of the Organization for Human Brain Mapping.

Poster No 1035

Cerebro-cerebellar Functional Connectivity in Reading Networks in Bilinguals

Wei Ting Serena Chua[1], Chiao-Yi Wu[2], Beth O'Brien[2], Hsin-Yu Lin[1], Brenda Rapp[3], John Desmond[4], Kenichi Oishi[5], SH Annabel Chen[1,6,7]

[1]Centre for Research and Development in Learning, Nanyang Technological University, Singapore, Singapore, [2]National Institute of Education, Nanyang Technological University, Singapore, Singapore, [3]Department of Cognitive Science, Johns Hopkins University, Baltimore, MD, USA, [4]Department of Neurology, Johns Hopkins University, Baltimore, MD, USA, [5]Department of Radiology and Radiological Science, Johns Hopkins University, Baltimore, MD, USA, [6]Psychology, School of Social Sciences, Nanyang Technological University, Singapore, Singapore, [7]Lee Kong Chian School of Medicine, Nanyang Technological University, Singapore, Singapore

Introduction: In accordance with the Dual-Route Model of Reading, neuroimaging studies on the cerebral cortex have proposed that the sub-lexical route (mapping of letters to corresponding sounds) involves dorsal regions, while the lexical route (the retrieval of corresponding phonological forms for the whole written forms) implicates ventral regions (Coltheart et al., 2001; Jobard et al., 2003). Accumulating evidence further suggests the involvement of right cerebellar regions in reading, during phonological and semantic processing (D'Mello et al., 2020; Li et al., 2020). The differential involvement of cerebro-cerebellar connections in phonological and semantic processes in reading has been elucidated by a meta-analysis (Alvarez & Fiez, 2018). In view of some studies finding little support for the cerebro-cerebellar involvement in reading (Ashburn et al., 2020), we aimed to investigate the functional connectivity of the cerebro-cerebellar network in reading and delineate the involvement of cerebellar regions in the sub-lexical route (Fig 1a) and the lexical route (Fig 1b).

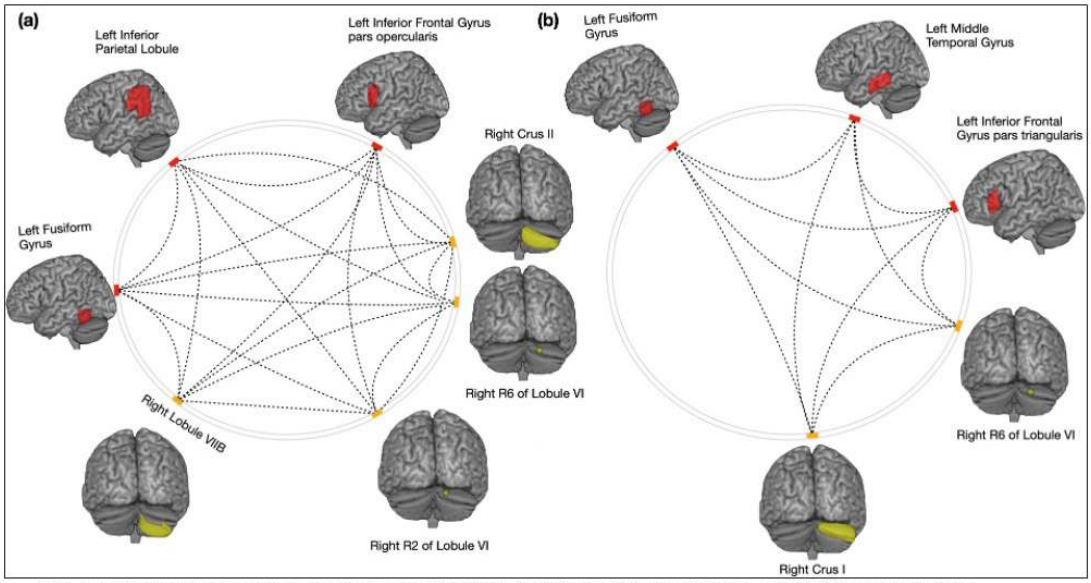

Fig. 1. Hypothesised cerebro-cerebellar connections in: **(a)** the sub-lexical route, and **(b)** the lexical route.

Methods: In an event-related fMRI paradigm, 32 Chinese-English and 33 Tamil-English adult bilinguals silently read words, pseudowords, and nonwords in a 3 Tesla MRI scanner. Following preprocessing, a generalised Psychophysiological Interaction approach (gPPI) was adopted at first-level analysis in CONN 21a (Whitfield-Gabrieli & Nieto-Castanon, 2012). Fisher-transformed r-to-z correlation values were extracted from each condition in their respective languages for each pairing hypothesised in the sub-lexical route and the lexical route. These values were entered in linear mixed effects models within each bilingual group with language type and word type as variables of interest, and language use (entropy for social contexts and modalities respectively; Gullifer & Titone, 2020) and reading proficiencies as covariates.

Results: For the sub-lexical route, greater functional connectivity between the left fusiform gyrus (FFG) and the right R6 sub-region of the cerebellar lobule VI was correlated with reading English nonwords compared to reading English words, p=.042 (Fig 2a). Within the Chinese-English bilingual group, higher functional connectivity was found between the left inferior parietal lobule (IPL) and the pars opercularis of left inferior frontal gyrus (IFGope) in association with reading in English, versus reading in Chinese, p=.0005 (Fig 2b). Within the Tamil-English bilingual group, higher functional connectivity between the left FFG and right R6 sub-region was correlated with reading Tamil pseudowords as compared to reading Tamil words, p=.0171 (Fig 2c). Reading Tamil nonwords (versus English nonwords) was associated with higher functional connectivity between the right cerebellar lobule VIIB and the right R2 sub-region of the cerebellar lobule VI, p=.0057 (Fig 2d). For the lexical route, null findings were obtained.

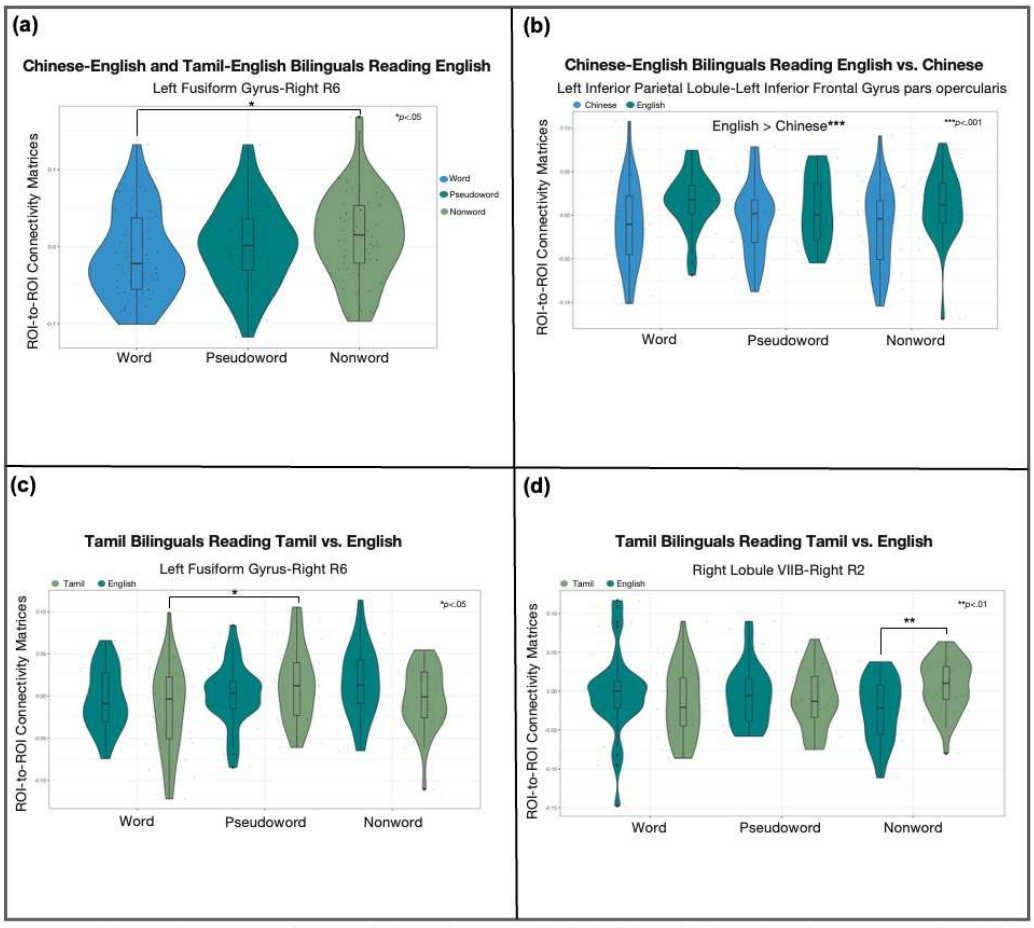

Fig. 2. Violin plots with embedded box plots to depict average Region-of-Interest to Region-of-Interest (ROI-to-ROI) connectivity for **(a)** the Left Fusiform Gyrus-Right R6 Pairing across all participants (English Nonword > English Word, $p < .05$), and **(b)** the Left Inferior Parietal Lobule-Left Inferior Frontal Gyrus pars opercularis within the Chinese-English bilingual group (English > Chinese, $p < .001$), **(c)** the Left Fusiform Gyrus-Right R6 Pairing within the Tamil-English bilingual group (Tamil Pseudoword > Tamil Word, $p < .05$), **(d)** the Right Lobule VIIB-Right R2 Pairing within the Tamil-English bilingual group (Tamil Nonword > English Nonword, $p < .01$).

Conclusions: This study provided supporting evidence for the involvement of cerebro-cerebellar connections in sub-lexical reading processes. The connectivity between left FFG and right R6 may be implicated in the sub-lexical route, whereby the left FFG could be involved in the letter encoding stages (Lochy et al., 2018) while the right R6 sub-region of Lobule VI in higher-level phonological processing. Similarly, the connectivity between the left IPL and left IFGope has been associated with sub-lexical processes such as letter-sound mapping (Junker et al., 2023). The results for the Lobule VIIB-right R2 sub-region pairing could be instead co-activation due to their proximity in location, rather than connectivity. The null findings for the

lexical route could be due to the low task demands in lexico-semantic processing. In sum, the findings underscore the need to clarify the cerebro-cerebellar connections implicated in reading processes to have a more comprehensive understanding of the neural mechanisms of reading.

References
1. Alvarez, T. A. (2018). Current perspectives on the cerebellum and reading development. Neuroscience & Biobehavioral Reviews, 92, 55-66.
2. Ashburn, S. M. (2020). Cerebellar function in children with and without dyslexia during single word processing. Human brain mapping, 41(1), 120-138.
3. Coltheart, M. (2001). DRC: a dual route cascaded model of visual word recognition and reading aloud. Psychological review, 108(1), 204.
4. D'Mello, A. M. (2020). Cerebellar contributions to rapid semantic processing in reading. Brain and language, 208, 104828.
5. Gullifer, J. W. (2020). Characterizing the social diversity of bilingualism using language entropy. Bilingualism: Language and Cognition, 23(2), 283-294.
6. Jobard, G. (2003). Evaluation of the dual route theory of reading: a metanalysis of 35 neuroimaging studies. Neuroimage, 20(2), 693-712.
7. Junker, F. B. (2023). The angular gyrus serves as an interface between the non-lexical reading network and the semantic system: evidence from dynamic causal modeling. Brain Structure and Function, 1-15.
8. Li, H. (2020). Functional parcellation of the right cerebellar lobule VI in children with normal or impaired reading. Neuropsychologia, 148, 107630.
9. Lochy, A. (2018). Selective visual representation of letters and words in the left ventral occipito-temporal cortex with intracerebral recordings. Proceedings of the National Academy of Sciences, 115(32), E7595-E7604.
10. Whitfield-Gabrieli, S. (2012). Conn: a functional connectivity toolbox for correlated and anticorrelated brain networks. Brain connectivity, 2(3), 125-141.

Poster No 1036

The effects of ROBO1 on Interhemispheric Connections in Neurotypical Adolescents and Young Adults

Nea Rinne[1], Patrik Wikman[1], Elisa Sahari[2], Juha Salmi[3], Elisabet Einarsdottir[4], Juha Kere[5], Kimmo Alho[1]

[1]University of Helsinki, Helsinki, Uusimaa, [2]University of Turku, Turku, Varsinais-Suomi, [3]Aalto University, Espoo, Uusimaa, [4]KTH-Royal Institute of Technology, Solna, Södermanland, [5]Karolinska Institutet, Huddinge, Södermanland

Introduction: Corpus callosum (CC) is a white matter (WM) structure in the human brain connecting the two hemispheres. It enables interhemispheric communication facilitating many cognitive functions. Maturation of the posterior CC, which connects areas critical in linguistic processing, may be related to the development of reading skills. Notably, the dyslexia susceptibility gene ROBO1 plays a role in axonal crossing between the hemispheres, suggesting that reduced hemispheric lateralisation in dyslexia might be due to genetic variation. The preregistered aim of this study was to determine, whether genetic variation in ROBO1 explains variation in the interhemispheric WM tracts. We conducted tractography for the middle posterior, posterior, and whole CC and studied whether five single nucleotide variations (SNVs) in ROBO1 explain differences in the number of CC streamlines.

Methods: The participants (n = 177) were healthy 13-to-25-year-olds with normal reading skills. Diffusion weighed images consisting of 70 slices were acquired using 64 diffusion gradients, with 3T MAGNETOM Skyra whole-body scanner in the Advanced Magnetic Imaging centre at the Aalto University. Diffusion tensor images (DTI) were analysed with the Explore DTI software (Leemans et al. 2019). Tractography through middle posterior, posterior and the whole CC was conducted based on FreeSurfer (http://surfer.nmr.mgh.harvard.edu/) parcellation. The number of WM tracts delineated from the middle posterior and posterior CC were normalised against the number of tracts derived from the whole CC tractography. The genotyping of five SNVs from ROBO1 (rs6770755, rs7651370, rs7631357, rs7637338, rs9853895) was performed at a certified core facility at Karolinska University Hospital, using the Agenda iPLEX platform. Mixed ANOVAs were employed to assess the relationship between the SNVs and the number of WM tracts.

Results: Two ROBO1 SNVs were significantly associated with the number of CC tracts: Variation rs7637338 was associated with the number of tracts in the whole CC ($F(1,172) = 6.49$, $p = 0.012$, $\eta 2 = 0.036$), whereas variation in rs7631357 was associated with the number of tracts in the posterior CC ($F(2,170) = 3.79$, $p = 0.025$, $\eta 2 = 0.043$).

Conclusions: The present results provide further evidence that the dyslexia susceptibility gene ROBO1 is important for the development of interhemispheric WM tracts. Our results suggest that the reduced hemispheric lateralization in developmental dyslexia may be attributed to genetic factors.

References
1. Leemans, A.J. (2019) 'ExploreDTI: a graphical toolbox for processing, analyzing, and visualizing diffusion MR data.', Proceedings of the International Society for Magnetic Resonance in Medicine, vol. 17, no. 1, pp. 3537

Organization for Human Brain Mapping

Advancing Understanding of the Human Brain

ORGANIZATION FOR HUMAN BRAIN MAPPING

www.humanbrainmapping.org

1935 County Road B2 W, Ste 165
Roseville, MN 55113
info@humanbrainmapping.org
952-641-2294